TRANSACTIONS
American Society for Metals
VOL. XLI 1949

TECHNICAL PROGRAM AND REPORTS OF OFFICERS AMERICAN SOCIETY FOR METALS — 30th ANNUAL CONVENTION, PHILADELPHIA, OCTOBER 23 to 29, 1948

FOR purposes of record and for the benefit of members who were not in attendance at the Thirtieth Annual Convention of the Society, held in Philadelphia, October 23 to 29, 1948, the Programs of the Technical Papers and Educational Lectures together with the Reports of Officers for 1948 are herewith published in full.

TECHNICAL PAPERS PROGRAM
Seminar on the Cold Working of Metals

SATURDAY, OCTOBER 23

Ballroom, Benjamin Franklin Hotel—9:30 A.M.
Chairman—M. Gensamer, Carnegie-Illinois Steel Corp.

Introduction, by M. Gensamer, Carnegie-Illinois Steel Corp.

Strain Hardening, Effects of Alloying Elements and Microstructure, by G. V. Smith, U. S. Steel Corp. Research Laboratories.

Residual Stresses (Macroscopic), by W. M. Baldwin, Jr., Case Institute of Technology.

Slip Lines and Slip Bands (Visual Effects of Cold Working), by R. D. Heidenreich, Bell Telephone Laboratories.

Ballroom, Benjamin Franklin Hotel—2:00 P.M.

Translation, Twinning and Banding (Crystallographic Mechanism), by C. S. Barrett, Institute for the Study of Metals, University of Chicago.

Deformation Textures, by R. M. Brick, University of Pennsylvania.

Recrystallization Textures, by C. G. Dunn, General Electric Co.

Ballroom, Benjamin Franklin Hotel—8:00 P.M.

Dislocation Theory, by W. Schockley, Bell Telephone Laboratories.

Nucleation Theory, by J. H. Hollomon, General Electric Co.

Effects of Mechanical-Thermal History on the Flow Stress, by J. E. Dorn, University of Michigan.

SUNDAY, OCTOBER 24

Ballroom, Benjamin Franklin Hotel—9:30 A.M.

Dynamics of Slip Bands, by C. Zener, Institute for the Study of Metals, University of Chicago.

Plastic After-Effects, by J. G. Leschen, General Electric Co.

Workhardening Under Combined Stresses, by L. R. Jackson, Battelle Memorial Institute.

Ballroom, Benjamin Franklin Hotel—2:00 P.M.

Creep, by J. D. Lubahn, General Electric Co.

Fatigue, by A. M. Freudenthal, University of Illinois.

Reactions in the Solid State, by B. L. Averbach, Massachusetts Institute of Technology.

MONDAY, OCTOBER 25

Heat Treatment Session

Ballroom, Benjamin Franklin Hotel—9:30 A.M.

Joint Chairmen—E. S. Davenport, United States Steel Corp., and R. F. Mehl, Carnegie Institute of Technology.

The Isothermal Decomposition of Martensite and Retained Austenite, by B. L. Averbach, Assistant Professor of Metallurgy, and Morris Cohen, Professor of Physical Metallurgy, Massachusetts Institute of Technology.

The Dimensional Stability of Steel—Part IV—Tool Steels, by B. S. Lement, Member of Staff, Department of Metallurgy, B. L. Averbach, Assistant Professor of Metallurgy, and Morris Cohen, Professor of Physical Metallurgy, Massachuseets Institute of Technology.

The Transformation and Retention of Austenite in SAE 5140, 2340 and T1340 Steels of Comparable Hardenability, by A. R. Troiano, Professor of Metallurgy, University of Notre Dame.

The Microstructure of Low Carbon Steel, by R. L. Rickett, Assistant Supervisor, Physical Metallurgy Section, and F. C. Kristufek, Research Laboratories, United States Steel Corp.

Heat Treatment Session

Ballroom, Convention Hall—2:00 P.M.

Joint Chairmen—R. A. Grange, United States Steel Corp., and Peter Payson, Crucible Steel Company of America.

Influence of Ni and Mo on Isothermal Transformation of Austenite in Pure Fe-Ni and Fe-Ni-Mo Alloys Containing 0.55% Carbon, by D. A. Scott, Instructor in Physical Metallurgy, W. M. Armstrong, Associate Professor of Physical Metallurgy, and F. A. Forward, Professor and Head, Department of Mining and Metallurgy, The University of British Columbia.

The Transformation Characteristics of Ten Selected Nickel Steels, by J. P. Sheehan, Associate Metallurgist, Armour Research Foundation, C. A. Julien, Patent Adviser, Naval Research Laboratory, and A. R. Troiano, Professor of Metallurgy, University of Notre Dame.

The Metallography and Heat Treatment of 8 to 10% Nickel Steel, by G. R. Brophy, Metallurgist in Charge of Steel Research, and A. J. Miller, Metallurgist, International Nickel Co.

Predicting the Effect of Complex Tempering Cycles, by J. L. Waisman, Metallurgist, Douglas Aircraft Co., and W. T. Snyder, Chief Engineer, Herff Jones Co.

TUESDAY, OCTOBER 26

Steel Ingots Session

Ballroom, Benjamin Franklin Hotel—9:30 A.M.

Joint Chairmen—J. H. Hollomon, General Electric Co., and E. C. Smith, Republic Steel Corp.

Distributions of Nonmetallic Inclusions in Some Killed Alloy Steel Ingots, by K. L. Fetters, Special Metallurgical Engineer, Youngstown Sheet and Tube Co., M. M. Helzel, Analytical Chemist, and J. W. Spretnak, Member of Staff, Metals Research Laboratory, Carnegie Institute of Technology.

Some Factors Affecting Subsurface Defects in Large Forging Steel Ingots, by E. A. Loria, Fellow, Mellon Institute of Industrial Research, and H. D. Shephard, Metallurgical Engineer, Kerchner, Marshall & Co.

Density Variations in Some Killed Steel Ingots, by C. F. Sawyer, Plant Metallurgist, Vanadium-Alloys Steel Co., and J. W. Spretnak, Member of Staff, Metals Research Laboratory, Carnegie Institute of Technology.

The Nature of Inclusions in Tensile Fractures of Forging Steels, by H. D. Shephard, Metallurgical Engineer, Kerchner, Marshall & Co., and E. A. Loria, Fellow, Mellon Institute of Industrial Research.

Nonferrous Alloys Session

Betsy Ross Room, Benjamin Franklin Hotel—9:30 A.M.

Joint Chairmen—E. H. Dix, Jr., Aluminum Company of America, and J. C. McDonald, Dow Chemical Co.

Fractographic Examination of Tungsten, by C. A. Zapffe and F. K. Landgraf, Consultants, Baltimore.

The Effect of Orientation on Knoop Hardness of Single Crystals of Zinc and Silicon Ferrite, by F. W. Daniels, Metals Section Laboratory, and C. G. Dunn, Research Physicist, General Electric Co.

The Effect of Single Addition Metals on the Recrystallization, Electrical Conductivity and Rupture Strength of Pure Aluminum, by R. H. Harrington, Research Metallurgist, General Electric Co.

Forming and Heat Treatment of Corrugated Diaphragms, by R. I. Jaffee, E. I. Beidler and R. H. Ramsey, Battelle Memorial Institute.

Mechanical Properties Session

Ballroom, Convention Hall—2:00 P.M.

Joint Chairmen—A. E. Focke, Diamond Chain Co., Inc., and V. H. Patterson, American Brake Shoe Co.

The Microstructure and Mechanical Properties of Cast Steels, by M. F. Hawkes, Assistant Professor of Metallurgical Engineering and Member of Staff, Metals Research Laboratory, and B. F. Brown, Graduate Student, Carnegie Institute of Technology.

Effect of Vanadium on the Properties of Cast Carbon and Carbon-Molybdenum Steels, by N. A. Ziegler, Research Metallurgist, W. L. Meinhart, Assistant Research Metallurgist, and J. R. Goldsmith, Metallurgical Engineer in Charge of Research Foundry, Crane Co.

Mechanical Properties, Including Fatigue, of Aircraft Alloys at Very Low Temperatures, by J. L. Zambrow, Research Engineer, and M. G. Fontana, Professor and Chairman, Department of Metallurgy, Ohio State University.

Influence of Low Temperatures on the Mechanical Properties of 18-8 Chromium-Nickel Steel, by D. J. McAdam, Jr., Metallurgist, G. W. Geil, Metallurgist, and Frances Jane Cromwell, Metallurgist, National Bureau of Standards.

WEDNESDAY, OCTOBER 27

ASM Annual Meeting

Ballroom, Benjamin Franklin Hotel—10:00 A.M.

Edward deMille Campbell Memorial Lecture, by Morris Cohen, Professor of Physical Metallurgy, Massachusetts Institute of Technology.

James P. Gill, Chairman

Engineering Properties Session

Ballroom, Convention Hall—2:00 P.M.

Joint Chairmen—A. L. Boegehold, General Motors Corp., and A. O. Schaefer, The Midvale Co.

Basic Reasons for Good Machinability of "Free Machining" Steels, by M. Eugene Merchant, Physicist, and N. Zlatin, Research Engineer, The Cincinnati Milling Machine Co.

An End-Quenched Bar for Deep Hardening Steels, by Gerrit deVries, Metallurgist, U. S. Naval Proving Ground.

Transverse Mechanical Properties in Heat Treated Wrought Steel Products, by Cyril Wells, Metals Research Laboratory, and R. F. Mehl, Director, Metals Research Laboratory, Carnegie Institute of Technology.

Residual Stresses and Microstructure in Hollow Cylinders, by H. B. Wishart, Chief Development Metallurgist, and R. K. Potter, Metallurgical Inspector, Carnegie-Illinois Steel Corp.

THURSDAY, OCTOBER 28

Stainless Steels Session

Ballroom, Convention Hall—9:30 A.M.

Joint Chairmen—C. L. Clark, Timken Roller Bearing Co., and V. N. Krivobok, International Nickel Co.

Resistance to Sensitization of Austenitic Chromium-Nickel Steels of 0.03% Max. Carbon Content, by W. O. Binder, Metallurgist, and C. M. Brown, Metallurgist, Union Carbide and Carbon Research Laboratories, and Russell Franks, Chief Metallurgist, Electro Metallurgical Co.

Mechanism of the Rapid Oxidation of High Temperature, High Strength Alloys Containing Molybdenum, by W. C. Leslie, Research Fellow, and M. G. Fontana, Professor and Chairman, Department of Metallurgy, Ohio State University.

Stabilization of Austenitic Stainless Steel, by Samuel J. Rosenberg, Senior Metallurgist, and John H. Darr, Scientific Aid, National Bureau of Standards.

Delta Ferrite Formation and Its Influence on the Formation of Sigma in a Wrought Heat Resisting Steel, by John J. Gilman, Instructor in Metallurgical Engineering, Illinois Institute of Technology, Pun Kien Koh, Research Metallurgist, Allegheny Ludlum Steel Corp., and Otto Zmeskal, Director, Department of Metallurgical Engineering, Illinois Institute of Technology.

Nonferrous Alloys Session

Room 300, Convention Hall—9:30 A.M.

Joint Chairmen—W. M. Baldwin, Jr., Case Institute of Technology, and F. N. Rhines, Carnegie Institute of Technology.

The Indium-Bismuth Phase Diagram, by E. A. Peretti, Associate Professor of Metallurgy, and S. C. Carapella, Jr., Teaching Fellow, Department of Metallurgy, University of Notre Dame.

Manganese-Zinc Phase Diagram from 0 to 50% Zinc, by E. V. Potter, Electronics Engineer, U. S. Navy Electronics Lab., and R. W. Huber, Bureau of Mines, U. S. Dept. of Interior.

Dilatometric Effects of Hardening and Recrystallization in the 60 Copper–20 Nickel–20 Manganese Alloy, by C. H. Samans, Chief, Metallurgical Section, Research Laboratory, C. C. Brayton, Technical Assistant, H. L. Drake, Technical Assistant, and L. Litchfield, Technical Assistant, American Optical Co.

Beta Laminations in Cartridge Brass, by Ralph L. Dowdell, Head, Department of Metallurgy, University of Minnesota, Charles A. Nagler, Associate Professor, Physical Metallurgy, Wayne University, Morris E. Fine, Member Technical Staff, Bell Telephone Labs., Harold P. Klug, Head, Department of Research in Chemical Physics, Mellon Institute of Industrial Research, and Gust Bitsianes, Instructor in Metallurgy, University of Minnesota.

High Temperature Alloys Session

Ballroom, Convention Hall—2:00 P.M.

Joint Chairmen—H. C. Cross, Battelle Memorial Institute, and J. J. Kanter, Crane Co.

Aging in Gas Turbine-Type Alloys, by Nicholas J. Grant, Associate Professor of Metallurgy, and J. R. Lane, Research Assistant, Massachusetts Institute of Technology.

Nickel-Base Alloys for High Temperature Applications, by A. G. Guy, Associate Professor of Mechanical Engineering, North Carolina State College.

Short-Time High Temperature Deformation Characteristics of Several Sheet Alloys, by James Miller and Glen Guarnieri, Research Metallurgist, Cornell Aeronautical Laboratory.

Stability of Steels at Elevated Temperatures, by A. B. Wilder, Chief Metallurgist, National Tube Co., and J. O. Light, Chief Metallurgist, Lorain Works, National Tube Co.

FRIDAY, OCTOBER 29

Physics of Metals Session

Ballroom, Convention Hall—9:30 A.M.

Joint Chairmen—C. G. Johnson, Worcester Polytechnic Institute, and M. F. Judkins, Firth Sterling Steel Co.

Application of the Theory of Diffusion to the Formation of Alloys in Powder Metallurgy, by Pol Duwez, Associate Professor of Mechanical Engineering and Chief of Materials Section of Jet Propulsion Laboratory, and Charles B. Jordan, Research Engineer, Jet Propulsion Laboratory, California Institute of Technology.

Thermodynamics in the Decarburization of Steel with Mill Scale, by W. A. Pennington, Chief Chemist and Metallurgist, Carrier Corp.

Cause and Cure of Inverse Chill and Hard Spots in Cast Iron, by C. A. Zapffe and R. L. Phebus, Consultants, Baltimore.

Some Wetting Properties of Metal Powders, by Bernard Kopelman, Section Head of Basic Metallurgical Research, and C. C. Gregg, Metallurgical Research and Development Laboratory, Sylvania Electric Products, Inc.

Testing Session

Ballroom, Convention Hall—2:00 P.M.

Joint Chairmen—H. B. Osborn, Jr., Ohio Crankshaft Co., and C. A. Zapffe, Consultant.

A Versatile Vacuum-Fusion Apparatus, by Manley W. Mallett, Research Engineer, Battelle Memorial Institute.

The Abrasion Resistance of Metals, by R. D. Haworth, Jr., Supervisor, Abrasion Research, Armour Research Foundation.

Solder Flow Tester for Tinplate, by J. J. Sperotto, General Research Laboratories, American Can Co.

Nature and Detection of Grinding Burn in Steel, by L. P. Tarasov, Metallurgical Engineer, and C. O. Lundberg, Assistant Metallurgical Engineer, Norton Co.

EDUCATIONAL LECTURES

Properties of Metals in Materials Engineering

MONDAY, OCTOBER 25

Convention Hall—4:15 P.M.

Chairman—C. R. Austin, Meehanite Metal Corp.

Introduction, by R. L. Templin, Assistant Director of Research and Chief Engineer of Tests, Aluminum Company of America.

Fundamental Concepts, by M. Gensamer, Assistant to Director of Research, Carnegie-Illinois Steel Corp.

Convention Hall—8:00 P.M.

Chairman—J. G. Jackson, William Steell Jackson & Son.

Properties of Metals Under Direct or Non-Reversed Loading, by John R. Low, Jr., General Electric Laboratories.

Application of Fatigue Data to the Machine Design, by R. E. Peterson, Manager, Mechanics Dept., Westinghouse Research Laboratories.

TUESDAY, OCTOBER 26

Convention Hall—4:15 P.M.

Chairman—J. F. Kahles, University of Cincinnati.

Determination of the State of Stress (Instrumentation), by W. M. Murray, Professor, Massachusetts Institute of Technology.

Analysis of Stress in Aircraft Engines, by W. T. Bean, Jr., Project Engineer, Continental Aviation Corp.

Convention Hall—7:30 P.M.

Chairman—C. R. Austin, Meehanite Metal Corp.

Testing to Specific Deflections (Buckling), by E. C. Hartmann, Chief, Engineering Design Div., Aluminum Research Laboratory.

Design for Energy Absorption, by Wendell P. Roop, Research Consultant, Structural Research Laboratory, Swarthmore College.

Metallurgy and Magnetism

By J. K. Stanley

Magnetic Department, Westinghouse Electric Corp.

MONDAY, OCTOBER 25

Convention Hall—5:15 P.M.

Chairman—G. R. Fitterer, University of Pittsburgh.

Magnetic Theory and Definitions

Types of Magnetic Material

TUESDAY, OCTOBER 26

Convention Hall—5:15 P.M.

Chairman—G. R. Fitterer, University of Pittsburgh.

Factors Affecting Magnetic Properties

WEDNESDAY, OCTOBER 27

Convention Hall—5:15 P.M.

Chairman—H. B. Knowlton, International Harvester Co.

Magnetic Analysis—A Metallurgical Tool

Grain Control in Industrial Metallurgy

TUESDAY, OCTOBER 26

Convention Hall—8:30 P.M.

Chairman—C. R. Austin, Meehanite Metal Corp.

Fundamentals of Grain Growth and Recrystallization, by J. E. Burke, Institute for the Study of Metals, University of Chicago.

WEDNESDAY, OCTOBER 27

Convention Hall—4:15 P.M.

Chairman—G. M. Cover, Case Institute of Technology.

Recrystallization in Iron and Iron Alloys with Suitable Reference to Practice, by R. L. Kenyon, Associate Director, Research Laboratory, Armco Steel Corp.

Convention Hall—8:00 P.M.

Chairman—H. B. Knowlton, International Harvester Co.

Working and Grain Control in the Copper Base Industry, by H. L. Burghoff, Research Metallurgist, Chase Brass & Copper Co.

THURSDAY, OCTOBER 28

Convention Hall—4:15 P.M.

Chairman—J. F. Kahles, University of Cincinnati.

Grain Control in the Light Metal Industry, by J. T. Hobbs, Metallurgist, Aluminum Research Laboratories.

ANNUAL MEETING OF AMERICAN SOCIETY FOR METALS

Philadelphia, Wednesday, October 27, 1948

The meeting was called to order by President F. B. Foley, who announced that the first order of business was the President's report. He then asked Vice-President H. K. Work to occupy the chair while he read his report. This is published in full beginning on page 9 of this volume of TRANSACTIONS.

VICE-PRESIDENT WORK: You have heard the report of the President. There being no objections, the report will stand approved as read. I now return the chair to the President.

PRESIDENT FOLEY: The next order of business will be the annual report of the treasurer, E. L. Spanagel.

Treasurer Spanagel presented his report which appears in full beginning on page 13.

PRESIDENT FOLEY: You have heard the report of the Treasurer. There being no objections, it will stand as read. The next order of business is the report of the Secretary.

Secretary Eisenman presented his report which appears in full beginning on page 17.

PRESIDENT FOLEY: You have heard the report of the Secretary. There being no objections, it will stand as read.

PRESIDENT FOLEY: I am now pleased to recognize Trustee A. E. Focke, representative of the Board of Trustees on the Constitution and By-Laws Committee. Dr. Focke then gave an explanation of the proposed changes in the constitution of the Society, as follows:

"To conform with the present method of distributing the TRANSACTIONS of the American Society for Metals, a change in the constitution and by-laws of the national Society is proposed. Originally, the TRANSACTIONS was published as a monthly and mailed to all members of the Society in good standing. The paper shortage and rapidly rising publication costs of the war and postwar years have made it expedient to publish the TRANSACTIONS as an annual volume and to send it only to those members who request it.

"However, the constitution of the American Society for Metals requires that the annual reports of the president, the secretary and the treasurer (heretofore published only in the TRANSACTIONS) shall be brought to the attention of *all* members of the Society. The proposed change in the constitution will permit that these reports be

printed in other publications of the Society, which normally go to all members, as well as in the TRANSACTIONS.

"The proposed change in the constitution has been approved by both the Board of Trustees and the Constitution and By-Laws Committee.

"The members of the Constitution and By-Laws Committee are: D. D. Beach, chairman (Georgia Chapter), R. F. Harvey (Rhode Island Chapter), Milo J. Stutzman (Kansas City Chapter), A. S. Jameson (Chicago Chapter), William W. Wight (Hartford Chapter), and Arthur E. Focke, representing the Board of Trustees.

"The wording of the present constitution is shown in the left-hand column below, with the revised wording in the right-hand."

ARTICLE XI

PUBLICATIONS OF THE SOCIETY

Present Constitution	*Proposed Changes*
Publications	**Publications**
Section 1. The Board of Trustees shall publish a journal to be known as TRANSACTIONS which shall be mailed to all members of the Society in good standing or to designated representatives of member firms or corporations. TRANSACTIONS shall be the official paper of the Society. The Board of Trustees may publish and distribute such other publications or literature as it may from time to time determine.	Section 1. The Board of Trustees shall publish TRANSACTIONS and may publish and distribute such other publications and literature as it may from time to time determine. At least one publication of the Society shall be distributed, not less frequently than once each month, to all members of the Society in good standing or to designated representatives of member firms or corporations.
Subscriptions	**Subscriptions**
Section 2. The Board of Trustees may accept subscriptions to TRANSACTIONS and other publications of the Society from persons who are not members of the society and shall fix the prices of such subscriptions.	Section 2. The Board of Trustees may accept subscriptions to publications of the Society from persons who are not members of the Society and shall fix the prices of such subscriptions.
Contents of Official Paper	**Contents of Publications**
Section 3. *Transactions* shall contain the annual report of the president, secretary and treasurer, together with such other scientific articles and such other items of interest and usefulness as shall be approved by the Publications Committee.	Section 3. The publications of the Society shall contain such scientific articles and such other items of interest and usefulness as shall be approved by the Board of Trustees or by such committees as the Board may appoint. The annual reports of the president and the secretary and the treasurer shall be published in the TRANSACTIONS and also in one of the publications of the Society which reaches all members of the Society as referred to in Section 1 above.

DR. FOCKE: I move that the proposed changes in the constitution be adopted.

PRESIDENT FOLEY: There being no discussion to the proposed amendment, the motion is unanimously approved.

The next order of business is the election of officers. (See page 24.)

ANNUAL ADDRESS OF THE PRESIDENT

FRANCIS B. FOLEY, *President*

Thirtieth Annual Meeting, Philadelphia, October 27, 1948

SEVENTY-FIVE years ago in 1873 the first steel bridge to be constructed in the United States was built across the Mississippi River at St. Louis. It is usually referred to as the Eads Bridge after the Captain Eads who was the designing engineer. Some of the bridge members were made of chromium steel melted in crucible pots in this city at the Midvale Steel Works. The contract for steel for this bridge called for 2800 tons. Although the chromium content of the steel was but 0.60 to 0.70%, it marks the first use of alloy steel in engineering construction.

In a paper read before the Iron and Steel Institute in London in 1886, Henri Brustlein states, "I believe that to the United States is due the first introduction of chromium steel for industrial purposes, at any rate when, in 1875 I had commenced my experiments in France with the manufacture of chromium iron and steel, I had read that in the United States chromium steel of considerable strength had already been manufactured."

Thus the use of constructional alloy steels began 75 years ago in this country, an event which your Society celebrates in this year's Metal Congress, appropriately enough in the city of Philadelphia. It is interesting to view the state of the art of steel manufacture in this country at about this time. Prior to 1865 all cast steel was made by the crucible process. The great Civil War had hardly ended in 1865 when the two Martins made the first commercially successful heat of open-hearth steel at the Sireuil Works near Paris under Siemens license and Durfee in the same year working under the Kelley and Mushet patents produced the first Bessemer steel in the

United States at Wyandotte, Michigan, from which the first steel rails rolled in this country were produced.

It was not until 1868, three years after the close of the Civil War, that Cooper, Hewitt & Co. tapped the first heat of open-hearth steel in this country from a 5-ton furnace at Trenton, N. J., a short distance up the Delaware River from here.

By the time the Eads Bridge was built the yearly production of open-hearth steel had attained, in 1874, 7000 tons, an amount which was produced in less than one hour in the steel mills of the United States in 1947.

It wasn't until 1903 that open-hearth steel production exceeded that of Bessemer steel which had been depended upon for tonnage production of steels for railroads, bridges, and other industrial uses.

Extensive use was not made of alloy steels until early in the 1890's when steel navies were being built and there was demand for guns, projectiles and armor. It was then that heat treatment, an essential adjunct of alloy steels, began to be applied to develop the strength and toughness necessary in alloy steels for such service. Excellent physical properties were developed in these steels quite some time before a rational explanation of the phenomena underlying the hardening and tempering processes had been arrived at by authorities who were devoting their time to such studies. The early days of automobile building found ready at hand a fairly well developed metallurgy and heat treatment of the alloy steels upon which it came to depend as that industry developed.

Our Civil War was fought with cast iron and wrought iron. Facilities for producing cast iron were greatly expanded so that a peacetime outlet for the product was keenly sought when the end of hostilities stopped the war demand. The great increase in the use of cast iron trellises and in the use of cast iron for other ornamental purposes, including cast iron animal figures for the adornment of lawns and cast iron hitching posts, during the years following the war attest the lengths to which cast iron merchants were forced to find a market for their product. The war had the other effect, as we have already observed, of quickening our interest in the bessemer and open-hearth methods of producing cast steel.

Skipping lightly over the short Spanish-American War, in which modern war vessels carrying alloy steel armor and guns got their first—however inadequate—trial in battle, we come to the first World War, which provided a tremendous incentive to the

production and heat treatment of alloy steels and steels of all kinds. It was to this widespread interest that we owe the beginning of the present American Society for Metals. It was the urgent need of the men engaged at that time to get together for the exchange of ideas that produced the nucleus which has grown to the present-day membership of over 20,000 with 76 chapters throughout the States and Canada.

It has been stated that more metal has been produced during the past 40 years than during all previous recorded time. This, of course, means that your Society has played an active part, during its 30 years of existence, in that astonishing feat, for it is the United States that has made this astonishing feat possible.

That there was a need for such an organization as ours is amply shown by its phenomenal growth. The past year has seen the addition of the Utah Chapter in Salt Lake City, increasing the ASM family to 76 chapters. Of these chapters it has been the pleasant duty of the President to visit some 40 during the past year, including two large group chapter meetings. In all his visits he found a cordial welcome, and witnessed very active interest in the Society's work and in the educational activities so valuable to the membership.

Not the least, by any means, of the educational activities of the Society is the issuance from time to time of the METALS HANDBOOK. The volume issued during the past year after many delays due to strikes had to be published in a larger leaf size than its predecessors. The material was completely revised and the contents expanded so that the old size was impractical. It is an encyclopaedia of metallurgical information.

Never before has there been so much authoritative metallurgical data placed between two covers. It is not practical here to record individually the names of all who, by serving in the many subcommittees of the HANDBOOK, have made this publication possible. The Society as a whole is deeply indebted to them. Opportunity is taken, however, to record the work of George V. Luerssen, chairman of the HANDBOOK Committee, and of Dr. Taylor Lyman, its editor.

Another contribution by the Society to progress in metallurgical education during the year was the issuance of the brochure "Your Career in the Metallurgical Profession" by the Committee on Education. This booklet, under the authorship of Dr. John W. W.

Sullivan, was written for the guidance of high school and preparatory school students and distributed to the schools throughout the nation.

Last year an innovation in the form of sessions on Saturday and Sunday, immediately preceding the opening of the Metal Congress and Exposition, devoted to the purely scientific appraisal of the behavior of metals in the solid state was tried. The resulting papers and discussions were published by the Society as part of its TRANSACTIONS. The venture proved such a success that it has been repeated this year with very gratifying results. The Society welcomes the opportunity to provide a medium of publication in a separate volume of its TRANSACTIONS of the proceedings of these meetings which have proved of widespread interest.

The dedication in August of the Sauveur Memorial Room at Headquarters was an interesting event of the year. This room serves not only to commemorate the work of Dr. Sauveur, but will remain as an inspiration to those engaged in the profession in which he was engaged so long and so brilliantly. To this end it will be kept alive as a museum and repository for the recording of progress in metallurgical art and science.

It is with deep regret that we record the death during our last meeting of William H. Phillips, a Past President of the Society, and of Prof. Charles Y. Clayton of Rolla, Mo., a former trustee of the Society, in June of this year.

During the last Metal Congress the Past President's Medal was awarded to Dr. Charles H. Herty, Jr. The Howe Medal was awarded to W. A. Pennington. The American Society for Metals Gold Medal award was conferred on Prof. C. H. Mathewson, its Medal for Advancement of Research on Charles R. Hook, and its Sauveur Achievement Award presented to F. P. Zimmerli.

The Board of Trustees held four meetings during the year, on October 24, 1947, April 30, August 20, and October 26, 1948.

May I now close by expressing my appreciation of the fine cooperation and help of the Officers and Board of Trustees of the Society, of its outstanding Secretary, Mr. Eisenman, and of the very warm welcome from the various chapters throughout the country, which it was my pleasure to visit during the year.

TREASURER'S REPORT

E. L. SPANAGEL, *Treasurer*

Your Treasurer takes pleasure in submitting this report covering our Society's fiscal year ended August 31, 1948. From a financial standpoint, this has been a rather unusual year in that the gain in income over expense was at the lowest level since 1940. It should be quite evident, however, that this situation has been occasioned by the completion and distribution of the 1948 METALS HANDBOOK. In that regard there has been a total of $230,000 expended on the publication of the new METALS HANDBOOK over the past four years, and $132,500 of this total was spent within the past fiscal year. As was anticipated, an abnormal expense of this magnitude could only result in a deficit in the normal operating cost of the Society. However, the 1947 National Metal Exposition, held in Chicago, made possible the following statement of total income and expense for the past year.

Income	$914,395.67
Expense	865,238.50
Excess of Income over Expense	$ 49,157.17

Gross income from membership dues amounted to $220,937.31, of which amount $90,519.37 was returned to the Chapters, both all-time high figures, indicating continued growth in our membership.

Income from METAL PROGRESS decreased 11.5% this year as compared to the prior year, whereas the expense of publishing METAL PROGRESS decreased only 3% with the result that the excess over expenses was only 50% of that of last year. In spite of these decreases, however, income from METAL PROGRESS represented about 36% of the total income of the Society and was an important factor in the over-all net gain for the year.

TRANSACTIONS and the METALS REVIEW are, of course, not self-sustaining and cost the Society net sums of approximately $23,400 and $36,100 respectively.

Sales of books published, including *The Review of Metal Literature* book, resulted in an excess of income over expense of approximately $16,000.

A condensed comparative balance sheet which reflects the financial condition of the Society at the close of the 1947 and 1948 fiscal years follows:

ASSETS	August 31, 1948	August 31, 1947	Increase Decrease*
Cash	$ 119,598.07	$ 243,180.55	$123,582.48*
Securities	1,314,907.56	1,213,187.25	101,720.31
Cash surrender value of life insurance	69,411.46	67,579.33	1,832.13
Accounts receivable	60,000.57	63,867.02	3,866.45*
Inventories	97,090.66	68,012.26	29,078.40
Other assets	9,329.14	4,933.17	4,395.97
Real estate	63,939.04	67,220.56	3,281.52*
Office furniture, fixtures, and equipment	58,609.49	39,479.86	19,129.63
Deferred charges	51,162.70	31,368.52	19,794.18
	$1,844,048.69	$1,798,828.52	$ 45,220.17
LIABILITIES, RESERVES, AND SURPLUS			
Accounts payable	$ 43,671.70	$ 47,863.65	$ 4,191.95*
Reserves	153,777.50	135,000.00	18,777.50
Deferred income	175,960.00	194,482.55	18,522.55*
Surplus	1,470,639.49	1,421,482.32	49,157.17
	$1,844,048.69	$1,798,828.52	$ 45,220.17

*Indicates red figures

During the past year new members have been assessed $5.00 in addition to the regular membership dues for the first year to defray partially the cost of the new METALS HANDBOOK. These moneys, amounting to $18,777.50, have been set aside in a special reserve for METALS HANDBOOK which has been established to provide for the cost of printing additional editions and eventual revision of the METALS HANDBOOK. Note also in the above balance statement that the security holdings of the Society were increased by $101,720. This increase is represented by new holdings of $70,000 par value United States Government Bonds and some $31,000 worth of Common Stock holdings in Columbia Gas and Electric Corporation, Cleveland Illuminating Company and American Tobacco Company. These investments were made on recommendation of the ASM fiscal agents, the Cleveland Trust Co., with whom your Finance Committee and Board of Trustees keep in constant touch and thereby maintain a close contact with the investment market.

Distribution of the Society's investment portfolio now is:

	As of August 31, 1948	% of Total
U. S. Government Bonds	$ 835,554	63.9
Canadian Government Bonds	10,000	0.8
Railroad Bonds	16,547	1.3
Public Utility Bonds	31,990	2.4
Industrial Bonds	17,524	1.3
Common Stocks	330,825	25.4
Preferred Stocks	18,694	1.4
Land Trust Certificates	46,382	3.5
	$1,307,516	100.0

As of August 31, 1948, the Society's investments had a market value of approximately $1,356,800. Interest and dividends earned on the above investments amounted to $47,141.58 or 3.6% as compared to $40,064.15 and 3.3% for the previous year.

In addition to the above investment portfolio, the Society's assets include real estate represented by the National Headquarters at $63,939, inventories in books, furniture and equipment totaling $155,700, and cash on deposit amounting to $119,598.

At the end of the 1947-48 fiscal year, the total assets of the Local Chapters amounted to approximately $188,000, an increase of about $9,000 over the previous year. This substantial reserve constitutes a definite guarantee of continued service, activity and progress in the various Local Chapters.

Your Treasurer gratefully acknowledges the splendid cooperation and able assistance given by the members of the Finance Committee, Secretary William H. Eisenman, Assistant Treasurer A. A. Hess, and Mr. A. W. Martèn of the Cleveland Trust Co.

AUDITED BALANCE SHEET

AMERICAN SOCIETY FOR METALS

August 31, 1948

ASSETS			
CASH (includes $4,137.74 of Canadian funds at par)...			$ 119,598.07
SECURITIES (approximate market prices aggregate $1,356,833.12)			
Bonds and stocks—at cost		$1,307,515.97	
Accrued interest.....		7,391.59	1,314,907.56
CASH SURRENDER VALUE OF LIFE INSURANCE			69,411.46
ACCOUNTS RECEIVABLE			
Advertising accounts.....	$22,886.44		
National Metal Exposition, Philadelphia—October, 1948.....	22,801.25		
Miscellaneous.....	16,312.88	$ 62,000.57	
Less reserve.....		2,000.00	60,000.57
INVENTORIES—at cost or lower			
Bound and unbound publications, books, paper stock, etc.		$103,090.66	
Less reserve.....		6,000.00	97,090.66
OTHER ASSETS			
Officers, employees, and sundry accounts and deposits.			9,329.14
REAL ESTATE (at cost less reserves for depreciation)..			63,939.04
OFFICE FURNITURE, FIXTURES, AND EQUIPMENT (at cost less reserves for depreciation).....			58,609.49
DEFERRED CHARGES			
Prepaid exposition expenses.....		$ 38,402.55	
Prepaid publication and sundry expenses.....		10,482.89	
Prepaid insurance.....		2,277.26	51,162.70
			$1,844,048.69

LIABILITIES, RESERVES, AND SURPLUS

ACCOUNTS PAYABLE		
For purchases, expenses, etc.	$ 39,135.48	
For apportionment of dues to local chapters	3,065.62	
Withholding tax	1,470.60	$ 43,671.70
RESERVES		
For conventions	$ 60,000.00	
For dues paid in advance	50,000.00	
For METALS HANDBOOK	18,777.50	
Campbell Memorial lecture fund	15,000.00	
H. M. Howe medal fund	5,000.00	
Sauveur achievement award	5,000.00	153,777.50
DEFERRED INCOME		
National Metal Exposition—Philadelphia—October, 1948		175,960.00
SURPLUS		
Balance at September 1, 1947	$1,421,482.32	
Add net income for the year	49,157.17	1,470,639.49
		$1,844,048.69

AUDITED INCOME AND EXPENSE STATEMENT

AMERICAN SOCIETY FOR METALS

Year Ended August 31, 1948

INCOME		
METAL PROGRESS—monthly publication		$ 334,345.01
Metal Exposition		227,182.22
Memberships		130,827.44
ASM METALS HANDBOOK		66,588.90
The METALS REVIEW—monthly publication		18,328.81
TRANSACTIONS		9,522.31
Books published (includes sales of *The Review of Metal Literature* Book amounting to $14,634.50)		61,697.19
Interest and dividends earned		47,141.58
General reprints and index		7,100.85
Discount earned		6,894.93
Sundry sales, etc.		2,429.69
Increment in cash value and dividends on life insurance		1,832.13
Books purchased for resale		426.92
Profit on sale of securities		77.69
TOTAL INCOME		$ 914,395.67
EXPENSES		
METAL PROGRESS—monthly publication	$ 301,793.21	
ASM METALS HANDBOOK	154,706.25	
National Metal Exposition—Chicago—October, 1947	136,371.80	
The METALS REVIEW—monthly publication	54,461.58	
Books published	45,756.92	
Memberships	35,645.80	
TRANSACTIONS	32,920.84	
General expenses	28,971.41	
Secretary's office	22,147.87	
Headquarters	16,492.59	
Accounting department	13,538.19	
National Committees	4,975.76	
President's office	4,299.77	
Trustees	3,270.67	
Technical books	817.40	
General reprints and index	5,488.87	
Medals and awards	883.85	
Miscellaneous merchandise, etc.	821.32	
Library salaries, supplies, etc.	742.76	
Lectures	520.00	
Research and educational contributions	375.00	
Medal fund	236.64	
TOTAL EXPENSES		$ 865,238.50
NET INCOME		$ 49,157.17

Board of Trustees,
American Society for Metals,
Cleveland, Ohio.

We have examined the balance sheet of American Society for Metals as of August 31, 1948, and the statements of income and expense and surplus for the year then ended, have reviewed the accounting procedures of the Society and, without making a detailed audit of the transactions, have examined or tested accounting records of the Society and other supporting evidence, by methods and to the extent we deemed appropriate. Our examination was made in accordance with generally accepted auditing standards applicable in the circumstances and included all procedures which we considered necessary.

During the year a Reserve for METALS HANDBOOK, amounting to $18,777.50, was established to provide for the cost of printing additional editions, and eventual revision of the new METALS HANDBOOK.

A non-profit company was incorporated during the year as Science Education Foundation, Inc., for the stated purpose, among other things, of advancing scientific and technical knowledge, through research, education and the dissemination of information for the benefit of the general public, including the power to own, control and operate facilities for broadcasting by radio, radio-telegraph, television and similar processes. At August 31, 1948, the only recorded asset of the corporation was a commercial account of $1,000.00 at The Cleveland Trust Company, Cleveland, Ohio. Organization expenses of the new corporation have been included as general expenses of the Society.

In our opinion, the accompanying balance sheet and related statement of income and expense present fairly the position of American Society for Metals at August 31, 1948, and the results of its operations for the year, in conformity with generally accepted accounting principles which, except as referred to in the second preceding paragraph, have been applied on a basis consistent with that of the preceding year.

Cleveland, Ohio
September 17, 1948

ERNST & ERNST
Certified Public Accountants

ANNUAL REPORT OF THE SECRETARY

WILLIAM H. EISENMAN, *Secretary*

The American Society for Metals on October 1, 1948, had a total membership of 20,037. Of this number 17,324 or 86.5% were the member classification; 1650 or 8.2% were sustaining members; while 1030 or 5.1% were junior members. There were 32 honorary and founder members.

TRANSACTIONS

Since the last National Metal Congress, Vol. 40 and Vol. 40A of the TRANSACTIONS were published and distributed to the member-

ship in April 1948. Vol. 40 totals 1164 pages and constitutes 42 articles with their discussions. It contains all of the papers presented at the October 1947 Convention held in Chicago together with other interim papers received during the year. The president, secretary and treasurer's report for 1947 and other current items of record were included in Vol. 40 together with a report of the Convention.

Vol. 40A contains the nineteen papers (312 pages) presented at the seminar on "Fracturing of Metals" held on Saturday and Sunday, October 18 and 19, 1947, during the National Metal Congress and Exposition, Chicago. This seminar was sponsored by the American Society for Metals, and coordinated by members of the metallurgical staff of Case Institute of Technology, under the direction of George Sachs.

Metal Progress

A tabulation of total editorial and advertising pages published annually in Metal Progress for the past eight years follows:

Fiscal Year	Editorial Pages	Revenue Advertising	Net Paid Circulation*
1941	645	1078	13,018
1942	699	1276	15,412
1943	688	1592	16,363
1944	648	1937	18,774
1945	674	2045	20,410
1946	832	2024	20,708
1947	722	1676	20,158
1948	628	1452	20,660

*Audit Bureau of Circulation figure for June. Print order is about 15% larger.

This table charts the vital statistics of your monthly magazine through the war and postwar years. It indicates the peak in advertising patronage during 1944, 1945 and 1946, and the rather alarming drop in 1947 and 1948. While this course of events has affected other engineering and technical publications in a similar way, the ASM cannot make, as readily, the conventional adjustments in its operations as can a commercial publishing house. The number of editorial pages, for example, has for years been fairly close to 650. That is none too many for a reasonably good job of covering the field of quality metals. If that number were sharply restricted in an effort to establish some constant relationship to advertising patronage, the value of the publication to our members would suffer disproportionately. Likewise it is impossible to restrict the print order, for the membership remains fairly close to its wartime peak—

a matter which, on practically all other counts, is a cause for gratification. The most pronounced effect on the balance sheet, however, has been the large increase in costs of typesetting, engravings and printing, that went into effect at the turn of the year, and a steady increase in paper costs. Compare, for example, costs in fiscal 1943 and fiscal 1948, years of comparable volume of production: In 1943, the necessary paper cost $36,000; last year it cost $54,000. In 1943 the printer's and engraver's bills came to $71,000; last year they amounted to $109,000.

Nevertheless, the Board of Trustees is resolved that the quality and coverage of METAL PROGRESS must be maintained—indeed, improved. We confidently expect that a major step in that direction has been taken with the assignment of Dr. Taylor Lyman, now that his work on the ASM METALS HANDBOOK has been completed, to be associate editor of METAL PROGRESS, thus reinforcing the efforts of Mr. Thum who has carried the editorial responsibility single handedly since the first issue in 1930.

METALS REVIEW

The biggest improvement made in METALS REVIEW during the past twelve months was the adoption of smooth coated stock instead of the rough newsprint heretofore used. The consequent improvement in legibility, appearance and durability excited many favorable comments from readers. At the same time a heavy cover in two colors was added, further enhancing the appearance and also presenting an opportunity to carry advertising and thus help defray the cost of these improvements.

The Review of Current Metal Literature continues to expand, and now runs to some 800 articles listed and annotated per month. This expansion is largely in the field of foreign literature, which is reaching this country in an ever-increasing flow. To accommodate these additional annotations, the size of the book was increased from 56 to 64 pages per issue.

METALS REVIEW continues to carry two feature articles in a specific field each month—one surveying the literature in that field published during a certain period, and the other describing new products and equipment introduced by the manufacturers in that same field. These feature articles were not carried in the September issue, the space being devoted instead to a preview of the National Metal Congress and Exposition.

As a news magazine, METALS REVIEW devotes a large portion of its space to reports of ASM chapter activities, news of national affairs, and the doings and accomplishments of members. The number of reports of chapter meetings alone published during the past twelve months totaled 333—an increase of 20% over the corresponding period last year. This extended coverage of local meetings would not be possible without the faithful efforts of chapter reporters and publicity chairmen.

An additional feature, started last March and now running into seven installments, is a Bibliography of Metallurgical Books Published in the Period 1936 to 1946. The bibliography will be completed in the November issue, and will then be reprinted as a separate pamphlet accompanied by an author index.

METALS HANDBOOK

The 1948 edition of the METALS HANDBOOK was published June 16, 1948. The 1948 edition is a thorough revision and substantial enlargement of the 1939 edition. Much new material has been added. The 1948 edition is almost 40% larger than the 1939 edition.

As the number and diversity of metallurgical subjects have increased, the range of authorship of the METALS HANDBOOK has widened correspondingly until, in the present edition, 68 subcommittees and 603 individuals are named as contributors. The accuracy and authority of the material included in the METALS HANDBOOK are assured by the names of the contributors. All are specialists who represent the best metallurgical learning of the day.

Important changes have been made in the scope, form and arrangement of the subject matter in the METALS HANDBOOK. The volume has a new, larger page size: 8¼ by 10¾ inches. This greatly facilitates the use of the book, for illustrations and tabular matter can be placed on the same page as the text matter that discusses them.

The Nonferrous Section has been almost entirely rewritten and has been expanded and changed greatly in form. Specific data for 220 nonferrous metals and alloys have been presented according to a new, semitabular arrangement.

The first extensive collection of alloy phase diagrams to be published in America is a part of this edition of the METALS HANDBOOK. This section comprises the last 124 pages of text. All of

the 284 phase diagrams are arranged alphabetically in this section.

Much time and effort have been expended to increase the usefulness of the index, which now contains five times as many entries as before. A separate folder, included with each copy of the METALS HANDBOOK, gives specific suggestions for using the book—and especially the index—to best advantage.

Since publication of the 1948 edition, about half the members have returned their old METALS HANDBOOKS in exchange for the new edition. In addition, 2155 copies have been sold.

BOOKS

During the past fiscal year, a total of 17,560 books published by the Society was sold to members and others. This figure includes 314 1939 METALS HANDBOOKS and 1363 1948 METALS HANDBOOKS. During this period six new titles were added to the list. These are:

ASM Review of Metal Literature—Vol. 4
1948 ASM Metals Handbook
Copper and Copper Alloys—By Owen W. Ellis
Fracturing of Metals—By 21 different authors
Chapter Know-How—By W. H. Eisenman
Your Career in the Metallurgical Profession—By John W. W. Sullivan

The following titles are now in process of preparation:

Physical Metallurgy of Aluminum—By 5 authors
Sleeve Bearing Materials—By 19 authors
Metallurgy and Magnetism—By J. K. Stanley
Symposium on Mechanical Wear—M.I.T.
Properties of Metals in Material Engineering
Grain Control in Industrial Metallurgy
Story of Magnesium

Many of the previous titles were reprinted.

PUBLICATIONS COMMITTEE

The Publications Committee for the year 1947-48 was made up of the following personnel: A. O. Schaefer, Chairman; R. H. Aborn, C. T. Evans, Jr., A. L. Feild, M. G. Fontana, J. H. Hollomon, H. B. Osborn, Jr., W. A. Pennington, F. N. Rhines, E. S. Rowland, L. E. Simon, H. Solakian, A. R. Troiano, H. S. VanVleet, C. A. Zapffe, and Ray T. Bayless, Secretary.

During the year the Committee has reviewed 51 papers of which 44 were approved for preprinting and presentation at this Convention; 4 were rejected; 2 were returned to authors for revisions; and 1 will be published in METAL PROGRESS. Four papers are now in the process of review.

The Publications Committee held one formal meeting on June 15 and 16, 1948, at which time the final arrangements for the technical program at this Convention were made.

Preprints

The forty-four papers being presented at this Convention were prepared in preprint form and distributed to those members of the Society who requested them. The total number of pages for the 1948 preprints is 1129. A total of 45,000 preprint copies was distributed free to the membership.

Educational Committee

The Educational Committee for the year 1948 was composed of the following personnel: C. R. Austin, Chairman; G. M. Cover, G. R. Fitterer, H. L. Grange, J. G. Jackson, J. F. Kahles, H. B. Knowlton, R. D. Stout, and Ray T. Bayless, Secretary.

This Committee held one formal meeting on November 18, 1947, at which time the three educational lecture courses for the 1948 Convention were selected and planned. These lectures are:

1. "Properties of Metals in Materials Engineering", by 8 authors—R. L. Templin, M. Gensamer, J. R. Low, Jr., R. E. Peterson, W. M. Murray, W. T. Bean, Jr., E. C. Hartmann, and W. P. Roop.
2. "Metallurgy and Magnetism", by J. K. Stanley.
3. "Grain Control in Industrial Metallurgy", by 4 authors—J. E. Burke, R. L. Kenyon, H. L. Burghoff, and J. T. Hobbs.

Ten-Year Secretary

The Society has the privilege this year of honoring William J. Parsons, who has given long and faithful service to the Los Angeles Chapter of the ASM. The arduous duties of a local secretary are well known to many of you, and it is certainly an indication of exceptional ability for Mr. Parsons to have been able to sustain activities for a ten-year period. However, in recognition of his endeavors, he is this year attending the congress as a guest of the Society.

FM Radio Station

With the broadening of the articles of incorporation of the Society, which were unanimously adopted at the annual meeting in Chicago last year, the board of trustees petitioned the Federal Communications Commission for a license to establish an FM radio

station for the purpose of advancing the educational facilities of the Society as well as to establish the ASM as a science service organization whose technical and educational programs would be available for distribution and use to the 4000 other FM and AM stations in the United States and Canada.

We are pleased to announce that the Federal Communications Commission has granted the application for the allocation of an FM channel and the Society only awaits the completion by the Federal Communications Commission of the examination and approval of the engineering features of the station so that then a constructional permit will be granted.

Seminar Committee

The Seminar Committee, consisting of John Chipman, Chairman (Boston), R. M. Brick (Philadelphia), J. E. Dorn (Golden Gate), J. H. Hollomon (Eastern New York), R. F. Mehl (Pittsburgh), G. Sachs (Cleveland), has been responsible for the selection of the subject of Cold Working of Metals presented during five sessions on October 23 and 24, 1948. After the selection of the subject the responsibility for correlating the program rested with Dr. M. Gensamer and Dr. J. H. Hollomon, and they received helpful cooperation from numerous individuals interested in this subject.

The Seminar presented has been an outstanding success, and reflects credit upon the organizers as well as the contributors and marks such a successful two-day meeting that the continuance of this activity is a foregone conclusion.

1948 National Metal Congress and Exposition

It is almost an axiom that each year it is my privilege to report another successful National Metal Congress and Exposition.

The ideal facilities afforded by the Convention Halls and Commercial Museum in Philadelphia assist in supplying those conditions which are conducive to a successful installation, a pleasant opening, and a satisfactory five-day operation.

The exhibitors participating in this year's Exposition have presented displays that have aroused enthusiastic comments and degrees of extreme satisfaction. It is conceded that the entire ensemble gives a most striking and harmonious presentation.

The central theme of the Congress this year has been "A Salute to Alloy Steel" and the Society is very grateful indeed to the dis-

tinguished group of executives and scientific personnel who have contributed so liberally of their valuable time in the work of the various committees. The Society acknowledges its gratitude to Mr. Robert Wheeler, Director of Publicity of the International Nickel Co., who, as chairman of the "Committee on the Visualization of 75 Years of Progress of Alloy Steel", with the cooperation of the members of the Committee, has presented on the stage of Convention Hall a remarkable dramatization of the progress of this great engineering material.

The Society also appreciates the conscientious and careful work of the Committee on Awards of the Salute to Alloy Steel, under the able leadership of J. M. Schlendorf, Vice-President of Republic Steel Corp. This committee assisted in the selection of the seventy-five distinguished American and Canadian metal men who will receive Distinguished Service Awards citing their valuable contributions to the advancement and progress of Alloy Steel.

The ASM is pleased to have sponsored this salute because among its 20,000 members the Society represents *all* the producers and *most* of the consumers of alloy steel and at the same time it may be stated that the principal progress and development in alloy steels have paralleled the progress and development of the Society.

The ASM hopes to continue to serve the metal industry in the future as it has in the past.

ELECTION OF OFFICERS

PRESIDENT FOLEY: We will now proceed with the election of officers. Complying with the constitution, I appointed in March, 1948, the following nominating committee, selected from the list of candidates suggested by eligible chapters prior to March 1, 1948:

J. B. Austin, Chairman—New York

G. M. Cover, Cleveland	K. L. Fetters, Mahoning Valley
F. A. McCoy, Kansas City	M. A. Scheil, Milwaukee
W. W. Farrar, Los Angeles	W. E. Ruder, Schenectady
F. C. Smith, Louisville	R. A. Johnson, Worcester

The committee met in Columbus on May 19, 1948, and made the following nominations for the following offices:

FOR PRESIDENT

Harold K. Work, Director of Research, Jones & Laughlin Steel Corp., Pittsburgh—1 year.

FOR VICE-PRESIDENT
Arthur E. Focke, Research Metallurgist, Diamond Chain Co. Indianapolis—1 year.

FOR TRUSTEES
Harry P. Croft, Vice-President in Charge of Development, Wheeling Bronze Casting Co., Moundsville, W. Va.—2 years.
Fred J. Robbins, President, Sierra Drawn Steel Co., Los Angeles—2 years.

The committee for nominating a secretary as provided for in the constitution was composed of the following:

F. B. Foley, Chairman

Past President A. L. Boegehold	Past President M. A. Grossmann
Past President Charles H. Herty, Jr.	Past President H. J. French
Past President Kent R. VanHorn	Past President Bradley Stoughton

This committee unanimously nominated W. H. Eisenman for Secretary for a 2-year term.

A report of these nominations duly appeared in the METALS REVIEW, June 1948.

I have been informed by the Secretary that no additional nominations were received prior to July 15, 1948, for any of the vacancies occurring on the Board of Trustees. Consequently, the nominations were closed. I now call upon the Secretary to carry out the provisions of the constitution in respect to the election of officers.

SECRETARY EISENMAN: Conforming with the provisions and requirements of the constitution of the American Society for Metals, I hereby cast the unanimous vote of the members for the election of the aforenamed candidates who were regularly nominated May 19, 1948.

PRESIDENT FOLEY: I declare the nominees as duly elected to their respective offices.

President Foley then introduced the newly-elected officers, at which time President-Elect Work gave a few words of acceptance.

President Foley awarded a certificate to William J. Parsons, who has served ten years as secretary of the Los Angeles Chapter.

PRESIDENT FOLEY: Has anyone present anything to bring before this meeting? If not, a motion to adjourn is in order.

President Foley then introduced Past President James P. Gill, Chairman of the Campbell Memorial Lecture meeting, who in turn introduced the lecturer, Dr. Morris Cohen, Professor of Physical Metallurgy, Massachusetts Institute of Technology, Cambridge, Mass., who presented his lecture entitled "Retained Austenite", which is published in full in this volume of TRANSACTIONS.

ASM ANNUAL DINNER

On Thursday evening, October 28, members and guests assembled in the Ballroom of the Benjamin Franklin Hotel for the Annual Dinner of the Society. The attendance was well over 700.

Those persons seated at the speakers' table were: W. J. DeMauriac, Philadelphia Electric Co., Philadelphia—Chairman, Philadelphia Chapter, ASM; H. P. Croft, Wheeling Bronze Casting Co., Moundsville, W. Va.—Trustee-Elect, ASM; F. J. Robbins, Sierra Drawn Steel Corp., Los Angeles—Trustee-Elect, ASM; C. M. Carmichael, Shawinigan Chemicals, Ltd., Montreal—Trustee, ASM; Morris Cohen, Massachusetts Institute of Technology, Cambridge—1948 Campbell Memorial Lecturer; A. E. Focke, Diamond Chain Co., Indianapolis—Trustee and Vice-President-Elect, ASM; J. W. Spretnak, Ohio State University, Columbus—Recipient of Howe Award; Earl Shaner, *Steel,* Cleveland; A. L. Boegehold, General Motors Corp., Detroit—Past President, ASM; A. E. White, University of Michigan, Ann Arbor—Past President and a Founder Member, ASM; W. H. Dow, Dow Chemical Co., Midland, Mich.—Recipient of ASM Medal for the Advancement of Research; E. A. Mowrer, Principal Speaker; F. B. Foley, The Midvale Co., Nicetown, Philadelphia—President, ASM; F. C. Frary, Aluminum Company of America, New Kensington—Recipient of ASM Gold Medal; K. R. VanHorn, Aluminum Company of America, Cleveland—Past President, ASM; H. K. Work, Jones & Laughlin Steel Corp., Pittsburgh—Vice-President and President-Elect, ASM; J. L. Cox, The Midvale Co., Nicetown, Philadelphia—Recipient of Distinguished Service Award; R. E. Zimmerman, U. S. Steel Corp., Pittsburgh—Vice-Chairman Distinguished Service Awards Committee; F. J. Griffiths, Steel Consultant, Massillon, Ohio—Recipient of Distinguished Service Award; T. W. Lippert, *Iron Age,* New York; R. A. Wheeler, International Nickel Co.—Chairman, Committee to Visualize Alloy Steel Progress; E. L. Spanagel, Rochester Gas & Electric Co.—Treasurer, ASM; D. M. McCutcheon, President, Society for Non-Destructive Testing; W. J. Parsons, Pacific Scientific Co., Los Angeles—Ten-Year Secretary, Los Angeles Chapter, ASM; Frederick Cooper, Vanadium-Alloys Steel Co., Narberth, Pa.—Secretary, Philadelphia Chapter, ASM; W. H. Eisenman, Secretary, American Society for Metals, Cleveland.

Presentation of President's Medal

The annual presentation of the President's Medal was made by F. B. Foley to A. L. Boegehold, the twenty-seventh president, who served the Society so ably in 1947.

Presentation of Howe Medal

In honor of Dr. Henry Marion Howe, the distinguished scientist, often called the dean of American metallurgists, the Board of Trustees in 1922 established the first of its medals. The rules governing the award of this medal make the provision that it be awarded to the author or authors of the paper judged of highest merit, presented before the ASM and published during any one year in the TRANSACTIONS of the Society.

The 1948 medal was awarded to the author of the paper entitled "Kinetics of Solidification of Killed Steel Ingots" which was published in Vol. 39 of TRANSACTIONS, 1947, page 569. The author who was honored is J. W. Spretnak, who was presented a certificate, a gold medal and a bronze replica.

Edward DeMille Campbell Memorial Lecture

In 1926 the Society established the Edward deMille Campbell Memorial Lecture and each year since that time has invited a distinguished scientist to present this lecture. The 1948 lecturer was Dr. Morris Cohen, Professor of Physical Metallurgy, Massachusetts Institute of Technology, and to commemorate this lecture a certificate certifying to that event was presented to Dr. Cohen.

Conferring of the ASM Medal for the Advancement of Research

The 1948 ASM Medal for the Advancement of Research was awarded to Willard Henry Dow, president of the Dow Chemical Company, in recognition of his consistent sponsorship, foresight, and influence in financing and prosecuting metallurgical research, which have helped substantially to advance the arts and sciences relating to metals.

In presenting Dr. Dow, Col. A. E. White read the citation engrossed on the scroll which accompanies the medal. President Foley then conferred the award. The citation is:

> "Trained as a chemical engineer and with a natural scientific bent Dr. Willard H. Dow has maintained personal direc-

tion of the research activities of the Dow Chemical Company while at the same time serving as its President and General Manager. Developments in the production and metallurgy of magnesium have always had Dr. Dow's particular interest.

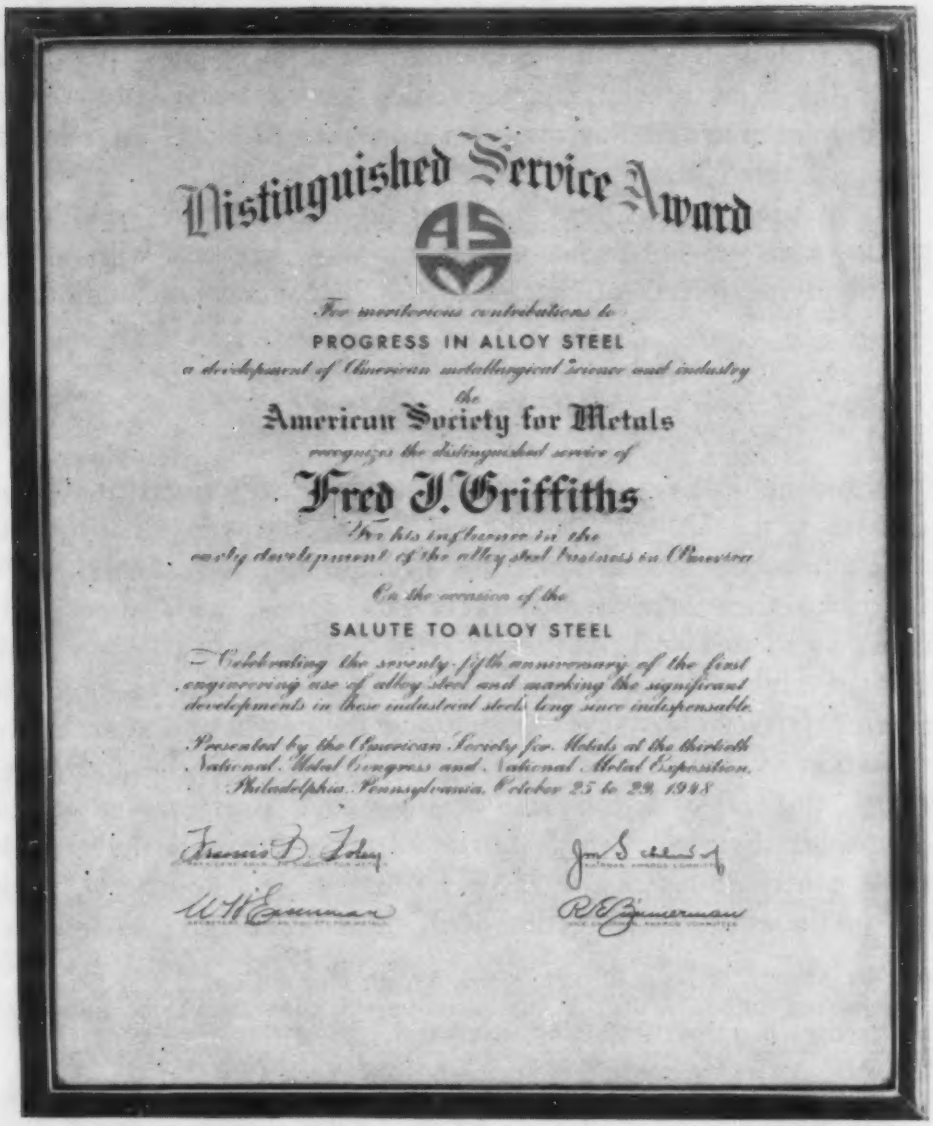
"His broad vision has given rise to research programs which have resulted in continuing reduction of costs in the magnesium industries and have made possible accomplishments such as the commercial production of magnesium metal from sea water, the reverberatory furnace melting of magnesium, the mechanical handling of molten magnesium with pumps and pipes, the continuous casting and rolling of slabs, the production of controlled-purity alloys of magnesium, the use of magnesium as an anode for electrolytically protecting iron and steel against corrosion, and the routine determination, by means of the Dow direct-reading spectroscope, of seven constituents of a magnesium alloy in two minutes.

"The Nation stands deeply indebted to Dr. Dow for his activities which enabled the filling of the unprecedented wartime demand for strategic magnesium."

Conferring of Gold Medal of ASM

The Gold Medal of the ASM, established in 1943, recognizes the recipient for outstanding metallurgical knowledge and great versatility in the application of science to the metal industry, as well as exceptional ability in the diagnosis and solution of diversified metallurgical problems. Dr. Kent R. VanHorn presented Francis Cowles Frary, Director of Research, Aluminum Company of America, as the candidate for the 1948 award. In presenting him, Dr. VanHorn read the citation engrossed on the scroll which accompanies the medal. President Foley then conferred the medal award upon Dr. Frary. The citation is as follows:

"Francis Cowles Frary builded Aluminum Research Laboratories and for thirty years had guided its activities with outstanding leadership. Frary has been personally active in all phases of research on aluminum, from the processing of bauxite and the production of the metal to its applications. Frary has made important contributions in such diverse fields as the electrothermal production of alumina, the electrothermal production of aluminum alloys, electric calcination of coke for



Distinguished Service Award

For meritorious contributions to
PROGRESS IN ALLOY STEEL
a development of American metallurgical science and industry
the
American Society for Metals
recognizes the distinguished service of
Fred J. Griffiths
For his influence in the
early development of the alloy steel business in America
On the occasion of the
SALUTE TO ALLOY STEEL
Celebrating the seventy-fifth anniversary of the first
engineering use of alloy steel and marking the significant
developments in these industrial steels long since indispensable
Presented by the American Society for Metals at the Thirtieth
National Metal Congress and National Metal Exposition
Philadelphia, Pennsylvania, October 25 to 29, 1948

Francis B. Foley
W. H. Zimmerman
Jos. S. Seidl
R. E. Zimmerman

Reproduction of one of the Distinguished Service Award Certificates Presented to 75 Individuals. The Certificates were 11 by 14 inches in size and mounted in a stainless steel frame.

the production of electrodes, molding sands used for casting magnesium alloys, and aluminum alloys.

"Frary Metal, his first significant contribution to metallurgy, was a lead alloy for bearings, hardened with calcium and barium. Developed in 1914 with Sterling Temple, the alloy exhibited the then unique phenomenon of age hardening, a fact which did not escape Frary's observation.

"Working with William Hoopes, Frary produced in 1920

the first aluminum of 99.99% purity by a unique method of electrolytically refining aluminum in a three-layer fused salt bath. The special characteristics of electrolytically refined aluminum are finding application in such products as reflectors and cable sheathing. Electrolytically refined aluminum has been used by his research staff to establish the equilibrium diagrams of important aluminum alloy systems without the modifying effects of the impurities in commercial aluminum."

Distinguished Service Awards
"Salute to Alloy Steel"

President Foley presented Dr. Rufus E. Zimmerman, Vice-President of the United States Steel Corp., and Vice-Chairman of the Committee on Awards for the "Salute to Alloy Steel". Dr. Zimmerman then presented to President Foley, with appropriate remarks as to the work of the Awards Committee, two individuals each to receive a Distinguished Service Award, John L. Cox and Frederick J. Griffiths. President Foley then indicated that in the presentation of the certificates to the two pioneers in the alloy steel industry, this act is symbolical of the actual presentation of the Distinguished Service Awards to the 73 other men who have made valuable contributions to the 75-year progress of Alloy Steel. The names of the recipients, together with the citations, are as follows:

ROBERT R. ABBOTT, director of metallurgy, White Motor Co.
A pioneering authority on the intelligent use of alloy steel, who influenced practices in many consuming industries.

OTHMAR H. AMMANN, consulting engineer, New York City
For extensive application of the strong structural steels to long-span highway bridges.

ROBERT S. ARCHER, vice-president, Climax Molybdenum Co. of Michigan
For systematization of knowledge basic to the science of metals.

WILBUR H. ARMACOST, vice-president, charge of engineering, Combustion Engineering Co., Inc.
For promoting the use of low-alloy steels for boilers and auxiliaries in high-temperature service.

EDGAR C. BAIN, vice-president, Carnegie-Illinois Steel Corp.
Investigator, author, advisor, administrator in many phases of alloy steel development.

HILAND G. BATCHELLER, president, Allegheny Ludlum Steel Corp.
For supporting a lengthy program of development of electrical sheets of improved magnetic properties.

QUINCY BENT, formerly vice-president, Bethlehem Steel Co.
For leadership in the conservation of strategic alloys in World War II.

ALFRED L. BOEGEHOLD, head, metallurgy department, Research Laboratories Division, General Motors Corp.
For his early application of the principles of hardenability to the more intelligent use of alloy steels.

HYMAN BORNSTEIN, director of laboratories, Deere & Co.
Pioneering metallurgist in the farm implement industry, responsible for many applications of special steels.

D. K. BULLENS, president, New England Auto Products Corp.
For his inspirational work in collecting and publishing American practices in "Steel and Its Heat Treatment".

HENRY T. CHANDLER, vice-president, Vanadium Corp. of America.
For early development of chromium-molybdenum and vanadium steels and their application to automobiles.

JOHN L. COX, Midvale Co.
For early adaptation of alloy steels for armor and projectiles to industrial purposes.

EDMUND S. DAVENPORT, assistant to vice-president, United States Steel Corp. of Delaware.
For his revealing studies on isothermal transformation, leading to greatly improved heat treating techniques.

C. NEWMAN DAWE, retired from the Vanadium Corp. of America.
For development of nickel-molybdenum steels and their application to automotive parts.

ENSLO S. DIXON, metallurgist, Texas Co.
For early and extensive application of chromium steels in oil refinery equipment.

BENJAMIN F. FAIRLESS, president, United States Steel Corp.
For support of many projects that improved the quality and widened the utility of alloy steels.

C. B. FRANCIS, consulting chemist and metallurgical engineer.
Author of the most inclusive and authoritative work on American practices in steel manufacture and treatment.

HERBERT J. FRENCH, vice-president, International Nickel Co., Inc.
For promoting the industrial uses of engineering alloy steels.

EMIL GATHMANN, president, Gathmann Engineering Co.
For conservation of alloys and alloy steel by improved ingot mold designs.

H. W. GILLETT, chief technical advisor, Battelle Memorial Institute.
Investigator, author, critic, organizer of research into alloy steels.

FRANK P. GILLIGAN, secretary-treasurer, Henry Souther Engineering Co.
For pioneer guidance and 25-year chairmanship of the S.A.E. Committee on Steel Specifications.

NORMAN P. GOSS, consulting physicist, Cold Metal Products.
For discovering a commercial process for inducing directional crystallization in transformer and electrical sheet.

H. W. GRAHAM, vice-president and director of technology, Jones & Laughlin Steel Corp.
For perfecting manganese steels used widely for oil field equipment, armor and other heat treated parts.

HENRY B. GREENSTED, metallurgical consultant, Algoma Steel Corp.
For applying alloy steels to a wide variety of industrial purposes in Canada.

FREDERICK J. GRIFFITHS, steel consultant.
For his influence in the early development of the alloy steel business in America.

MARCUS A. GROSSMANN, director of research, Carnegie-Illinois Steel Corp.
For evaluation of the influence of specific elements on the hardenability of steels.

THOMAS W. HARDY, technical representative in Canada, Climax Molybdenum Co.
Canadian metallurgist, for early recognition of the advantages of fine grain in alloy steels for severe services.

ISAAC HARTER, chairman, Babcock & Wilcox Tube Co.
For continuous improvement of steam boilers and auxiliaries through correct application of alloy steels.

WALTER G. HILDORF, chief metallurgical engineer, western division, Timken Roller Bearing Co.
For research and steelmaking developments that extended the use of alloy steels in high-temperature equipment.

ZAY JEFFRIES, vice-president, General Electric Co.
For his early systematization of knowledge basic to the science of metals.

CHARLES MORRIS JOHNSON, chief chemist, Park works, Crucible Steel Co. of America.
For early perfection of analytical methods for chemical control of alloys in steel.

J. B. JOHNSON, chief, materials laboratory, United States Air Force.
For establishing and maintaining quality standards in the aircraft and air engine industries.

WALTER E. JOMINY, staff engineer, Chrysler Corp.
For devising the hardenability test bearing his name.

AUGUSTUS B. KINZEL, president, Union Carbide and Carbon Research Laboratories, Inc.
For early work on high yield strength steels and for leadership in studying the weldability of alloy steels.

ALAN KISSOCK, mining engineer, Alan Kissock and Co.
For devising correct steelmaking processes, especially for the molybdenum alloys.

HARRY B. KNOWLTON, supervisor, materials engineering, International Harvester Co.
For applying alloy steels to agricultural implements and farm tractors.

FRED A. LOOSLEY, vice-president and manager, Dominion Foundries & Steel, Ltd.
Inventor and producer of alloy steel of improved machinability, largely used in Canadian armored vehicles.

WILLIAM J. MACKENZIE, manager, alloy steel sales, Youngstown Sheet & Tube Co.
For promoting the use of alloy steels throughout American industry.

FRANK M. MASTERS, owner, Modjeski and Masters.
For pioneering use of strong structural steels in long-span railroad bridges.

FRED E. MCCLEARY, retired chief metallurgist, Chrysler Corp.
For developing molybdenum and chromium-vanadium steels and extending their automotive applications.

JOHN MCCONNELL
For pioneering the production of alloy steels in the open-hearth furnace.

HARRY W. MCQUAID, consulting metallurgist.
For distinguishing between abnormal and normal steels and interpreting the relationship between grain size and hardening properties.

JOHN MITCHELL, assistant to the manager of alloy sales division, Carnegie-Illinois Steel Corp.
For leadership in the development of National Emergency Alloy Steels.

NORMAN L. MOCHEL, manager of metallurgical engineering and consulting engineer, Westinghouse Electric Corp.
For promoting the use of low-alloy steels in heavy electrical generating and transmission equipment.

WILLIAM ARTHUR NEWMAN, manager, department of research, Canadian Pacific Railway.
For the application of alloy steels to severe services on Canadian railroads.

J. HEBER PARKER, chairman of the board, Carpenter Steel Co.
For devising and producing alloy steels acceptable to the U. S. Navy and the budding automotive industry.

CHARLES FREDERICK PASCOE, assistant general manager, foundry division, Canadian Car & Foundry Co., Ltd.
For improvement and development of alloy cast steels for general engineering use in Canada.

W. E. RUDER, head, Metals Research, General Electric Co.
For applying superior alloy irons and steels to electrical equipment and large steam turbines.

ADOLPH O. SCHAEFER, executive engineer, The Midvale Co.
For development of many special alloy steels for use in ordnance and the heavy industries.

ROBERT B. SCHENCK, chief metallurgical engineer, Buick Motor Div., General Motors Corp.
For devising inspection and production methods whereby manganese steels could be widely used for automotive parts.

J. M. SCHLENDORF, vice-president in charge of sales, Republic Steel Corp.
For pioneering and continuing efforts to promote the use of alloy steels throughout American industry.

ROBERT W. SCHLUMPF, chief metallurgist, Hughes Tool Co.
For utilization of alloy steel in oil well drilling equipment.

MARTIN H. SCHMID, manager of sales, alloy steel division, Republic Steel Corp.
For promoting the intelligent use of alloy steels throughout American industry.

T. D. SEDWICK, engineer of tests, Chicago, Rock Island & Pacific R.R. Co.
For pioneering and constructive work in applying alloy steels to locomotive forgings.

CHAS. H. SHAPIRO, chief metallurgist, Metal Window Products Co.
For utilization of alloy steel in oil well drilling equipment.

BENJAMIN FRANKLIN SHEPHERD, chief metallurgist, Ingersoll-Rand Co.
For developing the martempering technique.

FRANK THAYER SISCO, director, Alloys of Iron Research.
For carrying through the monumental review of literature concerning the alloys of iron.

EARLE C. SMITH, chief metallurgist, Republic Steel Corp.
For applying science to the manufacture and use of alloy steels.

HOWARD J. STAGG, JR., metallurgist, Sanderson-Halcomb works, Crucible Steel Co. of America.
Lifelong proponent of intelligent use of alloy steel who influenced practices in many consuming industries.

OSCAR L. STARR, vice-president, Caterpillar Tractor Co.
For early recognition of those properties of alloy steels that are indispensable to diesel engines.

BRADLEY STOUGHTON, consulting engineer, Lehigh University.
Educator of two generations of makers and users of fine alloy steels.

JEROME STRAUSS, vice-president and technical director, Vanadium Corp. of America.
For pioneer work in the application of wrought and cast alloy steels to naval ordnance.

ERNEST E. THUM, editor, *Metal Progress.*
For gathering, interpreting and presenting information about alloy steels in all their aspects.

HENRY H. TIMKEN, JR., vice-president and chairman of the board, Timken Roller Bearing Co.
For vigorous support of efforts that widely extended the use of alloy steels throughout all industry.

RUFUS S. TUCKER, manager of sales, alloy division, Bethlehem Steel Co.
For continuous efforts toward promoting the use of alloy steel throughout American industries.

JOHN F. WANDERSEE, metallurgical engineer, Ford Motor Co.
For his pioneering work with alloy steel in automotive applications.

JOHN MITCHELL WATSON, retired from Hupp Motor Car Co.
For active promotion of the use of alloy steels in motor cars.

BLAINE B. WESCOTT, assistant to executive vice-president, Gulf Research & Development Co.
For application of alloy steels and irons in oil field and refinery equipment.

ALBERT EASTON WHITE, director, Engineering Research Institute, University of Michigan.
For contributions in the development, promotion and selection of steels for high-temperature service in power plants.

WILLIS RODNEY WHITNEY, retired director of research, General Electric Co.
For initiating and supporting research into many branches of alloy steel metallurgy.

CLYDE WILLIAMS, director, Battelle Memorial Institute.
For directing the War Metallurgy Committee's researches into alloy steels.

KARL D. WILLIAMS, chief engineer, metallurgical, Bureau of Ships, Navy Department.
For his efforts toward steady improvement of naval propulsion systems by the use of alloy steels.

WILLIAM PARK WOODSIDE, chairman, board of directors, Park Chemical Co.
For promoting the interchange of information about heat treatment and use of alloy steel during World War I.

WILLIAM H. WORRILOW, president, Lebanon Steel Foundry.
For promoting the use of alloy steel castings throughout American industry.

TRYGVE D. YENSEN, manager, magnetic department, Westinghouse Research Laboratories.
For researches resulting in large improvement of the magnetic properties of iron alloys.

Address of the Evening

Edgar Ansel Mowrer, writer and foreign correspondent, presented the main address of the evening entitled "We and the Russians".

RETAINED AUSTENITE

(1948 Edward DeMille Campbell Memorial Lecture)

By Morris Cohen

Introduction

IN 1925, within two and one-half months after the death of Edward DeMille Campbell, this Society saw fit to memorialize his achievements for all time by inaugurating a series of annual lectures, to be given each year at the National Metal Congress. It is a distinguished honor to be invited to participate in this series, and today I have the privilege of presenting the twenty-third Campbell Memorial Lecture.

It was not my good fortune to know Professor Campbell, except through his many students and prolific writings. Even had I attended the University of Michigan, where he graced the faculty for thirty-five years, our paths could not have crossed in point of time because he died some four years before I was ready to enter college. There are literally two generations separating our metallurgical careers.

On the other hand, I do know that the intervening years have not dimmed the impressive stature of this man, as an inspiring educator, as a versatile investigator and, above all, as a lasting example of indomitable courage. For, if I may remind you, Professor Campbell was only twenty-eight years old when a laboratory experiment exploded in his face, and he lost the sight of both eyes. A. H. White (1)[1] relates that "Ten days later, ... (Professor Campbell) was back at his desk, a broad white bandage over his eyes, conducting classes and supervising laboratory work." From then on, in total darkness and with deafness descending upon him in later life, he energetically pursued his professional career, organizing new courses, directing research, training students, and publishing no less than seventy-seven papers in the metallurgical and chemical literature.

It is clear from Professor Campbell's writings that he was greatly interested in the constitution and heat treatment of steel. He was particularly concerned with the nature of *hardened* steel, and

[1]The figures appearing in parentheses pertain to the references appended to this paper.

This is the twenty-third Edward DeMille Campbell Memorial Lecture, presented by Dr. Morris Cohen, professor of physical metallurgy, Massachusetts Institute of Technology, Cambridge, Mass. The lecture was presented October 27, 1948, during the Thirtieth Annual Convention of the Society, held in Philadelphia.

this leads me to the subject of today's discussion, for I am going to speak about *retained austenite:* that elusive constituent in hardened steel which has aroused speculation and defied explanation for so many years.

We are quite familiar with the fact that austenite, the high-temperature phase in steel, decomposes during cooling into such products as ferrite, carbide, pearlite, bainite or martensite (Fig. 1), depending on the cooling conditions and the composition of the steel. The characteristics of these products are of direct concern to us

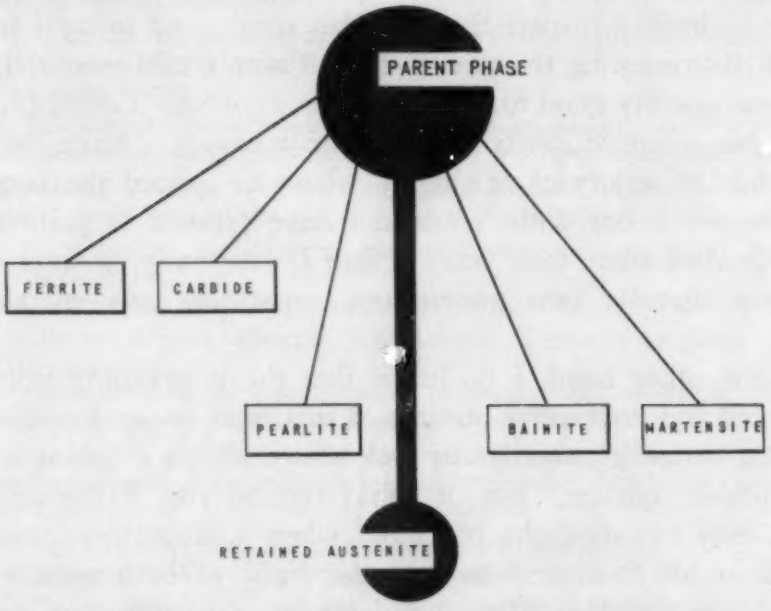


Fig. 1—Schematic Representation of Austenite and Its Transformation Products.

because they control the properties of the steel as we use it. Furthermore, because the austenite is largely consumed in giving birth to its progeny, we are naturally inclined to dote on the offspring and regard the parent solely as a means-to-an-end. However, we are now aware that the parent phase is peculiarly reluctant to sacrifice itself completely for its martensitic descendant. Thus, in the hardening of steel, part of the austenite frequently survives the quenching operation that leads to martensite formation, and remains with the martensite at room temperature to play a significant role, both during subsequent tempering and in later service. It can be said that retained austenite stands at the crossroads between hardening and tempering, and provides one of the main links connecting these two important technological processes.

To treat the problem of retained austenite in a fundamental manner, we must consider such key questions as: What is the nature of this constituent? How does it originate? Why is it so persistent? What are the factors that govern its amount? What happens to it during aging *at* room temperature, during cooling *below* room temperature, and during tempering *above* room temperature? How does it respond to stress and strain?

Merely from a listing of these searching questions, whether suitable answers are available or not at the moment, it becomes obvious that the complexities of retained austenite cannot possibly be unraveled unless the problem is approached on a broad front. Truly, the matter is one that calls for a comprehensive understanding of the phase transformations that underlie the practical heat treatment and industrial utilization of steel. I feel sure that Professor Campbell, were he with us today, would agree that such a subject is certainly worthy of our serious consideration.

Can the foregoing questions be answered? I have been thinking about them for a long time, and now wish to bring some of this thinking up to date in the light of our most recent knowledge. Admittedly, the answers will not prove completely satisfying, but perhaps I can at least excite your interest in some facet of the subject. Should this happen, you have my cordial invitation to join in the theorizing and researching for better answers. I can promise you a fascinating experience.

Acknowledgments

At this point I must stop to pay tribute to my colleagues at Massachusetts Institute of Technology who closed ranks so effectively behind me, and allowed me to concentrate on the preparation of this Lecture. Their fine cooperation, operating inevitably in the background, is one of the warm memories that I shall carry away from this interlude.

It is also my pleasant duty to acknowledge the debt that I owe my research associates and students who worked so brilliantly and diligently to provide much of the foundation upon which this Lecture is based. Not only have I borrowed liberally from their investigations, but these young men have proved a great source of pride and stimulation to me. In particular, I wish to thank Dr. B. L. Averbach, Mr. V. G. Paranjpe, Mr. S. A. Kulin, Mr. B. S. Lement, Mr. R. Balluffi, Dr. W. J. Harris, Jr., Mr. E. S. Machlin, Dr. R. T. How-

ard, Jr., Mr. A. G. Molinder, Mr. L. S. Castleman, and Mr. I. D. Bakalar.

Professor A. R. Troiano of the University of Notre Dame and Mr. Peter Payson of the Crucible Steel Company were kind enough to place unpublished information at my disposal.

And, finally, I must express my gratitude to my family and secretary who were so patient in putting up with it all.

The Nature of Austenite

Austenite is a solid solution of carbon and/or other solute atoms in face-centered cubic iron. It is definitely established that the carbon atoms occupy interstitial positions in the lattice. The atomic radius of carbon is about six-tenths that of iron (0.77 versus 1.27 A.U.) and, therefore, if carbon were to replace iron on points of the face-centered cubic lattice, a contraction of the lattice should result. Yet, as demonstrated in Fig. 2, the lattice parameter of austenite increases progressively with the carbon content. From this, we may infer that the carbon atoms make room for themselves in the interstitial pockets among the iron atoms, which are otherwise close-packed.

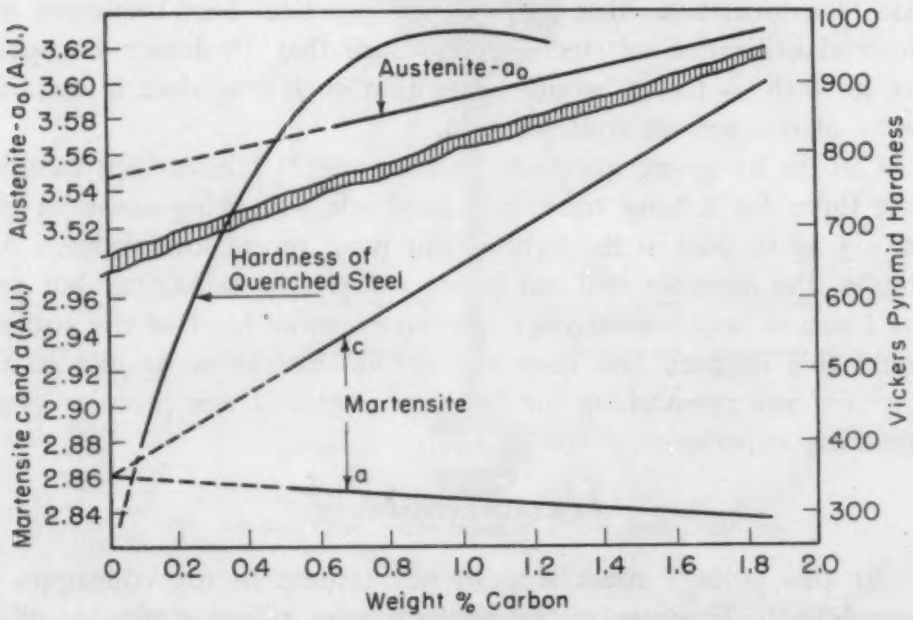


Fig. 2—Lattice Parameters (2, 3, 4) of Face-Centered Cubic Austenite and Body-Centered Tetragonal Martensite in Steel as a Function of Carbon Content. Axial ratio of tetragonal martensite extrapolates to unity at zero carbon. Hardness (5) of quenched steel increases with the carbon content of the martensite, but goes through a maximum because of the increasing quantities of retained austenite.

Of the various possible interstitial sites in the face-centered cubic lattice, the centers of the unit cells and the equivalent positions at the midpoints of the cube edges can house the carbon atoms with the least amount of distortion, and Petch (6) has shown unequivocally by X-ray intensity measurements that these are the actual locations of the carbon atoms in austenite.

There are four of these interstitial sites per unit cell: the twelve cube-edge midpoints indicated in Fig. 3 are each shared by four

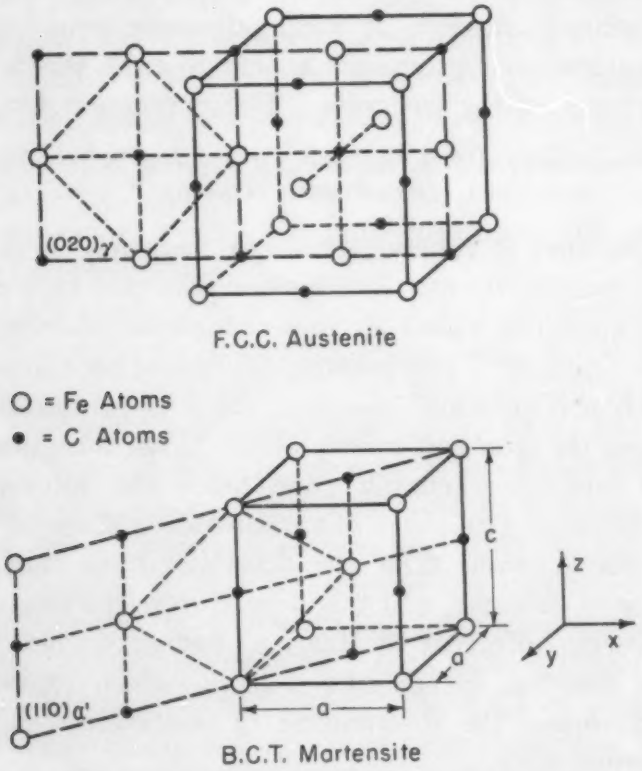


Fig. 3—Interstitial Carbon Sites in Face-Centered Cubic Austenite (6) and Body-Centered Tetragonal Martensite (7, 8). In 1% carbon steel, only about 4.7% of these positions are actually occupied.

adjacent cells, thus averaging three per cell, and the pocket in the cube center makes four. There are also four iron atoms per unit cell, and thus we find one interstitial site per lattice point. This means that if all the interstitial pockets shown in Fig. 3 were occupied by carbon atoms, the structure would contain 50 atomic per cent or 17.7 weight per cent carbon. Actually, the carbon content of austenite reaches a maximum at about 1.7 weight per cent, in which case only one interstitial site in twelve is occupied. In a 1% carbon steel,

just one in twenty-one of these positions is filled. There is no housing shortage for carbon in the austenite lattice!

It should be emphasized in passing that the above interstitial arrangement of the carbon atoms prevails irrespective of the source of the carbon, that is, whether the austenite receives its carbon from cementite, graphite, or a carbon-rich liquid phase. We do not find accommodation in the lattice for specific molecules or crystallites of the coexisting phases. On the other hand, there is reason to believe (as I shall discuss later) that the carbon distribution in austenite is not absolutely random at thermodynamic equilibrium. Carbon-rich and carbon-poor groupings appear to exist which help minimize the free energy of the austenite. The expression for free energy is

$$\text{Free energy} = (\text{internal energy}) + (\text{pressure} \times \text{volume}) - (\text{temperature} \times \text{entropy}) \qquad \text{Equation I}$$

and the pressure $\times$ volume term can be safely neglected in these solid-state considerations. We further note that on equilibrium cooling of the austenite, either an iron-rich phase (ferrite) or a carbon-rich phase (carbide*) precipitates, depending on composition. Even before such precipitation, however, there is presumably an association between the iron and carbon atoms in the austenite that tends to lower the interaction energy (and hence the internal energy) by forming statistical groupings of carbon-rich and carbon-poor concentrations. At the same time, the departure from randomness causes the entropy to decrease, and this acts to raise the free-energy counter to the lowering effect of the internal energy term. The particular balance of internal energy and entropy which minimizes the free energy determines the distribution of concentrations characterizing the equilibrium state.

It is evident from the explicit presence of temperature in Equation I that the entropy term exerts more influence the higher the temperature, and the equilibrium distribution moves toward randomness and statistical uniformity as the temperature is raised. Coincidentally, the favored bonding arrangement is progressively broken up, and this has its repercussions in the austenite-martensite reaction, as we shall see.

Hydrogen, nitrogen and probably boron dissolve interstitially in austenite. On the other hand, the atoms of the common alloying elements, such as manganese, nickel, chromium, vanadium, tungsten,

*Graphite is a more stable form of carbon than the carbide, but is more difficult to nucleate.

Table I
Comparative Diffusion Rates of Interstitial and Substitutional Elements in Austenite (0.6% Carbon – 4% Nickel)

Diffusing Element	Heat of Diffusion (Q)	Frequency Factor (D_o)	Diffusion Coefficient* (D) At 1800 °F (1256 °K)	Diffusion Coefficient* (D) At 68 °F (341 °K)
Carbon (9)	32,000 cal/mol	0.11 cm²/sec	3×10^{-6} cm²/sec	2×10^{-32} cm²/sec
Nickel (10)	65,500	0.46	5×10^{-11}	2×10^{-43}

*$D = D_o e^{-Q/RT}$ = grams of element that will move in one second through a cross section of one square centimeter under the influence of a unit concentration gradient (one gm/cm³/cm).

molybdenum, etc., are too large to fit comfortably in the interstitial pockets, and create less disturbance by substituting for iron atoms on the lattice points. It is generally recognized that interstitial elements enjoy much greater atomic mobility in solid solution than do the substitutional elements. An illuminating comparison is given in Table I. At 1800 °F, carbon diffuses sixty thousand times faster than nickel in austenite, while at room temperature, this ratio is increased to one hundred billion.

There is much evidence in the literature to indicate that austenite is relatively soft and ductile, compared to the hard, brittle martensite. These characteristics are clearly shown by the familiar austenitic stainless and Hadfield's manganese steels (11, 12). However, we are still justified in wondering whether the type of austenite retained in hardened steel enjoys similar properties. This question cannot be answered in a direct manner inasmuch as the predominating martensitic phase makes it difficult to examine the mechanical behavior of the retained austenite. Nevertheless, we may acquire a preliminary insight into the problem by exploring high carbon, high chromium steels which can be rendered substantially austenitic if quenched from above 2000 °F. With the aid of refrigeration, various martensite-austenite ratios can then be obtained for testing, without changing the composition.

Fig. 4, taken from the work of Mr. Kulin (13), presents the true stress – true strain curves (tested at room temperature) for

Table II
Mechanical Properties of 1.5% Carbon – 12% Chromium Steel

Austenitized at 2050 °F and refrigerated as shown. (Tested at room temperature.)

Refrigeration Temperature, °F	% Martensite Start of Test	% Martensite End of Test	% Martensite Formed in Test	Ultimate Strength, Psi	% Elongation	Stress at 0.5% Strain
84	5	30.5	25.5	100,000	3.4	31,000
45	18	36	18	123,000	3.1	68,000
32	22	32	10	120,000	2.1	84,000
22	37	41	4	137,000	1.4	104,000

specimens containing initially 5, 18, 22 and 37% martensite. The strength increases and the ductility decreases as the amount of martensite increases (Table II). The yield strength (taken as the stress at 0.5% strain) is particularly sensitive to the presence of martensite.

Refrigeration Temperature °F	Martensite % At Start	Martensite % At End	Martensite % Formed During Test
84	5	30.5	25.5
45	18	36	18
32	22	32	10
22	37	41	4

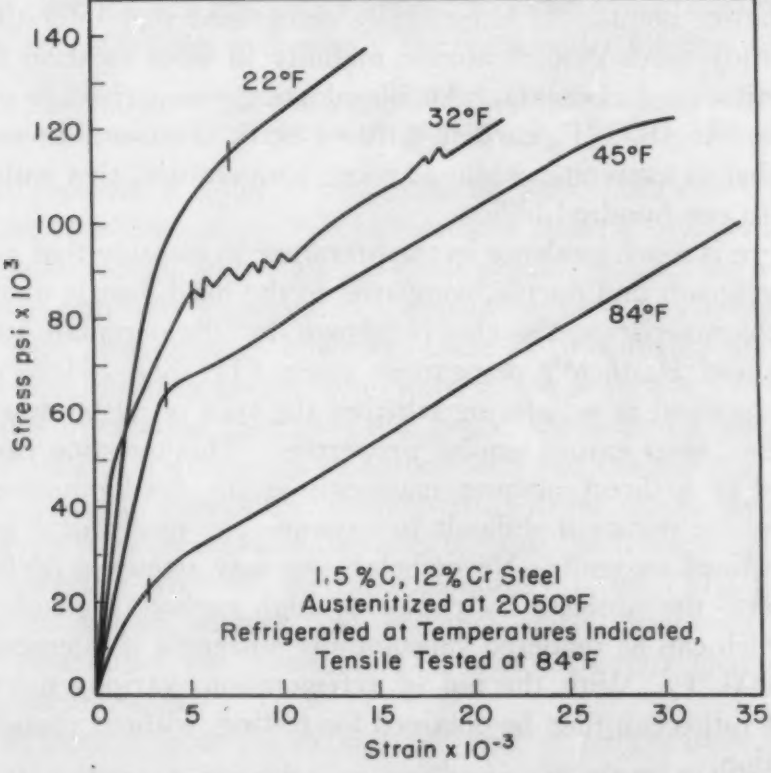


Fig. 4—True Stress – True Strain Characteristics of 1.5% Carbon – 12% Chromium Steel, Austenitized at 2050 F, and Refrigerated to Different Temperatures to Produce Different Amounts of Martensite (13). Tested at room tempertaure (84 °F). Markers on curves indicate where appreciable decomposition of austenite sets in during the test.

However, the amount of martensite does not stay constant during the tensile test, the extent of transformation becoming larger the less martensite that is present to begin with. Under such circumstances, we may certainly deduce that, if the austenite could withstand decomposition during the test, it would display higher ductility and lower hardness (yield strength) than the data indicate.

Thus, we see that the mechanical behavior of retained austenite depends not only on its intrinsic properties, but also on the extent to which it undergoes transformation in testing or in service. In addition, the magnitude of such transformation depends upon the amount of martensite already present. Still another important variable is the composition of the austenite, because this controls its stability relative to martensite. But let us postpone consideration of these details until we have delved further into the nature of the austenite-martensite reaction.

The Origin of Retained Austenite

Kinetics of the Austenite-Martensite Reaction

In the hardening of steel, the desired transformation product is martensite, and the cooling rate is made sufficiently rapid to prevent the austenite from decomposing into any of the other possible prod-

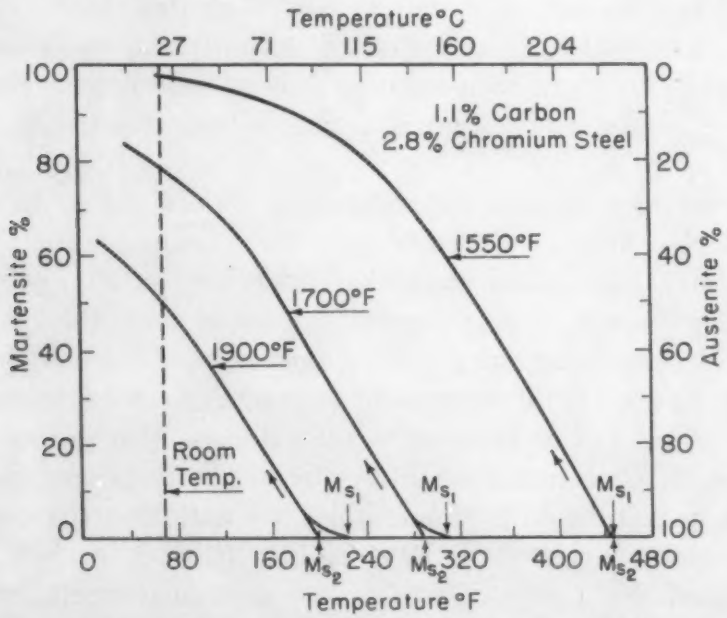


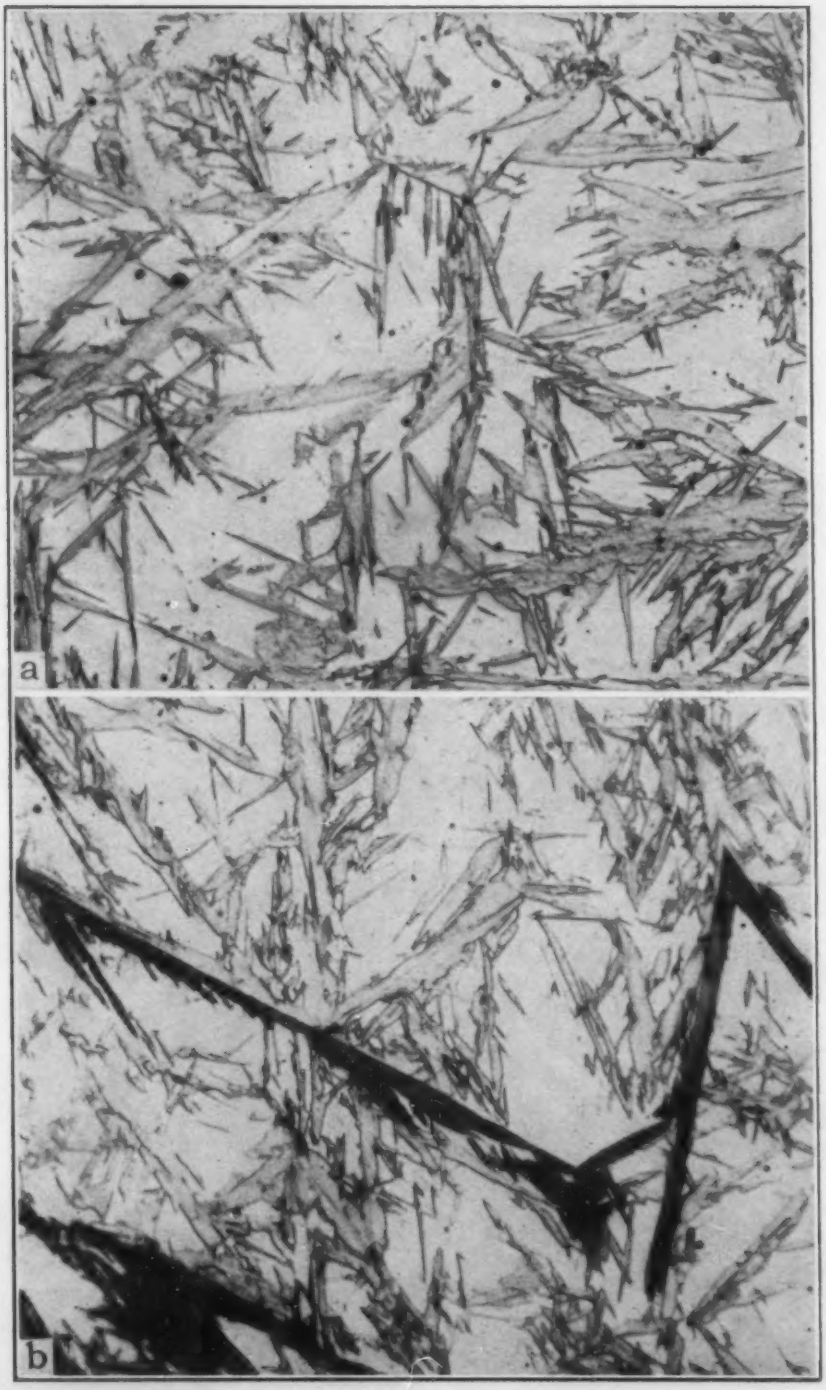
Fig. 5—Martensite Transformation Curves for 1.1% Carbon – 2.8% Chromium Steel, After Austenitizing at 1550, 1700 and 1900 °F (15). Percentages are based on volume of the steel matrix.

ucts. Fortunately, time is a major factor in the formation of these other products, and so they can be suppressed by fast cooling through the temperature ranges where they characteristically form. Thus, it is possible to supercool the austenite to the particular range where martensite is produced.

The birth of martensite out of the parent phase is quite a different event from that of the other progeny. The contrast is really startling when it is noted that cooling rates of the order of a few hundred degrees Fahrenheit per second are usually sufficient to avoid the pearlite and bainite transformations, but the martensite transformation cannot be suppressed with the fastest attainable cooling rates. The maximum cooling rate reported in the literature (14) (28,000 °F/sec) shows no evidence of being able to avoid this remarkable event or even to depress the temperature (M_s) at which it starts.

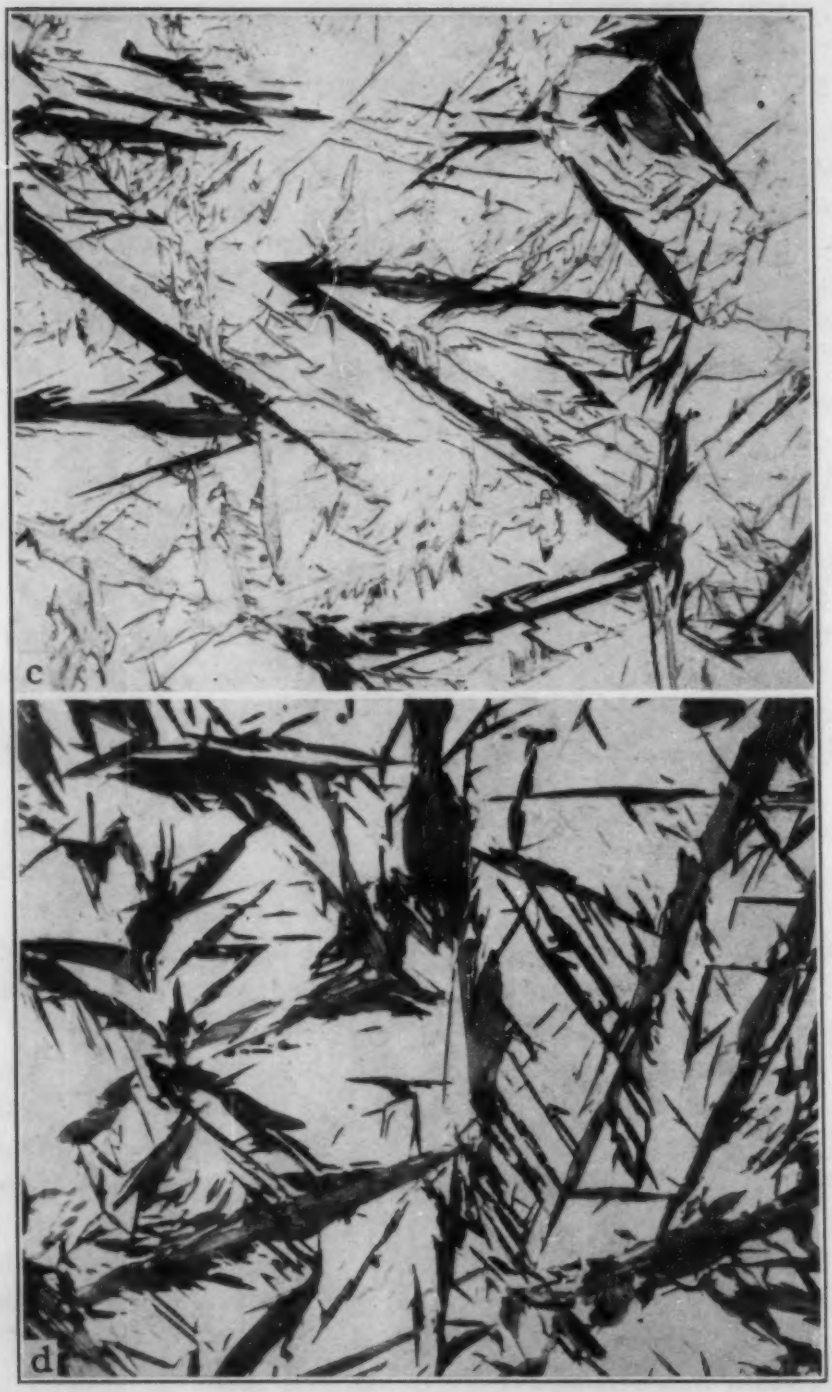
The quantitative course of the austenite-martensite reaction on cooling below M_s is shown in Fig. 5 for a sample steel (1.1% carbon – 2.8% chromium) austenitized at three temperatures (15). Curves such as these are determined by the well-known metallographic technique of Greninger and Troiano (16), in which small specimens are quenched into liquid baths at various temperatures for a brief period, then reheated (to 630 °F in this case) to "darken" any martensite that may have formed during the quench, and finally cooled rapidly to room temperature. These specimens are examined metallographically, and a typical series of microstructures is shown in Fig. 6.

On cooling to a bath temperature of 225 °F (Fig. 6a), we see that no martensite is produced because the reheating to 630 °F yields no dark martensite. The martensite appearing in Fig. 6a is of the light-etching variety, having formed on cooling from the "darkening" treatment. If the quenching-bath temperature is lowered to 194 °F (Fig. 6b), about 1% of martensite is produced, as evidenced by the darkened plates. The light-etching martensite that comes in *after* the "darkening" treatment is still apparent. With progressive lowering of the quenching-bath temperature, we note that the quantity of dark martensite increases to 19% at 140 °F, 35% at 104 °F, 53% at 50 °F and 86% at −320 °F. The light martensite has disappeared in Fig. 6d and below. This signifies that after quenching to somewhere between 140 and 104 °F, the subsequent heating at 630 °F stabilizes all the available austenite against transformation during cooling to room temperature. We shall have more to say about this stabilizing process. For the moment, it is extraneous, because we are concerned only with the amount of *dark* martensite in the structure: this is what traces the course of the transformation during quenching.



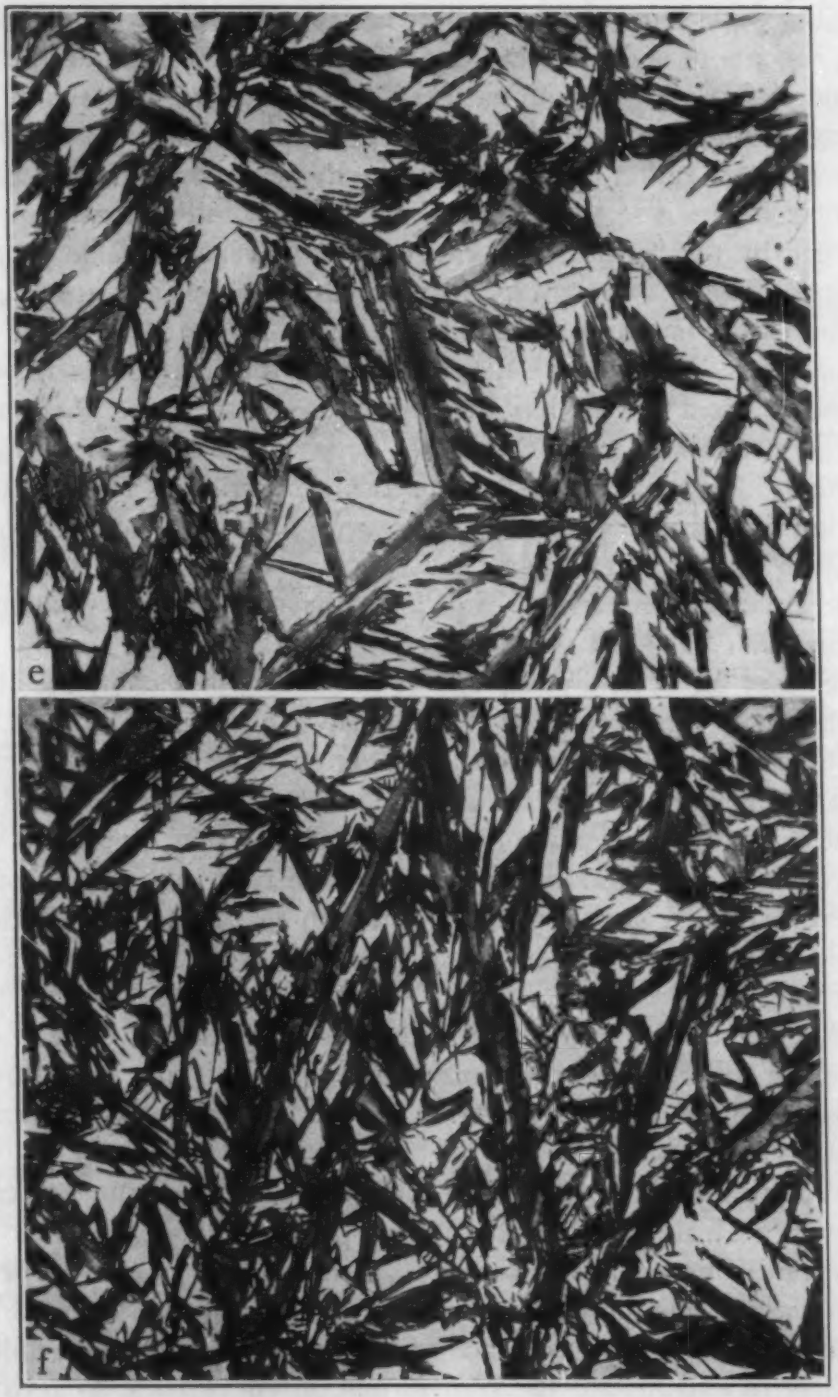
Figs. 6a and 6b—Photomicrographs of 1.1% Carbon – 2.8% Chromium Steel, Austenitized at 2000 °F for 30 Minutes, Quenched Into Liquid Baths at Designated Temperatures (T_q) for 10 Seconds, Reheated to 630 °F for 10 Seconds to "Darken" Martensite Formed, Then Quenched to Ambient of 77 °F. Etched with 4% nital containing 1% Zephiran chloride. × 750. *Molinder* (19a).

	T_q	Dark Martensite	Light Martensite
(a)	225 °F	0%	49%
(b)	194 °F	1%	46%



Figs. 6c and 6d—Photomicrographs of 1.1% Carbon – 2.8% Chromium Steel, Austenitized at 2000 °F for 30 Minutes, Quenched Into Liquid Baths at Designated Temperatures (T_q) for 10 Seconds, Reheated to 630 °F for 10 Seconds to "Darken" Martensite Formed, Then Quenched to Ambient of 77° F. Etched with 4% nital containing 1% Zephiran chloride. × 750. *Molinder* (19a).

	T_q	Dark Martensite	Light Martensite
(c)	140 °F	19%	21%
(d)	104 °F	35%	0%



Figs. 6e and 6f—Photomicrographs of 1.1% Carbon – 2.8% Chromium Steel, Austenitized at 2000 °F for 30 Minutes, Quenched Into Liquid Baths at Designated Temperatures (T_q) for 10 Seconds, Reheated to 630 °F for 10 Seconds to "Darken" Martensite Formed, Then Quenched to Ambient of 77 °F. Etched with 4% nital containing 1% Zephiran chloride. × 750. *Molinder* (19a).

	T_q	Dark Martensite	Light Martensite
(e)	59 °F	53%	0%
(f)	−320 °F	86%	0%

The individual martensite plates form with tremendous speed by a process of sudden shear occurring within a ten-thousandth of a second (17). More and more of these sudden shears take place during cooling and so the reaction proceeds primarily by the birth of new plates rather than by the growth of previous ones. A vivid example of the discrete nature of these rapid internal movements is afforded by the "clicks" that can be heard over a suitable acoustical pick-up. There is enough momentum or kinetic energy in each shear to send elastic impulses of audible frequency racing through the specimen. It may be said with due seriousness that martensite formation is a noisy event! This has nothing to do with the fact that there is a large expansion ($\Delta V/V = 0.042$ referred to room temperature) attending the austenite-martensite transformation. The martensite reaction in lithium (18) clicks energetically, and yet the volume change is less than one-tenth that of steel ($\Delta V/V = 0.003$). And in the zirconium-martensite transformation (19), there is actually a contraction ($\Delta V/V = -0.002$).

Except for second-order effects to be discussed later, the austenite-martensite transformation ceases when the cooling is stopped. We can summarize this characteristic by saying that the reaction depends primarily on temperature rather than on time. In other words, the extent of the transformation is controlled by the temperature to which the steel is cooled; and because of the fantastic speed with which the martensite plates can propagate, the course of the transformation is able to pace the dropping temperature, even during the fastest quenching.

The per cent of dark martensite in the structure is directly equal to the per cent of austenite transformed, and is measured by the method of lineal analysis (20). The percentages thus determined are on a volume basis.

We are now in a position to return to the transformation curves in Fig. 5. Clearly, the martensite temperature range depends upon the austenitizing temperature. For each curve, M_s can be defined in two ways. The more common procedure is to take M_s as the temperature at which the first trace of martensite is detected, while the second is to extrapolate the transformation curve back to zero in a linear fashion. Both M_s values are indicated in Fig. 5, and we shall refer to them as M_{s_1} and M_{s_2} respectively. The first is easier to determine, but suffers from the fact that the initial plates of martensite may not form in truly representative areas. The second

method requires quantitative measurements, but has the advantage of providing a convenient zero-point for fitting equations to the transformation curves. With the latter procedure, it is found that the three curves in Fig. 5, as well as a host of others, conform to the following empirical equations:

$$\text{Per cent martensite} = 100 - 3.05 \times 10^{-14}\left[820 - (M_{s_2} - T_q)\right]^{5.32} \qquad \text{Equation II}$$

$$\text{Per cent austenite} = 3.05 \times 10^{-14}\left[820 - (M_{s_2} - T_q)\right]^{5.32} \qquad \text{Equation III}$$

$$\text{Per cent retained austenite} = 3.05 \times 10^{-14}\left[820 - (M_{s_2} - 68\,^\circ\text{F})\right]^{5.32} \qquad \text{Equation IV}$$

where T_q is the quenching-bath temperature in degrees Fahrenheit, and the percentage values are based on the matrix structure (not the total structure) when undissolved carbides are present.

Equations II, III and IV hold satisfactorily for a wide variety of steels containing 0.75 to 1.35% carbon (21), up to 2.8% chromium (15) and up to 5.4% nickel (21), austenitized at temperatures throughout the range of 1550 to 1900 °F. The relationships may well apply beyond these limits, but the extent has not been established as yet. It is known, however, that these equations do not hold for high speed and high carbon, high chromium steels. This is immediately evident from the fact that the transformation curves for the latter materials and plain carbon tool steel cross one another (Fig. 7). A change of constants is required to fit the high alloy steel curves, and signifies that, while M_s may be the primary factor governing the amount of austenite retained at room temperature, composition does exert some influence in extreme cases over and above its effect through M_s. Within the composition limits cited, despite the variations in carbide solution and grain size produced by different austenitizing treatments, the course of the martensite transformation can be ascertained once M_{s_2} is known, and the austenite remaining at any temperature as well as at room temperature can be calculated.

Grain size is a factor in the austenite-martensite reaction that is deserving of attention. Barnett and Troiano (25) have reported that in SAE 2340, 4140, and 0.40% carbon – 3% chromium steels, M_{s_1} is raised by 15, 50 and 49 °F, respectively, when the grain size is increased from ASTM No. 7-9 to 1-2.* In higher carbon steels, the grain size effect is smaller, so that, as a practical matter, grain size is not an important variable in the retention of austenite. However, from a scientific standpoint, we must keep in mind that martensite

*This change corresponds to a factor of about 9 in average grain diameter.

formation is favored by *coarse* grain size, and the corresponding tendency is for less retained austenite to result. This is to be contrasted with the pearlite reaction which is favored by *fine* grain size.

Clearly, room temperature holds no particular charm for the austenite-martensite reaction. It is merely a convenient stopping point for the hardening quench in practice, and so we pay particular attention to it. Actually, however, as Figs. 5 and 7 show, the transformation curves extend smoothly to subzero temperatures. In all

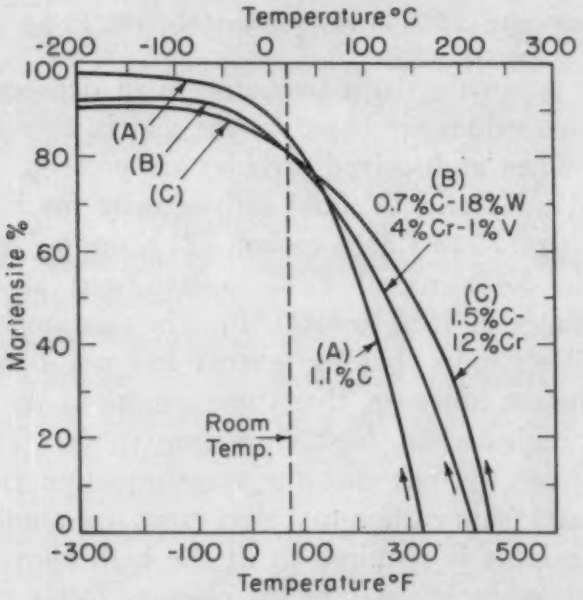


Fig. 7—Martensite Transformation Above and Below Room Temperature in (a) 1.1% Carbon Steel (15, 22), (b) 18-4-1 High Speed Steel (23), and (c) High Carbon, High Chromium Steel (24) Austenitized at 1550, 2350 and 1800 °F Respectively.

the cases that we have investigated carefully so far, the subzero transformation is essentially self-stopping; that is, it peters out (even during continuous and rapid cooling) short of completion by amounts that are well beyond the experimental error of the X-ray (26) and dilatometric methods (22) that have been brought to bear on the problem. According to these techniques, plain carbon and low alloy steels (0.70 to 1.25% carbon) cease transforming at about —250 °F with 0.5 to 5% austenite still available. High speed and high carbon, high chromium steels stop transforming at about —150 °F with 8 to 15% austenite remaining.

If hardened steel is aged at room temperature prior to subcooling, the retained austenite becomes stabilized against subzero trans-

formation. The characteristics of this process are shown in Fig. 8. In the first place, some isothermal decomposition of the retained austenite occurs during the stay at room temperature. This causes the small vertical line at 68 °F. The course of the subsequent cooling transformation is shown after 1, 10 and 50 hours at room temperature, in comparison with the normal transformation for continuous cooling through room temperature. It is evident that, as a result of the stabilizing process, there is a temperature interval in each case down to the point labeled M_s' during which no detectable transforma-

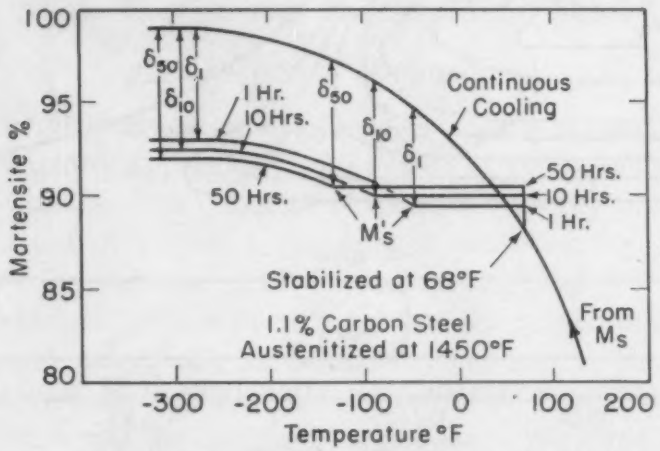


Fig. 8—Retained Austenite Transformation in 1.1% Carbon Steel, Austenitized at 1450 °F, on Continuous Cooling Through Room Temperature and After Aging 1, 10 and 50 Hours at Room Temperature. δ values indicate degree of stabilization caused by aging at room temperature.

tion occurs. Below M_s', the austenite-martensite reaction sets in, and follows rather parallel to the master curve, but displaced from it by approximately the amount of transformation (δ) that would occur between room temperature and M_s' if the stabilization had not taken place. The stabilized curves flatten out at the same temperature as does the unstabilized curve, and this indicates that stabilization does not displace the transformation to lower temperatures. Rather, there is almost a quantitative displacement in the vertical direction, just as though the percentage of austenite (δ) that does not transform on cooling to M_s' remains lost to the transformation even on cooling to temperatures well below M_s'. δ then becomes a quantitative measure of the extent of stabilization. It should be emphasized that the amount of isothermal transformation that takes place at room temperature is much too small to account for the stabilizing phenomenon.

Fig. 8 shows that δ increases, or M_s' is depressed, the longer

the holding time at room temperature. If the hardened steel is aged at elevated temperatures, instead of at room temperature, prior to refrigeration, the stabilization is even more marked and occurs more rapidly. The temperature-dependence of the rate of stabilization may be expressed as a heat of activation of 22,000 cal/mol for high carbon, low alloy steels (27, 28).

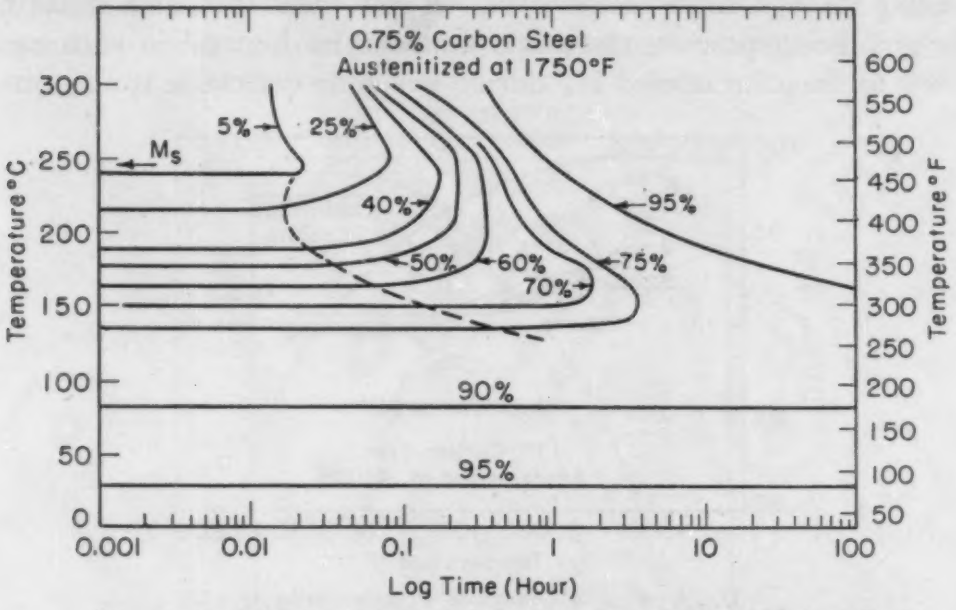


Fig. 9—Austenite Decomposition Diagram (21) for 0.75% Carbon Steel, Austenitized at 1750 °F. Horizontal lines represent martensite formation on cooling, curved lines show bainite formation on isothermal holding. Dashed line indicates beginning of isothermal transformation below M_s.

Kinetics of the Austenite-Bainite Reaction Below M_s

When the cooling of steel is interrupted at some temperature below M_s, the austenite remaining from the martensite transformation becomes available for isothermal decomposition into bainite. Fig. 9 illustrates the blending of the bainite and martensite reactions in a 0.75% carbon steel (21).

Above M_s, the time for bainite formation increases with decreasing temperature in accordance with the well-known C-curve behavior. Below M_s, the bainite curves are intercepted by a family of horizontal lines representing the insuppressible martensite transformation. The martensite lines remain horizontal in point of time until the isothermal decomposition of the remaining austenite commences, and then bend upward to meet the corresponding bainite lines extending down from higher temperatures. The dashed line in Fig. 9 denotes the locus of times at which bainite begins to appear on holding below

M_s. The shape of this line signifies that the bainite reaction is accelerated by the coexisting martensite, but this stimulating effect fades out at longer times and at lower temperatures, where the bainite curves tend to resume their original shape, as projected down from above M_s. At temperatures near the ambient, the austenite surviving the martensite transformation is so sluggish with respect to bainite formation that the latter does not form in any detectable amount for thousands of hours. At these low temperatures, retained austenite is remarkably persistent.

Explanation of the Retention of Austenite

Discarded Attempts

We are relatively unimpressed by the fact that retained austenite does not transform appreciably into *bainite* at room temperature. The bainite reaction, as in the case of pearlite, is typically time-dependent, and it is natural to expect a vanishingly small reaction rate at sufficiently low temperatures. This is exactly what Fig. 9 indicates. On the other hand, it is quite surprising that the austenite resists transformation into *martensite* on isothermal holding, when one remembers that martensite plates are able to form in a flash, even at subzero temperatures, while the cooling is underway. We must seek the key to this striking phenomenon, for it holds the explanation of the retention of austenite. Surely, if martensite could form isothermally with the same proficiency that it does while the temperature is dropping, there would be no retained austenite in hardened steel.

It is conceivable that, if the martensite were to have a slightly different composition from that of the parent austenite, the resulting change in composition of the remaining austenite might increase its stability relative to the martensite at a given temperature, and thus necessitate further cooling to keep the reaction going. This situation would be analogous to cooling an alloy through a two-phase field in which the phase compositions change with temperature, thus determining the relative amounts of the two phases that may coexist. If this hypothetical alloy were endowed with the faculty of quickly attaining equilibrium at any temperature, obviously the transformation of one phase into the other could not proceed unless the temperature were lowered. But such a process involving partition of concentrations would require that diffusion play a controlling role in the austenite-martensite reaction, and there is convincing evidence that this is not the case.

In the first place, the fact that martensite plates propagate with great speed, even at low temperatures where diffusion rates are extremely small, leads us to the important conclusion that martensite formation does not have to wait for diffusion, as do the familiar nucleation and growth reactions. Furthermore, lattice parameter measurements (which are sensitive functions of dissolved carbon in austenite and martensite, as shown by Fig. 2) invariably indicate that martensite and retained austenite in the same specimen have exactly the same carbon content, unless parasitic tempering reactions are allowed to occur. Knowing that interstitial carbon is able to diffuse ever so much more rapidly than substitutional elements (Table I), we are justified in assuming that if the carbon does not concentrate in one phase or the other, the alloying elements certainly do not either.*

In fact, there is good reason to believe that the carbon atoms do not even move out of their interstitial sites during the shear mechanism that generates the body-centered tetragonal martensite lattice. According to Fig. 2, the degree of tetragonality is a direct function of the carbon content. At zero carbon, the axial ratio becomes unity, and the body-centered tetragonal lattice degenerates to the body-centered cubic lattice of ferrite. The interstitial sites of the body-centered cubic lattice (Fig. 3) lie at the centers of the cube faces and at the midpoints of the cube edges. There are six of these sites per unit cell (six face positions shared by two cells each, and twelve edge positions shared by four cells each). The body-centered cubic lattice also contains two iron atoms per unit cell, or three interstitial pockets per lattice point. This is three times as many as there are in the face-centered cubic austenite.

It is obvious that if the interstitial sites in the body-centered cubic lattice were occupied at random by carbon atoms, the resulting lattice would be expanded, but would remain cubic, as in the case of austenite. The tetragonal structure of martensite can be accounted for if the carbon atoms are confined to one-third of the possible pockets (Fig. 3). This arrangement stretches the cell in the Z-direction and leads to tetragonality (7, 8). Now Greninger and Troiano (30) have found that, among other crystallographic comparisons, the (020) plane of the austenite becomes the (110) plane of the martensite. Lyman (31) points out that all the carbon atoms in the austenite lie on (020) planes, and hence if the carbon

*Moreover, the martensite transformations that occur in relatively pure lithium (18), cobalt (29) and zirconium (19) are presumably not controlled by concentration differences.

atoms actually maintain their original positions relative to the iron atoms during the transformation, they should find themselves exclusively on the (110) planes in the martensite. This, in turn, is found to produce exactly the preferential arrangement of carbon atoms required for stretching the body-centered cubic lattice of ferrite into the body-centered tetragonal lattice of martensite. Therefore, we may suspect that during the martensite reaction, the carbon atoms do not even escape into alternate interstices (to any appreciable degree), let alone diffuse sufficiently to cause a concentration difference between the austenite and martensite.

The prevailing "stress-theory" of martensite formation must also be discarded. According to this picture, the large volume expansion attending the austenite-martensite reaction exerts a constraining pressure on the remaining austenite and hence curtails its ability to undergo further transformation. Any factor that relieves this opposing pressure, or facilitates expansion, favors the continuation of the transformation. The thermal coefficient of contraction of austenite is large compared to that of martensite, and it has been proposed that (during cooling) the contraction of the austenite relative to the martensite enables the transformation to continue without necessitating much expansion of the over-all specimen. Undoubtedly, these stress effects do operate to some extent during the austenite-martensite reaction, for they are in accord with the LeChatelier principle, which states that if a condition of equilibrium in a system is changed (pressure, temperature, etc.), the equilibrium shifts in the direction which tends to undo the effect of the imposed change. However, we now have sufficient data to prove conclusively that these stress effects neither control nor explain the salient features of the austenite-martensite reaction.

It is convenient to differentiate between macrostresses and microstresses in this argument. *Microstresses* are those that exist on a localized scale between martensite plates and their immediate environment, and arise from the volume change of the transformation. *Macrostresses* are those that exist on a long-range scale between different parts of a specimen, and arise from both the phase change and the thermal gradients set up during the quenching. We can deal the macrostress factor a fatal blow by noting that specimens may be quenched into brine directly from the austenitizing temperature, as well as from just above M_s, and the amount of retained austenite is identical in the two cases. Yet the thermal gradients

and macrostress conditions are obviously quite different. Also, Troiano (32) has observed that the retained austenite contents along the length of a Jominy bar are the same as found in small specimens cooled at corresponding rates. Here again the macrostress conditions are quite different. Finally, as Carpenter (33) and Robertson (34) point out, hardened steel usually contains a gradient of stress ranging from compression in the core to tension at the surface, but no resultant gradient of retained austenite exists. In fact, steels that are largely austenitic in the as-quenched state have the opposite stress gradient: tension in the core and compression at the surface. Hence, contrary to the theory, we find high contents of retained austenite even in the presence of tensile stresses.

And what about the microstress factor? This explanation also crumbles in the light of the lithium (18) and zirconium (19) martensite reactions which produce virtually no change in volume. Furthermore, the argument that the differential thermal contraction of the austenite with respect to the martensite allows the transformation to proceed without causing much expansion is fallacious, because quenching dilatometer experiments disclose very large over-all expansions during the transformation (35). In other words, martensite is quite able to form despite such opposing back pressure that may exist in steel. It is a delusion, then, to rely upon this factor for inhibiting the transformation during isothermal holding.

It may be added that according to Laszlo (36) the back pressure, which theoretically hinders the reaction, increases to a maximum at about 50% transformation and then diminishes as the material becomes more homogeneous. Hence, if microstresses due to volume changes were controlling the reaction, martensite formation should speed up beyond 50% transformation. Actually, the reverse is true; the transformation curves exhibit a marked retardation of the reaction per degree of dropping temperature during the latter stages of the reaction.

And finally, the back-pressure theories cannot explain the fact that the M_s temperature lies several hundred degrees Fahrenheit below the critical range. It turns out that the amount of strain energy associated with the volume change of the transformation is only about 15 cal/mol (36), and this could account for a lowering of the equilibrium temperature of hardly more than 20 °F.

Theory of the Austenite-Martensite Reaction

It should now be evident that we shall not understand the retention of austenite without coming to grips with the fundamentals of the martensite reaction. The one cannot be grasped without the other, for both are part and parcel of the same problem. Having already rejected some of the existing notions about this transformation, let us see whether we can do something more constructive.

Bearing in mind that the austenite-martensite transformation involves a shear mechanism that does not have to wait for diffusion, we may postulate that two conditions must be fulfilled in order for the reaction to occur:

(a) The thermodynamic factors must be such that an over-all decrease in free energy attends the martensite formation; otherwise the transformation cannot proceed spontaneously.

(b) Activated regions must exist in the austenite where the formation of martensite plates can start.

Stated another way, we are going to assume that the shears, which generate the martensitic phase, propagate from nuclei in the austenite, but that the nuclei do not become active unless the driving force for the transformation is powerful enough to overcome all the obstacles that tend to resist the shearing process.

Although a given martensite plate may be born within a ten-thousandth of a second, we find difficulty in visualizing it as forming all at once. The major dimension of the largest plate is of the order of the austenite grain diameter, and this means that literally trillions of atoms would have to decide to move in the same direction at the same time (Fig. 10A). If we had to wait for such an improbable circumstance, martensite formation would be a very rare event indeed.

As illustrated in Fig. 10, it is much more likely that the shear originates at a nucleus and travels quickly across the austenite grain to generate the martensite plate. Two modes of nucleation should be considered. In Fig. 10B, the nucleus is portrayed as an incipient particle of martensite which grows rapidly at the expense of the austenite. Under such circumstances, we should have no hesitation in classing the martensite reaction as a process of nucleation and growth. However, there is a subtle difficulty with this picture. Grain boundaries (and also slip bands) are known to act as barriers to the martensite shear even though the nucleation may occur there. A small austenitic grain size actually makes it more difficult for martensite to form, and this is why the start of the transformation has to

wait for lower temperatures (M_s is depressed) in the presence of such obstruction. The incipient martensite particle appears to sense in advance the barrier conditions that lie in its potential path ahead, and these conditions enter into the decision as to whether the shear will materialize or not at a given temperature. Obviously, the nucleation and growth process in Fig. 10B is not endowed with such anticipatory powers.

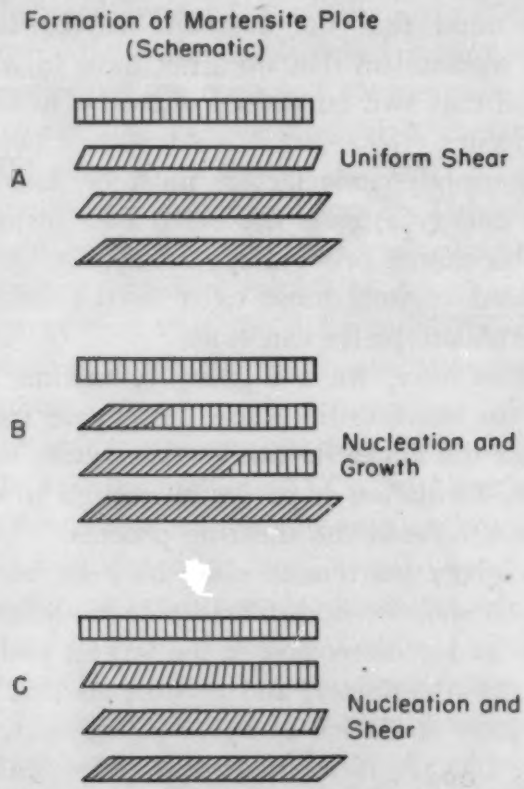


Fig. 10—Schematic Representation of Martensite Formation by (A) Uniform Shear, (B) Nucleation and Growth, and (C) Nucleation and Shear.

This dilemma disappears in the nucleation and shear process depicted in Fig. 10C. Here, the nucleus, in attempting to shear into martensite, transmits a force (or displacement) that travels ahead through the austenite with the speed of a sound wave. The interaction of this force with any obstacle, even far removed, is transmitted back to the nucleus, again at the velocity of sound; and in this way, the nucleus receives a signal as to the nature of the road ahead. If the conditions are favorable, that is, if the driving force of the reaction is large enough to overcome the existing barriers, the shear propagates in wave fashion, and a plate of martensite is born. If

the driving force is inadequate, the shear does not progress and the potential nucleus remains inactive, until at some lower temperature the driving force becomes sufficiently large.

The criterion of driving force that we shall use here is $F^A - F^M$, the excess in chemical free energy per mol of austenite over that of martensite of the same composition. Mr. Paranjpe (37) has calculated this driving force numerically as a function of carbon content and temperature, extrapolating the carbon activity data of Smith (38) and applying a few assumptions which need not be discussed here.

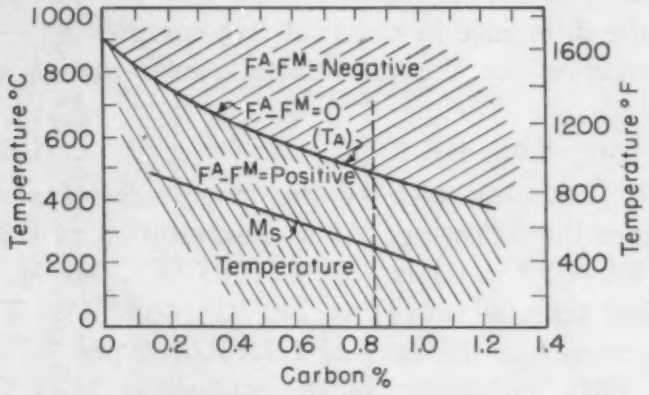


Fig 11—Effect of Temperature and Carbon Content on Driving Force (FA — FM) of Austenite-Martensite Transformation. Driving force is positive below temperature T_A, but reaction occurs only below M_s (43). FA — FM increases at rate of 1.3 cal/mol/°C with dropping temperature in 0.85% carbon alloy (37).

Fig. 11 shows the effect of carbon content and temperature on the relative stability of austenite and martensite. Below T_A, $F^A - F^M$ becomes positive and there is a finite driving force favoring the transformation of austenite into martensite. This is essentially the type of diagram first conceived by Johansson (39), and more rigorously extended by Zener (40).

The austenite-martensite transformation does not start just below T_A, where the driving force first becomes positive, because of the barrier conditions just alluded to. First, as we have previously noted, a small amount of strain energy (ΔF_ϵ) is produced by the attendant volume change, and this—about 15 cal/mol (36)—must be supplied by the difference in chemical free energies $F^A - F^M$. Secondly, new interfaces are evolved, and these require energy. If coherency exists between the austenite and martensite, the interfacial energy is in the form of elastic strain; if true surfaces exist, then there is surface energy. For the present purposes it is not

necessary to distinguish between these two forms of interfacial energy; they can be lumped into a single term (ΔF_r), the increase in interfacial energy per mol of martensite produced. The subscript r represents a specific size of martensite plate. As r becomes smaller, the amount of interfacial area per mol of martensite increases and so does ΔF_r.

Thirdly, the martensite shear does not take place reversibly. We know this from the fact that the movement has sufficient momentum to make the transformation noisy. The associated kinetic energy (K.E.*) is dissipated into heat, and this energy must also come from the difference in chemical free energies $F^A - F^M$. Thus, our first condition for the martensite transformation can now be written:

$$F^A - F^M \geqslant \Delta F_\epsilon + \Delta F_r + \text{K.E.} \qquad \text{Equation V}$$

We can obtain an idea of the magnitude of some of these quantities from the following: At a concentration of 0.85% carbon, T_A (where $F^A - F^M = 0$) is 485 °C (905 °F), but M_s (where the transformation actually starts) is 240 °C (465 °F). The quantity $F^A - F^M$ increases at the rate of 1.3 cal/mol per °C of dropping temperature (37), and hence is 320 cal/mol at M_s. Thus

$$\text{At } M_s: 320 \text{ cal/mol} \geqslant \Delta F_\epsilon + \Delta F_{r_s} + \text{K.E.} \qquad \text{Equation VI}$$

$$\Delta F_\epsilon \sim 15 \text{ cal/mol}$$

$$\text{or } 305 \text{ cal/mol} \geqslant \Delta F_{r_s} + \text{K.E.} \qquad \text{Equation VII}$$

where r_s indicates the size of the first martensite plates. While we are not able to calculate ΔF_{r_s} and K.E. separately, it is interesting to note that the ΔF_ϵ term is only about 5% of $F^A - F^M$, and hence is not an important factor in controlling M_s. We shall, therefore, drop it from further discussion.

The course of the martensite reaction can now be presented in terms of these concepts. In Fig. 12, the chemical free-energy curves for martensite and austenite of a given composition are shown schematically as a function of temperature. The ΔF_r and K.E. relationships are also indicated, the latter being taken as constant throughout the course of the reaction. ΔF_r has the initial value ΔF_{r_s}, which is larger the smaller the austenitic grain size. The temperature at which the driving force $F^A - F^M$ becomes large enough to exceed ΔF_{r_s} + K.E. determines the M_s temperature. However, in the presence of a general amount of martensite (P), the remaining austenite is blocked off into small volumes by the

*This term may also be considered to contain all other irreversible factors.

existing martensite, and so the effective size of the new plates to form must be smaller than r_s. This, in turn, means that ΔF_r is larger than ΔF_{r_s}, and the reaction does not proceed until the temperature is lowered to the point where $F^A - F^M$ exceeds the greater barrier condition. When this happens, ΔF_r becomes still larger, and throttles the reaction unless $F^A - F^M$ is increased again by further cooling.* Physically, the barrier is not "broken down"

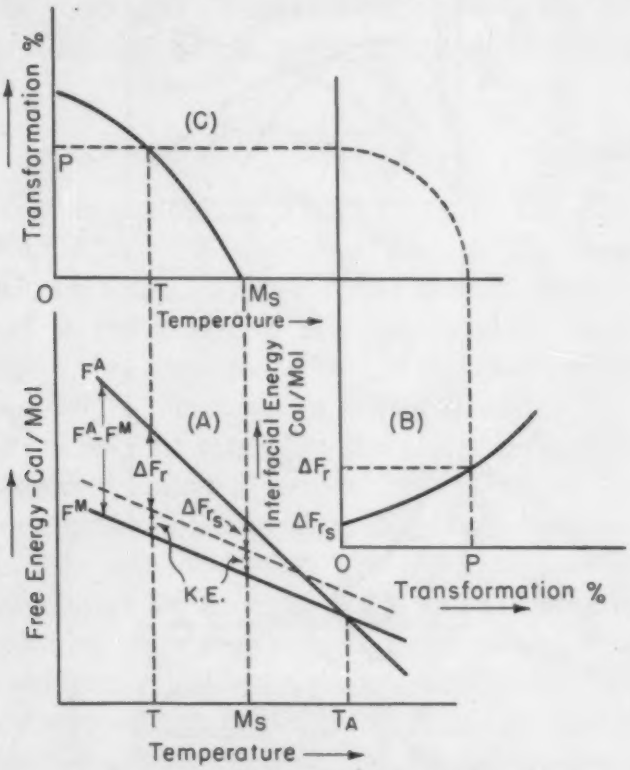


Fig. 12—Relationships Between Chemical Free Energies (FA and FM) and Nonchemical Energy Requirements (ΔF_r and K.E.) of the Austenite-Martensite Reaction.

by the driving force, but compels the new martensite to form in smaller and smaller units, necessitating larger and larger values of $F^A - F^M$ for the continuance of the transformation.

In these thermodynamical considerations, we have presupposed that nuclei are available in sufficient numbers to allow the over-all free-energy conditions to govern the start and course of the martensite transformation. Where do such nuclei come from? Obviously

*This thermodynamic picture is equally applicable to the martensite transformations of nonferrous systems (41) and readily accounts for the reverse transformation that is frequently observed on heating. In the case of steel, the reverse transformation does not take place because the martensite decomposes via tempering reactions.

they do not originate during the quenching process because, then, M_s would be generally sensitive to the cooling rate. Fisher, Hollomon and Turnbull (42) have recently offered the ingenious suggestion that potential nuclei (called embryos) actually exist in the parent phase at the austenitizing temperature, are frozen in during

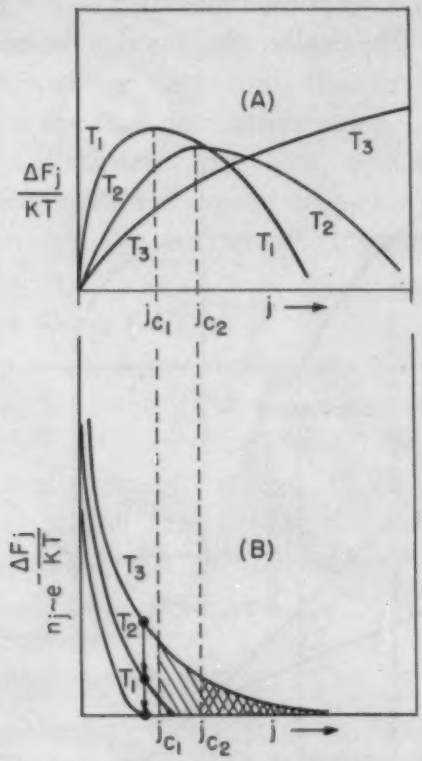


Fig. 13—Equilibrium or Steady-State Distribution of Embryos at Three Temperatures: T_1 and T_2 in Martensite Range, T_3 Above Critical Range ($T_1 < T_2 < T_3$). (A) Free energy of embryo formation as a function of number of atoms (j) in embryo. (B) Number of embryos (n_j) as a function of j. Shaded areas indicate number of embryos existing at T_3 that become potential nuclei at T_2 and at T_1. *Fisher, Hollomon and Turnbull* (42).

the quench, and are thus on hand for duty when the martensite range is reached. The increase in free energy accompanying the formation of an embryo containing a given number of atoms (j) is sketched hypothetically in Fig. 13A for one temperature (T_3) at which austenite is stable, and for two temperatures (T_2 and T_1) below M_s. At the latter temperatures, the curves pass through maxima, and hence embryos exceeding the critical size (j_c) are able

to grow spontaneously into a second phase. Such embryos are called nuclei, and it will be noted that the critical size decreases with decreasing temperature. At T_3, the free-energy curve increases without limit, and hence none of the embryos can become nuclei of a second phase at this temperature.

At each temperature, whether austenite is the stable phase or not, there tends to be an equilibrium or steady-state distribution of embryos in the austenite. The number of embryos of any given size (j) varies approximately with ΔF_j and the temperature as follows:

$$n_j \sim e^{-\Delta F_j/kT} \qquad \text{Equation VIII}$$

This relationship is plotted in Fig. 13B, with the $\Delta F_j/kT$ values taken from Fig. 13A. It is evident that at T_3 there are many embryos which exceed j_{c_3} in size and which, therefore, become potential nuclei if the austenite is cooled rapidly from T_3 to T_2. At T_1, since $j_{c_1} < j_{c_2}$, even more of the high-temperature embryos would be promoted to the status of potential nuclei.

The embryos may be related to the statistical groupings of iron and carbon atoms mentioned earlier, although they may also be looked upon as transient structural units, or even momentary energy concentrations. In any case, they are small regions that exist in the stable austenite at high temperatures and are endowed with the ability of activating martensitic shears when the temperature is lowered sufficiently to fulfill two separate conditions: (a) the driving force must be large enough to satisfy Equation V, and (b) some of the original embryos must exceed the critical nucleus size at the lower temperature. The fulfillment of condition (b) alone leads to potential nuclei, which cannot propagate into martensite until condition (a) is satisfied.

It is highly improbable that both of these conditions will become satisfied simultaneously at the same temperature during cooling. Therefore, in general, the first condition to be fulfilled only "cocks" or sets the stage for the transformation, while the second condition to be fulfilled "triggers" or controls the reaction. Is it possible to ascertain which is the second or controlling condition? The answer is: yes, by means of critical studies of the stabilization process, previously discussed in connection with subzero transformations. Suppose the hardening quench is interrupted at some temperature T_2 below M_s for an appreciable length of time, but not long enough

to form bainite. At T_2, there will be a tendency for the austenite to lose embryos (not already consumed by the existing martensite) as the distribution shifts from that of T_3 to that characteristic of T_2 (note arrows in Fig. 13B). Such a shrinkage of embryos involves diffusion, and its rate would be expected to depend upon temperature and time. Now if the available number of potential nuclei is quite limited, stabilization should be observed because the loss of potential nuclei during the holding treatment will inhibit the continuance of the transformation on further cooling, despite the increased driving force, until a temperature is reached where the critical size is small enough to promote the largest of the remaining embryos to the status of nuclei. Then the transformation can proceed. On the other hand, suppose that at the holding temperature the potential nuclei are plentiful. Then, the loss of some will not materially affect the course of the subsequent transformation when the cooling is resumed and no stabilization should be observed. We would conclude in this case that the transformation is controlled primarily by the over-all free-energy change because potential nuclei are available in ample supply.

Let us now consider the phenomenon of stabilization in this new light.

Stabilization of the Austenite-Martensite Reaction

Fig. 14 shows the effect of arresting the hardening quench of a 1.1% carbon – 1.5% chromium steel for 30 minutes at various temperatures within the martensite range before cooling to the ambient (15). If, for example, the hardening quench is stopped at 130 °F, the steel contains 51% martensite on reaching this temperature. After the hold of 30 minutes, the cooling transformation is completely inhibited down to about 115 °F, where it sets in and follows parallel to the normal transformation curve. During the cooling between 130 °F (T_h = the holding temperature) and 115 °F (M_s'), approximately 6% of austenite would have transformed into martensite, were it not for the stabilizing effect at T_h, and 6% remains lost to the transformation in view of the fact that the stabilized curve is displaced vertically from the unstabilized curve by just this amount.

The conclusion that we may reach in the light of the foregoing results is that enough potential nuclei disappear during the holding treatment at T_h to interfere with the progress of the subsequent cooling transformation. Thus, the transformation must wait until

the temperature is lowered to the level where the critical nucleus size becomes commensurate with that of the largest remaining embryos. As an alternative explanation, it might be argued that the same process which permits the shrinkage of embryos during the holding period may also lessen the driving force $F^A - F^M$, and that the austenite becomes somewhat more stable (in a thermodynamic sense) with respect to martensite. However, whether this

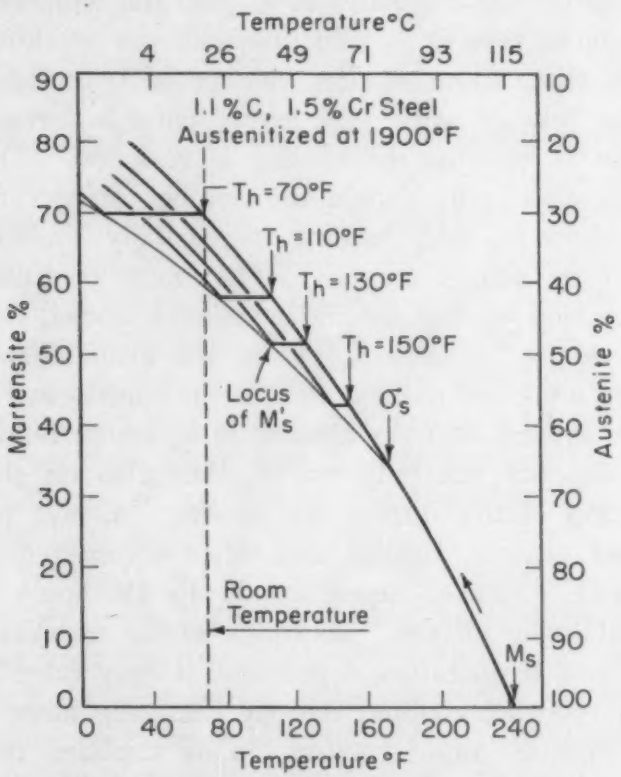


Fig. 14—Martensite Transformation in 1.1% Carbon – 1.5% Chromium Steel, Austenitized at 1900 °F, During Continuous Cooling and After Holding ½ Hour at T_h = 150, 130, 110 and 70 °F (15).

effect occurs or not, it does not exert a controlling influence on the reaction because then the stabilized curve would be displaced horizontally to lower temperatures. Actually, the displacement is in the vertical direction, as previously emphasized.

It appears from Fig. 14 that the extent of stabilization occurring in 30 minutes increases as the holding temperature is decreased. At first glance, this seems like a contradiction of an earlier statement (page 52) to the effect that stabilization takes place faster the higher the temperature. The latter represents the true temperature-

dependence of stabilization where the amount of coexisting martensite is constant. However, stabilization is greatly affected by the presence of martensite; the more martensite, the more readily stabilization occurs. This factor predominates in Fig. 14 and explains the anomalous increase of stabilization with decreasing temperature.

There is a temperature, which we shall call σ_s, above which no measurable stabilization is caused by a 30-minute hold. The locus of M_s' temperatures extrapolates to σ_s, and the temperature interval $T_h - M_s'$ becomes zero at σ_s. In line with our working theory, we may conclude that, above σ_s, the number of potential nuclei is so large that the loss of some still leaves enough for activating the transformation as soon as the cooling is resumed. This poses the interesting question: why should the number of potential nuclei be so plentiful above σ_s and become increasingly limited below σ_s? There is a very simple answer. The mere continuance of the martensite reaction during cooling consumes nuclei, by starting at some and sweeping out others. Thus, the availability of potential nuclei becomes more and more critical as the transformation proceeds.

It is now evident that the amount of austenite retained at room temperature depends not only on M_s, but also on the degree of stabilization that occurs during the cooling (always presupposing, of course, that pearlite, bainite and other nonmartensitic products are suppressed). Hence, Equations II to IV apply only in the absence of stabilizing effects. Inasmuch as the stabilization process is both time and temperature-dependent, it may have a chance to set in during retarded cooling, thereby retaining more austenite at the ambient than on rapid cooling. This explains the fact, long known in practical heat treatment, that oil quenching of tool steels frequently leads to more retained austenite than water quenching. We shall see that martempering, which involves air cooling through the martensite range, results in still more retained austenite.

Can we be sure that the increment of excess austenite retained by slower cooling is caused by the stabilization process, rather than by a variation in quenching stress? Let us compare the effect of quenching medium on two steels: 1.1% carbon – 1.5% chromium and 1.1% carbon – 5.4% nickel. As shown in Table III (15), when these steels are hot-quenched to 450 °F (above M_s in both cases) and then cooled in brine, oil and air, the slower cooling rates definitely increase the retained austenite in the chromium steel ($\sigma_s = 176$ °F), but not in the nickel steel which is insensitive to

stabilization above room temperature ($\sigma_s = 77$ °F). Clearly, the variation in cooling rate is operative only insofar as it affects the stabilizing process.

Table III
Effect of Quenching Medium on Retained Austenite at 77 °F (15).

Austenitizing temperature = 1900 °F. Hot-quenched to 450 °F, and then cooled to 77 °F as shown.

Steel	M_s, °F	σ_s °F	Per Cent Austenite Brine	Oil	Air	Per Cent Austenite Stabilized Oil-Brine	Air-Brine
1.1% C – 1.5% Cr	240	176	31	33	40	2	9
1.1% C – 5.4% Ni	155	77	66	66	66	0	0

When the austenite is highly alloyed, the tendency toward stabilization becomes so marked that it can occur even in the absence of martensite. In such cases, σ_s lies above M_s. For example, in certain high carbon, high chromium steels, stabilization sets in if the cooling rate in approaching M_s is retarded ever so slightly, and extremely rapid cooling must be invoked in order to prevent the M_s temperature from being depressed by the encroaching stabilization (44). These findings suggest that potential nuclei are in short supply in high alloy austenites, and that if some are lost by slow cooling, even in the absence of martensite, the transformation is inhibited. High speed steel occupies an intermediate position in that σ_s lies very slightly below M_s (45). Here, the supply of potential nuclei is adequate to make M_s insensitive to cooling rate, but the formation of several per cent martensite wipes out enough of these nuclei so that stabilization effects can then be observed. As we have seen, with lower alloy steels appreciably more martensite must form before the nucleus supply becomes the limiting factor.

It should be mentioned that, even below σ_s, stabilization in ordinary hardening can be avoided by rapid cooling because of its time-dependent nature. However, the theory predicts that, toward the latter stages of transformation, the stabilization should become insuppressible because of the loss of nuclei, not by time-dependent shrinkage, but by consumption in the transformation. At subzero temperatures, the critical nucleus size does not decrease rapidly with decreasing temperature, and the reaction can proceed during cooling only as fast as existing embryos become advanced to the status of nuclei by the dropping temperature. This explains why the reaction becomes essentially self-stopping at subzero temperatures. It also accounts for the fact that the reaction in low alloy steel

ceases at lower temperatures with less austenite remaining than in the case of high alloy steels, for we have seen that the latter behave as though their supply of available nuclei is more limited.

One might also venture the guess on these grounds that the self-stopping should not become absolutely complete, even at the lowest subzero temperatures previously mentioned, because at least a few more nuclei should become available at still lower temperatures. Some preliminary runs were recently made down to liquid helium temperatures (−452 °F = 4 °K) by Mr. Lement (46) using a precision-length technique (47) for measuring the extent of transformation. Until these experiments, the lowest temperature reached in this type of work was that of liquid nitrogen (−321 °F = 77 °K). In a low alloy tool steel, about one-third of the 2% austenite available at −321 °F was found to transform on cooling to −452 °F; while in high speed steel, the corresponding figures were one-fifth of the available 8%.

Quantities of Retained Austenite

Effect of Chemistry

Retained austenite contents at room temperature range all the way from 100% in the austenitic steels down to nil in the plain low carbon steels. Stainless steel of the 18% chromium – 8% nickel type and Hadfield's steel containing 1.2% carbon – 12.5% manganese are the classical examples of commercial austenites having their M_s below room temperature. Going down the line in retained austenite contents, we find 25 to 35% austenite in commercially hardened 1% carbon – 5% chromium die steel, 15 to 30% austenite in the 1.5% carbon – 12% chromium die steels, 15 to 25% austenite in high speed steels, and 3 to 15% in low alloy tool steels. Commercially hardened plain carbon tool steels retain about 5 to 10% austenite. The above values are subject to considerable variation because of the influence of austenitizing conditions and cooling rate effects.

As shown in Fig. 15, the quantity of retained austenite is markedly dependent upon the *dissolved* carbon content. It is surprising to observe than even in 0.2% carbon steel (brine-quenched from above A_3), we find up to 2% retained austenite. The extrapolation of the band in Fig. 15 suggests that traces of retained austenite may even be present in very mild steel.

We have seen that over an appreciable range of carbon and alloy contents, there exists a quantitative relationship between

retained austenite and M_s. Qualitatively, there is good correspondence between these two factors over much wider limits. Table IV lists nine elements in order of their effect on M_s, and it is evident that the same order applies to their effect on austenite retention. As might be expected, the two elements, cobalt and aluminum, which raise M_s also lower the amount of retained austenite.

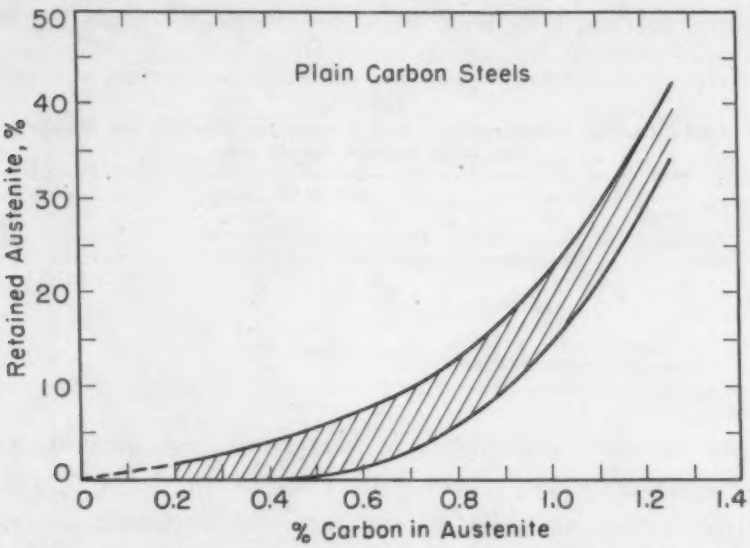


Fig. 15—Effect of Carbon Content on Retained Austenite in Plain Carbon Steels. Austenitized above Ac_3 and A_{cm}, and quenched in water or brine.

Carbon is, by far, the most potent element of those listed in its effect on austenite retention. The value shown in Table IV is estimated from the slope of the band in Fig. 15 at the 1% carbon level. Of course, all the factors in Table IV are approximations, and should be regarded merely as rough guides. They apply only to the chemistry of the austenite, and not to the composition of the steel as a whole when undissolved carbide or ferrite is present.

Table IV
Relationship Between the Effects of Elements on M_s and on Propensity for Retaining Austenite

Element	Change of M_s per 1% of Element (48)	Change of Retained Austenite* per 1% of Element (49)
Carbon	−540 °F	+50%
Manganese	− 60	+20
Chromium	− 40	+11
Nickel	− 30	+10 (15)
Molybdenum	− 20	+ 9
Tungsten	− 20	+ 8
Silicon	− 20	+ 6
Cobalt	+ 10 (49)	− 3
Aluminum	+ 30 (49)	− 4

*In presence of 1% carbon.

Effect of Austenitizing Temperature

It is well known that the austenitizing temperature has a large effect on M_s, and therefore on austenite retention, because the chemistry of the austenite changes with increasing carbide (or ferrite) solution. This factor is of major importance in the commercial heat treatment of high carbon steels, where carbides are deliberately left undissolved to some extent. In Table V, the amounts of retained austenite are presented as a function of austenitizing temperature and chromium content in 1.1% carbon steels. After austenitizing at 1550 °F, the retained austenite decreases with increasing chromium because the latter reduces the carbide solubility. However, once the carbides are substantially dissolved (1900 °F), the retained austenite increases with the chromium content as expected. Austenitizing at 1700 °F produces intermediate results.

Table V
Effect of Austenitizing Temperature* and Chromium Content on Retained Austenite in 1.1% Carbon Steels (15)

Per Cent Chromium in Steel	1550 °F		1700 °F		1900 °F	
	% Retained Austenite	% Undissolved Carbide	% Retained Austenite	% Undissolved Carbide	% Retained Austenite	% Undissolved Carbide
0	16	0.5	20	0	20	0
1.5	7	4.5	22	1.6	31	0
2.8	2	6.9	21	3.5	51	1.1

*All specimens brine-quenched to 77 °F.

There is another effect of austenitizing temperature over and above that of composition change. This phenomenon can be observed particularly well in the 5% nickel steel that we shall use as an example. In Fig. 16, we note that the retained austenite content continues to increase by a large amount, even beyond the point of complete carbide solution. Austenitizing at 1550 °F for ½ hour dissolves all the carbide in this 1.1% carbon – 5.4% nickel steel, and 39% austenite is retained on brine quenching. Yet austenitizing at 1900 °F yields 70% austenite without any further change in the composition of the austenite.

It would be quite natural to suspect at first glance that submicroscopic carbides continue to dissolve on heating from 1550 to 1900 °F; but surely the extent of such solution could hardly account for an increase in retained austenite of some 30%. In fact, lengthening the soaking time at 1550 °F by a factor of ten does not change the austenite percentage shown by the curve in Fig. 16. Further-

more, this phenomenon cannot be explained by the progressive disappearance of residual concentration gradients because the effect is essentially *reversible*. If the steel is first austenitized at 1900 °F, then cooled to 1580 °F (above the carbide precipitation temperature) and held for a sufficiently long time, the per cent of retained austenite gradually decreases and overtakes the value obtained when the steel is austenitized at 1580 °F in the first place.

I believe that this reversible phenomenon offers evidence of the statistical concentration distributions discussed earlier. It turns out

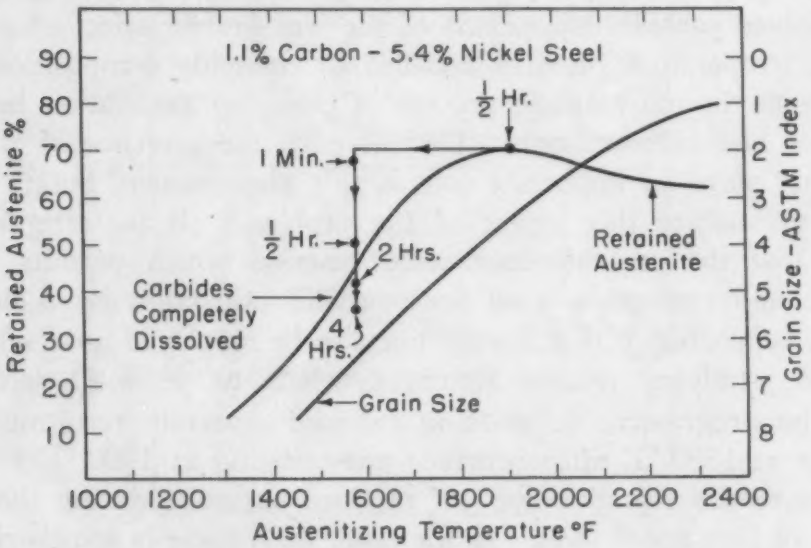


Fig. 16—Effect of Austenitizing Temperature on Retained Austenite and Grain Size in 1.1% Carbon – 5.4% Nickel Steel, Brine-Quenched to 70 °F. Heating time = ½ hour, except where shown (13).

that the driving force $F^A - F^M$ is vitally dependent on the carbon activity in the austenite. At any given temperature in the martensite range, $F^A - F^M$ increases with decreasing carbon activity. However, the carbon activity is not only dependent upon the carbon content, but also upon the degree of association with the iron, and is in turn affected by the statistical distribution in the iron lattice. Since the over-all carbon content remains constant on holding at 1580 °F after the complete carbide solution at 1900 °F, the decrease in retained austenite appears to result from the increasing "separation" of high and low carbon groupings that are stable at 1580 °F compared to the distribution that is stable at 1900 °F. The fact that the phenomenon at 1580 °F is time-dependent suggests that diffusion is involved, and this is certainly necessary for the postu-

lated grouping process. On the other hand, time would not be an important factor if the effect were simply due to a change in bonding energy of the atoms in place.

If the steel is first soaked at 1580 °F and then heated further, the equilibrium distribution characteristic of the temperature is gradually dispersed by the randomizing influence of entropy, the atomic interaction energy is increased and so is the relative activity of the carbon. This lessens the driving force behind the martensite reaction, and more austenite is retained.

It is quite likely that even in the temperature range where undissolved carbides exist, part of the well-known effect of austenitizing temperature hitherto ascribed to changing composition may be due to the more subtle process of changing association between the iron and carbon atoms. Undoubtedly, the presence of alloying elements plays an important role in this phenomenon, but it is too early to analyze this aspect of the problem. It is intriguing to think that the austenite-martensite reaction which permits us to harden and strengthen steel for practical utilization is so delicate and so reproducible that it may likewise be employed as a sensitive tool for studying elusive atomic distributions in solid solutions.

The progressive decrease in retained austenite resulting from holding at 1580 °F after previous austenitizing at 1900 °F is reminiscent of the "conditioning" of retained austenite during the tempering of high speed steel. In the latter case, there is some evidence that carbides precipitate from the austenite, and the resulting depletion renders the austenite more amenable to transformation on cooling back to room temperature. Now we see that it is quite possible to "condition" austenite for subsequent transformation *without* actual carbide precipitation. We shall make use of this fact later in connection with the tempering of high alloy steels.

It may be assumed that the distribution of embryos also changes with the above variations in austenitizing treatments. However, since σ_s lies well below M_s for the steel at hand and since the cooling to room temperature is rapid enough to avoid stabilization effects (15), the transformation is controlled by the driving force factor, and not by a limited supply of potential nuclei. Hence, these austenitizing effects are believed to operate through the changes that are caused in the free-energy difference $F^A - F^M$.

It remains to explain the decrease in retained austenite after austenitizing above 1900 °F. This appears to be the result of

increasing grain size which favors the formation of martensite. The effect is rather small compared to the other austenitizing variables and tends to be obscured by them, except at the higher temperatures after the other factors have expended themselves somewhat. The grain size effect also accounts for the fact that on prolonged heating at 1580 °F after austenitizing at 1900 °F, the retained austenite drops *below* the value obtained by direct heating at 1580 °F. Although the same distribution of iron-carbon groupings may be

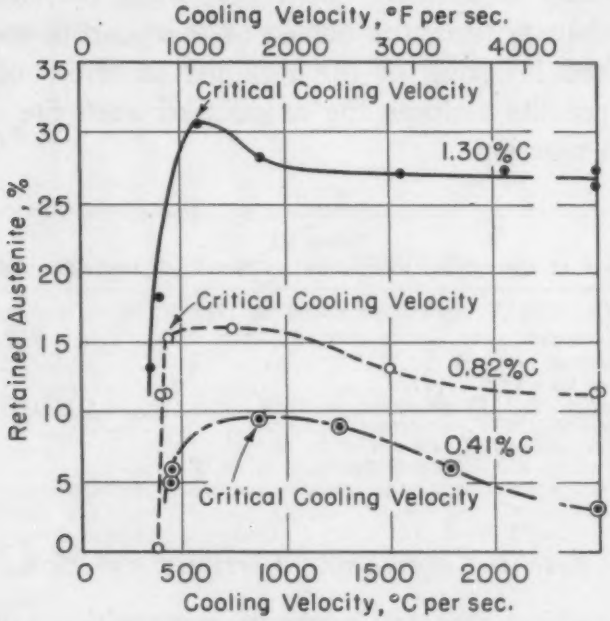


Fig. 17—Effect of Quenching Rate on Retained Austenite in 0.41, 0.82 and 1.30% Carbon Steels (50). The austenite contents shown appear to be somewhat high in the light of more recent determinations, but the trends are significant.

attained at 1580 °F, whether this temperature is approached from above or below, the grain size variations are not reversible. The grain size is much larger in the samples that are first heated to 1900 °F, and thus they arrive at lower austenite contents than the finer grained samples that are heated directly at 1580 °F.

Effect of Quenching Rate

In considering the foregoing data, we must remember that the cooling rate has some influence on the quantity of retained austenite in those steels that are capable of being stabilized. Table VI illustrates this effect for a low alloy tool steel austenitized at 1550 °F. Oil quenching retains more austenite than water quenching, and air

cooling retains more than oil quenching. In the air-cooling experiments, the steel was quenched into liquid baths to avoid non-martensitic reactions. The quench to 450 °F followed by air cooling corresponds to martempering, and retains some 4.5% more austenite than water quenching, whether the latter is conducted from 450 °F or directly from the austenitizing temperature.

More complete data on the effect of quenching rate are given in Fig. 17. It is evident that the retained austenite increases with decreasing velocity of cooling. However, when the cooling velocity becomes less than critical, the entrée of the pearlite transformation causes a marked lowering of the retained austenite content. The formation of pearlite reduces the amount of austenite available for the martensite reaction.

Table VI
Effect of Quenching Procedure on Retained Austenite (26)

1.0% C, 1.5% Cr, 0.2% V steel, austenitized at 1550 °F. 4.0% undissolved carbide.

Treatment	% Retained Austenite
Water-quenched to 68 °F	5.8
Oil-quenched to 68 °F	7.0
Oil-quenched to 120 °F, air-cooled to 68 °F	9.0
Oil-quenched to 250 °F, air-cooled to 68 °F	9.5
Salt-quenched to 450 °F, air-cooled to 68 °F	10.6
Salt-quenched to 450 °F, water-quenched to 68 °F	6.1

Effect of Carbide and Ferrite Formation

If the quenching rate and austenite composition are such as to permit either carbide or ferrite to precipitate during cooling, there is a corresponding change in the chemistry of the austenite that goes into the martensite transformation and the amount of retained austenite is affected accordingly. This behavior is nicely demonstrated in Fig. 18 for a series of 4.8% nickel steels, austenitized at 1700 °F and cooled at various rates (51).

Among the samples cooled in water, oil and air, the percentage of retained austenite increases as the carbon content increases, which is to be expected, but the lime-cooled samples exhibit the reverse trend. The reason for this apparent anomaly is that, in the latter series, enough proeutectoid ferrite is precipitated from the 0.62% carbon austenite to increase its carbon content to 1.2%,* while in the 1.0% carbon austenite, enough proeutectoid carbide is precipitated to decrease the carbon content to about 0.8%.*

*Determined from lattice parameter measurements.

In the water, oil and air-cooled series, the retained austenite content increases with decreasing cooling rate, as expected. The only exception is the 1.0% carbon steel, in which air cooling yields slightly less austenite than oil cooling, and is probably due to a small amount of carbide precipitation taking place during the slower cooling.

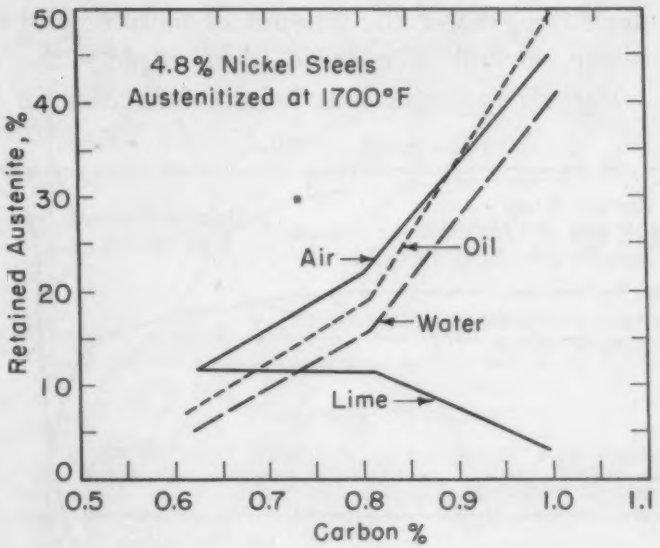


Fig. 18—Effect of Carbon Content and Cooling Rate on Retained Austenite in 4.8% Nickel Steel (51). Austenitized at 1700 °F, cooled as shown.

Effect of Bainite Formation

If the bainite reaction sets in before the martensite range is reached, the effect on the amount of retained austenite is rather complex. It depends on the nature of the steel, the quantity of bainite formed, and the temperature at which it forms. Acicular bainite acts like martensite in partitioning the austenite grains and limiting the size of the martensite plates to form later. Moreover, potential nuclei that might otherwise be available to the martensite are swept up by the bainite. The operation of these two factors alone should allow the existing bainite to substitute for that much martensite, leaving the quantity of retained austenite unchanged.

This is exactly what is found in plain carbon steel, as demonstrated in Fig. 19. The production of bainite at 500 °F detracts from the amount of martensite developed on cooling to room temperature, but the retained austenite content remains substantially

constant. Of course, the latter eventually decreases when too much of the austenite is consumed by the bainite reaction.

On the other hand, in alloy steels containing a more restricted supply of potential nuclei, the formation of bainite may reduce their number sufficiently to make the remaining austenite sensitive to stabilizing effects. In other words, the influence of any shrinkage of embryos that occurs simultaneously with bainite formation will be more pronounced the greater the amount of bainite; and for a given amount of bainite, it will take place more rapidly the higher the temperature. Fig. 20 indicates that bainite formation in high speed

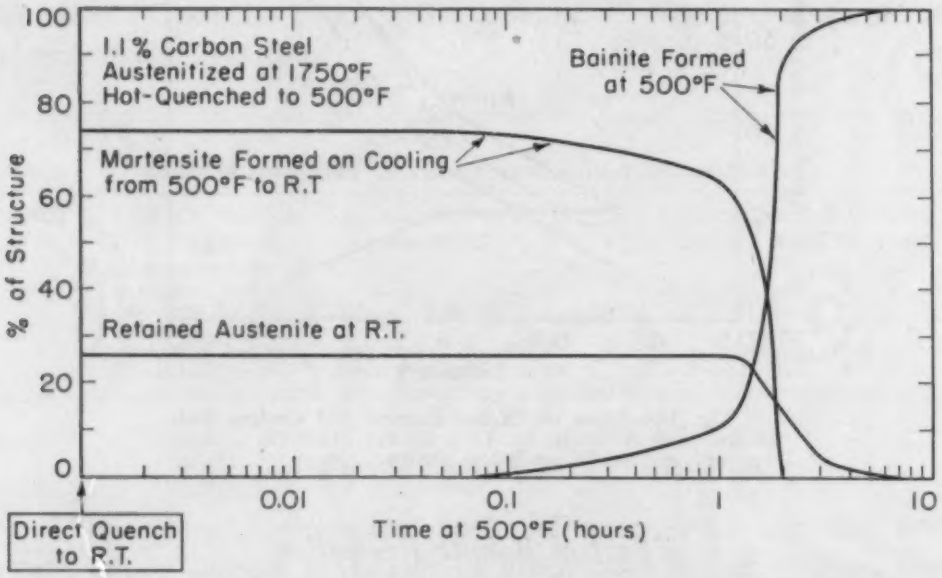


Fig. 19—Effect of Bainite Formation at 500 °F on Amounts of Martensite and Retained Austenite in 1.1% Carbon Steel (52). Austenitized at 1750 °F and hot-quenched to 500 °F.

steel during isothermal holding at 600 °F not only reduces the amount of martensite produced on cooling to room temperature, but also increases the amount of retained austenite. This is a true stabilizing effect. In fact, Gulyaev (54) has demonstrated that the stabilizing process may go on in high alloy steels even after the bainite reaction ceases, as in Fig. 21. Thus, it appears that the stabilization which attends bainite formation is not caused by this reaction per se, but is fundamentally attributable to the same embryo-shrinkage process that occurs on holding in the martensite range. In both cases, the presence of bainite or martensite intensifies the effect of this process on the subsequent martensite transformation

by limiting the availability of potential nuclei. But the stabilization is likely to be more striking in the bainite range than in the martensite range because of the higher temperatures involved.

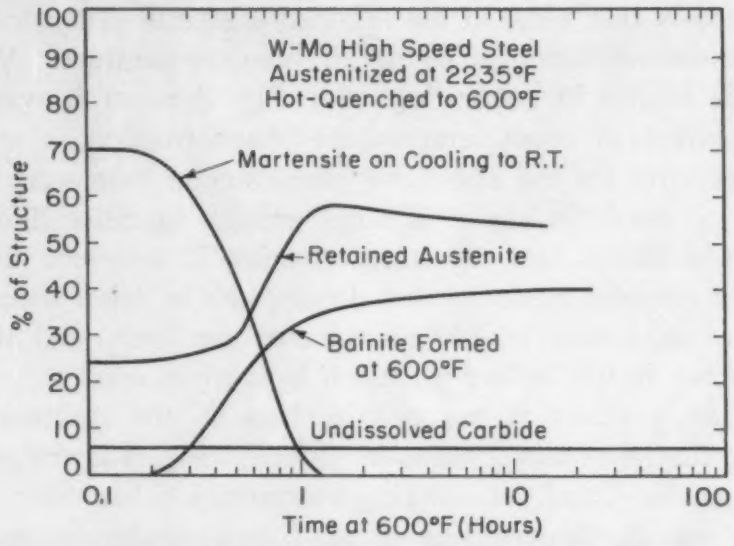


Fig. 20—Effect of Bainite Formation at 600 °F on Amounts of Martensite and Retained Austenite in Tungsten-Molybdenum High Speed Steel (53). Austenitized at 2235 °F and hot-quenched to 600 °F.

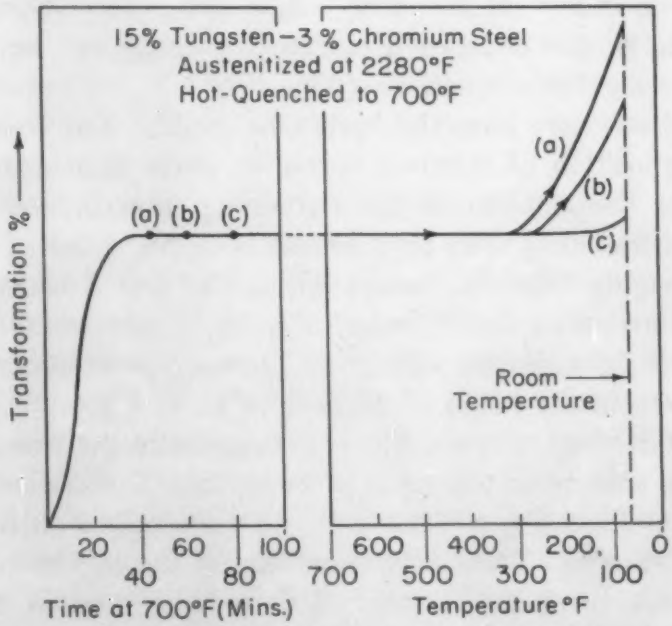


Fig. 21—Effect of Holding at 700 °F After Cessation of Bainite Transformation on Subsequent Cooling Transformation Into Martensite (54). Steel composition = 0.7% carbon, 15% tungsten, 3% chromium. Austenitized at 2280 °F and hot-quenched to 700 °F.

Decomposition of Retained Austenite During Tempering

Decomposition at Room Temperature

Recent experiments by Dr. Averbach (35) have demonstrated unambiguously that some of the retained austenite in hardened steel undergoes decomposition on aging at room temperature. We mentioned this briefly in connection with Fig. 8 when it was shown that the extent of room temperature transformation is much too small to account for the stabilizing phenomenon that occurs during such aging. Nevertheless, it is large enough to cause dimensional changes, and this is how the transformation is detected. For each per cent of retained austenite that decomposes at room temperature, there is an expansion of 140 microinches per inch, and this conversion factor is not influenced much by carbon content.

But the problem is not simple, because the martensite that coexists with the retained austenite undergoes partial tempering at room temperature, and the resulting contraction either detracts from, or entirely masks, the expansion effect of the austenite decomposition. Nevertheless, the two processes can be disentangled by observing the changes in length (by precision methods) in two specimens: one as-hardened and the other refrigerated. Such a pair of specimens gives two mixtures of austenite and martensite, whose separate contributions to the changes in length on aging can be solved by simultaneous algebraic equations (35).

Data of this sort form the basis of Fig. 22. The room temperature decomposition of retained austenite starts immediately as the steel reaches the ambient in the hardening quench, and continues for weeks and weeks. The total extent is of the order of a few per cent, and roughly half of it occurs within the first 2 hours after the quench. The rate of this reaction is quite insensitive to the aging temperature. As indicated in Fig. 22, it proceeds at about the same pace anywhere in the range of 32 to 200 °F.

It is interesting to speculate on the nature of the transformation product. Its amount is too small to be studied X-ray-wise or metallographically. Thus far, one can only draw inferences on the basis of the reaction kinetics. These inferences lead to the conclusion that the product is not bainite. First of all, we have seen in connection with Fig. 9 that bainite formation at room temperature is a fantastically slow process. Secondly, the rate of bainite formation in this steel is highly temperature-dependent, while the reaction in question

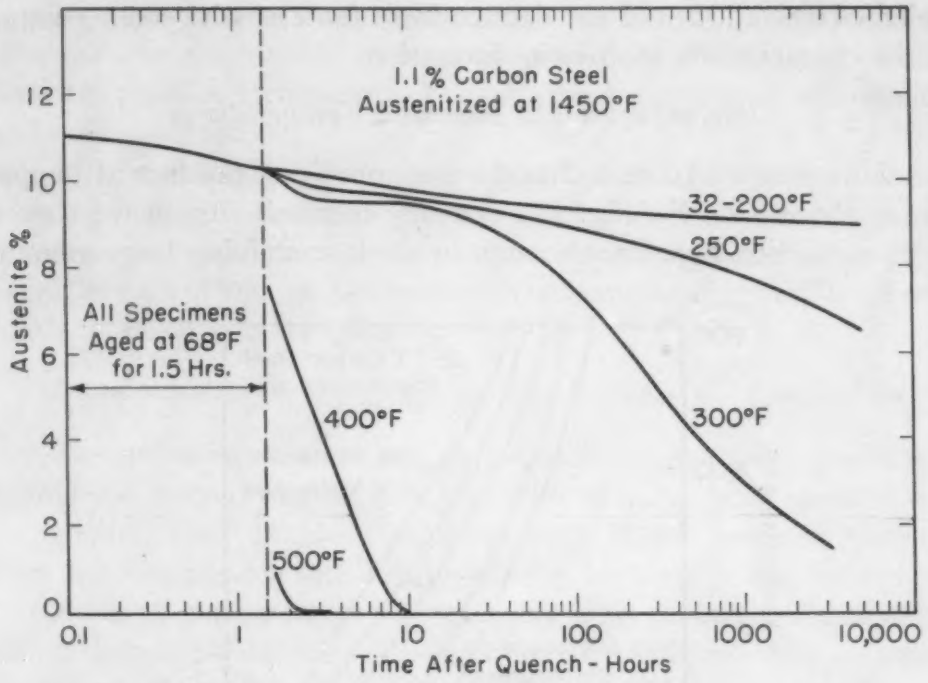


Fig. 22—Isothermal Decomposition of Retained Austenite in 1.1% Carbon Steel, Austenitized at 1450 °F and Water-Quenched (35).

is not. And thirdly, on aging the hardened steel at 250 °F and above, a second stage of decomposition sets in, and here the reaction kinetics are definitely characteristic of bainite formation. If the rate of the second-stage reaction is extrapolated back to room temperature, again we find that bainite formation proceeds too slowly to account for the transformation.

Considering various other possibilities, one cannot conceive that the product is pearlite or ferrite, while carbide precipitation would cause a contraction rather than the observed expansion. By a process of elimination, we are forced to the conclusion that the product is actually martensite. Perhaps the barriers that we have postulated are not absolutely fixed and slight relaxations allow the formation of some martensite plates that were just on the verge of propagating when the cooling was stopped. It is also possible that the existing martensite plates grow slightly in thickness because of the high energy interface existing between the martensite and austenite. The interfacial energy per mol of martensite would be lowered by such a growth process, since there would then be less interfacial area per unit volume of martensite. In any event, the isothermal formation of minor quantities of martensite is a second-

order effect and should not detract from the essential cooling nature of the characteristic martensite formation.

Decomposition at Elevated Temperatures

How can we be sure that the decomposition product at temperatures above 250 °F (Fig. 22) is really bainite? Again we have to rely on reaction kinetics, although in steels containing large amounts

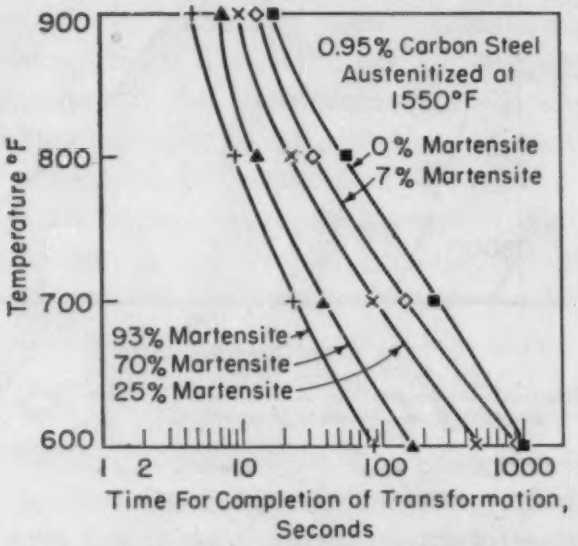


Fig. 23—Effect of Martensite on the Time-Temperature Relations for the Completion of the Bainite Transformation (55). 0.95% carbon steel, austenitized at 1550 °F.

of retained austenite, the product has been studied metallographically and identified as bainite (57). Fig. 23 taken from the work of Elmendorf (55) demonstrates how the time for the completion of the bainite reaction is influenced by the presence of martensite. The zero martensite curve is a part of the primary isothermal transformation diagram, while the others are obtained after arresting the initial quench at various temperatures below M_s to provide different amounts of martensite with the austenite.

When the primary transformation diagram exhibits a bainite "nose", the retained austenite displays similar characteristics. As an example, let us consider the retained austenite decomposition in a 1% carbon – 4% chromium steel. In Fig. 24 are superimposed the primary transformation curves of Lyman and Troiano (56), and the tempering transformation curves completed recently by Mr. Balluffi (57). Not only does the secondary transformation show a

bainite "nose" at the same temperature as the primary transformation, but there is similar correspondence in the carbide precipitation and the pearlite formation. These products can also be identified under the microscope.

It is now evident that the product of *retained* austenite decomposition is exactly the same as that which forms isothermally out of *primary* austenite in the widely-used hot quenching techniques. However, the rate of retained austenite decomposition is generally affected by the coexisting martensite.

Decomposition on Cooling from the Tempering Temperature

In tempering, we are not only concerned with the products of isothermal transformation, but also with reactions that occur during the cooling back to room temperature. If the retained austenite does not decompose into bainite during heating, it can be exposed to the "bay" temperatures for relatively long periods without appreciable decomposition into either bainite or pearlite. But something important does take place because the retained austenite becomes conditioned for transformation during the cooling back to room temperature. The time-temperature combinations for various degrees of conditioning are given in Fig. 25 for a 1% carbon – 5% chromium die steel, oil-quenched from three austenitizing temperatures (58).

The cooling product is definitely martensite. This is demonstrated by the microphotometer traces in Fig. 26 (58). For the as-hardened state, the X-ray pattern shows strong lines of austenite and the (110) – (101) doublet typifying tetragonal martensite. Tempering at 400 °F decomposes the tetragonal martensite, but the austenite lines remain undiminished in intensity. However, after prolonged tempering at 900 °F and cooling to room temperature, there is a marked decrease in the intensity of the austenite lines, and the tetragonal doublet of martensite reappears. Tempering once again at 400 °F destroys the tetragonality.

If the cooling from the conditioning treatment is very slow, or if it is interrupted, bainite may form out of the retained austenite and supersede the martensite transformation (59). Thus various mixtures of "secondary bainite" and "secondary martensite" may be produced (60).

The conditioning process operates through its effect on the martensite range of the retained austenite. This is clearly shown in high speed steel (Fig. 27). As the austenitized steel arrives at

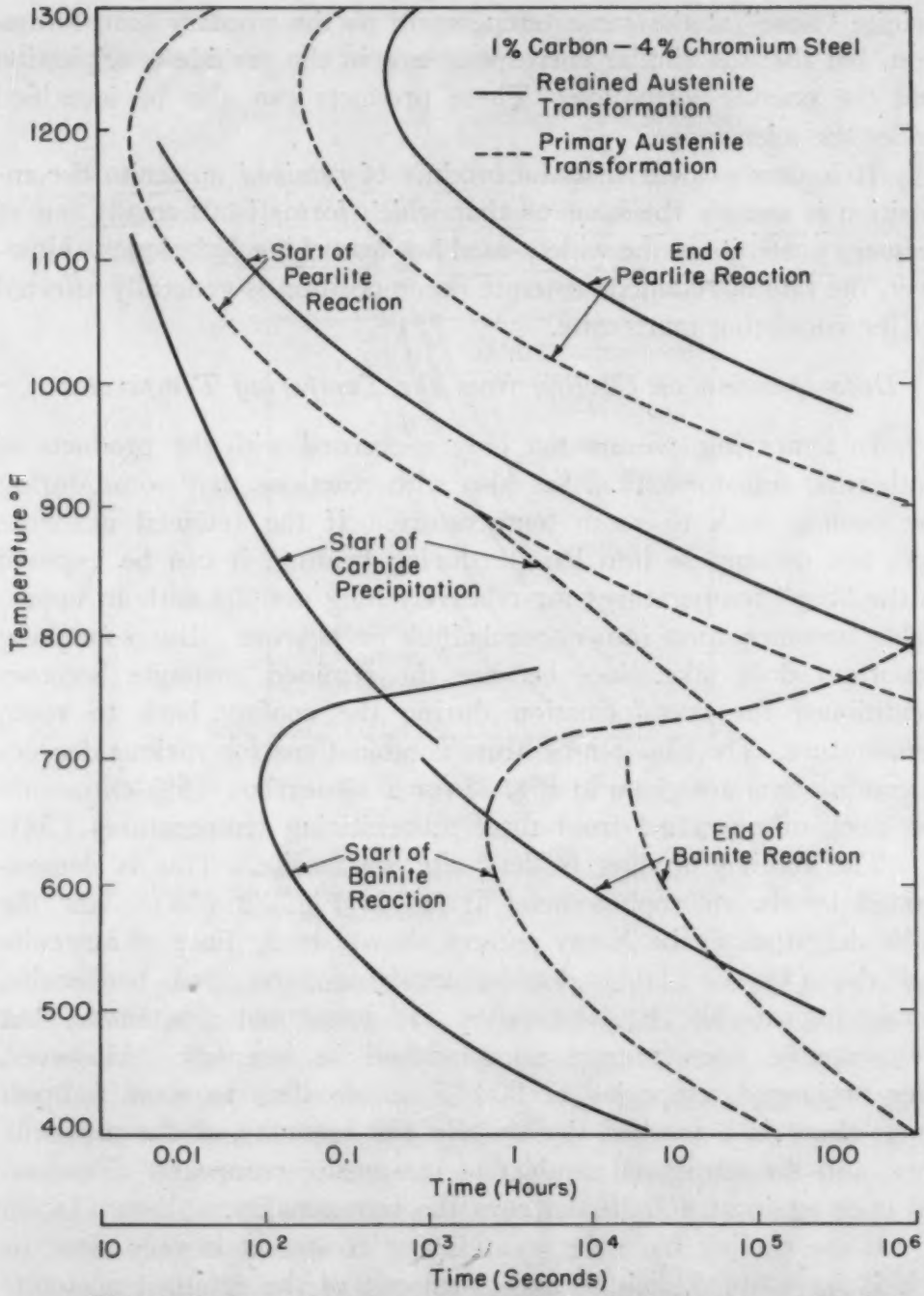


Fig. 24—Isothermal Transformation of Primary Austenite (56) and Retained Austenite (57) in 1% Carbon – 4% Chromium Steel. Primary transformation specimens hot-quenched from 2200 °F. Tempering transformation specimens austenitized at 2000 °F and refrigerated to yield 50% retained austenite. Hence the comparison is between 100% austenite on hot quenching and 50% austenite on tempering.

room temperature during the hardening quench, the martensite range of the remaining austenite extends below room temperature. If no stabilization sets in, M_s' lies at room temperature because the

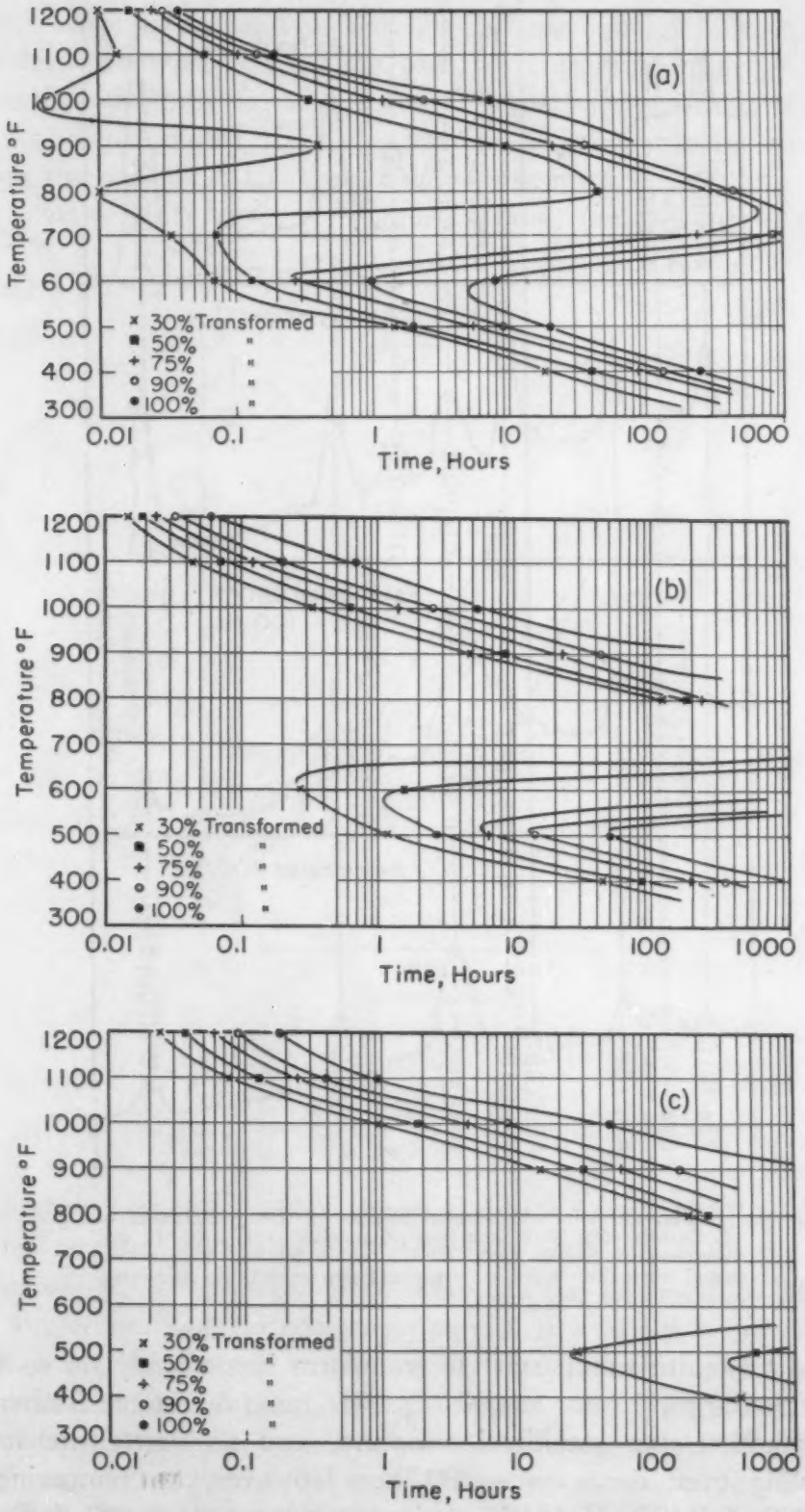


Fig. 25—Effect of Tempering Time and Temperature on Transformation of Retained Austenite in 1% Carbon – 5% Chromium Die Steel, Oil-Quenched from (a) 1700, (b) 1800 and (c) 2000 °F (58). Lower C-curves depict isothermal transformation into bainite; upper curves depict conditioning of retained austenite for transformation into martensite during cooling.

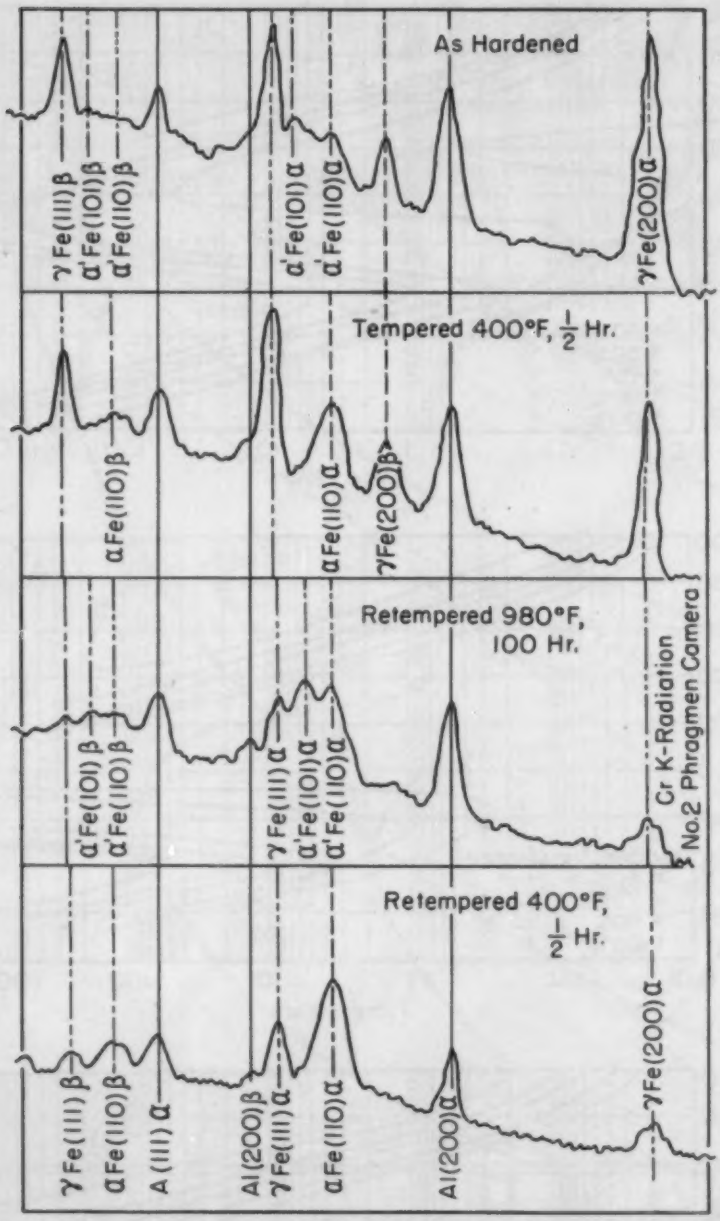


Fig. 26—Microphotometer Traces of X-ray Patterns of 1% Carbon – 5% Chromium Steel, Quenched from 2000 °F, and Tempered as Shown (58). αFe = cubic ferrite. γ'Fe = retained austenite. α'Fe = tetragonal martensite. Al = aluminum reference line.

retained austenite would start to transform immediately on cooling. On tempering for 1 hour at 600 °F, there is no detectable isothermal transformation, but stabilization occurs, and no martensite forms on cooling even down to —300 °F. However, on tempering at 950, 1000 and 1050 °F, M_s' is raised progressively to 40, 240 and

470 °F, respectively, and so the retained austenite is able to transform into martensite on cooling back to room temperature. If M_s' is raised sufficiently far above room temperature in this way, virtually (but not quite) all of the retained austenite can be converted during the cool from the tempering temperature.

Several years ago, we suggested that conditioning is due to

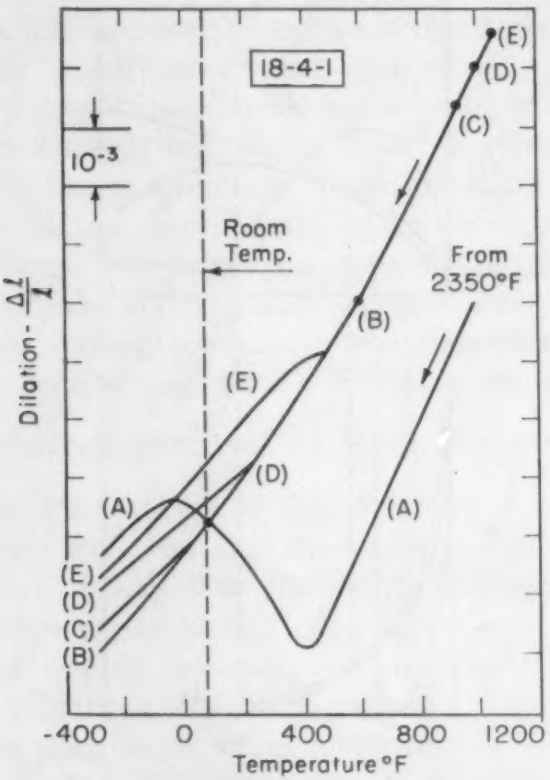


Fig. 27—Dilation Curves of 18-4-1 High Speed Steel on Cooling (A) from Austenitizing Temperature of 2350 °F, (B) from 1 Hour Tempering at 600 °F, (C) from 1 Hour Tempering at 950 °F, (D) from 1 Hour Tempering at 1000 °F, and (E) from 1 Hour Tempering at 1050 °F (64).

carbide precipitation, which depletes the carbon and alloy content of the retained austenite and makes it more amenable to transformation (61). However, we were always bothered by the fact that the amount of carbide precipitation, if it could be detected at all, was much too small to account for the extensive raising of M_s'. Even in the 1% carbon – 4% chromium steel (Fig. 24), which precipitates carbide conspicuously on tempering at 900 °F, there is hardly enough change in austenite composition to explain the observed conditioning. Now we know that actual carbide pre-

cipitation, though very helpful, is not the only factor at play in conditioning; for, in the nickel steel of Fig. 16, we find that conditioning may occur at temperatures where carbides cannot possibly form. It seems likely that, during the conditioning of high speed and high chromium steels, the distribution of atomic groupings (perhaps in preparation for carbide precipitation) shifts away from

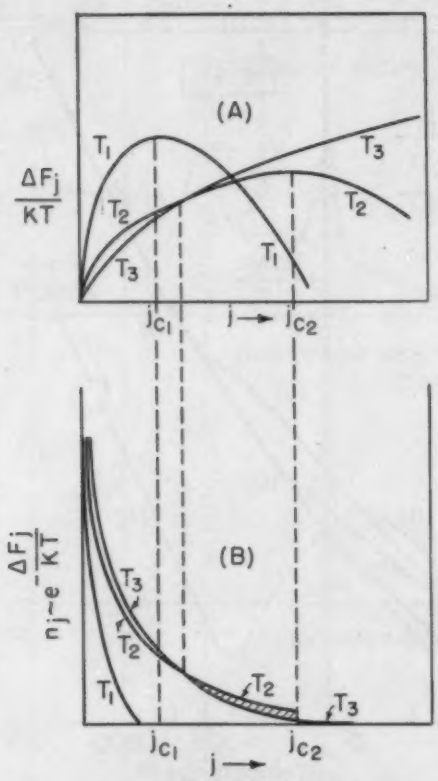


Fig. 28—Equilibrium or Steady-State Distribution of Embryos at Three Temperatures: T_1 in the Martensite Range, T_2 in the Conditioning Range, T_3 Above the Critical Range. Shaded area indicates embryo sizes existing at T_3 that increase in number at T_2. Compare with Fig. 13. *Fisher, Hollomon and Turnbull* (42).

that characteristic of the austenitizing temperature and thereby lowers the thermodynamic activity of the carbon and alloying elements just as though their concentrations were being depleted by actual precipitation. This increases the tendency toward martensite formation.

But the conditioning process must also furnish new potential nuclei to compensate for those lost during stabilizing at the lower temperatures, otherwise the increased driving force may be of no avail. Fisher, Hollomon and Turnbull (42) have shown how this

is possible at sufficiently high temperatures (but still below the equilibrium temperature). At temperature T_2 in Fig. 28, the steady-state distribution of embryos calls for more of the larger sizes than are on hand from the austenitizing temperature (T_3). Hence, aging at T_2 permits the larger sizes to form progressively and thus replenishes the supply of potential nuclei.

The rate of conditioning is accelerated by the presence of martensite, possibly because the extra interfaces provide good locations for atomic redistributions that tend to occur, as well as for actual carbide precipitation. Hence, conditioning of *retained* austenite is more pronounced than that of *primary* austenite. This also accounts for the fact that multiple tempering usually converts more retained austenite than single tempering for an equal length of time (45). With single tempering, the conditioning is aided only by the martensite present in the as-hardened steel, whereas with multiple tempering, each cooling produces a new increment of martensite which aids the conditioning process during subsequent tempers.

Mechanical Behavior of Retained Austenite

The stress-strain curves in Fig. 4 for the 1.5% carbon – 12% chromium steel with various martensite : austenite ratios were obtained in such a way that changes in magnetization could be measured throughout the tests (13). The magnetic readings were then translated directly into per cent martensite by virtue of an independent calibration with lineal analysis. The course of transformation as a function of strain and stress is shown in Figs. 29 and 30, respectively. The curves start at different levels in accordance with the amount of martensite present at the beginning of the test.

While the induced transformation proceeds more or less generally with the strain, the dependence on stress is particularly striking. In the latter case, the reaction is inhibited up to a fairly critical value of the stress, and then proceeds rapidly with further increase of stress. The critical stress (say, to induce 1% transformation) increases significantly with the amount of martensite already present. As indicated by the band in Fig. 30, there seems to be a definite tendency for the curves to track along together, once the reaction sets in.

The driving force $F^A - F^M$ is the same for the four specimens in this series at the common testing temperature, while the barrier

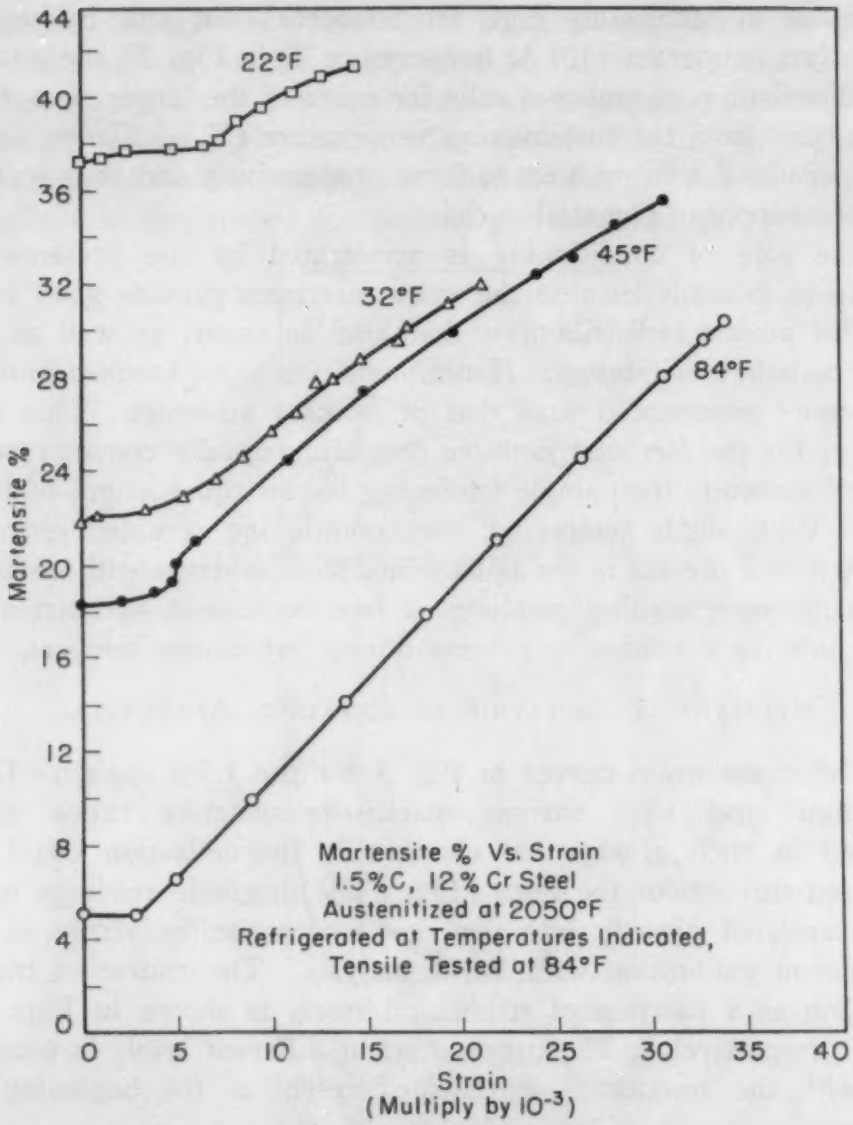


Fig. 29—Relationship Between Transformation and True Strain in Tensile Test of 1.5% Carbon – 12% Chromium Steel, Austenitized at 2050 °F, and Refrigerated to Produce Various Amounts of Martensite to Start With. Tensile tested at 84 °F (13).

condition imposed by the existing martensite is the important variable. To study the effect of changing $F^A - F^M$ in the presence of a given amount of martensite, it is necessary to austenitize the steels at different temperatures and then refrigerate to equalize the martensite : austenite ratios. Such comparisons show that the austenites with higher dissolved carbon and chromium (lower $F^A - F^M$) require larger stresses to induce 1% of transformation at room temperature than do the "leaner" austenites. For example,

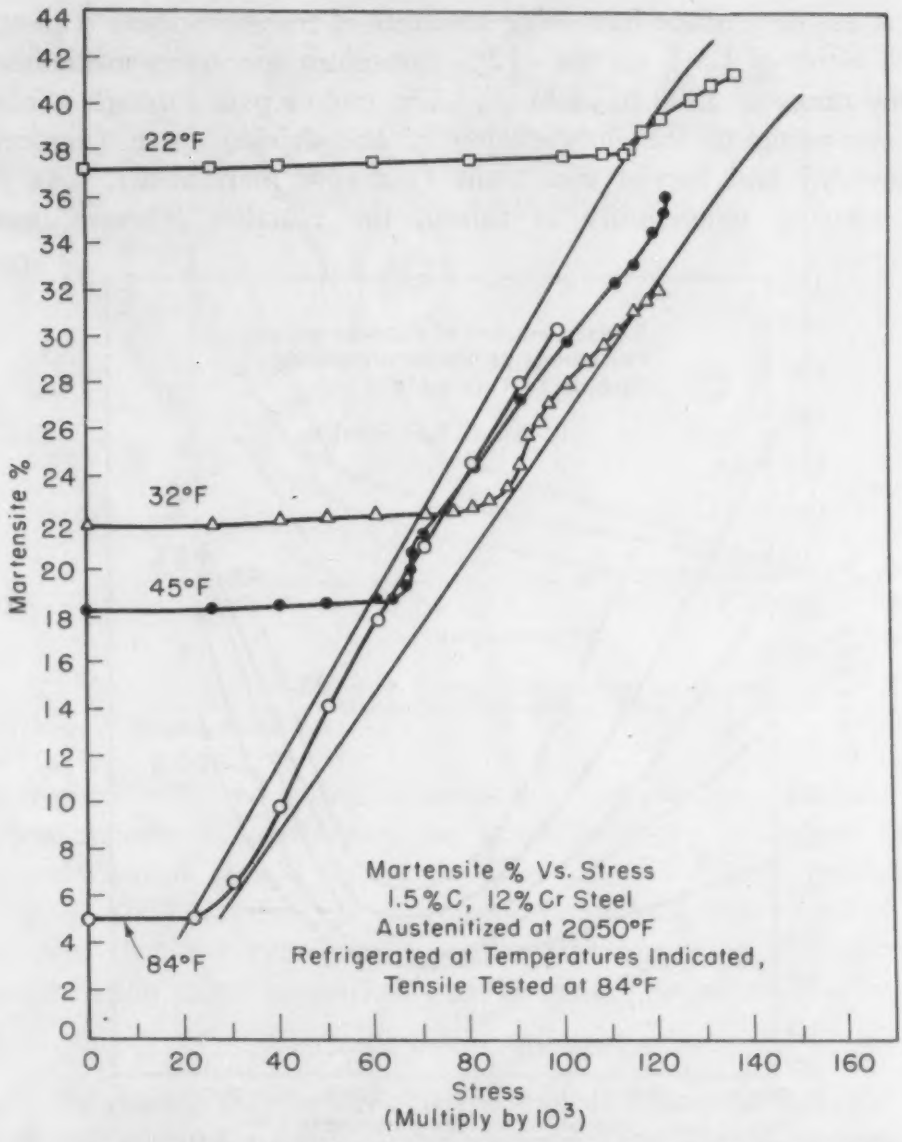


Fig. 30—Relationship Between Transformation and True Stress in Tensile Test of 1.5% Carbon – 12% Chromium, Austenitized at 2050 °F, and Refrigerated to Produce Various Amounts of Martensite to Begin With. Tensile tested at 84 °F (13).

the 1.5% carbon – 12% chromium steel under discussion yields about 35% of martensite when quenched from 2000 °F to the ambient, and also when quenched from 2050 °F and subcooled to 22 °F. The stress to form an additional 1% of martensite at room temperature is 29,000 psi for the first state and 115,000 psi for the second.

When the driving force and barrier conditions are allowed to vary simultaneously, the situation shown in Fig. 31 is found. Here

the stress to produce increasing amounts of transformation is plotted for a series of 1.5% carbon – 12% chromium specimens austenitized in the range of 1900 to 2100 °F. The curves pass through minima corresponding to the interrelation of the driving force (austenite chemistry) and barrier conditions (per cent martensite). As the austenitizing temperature is raised, the reaction proceeds more

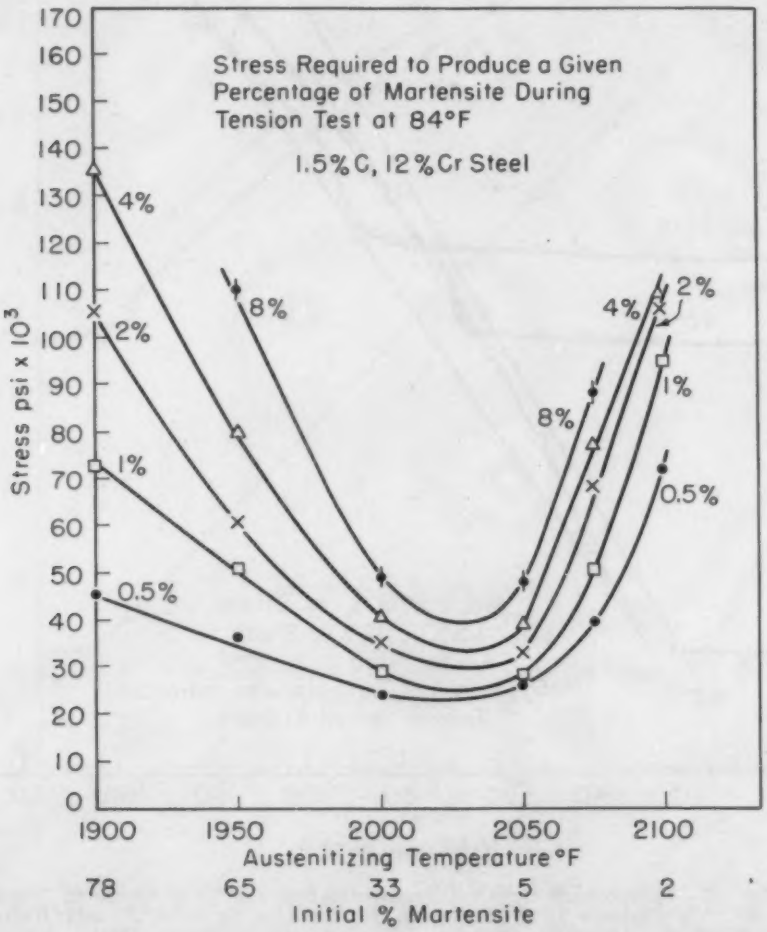


Fig. 31—Effect of Stress on Transformation in Tensile Test at 84 °F. 1.5% carbon – 12% chromium steel, austenitized as shown (13).

readily under stress because of the decreasing barrier factor. At the same time, the driving force factor is also decreasing and eventually predominates to reverse the trend of the curves.

Unfortunately, no experiments with the 1.5% carbon – 12% chromium steel have been performed as yet at different testing temperatures. The indications are, however, that this variation will be predictable in terms of the present findings. The driving force

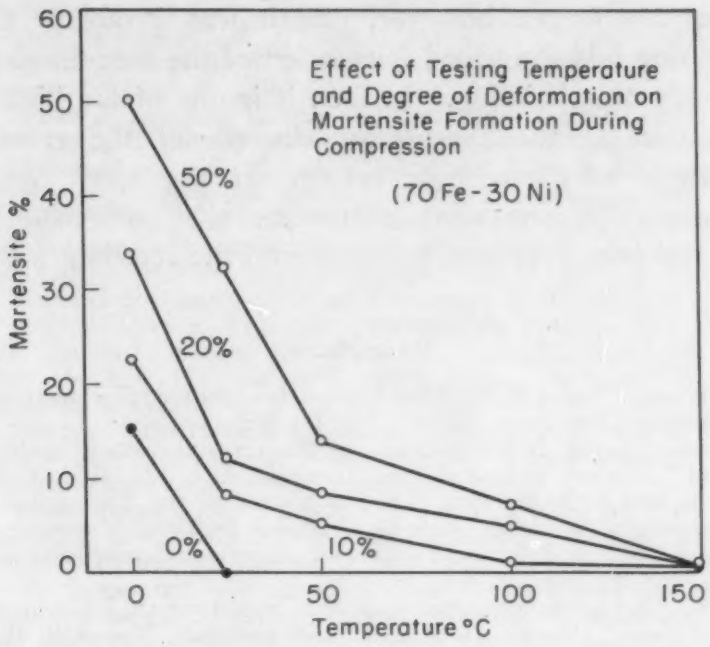


Fig. 32—Effect of Testing Temperature and Degree of Compression on Martensite Formation in Iron-Nickel Alloy (30% Nickel) (62).

increases with decreasing temperature and, in the presence of a given amount of martensite, the stress necessary to induce further transformation should decrease. This trend is already indicated in Fig. 32 (62) for the case of iron-nickel alloys (30% nickel). It is evident that the extent of austenite transformation during plastic deformation increases markedly as the testing temperature is lowered.

Concluding Remarks

In closing this twenty-third Campbell Memorial Lecture, I do not feel obliged to enumerate an impressive list of summarizing statements. Instead, I merely hope that you have found some interest in this working picture of the factors which lead to *retained austenite,* which govern its amount, and which control its behavior. We may not be completely satisfied with our present position, but at least we can appreciate that progress has been made. In my opinion, one of the major contributions to this progress has been the growing awareness of the need for *quantitative* information. Many of the scientific principles involved here were available in Professor Campbell's time, but precise data were lacking. Some of the key phenomena that I have discussed cannot even be detected, let alone understood, without exacting experimentation.

Let us not forget, however, that it was Professor Campbell's generation that laid the broad foundation of the metallurgical science which we are now building. In fact, it is one of the high purposes of this Annual Lecture Series to acknowledge the great achievements of those who have gone before. In this spirit, we can prepare ourselves for the next generation that will stand on our shoulders and peer over new horizons into the receding metallurgical unknown.

References

1. A. H. White, "Edward DeMille Campbell—Obituary," *Industrial and Engineering Chemistry*, Vol. 17, No. 11, 1925, p. 124.
2. E. Ohman, "X-ray Investigations on the Crystal Structure of Hardened Steel," *Journal*, Iron and Steel Institute, Vol. 123, 1931, p. 445.
3. K. Honda and Z. Nishiyama, "On the Nature of the Tetragonal and Cubic Martensites," *Science Reports*, Tohoku Imperial University, Vol. 21, Ser. 1, 1932, p. 299; TRANSACTIONS, American Society for Steel Treating, Vol. 20, 1932, p. 464.
4. G. Hagg, "X-ray Investigation on the Structure and Decomposition of Martensite," *Journal*, Iron and Steel Institute, Vol. 130, 1934, p. 439.
5. E. C. Bain, "Functions of Alloying Elements in Steel," published by American Society for Metals, 1939.
6. N. J. Petch, "The Positions of the Carbon Atoms in Austenite," *Journal*, Iron and Steel Institute, Vol. 145, 1942, p. 111.
7. N. J. Petch, "The Positions of the Carbon Atoms in Martensite," *Journal*, Iron and Steel Institute, Vol. 147, 1943, p. 221.
8. H. Lipson and A. M. B. Parker, "The Structure of Martensite," *Journal*, Iron and Steel Institute, Vol. 149, 1944, p. 123.
9. C. Wells and R. F. Mehl, "Rate of Diffusion of Carbon in Austenite in Plain Carbon, in Nickel and in Manganese Steels," *Transactions*, American Institute of Mining and Metallurgical Engineers, Vol. 140, 1940, p. 279.
10. C. Wells and R. F. Mehl, "Rate of Diffusion of Nickel in Gamma Iron in Low-Carbon and High-Carbon Nickel Steels," *Transactions*, American Institute of Mining and Metallurgical Engineers, Vol. 145, 1941, p. 329.
11. O. K. Parmiter, "Wrought Stainless Steels," A.S.M. METALS HANDBOOK, 1948, p. 553.
12. H. S. Avery and M. J. Day, "Austenitic Manganese Steel," A.S.M. METALS HANDBOOK, 1948, p. 526.
13. S. A. Kulin, Unpublished research at Massachusetts Institute of Technology, under ONR Contract N5ori-07814, 1948.
14. H. Esser, W. Eilender and E. Spenle, "Das Hartungsschaubild der Eisen-Kohlenstoff-Legierungen," *Archiv f.d. Eisenhüttenwesen*, Vol. 6, 1933, p. 389.
15. W. J. Harris and M. Cohen, "Stabilization of the Austenite-Martensite Transformation," *Metals Technology*, T.P. 2446, September 1948.
16. A. B. Greninger and A. R. Troiano, "Kinetics of the Austenite to Martensite Transformation in Steel," TRANSACTIONS, American Society for Metals, Vol. 28, 1940, p. 537.
17. F. Förster and E. Scheil, "Untersuchung des zeitlichen Ablaufes von Umklappvorgangen in Metallen," *Zeit. f. Metallkunde*, Vol. 32, 1940, p. 165.
18. C. S. Barrett and O. R. Trautz, "Low-Temperature Transformations in Lithium-Magnesium Alloys," *Metals Technology*, April 1948, T.P. 2346.
19. W. G. Burgers, "On the Process of Transition of the Cubic-Body-Centered

Modification into the Hexagonal-Close-Packed Modification of Zirconium," *Physica,* Vol. 7, 1934, p. 561.

19a. G. Molinder, Unpublished research at Massachusetts Institute of Technology, 1948.

20. R. T. Howard and M. Cohen, "Quantitative Metallography by Point-Counting and Lineal Analysis," *Metals Technology,* August 1947.

21. R. T. Howard and M. Cohen, "Austenite Transformation Above and Within the Martensite Range," *Metals Technology,* September 1947.

22. S. G. Fletcher and M. Cohen, "The Dimensional Stability of Steel. Part I —Subatmospheric Transformation of Retained Austenite," TRANSACTIONS, American Society for Metals, Vol. 34, 1945, p. 216.

23. M. Cohen and P. Gordon, "Heat Treatment of High Speed Steel," *The Iron Age,* Part I, Vol. 157, February 28, 1946, p. 42. Part II, Vol. 157, March 7, 1946, p. 52. Part III, Vol. 157, March 14, 1946, p. 68. Part IV, Vol. 157, March 21, 1946, p. 61. Part V, Vol. 157, March 28, 1946, p. 55.

24. R. D. Potter, "The Transformation of Retained Austenite in High-Carbon High-Chromium Steel at Subatmospheric Temperatures," S. M. Thesis, Massachusetts Institute of Technology, 1941.

25. W. J. Barnett and A. R. Troiano, "The Effect of Grain Size on the Martensite Transformations," *Metals Technology,* August 1948.

26. B. L. Averbach and M. Cohen, "X-ray Determination of Retained Austenite by Integrated Intensities," *Metals Technology,* February 1948.

27. J. H. Hollomon, L. D. Jaffe and D. C. Buffum, "Stabilization, Tempering and Relaxation in the Austenite-Martensite Reaction," *Journal of Applied Physics,* Vol. 18, 1947, p. 780.

28. S. G. Fletcher, B. L. Averbach and M. Cohen, "The Dimensional Stability of Steel. Part II—Further Experiments on Subatmospheric Transformations," TRANSACTIONS, American Society for Metals, Vol. 40, 1948, p. 703.

29. A. R. Troiano and J. L. Tokich, "The Transformation of Cobalt," *Metals Technology,* April 1948, T.P. 2348.

30. A. B. Greninger and A. R. Troiano, "Mechanism of Martensite Formation," *Transactions,* American Institute of Mining and Metallurgical Engineers, Vol. 145, 1941, p. 91.

31. T. Lyman, Discussion of reference (7).

32. A. R. Troiano, "The Transformation and Retention of Austenite in SAE 5140, 2340 and T1340 Steels of Comparable Hardenability," TRANSACTIONS, American Society for Metals, Vol. 41, 1949.

33. H. Carpenter and J. M. Robertson, "Metals," Oxford University Press, Vol. II, 1939, p. 884.

34. J. M. Robertson, "The Transformation of Austenite Below the Critical Range," *Carnegie Scholarship Memoirs,* British Iron & Steel Institute, Vol. 20, 1931, p. 1.

35. B. L. Averbach and M. Cohen, "The Isothermal Decomposition of Martensite and Retained Austenite," TRANSACTIONS, American Society for Metals, Vol. 41, 1949.

36. F. Laszlo, "Tessellated Stresses, Part II," *Journal,* Iron and Steel Institute, Vol. 148, 1943, p. 137.

37. V. G. Paranjpe, Unpublished research at Massachusetts Institute of Technology, 1948.

38. R. P. Smith, "Equilibrium Mixtures of Iron-Carbon Alloys with Mixtures of CO-CO_2 and CH_4-H_2," *Journal,* American Chemical Society, Vol. 68, 1946, p. 1163.

39. C. H. Johansson, "Thermodynamisch begrundete Deutung der Vorgänge bei der Austenit-Martensit-Umvandung," *Archiv f.d. Eisenhüttenwesen,* Vol. 11, 1937-38, p. 241.

40. C. Zener, "Equilibrium Relations in Medium-Alloy Steels," *Transactions,* American Institute of Mining and Metallurgical Engineers, Vol. 167, 1946, p. 513.

41. A. R. Troiano and A. B. Greninger, "The Martensite Transformation," A.S.M. METALS HANDBOOK, 1948, p. 263.
42. J. C. Fisher, J. H. Hollomon and D. Turnbull, "Nucleation of Phase Transformations," *Journal of Applied Physics*, Vol. 19, August 1948.
43. A. B. Greninger, "The Martensite Thermal Arrest in Iron-Carbon Alloys and Plain Carbon Steels," TRANSACTIONS, American Society for Metals, Vol. 30, 1942, p. 1.
44. E. P. Klier and A. R. Troiano, "Ar" in Chromium Steels," *Transactions*, American Institute of Mining and Metallurgical Engineers, Vol. 162, 1945, p. 175.
45. P. Gordon, M. Cohen and R. S. Rose, "Effect of Quenching-Bath Temperature on the Tempering of High Speed Steel," TRANSACTIONS, American Society for Metals, Vol. 33, 1944, p. 411.
46. B. S. Lement, Unpublished research at Massachusetts Institute of Technology, 1948.
47. B. L. Averbach, M. Cohen and S. G. Fletcher, "The Dimensional Stability of Steel. Part III—Decomposition of Martensite and Austenite at Room Temperature," TRANSACTIONS, American Society for Metals, Vol. 40, 1948, p. 728.
48. P. Payson and R. A. Grange, "The Temperature Range of Martensite Formation in Steel," A.S.M. METALS HANDBOOK, 1948, p. 611.
49. V. Zyuzin, V. Sadowski and S. Baranchuk, "Influence of Alloying Elements on Position of Martensite Point, the Amount of Retained Austenite, and Its Stability on Tempering," *Metallurg*, Vol. 14, 1939, p. 75.
50. H. Esser and H. Cornelius, "Die Vorgänge beim anlassen abgeschreckter Stähle," *Archiv f.d. Eisenhüttenwesen*, Vol. 7, 1934, p. 693.
51. F. S. Gardner, M. Cohen and D. P. Antia, "Quantitative Determination of Retained Austenite by X-rays," *Transactions*, American Institute of Mining and Metallurgical Engineers, Vol. 154, 1943, p. 306.
52. R. T. Howard, "The Kinetics of the Austenite-Martensite Reaction," Sc.D. Thesis, Massachusetts Institute of Technology, 1947.
53. P. Gordon, M. Cohen and R. S. Rose, "The Kinetics of Austenite Decomposition in High Speed Steel," TRANSACTIONS, American Society for Metals, Vol. 31, 1943, p. 161.
54. A. Gulyaev, "Decomposition of Austenite in High Speed Steel at Constant Temperature," *Metallurg*, Vol. 15, 1940, p. 43.
55. H. J. Elmendorf, "The Effect of Varying Amounts of Martensite Upon the Isothermal Transformation of Austenite Remaining After Controlled Quenching," TRANSACTIONS, American Society for Metals, Vol. 33, 1944, p. 236.
56. T. Lyman and A. R. Troiano, "Transformation of Austenite in One Percent Carbon High-Chromium Steels," *Transactions*, American Institute of Mining and Metallurgical Engineers, Vol. 162, 1945, p. 196.
57. R. Balluffi, Unpublished research at Massachusetts Institute of Technology, 1948.
58. O. Zmeskal and M. Cohen, "The Tempering of Two High-Carbon High-Chromium Steels," TRANSACTIONS, American Society for Metals, Vol. 31, 1943, p. 380.
59. M. Cohen, "Tempering of Toolsteels," METAL PROGRESS, Part I—Vol. 51, May 1947, p. 781; Part II—Vol. 51, June 1947, p. 962.
60. C. K. Baer and P. Payson, "The Bainitic Hardening of High Speed Steel," TRANSACTIONS, American Society for Metals, Vol. 39, 1947, p. 488.
61. P. Gordon and M. Cohen, "The Transformation of Retained Austenite in High Speed Steel at Subatmospheric Temperatures," TRANSACTIONS, American Society for Metals, Vol. 30, 1942, p. 569.
62. M. Cohen and P. K. Koh, "The Tempering of High Speed Steel," TRANSACTIONS, American Society for Metals, Vol. 27, 1939, p. 1015.
63. E. Scheil, "Über die Umwandlung des Austenits in Martensit in Eisen-Nickellegierungen unter Belastung," *Zeitschrift anorganische und allgemeine Chemie*, Vol. 207, 1932, p. 21.

AGING IN GAS TURBINE-TYPE ALLOYS

By Nicholas J. Grant and Joseph R. Lane

Abstract

Four high temperature alloys were investigated to determine their aging characteristics. Included were low carbon Vitallium, modified high carbon Vitallium, the nickel-cobalt-chromium-molybdenum alloy designated 6059, and a slight modification of the Multimet alloy N-155. Aging was studied with the help of a wide variety of techniques, including X-ray diffraction, stress-rupture testing, microscopic examination, the use of the dilatometer and magnetometer, and the measurement of electrical resistivity.

The lowest temperature for a precipitate to form, the temperature of maximum precipitation, and the resolution temperature for each alloy were determined. The rates of the precipitating reactions at temperatures ranging from 1000 to 1650 °F (540 to 900 °C) were also studied. The effect of aging on mechanical properties was evaluated by means of stress-rupture testing.

Introduction

IT is now generally accepted by those working in the field of alloys suitable for operation at high stresses in the range of 1350 to 1800 °F (730 to 980 °C) that aging, the precipitation of a second phase from a metastable solid solution, is of great importance in determining both the room temperature and high temperature physical properties.

Because aging is of such extreme importance in the determination of alloy behavior, it was decided to select for study four alloys which are broadly representative of a large variety of probable gas turbine and jet-engine types of alloys intended for use as turbine blades.

These four alloys are given in Table I.

This work was part of a program sponsored by the U. S. Navy, Bureau of Ships. The opinions expressed are strictly those of the authors.

A paper presented before the Thirtieth Annual Convention of the Society, held in Philadelphia, October 23 to 29, 1948. Of the authors, Nicholas J. Grant is associate professor of metallurgy, and Joseph R. Lane is research assistant, Massachusetts Institute of Technology, Cambridge, Mass. Manuscript received December 2, 1947.

Table I

	C	Mn	Si	Ni	Cr	Co	Mo	W	Ta	Fe
25 V-0	0.25	1.0	...	..	23	68	6	...	..	...
45 R-6	0.45	1.0	...	32	26	33	6	...	..	...
100 NT-2	1.0	1.5	0.5	30	20	20	3	2.2	2	Bal.
111 VT 2-2	1.1	...	...	..	23	67	6	...	2	...

Alloy 100NT-2 is a modified high carbon N-155 alloy; alloy 25V-0 is essentially Vitallium; 45R-6 is standard 6059 alloy; and 111VT2-2 is a modified high carbon Vitallium. Thus we have two high carbon alloys, and one each of low and medium carbon. Represented are the nickel-chromium-cobalt-iron, the cobalt-chromium-molybdenum and the cobalt-nickel-chromium-molybdenum types of alloys in several modifications. From these four alloy compositions it is hoped that a fairly representative picture of aging can be presented.

The compositions shown in the table are the proportions of each element added to the melt, without consideration of elements present as impurities in the additions.

In general, high temperature-type alloys are not in equilibrium in the cast condition, and subsequent heating can result in the precipitation of an aging constituent with or without a solution treatment. Of the above alloys 100NT-2 was solution treated at 2260 °F (1240 °C) for one-half hour, followed by water quenching. The others were "as cast".

The following variables were studied.

1. Temperature at which aging is first detected.
2. Temperature of maximum aging.
3. Overaging temperature.
4. Re-solution temperatures.
5. Time for initiation of aging.
6. Time for completion of aging.
7. Effect of aging on physical properties.

Experimental Procedure

Test bars were prepared with considerable care for each particular type of test. These tests are summarized below:

Hardness—Room temperature hardness measurements have long been used as a means of detecting aging, the relative degree of aging and overaging. It is a simple test, but for these particular alloys there were several disadvantages. Regular Rockwell or Brinell

readings generally are not sensitive enough to properly detect changes in hardness, due to the fact that the alloy structures are composed of hard carbide particles embedded in a relatively soft matrix. As the carbon content increases, more and more carbide of a more continuous nature determines the hardness reading. The increase in hardness of the austenitic matrix is lost, therefore, to a large extent to the greater hardness of the carbides under the hardness indentor. Furthermore, aging within the austenitic zones is far from uniform in most of the alloys; this is readily noted in Fig. 7, in which the structure of alloy 111VT2-2 after aging at 1350 °F (730 °C) for 48 hours is shown. Despite these difficulties, hardness has been used with some success to detect aging; however, the method is not very sensitive to small significant changes.

Because regular hardness measurements appeared to be insufficiently sensitive to aging in these alloys, an attempt was made to use the Knoop hardness tester, which produces an indentation on a microscale, and can be located as desired in any portion of the field. Here too, however, certain discrepancies arose which made it a less useful tool than had been anticipated. It was found that the hardness varied across any given austenitic field in one grain, depending on the amount of aging constituent encountered. It was found, too, that the orientation of each grain was a strong factor in the hardness reading obtained. Thus, readings from one grain to another differed sufficiently to obscure the real change in hardness due to aging.

Very early in high temperature research (1941), hot hardness was found to bear no relationship to high temperature strength or ductility from alloy to alloy and was accordingly not considered as a useful tool in aging studies, nor as a means of comparing alloys from a high temperature strength viewpoint.

On the basis of these considerations, hardness changes were not used in this aging study beyond the preliminary work with NT-2 and VT2-2-type alloys, which indicated the lack of sensitivity of the measurements. Typical results for alloys 87NT-2 and 95VT2-2 (resembling 100NT-2 and 111VT2-2, but slightly lower in carbon) are shown in Fig. 1. The average of a large number of hardness readings is shown, together with the extreme values obtained by measuring the hardness of several grains.

Magnetometer Testing—The detection of changes in the magnetic characteristics of alloys with changes in alloy structure such as might be produced by aging, for example, has been known often

to be a sensitive measurement. Unfortunately, it was found that only the iron-bearing 100NT-2 alloy showed measurable changes in magnetic susceptibility with aging. The cobalt-chromium alloys showed little or no deviation in magnetic properties with changes occurring during aging and accordingly could not be readily studied by this means. All tests were made at room temperature following

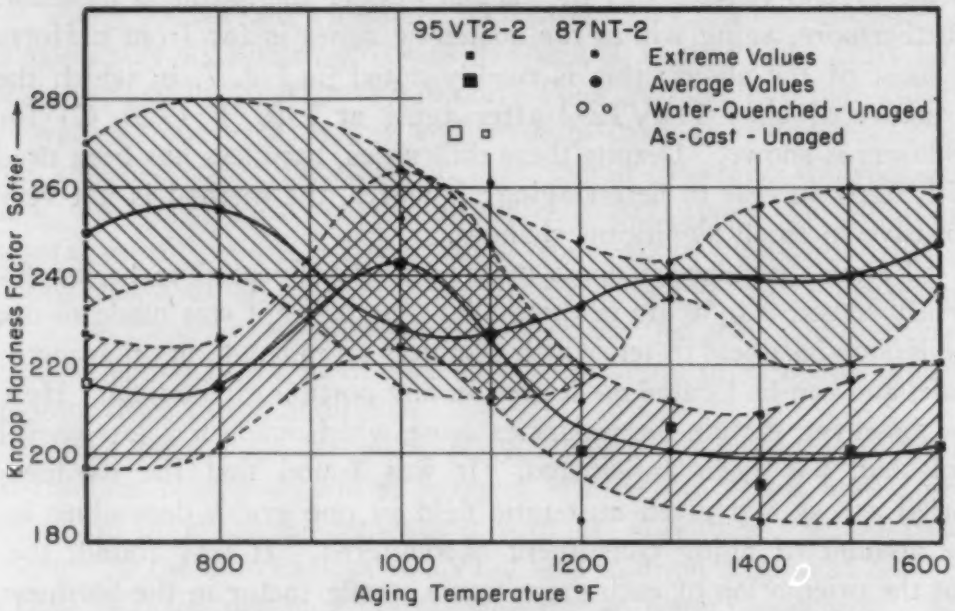


Fig. 1—The Variation of Hardness with Aging Temperature of Alloys 87NT-2 and 95VT-2 is Shown. The cross-hatched area illustrates the spread of hardness values obtained on the same specimen.

each aging treatment. Because of experimental difficulties, testing was discontinued after the 1400 °F (760 °C) treatment.

Microscopic Analysis—Cast bars, similar to those used in magnetic and resistance testing (¼ inch round, 4½ inches long), were charged into the furnace and a ½-inch length was cut off after each treatment. Through 1600 °F (870 °C) the duration of heating was 48 hours. The time was 24 hours at 1700 and 1800 °F (930 and 980 °C), 6 hours at 1900 and 2000 °F (1040 and 1095 °C), 4 hours at 2100 and 2200 ° F (1150 and 1205 °C), and 3 hours at 2250 °F (1230 °C) and above. In this way, each specimen had received the treatments at each lower temperature in the same way as the X-ray and resistance specimens with which they were later compared. All specimens were mechanically polished, and electrolytically etched in 10% HCl. Because of the large grain size, the microstructure varied considerably from one point to another. Characteristic sections and an exceptional single grain are shown in Fig. 2. This large

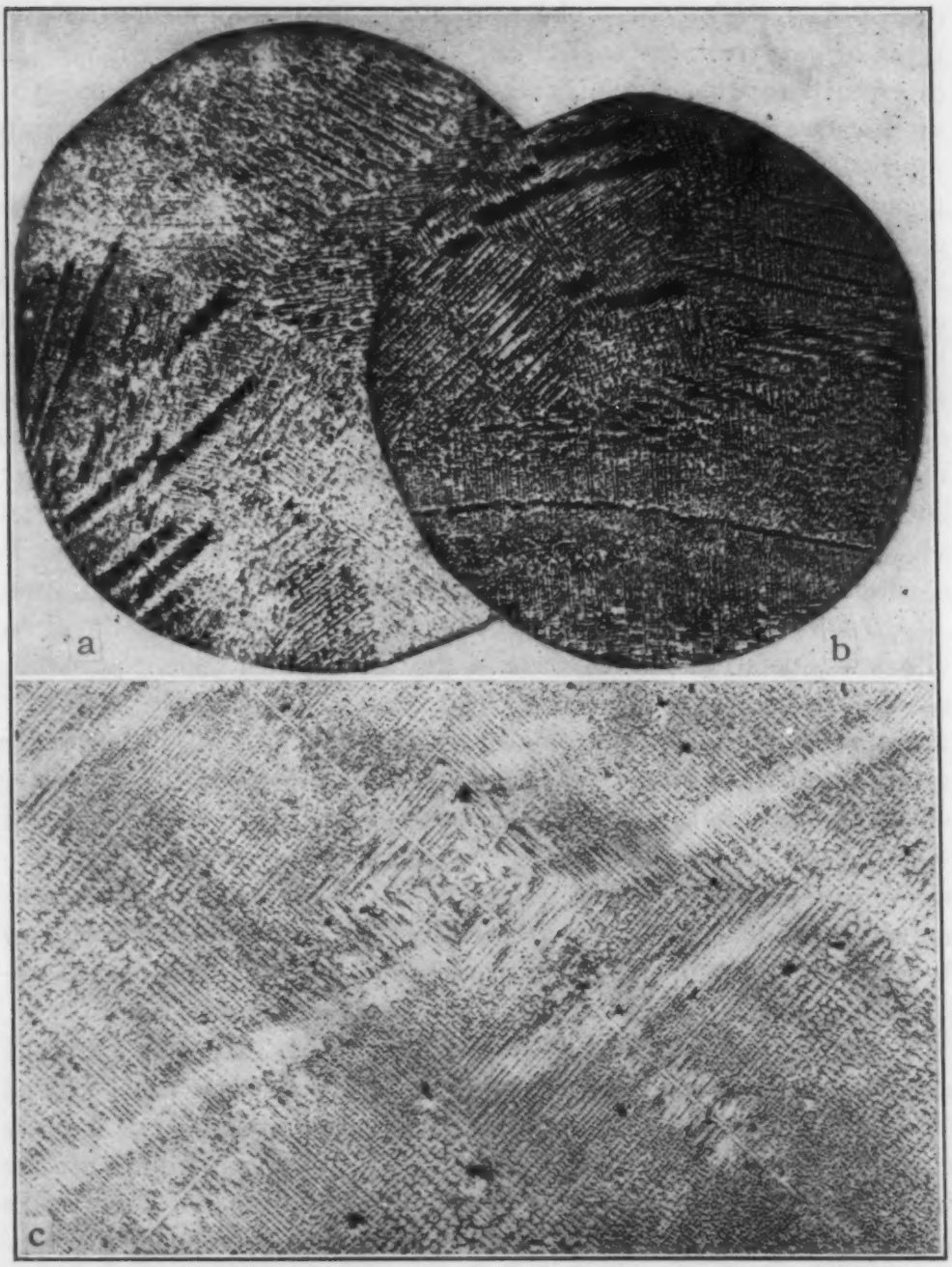


Fig. 2—a and b, Etched Sections of the Entire ¼-Inch Rod of Alloys 100 NT-2 (Fig. 2b) and 111 VT2-2 (Fig. 2a) Illustrate the Large Grains Typical of High Temperature Alloys. Alloy 45 R-6 is shown in Fig. 2c. This specimen happens to be a single grain across the entire ¼-inch section, illustrating the coarseness of grain which is sometimes obtained. × 25.

grain size accounts for the disparity in the appearance of photomicrographs in a series; however, an attempt was made to select a characteristic location of each sample.

X-Ray Diffraction—The four alloys were examined after two types of heat treatments. Debye-Sherrer photograms were made (a) after each treatment at progressively higher temperatures, and (b) after each treatment at the same temperature, with increasing time intervals. By means of the data accumulated, it was hoped that the times and temperatures necessary to produce aging could be found, and any phase transformations detected.

The failure to detect a precipitate by X-ray diffraction is not conclusive. A certain minimum quantity of the second phase must be present before it can be detected, and even then fine particle size, or strain, might widen the lines to the point where they cannot be observed. Furthermore, the formation of an intermediate phase, as in the case of duralumin, can render interpretation more difficult, for such a phase is apt to have a complicated structure which would not yield a strong X-ray pattern. The presence of a new set of lines in a pattern is conclusive evidence for the existence of another phase.

Dilatometric Survey—The expansion coefficient of the four alloys was determined. Because of the aging which takes place when an alloy is heated for the first time, the expansion curve is usually not smooth but has discontinuities at those temperatures at which precipitation is taking place. In addition, the slope of the curve changes after aging takes place, for the expansion characteristic of the original material differs from that of the aggregate containing the precipitate in addition to the matrix. For these reasons, the expansion coefficients given are for the metal which had previously been heated through the aging temperature range, as these measurements are considered to be of more general usefulness.

The expansion characteristics of these alloys are complicated by the formation of a precipitate on heating for the first time. In all cases, the alloy was essentially stabilized after the original heating cycle. These results suggest the advisability of pre-aging turbine blade materials before final fitting and the application of stress. This is true whether attachment is made by means of welding or mechanical fit, in order to minimize dimensional and structural instability.

In addition to measurements made on the dilatometer, the change in length produced by the aging of each alloy was directly measured. Bars 4 inches long were prepared with spherical ends, and carefully measured before and after aging at 1500 °F (815 °C). Further heat treatments at the same or lower temperature had no effect on the dimensions as measured in this way.

Electrical Resistance—Electrical resistance measurements were made upon ¼-inch bars, centerless ground to a uniform cross section, using a 2-inch gage length. Readings were made on a Kelvin double bridge, with a reflecting-type galvanometer.

Resistivity is a function of the resistance of the matrix, of the carbides, and of the aging precipitate. A change in the relative amounts of the separate phases will affect the over-all resistance, as will an alteration in the composition of one or more of the separate phases. Because two or more phases are always present, and since the exact composition of any of the phases is not known, the cause or direction of change of resistivity cannot be predicted. However, it has been found that electrical resistance measurements are a sensitive indication of the degree of aging as indicated by other measurements. The change of resistivity with aging was greater with the lower carbon alloys. This is very likely due to the presence of a relatively greater amount of carbide in the alloys higher in carbon, so that the addition of the aging precipitate has a smaller effect in changing the resistivity.

Stress Rupture—Standard stress-rupture tests were made on these four alloys, or on alloys which are slight modifications thereof. All these tests were conducted at 1500 °F (815 °C) and serve to illustrate the extreme importance of prior aging treatments on the 1500 °F (815 °C) rupture performance. The test specimens were 1¼-inch gage length, 0.250-inch diameter bars, cast by the same precision casting technique used for the preparation of all the other specimens.

Further changes in rupture life might result by the use of aging times greater than the 48 hours used here. This time was chosen since it was known that aging appeared to be complete within even a much shorter time. Tests on the cobalt-base alloy 70J (1)[1] showed that while aging at 1350 °F (730 °C) for times longer than 5 hours resulted in a small increase of rupture strength when tested at 1500 °F (815 °C), extended aging up to 200 hours did not improve the rupture properties when tested at 1350 or 1800 °F (730 or 980 °C).

Aging Behavior

Microscopic Analysis—All four alloys, as cast, contain at least three of what appear to be five distinct phases. As shown in Fig. 3,

[1]The figures appearing in parentheses pertain to the references appended to this paper.

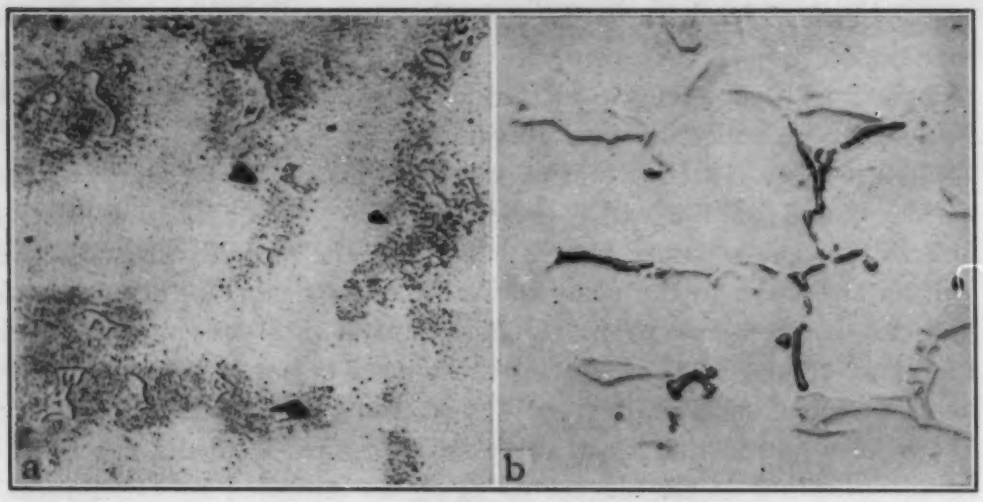


Fig. 3—The Above Photomicrographs Show Three of the Phases Existing in These Alloys. At left, the white areas are the prevalent dendritic carbides; the three dark grains are the phase referred to in the text as resembling MnS. The photomicrograph on the right is unetched. The lighter dendritic carbides surround a darker phase of similar shape. This latter is probably TaC. × 500.

these are (a) the continuous phase (a face-centered cubic and/or hexagonal structure, called austenite), (b) a globular or dendritic material referred to as carbide. The two remaining constituents, present in much smaller amounts, in part resemble this carbide. (c) One of the components darkens slightly when etched electrolytically in 10% HCl, and when in the form of discrete particles resembles manganese sulphide inclusions in steel. Often, however, these particles are continuous with the normal carbides, no distinct boundary being present—only the noted change in color. (d) The fourth phase is called the "A" constituent. It is not revealed by etching with an electrolytic oxalic acid etchant, but is distinguishable from the more prevalent carbides by the ease with which it darkens when etched electrolytically with HCl. When the specimen is properly etched to reveal aging, the "A" constituent has been attacked to such a degree that it cannot be readily distinguished from a pit. This is in contrast to the constituent resembling MnS previously described, where etching darkens, but does not dissolve it. (e) When columbium or tantalum is present (100NT-2), CbC or TaC form. In appearance they resemble most the chromium carbides. Figs. 4 through 7 show the structures of the alloys after aging at temperatures from 1200 °F (650 °C) to 2300 to 2400 °F (1260 to 1315 °C). At 2300 °F (1260 °C), which is within 100 to 150 °F of the fusion temperature, the matrix of all alloys had the same structure as at all

lower temperatures. Alloys 25V-0 and 45R-6 were seen to contain three phases: the matrix, dendritic carbides, and a smaller amount of the "A" constituent. None of the "MnS" phase was detected. Typical appearance of the "A" constituent, in an alloy composition in which it is more prevalent, is shown in Fig. 8 (1). The photomicrograph for alloy 100NT-2 at 1350 °F (730 °C) was taken near the edge of the specimen. It can be seen that the precipitate formed either along slip planes (caused by the cold work of cleaning off the oxide after the previous treatment and by the drastic quench) or along atomic planes in the manner of Widmanstätten structure. In general, the first precipitation was not uniform. This is clearly shown in Fig. 7.

Treatment at higher temperatures caused heavier aging, until the precipitation was a maximum at 1550 to 1600 °F (845 to 870 °C) for the two low carbon alloys, 1700 °F (925 °C) for 100NT-2, and 1600 to 1700 °F (870 to 925 °C) for 111VT2-2. Above these ranges, and especially above 1800 °F (980 °C), agglomeration of the precipitate began, together with some re-solution of the precipitate. By 2100 °F (1150 °C) practically all of the aging precipitate in alloys 25V-0 and 111VT2-2 had been redissolved, 2200 °F (1205 °C) being required for 45R-6 and 2250 °F (1230 °C) needed for alloy 100NT-2. Some spheroidization of the carbide particles was noticeable in alloy 25V-0 at 2100 °F (1150 °C). At or above 2300 °F (2250 °F for 111VT2-2), many of the carbide particles melted, forming characteristic star-shaped and square particles. Very frequently these carbides contain inclusions. As will be mentioned later, X-ray diffraction patterns gave no indication that these new carbide shapes were a new phase, although they differed considerably in appearance and distribution.

X-Ray Diffraction—A comparison of the diffraction patterns of the different alloys showed considerable similarity. In the as-cast condition, the patterns of 25V-0 and 45R-6 were the same. This was also the pattern produced by 100NT-2 after a solution treatment and quench (additional lines were present in the as-cast condition). 111VT2-2 also had this basic structure, but with an additional pattern superposed. These patterns were those of the face-centered cubic solid solution on which were superposed lines from varying amounts of hexagonal close-packed cobalt, and lines from the carbides and aging constituents. Not only were the matrix-plus-carbide patterns of the four alloys generally similar, but the patterns pro-

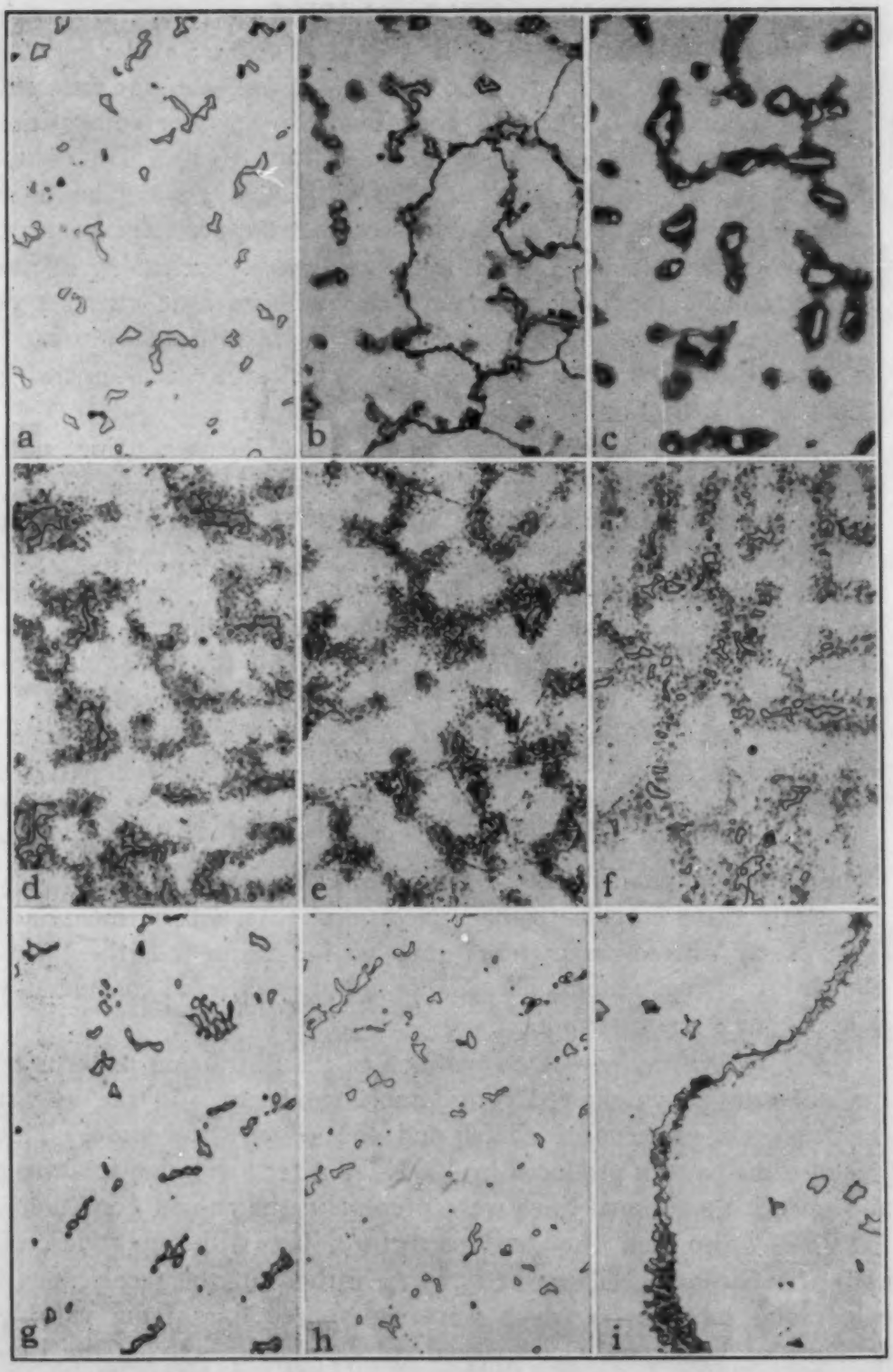


Fig. 4—Alloy 25 V-0. × 250. Aged progressively. a—1200 °F. b—1400 °F. c—1500 °F. d—1600 °F. e—1800 °F. f—2000 °F. g—2100 °F. h—2200 °F. i—2400 °F.

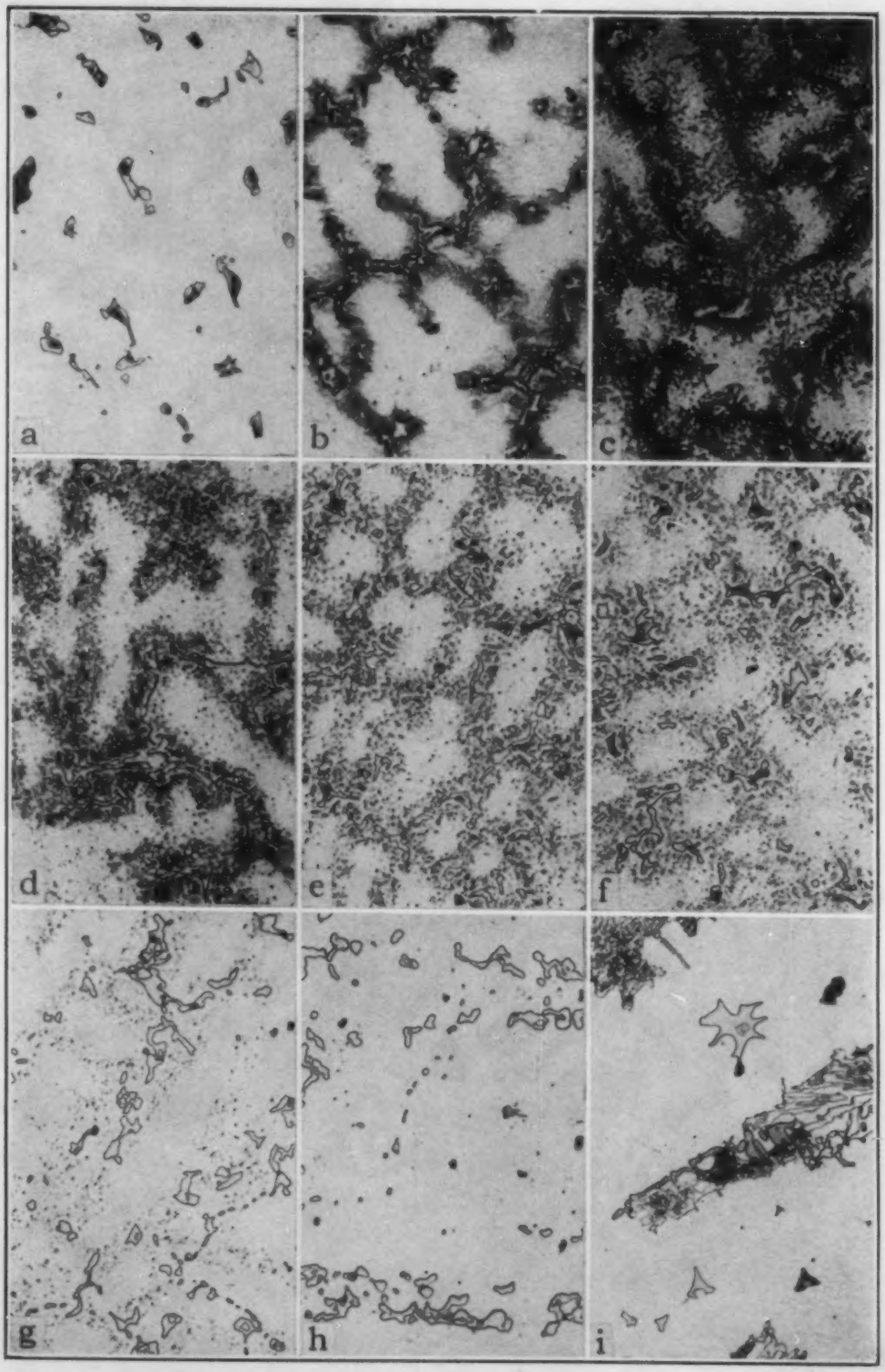


Fig. 5—Alloy 45 R-6. × 250. Aged progressively. a—1200 °F. b—1400 °F. c—1500 °F. d—1600 °F. e—1800 °F. f—2000 °F. g—2100 °F. h—2200 °F. i—2400 °F.

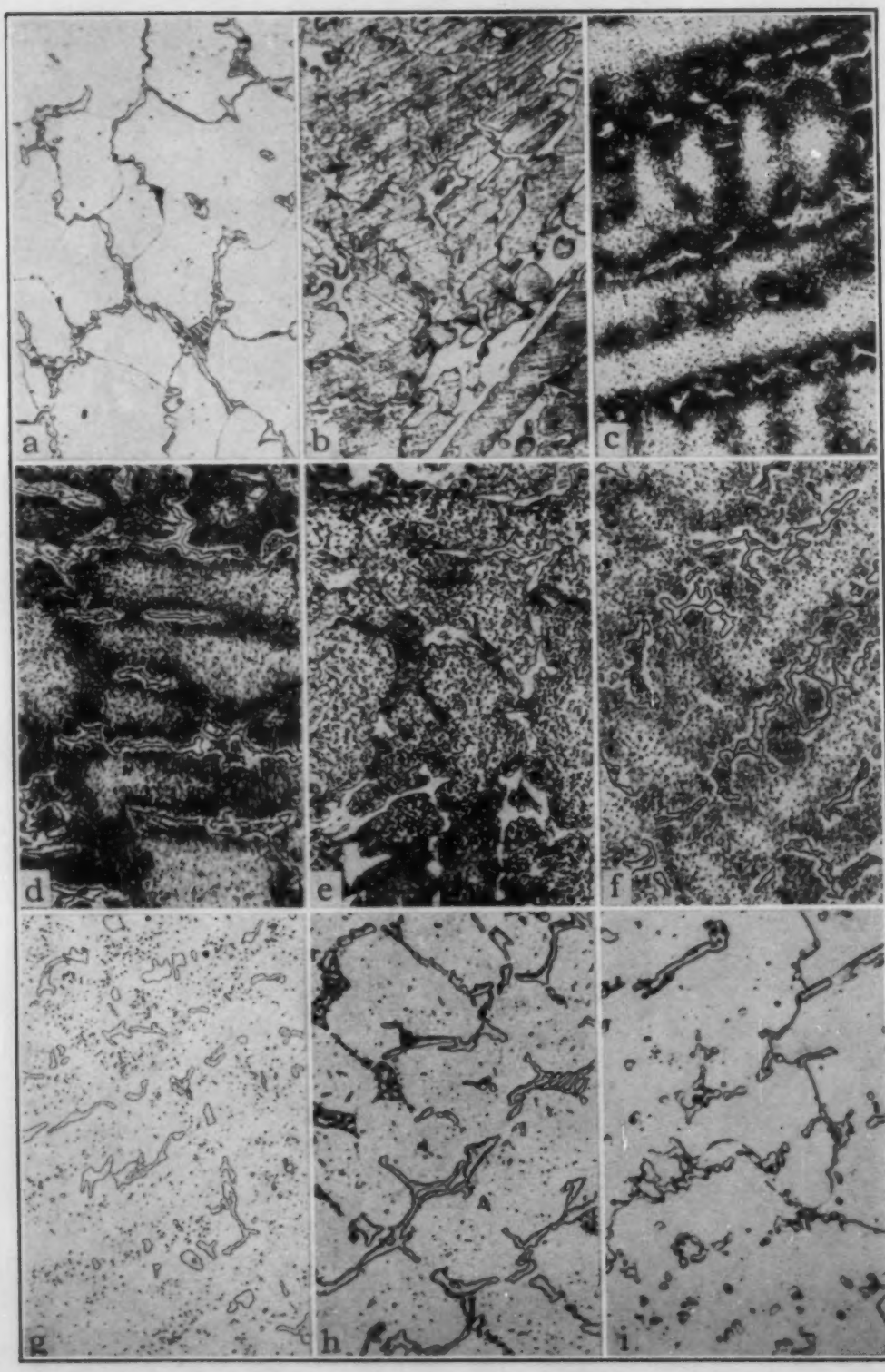


Fig. 6—Alloy 100 NT-2. × 250. Aged progressively. a—1200 °F. b—1350 °F. c—1500 °F. d—1600 °F. e—1800 °F. f—2000 °F. g—2100 °F. h—2200 °F. i—2300 °F.

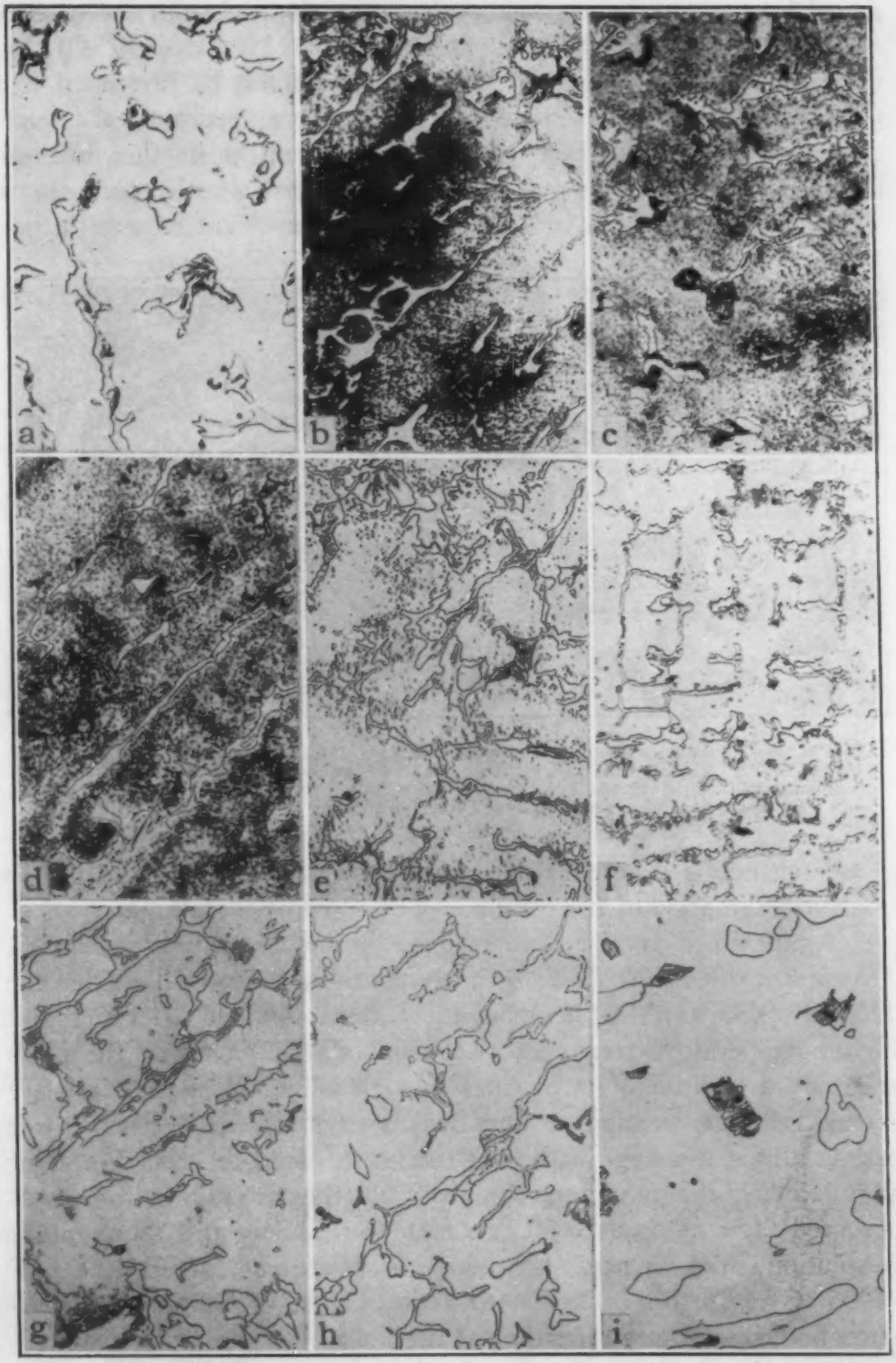


Fig. 7—Alloy 111 VT 2-2. × 250. Aged progressively. a—1200 °F. b—1350 °F. c—1500 °F. d—1600 °F. e—1800 °F. f—2000 °F. g—2100 °F. h—2200 °F. i—2300 °F.

duced by the aging constituents also were the same (in the case of alloy 100NT-2, this was true after aging at 1350 °F (730 °C), but not true when aged at 1000 °F). It should not be presumed that since the structures of some of the phases were apparently the same, the compositions of these phases were identical in the different alloys. No attempt was made to detect changes in lattice parameters. This information might provide a clue to the extent of substitution

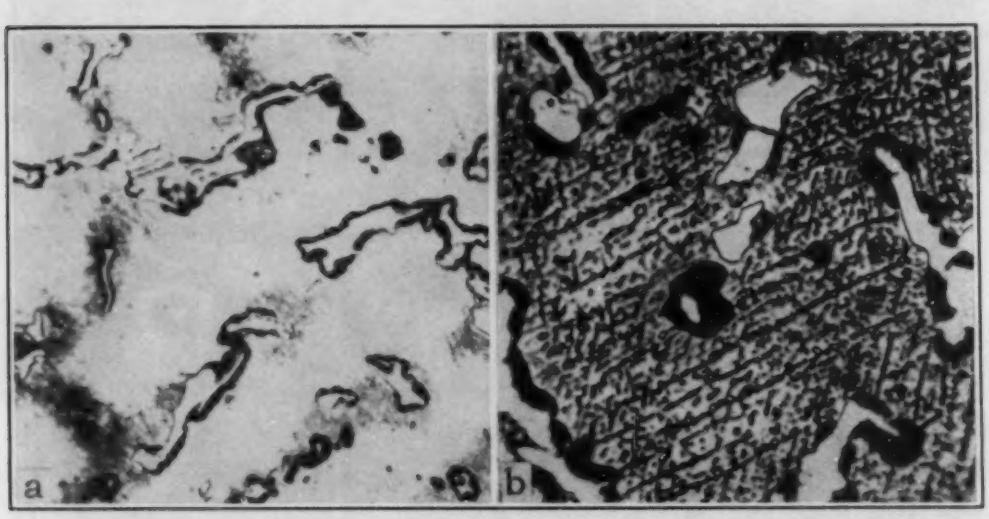


Fig. 8—Microstructure of a Modified Vitallium (70J) Which Contains a Larger Amount of "A" Constituent. Light areas are carbides, diagonal streaks are the aging precipitate, and black regions are the "A" constituent. Specimen on right is from a broken stress-rupture specimen. Etched electrolytically in 10% HCl.

of one element for another in a given structure, which would not be improbable in view of the complexity of some of the alloys.

Aging times were the same as for the metallographic specimens. Except for alloy 100NT-2, no precipitate was discernible after the 1200 °F (650 °C) treatment but the pattern obtained after the next higher temperature treatment (1350 or 1400 °F) showed the presence of an additional set of lines in each alloy. While the relative intensity of the precipitate lines was always low in the two lower carbon alloys, a change with heat treatment could be observed. For alloy 25V-0, the maximum intensity of the precipitate lines was observed after aging at 1600 °F (870 °C). Above this temperature re-solution took place, becoming complete at about 2000 °F (1095 °C). In this case, the formation of the precipitate was indicated both by the intensification of the lines of a phase already present (probably carbide) and by the appearance of new lines. The appearance of the films of alloy 45R-6 was essentially similar, except

that the intensity of the precipitate lines was approximately constant over the 1600 to 1900 °F (870 to 1040 °C) range of treatments.

Alloy 100NT-2 differed from others in the series by its response to solution heat treatment. X-ray patterns clearly show that quenching from an elevated temperature retains in metastable solid solution a phase which would separate on cooling under equilibrium conditions. All work on this alloy was preceded by a quench from 2260 °F (1240 °C), the solution treating temperature found to give the best strength in stress-rupture at 1500 °F (815 °C) and above (3). On reheating the quenched alloy, lines of a new phase began to appear at 1000 °F (540 °C). These precipitate lines began to become faint after the 1800 °F (980 °C) treatment, but were still present at 2100 °F (1150 °C). They could not be detected after heating to 2200 and 2300 °F (1205 and 1260 °C).

Diffraction patterns of alloy 111VT2-2 showed that precipitation had taken place at some temperature between 1200 and 1350 °F (650 and 730 °C). In this case, the intensity of the precipitate lines remained relatively constant after heat treatments up to 2000 °F (1095 °C). Above this temperature not only did the precipitate lines disappear, but a set of lines from a phase present in the cast alloy also vanished as it too went into solution.

In addition to progressive heating, specimens were X-rayed after increasing times at constant temperatures. These temperatures were 1500 °F (815 °C) for alloys 25V-0 and 45R-6, and 1000, 1350 and 1500 °F (540, 730 and 815 °C) for alloys 100NT-2 and 111VT2-2. Aging in 25V-0 and 45R-6 was noted to have started at a time between 5 and 20 minutes. The intensity of these lines in 25V-0 increased with additional time at temperature, the maximum not having been reached after 28⅓ hours. In both cases, the precipitate which formed isothermally at 1500 °F (815 °C) had the same structure as the one formed by slow progressive heating.

Isothermal treatment of alloy 100NT-2 produced interesting and unexpected results, which are tabulated below.

1000 °F—Precipitate lines appeared at about 1½ hours. X-ray indications of the precipitate phase were faint even after an accumulated time of 203.6 hours at temperature. The structure of the precipitate was the same as that which appeared when the alloy was heated at progressively higher temperatures from room temperature.

1350 °F—The pattern taken after 1⅓ hours at temperature showed an additional phase which differed from that obtained at 1000 °F (540 °C). The pattern was considerably stronger after an

accumulated time of 12⅓ hours at temperature, but changed little after an additional 4 days.

1500 °F—Aging had begun by 5 minutes, the precipitating phase having a structure similar to that obtained at 1350 °F (730 °C). The lines of the second phase were strongest after a total time of 28⅓ hours, and were changed but little after an additional 48 hours.

Treatment of alloy 111VT2-2 at constant temperature indicated no aging after a total time of 64.5 hours at 1000 °F (540 °C). At 1350 °F (730 °C) aging was observed to begin between 4⅓ hours and 12⅓ hours at temperature, while at 1500 °F (815 °C) aging began between 1⅓ and 9⅓ hours. The precipitate appeared to have the same structure in each case.

Because of the limited number of lines obtained with chromium radiation, it was not possible to index them with certainty. The possibility of an allotropic change in the structure of the matrix, which accompanies the formation of the aging precipitate, must be considered in the interpretation of the patterns obtained from cobalt-base alloys since both the hexagonal close-packed and face-centered cubic structures are definitely known to co-exist.

Linear Expansion—The curves in Fig. 9 show the manner in which the alloys change in length, upon the original heating, upon cooling, and when subsequently reheated. Except for an apparent slight interruption in the original expansion of alloy 25V-0 at 950 to 980 °F (510 to 525 °C), the curves are smooth although with some change in slope, up into the temperature region where aging is unquestionably known to occur. That these changes are associated with aging is evident from the absence of an inflection when the same specimen is reheated. A pronounced break in the curve (at 1400 to 1480 °F) occurs only with alloy 100NT-2, indicating rapid aging when this temperature is reached.

Table II

Temperature or Temp. Range—°F	Average Coefficient of Linear Expansion × 10^{-6} per °F			
	25 V-0	45 R-6	100 NT-2	111 VT 2-2
1500	10.8	10.3	10.2	8.7
1600	11.6	10.8	10.3	8.7
70 to 1200	9.2	8.7	8.5	8.75
70 to 1300	9.3	8.7	8.65	8.9
70 to 1400	9.3	...	....	8.9
70 to 1500	9.4	8.8	9.0	9.0
70 to 1600	9.6	9.0	9.0	9.0
70 to 1800	10.0	...	9.25	...

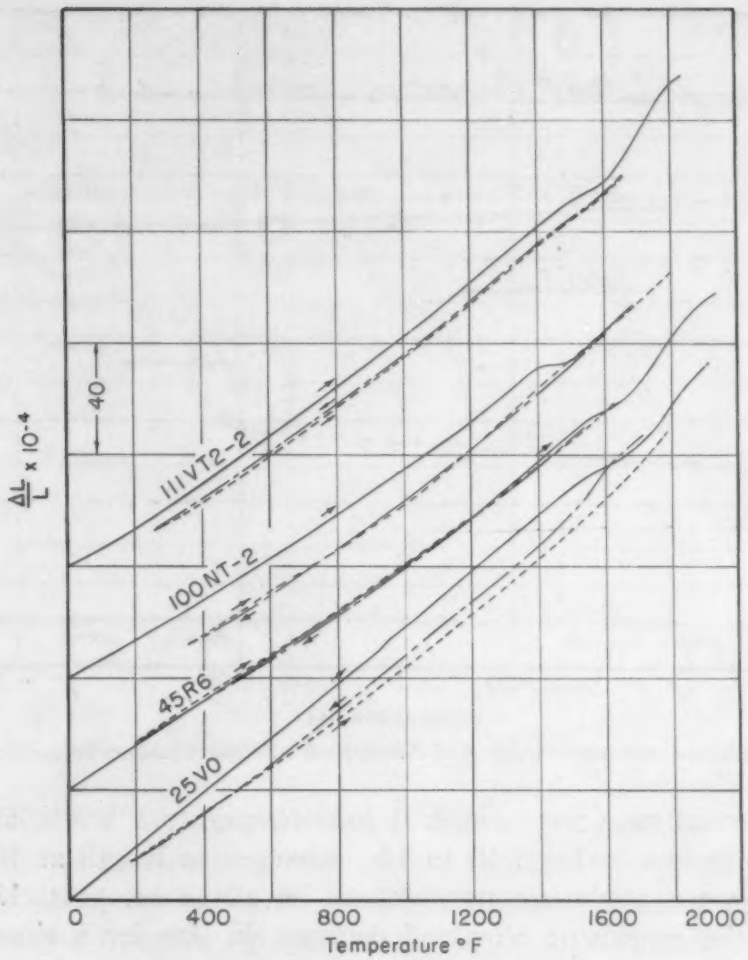


Fig. 9—Dilation Curves of the Four Alloys.

The expansion coefficients for metal which had previously been heated to 1700 to 1900 °F (925 to 1040 °C) are listed in Table II. Also, cast bars, 4 inches long, were measured before and after heat treatment. The change in length is expressed as inches per inch.

Alloy	Change in Length After Heat Treatment Inches Per Inch—Aging at 1500 °F for 8 Hours
25V-0	—0.00045
45R6	Not Measurable
100NT-2	+0.0013 (after solution treatment at 2260 °F) +0.00077 (after aging solution-treated bar)
111VT2-2	Not Measurable

Aging caused a shrinkage of the solution-treated 100NT-2, but it was still longer after aging than it was as-cast. The other alloys were not solution-treated.

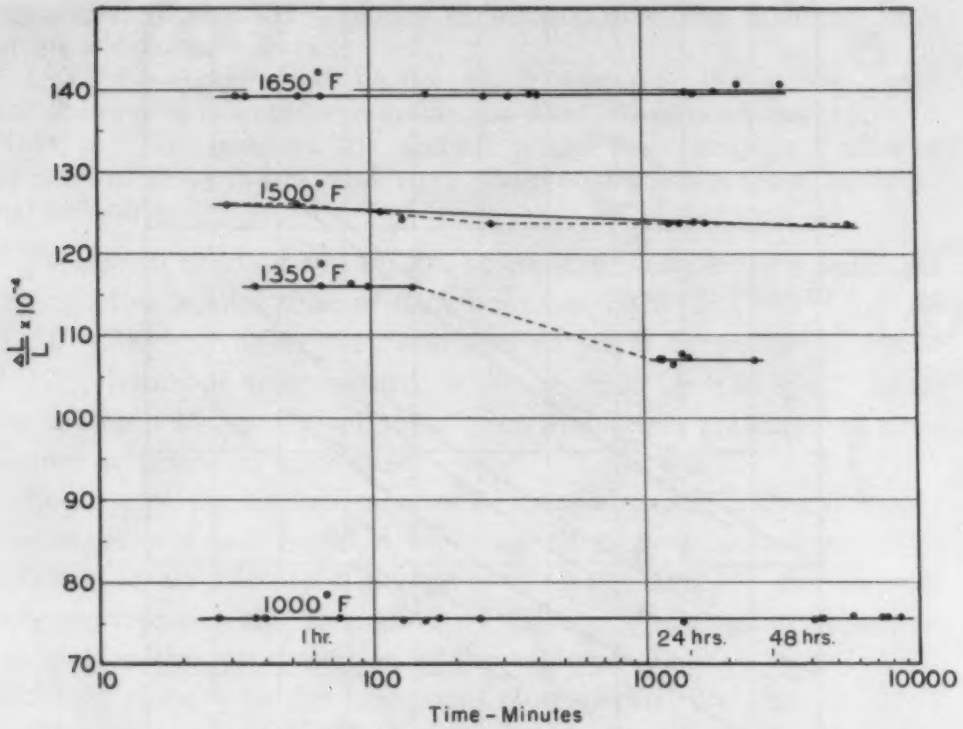


Fig. 10—Change in Length of Alloy 25V-0 at Each of Four Constant Temperatures.

Isothermal runs were made at four temperature levels, and the results are shown in Figs. 10 to 13. Changes in length at 1000 °F (540 °C) were slight or nonexistent in all cases. At 1350 °F (730 °C) the specimens remained constant in size for a time, then began to contract. Measurements of alloys 45R-6 and 100NT-2 were not obtained at short time periods, due to difficulties in stabilizing the temperature after rapid heating, but it is likely that these too would have shown an initial inoculation period before shrinkage began. At 1500 °F (815 °C), much of the aging had occurred while heating up to temperature, for these curves were flatter than those for 1350 °F (730 °C) aging. At 1650 °F (900 °C), precipitation reactions undoubtedly took place while the sample was being heated.

Fig. 9 shows a break in the curve of three of the alloys at 1600 °F (870 °C), and at a slightly lower temperature in the fourth. Undoubtedly the reaction associated with this change would occur at a lower temperature if more time were allowed. Thus, if a specimen were held at a lower temperature, 1350 or 1500 °F (730 or 815 °C), for example, and then heated higher, a less marked change would be expected over the 1500 to 1700 °F (815 to 925 °C) range (except for 100NT-2). However, if a specimen were heated directly to

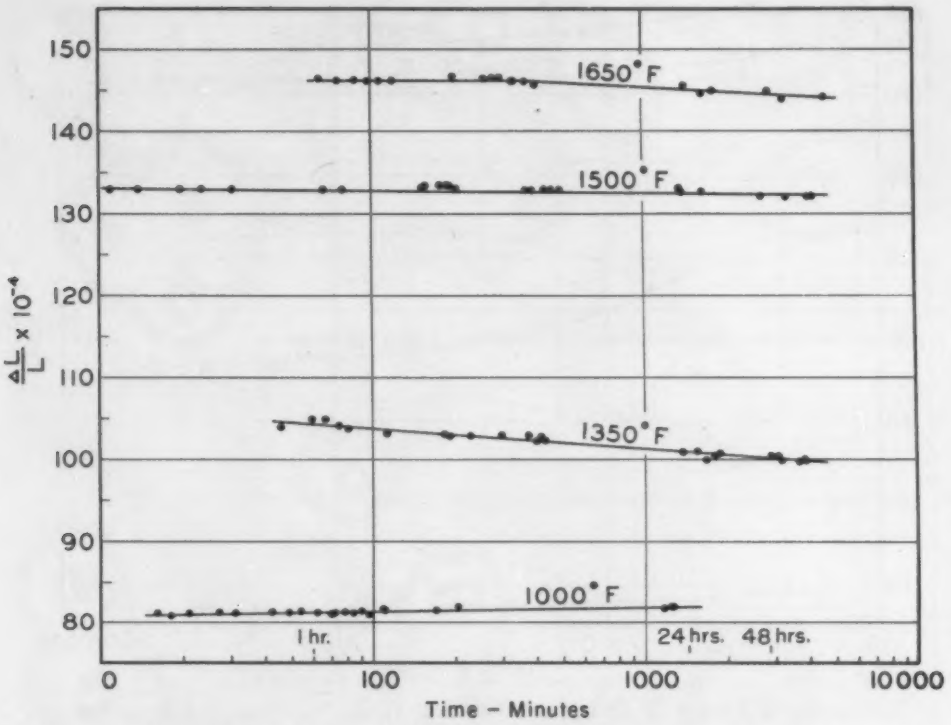


Fig. 11—Change in Length of Alloy 45R-6 at Each of Four Constant Temperatures.

1650 °F (900 °C), length changes due to precipitation would occur rapidly, and its length at temperature could not be predicted from a knowledge of the expansion coefficient alone. This is the explanation for the irregular spacing of the isothermal curves. They indicate only a small increase in length at 1650 °F (900 °C) over the length at 1500 °F (815 °C), and in alloy 100NT-2, where the break in the expansion curve is the sharpest (Fig. 9), this increase is the least. Any changes in length which do occur at 1650 °F (900 °C) are likely due not only to further slight precipitation but probably are associated with the coalescence of the precipitate and carbide particles.

Electrical Resistivity—Resistance specimens were aged for various lengths of time, as shown in the introduction, under microscopic analysis. As shown in Fig. 14, electrical resistivity, as measured after each aging treatment, changed very little between room temperature and 800 °F (425 °C). Beyond 1000 °F (540 °C) the resistivity of every alloy decreased, generally to the range of aging temperatures where the greatest precipitate was seen microscopically. As the aging precipitate was taken back into solution, the resistivity again rose. The cause for the inflection in the curve at 800 to

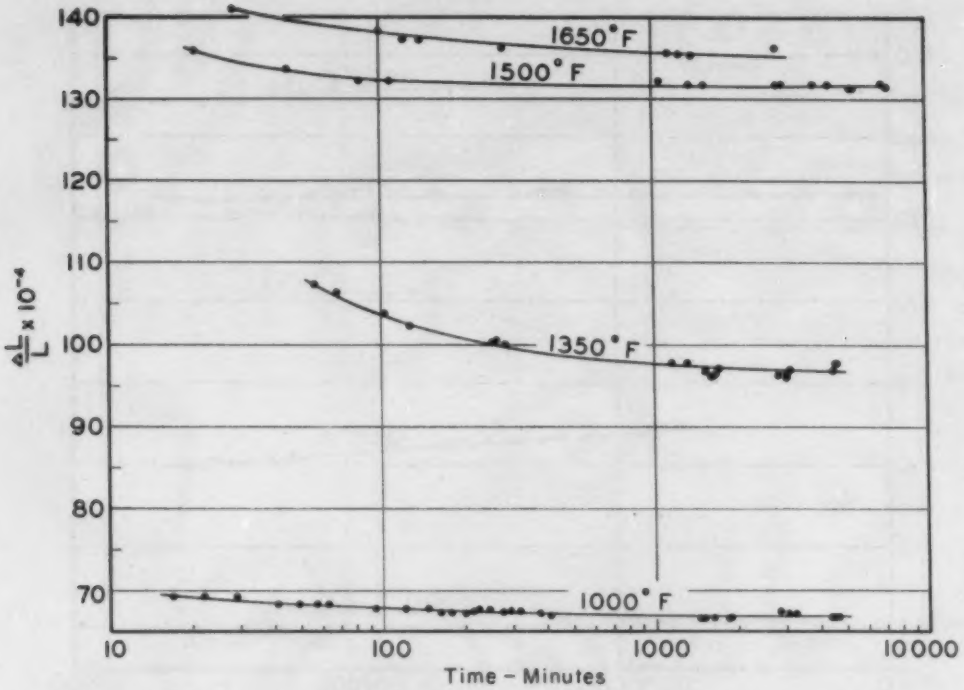


Fig. 12—Change in Length of Alloy 100 NT-2 at Each of Four Constant Temperatures.

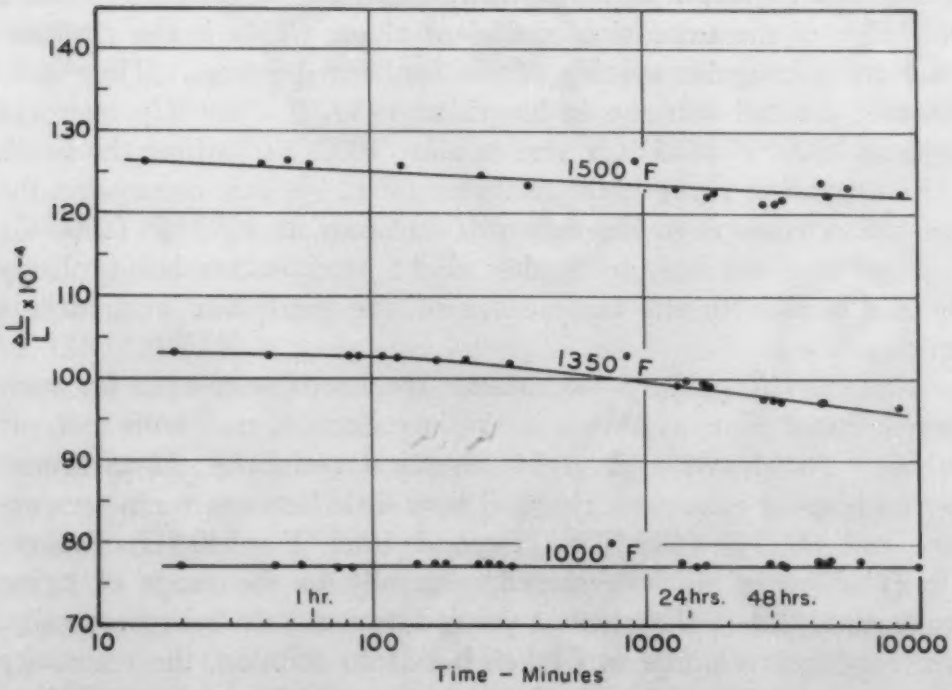


Fig. 13—Change in Length of Alloy 111 VT 2-2 at Each of Three Constant Temperatures

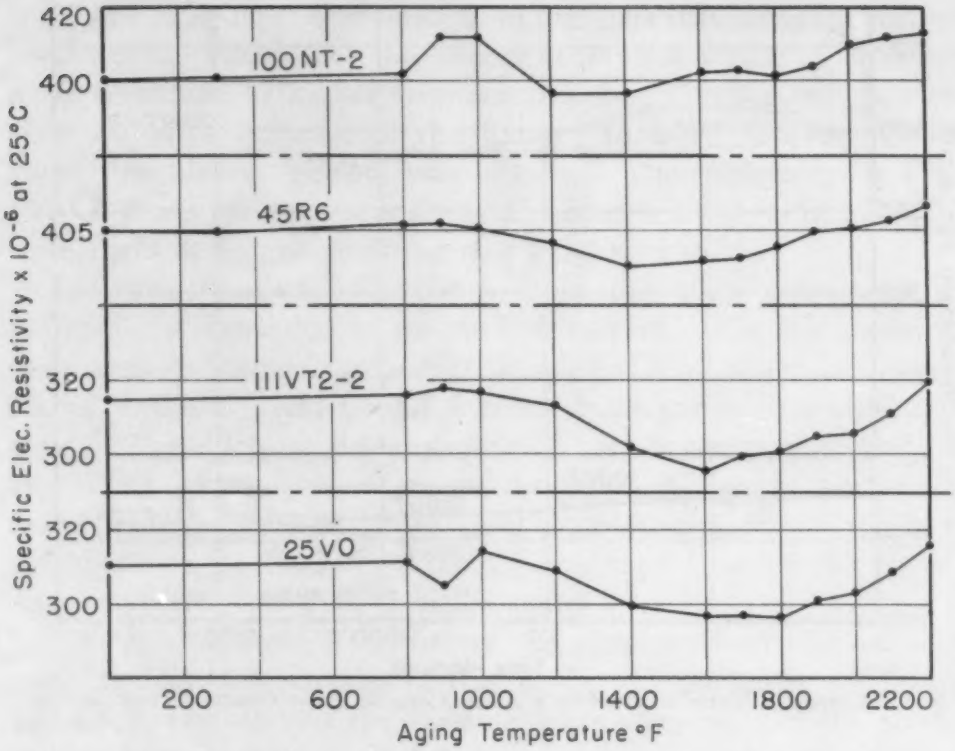


Fig. 14—Variation of Electrical Resistivity with Aging Temperature.

1000 °F (425 to 540 °C) is not clear. A pre-precipitation phenomenon may be involved, since the magnetic properties of 100NT-2 change at the same temperatures, and in one alloy (25V-0) there is a corresponding slight break in the expansion curve. However, these changes might well be caused by stress-relief. It had been found that filings had to be annealed at above 1000 °F (540 °C) to produce sharp X-ray diffraction lines, showing that this is the temperature range which provides stress-relief.

The presence of elements in solid solution in general increases resistivity. The curves in Fig. 14 show this trend. In general, there is no significant decrease in resistance below that of the cast material until the 1200 to 1400 °F (650 to 760 °C) treatments. Re-solution of the precipitate is likewise indicated by the increase in resistance above 1600 to 1800 °F (870 to 980 °C).

Prolonged heat treatment at elevated temperatures helped to show, by the change in resistivity, the stability of two of the alloys. As shown in Fig. 15, resistivity of 100NT-2 and 111VT2-2 after aging at 1000 °F (540 °C) remained unchanged, except for a 5 to 25-minute period of adjustment in the case of 100NT-2. That this slight change

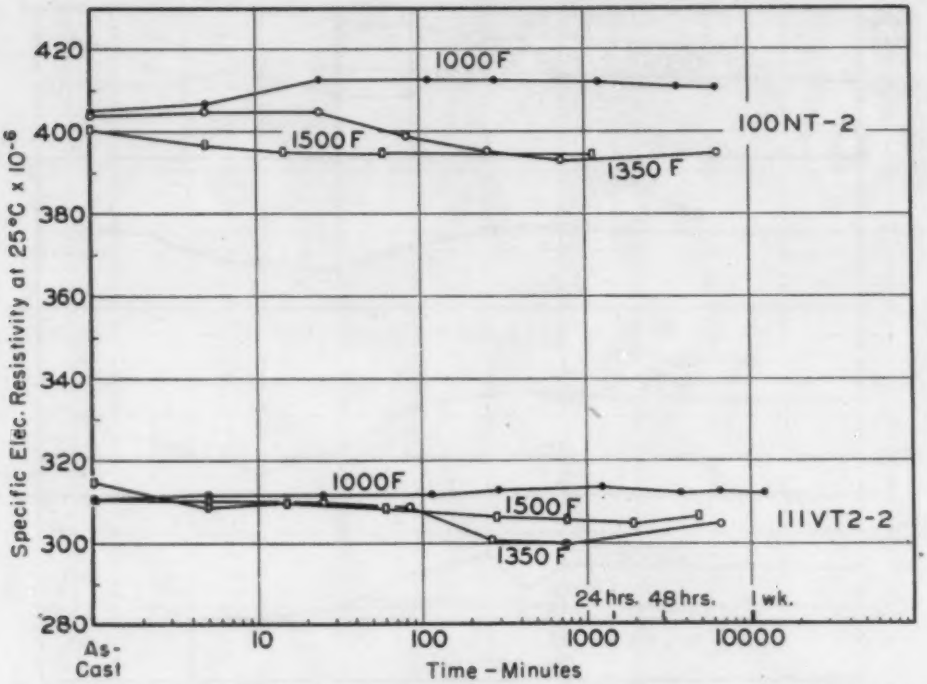


Fig. 15—Change in Electrical Resistivity After Aging at Three Constant Temperatures.

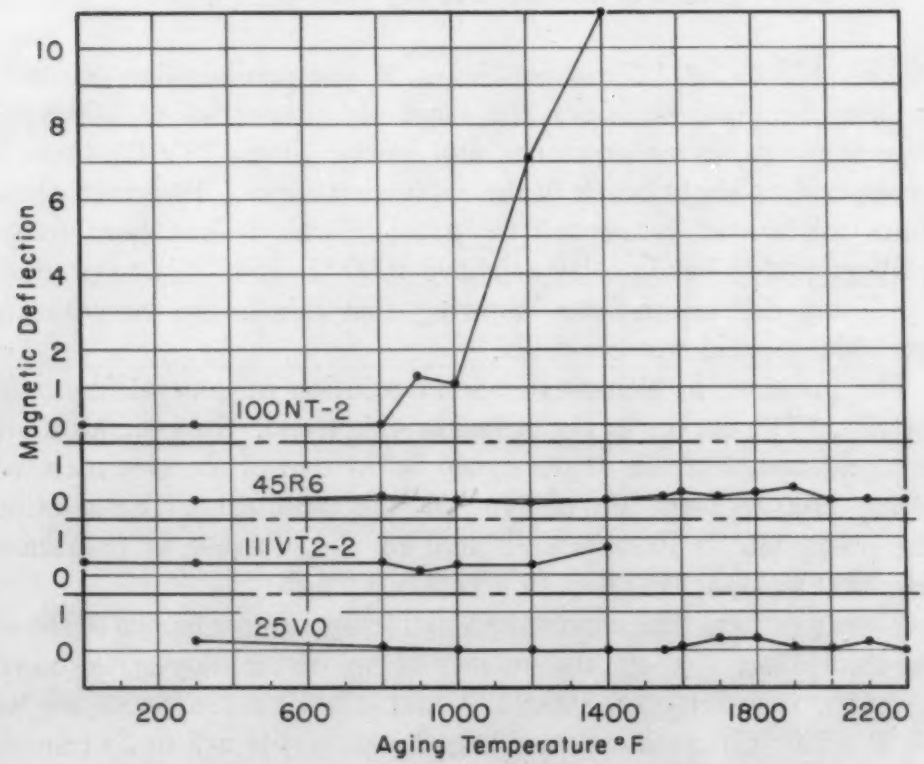


Fig. 16—Variation of Magnetic Deflection with Aging Temperature.

is not due to aging is presumed from the facts that no aging was seen microscopically and that the change was an increase of resistivity, while treatment at higher temperatures where aging certainly took place caused a decrease of resistivity. At 1350 °F (730 °C) this initial inoculation period was absent. The resistivity of alloy 100NT-2 was constant after aging 15 minutes. Changes in 111VT2-2 were slight and inconclusive at that temperature.

Magnetic Susceptibility—Only the alloy containing iron (100NT-2) responded to magnetic treatment. Fig. 16 shows that there was no change up to 800 °F (425 °C), a slight inflection at 900 °F (480 °C), and a rapid increase in magnetic susceptibility beyond. The increase in susceptibility is discontinuous, and this anomalous behavior may be caused by the relief of internal stress at a temperature between 900 and 1400 °F (480 and 760 °C). In the neighborhood of 1400 °F (760 °C) the rapid rise of the curve is associated with the onset of visible aging.

Stress-Rupture—Even before the supplementary data were accumulated for the purpose of this study, rupture tests, wherein the aging temperature was the variable, were showing that the strength at high temperatures as well as the ductility were greatly influenced by the prior aging treatment (2). In some cases the data were for similar but not identical alloys. The tests were not repeated because it was known that none of the alloying elements was nearly as important as carbon in influencing aging behavior, and only alloys with similar carbon contents were compared.

Alloy 25V-0

While no results are available on the regular Vitallium alloy, a modified Vitallium wherein 2% manganese is present instead of the usual 0.5 to 1% clearly shows the changes in high temperature properties (at 1500 °F) with increasing aging temperature. All aging times were set at 48 hours. Fig. 17 shows that maximum strength and minimum ductility at 1500 °F (815 °C) and 20,000 psi occur for the alloy when aged 48 hours at 1350 °F (730 °C) prior to testing. It therefore appears that the particle size and its mode of distribution are at some optimum value for attaining maximum strength when aging occurs for 48 hours without load at 1350 °F (730 °C). Quite apparently heating at 1600 °F (870 °C) causes the formation of a particle size and distribution of the precipitate characteristic of overaging.

While no evidence of precipitation at 1000 °F (540 °C) was detected microscopically or by X-ray, stress-rupture results showed that a change had taken place. Fig. 17 showed that the rupture time increased from 90 hours in the cast condition to 137 hours after aging 48 hours at 1000 °F (540 °C). Aging at a higher temperature, of course, increased the strength considerably. If a precipitate

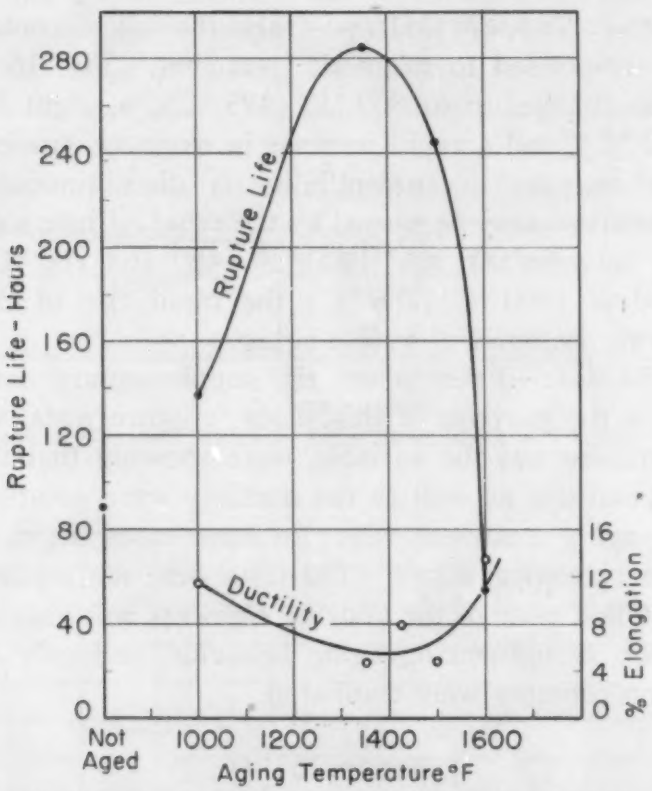


Fig. 17—Rupture Life as a Function of Aging Temperature for Alloy 27V-3. Test temperature was 1500 °F and stress was 20,000 psi.

actually forms at 1000 °F (540 °C), the particles are too small to be observed microscopically, and are too small a portion of the total mass to be observed by X-ray diffraction.

45R-6

Again as with low carbon Vitallium, no rupture results are available on regular 6059, but data are available on alloy 49T-6, a 6059 composition modified by the addition of 1% of titanium. Table III gives rupture life and ductility values at 25,000 psi and 1500 °F (815 °C) as a function of the aging temperature. Aging time was

48 hours at the indicated temperature. In some cases duplicate determinations were made.

Table III
Rupture Life and Ductility of Alloy 49T-6 at 25,000 psi at 1500 °F

	Stress, psi	Hours to Rupture	% Elongation	% Reduction of Area
As-cast—48 hours, 1000 °F	25,000	48.2	14.1	19.6
As-cast—48 hours, 1350 °F	25,000	65.1	28.3	20.3
As-cast—48 hours, 1350 °F	25,000	83.6	15.9	15.0
As-cast—48 hours, 1500 °F	25,000	84.4	23.0	18.6
As-cast—48 hours, 1500 °F	25,000	126.6	23.0	16.3
As-cast—48 hours, 1600 °F	25,000	36.1	22.2	13.4

In spite of the fact that alloy 6059 is quite irregular in performance in rupture tests at 1500 °F (815 °C), the table shows sufficient trend to indicate that maximum strength and ductility are attained by the 1500 °F (815 °C) aging treatment. As usual, the degree of improvement attained by selecting the proper aging treatment is appreciable.

100NT-2

Despite the fact that all the supplementary data show that alloy 100NT-2 ages on exposure of the solution-treated specimen to temperatures in the range 1350 to 1800 °F (730 to 980 °C), none of the rupture tests shows any improvement with aging treatments in the range of 1350 to 1600 °F (730 to 870 °C). Probably the reason for this is that the carbides contribute so very much to the strength of the alloy that any benefits imparted to the matrix through aging are not apparent. The change in rupture life due to aging treatments is no greater than the difference in rupture lives of two specimens from the same heat or from different heats (3). In low carbon alloys where the massive carbides constitute but a small area of any cross section and are far from complete in any given path in the structure, aging benefits imparted to the austenitic matrix are large and are readily apparent in any rupture test. Compare the structures of Figs. 4 and 6, a high and low carbon alloy respectively.

111VT2-2

As with alloy 100NT-2, while aging is known to occur in this alloy, the effects are not obvious in a rupture test at 1500 °F

(815 °C) (3). Again the path of the carbides is so great and the carbides are correspondingly so strong, that any strengthening effect on the austenitic matrix through aging is not perceptible. Table IV shows this effect directly in a group of high carbon VT2-2 alloys and in several modifications of it, at 30,000 psi and 1500 °F (815 °C).

Table IV

Alloy	Hours to Rupture	% Elongation	% Reduction of Area
91 VT 2-2* As-cast—No aging	180.0	7.9	4.1
As-cast—48 hours—1500 °F	174.3	15.3	8.6
93 VT 2-2* As-cast—No aging	213.8	4.7	2.6
As-cast—48 hours—1500 °F	179.4	3.1	2.8
102 VT 2-2* As-cast—No aging	174.0	6.4	4.1
As-cast—48 hours—1350 °F	173.3	5.6	4.5
114 VT 6-2* As-cast—No aging	114.6	7.2	4.5
As-cast—48 hours—1350 °F	101.7	6.4	4.1
109 VN 4-2* As-cast—No aging	169.4	18.9	8.7
As-cast—48 hours—1350 °F	157.6	14.4	11.3

*The first three are VT 2-2 alloys with carbon contents ranging from 0.91 to 1.02%, having the composition shown in Table I.
114 VT 6-2 contains 1.14 C, 23 Cr, 63 Co, 6 Mo, and 6% Ta.
109 VN 4-2 contains 1.09 C, 4 Ni, 23 Cr, 65 Co, and 6% Mo.

Without attaching too much significance to the exact results, the table above shows that aging at 1350 or 1500 °F (730 or 815 °C) does not strengthen the alloy and apparently, on the average, decreases the ductility slightly.

Conclusions

The results of all the measurements made show that these four alloys are stable up to 900 or 1000 °F (480 or 540 °C). While no reaction at this temperature can be observed microscopically, the results of several different types of measurements indicate that some sort of change is taking place in this temperature region. The first definite precipitation was noticed in all four alloys at close to 1350 °F (730 °C). The maximum amount of aging was at 1550 to 1600 °F (845 to 870 °C) in the two low carbon alloys, and at 1600 to 1700 °F (870 to 925 °C) in the high carbon alloys. In all cases agglomeration of the precipitate began at around 1700 °F (925 °C), and by 2100 to 2200 °F (1150 to 1205 °C) practically all of it was back in solution. The carbides were observed to have a melting point slightly lower than the rest of the alloy.

An effort was made to determine the rate of the precipitating

reaction. The study was made at four temperatures: 1000, 1350, 1500, and 1650 °F (540, 730, 815, and 900 °C). In spite of indications of a possible reaction at 1000 °F (540 °C), all of the alloys were quite stable at that temperature. The temperature of least stability (i.e., greatest reaction rate) was 1350 °F (730 °C). Alloys 25V-0 and 111VT2-2 were stable for about 2 hours at this temperature before a noticeable change took place. In many cases the reaction proceeded in a logarithmic manner for the duration of the test (up to 6 days); in others, the curve became asymptotic after a time. In general, the iron-bearing 100NT-2 behaved in the latter fashion. This initial inoculation period was not present at 1500 and 1650 °F (815 and 900 °C); doubtless, reactions which were delayed at lower temperatures were accelerated or completed while heating up to the higher test temperatures.

Perhaps one of the more surprising results of this investigation was the discovery that alloys differing so widely in composition behaved so much alike. The carbon content ranged from 0.25 to 1.1%, cobalt from 20 to 68%, and iron from impurity amounts to 20%, yet the temperatures for an aging precipitate to form, and to go back into solution, were nearly identical.

The ultimate purpose of the investigation was to enlarge our understanding of high temperature alloy behavior, with the aim of producing even stronger alloys. The aging reaction is known to be an important one in producing the optimum structure for highest strength. However, it was found that the additional strength imparted to an alloy by aging was of importance only if the metal did not already possess a nearly-continuous carbide network. The presence of such a network was a function not only of the carbon content, but also of the amount of carbide-forming elements, such as tantalum, columbium, molybdenum, and tungsten. In general, aging is of special importance in the lower carbon alloys where the austenite matrix is not broken up by semicontinuous carbide meshes.

Test and performance results have shown that the strength of the N-155-type alloy, compared with other alloys, does not drop off as greatly when the temperature, and especially when the time is increased. This observation can be correlated with the results of the aging tests. Table V below shows approximate temperatures for aging to appear, reach a maximum, for visible agglomerations to take place, and for the precipitate to dissolve. The temperature for carbide change included both extensive coalescence and melting. While

the temperatures for aging to appear and reach a maximum, and for agglomeration to begin are commensurable for all the alloys, solution of the aging precipitate in alloy 100NT-2 is not complete until a higher temperature is attained. The change of electrical resistivity with aging temperature, Fig. 7, substantiates this difference in behavior.

Table V

Alloy	Beginning of Visible Aging °F	Max. Aging °F	Agglomeration °F	Re-solution °F	Carbide Change °F
25 V-0	1300	1550–1600	1600	2100	2300
45 R-6	1300	1550	1600	2200	2300
100 NT-2	1300	1700	1700–1800	2250	2300
111 VT 2-2	1300	1600–1700	1700–1800	2100	2250

ACKNOWLEDGMENT

This work was considerably aided by the help of members of the Division of Industrial Cooperation Staff, especially Catherine Cathey, Ava Hamilton and Dr. S. C. Sun. Mr. F. J. Radavich obtained the data in Fig. 1. Sincere appreciation is expressed to the Bureau of Ships for sponsorship of the research.

References

1. N. J. Grant, "The Cobalt-Chromium J Alloy at 1350 to 1800 °F," TRANSACTIONS, American Society for Metals, Vol. 40, 1948, p. 585.
2. N. J. Grant, "The Effect of Composition and Structural Changes on the Rupture Properties of Certain Heat Resistant Alloys at 1500 °F," TRANSACTIONS, American Society for Metals, Vol. 39, 1947, p. 368.
3. N. J. Grant, "The Stress Rupture and Creep Properties of Heat Resistant Gas Turbine Alloys," TRANSACTIONS, American Society for Metals, Vol. 39, 1947, p. 281.

DISCUSSION

Written Discussion: By George C. Deutsch and Charles Yaker, Engine Performance and Materials Division, National Advisory Committee for Aeronautics, Cleveland.

Although high-temperature alloys of the types investigated have been in use for a number of years, large gaps in fundamental metallurgical data concerning these alloys still exist. In making this very comprehensive investigation, the authors have materially contributed to gas-turbine-alloy research.

In this paper the effects of changes in the face-centered-cubic and hexagonal-close-packed matrix phases on the physical properties have been considered simultaneously with the effect on the physical properties produced by the precipitation of microconstituents. From the standpoint of

improving the properties of alloys, it would be of considerable interest to have these two effects separated. Badger and Sweeny[2] point out that, in the range of aging temperatures of Vitallium, there would be an increase in the per cent of the hexagonal phase in the cubic matrix. A study of the cobalt-chromium equilibrium diagram shows that at higher temperatures (above approximately 1700 °F) a second-phase transformation, back to cubic, which would act as a re-solution, takes place. Thus the analogy between phase changes in the matrix and the precipitation and solution of microconstituents is complete. Also, alloy 25 V-0 contained no nickel. Inasmuch as commercial Vitallium, the alloy that is most similar to 25 V-0, has approximately 2.5% nickel and it is known that nickel tends to inhibit the transformation to the hexagonal-close-packed phase, it is possible that the effects observed in 25 V-0 would not be as pronounced in Vitallium.

This investigation showed a remarkable increase in rupture life caused by aging low-carbon Vitallium alloy 27 V-3 containing 2% manganese; however, Grant (2) has shown in curves of rupture life versus per cent manganese at the same test conditions that the rupture lives for aged Vitallium in the range of 0.5 to 1% manganese (the manganese range for commercial Vitallium) are much lower than the values presented for the alloy with the 2% manganese content. In the same reference, the range of results obtainable for the aged Vitallium with 0.5 to 1% manganese is roughly the same as that reported in the literature for as-cast Vitallium. Thus it appears that the alloy investigated shows greater susceptibility to age hardening and is superior for the lives shown than is commercial Vitallium.

Dr. Grant (2) also presents rupture data on 45 R-6, which is the alloy discussed in the present paper. This alloy shows only a slight and perhaps nonsignificant increase in rupture life on aging. Inasmuch as this alloy more nearly resembles commercial alloy 6059 than does alloy 49 T-6, for which data are presented in this paper, it would be hazardous to generalize for alloy 6059 on the basis of the data presented for alloy 49 T-6. It is possible that the 1% titanium additionally present in alloy 49 T-6 causes a precipitation phenomenon which is not so marked or is absent in regular 6059.

The photomicrographs in this paper show that, at the highest aging temperatures (2200 and 2300 °F), the secondary carbides have dissolved and the primary carbides are dissolving into the matrix solid solution. Because the quantity and speed of precipitation of carbides is a function of the total amount of carbides in solution, it would be reasonable to expect that more pronounced aging effects than were reported would be observed if the maximum carbide solution had been achieved prior to aging. Therefore, it would be of interest to study the aging of alloys 25 V-0, 45 R-6, and 111 VT 2-2 after a solution treatment selected to give maximum carbide solution.

---

[2]F. S. Badger, Jr. and W. O. Sweeny, Jr., "Metallurgy of High-Temperature Alloys Used on Current Gas Turbine Designs," *Symposium on Materials for Gas Turbines*, American Society for Testing Materials, 1946, p. 99.

Authors' Reply

The possible effect of the cobalt transformation was pointed out in the paper, but no data were presented because of our inability to obtain reliable measurements on relative proportion of cubic and hexagonal structures in the coarse-grained cast material. Subsequent X-ray measurements on heavily cold-worked filings showed that most alloys were face-centered cubic, an exception being the Vitalliums. Irrespective of carbon content, filings from cast Vitallium were completely hexagonal, while after aging the structure was completely cubic. In the Badger and Sweeny article referred to, the alloys were aged after a solution treatment at 2125 °F (1165 °C). The initial condition was not stated but probably was cast. They found that solution-treated Vitallium was completely cubic, and that subsequent aging caused the appearance of a mixed hexagonal-cubic structure. Notice the two important differences in treatment; our alloy specimens were not solution-treated, and were heavily cold-worked before aging. Before aging our alloys (for X-ray examination), we started with the stable low temperature hexagonal form. Badger and Sweeny retained the metastable high temperature configuration before aging their alloys. Thus, the only discrepancy is that our aged alloys were completely cubic, while theirs were a mixture of phases after aging. It is entirely possible that the phase transformation referred to by Deutsch and Yaker may help account for the difference. However, the binary cobalt-chromium system is not applicable, since other elements present, especially carbon and nitrogen, have such an important effect on this system and tend to lower the two-phase field. It is probable that most highly-alloyed cobalt-chromium alloys are cubic at all times because of the effect of these alloying elements on lowering the hexagonal → cubic transformation. This lowering is also true of nickel additions.

Our work, done over two years ago, was only a survey of the aging problem. The complication just discussed is of importance, and we are now calibrating a high temperature X-ray camera, which, we hope, will throw further light on the subject.

With regard to the rupture data on alloys similar, but not precisely the same, to Vitallium and 45 R-6 (6059), our intent was to show that a marked difference in rupture life resulted from aging at various temperatures; the precise values are of little consequence.

It is true, as pointed out by Deutsch and Yaker, that aging effects probably are more pronounced after aging a solution-treated alloy than when aging a cast alloy. However, the rupture strengths of these alloys are usually greater when aged in the cast condition, and this fact explains our choice of treatment. Vitallium, solution-treated at 2200 °F (1095 °C) or higher, takes the primary carbides into solution. On subsequent aging, a very heavy precipitate is formed, frequently at the grain boundaries, yielding a more brittle alloy. This is shown in reference (2) of this paper. Lower solution temperatures than 2200 °F (1095 °C) can possibly improve the alloy when cooling after solidification is too slow and permits some excess phase precipitation at temperatures other than 1350 °F (730 °C).

NICKEL-BASE ALLOYS FOR HIGH TEMPERATURE APPLICATIONS

By A. G. Guy

Abstract

Information is given on a new series of cast, nickel-base high temperature materials containing aluminum, molybdenum, and chromium as the principal alloying elements. Rupture test data at 1500 °F (815 °C) show that a number of the alloys in the series have higher rupture strengths than the best of the cobalt-base materials now in use.

As industrial machines operating at temperatures in the vicinity of 1500 °F (815 °C) become larger and more widely used, the importance of a relatively inexpensive construction material will increase. The high price of cobalt makes alloys using this metal as a base unavoidably expensive, but at present these compositions are the principal choice for exacting applications. Iron-base alloys, from a cost standpoint most desirable, appear to be incapable of meeting the strength and oxidation resistance requirements. Intermediate in cost are the nickel alloys, and compositions now on the market demonstrate the excellent oxidation resistance of these alloys, although the high temperature strengths are not so good as those found in cobalt-base materials.

The object of the present work was the development of a nickel-base alloy having superior rupture strength at 1500 °F (815 °C).

Preparation and Testing of Alloys

All of the compositions were made from commercially pure metals and were melted in the small arc furnace described by Epremian (1).[1] The order of melting was nickel, molybdenum, chro-

[1]The figures appearing in parentheses pertain to the references appended to this paper.

A paper presented before the Thirtieth Annual Convention of the Society, held in Philadelphia, October 23 to 29, 1948. The author, A. G. Guy, is associate professor of metallurgy, Mechanical Engineering Department, North Carolina State College, Raleigh, North Carolina. This work was done in the Research Laboratory, General Electric Co., Schenectady, N. Y. Manuscript received February 6, 1948.

mium, ferrocolumbium, silicon and manganese, ferroboron, and aluminum. The bar of aluminum was added about 30 seconds before casting the 2-pound heat at about 2910 °F (1600 °C) into a ceramic precision casting mold at 1470 °F (800 °C). The 0.253-inch diameter, 2-inch gage length specimens produced by this casting process were rupture tested without further heat treatment. X-ray inspection was used to insure the soundness of test bars. The same equipment and procedure used by Epremian (1) were used to obtain rupture data.

Results

Although a wide variety of nickel-base alloys were investigated in a tentative manner, effort was soon concentrated on a composition range suggested by examination of the aluminum-molybdenum-nickel ternary diagram given by Jaenecke (2). To the solid solution nickel-base alloy containing 6% aluminum and 6% molybdenum, 20% chromium was immediately added for oxidation resistance. This composition was found to have a 1500 °F (815 °C) 100-hour rupture strength of 26,000 psi, a strength comparable to that of the better cobalt-base alloys, and much superior to previously used nickel-base alloys. Extensive tests showed that the rupture strengths of alloys in this range were considerably improved by the addition of 0.5% boron and 2% columbium to the melt.

The results of a fairly complete survey of the rupture strengths of compositions in this range are given in Figs. 1 to 10. All of the alloys had the following nominal analysis in addition to the aluminum, molybdenum, and chromium contents noted in the figures:

Boron	0.5%
Columbium	2.0%
Iron	4.5%
Silicon	0.5%
Manganese	0.5%
Nickel	Balance

Chemical analyses for each of the elements except boron were obtained for two of the compositions. In each instance the actual analysis was very nearly the same as the nominal analysis as shown in Table I.

Figs. 1 to 3 show that the best combination of 100-hour rupture strength and elongation is obtained in alloys containing about 6% aluminum. Fig. 4 shows that in the 6% aluminum, 10% chromium

Table I

Actual Analysis Alloy B129		Nominal Analysis	Actual Analysis Alloy B132	
0.06	0.1	C	0.1	0.20
14.24	15.0	Mo	5.0	4.68
65.38	66.0	Ni	71.0	70.63
5.47	6.0	Al	6.0	5.55
0.40	0.5	Mn	0.5	0.46
0.42	0.5	Si	0.5	0.71
2.32	2.0	Cb	2.0	2.28
0.82	0.0	Co	0.0	0.54
4.11	4.5	Fe	4.5	4.23
4.86	5.0	Cr	10.0	9.69
98.08	99.6		99.6	98.97

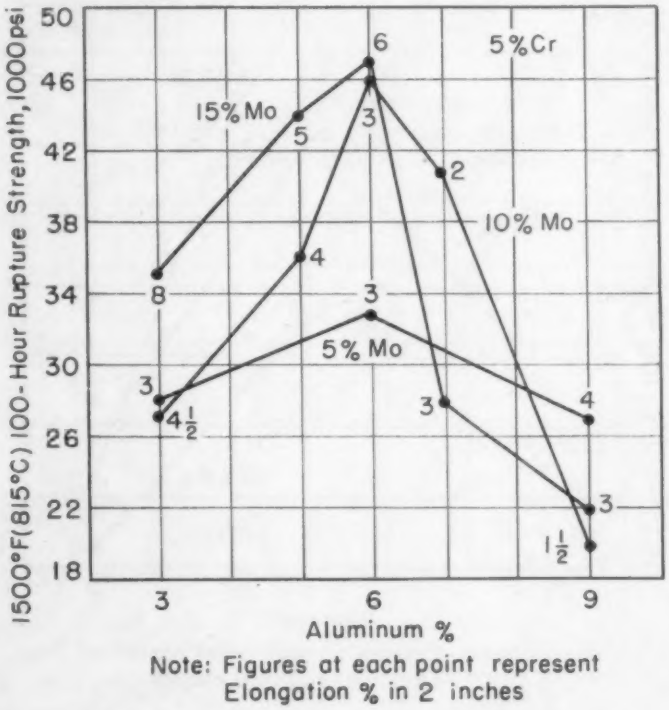


Fig. 1—Effect of Aluminum Content on the 100-Hour Rupture Strength of Alloys Containing 5% Chromium and 5, 10, or 15% Molybdenum.

alloys, a maximum 100-hour rupture strength is attained at 5 to 7% molybdenum. Fig. 5 shows that a number of chromium-molybdenum combinations produce high strengths.

The 1000-hour rupture strength data, Figs. 6 to 10, give nearly the same results as the 100-hour rupture strength data. However, the maximum in the 5% molybdenum curve of Fig. 10 indicates that the best material in this series has the composition range:

Chromium	12-15%
Molybdenum	5- 6%
Aluminum	5.5- 7%
Columbium	2%
Boron	0.5%
Iron	4.5%
Manganese	0.5%
Silicon	0.5%
Nickel	Balance

Preliminary tests on alloys of this series have given the following tentative information:

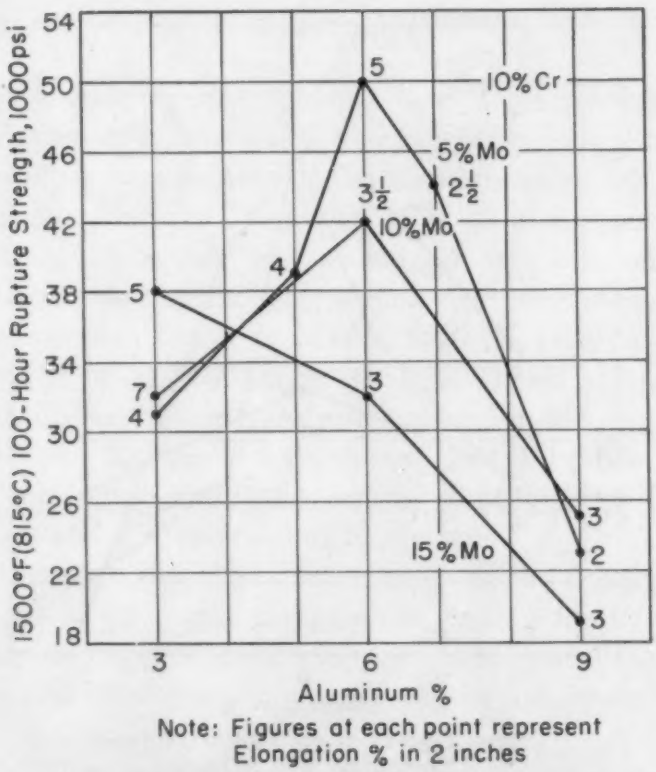


Fig. 2—Effect of Aluminum Content on the 100-Hour Rupture Strength of Alloys Containing 10% Chromium and 5, 10, or 15% Molybdenum.

Age hardening. No appreciable hardening occurs at aging temperatures near 1500 °F (815 °C). The room-temperature hardness is about Rockwell C-40.

Impact strength. Unnotched 0.250-inch square Charpy bars absorbed 5 foot-pounds at 1500 °F (815 °C).

Fatigue strength. The fatigue strength appears to be comparable to that of Vitallium-type cobalt-base alloys.

Tensile strength. The room-temperature tensile strength is

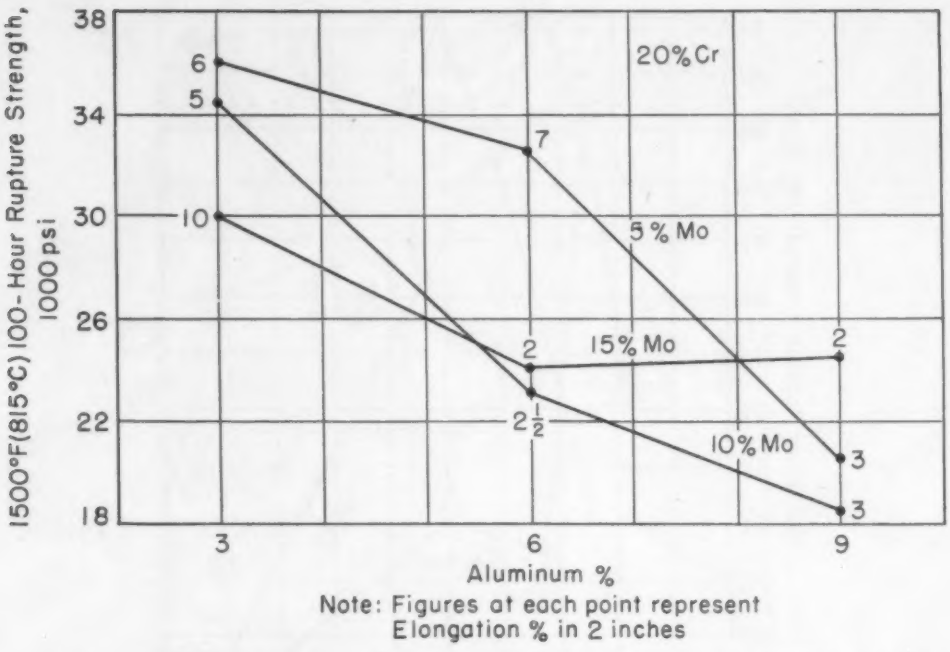


Fig. 3—Effect of Aluminum Content on the 100-Hour Rupture Strength of Alloys Containing 20% Chromium and 5, 10, or 15% Molybdenum.

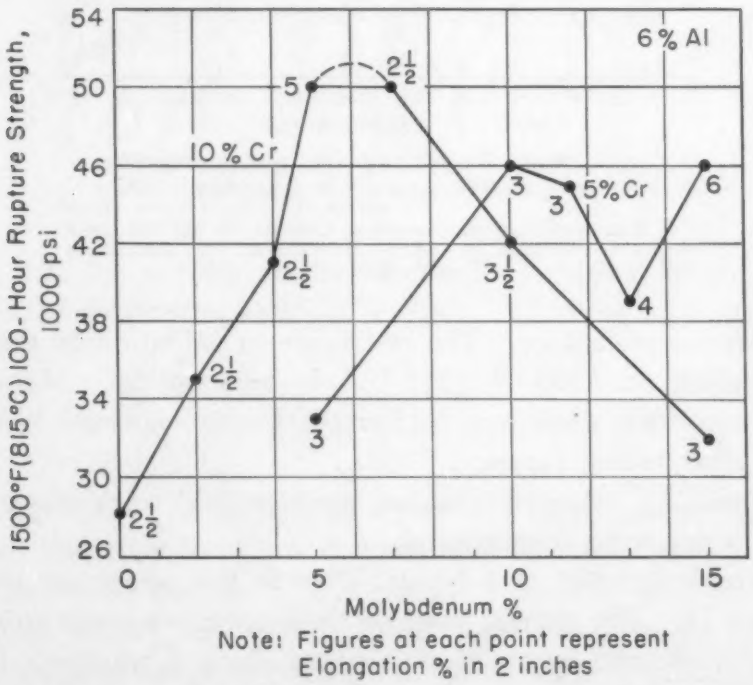


Fig. 4—Effect of Molybdenum Content on the 100-Hour Rupture Strength of Alloys Containing 6% Aluminum and 5 or 10% Chromium.

about 140,000 psi, while the value at 1500 °F (815 °C) is 100,000 psi.

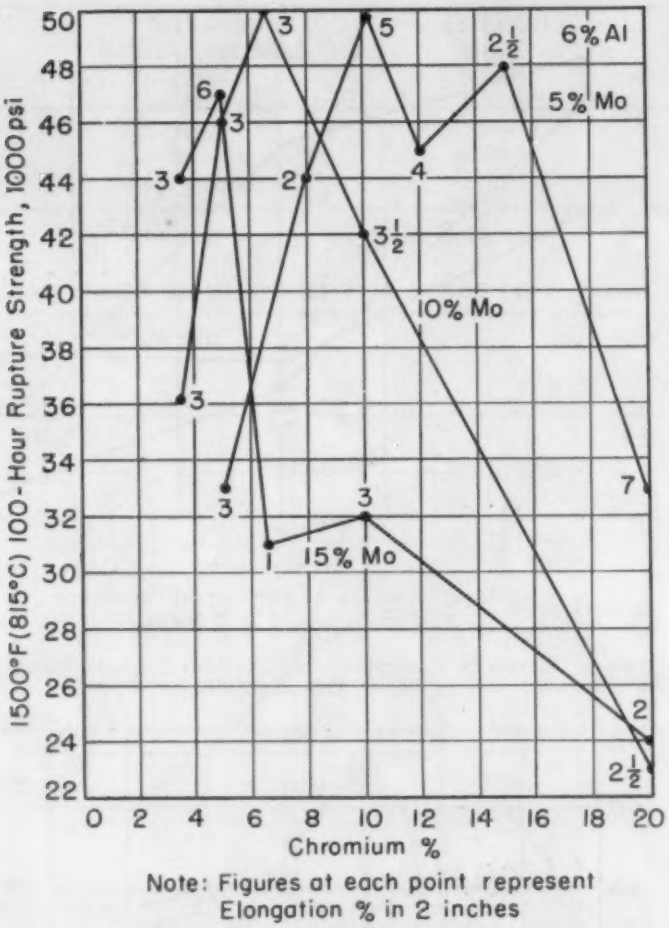


Fig. 5—Effect of Chromium Content on the 100-Hour Rupture Strength of Alloys Containing 6% Aluminum and 5, 10, or 15% Molybdenum.

Oxidation resistance. The resistance to oxidation by the atmosphere at 1500 °F (815 °C) is outstanding. Many specimens were still bright after 100 hours' exposure in the rupture testing furnace.

Forgeability. Attempts to hot work or cold work alloys of this series were unsuccessful.

Photomicrographs of a typical alloy in this series are shown in Figs. 11 to 14. The etchant used on these specimens was an aqueous ferrous chloride and hydrochloric acid solution. Comparing Figs. 12 and 13, it is evident that a constituent precipitates from the solid solution on heating at 1470 °F (800 °C). Thus, it is likely that age hardening would occur if the aging temperature were sufficiently low. The high strength of this material is undoubtedly due in part to the second phase widely distributed in the matrix, Fig. 12. Fig.

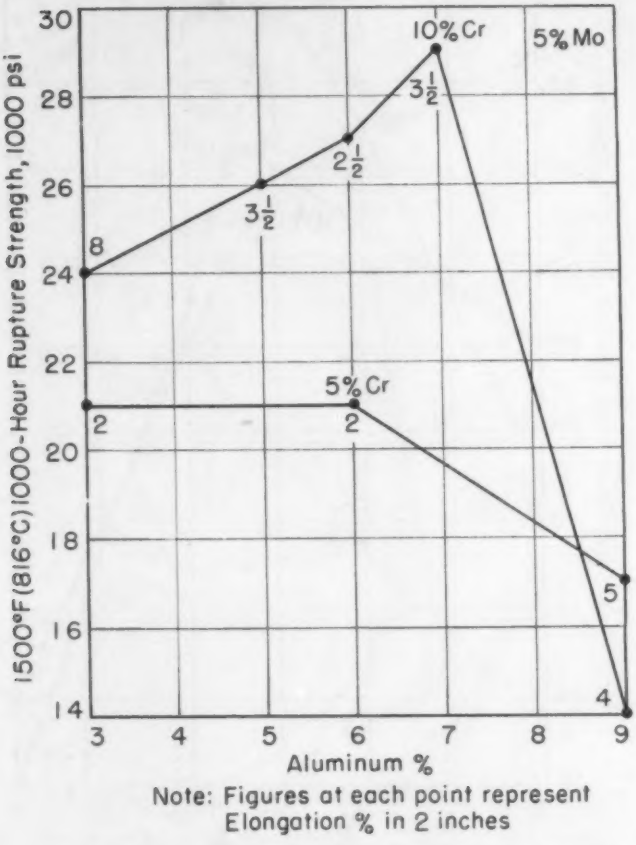


Fig. 6—Effect of Aluminum Content on the 1000-Hour Rupture Strength of Alloys Containing 5% Molybdenum and 5 or 10% Chromium.

14 shows that the microstructure of the cast material is not appreciably affected by heating at 1500 °F (815 °C) under high stress for long periods.

Discussion

Applications of alloys in this series will be somewhat restricted by the fact that they have low ductility and that they have not been successfully hot-worked or cold-worked. However, modern casting and forming techniques should permit their use in most instances where the need for exceptional high temperature strength and oxidation resistance is great.

It is unlikely that these alloys would be chosen for service at temperatures below about 1300 °F (705 °C) in view of the satisfactory properties of iron-base materials in this range. However, in the neighborhood of 1500 °F (815 °C) the best alloys in this

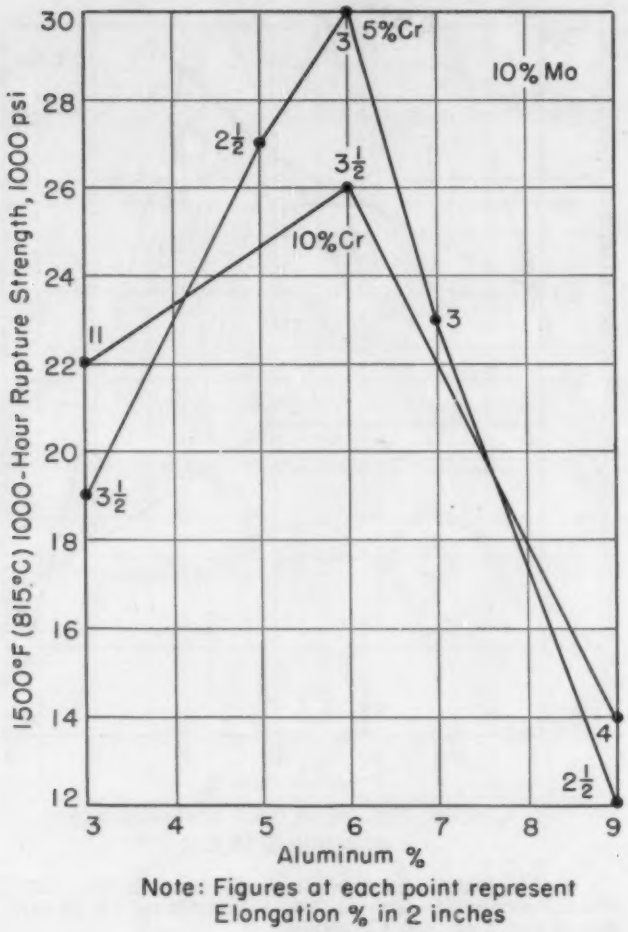


Fig. 7—Effect of Aluminum Content on the 1000-Hour Rupture Strength of Alloys Containing 10% Molybdenum and 5 or 10% Chromium.

series have rupture strengths and oxidation resistance unexcelled by any material now in use.

The behavior of the alloys during attempts at hot working suggests that they would have moderate strength at temperatures in the neighborhood of 2000 °F (1095 °C). In a few rupture tests run at 1700 °F (925 °C) the oxidation resistance was good and the 100-hour rupture strength was in the 15,000 to 20,000 psi range.

The presence of about 6% aluminum in these alloys causes some difficulty in melting. The oxidation of the aluminum produces a viscous slag in the melting furnace and also reduces the aluminum content of the final alloy. Although the melting procedure used in the present work minimized these difficulties, it is likely that remelting of these alloys would present some problems.

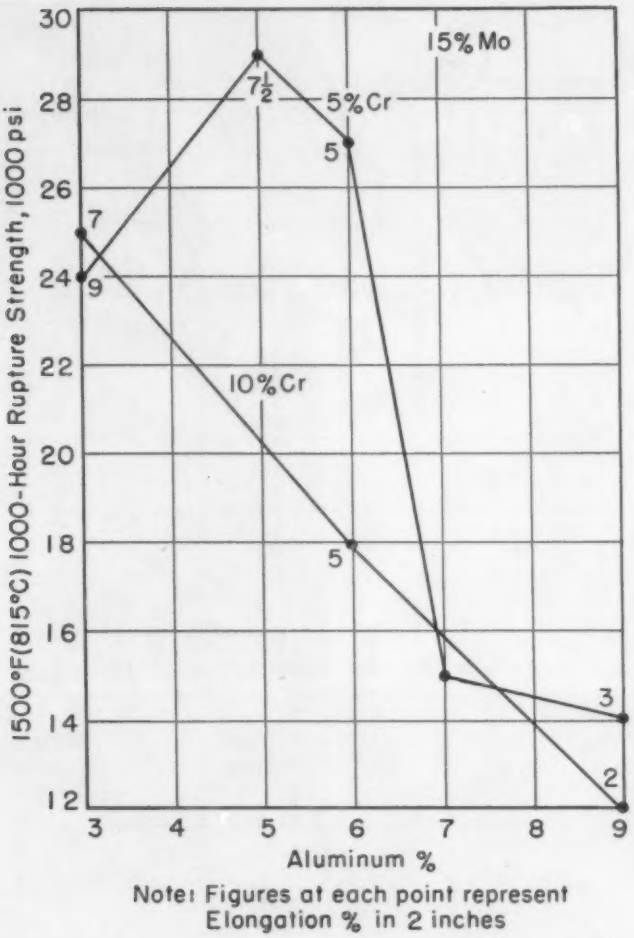


Fig. 8—Effect of Aluminum Content on the 1000-Hour Rupture Strength of Alloys Containing 15% Molybdenum and 5 or 10% Chromium.

Summary

The result of this investigation has been the discovery of a group of nickel-base alloys having unusually high rupture strengths at 1500 °F (815 °C). These alloys also have excellent oxidation resistance, and moderate fatigue strength. Although, compared to cobalt-base materials, these alloys have low elongation and impact resistance, it is probable that they are suitable for many industrial applications.

Acknowledgments

The aid of the following members of the General Electric Research Laboratory is gratefully acknowledged: Mr. E. Epremian,

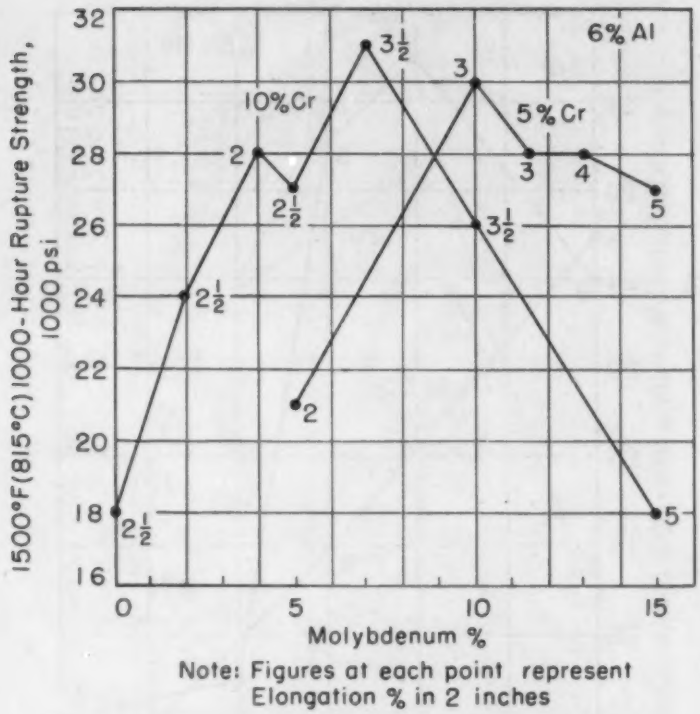


Fig. 9—Effect of Molybdenum Content on the 1000-Hour Rupture Strength of Alloys Containing 6% Aluminum and 5 or 10% Chromium.

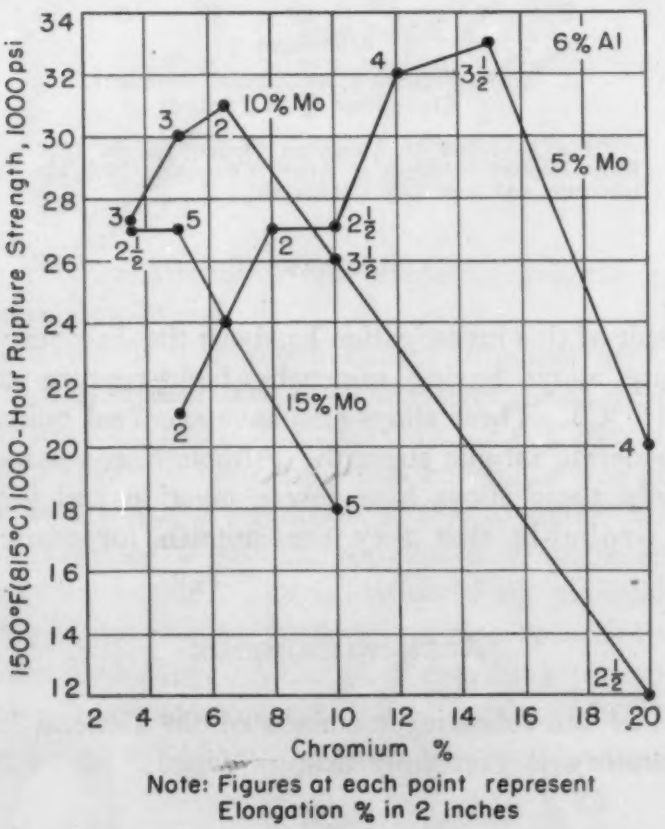


Fig. 10—Effect of Chromium Content on the 1000-Hour Rupture Strength of Alloys Containing 6% Aluminum and 5, 10, or 15% Molybdenum.

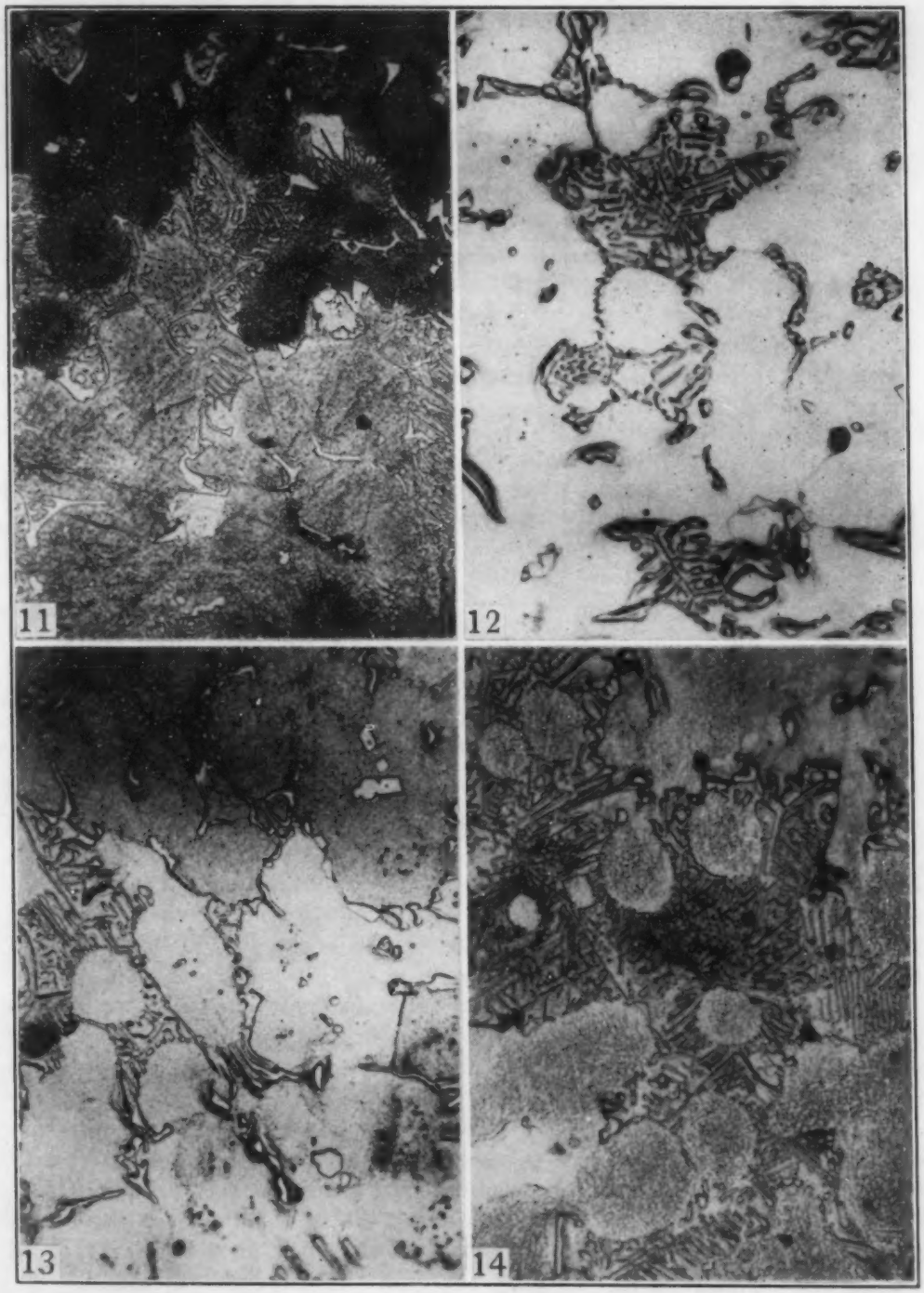


Fig. 11—Alloy B 85 (6% Aluminum, 10% Molybdenum, 5% Chromium) As-Cast. × 500.

Fig. 12—Alloy B 85 Water-Quenched From 2190 °F (1200 °C). × 500.

Fig. 13—Alloy B 85 Water-Quenched From 2190 °F (1200 °C) and Heated 20 Hours at 1472 °F (800 °C). × 500.

Fig. 14—Alloy B 85 As-Cast and Rupture Tested at 1500 °F (815 °C) Under 40,000 Psi for 193 Hours. × 500.

Miss M. J. Field, Mr. E. J. McMullen, Mr. W. E. Ruder, and Miss J. Wdowinski. Mr. R. B. Johnson of the Thomson Laboratory, General Electric Company, Lynn, Massachusetts, checked some of the data in his program to investigate these alloys further.

References

1. E. Epremian, "The Development of a Turbosupercharger Bucket Alloy," TRANSACTIONS, American Society for Metals, Vol. 39, 1947, p. 261-280.
2. E. Jaenecke, "Kurzgefasstes Handbuch Aller Legierungen," 1937, p. 358. Otto Spamer Verlag, Leipzig.

DISCUSSION

Written Discussion: By H. V. Kinsey, metallurgical engineer, Bureau of Mines, Ottawa, Ont., Canada.

Dr. Guy's paper giving some stress-rupture properties of cast nickel-base alloys containing chromium, molybdenum and aluminum as major alloying elements and columbium and boron as minor alloying elements is of particular interest to us since we have been engaged in a similar alloy development program at the Physical Metallurgy Research Laboratories of the Canadian Bureau of Mines, for the past three years.

Our work has developed along somewhat different lines and at probably a little slower pace than the work reported on in this paper. We are investigating several simple ternary alloy systems of which the nickel-aluminum-molybdenum system is one. Alloys belonging to this system have to date shown the most promise when evaluated on the basis of creep-rupture properties at 1500 °F (815 °C). The best alloy of this system that we have produced and tested to date is considerably below Dr. Guy's alloys in its stress-rupture properties. This alloy, which has an analysis of 66.5% nickel, 7.0% aluminum and 25.5% molybdenum, when tested at 1500 °F (815 °C), using a stress of 40,000 psi, broke in 100 hours with a total elongation of 4%.

The fact that Dr. Guy shows that the addition of chromium to certain nickel-aluminum-molybdenum alloys is beneficial is most interesting. Our work indicated that the simple nickel-aluminum-chromium system was not particularly promising.

It is interesting to note also that Dr. Guy has found that the addition of boron and columbium are beneficial to the stress-rupture characteristics of these alloys. Do these elements act independently or is it necessary to have both of them present to obtain these benefits? Is the boron present in solid solution or does it exist in the alloy as a boride? Could we have some quantitative data on the effect of these two elements?

From an analysis of the data presented it would appear that molybdenum and chromium are, to a limited extent, complementary in these alloys, and that when the molybdenum plus chromium content is between 15 and 20% of the total alloy, optimum stress-rupture characteristics are realized. The similarity in stress-rupture properties of alloys having a molybdenum plus chromium content of 17% is rather striking.

It is interesting to note that the results of Dr. Guy's work confirm our own findings on the influence which variations in aluminum content will have on the creep-rupture properties of these alloys. There is an optimum aluminum content above which increasing aluminum causes a deterioration of creep-rupture properties. In our work we have been able to correlate this falling off of creep-rupture properties with the appearance of a phase that we have identified as the intermetallic compound, NiAl. In the simple ternary nickel-aluminum-molybdenum system this phase begins to occur when the Ni:Al ratio is between 7:1 and 6:1. We have found this a rather useful method of roughly classifying this type of alloy.

We melt our alloys in a high-frequency induction furnace and cast centrifugally. It is our experience that neither the melting nor the remelting of these alloys presents any great problem, as long as the proper corrections are made for aluminum losses and suitable fluxes are used.

We wish to compliment Dr. Guy on the very interesting paper he has presented and look forward to hearing of future work by Dr. Guy and his successors with these alloys.

Written Discussion: By N. J. Grant, associate professor, Massachusetts Institute of Technology, Cambridge, Mass.

Dr. Guy has introduced a series of alloys of considerable interest because of the high-strength short-life characteristics. This is just another example of the great improvement which may be accomplished in a relatively soft element such as nickel through balanced alloying. It predicts an even greater future for cast alloys based on metallic elements of higher recrystallization temperatures than nickel—for example, titanium, chromium, zirconium, and molybdenum.

It is not evident from Dr. Guy's paper that these alloys have steep curves on the log stress or log rupture time curves. They do, and because of this the superiority does not exist at 1000 hours (with the accompanying lower ductility). The results are shown in Table II.

Table II
Stress and Elongation for Rupture Life

Alloy	Test Temp., °F	100 Hours	1000 Hours
5 Cr – 15 Mo – 6 Al	1500	47,000 (6)	27,000 (5)
10 Cr – 5 Mo – 6 Al	1500	50,000 (5)	27,000 (2.5)
422-19 (Co base)	1350	47,000 (23)	36,300 (11.5)
MIT-J Alloy (Co base)	1350	52,500 (7)	40,500 (7)
MIT-J Alloy (Co base)	1500	34,800 (13)	28,000 (10)
X-40 (Co base)	1500	28,000 (12)	23,200 (7)

The experience with boron-containing alloys is that large increases in high temperature strength may readily be realized. The increase is not uniform from heat to heat, however, since apparently the boron content is critical. With 6% aluminum, boron recovery is probably fairly good compared to aluminum-free alloys, and this may be the means of getting good recovery. Without chemical analysis this remains an important consideration.

In Table III are listed some rupture values for high carbon (0.60 to 0.80%) N-155 alloys containing 0.1 to 0.5% added boron.

Table III
Stress-Rupture Values at 30,000 Psi and 1500 °F

Alloy	Solution Temp. °F	Rupture Time	% Elong.
No. 1 (0.1B)	2100-WQ	363	6.4
No. 2 (0.2B)	2100-WQ	266	8.2
No. 3 (0.2B)	2100-WQ	180	4.5
No. 4 (0.2B)	2200-WQ	918	4.0
	2200-WQ	529	...

The spread of values is large. The best values for the same alloy without boron are about 70 to 80 hours with 6% elongation. Subsequently, other heats were cast which showed rupture lives of only 40 to 100 hours at the same combination of stress and temperature.

It would certainly be interesting to know the effect of removing all the boron from the alloy.

Written Discussion: By E. Epremian, graduate student, Carnegie Institute of Technology, Pittsburgh.

Dr. Guy is to be complimented for his discovery of a new type of alloy for high temperature service. The mechanical properties of these materials are far superior to those of the conventional cobalt-base alloys. There are a few minor points which I should like to question. Are both columbium and boron necessary for the high strength at elevated temperatures? I have found that boron is a potent strengthener in cobalt-base alloys, but the further addition of columbium contributes little to the mechanical properties. Also, it would appear unnecessary to deoxidize with manganese and silicon since relatively large additions of aluminum are made.

Written Discussion: By E. N. Skinner, Development and Research Division, International Nickel Co., Inc., New York, and A. M. Talbot, Research Laboratory, The International Nickel Co., Bayonne, N. J.

It is most gratifying to find in this paper attention focussed upon one of the more common and less expensive elements for the matrix of high strength–high temperature materials. The stress-rupture data presented by the author are most interesting and certainly would seem to warrant further investigation and close scrutiny by those concerned with applications in which this property, together with excellent resistance to oxidation, is important.

We have, at one time or another, briefly examined the potentialities of aluminum-containing nickel and nickel-chromium compositions. Our enthusiasm regarding the good high temperature strength and well-known excellent resistance to oxidation and other forms of high temperature corrosion has been considerably dampened on finding that these alloys containing more than 3 to 4% aluminum possess greatly impaired ductility over a range of temperatures. This loss of ductility, which precludes hot working on a commercial scale and, at higher aluminum contents, even

mild cold working, is believed to be associated with the formation of an intermetallic compound, possibly Ni_3Al, which is hard and brittle and predisposed to location in the grain boundaries.

Whatever the cause of room temperature brittleness, it has become apparent in some cases that acceptable levels of ductility may nevertheless be secured under prolonged application of stress at high temperature as in the stress-rupture test. Conversely, there is no assurance that a useful level of ductility obtaining at high temperatures will still be in evidence at room temperature. There have been experimental precision casting compositions which we have tested that have shown promising stress-rupture properties but at room temperatures developed a glass-like brittleness, especially under impact, which would effectively eliminate them from practical consideration, at least in their present status.

In the present paper, elongation of 2 to 4%, and in one case (15 Mo–5 Al–5 Cr) as high as 7.5%, are reported for 1000-hour rupture at 1500 °F (815 °C). We would very much like to know whether, in these alloys containing substantial amounts of molybdenum, this level of ductility was maintained at room temperature and whether the impact strength was similarly unaffected.

Author's Reply

It is especially gratifying to learn of the work Mr. Kinsey is doing on the nickel-aluminum-molybdenum system. When he finishes this research Mr. Kinsey will be in an excellent position to answer many of the questions that are being asked about the alloys reported on here. In view of the developmental nature of the present investigation, only fragmentary information was obtained on matters not directly related to the achievement of high rupture strength values. For this reason many of the following answers are incomplete.

The effect of removing both boron and columbium from an alloy of this series was determined for the composition 10% chromium, 6% molybdenum, 6% aluminum. The 100-hour rupture strength dropped from 48,000 psi (4% elongation) to 29,500 psi (1.5% elongation), and the 1000-hour rupture strength dropped from 29,000 psi (3% elongation) to 23,000 psi (2% elongation). Qualitative results suggest that the removal of either boron or columbium separately would give an intermediate rupture strength value. No information was obtained on the form in which boron is present in the alloys.

Short-time tensile tests were run on only a few of the compositions that were also rupture tested. The elongation values in these instances were about 1%. Room temperature impact strength was determined for the 10% molybdenum, 6% aluminum, 5% chromium alloy and was found to be about half as great as at 1500 °F (815 °C). In my estimation this measurable ductility removes these alloys from the "glass-like" group of brittle alloys.

Deoxidation with manganese and silicon was carried out before making the boron and aluminum additions in an effort to insure a high

and uniform recovery of the latter elements. It is encouraging that Mr. Kinsey has not experienced unusual difficulty in melting and remelting his aluminum-containing alloys.

As Dr. Grant points out, it is true that these nickel-base alloys generally have steep log stress versus log time curves compared to cobalt-base alloys. However, the best of these alloys on a 1000-hour rupture strength basis, containing 15% chromium, 5% molybdenum, and 6% aluminum, has a 100-hour rupture strength of 48,000 psi (2.5% elongation) and a 1000-hour rupture strength of 33,000 psi (3.5% elongation). This decrease is not much greater than that shown by the cobalt-base alloy 422-19 at 1350 °F (730 °C) in the same stress range. The reproducibility of the rupture values was satisfactory as is indicated by the generally gradual change of rupture strength with composition.

STABILITY OF STEELS AT ELEVATED TEMPERATURES

By A. B. Wilder and J. O. Light

Abstract

The stability of over one hundred different types of steel at 900, 1050 and 1200 °F (480, 565 and 650 °C) is being evaluated over a period of 11 years. Welded samples are included in the investigation. The results obtained in an examination of twenty of these steels for evidence of structural changes, oxidation characteristics and impact properties after exposure for 10,000 hours are presented.

The influence of zirconium, columbium and titanium on graphitization in molybdenum-bearing steels without chromium is discussed. Graphite observed in zirconium-molybdenum steel in the weld heat-affected zone was associated with a grain boundary phenomenon and, in some respects, was similar to chain graphite. Graphite was also observed in the zirconium and molybdenum steels, but not in the titanium-molybdenum or columbium-molybdenum steels. The Charpy impact properties of the zirconium steels were not appreciably changed by graphitization, but these steels were severely oxidized and decarburized at 1200 °F (650 °C).

The microstructure of the 12% chromium ferritic stainless steels was essentially unchanged after exposure. Oxidation of these steels after exposure was nil and the Charpy impact properties are being further investigated before definite conclusions are presented. The microstructure of the 17% chromium steel was not appreciably changed, but after 10,000 hours at 1200 °F (650 °C) a new constituent near the weld metal - base metal interface was observed which may be sigma phase, due to alloy diffusion. Further testing will be required to establish definite conclusions. This steel was embrittled after exposure for 10,000 hours at 900 to 1200 °F (480 to 650 °C). Sigma phase is discussed with reference to the 27 chromium steel after exposure. This particular steel was brittle before and after exposure. Oxidation after exposure was essentially nil in both the 17 and 27 chromium steels.

A paper presented before the Thirtieth Annual Convention of the Society, held in Philadelphia, October 23 to 29, 1948. Of the authors, A. B. Wilder is chief metallurgist, National Tube Company, U. S. Steel Corporation Subsidiary, Pittsburgh, and J. O. Light is chief metallurgist, National Tube Company, Lorain Works, Lorain, Ohio. Manuscript received May 8, 1948.

The 18% chromium–8% nickel, 18% chromium–8% nickel free machining (18-8 FM), and 18% chromium–8% nickel-molybdenum steels were observed to contain carbide precipitation at the grain boundaries after exposure, which resulted in lowering the Charpy impact strength. Sigma phase was observed in the exposed 18% chromium–8% nickel-columbium and titanium steels. The impact properties of these two steels were also lowered by exposure. Oxidation after exposure of the austenitic stainless steels was essentially nil.

Introduction

FOR the past five years a considerable amount of experimental work on the graphitization of steels has been conducted by a large group of independent investigators. Most of the experimental work has been confined to plain carbon and low alloy steels, some of which are, under certain conditions, susceptible to graphitization. The stability of steels at elevated temperatures reported in this paper is part of an extensive investigation (1)[1] of a large number of steels now under exposure which will continue for a period of 11 years. Alloy steels generally used for high temperature service contain chromium and frequently molybdenum. In a recent paper (2) the structural characteristics of steels containing less than 12% chromium after 10,000 hours' exposure were discussed. Although chromium has won recognition as an inhibitor of graphitization, other alloying elements such as columbium, zirconium, and titanium may also behave as stabilizers. The structural characteristics and properties of these special alloying elements in the absence of chromium have been investigated and the results after 10,000 hours' exposure are discussed.

The properties of steel after long periods of exposure at elevated temperature depend, in a large measure, upon the structural stability of the material. Although graphitization may appreciably influence the strength characteristics, particularly in the heat-affected zone of a weld, other structural changes may be of equal significance. It is desirable, therefore, to evaluate more thoroughly the stability of steels not normally susceptible to graphitization. Among those investigated after 10,000 hours' exposure are the ferritic and austenitic stainless steels which are widely used for high temperature service. The properties of stainless steels after exposure at temperatures in excess of

[1]The figures appearing in parentheses pertain to the references appended to this paper.

1200 °F (650 °C), although of considerable importance, are beyond the scope of this investigation. In addition to the structural changes in the parent metal and in the heat-affected zone of welds, the oxidation resistance, hardness and impact properties are reported. Other properties under investigation include creep rupture strength, tensile properties, intergranular corrosion and impact transition temperature. These results will be reported in a later paper.

Materials Investigated

Chemical composition with residual alloy content and deoxidation treatment of the zirconium, titanium, columbium and stainless steels exposed for 10,000 hours at 900, 1050 and 1200 °F (480, 565 and 650 °C) are shown in Table I. The term "deoxidation" is not strictly applicable to the stainless steels. The treatment indicated represents final additions to the steel. Heat treatment of the material prior to exposure and type of electrode used for the bead welds are shown in Table II. The steels were forged to a 1 by 1-inch bar and surface ground prior to exposure. All of the low alloy steels had a fine austenitic grain size of 5 to 8 after carburizing for 8 hours at 1700 °F (927 °C) and the grain size before carburizing was uniform. The grain size of the stainless steels was not uniform in all the materials tested. Where lack of uniformity existed, areas representative of the predominant condition were chosen for the metallographic studies.

Testing Procedures

Weld Bead Tests

Two 6-inch weld beads with different heat inputs were deposited on opposite sides of each bar as previously described (2). The weld beads were deposited at the U. S. Steel Corporation Research Laboratory with automatic welding equipment in order to eliminate the variables involved in hand welding procedures. Structural changes are reported for the small weld beads only; the results of the tests on the large weld beads will be reported later. The small weld bead was deposited with a ⅛-inch diameter electrode using 100 amperes at 24 volts and an arc travel speed of 10 inches per minute. No preheating or postheating was employed. The electrodes used are shown in Table II. This small weld bead can be considered repre-

Table I
Chemical Composition of Steels

Code No.	Steel Designation	Mfg. Process*	Deoxidation	C	Mn	P	S	Si	Cr	Ni	Mo
60	Mo	I	2.5# Al/Ton	0.08	0.50	0.016	0.028	0.293			0.57
61	Ti-Mo	I	2.5# Al/Ton	0.09	0.60	0.018	0.029	0.425			0.56
62	Ti-Mo	I	2.5# Al/Ton	0.10	0.60	0.018	0.030	0.348			0.95
63	Ti-Mo	I	2.5# Al/Ton	0.09	0.61	0.016	0.027	0.359			0.53
64	Ti-Mo	I	2.5# Al/Ton	0.09	0.61	0.016	0.029	0.344			1.05
65	Cb-Mo	I	2.5# Al/Ton	0.08	0.60	0.015	0.027	0.378			0.52
66	Cb-Mo	I	2.5# Al/Ton	0.08	0.62	0.016	0.028	0.434			0.98
44	Zr	I	16.2# Si-Ti-Zr†/Ton	0.20	0.58	0.006	0.022	0.222	0.014	0.059	0.03
45	Zr-Mo	I	16.2# Si-Ti-Zr†/Ton	0.19	0.49	0.006	0.023	0.290	0.011	0.061	0.51
46	12 Cr (410)	E	Silicon‡	0.10	0.35	0.016	0.005	0.738	12.72	0.38	0.03
53	12 Cr FM (416)	E	6.6# Si/Ton	0.11	0.73	0.015	0.336	0.440	13.39	0.23	0.03
47	12 Cr Al (405)	E	19# Al/Ton	0.07	0.34	0.031	0.011	0.278	12.95	0.21	0.05
48	12 Cr Mo (410 Mo)	E	3.8# Si(CaSi)/Ton	0.07	0.40	0.027	0.007	0.295	12.26	0.27	0.49
49	17 Cr (430)	E	2.8# Si(CaSi)/Ton	0.09	0.41	0.010	0.014	0.237	16.87	0.15	0.02
50	27 Cr N (446)	E	None	0.24	0.89	0.020	0.003	0.546	26.45	0.48	0.04
23	18-8 (304)	E	None	0.05	0.53	0.008	0.005	0.610	18.53	10.72	0.068
54	18-8 FM (303)	E	1.9# Si(FeSi)/Ton	0.09	0.77	0.146	0.008	0.255	18.33	8.98	0.04
51	18-8 Mo (316)	E	2.2# Si(FeSi)/Ton	0.07	1.32	0.013	0.011	0.315	18.27	10.59	2.16
24	18-8 Ti (321)	E	1.2# Al/Ton	0.07	0.52	0.021	0.003	0.386	17.97	10.40	0.071
25	18-8 Cb (347)	E	5.1# Si(FeSi)/Ton	0.06	1.43	0.018	0.006	0.444	17.80	11.16	0.076

Code No.	Steel Designation	Mfg. Process*	Deoxidation	Zr	Cb	Ti	Al	N	Cu	Se
60	Mo	I	2.5# Al/Ton				0.029			
61	Ti-Mo	I	2.5# Al/Ton			0.47	0.031			
62	Ti-Mo	I	2.5# Al/Ton			0.50	0.032			
63	Ti-Mo	I	2.5# Al/Ton			0.25	0.034			
64	Ti-Mo	I	2.5# Al/Ton			0.25	0.033			
65	Cb-Mo	I	2.5# Al/Ton		1.08		0.047			
66	Cb-Mo	I	2.5# Al/Ton		1.12		0.046			
44	Zr	I	16.2# Si-Ti-Zr†/Ton	0.10		0.023	0.007	0.006	0.02	
45	Zr-Mo	I	16.2# Si-Ti-Zr†/Ton	0.13		0.032	0.006	0.007	0.06	
46	12 Cr (410)	E	Silicon‡			0.002	0.006	0.039	0.02	
53	12 Cr FM (416)	E	6.6# Si/Ton			0.002	0.007	0.029	0.06	
47	12 Cr Al (405)	E	19# Al/Ton			0.0003	0.27	0.034	0.07	
48	12 Cr Mo (410 Mo)	E	3.8# Si(CaSi)/Ton			0.0003	0.004	0.029	0.02	
49	17 Cr (430)	E	2.8# Si(CaSi)/Ton			0.0003	0.004	0.078	0.02	
50	27 Cr N (446)	E	None			0.001	0.003	0.222	0.01	
23	18-8 (304)	E	None			0.0005	0.005	0.028	0.04	
54	18-8 FM (303)	E	1.9# Si(FeSi)/Ton			0.002	0.005	0.029	0.04	0.16
51	18-8 Mo (316)	E	2.2# Si(FeSi)/Ton			0.0003	0.009	0.030	0.16	
24	18-8 Ti (321)	E	1.2# Al/Ton			0.58	0.069	0.011	0.04	
25	18-8 Cb (347)	E	5.1# Si(FeSi)/Ton		0.77	0.001	0.010	0.027	0.01	

*I—Induction Furnace
E—Electric Arc Furnace
†Si 45.3%, Zr 29.4%, Ti 6.5%, Al 0.5%
‡Silicon deoxidation with 50% ferrosilicon

Table II
Prior Heat Treatment and Welding Electrodes

Steel Designation	Heat Treatment Prior to Exposure	Welding Electrode Employed
Mo	1650 °F Air Cool	E-7010
Ti-Mo (No. 61)	1650 °F Air Cool	E-7010
Ti-Mo (No. 62)	1650 °F Air Cool	E-7010
Ti-Mo (No. 63)	1650 °F Air Cool	E-7010
Ti-Mo (No. 64)	1650 °F Air Cool	E-7010
Cb-Mo (No. 65)	1650 °F Air Cool	E-7010
Cb-Mo (No. 66)	1650 °F Air Cool	E-7010
Zr	1650 °F Air Cool	E-6010
Zr-Mo	1650 °F Air Cool	E-7010
12 Cr (410)	1525 °F Furnace Cool to 1100 °F	Type 310
12 Cr FM (416)	1450 °F Air Cool	Type 310
12 Cr Al (405)	1425 °F Air Cool	Type 310
12 Cr Mo (410 Mo)	1450 °F Air Cool	Type 310
17 Cr (430)	1425 °F Air Cool	Type 310
27 Cr N (446)	1600 °F Water Quench	Type 310
18-8 (304)	1900 °F Water Quench	Type 308
18-8 FM (303)	1950 °F Water Quench	Type 308
18-8 Mo (316)	1950 °F Water Quench	Type 316
18-8 Ti (321)	1900 °F Water Quench Draw 1550 °F	Type 347
18-8 Cb (347)	1900 °F Water Quench Draw 1550 °F	Type 347

sentative of the most severe welding condition that may be experienced insofar as the thermal gradient of the heat-affected zone is considered. The results with weld bead samples are not always applicable to commercial welding conditions which vary considerably, and they should, therefore, be interpreted with this reservation.

Exposure Furnaces and Graphitization Chart

The electric furnaces employed for exposing the specimens, and the graphitization rating chart previously described (1, 2), were used in this investigation. All samples were exposed at 900, 1050 and 1200 °F (480, 565 and 650 °C) for 10,000 hours (approximately 60 weeks). The graphitization chart contains designations A, B, C, etc. (A being the smallest size particle), which are used with a prefix. A rating of 10C, for example, indicates 10 particles of dispersed graphite with an average size C in a 4 by 5-inch field at 500 magnification.

A transverse section of the weld bead samples was examined microscopically as follows: Zone 1, in the coarsened grain structure immediately beneath the weld metal; Zone 2, in the relatively fine grain structure beneath Zone 1; Zone 3, near the boundary of the heat-affected zone where the grain size is similar to the parent metal; and Zone 4, in the unaffected parent metal.

Impact and Oxidation Tests

Charpy impact tests were made in accordance with ASTM designation E-23-41T. A standard keyhole notched specimen was used and results reported are the average of two specimens tested at ordinary temperature. Impact tests of the parent metal were made on the zirconium, zirconium-molybdenum, and stainless alloys. Impact tests of welded specimens were not included in the investigation.

Oxidation resistance in air was determined by descaling unwelded 1 by 1 by 20-inch bars after exposure in the electric furnaces. The bars were racked (1) to permit exposure on all four sides except where each end of the bar is supported on the heat resisting rack. The sodium hydride bath at Wood Works, Carnegie-Illinois Steel Corporation, was used for descaling. The bars were not dipped in the acid brightening tanks subsequent to descaling, in order to reduce metal loss. Results are reported as per cent of weight loss and also as the average depth of scaling calculated from dimensional losses during exposure. Scale loss determinations and impact tests were not made on the titanium and columbium steels, due to lack of sufficient bar stock for exposure.

Metallographic Practice

The low alloy steels were etched with picral-nital, 4% picric acid and 2% nitric acid in alcohol. Special etching reagents were used for the stainless steels and frequently the metallographic specimens were intermittently polished during etching. All electrolytic etching was carried out with the specimen as the anode and an emf of 3 volts. The following etching reagents were used at ordinary temperature with the stainless steels:

Chromic Acid—10% aqueous solution, electrolytically. This reagent was used to reveal the structure of ferritic and austenitic stainless steels. Carbide and sigma phases were rapidly attacked.

Sodium Cyanide—10% aqueous solution, electrolytically. This reagent was used to distinguish between carbides and sigma phase in the ferritic and austenitic stainless steels. An etch for approximately 1 second outlined sigma, and 5 seconds or more darkened the carbides and further etched sigma.

Oxalic Acid—10% aqueous solution, electrolytically. The use of this reagent was confined, primarily, to unexposed stainless steels to develop grain size characteristics.

Murakami's Reagent—10% potassium ferricyanide, 10% potassium hydroxide in aqueous solution. This reagent was used at ordinary temperature for approximately 1 minute to darken carbides in austenitic stainless steels. The sigma phase was not attacked.

Marble's Reagent—4 grams cupric sulphate, 20 cubic centimeters hydrochloric acid and 20 cubic centimeters water. This reagent was used to develop the grain structure of austenitic stainless steels.

Vilella's Reagent—Alcoholic solution of 1% picric acid and 5% hydrochloric acid. This reagent, which etches austenite, was used approximately 1 minute with the austenitic stainless steels, the sigma phase being unattacked as shown in relief.

Sigma phase (3, 4, 5, 6) in this investigation was identified by the metallographic method. The specimen was etched with Murakami's reagent to darken the carbides, repolished and etched with Vilella's reagent, which outlined sigma phase and attacked both austenite and carbides. The same field was examined after each etching treatment. A similar technique was used with the sodium cyanide etch by varying the etching time. It is recognized that the X-ray method offers a more positive means for identification of sigma phase. This technique will, therefore, be used to further establish the presence of sigma phase, and the results will be reported when tests have been completed for longer periods of exposure. The results in this investigation with respect to sigma phase should, therefore, be accepted with the reservation that only the metallographic technique was employed for identification. After longer periods of exposure, the occurrence of ferrite in the austenitic alloys will also be investigated to determine if sigma phase is associated with ferrite. The magnetic method will be used.

Graphitization of Zirconium, Columbium, Titanium Alloy Steels

The molybdenum, zirconium, titanium-molybdenum, columbium-molybdenum and zirconium-molybdenum steels included in this investigation were laboratory induction furnace heats. Because of scaling and decarburization after 10,000 hours' exposure at 1200 °F (650 °C), results are not reported for this treatment. The molybdenum and zirconium steels were included for control purposes. Graphite ratings of these steels in the welded and parent metal are

Table III
Graphite Rating of Bead Welded Low Alloy Steels
(10,000 Hours' Exposure)

	Exposure Temperature									
	900 °F					1050 °F				
Steel Designation	Weld Metal	(1)*	(2)**	(3)†	(4)‡	Weld Metal	(1)	(2)	(3)	(4)
Mo	0	0	0	0	0	0	0	0	10A	3A
Ti-Mo (No. 61)	0	0	0	0	0	0	0	0	0	0
Ti-Mo (No. 62)	0	0	0	0	0	0	0	0	0	0
Ti-Mo (No. 63)	0	0	0	0	0	0	0	0	0	0
Ti-Mo (No. 64)	0	0	0	0	0	0	0	0	0	0
Cb-Mo (No. 65)	0	0	0	0	0	0	0	0	0	0
Cb-Mo (No. 66)	0	0	0	0	0	0	0	0	0	0
Zr	0	0	2G	0.5J	0.2J	0	0	0	1G	0.2J
Zr-Mo	0	0	0	0	0	0	0	0	75D	1F

*Zone 1, immediately beneath weld
**Zone 2, beneath Zone 1
†Zone 3, near boundary of heat-affected area
‡Parent metal

shown in Table III. After 10,000 hours' exposure at 1050 °F (565 °C) graphitization was observed in the molybdenum, zirconium and zirconium-molybdenum steels. The zirconium steel also contained graphite at the 900 °F (480 °C) exposure temperature. Graphite was not observed in any of the steels after 1000 hours' exposure.

The structure of the titanium-molybdenum (No. 62) parent metal shown in Fig. 1a consists of titanium carbide in a ferrite matrix with no evidence of pearlite. In the weld heat-affected zone before exposure, a similar carbide structure was observed and, in addition, a change in grain structure. Immediately beneath the weld metal, a coarse-grained structure was present and, adjacent to this zone, fine-grained recrystallized parent metal which merged into the unaffected parent metal. After exposure, there was no appreciable change in the grain structure of either the weld heat-affected zone or the parent metal. The microstructures of the molybdenum and columbium-molybdenum steel were similar to the titanium-molybdenum steels except that columbium carbide was present before exposure in the columbium-molybdenum steels and pearlite in the molybdenum steel. In the molybdenum steel, pearlite spheroidized after exposure and some graphite was observed. The small particle size of graphite in this steel may be associated with the low carbon content of the material. A stabilizing influence due to columbium and titanium is indicated. Longer exposure periods will be required to further establish the carbide stability of titanium-molybdenum and columbium-molybdenum steels.

The zirconium steels before exposure were similar in structure to the molybdenum steel in the parent metal and heat-affected zone. The parent metal structure of the zirconium-molybdenum steel before exposure is shown in Fig. 1b. The zirconium-molybdenum steel contained a narrow band of graphite in the weld heat-affected zone after exposure for 10,000 hours at 1050 °F (565 °C). Fig. 1c illustrates the structure observed which is the nearest approach to chain graphite encountered to date in this program. This narrow band of graphite clearly indicates the presence of a critical zone induced by welding. Fig. 1d, the same area as Fig. 1c but at higher magnification, shows the graphite to be at the ferrite grain boundaries. This same zirconium-molybdenum steel exposed at 900 °F (480 °C) contained no graphite. At 1200 °F (650 °C) very large particles of graphite were present, but due to decarburization, the specimens were not classified.

The zirconium steel contained dispersed graphite in the weld heat-affected zone and parent metal after exposure at 900 and 1050 °F (480 and 565 °C). The addition of 0.5% molybdenum to this steel apparently inhibited graphitization only at 900 °F (480 °C) during 10,000 hours' exposure.

Structural Changes in Ferritic Stainless Alloy Steels

The unexposed structures of 12% chromium, 12% chromium FM, 12% chromium-aluminum and 12% chromium-molybdenum parent metal are illustrated in Figs. 2a to 2d. In the weld heat-affected zone before exposure of the 12% chromium and 12% chromium-molybdenum steels, a smaller grain size was observed compared to parent metal. This condition was not observed in the 12% chromium FM and 12% chromium-aluminum steels. The structural characteristics of all these steels were essentially unchanged after 10,000 hours' exposure at the various temperatures.

No changes in structural characteristics of the 17% chromium parent metal after exposure were observed. The original structure of the parent metal is shown in Fig. 3a. A fine-grained network structure is shown. The structure of the weld heat-affected zone before and after exposure at 900 °F (480 °C) was unchanged and similar to the parent metal. After 10,000 hours' exposure at 1050 and 1200 °F (565 and 650 °C), the grain boundaries in the weld heat-affected zone could not be developed with the etching technique em-

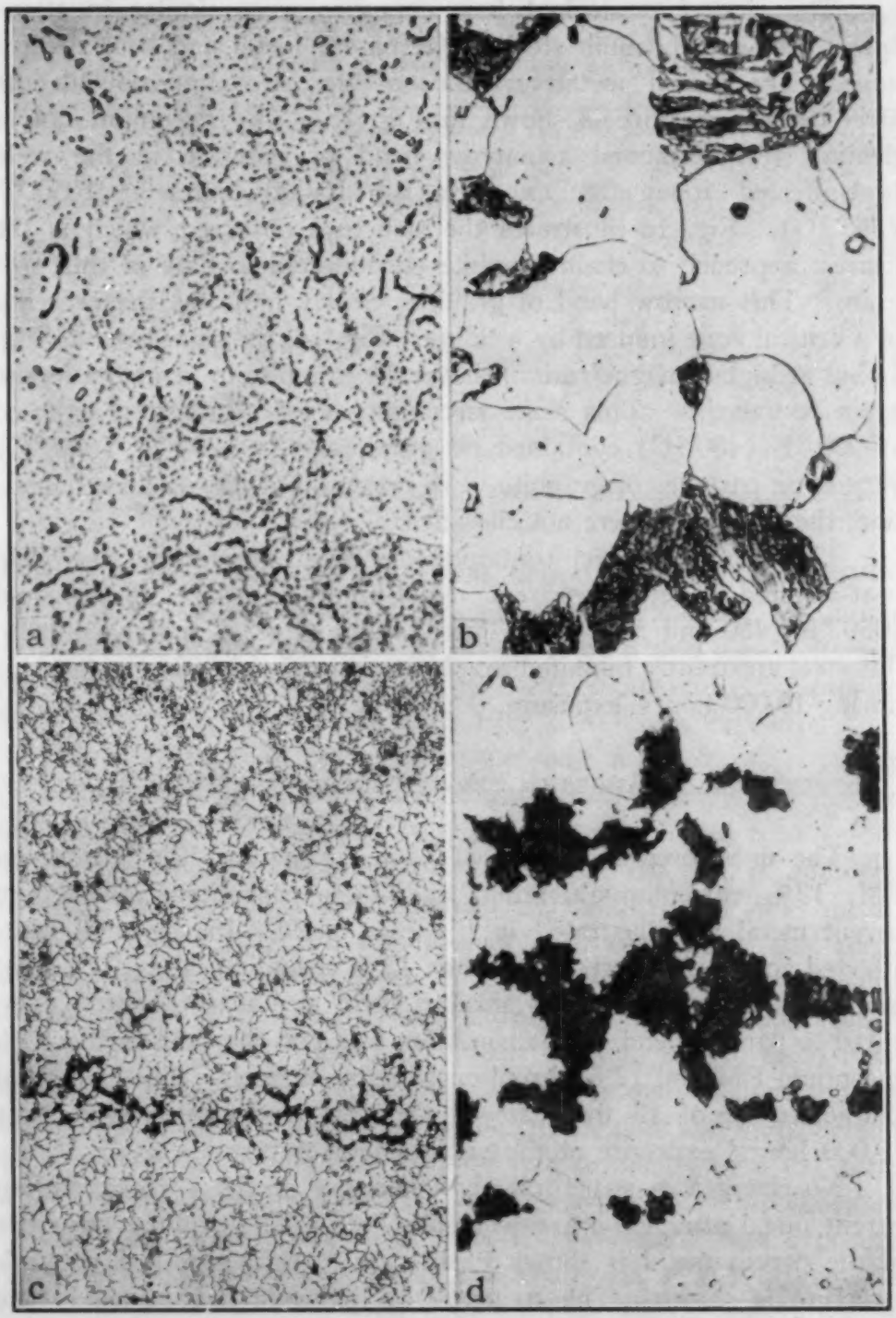


Fig. 1—Zirconium-Molybdenum and Titanium-Molybdenum (No. 62) Steels, Picral-Nital Etch. (a) Unexposed parent metal titanium-molybdenum steel showing titanium carbide. × 1000. (b) Unexposed parent metal zirconium-molybdenum steel showing carbide structure. × 1000. (c) Weld heat-affected zone zirconium-molybdenum steel exposed 10,000 hours at 1050 °F showing chain-like graphite. × 100. (d) Same as (c) except × 1000 showing graphite at grain boundaries.

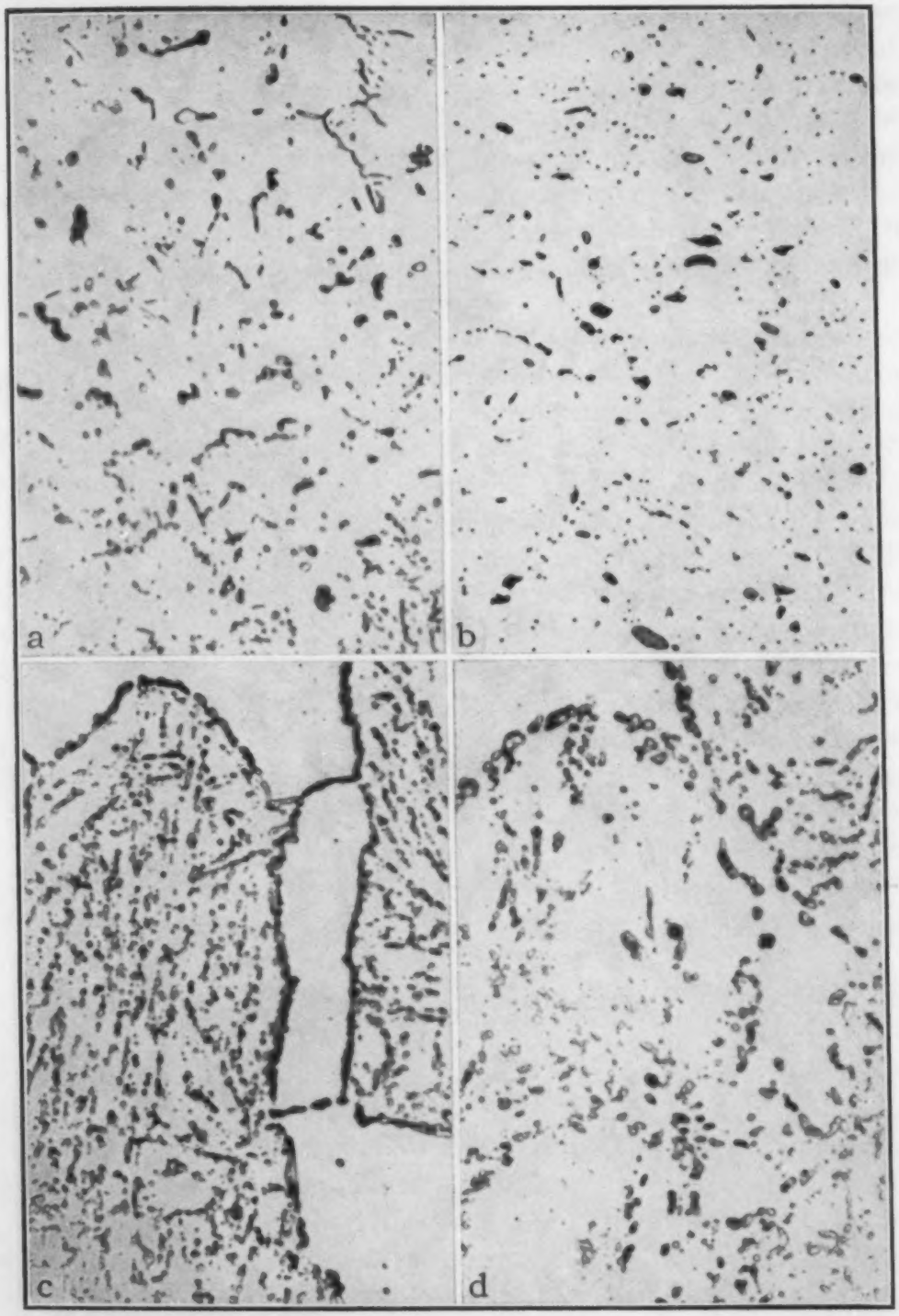


Fig. 2—12% Chromium Steels, Unexposed Parent Metal Showing Carbide Structure; Oxalic Acid Etch. × 1000. (a) 12% chromium, (b) 12% chromium FM, (c) 12% chromium-aluminum, (d) 12% chromium-molybdenum.

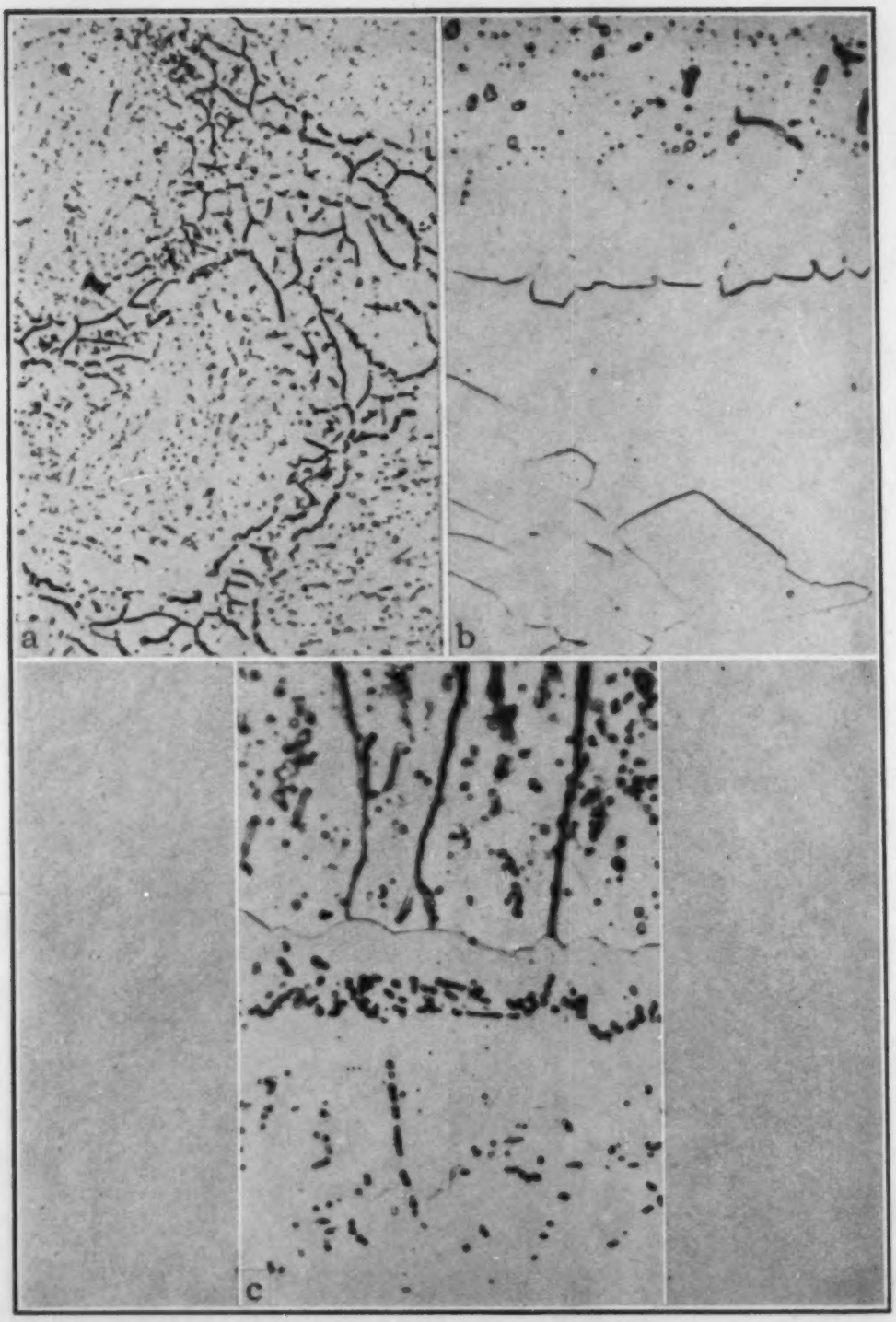


Fig. 3—17% Chromium Steel. × 1000. (a) Unexposed parent metal showing fine-grained network, oxalic acid etch. (b) Unexposed weld metal - base metal juncture, chromic acid etch. (c) Same location as (b) but after 10,000 hours' exposure at 1200 °F showing presence of a new phase in base metal, chromic acid etch.

ployed. In the weld heat-affected zone at the weld metal - base metal interface, a new constituent was observed after exposure at 1200 °F (650 °C) which may be sigma phase. The microstructure at this location of unexposed and exposed specimens is shown in Figs. 3b and 3c. Weld metal is shown in the upper part of the photomicrographs. Grain boundaries are not shown, due to the etchant used. The possible occurrence of sigma phase may be due to alloy diffusion into the base metal and will require longer periods of exposure for confirmation.

A structural change involving formation of sigma phase occurred in the parent metal and weld heat-affected zone of the *27%* chromium steel after 10,000 hours' exposure at 1050 and 1200 °F (565 and 650 °C). The unexposed parent metal is shown in Fig. 4a. A high concentration of sigma phase formed as a narrow band in the weld heat-affected zone as illustrated in Fig. 4b. Figs. 4c and 4d are the same field of the parent metal after 10,000 hours at 1200 °F (650 °C), the former showing only the carbide phase while the latter depicts both carbides (darkened) and sigma phase. Grain size characteristics of the weld heat-affected zone before and after exposure were similar to the original and exposed parent metal. There were no visible structural changes in parent metal or weld heat-affected zone after exposure for 1000 hours or at 900 °F (480 °C) after 10,000 hours' exposure. The occurrence of a high concentration of sigma phase in the weld heat-affected zone of the *27%* chromium steel subjected to temperatures over 900 °F for extended periods of time is of considerable commercial significance and will be further evaluated after longer periods of exposure.

Structural Changes in Austenitic Stainless Alloy Steels

The microstructure of 18-8, 18-8 FM and 18-8 Mo unexposed parent metal were generally similar. The structure of the 18-8 Mo steel is shown in Fig. 5a. The structure of the 18-8 FM steel containing the selenium-phosphorus constituent is depicted in Fig. 5b. Grain structures of the weld heat-affected zone of these steels before exposure were similar to the parent metal.

The occurrence of titanium carbide in the 18-8 Ti and columbium carbide in the 18-8 Cb unexposed parent metal are shown in Figs. 5c and 5d. Grain structure of the weld heat-affected zone of these steels before exposure had a tendency to have a columnar structure normal to the weld metal junction.

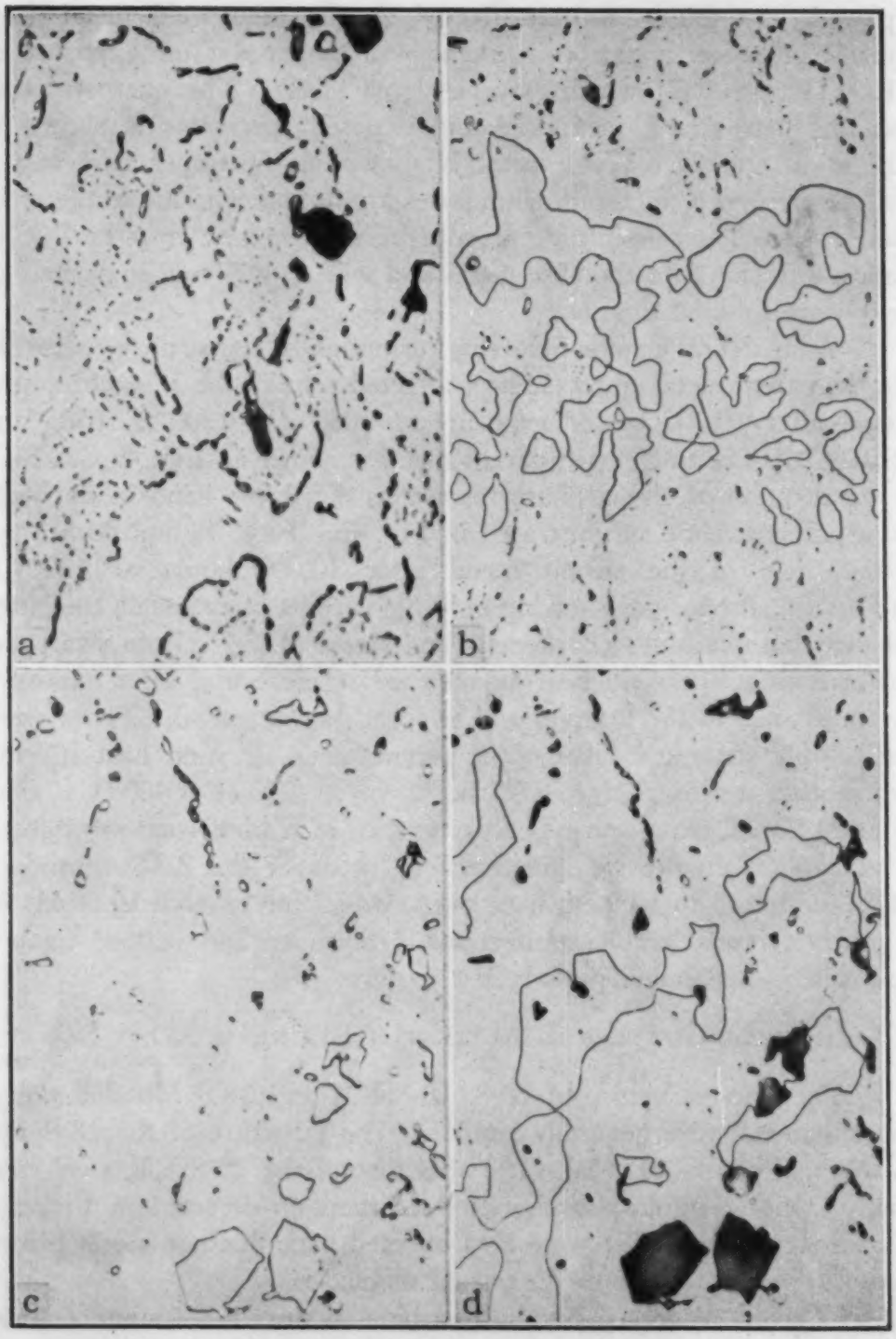


Fig. 4—27% Chromium Steel, Sodium Cyanide Etch. × 1000. (a) Unexposed parent metal showing carbide structure. (b) Exposed weld heat-affected zone, 1200 °F for 10,000 hours, showing sigma phase. (c) Exposed parent metal, 1200 °F for 10,000 hours, showing carbide phase. (d) Same as (c) but longer etch showing carbide (darkened) and sigma phases.

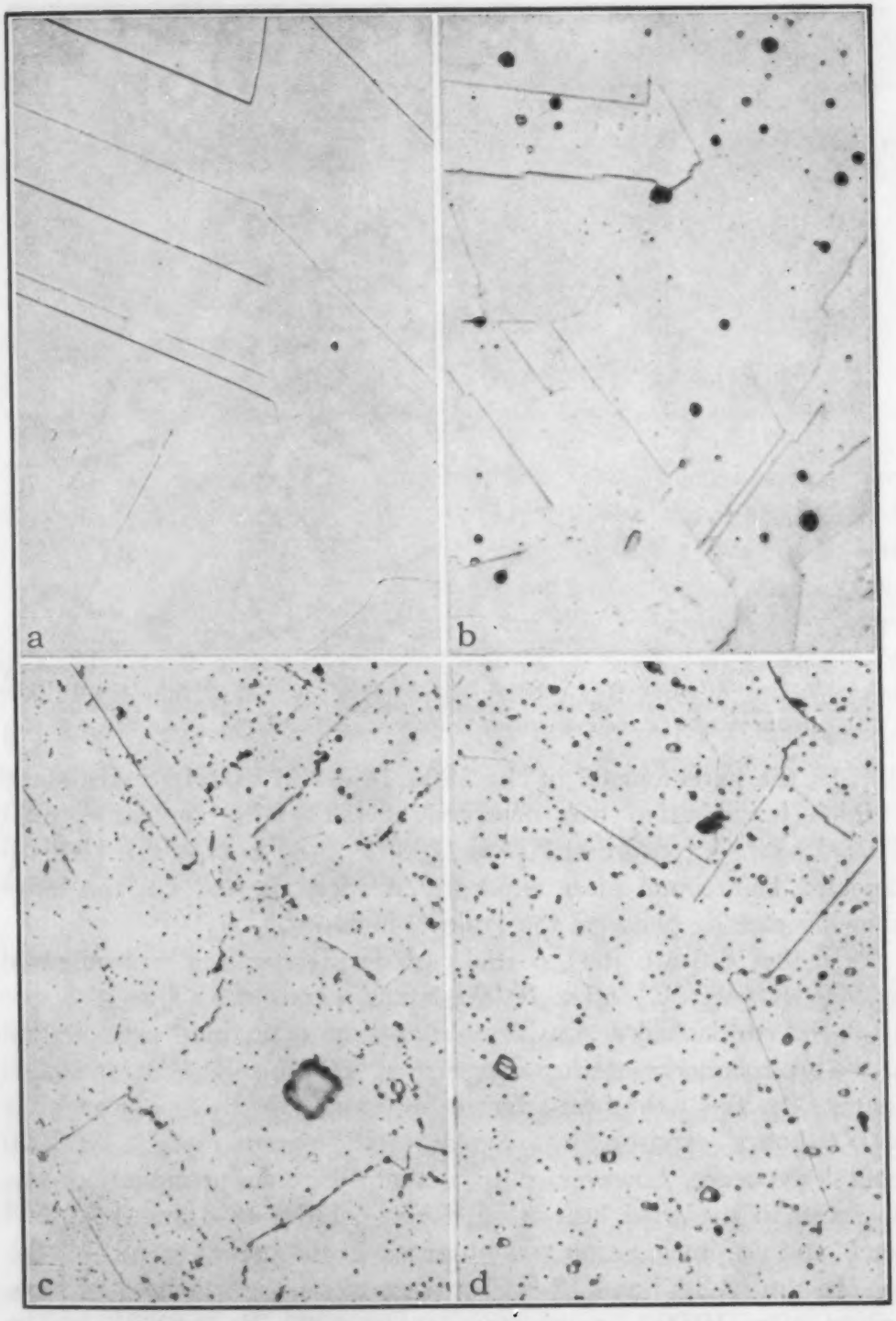


Fig. 5—18% Chromium – 8% Nickel Steels, Unexposed Parent Metal, Oxalic Acid Etch. × 1000. (a) 18-8 molybdenum showing austenite twins. (b) 18-8 FM showing selenium-phosphorus constituent. (c) 18-8 titanium showing titanium carbide. (d) 18-8 columbium showing columbium carbides.

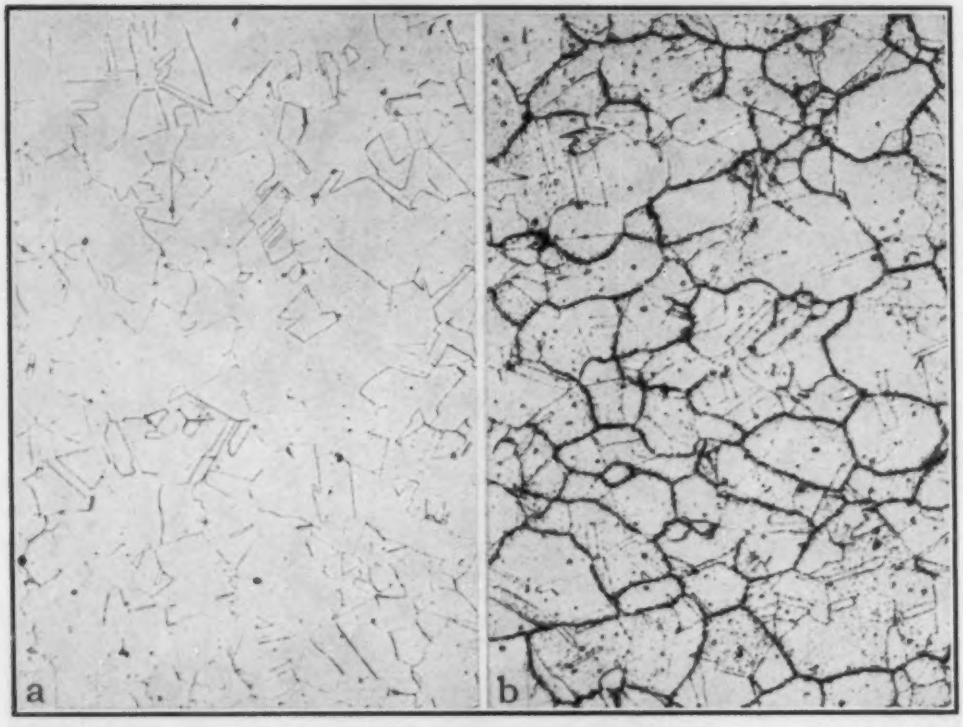


Fig. 6—18% Chromium – 8% Nickel-Molybdenum Steel, Parent Metal. × 100. (a) Unexposed showing grain structure, Marble's reagent etch. (b) After exposure for 10,000 hours at 1200 °F showing carbide phase at grain boundaries, oxalic acid etch.

In the parent metal of the 18-8, 18-8 FM and 18-8 Mo steels carbide precipitation was observed at the grain boundaries after 10,000 hours' exposure at 900 to 1200 °F (480 to 650 °C). This is depicted before and after exposure in Figs. 6a and 6b, the latter showing carbide phase at the grain boundaries.

In the 18-8 Mo steel, partial carbide precipitation was observed at 900 °F (480 °C) after 10,000 hours' exposure. The 18-8 and 18-8 FM steels had a considerable amount of carbide precipitation at the grain boundaries after exposure at 900 °F (480 °C) for 10,000 hours. In the weld heat-affected zone, carbide precipitation after 10,000 hours' exposure was similar to the parent metal. At 1000 hours' exposure, however, only a slight carbide precipitation was observed in the weld heat-affected zone of the 18-8 and 18-8 FM steels and no precipitation was observed in the parent metal.

In the 18-8 Ti and 18-8 Cb parent metal, sigma phase was observed after 10,000 hours' exposure at 1200 °F (650 °C). The occurrence of this phase was questionable at 1050 °F (565 °C) and was not observed at 900 °F (480 °C). Sigma phase in the 18-8 Ti steel is illustrated by comparison of Figs. 7a and 7b.

Table IV
Impact Properties

Steel Designation	Charpy Full Size Keyhole Notch Specimen, Foot-Pounds						
	Before Exposure	Exposed 1000 Hours			Exposed 10,000 Hours		
		900 °F	1050 °F	1200 °F	900 °F	1050 °F	1200 °F
Zr	42	46	41	43	42	50	..
Zr-Mo	30	29	35	..	37	25	..
12 Cr (410)	33	..	41	27	39	..	21
12 Cr FM (416)	42	36	42	37	26	27	36
12 Cr Al (405)	35	..	36	22	..	39	34
12 Cr Mo (410 Mo)	45	44	..	49	56	56	54
17 Cr (430)	46	..	32	34	1	3	4
27 Cr N (446)	1	..	1	1	½	½	½
18-8 (304)	91	87	75	60	79	62	47
18-8 FM (303)	62	57	61	41	59	29	32
18-8 Mo (316)	80	86	72	44	87	49	32
18-8 Ti (321)	107	101	90	69	88	72	62
18-8 Cb (347)	56	60	55	49	63	51	32

Sigma phase was observed in the weld heat-affected zone of the 18-8 Ti and 18-8 Cb steels after 10,000 hours' exposure at 1050 and 1200 °F (565 and 650 °C). A larger quantity of the constituent was present in the weld heat-affected zone than in the parent metal.

The use of two metallographic methods for identifying sigma phase in austenitic stainless steels is illustrated in Fig. 7. Figs. 7a and 7b are the same field, the former etched with Murakami's reagent to bring out the carbides, and the latter etched with Vilella's reagent after repolishing to leave the sigma in relief. Figs. 7c and 7d are also the same field, the former with a light sodium cyanide etch to outline the sigma phase, and the latter a heavier etch, which darkens the sigma and brings out the carbides.

Impact and Hardness Properties

Impact and hardness properties before and after 1000 and 10,000 hours' exposure at 900, 1050 and 1200 °F (480, 565 and 650 °C) are shown in Tables IV and V. Results are not reported for the molybdenum, titanium-molybdenum and columbium-molybdenum steels as only the structural characteristics of these steels were investigated.

Impact properties of the zirconium and zirconium-molybdenum steels were essentially unchanged after 10,000 hours' exposure at 900 and 1050 °F (480 and 565 °C). Results are not reported for 10,000 hours' exposure at 1200 °F (650 °C), due to decarburization. Although graphitization was observed in these steels after exposure, due to random distribution and carbide spheroidization, the impact properties were not adversely affected.

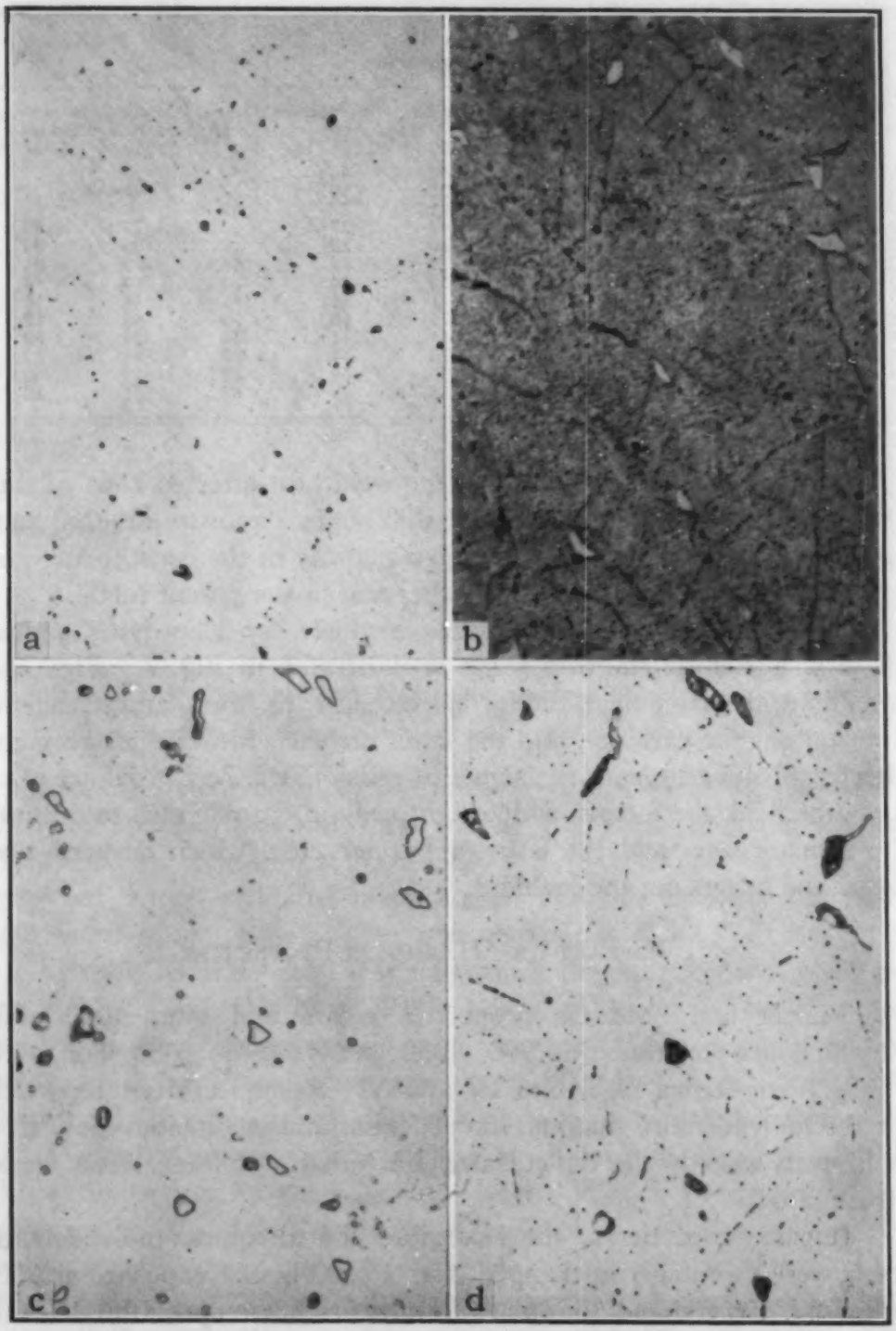


Fig. 7—18% Chromium – 8% Nickel-Titanium Steel. Parent metal after exposure of 10,000 hours at 1200 °F showing development of sigma phase. × 1000. (a) Murakami's reagent showing carbides. (b) Same field as (a) after repolishing and etching with Vilella's reagent showing carbides and sigma phase. (c) Light sodium cyanide etch showing sigma phase. (d) Same field as (c) with heavier sodium cyanide etch showing sigma and carbides.

Table V
Hardness Properties

Steel Designation	Rockwell B Hardness						
	Before Exposure	Exposed 1000 Hours			Exposed 10,000 Hours		
		900 °F	1050 °F	1200 °F	900 °F	1050 °F	1200 °F
Zr	71	72	65	65	69	59	..
Zr-Mo	76	80	80	..	83	74	..
12 Cr (410)	81	..	72	78	81	80	78
12 Cr FM (416)	80	79	80	76	78	78	80
12 Cr Al (405)	79	..	78	76	..	78	76
12 Cr Mo (410 Mo)	78	74	75	73	78	78	76
17 Cr (430)	88	..	88	86	104	85	82
27 Cr N (446)	92	..	92	91	109	100	100
18-8 (304)	75	77	76	76	83	81	75
18-8 FM (303)	83	86	87	90	87	94	92
18-8 Mo (316)	80	80	76	84	79	81	84
18-8 Ti (321)	81	77	78	86	82	83	80
18-8 Cb (347)	88	80	86	83	81	85	84

Impact properties of the various 12% chromium steels were, in many instances, not appreciably affected by exposure at the elevated temperatures. In certain cases the impact strength was decreased, but the significance of these results cannot be evaluated at the present time since no accompanying changes in the microstructure were observed. Impact values were not reported for all test conditions due to erratic results which may possibly be associated with undetected variations in microstructure. Additional specimens selected from different heats of steel are being exposed and the impact properties will be reported.

The 17% chromium steel was brittle after exposure for 10,000 hours at 900, 1050 and 1200 °F (480, 565 and 650 °C). No change in microstructure was observed with the exception of the possible formation of a finely dispersed phase. Evidence to support the presence of this new phase must await longer periods of exposure.

The 27% chromium-nitrogen steel was brittle before and after exposure. However, it should be recognized that all impact tests were conducted at ordinary temperatures which may be below the transition range for the material. A carbide phase was present in all the specimens and no structural change in the parent metal after 1000 hours' exposure was observed. After 10,000 hours' exposure at 1050 and 1200 °F (565 and 650 °C) sigma phase was observed. There was no observed structural change after exposure at 900 °F (480 °C) for 10,000 hours.

A carbide phase at the grain boundaries was observed in the 18-8 and 18-8 FM steels after exposure for 10,000 hours at 900, 1050 and 1200 °F (480, 565 and 650 °C). In the 18-8 Mo steel, the

grain boundary carbides were observed only at 1050 and 1200 °F (565 and 650 °C). The occurrence of this phase at the grain boundaries would account for the lower impact strength. With respect to the 18-8 Ti and 18-8 Cb steels, the lowered impact strength observed after 10,000 hours' exposure at 1200 °F (650 °C) was associated with the presence of sigma phase.

Hardness changes are presented in Table V. The hardness of the zirconium and zirconium-molybdenum steel remained virtually unchanged, with the exception of the zirconium steel after 10,000 hours at the 1050 °F (565 °C) exposure temperature. The 12% chromium steels exhibited no change in hardness after exposure at any of the temperatures involved. The 17% chromium steel after 10,000 hours' exposure at 900°F (480 °C) increased substantially in hardness, probably due to a submicroscopic precipitate unobservable under the microscope. At higher exposure temperatures, a slight decrease in hardness is evident. An increase in hardness at all temperatures occurred in the 27% chromium steel. This was probably associated with the formation of a new constituent. After exposure at 900 °F (480 °C) no changes in microstructure were observed and the hardening may therefore be related to a submicroscopic precipitate.

The 18-8 austenitic stainless steels became slightly harder at some exposure temperatures. No correlation could be detected between the observed changes in structural characteristics and the hardness values obtained. The changes observed were probably associated with carbide precipitation.

After longer periods of exposure, it will be possible to associate more clearly certain phase changes with changes in hardness and impact strength. In this investigation, it is planned to expose additional heats of steel to confirm results which are indicative of properties which have not been observed in other investigations.

Oxidation Characteristics

The degree of oxidation of the zirconium, zirconium-molybdenum and stainless alloy steels exposed to air for 10,000 hours at 900 to 1200 °F (480 to 650 °C) is shown in Table VI. It will be observed that the zirconium-bearing low alloy steels were appreciably susceptible to oxidation at 1200 °F (650 °C), very little oxidation was observed at 1050 °F (565 °C) and at 900 °F (565 °C) oxida-

Table VI
Oxidation After 10,000 Hours' Exposure

Steel Designation	Weight Loss, %			Depth of Metal Loss Due to Scale—Inches		
	900 °F	1050 °F	1200 °F	900 °F	1050 °F	1200 °F
Zr	0.8	1.7	15.7	0.0003	0.0020	0.0350
Zr-Mo	0.8	1.6	15.6	0.0003	0.0023	0.0370
12 Cr (410)	0.6	0.5	0.6	0.0000	0.0000	0.0000
12 Cr FM (416)	0.5	0.5	0.6	0.0000	0.0000	0.0000
12 Cr Al (405)	...	0.4	0.6	.....	0.0000	0.0000
12 Cr Mo (410 Mo)	0.6	0.6	0.5	0.0000	0.0000	0.0000
17 Cr (430)	0.6	0.6	0.6	0.0000	0.0000	0.0000
27 Cr N (446)	0.6	0.6	0.6	0.0000	0.0000	0.0000
18-8 (304)	0.7	0.7	0.7	0.0000	0.0000	0.0003
18-8 FM (303)	0.6	0.6	0.7	0.0003	0.0003	0.0005
18-8 Mo (316)	0.6	0.5	0.5	0.0000	0.0000	0.0000
18-8 Ti (321)	0.7	0.7	0.7	0.0000	0.0000	0.0000
18-8 Cb (347)	0.7	0.7	0.7	0.0003	0.0000	0.0003

tion was essentially nil. The ferritic and austenitic high alloy steels exhibited no appreciable oxidation at any of the temperatures used. Due to the high alloy content of the stainless alloys and the relatively low temperatures of exposure, the results obtained are consistent with expectation.

Oxidation data of the type under discussion are limited in application and should be used with caution. In general, stainless alloys are used in special atmospheres at elevated temperature and, therefore, oxidation characteristics may vary considerably with actual exposure conditions.

Conclusions

1. The titanium and columbium-molybdenum steels did not graphitize during 10,000 hours' exposure at either 900 or 1050 °F (480 or 565 °C), while both the parent metal and weld heat-affected zone of the molybdenum and zirconium steels graphitized. Graphite was observed as a chain-like structure in the weld heat-affected zone of the zirconium-molybdenum steels.

2. The 12% chromium steels appeared to be the most stable with respect to microstructure, impact properties and hardness at all temperatures.

3. Sigma phase was observed metallographically in the 27% chromium-nitrogen steel after exposure at 1050 and 1200 °F (565 and 650 °C), both in the parent metal and weld heat-affected zone, with a high concentration in the latter. The hardness of the parent metal increased during 10,000 hours' exposure at all three temperatures.

4. Carbide precipitation in the grain boundaries was observed in the austenitic 18-8, 18-8 FM and 18-8 Mo steel in both the parent metal and weld heat-affected zone after 10,000 hours' exposure at all three temperatures. This first occurred in the weld heat-affected zone. Carbide precipitation lowered the Charpy impact strength of the parent metal, particularly as exposed at 1050 and 1200 °F (565 and 650 °C).

5. After 10,000 hours' exposure at 1200 °F (650 °C), sigma phase was observed metallographically in the parent metal of the 18-8 Ti and 18-8 Cb steels and in the weld heat-affected zone as exposed at 1050 and 1200 °F (565 and 650 °C). The lower impact properties in the parent metal after exposure at 1200 °F (650 °C) were associated with sigma phase.

6. The Charpy impact strength of the zirconium steels' parent metal was not appreciably affected by graphitization after 10,000 hours' exposure at 900 and 1050 °F (480 and 565 °C).

7. The 17% chromium steel parent metal was embrittled by exposure for 10,000 hours at 900 to 1200 °F (480 to 650 °C) and an appreciable increase in hardness was observed after 10,000 hours' exposure at 900 °F (480 °C).

8. Oxidation of the parent metal in the stainless alloys after exposure in air for 10,000 hours at 900 to 1200 °F (480 to 650 °C) was essentially nil. The low alloy steels containing zirconium were appreciably oxidized after exposure at 1200 °F (650 °C).

Acknowledgment

The authors wish to express their appreciation for the assistance received from the management and operating personnel of National Tube Company, the U. S. Steel Corporation Research Laboratory, and Carnegie-Illinois Steel Corporation. They are particularly indebted to Mr. D. B. Collyer of Lorain Works, under whose direction the experimental work was conducted. Dr. R. E. Zimmerman, Vice-President, Research and Technology, of the United States Steel Corporation of Delaware, suggested the titanium and columbium-molybdenum steels. The zirconium steels were received from Union Carbide and Carbon Research Laboratories, Inc.

References

1. A. B. Wilder and J. D. Tyson, "Stability of Steels at Elevated Temperatures," *Steel,* October 20, 1947, p. 86.
2. A. B. Wilder and J. D. Tyson, "Graphitization of Steel at Elevated Temperatures," TRANSACTIONS, American Society for Metals, Vol. 40, 1948, p. 233.
3. Francis B. Foley, "The Sigma Phase," Alloy Casting Bulletin No. 5, July 1945.
4. H. D. Newell, "Properties and Characteristics of 27% Chromium Iron," METAL PROGRESS, American Society for Metals, Vol. 49, No. 5, 1946, p. 977.
5. Peter Payson and Charles H. Savage, "Changes in Austenitic Chromium-Nickel Steels During Exposures at 1100 to 1700 °F," TRANSACTIONS, American Society for Metals, Vol. 39, 1947, p. 404.
6. W. J. Barnett and A. R. Troiano, "X-Ray Identification of Sigma Phase in 25-20 Cr-Ni Stainless," METAL PROGRESS, American Society for Metals, Vol. 33, No. 3, March 1948, p. 366.

DISCUSSION

Written Discussion: By G. F. Comstock, assistant director of research, Titanium Alloy Manufacturing Division, National Lead Co., Niagara Falls, N. Y.

This paper is an interesting record of test results, presented in a straight-forward and orderly manner, and should be very useful for reference. The data indicating absence of graphitization in the titanium-molybdenum steels at 900 and 1050 °F (480 and 565 °C) are in agreement with results that we have obtained at 1100 °F (595 °C) on similar steels containing more than twice as much titanium as carbon. These steels, like those described in this paper, were fully killed with aluminum. With a lower ratio of titanium to carbon, however, some graphitization may be expected under favorable conditions, because of the presence of considerable carbon not stabilized by titanium, or in other words, occurring as iron carbide.

It should be noted that in the zirconium steels, which graphitized, the ratio of zirconium to carbon was much lower, or below one. The difference in graphitizing tendency between these steels and the titanium or columbium steels should therefore not be ascribed to the different alloy additions, as might be implied from Conclusion No. 1, but is most probably due to the different unstabilized carbon content, this being much higher in the zirconium steels. It is interesting, however, to note that the zirconium steels graphitized in spite of their very low aluminum contents.

The illustrations of sigma phase in the stainless steels are interesting, and agree with our own experience. The amount found in the Type 321 steel apparently had appreciably less effect on the notch-toughness of that steel than the sigma formation in the other 18-8 steels, because after 10,000 hours at 1200 °F (650 °C) the impact value of the Type 321 steel was nearly twice as great as the impact values of the other steels after the same exposure. This seems to have escaped mention in the text of the paper, or in Conclusion No. 5.

The authors deserve commendation for bringing their interesting data to the attention of the American Society for Metals in such a concise and readable form.

Written Discussion: By John J. B. Rutherford, metallurgist, The Babcock & Wilcox Tube Co., Beaver Falls, Pa.

The design engineer is faced with many problems in selecting materials applicable for chemical processing at elevated temperatures. Oxidation and creep tests have been performed on steel for over 25 years but many of the earlier data appear irrelevant, mainly because of the short periods involved in testing. There is the very natural tendency to cover numerous tests of short duration in preference to a few tediously-long tests. We were pleased to see the authors' work continued out to times in the order of a year, which begins to approach an industrial life-expectancy.

The most important feature to learn about a material for use at elevated temperatures is its strength and suitability to be used as a material of construction. However, in exploring the field of alloy components, it is desirable to study first the subject of stability, as observed at the surface and the internal structure. This is what the authors have contributed in an admirable manner. Since these results are preliminary to studies of much wider scope, comments must be restricted to this initial part of the work, even though we are interested in learning the effect of these structural changes on the mechanical properties at elevated temperatures.

We are quite disappointed in the failure of zirconium to stabilize carbide against graphite formation. Among the low alloy steels tested, Nos. 44 and 45 have twice as much carbon as the others which would naturally increase the tendency to graphitization. Have the authors experimented with zirconium in the higher chromium alloys to measure its effect on carbide stabilization? The structural changes observed in the stainless steels are obviously very complex, and might be more amenable to interpretation when studied in conjunction with their effect on the mechanical properties. We await eagerly the publication of other phases of these studies.

Written Discussion: By A. M. Hall, metallographer, and S. L. Hoyt, technical adviser, Battelle Memorial Institute, Columbus, Ohio.

We have been following closely the unusually comprehensive stability testing program in progress at the Lorain Works of the National Tube Company, and have read with great interest this report by Dr. Wilder and Mr. Light, covering certain of the findings to date.

Considering first the results of graphitization tests on the low-alloy ferritic steels, the findings seem generally consistent with expectations. The stabilizing influence of titanium, reported in this paper, confirms the results of graphitization tests made at Battelle and reported to the ASME.[2,3] The Battelle tests covered two titanium-molybdenum steels

[2]S. L. Hoyt and A. M. Hall, "Continuation of Joint EEI-AEIC Investigation on Graphitization of Piping," *Transactions*, American Society of Mechanical Engineers, 1947.

[3]A. M. Hall and S. L. Hoyt, "Further Investigation on the Graphitization of Piping for the EEI and AEIC," *Transactions*, American Society of Mechanical Engineers, 1948.

and two titanium-deoxidized carbon-molybdenum steels. The analyses are as follows:

Specimen No.	C	Mn	Si	Mo	Ti	Al
G40D	0.14	0.41	0.29	0.57	0.30	0.025
G40E	0.14	0.42	0.29	0.61	0.75	0.025
G53	0.15	0.36	0.13	0.55	0.048	.....
G54	0.14	0.42	0.12	0.58	0.035	.....

The Battelle tests were of considerably shorter duration than those reported here. Nonetheless, the absence of graphite in these steels, particularly in the carbon-molybdenum steel containing only 0.035% titanium, after 1700 hours at 1025 °F (550 °C), plus 5000 hours at 1125 °F (605 °C), was considered significant.

The stabilizing effect of columbium on the one hand and the graphitization of the steels containing zirconium on the other, reported by the authors, are matters of great interest. Columbium, along with titanium, is of course a very powerful carbon fixing agent. Zirconium, on the other hand, is not usually considered as a carbon stabilizer. A rough classification of the effect of various alloying elements on graphite formation may perhaps be permissible on such a basis as ability to fix carbon.

The structural changes found by the authors in the 17% chromium steel and in the Type 321 and Type 347 austenitic stainless steels, after long exposure at 1200 °F (650 °C), mark what may become a most important aspect of their program. The authors contemplate an unusually long test period, which will undoubtedly produce much very unique and valuable data on surface and structural stability. Moreover, it will have the advantage of involving little extrapolation. We may be obliged to alter our ideas, particularly on the structural stability of some of the stainless steels.

The performance of the 12% chromium steel is noteworthy, particularly the aluminum and molybdenum types, since this steel has been used extensively for lining equipment which operates at elevated temperatures.

In view of the long-time program, the writers would suggest that the inclusion of samples of the extra low-carbon type of the 18-8 steel would make an interesting addition to the series being tested.

Authors' Reply

The authors wish to express their appreciation for the discussions which this paper occasioned.

In reply to the first point raised by Mr. Comstock, the implication from the first conclusion of the paper that the zirconium and the titanium and columbium steels were compared directly is unfortunate. The authors plead guilty to drawing conclusions based, in part, on data not included in this paper but included in the paper presented last year. In order to rectify this circumstance, the following supplementary comparisons are made. In the interest of brevity, only the ratings for Zone 3 after 10,000 hours' exposure at 1050 °F (565 °C) are included:

	Steel Designation	Graphitization Rating
(1)	0.20% C, low Al	1 H
	0.20% C, 0.10% Zr, low Al	1 G
(2)	0.16% C, 0.51% Mo, low Al	0
	0.19% C, 0.51% Mo, 0.13% Zr, low Al	75 D
(3)	0.13% C, 0.52% Mo, high Al	100 B
	0.14% C, 0.51% Mo, 0.48% Cr, high Al	0
	0.09% C, 0.53% Mo, 0.25% Ti, high Al	0
	0.09% C, 0.56% Mo, 0.47% Ti, high Al	0
	0.08% C, 0.52% Mo, 1.08% Cb, high Al	0
(4)	0.14% C, 0.97% Mo, high Al	75 B
	0.09% C, 1.05% Mo, 0.25% Ti, high Al	0
	0.10% C, 0.95% Mo, 0.50% Ti, high Al	0
	0.08% C, 0.98% Mo, 1.12% Cb, high Al	0

These data constitute the basis of the authors' conclusion that both titanium and columbium inhibited graphitization, whereas zirconium had no such effect, and actually appeared to promote graphitization in the 0.5% molybdenum steel.

The second point raised by Mr. Comstock relative to the high impact value of the Type 321 steel after the severest exposure condition was not mentioned by the authors because percentagewise the losses in impact value of all the 18-8 steels except the 18-8 molybdenum were similar:

Steel Designation	Loss in Impact Value After 10,000 Hours at 1200 °F
18-8	48%
18-8 FM	48%
18-8 Mo	60%
18-8 Ti	42%
18-8 Cb	43%

The reply to Mr. Comstock's first point also serves as a partial reply to Mr. Rutherford's comments. The authors are sorry to advise Mr. Rutherford that no zirconium-chromium low alloy steels are included in the test program.

They are pleased, however, to be able to advise Messrs. Hall and Hoyt that samples of extra low carbon 18-8 steels have already been added to the investigation. It is encouraging that so many of the conclusions to date in this investigation have been in conformance with the Battelle test results.

SHORT-TIME HIGH TEMPERATURE DEFORMATION CHARACTERISTICS OF SEVERAL SHEET ALLOYS

By James Miller and Glen Guarnieri

Abstract

From short-time constant rate tensile tests at elevated temperatures true stress – true strain characteristics have been determined for five different types of alloys over a range of temperatures and strain rates. The alloys were selected to include SAE 1020 steel as a reference material; Regular Inconel to represent a comparatively stable annealed material; Inconel X, a fully-aged alloy; and S-816, both annealed and cold-rolled, to represent an alloy susceptible to age hardening in both the annealed and cold-rolled conditions. The true stress – true strain plots are used to yield information on the changes effected in the properties of the alloys as they undergo high temperature plastic deformation.

An attempt was made to use the data as a means of learning more about the mechanics of deformation at elevated temperatures through determination of the activation energies involved. The increase in such energy values with decrease in stress, as was found for all materials, was attributed to the effect of elastic distortion on the crystal lattice. A simplified mechanism of deformation is described using these characteristics and the relationship of the flow process to metallic diffusion pointed out.

Introduction

THE rapid development and adaptation of many new heat-resistant alloys for gas turbine and jet engine service have been accomplished through the accelerated test programs of the recent war years. While limited time or facilities were available for investigating fundamental principles or underlying causes for the superiority of certain compositions, the empirical test methods used were successful in meeting the immediate demands of the turbine and engine designers. As the metallurgist continues the search for materials capable of resisting even more intense heat and load conditions, no doubt his

A paper presented before the Thirtieth Annual Convention of the Society, held in Philadelphia, October 23 to 29, 1948. The authors, James Miller and Glen Guarnieri, are associated with Cornell Aeronautical Laboratory, Inc., Buffalo, N. Y. Manuscript received April 16, 1948.

activities can be guided more profitably by consideration of basic principles involved in high temperature deformation processes. This should be particularly so if results are to be achieved with leaner alloys containing fewer and smaller amounts of strategic metals.

In the course of evaluating the short-time load carrying ability of a number of available sheet alloys in the temperature range of 1200 to 1800 °F (650 to 980 °C), attempts were made to study the deformation characteristics of each with the intent of becoming more familiar with the basic mechanisms associated with high temperature flow. The accumulated experience of many investigators in this field has defined the variables of stress, strain, strain rate, and temperature as those factors primarily controlling the flow properties of a particular metal or alloy. In fact, these variables have been related (1)[1] and (2) in a single equation of state represented symbolically as $S = S(\varepsilon, \varepsilon', T)$ where S and ε represent true stress and true strain, ε' strain rate, and T the absolute temperature.

In spite of the complexity of such an equation of state, requiring six constants to define the behavior of a particular alloy under idealized conditions of microstructural stability, such an analysis serves a definite purpose in systematizing the study of the high temperature materials problem. Unfortunately, a large number of service applications exist where conditions of temperature, time, and strain give rise to such microstructural disturbances as recrystallization, spheroidization, precipitation, and phase changes. Fisher and MacGregor (3) have attempted to extend the equation of state concept to include the condition of tempering through introduction of a fifth variable resulting in a relationship of the form $S = S(\varepsilon, \varepsilon', T, P)$ where P is a parameter representing the degree of tempering.

Conceivably this type of relationship could be expanded eventually to include a variety of nonequilibrium conditions. While such mathematical analyses of the deformation process may proceed on the one hand, there exists on the other a definite need for interpretation of such results in terms of more familiar metallurgical fundamentals. In this investigation an attempt has been made to analyze tensile deformation data from this latter viewpoint.

Methods of Data Analysis

True stress – true strain data were obtained from tension tests conducted over a range of strain rates and temperatures so selected

[1]The figures appearing in parentheses pertain to the references appended to this paper.

that marked strain hardening was induced in the specimen at the lower test temperatures while appreciable annealing and recrystallization occurred at the higher end of the temperature range. The true stress – strain diagram provides a highly useful and sound basis for displaying the actual flow conditions existing in a stressed material at least up to the point where necking or nonuniform straining of the specimen occurs. The slope of such a plot on log-log coordinates serves as an index to the degree of hardening occurring during straining and, in the more familiar case of room temperature deformation, this positive slope is usually characteristic of the strain hardening properties of the material. At both room and elevated temperatures, the strain hardening process may be supplemented by precipitation hardening and phase changes[2] or counteracted by simultaneous recovery, recrystallization, tempering, and overaging. All such events contribute characteristic effects to the true stress – strain properties of an alloy, but their individual identification is not always possible where several such alterations are occurring simultaneously.

A further attempt has been made to disclose features of the high temperature deformation process through consideration of the activation energies associated with such flow. It is well agreed that all plastic deformation occurs as a shearing process in which one layer of a body slides past an adjacent layer. On an atomic scale we may picture this shear action as the squeezing and slipping of the individual atoms past their neighbors as they progress from one lattice position to another. In order for a particle to accomplish this transposition it must attain sufficient energy to overcome its restraining forces, and the magnitude of such an energy barrier becomes a major factor in determining the resistance of a material to plastic flow.

Analysis of the flow and creep problem from this viewpoint by Eyring (5), Dushman (6), Kanter (7), and Kauzman (8), has revealed that determination of the activation energies associated with plastic deformation may be made by consideration of the relationship between the variables of temperature and rate of flow. Results obtained from analogous systems, involving atomic interchange processes such as metallic diffusion and chemical reactions, provide a basis for expecting the rate at which atomic shear progresses to depend upon the probability of an atom being activated to the energy level

[2]As an example of this type of auxiliary hardening, the case of the 18 Cr – 8 Ni stainless steels may be cited in which the transformation of austenite to martensite during cold working enhances hardening.

necessary to permit its change of position. This probability may be represented by the term $e^{-Q/RT}$ where e is the natural logarithm base, Q the activation energy, R the universal gas constant, and T the absolute temperature.

The relationship $\varepsilon' = Ae^{-Q/RT}$ has been found to apply favorably to high temperature deformation results within the accuracy of the available data. Here ε' refers to the strain rate and A is a constant. Thus Q may be evaluated from the slope of the straight lines formed on a plot of log strain rate versus reciprocal of the absolute temperature for constant stress and strain parameters. The tensile data reported herein have been examined in this manner with the intent of evaluating the Q quantity for the several alloys studied and with the hope of learning more about the nature of the flow process.

Materials and Specimens

The sheet materials tested were selected to include an annealed alloy (Inconel Regular), an age-hardened alloy (Inconel X), an annealed alloy susceptible to age hardening (S-816 annealed), and a cold-worked alloy susceptible to age hardening (S-816 cold-worked). In addition an SAE 1020 steel was tested after treatment at 1250 °F (675 °C) to produce a relatively stabilized structure with respect to the test temperatures used. Both types of Inconel were supplied in sheet form by the International Nickel Company and the S-816 was supplied in sheet form by the Allegheny Ludlum Steel Corporation. The alloys and treatment received before testing are listed in Table I, together with the sheet thicknesses.

Table II gives the chemical analysis of the alloys tested. Specimens for all materials were machined from strips 1 by 16 inches and had a gage section 2 inches long by ½ inch wide.

Experimental Methods and Equipment

In order that the range of test temperatures would extend from temperatures where recrystallization and recovery were negligible

Table I

Alloy	Sheet Thicknesses	Treatment
SAE 1020	0.052 Inch	1 hour at 1250 °F air-cooled
Inconel Regular	0.042 Inch	Annealed at 1950 °F air-cooled
Inconel X Aged	0.052 Inch	Annealed at 2000 °F air-cooled 24 hours at 1550 °F air-cooled 20 hours at 1300 °F air-cooled
S-816 annealed	0.042 Inch	Steam quenched after 15 min. at 2200 °F
S-816 cold-worked	0.044 Inch	Annealed before cold rolling

Table II
Composition of Alloys Tested

Alloy	C	Mn	Si	S	P	Fe	Cr
SAE 1020	0.20	0.4	....	0.04	0.04	....	.....
Inconel Regular	0.06	0.16	0.33	0.007	.....	6.77	14.04
Inconel X	0.04	0.42	0.41	0.007	.....	6.58	14.84
S-816 Annealed	0.30	0.50	0.45	0.015	0.015	3.58	20.26
S-816 Cold-worked	0.36	0.99	0.31	0.014	0.016	2.54	19.74

Alloy	Ni	Co	W	Mo	Cu	Al	Cb	Ti
SAE 1020	.....	.....	....	....	....	....	....	....
Inconel Regular	78.16	.....	....	....	0.45	....	....	....
Inconel X	73.46	.....	....	....	0.02	0.64	1.00	2.54
S-816 Annealed	19.90	43.65	4.65	4.16	....	....	3.63	....
S-816 Cold-worked	19.99	44.52	4.08	3.79	....	....	3.65	....

factors to those where recrystallization was important, and also include temperatures where precipitation and coalescence could occur, the high temperature alloys were tested at 1200, 1400, 1600, and 1800 °F (650, 760, 870, and 980 °C) and the SAE 1020 at 600, 800, 1000, and 1200 °F (315, 425, 540, and 650 °C). In general, for any alloy, three tensile tests were made at each temperature at different constant strain rates varying from about 0.03% per minute to about 3% per minute.

The tests were conducted in a 60,000-pound capacity hydraulic-type tensile machine with controllable head speed. Heat was supplied to the specimen by a resistance-wound furnace capable of maintaining the temperature within 4 °F of the nominal value over the 2-inch gage length of the specimen. Thermocouples attached to each specimen insured that this variation in temperature was not exceeded throughout the test. Specimens were held at the testing temperature approximately 1 hour before loading, to allow stabilization of the temperature.

Strain measurements were made using a system having a sensitivity of 0.0001 inch and so designed as to permit convenient measurement of strain rate. In this system elongation of the gage length is transferred outside the furnace by extensometer arms attached to the ends of the gage length as illustrated in Fig. 1. Engaging the ends of the arms are small cantilever beams on which are mounted wire strain gages (9). These wire strain gages are connected in the bridge circuit of an SR-4 strain indicator unit in such a manner that the unbalanced current in the bridge is proportional to the average elongation in the gage length of the specimen. This unbalanced current after being suitably amplified is automatically registered on a milliammeter recorder. An auxiliary margin pen is used to indicate

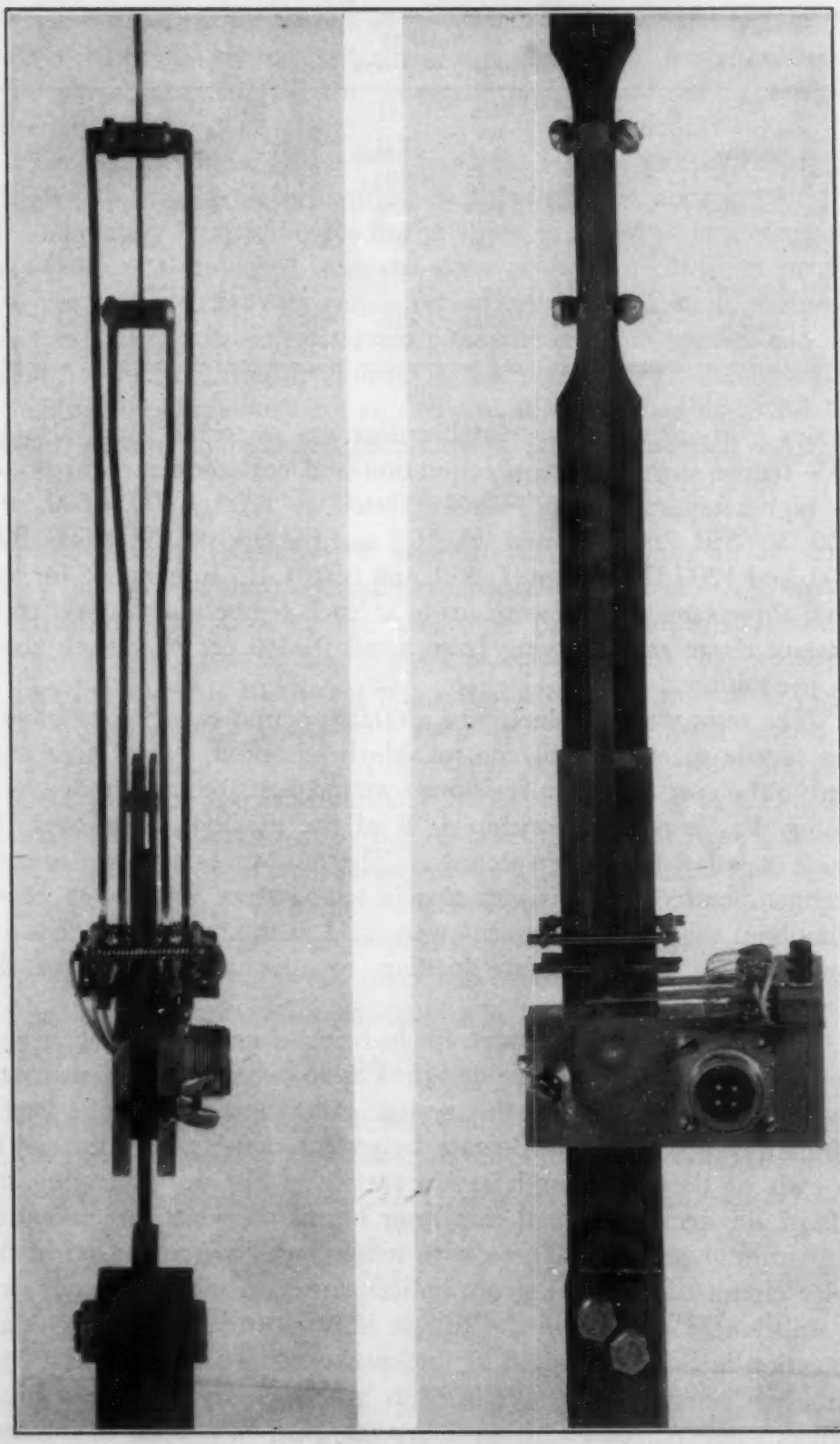


Fig. 1—Tensile Test Specimen With Extensometer Arms Attached and Cantilever Strain Gage in Position. Front and side view.

loads, and as the paper speed is constant, a complete record of strain, load, and time is obtained on a single chart.

Since the slope of the line formed on the milliammeter recorder is a measure of the strain rate, it is feasible, by means of close observation of the line as it is formed and simultaneous adjustment of the head speed of the tensile machine, to maintain a constant rate of strain up to the point at which necking of the specimen sets in. When local deformation or necking occurs, this method is, of course, no longer valid since the rate of strain is no longer uniform throughout the gage length. Hence, in this investigation true stress – true strain curves for constant strain rate were plotted only up to the point where it was known that an insignificant amount of necking had occurred. Except for the SAE 1020 carbon steel, the majority of the tests conducted displayed negligible necking to fracture so that complete stress-strain diagrams were plotted in such instances.

It was found that in some specimens a falling off in load occurred long before necking. Wherever this was known or suspected to be the case, the tests were discontinued at some point before failure. If measurements on the specimen showed the effects of local deformation to be negligible, the data were used out to the point where the test was discontinued. Wherever possible, the final points on the stress-strain diagram were checked by the actual cross section measurements on the specimen, and these values (indicated by * on the diagrams) were in good agreement with values obtained from the strain measuring system.

All stress values represent load divided by the actual cross sectional area as calculated from elongation data assuming plastic deformation occurring at constant volume. Elongation was converted to true strain by the equation $\varepsilon = \int_{l_o}^{l} \frac{dl}{l} = \ln \frac{l}{l_o}$ where l and l_o represent the instantaneous and original gage lengths. A constant conventional strain rate was considered adequate since the difference between it and the corresponding true strain rate would not be enough to affect stress significantly even at the larger values of strain.

True Stress – True Strain Results

Initial reference to the stress-strain data for the SAE 1020 steel (Fig. 2) serves to indicate some of the general features of these high temperature diagrams. The straight lines, plotted on a log-log scale

to the point at which necking occurs, are typical of the exponential relation usually found for these variables (4). Since the slopes and positions of these lines represent the degree to which a specimen hardens during the course of testing, it is not surprising to find a decrease in such coefficients as the temperature rises. This expresses the condition that more rapid stress relieving or annealing occurs at the higher temperatures, resulting in less net strain hardening.

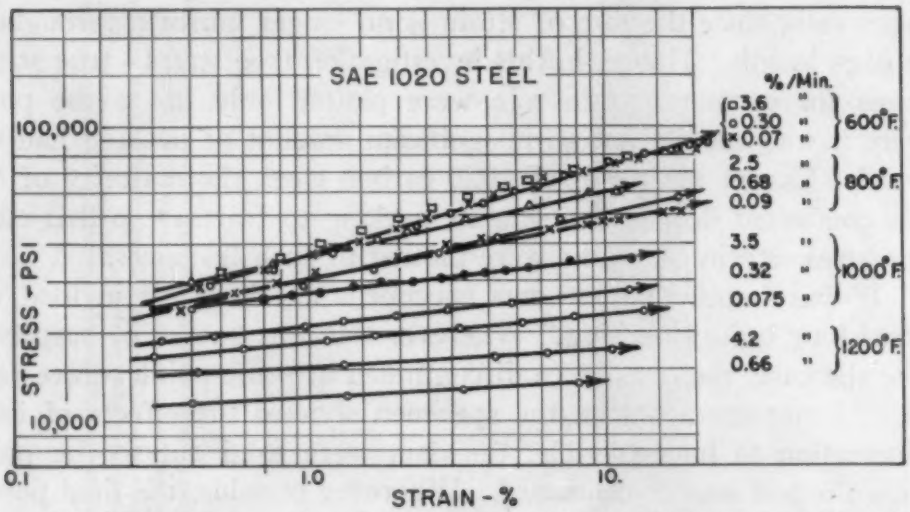


Fig. 2—True Stress – True Strain Characteristics of SAE 1020 Steel Plotted to Maximum Load.

At a particular temperature, this net quantity of strain hardening will also be reduced for slower strain rates since more time will be available for the annealing action to proceed. It will be noted that at 600 °F (315 °C) strain rate has no effect on the stress values over the range of rates investigated for the SAE 1020 steel. In this temperature range and below, the rate of annealing has been reduced to such a small value that time is of little significance in determining the net degree of strain hardening. With these characteristic features of the stress-strain – temperature-rate relationships in mind, examination of the data for the more complex alloys may be made.

Comparison of the S-816 annealed and cold-worked alloys (Figs. 3 and 4) shows that the latter reaches higher stress levels at all temperatures below 1800 °F (980 °C). Pronounced strain hardening is apparent in the 1200 and 1400 °F (650 and 760 °C) tests of the annealed material and at 1200 °F (650 °C) in the cold-worked material. Outstanding differences in the true stress-strain characteristics of the two materials are the pronounced negative slopes found

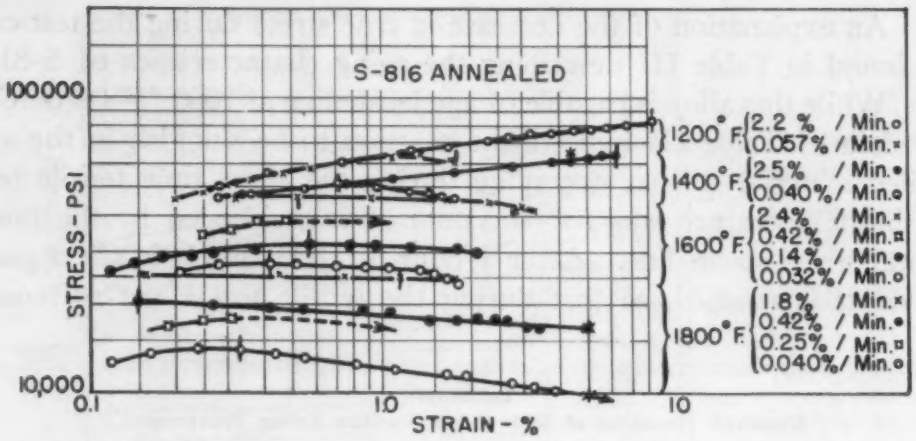


Fig. 3—True Stress - True Strain Characteristics of Annealed S-816. Maximum load indicated by vertical marker. * represents point obtained from final load and cross sectional area.

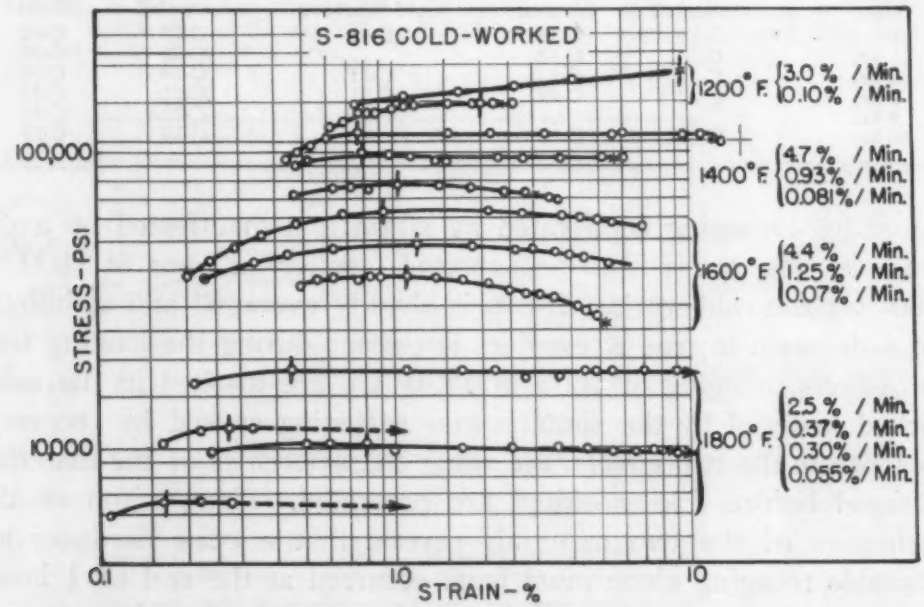


Fig. 4—True Stress - True Strain Characteristics of Cold-Worked S-816. Maximum load indicated by vertical marker. * represents point obtained from final load and cross sectional area.

only at 1800 °F (980 °C) in the annealed stock and at 1600 °F (870 °C) in the cold-worked stock. Cracking was eliminated as a cause of this phenomena on the basis of macro and microexamination. Necking was not responsible since, in all curves, the amount of necking before discontinuation was negligible (less than 2% in the case of the slow test at 1800 °F (980 °C) on the annealed S-816). Moreover, the final point is based on the final minimum cross section and load.

An explanation of the decrease in true stress during the test can be found in Table III describing the aging characteristics of S-816.

While this alloy is capable of age hardening at 1600 °F (870 °C), the data of Table III indicate the reaction to be sluggish in the annealed material so that overaging during the short time tensile test at this temperature was not encountered as evidenced by the horizontal stress-strain line. After 1 hour at 1800 °F (980 °C) a peak hardness is reached, so that during the tensile test a net softening

Table III
Rockwell Hardness of S-816 After Various Aging Treatments

	Aging Temperature				
	1600 °F			1800 °F	
Aging Time	Annealed	Cold-Worked	Overaged at 1800 °F 20 Hr. Before Cold Working	Annealed	Cold-Worked
0	C-18	C-42	C-42	C-18	C-42
½ hr.	C-20	C-42	..	C-21	C-34
1 hr.	C-22	C-42	C-31	C-24	C-31
2 hr.	C-22	C-42	C-31	C-21	C-31
4 hr.	..	..	C-31	C-21	C-31
20 hr.	C-26	C-34	..	C-18	C-30

caused by overaging accelerated by strain and manifested by a decrease in true stress is to be expected. After an hour at 1800 °F (980 °C) the cold-worked S-816 is already overaged and stabilized, and a decrease in true stress does not occur during the loading test. The effects of aging at 1600 °F (870 °C) are masked in the cold-worked material by the simultaneous softening caused by recovery. To separate the two effects, the aging characteristics of the material, overaged before cold working, are presented. Comparison of the hardnesses of the two materials reveals that a peak hardness attributable to aging alone must have occurred at the end of 1 hour. Hence, overaging accelerated by strain accounts for the negative slopes found in the 1600 °F (870 °C) stress-strain curves for S-816 cold-worked.

The stress-strain relationships for Inconel Regular (Fig. 5) show the same general characteristics as those for SAE 1020, although the straight line exponential relationship is not followed quite as closely. The strain hardening exponents, represented by the slopes of the lines, become less at higher temperatures and lower strain rates until at the lowest rate at 1800 °F (980 °C) the line is actually horizontal indicating that softening by recrystallization proceeds at the same rate as strain hardening. The negative slope at the end

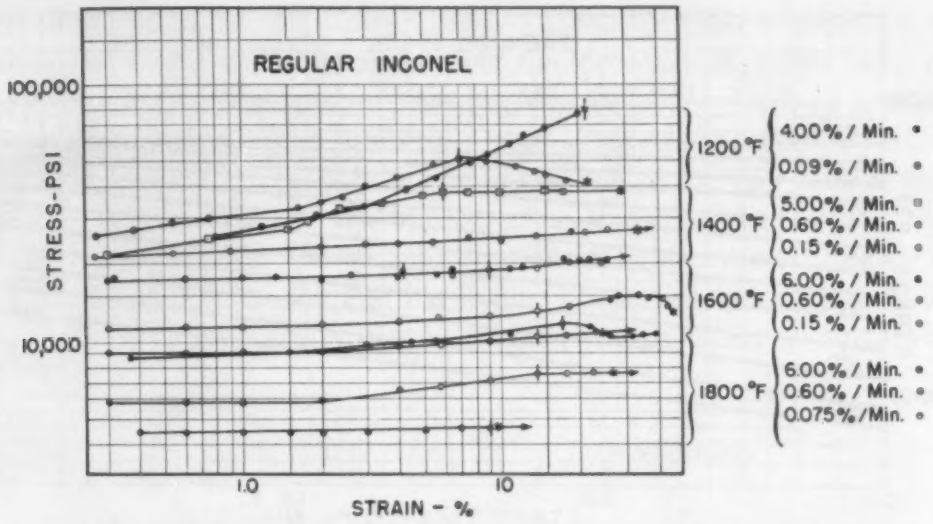


Fig. 5—True Stress - True Strain Characteristics of Regular Inconel. Maximum load indicated by vertical marker. * represents point obtained from final load and cross sectional area.

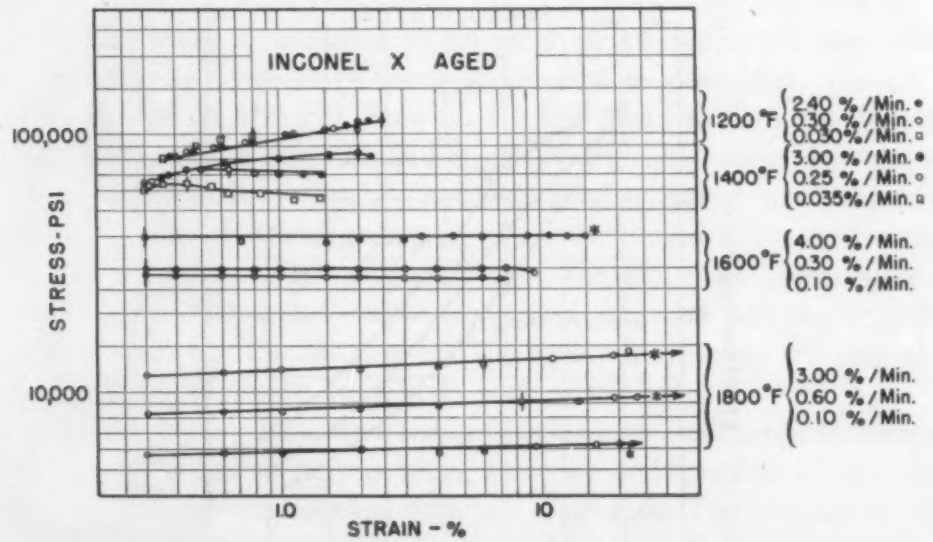


Fig. 6—True Stress - True Strain Characteristics of Aged Inconel X. Maximum load indicated by vertical marker. * represents point obtained from final load and cross sectional area.

of the stress-strain line for 1200 °F (650 °C) at 0.09% per minute was found, upon inspection of the fractured specimen, to be due to the gradual enlargement of a crack which was apparently initiated some time before actual failure, and which reduced the true cross sectional area.

Examination of the stress-strain characteristics for the aged Inconel X (Fig. 6) reveals the following. The magnitude of the

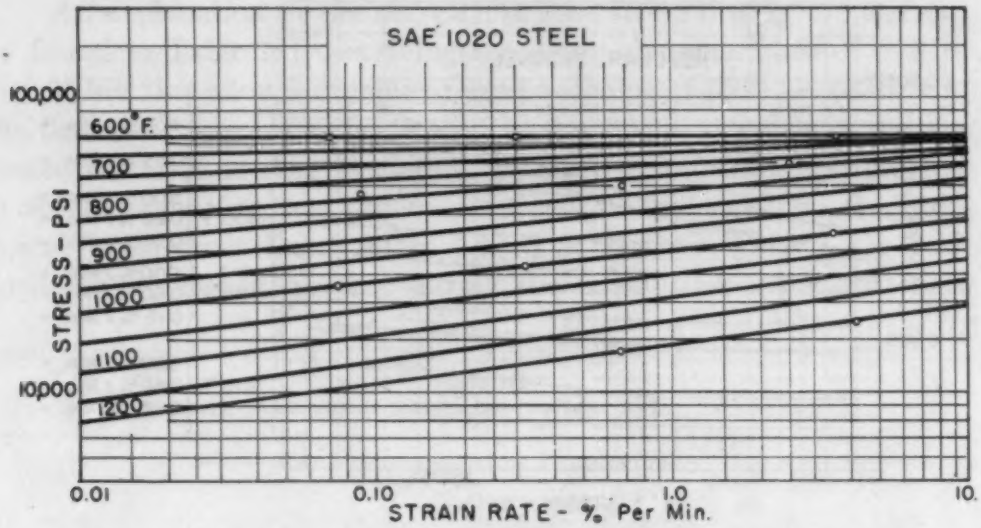


Fig. 7—Effect of Strain Rate on Stress at 10% Strain for SAE 1020 Steel.

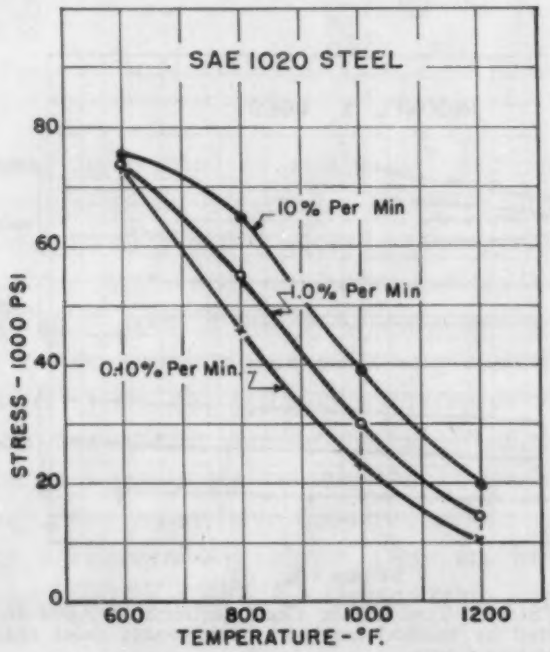


Fig. 8—Variation of Stress at 10% Strain With Temperature for Strain Rates of 10, 1.0, and 0.10% per Minute. SAE 1020 steel illustrated.

flow stress for any particular strain is unaffected by strain rate at 1200 °F (650 °C), indicating that, aside from strain hardening, no structural changes affecting resistance to flow are occurring during the test. At 1400 °F (760 °C), however, not only is the flow stress dependent on rate, but an actual decrease in stress occurs with in-

creasing strain in the slower tests. Metallographic studies of the material led to the conclusion that the decrease in stress was due to overaging of the specimen during the test. No form of cracking could be detected. The practically zero slope of the 1600 to 1800 °F (870 to 980 °C) stress-strain curves are due to the fact that at these higher temperatures strain hardening is being relieved at the same rate it is produced. Furthermore, at these temperatures the precipitate responsible for the age hardening properties becomes stabilized during the 1-hour holding time at temperature prior to application of the load.

Activation Energies of Deformation

In transposing the original stress-strain data to the reciprocal absolute temperature versus strain rate plots capable of evaluating Q, intermediate charts of strain rate versus stress for constant strain and temperature were prepared. Fig. 7, representing the data for the SAE 1020 steel, is included as an example of the strain rate versus stress diagrams. It is of passing interest to note that, for all the materials tested, straight lines on log-log coordinates were found to represent best the strain rate – stress relationship over the range of strain rates used. Such diagrams further serve to demonstrate primarily the character of the strain hardening versus annealing process at various temperatures. As the slope of these lines approaches the horizontal, temperatures are reached where the softening and recrystallization rate are negligibly slow, thus causing stress at a constant strain to vary little with strain rate.

In all such plots, interpolated values at intermediate temperatures were added to permit more accurate construction of the strain rate – reciprocal absolute temperature diagrams. The method of interpolation is illustrated by Fig. 8 for the SAE 1020 steel. Here stress versus temperature lines for three strain rates have been constructed from which stress values at intermediate temperatures were selected and returned to the rate-stress charts for construction of the additional temperature lines.

Figs. 9 to 13 represent the curves of strain rate versus reciprocal absolute temperature obtained by cutting the rate-stress lines at selected stress levels. It is evident that regardless of the alloy considered there is a wide range of conditions over which the probability relationship of $\varepsilon' = Ae^{-Q/RT}$ satisfies the data and from

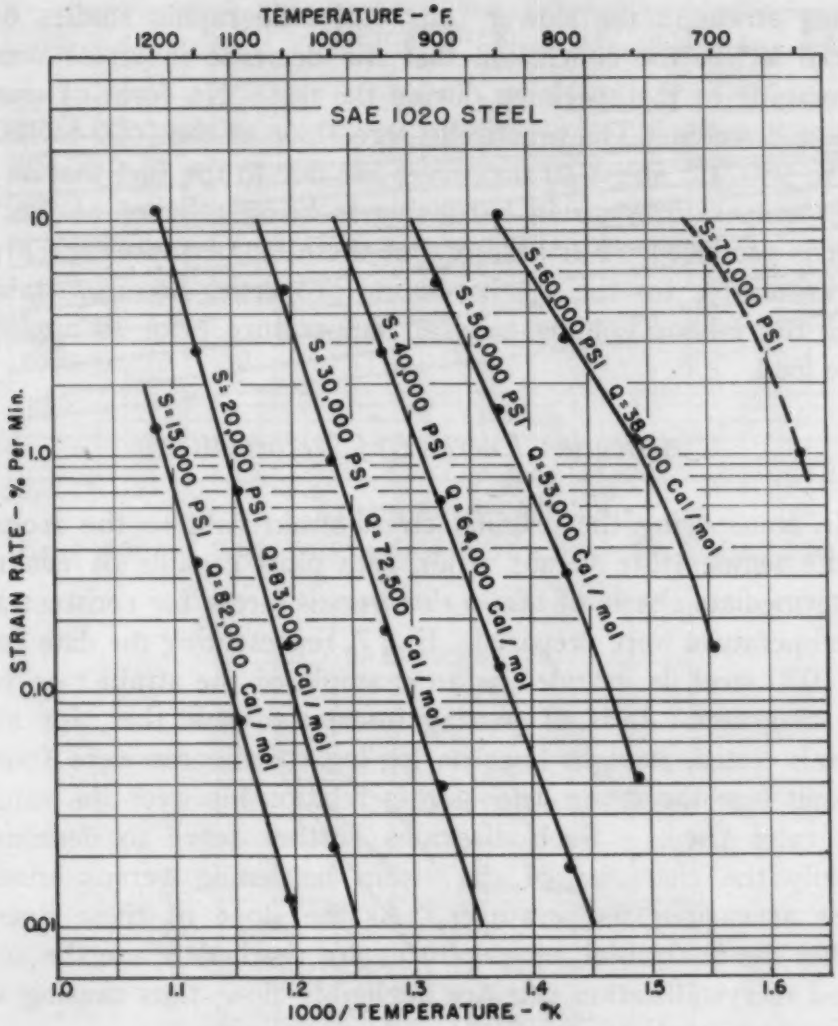


Fig. 9—Relationship Between Strain Rate and Reciprocal of the Absolute Temperature for Constant Stress at 10% Strain.

which activation energies (Q) may be calculated. It is equally evident that departure from this relationship exists under certain circumstances. An increasing Q value is noted consistently in all cases for decreasing stresses. This latter characteristic is summarized in Fig. 14, illustrating the variation of Q with stress at constant strain for the alloys tested.

Plastic Flow From the Activation Energy Viewpoint

It appears possible to picture a simplified working model of the deformation process incorporating some of the characteristic features

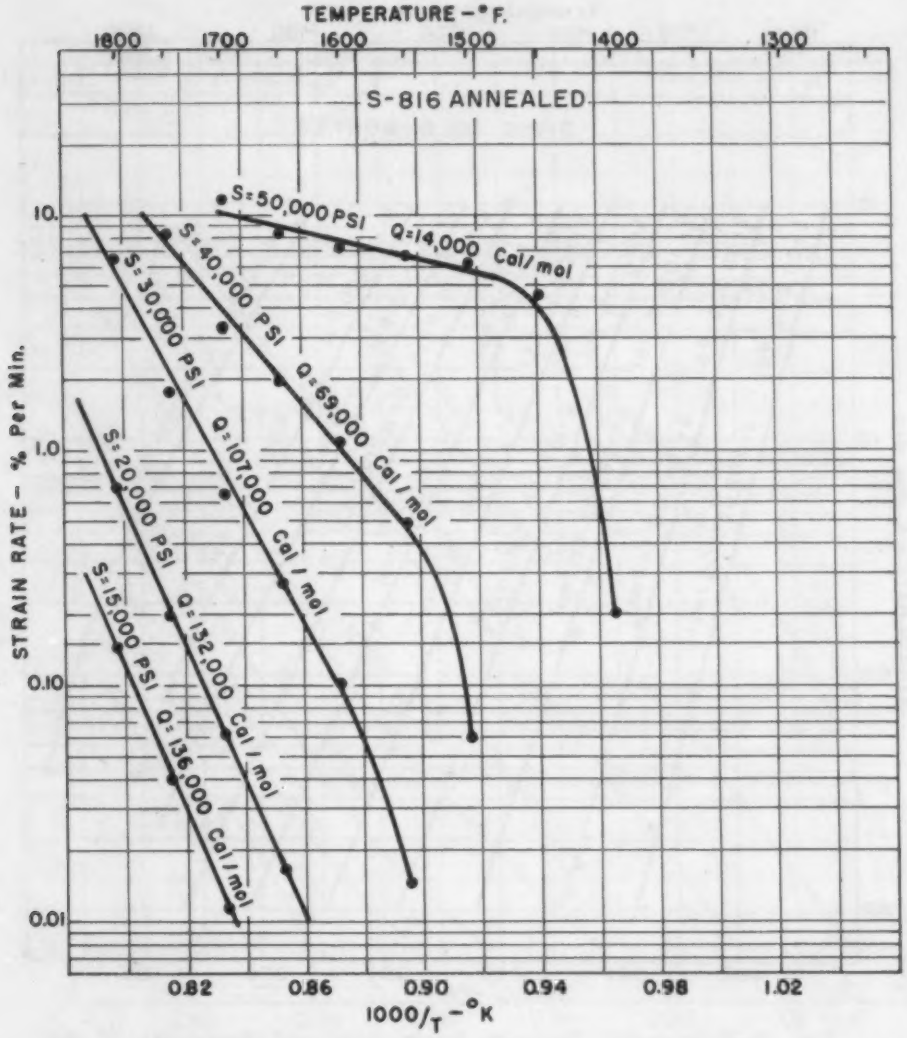


Fig. 10—Relationship Between Strain Rate and Reciprocal of the Absolute Temperature for Constant Stress at 1.0% Strain.

of the type of data presented. Fig. 15a illustrates several layers of atoms subjected to low tension stress and along which slip or relative movement may occur. The term slip, as used in this discussion, refers to the summation of a number of individual atomic shearing actions occurring on a plane in a certain direction and not to block movement or simultaneous displacement of groups of atoms (10). The potential energy curve associated with this atom configuration of Fig. 15a represents schematically the extent to which the atoms of the middle layer must be energized before they can move past their neighbors and be displaced in the slip direction. The peak height of this energy barrier may be considered to be influenced by

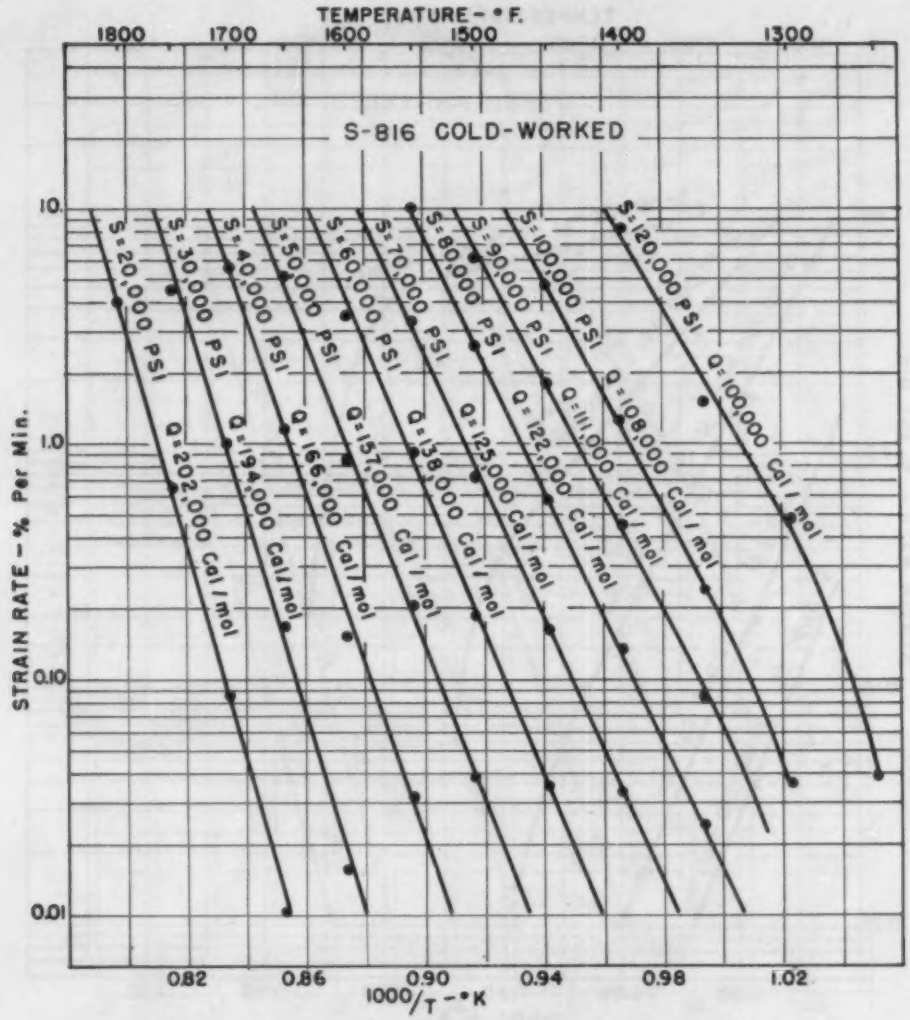


Fig. 11—Relationship Between Strain Rate and Reciprocal of the Absolute Temperature for Constant Stress at 1.0% Strain.

the density of packing of the atoms in a given metal or alloy, by the presence of foreign or dissimilar atoms distributed throughout the lattice (solid solution and precipitation hardening), and by the degree of distortion existing in the atomic layers (cold work).

Upon application of a greater load (Fig. 15b), it is reasonable to assume that the spacing between the atoms will be widened by additional elastic strain, with the net result that the atomic shear process may proceed with less difficulty. Restated from the energy viewpoint, when load is applied, the particles will require activation to a lower energy value in order to surmount the energy barrier and attain a permanent change in position. While in all cases, the curves of Fig. 14 bear out this effect of stress on the Q value, the

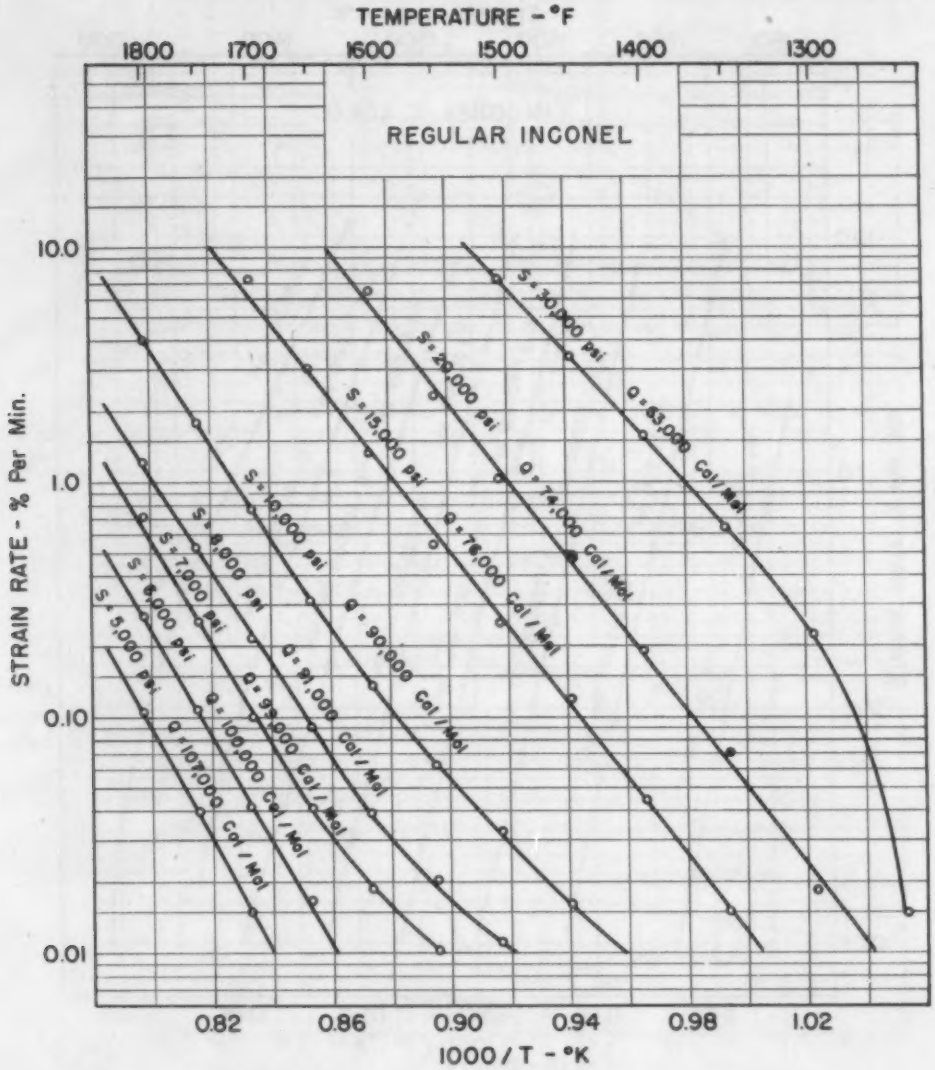


Fig. 12—Relationship Between Strain Rate and Reciprocal of the Absolute Temperature for Constant Stress at 10% Strain.

degree and nature of the variation is not the same from one alloy to the next.

The exact manner in which Q will vary with applied stress for strain rates of similar magnitude in a given material may depend upon several factors. From the picture illustrating the greater ease with which atomic shear can progress when the lattice is dilated by elastic strain, we would expect the activation energies required for shear to depend to some extent upon the elastic constants of the lattice. If, during the course of deforming a polycrystalline material, the slip direction changes or is transferred to planes of different

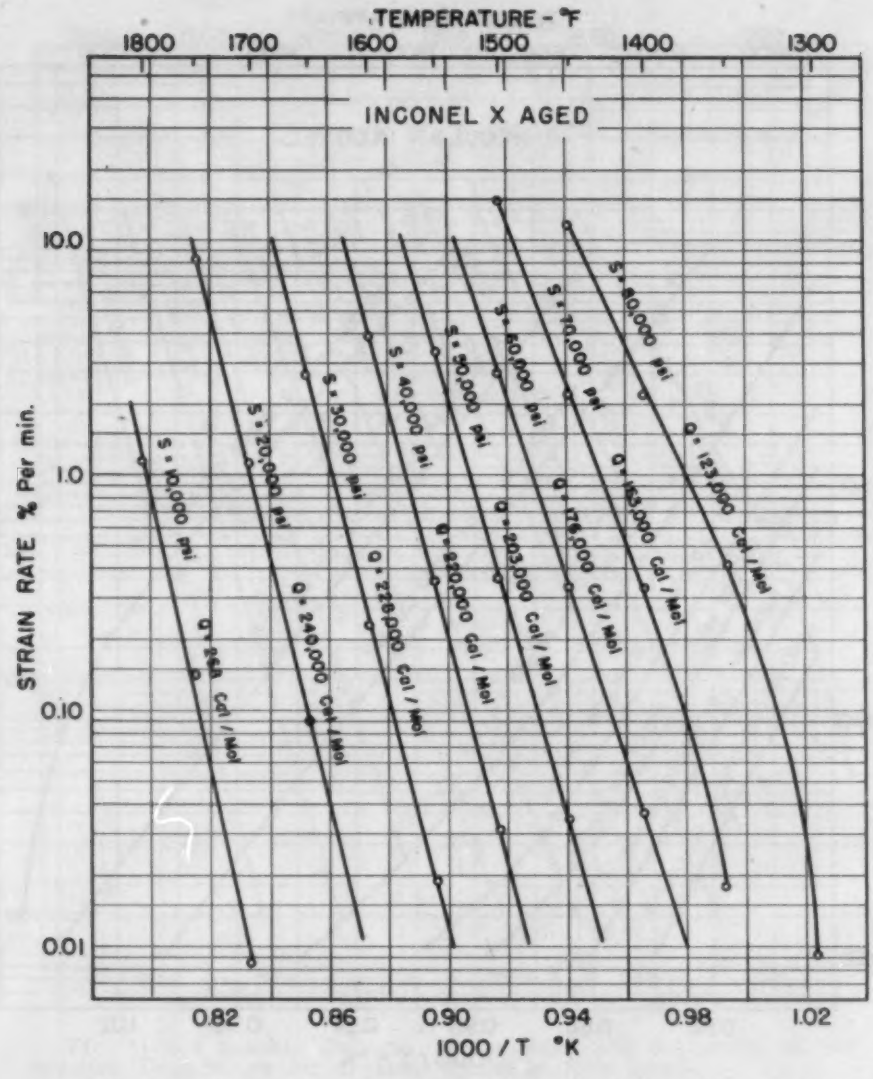


Fig. 13—Relationship Between Strain Rate and Reciprocal of the Absolute Temperature for Constant Stress at 1.0% Strain.

orientation with respect to the applied load, the elastic strain of the lattice in the slip direction would change. At the same time altogether different energy barriers could be anticipated due to the different configuration of atoms encountered in different directions of the lattice. Where microstructural changes occur from one temperature to another, Q values could be expected to vary with stress for a similar range of strain rates since a range of temperatures are involved for such a combination of variables.

If reference be made to the reciprocal absolute temperature charts (Figs. 9 to 13), it will be noted that at the lower temperature

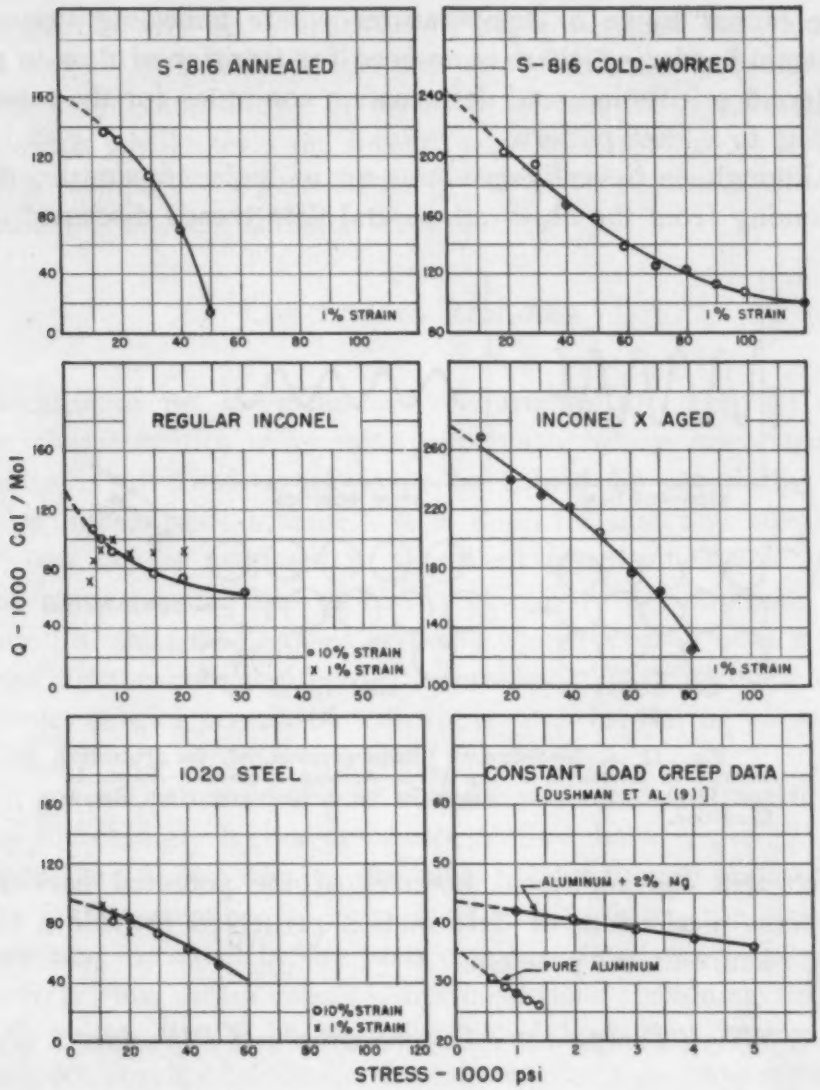


Fig. 14—Effect of Stress on Activation Energies at the Constant Strain Values Indicated.

end of the diagrams, the constant stress lines deviate from the straight line relationship, thereby suggesting a change in the nature of the deformation process. As can be determined from the original stress-strain diagrams, this departure of the Q lines from a constant slope occurs in a temperature range where the specimens are undergoing appreciable strain hardening during the entire tensile test. Under these conditions, in which the flow is transferred from one direction to another and possibly even to new sets of crystallographic planes, Q values would be encountered different from those obtained for the constant mode of deformation at the higher temperatures.

In the higher range of temperatures where annealing keeps pace with strain hardening, there is no need for transfer of flow to planes of different orientation, and deformation continues for the most part according to a fixed pattern.

Although no basically new concept of high temperature flow is forthcoming from the observations and data trends discussed above,

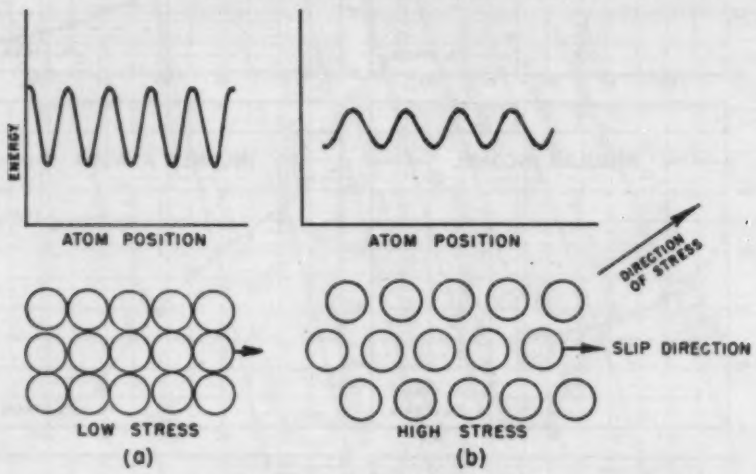


Fig. 15 a, b—Schematic Representation of the Potential Energy of Atoms in a Slip Plane Arising From the Atoms in the Planes Above and Below It for a Low and High Stress Condition.

it is felt that the additional features of the potential barrier and rate-process mechanism of deformation presented provide a clearer physical picture of the problem.

High Temperature Deformation and Diffusion

From consideration of constant load creep test results, Kanter (7) has likened the creep mechanism to that of metallic diffusion. In the Q versus stress plots (Fig. 14), the curves have been extrapolated to the zero stress axis to define activation energies of diffusion associated with the atoms or groups of atoms involved in the deformation of the various alloys. Data obtained from constant load creep tests by Dushman, Dunbar, and Huthsteiner (11) for pure aluminum and an aluminum alloy are included. A self-diffusion Q value for pure alpha iron is available from the work of Birchenall and Mehl (12). This diffusion value of 78,000 cal/mol for the alpha iron and the extrapolated zero stress value of 95,000 cal/mol for the SAE 1020 steel of this investigation would seem to be con-

sistent, particularly if comparison be made between the values of 35,000 and 43,000 cal/mol for the pure aluminum and aluminum plus 2% magnesium alloy. It would be of interest to conduct high temperature tensile tests on several pure metals such as iron and copper to compare the zero stress Q values so obtained with those determined from self-diffusion experiments.

Concluding Remarks

Because of the large number of variables affecting the deformation characteristics of metals, particularly where microstructural instability is involved, much is to be gained by correlating these variables into a basic scheme. It is doubtful that any single flow mechanism can be proposed in simplified form which will account for the many peculiarities of high temperature deformation. Consideration of the unit particles involved would seem to offer a means of reducing the complexity of the problem. Measurement of the activation energies associated with these particles during plastic flow provides a means of observing their behavior.

In general, it would appear that materials and treatments which display increasingly higher resistance to flow have larger Q values. However, this is not always the case. Even though an atom may require little activation to jump to a new position, the unit jump distance may be small in the particular slip direction, giving rise to a relatively slow strain rate. Other conditions remaining the same, high Q values should be an indicator of high flow strength. In this respect, result of diffusion experiments both on pure metals and alloys should be of interest to the metallurgist developing high temperature alloys since such data are capable of measuring the mobility of the constituent particles involved in the deformation process.

Acknowledgment

Appreciation is expressed to the U. S. Navy Department (Office of Naval Research and Bureau of Aeronautics) for their interest in sponsoring this work under project Squid. Thanks are due to the Metallurgy Section of the Cornell Aeronautical Laboratory, Inc., for helpful comments and discussion.

References

1. J. H. Hollomon, "The Mechanical Equation of State," *Metals Technology,* Vol. 13, September 1946, T.P. 2034.
2. J. H. Hollomon and J. D. Lubahn, "The Flow of Metals at Elevated Temperatures," *General Electric Review,* Vol. 50, February 1947, p. 28-32 and April 1947, p. 44-50.
3. J. C. Fisher and C. W. MacGregor, "Tempering Effects and the Mechanical Equation of State," TRANSACTIONS, American Society for Metals, Vol. 40, 1948, p. 302-314.
4. J. H. Hollomon, "Tensile Deformation," *Metals Technology,* Vol. 12, June 1945, T.P. 1879.
5. H. Eyring, "Viscosity, Plasticity, and Diffusion as Examples of Absolute Reaction Rates," *Journal of Chemical Physics,* Vol. 4, 1936, p. 283-291.
6. Saul Dushman, "Cohesion and Atomic Structure," *Proceedings,* American Society for Testing Materials, Vol. 29, 1929, p. 7-64.
7. J. J. Kanter, "The Problem of the Temperature Coefficient of Tensile Creep Rate," *Transactions,* American Institute of Mining and Metallurgical Engineers, Vol. 131, 1938, p. 385-418.
8. Walter Kauzman, "Flow of Solid Metals from the Standpoint of the Chemical Rate Theory," *Transactions,* American Institute of Mining and Metallurgical Engineers, Vol. 143, 1941, p. 57-81.
9. G. Guarnieri and J. Miller, "A Cantilever Strain Gage for High Temperature Tensile and Creep Testing of Sheet Materials," to be published in METAL PROGRESS, 1948.
10. F. Seitz, "The Physics of Metals," McGraw-Hill Book Company, Inc., New York, 1943, p. 85-101.
11. S. Dushman, L. W. Dunbar and H. Huthsteiner, "Creep of Metals," *Journal of Applied Physics,* Vol. 15, February 1944, p. 108-124.
    Clarence Zener and J. H. Hollomon, "Problems in Non-Elastic Deformation of Metals," *Journal of Applied Physics,* Vol. 17, No. 2, February 1946, p. 69-82.
12. C. E. Birchenall and R. F. Mehl, "Self Diffusion in Iron," *Mining and Metallurgy,* Vol. 28, November 1947, p. 555.

DISCUSSION

Written Discussion: By J. J. Kanter, materials research engineer, Crane Co., Chicago.

The carefully determined values for short-time high temperature tensile stress of alloys made available by this paper should prove useful, as the authors propose, for learning more about the mechanics of deformation at elevated temperatures.

In their Figs. 9 to 13, the authors show "activation" energies for constant stress and strain which they point out decrease as stress increases. A number of the constant stress reciprocal temperature plots markedly depart from linearity for the lower temperatures of the observed range. Thus it might be argued that the activation energies also vary with temperature, if the slopes of tangents to these curves might be so interpreted.

It would be no more arbitrary to freely discuss all of the tangents to reciprocal temperature plots as activation energies than it is to discuss only those applying to the linear leg of the plot. If the change in slope from stress to stress be attributed to a progressive change in solid state affecting activation, then it must also be recognized that the crystalline

state for constant strain varies with the temperature at which that strain is produced in a tensile test. If such be the case, merely the constancy of stress and strain does not imply constancy of state. The linearity of portions of the reciprocal absolute temperature plots of such tensile strain data may be fortuitous to the conditions of test and may not warrant some of the interpretations which have been made.

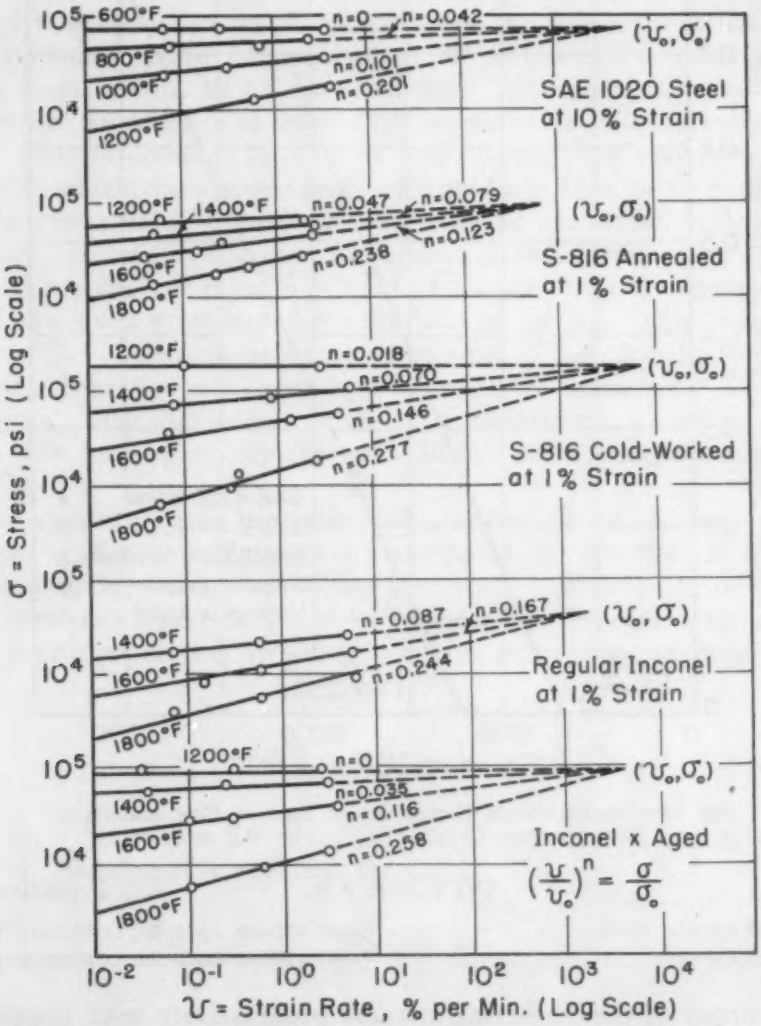


Fig. 16—Tensile Stress Versus Strain Rate of Five Materials.

In their Fig. 7, the authors show the effect of strain rate on stress for SAE 1020 steel, plotted logarithmically. The writer has replotted the data for the five materials reported by the authors on this basis as summarized in Fig. 16. This is done for the purpose of directing attention to the striking manner in which the isothermal curves all converge as strain rates increase and when produced intersect at a common point. Thus the strain rate – constant stress relationship may be very simply expressed by the equation

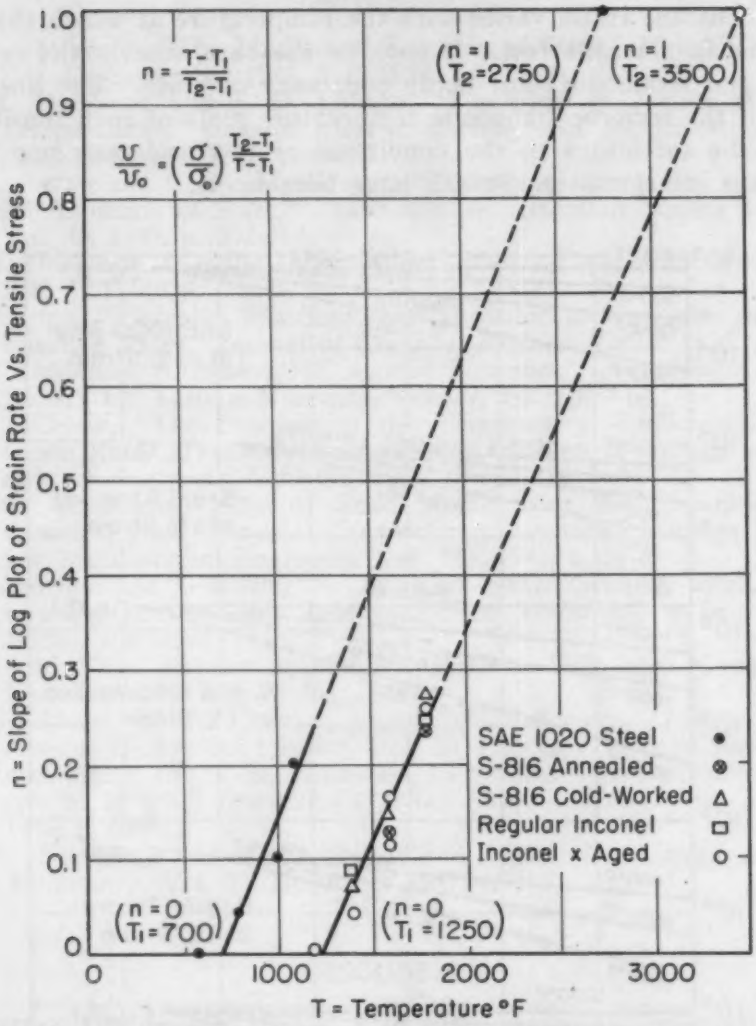


Fig. 17—Tensile Stress Versus Strain Rate of Five Materials.

$$(V/V_o)^n = \sigma/\sigma_o \qquad \text{Equation 1}$$

where V = strain rate, V_o = strain rate at common point
σ = stress, σ_o = stress rate at common point

Since the slopes of the isotherms increase progressively with temperature, the constant n furnishes a temperature parameter. Plotting the values of n versus temperature, as shown in Fig. 17, for the five materials reported by the authors, it appears that this parameter is fitted by the equation

$$n = \frac{T - T_1}{T_2 - T_1} \qquad \text{Equation 2}$$

where T = temperature of constant strain rate
T_1 = temperature of initial speed effect
T_2 = temperature at which $n = 1$

from which it is apparent that

$$V/V_o = (\sigma/\sigma_o)^{\frac{T_2 - T_1}{T - T_1}} \qquad \text{Equation 3}$$

The maximum temperature (T_1) at which there is no speed effect on stress, σ_o, seems to occur where the heat content of the alloy is of the order of that of fusion. This would mean the general level of activation is at this temperature just equivalent to that which is requisite for the viscous displacement of atoms from their lattice bonds. The calculated temperature at which n is unity (T_2) seems to be in excess of the fusion point. The difference ($T_2 - T_1$) is more nearly the fusion temperature, a point at which the viscous mode of flow ($n = 1$) is to be expected.

The stress value σ_o may in some way be associated with an amount of energy involved in the heat of fusion. A unit strain, such as might be imagined for the condition $n = 1$, at the stress σ_o is an appreciable fraction of the work represented by the heat of fusion. This being the case the value $T_2 - T_1$ would be expected to bear all but that small part of the activation energy contributed by the work of straining. The straining velocity V_o may be looked upon as a theoretical situation where slip strains are formed as rapidly as a fusion point temperature dissipates them.

The significance of the ratio V/V_o, under the rapid shearing mode of straining studied, would be as a measure of the fraction of the material participating in the action at any moment, and as such represents the probability that a particle would be energized to the extent of participating in the action promoting strain. Upon this conception we may write,

$$e^{-(Q - H_F)/RT} = V/V_o = (\sigma/\sigma_o)^{\frac{T_2 - T_1}{T - T_1}} \qquad \text{Equation 4}$$

where Q = Activation Energy, R = Gas Constant, and T = Absolute temperature. Solving this equation for Q,

$$Q = -RT \frac{T_2 - T_1}{T - T_1} \log e \ (\sigma/\sigma_o) \qquad \text{Equation 5}$$

Using the constants determined from the charts plotted in Figs. 16 and 17, values for Q for the five materials reported on by the authors are shown in Fig. 18 as functions of stress (σ) at various temperatures investigated. Activation energy values found by this approach, for the stress ranges reported in the paper, are of the magnitude heat of "liquification" rather than the larger "vaporization" heats obtained by the authors' analysis.

In rapid straining it would seem more reasonable to attribute the effects manifested to coordinated activations of groups of particles aligned

on slip planes rather than to the independent activities of atoms as may be the case in micro-creep. (The n values for a given temperature in the case of micro-creep are more nearly representative of viscous flow than for the present straining data.) The probability that a system of atoms entering slip deformation could be activated to "vaporization" energies

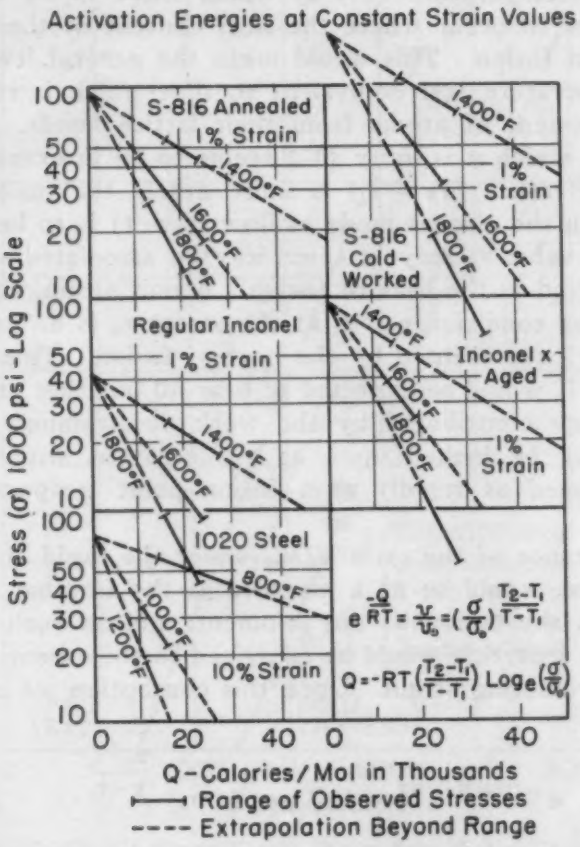


Fig. 18—Tensile Stress Versus Strain Rate of Five Materials.

would seem indeed remote as compared to that for activation to "liquification" energy through stress raisers and micro-localization of the heat of straining.

Authors' Reply

In that part of the paper which concerned an appraisal of the activation energies associated with high temperature deformation, the authors made several interpretations of the results which applied to temperature ranges over which the activation energy (Q) was constant for constant stress and strain. Mr. Kanter has attempted a more general analysis of the data so as to include the variation of Q with temperature as implied by the nonlinear portions of the strain rate – reciprocal absolute temperature plots (Figs. 9 to 13). While there are certain features of his discus-

sion which appeal to the writers, we cannot agree with the final equation 5 relating Q with temperature and stress nor with the activation energies so calculated.

Fig. 7 of the paper illustrates the type of plots obtained in general upon relating log stress with log strain rate. At sufficiently low temperatures, where the annealing rate is no longer significant, the lines are horizontal. With increasing temperature their slopes increase and tend to approach a constant value. Mr. Kanter has plotted this variation of slope (n) with temperature in Fig. 17 but it is questionable whether or not a linear relationship may be assumed even over the range of variables considered. Consequently the evaluation of n (equation 2) and the substitutions made in equations 3, 4, and 5 are not convincing.

The significance attached to the ratio V/V_o by Mr. Kanter as a measure of the fraction of material participating in the strain process at any moment is of interest. At some low value of this ratio, depending on temperature, deformation may be assumed to be occurring with a minimum number of particles cooperating. It is felt that a locus drawn through the points on the reciprocal temperature charts (Figs. 9 to 13) at which the Q lines depart from linearity define a range of temperature, strain rates, and stress conditions over which a diffusion-type strain mechanism predominates.

APPLICATION OF THE THEORY OF DIFFUSION TO THE FORMATION OF ALLOYS IN POWDER METALLURGY

By Pol Duwez and Charles B. Jordan

Abstract

A simple theoretical discussion is first given, by means of which it is possible to predict approximately the time and temperature required for complete homogenization by diffusion of a mixture of two metal powders. The theory is first developed for one-dimensional diffusion in a stack of interleaved thin sheets of two metals, which arrangement has recently been investigated in France by Chevenard and Waché. With the aid of an analysis by Weinbaum of diffusion in a simple model of a mixture of powders, it is then shown that the method of predicting time and temperature of homogenization can be extended to this three-dimensional case. The method involves only consulting a pair of charts which are given; no calculations are necessary.

An experimental investigation of the progress of diffusion in compacts of mixed copper and nickel powders is next described. In these experiments, the compacts were heated for various lengths of time at different temperatures, and the degree of diffusion thereby produced measured by means of X-ray diffraction. A discussion of experimental errors is given. When the results of the measurements are compared with those predicted by theory, it is found that the agreement is qualitatively correct, and that the quantitative deviations are quite understandable in view of the range of experimental variables involved.

Introduction

In a recent paper, Chevenard and Waché (1)[1] describe an ingenious experimental method of studying intermetallic diffusion

[1]The figures appearing in parentheses pertain to the references appended to this paper.

A paper presented before the Thirtieth Annual Convention of the Society, held in Philadelphia, October 23 to 29, 1948. Of the authors, Pol Duwez is associate professor of mechanical engineering and chief of the Materials Section of Jet Propulsion Laboratory, and Charles B. Jordan is research engineer, Jet Propulsion Laboratory, California Institute of Technology, Pasadena, Calif. Manuscript received April 19, 1948.

in a pile of alternating plates of two different iron-nickel alloys. The magnetic properties of these alloys make it possible to follow the progress of diffusion by determining the change in the Curie point of the aggregate as homogenization proceeds. Moreover, it is not difficult to give a theoretical analysis of diffusion in such an aggregate of interleaved sheets, and Chevenard and Waché were able to obtain very good agreement between experimental and theoretical results. In this paper, it will be shown that the analysis can be extended to give an approximate relation between the temperature and the duration of heating required to attain a given state of homogenization in a compact of two metal powders. It will also be shown that there is fair agreement between the results of such an analysis and the results of experiments with copper and nickel powders which will be described.

Diffusion in a Pile of Alternating Plates

Since the paper of Chevenard and Waché is rather inaccessible in this country, it will be appropriate first to review briefly the case of one-dimensional diffusion investigated by them. Consider a system made of a large number of alternating plates of two different metals. If the thickness of the plates is small compared with their other dimensions, the end effects may be neglected and the problem of diffusion is a one-dimensional one. Consequently, the classical Fick's equation for one dimension

$$\frac{\partial c}{\partial t} = D \frac{\partial^2 c}{\partial x^2} \qquad \text{Equation 1}$$

may be applied to this case. In this equation, c is the concentration at a distance x from the interface between two adjacent plates, D is the diffusion coefficient, and t is the time. Since this equation is formally equivalent to the equation of heat conduction, it is possible to apply the solution of heat conduction problems to the analogous situations in diffusion theory. In the present instance, the equivalent thermal situation is that of a large flat slab which is suddenly immersed in a medium having a different temperature. The solution of this problem may be found in several treatises on heat conduction (2). The concentration distribution in any one plate turns out to be

$$\frac{c}{c_0} = \frac{4}{\pi}\left[e^{-t/\theta} \sin\frac{\pi x}{\eta} + \tfrac{1}{3} e^{-9t/\theta} \sin\frac{3\pi x}{\eta} + \ldots\ldots\right] \qquad \text{Equation 2}$$

where c is related[2] to the concentration of one of the metals at a point x; c_o is related to the initial concentration of the same metal; θ is a characteristic time given by

$$\theta = \frac{\eta^2}{\pi^2 D} \qquad \text{Equation 3}$$

and η is the thickness of each plate. It should be pointed out that this solution is valid only if D is not a function of concentration, which assumption is only approximately true in the case of intermetallic diffusion.

Curves of c/c_o versus x/η have been plotted for different values of the ratio t/θ and are presented in Fig. 1. When $t = 0$, $c = c_o$ for all values of x. For small values of t/θ the concentration distribution curve is very steep near $x = 0$, c/c_o remaining equal to 1 in the center of the plate. For $t/\theta > 1$, the first term of the series of Equation 2 predominates, and the concentration distribution curve becomes sinusoidal. For large values of t/θ (i.e., for $t/\theta > 5$) the sine curve flattens out to coincide with the axis of abscissae and homogeneity is practically achieved.

The progress of diffusion in a pile of alternating plates can be conveniently represented by the variation with time of the value of c/c_o at the center of a plate. This variation may be computed from Equation 2 by setting $x/\eta = \frac{1}{2}$ and calculating c/c_o as a function of t/θ. The value of c/c_o for $x/\eta = \frac{1}{2}$ will be designated by K for convenience, and t/θ will be designated by τ. A plot of K versus τ is presented in Fig. 2. Since the curve relates two dimensionless parameters, it is universal.

On the basis of this theory, complete homogeneity is achieved only for an infinite value of τ. For practical purposes, however, homogenization may be considered complete when $K = 0.01$, at which point $\tau = 5$ approximately. Therefore, the time required to attain practically complete homogeneity at any given temperature will be given simply by $t = 5\theta$, and hence can be calculated when θ is known.

To obtain θ, the procedure is as follows: The diffusion coefficient D is first computed at the temperature T by the well-known formula

$$D = D_\infty e^{-Q/RT} \qquad \text{Equation 4}$$

in which D_∞ and Q are constants which have been experimentally

[2]For the exact significance of c and c_o, see Appendix.

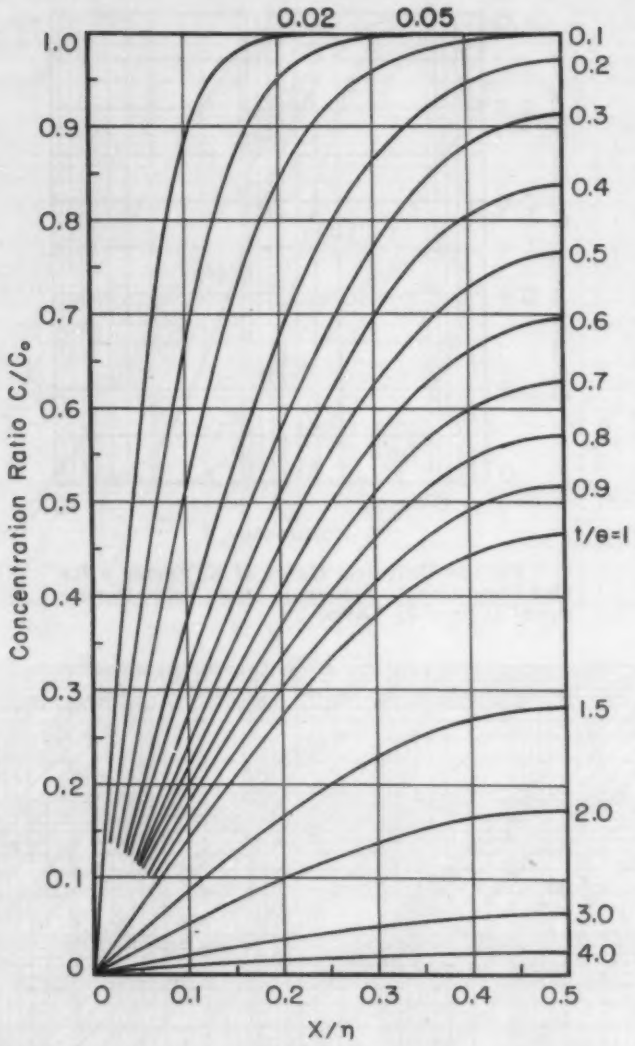


Fig. 1—Concentration Ratio c/c_0 Versus x/η for Different Values of the Ratio t/θ.

determined for various pairs of metals (3). Having D, θ can be computed from Equation 3.

The relation between thickness η, temperature T, and time t required to attain (practically) complete diffusion may be conveniently represented by two diagrams which are graphs of Equations 3 and 4. Fig. 3 is a graph of Equation 3, showing that log θ is a linear function of log D for a given value of η. Values of η from 1 micron to 1000 microns, and values of θ from 10 seconds to 10 days, are represented in the figure. Equation 4 is represented by a straight line if log D is plotted against 1/T. Fig. 4 shows this relation for some metals for which the constants D_∞ and Q have been determined.

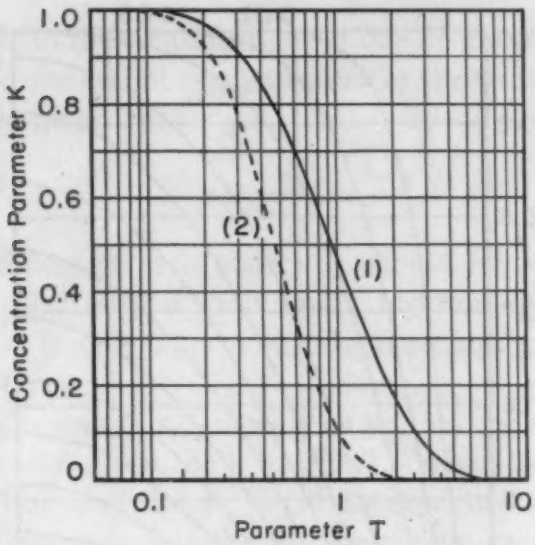


Fig. 2—Universal Curve of K Versus τ for One-Dimensional (Curve 1) and Three-Dimensional (Curve 2) Cases.

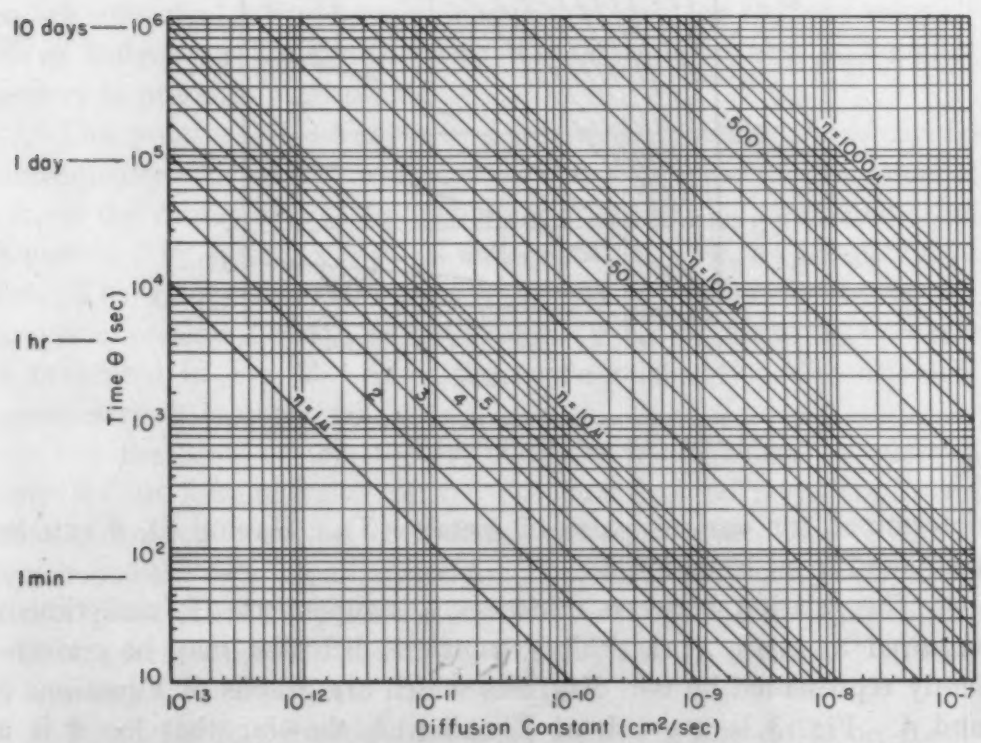


Fig. 3—Graph of Time θ Versus Diffusion Constant D for Various Thicknesses η of Plates.

The horizontal axis of 1/T has been ruled with a scale of T in order to facilitate use of the graph.

An example will illustrate the use of the two charts. Suppose

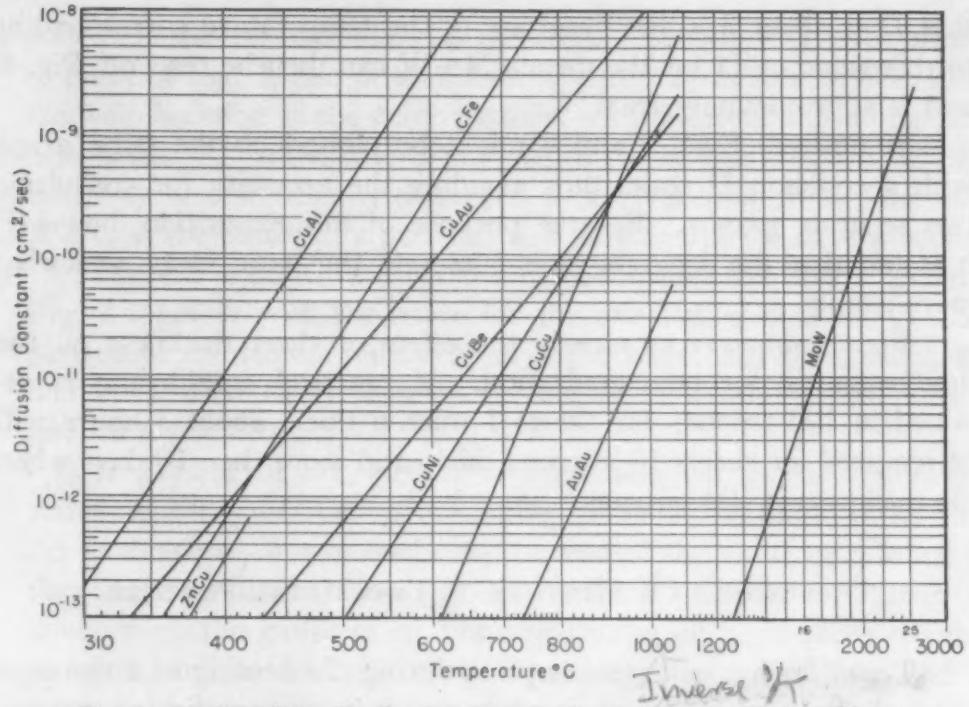


Fig. 4—Graph of Diffusion Constant Versus Temperature for Various Metals.

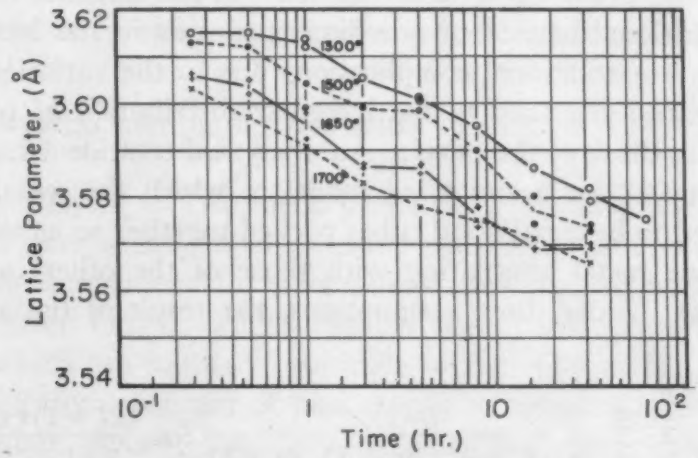


Fig. 5—Lattice Parameter Versus Sintering Time at Various Constant Temperatures for Mixture No. 1.

it is desired to estimate the temperature at which a pile of interleaved sheets of molybdenum and tungsten, each sheet 10 microns thick, should be heated in order to achieve practically complete homogeneity in 5 hours. First, D is read off Fig. 3 from the intersection of the horizontal line $\theta = 1$ hour ($\theta = t/5$ at homogeneity as discussed above) with the diagonal line $\eta = 10$ microns. The result is

that D is about 3×10^{-11} cm²/sec. The temperature corresponding to this value of D for the metals Mo-W can then be read off Fig. 4, and is approximately 1800 °C.

If desired, Figs. 3 and 4 might be plotted on the same graph with a common D scale, thus avoiding the necessity for consulting two separate graphs. For the purpose of this exposition, however, it is felt that the separate plots illustrate the basic ideas somewhat more simply.

Fig. 3 shows very clearly the effect of sheet thickness on the time required for homogenization. If practical equilibrium is attained in 100 seconds for sheets 1 micron thick, about 3 hours will be required for sheets 10 microns thick, and more than 10 days when the thickness is 100 microns.

Diffusion in a Mixture of Two Metal Powders

The diffusion which takes place during the heating of a compact of two metal powders is obviously a much more complicated process than that involved in the homogenization of a pile of thin plates discussed in the previous section. In the former case the diffusion is three-dimensional instead of one-dimensional as in the latter; moreover, there are additional complications due to the variations of particle shape and size, and to the irregular distribution of particles of one metal in those of the other. An analytical treatment has recently been given (4) for a simplified model in which the metal particles are assumed to be equal sized cubes packed together so as to fill space, those of one metal alternating with those of the other in all three dimensions. Under these assumptions, the result of the analysis of Reference 4 is:

$$\frac{c}{c_0} = \frac{64}{\pi^3} \sum_{0}^{\infty} \sum_{0}^{\infty} \sum_{0}^{\infty} \frac{(-1)^{l+m+n}}{(2l+1)(2m+1)(2n+1)} \cos \frac{(2l+1)\pi x}{\zeta} \cos \frac{(2m+1)\pi y}{\zeta} \cos \frac{(2n+1)\pi z}{\zeta} e^{-k^2 Dt} \qquad \text{Equation 5}$$

where

$$k^2 = \frac{\pi^2}{\zeta^2}\left[(2l+1)^2 + (2m+1)^2 + (2n+1)^2\right]$$

and ζ is the edge of a cube.

Equation 5 is the three-dimensional analog of Equation 2, and

may be used to compute concentration distribution curves similar to those of Fig. 1, except that a set of such curves now applies along any *one* direction in the cubic particle, with different sets along other directions. As in the case of the pile of plates, the progress of diffusion may be conveniently measured by the variation of K (the value of c/c_o at the center of a particle) as a function of the time parameter τ.[3] The curve of K vs τ for the three-dimensional case is given in Fig. 2 together with the curve for the one-dimensional case. Comparison of the curves indicates, as might have been anticipated, that homogenization takes place more rapidly in a mixture of powders than in a pile of plates.

If a value of $c/c_o = 0.01$ is again adopted as the criterion of complete diffusion, the corresponding value of τ is found to be about 2.5 in the three-dimensional case, instead of the value of 5 found for the one-dimensional case. It is therefore possible to extend the analysis to the problem of homogenization of a mixture of metal powders, and to find the relation between the temperature and the time which are necessary in order to achieve complete diffusion for powders of a given particle size. The charts of Figs. 3 and 4 may again be used, the only modification of the procedure lying in the use of $t = 2.5\theta$ at complete homogenization instead of $t = 5\theta$.

Experimental Study of Diffusion in Nickel-Copper Compacts

The alloying of two metal powders by intermetallic diffusion in the solid state is subject to the same restrictions as if the metals had been melted together: the same phases must appear, within the same concentration limits. Thus diffusion cannot take place between two metals which are mutually insoluble in the solid state; moreover, if the equilibrium diagram of two metals is complex, showing several intermediate phases, these phases will also appear under suitable conditions as the result of diffusion. Clearly the simplest case in which diffusion can be studied is that of two metals which form a complete series of solid solutions with each other. As is well known, the crystal structure of such intermediate solid solutions is the same as that of the two metals forming them, except for the size of the unit cell, which is a continuous and approximately linear function of concentration. Consequently, the X-ray powder patterns of such

[3] The appropriate definition of τ in three dimensions is $\tau = t/\theta$ where $\theta = \frac{\zeta^2}{\pi^2 D}$

solid solutions are the same as those of the constituent metals except for the spacing of the lines, which shows a small gradual shift with concentration corresponding to the variation of unit cell size. The copper-nickel system was chosen for the following experimental study because it satisfies the requirement of forming a complete series of solid solutions, and because copper and nickel powders are readily obtainable.

Preparation of Specimens—Two mixtures of copper and nickel powders were prepared, each consisting of equal atomic percentage of the two metals, but differing in the range of particle size included. Mixture No. 1 was made up of powders which had been classified by sifting between 200-mesh and 325-mesh screens; mixture No. 2 was made of powders as furnished by the vendor and not further classified. Of the latter mixture, the copper powder is known to be all of particle size smaller than 325 mesh, while of the nickel powder approximately 5% is between 150 and 200 mesh, 17% is between 200 and 325 mesh, and the remainder is smaller than 325 mesh. Both mixtures were mixed mechanically for 48 hours.

The mixed powders were then pressed into disks 1 inch in diameter, 5 grams of mixture being weighed out for each specimen. A pressure of 80,000 psi was used throughout.

Special furnaces were constructed for sintering the specimens thus prepared. The basic design requirement of these furnaces was the provision for means of rapid quenching. This requirement was fulfilled by constructing each furnace in the form of a vertical silica tube (inside diameter $1\frac{7}{16}$ inches, outside diameter $1\frac{7}{8}$ inches, length 30 inches) mounted coaxially with a surrounding ceramic tube (inside diameter 4 inches, outside diameter 5 inches, length 21 inches), the annular space between the two cylinders being filled with asbestos fiber. Heating was provided by a Nichrome wire resistance wound on the silica tube. Both ends of the silica tube were closed with rubber stoppers through which inlet and outlet tubes for providing hydrogen atmosphere were introduced, as well as a chromel-alumel thermocouple. The couple was completely surrounded inside the furnace by a ceramic tube, which prevented direct exposure of the couple to the hydrogen atmosphere. Provision was made for water cooling the metal base of the furnace, to prevent both deterioration of the bottom rubber stopper and possible injury to the operator when quenching a specimen. During sintering, the copper-nickel disks were suspended in the furnace by a wire support so that they

were held in the center of that portion of the length of the silica tube on which the Nichrome winding was wrapped. The wire support was itself held at the top of the silica tube by being gripped between stopper and tube. The entire furnace stood over a vessel of water, so that quenching was quickly accomplished at the end of a test by flushing the furnace with nitrogen, then removing the bottom stopper and loosening the top stopper, thus allowing specimen and wire support to fall into the water.

Specimens of mixture No. 1 were sintered at 1300, 1400, 1500, 1600, 1650, and 1700 °F (705, 760, 815, 870, 900, and 925 °C); those of mixture No. 2 at 1100, 1200, 1300, 1400, and 1500 °F (595, 650, 705, 760, and 815 °C). At each temperature, a separate specimen was sintered for each of the following time intervals: 15 minutes, 30 minutes, 1, 2, 4, 8, 16, and 32 hours.

In preparation for taking X-ray diffraction patterns, each specimen was given a clean flat surface by abrading with emery cloth, usually on a belt sander, although a few were cleaned by hand. The effect of surface preparation was checked by subjecting each of several specimens to a succession of different treatments, such as cleaning by hand with abrasive paper, belt sanding, polishing, and etching, and taking a diffraction pattern after each step.

X-Ray Diffraction Analysis—A North American Philips X-ray Spectrometer was used with copper radiation filtered through a nickel foil. The Geiger counter was moved 2 degrees per minute and the pattern was recorded automatically on a Brown Recorder with a chart speed of 30 inches per hour.

The angular range of diffracted beams which can be measured on the Norelco unit is such as to include the (111), (200), and (220) reflections from pure copper, pure nickel, and any solid solution of the two. Accordingly, the general procedure was to measure these three interplanar spacings on each Norelco chart for the copper-rich solid solution present in each specimen after sintering, to calculate the lattice parameter from each of the three spacings, and to average the three values of the parameter thus obtained. For reasons discussed below, it was not always possible to measure all three reflections, and in such cases only one or two were measured.

More accurate location of the diffraction peaks was carried out in the case of specimens of mixture No. 1 which were sintered at 1300, 1500, 1650, 1700, and 1800 °F (705, 815, 900, 925, and 980 °C). This work was done either by hand scanning (taking the

average of three readings of intensity at each angular setting, the latter being taken at intervals of 0.05 degree) or by automatic scanning at slow speed (in which the Geiger counter scanned at the rate of 0.25 degree per minute). These two methods are considered to be equivalent as regards the degree of accuracy with which the diffraction maxima can be located. In either case, only the (200) reflections were scanned.

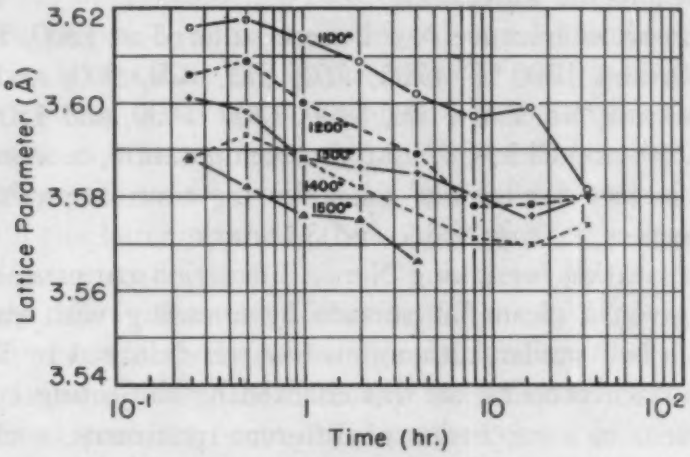


Fig. 6—Lattice Parameter Versus Sintering Time at Various Constant Temperatures for Mixture No. 2.

The measured values of the lattice parameters are plotted as functions of sintering time at constant sintering temperature in Figs. 5 and 6. It was found that the different types of surface preparation tested had no measurable effect on the location of the diffraction maxima.

Relation Between Concentration and X-Ray Diffraction Measurement

The changes in the X-ray diffraction patterns observed at different stages of diffusion may be described as follows: Before diffusion, the X-ray pattern of the mixture is simply the superposition of the patterns of copper and of nickel (Fig. 7a). As diffusion progresses, some nickel diffuses into the particles of copper to form copper-rich solid solution, and vice versa. Since, however, the concentration is not uniform at this stage, there will be produced a series of copper-rich solid solutions and a series of nickel-rich solid solutions. Each series produces a set of broadened lines on the X-ray pattern (Fig. 7b). Eventually the nickel-rich series merges with

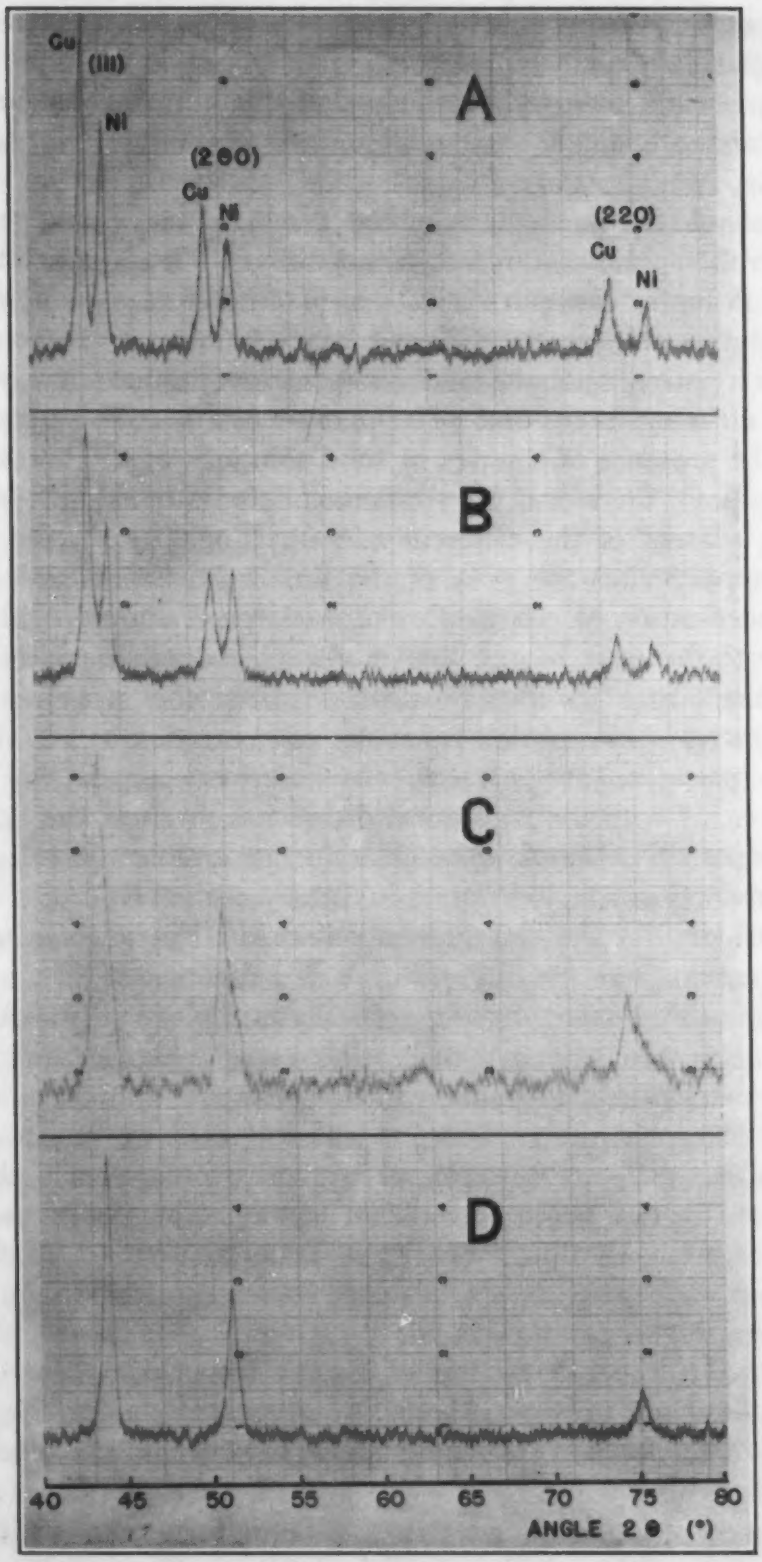


Fig. 7—X-Ray Diffraction Patterns of Copper-Nickel Compacts Showing the Progress of Diffusion.

the copper-rich series, producing a pattern of lines which are at first very broad (Fig. 7c) (corresponding to the wide range of concentration present), then progressively sharper, ultimately becoming the pattern of the homogeneous solid solution of equilibrium concentration (Fig. 7d).

It should be particularly noted that at intermediate stages of diffusion the specimens are not homogeneous, but contain solid solutions of different concentrations, i.e., of different lattice parameters. Solid solutions having the different lattice parameters are present in different relative amounts, and consequently produce X-ray reflections of different intensities. The contour of a broadened X-ray line due to the presence of a series of solid solutions of neighboring concentrations is, therefore, an approximate indication of the relative amounts present of the different concentrations, i.e., lattice parameters; in particular, the peak of the broadened line corresponds to that concentration which is present in largest amount. Since the position of the peak of the line is always measured on the X-ray charts, the lattice parameter calculated from the measurements is always the parameter of that particular concentration of solid solution which is predominantly present. In order to compare the experimental results with the theoretical discussion given at the beginning of the paper, it is therefore necessary to determine the relation between predominant concentration and the parameter K.

Consider first the one-dimensional case. For a given value of τ, the equation gives the concentration as a function of distance. Let this relationship be thought of graphically as a plot of distance versus concentration. According to the well-known Vegard's Law, the lattice parameter of a solid solution is, to a good approximation, a linear function of concentration; hence the plot of distance versus concentration also represents distance versus lattice parameter if the scale of abscissas be changed by a constant factor. Now, along the direction of diffusion, the linear density of material within a single plate is constant and, therefore, the distance traversed along this direction from some origin, say the boundary between two adjacent plates, is proportional to the total number of crystals traversed. Consequently, if the scale of ordinates be changed by a constant factor, the plot of distance versus lattice parameter also represents the total number of crystals between the origin ($x = 0$) and the variable point ($x = x$) as a function of lattice parameter. Let the lattice parameter of those crystals at $x = 0$ be called a_o, and the lattice parameter at $x = x$ be

called a. Then the total number of crystals between $x = 0$ and $x = x$ is also the total number N having a lattice parameter between a_o and a. Therefore, the relative number of crystals having a lattice parameter between a and $a + da$ is measured by dN/da, or the slope of the N versus a curves. The preceding argument shows that these slopes are equivalent to those of the distance versus concentration curves. Hence, finally, the predominant concentration is the concentration at that point where the slope of the distance versus concentration curves is a maximum. In order, therefore, to compare the theoretical with the experimental results, it is necessary to determine from the curves of Fig. 1 the value of c at which the slope dx/dc is a maximum.

The argument in the three-dimensional case is similar to the foregoing, except that now the concentration is a function of three spatial variables instead of one. In finding the predominant concentration, therefore, it is necessary to determine the concentration for which the slope of the c versus distance curves is a maximum for all directions in space. It turns out that this predominant concentration is that which is present at the centers of the particles (4) and, analogously, that in the one-dimensional case the predominant concentration is that at the centers of the plates.

These concentrations are just those denoted by K in the theoretical discussion, where they were used as a convenient measure of the progress of diffusion, and universal curves given (Fig. 2) for their variation with temperature, time, and particle size (as expressed in the parameter τ). Therefore, the experimental points of predominant lattice parameter, when converted to predominant solid solution concentration by means of Vegard's Law, and plotted as a function of τ, should fall on the theoretical universal curves, if the assumptions on which the latter were derived are a fair approximation of the actual conditions.

Comparison of Results With Theory

Figs. 8 and 9 show a number of the experimental data plotted on the same graph with the two theoretical universal curves. The agreement, while not quantitatively precise, does indicate that the general trend and order of magnitude of the dependence of K on τ is at least qualitatively correct. It should be emphasized that there are several approximations in the theoretical development which are

not accurately fulfilled in the actual conditions of the experiment; for example, the assumption that the diffusion constant D is independent of concentration, or that the metal particles are all of equal size and arranged in a very regular manner. The fact that there is a range of particle sizes present, particularly wide in the case of

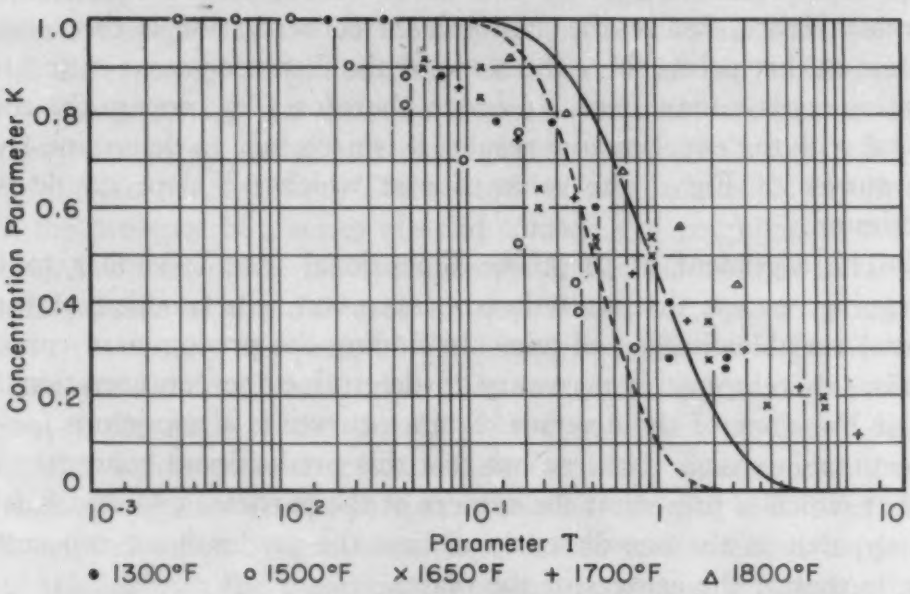


Fig. 8—Concentration Parameter K Versus Parameter τ for Mixture No. 1.

mixture No. 2, is alone sufficient to account for much deviation of the experimental points from the theoretical curve. In order to obtain an idea of the magnitude of this effect, the value of τ was calculated for particle sizes of 1 micron and of 43 microns, corresponding roughly to the spread present in mixture No. 2. (In calculating the plotted points an average value of 20 microns was taken.) The ratio of these two values of τ is independent of time, temperature, and material; hence, on the logarithmic scale of abscissas used in plotting the universal curves, the horizontal spread is constant. This spread is large compared to the deviation of the experimental points from the curve; consequently, the observed deviations are not a disproof of the theory.

Sources of Experimental Error

It is also necessary to consider the experimental errors as such, without reference to agreement with any theoretical treatment. One

troublesome source of error lay in the deviation from flatness of the sintered specimens. It was found that departures of only a few thousandths of an inch from planarity were sufficient to produce measurable shifts in the positions of the diffraction maxima. Because of the excessive time and labor which would have been required

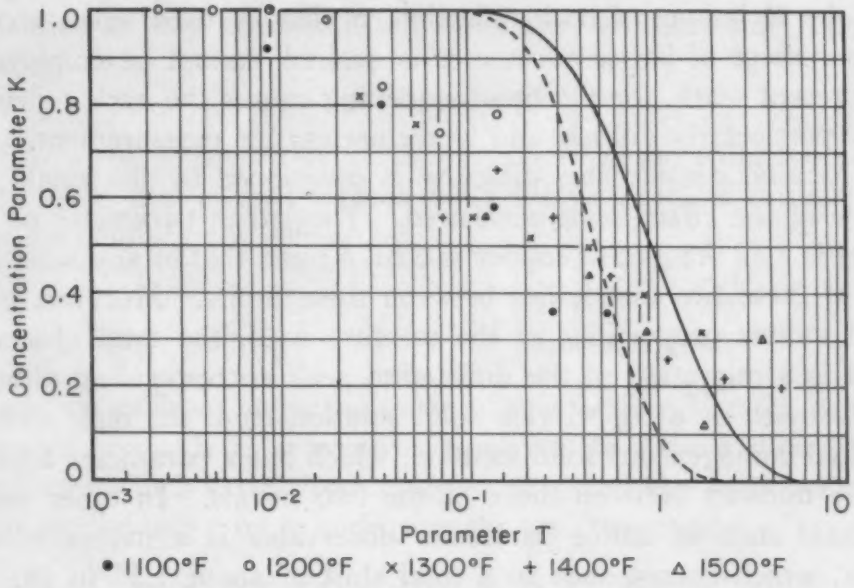


Fig. 9—Concentration Parameter K Versus Parameter τ for Mixture No. 2.

to mount all the specimens in plastic and grind accurately flat, this preparation was employed only for those specimens scanned by hand or by slow-speed automatic scanning.

A second source of error was the presence of random fluctuations in the intensity of output from the X-ray tube, which produced a corresponding unsteadiness in the record traced on the charts, thus making for uncertainty in locating the diffraction maxima accurately.

Probably the source of largest error is the presence of a range of particle sizes in both mixtures, as already mentioned above. It would certainly be very desirable to control this variable closely, that is, to conduct the experiment with powders of a small range of particle sizes. At the time of the experimental work described herein, the only accurate sizing technique available to the authors was that of water elutriation, which is a very slow process at best, and particularly so in the case of metals because of their high density. Hence, it was not feasible to size the particles more closely than can be done by screening.

Regardless of how precisely the experimental conditions are controlled, it is inevitable that during the intermediate stages of sintering there should be present a series of solid solutions of varying concentrations. The X-ray diffraction lines will thereby be broadened, as discussed above, making for uncertainty in locating the peaks, and hence to a lack of precision in the results. It is because of this effect that the technique of back-reflection, ordinarily used when accurate measurement of lattice parameter is desired, cannot be employed in the present work, for the line broadening causes the back reflections to be particularly diffuse, and hence useless for measurement.

Finally, considerable difficulty is occasioned by the small magnitude of the effect being measured. The lattice parameter of pure nickel is 3.52 Å; that of copper is 3.61 Å; and that of any solid solution of these two metals lies between these limits. Morever, in the equal atomic proportions of the mixture used, the total observable effect is a migration of the diffraction peak corresponding either to a nickel-rich or a copper-rich solid solution from the pure metal to the final homogeneous solid solution, which has a parameter approximately midway between those of the two metals. In other words, the total shift in lattice parameter observable is a matter of only 0.05Å, which corresponds to a total shift of about 1.5° in 2θ. On this basis, it might be thought more advantageous to have carried out the investigation using two metals which differ more widely in their lattice parameters. Unfortunately, it is a general rule that if the lattice parameters of two metals differ by more than about 15%, the two will not form a complete series of solid solutions, and the latter condition is essential in order to have a simple, well-defined means of following the diffusion process.

Acknowledgment

This work was done at the Jet Propulsion Laboratory, California Institute of Technology, under contract with the Army Ordnance Department, Washington, D. C. The authors wish to thank this agency for the permission to publish the results of this investigation.

Appendix

A measure of concentration appropriate for use in the study of diffusion may be arrived at by means of the following considerations,

in which all concentrations will be expressed as weight fractions. Consider diffusion between two alloys, I and II, and let c_1 be the initial concentration of one of the metals in I, and c_2 its initial concentration in II. Then at equilibrium the concentration throughout will be $c_0 = \frac{1}{2}(c_1 + c_2)$, assuming, for convenience, that equal weights of alloys I and II were taken. Now let c^* be the variable concentration at any point and any time during diffusion. Then the quantity

$$c^* - \tfrac{1}{2}(c_1 + c_2)$$

measures the departure of the actual concentration from the equilibrium value, and is thus a measure of the progress of diffusion. If now the quantity c is defined by

$$c = \left[c^* - \tfrac{1}{2}(c_1 + c_2) \right] \frac{c_1 + c_2}{|c_1 - c_2|}$$

then c varies from an initial value of c_0 in either I or II to a final value of zero. It is convenient, however, to have a dimensionless parameter which varies from unity to zero, and this can obviously be done by dividing c by c_0 and using the resulting ratio

$$\frac{c}{c_0} = \left[\frac{c^* - \tfrac{1}{2}(c_1 + c_2)}{\tfrac{1}{2}(c_1 + c_2)} \right] \frac{c_1 + c_2}{|c_1 - c_2|}$$

as is done in the text.

References

1. P. Chevenard and X. Waché, "Etude Expérimentale de la Diffusion Métallique par la Méthode Thermomagnétique Appliquée à des Agrégats Multilames," *Revue de Métallurgie*, 1945.
2. H. S. Carslaw and J. C. Jaeger, "Conduction of Heat in Solids," 1947, p. 77. Oxford University Press.
3. R. M. Barrer, "Diffusion in and Through Solids," 1941, p. 275. Cambridge University Press.
4. S. Weinbaum, "Alloying of Metal Powders by Diffusion." (Submitted for publication.)

DISCUSSION

Written Discussion: By Harry Udin and Amos J. Shaler, Massachusetts Institute of Technology, Cambridge, Mass.

The present paper of Duwez and Jordan shows that during the sintering of a mixture of copper and nickel powder homogenization behaves qualitatively according to the classical viewpoint of diffusion.

That homogenization is initially more rapid than is predicted by theory may be attributed to the contribution of the finer fraction of the powders. Likewise, it appears that the process approaches completion more slowly than the theoretical process since a larger size fraction of powders is also present.

Quantitatively, the results seem somewhat anomalous. In Fig. 9 homogenization even of the largest particle size is nearly complete at a time when theory predicts only that the mean particle size is approaching complete homogenization. This occurs in spite of the fact that at less than 100% density homogenization by diffusion would be retarded since the interfacial area available for diffusion is correspondingly less.

To account for this anomaly, it is necessary to consider that sintering is always a concomitant of diffusion until the powder mass is of 100% density. Until such a density is achieved, there must be a mass movement of metal toward the interior. The driving force for such motion has been attributed to surface tension. Nevertheless, such a motion, like diffusion,[4] is also atomic in nature. As a consequence, it is to be expected that the atoms of copper move at a different rate from those of nickel, due to their different mobilities, although the driving force is approximately uniform. Thus an increment of homogenization will be superimposed on that due to diffusion.

The simple cubic array of Weinbaum[5] can decrease its free energy only by increasing its entropy, whereas an actual compact of unlike powders has superimposed upon this entropy effect some excess surface energy which can be dissipated by an atomic motion which likewise leads to homogenization.

Authors' Reply

We wish to thank Messrs. Udin and Shaler for their interesting discussion. As they point out, the porosity in an actual powder compact will retard diffusion below the rate calculated on the basis of Weinbaum's model, which is nonporous. Moreover, as shrinkage proceeds, the increasing area of interfacial contact will accelerate diffusion. However, it is not clear to us that shrinkage can affect homogenization in any way other than by this increase in contact area. From the phenomenological viewpoint, it is certainly true that the free energy of an actual compact can decrease by the dissipation of surface energy as well as by the increase of entropy resulting from homogenization, for otherwise shrinkage would not take place. It does not seem evident to us, however, that this decrease in free energy is not just that required to bring about shrinkage, leaving no remainder to produce homogenization. The situation appears even less clear from the atomic viewpoint in the absence of a clearly established picture of the atomic mechanisms of diffusion, sintering, and shrinkage.

---

[4] A. J. Shaler and John Wulff, "On the Mechanism of Sintering," *Industrial Engineering Chemistry*, Vol. 40, 1948, p. 838.

[5] Authors' reference (4).

THERMODYNAMICS IN THE DECARBURIZATION OF STEEL WITH MILL SCALE

By W. A. Pennington

Abstract

Experiments have been conducted to show that the decarburization of ferrous alloys with mill scale is effected through two chemical reactions involving gases. One of these reactions causes an expansion in volume, at constant pressure, and therefore causes gases to escape from a heat treating chamber where decarburization is taking place.

A technique of following the effect of different variables on decarburization with mill scale has been established which is based upon volume measurements of the gases collected. The method is unique in that good results for the average specimen are available continuously throughout a run.

Chemical thermodynamics has been applied to calculate the end-point carbon for various conditions. Supporting experimental evidence has been presented to demonstrate the reliability of the calculations where they are made on the proper basis.

Among the factors investigated are: (a) total pressure of CO and CO_2, (b) effect of inert gases, (c) type of scale, (d) composition of steel, (e) temperature, (f) thickness of steel, and (g) catalysts.

Some suggestions have been made pertaining to decarburization in mill practice.

Introduction

MOST of the experimental investigations pertaining to the decarburization of steel, which have been reported in the literature, have been prompted either by academic interest or the practical hope of finding a means of preventing the loss of carbon. There are some few scientists, however, who are carrying on a very active program of research with the specific intention of discovering better

A paper presented before the Thirtieth Annual Convention of the Society, held in Philadelphia, October 23 to 29, 1948. The author, W. A. Pennington, is chief chemist and metallurgist, Carrier Corporation, Syracuse, N. Y. Manuscript received March 10, 1948.

and cheaper ways of effecting decarburization of steel strip in plant production. Notably among these are metallurgists, and a few chemists, who have the responsibility of producing magnetic steels of the highest quality.

It is well known that these steels, which contain silicon up to some 5%, are superior where a state of preferred orientation of the grains exists. Such a condition can be obtained with considerably more ease through decarburization to some very low level of carbon.

The writer some years ago set out to produce decarburized steel strip for an entirely different reason. There was a definite need for a dead soft steel with considerable corrosion resistance. The particular processing of the strip required a heating to some 1550 °F (845 °C) which, of necessity, was followed by a cooling to room temperature in a matter of 20 to 30 minutes.

Ordinary steel, such as may be used for hot-dipped galvanizing, can be rendered dead soft through a box anneal at some 1275 °F (690 °C) over a fairly long period with, of course, a slow cool. The iron carbide becomes spheroidal and no longer makes a substantial contribution to the hardness.

The new problem was further complicated by the fact that every addition which could be made to the steel to enhance corrosion seemed to induce a greater degree of hardness. To have a steel which would compare favorably with dead soft galvanized steel, and with the other required properties, it appeared that it would be necessary to make the steel with a carbon content around 0.05% and then to reduce this value to something like 0.007% through strip decarburization. Needless to say, the method would have to be cheap, which precludes the use of moist hydrogen and other similar possibilities.

Knowing that steel strip sometimes suffers from surface decarburization where heat treated with the mill scale intact, it was decided to attempt to make use of this principle in developing a practical method. Early in the investigation, it was realized that a thorough understanding of the chemical thermodynamics would lead to the desired goal. The principles discovered in the various research investigations are so fundamental that they are reported here in the hope that they may be of help to some of those interested in plant methods of decarburization.

In a previous paper (1)[1], the writer was particularly concerned

[1]The figures appearing in parentheses pertain to the references appended to this paper unless their significance is otherwise indicated.

with the mechanism of decarburization of steel as it involves the migration of carbon within the body of the steel. The position was taken that the chemical reactions, whatever they are, take place at the surface and therefore all equilibria within the steel can be regarded as being physical rather than chemical. Having thus disposed of the possibility of decarburizing chemical reactions taking place within the metal, concentration was put upon the nature of the diffusion of carbon, particularly as it takes place in a two-phase system.

With the mechanism of diffusion clearly in mind, it is time to consider the chemical reactions which take place at the surface of the steel. These reactions, like all others, are governed as to rate by kinetics and as to extent by thermodynamics.

Inasmuch as the mill scale is to be used as the decarburizing agent, it is necessary to discuss its nature and to show how it functions. Once this has been accomplished, free energy data can be derived which can be used to determine the extent of decarburization which may be expected and indeed to determine whether there will be any appreciable decarburization. In the application of the free energy data, it was necessary to have information on the solubility of carbon in α-iron. Not being satisfied with the data at hand, experiments were conducted designed to measure directly the solubility of carbon in α-iron at a few temperatures.

Many factors have been found which affect both the rates and the end value of decarburization. Among those which will be discussed are: (a) total pressure of CO and CO_2, (b) effect of inert gases, (c) type of scale, (d) composition of steel, (e) temperature, (f) thickness, and (g) effect of catalysts.

It should be reiterated that the purpose of this work is to develop certain thermodynamic principles which will allow the metallurgist or physical chemist to calculate with certainty results which may be obtained in plant practice as well as in the laboratory.

Nature of Mill Scale

Mill scale consists primarily of iron and oxygen and is formed upon the surface of steel as it is handled hot in the steel mill, and hence the name. The proportions of iron and oxygen are such as to correspond almost precisely to the formula Fe_3O_4.

Where certain steels are heated above some critical temperature, the oxygen in some way becomes available as an agent for carbon

removal with an accompanying depletion of oxygen in the mill scale. The reduction of mill scale may be regarded to take place in two steps; namely, the formation of ferrous oxide and then a final reduction to metallic iron. Jette and Foote (2) have found that FeO is often, if not always, associated with dissolved oxygen. This solid solution, known as wüstite, has an average of 0.95 iron atom associated with each atom of oxygen. On duly considering this solid solution, one can regard the reduction of Fe_3O_4 as first going to wüstite and then to elementary iron.

Inasmuch as the intermediate reduction product, whatever it is, is always present as long as the decarburization is taking place, it is only necessary to consider it in the thermodynamic considerations involving chemical equilibria. Herein wüstite has been accepted as the choice of intermediate product, but it is felt that almost precisely the same quantitative values would have been arrived at if the intermediate product had been taken as FeO.

Chemistry of the Cycle

It is well known that ordinary scaled steel can be bright annealed by heating it in a closed container to some temperature above 1275 °F (690 °C). At the same time that the scale is being converted into bright metal, the stock will lose carbon and the gas pressure will increase in the container unless provision is made for "outward breathing". If such provision is made, gas will escape as long as the decarburization proceeds. However, there comes a time at which the carbon of the steel will be in equilibrium with the oxygen of the scale and absolutely no further decarburization will take place.

If consideration be restricted to low carbon steels, say with no more than 0.085% carbon, there will nearly always be an excess of scale and the chemical activity of the wüstite may be considered as unity. As the reactions proceed the activity of carbon gets less and less until the action comes to a dead end and no further gas will ever come from the container even though there are still scale and carbon present within.

The volume of gas which comes from the container can be easily measured and serves as a basis for measuring the amount of carbon removed. Further attention will be given to this point later.

How does the scale react with the carbon? Already it has been established that both the carbon and oxygen are present in solid sub-

stances. Do they react with each other or does the reaction proceed through the benefit of some intermediate gaseous reactions? Several experiments were conducted to ascertain the chemical mechanism. The results of one of these will suffice to answer the above questions.

A steel containing 0.062% carbon, which was available in 18 gage in the hot-rolled condition, was first cut into strips 3 by 5 inches and then normalized using a so-called neutral atmosphere. Some of the specimens were left in this condition to serve as one group, but others were pickled electrolytically as a cathode in clean, 10% sulphuric acid. It was desired to have both types of specimens in ex-

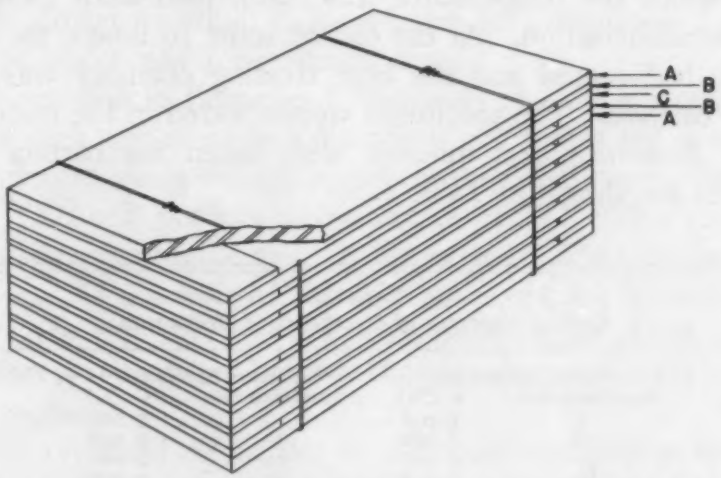


Fig. 1—Type of Pack Assembly Containing Scaled and Descaled Specimens. A = Scaled Specimen; B = Spacer; C = Unscaled Specimen.

actly the same condition except for the surface oxide. The pickled specimens were heated in boiling water and dried with absolute alcohol.

A pack was made with alternate scaled and descaled specimens, there being 16 scaled and 15 descaled specimens. To prevent the oxide of the scaled specimens from touching those which had been pickled, a 22-gage ingot iron spacer was introduced between the various pairs of specimens at either end of the pack. Fig. 1 illustrates how the specimens were assembled.

The pack was wired at either end with a soft steel wire and introduced into a heat treating box made of low carbon steel provided with a ⅛-inch gas pipe to lead off the gases. The box was welded gas-tight and then put into a furnace so that the specimens were horizontal. The lead-off gas pipe was so connected as to deliver the gases formed into an inverted graduate by downward dis-

placement of a solution made by saturating a 5% sulphuric acid solution with sodium sulphate. No appreciable amount of carbon dioxide will dissolve in this solution.

As soon as the temperature of the furnace began to rise, gases were expelled from the heat treating chamber. At first this evolution was caused by the expansion of air in the chamber due to the rise in temperature. The flow of gas became slower and slower, with a given temperature rise, until some point around 1300 °F (705 °C) was reached. Here the decarburization really got under way and continued quite satisfactorily at 1450 °F (790 °C), the point at which the temperature was maintained until there was no further decarburization. At the end of some 16 hours, the evolution of carbon had ceased and the heat treating chamber was removed from the furnace. The specimens were sheared in the middle across the short dimension and millings were taken for carbon analyses. The results are shown in Table I.

Table I
Carbon Analyses of Decarburized Specimens

Scaled Specimens		Pickled Specimens	
Specimen No.	C (%)	Specimen No.	C (%)
1	0.009	2	0.009
9	0.009	10	0.010
17	0.008	16	0.009
23	0.010	22	0.009
31	0.009	30	0.009

Obviously both sets of samples were decarburized to the same equilibrium value, but perhaps not with the same speed. There was no solid oxide in contact with the pickled specimens and consequently there could have been no solid reaction of scale with the carbon in the steel.

Since the only oxidizing substance present was the scale on the odd-numbered pieces, it becomes necessary to picture the decarburization as being effected by gaseous reactions. Some gas must act as a carrier to get the oxygen from the scale to the surface of the pickled specimens. The question now arises as to what gases may be involved. An earlier experiment in which gray iron turnings were decarburized with mill scale at 1700 °F (925 °C) gave a gas, after all air had been expelled, which contained 85% CO and 15% CO_2. It is necessary to consider these two gases only to arrive at a mechanism.

It has long been known that CO_2 is a decarburizer as shown by the reaction given in Equation I

$$C \text{ (in Fe)} + CO_2 = 2CO. \qquad \text{Equation I}$$

Carbon monoxide thus formed is a reducing agent quite capable of reducing iron oxide or wüstite. This reaction is illustrated in Equation II,

$$\underbrace{0.95\,FeO + 0.025\,O_2}_{\text{wüstite}} + CO = 0.95\,Fe + CO_2. \qquad \text{Equation II}$$

The carbon dioxide formed by the reaction now becomes available for further decarburization in accordance with Equation I and the cycle will be under way for a second time.

In the reaction in Equation I, two mols of carbon monoxide are formed for each mol of carbon dioxide which reacts and, since equal mols of different gases occupy approximately the same volume, one volume of CO_2 will produce two volumes of CO. This increase in volume causes some of the gases to be expelled from the heat treating chamber. As a matter of fact, the gases coming from the chamber, where gray iron turnings are being decarburized, burn with considerable force, if they are lighted, showing that much gas is coming from the container.

Having reviewed the nature of mill scale and having established the nature of the decarburizing chemical reactions, it is now appropriate to develop and compile the free energy data needed to understand quantitatively the effect of the various factors which are to be discussed later.

Free Energy Data

There are two important mathematical relations among the free energy change of a chemical reaction, the equilibrium constant, and the concentrations of the involved substances. One relation gives the free energy change in terms of the equilibrium constant; the other gives the constant in terms of the concentrations. Free energy data then serve as a basis for the calculation of an unknown concentration.

Let us take the general equation,

$$bB + cC = dD + eE, \qquad \text{Equation III}$$

where the capital letters represent the compounds and the small let-

ters the number of mols. According to the law of mass action, the equilibrium constant for this general equation may be given as

$$K = \frac{A_D^d \, A_E^e}{A_B^b \, A_C^c}. \qquad \text{Equation IV}$$

The capital A denotes chemical activity and is usually proportional to concentration. The activity of a gas then is proportional to its pressure. In practical measurements, the equilibrium constants are so evaluated that the chemical activities of pure liquids or solids are equal to unity and hence disappear from the equation.

The relation of the equilibrium constant and free energy may be found in any text of physical chemistry as

$$\Delta F^\circ = -RT\ln K. \qquad \text{Equation V}$$

Here ΔF° is the free energy change in the selected standard state, R is the gas constant, T is the absolute temperature, and K is the equilibrium constant.

With these basic relations for the general equation, it is time to turn to the two equations which are involved in the decarburization of steel with mill scale. For Equation I

$$K_1 = \frac{A_{CO}^2}{A_C \; A_{CO_2}} \qquad \text{Equation VI}$$

or since the activities of the gases are proportional to their pressures,

$$K_{1P} = \frac{P_{CO}^2}{A_C \; P_{CO_2}}. \qquad \text{Equation VII}$$

The subscript "1P" is used to denote a second constant not necessarily the same as the first but proportional to it in any event.

The equilibrium constant for Equation II becomes

$$K_2 = \frac{A_{Fe}^{0.95} A_{CO_2}}{A_{Wu} \; A_{CO}}. \qquad \text{Equation VIII}$$

Wu is not to be regarded as a chemical symbol but rather an abbreviation of wüstite. Since the activities of solid iron and wüstite are equal to unity and the activity of each gas is proportional to its pressure,

$$K_{2P} = \frac{P_{CO_2}}{P_{CO}} . \qquad \text{Equation IX}$$

If the two equilibrium constants for Equations VII and IX are known and the pressure of the gases measured, then it is simple to calculate A_C and to estimate the end carbon at equilibrium. If the equilibrium constants are not known, but the free energy changes are, the constants can be calculated by Equation V.

Once K_{2P} is known, the ratio of CO_2 to CO can be calculated and if the total pressure of the carbon gases is known, A_C can be calculated with no need for experimental measurements in addition to those already made for an evaluation of the free energy change.

For theoretical considerations, a free energy equation is needed for the reaction in Equation II. This equation can be derived by the law of summation involving other reactions. Chipman and Marshall (3) give

$$FeO\ (w\ddot{u}stite) + H_2(g) = 0.95\ Fe\ (\alpha) + H_2O(g)\ ; \qquad \text{Equation X}$$
$$\Delta F^\circ = 7457 + 7.24\ T\ln T - 0.00321T^2 - 52.628T. \qquad \text{Equation Xa*}$$

Chipman (4) gives results for a second equation which can be used with Equation X:

$$CO(g) + H_2O(g) = H_2(g) + CO_2(g)\ ; \qquad \text{Equation XI}$$
$$\Delta F^\circ = -10{,}020 - 0.40\ T\ln T - 0.0018T^2 + 0.25 \times 10^{-6}T^3 + 13.63T. \qquad \text{Equation XIa}$$

If Equation X is added to Equation XI, Equation XII will be obtained:

$$FeO\ (w\ddot{u}stite) + CO(g) = 0.95\ Fe\ (\alpha) + CO_2(g). \qquad \text{Equation XII}$$

Likewise Equation Xa may be added algebraically to Equation XIa to obtain a free energy equation to correspond with Equation XII:

$$\Delta F^\circ = -2563 + 6.84\ T\ln T - 0.00501T^2 + 0.25 \times 10^{-6}T^3 - 38.998T. \qquad \text{Equation XIIa}$$

The free energy data for the conversion of α- to β-iron has been taken from Chipman and Murphy (5):

$$0.95\ Fe\ (\alpha) = 0.95\ Fe\ (\beta)\ ; \qquad \text{Equation XIII}$$
$$\Delta F^\circ = -1948 - 5.65\ T\ln T + 0.00323T^2 + 37.782T. \qquad \text{Equation XIIIa}$$

By adding Equation XII to Equation XIII and Equation XIIa to Equation XIIIa the following are obtained:

*Throughout this paper an "a" in the equation number will denote a free energy equation.

$$FeO\ (w\ddot{u}stite) + CO(g) = 0.95\ Fe\ (\beta) + CO_2(g); \qquad \text{Equation XIV}$$
$$\Delta F^\circ = -4511 + 1.19\ T\ln T - 0.00178T^2 + 0.25 \times 10^{-6}T^3 - 1.216T. \qquad \text{Equation XIVa}$$

It remains to obtain an equation involving γ-iron. Chipman and Marshall (3) give:

$$0.95\ Fe\ (\alpha) = 0.95\ Fe\ (\gamma); \qquad \text{Equation XV}$$
$$\Delta F^\circ = 105 - 3.47\ T\ln T + 0.00269T^2 + 21.230T. \qquad \text{Equation XVa}$$

The desired equation can be found by adding Equation XV to Equation XII and Equation XVa to Equation XIIa:

$$FeO\ (w\ddot{u}stite) + CO(g) = 0.95\ Fe\ (\gamma) + CO_2(g); \qquad \text{Equation XVI}$$
$$\Delta F^\circ = -2458 + 3.37\ T\ln T - 0.00232T^2 + 0.25 \times 10^{-6}T^3 - 17.768T. \qquad \text{Equation XVIa}$$

Equations XIIa, XIVa, and XVIa are the desired free energy equations involved in the reduction of wüstite.

There is yet need for an equation for the decarburization reaction itself, from which the equilibrium constants can be calculated or, better yet, a need for the equilibrium constants themselves. Austin and Day (6) have favored the science with a list of equilibrium constants at 50-degree intervals from 400 to 950 °C (725 to 1740 °F) for the reaction under consideration. The data conform to the following relation:

$$\text{Log } K_{1P} = 9.34091 - 9090.9(1/T), \qquad \text{Equation XVII}$$

where T is the absolute temperature on the Centigrade scale. The data given in Table II were calculated through the use of this equation.

The data given in Table III have been calculated through the solution of Equations XIIa, XIVa or XVIa with Equation V as

Table II
Equilibrium Constants for Decarburizing Reaction

Temperature			
°F	°C	°T	K_{1P}
1250	677	950	0.591
1300	704	977	1.086
1350	732	1005	1.974
1400	760	1033	3.471
1450	788	1061	5.925
1500	826	1089	9.84
1550	843	1116	15.67
1600	871	1144	24.79
1650	899	1172	38.39
1700	927	1200	58.23
1750	954	1227	85.48
1800	982	1255	125.1

pairs of simultaneous equations. Assuming that primary interest should center around a condition of atmospheric pressure, the partial pressure of CO and CO_2 have been calculated and are included in Table III.

The two tables contain the equilibrium constants needed for the theoretical considerations. No attempt has been made to review all of the literature or to make a critical review of different data. These serve the purpose quite well. However, it should be pointed out that Stanley (7) has made a rather complete coverage of carburization and decarburization as far as the equilibrium constants are concerned.

Perhaps it is in order to show clearly how the data of columns 6 and 7 of Table III were obtained. It is realized that P is the total pressure and is equal to the sum of the partial pressure of CO and CO_2. If P is restricted to unity then

$$P_{CO} + P_{CO_2} = 1, \qquad \text{Equation XVIII}$$

but according to Equation IX

$$K_{2P} = \frac{P_{CO_2}}{P_{CO}}.$$

The values of K_{2P} (column 4) were substituted in Equation IX and the resulting equation solved simultaneously with Equation XVIII.

With the equilibrium constants known, it is a simple matter to use Equations VII and IX to calculate the activity of carbon in iron at equilibrium. In other words, one can calculate the minimum to which the chemical activity can be reduced during decarburization.

Table III
Equilibrium Constants for Deoxidizing Reaction

Form of Fe	Temperature °F	Temperature °T	K_{2P}	P (Atm.)	P_{CO}	P_{CO_2}
α	1250	950	0.712	1	0.584	0.416
α	1300	977	0.661	1	0.602	0.398
α	1350	1005	0.617	1	0.618	0.382
α	1400	1033	0.577	1	0.634	0.366
α	1450	1061	0.544	1	0.648	0.352
β	1500	1089	0.514	1	0.661	0.339
β	1550	1116	0.489	1	0.672	0.328
β	1600	1144	0.468	1	0.681	0.319
β	1650	1172	0.446	1	0.692	0.308
γ	1700	1200	0.434	1	0.697	0.303
γ	1750	1227	0.418	1	0.705	0.295
γ	1800	1255	0.403	1	0.713	0.287

What does this chemical activity mean with respect to concentration? It has already been assumed that the activity is proportional to the concentration. As far as γ-iron is concerned, the solubility data are adequate for converting chemical activity to per cent carbon. For example, austenite containing 1.1% carbon at saturation has a chemical activity of unity, but changes to 0.5 at 0.55% carbon, a mere matter of proportionality.

It has been shown how the activity of dissolved carbon can be calculated quite accurately, but this does not give the concentration which, after all, is what is desired. The activity at saturation is unity and at other levels proportional to the concentration. Since satisfactory data were not at hand on the solubility of carbon in α-iron, an experiment was conducted to measure the saturation values at a few temperatures.

Solubility of Carbon in α-Iron

Small ingots (4 by 8 by 1-inch) of eutectoid steel were made through the use of an Ajax induction furnace, the steel being poured into gray iron molds. Commercially pure iron stock was used and graphite added to supply the carbon. Some little aluminum was added just before pouring to kill the steel so that better ingots would be obtained and also that the decarburization, which was to be effected later, could be carried out faster.

The small ingots were sand blasted and then forged to 0.5-inch thickness. The forgings were hot-rolled to 0.062 inch, normalized, and pickled at the cathode in sulphuric acid. Specimens 3 by 5 inches were subjected to decarburization at different temperatures with hydrogen containing 20% water vapor until the center band (γ-iron) was no closer than 0.020 inch to the surface. At the desired point of decarburization, the pieces were removed from the furnace and sweated to a parallel block with soft solder so that successive layer cuts could be taken with a shaper. Use was made of a tensile machine to exert pressure upon the piece while it was being soldered in order that there would be reasonable flatness.

When this program was started it was intended that measurements would be made at quite a few temperatures, but after three runs had been made at 1400, 1450, and 1500 °F (760, 790, and 815 °C) the work was temporarily abandoned and, because of the terrific time and inconvenience involved in such experimentation, has

Table IV
Carbon Analyses of Layer Cuts

Layer No.	Thickness (In.)	1400 °F	1450 °F	1500 °F
2	0.005	0.026	0.020	0.014
3	0.005	0.025	0.020	0.014
4	0.005	0.026	0.019	0.014
5	0.005	0.38	0.22	0.11

not been resumed. In Table IV will be found data which are typical. In a previous publication (1) similar results were given for another steel at 1400 and 1500 °F (760 and 815 °C). The postulation was made that the carbon, in the ferrite layer, is practically constant and that decarburization is the best means of obtaining the ferrite solubility. It does not particularly matter about the time of decarburization as long as the time is between some rather broad limits. The temperature, of course, must be held fairly close to the desired point, but still it is not too sensitive.

Along with the data of Table IV one may make use of the fact that α-iron at some 1660 °F (905 °C) contains zero per cent carbon. By using the technique of finite differencing with Newton's law of expansion, the following equation may be obtained:

$$y = 0.3936 - 0.000403t + 0.0000001t^2, \qquad \text{Equation XIX}$$

where y is the per cent carbon and t is degrees Fahrenheit. If the equation is solved for t where y is set at zero, a value of 1663 will be found. This is the top limit of t for which the equation is valid. This differs from 1660 because of the slight error in curve fitting. The equation is not valid below 1333 °F, at which point y is 0.034%.

While the data, on which Equation XIX is based, are not as complete as would be desired, the equation is still probably fairly accurate and, of course, can be justifiably used until something better is at hand. With its use one is able to calculate the carbon content corresponding to any chemical activity which occurs in the ferrite range.

Equilibrium or End Carbon

Let us now turn to the question of how low the carbon can be reduced at some specific temperature where the total pressure of CO and CO_2 is 1 atmosphere. For the purpose of illustration, a condition where the total pressure of the carbon gases is 1 atmosphere

(29.92 inches of mercury) and the temperature for the heat treatment is 1450 °F (790 °C) has been selected.

From Table II, it may be found that, for the condition at hand, K_{1P} is 5.925 and therefore

$$\frac{P_{CO}^2}{A_C \, P_{CO_2}} = 5.925. \qquad \text{Equation XX}$$

In Table III, the values for P_{CO} and P_{CO_2} are 0.648 and 0.352 respectively. Substitution of these values in Equation XX yields a value for A_C of 0.201. The next step is to learn whether this activity corresponds to α- or γ-iron. At this point, it is desirable to determine the activity of austenite containing minimum carbon at 1450 °F (790 °C). Throughout this discourse such values have been taken from the iron-carbon equilibrium diagram occurring in METAL PROGRESS, Vol. 30, 1936, p. 49. In fact, all general references to the iron-carbon diagram will be to this specific diagram. At 1450 °F (790 °C), the A_3 value (minimum carbon) is 0.35; the A_{cm} value (maximum carbon) is 0.94. Since the chemical activity of a saturated solution is the same as the pure dissolved substance, the activity of the saturated solution is the same as free cementite which is practically the same as that of graphite itself. Inasmuch as pure graphite is the standard state used in the determination of K_{1P}, its chemical activity is equal to unity and so the solution saturated with carbon also has unit activity. It follows then that the chemical activity of austenite containing 0.35% carbon is 0.372.

If one finds that the activity is greater than 0.372 for solid-gas equilibrium, then austenite must exist; if the activity is less than 0.372, then ferrite will exist. If the activity is precisely 0.372, there may be either or both phases present.

In the calculation made above, it was found that the lower limit of activity which would be attained at equilibrium would be 0.201. This value is less than 0.372 and hence the steel must be ferritic at 1450 °F (790 °C) at the end point. What will be the limiting percentage carbon to which the steel can be reduced? According to Equation XIX, ferrite, in equilibrium with austenite at this temperature, contains 0.0195% carbon. Its activity must be the same as the minimum carbon austenite because of being in equilibrium with it. Consequently, ferrite containing 0.0195% carbon has an activity of 0.372. On a proportionality basis a steel whose activity is 0.201 will contain 0.0105% carbon.

Table V
Equilibrium Carbon Values at Different Temperatures for Pure Iron-Carbon Alloys

Temp. (°F)	γ-Fe Max. %C	γ-Fe Min. %C	Solid-Solid Equil. Activity	α or β-Fe Max. %C	Solid-Gas Equil. Activity	End %C
1250	....	....	.....	0 032	1.387	No Decarb.
1300	....	....	.....	0.032	0.839	0.028 (about)
1350	0.84	0.71	0.845	0 0331	0.507	0.0199
1400	0.89	0.51	0.573	0.0254	0.316	0.0140
1450	0.94	0.35	0.372	0.0195	0.201	0.0105
1500	0.995	0.24	0.241	0 0141	0.131	0 0077
1550	1.05	0.15	0.143	0.0092	0.088	0.0057
1600	1.10	0.08	0.073	0.0048	0.0586	0 0039
1650	1.15	0.03	0.026	0.0009	0.0405	0.0466
1700	1.21	....	.....	.....	0.0275	0.0333
1750	1.28	....	.....	.....	0.0197	0.0252
1800	1.33	....	.....	.....	0.0142	0.0189

Any steel which has a composition such that the ordinary iron-carbon diagram may be applied will decarburize to 0.0105% dissolved carbon in the presence of mill scale or iron oxide. There are some substances such as titanium and vanadium which form insoluble carbides and therefore the total carbon may be higher than 0.0105 where these substances are present. Each alloy has its own equilibrium diagram and it would be helpful if it were known. However, it is not always necessary, because there are compensating factors which make it possible to use the classical diagram. For example, in certain experiments nickel, which lowers the diagram, and silicon, which raises it, both gave an end carbon practically identical with that of a pure iron-carbon alloy and also with that calculated through the use of the diagram. Extreme discretion must be exercised because there is a point of alloy composition where the actual decarburization with mill scale does not take place at certain temperatures. There are compositions which do not decarburize at all in the presence of mill scale and appreciable quantities of CO and CO_2.

Similar calculations have been made for other temperatures and the results compiled in Table V. The reader must be aware that the total pressure of CO and CO_2, for the conditions represented, is 1 atmosphere. It will later be shown that a change in the total pressure of these gases will change the end carbon terrifically. It becomes necessary, at this point, to differentiate between two kinds of equilibria encountered in decarburization. Reference is made to both kinds in Table V. First, there is a condition of equilibrium which exists involving α- and γ-iron only. This type will be referred to as solid-solid equilibrium. Secondly, there is finally attained a condition of equilibrium between the solid steel, as a whole, and the

decarburizing gas phase. This type will be called solid-gas equilibrium.

The carbon contents for the solid-solid equilibrium can be read from the iron-carbon diagram, being on the ferrite and the A_3 line. Through the use of other thermodynamic data, the carbon content of the steel for the solid-gas equilibrium can be ascertained and this value constitutes the lower or end-point carbon. The last four values in column 7 of Table V are for carbon in γ- rather than α-iron. An iron or steel which adheres to the classical diagram cannot be decarburized below 0.0466% carbon at 1650 °F (900 °C). In other words, a steel containing 0.05% carbon cannot be decarburized with mill scale to 0.005%, but it can be at 1600 °F (870 °C), though such an attainment may come very slowly.

After some of the preliminary experiments, which have been described, had been performed, a special technique of following decarburization was developed and was used throughout the work reported here. A description of this technique will now be given.

Equipment and Technique

The Heat Treating Chamber—Already in another part of this paper an experiment was described in which scaled and descaled specimens were decarburized. The progress of decarburization was followed by volume measurements of the gases expelled from the heat treating chamber. Later in the experimental work conveniences were added and refinements made. The method is so useful in studying many problems connected with decarburization that it will be described here in some detail.

The heat treating chamber consisted of a steel box 5 by 7 by 5 inches made of 11-gage low carbon steel with the exception that the end to which the exit pipes were attached was ¼-inch plate. The box was made of welded construction, the end opposite the exit pipes being put on after the work was introduced.

The specimens were usually no more than 5 inches long so that they could be some 2 inches away from the sealing plate when it was welded on. In this way there was no danger of getting premature decarburization.

As it is shown in Fig. 2, there were two gas pipes going into the lead-off face of the box. Both were about 30 inches long. The top one was the standard ⅛-inch pipe and served to lead off the

gases produced in excess of the pressure of the outside atmosphere. The inner end of this pipe was flush with the inside of the lead-off plate. The other pipe was the standard ½-inch gas pipe and extended into the center of the box. It was so placed that it could serve as a conduit for an iron-constantan thermocouple whose welded connection was at the center of the box. A reducer ¾ to ½ inch was screwed to the end of this pipe. It was so machined on the

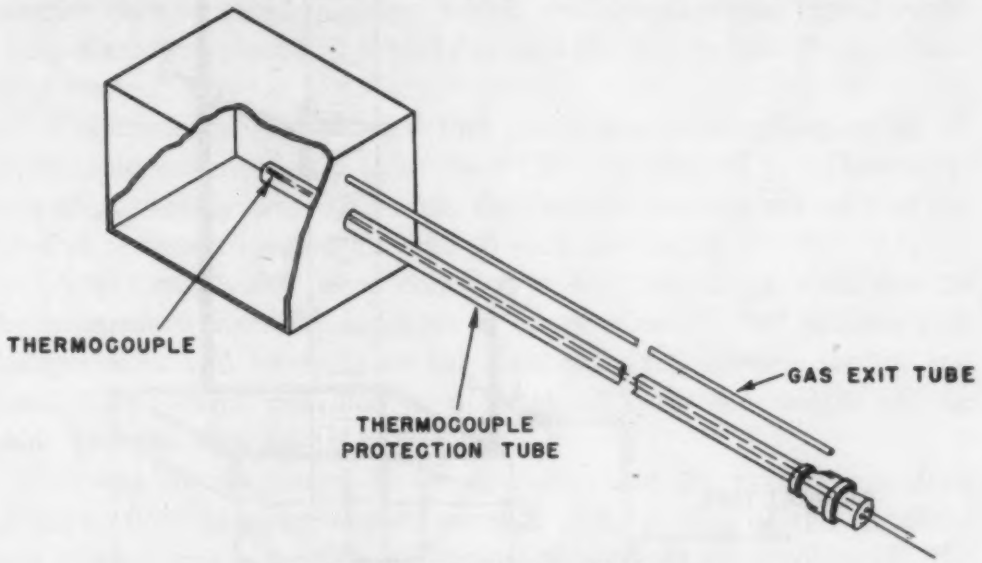


Fig. 2—The Heat Treating Chamber.

¾-inch side that a rubber stopper could be inserted to secure gas tightness. The thermocouple wires were inserted through holes in the rubber stopper which had been made by driving a small nail through the rubber. The fit was snug and there was never any gas leak around the wires. Sometimes a glass tube was used through the rubber stopper for the purpose of leading in some desirable gas.

The boxes were decarburized with mill scale on the inside before they were used in the tests.

The Furnace—Once the boxes were welded tight, they were placed in a Hoskins electric furnace in such a way that the pipes came out of the door space through a network of fire bricks and fibrous insulating material. Usually three boxes were included in each run. It was found advisable to protect the heat treating boxes from oxidation with a reducing atmosphere.

Quite uniform conditions could be maintained in the heat treating chamber throughout the run. The furnace controls were set so as to get a desired temperature in the center of the box, as indicated

by the thermocouple measurements. There was little, if any, difference in the temperature within any of the boxes at any specific time during a single run.

Gas Collection—The gases were led, as shown in Fig. 3, from the ⅛-inch gas pipe through the trap and on through rubber and glass tubing to a delivery point inside a battery jar and underneath

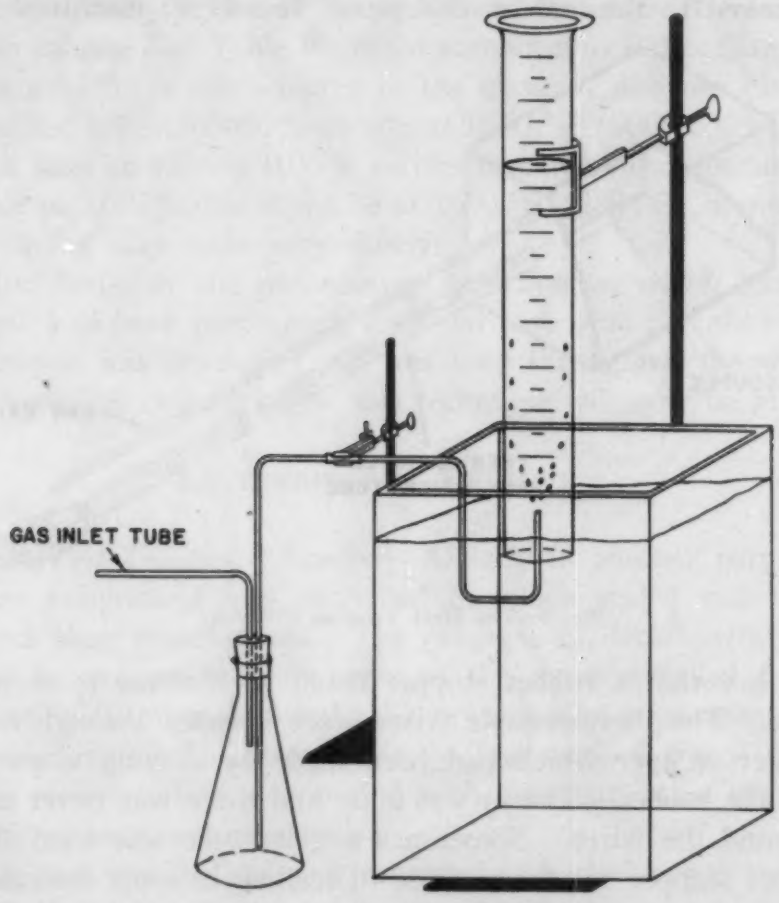


Fig. 3—Gas Collecting Apparatus.

an inverted graduate. A solution, made by saturating a 5% solution of sulphuric acid with sodium sulphate, was used as the displacement liquid. It almost filled the battery jar and completely filled the inverted graduate before the collection of the gas was started.

A piece of glass tubing, through a cork float, was connected by rubber tubing to a rubber aspirator bulb. This assembly was used to fill the graduate with the salt-acid solution.

Sometimes a 1-liter graduate was used; at other times one of 2-liter capacity was used. In many cases it was necessary to shift

the gas delivery tube to another set-up because the first graduate had been completely filled. Sometimes as many as six graduates were filled with the gases from a single box. In general, it was found that four battery jar set-ups were enough to keep the three collections going in order.

Making the Run—There was considerable time involved in getting everything ready for a run and therefore it was expedient to exercise care to avoid mistakes which would necessitate repeat runs. The boxes were placed in a cold furnace the day before the run was to be made.

Experiments soon showed that there was no decarburization of appreciable magnitude up to at least 1275 °F (690 °C). Therefore, once the assembly was connected, the furnace was turned on and set for this temperature and allowed to soak overnight.

Any gases which were collected during the night were due to the expansion from the increase in temperature. This volume and the gas laws can be used to calculate the free volume within the box. The volume can also be ascertained from the weight of the work and the dimensions of the box.

It was always found, in the morning, that the system was dead as far as flow of gases was concerned. The setting of the temperature control was immediately changed to some desired point. If the new setting was at 1375 °F (745 °C), the temperature would be attained in no more than a single hour. The increase in temperature would at once cause the flow of some little gas due to expansion and, at some temperature, perhaps slightly above 1300 °F (705 °C), the gases produced by decarburization would begin to form and the speed of gas flow would noticeably increase, soon reaching a maximum either before or at the attainment of the leveling off of temperature.

In order to know the volume of gas so as to have it related definitely to mass, it was necessary to correct the volume to some standard condition. As customary, 0 °C (32 °F) and 760 millimeters (29.92 inches) of mercury pressure were used. The height of the liquid in the graduate over that in the battery jar was measused with a foot-ruler so that the pressure of this liquid could be subtracted from the barometric pressure to obtain a more correct value of the pressure of the gas over the liquid.

From the laws pertaining to gas volume, pressure and temperature, the volume of gas collected by expansion could be calculated

and, hence, it was known precisely when the decarburization started.

It is appropriate to ask what relation is there between the volume of gas collected and the amount of carbon removed from the work in the heat treating box. Under the conditions of pressure and temperature being considered, one gram-molecule of any pure gas, based on the ideal gas law, will occupy 22,400 milliliters. This volume then is the gram-molecular volume (S.T.P.).* It should be remembered that a gram-molecule is an amount of material which weighs the same number of grams as the molecule weighs in atomic weight units.

One gram-molecule of CO_2 weighs 44 grams and contains 12 grams of carbon; one gram-molecule of CO weighs 28 grams, but it also contains 12 grams of carbon. It follows that CO and CO_2 can be mixed in any proportions and still a gram-molecular volume will contain precisely 12 grams of carbon. This is fortunate for the particular situation at hand because the volume of gas produced through the decarburization becomes an accurate measure of the amount of carbon taken from the steel, regardless of the relative amounts of CO and CO_2. One milliliter will represent 0.000536 grams of carbon. If a 5000-gram sample of steel is used, then 1 milliliter of gas will represent approximately 0.00001% carbon. It is believed that the volume measurements were well within 10 milliliters of the true value and therefore the carbon removed from a 5000-gram sample could possibly be within 0.0001% of the true value.

If the carbon content of a steel is known as it goes into the heat treatment, there are three ways of finding out what the carbon is at the dead end of decarburization: (a) calculations through the use of thermodynamic data, (b) calculations involving gas volume measurements, and (c) actual chemical analyses by some other accepted procedure such as the combustion method. It will be interesting to learn that the three agree almost perfectly.

Confirmation of Theory

A fairly pure iron-carbon alloy made in the laboratory, rolled to 0.062 inch and normalized, was used to check the theoretical considerations; this steel was killed with aluminum. The carbon content as hot-rolled was 0.054%, but the normalizing treatment reduced the carbon to 0.048%. This is the carbon concentration as the various runs with this material were started. In the first few runs, the end-

*Standard temperature and pressure.

Table VI
End Carbon at 1450 °F (Low Carbon Steel)

Method	% C
Gas Evolution	0.0106
Thermodynamic Calculation	0.0105
Combustion	0.0103
Average	0.0105

point carbon was something like 0.0085, but the thermodynamic value was 0.0105 which is not to be considered as satisfactory agreement.

These first runs were made simply by putting the air-filled boxes in the furnace. Nitrogen was used later with the same result. However, where the boxes were filled initially with a gas, produced by decarburization of other steel, the end result did check quite well with the thermodynamic value.

It was found on a little closer scrutiny that the total pressure of CO and CO_2 had been erroneously assumed to be unity. There was not enough carbon in the steel to drive out all the nitrogen before the end point was reached. The thermodynamic value then had been calculated for a condition which did not exist. It will be shown later that the agreement between theory and practice is all that can be asked when the actual total pressure of CO and CO_2 is duly considered.

The results for one of the runs will be described. Enough of the 3 by 5 by 0.062-inch pieces were put in the box to amount to 3464 grams. A mixture of some 85% CO and 15% CO_2 (volume per cent) was passed through the cold box containing the work for some 15 minutes so as to displace all the air. This mixture is approximately the same composition as the end-point gas and therefore the total pressure of CO and CO_2 at the end of the run was equal to the pressure of the atmosphere which was very close to 758 millimeters when the run was made.

Fig. 4 is presented to show the results graphically and to illustrate how smooth a curve can be obtained using this technique. One knows at any time just how far the decarburization has proceeded and consequently how far it yet has to go to reach the thermodynamic end point.

Six of the specimens were taken for chemical analyses at the end of the run. Four values were 0.010 and two were 0.011, making an average of 0.0103. For convenient comparison the end result is

shown in Table VI as arrived at by three different methods. It should be pointed out that the gas evolution carbon value depends upon a beginning carbon determined by the combustion method and therefore could differ as much or more than 0.0005 from the true value.

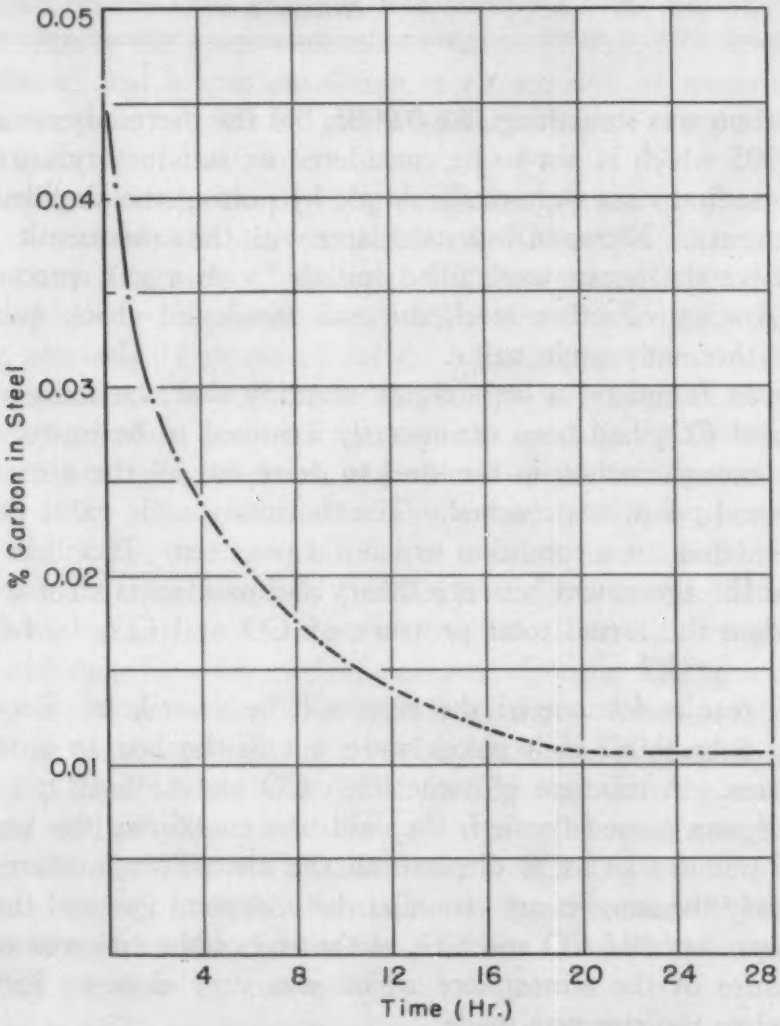


Fig. 4—Decarburization Curve for a Low Carbon Steel Decarburized at 1450 °F.

A modification of this experiment can be used conveniently to determine the per cent carbon in the original steel. The carbon removed was 0.0374%. If this value is added to the thermodynamic value of 0.0105 at the end point, 0.0479 will be obtained as the original carbon of the normalized piece. It is believed possible to set up a micro method using copper cylinders where many carbon analyses could be run in a day's time with a single furnace. There would

probably be no advantage over the combustion method for an expert in the combustion technique, but for someone trying to get accurate values for a few determinations only, there might be some merit in the use of such a method.

At this stage of experimentation, other temperatures were tried, particularly 1375 and 1550 °F (745 and 845 °C). In all cases where 1375 °F (745 °C) was used, good checks were obtained among the three values for end-point carbon. However, they did not always agree as well as the results shown in Table VI.

At 1550 °F (845 °C), a seemingly peculiar phenomenon was encountered—the steels tested, all containing nickel and manganese, did not decarburize at all except in going through the lower temperature range. It was feared at the time that the thermodynamics was so complicated that the results could not be explained. Later, they were found to be in perfect harmony with the thermodynamic considerations where the correct equilibrium diagram was used. As a matter of fact, the thermodynamics is so well understood at this point, that it is in order to discuss some of the factors which affect decarburization with mill scale.

Effect of Total Pressure of Carbon Gases

First, let us examine again the reactions in Equations I and II. In the latter, no change in pressure occurs as the reaction proceeds because one mol of CO produces exactly one mol of CO_2. Since there is no change in pressure, which results from a tendency for a volume increase, a change in the total pressure of CO and CO_2 can have no effect on the equilibrium. K_{2P} is a ratio of the pressure of CO_2 to the pressure of CO. If both values were doubled, the ratio would still be the same.

An entirely different situation, however, is found for the reaction in Equation I. Here one mol of CO_2 forms two of CO. There is a tendency toward a volume change and therefore the total pressure of the two gases will have an effect. An increase in pressure, not of inert gases but of CO and CO_2, will tend to force the equilibrium to shift toward the smaller volume or toward more CO_2. This direction is opposite to that of decarburization; consequently, an increase in the total pressure of CO and CO_2, as long as the ratio of the two remains the same, will result in a higher end-point carbon. The ratio of P_{CO_2} to P_{CO} is controlled by the deoxidizing reaction and

is unaffected by the total pressure of the two gases. In other words, as long as there is wüstite present the ratio, P_{CO_2}/P_{CO}, must be constant at equilibrium, regardless of the total pressure. A reduction then in the total pressure of the carbon gases should result in a lowering of the end-point carbon.

As a matter of interest, the end-point carbon values have been calculated for an iron-carbon alloy decarburized with mill scale at 1375 °F (745 °C) with pressures varying from 0.01 to 5.12 atmospheres.

Through the use of Equations XIIa and V, K_{2P} was found to be 0.596 at 1375 °F (1019 °T). Equation XVII gives a value of 2.627 for K_{1P}.

In all cases, regardless of pressure

$$\frac{P_{CO_2}}{P_{CO}} = 0.596$$

and P_{CO_2} and P_{CO} together will equal the pressure as given in the first column of Table VII. Two equations are thus obtained, whose solution gives the values for P_{CO} and P_{CO_2} occurring in columns 2 and 3. Equations VII and IX can now be used to get

$$A_C = 0.639\ P_{CO}, \qquad \text{Equation XXI}$$

a very convenient equation for obtaining the solid-gas equilibrium activity of carbon. These activity values are given in column 4.

The minimum carbon (iron-carbon diagram) for austenite at 1375 °F (745 °C) is 0.60%; the maximum is 0.85%; consequently, the activity of austenite in equilibrium with ferrite is 0.60 to 0.87 or 0.690. Ferrite with this activity, by Equation XIX, contains 0.0286% carbon. It is a matter of simple proportion to get the values in column 5.

The physical properties of a decarburized steel change very much on reducing the carbon from some point around 0.014 to 0.007%. A good grade of softness can be obtained with the lower carbon content; at 0.014% the hardness may be almost twice as high on the Rockwell B scale. Table VII shows that softness can be obtained in the laboratory or in the plant because a carbon content of only 0.0053% can be obtained at 1375 °F (745 °C), if the total pressure (P) of the carbon gases is 0.32 atmosphere at the end point.

While the end-point carbon becomes less with a decrease in P,*

*Total pressure of carbon gases.

Table VII
End-Point Carbon Variation With $P_{CO} + P_{CO_2}$ at 1375 °F

$P_{CO} + P_{CO_2}$	P_{CO}	P_{CO_2}	Ao	C (%)
0.01	0.00627	0.00373	0.00401	0.00017
0.02	0.01253	0.00747	0.00801	0.00033
0.04	0.02506	0.01494	0.01601	0.00066
0.08	0.05013	0.02987	0.03203	0.0013
0.16	0.1003	0.0597	0.06409	0.0026
0.32	0.2005	0.1195	0.1281	0.0053
0.64	0.4010	0.2390	0.2562	0.0106
1.28	0.8020	0.4780	0.5125	0.0212
2.56	1.604	0.956	1.0250	No decarb.
5.12	3.208	1.912	2.0499	No decarb.

the rate of reaction probably also decreases. There is not much CO_2 to do the decarburizing, at some total pressure of 0.01 atmosphere, and it is expected that a very long time indeed would be required to reach the low value of 0.00017% carbon.

Data were obtained which substantiated the conclusions drawn from the theoretical considerations above. It was suspected from previous observation that the mass of steel in the box, the per cent carbon in the steel, and the volume of the box all had something to do with the end-point carbon, if the box, at the start of the run, contained nitrogen or some other inert substance as the only gas. With the same box and the same steel, mass is the only one of these variables left to be considered. Three different weights were used in an experimental run.

The steel used was an experimental one in 16 gage containing 0.52% manganese and 0.46% nickel, the carbon being 0.046% after it was normalized. Boxes 1, 2 and 3 contained enough 3 by 5-inch pieces to amount to 2035, 4960 and 8005 grams, respectively. The decarburization curves are shown in Fig. 5, as obtained for a heat treatment at 1375 °F (745 °C). A summary of the important data is given in Table VIII.

One can estimate the end-point carbon by a reference to Table VII for the case where all gases present at the end were CO and CO_2. The barometer reading was 750 millimeters which is 0.987 atmosphere. By interpolating in Table VII the end carbon for this value of P will be 0.0163. This theoretical value corresponds to the condition which existed in box No. 3 and is a satisfactory check with the value of 0.0170 obtained experimentally. The end-point carbon, as given in Table VIII, was arrived at from the volume of gas expelled and collected. Samples were analyzed by the combustion method and no single one differed more than 0.0016 from the

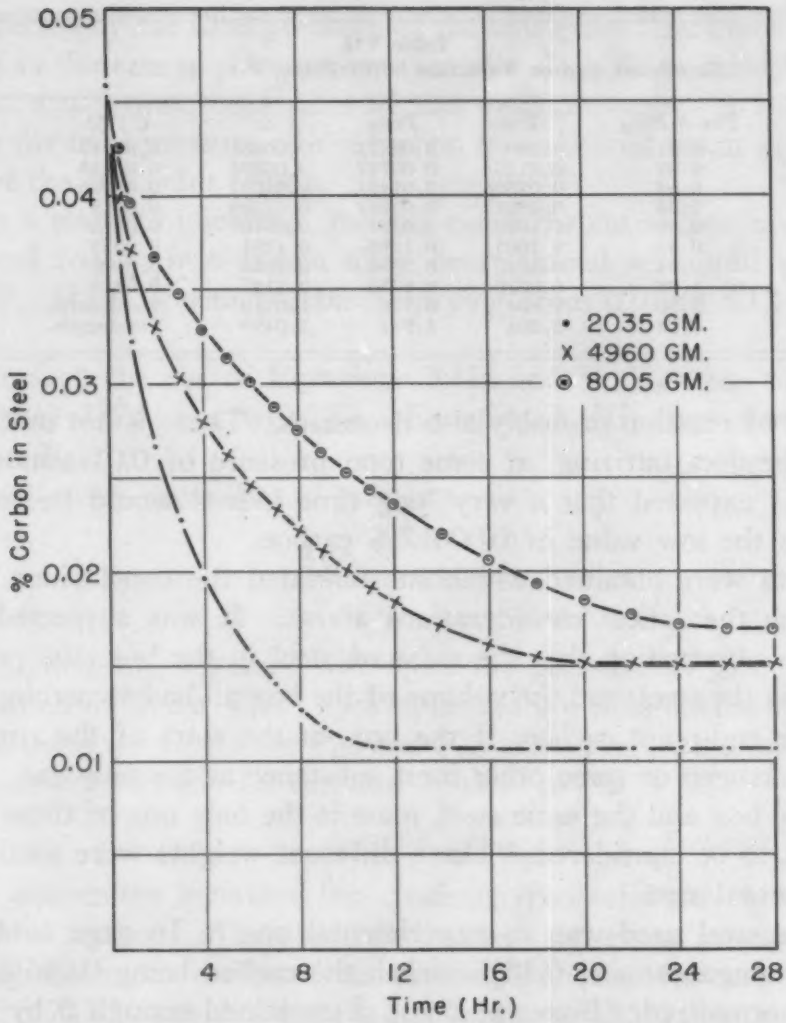


Fig. 5—Effect of Mass of Steel on Decarburization at 1375 °F.

values given in the table. The amount of carbon obtained by the two chemical methods agreed quite well. Now how about the thermodynamic values?

Above, it was shown that the thermodynamic value was reasonably close to the experimental value for box No. 3. This theoretical value was obtained on the basis of the assumption that all gases in the box at the end were CO and CO_2. Certainly this was not true for box No. 1 and it will be advisable to calculate how much of the gas was CO and CO_2. To accomplish this feat, it is expedient to derive an equation which will give the percentage (by volume) of nitrogen or other inert gas in terms of the volume of gases collected and the original free gas volume of the heat treating chamber. In the deriva-

Table VIII
Effect of Mass on Decarburization

Box No.	Wt. of Steel (gm.)	End Point C (%)	Total Time (Hr.)
1	2035	0.0106	11.33
2	4960	0.0151	19.25
3	8005	0.0170	25.25

tion, all volumes of gases were converted to correspond to the temperature and pressure existing in the heat treating chamber. It has been assumed that carbon gases are generated at all possible points within the box at a constant rate. This assumption means that the composition of the gas in the box is uniform at any time. Strictly speaking, this condition is not realized, but perhaps is fairly closely approached.

Let A = free volume in box (a constant),
y = % N_2 in box at any time,
x = volume of gases collected (converted to 1375 °F),
dy = change in % N_2 for dx expansion, and
dx = change in volume of gases collected.

It may be shown that

$$-Ady = ydx. \qquad \text{Equation XXII}$$

On integrating between limits,

$$-2.303A \log y \Big]_{100}^{y} = x \Big]_{o,}^{x} \qquad \text{Equation XXIII}$$

and

$$\log y = 2 - \frac{x}{2.303A}. \qquad \text{Equation XXIV}$$

The percentage nitrogen in the different boxes has been calculated through the use of Equation XXIV, and the results occur in Table IX along with the end-point carbon values. In most experiments, the calculated and observed values agreed almost perfectly, but extreme care had to be used in order for the conditions to be controlled and known. The results presented may be considered typical.

Further experiments were conducted on other steels using three boxes simultaneously with approximately 5000 grams of steel in each charge. At the end points, different volumes of nitrogen were introduced into two of the boxes, the third being removed from the furnace so that the final carbon could be checked chemically. The end-point carbon was lower with a higher percentage of nitrogen and

Table IX
Percentage Nitrogen in Box and Carbon in Steel at End Point

Box No.	A (ml.)	Vol. of Gases at 1375 °F	% N_2 (y)	% C	
				Obs.	Calc.
1	2500	5023	33.3	0.0106	0.0109
2	2135	10689	0.67	0.0151	0.0162
3	1655	16170	0.0057	0.0170	0.0163

agreed with the thermodynamic value as well as the experimental technique would warrant.

It is absolutely clear from the foregoing that steel strip cannot possibly be decarburized with mill scale, in a plant box anneal at 1375 °F (745 °C), to a value as low as 0.007% if the total pressure of CO and CO_2 approaches one atmosphere. Either the amount of steel and the carbon in it will have to be small enough that much of the original nitrogen in the box will not be driven out, or an inert gas will need to be introduced, or a partial vacuum applied. The last suggestion is probably quite impractical, due to the likelihood of collapsing the annealing cover.

Effect of Inert Gases

The portion of the paper immediately above has dealt coincidentally with this subject rather extensively. Perhaps, however, it is in order to make a summary more pointedly with respect to the effect of inert gases.

Considerable confusion has existed throughout the years as to what is and what is not a decarburizer. In the case where hydrogen and water vapor are used, some are inclined to regard hydrogen as the decarburizer; others are just as certain that water is the active chemical. In any event, one should be inclined to regard the chemical which actually reacts with the carbon to produce a gas as the decarburizing agent.

Nitrogen carrying moisture may be used to effect decarburization, yet nitrogen is not a decarburizer, but rather an agent to carry the water vapor and to help keep up the pressure. The nitrogen certainly aids in the decarburization. So does the heat and it is not considered to be a decarburizer.

As far as the decarburization with mill scale is concerned, nitrogen or other inert gas will act just like so much vacuum in its effect upon the end-point carbon. As to rate, it may not have the same ef-

fect as a vacuum, due to the hindering effect of the nitrogen molecules to free movement of the carbon gases.

Type of Scale

In the early part of the work involving quantitative decarburization, before the gas collecting technique was employed, individual specimens were studied where the reaction was carried out for different lengths of time. In general, the hot-rolled product was used. It was not unusual to find some specimen which had been heated 16 hours with more carbon than another, from the same sheet, which had been heated for only 12 hours. At the time, this variation was accepted as something unavoidable. However, it was later found that uniform results could be obtained if the strip or sheet was first normalized.

With the development of the gas collecting technique, it became a simple matter to compare the decarburization rates for hot-rolled and normalized stock. The data shown in Fig. 6 are for a steel containing approximately 0.5% nickel and 0.5% manganese. About 5000 grams of 16-gage stock was used in both cases. Normalizing the steel increased the rates of decarburization. The end point was about the same for both cases, but 1½ times as much time was required for the hot-rolled steel. The beneficial effect of the normalizing treatment was even more pronounced with some other steels.

It was decided to return to a study of individual specimens to learn if there was any difference in behavior of the different pieces. This study was carried out by wrapping the specimens with a very light gage, low carbon steel so as to have at least three thicknesses of metal on either side. The ends were folded over and the package flattened with a hammer. There was little chance for inward breathing and yet the CO and CO_2 produced could be pushed out as the pressure tended to rise above that of the atmosphere.

In general, all specimens were wrapped and introduced into the furnace, one of each material being put in every 4 hours. All were removed at the same time. The data for two low alloy steels heated at 1450 °F (790 °C) are given in Table X. It is immediately obvious that the decarburization is much more uniform and reliable where the sheet or strip is first normalized before the anneal. One can rely on the normalized stock to behave uniformly, but the hot-

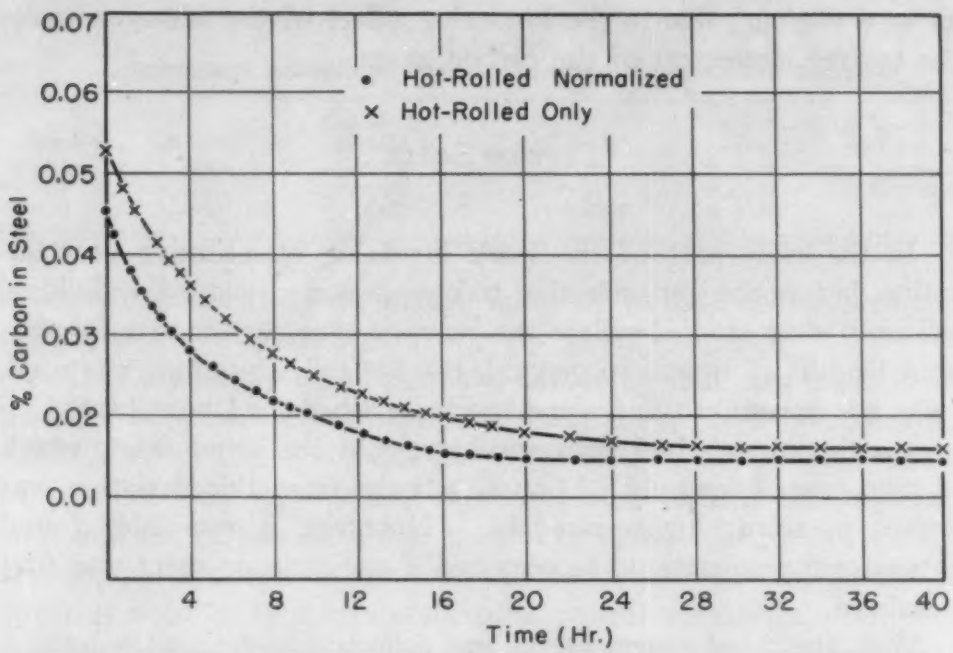


Fig. 6—Effect of Normalizing Hot-Rolled Steel.

rolled can and does give wide variations. Should one attempt to decarburize a hot-rolled coil in the plant by a box anneal lasting 24 hours, there might be found many places in the strip where the carbon was as low as 0.006%, yet there might be other places where the carbon would be much higher. The normalized coil when decarburized can be expected to be fairly uniform from one end to the other.

The results shown in column 2 of Table X were so irregular, it was decided to try another steel with about the same carbon, and heat treat all specimens for 24 hours. The steel was of low alloy composition, containing 0.084% carbon, and was 0.073 inch thick. An examination of Table XI will reveal the effectiveness of the normalizing treatment. It was somewhat of a surprise to get such uniformity among the hot-rolled specimens. Obviously the hot-rolled steel had not even come close to equilibrium. A more thorough investigation of the normalized stock revealed that it was at the minimum carbon level somewhere between 14 and 16 hours. The hot-rolled steel would perhaps require much more than 30 hours.

From the results involving many steels ranging in carbon from 0.024 to 0.086%, it was concluded that the normalizing treatment was most effective on the higher carbon steels. In some cases, there

Table X
Effect of Normalizing on Rates of Decarburization (1450 °F)

Time (Hr.)	% C Steel A		% C Steel B	
	Hot-Rolled	Normalized	Hot-Rolled	Normalized
0	0.081	0.077	0.060	0.055
4	0.067	0.055	0.051	0.039
8	0.054	0.040	0.035	0.027
12	0.042	0.020	0.027	0.009
16	0.029	0.006	0.006	0.005
20	0.037	0.005	0.010	0.005
24	0.006	0.006	0.008	0.004

seemed to be little difference in the rates for the two treatments. Where there was little difference, the carbon content was always in the low part of the range, perhaps from 0.024 to 0.032%. It is predicted that, in any plant decarburization with mill scale where a carbon as low as 0.006% is desired, it will be expedient to normalize the coil before it is heat treated for the decarburization.

Composition of the Steel

Very little experimenting on the decarburization of low carbon steels is usually done before one learns that a steel containing silicon will decarburize much faster than some which do not contain this element. There are other elements, such as aluminum, which have the same effect. It may well be that a steel which has been deoxidized will decarburize faster, regardless of the deoxidizer used, except where there may be carbide precipitation. While the decarburization may go faster, it does not follow that the end point will be the same for the different elements. In the first place, the elements' effect upon the equilibrium diagram must be considered and, in the second place, insoluble carbides may be formed. The activity of carbon is determined by the amount dissolved, not upon that which may be precipitated as a carbide of a metal like titanium.

The effect of aluminum is well shown by the data in Table XII. Varying percentages of aluminum were added to small experimental heats of commercially pure iron and the 16-gage strip was decarburized by the box-anneal technique at 1375 °F (745 °C). There is a great deal of difference in time for attaining equilibrium for the material to which 0.02% aluminum was added and that to which 0.05% was added. A further increase to 0.20% had little effect, indicating that the phenomenon was one of deoxidation. On one occasion, 8000 grams of an iron containing as much as 0.05% dis-

Table XI
Effect of Normalizing on Decarburization in 24-Hour Anneal at 1450 °F

Specimen No.	Hot-Rolled C (%)	Normalized C (%)
1	0.033	0.005
2	0.030	0.008
3	0.034	0.005
4	0.029	0.005
5	0.033	0.006
Average	0.0318	0.0058

solved oxygen and 0.032% carbon evolved gases for 48 hours at 1375 °F (745 °C), without reaching an equilibrium.

As a result of the finding in connection with aluminum, it was decided to study other metals as additions, but not as deoxidizers. Each experimental heat was made from commercially pure iron as the base stock and was deoxidized with 0.05% aluminum just before the other alloying addition was made to prevent the other metal being used up in the deoxidation. All heats were hot-rolled to 16 gage and normalized before the decarburization treatment at 1375 °F (745 °C). Unfortunately, the initial carbon was not uniform in piece to piece and the amount of material used was not the same, so there is little comparison to make of time required to reach equilibrium. There were some interesting observations (see Table XIII) made regarding the end-point carbon for the different alloys all decarburized at 1375 °F (745 °C). The observed final value was obtained by the combustion method; the original, by adding to the final value an equivalent to the volume of gas collected. The calculated value was made on the same thermodynamic basis as previously described with due consideration to the total pressure of CO and CO_2 at the actual end point.

In calculating the thermodynamic end point, no consideration was given to the effect of the alloying element on the equilibrium diagram. It was assumed, for the sake of the calculation, that all the carbon was dissolved as Fe_3C or, if not, as some carbide which would readily be converted into Fe_3C as the decarburization proceeded. The assumption seemed to be in order except for the last three elements listed in Table XIII.

At least two of them, titanium and vanadium, are known to form insoluble carbides. The thermodynamic value in the table is for the carbon which is dissolved and has nothing to do with that which may be present as inclusions. The carbon remaining in the

Table XII
Effect of Added Aluminum on Decarburization at 1375 °F

	Percentage Carbon			
		Final		
Al (%) Added	Initial	Analyzed	Thermodynamic	Time (Hr.)
0.02	0.027	0.010	0.0096	17
0.05	0.028	0.011	0.0110	9
0.20	0.031	0.012	0.0107	8

steel after decarburization, which is in excess of the thermodynamic value, must occur in precipitated carbides. Decarburization can then be used as a laboratory technique to establish the chemical formula of the inclusions if the percentage of titanium or vanadium is known. In the case at hand, the carbides would be Ti_2C and V_2C if none of the metals were lost in making the ingots.

If there was roughly 50% melting efficiency with respect to the added metals, the formulas would be TiC and VC.

Boron is extremely effective in preventing the loss of carbon. Alloy 14, which probably contained considerably less than 0.05% boron, decarburized only down to 0.048% carbon. One naturally wonders what effect this element would have in preventing undesirable decarburization of higher carbon steels heat treated at temperatures higher than that used in this experiment.

All steels listed in Table XIII were decarburized overnight in hydrogen containing 20% by volume of water vapor. With the exception of the ones containing titanium and vanadium, none contained more than 0.005% carbon; the one containing boron was down to 0.003%. The titanium alloy was down to 0.012%, but the one containing vanadium had decarburized only to 0.021% carbon.

The decarburized pieces were cold-reduced from 16 to 22 gage and box-annealed at 1300 °F (705 °C) for 12 hours. The specimen containing boron, in spite of the low carbon, had a hardness around Rockwell B-52, which was about the same as that for the one containing titanium and was much higher than the others; that containing vanadium, even though its carbon was 0.021%, had a value of about B-39, in the same range in which most of the alloys fell even though they had very low carbon content.

Temperature

On leaving the 1375 °F (745 °C) point for an exploration at

Table XIII
Effect of Some Alloying Elements on End-Point Carbon at 1375 °F

Alloy No.	Element Added	% Added	Percentage Carbon		
			Initial	Final	
				Obs.	Calculated
1	Cu	0.25	0.030	0.013	0.0147
2	Ni	0.25	0.028	0.013	0.0141
3	Cr	0.25	0.036	0.012	0.0160
4	Mn	0.25	0.029	0.012	0.0135
5	Zr	0.25	0.044	0.013	0.0160
6	Co	0.25	0.025	0.014	0.0130
7	Mo	0.25	0.054	0.017	0.0161
8	W	0.25	0.044	0.014	0.0158
9	As	0.05	0.032	0.012	0.0145
10	P	0.20	0.021	0.007	0.0097
11	Si	0.20	0.019	0.006	0.0062
12	Ti	0.25	0.052	0.039	0.0134
13	V	0.25	0.048	0.037	0.0097
14	B	0.05	0.063	0.048	0.0130

other temperatures, it was decided to pass up the 1450 °F (790 °C) level, where some little work had already been done, in favor of an investigation at 1550 °F (845 °C). The first experiment was carried out according to the standard technique, using a steel with nominally 0.50% of nickel and the same amount of manganese. As usual, the boxes and furnaces were allowed to soak overnight at 1275 °F (690 °C).

On going through the familiar range from 1275 to 1450 °F (690 to 790 °C), all three boxes containing different amounts of steel gave forth gases as would be expected from the experience gained up to this point. However, at some temperature just lower than 1550 °F (845 °C), the flow of gas stopped completely for all three boxes. This same thing had happened at the lower temperature for a single box and the cause had been traced to the development of a hole in the weld due to oxidation. In the case at hand, a protective atmosphere was being used and therefore it did not seem that the boxes which had previously been found to be gas-tight could possibly be leaking. It was too much to think that all three should come to a dead end at about the same time.

The furnace temperature was held constant at 1550 °F (845 °C) for as much as 2 hours with no gas leaving the chamber for the last 1½ hours. At the last moment, it was decided to reduce the temperature to some 1450 °F (790 °C) and determine if there were leaks in the boxes. If there were not, there would be a tendency to suck the solution back into the delivery tubes because of the cooling. This move proved to be a good one because, when the tempera-

ture was lowered some substantial amount, gases were again evolved as fast as usual at the same stage of decarburization. The temperature was kept at 1450 °F (790 °C) until the decarburization reached the end point. The usual amount of gas was collected and the end point was about what one would expect. The gases stopped flowing out of the box at 1550 °F (845 °C) simply because there was no longer any chemical reaction which produced gas. The decarburization had stopped completely for thermodynamic reasons.

According to Table V, the end-point carbon should have been 0.0057% at 1550 °F (845 °C), but it was nowhere near this value showing that a wrong thermodynamic value had been calculated. One should at all times be aware that the use of the wrong diagram might prove to be fatal, and be on the lookout for a case to justify the suspicion. Here it is! A low alloy steel containing nickel and manganese to the extent of some 0.5% of each, along with the residuals of other elements, will not decarburize to a low level at 1550 °F (845 °C) even though it will at 1450 and 1800 °F (790 and 980 °C), where the decarburization is effected by mill scale in a closed container.

By using the correct equilibrium diagram for this particular alloy, the correct thermodynamic value would have been obtained and it could have been predicted that the material would not decarburize at 1550 °F (845 °C).

The diagram is not readily available, but it can be estimated that this amount of nickel and manganese will lower the equilibrium diagram for pure iron-carbon alloys about 50 °F. There is also a shifting toward the left, but this shift is small compared with the downward shift and therefore can be neglected. It is now necessary to make some adjustments for Table V. The values in columns 2, 3, 4 and 5 should all be shifted upward so that the value for some temperature, after the adjustment, will be the same as those for a temperature 50 °F higher. These adjustments occur in Table XIV along with the more proper end-point values. It should be mentioned that the solid-gas equilibrium activity remains practically the same and therefore these values have been regarded as being constant for a particular temperature even where the diagram is somewhat different from the classical diagram.

The end-point carbon values, calculated on this basis, are in general higher than those for the pure iron-carbon alloys and the range in which low carbon values can be obtained is much more

Table XIV
Equilibrium Carbon Values for an Iron-Carbon Alloy Containing 0.50% Ni and 0.50% Mn

Temp. (°F)	γ-Fe Max. %C	γ-Fe Min. %C	Solid-Solid Equil. Activity	α or β-Fe Max. %C	Solid-Gas Equil. Activity	End %C
1250	....	....	.....	0.032	1.398	No decarb.
1300	0.84	0.71	0.845	0.0331	0.839	0.0329
1350	0.89	0.51	0.573	0.0254	0.507	0.0225
1400	0.94	0.35	0.372	0.0195	0.316	0.0166
1450	0.995	0.24	0.241	0.0141	0.203	0.0119
1500	1.05	0.15	0.143	0.0092	0.131	0.0084
1550	1.10	0.08	0.073	0.0048	0.088	0.0968
1600	1.15	0.03	0.026	0.0009	0.0586	0.0674
1650	1.21	....	.....	.....	0.0405	0.0490
1700	1.28	....	.....	.....	0.0275	0.0352
1750	1.33	....	.....	.....	0.0197	0.0262

narrow. It is interesting to note that at 1300 °F (705 °C) there is only a very slight difference in the solid-solid activity and the solid-gas activity, the latter being smaller, indicating that α-iron can be formed. With a slight lowering of the diagram by further alloy addition, the solid-gas activity would be higher than the solid-solid activity and the carbon could not be reduced below about 0.80%.

If alloys are added to the steel until the diagram is lowered 100 °F, it may be possible that there can be no decarburization of a steel already containing fairly low carbon during a heat treatment where the steel is in a closed container with mill scale.

Table XV has been obtained, in the same way that Table XIV was, with a further 50 °F shift. It is interesting to note that there is no longer a range within the critical where low carbon values can be obtained.

After considering the effect of manganese and nickel as elements which lower the diagram, it is only natural to consider some of those which raise the diagram. It has already been pointed out that silicon promotes decarburization, particularly insofar as rates of reaction are concerned. It has been thought that its effect was in some way due to its deoxidizing power. Possibly its effect may be associated with the fact that the diagram is raised.

Aside from the effect on the end-point carbon, temperature also has an influence upon the rates of decarburization. Any ordinary low carbon steel will decarburize faster around 1450 to 1500 °F (790 to 815 °C) in any atmosphere which was tried.

Thickness

While no accurate comparisons were made for steels of differ-

Table XV
Equilibrium Carbon Values for Steel Whose Critical Range Is 100 °F Lower Than the Normal

Temp. (°F)	γ-Fe Max. %C	γ-Fe Min. %C	Solid-Solid Equil. Activity	α or β-Fe Max. %C	Solid-Gas Equil. Activity	End %C
1250	0.84	0.71	0.845	0.0331	1.398	No decarb.
1300	0.89	0.51	0.573	0.0254	0.839	0.747
1350	0.94	0.35	0.372	0.0195	0.507	0.477
1400	0.995	0.24	0.241	0.0141	0.316	0.314
1450	1.05	0.15	0.143	0.0092	0.203	0.213
1500	1.10	0.08	0.073	0.0048	0.131	0.144
1550	1.15	0.03	0.026	0.0009	0.088	0.101
1600	1.21	....	.....	.....	0.0586	0.071
1650	1.28	....	.....	.....	0.0405	0.052
1700	1.33	....	.....	.....	0.0275	0.037

ent thicknesses, where the decarburization was done with mill scale, it is believed that the relative order of results would be similar to those obtained by any other means of decarburizing.

Different thicknesses of the steel, described in a previous publication (1), were subjected to decarburization at 1500 °F (815 °C), in hydrogen containing 20% by volume of water vapor, to determine the time necessary to render the eutectoid steel completely ferritic. The results are shown in Table XVI for specimens with a ground finish.

The complete data, of which those in Table XVI are a part, were fitted with empirical equations giving the number of grams lost (y) for a specimen 0.7 by 4.0 inches in terms of total time (t). The relation of these equations for different thicknesses was apparently simple enough to justify the introduction of thickness (x) as a parameter in obtaining

$$y = 0.053 + (0.05635 + 0.106x) \log t + (0.02215 + 0.344x) (\log t)^2.$$

Equation XXV

This equation gives 1.3 hours as the time necessary to decarburize this steel, where the thickness is 0.020 inch. If the thickness is only 0.010 inch, a matter of only 15 minutes will be required. A piece ¼ inch thick will require perhaps as much as 178 hours.

Effect of Catalysts

Various investigators have observed the silica and alumina inclusion in steel due to surface infiltration of oxygen. Notably among these are Welchner and Roush (8). These inclusions were recognized some time ago in the surface of silica steels which had been

Table XVI
Effect of Thickness on Time for Decarburization of Eutectoid Steel

Thickness (In.)	Temperature (°F)	Total Time (Hr.)
0.040	1500	6.4
0.048	1500	9.4
0.056	1500	13.2
0.064	1500	19.1

decarburized with mill scale and even some which had been decarburized with moist hydrogen. It has been found many times that silicon in itself speeds up decarburization, but if the amount of silicon becomes higher and higher, the over-all effect of silicon reaches a maximum long before 4.5% is reached. There are really two factors at work: (a) The beneficial effect of silicon as an alloying element, and (b) the hindering effect of silica inclusions formed by the diffusion of oxygen into the steel.

In the decarburization of ordinary steel with moist hydrogen, faster reaction is obtained with the hydrogen present, even though water vapor is the decarburizer, than where water vapor alone is present. The hydrogen serves to prevent oxidation of the elementary iron itself with subsequent inward diffusion of iron oxide which would interfere with the diffusion of carbon.

Likewise, some substance which will prevent the oxidation of silicon within the metal should act as an aid in speeding up decarburization of steels high in silicon. Knowing that hydrofluoric acid attacks silica and glass, it was decided to use a fluoride. Perhaps due to its availability, sodium fluoride was selected and applied to the surface of the work with a paint brush using a slurry made with water. The coating was painted right over the normalized scale.

High silicon steels responded even beyond expectation, but the product produced was quite brittle and hardly suitable for cold rolling. There is a bare possibility that this condition could be taken care of, if the steel were decarburized in coils or strip and then hot-rolled to some thinner gage to eliminate the brittleness.

Suggestions Relative to Plant Operations

There is an interesting point for discussion in Table V. At temperatures almost up to 1300° F (705 °C), the solid-gas equilibrium activity exceeds unity. What is the physical significance of such an activity?

Actually, the theoretical activity is higher than that for pure graphite or pure cementite. It is known that graphite or cementite dissolves in α-iron to saturate it at some low value at 1275 °F (690 °C). Perhaps there might be 0.028% carbon in the saturated solution whose activity, of course, is unity. Now, since the theoretical equilibrium activity is in excess of the saturated solution, there will be a tendency to form free cementite particles in the surface of the steel. It may be possible to find, underneath the oxide coating on a steel heat treated at 1275 °F (690 °C), free cementite particles which may cause primary boiling where the steel is later coated with enamel. Such a formation of carbides presupposes that a carburizing material is present in the furnace atmosphere. If this theory is correct a raise of 50 °F in the heat treating temperature will eliminate the difficulty.

In the way of summarizing some of the effects upon the end-point carbon, two problems will be solved.

First, how much steel can be used in a box anneal at 1400 °F (760 °C) and get an end-point carbon of 0.007% if the original normalized steel contains 0.05% carbon and the box has 250 cubic feet of free gas space? The chemical activity of a steel with respect to carbon which contains 0.007% carbon can be found by simple proportion to be 0.158. This activity should be substituted in Equation VII along with a value for K_{1P} obtained from Table II. Thus a value for P^2_{CO}/P_{CO_2} may be obtained. From Table III can be obtained a value for P_{CO_2}/P_{CO}. The two equations obtained in this manner can be solved simultaneously for P_{CO} and P_{CO_2}. If the atmospheric pressure is 740 millimeters (0.974 atmosphere), the pressure of nitrogen may be found by subtracting $P_{CO} + P_{CO_2}$ from 0.974. The volume percentage of nitrogen will be 48.8. This value can now be used in Equation XXIV to solve for x, the volume of gas evolved from the sand-sealed box. The calculation gives, for the problem at hand, 179.4 cubic feet at 1400 °F (760 °C) and 740 millimeters. At 32 °F and 29.92 inches of mercury the volume will be 46.21 cubic feet. The pound-atom of carbon in mixtures of CO and CO_2 occupies 359.1 cubic feet, under this standard condition, and contains 12 pounds of carbon; 46.21 cubic feet then contains by proportion 1.544 pounds of carbon. The carbon to be removed is 0.043% of the total weight and is 1.544 pounds. One hundred per cent then will be 3590 pounds, the amount of the steel which can be charged into the box if 0.007% carbon is expected at

the end point. With less steel, the end point will be lower; with more, it will be higher.

The second problem involves the calculation of the end-point carbon where 20,000 pounds of the steel is charged into the box which holds 250 cubic feet. The volume of the steel can no longer be neglected. In this case it amounts to about 41 cubic feet and, therefore, there will be about 209 cubic feet of free gas space.

Let m = %C at equilibrium and
n = activity at equilibrium.

$$\frac{(20{,}000)\ (0.05 - m)}{100} = 10\text{-}200m = \text{lb. of C removed.}$$

By proportion,

$$\frac{m}{0.0254^*} = \frac{n}{0.573}, \qquad \text{Equation XXVI}$$

from which

$$n = 22.56m. \qquad \text{Equation XXVII}$$

By substituting the proper value for K_{1P} and the value of n for A_C in Equation VII,

$$3.471 = \frac{P^2_{CO}}{(22.56m)\ P_{CO_2}}, \qquad \text{Equation XXVIII}$$

from which

$$\frac{P^2_{CO}}{P_{CO_2}} = 78.31m. \qquad \text{Equation XXIX}$$

For the same conditions Equation IX yields:

$$\frac{P_{CO_2}}{P_{CO}} = 0.577. \qquad \text{Equation XXX}$$

Multiply Equation XXIX by Equation XXX and

$$P_{CO} = 45.18m. \qquad \text{Equation XXXI}$$

From Equation XXX,

$$P_{CO_2} = 0.577\ CO \qquad \text{Equation XXXII}$$

*See Table V.

Assuming that the total pressure is 1 atmosphere, the volume percentage of nitrogen will be 100 $(1 - P_{CO} - P_{CO_2})$. By appropriate substitutions, first from Equation XXXII and then from Equation XXXI, the percentage of nitrogen simplifies to $100 - 7125m$. This value is now ready for substitution in Equation XXIV. A and **x** must be evaluated so that their values may be substituted in the same equation.

Above, it was found that $10 - 200m$ pounds of carbon must be removed to reach the end point. Since 1 pound of carbon in carbon gases will occupy 29.93 cubic feet under standard conditions (S.T.P.), the amount with which we are concerned will occupy $29.93\ (10 - 200m)$ cubic feet at 32 °F and 29.92 inches of mercury. Recapitulating for substitution in Equation XXIV:

$$\log \mathbf{y} = \log\ (100 - 7125m),$$
$$\mathbf{x} = 1132 - 22640m, \text{ and}$$
$$\mathbf{A} = 209.$$

Carrying out the substitutions in Equation XXIV:

$$\log\ (100 - 7125m) = 2 - \frac{1132 - 22640m}{(2.303)\ (209)}. \qquad \text{Equation XXXIII}$$

The equation can best be solved for an approximate value by trial and error. In this way, it is found that

$$m = 0.0138.$$

For quantities of steel where the volume of carbon gases is large, the equilibrium value can be read in Table V; for smaller amounts, it is more appropriate to make a calculation such as that just shown.

Where special properties are desired, a carbon value of 0.014% may be far too high. Three samples of a low alloy steel, decarburized to 0.014, 0.013 and 0.013% carbon, respectively, in 0.072-inch thickness and finally cold-rolled to 0.030 inch, gave, after a 1500 °F (815 °C) heat treatment, an average yield strength of 42,300 psi. Three other samples, where the carbon was reduced to 0.007, 0.006 and 0.007%, gave an average yield strength of 31,960 psi. If one is seeking a low yielding, soft material in this type of steel, 0.014% carbon cannot be considered as being satisfactory.

On the other hand, it is not economically practical to reduce the size of the charge to some such small amount as 4000 pounds.

If the box containing the 20,000 pounds of steel could be partially evacuated near the end of the run, the carbon could be reduced to a lower value. This suggestion is not very practical because, due to the high temperature, the box will collapse unless made of quite heavy material. The total pressure of the carbon gases can best be diminished by flushing the box with nitrogen or compressed air which has been led through a box of hot coke, charcoal, or graphite. This container can well be placed inside the annealing cover. If the flushing is to be done with tank nitrogen, it should be used near the usual end point. Should the other alternative be used, the air can be turned on at a fairly slow flow at any time the anneal is under way.

It has been the writer's experience that a steel containing a fairly high carbon, say around 0.080%, cannot be decarburized with mill scale to have a yield strength as low, after cold rolling and heat treating at 1550 °F (845 °C), as can be obtained with the lower carbon steels, containing no more than 0.050% initially. In fact, the yield strength of the steel originally containing 0.080% may be as much as 1½ times as high after the completed processing. If the final carbon analyses are the same for two steels, that having the higher carbon originally will have the higher yield strength and will be harder.

Conclusions and Summary

1. Decarburization of steel with mill scale is effected by two gaseous reactions.
2. CO reduces the mill scale; CO_2 oxidizes the carbon at the surface of the steel.
3. Pickled specimens can readily be decarburized by the scale on other pieces even though there is no solid contact.
4. Equilibrium constants and free energy data have been used in thermodynamic considerations involving decarburization.
5. To use thermodynamic principles with a good degree of accuracy, it was necessary to establish the carbon solubility in ferrite within the critical range.
6. It has been found experimentally and thermodynamically that, where decarburization is effected with mill scale, a dead end point is reached with both mill scale and carbon still present.
7. An experimental technique has been developed which can be used to measure continuously the progress of decarburization.

8. A measure of the volume of gas expelled from the reaction chamber can be used as a method for carbon analysis.
9. The thermodynamic end-point carbon is dependent upon the total pressure of CO and CO_2. The higher this pressure, the higher is the end point.
10. At any temperature, there is a total pressure of CO and CO_2 above which a given steel will not decarburize.
11. A lowering of the total pressure of CO and CO_2 can be effected by diluting the gas with nitrogen. Such a dilution tends toward lower carbon content.
12. Mass of steel decarburized is sometimes a factor for consideration due to the expulsion of different quantities of nitrogen from the chamber.
13. Likewise, the amount of carbon in the steel has its effect.
14. Neither the mass of steel nor per cent carbon has an effect upon the end point if the heat treating chamber is filled with a gas consisting of 85% CO and 15% CO_2 at any time during the heat treatment.
15. An equation has been derived which is useful to determine the amount of nitrogen or inert gas remaining in the heat treating chamber at any time.
16. Inert gases aid in lowering the end-point carbon, but only because they serve to lower the total pressure of CO and CO_2.
17. Decarburization of steel which has been hot-rolled-normalized proceeds much more uniformly than does that hot-rolled only.
18. Deoxidizing agents, such as silicon and aluminum, where dissolved in the steel, increase the rates of decarburization.
19. Titanium, vanadium and boron raise the end-point carbon beyond the calculated value, unless insoluble carbides be taken into consideration in the calculations.
20. It has been suggested that decarburization can be used to establish the chemical formulas of insoluble carbides.
21. Some vanadium steels can be made quite soft even though as much as 0.02% carbon is still present.
22. The fastest decarburization of low carbon steels seems to take place somewhere around 1450 °F (790 °C).
23. No appreciable amount of decarburization with mill scale will take place at a temperature as low as 1275 °F (690 °C).
24. One steel tested did not decarburize at 1550 °F (845 °C), but it would at 1450 °F (790 °C) or at 1800 °F (980 °C).

25. It has been postulated that no steel, whose equilibrium diagram is 100 °F lower than the classical diagram, will decarburize into the α-iron region where mill scale is present and the steel is in a closed container.
26. A mathematical relation of thickness to amounts of carbon removed has been presented where hydrogen and water vapor are involved.
27. It has been found that high silicon steels and irons decarburize faster where a fluoride catalyst is used.
28. The suggestion has been offered that it is possible to form free cementite particles in the surface of a steel covered with scale if it is heat treated at 1275 °F (690 °C).
29. Free cementite could not form at 1325 °F (720 °C) in the surface of a steel covered with mill scale, because this temperature is well within the decarburizing range for ordinary steels.

Acknowledgment

In the course of the last several years, the writer has received many helpful suggestions, in connection with decarburization, from associates in the field of metallurgy; so many, in fact, that it is impossible to mention them all here.

Part of the work reported here was done in Mellon Institute while the author was the incumbent of the industrial fellowship on foundry practice.

The writer is also indebted to friends in Carrier Corporation who have helped to complete this work.

References

1. W. A. Pennington, "A Mechanism of the Surface Decarburization of Steel," TRANSACTIONS, American Society for Metals, Vol. 37, 1946, p. 48-109.
2. Eric R. Jette and Frank Foote, "A Study of the Homogeneity Limits of Wüstite (FeO) by X-Ray Methods," *Transactions,* American Institute of Mining and Metallurgical Engineers, Vol. 105, 1933, p. 276-289.
3. John Chipman and Shadburn Marshall, "Equilibrium $FeO + H_2 = Fe + H_2O$ at Temperatures up to Melting Point of Iron," *Journal,* American Chemical Society, Vol. 62, 1940, p. 299-305.
4. John Chipman, "Free Energy of Water, Carbon Monoxide, Carbon Dioxide, and Methane," *Industrial and Engineering Chemistry,* Vol. 24, 1932, p. 1013-1017.
5. John Chipman and Donald W. Murphy, "Free Energy of Iron Oxides," *Industrial and Engineering Chemistry,* Vol. 25, 1933, p. 319-327.
6. J. B. Austin and M. J. Day, "Chemical Equilibrium and the Control of

Furnace Atmospheres," *Industrial and Engineering Chemistry,* Vol. 33, 1941, p. 23-31.
7. J. K. Stanley, "Steel Carburization and Decarburization; a Theoretical Analysis," *Iron Age,* Vol. 151, 1943, p. 31-35, 36-39, 49-55.
8. J. Welchner and R. W. Roush, "Supposed Graphite in Carburized NE and S.A.E. Steels; Effect of Calcium and Barium," METAL PROGRESS, Vol. 43, 1943, p. 889-896.

DISCUSSION

Written Discussion: By F. R. Morral, associate professor, Department of Materials Engineering, Syracuse University, Syracuse, N. Y.

Dr. Pennington's paper was very interesting and he is to be congratulated for his painstaking work and his detailed presentation, a suitable sequel to his former paper.

I wonder if Dr. Pennington has treated steel pieces thicker than 0.062 inch and made carbon analyses on successive 0.005-inch layers. The carbon analyses of the fifth layer in Table IV are consistently 0.13% carbon lower than the carbon should be according to his Table V. Is there any significance in this?

I am somewhat surprised to note that Dr. Pennington takes the 1936 METAL PROGRESS Iron-Carbide Diagram as a reference. He will note on comparing it with the October 1947 diagram (or the 1948 ASM METALS HANDBOOK, page 1182), that some changes have been agreed upon. Furthermore, the diagram used may be somewhat difficult for the younger generation to find.

Dr. Pennington has calculated an equation to determine the time necessary to decarburize a given thickness of steel if the amount of carbon which should be removed is established. A set of curves could be drawn showing the relationship between thickness of the steel to be decarburized and rate of decarburization to ferrite at various temperatures. These curves probably will be straight lines. Such a graph may be useful.

Author's Reply

The points to which Dr. Morral has devoted attention are indeed apropos.

The author does not recall having made layer cuts from decarburized specimens whose thickness was more than the nominal 0.062 inch. Thicker specimens should give more convincing results.

As far as physical chemistry is concerned, there is no significance to the fact that the carbon values of layer 5 in Table IV are consistently 0.13% lower than the values in column 3, Table V. However, there is a probable psychological significance in that the author, in selecting typical data for Table IV, subconsciously chose those nearest to a 3:2:1 relationship for the fifth layer. It would have been more realistic had another set of data been presented for the 1400 °F (760 °C) treatment where the fifth layer had 0.092% carbon.

The layer cut which contains the interface between ferrite and what

was austenite at the operating temperature can have, for the 1400 °F (760 °C) treatment, any carbon content from 0.026 to 0.51%, depending upon the location of the interface within the layer. It should be pointed out that the experimenter can control the depth of the interface quite accurately by stopping the decarburization at a desired point. It is not at all difficult to stop the reaction within 0.01% carbon of a desired value. In this way, one can always have the interface within the layer desired and, furthermore, can have the interface at a desired plane within the layer.

All the calculations in this paper were made some time before the 1947 diagram was available. It did not occur to the writer that the new diagram could cause much difference. The main difference in the two diagrams is the solubility of carbon in austenite; it is most difficult to understand how, in the modern era, there could be a line so wrong as one of the Acm lines must be.

It was stressed in the paper that the diagram being used was not necessarily that of a particular steel being tested, but served as a type. The exact diagram would be desirable for extremely accurate calculations. One can, however, solve practical problems by making use of any diagram which is approximately correct.

As to the suggested curves for time to decarburize different thicknesses to complete ferrite at different temperatures, data in Table XVI are convincing that the thickness-time curve, at a particular temperature, is not a straight line. Multiplying the thickness, in the case of 0.040-inch material by 1.6, multiplies the time by almost exactly 3.0.

Informal discussions of the paper since its presentation have revealed that some are inclined to get the wrong impression with regard to the effect of mass on the thermodynamic end-point carbon. As such, mass has no effect. Indirectly, it may control the compositions of the gases in the box and thus indirectly change the thermodynamic end-point.

CAUSE AND CURE OF INVERSE CHILL AND HARD SPOTS IN CAST IRON

By C. A. Zapffe and R. L. Phebus

Abstract

Abnormal conditions of "inverse chill" in gray cast iron and zones of retarded graphitization—"hard spots"—in malleable iron are studied from the standpoint that both conditions follow directly from hydrogen segregation similar to that causing "flakes" in forgings, "white spots" in castings, and "fisheyes" in welds.

Based upon the known stabilization of cementite by hydrogen, the study proceeds to disclose the thermodynamic nature of stabilization in general, and stabilization by hydrogen in particular, the relationship of hydrogen concentration across the area of segregation both to the cementite in the chill and to a secondary phenomenon of abnormal graphitization adjacent to the chill, and methods for prevention of the defects.

Introduction

FOR at least a quarter of a century (1),[1] there has continued published discussion of a phenomenon which causes gray cast iron to develop anomalous chill areas away from the chill surface, and malleable iron to show internal zones of retarded graphitization.

In the case of gray iron, these areas often appear near the center of the section as a cementitic zone surrounded by a graphitic rim, exactly opposite to the expected occurrence of chill at the surface, where cooling is necessarily most rapid. The phenomenon is accordingly called "inverse chill". X-ray studies of ring castings have revealed small shrinks and voids which, on metallographic examination, are found in almost every case to be associated with an adjacent zone of "inverse chill" (2). Morrogh and Williams (3), in their

[1]The figures appearing in parentheses pertain to the references appended to this paper.

Research conducted in conjunction with an Office of Naval Research contract on gas-metal systems.

A paper presented before the Thirtieth Annual Convention of the Society, held in Philadelphia, October 23 to 29, 1948. The authors, C. A. Zapffe and R. L. Phebus, are consultants, Baltimore. Manuscript received May 14, 1948.

recent exhaustive discussion of cast iron, state that . . . "No satisfactory explanation has been given for inverse chill."

In malleable iron, similar centers of stabilized cementite occasionally appear, resulting in similar difficulties, particularly in machining, such that in both the malleable and the gray iron industries "hard spots" constitute a well-known nuisance.

While these two phenomena are commonly discussed separately, it is the purpose here to show that they are in fact one, and that they have both a ready explanation and a ready cure.

Observations

In the research laboratory of the Piston Ring Division of the Koppers Company in Baltimore, under the direction of Dr. T. C. Jarrett, there was produced a ring cylinder of cast iron typically sensitive to the defect in question. The following material constituted the charge, melted in an induction furnace:

Pig Iron	40 pounds
Return Scrap	60 pounds
85% Ferrosilicon	0.31 pounds
Graphite	0.12 pounds

The ferrosilicon and graphite were added as inoculants at a temperature of 2850 °F (1565 °C), which later rose to 2900 °F (1595 °C). The melt was then covered with a mixture of silica sand with approximately 10% borax glass and was poured between 2760 and 2725 °F (1515 and 1495 °C) from beneath this cover. None of the materials was previously dried. Analysis of the resulting iron follows:

Total Carbon	3.79%
Graphitic Carbon	3.05%
Combined Carbon	0.74%
Silicon	2.82%
Sulphur	0.047%
Phosphorus	0.51%
Manganese	0.51%

Typical "hard spots" were found. In Fig. 1 a ring section is shown ground to one-half thickness and etched with nitric acid. The centrally located flecks of unetched carbide disclose "inverse chill". An enlargement in Fig. 2 makes the practical importance of these cementitic areas more obvious. Machining such a ring understandably leads to much difficulty.

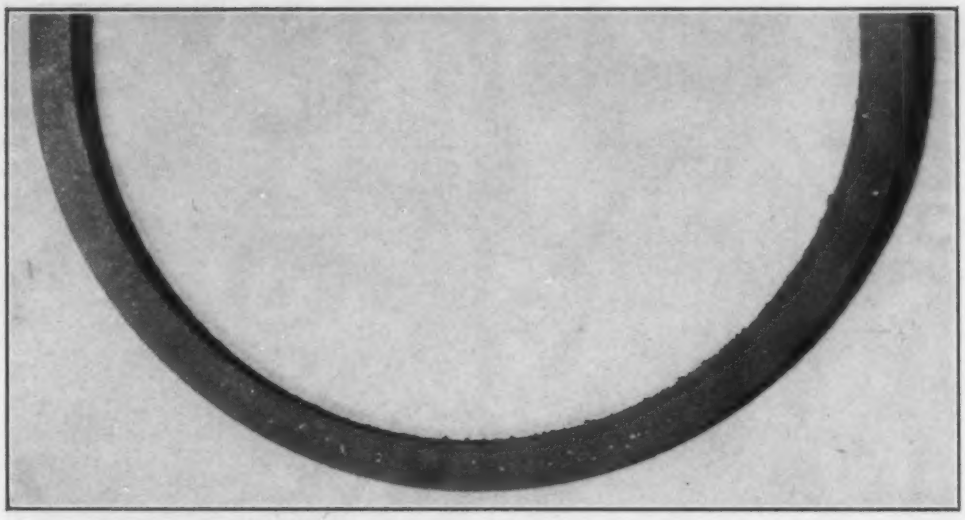


Fig. 1—Cross Section of Part of a Gray Iron Piston Ring Ground to One-Half Thickness and Etched With HNO_3. The centrally located flecks of unetched carbide disclose "inverse chill". × 1.0. (Courtesy Piston Ring Division, Koppers Co.)

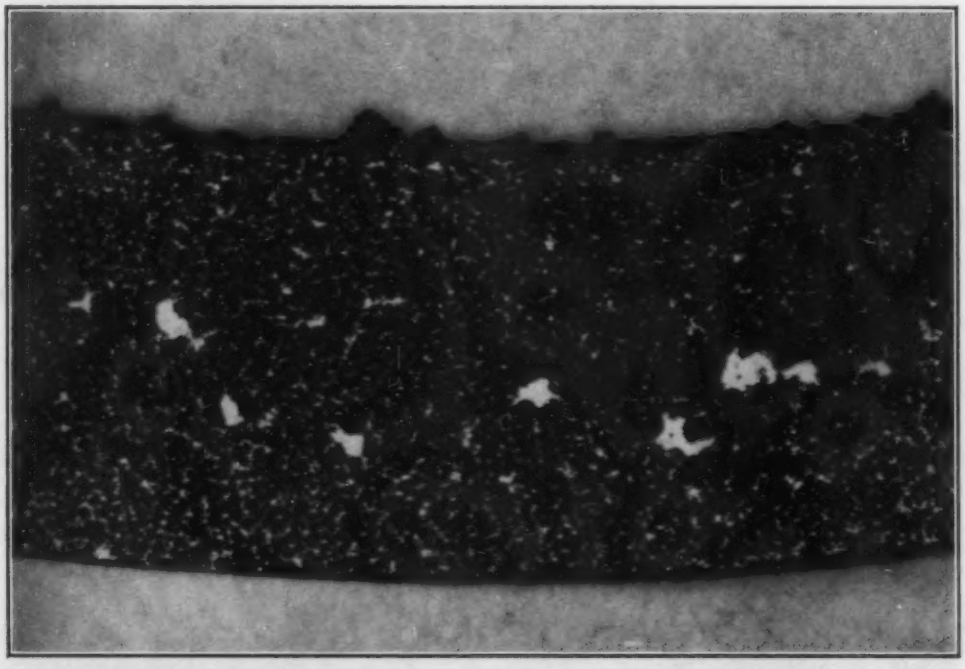


Fig. 2—Enlargement of Fig. 1. × 10. (Courtesy Piston Ring Division, Koppers Co.)

Under the microscope the "hard spot" is readily detected as an accumulation of fine eutectic carbide characteristically associated with Type D, or undercooled, graphite, as illustrated in Fig. 3. This carbide form can be contrasted to the eutectic carbide found in areas of normal chill. (See Fig. 4.) An interdendritic disposition is

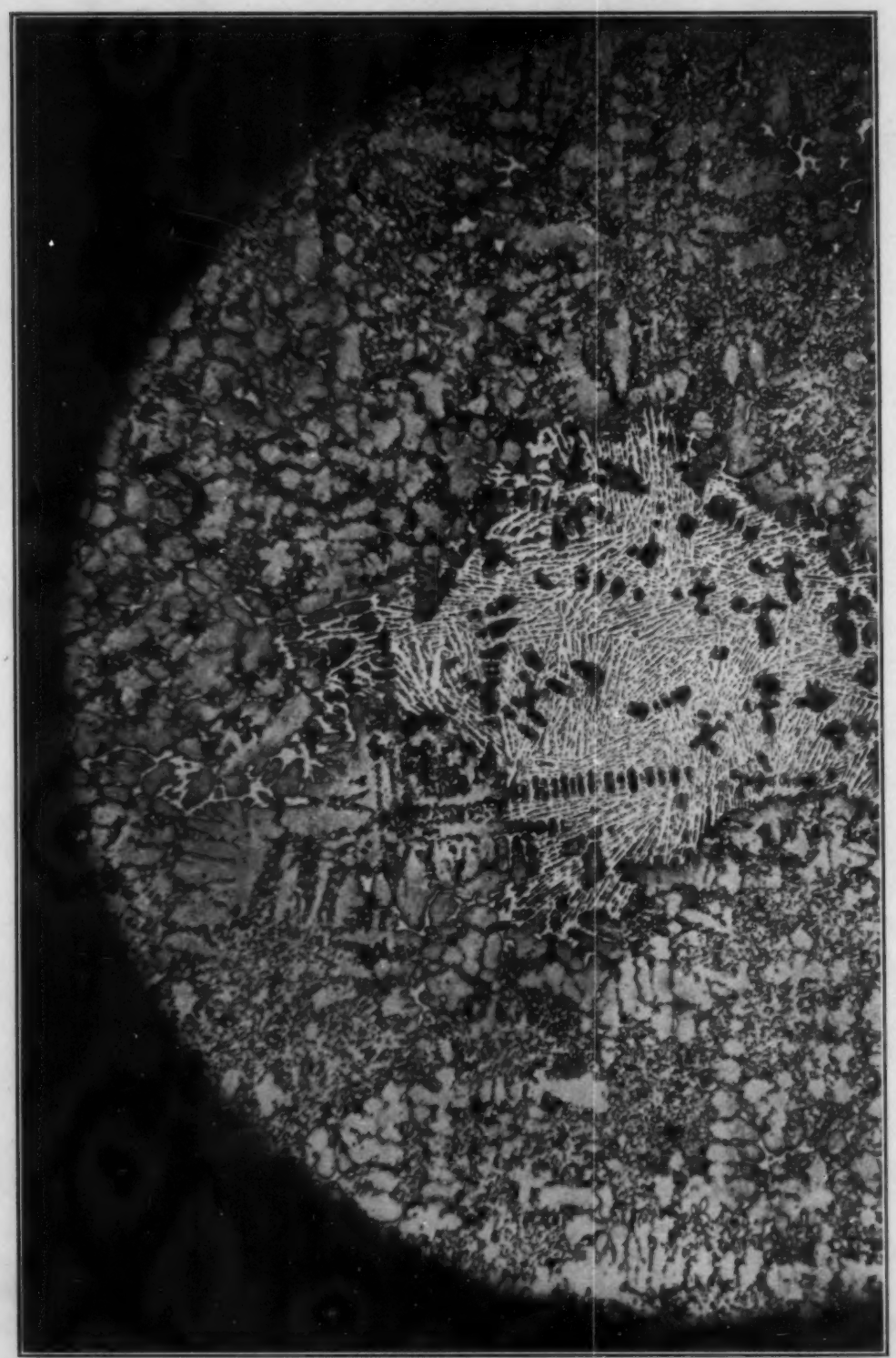


Fig. 3—Photomicrograph of an Area of Inverse Chill. Note the typical eutectic laminar carbide in a local matrix of austenitic-pearlitic dendrites and Type D, or undercooled, graphite. Picral etch. × 250. (Courtesy Piston Ring Division, Koppers Co.)

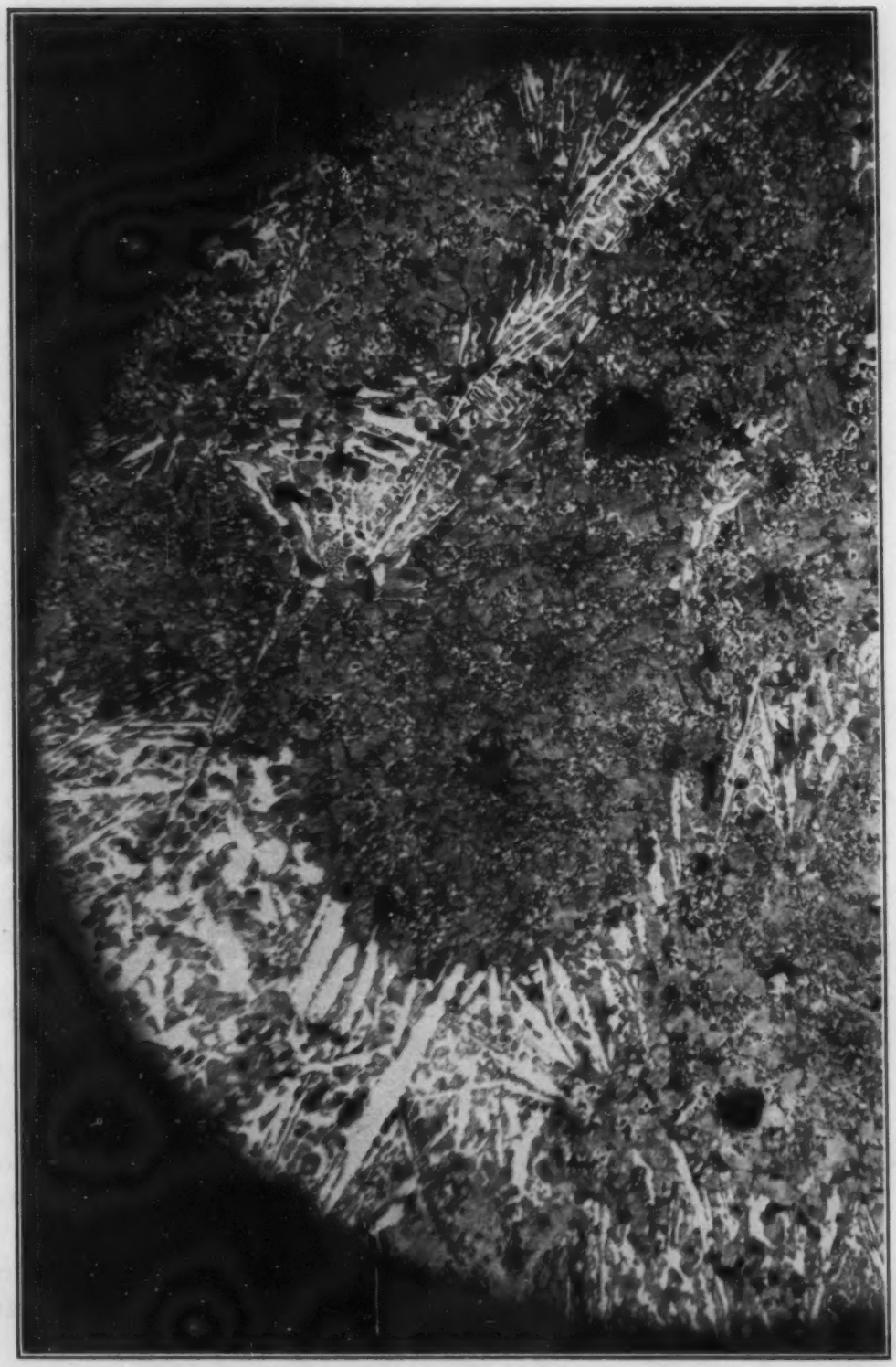


Fig. 4—Photomicrograph of Normal Chill, Partly Decomposed. Large eutectic laminae project as primary structures into a eutectic matrix which subsequently decomposed to form pearlite, ferrite, undercooled graphite, also some nodular graphite. Picral etch. × 250. (Courtesy Piston Ring Division, Koppers Co.)

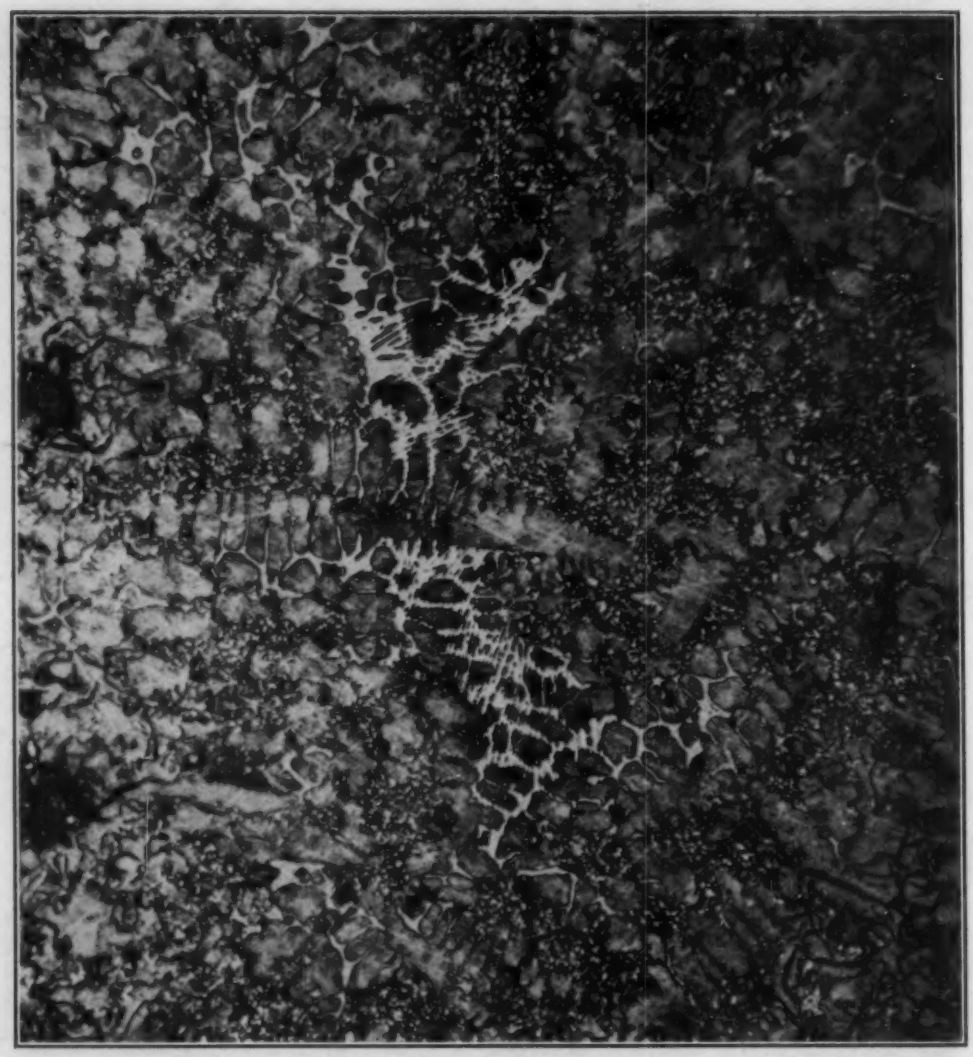


Fig. 5—Photomicrograph of a Less Massive Area of Inverse Chill. Note (a) the pronounced interdendritic disposition of the carbide, (b) the surrounding austenitic-pearlitic dendrites with undercooled graphite, and (c) the occasional graphite nodule. Picral etch. × 250. (Courtesy Piston Ring Division, Koppers Co.)

especially evident in less massive occurrences, such as that shown in Fig. 5, and this gives rise to a characteristic dendritic pattern of decomposed austenite generally coinciding with occurrence of the defect.

In Fig. 6 there appear all the structures characteristically associated with inverse chill; and, in addition, normal flake graphite can be seen surrounding the defective zone.



Fig. 6—Photomicrograph of an Area of Inverse Chill. In addition to all characteristic structures, the normal flake graphite structure can be seen bounding the zone of the defect. Picral etch. × 250. (Courtesy Piston Ring Division, Koppers Co.)

Previous Theories

The Segregation Theory

Twenty-eight years ago, Osann (1) described "hard white spots" found in cast iron rolls and ascribed them to carbon segregation.

In 1939, however, Fisher (4) published a detailed consideration of inverse chill with data which disprove not only the theory of carbon segregation, but any theory having to do with the segregation of commonly analyzed elements. For example, the following is an analysis given by Fisher for the gray rim and the white core, respectively, of a section showing inverse chill:

	Total Carbon	Graphitic Carbon	Combined Carbon	Mn	P	S	Si
Outside (gray)	3.40	3.40	....	0.36	0.60	0.106	2.61
Inside (chill)	3.29	0.25	3.04	0.19	0.74	0.102	3.16

One will note that, although there is less total carbon in the chill area, the carbon equivalent lies considerably toward the graphitizing side.

As for other elements, there stands in this analysis a remarkable disproof of any existing segregation theory. Thus, the graphitizing elements, silicon and phosphorus, show a concentration in the chill area which is greater by more than 20%, and the only other element showing segregation at all is manganese, which is a "retarder" element and shows, contrarily, less concentration in the area which is retarded.

The Pressure Theory

Fisher (4) and Fielden (5) both discuss pressure as a cause of inverse chill, the pressure presuming to originate in the contraction of the surface during cooling.

Since "inverse chill" has been observed associated with porosity and shrinkage, the pressure theory immediately becomes untenable. Fisher's own photographs show shrinkage cavities centrally located within the chill (4).

Other Theories

A so-called "oxygen theory" was originated by Scheil, Ruff and

Schulz, according to Fisher (4), in which oxidation during pouring presumably formed "unfavorable" oxide nuclei, whatever they might be. Touceda (6) seems also to have had in mind an oxygen theory.

Among other theories, there is one attributed by Fisher (4) to Moly Matrix in 1938 involving overdosage of ferrous sulphide in the ladle. While sulphur can favor retention of cementite, the defects in question certainly do not depend on sulphur manipulations; and sulphur, therefore, is not the fundamental cause.

Still another theory, utterly untenable, claims that high pouring temperature, which is known to favor inverse chill, provides an excess of heat to the mold sand which later anneals the rim and leaves the core white (4)! A very simple explanation for the known effect of high pouring temperature will follow from the present study.

Summary

As late as 1946, Crome (7) described inverse chill at length, but without explanation. Fisher's conclusion probably provides a fair summary, that there is today no satisfactory explanation for "the rather common mystery of the inverse chill in gray cast iron".

The Hydrogen Theory

General Statement

Both "inverse chill" in gray iron and "hard spots" in either gray or malleable iron are nothing other than the result of a segregation of hydrogen. This is the claim of the present paper. It applies to the systemic defect previously described, of course, which should not be confused with chance segregations of such elements as chromium or phosphorus, whose dispositions are readily analyzed and known.

Hydrogen is present in all irons to greater or less degree. During solidification of the iron, the hydrogen markedly segregates between growing dendrites because its solubility is greatly decreased in solid iron and because it has perhaps the greatest mobility of all impurities dissolved in the iron.

In the case of gray iron, this segregated hydrogen prevents decomposition of the concurrent eutectic iron carbide during the freezing and cooling period in which that carbide would normally decompose to form graphite; and in malleable iron, exactly the same phenomenon reveals itself during the subsequent malleableizing cycle when

hydrogen-rich areas concealed within the white iron matrix resist decomposition. In both cases, "hard spots" are observed, particularly during subsequent machining.

Hydrogen as a Stabilizer of Cementite

Previous Observations—At least as early as 1910 it was known that hydrogen stabilizes the cementite in cast iron, for Wüst (8) and Wüst and Sudhoff (9) discuss that fact. Later, Honda and Murakami (10) in 1920 and Sawamura (11) in 1928 flushed melts of iron-carbon alloys with such gases as CO_2, CO, O_2, air, N_2, NH_3, CH_4, and H_2 and proved that all gases containing hydrogen stabilized cementite, and that none of the other gases had that effect. In 1930, Norbury and Morgan (12), (13) conducted similar research. In 1935 Baukloh (14) described further the nature of carbide stabilization by hydrogen. From 1937 to 1939, Boyles (15-17) extended these studies up to H_2 pressures of 300 psi.

Later, Schwartz and his associates (18), (19) and Lorig and Samuels (20) demonstrated the strong effect of hydrogen on the decomposition of cementite during malleableizing. And Houdremont and Heller (21), injecting the gas by annealing in an atmosphere of hydrogen at 1000 °C (1830 °F), found that the cementite in cast iron was stabilized, also that the hardenability of steel was increased.

Thermodynamic Explanation for Stabilization by Hydrogen—In its simplest fundamentals, the behavior of carbon in iron follows the thermodynamic dictates of its fugacity, or "escaping tendency". When the fugacity of carbon dissolved in iron is greater than its fugacity as graphite, the carbon tends to escape from the iron and form graphite, and vice versa.

Expressing the fugacity of the carbon in terms of its vapor pressure, P_C, graphite can form only under such conditions that:

$$P_C > (P_C)_{\text{Graphite}} \qquad \text{Equation 1}$$

where P_C is the carbon pressure of the system in question at any given temperature and $(P_C)_{\text{Graphite}}$ is the carbon pressure over free graphite at that same temperature. The term on the left is some function of carbon concentration in the iron, whereas the term on the right is a constant at constant temperature.

For the internal reaction expressing the dissociation of iron carbide into free iron and dissolved carbon:

$$[Fe_3C] = 3\,Fe + [C] \qquad \text{Equation II}$$

where brackets represent solution in iron. The total dissolved carbon, therefore, includes the free carbon [C] plus the portion associated with Fe as Fe_3C:

$$\Sigma[C] = [C] + [C]_{Fe_3C} \qquad \text{Equation III}$$

The vapor pressure, P_C, is measured directly by the free carbon [C], the portion statistically bound as Fe_3C being unable to "escape" and therefore unable to contribute further to the fugacity. Consequently, for any given total carbon content showing in an analysis of liquid iron or of graphite-free white iron:

$$[C] = f(P_C) = \Sigma C - [C]_{Fe_3C} \qquad \text{Equation IV}$$

where $f(P_C)$ expresses the functional relationship between [C] and P_C.

Accordingly, P_C for any system becomes further decreased by additional chemical bonds which may develop within the matrix. Strong bond attractions do exist between H and C, and hence not unexpectedly between [H] and [C] within the iron matrix, even though they are certainly greatly weakened at high temperatures. The affinity can be generally expressed as:

$$[C] + x[H] = [CH_x] \qquad \text{Equation V}$$

where x is the ratio H/C in the compound in question and [C], as before, concerns only that portion of dissolved carbon which is statistically "free". Methane, CH_4, is the combined form commonly considered; but fixing $x = 4$ is unnecessary, and may be misleading, particularly at high temperatures.

For an iron-carbon system containing hydrogen, therefore, internal association of carbon exists both with iron and with hydrogen. The total carbon includes at least three fractions:

$$\Sigma[C] = [C] + [C]_{Fe_3C} + [C]_{CH_x} \qquad \text{Equation VI}$$

This expression does not include CH_x as an occluded gas phase, but only as an associated phase in solution.

Since $\Sigma[C]$ is arbitrarily a constant in the systems under comparison, where one iron graphitizes and the other does not:

$$[C]^* = [C] - [C]_{CH_x} = \Sigma[C] - \left\{ [C]_{Fe_3C} + [C]_{CH_x} \right\} \qquad \text{Equation VII}$$

where [C], as before, measures the vapor pressure P_C of the hydrogen-free alloy, and [C]* that of the hydrogeniferous alloy. Hence $P^*_C < P_C$.

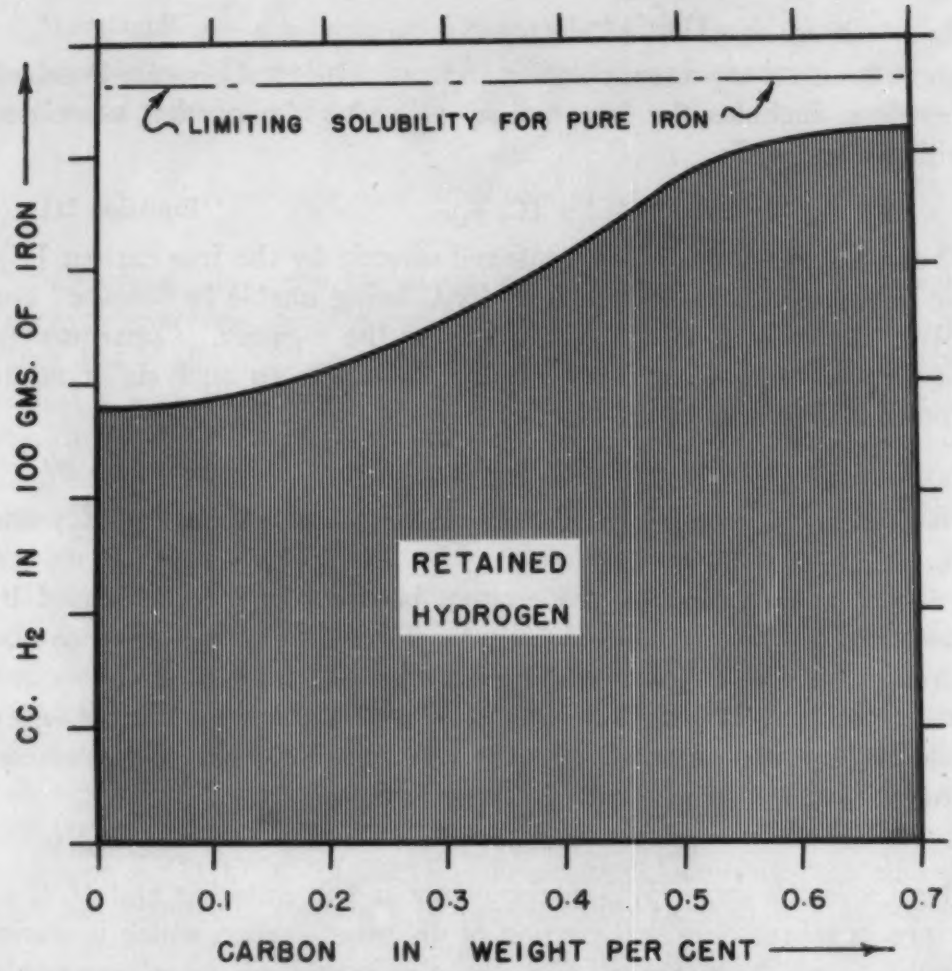


Fig. 7—Effect of Carbon Content on Retention of Hydrogen by Iron During Freezing and Cooling. Iron melts with increasing carbon contents were held under hydrogen at 1 atmosphere pressure for a fixed period of time and were then chill-cast and analyzed for hydrogen. The quantity of residual hydrogen increased as shown with increasing carbon content. (Bardenheuer and Keller, Ref. 29.)

Hydrogen remains one of the last important alloy elements whose analysis and control are still largely neglected in modern industry. Those conditions then understandably arise wherein two presumably duplicate irons, or two presumably identical zones within a given iron, respond oppositely with regard to graphitization. Their two responses, however, conform to the simple stipulations of Equation I; and for the two conditions, we may therefore write:

Normal Iron (Hydrogen-free):

$$P_o > (P_o) \xrightarrow[\text{Graphite}]{} \text{graphitization} \qquad \text{Equation VIII}$$

Abnormal Iron (Hydrogeniferous):

$$P^*_C < (P_C) \xrightarrow[\text{Graphite}]{} \text{retention of cementite} \qquad \text{Equation IX}$$

In other fields of metallurgy this fact of internal association of [C] and [H] is amply demonstrated as an increasing resistance to diffusion of hydrogen through iron as the carbon content increases (22), as a difficulty in removing hydrogen during analysis of irons and steels high in carbon (23), as blistering of vitreous enamel on cast iron from hydrogen being released by cementite during graphitization (24-28), and as a tendency of carbon to hold hydrogen in solution during the freezing of iron-carbon alloys. (See Fig. 7.)

Hydrogen as a Segregating Element

With the establishment of hydrogen as a stabilizer of cementite, both by fact and by principle, all features of "inverse chill" and "hard spots" become simply explained, for hydrogen transcends every known element in its ability to segregate.

No more need be said here than to point to the segregation phenomena of hydrogen in steel known variously as "flakes" or "shatter cracks" in forgings (30), as "white spots" in cast steel (31), as "fisheyes" in weld metal (32, 33), as "cluster blisters" overlying carbide patches when vitreous enamel is fired on steel and cast iron (25-27), and as blisters in steel sheet (25). As for the chemical principles of hydrogen segregation, they are amply described in these other references.

In Fig. 8, the photomacrograph of "white spots" in a low-alloy steel is extremely suggestive of the "inverse chill" seen in Figs. 1 and 2; and the condition of "silver streaks" and "fisheyes" on the weld fractures in Fig. 9 could easily be mistaken for the inverse chill occurring, for example, along the centerline shrink of cast iron stove plates (4). These are demonstrations of hydrogen segregation.

In steel, high concentration of hydrogen at the site of a segregation leads to local loss of ductility from interference with the slip mechanism.

In cast iron, the segregation shows instead as a zone of stabilized carbide.

Moisture as an Observed Source of Hydrogen

In the steel industry, moisture has been universally indicated

as the prime carrier of hydrogen to the metal and, therefore, as the origin of numerous defects.

In the cast iron industry, moisture has similarly long been identified with the defects in question. Fisher (4) blames inverse chill on green or damp ladles and damp cupola hearths; Dietert and

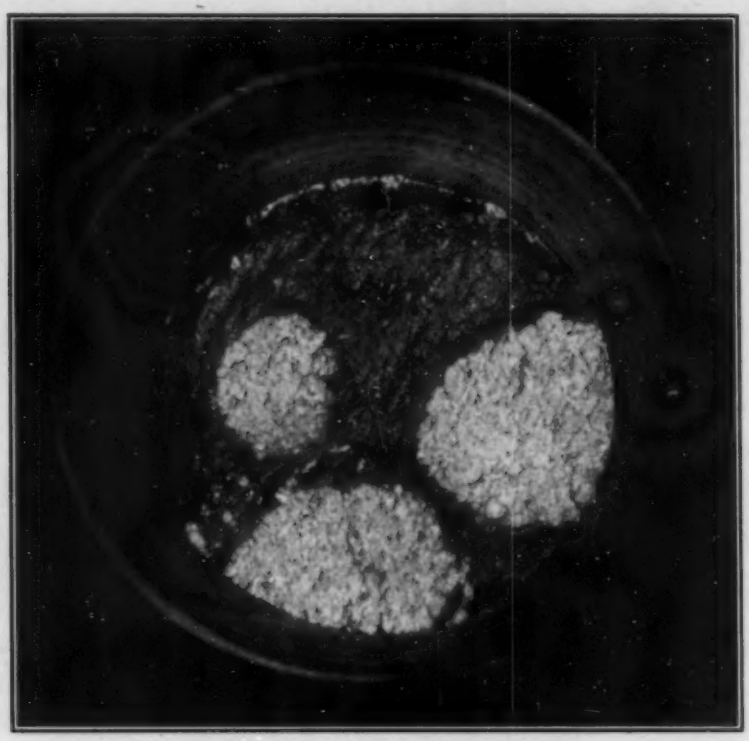


Fig. 8—"White Spots" Appearing on the Face of a Tensile Fracture of Low Alloy Steel. This phenomenon results from the segregation of hydrogen, and its appearance is suggestive of the phenomenon of "inverse chill" shown in Figs. 1 and 2. × 3. (Courtesy of F. B. Foley.)

Woodliff (34) on moisture in the mold; Bales and McCarthy (35) on moisture in new ladle linings; Schwartz (36) and Cowan (37) on moisture in the blast.

However, the literature on inverse chill and hard spots largely neglects the relationship between moisture and hydrogen absorption; and where the relationship is recognized, its chemical principles are misapplied to such an extent that incorrect conclusions are drawn.

Thus, Touceda (6) and many others seem to have believed that the principal action of moisture was to oxidize the iron (4), (38). Dietert and Woodliff (34) even go so far afield as to propose that the moisture in the mold promotes inverse chill by its quenching

action. Touceda (6) and Fielden (5) both relate inverse chill to conditions of unsoundness from absorbed gas, virtually describing phenomena of hydrogen absorption (39), yet placing the blame elsewhere.

Steam injected in the blast furnace is known to increase combined carbon (40), a fact having obvious implication for hydrogen, rather than for oxygen, a known graphitizer; and Schwartz (36)

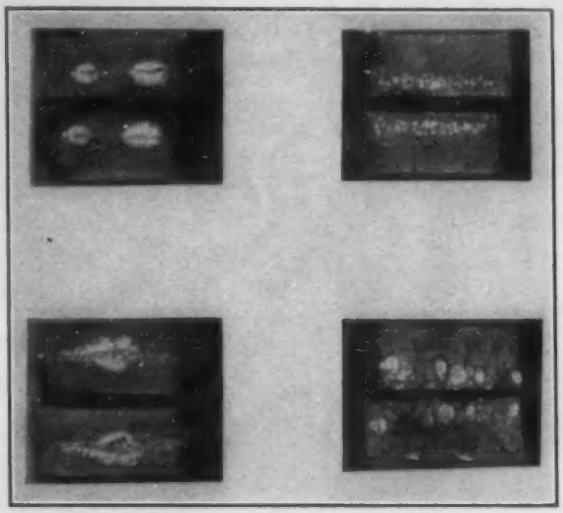


Fig. 9—"Silver Streak" and "Fisheyes" Appearing Along the Interbead Junction on the Fractures of Steel Welds. An expression of hydrogen segregation, these defects resemble respectively in appearance and location the "inverse chill" observed along the centerline shrink of gray iron castings, and the "hard spots" previously shown in Figs. 1 and 2. Natural size.

recently patented a malleable iron process using a dry blast because he could show that the hydrogen resulting from the steam-iron reaction decreased the elongation, tensile strength, and graphitization of malleable iron and increased the required annealing time. Cowan (37), similarly recognizing moisture as a hydrogenizer, states that increasing the moisture in the cupola blast from 3 grains per cubic foot to 10 grains will change a gray iron to white iron. None of these investigators, however, has described the principles which underlie the efficacy of moisture as a hydrogenizer of iron and steel.

Cause of Inverse Chill and Hard Spots

Moisture—The Indirect Cause

First, there stands the fact that moisture predominates as the

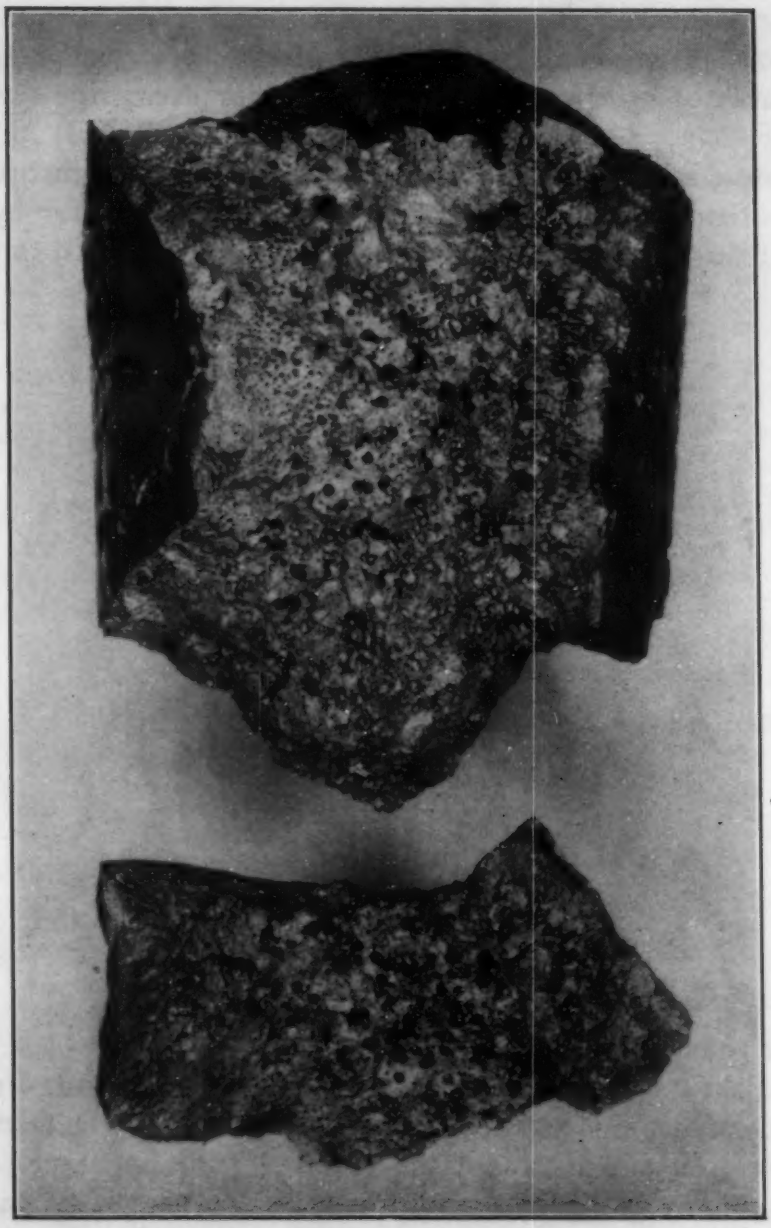


Fig. 10—Cast Iron Containing 15% Silicon Poured in a Crucible With a New Lining and Subsequently Chill-Cast. The gassiness was derived from hydrogen provided by moisture in the lining.

indirect cause of the defects in question. If the direct cause is assumed to be hydrogen, and not oxygen, contributed by the moisture, all previous relationships to green ladles, damp molds, and so forth, become immediately explained. Moldenke, according to Fisher (4), related inverse chill to the first cast of a cupola heat. In Fig. 10 the effect of hydrogen pickup from the moisture in a new crucible

lining is illustrated as gassiness in a high-silicon cast iron. Melted in an induction furnace, the iron was poured half in a new clayed crucible dried by usual burning with a gas flame and half in a used crucible, both halves subsequently being chill cast. The half cast in the used crucible was sound; the other half developed the gassiness evident in the figure, illustrating the value of "drying" the ladle with a wash heat. Bales and McCarthy (35) state that foundry clay contains 6 to 12% H_2O, that much is eliminated at 500 °C (930 °F), but that some still remains at 800 °C (1450 °F). This fact is well known in the vitreous enameling industry, where the residual moisture combined in the clay of the enamel plays an important role during enamel firing at temperatures up to 900 °C (1650 °F) (25-27).

Because hydrogen already in the metal at the time of casting will have greater opportunity to segregate in thicker castings, Touceda's (6) observation becomes explained that inverse chill is more common in thicker castings, in spite of their slower cooling.

However, since hydrogen is also derived from moisture in the mold, there will be those conditions in which thinner sections will become more liable because a large mold area is injecting hydrogen into a proportionately smaller volume. This condition, of course, tends to move the chill surfaceward, until it shows as a deepened normal chill.

Now many of the "unusual aspects of malleable iron melting" (38) can be clarified. An induction furnace is likely to produce a gray iron which would be white if melted in the cupola because the melting conditions of the induction furnace are much less conducive to hydrogenizing. Fe_3O_4 additions may cause graphitization, and Fe_2O_3 stabilization (38), if the Fe_2O_3 contains water of hydration. Increasing superheat will favor white iron, not only because of changed nucleating conditions, but because the solubility of hydrogen in iron rapidly increases with increasing temperature of the melt. And the puzzling fact that two "apparently identical" pig irons can result in importantly different cast irons (41) can be understood on the basis of their differing hydrogen contents.

As for the effects of steam (38), the resulting white iron follows, not from iron oxide, but from hydrogen:

$$H_2O + Fe = [O] + 2\,[H] \qquad \text{Equation X}$$

where brackets again represent solution in the iron. Note that *two*

atoms of hydrogen are produced for every atom of oxygen.

Error in previous conclusions drawn for such systems seems to follow from supposing that the solubilities [O] and [H] depend directly upon the macrothermodynamic system of environmental gas proportions (38), (42-44), such as the composition of gases in a welding atmosphere.

Quite to the contrary, the best measurements of environmental gas pressures would only represent a poor approach to the potentials which generate them at the metal's surface. There is instead involved a dynamic state which can only be properly understood on the basis of a microsystem taken immediately adjacent to the surface of the metal. There the true fugacities are likely to be quite different from the measured fugacities of the external system where partial pressures balance to a total pressure of one atmosphere, without regard to the pressure that would develop if the reactions progressed in a closed system.

These principles are discussed at length elsewhere (45), and the reader is referred to that reference. Only a few brief statements will be made here. Both hydrogen and oxygen dissolve atomically. They therefore stand in direct relation to the partial pressures of atomic oxygen and atomic hydrogen at the metal surface:

$$[O] = k \cdot P_O \qquad \text{Equation XI}$$

$$[H] = k' \cdot P_H \qquad \text{Equation XII}$$

and only indirectly to the environmental pressures, just mentioned, of the resulting molecular gases P_{O_2} and P_{H_2}.

In the case of the steam-iron reaction, the surface conditions can be evaluated by considering a microsystem taken at the interface. The reaction:

$$[FeO] + H_2 = H_2O + Fe \qquad \text{Equation XIII}$$

is a modification of Equation X. The mass action constant (46, 47):

$$K = \frac{H_2O}{H_2[FeO]} \qquad \text{Equation XIV}$$

$$\log K = \frac{10{,}200}{T} - 5.50 \qquad \text{Equation XV}$$

shows that for any given oxygen content of the metal, expressed here as [FeO]:

$$K' = \frac{P_{H_2O}}{P_{H_2}} \qquad \text{Equation XVI}$$

and

$$P_{H_2} = K'' \cdot P_{H_2O} \qquad \text{Equation XVII}$$

When P_{H_2O} is fixed at 1 atmosphere, as in bubbling steam through liquid metal, or as is perhaps approximated locally where moisture in the mold, for example, meets hot iron and vaporizes:

$$P_{H_2} = \frac{1}{K \cdot [FeO]} \qquad \text{Equation XVIII}$$

$$\log P_{H_2} = 5.50 - \frac{10{,}200}{T} - \log [FeO] \qquad \text{Equation XIX}$$

In Fig. 11, the hydrogenizing values for the steam-iron microsystem with P_{H_2O} fixed at 1 atmosphere are expressed in terms of P_{H_2} potentials for liquids of several oxygen fugacities varying from 0.0001 to 0.1 weight per cent [FeO]. It will be noted that even for the highest [FeO] value shown, 0.1%, the steam is equivalent in hydrogenizing potential to more than 10 atmospheres of H_2 at 1600 °C (2912 °F).

In cast iron, of course, silicon and carbon pre-empt the oxygen and drive its fugacity within the iron to very low values by the reactions:

$$FeO + C = Fe + CO \qquad \text{Equation XX}$$

$$FeO + CO = Fe + CO_2 \qquad \text{Equation XXI}$$

and (48), (49)

$$FeO + Si = Fe + SiO \qquad \text{Equation XXII}$$

$$FeO + SiO = Fe + SiO_2 \qquad \text{Equation XXIII}$$

Consequently, steam contacting cast iron encounters much lower oxygen fugacities, and accordingly becomes much more potent as a hydrogenizer. While oxygen values for cast iron are not yet known accurately, they rather certainly enter the range, expressed in terms of [FeO], of 10^{-3} and 10^{-4}%. In Fig. 11 the P_{H_2} values for such microsystems are seen to exceed 10,000 atmospheres. Little wonder that moisture leads to hydrogen-caused defects in cast iron!

While the actual values in the plot have only qualitative sig-

nificance, they definitely indicate that steam contacting molten iron contributes more hydrogen to the iron than does an equal pressure of H_2; and that in irons containing such great quantities of "deoxidizer" elements (silicon and carbon) as cast iron, the hydrogenizing pro-

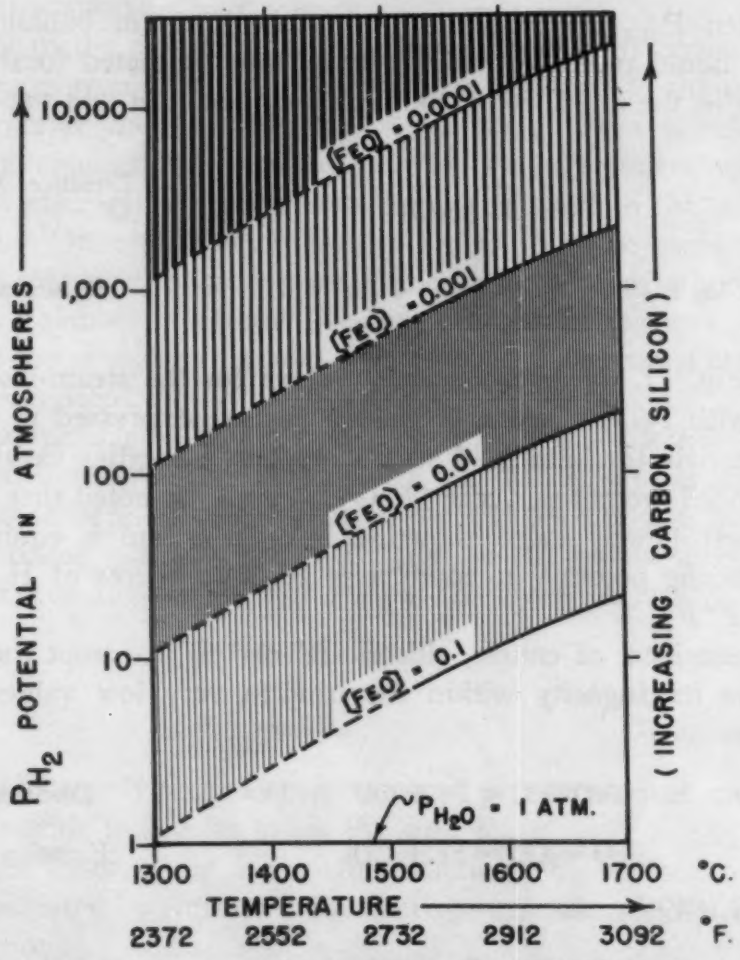


Fig. 11—Potential Hydrogen Pressures Resulting From Steam at 1 Atmosphere Pressure Contacting Molten Irons Having Oxygen Activities as Indicated by Four Typical Curves. Effects of increasing temperature and increasing carbon and silicon content are both seen to increase greatly the hydrogenizing potential of steam.

pensity of the steam is immensely increased, such that the majority of its hydrogen content can be expected to enter the iron under favorable conditions. As indicated on the right-hand side of the plot, increasing carbon and silicon contents are equivalent to decreasing [FeO].

Actual observations in the foundry, the steel plant, and all

secondary industries in general, which employ heated iron and steel in contact with moisture, bear witness to these statements.

The observation that inverse chill results from heavy ladle additions of ferrosilicon (2)—a graphitizer—falls immediately in line with what has just been said regarding silicon as an aggravator of the "hydrogen potential". Such late additions provide heavy local concentrations of superdeoxidized metal, which will have the greatest ability for breaking down any residual moisture in slag, ladle lining, or atmosphere.

Hydrogen Segregation—The Direct Cause

In the diagrammatic sketch of Fig. 12, the relationship between hydrogen segregation and the defects in question is explained. The ordinate at the left is placed at the center of the "hard spot" shown in the previous Fig. 6 and measures in a qualitative manner the hydrogen content across the typical section being considered. Thus, the maximum hydrogen content extends across Zone C, everywhere in this zone of "inverse chill" being greater than the critical H** value necessary for retaining cementite under the conditions of the particular specimen.

From H** to H* (Zone B) the hydrogen content lacks the ability to stabilize the cementite; but it is sufficient to produce the abnormal boundary area of undercooled graphite and dendrites of decomposed austenite characteristic of zones of inverse chill.

At a still greater distance from the seat of segregation, the hydrogen content falls below H*, which is the minimum necessary to produce the effect in Zone B. Zone A of normal graphitic iron results.

Cure of Inverse Chill and Hard Spots

Since the defects in question are caused by hydrogen, their cure is straightforward and not too difficult. It will be observed from Fig. 12 that a minimum quantity of hydrogen is necessary for causing either chill or abnormal graphitization. This "critical quantity" aspect of hydrogen is quite common to all its activities (50).

Consequently, total removal of the gas, which is impossible anyway, is not necessary. The hydrogen content need only be reduced.

This can be effected by taking proper precautions during melting, tapping and casting, such that hydrogen carriers, particularly

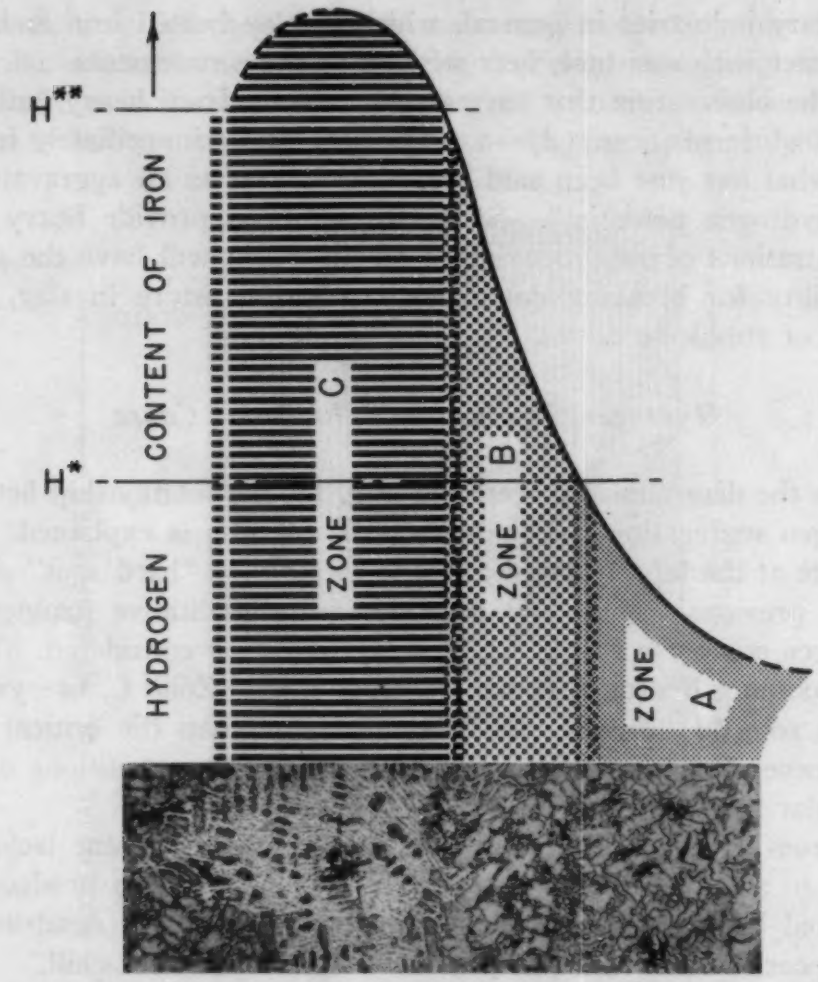


Fig. 12—Diagrammatic Sketch of Hydrogen Segregation Providing Inverse Chill. The micrograph from Fig. 6 is superimposed on a graph indicating hydrogen content across the section shown. In Zone C the hydrogen content exceeds a minimum H** critical for cementite retention; in Zone B lesser quantities still exceed an H* critical content necessary for promotion of undercooled Type D graphite; but in Zone A the hydrogen content is not great enough to prevent the formation of relatively normal flake graphite. Photomicrograph—X 250.

moisture, will be reduced to the required minimum. The "hard spots" shown in this paper were obtained by deliberately not drying the materials in the charge.

With careful selection and drying of materials for the charge and avoidance of subsequent conditions of undue moisture in crucible or mold, rings are readily obtained which are free from the defect. This was demonstrated by experiment.

With the cupola furnace, or any gas-fired furnace, of course, hydrogen is always present. Boegehold (38) remarks that an analysis which freezes white from a cupola melt will freeze gray from a

melt made in an induction furnace. This is consistent with the generally lesser hydrogenizing conditions of induction melting.

As far as hydrogen is concerned, however, another answer to the problem stands in flushing the melt with a hydrogen-free gas (39). With this technique, melting can be conducted with an utter disregard for hydrogen pickup. Just before casting, the harmful gas can be removed by a simple flushing treatment (39); and thereby a great disadvantage of cupola melting becomes surmounted.

Conclusions

The principal contributions of this paper can be stated as follows:

1. "Inverse chill" in gray iron and a type of graphitization-resistant zones ("hard spots") in malleable iron are probably one and the same phenomenon.
2. Hydrogen segregations within the body of the iron are the cause of this phenomenon.
3. Stabilization of cementite by hydrogen requires some critical quantity of the gas under any given set of conditions.
4. Stabilization in general follows from simple thermodynamic considerations of P_C—the fugacity of the carbon in solution—with respect to its fugacity as graphite.
5. A secondary phenomenon of abnormal graphitization (Type D graphite) follows from lesser concentrations of hydrogen and occurs adjacent to the chill zone. When found alone, it frequently indicates a condition of approaching inverse chill.
6. Moisture is the principal source of the hydrogen in question.
7. The efficacy of moisture as a hydrogenizer follows from its thermodynamic equivalence to hydrogen in the Fe-O-H system and the fact that the thermodynamic relationships make a given concentration of H_2O equivalent to many times that concentration of H_2, so far as hydrogenizing is concerned.
8. This factor of equivalence becomes greatly increased by the presence of elements producing low oxygen pressures such as the silicon and carbon in cast iron. Steam contacting cast iron, for example, can theoretically hydrogenize surface layers (microsystems) of the iron as effectively as 10,000 atmospheres of pure H_2.
9. The cure for "inverse chill" and "hard spots" accordingly lies

in the control of the hydrogen content of the iron—in effect, the control of moisture contacting the iron.

10. Induction melting may be preferred over melting in the cupola or in gas-fired furnaces, since, in the latter, hydrogen in great quantities is always present. However, that differential can be erased by removing hydrogen from cupola-melted iron by means of a ladle treatment.
11. In induction melting, care in reducing the moisture content of the charge can suffice to prevent the defects; but, with any melting process, the simplest advisable precaution concerns flushing the melt with a hydrogen-free gas shortly before casting.

ACKNOWLEDGMENT

Grateful acknowledgment is due the Office of Naval Research for their sponsorship of the research project on hydrogen in metals from which the present paper stems as a special study.

The Koppers Company, Incorporated, Piston Ring Division, has been most helpful in providing both photographs and information used in this paper. Particularly do Dr. Tracy C. Jarrett, director of research for that organization, and Mr. A. B. Shuck, assistant to Dr. Jarrett, deserve acknowledgment for their friendly co-operation. Similarly, Mr. Dallas Lunsford, research metallurgist for The Perfect Circle Company of New Castle, Ind., is to be thanked for helpful contributions.

References

1. B. Osann, "Segregation and Hard Spots in Castings Caused by It," *Stahl u. Eisen,* Vol. 40, 1920, p. 145-148.
2. Private correspondence with D. Lunsford, New Castle Plant of The Perfect Circle Co., New Castle, Ind.
3. H. Morrogh and W. J. Williams, "Graphite Formation in Cast Irons and in Nickel-Carbon and Cobalt-Carbon Alloys," *Journal,* Iron and Steel Institute, Vol. 155, 1947, p. 321-372.
4. F. E. Fisher, "Inverse Chill," Pig Iron Rough Notes (Sloss), p. 12-13, 22, Autumn 1939.
5. M. Fielden, "Some Effects of P on Cast Iron," *Iron and Steel,* London, Vol. 16, 1942, p. 214-217.
6. E. Touceda, "Inverse Chill in Malleable Iron," *Transactions,* American Foundrymen's Association, Vol. 48, No. 3, 1941, p. 449-461; discussion, p. 461-464.
7. L. Crome, "Some Notes on Graphitization," *Foundry,* Vol. 74, No. 4, 1946, p. 98-101, 232.
8. F. Wüst, "Influence of Hydrogen and Nitrogen on the Iron-Carbon System," *Metallurgie,* Vol. 7, 1910, p. 261-264.
9. F. Wüst and E. Sudhoff, "On the Effect of Hydrogen and Nitrogen on

Malleable Cast Iron at Different Temperature," *Metallurgie,* Vol. 7, 1910, p. 261-264.

10. K. Honda and T. Murakami, "Graphitization of Iron-Carbon Alloys," *Journal,* Iron and Steel Institute, Vol. 102, 1920, p. 287.
11. H. Sawamura, "Influence of Various Gases Upon the Graphitization of Cast Iron," *Iron and Steel,* Vol. 14, 1928, p. 741-755.
12. A. L. Norbury and E. Morgan, "The Effect of Melting Conditions on the Microstructure and Mechanical Strengths of Gray Cast Iron Containing Various Amounts of Carbon and Silicon," *Journal,* Iron and Steel Institute, Advance copy No. 11, 1930, p. 1-20.
13. A. L. Norbury and E. Morgan, "Effect of Melting Conditions on Gray Cast Iron," *Fuels and Furnaces,* Vol. 8, 1930, p. 1083-1084.
14. W. Baukloh, "On the Influence of Hydrogen on Cast Iron," *Giesserei,* Vol. 22, 1935, p. 406-409.
15. A. Boyles, "The Freezing of Cast Iron," *Transactions,* American Institute of Mining and Metallurgical Engineers, Vol. 125, 1937, p. 141-203.
16. A. Boyles, "Formation of Graphite in Cast Iron," *Transactions,* American Foundrymen's Association, Vol. 46, 1938, p. 297-340.
17. A. Boyles, "Influence of Atmosphere and Pressure on Structure of Iron-Carbon-Silicon Alloys," *Metals Technology,* Vol. 6, 1939, T.P. 1046.
18. H. A. Schwartz and G. M. Guiler, "Hydrogen in Solid White Cast Iron," *Transactions,* American Foundrymen's Association, Vol. 47, 1939, p. 742.
19. H. A. Schwartz, G. M. Guiler and M. K. Barnett, "The Significance of Hydrogen in the Metallurgy of Malleable Cast Iron," TRANSACTIONS, American Society for Metals, Vol. 28, 1940, p. 811-829; discussion, p. 829-831.
20. C. H. Lorig and M. L. Samuels, "Some Effects of Hydrogen on the Time of Malleableization," American Foundrymen's Association Preprint No. 42-7, 1942, 19 p.
21. E. Houdremont and P. A. Heller, "Hydrogen as an Alloying Element," *Technische Mitteilungen, Krupp Forschungsber,* Vol. 4, 1941, p. 117-126.
22. P. Bardenheuer and G. Thanheiser, "Investigations on the Pickling of Low Carbon Steel Sheet," *Mitteilungen, Kaiser-Wilhelm Institut für Eisenforschung,* Düsseldorf, Vol. 10, 1928, p. 323-342.
23. F. Körber and H. Ploum, "The Absorption of Hydrogen by Iron in Its Treatment With Acid and the Content of the Hydrogen in This Metal," *Mitteilungen, Kaiser-Wilhelm Institut für Eisenforschung,* Düsseldorf, Vol. 14, 1932, p. 229-248.
24. E. P. Poste, "Chemistry and Vitreous Enamels," *Industrial and Engineering Chemistry,* Vol. 32, No. 1, 1940, p. 9-15.
25. C. A. Zapffe and C. E. Sims, "The Relation of Defects in Enamel Coatings to Hydrogen in Steel," *Journal,* American Ceramic Society, Vol. 23, 1940, p. 187-219; discussion, p. 291-300.
26. C. A. Zapffe and C. E. Sims, "Cause of Pinholes and Some Related Defects in Enamel Coatings on Cast Iron," *Journal,* American Ceramic Society, Vol. 24, 1941, p. 249-253; discussion, p. 254-256.
27. C. A. Zapffe, "Cause of Defects in Enamel Fired on Cast Iron at Temperatures Above 725 °C," *Journal,* American Ceramic Society, Vol. 25, 1942, p. 175-180.
28. W. N. Harrison, C. M. Saeger and A. I. Krynitsky, "Progress Report on Cast Iron for Enameling Purposes," *Journal,* American Ceramic Society, Vol. 11, 1928, p. 595-608.
29. P. Bardenheuer and E. H. Keller, "The Effect of Hydrogen Absorbed by Steel During Melting," *Mitteilungen, Kaiser-Wilhelm Institut für Eisenforschung,* Düsseldorf, Vol. 18, 1936, p. 227-237.
30. C. A. Zapffe and C. E. Sims, "Hydrogen, Flakes, and Shatter Cracks,"

Metals and Alloys, Vol. 11, 1940, p. 145-151, 177-184; Vol. 12, 1940, p. 44-51, 145-148.

31. C. A. Zapffe, "Defects in Cast and Wrought Steel Caused by Hydrogen," METAL PROGRESS, Vol. 42, 1942, p. 1051-1056.
32. C. A. Zapffe and C. E. Sims, "Defects in Weld Metal and Hydrogen in Steel," *Welding Journal Supplement,* Vol. 19, 1940, p. 377-s to 395-s.
33. C. A. Zapffe, " 'Fisheyes' in Steel Welds Caused by Hydrogen," METAL PROGRESS, Vol. 42, 1942, p. 201-206.
34. H. W. Dietert and E. E. Woodliff, "Sand Affects Physical Properties of Gray Iron," *Transactions,* American Foundrymen's Association, Vol. 48, 1940, p. 393-424.
35. C. E. Bales and F. McCarthy, "Dry Foundry Ladles Through Eliminating Boiling Produce More Salable Castings," *American Foundryman,* Vol. 6, No. 11, 1944, p. 2-5.
36. H. A. Schwartz, "Malleable Iron Process," U. S. Patent 2,245,876, June 17, 1941.
37. R. J. Cowan, "Effect of Moisture in Blast Air," *Iron Age,* Vol. 150, 1942, No. 20, p. 43-50; No. 21, p. 46-50.
38. A. L. Boegehold, "Some Unusual Aspects of Malleable Iron Melting," Campbell Memorial Lecture, TRANSACTIONS, American Society for Metals, Vol. 26, 1938, p. 1084-1121.
39. C. A. Zapffe and C. E. Sims, "Hydrogen and Nitrogen as Causes of Gassiness in Ferrous Castings," *Transactions,* American Foundrymen's Association, Vol. 51, 1944, p. 517-556; discussion, p. 557-562.
40. J. J. Alexander, "Blast-Furnace Moisture Control," *Blast Furnace and Steel Plant,* Vol. 32, 1944, p. 1213-1219.
41. H. G. Hall, "Malleable Cast Iron," *Foundry Trade Journal,* Vol. 81, 1947, p. 53-57.
42. M. W. Mallett, "The Water-Gas Reaction Applied to Welding-Arc Atmospheres," *Welding Journal,* Research Supplement, Vol. 11, No. 7, 1946, p. 396-s to 399-s.
43. L. Reeve, "The Relation Between the Hydrogen Content of Weld Metal and Its Oxygen Content," Iron and Steel Institute, Advance copy, June 1945; also, *Welding Journal,* Research Supplement, Vol. 10, 1945, p. 618-s to 623-s.
44. S. A. Herres, "Practical Importance of Hydrogen in Metal-Arc Welding of Steel," TRANSACTIONS, American Society for Metals, Vol. 39, 1947, p. 162.
45. C. A. Zapffe, "Concept of the Hydrogen Potential in Steam-Metal Reactions," TRANSACTIONS, American Society for Metals, Vol. 40, 1948, p. 315-352; discussion, p. 352-354.
46. J. Chipman and M. G. Fontana, "Determination of Oxygen and Nitrogen in Steel: Improvements in Vacuum-Fusion Method," *Industrial and Engineering Chemistry,* Analytical Edition, Vol. 7, 1935, p. 391-395.
47. J. Chipman and A. M. Samarin, "Effect of Temperature Upon Interaction of Gases With Liquid Steel," *Metals Technology,* Vol. 4, T.P. 784, 1937, 15 p.
48. C. A. Zapffe and C. E. Sims, "Silicon-Oxygen Equilibria in Liquid Iron," *Transactions,* American Institute of Mining and Metallurgical Engineers, Vol. 154, 1943, p. 192-221; discussion, p. 221-227.
49. C. A. Zapffe and C. E. Sims, "Silicon Monoxide," *Iron Age,* Vol. 149, No. 4, 1942, p. 29-31; No. 5, 1942, p. 34-39.
50. C. A. Zapffe and C. E. Sims, "Hydrogen Embrittlement, Internal Stress, and Defects in Steel," *Transactions,* American Institute of Mining and Metallurgical Engineers, Vol. 145, 1941, p. 225-261; discussion, p. 261-271.

DISCUSSION

Written Discussion: By R. Schneidewind, professor, University of Michigan, Ann Arbor, Mich.

The writers have very ably demonstrated that hydrogen can promote the production of hard spots and inverse chill in gray irons. This view is in keeping with the known tendency of hydrogen to stabilize carbides in iron-carbon-silicon alloys.

The paper contains some statements, however, which perhaps could be further clarified. On page 267, "In the case of gray iron, the segregated hydrogen prevents decomposition of the concurrent iron carbide during the freezing and cooling period in which that carbide would normally form graphite"—do not the authors intend that "hydrogen promotes the formation of eutectic cementite" since normal flake graphite formation is generally considered to take place directly from the melt?

On page 279, the authors regard silicon additions as promoters of inverse chill because they produce "superdeoxidized metal". In practice, ferrosilicon additions, alone or in combination with graphite, are frequently used to correct the condition of inverse chill. Best results are obtained with silicon or other similar alloy if these alloys contain calcium. Crosby and Herzig[2] made a series of irons averaging 2.10% silicon. In the first of these, all the silicon was in the charge; in others, a part was charged and the remainder was added as ferrosilicon before pouring; in the last heat 0% silicon was in the charge and 2.13% was added as ferrosilicon. No tendency toward chilling was observed.

Conclusions 10 and 11 would indicate that induction furnace melting is conducive to "grayness" and cupola melting to a white tendency. This is contrary to the experience of most people in the foundry field who have found that the induction melt is most liable to be chilled whereas a properly operated cupola is most apt to produce a gray iron. Could some other condition such as furnace lining or moisture in the raw materials be responsible for this seeming contradiction?

Written Discussion: By H. A. Schwartz, manager of research, National Malleable and Steel Castings Co., Cleveland.

This commentator is interested in the authors' further development of the effect of hydrogen in the metallurgy of the various cast irons. They have presented an interesting discussion showing that inverse chills and related phenomena may be due to hydrogen segregation. Since their conclusions are not supported by any actual data as to hydrogen content, either on the metal as a whole or on segregated metal, the paper appears to be somewhat speculative in character.

Having had some considerable contact with the determination of hydrogen in cast irons, this writer realizes quite fully that asking Messrs. Zapffe and Phebus to support their theory by actual determination showing that hydrogen did, in fact, segregate, would set them a somewhat impossible task.

---

[2]V. C. Crosby and A. J. Herzig, "Late Silicon Additions to Cast Iron," *Foundry*, Vol. 66, 1938, p. 28-35.

The omission of any reference to the work of Ham and his associates, who dealt with actual measurements of the migratory rate of hydrogen through iron, is unfortunate.

Written Discussion: By Tracy C. Jarrett, manager of research and engineering, Koppers Co., Inc., Baltimore.

The authors are to be congratulated for introducing a new concept of the cause of inverse chill in cast iron. From the foundry operator's standpoint, the problem of inverse chill has been an elusive one. The ordinary measures for chill reduction have little effect. The trouble may suddenly appear in large numbers of castings, then as suddenly disappear. The piston ring foundry may run for months with very few rejections from this defect, then suddenly have a day or several days when no castings are shipped because of hard spots. In studying the defect in our foundry, we have made the following observations:

1. Increasing the carbon-silicon level of a metal which produces inverse chill does not eliminate hard spots.
2. The common silicon-containing inoculants produce little improvement when the difficulty is encountered.
3. Natural graphite in very heavy inoculating additions (6-8 ounces for 100 pounds) improves the condition, providing the graphite is completely dry.
4. The use of cold ladles or improperly dried, patched ladles or cupola spouts will result in the appearance of the defect, even in metals prone to inverse chill.
5. Bad pouring practices and poorly stacked or gated molds increase the prevalence of the inverse chill defect.
6. Certain lots of pig iron in scrap have a greater tendency to produce inverse chill and hard spots than other lots.

The hydrogen theory of the cause of inverse chill may be used to explain some of these observations. We believe, however, that hard spots may be the result of accumulation of factors including the absorption of hydrogen.

Written Discussion: By H. Morrogh, The British Cast Iron Research Association, Birmingham, England.

It is certainly timely that attention is drawn to the phenomenon of inverse chill in cast iron and it is my opinion that the solution of this problem will automatically provide information of far-reaching importance regarding the solidification of cast irons. I have also given some thought to this problem and as a result of the authors' paper I am provoked to suggest a few simplying features and to disagree strongly with some of their ideas.

The authors have suggested that hydrogen is the cause of inverse chill in cast iron and in view of the elaboration of their theory one would think that they had some experimental support for their ideas. However, on close reading it appears that a high hydrogen content in the region of the inverse chill is a purely hypothetical idea and no proof has been given or attempted. One forms the impression that once the authors

had conceived a hydrogen theory they chose a few convenient facts and ignored some fundamental observations.

The authors quote Morrogh and Williams as saying that no satisfactory explanation has been given for inverse chill. This is quite correct but the authors have conveniently ignored the other observations made by Morrogh and Williams. These observations are confirmed by Zapffe and Phebus but apparently not much importance is attached to them. I refer particularly to the fact that the type of inverse chill under discussion always occurs associated with undercooled graphite and that the carbide structure has an unusual acicular structure. (Morrogh and Williams also described a form of inverse chill arising when a white iron was inoculated by molding sand at the edge of a casting.) Furthermore, Morrogh and Williams, confirming the work of Eash, showed that irons having undercooled graphite solidify white and graphitize after solidification and that this white iron, if preserved by quenching after solidification, shows the acicular carbide structure which characterizes inverse chill. It might therefore be assumed that the carbide of inverse chill represents the same carbide structure as that normally giving undercooled graphite. Any theory of inverse chill must take into account firstly, its association with undercooled graphite and secondly, its acicular structure. The hydrogen theory of Zapffe and Phebus completely ignores this point.

Morrogh and Williams also showed that nodular graphite was frequently associated with inverse chill and in a more recent paper[3] they have shown that cerium-treated nodular cast irons are particularly prone to the formation of inverse chill. Now nodular cast irons as well as undercooled graphite irons solidify white and graphitize after solidification, and again, therefore, we have the importance of this condition emphasized.

One way of confirming the validity of a theory for the mechanism of a process is to be able to reproduce and control the phenomenon on the basis of the theory. It is our experience in the laboratories of the British Cast Iron Research Association that if we wish to produce inverse chill easily we must meet the following requirements:

1. Make the iron solidify white and graphitize after solidification either by producing an undercooled graphite structure or by producing a nodular graphite structure.
2. Use an iron of relatively high carbon content.
3. Cast into a fairly thin section.

We find requirement No. 1 to be absolutely essential but we can produce the undercooled graphite in a variety of ways, for instance by rapid cooling, by superheating, by treatment with titanium and carbon dioxide, by treatment with zirconium and by vacuum melting which may be accompanied by superheating and/or rapid cooling. In this context it is important to note that two of these methods of producing undercooled graphite, namely bubbling with carbon dioxide and vacuum melting, are also methods of eliminating hydrogen from the melt. This point alone makes the acceptance of the hydrogen theory difficult.

[3]H. Morrogh and W. J. Williams, "Production of Nodular Graphite Structures in Cast Iron," *Journal*, Iron and Steel Institute, Vol. 158, March 1948, p. 306.

The use of a high carbon content is not essential but it appears to facilitate the production of inverse chill and it is interesting to observe that the analysis quoted on page 260 of the paper by Zapffe and Phebus is actually hypereutectic. Furthermore, all the cerium-treated nodular irons in which inverse chill is readily formed are hypereutectic.

With regard to section size, it is the writer's experience that inverse chill is rarely seen in sections greater than 1 inch and most frequently in sections up to ¼ inch. Again the ring example given by Zapffe and Phebus has a small section size.

From the foregoing it is apparent that inverse chill can be produced under conditions where one would not expect to find any abnormal concentrations of hydrogen and in fact it can be produced when hydrogen has been eliminated from the melt.

If the hydrogen theory is unsatisfactory is there an alternative theory which fits the observed facts more closely? It is the writer's opinion that there is and in what follows an attempt is made to describe this theory very briefly. When an iron solidifies white and graphitizes after solidification there should be an expansion corresponding to this graphitization and this expansion should be greater the higher the total carbon content. With castings of thin section giving undercooled graphite the time interval between the solidification of the outer surface of the section and the center of the section is so small that the whole of the section is solid before graphitization has begun. Graphitization will begin first at the edge of the section but as the mold is to be considered as filled with a solidified white cast iron there must be an outward expansion. Since the section is small and since the casting is cooling rapidly, the outer graphitized and expanded layers will possess considerable strength when the central zones begin to graphitize and hence will tend to restrain the expansion of the central zones, and by virtue of their own expansion they will tend to exert pressure on the central zones. There is good reason to believe that the stability or persistence of iron carbide is increased at higher pressures. It is obvious that the expansion effect, and hence the pressure, will be greater the higher the carbon content.

With relatively heavy sections the outer layer of metal will have solidified white and begun to graphitize before the central zones have begun to solidify. In this case the resulting expansion, consequent upon the graphitization of the outer layers, takes place by the gradual displacement of the liquid at the center. This displacement of the liquid at the center can cause exudations or "bleeding", which is a common occurrence in irons having undercooled graphite structures (and must not be confused with hydrogen bleeding which is accompanied by blowhole formation) or, in the case when feeding of the casting is not very good, the displacement of the liquid by the expansion of the outer layers merely compensates for the shortage of liquid metal and so prevents the formation of porosity cavities. It is common experience that irons having undercooled graphite structures are much less prone to porosity than normal flake graphite irons. Due to the fact that the expansion of the outer layers displaces the internal liquid and compensates for porosity cavities, no pressure is

exerted up to the central zones and hence there is no stabilization of the carbide and no inverse chill.

Since the carbide of inverse chill corresponds to the carbide which will normally give undercooled graphite, it is not surprising that it has an acicular structure since, by quenching, Morrogh and Williams have shown the carbide giving undercooled graphite to have an acicular structure.

It is believed that the theory briefly outlined above permits the explanation of the normal cases of inverse chill and in particular accounts for its association with undercooled graphite and its acicular structure. The production of inverse chill in cases of vacuum melting and after bubbling hydrogen through the melt makes the acceptance of the hydrogen theory difficult. It is pertinent to inquire whether inverse chill can be produced by treatment of a melt with hydrogen. Norbury and Morgan[4] have demonstrated that bubbling hydrogen through molten cast iron immediately prior to casting gives coarse flake graphite whereas inverse chill is associated with undercooled graphite.

It is not the intention of the writer to disagree with Zapffe and Phebus upon the carbide stabilizing effect of hydrogen. This is a well established fact. It is, however, suggested that they have not brought forward any scientific evidence that hydrogen stabilizes inverse chill and furthermore, that they have ignored certain features which are contradictory to their theory. The apparent similarity of the white spots on the tensile fracture of a steel sample and the fracture of cast iron having inverse chill, even if it really existed, could not be accepted as scientific evidence for a common cause for the two phenomena.

It is extremely unfortunate, and likely to be very misleading, that Zapffe and Phebus should have embroidered their interesting idea with such a complicated appearance of theoretical finality.

Authors' Reply

Perhaps the title of this paper would have been better stated, as the discussions rather uniformly suggest, along the lines of "A Theory For . . ., etc." However, one will note on page 280 the statement that: "This was demonstrated by experiment". Further elaboration was omitted, first, for reasons of professional confidences, but also because there is little else to report when the experiment described in the first part of the paper to produce inverse chill by using undried materials is repeated with dried materials, and no inverse chill occurs. It should be sufficient to present the first six photomicrographs concerning the experimentally produced inverse chill, formulating the principles which explain an already widely agreed relationship of inverse chill to the presence of moisture during melting, and then stating, along with the collected identical records of many other observers, that the same iron was made free of inverse chill by prohibiting hydrogen pickup from moisture during melting and casting.

[4]A. L. Norbury and E. Morgan, "The Effect of Nonmetallic Inclusions on the Graphite Size of Grey Cast Iron," *Journal*, Iron and Steel Institute, Vol. CXXXIV, No. 2, 1936, p. 327.

Further confirmation now appears in Dr. Jarrett's discussions; and one should especially note that this authority relates the defect to improperly dried ladle and spout linings, and even to the moisture carried in improperly dried natural graphite deliberately added because of its expected promotion of graphitizing.

Dr. Schwartz recognizes the difficulty in analyzing the inverse chill area for hydrogen; and the authors gladly leave such an experiment for other investigators. The principle of hydrogen segregation at isolated loci within iron-base alloys has been so well demonstrated by such phenomena as those shown in the deprecated Figs. 8 and 9, and described in the literature briefly mentioned, that Mr. Morrogh's accusation would be better turned to ask why he was not aware of both the principle and the facts. A concentration of hydrogen can readily develop at a nucleation point within moderately hydrogenized iron, such that one could not attain the equal melting of the metal under a thousand atmospheres pressure of H_2. So why compare localized inverse-chill structures with general constitutional structures obtained in iron melted under only 1 atmosphere of hydrogen? Boyles' work hits nearer to the mark when he increases the pressure toward 300 atmospheres and the structure becomes white.

Professor Schneidewind's comments are well made; and we can agree with his suggested rewording, although we are referring essentially to the same thing from the fundamental standpoint of carbon atomically dissolved in the liquid and failing to create a graphite phase at any time thereafter because its fugacity remains less than the fugacity of free graphite.

As for the effects of silicon, these are twofold and competing. Silicon is a graphitizing agent; but, in contact with moisture, it can cause an absorption of hydrogen which then counteracts the effect of the silicon.

Upon first reading Mr. Morrogh's thorough discussion, the authors were discouraged into believing they had committed an enormous error; for Mr. Morrogh's position as an authority in the field of cast iron is well attested by his magnificent writings.

On more careful study, however, his arguments deteriorate. In the first place, the criticism of the principles of hydrogen segregation in ferrous metals, as already explained, is perhaps a case of neglect on the part of previous writers, rather than a spurious accumulation of data on ours. The gas is notorious for exactly this type of action; and metallurgists working with cast iron should long ago have searched for its applications in that metal.

Second, his alternative pressure theory was earlier proposed by Fisher and by Fielden, and is disposed of on page 266 because it cannot apply to those cases where inverse chill surrounds a cavity. As for cases where a cavity is not visible, the characteristics of "fisheyes" in steel remind us that a planar microsection through the affected area need not disclose the cavity nucleating the gas concentration; "fisheyes" and "white spots" often develop on fractures passing off-center through the embrittled zone and therefore fail to expose the nuclear hiatus. One can slice a peach without exposing the seed.

Consequently, the pressure theory clearly fails to apply in certain instances where the hydrogen theory is particularly adaptable. On the other hand, the authors are willing to admit that there can be other causes for other occurrences of a similar phenomenon. Their principal point is that hydrogen is theoretically able to cause the phenomenon, and that its removal prevents occurrences which are otherwise very common. For example, tellurium mold washes can produce extreme inverse or "migrating" chill.[5] However, the hydrogen theory must still be borne in mind here, for tellurium has proved its ability in acid pickling phenomena to increase hydrogen absorption by many, many times.[6]

Mr. Morrogh's experiments producing inverse chill from vacuum melting and from metal flushed with CO_2 certainly appear to contradict the hydrogen theory. On the other hand, his wording is not clear. If "titanium and carbon dioxide" were added together, the stabilizing effect of titanium might have prevailed to augment the sensitivity to chill. And if the vacuum melting produced the phenomenon only on superheating or on rapid cooling, as his text allows, one could submit that, while the H content was probably lessened, the superheating would counteract H removal, and rapid cooling would increase the sensitivity to chill factors.

As for the association of inverse chill with undercooled graphite and with acicular cementite, these characteristics are amply brought out in both text and photomicrographs. In our opinion, these are constitutional forms expressing delayed decomposition of the iron-carbon solution; and hydrogen in the case of inverse chill is the probable cause of the delay. Perhaps the same constitutional forms could occur elsewhere with other factors operating.

Mr. Morrogh's remarks on bleeding and porosity are to be handled gingerly. Is he certain that the bleeding is not associated with a microscopic porosity—in keeping with the near-solid late-stage decomposition? Also, one must bear in mind that gas escaping from the metal to develop porosity is no longer within the metal to cause constitutional changes. Several stages of gas condition must be recognized: (a) High gas content with no nucleation of porosity, in which condition the gas remains dissolved in the metal to cause a maximum constitutional change; (b) High gas content with nucleation of porosity, such that the gas escapes and a metal remains, porous but constitutionally gas-free; and (c) Excessive gas content which not only causes porosity, but fills the pores with sufficient pressures of gaseous precipitate to support constitution-changing concentrations within the adjoining walls.

Certainly Mr. Morrogh's detailed criticisms warrant close attention, particularly in view of his proved incisive thinking on other aspects of this field. The authors are content, however, to leave the discussion as presented in this paper until further experiment will clearly prove or dis-

[5]J. O. Vadeboncoeur, "Tellurium Corewashes," TRANSACTIONS, American Society for Metals, Vol. 37, 1946, p. 303-308.

[6]W. Baukloh and G. Zimmermann, "Diffusion of Hydrogen through Steel during Electrolytic Pickling," *Arch. Eisenh.*, Vol. 9, 1936, p. 459.

prove the theory. It is believed to be a valid theory, and one not previously considered. It has been presented purely in an attempt to bring to the cast iron field some assistance with an important problem. The theory was conceived eight years ago by the senior author when he, in the course of a study of gas-metal systems, read of the problem of inverse chill. Since then his interests have been in other fields than cast iron; but a continuing resurgence of the problem in consulting work and in the press—on an important scale during the recent war—finally moved him to take time off to present his views to the industry for whatever aid it might bring them.

As Mr. Morrogh states, the proof of a theory is whether it works. One plant has already used the theory, and it works.

SOME WETTING PROPERTIES OF METAL POWDERS

By Bernard Kopelman and C. C. Gregg

Abstract

The wetting characteristics of a series of metal and inorganic powders were investigated qualitatively by the examination of suspensions of the powders in the two-phase systems, kerosene-water and water-carbon tetrachloride. Additional tests were made in which the wetting properties of the liquids were modified by addition of small amounts of hydrogen peroxide and other wetting agents in the case of the water phase and oleic acid in the case of the oil phase.

In general, it was found that metal powders are poorly wetted by water and organic liquids and are thus difficult to disperse in liquid media. Results indicated that the more refractory metal powders are most difficult to disperse. On the basis of wetting behavior, metal powders may be classified into two groups: the lower melting metals and the refractory metals. Titanium powder exhibited properties intermediate between the two classes, while the behavior of graphite powder is unique.

The data indicate that the lower melting metals can be made dispersible in organic liquids by the addition of approximately 1% oleic acid. The addition of commercial surface-active agents improves the wetting behavior of the refractory metals in water and in some cases makes the lower melting metals dispersible in organic liquids. Hydrogen peroxide in small amounts does not affect the wetting behavior of metal powders.

In general, the higher oxides of multivalent metals and the oxides of monovalent metals were found to be hydrophilic while the lower oxides of multivalent metals and the metals themselves were not water-dispersible.

THE wetting of powders is of prime importance in many industries, such as the paint or ink fields where elaborate steps are taken to insure thorough wetting of the powder by the liquid in

A paper presented before the Thirtieth Annual Convention of the Society, held in Philadelphia, October 23 to 29, 1948. The authors, Bernard Kopelman and C. C. Gregg, are associated with the Metallurgical Research and Development Laboratory, Sylvania Electric Products, Inc., Bayside, N. Y. Manuscript received February 25, 1948.

which it is to be dispersed. Within the last decade or two, literally hundreds of wetting agents have appeared on the market, designed to increase, and thereby hasten, the wetting of the powder involved.

Two distinct types of powders are recognized: organophilic, or those that wet readily by organic liquids, and hydrophilic, those that wet readily by water. Most of the powders fall within these extremes, and require considerable mixing or grinding for adequate dispersion.

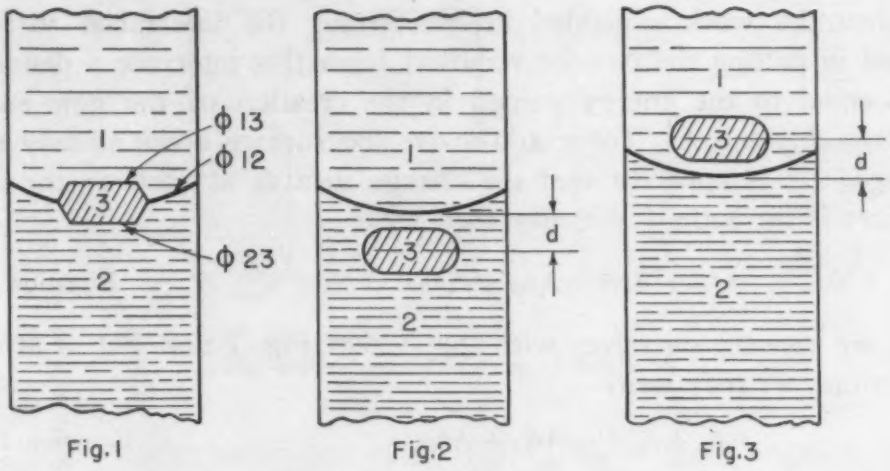
Except for aluminum and bronze powders, little attention has been paid to the wetting properties of metal powders. This phenomenon has been studied in a simple way and the results obtained may be of interest to those concerned in handling metal powders in a wet condition.

Theory of the Experiments

If two immiscible liquids, such as water and kerosene, or water and carbon tetrachloride, are placed in a vessel, say a glass test tube, two distinct layers are formed, the liquid with the higher density comprising the lower layer. If to a set of two such liquids we add a small amount of fine powder and shake the contents vigorously, the powder will assume, after settling, any one of the following positions in this system:

a. It will be found at the bottom of the upper layer and, upon slight shaking, will disperse as a fine powder in the upper layer.
b. It will be found at the bottom of the lower layer and, upon slight shaking, will disperse as a fine powder in this lower layer.
c. It will be found at the interface of the two liquids and, upon slight shaking, will remain at this interface with no free motion of the particles but appearing as trapped at the interface.
d. It will be found around the surface of the glass vessel in the upper layer, with no motion of the particles upon shaking.
e. It will be found around the surface of the glass vessel in the lower layer, with no motion of the particles upon shaking.
f. It will be found in the lower layer as a glob of metal, apparently containing a coating of the liquid of the upper level, and will not disperse upon shaking.

It is obvious that the powder will seek a position where it is most compatible, and this position is where, of all the liquids or solids involved, its interfacial tension with any one of the substances present is lowest. Of course, if the particles are large enough they will always sink to the bottom of the lower layer, since gravitational forces will overcome the forces of interfacial tension.



Figs. 1, 2, 3—Adhesion of Solid Between Two Liquids.

This concept was handled in a qualitative way by Freundlich (1)[1] and later by Hofmann (2). Their treatment described the conditions necessary for the powder to cling to the interface, or be dispersed in the lower layer, but did not include the requisites for suspension in the upper layer. Conditions defining this latter state may be easily expanded from their treatment.

Fig. 1 illustrates the two-liquid layers with the solid at the interface. This system may or may not be at equilibrium. Fig. 2 shows the powder in the lower layer, either by virtue of a necessary force applied or because the system is more stable under these conditions. Fig. 3 shows conditions similar to Fig. 2 except that the powder is in the upper layer. Let us apply the following symbols:

ϕ_{12}—interfacial tension between upper and lower liquids.

ϕ_{13}—interfacial tension between the powder and the upper liquid.

ϕ_{23}—interfacial tension between the powder and lower liquid.

A—change in area of any of these interfaces as a result of motion of the powder.

[1]The figures appearing in parentheses pertain to the references appended to this paper.

d—the distance the powder moves from the interface to its new position either into the upper or lower layer.

F_a—the force required to move the powder from its position at the interface to its new position in the lower layer.

F_b—the force required to move the powder from its position at the interface to its new position in the upper layer.

Equilibrium between the systems Fig. 1 and Fig. 2 is reached when the work expended in overcoming the interfacial force ϕ_{13} and in pulling the powder removed from this interface a distance d is equal to the energy gained in the creation of the new surface areas A_{12} and A_{23} (over and above the surface areas already existing). It is apparent that the change in area at each of the interfaces is the same. We may then write—

$$A\phi_{13} + F_a d = A\phi_{12} + A\phi_{23} \qquad \text{Equation I}$$

If we concern ourselves with the system Fig. 1 and Fig. 3 at equilibrium, we may write—

$$A\phi_{23} + F_b d = A\phi_{12} + A\phi_{13} \qquad \text{Equation II}$$

If we combine Equations I and II, and then simplify, we arrive at

$$\frac{F_a}{F_b} = \frac{\phi_{12} + \phi_{23} - \phi_{13}}{\phi_{12} - \phi_{23} + \phi_{13}} \qquad \text{Equation III}$$

We may write this in the form

$$\frac{F_a}{F_b} = \frac{\phi_{12} + (\phi_{23} - \phi_{13})}{\phi_{12} - (\phi_{23} - \phi_{13})} \qquad \text{Equation IV}$$

From Equation IV, we may deduce the following:

a. When $\phi_{23} > \phi_{13}$, $F_a > F_b$, and thus less force is required to pull the solid into liquid 1.

   1. Under conditions of (a), as long as F_a/F_b remains positive, partial wetting of the solid by both liquids exists, with preferential wetting by liquid 1. This means that most of the solid at equilibrium will remain at the interface, with some of it possibly being dispersed in liquid 1. The higher the ratio, the less solid at the interface, and the more dispersion of solid in liquid 1.
   2. Under conditions of (a), if F_a/F_b becomes negative, the solid will spontaneously go into liquid 1, for F_b is negative.

b. When $\phi_{23} < \phi_{13}$, $F_b > F_a$, and thus less force is required to pull the solid into liquid 2.
   1. Under conditions of (b), as long as F_a/F_b remains positive, partial wetting of the solid by both liquids exists, with preferential wetting by liquid 1. The consequences are inverse to those stated under (a) 1.

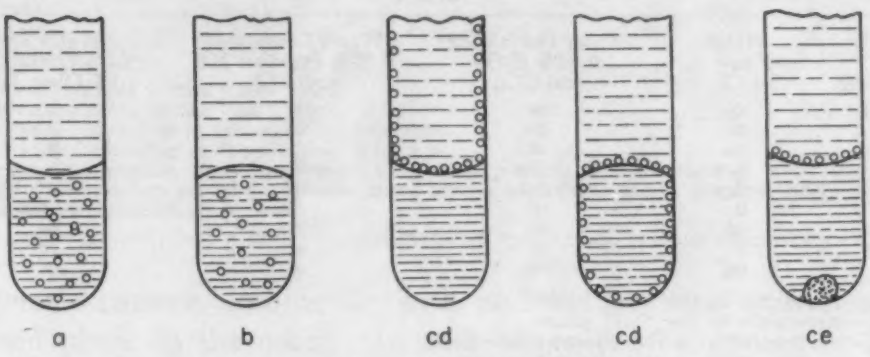


Fig. 4—Preferential Wetting of Solids.

   2. Under conditions of (b), if F_a/F_b becomes negative, the solid will spontaneously go into liquid 2, for F_a is negative.

c. Of course when $\phi_{23} = \phi_{13}$, then $F_a/F_b = 1$, and equal wetting occurs, with the solid held solely at the interface of the two liquids.

It should be recognized that the above treatment is somewhat approximate, since the angle of wetting of the solid by the liquids is of importance. However, a stricter mathematical treatment of the conditions will yield identical results. This treatment can be still further expanded to include the interfacial tensions of the solid powder with the glass walls. However, the concept may be summed up as the simple fact that the powder will situate itself with whatever material will result in minimum interfacial tension for the system.

Experimental Treatment

Two sets of conditions have been used: one in which the upper layer is water and the other in which the lower layer is water. Thus, one system is water-carbon tetrachloride, the other is kerosene-water. Approximately 7 cubic centimeters of each of the two liquids is

placed in a test tube, and approximately 0.03 cubic centimeter of powder is added and the contents then shaken vigorously. It makes no difference to the final equilibrium whether the powder has been added first to the water or the organic liquid, the result is the same. The test tubes are shaken three or four times over a period of a

Table I

Powder	Water and CCl_4	Water Containing 0.25% H_2O_2 and CCl_4	Water Containing 0.25% Dupanol ME and CCl_4	Water and CCl_4 Containing 1% Oleic Acid
Al	ca	ca	b	b
Mg	ca	ca	b	b
Cu	ca	ca	b	b
Ni	dca	dca	b	b
Ti	dca	dca	cd	cd
Mo	d	cd	de	cd
Ta	cd	cd	d	cd
Pt	d	cd	d	ce
C	cd	cd	a	cd

a—dispersible in the water phase
b—dispersible in the "oil" phase
c—nondispersible at the oil-water interface
d—nondispersible at the glass-oil interface
e—nondispersible, either as powder or glob of powder, in the bottom of lower layer.
In a designation containing two or more letters, all effects occur, the first letter denoting the strongest behavior.

Table II

Powder	Water and Kerosene	Water Containing 0.25% H_2O_2 and Kerosene	Water Containing 0.25% Dupanol ME and Kerosene	Water and Kerosene Containing 1% Oleic Acid
Al	cd	ce	c	b
Mg	ce	e	c	b
Cu	ce	c	ce	b
Ni	cde	cd	c	b
Ti	cd	cd	cd	cd
Mo	ce	ce	a	ce
Ta	cd	cd	a	cd
Pt	ce	ce	a	cd
C	cd	cd	b	cd

a—dispersible in the water phase
b—dispersible in the "oil" phase
c—nondispersible at the oil-water interface
d—nondispersible at the glass-oil interface
e—nondispersible, either as powder or glob of powder, in the bottom of lower layer.
In a designation containing two or more letters, all effects occur, the first letter denoting the strongest behavior.

day to insure good wetting of the powder by the two liquids involved, allowed to stand overnight, and are observed the following day. Extensive tests on paint pigments were carried out utilizing this technique in the laboratories of H. A. Gardner (3). The results are listed in Tables I, II and III.

In each case water is one of the liquid phases. Carbon tetrachloride, immiscible with and heavier than water, is the second phase in one

Table III

Powder		Water and CCl_4	Water and Kerosene
Tungsten	(W)	cd	ce
Tungsten dioxide	(WO_2)	cd	c
Tungsten oxide	(W_4O_{11})	a	acd
Tungsten trioxide	(WO_3)	a	acd
Uranium dioxide	(UO_2)	a	a
Manganous carbonate	($MnCO_3$)	a	ca
Zinc oxide	(ZnO)	a	cd
Lead oxide	(PbO)	cd	ce
Titanium oxide	(TiO_2)	a	a

a—dispersible in the water phase
b—dispersible in the "oil" phase
c—nondispersible at the oil-water interface
d—nondispersible at the glass-oil interface
e—nondispersible, either as powder or glob of powder, in the bottom of lower layer.
In a designation containing two or more letters, all effects occur, the first letter denoting the strongest behavior.

system; kerosene, immiscible with and lighter than water, is the second phase in the other. In addition to distilled water, and the pure organic liquids as the two phases in each case, additional components have been added to modify its properties. One-quarter per cent hydrogen peroxide has been added to the water in the expectation that by increasing the oxidizing properties of the water, the wetting properties will be enhanced.

Also, to the water, one-quarter per cent Duponol ME has been added. This is one of the more potent of the hundreds of commercially available surface-active agents whose function is to increase the wetting properties of water primarily by decreasing its surface tension. Duponol ME is a pure sodium lauryl sulphate marketed by DuPont, and in the percentage used here will reduce the surface tension of water to less than one-half of its original value.

One per cent of oleic acid has been added to the oil phase. This acid is a long straight chain organic acid, showing nonpolar properties because of its long hydrocarbon chain, and polar properties because of its acid group. The acid group is not sufficiently powerful to counteract its long chain and the material is not water soluble. (If the acid group is converted to its sodium salt merely by mixing the oleic acid with a solution of caustic soda, pure soap is formed, which is water soluble, and has the property of reducing the surface tension of water.) A substance such as oleic acid will thus show directional properties in that either its polar or nonpolar groups can behave as the wetting medium.

Examination of the data listed in the tables reveals that—

1. Some metal powders may show the unique property of being hardly wetted by either water or oil, and are repelled to the glass walls of the container (Mo, Ta, Pt). Such metals would be described as both hydrophobic and organophobic. This behavior had not been reported previously in the case of inorganic materials.

2. The powders group themselves into two classes, with graphite exhibiting an even different behavior. One group consists of Al, Mg, Cu, Ni and the other Mo, Pt and Ta. Titanium seems to be the borderline material separating the two classes, since in some cases it is in the first group, and in the other cases in the latter group.

3. The behavior of each of these two groups (and also of graphite) is a function of the particular organic liquid being used.

4. Duponol ME, considered a powerful agent in making inorganic materials water wettable, can apparently make one of these metal groups dispersible in oil, in certain cases. This emphasizes the difference in behavior between metal and inorganic powders.

5. Hydrogen peroxide is essentially without effect on these powders, in the percentage studied.

6. Oleic acid will make one of these groups oil dispersible, but not the others.

7. The higher oxides of tungsten are wetted by water, whereas the lower oxide and the metal itself are not.

8. Tungsten powder will apparently fall into the class occupied by the other more refractory metals.

Wetting of powders is essentially a surface phenomenon and one would expect it to be affected by one or more of the following factors:

a. Method of preparation of the metal powders.
b. Whether the oxide skin formed on the metal on standing is of the so-called protective type.
c. The surface tension of the metal powders.

Table IV lists these properties. The information as to whether the metal forms a protective oxide, column 3, has been taken from Seitz (4). Surface tension data with an asterisk have been estimated by Kuczynski (5). The remaining surface tension data have been taken from Bircumshaw (6).

It is apparent that classification of these powders into two groups occurs mainly by virtue of their surface tensions, the higher surface tensions in one group, the lower in the other group. It is

Table IV

Metal Powder	Particle Size Range, Microns	Method of Preparation	Protective Oxide Coating	Surface Tension Dynes/Cm
Aluminum	60-90	Atomized	yes	765*
Magnesium	300-500	Chip Cuttings	no	
Copper	5-15	Hydrogen Reduced	yes	1103
Nickel	20-70	Carbonyl	yes	1480*
Titanium	8-35	Mechanical Grinding		
Platinum	13-33	Chemical Reduction		1819
Molybdenum	60-100	Hydrogen Reduced	no	2100*
Tantalum	5-20	Electrolysis of Fused Salt		
Tungsten	1-3	Hydrogen Reduced	yes	2500*

*Estimated by Kuczynski (5).

somewhat surprising that the protective oxide coating does not play a more significant role. One would suspect that if the oxide were truly protective, the metal powder would behave exactly as its oxide. That this is not the case is shown in Table V.

Table V

Water and		Carbon Tetrachloride	Kerosene
Aluminum oxide	(Al_2O_3)	a	a (c)
Magnesium oxide	(MgO)	a	a
Titanium oxide	(TiO_2)	a (d)	a
Tungsten oxide	(WO_3)	a	acd

a—dispersible in the water phase
b—dispersible in the "oil" phase
c—nondispersible at the oil-water interface
d—nondispersible at the glass-oil interface
e—nondispersible, either as powder or glob of powder, in the bottom of lower layer.

In a designation containing two or more letters, all effects occur, the first letter denoting the strongest behavior. If a letter is in parentheses, the effect is very weak.

It may be seen that all of these powders show hydrophilic properties. Indeed, it would appear that in general the higher oxides of multivalent metals, and the lone oxides of univalent metals, are hydrophilic. Titanium oxide, found to be water wettable, is generally considered to be an oil pigment, and wetted by oil. It is possible that prolonged shaking would have transposed this titania to the oil phase. It was not totally unexpected to find that metal powders are wetted as poorly by both water and organic liquids because of their exceedingly high surface tensions.

Organic materials, containing essentially covalent bonds between the atoms, are found to have very low surface tensions, usually between 20 and 50 dynes per centimeter. Inorganic materials, generally consisting of mixed covalent and ionic bonds, have somewhat higher surface tensions, of the order of 70 to 200 dynes per centimeter.

In the case of metals, the surface tensions of the lower melting metals are about 350, extending to over 2000 for the refractory metals. The high interfacial tension between metal and water or organic liquid implies poor wetting of metal powders in liquids.

Summary

It has been found experimentally, as one would expect from surface tension considerations, that metal powders are wetted poorly by water or organic liquids, and thus are difficult to disperse in liquid media. Further, the more refractory the metal, the more difficult the dispersion, and metal powders thus group themselves, as regards wetting behavior, into the lower melting and the refractory classes.

The data indicates that the lower melting metals can be made dispersible in organic solvents if about 1% oleic acid is added to the solvent. Further, the refractory metals can have their wetting properties in water improved by the addition of surface-active agents.

Acknowledgment

Acknowledgment is made to Sylvania Electric Products, Inc., for permission to publish the results of this work, and to Mr. W. E. Kingston, manager of metallurgical research and development, for his support of this project.

References

1. "Kapillarchemil," Leipzig Akad. Verlagagesellsch, 1909, p. 175.
2. *Zeitschrift Physikalische Chemie,* Vol. 83, 1913, p. 385-423.
3. H. A. Gardner, "Physical and Chemical Examination of Paints, Varnish and Lacquers."
4. F. Seitz, "Physics of Metals," 1943, p. 189.
5. Calculated by G. Kuczynski of this laboratory.
6. *Philosophical Magazine,* Vol. 17, 1934, p. 181.

DISTRIBUTIONS OF NONMETALLIC INCLUSIONS IN SOME KILLED ALLOY STEEL INGOTS

By K. L. Fetters, M. M. Helzel and J. W. Spretnak

Abstract

The nonmetallic inclusions in nine alloy steel ingots were studied by metallographic methods and by petrographic examination of inclusions obtained by acid extraction. The metallographic examination revealed the following general types of inclusions: globular silicates, complex silicates, globular oxides, eutectic, angular, duplexed, and globular sulphides. The inclusions were fairly uniformly distributed in the ingot. There was a trend for increasing size of sulphides toward the top of the ingot, and increasing size of oxides and silicates toward the bottom of the ingot.

The petrographic studies of the extracted residues revealed the following types of inclusions: alumina clusters and grains, oxide and clear glass, ferrous aluminate, mullite, oxide crystal phase, quartz, and aggregates of quartz and alumina. The average inclusion contents in the nine ingots varied widely. As a generality, the alumina-type inclusions were predominant in the bottom portion of the ingots, and the silicate and oxide glass types toward the top of the ingots.

Little or no correlation is evident between the size, type, distribution, or amount of nonmetallic inclusions and the occurrence of bore defects in heavy-walled seamless tubes.

THIS paper is another of a series of papers (1)[1] on the study of the influence of various factors in ingot freezing and structural characteristics of killed alloy steel ingots on the resulting quality

[1]The figures appearing in parentheses pertain to the references appended to this paper.

Contribution from the Metals Research Laboratory, Carnegie Institute of Technology, Pittsburgh. The work presented is a portion of the research carried on by NDRC Research Project NRC-39 under Contract OEMsr-755.

A paper presented before the Thirtieth Annual Convention of the Society, held in Philadelphia, October 23 to 29, 1948. Of the authors, K. L. Fetters is special metallurgical engineer, Youngstown Sheet and Tube Co., Youngstown, Ohio; M. M. Helzel is analytical chemist, Metals Research Laboratory, Carnegie Institute of Technology, Pittsburgh, and J. W. Spretnak, who, at the time of this work, was member of staff, Metals Research Laboratory, Carnegie Institute of Technology, is now associate professor of metallurgy, Ohio State University, Columbus, Ohio. Manuscript received April 14, 1948.

of heavy-walled seamless tubes processed from these ingots. These cylinders were subsequently converted into cannon tubes. The factors already considered in previous papers are the following:

1. Kinetics of solidification
2. Relationship between the solidification kinetics and primary ingot structure
3. Relationship between primary ingot structure and the subsequent bore surface quality and mechanical properties
4. Distribution of oxygen and nitrogen in the ingot
5. Macrosegregation in the ingot.

In the initial paper of this series, the bore surface defects encountered were described. Another problem which arose was the quench cracking of these tubes during heat treatment. A significant observation made was that over 75% of the rejections for these causes occurred in tubes processed from the bottom thirds of the ingots.

It seemed logical to consider that the above-mentioned "deficiencies" in properties of the lower portion of the ingot are associated with the solidification structure of the ingot and that the amount, type, size, and distribution of nonmetallic inclusions are of consequence in the problem.

This paper gives the results of a thorough investigation on the nature and distribution of nonmetallic inclusions in nine fully killed alloy steel ingots which were furnished by the co-operating companies. Each of these ingots had been split longitudinally and macroetched for visual examination, and in each case one half of the ingot was sent to the Metals Research Laboratory for further study. The experimental methods used in this study were the standard metallographic methods and petrographic examination of the acid-extracted inclusions.

Description of Ingots

Split ingots were furnished by Producers A, B, C, D, E, G, H, and N. The ingots of Producers A, C, E, G, and H were representative of the ingots cast by these producers for the 40 and 75-millimeter seamless gun tubes. The Producer B ingot was used for 37-millimeter and the Producer N ingot for the 75-millimeter forged and bored gun tubes. The Producer D ingot was typical of those used in the production of the 3-inch Navy gun tubes. The molds used

Table I

Producer	Melting Method	Composition	Ingot Dimensions	Ingot Weight Lb.	L/W*	Taper % on Diameter	Deoxidation Practice
A	BOH	SAE 4340 S	21 in. fluted ø x 73¾ in.	6160	3.2	4.35	CaSi-Al
B	BE	SAE 4340	20 in. fluted ø x 50½ in.	5000	2.1	5.80	CaSi-Al
C	BOH	SAE 4340 S	22 x 25 x 71 in.	6600	2.7	2.08, 6.04	CaSi-Al
D	AOH	0.32 Mo-0.12 V	22 in. fluted ø x 77 in.	6500	3.0	4.40	Mn-Si
E	BOH	SAE 4340 S	22 x 24 x 60 in.	6500	2.5	5.70	Si-Al
G-26 in.	BOH	SAE 4340	26½ x 26½ x 66½ in.	9500	2.3	19.60, 6.73	CaSi-Al
G-21 in.	BOH	SAE 4340	21⅜ in. fluted ø x 73¼ in.	9225	3.4	11.10, 5.55	CaSi-Al
H	BOH	SAE 4340 S	22 x 22 x 72 in.	6100	3.1	5.24	CaSi-Al
N	BE	0.60 Cr, 1.55 Ni, 0.24 Mo	13 in. dodecagon x 74 in.	3100	5.7	3.93	CaSi-Si-Mn

*Ratio of length to average cross sectional dimension.

to produce these ingots were all standard cast-iron, "big-end-up", hot-topped molds. Table I describes the ingots studied.

Each of these split ingots was machined and macroetched for examination. There was some variation in the appearance of the ingots, particularly in degree of central porosity, but no significance could be attached to the observed differences.

The ingots produced by A and E showed pronounced herringbone patterns. These patterns or structures, which are areas of porosity in the form of "V's", extended almost the complete length of the center section, whereas most of the others showed this to a much lesser degree. Variations in etching methods, temperatures, etc., among the various steel producing plants likely have had something to do with these differences. However, since "herringbone" formation is known to be caused by factors which disturb the progressive freezing of the ingot from bottom to top, mold size and shape must have some influence. It seems likely that molds with smaller L/W ratios and steep tapers, both factors promoting progressive solidification, would tend to decrease "herringbone" formation. The data collected during these studies substantiate this to some degree, but no correlation was found between herringbone structures and defects found in gun tubes.

Sampling of Ingots

In each case the ingot was quartered longitudinally and one quarter was used by the laboratory for metallographic and acid

extraction studies. For this purpose the quarter ingot was cut into 3-inch transverse slices. The metallographic samples were chosen representing edge (1 inch in from the ingot edge), quarter and center of the ingot (the center sample was approximately on the ingot center line). The acid extraction samples were selected only from the center and edge positions and were ½ inch farther away from the center and the edge, respectively, than were the metallographic samples.

Methods of Investigation

Metallographic

Standard metallographic preparation procedures were used. The samples were ground, polished through 1, 0, 00, 000 papers, polished on a wax wheel with 600-mesh carborundum, and finished with "gamal" alumina on a "gamal" cloth. Care was taken to preserve the inclusions through the polishing operations.

Acid Extraction

In the following will be found a brief description of the techniques of acid extraction and petrographic examination of the residues. The sample, selected to represent the desired ingot location and consisting of 100 grams of medium fine drillings or millings, is prepared, washed with ether and weighed.

The sample is placed in a liter beaker and covered with 800 milliliters of 20% hydrochloric acid. The beaker is covered with a watch glass and held at 130 to 150 °F for 1 day. The used acid is poured off into another liter beaker and 800 milliliters of fresh acid is added to the original beaker which is heated again for 1 to 2 days. As the sample goes into solution the acid changes can be less frequent and in smaller quantity. The solids in the spent acid are allowed to settle and the supernatant liquid is siphoned off. When solution of the sample is completed (approximately 1 week is required), the solids are centrifuged from the acid after siphoning off the supernatant liquid.

When all of the solids, inclusions, and carbides are in the bottom of the centrifuge tube, they are washed into a 400-milliliter beaker with 150 to 200 milliliters water, and 100 milliliters concentrated HCl

is added. The solution is heated slightly and 10 grams ammonium persulphate is added. This mixture is boiled from 3 to 4 minutes. The persulphate solution is centrifuged and siphoned in the same manner as the acid. This treatment is repeated until the residue clears and shows no further change in color. When the residue in the centrifuge tube has lightened, it is washed with water by placing a cork in the tube and shaking. It is then recentrifuged and the liquid is siphoned off. The residue is returned to the beaker with 100 milliliters of water, and 50 milliliters of 10% sodium hydroxide solution is added to remove silicic acid. It is warmed (180 to 200 °F) and stirred for several minutes, then removed from the hot plate and stirred vigorously. It is centrifuged and siphoned until the solution is removed. This treatment is repeated if necessary.

The solids are washed and centrifuged with hot dilute HCl (1 : 3) several times. The residue is rinsed onto a Whatman 42 filter paper and washed with water 4 to 5 times. The filter paper is placed in a weighed platinum crucible. The paper is charred carefully and ignited to a constant weight at 1000 °C (1830 °F). The total percentage of inclusions is calculated from the sample weight.

The method of acid extraction of inclusions is subject to certain errors since not all nonmetallics are acid insoluble, and the various chemical steps in the extraction procedure can readily cause the formation of new phases. The method retains mainly the higher melting point inclusions of the alumina, aluminate, and silicate types, while sulphides in particular are dissolved by the acid. Iron oxides of several types may be formed during the chemical extraction and the final ignition of the inclusions could also effect changes in state of the constituents. For these reasons, acid-extraction results can best be correlated only within a heat of steel where the inclusions are of the same type and general distribution.

Petrographic

The residues obtained from the acid extraction were studied with a polarizing mineralogical microscope by which the approximate mineral composition of each of the phases was determined. It was also possible to estimate the relative percentage of the several phases.

It is not the purpose of this paper to discuss the details of the petrographic study of nonmetallic inclusions, but it does seem in order to include the basic fundamentals of procedure by means of

which these studies were carried out. Further details may be found in standard textbooks on the subject (2).

Microscope slides were prepared by placing one or two drops of an oil of known refractive index in the center of a glass slide. A very small quantity of the extracted inclusions was dropped onto the oil and a cover glass placed over it. Care is taken not to clutter the field as this complicates the determination of the optical properties.

It is the purpose of the microscopic studies to determine enough of the optical properties of the minerals to ascertain their identity in accordance with the standard tables of the optical properties of minerals. The Tables of Larsen and Berman (2) were used in this work. The acid-extractable residues were examined for the following optical properties: isotropic or anisotropic, uniaxial or biaxial, refractive index, positive or negative optical sign, angle of extinction and pleochroism.

Results and Discussion

Metallographic Examination

Producer A Ingot—The majority of the inclusions were angular or irregularly shaped sulphides and duplexed sulphides and were distributed fairly evenly throughout the ingot. Particularly along the center line of the ingot were found occasional spherical and irregularly shaped inclusions thought to be exogenous in origin. Figs. 1 and 2 show the predominant types of inclusions found in the ingots studied.

Producer B Ingot—Both angular and some duplexed sulphides were the major types of inclusions encountered. Some dark globular oxides were also observed. In the bottom center positions the sulphides were of the eutectic type, indicative of the effect of a "critical amount of aluminum" in deoxidation. The sulphides increased in size toward the top while the oxides were largest in the bottom portion.

Producer C Ingot—The inclusions in this ingot closely resembled those in Ingot A. The angular sulphides predominated, with some duplexed sulphides also present. No trends were apparent as to size, type, or distribution of inclusions in this ingot.

Producer D Ingot—The inclusions were mainly complex sili-

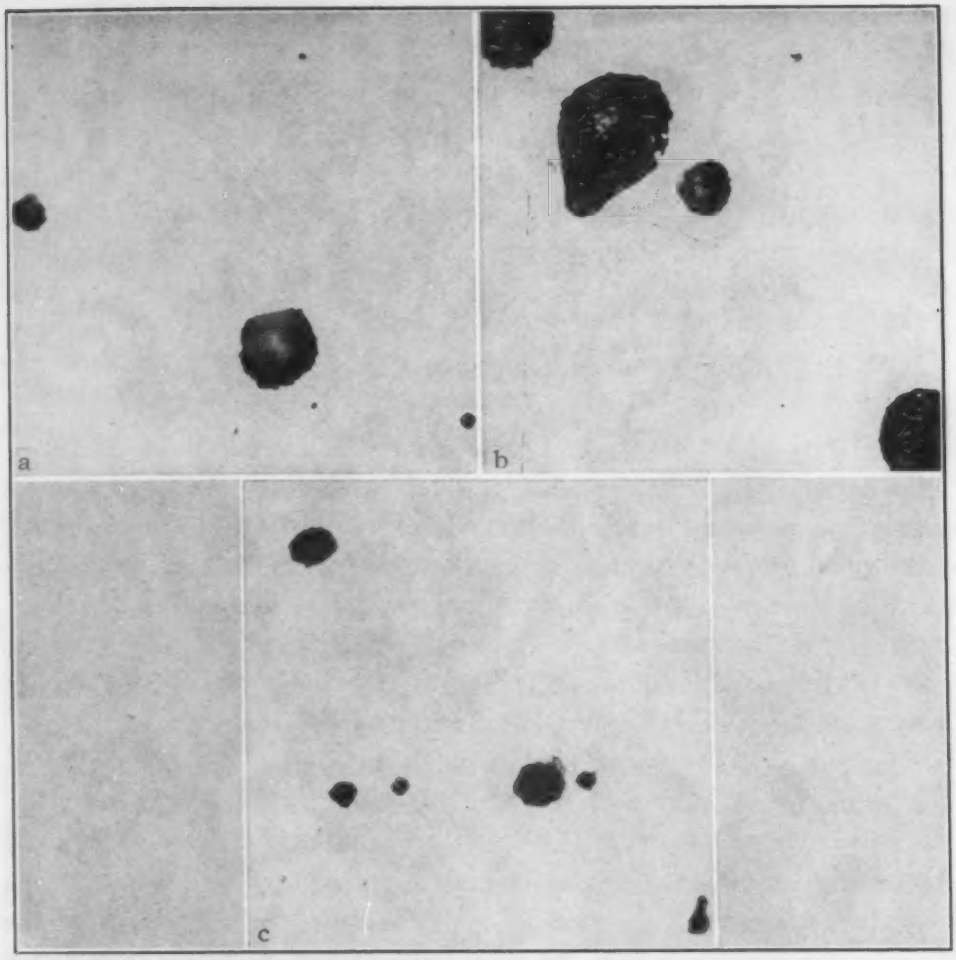


Fig. 1—Typical Inclusions Studied by Metallographic Examination. × 500.
a—Globular silicate. b—Complex silicate. c—Globular oxides.

cates and duplexed sulphides. The silicates and sulphides were both globular and irregular in shape. The silicates varied greatly in size, with a few large enough to indicate that they were probably exogenous.

Producer E Ingot—The majority of the inclusions in this ingot were sulphides; in the center positions they were of the eutectic type, outlining the grains, and at the edge positions they were angular. Dark globular oxides were found in all positions, decreasing in size from bottom to top.

Producer G 26-Inch Ingot—The inclusions in this ingot were all globular in shape. The sulphides and duplexed sulphides increased in size toward the top and center. The oxides and silicates increased in size toward the bottom and from edge to center.

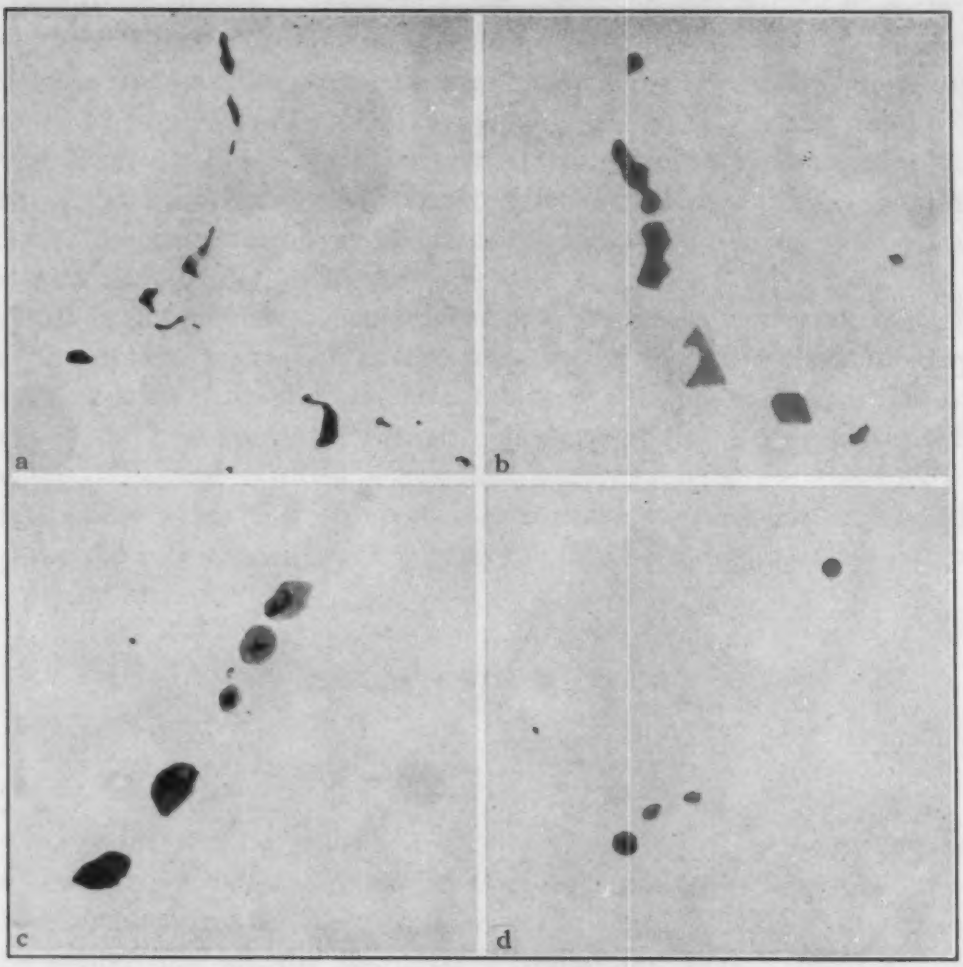


Fig. 2—Typical Inclusions Studied by Metallographic Examination. × 500. a—Eutectic sulphide. b—Angular sulphide. c—Duplexed sulphides. d—Globular sulphide.

Producer G 21-Inch Ingot—The inclusions in this ingot were also globular in shape. The sulphides and duplexed sulphides increased in size toward the top of the ingot. The oxides and silicates did not show a trend in size or distribution. In the bottom slices an occasional oxide or silicate was found which appeared two to five times larger than the average size.

Producer H Ingot—Angular sulphides, angular duplexed sulphides, globular silicates, and dark globular oxides were found in this ingot. All of these inclusions increased in size from edge to center, but there was no appreciable difference in size from the top to the bottom of the ingot. The various types of nonmetallics were observed to be evenly distributed.

Producer N Ingot—This ingot was the only bottom poured ingot studied. The inclusions were all globular in shape. The sulphides and duplexed sulphides were slightly larger in the middle third of the ingot, with no differences from the edge to the center. In the bottom center very few oxides and sulphides were observed which were not duplexed. In the top three-quarters of the ingot an occasional globular complex silicate of considerably larger size than the average was found.

Acid Extraction—Petrographic Studies

The most prevalent nonmetallic phases found in the ingots by examination are shown in the photomicrographs of Figs. 3 and 4. They are oxide and clear glass, ferrous aluminate, alumina clusters, alumina grains, and mullite. The less frequently occurring phases, quartz, and quartz combined with alumina, are also seen in this figure. The oxide crystal phase ($n = 1.70$) was present in minute quantities in only three ingots and was not photographed.

The percentages of extracted inclusions for each ingot according to slice number and position, whether center or edge, are tabulated in Table II. The percentages according to types of inclusions found in each ingot are presented in Table III.

In order to compare the inclusion distribution as judged from the acid extraction results, Fig. 5 was constructed to show the relative inclusion content of the various zones of the ingots studied. In order that these sketches may be comparable, a relative cleanliness legend has been used, since, as pointed out earlier, it is quite difficult to compare directly actual inclusion contents for ingots made from various heats and with varying deoxidation practices. Table IV gives the percentage ranges of inclusion content for the legends used in Fig. 5.

The types and amounts of the inclusions in these ingots are discussed in the following:

Producer A Ingot—As already stated, the acid extraction method retains mainly the higher melting point inclusions of the alumina, aluminate and silicate types. Acid-extraction analysis indicated the percentage of acid-extractable inclusions to be greater at the edge position than at the center, except at the position just under the hot top. Along the center line of the ingot, results from slice to slice were more variable than those from the edge position. The average

Table II
Percentage of Extracted Inclusions by Ingot Positions

Ingot* Slice No.	Producer A		Producer B		Producer C		Producer D		Producer E		Producer G 26 in.		Producer G 21 in.		Producer H		Producer N	
	Center	Edge	Center	Edge	Center	Edge	Center	Edge	Center	Edge	Center	Edge	Center	Edge	Center	Edge	Center	Edge
1	0.0081	.....	0.0197	.....	0.0083	.....	.....	.....	0.0126	.....	0.0183	0.0168	0.0088	0.0135	0.0104	0.0161	0.0052	0.0075
2	0.0192	.....	0.0174	0.0101	0.0069	.....	0.0259	.....	0.0049	.....	0.0153	0.0159	0.0099	.....	0.0055	.....	.....	.....
3	0.0154	0.0256	0.0183	0.0118	0.0090	0.0123	0.0399	0.0219	0.0133	0.0095	0.0104	0.0158	0.0108	0.0130	0.0155	0.0139	.....	.....
4	0.0225	0.0258	0.0099	.....	0.0040	0.0099	0.0421	0.0054	0.0073	.....	0.0103	0.0159	0.0114	.....	0.0088	.....	0.0058	0.0078
5	0.0138	.....	0.0140	.....	0.0086	.....	0.0454	.....	0.0134	.....	0.0096	0.0148	0.0100	0.0151	0.0095	0.0165	.....	.....
6	0.0093	0.0187	0.0113	0.0114	0.0043	.....	0.0401	.....	0.0080	.....	0.0079	0.0186	0.0122	.....	0.0090	.....	.....	.....
7	0.0143	0.0239	0.0127	0.0125	0.0096	.....	0.0300	.....	0.0090	.....	0.0066	0.0191	0.0129	0.0144	.....	0.0138	0.0064	0.0065
8	0.0153	.....	0.0137	.....	0.0068	.....	0.0305	.....	0.0075	.....	0.0065	0.0130	0.0125	.....	0.0100	.....	.....	.....
9	0.0186	0.0255	0.0123	.....	0.0075	0.0126	0.0193	0.0193	0.0069	0.0079	0.0225	0.0170	0.0095	.....	.....	.....	.....	.....
10	0.0082	.....	0.0113	0.0094	0.0060	0.0143	0.0182	0.0180	0.0092	.....	0.0094	0.0156	0.0080	0.0152	0.0142	0.0160	0.0043	.....
11	0.0200	.....	0.0053	0.0137	0.0056	.....	0.0281	.....	0.0145	.....	0.0122	0.0171	0.0088	.....	.....	.....	.....	.....
12	0.0173	.....	.....	.....	0.0045	0.0104	0.0275	.....	0.0057	.....	.....	.....	0.0122	.....	0.0110	.....	.....	.....
13	0.0240	0.0117	.....	.....	0.0086	0.0220	0.0242	.....	0.0066	.....	.....	.....	0.0168	0.0150	.....	0.0142	0.0038	0.0046
14	0.0134	.....	.....	.....	Pitted 0.2067	0.0126	0.0177	0.0213	0.0106	0.0095	.....	.....	0.0106	.....	0.0091	.....	.....	.....
15	0.0173	0.0201	.....	.....	0.0074	.....	0.0176	0.0935	0.0064	0.0125	.....	.....	0.0128	.....	.....	.....	.....	.....
16	0.0144	0.0212	.....	.....	0.0081	.....	.....	.....	.....	.....	.....	.....	0.0139	0.0105	0.0068	0.0142	.....	.....
17	.....	.....	.....	.....	0.0091	0.0162	.....	.....	.....	.....	.....	.....	0.0119	.....	.....	.....	0.0026	0.0046
18	.....	.....	.....	.....	.....	.....	.....	.....	.....	.....	.....	.....	0.0116	.....	.....	.....	.....	.....
19	.....	.....	.....	.....	.....	.....	.....	.....	.....	.....	.....	.....	.....	.....	.....	.....	.....	.....
20	.....	.....	.....	.....	.....	.....	.....	.....	.....	.....	.....	.....	.....	.....	.....	.....	0.0038	.....

*The ingot slices are numbered in order from bottom to top of ingot.

Table III
Percentage of Various Nonmetallic Inclusions Found in Split Ingots

Phases of Nonmetallic Inclusions	Producer A	Producer B	Producer C	Producer D	Producer E	Producer G 26 in.	Producer G 21 in.	Producer H	Producer N
	Per Cent				Per Cent				
Alumina				Extracted inclusions were coated by oxide which made microscopic analysis difficult. Petrographic examination, however, showed that approximately 95% of the inclusions were of the silicate type.					
(Clusters)	40-55	30-55	15-55		5-15	25-50	60-70	35-55	55*
(Individual grains)	25-30	15-40	22-50		25-35	45-65	22-37	15-30	42*
Ferrous Aluminate (hercynite)	3-10	Trace to 3	2-7		30-40				
Oxide Glass (yellow, brown, red, orange) n = 1.58 — 1.68	3-8	2-15	2-20		7-55	2-5	1-6	1-15	82-94†
Mullite ($3Al_2O_3 \cdot 2SiO_2$)	7-12	1-10	1-5		Trace to 5		1-2	Trace to 3	
Clear Glass n = 1.50 — 1.58	2-10	14-29	3-40		Trace to 5	0-5	1-5	1-3	2-15
Oxide Crystal Phase n = 1.70		Trace to 2				0-2	2		
Quartz						0-3		2-25	1-10
Quartz and Alumina								8-33	

*Bottom edge only.
†Glasses, small particles, oxide coated. None in bottom edge sections.

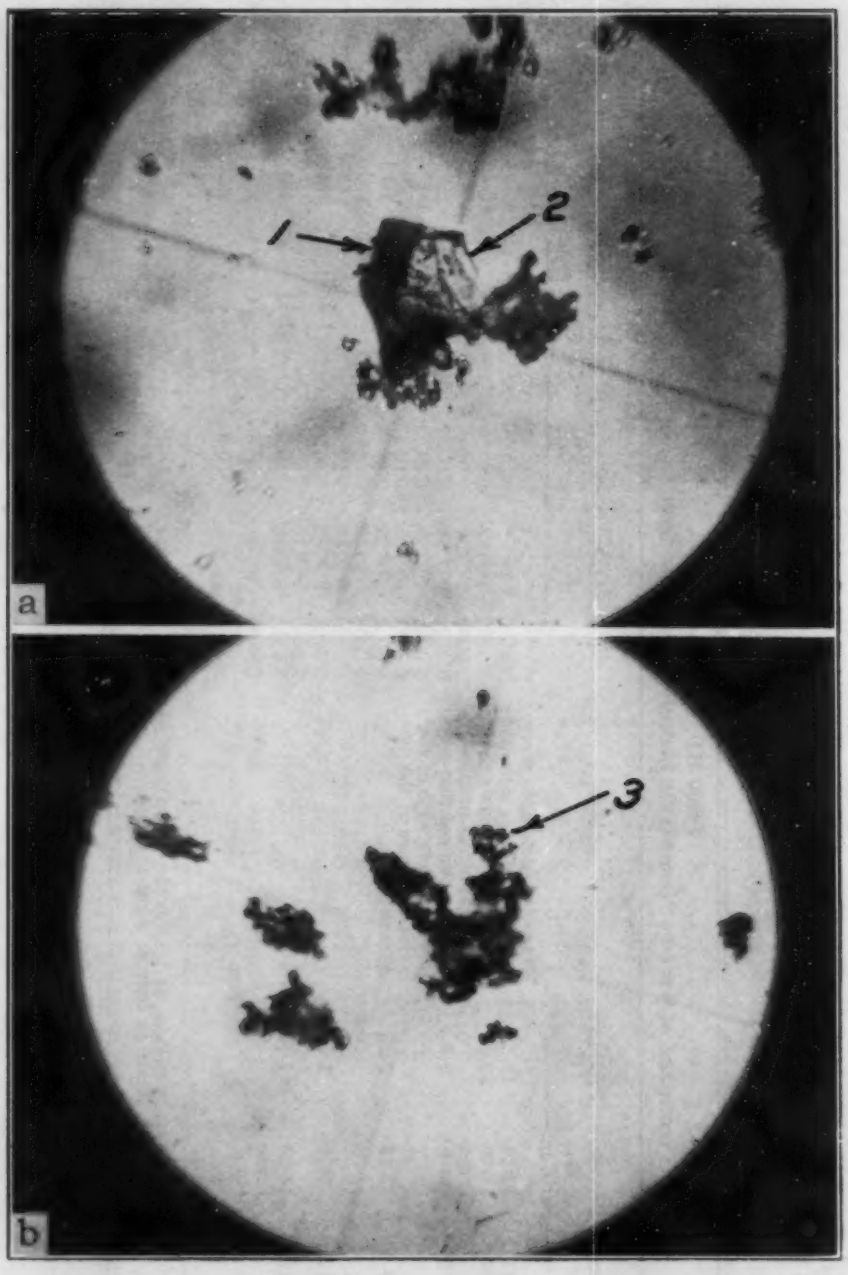


Fig. 3—Acid Extraction Inclusions Studied by Mineralogical Examination. (Original magnification × 350.) a—Oxide (1) and clear glass (2). b—Ferrous aluminate (3).

percentage of acid-extractable inclusions for the ingot is 0.0177%. The nonmetallics were distributed quite evenly from bottom to top of the edge and center sections. Ferrous aluminate was concentrated mostly in the bottom three slices of the edge and center sections and the top edge.

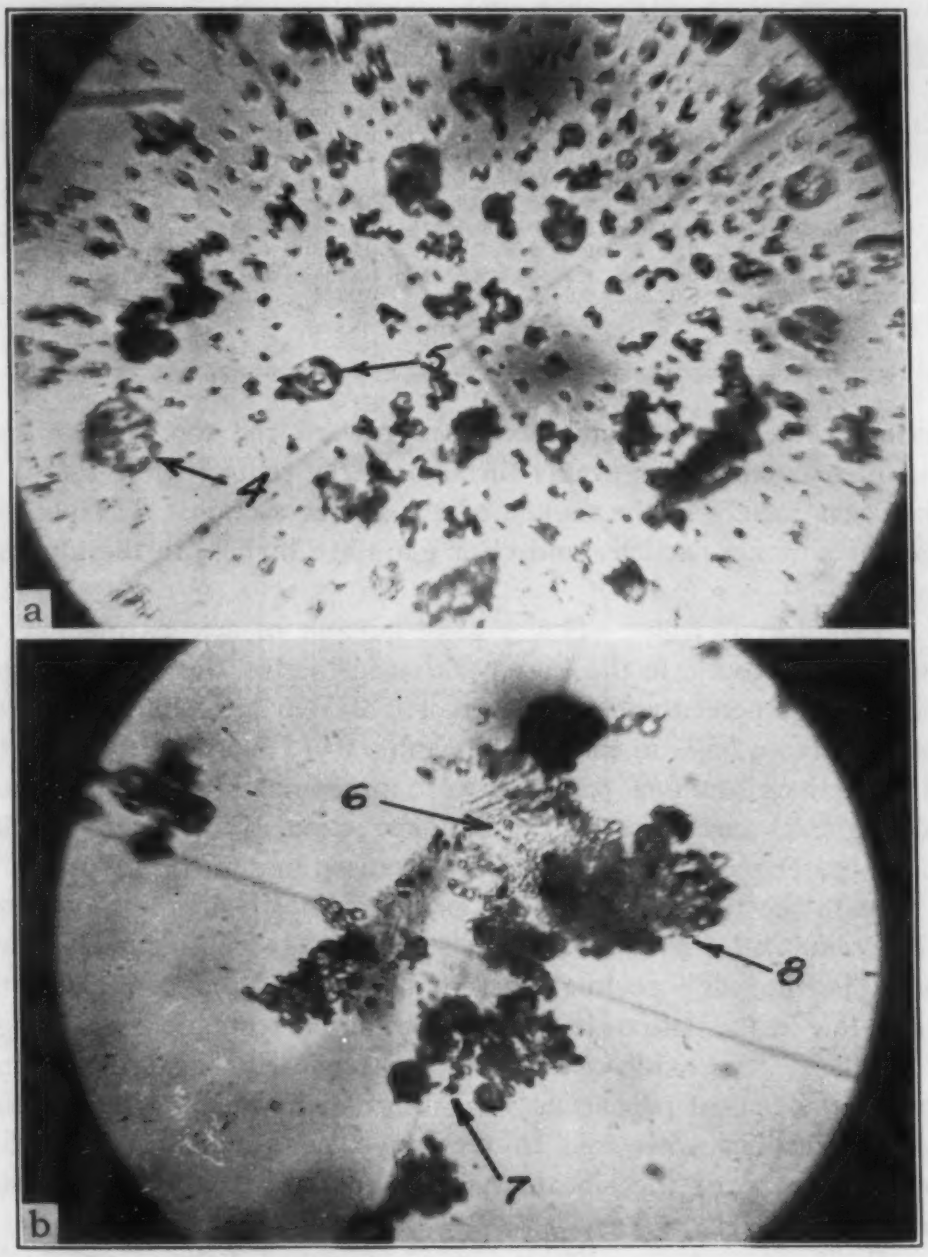


Fig. 4—Acid Extraction Inclusions Studied by Mineralogical Examination. (Original magnification ×350.) a—Quartz (4) and quartz and alumina (5). b—Alumina grains (6), alumina clusters (7), and mullite (8).

Producer B Ingot—The highest concentration of nonmetallics was in the center position of the bottom third of the ingot. In the edge samples the inclusions were concentrated toward the top of the ingot. The average percentage of extractable inclusions for the ingot is 0.0126%. Alumina clusters were heavily concentrated in the

Table IV

	Producer								
	A	B	C	D	E	G–26 in.	G–21 in.	H	N
1	0.0080 to 0.0125	0.0050 to 0.0100	0.0040 to 0.0085	0.0050 to 0.0150	0.0045 to 0.0073	0.0065 to 0.0105	0.0080 to 0.0103	0.0050 to 0.0080	0.0020 to 0.0035
2	0.0125 to 0.0170	0.0100 to 0.0130	0.0085 to 0.0130	0.0150 to 0.0250	0.0073 to 0.0097	0.0105 to 0.0145	0.0103 to 0.0126	0.0080 to 0.0110	0.0035 to 0.0050
3	0.0170 to 0.0215	0.0130 to 0.0160	0.0130 to 0.0175	0.0250 to 0.0350	0.0097 to 0.0121	0.0145 to 0.0185	0.0126 to 0.0149	0.0110 to 0.0140	0.0050 to 0.0065
4	0.0215 to 0.0260	0.0160 to 0.0200	0.0175 to 0.0220	0.0350 to 0.0450	0.0121 to 0.0145	0.0185 to 0.0225	0.0149 to 0.0172	0.0140 to 0.0170	0.0065 to 0.0080
5	....	....	....	0.0450 to 0.0935	....	....	....	....	....

bottom center section and decreased toward the top. Clear glass was distributed rather evenly throughout the center, while the oxide glass was mostly in the middle of the center section. The percentages of alumina particles and clear glass are highest in the top edge position.

Producer C Ingot—The greatest amount of acid-extractable inclusions was found in the edge position in the top third of the ingot. The average percentage for the ingot is 0.0096%. Alumina clusters decrease from 55% in the bottom center to 15% in the top. In the edge sections alumina particles were predominant, with clear and oxide glasses increasing in the middle section of the edge samples. In the center sections, oxide glasses increased in percentages from the bottom to the top. Clear glass was found mostly in the top center.

Producer D Ingot—The highest percentage of nonmetallics was found in the edge position just under the hot-top and along the center line in the bottom half. The average percentage for the ingot is 0.0285%. An oxide coating over the inclusions made determination of the optical properties very difficult; however, after treating the nonmetallics with acid to remove some of the coating, 95% appeared to be of the silicate type, as might be expected for acid open-hearth steel.

Producer E Ingot—There were no marked differences in acid-extractable inclusion content from edge to center or from bottom to top in this ingot. The variation in percentages of inclusions was less marked in the edge position as compared with the center positions. The average percentage of inclusion content for the ingot is 0.0092%. The presence of alumina particles decreased from bottom to top of the center and edge sections. The concentration of ferrous aluminate and clear and oxide glasses increased greatly from the bottom to the top in both positions.

Producer G 26-Inch Ingot—The nonmetallic inclusion content was consistently higher in the edge positions, except for the extreme bottom slice. The percentages were quite uniform from bottom to top in the edge positions; however, in the center positions the

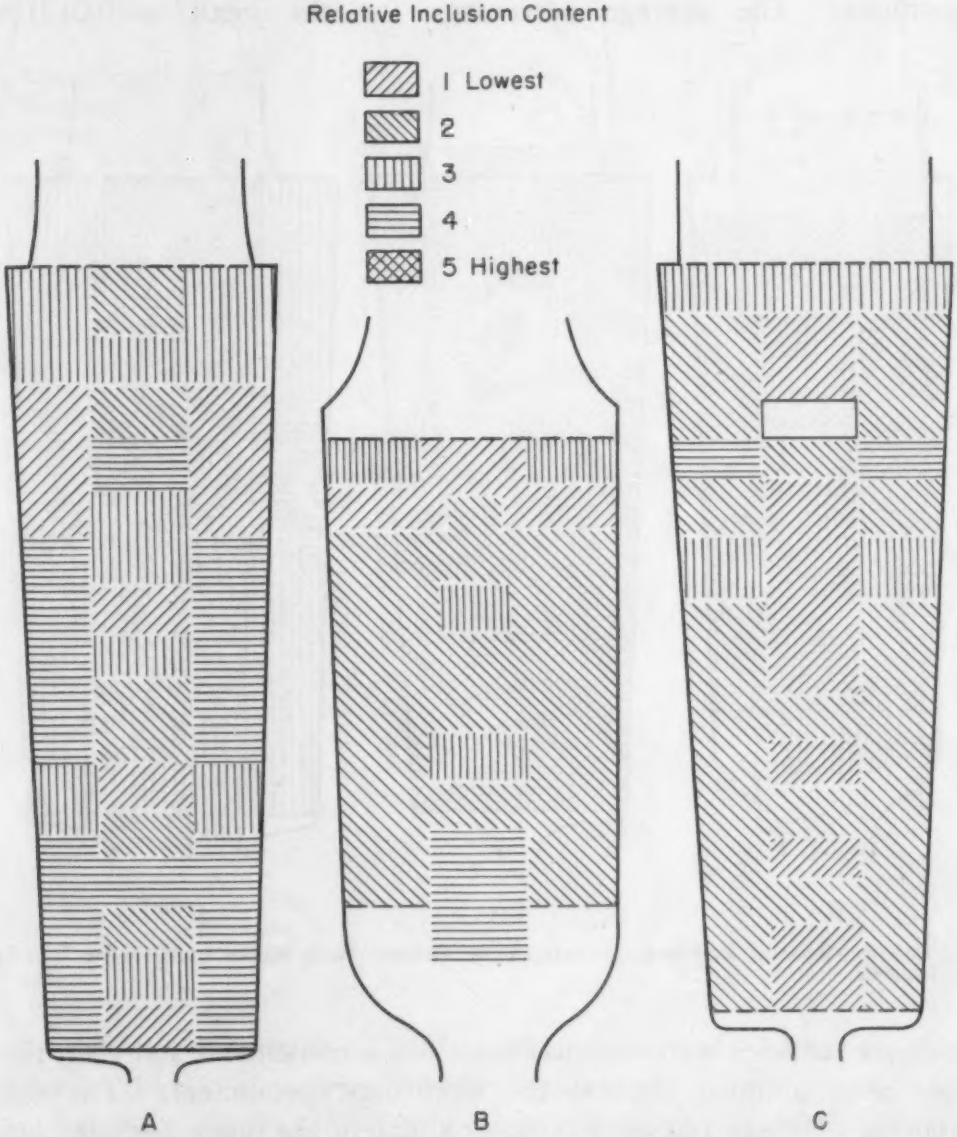


Fig. 5a—Relative Inclusion Contents in the Various Zones of the Ingots.

inclusions decreased from bottom to top. The average percentage for the ingot is 0.014%. Alumina particles constitute the major inclusion phase in all positions of the ingot, averaging around 60% of each sample studied. Alumina clusters constitute another major

phase. Small amounts of clear glass, oxide glass, quartz and the oxide crystal phase were found throughout the ingot.

Producer G 21-Inch Ingot—The percentage of acid-extractable inclusions was higher along the edge than in the center; however, the percentages were fairly uniform from top to bottom in both positions. The average percentage for the ingot is 0.0121%.

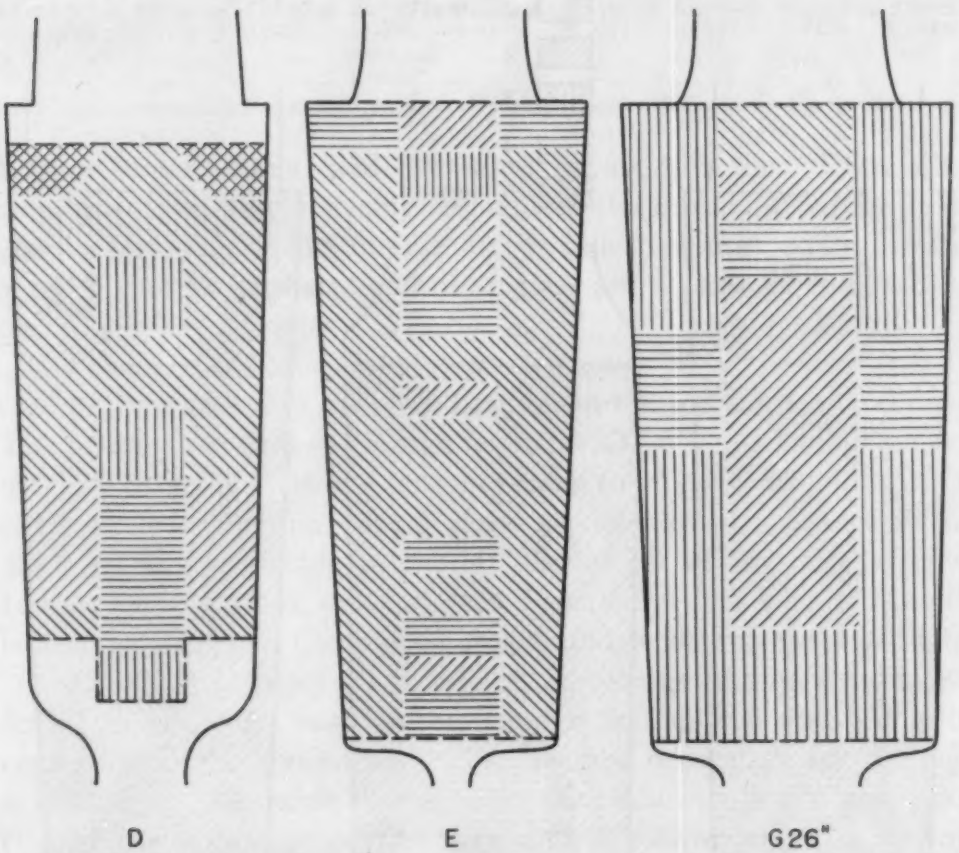


Fig. 5b—Relative Inclusion Contents in the Various Zones of the Ingots. See Fig. 5a for Legend.

Alumina particles were the major inclusion constituent found in this ingot with alumina clusters the next most prominent. The distribution of these phases was approximately the same for all positions in the center and edge except for the top edge where the percentage of oxide and clear glasses increased to about 8%.

Producer H Ingot—Higher concentration of nonmetallics was found in the edge position. The distribution was fairly uniform from bottom to top. The average percentage of inclusions for the ingot is 0.0119%. Alumina particles and clusters were the pre-

dominant constituents. The percentages increased from the bottom to the top in both center and edge. There was about 25% quartz in the bottom center positions and a combined quartz and alumina phase which increased in quantity from the bottom to the top edge samples.

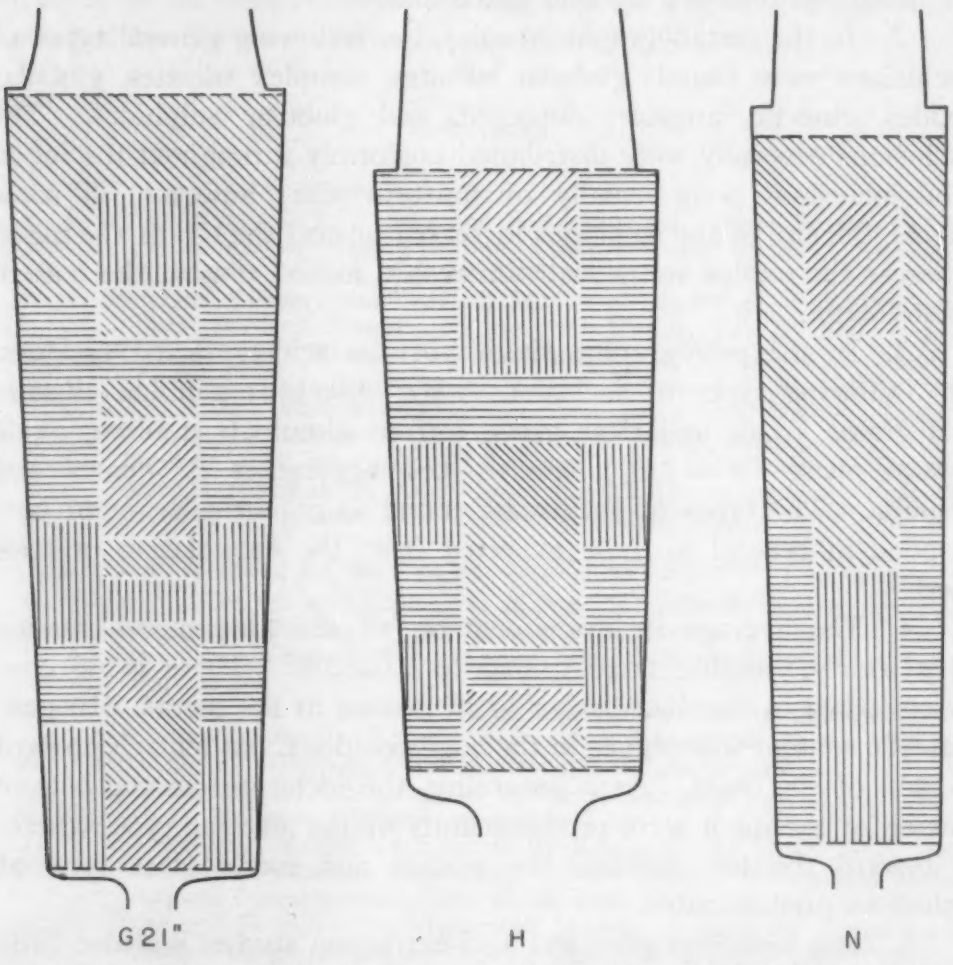


Fig. 5c—Relative Inclusion Contents in the Various Zones of the Ingots. See Fig 5a for Legend.

Producer N Ingot—The largest quantity of inclusions was found in the edge positions in the bottom half of the ingot. All edge positions were consistently higher than the center positions. Small particles of oxide-coated glasses and high alumina glass constituted the major portion of the nonmetallics in all sections, except in the bottom edge where alumina clusters and particles made up about 97% of the inclusions. The inclusions in both positions decreased from bottom to top. The average percentage for the ingot is 0.0055%, the lowest of all the ingots studied.

Summary

1. The nonmetallic inclusions in nine alloy steel ingots were studied by metallographic methods and by petrographic examination of inclusions obtained by acid extraction.

2. In the metallographic studies, the following general types of inclusions were found: globular silicates, complex silicates, globular oxides, eutectic, angular, duplexed, and globular sulphides. The inclusions generally were distributed uniformly throughout the ingot. The inclusions were usually of uniform size; however, in some ingots, the size of the sulphides increased toward the top of the ingot, whereas the oxides and silicates increased in size toward the bottom of the ingot.

3. In the petrographic studies of the acid-extracted residues, the following types of inclusions were observed: alumina clusters and grains, oxide and clear glass, ferrous aluminate, mullite, oxide crystal phase ($n = 1.70$), quartz, and aggregates of quartz and alumina. The types of inclusions found in a particular ingot correspond in general to those expected from the deoxidation practice used.

4. The average inclusion contents of the nine ingots studied vary widely, ranging from 0.0055 to 0.0285%. There is no consistent trend in the distribution of inclusions in the ingots. In general, the content was higher in the edge positions, particularly toward the top of the ingot. As a generality, the inclusions in the bottom portion of the ingot were predominantly of the alumina type, whereas toward the top portion, the silicate and oxide glass type of inclusions predominated.

5. The metallographic and acid-extraction studies revealed little or no correlation between the size, type, distribution, or amount of nonmetallic inclusions with the occurrence of bore defects in seamless 75 and 40-millimeter tubes. This general lack of correlation leads to the conclusion that there were other factors, considerably more potent than nonmetallic inclusions alone, operating to cause the formation of bore defects in these heavy-walled seamless tubes.

Acknowledgments

The authors wish to acknowledge the contribution of Dr. R. F. Mehl, Head of the Department of Metallurgy and Director of the

Metals Research Laboratory, as Official Investigator for NDRC Research Project NRC-39.

The work on this project was assisted by the co-operation of the Project Advisory Committee. The members of this committee are listed in the first reference of this paper. The split ingots were furnished by the co-operating companies of the project.

References

1. *References in present series on ingots*
   a. J. W. Spretnak, K. L. Fetters and E. L. Layland, "Ingot Factors in the Production of Seamless Gun Tubes," TRANSACTIONS, American Society for Metals, Vol. 39, 1947, p. 627.
   b. V. Paschkis, "Theoretical Thermal Studies of Steel Ingot Solidification," TRANSACTIONS, American Society for Metals, Vol. 38, 1947, p. 117.
   c. J. W. Spretnak, "Kinetics of Solidification of Killed Steel Ingots," TRANSACTIONS, American Society for Metals, Vol. 39, 1947, p. 569.
   d. J. W. Spretnak, "Macrosegregation in Some Alloy Steel Ingots," TRANSACTIONS, American Society for Metals, Vol. 40, 1948, p. 897.
   e. C. F. Sawyer, J. W. Spretnak and G. Derge, "The Distribution of Oxygen and Nitrogen in an Alloy Steel Ingot," TRANSACTIONS, American Society for Metals, Vol. 40, 1948, p. 922.

2. *References pertaining to study on nonmetallic inclusions*
   a. Emile M. Chamot and Clyde W. Mason, "Handbook of Chemical Microscopy," Volumes I and II.
   b. Alexander N. Winchell, "Elements of Optical Mineralogy," Part I and Part III.
   c. E. S. Larson and H. Berman, "The Microscopic Determination of Non-Opaque Minerals, Bulletin 848, U. S. Geological Survey (1934).
   d. Alexander N. Winchell, "The Microscopic Characters of Artificial, Inorganic, Solid Substances or Artificial Minerals."
   e. Charles P. Shillaber, "Photomicrography."
   f. G. R. Fitterer, "Method of Electrolytic Extraction of MnO, MnS, FeS, and SiO_2 Inclusions from Plain Carbon Steels," Mining and Metallurgical Investigations, Nos. 46-59, 1930-32.
   g. O. Hare and G. Soler, "An Improved Method of Studying Inclusions in Alloy Steels," *Metals and Alloys,* Vol. 8, 1937, p. 169-172.
   h. C. H. Herty, Jr., G. R. Fitterer and W. E. Marshall, Jr., "Theoretical Considerations in the Electrolytic Determination of Non-Metallic Inclusions in Steel," *Mining and Metallurgical Investigations,* No. 35-45.
   i. "Determination of Slag and Oxides by the Iodine Method," *Proceedings,* American Society for Testing Materials, 28th Meeting, Vol. 25, 1925, p. 80-81.
   j. J. H. S. Dickenson, "A Note on the Distribution of Silicates in Steel Ingots," *Journal,* Iron and Steel Institute, Vol. 113, 1926.
   k. J. T. Whiting, "Microscopic & Petrographic Studies of Blast Furnace Materials," A.I.S.I., *Blast Furnace and Steel Plant,* Vol. 26, 1938, p. 585-589, 632, 694-696, 715.
   l. Klinger and Koch, "Electrolytic Extraction of Inclusions," Translated from *Technische Mitteilungen Krupp, Forschungs,* Report No. 3, May 1938.

DISCUSSION

Written Discussion: By R. L. Wilson, director of metallurgy, and D. J. Girardi, research metallurgist, The Timken Roller Bearing Co., Canton, Ohio.

The problem of inclusion studies is always a difficult one and an extensive survey such as is set forth in this paper is welcomed. Because of the uncertainties involved in the acid extraction of inclusions, it is difficult to compare directly acid-extraction results among heats varying in melting, deoxidation and mold practices. However, it is in such instances that one is frequently interested in making direct comparisons. One wonders about the significance of an average percentage of acid-extractable inclusions of 0.0285% in the case of Producer D ingot and an average of 0.0055% in the case of Producer N ingot.

The lack of correlation between the size, type distribution and amount of nonmetallic inclusions and the occurrence of bore defects in heavy-walled seamless tubes does emphasize the importance of considering other factors.

Written Discussion: By S. F. Urban, director of research, Titanium Alloy Mfg. Division, National Lead Co., Niagara Falls, N. Y.

On perusing this paper, it is obvious that many weary hours were spent in obtaining the detailed data regarding the percentage, distribution and nature of the inclusions in various positions of ingots made by various producers. It is unfortunate that in spite of the scope of the investigation, no correlation is found between the factor studies and rejections of gun tubes from the bottom third of ingots converted into gun tubes.

Since the bottom third portion of an ingot has been known to be a contrary position in an ingot, it is perhaps in order to make the suggestion which is admittedly not a new one but should definitely be considered. There is enough information available to indicate that the inverted V in the bottom portion of an ingot might be eliminated by the use of a heated bottom or some means of delaying bottom solidification other than by ingot mold design.

Written Discussion: By J. V. Russell, director, Metallurgical Laboratory, Republic Steel Corp., Chicago.

The authors are to be complimented on what is evidently a very large amount of work and on the completeness of the data presented. It is undoubtedly an oversight but they failed to indicate whether the samples are numbered from top to bottom or bottom to top as taken from the ingot. We were particularly interested in their conclusion that sulphides were, in general, evenly distributed throughout the ingot. Our experience on similar steels and on resulphurized steels indicates about the same condition. Is not this fact considerable evidence for the belief that sulphides form as such out of the liquid steel at a temperature near or even below the solidification point? We were also interested in their observation that the eutectic-type sulphide inclusions were observed to occur only in the lower part of the ingot. This is associated by them with the use of "critical amounts of aluminum". We would like to ask why it is that

the condition will be in only a part of the ingot since it is generally thought that the addition of aluminum affects equally all parts of the ingot. Is there a possibility, in this case, that aluminum would have been added to the ingot as it was being poured rather than as a ladle or furnace addition, which is the usual practice for heats of the type studied? We would also like to know if the authors care to advance any explanation of the fact that the inclusion type changes from alumina in the bottom portion of an ingot to silicates and oxide types in the upper portion.

Written Discussion: By T. R. Gaulke, metallurgist, and M. A. Scheil, director of metallurgical research, A. O. Smith Corp., Milwaukee.

The authors are to be complimented on their thorough job dealing with a subject of such comprehensive scope. It is also gratifying to learn that their results are in close agreement with similar work conducted at the A. O. Smith Corp. in 1944.

The work at A. O. Smith, too, was instigated under similar circumstances and involved the welded fabrication of torpedo air flasks for the U. S. Navy. These flasks were made of 4340 steel plate rolled from slab-type ingots fortified with a small amount of vanadium for grain size control and to permit higher drawing temperatures. This steel was subjected to a rigid quality control program which included the keeping of accurate records to permit us to trace all rejections back to the responsible location in ingot and slab. Practically all the rejections were occasioned by laminations uncovered during machining. Of all the steel rejected, it was found that about 90% was in plate material rolled from the bottom slabs of the ingots. It was thought that improper mold design was at least partly responsible for the poor showing of these bottom slabs and, consequently, an investigation was undertaken to thoroughly study the product of one 65-ton electric furnace heat poured into open bottom molds and closed bottom molds.

The closed bottom mold represented the new type mold with rounded bottom designed to effect a change in the pattern of segregation through the ingot. The top and bottom dimensions of the two type molds were the same: 28⅜ by 61¾ inches at the top and 26⅜ by 59¾ inches at the bottom. Pouring height usually reached about 62 inches. The closed mold had a 6½-inch radius joining the closed bottom to the side walls and the plug hole centrally located in the bottom was 6⅛ inches in diameter. The height of the curved bottom from the straight side wall section to the plug hole level was 13¾ inches.

One 30,000-pound ingot of each design was rolled to slab and the bottom slab was quarter-sectioned for examination. One 30,000-pound ingot of each design was slow-cooled and quarter-sectioned for examination. The fifth ingot from an open bottom mold was processed into plate for performance observation. Extensive etch tests, chemical analyses, spectrographic analyses, microexamination and radiographic inspections were carried out on the sectioned ingots and slabs. Ten core-drilled specimens, ⅞ inch in diameter by 6 inches long, were removed from choice locations in the quarter-sectioned closed bottom ingot. It was from the drilled cores of the ingot and segregated areas of the bottom slabs of the

ingot that our microexamination dealing with inclusions was conducted.

Globular sulphides, duplex oxide-sulphide combinations and globular oxides were found to predominate. Sulphur printing of the drilled cores gave a fine picture of relative size and distribution of sulphide inclusions in the ingot. Cores drilled near the ingot surface showed small, finely dispersed sulphides, while those approaching the top center of the ingot showed larger sulphides with a tendency to form clusters. This was verified by microexamination. The oxides resulting from deoxidation with aluminum were found in abundance in the bottom central portion of the 30,000-pound ingot.

The segregated areas in the bottom slabs showed the presence of (Fe,Mn)S and spheroidized carbides. This segregation, however, was very slight and usually observed between the case and core where the lower melting point impurities were rejected from the solidifying columnar grains.

Generally speaking, we could find no difference in the product of the two types of mold. The heat investigated proved to be of exceptionally high quality. But the investigation did result in our dropping the micro-cleanliness ratings as a standard of quality and placing more reliance on the development of a set of deep-etch standards for quality control.

Written Discussion: By Edward A. Loria, Fellow, Mellon Institute of Industrial Research, Pittsburgh.

In this series of papers on gun steel ingot practice the authors refer to the occurrence of bore defects which were found in partially and often completely machined tubes, but have not given an explanation for their existence. It was stated that metallographic studies indicated that inclusions were not the primary cause of these defects although they may have acted in some manner to initiate them. The bore defects concerned were not quenching cracks, nonmetallic inclusions or flakes. They were usually quite shallow and possibly could have been internal ruptures caused by hot working. In the present paper, it is stated that some of the ingots showed pronounced herringbone patterns or areas of considerable porosity and there is the possibility that the extension of the original porous area by actual tearing into an originally sound adjacent area during hot working may have produced this defect. Porosity, as a rule, is not evident until machining operations have been fairly well advanced and is resultant from weakness along the secondary segregation, this weakness being caused usually by cold metal from the furnace or by insufficient mold design. During forging, small cavities or cracks are formed at this point in the ingot and appear when the center portion of the forging is bored. It is interesting to note that when ingots are split longitudinally the polished section does not usually show many cracks in the position of the V segregate. Macroetching, however, may result in discontinuities being found at this position because of the removal of nonmetallic inclusions during the process, and evidently these inclusions form lines of weakness which, on forging, rupture to form cavities. Therefore, it follows that the condition of the V segregate is the determining factor in their existence. The presence of a V segregate at the position of the cavities may

be detected by sulphur printing or macroetching. These defects can be minimized by increasing the taper on the ingot body to allow better shrinkage conditions. In the last paper of the series the authors showed that the center positions of the split ingots had the lowest densities and the greatest variations in density. There was a definite trend in the center positions of decreasing density toward the top of the ingot. Thus, density had a positive correlation with frequency of bore defects.

It would be well to point out that the authors have based their conclusions on a study of the inclusions in small ingots of 13 to 26 inches cross-sectional dimension. In larger ingots the size and amount of the inclusions increase and the tendency to form a mixture of large and small inclusions is accentuated along with the danger of producing an unfavorable inclusion distribution. The total nonmetallic content may affect the quality of gun tubes produced from the latter to a greater extent than the former, notwithstanding the fact that the quality of gun tubes may not be so much related to the amount of inclusion material as to the distribution of that inclusion material.

The RAT values obtained from test specimens taken from various sections in these ingots would evaluate their cleanliness and provide some indication of their quality since gun tubes processed from ingots with the fewest inclusions would probably be the best in service. Both discontinuous and continuous stringer-type inclusions are known to exert a detrimental influence on the transverse ductility of quenched and tempered gun tubes; the presence of untempered martensite or slack-quenched structures may also produce inferior physical properties. Do the authors have tensile test data taken from various positions in their nine alloy steel ingots? If the data are included as a part of the recent investigation by Wells and Mehl,[2] where in that study can the results be found? Perhaps the results are not only complicated by the difficulty of determining any measure of inclusion distribution but also by the difficulty of determining to what extent defects are aggravated or minimized by unfavorable or favorable hot working conditions.

Authors' Reply

The authors wish to thank those who have discussed this paper and offer the following comments on the questions and points that have been raised.

The question as to the significance of the quantitative amount of inclusions which was raised by R. L. Wilson and D. J. Girardi is of particular interest in any evaluation of the acid-extraction method of inclusion determinations. In the case of ingot D which was made in the acid open-hearth, it would be expected that the prevailing inclusion types would be silicates and since silicates are not likely to be altered or dissolved in acid extraction it is not surprising to find the highest inclusion content in this ingot 0.0285%. Ingot N which was made in the basic electric

[2]C. Wells and R. F. Mehl, "Transverse Mechanical Properties in Heat Treated Wrought Steel Products," TRANSACTIONS, American Society for Metals, Vol. 41, 1949, p. 715.

furnace has the lowest inclusion content 0.0055% which may either represent a substantiation of the traditional cleanliness of properly made electric furnace steel or at least its freedom from inclusions retained by acid extraction. It should be noted that the deoxidation practice of this ingot differs principally from the other electric furnace ingot (B which had 0.0126%) in that aluminum was not used in the deoxidation of N, and that alumina inclusions are quite likely to be retained in acid extraction.

Mr. J. V. Russell brings up the question of the significance of the greater occurrence of alumina-type inclusions in the lower part of the ingot and the predominance of silicate and oxide types in the upper part of the ingot. The authors believe this is the result of the ease with which the silicate and oxide types may be fluxed with resultant agglomeration and greater particle size which, according to Stokes' law, would explain their prevalence relatively in the upper portion of the ingot.

The discussion of Mr. Loria regarding central porosity as related to forging defects is particularly interesting since it is the authors' opinion that the relatively greater prevalence of bore defects in guns made from seamless tubes must in some way be related to the macro-inhomogeneities which were often observed in the lower part of the ingot. Now that several years have passed since this study, it no longer seems so surprising that no correlation could be found between relative inclusion content and bore defects. For the most part bore defects which were uncovered during the machining of the inside of the tubes were quite small and their origin may be considered to have been ruptures that occurred during hot working (piercing). It is not necessarily the amount of inclusions, but the possible coincidence of inclusions with the points of maximum stress during piercing that likely caused the ruptures. It is well known that in piercing tubes the stress system is enormously complex and that the setting of the mills and the condition of the piercer points in the piercer and the balls in the high mill are all related to the resultant inside surface of the tube. How then to explain the greater prevalence of bore defects in the tubes made from the lower third of the ingot? Assume first that since tubes were not pierced separately as to position from which they came in the ingot there was no controllable variable in piercing that could explain the relation between ingot position and defects. It is also evident that unknown and uncontrollable variations did occur in mill settings and seamless "tools". When these variations were such as to cause an unfavorable distribution of stresses, relatively minor inclusions could easily be the point of origin of hot ruptures while with a more favorable system of stresses the same inclusions would not be related to defects. This then would easily "mask" the correlation between inclusions and bore defects. Note also that the conclusion was reached that alumina inclusions predominate in the lower portion of the ingot. The refractory nature of alumina inclusions and their frequent sharp edges would create ideal stress raisers to serve as the origin of hot ruptures. Note that the ingots of producers A, C, E, G, and H were the ones which were used for seamless tubes. The following remarks were made in the paper in describing the results of the petrographic studies of these ingots.

A. "Ferrous aluminate was concentrated mostly in the bottom three slices of the edge and center sections and the top edge."

C. "Alumina clusters decrease from 55% in the bottom center to 15% in the top."

E. "The presence of alumina particles decreased from bottom to top of the center and edge sections."

G. 26-inch ingot. "Alumina particles constitute the major inclusion phase in all positions of the ingot, averaging around 60% of each sample studied."

G. 21-inch ingot. "Alumina particles were the major inclusion constituent found in this ingot with alumina clusters the next most prevalent."

H. "Alumina particles and clusters were the predominant constituents."

If we consider that the conditions necessary for a hot rupture are stress raisers combined with an unfavorable stress distribution these conditions will be met in normal seamless operation most frequently where alumina inclusions are small, angular and most plentiful, namely, the lower third of the ingot. Perhaps we found the qualitative explanation of bore defects though the quantitative explanation was missed in the mass of unmeasurable variables in these studies.

SOME FACTORS AFFECTING SUBSURFACE DEFECTS IN LARGE FORGING STEEL INGOTS

By E. A. Loria and H. D. Shephard

Abstract

The defects which occur at or near the ingot surface in several large steel forging ingots of a particular acid open-hearth grade were examined critically by means of transverse macroetch tests, sulphur prints, magnaflux and microscopy in an effort to determine the factors affecting their formation. Specifically considered were subsurface cracks, subsurface porosity and other defects caused by the presence of nonmetallic inclusions. Subsurface cracks in forging ingots are initiated by segregates of nonmetallic inclusions. Cracking occurs as the result of lowered crystal-to-crystal cohesion in the case of inclusions which form continuous layers of liquid during forging, whereas inclusions which are solid at forging temperatures as little prisms at the grain edges lower the fracture stress by acting as areas for stress concentration. Data were obtained regarding the position and occurrence of subsurface porosity and some theories concerning its cause are discussed. The important aspect of these mechanisms is that either inclusions or porosity may exist in the ingot subsurface, depending upon the manner and extent of deoxidation. Small seams on the machined surface of round forgings which were exposed by magnafluxing the periphery after machining 1½ inches below the surface of the original ingot arise from stringer-type inclusions. General trends of inclusion distribution in the microscopic examination of the top, middle, and bottom transverse sections of several 36-inch forging ingots are presented. Sulphur prints reveal the segregation of inclusion stringers within the outer (chill) zone of forging ingots interspersed among an otherwise even distribution of minute sulphides. In general, it has been observed that where such stringer inclusions occur within a zone of relatively minute inclusions internal tears are most likely to occur on processing the ingot. The difference in conformation of sulphides

A paper presented before the Thirtieth Annual Convention of the Society, held in Philadelphia, October 23 to 29, 1948. Of the authors, E. A. Loria is Fellow, Mellon Institute of Industrial Research, Pittsburgh, and H. D. Shephard was formerly metallurgist, Mesta Machine Company, now metallurgist, Kerchner, Marshall & Company, Pittsburgh. Manuscript received October 13, 1947.

in the ingot subsurface is believed responsible for this type of defect because the sulphide stringers are incapable of dispersion or diffusion within the minute, even distribution of globular sulphides and therefore act as points for stress concentration during hot working.

Introduction

OVER the past several years, the importance of controlling surface and subsurface defects in steel ingots and forgings has been recognized. Many methods have been developed to avoid the occurrence of surface defects during steel processing and to improve the surface condition of ingots for appearance and serviceability. The attributable factors which have been dealt with are deoxidation technique, ingot mold design, temperature of molten metal and ingot mold at time of pouring, pouring technique, mold practice, and pit practice. While satisfactory methods have been devised for improving the surface conditions of ingots, much less information has been made available on the problem of evaluating the factors contributing to the occurrence of subsurface defects in certain forging grades of steel ingots; hence the purpose of the investigation reported herein was to assemble suitable data from which conclusions regarding the origin of subsurface defects could be drawn.

The conventional forging steel ingots are subject mainly to defects in the following categories: (a) cracks, (b) porosity, (c) defects caused by the presence of nonmetallic inclusions, (d) pipe and bursts, and (e) macrosegregation. When observed in transverse sections of ingots these defects are found in certain definite locations and can therefore be classified as surface, subsurface and center defects.

Type (a) defects are actual discontinuities in the ingot and, depending on their nature and distribution, may make the steel unfit for use unless they are removed by further hot reduction. Surface cracks as revealed by deep etching usually follow an irregular path and may result from improper handling during heating, forging, or during cooling from the finishing temperature. Internal cracks, sometimes called flakes, cooling cracks or thermal checks, can also be detected by the macroetch test and their identity verified by a fracture test of a hardened specimen on which they are revealed as brightly crystalline spots. Type (b) defects can be found in widely varying degrees within the ingot and the question of whether the

steel should or should not be used is one of experienced judgment. These include center looseness or shrinkage, subsurface porosity, blowholes and unsound steel in general. Center porosity may be the result of an actual discontinuity within the metal in which case it is probably more proper to classify the defect as a pipe. Usually, however, porosity is of such a nature that it is not visible until the specimen is subjected to a deep etch. The type (c) defects occur in various sizes and shapes. The inclusions may be the products of deoxidation, or may be exogenous in origin. The inclusion type of defects which are generally discovered on machining are referred to as seams, slag, porous metal, pits and sand splits. Seams in forged material generally follow the contour of the forging and the flow of the metal. This most detrimental effect is avoided if, during processing, the surface is machined to a sufficient depth to remove the seams. Type (d) defects are visible after deep etching and can generally be distinguished from each other by the degree of sponginess surrounding the defect. Piped material usually shows considerably more sponginess than burst material. Pipes are internal cavities formed during ingot solidification and are invariably associated with segregated impurities which are deeply attacked by the etching reagent. Cavities in the center not associated with deeply attacked impurities are often mistaken for pipe but such cavities are usually traced to bursts caused from improper handling of the steel during forging. Type (e) defects consist of composition variations over comparatively large distances in the ingot, such as from the sides to the center and from bottom to top.

Determining the factors affecting defects in forging ingots is complicated by many attributable variables which occur during the steelmaking process. Review of the literature with respect to large steel forging ingots confirms this contention, for most investigators have concluded that such defects were the result of a combination of variables. Latta and his collaborators (1)[1] stressed the importance of the condition of the furnace, the charge, duration of melt, time of ore addition, time deoxidation additions are made prior to tap, duration of tap, and pouring practice on the quantity of nonmetallic inclusions in large steel forging ingots. Their belief that the danger of unfavorable inclusion distribution increases with the size of the ingot was based on the fact that with increasing quantities of steel it becomes more and more difficult to pour within a definite restricted

[1]The figures appearing in parentheses pertain to the references appended to this paper.

range of temperature due to the longer time of pouring. In this respect pouring technique was deemed particularly important by these investigators; their contention being that too high a pouring temperature is as detrimental as a too low one, inasmuch as this can be remedied by changing the velocity of pouring to a limited extent only. Accordingly, the proper way to specify the rate of pouring is to state the rate of rise, taking into consideration the ingot cross section. If the pouring temperature is too high, one is inclined to correct this by reducing the rate of pouring. When reducing the velocity of pouring, a point is reached where an oxide film forms on the top surface of the steel already in the mold. This surface oxidation of steel may be a main source of sand inclusions. In the case of too low temperatures, these influences prove to be still more harmful and cannot be corrected by speeding up the pouring, without committing other grave errors.

After correlating his data on how to avoid defects in medium and large ingots of basic open-hearth steel, Wulffert (2) concluded that the three important factors which influence the condition of the steel along the ingot axis were the content of the total iron in the final slag, the rate of carbon elimination and the pouring temperature. Wulffert disproves the contention that increased pouring temperatures may exert a detrimental effect on the occurrence of segregations and maintains that it does not apply to ingots of medium and large size.

Kerpely (3) examined the defects in forged crankshafts due to sand inclusions (seams) and based their occurrence primarily on the quality of the open-hearth pig in the charge, the degree of fluidity of the steel, pouring temperature and the regulation of the pouring velocity. The reaction products from deoxidation also made their appearance in the samples taken from the pins of discarded crankshafts and the author observed that the occurrence of a thin and high FeO slag was invariably accompanied by an increase in the number of sand seams in the steel. To avoid their occurrence, a rather fluid slag had to be maintained during the course of the heat. On studying the distribution of inclusions over the ingot cross section Kerpely found that they were by no means equally distributed and assumed that in such a case the crystallization of the ingot plays a role insofar as slags tend to appear in the neighborhood of the ingot center with conditions of pouring and cooling conducive to pronounced transcrystallization; whereas with uniform crystallization, the inclusions

were found in regular distribution over the entire cross section of the ingot.

An excellent survey of the literature on the subject of ingot solidification and some interesting experimental results on solidification kinetics from a study of small ingots and a few large ingots has been made recently by Spretnak (4). The importance of the primary ingot structure[2] in ingots which undergo severe combined stressing in processing or application is indicated. In another paper dealing with the ingot factors in the production of seamless gun tubes, Spretnak (5) commented that there was no doubt that the size, amount, and distribution of nonmetallics are closely related to the defects in gun tubes and pointed out the pertinent fact that the overall problem (with respect to the entire ingot) is not only complicated by the difficulty of determining any measures of inclusive distribution, but also by the difficulty of determining to what extent defects are aggravated or minimized by unfavorable or favorable hot-working conditions.

In order to confine the problem it was necessary to restrict most of this investigation to defects which occurred in the subsurface or outer portion of forging ingots since it was felt that the analysis of these defects would be of particular importance in the case of ingots which must undergo severe processing operations. The subsurface defects specifically considered were the types (a), (b), and (c) listed above in instances where these defects occurred in the subsurface or outer portion of the ingot. Thus, defects which occur in the central portion of an ingot such as, for example, center porosity or shrinkage (type b defects) are not specifically considered in this paper.

To this end, transverse macroetch tests, sulphur printing, magnaflux and metallographic examination of several acid open-hearth ingots and forged sections were made. Data were obtained from a forging grade of the nominal composition: 0.38% carbon, 0.67% manganese, 0.041% phosphorus, 0.021% sulphur, 0.27% silicon. Producers of forging steels recognize the importance of chemical composition in relation to the hot-working properties and the typical defects found in their product. Soler (6) has discussed the decided effect of chemical composition of killed steel on hot-working properties and surface characteristics through its influence on the state of

---

[2]The term "primary ingot structure" is used to designate the solid structure resulting from the precipitation from the melt of dendritic crystals, which may occur either as equiaxed crystals of varying size, or columnar crystals which are elongated and possess preferred orientation in one direction (4).

deoxidation, gas content, freezing range and phase structure. Accordingly the scope of this investigation was necessarily limited to the evidence obtained by the aforementioned test procedures on one particular acid open-hearth forging grade which was customarily tapped in the range 2900 to 3000 °F (1593 to 1649 °C), deoxidized with manganese-silicon, and poured at 2800 to 2850 °F (1538 to 1565 °C) into various big-end-up fluted molds producing 32 to 48-inch ingots. The steel was forged between 2100 and 2350 °F (1150 and 1290 °C), the macroetched sections shown throughout the paper representing in most instances a reduction S ÷ s, ingot to forging, of 4.

Subsurface Cracks in Forging Ingots

Inasmuch as the objective of this investigation was that of determining the cause of cracks created under the ingot skin, an understanding of the cracking phenomenon in forging steels in general was highly desirable. As pointed out in the introduction, defects which have been designated as flakes or shatter cracks are not a part of this study since the outstanding characteristics of such defects usually occur in a zone which is intermediate between surface and core. The distance of the zone from the surface depends upon the size of the forging and its past treatment, and the defects produce a so-called "picture-frame" effect, especially in large forgings. Zapffe and Sims (7) maintain that hydrogen embrittlement, caused by accumulation of the gas at some discontinuity within the forging, is the seat for the defect, and some superimposed internal stress operating across this brittle zone is the cause of the fissure. It is also known that cooling cracks occur in ingots and that they are found to be intercrystalline. However, such cracks are not found in the outer inch or two of the section through a forging. This is despite the fact that the outer layers of the forging cool most rapidly, although slow cooling is known to prevent the occurrence of cooling cracks. Nevertheless, it is within the slow cooling interior of the forging that cooling cracks actually occur. Foley (8) has associated coarse austenite grain size and thermal stresses as prerequisites for the development of such cracks in ingots and forgings. In view of these observations, it is quite evident that the type of cracking discussed herein can be classified as a separate cracking phenomenon.

There are a number of ways in which cracks, whatever their origin, can be detected in the surface of a steel ingot. Macroetching, sulphur printing, magnetic-powder method and microscopic observa-

tion have all been used advantageously. The macroetch test reveals readily and quickly many of the characteristics of steel. The results obtained on properly etched samples are of great value if correctly interpreted. Surface seams, internal cracks and pipe are easily recognized. Crystallization pattern, unsound steel, nonmetallic inclusions and metallic segregates are also quite evident. Numerous pinholes and nonmetallic inclusions visible as a result of the deep etch are usually indicative of both gases and oxides being distributed in the steel at the time of casting. However, in the ingot subsurface it is at times difficult to differentiate between them, for nonmetallic inclusions usually appear as pits also, and furthermore every pit developed does not even indicate the occurrence of an inclusion, since pitting may also occur as a result of acid attack around carbide particles (etching out of metallic segregates). When nonmetallic inclusions are suspected in alloy steels which may contain metallic segregates, a comparison can be made of an annealed specimen and a hardened specimen etched alike. If the etching pits are the result of nonmetallic inclusions, they will appear similarly in both the annealed and hardened specimens, whereas if they are the result of a metallic segregate they will differ, since carbides will go into solution during heating for hardening, provided the austenitizing temperature is high enough. Segregation as revealed by macroetching is not always an indication of defective material. Such segregation can be identified by examining a polished specimen under the microscope to determine if it is metallic segregation, crystalline arrangement, or a concentration of impurities. The microscopic identification of segregation may also be supplemented by chemical means; such as analysis of ingot drillings for carbon, phosphorus and sulphur, or by analysis of inclusions after chemical extraction of same.

It is known that ingot cracks as revealed by deep etching usually follow an irregular path and may result from improper handling during heating, forging, rolling, or during cooling from the finishing temperature. With heat treated material, surface cracks may be caused by improper treatment, by improper grinding after hardening, or by service stresses. The type of cracking with which this paper is concerned is shown in Figs. 1 to 4 which represent transverse macroetch tests on various 36-inch forging ingots. The section depicted in Fig. 1, taken from the top third of the ingot, is a typical example of several samples which have been examined, and shows clearly the nature and location of the cracks in the outer portion of the cross

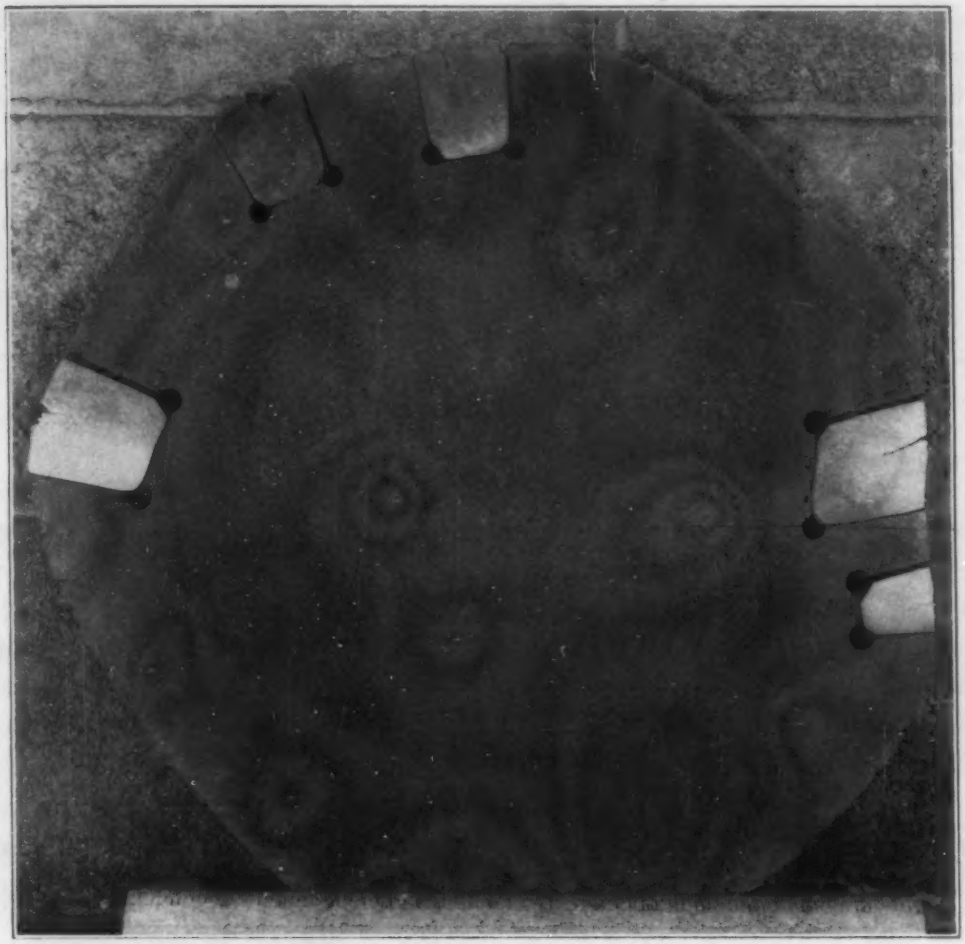


Fig. 1—Transverse Macroetch of 36-Inch Forging Ingot Taken From Top Third of Ingot. Note polished sections for metallographic examination where fully developed cracks occurred on forging, and fine internal cracks in bottom portion which opened up on etching. Originally × 0.4, reduced 50% in reproduction.

section. The fully developed cracks which extend to the surface and the fine subsurface cracks which opened up on etching are obvious. Observation of these cracks in several ingots indicated that they are not confined to any particular portion of the ingot but occur indiscriminately therein. The cracks are typical of those usually associated with the "corner ghost". Those experienced with large forging ingots will recognize that such indications on macroetching, if they do not extend to the ingot surface similar to the two in the lower corners of the photograph, vary greatly in character. They sometimes are actual cracks, but such indications sometimes are caused by segregations of either a metallic or nonmetallic character.

To ascertain the possible cause for this type of cracking, several

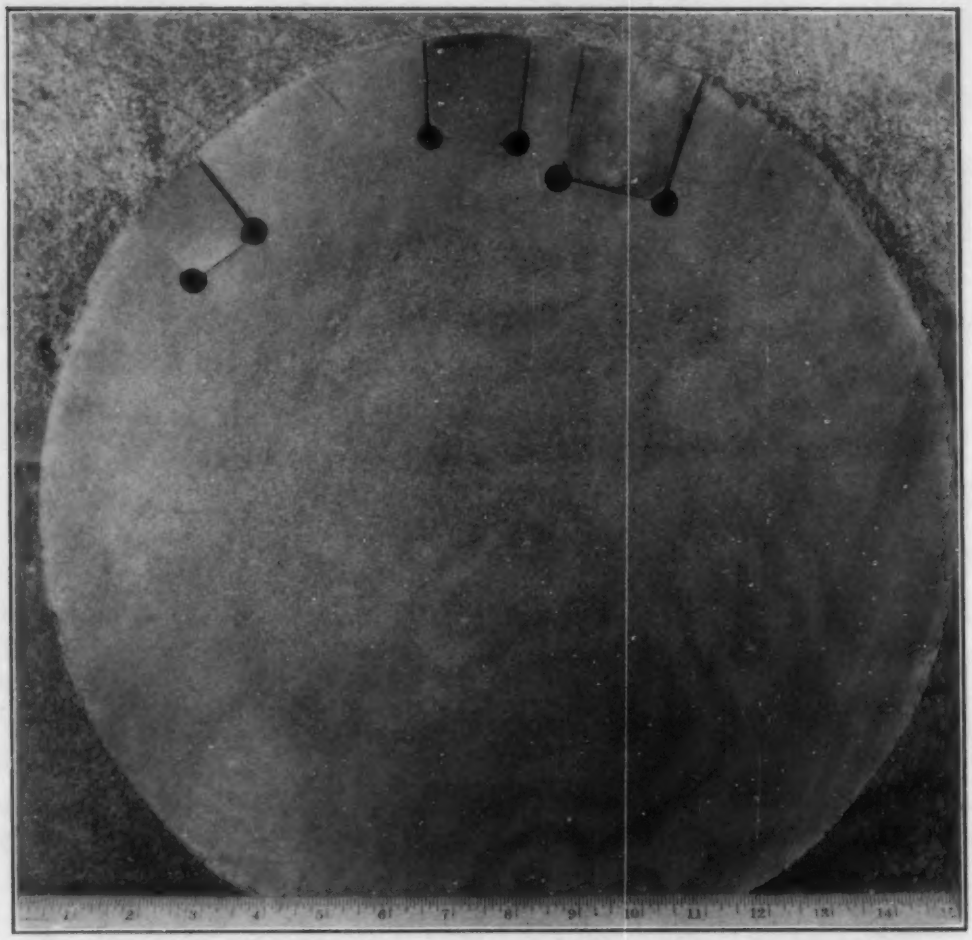


Fig. 2—Transverse Macroetch of 36-Inch Forging Ingot Taken From Top Third of Ingot. Note fine cracks at or near surface and pattern effect in central portion. Originally × 0.4, reduced 50% in reproduction.

sections were cut out of ingots where fully developed cracks occurred on forging (as shown in Figs. 1 to 4) and prepared for metallographic examination. Representative microstructures in areas where subsurface cracks occurred in the transverse section of the forging ingot shown in Fig. 1 are presented in Fig. 5. In micrographs (a) and (b) the oxidized condition at the edge of a crack resulting in oxide penetration and the oxide layers at both edges of another crack and the dispersion of fine particles beneath are illustrated. Micrograph (c) of the unetched structure taken directly below an area where cracking occurred reveals fine precipitate particles and stringer inclusions. Micrograph (d), another view in the vicinity of a crack, shows streaks of fine inclusions below the surface where cracking occurred.

The foregoing illustrations show that ingot cracks are rimmed

by ferrite containing dot-like inclusions of oxides. Furthermore, the concentration of other fine precipitate particles, nonmetallic inclusions and carbides, partly oriented in streaks in the vicinity of such cracks, is observed. Usually the cracks are not uncovered in the early processing of an ingot since they actually originate below the ingot surface and are detected only during forging, resulting in the formation of an oxide layer at the surface of the crack and some internal oxidation and decarburization. Microscopic examination of the structures occurring in areas below the cracks which opened up on macroetching the transverse section of the forging ingot shown in Fig. 1 provides further evidence of the segregate of inclusions and carbides. Representative microstructures which have been observed in several samples are presented in Fig. 6. Photomicrograph (a) shows the segregation of fine particles and larger, angular inclusions, and photomicrograph (b) depicting the same field at higher magnification identifies the inclusions as complex sulphides and silicates and reveals the presence of both spheroidal and angular carbides mainly in the ferrite grain boundaries. Another view at the same magnification, micrograph (c) confirms the concentration of globular oxide-sulphides and oxide-silicates, spheroidal carbides and partially spheroidized pearlite. Dark field illumination of this same area, micrograph (d) identifies some of the larger inclusions as silicates and the smaller cross-bearing ones as silica particles.

The type of subsurface cracking in forging ingots which has been described can occur as the result of a combination of factors. However, the observation that segregates of nonmetallic inclusions are found in areas where such cracking occurs is a significant one and bears on the importance of metallurgical structure in promoting potential areas of weakness for the propagation of subsurface cracks on forging the ingot. The primary ingot structure, the distribution of stress on forging, temperature, strain rate and inclusion segregates are all significant factors affecting rupture. In the case of subsurface cracking, inclusion segregates are an important cause. Admittedly, the effect of forging on inclusion segregates depends on the type of inclusion, its plasticity and melting point, the amount of the reduction, and the forging temperatures; nevertheless the end result insofar as initiation of cracking is concerned is the same. Inclusions which are plastic or liquid at the forging temperature form continuous layers which prevent the welding of adjoining grains during forging. The greater the amount of reduction the greater will be the tendency for

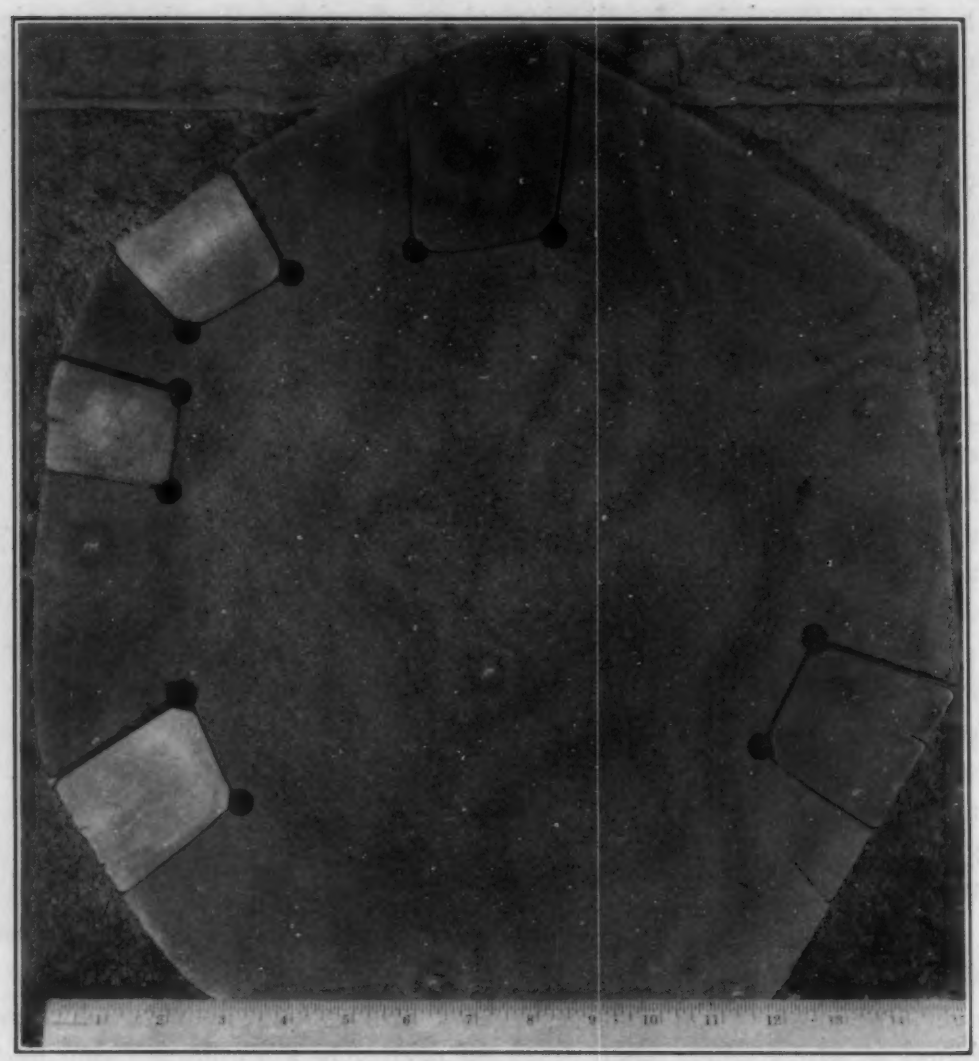


Fig. 3—Transverse Macroetch of 36-Inch Forging Ingot Taken From Top Third of Ingot. Note cracks, extent of pattern effect and evidence of subsurface porosity in lower left portion. Originally × 0.4, reduced 50% in reproduction.

crack propagation since the liquid will have greater opportunity to spread entirely around grain boundaries, resulting in an area which is extremely brittle both hot and cold. The hot shortness of steels and many nonferrous alloys with common impurities is directly attributable to the presence of liquid that wets grain boundaries. On the other hand, inclusions with melting points above that of steel also lower the fracture stress during forging by forming little prisms at the grain edges instead of harmful continuous layers of liquid. The effect of such a segregate located in the ingot subsurface as a stress-raiser during forging is bad and the lack of forgeability in

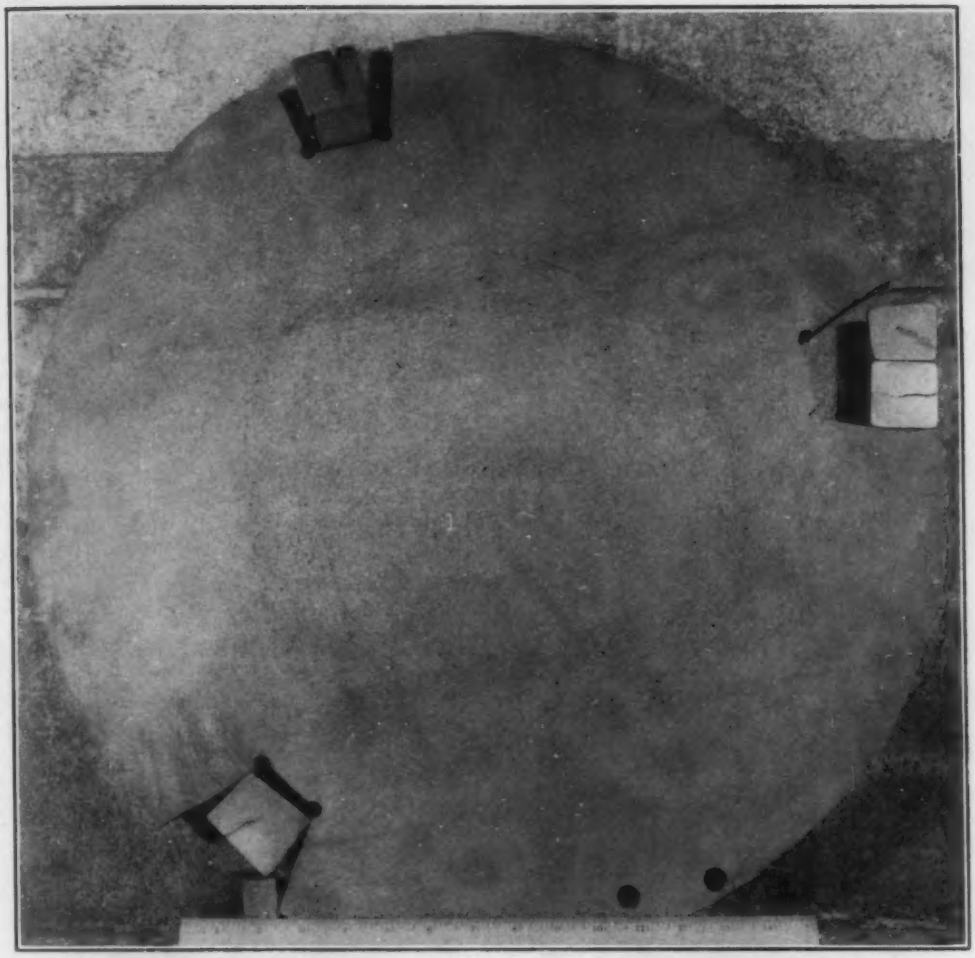


Fig. 4—Transverse Macroetch of 36-Inch Forging Ingot Taken From Middle Section of Ingot. Note fine, subsurface cracks and compare pattern effect with sections shown in Figs. 1-3. Originally × 0.4, reduced 50% in reproduction.

such an area is not surprising even though such inclusions may not interfere with the crystal-to-crystal cohesion to an appreciable extent.

It is difficult to predict that inclusions can increase the resistance to flow; it seems more logical to assume that they reduce the resistance to rupture and thus decrease the amount of plastic deformation which can take place before cohesive failure occurs. Once localized fracture has occurred at the position of an inclusion segregate, a sharp notch (crack) is formed which produces stress conditions more favorable to cohesive failure than to plastic deformation. Even in some areas where the metal has not ruptured, the concentration of inclusions is still great enough that the transverse section etches like a crack and the steel is in effect "hot short".

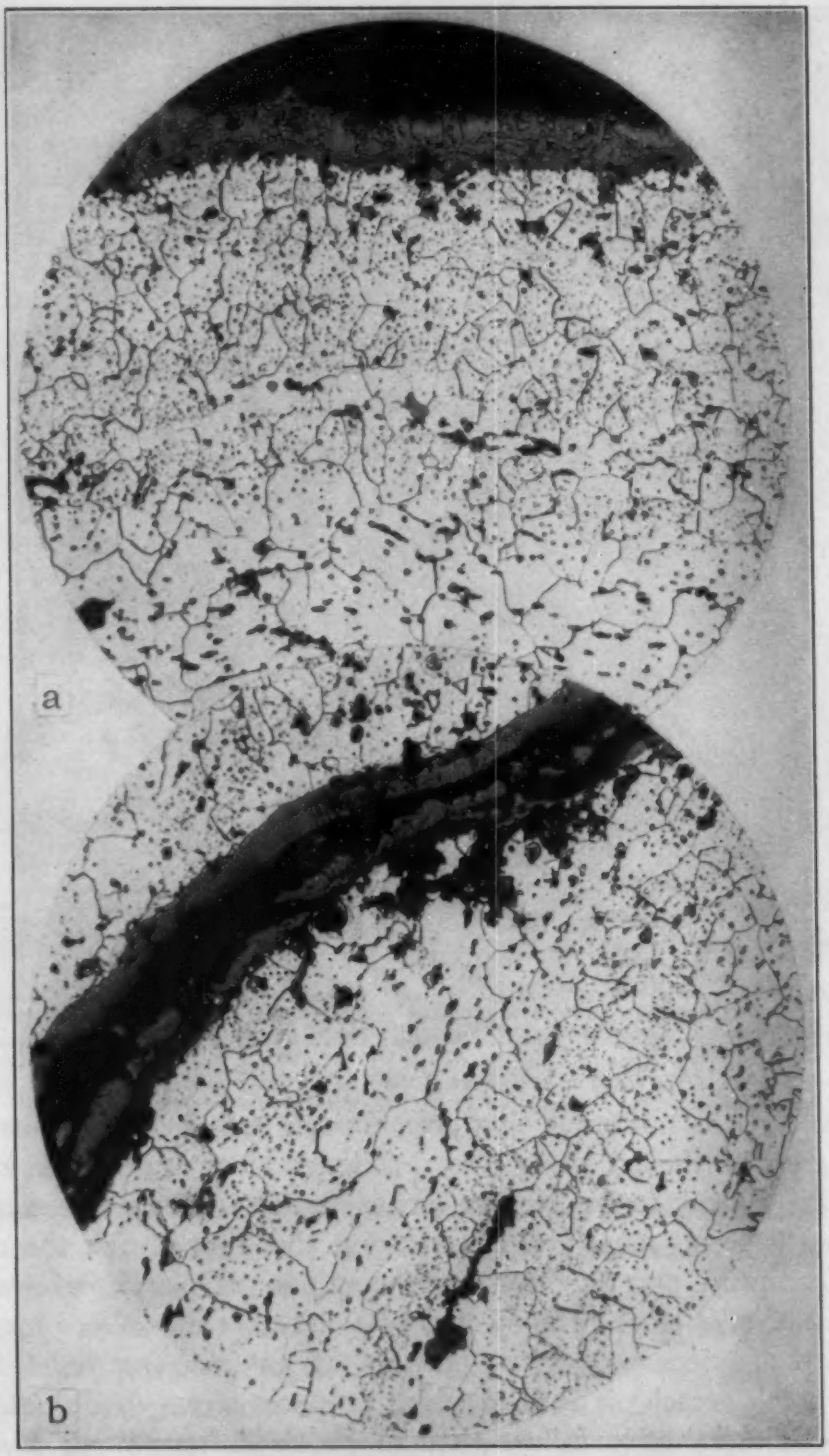


Fig. 5—Structures in Areas Where Subsurface Cracks Occurred in Transverse Section of Forging Ingot Shown in Fig. 1. a—Oxidized condition at crack resulting in oxide penetration. b—Oxide layers at surfaces of crack and dispersion of fine particles.



Fig. 5—Structures in Areas Where Subsurface Cracks Occurred in Transverse Section of Forging Ingot Shown in Fig. 1. c—Unetched structure below crack shows precipitate particles and stringer inclusions. d—Streaks of inclusions below area where cracking occurred. Nital etch. × 100.

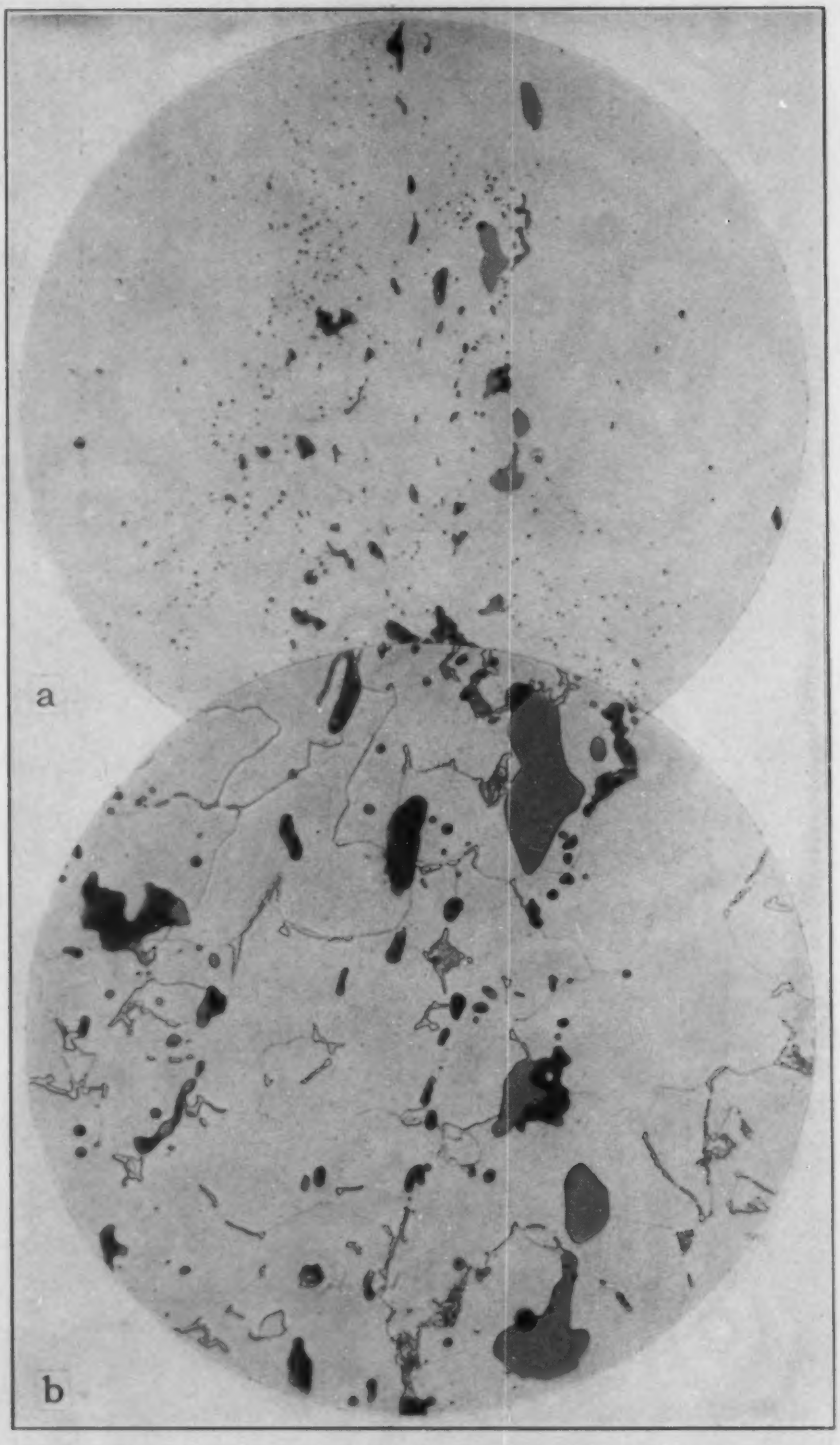


Fig. 6—Structures in Areas Below Cracks Opened Up on Macro-etching Transverse Section of Forging Ingot Shown in Fig. 1. a—Segregate of fine particles and larger, angular inclusions at × 100. b—Same field at × 500 shows sulphides and silicates.

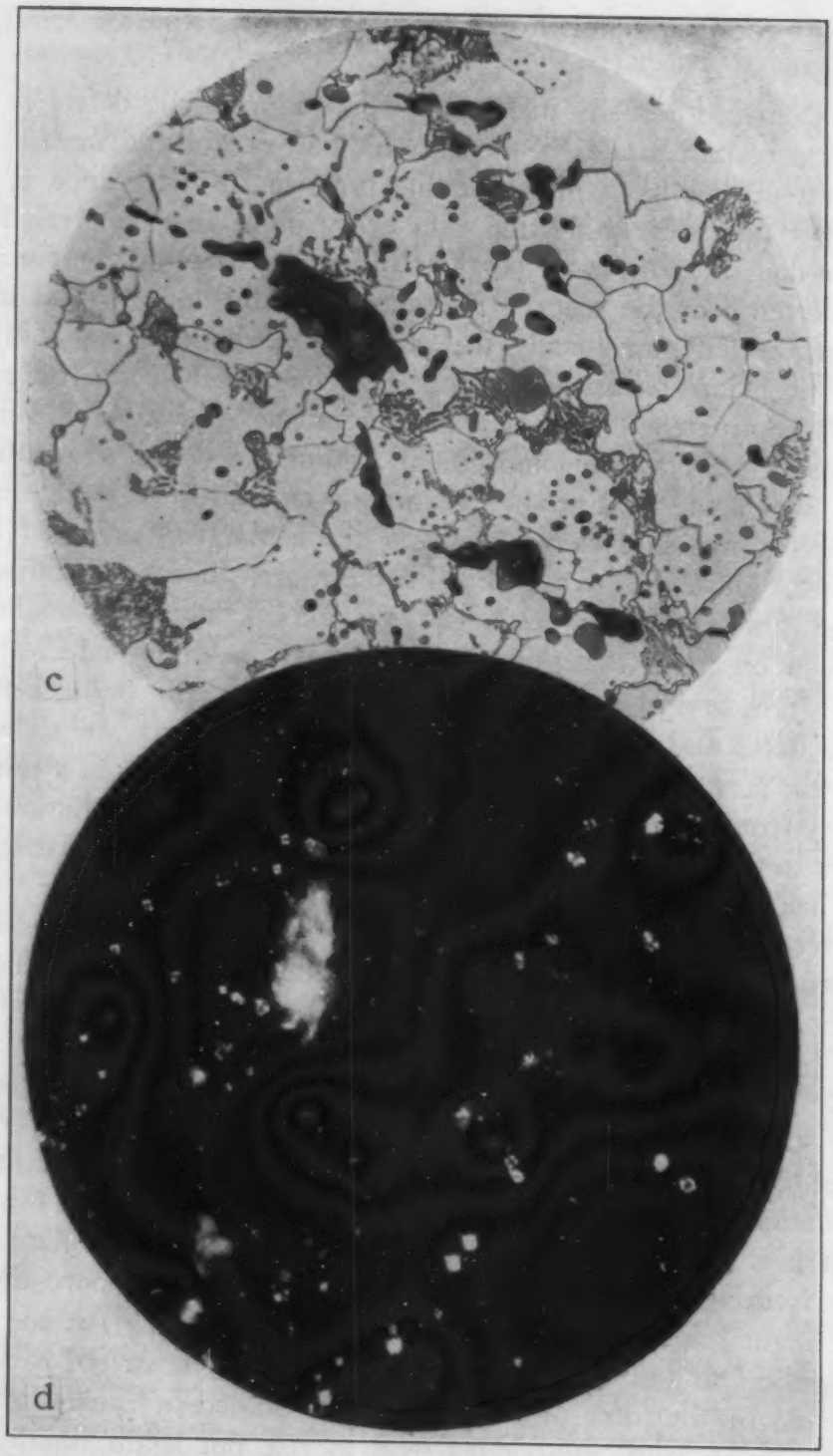


Fig. 6—Structures in Areas Below Cracks Opened Up on Macro-etching Transverse Section of Forging Ingot Shown in Fig. 1. c—Another view at × 500 shows fine particles as globular oxide-sulphides and oxide-silicates. d—Dark field illumination identifies silicates and smaller silica inclusions at × 500.

Subsurface Porosity in Forging Ingots

Subsurface porosity in forging ingots is a unique defect in that it affects certain grades of steel more than others and occurs only intermittently within a given melting practice. For instance, it may not show up in every heat, nor in every ingot from a given heat; neither does it show in all portions of an ingot nor on the complete circumference of the ingot. The defect usually appears just under the surface but occasionally the pits may be as deep as 2 inches. Also, subsurface porosity does not show on unetched macrosamples. When deeply etched with acid in the transverse section, the defect consists of pits; in the longitudinal section the defect shows up as seams, and if the final product requires a smooth finish with enough of the forging surface removed to reach the contaminated area, the metal must be scrapped. Furthermore, in steels poured in tapered-flute molds for better surface and metallurgical quality, it has been observed that subsurface porosity is found half way between flutes and also that such porous areas usually occur between all the flutes and not just one pair. Two such areas are shown in the lower part of Fig. 10 depicting a transverse slice taken a third of the way from the top of a 48-inch ingot. No definite correlation with respect to the frequency of this defect with change in deoxidation and ingot height was found.

Recently Altman (9) has discussed the many possible causes of subsurface porosity in certain forging grades of steel ingots and has shown that, regardless of the theoretical causes for the defect, it could be overcome by the proper application of an aluminum mold wash. Thus, insufficient deoxidation was deemed the most important factor, though the rate of fill, mold wash, and pouring temperature all had their effect on the amount of porosity encountered. Assuming deoxidation is complete, the consistent location of the defects indicates that it is a mold surface – ingot surface reaction taking place early in the freezing stages that is responsible for subsurface porosity. In killed ingots, where much oxide material rises to the surface early during the filling of the mold, this top scum may be stirred back into the liquid by the force of the stream (or "folded in" near the mold walls). Such oxide aggregates tend to rise out again rapidly, but where they reach zones near the mold wall they can be caught by the dendrites growing inward rapidly from the ingot surface. This effect may thus be responsible for part of the surface or subsurface

seams in such ingots. On the other hand, the subsurface of an ingot freezes early, thereby lacking certain degassing advantages which act to minimize gas in top sections; and the subsurface represents the early portion of the cast, which has first contact with the mold wash, an obvious source for considerable quantities of gas. The mold gas may enter the ingot when the skin is already partly solidified by passing through surface inclusions which are still liquid; upon coming in contact with the molten metal at the interior the gas expands to form porous areas.

Indeed, the use of a strong deoxidizer such as aluminum in the mold wash is warranted. The important aspect of these mechanisms is that either inclusions or pinholes may exist in the ingot subsurface, depending upon the manner and extent of deoxidation.

A very recent contribution on the distribution of oxygen and nitrogen in a large alloy steel ingot by Sawyer and collaborators (10) confirms the surprising degree of local heterogeneity existing in the distribution of oxygen in an ingot. The highest concentration of nonmetallic inclusions (oxides) was found to be in the bottom third of the ingot at the quarter cross section and the high oxygen values obtained in this position where rapid solidification occurs were termed by the authors to be the result of oxygen-bearing nonmetallic inclusions. The concentration of inclusions in the quarter section is also evident in several of the illustrations in this paper and its importance in initiating internal tears is discussed later. The fact that concentration of inclusions and carbides can occur near the ingot surface designates the necessity of exercising caution in interpreting from a macroetch or sulphur print that subsurface porosity actually occurs in an ingot since, as previously stated, it is difficult to differentiate pinholes from pits which were formerly segregates of nonmetallics and carbides because the latter will also appear as pits as a result of acid attack. Actually, in a number of ingots the defect was caused by the presence of nonmetallic segregates instead of porosity from the entrapment of gases.

In regard to center porosity, it has been observed that there may be a definite trend in the center position of decreasing density toward the top of the ingot. Of interest in this connection is the configuration of the central pattern of segregates in the various forgings shown throughout the paper and the observation that the pattern effect is generally more pronounced in transverse macroetch

tests taken from the top section as compared to the bottom section of the ingot where there may be little or no evidence of its occurrence. Thus, the concentration of inclusion and metallic segregates in the central area as revealed by the extent of the pattern follows the same trend as the variation in density which may occur in these ingots. Pattern effect will be discussed further in the next section.

State of Deoxidation and Type of Inclusions

In steelmaking, the state of deoxidation is limited by the final chemical analysis desired in the finished product and is controlled primarily by carbon, manganese, silicon and aluminum, and to a lesser extent by other deoxidizing elements. The degree of deoxidation affects the density of the cast structure and broadly classifies the steel as killed, semi-killed, or rimming. This in turn manifests itself in surface and subsurface characteristics. The manner and extent of deoxidation also control the amount, type, and distribution of nonmetallic inclusions formed. The exposure of liquid steel to the oxygen of the air during tapping and pouring and the consequent reaction have been mentioned as a source of the formation of inclusions, and, further, the admixture of furnace slag during tapping or of refractory material from various sources has also been considered. Silicate inclusions are often referred to as the natural and inevitable reaction product on adding silicon or silicon and manganese to the bath as deoxidizers. Under suitable conditions a certain amount of inclusions are removed from the bath by rising, particularly when the product is easily fusible, because it will then coagulate more readily.

In the great majority of cases, macroscopic examination of inclusions in the solidified ingot is of greater importance than microscopic methods because the interest is not in the small uniformly distributed inclusions observed only microscopically, but in the larger inclusions and segregates which can also be detected macroscopically. These larger inclusions and segregates are not uniformly distributed but are scattered at random throughout the steel, so that examination of large areas by means of macroetch, step-down, sulphur prints and magnaflux tests is necessary. Such inclusions in forging ingots are detrimental to service life only when they occur in certain strategic positions, notably at or near the surface. The presence of small seams on the machined surfaces of round forgings presents such a

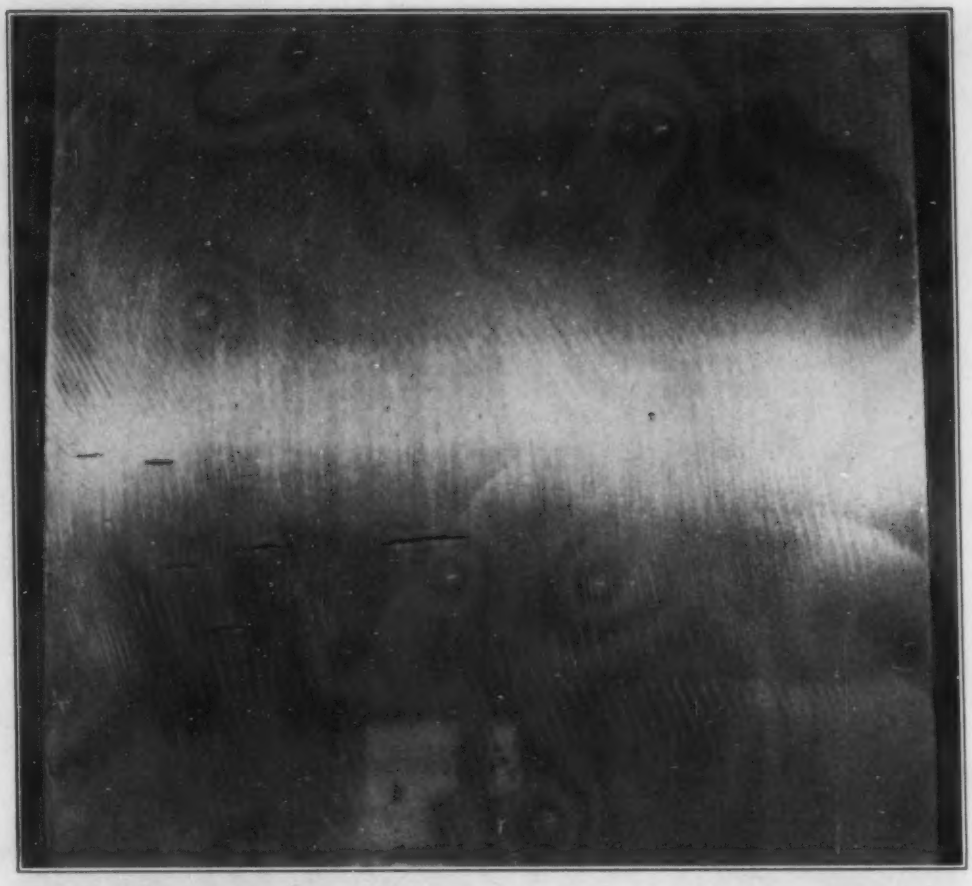


Fig. 7—Magnaflux Pattern on Periphery of Forgings Showing Defects Exposed 1½ Inches Below Surface of Original Ingot. Actual size.

problem. Figs. 7 and 8 show the type of defect which is exposed by magnafluxing the periphery of a forging after machining 1½ inches below the surface of the original ingot. Because steel is very highly permeable to magnetic flux as compared to air or any non-metallic solid, the magnetic lines of force will spread out at any discontinuity in the steel, whether caused by a crack, a hole, or an inclusion. The magnetic powder being also highly permeable will be drawn-in in an attempt to bridge the gap and thus produces a concentration outlining the defect. This type of subsurface defect has been observed and studied from the standpoint of length, total number, general position and color of the material in the seam. To do this, longitudinal specimens were cut out of the affected areas, polished metallographically and examined under the microscope.

Fig. 9 shows that the seams revealed by the magnaflux test really arise from stringer-type inclusions. An estimate of their

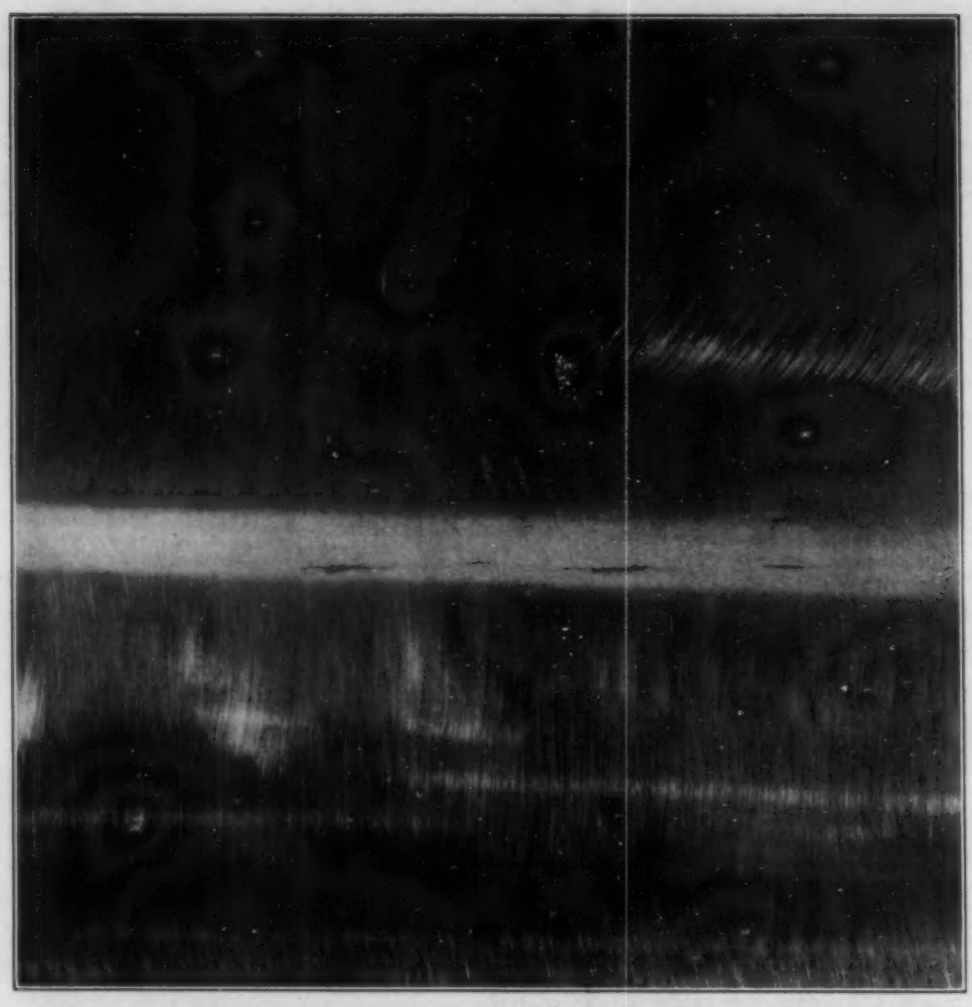


Fig. 8—Magnaflux Pattern on Periphery of Forgings Showing Defects Exposed 1½ Inches Below Surface of Original Ingot. Actual size.

size varies from ⅛ to ½ inch in length and their appearance would classify them as oxide-silicates. When located and observed visually on the machined surface these seams appear as yellowish-white streaks but under the microscope they are dark brown in color and opaque. Their general location is confined to the ingot subsurface, usually within 3 inches of the rim. All these factors contribute to the general conclusion that this type of seam is caused by the probable trapping of products of deoxidation occurring during the finishing of the heat, or products of oxidation from pouring. To date no connection whatsoever has been found between the frequency of these seams and mold life.

Sulphides constitute well over 50% of all the natural or precipi-

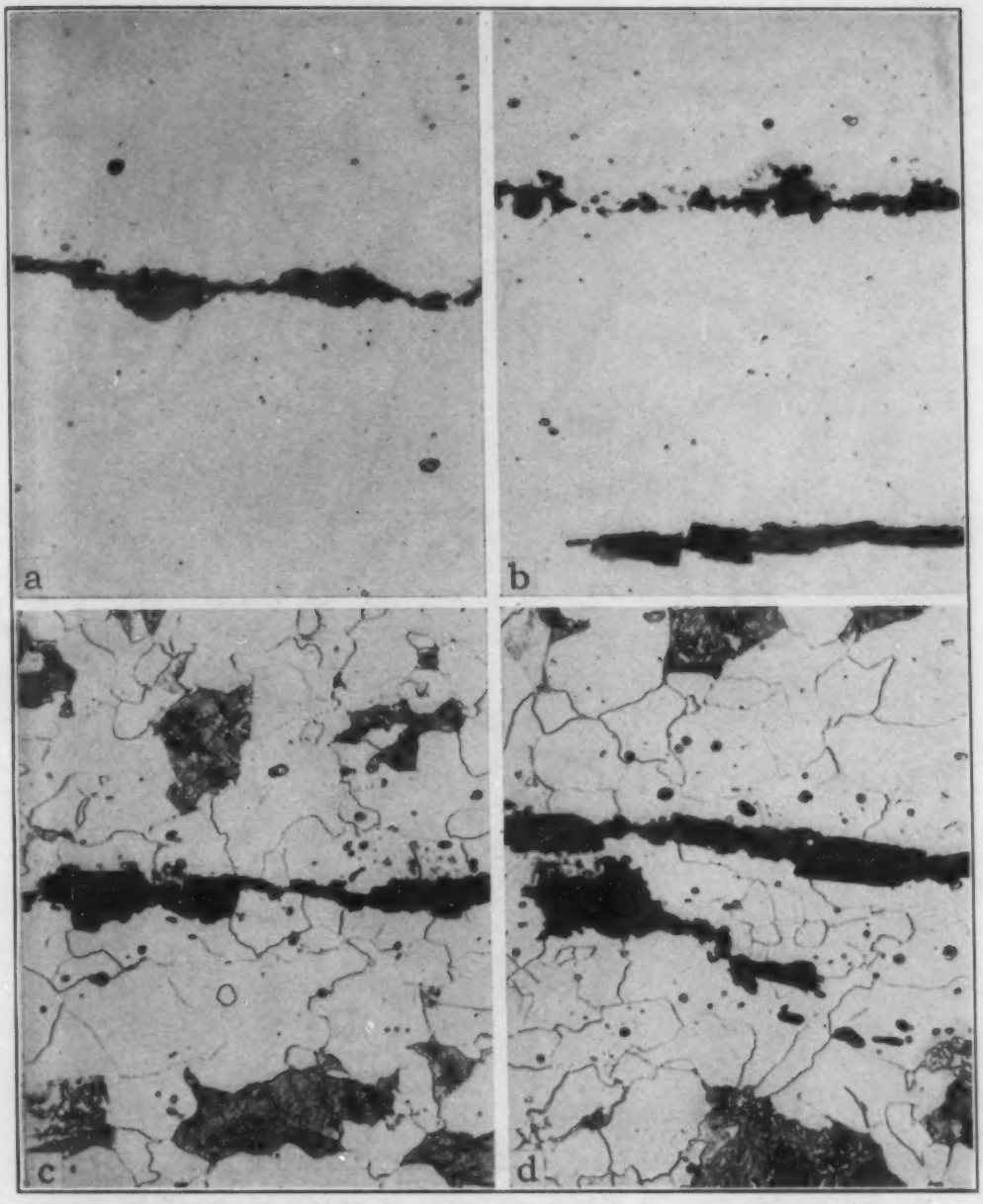


Fig. 9—Types of Stringer Inclusions Affecting Defects on Periphery of Forgings Shown in Figs. 7 and 8. Nital etch. × 100.

tated inclusions present in most steels. Inasmuch as practically all the sulphur forms sulphide inclusions, one of the most profitable means of reducing the inclusion count is to keep sulphur as low as possible. It has long been recognized that the amount and distribution of sulphides in acid open-hearth forging steels are important causes of defects initiating rupture during the processing of ingots and that the analysis of steel for sulphur does not tell much about

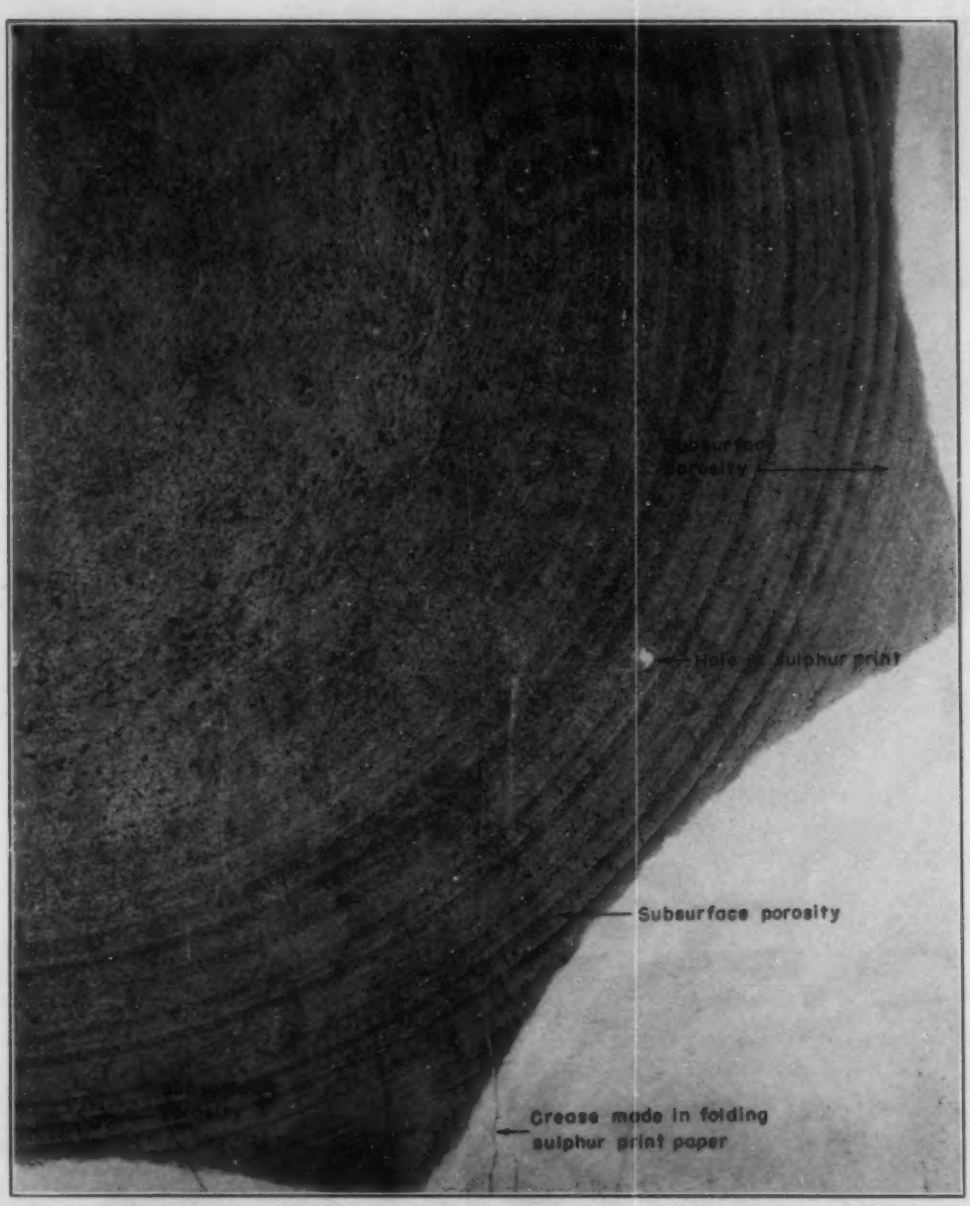


Fig. 10—Sulphur Print of Transverse Section of 48-Inch Forging Ingot Taken From Top Third of Fluted Round Ingot. Observe areas of subsurface porosity halfway between flutes and location of sulphides in a concentric band in central portion of ingot. Originally × 0.4, reduced 50% in reproduction.

the distribution of the sulphide particles present. To study segregation, or distribution of sulphide particles, recourse is made to the process known as sulphur printing. By this method, a record of the position of sulphides and phosphides in the section examined is thus obtained, the points on the specimen which were high in sulphur being represented on the print by dark brown areas.

Fig. 10 represents part of a large sulphur print of the transverse section of a 48-inch forging ingot taken from the top third of a fluted round ingot. The area of subsurface porosity halfway between flutes has already been discussed but the concentration of sulphides grouped in a concentric pattern midway between the center and rim of the ingot is also of interest. Pattern effect in ingots is almost wholly the result of the crystallization of the ingot and generally results from that part of the ingot containing the columnar structure etching differently from that part which was the granular structure of the ingot. Should the steel contain considerable sulphide and silicate inclusions, then the area of contact between the columnar structure and the granular structure may be particularly noticeable. In the absence of large amounts of sulphides and silicates, the pattern effect probably is of no serious consequence. On forging, the internal pattern as revealed by the macroetch test is dependent on the amount of reduction incurred by the section; the center pattern usually acquires a more rounded appearance in heavily forged sections as shown, for example, in Fig. 4. A relatively light amount of reduction leaves the inclusions in the same general area which they occupied in the raw ingot. The location of the concentric band of inclusion segregate (mainly sulphide) midway between center and rim of the section shown in Fig. 11 results from the insufficiency of the relatively light amount of reduction (S ÷ s, ingot to forging, of 2.5) in breaking up the initial as-cast distribution of these inclusions. Usually such a pattern is moved inward with heavier reduction but on occasion the same configuration has persisted in sections forged as high as 6 (reduction S ÷ s, ingot to forging) so that no conclusions pertaining to its definite location within a forged section can be made.

Microscopic examination of the top, middle, and bottom transverse sections of several 36-inch forging ingots cast in big-end-up molds revealed that the inclusions were mainly complex silicates and duplexed sulphides. The silicates varied greatly in size, with some large enough to indicate that they were probably exogenous. General trends observed in the ingots as to the size, type and distribution of nonmetallics can be summarized:

a. Top Section—Near the surface corresponding to the chill or that part of the ingot containing the columnar structure were found the finest dispersion of inclusions and the occasional segregation of inclusions in stringer-like arrangement. At the junction

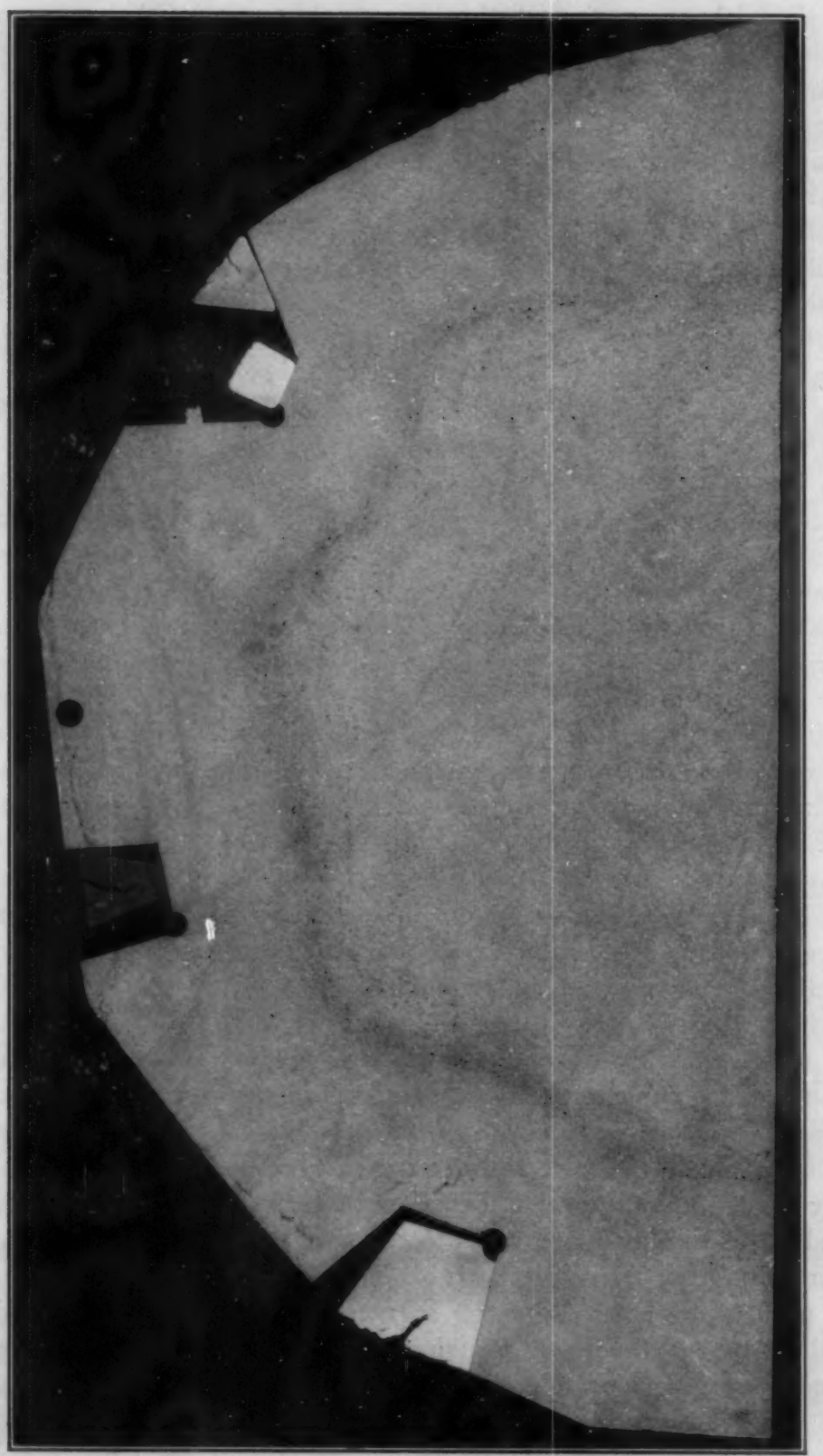


Fig. 11—Transverse Macroetch of 48-Inch Forging Ingot Taken From Middle of Ingot. Note fine internal structure and concentric band of inclusion segregate midway between center and rim of section. Originally × 0.5, reduced 30% in reproduction.

between rim and core corresponding to the junction of columnar and granular crystallization structure, the inclusions were chiefly sulphide and were larger and more numerous. In the core the inclusions were chiefly oxide-sulphide and sulphides with only occasional oxide-silicate reaction products.

b. Middle Section—The size, number, type and distribution of the inclusions were very similar to those in the top section. At the junction between rim and core they became noticeably larger and more numerous. The segregates in the core were somewhat larger than in the top sections, as seen from sulphur prints.

c. Bottom Section—The sulphide inclusions in the rim and core were similar in size, nature and distribution to those in the top and middle sections but were not so numerous. There was again an increase in sulphides in the intermediate zone between rim and core. The sulphide inclusions in the core were less abundant than in the other two sections, whereas the oxide-silicate inclusions were more numerous throughout the transverse section than in either the top or middle cuts.[8]

Returning to the main thesis of the paper, attention is focused on the observation that inclusion stringers are located within the outer (chill) zone of forging ingots interspersed among an even distribution of minute sulphides. As a typical illustration, Fig. 12 depicts a sulphur print of a transverse section of a 36-inch forging ingot, taken from the top third of the ingot. The segregation of sulphides in the central portion of the ingot and the presence of inclusion stringers within the ingot subsurface (indicated by arrows) are evident. The appearance of deep internal tears in this localized region of the ingot can also be seen. In general, it has been observed that where such stringer inclusions occur within a zone of relatively minute inclusions, fissures or tears are most likely to occur on processing the ingot. This association of inclusion stringers and tears located in the ingot subsurface is further substantiated by the presence of bits of stringer particles in the newly formed edges produced by the tear. The difference in conformation of sulphides in the ingot subsurface is believed responsible for this type of defect in forging ingots, because the sulphide stringers are incapable of dispersion or diffusion within an otherwise minute, even distribution of globular

[8]The inferior physical properties of transverse test specimens taken from the bottom third of a forging ingot may not be so much related to the amount of inclusions as to the distribution of that inclusion material. It has been established (11) that distribution can be radically affected by the type of deoxidation practice employed, resulting in a marked decrease in the difference between longitudinal and transverse tensile properties.

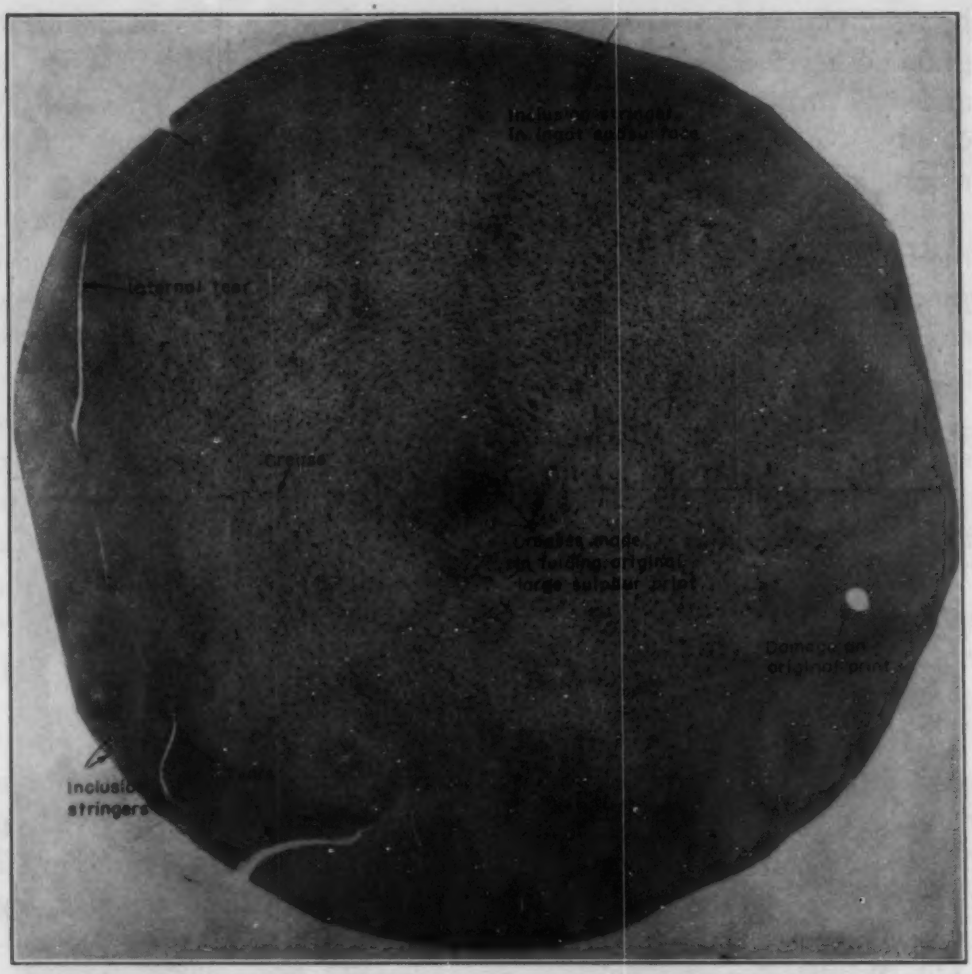


Fig. 12—Sulphur Print of Transverse Section of 36-Inch Forging Ingot Taken From Top Third of Ingot. Observe segregation of sulphides in central portion of ingot and sulphide stringers in ingot subsurface. Originally × 0.4, reduced 50% in reproduction.

sulphides and act as points for stress concentration during hot-working. Also these elongated stringers may act as effective barriers to heat flow, the interface being a likely site for the initiation of tensile stress and internal tearing due to the unequal expansion occurring between the internal and external zones of the ingot.

Deoxidation practice can be a potent factor in promoting a difference in the character of the sulphides and thereby affecting forgeability. As an example, Fig. 13 shows the same type of forging ingot as Fig. 12, the sulphur print being taken from an identical position. This ingot was obtained from a heat deoxidized with silicon carbide. The very fine, even distribution of sulphides throughout the greater portion of the ingot and the decreased amount of segre-

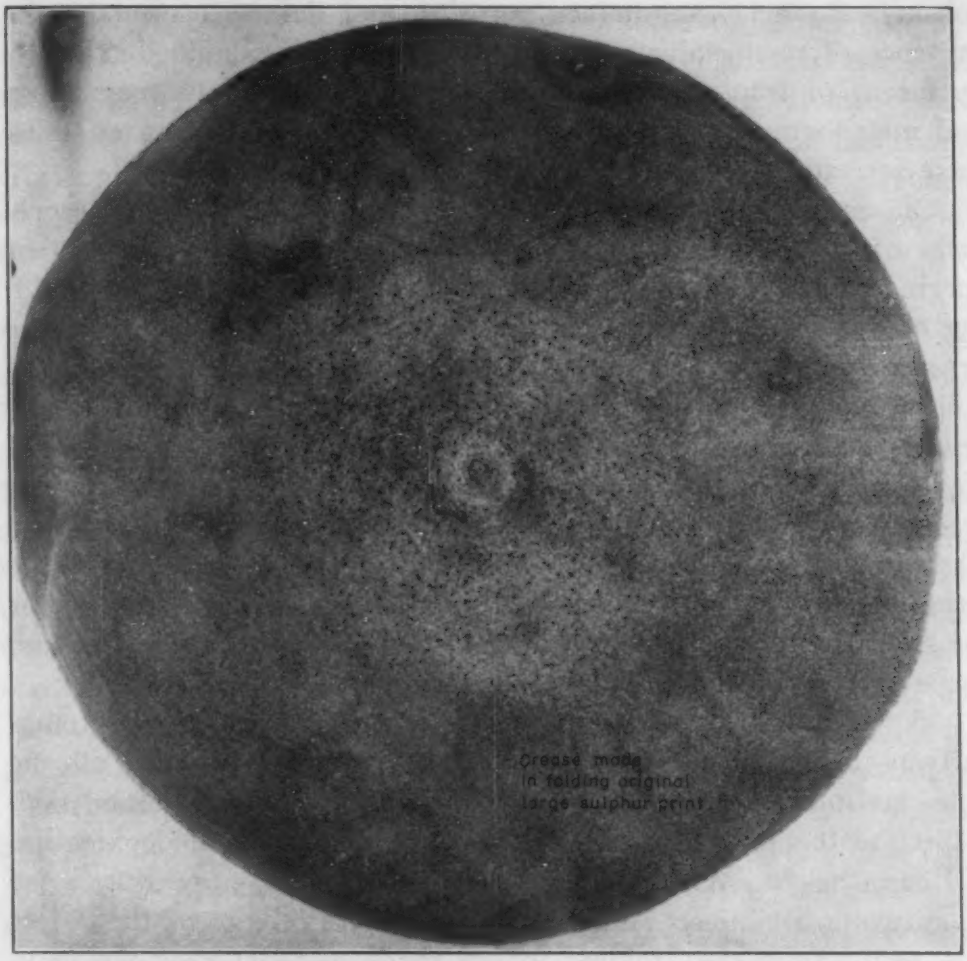


Fig. 13—Sulphur Print of Transverse Section of 36-Inch Forging Ingot Taken From Top Third of Ingot. Heat deoxidized with silicon carbide. Observe very fine, even distribution of sulphur and decreased amount of segregate in the central portion of ingot. Originally × 0.4, reduced 50% in reproduction.

gate in the central area of the ingot are evident. Also, perhaps the formation of carbon monoxide as one of the reaction products arising from the addition of this deoxidizer and its bubbling through the liquid steel while it is in the ladle effectively eliminates any hydrogen which may be present, doing this at the most opportune time insofar as ease of removal is concerned.

Summary

1. This paper reports the results of an investigation of the subsurface defects in several large steel forging ingots of SAE 1040 acid open-hearth grade. The defects specifically considered were

subsurface cracks, subsurface porosity, and defects caused by the presence of nonmetallic inclusions. These were examined critically by means of transverse macroetch tests, sulphur prints, magnaflux, and metallography, in an effort to determine the factors effecting their formation.

2. Subsurface cracks in forging ingots were initiated by segregates of nonmetallic inclusions. Inclusions which are liquid at the forging temperature form continuous layers which prevent the welding of adjoining grains. The greater the amount of reduction the greater will be the tendency for crack propagation since the liquid will have greater opportunity to spread entirely around grain boundaries, resulting in an area which is extremely brittle both hot and cold. Inclusions with melting points above that of steel lower the fracture stress during forging by forming little prisms at the grain edges instead of continuous layers of liquid. By acting as areas for stress concentration, such segregates lower the rupture strength of the steel and the magnitude of the lowering depends on the size and shape of the included particles.

3. In the forging ingots studied, subsurface porosity was found halfway between the flutes and usually occurred between all the flutes and not just one pair. No definite correlation was found with respect to the frequency of this defect with change in deoxidation and ingot height. The cause of subsurface porosity appears to arise from two possibilities. Assuming deoxidation is complete, the defect may result from the "folding in" of oxide material near the mold walls after it had arisen to the surface and had been stirred back into the liquid steel by the force of the pouring stream. The other possibility lies in the fact that the subsurface of an ingot freezes early, thereby lacking certain degassing advantages which act to minimize gas in the top sections. The subsurface represents the early portion of freezing which has first contact with the mold wash, an obvious source for considerable quantities of gas. The mold gas may enter the ingot when the skin is already partly solidified by passing through surface inclusions which are still liquid; upon coming in contact with the molten metal at the interior the gas expands to form porous areas. Actually, in a considerable number of transverse sections the defect observed in sulphur prints or macroetch tests was caused by the presence of nonmetallic segregates which were removed by acid attack instead of porosity from entrapped gases.

4. Small seams on the machined surfaces of round forgings which were exposed by magnafluxing the forging periphery after machining 1½ inches below the surface of the original ingot were examined microscopically and found to be stringer-type inclusions. Observations indicate that the defect is caused by the probable trapping of deoxidation products occurring during the finishing of the heat or products of oxidation from pouring.

5. The pattern effect in transverse sections is predominant in the top portions of the ingots studied and appears to follow the same trend as density variations in the center positions of split ingots. On forging, the configuration of the internal pattern is dependent on the amount of reduction. Inclusion segregates in areas midway between center and rim of a section reflect the as-cast distribution and insufficient forging reduction. Usually such a segregate is moved inward with heavier reduction but no conclusion pertaining to its definite location within a forged section can be made. General trends of inclusion distribution observed in the microscopic examination of the top, middle, and bottom transverse sections of the 36-inch forging ingots cast in big-end-up molds are presented.

6. Sulphur prints reveal the segregation of inclusion stringers within the outer (chill) zone of forging ingots interspersed among an even distribution of minute sulphides. In general, it has been observed that where such stringer inclusions occur within a zone of relatively minute inclusions, fissures or tears are most likely to occur on processing the ingot. The difference in conformation of sulphides in the ingot subsurface is believed responsible for this type of defect in forging ingots, because the sulphide stringers are incapable of dispersion or diffusion within an otherwise minute, even distribution of globular sulphides and act as points for stress concentration during hot-working.

References

1. F. Latta, E. Killing and F. Sauerwald, "Nonmetallic Inclusions in Large Steel Forging Ingots," *Stahl und Eisen,* Vol. 53, 1933, p. 313-326.
2. E. Wulffert, "Avoidance of Defects in Medium and Large Ingots of Basic Open Hearth Steel," *Stahl und Eisen,* Vol. 60, 1940, p. 833-839.
3. K. von Kerpely, "Defects in Forged Crankshafts Due to Sand Seams," *Stahl und Eisen,* Vol. 54, 1934, p. 1153-1186.
4. J. W. Spretnak, "Kinetics of Solidification of Killed Steel Ingots," TRANSACTIONS, American Society for Metals, Vol. 39, 1947, p. 569-626.
5. J. W. Spretnak, K. L. Fetters and E. L. Layland, "Ingot Factors in the Production of Seamless Gun Tubes," TRANSACTIONS, American Society for Metals, Vol. 39, 1947, p. 627-650.

6. G. Soler, "Influence of Chemical Composition on the Hot-Working Properties and Surface Characteristics of Killed Steels," *Transactions*, American Institute of Mining and Metallurgical Engineers, Vol. 145, 1941, p. 194-212.
7. C. A. Zapffe and C. E. Sims, "Hydrogen Embrittlement, Internal Stress and Defects in Steel," *Transactions*, American Institute of Mining and Metallurgical Engineers, Vol. 145, 1941, p. 225-271.
8. F. B. Foley, "Cause of Cooling Cracks," Open Hearth Proceedings, American Institute of Mining and Metallurgical Engineers, Vol. 27, 1944, p. 370-371.
9. A. R. Altman, "Subsurface Porosity in Ingots," Open Hearth Proceedings, American Institute of Mining and Metallurgical Engineers, Vol. 28, 1945, p. 405-415.
10. C. F. Sawyer, J. W. Spretnak and G. Derge, "The Distribution of Oxygen and Nitrogen in an Alloy Steel Ingot," TRANSACTIONS, American Society for Metals, Vol. 40, 1948, p. 922-934.
11. E. A. Loria and A. P. Thompson, "Ladle Deoxidation of Killed Steel With Silicon Carbide and Its Effect on Physical Properties and Hardenability," TRANSACTIONS, American Society for Metals, Vol. 39, 1947, p. 651-669.

DISCUSSION

Written Discussion: By R. M. Allen, chief control metallurgist, Carnegie-Illinois Steel Corp., Homestead District Works, Homestead, Pa.

We have read this paper with particular interest, since it so closely parallels some of our experiences in the production of large forgings from both basic open-hearth and electric furnace ingots. The authors' illustrations of inclusions associated with forging cracks are noteworthy, and it is believed that there can be general agreement that inclusions may cause cracking either by the formation of liquid envelopes around grain boundaries or by reducing the forgeability of the steel by acting as stress raisers. From this premise it would appear that the future problem lies in the more positive identification of the harmful inclusions and the means necessary for their elimination.

We would like to point out that, in our opinion, a discussion of cracks in forging ingots is not complete without some reference to the control of pouring temperature, to control of teeming speed, and to the type of mold coating. Although the first of these three points is certainly interrelated with the occurrence of inclusions, the latter two can control the degree of cracking independently of steel cleanliness.

The authors state that the use of aluminum as a mold coating was helpful in the elimination of pinhole type defects caused by nonmetallics on the surface of the forgings. This is in contradiction to experiences at our plant where it was recently developed that, other factors being held constant as is practicable, the use of aluminum as a mold coating in the production of forgings which require a high surface finish was detrimental. It was found that the use of tar as a more active mold coating minimized the occurrence of these defects. Although it would be possible to theorize at some length on this apparent contradiction, it is probable that the real

difference lies in the degree of perfection of the finished surface. We can, however, report that results from the same study do confirm the authors' experience with sulphur, in that our results show a direct correlation between the final sulphur content and the occurrence of pinhole type defects.

The occurrence of nonmetallics in the outer portion of a forging ingot can be significant from a quality standpoint, not only in the occurrence of cracking or surface imperfections, but in the effect on transverse properties. It is coincidental that during the past several months we have had occasion to make a fairly extensive investigation into this effect. Our investigation showed that the inability to develop satisfactory transverse ductility was in a large part due to the presence of nonmetallic material visible in the fractured face of the tensile specimen. We might point out that this same experience is reported on in a succeeding paper to be delivered this morning by the same authors.[4] The nonmetallic material in our samples was identified as products of deoxidation occurring in the outer portion of the ingot as cast. There was no noteworthy history of forging cracks or surface imperfections in connection with the processing of these forgings.

We feel that the authors should be commended on their presentation of a subject which will be of particular interest to everyone handling large forging ingots, and that its discussion will stimulate interest and further work along the lines suggested.

Written Discussion: By A. R. Altman, open-hearth superintendent, Heppenstall Co., Pittsburgh.

The authors are to be congratulated on their presentation of an excellent paper of compiled and original data.

The improvement of large forging ingots to any degree is a very important achievement. Many times, the internal defects do not become apparent until considerable time and/or money has been expended. Quite often, the defect results in the scrapping of the product. As the rejection occurs late in the process, the expense is much greater than if it were merely an ingot. Naturally, anything we may do to improve the ingot, as cast, will benefit all the way to the finished product.

Prior to 1945, we were in considerable difficulty with subsurface porosity.

As stated in a paper presented in 1945 Open-Hearth Proceedings, decided improvement resulted from the use of aluminum mold wash. Since that time, and to the present, the benefits have continued. Although the wash is expensive, the rejections are extremely low.

In the summary of Messrs. Loria and Shephard's paper, they mention two possible causes of subsurface porosity. A third one may be added—excessive splash from a "ragged" pour.

If enough mold wash is applied, that is, several coats, one on the other, the ill effects from an excessive splash from a "ragged" pour may be overcome by, we suggest, local or simultaneous deoxidation.

[4]H. D. Shephard and E. A. Loria, "The Nature of Inclusions in Tensile Fractures of Forging Steels," TRANSACTIONS, American Society for Metals, Vol. 41, 1949, p. 375.

Prior to 1946, we were greatly concerned with cracks extending from the surface into the ingot. These cracks were discovered upon macroetching transverse sections of large ingots.

Silicon carbide (sold as Ferrocarbo-S) was proposed and tried. Considerable improvement was observed. So much so that we increased its use until, at the present time, we use it in all heats which are to be cast into large ingots.

The occurrence of corner cracks in macroetched transverse sections of large ingots is practically eliminated.

We were at a loss to understand the improvement. Possibly Messrs. Loria and Shephard, on page 355 of their paper, have the answer, as follows, "Perhaps the formation of carbon monoxide as one of the reaction products resulting from the use of this deoxidizer may have a beneficial effect in helping to eliminate hydrogen". Also, "performing this function at a most opportune time insofar as ease of removal is concerned".

I would like to ask the following questions:

1. How could the "quality" of the open-hearth pig in the charge affect the "sand" inclusions in the forging? [Page 331, Kerpely (3)].

2. In description of Fig. 13, it states, "Heat deoxidized with Silicon Carbide". Does this mean wholly, partially or finally deoxidized with silicon carbide?

Written Discussion: By Philip Melara, supervisor, Inspection Laboratories, Grumman Aircraft Engineering Corp., Bethpage, L. I., N. Y.

The authors are to be congratulated for a very informative and excellent paper. In our company, we have found inclusions to be troublesome in forming, welding, and plating. It may be interesting to cite a few specific cases and problems.

We have had failures in bending material that was completely of banded structure, and which contained a great number of inclusions as determined by the hot acid deep etch test. The solution to this problem was in the complete spheroidization of the microstructure of the steel.

Oxide inclusions of great magnitude and quantity gave poor weld quality when the material was welded with acetylene gas. It was decided that the gas excited the oxide particles to spark considerably with resultant porosity. The material was successfully welded without porosity and sparking with electric arc welding.

Forgings which contained large inclusion segregate areas have been found to fail in proof loading after hard chromium plating. The hard chromium plating was about 0.040 inch thick. The proof load was only two-thirds of the ultimate load as determined by the heat treatment of the forgings and its cross-sectional area. Our laboratory, after many microscopic tests of several failures, decided that the atomic hydrogen which evolved during plating was able to concentrate and produce stresses at the segregate inclusion areas; and this localized form of embrittlement then produced premature rupture.

Examination of several fractures revealed flat areas (suggesting embrittlement and perpendicular to the direction of loading) which appeared to contain inclusions. These brittle inclusion areas acted as stress raisers

to cause premature failure in the forging which was designed to be a hook. Failure always occurred in the throat of the hook.

We made sub-size tensile coupons of a ruptured hook, and they gave satisfactory physical properties. Therefore, we concluded that inclusion areas in the vicinity of severe fiber stress are detrimental; and any subsequent plating operation which evolved atomic hydrogen for long periods of time added to the brittle nature of the inclusion segregates.

Authors' Reply

The authors wish to express their appreciation for the submitted discussions. The 36-inch fluted round ingots were 120 inches long and weighed 50,000 pounds, whereas the 48-inch fluted round ingots were the same length but weighed about 100,000 pounds. The heats were made in a 125-ton furnace and were poured within the range 2800 to 2850 °F (1538 to 1565 °C). A 1½-inch nozzle was used for pouring the 36-inch ingots and a 1¾-inch nozzle for the 48-inch ingots. The pouring time to hot top required about 12 to 15 minutes and graphite was used as a mold coating. We agree with Mr. Allen's opinion that a discussion of cracks in forging ingots is not complete without some reference to the control of pouring temperature, teeming speed, and mold coating. Whatever be the scientific explanation of cracking, it is found in practice to be related to teeming rate, ingot shape, composition and steel quality.

The paper illustrates that inclusion segregates initiate subsurface cracking during forging operations. Such cracks have been associated with the corner ghost, corner weakness or corner segregation and a general hypothesis regarding their formation would be appropriate. When metal is poured into an ingot mold, generally made of cast iron or similar material of good thermal conductivity, a thin wall of solid metal is quickly formed by contact with the relatively cool mold. As a result of further heat conduction, a contraction of this solid skin takes place, accompanied by an expansion of the mold itself, resulting in a small air gap being formed between the ingot chill skin and the mold wall. This relatively thin metal wall has to withstand considerable hydrostatic pressure from the liquid metal enclosed, this pressure being especially great toward the bottom end of the ingot. While the ingot wall is in contact with the mold wall, there is no possibility of any rupture resulting from this procedure, but when the air gap is formed, there is a tendency for the liquid steel pressure to expand the envelope enclosing it. This results in the formation of cracks in the solid metal at the corners of the ingot, as shown in Fig. 14. The crack is then filled with metal containing a relatively high proportion of nonmetallic matter rejected by the solidifying steel. An additional contraction of the entire ingot during further solidification results in a partial closing of the crack formed and, finally, the formation of a discontinuous line of nonmetallics extending inward from the corners of the ingot.

In addition to the stresses set up by the pressure of the liquid metal, there are other stresses acting in the same manner. When the gap is

formed by the contraction it is filled with air or, at least, with gases which are relatively nonconducting. This change in the wall of the ingot, from being in contact with a surface which is conducting heat away rapidly, to contact with gases which are relatively nonconducting, alters the temperature gradient between the center of the ingot and the outside so that reheating of the outside of the ingot takes place by conduction from the hotter molten metal in the center causing a further tendency to expan-

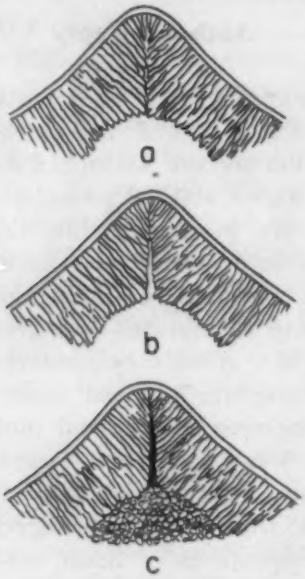


Fig. 14—Development Mechanism for Subsurface Cracking in Forging Ingots.
a—Formation of air gap.
b—Rupture at corner.
c—Partial closing in and retention of nonmetallics.

sion. This expansion may only take place by rupture of the solid wall at the corners from the inside, thus adding to the effect produced by the pressure of the liquid metal. In view of this mode of formation, the segregate area does not extend from the outside of the ingot and in many instances, does not appear as a crack until shaping operations and if not pronounced, may never appear as a definite crack.

This explanation for the development of subsurface cracking is analogous to that set forth by Thomson and Campbell.[5] Also, these investigators mention ways of minimizing its occurrence. One method is to heat the mold locally on the outside to a temperature of about 300 °C. The effect of this is to expand the mold, prior to teeming, in the hope that when the ingot wall is formed, the air gap between it and the mold will be minimized. The question of mold design also arises, since by altering the angle of the mold corner it is possible to increase locally the thickness of the ingot wall and increase its resistance to the stresses set up. The

[5]J. Thomson and G. Campbell, "Defects in Acid Open Hearth and Basic Electric Steel Ingots," *Journal*, West of Scotland Iron and Steel Institute, Vol. 158, 1942, p. 79-87.

fluted or corrugated mold is an improvement in this respect. Another method consists of progressively filling the air gap with molten lead in order to give some support to the ingot chill skin and eliminate the nonconducting gaseous layer. Thomson and Campbell state that some degree of success has been obtained by the use of this method.

In a very recent paper, Stephenson[6] has shown that the cause of cracking can be associated with the boundaries between the ingot's columnar crystals, which are weakened either because of the precipitation of nonmetallics or the concentration of shrinkage stresses at that point. Any factors such as the formation of folds or variations in solidification pattern tending to extend the continuity of these boundaries provide an ingot condition conducive to cracking.

Messrs. Allen and Altman have related the respective merits of tar and aluminum mold coatings. In this paper no preference was made between the two of them although the deoxidizing action of aluminum was mentioned in connection with subsurface porosity. Actually a graphite mold coating was employed in the forging ingots studied. We agree with Mr. Altman that excessive splash from a ragged pour may produce subsurface porosity. The bottom end of an ingot is sometimes found to be considerably splashed due to the initial stream striking the bottom of the mold and deflecting on to the sides. This splash chills quickly and if it is very thick it may bend away from the mold wall toward the center of the mold and be trapped in this position by the rising of the metal. At times the ingot may even be forged without the defect becoming apparent.

In most cases, porosity in large forgings is not evident until machining operations have been fairly well advanced and results from weakness along the secondary segregation, this weakness being caused usually by cold metal from the surface or by insufficient feeding from the head as a result of unsatisfactory mold design. During forging, small cavities or cracks are formed at this point in the ingot and appear when the center portion of the forging is bored or exposed in some manner. In many instances, this type of defect cannot be observed, either because this particular part of the ingot is not exposed, even after final machining, or because the V segregation is removed. When such ingots are split longitudinally the polished section does not, as a rule, show many cracks in the position of the V segregate. Macroetching, however, may reveal discontinuities at this position because of the removal of nonmetallic inclusions during the process and evidently these inclusions formed areas of weakness which on forging ruptured to form cavities. It, therefore, follows that the condition of the V segregate is the determining factor in their existence. In their discussion Thomson and Campbell maintain that these defects can be minimized by increasing the taper on the ingot body to allow better shrinkage conditions. Notwithstanding, the problem is complex for, along with porosity, the length of columnar crystals, quantity and size of equiaxed crystals, inverted V segregation, core of vertical solidification, width

[6]R. L. Stephenson, "Problems Associated with the Production of Sound Ingots," *Electric Furnace Steel Proceedings,* American Institute of Mining and Metallurgical Engineers, Vol. 5, 1947, p. 32-42.

of vertical core, and axial V segregation are also subject to changes with changes in mold design as influencing relative transverse and vertical solidification rates.

In reply to Mr. Altman's first question, the Kerpely paper which was published in 1934 explained that due to the varied production schedule set up for the blast furnace the silicon and manganese contents of the pig varied from the limits: 3.5 to 4.0% carbon, 0.5 to 1.0% silicon, 2.5 to 3.5% manganese, 0.1 to 0.3% phosphorus, 0.045 to 0.050% sulphur. When the silicon and manganese were below the minimum the heat produced inclusion defects in the forged crankshafts, the unfavorable effect of too low a silicon on the course of the heat being particularly noticeable. The effects of a low grade pig iron, by which he meant an iron with less than 0.5% silicon and 2.5% manganese, were longer melt-down periods, poorer refining conditions, poorer slag quality, etc. Moreover, in agreement with the results by Daeves,[7] the lower fluidity of such steel was conducive to an increase in the number of sand inclusions. In his paper, Daeves produces curves which show the relative decrease in rejected forgings with increasing per cent manganese or per cent silicon in the charge. In answer to the second question, the heat from which the forged section depicted in Fig. 13 was taken was finally deoxidized (in ladle) with 4 pounds silicon carbide per ton of steel.

[7]K. Daeves, "Causes and Avoidance of Sand Seams in Large Forgings," *Stahl und Eisen*, Vol. 52, 1932, p. 1162-1168.

DENSITY VARIATIONS IN SOME KILLED STEEL INGOTS

By C. F. Sawyer and J. W. Spretnak

Abstract

A density survey of five killed alloy steel ingots has been made. A considerable variation in density from position to position was found indicating differences in the degree of microshrinkage in the ingot. The lowest average density was found in the center of the top two-thirds of the ingots where the highest yield of heavy-walled seamless tubes free from bore defects and quench cracks was obtained.

THIS paper is the last of a series of papers (1), (2), (3), (4), (5), (6)[1] dealing with a study of the influence of various factors in ingot freezing and structural characteristics of killed alloy steel ingots on the resulting quality of heavy-walled seamless tubes processed from these ingots. These cylinders were subsequently converted into cannon tubes. The factors reported on in previous publications are the following:

1. Kinetics of solidification
2. Relationship between the solidification kinetics and primary ingot structure
3. Relationship between primary ingot structure and the subsequent bore surface quality and mechanical properties
4. Distribution of oxygen and nitrogen in the ingot
5. Macrosegregation in the ingot
6. Distribution of nonmetallic inclusions.

The problem motivating this work was the rejection of these tubes for bore surface defects (1). A problem of quench cracking

[1]The figures appearing in parentheses pertain to the references appended to this paper.

Contribution from the Metals Research Laboratory, Carnegie Institute of Technology, Pittsburgh. The work presented is a portion of the work carried on by NDRC Research Project NRC-39 under Contract No. OEMsr-755.

A paper presented before the Thirtieth Annual Convention of the Society, held in Philadelphia, October 23 to 29, 1948. Both authors were formerly associated with the Metals Research Laboratory, Carnegie Institute of Technology, Pittsburgh. C. F. Sawyer is now plant metallurgist, Vanadium-Alloys Steel Co., Latrobe, Pa., and J. W. Spretnak is associate professor of metallurgy, Ohio State University, Columbus, Ohio. Manuscript received April 9, 1948.

was also encountered later in the practice. Significantly, over 75% of the rejections for these causes occurred in tubes processed from the bottom thirds of ingots. This paper presents the results of a study of the variation of density in various positions of five fully-killed alloy steel ingots, representative of the practice, in order to evaluate the significance of an additional factor which may have contributed to the high frequency of rejections of these tubes processed from the bottom thirds of ingots.

Although the results obtained were negative in terms of explaining this bottom effect, it was thought that the data obtained might be of fundamental interest in contributing to a better understanding of the process of ingot solidification. Data on steel densities in the ingot stage are very limited in the literature.

Ingots Studied

Five ingots available as representative of those used in the production of gun tubes were used in the density survey. The molds used to produce these ingots were all standard cast iron, "big-end up," top poured, hot-topped molds. Table I gives the pertinent data on these ingots.

Table I

Ingot	Melting Method	Composition	Ingot Dimensions	Weight Lb.	L/W*	Taper % on Diameter	Deoxidation Practice
A	BOH	SAE 4340	21 in. fluted ø x 73¾ in.	6160	3.2	4.35	CaSi-Al
B	BE	SAE 4340	20 in. fluted ø x 50½ in.	5000	2.1	5.80	CaSi-Al
C	BOH	SAE 4340	22 x 25 x 71 in.	6600	2.7	2.08, 6.04	CaSi-Al
D	AOH	0.32 Mo-0.12 V	22 in. fluted ø x 77 in.	6500	3.0	4.40	Mn-Si
E	BOH	SAE 4340	22 x 24 x 60 in.	6500	2.5	5.70	CaSi-Al

*Ratio of length to average cross sectional dimension.

After slow cooling, the ingots were sectioned longitudinally along the midplane. Each half was then sawed into transverse slices about 3 inches thick. Samples of 20 to 40 grams each were taken from the edge, quarter, and center position in each slice. The samples were cut in the shape of right rectangular parallelepipeds and all the faces were carefully polished before the determinations. For the most part, densities were determined on duplicate samples. Samples from the center positions in the region of the secondary pipe with visible holes were discarded and new samples were cut

from the immediately adjacent material. Fig. 1 shows the positions of the samples in the center plane of the ingots. In all cases the slices are numbered starting with slice 1 at the bottom or butt of the ingot.

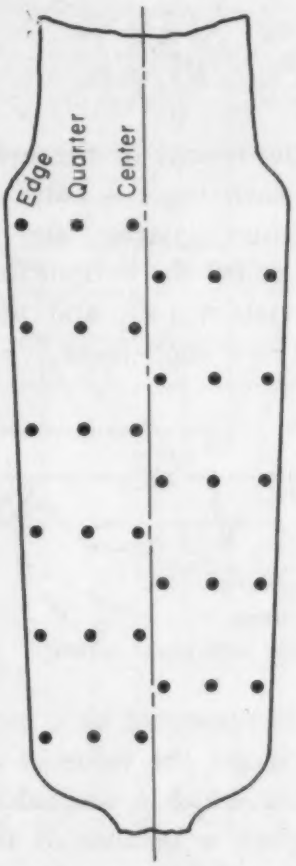


Fig. 1—Position of the Samples in the Ingots.

Method of Density Determination

The density of the samples in grams per cubic centimeter was determined by the weight in air, weight in water technique, wherein

$$\text{Density} = \frac{W_a \cdot d_w}{W_a - W_w}$$

W_a is the weight of the specimen in air, d_w is the density of water at the temperature used (d_w is taken from handbook tables), and W_w is the weight of the specimen in water. A detailed description of the experimental technique of density or specific volume determina-

tions has been published (7). In this study, relatively gross variations in density were of interest; therefore, the calculations have been rounded off in the second decimal place. The experimental technique used would yield an accuracy of at least 0.001 gram per cubic centimeter.

Results

In Figs. 2 and 3, the results of the individual density determinations are plotted for each ingot. Table II lists the arithmetical average ($\overline{X}$) for the center, quarter, and edge positions for each ingot as a whole as well as for the bottom third and for the top two-thirds, the standard deviation (σ), and the average of the three standard deviations ($\overline{\sigma}$) for each ingot. σ is calculated from the formula

$$\sigma = \sqrt{\frac{\sum_{i=1}^{i=n} X_i^2}{N} - \overline{X}^2}$$

where N = the number of samples
X_i = the individual values
$\overline{X}$ = the average of the individual values.

The standard deviation is presented as a measure of the dispersion of the data; that is, the larger the value of σ, the greater the range of density in the group for which σ was calculated.

Ingot E has the highest $\overline{\sigma}$ because of the several low densities near the top in the region of the secondary pipe. Ingot A has the second highest $\overline{\sigma}$ since there is no position with a low σ value. It is interesting to note that the edge position, where the metal is generally considered quite sound in a killed steel ingot, has the lowest σ (the least spread in individual density values) in Ingot B only, and Ingot A actually has a higher σ in the edge position than in either the center or quarter.

Considering the averages, in all five ingots the density is least in the center position. The quarter position has a lower average density than the edge in Ingot D only. Thus, four times in five, the highest average density is found in the quarter position. The highest average density for any position in the five ingots is the quarter position in Ingot B.

The average of the bottom third in the center position for each

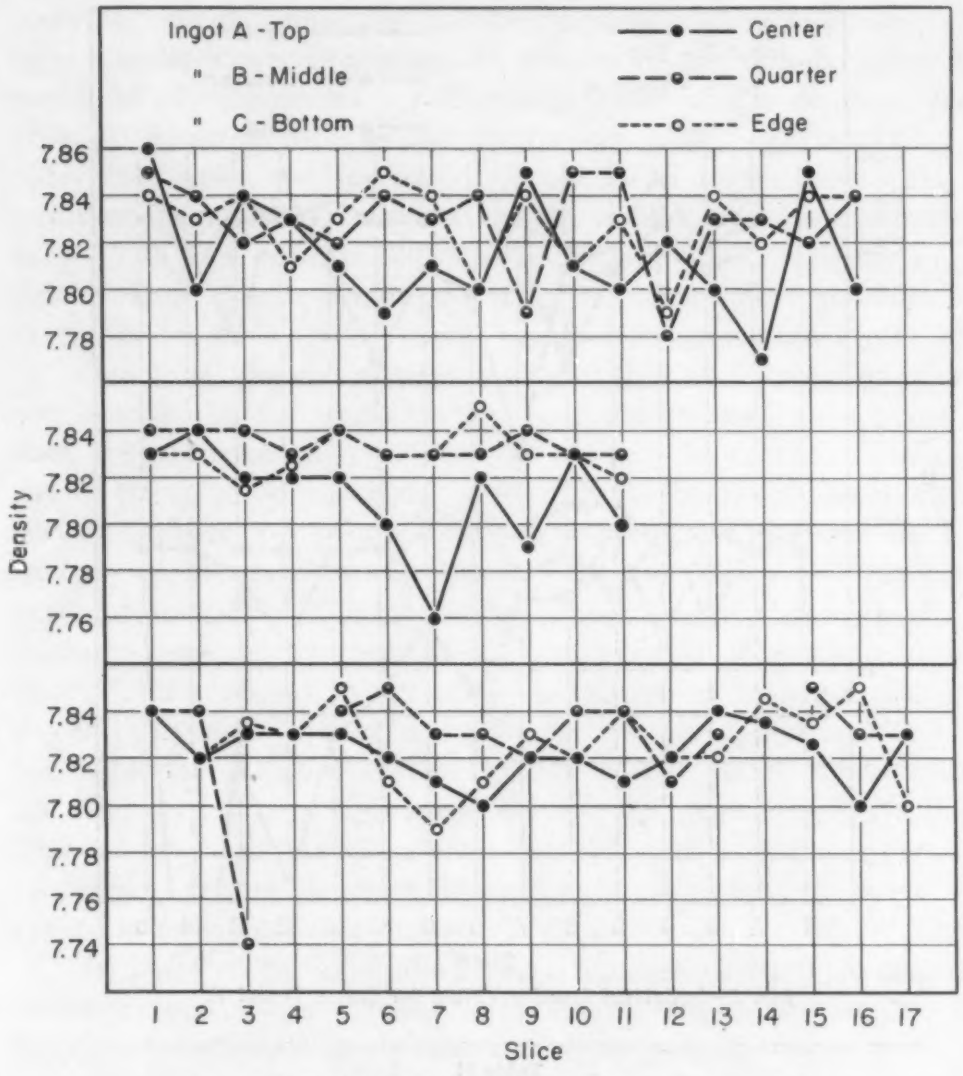


Fig. 2—Individual Density Values for Ingots A, B and C.

of the ingots shows a higher density than that of the center position for the top two-thirds. In Ingots A, B, and E, the average density of the bottom third in the quarter position is greater than that of the top two-thirds.

Discussion

There is a considerable variation in individual density values in these five ingots. Killed steel ingots are generally considered to be of quite uniform density except as the center may contain secondary pipe. Actually, there must be considerable microshrinkage

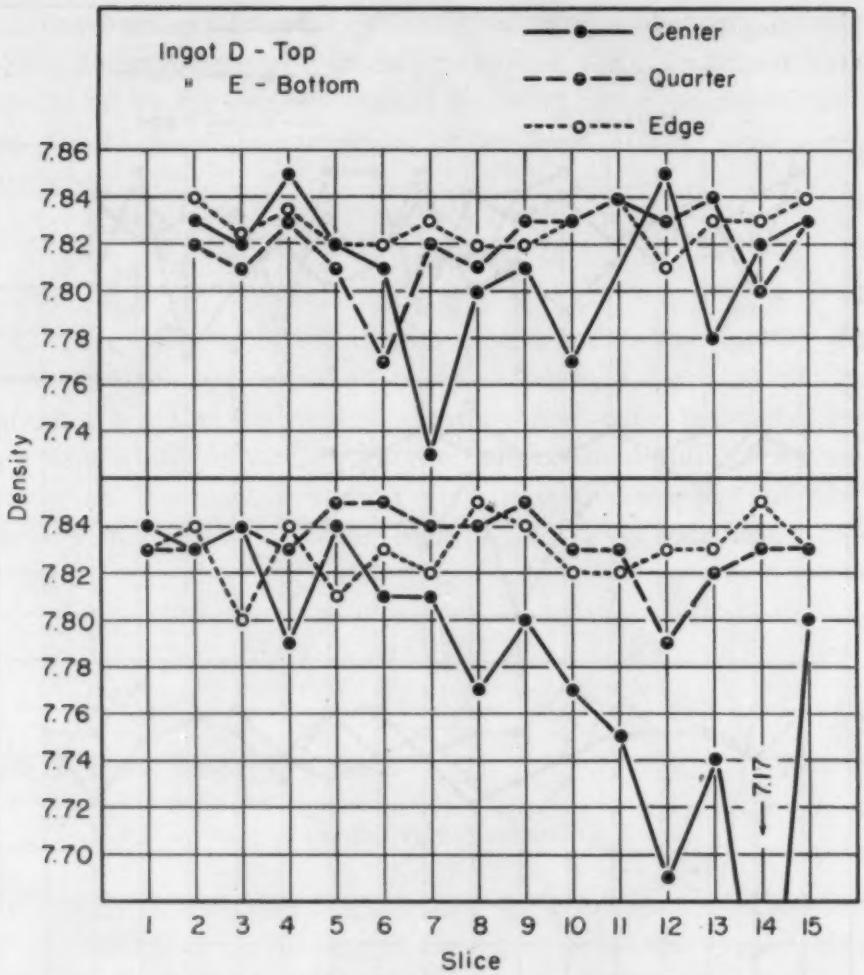


Fig. 3—Individual Density Values for Ingots D and E.

Table II

Ingot	Position	Bottom Third $\bar{X}$	Top Two-thirds $\bar{X}$	σ	$\bar{\sigma}$
A	Center	7.828	7.800	0.0245	
A	Quarter	7.832	7.827	0.0200	0.0237
A	Edge	7.830	7.827	0.0265	
B	Center	7.828	7.803	0.0283	
B	Quarter	7.838	7.833	0.0265	0.0216
B	Edge	7.825	7.833	0.0100	
C	Center	7.828	7.819	0.0118	
C	Quarter	7.822	7.831	0.0245	0.0188
C	Edge	7.831	7.824	0.0200	
D	Center	7.826	7.802	0.0265	
D	Quarter	7.812	7.826	0.0100	0.0168
D	Edge	7.828	7.838	0.0140	
E	Center	7.828	7.711	0.1600	
E	Quarter	7.836	7.831	0.0173	0.0379
E	Edge	7.824	7.832	0.0265	

occurring during solidification. Segregation of the important elements in the ingots (4) is not of sufficient magnitude to cause the noted density deviations. The configuration of the dendrite arms growing into the melt as the steel cools could, by restricting to different degrees the feeding of liquid metal to the interstices as solidification proceeds, cause the density of the individual samples to vary. The edge position seems to be as susceptible to density modification from this source as any other region of the ingot with the exception of the very last metal to solidify around the center line.

Gun tubes pierced from the bottom thirds of ingots showed a considerably higher frequency of bore defects and quench cracks than did gun tubes pierced from the top two-thirds (1). The density of the longitudinal center of the ingot is of interest in this connection because this portion of the ingot becomes the bore or I.D. surface of the tube during the piercing operation. The average center density of all the ingots was highest in the bottom third. It might be expected that because the frequency of defects was highest in products produced from the bottom portion of the ingot, the density in this position would be the lowest. However, the rejections for bore defects and bore surface quench cracks varied directly with the density, i.e., the higher the density, the higher the rejections. This behavior can be construed as further evidence of the importance of primary crystal structure in the bottom portion of the ingot discussed in previous publications (1), (2), (3).

In the five ingots studied, there appears to be no correlation between average density and variation in density with either the length-to-width ratio or the amount of taper in the ingot.

Summary

1. A density survey of five killed alloy steel ingots has been made.
2. A wide variation in density from sample to sample was found.
3. The samples of lowest density were found along the center in the region of the secondary pipe in the top two-thirds of the ingots.
4. Certain configurations of the dendrite arms growing into the melt could, by limiting to various degrees the feeding of liquid metal into the interstices, probably cause the noted deviations in density.
5. The top two-thirds of the ingot where the density of the center

has the lowest average gave the highest yield of pierced seamless gun tubes free from bore defects or bore surface quench cracks.

ACKNOWLEDGMENTS

The authors wish to acknowledge the contribution of Dr. R. F. Mehl, Head of the Department of Metallurgy and Director of the Metals Research Laboratory, as Official Investigator for NDRC Research Project NRC-39.

Mrs. Jean Brink Barclay and Mrs. Lucile Roberts carried out the density determinations.

The work on this NDRC project was assisted by the co-operation of the Project Advisory Committee. The members of this committee are listed in the first reference of this paper. The split ingots were contributed by the co-operating companies of the project.

References

1. J. W. Spretnak, K. L. Fetters and E. L. Layland, "Ingot Factors in the Production of Seamless Gun Tubes," TRANSACTIONS, American Society for Metals, Vol. 39, 1947, p. 627.
2. V. Paschkis, "Theoretical Thermal Studies of Steel Ingot Solidification," TRANSACTIONS, American Society for Metals, Vol. 38, 1947, p. 117.
3. J. W. Spretnak, "Kinetics of Solidification of Killed Steel Ingots," TRANSACTIONS, American Society for Metals, Vol. 39, 1947, p. 569.
4. J. W. Spretnak, "Macrosegregation in Some Alloy Steel Ingots," TRANSACTIONS, American Society for Metals, Vol. 40, 1948, p. 897.
5. C. F. Sawyer, J. W. Spretnak and G. Derge, "The Distribution of Oxygen and Nitrogen in an Alloy Steel Ingot," TRANSACTIONS, American Society for Metals, Vol. 40, 1948, p. 922.
6. K. L. Fetters, M. M. Helzel and J. W. Spretnak, "Distribution of Nonmetallic Inclusions in Some Killed Alloy Steel Ingots," American Society for Metals Preprint No. 9, October 1948.
7. S. G. Fletcher and M. Cohen, "The Effect of Carbon on the Tempering of Steel," TRANSACTIONS, American Society for Metals, Vol. 32, 1944, Authors' Reply to Discussion, p. 358.

DISCUSSION

Written Discussion: By C. E. Sims, Battelle Memorial Institute, Columbus, Ohio.

The authors have given convincing evidence of a complete lack of correlation between the variations in density of an ingot and the prevalence of bore defects in a pierced tube made from it. In the absence of blowholes or definite pipe, the lower density is a manifestation of the inability of liquid steel to feed through a maze of dendrites to compensate for all of the solidification shrinkage of freezing steel. Judging from results on cast steel forging blanks where the hot working was very slight, it requires a reduction of only about 5 to 10% to eliminate micro-

shrinkage and to realize the ultimate mechanical properties of a steel. It can be deduced, therefore, that by the time an ingot is rolled to a billet ready for piercing, all effects of microshrinkage have been erased, and no correlation with original density should be evident.

Written Discussion: By S. F. Urban, director of research, Titanium Alloy Manufacturing Division, National Lead Co., Niagara Falls, N. Y.

Though this paper depicts some general trends in density variations in killed ingots, it turned out, as stated in the paper, there is no correlation between these density variations and rejections of gun tubes. This task obviously needed doing and now that it has been done and unfortunately came up negative, it appears that density studies are not going to be particularly enlightening unless they are made with an extremely high degree of precision. This reasoning in this instance is that, with approximately 0.03% maximum inclusion content by weight, the effect of this amount of nonmetallic matter or 0.01% will be so small on calculated densities that it is doubtful whether determinations can be made in a sufficiently high degree of precision to allow valid interpretation.

Written Discussion: By R. L. Wilson, director of metallurgy, and D. J. Girardi, research metallurgist, The Timken Roller Bearing Company, Canton, Ohio.

The authors are to be complimented for contributing density data on steel in the ingot stage. As mentioned in this paper, such information is noted for its paucity. In examining Figs. 2 and 3 there appears to be some tendency for the center density values to be on the low side in the range of ingot slices 6 to 8 and I wonder if the authors place any significance on this point. It is interesting to note that the top two-thirds of the ingot with a lower average center density gave the highest yield of pierced seamless gun tubes free from bore defects or bore surface quench cracks.

Written Discussion: By A. B. Wilder, chief metallurgist, National Tube Co., United States Steel Corp. Subsidiary, Pittsburgh.

It is concluded by the authors that, "the top two-thirds of the ingot where the density of the center has the lowest average gave the highest yield of pierced seamless gun tubes free from bore defects or bore surface quench cracks." Our understanding is that the upper part of ingots of this type of steel also contain fewer alumina inclusions. We would appreciate comments of the authors with reference to the influence of hydrogen in the presence of alumina inclusions on the defects encountered in the bottom third of the ingot.

Authors' Reply

The authors agree with Mr. Sims that the rolling of the ingot into billets ready for piercing should eliminate variations in the density found in the ingot. Whether this elimination of density variations also eliminates all effects of microshrinkage is somewhat open to question since the most frequent occurrence of bore defects and quench cracking occurred in gun tubes processed from the bottom one-third of the ingots.

It may be that the common mechanical tests are not adequate to predict the behavior of steel during piercing and heat treating.

Mr. Urban points out the difficulties encountered in attempting to determine the inclusion content of steel by use of density measurements. The inclusion content of these ingots was studied by other methods (6).

In answer to Mr. Wilson and Mr. Girardi, there is probably some tendency for the ingots to bridge over during solidification, which could cause a lowering of the center density values in certain locations.

The authors have no data with which to answer Dr. Wilder on the effect of hydrogen in the presence of alumina inclusions.

THE NATURE OF INCLUSIONS IN TENSILE FRACTURES OF FORGING STEELS

By H. D. Shephard and E. A. Loria

Abstract

Procedures are described for studying the nature of flaws in steel by observing the appearance of tensile fractures under polarized light and providing an interpretation of the reflecting constituents contained therein, based on a careful metallographic examination of the tensile test specimen made at or in the vicinity of the fracture. Under consideration were test specimens of two acid open-hearth forging grades that produced somewhat angular, fibrous fractures, ductile cup-cone, silky fractures, and flat, crystalline-appearing fractures. Making use of both reflected polarized light and bright field illumination, a study of the structure of the major inclusions in these fractures together with their correlation with tensile ductility is presented. Actually, most of the fractures shown are not indicative of the normal tensile fractures obtained in these steels, but have been selected in order to denote the distribution of inclusions where fractures of intermediate or poor tensile ductility occur. In such cases, this method of examination reveals the importance of inclusions in initiating rupture and the consequent necessity for revisions in melting practice or ingot design.

Introduction

In their report on the fracture of metals, Gensamer and his collaborators (1)[1] indicated the need for further research on the nature of flaws in steel and suggested the examination and classification of fractures as a logical starting point in such a study. A significant step in this direction had already been taken by Zapffe (2), who had improved the technique of examining the cleavage surfaces of metals and interpreted their relationship to the mechanism of fracture. The present paper considers another approach to the problem

[1]The figures appearing in parentheses pertain to the references appended to this paper.

A paper presented before the Thirtieth Annual Convention of the Society, held in Philadelphia, October 23 to 29, 1948. Of the authors, H. D. Shephard was formerly metallurgist, Mesta Machine Company, now metallurgist, Kerchner, Marshall & Company, Pittsburgh; E. A. Loria is Fellow, Mellon Institute of Industrial Research, Pittsburgh. Manuscript received April 10, 1948.

by observing the appearance of tensile fractures under polarized light and provides an interpretation of the reflecting constituents contained therein, based on a careful metallographic examination of the tensile test piece made at or in the vicinity of the fracture.

Perhaps the best theory on the mechanism of metal fracture yet formulated involves the concepts of resistance to flow and resistance to fracture (3). The theory postulates that, if the stress required for fracture is greater than that required for flow, plastic deformation will occur; conversely, if the stress required for flow is greater than that required for fracture, rupture will take place. Flow may terminate in either shear or cleavage separation with the former characterized by high ductility, a fibrous or silky-appearing fracture generally at 45 degrees to the direction of applied load, and high energy absorption; and with the latter, by relatively low ductility, a granular or crystalline-appearing fracture generally normal to the direction of applied load, and in most cases low energy absorption. Cleavage fracture may occur, and often does, after appreciable flow; the term refers to a mode of separation and is not intended to apply only to completely brittle fracture without measurable deformation, although this case is obviously included. The appearance of both granular and intergranular fractures under plane polarized light will be given attention in this paper.

There are few critical observations available on the structural aspects of the fracture of polycrystalline materials. Metals that break brittlely are believed by many to fail by the same cleavage type of fracture as do single crystals, while ductile polycrystalline aggregates are thought to fail by the shearing or slipping process. The broken surface of steel appears to consist of bright reflecting facets believed to be the cleavage planes of the ferrite; whereas a shear type of failure is supposed to result where it breaks as a ductile material in simple tension. Photographs of the fractured edges of ductile and brittle steels have been shown in recent contributions by Hollomon (4) and Grossmann (5).

It is a well-known fact that nonmetallic inclusions significantly affect the fracture stress of steel. Although no quantitative studies have been made, it is also known that the magnitude of the lowering of the fracture stress depends on the size, shape and distribution of the included particles (6). For example, the orientation of inclusions during deformation at high temperatures causes the fracture stress of steels of any structure to vary markedly in different directions.

Both tensile ductility and notched-bar impact toughness are decreased for specimens taken transverse to the direction of working and are increased for specimens taken parallel to the direction of principal rolling or forging elongation. Such transverse tests are not only affected by the degree of reduction but also by the original ingot heterogeneities. The variation between values obtained from longitudinal and transverse test specimens is generally not noticeable in the tensile strength but is evident in the ductility (as measured by elongation and reduction of area in the tensile test).

The use of reflected polarized light in the study of inclusions in polished sections of steel was demonstrated years ago by Hoyt and Scheil (*7*), but to the authors' knowledge no previous work has appeared on the examination made directly upon the fracture surface employing reflected plane polarized light with crossed nicols as the explorative medium. Such surfaces are neither etched nor polished and thus are unaffected by chemical attack or physical distortion. Making use of both reflected polarized light and bright field illumination in a study of the structure of some inclusions occurring in various types of fractures and attempting a correlation between these fractographs and the tensile ductility comprises the scope of the present paper. Actually, most of the tensile fractures shown herein are not indicative of the normal tensile fractures obtained in the steels under consideration but have been selected in order to demonstrate what one can look for in the way of inclusion distribution where fractures of intermediate or poor tensile ductility occur. By establishing an analytical approach to the effects of such inclusions on the type of fracture and on ductility, the metallurgist may revise his melting practice or ingot design if observations comparable to those shown in this paper are obtained. In addition to proper steelmaking practice, the importance of primary ingot structure in ingots used for products that undergo severe combined stresses in processing or application has been emphasized, for molds should be designed to produce the desired primary ingot structure.

Materials and Test Procedure

The chemical composition range of the steels used in this investigation is given in the following tabulation:

Steel	C	Mn	Si	P	S	V
A	0.35-0.45	0.40-0.80	0.15-0.35	0.05	0.05	0.08-0.12
B	0.32-0.38	0.60-0.90	0.15-0.30	0.04	0.04	

Both steels are forging grades made by the acid open-hearth steelmaking process. Ferrosilicon but no aluminum was employed for ladle deoxidation, and vanadium was added for fine grain size specification in the case of steel A. In order to discern more readily the appearance of nonmetallic inclusions in the tensile fractures under polarized light, some of the test specimens for steel A and all of those for steel B were cut out of forgings processed from the top third of various ingots, which is ordinarily known to be the dirtiest portion of an ingot. The other tensile specimens for steel A were selected at random. In all instances, however, the specimens were taken parallel to the axis of compression so that the defects were oriented perpendicular to the axis of the transverse specimen by the prior compressive deformation (hot work). Thus, really under consideration in three separate categories were the test specimens of somewhat dirtier than normal steel producing somewhat angular, fibrous fractures, a second group consisting of more ductile cup-cone, silky fractures, and a third group of flat, crystalline-appearing fractures obtained from heavily forged steel.

The test specimens were drilled out of different forgings where cooling slots were necessary. The steels were either normalized or quenched from 1550 to 1650 °F (845 to 900 °C) and then tempered at temperatures varying from 850 to 1200 °F (455 to 650 °C). Thus treated they were subjected to metallographic examination and tensile testing, standard 0.505-inch diameter by 2.0-inch gage length test bars being machined from each coupon.

Just as soon as a tensile test specimen was broken it was mounted by means of plasticine in a 1-inch diameter ring with the broken end projecting outward so that it could then be fitted into the annular opening in the stage of the inverted microscope. The specimen, thus supported from above by the temporary mount, has its fracture surface practically horizontal to the beam of plane polarized light projected through the objective lens of the microscope.

The polarizing microscope as used with reflected light has been sufficiently described in the literature (8) and need not be fully discussed here. Aside from noting that the instrument was a Zeiss model, only a few of the more pertinent points will be covered. The polarizing microscope differs from an ordinary microscope chiefly in having a polarizing prism in the vertical illuminator for producing plane polarized light, and an analyzer above the objective for analyzing the light that is reflected from the surface of the specimen. A

specimen illuminated by plane polarized light appears the same as if ordinary light were employed, but with the analyzer any effect that the specimen may have upon the original plane of vibration of the light can be rendered strikingly evident. The analyzer is rotatable and, in the crossed position, the planes of vibration of the two prisms are perpendicular to each other, and the analyzer stops all the light that the polarizer normally transmits. Thus the metallic portion of the specimen appears dark, whereas an inclusion that alters the plane of vibration of the incident illumination appears illuminated because the analyzer permits that light to pass through. The fractographs were depicted at the minimum magnification permitted by the metallograph, and the exposure times for the photographic plates varied from 2 to 5 minutes, i.e., until a good image of the structure, such as shown in Figs. 1 and 2, was obtained.

In order to avoid any oxidation of the surface of the tensile fracture, the fractographic examination under polarized light and the polished surface examination under bright field illumination were made in immediate sequence. Just as soon as a test specimen had been examined under the polarizing microscope and the structural aspects of the fracture noted, it was then dry ground until the polished microsection produced the exact configuration of the nonmetallic constituents in the fracture. The preparation of the polished microsections required careful attention, and frequent observation of the microstructure at various stages of dry polishing was necessary in order to find and preserve a desirable area for illustration. Actually, two methods of examination were considered. The first procedure consisted in mounting a portion of the broken tensile test piece sideways so that the surface perpendicular (transverse) to the fracture would be exposed to grinding. Thus a cross sectional view of the inclusions at the surface of the fracture would be obtained. Typical photomicrographs are presented in Figs. 3 to 6. The second procedure was to polish the face of the fracture slowly and carefully, with frequent observation of the polished section under the microscope in order to detect the presence of nonmetallic inclusions at or just below the fracture surface. Figs. 6 and 8 are representative of this procedure.

Results and Discussion

The experimental observations are concerned mainly with the appearance and characteristics of tensile fractures under polarized

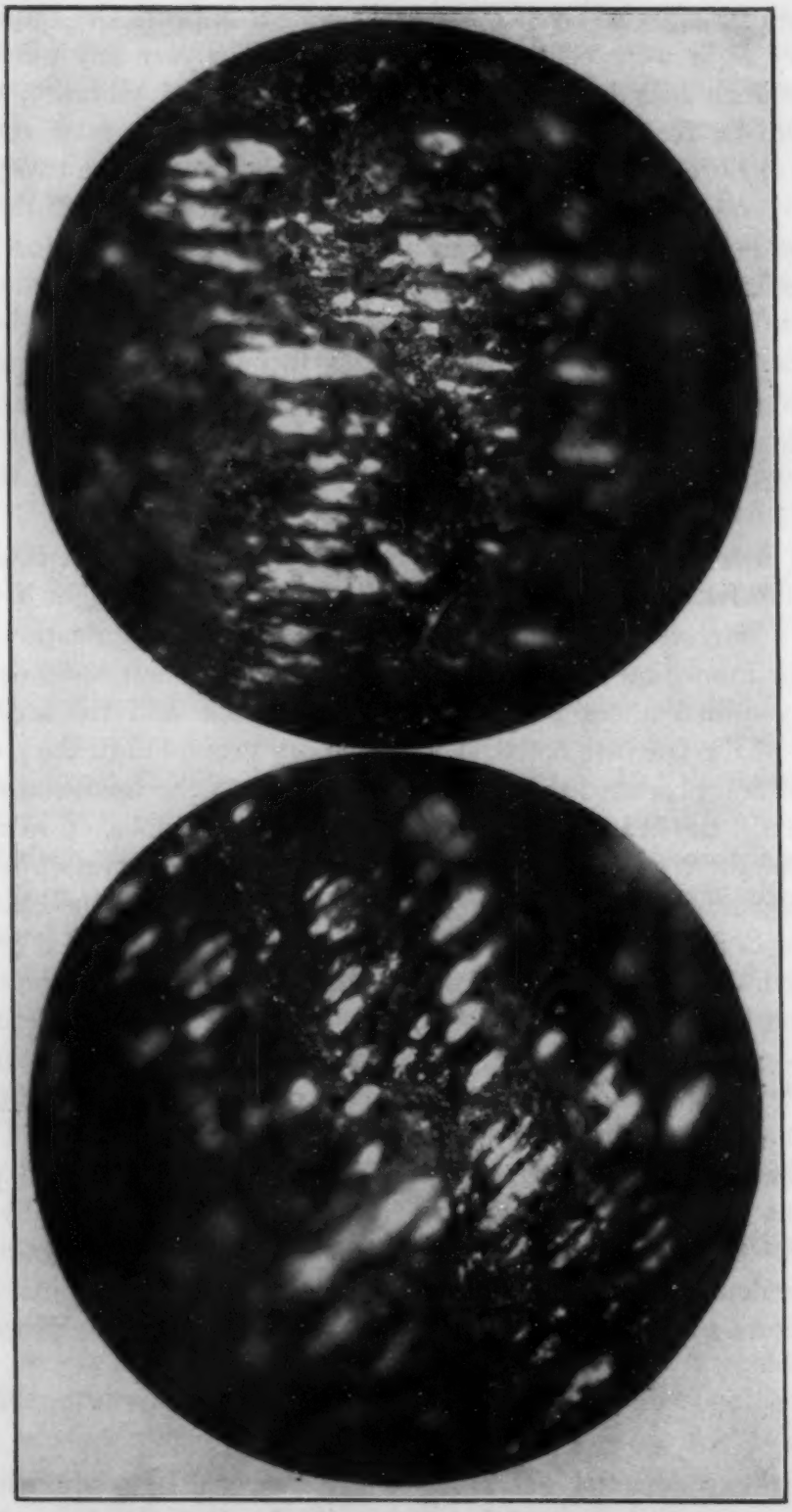


Fig. 1—Tensile Fractures of Steel A by Polarized Light Between Crossed Nicols. Angular, fibrous types showing white elongated particles. × 40.



Fig. 2—Tensile Fractures of Steel A by Polarized Light Between Crossed Nicols. Angular, fibrous types showing white elongated particles. × 40.

light and the morphology of inclusions in polished sections taken at or near the surface of these fractures. For complete recording, the relationship between the translucent particles or areas in the tensile fractures and the inclusions observed in polished sections are illustrated in appropriate photomicrographs.

Figs. 1 and 2 portray the fractures of several transverse tensile test specimens of steel A taken from the top sections of various ingots. All these fractures were angular and fibrous in appearance. The type of fracture is specified according to a nomenclature which, in the absence of accepted standards, is intended merely to be descriptive to those familiar with the appearance of fractures and denotes no scientific analysis of the crystalline mechanism of fracture. Thus "fibrous" refers to all fractures occurring after extensive plastic deformation and generally associated with high ductility. Usually "angular" refers to fractures tending to occur as a shear on a single plane at about 45 degrees to the axis of the tensile specimen and generally associated with intermediate ductility. The fractures shown in Figs. 1 and 2 are classified as both fibrous and angular in that there is a slight tendency for the fractures to occur at an angle to the tension axis though the angle nowhere near approaches the 45-degree shear mentioned above. The transverse ductility values for these fractures were in the range of 18 to 20% reduction of area. The reduction S ÷ s, ingot to forging, was 4.

Examination of the tensile fractures by reflected polarized light between crossed nicols discloses white elongated particles aligned parallel to the forging direction in each specimen. Observed under a low-power binocular these surfaces showed olive or white spots that would indicate the presence of silicates. In order to identify the elongated particles found on the surface of each fracture under polarized light, cross sectional views of these surfaces were prepared. A typical observation at a magnification of 125 diameters is set forth in Fig. 3. This specimen was dry polished carefully until the desired area portrayed was reached. Such a procedure was followed in order to avoid oxidation or corrosion of the fracture surface and tarnish of any inclusions therein by water attack during polishing. Also, no etching was resorted to in order to avoid staining or producing a void between the inclusion segregate and the "Lucite" mounting medium. Furthermore, it is not advisable to etch a specimen before examination in polarized light. Such etching tends to attack and roughen the surfaces of the inclusions and sometimes



Fig. 3—Nonmetallic Inclusions in Tensile Fracture of Steel A. View shown is transverse to the fracture surface. Unetched. × 125.

attacks the matrix surrounding the inclusion to produce a certain transparency to the inclusion and so make its identification less positive. The upper (dark) portion of Fig. 3 depicts the "Lucite" mounting medium whereas the lower (white) portion is the steel base. The elongated inclusion segregate at the fracture interface corresponds to one of the white elongated particles observed under polarized light on the face of the tensile fracture. Of particular interest is the complex nature of the inclusion segregate that appears to be broken up into irregularly shaped blocks with particles of a second constituent interspersed in a eutectic fashion therein. Fig. 4 shows the polished section at the higher magnification of 500 diameters and under both bright field illumination and polarized light between crossed nicols. The eutectiform constituent is gray in color compared to the dark brown of the matrix and appears in a continuous fashion, transcending from one fragment to another and indicating that the matrix may have been fragmented during the polishing process. Under polarized light the fragmented blocks appear bright or milky white, whereas the interspersed constituent is opaque or dark in color. The metallic surface of a specimen is always dark but the inclusions may be dark or light, depending upon their type but independent of their size. In one group, characterized broadly as opaque or dark inclusions, are iron oxide, manganese

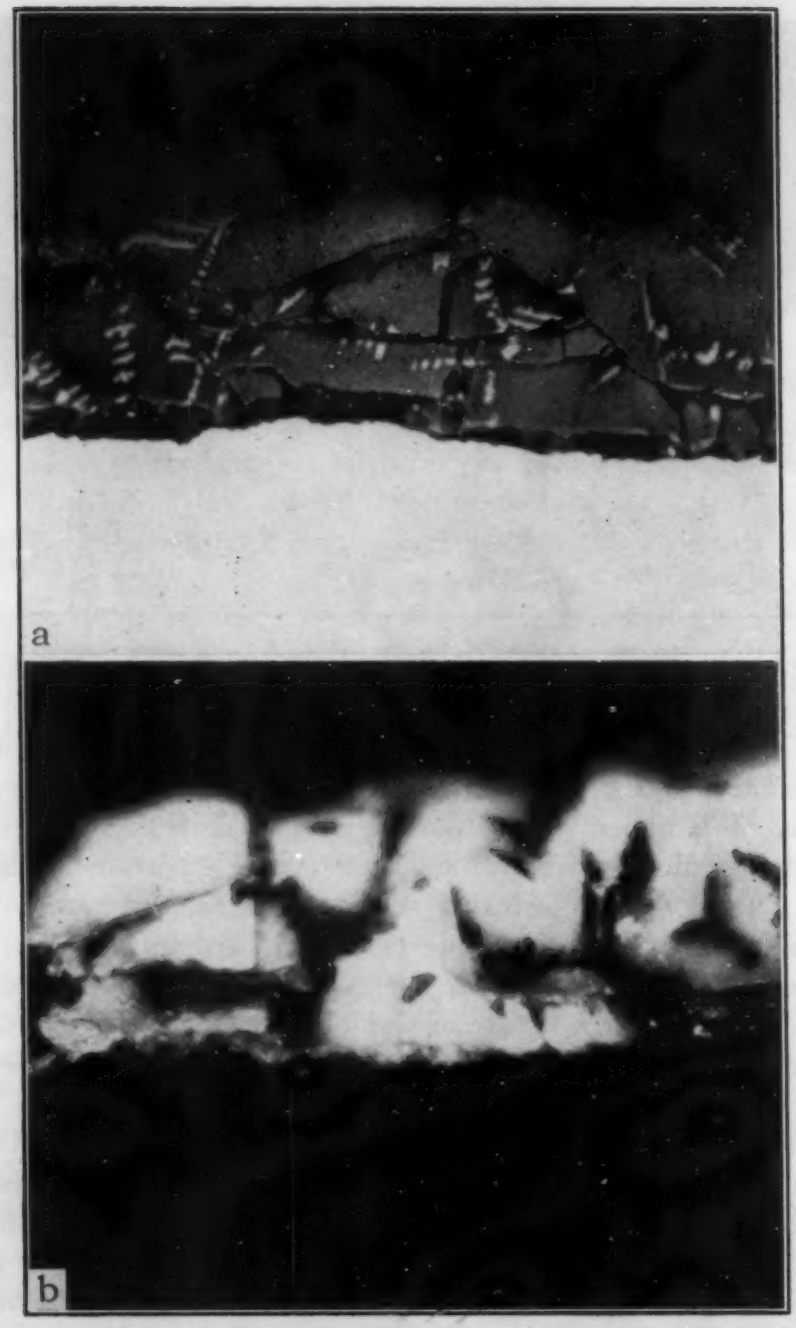


Fig. 4—Nonmetallic Inclusions in Tensile Fracture of Steel A. Views shown are transverse to the fracture surface. (a) Bright field illumination; (b) Under polarized light. Unetched. × 500.

oxide, iron sulphide, and manganese sulphide. In the second group of transparent or bright inclusions are the silicates that can be more closely distinguished by means of their coloring and optical effects. At times transparent silicates may be slightly contaminated with

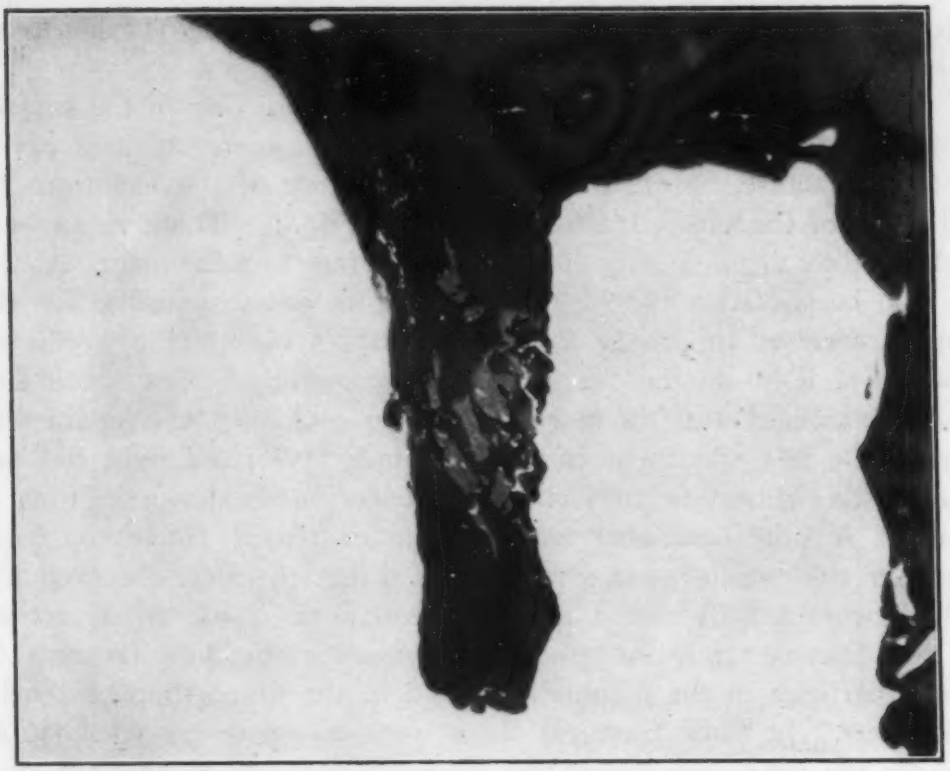


Fig. 5—Inclusion Segregate in Cavity of Tensile Fracture of Steel A. View shown is transverse to the fracture surface. Unetched. × 125.

metallic oxides that are miscible in the silicates, and this produces a coloration in polarized light with crossed nicols. Such contamination of silicate inclusions tends to reduce their clear transparency to a milkiness. Hoyt and Scheil (7) observed that siliceous inclusions in wrought steels usually are contaminated with oxides, which lower the melting point and make them more plastic at the rolling or forging temperature, so that usually they appear in elongated shapes. As the amounts of these contaminating oxides increase, iron and manganese silicates are encountered. Even now quantitative methods in use cannot distinguish between iron oxide and manganese oxide, which occur as separate phases or as duplex inclusions, nor between iron oxide and manganese oxide which are in combination as silicates, but this distinction can be readily made by examination with reflected polarized light. Fig. 4 shows that the opaque iron oxide or manganese oxide eutectic occurs as a separate phase but still as a constituent part of a duplex inclusion, notwithstanding the fact that the milkiness of the silicate would indicate further contamination of the matrix phase. Accordingly, it is believed that the duplex inclusions

found in the tensile fractures of test specimens of steel A taken from the top sections of ingots are complex oxide-silicates.

Fig. 5 presents another view taken perpendicular to the surface of a tensile fracture and reveals an inclusion segregate in a cavity of the fracture. More evidence of the nature of the inclusions on the face of the tensile fracture is found in Fig. 6. These views were obtained by dry polishing the irregular surface to a flat plane. Again, it can be seen that the inclusion segregates are responsible for the appearance of the white elongated particles observed by reflected polarized light on the fracture face of the tensile test specimens.

Examination of the more ductile, cup and cone type of fracture in tensile test specimens of steel A under polarized light did not reveal the same type of inclusion distribution as shown in Figs. 1 and 2 for the somewhat angular type of tensile fracture. As a general rule, much fewer white elongated particles were observed and these were usually found in the central area of the cross section. There was certainly no tendency whatsoever for the alignment of such particles in the manner disclosed in the first group of tensile fractures. In some fractures there were no white particles visible under the polarizing microscope. Fig. 7 is a typical example of a cup and cone fracture under polarized light with crossed nicols. The reduction of area for this particular test specimen was 45% (reduction of S ÷ s, ingot to forging, of 4). The view is the cup side of a silky fracture and it contains but a few white elongated particles at the very depression or center of the cup. Careful dry polishing of this face to an even flat surface produced the inclusion structures shown in Fig. 8. These inclusions were found in the same area where the white elongated particles were observed in the fracture and no doubt are responsible for such an observation under polarized light. These inclusions are complex in nature, possessing a darker interior, part of which is in the form of needles or spines. Under bright field illumination their color varies from the black of the needles to the brown of the matrix. These inclusions are believed to be complex silicates, but their constituency is certainly different from those shown in Figs. 3 to 6 and associated with the somewhat angular fractures possessing intermediate ductility.

The third group of tensile fractures examined was taken from test specimens of heavily forged steel B. The effects of considerable hot work on the configuration of inclusions are varied. They depend on the type of inclusions, the amount of the reduction, and the tem-

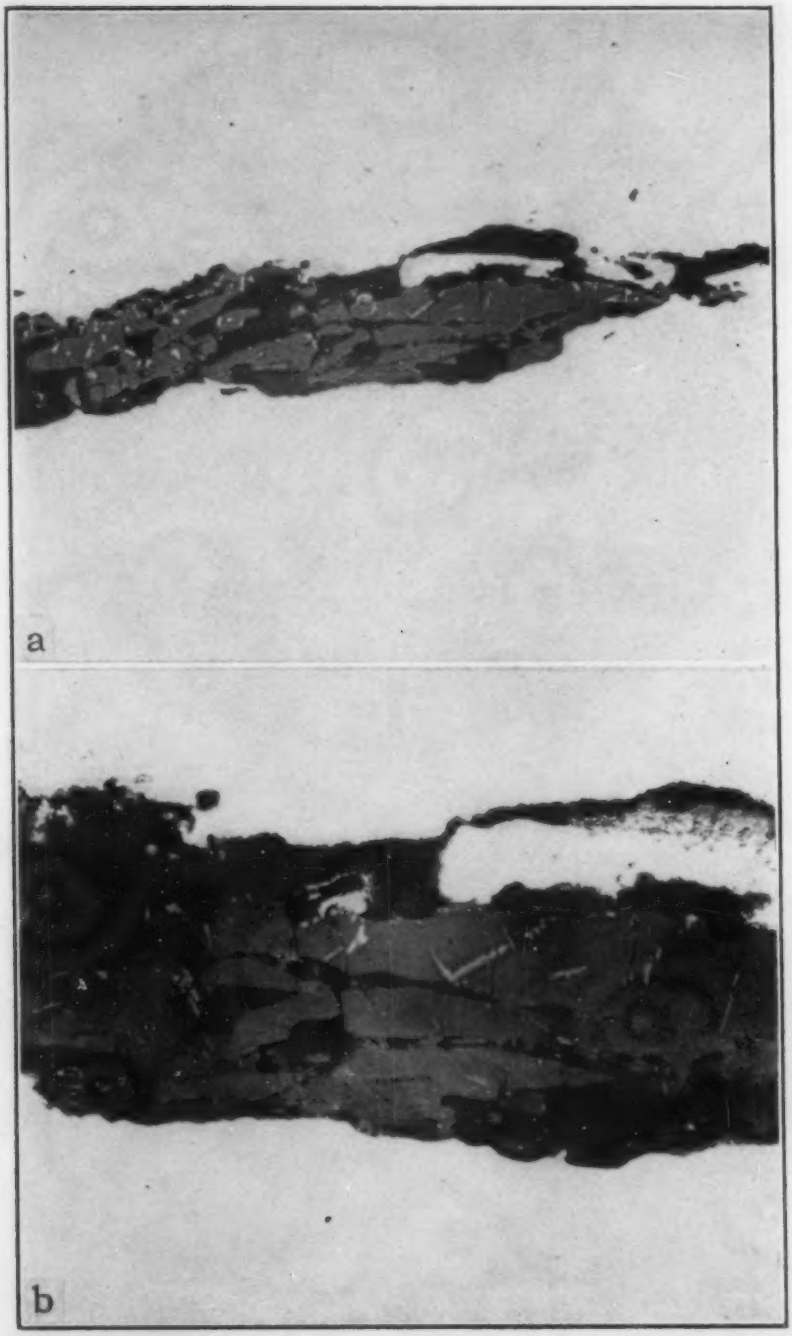


Fig. 6—Inclusion Segregate on Grinding Surface of Tensile Fracture of Steel A. Unetched. (a) × 125; (b) × 500.

perature at which it is conducted. The extent to which an inclusion is elongated and spread will depend on its plasticity at the temperature of reduction, and this in turn is related to the melting point or softening range of the inclusion. As inclusions approach their melt-

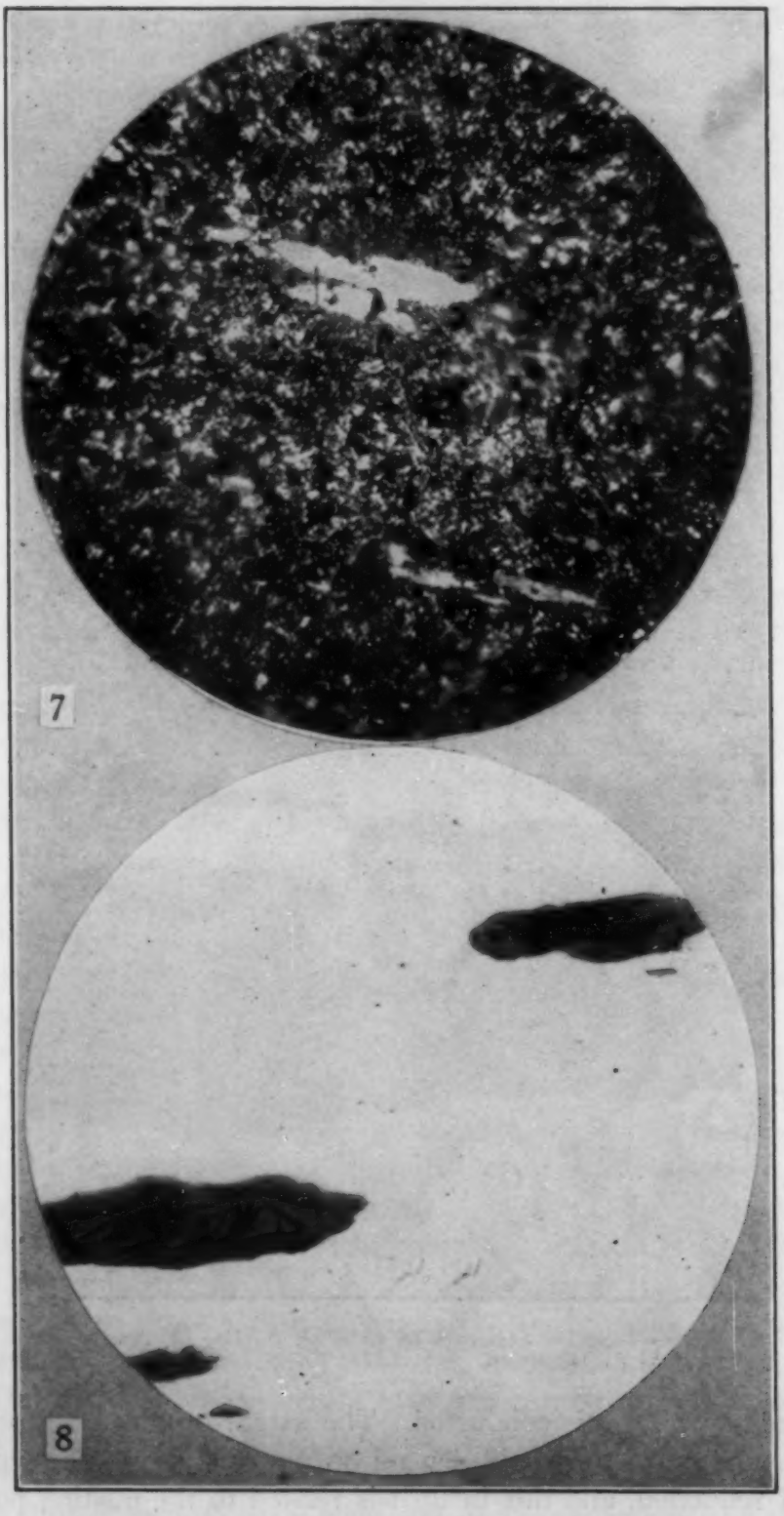


Fig. 7—Nonmetallic Inclusions in Tensile Fracture of Steel A Under Polarized Light. Cup side of a cup and cone, silky fracture containing white elongated particles in center of fracture. × 40.

Fig. 8—Nonmetallic Inclusions in White Area of Fig. 7 on Grinding Surface of Tensile Fracture. Unetched. × 100.

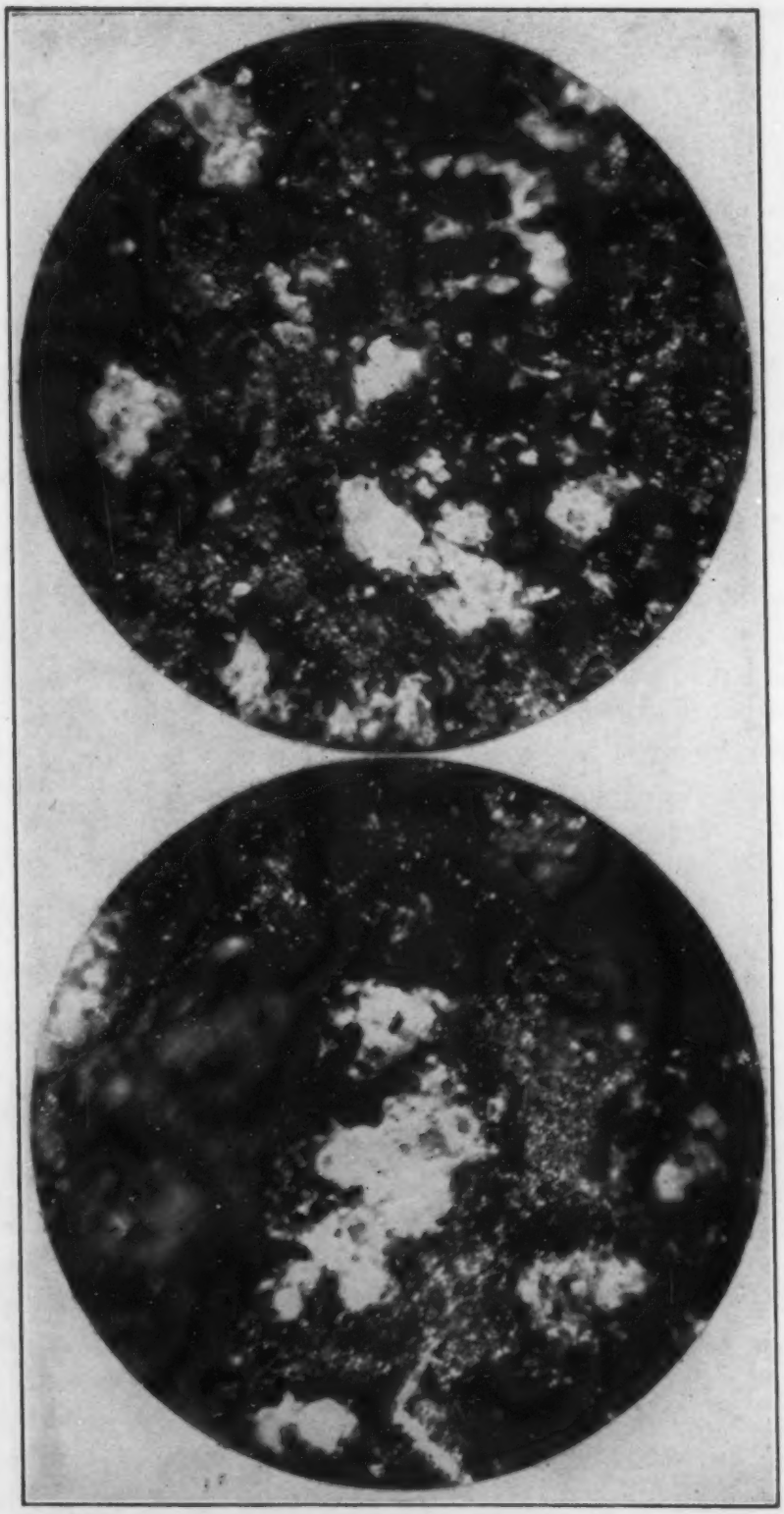


Fig. 9—Tensile Fractures of Steel B Under Polarized Light Between Crossed Nicols. Considerable hot work has flattened the white areas into irregular shapes. × 35.

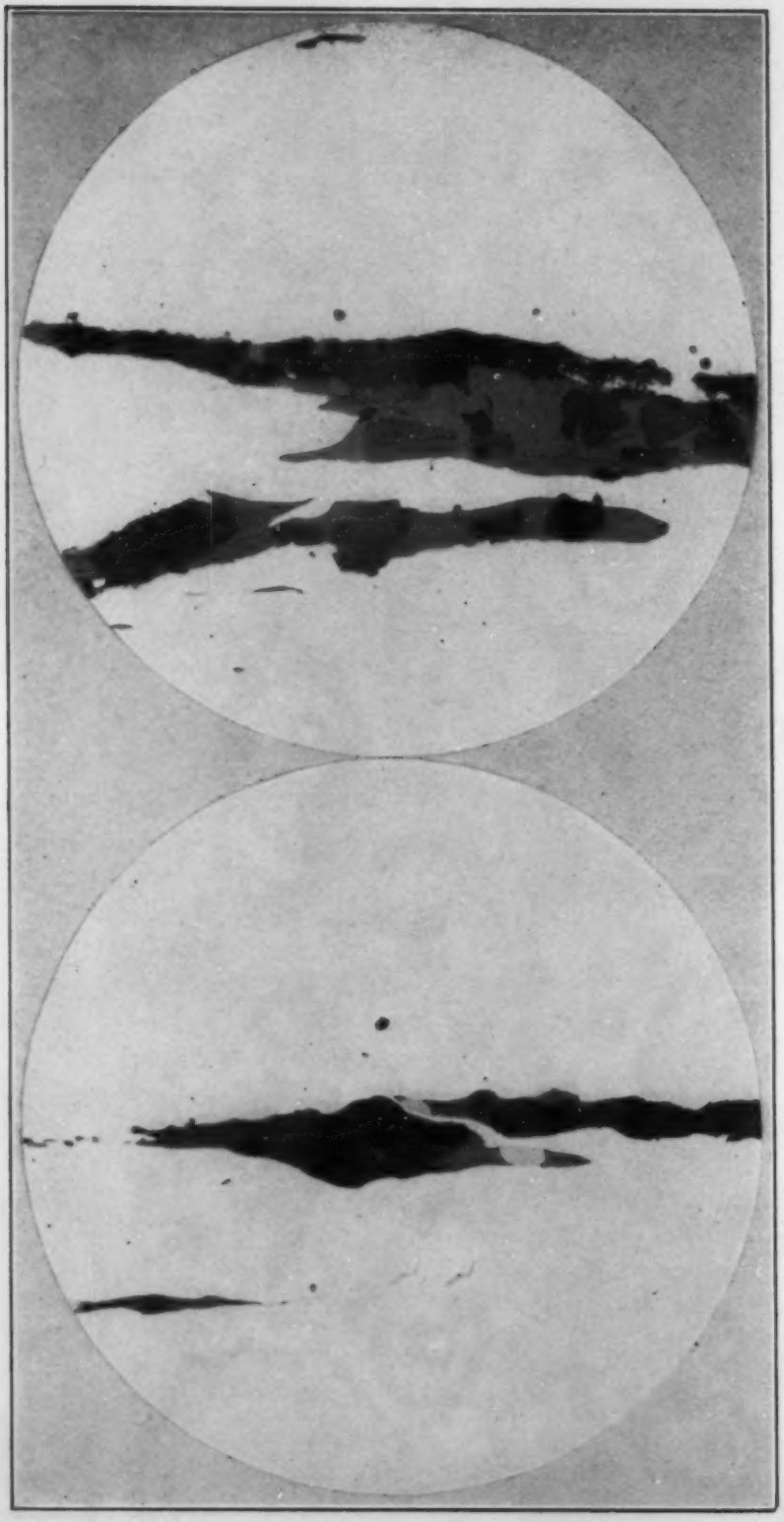


Fig. 10—Duplex Inclusions in Tensile Fractures of Steel B. Views shown are transverse to the fracture surface. Unetched. × 200.

ing points their plasticity becomes greater; however, the extent of the softening range below the melting point varies with the type of inclusion. In general, the silicates have wider ranges of plasticity than do the other common inclusions.

Fig. 9 presents two typical tensile fractures of steel B under polarized light between crossed nicols. The considerable amount of hot work performed on these steels (reduction S÷s, ingot to forging, of 12) flattened or pancaked the white, usually elongated particles into irregular shapes. These areas run perpendicular or transverse to the axis of the tensile test specimen. Observed visually these fractures are crystalline in appearance and under a low-power binocular the white areas still appear as minute white spots. Actually the fractures are flat breaks and their relative degree of flatness permits a greater area of the fracture face to be in focus (as can be seen by comparing Fig. 9 with Figs. 1 and 2). Both specimens broke at what might be termed their yield point and consequently possessed 0% reduction of area. Fig. 10 provides two bright field illumination views taken transverse to the fracture surface and shows that duplex inclusions produce the milky white, irregularly shaped areas observed in the tensile fractures under polarized light. The upper photomicrograph taken at a magnification of 200 diameters shows an elongated iron oxide or manganese oxide-silicate combination (brown color variations), whereas the lower photomicrograph is predominantly dark brown silicate with two light gray still somewhat rounded sulphide inclusions attached thereto.

Summary

A procedure has been suggested that will enable the examination and classification of tensile fractures according to the nature and distribution of the predominant inclusions. Employing plane polarized light with crossed nicols as the explorative medium, a microscopic study of the reflecting constituents in fracture surfaces has been made and correlated with a careful metallographic examination of the polished surfaces at or in the vicinity of each fracture. Under consideration were transverse tensile test specimens of two particular acid open-hearth forging grades that produced fractures in three distinct categories. Notwithstanding this fact, the analytical method described can be made applicable to any particular grade of steel. Most of the depicted fractures are not indicative of the normal tensile fractures obtained in these steels, but have been selected in order to

show the nature of the inclusions in fractures of intermediate or poor tensile ductility. In such cases, the method of examination reveals the importance of inclusions in initiating rupture and the consequent necessity of revisions in melting practice or ingot design.

In tensile fractures of steel A of intermediate ductility, which were classified as somewhat angular and fibrous in appearance, examination by reflected polarized light between crossed nicols disclosed white elongated particles aligned parallel to the forging direction in each specimen (reduction S÷s, ingot to forging, of 4). In order to identify these particles, both cross sectional and parallel views of the fracture surface were prepared and the polished surfaces were observed under bright field illumination and polarized light between crossed nicols. Inclusion segregates, believed to be complex oxide-silicates, were found at the fracture interface in areas corresponding to the white elongated particles observed under polarized light.

Similar examination of the more ductile, cup and cone type of fracture in tensile test specimens of steel A displayed much fewer white elongated particles that were usually confined to the central area of the fracture. There was no tendency whatsoever for the alignment of such particles in the manner shown in the previous group of tensile fractures. In some of these fractures there were no white particles at all visible under the polarizing microscope. A study of polished surfaces where such particles did exist uncovered complex silicates, whose constituency was obviously different from those associated with the somewhat angular fractures possessing intermediate ductility.

In the third category, tensile fractures of heavily forged steel B, which were actually flat, crystalline breaks possessing no measurable ductility index, were subjected to examination by polarized light between crossed nicols and proved that the considerable amount of hot work (reduction S÷s, ingot to forging, of 12) flattened the white, usually elongated, particles into irregular shapes. These areas, which run perpendicular or transverse to the axis of the tensile test specimen, are responsible for its premature rupture. Bright field illumination views of these areas showed them to be elongated oxide-silicates with occasional rounded sulphides attached thereto.

References

1. M. Gensamer, E. Saibel and J. T. Ransom, "Report on the Fracture of Metals," Part I, Welding Research Supplement, American Welding Society, Vol. 12, No. 8, August 1947, p. 443-472.

2. C. A. Zapffe and M. Clogg, "Fractography—A New Tool for Metallurgical Research," TRANSACTIONS, American Society for Metals, Vol. 34, 1945, p. 71-98.
3. M. Gensamer, "Strength of Metals Under Combined Stresses," American Society for Metals, 1941.
4. J. H. Hollomon, "The Problem of Fracture," Welding Research Supplement, American Welding Society, Vol. 25, No. 9, September 1946, p. 534-583.
5. M. A. Grossmann, "Toughness and Fracture of Hardened Steels," *Transactions,* American Institute of Mining and Metallurgical Engineers, Vol. 167, 1946, p. 39-79.
6. J. C. Fisher and J. H. Hollomon, "A Statistical Theory of Fracture," *Metals Technology,* Vol. 14, No. 5, August 1947.
7. S. L. Hoyt and M. A. Scheil, "Use of Reflected Polarized Light in the Study of Inclusions in Metals," *Transactions,* American Institute of Mining and Metallurgical Engineers, Vol. 116, 1935, p. 405-424.
8. R. W. Dayton, "Theory and Use of the Metallurgical Polarization Microscope," *Transactions,* American Institute of Mining and Metallurgical Engineers, Vol. 117, 1935, p. 119-155.

DISCUSSION

Written Discussion: By Francis W. Boulger, supervising metallurgist, Battelle Memorial Institute, Columbus, Ohio.

It is always interesting to learn about the application of new methods to the study of inclusions and their effects on the properties of steel. The authors are to be complimented on applying new techniques to the study of nonmetallics found on the fracture surface of certain tensile specimens. The term inclusions is a broad one, however, and care must be exercised in generalizing on their effects on mechanical properties.

The inclusions found in steel have two origins. Some result from reactions occurring during cooling and solidification of the steel, others result from entrapment of material with which the liquid steel has been in contact. The former are naturally occurring, indigenous inclusions characteristic of the steel composition and the deoxidation practice employed. The latter are accidental or exogenous inclusions and do not necessarily bear any relationship to composition.

Although indigenous inclusions vary in size with the steel section in which they form, they are ordinarily very much smaller than those found by the authors. Usually, large indigenous silicate inclusions are less than one-eighth as big as those shown in the photomicrographs. In most cases, sulphides comprise at least half of the inclusions occurring naturally in steel. In this paper, the authors refer to sulphides only as the minor portion of the mixed inclusion shown in Fig. 10. From the size and composition of the inclusions studied, it appears to the writer that they were probably accidental or exogenous inclusions, which are conceded to be harmful. If this be true, then their examination did not show "the necessity of revisions in melting practice or ingot design" as suggested by the authors.

The authors cautioned the reader that the tensile fractures they studied were abnormal. It may also be advisable to suggest that the inclu-

sions studied were not characteristic of steels in general, and the conclusions drawn about their embrittling effects may be of limited application.

In closing, it might also be mentioned that the generalization that "the top third of an ingot is generally known to be the dirtiest portion" does not always hold. For example, Fetters, Helzel and Spretnak[2] reported at this meeting that the inclusions were usually distributed uniformly in the nine ingots they examined.

Authors' Reply

The inclusions depicted in this paper are not exogenous as Mr. Boulger would surmise. They are really endogenous inclusions which originate spontaneously in steel ingots weighing anywhere from 80,000 to 250,000 pounds. Because of their large size and relatively slow solidification rate, the inclusions therein can grow to much larger sizes than those usually encountered in smaller ingots.

The observation that the top third of the ingot is generally the dirtiest portion holds true when one is aware of the fact that these massive ingots require anywhere from 4 to 24 hours to solidify. No real comparison of inclusion distribution can be made between 36- to 84-inch diameter ingots and Spretnak's 22-inch diameter ingots. Nevertheless, in the single acid open-hearth forging ingot which Spretnak examined (designated as ingot D) he found the highest percentage of nonmetallics in the edge positions just under the hot top and the next highest content in the center of the top third of the ingot.

The nature of some inclusions in the tensile fractures of transverse test specimens taken from large forgings has been shown and it is significant to note that even in the case of the more ductile, cup-cone fracture (Fig. 7) a careful metallographic examination will reveal an inclusion segregate at the center of the cup (Fig. 8) in at least 50% of such fractures. Fig. 11 presents the same field as Fig. 8 at the higher magnification of 300 diameters under both bright field illumination and polarized light between crossed nicols. The needles or spines are quite in evidence and under polarized light the entire mass is more or less transparent though the needle outlines are still apparent.

The occurrence of inclusions in the outer portion of forging ingots can be significant from a quality standpoint, not only in the occurrence of cracking or surface imperfections on machining,[3] but in the effect on transverse mechanical properties. The inability to develop satisfactory transverse ductility is, in large part, due to the presence of nonmetallic material visible on the fracture face of the tensile test specimen. On the influence of ingot size on transverse ductility, it can be said that the amount and size of inclusions and the tendency to form a mixture of large and small inclusions increases in large ingots thereby accentuating the

[2]K. L. Fetters, M. M. Helzel and J. W. Spretnak, "Distribution of Nonmetallic Inclusions in Some Killed Steel Ingots," TRANSACTIONS, American Society for Metals, Vol. 41, 1949, p. 303.

[3]E. A. Loria and H. D. Shephard, "Some Factors Affecting Subsurface Defects in Large Forging Steel Ingots," TRANSACTIONS, American Society for Metals, Vol. 41, 1949, p. 328.

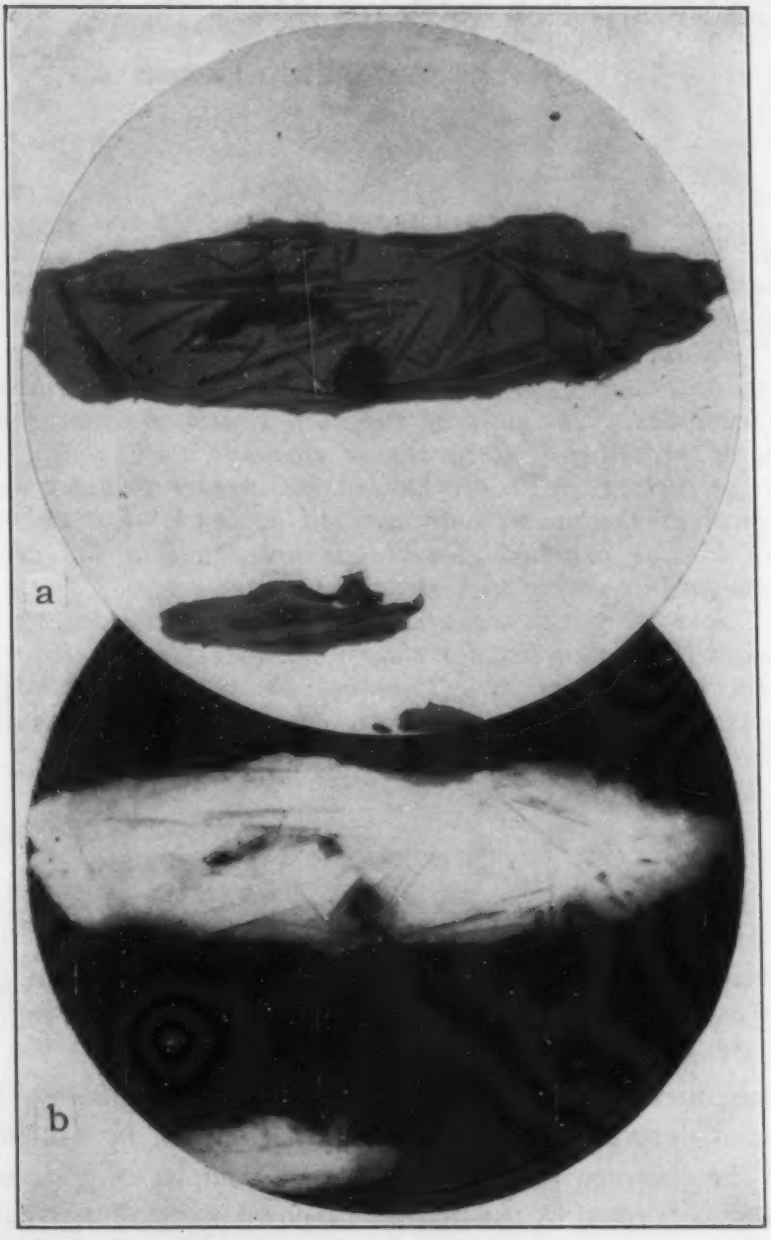


Fig. 11—Nonmetallic Inclusions in Tensile Fracture of Steel A on Grinding Surface of Tensile Fracture. Same field as Fig. 8. a—Bright field illumination. b—Under polarized light. Unetched. × 300.

possibility of producing an unfavorable distribution. The amount of decrease of transverse ductility with a given increase of forging reduction is frequently largely determined by those inclusions which are drawn out into stringers during forging and have a detrimental effect on transverse ductility.

FRACTOGRAPHIC EXAMINATION OF TUNGSTEN

By C. A. Zapffe and F. K. Landgraf

Abstract

The technique of fractography is applied to the cleavage facets of cast carboniferous tungsten, cast aluminiferous tungsten, and pure tungsten made by the methods of powder metallurgy.

With carbon present, the cast material shows a distinctive fracture, principally transgranular, with evidence of carbides. Carbon-free tungsten containing aluminum shows prominent intergranular cleavage with characteristic structures. Transgranular fractures reveal patterns typical of the metal, with marked evidence of distortion and lineage growth. Small gas holes within the grain show an interesting wall structure.

Tungsten rod manufactured by the hot-swaging of reduced tungsten powder clearly discloses on its cleavage facets the degree of attainment of fusion and homogeneity, such that the technique can be recommended for control and evaluation of the processing.

Introduction

TUNGSTEN is an extremely refractory metal which has long served in the electrical field, but which is now coming under renewed examination through the present emphasis in engineering on metals for high-temperature service.

Some interest, therefore, attaches to registrations of crystal growth and deformation mechanisms as disclosed by fractographic study of the cleavage facets of tungsten. Samples of tungsten both as cast and as formed by the process of powder metallurgy have been studied; and typical fractographs are presented in this paper. The study is necessarily introductory only, serving principally to call attention to several informative and characteristic structures in tung-

From research conducted in the laboratory of the senior author under contract with the Office of Naval Research.

A paper presented before the Thirtieth Annual Convention of the Society, held in Philadelphia, October 23 to 29, 1948. The authors, C. A. Zapffe and F. K. Landgraf, are consultants, Baltimore, Md. Manuscript received May 28, 1948.

sten, and to fractography as an efficient technique for disclosing these structures.

General Remarks on Tungsten

Crystallographic and physical features of the metal pertinent to the present study are as follows:

Property	Remarks (1), (2), (3), (4)[1]
Melting point	3370 °C (7000 °F)
Boiling point	5900 °C (10,620 °F)
Specific gravity	19.3
Atomic number	74
Atomic weight	184
Electron Orbitals	[1-, 2-, 3-, 4-] $(5_s)^2$, $(5_p)^6$, $(5_p)^4$, $(6_s)^2$
Crystal Structure	
[α]*	"Cubic": Ewald-Hermann Type No. A15 $a_o = 5.038$
β	BCC: (A2) $a_o = 3.1583$
Slip	{112}, [111]
Twinning	{112}, [111]
Planes developed by etching	{110}

*A form not well understood.

Tungsten occurs as oxides (5):

WO_3
W_2O_5
WO_2

The metal is commonly prepared by reduction of the oxide with carbon, aluminum, or hydrogen. Each of these elements was involved in the preparation of the present specimens. The carbides are believed to be (6), (7), (8), (9), (10):

Carbide	Temperature Range	Crystal Form
W_6C_2	.....	.....
*αW_2C (W_4C_2?)	1900-2400 °C	Hexagonal close-packed
βW_2C (W_4C_2?)	>2400 °C	Hexagonal close-packed
W_2C_2	.....	.....
*WC (W_2C_2?)	<1900 °C	Hexagonal CdI type

*Principal forms

No information is at hand on the W-Al system; and the W_xO_y-H_2 equilibrium is not important to discuss at this time.

[1]The figures appearing in parentheses pertain to the references appended to this paper.

Specimens

Specimen*	Remarks
No. 14	0.4% carbon added during melting
No. 15	1.0% aluminum added during melting
L-7523	99.9+% W with $R_2O_3 < .02\%$

*Designation of supplier

Through the courtesy of S. A. Herres and C. H. Lorig of Battelle Memorial Institute there were supplied samples of tungsten cast by an electric-arc process similar to that described by Parke and Ham for molybdenum (11).

In addition, a rod 0.187 inch in diameter of tungsten manufactured by the process of powder metallurgy was supplied through courtesy of F. H. Driggs, L. F. Yntema, and D. Heckinger of the Fansteel Metallurgical Corporation. This material is a compress of reduced tungsten powder; and some illumination will accordingly be thrown by the fractographs on the success of the method with regard to fusion and homogenization.

Observations

Carboniferous Tungsten

Particular interest attaches to the carboniferous sample No. 14 because of a possible analogy with carboniferous molybdenum (12), (13).

Fracture promptly discloses a difficult traverse for cleavage, suggestive of carboniferous molybdenum. Facets are small and rough. A typical example in Fig. 1 discloses distortion and complex growth characteristics of the crystal. In Fig. 2, the pattern of multiple growth nuclei resembles a similar instance in the transgranular fracture of molybdenum (13).

Intergranular fracture is not so distinct from the transgranular as in carbon-free specimens later to be discussed. Fig. 3 probably represents intergranular separation across the light-colored field, though this was not proved. The fractograph is particularly presented because of the aligned tufted markings on the light field. These have some resemblance to the "carbide feathers" found in



Fig. 1—Transgranular Cleavage in Cast Carboniferous Tungsten Disclosing Distortion and Complex Growth Characteristics of the Crystal. × 725.



Fig. 2—Transgranular Cleavage in Cast Carboniferous Tungsten Revealing Multiple Growth Nuclei Within the Crystal. × 450.



Fig. 3—Fractograph of Cast Carboniferous Tungsten Possibly Disclosing a Carbide Form Similar to That Found in Molybdenum. × 450.

carboniferous molybdenum (11), (12); and they are rather commonly observed here.

Further evidence for some form of tungsten carbide may stand in the following two fractographs. In Fig. 4 one sees at high magnification the interesting detail of certain minute patterns not uncommonly found. The long, smooth spines with lateral needles are a

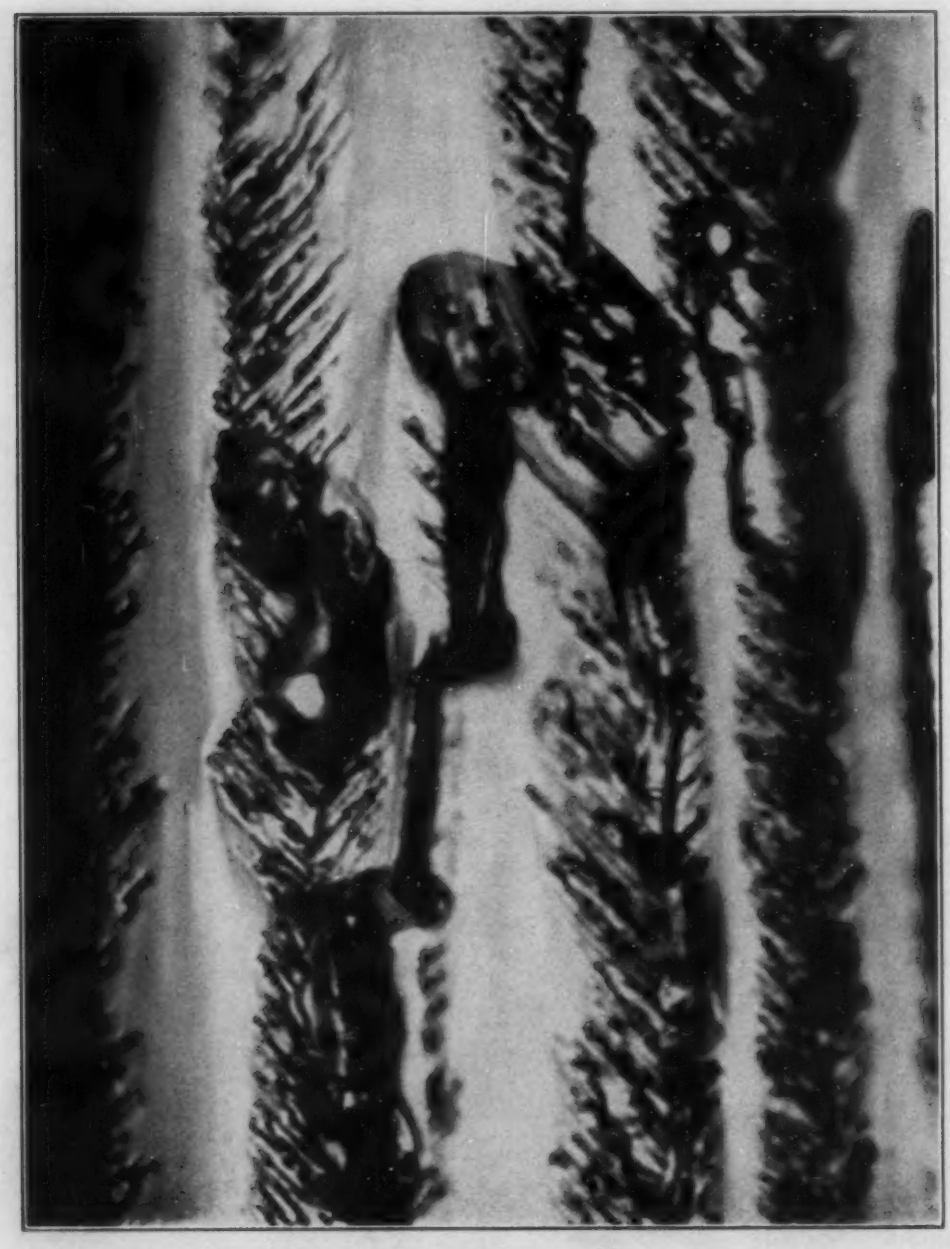


Fig. 4—Fractograph at High Magnification Showing the Characteristic Detail of a Certain Fine Structure Found in Cast Carboniferous Tungsten. × 2000.

marked characteristic which is absent in the carbon-free tungstens. In Fig. 5 an isolated marking of this type more clearly reveals the structure, the angular displacements at 41 degrees being particularly interesting. This is certainly suggestive of the "carbide feather" found in carboniferous molybdenum. There is a strong resemblance in type, but a marked difference in detail. The significant angularity

also indicates that this is a crystal plane that is exposed, whereas in molybdenum the precipitate is uniformly intergranular.

On the other hand, the matter of carbide structures in tungsten

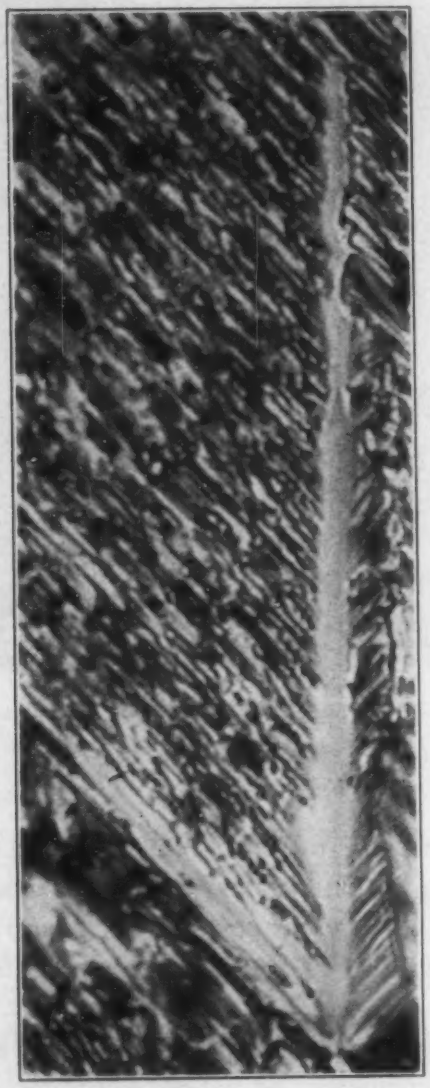


Fig. 5—Fractograph at High Magnification Believed to Disclose a Pattern Relating to Tungsten Carbide. The smooth spine with needle-like structure at 41 degrees resembles the "carbide feathers" in cast carboniferous molybdenum. × 1900.

and molybdenum, also chromium, has indicated sufficient complexity to warrant subsequent separate study; and conclusions here shall only be tentative.

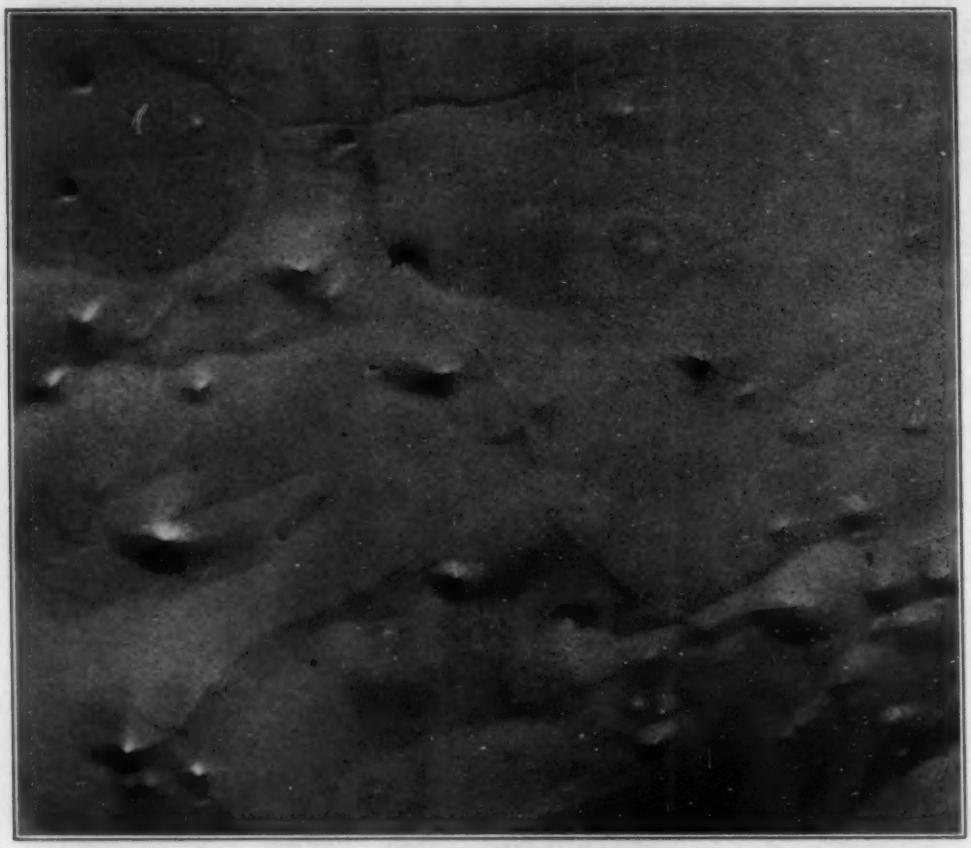


Fig. 6—Fractograph of Typical Intergranular Facet in Aluminiferous Tungsten. × 200.

Aluminiferous Tungsten

In marked contrast to the preceding specimen, the tungsten deoxidized with aluminum discloses a combination of intergranular and transgranular cleavages, each highly distinctive, and both readily distinguishable from the patterns of the tungsten deoxidized with carbon.

First, the intergranular cleavage is apparent even to macroscopic observation as a separation of large columnar growths extending from rim toward center. Though heavily deoxidized with 1% of aluminum added during melting, the fracture is not unlike that of oxygenized cast molybdenum.

At higher magnification, however, these surfaces are readily distinguished from those of molybdenum. A typical example is shown in Fig. 6 at 200 diameters, the expansiveness of the field indicating the large size of the crystal. Unlike molybdenum, this metal is typically barren of precipitated forms on the grain surface. Small

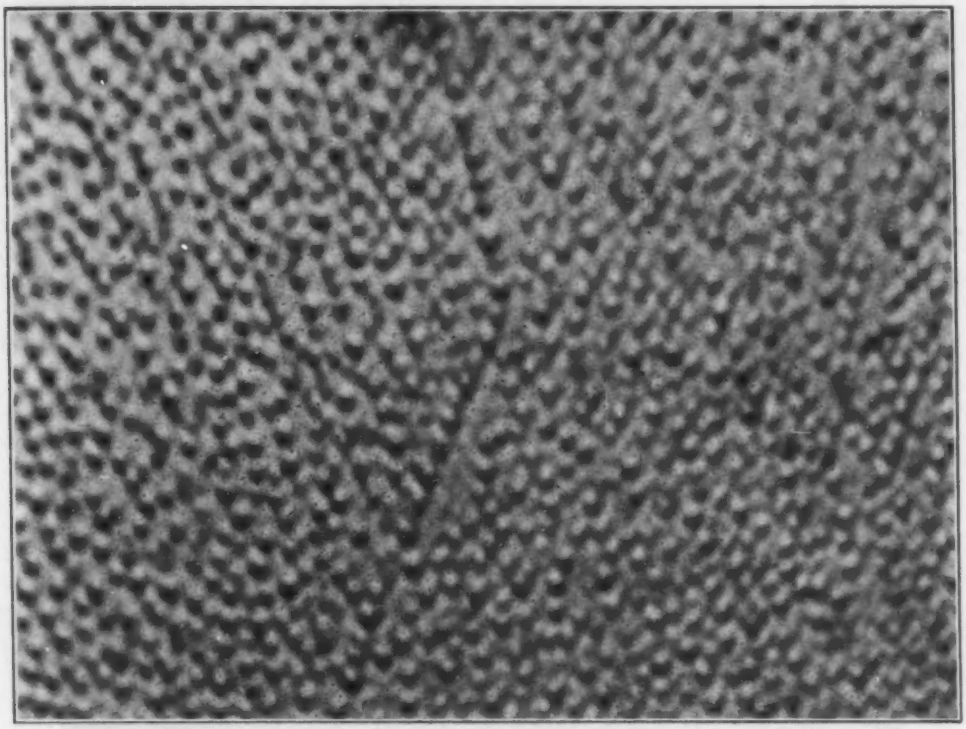


Fig. 7—Fractograph at High Magnification Showing Typical Pitted Structure on Intergranular Facet. × 3400.

hummocks characteristically appear, however, which are similar to the appearance of grain-boundary inclusions in steel (14).

At very high magnification, a second characteristic is everywhere evident—a fine, pitted structure, as shown in Fig. 7.

Occasionally, an angular structure appears on the pattern, as shown in Fig. 8. The nature of these markings is not known, but they suggest an association with the aluminum content because of their absence in other specimens. There also appear in Fig. 8 several parallel markings which traverse the entire field with such disregard for surface undulations that they probably simultaneously define themselves as deformation markings and the entire field as belonging to one crystal.

In Fig. 9, transition from this intergranular separation to transgranular cleavage is shown. The pitted structure is faintly visible on the intergranular facet toward the right. A similar instance of these two types of cleavage within a single field has been shown for molybdenum (12).

In Fig. 10, transgranular cleavage is displayed as the cross-fracture of one of the elongated grains. There is evidence here of



Fig. 8—Intergranular Facet Containing an Unknown Registration, Perhaps Associated With the Aluminum Content. Deformation markings are also visible, traversing the entire field as straight, parallel lines. × 475.

a pattern of grain growth nucleated in the lower right-hand corner and considerably distorted; and there is an approach to significant angularity disclosing the crystallography of the crystal. The pattern is readily distinguished from that of carboniferous tungsten, and also from that of molybdenum (13).

Gas holes are numerous in this material, which raises some question as to the nature of the gas evolving in the presence of so much aluminum. The interior of one of these gas holes is shown in



Fig. 9—Fractograph Showing Transition From Intergranular to Transgranular Cleavage. × 825.

Fig. 11. This is a characteristic pattern for the porosities in the aluminiferous tungsten, and is distinct from the pattern for porosities in the carboniferous tungsten. The latter resist successful photographing and are not shown. They have a much finer design and lack the strict polygonal characteristics shown in Fig. 11.

A third type of fracture pattern is presented in Figs. 12 and 13. Comparing these with Figs. 6 and 8, one will observe that the elon-



Fig. 10—Typical Transgranular Cleavage in Aluminiferous Tungsten, Disclosing Grain Nucleation in the Lower Right, Gas Holes, and Near-Crystallographic Markings. × 375.

gated grains of typical intergranular cleavage are indicated, but that the surfacial markings are absent; and comparing them with Fig. 10, one also finds some lack of conformity with the transverse fracture of the columnar grain. This pattern type may therefore represent *longitudinal transgranular* fracture, in contradistinction to the *transverse transgranular* failure in Fig. 10; or it may possibly represent longitudinal intergranular fracture in a section of the metal where



Fig. 11—Interior of Gas Hole in Aluminiferous Tungsten Showing the Typical Polygonal Wall-Pattern. × 825.

the intergranular surfaces are much more adhering. The first possibility implies the existence of a second cleavage family, providing primary and secondary cleavage patterns as found in antimony (15). The second possibility is reduced by the lack of typical surfacial residues characterizing intergranular failures in general—with the one possible exception of the left facet in Fig. 13. Perhaps this is a subgranular or "lineage" separation, but the matter will not be pursued here.

In closing the discussion of aluminiferous tungsten, Fig. 14 is included as an anomalous pattern infrequent and unidentified.



Fig. 12—Fractograph Showing Cleavage Apparently Along Longitudinal Axis of the Grain, but Lacking Either Intergranular or Transverse Transgranular Characteristics. × 875.

Extruded Tungsten Powder

Fracture of the tungsten rod produced by hot-swaging of reduced tungsten powder ingots clearly reveals the degree of success attained by this method with respect to fusion and homogenization.

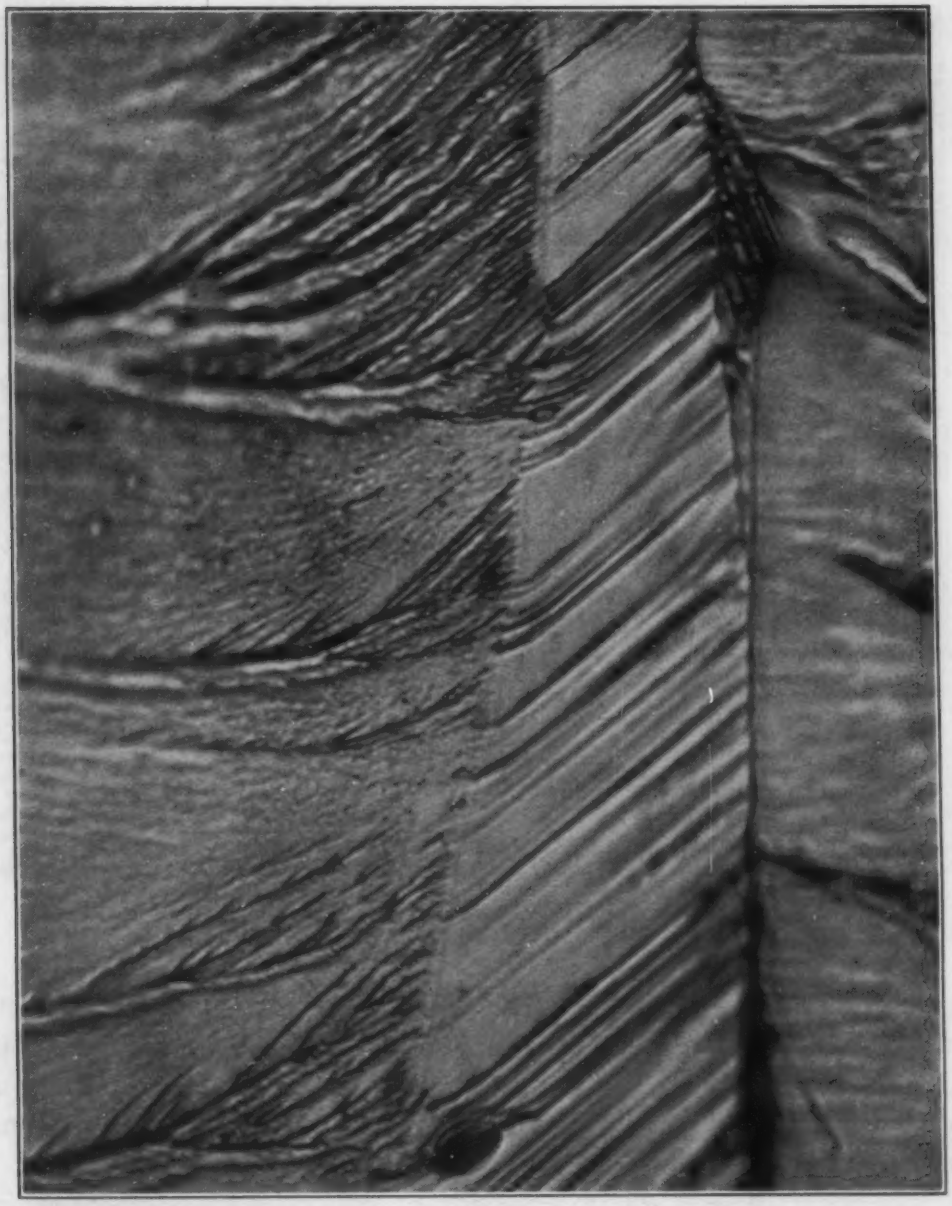


Fig. 13—Cleavage Similar to That in Preceding Figure, But With Some Indication of Surfacial Roughness on the Facet on the Left. × 875.

In Figs. 15 and 16 one sees typically transgranular patterns, but generally surcharged with a smut undoubtedly representing incomplete fusion of the powder. Some facets are homogeneous to a point of close resemblance with cast metal. Fig. 15 shows this condition both toward the top and toward the bottom. Fig. 16, however, discloses much less attainment in this respect.

In Fig. 17 the lack of fusion displays itself as small islands of

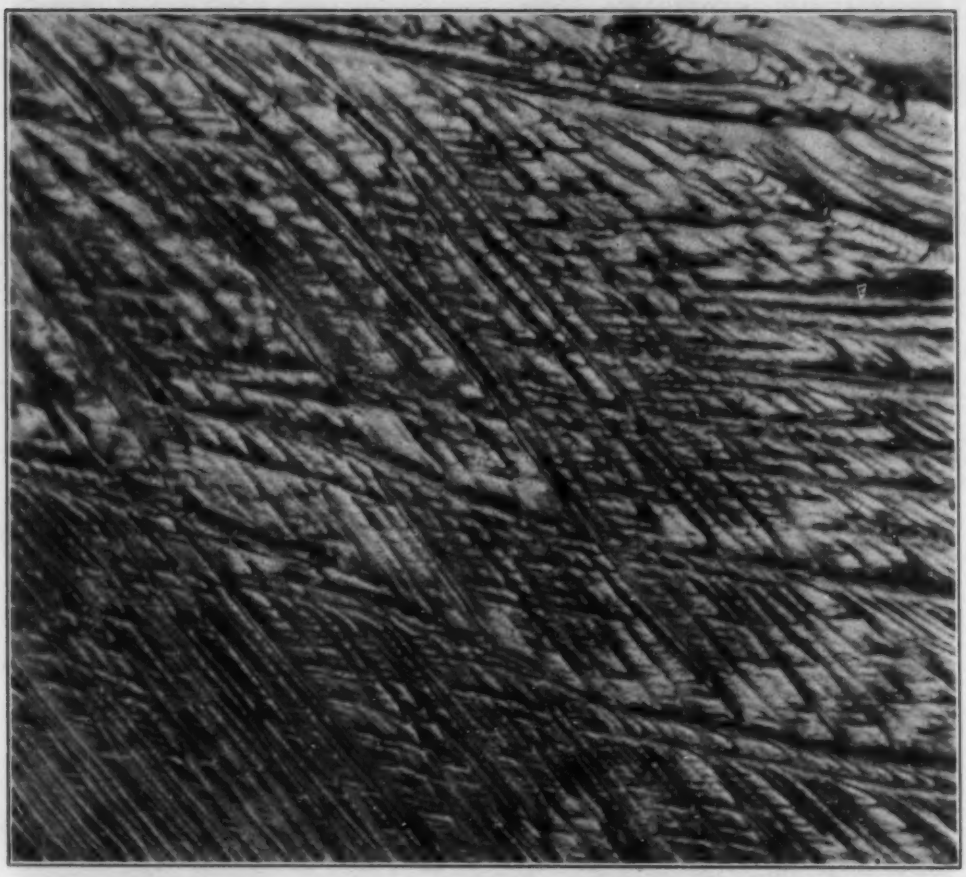


Fig. 14—Anomalous Pattern in Aluminiferous Tungsten, Infrequent and Unidentified. × 825.

coalesced powder not yet joined to the major grain. While assignment of patterns in this material as intergranular or transgranular is difficult, it is believed that the surface in Fig. 17 simulates a grain surface and that the pattern, therefore, may be classed as intergranular.

In view of the direct evidence of inhomogeneity exposed in these fractographs, one is led to suggest that the technique of fractography be applied to the fabrication of tungsten from powder much as it is to the casting and forging of molybdenum (11). Certainly the factors of temperature, particle size, purity of powder, pressure, atmosphere, and so forth, could be readily assessed by observing the variations in these patterns with the variation of the particular factor.

Conclusions

From this preliminary examination of the cleavage patterns of



Fig. 15—Fractograph of Pure Tungsten Fabricated by the Hot-Swaging of Reduced Tungsten Powder Ingots. Toward the top and toward the bottom this grain evidences good fusion and the characteristics of cast metal. Incomplete fusion is evident in the center. × 1100.

tungsten, the following conclusions can be tentatively drawn:

1. Cast tungsten containing carbon fractures principally transgranularly, and the pattern is distinctive;

2. Carbides in carboniferous tungsten are probably identified by a spine-and-needle structure resembling the "carbide feathers" in carboniferous molybdenum;



Fig. 16—Fractograph Similar to Preceding, Showing Marked Inhomogeneity. × 1100.

3. Cast tungsten containing aluminum fractures both intergranularly and transgranularly, and patterns of both are highly distinctive;

4. Intergranular fracture of aluminiferous tungsten is characterized by an undulating, crystallographically structureless surface covered with fine pits;



Fig. 17—Fractograph of Powder-Metallurgy Tungsten Disclosing Islands of Coalesced Powder Not Yet Homogenized Into the Major Grain. × 850.

5. Transgranular fracture of aluminiferous tungsten reveals growth characterisitcs of the grain, a typical surfacial pattern, near-crystallographic markings, and often gas holes;

6. The interior of the gas holes shows a polygonal wall-pattern

characteristic of the metal and unlike the pattern found in gas holes in carboniferous tungsten;

7. An unidentified type of cleavage in aluminiferous tungsten may represent: a) transgranular cleavage on a second family of planes (parallel to the growth axis of the crystal), b) a modified intergranular cleavage, or c) interlineage cleavage;

8. Tungsten rod manufactured by hot-swaging of reduced tungsten powder ingots clearly discloses in fractographs the degree of attainment of fusion and homogeneity of the powder;

9. Fractography can, therefore, be applied to an evaluation of the factors controlling the process much as it is now applied in the casting and forging of molybdenum.

ACKNOWLEDGMENT

The authors gratefully extend acknowledgment to S. A. Herres and C. H. Lorig of Battelle Memorial Institute for supplying the specimens of cast tungsten; to F. H. Driggs, L. F. Yntema, and D. Heckinger of the Fansteel Metallurgical Corporation for supplying the tungsten rod; and particularly to the Office of Naval Research, under whose sponsorship this study was conducted.

References

1. C. S. Barrett, "Structure of Metals," McGraw-Hill Book Co., Inc., New York, 1943, 567 p.
2. L. Pauling, "The Nature of the Chemical Bond," Cornell University Press, New York, 1945, 451 p.
3. G. L. Clark, "Applied X-Rays," McGraw-Hill Book Co., New York, 1940, 674 p.
4. Correspondence with Fansteel Metallurgical Corporation.
5. M. de K. Thompson, "The Total and Free Energies of Formation of the Oxides of Thirty-Two Metals," Electrochemical Society, New York, 1942, 89 p.
6. K. K. Kelley, "Contributions to the Data on Theoretical Metallurgy. VIII. The Thermodynamic Properties of Metal Carbides and Nitrides," *Bureau of Mines Bulletin*, No. 405, 1935, 66 p.
7. K. Becker, "The Constitution of Tungsten Carbides," *Z. Elektrochem.*, Vol. 34, 1928, p. 640-642.
8. G. Hägg, "Characteristics of the Phases of Transition Elements in Binary Systems With Boron, Carbon, and Nitrogen," *Z. physik. Chem.*, Vol. 6B, 1930, p. 221-232.
9. A. A. Ravdel, "Carburization of Metals," *Journal*, Russian Physical Chemistry Society, Vol. 62, 1930, p. 515-522.
10. J. L. Gregg and C. W. Küttner, "A Metallographic Study of Tungsten," American Institute of Mining and Metallurgical Engineers, T.P. No. 184, 1929, p. 3-12.
11. R. M. Parke and J. L. Ham, "The Melting of Molybdenum in the Vacuum Arc," *Metals Technology*, Vol. 13, T.P. 2052, 1946, 12 p.

12. C. A. Zapffe, F. K. Landgraf and C. O. Worden, "Fractographic Study of Cast Molybdenum." To be published by American Institute of Mining and Metallurgical Engineers.
13. C. A. Zapffe, F. K. Landgraf and C. O. Worden, "Transgranular Cleavage Facets in Cast Molybdenum." To be published in METAL PROGRESS.
14. C. A. Zapffe, "Boiler Embrittlement," *Transactions*, American Society of Mechanical Engineers, Vol. 66, 1944, p. 81-117; discussion, p. 117-126.
15. C. A. Zapffe and F. K. Landgraf, "Fractographic Structures in Antimony," METAL PROGRESS, Vol. 53, No. 3, 1948, p. 377-381.

DISCUSSION

Written Discussion: By J. Chelius, tungsten metallurgist, and R. W. Yancey, chief metallurgist, Fansteel Metallurgical Corp., North Chicago, Ill.

We wish to commend Dr. Zapffe and Mr. Landgraf for their interesting paper on the examination of tungsten by the fractographic technique.

Although we have had very little experience with cast tungsten our work with pressed and sintered tungsten powder has never shown that islands of coalesced powder were present as shown on their fractograph, Fig. 17. It is difficult for us to understand just how this condition could exist in view of the previous hot working operations which are performed on a 0.187 inch diameter rod. We would like to suggest that the islands of coalesced powder as shown on the fractograph, Fig. 17, might possibly be a group of individual grains. We have found that in heating to the recrystallization temperature some grains exhibit a tendency toward excessive grain growth. Between some of the large grains we oftentimes find innumerable small grains.

The authors' description of the fractures as shown in Figs. 15 and 16 does not mention the possibility of the presence of various addition agents which are added intentionally for grain size control. Conventional metallographic preparation of sintered tungsten does not show an intragranular material described by the authors as smut. We sometimes find an intergranular substance present.

The fractographic technique opens up a new field in the study of the metallurgy of tungsten, especially when supplemented with conventional metallography and X-ray diffraction methods.

Written Discussion: By E. H. Dix, Jr., assistant director of research, Aluminum Company of America, New Kensington, Pa.

The study of the path of fracture is very important in diagnosing types of failure which occur in service. For example, a fatigue failure is quite characteristic and can be distinguished from a tension failure. Also, in developing alloys to have higher creep properties at elevated temperatures, the path of fracture is important. I would like to ask the authors if they can see anything in this new method of fractography which would be helpful in these problems.

Authors' Reply

Certainly the suggestions of Messrs. Chelius and Yancey regarding the identity of the blobs in the pattern of Fig. 17 are as good as any we can make. We believe that Figs. 15 and 16 represent transgranular cleavage, and the "smut" therefore intragranular imperfection; but the cleavage of Fig. 17 may be intergranular, and the small islands possibly small grains of either tungsten or addition agent, or an alloy of both.

To answer Mr. Dix, we will point out that the fractographic technique is based upon direct examinations of the microscopic path of cleavage, and that it therefore provides firsthand observations of those intragranular structures which are involved in deformation and cleavage, and upon which deformation and cleavage in turn depend.

THE EFFECT OF ORIENTATION ON KNOOP HARDNESS OF SINGLE CRYSTALS OF ZINC AND SILICON FERRITE

By F. W. Daniels and C. G. Dunn

Abstract

An investigation of the effect of crystal orientation on Knoop hardness of single crystals of silicon ferrite and zinc was undertaken. A single crystal of silicon ferrite with the (001), (110), and (111) planes exposed was tested with a Tukon hardness tester. The (0001) and $(14\bar{3}0)$ planes of zinc were likewise tested. Hardness was found to vary periodically with direction of the long diagonal of the Knoop indenter with respect to the crystal. Over the range of orientations investigated the hardness variations were large. A method was determined for obtaining a significant Knoop hardness number of body-centered cubic crystals of unknown orientation. An attempt was made to explain hardness variations on the basis of resolved shear stress on the slip planes of the metal. Fair agreement of theory with experiment was obtained for all test planes except the (0001) plane of zinc.

Introduction

IT is well known that the capacity of a metal to deform plastically is a directional or anisotropic property. Since penetration hardness involves plastic deformation, it is readily understandable that such hardness may also be a function of the orientation of the crystal or crystals upon which an indenter is imposed. Early work with the Brinell penetrator did not reveal directional effects of any consequence. O'Neill (1),[1] for instance, found but a small difference in hardness of the {100}, {110}, and {111} planes of aluminum, and Pfeil (2) concluded that the Brinell hardness of a single crystal of

[1]The figures appearing in parentheses pertain to the references appended to this paper.

A paper presented before the Thirtieth Annual Convention of the Society, held in Philadelphia, October 23 to 29, 1948. The authors, F. W. Daniels and C. G. Dunn, are connected with the Metals Section of the Laboratory, General Electric Co., Pittsfield, Mass. Manuscript received March 17, 1948.

iron is the same for all crystallographic planes. With the Knoop indenter, however, directional hardness of minerals has been noted by Winchell (3) and by Thibault and Nyquist (4).

Except for the unpublished work of Guy (5) the authors know of no data which show variation in Knoop hardness with orientation of metallic single crystals. Directional hardness of metals, however, is quite pronounced as was recently noticed in another investigation at the General Electric Company Laboratories. Several single crystals of silicon ferrite had been cold-rolled and subsequently annealed at high temperature. In certain instances the annealed samples would yield higher Knoop hardness numbers than samples in the cold-rolled condition if the crystal orientation of the test surfaces were not held constant. This example is cited to show that directional hardness variations may be of such magnitude as to cause misinterpretation of hardness data.

The purpose of the present investigation was to determine the Knoop hardness of single crystals of silicon ferrite and zinc for various orientations of the crystals. A further objective was to explain, if possible, the results in terms of shear stress on the slip systems of these metals. Silicon ferrite was chosen because large single crystals were readily available, and zinc, because its simple slip system would supposedly aid in the theoretical explanation of results.

Experimental Procedure

Since it was impossible to perform hardness tests on all possible crystallographic planes of silicon ferrite or zinc, a few of the important planes of each metal were selected for experiment. With each plane Knoop hardness numbers (KHN) were found for various angular positions θ of the long diagonal of the indenter with respect to an arbitrary reference or index direction on the plane of the sample.

More specifically, the procedure was as follows: There was available a large crystal of silicon ferrite (3.5% silicon) of known orientation. By suitable cuts this crystal was divided into three specimens, with known crystallographic planes exposed: namely, (001), (110), and (111). Each specimen was mounted in plastic and carefully polished metallographically, disturbed surface metal being eliminated by electropolishing. Orientations were rechecked by back-reflection X-ray methods. Hardness indentations were made

Table I
Average Knoop Hardness Number for Silicon Ferrite and Zinc

Metal	Plane	Average KHN
Silicon Ferrite	(001)	205.9
	(110)	207.9
	(111)	206.2
Zinc	(0001)	16.7
	$(14\bar{5}0)$	32.9

with a Wilson Tukon tester equipped with a Knoop indenter. A load of 500 gms. was used throughout the experiments. The indentations were measured by means of a Bausch and Lomb filar microscope attached to the Tukon tester. A specimen jig calibrated in degrees permitted rotating the mounted sample about a vertical axis to any desired position; thus indentations could be placed on the specimen surface, the long diagonal of the indenter being positioned at any angle to an index line on the sample. For each of the exposed (001), (110), and (111) planes, measurements were made at 10-degree intervals about the vertical axis commencing with the long diagonal of the indenter parallel to a <110> direction, the only direction common to all three planes.

With a few exceptions, the procedure outlined above was used for a pure (99.99%) zinc crystal.[2] Planes exposed were the (0001) and $(14\bar{5}0)$.[3] Deep etching, rather than electropolishing, served to eliminate disturbed surface metal. In the case of the cleaved surface, (0001) plane, no polishing whatsoever was necessary, as back-reflection X-ray photographs revealed little evidence of surface distortion. The index lines for the (0001) and $(14\bar{5}0)$ planes were the $[11\bar{2}0]$ and [0001] directions respectively.

Experimental Results

The measurements, converted to Knoop hardness numbers (KHN), were plotted against the angular displacement θ of the indenter from the index line on the sample. Results for the (001), (110), and (111) planes of silicon ferrite are shown in Figs. 1, 2, and 3 respectively. Figs. 4 and 5 show the results for the (0001) and $(14\bar{5}0)$ planes of zinc respectively.

[2]Obtained through the kindness of E. A. Anderson of the New Jersey Zinc Co.

[3]The $(14\bar{5}0)$ plane is tilted 10°50′ to the $(01\bar{1}0)$ plane. The poles of both planes lie in the (0001) plane.

An average hardness for each plane was obtained by adding the values at 10-degree intervals over a range of degrees that included all possible crystallographic directions and dividing by the number of values. Results for silicon ferrite and zinc are given in Table I.

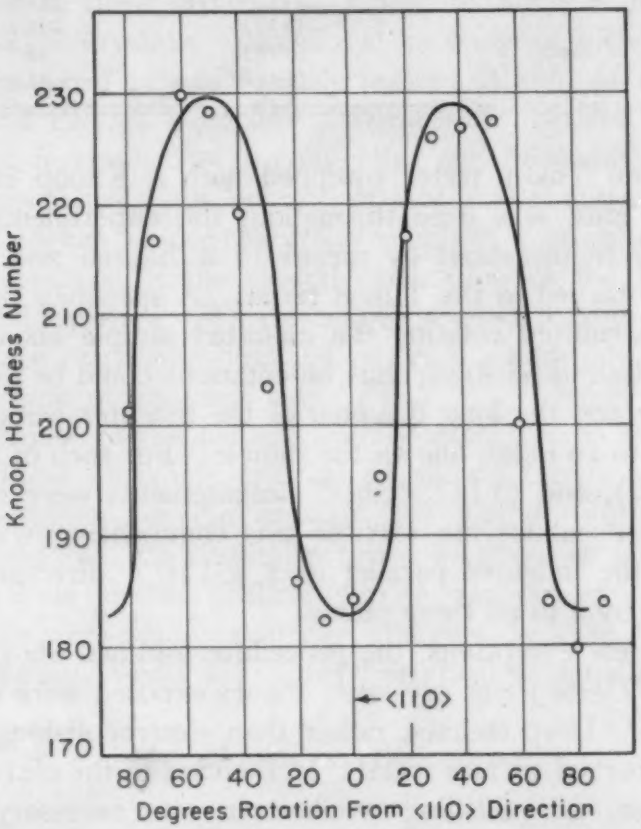


Fig. 1—Knoop Hardness Versus θ for the (001) Plane of Silicon Ferrite.

THEORETICAL

The Effective Resolved Shear Stress—A complete explanation of the experimental results would involve such factors as resolved shear on slip planes, twinning, work hardening, and friction. Disregarding twinning, it would seem that resolved shear alone should play the major role in determining hardness variations, because work hardening and friction should be roughly constant for equal depths of penetration. An explanation, therefore, will be attempted on the basis of resolved shear with hardness treated as an inverse function of the ease of slip (i.e., a large indentation accompanies high resolved shear on the slip planes).

Consider first the deformation produced by a Knoop indenter (the indenter is a pyramid having four facets with an included longitudinal angle of 172°30′ and an included transverse angle of 130°00′). During load application the indenter acts as a wedge imposing on the metal forces which cause some of the metal to move to the surface around the indent. The force for a single facet which

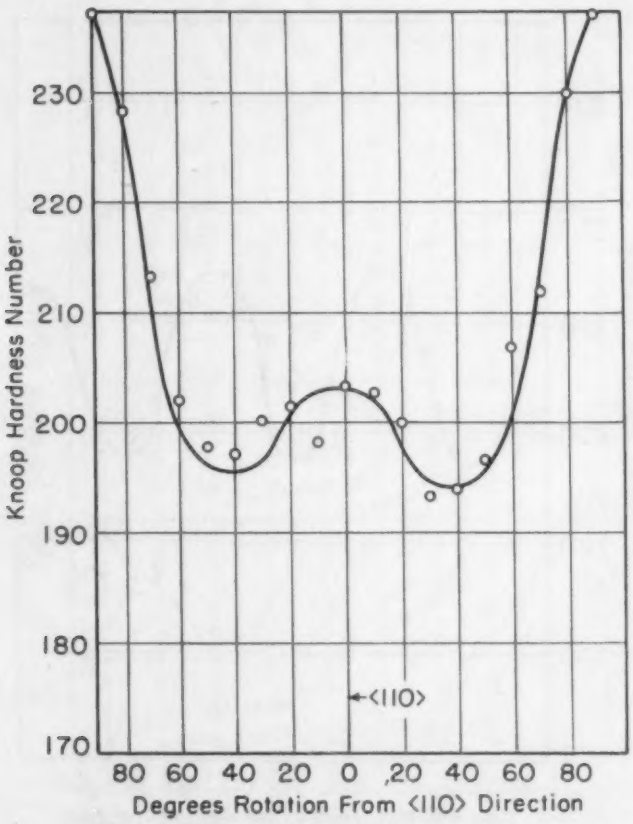


Fig. 2—Knoop Hardness Versus θ for the (110) Plane of Silicon Ferrite.

causes such displacement of metal is assumed to be parallel to the steepest slope of that facet, as illustrated in Fig. 6. Further, the metal tending to deform may be considered as a number of very small cylinders parallel to the deforming force F, each cylinder tending to elongate towards the surface. The ease of deformation of each cylinder is dependent upon two factors: (a) the position of the slip plane and slip direction, and (b) the constraints exerted on each cylinder by neighboring cylinders.[4] Both these factors in turn are dependent on crystal orientation.

[4]At the interface between the indenter and the metal, the indenter itself is a constraining factor.

Omitting the constraining factor for the moment, the resolved shear tending to deform a cylinder is expressed by the well known formula:

$$\text{Resolved shear} = F/A \cos\lambda \cos\phi \qquad \text{Equation I}$$

where A is the cross sectional area of the cylinder, λ is the angle

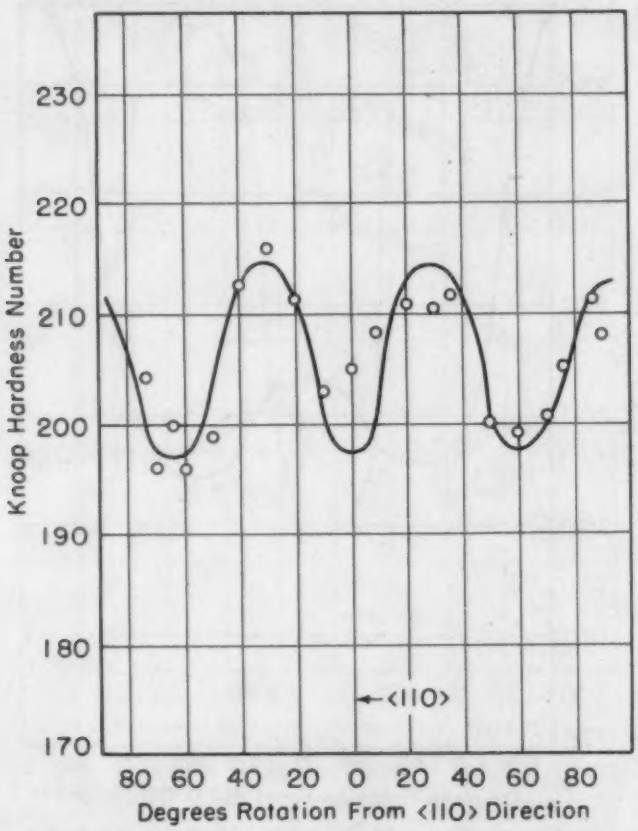


Fig. 3—Knoop Hardness Versus θ for the (111) Plane of Silicon Ferrite.

between the slip direction and the force F, and ϕ is the angle between the normal to the slip plane and the force F.

Constraints modify the tendency to slip (as expressed in Equation I) according to the position of the axis of rotation of the slip plane. This may be seen to advantage by considering the changes that occur during plastic deformation. As each cylinder elongates by slip and lattice rotation, the cross sectional area must reduce and change from a circular to an elliptical shape. Because the extruded metal at the surface is continuous (i.e., cylinders must not be separated) the ellipse axis perpendicular to F and parallel to

the indenter facet must remain unchanged in length while the ellipse axis perpendicular to F and perpendicular to the indenter facet must decrease. Such limitations on the change of shape, in actuality, may require simultaneous slip on more than one slip system; but our calculations are aimed towards an evaluation only of the tendency to slip on a single slip plane per facet for a small constant depth of

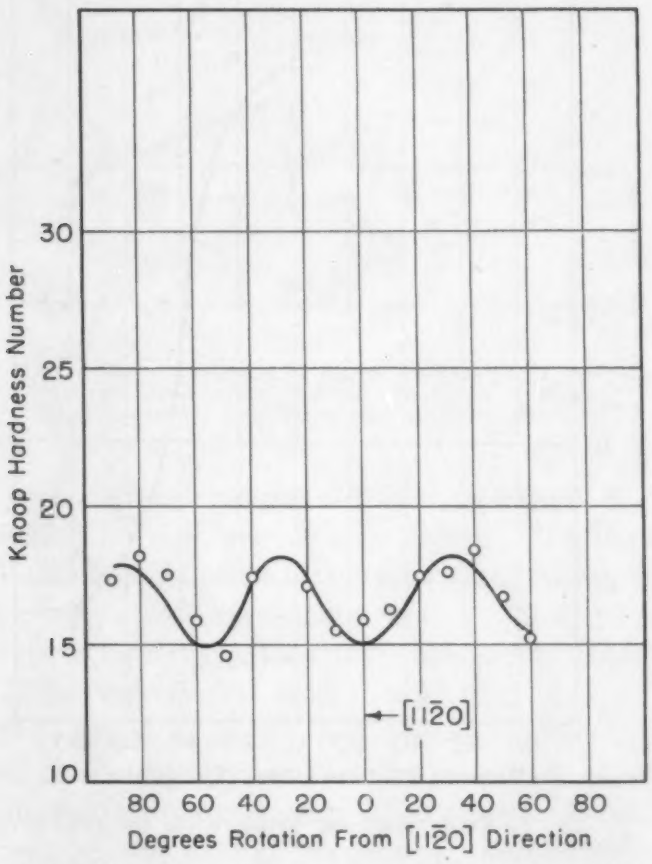


Fig. 4—Knoop Hardness Versus θ for the (0001) Plane of Zinc.

penetration and for a fixed position of the indenter with respect to the crystal.

From the above it is seen that a factor should be introduced into the resolved shear (Equation I) which evaluates the tendency of the lattice to rotate under constraint. A particular slip plane will tend to rotate about an axis AR in the slip plane SP and perpendicular to the slip direction SD as illustrated by Fig. 6. Due to constraints, the force F has a maximum rotational effect about an axis H perpendicular to F and parallel to the indenter facet. Call

the angle between these two axes Ψ. When Ψ is large the constraint is large; therefore, the resolved shear effective in promoting deformation must be small. At $\Psi = 90$ degrees the effective resolved shear should be zero so that rotation does not occur and change the cross sectional axis of the cylinder paralled to H. At $\Psi = 0$ degrees the

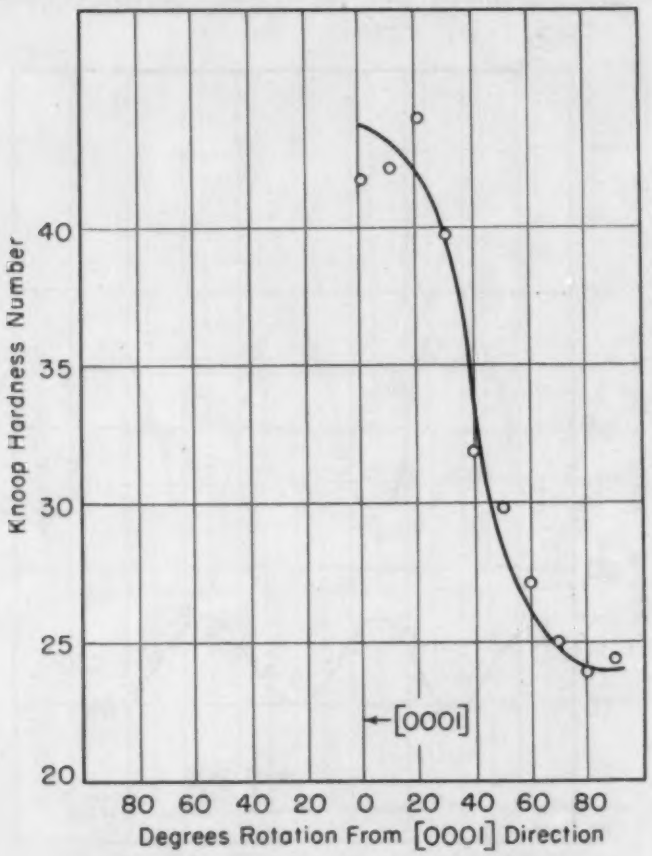


Fig. 5—Knoop Hardness Versus θ for the $(14\bar{5}0)$ Plane of Zinc.

rotational effect reaches a maximum. A modifying function which would decrease the resolved shear as Ψ increases from 0 to 90 degrees is cos Ψ. Multiplying Equation I by cos Ψ, an effective resolved shear (ERS) is obtained.

$$\text{ERS} = F/A \cos \lambda \cos \phi \cos \Psi \qquad \text{Equation II}$$

The value of cos λ cos ϕ cos Ψ changes if the orientation is changed. ERS, therefore, is a function of the angle θ between the long diagonal of the indenter and the index line on the sample. F/A will be assumed constant for all crystal orientations; cos λ cos ϕ cos Ψ hereafter will be referred to as ERS.

The determination of the angles λ, ϕ, and Ψ may be expedited through use of a stereographic projection. First the plane of projection is made coincident with the test plane of the sample. The normal (SP) to the slip plane, the slip direction (SD), and the axis of rotation (AR) are located with the aid of a Wulff net to give the plot shown schematically in Fig. 7. The indenter is likewise plotted from the known angles of the indenter: namely, 172°30′ and

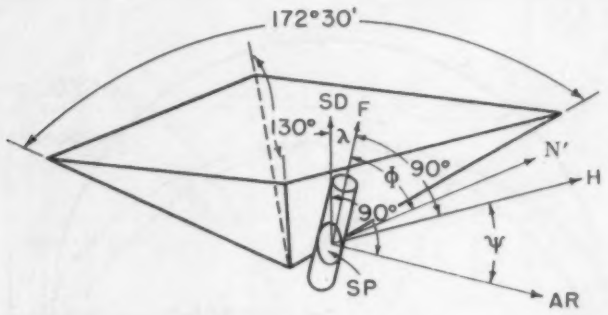


Fig. 6—Diagram of Knoop Indenter and Cylinder of Deformation Showing Positions of Force, Slip Direction, Slip Plane, and Axes of Rotation.

130°00′. These angles determine the four directions A, B, C, and D —the intersection lines of the indenter facets. The lines connecting A and B, B and C, etc. (arcs of great circles) locate the planes of facets. For example, AB represents facet 1. The extension of AB to the basic circle locates the direction, marked H, which is parallel to the line of intersection of facet 1 with the plane of the sample (Fig. 6). The normal to facet 1 is a direction (point N) 90 degrees from A and 90 degrees from B. The direction of steepest slope (also F) is diametrically opposite to N as shown. Facets 2, 3, and 4 may be treated similarly. The index line and the direction of the long diagonal of the indenter lie in the basic circle. Having located all directions necessary to determine λ, ϕ, Ψ, and θ, actual values of the angles may be read with the aid of a Wulff net.

Before values of effective resolved shear can be calculated it is necessary to consider the slip systems for silicon ferrite and zinc. Barrett, Ansel and Mehl (6) have shown that slip in body-centered cubic silicon ferrite (below 4% silicon) may occur on planes of the type {110}, {112} and {123} but only in <111> directions. For zinc, Schmidt and Boas (7) have reported that slip occurs on (0001) planes in the $<11\bar{2}0>$ directions.

There is a good possibility that no single slip system (for one

indenter facet) operates alone; rather several systems may operate simultaneously or in succession. Also it is possible that slip may change from one type slip system to another as θ varies. In the case of silicon ferrite with its 48 slip systems, analysis would be extremely complicated without some simplification. Therefore, the assumption is made that the indenter will tend to cause slip on only one type slip system. The authors, however, know of no data that indicate

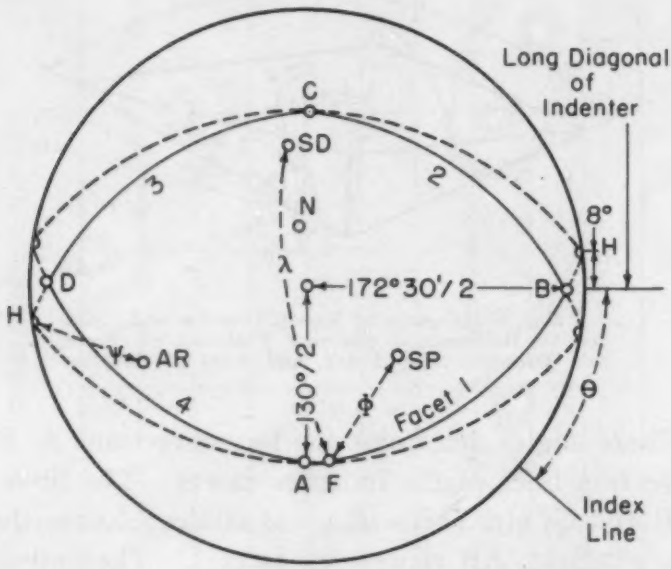


Fig. 7—Stereographic Projection Showing Schematically the Positions of the Indenter Facets and Their Intersections with the Surface of the Sample. Also shown are the directions of the force, slip direction, slip plane, and axes of rotation.

which type of system tends to operate during the indenting period; consequently, calculations for each of the three types were performed.

Calculations—In discussing the mechanics of the calculations, the (001) plane of silicon ferrite with slip on {112} planes is taken as exemplary, the same method being employed for all test planes and slip systems of both zinc and silicon ferrite.

Calculated values of effective resolved shear for the four facets of a Knoop indenter are obtained by synthesis of the values for one facet.

For a single facet, values of λ, ϕ, and Ψ may be read from a stereographic projection (see Figs. 6 and 7) for various angles α[5]

[5] α is analogous to θ for the indenter and differs from θ by 8 degrees.

between an index line[6] on the sample and the line H formed by the intersection of the facet with the surface of the sample. ERS or $\cos \lambda \cos \phi \cos \Psi$ can then be computed. It is assumed that the slip system which tends to act has greater ERS values than all other slip systems of the same type. Therefore, in Fig. 8, which is a plot of ERS versus a for the (001) plane of silicon ferrite with slip on

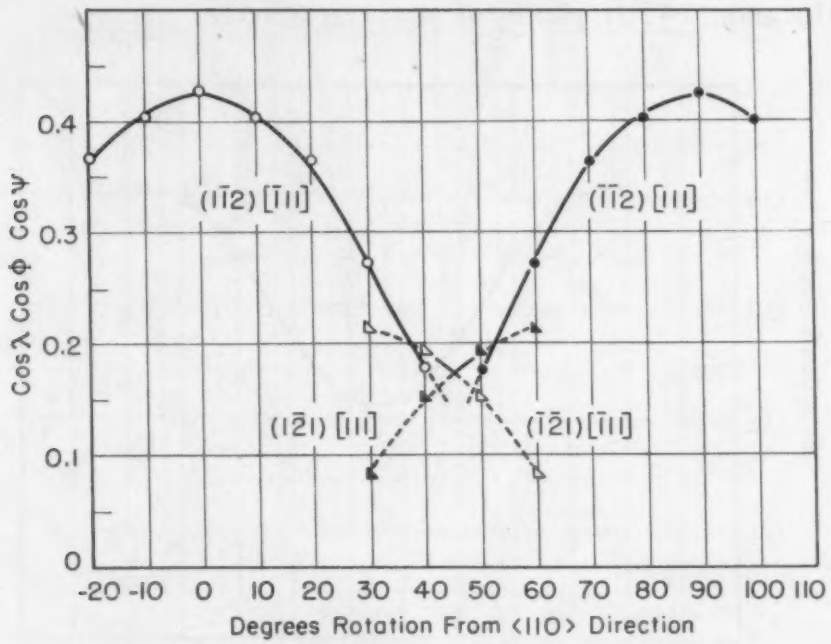


Fig. 8—Effective Resolved Shear Stress Versus a for Indentations on the (001) Plane of Silicon Ferrite with Slip on {112} Planes. The four curves are for one facet only.

{112} planes, the slip system (1$\bar{1}$2) [$\bar{1}$11] tends to operate from −37 to +37 degrees, the ($\bar{1}$2$\bar{1}$) [$\bar{1}$11] from 37 to 45 degrees, etc. Other slip systems of the {112} <111> type were quickly ruled out on the basis of high values of λ, ϕ, or Ψ. The range of a never need exceed 180 degrees, and 90 degrees is usually sufficient because of crystal symmetry.

Because facets of the indenter are inclined to one another, the calculated ERS values of one facet may be extended to include all four facets by simply shifting the abscissa plus or minus 8 degrees and reading ordinate values at the proper points. The values for each facet are added and the total divided by four because numerically

[6]The index lines are <110> directions for all planes of silicon ferrite. For the (0001) and (14$\bar{3}$0) planes of zinc the indices are [11$\bar{2}$0] and [0001] directions respectively.

cos λ cos ϕ cos Ψ must be in the range 0 to ½. In Fig. 9 averaged ERS values are plotted against θ for the (001) plane of silicon ferrite.

Calculations, as described above, were made for all three types of slip planes of silicon ferrite and the one slip plane of zinc. Curves appear in Figs. 10, 11, and 12 for the (001), (110) and (111) planes of silicon ferrite respectively and in Figs. 13 and 14 for the (0001) and $(14\bar{5}0)$ planes of zinc respectively.

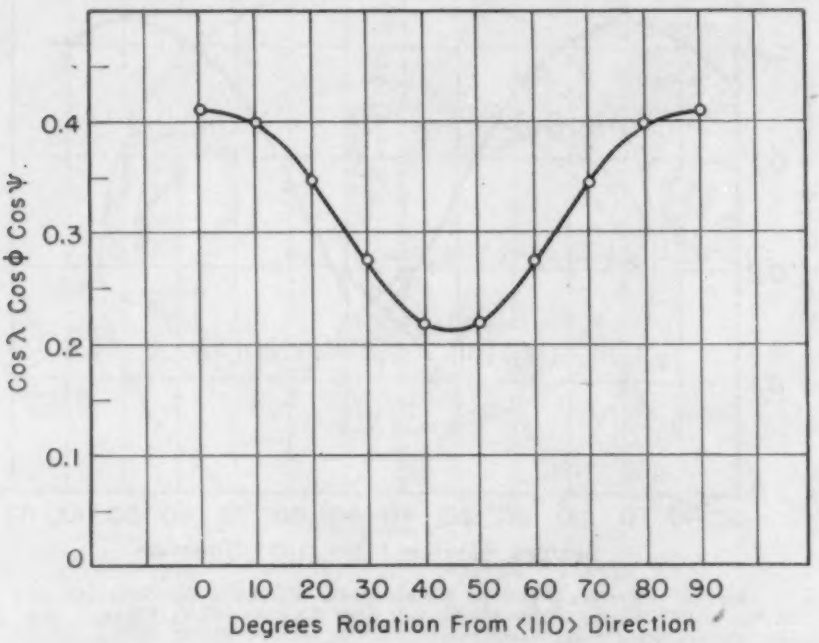


Fig. 9—Effective Resolved Shear Stress Versus θ for Indentations on the (001) Plane of Silicon Ferrite with Slip on {112} Planes.

In order to compare calculated and experimental data it is convenient to plot hardness in the reciprocal form: constant/KHN. Furthermore, another arbitrary constant is used implicitly to locate the position of the curve on the ordinate scale. It varies slightly from one crystallographic plane to another for silicon ferrite and quite appreciably for zinc.

For silicon ferrite 7000/KHN (KHN being obtained from the experimental curves) is plotted against θ for comparison with ERS versus θ. See Figs. 10, 11, and 12. For zinc 850/KHN is plotted similarly for comparison purposes in Figs. 13 and 14.

As a matter of interest it was desirable to know how cos λ cos ϕ plotted against θ would agree with experimental data. Illustrative

curves of cos λ cos ϕ as given in Figs. 14 and 15 show that this double product is in poorer agreement with experimental facts than is the triple product cos λ cos ϕ cos Ψ. The experimental results, therefore, justify the inclusion of the constraining factor cos Ψ.

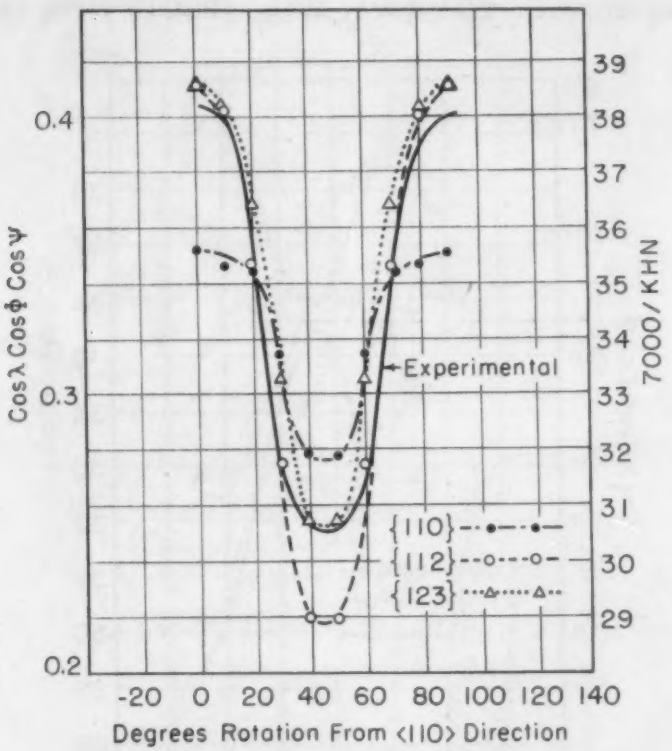


Fig. 10—Effective Resolved Shear Stress Versus θ for Indentations on the (001) Plane of Silicon Ferrite with Slip on {110}, {112}, and {123} Planes Respectively. Also curve of experimental data.

Discussion

Experimental Results—The Knoop hardness of single crystals of silicon ferrite and zinc is highly dependent upon orientation as evidenced by the several curves KHN versus θ shown in Figs. 1 through 5. For example, the hardness of silicon ferrite in the range of orientations investigated shows a 29% variation from a minimum of 183 to a maximum of 237. In the case of zinc the difference from the minimum value of 15.5 to the maximum value of 44.0 is an increase of 184%.

In addition to the large changes in hardness depending on crystal orientation there is a regularity to the variation of hardness for each

plane consistent with crystal symmetry. In the (001) plane of silicon ferrite (4 fold symmetrical) hardness values repeat every 90 degrees. For the (110) plane (2 fold) repetitions occur every 180 degrees. Finally, for the (111) plane (3 fold, actually 6 fold with respect to the indenter) repetitions occur every 60 degrees. For zinc, hardness repeats every 60 degrees in the (0001) plane (6 fold), and

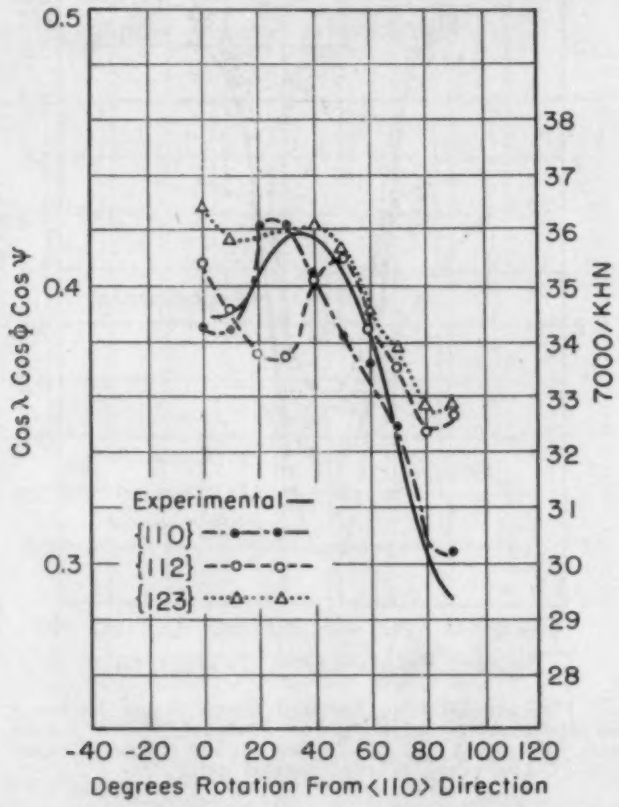


Fig. 11—Effective Resolved Shear Stress Versus θ for Indentations on the (110) Plane of Silicon Ferrite with Slip on {110}, {112}, and {123} Planes Respectively. Also curve of experimental data.

every 180 degrees in the $(14\bar{5}0)$ plane (2 fold with respect to the indenter). Furthermore, the magnitude of the variation from minimum to maximum value for a single plane is different for different planes. Thus the variation in hardness in the (111) plane of silicon ferrite is much less than in the (001) and (110) planes. Likewise, the variation of hardness in the (0001) plane of zinc is small compared with the variation in the $(14\bar{5}0)$ plane. Interesting too is the fact that maxima and minima hardness in each plane occur in the vicinity of simple crystallographic directions.

The over-all dependency of hardness upon crystal orientation as noted above indicates that in reporting the Knoop hardness of a single crystal it is essential to specify the crystallographic plane of test and the direction of the long diagonal of the indenter. Further, the effect of orientation should be carefully considered in any case where an unsymmetrical indenter is employed. In this connection

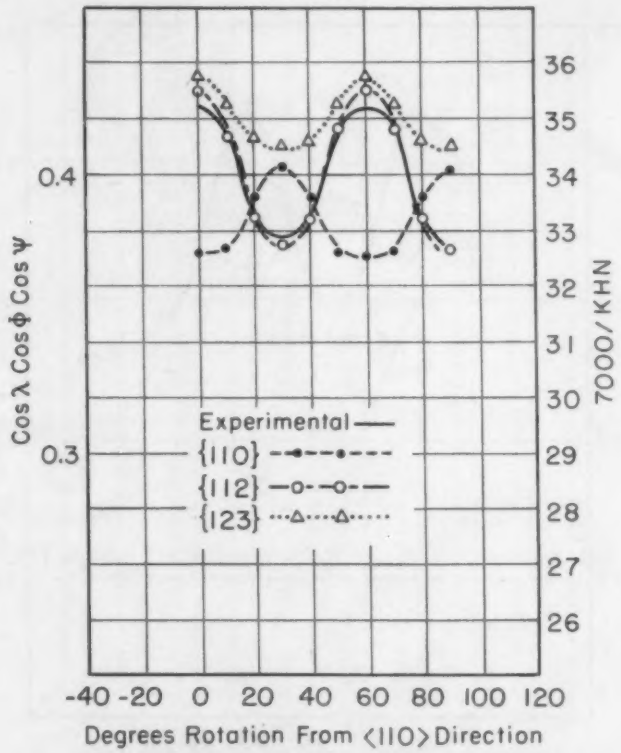


Fig. 12—Effective Resolved Shear Stress Versus θ for Indentations on the (111) Plane of Silicon Ferrite with Slip on {110}, {112}, and {123} Planes Respectively. Also curve of experimental data.

a more symmetrical indenter than the Knoop would in general decrease the magnitude of hardness variations. A square based pyramidal indenter such as the Vickers, however, would not decrease the variations in the (001) plane of silicon ferrite since each facet would penetrate metal at equivalent orientations.

In reporting hardnesses of silicon ferrite it may be possible to circumvent the necessity of specifying crystal plane and indenter direction by employing an averaging process suggested by the experimental results. A glance at Table I reveals that the average hardness of all three planes of silicon ferrite is the same within experimental error. This indicates that for silicon ferrite the average hard-

ness is independent of crystal plane. If desirable, then, the hardness of two different crystals of unknown orientations may be compared by taking measurements at close angular intervals and averaging over 180 degrees.[7]

It should be remembered that the average hardnesses reported herein are obtained from measurements at 10-degree intervals. Values

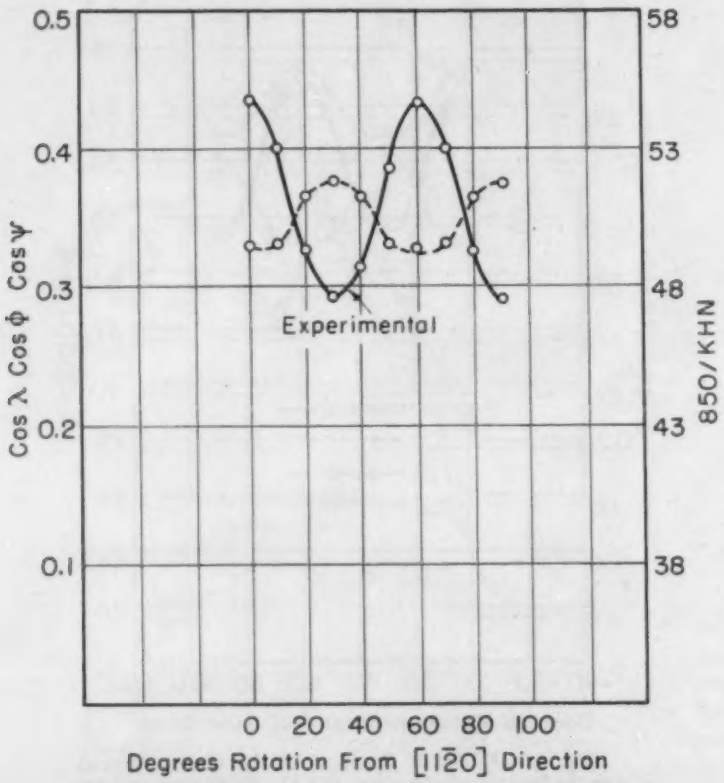


Fig. 13—Effective Resolved Shear Stress Versus θ for Indentations on the (0001) Plane of Zinc and Curve of Experimental Data.

taken at smaller intervals from the curve would yield a more accurate average; and of course $\int_0^{\pi} \frac{KHN\, d\theta}{\pi}$ would represent the best average for any plane. Results computed from this expression would be compatible with those obtained with a Brinell penetrator. In this connection the constancy of hardness for the three planes of silicon ferrite constitute good agreement with the work of Pfeil (2) previously mentioned. In the case of zinc, however, the results given

[7] 180 degrees will always include all possible types of crystallographic directions, because the indenter has 2-fold symmetry.

in Table I indicate that average hardness does depend upon crystallographic plane. In general, average hardness values for body-centered and face-centered cubic lattices in metals appear to be independent of the plane tested, whereas in other types of lattices this probably is not true.

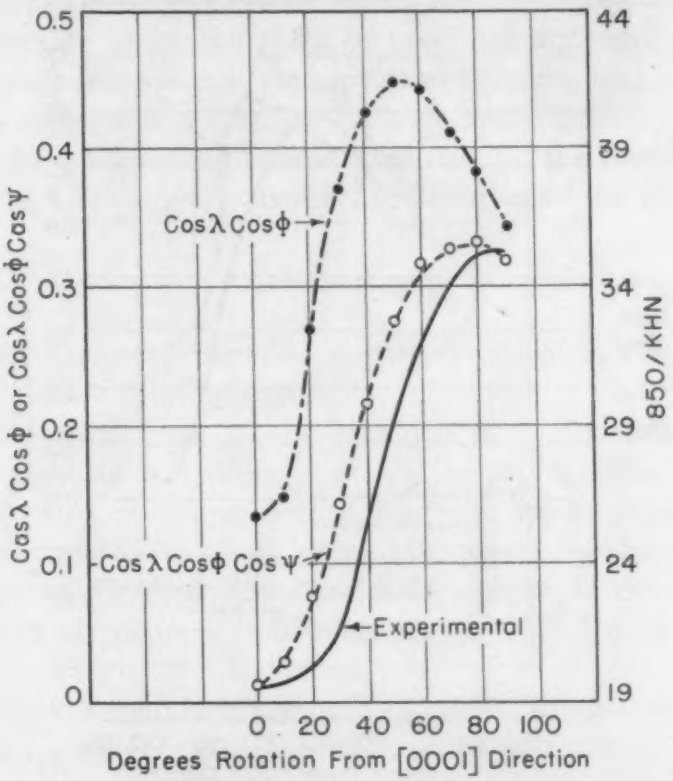


Fig. 14—Effective Resolved Shear Stress, Experimental Data, and Resolved Shear Stress for the (14$\bar{5}$0) Plane of Zinc.

Theoretical Results—Effective resolved shear, like hardness, is dependent upon crystal orientation. The per cent variation in ERS estimated from Figs. 10, 11, and 12 for silicon ferrite and Figs. 13 and 14 for zinc is even larger than the per cent variation in hardness previously mentioned; therefore, ERS values appear adequate to account for the magnitude of the experimentally determined hardness variations.

In regard to the shape of the calculated curves, by proper selection of slip planes good agreement can be found between theory and experiment for all cases except the (0001) plane of zinc.

For the (001) plane of silicon ferrite all three curves based on each type of slip system agree with experiment (see Fig. 10). For the (110) test plane, agreement is best for slip on {110} planes (Fig. 11). Finally for the (111) test plane, good agreement is obtained with slip on either the {112} or {123} planes (Fig. 12).

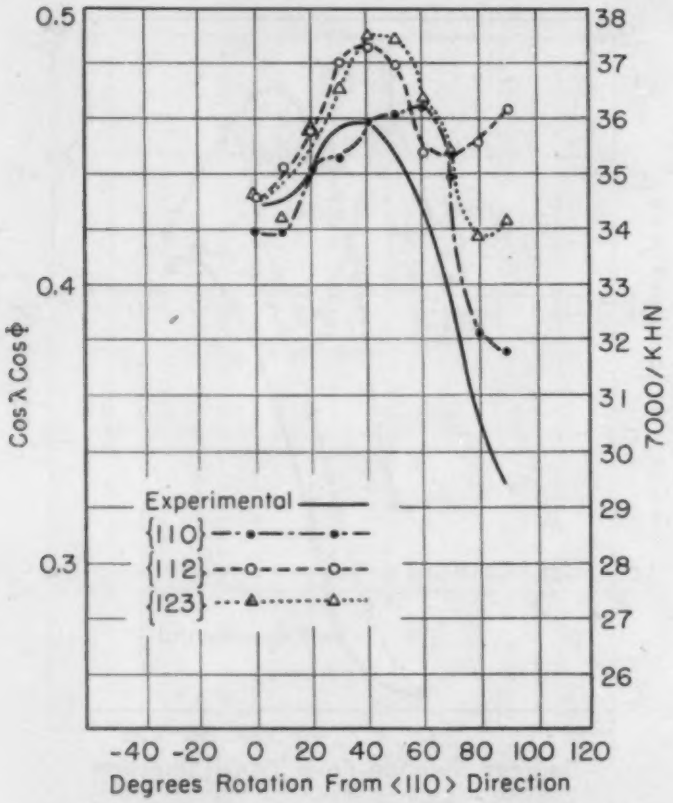


Fig. 15—Resolved Shear Stress Versus θ for Indentations on the (110) Plane of Silicon Ferrite with Slip on {110}, {112}, and {123} Planes Respectively. Also curve of experimental data.

For the $(14\bar{5}0)$ plane of zinc, agreement of theory and experiment was reasonably good, but in the case of the (0001) plane theoretical curves were 30 degrees out of phase with experimental curves.

Experimentally, markings indicative of some twinning were observed adjacent to the indents on the zinc crystal. A consideration of a stereographic projection of the (0001) plane would show that twinning can move metal toward the surface in a direction parallel to F; so deformation by twinning may be quite favorable. Further, a phase shift as mentioned in the preceding paragraph could conceivably be expected if twinning rather than slip predominated in

tests on a (0001) plane. Zinc was chosen for experiment because of its simple slip system; actually the theoretical treatment is complicated by the presence of twinning.

Although in some respects the theoretical treatment proves inadequate, effective resolved shear does seem capable of explaining directional hardness effects in a qualitative manner.

Furthermore, the expression for ERS could conceivably be modified to eliminate anomalies between predicted and experimental results by introducing some of the aspects of twinning and simultaneous slip on two or more slip systems. Also a determination of the active slip planes to compare with those predicted by the theory would be of interest and of value for further modification of the theory.

Conclusions

1. The Knoop hardness of single crystals of silicon ferrite and zinc varies with crystal orientation.

2. The cyclic form of the variation in Knoop hardness for a particular plane of test depends on the crystallographic plane. On the (001) plane of silicon ferrite, hardness values repeat every 90 degrees; on the (110) plane, every 180 degrees; and on the (111) plane, every 60 degrees. On the (0001) plane of zinc, hardnesses repeat every 60 degrees, while on the $(14\bar{5}0)$ plane, every 180 degrees.

3. When Knoop hardness values, taken at equal small angular intervals on a given plane, are averaged, the average hardness is independent of plane for silicon ferrite and dependent on plane for zinc.

4. In general the form of the experimental results can be explained qualitatively by means of a modified resolved shear stress formula.

Acknowledgments

The authors wish to express their appreciation to Miss Mary P. Burdette, who assisted in the experimental work, and to Mr. William W. Martin, who contributed to the theoretical treatment.

References

1. H. O'Neill, "Hardness Tests on Crystals of Aluminum," *Journal*, Institute of Metals, Vol. 30, 1923, p. 299.

2. L. B. Pfeil, "The Effect of Cold Work on the Structure and Hardness of Single Iron Crystals and the Changes Produced by Subsequent Annealing," Carnegie Memoirs, Iron and Steel Institute, Vol. 16, 1927, p. 153.
3. H. Winchell, "The Knoop Microhardness Tester as a Mineralogical Tool," *American Mineralogist*, Vol. 30, 1945, p. 583.
4. N. W. Thibault and H. L. Nyquist, "The Measured Knoop Hardness of Hard Substances and Factors Affecting Its Determination," TRANSACTIONS, American Society for Metals, Vol. 38, 1947, p. 271.
5. A. A. Guy, "Study of the Mechanism of Precipitation From Solid Solution in Copper Beryllium and Copper Iron Alloys," Appendix I, Doctors Thesis deposited in Library of Carnegie Institute of Technology, 1946.
6. C. S. Barrett, G. Ansel and R. F. Mehl, "Slip Twinning and Cleavage in Iron and Silicon Ferrite," TRANSACTIONS, American Society for Metals, Vol. 25, 1937, p. 702.
7. E. Schmidt and W. Boas, Kristallplastizitat, p. 90, Berlin, 1935, Springer.

DISCUSSION

Written Discussion: By H. C. Vacher, metallurgist, National Bureau of Standards, U. S. Department of Commerce, Washington, D. C.

I have read the authors' paper with considerable interest because we have a similar investigation in progress and have obtained similar results. Our work has been confined principally to copper. The results for copper showed 2, 4, and 6-fold symmetry for the (110), (100) and (111) planes respectively with the maxima and minima corresponding to the orientations shown in this paper for silicon ferrite.

Copper is particularly interesting theoretically because slip lines near the indents are readily observable. I have applied the authors' Equation II to results obtained on a surface approximately parallel to the (110) plane and with the long diagonal approximately parallel to a (110) direction. The four highest ERS values were obtained for slip-system-facet combinations whose slip planes were indicated by slip lines near the indent. We hope to be able to publish a report on our results in the near future.

Written Discussion: By Horace Winchell, Mineralogical Laboratory, Yale University, New Haven, Conn.

This exceedingly fine paper is the first in my experience that brings some degree of order to the theory of hardness testing with an asymmetrical point. The authors' use of resolved shear stress in their calculations sheds light upon the problem of continuous variation of hardness with changing azimuth of the long axis of the indenter, when we all know very well that the crystal structure of a plane surface is discontinuous with reference to a variable direction. It seems as if perhaps the time is at last ripe for an experiment where a large model of the indenter point is pushed against an atomic packing model of a crystal, to observe whether the slip systems brought into play actually do agree with those postulated. Even if the experimental conditions cannot duplicate those in the crystal very closely, the chances of interesting and worthwhile results seem good.

As a footnote to the results quoted by these authors, I should add here that similar results have been obtained in preliminary experiments on brittle mineral crystals. We used a much lighter load, but otherwise nearly the same setup as described by the authors.

Congratulations for a most enlightening bit of research!

Written Discussion: By A. G. Guy, associate professor, Department of Mechanical Engineering, North Carolina State College of Agriculture and Engineering, University of North Carolina, Raleigh, N. C.

The authors are to be complimented on their success in explaining such a complex phenomenon as a hardness test in terms of the fundamental slip process. The anisotropy of hardness in single crystals was observed in 1942 at the Carnegie Institute of Technology in a series of Tukon tests on copper-beryllium alloys. Data were then obtained on suitably oriented single crystals of pure aluminum, but attempts at analysis of these data were unsuccessful. The procedure used in the study of the copper-beryllium alloys to avoid orientation effects was to maintain the orientation constant.

The method of analysis used by the authors has been applied to the Tukon testing of aluminum single crystals with the result shown in the table. For tests on a given crystal plane there is very nearly the desired inverse proportion between the cosine factor and the hardness number. However, the correlation for hardness tests on the two different planes is not good. Since there is nothing in the method of analysis that suggests this correlation should not be expected, it appears that the analysis might be improved.

One of the difficulties is undoubtedly that slip occurs on slip systems in addition to the one with the highest cosine factor. Photomicrographs of the Tukon indents in aluminum single crystals show that this is true at least in the instances of the last three of the four tests given in Table II.

Table II

Crystal Plane on Which the Test Was Made	Crystal Direction of the Long Axis of the Indenter	KHN	$\frac{KHN}{18.0}$	$\cos\lambda\cos\phi\cos\Psi$	$\frac{0.277}{\cos\lambda\cos\phi\cos\Psi}$
(001)	[010]	17.8	0.989	0.277	1.000
(001)	45° from [010]	12.1	0.672	0.353	0.785
(101)	[010]	18.0	1.000	0.310	0.894
(101)	90° from [010]	14.3	0.795	0.368	0.753

Written Discussion: By L. P. Tarasov, metallurgical engineer, Norton Company Research Laboratories, Worcester, Mass.

The authors have shown that for a given crystallographic plane the Knoop hardness numbers of silicon ferrite and of zinc vary significantly with the crystallographic direction of the long diagonal of the indentation lengths. It would be interesting to know to what extent the ratio of the long and short diagonals varied with crystallographic direction and whether the hardness numbers calculated from the indentation areas

differed appreciably from the ones calculated in the ordinary manner from the lengths alone. Such variations in the ratio of the diagonals are known to occur in very hard substances of a nonmetallic nature, and they are attributed to differences in the elastic recovery with crystallographic direction.

A point worth mentioning is that the unrecovered hardness, which is the hardness number calculated before any elastic recovery of the indentation has taken place, should show the same sort of anisotropy as that found by the authors. This is because the unrecovered indentations, such as exist before the load is removed, must have the theoretical ratio of long to short diagonal lengths derived from the geometry of the indenter, and this same ratio is used in the calculation of the measured (or recovered) hardness numbers involving the indentation lengths alone.

Written Discussion: By Russell W. Mebs, metallurgist, National Bureau of Standards, Washington, D. C.

The authors present an interesting interpretation of the effect of crystal orientation on the resistance to deformation by indentation for metal single crystals. They re-emphasize the fact often ignored that individual crystals have directional characteristics, and therefore, when properties are measured in terms of one or a small number of crystals, account should be taken of such anisotropic effects.

A serious defect in the theoretical calculations lies in the assumption that each indenting facet produces a tensile stress in the adjacent metal parallel to the direction of the steepest slope of the facet. Basic mechanical principles dictate that each facet should produce a large compressive stress in the adjacent metal in a direction normal to the contact plane, plus a small frictional shear stress component parallel to the plane and in a downward direction. The compressive stress may be resolved as a hydrostatic compressive stress, which would produce no plastic flow, plus a shear stress along planes diagonal to the parallel and normal directions. The total resolved shear stress, which includes the frictional component, would also lie along diagonal planes, only slightly altered in directions from those indicated above. Hence flow would take place by multiple shear along certain crystal planes preferentially oriented with respect to the above planes of total shear stress, so as to produce flow in the direction of least constraint. Thus is produced the bulging adjacent to each edge of the impression. I cannot conceive a mechanism whereby a compressive force normal to the surface of a metal would be translated to a lateral tensile stress a short distance beneath that surface. On the other hand, lateral flow can occur although the transverse component of principal stress be small or zero.

Because of the anisotropy of a single crystal, the stress distribution under load is probably equally or more complex than that shown by Heyer[8] in the Brinell hardness testing of polycrystalline metals. Furthermore, plastic flow might be expected to produce crystal fragmentation,

[8]Robert H. Heyer, "Analysis of the Brinell Hardness Test," *Proceedings*, American Society for Testing Materials, Vol. 37, Part II, 1937, p. 119-141.

rotation, and possibly a new preferred orientation in the more severely deformed portions of the metal.

Thus the analysis of the authors is believed to require considerable modification and amplification in order to explain the observed anisotropy in hardness measurements.

It is hoped the authors will extend their careful measurements of the effect of crystal orientation on Knoop hardness numbers to single crystals of other metals.

Written Discussion: By Robert I. Jaffee, Battelle Memorial Institute, Columbus, Ohio.

The results given in this fine paper help to explain the wide variation in Knoop hardness readings obtained on testing polycrystalline material. Usually, the entire Knoop impression is located entirely within a single grain, and the average Knoop hardness of a polycrystalline material is taken as the average of many grains of different orientation. Thus, the scatter of results is wide in polycrystalline material, whereas the results given in the present paper appear to be remarkably consistent.

The unidirectional nature of the Knoop indenter helps to accentuate orientation effects. From a practical point of view, this is disadvantageous when one is working with polycrystalline materials. The effect of orientation on hardness would diminish, but not be entirely eliminated, if a square impression such as is obtained with a Vickers diamond were used. Therefore, it appears that the micro-Vickers would be a more useful hardness test for polycrystalline materials than the Knoop.

Authors' Reply

We wish to thank all those who have commented on the paper. It is encouraging to know that others are interested in the anisotropy of hardness and are appreciative of its importance in hardness testing.

We share Mr. Vacher's hope that he will soon publish his work on single crystals of copper. Copper, incidentally, provides a more simple case for theoretical treatment than silicon ferrite because it has but one type slip system. Also copper does not twin as easily as zinc, which also is an advantage in theoretical treatment.

Dr. Winchell's suggestion of a study of an atomic model under influence of a large-scale indenter presents interesting possibilities.

Dr. Guy, who pioneered some of the early theory on the anisotropy of Knoop hardness, has made some well considered remarks. As he points out, rather poor correlation of theoretical and experimental data may exist because the slip planes actually in operation were not determined. We recognized this (page 437), but our initial attempts to determine the slip systems by microscopic examination were unsuccessful. For this reason all possible slip systems were dealt with in the case of silicon ferrite.

With regard to Dr. Tarasov's comments on recovery, we feel that directional variations in elastic recovery are very small in the relatively soft metals used in this investigation. In harder materials, however,

directional variation of the ratio of long to short diagonal is a factor to be considered.

Mr. Mebs in his analysis of the forces producing motion of metal to the surface has, we believe, made an important contribution to the theoretical treatment. First we should state that the force F (see Fig. 6) was assumed solely on the basis that the metal is actually moved toward the surface. The origin of the force was considered as a reaction force of hydrostatic nature similar to the forces about a wedge being pushed into an amorphous solid.

We realize that Equation II was not rigourously derived. Mr. Mebs has raised a legitimate objection concerning the detailed nature of the resolved forces. Perhaps the method of calculation could be altered so as to be more consistent with the forces involved. This might be accomplished by using a force parallel to N (Fig. 7) as the force causing deformation. Then if the same small cylinders of metal are assumed beneath the indenter, only the values of λ will be altered. Whether such a change will yield correlative results can only be determined by mechanically carrying out the calculations. In some positions of the indenter the trends of variation would be similar to those already calculated. In general, however, different results would be expected.

THE EFFECT OF SINGLE ADDITION METALS ON THE RECRYSTALLIZATION, ELECTRICAL CONDUCTIVITY AND RUPTURE STRENGTH OF PURE ALUMINUM

By R. H. Harrington

Abstract

Of eleven addition metals, the individual alloying effects of iron, magnesium and zirconium proved most important. The electrical conductivity of "pure" aluminum is about 64% of that of pure copper. In both annealed and cold-worked conditions, the addition of 0.35% zirconium gave outstanding rupture strength but the electrical conductivity for the cold-worked condition was lowered to 53%. Zirconium also raised the recrystallization temperature to about 600 °C (1110 °F), just below the melting point. The addition of 1% iron, usually regarded as an undesirable impurity, yielded outstanding rupture strength for the annealed condition while maintaining a high electrical conductivity of 61% and raising the recrystallization temperature to about 450 °C (840 °F). Of the high conductivity materials (61.6%), the addition of only 0.2% magnesium gave the highest rupture strength for the cold-worked condition while raising the recrystallization temperature slightly from about 275 °C (525 °F) to about 320 °C (610 °F). This program was basic to the development of more complex compositions having high electrical conductivity and creep strengths much superior to that of commercial E. C. Grade aluminum.

Introduction

LARGE high speed electric generators have in some cases suffered plastic deformation of the copper or aluminum rotor windings, caused by stresses produced by restrained expansion. Such deformation takes place gradually, and seems to be associated with repeated cycles of service and shutdowns. The cumulative result, after years of service, may be short circuiting some of the turns, or grounding, of the winding. Many large 3600-rpm generators with very long rotors were built with field coils of aluminum, for its more

A paper presented before the Thirtieth Annual Convention of the Society, held in Philadelphia, October 23 to 29, 1948. The author, R. H. Harrington, is research metallurgist, General Electric Research Laboratories, Schenectady, N. Y. Manuscript received May 6, 1948.

favorable ratio of conductivity to weight, so as to reduce centrifugal stresses and permit the use of large diameter rotors. The best commercial aluminum ("electrical conductivity" or E.C. Grade) consists of a minimum of 99.45% aluminum, with the chief impurities being 0.25 to 0.45% iron and about 0.10% silicon. Its electrical conductivity may range from 61.5 to 62.5% (conductivity of pure copper — 100%). Improvement of the elastic and creep strengths of this aluminum is greatly desired.

To develop a stronger aluminum, it was necessary to undertake a basic program of research to determine the effect of single addition metals on the recrystallization, electrical conductivity, and rupture strength of "pure" aluminum. A search of the literature showed that various "pure" aluminums have given electrical conductivities ranging from 63.5 to 65.4%. A few references cited the effects of one or two addition metals on the electrical conductivity of "pure" aluminum. Published reports on the effects of addition metals on the recrystallization and rupture strengths of aluminum appeared to be completely lacking.

Composition and Preparation of the Alloy Materials

In some cases, the quantities of added metals were judged from standard equilibrium diagrams and, in a number of cases, were determined by logical assumptions. In each case the goal was to add as much of the second metal as possible to contribute strength without unduly lowering the electrical conductivities. The chosen compositions, types of materials added, and the actual compositions by spectrographic or chemical analysis are given in Table I.

Table I
Composition of Materials

Alloy No.	% by Addition	Material Added	Spectrographic Analysis	Chemical Analysis
A	99.95% Al	none*		
1	0.3 Ag	fine silver	....	0.28–0.28
2	0.3 Be	5 Be – 95 Al	0.31	.....
3	0.2 Cr	98 Cr – 2 Fe	0.20	.....
4	0.3 Cu	tough pitch Cu	0.30	.....
5	1.0 Fe	elec. Fe powder	....	1.09–1.09
6	0.2 Mg	pure Mg	0.19	.....
7	0.05 Mn	elec. Mn	0.089	.....
8	0.5 Ni	shot Ni	....	0.48–0.47
9	1.0 Si	99.53 Si – 0.47 Fe	0.82	0.82–0.83
10	0.05 Ti	+Al pressed powder	0.03	.....
11	0.5 Zr	+Al pressed powder	....	0.36–0.35

*Alloy consists of 99.95% Al, impurities by spectrographic analysis consisting of traces of Cu and Si, with Fe, Mg, Cr, and Ti reported as nil.

The base aluminum of 99.95% purity was furnished by the Aluminum Company of America. In each case the aluminum charge was first melted in a resistance heated graphite crucible, heated to about 800 °C (1470 °F), and the alloying material was then added. The melt was then cooled to about 700 °C (1290 °F) whereupon it was poured into preheated graphite molds giving cast rods of about 450 mils diameter. The metal charged in each case was about 2.5 pounds and the total time for melting and pouring was about 10 minutes. Types of fractures and microstructures of the as-cast materials will be discussed later.

For the series of "aluminums", described in Table I, all materials were treated practically identically according to the following schedule:

1. Rods cast to 450 mils diameter.
2. Cast rods cold-swaged about 25% reduction to 400 mils diameter.
3. All rods then annealed for 4 hours at 400 °C (750 °F) with the exception that Alloy 11 (0.35% zirconium) was annealed 10 hours at 500 °C (930 °F).
4. All annealed 400-mil rods were then cold-swaged a uniform reduction of 60% to 250 mils diameter.
5. For rupture tests in the annealed state, the cold-swaged 250-mil rods were annealed for ½ hour at 500 °C (930 °F) in pure dry nitrogen atmosphere.

Recrystallization-hardness studies were made of the 60% cold-worked 250-mil diameter rods. Electrical conductivity tests were made on these rods as cold-swaged 60% and after 400 and 500 °C (750 and 930 °F) anneals of the same stocks. Rupture tests were conducted on the 250-mil diameter rods as cold-swaged and after annealing at 500 °C (conditions 4 and 5). Microstructures of the annealed 250-mil diameter rods (condition 5) were compared with the "as-cast" structures.

Qualitative "Hand-and-Eye" Tests of the Alloys

Although qualitative tests must be held suspect for future proof, they are nevertheless of real value in establishing predictions and in focussing attention on nonconformists in the group. Research, in its strictest sense, usually ignores purely qualitative tests with a result somewhat similar to the eating of perfectly cooked, but unseasoned, food.

Table II lists the fracture structures and relative "ductility" of these fractures of the as-cast materials, from samples broken by impact, using the hand-hammer-and-vise method.

Table II
Fracture Studies of This Aluminum Series (As-Cast)

Alloy No.	% Comp.	Impact Fracture Comments	
		Fracture Structures	Impact Ductility
A	"pure"	radial dendrites	very ductile
1	0.3 Ag	radial dendrites	slightly ductile
2	0.3 Be	dend. rim, fine-grained core	ductile, tough
3	0.2 Cr	radial dendrites	brittle, bright
4	0.3 Cu	radial dendrites	slightly ductile
5	1.0 Fe	radial dendrites	ductile, dull
6	0.2 Mg	radial dendrites	very ductile
7	0.1 Mn	cellular	very ductile
8	0.5 Ni	radial dendrites	slightly ductile
9	0.8 Si	radial dendrites	brittle
10	0.05 Ti	radial dendrites	very ductile
11	0.35 Zr	radial dendrites	medium ductile

The 60% cold reduction of the annealed 400-mil rods, finishing to 250 mils diameter, gave a good opportunity to rate this series as to cold workability. It was also found that if 24-inch lengths of the cold-worked 250-mil rods were grasped with the hands at the two ends, differences in stiffness could be judged qualitatively by hand flexing or bowing the rods. In this way flexibility (elastic bending) and stiffness for this series were rated on the basis of 10 for the "stiffest" alloy and recorded in Table III. As is well known, there is no direct relationship between impact ductility and most methods of cold forming, or cold workability. This is further indicated by comparing "impact ductility" of Table II with "cold workability" of Table III.

Table III
Cold Workability and Stiffness of Wrought Materials

Alloy No.	% Comp.	Flexibility	Stiffness Factor	Cold Workability
A	"pure"	bends very easily	½	very good
1	0.3 Ag	bends very easily	1	very good
2	0.3 Be	very stiff	10	very good
3	0.2 Cr	bends quite easily	2	fair
4	0.3 Cu	bends very easily	1	fair
5	1.0 Fe	very stiff	8	very good
6	0.2 Mg	bends quite easily	2	very good
7	0.1 Mn	bends very easily	1	very good
8	0.5 Ni	somewhat stiff	3	fair
9	0.8 Si	flexes quite easily	2	poor
10	0.05 Ti	bends very easily	1	very good
11	0.35 Zr	very stiff	10	good

The results of qualitative tests, as given in Tables II and III, call attention to Alloys 2, 5 and 11 (Be, Fe and Zr, respectively). Subsequent rupture tests prove some value to these qualitative leads. However, the beryllium alloy proves to be a disappointment in this property while the magnesium alloy proves to be a "sleeper" of surprising value.

Recrystallization-Hardness Studies for the Binary Series

Individual samples of each of the 12 members of the alloy series, cut from the 60% cold-worked rods, were heated for 4 hours at each of a series of temperatures ranging from 125 to 400 °C (and to 500 °C for the Fe, Be, and Zr alloys). Rockwell H hardness tests were made on the flat rectangular (axial) surfaces of the half cylinders (cut axially previous to the aging treatments). The samples had been cut from the 250-mil diameter rod stock with a very thin cut-off wheel while the cylinder-sample was continually drenched in cold water. The Rockwell H hardness values were then plotted against the aging temperature. Since the Rockwell scale is purely empirical, negative scale readings are as valid as positive ones.

The results fall into three alloy groups: (a) The first group includes those addition metals which do not appreciably alter the recrystallization-hardness curve for "pure" aluminum; (b) the second group contains those addition metals which show more work hardening than does pure aluminum, which also show appreciable age hardening previous to recrystallization, and which have recrystallization temperatures somewhat higher than that for pure aluminum; and (c) the third group includes those addition metals which show marked work hardening for the same amount of cold work as was applied to the pure aluminum, which show marked thermal stability before recrystallization, and which, with one exception, exhibit phenomenally high recrystallization temperatures. The results are plotted respectively in Figs. 1, 2 and 3. In each figure the recrystallization-hardness curve for pure aluminum is reproduced for purposes of comparison. It should be remembered that all alloy materials had received, as nearly as possible, identical treatment, finishing with 60% cold reduction (in cross section area).

Group 1. The Addition Metals Ag, Mn, and Ti. (Fig. 1)

The curve for the basic 99.95% pure aluminum shows a continuous downward trend at all temperatures above room temperature. This

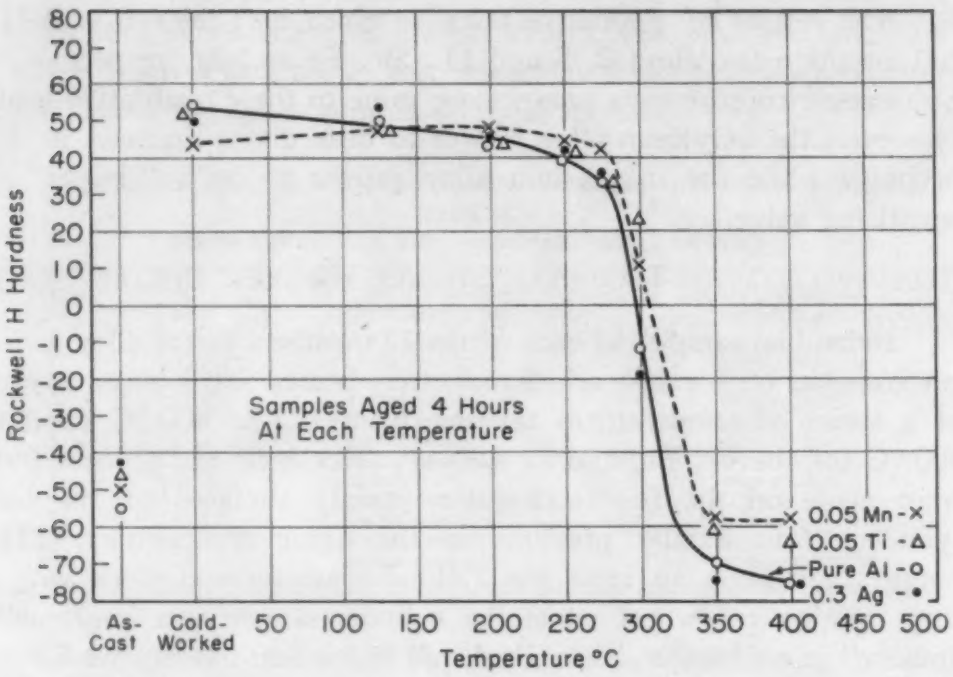


Fig. 1—Recrystallization-Hardness Curves for Group 1. (Manganese, Titanium, Silver.)

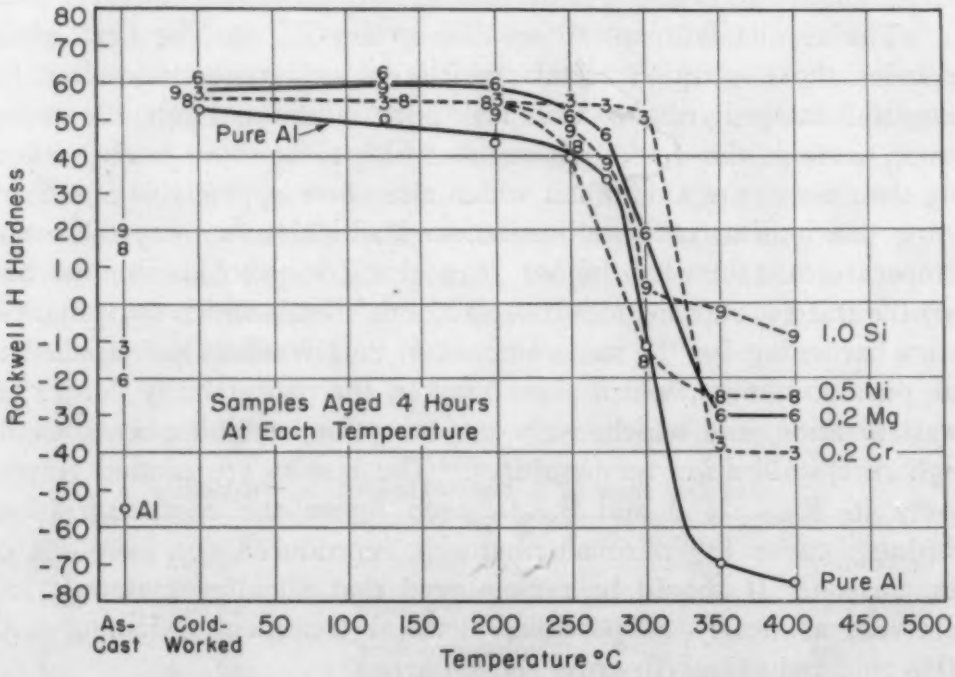


Fig. 2—Recrystallization-Hardness Curves for Group 2. (Chromium, Magnesium, Nickel, Silver.)

indicates that cold-worked pure aluminum possesses no true thermal stability and that, theoretically, it tends to recrystallize *even at room*

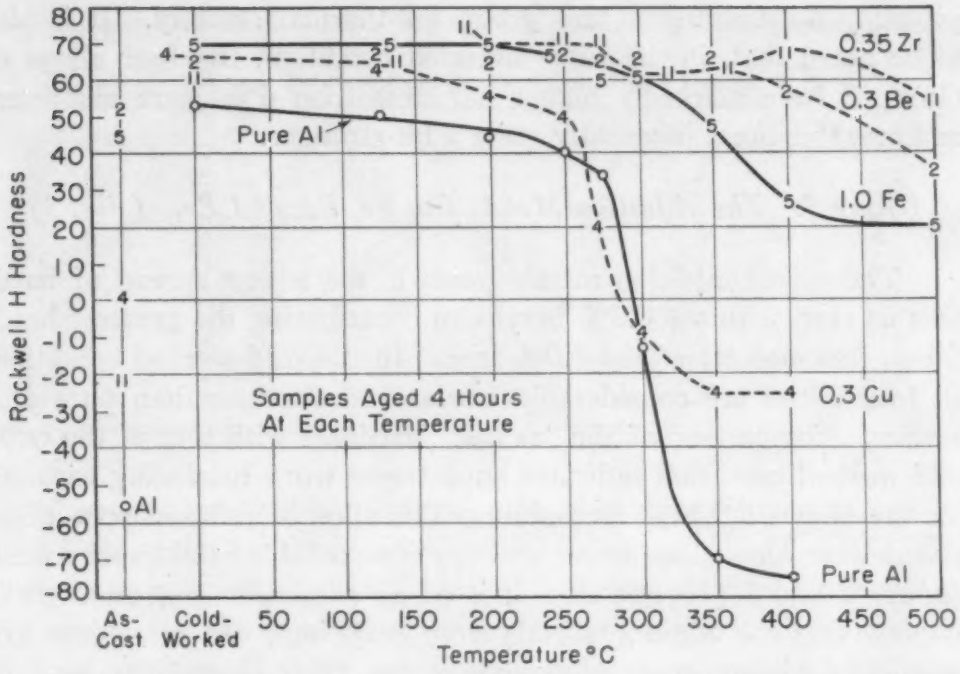


Fig. 3—Recrystallization-Hardness Curves for Group 3. (Copper, Iron, Beryllium, Zirconium.)

temperature. The curve for the 0.05% titanium alloy is nearly identical with that for pure aluminum. Both the 0.3% silver and the 0.1% manganese alloys show very slight age hardening previous to recrystallization and thus are more thermally stable than either the 0.05% titanium alloy or the pure aluminum. All four of these materials have nearly identical "recrystallization temperatures".

Group 2. The Addition Metals Cr, Mg, Ni, and Si. (Fig. 2)

Whereas in Group 1 the hardness for the four alloys in the "as cast" condition was nearly identical, the four addition metals in Group 2 cause quite a spread in hardness, as cast. In contrast with the curve for pure aluminum, the recrystallization-hardness curves for these addition metals show definite age-hardening and real thermal stability at temperatures below those that result in normal recrystallization-softening. The 0.5% nickel alloy has a slight tendency for a lower recrystallization temperature than for pure aluminum. The additions of 0.8% silicon, 0.2% magnesium and 0.2% chromium tend to give recrystallization temperatures in the range of 50 degrees above that for pure aluminum. The 0.2% magnesium and the 0.2% chromium alloys have the highest curve-knees and therefore are

probably outstanding in this group for thermal stability. It is also to be noted that, in the fully annealed condition, the four alloys of Group 2 have markedly higher hardness than does pure aluminum and are, therefore, inherently quite a bit stronger.

Group 3. The Addition Metals Cu, Fe, Be, and Zr. (Fig. 3)

These four addition metals result in the widest spread of hardness as cast, with the 0.3% beryllium contributing the greatest hardening, followed closely by 1.0% iron. In the cold-worked condition, all four alloys are considerably harder and stronger than pure aluminum. Comparison of the "as cast" hardness with that of the 60% cold-worked condition indicates an extreme work hardening capacity for the alloy of 0.35% zirconium. The alloy of 0.3% copper gives a somewhat anomalous curve and appears to bridge the gap between Groups 2 and 3 (beyond that, it is of no particular interest). It is obvious that the addition metals iron, beryllium, and zirconium are practically phenomenal in extending the thermal stability and in raising the recrystallization temperature of pure aluminum (by 100 to 300 °C). The recrystallization-hardness curve for the 1.0% iron alloy is practically normal. It must be remembered that iron has generally been regarded as an undesirable impurity (as it really is in *some* aluminum alloys). The addition of 0.3% beryllium produces a slight tendency for two age hardening maxima, and aging at 500 °C does not quite completely anneal this material. The most startling effect is that of 0.35% zirconium, resulting in two very real age hardening maxima (at 275 and at 400 °C). All the data of the three groups show that all of the other alloys, when fully annealed, have hardnesses appreciably below those for their "as cast" conditions. Consider then the case of the 0.35% zirconium alloy: it has only begun to soften at 500 °C (930 °F)! Our earlier roughly qualitative tests pointed to the addition metals iron, beryllium, and zirconium as most interesting and it seems as though this prophecy would be proven. But wait! There will finally be one disappointment in the three and there still is the "sleeper".

The Effect of the Addition Metals on Electrical Conductivity

The electrical conductivities were measured for the 250-mil diameter (60% cold-worked) rods of the alloys in each of three

Table IV
Effect of Treatment on the Electrical Conductivities

Alloy No.	% Comp.	60% Cold-Worked	Annealed 4 Hrs. 400 °C	Annealed 10 Hrs. 500 °C
A	"pure"	64.1	64.4	64.2
1	0.3 Ag	65.0	62.3	62.4
2	0.3 Be	62.5	63.4	63.4
3	0.2 Cr	50.1	49.8	50.1
4	0.3 Cu	60.9	61.0	60.8
5	1.0 Fe	60.8	61.2	61.7
6	0.2 Mg	61.6	61.3	61.6
7	0.1 Mn	58.6	58.6	58.6
8	0.5 Ni	62.9	63.2	63.1
9	0.8 Si	Surface and internal cracks prevented tests.		
10	0.05 Ti	62.2	62.4	62.4
11	0.35 Zr	53.3	55.9	60.5

conditions: (a) as cold-worked, (b) after annealing 4 hours at 400 °C (750 °F), and (c) after annealing 10 hours at 500 °C (930 °F). The results are presented in Table IV. The variation of conductivity with treatment of the material seems in many cases to be anomalous. Still, in most cases, there are possible reasons. The electrical conductivity of "pure" aluminum is very high and checks well with the maximum of 0.05% of impurities. With annealing of cold-worked material, it is normal to expect the conductivity to increase due to reduction of lattice distortion from the cold working. However, for "pure" aluminum, the conductivity is lower after annealing at 500 °C (930 °F) than after annealing at 400 °C (750 °F) (and still higher than for the cold-worked condition). One explanation could be that the cold work lattice-distortion induced precipitation of some of the minute impurities during annealing at 400 °C (750 °F) and that re-solution took place at 500 °C (930 °F). The quantity of precipitation involved would be far too small to cause measurable strengthening and yet the hardness after aging at 400 °C (750 °F) is further very slightly lowered by annealing at 500 °C (930 °F). In comparison with other pure metals (as for copper), it is surprising that 60% cold work should have so little effect on the conductivity of annealed pure aluminum. The marked *maximum* of conductivity for the 0.3% silver alloy in the 60% cold-worked condition remains a true anomaly at this time. The conductivity variations for the 0.35% zirconium alloy have a possible explanation: (a) The conductivity after aging at 400 °C (750 °F) is higher than for the cold-worked condition although aging at 400 °C (750 °F) develops the second hardness maximum for this alloy, higher hardness than for the cold-worked condition; (b) this combination of

effects suggests lattice-strain induced precipitation with lattice distortion still pronounced; and (c) although further aging at 500 °C (930 °F) would tend to cause re-solution of the precipitated phase, the further relief from lattice distortion could result in further actual increase in conductivity as indicated by the data in Table IV. Thus some of the anomalies in the conductivity data are explainable while others remain as true anomalies. Consider the case of the alloy containing 0.10% manganese: that so small an amount of alloy metal should lower the conductivity so much and then to have the conductivity constant for all conditions, cold-worked or annealed! It is to be noted for the alloy of 0.35% zirconium that, while its cold-worked hardness and strength and its thermal stability are so promising, in the plain cold-worked condition its electrical conductivity is too low to permit rating it as a truly high conductivity material: to achieve a high conductivity the cold-worked alloy must be aged at 500 °C (930 °F).

Standard Rupture Tests of the Binary Aluminum Series

The rupture test bars used for this program were 2 inches long with about 1 inch gage length, 250 mils in diameter at the threaded ends and 159 mils in diameter over the gage length. These bars were machined from the 60% cold-worked 250-mil diameter rod stock previously described. For rupture tests of the alloys in the annealed condition, the required test bars were annealed for ½ hour at 500 °C (930 °F) in an atmosphere of pure dry nitrogen.

The temperature for rupture testing was chosen as 125 °C (255 °F) to represent the effective operating temperature in the generator windings. The rupture test (as usual) consisted of loading the bars to various specified chosen stresses and heating the bars under those stresses continuously at 125 °C (255 °F) until the bar either fractures or bears the load without fracture for so long a time that the test is discontinued (usually more than 1000 hours). Thus *rupture strength* is the maximum stress borne without fracture for a specified time (such as 1000 hours) at a given temperature. Similarly, alloys may be compared on the basis of *rupture life*: the number of hours to fracture under the same stress at the same temperature. The chief value of the rupture test is to qualitatively sort materials into those alloys which would have low creep strength from those promising high creep strength. Since there is no direct

relation between rupture strength (or rupture life) and actual creep strength, the rupture test merely indicates those alloys that merit the time and cost involved in determining their creep strength. A summary of the rupture tests for the annealed binary aluminum series is given in Table V.

Table V
Rupture Test Results for the Annealed Binary Aluminum Series

Alloy No.	% Comp.	Life in Hours at 125 °C (Stresses Below) 4500 psi	5250 psi	6000 psi	6750 psi	7500 psi	8250 psi	9000 psi	10,500 psi
A	"pure"	60	....	0.6	...	0.03	...	....	..
1	0.3 Ag	28	3.6	1.4	...	0.03	...	....	..
2	0.3 Be	...	....	729	256	5.2	...	0.55	..
3	0.2 Cr	...	0.05	....	...	†	...	....	..
4	0.3 Cu	...	....	70	...	3.8	...	0.05	..
5	1.0 Fe	...	....	....	...	1008*	108	3.7	..
6	0.2 Mg	...	....	675	...	0.15	...	....	..
7	0.1 Mn	17	....	†	...	....	...	....	..
8	0.5 Ni	...	....	58	...	0.55	...	....	..
9	0.8 Si	...	....	....	...	....	...	....	..
10	0.05 Ti	117	....	0.20	...	0.03	...	....	..
11	0.35 Zr	...	....	....	...	....	...	1875*	74

*Test stopped at time indicated without failure.
†Broke loading.

Inspection of Table V quickly indicates that the 0.35% zirconium alloy is outstanding in rupture strength. Among the high conductivity materials, the 1% iron alloy is outstanding with the 0.3% beryllium alloy well behind in second place and the 0.2% magnesium alloy a close third among the annealed materials.

Table VI
Rupture Test Results for the Cold-Worked Binary Aluminum Series

Alloy No.	% Comp.	Life in Hours at 125 °C (Stresses Below) 7500 psi	8250 psi	9000 psi	10,500 psi	10,875 psi	11,250 psi	12,000 psi	13,500 psi
A	"pure"	148	58	89	0.05	...	...	....	....
1	0.3 Ag	1078*	139	6	0.15	...	...	....	....
2	0.3 Be	1823*	749	94	8	...	...	....	....
3	0.2 Cr	....	...	1364*	35	0.6	...	....	....
4	0.3 Cu	....	...	778	237	...	...	5	0.53
5	1.0 Fe	....	...	1897*	316	...	102	38	2
6	0.2 Mg	....	...	....	2954*	...	...	366	2
7	0.1 Mn	0.04	...	....	0.03	...	...	....	....
8	0.5 Ni	266	...	0.70	0.55	...	...	0.10	....
9	0.8 Si	3	...	100	3.7	...	...	....	....
10	0.05 Ti	1435	...	40	0.75	...	...	0.02	....
11	0.35 Zr	....	...	....	2020*	...	867	246	0.10

*Test stopped at time indicated without failure.

Inspection of Table VI yields the startling disclosure that the 0.2% magnesium alloy (the "sleeper"), in the cold-worked condition,

has the highest rupture strength of all the materials, with 0.35% zirconium a close second, followed by the 1% iron and 0.2% chromium materials, in that order. The 0.2% chromium alloy, cold-worked, is also something of a surprise. It has been recent practice to add about 0.2% chromium to several aluminum alloys to improve their corrosion resistance and it is now evident that, under certain conditions, chromium may be otherwise beneficent. The effect of the addition of magnesium appeared to be so far out of line that it seemed probable that the test bars had been improperly identified. However, analysis of the actual tested bars proved them to be from the magnesium stock.

Microstructures of the Binary Aluminum Series

The microstructures were studied for two conditions for each of the 12 aluminum materials: (a) as-cast and (b) after annealing 10 hours at 500 °C (930 °F) of the 60% cold-worked rod stock. The surfaces of the samples were prepared by electrolytic polishing in a bath of DeSy and Haemers solution and examined at a magnification of 250 diameters. All of the "as-cast" structures show either a mottling due to solute metal segregation in solid solution or else a clearly defined dendritic structure. The following is a summary of the microstructures:

99.95% Aluminum. No second phase. A few etching pits.
Aluminum Plus 0.3% Silver. Traces of second phase in boundaries.
Aluminum Plus 0.3% Beryllium. A second phase in the grain boundaries and indications of precipitation.
Aluminum Plus 0.2% Chromium. No second phase. A few etching pits.
Aluminum Plus 0.3% Copper. Traces of a second phase.
Aluminum Plus 1.0% Iron. False (?) appearance of two phases present in equal amounts.
Aluminum Plus 0.2% Magnesium. No second phase. A few etching pits.
Aluminum Plus 1.0% Manganese. No second phase. A few etching pits.
Aluminum Plus 0.5% Nickel. A discrete second phase.
Aluminum Plus 0.8% Silicon. Sharply angled second phase showing as voids in photomicrographs. Explains brittleness of this material.
Aluminum Plus 0.05% Titanium. No second phase. Etching pits.
Aluminum Plus 0.35% Zirconium. Traces of second phase, especially in grain boundaries of annealed material, discontinuous. Also etching pits.

Figs. 4, 5, 6 and 7 are examples of the observed structures.

Examples of Complex Derived Alloys

Of a number of more complex compositions, derived from the

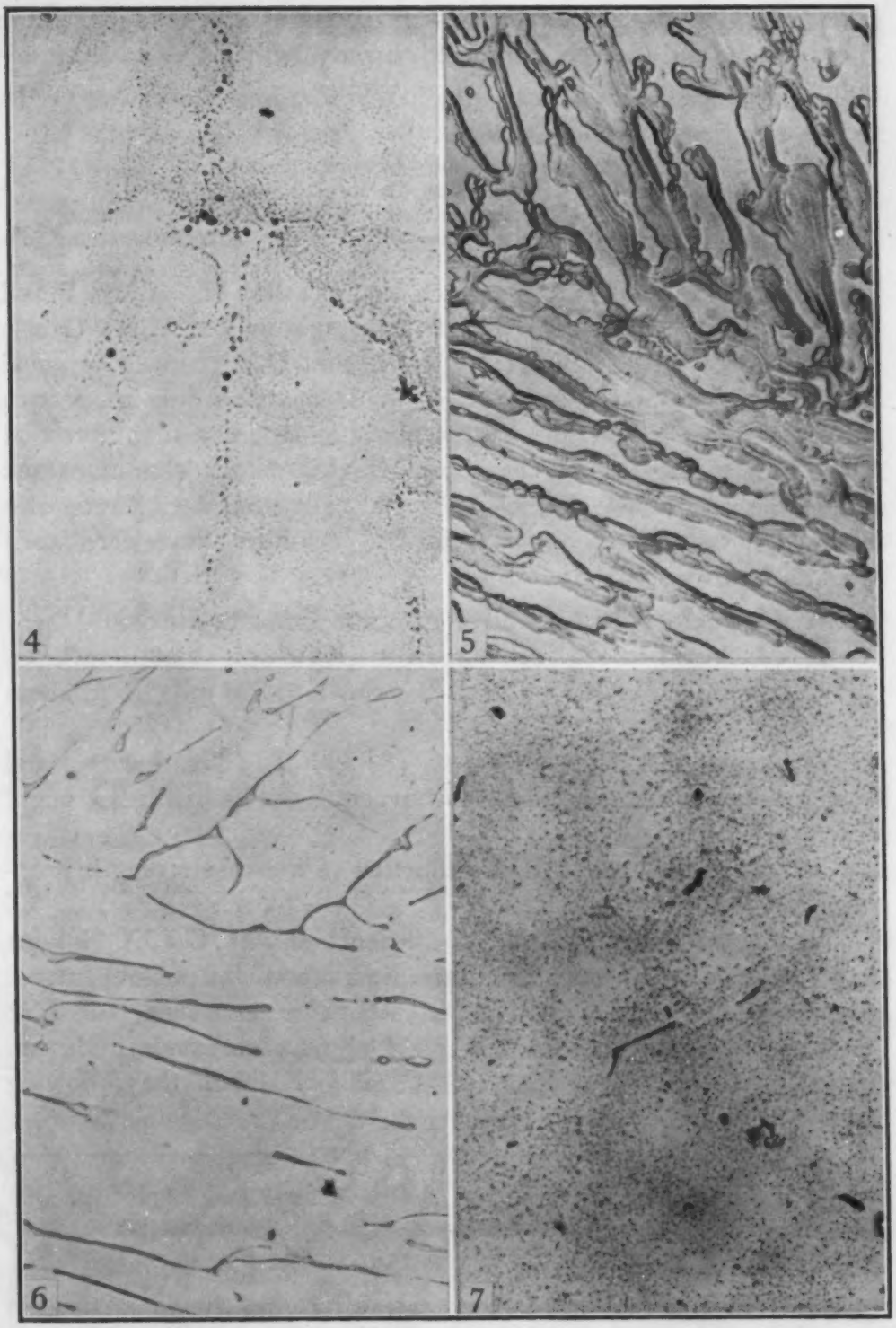


Fig. 4—Aluminum 99.95% Plus 0.3% Silver, Annealed. × 250.
Fig. 5—Aluminum 99.95% Plus 1.0% Iron, As-Cast. × 250.
Fig. 6—Aluminum 99.95% Plus 0.5% Nickel, Annealed. × 250.
Fig. 7—Aluminum 99.95% Plus 0.8% Silicon, Annealed. × 250.

basic information obtained for the binary series, the following three alloys, A, B, and C, were compared directly with E.C. Grade aluminum (Alloy D):

Alloy	Composition
A	1.05% iron–0.32% magnesium–balance aluminum
B	0.53% iron–0.29% magnesium–balance aluminum
C	0.43% iron–0.32% magnesium–0.10% silicon–balance aluminum
D	0.41% iron–0.005% magnesium–0.10% silicon–balance aluminum

Alloy A contains twice as much iron as Alloy B. Alloys B and C have similar contents of iron and magnesium but Alloy C also contains about 0.10% silicon. Alloys C and D contain about equal amounts of iron and silicon but Alloy D contains only a spectrographic trace of magnesium. It is of particular interest to note that Alloy C was made simply by remelting E.C. Grade aluminum and adding the magnesium. Alloy D is plain remelted E.C. Grade aluminum (the same stock as for Alloy C). All four alloys were fabricated as follows:

1. Cast into 1¼-inch square ingots in graphite molds.
2. Machined to 1⅛ inch square to give clean, smooth surfaces.
3. Hot-rolled at 400 °C (750 °F) down to 390 mils thick, about 1⅛ inches wide.
4. Annealed 4 hours at 450 °C (840 ° F). (Treatments 3 and 4 completely replace the initial cast structure with a typical wrought structure.)
5. Finish cold-rolled 10% reduction to increase strength properties for generator winding use.
6. Aged 5 hours (1 hour is sufficient) at 200 °C (390 °F) for standard strain relief and to stabilize the material for subsequent use at temperatures up to about 150 °C (300 °F).

Compression creep tests for all 4 alloys were made under an applied stress of 5130 psi at 140 °C (285 °F) with the following results:

	Alloys			
	A	B	C	D
	1.05% iron 0.32% magnesium	0.53% iron 0.29% magnesium	E.C.+ 0.32% magnesium	Plain E.C.
Creep rate:*	475	375	94	986

By ratios of the respective creep rates it is clearly apparent that Alloy A gives half the creep rate of E.C. Grade aluminum, Alloy B is somewhat better than A while Alloy C has the very low creep rate

*Micro-inches per inch per 1000 hours.

of less than $\frac{1}{10}$ that of the standard E.C. Grade aluminum. The first (or rapid) stage of creep for Alloy C also results in only about $\frac{1}{10}$ of the extension of the first stage for E.C. Grade aluminum.

Proportional limits in compression at room temperature and at 140 °C (285 °F) for Alloys C and D were measured with the following results:

	Alloys	
	C	D
	E.C.+ 0.3% magnesium	E.C. Grade
Compression P.L. at 23 °C	12,500 psi	5,700 psi
Compression P.L. at 140 °C	8,500 psi	2,500 psi

Thus, at room temperature, Alloy C has the same "elastic strength" as does cold-rolled copper. At 140 °C (285 °F) Alloy C has more than 200% advantage over E.C. Grade aluminum. Alloy C also has greater thermal stability.

Hardness tests gave the following results for Alloys C and D:

	Alloy C	Alloy D
	E.C.+ 0.3% magnesium	Plain E.C.
After annealing:	45 R.H.* 25 Brinell	23 R.H.* 20 Brinell
After 10% cold rolling:	76 R.H. 34.4 Brinell	62 R.H. 27 Brinell
After strain-relief, 5 hours at 200 °C:	88 R.H. 42.4 Brinell	57 R.H. 25 Brinell

The above treatments are in correct sequence for producing finished stock for generator winding. These data show that the hardness and strength are lowered for strain-relief treated E.C. Grade aluminum while Alloy C has its hardness and strength properties *increased* by "strain-relief". The hardness effects further indicate that Alloy C has excellent thermal stability whereas E.C. Grade aluminum has relatively poor thermal stability. In still other words, Alloy C possesses a considerably higher maximum service temperature than does E.C. Grade aluminum. This may be due to strain-induced precipitation of Mg_2Si in Alloy C.

The electrical conductivities for Alloys A, B, C and D were found to be as follows:

*R.H. = Rockwell Hardness, H scale.

	Alloys			
	A	B	C	D
	1.05% iron 0.32% magnesium	0.53% iron 0.29% magnesium	E.C.+ 0.3% magnesium	E.C. Grade
*Electrical Conductivities:**				
Cold-rolled	60.7	61.0	58.6-60	61.0
Annealed	61.2	61.5	60.5-61	61.5

*Conductivities in %, relative to pure Cu = 100%.

The range of conductivity given for Alloy C results from the ratio of silicon to magnesium as silicon may vary from 0.05 to 0.15%.

Summary

The effects of binary additions of 0.3% silver, 0.3% beryllium, 0.2% chromium, 0.3% copper, 1.0% iron, 0.2% magnesium, 0.1% manganese, 0.5% nickel, 0.8% silicon, 0.05% titanium, and 0.35% zirconium on the recrystallization, electrical conductivity and rupture strength of pure aluminum were determined and abstracted as follows:

1. The results of the recrystallization-hardness study are best given in Table VII:

Table VII
Summary of Recrystallization-Hardness Data

Alloy No.	% Comp.	Upper Knee, °C	Inflection Point, °C	Lower Knee, °C
A	"pure"	200?	300	350
1	0.3 Ag	250	300	350
2	0.3 Be	350	450	550?
3	0.2 Cr	300	325	350
4	0.3 Cu	250	275	350
5	1.0 Fe	325	375	450
6	0.2 Mg	275	315	350
7	0.1 Mn	275	315	350
8	0.5 Ni	200	270	350
9	0.8 Si	200	290	350
10	0.05 Ti	250	315	350
11	0.35 Zr	400	530	600?

It must be remembered that Table VII is based on data from 4-hour heating periods. The upper knee is indicative of thermal stability and comparative maximum service temperatures. The lower knee is indicative of practically complete structural recrystallization. It is of interest to note that all the alloys, except for those of 0.3% beryllium, 1.0% iron and 0.35% zirconium, have about the same temperature for practically complete recrystallization.

2. Relative to electrical conductivity, the stated additions of silver, beryllium, copper, iron, magnesium, nickel and titanium yielded conductivities above 60% for the cold-worked condition while the binary alloys with chromium, manganese, and zirconium gave conductivities below 60%. The same two classifications hold for the annealed materials with the exception that the alloy of 0.35% zirconium, if annealed at 500 °C (930 °F), will reach a conductivity rating of 60.5%.

3. For rupture strength in the annealed condition, the alloys of 0.35% zirconium and 1.0% iron are markedly outstanding. In the cold-worked condition, the binary alloy of 0.2% magnesium is superior to that of zirconium, with those of 1.0% iron, 0.2% chromium and 0.3% beryllium following zirconium in that order.

Further superiority in creep life and creep strength is shown by certain more complex alloys, derived from results of tests of the binary series. Among the superior alloys covered by patent applications filed with the U. S. Patent Office are those essentially of aluminum-magnesium, aluminum-zirconium, and of the class aluminum-iron-magnesium-silicon. Uses would be for "high strength" conductors, high conductivity structural materials, generator windings, etc.

Acknowledgments

All rupture tests were conducted by E. A. Smith of the General Electric Research Staff. The compression creep and proportional limit tests were conducted by L. B. Barker of General Electric's Schenectady Works Laboratory. Acknowledgment is also due Mrs. John Freeburg, formerly of the General Electric Research Staff, for the photomicrographs.

FORMING AND HEAT TREATMENT OF CORRUGATED DIAPHRAGMS

By R. I. Jaffee, E. I. Beidler and R. H. Ramsey

Abstract

The amount of cold deformation resulting from forming corrugated diaphragms of beryllium-copper, 60:20:20 copper-nickel-manganese, titanium-Elinvar (Ni-Span C), and Grade A phosphor bronze was evaluated and found to consist of a small over-all elongation which was made up of larger localized elongations of 5 to 10% maximum reduction at the tops of corrugations and smaller localized contractions at the bottoms of corrugations.

The specific effect of cold work on the age hardening response was determined on sheet material. Tensile tests on material age-hardened in the as-received condition and with an additional cold reduction of the order of 10% reduction of thickness indicated that the effect of this amount of cold work was negligible insofar as the time dependence of the aging curves was concerned.

The conclusion is drawn that as far as mechanical properties are concerned, a diaphragm can be heat treated according to the age hardening curve of the unformed sheet stock without danger of overaging the most deformed sections of the diaphragm.

PRESSURE-RESPONSIVE devices, such as altimeters for aeronautical work, are frequently made of two corrugated diaphragms joined together into capsule form by soft soldering, silver soldering, or, less frequently, welding. As barometric or aneroid capsules, the inside is evacuated and the thickness of the capsule decreases or increases with rise or fall of atmospheric pressure. Fig. 1 shows a typical double aneroid capsule, such as is used in altimeters or radio sondes, and a cross section of a diaphragm from which such capsules are made.

This investigation was sponsored by The Signal Corps Engineering Laboratories, Bradley Beach, New Jersey.

A paper presented before the Thirtieth Annual Convention of the Society, held in Philadelphia, October 23 to 29, 1948. The authors, R. I. Jaffee, E. I. Beidler and R. H. Ramsey, are associated with Battelle Memorial Institute, Columbus, Ohio. Manuscript received December 13, 1947.

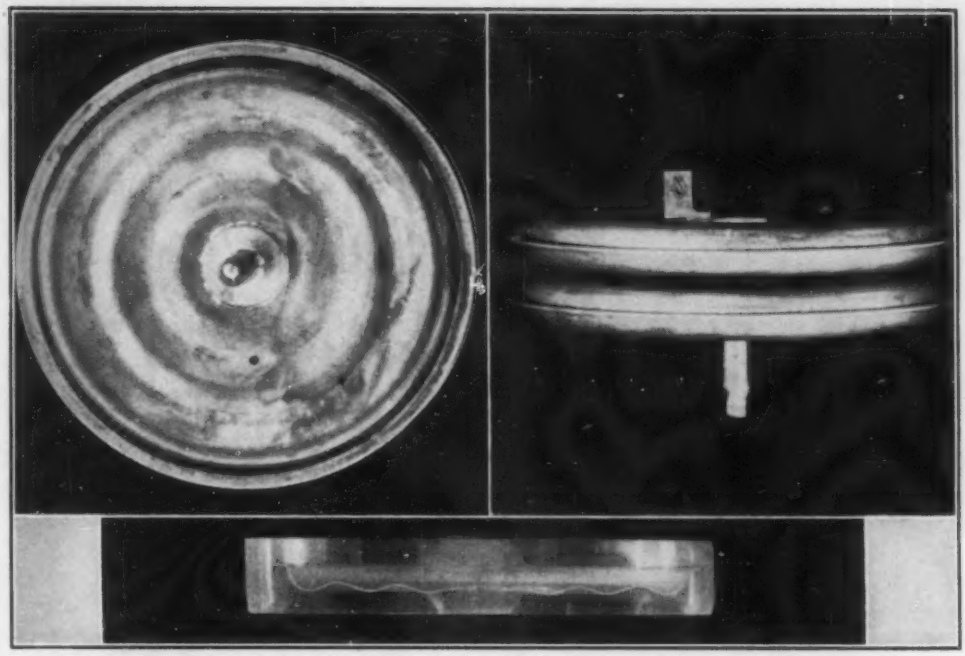


Fig. 1—Upper—An Example of a Double Aneroid Capsule, Each Section Composed of Two Diaphragms Soft Soldered Together. Lower—A section of a diaphragm mounted in lucite. Diameter of diaphragms approximately 2½ inches.

Diaphragms are most frequently made from age hardening alloys, such as beryllium-copper or 60:20:20 copper-nickel-manganese, or cold-worked alloys like phosphor bronze. In the case of age hardening alloys, there is some uncertainty in the heat treatment of the diaphragms to maximum mechanical properties because they receive a variable and indeterminate amount of cold working during the forming operation, which in turn affects the aging response. The general effect of cold work on the aging response is illustrated in Fig. 2, which shows the results of aging tests at three different temperatures on solution-annealed and on full-hard (37% reduction), 0.006-inch, 2% beryllium-copper sheet (Berylco 40 alloy, nominally containing 2% beryllium, 0.3% cobalt, balance copper, obtained from the Beryllium Corporation, Reading, Pennsylvania). Besides producing higher tensile strengths, the full-hard sheet ages to peak strength in a shorter time than the soft, annealed sheet. Thus, an aging time corresponding to peak strength on annealed stock will overage full-hard stock, particularly where the aging peak is sharp, as it is at 675 and 725 °F (355 and 385 °C).

It was the object of the work reported here to evaluate the actual amount of cold work put into the diaphragms during forming

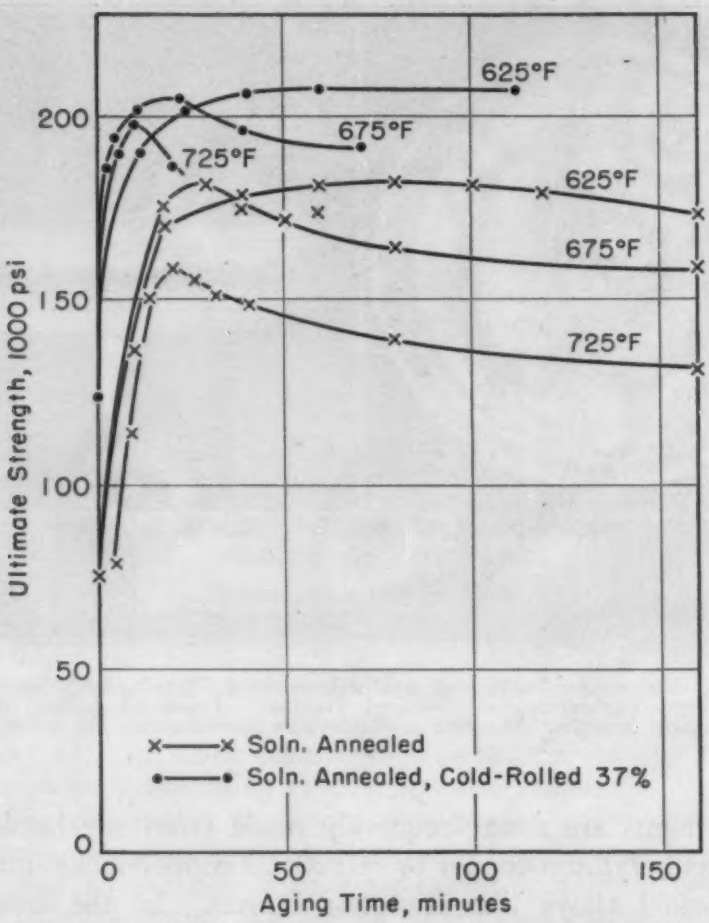


Fig. 2—Aging Response of Annealed and Full-Hard Commercial 2% Beryllium-Copper Sheet at Various Temperatures.

and to determine the effect of the amount of forming on the time dependence of the aging response so that the age hardening treatment might be adjusted to compensate for the forming operation. It was found experimentally that the amount of cold work induced by forming was actually quite small, equivalent to about 5 to 10% reduction in thickness, and that this amount of cold work does not change the time dependence of the aging response enough to make adjustment of the heat treating time, determined on the original stock, necessary.

Method of Evaluating Cold Work

Concentric circles were scribed on the diaphragm blanks with a pair of dividers. The initial diameters of the circles were measured by means of an optical comparator. After forming the diaphragm, the diameters of the circles were again measured to give data from

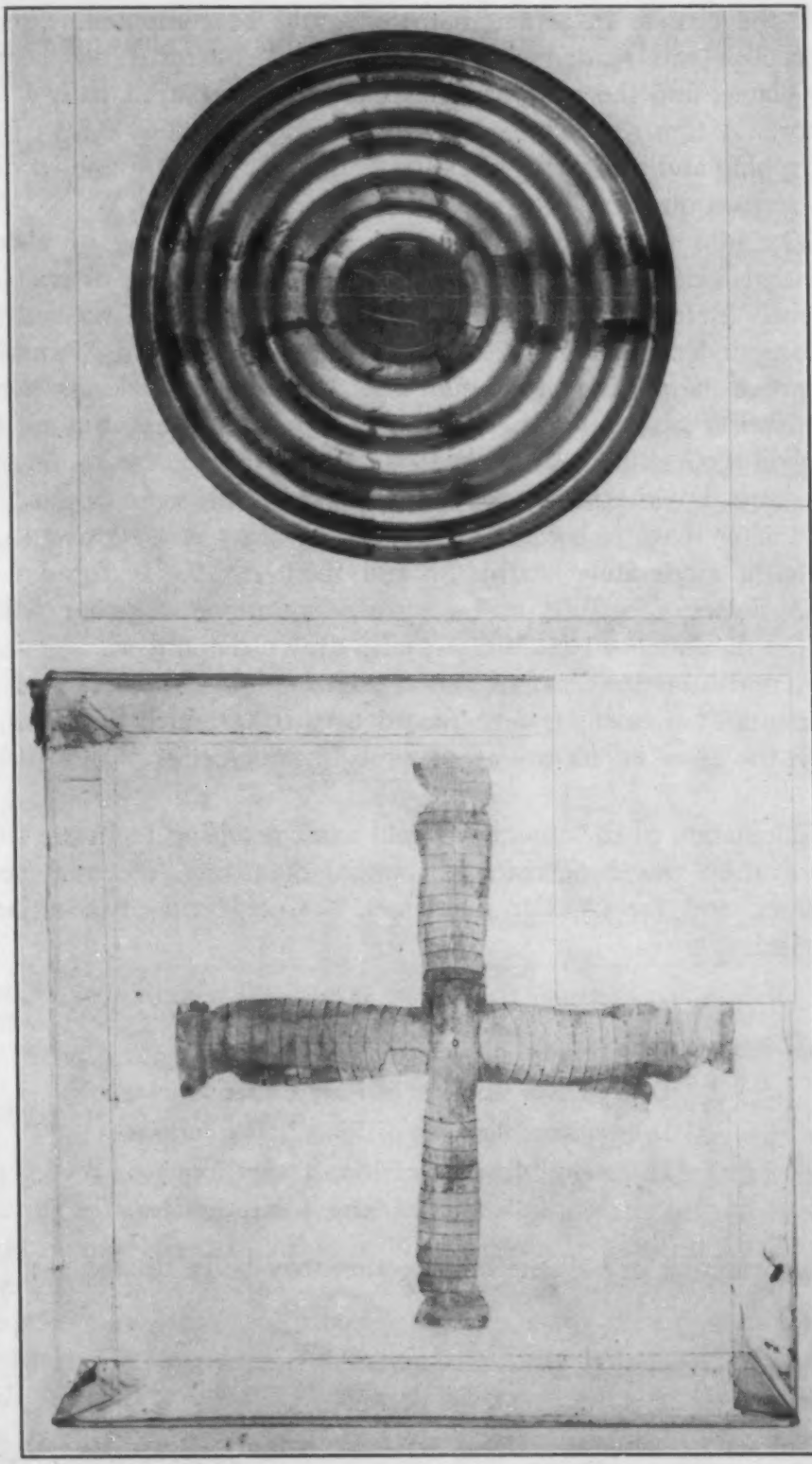


Fig. 3—Scribed Diaphragm and Film Stripped from Diaphragm Mounted Between Glass Plates.

which the change in actual diameter could be computed. Then a film replica was made, which was stripped, mounted flat between glass plates, and the contour diameters were measured with a comparator. A film shrinkage correction of approximately 0.5%, found by stripping and measuring the film from blanks having known diameters scribed on them, was applied to the readings.

The film was formed by drying a dope consisting of about 1 volume of lucite molding powder dissolved in 3 volumes of trichloroethylene. Before applying the film, the diaphragm was washed with trichloroethylene and swabbed with a small amount of "Aquadag" to improve the parting of the film and to make the markings clearer. The diaphragm was thoroughly dried at room temperature, and then diametral sections parallel to the grain and perpendicular to the grain were painted with the dope. Usually two coats were applied, the second after the first became tacky. The coating was allowed to dry slightly in moderately warm air and then at 210 °F for 1 hour. Fig. 3 shows a scribed and formed diaphragm, together with a mounted film stripped from a partially drawn diaphragm.

Actual measurements of actual and contour diameters and displacements of diameters were recorded to 0.0001-inch precision, although the absolute accuracy was probably not better than ±0.0003 inch.

Calculation of the amount of cold work resulting from the forming operation was done using the initial diameters, the final actual diameters, and the contour diameters. Considering two adjacent rings, let:

D_1 = original diameter of Ring 1.
D_2 = original diameter of Ring 2.
D_1' = contour diameter of Ring 1 after forming.
D_2' = contour diameter of Ring 2 after forming.
D_1'' = actual diameter of Ring 1 after forming.
D_2'' = actual diameter of Ring 2 after forming.

The deformation in a diametral direction may be calculated as:

$$\% \text{ diametral change, } E_D = \frac{(D_2' - D_1') - (D_2 - D_1)}{D_2 - D_1} \times 100$$

$$E_D = \frac{(D_2' - D_2) - (D_1' - D_1)}{D_2 - D_1} \times 100 \qquad \text{Equation I}$$

The deformation in a single ring in a circumferential direction may be calculated as:

$$\% \text{ circumferential change, } E_c = \frac{\pi D_n'' - \pi D_n}{\pi D_n} \times 100$$

$$E_c = \frac{D_n'' - D_n}{D_n} \times 100 \qquad \text{Equation II}$$

Forming

A design for a diaphragm, which was developed by Wildhack and Goerke[1] of the Bureau of Standards, for the NACA was used in this work. It is shown diagrammatically in Fig. 4. In the present case, D = 2.188 inches, and the flange width was $\frac{3}{32}$ inch.

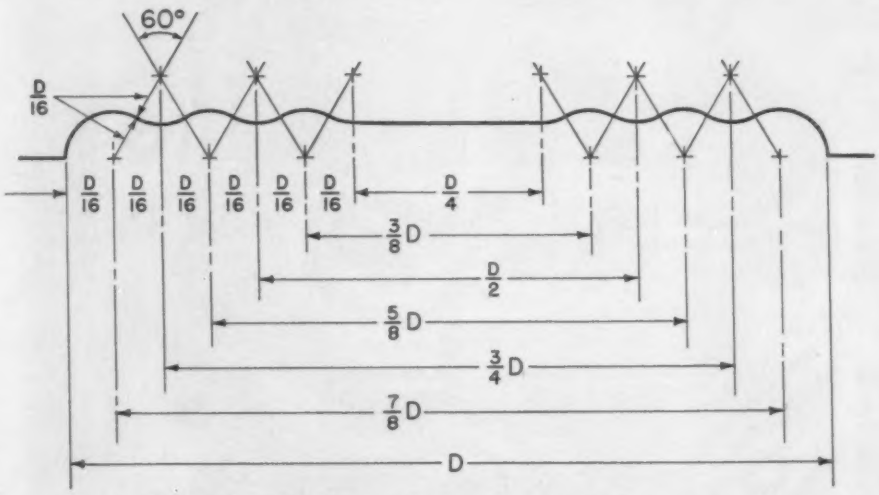


Fig. 4—NACA Design of Diaphragm, After Wildhack and Goerke (1).

The forming press and dies used in forming the diaphragms are shown in Figs. 5 and 6, respectively. The radius of the shoulder over which the blank was drawn is $\frac{1}{32}$ inch. Wrinkling of the flange was avoided by use of hold-down pressure applied by a torque wrench. About 100 foot-pounds applied to the wrench served this purpose. A stop ring attached to the main thread controlled the amount of draw. The height of the formed diaphragm was 0.143 inch, which corresponded to a punch movement of 0.137 inch and the 0.006-inch thickness of stock.

[1]W. A. Wildhack and V. H. Goerke, "The Limiting Useful Deflections of Corrugated Metal Diaphragms," NACA Technical Note No. 876.

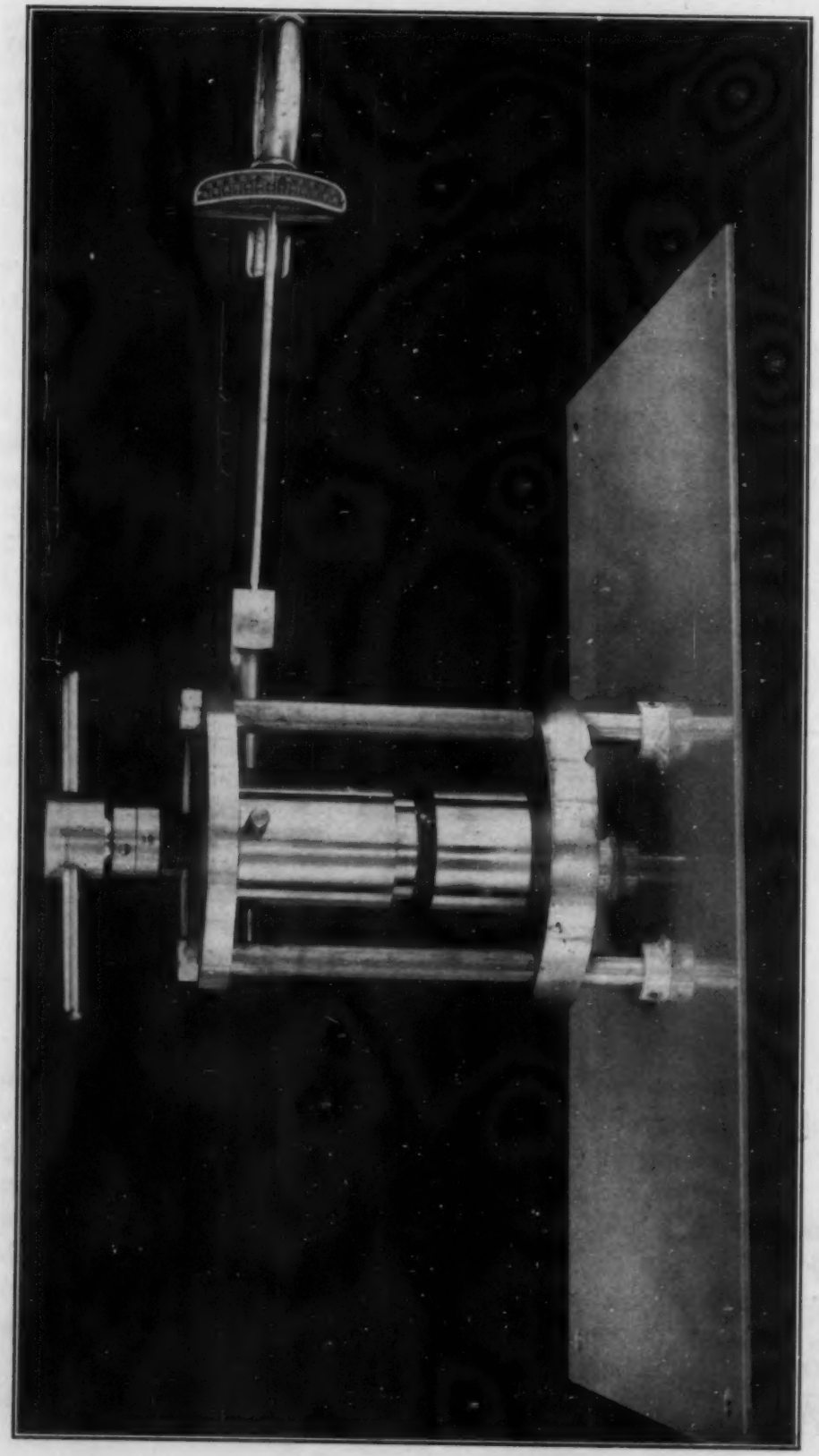


Fig. 5—Press for Forming Diaphragms. Torque wrench shown is for regulation of hold-down pressure on flange (shown turned 90 degrees from operating position).



Fig. 6—Punch and Die Set for Forming Diaphragms. (¼ normal size.)

Stages of Forming

Two stages of forming were investigated: (a) a shallow draw to the point just before the convolutions were formed, corresponding to a diaphragm height of 0.100 inch, and (b) a full draw to a diaphragm height of 0.143 inch, in which the complete convolutions were formed.

Alloys Tested

Four kinds of sheet, approximately 0.0065 inch thick, were investigated.

1. 2% beryllium-copper, quarter-hard, 10% reduction after solution anneal (Berylco 25, diaphragm stock); tensile strength, 81,000 psi; elongation in 2 inches, 34%.
2. 60:20:20 copper-nickel-manganese, quarter-hard, 10% reduction after solution anneal (Chace 720); tensile strength, 99,000 psi; elongation in 2 inches, 33%.
3. Titanium-Elinvar, solution-annealed according to manufacturer (Ni-Span C alloy. Nominal analysis: 42% nickel, 5.5% chromium, 2.5% titanium, balance iron); tensile strength, 109,000 psi; elongation in 2 inches, 15%.
4. Grade A phosphor bronze, extra hard temper, 50% reduction (Elephant Brand No. 16 metal, 4% tin, trace phosphorus); tensile strength, 87,000 psi; elongation in 2 inches, 4%.

Results of Deformation Studies

Figs. 7, 8, 9, and 10 show for diaphragms of beryllium-copper, Chace 720 alloy, Ni-Span C, and Grade A phosphor bronze, respectively, the results of the deformation measurements. In the upper part of each figure the changes in the actual diameters of the rings, $D'' - D$, on forming a complete diaphragm are plotted. In the lower part of each figure the changes in the contour diameters, $D' - D$, on partial and complete forming are plotted. Below both plots is a drawing of a diaphragm partially and completely formed, with arrows issuing from the completely formed diaphragm to the approximate location of the original diameters on the blank from which the diaphragm was drawn.

Comparable results were obtained for all of the diaphragms. Therefore, a detailed discussion of Fig. 7, for beryllium-copper, will serve to illustrate the general deformation of all of the diaphragms.

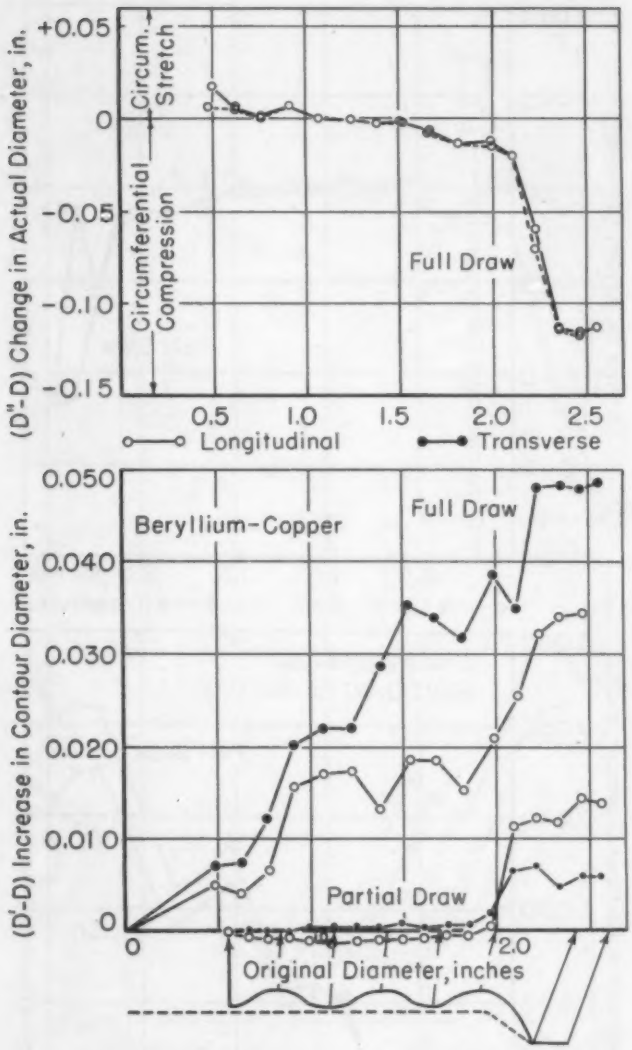


Fig. 7—Deformation in Forming Diaphragms from Quarter-Hard Beryllium-Copper.

Referring to the upper part of Fig. 7, the changes in actual diameter are greatest at the flange, where they are negative in sign. They decrease in magnitude rapidly from the flange to the top of the outer convolution, and then more slowly, crossing over to positive changes in actual diameter at about the middle convolution. Negative changes in actual diameter correspond to circumferential shrinkage or compression, and positive changes to circumferential stretching or expansion. The magnitude of the circumferential shrinkage at the flange amounts to a maximum of $100\,\frac{D'' - D}{D} = 100 \times \frac{0.115}{2.35} = 4.9\%$; the circumferential shrinkage at the outer convolution is $100 \times$

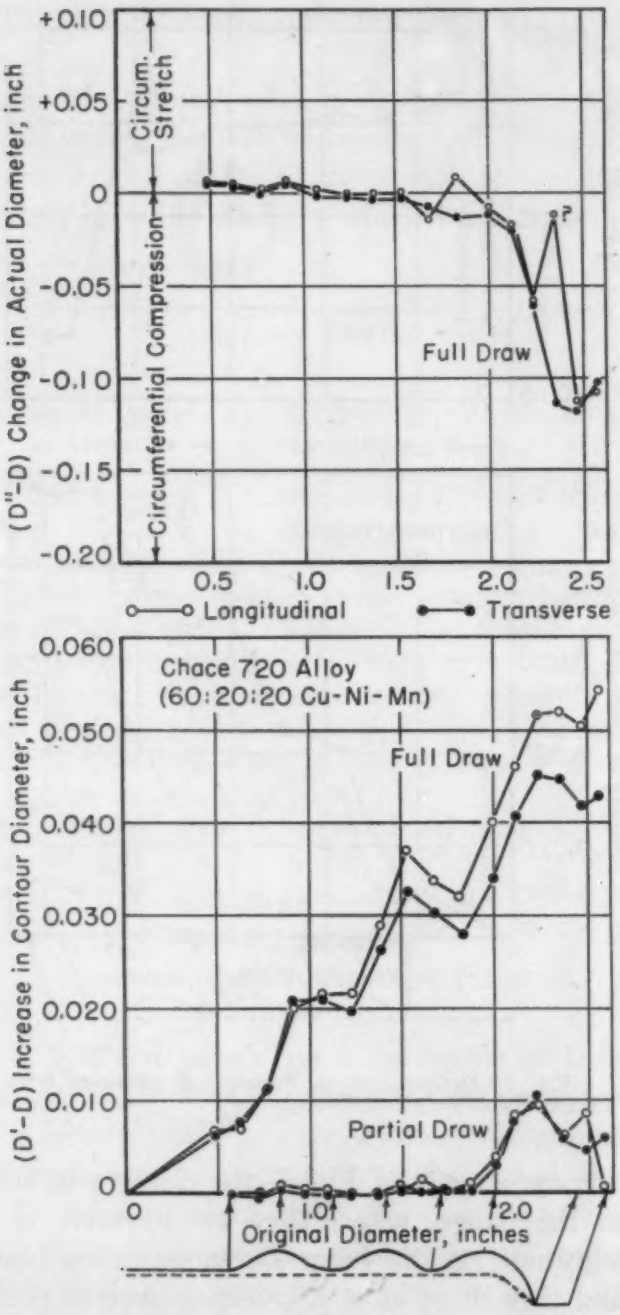


Fig. 8—Deformation in Forming Diaphragms from Annealed Chace 720 Alloy.

$\frac{0.015}{2.0} = 0.75\%$; the neutral middle ring, where neither stretching nor shrinking takes place, has no circumferential deformation; and, finally, the circumferential stretching is a maximum at the edge of the central flat zone, amounting to 1 to 3%.

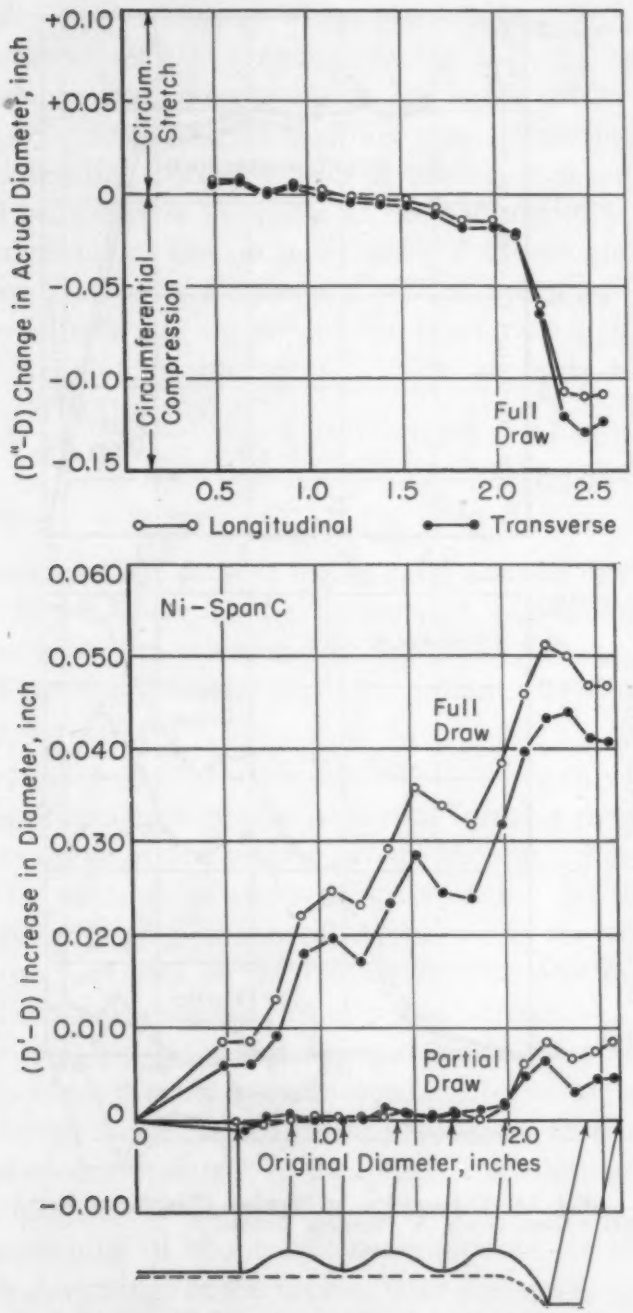


Fig. 9—Deformation in Forming Diaphragms from Annealed Ni-Span C.

Diametral deformation was measured by means of the changes in contour diameter, D′ — D. It will be noted, first, that with the partially formed diaphragm practically all of the deformation takes place in the deep drawn section. The top of the cup is virtually unchanged. In the case of the completely formed diaphragm, the

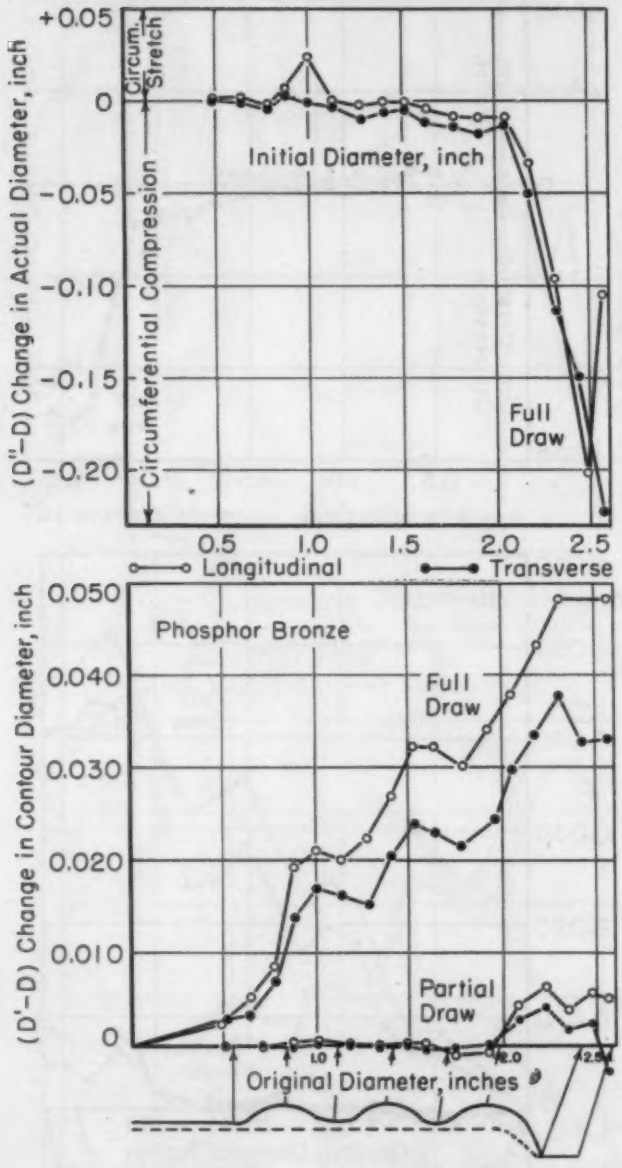


Fig. 10—Deformation in Forming Diaphragms from Extra-Hard Grade A Phosphor Bronze.

change in contour diameter is irregular, consisting of steep sections with positive slope and other sections with flat or negative slopes. The steep sections with positive slope correspond to the tops of corrugations, which were subjected partly to tensile bending during forming. The sections that are flat or have negative slope correspond to the bottoms of corrugations, which were subjected partly to compressive bending during forming. Since the curves of D′ — D pro-

ceed generally upward, away from the abscissa line, there is an over-all diametral tensile straining during forming. The over-all diametral stretching amounts to about 2% in the transverse direction and about 1.5% in the longitudinal direction. Superimposed on this are localized bending forces, tensile in nature at the tops of corrugations, and compressive in nature at the bottoms of corrugations.

The magnitude of the surface diametral deformation can be calculated by application of Equation I. Thus, the steepest part of the contour curves occurs at the top of the inner corrugation parallel to the rolling direction of the sheet. This amounts to a diametral stretching of $\frac{0.0157 - 0.0067}{0.9093 - 0.7640} \times 100 = 6.2\%$. At this point there is a circumferential stretching of $\frac{0.007}{0.9} \times 100 = 0.8\%$. The total surface deformation, then, is close to the value for the diametral stretch. The diametral shrinking at the bottoms of corrugations is smaller in magnitude than the stretching at the tops. Thus, at the bottom between the outer and middle corrugation there is a diametral shrinkage of $\frac{0.0319 - 0.0353}{1.8178 - 1.5246} \times 100 = 1.2\%$.

It is significant to note that in partial forming there is no appreciable deformation of the section where the convolutions are to be formed. This means that the results found for the outside surface of the diaphragm apply in general to the inside surface, except that the tops of corrugations on the outside surface now become bottoms of corrugations with respect to the inside surface.

The general picture of the deformation in forming a diaphragm of beryllium-copper is: (a) there is circumferential compression of about 5% at the flange, which decreases rapidly at the corrugations, where a small compression at the outer convolution changes to a small stretching at the inner convolution; (b) there is an over-all diametral stretching of about 2%, superimposed on which are localized surface stretchings at the tops of convolutions ranging up to 6%, and localized surface compressions up to 1 to 2% at the bottoms between corrugations; (c) the conditions on the inner surface of the diaphragm are probably similar to those on the outer surface, with the positions of the top and bottom corrugations reversed.

The largest deformations, those of diametral stretching at the tops of corrugations, usually the inner one, and circumferential compression at the flange are given for the four diaphragms in Table I.

Table I
Deformation in Forming Diaphragms

Material	Over-all Stretch, % Long.	Over-all Stretch, % Trans.	Diametral Stretch, Top of Inner Convolution, % Long.	Diametral Stretch, Top of Inner Convolution, % Trans.	Circumferential Compression at Flange, % Long.	Circumferential Compression at Flange, % Trans.
Beryllium-copper	2.0	2.7	6.0	5.9	4.9	4.9
Chace 720	3.1	2.4	6.6	6.9	4.5	4.8
Ni-Span C	2.7	2.3	6.5	6.4	4.4	5.2
Phosphor bronze	2.0	1.3	10.2	6.5	8.2	8.7

It can be seen from these results that the maximum localized deformation is in the order of 5 to 10% reduction in thickness, which is not a particularly large figure. Since finite circles were scribed, the results found probably are somewhat lower than the true maximum localized deformation, but because the materials tested had not approached imminent fracture, it is felt that they are of the correct order of magnitude. The only material which could be cracked during the forming operation was the extra hard temper, Grade A phosphor bronze sheet, which after full forming tended to crack in line with the top of the first corrugation in a direction parallel to the grain. Here, the values given may be considerably low.

Effect of Deformation on the Aging Characteristics

Since it was found that the deformation in forming diaphragms consisted of both stretching and contraction, all within 10% reduction of thickness, it was of interest to ascertain by how much the aging characteristics (particularly in regard to time) of the alloys were altered by a 10% deformation. If the characteristics were unaltered, one could age harden the diaphragms according to the aging curve of the original stock without any uncertainty as to its applicability to the formed diaphragm.

The stocks of the age hardening alloys, from which the diaphragms were formed, were cold-rolled an additional 10% reduction in thickness (also 20% reduction in the case of beryllium-copper), and the aging characteristic, tensile strength versus time at aging temperature, was run on the two conditions. Beryllium-copper and the copper-nickel-manganese alloy were heat treated in a salt bath of Houghton No. 430 salt (nitrate bath), and Ni-Span C and phosphor bronze were heat treated in an atmosphere of dry hydrogen.

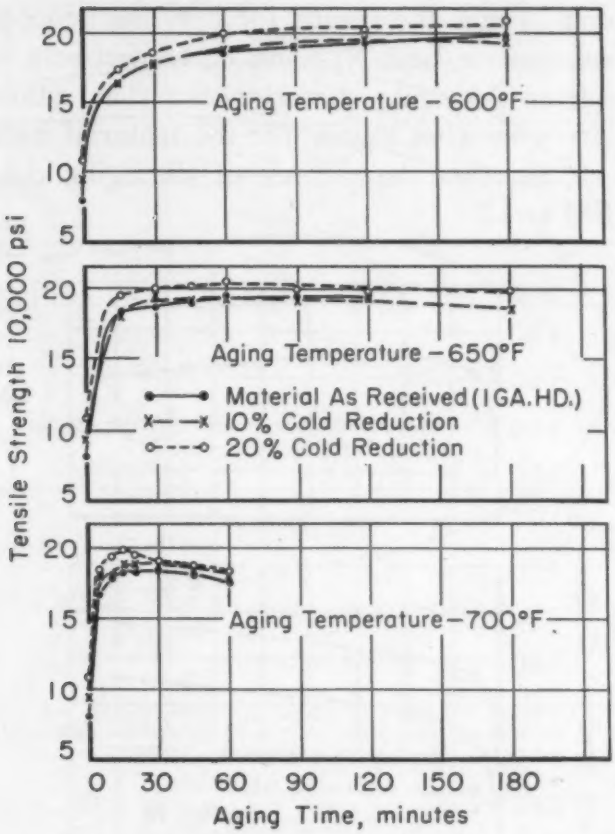


Fig. 11—Effect of Cold Work on Aging Characteristics of Berylco 25 Sheet Material.

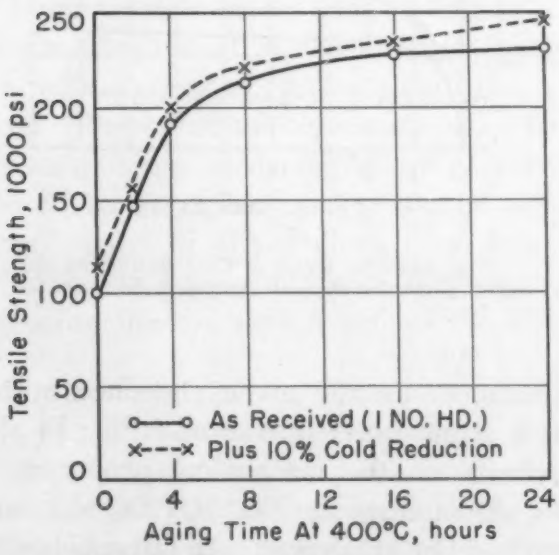


Fig. 12—Effect of Cold Rolling on the Aging Characteristics of 60:20:20 Cu-Ni-Mn Alloy.

Figs. 11, 12, and 13 give the results for beryllium-copper, 60:20:20 copper-nickel-manganese, and Ni-Span C, respectively.

It is seen from the aging characteristics that, although the tensile strengths are somewhat higher for the material with 10% additional cold work, the time dependence of the aging characteristic is scarcely modified at all.

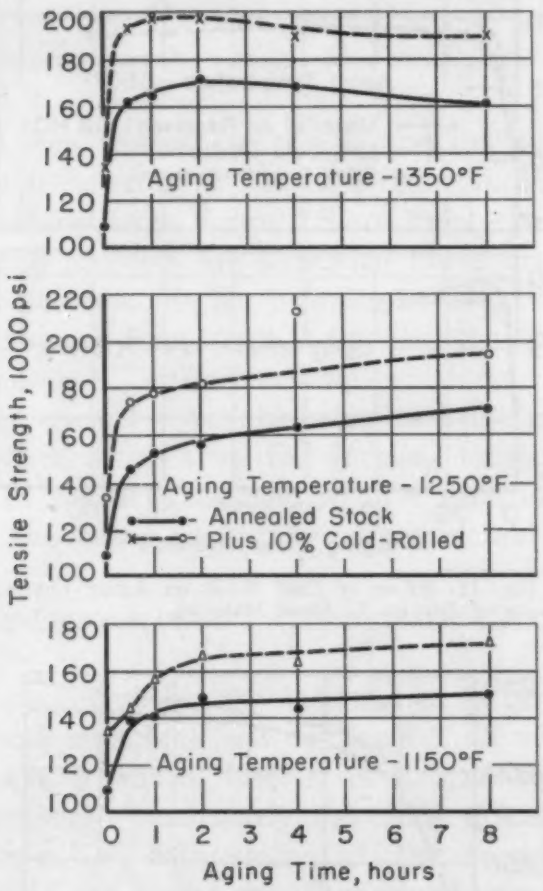


Fig. 13—The Effect of Cold Rolling on the Aging Characteristics of Annealed Ni-Span C.

The heat treatment usually given phosphor bronze diaphragms after forming is a strain-relief operation. Fig. 14 shows the effect of 30-minute reheats on the mechanical properties of this stock. From these data, 30 minutes at 390 °F (200 °C) would appear to be a suitable strain-relief treatment. It is probable that this figure would not be changed by the additional cold work in forming.

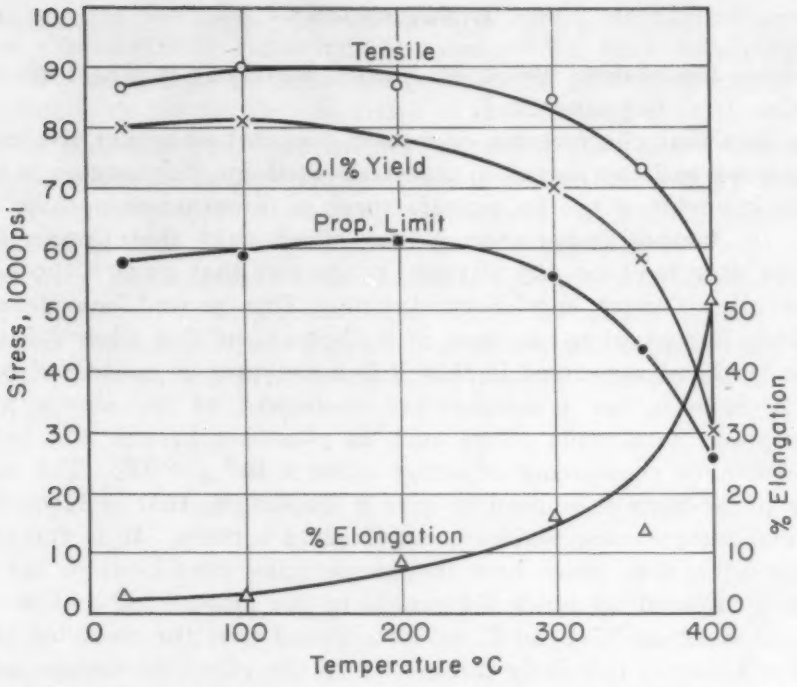


Fig. 14—Strain Relief of Grade A Phosphor Bronze Cold-Rolled 50% Reduction. Effect of 30-minute reheats on mechanical properties.

Conclusions

The cold work involved in forming diaphragms according to the NACA model is very small on an over-all basis. Locally, there is stretching equivalent to 5 to 10% reduction in thickness at the tops of corrugations, with somewhat smaller contraction at the bottom of the corrugations. The effect of deformations of this order on the aging characteristics of age hardening alloys of three common types has been found to be negligible insofar as the time dependence is concerned. Diaphragms of these alloys may then be heat treated according to the age hardening curve of the original stock without danger of decreasing the mechanical properties as a result of over-aging.

Acknowledgments

The authors are grateful to the Signal Corps Engineering Laboratories, Bradley Beach, New Jersey, for permission to publish this work, and to Dr. C. J. Brasefield and Mr. W. D. Huston of that laboratory for their encouragement and suggestions.

DISCUSSION

Written Discussion: By A. M. Talbot, metallurgist, The International Nickel Co., Inc., Bayonne, N. J.

The fact that the forming operation does not endanger the mechanical properties to be expected in materials used for diaphragms is of considerable importance to the manufacturer of pressure-responsive instruments. Of further importance is the effect that these same forming operations may have on any physical properties that govern the behavior of these alloys under service conditions. This second consideration is particularly important in the case of Ni-Span C as this alloy differs from the other three alloys tested in that it is a constant or controlled modulus alloy. Ni-Span C has a temperature coefficient of the elastic modulus which is about zero while alloys such as phosphor bronze and beryllium copper will have coefficients of about -200×10^{-6} per °F. The constant modulus of Ni-Span C is used to give a diaphragm that is insensitive to the normal temperature variation expected in service. It is therefore of particular interest to know how the temperature coefficient of the elastic modulus is affected by small differences in the amount of cold work.

In our work on Ni-Span C we have found that the so-called thermoelastic coefficient is relatively insensitive to the effect of various amounts of cold work. Table II shows the results obtained on one heat of Ni-Span C wire.

Table II

Hardening Treatment	0.2% Offset Yield Str. psi	Tensile Strength psi	Thermoelastic Coefficient per °F
4 hr. 1100 °F	68,000	142,000	-2×10^{-6}
34% cold drawn, 4 hr. 1100 °F	174,000	183,000	-7×10^{-6}
2 hr. 1300 °F	99,000	164,000	$+7 \times 10^{-6}$
34% cold drawn, 1 hr. 1300 °F	190,000	207,000	$+8 \times 10^{-6}$

It will be observed that the change in the thermoelastic coefficient due to the presence of 34% cold work prior to aging is of a small order of magnitude. This indicates that the introduction of about 10% additional cold work in certain areas during the formation of diaphragms will not materially affect the thermoelastic characteristics of Ni-Span C.

A point of minor importance is the properties given in the paper for annealed Ni-Span C. In general, the alloy is furnished for diaphragms with about 10 to 15% cold work and the tensile properties listed for the annealed material seem to be more nearly those of material with about 10% cold work.

Authors' Reply

Mr. Talbot's data on the effect of prior cold work on the thermoelastic modulus of heat treated Ni-Span C alloy make a very welcome supplement to the data presented on the alloy in the paper. The problem

of heat treating Ni-Span C diaphragms to peak mechanical properties and low thermoelastic coefficient appears to be very straightforward, indeed. We agree that an initial temper of 10% cold work appears to be more in line with the tensile properties of the Ni-Span C stock used.

The information published in this paper is a part of a comprehensive research program on aneroid capsules sponsored at Battelle by the Signal Corps. A stress analysis of the aneroid capsule has been published.[2] An investigation of drift and hysteresis of aneroid capsules at room temperature has been in progress for a considerable time, and a paper on the findings to date will be published at a future time. Work is now in progress on the temperature dependence of aneroid capsules and capsule materials. This should provide data on some of the points Mr. Talbot brought up.

[2]H. J. Grover and J. C. Bell, "Some Evaluations of Stresses in Aneroid Capsules," *Proceedings*, Society for Experimental Stress Analysis, Vol. 5, No. 2, 1948.

MECHANICAL PROPERTIES, INCLUDING FATIGUE, OF AIRCRAFT ALLOYS AT VERY LOW TEMPERATURES

By J. L. Zambrow and M. G. Fontana

Abstract

Aluminum and aluminum alloys, a magnesium alloy, low alloy steels, 18-8S stainless steel, Stainless "W", an 8½% nickel steel and aluminum bronze were subjected to mechanical tests in the temperature range—room temperature to —253 °C (—423 °F). Data on the following are reported: fatigue tests at 25, —78 and —196 °C; impact tests at 25, —78, —127, —192 and —253 °C; hardness tests at 25, —78 and —192 °C; and tensile tests at 25, —78 and —196 °C. Equipment, techniques and precautions used in performing these tests are described.

Introduction

THE interest in materials and equipment to operate at very low temperatures has increased tremendously in recent years. However, relatively few data are available in the literature (3)[1] on the mechanical properties of metals and alloys at low temperatures, particularly at temperatures below —78 °C (—108 °F). For example, there is very little information available on fatigue properties at temperatures below freezing and practically none at or below —78 °C (—108 °F). Very little data useful for engineering design are available on low temperature mechanical properties.

This paper covers an investigation of mechanical properties primarily in the temperature range —78 °C (—108 °F) to —196 °C (—320 °F) but some tests were made at —253 °C (—423 °F). Tests at room temperature were also made for comparison purposes.

One purpose in presenting this paper is to make available information that should have widespread interest at the present time. Another purpose is to describe the techniques used which may be of interest to other investigators in this field. Conventional test equip-

[1]The figures appearing in parentheses pertain to the references appended to this paper.

A paper presented before the Thirtieth Annual Convention of the Society, held in Philadelphia, October 23 to 29, 1948. Of the authors, J. L. Zambrow is research engineer, Ohio State University Research Foundation, and M. G. Fontana is professor of metallurgical research, and chairman, Department of Metallurgy, The Ohio State University, Columbus, Ohio. Manuscript received April 30, 1948.

Table I
Composition of the Nonferrous Metals and Alloys

Material	Specifications	Per Cent									
		Si	Fe	Cu	Mn	Al	Mg	Zn	Cr	Ni	Other
2 S Aluminum	QQ-A-4116	0.37	0.37	0.15	0.03*	bal.	0.03*	0.03*	....	0.03*	*0.03 Ti
24 S-T Aluminum	QQ-A-354	0.16	0.43	3.8–4.4	0.6–0.9	bal.	1.2–1.7	0.10*	....	0.05*	*0.05 Bi, Pb
61 S-T Aluminum	QQ-A-325	0.5–0.7	0.41	0.19–0.27	0.15*	bal.	0.8–1.0	0.08	0.19–0.28	....	*0.15 Ti
75 S-T Aluminum[1]	AN-A-9a	0.20	0.45	1.50	0.15	bal.	2.80	5.70	0.30	....	0.05 Ti
FS-1 Magnesium	AN-M-27	0.01*	0.001*	0.01*	0.49	3.10	bal.	1.05	....	0.001*	....
Aluminum Bronze	QQ-B-666	0.02	0.66–1.45	bal.	0.03	9.0	....	....	....	0.50	0.50 Sn

*Less than.
[1]Procured from stock as "commercial heat treated and aged (at 250°F)".

Table II
Composition of the Steels

Steel	Specification	Per Cent									
		C	Mn	P	S	Si	Ni	Cr	Mo	Al	Ti
SAE 2330[1]	AN-QQ-S-689	0.28–0.33	0.60–0.80	0.026*	0.30*	....	3.25–3.75	....	....	....	....
NE 8630[2]	AN-S-14a	0.27–0.33	0.70–0.90	0.022*	0.033*	0.20–0.35	0.48–0.67	0.49–0.56	0.18	....	....
Type 304 Stainless (18-8)[3]	.....	0.054	0.49	0.019	0.015	0.42	8.82	18.50	....	....	....
Type 322 Stainless "W"[4]	.....	0.07	0.43	0.013	0.003	0.53	6.5	17.0	....	0.12	0.37
8½% Nickel[5]	.....	0.10	0.77	0.010	0.024	0.23	8.60	....	....	0.05	0.05

*Less than.
[1]Procured from stock as normalized material. Heat treated material quenched in oil from 1500°F and drawn at 925°F to Rc 33-35.
[2]Procured from stock as normalized material. Heat treated material quenched in oil from 1500°F and drawn at 850°F to Rc 33-35.
[3]Cold-rolled to 210,000 psi tensile strength.
[4]Air-cooled from 1900°F and aged at 1000°F for 40 minutes. Tensile strength 188,000 psi.
[5]Heat treated as follows: 1 hr. at 1650°F—air cool; 1 hr. at 1450°F—air cool; 2 hr. at 1050°F—air cool.

ment is generally used, but some modification, special techniques and precautions are required for testing at very low temperatures. Methods of testing and also methods for attaining and maintaining these temperatures are described. The work reported in this paper was carried out at the Engineering Experiment Station under a contract between the Ohio State University Research Foundation and the Materials Laboratory, Engineering Division, Air Materiel Command, Wright-Patterson Air Force Base, Dayton, Ohio.

Materials

The materials studied are all commercially available and they included 2S-¾H, 24S-T, 61S-T, and 75S-T aluminum alloys,

Dowmetal FS-1 (magnesium alloy), SAE 2330 steel, normalized and also heat treated to about 150,000 psi tensile strength, NE 8630 steel, normalized and also heat treated to 150,000 psi tensile strength, 18-8 stainless steel (Type 304), severely cold drawn to 210,000 psi tensile strength, and also annealed at three temperatures, age-hardened Stainless "W" (Type 322), and aluminum bronze. Tables I and II show the chemical compositions of the materials tested, the specification under which the materials were bought, and the heat treatment. All of the material was in the form of ¾-inch rounds, and most of it was furnished by Wright Field.

Apparatus

Fatigue Tests—Krouse reciprocating-cantilever-beam machines of the constant deflection type were redesigned for this work. This type of machine is often used for the fatigue testing of plate specimens. The principal modification for our work consisted of a 90-degree rotation of the supporting beam for the vise so that the specimen was in a vertical position instead of horizontal. The speed of the machine was adjustable over the range of 750 to 2000 cycles per minute. For the low temperature tests the specimen was surrounded by a split metal Dewar filled with a liquid coolant. By Dewar, we mean a double-walled vessel with the space between the walls evacuated for thermal insulation. Fig. 1 shows the fatigue unit being loaded and one-half of the Dewar in position. Fig. 2 shows the apparatus just prior to starting a run. Frosting on the outside of the Dewar is just beginning.

The advantages of this type of machine can be summarized as follows:

(a) The specimen is vertical and the coolant can easily be contained in the Dewar surrounding the specimen.

(b) All bearings are a considerable distance from the coolant.

(c) Less heating of the specimen occurs because the maximum stress is applied only to a small portion of the specimen.

(d) No stuffing boxes are required to seal the Dewar. The seal is stationary and rotating seals are not required.

(e) A thermocouple can be attached to the neutral axis of the specimen for a direct measurement of the temperature of the specimen.

The desired stress was applied to the specimen by hanging the

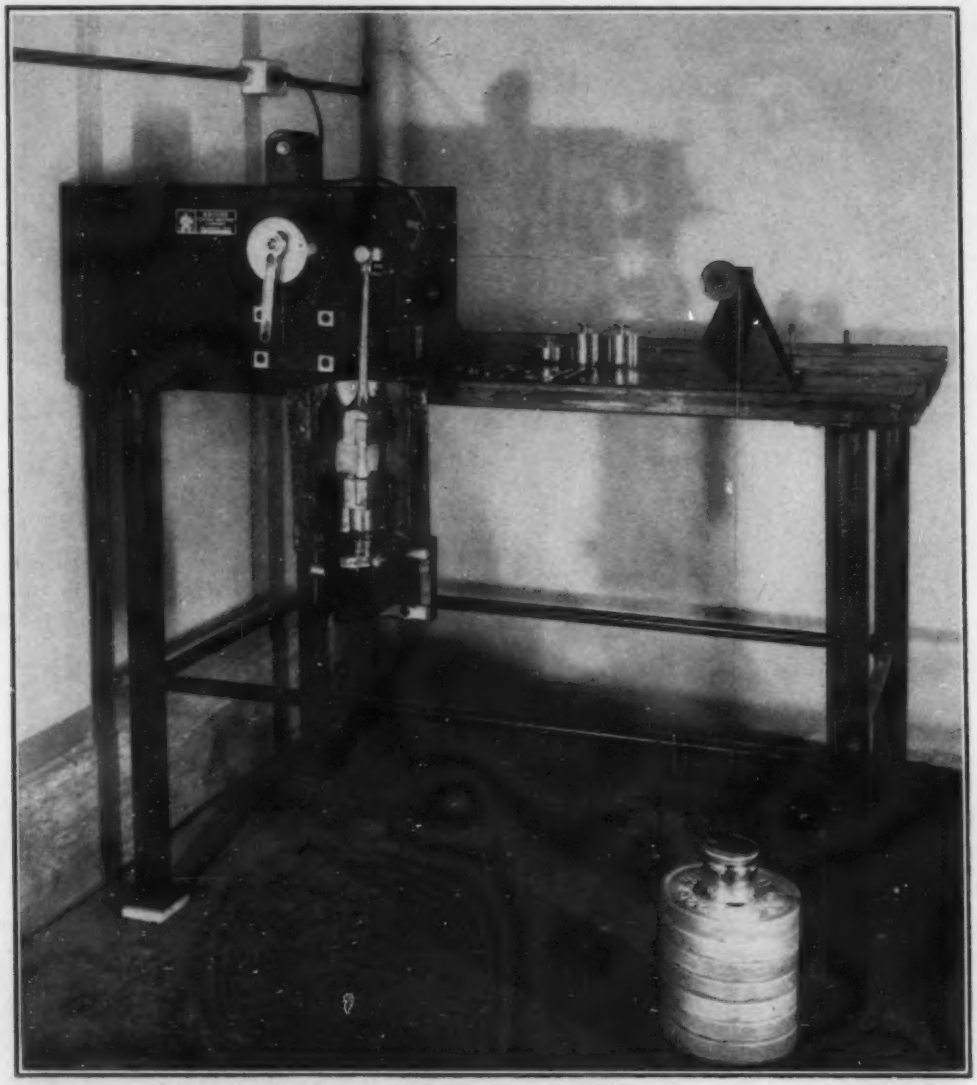


Fig. 1—Reciprocating Beam Fatigue Machine.

corresponding dead weight from the connecting rod bearing (Fig. 1), and an electronic indicator was used to indicate the point to which the beam deflected under the given load. The connecting rod was then attached to the beam and the eccentric was adjusted to produce the same deflection. The specimen was carefully aligned in the machine so that the reversed stress (compression) was of the same magnitude. The machine was occasionally stopped for a few minutes during a test to check the loading of the specimen.

The dynamic loading of the specimen was checked with an electric strain gage by the manufacturer of the machine. The results of these tests indicated that the dynamic stress was within 2% of the

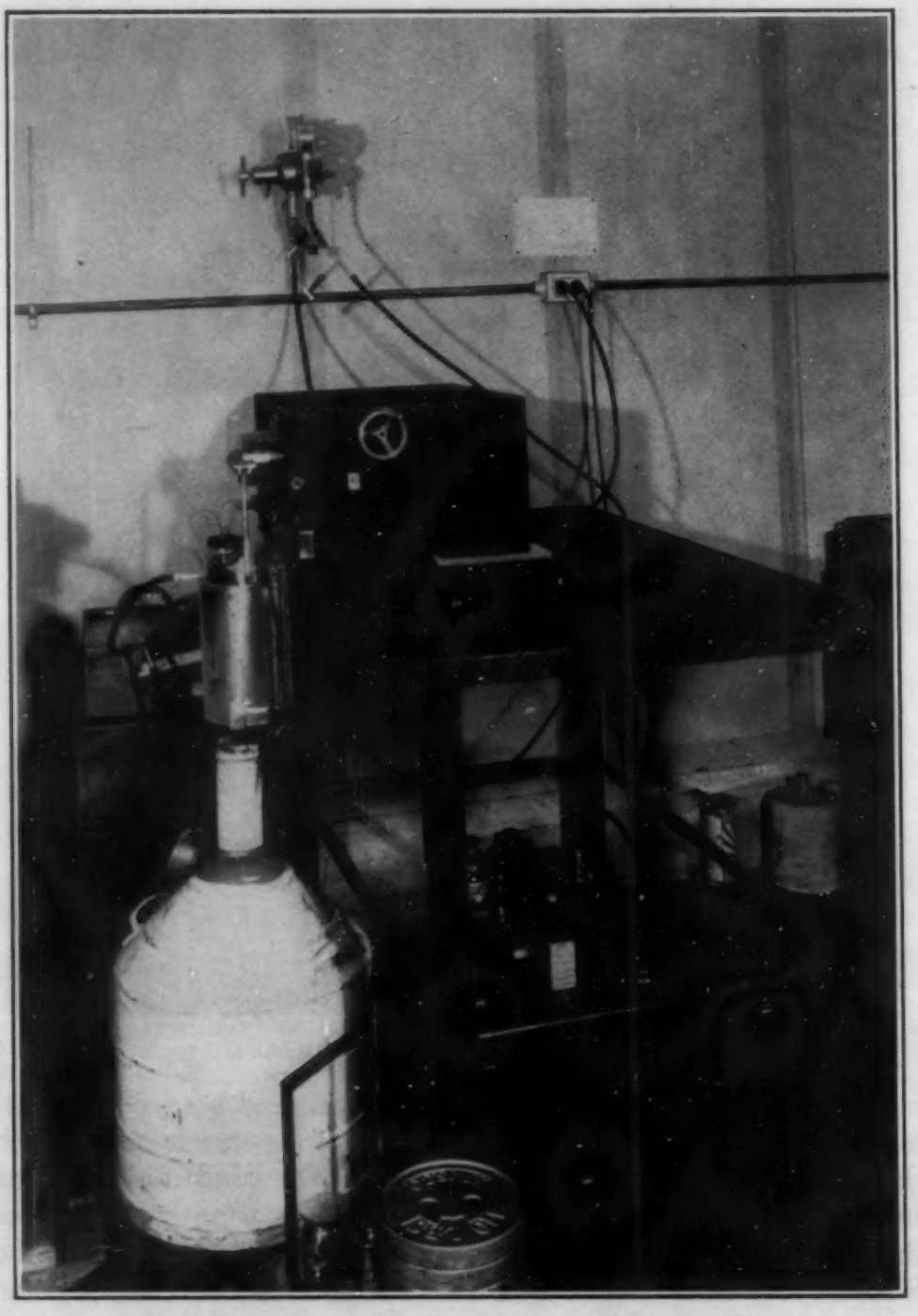


Fig. 2—Apparatus for Low Temperature Fatigue Testing.

static stress over the range of speeds available and within the limit of stress which could be checked with this gage (approximately 30,000 psi).

Since most of the investigations on the fatigue of metals have been carried out with rotating-beam machines, it was decided to determine whether or not the reciprocating-beam machine would yield similar results. A few tests were made with a rotating-beam machine for comparison.

The machine used was an R. R. Moore type which had been designed for high temperature work. Tests were made at room temperature and —78 °C. For the tests at —78 °C, the specimens were placed in the Dewar shown in Fig. 3 and immersed in a coolant consisting of methylcyclohexane and dry ice. The sealing of the Dewar was accomplished by pulleys which were fastened to the specimen with set screws. It was necessary to add a small quantity of motor oil to the methylcyclohexane to reduce the surface tension before the seal became effective. Obviously, this method of sealing was effective only while the specimen was rotating at high speed. It was too inefficient for use at lower temperatures.

Impact Tests—Almost all of the impact tests were made on a Riehle impact testing machine using the 220 ft-lb initial position (18.1 feet per second). A few tests were made on an Amsler impact testing machine using the 35 ft-lb initial position (9.6 feet per second).

Hardness Tests—A Vickers machine was used for the hardness tests in this investigation. The specimen was contained in a metal dish with a bottom rigid enough to withstand the necessary loads. When liquid air or dry ice was used as a coolant, the considerable gas released agitated the liquid and the specimen was efficiently cooled. The simple metal-lined wooden dish shown in Fig. 4 was a satisfactory container for the coolant and specimen.

Tensile Tests—A four-screw, 60,000-lb capacity, Olsen Universal testing machine was used for the tensile tests. It is a mechanically-loaded type equipped with a pendulum-lever weighing system, an electric extensometer, and an autographic recorder. For low temperature tests, the specimen was surrounded by a metal Dewar as shown in Fig. 5. This figure shows a test in progress to determine ultimate strength at —253 °C (—423 °F) using liquid hydrogen as the cooling medium. The hood and exhaust blower system are provided for safety.

Strain measurements were made with a Tuckerman gage fitted with extension arms. An open view of this apparatus is shown in Fig. 6.

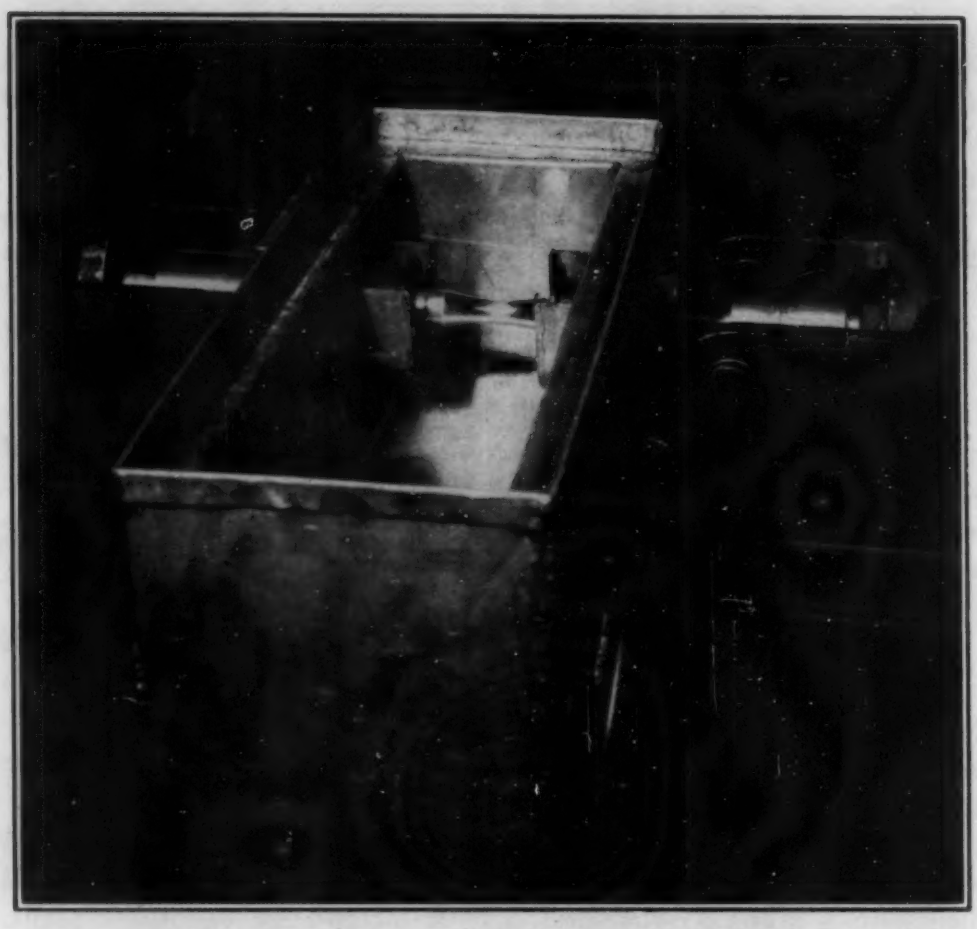


Fig. 3—Dewar for Rotating Beam Machine.

All temperature measurements were made with a copper-constantan thermocouple used in conjunction with a Leeds and Northrup potentiometer indicator.

Fatigue Tests—A sketch of the finished fatigue specimens is shown in Fig. 7. The reduced sections were either 0.50 or 0.30 inch in diameter, and the radii of the profiles of the reduced sections were 4 and 2⅝ inches respectively. The bars as received were cut into sections 5 inches long. The center portions of these bars were then turned down, leaving about 0.004 inch on the diameter for polishing. The reduced section was then highly polished with a polishing wheel, having the same radius as the specimen profile, using 180-grit abrasive and keeping the plane of the wheel parallel to the longitudinal axis of the specimen.

Fatigue tests were made at room temperature, —78 °C (temperature of dry ice), and at —196 °C (temperature of liquid nitro-

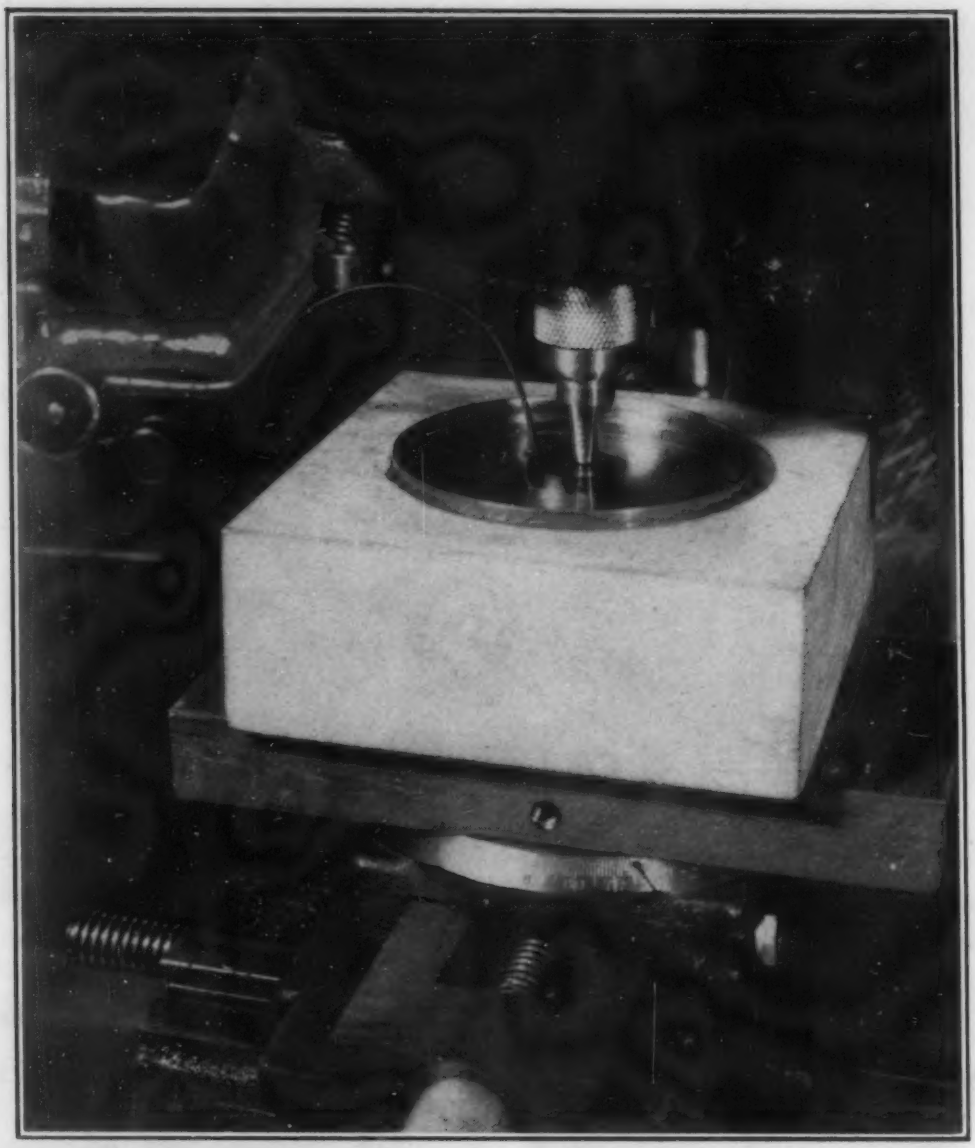


Fig. 4—Apparatus for Low Temperature Vickers Hardness Tests.

gen). In the room temperature tests at high stress levels, the specimens (particularly the steels) became quite hot, but only for short periods of time because the machine was frequently stopped for calibrating. In the low temperature tests, no temperature rise was observed in the specimens at any time. Apparently, all the heat generated was readily absorbed by the bath.

The initial plan of the fatigue portion of this work was to determine the endurance limit of the materials over the low temperature range described above. However, emphasis was subsequently placed

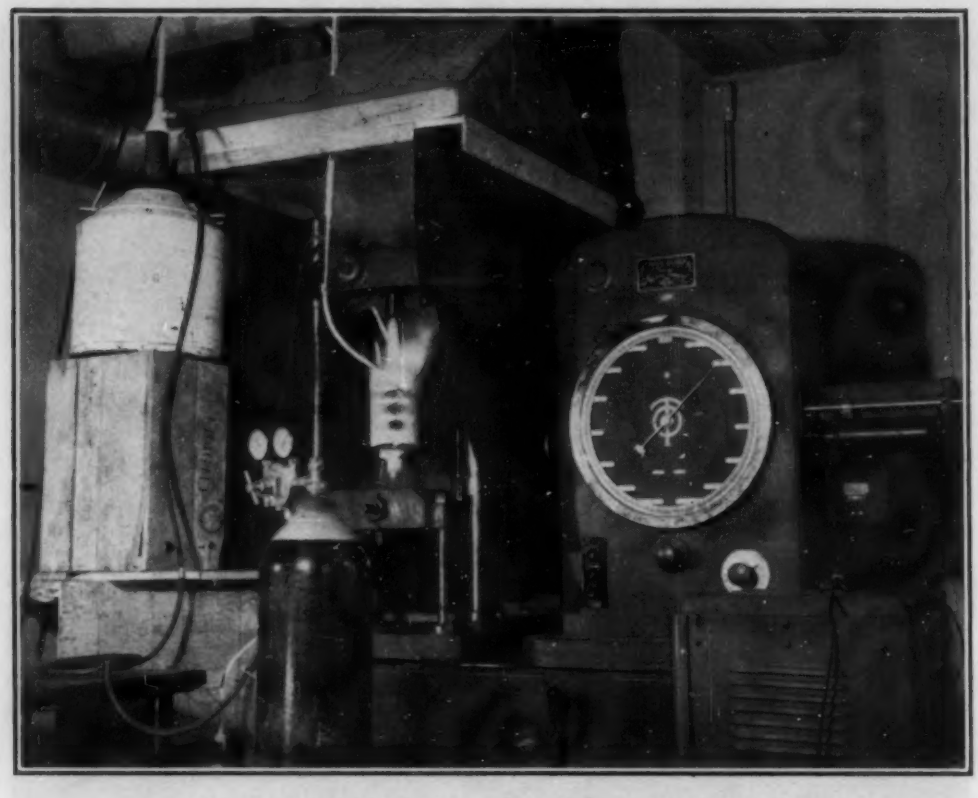


Fig. 5—Apparatus for Low Temperature Tensile Tests.

on tests in the high stress-low cycle region and, accordingly, a large portion of the data presented herein concerns the "left-hand" portion of the S-N curve.

The nominal stress for the tests was based on the relation $M = S \frac{I}{c}$; where M is the moment in inch-pounds, S is the stress in psi, and $\frac{I}{c}$ is the section modulus. Since many of the tests were performed above the yield point, the value of S thus obtained was not the true stress, but it did furnish a quantitative basis on which to evaluate the results.

Although the machine was a constant-deflection type, it was desirable to maintain the stress as nearly constant as possible during the test. Some of the materials were very susceptible to work hardening, so it was necessary to adjust the eccentricity at intervals during the test. A series of tests indicated that only a few cycles were required to accomplish the major portion of the work hardening, and that thereafter the deflection for a given moment was fairly constant.

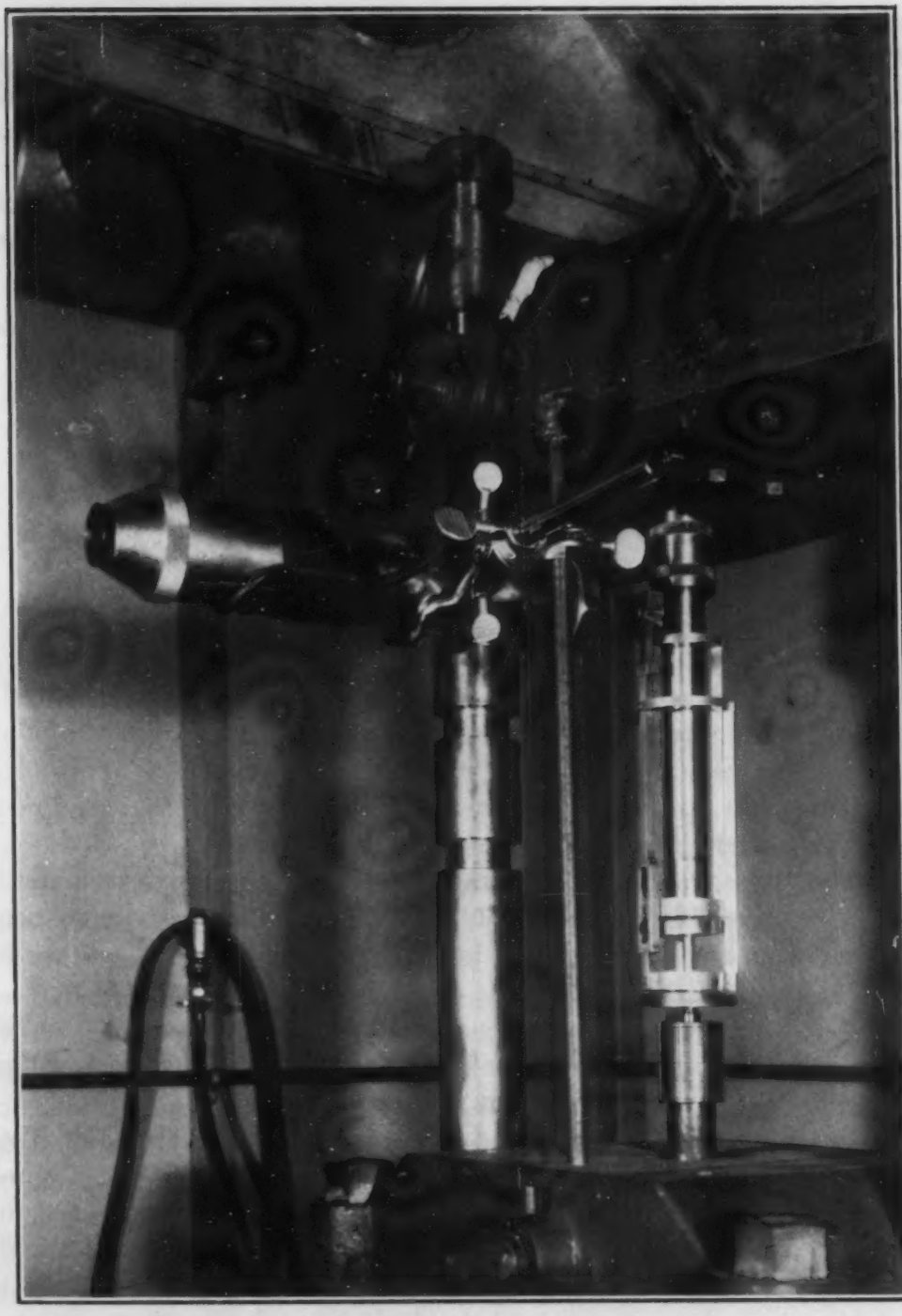


Fig. 6—Tuckerman Gage and Extension Arms.

The following procedure was, therefore, adopted for all high stress tests. After the initial deflection for a given load was determined, the machine was turned about 10 cycles manually and another

calibration made. If there was an appreciable change in the deflection, the procedure was repeated until the deflection approached a constant value. The motor was then used to drive the machine and checks were made at progressively longer intervals until the deflection was constant or the specimen failed.

The initial test for any alloy was usually made at a nominal stress of about the same magnitude as the ultimate strength of the

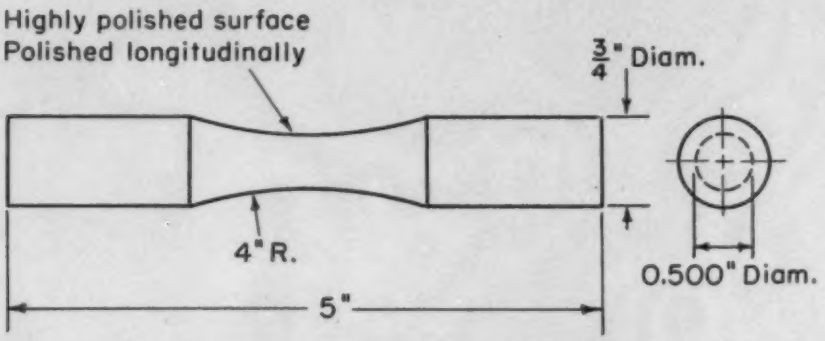


Fig. 7—Specimen for Low Temperature Fatigue Tests.

alloy. The specimen was then run until a visible crack appeared. This was done because the specimen was not visible in the low temperature tests and a definite indication of failure was desirable. In many cases, the crack progressed so rapidly that the specimen failed completely before the machine came to a stop.

The stress was raised progressively for the successive tests until failure occurred between 1000 and 2000 cycles. The stress was then lowered from that used for the initial test until the specimen withstood at least 100,000 cycles.

The rotating-beam machine was a constant-stress type so the desired moment was obtained and maintained simply by placing the corresponding dead weight on the weight pans. For the low temperature tests of the steel, the weights were placed on the pans after the machine was started. For the low temperature tests of the aluminum alloy at stress above the yield point, however, the loads used to obtain the desired stresses resulted in a greater deflection than could be accommodated without adjusting the position of the Dewar. It was, therefore, necessary to load the specimens at room temperature. The loaded specimens were then chilled before starting the test.

Charpy Impact Tests

Standard Charpy bars with a keyhole notch were used for most

of the impact tests (ASTM Designation: E23-41T, Fig. 3B). Each specimen was cut from the center of the bar to assure uniformity of test conditions. After machining, the specimens were polished so all scratches were longitudinal.

Test Conditions—The specimens were tested at room temperature; at the temperature of an acetone-dry ice mixture (—78 °C);

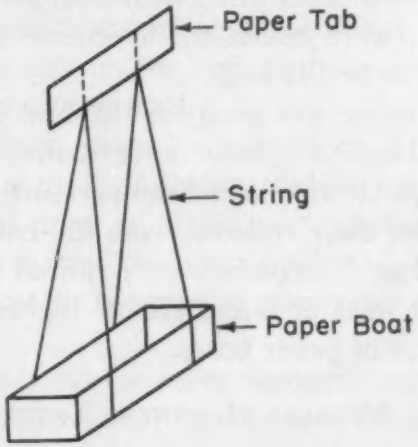


Fig. 8—Paper Boat Used to Transfer Low Temperature Specimens From Container to Impact Testing Machine.

at the melting temperature of methylcyclohexane (—127 °C); at the temperature of liquid air (—192 °C); and at the temperature of liquid hydrogen (—253 °C). The steel specimens were tested at —10 and —30 °C, also, to trace the steep drop in impact strength which occurred between room temperature and —78 °C. The specimens were immersed in the bath at the desired temperature for half an hour before testing. The bath for —10 and —30 °C was methylcyclohexane which had been chilled to, and was maintained at, the desired temperature with liquid air.

Technique—The specimens that were tested at the temperature of liquid hydrogen were cemented into paper boats before being immersed. The boat served as a container for the liquid hydrogen while the specimen was transferred from the hydrogen container to the testing machine, thus preventing a rise in the temperature of the specimen during the transfer. The boats were constructed as shown in Fig. 8. A perforated paper cover was placed over the boat before immersing to keep the hydrogen from bubbling out during the trans-

fer. The strings and paper tab were used to facilitate the immersion and withdrawal of the specimens from the Dewar flask.

After the specimen had soaked for ½ hour, the boat was withdrawn and placed on the anvil of the testing machine. As soon as the boat was positioned, the strings were cut and the pendulum was released. About 5 seconds were required for this operation.

The use of the boat introduced a correction into the absorbed energy reading, so two boats filled with liquid hydrogen, but with no specimens in them, were tested to determine the correction factor. It was determined to be 0.2 ft-lb.

A similar technique was used for the first impact tests at liquid air temperature. However, tests were made which indicated that there was no perceptible rise in the temperature of the specimens for about 7 seconds after their removal from the bath without the use of boats. Since less than 5 seconds were required to position the specimen, all subsequent tests at liquid air, or higher, temperatures were made without the use of paper boats.

Vickers Hardness Tests

Cylinders about ½ inch long were cut from the ¾-inch diameter bars for hardness test specimens. The ends were faced in a lathe and polished down to a 2/0 grit paper.

Five impressions were made with a diamond pyramid at regular intervals along two radii of the specimen, at 90 degrees to each other. The average hardness number for these ten impressions was then taken as the hardness number for the specimen.

Impressions were made at room temperature, —78 and —192 °C (—108 and —313 °F). In the low temperature tests, the specimen was placed in the metal-lined wooden dish shown in Fig. 4. The impressions were made while the specimens were immersed in a coolant (acetone and dry ice for —78 °C (—108 °F), and liquid air for —192 °C), and the impressions were measured after the specimens were brought back to room temperature. Tests were made in which the impressions were made and measured while the specimen was immersed in liquid air. These tests indicated that the increase in diagonal length caused by thermal expansion did not significantly change the hardness number.

Tensile Tests

The modulus of elasticity was determined by taking strain read-

ings with the Tuckerman gage at 500-pound increments of load until a total load of 5000 pounds or one-half the yield strength (whichever was the least) was reached. The machine was stopped for each reading. Modulus of elasticity determinations were made at room temperature and —78 °C (—108 °F). The same specimens were used for both temperatures because it was felt that the variation in modulus from one specimen to the next might mask the effect of the temperature. Previous hardness tests had indicated that no permanent structural changes occurred in these alloys as a result of the relatively short exposures to low temperatures which the specimens were subjected to during the tests.

Standard 0.505-inch diameter specimens (ASTM designation E8-46) were used for most of the tensile tests in this investigation. Because of the limited capacity of the machine, the specimens for the tests of the high strength alloys were made 0.357 inch in diameter. The per cent elongation for the smaller specimens was based on a gage length of 1.4 inches.

Tensile tests were made at room temperature, —78 °C (dry ice) and —196 °C (liquid nitrogen). At the low temperatures, the specimens were soaked in the bath for about 15 minutes before starting the test.

Strain measurements for the determination of the yield strength were also made with the Tuckerman gage. Readings were taken at sufficiently small intervals to definitely establish the stress-strain curve. In each case the yield point was determined by a 0.2% offset.

It was necessary to remove the extension arms from the specimen after the yield strength had been determined to avoid breaking the pointed screws with which the arms were attached to the specimen. In order to do this, the load had to be released, and the specimen taken out of the bath. The specimen was immediately replaced in the machine and loaded to failure.

All measurements for the determination of the elongation and the reduction of area were made after the test specimens returned to room temperature.

Results and Discussion

The results of the rotating-beam and reciprocating-beam fatigue tests of the normalized SAE 2330 steel at room temperature and —78 °C (—108 °F) are illustrated in Fig. 9. The tests were car-

ried only to 85,000 psi because that was the maximum capacity of the rotating-beam machine. The results of similar tests of the 24S-T aluminum are illustrated in Fig. 10.

The slope of the S-N curve for the room temperature reciprocating-beam tests of the normalized SAE 2330 steel was steeper than that for the rotating-beam tests. The difference in the curves was probably caused by the difference in the stress patterns which were developed in the specimens in the two tests. A greater portion of the section was stressed to the nominal value in the rotating-beam tests than in the reciprocating-beam tests, thus increasing the probability of stressing a "defective" or "susceptible" area, and also causing the generation of a greater amount of heat. No temperature measurements were made in the rotating-beam tests (at room temperature), but at the higher stress levels the specimens became hot, whereas in the reciprocating-beam tests at the same stress levels the specimens reached a temperature of only a few degrees above room temperature. At —78 °C there was considerable scatter in the results obtained with both machines, but the curves appeared to be approximately parallel to the room temperature curves. It was noted that at the lower stress levels above the endurance limit there was little difference in the values obtained with both machines, and also there was only a slight difference in the values obtained for the endurance limit.

The curves for the room temperature tests of the 24S-T aluminum obtained with the two machines were almost identical. Also, there appeared to be no difference between the curves obtained with the rotating-beam machine at room temperature and —78 °C. The specimens were loaded at room temperature and then chilled to —78 °C before the test was started and this was believed to be the cause of the similarity of the curves.

The results of the reciprocating-beam fatigue tests of the normalized and hardened SAE 2330 steel, normalized and hardened NE 8630 steel, cold drawn 18-8S stainless (Type 304), hardened Stainless "W" (Type 322), and 8½% nickel steel at room temperature, —78 °C (—108 °F), and —196 °C (—321 °F) are illustrated in Figs. 11 to 17 respectively. In each case the fatigue strength at the high stress levels increased with decreasing temperature. It appeared that the curves for the SAE 2330 steel converged at the lower stress levels and that the endurance limit at —78 °C was only slightly greater than at room temperature. At —196 °C, however, the curve

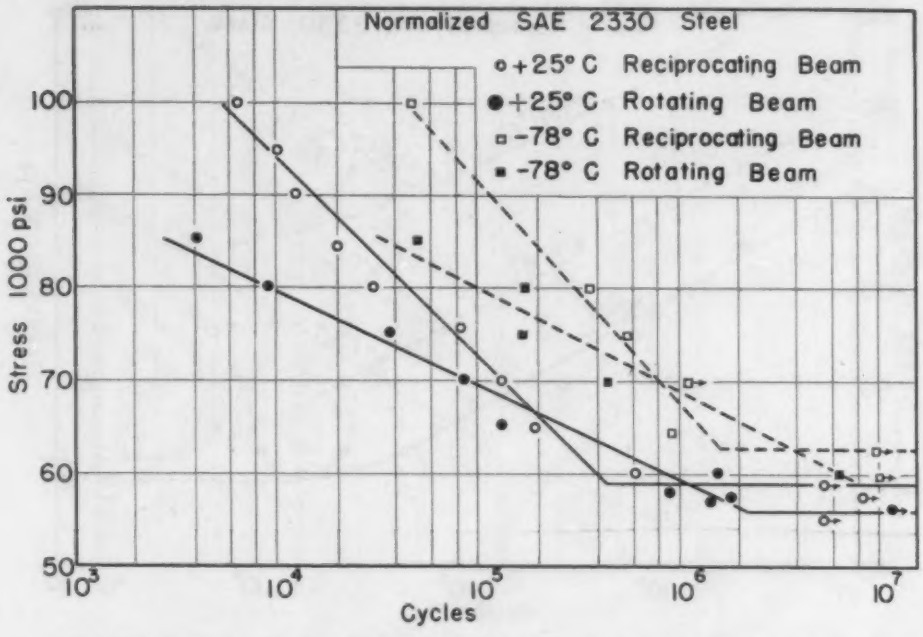


Fig. 9—Fatigue Tests of Normalized SAE 2330 Steel at Room Temperature and —78 °C.

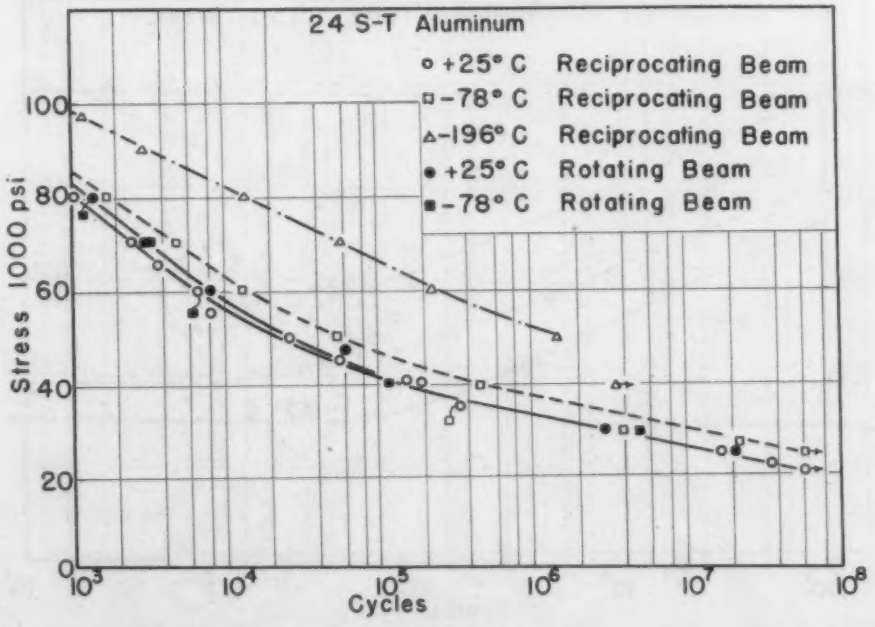


Fig. 10—Fatigue Tests of 24 S Aluminum at Various Temperatures.

was much higher than at —78 °C and appeared to be substantially parallel to the room temperature curve.

The hardened SAE 2330 steel showed a definite increase in endurance limit (75,000 psi at room temperature to about 90,000 psi

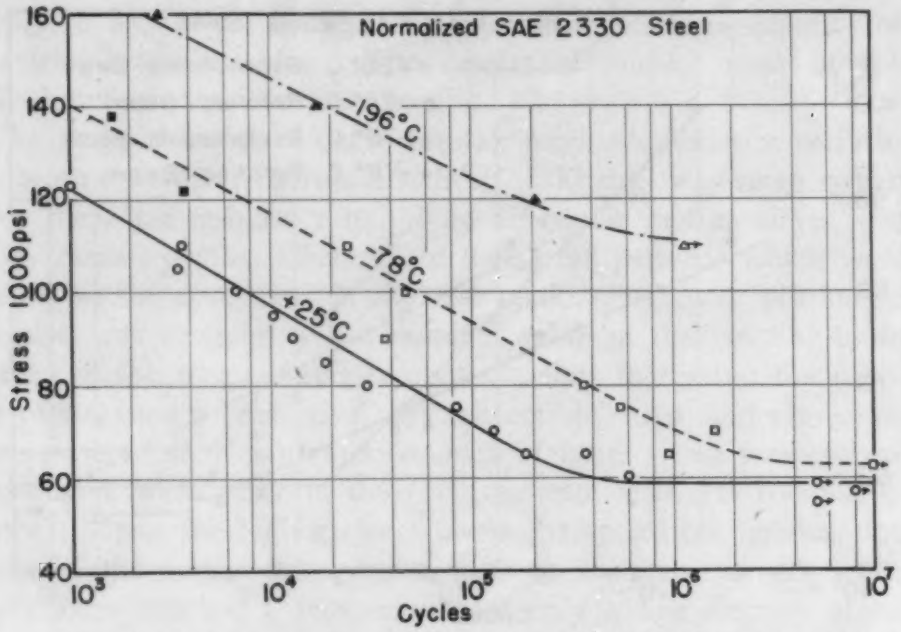


Fig. 11—Reciprocating Beam Fatigue Strength of Normalized SAE 2330 Steel at Various Temperatures.

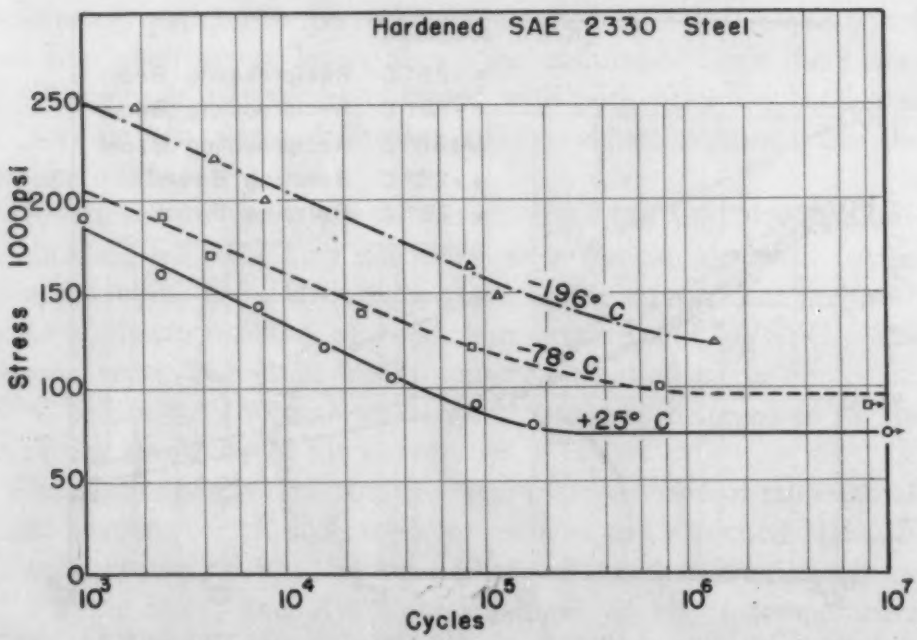


Fig. 12—Results of Reciprocating Beam Fatigue Tests of Hardened SAE 2330 Steel at Various Temperatures.

at −78 °C), although the increase was not as great as anticipated from the results of the high stress tests.

The curve for the NE 8630 steel at −78 °C was higher than that for room temperature, but it did not have a sharp "knee" and

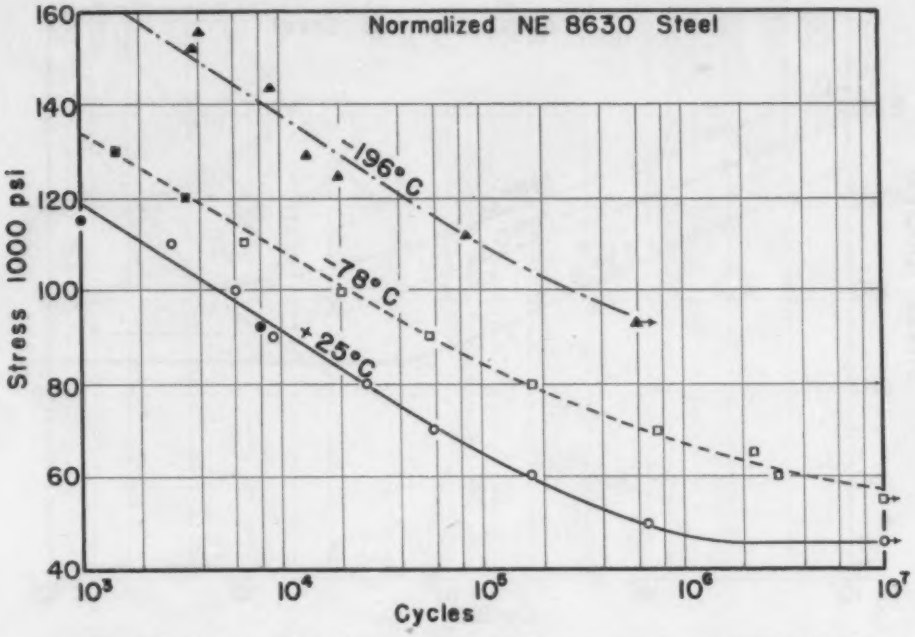


Fig. 13—Reciprocating Beam Fatigue Strength of Normalized NE 8630 Steel at Various Temperatures.

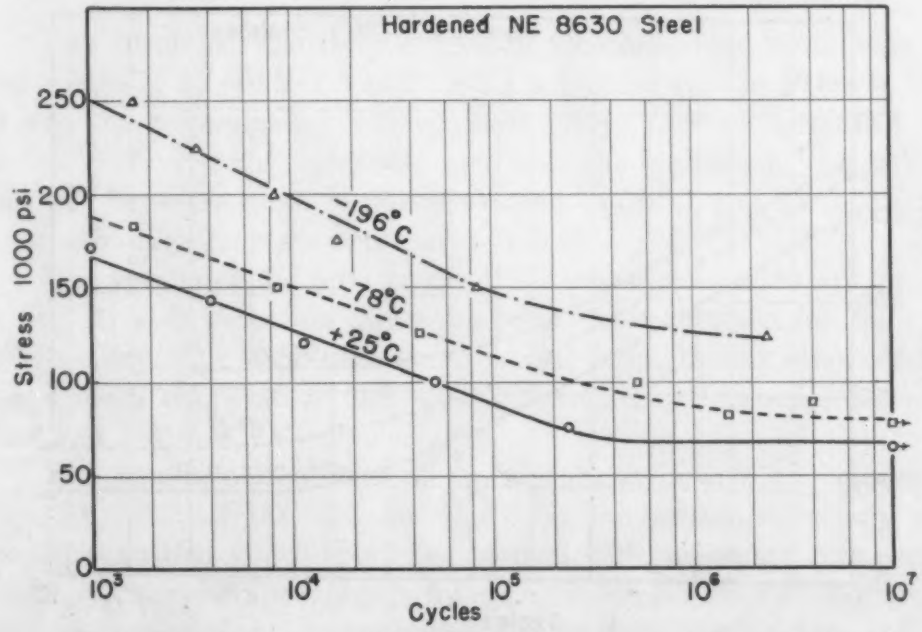


Fig. 14—Results of Reciprocating Beam Fatigue Tests of Hardened NE 8630 Steel at Various Temperatures.

appeared to be converging on the room temperature curve. The curve for —196 °C was considerably higher than the curve for —78 °C and was parallel to it within the range of stresses tested.

The curves for the hardened NE 8630 steel and the stainless

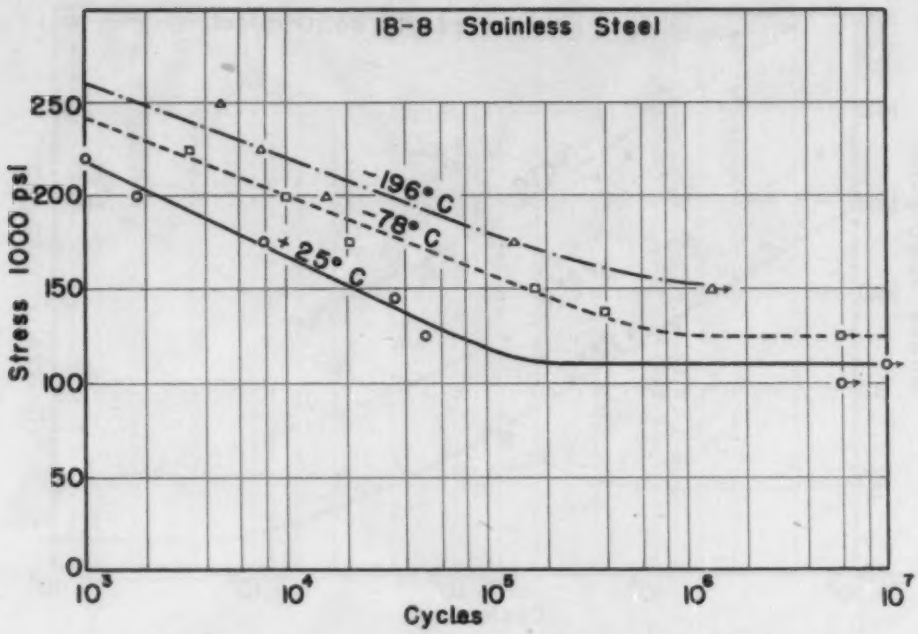


Fig. 15—Reciprocating Beam Fatigue Strength of 18-8 Stainless Steel at Various Temperatures.

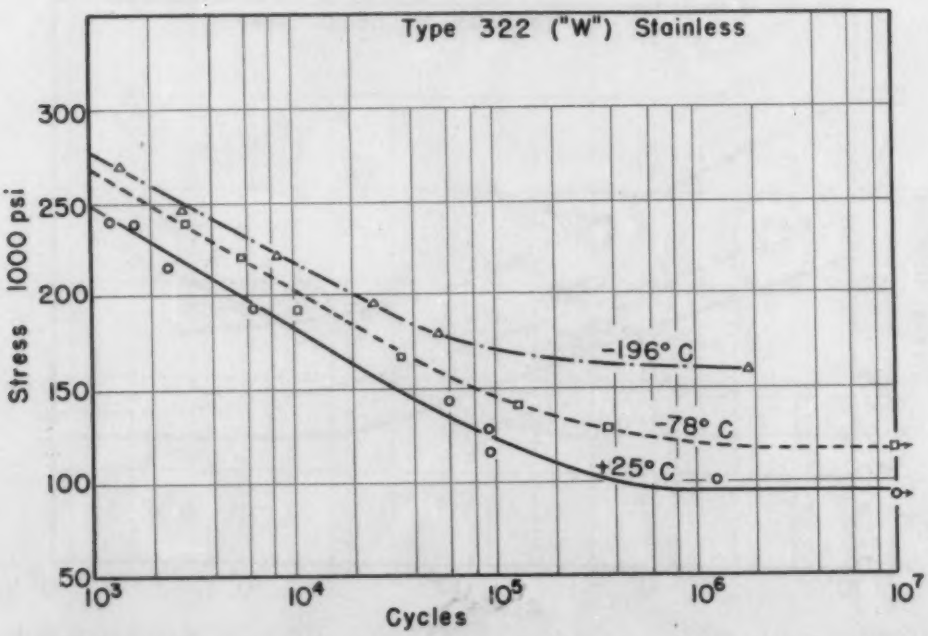


Fig. 16—Results of Reciprocating Beam Fatigue Tests of Type 322 ("W") Stainless Steel at Various Temperatures.

steels were similar to those for the hardened SAE 2330 steel. There appeared to be a definite increase in endurance limit with falling temperature, the increase between —196 °C and —78 °C being slightly greater than that between —78 °C and room temperature.

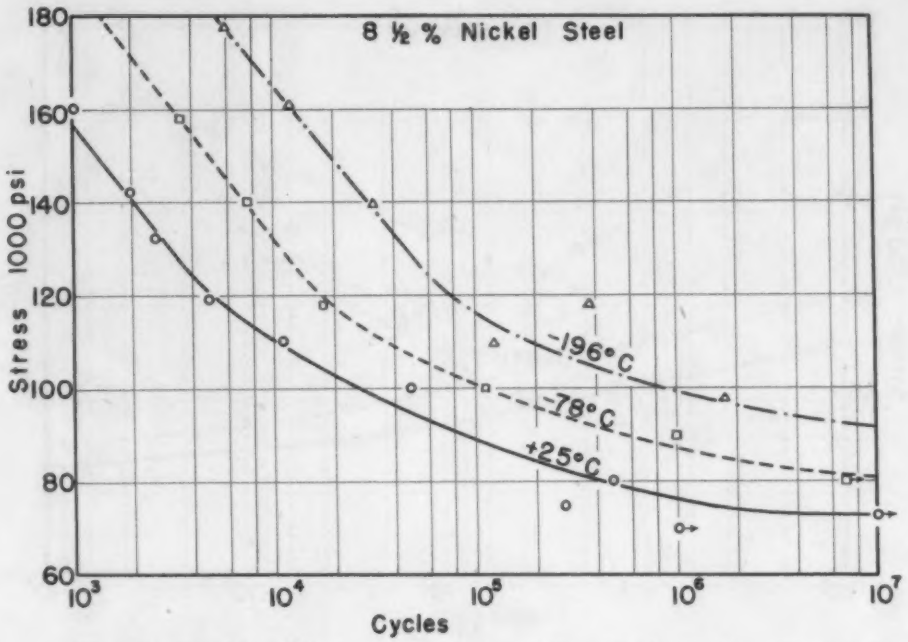


Fig. 17—Results of Reciprocating Beam Fatigue Tests of Normalized 8.5% Nickel Steel at Various Temperatures.

The results of the fatigue tests of aluminum and aluminum alloys (24S-T, 2S, 61S-T and 75S-T) are illustrated in Figs. 10, 18, 19 and 20 respectively. All of these alloys showed a similar behavior in the tests. There was only a slight increase in the fatigue strength between room temperature and —78 °C and then a comparatively large increase between —78 and —196 °C.

The results of the tests of the FS-1 magnesium alloy are shown in Fig. 21 and were just the opposite of those obtained for the aluminum alloys. A large increase in fatigue strength was observed between room temperature and —78 °C and a small increase between —78 and —196 °C.

The results of the tests of the aluminum bronze are shown in Fig. 22. At 100,000 psi and —78 °C the initial deflection was greater than that which could be obtained with maximum cam eccentricity. After the specimen had been stressed for 10 cycles, the deflection decreased to a value within the limits of the machine. Continual stressing at the maximum cam eccentricity did not work harden the specimen sufficiently to withstand stresses greater than 100,000 psi, so that was the maximum stress used.

Impact Tests

Fig. 23 summarizes the Charpy impact tests. The materials

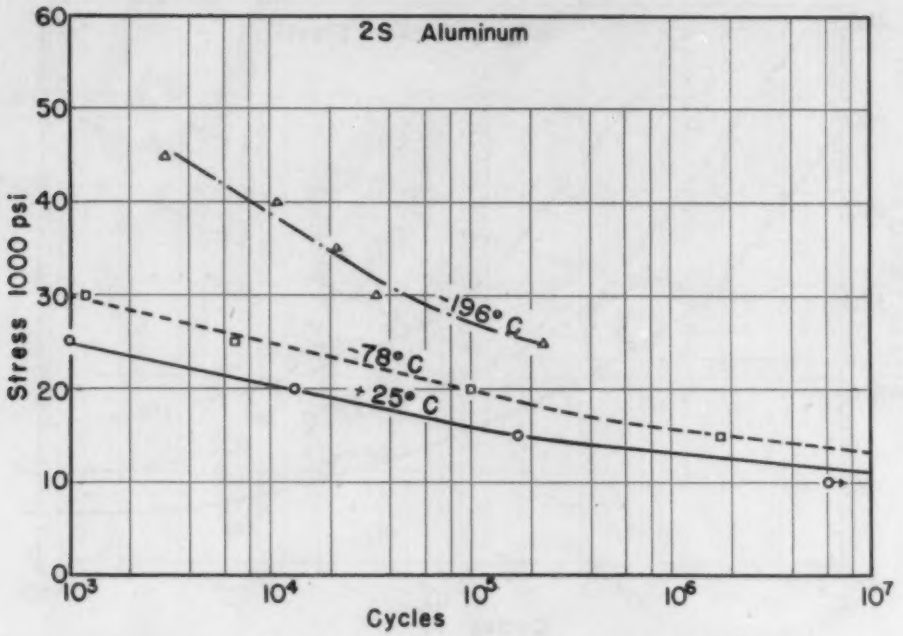


Fig. 18—Reciprocating Beam Fatigue Strength of 2S Aluminum at Various Temperatures.

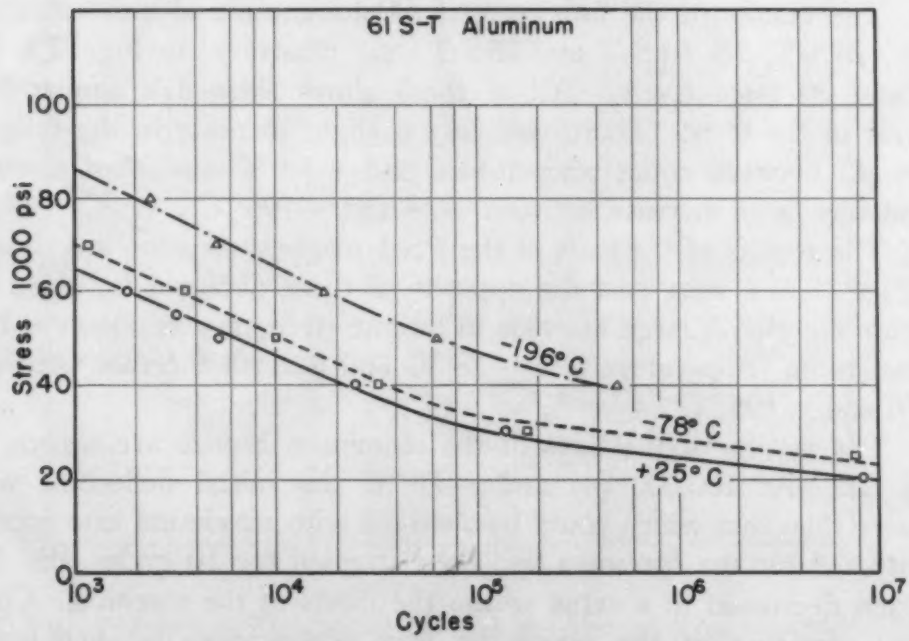


Fig. 19—Reciprocating Beam Fatigue Strength of 61S Aluminum at Various Temperatures.

indicated in this chart are arbitrarily placed from left to right in the order of decreasing impact strength at room temperature.

The 18-8 stainless steel exhibited the highest impact values at

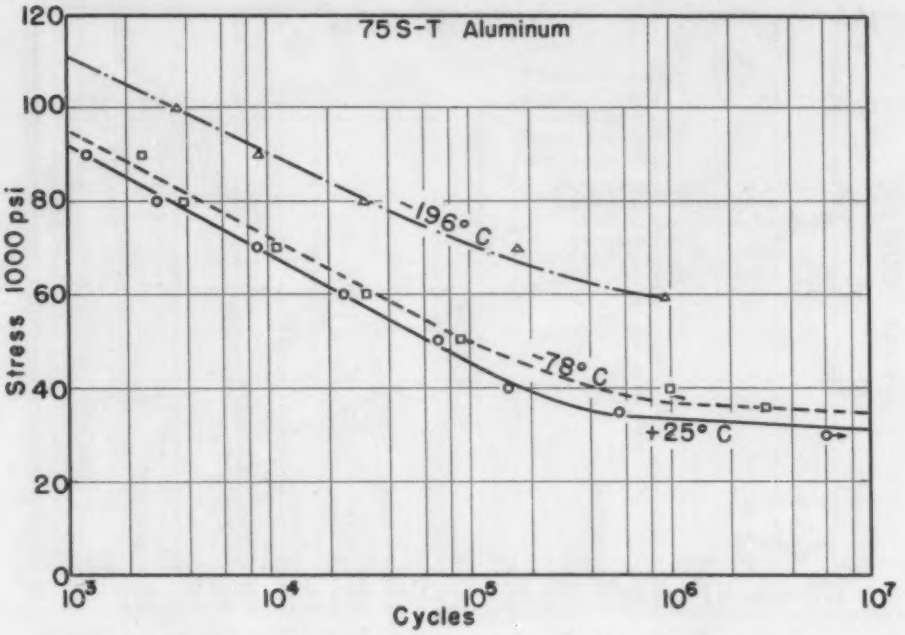


Fig. 20—Reciprocating Beam Fatigue Strength of 75S Aluminum at Various Temperatures.

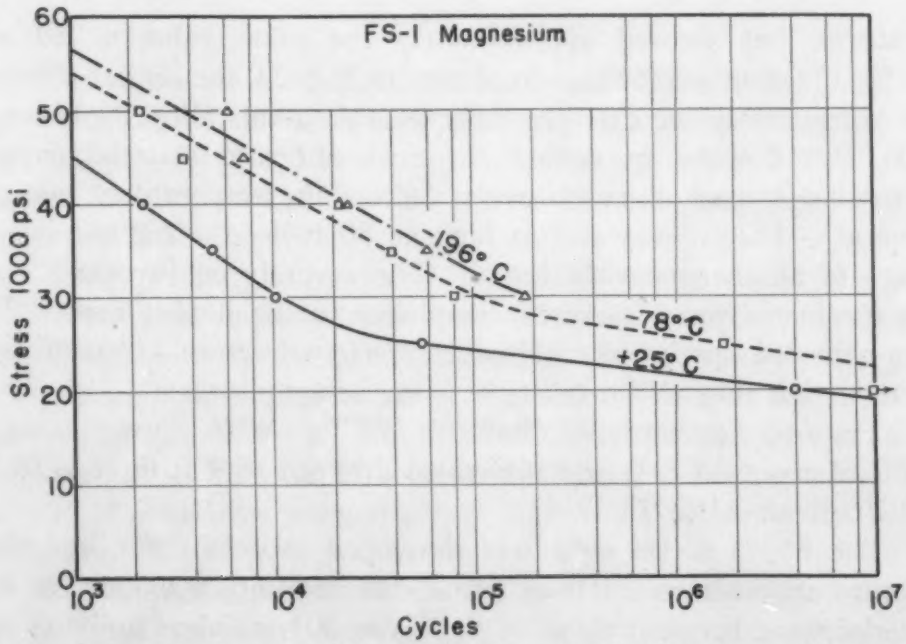


Fig. 21—Reciprocating Beam Fatigue Tests of FS-1 Magnesium at Various Temperatures.

the low temperatures, with the quench-annealed 18-8S showing the highest values of all the materials tested.

Impact values for the Type 304 stainless steel, cold drawn to a tensile strength of 210,000 psi, increased slightly at intermediate tem-

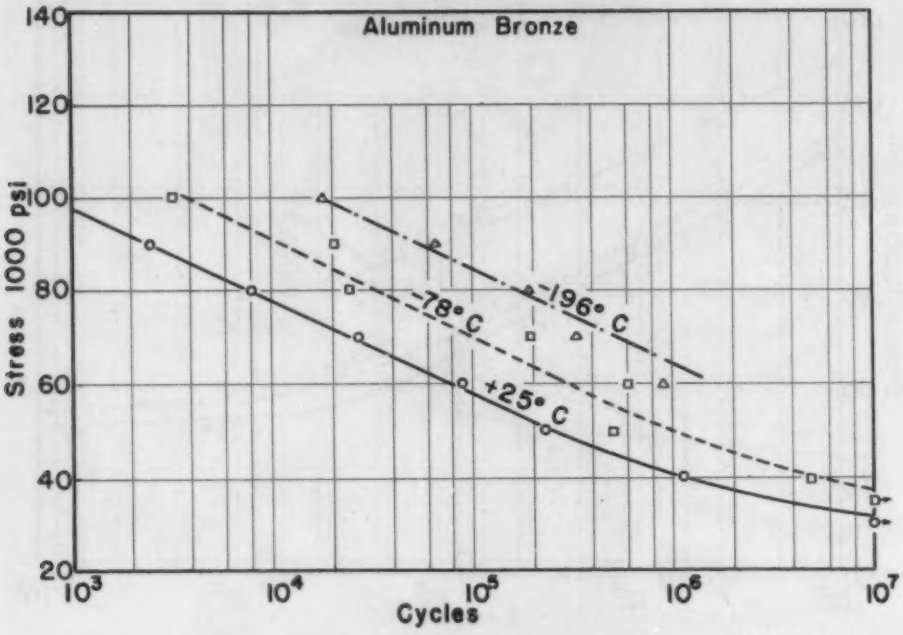


Fig. 22—Reciprocating Beam Fatigue Tests of Aluminum Bronze at Various Temperatures.

peratures, but showed approximately the same value at 20 and —253 °C (about 25 ft-lb). As shown in Fig. 23, the impact strength was considerably increased by fully annealing this alloy (4 hours at 2000 °F and water quenching). Such annealed material showed decreasing impact strength with decreasing temperature, but the value at —192 °C was still as high as 80 ft-lb—the highest impact values of all the materials tested. The severely cold-worked Type 304 specimens were fractured completely in the impact tests. The fully-annealed specimens did not completely fracture at room temperature, but they all broke at the lower temperatures.

Tests on age-hardened Stainless "W" gave an impact value at 25 °C of about 14 ft-lb and this value dropped to 4 ft-lb at —78 °C and 2 ft-lb at —192 °C.

The 8½% nickel steel was developed especially for low temperature applications. It was found that the impact values for this material were between those of the Type 304 stainless and the low alloy steels as shown in Fig. 23. The results of the tests indicated that there was a slight increase in impact strength when the temperature was lowered to —40 °C and then a decrease when the temperature was lowered to —78 °C. The drop was steeper between —78 and —127 °C, and finally a more gradual drop to 22 ft-lb at —196 °C.

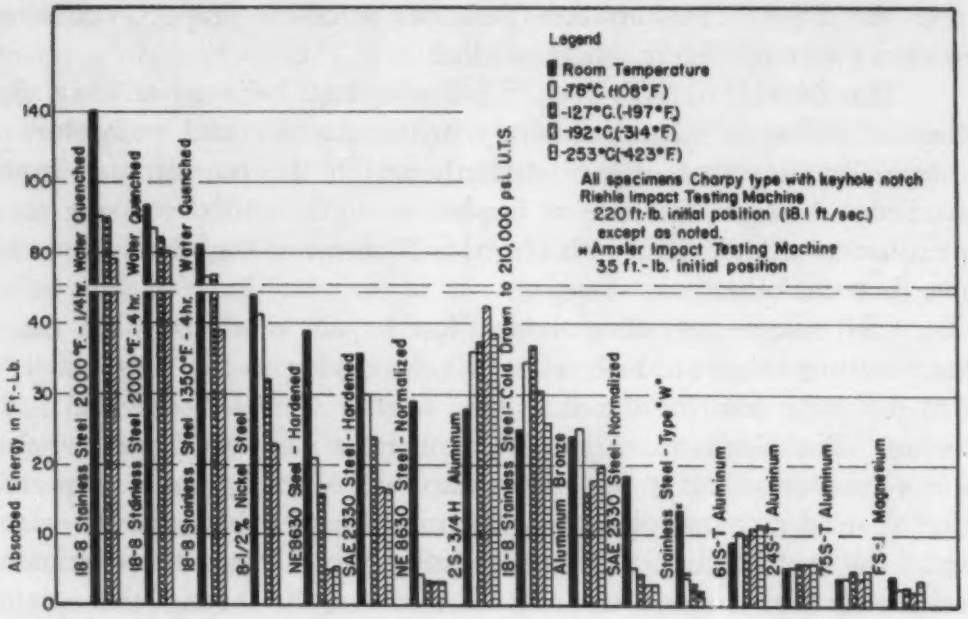


Fig. 23—Results of Charpy Impact Tests of Aircraft Alloys at Room and Very Low Temperatures.

The values for normalized and hardened NE 8630 steel, and also for normalized SAE 2330, dropped sharply as the temperature was lowered to —78 °C, showing about 5 ft-lb or less at —78 °C and about 3 ft-lb at —253 °C. The rate of decrease was more gradual for the SAE 2330.

The superiority of hardened SAE 2330 over hardened NE 8630, as far as loss in impact values with decreasing temperatures is concerned, is shown by the fact that the NE 8630 steel showed a practically straight-line drop to about 5 ft-lb at —192 °C and had this same value at —253 °C. The SAE 2330 steel had the same notch toughness at —10 °C as at room temperature, a more gradual drop to —192 °C and the comparatively high value of about 16 ft-lb at —192 and —253 °C.

The impact strength of the 2S-3/4H aluminum increased as the temperature was decreased to —192 °C and decreased at —253 °C. These results, however, are not particularly quantitative and not reliable for comparative purposes, because all specimens bent with partial fracture in the impact tests. In fact, it is not strictly correct to report the results for 2S as the "impact strength" of this material as we are doing in this paper. This point should be kept in mind when studying the data. Perhaps all that should be said is

that the 2S-3/4H aluminum possesses excellent impact resistance within the temperature range studied.

The 24S-T, 61S-T, and 75S-T alloys all behaved alike in that they all failed in a comparatively brittle manner and each showed essentially the same impact strength within the temperature range studied. A slight increase in impact strength with decreasing temperature was indicated, with the 61S-T showing slightly higher values than the other two alloys.

FS-1 magnesium alloy showed low impact values over the entire temperature range studied, with all values lying in the range of 2 to 4 ft-lb. The data for the aluminum bronze were a "shotgun" scattering. The blocks for Fig. 23 were merely made to the average of the values obtained at each temperature. Metallographic examination showed a coarse plate-like structure; the material was in essentially the cast condition. Profile studies showed that the specimens exhibiting high impact values fractured largely through the plates of alpha bronze, whereas those showing low values fractured largely through the dark-etching matrix material. The impact value was also dependent on whether the fracture occurred parallel to or at right angles to the plates. Results would probably have been more consistent on completely wrought material.

Hardness

All of the materials investigated showed an increase in hardness with a decrease in temperature. The data are shown in Table III. Hardnesses were determined at only the three temperatures noted. Hardness tests were made on specimens before, during, and after exposure to the low temperatures and it was found that the hardness increased with decreasing temperature, and then reverted to its initial value when the specimen was returned to room temperature. The hardness appeared to be dependent upon the heat treatment which the specimen had undergone as well as upon the temperature over the entire range of test temperatures. For example, the hardened SAE 2330 was harder at +25 °C than the normalized material and continued to be harder as the temperature was lowered.

Tensile Tests

The results of the tensile tests are summarized in Figs. 24 to 26. The values shown for the yield strength at —78 °C and all the values for the tests at —196 °C are for single specimens. The remaining

values are averages of two tests. The moduli of elasticity at room temperature and —78 °C are listed in Table IV. Almost all of the materials showed a slight increase in the modulus of elasticity.

There appeared to be a good correlation between the ultimate tensile strength and the fatigue strength at high stress levels. For example, the aluminum alloys showed only a slight increase in tensile strength between room temperature and —78 °C and there was likewise only a small increase in the fatigue strength. Between —78 and —196 °C there was a comparatively large increase in tensile strength and a correspondingly large increase in the fatigue strength. The differences for the tensile strengths of the steels were less pronounced, and likewise the difference between the fatigue curves was less pronounced. The FS-1 magnesium was an exception to this rule. The tensile strength changed more between —78 and —196 °C than between room temperature and —78 °C, yet almost the entire increase in fatigue strength occurred between room temperature and —78 °C and only a small increase between —78 and —196 °C. All the steels showed an increase in tensile strength with decreasing temperature. In general, the increase between room temperature and —78 °C was somewhat less than that between —78 and —196 °C, e.g., the ultimate tensile strength of the SAE 2330 increased from

Table III
Results of Vickers Hardness Tests at Various Temperatures

Material	Vickers Pyramid Hardness		
	+20 °C	−78 °C	−192 °C
2S Aluminum	44	50	60
24S-T Aluminum	143	151	166
61S-T Aluminum	181	193	214
FS-1 Magnesium	104	114	130
Aluminum Bronze	56	62	69
SAE 2330 Steel			
Normalized	245	286	314
Hardened[1]	321	359	384
NE 8630 Steel			
Normalized	217	252	288
Hardened[2]	302	327	377
8½% Nickel Steel[3]	253	294	372
Stainless W[4]	423	460	560
Type 304 Stainless[5]	422	480	610
Quenched from 1350 °F[6]	233	310	400
Quenched from 2000 °F[7]	162	205	340
Quenched from 2000 °F[8]	145	215	255

[1]Oil-quenched from 1500 °F, drawn at 925 °F.
[2]Oil-quenched from 1500 °F, drawn at 850 °F.
[3]Air-cooled from 1650 °F, air-cooled from 1450 °F, air-cooled from 1050 °F.
[4]Air-cooled from 1900 °F, aged 40 minutes at 1000 °F.
[5]Cold-rolled to 210,000 psi tensile strength.
[6]Water-quenched after 4 hours at 1350 °F.
[7]Water-quenched after 15 minutes at 2000 °F.
[8]Water-quenched after 4 hours at 2000 °F.

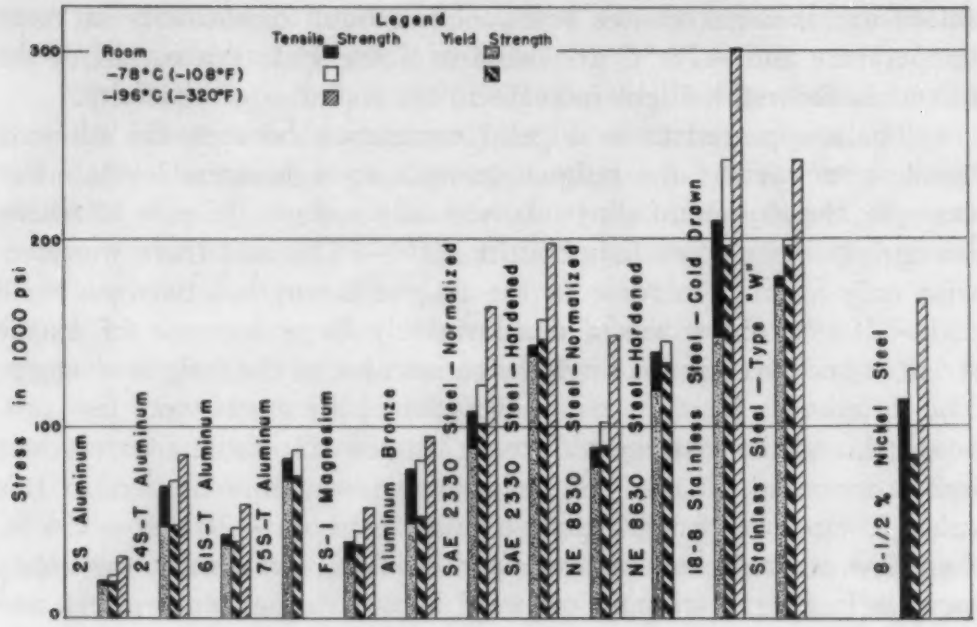


Fig. 24—Tensile and Yield Strengths of the Aircraft Alloys at Various Temperatures.

109,000 psi at room temperature to 123,000 psi at —78 °C and then to 165,000 psi at —196 °C. With the exception of the Type "W" stainless and the normalized SAE 2330, all the steels showed an increase in elongation when the test temperature was lowered to —78 °C. The steels also showed a decrease in the reduction of area with falling temperature with the exception of the 8½% nickel steel which showed a slight increase.

The behavior of the 18-8 stainless steel in the tensile test at the

Table IV
Modulus of Elasticity of Aircraft Alloys at Room Temperature and —78 °C

Material	Modulus of Elasticity, psi × 10^{-6}	
	+25 °C	—78 °C
2S Aluminum	10.05	11.25
24S Aluminum	10.87	11.11
61S Aluminum	10.08	10.62
75S Aluminum	10.21	10.75
FS-1 Magnesium	6.58	6.83
Aluminum Bronze	19.21	19.77
Normalized SAE 2330 Steel	29.46	30.71
Hardened SAE 2330 Steel	32.30*	33.19*
Normalized NE 8630 Steel	28.38	30.10
Hardened NE 8630 Steel	31.87*	31.75*
Type 304 (18-8) Stainless Steel	24.19*	26.53*
Type 322 ("W") Stainless Steel	30.55	28.78
8½% Nickel Steel	28.55	30.15

*Tentative.

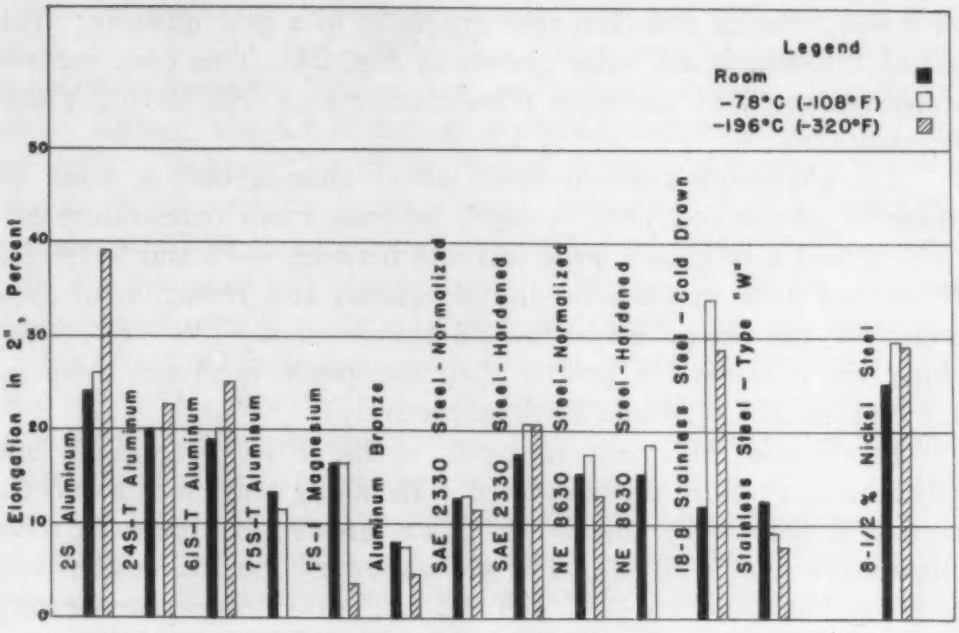


Fig. 25—Per Cent Elongation in 2 Inches of the Aircraft Alloys at Various Temperatures.

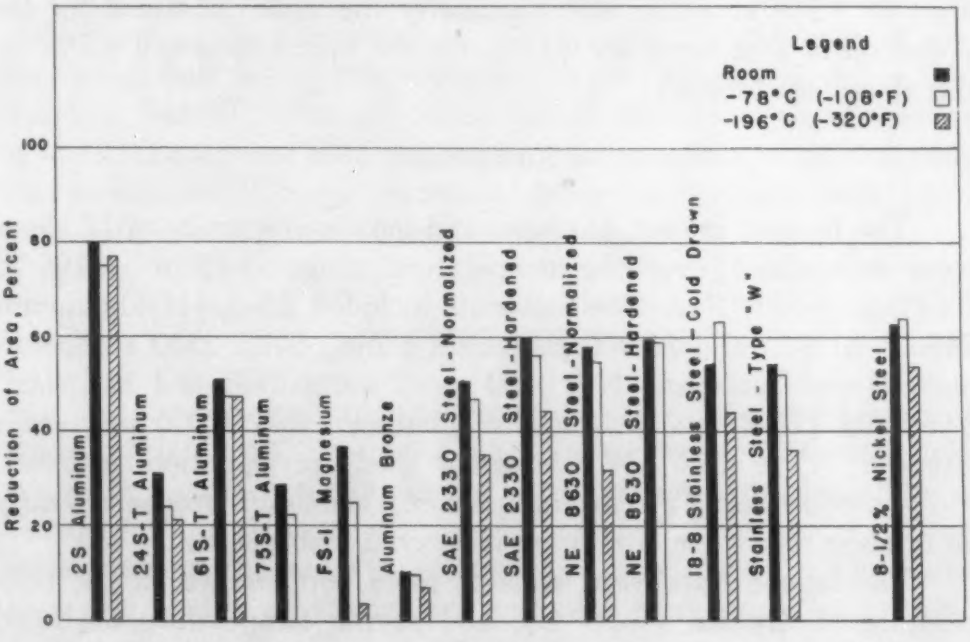


Fig. 26—Per Cent Reduction of Area of the Aircraft Alloys at Various Temperatures.

low temperature was unique. At —78 °C the load dropped rapidly for a short period after the ultimate strength was reached, then leveled off, and finally dropped again in the usual manner just before failure. At —196 °C, the load dropped very sharply after the ulti-

mate was reached, and then rose gradually to a new ultimate. This second ultimate is the value shown in Fig. 24. This behavior was probably caused by austenite transforming to ferrite during plastic deformation.

The aluminum and aluminum alloys showed only a small increase in tensile and yield strength between room temperature and —78 °C and a relatively large increase between —78 and —196 °C. There was little variation in the elongation and reduction of area, except for the elongation of the 2S aluminum at —196 °C (39%) which was considerably greater than the values for room temperature and —78 °C (24 and 26% respectively).

The tensile and yield strengths of the FS-1 magnesium and the aluminum bronze also increased with falling temperature and the increase between —78 and —196 °C was greater than between room temperature and —78 °C. The elongation of the magnesium was fairly good at +25 and —78 °C (16.5%), but it dropped to the very low value of 3.5% at —196 °C. The elongation for the aluminum bronze was quite low at all the test temperatures (8% at room temperature to 4.5% at —196 °C). Similarly the values obtained for the reduction of area were low (3.0% for the magnesium and 6.5% for the aluminum bronze).

Summary

The fatigue, impact, hardness and tensile properties of 12 alloys were determined over the temperature range +25 to —196 °C (+70 to —321 °F). The materials included 2S-3/4H aluminum; 24S-T, 61S-T, and 75S-T aluminum alloys; SAE 2330 steel, normalized and hardened; NE 8630 steel, normalized and hardened; Type 304 (18-8) stainless steel, cold drawn to 210,000 psi tensile strength; Type 322 (W) stainless steel, precipitation-hardened; 8½% nickel steel; FS-1 magnesium; and aluminum bronze. Nearly all of these alloys are often used in aircraft construction.

The fatigue tests were made at room temperature, at the temperature of dry ice (—78 °C), and at the temperature of liquid nitrogen (—196 °C). Liquid nitrogen was used instead of liquid air or oxygen in many of the tests for safety reasons. Many of the tests were made at stress levels above the yield point of the metals tested. Without exception, the alloys showed an increase in fatigue strength with falling temperature. The fatigue strength appeared to be related to the tensile strength.

Charpy impact tests were made over the temperature range +25 °C to —253 °C (—423 °F). These tests showed no general correlation between temperature and impact values. The ferritic steels showed a sharp decrease in impact values with falling temperature; the austenitic steels showed a gradual decrease; the 2S aluminum showed an increase; and the values for the remaining aluminum alloys and the FS-1 magnesium remained fairly constant over the range of test temperatures. The results for the aluminum bronze were widely scattered so a definite trend was not established.

Vickers hardness tests were made at room temperature, —78 °C and —192 °C (liquid air). The hardness of all the materials increased with falling temperatures. Hardness tests were made before, during, and after exposure to the low temperatures, which indicated that the hardness was dependent on the prior heat treatment of the specimen as well as the test temperature. No evidences of phase changes were observed for these relatively short exposures to the low temperatures since, in every case, the hardness reverted to its initial value when the specimen was warmed to room temperature.

Without exception, the tensile strength and yield strength increased with falling temperature. In general, the reduction of area decreased with falling temperature. The exceptions were the 18-8 stainless and 8½% nickel steels which showed a slight increase at —78 °C over that obtained at room temperature. The elongation was inconsistent. Some materials showed an increase with falling temperature, and others showed a decrease.

Acknowledgment

The interest and support of the Materials Laboratory is greatly appreciated. The Ohio State University Cryogenic Laboratory conveniently furnished the liquid air, nitrogen and hydrogen. The assistance of Mr. Howard E. Brooks and Mr. Emerson H. Wright in conducting the tests is gratefully acknowledged. The metallographic studies on the impact specimens were made by Professor J. O. Lord and Mr. C. A. Carman.

References

1. J. L. Everhart, W. E. Lindlief, J. Kanegis, P. G. Weissler and F. Siegel, "Mechanical Properties of Metals and Alloys," Circular of the National Bureau of Standards C447, Dec. 1, 1943.

2. E. W. Colbeck, M. A. MacGillivray and W. R. D. Manning, "Mechanical Properties of Some Austenitic Steels at Low Temperatures," *Transactions,* Institute of Chemical Engineers, Vol. II, 1933, p. 89.
3. W. J. DeHaas and R. A. Hadfield, "The Effect of the Temperature of Liquid Hydrogen on the Tensile Properties of Forty-One Specimens of Metals," *Philosophical Transactions,* Royal Society, Series A, Vol. 232, 1933, p. 297-332.
4. J. B. Johnson and T. Oberg, "Mechanical Properties at —40 °F of Metals Used in Aircraft Construction," *Metals and Alloys,* March 1933, p. 25.
5. W. D. Boone and H. B. Wishart, "High-Speed Fatigue Tests of Several Ferrous and Non-Ferrous Metals at Low Temperatures," *Proceedings,* American Society for Testing Materials, Vol. 35, 1935, Pt. II, p. 147.
6. D. J. McAdam, Jr. and R. W. Mebs, "The Technical Cohesive Strength and Other Mechanical Properties of Metals at Low Temperatures," *Proceedings,* American Society for Testing Materials, Vol. 43, 1943, p. 661.
7. C. H. Herty and D. L. McBride, "Effect of Deoxidation on the Impact Strength of Carbon Steels at Low Temperatures," Cooperative Bulletin 67, Mining and Metallurgy Advisory Board (1934).
8. R. K. Hopkins, "Impact Resistance of Some Welds at Sub-Zero Temperatures," *Welding Journal,* Vol. 13, 1934, p. 16.
9. J. J. Egan, W. Crafts and A. B. Kinzel, "Low-Temperature Impact Strength of Some Normalized Low-Alloy Steels," TRANSACTIONS, American Society for Steel Treating, Vol. 21, 1933, p. 1136.
10. North American Aviation, Inc., "Properties of Various Alloys at Sub-Zero Temperatures," *Iron Age,* Vol. 158, No. 20, Nov. 14, 1946, p. 75.
11. T. N. Armstrong and A. P. Gagnebin, "Impact Properties of Some Low Alloy Nickel Steels at Temperatures Down to —200 Degrees Fahr.," TRANSACTIONS, American Society for Metals, Vol. 28, March 1940, No. 1, p. 1-19.
12. M. G. Fontana and J. L. Zambrow, "Impact Strength and Hardness of Aircraft Alloys Down to —423 °F.," METAL PROGRESS, January 1948, p. 97-101.

DISCUSSION

Written Discussion: By G. N. Krouse, Krouse Testing Machine Co., Columbus, Ohio.

The authors are to be congratulated on this excellent piece of research which contributes a great deal of useful data for design purposes.

The scope of this work covered practically the whole low temperature range which engineers will probably encounter in mechanical designs and indicates the trend for the remaining small range of lower temperatures.

In order to more nearly simulate service conditions this excellent work might very well be extended to cover the effects of notches on fatigue strengths and the effects of range of stress on these notched materials.

There has been a tendency to assume that a given type notch produces a fixed stress concentration value without due consideration being given the inherent notch susceptibility of materials or the effects of stress

range on the damaging stresses. These factors are extremely important when dealing with narrow design limits.

Written Discussion: By Thomas J. Dolan, research professor, Theoretical and Applied Mechanics, University of Illinois, Urbana, Ill.

In recent years there has been propounded a great deal of speculation (including some erroneous concepts) regarding the mechanical properties of metals at low temperatures. The evolution of many new mechanisms which must operate at very low temperatures has made it a necessity that we obtain more exact knowledge regarding the resistance of structural metals to the various types of loading conditions and environment that may be encountered in service. In addition, it is becoming increasingly evident that before fundamental laws of the mechanical behavior of a material can be formulated (such as a quantitative "mechanical equation of state") a great deal more must be known about the manner in which temperature enters as a parameter in contributing to the structural actions of commonly used metals. It is, therefore, gratifying that the authors have been able to overcome many of the difficulties of techniques of testing at low temperature, and have been fortunate enough to have had available the large quantities of liquefied gases necessary to produce the extremely low temperatures involved in the test program.

Unless extreme precautions are taken, great fire and explosion hazards exist in the use of some of these coolants (such as liquid air and liquid hydrogen) employed by the authors. Minute quantities of oxidizable substances in contact with liquid air become very unstable powerful explosives. It might be of great benefit to some of the readers who may contemplate further research at low temperatures if the authors could outline briefly some of the safety precautions they found necessary in their tests.

The popular fad in recent years among materials engineers has been the testing of a wide variety of specimens to determine the temperature of transition from brittle to ductile fracture or the energy-absorbing characteristics in the range from values just above room temperature to perhaps minus 100 °F. The emphasis placed on this type of information has led to the popular impression that metals are inherently brittle and have practically no energy-absorbing characteristics at very low temperatures. The authors' data in this regard are rather reassuring, since they indicate that without exception the tensile strength and yield strength increased with falling temperature. Moreover, though the per cent elongation and per cent reduction of area decreased to some extent at low temperatures, the plastic deformations still remained appreciably large (that is, the tensile specimens did not exhibit the brittle "glass-like" fracture without ductility, that has been falsely attributed to many of these metals at low temperature). In fact, for several of the metals, including the aluminum alloys and some of the steels, the per cent elongation in the tensile test was greater at these extremely low temperatures than that observed at room temperature.

As one result of the emphasis that has been given to tests involving the position of the transition temperature for brittle fracture, it has been

postulated[2] that perhaps fatigue fracture occurs when the transition temperature of a steel increases during the test and becomes equal to the testing temperature. In contrast with this concept it is particularly reassuring to find that in the authors' tests the fatigue strengths of the steels tested all continued to increase even though the temperatures were depressed to values far below those normally considered to be below the transition temperature for brittle fracture in various static and impact tests.

The fact that the fatigue strength, static tensile strength and hardness of the twelve alloys consistently increased as the temperature was decreased from plus 25 °C to minus 196 °C would lead one to suggest that some functional relationship may exist between these properties and the temperature. A further study of the data might yield valuable information regarding the fundamental structural actions involved; this information could be used to check the validity of present theories of the behavior of material, or to further modify existing hypotheses of the elastic and inelastic behavior of metals.

The data shown in the authors' Figs. 9 and 10 indicate that slightly higher endurance limits were obtained from fatigue tests in a reciprocating or vibratory bending machine as compared with test results from the rotating beam machine. This is in agreement with the data obtained in previous tests[3] in which consistently higher values of fatigue strength (and of finite fatigue life) were obtained in round specimens tested in a vibratory bending machine of the same type as that employed by the authors. This apparently, then, is an inherent quality of the type of test that might possibly be associated with the greater volume of material subjected to peak stress in the rotating beam test as suggested by the authors. A similar discussion of this point has been presented by Peterson.[4]

The authors have pointed out that in general the per cent reduction of area in the tensile test decreased with falling temperature, whereas some metals exhibited an increase and some a decrease in elongation as a result of lowering the temperature. This fact further emphasizes the differences in the character of these two commonly used measures of ductility. Furthermore, one might also question the adequacy of the ordinarily determined tensile strength as commonly obtained in standard acceptance tests. The tensile strength is not necessarily a unique fundamental property of a metal but must in turn be determined by the load per unit of actual area at which localized necking of the specimen begins (the condition for which the total load applied to the specimen begins to decrease). Thus, the load per unit of original area may have no real significance; the specimens may begin local necking at different values

---

[2]C. W. MacGregor and N. Grossman, "Some New Aspects of the Fatigue of Metals Brought Out by Brittle Transition Temperature Tests," Welding Research Supplements, March 1948, p. 132, and discussions, Aug. 1948, p. 428-432.

[3]Thomas J. Dolan's discussion of "Fatigue Characteristics of Rotating Beam Versus Rectangular Cantilever Beam Specimens of Steel and Aluminum Alloys," *Proceedings*, American Society for Testing Materials, Vol. 47, 1947, p. 673-676.

[4]Same reference, p. 673.

of "true stress" which in turn are influenced by the temperature of testing. A somewhat more useful concept, and one regarding which it would be desirable to have further information, would be the so-called "true-stress at rupture" or fracture stress. While the method of measurement of strains employed by the authors does not permit the drawing of a complete true-stress, natural-strain curve, it would be desirable to know whether they recorded the loads at fracture from which a computation could be made to determine the fracture stress for each of the metals at each of the testing temperatures. Though the tensile strength increased as the temperature was depressed, the reduction of area also decreased, and hence the fracture stress may have remained fairly constant over a wide range of temperature. It would form a valuable addition to the paper if in their closing discussion the authors could present values of true-stress at fracture for a range of temperatures if such data are available.

Written Discussion: By Charles A. Nagler, associate professor, Department of Chemical and Metallurgical Engineering, Wayne University, Detroit.

The authors are to be complimented on their paper concerned with physical properties of aircraft alloys at low temperatures. In the conclusion of the paper the statement appears "the fatigue strength appeared to be related to the tensile strength." From the stress-cycle curves and the tensile strength, data that appear in Table V were taken and the

Table V

	−196°C			−78°C			+25°C		
Alloy	Endurance Limit	Tensile Strength	Endurance Limit, %	Endurance Limit	Tensile Strength	Endurance Limit, %	Endurance Limit	Tensile Strength	Endurance Limit, %
2 S	24,000	55,000	68	13,000	25,000	52	11,000	23,000	48
24 S-T	50,000	88,000	57	22,000	75,000	29	21,000	70,000	30
61 S-T	40,000	60,000	67	26,000	48,000	54	20,000	45,000	44
75 S-T	58,000	.....	..	35,000	.....	..	31,000	.....	..
FS-1	30,000	60,000	50	22,000	46,000	48	18,000	40,000	45
Al-Bronze	60,000	95,000	63	38,000	85,000	45	32,000	80,000	40
SAE 2330 N	111,000	165,000	67	65,000	125,000	52	59,000	110,000	54
SAE 2330 H	120,000	197,000	61	95,000	158,000	60	80,000	143,000	56
NE 8630 N	94,000	148,000	63	57,000	103,000	55	45,000	90,000	50
NE 8630 H	120,000	.....	..	80,000	145,000	55	65,000	140,000	46
18-8 C.D.	155,000	300,000	52	125,000	240,000	52	110,000	220,000	50
18-8 W	160,000	242,000	66	115,000	200,000	57	91,000	182,000	50
8½% Ni Steel	92,000	168,000	55	81,000	132,000	61	73,000	118,000	62

endurance limit determined as a per cent of the tensile strength of conditions of test at +25, −78, and −196 °C.

The average endurance limit of the material tested at temperatures of +25, −78, and −196 °C was found to be 47, 52, and 60%. The value of this calculation lies in the fact that we have an approximate increase of 13% in the endurance limit under conditions of test at −196 °C.

Written Discussion: By R. C. A. Thurston, metallurgical engineer, Bureau of Mines, Ottawa, Ontario, Canada.

The authors are to be complimented on the notable addition they have made to the relatively small amount of data available on mechanical properties of metals at very low temperatures, particularly as regards resistance to alternating stresses. This field of research is becoming of increasing importance and the author's description of the different techniques they have adopted will undoubtedly be of considerable value to other research investigators working in the same direction.

In this connection, I would like to ask for further information on one or two points. How was the temperature measured in the R. R. Moore tests and what was the degree of control in general? No temperature rise was observed in the low temperature fatigue tests at high stresses; did the authors make any measurement at the points of maximum stress? What was the speed of testing adopted in the Krouse and R. R. Moore fatigue tests?

The results obtained follow the general trend of those reported by previous investigators mentioned in the list of references. With the exception of the 2 S aluminum, the S/N curves are of similar form at the three temperatures of the tests. The 2 S aluminum at −196 °C, however, has a steeper slope or longer endurance at the higher stresses than one might expect. This is of particular interest since it agrees with some earlier work described by W. Hofmann.[5] The results of his fatigue tests under direct stresses on aluminum at +20, −55 and −160 °C bear a marked resemblance to those plotted in Fig. 18. Can the authors suggest any explanation for this behavior?

In conclusion, it is to be hoped that the authors will continue their work by investigating the effect of notches in fatigue at low temperatures since reliable data on this subject are very difficult to find.

Authors' Reply

The authors wish to thank Mr. Krouse, Professor Dolan, Professor Nagler, and Mr. Thurston for their discussions of the paper and suggestions for future work.

In answer to Mr. Krouse, fatigue and tensile tests of notched specimens are on the program and we hope to start this work in the near future.

Professor Dolan has pointed out the hazards of working with some liquefied gases. We used liquid nitrogen for the fatigue tests because it is relatively inert. Liquid air becomes dangerous if the tests are long, and the oxygen concentration builds up. The concentrated liquid in contact with a combustible material such as oil or grease can explode. We used liquid air for most of the tensile tests because they were relatively short. All of the specimens were carefully cleaned prior to cooling.

In the tests where liquid hydrogen was used, the specimens were

[5]W. Hofmann, "The Stress Resistance of Light Alloys at Low Temperatures," Z. W. B. Report No. F.B.2024, 1944.

Table VI
Mechanical Properties of Aircraft Alloys at Various Temperatures

Material	Hardness			Impact Test				Tensile Test		
	Vickers Hardness No.			Absorbed Energy, Ft-Lb.				Ultimate Tensile Strength, psi		
Temperature, °C	+25	−78	−192	+25	−78	−192	−253	+25	−78	−192
2 S Aluminum	43.5	49.7	59.7	28.0	36.0	42.5	38.5	19,500	21,600	31,900
24 S-T Aluminum	143	151	166	5.5	5.5	6.0	6.0	69,900	72,300	87,300
61 S-T Aluminum	104	114	130	9.0	10.2	11.0	11.5	44,200	47,800	56,000
75 S-T Aluminum	181	193	214	4.0	5.0	6.0	5.0	83,900	88,600	99,500
125 S-T Aluminum	...	...	...	...	...	...	...	94,800	.....	.....
FS-1 Magnesium	55.9	61.9	68.9	4.2	2.6	2.0	3.7	40,100	45,600	62,800
Aluminum Bronze	142	154	168	23.9	25.2	17.7	19.8	78,300	84,000	96,000
SAE 2330 Steel										
Normalized	246	284	315	18.6	5.6	3.0	3.1	108,600	121,100	162,900
Hardened	322	358	384	35.8	30.0	16.8	16.4	145,300	159,200	186,300
NE 8630										
Normalized	217	252	289	29.0	4.4	3.4	3.5	89,800	104,200	150,300
Hardened	302	332	376	39.1	21.0	5.0	5.4	142,000	154,500	192,100
18-8 S Stainless	440	492	596	24.7	34.5	30.3	25.9	212,400	241,100	296,250
Stainless W	423	459	560	13.5	4.1	1.4	....	181,900	203,300	240,800
8½% Nickel	252	291	350	44.0	41.4	22.6	21.0	117,300	136,000	169,500

Table VI—(Continued)
Mechanical Properties of Aircraft Alloys at Various Temperatures

Material	Tensile Test											
	True Ultimate Strength, psi			Yield Strength, psi			Elongation, %			Reduction of Area, %		
Temperature, °C	+25	−78	−192	+25	−78	−192	+25	−78	−192	+25	−78	−192
2 S Aluminum	.....	44,700	80,000	17,500	18,200	20,600	24.0	26.5	42.0	80.5	77.0	73.5
24 S-T Aluminum	96,100	94,600	107,000	48,500	51,100	63,100	20.0	21.0	21.5	30.5	25.5	20.5
61 S-T Aluminum	70,800	70,400	89,000	38,400	41,400	42,500	19.0	21.0	25.5	51.0	50.5	47.0
75 S-T Aluminum	111,300	110,500	116,700	72,200	78,100	89,500	13.5	12.5	12.0	28.0	22.5	15.0
125 S-T Aluminum	106,700	.....	.....	85,250	.....	.....	9.0	....	....	9.5	....	....
FS-1 Magnesium	56,600	58,200	69,300	29,900	39,600	48,400	16.0	15.0	6.5	36.5	22.5	8.0
Aluminum Bronze	86,800	92,500	101,000	50,000	54,700	65,000	8.5	8.0	5.0	10.0	10.0	4.5
SAE 2330 Steel												
Normalized	162,600	176,000	214,000	88,700	104,800	141,000	12.5	11.5	13.0	50.0	46.5	33.0
Hardened	243,500	260,000	291,000	139,300	146,400	186,300	17.5	20.5	20.5	59.0	56.0	40.0
NE 8630												
Normalized	150,400	174,000	189,200	80,500	91,500	134,100	16.0	18.5	11.5	58.5	57.0	28.5
Hardened	239,000	280,000	307,500	121,500	126,800	166,500	15.5	17.0	12.5	59.5	57.0	50.0
18-8 S Stainless	301,000	392,000	538,700	148,800	180,000	189,000	12.0	14.5	23.5	54.5	62.0	45.5
Stainless W	266,000	288,500	326,300	176,500	198,000	236,800	12.5	9.5	8.0	54.0	55.0	38.0
8½% Nickel	220,000	240,000	284,000	87,800	88,000	133,200	25.0	27.5	30.0	62.5	60.5	55.0

Table VII
Mechanical Properties of Aircraft Alloys at Various Temperatures

Material	Modulus of Elasticity, psi ×10						Compression Tests								
	Tension			Compression			Ultimate Strength, psi			Yield Strength, psi			Fatigue Strength, psi		
Temperature, °C	+25	−78	−192	+25	−78	−192	+25	−78	−192	+25	−78	−192	+25	−78	−196
2 S Aluminum	10.05	11.25	11.46	.....	.....	.....	.....	.....	.....	.....	.....	.....	11,000[2]	13,000[2]	23,000[1]
24 S-T Aluminum	10.87	11.11	11.97	10.75	13.41	13.22	66,500	64,600	79,600	46,150	49,700	57,350	20,000[2]	25,000[2]	43,000[2]
61 S-T Aluminum	10.08	10.62	10.77	.....	.....	.....	.....	.....	.....	.....	.....	.....	20,000[2]	23,000[2]	38,000[1]
75 S-T Aluminum	10.20	10.79	11.55	10.43	12.28	12.90	82,400	86,500	105,900	72,750	78,300	83,200	28,000[2]	30,000[2]	58,000[1]
125 S-T Aluminum	10.04	.....	.....	.....	.....	.....	.....	.....	.....	.....	.....	.....	.....	.....	.....
FS-1 Magnesium	6.36	6.58	7.3	6.66	7.80	7.91	53,450	54,950	70,350	16,900	18,100	23,200	19,000[2]	23,000[2]	28,000[1]
Aluminum Bronze	18.6	19.86	20.27	.....	.....	.....	.....	.....	.....	.....	.....	.....	32,000[2]	36,000[2]	64,000[1]
SAE 2330 Steel															
Normalized	26.88	28.08	30.8	.....	.....	.....	.....	.....	.....	.....	.....	.....	59,000[2]	63,000[3]	112,000[1]
Hardened	29.18	30.02	31.59	29.94	32.87	32.15	139,300	145,950	192,950	138,000	144,150	192,950	75,000[2]	95,000[2]	125,000[1]
NE 8630 Steel															
Normalized	27.14	28.86	31.66	.....	.....	.....	.....	.....	.....	.....	.....	.....	46,000[2]	58,000[2]	93,000[1]
Hardened	29.77	31.09	32.28	.....	.....	.....	.....	.....	.....	.....	.....	.....	70,000[2]	80,000[2]	125,000[1]
18-8 S Stainless	23.57	25.49	27.66	25.43	27.37	27.74	170,000	176,850	223,000 241,000	131,100	150,750	175,500	110,000[2]	125,000[2]	155,000[1]
Stainless W	29.05	30.45	31.65	.....	.....	.....	.....	.....	.....	.....	.....	.....	95,000[2]	120,000[2]	155,000[1]
8½% Nickel	27.62	28.33	29.95	.....	.....	.....	.....	.....	.....	.....	.....	.....	73,000[2]	80,000[2]	100,000[1]

[1] = 10^6 Cycles.
[2] = 10^7 Cycles.
[3] = 10^8 Cycles.

first chilled with liquid nitrogen. We tried to keep frozen air and water vapor from contacting the hydrogen but in tests of this nature, it was difficult. The laboratory is equipped with a blower system to immediately draw off the hydrogen which is liberated, and thus reduce the hazard.

In regard to the true stress, the tests were not set up for such determinations. However, the breaking loads were recorded so some data are available. These are listed in Tables VI and VII as the true ultimate stress (breaking load divided by reduced area). These tables summarize the data which were obtained in the investigation and include many results which were obtained after the paper was submitted for publication. All the alloys showed an increase in the true ultimate stress with falling temperatures. The aluminum alloys were unusual in that they showed little change, or a slight decrease, between room temperature and —78 °C, and then a pronounced increase between —78 and —192 °C.

In reply to Mr. Thurston, no measurements of the specimen temperature were made in the tests with the R. R. Moore machine. The bath temperature only was measured in these tests and it varied from —74 to —78 °C, depending on the amount of dry ice present. In the tests with the Krouse machines, the temperature measurements were made at the neutral axis of the specimen. No attempts were made to measure the temperature at the point of maximum stress because of the danger of scratching or otherwise altering the specimen. The tests, with both machines, were made at a speed of 2000 rpm.

The behavior of the 2S aluminum in the fatigue test appeared to be related to the true ultimate tensile strength. All the aluminum alloys showed a pronounced increase in the true ultimate tensile strength between —78 and —196 °C, but in the case of the 2S aluminum, it was particularly large (44,700 to 80,000 psi). This may be a partial explanation for the unusual behavior of this material in the fatigue tests.

THE MICROSTRUCTURE AND MECHANICAL PROPERTIES OF CAST STEELS

By M. F. Hawkes and B. F. Brown

Abstract

The microstructures of a large number of plain carbon, low alloy, and medium alloy, cast steels were studied after various annealing and normalizing treatments. The temperature at which austenite transforms on cooling is the fundamental variable controlling microstructure; it was found that as this temperature is lowered by virtue of increased cooling rate or hardenability, the structures observed are successively:

1. *Dendritic blocky ferrite plus pearlite*
2. *Random blocky ferrite plus pearlite*
3. *Widmanstätten ferrite plus pearlite*
4. *Martensite*

Mixtures of these structures are usually observed because transformation on cooling extends over a range of temperatures. Another important factor causing mixed structures is dendritic segregation of alloying elements. It is shown that the relative severity of segregation cannot be inferred by comparing single conventional photomicrographs of specimens of two cast steels cooled in a similar manner.

When comparing many cast steels having about the same strength, the wide variation observed in microstructure does not show good correlation with mechanical properties; other factors such as porosity, inclusion type, steelmaking variables and, undoubtedly, gases are equally important. In any one cast steel successively better ratios of ductility to strength are shown to be obtained by faster cooling, which leads to the succession of structures listed in the preceding paragraph. Little or no loss in ductility and appreciable gain in strength are obtained by using moderately rapid cooling, which produces Widmanstätten ferrite, instead of slow cooling, which produces blocky ferrite.

This article sets forth the results of research conducted by Carnegie Institute of Technology and supported by the Steel Founders' Society of America.

A paper presented before the Thirtieth Annual Convention of the Society, held in Philadelphia, October 23 to 29, 1948. Of the authors, M. F. Hawkes is assistant professor of metallurgical engineering and member of staff, Metals Research Laboratory, Carnegie Institute of Technology, and B. F. Brown is graduate student and, at the time of this investigation, research assistant, Metals Research Laboratory, Carnegie Institute of Technology, Pittsburgh. Manuscript received April 15, 1948.

Part I: Microstructure of Annealed and Normalized Cast Steels

THE variety and complexity of microstructures exhibited by cast steels is well known to the metallographer doing routine work in that field. Unlike the case with wrought steels, however, little has been done to explain or classify these structures, and the text-books give little information about them. This paper presents a study of one important portion of that field and a few remarks on cast steel structures in general.

To be specific, it was found early in this study that as-cast microstructures vary widely, depending upon production variables which are difficult to control and not completely understood. Fortunately, however, these structures bear little direct relation to structures found after reheating a steel casting, and, since nearly all castings are heat treated in some fashion, the importance of as-cast structure is much less than might be imagined. Reheated castings may be divided arbitrarily into two groups: those subsequently quenched rapidly enough to harden (i.e., transform to martensite) and those cooled more slowly so that other structures are obtained. From the structure standpoint, there is little to be said about the first group; martensite is a single constituent, it is always tempered to increase ductility, and this can result only in the formation of a fine dispersion of ferrite and carbide which becomes relatively coarser yielding higher ductility as the tempering temperature is increased. There is little to say about this structure or its effect upon mechanical properties that has not already been said. For this reason not much emphasis was placed on quenched and tempered steels. Instead major emphasis was centered on normalized or annealed cast steels which exhibit an amazing variety and complexity of structures in contrast with wrought steels.

Part I of this paper deals with those types of cast steel produced in the greatest tonnages today. These are low and medium carbon steels with or without moderate amounts of alloying elements and they do not possess high hardenability; therefore, on annealing or normalizing them, a structure consisting of ferrite and pearlite is formed. The case of higher alloy steels which transform to a variety of intermediate products will not be considered. Part II of this paper deals with relationship between the structures observed in annealed or normalized steel castings and the mechanical properties of such castings.

The Microstructure of Annealed and Normalized Steel Castings

In all low and medium carbon steels heated into the austenite range and allowed to transform on cooling, the ratio of pearlite to ferrite formed increases, and the pearlite becomes finer as the cooling rate increases. Furthermore, in all such steels, ferrite forms before pearlite as transformation of austenite occurs on cooling. Therefore, the ferrite pattern determines the type of microstructure finally observed at room temperature. The pearlite is formed last, and thus it is found merely in those places within the former austenite grains which had not already transformed to ferrite. Thus the succeeding discussion obviously must emphasize ferrite distribution.

In cast steels, other factors compete with cooling rate to influence markedly the type of ferrite-pearlite distribution. This leads to the greater variety of microstructures found in annealed or normalized cast steels than found in comparable wrought steels. Studies on approximately ninety commercial heats of varying composition and manufacture have led to the conclusion that the most important factor causing the multiplicity of structures in cast steels is dendritic segregation of alloying elements (including "residual" elements and phosphorus). The steps in this reasoning will be more apparent as the following analysis of these structure types unfolds.

In cast steels, fast cooling velocities (up to the "critical cooling velocity" which is that at which only martensite forms) almost always promote a pronounced plate-like, geometrical array of ferrite grains which will be called Widmanstätten ferrite in subsequent discussion. On the contrary, slowly cooled (annealed) cast steels exhibit a variety of microstructures which are all based upon larger, relatively equiaxed grains of ferrite to be called blocky ferrite hereinafter. This ferrite may be distributed in grain boundary, random, or dendritic fashion; this depends upon various factors and will be elaborated on in later paragraphs.

The fundamental variable, through which all other factors operate to influence microstructure, will be shown to be the temperature at which the austenite (formed on heating) transforms to ferrite on cooling. This is illustrated in Fig. 1, which shows schematically the ferrite portion of a "cooling S-curve" over which are drawn cooling curves representing treatments varying from rapid water quenching to slow furnace cooling. These cooling curves are drawn starting at the A_3 temperature because no transformations

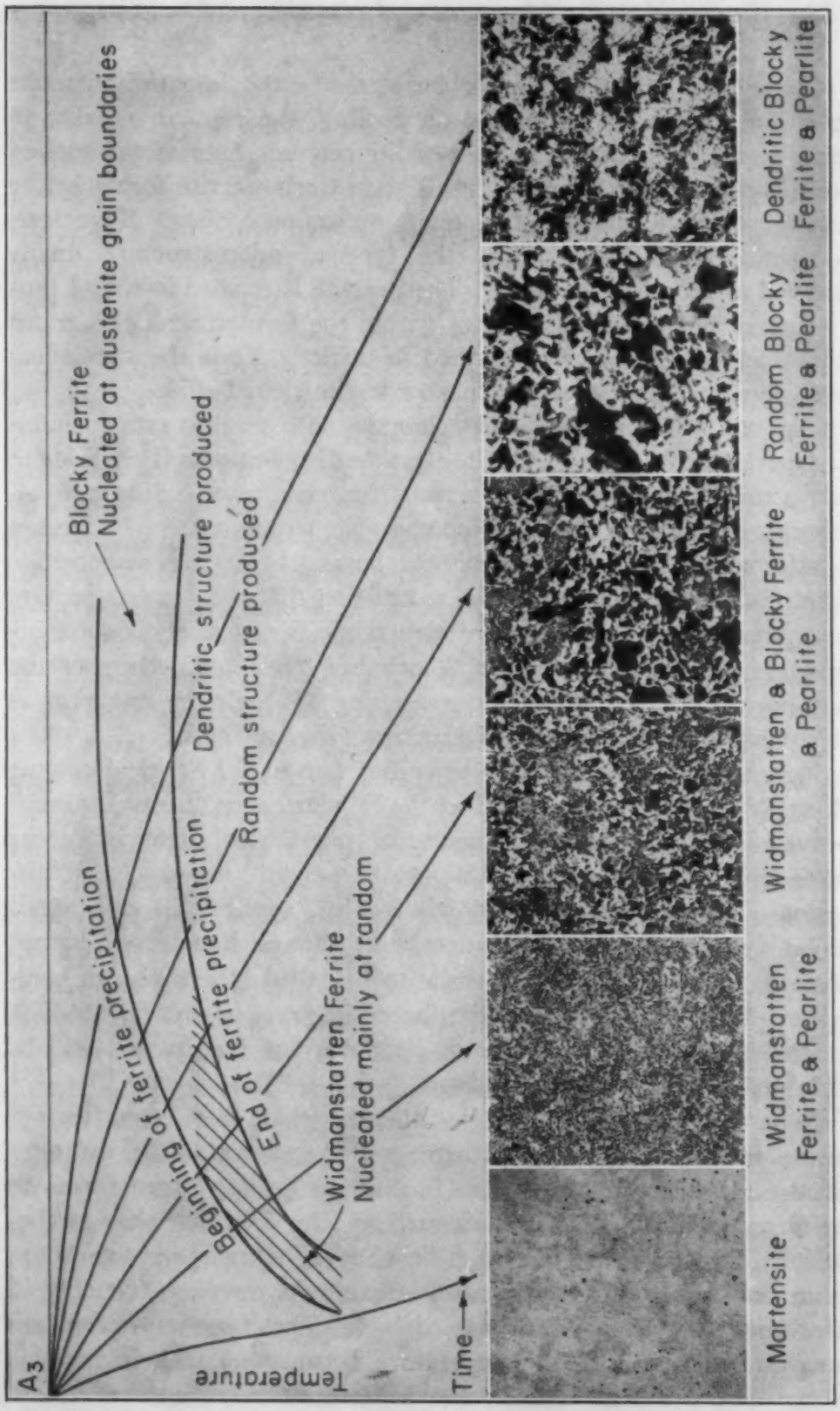


Fig. 1—Schematic Diagram Showing Effect of Cooling Rate on Structure. Illustrated photomicrographs of low alloy 0.30% carbon cast steel. All photomicrographs originally × 100, reduced 50% in reproduction; nital etch.

occur during cooling of the austenite above this temperature, regardless of time of cooling.

The curves are drawn to illustrate what has happened in an actual experiment where a typical alloy cast steel was cooled at various rates. The photomicrographs at the bottom show the final structure obtained as a result of each different cooling rate. The steel was from a commercial basic electric heat containing approximately 0.30% carbon, 1.00% manganese, 0.50% chromium, and 0.70% nickel; it had been deoxidized with Ca-Mn-Si. Half-inch sections of the as-cast steel were heated 1 hour at 1600 °F (870 °C) and were cooled respectively in water, air, powdered asbestos, an open furnace, a closed furnace, and a furnace with power partially on. These treatments produced the structures illustrated from left to right.

The water quench exceeded the critical cooling velocity of the steel and thus caused the austenite to transform at a very low temperature to simple martensite which is outside the subject under discussion. Air cooling caused the transformation to occur at a fairly low temperature—in the neighborhood of 1100 °F (595 °C)—near the knee of the S-curve. This is the criterion for the formation of Widmanstätten ferrite which is illustrated in the second photomicrograph. Examination at high magnification reveals a considerable amount of fine pearlite in the small spaces left between the ferrite plates. Interrupted cooling studies show some tendency for the first few ferrite plates which form to be nucleated at austenite grain boundaries. However, the great majority of ferrite plates are nucleated at random, once transformation of austenite is underway.

This is in sharp contrast with the formation of blocky ferrite in its various forms; this product is nucleated primarily at austenite grain boundaries. It should also be emphasized at this point that earlier views (1)[1], which postulated that Widmanstätten ferrite was most likely to form at intermediate cooling rates, are in error and that actually the tendency for this pattern to occur (in cast steels, at least) becomes more and more pronounced as the cooling velocity approaches the critical cooling velocity. No exceptions to this rule have been found in hundreds of gradient-quenched specimens studied. The importance of knowing the conditions under which the Widmanstätten distribution is produced will become evident in Part II of this paper which deals with the relation of structure to mechanical

[1]The figures appearing in parentheses pertain to the references appended to this paper.

properties. Furthermore, it is important to understand that this Widmanstätten pattern is a normal structure for cast steels, has good mechanical properties as will also be shown in Part II, and is not indicative of overheating or coarse austenite grain size as is often the case in wrought steels.

It is also important to emphasize that the Widmanstätten ferrite referred to in this work must not be confused with so-called acicular ferrite or "X-constituent" found just below the hardened rim of some slack-quenched alloy steels. The microstructure of this constituent often resembles somewhat that of Widmanstätten ferrite, but actually it is a ferrite supersaturated with carbon[2] and one which forms only well below the knee of the S-curve. Widmanstätten ferrite can be produced slightly below the knee in some steels, but its usual temperature range of formation is above the knee. Steels in which intermediate products of the "X-constituent" type are found will not be discussed in this paper.

Referring to Fig. 1, it is seen that when the cooling velocity is decreased, as, for instance, by furnace cooling, ferrite forms at a higher temperature and has a blocky appearance; the next to the last photomicrograph in the series is a good illustration of this type of ferrite randomly distributed.

There is an obvious and sharp distinction between the appearance of Widmanstätten and blocky ferrite but not between the cooling rates at which they form. This, and the fact that three modifications of blocky ferrite exist and may coexist, are results of the dendritic type of segregation already mentioned. The former fact is illustrated by the third and fourth photomicrographs of Fig. 1. They show that, over a wide range of cooling rates, both Widmanstätten and blocky ferrite may be found in the same microspecimen, and that a large change in cooling rate is necessary to effect a change from one pure type to the other. This results from the fact that the "cooling S-curve" for a steel shifts to the right as one goes from the low alloy core of a former dendrite to the alloy-rich interdendritic region. Thus the core regions transform first and at higher temperatures to blocky ferrite (nucleated at austenite grain boundaries), and the interdendritic regions transform later at lower temperatures which produce Widmanstätten ferrite (nucleated at random within what is left of the remaining austenite grains).

This behavior is well illustrated in Fig. 2 where photomicro-

[2]Widmanstätten ferrite on the other hand is a normal low-carbon ferrite.

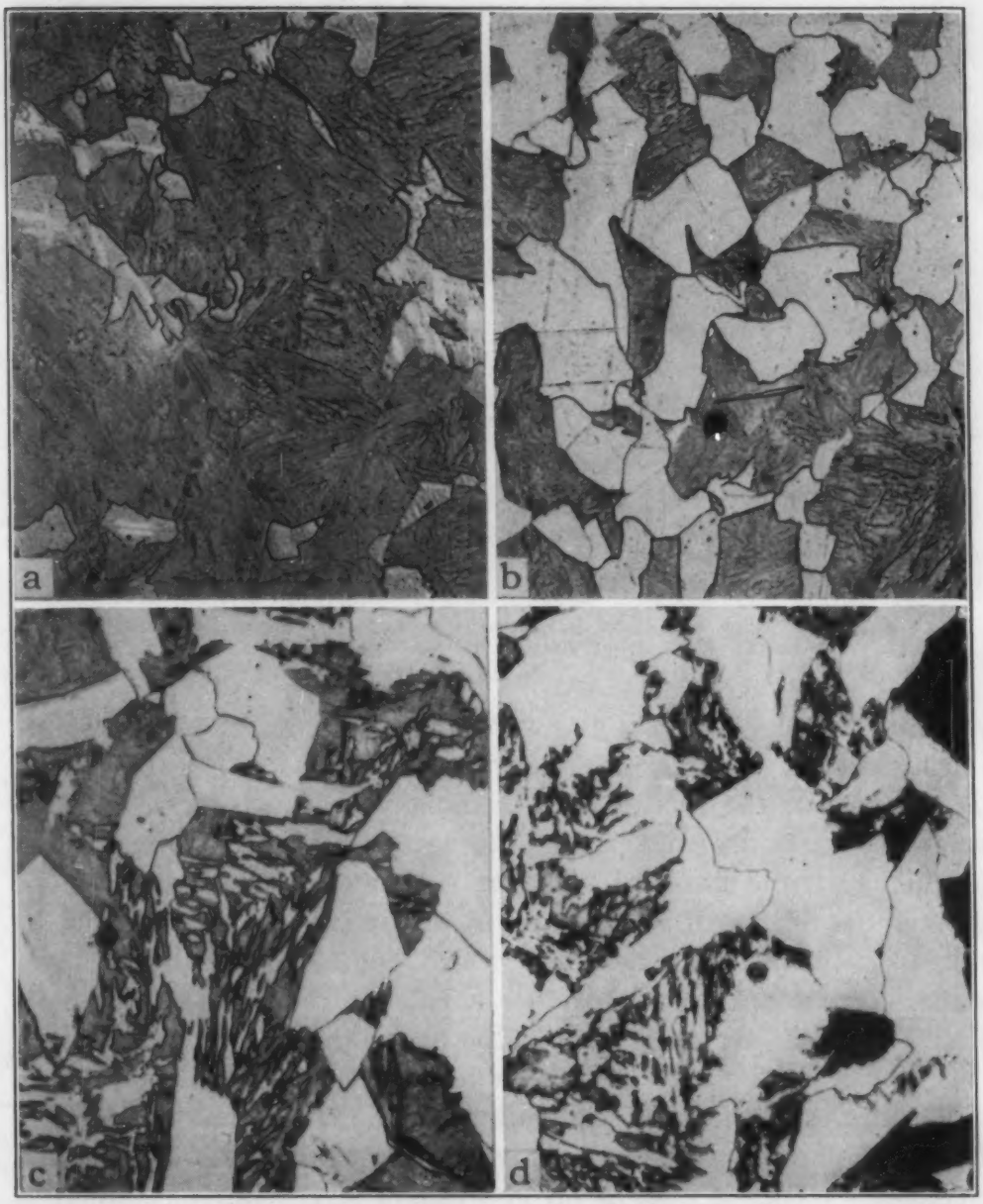


Fig. 2—Progress of Transformation of Typical Low Alloy Cast Steel on Cooling. Quenched at following temperatures and times: a—1120 °F, 1 minute; b—1070 °F, 3 minutes; c—810 °F, 12 minutes; d—660 °F, 24 minutes. All photographs at × 500; nital etch.

graphs show the progress of transformation at various stages during the air cooling of a typical low alloy cast steel. This was a commercial acid open-hearth steel containing approximately 0.20% carbon, 0.80% manganese, 0.60% chromium, 0.60% nickel, and 0.15% molybdenum; it was deoxidized with Ca-Mn-Si. Small as-cast samples were heated 1 hour at 1550 °F (845 °C) (in order to

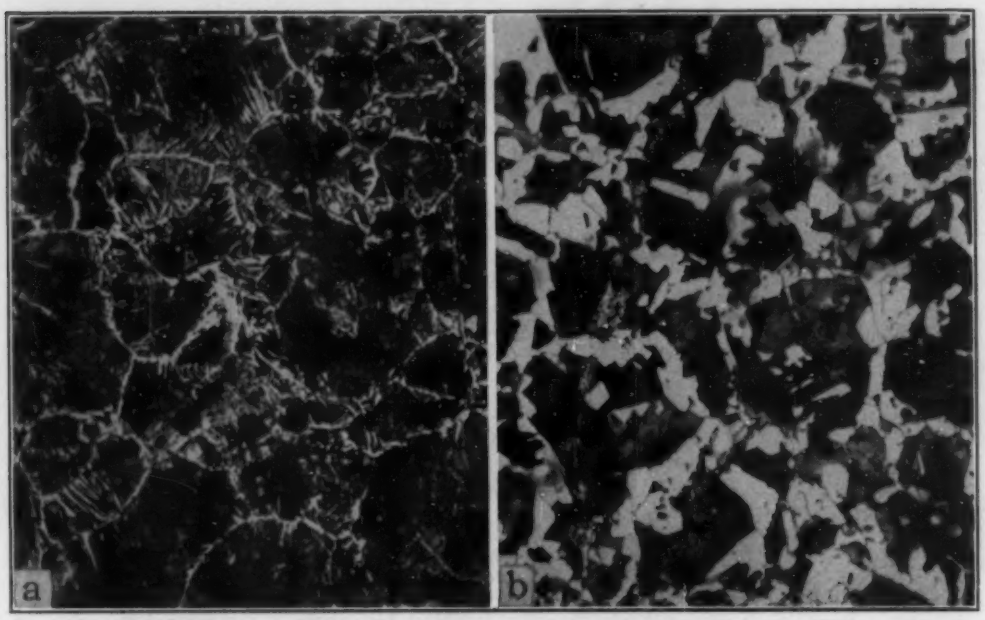


Fig. 3—Low Alloy Cast Steel Exhibiting Pronounced Tendency for Grain Boundary Ferrite Outlining. Both photographs at × 100; nital etch.
a. Normalized b. Annealed

minimize homogenization) and were brine-quenched at various stages during cooling in order to follow the progress of transformation. The nature of the ferrite (and eventually pearlite) formed at any stage is clearly shown against a background of martensite (representing austenite untransformed at the time of quenching). The greater the degree of segregation in a cast steel, the greater is the range of cooling velocities over which both blocky and Widmanstätten ferrite are found together. Thus this type of structure is found in some cast steels both in the normalized and annealed state.

Blocky ferrite may exist in at least three modifications because of the effects of dendritic segregation. The first of these is probably found only when there is relatively little segregation of alloying elements. Hence it is common in wrought steels, fairly common in plain carbon cast steels, and rare in alloy cast steels. It is the grain boundary type illustrated in Fig. 3 which shows photomicrographs of a low alloy cast steel cooled at various rates. This was a commercial acid open-hearth heat containing 0.30% carbon, 1.5% manganese, and no additional elements other than "residuals"; it was silicon-killed and had a coarse austenite grain size. The latter property also has a slight effect in promoting the grain boundary type of ferrite. More important than this, however, is the freedom that exists from dendritic segregation of alloying elements; these

are slow to diffuse at any temperature and remain segregated long after the steel has been homogenized with respect to carbon. Hot working apparently gives appreciable improvement, however. In any event, when most wrought steels are normalized, the ferrite nucleates chiefly at austenite grain boundaries as transformation occurs during cooling. Austenite then continues to transform to ferrite more by the mechanism of growth of existing grain boundary ferrite nuclei than by new nucleation within austenite grains. This likewise occurred in the cast steel of Fig. 3.

On the other hand, in most cast steels, as the cooling rate becomes too slow to allow Widmanstätten ferrite to form, the blocky ferrite takes on a more or less random pattern. The third alternative, favored by a high degree of dendritic segregation and also by very slow cooling, is a very dendritic pattern formed by the blocky ferrite.[3]

These modifications are explained in the following way: it is a general principle that transformations in single-phase solid alloys tend to be nucleated at the grain boundaries of the decomposing phase (austenite in the case of steels). Dendritic segregation in steels introduces an additional influence on nucleation, however, for low alloy dendrite cores have S-curves shifted to the left with respect to the S-curves of the high alloy regions between dendrite branches. Reheating produces many new austenite grains within the region of each original dendrite (2), so there are as many grain boundaries in the dendrite cores as elsewhere. Furthermore, the shift of the S-curve to the left means a tendency for ferrite to nucleate sooner. Thus a reasonable balance between the grain boundary and the segregation influences on nucleation can result in a structure which appears to have a more or less random distribution of ferrite; such a structure was shown in the next to the last photomicrograph of Fig. 1

On the other hand, if the degree of segregation is very high, this will be the dominating factor, and the ferrite formed will delineate the dendritic pattern. Such a structure was shown in the last photomicrograph of Fig. 1. Furthermore, this pattern has been observed in all the cast steels (including plain carbon heats) studied when the cooling was sufficiently slow. This occurs because the higher the temperature of transformation, the greater is the ratio of rate of growth of ferrite to rate of nucleation of ferrite. In

---

[3]This is analogous to ferrite banding in slowly cooled alloy wrought steels. Here dendritic segregation has been rolled into bands but not removed.

other words, once a few nuclei have formed, ferrite grains grow out rapidly from these sites, and carbon atoms diffuse rapidly away from the advancing interface because of the high temperature. This builds up a high carbon concentration in the remaining austenite which inhibits new nucleation of ferrite. Ferrite continues to grow, however, until the carbon concentration of the remaining austenite reaches approximately the eutectoid composition. At this point pearlite nucleates and grows until all the austenite has transformed.

The various stages in the formation of a dendritic-type blocky ferrite structure are shown in Fig. 4. This is a series of photomicrographs similar to that of Fig. 2 except that furnace cooling instead of air cooling was used in order to have all ferrite in the blocky form. For this study, the steel was a commercial basic electric heat containing approximately 0.30% carbon, 0.80% manganese, 0.70% chromium, 0.80% nickel, and 0.20% molybdenum; it was deoxidized with aluminum and ferrotitanium. As-cast specimens were austenitized 1 hour at 1600 °F (870 °C) before the furnace cooling was started. Again, the martensite in these photomicrographs represents austenite untransformed at that particular stage in cooling. Note in Fig. 4b that, as transformation proceeded, the martensite etched more unevenly; this is evidence that during transformation on slow cooling, carbon diffuses through the austenite away from the growing ferrite as explained in the previous paragraphs.

In spite of the fact that, early in this section, temperature of transformation was stated to be the fundamental variable controlling microstructure, the discussion has centered around experiments in which cooling rate was the variable. To emphasize the fact that temperature *is* the fundamental variable, Fig. 5 is included. These photomicrographs illustrate a study in which the progress of isothermal transformation of the same steel used for Fig. 2 is followed by quenching thin specimens after holding them in a lead bath for various lengths of time at various constant temperatures (the usual isothermal S-curve technique). All specimens were heated 1 hour at 1600 °F (870 °C) before transferring to the lead bath.

At temperatures slightly below the critical range, only blocky ferrite forms, and, as can be seen from the top horizontal row of photomicrographs, nucleation occurs primarily at former austenite grain boundaries; growth of ferrite then proceeds largely from those nuclei. As before, the background phase is martensite formed on

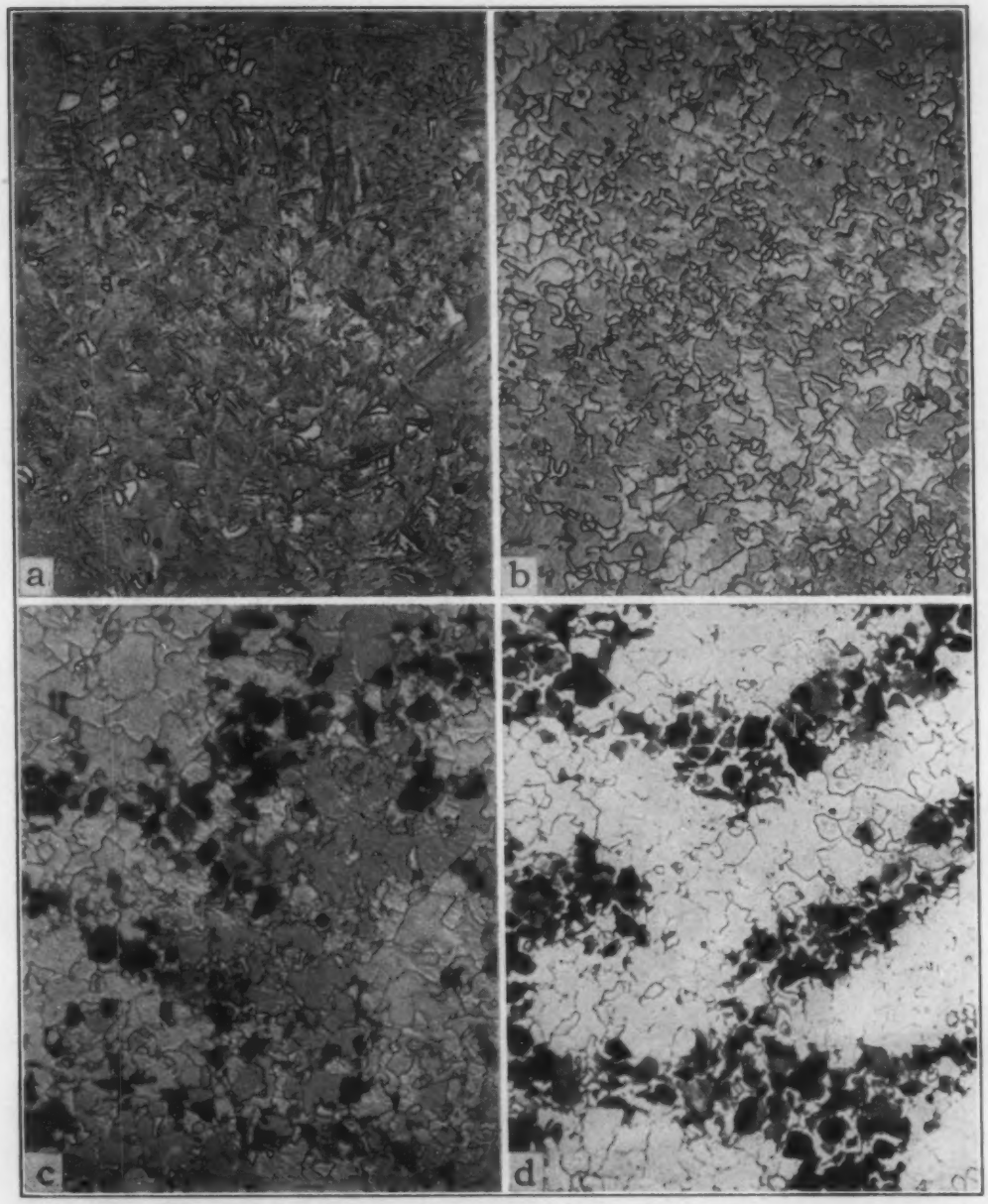


Fig. 4—Progress of Transformation of Low Alloy Cast Steel to Dendritic Blocky Ferrite on Slow Cooling. Quenched at following temperatures and times: a—1380 °F, 20 minutes; b—1280 °F, 64 minutes; c—1180 °F, 80 minutes; d—1140 °F, 90 minutes. All photographs at × 250; nital etch.

the quench from 1280 °F (695 °C), and it represents austenite untransformed up to the time indicated below the photomicrographs. Although the effect of dendritic segregation is less pronounced on isothermal transformation than it is on cooling, nevertheless that effect is enough to produce an apparently random structure.

At 1200 °F (650 °C), the structure is still random blocky fer-

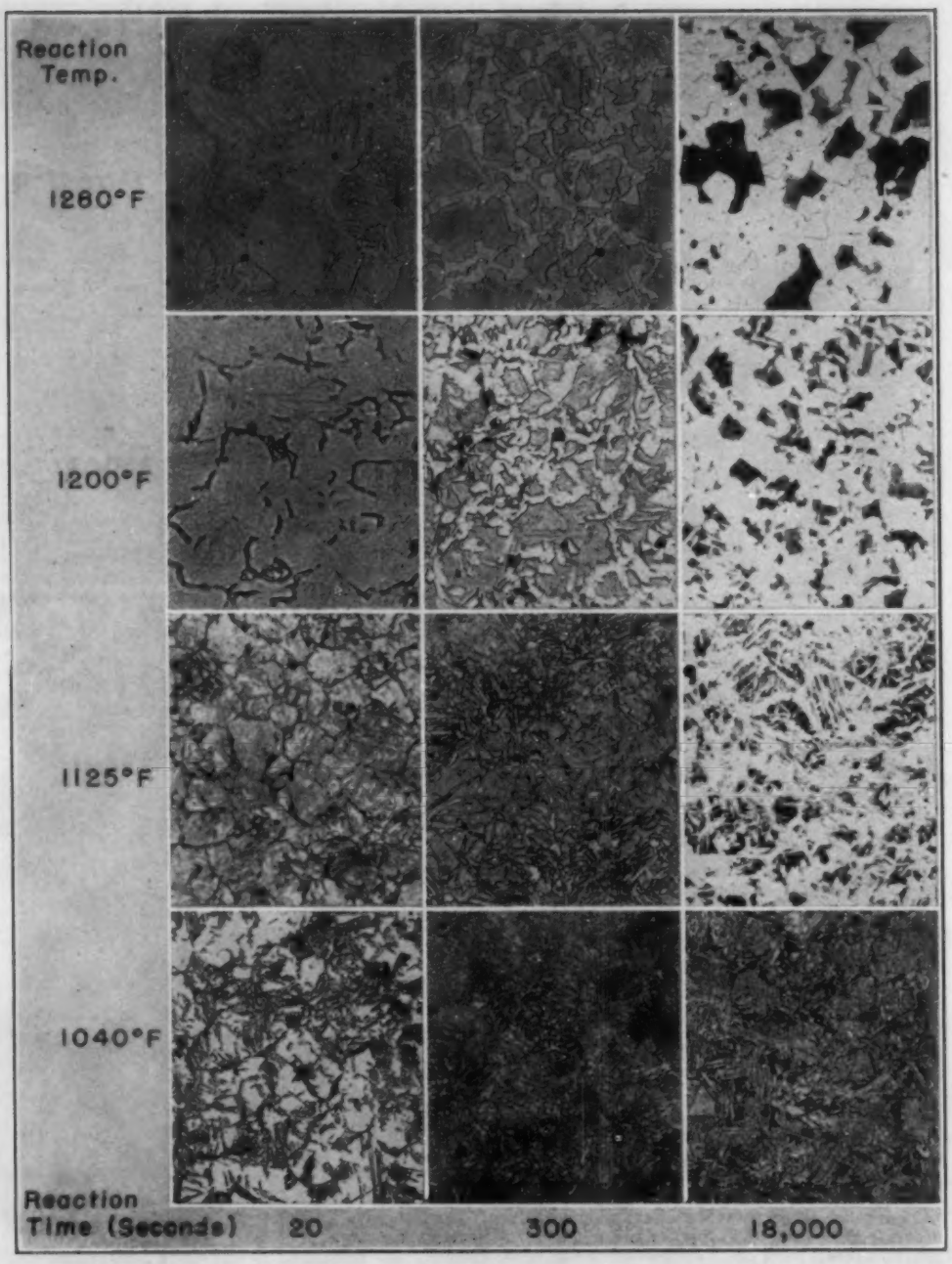


Fig. 5—Effect of Temperature at Which Austenite Transforms Upon Microstructure. Cast NE 8620 steel used for illustration. Original magnification × 100, reduced 25% in reproduction; nital etch.

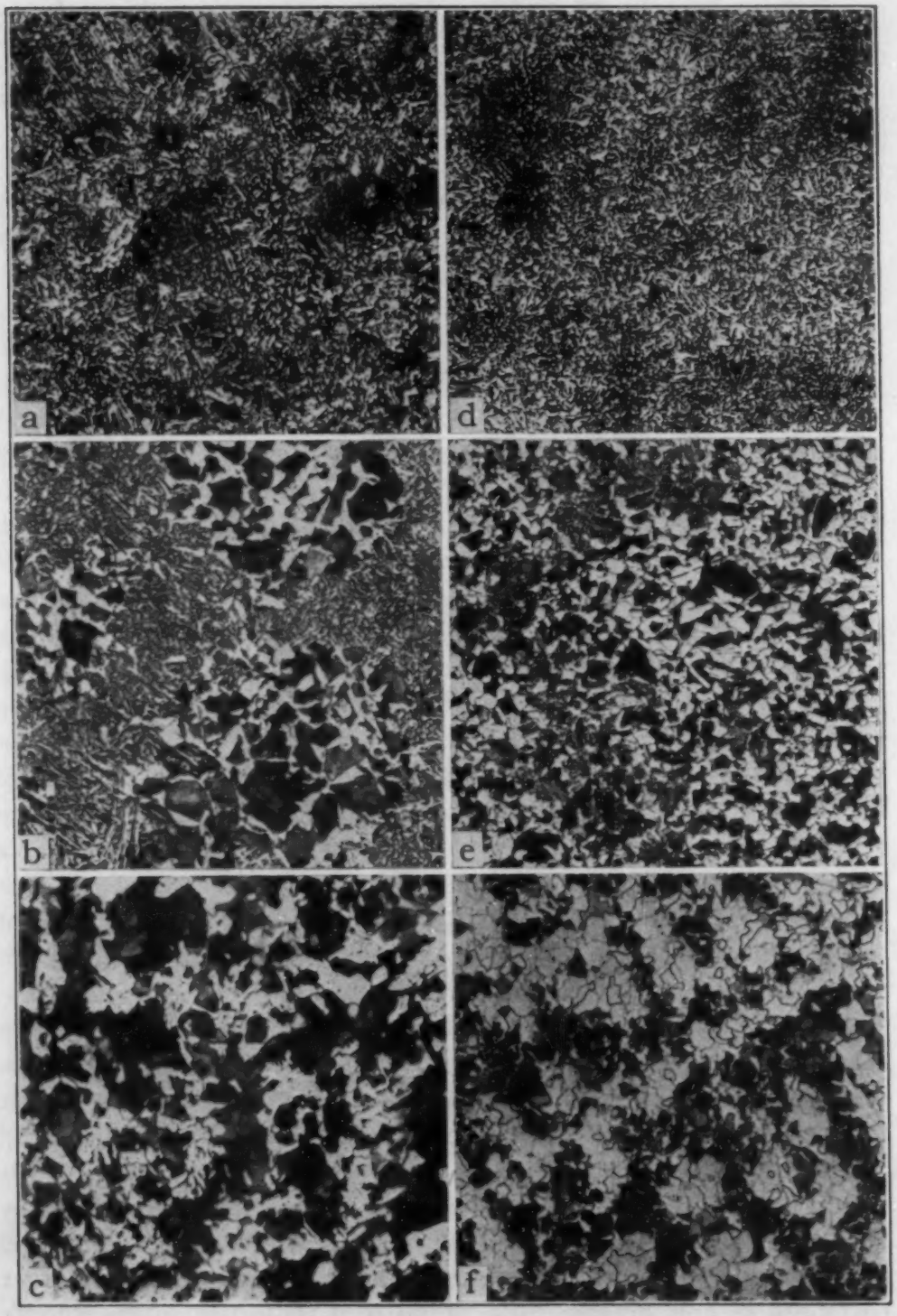
rite, but the particle size is finer because the rate of nucleation has increased more than the rate of growth. At 1125 °F (605 °C), even though the first nuclei form at austenite grain boundaries, subsequent transformation is chiefly to Widmanstätten ferrite nucleated at

random. At 1040 °F (560 °C), the structure is essentially all Widmanstätten ferrite.

When one keeps in mind the slight effect of dendritic segregation and the ever-present tendency for the first few nuclei to form at grain boundaries, the chart illustrates that a uniform and characteristic microstructure is produced when transformation occurs at any one constant temperature; it also shows that a rather abrupt change from formation of blocky ferrite to formation of Widmanstätten ferrite occurs when the temperature of transformation becomes sufficiently low.

Similar isothermal studies were made on several other cast steels with the same result. As always, high transformation temperatures promote the formation of blocky ferrite while, at low temperatures approaching the knee of the S-curve, Widmanstätten ferrite is formed. It was also observed that with steels of lower carbon content, the temperature range over which Widmanstätten ferrite is produced extends to a slightly higher value. Mixed structures form in a narrow intermediate transformation temperature range which is wider the greater the degree of dendritic segregation.

It should be emphasized at this point that the examination of a single microspecimen of annealed or normalized cast steel does not yield suitable evidence for determining degree of segregation. This is because transformation occurs on cooling, and thus more than one type of ferrite may form, and because dendritic segregation is evidenced in different ways in the different types of structure. This can best be shown by a comparison of two cast steels cooled at several different cooling rates as illustrated in Fig. 6. When both steels were air-cooled together at a fairly rapid rate, fine Widmanstätten patterns were formed and steel 34 appears to show more segregation. This is an etching effect where segregation has produced areas of finer ferrite plates and finer pearlite (due to lower transformation temperature); these areas have etched darker than the remainder of the structure. On the other hand, when both steels were air-cooled together at a slower rate, mixed structures of blocky and Widmanstätten ferrite resulted because of segregation, and steel 31 appears to be more severely segregated because of the larger particle size and greater ratio of pearlite to ferrite in the blocky areas. Finally the effect is once again reversed when annealing was the treatment used. Here steel 34 appears more acutely segregated, probably because its lower hardenability caused transformation to



Steel No. 31 (NE9430) Steel No. 34 (NE8630)

Fig. 6—Two Cast Steels Compared for Evidence of Dendritic Segregation. × 100. Nital etch. a—Rapid normalize. b—Slow normalize. c—Annealed. d—Rapid normalize. e—Slow normalize. f—Annealed.

occur at a higher temperature, or possibly because it may actually be segregated to a greater extent.

Summary

The type of structure found in normalized or annealed cast steels is determined by the temperature at which the steels transform on final cooling. This temperature is governed chiefly by the relation between cooling rate and hardenability of the steel. The latter factor is in turn influenced by dendritic segregation. Carbon content and possibly alloy content have a slight direct effect on the type of structure formed at a given temperature. They exert an important indirect effect, on the other hand, by being the principal factors governing hardenability.

Part II: The Relationship Between Microstructure and Mechanical Properties of Cast Steels

One approach to a study of the effect of microstructures on mechanical properties is obviously to compare the structures and properties of a great number of steels made under unlike conditions. Such a study, even if superficially made, clearly demonstrates that other variables, difficult to control in a laboratory study of commercial heats of steels, overshadow the structure influence. Among these are design and section size of test coupons, melting, tapping, and pouring practice, deoxidation practice, inclusions, and porosity. (Variables such as composition, thermal history, and austenite grain size are obviously of major importance too, but they can be kept under control easily.) This situation is so pronounced that only very large-scale sampling and rigid statistical analysis will suffice if the influence of the structure variable alone is to be determined accurately. Such a treatment was not within the scope of this project, although semi-statistical studies were made on the heats available and later will be mentioned briefly.

On the other hand, most of the common microstructures observed in commercial cast steels can be produced in a single heat of steel by suitable heat treatment; this eliminates all extraneous variables except the inhomogeneities characteristic of cast steel and the small differences found among coupons taken from different test blocks of a given heat. Seven such heats of cast steel, and one heat

of wrought steel for comparison purposes, were studied intensively. The chemical analysis and deoxidation practice for each of these steels appears in Table I.

In the study, samples from each individual heat were removed from equivalent positions in 1-inch test coupons, flame-cut surfaces being avoided. The samples were approximately ½ by ½ by 6 inches in size, providing stock for a 0.252-inch tensile specimen, a metallographic section, and a standard keyhole Charpy notch impact specimen. The wrought steel was supplied in the form of a ¾-inch round hot-rolled bar. All samples of a given steel received identical austenitizing treatments which are listed in Table I. They were cooled from this temperature at various rates (from water quenching to furnace cooling) to develop different structures. Cooling rates were estimated by noting the time required to cool from the austenitizing temperature to half that figure and then converting these times to cooling rates in degrees F per minute. Regardless of cooling rate, a metallographic section showed an essentially uniform structure over the cross section of these small samples.

In most instances it appeared desirable, from the standpoint of machinability and testing, to temper certain specimens of a series. In such cases, the entire series was given the same tempering treatment, shown in Table I, after which the specimens were air-cooled. This was done for the sake of uniformity even though tempering of annealed steel is not common practice and does not appreciably affect mechanical properties.

Tension tests showed that tensile strength increases regularly with cooling rate. As the tensile strengths of steels are varied, the other common mechanical properties also vary regardless of what factors cause the change in tensile strength. Therefore the results to be described are presented as graphs in which the various other properties are plotted as functions of tensile strength.

Results of Mechanical Property Tests

The data from the seven cast steels are presented graphically in Figs. 7 through 13. Each figure corresponds to a particular heat of steel and is divided into four graphs; the top one is a graph of tensile strength against reduction of area, the second against elongation, the third against Charpy impact strength, the fourth against yield strength. The cooling rates used to get the various tensile

Table I
Steels Used in Study of Effect of Microstructure on Mechanical Properties

Steel No.	Type	C	Mn	Si	P	S	Cr	Ni	Mo	Inclusion Type	Deoxidation	Austenitizing Temp., °F	Time at Temp.	Tempering Temp., °F	Tempering Time	Section Treated
426	Cast Plain Carbon	0.30	0.66	0.37	0.048	0.036	0.09	0.10	0.06	I	FeMn FeSi	1610	1 hr.	1000	1 hr.	½-in. square bars
783	Cast Plain Carbon	0.23	0.62	0.32	0.037	0.032	....	....	....	I	.....	1600	1 hr.	1000	1 hr.	1-in. bar
	Wrought Plain Carbon	0.34	0.76	0.22	0.009	0.028	0.09	0.02	....	...	.....	1600	1 hr.	1000	1 hr.	¾-in. round bars
5	Cast NE 1330	0.30	1.61	0.44	0.012	0.020	0.03	0.05	0.02	I	5 lb. Ferro-titanium per ton	1600	1½ hr.	1000	1 hr.	½-in. square bars
17	Cast NE 8030	0.30	1.26	0.41	0.013	0.020	0.04	0.10	0.14	III	1.6 lb. Aluminum per ton	1650	1½ hr.	1000; also 1 series untempered.	1½ hr.	½-in. square bars
16	Cast NE 8620	0.20	0.78	0.32	0.033	0.037	0.60	0.60	0.16	I	2 lb. CaMnSi per ton	1600	1½ hr.	1000	1 hr.	½-in. square bars
25	Cast NE 8630	0.29	0.95	0.52	0.039	0.018	0.55	0.62	0.17	I	2 lb. FeTi 3 lb. CaMnSi	1640	1½ hr.	1000	1½ hr.	1-in. square bars
31	Cast NE 9430	0.30	1.11	0.33	0.016	0.021	0.48	0.67	0.12	I	4 lb. CaMnSi per ton	1600	1 hr.	....	....	½-in. square bars

strengths are indicated along the top of the yield strength curves. The effect of microstructure upon reduction of area will be discussed first, using the graphs of tensile strength against reduction of area for all of the steels studied. The other properties will be treated later in the same manner.

Reduction of Area—A typical example of the reduction of area curves is illustrated in Fig. 7, which represents an NE 8030 cast steel cooled to room temperature at various rates and then tempered at 1000 °F (540 °C). The two highest strengths were obtained by water quenching and the structure corresponding to the two points (essentially duplicate data) is tempered martensite. Oil quenching gave structures consisting of Widmanstätten ferrite plus fine pearlite and tempered martensite. This leads to lower tensile strength and higher reduction of area. With progressively less violent oil quenching and various types of air cooling, the Widmanstätten structures became progressively coarser and the martensite disappeared. As a result, the tensile strength decreases but the reduction of area levels off.

Slower cooling rates produce random ferrite which, as will be shown better in other examples, is at first associated with a decrease in reduction of area, even though the tensile strength decreased. Further slow cooling once again increased the reduction of area as long as a random structure was produced. However, at a cooling rate of about 40 °F per minute, a dendritic blocky ferrite structure developed, and, as the cooling rate was further decreased, the dendritic pattern grew progressively more pronounced. It is very interesting to note that at these slow cooling rates, as the tensile strength continued to decrease, the reduction of area also dropped off sharply. In order to check this drop in reduction of area with untempered specimens, the lower portion of the curve was repeated and was found to be almost superimposed upon the curve for the tempered specimens.

A lower carbon NE 8620 cast steel was treated similarly to the NE 8030 cast steel, with cooling rates varied as before; the resulting data are plotted in Fig. 8. Again reduction of area drops off with the appearance of blocky ferrite but rises again over the range of cooling rates where only random blocky ferrite and pearlite are formed. Once again the reduction of area drops off with appearance of dendritic blocky ferrite.

An NE 9430 cast steel was studied using specimens which were

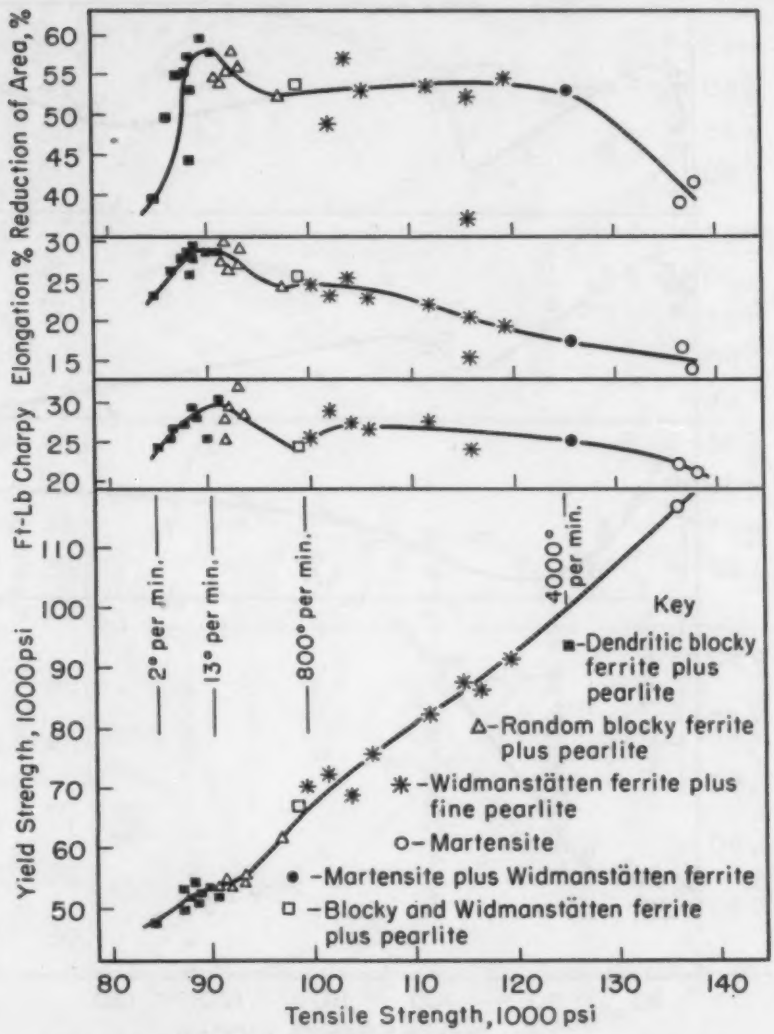


Fig. 7—Effect of Structure on Mechanical Properties of an NE 8030 Cast Steel 17.

untempered. It was observed that the specimens with ferrite of only the Widmanstätten type had martensite as well as fine pearlite in the matrix, which, in general, led to more scatter in ductility at high tensile strengths. The data for this series are presented in Fig. 9. Here it is seen that the ductility of Widmanstätten ferrite aggregates increased rapidly as the martensite in the matrix was replaced entirely by fine pearlite. There was observed the customary leveling off in reduction of area or perhaps a slight drop with the appearance of large quantities of random blocky ferrite. The rest of the curve follows the general pattern of those previously described, with scattering and drop in ductility as the dendritic pattern devel-

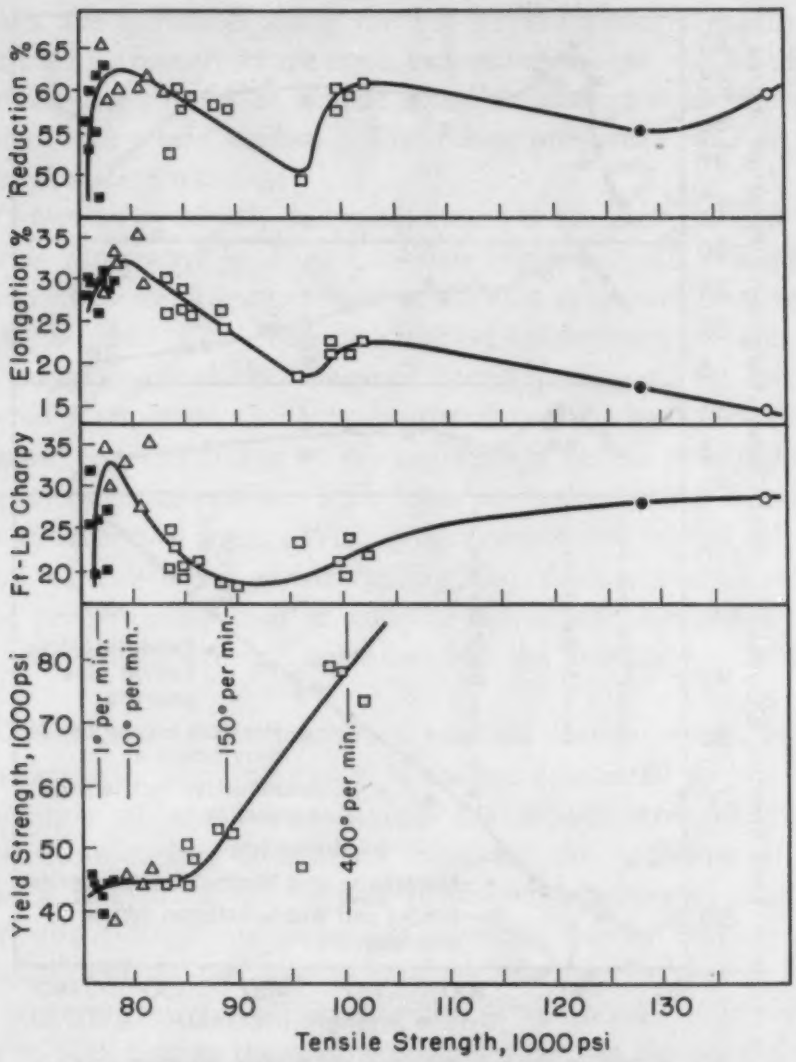


Fig. 8—Effect of Structure on Mechanical Properties of an NE 8620 Steel 16. (For key to symbols, refer to Fig. 7.)

oped. Since untempered high strength steels are rarely used, and since tempering of annealed steel, though equally rare, does not appreciably affect properties, the rest of the steels were all tempered at 1000 °F (540 °C).

The NE 1330 cast steel was one in which the structure as-cast and after most heat treatments showed a pronounced tendency for the ferrite to form preferentially at the austenite grain boundaries. See Fig. 10. No pure Widmanstätten ferrite (free from grain boundary ferrite) was formed. The curve has the same general shape as those previously described, except that the drop in ductility seems to come before the dendritic pattern is well developed.

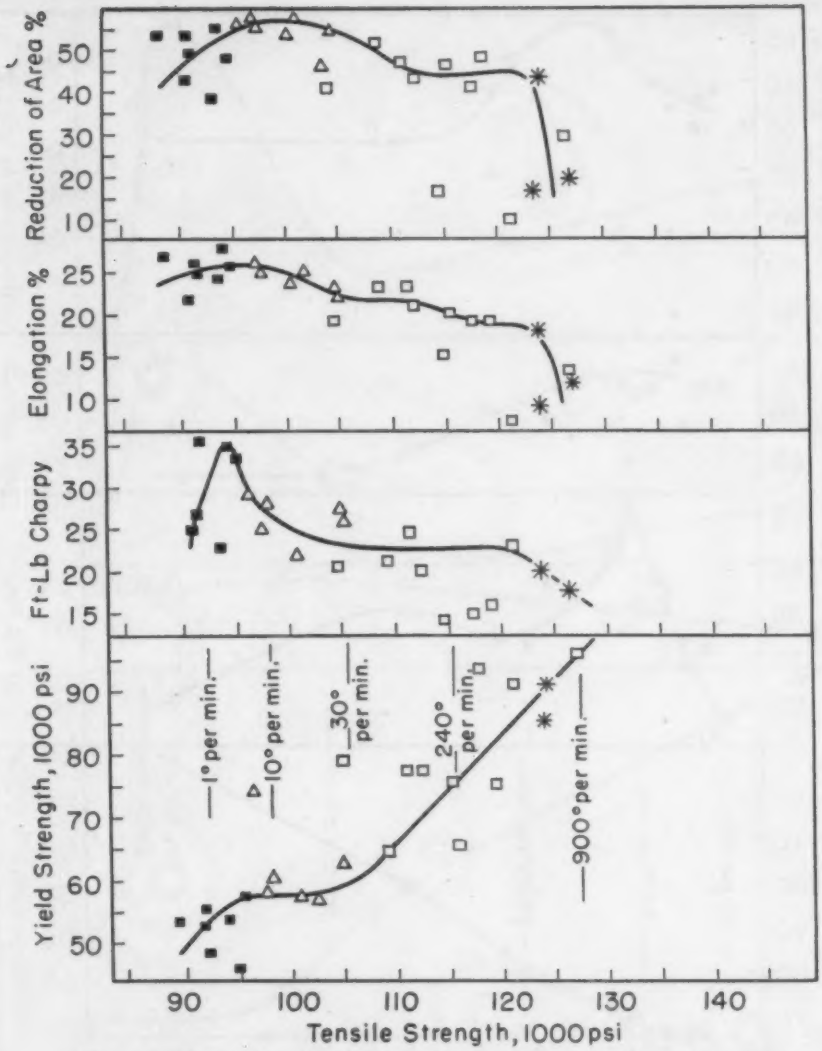


Fig. 9—Effect of Structure on Mechanical Properties of an NE 9430 Steel 31. (For key to symbols, refer to Fig. 7.)

The next series studied was the plain carbon steel 426, data for which are illustrated in Fig. 11. Water quenching produced a martensitic specimen represented by the highest tensile strength on the curve. Oil quenching produced Widmanstätten plus grain boundary blocky ferrite. Hence the graph does not show the drop in ductility between Widmanstätten ferrite and essentially blocky ferrite. The shape of the curve from there on down to the slowest cooling velocities follows the usual trend. The change in microstructure differs, however, in that a strong dendritic pattern comparable to those in the previously discussed low alloy cast steels never develops. A slight pattern is seen at the slowest cooling rates, but the structure

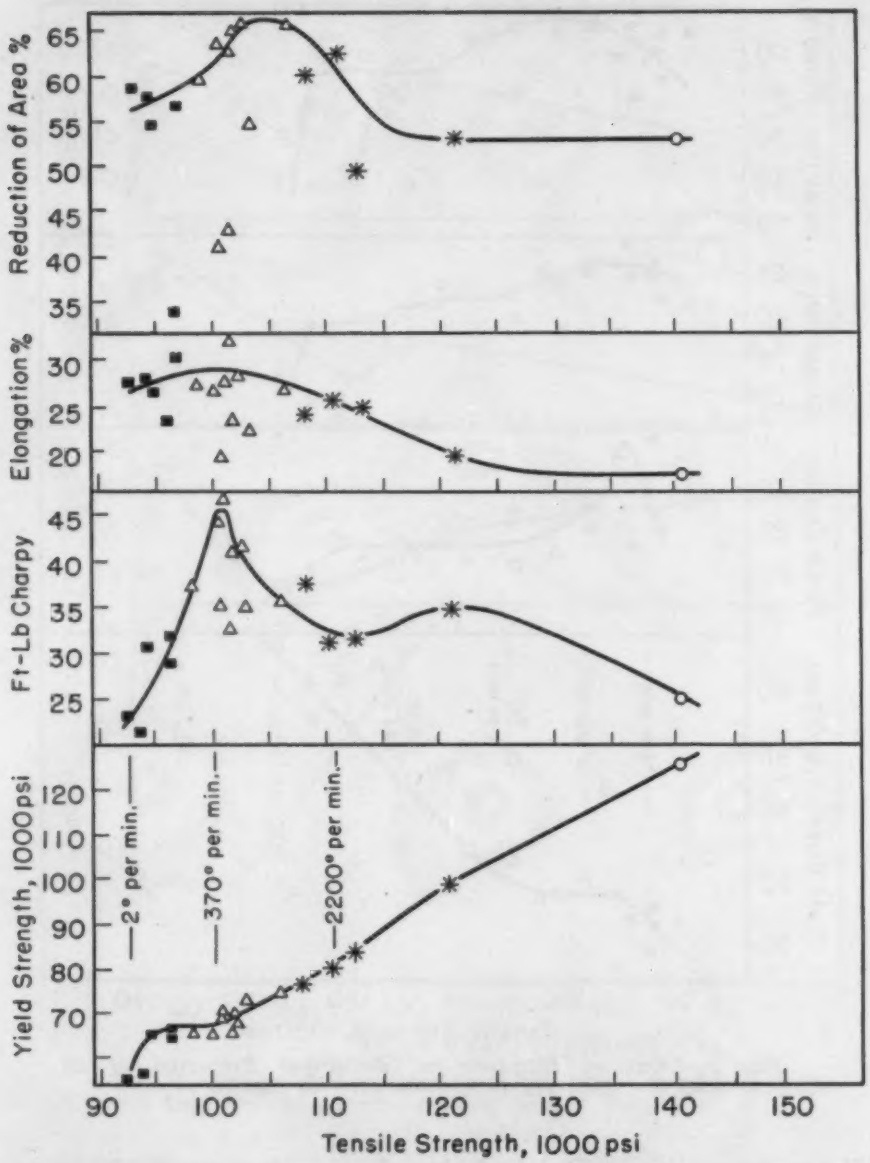


Fig. 10—Effect of Structure on Mechanical Properties of an NE 1330 Cast Steel 5. (For key to symbols, refer to Fig. 7.)

is best described as random and is so indicated on the chart. An additional factor which may contribute to the rapid decrease in reduction of area at the slowest cooling rates is a tendency for some of the ferrite in annealed samples of this steel to form a very coarse outline, possibly at sites of former as-cast austenite grain boundaries.

Specimens of another plain carbon cast steel 783 were treated and tested in the usual way. See Fig. 12. The steel did not quench out, and hence no point for martensite appears. There is the cus-

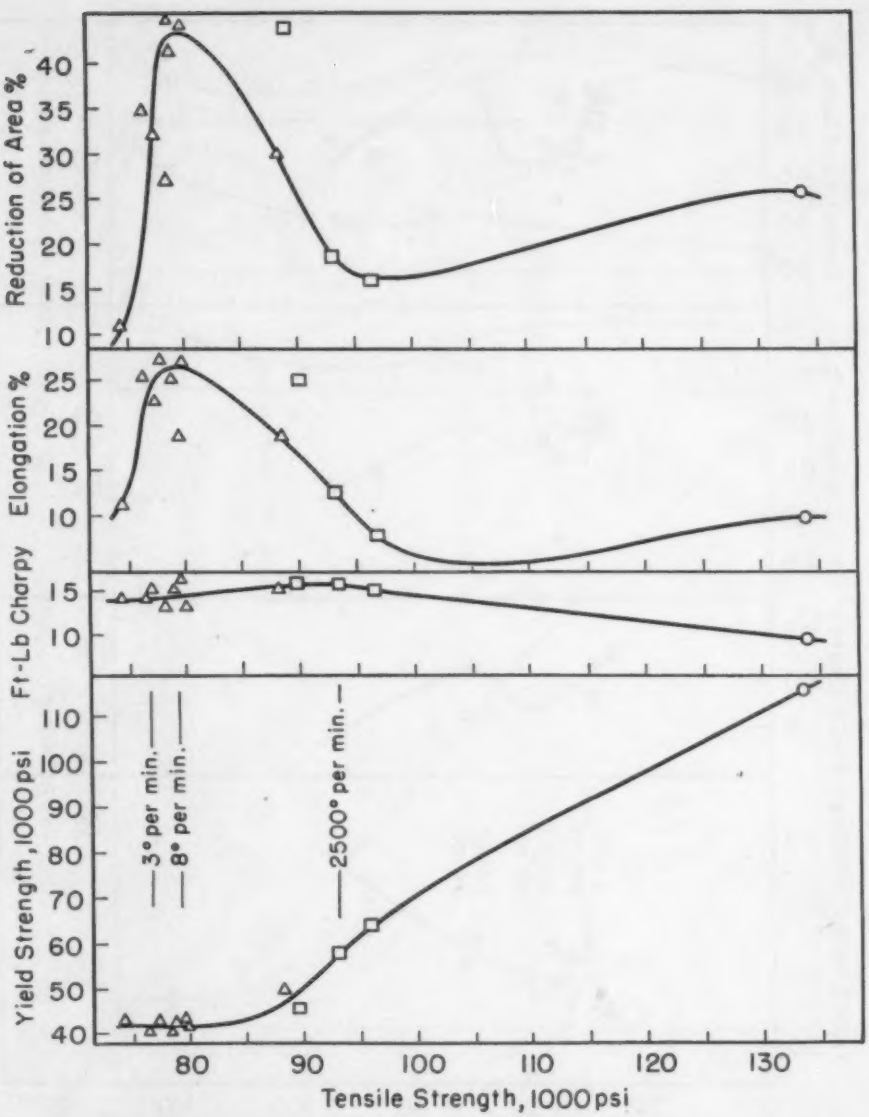


Fig. 11—Effect of Structure on Mechanical Properties of Plain Carbon Steel 426. (For key to symbols, refer to Fig. 7.)

tomary drop in reduction of area as quantities of blocky ferrite appear in conjunction with the Widmanstätten ferrite. In this steel, reduction of area continues to rise at the slowest cooling rates in spite of the fact that a pronounced dendritic pattern is formed. A possible reason for this may be the fact that, even at the slowest cooling rates, an appreciable quantity of Widmanstätten ferrite is found interspersed throughout the dendritic pattern.

The one other exception to the trend for ductilities to drop as dendritic patterns develop is illustrated by an NE 8630 cast steel,

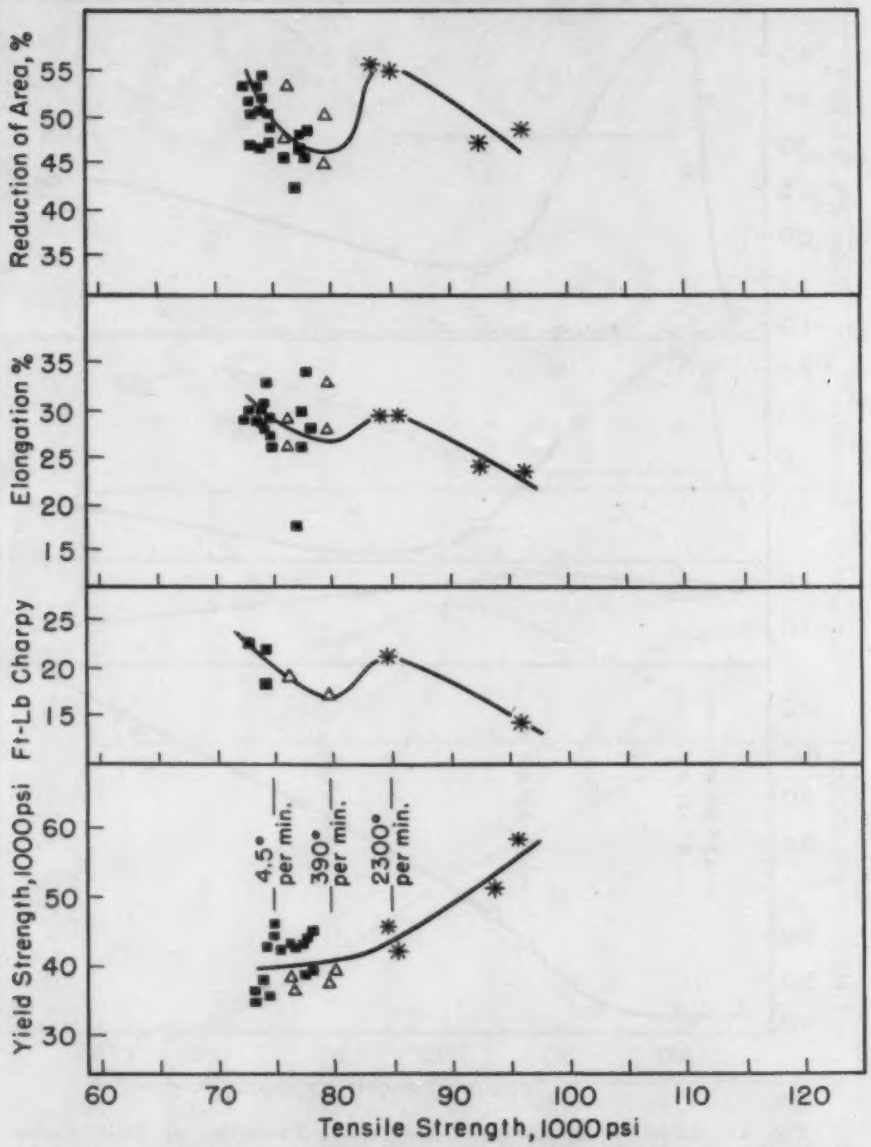


Fig. 12—Effect of Structure on Mechanical Properties of Plain Carbon Steel 783. (For key to symbols, refer to Fig. 7.)

Fig. 13. The rest of the curve is normal. The fact that some anomalies, however, do exist at slowest cooling velocities, as has been shown, led to the attempt to discover new variables as discussed in Appendix I.

A hot-rolled plain carbon steel was given a series of heat treatments similar to those given the preceding cast steels; specimens were similarly tested and the data are plotted in Fig. 14. Here it is seen that, for both the tempered and untempered series, the reduction of area decreased as the cooling rate and tensile strength were de-

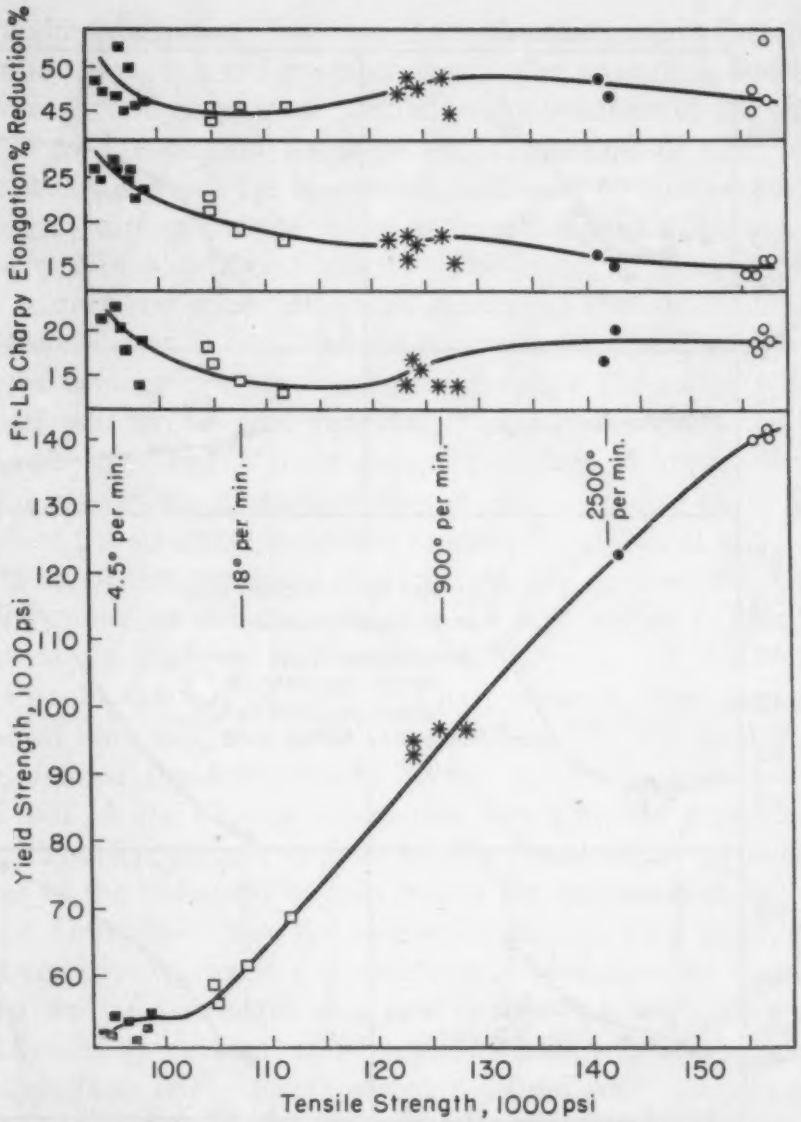


Fig. 13—Effect of Structure on Mechanical Properties of an NE 8630 Cast Steel 25. (For key to symbols, refer to Fig. 7.)

creased. The structure changed from Widmanstätten to random blocky ferrite to banded blocky ferrite as the cooling rates were decreased from a water quench to an oil quench to furnace cooling at various rates. The gradually decreasing reduction of area accompanying this change in microstructures is familiar to metallurgists experienced in heat treating plain carbon wrought steels. As mentioned before, the banded ferrite in wrought steels is analogous to the dendritic blocky ferrite in cast steels.

Elongation—In general, the per cent elongation obtained in a tensile test is much less sensitive to changes in microstructure than

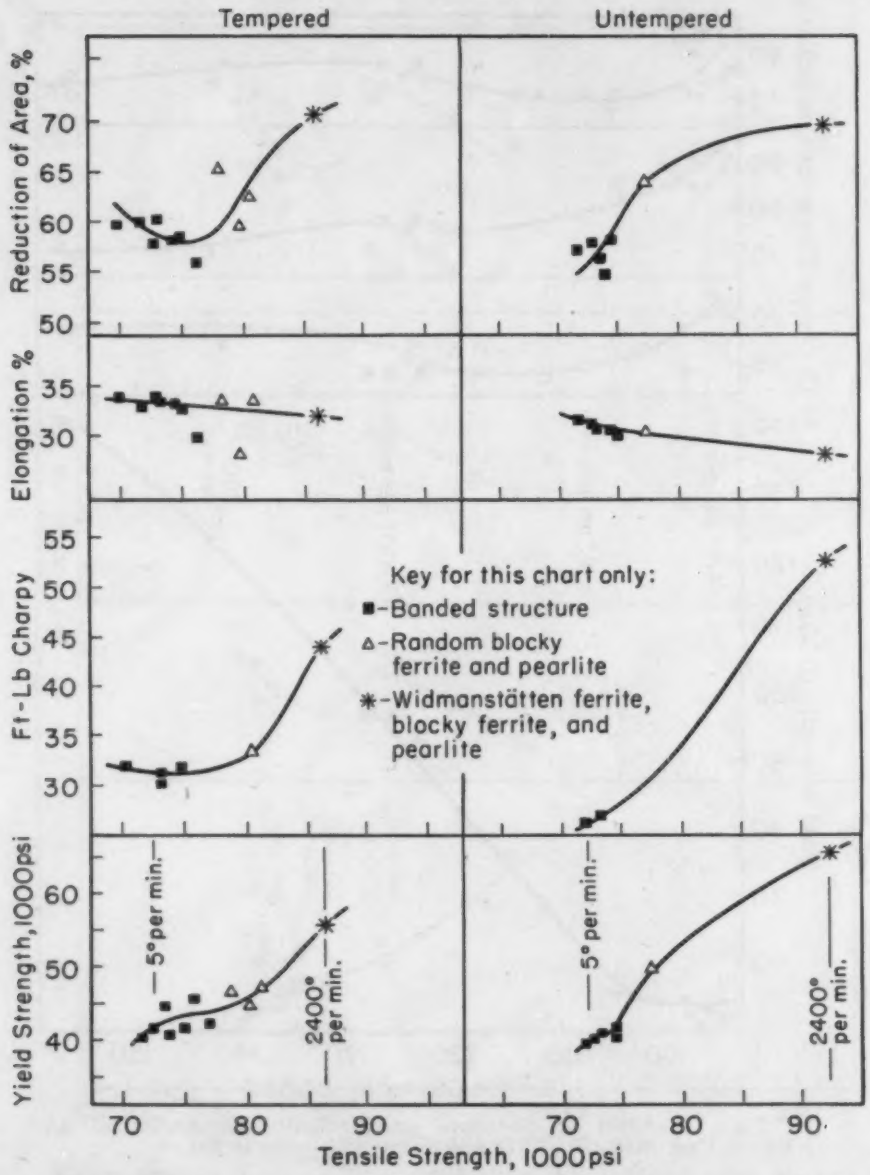


Fig. 14—Effect of Structure on Mechanical Properties of a Hot-Rolled Plain Carbon Steel.

is either reduction of area or Charpy impact strength. Graphs of elongation as a function of tensile strength appear in Figs. 7 through 14, Figs. 7 and 8 being typical and complete. In these figures, it may be seen that the elongation follows the same general trend as reduction of area. Elongation increases as the tensile strength of Widmanstätten aggregates decreases, and it levels off or drops with the appearance, in quantity, of blocky ferrite.

Once again it rises with decreasing strength as long as the struc-

ture is random, but when dendritic blocky ferrite appears, it falls off in the same manner as reduction of area. The anomalies which appeared in reduction of area are parallel to the behavior of the elongation. The one exception to these generalizations is that of the wrought steel, in which the elongation continued to rise very slowly but uniformly throughout the range as tensile strength decreased.

Charpy Notch Impact Strength—The curve of Charpy impact strength follows the same pattern in general as that of reduction of area. This is shown in Fig. 7 where it is seen that the Charpy values rose as the cooling rate was decreased through the range where a Widmanstätten ferrite plus pearlite structure was produced. As blocky ferrite appeared in large quantities, a drop in impact strength was noted as was the customary rise at slower cooling rates in the range where the structure remained random. Likewise, at still slower cooling rates which produced dendritic blocky ferrite, the Charpy values fell much as did the reduction of area values. This same behavior may be observed in Figs. 9 and 10.

In Fig. 11 there is no drop in Charpy values, even though the reduction of area drops; it will be remembered in this steel that no strongly defined dendritic blocky ferrite structure developed. In Figs. 12 and 13, the Charpy values rise even with the appearance of a strong dendritic pattern at low cooling rates. This parallels the anomalies in the reduction of area values for the same steels.

Yield Strength—Of all the properties studied, yield strength was the least sensitive to changes in structure. As is common knowledge (3), (4), the yield strength of a steel decreases continuously as the tensile strength is lowered, and the yield-tensile ratio also decreases. The general form of the tensile strength versus yield strength curves obtained in this study is well illustrated by Fig. 7. At higher strength levels the curve is virtually a straight line which continues down to some value in the range of 40,000 to 55,000 psi, where the yield strength levels off for a short space and then apparently turns down slightly. Presumably these shelves would be observed in all steels if the yield strength were reduced to this range.

There is no particular correlation between changes in type of microstructure and this leveling off of yield strength. Rather, it appears that at some very low strength range, any steel will maintain a nearly constant minimum yield strength as long as the microconstituents are uniformly distributed. Dendritic segregation may be the cause for the final slight drop. Except for the position of

these shelves in the lower ranges, nearly all the tensile strength versus yield strength curves superimpose nicely on one another.

Generalizations

Some interesting general conclusions can be drawn from the studies which have just been described in detail. To illustrate these clearly, an idealized set of curves, typical of the foregoing experimentally determined ones, is shown in Fig. 15. Once again, changes in the four other mechanical properties are related to tensile strength to give a rational basis for comparison.

Reduction of Area—The effect of microstructure on reduction of area is shown in the top curve of Fig. 15. The dotted line in this and the other graphs in the figure represent the trend for martensite tempered back to various strengths. These were drawn from data taken from a previous paper (3) and are in agreement with a smaller amount of data taken on tempered martensite in the current work. These dotted curves are included merely to emphasize once again that all the common mechanical properties of tempered martensite (resulting from liquid quenching) are superior to those of other structures of the same tensile strength.

This is illustrated by the slope of that portion of the solid line lying just below the dotted line in the reduction of area graph. Oil quenching and rapid air cooling were used to produce the Widmanstätten ferrite which gives the reduction of area represented by this portion of the line. At the fastest cooling rates some martensite is included in this structure, and as the cooling velocity decreases, it is replaced by pearlite; also within this range the Widmanstätten ferrite plates become coarser. Thus, although the reduction of area continues to increase with decreasing tensile strength, the rate of increase is less in the lower strength range.

On the other hand, at still slower cooling rates, the occurrence of blocky ferrite mixed with the Widmanstätten ferrite actually causes the reduction of area to decrease at the same time the tensile strength is dropping. Eventually, at still slower cooling velocities, random ferrite only is obtained, and the reduction of area again rises with decreasing tensile strength. This continues as long as the structure remains random, and eventually a value is reached which is as high or slightly higher than the best reduction of area for the Widmanstätten pattern.

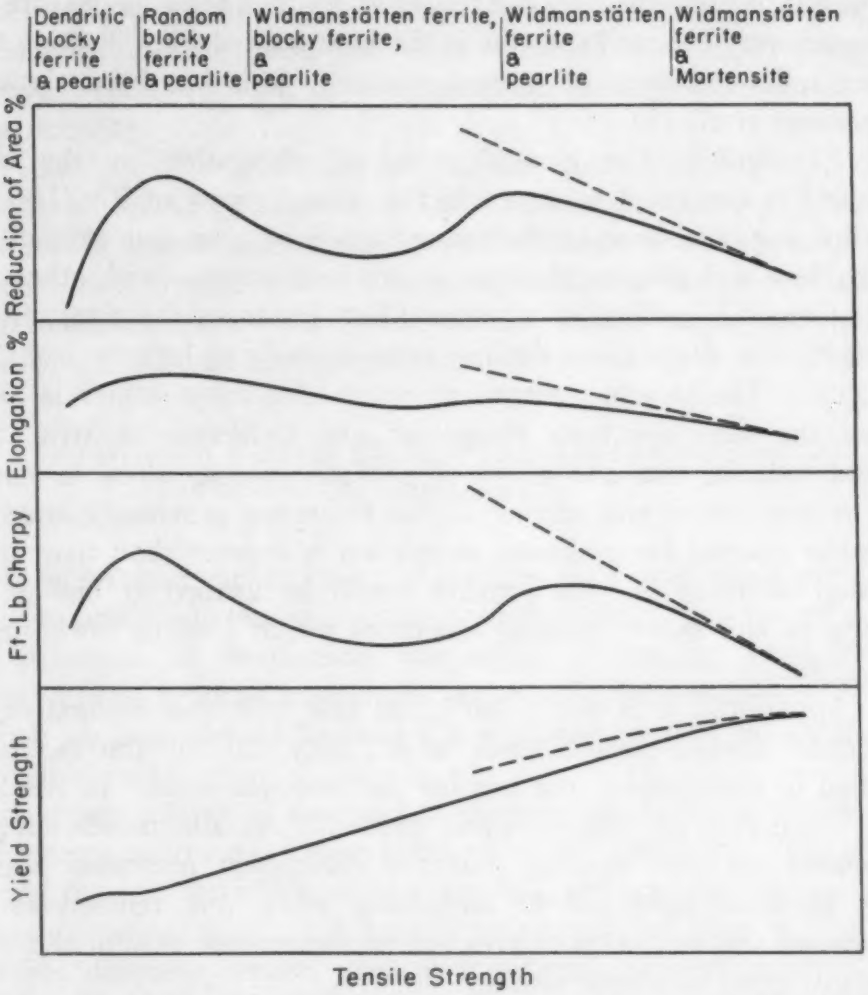


Fig. 15—Idealized Diagram Showing the Effect of Structure on Mechanical Properties of Cast Steel.

Thus there is available a wide range of cooling rates and a correspondingly wide range of tensile strengths (e.g., 30,000 psi) in which satisfactory ductility can be obtained. Furthermore, frequently better ductility can be obtained with the higher strength Widmanstätten structure than with any other structure except tempered martensite. In any event, the appearance of some Widmanstätten ferrite in a microstructure should not cause apprehension.

Finally, the appearance of dendritic blocky ferrite at very slow cooling rates is concurrent with a drop in reduction of area (frequently from about 60% down to about 45%). At the same time, a grain boundary precipitate (discussed in Appendix I) appears. A third influence possibly contributing to this decrease in reduction of

area with decreasing tensile strength is the fact that, as pearlite itself becomes very coarse (and this is the case with these annealing treatments), its reduction of area decreases. This has been shown by Gensamer et al. (5).

Elongation—The general trend of elongation as the tensile strength is decreased is shown in the second graph of Fig. 15. It is qualitatively the same as that of reduction of area, but elongation is much less sensitive to changes in microstructure (and other variables) than is reduction of area. For instance, the final drop in elongation at the slowest cooling rates is likely to be only from 30% to 25%. The tensile strength at which this drop occurs is always about the same for both elongation and reduction of area. This would indicate that the effect of pearlite spacing alone is not the major one, for it was shown in the reference previously cited (5) that the spacing for optimum elongation is coarser than that for reduction of area; i.e., the pearlite would be formed at higher temperatures and slower cooling velocities which lead to lower tensile strengths.

Apparently it is not a hard and fast rule that elongation and reduction always parallel each other; they did for the cast steels studied in this project, but not for the wrought steel. In the latter case, reduction of area dropped gradually as the tensile strength decreased on slow cooling, but the elongation increased slightly. This situation need not be surprising when one remembers that elongation and reduction of area are measurements of similar but not identical types of plastic strain.

Charpy Impact Strength—Impact strength also follows the same general trend as reduction of area and appears to be intermediate between elongation and reduction of area in sensitivity to microstructure. For instance, the decrease at the slowest cooling rates for a typical steel might be from 35 to 25 ft-lb. The general shape of the curve is illustrated in Fig. 15.

It is not inferred that Charpy impact strength always parallels reduction of area and elongation. In fact, in plain carbon cast steel 426 it did not do so at the slowest cooling velocities. This may indicate that Charpy impact strength is more sensitive to changes in microstructure and less sensitive to possible grain boundary precipitates or other variables poorly understood than are reduction of area and elongation.

What is certain, however, is that relatively fast cooling rates

can be used to obtain higher tensile strengths without necessarily sacrificing notch toughness. In other words, Widmanstätten ferrite structures (and, of course, tempered martensite) give good all-round ductility.

Yield Strength—As illustrated at the bottom of Fig. 15, yield strength is relatively insensitive to microstructure. It decreases continuously with tensile strength, as is common knowledge, and so also does yield-tensile ratio. The yield-tensile curve is essentially a straight line except for the "shelf" at low tensile strengths and the final drop-off. These have already been discussed.

Comparison of Various Heats of Cast Steel on the Basis of Microstructure

It was stated earlier that nothing less than large-scale sampling and rigid statistical analysis would suffice to determine the effect of microstructure on mechanical properties by making comparisons among various heats of steel made under different conditions. Brief mention at least should be made here of the studies which led to this conclusion.

A great volume of mechanical property data was available (3) for 32 heats of low alloy cast steels made commercially. The steels differed in such variables as composition, steelmaking process, and method of deoxidation. Mechanical properties had been determined for three different section sizes after several different programs of heat treatment. In the present investigation, microstructures of these steels were observed and correlation with mechanical properties was attempted in the following manner:

For each combination of a particular section size, a particular heat treatment, and a particular mechanical property, that property was plotted as a function of tensile strength for all the steels.[4] Over every point on each chart was pasted a photomicrograph of the corresponding structure for the steel.

Because of the variation in hardenability among the steels, a good spread in tensile strength and other properties was obtained. The general trend of yield strength increasing and ductility properties decreasing with increase in tensile strength was observed. It

---

[4]The charts thus differed from those previously presented in this paper in that each point represents a different steel, with other variables as well as structure varying, instead of representing the same steel with "heat variables" constant and structure changing by virtue of varying cooling rate.

was also observed that, in general, the steels of higher strengths contained little or no blocky ferrite.

For any given tensile strength, considerable scatter occurred in all charts for the property being plotted (with the exception of yield strength). This scatter could not be rationalized on the basis of microstructure; thus, using statistical criteria it was just as probable to find blocky ferrite corresponding to high points on a reduction of area plot as it was to find Widmanstätten ferrite. Obviously other variables were masking the effect of microstructure and much larger-scale sampling would be necessary to identify any one of them. The same approach was tried with many different variables with but little success. In general, high phosphorus and Type II (intergranular sulphide) inclusions were associated with lower ductility, but there were exceptions.

Summary

Microstructure is only one of several important variables governing the mechanical properties of cast steels, and it is the only one which was studied intensively in this investigation. To isolate its effect from that of other variables it was necessary to compare the properties associated with different microstructures by producing these microstructures in individual heats of cast steel by varying the heat treatments given to the specimens.

The results of such studies indicate the following:

1. In any one cast steel successively better ratios of ductility to strength are obtained as faster and faster cooling rates are used. This leads to the formation of different types of microstructure in the following progression:
   a. Dendritic blocky ferrite plus pearlite
   b. Random blocky ferrite plus pearlite
   c. Widmanstätten ferrite plus pearlite
   d. Martensite (must be tempered, of course)
2. The maximum ductility obtainable in a cast steel is gained by quenching the steel to martensite and then tempering it at a high temperature.
3. Little or no loss in ductility and appreciable gain in strength are obtained by moderately rapid cooling (e.g., in air), which forms Widmanstätten ferrite, in place of slow cooling, which forms blocky ferrite.

These are the criteria for obtaining the best mechanical properties in *any one heat* of cast steel.

On the other hand it should be stated emphatically that a selection among *various heats* of cast steel cannot be made on the basis of microstructure alone. Thus one steel may have a better combination of strength and ductility when heat treatment results in a blocky ferrite structure than does *another* heat of similar composition heat treated to give a Widmanstätten structure. Indeed, even an apparently pronounced dendritic structure alone is not a valid cause for rejection, because the other important variables governing mechanical properties may all be favorable. Furthermore, a steel is found occasionally which shows better ductility with a dendritic blocky ferrite structure than it does with any other type of structure formed on annealing or normalizing.

Appendix I

Results of Investigation Using Zephiran Chloride Etchant

In the metallographic work on the specimens used for the determination of the effect of microstructure on mechanical properties, the standard etching reagents were supplemented by a special etchant consisting of an ether solution of picric acid and Zephiran chloride (an organic chloride). This etchant was developed[5] primarily to detect an unidentified precipitate in quenched and tempered steels susceptible to temper brittleness. It was used in the present study on the premise that the solubility phenomena which cause the precipitation of a grain boundary constituent in the ferrite of tempered martensite might also occur in slowly cooled blocky ferrite.

As brought out in the reference cited, the etchant discloses that a precipitate forms in temper-brittle alloy steels cooled slowly through the temperature range of 1100 °F (595 °C) and somewhat below. Presumably the precipitate may be present to some extent also in steels which are not temper brittle, but the common features of the structure which are also brought out by this etchant make a comparison of the two cases difficult. A clear distinction is obtained, however, by repolishing any unknown specimen after mounting it in bakelite with a "blank" specimen known to be free of embrittlement. Such treatment will remove the ordinary features of the microstruc-

[5] J. B. Cohen, A. Hurlich and M. Jacobson, "A Metallographic Etchant to Reveal Temper Brittleness in Steel," Transactions, American Society for Metals, Vol. 39, 1947, p. 109.

ture of a temper-brittle specimen but will leave the grain boundary precipitate readily apparent. On the other hand, neither ordinary structure nor precipitate will be apparent in the "blank" specimen.

The same technique was tried in the present study to investigate the very slowly cooled specimens which suffered a decrease in ductility usually concurrent with the appearance of a dendritic blocky ferrite pattern. The "blank" was always a specimen of the same steel cooled slightly faster to produce random ferrite with good ductility. Careful polishing and microscopy were necessary, but positive results were obtained on the four steels, 5, 16, 17 and 31, in which no anomalous mechanical property results had been observed. The slowest cooled specimens with low ductility all showed a precipitate which remained after repolishing; the corresponding "blank" specimen (with random ferrite) repolished simultaneously in the same bakelite mount showed no precipitate.

These slowly cooled steels owe their dendritic appearance to the fact that some areas have a greater ratio of pearlite to ferrite than others. It is in these pearlite-rich areas that the precipitate is more pronounced. Fig. 16 is a photomicrograph taken at high magnification in a pearlite-rich area of an annealed cast steel. It was taken before repolishing, however, and shows how the precipitate outlines pearlite colony boundaries and extends partially out into the ferrite before disappearing as a chain of dots. Note that in these slowly cooled steels the precipitate forms a finer grain boundary outline than it would if it were confined to austenite grain boundaries as appears to be the case in quenched and tempered steels.

In addition, a very slowly cooled specimen of steel 16 containing the precipitate was cut in three pieces; one piece was untreated, and the other two pieces were reheated 2 hours at 1175 °F (635 °C); one of these two pieces was then slowly cooled again, while the other was instead quenched. All three pieces were then mounted together in bakelite, etched with Zephiran chloride, and repolished. The original piece, and the piece which was reheated and slowly cooled, both showed the precipitate, but the rapidly cooled specimen did not. The precipitate in the reheated and slowly cooled specimen appeared identical with that in the original piece. Thus this precipitation is a reversible phenomenon and is not associated with the transformation of austenite.

The effect of this unidentified phase on mechanical properties has not been established, and it is not certain whether it or the

dendritic pattern is responsible for the decreases in ductility reported at very slow cooling rates. The precipitate was not observed in plain carbon cast steels.

The precipitate may have some bearing on the aforementioned anomalous behavior of ductility of specimens of steel 25 cooled at the slowest rates. The results are inconclusive, however. In this steel, the

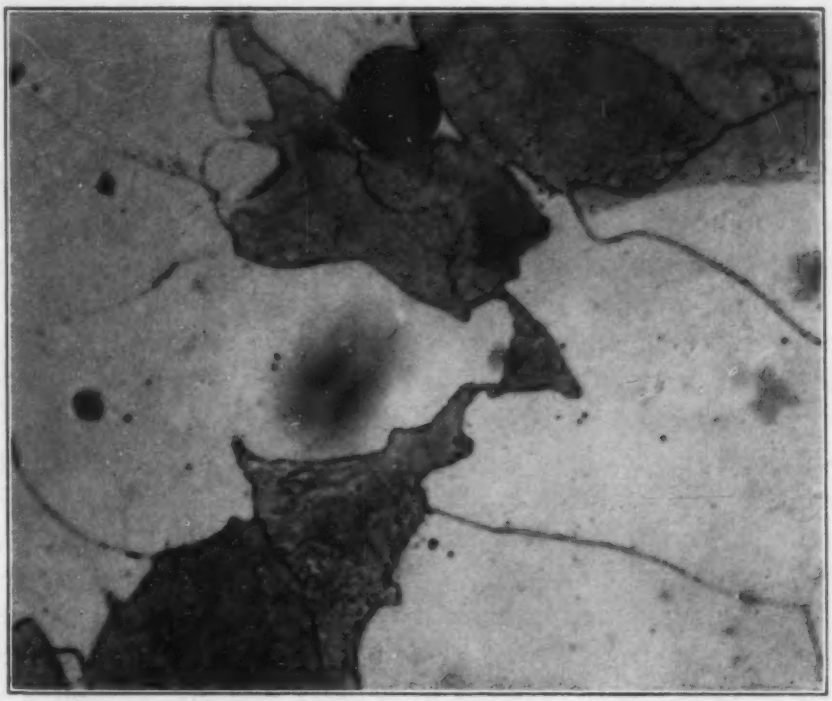


Fig. 16—Distribution of Intergranular Precipitate in Slowly Cooled Low Alloy Cast Steel. Zephiran chloride etchant, not polished after etching. × 1500.

precipitate found in a slowly cooled dendritic sample polished out in the same length of time as that found in a more rapidly cooled sample with a random structure. A rather heavy precipitate was observed with both cooling rates, however; also it will be noted that the ductility of this steel is somewhat low regardless of cooling rate, nor were there assignable causes for this, such as Type II inclusions. Thus, if the precipitate is a factor influencing ductility, it still is not clear for steel 25, whether it is in a form which is equally harmful at all cooling rates or in a form not harmful at all.

In summary, a new precipitate in very slowly cooled alloy cast steels has been detected using the Zephiran chloride etching reagent. Its occurrence in such steels has paralleled the development of a

dendritic blocky ferrite microstructure. Both of these features occurred simultaneously with an unexpected decrease in ductility. Either, both, or neither may be the cause of this decrease, but, in any event, it is felt that the Zephiran chloride reagent should be given a trial by future investigators working on similar problems in cast steels.

Appendix II

Note on As-Cast Structure and Grain Size

The same general features of microstructure observed in normalized and annealed cast steels are found also in as-cast structures. However, classification and prediction of these structures is much more complex because of the influence of additional variables such as cooling rate and temperature gradients during freezing, temperature at which castings are removed from their molds, and undoubtedly other production variables not well understood.

Although this leads to a bewildering variety of as-cast structures in apparently similar heats of steel, close examination shows them to consist of various forms and combinations of Widmanstätten, grain boundary, and random ferrite, together with pearlite. As always, faster cooling rates and greater hardenability favor the Widmanstätten patterns. In addition, alloying elements have a pronounced tendency to cause these patterns to be very fine and exhibit a striking geometric array of ferrite plates in contrast with the very coarse ill-defined Widmanstätten patterns common to plain carbon cast steels.

Studies, made in the attempt to correlate as-cast microstructure with microstructure or mechanical properties after heat treatment, showed no significant relationships. There is much less variability in annealed and normalized microstructures, and the principles governing their morphology, as outlined in Part I of this paper, remain unaffected over the wide range of initial as-cast structures.

A frequently disturbing feature of the microstructure of as-cast steels is the huge austenite grain size which is sometimes well delineated by grain boundary ferrite. Furthermore, near the surface of a casting, these grains, which formed during freezing of the casting, usually have a pronounced columnar shape with the length of the grain being several times greater than the other two dimensions. That

this grain size is readily refined to ASTM ratings in the range of 5 to 8 for both silicon- and aluminum-killed cast steels by customary single annealing or normalizing operations was demonstrated conclusively in a previous paper (2). Evidence was also presented indicating that there is no correlation between as-cast and subsequent grain size. In the present investigation, the latter study was repeated using improved technique to eliminate all possible disturbing variables such as columnar crystallization. New data are presented in Fig. 17

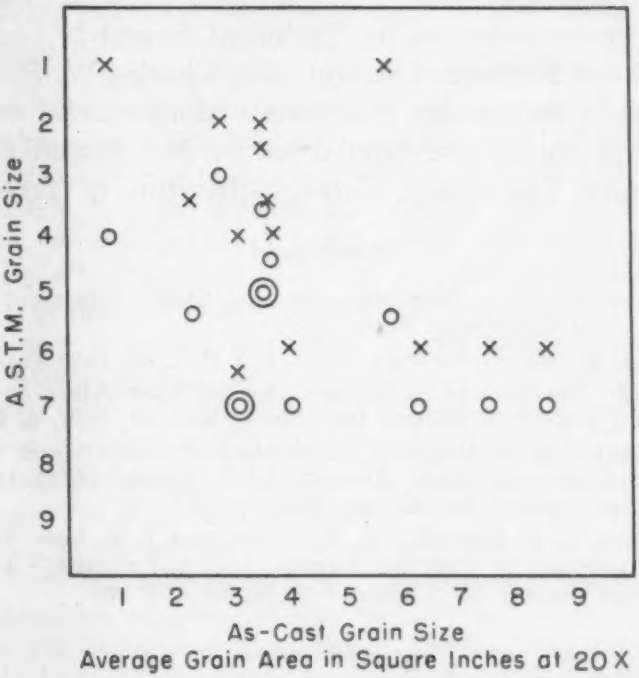


Fig. 17—As-Cast Austenite Grain Size and Grain Size After Heat Treatment of Fourteen Cast Steels.

which confirms the fact that the austenite grain size developed by a single reheating operation is not influenced by the previous as-cast austenite grain size. Measurements of both grain sizes were made on the same centerline plane (giving equiaxed grain contours) through test coupons of 14 silicon- and aluminum-killed cast steels. These represented all the available steels which showed a continuous grain boundary ferrite envelope in the as-cast microstructure; only in such steels can the as-cast austenite grain size be determined satisfactorily.[6]

[6]M. F. Hawkes, discussion to paper by E. A. Loria, "Detection of As-Cast Austenite Grain Size in Heat Treated Cast Alloy Steels," TRANSACTIONS, American Society for Metals, Vol. 40, 1948, p. 693.

The circles in Fig. 17 refer to the grain size after austenitizing at 1550 °F (845 °C), and the X's refer to the grain size after austenitizing at 1700 °F (925 °C). There is obviously no correlation between the austenite grain size obtained on reheating to either of these temperatures and the previous as-cast austenite grain size.

Acknowledgment

This research was made possible by the Steel Founders' Society of America, Cleveland, Ohio. The authors profited greatly through the friendly co-operation of its Technical Research Committee and its Technical and Research Director, Mr. Charles W. Briggs. Steels were supplied by its member foundries. Much careful metallography and mechanical testing was carried out by Mr. Joseph Danko of the Metals Research Laboratory, Carnegie Institute of Technology.

References

1. Albert Sauveur, "The Metallography and Heat Treatment of Iron and Steel," The University Press, 1926.
2. M. Hawkes, *Metals Technology,* Vol. 14, T.P. 2170, June 1947.
3. M. Hawkes, "Mechanical Properties of Cast Low Alloy Steels," TRANSACTIONS, American Society for Metals, Vol. 39, 1947, p. 1.
4. E. J. Janitzky and M. Baeyertz, "The Marked Similarity in Tensile Properties of Several Heat Treated SAE Steels," METALS HANDBOOK, American Society for Metals, 1939, p. 515.
5. M. Gensamer, E. B. Pearsall, W. S. Pellini and J. R. Low, Jr., "The Tensile Properties of Pearlite, Bainite, and Spheroidite," TRANSACTIONS, American Society for Metals, Vol. 30, 1942, p. 983.

DISCUSSION

Written Discussion: By G. A. Lillieqvist, research director, American Steel Foundries, East Chicago, Ind.

I have read with great interest the subject paper by Messrs. Hawkes and Brown. I wish to congratulate the authors on this excellent paper and feel that they have made a great contribution to the steel castings industry. In the past, we have also observed these various microstructures, but have never been able to use the proper terminology. Out of the confusion the authors have brought some order in terminology for the microstructure and in outlining the basic factors contributory to their formation.

I have noted that the deoxidation practice for the investigated steels varies to a considerable degree. Some of the steels were deoxidized with calcium-manganese-silicon only; while other steels were deoxidized with aluminum and ferrotitanium. It is a recognized fact that deoxidation

practice plays a very important part in regard to dendritic segregation as well as in regard to grain growth characteristics. It would be of great interest if the deoxidation practice would be known of steels 31 and 34. The microstructure of these steels appears on page 532. I would assume that the same deoxidation practice was not used for the steels.

I was especially interested in Appendix 1, "Results of Investigation Using Zephiran Chloride Etchant". I believe that an intensive study of this condition should be made as it may lead to different and important conclusions.

Again, I wish to congratulate the authors for their splendid contribution.

Written Discussion: By Edward A. Loria, Fellow, Mellon Institute of Industrial Research, Pittsburgh.

The authors have competently evaluated the effect of microstructure on mechanical properties of cast steel, major emphasis being placed on the relative effects of grain boundary, random and Widmanstätten distribution of ferrite on the tensile and impact properties of annealed and normalized carbon, low and medium alloy steels. The simple relationship to be expected between strength and ductility was found to be valid in cast steels only when the type of ferrite distribution remained the same. Changes in type produced several maxima and minima in the curves. The question now arises as to whether or not wrought steels cooled at various rates also show this behavior.

Of interest are the earlier results of Piwowarsky and Evers[7, 8] on numerous tests of unalloyed and alloyed cast steel melted in acid and basic furnaces, which indicated the importance of microstructure on mechanical properties. The difference in structure between air cooling and furnace cooling of a number of cast steels showed that the impact, yield point and tensile strength were lower with furnace cooling, while elongation and reduction of area did not conclusively establish a superiority of the one or the other cooling practice. Their rapidly cooled structures were Widmanstätten and blocky ferrite plus pearlite, whereas the furnace-cooled specimens had the characteristic dendritic blocky ferrite and pearlite. The present authors have refined the effects of microstructure on mechanical properties to a far greater extent.

The writer would like to know if the test specimens used in this study were cast into shapes where solidification was under close control. The solidification pattern and the degree of segregation of alloying elements which are dependent upon the rate of solidification have been found to exert an important influence upon the ductility of cast steel at a given hardness, chiefly through their effects upon hardenability and the distribution of microconstituents. Also, what effect would the direction of the columnar dendritic crystallization have on the results? The orientation of dendritic pattern probably produces angular fractures, but since

[7]A. Evers and E. Piwowarsky, "The Annealing of Cast Steel," *Archiv für das Eisenhüttenwesen*, Vol. 17, 1943, p. 35-42.

[8]E. Piwowarsky and A. Evers, "Notched Bar Impact Strength of Cast Steel," *Stahl und Eisen*, Vol. 64, 1944, p. 142-144.

such orientations are determined by chance, the occurrence of angular fracture in cast steels may not always be generally associated with intermediate ductility. The columnar dendritic structure often found at the surfaces of steel castings, when sound, has been found to possess higher hardenability than the interior, equiaxed or granular structure of the same casting.[9] The distribution of the alloying elements is more uniform and the solidification pattern is finer.

The authors correlate the loss of ductility with the appearance of dendritic blocky ferrite and the grain boundary precipitate in slowly cooled steels and mentioned that Charpy impact strength is more sensitive to changes in microstructure and less sensitive to possible grain boundary precipitation or other variables than are reduction of area and elongation. This is undoubtedly true, the change in type of ferrite distribution having produced the maxima and minima in the curves. For example, the decrease in Charpy impact in a structure consisting of small amounts of Widmanstätten ferrite and martensite lies in the contribution of the ferrite in lowering the fracture strength. Considering the stress situation in this case, it is apparent that there are relatively large volumes of very hard martensite bonded together by thin layers of soft ferrite. The ferrite consequently has no opportunity to flow, since it is bonded, as a thin layer, between hard masses of martensite. Had the ferrite been able to flow, it would have absorbed energy in the flow process, and consequently would have contributed to greater toughness, rather than brittleness. The minima in Charpy impact in structures containing both Widmanstätten ferrite and blocky ferrite arise from the presence of ferrite in the interdendritic boundaries. Probably the incipient fractures are seen to occur most frequently in or adjacent to patches of blocky ferrite. Perhaps several ruptures began in a single large patch of ferrite, the main path of fracture as well as branch fractures being through these patches or islands of blocky ferrite.

The authors have shown that there is no apparent relationship between as-cast and subsequent grain size in cast steels which developed ferrite outlining of the as-cast grains. Employing the basic ingredients of Austin's reagent to detect burning in alloy steels, the writer[10] has developed an etchant consisting of 2 parts of water in 1 part of sulphuric acid and 2 parts of nitric acid which has been used successfully in illustrating the as-cast grain pattern in alloy steels which do not show ferrite outlining. Figs. 18 and 19 depict the as-cast grains and dendritic structure developed during metal solidification in a manganese-molybdenum steel and a nickel-chromium-molybdenum steel. It is apparent that the etchant provides grain contrast, use being made of the circumstance that each former austenite grain had a definite crystalline orientation differing from that of its neighbors, and that the orientation of the decomposition products is fixed by the orientation of the austenite grains from which they arise. The rate of chemical attack by the reagent varies greatly

[9]G. A. Timmons, "Factors Affecting the Ductility of Cast Steel," *Transactions*, American Foundrymen's Association, Vol. 51, 1943, p. 417-480.

[10]E. A. Loria, Unpublished research.



Fig. 18—As-Cast Macrostructure of Alloy Cast Steel Containing 0.31% Carbon, 1.44% Manganese, 0.26% Molybdenum. Modified nitro-sulphuric etch. × 5.

with the orientation of the grains, thus producing a typical grain-contrast etch. Notwithstanding, it does not develop the as-cast grain structure in steels such as plain carbon (Grade B) and nickel steels whose grain size is well delineated by grain boundary ferrite. The etching procedure is tedious and several attempts may be necessary in order to produce the desired structure. The amounts specified above must be rigidly adhered to if satisfactory results are to be obtained. Specifically, the polished specimen is immersed in the solution for 5 to 20 seconds, depending on its freshness. Soon after immersion, there is a bubbling action around the periphery of the specimen and an evolution of brownish fumes. Upon removal, the pronounced smudge or precipitate formed on the polished face is removed quickly by wiping with cotton under water. Then, after rinsing in alcohol the specimen is dried under an air blast. The reagent becomes cloudy after it has been used a few times and loses its effectiveness.

No doubt the authors are referring to annealed and normalized cast steels when they state that only in steels which show a continuous grain boundary ferrite envelope can the as-cast austenite grain size be determined satisfactorily. The as-cast grain pattern can be shown in speci-

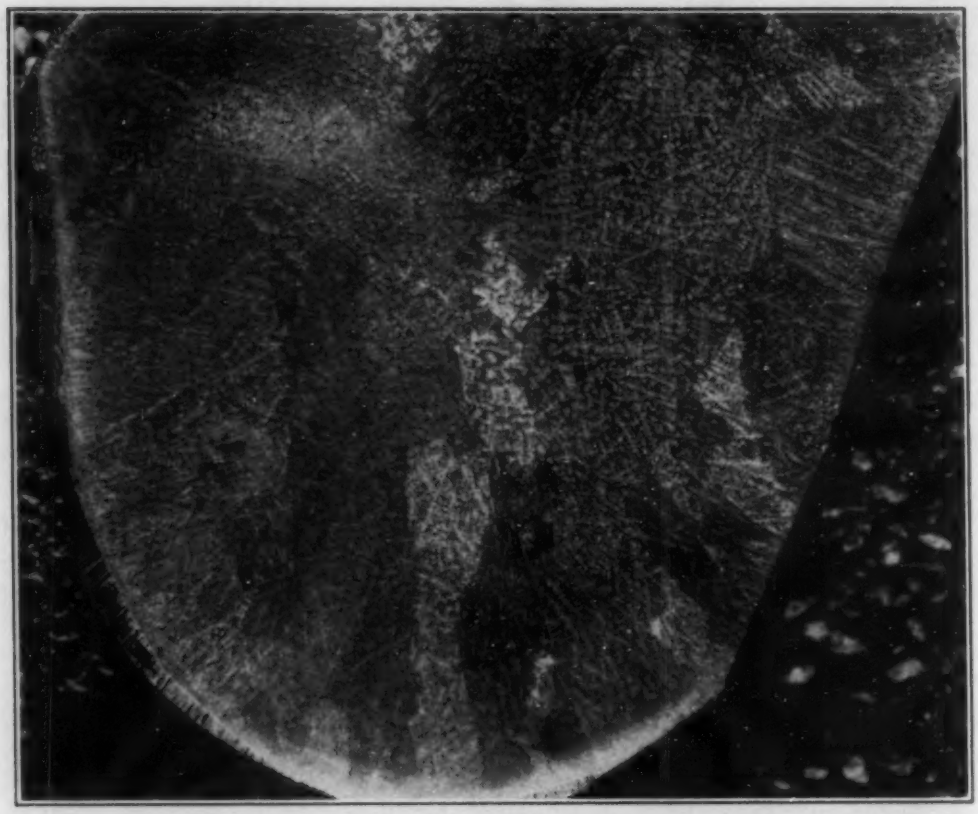


Fig. 19—As-Cast Macrostructure of Alloy Cast Steel Containing 0.29% Carbon, 1.21% Manganese, 0.61% Nickel, 0.54% Chromium, 0.22% Molybdenum. Note dendritic pattern within the grains. Modified nitro-sulphuric etch. × 5.

mens possessing a martensitic structure by etching with the zephiran chloride – picric acid reagent, preferably after a low temperature tempering treatment. In cast armor plate, water-quenched at 1600 °F (870 °C) and tempered at various temperatures to produce the desired fibrous fracture for ballistic specifications, etching with ordinary nital-picral will yield over-all grain contrast and a clear delineation of the grains in a section with a martensitic or acicular structure tempered at 1000 °F (540 °C) and below. Recently Lorig and Elsea[11] have shown that hairline cracks developed by deep etching in a hot 38% hydrochloric, 12% sulphuric acid solution outlined the primary austenite grain boundaries in certain alloy steels. The modified nitro-sulphuric reagent described above will now provide additional means of detecting the austenite grain size in cast alloy steels.

The use of the ether solution of picric acid and Zephiran chloride to delineate an unidentified precipitate in annealed low alloy cast steels possessing a dendritic blocky ferrite structure is very interesting and invites some thought as to its nature and mode of formation. It is a

[11]C. H. Lorig and A. R. Elsea, "Occurrence of Intergranular Fracture in Cast Steels," *Transactions*, American Foundrymen's Association, Vol. 55, 1947, p. 160-174.

well-known fact that annealing is a manifestation of a trend toward equilibrium and away from some unstable condition set up by rapid cooling and that various constituents have an appreciable solubility in austenite, one that varies with temperature and is much decreased when the austenite transforms to ferrite on cooling. These phenomena illustrate that the precipitate is really inherent in the rate of cooling through the solvus of the iron-carbon diagram or, more appropriately, on cooling through the solvus surface of the iron-carbon-manganese or perhaps the iron-carbon-nitrogen systems, since it was stated that the precipitate was not observed in plain carbon cast steels and suggests the possibility that elements such as manganese have an effect. Thus if one cools slowly through the solvus inclusion films, intermetallic compounds, carbon, nitrogen or other elements will precipitate at the boundaries of the large equiaxed grains whereas with fast cooling there is no opportunity for these constituents to form a continuous network because of the rapid cooling rate and the resultant mode of formation of the matrix structure. The formation of the precipitate is therefore intimately associated with the type of ferrite that is produced and has its greatest opportunity of forming a fairly continuous network in dendritic blocky ferrite and pearlite formed on slow cooling. A Widmanstätten ferrite nucleated at relatively fast cooling velocities would present a plate-like, geometrical array of ferrite grains among which the precipitate particles (if formed) would be dispersed to such an extent that they would not be a factor in lowering ductility.

The intergranular precipitate is not basically different from those already observed in temper-brittle chromium steels and in boron steels. It can be identified as consisting of any or possibly a combination of the constituents mentioned above. Carbon and nitrogen have been shown definitely to give rise to precipitation or aging effects when present in amounts ordinarily found in low carbon steel. The solubility of nitrogen in ferrite at room temperature is not more than 0.001% so precipitation effects caused by nitrogen may occur in steel containing more than this amount. Since carbon has a much higher solubility in austenite than in ferrite, the transformation of austenite to ferrite leads to a precipitation of carbide and to hardening. Have the authors observed the precipitate in low alloy cast steels in the as-cast state, perhaps in the ferrite network or in the precipitation of massive cementite in the primary grain boundaries, two phases in themselves to which the cause of brittle fracture may sometimes be ascribed?

It would be of interest to determine the maximum temperature above which no precipitation occurs regardless of the initial composition of the ferrite and if the precipitate can form during tempering below the equilibrium temperature for precipitation. This maximum temperature would be the temperature at which the solubility of the constituents in ferrite would be equal to the initial concentration in ferrite and would be expected to vary appreciably with the composition of the steel, for the initial concentration of the constituents would be expected to vary. Also

such samples of one steel on being partially transformed to various small percentages of ferrite at various temperatures and then quenched to martensite and tempered would provide data on the effect of ferrite on the impact strength of hardened cast steel, the amount and type of ferrite formed (free from the associated fine pearlite obtained when continuous cooling is employed) being correlated with the resulting Charpy impact strength.

The writer is using 1% Zephiran chloride in 4% nital in a further study of the intergranular precipitate. In general, nital is a better grain boundary delineator than picral and the addition of the wetting reagent, Zephiran chloride, increases the sensitivity of the nital and the speed of etching. The nital is thus considerably improved by the addition of Zephiran chloride.

Written Discussion: By Max Bolotsky, metallurgist, Aberdeen Proving Ground, Aberdeen, Md.

The writer wishes to submit a concept of temper brittleness for use in the evaluation of the data presented by Hawkes and Brown. This concept was evolved at the outset of the 1947 National Metal Congress in Chicago, but was not presented heretofore because of the hope (not realized at this date) that the writer could secure direct evidence that would confirm the concept, which is based upon what appears to the writer to be much indirect experimental data.

Since the 1947 National Metal Congress the writer has not seen data in contradiction to his views. The concept, as written on November 2, 1947, is as follows:

Temper brittleness in steel is caused primarily by the precipitation of a carbide into the grain boundaries during cooling from the critical range. Additional embrittlement results by tempering in the "embrittlement range", which depends upon the composition of the steel, or by slow cooling from or above the "embrittlement range".

In steels containing no elements but carbon, silicon, phosphorus, sulphur, and aluminum, the precipitate is the small amount of iron carbide that is insoluble in alpha iron, as shown by the iron-carbon diagram (see ASM METALS HANDBOOK).

The addition of manganese to the above elements either increases the tendency of the above described iron carbide to precipitate into the grain boundaries or causes greatly increased precipitation due to one or more carbides of manganese or to complex iron-manganese carbides.

The addition of molybdenum to the above elements reduces the precipitation of carbides into the grain boundaries, either by affecting the solubility of the above described iron carbide or by the formation of carbide of molybdenum that resists precipitation into the grain boundaries.

When the manganese content is sufficiently high, the ability of molybdenum to retard grain boundary carbide precipitation is greatly reduced.

Apparently vanadium acts similarly to manganese, and columbium and titanium have an effect similar to that of molybdenum.

The higher the carbon content, the more the embrittling constituent resulting from a specified heat treatment.

For a steel of specified chemical content, the faster the cooling rate from the critical range, the less the amount of embrittling grain boundary carbide precipitate. The superiority in impact toughness of tempered martensite over tempered or untempered bainite, and the superiority in impact toughness of tempered or untempered bainite over tempered or untempered pearlite are due primarily to the difference in the amounts of embrittling precipitate caused by the differences in the cooling speeds rather than because of the microstructures themselves. For example, a medium carbon, plain carbon steel heat treated to produce tempered martensite has superior impact properties to the impact properties of the same steel in the as-rolled condition, not because of differences in microstructure (i.e., tempered martensite versus pearlite) but because of differences in amount of embrittling grain boundary carbide caused by the differences in cooling rate from the critical range.

The larger the grain size the worse the effect of a specified amount of precipitate because the less is the grain boundary area and therefore the higher is the concentration of precipitate per unit of grain boundary area.

Authors' Reply

Mr. Lillieqvist is correct in presuming that the two steels of Fig. 6 did not have the same deoxidation treatment; steel number 34 was deoxidized with 2 pounds per ton of aluminum and 5 pounds per ton of ferrotitanium, while steel number 31 was deoxidized with 2 pounds per ton of calcium-manganese-silicon in the furnace and the same amount in the ladle.

Mr. Loria has added some information from two papers by Evers and Piwowarsky, of which only the first had been surveyed before writing this current paper. Inasmuch as Evers and Piwowarsky varied other (and more potent) factors than simple microstructure, no structure-property correlations can be made from their publication. It is interesting to note that those authors apparently considered the appearance of Widmanstätten ferrite (in aluminum-killed steels austenitized at 880 to 910 °C) an indication of overheating.

In reply to the question of control of solidification, it should be noted that all the specimens of a given series were cast in effectively identical sand molds. For one early study of directional properties in columnar cast steel, Mr. Loria is referred to the publication of Piwowarsky, Bosic and Soenchen.[12] The present authors did not make such studies.

Mr. Loria's adaptation of Austin's reagent for delineating as-cast austenite grains is a welcome addition to the tools available for the metallography of cast metals. His confirmation of the reported lack of

[12]Piwowarsky, Bosic and Soenchen, *Archiv für das Eisenhüttenwesen*, Vol. 7, 1933.

correlation between as-cast and subsequent grain size is welcomed. It is becoming evident that the factors controlling heat treated grain size are not operating to control as-cast grain size, and if one is interested in controlling as-cast grain size, he will have to look to other influences than deoxidation practice. It has been suggested that degree of superheat may be one such influence.

It is gratifying to note the interest evidenced in the precipitate observed by using Zephiran chloride etching reagent. The limited number of observations on the behavior of this precipitate indicate that it acts like other phases which come out of solid solution during precipitation hardening, and hence the speculations of Messrs. Bolotsky and Loria are for the most part quite plausible. In considering this precipitation and the effects of alloy additions, we might profitably draw upon observations made on aluminum-copper precipitation hardening kinetics where it is noted that small amounts of manganese and magnesium, while affecting solubility limits very little, strongly accelerate the precipitation. Further study of this precipitate is underway currently at Carnegie Institute of Technology. The authors prefer to await the results before making positive statements about the effect of the precipitate on mechanical properties. No metallographic studies using Zephiran chloride have been made on as-cast steel by the authors.

Mr. Bolotsky's statement discounting the effect of differences in microstructure upon impact strength does not seem reasonable to the present authors. If the curves of Figs. 7 to 11 in the paper are to be explained, a very odd relationship would have to exist between cooling velocity and the amount of postulated grain boundary carbide.

EFFECT OF VANADIUM ON THE PROPERTIES OF CAST CARBON AND CARBON-MOLYBDENUM STEELS

By N. A. Ziegler, W. L. Meinhart and J. R. Goldsmith

Abstract

An investigation was made of (a) carbon, (b) 0.5% molybdenum and (c) 1% molybdenum cast steels, in which vanadium ranged from 0 to 0.3% and carbon from 0.05 to 0.3% in each group. Results obtained in the various tests on characteristics and properties are presented.

Thermal sluggishness was increased by the combined effects of carbon, molybdenum and vanadium, but not by vanadium alone in the carbon steel group. Some residual delta ferrite (untransformed) was found in the structure of the low carbon, high molybdenum, high vanadium compositions. Increasing vanadium contents reduced the pearlite grain size and produced some extremely fine spheroidal carbides.

Vanadium moderately increases the tensile strength, yield point, proportional limit and hardness, slightly reduces the ductility and to a considerable extent reduces the impact resistance.

Metal arc welding of these steels presented no difficulties with regard to cracks and voids. Ductility of the resultant weld assemblies, however, was decreased by the combined effect of carbon, molybdenum and vanadium.

Vanadium-bearing steels in the "as cast" condition appear more brittle than similar compositions without vanadium. When properly heat treated this brittleness is eliminated, nevertheless impact resistance is lower and greater care is required than for carbon and carbon-molybdenum steels.

Introduction

THE most popular application of vanadium as an alloying element is in various types of tool steels. That subject, however, is outside the scope of the present article. In making low alloyed

A paper presented before the Thirtieth Annual Convention of the Society, held in Philadelphia, October 23 to 29, 1948. Of the authors, N. A. Ziegler is research metallurgist, W. L. Meinhart is assistant research metallurgist, and J. R. Goldsmith is metallurgical engineer in charge of research foundry, Crane Co., Chicago. Manuscript received April 29, 1948.

steels, vanadium is used less frequently than such metals as chromium, nickel and molybdenum. Nevertheless, Knowlton (1)[1] over 20 years ago wrote that vanadium acts as a cleaner and in addition it strengthens the ferrite and makes cementite more stable. He also pointed out that vanadium acts as a grain refiner. According to him carbon-vanadium steels are used in the manufacture of large forgings and castings, particularly those used in locomotive construction, and carbon-chromium-vanadium steels are used in automotive construction.

In view of the fact that vanadium belongs to the class of less popular alloying elements (which is particularly true about low-alloyed steels), its various effects on the properties of steel are less well known than those of the more widely used metal additions. Nonetheless, the references indicate the amount of work done on this subject. Among other things, it is known (2) that up to about 30% vanadium (which itself has a body-centered cubic structure) and alpha iron are isomorphous and form a continuous series of solid solutions.

Vanadium belongs to the class of "gamma-loop-forming" elements, in which respect it acts in the same direction as chromium, molybdenum and silicon, and opposite to that of manganese, nickel, carbon and copper. According to the information available (2), it takes somewhere between 1.1 and 2.5% vanadium to eliminate the gamma state in "pure" iron.

Within the last few years, small additions of vanadium to steel castings have been advocated for the purpose of improving their creep resistance, and making carbides more stable, thus reducing their susceptibility to graphitization in superheated steam service. While the first effect is fairly well established, the second one requires further confirmation.

The authors thus undertook a broad survey of the effect of vanadium on various properties of cast carbon and carbon-molybdenum steels. The present paper describes the results of this work and is another step in our attempts to determine the effect of one isolated variable at a time on thermal characteristics, physical properties, hardenability and, to some extent, weldability of cast carbon and low alloyed steels. Our previous publications dealt with the effect of copper (3), chromium and molybdenum (4), nickel (5), manganese (6), and silicon (7).

[1]The figures appearing in parentheses pertain to the references appended to this paper.

Experimental Procedure

The experimental technique used in this work is quite similar to that described in our previous publications (3, 4, 5, 6 and 7).

A series of experimental melts was made in a 200-pound high frequency induction furnace, using low carbon steel scrap as raw material and conventional melting and deoxidizing technique. Each heat was killed by the addition of about 2 pounds of aluminum per ton, tapped into a 250-pound capacity ladle, and cast into (a) keel coupon blocks and (b) welding plates, using green sand molds.

These steels are divided into three groups: (a) plain carbon-vanadium, (b) carbon-vanadium containing 0.5% molybdenum, and (c) carbon-vanadium containing 1% molybdenum. Tables I, II and III give the nominal compositions and chemical analyses of steels belonging to each one of these groups respectively. Each group is subdivided into three subgroups: (a) steels containing under 0.1% carbon, (b) steels containing about 0.15% carbon, and (c) steels containing about 0.3% carbon. Each subgroup consists of four or more steels with vanadium ranging from 0 to about 0.3%.

Each keel coupon block was sectioned into test bar blanks and heat treated by normalizing from 1750 °F (955 °C) and drawing at 1250 °F (675 °C). The welding plates were heat treated similarly.

All of these compositions were subjected to tensile,[2] Vickers hardness and Charpy impact[3] testing. The latter was performed: (a) at room temperature, and (b) at —25 °F (—32 °C).

Most of these compositions were also subjected to dilatometric thermal analysis. The final hardnesses of the dilatometer samples are incorporated in Tables I, II and III. The data from physical testing were omitted to conserve space; however, results are presented in graphical form.

As shown in Tables I, II and III, the minor elements (silicon, manganese, sulphur and phosphorus), as well as molybdenum in Tables II and III, in all of these experimental steels are reasonably uniform. Carbon content within each subgroup may be considered as constant. Vanadium content within each subgroup (as previously pointed out) ranges between 0 and about 0.3%, thus permitting certain conclusions to be drawn concerning its effect on properties.

[2]Standard 0.505-inch diameter, 2-inch gage test bar.
[3]Standard Charpy test bar with keyhole notch.

Table I
Carbon-Vanadium Series
Chemical Analysis and Dilatometer Data

Serial No.	Nominal Composition C	V	Chemical Analysis Si	Mn	S	P	C	Ni	Cr	Mo	V	Hardness of Dilatometer Specimens V.P.N. 5-Hr. Cool	Air Cool
1	0.1 max.	0	0.20	0.54	0.016	0.019	0.07	....	0.03	....	0	103	111
2	0.1 max.	0.05	0.23	0.62	0.017	0.019	0.06	....	0.03	....	0.08	103	130
3	0.1 max.	0.15	0.21	0.60	0.018	0.020	0.08	....	0.03	....	0.16	126	141
4	0.1 max.	0.30	0.20	0.64	0.015	0.019	0.09	....	0.03	....	0.25	135	151
5	0.15	0	0.32	0.80	0.020	0.036	0.15	....	0.03	....	0	132	141
6	0.15	0.05	0.42	0.94	0.021	0.020	0.14	....	0.05	....	0.08	141	148
7	0.15	0.15	0.34	0.57	0.024	0.016	0.17	....	0.03	....	0.16	141	155
8	0.15	0.30	0.31	0.55	0.021	0.017	0.15	....	0.03	....	0.24	148	175
9	0.30	0	0.45	0.70	0.017	0.024	0.29	....	0.08	0.03	0	156	160
10	0.30	0.05	0.47	0.71	0.018	0.022	0.30	....	0.03	0.03	0.10	154	156
11	0.30	0.15	0.39	0.66	0.024	0.026	0.25	0.10	0.05	0.05	0.17	160	199
12	0.30	0.30	0.45	0.71	0.023	0.014	0.27	....	0.05	....	0.25	188	238

Table II
Carbon – 0.5% Molybdenum-Vanadium Steels
Chemical Analysis and Dilatometer Data

Serial No.	Nominal Composition C	Mo	V	Chemical Analysis Si	Mn	S	P	C	Ni	Cr	Mo	V	Hardness of Dilatometer Specimens V.P.N. 5-Hr. Cool	Air Cool
1	0.1 max.	0.5	0	0.25	0.52	0.011	0.020	0.08	....	0.03	0.61	0	115	125
2	0.1 max.	0.5	0.05	0.26	0.54	0.012	0.018	0.09	....	0.03	0.59	0.07	119	145
3	0.1 max.	0.5	0.15	0.33	0.60	0.009	0.018	0.08	....	0.03	0.55	0.15	128	131
4	0 1 max.	0.5	0.30	0.30	0.55	0.007	0.019	0.05	....	0.05	0.62	0.25	106	123
5	0.15	0.5	0	0.33	0.68	0.016	0.022	0.14	....	0.03	0.57	0	140	153
6	0.15	0.5	0.05	0.34	0.78	0.016	0.021	0.15	....	0.03	0.58	0.08	135	172
7	0.15	0.5	0.15	0.30	0.69	0.025	0.024	0.13	....	0.05	0.56	0.15	141	173
8	0.15	0.5	0.30	0.40	0.81	0.023	0.013	0.17	....	0.10	0.56	0.25	182	276
9	0.30	0.5	0	0.39	0.56	0.022	0.021	0.28	....	0.03	0.61	0	158	202
10	0.30	0.5	0.05	0.43	0.69	0.023	0.024	0.25	....	0.28	0.61	0.06	181	198
11	0.30	0.5	0.15	0.45	0.73	0.023	0.018	0.26	....	0.03	0.59	0.18	171	264
12	0.30	0.5	0.30	0.46	0.78	0.019	0.020	0.25	....	0.03	0.52	0.25	196	336

Thermal Analysis and Microexamination

Four steels with increasing vanadium content within each subgroup (Tables I, II and III) were subjected to thermal analysis using a self-recording differential dilatometer. In each case a specimen[4] was heated in vacuum to 1830 °F (1000 °C) in 2 hours, and then cooled to room temperature (a) in 5 hours[5] and (b) in air.[6]

[4] 50 millimeters long and 4 millimeters in diameter.

[5] An average cooling rate of 3.2 °C per minute or 5.8 °F per minute.

[6] An average cooling rate of 50 °C per minute or 90 °F per minute.

Table III
Carbon – 1.0% Molybdenum-Vanadium Steels
Chemical Analysis and Dilatometer Data

Serial No.	Nominal Composition C	Mo	V	Chemical Analysis Si	Mn	S	P	C	Ni	Cr	Mo	V	Hardness of Dilatometer Specimens V.P.N. 5-Hr. Cool	Air Cool
1	0.1 max.	1.0	0	0.44	0.46	0.032	0.019	0.05	....	0.03	1.09	0	131	141
2	0.1 max.	1.0	0.05	0.41	0.39	0.029	0.019	0.06	....	0.03	1.04	0.07	132	137
3	0.1 max.	1.0	0.15	0.50	0.40	0.026	0.021	0.06	....	0.03	1.15	0.19	147	148
4	0.1 max.	1.0	0.30	0.45	0.38	0.025	0.019	0.06	....	0.03	1.07	0.26	139	146
5	0.15	1.0	0	0.38	0.72	0.033	0.018	0.14	....	....	1.08	0	160	185
6	0.15	1.0	0.05	0.44	0.87	0.032	0.018	0.15	....	....	1.08	0.09	176	212
7	0.15	1.0	0.15	0.51	0.78	0.026	0.027	0.15	....	....	1.12	0.17	177	219
8	0.15	1.0	0.30	0.46	0.86	0.038	0.022	0.16	....	0.05	1.16	0.27	184	279
9	0.30	1.0	0	0.48	0.67	0.035	0.023	0.29	....	0.03	1.17	0	219	299
10	0.30	1.0	0.05	0.39	0.58	0.031	0.021	0.30	0.02	0.06	1.14	0.09	...	...
11	0.30	1.0	0.05	0.45	0.75	0.031	0.018	0.29	....	0.03	1.10	0.12	243	285
12	0.30	1.0	0.15	0.49	0.59	0.034	0.018	0.29	....	0.03	1.04	0.18	228	302
13	0.30	1.0	0.30	0.54	0.65	0.035	0.019	0.25	....	0.03	1.12	0.26	221	317

The results thus obtained are presented in Figs. 1 and 2 (for plain carbon-vanadium steels), Figs. 3 and 4 (for carbon – 0.5% molybdenum-vanadium steels) and Figs. 5 and 6 (for carbon –1% molybdenum-vanadium steels). Moreover, Figs. 1, 3 and 5 are compilations of the dilatometer curves obtained on slow cooling (5 hours) and Figs. 2, 4 and 6 are those obtained on more rapid cooling (in air). The chemical analysis and final Vickers hardness of the specimen are given adjacent to each curve in each of the above figures. Vickers hardnesses are also graphically represented, as functions of vanadium content, in Figs. 16, 17 and 18.

In Figs. 1, 2, 3, 4, 5 and 6, the curves are arranged into three subgroups: those representing (a) steels containing under 0.1% carbon, (b) steels containing about 0.15% carbon, and (c) steels containing about 0.3% carbon. Within each subgroup they represent four steels ranging in vanadium between 0 and about 0.3%.

After the completion of the thermal cycle, each dilatometer specimen was subjected to microexamination.

Plain Carbon-Vanadium Group—Vanadium, as already known, tends to raise the transformations on heating. This trend, however, is very slight within the vanadium contents investigated (Figs. 1 and 2). There is a tendency for the hardness of the dilatometer specimens to increase with increasing vanadium. This tendency becomes more pronounced with the increase in carbon and is particularly

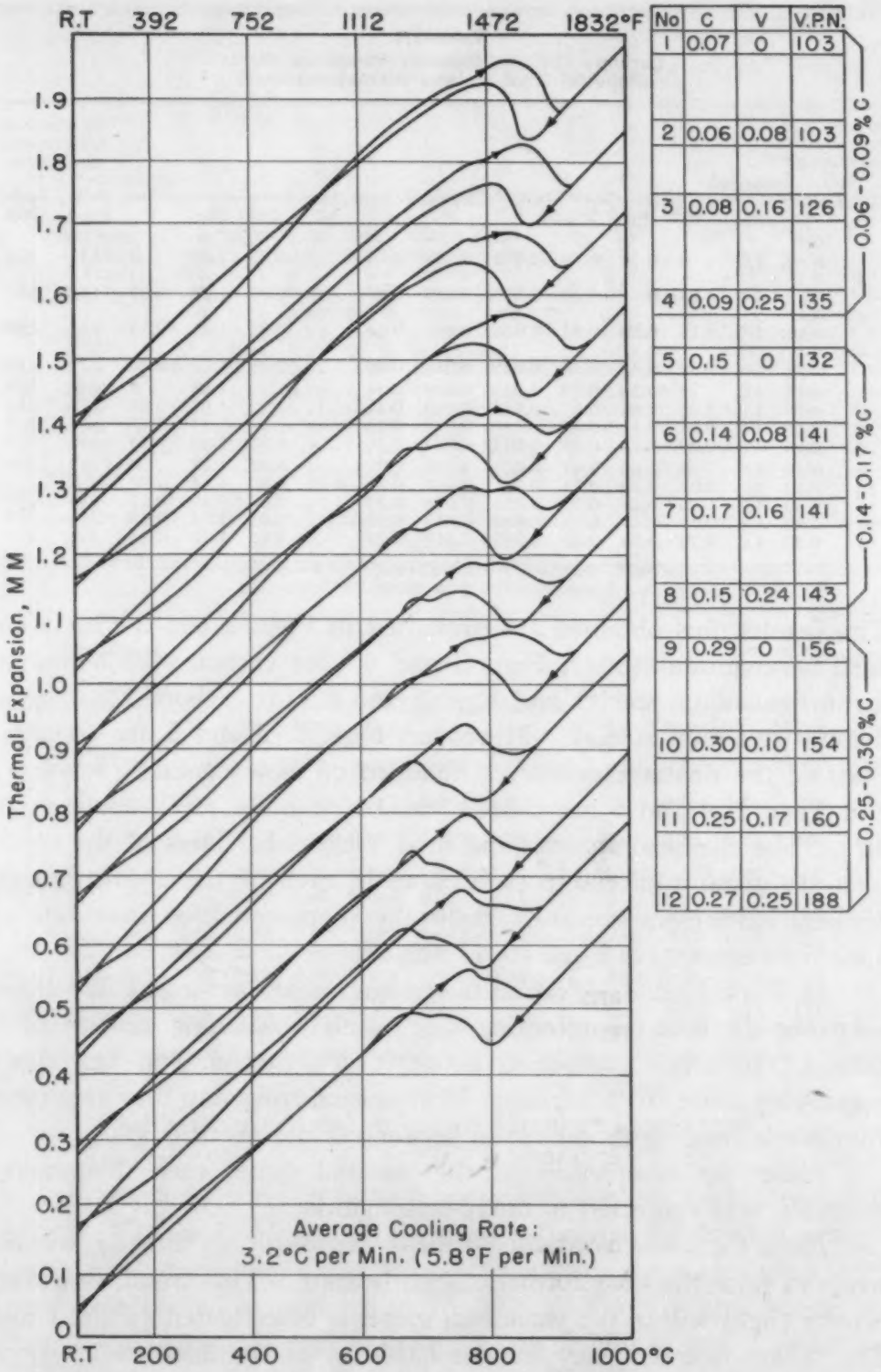


Fig. 1—Thermal Curves of Carbon-Vanadium Steels. (Slow cooling rate.)

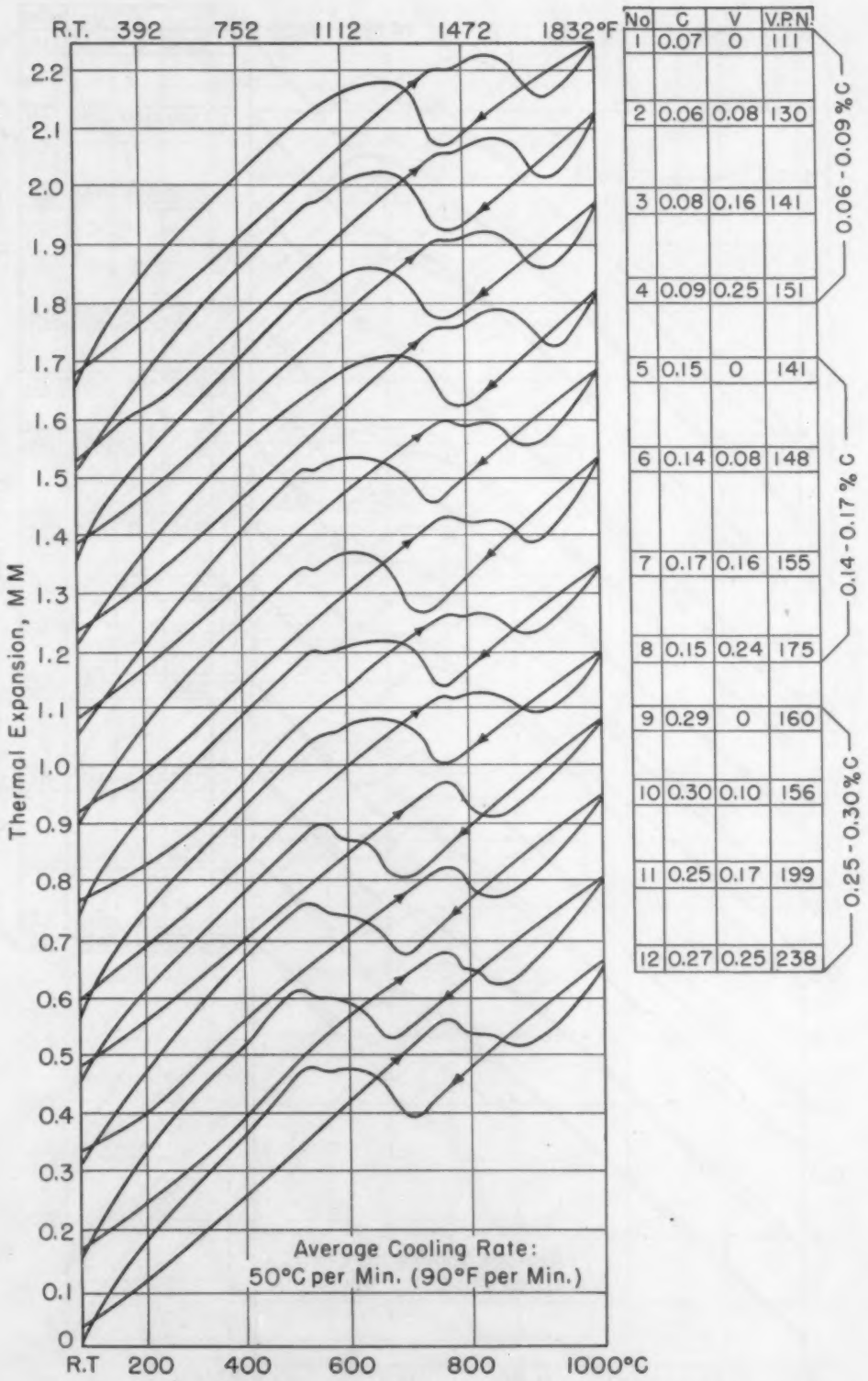
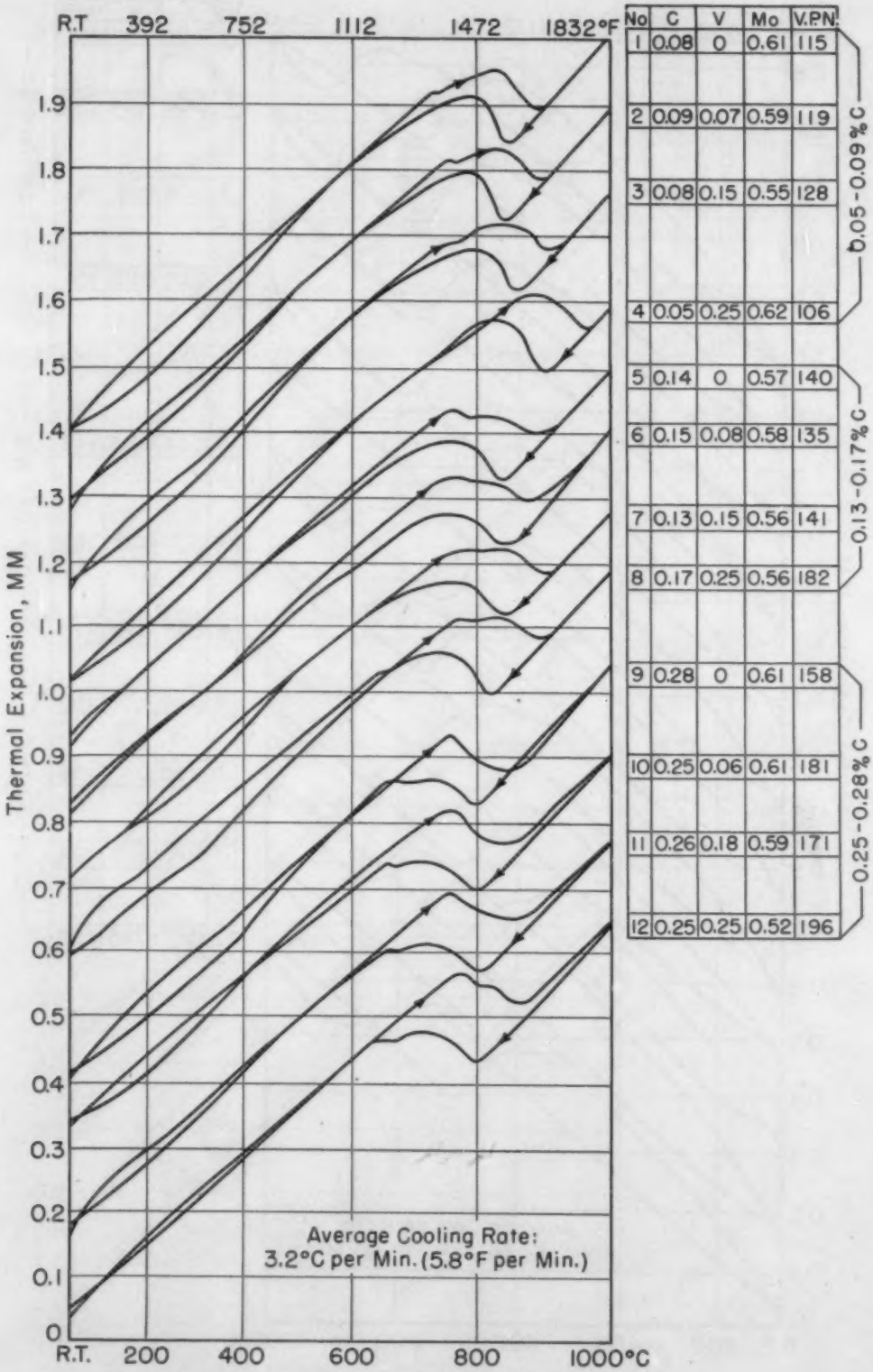


Fig. 2—Thermal Curves of Carbon-Vanadium Steels. (Rapid cooling rate.)



No	C	V	Mo	V.P.N.
1	0.08	0	0.61	115
2	0.09	0.07	0.59	119
3	0.08	0.15	0.55	128
4	0.05	0.25	0.62	106
5	0.14	0	0.57	140
6	0.15	0.08	0.58	135
7	0.13	0.15	0.56	141
8	0.17	0.25	0.56	182
9	0.28	0	0.61	158
10	0.25	0.06	0.61	181
11	0.26	0.18	0.59	171
12	0.25	0.25	0.52	196

Fig. 3—Thermal Curves of Carbon-Vanadium – 0.5% Molybdenum Steels. (Slow cooling rate.)

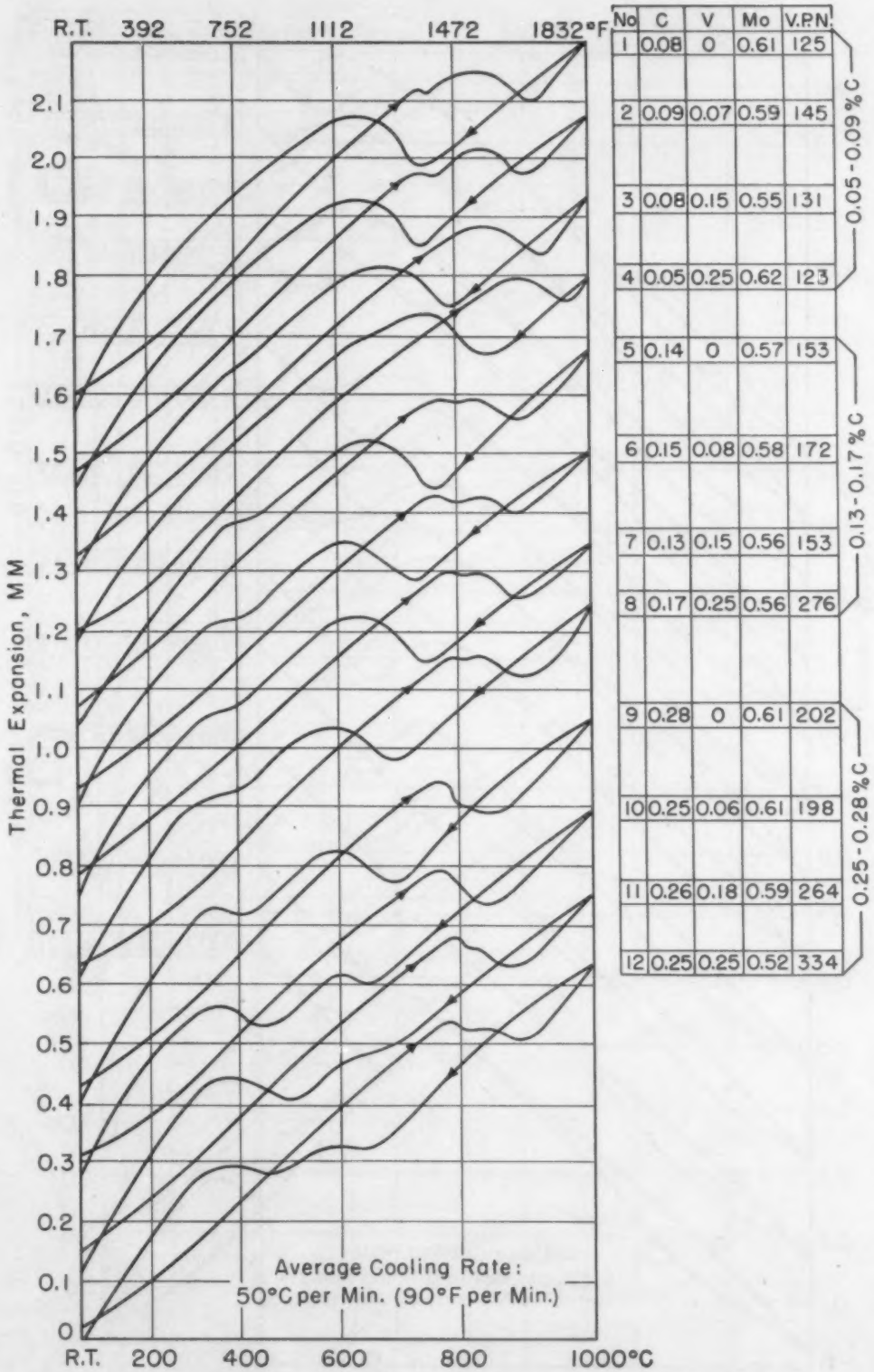


Fig. 4—Thermal Curves of Carbon-Vanadium – 0.5% Molybdenum Steels. (Rapid cooling rate.)

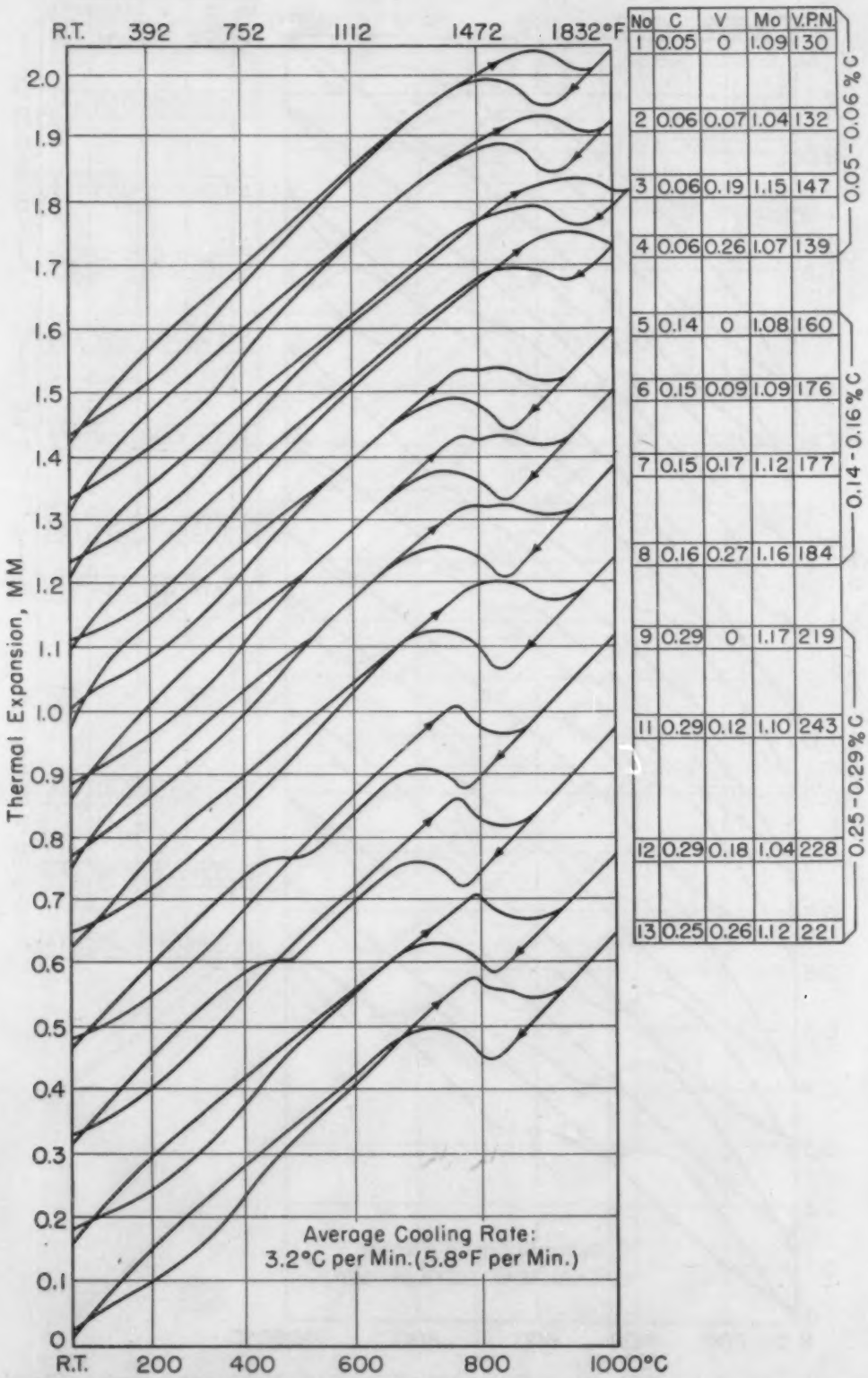
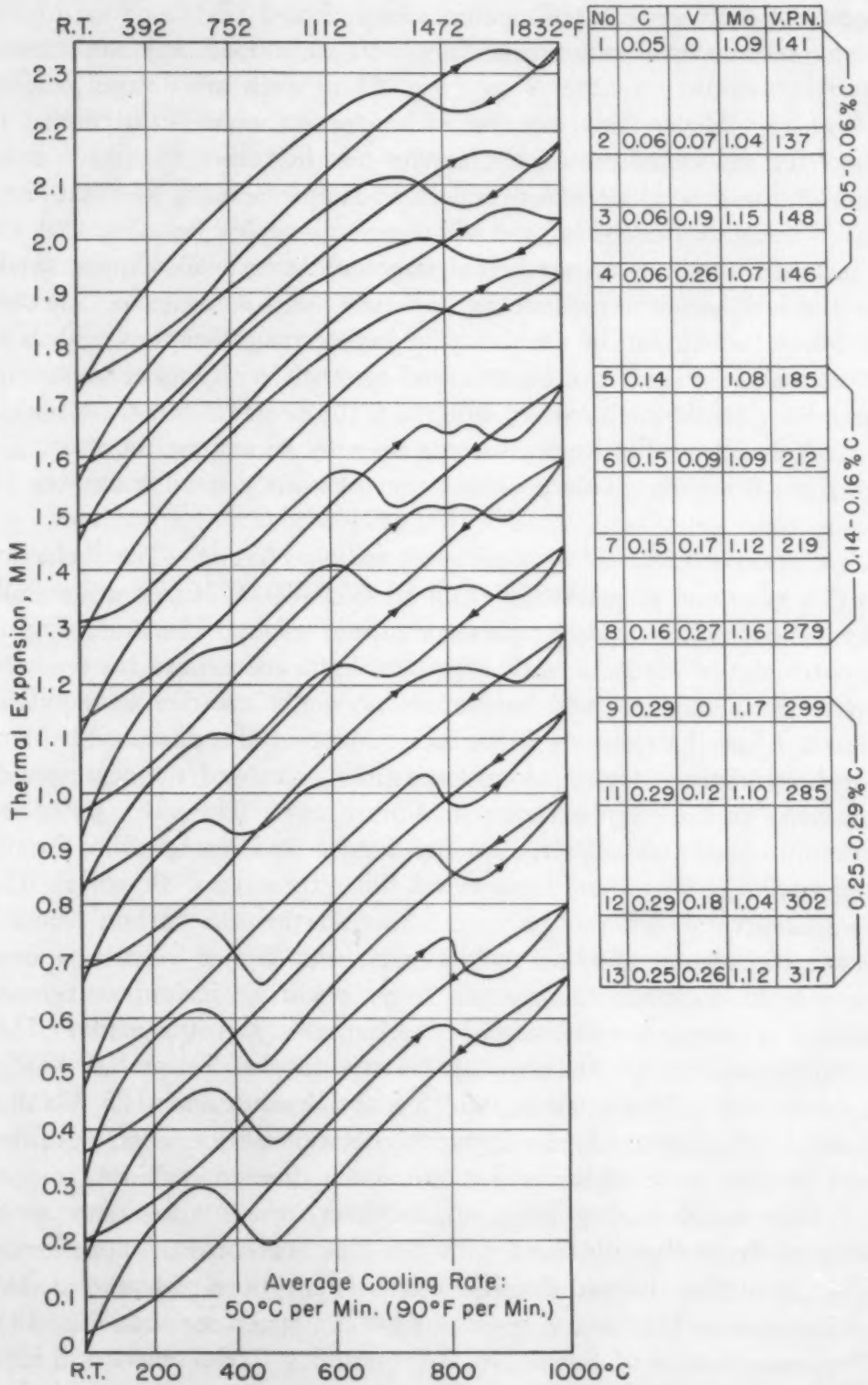


Fig. 5—Thermal Curves of Carbon-Vanadium – 1.0% Molybdenum Steels. (Slow cooling rate.)



No	C	V	Mo	V.P.N.
1	0.05	0	1.09	141
2	0.06	0.07	1.04	137
3	0.06	0.19	1.15	148
4	0.06	0.26	1.07	146
5	0.14	0	1.08	185
6	0.15	0.09	1.09	212
7	0.15	0.17	1.12	219
8	0.16	0.27	1.16	279
9	0.29	0	1.17	299
11	0.29	0.12	1.10	285
12	0.29	0.18	1.04	302
13	0.25	0.26	1.12	317

Fig. 6—Thermal Curves of Carbon-Vanadium – 1.0% Molybdenum Steels. (Rapid cooling rate.)

apparent with more rapid cooling (Figs. 2 and 17C). None of the plain carbon-vanadium steels, however, developed any suppressed transformations on either slow (Fig. 1) or even more rapid cooling (Fig. 2). Hence, this increase in hardness should be attributed to the effect of vanadium on the ferrite matrix rather than to formation of the martensite-like products of suppressed transformations.

Microexamination of the dilatometer samples revealed that the effect of vanadium on structural characteristics is also quite small. In the low and intermediate carbon subgroups some extremely fine carbides (which can be seen only at higher magnifications), such as illustrated in Fig. 7, can be observed in steels with higher vanadium contents. In the high carbon subgroup, the pearlite structure, typical of cast and annealed steels, is made finer by vanadium, as illustrated by Figs. 8 and 9. This confirms the previously cited statement by Knowlton.

Carbon – 0.5% Molybdenum-Vanadium Group—The behavior of this group on slow cooling from 1830 °F (1000 °C) is quite similar to that of the plain carbon-vanadium group. In fact, Fig. 3 appears almost identical with Fig. 1. Slight differences between the corresponding curves and hardnesses no doubt are due to molybdenum and small variations in carbon. Most of the dilatometer samples have microstructures closely resembling those of the corresponding steels in the plain carbon-vanadium group. However, there are more fine carbides scattered in the ferrite and less pearlite in the 0.15 to 0.3% vanadium samples of this group (not shown). The chief structural differences were found in the low carbon samples where the combination of molybdenum and higher vanadium contents tends to close the gamma loop, resulting in untransformed (delta) ferrite, more fine carbides and elimination of pearlite. This is illustrated by Fig. 10 (showing the structure of Serial No. 4, Fig. 3, containing 0.05% carbon, 0.62% molybdenum, and 0.25% vanadium). The structure is apparently composed of coarse-grained delta ferrite, some alpha ferrite and finely divided carbides.

More rapid cooling (Fig. 4), however, presents a picture quite different from that obtained with the plain carbon-vanadium group (Fig. 2) in that thermal sluggishness is much more pronounced, and the increase in hardness is greater (for the latter see also Fig. 18). Microexamination of Serial No. 2 (containing 0.09% carbon, 0.59% molybdenum and 0.07% vanadium) reveals small amounts of a suppressed transformation product with Widmanstätten structure

(Fig. 11) even though the corresponding dilation was hardly noticeable on the cooling branch of the corresponding dilatometer curve (Fig. 4, Serial No. 2).

This increase in thermal sluggishness results from the combined effect of carbon and molybdenum plus some effect due to vanadium. Thus in the intermediate carbon subgroup even Serial No. 5 (0.14% carbon, 0.5% molybdenum and 0% vanadium) contains some pearlite and suppressed transformation product (structure not shown). In Serial No. 8, containing practically the same percentages of carbon and molybdenum, but also 0.25% vanadium, pearlite disappears and is replaced by bainite and carbides (Fig. 12).

Likewise in Serial No. 12 (0.25% carbon, 0.52% molybdenum, 0.25% vanadium), from the high carbon subgroup even the free ferrite is present in small amounts, and the predominating constituents are upper and lower bainite (Fig. 13).

Carbon – 1% Molybdenum-Vanadium Group—In this group the dilatometer curves obtained on slow cooling (Fig. 5) are quite different from those of the two preceding groups (Figs. 1 and 3) although the resultant hardnesses are comparable to those of the corresponding ones in the carbon – 0.5% molybdenum-vanadium group.

In the low carbon subgroup, the combined effect of molybdenum and vanadium raises transformations on heating to quite high temperatures. Moreover, the combined effect of these two elements promotes the previously mentioned spheroidization of carbides to such an extent that the pearlite constituent frequently is completely absent. Fig. 14 illustrates the structure of the slowly cooled specimen, Serial No. 4 (0.06% carbon, 1.07% molybdenum, 0.26% vanadium), composed of a mixture of alpha and residual delta ferrite, impregnated with fine spheroidal carbides. This structure is similar to that shown in Fig. 10 for the 0.05% carbon, 0.62% molybdenum, and 0.25% vanadium slowly cooled (Serial No. 4) sample.

A slight suppressed transformation, associated with the appearance of Widmanstätten pattern in the resultant structure, can be observed in Serial No. 6 (0.15% carbon, 1.09% molybdenum, 0.09% vanadium) (structure not shown). In all subsequent steels slow cooling recorded in Fig. 5 produces a certain degree of thermal suppression, associated with corresponding amounts of bainite (structures not shown).

With more rapid cooling (Fig. 6), the low carbon subgroup does not develop any well pronounced suppressed transformations. How-

ever, in the steel Serial No. 2 containing 0.07% vanadium, microexamination (Fig. 14) reveals some constituent with martensite-like structure, which has a strong resemblance to some of the structures observed by the authors in high silicon-molybdenum steels (7). Apparently, this constituent is a product of the suppressed transformation, but its amount is so small that the corresponding dilation on the cooling branch of the dilatometer curve (Fig. 6, Serial No. 2) is hardly noticeable.

When vanadium content of the low carbon subgroup increases to 0.26% (Fig. 6, Serial No. 4), a differently appearing constituent (Fig. 16) is formed by the rapid cooling. It apparently also is a product of a hardly noticeable (Fig. 6) suppressed transformation, closely related to lower bainite, and perhaps influenced in its formation by the residual delta ferrite. Incidentally, it may be noted that Figs. 14 and 16 represent structures of the same steel, obtained by a slow and more rapid cooling respectively.

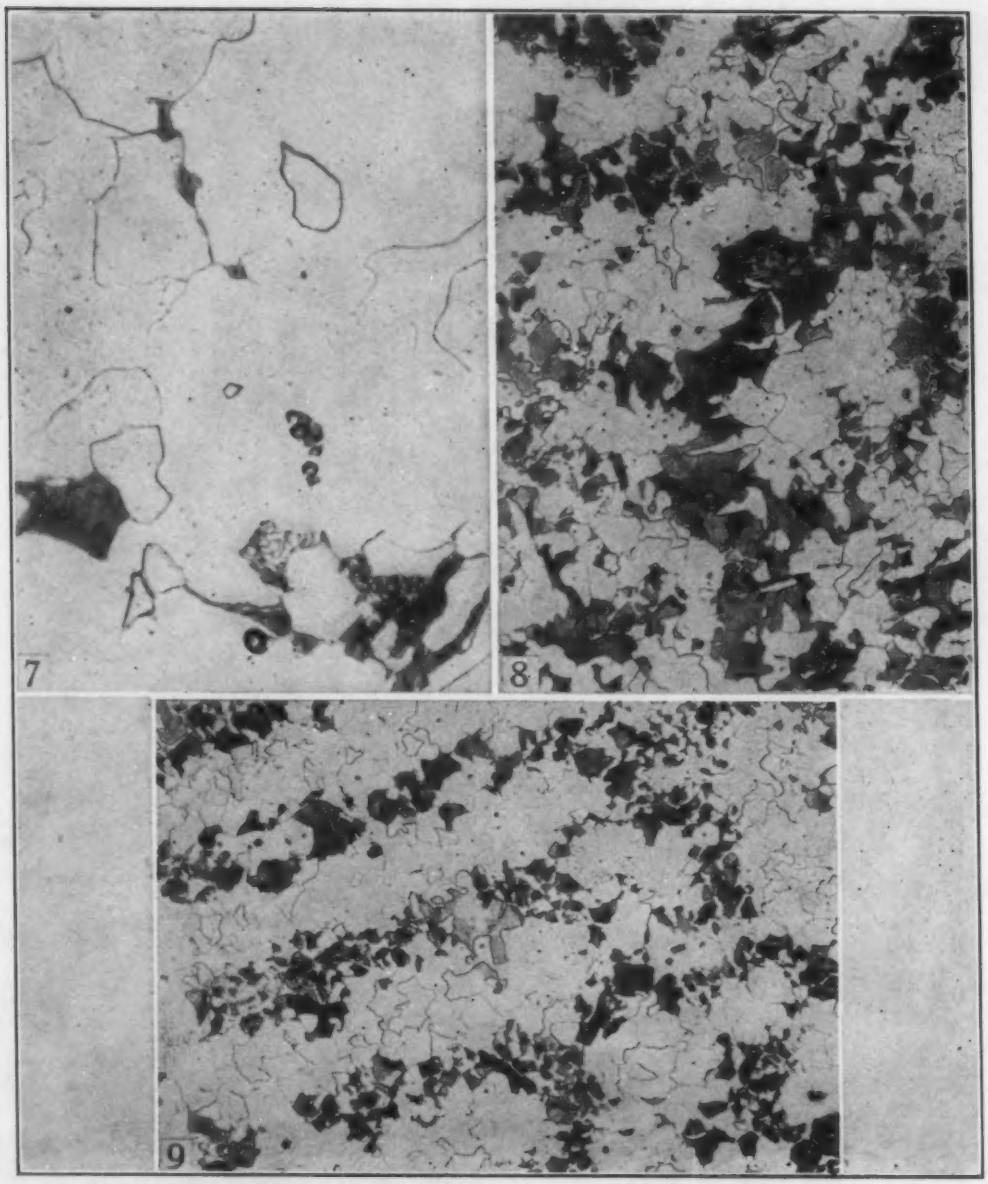
The dilatometer curves of the intermediate and high carbon subgroups have more conventional shapes (Fig. 6): in the case of the former, transformations on cooling are split, and in the case of the latter are completely suppressed. Consequently, the structures consist of (a) pearlite, ferrite and bainite for the intermediate carbon subgroup, and (b) bainite and martensite for the high carbon subgroup (structures not shown). Hardnesses of the more rapidly cooled dilatometer specimens of all this group, on the other hand, are not very different from the corresponding ones in the carbon–0.5% molybdenum-vanadium group (compare Fig. 6 with Fig. 4, and Fig. 18 with Fig. 19).

Physical Properties

Figs. 17, 18 and 19 are graphic representations of physical data averaged from two or more tests. Each figure consists of three separate graphs (A, B and C) for the low, intermediate and high carbon contents respectively. Within each graph, each physical property is plotted as a function of the vanadium content.

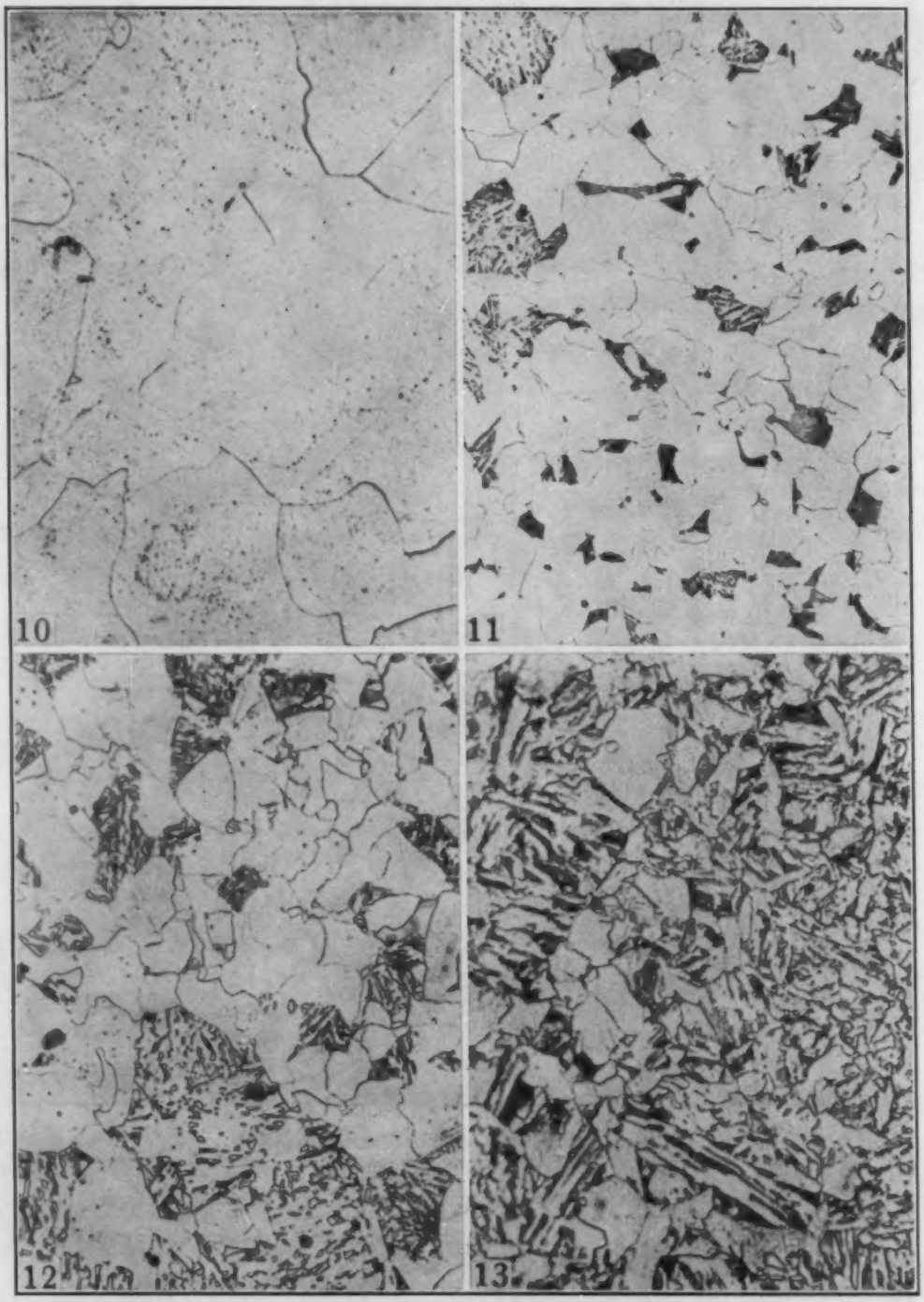
The following general observations can be made:

Vanadium increases the tensile strength, yield point and proportional limit. In the case of the plain carbon-vanadium steels (Fig. 17A, B and C), as well as of the low carbon subgroups of the molybdenum-bearing steels (Figs. 18A and 19A), this increase is not very great.



Figs. 7, 8, 9—Plain Carbon-Vanadium Steels.
Fig. 7—Serial No. 4. 0.09% carbon, 0.25% vanadium. 5-hour cool from 1830 °F (1000 °C). Etched in picral. × 500.
Fig. 8—Serial No. 9. 0.29% carbon, 0% vanadium. 5-hour cool from 1830 °F (1000 °C). Etched in picral. × 150.
Fig. 9—Serial No. 12. 0.27% carbon, 0.25% vanadium. 5-hour cool from 1830 °F (1000 °C). Etched in picral. × 150.

In the case of the intermediate and high carbon subgroups of molybdenum-bearing steels (Figs. 18B and C, and 19B and C) it is appreciable. Ductility, as represented by the elongation and the reduction of area, is affected in the reversed direction. Hardness,



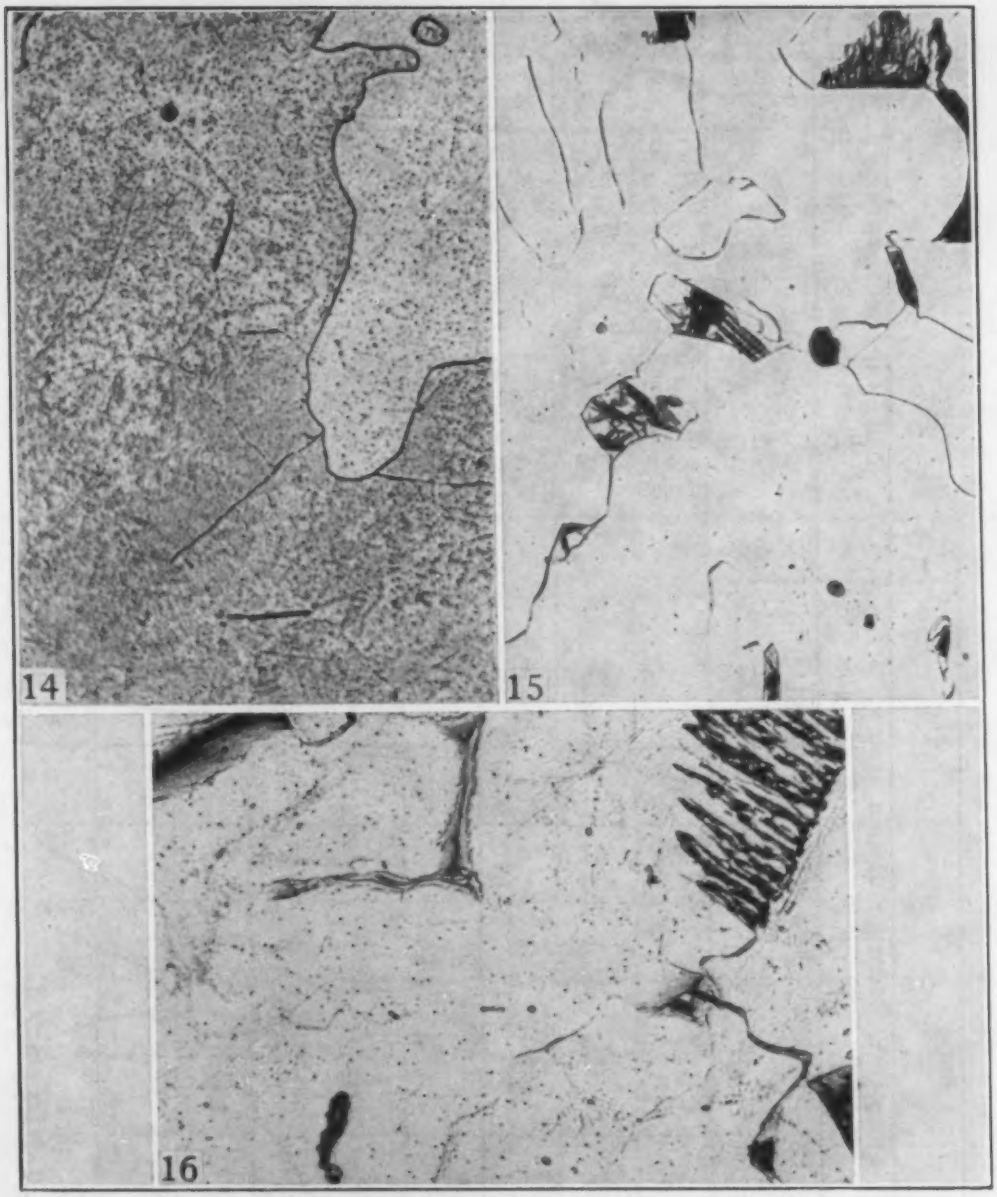
Figs. 10, 11, 12, 13—Carbon – 0.5% Molybdenum-Vanadium Steels.

Fig. 10—Serial No. 4. 0.05% carbon, 0.62% molybdenum, 0.25% vanadium. 5-hour cool from 1830 °F (1000 °C). Etched in picral. × 500.

Fig. 11—Serial No. 2. 0.09% carbon, 0.59% molybdenum, 0.07% vanadium. Air cool from 1830 °F (1000 °C). Etched in picral. × 150.

Fig. 12—Serial No. 8. 0.17% carbon, 0.56% molybdenum, 0.25% vanadium. Air cool from 1830 °F (1000 °C). Etched in picral. × 500.

Fig. 13—Serial No. 12. 0.25% carbon, 0.52% molybdenum, 0.25% vanadium. Air cool from 1830 °F (1000 °C). Etched in picral. × 500.



Figs. 14, 15, 16—Carbon – 1.00% Molybdenum-Vanadium Steels.
Fig. 14—Serial No. 4. 0.06% carbon, 1.07% molybdenum, 0.26% vanadium. 5-hour cool from 1830 °F (1000 °C). Etched in picral. × 500.
Fig. 15—Serial No. 2. 0.06% carbon, 1.04% molybdenum, 0.07% vanadium. Air cool from 1830 °F (1000 °C). Etched in picral. × 500.
Fig. 16—Serial No. 4. 0.06% carbon, 1.07% molybdenum, 0.26% vanadium. Air cool from 1830 °F (1000 °C). Etched in picral. × 500.

as previously pointed out, is increased in about the same proportion as the strength.

The impact resistance, and particularly that at —25 °F (—32 °C), is affected more than any other property. When vanadium content increases to about 0.3%, the impact resistance at

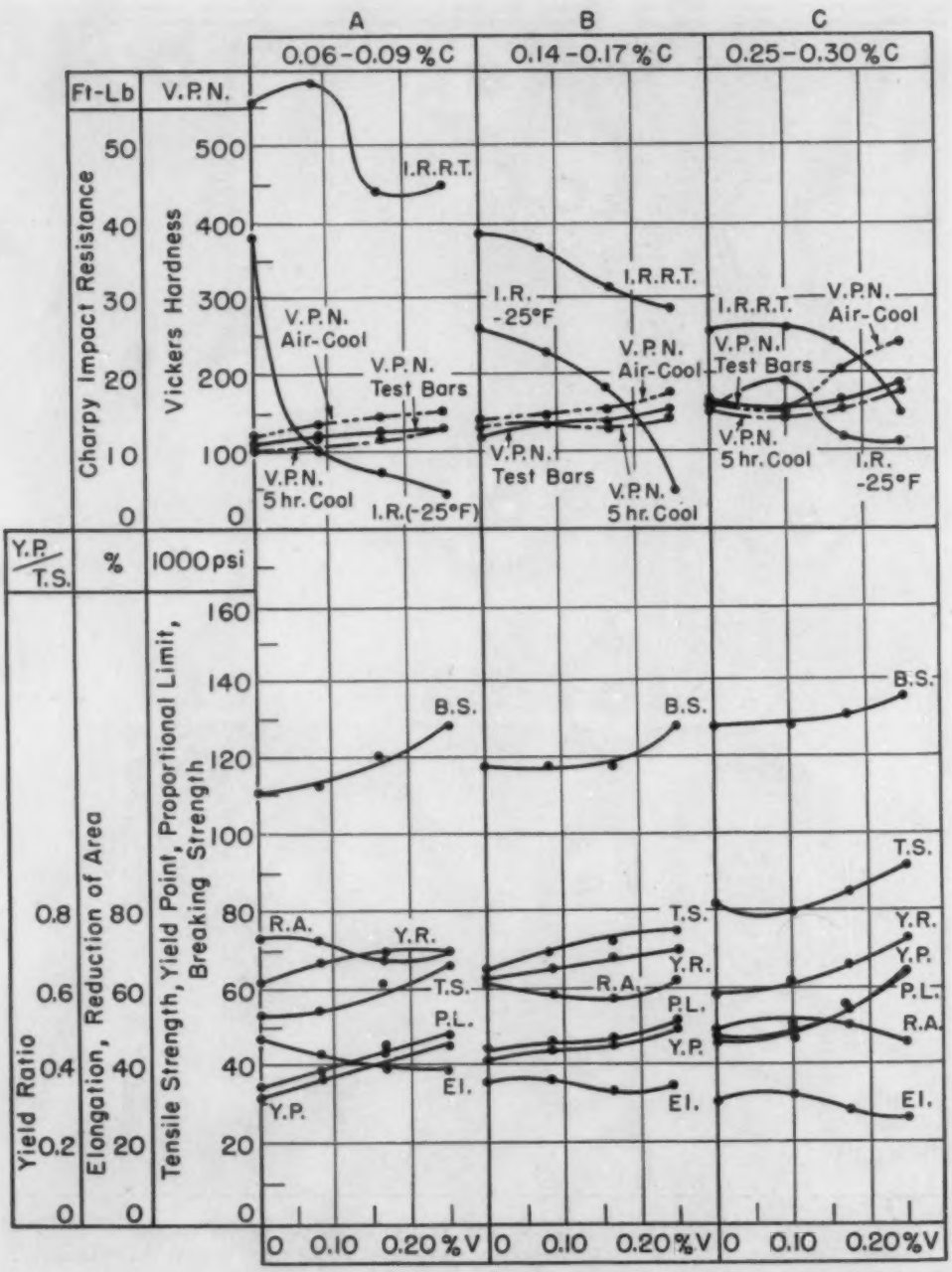


Fig. 17—Effect of Vanadium on Physical Properties of Carbon Steels.

—25 °F (—32 °C) decreases to rather low values. This observation is similar to that made by the authors in connection with the high silicon steels (*7*). While steels with high vanadium content still have good ductility as expressed by the elongation and the reduction of area, their impact resistance, and particularly that at —25 °F (—32 °C) is quite low. This embrittlement might have

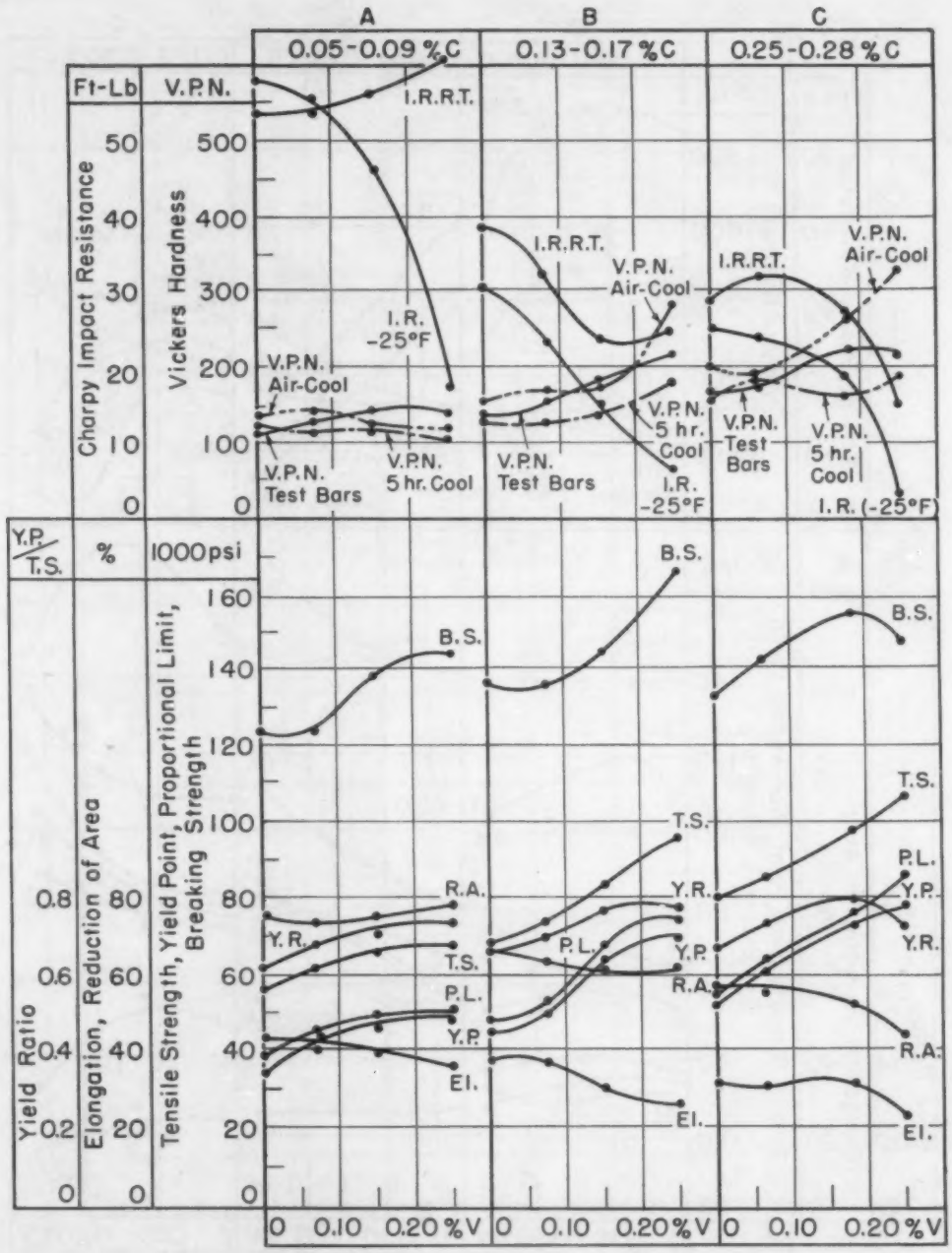


Fig. 18—Effect of Vanadium on Physical Properties of Carbon – 0.5% Molybdenum Steels.

resulted from the presence of residual delta ferrite in the structure and also from the tendency for vanadium to form stable carbides.

Aging Experiments

Some selected compositions from the plain carbon-vanadium and carbon – 0.5% molybdenum-vanadium groups were subjected to

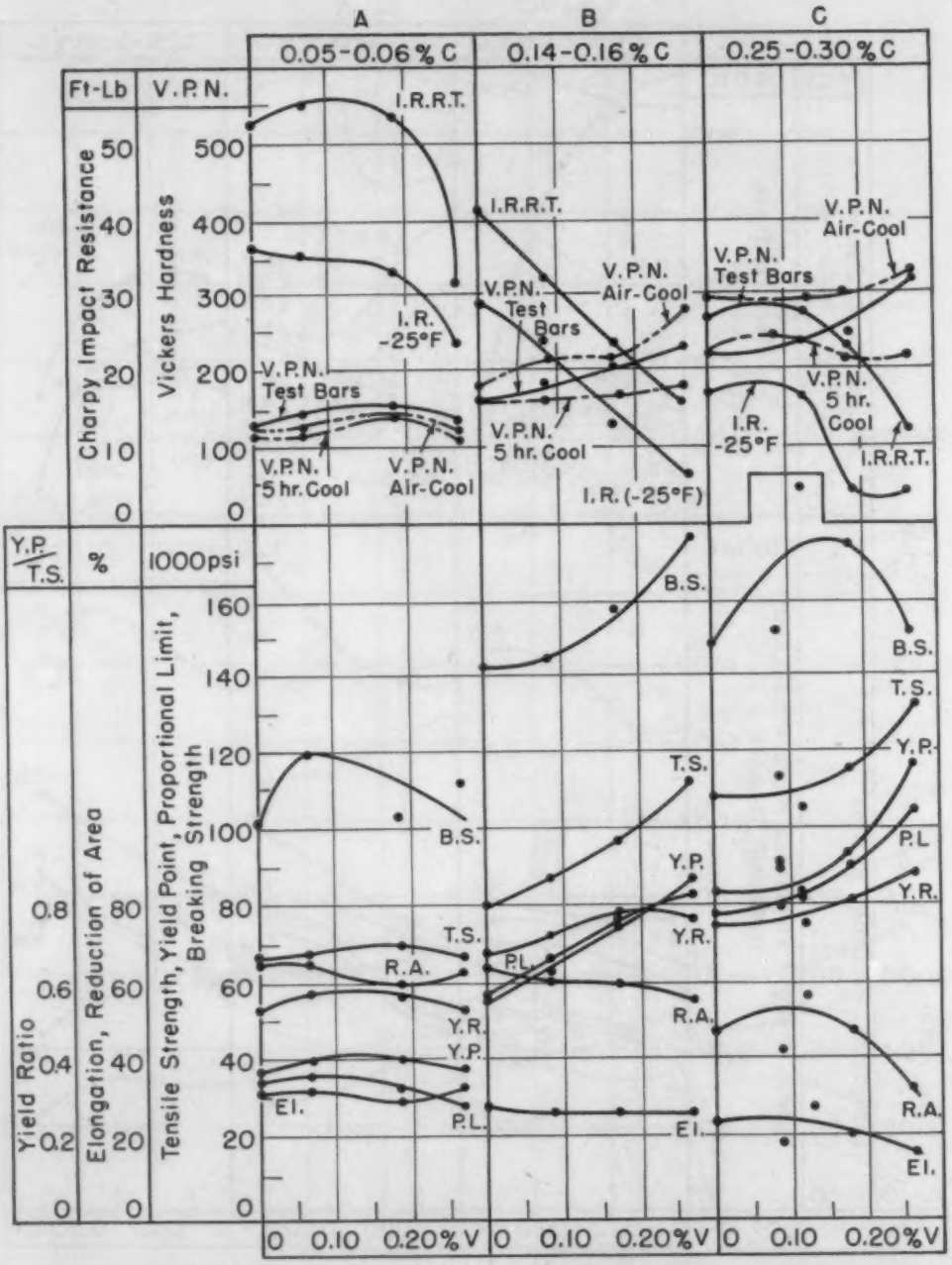


Fig. 19—Effect of Vanadium on Physical Properties of Carbon – 1.0% Molybdenum Steels.

aging at 1150 °F (620 °C) for 2000 hours.[7] The aging temperature was selected arbitrarily. It is appreciated by the authors that it is not the best one to promote graphitization and other phenomena occurring in this type of steels in superheated steam service. After

[7]The carbon – 1% molybdenum-vanadium group was not aged.

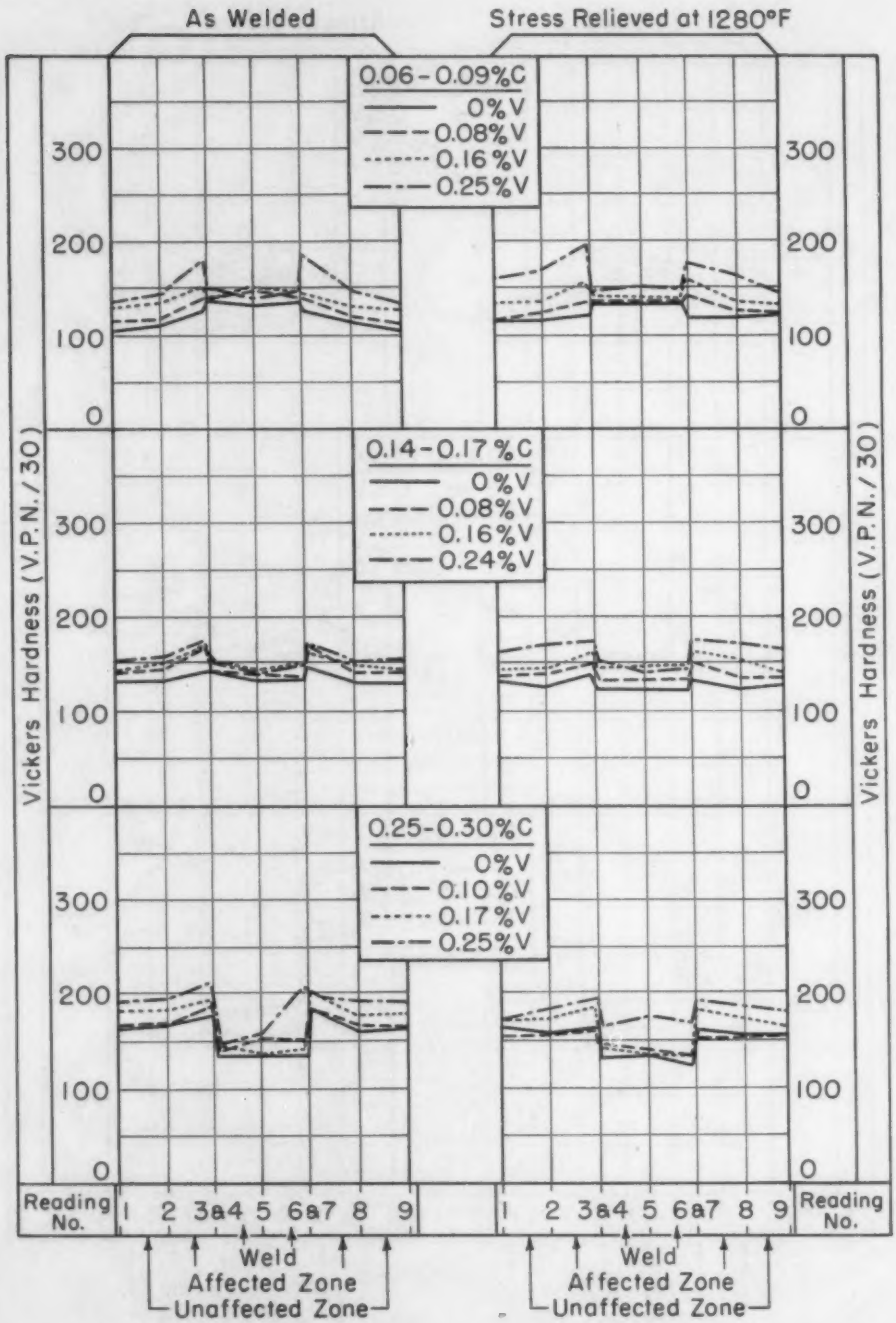


Fig. 20—Hardness Distribution Across the Weld and the Affected Zone in Carbon-Vanadium Steels.

this aging treatment samples were tested for tensile properties[8] and Charpy impact resistance.[9] The latter was performed at room temperature and (a) at 750 °F (400 °C) for the plain carbon-vana-

[8]2-inch gage, 0.505-inch diameter.

[9]Keyhole notch.

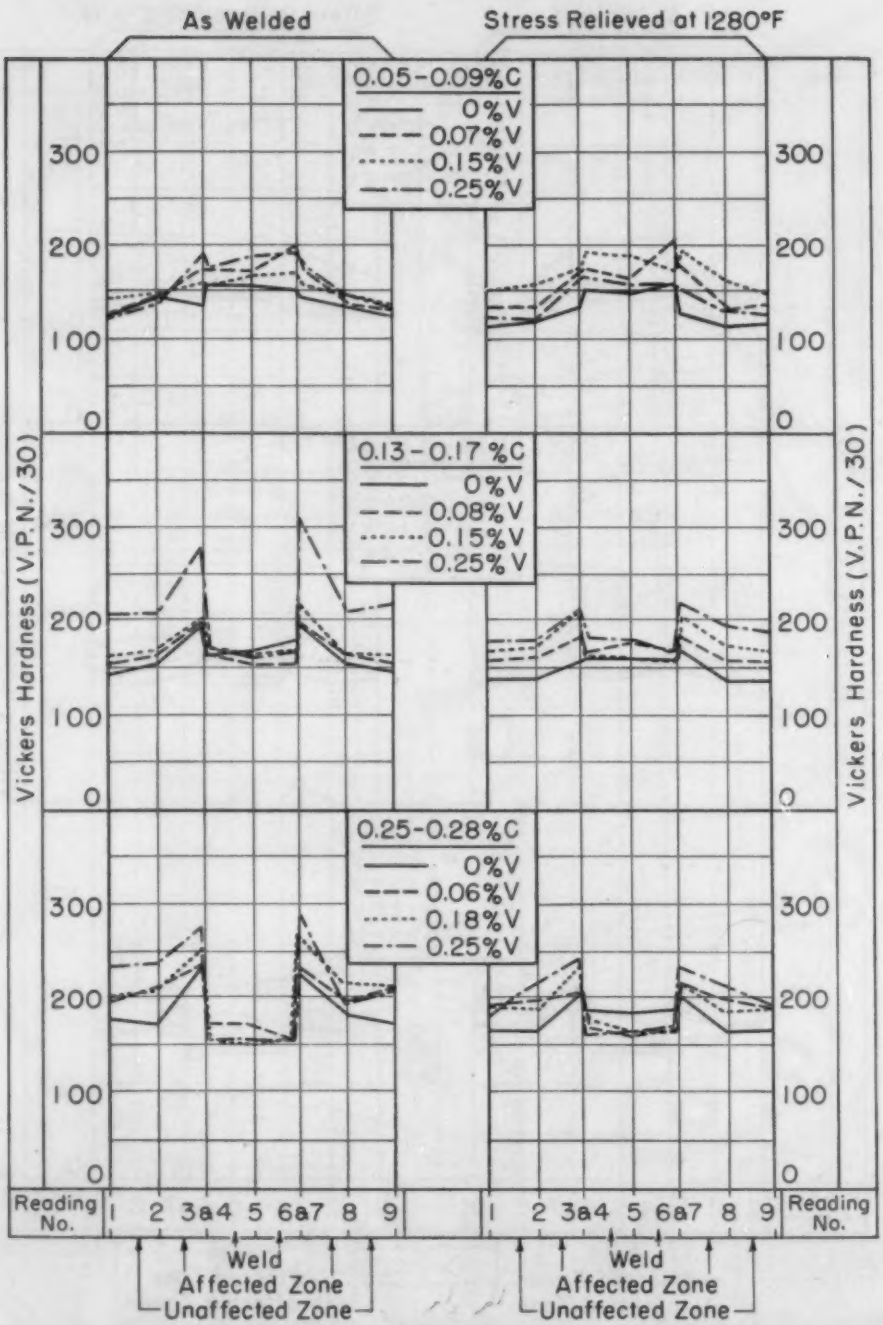


Fig. 21—Hardness Distribution Across the Weld and the Affected Zone in Carbon–0.5% Molybdenum-Vanadium Steels.

dium steels and (b) at 1000 °F (540 °C) for the carbon–0.5% molybdenum-vanadium steels.

From each subgroup only two steels were aged: (a) with no vanadium and (b) with the highest (about 0.3%) vanadium. By

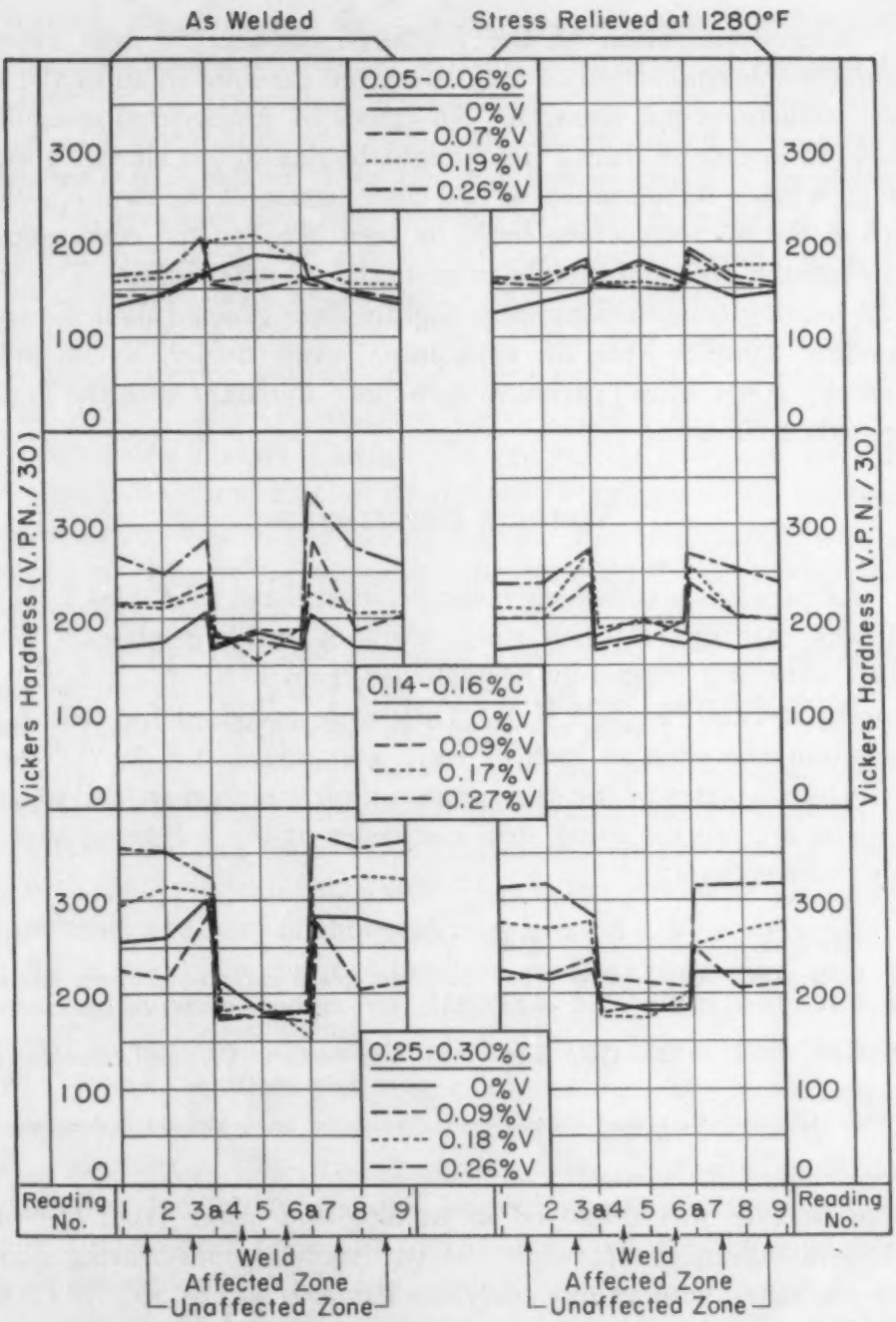


Fig. 22—Hardness Distribution Across the Weld and the Affected Zone in Carbon–1.0% Molybdenum-Vanadium Steels.

comparing their physical properties (not given) with those from the corresponding original tests presented in Figs. 17 and 18, it was found that aging in most cases reduced the tensile strength, yield point, proportional limit and hardness, while raising the elongation and particularly reduction of area and impact resistance.

Microexamination of the fractured impact test bars revealed complete spheroidization of the constituent carbides in all of the samples (structures not shown). No traces of graphitization could be observed in any of them. This might be due to too short a time, or too high aging temperature, or to a combination of the two. No difference in the microstructure could be seen between the corresponding molybdenum-free and molybdenum-bearing compositions. The vanadium-bearing compositions were slightly finer grained than the corresponding samples free of vanadium. And finally, as should be expected, spheroidized carbides were more abundant with the increasing carbon content.

Welding Experiments

As previously stated, each composition listed in Tables I, II and III was cast into 7/8-inch thick pairs of welding plates,[10] all of which were heat treated by normalizing from 1750 °F (955 °C) and drawing at 1250 °F (675 °C). They were prepared for welding by machining one edge of each to form a standard A.S.A. "U" bevel. Each pair of plates of the same composition was then welded together by metal arc process using steel electrodes of the following approximate compositions:

Si	Mn	S	P	C	Mo	V	
0.14	0.28	0.025	0.022	0.06	....	....	for plain carbon-vanadium steels*
0.04	0.31	0.027	0.019	0.10	0.51	0.11	for carbon – 0.5% molybdenum-vanadium steels
0.04	0.28	0.037	0.021	0.06	0.96	0.13	for carbon – 1% molybdenum-vanadium steels

*No carbon-vanadium steel electrodes were available, hence straight carbon steel was used.

No preheating was employed in welding the plates from the plain carbon-vanadium group, while the two molybdenum-bearing groups were preheated with an oxy-acetylene flame to 400 to 500 °F (200 to 260 °C).

Radiographically sound welds were made in 7 to 8 passes on assemblies 7/8 inch thick with a 7-inch running length of welding. Standard tensile[11] and Charpy[12] impact bars were machined from the welds which had not been given any stress-relieving treatment. In

[10]The description of these plates is given in a previous publication (6).
[11]2-inch gage, 0.505-inch diameter.
[12]Keyhole notch.

the former, the weld and the affected zone were left between the gage marks. In the latter, the keyhole notch was cut through the weld metal to the fusion line in an attempt to force the break in the heat-affected zone adjacent to the weld, as illustrated in a previous publication (6). All of these test bars were subjected to physical testing, but resultant data were omitted to conserve space.

From each weld, two strips (3/8 by 7/8 by 10 inches) were cut and used for side bend tests: one "as-welded" and the other stress-relieved at 1280 °F (690 °C). Each weld was also subjected to hardness distribution studies, across the weld and the affected zone: (a) "as-welded" and (b) stress-relieved at 1280 °F (690 °C).

Tensile and Impact Testing—In general the test data from the weld assemblies show that all of the tensile properties of the welds are inferior to those of the parent metals. For this reason, with the exception of the low carbon subgroups, most of the tensile test bars broke through the welds.

Keeping in mind that the weld assemblies were not stress-relieved before testing, it might be stated that their physical properties compare favorably with those of the parent metals.

Bend Tests—Bend tests were made on all assemblies, both in the 1280 °F (690 °C) stress-relieved and "as-welded" conditions. Longitudinal sections for the side bend tests were prepared in accordance with the American Standards Association procedure piping code requirements and bent at the weld zone around a 1-inch mandrel.

All of the plain carbon-vanadium steel weld samples bent 180 degrees without cracking. Some failures in the other two groups occurred in the weld metal and none in the parent metal affected zones. Results indicate that the combined increase in percentages of carbon, molybdenum and vanadium reduces the ductility of the weld assemblies. The stress-relieving heat treatment used helps the situation, but probably should be performed at a higher temperature or for a longer period of time, particularly for the composition high in carbon and the alloying elements.

Hardness Distribution Studies—A cross section from a weld of each composition was subjected to hardness distribution survey across the weld and the affected zone (using a Vickers pyramid hardness tester with a 30-kilogram load), (a) in the "as-welded" condition and (b) stress-relieved at 1280 °F (690 °C).

The three sets of test data are graphically represented in Figs. 20, 21 and 22 for plain carbon-vanadium, carbon – 0.5% molybde-

num-vanadium and carbon – 1% molybdenum-vanadium groups respectively, both "as-welded" and stress-relieved.

In studying these three figures, the following observations can be made. In general, over-all hardness distribution curves raise to higher levels, particularly in the heat-affected zones, with increase in carbon, vanadium and/or molybdenum. In the low carbon subgroups, with low vanadium content, the welds are harder than the affected zones. However, when the vanadium content increases to about 0.15% or higher, the affected zones become harder than the weld. In the intermediate and high carbon subgroups, the affected zones are harder than the welds, regardless of the vanadium content. In the higher molybdenum and higher carbon steels, the effect of vanadium (increasing the hardness of the parent metal) is much stronger than in those with lower carbon and/or molybdenum. In all cases increasing vanadium raises the hardness of the heat-affected zone, except where it promotes the formation of delta ferrite (Fig. 21, 1% molybdenum low carbon subgroup). Stress-relieving reduces the hardness somewhat, but its effect is small. This applies particularly to the higher molybdenum-vanadium carbon compositions.

This checks and confirms our statement made above, that a stress-relieving treatment at 1280 °F (690 °C) may be insufficient to draw, stress-relieve and soften the higher vanadium compositions.

Embrittlement of the Vanadium-Bearing Steels

During the course of this work it was noticed that some of the vanadium-bearing steels are quite brittle in the "as-cast" condition. The gates of some of the vanadium-bearing castings, when shaken out of the molds, could be broken off with a sledge hammer, which is not the case with respect to similar compositions, but not containing vanadium.

Four heats were thus made, all containing 0.15 to 0.20% carbon, about 0.5% molybdenum and 0.20 to 0.26% vanadium. This composition was selected, because it was believed that it would be of greatest interest for industrial applications. Analyses of all of them were kept as constant as possible. Two of them were killed in the conventional manner with aluminum, while the other two were killed with silicon only. All of them were cast into keel coupon blocks.

All four of these heats were tested:

a. "As-cast".

b. Normalized at 1750 °F (955 °C) and drawn at 1250 °F (675 °C).
c. Normalized at 1750 °F (955 °C) and drawn at 1375 to 1400 °F (746 to 760 °C).
d. Annealed at 1850 °F (1010 °C), normalized at 1750 °F (955 °C) and drawn at 1325 °F (718 °C).

Steels "as-cast" were tested for Charpy impact resistance (room temperature) and Vickers hardness only, while those subjected to "b", "c" and "d" heat treatments were tested for tensile properties as well. Test data thus assembled are graphically represented in Fig. 23.

The following observations can be made: In the "as-cast" condition, all four steels are quite brittle. The conventional heat treatment by normalizing and drawing ("b") improved the impact resistance.

Normalizing at the same temperature (1750 °F or 955 °C), followed by a higher temperature draw (1375 to 1400 °F or 746 to 700 °C) ("c") reduced the tensile strength, yield point and hardness, but did not appreciably affect the ductility. At the same time there was a considerable increase in the impact resistance.

On the other hand, annealing at 1850 °F (1010 °C) followed by normalizing at 1750 °F (955 °C) and drawing at 1325 °F (718 °C) ("d") resulted in physical properties not very different from those produced by the heat treatment ("b").

Moreover, the aluminum-killed steels appear to be a little stronger, while those silicon-killed have a slightly higher impact resistance. All four steels were subjected to dilatometric analysis. The resultant curves are alike and quite similar to those of Serial Nos. 7 and 8, Figs. 3 and 4. No suppressed transformations are developed in slow cooling, but the more rapid cooling rate results in split transformations.

All four heats were subjected to microexamination, using broken impact bars, "as-cast" as well as heat treated in three different ways. Some variations in structure were observed in samples from the different heats of the "as-cast" steels. However, all four looked very much alike structurally when heat treated in the same way, but each heat treatment produced definite differences.

In the "as-cast" conditions two of the steels revealed some products of suppressed transformation (Fig. 24), while the others had primarily pearlite and ferrite structures. This observation, however, might not be very significant, because the former castings might have

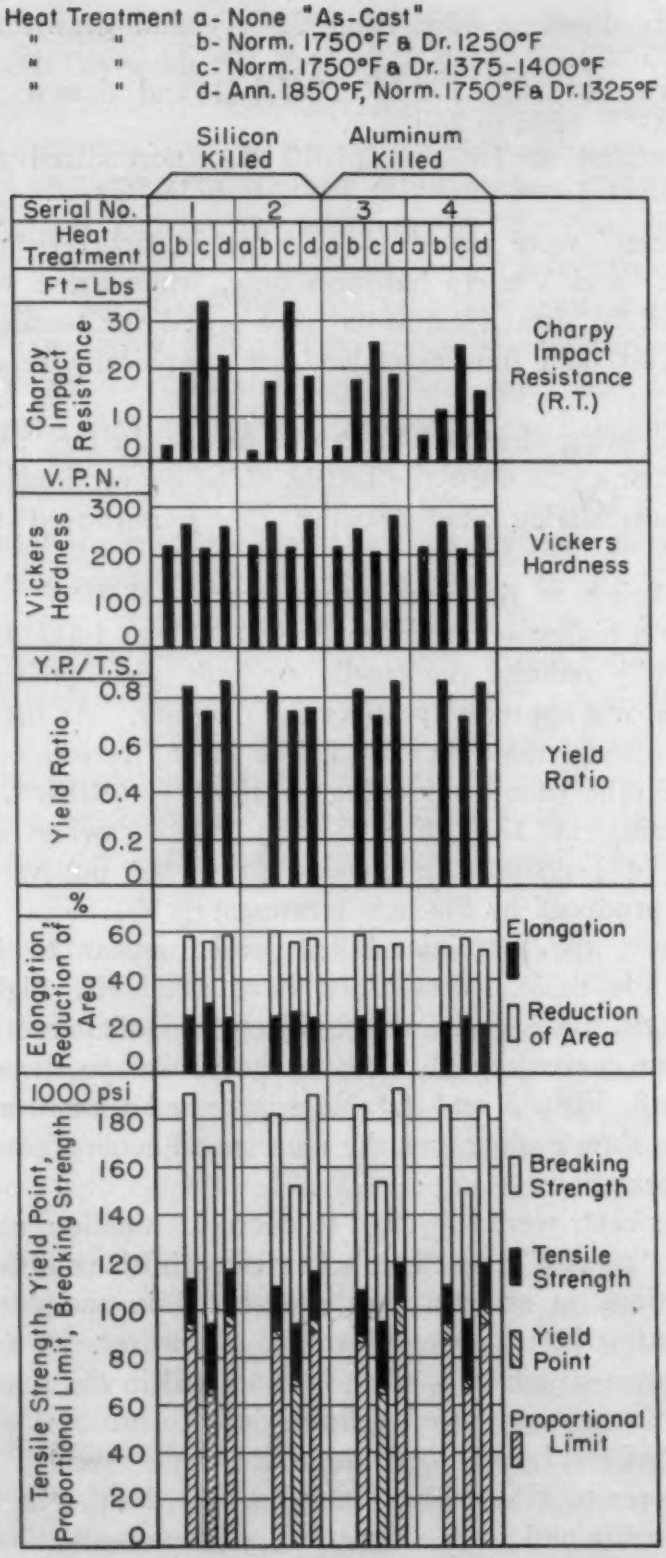
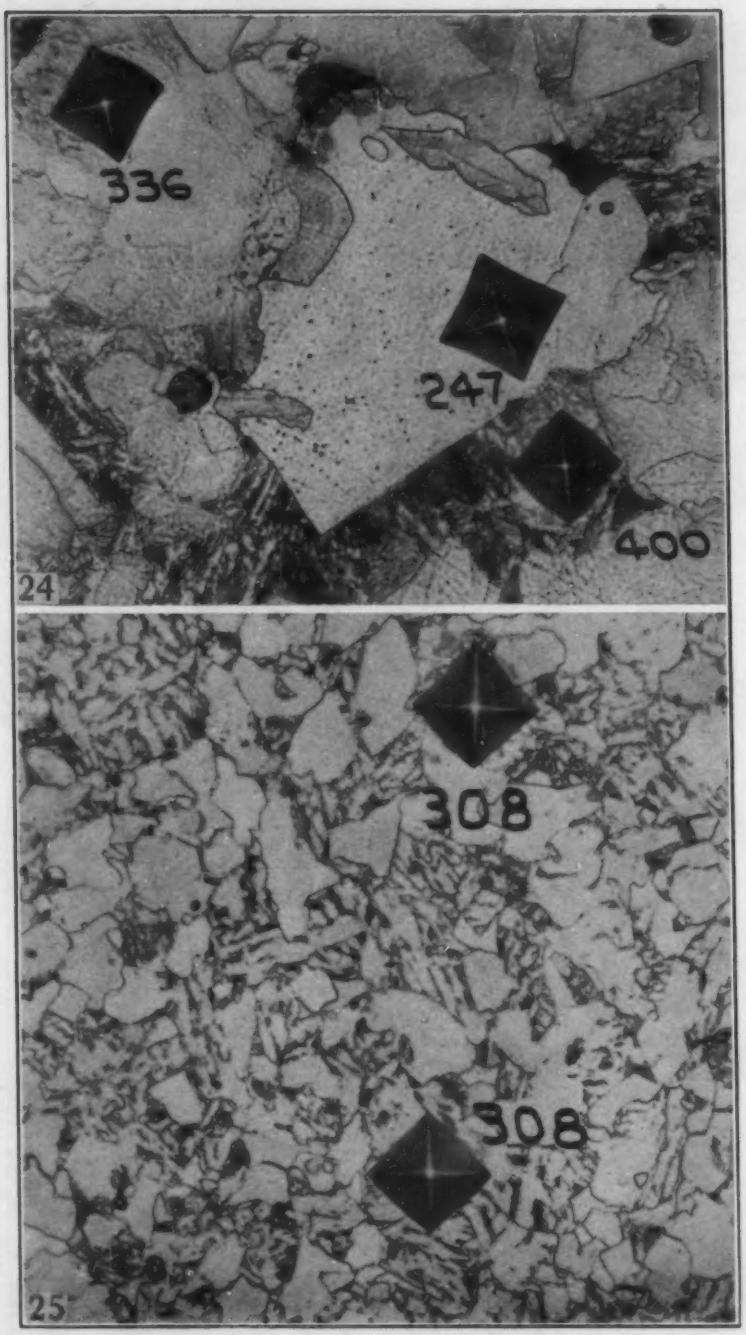
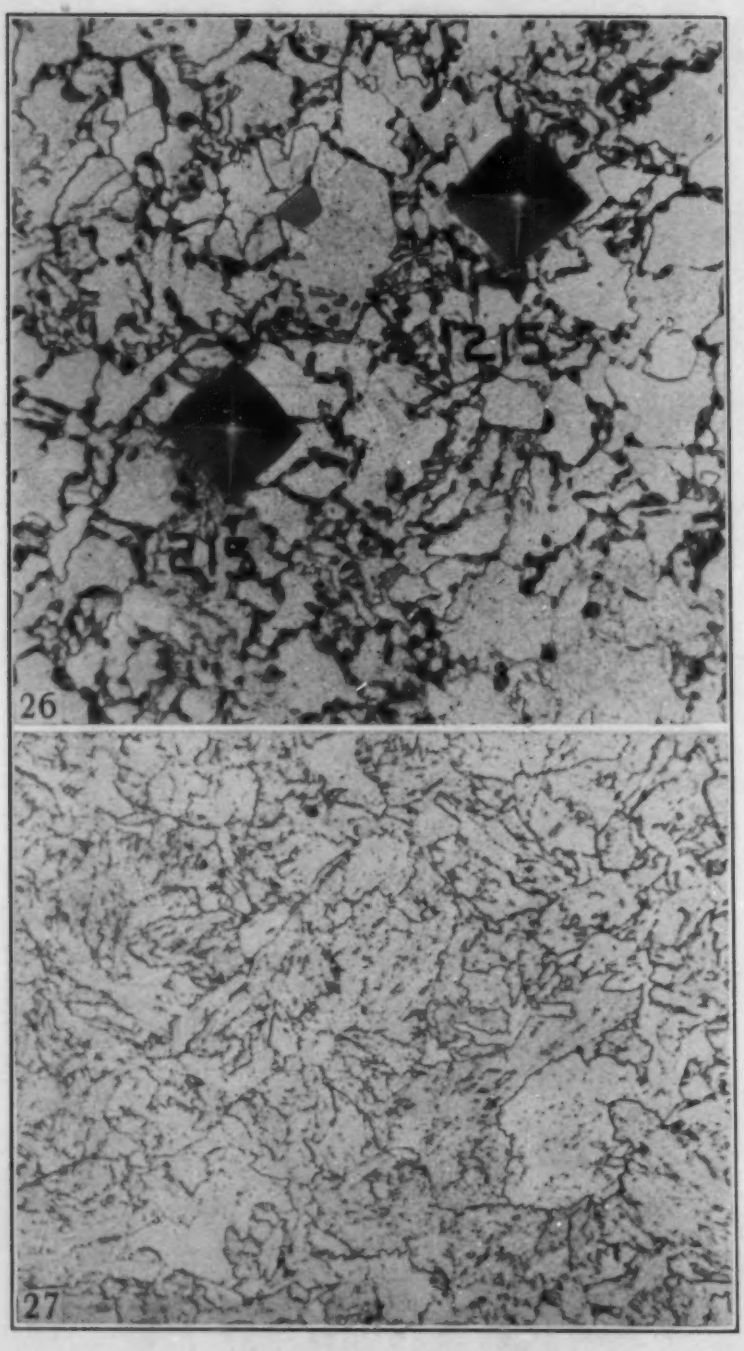


Fig. 23—Effect of Heat Treatments on Physical Properties of 0.15% Carbon – 0.5% Molybdenum – 0.25% Vanadium Steels.



Figs. 24, 25—0.15 to 0.20% Carbon, 0.5% Molybdenum, 0.20 to 0.26% Vanadium Steel.
Fig. 24—Serial No. 1. As cast. Etched in picral. × 500.
Fig. 25—Serial No. 3. Normalized 1750 °F, Drawn 1250 °F. Etched in picral. × 500.

been shaken out of the molds hotter than the latter. A highly segregated condition particularly in the grain boundaries, as well as in the cleavage planes, might be the explanation of the low impact resistance



Figs. 26, 27—0.15 to 0.20% Carbon, 0.5% Molybdenum, 0.20 to 0.26% Vanadium Steel.

Fig. 26—Serial No. 3. Normalized 1750 °F, Drawn 1375 to 1400 °F. Etched in picral. × 500.

Fig. 27—Serial No. 4. Annealed 1850 °F, Normalized 1750 °F, Drawn 1325 °F. Etched in picral. × 500.

in the "as-cast" state. The strongly pronounced cleavage planes, Fig. 24, may be due to the segregation of vanadium carbides because

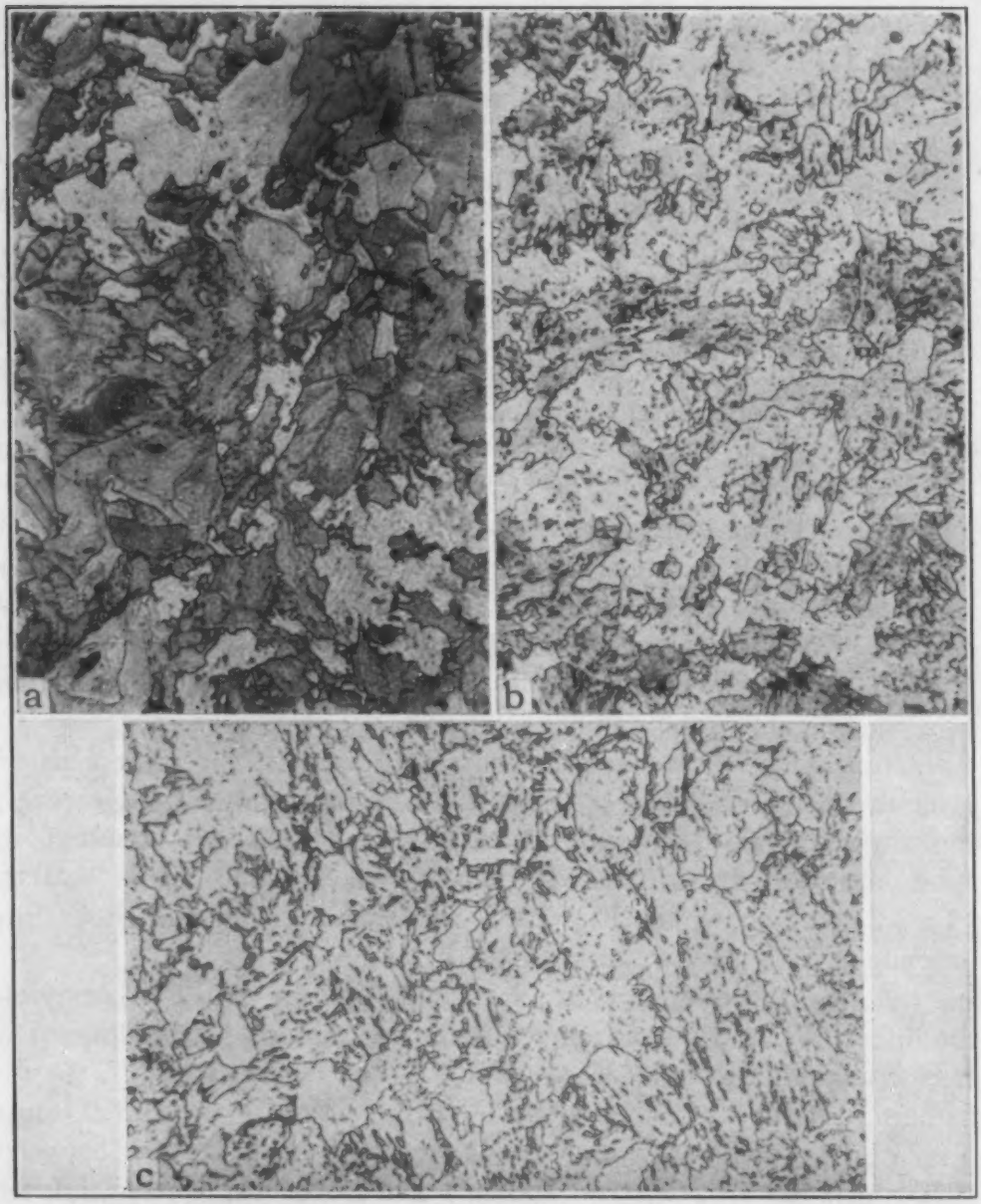


Fig. 28—Serial No. 8. Carbon – 1.0% molybdenum-vanadium group, containing 0.16% carbon, 1.16% molybdenum and 0.27% vanadium. Normalized from 1750 °F (955 °C) and drawn at different temperatures. Etched in picral. × 500. (a)—1250 °F (675 °C) Draw. (b)—1350 °F (730 °C) Draw. (c) 1400 °F (760 °C) Draw.

this "as-cast" structure and brittleness never have been observed in steels of similar composition but free from vanadium. Apparently this potential brittleness of vanadium steels has been recognized by other investigators. The tentative ASTM specification for Grade WC8 (0.20% carbon max., 0.95 to 1.25% molybdenum, 0.15 to 0.25% vanadium) requires only 15% minimum elongation (36).

This composition is comparable to our Serial Nos. 7, 8, 12 and 13 (Table III). Elongation of these steels (Fig. 19) ranges between 15 and 24.5%. For all other grades of "alloy steel castings suitable for fusion welding for high temperature service", the same specification requires a minimum elongation of at least 20% or higher.

Conventional normalizing and drawing (1750 °F or 955 °C and 1250 °F or 675 °C) resulted in the finer-grained structure shown in Fig. 25. Products of a suppressed transformation modified by drawing are in evidence. Their distribution and microhardness are much more uniform than in the "as-cast" structure, thus resulting in a considerable improvement in impact resistance.

Normalizing at 1750 °F (955 °C) followed by drawing at 1375 to 1400 °F (746 to 760 °C) resulted in a structure shown in Fig. 26. The high draw temperature apparently reached the lower edge of the critical range, causing a partial transformation. This is indicated by the rounded pearlite-like grains instead of the usual modified Widmanstätten structure. At the same time the untransformed portion was softened by this drawing treatment, resulting in a considerable improvement in the impact resistance.

Annealing followed by normalizing developed the same type of structure as normalizing alone (structure not shown). However, the higher draw temperature (1325 °F or 718 °C) resulted in spheroidization of carbides of the original Widmanstätten pattern (Fig. 25) as shown in Fig. 27. This may explain the slight improvement in impact resistance.

Another experiment was performed with the object of studying the effect of the drawing temperature on the impact resistance of a steel containing 0.16% carbon, 1.16% molybdenum and 0.27% vanadium. After normalizing at 1750 °F (955 °C) individual samples were drawn at progressively higher temperatures, between 1250 and 1400 °F (675 and 760 °C) and tested for Charpy impact resistance (duplicate test bars). Drawing at 1250 °F (675 °C) resulted in 17.0 foot-pounds impact resistance. No improvement could be observed until the drawing temperature reached 1350 °F (730 °C) when the impact resistance increased to about 23 foot-pounds.

Microexamination substantiates these observations. Fig. 28a is the structure of the sample drawn at 1250 °F (675 °C), which is composed of ferrite and products of a suppressed transformation, decomposed to some extent by the drawing treatment.

Higher drawing treatments tend to spheroidize more and more

the suppressed transformation product until at 1350 °F (730 °C) this spheroidization has progressed to a rather considerable degree, as can be seen in Fig. 28b. Still higher drawing temperature of 1400 °F (760 °C) brings the spheroidizing process to completion, as shown in Fig. 28c. Moreover, along with the latter structure, many fine grains at still higher magnifications display an internal bainite-like structure similar to those shown in Fig. 15. Apparently, the temperature of 1400 °F (760 °C) touches the beginning of the transformation on heating (see dilatometer curves, Serial No. 8 (Figs. 5 and 6) so that small localized regions in the steel become austenitic.

Summary

1. The effect of increasing vanadium content between 0 and 0.30% on the properties of: (a) plain carbon, (b) carbon – 0.5% molybdenum, and (c) carbon – 1% molybdenum cast steels has been investigated. Carbon contents within each of these groups ranged between about 0.05 and 0.30%.
2. Dilatometric analysis and microexamination show that vanadium tends to raise transformation temperatures on heating, particularly for low carbon steels.
3. None of the plain carbon-vanadium steels developed any suppressed transformations (thermal sluggishness) when cooled at the slow (3.2 °C or 5.8 °F per minute) or more rapid (50 °C or 90° F per minute) rates.
4. Rapid cooling of the 0.5% molybdenum steels revealed that they were more thermally sluggish than the plain carbon group. This increase in thermal sluggishness was accentuated by the combined effects of carbon, molybdenum and vanadium.
5. In the group of steels containing 1% molybdenum, a split transformation can be observed in all the higher carbon steels, even on slow cooling, revealing that they are more thermally sluggish than the corresponding 0.5% molybdenum steels. Increasing vanadium in the low carbon steels of this group tends to close the gamma loop, resulting in some delta ferrite in the structure and reduced thermal sluggishness. However, microexamination indicates small amounts of bainite along with the delta ferrite.
6. Vanadium in amounts of 0.15% and higher is responsible for the presence of extremely fine spheroidal carbides, the amount of which increases with increasing carbon content.
7. Vanadium reduces the pearlite grain size in the "annealed" structures.
8. Vanadium moderately increases the tensile strength, yield point, proportional limit and hardness. It slightly reduces elongation

and reduction of area, and considerably decreases impact resistance. These effects are more pronounced with higher carbon and molybdenum.

9. Aging of some carbon-vanadium and carbon – 0.5% molybdenum-vanadium steels at 1150 °F (620 °C) for 2000 hours completely spheroidized their structures, but did not produce any graphitization.
10. Welding all of these compositions by the metal arc process employing heavy coated electrodes did not present any particular difficulties with respect to cracking or voids in the weld deposits. However, obtaining satisfactory ductility becomes more of a problem as the molybdenum, vanadium and carbon contents are increased in these steels. This is indicated by the higher percentage of failures encountered in the limited number of side bend tests made.
11. Hardness distribution studies across the weld and the affected zone show that in the low carbon, low vanadium compositions the welds are harder than the parent metal. With increasing carbon, molybdenum and vanadium the over-all hardness increases and in the affected zones reaches rather high values, indicating potential difficulties connected with welding.
12. Stress-relieving treatment of vanadium-bearing steels is less effective than when applied to other steel compositions previously investigated by the authors. This may be due to a high stability of vanadium carbides.
13. Vanadium-bearing steels in the "as-cast" condition appear to be more brittle than similar compositions free from vanadium. A proper heat treatment (normalizing at 1750 °F or 955 °C) and draw at 1325 to 1350 °F (720 to 730 °C) eliminates this brittleness and brings the impact resistance to fairly high values.
14. It is hoped, by the authors, that this paper establishes certain trends, thus giving some clues to future investigators in solving their problems connected with carbon-molybdenum-vanadium steels. No attempt is being made to recommend any definite composition for a specific application.
15. Many of the compositions presented in this paper at present are being studied from the viewpoint of graphitization, and it is hoped that the resultant data will be available in due time.

Acknowledgments

The authors wish to express their appreciation to Crane Co. for permission to publish this work; to A. F. Lahr, B. F. Grant, H. A. Peterson, J. A. Harlan, B. E. Jenkins, R. A. Mueller and P. Hjulin of the Research Laboratory for their assistance in preparation of samples and help with the various tests; and to the Control Laboratory for making chemical analyses.

References

1. H. B. Knowlton, "Facts and Principles Concerning Steel and Heat Treatment," TRANSACTIONS, American Society for Steel Treating, Vol. 12, No. 3, September 1927, p. 479.
2. METALS HANDBOOK, American Society for Metals, 1939 Edition, p. 403, 592.
3. N. A. Ziegler and W. L. Meinhart, "The Effect of Copper on the Properties of Cast Carbon-Molybdenum Steels," *Transactions,* American Foundrymen's Association, Vol. 52, No. 4, June 1945, p. 1151.
4. N. A. Ziegler and W. L. Meinhart, "Characteristics and Properties of Some Cast Chromium-Molybdenum Steels," TRANSACTIONS, American Society for Metals, Vol. 34, 1945, p. 589.
5. N. A. Ziegler and W. L. Meinhart, "Effect of Nickel on Physical Properties and Thermal Characteristics of Some Cast Chromium-Molybdenum Steels," TRANSACTIONS, American Society for Metals, Vol. 37, 1946, p. 360.
6. N. A. Ziegler, W. L. Meinhart and J. R. Goldsmith, "The Effect of Manganese on the Properties of Cast Carbon and Carbon-Molybdenum Steels," TRANSACTIONS, American Society for Metals, Vol. 38, 1947, p. 398.
7. N. A. Ziegler, W. L. Meinhart and J. R. Goldsmith, "The Effect of Silicon on the Properties of Cast Carbon and Carbon-Molybdenum Steels," TRANSACTIONS, American Society for Metals, Vol. 40, 1948, p. 617.
8. A. Heinzel, "The Effect of Different Elements on the Polymorphism of Iron," *Zeitschrift für Tech. Physik,* Vol. 10, No. 4, 1929, p. 137.
9. G. L. Norris, "Vanadium Steels for Railroad Equipment," *Iron Age,* Vol. 125, No. 4, Jan. 23, 1930, p. 297.
10. N. Petinot, "Vanadium Additions Improve Steel," *Steel,* Vol. 87, Nos. 8, 9, 10, Aug. 21, 1930, p. 43; Aug. 28, 1930, p. 47; Sept. 4, 1930, p. 56.
11. M. Oya and K. Honda, "Iron-Vanadium Diagram," METAL PROGRESS, Vol. 18, No. 4, October 1930, p. 84.
12. B. Schulz, "Research on Vanadium Steels and Their Significance in Heat Technique," *Brennstoff und Waermetechnik,* Vol. 13, January 1931, p. 7.
13. R. Vogel and E. Martin, "On the Ternary System, Iron-Carbon-Vanadium," *Archiv. für das Eisenhüttenwesen,* Vol. 4, No. 10, April 1931, p. 487; *The Metallurgist,* June 1931, p. 91; July 1931, p. 98.
14. H. Hougardy, "Contribution to Study of Iron-Carbon-Vanadium System," *Archiv. für das Eisenhüttenwesen,* Vol. 4, No. 10, April 1931, p. 497; *Journal,* British Iron and Steel Institute, Vol. 74, No. 2, 1931, p. 716; *The Metallurgist,* July 31, 1931, p. 98.
15. K. Honda, "Vanadium Steel from Sponge Iron," METAL PROGRESS, Vol. 20, No. 2, August 1931, p. 89.
16. A. B. Kinzel and C. O. Burgess, "Effect of Vanadium in High Speed Steel," *Proceedings,* Iron and Steel Division, American Institute of Mining and Metallurgical Engineers, Vol. 100, 1932, p. 257.
17. Anonymous, "Tempering of Steels Containing Vanadium," *The Metallurgist,* Sept. 30, 1932, p. 134.
18. C. H. Mathewson, E. Spireand and C. H. Samans, "Division of the Iron-Vanadium-Oxygen System into Some of its Constituent Binary and Ternary Systems," TRANSACTIONS, American Society for Steel Treating, Vol. 20, No. 4, October 1932, p. 357.
19. E. Houdremont, H. Bennek and H. Schrader, "Studies of Vanadium Alloys," *Revue de Metallurgie,* Vol. 30, No. 4, April 1933, p. 152.
20. J. Strauss, "Vanadium in Steel Castings," *Transactions,* American Foundrymen's Association, Vol. 4, No. 3, October 1933, p. 225.
21. H. H. Abram, "Vanadium in Carbon and Alloy Steels," *Journal,* British Iron and Steel Institute, Vol. 130, No. 2, 1934, p. 351.
22. E. Houdremont, H. Bennek and H. Schrader, "Hardening and Tempering of Steels Containing Carbides of Low Solubility, Especially Vanadium

Steels," *Proceedings,* Iron and Steel Division, American Institute of Mining and Metallurgical Engineers, Vol. 116, 1935, p. 260.
23. Anonymous, "Vanadium Steels and Cast Irons," Vanadium Corporation of America, 1937.
24. H. H. Abram, "The Influence of Vanadium on Nickel-Chromium and Nickel-Chromium-Molybdenum Steels," *Engineering* (London), Jan. 8, 1937, p. 53.
25. T. G. Zimmerman, R. H. Aborn and E. C. Bain, "Some Effects of Small Additions of Vanadium to Eutectoid Steel," TRANSACTIONS, American Society for Metals, Vol. 25, No. 3, September 1937, p. 755.
26. H. H. Burton and T. F. Russell, "Precipitation Hardening of Three Steels Containing Vanadium," *Journal,* British Iron and Steel Institute, Vol. 138, No. 2, 1938, p. 57.
27. I. W. J. Priestley, "Vanadium in Steel and Iron," *Metals and Alloys,* Vol. 9, No. 8, Part I, August 1938, p. 93; Part II, Vol. 9, No. 9, September 1938, p. 237.
28. W. Köster and K. Lang, "The System Iron-Cobalt-Vanadium," *Zeitschrift für Metallkunde,* Vol. 30, No. 9, September 1938, p. 352.
29. F. Wever and A. Rose, "The Influence of Rate of Cooling on the Transformations of Vanadium Steels," *Mitteilungen aus dem Kaiser-Wilhelm Inst. für Eisenforschung,* Vol. 20, No. 16, 1938, p. 213.
30. G. F. Comstock, "Effect of Titanium and Vanadium on Forged Pearlitic Manganese Steel," *Iron Age,* Vol. 143, No. 7, Feb. 16, 1939, p. 27.
31. P. Hidnert, "Thermal Expansion of Some Chromium-Vanadium Steels," *Journal of Research,* National Bureau of Standards, Vol. 24, January 1940, p. 25.
32. Anonymous, "Vanadium in Iron and Steel" (a composite abstract), *Metals and Alloys,* Vol. 11, No. 6, June 1940, p. 316.
33. Anonymous, "The Influence of Vanadium on the Scaling of Steel," *The Metallurgist,* October 1941, p. 35.
34. R. G. McElwee and T. E. Barlow, "Vanadium in Gray Iron Castings," *The Foundry,* Vol. 72, No. 12, 1944, p. 88.
35. F. F. Franklin, "Chromium-Vanadium Carburizing Steel," *Materials and Methods,* Vol. 23, No. 6, June 1946, p. 1564.
36. 1947 Supplement to Book of A.S.T.M. Standards Including Tentatives, Part I-A, Ferrous Metals, p. 268-273.

DISCUSSION

Written Discussion: By A. B. Wilder, chief metallurgist, National Tube Co., U. S. Steel Corp. Subsidiary, Pittsburgh.

The authors have contributed very helpful information with reference to the properties of cast carbon-molybdenum-vanadium steels. The stability of these steels at elevated temperatures, particularly with regard to graphitization, is of importance. Results of this nature to be published in the future will be of interest. It would also be desirable to have information regarding creep properties.

In our work[18] with the wrought carbon, 1.50% molybdenum, 0.16% vanadium steels, graphitization has been observed in the weld heat-affected zone after exposure at 1050 °F (565 °C) for 10,000 hours. The steels examined contained 0.45% silicon and were melted in a laboratory induction furnace. Graphitization was observed only in the heat-affected zone of the weld.

[18] A. B. Wilder and J. D. Tyson, "Graphitization of Steel at Elevated Temperatures", TRANSACTIONS, American Society for Metals, Vol. 40, 1948, p. 233

Recently, several commercial heats of wrought carbon, 1% molybdenum, 0.25% vanadium steels and an induction furnace heat of a similar type of steel containing, in addition, 0.5% chromium were examined after 4000 hours' exposure at 900, 1050 and 1200 °F (480, 565 and 650 °C). Graphitization was not observed.

Written Discussion: By Walter Crafts, chief metallurgist, Union Carbide and Carbon Research Laboratories, Inc., Niagara Falls, N. Y.

This paper extends the series of valuable papers that the authors have contributed on the effects of alloys in steel castings. In this paper they have reported a tendency toward low impact strength in the 0.15 to 0.30% vanadium steels that is rather surprising. Two causes of low impact strength in vanadium steels have long been recognized. The suppression of the austenite loop and resulting presence of delta ferrite in low-carbon steels, especially those containing molybdenum, was observed by the authors. Intergranular vanadium carbide is also sometimes found in steels of higher vanadium content than those tested by the authors. Both of these structures lead to low impact strength, but do not explain the low values found in 0.15 to 0.30% carbon, 0.15 to 0.30% vanadium steels.

A clue to this unexpected low impact strength is observable in the microstructures. In steels that reject ferrite during cooling there is a tendency toward a stabilization of the residual austenite that is similar to that described for bainite by Klier and Lyman,[14] but of much greater magnitude and serious character. The condition in an aggravated form produces the structure called "fibrous pearlite" by Crafts and Lamont[15] and which seems to be present in Fig. 12. It is presumed that this structure is of a bainitic character and of a nature comparable with that described by Klier and Lyman. It tends to form when there is an appreciable ferrite rejection and tends to contain fairly stable residual austenite. It is promoted by the presence of carbide-forming alloys, such as molybdenum, chromium, manganese and vanadium, and results in low ductility and impact strength, as well as low yield strength, except in the steels containing vanadium, titanium, etc., that have limited carbide solubility.

The residual austenite may be quite stable and the same quality that increases the high temperature strength of vanadium steels may be expected to retard decomposition of the austenite. If this austenite is sufficiently stable to resist transformation while the steel is at the tempering temperature, it may be expected to transform to martensite on cooling and cause embrittlement. A second tempering treatment would then be expected to increase the toughness materially. Similarly, a long tempering treatment or one at a higher temperature might also be expected to have the beneficial effect that was actually found by the authors. It is, therefore, considered probable that the reported low impact strength is a result of inadequate tempering rather than an inherent deficiency of vanadium steel.

[14]E. P. Klier and Taylor Lyman, "The Bainite Reaction in Hypoeutectoid Steels", *Transactions*, American Institute of Mining and Metallurgical Engineers, Vol. 158, 1944, p. 394.

[15]Walter Crafts and John L. Lamont, "Hardenability of Low Chromium Steels", HARDENABILITY OF ALLOY STEELS, published by American Society for Metals, 1939, p. 197.

As pointed out by the authors, the molybdenum-vanadium steel, WC8, is of practical interest for high temperature steam service, so that the results of their long-time tests would be quite helpful and it is hoped that they will include the data in their reply to discussion. In connection with their discussion of low ductility in WC8-type steels, it should be pointed out that steels Nos. 12 and 13 are well outside of the specification with respect to carbon, and that steels Nos. 7 and 8, which are within the specification, have high ductility.

The authors are to be congratulated on their investigation of a well-planned series of vanadium steels and it is hoped that they will continue it with a more comprehensive study of the effects of heat treatment.

Written Discussion: By Jerome Strauss, vice-president, Vanadium Corporation of America, New York.

In view of present interest in and rapidly extending use of molybdenum-vanadium steels in power plant equipment operating at moderately elevated temperatures, this paper is timely and of interest, in that it represents a very large amount of investigative work on a group of steels on which very little data have been published. This appears even more important than the fact that it constitutes one of a series of continuing investigations on the properties of certain low alloy cast steels. However, examination of the steels employed and the conditions of testing raises some significant questions.

Conditions of steelmaking must have been quite variable to have resulted in silicon contents ranging from 0.20 to 0.54% and manganese contents from 0.38 to 0.94%. The range of silicon in any one subgroup of four steels seems not overly large, but because of their influence on quality these steelmaking conditions must be reflected in the mechanical properties, and general comparisons of these properties can lead to erroneous conclusions.

On the other hand, the manganese range, no doubt also the result of variation in steelmaking from heat to heat, covers ranges in individual subgroups as great as 39 points. In addition to the meaning in respect to steel quality, this spread in manganese has tremendous effect on hardenability in view of the well-known fact that manganese influences this property to a greater extent per unit of weight than any common alloying metal. Observe, for example, the influence on hardness after cooling from 1830 °F (1000 °C) as shown in Table I. When slowly cooled the full vanadium content of 0.25% raises the hardness of the 0.06 to 0.09% carbon, plain carbon steels, 32 units; in the 0.25 to 0.30% carbon steels there is likewise a hardness increase of 32 but in the 0.14 to 0.17% carbon steels only 16 points result from the full increase of vanadium—the effect being due to sharp lowering of manganese content. Air-cooled, the low carbon steels show a change of 40 points, the high carbon steels 78, but the intermediate carbon steels only 34; again the manganese is suspect. In the second and third groups of the 0.5% molybdenum steels, one wonders whether the effects result from the vanadium alone or are colored by the difference in manganese.

In one other respect, steelmaking conditions may have exerted a pronounced influence, but no evidence is in the data presented to permit evaluation. It is observed that the sulphur content of these steels varies from 0.007 to 0.038% and that the third group with its 1% molybdenum content contains a higher sulphur content than any of the other heats used in the preparation of these data, with the single exception of one of the plain carbon heats. Yet in the making of all of the steels, regardless of both carbon and sulphur, a uniform addition of 2 pounds of aluminum per ton was made. The distribution of inclusions and particularly at the grain boundaries is not detectable from any of the photomicrographs nor is it recorded, but should there be chain-type inclusions in these steels they would play particular havoc with the mechanical properties when normalized and tempered, especially under tempering conditions not producing spheroidization of the carbide. The detrimental effect on ductility and impact strength would increase as the basic hardness of the composition increased.

The selection of heat treatment temperatures was no doubt dictated by definite reasons, but their omission from the presentation raises questions in the mind of the reader. It is assumed, perhaps erroneously, that these studies were intended solely to guide the development of steels for use at elevated temperatures. However, the effects of carbon, manganese, molybdenum, and vanadium on the normalizing temperature, especially with reference to solution of carbides in the presence of vanadium and the slow grain coarsening that results as the temperature rises, may have been neglected. For the best creep strength, it appears desirable to take some carbide into solution, but other investigators have preferred higher temperature in order to obtain a more significant effect upon this property. These are not, however, the conditions that result in good impact properties either at room temperature or below; this objective is attainable by the use of normalizing temperatures not too much above the end of the A_3 range, and preferably with the prior use of a homogenizing treatment in accordance with the suggestion by Krivobok when discussing a previous paper in this series. The fixed temperature selected for this investigation is neither in the best interest of creep strength nor of low temperature impact strength.

It appears, therefore, that the heat treatment conditions have not been selected with due regard to the metallurgy of this series of steels. This leads to the necessity of expressing conclusions, particularly with regard to the mechanical properties, with proper limitations, namely within the confines of the experimental procedure used.

Some of the conclusions drawn may perhaps lead to misinterpretation due to insufficient comparisons. For example, the statement is made that vanadium increases the elastic limit, yield point, and tensile strength, but that the increase is not very great, and yet the data show that 0.25% vanadium in all three groups increases these properties in every instance to a greater degree than that resulting from 0.50 to 0.60% molybdenum and to values not far below those for 1.00 to 1.20% molybdenum, so that in this respect there is an equivalence of at least about

3:1 based upon weight percentage. Review of these data calls attention to the graphs displaying proportional limit higher than yield point in most instances, and to this the authors may desire to add comment.

Mention has been made above of the influence of heat treatment on impact strength. On pages 581 and 582 the authors discuss this question of impact strength and make comparisons of the effects of vanadium and silicon. The influence of silicon on low alloy cast steels is well known, namely, that at amounts in the vicinity of 0.75% a decrease in impact strength occurs that is not too greatly dependent upon alloy composition or heat treatment procedure and which becomes more rapid as the silicon content rises above this level. In the case of vanadium, definite improvement in impact resistance may be obtained with the use of properly selected heat treatment conditions applied to many low alloy steels and this fact is responsible for the use of the numerous cast types containing this element. The writer sees no reason for these carbon-molybdenum steels being different in this respect from other types previously investigated in considerable detail, but of course has not had time to check the data presented. However, it is very definite that heat treatment conditions exert a tremendous influence upon impact strength at room and low temperatures and in any event statements with respect to change in ductility or impact strength must be made with due regard for, and a statement of, the change in tensile strength or hardness. It should, perhaps, be repeated that the heat treatment conditions for best strength properties at elevated temperatures are not those for best impact properties when high temperature is not involved, while it may be added that, in general, high creep strength is opposed to high room temperature ductility not only in highly alloyed steels but in many low alloy steels as well.

Taking into consideration the available welding electrodes and the limited recorded data, it is not possible to comment in much detail on this phase of the investigation; however, the charts of the hardness surveys indicate that the last statement in this section on page 590 should have been more properly modified to indicate that higher temperature may be required for the higher molybdenum compositions and not the higher vanadium compositions, in view of the fact that the stress relief on the lower molybdenum steels, whether of low or high vanadium, appears to be adequate for all engineering purposes. It seems likely, based upon other statements in the paper and this same lack of details, which admittedly might have made the paper very long, that the comment on the side bend tests on page 589 and in Conclusion 10 may refer only to the one composition with the maximum of all the hardening elements.

The molybdenum-vanadium steels of the higher alloy contents, at least the 1.00% molybdenum, 0.25% vanadium now in commercial use, do exhibit low impact strength in the as-cast state. Properties at elevated temperatures are, however, of such great value, that this minor difficulty has exerted no restraint on its use, and the problem is believed by those working with it to be amenable to solution. The authors leave the impression that the fault lies with the vanadium but, not having mentioned that the carbon-vanadium steels are brittle (which would belie

forty years of extensive commercial use), the responsibility could equally be placed upon the molybdenum. Would it not be more strictly correct to refer specifically to the full composition of those steels to which the observations actually apply?

It is noted that the authors, on pages 591, 593, 594, and 595, present very indecisive statements regarding the cause while admitting that the cooling rate may have been responsible; perhaps not only the cooling rate but also the metal condition and pouring temperature should be given consideration. On page 595 reference is made to the fact that in ASTM Tentative Specification A-217-47T the minimum elongation required for the molybdenum-vanadium steel is 15%, which is 5% less than for the other steels listed. It should be observed first that only one of the other steels is required to have the same minimum tensile strength. It should be observed, further, that of the four steels prepared initially by the authors, only one shows 15% elongation, the others all being 20% or more, and that the four subsequent heats made show in all three sets of heat treatments a minimum of 20% elongation. Consequently, the statement at the top of page 596 that "elongation .... ranges between 15 and 24.5%" should be in more detail to avoid misunderstanding, to which it may be added that heat treatment properly designed for the one steel with the maximum of hardening elements would no doubt have brought it well within the 20% elongation minimum.

In the Conclusions as in the text, the terms "potential" and "might" indicate that even in the authors' own opinion they have not done enough with these steels to warrant thorough understanding of their behavior. As pointed out above, difficulties in the as-cast state have not been so great as to hamper extensive commercial use and in the heats recorded here were possibly exaggerated by the authors' steelmaking, deoxidation and casting practices. As available hardness gets higher, all pearlitic steels, regardless of composition, may be expected to require somewhat closer control, which if not provided may result in some troubles of greater or lesser magnitude. Similarly, the statement of the possibility of welding troubles does not in any degree conform to actual experience with vanadium steels of even higher hardening capacity than those dealt with in this paper. It would appear, therefore, very much in the interest of both producer and user for the authors to continue in their study of these compositions but with steelmaking and thermal treatment adapted to the metallurgy of the compositions, rather than to employ uniformly an arbitrarily selected procedure.

It seems pertinent to add some comments on the authors' general remarks regarding vanadium.

What they mean by the term "popular" is not certain, but at least the background of application for any of the alloying elements cannot be covered in a single word. Their use is always the result of a combination of metallurgical and economic factors. There are today very many low alloy constructional steels containing vanadium in amounts from about 0.02 to about 0.25% and even slightly higher, and quite a number of these are in the form of castings.

As to the "popularity" being confined to tool steels, it might be commented that while some of the tool steels (i.e., high speed steels) function not nearly so well if at all without their vanadium content, likewise a number of constructional steels (i.e., turbine motors, very high strength guns, heavy leaf springs) cannot be caused to function properly without their vanadium content. Additionally, during the last 30 or more years the distribution of vanadium between tool steels and constructional steels has varied back and forth between about 20:80 tool:constructional to 70:30, and the fluctuation continues. The sole factors mitigating against more widespread use of vanadium in low alloy constructional steels are availability and cost and these are in major part out of man's control, namely, the location of the deposits and the chemistry of vanadium and of the elements with which it occurs.

No issue can be taken with the quotation from Knowlton, but since facts of the kind quoted change continuously with time, it is regretted that the authors did not include examination of earlier and later texts. The statements in the present paper regarding vanadium uses go back in some cases to almost 20 years before Knowlton's comments, while the uses have altered considerably since that time. There is most limited application today of vanadium as a "cleaner", if by that term the authors refer to combination with oxygen and nitrogen, more particularly the former. There is no economy in using a $3.00 element as a deoxidant when 10 to 20-cent elements will carry oxygen contents even lower. In a very few instances, for example in the new vanadium rimming steels, ferrovanadium is most effectively used for oxygen and nitrogen control, but even in this case preliminary deoxidation depending upon steelmaking conditions is undertaken with silicon or aluminum.

Authors' Reply

The authors wish to thank Messrs. Wilder, Crafts and Strauss for their constructive discussions.

With regard to Dr. Wilder's remarks on graphitization, our preliminary work on cast steels confirms the results he has obtained on wrought steels. Vanadium in the amounts used may retard, but does not prevent graphitization at 1025 and 1050 °F (550 and 565 °C). In aluminum-killed steels containing about 0.2% carbon and 0.15 to 0.25% vanadium, some samples started to graphitize in the heat-affected zones of welds after 7500 to 10,000 hours at 1025 °F (550 °C). Other similar samples treated in the same way resisted graphitization. Steels with 0.25% vanadium resisted graphitization longer than those of lower vanadium contents, other factors being equal.

The work on high temperature properties is being performed by another group in our laboratory. They find that these steels normalized at 1750 °F (955 °C) and drawn at 1250 °F (675 °C) show an appreciable increase in creep resistance over that of carbon-molybdenum steels tested in the 900 to 1100 °F (480 to 595 °C) temperature range. However, room temperature impact resistance of the original samples was reduced during

the creep cycle, which appeared to have been caused by some precipitation. This effect was most pronounced in the 0.25% carbon, 0.25% vanadium compositions. In lower carbon (about 0.15% carbon) steels this embrittlement is less pronounced.

Mr. Craft's remarks concerning the causes of brittleness in vanadium steels are very interesting. However, it seems somewhat doubtful that any austenite could be retained in these steels at room temperature, as has been found in higher carbon low alloy steels subjected to faster cooling rates from austenitizing temperatures. Detailed study of the original dilatometer curves and metallographic samples did not reveal the presence of any retained austenite. Increasing the vanadium content from 0.05 to 0.25% does not by itself have any marked effect on thermal sluggishness; however, hardness is raised and impact resistance lowered progressively in the heat treated steels. Evidently the stability and segregation of the vanadium carbides are mainly responsible for this situation. It can be corrected by a suitable heat treatment, as shown in the paper.

In reply to Dr. Strauss' discussion, it may be stated that conditions of steelmaking in our 200-pound induction furnace are more closely controlled than they are in an average production shop. On the other hand, our furnace is sufficiently large to insure a higher degree of homogeneity than may be expected from a small laboratory furnace of a few pounds capacity. The melting stock is ingot iron for lower carbon steels and SAE grade steels for higher carbon compositions.

When ingot iron is used, some ferrosilicon must be added to the furnace during the melting period, to reduce boiling caused by the reaction between iron oxide and carbon. This addition is not necessary with SAE scrap. To obtain the desired silicon content in the resultant steel, the major part of it is added to the tapping stream of the metal. The calculated amounts of manganese are added to the furnace. Most of the aluminum is added to the furnace, and a small part to the tapping stream.

Some experiments performed by our engineers show that 2 pounds of aluminum per ton of steel give the desired results. This amount produces complete deoxidation associated with the absence of undesirable necklace type of inclusions which might be caused by overdosing with aluminum.

All of these techniques are well established by foundry practice and are necessary in producing good sound steels. On the other hand, it is very difficult to adjust the metalloid additions so that their amounts in the resultant steels would be within closer tolerances than those found in our experimental steels. It is true that some of these steels exceed the specified (WC8) maximum of 0.7% for manganese, but the differences noted, as is clearly shown in one of our previous papers (6), should not produce much effect on hardenability. Likewise, the variations in silicon content (none of which exceeds the specified 0.6% maximum) should not have any effect on any of the physical properties. This also was sufficiently well demonstrated in one of our previous publications (7). The

same should apply to the sulphur and phosphorus contents, which again never exceed the specified maximums of 0.06 and 0.05% respectively.

We quite agree with Dr. Strauss that the effect of vanadium, no doubt, is an indirect one. The same applies equally well to any other alloying element. In our previous publications, as well as in the present one, it is sufficiently well demonstrated, it is hoped, that carbon associated with the alloying elements is the principal factor determining properties of steel. However, direct or indirect, in this particular case we are dealing with the effect of vanadium.

Heat treatment, as shown in the section of the paper covering "embrittlement", has a profound effect on physical properties. This applies equally well to any ferritic steel. Moreover, it is true that a different heat treatment should be used to develop some specific property. Our heat treatment was selected on the strength of previous experience to bring out with some compromise the most desirable room temperature properties.

With regard to homogenization, Marcotte and Eddy[16] have shown that these heat treatments have a negligible effect on the hardenability and impact resistance of cast carbon and SAE 4330 types of steel.

Occurrence of proportional limit higher than yield point is quite common for cast steels, particularly with low carbon. It is due to the peculiarities of the stress-strain diagram and has nothing to do with the vanadium.

Regarding weldability of vanadium-bearing steels, all that can be said at present is that there is not enough information on this subject. There is no doubt that with sufficient skill almost any steel can be welded. Our limited experiments indicate rather definitely that vanadium-bearing steels are a little bit more difficult to weld than similar ones, but without vanadium. This, however, in no way means that it cannot be done.

Any further discussion concerning the general remarks or terminology on the effect and use of vanadium, such as "moderate" increase in some of the physical properties or relative "popularity" of vanadium, does not appear warranted.

In conclusion it may be stated that this paper never was intended to be a thesis on vanadium steels. It merely presents the results of some experiments related to the problems of the steel casting industry. The results obtained are obvious, but their interpretation is a matter of personal opinion. It is gratifying to know that such a lively interest was taken in them.

---

[16]R. J. Marcotte and C. T. Eddy, "The Effect of Homogenization on Cast Steels", TRANSACTIONS, American Society for Metals, Vol. 40, 1948, p. 649.

INFLUENCE OF LOW TEMPERATURES ON THE MECHANICAL PROPERTIES OF 18-8 CHROMIUM-NICKEL STEEL

By D. J. McAdam, Jr., G. W. Geil and Frances Jane Cromwell

Abstract

By means of tension tests of notched and unnotched specimens an investigation has been made of the mechanical properties of various 18-8 chromium-nickel steels between room temperature and —188 °C (—306 °F). One of the steels was ferritic; the others were of the metastable austenitic type. Plastic deformation of the metastable austenitic alloys causes a phase change and thus hardens the alloy. The rapidity of this change increases with decrease in temperature. At low temperatures the hardening due to the phase change is so rapid that the load-extension curve sometimes has two maxima. For this reason six important strength indices sometimes are required to evaluate the mechanical properties.

Introduction

In a series of papers, the authors and their associates have presented results of a general investigation of the influence of low temperatures on the mechanical properties of ferrous and nonferrous metals (7-12).[1] However, the only steels studied were ferritic, and the only stainless steel was a 13-2 chromium-nickel steel (7, 8). Of the chromium-nickel alloys generally classed as austenitic there are two groups; in one group, the austenite is stable at room temperature; in the other group, the austenite is metastable. When alloys of the metastable or "marginal" group are cooled rapidly from about 1900 °F (1040 °C), they are austenitic. The austenite, however, tends to change partially to ferrite when the alloy is plastically deformed at room temperature. Because the ferrite thus formed contains carbon in supersaturated solution, it is sometimes called

[1]The figures appearing in parentheses pertain to the references appended to this paper.

A paper presented before the Thirtieth Annual Convention of the Society, held in Philadelphia, October 23 to 29, 1948. The authors are associated with the National Bureau of Standards, Washington, D. C. Manuscript received March 10, 1948.

martensite (14). In future reference to this phase, however, it will be designated as ferrite.

One of the most important of the marginal alloys contains about 18% chromium and 8% nickel and is generally known as 18-8 chromium-nickel steel. Generally the chromium content ranges between 17 and 19%, and the nickel content between 7 and 9%. Since the space lattice of chromium is body-centered and that of nickel is face-centered, an increase in the chromium content tends to make the alloy ferritic, and an increase in the nickel content tends to make it austenitic. For steels containing 18% chromium, about 13 to 15% of nickel generally is necessary to make the austenite stable at room temperature. An empirical formula was developed by Post and Eberly (16) to show the percentage of nickel necessary to make an alloy stable when cold-worked to 80% reduction in cross section. Since carbon, manganese and molybdenum have a marked effect on the stability of austenite, constants for these elements were also included in the formula. The formula was based entirely on results of experiments at room temperature. The boundary between the stable and marginal group, however, depends greatly on the temperature.

The influence of low temperatures on the properties of ferrous and nonferrous metals has been investigated by Colbeck, MacGillivray and Manning (4). An 18-8 chromium-nickel steel was included in their investigation. They report values for the yield stress, ultimate stress, and reduction of area at various temperatures between room temperature and the temperature of liquid air, but they give no values for the breaking stress. DeHaas and Hadfield (5) reported values for the same properties at room temperature and at the temperature of liquid hydrogen, —252.8 °C (—423 °F). Their values for ultimate stress are shown in Fig. 15, which will be discussed later.

Rosenberg (17) studied the tensile and impact properties of aircraft metals, including various alloys of the 18-8 type, at temperatures down to —78° C (—108 °F). In addition to plain 18-8 alloys, there were alloys containing small percentages of elements that are customarily added to prevent local depletion of chromium by carbide precipitation at elevated temperatures. Specimens from some of these heats of steel have been included in the investigation to be described in this paper, and a few of the results obtained by Rosenberg have been plotted in some of the figures.

Much of the literature on the properties of the chromium-nickel stainless steels is confined mainly to the study of the properties of the alloys at room temperatures and at elevated temperatures (1, 2, 3, 6, 14-16, 18-20). The present paper gives the results of an investigation of the effect of temperature, ranging from room temperature to that of liquid air, on the mechanical properties of 18-8 chromium-nickel alloys. The results obtained in this study also reveal the influence of plastic deformation and temperature on the transformation from austenite to ferrite and give information applicable qualitatively to the entire group of metastable alloys, including those that are much nearer than the 18-8 alloy to the boundary between the metastable and the stable austenitic group. A ferritic 18-8 steel of the precipitation hardening type also was included in this study (18, 20).

Materials, Method of Investigation, and Specimens

The alloys used in this investigation were all of the 18-8 type; the chemical compositions are given in Table I. The compositions of all but one of the alloys were such that the alloys were austenitic after quenching from 1900 °F (1040 °C); the alloy designated EH in Table I becomes ferritic after quenching from 1900 °F (1040 °C), and can then be hardened by reheating to cause precipitation. The heat treatments given to these alloys are described in Table II.

The alloys were received in the form of round rods of the sizes indicated in Table II. The rods of one of the alloys, designated by EF in Table I, had been annealed by the manufacturer. The annealing treatment doubtless was about the same as the austenitizing treatment given to alloys EA to EE (Table II). The rods of the other alloys were in cold drawn condition; the rods of two of the alloys (EB and EE) had been drawn two different amounts.

Table I
Description of Steels

Material Designation	Chemical Composition, Per Cent								
	Carbon	Manganese	Silicon	Chromium	Nickel	Molybdenum	Titanium	Columbium	Aluminum
EA	0.07	0.44	0.50	18.22	8.63	....	....	....	....
EB	0.10	0.47	0.35	18.82	9.38	....	....	....	....
EC	0.05	0.39	0.62	19.04	9.15	....	0.29	....	....
EE	0.075	0.64	0.61	18.61	10.16	....	....	0.93	....
EF	0.07	0.93	0.42	18.58	8.93	3.36	....	....	....
EG	0.07	0.73	0.48	18.41	7.88	2.80	....	....	....
EH	0.07	0.50	0.50	17.00	7.00	....	0.70	....	0.20

Table II
Heat Treatment of Steels

Material Designation	Rod Diameter, In.	Temperature, °F	Time Held, Hr.	Cooled in
EA to EE	0.625	1900	1	Water
EF	0.625	*	..	.....
EH	1.000	1900	½	Air
		1000	¾	Water

*Annealed by manufacturer.

For a description of the apparatus and the methods of testing at low temperatures, reference may be made to a previous paper (*7*). Most of the specimens used in this investigation were unnotched and of standard form. Deeply notched cylindrical specimens, however, were also used in obtaining the diagrams in Fig. 16. The notches were all about the same depth (k = about 0.16),[2] but the notch angle varied between 150 and 50 degrees. The notched specimens were about 5½ inches long. The ends of the specimens were threaded to ⅝ inch diameter. Between the threaded ends, each specimen was machined to a uniform diameter of ⅝ inch, and a circumferential V-notch was machined at the midsection. The notch was carefully machined to the selected angle, with the conical sides tangent to the arc at the root of the notch. Care was also taken to minimize heating, bending, or appreciable cold work during the machining.

Variation of the Nominal Stress with Tensile Extension

Automatic load-extension diagrams obtained in the tension tests of the 18-8 chromium-nickel steels gave clear evidence of phase changes during the plastic deformation. Typical curves derived from automatic load-extension diagrams obtained with unnotched specimens are shown in Figs. 1, 2, and 3. These curves show the influence of plastic extension on the nominal stress, that is, the stress value obtained by dividing the tensile load by the initial area of cross section.

Fig. 1 shows results of tension tests of annealed austenitic plain 18-8 alloy at three different temperatures. The curve obtained at room temperature is qualitatively similar to a curve obtained without phase change. The slope decreases continuously between the

[2]Notch depth is expressed in terms of the relative area ($k = b^2/B^2$) of the minimum cross section, where b and B represent the radii of the minimum and maximum cross section respectively. Thus, the greater the notch depth, the smaller is the value of k.

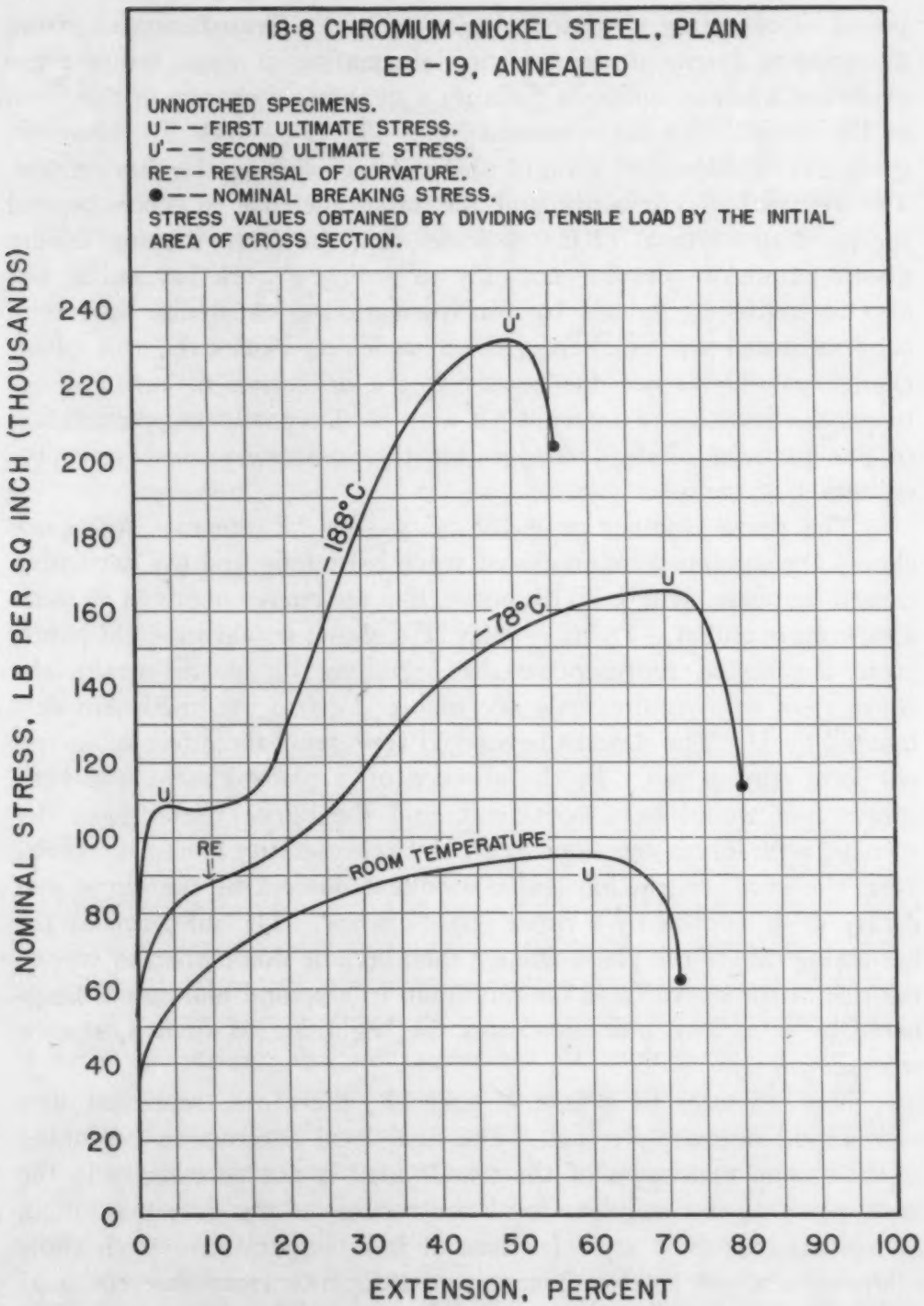


Fig. 1—Variation of Nominal Stress With Extension, Annealed 18-8 Chromium-Nickel Steel, Plain.

points representing yield and maximum load. Transformation from austenite to ferrite during plastic deformation at room temperature evidently was not sufficient to cause a qualitative change in the form of the curve. The curve obtained at —78 °C (—108 °F), however, gives clear evidence of a rapid phase change during the tension test. The reversal of curvature and the rapid increase in slope beyond the point of reversal (RE) indicates that the strengthening during plastic extension was due not only to ordinary work hardening, but also to hardening caused by transformation of austenite to ferrite supersaturated with carbon. The hardening caused by this phase change possibly is not due merely to the difference in hardness between the ferrite and austenite; it may be due partly to precipitation of fine particles of the ferrite within the austenite grains or to precipitation of carbides.

The curve obtained at —188 °C (—306 °F) reveals still more clearly the combined influences of work hardening and the hardening caused by phase change. This curve, like the curves obtained at room temperature and at —78 °C (—108 °F), shows no abrupt yield point; from the region representing the beginning of plastic strain, the curve rises with continuously decreasing slope to the maximum designated by U. The descent beyond U represents the effect of incipient local contraction. In the absence of a phase change the local contraction would have continued, and the curve would have descended with increasing slope to a point representing fracture. However, the local contraction and consequent descent of the curve evidently were stopped by a rapid phase change. The influence of the hardening due to the phase change then became dominant and caused the rise of the curve from the minimum to a second maximum designated by U′. This point indicates the beginning of final local contraction.

The ordinates of points U and U′, therefore, represent first and second ultimate stresses. The final local contraction beginning at the second maximum of the tensile load is not necessarily in the same place as the incipient local contraction at the first maximum. Specimens examined after fracture at low temperatures often show evidence of slight local contraction at a distance from the region of final contraction.

Fig. 2 shows results obtained with cold drawn rods of the same alloy that was used in obtaining Fig. 1. The metal designated EBM in Fig. 2 was cold drawn to approximately 49% reduction of area

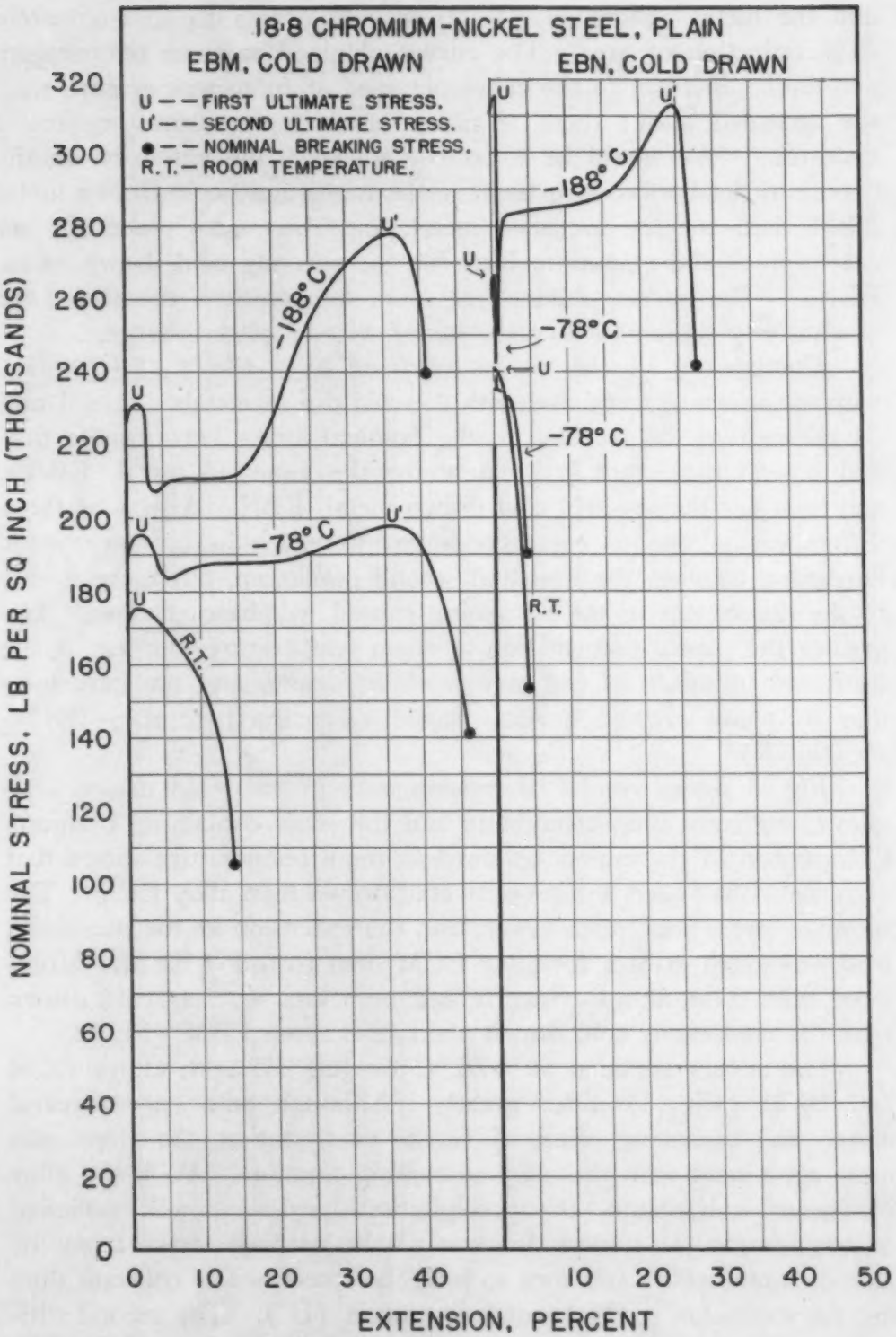


Fig. 2—Variation of Nominal Stress With Extension, Cold-Drawn 18-8 Chromium-Nickel Steels, Plain.

and the metal designated EBN was cold drawn to approximately 71% reduction of area. The curves obtained at room temperature are similar in form to the curve obtained at room temperature with the annealed alloy; there is no reversal in curvature or second maximum. As would be expected, however, the extension at the maximum load was much less for the moderately cold drawn metal EBM than for the annealed metal, and there was practically no extension at the maximum load for the severely cold drawn metal EBN. The curves obtained at room temperature, therefore, are qualitatively similar to curves obtained without phase change.

Comparison of the curves obtained at —188 °C (—306 °F) with the annealed metal and with the cold drawn metals (Figs. 1 and 2) shows that the increase in the nominal stress between the first and second maximum is greatest for the annealed metal, EB-19, and least for the severely cold drawn metal, EBN. A part of these differences is due to corresponding differences in ordinary work hardening between the first and second maximum, but more is due to the differences in the hardening caused by phase changes. The greater the plastic deformation at room temperature, the less is the combined influence of ordinary work hardening and the hardening due to phase change during plastic deformation at —188 °C (—306 °F).

Fig. 3 shows results of tension tests of two cold drawn 18-8 alloys, one containing columbium and the other containing titanium. Comparison of the curves obtained at room temperature shows that alloy ECM had been less severely cold drawn than alloy EEM. The ultimate stress was much lower, and the extension at the maximum load was much greater for alloy ECM than for alloy EEM. Moreover, both these alloys evidently had been less severely cold drawn than the moderately cold drawn plain 18-8 alloy, EBM (Fig. 2).

The curves obtained at —78 °C (—108 °F) with alloys ECM and EEM (Fig. 3) differ greatly. Although both curves reveal clearly the hardening effect of ferrite precipitation, the effect was more prominent with the alloy containing titanium. With the alloy containing columbium, the precipitation hardening was sufficient merely to stop the abrupt decrease of the nominal stress from the first maximum (U) and then to hold the stress nearly constant during the extension to the second maximum (U′). The second ultimate stress, therefore, was a little lower than the first. With the alloy containing titanium, however, the nominal stress increased

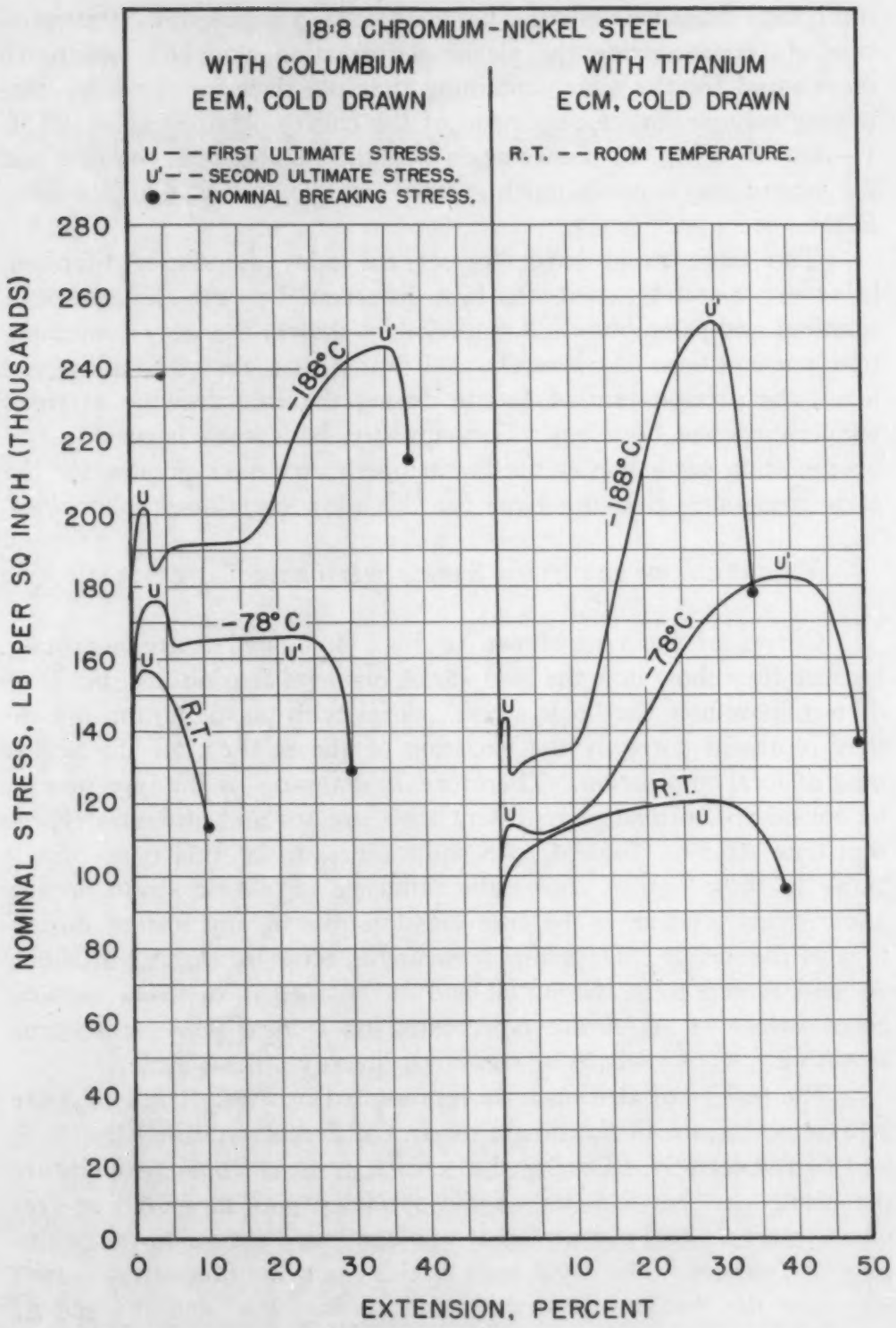


Fig. 3—Variation of Nominal Stress With Extension, Cold-Drawn 18-8 Chromium-Nickel Steels.

more than 50% between the first and second maximum. Precipitation of ferrite during the plastic deformation evidently was much more rapid for the alloy containing titanium than for the alloy containing columbium. Comparison of the curves obtained at —188 °C (—306 °F) (Fig. 3) shows again that the rise between the first and the second maximum is much greater for alloy ECM than for alloy EEM.

The more rapid hardening of the alloy containing titanium, however, cannot be attributed to a difference between the effects of titanium and columbium. As previously shown, the alloy containing titanium had been less severely cold drawn than the other alloy, and hence the precipitation of ferrite during the cold drawing at room temperature had been less. Consequently, both work hardening and precipitation hardening at the low temperatures were greater for the alloy containing titanium than for the alloy containing columbium.

Variation of the Flow Stress with the True Strain

Curves of the type shown in Figs. 1, 2, and 3 are important because they show how the load varies during a tension test, but they do not show how the "true stress" varies with plastic strain, nor do they represent correctly the variation of the strain after the beginning of local contraction. Therefore, in diagrams of the type now to be considered, ordinates represent true stresses and abscissas represent true strains. Figs. 4 to 8 show diagrams of this type. Each curve in these figures shows the influence of plastic strain on the "flow stress", which is the true tensile stress at any instant during flow of the metal. Strain is represented in terms of A_o/A,[3] in which A_o and A represent the initial and current areas of cross section. Since values of A_o/A are represented on a logarithmic scale, true strain ($\log_e A_o/A$) would be measured linearly on this scale.

The results of tension tests represented in Figs. 1, 2, and 3 are represented again in the diagrams of a different type in Figs. 4, 5, and 6, respectively. During the tension tests at room temperature the change in the diameter of the specimen was measured at frequent intervals, and measurement was continued almost to the beginning of fracture. The small open circles along the flow-stress curves represent the results of measurements during flow, and the end of

[3]The ratio A_o/A is designated the effective length ratio and represents the ratio of current to original length, had the specimen contracted uniformly at the same rate as at its minimum cross section.

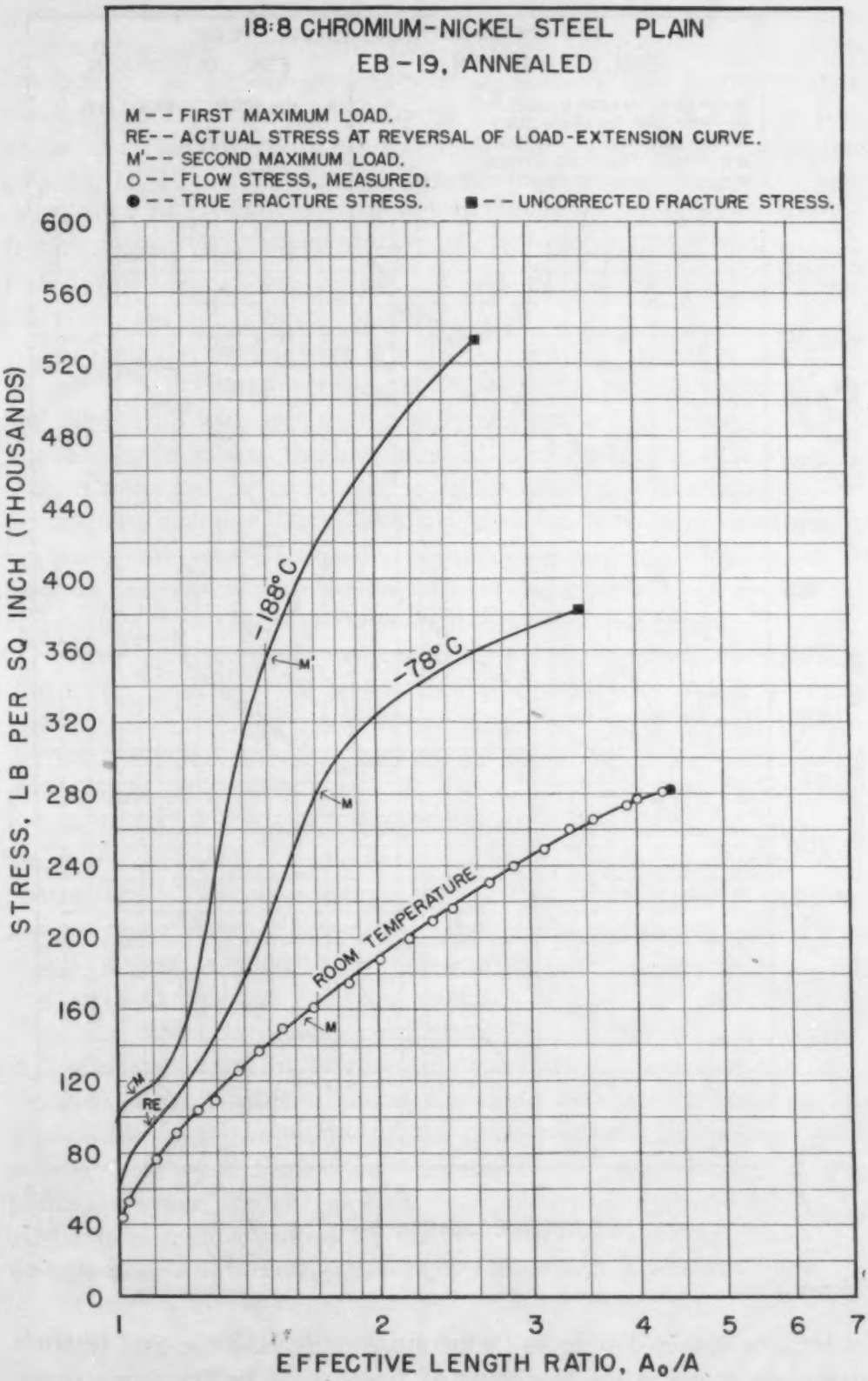


Fig. 4—Variation of True Stress With Strain, Annealed 18-8 Chromium-Nickel Steel, Plain.

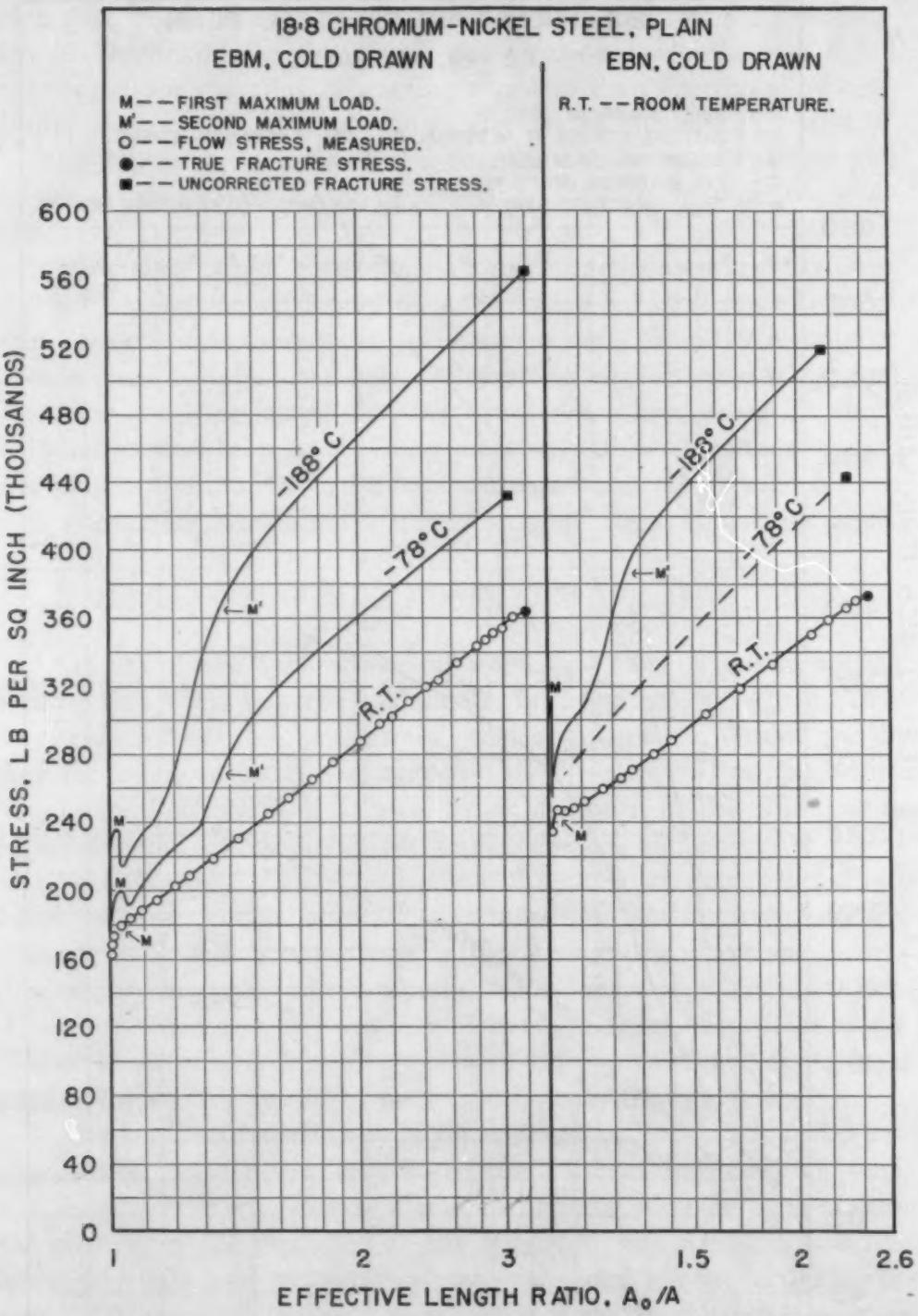


Fig. 5—Variation of True Stress With Strain, Cold-Drawn 18-8 Chromium-Nickel Steels, Plain.

each curve obtained at room temperature represents the true fracture stress, the stress at the beginning of fracture. The fracture stresses

were also determined in the usual way, by dividing the load at the beginning of fracture by the area of cross section measured after fracture. The area so determined is generally less than the area measured at the beginning of fracture, because the metal at the rim of the cross section continues to extend after fracture begins at the axis (8, 11, 12). With these 18-8 chromium-nickel steels, however, the difference between the uncorrected fracture stress and the true fracture stress was slight, even at room temperature. The uncorrected fracture stresses of the alloys tested at room temperature, therefore, are not indicated in the figures.

During the tension tests at —78 °C (—108 °F) and at —188 °C (—306 °F), no transverse measurements of the specimen were made, and the fracture stresses were determined in the usual way, by dividing the tensile load at the beginning of fracture by the area of cross section measured after fracture. Since the difference between the uncorrected fracture stress and the true fracture stress was slight even at room temperature, it probably was negligible at low temperatures. The uncorrected fracture stresses indicated in Figs. 4, 5, and 6, therefore, probably are not far from the true fracture stresses.

Since no transverse measurements of the specimens were made during the tests at —78 and —188 °C (—108 and —306 °F), the flow-stress curves for these temperatures (Figs. 4, 5, and 6) are derived from the corresponding curves representing the variation of the nominal stress with extension (Figs. 1, 2, and 3). The derivation is based on the simplifying assumption that each specimen remains cylindrical during the extension to the beginning of final local contraction. This assumption implies that, during this extension, the per cent difference between the flow stress and the nominal stress at any instant is equal to the per cent extension. In this way, the flow-stress curves for —78 and —188 °C (—108 and —306 °F) in Figs. 4, 5, and 6 have been constructed between the point representing yield and the point representing the final maximum of the load. Because of the local contraction, the curve between the point representing the final maximum and the point representing fracture cannot be determined from a load-extension diagram. Between these points, however, the curves have been drawn to represent the probable approximate variation of the flow stress at —78 and —188 °C (—108 and —306 °F).

The flow-stress curve obtained with annealed plain 18-8 alloy at room temperature (Fig. 4) is similar in form to curves obtained

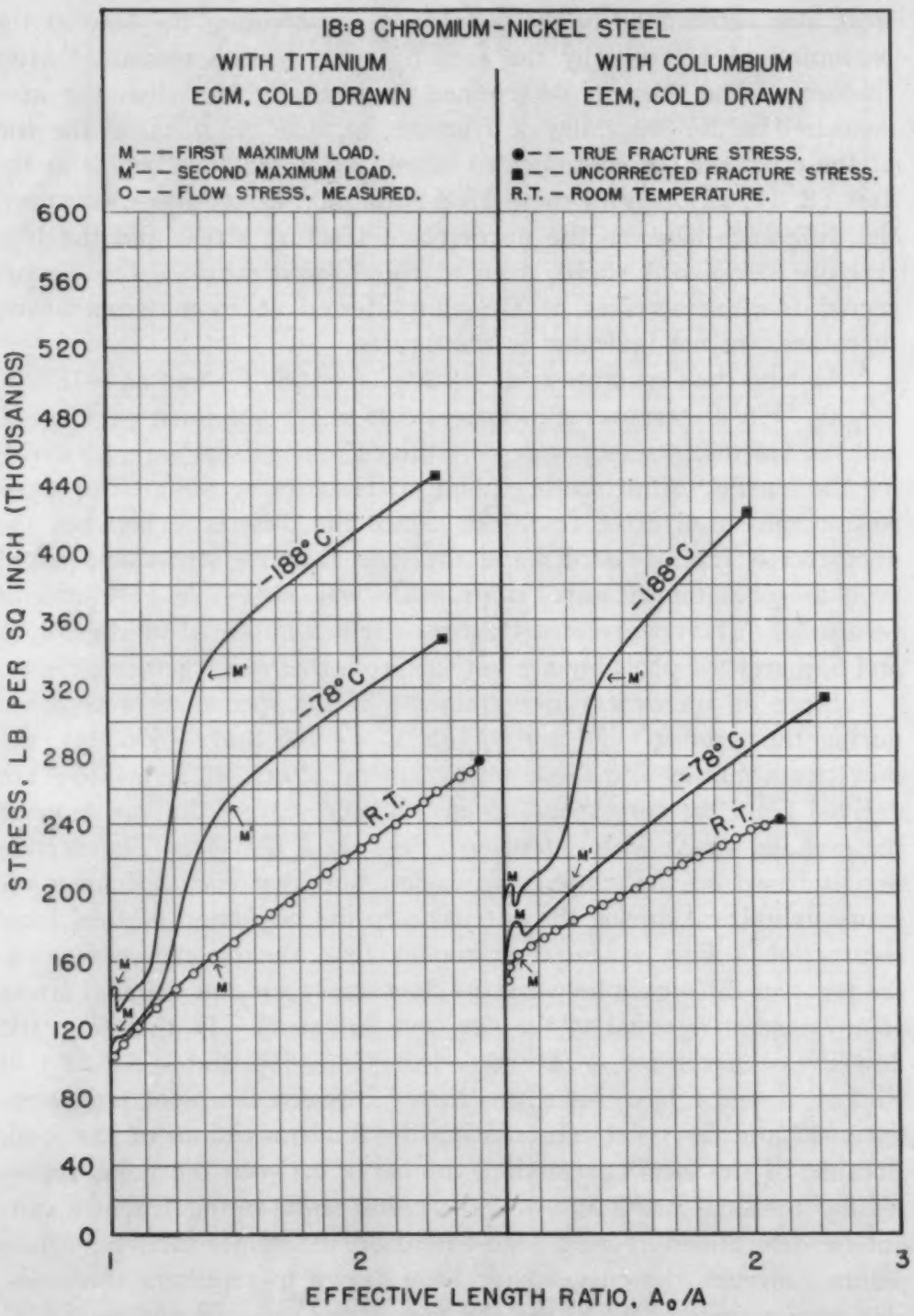


Fig. 6—Variation of True Stress With Strain, Cold-Drawn 18-8 Chromium-Nickel Steels.

with metal that is free from phase change during plastic deformation. As shown in previous papers (11, 12), the flow-stress line obtained

with some metals is nearly straight between the points representing maximum load and fracture, as in Fig. 6, but the line obtained with many metals rises with continuously decreasing slope, as in Fig. 4. The flow-stress lines obtained at room temperature with the cold drawn plain alloys (Fig. 5) rise with increasing slope, thus showing the effect of the precipitation hardening during the plastic deformation. The flow-stress curves obtained at low temperatures, like the corresponding curves in Figs. 1, 2, and 3, give clear evidence of the influence of phase change. The reversal of curvature and the steep ascent to the point representing the beginning of local contraction can be attributed only to the hardening caused by rapid precipitation of ferrite throughout the austenite.

Although the nominal-stress curve obtained with the annealed alloy at —188 °C (—306 °F) (Fig. 1) descends beyond the first maximum (U), the corresponding curve in Fig. 4 indicates that the flow stress rises continuously with plastic strain. The continuous rise of the flow stress is in accord with the previously expressed view that the descent of the nominal-stress curve beyond the first maximum in Fig. 1 does not represent a yield point, but represents incipient local contraction. Moreover, the curves obtained at —78 °C (—108 °F) with the annealed alloy show no indication of a yield point. However, all the curves obtained with the previously cold-worked alloys at the low temperatures apparently indicate an abrupt drop in the stress beyond the first maximum. Although this drop of the curves resembles somewhat the drop between the upper and lower yield points of ferritic steels, there are two reasons why the drop in the curves does not represent a yield point. One reason is that considerable plastic strain occurs during the test before the load reaches the first maximum, for all the alloys except the severely cold drawn plain alloy EBN (Fig. 5). The other reason is that no suggestion of a yield was obtained with the annealed alloy (Fig. 4). It seems probable, therefore, that there is no drop in the true flow stress for either an annealed or a cold drawn 18-8 alloy. The strains plotted in Figs. 4, 5, and 6 are *average* true strains, calculated on the assumption that the specimens remained cylindrical during the extension to the beginning of final local contraction. Actually, however, the true strain in the region of incipient local contraction may be considerably greater than is indicated by the average extension of the specimen. Moreover, inertia effects probably accentuate the abrupt drop of the load from the first maximum. The true flow

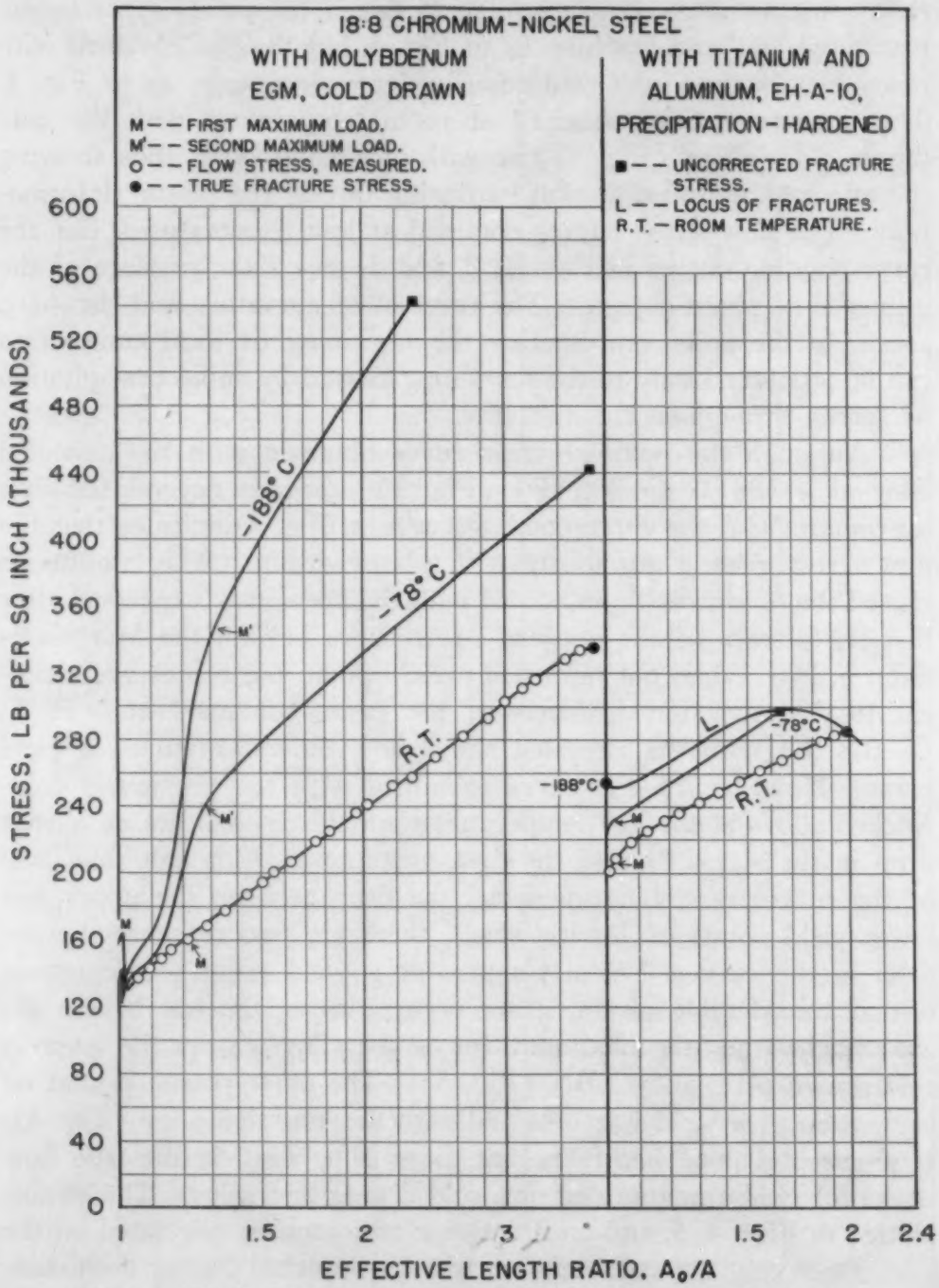


Fig. 7—Variation of True Stress With Strain, 18-8 Chromium-Nickel Steels.

stress, therefore, probably rises continuously with the plastic deformation of either annealed or cold drawn 18-8 alloys.

In Fig. 7, a comparison is made between a cold drawn metastable austenitic alloy containing molybdenum and a precipitation-hardened

alloy. The composition of the precipitation-hardenable alloy (EH) and the details of the heat treatment are given in Tables I and II. As shown in Fig. 7, the flow-stress curves obtained with the alloy (EGM) containing molybdenum are generally similar to the curves shown in Figs. 4, 5, and 6. The ductility of the metastable austenitic alloys evidently is not seriously affected by the rapid hardening caused by the phase change during plastic deformation at low temperatures (Figs. 4, 5, and 6). However, the effect of low temperatures on the ductility of the annealed plain 18-8 alloy (Fig. 4) was greater than the effect on the cold drawn alloys (Fig. 5). The adverse effect of a low temperature on the ductility evidently is greater when all the plastic deformation is at the low temperature than when part of it is at room temperature. Precipitation of ferrite from the austenite, therefore, evidently has considerable effect on the ductility. The good ductility exhibited by these alloys at low temperatures may be due partly to retention of some of the austenite.

At room temperature, the flow-stress curve for the ferritic alloy EH-A-10 (Fig. 7) was higher than that for the moderately cold drawn plain alloy EBM (Fig. 5) or the moderately cold drawn alloys containing titanium, columbium and molybdenum (Figs. 6 and 7), but was lower than that for the severely cold drawn plain alloy EBN (Fig. 5). The ductility of the ferritic alloy at room temperature (Fig. 7) was a little less than that of any of the cold drawn metastable austenitic alloys (Figs. 5, 6, and 7). With decrease in temperature the ductility of the ferritic alloy decreased rapidly, and a specimen tested at —188 °C (—306 °F) showed no ductility. To make sure that the brittleness at that temperature was not due to some defect in the specimen, another specimen was tested; the result was the same. The effect of low temperatures on the ductility of this alloy, therefore, evidently is similar to the effect on the ductility of annealed low-carbon steels. For use at low temperatures, the ductility possibly would be improved if some austenite were retained along with the ferrite and the precipitated constituent.

It has been shown that the influence of the total plastic deformation on the flow stress at a low temperature depends on the relative amounts of the plastic deformation at room temperature and at the low temperature. For a study of the influence of both the prior plastic deformation at room temperature and the total plastic deformation, results obtained with the same metal after various amounts of prior plastic deformation may be assembled in a single

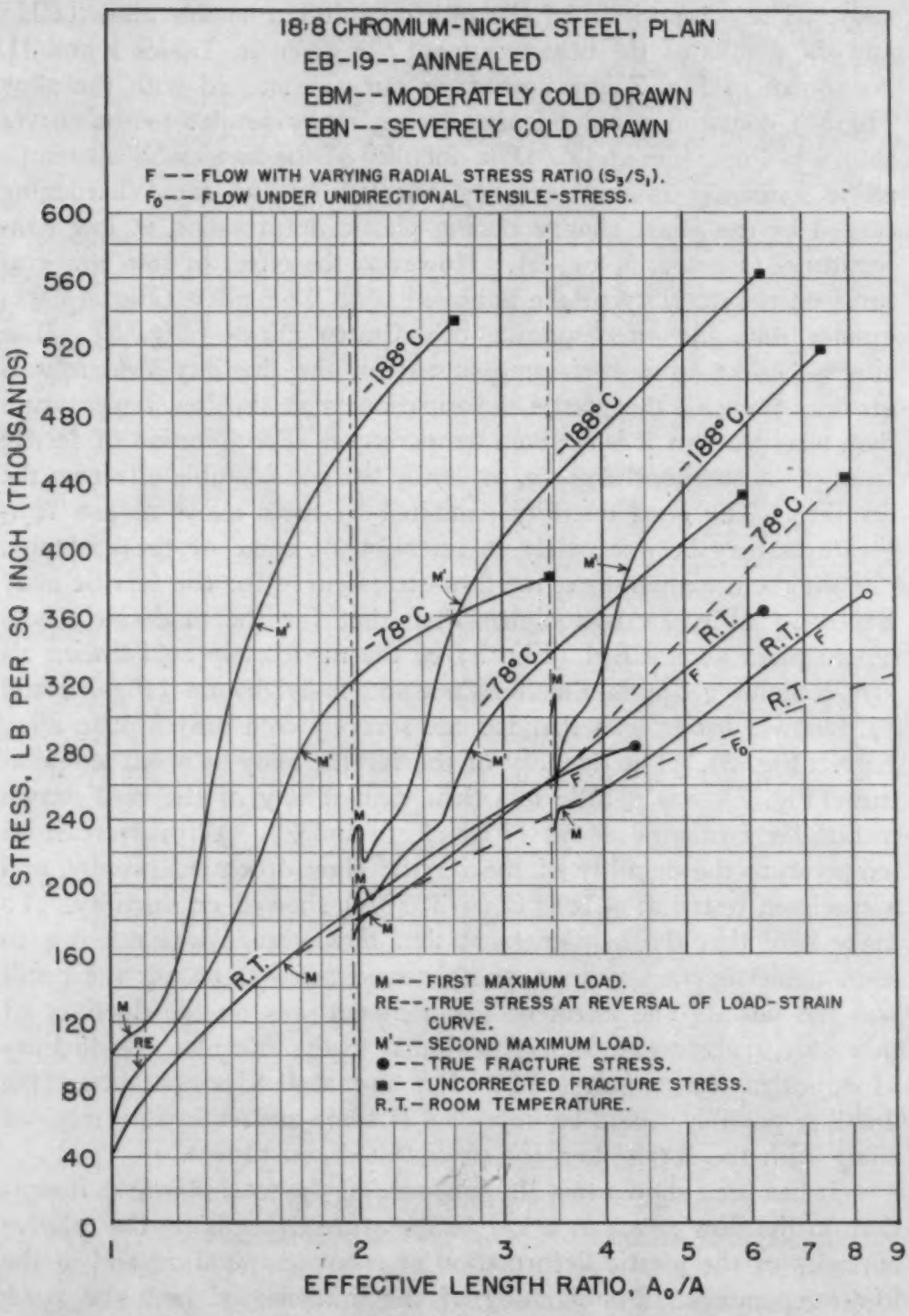


Fig. 8—Influence of Prior and Total Plastic Deformation on Flow Stress and Fracture Stress of Plain 18-8 Chromium-Nickel Steel.

diagram, in which abscissas represent values of the total plastic deformation (13). A diagram of this type is shown in Fig. 8, which is derived by assembling flow-stress curves reproduced from Figs. 4 and 5. Fig. 8 thus represents the influence of total plastic deformation on the flow stress and fracture stress of a plain 18-8 chromium-nickel steel. Since the true strains represented by the prior plastic deformation and the subsequent deformation during a tension test are directly additive, and since the abscissa and ordinate scales in Fig. 8 are the same as in Figs. 4 and 5, the flow-stress curves have been transferred directly from the basic diagrams to Fig. 8. In such a transfer, however, it is necessary to place the origin of each curve at an abscissa representing the corresponding amount of prior plastic deformation. The two vertical dot-and-dash lines in Fig. 8 represent the amounts of prior plastic deformation given to alloys EBM and EBN. Curve F_o represents approximately the tensile flow-stress curve that would be obtained if the stress could be kept unidirectional. The local contraction of a tension test specimen induces transverse radial tensile stress, and the ratio of the transverse to the longitudinal stress (radial stress ratio) increases with the local contraction. Because of the increasing radial stress ratio, curve F for the annealed alloy rises above the derived curve F_o. A method of deriving curve F_o is described in a previous paper (13) in which the relation between curves F_o and F is shown in diagrams. In Fig. 8, curve F_o has been drawn so as to be in approximately correct relation to curve F for the annealed alloy. It also has been drawn to pass through the first maximum points M on the flow-stress curves obtained with the cold drawn alloys EBM and EBN at room temperature. The diagram thus represents qualitatively the influence of prior and total plastic deformation and of low temperature on the flow stress and fracture stress.

The curves representing flow during local contraction at room temperature rise above curve F_o because of increasing transverse radial tensile stress induced by the local contraction. A curve similar to curve F_o could be drawn through points M on the flow-stress curves obtained at —188 °C (—306 °F). Since points M represent flow stresses after various amounts of plastic deformation at room temperature and only slight plastic deformation at —188 °C (—306 °F), a curve drawn through points M would approximately represent flow under unidirectional tensile stress entirely at —188 °C (—306 °F), but with the requirement that the precipitation harden-

ing was the same as at room temperature. A similar curve could be drawn to represent flow at —78 °C (—108 °F). The more rapid rise of the flow-stress curves obtained at —78 and —188 °C (—108 and —306 °F) (Fig. 8) is due to the more rapid precipitation hardening during flow at these temperatures. The rapid rise of these curves cannot be attributed to an increase in the radial stress ratio; the stress remains nearly unidirectional until the beginning of the final local contraction, designated by M′.

The rapid precipitation hardening during plastic deformation at low temperatures evidently increases the fracture stress nearly as rapidly as it increases the flow stress. If precipitation hardening were no more rapid at —188 °C (—306 °F) than at room temperature, the point representing fracture in a test entirely at —188 °C (—306 °F) would be on the previously discussed curve that could be drawn through the corresponding points M in Fig. 8. With sufficient increase in the prior plastic deformation at room temperature, the fracture stress at a low temperature would begin to decrease because of the decrease in the relative amount of plastic deformation at the low temperature and the accompanying decrease in the amount of precipitation hardening.

Changes in Magnetism of 18-8 Chromium-Nickel Steel with Plastic Deformation

Several investigations have been made of the change in magnetic properties of 18-8 alloys with plastic deformation (1, 2, 14, 16). In some investigations, quantitative studies of the transformation from austenite to ferrite have been made by measurement of magnetic permeability (2, 16). None of the specimens used in these previous investigations, however, had been plastically deformed at low temperature. Since the evidence in Figs. 1 to 8 shows that the hardening due to the phase change is more rapid at low temperatures than at room temperature, a brief qualitative investigation has been made to determine if these differences in precipitation hardening could be correlated with changes in magnetism. For this purpose, typical specimens that had been used in tension tests represented in Figs. 4 to 7 were explored by means of a small, strong, horseshoe magnet. These specimens included annealed, moderately cold drawn, and severely cold drawn metals. Some had been tested to fracture at room temperature, and some had been tested at low temperatures.

The specimens that had been tested to fracture at room temperature were slightly magnetic at the surface of fracture and in the adjacent locally contracted region, but the magnetic attraction was hardly noticeable elsewhere along the specimen. Moreover, the magnetic attraction was not appreciably greater for moderately cold drawn than for annealed metal. The attraction was a little greater for specimens of severely cold drawn metal, especially at the surface of fracture. However, the attraction was not strong enough to lift the specimens. The increase in magnetism in the locally contracted region is a result of the relatively large amount of plastic deformation occurring during the local contraction.

The specimens that had been tested at —78 and —188 °C (—108 and —306 °F) were only slightly magnetic at the threaded ends, which had not been plastically deformed at the low temperatures. Between the end fillet and the locally contracted region, however, each specimen was strongly magnetic; the attraction was strong enough to lift some specimens attached to both poles of the magnet. At the surface of fracture, the attraction was so strong that each specimen could be vertically suspended from one pole of the magnet. The magnetic attraction along the plastically extended side of the specimen, however, evidently was not so strong for the severely cold drawn specimens as for the moderately cold drawn or annealed specimens. The weaker magnetic attraction for the severely cold drawn alloy may be correlated with the relatively smaller amount of plastic deformation at low temperature. The method of investigation was not sensitive enough to detect differences in magnetism between specimens of annealed metal and specimens of moderately cold drawn metal, or to detect differences between specimens that had been plastically deformed at —78 °C (—108 °F) and those that had been deformed at —188 °C (—306 °F).

The results of these qualitative magnetic tests confirm the previously expressed view that the rapid rise of the flow stress with plastic deformation at low temperatures (Figs. 4 to 8) is due to a rapid transformation of austenite to ferrite.

The Variation of the Strength of 18-8 Chromium-Nickel Steels Between Room Temperature and —188 °C

Consideration will now be given to diagrams of a different type. In these diagrams, which are shown in Figs. 9 to 16, temperatures are plotted as abscissas and indices of strength are plotted as ordi-

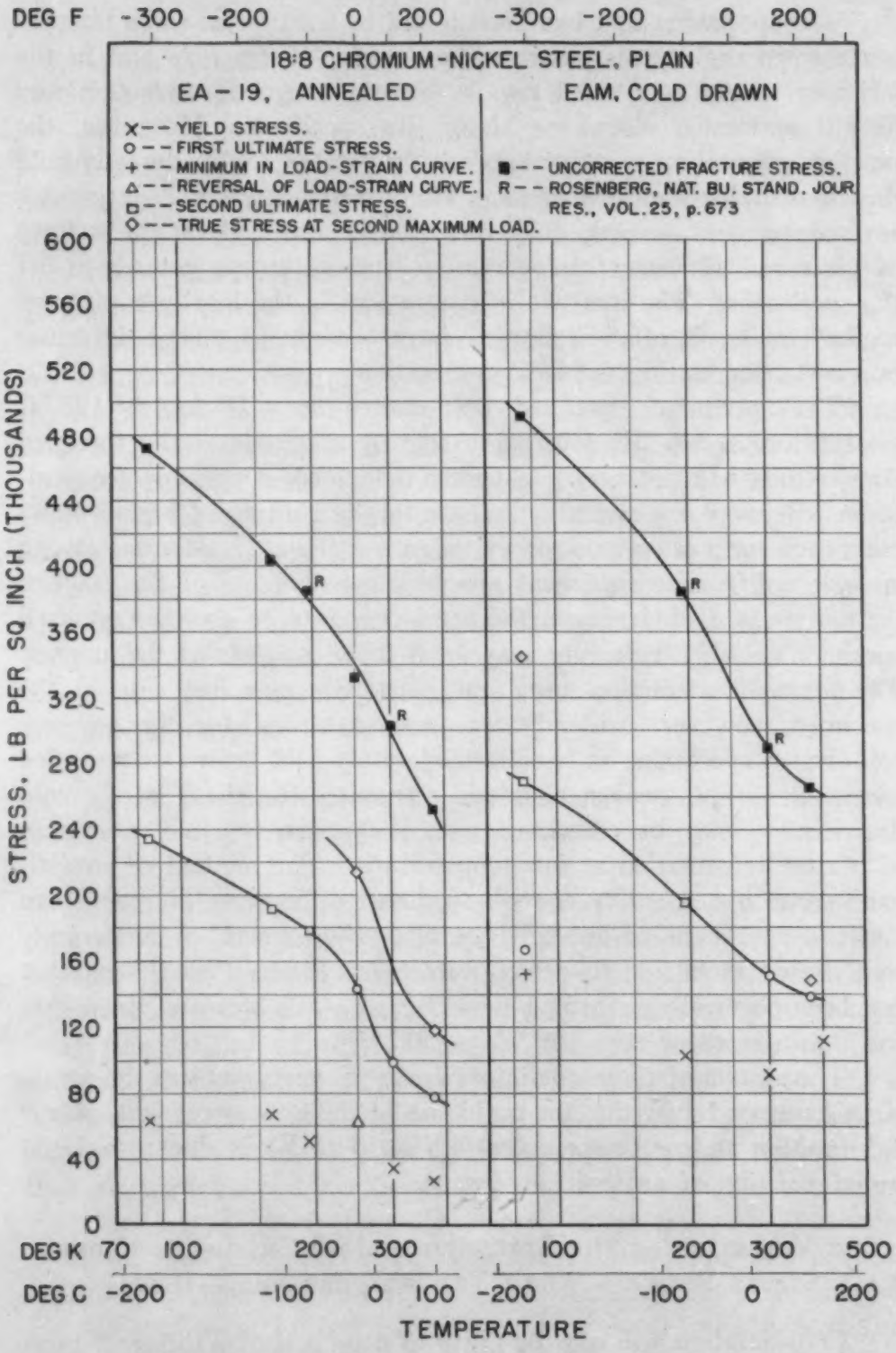


Fig. 9—Variation of the Strength of Plain 18-8 Chromium-Nickel Steels With Temperature.

nates. In these figures, the temperature scale is the same that has been used in previous papers by the authors and their associates (7-11). Temperatures in degrees K are plotted on a logarithmic scale. Since abscissas are proportional to the logarithm of the degrees K, the scale is the same in principle as Kelvin's original thermodynamic scale. This scale has been used because, as has been shown (7-11), it gives a linear relationship between temperature and the strength indices for various metals, in the absence of phase changes.

The strength of most metals can be evaluated by the use of only three indices, namely, the yield stress, ultimate stress, and fracture stress. For 18-8 chromium-nickel steels at low temperatures, however, six strength indices are important, although sometimes less than six are sufficient. As illustrated in Figs. 1 to 7, these indices are: yield stress, first ultimate stress, stress at a minimum in the load-extension curve, stress at a reversal of the load-extension curve, second ultimate stress, and true fracture stress. All these indices and the true stress at the second maximum load have been used in Figs. 9 to 14. Nominal-stress values, such as those represented in Figs. 1 to 3, have been used for the first ultimate stress, the minimum in a load-extension curve, the reversal of a load-extension curve, and the second ultimate stress.

Fig. 9 shows results obtained with a plain 18-8 alloy. This is not the same as the alloy used in obtaining Figs. 1, 2, 4, 5, and 8. Since most of the experiments represented in Fig. 9 were made several years ago, the importance of determining values for both the first and second ultimate stresses was not realized. Complete curves for the first ultimate stress, therefore, could not be obtained. As indicated by the symbols along the two ultimate-stress curves in Fig. 9, part of each curve shows the influence of a range of temperature on the first ultimate stress, and part shows the influence of a lower range of temperature on the second ultimate stress. However, the experiments have been made at enough different temperatures to establish definitely the form of the curves of variation of the ultimate stress and fracture stress.

Figs. 9 to 14 show the effect of temperature on the important strength indices. The effect of temperature on a strength index comprises the direct effect on the strength of the metal, and the superimposed effects on the amount of plastic deformation and the rate of hardening in the test made to determine the strength index.

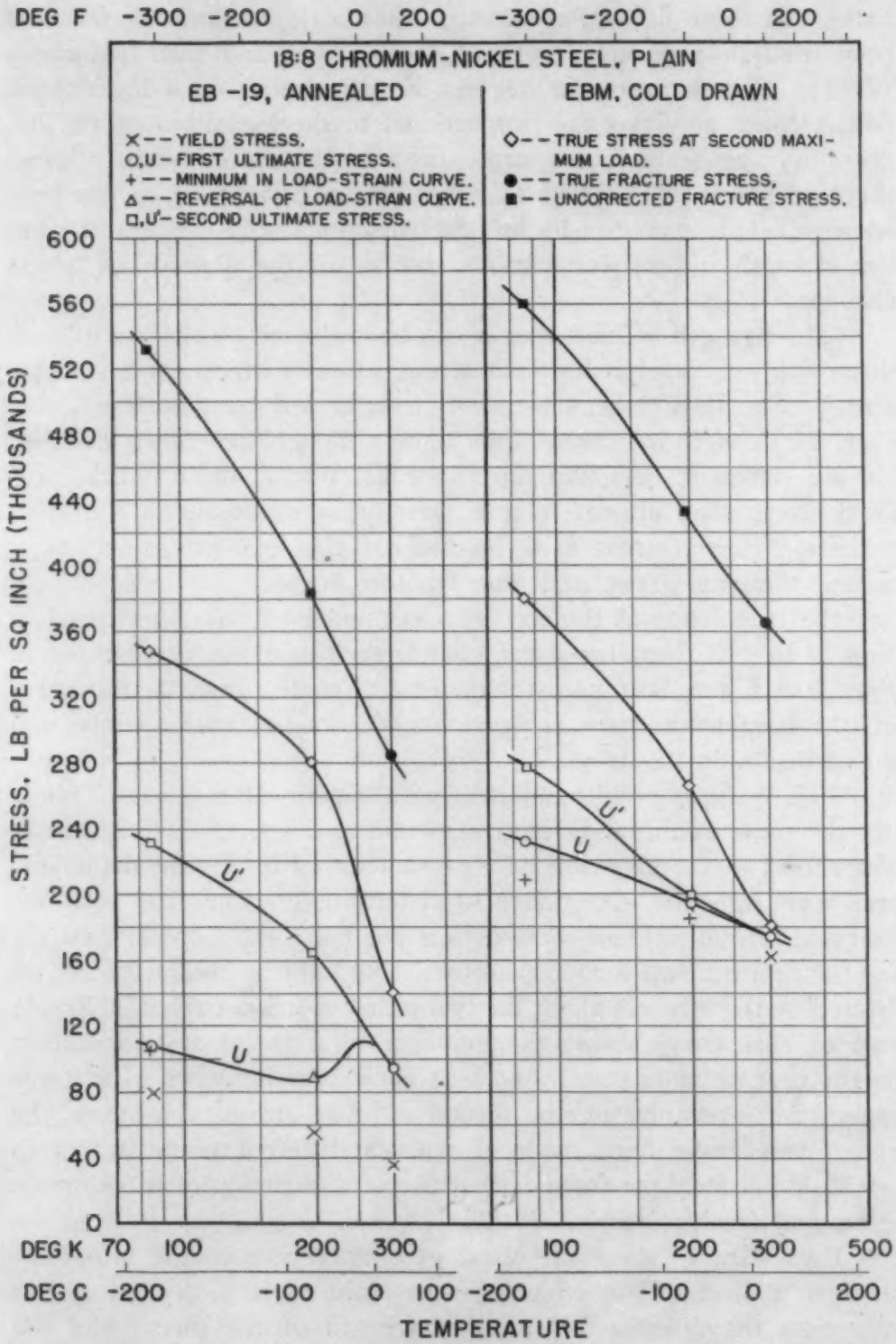


Fig. 10—Variation of the Strength of Plain 18-8 Chromium-Nickel Steels With Temperature.

For the 18-8 alloys, the superimposed indirect effects vary greatly with the temperature, and with the amount of plastic deformation required for determining the strength index. In studying the variation of the strength indices with temperature, therefore, consideration should be given to the relation between the direct and indirect effects of temperature on each index. The smaller the amount of plastic deformation required for determining the index, the less are the superimposed indirect effects, and the more nearly does the variation of the index with temperature represent the direct effect of temperature on the strength of the metal.

Since the yield stress represents the strength of the metal at approximately the beginning of plastic strain, the influence of temperature on this index generally represents approximately the direct influence of temperature on the strength of the metal. The yield stresses of the 18-8 alloys at room temperature were determined by means of transverse measurements during the tension tests. At low temperatures, the yield stresses were determined by means of the automatic load-extension diagrams. Because of the indefiniteness of the yield stress of the metastable austenitic alloys, the values obtained from the automatic diagrams are only approximate.

As shown in Figs. 9, 10, 12, 13, and 14, the increase in the yield stress with decrease in temperature is less rapid than the increase of any other index except the first ultimate stress. As would be expected, however, the greater the amount of *prior* plastic deformation, the less do the indices of resistance to plastic deformation diverge with decrease in temperature. After severe prior plastic deformation, the curves for the first and second ultimate stresses nearly coincide, as shown in the diagram for alloy EBN in Fig. 11.

The yield stress of the ferritic alloy (Fig. 11) rises much more rapidly with decrease in temperature than the yield stress of the metastable austenitic alloys (Figs. 9 to 14); the rise is about as rapid as for a carbon steel. As shown in a previous paper (9), a rapid increase of the yield stress with decrease in temperature is associated with a rapid decrease in ductility.

Next to the yield stress the first ultimate stress is the most suitable index for revealing the direct influence of temperature on the strength of an 18-8 alloy. However, when the curve of nominal stress versus extensions merely reverses without traversing a maximum, the nominal stress at the reversal may be used for the same purpose, and is nearly as satisfactory as the first ultimate stress. In

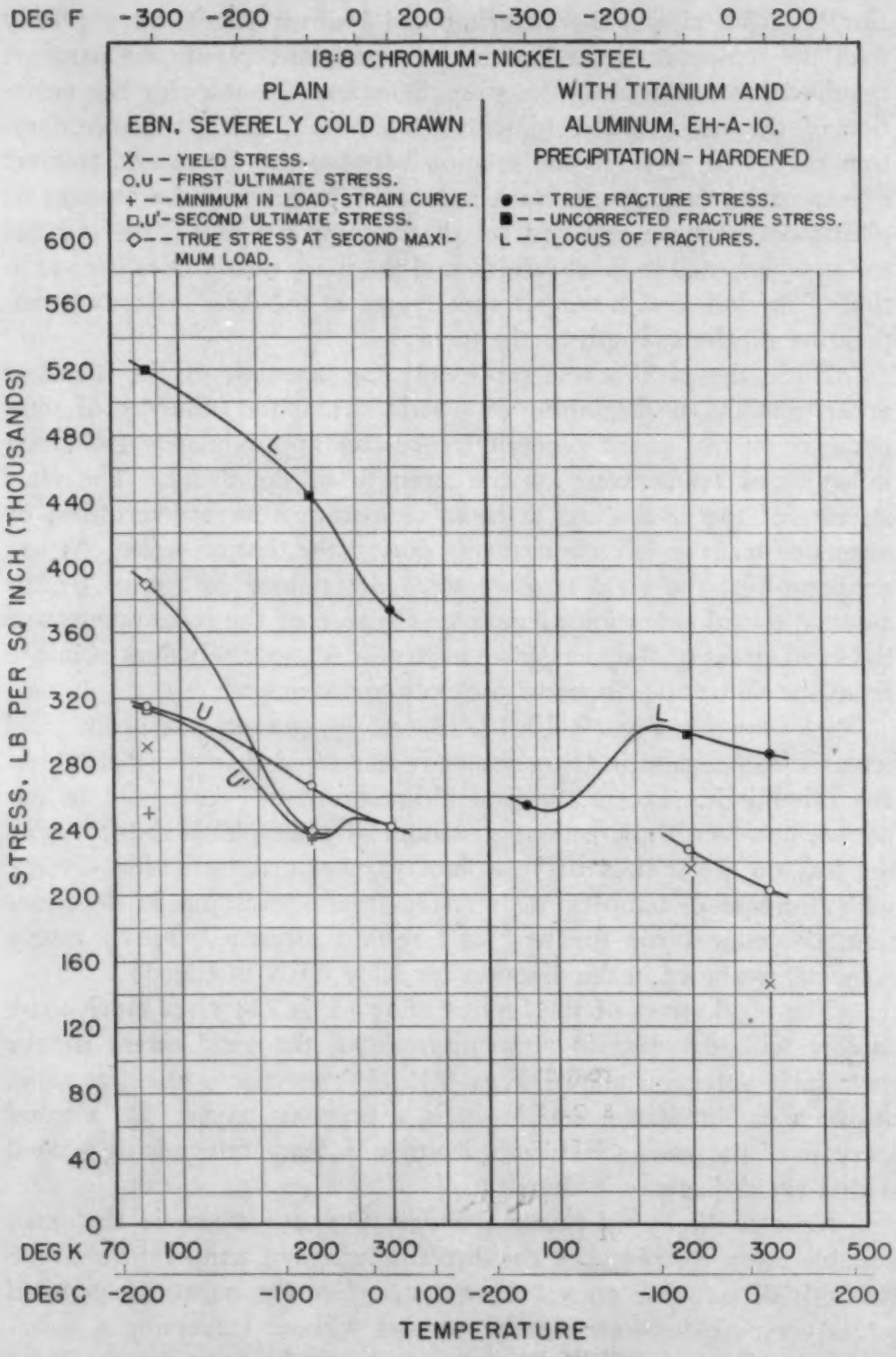


Fig. 11—Variation of the Strength of 18-8 Chromium-Nickel Steels With Temperature.

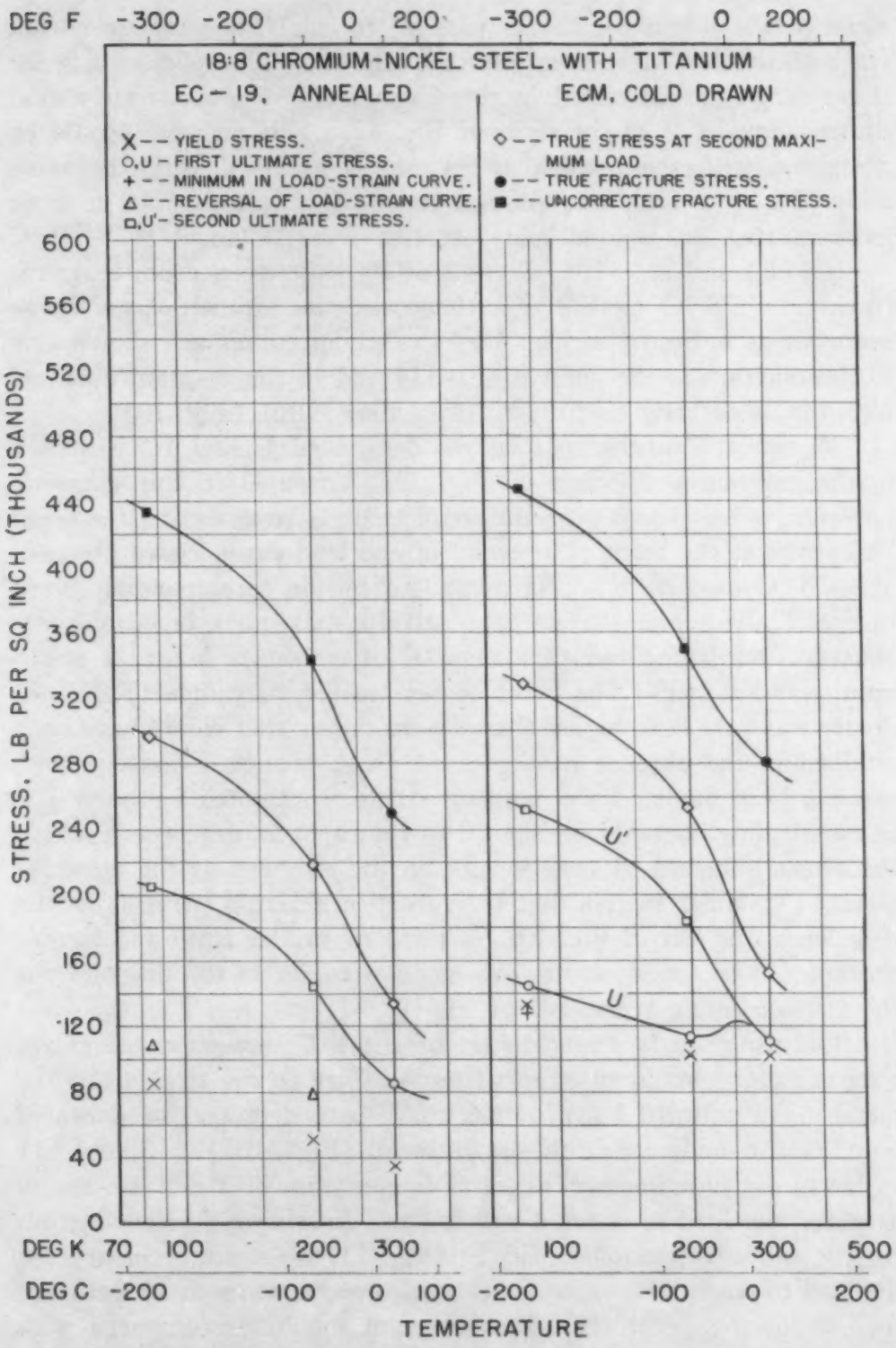


Fig. 12—Variation of the Strength of 18-8 Chromium-Nickel Steels With Temperature.

some of the diagrams, it was possible to establish complete curves for both the first and second ultimate stresses. The relation between these curves is illustrated in the diagram for the moderately cold drawn alloy ECM at the right of Fig. 12. This diagram should be compared with the nominal-stress curves obtained with the same alloy (Fig. 3). Only one ultimate-stress value was obtained at room temperature, but two ultimate stresses were obtained at —78 °C (—108 °F) and at —188 °C (—306 °F). Between room temperature and —78 °C (—108 °F), therefore, the ultimate-stress curve branches as indicated in Fig. 12. Branching curves are shown also in the diagram at the right of Fig. 14 and in the diagram obtained with the moderately cold drawn plain alloy EBM (Fig. 10).

A similar branching of curves designated U and U′ is shown in the diagram at the left of Fig. 10. Curve U in this diagram, however, is based partly on the small triangle representing the nominal stress at the point of reversal of the load-strain curve obtained at —78 °C (—108 °F). As illustrated by the corresponding curve in Fig. 1, the nominal stress approached a maximum, but rapid precipitation hardening caused a reversal of curvature before a maximum was attained. The point of reversal of curvature (RE) evidently was very little higher than the maximum that would have been attained in the absence of the rapid phase change. Consequently, use has been made of the nominal stress represented by point RE in establishing curve U in Fig. 10 to represent as nearly as possible the direct influence of temperature on the strength of the annealed metal. A similar method has been used in deriving curve U in the diagram at the left of Fig. 13. A curve of similar form and significance could be based on the two small triangles in the diagram for the annealed alloy at the left of Fig. 12.

Only the nearly straight part of curve U, however, represents approximately the direct effect of temperature on the strength of the metal. The upward bulge of the curve in a diagram for annealed metal or for moderately cold drawn metal (Figs. 10, 12, 13, and 14) is due to the superimposed effect of temperature on the strain necessary for the load to reach a maximum. As shown in the diagram for the annealed plain alloy EB-19 (Fig. 1), the strain necessary for the load to reach a maximum was much greater at room temperature than at low temperatures. This diagram should be compared with curve U in the diagram at the left of Fig. 10. A similar relationship is revealed by a comparison of the diagram at the right of Fig. 3

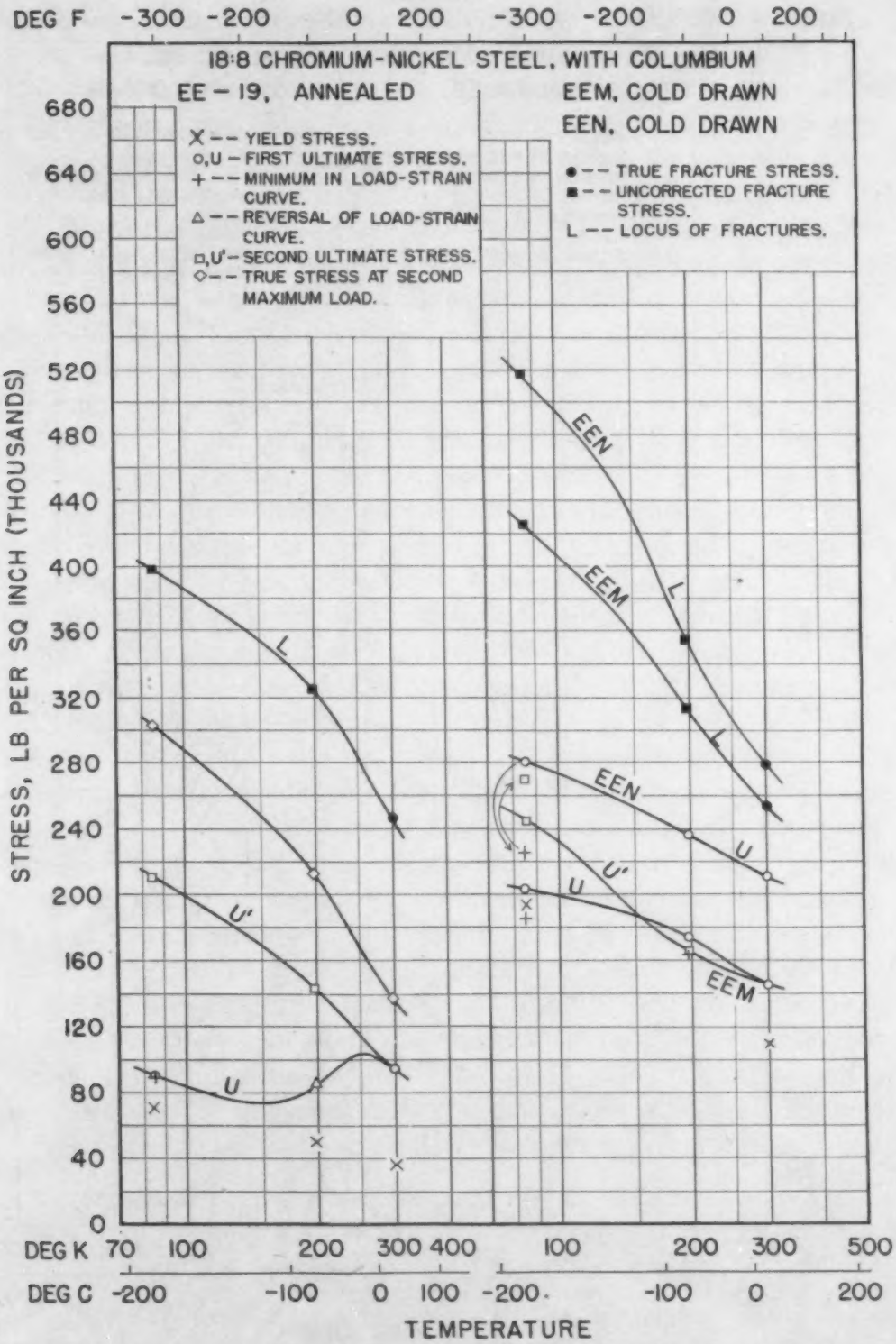


Fig. 13—Variation of the Strength of 18-8 Chromium-Nickel Steels With Temperature.

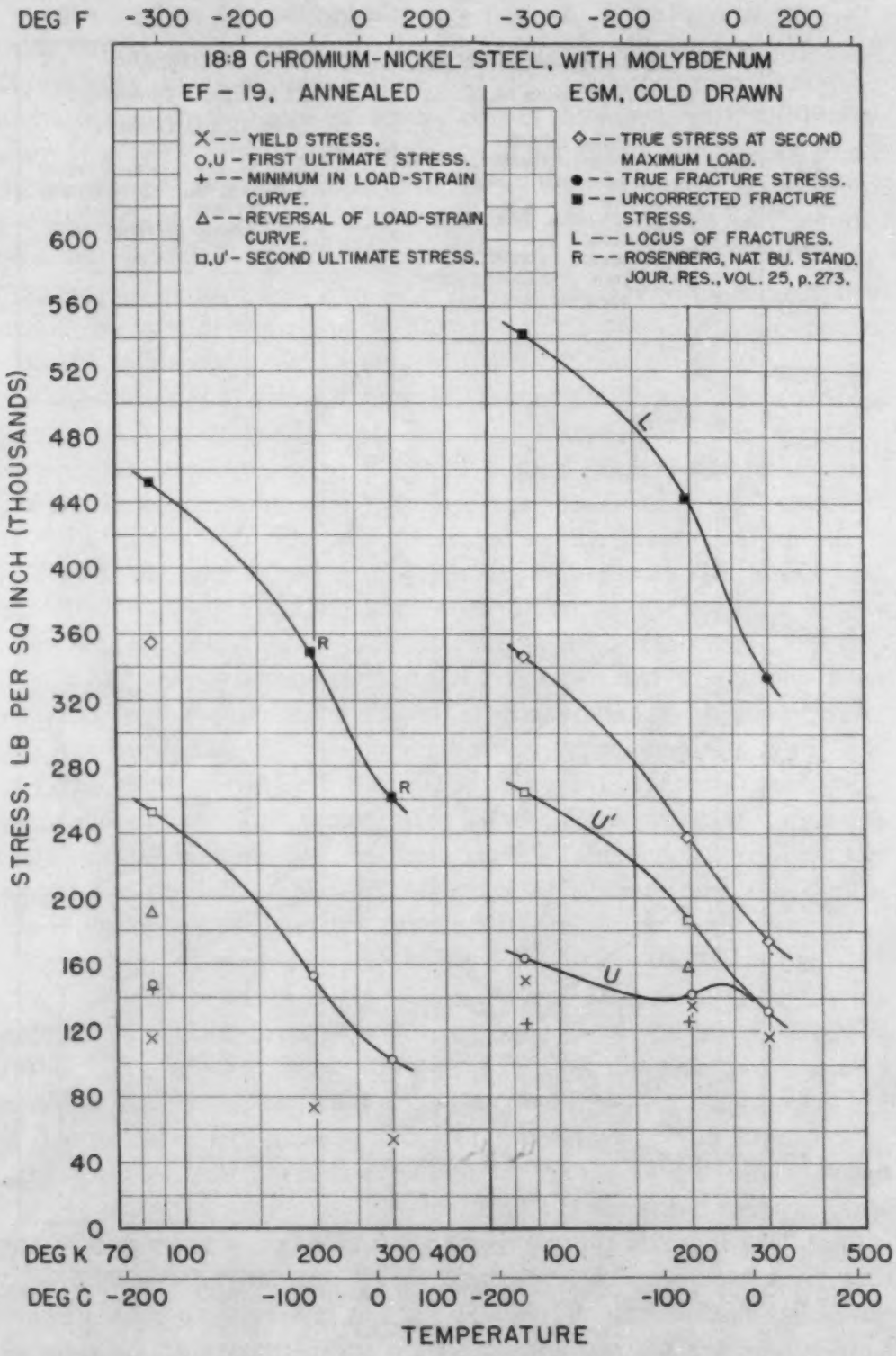


Fig. 14—Variation of the Strength of 18-8 Chromium-Nickel Steels With Temperature.

with curve U in the diagram at the right of Fig. 12, and by a comparison of the diagram at the left of Fig. 7 with curve U in the diagram at the right of Fig. 14. The upward bulge in curve U in diagrams for annealed alloys or for moderately cold drawn alloys, therefore, is due to hardening of the metal during the relatively great plastic deformation necessary for the load to reach a maximum.

When the prior cold work has been severe, the strain necessary for the load to reach a maximum is about as small at room temperature as at low temperatures. Illustrations of this relationship are shown in Fig. 2 and in the diagram at the left of Fig. 3.[4] Since the plastic strain at the first maximum load was small at room temperature and at low temperatures, the corresponding curves U in Figs. 10, 11 and 13 are practically free from effects of variable plastic deformation. Unlike the curves obtained with the less severely cold-worked alloys or with the annealed alloys, these curves rise continuously with decrease in temperature. If yield-stress curves were drawn in these figures, their slopes would differ little from the slopes of curves U and from the slopes of the nearly straight parts of curves U obtained with the softer alloys. These slopes represent approximately the direct effect of temperature on the strength of the 18-8 chromium-nickel steels.

All the curves of the variation of the second ultimate stress with temperature are affected by the phase changes induced by plastic deformation. In the absence of the rapid phase changes at low temperatures there would be no second ultimate stress. The divergence of curves U and U′ is greatest for the annealed metals, and decreases with increase in the amount of prior cold work. The influence of the rapid phase change at low temperatures is revealed most prominently by the steep rise of the curves representing the influence of temperature on the true stress at the second maximum and on the fracture stress. The course of each of these curves, however, indicates that with decrease in temperature below that of liquid air the influence of temperature on these strength indices gradually decreases.

The Variation of the Strength of 18-8 Chromium-Nickel Steel and of Some Other Metals Between Room Temperature and the Temperature of Liquid Hydrogen (—252.8 °C)

The only extensive investigation of the mechanical properties of metals at the temperature of liquid hydrogen was by DeHaas and

[4]Comparison of ultimate stresses shows that the prior cold work was more severe for these three alloys and for alloy EEN (Fig. 13) than for any of the other alloys used in the investigation.

Hadfield (5). Steels of many different compositions and a few nonferrous metals were included in their investigation. Only two chromium-nickel stainless steels were used. One was an 18-8 chromium-nickel steel; the other was a stable austenitic steel containing 14.4% chromium and 59.3% nickel. Yield stresses, ultimate stresses, and ductility values were determined at room temperature and at the temperature of liquid hydrogen, but fracture stresses were not determined.

In Fig. 15, results obtained by DeHaas and Hadfield at room temperature and at —252.8 °C (—423 °F) are compared with results obtained at the National Bureau of Standards within the range between room temperature and —188 °C (—306 °F). The diagram shows results obtained by DeHaas and Hadfield with monel metal, electrolytic copper, the 18-8 alloy, and the stable austenitic chromium-nickel steel. For comparison, curves obtained with monel metal and oxygen-free copper have been reproduced from a paper by McAdam and Mebs (7), and two curves obtained with the annealed plain 18-8 alloy EA-19 have been reproduced from Fig. 9. With the exception of the fracture stresses derived from Fig. 9, only ultimate stresses are represented in Fig. 15.

With the 18-8 chromium-nickel steel and the stable austenitic steel, DeHaas and Hadfield obtained almost identical results at room temperature. At —252.8 °C (—423 °F), however, the ultimate stress of the 18-8 alloy was about 50% greater than that of the stable austenitic alloy. The strength index reported for the 18-8 alloy at this temperature undoubtedly is the second ultimate stress. The ultimate-stress curve obtained with the 18-8 alloy EA-19 has been prolonged with little change of curvature, so as to pass through the point representing the result obtained by DeHaas and Hadfield with an alloy of the same type. Moreover, the fracture-stress curve obtained with alloy EA-19 has been prolonged with little change of curvature, so that an approximate estimate may be made of the probable breaking stress of this alloy at the temperature of liquid hydrogen. The value thus obtained is of the same order as the breaking stresses of some of the 18-8 alloys in liquid air (Figs. 10, 11, 13 and 14).

As shown in previous papers (7, 9, 10), and as illustrated in Fig. 15 by the curves for monel metal G-14 and copper N-8, the variation of the strength indices for many nonferrous metals on this temperature scale is nearly linear between room temperature and

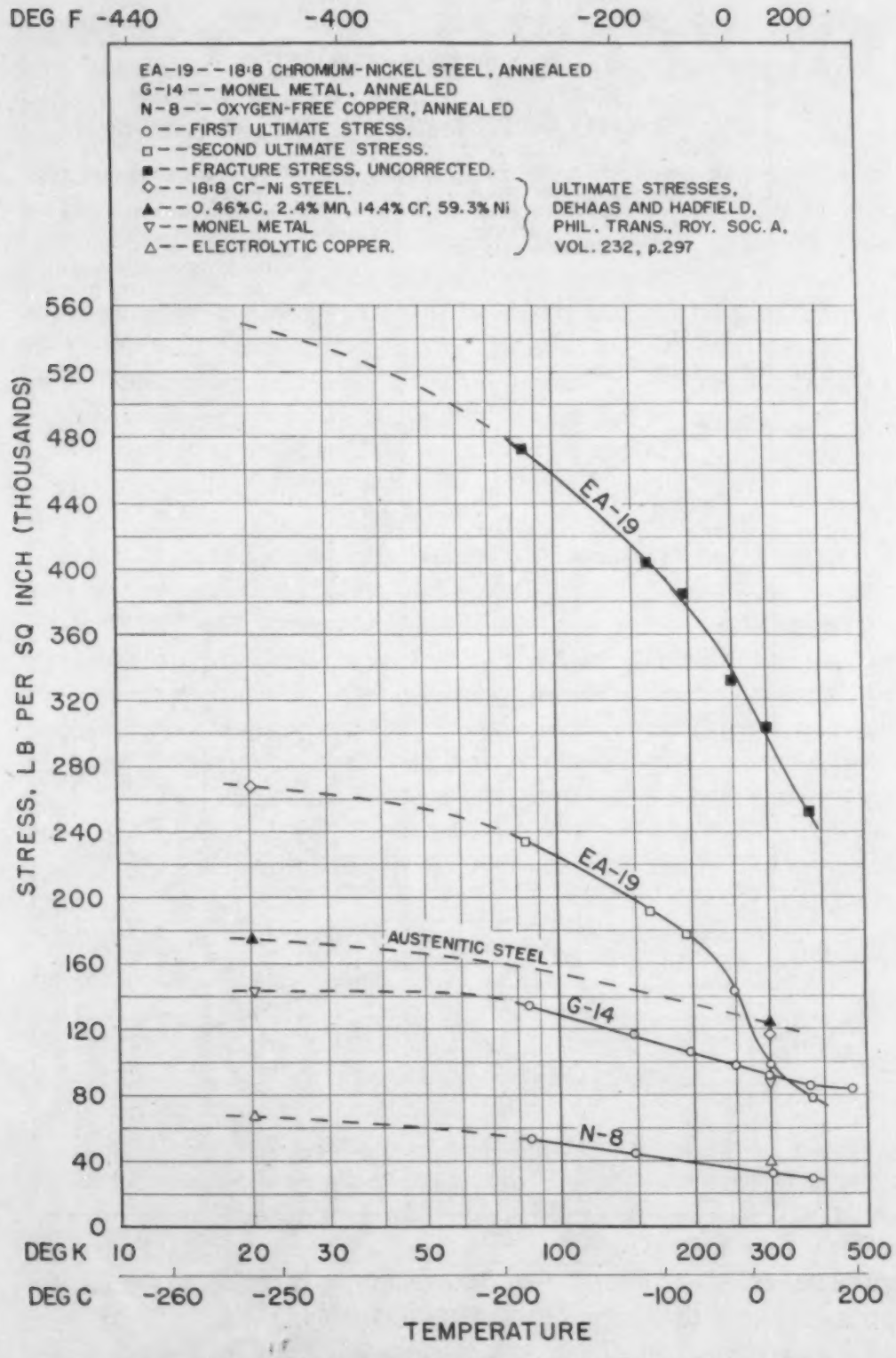


Fig. 15—Variation of the Strength of Various Metals With Temperature.

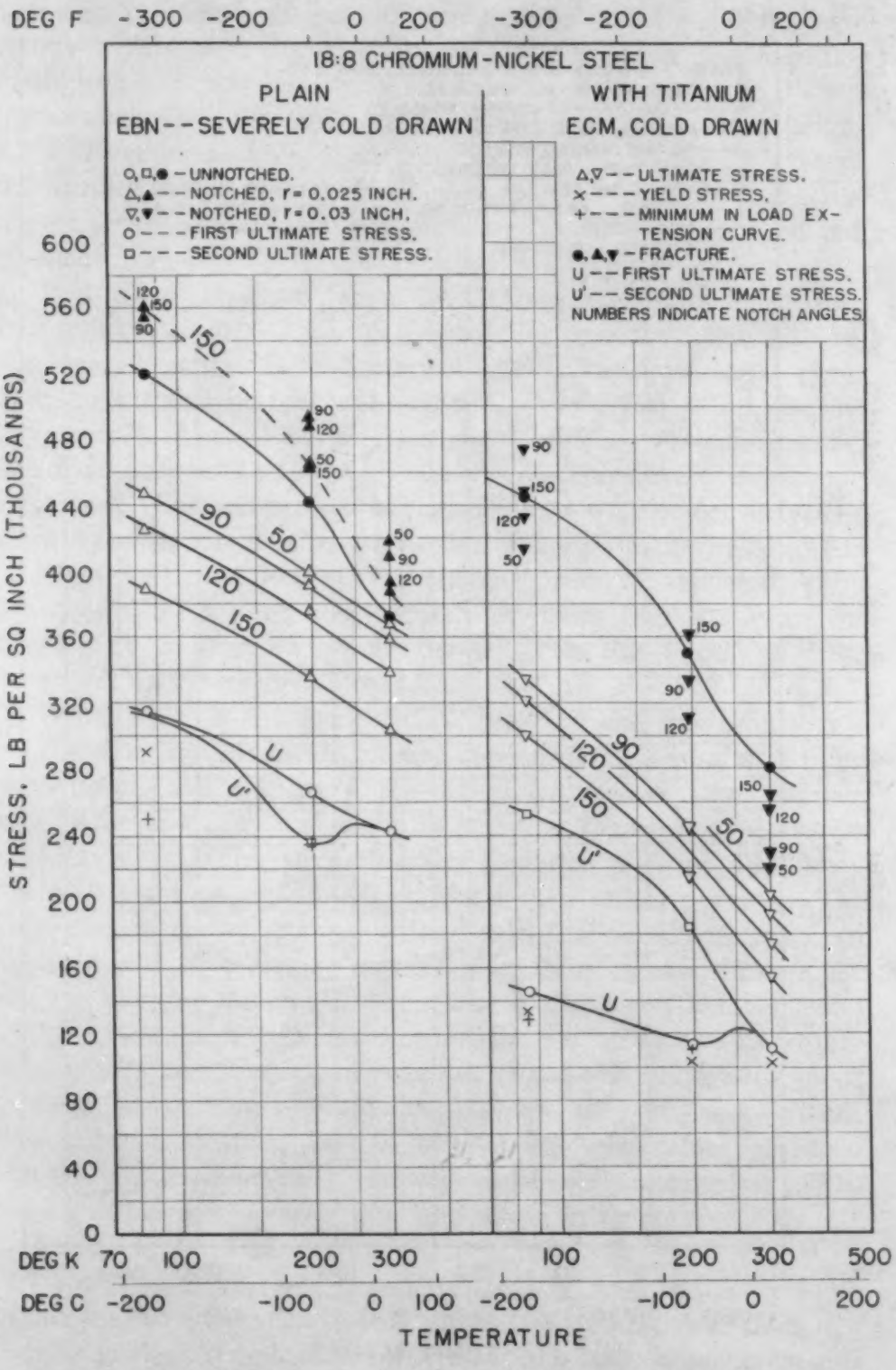


Fig. 16—Combined Influences of Notches and Low Temperatures on the Tensile Properties of 18-8 Chromium-Nickel Steel.

—188 °C (—306 °F). The results reported by DeHaas and Hadfield, however, indicate that the linear relationship does not continue between the temperatures of liquid air and liquid hydrogen. Although some of the reported ultimate stresses at the temperature of liquid hydrogen may be too low, the evidence indicates that the curves for the nonferrous metals and the stable austenitic alloy differ greatly in slope from the curve obtained with the 18-8 alloy. The evidence also indicates that the great difference in strength of these chromium-nickel alloys at the temperature of liquid air is due to a difference in the stability of the austenite. The austenite in the alloy containing 14.4% chromium and 59.3% nickel evidently retains its stability during plastic deformation at the temperature of liquid hydrogen.

If curves to represent the variation of the first ultimate stress of the metastable austenitic alloys with temperature were included in Fig. 15, the slope between room temperature and —188° C (—306 °F) would differ little from the slopes of the curves obtained with monel metal and copper, and from the probable slope of a curve obtained with the stable austenitic steel. The slopes of these curves represent approximately the direct effect of temperature on the strength of the metals. The difference between these slopes and the slope of the curves for the 18-8 alloy is due to the superimposed effect of the variation in the amount of phase-change with temperature. This variation becomes less with decrease in temperature, since the proportion of untransformed austenite remaining after deformation of the specimen in the tensile test becomes less as the temperature is lowered. As the temperature approaches that of liquid air, possibly all or nearly all of the austenite is transformed to ferrite by the plastic deformation.

Influence of Notches on the Mechanical Properties of 18-8 Chromium-Nickel Steel

Fig. 16 shows the results of a brief investigation of the influence of notches on the strength indices of 18-8 alloys throughout a range between room temperature and —188 °C (—306 °F). The alloys used in obtaining these two diagrams are the same that were used in obtaining the diagram at the left of Fig. 11 and the diagram at the right of Fig. 12. The curves representing results obtained with unnotched specimens are the same in Fig. 16 as in the corresponding diagrams of Figs. 11 and 12. A slight distinction between the first

and second ultimate stresses could be observed in some specimens with 150-degree notch angle, but no distinction could be made when the angle was smaller.

Even when the angle was 50 degrees, however, the plastic strain necessary for the load to reach a maximum at low temperatures was more than that for an unnotched specimen at the first maximum. Although the ductility decreased with decrease in the notch angle and with decrease in temperature, the combined influence of these two variables on the ductility was less for the 18-8 alloys than for pearlitic steels. At −188 °C (−306 °F), the strain at fracture of a 50-degree specimen was about 26% ($A_o/A = 1.26$). Moreover, the breaking stress of this specimen at −188 °C (−306 °F) was high, although the specimen fractured before the tensile load reached a maximum. These unusual properties suggest that the ultimate stresses of the notched specimens were appreciably increased by the phase change during plastic deformation. This phase change evidently contributes to the toughness of both notched and unnotched specimens.

Acknowledgment

Acknowledgment is due to Messrs. D. H. Woodard and W. D. Jenkins, to Mrs. Fannie Wilkinson and Miss Lavaria Weinrich for general assistance in the experiments and the preparation of the illustrations.

References

1. R. H. Aborn and E. C. Bain, "Nature of the Nickel-Chromium Rustless Steels," Transactions, American Society for Steel Treating, Vol. 18, 1930, p. 837-873.
2. J. B. Austin and O. S. Miller, "Magnetic Permeability of Some Austenitic Iron-Chromium-Nickel Alloys as Influenced by Heat Treatment and Cold Work," Transactions, American Society for Metals, Vol. 28, 1940, p. 743-755.
3. F. K. Bloom, G. N. Goller and P. G. Mabus, "The Cold Work Hardening Properties of Stainless Steel in Compression," Transactions, American Society for Metals, Vol. 39, 1947, p. 843-864.
4. E. W. Colbeck, W. E. MacGillivray and W. R. D. Manning, "The Mechanical Properties of Some Austenitic Stainless Steels at Low Temperatures," *Transactions,* Institute of Chemical Engineers, Vol. 11, 1933, p. 89-102.
5. W. J. DeHaas and Sir Robert Hadfield, "The Effect of the Temperature of Liquid Hydrogen on the Tensile Properties of Forty-One Specimens of Metals," *Philosophical Transactions,* Royal Society, A, Vol. 232, 1933-34, p. 297-332.
6. V. N. Krivobok and R. A. Lincoln, "Austenitic Stainless Alloys," Transactions, American Society for Metals, Vol. 25, 1937, p. 637-677.

7. D. J. McAdam, Jr. and R. W. Mebs, "The Technical Cohesive Strength and Other Mechanical Properties of Metals at Low Temperatures," *Proceedings,* American Society for Testing Materials, Vol. 43, 1944, p. 661-703.
8. D. J. McAdam, Jr., R. W. Mebs and G. W. Geil, "The Technical Cohesive Strength of Some Steels and Light Alloys at Low Temperatures," *Proceedings,* American Society for Testing Materials, Vol. 44, 1944, p. 593-644.
9. D. J. McAdam, Jr., G. W. Geil and R. W. Mebs, "The Effect of Combined Stresses on the Mechanical Properties of Steels Between Room Temperature and —188 °C," *Proceedings,* American Society for Testing Materials, Vol. 45, 1945, p. 448-485.
10. D. J. McAdam, Jr., G. W. Geil and R. W. Mebs, "Effects of Combined Stresses and Low Temperatures on the Mechanical Properties of Some Nonferrous Metals," TRANSACTIONS, American Society for Metals, Vol. 37, 1946, p. 497-537.
11. D. J. McAdam, Jr., G. W. Geil and R. W. Mebs, "Influence of Plastic Deformation, Combined Stresses, and Low Temperatures on the Breaking Stress of Ferritic Steels," American Institute of Mining and Metallurgical Engineers, T.P. 2220, *Metals Technology,* August 1947.
12. D. J. McAdam, Jr., G. W. Geil and W. D. Jenkins, "Influence of Plastic Extension and Compression of the Fracture Stress of Metals," *Proceedings,* American Society for Testing Materials, Vol. 47, 1947, p. 554-572.
13. D. J. McAdam, Jr., G. W. Geil and Frances Jane Cromwell, "Flow, Fracture and Ductility of Metals," American Institute of Mining and Metallurgical Engineers, T.P. 2296, *Metals Technology,* January 1948.
14. N. B. Pilling, "Some Effects of Nickel Content on Austenitic Iron-Chromium-Nickel Alloys," *Proceedings,* American Society for Testing Materials, Vol. 30, Pt. 2, 1930, p. 278-290.
15. L. B. Pfeil and D. G. Jones, "A Contribution to the Study of the Properties of Austenitic Steels," *Journal,* Iron and Steel Institute, Vol. 127, No. 1, 1933, p. 337-378.
16. C. B. Post and W. S. Eberly, "Stability of Austenite in Stainless Steels," TRANSACTIONS, American Society for Metals, Vol. 39, 1947, p. 868-888.
17. S. J. Rosenberg, "Effect of Low Temperatures on the Properties of Aircraft Metals," National Bureau of Standards, *Journal of Research,* Vol. 25, 1940, p. 673-701.
18. R. Smith, E. H. Wycke and W. W. Gorr, "A Precipitation-Hardening Stainless Steel of the 18 Per Cent Chromium, 8 Per Cent Nickel Type," American Institute of Mining and Metallurgical Engineers, T.P. 2006, *Metals Technology,* June 1946; *Transactions,* American Institute of Mining and Metallurgical Engineers, Vol. 167, 1946, p. 313-343.
19. THE BOOK OF STAINLESS STEELS, published by American Society for Metals, Cleveland, 1935.
20. H. H. Uhlig, "The Role of Nitrogen in 18-8 Stainless Steel," TRANSACTIONS, American Society for Metals, Vol. 30, 1942, p. 947-980.

DISCUSSION

Written Discussion: By M. G. Fontana, professor and chairman, Department of Metallurgy, The Ohio State University, Columbus, Ohio.

True stress curves are described by Dr. McAdam. Were the instantaneous diameters of the necked portions of the specimens measured during the tensile tests at low temperatures? If so, I would like to

have a description of the apparatus used for measuring these diameters. I am sure other investigators in the field of mechanical testing at low temperatures would like to have information on this point since it is a difficult measurement to make at low temperatures. A description of the apparatus in the discussion would add a lot to this good paper.

Authors' Reply

As stated in the paper, instantaneous diameters were measured during the tests at room temperature, but not at low temperatures. At that time, no apparatus had been developed at the National Bureau of Standards for similar measurements at low temperatures. As stated in the paper, the flow-stress curves for low temperature tests were constructed on the assumption that the specimen remained cylindrical until the final local contraction began. Mr. Geil informs me that an apparatus has now been developed for making diameter measurements at low temperatures.

Flow-stress curves obtained with this apparatus agree well with those constructed on the above-mentioned assumption. They show also that there is an actual drop in the true stress in cold drawn 18-8 alloy after the curve attains the first maximum. The results thus confirm the course of curves such as those in Fig. 5 of the paper. Consequently the suggestion on page 623 that the true stress probably does not drop beyond the first maximum must be abandoned. Sometimes there are repeated slight rises and descents of the flow stress as the curve approaches the second maximum.

BASIC REASONS FOR GOOD MACHINABILITY OF "FREE MACHINING" STEELS

By M. Eugene Merchant and Norman Zlatin

Abstract

The following treatments are known to improve the machinability of steels:

1. *Addition of sulphur*
2. *Addition of lead*
3. *Addition of sodium sulphite*
4. *Cold working*

A study has been made of the basic reasons for the improved machinability—reasons related to the mechanics of cutting. The effect of these four treatments on the three basic properties affecting the mechanics of cutting —(a) coefficient of friction between chip and tool, (b) mean shear strength of the metal in cutting, and (c) machining constant of the metal—has been evaluated. The effect of other less basic mechanical properties has also been considered. The reasons for the improved machinability have become apparent in each case as a result of this study.

Introduction

IT is well known that certain chemical and physical modifications of steels will impart improved machinability. The best known of these are:

1. Addition of sulphur
2. Addition of lead
3. Addition of sodium sulphite
4. Cold working

Steels so modified may be termed "free machining" in the very broadest sense of the term. (It is recognized, of course, that cold-worked steels are not considered to be free machining steels in the usual sense of the term.) In most cases there has been no clear

A paper presented before the Thirtieth Annual Convention of the Society, held in Philadelphia, October 23 to 29, 1948. Of the authors, M. E. Merchant is senior research physicist, and N. Zlatin is research engineer, Research Dept., The Cincinnati Milling Machine Co., Cincinnati. Manuscript received April 30, 1948.

Table I
Composition and Mechanical Properties of Steels Used in Tests

Material	Condition	Chemical Analysis										Brinell Hardness Number	Meyer Strain Hardenability Exponent
		C	Mn	P	S	Si	Cr	Ni	Pb	Cu	Mo	H	"n"
Stainless													
Type 303 (Sulphur)	Annealed	0.078	0.80	0.040	0.281	0.56	18.11	9.06	....	0.18	....	162	2.37
Type 304	Annealed	0.067	1.35	0.027	0.009	0.36	17.65	10.25	....	0.12	....	139	2.39
C-1022													
Leaded	Hot-Rolled	0.23	0.74	0.011	0.036	....	....	....	0.13	....	....	121	2.29
B-1113													
Sulphur	Cold Drawn	0.11	0.86	0.053	0.324	....	....	....	....	....	....	170	2.24
C-1019													
Plain	Hot-Rolled	0.20	0.97	0.013	0.035	....	....	....	....	....	....	147	2.20
A-8640													
Sulphite-Treated	Annealed and Cold-Finished	0.40	0.96	0.015	0.046	0.28	0.57	0.50	....	....	0.21	187	2.30
A-8640													
Plain	Annealed and Cold-Finished	0.41	0.86	0.013	0.015	0.26	0.47	0.50	....	....	0.28	191	2.30
SAE 52100	Cold Drawn	1.01	0.31	0.010	0.004	0.23	1.40	....	....	....	....	235	2.12
SAE 52100	Cold Drawn and Annealed	1.01	0.35	0.023	0.004	0.21	1.42	....	....	....	....	190	2.33

understanding of the reasons for the improved machinability imparted by such treatments as the above. Various mechanisms have been suggested but few have been proven by direct theory and experiment. It has been the purpose of the investigation described in this paper to study the basic reasons for the good machinability of free machining steels. Such information is needed if the knowledge of how to impart free machining properties is to advance. When we know the causes behind any action, we have a sound basis for improving that action.

First, a matter of definition. What is meant by the fact that free machining steels have good machinability? Actually this term may cover a multitude of performance characteristics; however, there are three main characteristics of which one or more are noticeably improved by free machining modifications. These are:

1. Tool life obtainable under given machining conditions (or alternatively, the cutting speed required to give a constant tool life).
2. Surface finish.
3. Tool forces and power consumption.

Steels Selected for Test

Five pairs of steels, each consisting of one normal and one free machining material, were selected for test. The pairs selected were:

1. Type 303 (sulphur) stainless and Type 304 stainless
2. AISI C-1022 leaded and AISI C-1019 (plain)
3. AISI B-1113 (sulphur) and AISI C-1019 (plain)
4. AISI A-8640 (sodium sulphite added) and AISI A-8640 (plain)
5. SAE 52100 cold drawn tubing and SAE 52100 cold drawn and annealed tubing.

(Note that one steel, the C-1019, is common to two of the pairs.) The chemical analyses and mechanical properties of these steels are listed in Table I. The microstructures in the unetched and etched states are shown in Figs. 1 to 5. The relative machinability, in practice, of the two members of each of the five pairs of steels may be judged from the data given in Table II. Tool life values given there are in some cases expressed in terms of the cutting speed required to give a constant tool life (known as "equivalent cutting speed") and in other cases as the elapsed cutting time between tool

Table II
Machinability Characteristics of Steels Used in Tests

Material	Relative Tool Life or Equivalent Cutting Speed	Relative Surface Finish Microinches rms.¶	Relative Cutting Force F_c, lb.§	Relative Thrust Force F_t, lb.§	Relative Power Consumption H.P. min./cu.in.§
Stainless					
Type 303 (Sulphur)	100–130 ft/min.*	20–30	167	98	0.94
Type 304	70– 90 ft/min.*	6–9	222	177	1.25
C-1022					
Leaded	160–190 ft/min.†	30–40	101	24	0.57
B-1113					
Sulphur	210–235 ft/min.†	25–35	106	37	0.60
C-1019					
Plain	120–140 ft/min.†	60–70	167	115	0.94
A-8640					
Sulphite-Treated	5 hr. per grind at 111 ft/min.**	65–85	199	148	1.12
Plain	2½ hr. per grind at 88 ft/min.**	65–85	206	157	1.16
SAE 52100					
Cold Drawn	90– 95 ft/min.‡	6–7	197	129	1.11
Annealed	85– 90 ft/min.‡	6–7	210	149	1.18

*From "Machining of Stainless Steels," Rustless Iron and Steel Division of American Rolling Mill Co.

**From "Metallurgical Aspects of Machinability," by F. J. Robbins, *Iron Age*, Vol. 157, No. 13, March 28, 1946, p. 47-51.

†From "A Discussion of Leaded Steels," by F. J. Robbins and G. R. Caskey, TRANSACTIONS of the American Society for Metals, Vol. 27, 1939, p. 887-915.

‡From recommendations made by producer of steel.

¶From cutting tests on actual material using a high speed steel tool, cutting speed = 95–110 ft/min., feed = 0.003 in./rev.

§From cutting tests on actual material using a sintered carbide tool. Same test conditions as for data in Table IV.

grinds. The tool life values are not comparable between the various pairs but only within each pair. However, the values given for surface finish, tool forces and power consumption are comparable between pairs as well as within them. (For the meaning of the terms "Cutting Force, F_c" and "Thrust Force, F_t" used in Table II, see Fig. 8.)

In the present study, each of the above steels was tested to determine the values of those basic properties which are known to influence its machinability.

Basic Properties That Influence Machinability

The authors do not wish to give the impression that all the basic properties which influence or control machinability are known or understood. This is probably far from true. However, certain basic properties are known which have considerable influence on machinability. Most of these can be expressed quantitatively. For

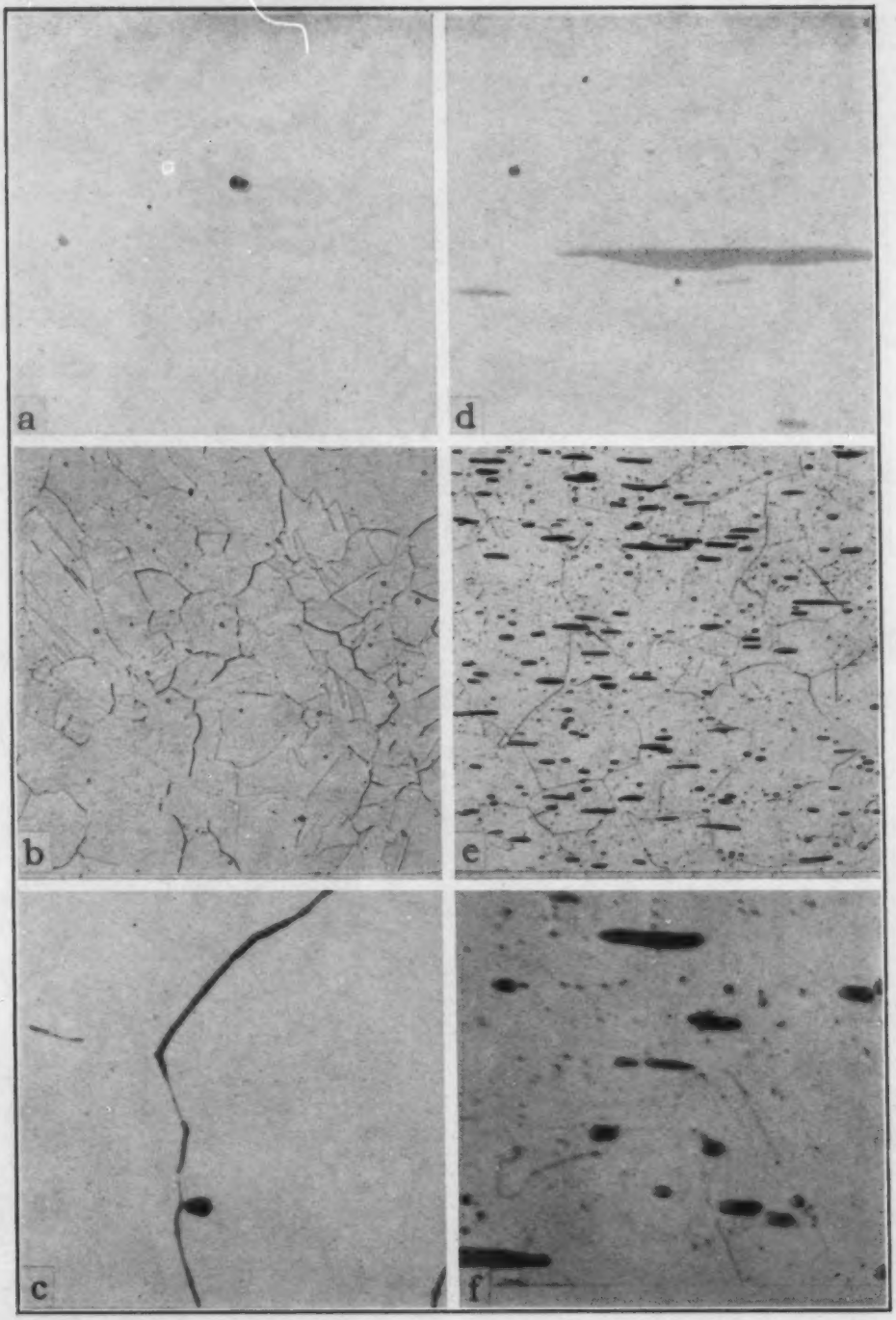


Fig. 1—Microstructures of Steels Used in Tests. a, b, c—Type 304 stainless. d, e, f—Type 303 (sulphur) stainless. a, d—Unetched, × 500. b, e—Etched, × 100. c, f—Etched, × 500.

purposes of discussion these properties can be divided roughly into two classes: 1. Properties that control the geometry and mechanics of chip formation. 2. Other mechanical properties.

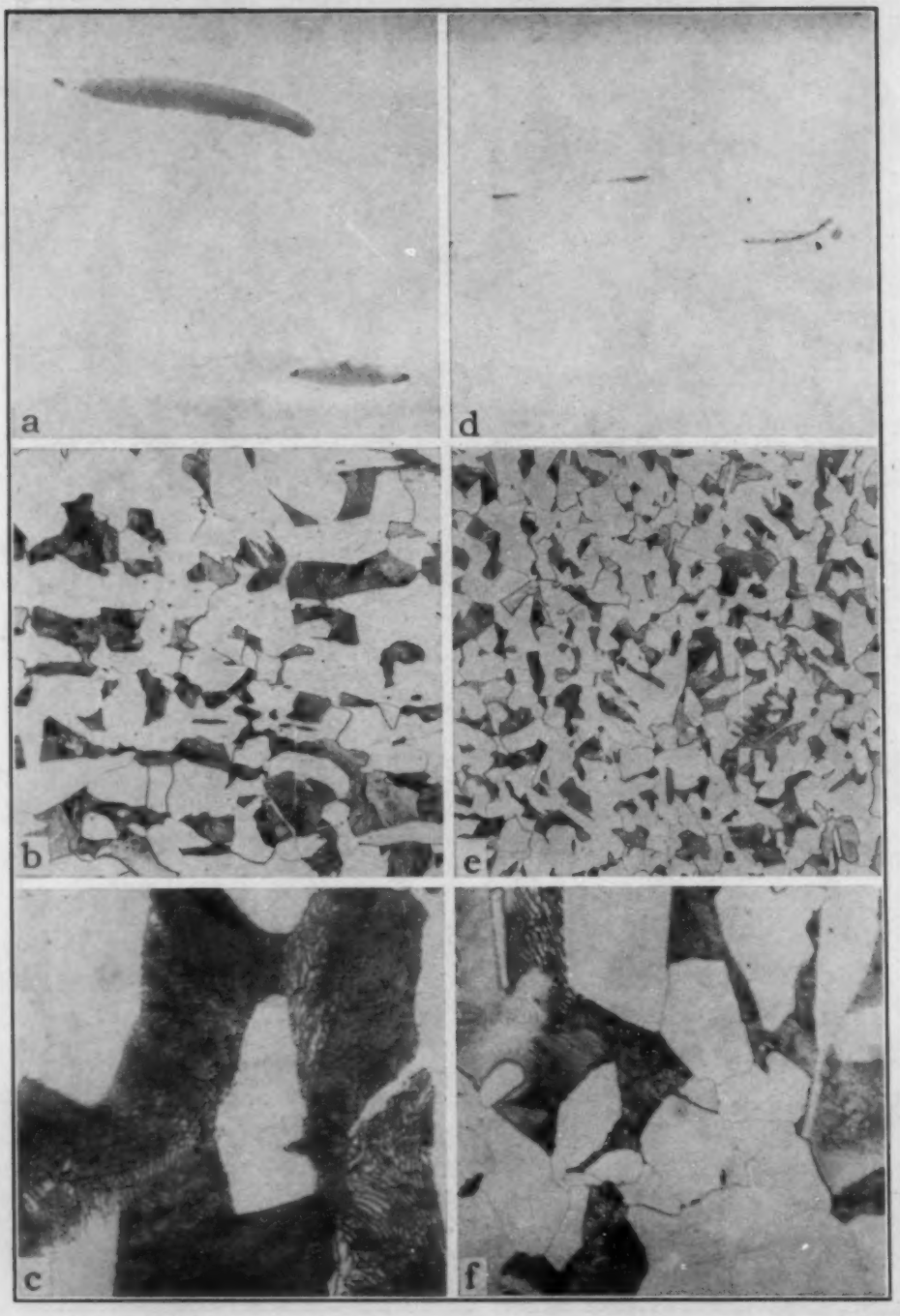


Fig. 2—Microstructures of Steels Used in Tests. a, b, c—AISI C-1022 H.R. (leaded). d, e, f—AISI C-1019 H.R. a, d—Unetched, × 500. b, e—Etched, × 100. c, f—Etched, × 500.

Properties That Control Chip Formation

Recent research (1), (2), (3)[1] has demonstrated that three

[1]The figures appearing in parentheses pertain to the references appended to this paper.

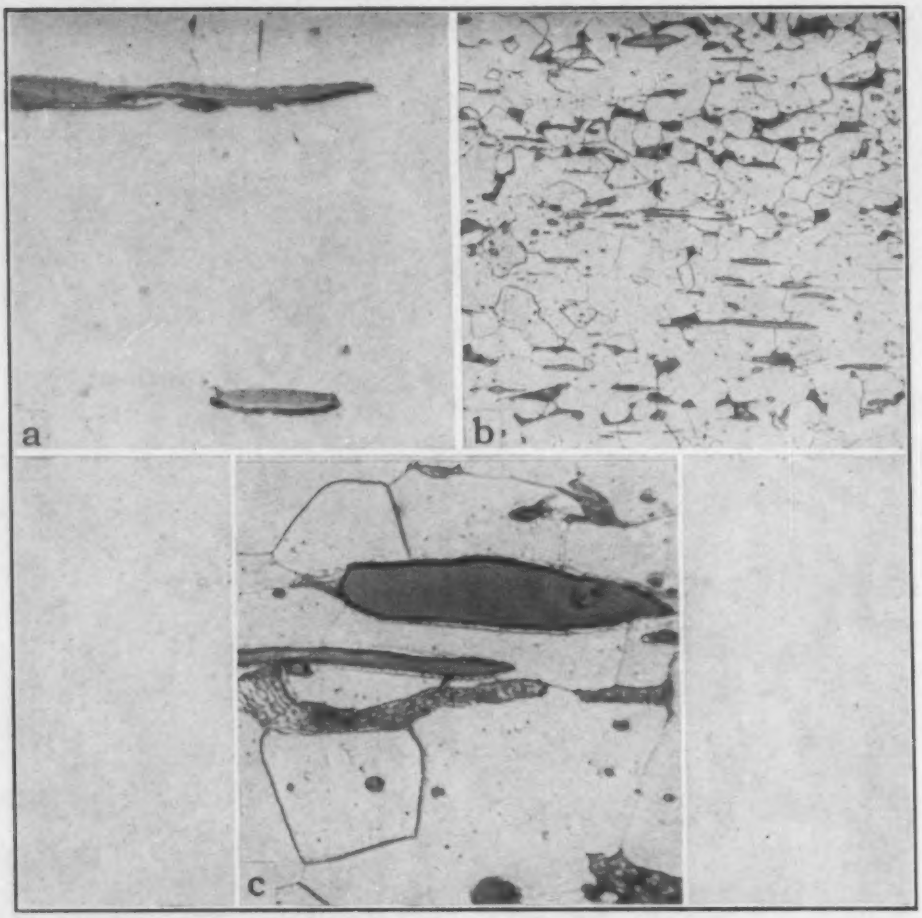


Fig. 3—Microstructures of Steels Used in Tests. AISI B-1113 C.R. a—Unetched, × 500. b—Etched, × 100. c—Etched, × 500.

basic properties are the main variables controlling the geometry and mechanics of chip formation. These are:

1. The coefficient of friction μ acting between chip and cutting tool.
2. The resistance of the material to plastic deformation during cutting as measured by its mean shear strength S_s.
3. An angle C that, in theory, is related to the rate of change of the shear strength of the material with applied compressive stress. This angle is known as the "machining constant" and is essentially a property of the work material alone. (See Fig. 6.)

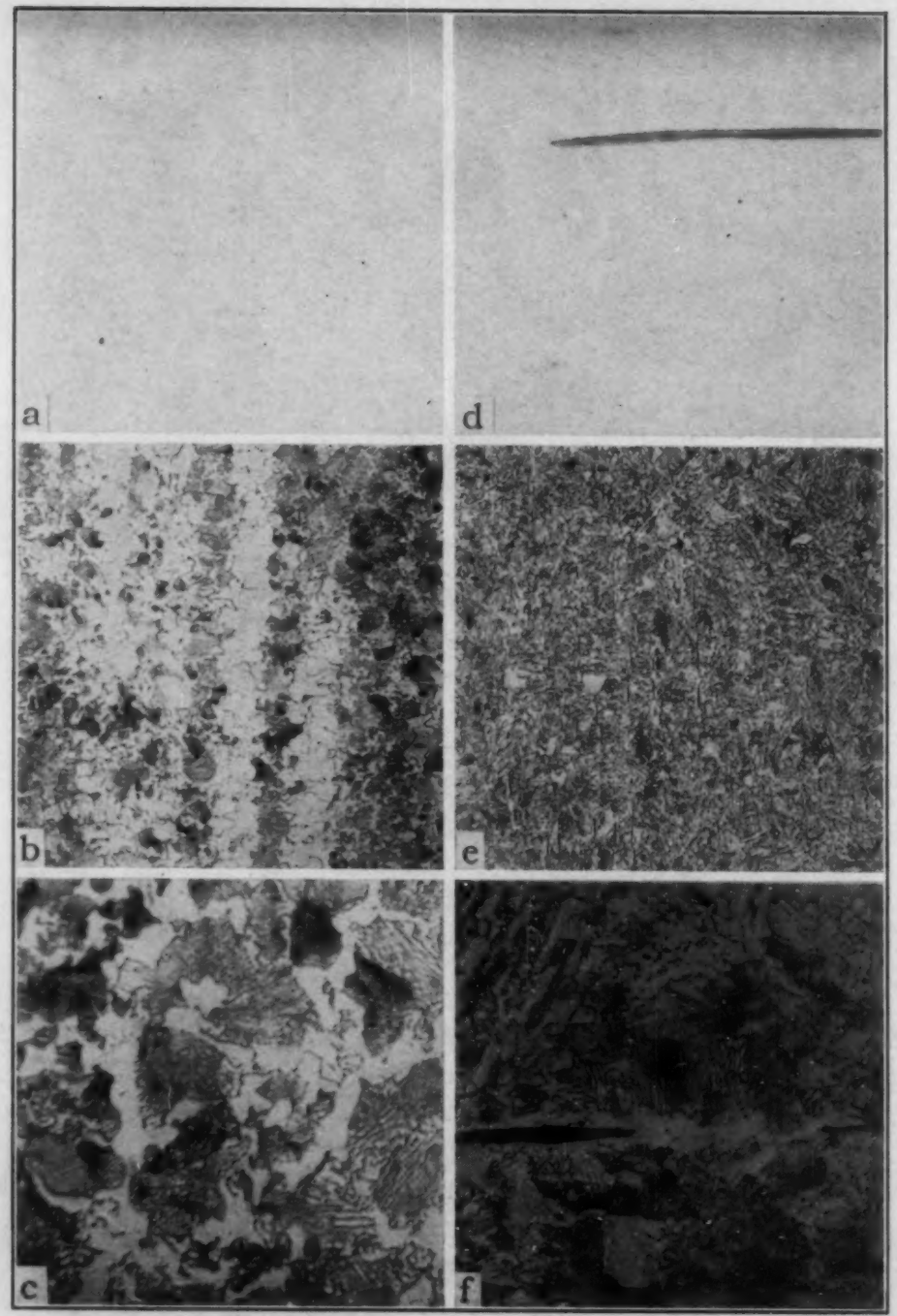


Fig. 4—Microstructures of Steels Used in Tests. a, b, c—Plain NE 8640. d, e, f—Sulphite-treated NE 8640. a, d—Unetched, × 500. b, e—Etched, × 100. c, f—Etched, × 500.

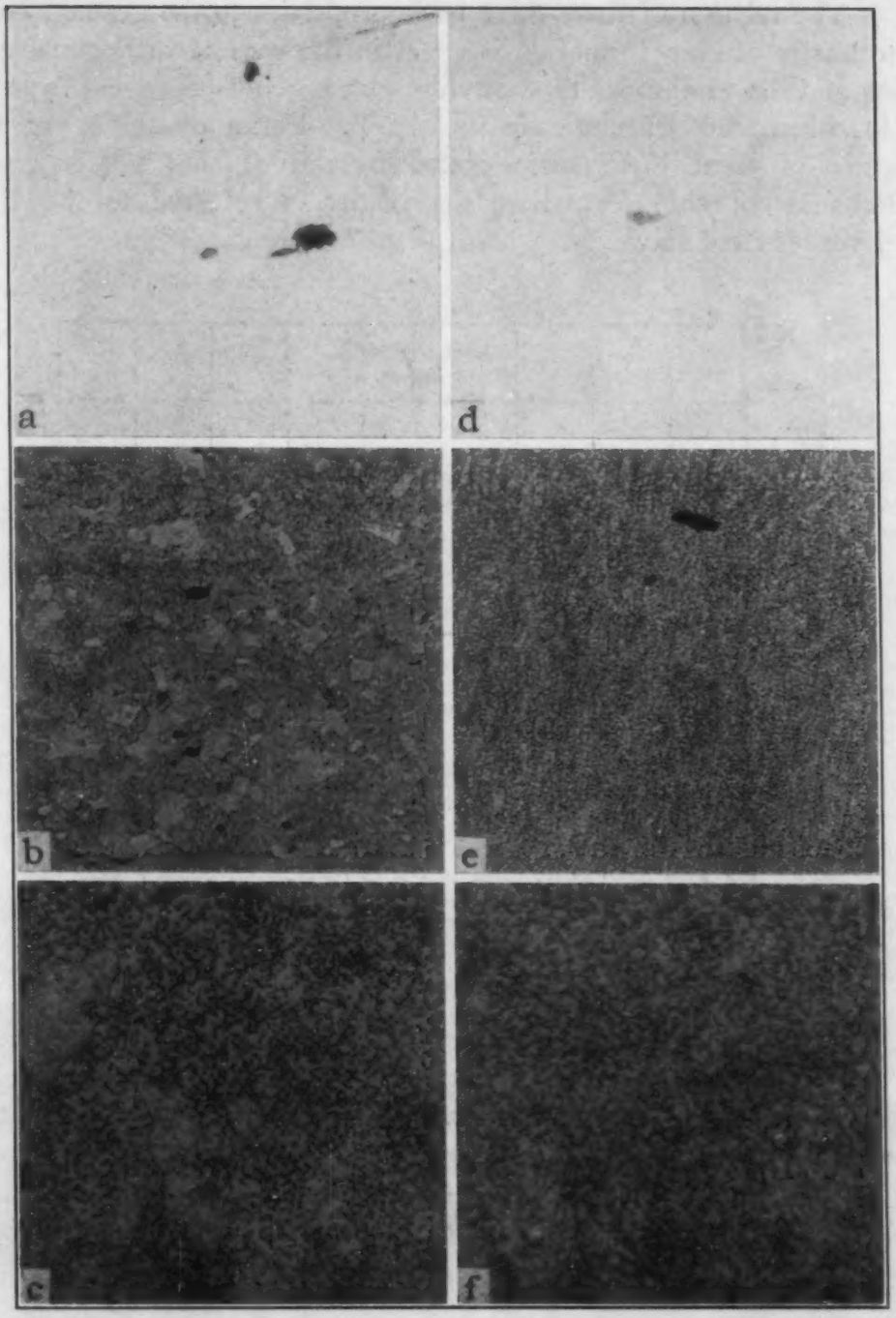


Fig. 5—Microstructures of Steels Used in Tests. a, b, c—SAE 52100 annealed. d, e, f—SAE 52100 cold drawn. a, d—Unetched, × 500. b, e—Etched, × 100. c, f—Etched, × 500.

The relation of these three basic properties to the geometry and mechanics of chip formation is exact in the case of orthogonal cutting and the continuous type of chip with no built-up edge (Type 2) (4), illustrated schematically in Fig. 7. For a discussion of the nature of these three basic properties and of the geometry and mechanics of chip formation, the reader is referred to the four references cited above.

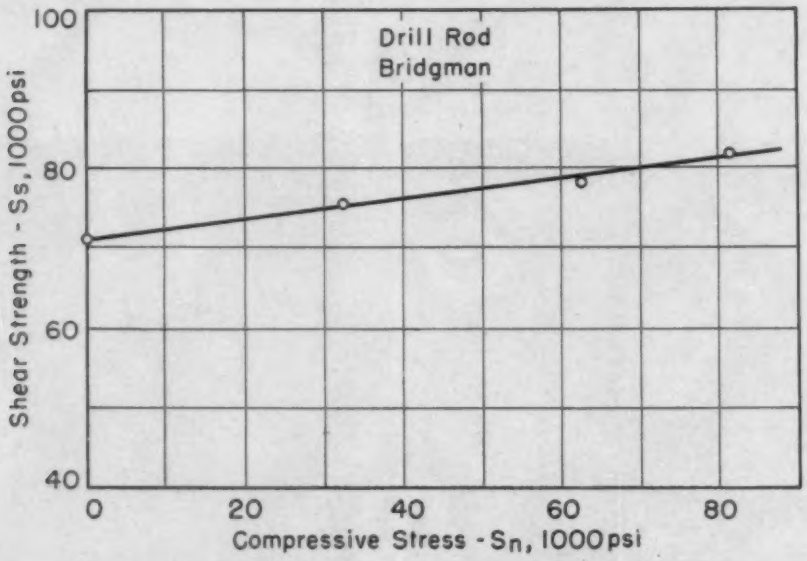


Fig. 6—Typical Shear Strength Versus Compressive Stress Curve, as Observed by Bridgman. The machining constant C is theoretically equal to the complement of the slope angle of this curve.

Relation of μ, S_s, and C to Machinability

The tool forces (and power consumption) are controlled almost entirely by these three properties. The force relationships for the case of the Type 2 chip and orthogonal cutting conditions are shown in Fig. 8. In this case the tool forces F_c and F_t are directly controlled by the values of the three basic properties μ, S_s, and C as follows:

$$F_c = A_o S_s \left[\tan\left(\frac{C+\tau-\alpha}{2}\right) + \cot\left(\frac{C-\tau+\alpha}{2}\right)\right] \quad \text{Equation I}$$

$$F_t = A_o S_s \left[\tan\left(\frac{C+\tau-\alpha}{2}\right) \cot\left(\frac{C-\tau+\alpha}{2}\right) - 1 \right] \quad \text{Equation II}$$

where:

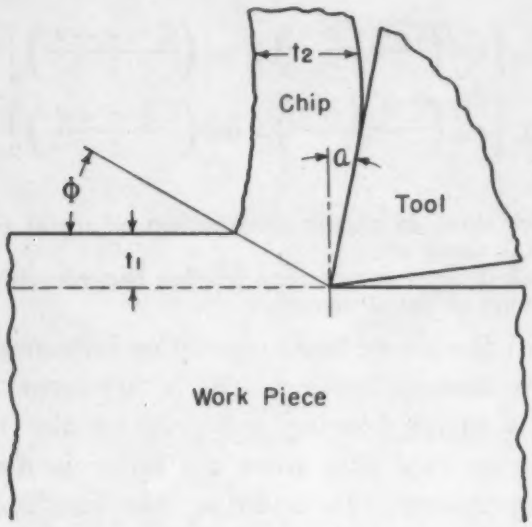


Fig. 7—Geometry of Type 2 Chip (Orthogonal Cutting).

A_o = cross sectional area of "chip" before removal
(= t_1 × width of cut)
a = true rake angle of tool (see Fig. 8)
τ = friction angle (= arc tan μ) (see Fig. 8)

Power consumption in cutting is also, in this case, directly controlled by μ, S_s, and C. The relationship is:

$$P_c = \frac{S_s}{396{,}000}\left[\tan\left(\frac{C+\tau-a}{2}\right)+\cot\left(\frac{C-\tau+a}{2}\right)\right] \quad \text{Equation III}$$

where:

P_c = horsepower consumed in cutting, per cubic inch of metal removed per minute, when S_s is expressed in pounds per square inch.
and the other quantities are as already defined.

It is evident from Equations I, II, and III that the force system and power consumption (in the case of orthogonal cutting and a Type 2 chip) are completely determined by the basic properties μ, S_s, and C, when the size of cut and rake angle are fixed.

Heat generation and tool temperatures are also controlled by μ, S_s, and C. In cutting, heat is generated at two different sources —first on the shear plane during deformation of the metal, then at the chip-tool interface as a result of the friction between chip and tool. In the case of orthogonal cutting and a Type 2 chip, the mechanical work done at the shear plane and at the tool face (per unit volume of metal removed), which is dissipated as heat, is related to the three basic quantities in the following manner:

$$W_s = S_s\left[\cot\left(\frac{C-\tau+\alpha}{2}\right)+\tan\left(\frac{C-\tau-\alpha}{2}\right)\right] \quad \text{Equation IV}$$

$$W_f = S_s\left[\tan\left(\frac{C+\tau-\alpha}{2}\right)-\tan\left(\frac{C-\tau-\alpha}{2}\right)\right] \quad \text{Equation V}$$

where:

W_s = work done in plastic deformation of metal per unit volume of metal removed.

W_f = work done in overcoming friction between chip and tool per unit volume of metal removed.

Thus, all three of the above basic quantities influence heat generation and temperature rise in cutting. It is apparent then that these quantities have a direct bearing not only on the forces acting on the tool but also on tool life, since the latter is directly influenced by the tool temperature. In addition, the finish obtained on the workpiece is considerably influenced by the coefficient of friction μ. In general, the higher the value of μ, the poorer is the finish. It is evident then that the basic quantities, μ, S_s, and C, play an important part in determining the machinability of a given material.

Evaluation of μ, S_s, and C

These quantities can be evaluated by calculation from experimental values, for the case of a Type 2 chip and orthogonal cutting conditions. The values which must be measured experimentally in order to make such calculations are the two force components F_c and F_t, and the shear angle ϕ (Fig. 8). The experimental methods used in obtaining such measurements have been described in detail in a previous publication (5). The equations for calculating values of the three basic quantities from these measured values are as follows:

$$\mu\ (=\tan\tau) = \frac{F_t + F_c\tan\alpha}{F_c - F_t\tan\alpha} \quad \text{Equation VI}$$

$$S_s = \frac{F_c\sin\phi\cos\phi - F_t\sin^2\phi}{A_o} \quad \text{Equation VII}$$

$$C = 2\phi + \tau - \alpha \quad \text{Equation VIII}$$

By means of such measurements and calculations, values for μ, S_s, and C have been determined for each member of the five pairs of steels under discussion in this paper, as will be described later.

Other Mechanical Properties

In addition to the three properties discussed in the foregoing

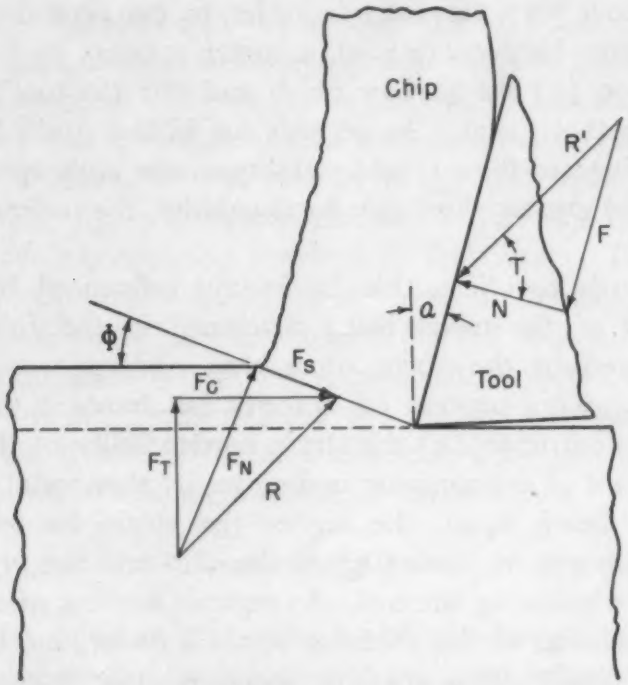


Fig. 8—Force System Acting on Type 2 Chip (Orthogonal Cutting).

section, several other fairly basic mechanical properties appear to have a direct bearing on the machinability of a given material. These are:

1. The strain hardenability of the material, as measured for instance by the Meyer strain hardenability exponent, n.
2. The bulk hardness of the material, as measured for instance by the Brinell hardness number, H.
3. The abrasiveness of the various constituents of the microstructure, for which there is no quantitative measure at present. Qualitative estimates may be obtained by examination of the microstructure.

The Meyer strain hardenability exponent, mentioned as a suitable measure of the first of the above properties, offers a means of evaluating the amount of strain hardening produced in a metal by a given amount of plastic deformation (6). It is measured in the following manner:

> Hardness indentations are made on the given material with a ball indenter at several different loads. When the diameters of the resulting indentations are plotted against load on double log paper, a straight line results. The slope of this line is the Meyer exponent n. The measurements and technique must be

carried out very carefully in order to get reproducible results.

The strain hardenability of a metal appears to have a direct influence upon (a) the surface finish and (b) the tool life obtained in machining that metal. As regards finish, the strain hardenability evidently influences the size and stability of the built-up edge. Thus, in general, the greater the strain hardenability, the poorer the surface finish.

As regards tool life, this is directly influenced by the strain hardenability of the metal being machined in the following way. Metal removed in the form of a chip undergoes severe plastic deformation. This process of deformation hardens the chip to a degree depending upon (a) the strain hardenability of the metal and (b) the amount of deformation undergone by that metal (7). Thus, other things being equal, the higher the strain hardenability, the greater the amount of hardening of the chip and the greater should be its abrasive action on the tool. As regards amount of deformation, this is proportional to the shearing strain ϵ undergone by the metal at the shear plane. This shearing strain is directly related (in the case of orthogonal cutting and a Type 2 chip) to the basic properties μ and C. The equation is as follows:

$$\epsilon = \cot\left(\frac{C - \tau + \alpha}{2}\right) + \tan\left(\frac{C - \tau - \alpha}{2}\right) \qquad \text{Equation IX}$$

where:

ϵ = shearing strain undergone by chip during process of removal.

The greater the shearing strain, the greater the amount of hardening of the chip and so the greater its abrasive action on the tool. Thus, the strain hardenability of the metal, when considered together with quantities μ and C, directly influences the rate of abrasion of the cutting tool.

The initial hardness of the metal being machined, as measured for instance by its Brinell hardness number H, also has a direct bearing on the rate of abrasion of the cutting tool. If two metals with equal strain hardenability undergo equal amounts of deformation in the process of chip formation, then naturally the metal with the higher initial hardness will produce the harder chip and so abrade the cutting tool the more rapidly. Thus, the strain hardenability, the shearing strain, and the initial hardness, taken together, determine the final hardness of the chip, which in turn influences directly the rate of abrasion of the cutting tool.

The rate of abrasion of the cutting tool is, however, influenced not only by the bulk hardness of the chip but also by the abrasiveness of the individual components of the microstructure. Thus, the presence of hard abrasive inclusions such as aluminates and silicates will ordinarily accelerate the rate of abrasion of the cutting tool.

It is evident from the above discussion that two types of abrasiveness of the material are involved in tool wear. These may be termed "inherent abrasiveness" and "induced abrasiveness". The "inherent abrasiveness" is characterized by the bulk hardness of the material and the abrasiveness of the microconstituents. The "induced abrasiveness" is that arising from the further hardening produced by deformation of the metal, as characterized by the strain hardenability of the metal and the amount of deformation.

Summarizing Table

Six different basic properties which are known to have a considerable influence on machinability have been introduced and discussed in this section of the paper. Table III summarizes the effect of these properties on the practical machinability characteristics of a material.

Test Methods

In order to study the basic reasons for the improved machinability of the free machining member of each of the five pairs of steels under study, measurements were made of the properties which have been discussed in the preceding section (with the exception of the abrasiveness of the microconstituents, which is not as yet subject to quantitative measurement). Cutting tests were run from which

Table III
Effect of Basic Properties on Machinability Characteristics

	A *decrease* in the given property has the following effect:		
Basic Properties	Probable Effect on Tool Life	Usual Effect on Surface Finish	Known Effect on Tool Forces and Power Consumption
1. Coefficient of friction, μ	Good	Good	Good
2. Shear Strength, S_s	Good	None	Good
3. Machining constant, C	Bad	?	Bad
4. Strain hardenability	Good	Good	——*
5. Hardness	Good	None	——*
6. Abrasiveness of microconstituents	Good	None	——*

*Forces and power consumption determined almost completely by values of μ, S_s, and C.

values of coefficient of friction, shear strength and machining constant could be calculated. Hardness tests were also run to obtain values of Brinell hardness and Meyer strain hardenability exponent.

Cutting Tests

The cutting tests were run using an orthogonal cutting arrangement in order to satisfy the first of the conditions necessary to make Equations VI through VIII applicable. In an orthogonal cutting arrangement the tool has a single straight cutting edge which is set at right angles to the direction of motion of tool relative to work. Such an arrangement can be conveniently obtained by using a tubular work piece and removing a chip continuously from the end of the tube. This arrangement is illustrated schematically in Fig. 9.

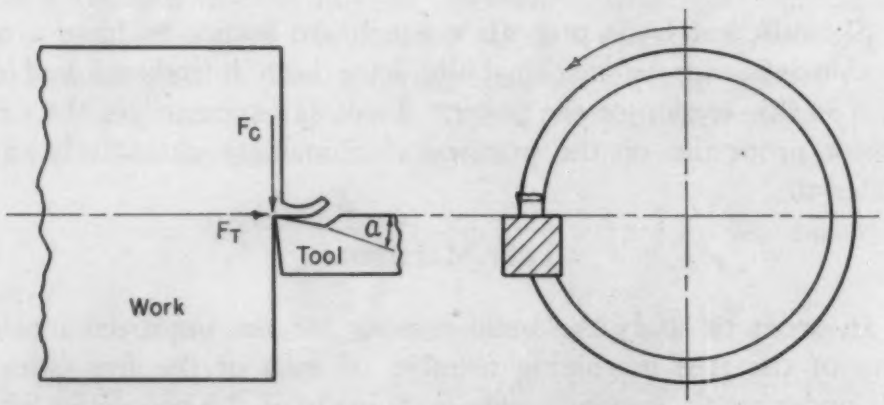


Fig. 9—A Convenient Orthogonal Cutting Arrangement.

In addition to using the orthogonal cutting arrangement, a steel cutting grade of sintered carbide tool was employed, together with cutting speeds greater than 200 feet per minute, in order to give a Type 2 chip. The presence of a Type 2 chip is the second condition needed to make Equations VI through VIII applicable.

Using the above arrangement, cutting tests were made on the five pairs of steels over a range of feeds and speeds. One series was made using a feed of 0.0018 inch per revolution and covering a range of speeds from approximately 300 to 900 feet per minute. A second series was made using a cutting speed of 350 to 450 feet per minute and covering a range of feeds from 0.001 to 0.007 inch per revolution. The rake angle (a) used on the carbide tool was

+10 degrees and the relief angle was 3 degrees. The wall thickness of the tubing (which corresponds to the depth of cut in a normal turning operation) was 0.25 inch. Measurements of cutting force F_c, thrust force F_t, and shear angle ϕ, were made in each series of tests. From the resulting data, values for coefficient of friction μ, shear strength S_s, and machining constant C were calculated by use of Equations VI through VIII.

Some of the more interesting of these sets of values are plotted in Figs. 10 to 16. These illustrations show the behavior of the coefficient of friction as influenced both by changes in speed and changes in feed for several of the pairs of steels under study. Values of shear strength as a function of compressive stress, as found from the data obtained in both the speed and feed runs, are also plotted for several of the pairs of steels.

It has been found that μ, S_s, and C are much less influenced by changes in cutting speed than in feed. (See also Figs. 10 to 13.) Therefore, in order to obtain good average values of these three quantities for all the steels tested, the individual values of these quantities obtained in the speed runs over a range of cutting speed from 300 to 900 feet per minute were averaged. These average values are given in Table IV.

Table IV
Average Values of Basic Properties Observed From Cutting Tests

Tool: Sintered carbide, rake angle (α) = +10 degrees, relief angle = 3 degrees
Cutting Speed: Readings averaged from data taken over range from 300 to 900 ft/min.
Feed: 0.0018 in./rev.
Width (depth) of cut: 0.25 in.

Material	Average Coefficient of Friction Between Chip and Tool μ	Average Shear Strength S_s lb/sq.in.	Average Machining Constant "C" deg.
Stainless Steels			
Type 303 (Sulphur)	0.87	107,000	92
Type 304	1.14	118,000	83
C-1022			
Leaded	0.49	85,000	72
B-1113			
Sulphur	0.54	79,000	74
C-1019			
Plain	0.97	89,000	74
A-8640 Steels			
Sulphite-Treated	1.05	106,000	78
Plain	1.09	110,000	80
SAE 52100 Steels			
Cold Drawn	0.94	105,000	73
Annealed	1.00	104,000	69

Measurement of Other Mechanical Properties

The hardness and strain hardenability of each of the steels was determined by use of a standard Brinell apparatus. Standard Brinell

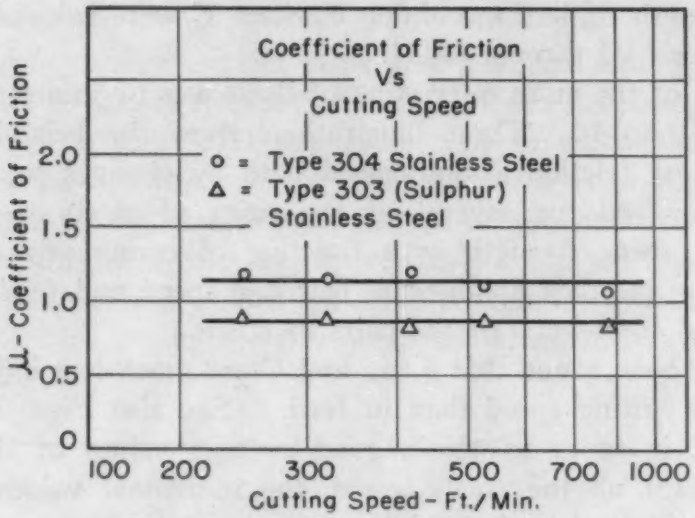


Fig. 10—Chip Friction Versus Cutting Speed for Plain and Sulphurized Stainless Steels.

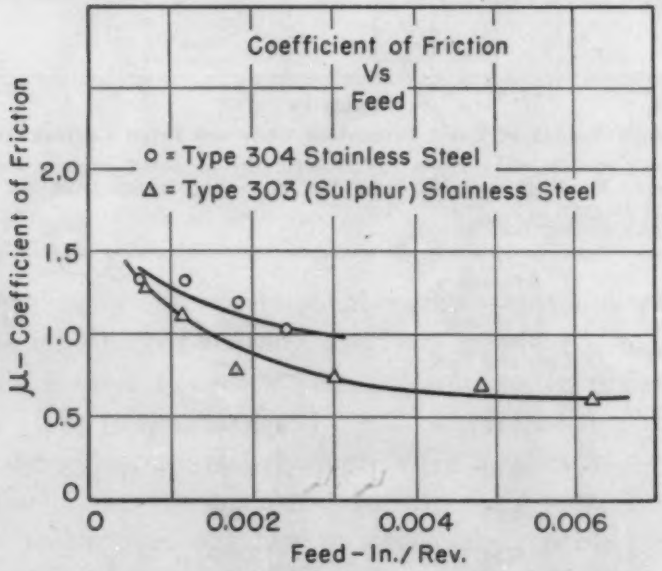


Fig. 11—Chip Friction Versus Feed for Plain and Sulphurized Stainless Steels.

hardness values were obtained using a load of 3000 kilograms. Hardness indentations were also made with loads of 1000 and 2000 kilograms in order to obtain the Meyer strain hardenability exponent

of the material in the manner described earlier in the paper. The observed values of hardness and strain hardenability are given in the last two columns of Table I.

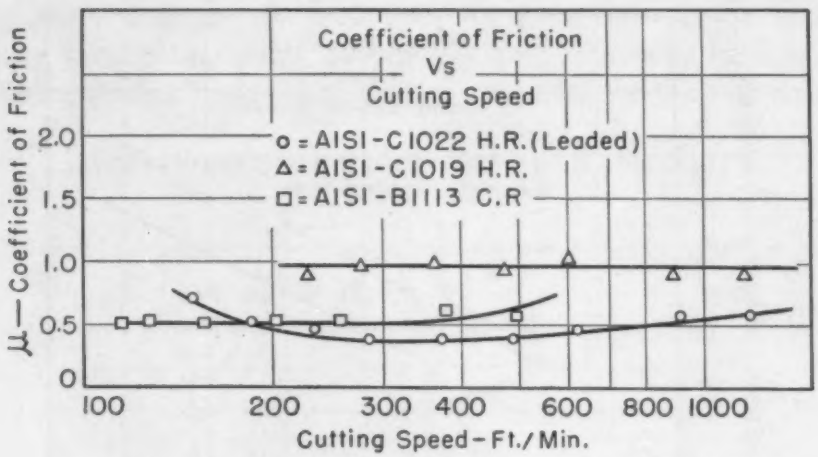


Fig. 12—Chip Friction Versus Cutting Speed for Plain, Sulphurized and Leaded Low Carbon Steels.

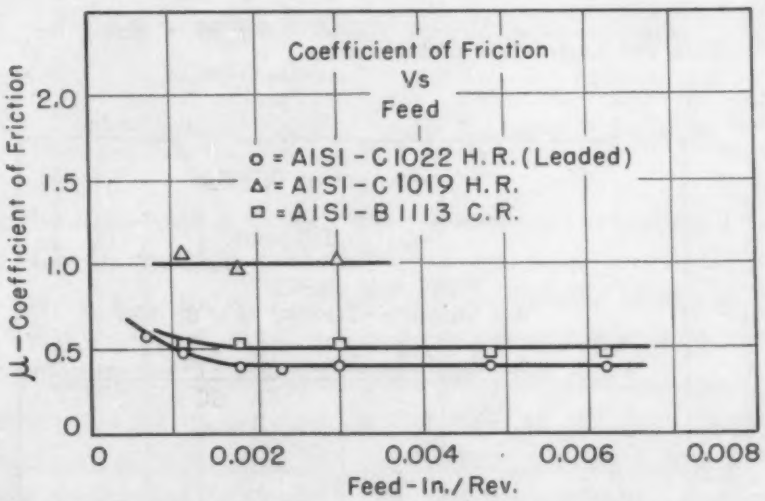


Fig. 13—Chip Friction Versus Feed for Plain, Sulphurized and Leaded Low Carbon Steels.

Conclusions

As a result of the above series of tests and measurements, the basic reasons for the good machinability of each of the five free machining steels under study have become apparent. These may be recognized from a study of Figs. 10 to 16 and the data presented in Table IV and in the last two columns of Table I.

In the case of the pairs of steels in which one member is high in sulphur and the other low (both the stainless steels and the plain carbon steels), the main reason for the improved machinability of

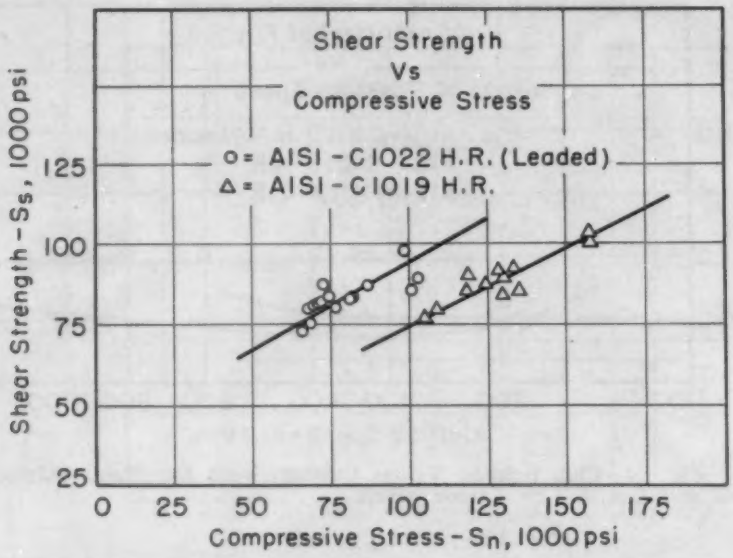


Fig. 14—Shear Strength Versus Compressive Stress for Plain and Leaded Low Carbon Steels.

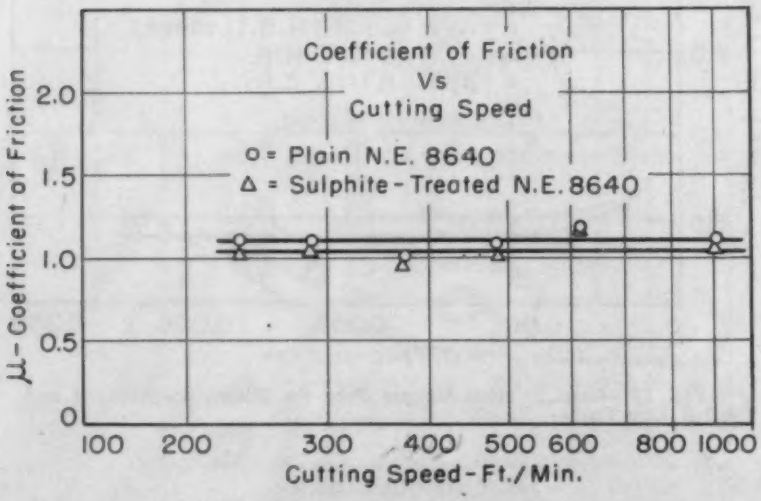


Fig. 15—Chip Friction Versus Cutting Speed for Plain and Sulphite-Treated A-8640 Steels.

the high sulphur steels is found in their much lower coefficient of friction of chip on tool. (See Figs. 10 to 13 and Table IV.) It may be noted, however, that sulphur appears to be more effective in reducing friction in the case of the plain carbon steels than in the

case of the stainless steels. This fact seems to be borne out quite generally by tests on various other types of sulphurized and non-sulphurized stainless steels and plain carbon steels.

The low values of coefficient of friction found for the high sulphur steels may be attributed to the behavior of the sulphide inclusions during the cutting process. These inclusions have a fairly low melting point compared to that of the steel; at the temperatures

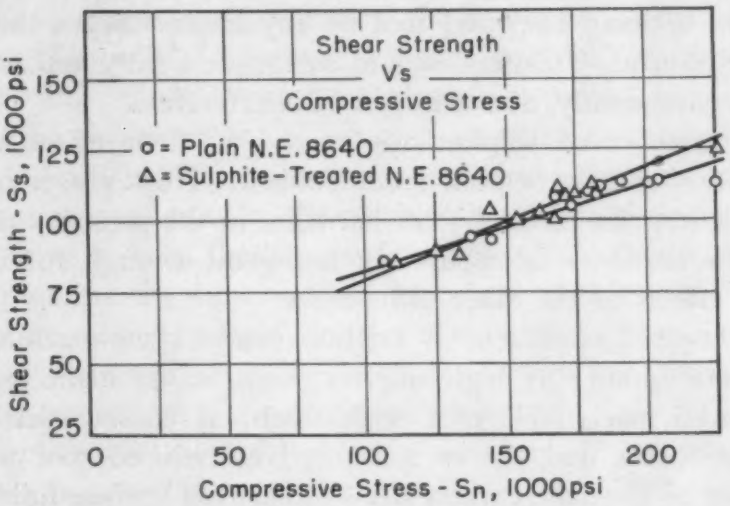


Fig. 16—Shear Strength Versus Compressive Stress for Plain and Sulphite-Treated A-8640 Steels.

found at the chip-tool interface during cutting they should be fairly soft and should tend to "smear" over the tool face. This action would provide a "sandwich-filling" of low shear strength material between chip and tool, thus helping to prevent metal-to-metal contact and allowing free sliding of the chip over the tool face.

It appears that in the case of the pair of stainless steels tested, the addition of sulphur also produced an appreciable increase in the machining constant (92 degrees for the high sulphur steel as compared with 83 degrees for the plain). This is a beneficial effect. The reason for the increase in this value in this case is not known. It does not appear to be general, either for other types of stainless steels or for plain carbon steels. However, it was quite marked in this particular case and may possibly be associated with the difference in grain size noticeable in Fig. 1.

It is particularly interesting to note that the addition of sulphur to the steels tested has only a slight effect on their shear strengths. Only a small decrease in shear strength is noted due to addition of

sulphur. Further, it was found during the tests that the sulphurized steels produced just as continuous a chip as the plain steels. No tendency of these materials to form a discontinuous or segmental chip was noted. Thus the idea held by some that the better machinability of sulphurized steels is due to reduced resistance to shear or an increased tendency for the chip to become discontinuous is disproved. The reason that high sulphur steels give well-broken-up chips in practice can be found in the fact that lowering the coefficient of friction between chip and tool by any means causes the chip to curl more tightly. This tendency to curl more tightly makes the chip break more frequently, due to increased interference.

The presence of sulphur apparently has little effect on strain hardenability, as may be seen from Table I. However, it seemingly does result in a somewhat higher hardness in the present case. This increase in hardness is apparently not great enough to offset the beneficial effects of the other differences.

The lowered coefficient of friction (and higher machining constant, where found) of high sulphur steels is the main reason for the improved machinability of such steels, as characterized by the lower tool forces and power consumption, reduced tool wear and (in the case of the plain carbon steels) improved surface finish shown in Table II.

The effect of lead in improving the machinability of a plain carbon steel is quite similar to that of sulphur. The main benefit again is a large reduction in coefficient of friction as may be seen from Figs. 12 to 14 and the data in Table IV. In fact, the lead seems to be a little more effective in reducing friction than does sulphur. The reason for the reduced friction again can be attributed to the smearing of the insoluble lead inclusions over the face of the tool, thus allowing free sliding of the chip. As in the case of sulphur, the lead produces little if any change in the machining constant and only a slight decrease in the average value of the shear strength. The chips obtained from the leaded steel (C-1022) were as continuous as those from the plain carbon steel (C-1019). The hardness and strain hardenability of the two steels are practically the same, as may be seen from Table I. As in the case of the sulphur, a reduced coefficient of friction brought about by the addition of lead results in increased tool life, improved surface finish, and decreased tool forces and power consumption, as may be seen from Table II. However, as is well known, the main advantage of

using lead instead of sulphur to impart free machining properties is that lead has little or no adverse effects on the performance characteristics of the steel in service.

Turning now to the pair of A-8640 steels, one of which has been modified by the addition of sodium sulphite, a quite different situation is found. Here we see no appreciable difference in any of the directly measurable basic properties found for these two steels. The values of coefficient of friction, shear strength and machining constant are practically the same for both, as may be seen from Table IV. (See also Figs. 15 and 16.) (Note particularly that the sulphite treatment does not reduce chip friction.) Further, the two members of the pair are alike as regards hardness and strain hardenability, as may be seen from the data in Table I. These facts are reflected in the machinability data given in Table II, where it may be seen that the surface finish, tool forces, and power consumption are the same for both members of this pair. However, the sulphite-treated sample is free machining in the sense that a considerably greater tool life is obtained with the sulphite-treated steel as compared with the untreated material. *Since all other basic properties are the same for the two members of the pair, the conclusion is that the long tool life found for the sulphite-treated steel is mainly due to the less abrasive character of its microconstituents.* It is well known that the addition of sodium sulphite to a molten steel fluxes out abrasive silicate and aluminate inclusions; the good machinability of sulphite-modified steels has been attributed to that fact (8). The present findings are in agreement with this conclusion. It is of interest to note that the good tool life given by the sulphite-treated steel would not be evident from "machinability" tests based on measurements of forces or power consumption alone; it is plain that exact reliance on such tests for measuring machinability is not justified.

The basic properties found for the two samples of SAE 52100 steel show no striking differences. However, the cold drawing process has produced a fairly appreciable increase in the machining constant (and possibly a slight decrease in coefficient of friction), as may be seen from the data in Table IV. It is interesting to note that cold working has not increased the mean shear strength of the steel. But, as would be expected, the strain hardenability has been decreased and the hardness has been increased by cold drawing, as may be seen from the data in Table I. These are the usual effects

of cold drawing, as has been confirmed by tests on a number of pairs of other types of steels consisting of a cold drawn member and a hot-rolled or annealed member.

All of these changes produced by cold drawing are beneficial, with the exception of the increased hardness which increases the abrasiveness of the steel. Therefore, small improvements in machinability are noted in the form of decreased tool forces and power consumption (and improved surface finish in the usual case, though that does not show up in the present tests), as seen from the data in Table II. Furthermore, small increases in tool life as a result of the cold drawing process are often noted in practice, as in the present case. However, this effect is not always found because the benefits derived from the small changes in machining constant and strain hardenability are sometimes offset by the accompanying increase in hardness. Again, as in the case of the high sulphur and the leaded steels, the chips obtained from the cold-worked and the annealed samples were equally continuous. The free machining obtained with cold drawn materials cannot be attributed to the production of a discontinuous chip. These results supply the answer to a question which has troubled many: Why should cold working, which hardens and strengthens the steel, improve its machining properties?

Summary

Summing up, it may be said that this study has established or confirmed the main basic mechanisms by which each of the four treatments discussed herein is able to improve the machinability of steels. The mechanisms are as follows:

1. High sulphur—This treatment considerably reduces the coefficient of friction between chip and tool and in some cases, apparently, increases the machining constant. The presence of sulphur does not reduce the shear strength nor produce a discontinuous chip. The reduced friction and increased machining constant are beneficial to all aspects of machinability. Sulphur is more effective in reducing friction when added to plain carbon steels than when added to stainless steels.

2. Lead—This treatment also greatly reduces the coefficient of friction between chip and tool. As with sulphur, no difference in shear strength or in chip type is noted in comparing a leaded with a nonleaded steel. Again all aspects of machinability are benefited.

3. Sodium sulphite—This treatment does not appreciably change those basic mechanical properties which are at present susceptible to direct measurement. The free machining properties obtained by sulphite treatment must, therefore, be attributed to a less abrasive microstructure. This fact merely helps to confirm a conclusion previously arrived at by others. Because only the abrasiveness of a steel is modified by the addition of sodium sulphite, the only aspect of machinability which is benefited is that of tool life.

4. Cold working—This treatment produces a slight increase in the machining constant, a decrease in the strain hardenability and an increase in the hardness. These effects oppose each other to some extent as regards their influence on tool life, but are beneficial to surface finish, tool forces and power consumption.

Acknowledgments

The authors wish to thank the firms that kindly supplied the steels used in this investigation. The stainless steels were supplied by the Rustless Iron and Steel Division of the Armco Steel Company; the C-1019 and A-8640 steels by the LaSalle Steel Company; and the 52100 steels by the Timken Steel and Tube Division of Timken Roller Bearing Company. Special thanks are due Mr. Glenn D. Boyer, Metallurgist, LaSalle Steel Company, for locating the piece of "pre-war" leaded C-1022 steel used in these tests.

The assistance of Miss Dorothy Meek, Research Technician, who carried out many of the cutting tests and calculations, is gratefully acknowledged. The authors also wish to thank Mrs. Joan Gailey, Mrs. Betty Startsman and Mrs. Betty Martin of the research staff for their assistance in the preparation of the paper.

References

1. M. Eugene Merchant, "Basic Mechanics of the Metal Cutting Process," *Journal of Applied Mechanics*, Vol. 66, 1944, p. A-168 to A-175.
2. M. Eugene Merchant, "Mechanics of the Metal Cutting Process—I. Orthogonal Cutting and a Type 2 Chip," *Journal of Applied Physics*, Vol. 16, 1945, p. 267-275.
3. M. Eugene Merchant, "Mechanics of the Metal Cutting Process—II. Plasticity Conditions in Orthogonal Cutting," *Journal of Applied Physics*, Vol. 16, 1945, p. 318-324.
4. Hans Ernst, "Physics of Metal Cutting," *Machining of Metals*, American Society for Metals, 1938, p. 1-34.
5. M. Eugene Merchant and N. Zlatin, "New Methods of Analysis of Machining Processes," *Proceedings of the Society for Experimental Stress Analysis*, Vol. 3, No. 2, 1946, p. 4-27.

6. H. O'Neill, "The Hardness of Metals and Its Measurement," Chapman and Hall, 1934, p. 49-62.
7. N. Zlatin and M. Eugene Merchant, "The Distribution of Hardness in Chips and Machined Surfaces," *Transactions,* American Society of Mechanical Engineers, 1947 (annual bound volume only); also *Iron Age,* Vol. 159, No. 21, May 22, 1947, p. 69-75.
8. Glen D. Boyer, "Effect of Sulphur on the Quality of Sulphite Treated Steels," *Steel,* Vol. 119, No. 2, July 8, 1946, p. 96-97, 120.

DISCUSSION

Written Discussion: By A. O. Schmidt and J. R. Roubik, Kearney & Trecker Corp., Milwaukee.

This paper is a welcome addition to the literature on metal cutting and machinability. The reasons for improvement in machinability with various treatments have been clearly indicated and explained.

Fig. 10 shows that with the stainless steels tested the coefficient of friction is independent of the cutting speed at least between the limits of 250 and 800 feet per minute. With some exception of the data for the leaded steel, substantially the same tendency can be observed in Fig. 12. This would indicate that the normal force and hence the relative cutting force and thrust force will not vary with cutting speed.

At feeds above 0.002 inch per revolution, Figs. 11 and 13 illustrate that the coefficient of friction remains constant while an increase is pictured at finer feeds. It should be pointed out that data for these finer feeds is difficult to evaluate properly. It is generally realized that grinding a truly sharp edge is no easy task. The grinding marks near the cutting edge and the tendency of the edge to become slightly rounded, roughened, or irregular are responsible for the deviation of the actual shape of the cutting edge from the theoretical shape. The percentage of error introduced by this deviation or variation is increased or more noticeable at the finer feeds. It appears to be reasonable that the coefficient of friction may increase under these circumstances.

A point which the authors bring out well is that machinability in terms of power is unrelated to machinability in terms of surface finish. Table II confirms the lack of relationship between tool life, surface finish, and power consumption. A material requiring high power consumption which might sometimes indicate "poor" machinability may show good surface finish which might be considered "good" machinability. However, it can generally be stated that materials showing better tool life also require lower cutting forces.

With a given material we have found that surface finish is a function of cutting speed and feed. For example, when milling SAE 1050 (200 Bhn) at 500 feet per minute and a constant feed with cutters having various radial-rake angles, profilometer readings of surface finish were about 30 microinches, r.m.s. When the cutting speed was reduced to about 100 feet per minute, all other conditions remaining unchanged, the surface finish was much rougher, measuring between 100 and 200 micro-

inches, r.m.s. The finer feeds also improved the surface finish readings.

Written Discussion: By Francis W. Boulger, supervising metallurgist, Battelle Memorial Institute, Columbus, Ohio.

The authors are to be congratulated on this interesting addition to the series of papers on metal cutting issued by their company. Their testing method gives quantitative values for several properties of a material, which influence its behavior in machining operations. Because of the complexity of cutting processes, it is not surprising that the method requires an interpretation of the relative importance of three properties determined in a machining operation as well as consideration of hardness and strain hardening characteristics. An expression by the authors on the relative importance of differences in shear strength, in friction coefficients, and in the constant "C" would be welcomed.

An estimate of the relative importance of the three properties seems necessary if one wants to use Table IV to compare the machinability of the nine samples. For instance, the lead-bearing C-1022 steel had a low shear strength and friction coefficient, which is desirable, but a comparatively poor machinability constant "C". The reverse was true for the sample of stainless steel Type 304. Should it be deduced from a comparison of Tables II and IV that the value of constant "C" is less important in determining machinability than the other properties? The problem of weighting the importance of the three "basic properties" also arises if one wishes to compare the A-8640 and SAE 52100 steels from the data in Table IV.

The conclusions regarding the mechanisms by which sulphur and lead improve the machinability of steel seem reasonable and well founded. The results obtained on the A-8640 steels, however, are a little disconcerting. Increasing the sulphur content of this steel from 0.015 to 0.046% should give an improvement in machinability, and this can be shown by other laboratory tests. Since sulphur combines with iron and manganese to form inclusions in the steel, it seems unlikely that the mode of addition would influence its effect on the friction coefficient and machining constant. Perhaps the unintentional variations in microstructure and composition of the two samples masked the effect of the increased sulphur content of the sulphite treated A-8640 steel.

Written Discussion: By T. M. Garvey, research associate, Carnegie-Illinois Steel Corp., Pittsburgh.

The authors of this paper are to be complimented for this valuable contribution concerned with establishing the relationships between the machinability of steels and their mechanical properties. This publication is a worthy supplement to that describing their earlier work on the mechanical factors inherent in metal cutting processes. The experimental evidence leading to an explanation of the effects of cold working on machinability is of valuable practical significance, and it is hoped that this phase of the work will be expanded to include the low carbon free machining grades of steel.

We would like to call particular attention to the comparison of the sulphite treated A-8640 steel with the untreated steel of the same grade.

Since no appreciable differences were found in any of the directly measured mechanical properties of these two steels, the authors concluded that the longer tool life in the case of the sulphite treated steel was primarily the result of less abrasive microconstituents. However, in order to prevent any misunderstanding of the role of the sulphite addition in enhancing machining properties, it might be advisable to point out that there is a significant difference in the sulphur content of these two steels. The data presented in the reference publication[2] disclosed that when sulphur, equivalent in amount to that added in the sulphite, was added as stick sulphur, a 12% increase in production was obtained, accompanied by a 50% increase in tool life. Although this improvement in tool life was appreciably less than that obtained with the sulphite treatment, it nevertheless represents a substantial increase in machinability.

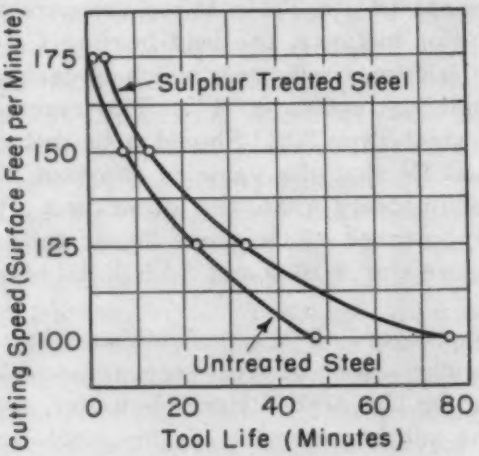


Fig. 17—Effect of Sulphur on the Machinability of AISI 4620 Steel.

As additional evidence of the beneficial effects of small additions of sulphur to alloy steels, Fig. 17 is presented. The data were produced by Messrs. R. Swanson and C. Armstrong, of the Gary Steel Works, and were based on tool life tests conducted with high carbon tool bits on annealed AISI 4620 steel. It is evident that at surface speeds similar to those reported for the production machining of the A-8640 steels, considerable improvement in tool performance has been obtained by the addition of a relatively small amount of sulphur. Similar results have been noted for other alloy steels machined with high speed cutting tools. In view of these data, we would like to receive the authors' comments relative to the benefits derived from sulphur additions apparently too small to influence the mechanical properties studied in their experiments. The question arises as to whether the coefficients of friction of chip-on-tool for the 0.046% sulphur steel and the 0.015% sulphur steel would be significantly different if plain carbon or high speed tools were used.

[2]F. J. Robbins, "Metallurgical Aspects of Machinability," *Iron Age*, Vol. 157, No. 13, March 28, 1946, p. 47-51.

Written Discussion: By William Wilson, Jr., research metallurgist, Armour Research Foundation of Illinois Institute of Technology, Chicago.

We had occasion to apply the authors' test to evaluating the machining constant of a heat treated alloy steel. In these tests an effort was made to study the effect of microstructure on the machining constant "C". Unfortunate circumstances interrupted the work at an early date; however, certain interesting observations were made. These are as follows:

MACHINING CONSTANT AND ROCKWELL HARDNESS OF STRUCTURES IN A MODIFIED "SAE 4350"

Structure	Rockwell "C" Hardness	Machining Constant—"C" degrees
Spheroidized martensite	18	66
Fine lamellar pearlite	20	68
Upper bainite	38	72
Lower bainite	37	74
Tempered martensite	45	80

I wonder if the authors would care to comment on these results and if they know of any other similar results obtained with this testing procedure.

Authors' Reply

The authors appreciate the comments and suggestions made by the various discussers. These serve to contribute additional information as well as to indicate where further work is needed.

Dr. Schmidt points out that in the case of many of the steels investigated, such as the stainless, the C-1019 and the NE 8640, the coefficient of friction of the chip on the cutting tool is essentially independent of cutting speed over the range investigated and thus the cutting force should also be independent of speed over that range. This was found to be essentially the case for these particular steels. However, in the case of those steels for which the friction coefficient varied with cutting speed, a corresponding variation in cutting forces was also observed, as might be expected.

Dr. Schmidt also draws attention to the fact that the coefficient of friction of chip on tool increases with decreasing feed and suggests that this may be due to the irregularity of the cutting edge. Whatever the cause, this behavior is practically universal in metal cutting, irrespective of the care with which the tools are sharpened. The coefficient of friction is always higher at low feeds than at high and it is this behavior which accounts for the well-known fact that more power is consumed in removing a unit volume of metal at low feeds than at high.

Mr. Boulger's discussion raises the question of how to predict machinability ratings from the basic properties dealt with in the paper. This was not the purpose of the present study. The primary reason for conducting the research reported in this paper is stated in the introduction: "to study the basic reasons for the good machinability of free machining steels". The aim was to single out and evaluate, insofar as possible,

each of the known basic factors that influence the machinability of each steel studied in order to analyze its cutting characteristics. By thus determining which basic characteristics of a given steel are poor from the point of view of machinability, one has a basis on which to work to improve its machinability.

Rating the machinability of the nine test samples was not the object of this paper. As a matter of fact there is no known single index number that adequately rates materials with respect to tool life, surface finish and power consumption. Most ratings are based solely on tool life tests. If a material has a high tool life rating but produces unsatisfactory surface finish it surely does not rate a high machinability index number, for many applications.

Mr. Boulger also raises the question as to why the increase in sulphur content of the A-8640 steel from 0.015 to 0.046% does not decrease the friction between the chip and tool, even though sulphur content of that order does affect machinability. The authors have recognized the fact in the paper that the presence of 0.046% sulphur does very definitely improve machinability in terms of increased tool life (see Table II) attributable to reduced abrasiveness. However, this is a very small quantity of sulphur compared to that present in the Type 303 stainless and the B-1113 steels and therefore it is not surprising that it does not cause any appreciable decrease in the chip friction, tool forces or surface roughness. However, it is interesting to note from the data given in Table IV or in Fig. 15 of the paper that there is an indication of very slightly lower friction in the case of the 0.046% sulphur steel, compared to the 0.015% sulphur steel.

The data which Mr. Garvey presents on the effect of low sulphur content added as stick sulphur is very interesting, and serves further to confirm the fact that small amounts of sulphur, even though not added in the form of sulphite, do serve to improve tool life to some extent. Since the authors' tests were made with carbide tools, and Mr. Garvey's tests with high speed steel tools, Mr. Garvey rightly inquires as to whether the presence of small amounts of sulphur might not show a significant decrease in chip friction if high speed steel tools were used. The authors do not have specific data on the A-8640 steels when cut with high speed steel tools. However, data obtained on the high sulphur B-1113 steel seemed to indicate that with high speed steel tools sulphur may be less effective in reducing friction than with carbide tools. These data are given in Table V of this closure. The effect may perhaps be attributed to the lower tool-face temperatures obtained with high speed tools, which should reduce the ability of the sulphide inclusions to smear over the tool face. In any event, the data suggest that it is not likely that lower friction coefficients would be found when cutting low sulphur steels with high speed steel tools than when cutting them with carbide tools. It appears rather that the benefits derived from small sulphur additions must be due mainly to a reduction of the abrasive action of otherwise harmful inclusions in the steel.

The data presented by Mr. Wilson on the relation of machining con-

Table V
Effect of Tool Material on Basic Properties of High Sulphur Steel

Tool: Rake angle (α) = +15°, relief angle = 3°
Cutting Speed: Readings averaged from data taken over range from 200 to 400 ft./min.
Feed: 0.003 in./rev.
Width (depth) of cut: 0.25 in.

Material	Average Coefficient of Friction Between Chip and Tool μ		Average Shear Strength S_s psi		Average Machining Constant "C" degrees	
	Carbide Tool	H.S.S. Tool	Carbide Tool	H.S.S. Tool	Carbide Tool	H.S.S. Tool
B-1113 (Sulphur)	0.56	0.78	70,000	72,000	75	76
C-1019 (Plain)	1.04	1.06	82,000	78,000	79	75

stant to structure in the case of the SAE 4350 steel are very interesting. The results appear to be in harmony with some preliminary tests made by the authors on similar types of steels. However, this work has not progressed far enough to allow any definite conclusions to be drawn. It is unfortunate that circumstances prevented Mr. Wilson from pursuing this study. The authors hope that he and others may find it possible to make further studies of this type in the future.

AN END-QUENCHED BAR FOR DEEP HARDENING STEELS

By Gerrit DeVries

Abstract

A test to give the relative hardenabilities of deep hardening steels is described. A 1-inch diameter bar 6 inches long was end-quenched from the austenitizing temperature in a fixture so constructed that the top of the bar was kept at approximately 1200 °F (650 °C) during the quench. This made the temperature in the bar a function of the distance from the quenched end and allowed the steel in the bar to transform isothermally at the various temperatures. After the bar had been in the fixture for an hour, it was taken out and given an over-all quench. The austenitic areas in the bar then transformed to martensite. The amount of transformation at each temperature was determined by making hardness measurements along the side of the bar and comparing the hardness at each position with the maximum hardness. By comparing the loss in hardness at various points with the temperature at those points during the quench the relative amount of transformation at any temperature could be estimated and thus the relative hardenability of different steels could be determined.

Introduction

MOST metallurgists are agreed that a structure of tempered martensite has the best physical properties. However, it is difficult to obtain a martensitic structure throughout a large size piece of steel because of the slow cooling rate of the piece. To overcome this difficulty steels which harden with slow cooling rates are used.

The measurement of the hardenability of these deep hardening steels is difficult because of the slow cooling rate needed. The best way is to heat treat various size pieces and observe the depth of hardening. However, the cost and difficulty of handling and heat treating

The statements or opinions in the article are those of the author and do not necessarily express the views of the Navy Department.

A paper presented before the Thirtieth Annual Convention of the Society, held in Philadelphia, October 23 to 29, 1948. The author, Gerrit DeVries, is metallurgist, United States Naval Proving Ground, Dahlgren, Va. Manuscript received April 15, 1948.

a number of very large pieces of steel is apparent. The estimation of the hardenability from isothermal transformation curves (S-curves) has the objection that a large amount of cost and work is needed to make the curves, the relation between the transformation at constant temperature and varying temperature is not completely known, and small size pieces of steel may transform at a different rate than large size pieces due to different amounts of strain.[1] Nevertheless, it is useful to know the differences in hardenability of two or more steels. Often steels of similar composition have great differences in hardenability and these differences may influence the physical properties. Therefore, a simple test giving the relative hardenabilities of deep hardening steels would be desirable. The test should use a small size sample, be capable of testing steels of the greatest hardenability, be easy to make and be reproducible in another laboratory.

The hardenability measurement of steels of low and medium hardenability can be done conveniently with the Jominy test; however, this test is not capable of distinguishing the difference in hardenability between steels of great hardenability. When Jominy bars of steels of great hardenability are tested, the bar hardens all the way to the end. To overcome this and permit a comparison of the hardenability of steels of great hardenability with relative ease, the Jominy test was modified by lengthening the bar 2 inches, making it 6 inches long and by keeping the top of the bar hot in a furnace while the end was being quenched. This allows the bar to be kept in the quenching fixture for any period of time. In the standard Jominy test the bar cools below the transformation temperature in less than 10 minutes.

Description of Test

The test piece was a round bar 1 inch in diameter and 6 inches long with a collar at the top to hold it in the quenching fixture. The quenching fixture consisted of a large galvanized can with a hole in the bottom to let the water drain and a pipe running up the center for the quenching jet. On top of the can in the center was a furnace which held the top 2 inches of the test piece. The furnace consisted of a 2⅜-inch diameter steel core, 2 inches long, with a 1.02-inch diameter hole in the center. The core was covered with alundum cement; then a coil of nichrome wire wrapped around it; this was

[1] G. K. Manning, "End Quench Hardenability Versus Hardness of Quenched Rounds," Metal Progress, Vol. 50, No. 4, October 1946, p. 647.

covered with more alundum cement; and the whole surrounded by insulating magnesia. The purpose of the core was to equalize the temperature in the furnace. A sketch of the furnace is shown in Fig. 1. The temperature of the furnace was controlled with a variac, but it would be better to have it automatically controlled because of the smaller temperature variation.

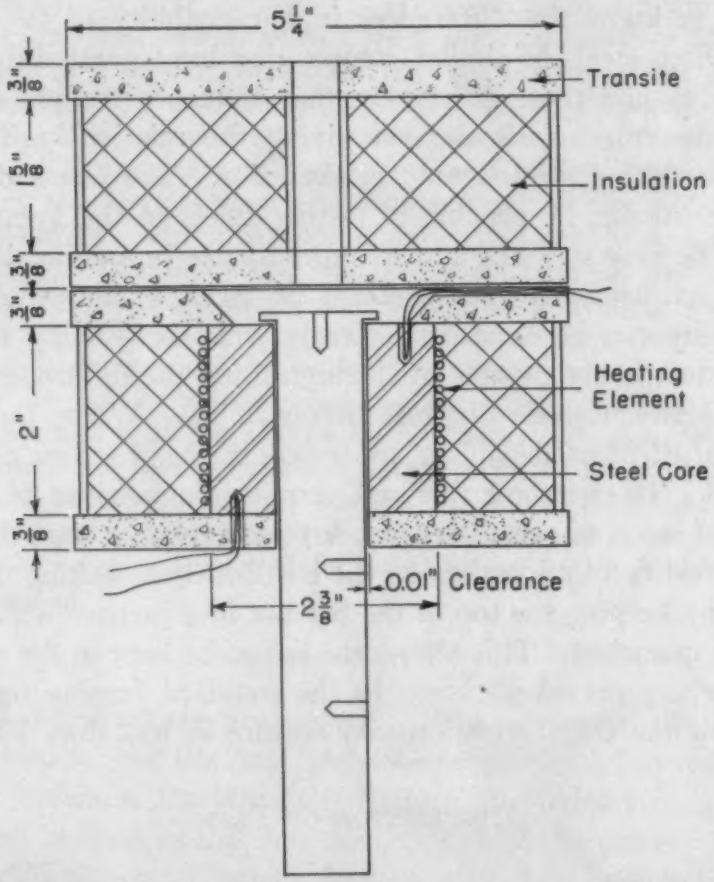


Fig. 1—Drawing of the Furnace Used to Keep the Top of the End-Quenched Bar Hot.

During the test the steel core was kept at approximately 1200 °F (650 °C) to keep the top 2 inches of the test piece hot. Thermocouples were placed in the steel core at the top and bottom and readings taken during the test. The bottom end of the test piece, which was ½ inch away from the top of the quenching jet, was struck by a ½-inch diameter, 2½-inch high, jet of tap water at approximately 70 °F. The test piece was kept in the fixture for 1 hour, then taken out and given an over-all water quench.

Experimental

Three test bars as described were made from each of three types of deep hardening steels. The steels were of the following composition:

Steel		C	Mn	P	S	Si	Ni	Cr	Mo	V
A		0.64	0.93	0.022	0.029	0.28	1.64	1.01	0.24	....
B	d	0.65	0.26	0.016	0.010	0.20	3.20	2.25	....	0.05
	e	0.64	0.38	0.018	0.018	0.43	3.38	2.22	0.08	....
C		0.35	0.69	0.012	0.010	0.24	3.25	1.32	0.48	0.27

All the steels had greater hardenability than could be measured

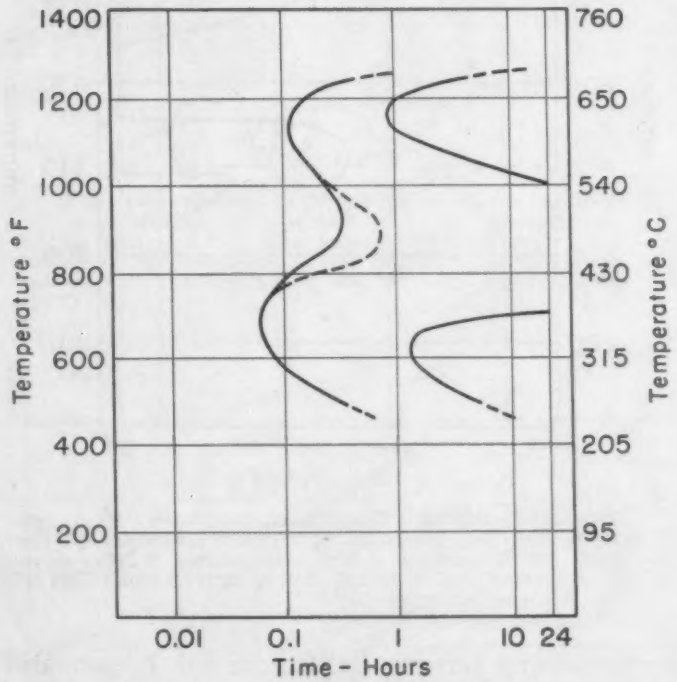


Fig. 2—Isothermal Transformation Curve of a Steel Similar to Steel A. Austenitizing temperature 1600 °F. Composition: 0.65% carbon, 0.79% manganese, 0.35% silicon, 1.00% chromium, 1.27% nickel, 0.29% molybdenum. Ms 445 ±5 °F. Mf approximately 100 °F.

with a Jominy bar. Isothermal transformation curves of steels similar to steels A and B and the isothermal curve of steel C are given in Figs. 2, 3 and 4. The test specimens of each steel were numbered 1, 2 and 3. Test specimen number 1 of steel B was made from heat d; specimens numbered 2 and 3 of steel B were made from heat e.

Three tests of each steel were made to determine the influence

of small differences in the steel core's temperature and other variables on the reproducibility of the test. Steels A and B were austenitized at 1600 °F (870 °C). Steel C was austenitized at 1700 °F (925 °C). To prevent decarburization, each bar was placed in a graphite cup and heated in a furnace with a carbon block. All the bars were held at the austenitizing temperature for 1 hour, then

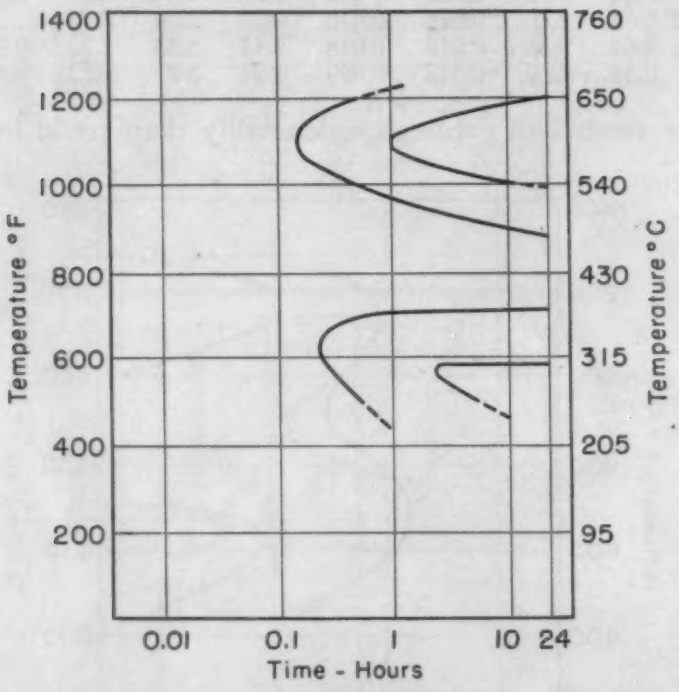


Fig. 3—Isothermal Transformation Curve of a Steel Similar to Steel B. Austenitizing temperature 1600 °F. Composition: 0.60% carbon, 0.37% manganese, 0.24% silicon, 2.14% chromium, 3.22% nickel, 0.07% molybdenum. Ms 395 ±5 °F. Mf approximately 70 °F.

placed in the quenching fixture, held there for 1 hour and then given an over-all quench in water. While the bars were in the fixture, temperature measurements were made in the bars at various positions. These measurements were made by inserting thermocouples into ⅛-inch diameter holes, ½ inch deep, drilled in the bars and reading the voltages at various times during the test.

The temperature of the steel core in the tests varied from 1200 °F by ±50 °F. Also, the temperature of the top of the bars varied by nearly that amount. However, since the temperature of the quenched end in all the tests was nearly the same, the differences in temperature near the quenched end of the specimens were less. Assuming that the steel core was kept at 1200 °F (650 °C), Fig. 5

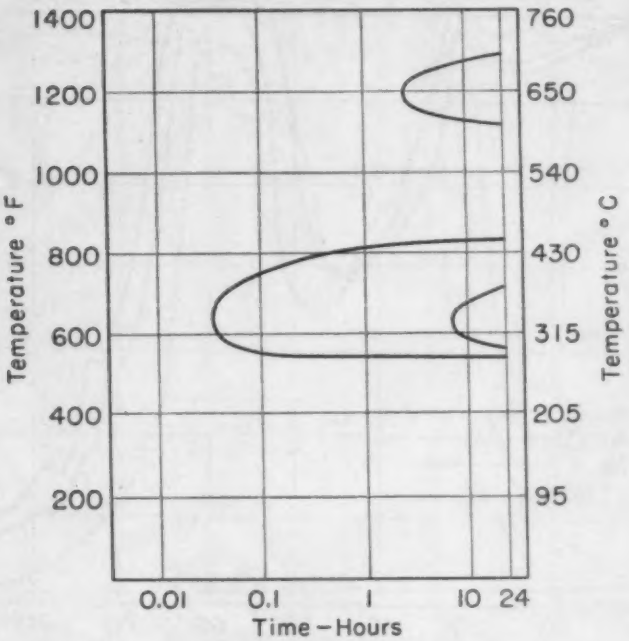


Fig. 4—Isothermal Transformation Curve of Steel C. Austenitizing temperature 1650 °F. Composition: 0.35% carbon, 0.69% manganese, 0.24% silicon, 3.25% nickel, 1.32% chromium, 0.48% molybdenum, 0.27% vanadium. Ms approximately 600 °F. Mf approximately 450 °F.

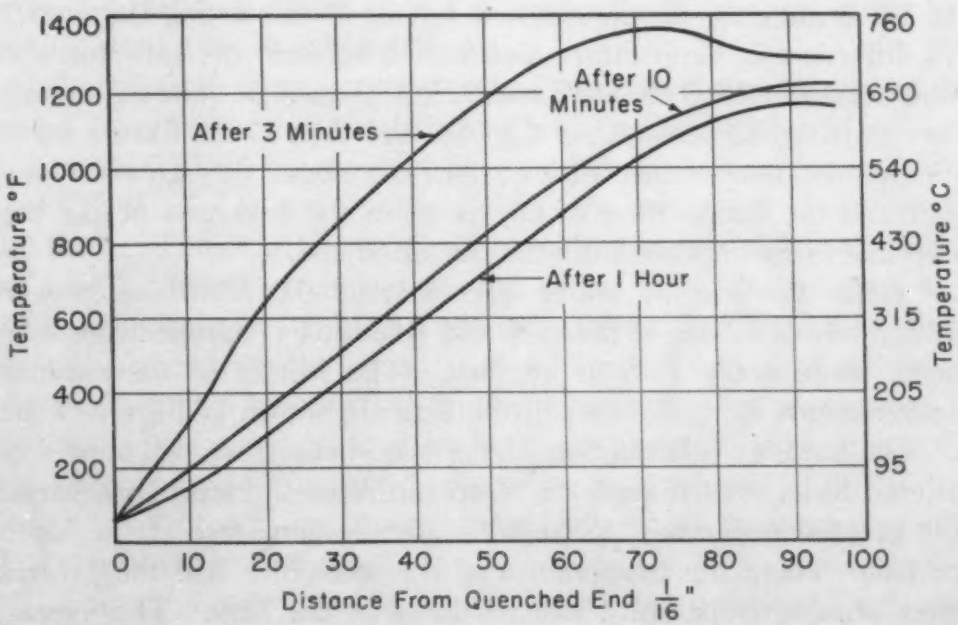


Fig. 5—Approximate Temperature Distribution in the Bar 3 Minutes, 10 Minutes and 1 Hour After the Start of the Quench.

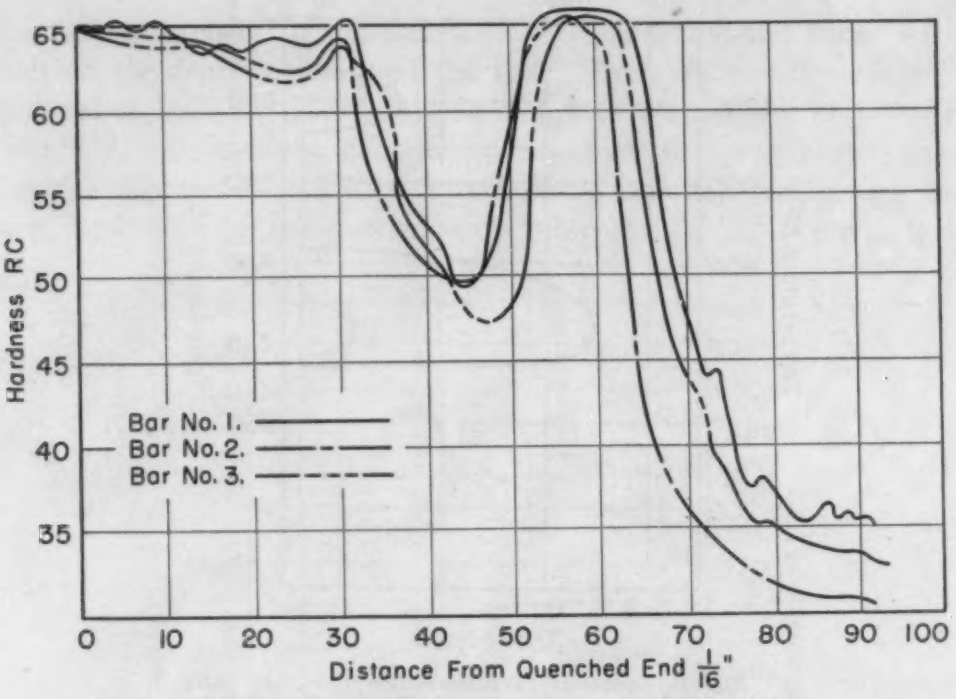


Fig. 6—Hardness Versus Distance From Quenched End of Three 1 by 6-Inch Bars of Steel A. End-quenched from 1600 °F with the top 2 inches of bar kept hot by a furnace. Average temperature ½ inch from top of bar for the last 40 minutes of the quench. Bar 1, 1140 °F; Bar 2, 1160 °F; Bar 3, 1130 °F.

shows the approximate temperature distribution along the length of the bar 3 minutes, 10 minutes and 1 hour after starting the quench. No difference in temperature distribution between the bars quenched from 1600 and 1700 °F (870 and 925 °C) could be found 3 minutes after starting the test. After the bars had been in the fixture for 20 minutes the temperature distribution was about the same as for 1 hour and the temperature of any point in the bars was nearly proportional to its distance from the quenched end.

After the over-all water quench, flats 0.015 inch deep were ground on both sides of the bars and Rockwell C hardness measurements made every 16th of an inch. The results of the hardness measurements along the flats of the bars are shown in Figs. 6, 7 and 8. The hardness distribution of the specimens from the same steel differed little, even though the temperature of the steel core varied. The greatest differences in hardness distribution were at the top of the bar. There the temperature of the steel core had the greatest effect on the temperature and hardness of the bars. The average temperature ½ inch from the top of the bars for the last 40 minutes of the test are given with Figs. 6, 7 and 8.

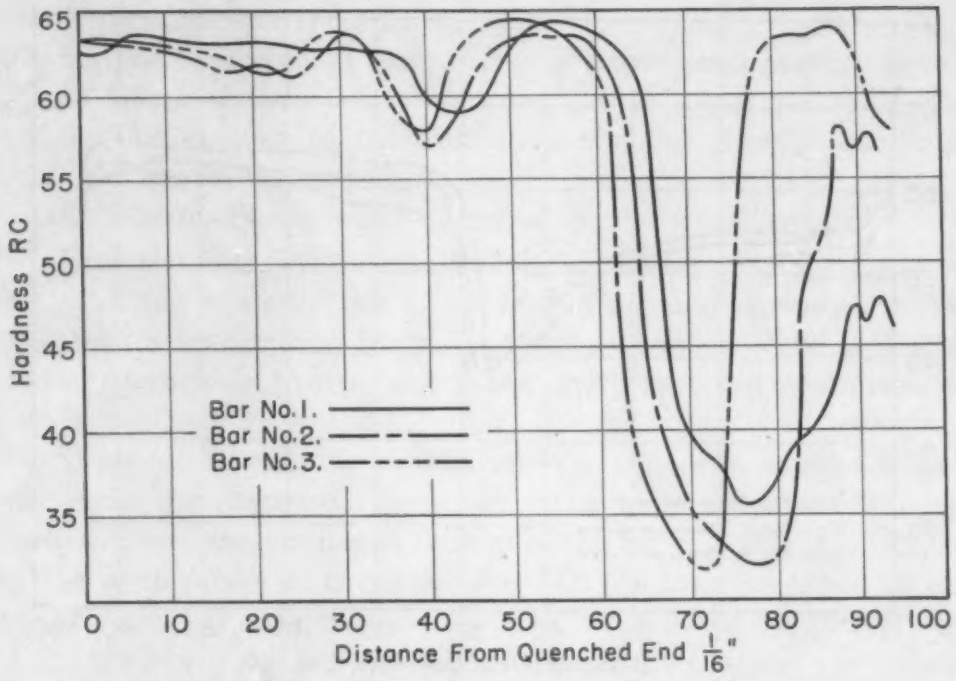


Fig. 7—Hardness Versus Distance From Quenched End of Three 1 by 6-Inch Bars of Steel B. End-quenched from 1600 °F with the top 2 inches of the bars kept hot by a furnace. Average temperature ½ inch from top of bar for the last 40 minutes of the quench. Bar 1, 1150 °F; Bar 2, 1165 °F; Bar 3, 1200 °F.

The effect of the temperature at the top of the bar can best be seen in Fig. 7; there the hardness at the top of the bar is proportional to the temperature. This shows the necessity for the top of the bar to be kept at a constant temperature.

The differences in hardenability of steels A, B and C can be estimated from a study of the hardness distribution as shown in Figs. 6, 7 and 8. These curves show that steel A has not as great a hardenability as steel B and that steel C has the greatest hardenability of the three. The form of the curve of each steel was different. Steel A had a big drop in hardness about 3 inches from the quenched end, then an increase in hardness and then another decrease in hardness about 5 inches from the quenched end. Steel B had a small drop in hardness about 3 inches from the quenched end, then an increase in hardness, then another drop in hardness about 5 inches from the quenched end and then another increase in hardness. Steel C had only a small drop in hardness about 3 inches from the quenched end. The rest of the bar was hard.

Using the curves in Fig. 5 showing the temperature distribution and Figs. 6, 7 and 8 showing the hardness distribution, the temperature and the amount of bainite and pearlite formation can be esti-

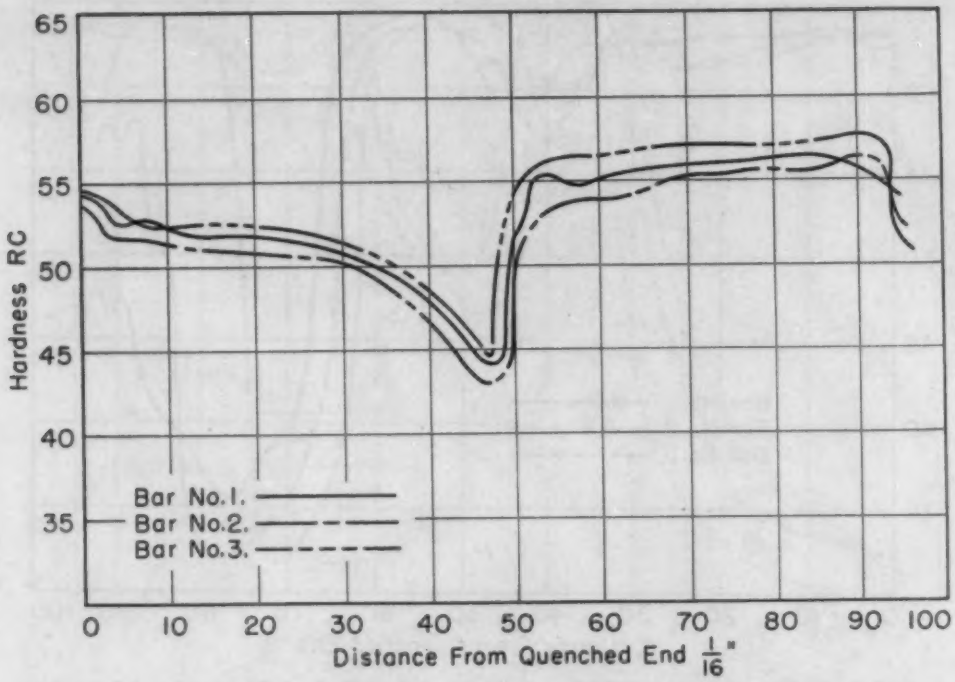


Fig. 8—Hardness Versus Distance From Quenched End of Three 1 by 6-Inch Bars of Steel C. End-quenched from 1700 °F with the top 2 inches of the bars kept hot by a furnace. Average temperature ½ inch from top of bar for the last 40 minutes of the quench. Bar 1, 1140 °F; Bar 2, 1150 °F; Bar 3, 1190 °F.

mated. The drop in hardness about 3 inches from the quenched end is at the temperature of bainite formation and the drop in hardness about 5 inches from the quenched end is at the temperature of pearlite formation. From the curve showing the temperature distribution after 1 hour and the curve showing the hardness distribution, steels A and C had the maximum rate of bainite formation at about 650 °F and steel B at about 600 °F. Steel A had the maximum rate of pearlite formation at about 1150 °F (620 °C), steel B at about 1100 °F (595 °C), and steel C had such great pearlite hardenability that no softening occurred in that range. This checks with the transformation characteristics as given in Figs. 2, 3 and 4.

Discussion

This test as described has the following advantages:

1. It is simple and inexpensive to make.
2. The results are reproducible.
3. A comparison of the hardenability of any two or more types of steels can be made.

4. A small size specimen is used.
5. The approximate temperature of bainite and pearlite formation is shown.
6. The amount of transformation for any selected length of time can be determined.
7. The maximum water-quenched hardness is given.

This test is only a little more expensive than a standard Jominy test. All that is needed is a 6-inch long end quench specimen, a furnace with a temperature-controlled steel core mounted on a regular Jominy quenching fixture, and a few more hardness measurements than a standard Jominy test.

It should be possible to duplicate the results in another laboratory since the apparatus is simple. The most important thing to control is the temperature at the top of the bar and this is controlled by the temperature of the steel core. In the tests described in this report there was a difference of 40 to 60 °F between the temperature of the steel core and the top of the bar. If the cover of the furnace had been heated, the difference in temperature between the steel core and bar would have been less. In tests at another laboratory, with another set-up, the temperature difference between the steel core and top of the bar may not be the same as in this report but by regulating the temperature of the steel core the temperature of the top of the bar could be the same. However, to get exactly the same temperature distribution in the bar the other furnace should be constructed like the furnace in this report.

The hardenability of any steel can be estimated by regulating the temperature of the steel core and the length of time the bar is in the quenching fixture. By leaving the bar for a long period of time in the fixture any steel will transform. It may be necessary with some new steels to make two or more tests in order to get all the information desired. As an example, to find the temperature of the pearlite formation of steel C, another test would have to be run for a longer time. The side of the bar could be polished, etched and examined with a microscope to determine the amount of transformation.

The minimum as-quenched hardness at the center of any size piece of steel can be estimated if the cooling rate is known and samples of the steel are tested by this test for the proper lengths of time. If a plate of steel C were quenched so that the temperature in the center remained in the transformation range for less than an hour, the hardness in the center would be greater than Rockwell C-43.

This test also gives the approximate temperature at which bainite and pearlite formation begins and ends and also the amount of transformation in a given period of time. By knowing the temperature of bainite and pearlite formation, the best temperature to hold for annealing, austempering and martempering can be determined.

Very little of the steel transforms until the temperature in the bar reaches a steady state. So the transformation of the steel is essentially at constant temperature. But, the steel in the bar reaches this constant temperature gradually, not abruptly as in isothermal transformation specimens.

Acknowledgments

The author wishes to express appreciation to E. W. Kern, F. E. Baird and Charles Burton for assistance in making the quenching jig; to Ronald Hayes and Edith Berry for assistance in making the hardness measurements; to W. Dale Parker for making the drawings and to Henry L. DeRocher for reviewing the paper.

DISCUSSION

Written Discussion: By C. A. Liedholm, quality manager, Piasecki Helicopter Corp., Morton, Pa.

Mr. DeVries has developed a new and important test of hardenability and annealing response, and has offered it to the metallurgical profession. It is my hope that the usefulness of this test will not be underestimated, but that it will be promptly adopted, used, developed further, and refined.

One cannot underestimate, for instance, the value to a metallurgical practitioner who is expected to find correct answers, and quickly, to complex metallurgical questions, of having access to a test which appears capable of locating the temperature of maximum reaction speed of the pearlite or the bainite transformation, or to compare the hardenabilities of two deep hardening steels in one run.

From a practical standpoint, the fact that the test piece cools fairly slowly has the apparent advantage that the effect upon the bainite reaction of prior transformation in the pearlite region is not blotted out to the same extent as in strictly isothermal reactions. However, the fact that the major part of the reactions occur isothermally at various temperatures, of course, involves hazards to the interpretation of the test results in terms of strictly continuous cooling cycles.

It is to be hoped that this aspect be subjected to an intense investigation to promote the correct interpretation of the test.

As to the application of this test to determinations of "isothermal"

annealing temperatures, both the optimum and the permissible range, it is obvious that the possibilities are excellent, and the test fills a real need of long standing. If the test conditions are properly chosen and controlled, a few runs should be able to produce results which formerly required knowledge of the complete end-of-transformation curve of the isothermal diagram.

The experimental technique can evidently be varied in an unlimited number of ways to suit the purpose of testing but, of course, much will be gained if the accuracy of the temperature readings is improved, which is no problem with the fast single and multiple-point recording potentiometers which are commercially available nowadays. Such refinements will greatly enhance the usefulness of the test.

I repeat that I hope this test will be much used and I look forward to seeing reports in the future on typical applications. I congratulate Mr. DeVries on this excellent and timely development.

Written Discussion: By F. C. Albers, staff metallurgist, Caterpillar Tractor Co., Peoria, Ill.

The author has done a commendable job in developing an end quench test to determine some of the hardening characteristics of deep hardening alloy steels. However, it appears that he has overcomplicated the problem, to some extent, by superimposing constant temperature transformation conditions upon conditions of continuous cooling. By using a furnace to maintain one end of the test specimen at a temperature of 1200 °F (650 °C), constant temperature transformation conditions are imposed upon one end of the bar while the other end is cooled continuously in a water jet. This makes it extremely difficult to determine a relationship between position on the test bar and cooling rate or expected hardness in a quenched round of a given size. The cooling conditions imposed upon the specimen in this test are not similar to those experienced by a quenched piece, and therefore the test may be of questionable value in predicting quantitatively the depth of hardening that will result from a given quenching operation.

In spite of the above objections, this test should be satisfactory for comparing the hardening properties of deep hardening alloy steels on a qualitative basis. It also has the advantage of supplying certain information about the time-temperature-transformation diagram for the steel being tested. In this connection it should be mentioned that the TTT curves, presented in the paper, in some cases do not support the end-quench hardness test results obtained. An example of this is exhibited by steel A. The end-quench hardness curves (Fig. 6) show a hardness peak at a distance of 60 sixteenths from the quenched end. Referring to the temperature distribution curves (Fig. 5) it is seen that at a distance of 60 sixteenths, after a period of 1 hour, the bar was at a temperature of about 900 °F (480 °C). The TTT curve for this steel (Fig. 2) shows that after holding a sample for 1 hour at 900 °F (480 °C) some transformation has taken place. If this were true, we would not expect to obtain maximum hardness at this point. Of course, the reason for this discrepancy, as the author has pointed out, lies in the fact that the

steels used for the end quench tests and those used to determine the TTT curves were similar but not of the same composition. It is interesting to note, however, how the end quench test results do render information on the isothermal transformation characteristics of the material being tested.

It would be of considerable interest to know how Mr. DeVries' end quench hardenability results compare with those obtained by other methods of determining the hardenability of deep hardening steels. Would the steels tested appear in the same order of merit if their hardenability were determined by the direct quenching of different size rounds? Or, another test that might be used for comparative purposes is the air hardenability test[2] developed by workers at the Carpenter Steel Co.

In closing I would like to ask Mr. DeVries how he explains the high hardness obtained on the upper end of the end quench samples from steel C. The hardness of that portion of the sample held at 1200 °F (650 °C) for 1 hour and then quenched is greater, by two or three points Rockwell "C", than the end of the sample quenched directly in water. Could this be due to more retained austenite in the end of the bar receiving the rapid quench?

Written Discussion: By William Wilson, Jr., research metallurgist, Armour Research Foundation of Illinois Institute of Technology, Chicago.

The development of a hardenability test for deep hardening steels was undertaken about two years ago, as a part of the A. Finkl and Sons Company research program. Although the air hardenability test developed by Post, Fetzer and Fenstermacher had been published at that time, the desirability of including the hardenability range of the Jominy test suggested the development of a new test similar in principle to the one developed by Mr. DeVries.

It suffices to say that the standard Jominy quenching conditions were applied to one end of the bar, and a furnace hindered the cooling of the other end of the bar to a prescribed cycle. The cooling curves for various points of this bar came rapidly to the temperatures predicted by the equation for heat conduction in a fin—during this portion of the cooling cycle, the cooling curves could not be modified by changing the prescribed cycle of the furnace. Below this steady-state temperature distribution of the bar, the cooling rates can only be adversely influenced by the prescribed cooling rate of the furnace.

If the furnace temperature is maintained constant, all points of the bar will cool rapidly to their respective steady-state temperature and remain at that temperature until the test is interrupted. The steels selected by Mr. DeVries have ideal diameters well in excess of the Jominy test limit and undoubtedly transform isothermally. However, steels which just exceed the hardenability limit of the Jominy test might transform during the initial rapid cooling portion of the test.

Complex deep hardening steels may be limited in hardenability either

[2] C. B. Post, M. C. Fetzer and W. H. Fenstermacher, "Air Hardenability of Steels," TRANSACTIONS, American Society for Metals, Vol. 35, 1945, p. 85-106.

by transformation in the pearlitic or bainitic temperature ranges or both. From the time-temperature-transformation diagrams and the author's hardness surveys, I would conclude that the limiting hardenability of steel B would be found in the pearlitic temperature range and the limiting hardenabilities of steels A and C would be found in the bainitic temperature range.

In view of the obvious limitations of predicting cooling transformations from isothermal transformation data, it would appear essential that the cooling curves should at least approximate the simplified solutions of the heat conduction equations. When this condition is not met by any hardenability test, reliable test results cannot be expected from that test. Obviously the hardenability tests mentioned in this discussion do not conform to the simplified solutions of the heat conduction equations.

The latest test developed for the A. Finkl and Sons Company uses a 1¼-inch diameter bar 11 inches long and this bar has its radial heat flow modified throughout almost its entire length. The details of this test will be published within the next year—a detailed description here would consume too much time. Measured cooling curves on this hardenability test bar approximately conform to the simplified solutions of the heat conduction equations. Hardenability can be studied successfully in steels with an ideal diameter less than 21. This is approximately three times the limit of the Jominy hardenability test.

Author's Reply

The author would like to extend his thanks and appreciation for the interest exhibited by the discussers in the preparation of written contributions and the constructive comments which they have presented.

As the discussers point out and as is mentioned in the introduction, the relation between transformation at constant temperature and transformation or continuous cooling is not exactly known and therefore caution should be used when the results of this test are applied to continuous cooling cycles.

Unfortunately, because of lack of material it was not possible to determine the hardenability of the steels by other tests as suggested by Mr. Albers. His last question, the high hardness of steel C at the upper end, may be explained by the difference in cooling rates of the bar. When the bar is removed from the fixture and given an over-all quench at the completion of the test, the cooling rate at 0.015 inch below the surface of the round is greater than the cooling rate obtained at $\frac{1}{16}$ inch from the quenched end of the bar in the test apparatus. Consequently, the austenite remaining in the bar at the completion of the test transforms to a harder product than that originally transformed at the quenched end of the specimen.

RESIDUAL STRESSES AND MICROSTRUCTURE IN HOLLOW CYLINDERS

By H. B. Wishart and R. K. Potter

Abstract

Compressive stresses can be produced on the surface of hollow cylinders by quenching in a suitable medium from austenitizing temperatures. Tensile or compressive stresses can be produced at the bore of the cylinder by quenching with plugged or open ends. The magnitude of the stresses is controlled within limits by the draw temperature.

The formation of an appreciable amount of martensite at the surface of the cylinders during water quenching materially lowered the surface compressive stresses when the cylinders were drawn, due to the volumetric change which occurs when martensite is tempered.

DURING the past several years the use of residual stresses to obtain increased resistance to fatigue failure in various items has materially increased. In specific applications such as shafts and axles subjected to flexural stresses, residual compressive stresses in the outer fibers of the member have been known to increase the fatigue resistance of the member. Since the magnitude of the tensile stress in the outer fibers of a shaft subjected to complete reverse bending governs the ability of the shaft to resist fatigue damage when no detrimental factors exist such as imperfections in the surface, then any residual compressive stress in the outer fibers in general tends to reduce this magnitude.

It is of course to be realized that for the residual stress to be beneficial in prolonging the life of any part, in the majority of cases the residual stress must be effective during the life of the part. While there is some question as to the lasting effect of residual stresses, particularly when occasional overloads or other adverse service conditions are encountered, the general indication is that if residual stresses are made use of in a conservative manner, beneficial

A paper presented before the Thirtieth Annual Convention of the Society, held in Philadelphia, October 23 to 29, 1948. Of the authors, H. B. Wishart is chief development metallurgist, and R. K. Potter is metallurgical inspector, Gary Steel Works, Carnegie-Illinois Steel Corp., Gary, Indiana. Manuscript received May 28, 1948.

results can be obtained. Moore (1)[1] has shown in a limited number of tests that residual stress is reduced by overloads, the degree of reduction varied with the condition of loading. In any given application it is therefore best to make a careful investigation of the beneficial effects to be derived in any part where residual stresses are to be used to give increased service life.

Zimmerli (2), Horger and Neifert (3), and Almen (4) have shown that a compressive stress can be produced in the outer fibers of steel members by shot peening and that improved fatigue resistance is obtained. Horger and others have shown that compressive stresses can also be developed by cold rolling and heat treatment. As the purpose of this investigation was to develop a satisfactory and relatively simple mill method of producing compressive stresses in the outer fibers of large diameter (7-inch) cylinders, the heat treating method was selected as being the most practical when all factors were carefully considered.

The determination of residual stresses in cylinders is not an easy problem. While some excellent work has been done in the past in measuring residual stresses and in determining stresses in various grades of steel subjected to different heat treatments by Scott (5) and others, the amount of equipment necessary for the accurate determination of such stresses was materially reduced and the process simplified with the development of the electric strain gage. All residual stress determinations reported in this paper were obtained by the use of such gages.

Specimens Used in Investigation

The hollow cylinders used in this program were obtained from three different grades of steel, SAE 1045, 1035, and 1020. The analyses of the steels used are shown in Table I. The cylinders,

Table I
Chemical Compositions of Cylinders

Grade of Steel	Analysis, Per Cent				
	C	Mn	P	S	Si
SAE 1045	0.46	0.68	0.016	0.028	0.23
SAE 1035	0.33	0.72	0.017	0.024	0.17
SAE 1020	0.20	0.49	0.016	0.025	0.25

[1]The figures appearing in parentheses pertain to the references appended to this paper.

18 inches in length and 7 inches in diameter, were machined from 7¼-inch diameter forged rounds. It was desired to use as long a cylinder as possible in order to eliminate end effects on stress determinations. Mechanical considerations were the limiting factor in using a longer cylinder. As Sachs (6) indicated that a length 2 to 3 times the diameter is sufficient in a cylinder to obtain reliable stress results, the 18-inch cylinders were considered to be satisfactory. A 4-inch diameter hole was bored longitudinally through the center of each cylinder before heat treating.

Heat Treatment of Cylinders

Compressive surface stresses can be produced by both subcritical quenching and by quenching under certain conditions from an austenitizing temperature when the cylinders are entirely heated or locally heated. Also many combinations of quenching media and quenching with open and closed ends are possible. The data contained in this paper pertain to fully heated cylinders some of which were quenched in water and some in oil, from an austenitizing temperature of 1600 °F (870 °C). The cylinders were quenched with open and closed or plugged ends. The plug consisted of a machined disk which was bolted to each end of the cylinder before heating.

In all cases the cylinders were heated to 1600 °F (870 °C) and allowed to remain in the furnace approximately 3 hours prior to quenching. A controlled atmosphere, obtained by passing air through burning charcoal in a Lindberg Hydrizing Unit, was used in the heating furnace to minimize scaling and decarburization. Microscopic examination of the surface of cylinders after heat treatment showed little indication of decarburization. In quenching in either water or oil the cylinders were suspended vertically in the quenching medium by an eyebolt which was attached to one end of the cylinder. By this method no tongs or cold material came in contact with the cylinders to give an uneven quench.

The cylinders were given a circular motion during quenching and were held in the quenching medium until cold. When the cylinder was quenched in oil, the oil at the beginning of the quench of each cylinder was 70 °F and the final temperature was 120 °F. When the cylinders were quenched in water, due to the limited amount of water in the quenching tank, crushed ice was used to prevent the water temperature from going above 90 °F. After the quenching

operation the cylinders were drawn for 8 hours at the temperatures shown in Table II and then air-cooled. In several instances the residual stress was determined in cylinders which were not drawn.

Method of Determining Residual Stresses

There are a number of methods which may be used to determine residual stresses such as the split ring method, disk method, and the triaxial method proposed by Sachs (6). A review of these methods and others is given both by Sachs (7) and Barrett (8). Inasmuch as the Sachs method considers all three principal stresses, this method was selected for evaluating the residual stresses in the cylinder.

The Sachs method consists in boring the interior of the cylinder out in steps and measuring the changes in length and circumference after each boring operation. By the use of the data obtained during the boring operation, longitudinal, circumferential and radial stresses can be calculated for the cylinder.

The following formulas were used for the calculation of the stresses by the boring-out method:

$$l = \frac{E}{1-v^2}\left[(F_b - F)\frac{dA}{dF} - A\right] \qquad \text{Formula I}$$

$$t = \frac{E}{1-v^2}\left[(F_b - F)\frac{d\Theta}{dF} - \frac{(F_b - F)}{2F}\Theta\right] \qquad \text{Formula II}$$

$$r = \frac{E}{1-v^2}\left[\frac{(F_b - F)}{2F}\Theta\right] \qquad \text{Formula III}$$

Where:

F_b = Complete cross sectional area of cylinder, including bore $= \pi R_b^2$.
F = Variable cross sectional area to position of cutting tool (to surface of last boring operation) $= \pi R^2$.
l, t, r = Respectively the longitudinal, tangential, and radial stresses in the cylinder after boring out a cross sectional area of F.
E = Modulus of elasticity (30,000,000 was used in these calculations).
v = Poisson's ratio (0.25 was used in the calculations).
$A = e_l + ve_e$
$\Theta = e_e + ve_l$
e_l = Cumulative strain measured by longitudinal strain gage on boring.
e_e = Cumulative strain measured by the circumferential strain gage on boring.

After each layer is bored out the strain gages are read and

Table II
Residual Stresses Developed in Cylinders

Cyl. No.	S.A.E. Steel	Type Quench**	Draw Temp. °F	Stress, psi × 1000, at Cross Sectional Areas of Cylinder Shown — 12.5 Sq. In. Represents Bore, 38.5 Sq. In. Is Circumference																				B.H.N.*** Average
				Longitudinal Stress							Tangential Stress							Radial Stress							
				12.5	15	20	25	30	35*	38.5	12.5	15	20	25	30	35*	38.5	12.5	15	20	25	30	35*	38.5	
PLUGGED ENDS																									
1	1045	W	None	115	100	50	5	−40	−85	−110	100	80	35	− 9	−50	−80	−100	0	5	15	15	11	7	0	
2	1045	W	600	27	45	50	−4	−52	−55	− 31	46	47	35	−18	−50	−58	− 37								372
3	1045	W	800	28	30	30	3	−26	−28	− 23	36	34	23	−17	−30	−22	− 14								305
4a	1035	W	600	46	48	48	15	−38	−50	− 35	40	39	40	− 8	−40	−44	− 31	0	3	8	8	5	2	0	365
5a	1035	W	800	17	18	28	0	−28	−19	− 12	17	18	25	− 8	−27	−18	− 2	0	2	5	5	3	1	0	258
64	1020	W	None	108	77	37	9	−35	−75	− 90	115	68	21	− 9	−49	−75	− 82	0	8	11	12	9	4	0	308
65	1020	W	600	31	40	29	12	−25	−42	− 46	31	39	16	− 5	−28	−37	− 39	0	2	6	9	5	2	0	214
66	1020	W	800	18	15	19	9	−16	−19	− 19	12	13	15	4	−22	−21	− 17	0	2	3	4	3	2	0	179
5	1045	O	None	63	60	38	10	−27	−66	− 80	53	51	28	0	−32	−61	− 80								250
6	1045	O	600	30	40	60	15	−27	−63	− 67	43	50	38	0	−40	−63	− 64								250
7	1045	O	800	19	24	21	2	−18	−32	− 35	15	20	23	0	−24	−31	− 33								250
2a	1035	O	600	38	36	25	8	−17	−40	− 50	25	30	20	− 3	−24	−38	− 40	0	2	5	7	5	2	0	193
3a	1035	O	800	19	16	15	4	−13	−23	− 26	6	8	10	5	−10	−18	− 18	0	1	2	3	3	1	0	203
68	1020	O	600	32	31	24	−4	−18	−26	− 33	29	27	19	− 9	−19	−27	− 29	0	2	5	5	2	1	0	142
67	1020	O	800	30	29	16	−2	−16	−21	− 21	30	21	11	− 8	−16	−19	− 15	0	2	5	5	3	2	0	145
OPEN ENDS																									
10	1045	W	600	−60	−55	43	36	10	−50	− 38	...	−40	35	−47	−32	−45	− 27								426
11	1045	W	800	−20	−18	18	20	− 7	−18	− 9	−27	−23	18	21	− 6	−16	− 8	0	−1	−2	0	2	5	0	313

*0.165 inch from surface or circumference of cylinder.
**Under this column "W" =water; "O" =oil.
***Average equivalent Brinell hardness taken on periphery of cylinder.

Table II (continued)
Residual Stresses Developed in Cylinders

Cyl. No.	S.A.E. Steel	Type Quench**	Draw Temp. °F	Stress, psi × 1000, at Cross Sectional Areas of Cylinder Shown — 12.5 Sq. In. Represents Bore, 38.5 Sq. In. Is Circumference — Longitudinal Stress 12.5	15	20	25	30	35*	38.5	Tangential Stress 12.5	15	20	25	30	35*	38.5	Radial Stress 12.5	15	20	25	30	35*	38.5	B.H.N.*** Average
OPEN ENDS																									
9a	1035	W	600	−95	−30	45	32	−14	−43	− 26	−130	−10	35	36	−20	−40	− 26	0	−3	−2	3	4	2	0	373
10a	1035	W	800	−85	−20	15	25	8	−21	− 14	− 80	−25	13	21	12	−11	− 6	0	−3	−3	−1	2	1	0	250
59	1020	W	600	−50	−15	29	39	− 5	−39	− 41	− 59	−23	37	39	− 5	−34	− 31	0	2	1	1	2	1	0	180
60	1020	W	800	−24	− 1	19	23	− 9	−19	− 16	− 45	0	19	21	−11	−11	− 10	0	−4	−2	8	17	14	0	198
14	1045	O	600	−46	−42	29	35	2	−37	− 52	− 30	−27	30	36	20	−30	− 39								245
15	1045	O	800	−30	−25	10	18	12	−20	− 34	− 56	−45	14	19	14	− 5	− 21								250
7a	1035	O	600	−80	−30	26	31	18	−40	− 53	− 95	−23	27	33	15	−17	− 53	0	−7	−5	0	2	2	0	222
8a	1035	O	800	−75	−28	16	19	9	−16	− 26	− 80	−30	17	24	17	− 3	− 15	0	−4	−4	0	1	2	0	206
62	1020	O	600	−25	−26	26	26	− 6	−31	− 35	- 35	−54	31	31	8	−28	− 32	0	−2	−4	0	3	3	0	156
63	1020	O	800	−60	−11	15	18	9	−10	− 11	−110	−15	28	24	15	−16	− 14	0	−8	−6	1	0	9	0	142

*0.165 inch from surface or circumference of cylinder.
**Under this column "W" =water; "O" =oil.
***Average equivalent Brinell hardness taken on periphery of cylinder.

averaged to give e_l and e_c, from which A and Θ are determined. Values of A and Θ then are separately plotted against F. By measuring the slopes at various points on these curves $\frac{dA}{dF}$ and $\frac{d\Theta}{dF}$ are found. The stresses l, t, and r are then calculated for the various values of F by Formulas I to III.

In order to obtain the changes in length and circumference as required by the Sachs method, SR-4 electrical strain gages were cemented to the outer surface of the cylinders when the cylinders had cooled to room temperature after the last heat treating operation. These gages were mounted midway along the cylinder length so that there was a set of longitudinal and tangential gages mounted at 90-degree intervals on some cylinders and on each side of the cylinder, 180 degrees apart on other cylinders. These gages were covered with wax to protect them from moisture and from cooling liquid used in the boring-out process.

During the process of boring, the cutting tools were kept sharp, coolant was used, and metal removed on any one cut was kept to a minimum in order to reduce the heating and cold working. In the boring operation the cross sectional area of the material was divided into fifteen equal concentric rings. Fourteen of these rings were removed in successive boring operations, leaving the fifteenth remaining as a shell.

After each boring-out step, the cylinder was removed from the lathe and allowed to cool in the laboratory overnight before the strain readings were made. This was to allow the cylinder to cool to room temperature so that changes in length due to temperature would not affect the strain readings. An SR-4 Baldwin strain indicator was used for obtaining the strain gage readings. Variations in laboratory temperature were compensated for by the use of dummy gages. The bore dimensions were obtained by a micrometer.

The respective changes in longitudinal and circumferential readings were averaged for each boring step before calculating the residual stresses. Considerable variation was noted at times between the comparative gage readings, possibly due to such items as a slight distortion occurring in the cylinder caused by uneven quenching and slight differences in wall thickness. Typical data for a water-quenched and an oil-quenched cylinder are shown in Table V. These averaged longitudinal and circumferential strain readings are further leveled out by plotting e_l, e_c, A and Θ and drawing smooth curves

through the plotted points to obtain $\frac{dA}{dF}$ and $\frac{d\Theta}{dF}$. The stress calculated by use of the Sachs equations were then plotted as shown in Figs. 1, 2, and 3. The stresses shown in the tables and Fig. 4 were obtained from such plots at the locations shown. The so-called

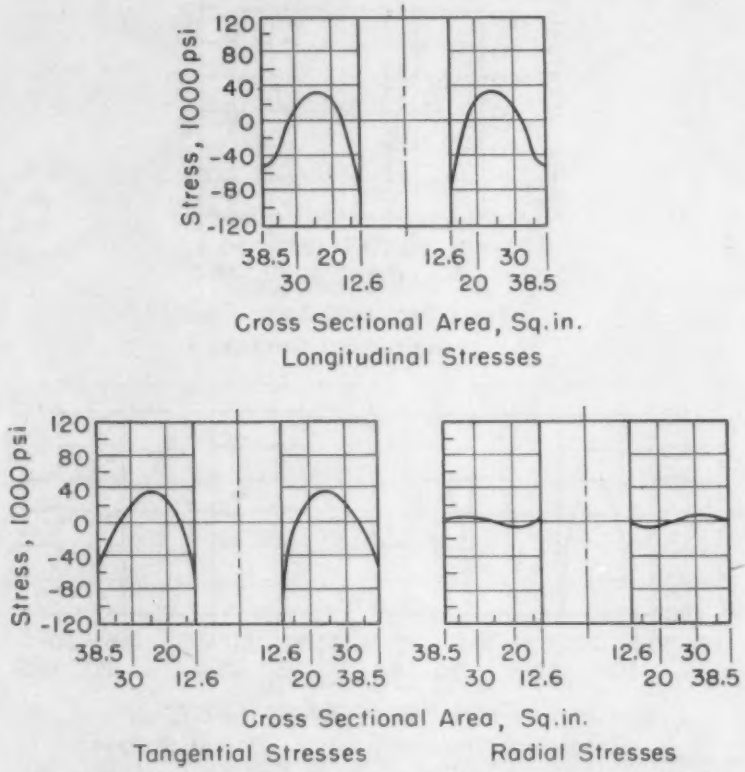


Fig. 1—Residual Stresses in a Hollow SAE 1035 Cylinder With Open Ends, Oil-Quenched and Drawn at 600 °F.

stresses at the circumference of the cylinders represent an extension of the curve from the last real value.

In order to check the reproducibility of this method two cylinders were treated identically, cylinder No. 6 (Table II) and cylinder No. 55 (not contained in this report). The surface stresses computed as previously described were —67,000 psi and —65,000 psi respectively for the two cylinders, which is a better check than would normally be expected.

The Sachs method of calculating stresses can be used by either mounting strain gages on the outside of the cylinder and boring out increments for determining the stresses in the cylinder or by mounting strain gages in the bore and turning the cylinder. Both methods were initially considered in this investigation. Due to the difficulty

involved in mounting the strain gages in the bore, the gages were mounted on the surface.

It is to be emphasized that at best the determination of residual stresses is a slow, time-consuming job. Every care must be taken in

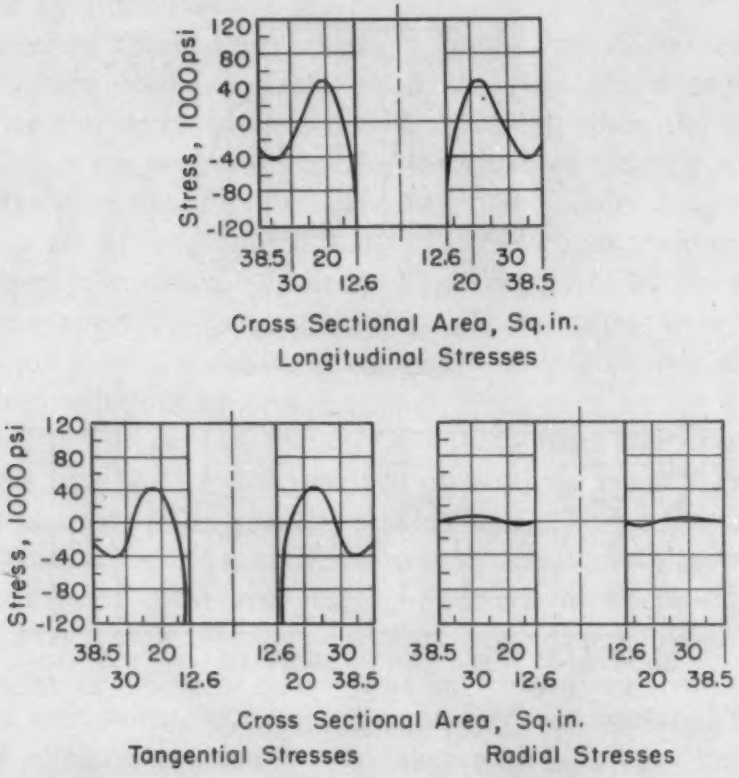


Fig. 2—Residual Stresses in a Hollow SAE 1035 Cylinder With Open Ends, Water-Quenched and Drawn at 600 °F.

the procedure and laboratory technique to insure that the values obtained are accurate and correct.

Test Data and Discussion

Data showing the residual stresses contained in twenty-seven cylinders from the bore to the circumference in the longitudinal, tangential, and radial directions are shown in Table II. Information pertaining to the grade of steel, quenching media, whether the cylinders were quenched with open or plugged ends, draw temperatures, and average equivalent Brinell hardness is also shown in the same table. Due to the curved surface of the cylinder, which made it impracticable to obtain Brinell readings direct, Rockwell hardness

readings were obtained and converted to Brinell values. These values are shown in a compact form in Table III.

Due to the large number of curves involved if data from Table II were to be plotted, three cylinders, 7a, 9a, and 4a, were selected

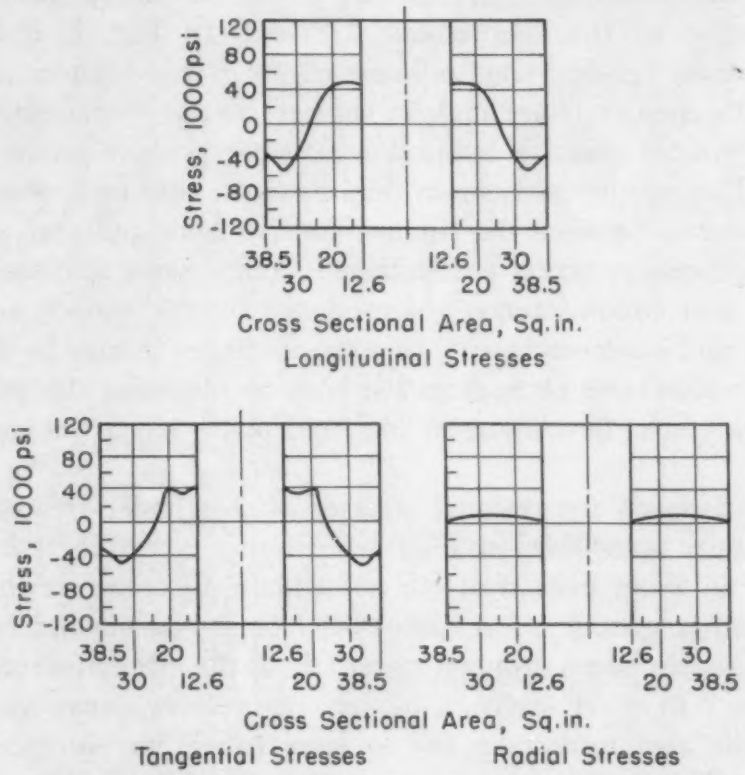


Fig. 3—Residual Stresses in a Hollow SAE 1035 Cylinder With Plugged Ends, Water-Quenched and Drawn at 600 °F.

as being representative of the group and the stress data plotted in graphical form as shown in Figs. 1, 2, and 3. In this group two cylinders were quenched with open ends, one in oil and the other in

Table III
Average Equivalent Brinell Hardness Taken on Periphery of Cylinder

Type Quench	Draw Temp., °F	SAE 1045 Steel		SAE 1035 Steel		SAE 1020 Steel	
		Open Ends	Plugged Ends	Open Ends	Plugged Ends	Open Ends	Plugged Ends
Water	None						
	600	426	372	373	365	180	214
	800	313	305	250	258	198	179
Oil	None		250				
	600	245	250	222	193	156	142
	800	250	250	206	203	142	145

water, while the third cylinder was water-quenched with the ends plugged.

Inasmuch as the residual longitudinal stresses are most important in increasing fatigue life in axles and shafting subjected to flexure, the discussion from this point on will be mainly devoted to a consideration of the longitudinal stresses. In Fig. 1, it is to be noted that the residual longitudinal stresses in this cylinder quenched in oil with open ends are high in compression at the circumference. Negative values indicate compressive stress; positive values, tensile stress. This compressive stress diminishes to zero and changes into a tensile stress between the surface and the bore and then develops into a compressive stress at the bore. Compressive stresses both at the bore and circumference are produced by the quench action on the inner and outer surfaces. In some instances it may be desirable to have compressive stresses in the bore to minimize the possibility of fatigue cracks developing at localized points of stress concentration.

Fig. 2 shows the residual stresses of a cylinder treated in the same manner as shown in Fig. 1 with the exception that it was quenched in water instead of oil. The main difference in the longitudinal and tangential stress curves between the two cylinders is that the compressive stress dropped materially at the circumference in the latter case. In other words, a higher compressive stress was developed in the area just under the surface than at the surface of the cylinder. This was an important finding in this investigation and will be discussed in greater detail later.

Fig. 3 shows the effect of plugging the ends of a cylinder before quenching. This cylinder was water-quenched. Here again the compressive stress at the surface is lower than obtained at a point slightly under the surface. The main difference between this curve and the one shown in Fig. 2, magnitude of stresses not being considered, is that tensile stresses are obtained at the bore of the cylinder.

By an inspection of the data shown in Table II, it is immediately apparent that the main general difference between the stress pattern of cylinders quenched with open ends and plugged ends is the compressive or tensile stresses developed at the bore. It is also to be noted that a comparative stress exists for a much greater distance from the surface toward the bore in the plugged-end-quenched cylinders than in the open-end-quenched cylinders.

Table IV

Longitudinal Stress, Psi × 1000, 0.165 Inch in From Circumference and at Circumference of Cylinders

Type Quench	Draw Temp., °F	Ends	SAE 1045 Steel: Stress Reading 0.165 Inch in From Circumference	SAE 1045 Steel: Circumferential Stress Reading	SAE 1045 Steel: Stress* Change	SAE 1035 Steel: Stress Reading 0.165 Inch in From Circumference	SAE 1035 Steel: Circumferential Stress Reading	SAE 1035 Steel: Stress* Change	SAE 1020 Steel: Stress Reading 0.165 Inch in From Circumference	SAE 1020 Steel: Circumferential Stress Reading	SAE 1020 Steel: Stress* Change
Water	None	Plugged	−85	−110	25				−75	−90	15
Water	600	Plugged	−55	−31	−24	−50	−35	−15	−42	−46	4
Water	800	Plugged	−28	−23	−5	−19	−12	−7	−19	−19	0
Water	600	Open	−50	−38	−12	−43	−26	−17	−39	−41	2
Water	800	Open	−18	−9	−9	−21	−14	−7	−19	−16	−3
Oil	None	Plugged	−66	−80	14						
Oil	600	Plugged	−63	−67	4	−40	−50	10	−26	−33	7
Oil	800	Plugged	−32	−35	3	−23	−26	3	−21	−21	0
Oil	600	Open	−37	−52	15	−40	−53	13	−31	−35	4
Oil	800	Open	−20	−34	14	−16	−26	10	−10	−11	1

*(−) Denotes decrease from stress reading 0.165 inch in from circumference.

Effect of Microstructure on Residual Stresses

Residual longitudinal stresses adjacent to the surface and at the surface of the cylinders shown in Table II have been compiled in Table IV. An additional column has been added to this table which

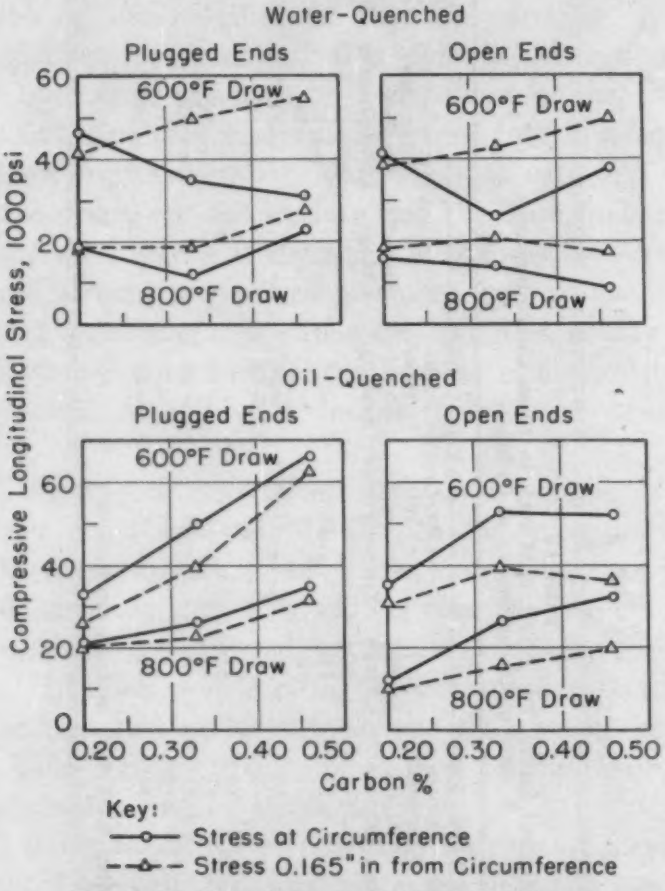


Fig. 4—Residual Stress in Cylinders at Circumference and 0.165 Inch in From Circumference.

shows the change in stress from an arbitrarily selected point 0.165 inch in from the surface to the stress at the surface. An inspection of this latter column shows that for the water-quenched and drawn SAE 1045 and 1035 cylinder the stress at the surface was always lower than the area adjacent to the surface. The lower the draw the higher the stresses and the greater the difference. In the oil-quenched cylinders of the same grades of steel the reverse was always true—that is, the stress was higher at the surface than adjacent to the surface. In both oil-quenched and water-quenched cylinders which were *not* drawn after quenching, the surface stresses were the highest.

Table V
Average Residual Stresses in 7-Inch Rounds, 4-Inch Bore SAE 1035 Cylinders Open Ends—Drawn 600 °F

Area of Bore Sq. In.	e_1* Average of 4 Gage Readings	Maximum Variation from Average in 4e_1 Gages	e_c* Average of 4 Gage Readings	Maximum Variation from Average in 4e_c Gages	Longitudinal Stress in psi	Tangential Stress in psi
			Water-Quenched			
12.56	0	0	0	0	−81,000	−214,000
14.80	−92	12	−150	40	−14,000	−11,000
16.63	−96	34	−168	47	7,000	+14,000
18.49	−37	48	−140	65	28,000	25,000
20.00	57	62	−89	46	46,000	34,000
21.70	156	64	−7	43	50,000	36,000
23.30	295	75	116	41	42,000	45,000
25.10	484	26	294	19	35,000	33,000
26.90	667	68	453	43	27,000	21,000
28.50	889	59	653	33	9,000	4,000
30.20	1020	50	778	54	−24,000	−22,000
31.90	1079	34	819	101	−40,000	−38,000
33.70	1026	51	794	101	−44,000	−42,000
35.22	977	58	716	179	−42,000	−38,000
36.84	976	89	636	259	−38,000	−33,000
			Oil-Quenched			
12.56	0	0	0	0	−160,000	−150,000
14.80	−119	19	−210	35	−19,000	−30,000
16.63	−145	25	−296	41	48,000	−3,000
18.49	−120	30	−312	42	21,000	21,000
20.00	−66	39	−304	49	27,000	27,000
21.70	−10	40	−262	68	31,000	32,000
23.30	+95	40	−211	64	27,000	35,000
25.10	178	48	−162	37	37,000	32,000
26.90	393	63	−41	59	27,000	28,000
28.50	534	69	50	50	23,000	22,000
30.20	766	81	241	46	15,000	15,000
31.90	1004	84	439	74	2,000	9,000
33.70	1158	69	581	96	−24,000	−8,000
35.22	1356	74	753	97	−41,000	−22,000
36.84	1404	139	920	90	−49,000	−35,000

*Microinches

The water and oil-quenched SAE 1020 steel cylinders did not show any marked change in surface stress with regard to quenching mediums used, such as was noted in the higher carbon steel cylinders.

The data contained in Table IV for cylinders drawn at 600 and 800 °F (315 and 425 °C) are plotted graphically in Fig. 4. In general the stresses at the surface of the oil-quenched cylinders decrease with decreasing carbon content of the steel. In the case of the water-quenched SAE 1045 and 1035 steel cylinders it is shown that the surface stresses in all cases are less than the stresses adjacent to the surface and in some instances are actually lower than the stresses developed on or near the surface of the SAE 1020 grade cylinders. With respect to the stresses near the surface, in general they have a tendency to decrease with carbon content.

In an effort to find an explanation for the dropping off of the

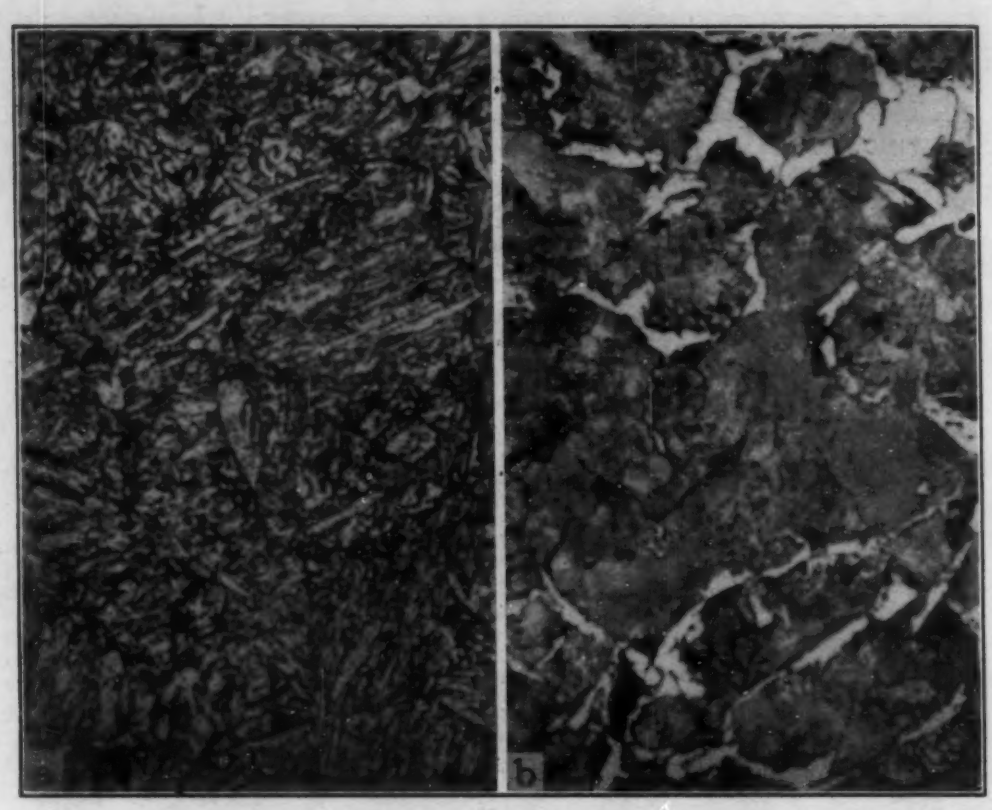


Fig. 5—Rims of SAE 1045 Cylinders Quenched With Plugged Ends. Picral etch. × 1000. a—Water-quenched and drawn at 800 °F. b—Oil-quenched and drawn at 800 °F.

surface stress in the water-quenched cylinders previously mentioned, a microscopic study was made of the oil-quenched and water-quenched cylinders at the circumference and adjacent to the circumference. Figs. 5, 6, and 7 contain photomicrographs of specimens cut from the circumference of oil and water-quenched cylinders of the three grades of steel. In all instances the cylinders from which the specimens were cut were drawn at 800 °F (425 °C).

The microexamination showed that a martensitic structure had been produced in the water-quenched cylinders at and near the surface. In the case of the SAE 1045 steel cylinders, the amount of martensite formed was sufficient to form almost a solid ring. The amount of martensite formed materially decreased with carbon content of the steels, so that only very small, infrequent patches were noted in the SAE 1020 cylinders. These patches are not apparent in Fig. 7. The martensite in the worst case, SAE 1045 steel, did not extend over one-eighth inch below the surface and except at the

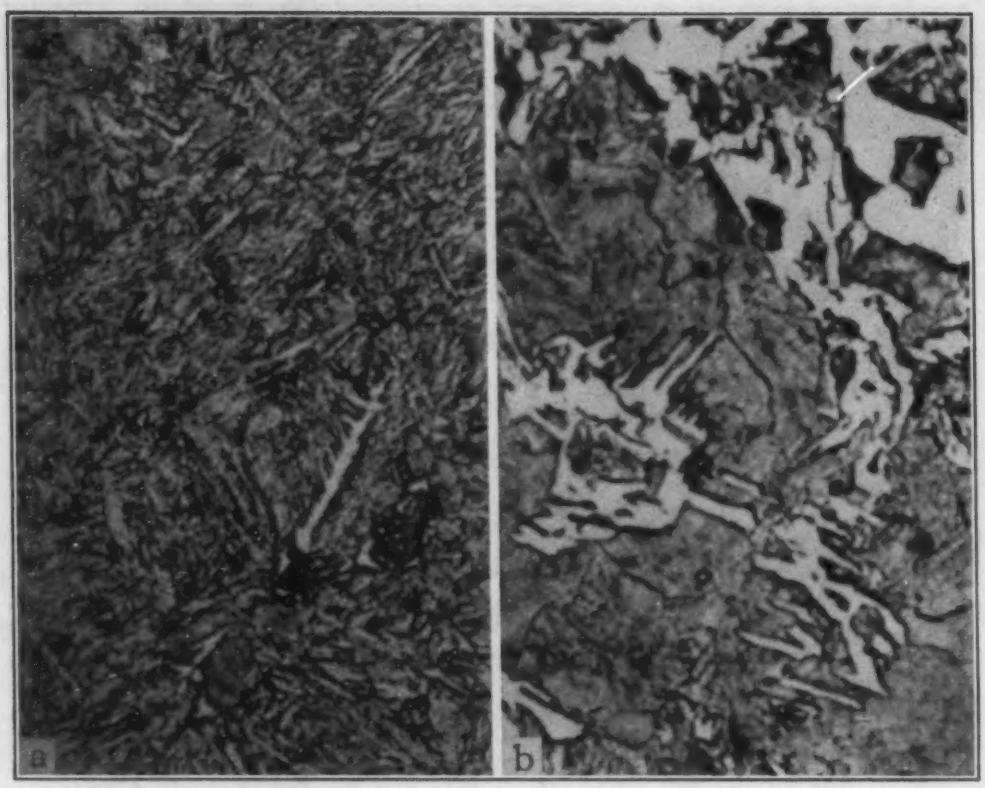


Fig. 6—Rims of SAE 1035 Cylinders Quenched With Plugged Ends. Picral etch. × 1000. a—Water-quenched and drawn at 800 °F. b—Oil-quenched and drawn at 800 °F.

surface occurred mostly in a "spotty" condition. No martensite was formed in any of the oil-quenched cylinders.

The fact that martensite was formed in the water-quenched cylinders does not necessarily mean that the compressive surface stress of the cylinders will be reduced. In Table IV the compressive stress at and near the surface of a water-quenched cylinder is shown which was not *drawn*. In this instance the surface stress was the maximum value. The explanation of the reduction of surface stresses in the water-quenched and drawn cylinders is the well-known fact that martensite when drawn undergoes a volume change. The amount of martensite existing in the SAE 1045 and 1035 cylinders was sufficient to cause, when drawn, an appreciable lowering of the surface stress, due to its volume change. This reduction of surface stresses was not apparent in the SAE 1020 steel cylinders, due to the insignificant amount of martensite formed.

It is apparent that if maximum compressive stresses are desired at the surface of quenched and drawn cylinders, then the quench

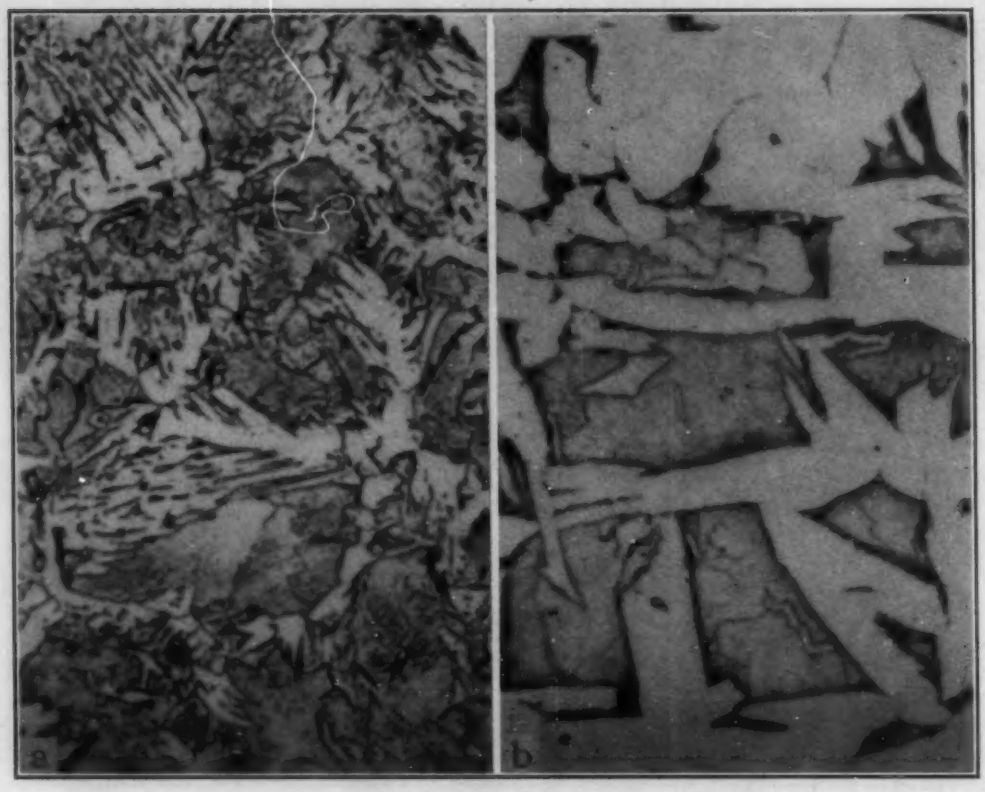


Fig. 7—Rims of SAE 1020 Cylinders Quenched and Plugged Ends. Picral etch. × 1000. a—Water-quenched and drawn at 800 °F. b—Oil-quenched and drawn at 800 °F.

must be so regulated as to prevent the formation of a layer of martensite. Where it is possible to machine the layer of tempered martensite from the quenched and drawn cylinder it has been found that control of the quench to prevent the martensite formation loses most of its importance. In stress analysis made on cylinders treated in this manner the compressive stress at the new surface was found to be slightly higher than the stress which existed at the same location before removing the layer containing tempered martensite.

Hardness Versus Stress

From a study of the data presented in this paper it is apparent that hardness of the steel and stresses contained in the steel have no direct relationship with each other. A good example of this non-relationship is shown in Table III by referring to the hardness values shown for the oil-quenched SAE 1045 plugged-end cylinders. For all three cylinders, one not drawn, one drawn at 600 °F (315 °C),

and the other drawn at 800 °F (425 °C), the surface hardness was the same. By noting the longitudinal compressive stresses for the same cylinders in Table IV, 80,000, 67,000, and 35,000 psi, it is apparent that the difference in draw temperature has appreciably affected the stress pattern without changing the hardness.

Conclusions

From the data contained in this paper it is to be concluded that longitudinal and tangential compressive stresses can be produced at the surface of steel cylinders by quenching the cylinders from an austenitizing temperature, the magnitude of the stresses being controlled by the draw temperature. The following items were found to be important in controlling the residual stresses produced in cylinders:

1. Cylinders quenched with plugged ends formed a tensile stress at the bore while a compressive stress was formed when the cylinders were quenched with open ends.
2. Appreciable amounts of tempered martensite formed at or near the surface of cylinders by quenching in water; drawing materially reduced the surface compressive stress due to the volumetric change which takes place when martensite is tempered. The surface stresses of the cylinders quenched in oil were not affected as the rate of quench was not sufficient to form martensite.
3. The effect of the ring of tempered martensite on the residual stresses can be eliminated by machining the area containing this constituent from the cylinder.
4. No direct relationship exists between changes in hardness and residual stresses.
5. The compressive stresses at or near the surface of the cylinders were in general lowered with decreasing carbon content of the steel where not influenced by the tempered martensite factor.

Acknowledgments

The authors wish to make acknowledgment to Messrs. L. E. White and E. L. Koehler, Gary Steel Works metallurgists, for their part in obtaining and calculating data reported in the paper, and to further acknowledge the helpful suggestions made by Mr. C. J. Hunter, chief metallurgist, Gary Works, and members of the Research and Technology Department during the preparation of this paper and to the management of Carnegie-Illinois Steel Corporation for permission to publish the paper.

References

1. H. F. Moore, "A Study of Residual Stresses and Size Effect and a Study of the Effect of Repeated Stresses on Residual Stresses Due to Shot Peening of Two Steels," *Proceedings,* Society for Experimental Stress Analysis, Vol. II, No. 1, May 1944, p. 170-177.
2. F. P. Zimmerli, "Shot-Blasting and Its Effects on Fatigue Life," SURFACE TREATMENT OF METALS, published by American Society for Metals, 1944, p. 261-278.
3. O. J. Horger and H. R. Neifert, "Improving Fatigue Resistance by Shot Peening," *Proceedings,* Society for Experimental Stress Analysis, Vol. II, No. 1, May 1944, p. 178-189.
4. J. O. Almen, "Shot Blasting to Increase Fatigue Resistance," *SAE Journal,* Vol. 51, No. 7, p. 249-268.
5. H. Scott, "Origin of Quenching Cracks," Bureau of Standards, 1925.
6. G. Sachs, "Der Nachweis-innerer Spannungen in Stangen und Rohren," *Z. Metallkunde,* Vol. 19, 1927, p. 352-357.
7. G. Sachs and G. Espey, "The Measurement of Residual Stresses in Metal," *The Iron Age,* Sept. 18, 1941, p. 63-71.
8. C. S. Barrett, "A Critical Review of Various Methods of Residual Stress Measurement," *Proceedings,* Society for Experimental Stress Analysis, Vol. II, No. 1, May 1944, p. 147-155.

DISCUSSION

Written Discussion: By Charles B. Bryant, chief engineer, Technical Board of the Wrought Steel Wheel Industry, Chicago.

The investigation described in this paper offers interesting and valuable information in regard to the development and control of residual stress patterns in cylindrical objects. In the manufacture of wrought steel wheels for heavy duty services, such as under Diesel locomotives or railroad passenger cars in high speed service, it has been the practice for some years to produce residual compressive stress in the tread and flange portions of the wheels. In fact, it would hardly be possible for wheels to give satisfactory and safe service for these purposes without such prestressing.

Compressive stresses are produced by quenching the tread portion of the wheel; the usual method being to mount the wheel at quenching temperature on a revolving mandrel and to cool the tread by water spray or by a combination of spraying and dipping in a trough. The values of compression at the surface produced by this method are of the same order as those described in the paper. The stress pattern below the surface is not well known; since, because of the geometry of a wheel, the Sachs boring-out method cannot be used.

The principal reason for such prestressing of wheels is to develop improved resistance to thermal cracking resulting from brake shoe heating. When heavily loaded wheels are severely braked, as in an emergency stop, the rate of energy dissipation amounts to hundreds of horsepower per wheel, and the tread of the wheel is strongly heated. The thermal expansion of the heated surface layer is resisted by the relatively cool metal beneath, and the surface layer is thus upset during the heating cycle.

After the brake shoe application is released and the wheel cools, this upset surface layer tries to contract. Through repetitions of this cycle, progressively increasing tension is set up in the tread of the wheel and when this reaches a sufficiently high value, thermal cracking occurs. By producing substantial residual compressive stresses in the wheel tread when it is new, the build-up of tension to the point where thermal cracking occurs is always greatly delayed and in most cases entirely prevented. Exact analysis of what goes on is complicated by metallurgical changes which occur when the heating is sufficient to exceed the critical transformation temperature and also by the fact that the surface is being continuously worn away by abrasion of rail and brake shoe. There is also cold working of the wheel tread because of the high unit pressures developed between tread and the rail.

Experience has amply demonstrated the value of initial residual compression in wheel treads.

Written Discussion: By E. L. Koehler, research metallurgist, Armour Research Foundation, Chicago.

I wish to congratulate the authors on the presentation of their material. Due to the great amount of work required by such testing, there is a scarcity of data of this sort. While the factors involved in the development of residual stresses are well known, as are qualitatively the stress distributions produced, the data presented give qualitatively the effects of a variety of heat treatments in large cylinders of plain carbon steels. Of special interest are the indications of effects of geometric shape on stress relief.

Perhaps a good starting point in illustrating this effect is Fig. 2 of this paper. The authors have shown the effects of tempering martensite existing at the surface on reducing the longitudinal and tangential stresses at the outer surface. It is likely, however, that a little more than this is involved. Since severity of quench is known to be even greater on the inside than on the outside of a hollow cylinder,[2] it must be assumed that martensite also existed at the inner surface. Instead of showing an equivalent effect on reduction of compressive stresses by contraction of the martensite on tempering, the stresses at the bore show remarkable resistance to relaxation. Others of the data presented likewise tend to indicate the following relationships:

1. Compressive stresses at the outer surface are readily relieved.
2. Tensile stresses at the inner surface are even more readily relieved.
3. Compressive stresses at the inner surface are not readily relieved.

The reason for this behavior is not too difficult to visualize. Stress relief is accomplished by a relaxation of shear stresses on plastic movement. The fact that the longitudinal and tangential stresses are in the same direction and about the same magnitude makes relaxation dependent on plastic flow in the radial direction. This is subject to the geometric limitation that flow toward the axis of the cylinder causes a decrease in diameter and therefore displaces the tangential stress in the compressive

[2] J. H. Hollomon and C. Zener, "Quenching and Hardenability of Hollow Cylinders," TRANSACTIONS, American Society for Metals, Vol. 33, 1944 p. 1.

direction. It is to be expected, therefore, that at the surface of the bore of the cylinder tensile stresses will be readily relieved while compressive stresses will be persistent. Likewise at the outer surface of the cylinder the compressive stresses are more readily relieved than tensile stresses would be. It can also be expected that the effect would be more noticeable at smaller diameters.

Written Discussion: By Thomas J. Dolan, research professor, Theoretical and Applied Mechanics, University of Illinois, Urbana, Ill.

The authors are to be commended for this careful study of the quenching stresses developed in hollow cylinders. Their logical explanations for the differences observed in water-quenched versus oil-quenched steel cylinders of different carbon content is a distinct contribution to our knowledge of some of the factors that are of importance in determining the final state of inherent stresses in a machine part.

The existence of a martensitic shell comprising the outer layers of the drastically quenched specimens of carbon steel, which resulted in surface residual stresses somewhat smaller than those below the surface, would lead one to predict that for large members of alloy steel this rim would be somewhat thicker due to the greater hardenability. This condition probably would exist even for slow quenching but would be accentuated to greater depth by rapid quenching. Thus for solid bars which have sufficient mass effect to prevent "through-quenching" to martensite, a rather complex (unknown) distribution of residual stresses is induced by quenching. Furthermore, unless exceedingly high drawing temperatures are employed, these residual stresses are not entirely removed by tempering but remain in some modified pattern in the final part as placed in service. Undoubtedly the residual stresses play an important part in affecting the final strength characteristics of a machine member; they may in many cases be fully as important as the stresses imposed by externally applied loads. The designer should therefore have at his disposal some means of estimating magnitude and distribution of the inherent stresses (whether they be beneficial or harmful) before he can produce with any assurance a safe, economical design.

In studying the data of Table II, it is of interest to note that after draw temperatures as high as 800 °F (425 °C) sustained for 8 hours, these metals still retained relatively high residual stresses (ranging from 19,000 to 28,000 psi compression). While these values are lower than the residual stresses observed for the "as-quenched" condition, they are still of considerable magnitude, and emphasize the futility of employing an ordinary low-temperature stress-relief heat treatment for cases in which an attempt is made to remove all harmful residual stresses. It is evident that much higher temperatures must be employed before an approach can be made to complete removal of residual stresses.

The authors have emphasized mainly the longitudinal stresses in connection with strengthening effects for shafts in fatigue. There are, of course, numerous other applications in which the circumferential or tangential stresses at the bore or at the outside diameter might be of particular importance. For pressure cylinders subjected to internal or to

external pressure, or for applications such as piston pins for internal combustion engines, hollow steel rollers, flywheels, etc., the data they have compiled have a direct application in at least a qualitative manner. The process of "auto-frettage" or cold working of cannon is employed to develop favorable (compressive) circumferential residual stresses in the bore. From the authors' data it appears probable that a carefully controlled process of heat treatment could develop a similar state of residual stress and make it unnecessary to resort to the use of the expensive equipment and tedious processing required to produce the desired residual stresses by "auto-frettage".

There is one other aspect of the problem that is not mentioned directly in the paper, but which is encountered in producing machine parts. In many manufacturing processes it is not possible to schedule the heat treatment to follow the machining to final dimensions; therefore, the usual sequence of operations requires stock to be removed from the surfaces of a member after heat treatment. Since the maximum residual stresses are at or near the surface, the machining operations will remove the most highly stressed layers. As a result, a redistribution of stress at interior points must occur to maintain equilibrium in the remaining metal. From this viewpoint, boring out layers of material having compressive stresses is equivalent to the addition of tensile stresses at the new bore surface; for known initial conditions the remaining residual stresses might be computed approximately for any particular case if inelastic action does not occur. However, it seems probable that the stresses at interior points after removal of surface layers could be evaluated accurately by simple super-position of the stresses obtained from the data recorded by the authors. It would be of interest if the authors could present in their closing discussion some concepts of the relative amount of residual stress remaining in the bore after the first surface layers had been removed, or those remaining on the outside diameter after the removal of a surface cut. These values would serve as a basis for estimating the amount of inherent stress to be expected in a finished part on which machining operations were necessary after final heat treatment.

Written Discussion: By H. J. Schrader, research professor, Theoretical and Applied Mechanics, University of Illinois, Urbana, Ill.

The authors have done a splendid job of determining the residual stresses in hollow cylinders and I feel that this paper is a fine contribution to engineering literature.

Abnormally high stresses, caused by accidental loads or localized heating, may eliminate some of the benefits of the residual compressive stresses on the surface. However, under normal operating conditions the stress situation may give an additional safety factor or, when the designer has reasonable assurance of no accidental high loads, a decrease in the size of a shaft may be possible.

Even though the determination of residual stresses is a tedious time-consuming proposition, I hope the authors will find it feasible to continue with this study, using solid cylinders. Applications of this method of heat treating for high surface compressive stresses would be numerous in the railroad industry, especially if applied to solid cylinders.

Authors' Reply

The authors wish to thank Messrs. Bryant, Koehler, Dolan, and Schrader for their comments on residual stresses. The discussions by the first two gentlemen require no answer.

It is quite possible as pointed out by Professor Dolan that the stress patterns in alloy steels may be quite complex. In some cases tension may be developed at the outer surface. A German paper[3] which we have recently examined has data which indicate such a condition was produced in 27.3-millimeter alloy bars.

Quench and draw treatments may be used for production of stress patterns for other applications than those mentioned originally by us. In any such application, it probably would be advisable to check the actual stress pattern by the Sachs method in order to be sure of the pattern actually produced.

In connection with the question asked about stress redistribution when layers are removed from the surface or bored from the interior, a study was made on one cylinder to determine the redistribution of stress when a given layer was removed from the surface. It was found that the stress at the new circumference was slightly higher in compression than it was at the same location before the turning operation. It was pointed out in the paper that the effect of tempered martensite toward reduction of the compressive stress on the surface of the cylinder could be practically eliminated if this area could be turned off.

Professor Schrader's comments regarding the possibility of removal of residual stresses by abnormally high stresses produced by external loading or heating are entirely valid. We have found that heat from a machining operation without the use of coolant may definitely affect stresses.

---

[3]H. Buhler and H. Buchholtz: "Uder die Wirkung von Eigenspannungen aug die Schwingungskestigkeit," *Mitteilungen aus dem Forschungs-Institut der Vereinigte Stahlwerke Aktiengesellschaft Dortmund*, Band 3, Lieferung 8, September 1933.

TRANSVERSE MECHANICAL PROPERTIES IN HEAT TREATED WROUGHT STEEL PRODUCTS

By Cyril Wells and Robert F. Mehl

Abstract

Average, variation, and degree of control of each of the properties—transverse reduction of area, transverse impact, and yield strength—have been determined for several units of heat treated wrought steel products. These units vary considerably in size: minimum, a part of a single tube or forging; maximum, several hundred tubes or forgings. Based on the quality and degree of control of quality observed per unit, specifications which operate more efficiently and economically for the acceptance of tubes for certain purposes have been developed.

Studies have been made of the effect on transverse ductility of (a) size of ingot, (b) forging reduction, (c) yield strength, (d) reheat treatment, and (e) nonmetallic inclusions. Relations between transverse reduction of area and transverse impact and between transverse impact and yield strength have been determined as has also the relation of angle between longitudinal axis and flow line direction in specimens to mechanical properties.

Significance of angular fracture and of porosity resulting from deep acid etching in relation to transverse reduction of area quality are discussed and evaluated.

Introduction

In a recent publication (1)[1] it was pointed out that as a result of research work done at the Carnegie Institute of Technology on gun tubes, three series of papers are to be written on the subjects of (a) Transverse Mechanical Properties in Heat Treated Wrought

[1]The figures appearing in parentheses pertain to the references appended to this paper.

This paper is based on work done for the Office of Scientific Research and Development under Contracts No. NDCrc-120, OEMsr-143, and OEMsr-771 with the Carnegie Institute of Technology in Pittsburgh.

A paper presented before the Thirtieth Annual Convention of the Society, held in Philadelphia, October 23 to 29, 1948. Of the authors, Cyril Wells is associated with the Metals Research Laboratory, and Robert F. Mehl is director of the Metals Research Laboratory, Carnegie Institute of Technology, Pittsburgh. Manuscript received April 15, 1948.

Steel Products, (b) Factors Affecting Steel Ingot Quality, and (c) Causes of and Remedies for Quench Cracking in Heat Treated Wrought Steel Products. So far, five papers in the second series, (1) to (5) inclusive, have been published.

The present paper, which is the first on the subject of "Transverse Mechanical Properties in Heat Treated Wrought Steel Products", consists primarily of a summary of material which is later to be reported in greater detail in other papers of the series. This procedure, while unusual, appears to be desirable, since it quickly brings together into one publication many pieces of interrelated information which are believed to be of immediate interest and value to many producers and purchasers of wrought steel products.

Studies of mechanical properties, especially yield strength, transverse reduction of area, and notched-bar transverse impact, were made primarily to secure such information as would be useful (a) in the development on sounder principles of specifications for the acceptance of wrought gun tubes, and (b) as a basis for improving metallurgical practices, especially with respect to heat treatment and inspection procedures. To reach this major objective, it was necessary to determine as quantitatively as possible many relationships of interest to design engineers and metallurgists generally. These determinations involved comprehensive statistical studies of thousands of suitable data. Actually about 250,000 tensile and impact data for specimens from heat treated wrought steel products of various sizes (minimum 2.5 to 5.5 inches O.D. and 85 inches long, and maximum 17 to 25 inches O.D., 8.5 inches I.D., and 340 inches long) were received from the armed services and industry; these, together with about 3000 laboratory data, were used in numerous investigations. The information obtained is presented and discussed in appropriate sections which follow: its usefulness (a) in the development of specifications for the acceptance of wrought gun tubes and (b) as a basis for improving metallurgical practices is indicated in sections on Specifications (page 794) and Modification of Heat Treatment Practice (page 798). A large number of data were used in statistical studies and considerable care was taken to avoid bias in sampling in order that confidence in conclusions subsequently drawn would be justified from a statistical point of view.[2]

---

[2]A discussion of statistical methods used in investigations referred to in this publication is given in a paper now being written by C. Wells and E. G. Olds on the subject, "The Use of Statistical Methods for the Evaluation of the Quality of Wrought Steel Products".

In the development of specifications for gun tubes, principles not previously used for this purpose were successfully applied; as a result, more efficient use has been made of available knowledge and better gun tube specifications have been written. Fortunately, the principles which guided the authors toward the solution of their problem are now being used with increasing frequency for solving other specification problems. The best solution depends on as complete a knowledge as possible of (a) the quality of material inspected with respect to each property specified, and (b) the relation between each specified property and service performance. Sometimes it is found that small units which form a larger unit are essentially alike with respect to a specified property; at other times it is found that the average quality among small units varies significantly, but the variation within one unit is essentially the same as that within any other. Such information as this is of considerable fundamental importance and if properly used by those responsible for the writing of specifications should result in the acceptance, with considerably greater certainty, of materials which should be accepted and the rejection of those which should be rejected. Specifications based on knowledge obtained in the present investigation should (and did) result in the saving of considerable effort consumed (a) in the making of unnecessary tests, unnecessary heat treatments and schedule changes, and (b) in the remanufacture of material to replace rejected tubes which should have been accepted.

Since wrought gun tubes are samples of heat treated low alloy wrought steel products,[3] the knowledge gained from a comprehensive statistical study of yield strength, transverse reduction of area, and transverse impact quality of heat treated wrought tubes should be of value to producers and consumers of heat treated low alloy wrought steel products generally. Application to other alloy products of many of the conclusions drawn as a result of this study is also justified.

Determination of Mechanical Properties

Standard procedures were followed for the determination of mechanical properties. Tensile specimens of standard geometry were used for the determination of tensile strength, yield strength (0.01%

[3]These were usually SAE steels with carbon generally above 0.30 and below 0.45% and total alloy content above 1.5 and below 4.5%. Steels of compositions lying between SAE 4330 and SAE 4340 were among those most commonly used for gun tubes in World War II.

or 0.1% offset), longitudinal elongation, transverse elongation, longitudinal reduction of area, and transverse reduction of area. Most of the specimens were 0.505 inch in diameter; some were 0.357 inch, and others 0.252 inch. Various rates of loading were used. The minimum was 2500 psi per minute and the maximum 100,000 psi per minute; usually the rate was about 90,000 psi per minute.

Specimens used for the determination of Charpy longitudinal and transverse impact values were 0.394 inch square and 2.165 inches long, and each contained a standard "V" notch; in transverse test bars the base of the notch was generally parallel with the direction of fiber. Test pieces were practically all broken at either 21 °C (70 °F) or —40 °C (—40 °F).

Unless stated to the contrary, it should be assumed that (a) tensile specimens are each 0.505 inch in diameter, (b) yield strength is measured at 0.01% offset, (c) the rate of loading is about 90,000 psi per minute, (d) impact specimens are broken at 70 °F, and (e) the base of the "V" notch is parallel with the direction of the fiber.

Definition of Transverse Yield Strength, Transverse Reduction of Area, and Transverse Impact Quality for a Unit of Product

The "true" quality of a unit of product with respect to a property such as transverse yield strength (measured at some selected "offset" value), transverse reduction of area, and transverse impact is arbitrarily defined as the distribution of values of the property for all transverse specimens of standard size which can be taken from the unit at specified positions. Thus, when a specification requires that the centers of transverse tensile specimens shall be always at midwall positions which are at least "A" inches from the ends of a gun tube, the quality of the unit, with respect to, say, transverse reduction of area, consists of the distribution of transverse reduction of area values (an infinite number) for specimens whose centers include all positions in the midwall of the tube which fall "A" inches or more from its ends. In this instance the quality of the unit and the tube of which the unit is a part are not identical, although for practical purposes the quality of both unit and gun tube is frequently sufficiently alike to be considered synonymous. However, the distinction between the quality of the unit and the quality of the tube

should be noted, and the possibility of the unit and tube having significantly different properties should not be overlooked.

The "determined" quality of a unit with respect to a property such as transverse yield strength, transverse reduction of area, and transverse impact is considered to be the distribution of values of the property for all specimens of a given size taken from the unit at specified positions. If only one transverse reduction of area value is available, then that value is the determined quality of the unit with respect to transverse reduction of area; if 60 values are available, then the distribution of the 60 values is the determined quality of the unit. Obviously, as the number of values increases, the probability that the "determined" quality will better represent the "true" quality increases also.

A unit may be part of a wrought gun tube, a complete wrought gun tube, a part of each of several wrought gun tubes, or several complete wrought gun tubes; a unit is thought of as consisting entirely of specimens, each one of which is separated from all others. In general, the units whose qualities have been determined in the present investigations consist essentially of the midwall material of (a) each of several gun tubes, and (b) each of several groups of gun tubes. This is because practically all specimens have been taken from midwall positions and specimens taken from these positions are truly representative only of midwall material.

Sampling

While it is impossible to determine the exact quality of a unit of product with respect to properties such as yield strength, reduction of area, and impact, one can determine quality within the accuracy normally desired through the use of a proper sampling plan. Such a plan requires that (a) the number of values per sample be large enough to insure the precision desired, and (b) the choice of specimens for which the values are obtained be as unbiased (random) as possible.

The large number of values available per sample and the small degree of bias associated with these values have enabled the authors to describe yield strength, transverse reduction of area, and transverse impact quality of each of many units with much more precision than usual. Obviously, the transverse reduction of area quality of the midwall material of Forging No. 1 from Company 12 is much

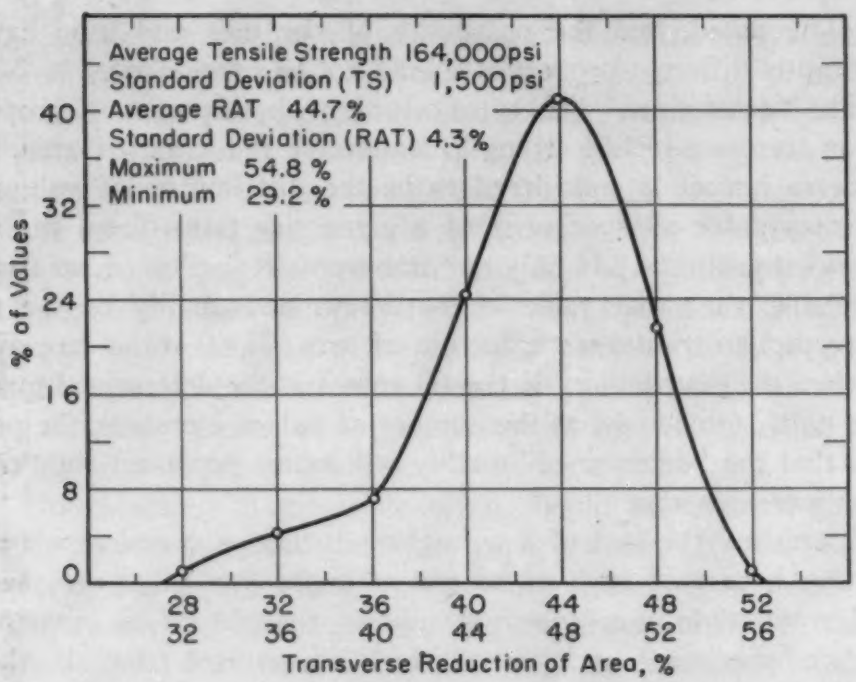


Fig. 1—Shows the Distribution of 277 Transverse Reduction of Area (RAT) Values for Specimens From Forging 1, Company 12. RAT is abbreviation for transverse reduction of area and TS is abbreviation for tensile strength.

more precisely represented by the distribution of the 277 values for the 0.252-inch diameter transverse tensile specimens (Fig. 1) than would be the case if values were available for only four such specimens.[4]

A brief discussion of the requirements for a representative sample and of measures of its reliability and significance is given by Arkin and Colton (6) as well as by many other authors of standard texts dealing with statistics. It is pointed out that standard error of the mean is given by the formula $\sigma_{\bar{x}} = \frac{\sigma}{\sqrt{N}}$ where $\sigma_{\bar{x}}$ is the standard error of the mean, σ is the standard deviation of the sample, and N is the number of values per sample. The standard deviation of the sample of 277 transverse reduction of area values referred to above is 4.3%, and the standard error of the mean is 0.26%. It is estimated that the determined average of 44.7% is correct to within $\pm$ 0.78% (three times the standard error of the mean) with a certainty of 99.7%.

[4]In commercial practice usually no more than four transverse reduction of area values are available per forging.

In investigations referred to here, transverse specimens were generally taken from midwall positions in heat treated tubes (Fig. 2) and from midradius positions in solid heat treated forgings (Fig. 3). With few exceptions, specimens were located at least two-thirds of a wall thickness from the ends of tubes and at least two-thirds of a diameter from the ends of solid forgings. Longitudinal test pieces also came from either midwall or midradius positions located at least two-thirds of the wall thickness (in tubes) or two-thirds of the diameter (in solid forgings) from the ends.

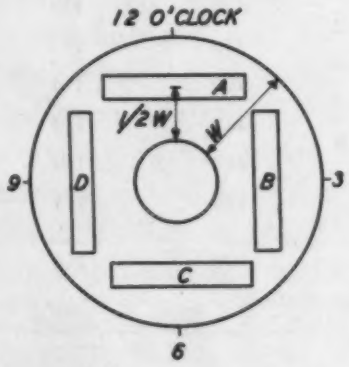


Fig. 2—Shows Positions of Transverse Tensile (or Impact) Specimens With Relation to Cross Section of Tubes. W—wall thickness.

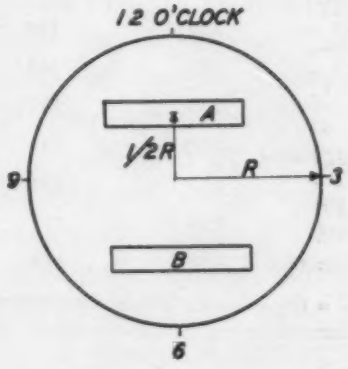


Fig. 3—Shows Positions of Transverse Tensile (or Impact) Specimens With Relation to Cross Section of Solid Forgings. R—radius.

The reason for taking specimens from midwall positions located at least two-thirds of a wall thickness from the ends of tubes is that the quality of material in such specimens is believed to be essentially the same as that existing in finished gun tubes and subjected to the most severe conditions in service. Mechanical properties of material in specimens taken from midwall positions, close to but at distances greater than two-thirds of a wall thickness from the ends of a tube, are usually considered to be about the same as the properties of material in specimens which may be taken from other midwall positions in the tube, provided they also are more than two-thirds of a wall thickness from the tube ends.

Most commercial data referred to in this paper are for specimens taken from midwall positions lying between about two-thirds and four wall thicknesses from the ends of tubes, while most laboratory data are for specimens taken from midwall positions frequently lying considerably beyond four wall thicknesses from the ends.

Table I
Effect of Rate of Loading on Tensile Properties

Specimen No.	No. of Pairs	Rate of Loading 2500 psi per Minute: Tensile Strength (1 unit = 1000 psi)	Rate of Loading 2500 psi per Minute: Yield Strength at 0.01% Offset (1 unit = 1000 psi)	Rate of Loading 2500 psi per Minute: RAT* %	Rate of Loading 100,000 psi per Minute: Tensile Strength (1 unit = 1000 psi)	Rate of Loading 100,000 psi per Minute: Yield Strength at 0.01% Offset (1 unit = 1000 psi)	Rate of Loading 100,000 psi per Minute: RAT %
1	1				132	116	46.0
1A		130	115	42.9			
2	2				129	113	44.8
2A		130	115	45.1			
3	3				131	115	44.8
3A		130	115	47.0			
4	4				130	113	47.7
4A		129	113	....			
5	5				130	115	45.3
5A		129	110	47.2			
6	6				129	113	43.6
6A		128	113	46.6			
7	7				129	114	47.3
7A		130	117	45.2			
8	8				129	113	47.7
8A		127	111	49.9			
9	9				128	113	45.3
9A		127	111	35.9			
10	10				128	111	46.1
10A		126	111	46.6			
	Average	129	113	45.2	129	114	45.9

*RAT is the abbreviation for transverse reduction of area.

Effect of Rate of Loading on Yield Strength and Transverse Reduction of Area Values

Information about the effect of rate of loading on yield strength and transverse reduction of area values was required for two reasons. Those responsible for the contents of Army specifications for gun tubes wished to know whether the maximum specified rate of loading requirement could be raised from 30,000 psi per minute to 100,000 psi per minute without significantly changing yield strength and transverse reduction of area values. Also, since the yield strength and transverse reduction of area data received from producers of gun tubes were for specimens subjected to various rates of loading up to a maximum of 100,000 psi per minute, it seemed advisable to determine whether or not the influence of variation of loading rate could logically be discarded as having no appreciable effect on the results of statistical studies discussed in this paper.

Results given in Table I show that an increase of rate of loading from 2500 to 100,000 psi per minute had no significant effect on either yield strength (measured at 0.01% offset) or on transverse reduction of area values for specimens taken from a heat treated gun tube. Ten pairs of specimens were taken from midwall positions

Table II
Effect of Specimen Size on Tensile Properties

Specimen Diameter* (Inches)	RAT, %		Yield Strength at 0.01% Offset (1 unit = 1000 psi)		Yield Strength at 0.1% Offset (1 unit = 1000 psi)		Tensile Strength (1 unit = 1000 psi)	
	Average	Standard Deviation	Average	Standard Deviation	Average	Standard Deviation	Average	Standard Deviation
0.505	39.6	2.65	143	2.39	150	0.76	164	0.63
0.252	41.8	2.85	136	1.73	148	1.19	164	1.89

*The geometry of the 56 specimens (28 of each size) was not changed. The 0.505-inch diameter specimens are standard; 0.252-inch diameter specimens are frequently used when it is not possible to obtain those of the larger size and are sometimes referred to as standard "sub-size" specimens. RAT is the abbreviation for transverse reduction of area.

in the tube. The difference between the centers of any two specimens constituting a pair (when in the tube) was not more than about three-fourths of an inch apart. Each tensile specimen had a standard geometry and its midlength diameter was 0.357 inch. A Peters averaging extensometer at the high rate of loading and a Tuckermann extensometer at the low rate of loading were used to measure extensions of tensile specimens under load. Data obtained by the authors but not included in this paper show that when the rate of loading was low, both types of extensometer gave the same yield strength values within the limits of statistical significance.

Effect of Specimen Size on Yield Strength and Transverse Reduction of Area Values

It is usually assumed that standard subsize specimens (0.252 inch in diameter) can be substituted for those of standard size (0.505 inch in diameter) without changing yield strength and transverse reduction of area values enough to be significant from a practical point of view. The present authors believe this assumption is frequently valid but wish to point out that, from a statistical viewpoint, the results given in Table II show the average of 28 yield strength values for 0.252-inch diameter specimens to be significantly lower than the average of the same number of values for 0.505-inch diameter specimens.[5] This is true whether yield strength measurements

[5]The difference between averages is considered statistically significant if

$$(\overline{X}_1 - \overline{X}_2) \Big/ \sqrt{\frac{\sigma_1^2}{n_1} + \frac{\sigma_2^2}{n_2}} > 3$$

where $\overline{X}_1$ and $\overline{X}_2$ are the two averages, σ_1 and σ_2 are the two standard deviations, and n_1 and n_2 are the number of tests per average. The difference between standard deviations is considered significant if $(\sigma_1 - \sigma_2) \Big/ \sqrt{\frac{\sigma_1^2}{2n_1} + \frac{\sigma_2^2}{2n_2}} > 3$. Many statisticians consider that when n_1 or n_2 is less than 30, the sample size is too small to justify the use of the tests of significance indicated above. The present authors have occasionally used these tests when n_1 or n_2 is as low as 16; however, this has only been done when either the "t" test (23) or other information also supports the conclusions drawn.

Table III
Effect of Specimen Size on Average Transverse Reduction of Area, Yield Strength, and Tensile Strength Values

Forging No.	Disk No.*	Average RAT for 0.252-in. and 0.505-in. Specimens (%)		Average Yield Strength (at 0.01% Offset) for 0.252-in. and 0.505-in. Specimens (1 unit = 1000 psi)		Average Tensile Strength for 0.252-in. and 0.505-in. Specimens (1 unit = 1000 psi)	
		0.252-in. Diameter	0.505-in. Diameter	0.252-in. Diameter	0.505-in. Diameter	0.252-in. Diameter	0.505-in. Diameter
1	1	47.8	45.7	101	102	126	125
	2	47.4	43.9	98	101	125	125
2	1	49.3	48.9	90	94	121	122
	2	47.8	42.9	95	97	127	127
3	1	40.3	38.4	106	113	138	136
	2	44.0	39.2	101	108	134	132
4	1	37.4	32.3	106	115	137	140
	2	43.2	38.0	105	108	134	134
	Average	44.6	41.2	100	105	130	130

*From each hollow disk (about 1 inch thick) were taken eight specimens, four of which were 0.252 inch and four 0.505 inch in diameter. All specimens came from close to midwall positions in the disks. Each forging from which the disks were cut was a heat treated gun tube supplied by Company 5.

are made at either 0.01 or 0.1% offset. Decreasing specimen size had no significant effect on standard deviation values based on transverse reduction of area and yield strength results. It is suspected that the relatively large difference between the two standard deviation values of 630 and 1890 psi (Table II) is not due primarily to specimen size effect.

The 56 specimens referred to above were obtained in pairs, each pair consisting of one 0.252-inch diameter and one 0.505-inch diameter specimen; the difference between the centers of any two specimens constituting a pair (when in the tube) was not more than 1 inch apart. All specimens came from midwall material of a heat treated gun tube.

On a basis of the results presented in Tables II and III, it is concluded that an increase of specimen size tends to increase average yield strength and decrease average transverse reduction of area values without affecting average tensile strength significantly.

Scope of Research Program

The major objective as previously indicated was to provide information which would lead to (a) the development on sounder principles of specifications for the acceptance of gun tubes, and (b) the consistent production of gun tubes of such quality, relative to specified properties, that they would practically always meet specifi-

cation requirements. It is believed that a complete quantitative knowledge of the quality of gun tubes produced with respect to each specified property, and a complete knowledge of the relationship between each specified mechanical property and performance in service, would provide a sound foundation on which to build a specification. Such a specification, based on adequate knowledge and properly designed, would accept only material which should be accepted, reject only material which should be rejected, and at the same time require only a minimum amount of testing to be done for the purpose of providing adequate evidence of acceptable or unacceptable quality.[6] It was obvious that if such a specification were written, the expenditure of effort and expense required for the production, processing, testing, and inspection of gun tubes would be significantly reduced.

The scope of the program planned to secure the required information involved the co-ordinated effort of a group of workers from (a) the Metals Research Laboratory at the Carnegie Institute of Technology, (b) companies involved in the production, processing, and heat treatment of gun tubes, (c) various NDRC committees, and (d) the armed services.[7] In general, the gun tube research program as executed at the Carnegie Institute of Technology required that (a) determinations be made of the average, variation, and degree of control of quality with respect to each specified property: yield strength, transverse reduction of area, and transverse impact, and (b) every effort be made by the Carnegie Institute of Technology in co-operation with Army Ordnance and NDRC to utilize the results obtained to best advantage in the writing of Army Ordnance specifications for the acceptance of gun tubes. The program also required that an effort be made to ascertain causes for variation of steel quality and to suggest practice changes which, if made, would increase the probability of acceptance of all material presented for inspection.

In addition, the research program included a limited study of the effect of transverse reduction of area (RAT) on the behavior of certain gun tubes; however, no exhaustive study was made on

---

[6]Evidence is considered adequate if it provides the inspector with enough information to be practically certain that he accepts only material which should be accepted and conversely. If it is 99.7% certain that the average quality of a forging with respect to a property lies between the limits of $\overline{X} \pm 3\sigma$, then it is assumed that it is practically certain the average lies between $\overline{X} + 3\sigma$ and $\overline{X} - 3\sigma$. Here $\overline{X}$ is considered to be the average of a large number of values of the property, and σ is the standard deviation of those values.

[7]See Acknowledgments.

the relation between RAT quality and performance, and no plans at all were made to determine the effect of either of the two specified properties, yield strength and transverse impact, on the behavior of gun tubes in service. The relation between each of the specified properties and performance has been studied by Army Ordnance personnel and decisions as to what should be the minimum quality

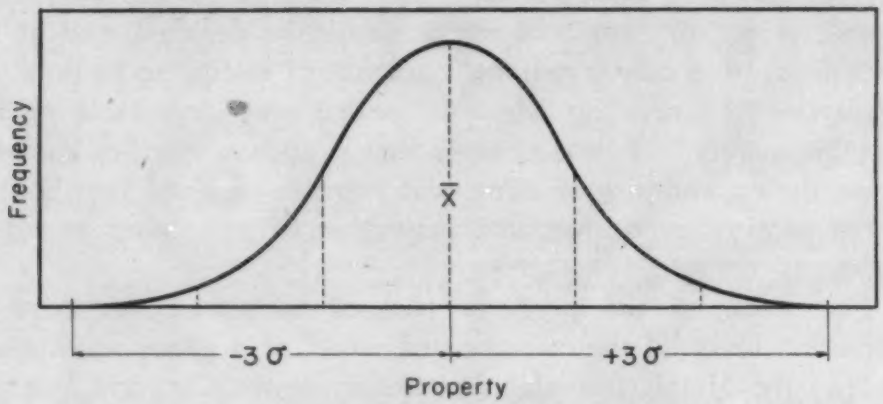


Fig. 4—Normal Curve Showing the Distribution of Property Values in a Normal Universe. $\overline{X}$—average; σ—standard deviation.

of acceptable material for gun tubes are based largely on their conclusions. It is readily admitted by all that the relation between each specified property and performance in service is not well known and considerable time will elapse before such relations can be determined sufficiently quantitatively to satisfy all concerned.

Average and Variation of Transverse Reduction of Area

It is well known that if a property varies in a unit in such a way as to be precisely represented by a normal curve (Fig. 4), then the quality of that unit with respect to the property considered is quantitatively described by average ($\overline{X}$) and standard deviation (σ) values. Obviously, when the average and standard deviation of a large number of transverse reduction of area values for representative samples are high, the average quality of the unit and the variation of quality within that unit are also high.

Actually, for many purposes the transverse reduction of area quality of a number of wrought steel products can be described with sufficient precision by average and standard deviation values. From the determined average ($\overline{X} = 44.7\% \pm 0.8$) and standard deviation $\sigma = 4.3\% \pm 0.55$) reported in Fig. 1, it is estimated that the mini-

Table IV
Chemical Composition of Forgings*

Company No.	Forging No.	Approximate Size of Forgings in Inches			Per Cent						
		Length	Max. O.D.	I.D.	C	Mn	Si	Ni	Cr	Mo	V
12	1	180	7.5	2.5	0.28	0.69	0.22	2.49	1.05	0.40	0.08
15	1	85	5.5		0.36	0.65	0.20	1.90	0.98	0.27	....
15	2	85	5.5		0.36	0.65	0.20	1.90	0.98	0.27	....
15	3	85	5.5		0.38	0.64	0.22	1.87	0.97	0.24	....
15	4	85	5.5	Solid	0.38	0.64	0.22	1.87	0.97	0.24	....
15	5	85	5.5	Forg-	0.34	0.60	0.18	1.96	1.14	0.25	....
15	6	85	5.5	ings	0.34	0.60	0.18	1.96	1.14	0.25	....
15	7	85	5.5		0.35	0.68	0.22	1.91	0.93	0.26	....
15	8	85	5.5		0.35	0.68	0.22	1.91	0.93	0.26	....
12	2	115	6.5	2.5	0.34	0.65	0.28	2.39	0.92	0.41	0.08
12	3	180	11.0	3.0	0.38	0.64	0.25	2.05	0.94	0.34	0.09
15	9	85	5.5	S.F.	0.34	0.60	0.25	1.86	0.89	0.25	....
5	1	340	25.0	8.5	0.35	0.72	0.24	0.22	1.40	0.50	0.17
5	2	340	25.0	8.5	0.38	0.80	0.21	0.41	1.51	0.44	0.15
15	10	85	5.5	Solid	0.34	0.63	0.20	1.91	0.95	0.27	....
15	11	85	5.5	Forg-	0.36	0.62	0.21	1.90	0.90	0.27	....
16	1	85	5.5	ings	0.35	0.64	0.25	2.15	0.93	0.31	....
13	1	160	10.0	2.5	0.36	0.72	0.26	1.51	0.85	0.33	0.09
13	2	100	10.0	3.5	0.36	0.74	0.31	1.93	0.85	0.38	0.08
15	12	85	5.5	...	0.34	0.63	0.20	1.91	0.95	0.27	....
5	3	340	25.0	8.5	0.34	0.84	0.21	0.47	1.22	0.49	0.16
7	1	100	7.5	2.0	0.37	0.60	0.27	0.35	0.89	0.23	....

*All steels were fine-grained; those to which vanadium was not added were aluminum-killed.
Note: P and S each below 0.03%.

mum and maximum among 277 transverse reduction of area values for 0.252-inch diameter specimens cut from Forging 1 of Company 12 should be on the average about 32.4 and 57.0%, respectively;[8] the observed minimum is 29.2% and the maximum 54.8%. Forging 1 from Company 12 was made from a fine-grained basic electric steel; its approximate dimensions and chemical composition are given in Table IV. The forging reduction was roughly 4 to 1.[9]

If a more precise description of transverse reduction of area quality is desired than is given by an average and standard deviation value, then a frequency curve such as that of Fig. 1 will serve. Such a curve representing the distribution of transverse reduction of area values for a large number of specimens (all of one standard size) is rarely normal but tends to be skewed as shown. The frequency curve given in the figure is typical of those drawn to show the distribution of transverse reduction of area values for specimens taken from high quality forgings which have been quenched essentially to martensite and subsequently tempered to a tensile strength of about

[8]These estimates are based on the assumption that samples are drawn from a normal population. According to Pearson, the mean range for a sample of 277 values is 5.70453 σ. Better estimates based on factors not considered here are given in Table VI and discussed on page 731.

[9]When the area of cross section of an ingot is reduced to one-quarter of its original value by forging, the forging reduction is said to be 4 to 1.

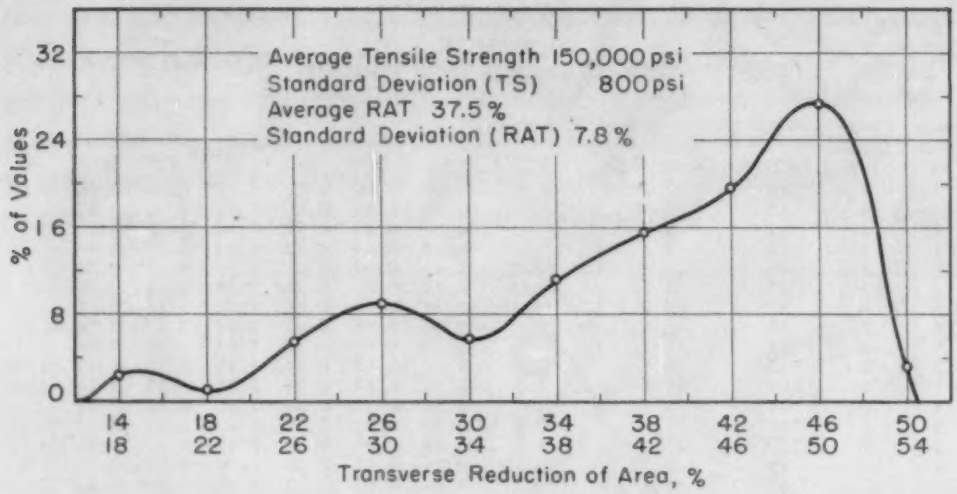


Fig. 5—Shows the Distribution of 162 Transverse Reduction of Area Values for Specimens From Forging 1, Company 15. RAT is abbreviation for transverse reduction of area and TS is abbreviation for tensile strength.

165,000 psi. A plot of values for specimens taken from a forging of poorer transverse reduction of area quality is given in Fig. 5. The data are for 0.252-inch diameter specimens from Forging 1 supplied by Company 15. This forging was quenched to martensite and tempered to a tensile strength of 150,000 psi. Chemical composition and forging dimensions are listed in Table IV. Minimum and maximum forging reduction was about 15 to 1 and 70 to 1, respectively.

Normally, one expects the variation of transverse reduction of area quality to be relatively low when the average is high, and conversely; therefore, it is not surprising to find the variation to be lower in Forging 1 from Company 12 than in Forging 1 from Company 15, since the former forging has a higher average than the latter. Sometimes, however, it was observed that the variation was significantly lower in a forging of lower than in one of higher average quality. Determined average transverse reduction of area and standard deviation values for one forging tempered to 146,000 psi are 19.8 and 4.9%, respectively, while corresponding values for another forging tempered to about the same tensile strength (151,000 psi) are 37.5 and 7.8%.

Results presented in Table V support the generally accepted belief that the average quality of forgings varies considerably. The determined average for one forging tempered to 146,000 psi is 19.8% while the average for another forging of the same size and compo-

Table V

Shows Transverse Reduction of Area Average and Variation of Quality Within Each of a Number of Forgings

Company No.	Forging No.	No. of Values	Tensile Strength* Average	Tensile Strength* Sigma	Transverse Reduction of Area, % Average	Transverse Reduction of Area, % Sigma
12	1	277	164	1.5	44.7	4.3
15	1	162	151	0.8	37.5	7.8
15	2	29	154	0.4	36.9	6.0
15	3	30	147	1.2	22.3	5.3
15	4	28	146	2.6	19.8	4.9
15	5	38	141	1.2	25.5	5.5
15	6	26	139	0.9	24.6	4.5
15	7	20	142	0.8	43.8	4.8
15	8	20	140	1.8	39.6	6.1
12	2	66	178	1.1	39.0	3.3
12	3	53	150	0.9	38.0	7.1
15	9	91	137	2.5	40.4	6.2
5	1	64	126	1.4	47.7	3.5
5	2	63	125	2.8	48.4	2.8
15	10	48	144	1.7	32.3	7.6
15	11	47	146	3.1	33.6	8.1
16	1	62	153	3.8	21.0	7.4
13	1	59	115	2.0	46.0	3.6
13	2	21	129	2.6	43.8	5.9
15	12	50	147	2.8	40.3	3.3
5	3	32	136	0.7	44.0	4.4
		Average	143	1.7	36.6	5.4

*Each unit = 1000 psi.

Sigma (σ) = standard deviation. $\sigma = \sqrt{\frac{\Sigma X^2}{n} - \overline{X}^2}$, where ΣX^2 is the sum of the squares of individual values, n is the number, and $\overline{X}$ is the average of the values.

Forgings were quenched in water and subsequently tempered. Tensile specimens were 0.252 inch in diameter.

sition and tempered to about the same tensile strength (142,000 psi) is 43.8%. Results also show that the variation of transverse reduction of area quality, especially in forgings of superior quality, is very much larger than is usually recognized. Determined standard deviation values reported in Table V lie between a minimum of 2.8% and a maximum of 8.1% (average 5.4%).

The observed maximum difference (range) among values for specimens from each of 21 forgings is listed in Table VI. Values equal to six times the determined standard deviation (6σ) are also given. These represent estimates of the magnitude of ranges which would be observed if values for 444 specimens were available per forging.[10] The lowest, average, and highest values of 6σ given in the table are 16.8% (Forging 5-2), 32.2% and 50.4% (Forging 15-11), respectively.

[10]Mean range values for samples of size "n" taken from a normal population are given in Pearson's tables. See *Tables for Statisticians and Biometricians*, Third Edition, Table XXII, p. 165. Cambridge University Press, 1931. When "n" = 444 (444 values per sample), the mean range is 6.00079σ.

Table VI

Presents Actual and Estimated Values for (a) Maximum RAT, (b) Minimum RAT, and (c) the Difference Between (a) and (b)

Company and Forging Number	No. of Values	Estimated RAT, %			Observed RAT, %			Values of 6σ, %
		Maximum	Minimum	Difference	Maximum	Minimum	Difference	
12-1	277	54.9	30.4	24.5	54.8	29.2	25.6	25.8
15-1	162	54.9	13.2	41.7	50.4	14.0	36.4	46.8
15-2	29	47.1	22.7	24.4	46.7	22.8	23.9	36.0
15-3	30	32.5	10.8	21.7	31.2	13.2	18.0	31.8
15-4	28	28.0	8.3	19.7	28.0	10.8	17.2	29.4
15-5	38	35.3	11.8	23.5	38.0	17.5	20.5	33.0
15-6	26	32.0	14.2	17.8	32.3	16.0	16.3	27.0
15-7	20	51.3	33.4	17.9	50.8	31.1	19.7	28.8
15-8	20	49.1	26.3	22.8	49.0	24.4	24.6	36.6
12-2	66	45.5	30.0	15.5	45.0	30.7	14.3	19.8
12-3	53	51.4	19.2	32.2	....	....	....	42.6
15-9	91	53.2	22.5	30.7	47.0	15.1	31.9	37.2
5-1	64	54.5	38.1	16.4	53.3	38.0	15.3	21.0
5-2	63	53.9	40.8	13.1	53.5	37.6	15.9	16.8
15-10	48	46.5	12.5	34.0	45.5	18.2	27.3	45.6
15-11	47	49.2	11.8	37.4	50.0	17.4	32.6	50.4
16-1	62	35.4	0.9	34.5	30.1	2.3	27.8	44.4
13-1	59	53.0	36.3	16.7	52.9	39.2	13.7	21.6
13-2	21	53.1	30.9	22.2	54.5	32.5	22.0	35.4
15-12	50	46.5	31.7	14.8	45.9	37.4	8.5	19.8
5-3	32	51.6	33.4	18.2	50.1	35.0	15.1	26.4
	Average	46.6	22.8	23.8	45.5	24.1	21.3	32.2

RAT is abbreviation for transverse reduction of area. Sigma (σ) = standard deviation.

If each forging had been cut up entirely into transverse tensile test specimens, and transverse reduction of area values had been determined for each specimen, then the observed difference between minimum and maximum among the values per forging would have been higher (in some instances much higher) than those reported. Larger sample size and more adequate sampling would both have tended to increase determined range values and would have allowed average and variation of forging quality to be described more quantitatively. Generally, in present investigations, only midwall material of tubes and midradius material of solid forgings were sampled; in addition, samples rarely included material located closer than two-thirds of a wall thickness from the ends of tubes or closer than two-thirds of a diameter from the ends of solid forgings. Considerable evidence is now available which shows that the average transverse reduction of area quality across a forging may be and frequently is quite large; for this reason it is believed that standard deviation figures based on samples coming from only midwall or midradius positions may be significantly lower than figures based on samples which are more representative of whole forgings and not of only midwall or midradius material.

Moderately good agreement exists between comparable estimated and observed values given in Table VI. Estimates of maximum, minimum, and range (difference between maximum and minimum) are based on (a) an assumption that the mean range of samples of size "n" taken from a normal population is approximately equal to the range (in terms of standard deviation) of samples of size "n" taken from a forging, (b) an assumption that usually about 0.416[11] of the range is above and 0.584 is below the average, and (c) determined average ($\overline{X}$) and standard deviation (σ) values. According to Pearson (7), the mean value when "n" = 277 is 5.070453 σ; therefore, the estimated range for the 277 transverse reduction of area values for Forging 12-1 (Table VI) is 24.5%, since σ = 4.3%, and the estimated maximum value is 0.416 × 24.5% + 44.7% = 54.9%, since $\overline{X}$ = 44.7%.

A discussion of the causes of variation of transverse reduction of area quality and of the significance of that variation, especially in its relation to specifications, is given in appropriate sections which follow.

Control of Transverse Reduction of Area Quality

The extent to which the transverse reduction of area quality of a product is controlled largely determines the amount of data needed to describe the quality of each unit of that product adequately. Obviously, when all units are alike, then the distribution of "n" data which adequately describes the transverse reduction of area quality of one unit also describes that of any other unit equally well.

Units are considered to be essentially alike when all of a sufficiently large number of "average" and "range" values for unbiased samples from these units fall between control limits.[12] Since all averages and ranges, except one for samples from midwall positions in disks cut from Forging 1 of Company 12, fall within control limits, it is concluded that the midwall material of each disk is essentially like that in any other. The evidence that Disk 53

[11] When the range (R) is 6 σ, it is assumed that usually the maximum is about 2.5 σ above and the minimum is 3.5 σ below the average, i.e., $\frac{2.5\,R}{6} = 0.416\,R$ is above and $\frac{3.5\,R}{6}$ is below the average.

[12] Tentatively any number of values above 60 (30 averages plus 30 ranges) are accepted as sufficient to indicate whether or not a number of units, properly sampled, are essentially alike. Each range is the difference between the maximum and minimum value in a sample, and each average is the sum of all the values in a sample divided by the number of values in it.

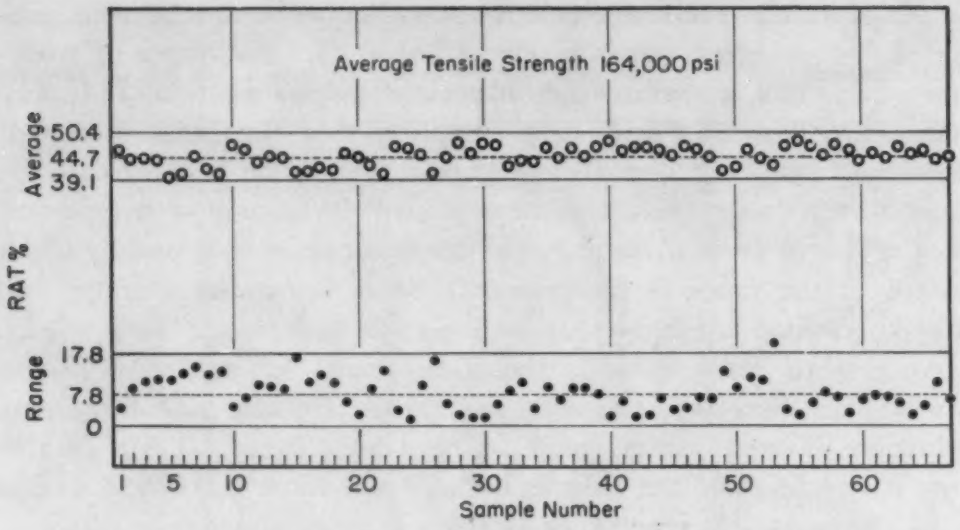


Fig. 6—Shows the Transverse Reduction of Area Quality of the Midwall Material in Each of 67 Disks From Forging 1, Company 12, to be Essentially Alike. * Sample 1 consists of four transverse reduction of area (RAT) values for 0.252-inch diameter specimens from Disk 1. Sample 2 consists of four RAT values for specimens from Disk 2, etc.

(Fig. 6) is of poorer transverse reduction of area quality than the others is too weak to be conclusive. One of the four values for specimens from Disk 53 is lower than that observed for any specimens from other disks. Nonmetallic inclusions are believed responsible for this unusually low value.

All disks referred to above are from the large end of the tube. These were about ¾ inch thick and were cut transverse to the longitudinal axis of the forging at positions of 17 inches (Disk 1), 17¾ inches (Disk 2) and so on to 68 inches (Disk 67) from the large end. Four transverse tensile test specimens were taken from midwall positions of each disk. The maximum difference among the four transverse reduction of area values for the specimens is a "range" (plotted as a closed circle); the average of the four values is plotted as an open circle, Fig. 6. Range control limits given in the figure are 0 and 17.8%, and average control limits are 50.4 and 39.1%.[13] The average of "ranges" is 7.8% and the average of "averages" is 44.7%.

From results given in Fig. 6, it is concluded that the control of transverse reduction of area quality of midwall material in Forging 1 from Company 12 is such that a large enough sample

[13]Calculated limits for "averages" are $\overline{X} \pm 0.729\ \overline{R}$ and limits for "ranges" are 0 and $2.282\ \overline{R}$. $\overline{X} = 44.7\%$ and $\overline{R} = 7.8\%$. When each sample consists of only two values, the limits for averages are $\overline{X} \pm 1.88\ \overline{R}$, and for ranges 0 and $3.268\ \overline{R}$.

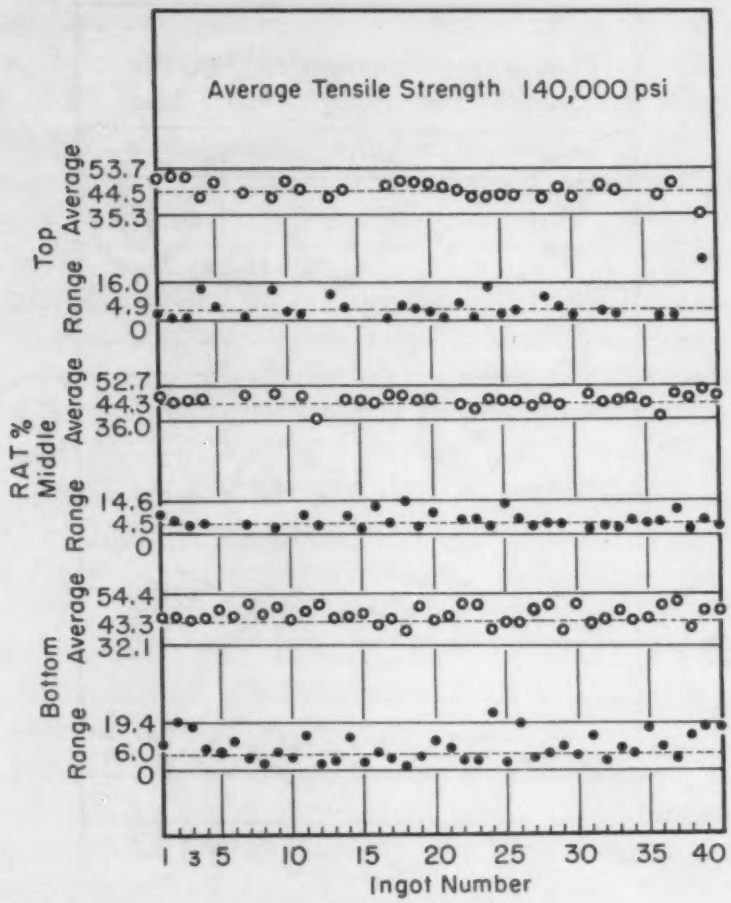


Fig. 7—Suggests From a Practical Point of View That Transverse Reduction of Area (RAT) Quality of All Tubes From Heat 1, Company 14, Is Essentially Alike. Each of 102 samples (one per tube) consists of two RAT values for 0.357-inch diameter specimens from a midwall position close to the small end of a rolled and pierced tube.

(number of values for specimens) taken from one midwall region between 17 and 68 inches from the heavy end is practically equal in quality to any other equally large sample taken from other positions between the limits mentioned. Probably, for most practical purposes, it is reasonable to assume that an adequate sample from the midwall material in one region of a forging is equivalent to a similar sample from the midwall material in any other region.[14] This assumption is generally (at least tacitly) accepted and is the basis for the conclusion that results for samples from the ends of forgings are adequate to describe the quality of forgings. However, there is reason

[14]This forging is believed to have been quenched essentially to martensite before being uniformly tempered and therefore there is no metallurgical reason to suspect that the transverse reduction of area quality of the ends is significantly different from that of other parts of the forging on account of heat treatment.

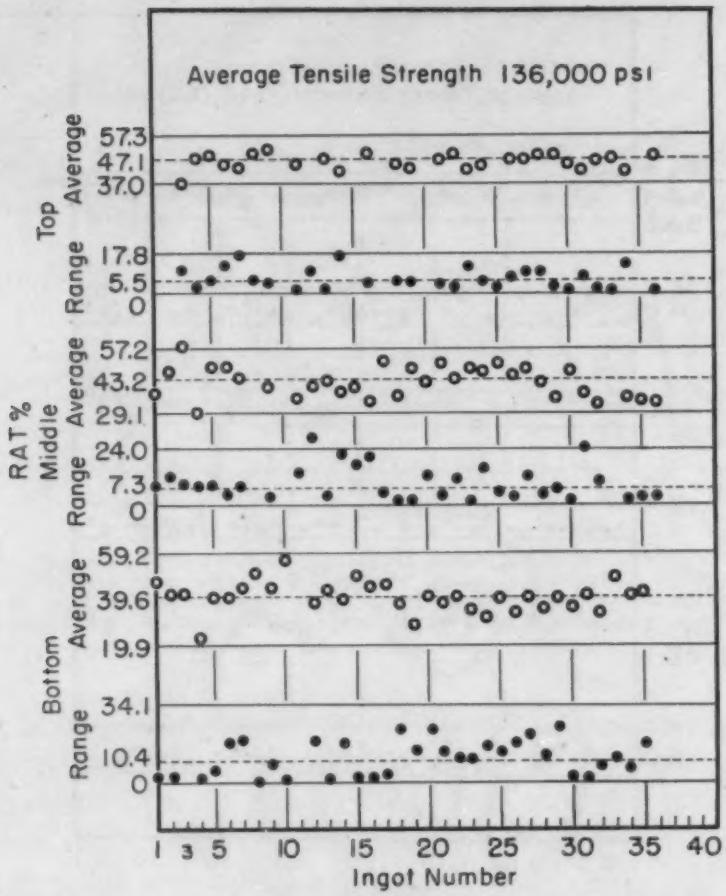


Fig. 8—Suggests That the RAT Quality of All Tubes From Heat 2, Company 14, and From One Ingot Position (Top, Middle, or Bottom) Is Alike. Each of 95 samples (one per tube) consists of two RAT values for 0.357-inch diameter specimens from a midwall position close to the small end of a rolled and pierced tube.

to suspect that the transverse reduction of area quality of midwall material, such as that not sampled in Forging 1 and consisting of steel from bottom thirds of ingots, is lower on the average than the quality of material from the adequately sampled regions. This suspicion is based on the fact that transverse reduction of area quality is frequently lower in material from bottom thirds of ingots.

From results plotted in the control charts of Figs. 7 and 8, it appears that all tubes from the same heat (Heats 1 and 2 from Company 14) and from a similar ingot position (top, middle, or bottom) are probably alike within the limits of practical significance. Out of about 100 averages and 100 ranges plotted in each of the above-mentioned figures, no averages (open circles) and two ranges (closed circles) are outside the control limits in Fig. 7, while one

average and two ranges are outside the limits shown in Fig. 8. It seems quite reasonable from these results to expect that all tubes made from Heat 2 would have been essentially alike in transverse reduction of area quality if one instead of three tubes had been made from each ingot. In this instance it is assumed that all the steel from an ingot which normally went into three tubes would have gone into only one.

Strong evidence supporting the belief that the transverse reduction of area quality of tubes varies with the position in ingots from which they come is given in Fig. 8; other evidence somewhat weaker but supporting the same belief is given in Fig. 7. Calculated average ($\overline{X}$) and standard deviation (σ) figures based on transverse reduction of area values for 0.357-inch diameter specimens from tubes from (a) tops, (b) middles, and (c) bottoms of ingots comprising Heat 2 are (a) 47.1 and 5.8%, (b) 43.2 and 8.1%, and (c) 39.6 and 9.2%; comparable figures based on values for specimens taken from tubes from (a) tops, (b) middles, and (c) bottoms of ingots comprising Heat 1 are (a) 44.5 and 4.3%, (b) 44.3 and 5.4%, and (c) 43.3 and 5.3%.[15]

Heats 1 and 2 from Company 14 consisted of fine-grained aluminum-killed basic open-hearth steel. This was cast into ingots (roughly 21 inches in diameter just below the hot top) and was subsequently rolled and pierced to give about 100 tubes per heat. Three tubes were made per ingot, one from each of top, middle, and bottom positions. Tubes were about 115 inches long and had an O.D. of about 7 inches for most of the length. The I.D. was approximately 2.5 inches. All tubes were quenched in water and tempered to a tensile strength of about 140,000 psi. Chemical composition of the heats was as follows:

	C	Mn	P	S	Si	Ni	Cr	Mo
Heat No. 1	0.36	0.84	0.014	0.018	0.25	1.86	0.85	0.37
Heat No. 2	0.36	0.80	0.015	0.017	0.24	1.89	0.76	0.38

Studies of a large number of transverse reduction of area data for specimens from tubes in each of several hundred heats have led to the conclusion that within the limits of practical significance all tubes in a heat have usually the same transverse reduction of area

[15]These standard deviation values are calculated from the formula $\sigma = \sqrt{\frac{\Sigma X^2}{n} - \overline{X}^2}$ and not from the relation $\sigma = \frac{\overline{R}}{1.128}$

quality. The variation of quality among tubes from each of most heats is believed to be much better represented by the results given in Fig. 7 than in Fig. 8.

Average and standard deviation data based on samples taken from individual forgings and from groups of forgings constituting heats are given in Table VII. It may be observed from these data that the maximum difference between any determined transverse reduction of area average for a sample from a group of forgings comprising a heat and for a sample from a tube in that heat is 3.3% (43.8 to 40.5%). It may also be observed from data given in the table that each difference between two determined standard deviation values, one based on a sample from a heat and the other on a sample from a tube from that heat, lies between a minimum of 0% (4.3 to 4.3%) and a maximum of 2.9% (7.4 to 4.5%); only one of these differences (2.9%) is so high as to indicate definitely a significant difference between the two standard deviations.[16] Much of the difference observed between the two averages or two standard deviations making up each pair considered above is frequently due to the combined effect of sampling error and the use of more than one specimen size.[17] If this effect were always absent, all the forgings in each of many heats investigated would appear to be much more nearly alike than they do now.

The results given in the control chart of Fig. 7 and Table VII are typical of thousands of others which support the conclusion that, with few exceptions, all tubes in a heat are essentially alike in transverse reduction of area quality. While the thousands of data referred to above are available and have been studied, they cannot be included here because of space restrictions.

Not only does it appear extremely probable that all similarly heat treated forgings from any arbitrarily selected heat will, if thoroughly tested, be found to have essentially the same transverse reduction of area quality, but it also seems quite probable that all forgings from any arbitrarily selected group of ten or even more

---

[16]It is assumed that the populations sampled are in sufficiently good control (in the control chart sense) and the samples are large enough to justify the conclusion that two standard deviations appear to be significantly different if $(\sigma_1 - \sigma_2) \Big/ \sqrt{\frac{\sigma_1^2}{2n_1} + \frac{\sigma_2^2}{2n_2}} > 3$. When $\sigma_1 = 7.4\%$, $\sigma_2 = 4.5\%$, $n_1 = 53$ and $n_2 = 26$, the value of the expression is 3.05.

[17]Sampling error is controlled largely by sample size and sample size is limited by economic factors. To increase sample size (number of values for specimens) when only a small amount of material was available, 0.252-inch diameter rather than 0.357-inch diameter or 0.505-inch diameter specimens were frequently used. The 0.252-inch diameter specimens were considered standard for laboratory work.

Table VII
Shows Degree to Which the Transverse Reduction of Area Quality Is the Same for an Individual Forging as for a Group of Forgings from the Same Heat

Heat and Company No.	No. of Forgings	No. of Values	Average TS	Transverse Reduction of Area, % Average	Sigma	Company and Forging No.	No. of Values	Average TS	Transverse Reduction of Area, % Average	Sigma
1-12	5	20	160	41.7	4.3	12-1 T	277	164	44.7	4.3
1-15	32	32	148	34.7	8.5	15-1 M	162	151	37.5	7.8
						15-2 T	29	154	36.9	6.0
2-15	38	38	147	22.8	5.8	15-3 M	30	147	22.3	5.3
						15-4 B	28	146	19.8	4.9
3-15	44	53	142	25.4	7.4	15-5 T	38	141	25.5	5.5
						15-6 M	26	139	24.6	4.5
4-15	44	44	145	40.5	6.9	15-7 M	20	142	43.8	4.8
						15-8 B	20	140	39.6	6.1
2-12	9	18	184	36.7	3.6	12-2 T	66	178	39.0	3.3
3-12	4	16	157	36.0	6.8	12-3 T	53	150	38.0	7.1
5-15	42	42	138	41.5	5.8	15-9 M	91	137	40.4	6.2
6-15	18	18	144	34.4	6.5	15-10B	48	144	32.3	7.6
7-15	21	21	147	36.8	5.3	15-11B	47	146	33.6	8.1
1-7	5	20	104	57.1	2.6	7-1 M	16	104	56.0	4.4
		Average	147	37.0	5.7		Average	146	35.6	5.7

TS = Tensile strength; each unit is 1000 psi.
T, M, or B (column 7) signifies specimens come from top, middle, or bottom third of the forged ingot.
All specimens from groups of forgings (column 2) were 0.357 inch in diameter except those from Heats 1 to 3, Company 12, and Heat 1, Company 7. Specimens from other groups were 0.505 inch in diameter. All specimens from individual forgings (column 7) were 0.252 inch in diameter.

consecutively made heats will, if thoroughly tested, similarly be found to have essentially the same transverse reduction of area quality. Hundreds of control charts have been plotted which, considered together, amply support this conclusion. One typical control chart, showing that all the forgings from seven consecutive heats made by Company 17 are probably alike within the limits of practical significance, is plotted in Fig. 9. These heats, numbered 1 to 7, were cast into ingots with a 24-inch round cross section just below the hot top. Ingots were subsequently made into forgings having a length of about 160 inches, a maximum O.D. of 10 inches, and an I.D. of 2.5 inches. These were quenched in water and tempered to a tensile strength of about 120,000 psi. All forgings are fine-grained and have chemical compositions lying between the following limits:

Per Cent of Element							
C	Mn	P	S	Si	Cr	Mo	V
0.28	0.71	0.012	0.012	0.25	0.97	0.47	0.10
0.30	0.80	0.019	0.014	0.31	1.02	0.51	0.13

Averages (open circles) and ranges (closed circles) plotted in the control chart of Fig. 9 all fall either within or quite close to control limits. Each average plotted in the chart consists of an average of four transverse reduction of area values for 0.505-inch

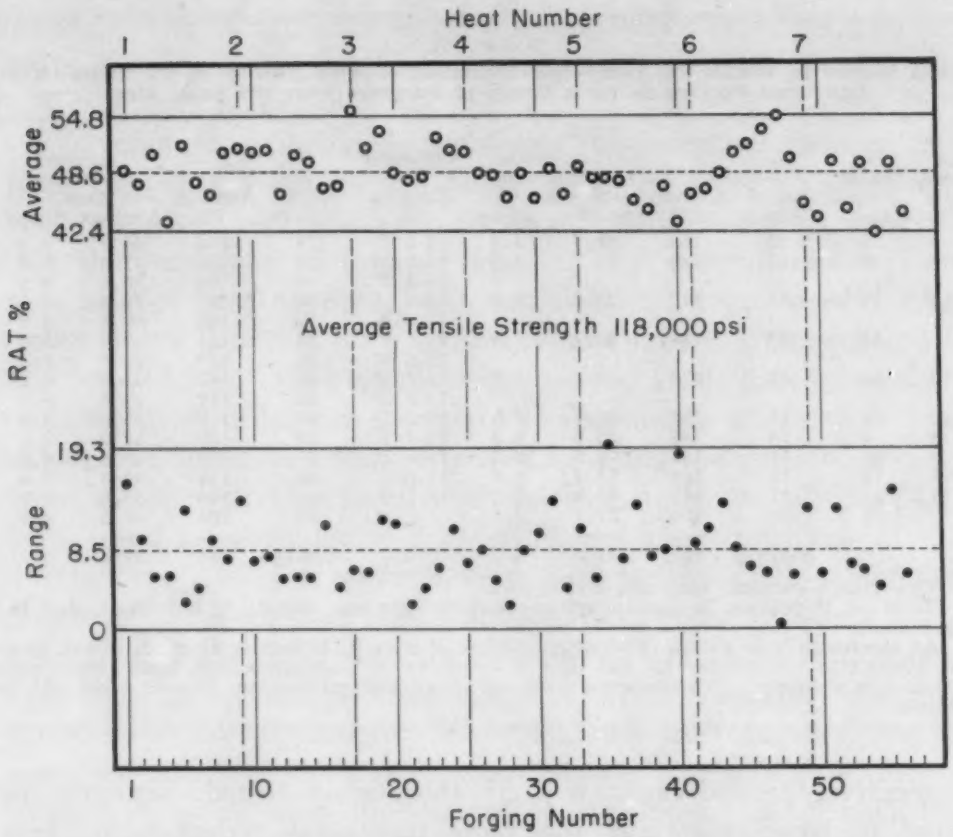


Fig. 9—Gives Evidence Showing That the Transverse Reduction of Area (RAT) Quality of All Forgings From Heats 1 to 7 (Company 17) Is Probably Identical Within Limits of Practical Significance. Values of four 0.505-inch diameter specimens (two from each end of a forging) constitute a sample. All specimens come from midwall positions located more than two-thirds of a wall thickness from the ends. Eight forgings constitute a heat.

diameter specimens from the midwall material in a forging and each range consists of the maximum difference among the four values. The average of 32 transverse reduction of area values for specimens consisting of midwall material taken from each group of eight forgings comprising a heat is 46.2% minimum (Heat 7) and 51.0% maximum (Heat 3); calculated standard deviation values are 3.5% minimum (Heat 4) and 5.2% maximum (Heat 5). The average of all 224 values (32 for each of 7 heats) is 48.6% and the standard deviation is 4.5%. From a statistical point of view the maximum difference of 4.8% (51.0 to 46.2%) among the averages is significant, but the maximum difference of 1.7% (5.2 to 3.5%) among the standard deviations is insignificant;[5] from a practical viewpoint, both maximum differences are insignificant.

In those instances where control chart evidence shows a variation

of transverse reduction of area quality in a practice beyond that normally expected, it is frequently found that (a) all forgings within certain heats have lower transverse reduction of area quality than usual and (b) the variation of transverse reduction of area quality within tubes in such heats is normal, but the average transverse reduction of area quality is lower than normal. Typical data supporting this conclusion are given in the control chart of Fig. 10.

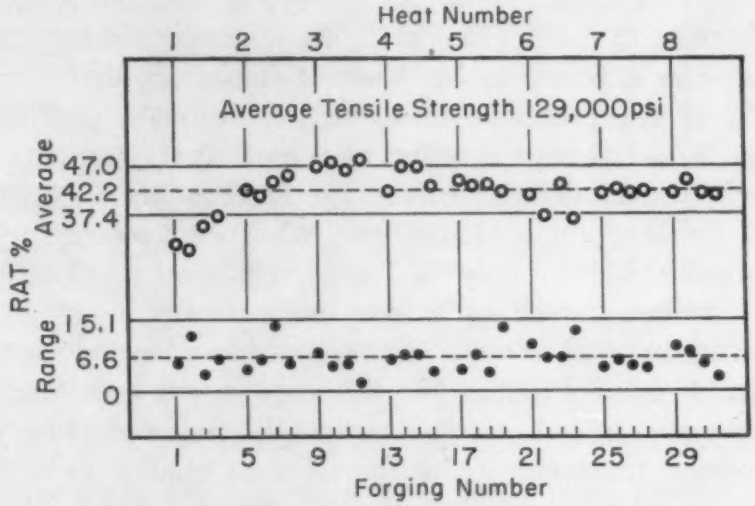


Fig. 10—Suggests (a) the Variation of Transverse Reduction of Area (RAT) Quality Within Any One Forging Is Practically the Same as That Within Any Other in These Eight Heats and (b) the RAT Quality of Forgings From Some Heats Is Significantly Different From That of Forgings From Other Heats. Values of four 0.505-inch diameter specimens (two from each end of a forging) constitute a sample. All specimens come from midwall positions located more than two-thirds of a wall thickness from the ends. Four forgings constitute a heat.

While all ranges (closed circles) fall within calculated control limits, averages (open circles) do not. Averages for samples from forgings from the first of the eight consecutive heats from Company 13 referred to in the figure are usually low; however, the ranges for the same samples all fall well within control limits.

Heats 1 to 8, inclusive, referred to in the above figure, were cast into ingots with a 34-inch square cross section just below the hot top. These ingots, consisting of basic electric fine-grained steel, were subsequently made into forgings having a length of about 210 inches, a maximum O.D. of 18.5 inches, and an I.D. of 7.5 inches. Each forging was quenched in water and tempered to a tensile strength of about 130,000 psi. A typical composition is as follows:

C	Mn	P	S	Si	Cr	Mo	V
0.34	0.74	0.012	0.010	0.31	0.85	0.38	0.08

From a practical point of view, the average transverse reduction of area quality of a product made by one company does not normally differ significantly from that of a similar product made by another company. Of six products consisting of forgings 160 inches long, 7.5 inches maximum O.D., and 2.5 inches I.D. and coming from Companies 5, 6, 8, 10, 11, and 13, respectively, none had a determined average lower than 30.9% (yield strength at 0.1% offset 152,000 psi) or higher than 35.3% (yield strength 145,000 psi). This difference of 4.4% (35.3 to 30.9%) is approximately the maximum normally expected to be observed among six determined averages such as those referred to above. Occasionally a difference of more than 10% has been observed as is evident from results included in Table VIII; the determined average for Product 1 (Company 1) is 50.3% (yield strength 115,000 psi) while the average for Product 15 (Company 15) is only 37.7% (yield strength 119,000 psi). Units of Product 1 were made from much smaller ingots and during forging were reduced in cross section much less beyond the optimum than were units of Product 15; this explains at least some of the large differences noted, since excessive forging reduction tends to lower average transverse reduction of area quality as is apparent from results included in the section entitled "Effect of Forging Reduction on Longitudinal and Transverse Reduction of Area Quality", page 754.

The conclusion that average transverse reduction of area quality of one product is usually about the same as that of any similar product is based on the assumption that each of the products considered consists of forgings which are quenched in water and tempered at least approximately to the same yield strength. Obviously, Product 4 (Company 4—Table VIII), tempered to a yield strength of 75,000 psi, is expected to and does have a higher average transverse reduction of area quality than Product 9 (Company 9), tempered to a yield strength of 93,000 psi. If the forgings constituting Product 9 had been tempered to a yield strength of 75,000 psi, it is probable that the determined average transverse reduction of area value would have been about 51.4%, a value only 3.6% lower than the figure listed for Product 4.[18]

Standard deviation data included in Table VIII (Column 9)

[18]It is assumed that when yield strength is raised by 5000 psi, transverse reduction of area is lowered by about 1.5%; evidence supporting the validity of this assumption is given under the subheading, "Relation between Transverse Reduction of Area and Yield Strength", page 743.

Table VIII

Average and Standard Deviation Figures Based on Transverse Reduction of Area Data for a Large Number of Forgings from Each of Several Companies

Company No	Ingot Cross Section Just Below Hot Top	Approx. Forging —Dimensions in Inches— Length	Max. O.D.	I.D.	Approx. No. of Heats	Approx. No. of Values	Transverse Reduction of —Area, %— Average	Sigma	Average YS at 0.01% Offset (psi)
1	10 in. square	85	5.5	S.F.*	72	600	50.3	3.5	115,000
2	12 in. square	85	5.5	S.F.	20	700	47.2	5.4	111,000
3	13 in. round	85	5.5	S.F.	10	200	43.1	4.1	109,000
4	13 in. round	50	7.0	2.5	102	4100	55.0	3.6	75,000
5	16 in. round	160	7.5	2.5	3	100	33.7	4.0	143,000
	43 in. round	410	20.0	7.0	45	720	39.5	3.6	109,000
	46 in. round	340	25.0	8.5	40	320	37.4	4.9	114,000
6	16 in. round	160	7.5	2.5	11	200	31.0	3.9	155,000
7	17 in. round	100	7.5	2.0	51	1500	54.3	3.0	74,000
8	18 in. round	160	7.5	2.5	5	36	30.9	4.3	152,000
	33 in. round	210	18.5	7.5	124	1500	41.9	4.3	109,000
9	18 in. round	50	7.0	2.5	8	1200	46.0	3.7	93,000
10	18 in. square	160	7.5	2.5	36	240	35.3	5.1	145,000
11	18 in. square	160	7.5	2.5	3	120	34.7	3.6	152,000
12	19 in. round	160	10.0	2.5	153	2450	46.1	5.5	108,000
13	21 in. round	160	7.5	2.5	30	1170	33.2	5.0	158,000
	34 in. square	210	18.5	7.5	75	1200	44.3	4.8	110,000
14	21 in. round	115	8.5	2.5	190	3400	44.3	4.1	117,000
15	20 in. x 23 in.	85	5.5	S.F.	30	1500	37.7	3.3	119,000
16	20 in. x 23 in.	85	5.5	S.F.	55	4500	34.1	6.6	135,000
17	24 in. round	160	10.0	2.5	45	1500	48.1	4.8	100,000
	42 in. round	410	20.0	7.0	33	280	41.5	5.0	108,000
	48 in. round	340	25 0	8.5	40	300	41.1	5.1	101,000
						Average	41.3	4.4	118,000

*S.F. = Solid forging.

Standard deviation (σ) values of column 9 have been calculated from the formula $\sigma = \frac{\overline{R}}{A}$; A is a constant which depends on sample size, $\overline{R}$ is the average range, and σ is the standard deviation. Unless stated to the contrary as in this instance, assume standard deviation values have been calculated from the formula $\sigma = \sqrt{\frac{\Sigma X^2}{n} - \overline{X}^2}$.

Chemical compositions of forgings referred to above usually lie between the following limits:

C	Mn	P	S	Si	Ni	Cr	Mo	V
0.25	0.50	<0.03	<0.03	0.20	0.20	0.50	0.20	0.00
0.45	1.00			0.40	3.00	2.00	0.60	0.20

All forgings were quenched in water and tempered.

support the belief that at least from a practical point of view the variation of transverse reduction of area quality within the midwall material of a typical forging (or heat unit[19]) produced in one practice is usually about the same as that in the midwall material of a typical forging (or heat unit) produced in any other of the many practices considered. In general, the variation is such as to be well enough represented for most practical purposes by a standard deviation of 4.5%.

Standard deviation (σ) values listed in the table were calculated

[19]A "heat unit" consists of all the forgings of the same dimensions made from a heat and subjected to the same treatment.

from data obtained as a result of using two procedures. In one procedure a sample consisted of two transverse reduction of area values, one for a 0.357-inch diameter specimen from a midradius position close to the large end of one solid forging and the other for a specimen from a similar midradius position in another solid forging from the same heat. The difference between the two values constitutes a range, and from "n" transverse reduction of area values available (one per forging) ½ n range data were obtained. The average of the ½ n range values is $\overline{R}$ (average range) and standard deviation values are calculated from the formula σ (standard deviation) $= \frac{\overline{R}}{1.128}$. In the second procedure a sample consisted of values for two 0.505-inch diameter specimens both taken from a midwall position close to one end of a forging. Of the data constituting samples, about 50% were for specimens from the large end and 50% were for specimens from the small end of forgings. As in Procedure 1, the difference between values in a sample constitutes a range, the average of all ranges is $\overline{R}$, and standard deviation values are calculated from the formula $\sigma = \frac{\overline{R}}{1.128}$. Standard deviation values calculated from this formula are sufficiently accurate for most purposes, providing "n" is large and the range values practically all fall within control limits. Usually, in the present investigation, "n" (the number of transverse reduction of area values used) was quite large (Table VIII) and more than 95% of all range values fell within control limits. Control limits used by the authors are 0 and 3.628 $\overline{R}$ when two, 0 and 2.114 $\overline{R}$ when four, and 0 and 2.004 $\overline{R}$ when six values constitute a sample.

The variation among standard deviation values and the average of these values based on data in Table VIII are lower than the variation and average based on data in Tables V and VII; this is to be expected since (a) many of the individual forgings referred to in Tables V and VII, for which a large number of transverse reduction of area data are available, were deliberately selected from "heat units" each of which varies in transverse reduction of area quality much more than normally, and (b) no such selection was made in the choice of forgings referred to in Table VIII. Part of the greater variation among the standard deviation figures in Tables V and VII may be due to larger sampling errors caused by sample size effect, since with few exceptions each of these figures is based

on only a small fraction of the data used in the determination of each of the standard deviation figures appearing in Table VIII.

It is believed that every standard deviation (σ) value listed in Table VIII (one per each of 23 practice units)[20] indicates sufficiently precisely for most practical purposes the variation of transverse reduction of area quality within the midwall material of forgings obtained in a practice. However, the authors suspect that the standard deviation figures listed are too low to describe accurately the excessive variation existing within an occasional forging coming from the 23 practices considered in the table. Enough lack of control of ranges was observed when suitable data were plotted on control charts to arouse this suspicion.

It is apparent from material presented in this section and from an enormous amount of other data available to the authors that sufficient control of transverse reduction of area quality exists within forgings, heat units and practice units to enable one to predict quite frequently and with ample certainty for most purposes (a) the transverse reduction of area quality of forgings using data for specimens taken only from positions close to the ends of forgings and (b) the transverse reduction of area quality of each forging in a heat (or practice) unit from a knowledge of the transverse reduction of area quality of the heat (or practice) unit; this conclusion is valid in many instances where transverse reduction of area values are available only for tensile specimens from a small fraction of the total number of forgings in the unit.

The importance of information, such as is presented in this section, to personnel responsible for the development of specifications which include a transverse reduction of area requirement and to metallurgists who have the responsibility of making a product which meets this requirement as frequently as possible will be considered in appropriate sections entitled "Specifications", page 794, and "Modification of Heat Treatment Practice", page 798.

Relation Between Transverse Reduction of Area and Yield Strength

It is well known that in a wrought steel product quenched to

[20] A "practice unit" consists of all the forgings made consecutively in a practice over an arbitrarily selected period of time; each forging has the same dimensions and is assumed to be treated like any other in the practice unit. Practice Unit 1 (Company 1, Table VIII) consists of 600 forgings from 72 heats; Practice Unit 2 (Company 2) consists of 700 forgings from 20 heats, and so on, to Practice Unit 23 which has in it 75 tubes from 40 heats.

martensite and subsequently tempered the transverse reduction of area quality varies inversely with yield strength; however, quantitative information about this relationship has remained quite meager until results presented in this section became available. Evidence presented here shows that an increase of 5000 psi in yield strength is accompanied by a decrease of about 1.5% in transverse reduction of area.

Materials used in the determination of the relation between

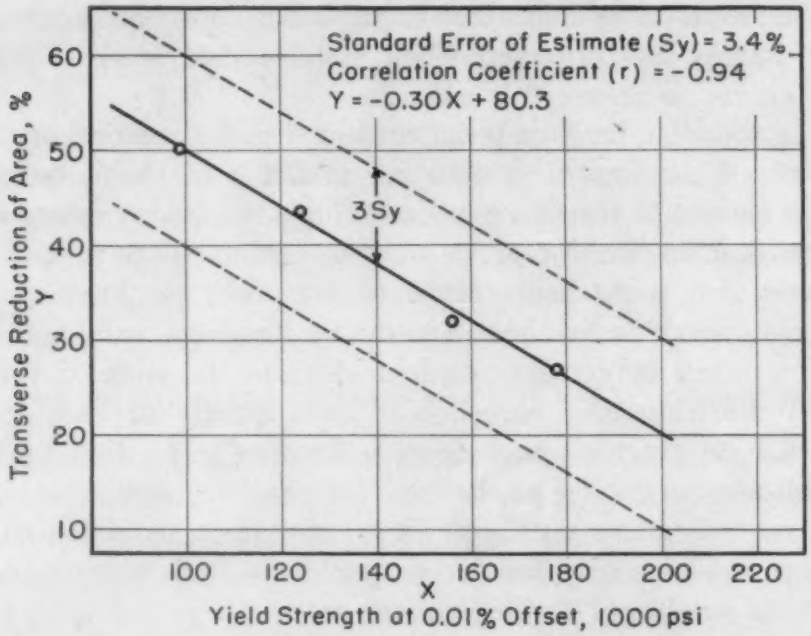


Fig. 11—Shows Relation Between Transverse Reduction of Area and Yield Strength in a Quenched and Tempered Seamless Tube (Tube No. 14-2). The Y coordinate of each of the four data points represents an average of 50 transverse reduction of area values for 50 specimens and the X coordinate represents an average of 50 yield strength values for the same 50 specimens.

transverse reduction of area and yield strength are described in Table IX and results are given in Table X and Fig. 11.

The three seamless tubes referred to in Table IX came from the top third of ingots while the forging consisted of an entire ingot except for top and bottom discard. Four sections, each between 1 and 2 feet long, were cut from a tube. All sections consisted of steel from the top third of ingots. Pieces were quenched to martensite and subsequently tempered. The four pieces from each tube were tempered to different yield strengths; minimum and maximum yield strength level values are given in Column 2, Table X. Values of all

Table IX
Data Describing Material Used in the Determination of the Relation Between Transverse Reduction of Area and Yield Strength

Company and Tube No.	Approx. Size of Tube in Inches			Type of Tube	Per Cent									Approx. Reduction by Forging or Rolling
	Lgth.	O.D.	I.D.		C	Mn	P	S	Si	Ni	Cr	Mo	V	
14-1	90	5	1.5	Seamless	0.36	0.78	0.02	0.02	0.17	1.89	0.81	0.41	....	20 to 1
14-2	90	5	1.5	Seamless	0.34	0.71	0.02	0.03	0.26	1.84	0.75	0.34	....	20 to 1
14-3	115	7	2.5	Seamless	0.38	0.78	0.01	0.03	0.31	1.96	0.85	0.36	....	15 to 1
12-2	115	6.5	2.5	Forging	0.34	0.65	0.01	0.01	0.28	2.39	0.92	0.41	0.08	3.4 to 1

Tubes 14-1, 14-2, and 14-3 were all made of basic open-hearth steel. Tube 12-2 was made of basic electric steel.

Reduction by forging or rolling is described by the ratio of cross section of ingot before to cross section after forging or rolling.

Each tube was quenched to martensite and drawn to various yield strength levels.

four levels to which sections from Tube 14-2 were tempered are indicated by X co-ordinates of center points of circles drawn in Fig. 11. From each of the four sections per tube were cut about fifty 0.252-inch diameter transverse tensile test specimens and a yield strength and transverse reduction of area value was obtained for each specimen. The 400 or so data per tube, together with appropriate formulas, were then used in calculations of a correlation coefficient (r), a regression line relating transverse reduction of area (Y) and yield strength (X), and a standard error of estimate (S_y). The formulas referred to are as follows:

$$r = \frac{\frac{\Sigma XY}{n} - \overline{X}\,\overline{Y}}{\sigma_x \sigma_y} \qquad \text{.....1.}$$

r = correlation coefficient
Y = transverse reduction of area values
X = yield strength values
$\overline{X}$ = arithmetic mean of X values
$\overline{Y}$ = arithmetic mean of Y values
n = total number of either X or Y values
σ_x = standard deviation of X values[21]
σ_y = standard deviation of Y values[21]

$$Y - \overline{Y} = \frac{\sigma_y}{\sigma_x} r\,(X - \overline{X}) \qquad \text{.....2.}$$

$$S_y = \sigma_y \sqrt{1 - r^2} \qquad \text{.....3.}$$

S_y = standard error of estimate.

[21] σ_x is calculated from the expression $\sigma_x = \sqrt{\frac{\Sigma X^2}{n} - \overline{X}^2}$ and σ_y from the expression $\sigma_y = \sqrt{\frac{\Sigma Y^2}{n} - \overline{Y}^2}$

Table X
Data Showing Relation Between Transverse Reduction of Area and Yield Strength

Company and Tube No.	YS Range (1 unit = 1000 psi)	No. of YS Values	No. of RAT Values	r (Correlation Coefficient)	Equation of Regression Line	S_Y %	Effect of Change of 5000 psi on RAT, %
14-1	102-177	199	199	−0.94	$Y = -0.33X + 79.1$	3.7	1.6
14-2	99-178	200	200	−0.94	$Y = -0.30X + 80.3$	3.4	1.5
14-3	106-186	199	199	−0.91	$Y = -0.27X + 74.7$	3.7	1.4
12-2	83-147	204	204	−0.89	$Y = -0.28X + 80.7$	3.5	1.4

YS = Yield strength.
RAT = Transverse reduction of area.
S_Y = Standard error of estimate (see page 31).
Y = Transverse reduction of area in per cent.
X = Yield strength at 0.01% offset in special units (1 unit = 1000 psi).

It is probable that the formulas given above are sufficiently self-explanatory to satisfy most readers; however, if more detailed information is needed, it can be found in Arkin and Colton's book (6) or in other standard texts.

A standard deviation has been calculated from transverse reduction of area values for the 50 specimens taken from each of the sections cut from the four tubes referred to in Table X; on the average these standard deviations support the conclusion that over a wide range of yield strength the variation of transverse reduction of area quality within a quenched and tempered forging is practically independent of yield strength level. One calculated standard deviation based on 50 values for specimens taken from a section of Forging 12-2 tempered to 83,000 psi is 2.9% while another based on 50 values for specimens from a section of the same forging tempered to 147,000 psi is 3.3%. Results given in Table VIII also support the same conclusion; the determined standard deviation based on transverse reduction of area values for specimens from forgings in one "practice unit" having an average yield strength of about 75,000 psi is 3.6% and based on values for specimens from forgings in another "practice unit" having a yield strength of about 155,000 psi, it is 3.9%. Since over a wide yield strength range the variation of transverse reduction of area appears to be as high in a forging drawn to one yield strength level as another, it appears reasonable to suppose that all three lines drawn in Fig. 11 should be parallel as shown.

All 200 yield strength and 200 transverse reduction of area values for specimens taken from Tube 14-2 fell (as expected) within the space between the two dashed lines in Fig. 11.

Information reported in this section made it possible to use

transverse reduction of area data for specimens from wrought steel products tempered to widely different yield strength levels much more effectively (a) in the development of certain specifications, (b) in the study of the effect of various factors on transverse reduction of area quality, (c) in the determination of the degree to which the transverse reduction of area quality of any Product A would differ from any other Product B if both had been tempered to the same yield strength instead of to different yield strength levels. Product A is here assumed to have actually a much higher (or lower) yield strength than Product B and each product is assumed to consist of any one of the following units: a forging, a heat unit, or a practice unit. Knowledge of the relation between transverse reduction of area and yield strength also resulted in a modification of heat treating practice which markedly increased the probability that each forging submitted for inspection would meet specification requirements. (See section entitled "Modification of Heat Treatment Practice", page 798.)

Effect of Reheat Treatment on Transverse Reduction of Area Quality

Many metallurgists believe that among forgings quenched and tempered to the same yield strength those which have been reheat treated are likely to have a significantly higher transverse reduction of area quality than those which have not. While in some instances this belief appears reasonable, data offered to support it are frequently so biased and misinterpreted that the conclusions drawn are quite erroneous. Bias results from a failure to obtain samples which adequately represent the transverse reduction of area quality of the product being considered. Much more bias exists among data than is generally realized because of the commonly accepted viewpoint that the variation of transverse reduction of area quality within forgings is much less than it really is. A correct interpretation of a sufficiently large amount of representative data leads to the conclusion that a reheat treatment consisting of either (a) a retemper or (b) a requench and temper over and above a normal quench and temper treatment probably has a small but usually insignificant effect on the transverse reduction of area quality of forgings, providing the forgings are tempered to the same yield strength before and after reheat treatment and during quenching the austenite is transformed

essentially to martensite. Results supporting this conclusion are given in Tables XII and XIII.

The possibility that the quality of very large forgings which obviously cannot be quenched essentially to martensite before the temper may in general be improved by reheat treatments is readily conceded. Some data are available which show the transverse reduction of area quality of very large reheat treated forgings to be much higher than the quality of the same forgings drawn to the same yield strength but not reheat treated. The authors believe that these data are not sufficient to justify the conclusion that the quality of large forgings is usually improved by reheat treatments, and for the present they have accepted the viewpoint that a drastic improvement of transverse reduction of area quality caused by reheat treatment is generally obtained only when the original treatment involving a quench and subsequent temper has been improperly executed.

Materials used in the study of the effect of reheat treatment on transverse reduction of area quality are referred to in Tables XII and XIII. Sizes are given in Tables IV and XIII and compositions in Tables IV and VIII. Heat treatments are described in Table XI.

Results given in Table XII show that neither retempering nor requenching and tempering significantly improved transverse reduction of area quality except by lowering yield strength. Details of heat treatments which each forging received are given in Table XI. Two forgings (15-11 and 5-3—Table XII) were retempered and two (15-12 and 5-2) were requenched and tempered. It is estimated that if the four forgings had been drawn to 120,000 psi, the determined averages per forging before and after reheat treatment would have been 37.2 and 39.0%, 39.2 and 39.8%, 40.9 and 41.9%, and 40.0 and 40.2%, respectively. Determined standard deviations before and after reheat treatment are 8.1 and 7.0%, 4.9 and 3.6%, 3.3 and 4.0%, and 2.7 and 2.7%

Additional data are given in Table XIII supporting the belief that (a) retempering and (b) requenching and tempering treatments which do not affect yield strength normally have little effect on average transverse reduction of area quality. Among the tubes referred to in this table, those in Groups 1B, 4, and 6 were all retempered and those in Groups 2B, 8, 10, and 12 were requenched and tempered. Details of heat treatments are given in Table XI. It is estimated that if all tubes had been tempered to a yield strength of 100,000 psi, determined group unit averages before and after reheat

Table XI
Description of Heat Treatments

Treatment No.	Heat Treatment—Approximate Prior Treatment 1 Temp., °F	1 Time at Temp., Hrs.	2 Temp., °F	2 Time at Temp., Hrs.	3 Temp., °F	3 Time at Temp., Hrs.	Quench Temp., °F	Quench Time at Temp., Hrs.	Temper Temp., °F	Temper Time at Temp., Hrs.
1	After forging, forging was cooled and heated for quench						1625	6	1080	10
2	Treatment same as 1 plus additional temper								1080	10
3	1640	21	1520	20	1200	14	1680	10	1200	12
4	Treatment same as 3 plus additional temper								1100	10
5	Same as 1 plus requench and temper						1625	6	1080	10
6	Same as 3 plus requench and temper						1680	10	1200	12
7	1640	14			1240	14	1600	8	1250	8
8	Same as 7 plus additional temper								1250	8
9	1700	5					1500	5	1175	10
10	Same as 9 plus additional temper								1175	10
11	1550	20					1600	10	1140	48
12	Same as 11 plus additional temper								1140	48
13	Same as 7 plus requench and temper						1600	8	1250	8
14	1700	24					1650	10	1300	24
15	Same as 14 plus requench and temper						1650	10	1300	24
16	Same as 9 plus requench and temper						1500	5	1175	10

After each prior treatment (1, 2, or 3), tubes were furnace-cooled or air-cooled to at least below their transformation range before being treated for the quench.
After tempering, tubes were either air or furnace-cooled.
Tempering temperatures listed are probably correct within ± 50°F (28°C).
All tubes were quenched in water.

treatment would have been 41.3 and 42.4% (Groups 1A and 1B), 41.8 and 44.4% (Groups 2A and 2B), 44.4 and 44.1% (Groups 3 and 4), 40.7 and 40.1% (Groups 5 and 6), 40.5 and 38.6% (Groups 7 and 8), 44.3 and 42.3% (Groups 9 and 10), and 32.4 and 33.5% (Groups 11 and 12).

Following is constitution of the group units referred to above:

The 58 tubes in Group 1A are the same as in Group 1B also and the 18 tubes in Group 2A are the same as in Group 2B. Group Unit 3 contains 2 tubes from each of 35 heats and 3 from each of 6 heats, 41 of these tubes from the same 41 heats constitute Group 4. Group 5 contains 6 tubes from each of 22 heats and 22 of these from the same 22 heats constitute Group 6. All tubes of Groups 7 and 8 come from the same heat. Group 9 consists of 14 tubes from each of 39 heats and 13 from each of 22 heats, 61 of these from the same 61 heats constitute Group 10. Group 11 consists of 4 tubes from each of 75 heats and 23 tubes from 23 of these heats constitute Group 12.

It is believed that (a) tubes from the same heat and (b) tubes from the same well controlled practice[22] are alike so frequently when

[22]Control charts based on the 1200 yield strength and 1200 transverse reduction of area values for specimens from tubes in Group 11 established the fact that Practice 17 used by Company 17 was well controlled. Less than 1% of all range and average values fell outside of control limits, and these were not far outside. Each sample consisted of 4 transverse reduction of area values for specimens from each of 300 tubes made consecutively in the practice; an average is an average of the 4 values per tube and a range is the maximum difference among the 4 values. The standard deviation calculated from the formula $\sigma = \frac{\overline{R}}{2.059}$ is 4.8% where $\overline{R}$ = the average of all range values and σ = standard deviation.

Table XII

Data Showing Effect of Reheat Treatments on the Transverse Reduction of Area Quality of Each of Four Forgings, Assuming the Forgings to be Tempered Always to the Same Yield Strength

Company and Forging No.	Treatment No.	Number of YS Values	Number of RAT Values	Average YS (1 unit = 1000 psi)	Average RAT %	Estimated RAT Average When YS is Assumed to be 120,000 psi, %	Standard Deviation %
15-11	1	47	47	132	33.6	37.2	8.1
	2	48	48	122	38.4	39.0	7.0
5-3	3	16	16	107	43.1	39.2	4.9
	4	16	16	103	44.9	39.8	3.6
15-12	1	50	50	122	40.3	40.9	3.3
	5	50	50	132	38.3	41.9	4.0
5-2	3	31	31	89	49.3	40.0	2.7
	6	32	32	95	47.7	40.2	2.7

Treatments 1 to 6 are described in Table XI. Treatments 1 and 3 are original treatments which include the first quench and temper; 2 and 4 are retemper treatments, while 5 and 6 are requench and temper treatments.

Compositions and sizes of forgings are given in Table IV.

YS = Yield strength at 0.01% offset.

RAT = Transverse reduction of area.

Estimated RAT averages (column 7) are based on the assumption that an increase of 5000 psi in yield strength causes a decrease of 1.5% in RAT and conversely. Evidence given in the sector entitled "Relation Between Transverse Reduction of Area and Yield Strength", page 29, shows this assumption to be quite reasonable.

Specimen size, 0.252 inch in diameter.

similarly heat treated as to justify the use of the above group units in present studies.

In Columns 8 and 9, Table XIII, are listed the number of yield strength and transverse reduction of area data available per group unit. In general, the same number of values per property comes from each tube in a group unit; occasionally a difference of one exists between the number of data from one tube and from another in the same group unit. When more values are available per tube than are to be used, those first determined are selected and all others are discarded. Among the data for each group unit there are about as many values for specimens from the top as from the bottom portion of ingots.

Acceptance of the conclusion that the transverse reduction of area quality of quenched and tempered wrought steel products of certain sizes and compositions are rarely improved by reheat treatments has already resulted in a drastic reduction of such treatments and in a modification of the design of certain specifications.

Relation of Angle Between Longitudinal Axis and Flow Line Direction in Specimens to Reduction of Area

It is well known that longitudinal tensile specimens taken from

Table XIII

Data Showing the Effect of Reheat Treatments on the Transverse Reduction of Area Quality of Tubes, Assuming All Tubes to be Tempered to the Same Yield Strength

Company No.	Approx. Size of Tubes in Inches —Maximum— Lgth.	O.D.	I.D.	No. of Tubes per Group	Group Unit No.	Treatment No.	No. of YS Values	No. of RAT Values	Average YS (1 unit = 1000 psi)	Average RAT %	Estimated RAT Average When YS Is Assumed to be 100,000 psi, %
5	240	14	4	58	1A	7	232	232	88	44.9	41.3
				58	1B	8	232	232	79	48.7	42.4
				18	2A	7	74	74	78	48.4	41.8
				18	2B	13	74	74	83	49.5	44.4
8	145	14	5.5	88	3	11	352	352	103	43.6	44.4
				41	4	12	164	164	101	43.8	44.1
12	160	10	2.5	132	5	9	720	720	104	39.5	40.7
				22	6	10	88	88	102	39.5	40.1
14	115	8.5	2.5	107	7	9	214	214	119	34.8	40.5
				52	8	16	104	104	117	33.5	38.6
15	85	5.5	S.F.	832	9	1	832	832	124	37.1	44.3
				61	10	5	61	61	124	35.1	42.3
17	300	16	5	300	11	14	1200	1200	72	40.8	32.4
				23	12	15	92	92	68	43.1	33.5

Treatments 1 to 16 are described in Table XI. Treatments 1, 7, 9, 11, and 14 are original treatments which include the first quench and temper; 8, 10, and 12 are retemper treatments, while 5, 13, 15, and 16 are requench and temper treatments.

Compositions of tubes referred to above fall between the limits noted in Table VIII.

Specimens for all tubes except those supplied by Companies 14 and 15 were 0.505 inch in diameter; specimens from tubes supplied by Companies 14 and 15 were 0.357 inch in diameter.

YS = Yield strength at 0.01% offset.

RAT = Transverse reduction of area.

S.F. = Solid forging.

wrought steel products which have flow lines parallel with their longitudinal axis give higher reduction of area values than do transverse specimens; therefore, one expects reduction of area values to be decreased as the angle between the direction of the longitudinal axis and the direction of flow lines in specimens is increased from 0 to 90 degrees. Brearley (8) using a rolled slab of 0.23% carbon Bessemer steel has observed that as the angle between the direction of the longitudinal axis and the direction of flow lines was increased from 0 (longitudinal) to 90 degrees (transverse), reduction of area values were decreased rapidly in the range 20 to 70 degrees but only insignificantly in the ranges of 0 to 20 degrees and 70 to 90 degrees. The present authors and their associates have now redetermined this relation much more quantitatively than hitherto, using materials listed in Table XIV. Results of this redetermination are given in the table and in Figs. 12 and 13.

As the angle between longitudinal axis and flow line direction in specimens from Tube 14-4 and Forging 21-1 was increased from 0 to 90 degrees, determined reduction of area averages were decreased and standard deviations were increased as shown by the data

Table XIV

Data Showing Relation Between Angle of Test and Reduction of Area in Tube 14-4 and Forging 21-1

Tube or Forging No.	Diameter of Specimens in Inches	Number of Reduction of Area Values	Angle of Test in Degrees	Average Reduction of Area Values, %	Standard Deviation %
14-4	0.252	15	0	60.4	0.7
	0.252	8	22	59.8	0.7
	0.252	16	36	58.4	1.7
	0.252	48	54	51.2	5.0
	0.252	48	68	40.9	4.7
	0.252	46	90	39.1	3.7
21-1	0.357	15	0	58.1	1.6
	0.357	15	18	59.3	0.8
	0.357	15	36	54.9	2.1
	0.357	60	45	42.7	11.3
	0.357	56	54	31.7	12.0
	0.357	55	72	25.1	8.2
	0.357	55	90	25.3	7.4

Seamless Tube 14-4 was quenched to martensite and tempered to a tensile strength of 166,000 psi (yield strength at 0.01% offset, 146,000 psi); this tube was about 115 inches long, 6 inches O.D., and 2.5 inches I.D.

Specimens from Forging 21-1 were quenched to martensite and tempered to a tensile strength of 150,000 psi (yield strength of 0.01% offset, 130,000 psi); the forging was a 6-inch round.

Reduction by hot working about 10 to 1 for forging and 20 to 1 for tube.

	Composition Per Cent of Element							
	C	Mn	P	S	Si	Ni	Cr	Mo
Tube 14-4	0.37	0.82	0.018	0.015	0.28	1.92	0.83	0.38
Forging 21-1	0.48	0.90	*	0.025	*	*	*	*

*P, Si, Ni, Cr, and Mo below 0.03, 0.17, 0.1, 0.1, and 0.1%, respectively.

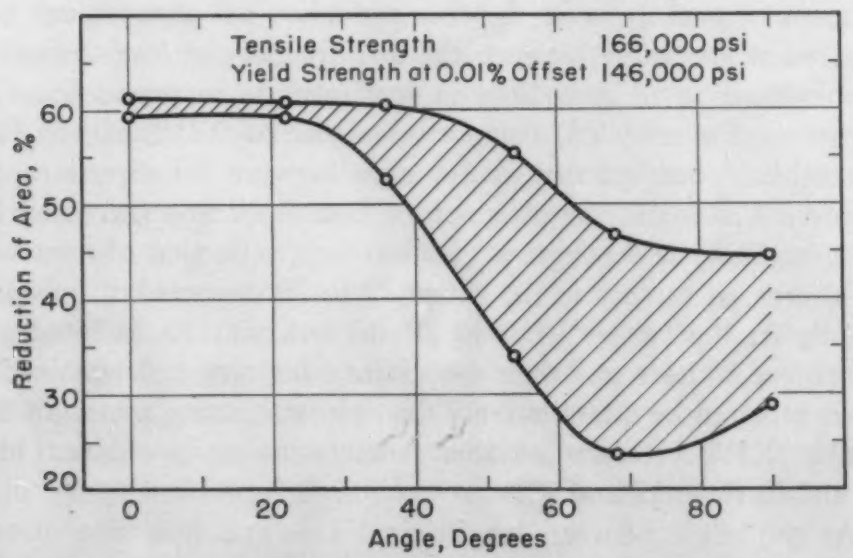


Fig. 12—Shows Relation of Angle Between Longitudinal Axis and Flow Direction in Specimens to Reduction of Area. (0°—Longitudinal, 90°—Transverse.) Maximum and minimum among reduction of area values (at each of several angles) are indicated by open circles. Tensile specimens were 0.252 inch in diameter and came from Tube 4, Company 14.

included in Columns 4, 5, and 6 of Table XIV.[23] Maximum and minimum among reduction of area values in each of six groups (one group per angle) are represented by open circles in Fig. 12; these maximum and minimum data show that the variation among reduction of area values within each group is quite small when the angle is less than 22 degrees, much larger when it is 36 degrees, and very large when it is 54 degrees or higher.

Obviously, the magnitude of the variation observed, especially

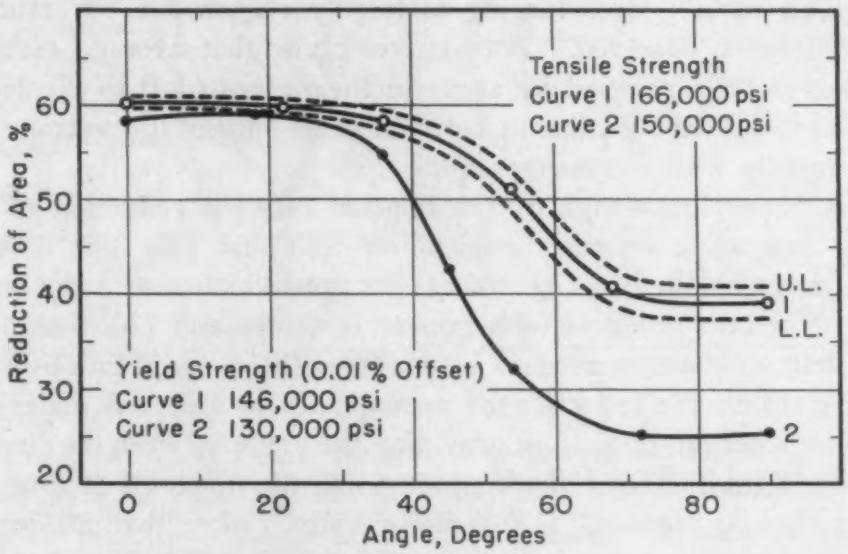


Fig. 13—Shows Relation of Angle Between Longitudinal Axis and Flow Direction in Specimens to Average Reduction of Area. Data for Curve 1 are for 0.252-inch diameter specimens from Tube 14-4, Company 14; data for Curve 2 are for 0.357-inch diameter specimens from Forging 21-1, Company 21. Forging 21-1 is an SAE 1045 steel and Tube 14-4 is an SAE 4334 steel. U.L.—Upper control limit. L.L.—Lower control limit.

among reduction of area values for specimens in which the angle between longitudinal axis and flow line direction is 54 degrees or higher, makes it impossible to represent the relation between angle and reduction of area by a single curve; this relation is represented in Fig. 12 by a shaded area. The connection between angle and determined reduction of area averages based on data for specimens from Tube 14-4 is shown in Fig. 13; each open circle represents the relation between an angle and a determined average and the dashed

[23]Data for Forging 21-1 were taken from a report entitled "Acceptance Tests for Plain Carbon Steel Gun Forgings and Other Ordnance Forgings", by R. F. Mehl and A. H. Grobe, Serial No. M-466, May 3, 1945. This report may be obtained on microfilm or as photostat copy through the Office of Technical Services, U. S. Department of Commerce, Washington 25, D. C.

curves represent the limits between which all true averages are expected to fall.[24]

Curves 1 and 2 of Fig. 13 considered together show the connection between angle and average reduction of area in two materials which were quenched to martensite before being tempered, one an SAE 4335 seamless tube (14-4) and the other an SAE 1045 forging (Forging 21-1). Apparently the variation of average reduction of area quality with angle is much more pronounced in the forging than in the tube. Probably the higher carbon and lower alloy content in the plain carbon steel forging is largely responsible for much of the difference observed. Both curves show that average reduction of area is little affected by angle in the ranges of 0 to 30 degrees and 70 to 90 degrees, but in between these ranges the average falls very rapidly with increasing angle.

A better knowledge of the relation between reduction of area values and angle between longitudinal axis and flow line direction has already resulted in (a) process changes which insure the acceptance of certain products with greater certainty and (b) the conclusion that no changes need to be made in those specifications which require transverse reduction of area quality in accepted material to be above a certain minimum, providing the angle between the direction of the longitudinal axis of the product and the direction of flow lines is less than 20 degrees. If this angle is much more than 20 degrees, the position of test specimen normally specified should probably be modified.

Effect of Forging Reduction on Longitudinal and Transverse Reduction of Area Quality

Most metallurgists are well aware of the general beneficial effect of optimum hot working on ductility and toughness in wrought steel products. Results presented in this section generally confirm what is already known and in addition show more quantitatively than hitherto the effect of forging reduction on longitudinal and transverse reduction of area quality in wrought steels which have been quenched at least partially to martensite and subsequently tempered to a given tensile strength.

[24] These upper and lower limits, designated U. L. and L. L. respectively, are calculated from the expression $\overline{X} + 3\sigma_{\bar{x}}$ and $\overline{X} - 3\sigma_{\bar{x}}$ where $\overline{X}$ is the determined average (arithmetical mean) and $\sigma_{\bar{x}} = \sigma/\sqrt{n}$; $\sigma_{\bar{x}}$ is the standard error of the average, σ is the determined standard deviation based on n, the number of individual reduction of area values.

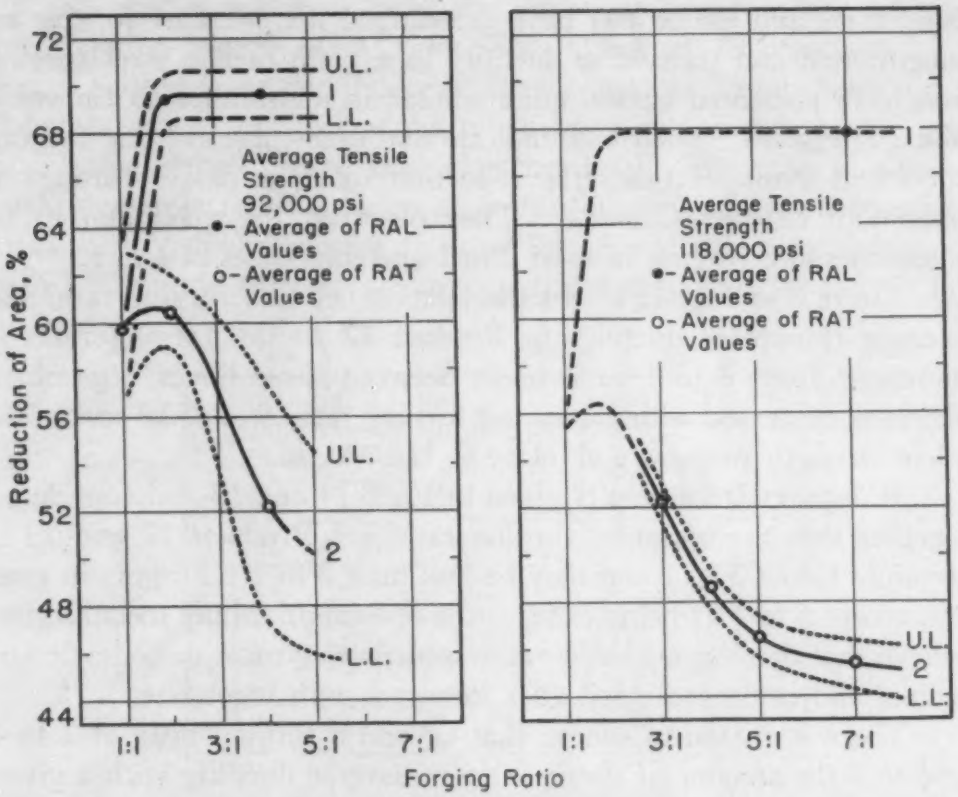


Fig. 14—Effect of Forging Reduction on Longitudinal and Transverse Reduction of Area Quality in Forgings From Company 19. RAL, RAT, U.L., and L.L. are abbreviations for longitudinal reduction of area, transverse reduction of area, upper limit, and lower limit. (See footnote on page 754.)

Fig. 15—Effect of Forging Reduction on Longitudinal and Transverse Reduction of Area Quality in Forgings From Company 17.

Curve 1 in Fig. 14 and Curve 2 in Figs. 14 and 15 show the effect of forging reduction on average longitudinal and average transverse ductility in forgings from Companies 17 and 19. Curves designated U. L. and L. L. represent upper and lower limits between which true averages are expected to fall. These limits are calculated from the expressions referred to and interpreted in footnote 24.

By increasing forging ratio—ratio of area of cross section of ingot before to that after forging—from 1 to 1 (no reduction) to 2 to 1, longitudinal ductility in Product 19 was increased practically to a maximum; at 1 to 1 the determined average of longitudinal reduction of area values for 0.252-inch diameter specimens taken from one of the unforged ingots in 59.5%, at 2 to 1 the average is 69.5% and at 4 to 1 it is 69.7%. At 1 to 1 the determined average of transverse reduction of area values is 60.0%, at 2 to 1 it is 60.4%, and at 4 to 1 it is 52.3%; all tensile strength values are close to 92,000

psi. Mehl and Grobe (9) have determined the effect of forging on longitudinal and transverse ductility in a plain carbon steel forging and have presented curves quite similar in appearance to Curves 1 and 2 in Fig. 14. Their data indicate that each curve relating forging ratio and average transverse reduction of area passes through a maximum as does Curve 2. They observed the maximum to be sometimes at a forging ratio of 2 to 1 and sometimes at 4 to 1.

Curve 2 of Fig. 15 shows the relation between forging ratio and average transverse ductility in Product 17 as the forging ratio is increased from 3 to 1 to 7 to 1; between these limits determined averages decreased with increasing forging ratio from 52.3 to 45.5%. Yield strength values are all close to 118,000 psi.

It appears from results given in Figs. 14 and 15 and considered together that the optimum forging ratio for Products 17 and 19 is certainly below 3 to 1 and may be less than 2 to 1. Forgers in general accept 3 to 1 as being close to the optimum. Many metallurgists believe that the forging ratio value contributing most to better longitudinal and transverse properties increases with ingot size.

There is reason to believe that beyond a forging ratio of 2 to 1 or 3 to 1 the amount of decrease of transverse ductility with a given increase of forging reduction is frequently largely determined by those nonmetallic inclusions which are drawn out into stringers during forging and have a detrimental effect on transverse ductility. Possibly if steels contained no nonmetallic inclusions, transverse ductility, like longitudinal ductility, would increase with forging reduction almost to a maximum (say at some low forging ratio like 2 to 1) and then stay practically constant or change only very slowly with additional forging reduction.

Frequency curves showing the effect of forging reduction on the distribution of transverse reduction of area values are given in Fig. 16; each curve is based on 340 values for 0.505-inch diameter specimens having tensile strengths between 113,000 and 123,000 psi (average 118,000 psi). Increasing the forging ratio lowered the average from 52.3 to 45.5% and raised standard deviation from 4.0 to 6.9%. The major portion of the increase of standard deviation is probably caused by inclusion stringers which are believed to be primarily responsible for specimens for forgings reduced 7 to 1 by hot work having transverse reduction of area values of less than 36%. Stringers produced by a 3-to-1 reduction are on the average shorter and presumably not as damaging.

Source, composition, and size of ingots used in the present investigation are given in Table XV. Product 19 consisted of 8 ingots poured from five induction furnace heats. Ingots were about 5 inches square just below the top discard, 4½ inches square just above the bottom discard, and 25 inches long. The cross section of each ingot was reduced by hammer forging to give two square sections, one having a forging ratio of 2 to 1 and the other a ratio of 4 to 1. Forging temperature was approximately 1204 °C (2200 °F).

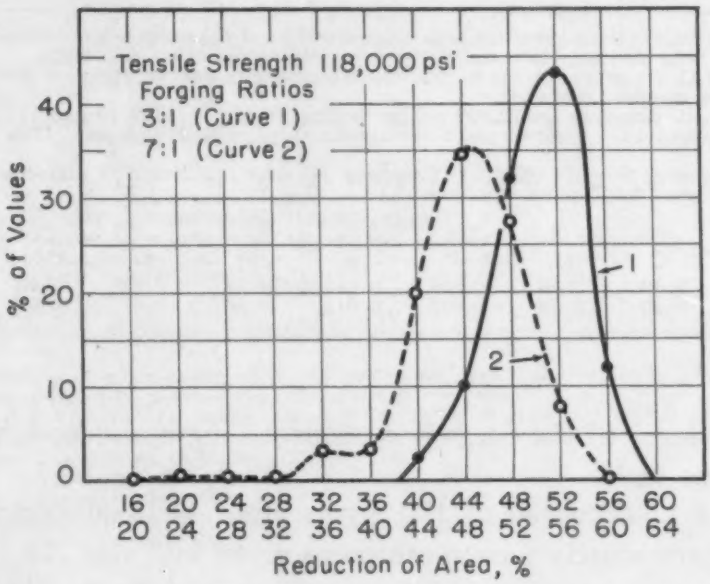


Fig. 16—Frequency Curves Showing Effect of Forging Reduction on Transverse Reduction of Area Quality. Each frequency curve is based on 340 values.

After forging, all pieces were air-cooled, reheated to 940 °C (1725 °F), normalized, reheated to 871 °C (1600 °F), quenched in water, and finally tempered to a tensile strength of 92,000 psi. Four transverse and four longitudinal tensile test pieces were cut from each of six ingots, while two transverse and two longitudinal test pieces were cut from two other ingots; half the pieces were from sections having a forging ratio of 2 to 1 and half were from sections having a forging ratio of 4 to 1. In addition, four specimens, two longitudial and two transverse, were cut from an unforged, heat treated section of an ingot; this section was a transverse slice about 2½ inches thick located just below the hot top of Ingot 1. Each specimen blank was cut so that its center was located midway between the long axis

Table XV

Results Showing Relation Between Forging Ratio and Reduction of Area Quality in Quenched and Tempered Forgings

Source of Material	Ingot Cross Section Just Below Top Discard	Ingot Cross Section Just Above Bottom Discard	No. of Values	Forging Ratio	Average RAT %	σ RAT %	Average RAL %	σ RAL
Company 19	5 in. square	4.5 in. square	2	1 to 1	60.0		59.5	
			28	2 to 1	60.4	2.6	69.5	1.9
			28	4 to 1	52.3	9.0	69.7	1.6
Company 17	26 in. round	18 in. round	340	3 to 1	52.3	4.0		
			340	4 to 1	48.6	6.0		
			340	5 to 1	46.5	5.6		
			340	7 to 1	45.5	6.9		
			2	7 to 1			67.8	

The forging ratio is the ratio of the area of cross section of the ingot before to that after forging; the forging ratio obviously approaches 1 to 1, no forging reduction, as a limit.

RAT and RAL are abbreviations for transverse and longitudinal reduction of area.

σ Designates standard deviation.

Average tensile strengths are 92,000 psi for forgings from Company 19 and 118,000 psi for those from Company 17. Yield strength average for forgings from Company 17 is 100,000 psi at 0.01% offset.

Tensile specimens from Product 19 (Company 19) were 0.252 inch in diameter and those from Product 17 were 0.505 inch in diameter.

	Approximate Composition—Per Cent of Element—							
	C	Mn	P	S	Si	Cr	Mo	V
Product 19	0.30	0.50	0.008	0.025	0.25	0.90	0.40	....
Product 17	0.30	0.76	0.013	0.012	0.26	1.01	0.49	0.10

and side surfaces of the forged or unforged ingot and several inches from the two ends.

Product 17 consisted of 170 ingots from 44 basic electric heats and had approximately a composition as given in Table XV. Ingots were forged into rounds; two forgings were made per ingot, one from the top and the other from the bottom half. The maximum forging temperature was about 1231 °C (2250 °F) and the minimum 1036 °C (1900 °F). After forging, the pieces were air-cooled, reheated to 953 °C (1750 °F), furnace-cooled, reheated to 912 °C (1675 °F), water-quenched, and finally tempered to a tensile strength of about 118,000 psi. The forging ratios at ingot positions located (before forging) 6, 40, 42, and 88 inches below the hot top were 4 to 1, 7 to 1, 3 to 1, and 5 to 1, respectively. Eight 0.505-inch diameter transverse tensile test specimens were cut from each ingot, two from each position at which the forging ratio was 4 to 1, 7 to 1, 3 to 1, and 5 to 1, respectively. Tensile test blanks were taken from midradius positions as indicated in Fig. 3, and each blank was located more than two-thirds of a diameter from the nearest end of the forging.

Table XVI

Data Showing Relation Between (a) Estimated Average Transverse Reduction of Area Quality of Quenched and Tempered Forgings and (b) Original Cross Sectional Area of Ingots, Assuming the Forging Ratio to be 3:1 and the Forgings to be Tempered to a Yield Strength of 115,000 psi

Company No.	Item No.	No. of Ingots	Forging Ratio	No. of RAT Values	Average YS at 0.01% Offset (1 unit = 1000 psi)	RAT Quality % Average	RAT Quality % σ	Original Area of Cross Section of Ingot "X" Ins. Below Hot Top in Square Ins.	Estimated Average RAT Quality, Assuming YS Is 115,000 psi and Forging Ratio Is 3:1 %
1	1	600	3.1:1	600	115	50.3	3.5	100	50.7
2	2	700	4.7:1	700	111	47.2	5.4	144	51.1
3	3	200	4.4:1	200	109	43.1	4.1	133	45.8
4	4	38	3.0:1	76	122	43.3	2.6	133	45.4
5	5a	50	3.5:1	100	143	33.7	4.0	202	44.0
	5b*	80	4.2:1	161	124	37.3	3.1	1450	44.0
	5c*	79	3.0:1	158	112	38.7	3.5	1660	37.8
6	6	47	3.5:1	94	154	31.1	3.9	202	44.7
7	7*	54	4.0:1	108	74	54.9	3.4	227	46.3
8	8a	18	4.5:1	36	152	30.9	4.3	254	46.8
	8b*	60	3.0:1	120	109	43.5	4.5	855	41.7
9	9	600	5.0:1	1200	93	46.0	3.7	254	45.2
10	10	59	5.7:1	118	145	34.6	5.0	324	49.9
11	11	28	5.7:1	56	152	35.4	3.6	324	52.8
12	12*	77	3.0:1	154	102	47.7	3.8	283	43.8
13	13a	289	6.1:1	578	156	32.8	4.6	345	51.6
	13b*	217	3.7:1	434	110	46.1	3.5	1156	47.2
15	15	500	15:1	500	120	38.5	3.5	460	48.0
16	16	1000	15:1	1000	134	34.6	6.0	460	48.3
17	17a*	170	4.0:1	340	100	48.5	4.2	452	47.7
	17b*	129	4.0:1	258	123	37.5	5.8	1380	43.6
	17c*	80	3.4:1	160	99	40.5	5.9	1810	37.6

*These items were assumed to be quenched essentially to bainite; all others were probably quenched to martensite before being tempered.

Material "X" inches below hot top of ingot is that for which forging ratio and transverse reduction of area quality have been determined.

RAT = Transverse reduction of area.

YS = Yield strength.

σ = Standard deviation.

Influence of Size of Ingot on Transverse Ductility in Forgings

It is generally agreed among those who have had wide experience in the making of forgings from ingots of extreme sizes that quenched and tempered forgings with the same forging ratio and yield strength are more likely to have higher transverse ductility if they come from small rather than large ingots. Results supporting this viewpoint are given in Table XVI and in Fig. 17.

The average and transverse reduction of area values for specimens taken from midwall positions (Fig. 2) in forgings receiving the same forging reduction and subsequently quenched and tempered to the same yield strength is usually higher when the forgings come from smaller ingots; however, variation among values for specimens from forgings produced in a single practice appears to be, at least approximately, independent of whether the forgings come from large

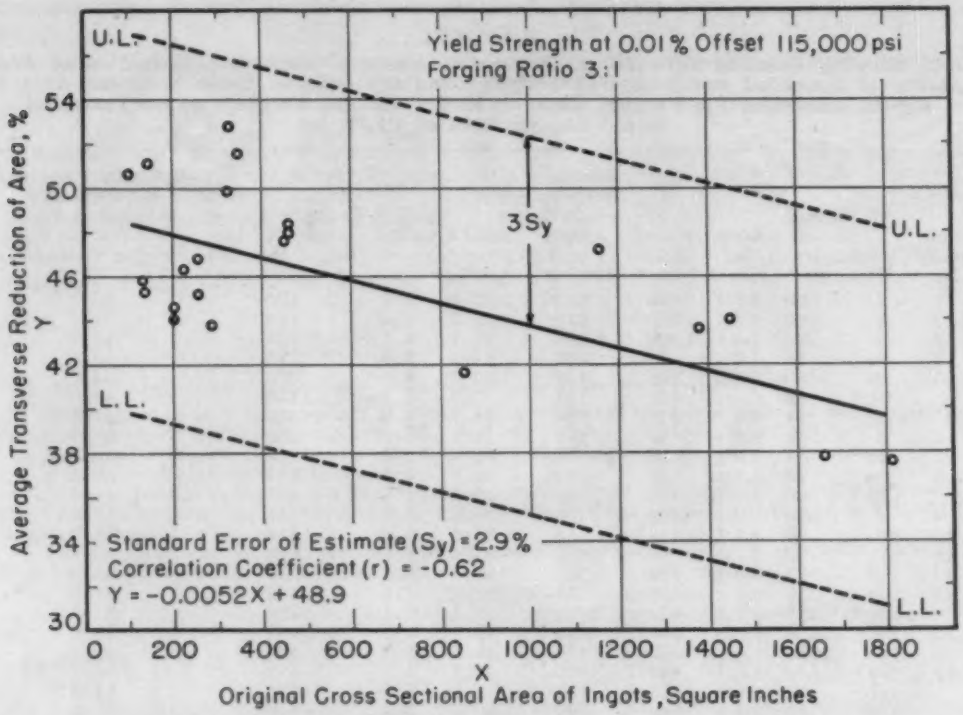


Fig. 17—Shows Relation Between (a) Average Transverse Reduction of Area Quality of Quenched and Tempered Forgings and (b) Original Cross Sectional Area of Ingots, Assuming the Forging Ratio to be 3:1 and the Forgings to be Tempered to a Yield Strength (at 0.01% Offset) of 115,000 Psi. U.L. and L.L. are abbreviations for upper and lower limit, respectively.

or small ingots. Data available for Products 1 (Item 1, Table XVI) and 5c and for Products 17a and 17c substantiate these conclusions.

Average and standard deviation figures based on 600 transverse reduction of area values for specimens from Product 1 are 50.3 and 3.5%, respectively; based on 158 values for specimens from Product 5c, the figures are 38.7 and 3.5%.[25] Specimens from both products consisted of material which had been reduced about 3 to 1 by forging and later quenched and tempered to a yield strength of approximately 115,000 psi. Product 1 was cast into ingots designated as 10-inch squares and Product 5c into ingots designated as 46-inch rounds.

The average of transverse reduction of area values for 340 specimens from Product 17a (Item 17a, Table XVI) is 48.5% and the average for 160 specimens from Product 17c is 40.5%; standard deviations are 4.2 and 5.9%, respectively. Both products were from the same company, received approximately the same forging reduction,

[25]This and other standard deviation figures given in Table XVI are approximate; they are calculated from the formula $\sigma = \bar{R}/A$ where A is a constant which depends on sample size, $\bar{R}$ is the average range based on samples of either 2 or 4, and σ is standard deviation.

and were quenched and tempered close to the same yield strength. Product 17a was cast into ingots designated as 24-inch rounds and Product 17c was cast into 48-rounds. Typical compositions are as follows:

	Per Cent of Element							
	C	Mn	P	S	Si	Cr	Mo	V
Product 17a	0.30	0.75	0.016	0.013	0.25	0.98	0.49	0.12
Product 17c	0.36	0.81	0.011	0.012	0.26	1.13	0.54	0.10

Specimens from these products were taken at least two-thirds of a wall thickness from the nearest end of forgings and from midwall positions (Fig. 2). The 340 specimens from Product 17a consisted of material which had been reduced 4 to 1 by forging, quenched and tempered to a yield strength of about 100,000 psi and came from the smaller ingots; the 160 specimens from Product 17c consisted of material which had been reduced 3.4 to 1, quenched and tempered to a yield strength of about 99,000 psi and came from the very large ingots.

All products referred to in Table XVI were made from fine-grained basic electric steels and had compositions lying between the limits given in Table VIII. Tensile specimens from Products 1, 2, 3, 15, and 16 were 0.357 inch in diameter; all others were 0.505 inch in diameter.

In an effort to utilize the data given in Table XVI to a maximum extent for the purpose of indicating, at least approximately, the effect of ingot size on transverse ductility in forgings, an estimate was made of the average transverse reduction of area quality to be expected in each product if the forging ratio were 3 to 1 and the yield strength after the quench and temper were 115,000 psi. Transverse reduction of area averages were estimated from data given in Columns 4, 6, and 7, using two assumptions which are: (a) an increase of 5000 psi in yield strength is accompanied by a decrease of 1.5% in transverse reduction of area, and (b) transverse reduction of area is decreased with increase of forging ratio beyond 3 to 1 as indicated by data plotted in Fig. 15. Evidence given in Table X shows the assumed relation between yield strength and transverse reduction of area to be valid over a very large range of yield strength in forgings quenched to martensite and subsequently tempered; however, it is conceded that in forgings quenched to bainite before being tempered, the range of yield strength over which the assumed relation

is valid may be quite small. With one exception,[26] determined averages of yield strength values for specimens from quenched and tempered forgings quenched to something other than martensite before being tempered were not more than 16,000 psi above or below 115,000 psi; therefore, as long as the assumed relation is approximately valid over this small yield strength range, estimated transverse reduction of area averages for such forgings tempered to 115,000 psi should be sufficiently accurate for use in present studies.

Data from Columns 9 and 10 (Table XVI) plotted in Fig. 17 show the relation between (a) original cross sectional area of ingots at "X" inches below the hot top[27] and (b) estimated average transverse reduction of area quality of quenched and tempered products reduced 3 to 1 by forging and tempered to a yield strength of 115,000 psi. As cross sectional area (size of ingot) increases, average reduction of area (transverse ductility) decreases as indicated by the regression line shown in the figure. Within a range of about 1700 square inches (100 minimum, 1800 maximum), an increase of 100 square inches in the cross sectional area of a round or square ingot may be expected to cause a decrease of about 0.5% in average transverse reduction of area in quenched and tempered forgings with a forging ratio of 3 to 1 and a yield strength of 115,000 psi. While this conclusion is probably only approximately correct, a tentative acceptance of it is believed justified, pending the availability of more precise information on the subject.

It is believed that if all ingots referred to in Table XVI had been reduced 3 to 1 in cross section by forging, and subsequently quenched to martensite before being tempered, the transverse reduction of area quality on the average would have been practically as high for midwall material in the large as in the small forgings. Also, it appears probable that if the ingots had been reduced 3 to 1 by forging, subjected to normal commercial quenching treatments and subsequently tempered to a low yield strength of 80,000 psi or so, both large and small forgings would have on the average about the same transverse reduction of area quality.

The average of 20 transverse reduction of area values for speci-

---

[26] One product (Item 7, Table XVI) with an SAE 4130 composition was quenched and tempered to a yield strength of about 74,000 psi; it is believed that the average transverse reduction of area of this product is practically the same as would have been obtained if it had been quenched to martensite before being subjected to the high temperature draw treatment necessary to give a yield strength of only 74,000 psi.

[27] Material "X" inches below hot top of ingot is that for which forging ratio and transverse reduction of area quality have been determined.

mens from a large forging (Forging 5-3) about 340 inches long, 25 inches maximum O.D. and 8.5 inches I.D., reduced 3 to 1 by forging and having a yield strength of 115,000 psi, is 39.0% and the average of 20 additional values for specimens from the same forging which were quenched to martensite and tempered to the same yield strength is 46.6%. Averages of transverse reduction of area values for specimens from small ingots reduced 3 to 1 by forging, quenched to martensite and tempered to a yield strength of 115,000 psi are quite frequently no higher than 46.6%. An average of 20 other transverse reduction of area values (a) for specimens retempered to a yield strength of 80,000 psi and (b) for specimens quenched to martensite and retempered to a yield strength of 80,000 psi is 55.6 and 54.2%, respectively. All specimens from the large ingot referred to in this paragraph were 0.252 inch in diameter and came from Forging 5-3. The original cross sectional area of the ingot at positions from which specimens were taken was 1660 square inches.

Relation Between Transverse and Longitudinal Reduction of Area at Various Yield Strength Levels

For many years metallurgists have known that both transverse and longitudinal reduction of area quality of quenched and tempered wrought steel products decreases with increasing yield strength; however, not until recently when results discussed in this section were first obtained did precise information about the relation between transverse and longitudinal reduction of area at various yield strength levels become available.

Regression lines (designated RAT and RAL in Fig. 18) and limit lines (designated U.L. and L.L.) when considered together show the relation (a) between yield strength and transverse reduction of area (RAT), and (b) between yield strength and longitudinal reduction of area (RAL) for a quenched and tempered seamless tube (Tube 14-2); calculated correlation coefficients are —0.94 and —0.99, respectively. Apparently, transverse ductility in such a hot-worked product quenched to martensite and subsequently tempered decreases more rapidly with increasing yield strength than does longitudinal ductility, and the variation of ductility at each yield strength level is very much larger in the transverse than the longitudinal direction. Within a considerable yield strength range, 180,000 psi maximum and 95,000 psi minimum, an increase of 5000 psi was accom-

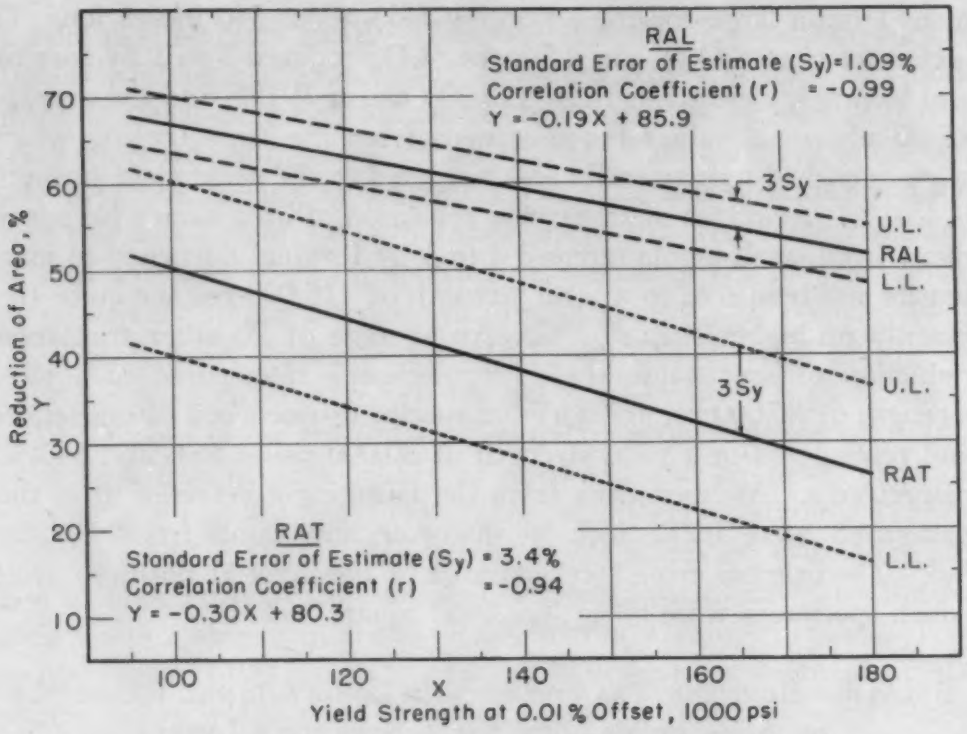


Fig. 18—Relation Between Transverse and Longitudinal Reduction of Area at Various Yield Strength Levels in a Quenched and Tempered Seamless Tube (Tube 14-2, See Table IX). RAT and RAL are abbreviations for transverse and longitudinal reduction of area.

panied by a decrease of about 1.5% in average transverse and 0.95% in average longitudinal reduction of area; thus, when at a yield strength of 95,000 psi, average transverse and longitudinal reduction of area values are known to be 51.8 and 67.8%, respectively (RAT/RAL ratio 0.76), then at 180,000 psi they are expected to be 26.3 and 51.7% (RAT/RAL ratio 0.51).[28]

Calculated standard deviations based on reduction of area values for transverse and longitudinal specimens from quenched and tempered tubes drawn to different yield strength levels support the conclusion that over a wide yield strength range the variation of reduction of area quality—longitudinal or transverse—in a hot-worked product quenched to martensite and subsequently tempered is, at least approximately, independent of yield strength level. As previously pointed out, standard deviations calculated from transverse reduction of area values for specimens from sections of Forging 12-2 drawn

[28]Results given by Janitzky and Baeyertz (10) show that over a wide yield strength range and in wrought SAE structural steels as a group an increase of 5000 psi in yield strength is usually accompanied by a decrease of about 1% in longitudinal reduction of area, providing the steels are quenched to martensite before being tempered.

to a yield strength of 83,000 psi and 147,000 psi are 2.9 and 3.3%. Standard deviations calculated (a) from 16 values for longitudinal specimens cut from Section A of Tube 14-2 drawn to a yield strength of about 180,000 psi and (b) from 16 values for specimens from Section B drawn to 100,000 psi are 1.2 and 1.0%, respectively.

Equations for the regression lines drawn in Fig. 18 and also upper and lower limits were calculated from yield strength and reduction of area data for 200 transverse and 48 longitudinal specimens, each 0.252 inch in diameter and coming from Tube 14-2. Formulas used for making these calculations are given on page 31.

Points representing yield strength and longitudinal reduction of area values for 48 longitudinal specimens from Tube 14-2 all fell as expected between the upper two of the four limit lines drawn in the figure; also points representing yield strength and transverse reduction of area values for 199 transverse specimens all fell between the lower two of the limit lines. One transverse reduction of area value for a specimen having a yield strength of 178,000 psi is 16.0% which is below the lower limit; occasional low values such as this have frequently been found to be caused by nonmetallic inclusions.

Correlation of Transverse Reduction of Area With Transverse Impact

Since values for impact tests reveal various types of brittleness —cold brittleness,[29] temper brittleness, and brittleness resulting from a quenching to something other than martensite before tempering— which are not evident from reduction of area values, it is obvious that a correlation between transverse reduction of area and transverse impact can be expected only for materials relatively free from such types of brittleness. In many practices the heat treatment is such as to insure that each unit of heat treated product is free from brittleness, at least at temperatures above —73 °C (—100 °F) or so. It is in materials from such practices in which the variations of both properties result primarily from the same causes (such as variation of deoxidation practice and of nonmetallic inclusion content) that one may expect to find a correlation between transverse reduction of area and transverse impact quality. Such a correlation has been ob-

[29] Over a narrow range of low temperatures impact but not reduction of area values for specimens from quenched and tempered wrought steels such as Product 14 fall very rapidly, frequently to less than 3 or 4 foot-pounds, as the temperature is lowered. At temperatures below this range, the steels are said to suffer from "cold brittleness."

served among values for specimens from Product 14 and from other products similarly heat treated, supporting the viewpoint expressed by McAdam and Clyne (11) that in the absence of cold brittleness reduction of area is a good index of the impact value obtainable.

Results given in Fig. 19 show the relation between average transverse reduction of area and average transverse impact quality in

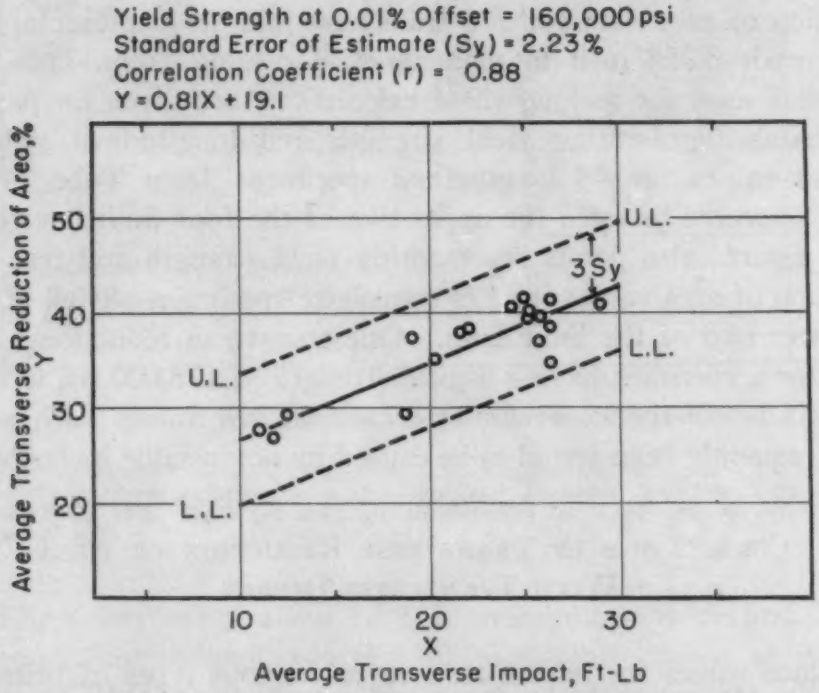


Fig. 19—Relation Between Average Transverse Reduction of Area and Average Transverse Impact Quality in Quenched and Tempered Seamless Tubes (Product 14, Company 14). The X coordinate of each circle represents an average of 24 transverse impact values and the Y coordinate an average of 24 transverse reduction of area values.

Product 14 consisting of seamless tubes quenched to martensite and tempered to a yield strength of about 160,000 psi; an increase of 1% in average transverse reduction of area is accompanied by an increase of about 1.2 foot-pounds in average transverse impact. Standard error of estimate and correlation coefficient values are 2.23 and 0.88%, respectively, and the equation for the regression line is Y (average transverse reduction of area in per cent) = 0.81 X (average transverse impact in foot pounds) + 18.4.

Calculations of standard error of estimate, correlation coefficient, and regression line equation were made using formulas described on page 745 and data plotted in Fig. 19. The X co-ordinate of the center point in each circle represents an average of 24 transverse reduction

of area values for specimens 0.357 inch in diameter taken from mid-wall positions (Fig. 2) in six tubes coming from the same heat, and the Y co-ordinate of the same point represents an average of 24 transverse impact values for standard "V" notch Charpy specimens coming from similar positions in the same six tubes. The two averages associated with one point are based on data from tubes in one heat; averages associated with any other point are based on data from tubes in another heat. Charpy specimens were broken at 70 °F and tensile tests were made at room temperature. Tubes were each about 160 inches long, 7.5 inches O.D., and 2.5 inches I.D., and had a typical composition as follows:

Per Cent of Element							
C	Mn	P	S	Si	Ni	Cr	Mo
0.37	0.80	0.015	0.015	0.27	1.85	0.82	0.38

Tubes all came from basic electric heats except for those of lowest transverse reduction of area and lowest transverse impact quality from three basic open-hearth heats.

Studies of microstructure and hardness of pieces from the quenched product and of impact data for specimens from the quenched and tempered product convinced the authors that each tube considered in this investigation was consistently sufficiently well heat treated to insure maximum toughness. Rockwell hardness values measured across a section cut from a quenched tube varied by only one or two points and "V" notch Charpy impact values for transverse specimens from a large number of quenched and tempered tubes were rarely less at —40 °C (—40 °F) than at 21 °C (70 °F) by more than 2 or 3 foot-pounds.

In a few instances the authors have used the relation given in Fig. 19 for estimating the maximum average impact quality expected to be developed in a unit of wrought steel product of known transverse reduction of area quality when it is properly heat treated. These estimates were made for materials having yield strengths between 140,000 and 165,000 psi. For example, determined transverse reduction of area averages are 44.7% for Forging 1, Company 12 (tensile strength 164,000 psi, yield strength approximately 145,000 psi), and 32.0% for Forging 14-2 (yield strength 156,000 psi), and estimated average transverse impact values are 32 and 17 foot-pounds; determined average transverse impact values are 30.2 and 18.7 foot-pounds, respectively.

Angular Fracture

It is generally assumed that transverse tensile test specimens from highest quality quenched and tempered wrought steel products should exhibit a cone and cup fracture (Fig. 20a and b) when broken in the tensile test. Occasionally, specimens show an angular fracture (Fig. 20c) in which the relation of fracture surface to fiber is as indicated diagrammatically in Fig. 21. Such a fracture causes

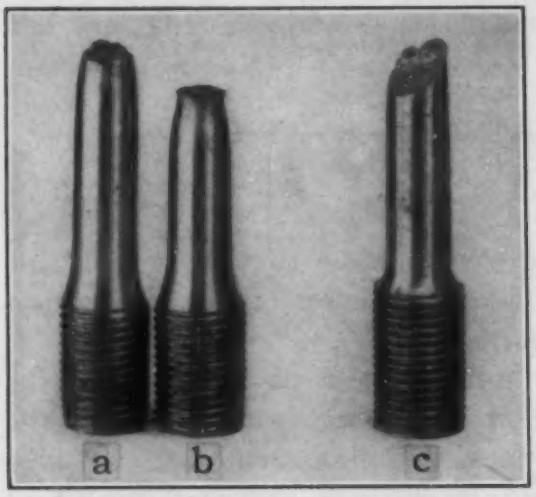


Fig. 20—Photograph of Broken Specimen With Cone and Cup Fracture (a and b) and of Part of Specimen With Angular Fracture (c).

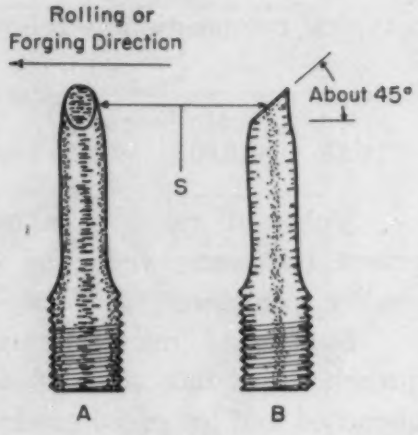


Fig. 21—Appearance of Macro-etched Broken Tensile Specimen With Angular Fracture—Shown Diagrammatically. Relation of fracture surface to fiber is indicated.

some concern among those producers who associate an angular break with low ductility. Results presented in Fig. 22 show that on the average transverse reduction of area values for test pieces having an angular break are lower than those for pieces having a cup and cone break, and there is some justification for believing that if the cause responsible for a particular angular fracture had been removed so that the broken test piece considered would have had a cup and cone fracture, then the transverse reduction of area value for that piece would have been higher. However, it is quite apparent from the figure that many transverse reduction of area values for test pieces with an angular fracture actually are higher than those for many other test pieces with a cup and cone fracture. For this reason it is concluded that (a) an angular fracture in itself is no certain criterion for low ductility and (b) there is little justification for suspecting the quality of a product simply because a specimen has an

angular fracture, especially if the transverse reduction of area value for that specimen is relatively high.

Data given in Table XVII show that the frequency of occurrence of angular fracture among broken transverse tensile test specimens from Product 14 and the frequency of occurrence of unusually low transverse reduction of area values for specimens having such a

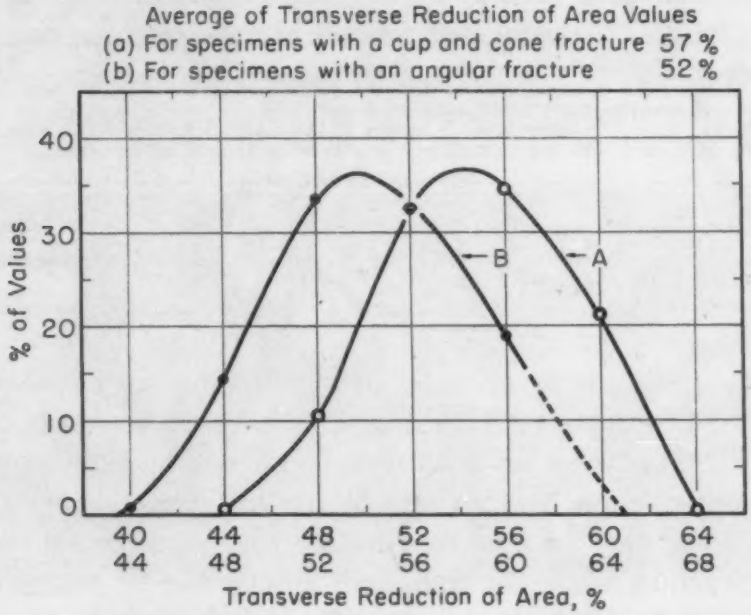


Fig. 22—Frequency Curves Showing the Distribution of Transverse Reduction of Area Values for Specimens 0.505 Inch in Diameter Which Broke to Give (a) a Cup and Cone Fracture —Curve A and (b) an Angular Fracture—Curve B. Number of values for specimens with a cup and cone fracture equals 400; number of values for specimens with an angular fracture equals 96. Forgings from which test pieces were taken were quenched and tempered to a yield strength of about 75,000 psi. Composition of forgings is approximately SAE 4140.

fracture is largely determined by the amount of nonmetallic inclusions present. As the steel becomes dirtier and the number of stringers consisting of small, hard, angular particles increases, the frequency of occurrence of specimens with angular fracture and low transverse ductility increases also. Out of 76 transverse tensile test specimens from seamless Tube 14-4 (Table XVII) containing an unusually large quantity of nonmetallic inclusions (SAE rating 3^{vd}-1^{52d}-A),[30] 12 have cup and cone and 64 have angular fractures;

[30] An SAE rating of 3^{vd}-1^{52d}-A signifies that in a surface having an area of 0.5 square inches and selected to be parallel with the direction of rolling or forging, 52 disconnected inclusions were observed which had a length of between 0.005 and 0.0075 inch (written as 1^{52d}). The longest inclusion was between 0.0125 and 0.0175 inch long and was very disconnected in appearance (written as 3^{vd}). "A" signifies that relatively few inclusions shorter than 0.005 inch were present. For a detailed description of SAE rating procedure, see *SAE Handbook* (12).

Table XVII

Data Showing Influence of Nonmetallic Inclusions on (a) Frequency of Occurrence of Angular Fracture and (b) Transverse Reduction of Area Values for Specimens Which Have an Angular Fracture

Company and Tube Number	Inclusion Rating (SAE Method)	Number of Fractures		Average RAT Values, %		Minimum RAT Values, %		Maximum RAT Values, %	
		Cup-cone	Angular	Cup-cone	Angular	Cup-cone	Angular	Cup-cone	Angular
14-4	3^{vd}-1^{sgd}-A	12	64	48.4	30.0	47.3	15.4	52.4	49.0
14-5	2^{d}-1^{4d}-A	93	2	58.7	53.0	49.6	50.6	63.1	55.3

RAT is abbreviation for transverse reduction of area.

Tensile and yield strength values for the tubes are about 125,000 and 105,000 psi, respectively. Specimens were 0.252 inch in diameter.

Both tubes, each 90 inches long, 5 inches O.D., and 1.5 inches I.D., were made from basic electric steel and had approximately the following typical composition:

Element in Per Cent							
C	Mn	P	S	Si	Ni	Cr	Mo
0.33	0.71	0.015	0.020	0.26	1.84	0.75	0.36

The method used for rating specimens for inclusions is that recommended by SAE and described in the SAE *Handbook* (12).

out of 95 specimens from Tube 14-5 containing an unusually small quantity of inclusions (SAE rating 2^{d}-1^{4d}-A), 93 have cup and cone and only 2 have angular fractures. The minimum among the 76 transverse reduction of area values for test pieces from the dirty steel is 15.4% and the specimen having this value broke to give an angular fracture while the minimum among the 95 values for test pieces from the clean steel is 49.6% and the specimen with this value broke to give a cup and cone fracture. The average of the transverse reduction of area values for 64 dirty steel test pieces with an angular fracture is only 30.0%, whereas the average of the values for the 2 clean steel test pieces with an angular fracture is 53.0%.

Not all specimens from steels which are normally considered as being unusually clean have a cup and cone fracture; some have an angular fracture. Out of 300 specimens, each 0.252 inch in diameter, taken from an SAE 4140 forging quenched and drawn to a tensile strength of 105,000 psi, 258 have a cup and cone and 42 have an angular fracture. This forging which came from Company 7 is clean (SAE rating 1^{d}-1^{3d}-A), and no transverse reduction of area value for any specimen is below 45.0%.

A study made to determine why tensile test specimens from highest quality, exceptionally clean, and properly heat treated steels should sometimes break to give an angular fracture led the authors to the conclusion that the type of fracture obtained when a specimen from such steels is broken depends to a large extent on the orienta-

tion of the dendritic pattern and on the degree of interlocking of the dendritic arms. This conclusion is based on the fact that out of 40 surfaces examined, one close to and parallel with the angular fracture surface in each of 40 specimens, 39 have Structure A (Fig. 23) and 1 Structure B, while out of 50 surfaces comparable with the 40 referred to above but associated with specimens wtih cup and cone fractures, only 19 have Structure A and 31 have Structure B.

Since angular fracture in highest quality wrought steel products depends on orientation of dendritic pattern and therefore on segregation, a homogenizing treatment is expected to reduce the percent-

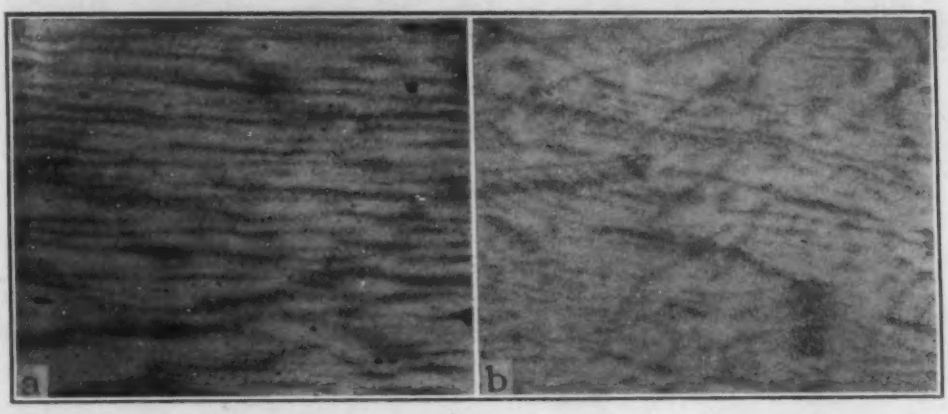


Fig. 23a—Structural Appearance of a Surface Approximately Parallel With Surface S (Fig. 21), a Specimen With an Angular Fracture. × 10. Fig. 23b—A cup and cone fracture. × 10. To obtain contrast broken specimens were made austenitic, partially transformed to bainite at about 350 °C, and subsequently quenched in water.

age of specimens having an angular fracture. Actually all high temperature, long-time homogenizing treatments did reduce the percentage of angular fractures quite significantly; in one instance the percentage was reduced from about 15.1 to 1.7%. In this case, 236 broken tensile specimens were examined; all had a yield strength of about 115,000 psi and came from a high quality quenched and tempered seamless tube. In homogenizing treatments steels were heated to 1350 °C (2462 °F) for 65 hours.

Insofar as angular fracture depends on the orientation of dendritic pattern and since orientations of dendritic pattern are determined by chance, the occurrence of some angular fractures even among specimens from high quality forgings is to be expected and should give little concern. Rejection of such high quality material because of angular fracture is unwarranted.



Fig. 24—Appearance of Deeply Etched Surface of a Disk Cut From Forging 17-1. Etchant caused deep pits in specimen blanks 4U, 5U, 6U, and 7U, respectively. On the average transverse reduction of area values are as high for specimens from these blanks as for specimens from others which are relatively free from pitting. The tensile strength of each test piece is close to 100,000 psi. Figures appearing on bottom of photograph are transverse reduction of area values in per cent. × 1.

Transverse Reduction of Area Quality of Forged Material Which Before Being Deeply Etched Appears Sound but Afterwards Appears Porous

It is assumed by many inspectors that, on the average, transverse reduction of area values for specimens taken from a forging are likely to be significantly lower if the specimens contain material which becomes porous when deeply etched. Results presented in Fig. 24 and others available to the authors show quite definitely that this assumption is frequently invalid. The average of transverse reduction of area values for specimens from Blanks 4U to 7U is 40.8% and for specimens from Blanks 8U to 11U, it is 40.3%. Blanks 4U to 7U showed large pits when deeply etched, while Blanks 8 to 11U did not.[31] After test pieces were broken, they were all subsequently etched; only those from Blanks 4U to 7U contained large pits. All specimens were 0.252 inch in diameter and had a tensile strength close to 100,000 psi.

The etched surface referred to in Fig. 24 is perpendicular to the longitudinal axis of the forging. The forging which was quenched and tempered consists of acid open-hearth steel, is about

[31] The etchant contained 38% HCl, 12% H_2SO_4, and 50% water. It was heated to 80 °C and pieces to be etched were kept in the hot solution for various times, depending on the severity of etching desired.

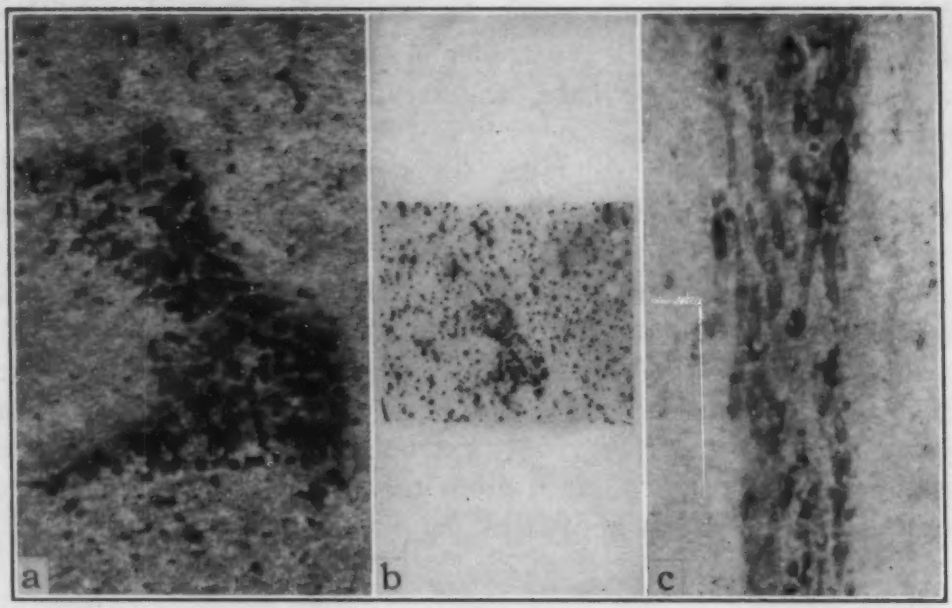


Fig. 25a—Photomicrograph of Deeply Etched Surface A. Surface A was developed by etching Surface B. × 8. Fig. 25b—Enlarged photograph of a sulphur print of Surface B. × 2. Fig. 25c—Photomicrograph of deeply etched Surface C which cuts Surface A in the severely pitted region and is perpendicular to it. Surface C is parallel with the longitudinal axis of the forging. × 8.

210 inches long, 18.5 inches maximum O.D., and 7.5 inches I.D., and has the following composition:

Per Cent of Element						
C	Mn	P	S	Si	Mo	V
0.41	0.74	0.039	0.023	0.31	0.42	0.22

Deep holes, frequently ⅛ inch in diameter and ¼ inch or more in depth, observed in etched disks from Forging 17-1 result from the preferential attack of hot etchant on sulphide-rich regions. In Surface B (Fig. 25) a sulphide-rich region was located. This surface was subsequently acid etched and it was observed that the located sulphide-rich region was etched more quickly than other material, giving rise to the development of, first, a large number of small holes clustered together (Fig. 25a), and later, one large hole. Regions attacked most vigorously contained segregated alloying elements and carbon, as well as sulphides. The longitudinal axis of the holes in etched disks is usually roughly parallel with the longitudinal axis of the forging. Cross sections of holes have different shapes but quite frequently they are approximately round.

Sulphides in Forging 17-1 are softer than the matrix—determined by scratch test—are dove gray in color, have roughly a cylin-

drical shape, and generally appear to consist of a single phase. These inclusions have a much less detrimental effect on transverse reduction of area than have the hard, angular, stringer type of inclusions referred to previously.

Frequently, when sulphides are segregated in the region of a tensile test specimen where rupture normally occurs, the specimen breaks at some distance away from that region. One specimen, with a cup and cone fracture and for which the transverse reduction of area value is 52.0%, broke three-eighths of an inch away from the position at which the fracture surface is usually expected. When etched, the large piece of the specimen showed a large hole about $\frac{3}{32}$ inch in diameter (Fig. 26), extending completely through the specimen and located $\frac{3}{8}$ inch from the fracture. The average of the transverse reduction of area values for 11 such specimens is

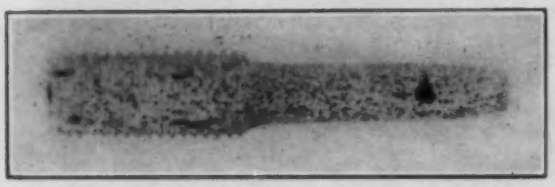


Fig. 26—Photograph of Part of a 0.252-Inch Diameter Transverse Tensile Test Specimen Deeply Etched After Being Broken. Material containing segregated sulphides was etched out giving a hole $\frac{3}{32}$ inch in diameter extending through the specimen and located $\frac{3}{8}$ inch from the fracture. Fracture type is cup and cone. The transverse reduction of area and tensile strength values for the specimen are 52% and 99,000 psi, respectively. × 1.

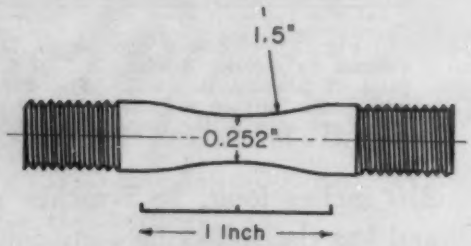


Fig. 27—Sketch of Specimen Designed to Limit Positions of Rupture to Sulphide-Rich Regions Located Close to a Plane Passing Through the Center and Perpendicular to the Longitudinal Axis of the Specimen.

43.2% and the average of values for 11 other specimens which when broken and etched were relatively free from deep pits is 46.0%. All test pieces had a tensile strength close to 95,000 psi and came from positions close together in the forging. Subsequently, several transverse tensile specimens were specially shaped (Fig. 27) so as to be sure they would break through their center when tested, whether they contained segregated sulphides or not. Average tensile strength and transverse reduction of area values are 98,000 psi and 39% for specimens which did, and 98,000 psi and 45% for specimens which did not, show pits when fracture surfaces were deeply etched. Since each average is based on only two data, the results are inconclusive, although they do suggest from a practical point of view that segregated sulphides in Forging 17-1 did not lower transverse reduction of area quality significantly.

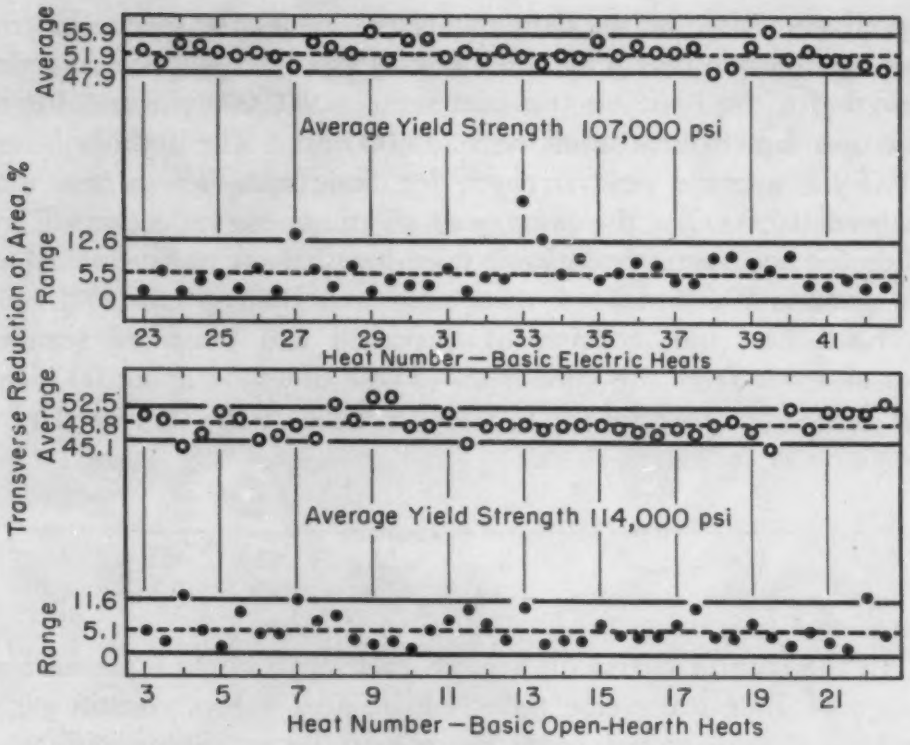


Fig. 28—Control Charts Showing the Difference Between the Transverse Reduction of Area Quality in Basic Electric and Basic Open-Hearth Heat Units to be Insignificant From a Practical Point of View. Each open circle represents an average of four transverse reduction of area values constituting a sample and each closed circle represents the maximum difference among the same four values.

Transverse Reduction of Area Quality of Basic Electric Versus Transverse Reduction of Area Quality of Basic Open-Hearth Wrought Steel Products

A general belief exists that, on the average, heat treated wrought steel products made of basic electric steel have better transverse ductility than comparable products made of basic open-hearth steel. Sometimes, however, as indicated by results presented in Fig. 28, the difference between the transverse reduction of area quality of a product made from basic electric and basic open-hearth steel is so small as to be practically insignificant.[32] Calculated average and standard deviation figures based on 160 transverse reduction of area values for specimens from basic electric heat units are 51.9 and 3.5%,

[32]A detailed account of (a) the basic open-hearth practice used for the making of the open-hearth steel referred to here and (b) factors which influence the quality of basic open-hearth steels is given by Mravec, Welchner, and Hildorf (13). Steels from both basic open-hearth and basic electric heats were cast into 21-inch diameter molds and were similarly processed and heat treated.

respectively; based on the same number of values for specimens from basic open-hearth heat units, they are 48.8 and 3.5%. Average yield strength for the basic electric heat units is 107,000 psi and for the basic open-hearth heat units, it is 114,000 psi. The authors believe that if the average yield strength for basic open-hearth heat units had been 107,000 psi, the average of all transverse reduction of area values for specimens from basic open-hearth heat units would have been close to 50.9%.

Each heat unit consists of quenched and tempered seamless tubes all made from the same heat. These tubes are about 90 inches long, 6 inches maximum O.D., and 1.5 inches I.D. A typical composition is as follows:

Per Cent of Element							
C	Mn	P	S	Si	Ni	Cr	Mo
0.35	0.82	0.015	0.013	0.25	1.80	0.75	0.36

In the control charts of Fig. 28 each open circle represents an average of four transverse reduction of area values constituting a sample, and each closed circle represents the maximum difference among the same four values. There are two samples per heat unit, one consisting of four values for specimens from tubes made from the first ingot and the other consisting of four values for specimens from tubes made from the last ingot. Of the specimens from each ingot, two came from the top third and two from the bottom third. All specimens were 0.357 inch in diameter and came from midwall positions (Fig. 2) in sections of tubes 6 inches in outside diameter.

Reducing slags which cannot be used in the making of basic open-hearth steel are normally considered largely responsible for the production of steels containing fewer nonmetallic inclusions and having higher transverse ductility. However, it is now possible through a careful control of the oxidizing condition of the basic open-hearth slag and through use of a proper deoxidizing practice (13) to produce basic open-hearth steels of such consistently high transverse reduction of area quality as to compare quite favorably with the best of basic electric steels.

Effect of Nonmetallic Inclusions on Transverse Ductility

For a very long time it has been known that nonmetallic inclusions lower transverse ductility in wrought steel products (14), (15)

and (16), and that the magnitude of this effect depends on the quantity and type of inclusions present (13). Many believe that the difference between transverse and longitudinal ductility in forgings is primarily due to the effect of nonmetallic inclusions on transverse ductility (14) and (17).

The most precise determinations of the relation between quantity of inclusions and transverse reduction of area quality and between type and quality have been made by Mravec, Welchner, and

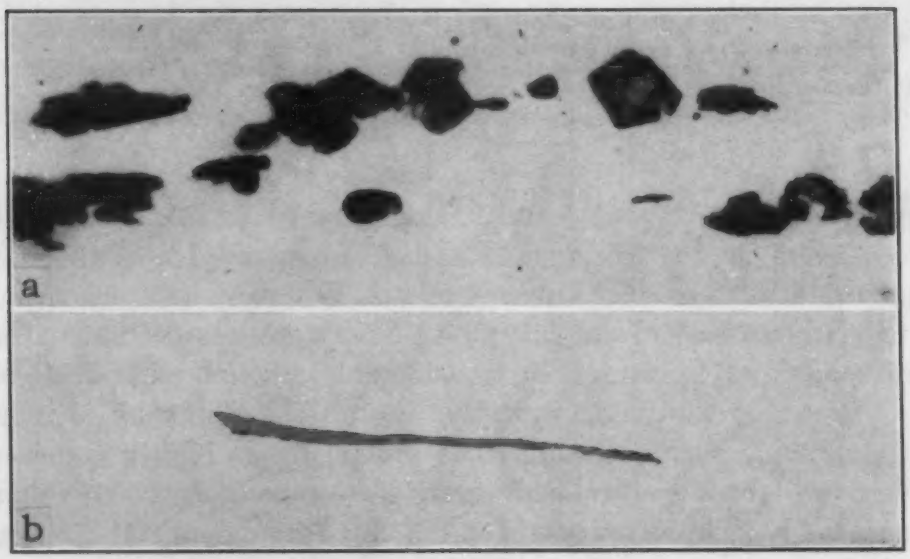


Fig. 29a—Hard Angular Particles Responsible for Low Transverse Reduction of Area Quality of Forging 4, Company 15. Unetched. × 1000. Fig. 29b—Continuous stringers which had no significant effect on transverse reduction of area values for specimens from Forging 2, Company 17. Unetched. × 250.

Hildorf (13). Four fundamentally different types were considered: A. Spherical silica glass type; B. Irregular particles, primarily isolated oxides; C. Discontinuous stringers, oxides, and brittle inclusions fragmented and given directional properties during rolling; D. Continuous stringers, silicates and sulphides malleable at steel rolling temperatures. Randomly distributed nonmetallic inclusions, Types A and B, were observed to be much less detrimental than stringers, Types C and D.

Discontinuous stringers, consisting of hard, angular particles such as those referred to in Fig. 29a, lower average and increase variation of transverse ductility. They, no doubt, are responsible for much of the difference observed between transverse reduction of

Table XVIII
Data Showing Influence of Nonmetallic Inclusions on Average and Variation of Transverse Ductility

Company No.	Tube (or Forging) No.	No. of Values	Inclusion Rating (SAE Method)	Average of RAT Values %	Standard Deviation %	Average of TS Values (psi)	Reduction by Hot Working
14	4	76	3^{vd}-1^{82d}-A	32.9	6.8	125,000	20 to 1
14	5	95	2^{d}-1^{4d}-A	58.6	2.4	125,000	20 to 1
15	4	28	4^{vd}-1^{48d}-C	19.8	4.9	146,000	15 to 1
15	7	20	1^{d}-1^{2d}-A	43.8	4.8	142,000	15 to 1
12	2	66	0-0-A	39.0	3.3	178,000	3.4 to 1
7	2	21	1^{d}-1^{3d}-A	59.1	2.6	103,000	4 to 1

Tubes and forgings were made of basic electric fine-grained steel and were quenched and tempered.
Specimens were 0.252 inch in diameter.
The method used for rating specimens is that recommended by SAE and described in the SAE *Handbook* (12).

area averages for Tubes 4 and 5, Company 14 (Table XVIII), between averages for Forgings 4 and 7, Company 15, and between standard deviations for Tubes 4 and 5, Company 14. Continuous stringers consisting of sulphides (Fig. 29b) are less detrimental and may sometimes be present in considerable amount without significantly lowering transverse ductility. Forging 2, Company 17, which contains many such inclusions, has practically as high a transverse reduction of area quality as Forging 2, Company 7, which is quite clean. SAE inclusion ratings for the two forgings are 3^{d}-1^{28}-B and 1^{d}-1^{3d}-A, respectively; averages of transverse reduction of area values are 54.8 and 59.1% and standard deviation figures are 2.0 and 2.6%. The minimum among 40 values for Forging 2, Company 17, is 51.1%, and among 21 values for Forging 2, Company 7, it is 52.6%.

Since nonmetallic inclusions lower average and increase variation of transverse ductility in a forging, it is expected and found that they lower the transverse reduction of area quality of some specimens more than others. Some dirt, especially if it consists of isolated randomly distributed particles free from sharp corners, appears to have an insignificant effect on quality (13). Occasionally discontinuous stringers are so distributed as to lower the transverse reduction of area quality of each specimen drastically and by approximately the same amount. This condition is believed to have caused the average for Forging 4, Company 15 (Table XVIII), to be so low and the standard deviation to be much less affected than expected. Quite often dirt in a forging drastically lowers the quality

of a few among a large number of specimens taken from it but has little effect on the rest. This situation, which is quite common, appears to be the one existing in Forging 13, Company 15. Curve A of Fig. 30 shows the distribution of transverse reduction of area values for 90 specimens taken from this forging. A few values, responsible for the "tail", were quite low because of discontinuous

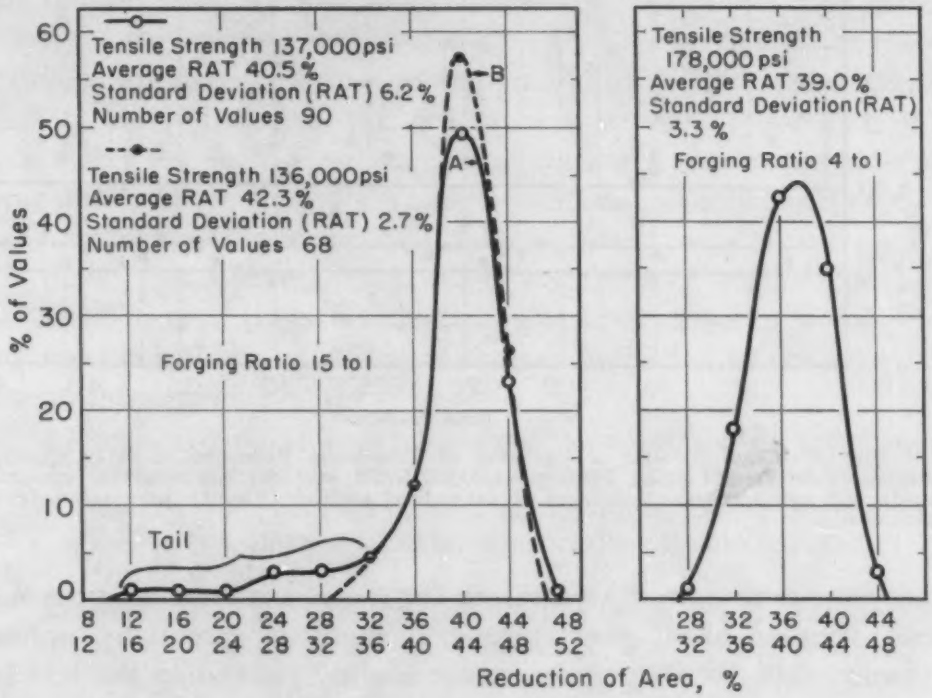


Fig. 30—Frequency Curves Showing the Distribution of Transverse Reduction of Area Values for 0.252-Inch Diameter Specimens From Forging 13, Company 15. This forging is much dirtier than that referred to in Fig. 31. RAT is the abbreviation for transverse reduction of area.

Fig. 31—Frequency Curve Showing the Distribution of 66 Transverse Reduction of Area Values for 0.252-Inch Diameter Specimens From Forging 2, Company 12. This forging is unusually clean.

stringers. The dashed curve shown in the same figure represents, at least approximately, the expected distribution if such stringers had been absent. It is inferred from the two curves considered together that, if clean, the specimen having lowest transverse ductility (15.1%) would have had a value above 32%, most likely 42.3% (the average), and less than 52%.

The 68 values used in the determination of Curve B (Fig. 30) are those which give averages and ranges falling within the control chart limits shown in Fig. 32. Justification for this procedure depends on the validity of the assumption that the distribution of

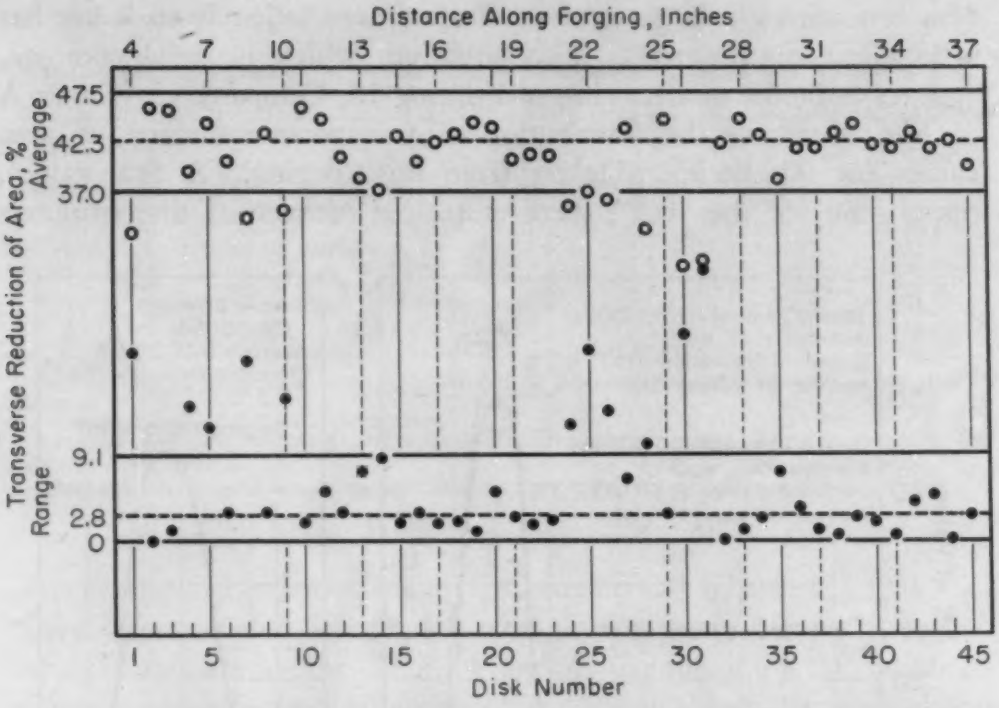


Fig. 32—Chart Showing a Variation of Transverse Reduction of Area Quality Among Disks From Forging 13, Company 15. Disks were cut and numbered consecutively and two specimens consisting of midradius material (Fig. 3) were taken from each disk.

transverse reduction of area values for specimens from an extremely clean forging of a given tensile strength is essentially normal. Actually, this distribution is usually slightly skewed to the left but is so close to being normal that all averages and ranges fall within control chart limits. A typical distribution is shown in Fig. 31. The control chart limits given in Fig. 32 were determined as follows: All 90 values for specimens from Forging 13, Company 15, were grouped into 45 pairs. Ranges and averages were determined and plotted and control limits were calculated.[33] Ranges and averages outside of limits were discarded and new limits were calculated from remaining data. This procedure was followed until all ranges and averages based on data not previously discarded fell within control limits. When this occurred, 34 averages and 34 ranges based on 68 transverse reduction of area values were within the limits. These 68 values are the ones selected and used in plotting Curve B, Fig. 30.

All specimens from Forging 13, Company 15, with values of less

[33]Incidentally, it is of metallurgical interest to observe that by use of a proper sampling procedure and by means of the control chart method of handling data it was possible to show that sections of Forging 13, Company 15, located 4 to 10 inches and 21 to 27 inches from one end were especially low in transverse reduction of area quality.

than 32% were found to contain discontinuous stringers. In general, the number and size increased with decreasing transverse reduction of area quality. Other randomly selected specimens with higher values were observed to contain either no discontinuous stringers or only a few short ones. However, the SAE inclusion rating for the specimen with highest transverse ductility is not so much lower than that for the specimen with lowest transverse ductility as was anticipated; the values are 2^{d}-1^{22d}-A and 2^{vd}-1^{34d}-A, respectively. Surfaces examined are generally close to and parallel with fractured surfaces. Each rating is based on the results of a survey of one-half of a square inch of surface, which is the standard area required when using the SAE method for rating inclusions. To obtain this area many surfaces per specimen had to be examined.

Belief that Curve B, Fig. 30, is a reasonably good estimate of the distribution of transverse reduction of area values to be expected if Forging 13, Company 15, were clean is supported by the following general information:

1. Standard deviations for transverse reduction of area values for specimens from unusually clean forgings are generally about 3% (Fig. 31); this is not significantly higher than 2.7%, the standard deviation for the 68 selected values referred to in Fig. 30.
2. 42.3% is the estimated average for Forging 13, Company 15, if it were clean. The determined average of Forging 2, Company 12, known to be unusually clean, is 39.0%. After due allowance is made for differences of tensile strength and forging ratio, the averages for the two forgings are alike well within the rather wide limits of error expected. The relation between tensile strength and transverse reduction of area is considered to be such that an increase of 5000 psi in tensile strength is associated with a decrease of 1.5% in transverse reduction of area (18) and the relation between forging ratio and transverse reduction of area is assumed to be such that a decrease from 15 to 1 to 3.4 to 1 in forging ratio increases transverse reduction of area by about 6.5% (Fig. 15). Estimated averages are 51.6 and 48.8% for Forgings 2 and 13, respectively, assuming a forging ratio of 3.4 to 1 and a tensile strength of 136,000 psi for both forgings.

Information relating to tubes and forgings mentioned in this section is given in Tables XVIII and XIX. A typical composition for Tubes 4 and 5, Company 14, is listed in Table XVII and compositions for Forgings 4 and 7 from Company 15 and Forging 2 from

Company 12 are included in Table IV. Those for Forging 2 from Company 7, Forging 13 from Company 15, and Forging 2 from Company 17 appear below.

Table XIX
Compositions of Forgings 2 and 13 From Companies 7, 15, and 17

Company	Forging No.	Per Cent of Element								
		C	Mn	P	S	Si	Ni	Cr	Mo	V
7	2	0.36	0.58	0.010	0.012	0.25	0.30	0.90	0.24	....
15	13	0.34	0.60	0.018	0.018	0.25	1.86	0.89	0.25	....
17	2	0.37	0.77	0.038	0.023	0.35	....	....	0.42	0.21

Forging 2, Company 17, consists of an acid open-hearth steel reduced 4 to 1 by hot work and subsequently quenched and tempered to a tensile strength of 97,000 psi.

Effect of Homogenizing Treatments on Transverse Ductility

Studies of the effect of homogenizing treatments on transverse ductility have been made (a) to determine whether or not a commercial homogenizing treatment might be used to advantage for improving transverse ductility in forgings and (b) in an effort to learn more about the factors responsible for ductility being lower in the transverse than the longitudinal direction. Results are given in Fig. 33.

It is concluded that (a) the severity of homogenizing treatment required to significantly improve transverse ductility is so drastic as to be impractical commercially and (b) elongated nonmetallic inclusions and the heterogeneous distribution of elements in solution are together largely responsible for transverse ductility of forgings being lower than longitudinal ductility. Since the separate effect of each of these two factors on forging quality has not been evaluated, it is not yet possible to state quantitatively how much of the total effect is due to each cause.

A very clean, high quality SAE 4140 forging quenched to martensite and tempered to 100,000 psi is expected to have a transverse reduction of area average of about 55%, a standard deviation of approximately 3%, a longitudinal reduction of area average of about 65% (19), and a standard deviation of 1% or so. Forging 2, Company 7, used in the present investigation is of unusually good quality. Determined transverse reduction of area average and standard deviation figures, each based on 21 values, are 59.1 and 2.6%, and determined longitudinal reduction of area average based on 12 values is

66.3%. Tensile strength is 103,000 psi. A homogenized section from this forging subsequently normalized, quenched, and tempered to a tensile strength of 96,000 psi has a transverse reduction of area average and standard deviation of 66.1 and 1.3% and a longitudinal reduction of area average based on only 4 values of 72.0%. After due allowance is made for a difference of tensile strength,[34] it appears

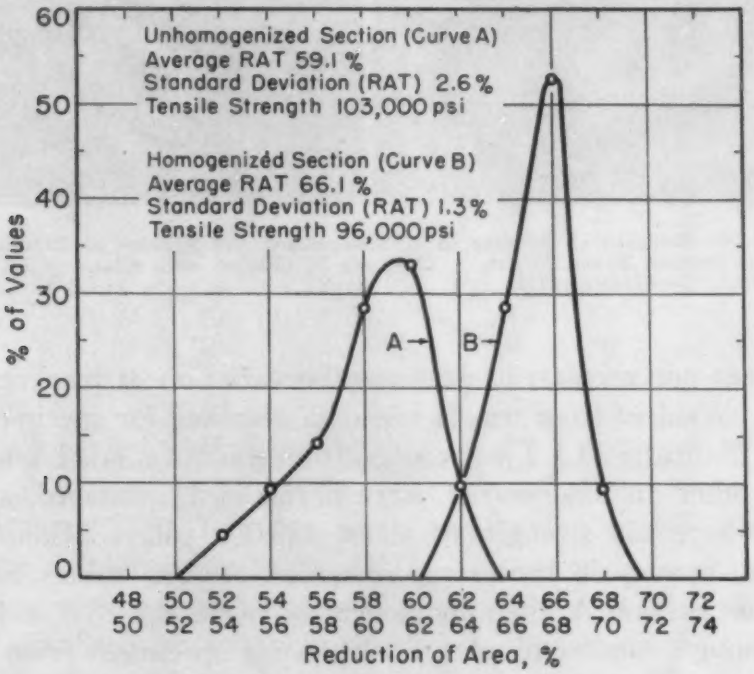


Fig. 33—Curves A and B Each Show the Distribution of 21 Transverse Reduction of Area Values for 0.252-Inch Diameter Specimens Taken From Forging 2, Company 7. Specimens A came from a heat treated unhomogenized section and Specimens B from a heat treated homogenized section of the forging.

that the homogenizing treatment raised the transverse reduction of area average by 4.9% (66.1 — 61.2%) and lowered standard deviation by 1.3% (2.6 — 1.3%).

The homogenizing treatment used, 1350 °C (2462 °F) for 65 hours, caused elements in solution to be more uniformly distributed, eliminated banding (Fig. 34), probably spheroidized some nonmetallic inclusions, and rounded the sharp corner of others. In addition, this treatment may have caused a small percentage of the inclusions to be dissolved and reprecipitated (20).

Heating a wrought steel product to 1350 °C (2462 °F) for 65

[34]It is assumed that a decrease of 7000 psi in tensile strength (from 103,000 to 96,000 psi) would be accompanied by an increase of 2.1% in average transverse reduction of area and 1.4% in average longitudinal reduction of area (18).

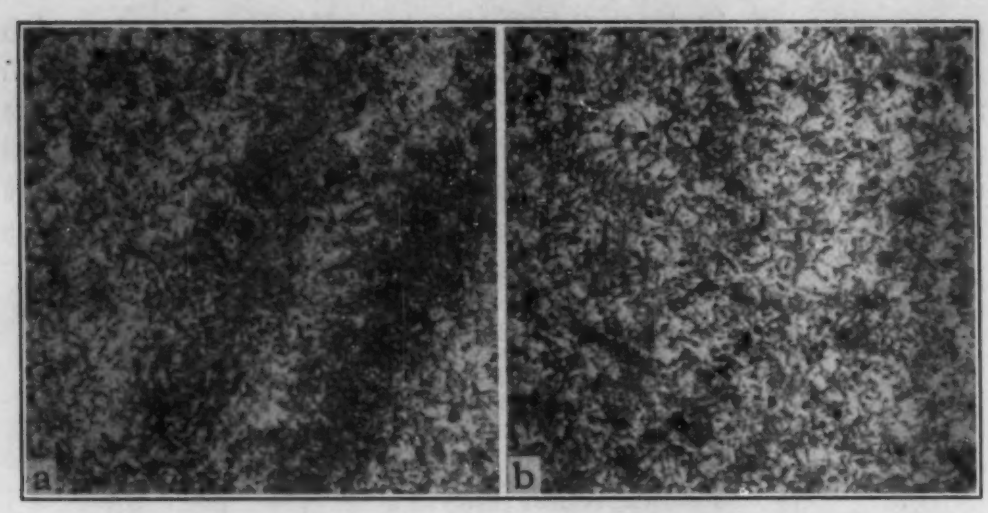


Fig. 34—Evidence of Banding in Unhomogenized and Absence of Banding in Homogenized Sections From Forging 2, Company 7. Etched with nital. × 75. a—Unhomogenized. b—Homogenized.

hours does not necessarily decrease the variation of transverse ductility as is evident from tensile test data obtained for specimens from Tube 6, Company 14. Two sections from this tube, one homogenized and the other unhomogenized, were normalized, quenched, and tempered to a tensile strength of about 125,000 psi. Minimum and maximum among 58 transverse reduction of area values for specimens from Section A, the unhomogenized piece, are 28.8 and 56.0%, while among a similar number of values for specimens from Section B, the minimum and maximum are 29.0 and 62.8%. Specimen A from unhomogenized Section A with a value of 28.8% and Specimen B from homogenized Section B with a value of 29.0% both contained discontinuous stringers and the particles in these stringers appeared to be as angular in Specimen B as in Specimen A. These data show that the probability of successfully decreasing the variation of transverse ductility in a wrought steel product by means of a homogenizing treatment is higher if the product is clean than if it contains discontinuous stringers consisting of angular particles which are so refractory that they remain apparently unaffected when exposed to severe homogenizing treatments.

Of the materials used in the present study, Forging 2 from Company 7 is a fine-grained basic electric steel cast into a 17-inch round ingot, reduced 4 to 1 by forging, and having the composition listed in Table XIX, while Seamless Tube 6 from Company 14 is a fine-grained basic open-hearth steel cast into a 21-inch round ingot,

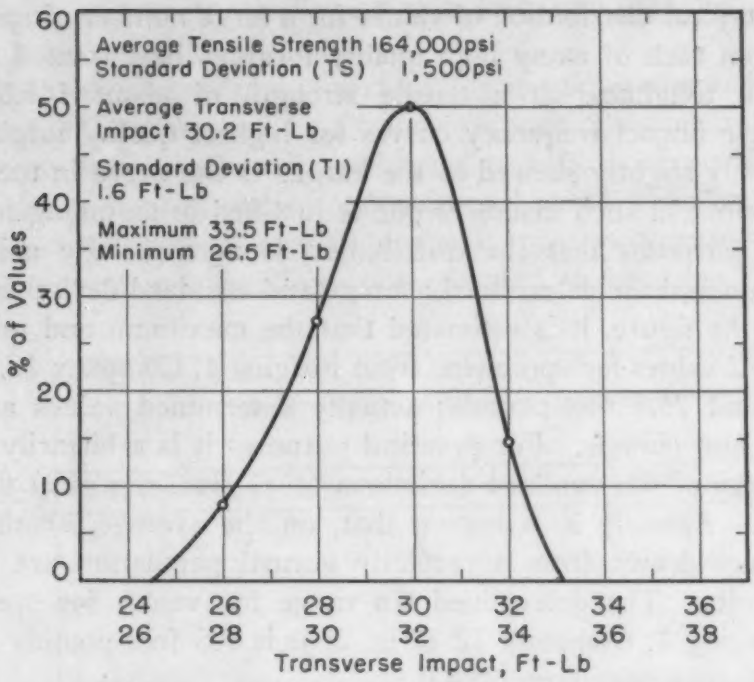


Fig. 35—Distribution of 172 Transverse Impact Values for Specimens From Forging 1, Company 12. TS is abbreviation for tensile strength, and TI is abbreviation for transverse impact.

reduced about 15 to 1 by hot work, and having a composition very much like that given in Table XVII.

Homogenizing treatments were made in a controlled atmosphere and decarburized material was discarded. Specimens were all 0.252 inch in diameter.

Average and Variation of Transverse Impact

Determinations of average and variation of transverse impact quality for each of a large number of tubes have been made using material in which maximum toughness at desired yield strength levels was practically always developed through the choice of proper compositions and by using appropriate heat treatments. Usual metallurgical precautions were taken to avoid temper brittleness and brittleness resulting from ineffectual quenching before the temper. Furthermore, all specimens were broken at 70 °F, a temperature considerably above that at which they are likely to suffer from "cold brittleness".[29]

The frequency curve of Fig. 35 shows the distribution of 172 transverse impact values for specimens from Forging 1, Company 12,

and is a typical distribution of values for a large number of specimens taken from each of many high quality forgings heat treated to have maximum toughness at a tensile strength of about 165,000 psi. Transverse impact frequency curves for highest quality forgings are usually only slightly skewed to the left, as is the curve in the figure, and therefore in such instances one is justified in assuming for most practical purposes that the distribution is normal. By using this assumption and the determined average and standard deviation values given in the figure, it is estimated that the maximum and minimum among 172 values for specimens from Forging 1, Company 12, should be 34.5 and 25.9 foot-pounds; actually determined values are 33.5 and 26.5 foot-pounds. For practical purposes it is arbitrarily agreed that a range of six standard deviations (6σ) shall represent the total variation. Actually it is known that, on the average, about 3 per 1000 values drawn from a perfectly normal population are outside of 6σ limits. The determined 6σ range for values for specimens from Forging 1, Company 12 (Fig. 35), is 9.6 foot-pounds (maximum 35.0 and minimum 25.4).

Standard deviations for transverse impact tend to decrease with increasing yield strength level. Values based on about 50 transverse impact data per yield strength level are 1.7, 2.1, 1.4, and 0.7 foot-pounds where the four levels are 99,000, 124,000, 156,000, and 178,000 psi, respectively. The data used are for specimens from sections of Tube 14-2. Each section was quenched and subsequently tempered to a different one of the four yield strength levels referred to above.

It is well known that the maximum transverse impact quality which can be developed in units of a wrought steel product varies considerably. Results given in Fig. 19 show averages for some tubes to be as low as 11 foot-pounds and averages for others to be as high as 29 foot-pounds. These tubes have roughly an SAE 4335 composition and were quenched to martensite before being tempered to a yield strength of about 160,000 psi. All evidence supports the opinion that the highest transverse impact quality possible was developed in each of the tubes. The relatively good correlation between average transverse reduction of area and transverse impact quality (Fig. 19) suggests that the primary cause of the variation of average transverse reduction of area quality among the tubes is also the primary cause of the average transverse impact quality variation. Discontinuous non-metallic inclusion stringers or conditions responsible for such stringers may be that primary cause.

Control of Transverse Impact Quality

Normally, transverse impact quality is sufficiently well controlled to justify the assumption that transverse impact values for specimens coming from midwall positions located two-thirds of a wall thickness from the ends of quenched and tempered tubes describe the quality of all midwall material as well on the average as do values for specimens from other midwall positions, located at distances greater than

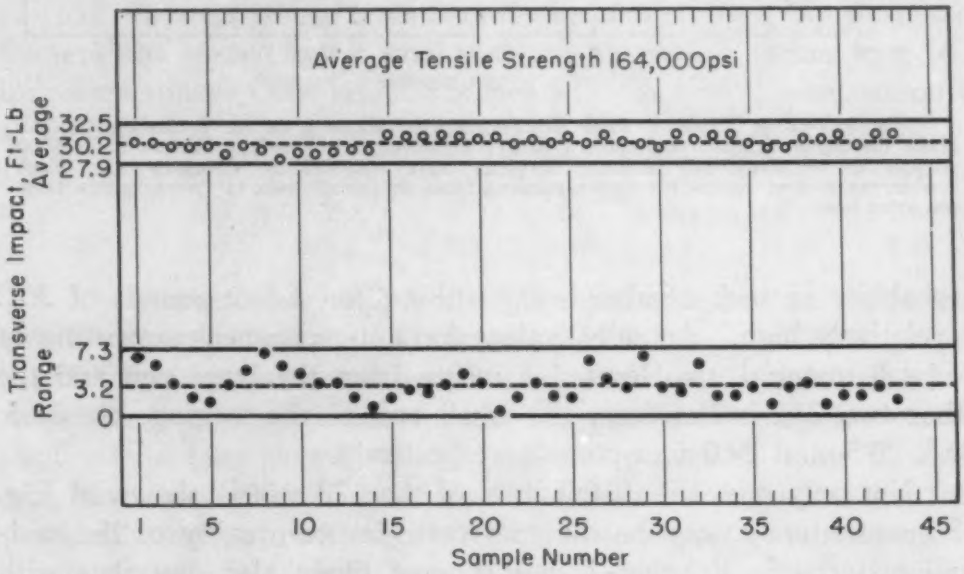


Fig. 36—Shows the Transverse Impact Quality of the Midwall Material in Each of 43 Disks From Forging 1, Company 12, to be Essentially Alike. Sample 1 consists of four transverse impact values for specimens from Disk 1. Sample 2 consists of four transverse impact values for specimens from Disk 2, etc.

two-thirds of a wall thickness from the ends. Considerable evidence which supports this conclusion is available but the greater part of it cannot be presented here because of space restrictions. Typical results are given in Fig. 36; these indicate that the transverse impact quality of midwall material located in 43 transverse disks cut consecutively from Forging 1, Company 12, does not vary significantly from disk to disk. It is probable that the distribution of transverse impact values (Fig. 35), which describes the quality of a unit consisting of all the midwall material in the 43 disks, also describes the quality of midwall material in each disk. The probability of a transverse impact value being less than 26.5 or above 33.5 foot-pounds for a specimen taken from the midwall material of a disk located two-thirds of a wall thickness from an end is quite low, but the

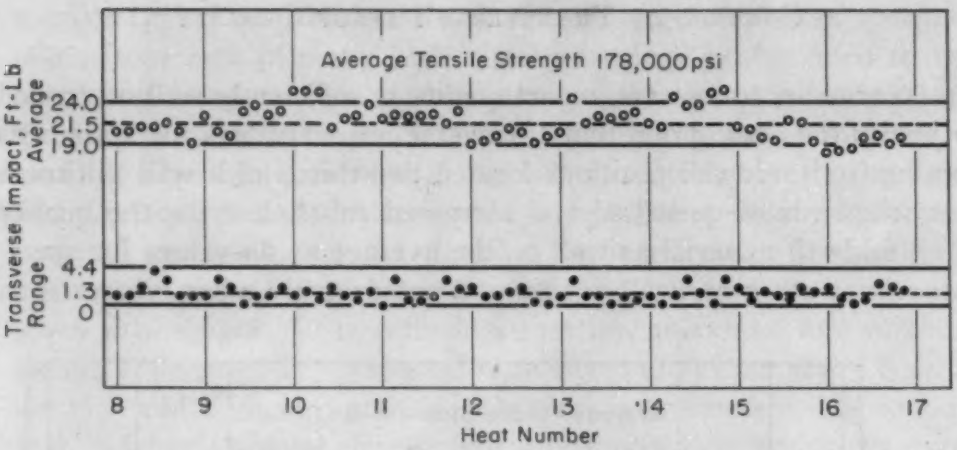


Fig. 37—Gives Evidence That All Forgings in Heats 8 to 16, Inclusive, Do Not Have the Same Transverse Impact Quality; However, All Forgings Within Each Heat Appear to be Essentially Alike. Forgings were supplied by Company 15. Each sample consists of values for two specimens from the small ends of two forgings from the same heat.

probability of such a value being within 2 or 3 foot-pounds of 30.2 is relatively high. Actually, values for four specimens consisting of midwall material, two located 3 inches from the large end and the other two 2½ inches from the small end of the forging, are 29.5, 30.5, 28.5, and 29.0 foot-pounds, respectively.

Not only does the distribution of the 172 values shown in Fig. 35 quantitatively describe the transverse impact quality of the midwall material in Forging 1, but it most likely also describes with about the same precision the quality of the midwall material in all other forgings which together comprise the "heat unit".[19] This conclusion is based on results which indicate that the frequency with which all tubes in a heat unit have essentially the same transverse impact quality is quite high. Data plotted in the control chart of Fig. 37 are typical. They show that the heat units (Heats 8 to 16 inclusive, Company 15) which make up the "practice unit"[20] do not all have the same transverse impact quality, but probably all tubes within each heat unit are essentially alike.

Usually when the primary reason for plotting a control chart is to determine whether or not the tubes in a heat unit are alike with respect to some property, two or more values per tube constitute a

[19] A "heat unit" consists of all the forgings of the same dimensions made from a heat and subjected to the same treatment.

[20] A "practice unit" consists of all the forgings made consecutively in a practice over an arbitrarily selected period of time; each forging has the same dimensions and is assumed to be treated like any other in the practice unit. Practice Unit 1 (Company 1, Table VIII) consists of 600 forgings from 72 heats; Practice Unit 2 (Company 2) consists of 700 forgings from 20 heats, and so on, to Practice Unit 23 which has in it 75 tubes from 40 heats.

sample. Since only one value per tube in each of the heat units referred to in Fig. 37 is available, each sample consists of one value from each of two tubes. However, since the average range value (1.3 foot-pounds) is as low as expected when samples consisting of two values per tube are used and since both averages and ranges all fall within control limits when an individual control chart is plotted per heat, it appears reasonable to accept the conclusion that the tubes in each of the 9 consecutive heats are probably alike within the limits of practical significance.

All forgings from Heats 8 to 16 inclusive (Fig. 37) consist of fine-grained basic electric steel and are about 115 inches long, 6.5 inches maximum O.D. and 2.5 inches I.D. A typical composition is as follows:

Per Cent of Element							
C	Mn	P	S	Si	Ni	Cr	Mo
0.35	0.65	0.012	0.013	0.20	1.95	1.05	0.35

These tubes were all quenched to martensite and tempered to a tensile strength of about 178,000 psi.

Information presented here has been used in the development of more efficient specifications for the acceptance of tubes for certain applications (see page 794). It has also proved of value to many who have the responsibility of making tubes of such quality that they practically always meet specified transverse impact requirements.

Relation Between Transverse Impact and Yield Strength

It is common knowledge that at 70 °F the maximum transverse impact quality which can be developed in a wrought steel product quenched to martensite and subsequently tempered increases with decreasing yield strength. As a result of the present investigation, the relation between transverse impact and yield strength is now known much more quantitatively than before.

Over a yield strength range lying between the limits of 80,000 and 180,000 psi, an increase of 5000 psi is believed on the average to be associated with a decrease of about 3 foot-pounds in transverse impact. This conclusion is based on results given in Table XX. A typical plot is given in Fig. 38. Tube 14-2 referred to in this figure and Tube 3 from Company 14 (also designated as 14-3) are described in Table IX while Forgings 1 and 2 from Company 12 are described in Table IV. Tube 5 from Company 13 is about 180

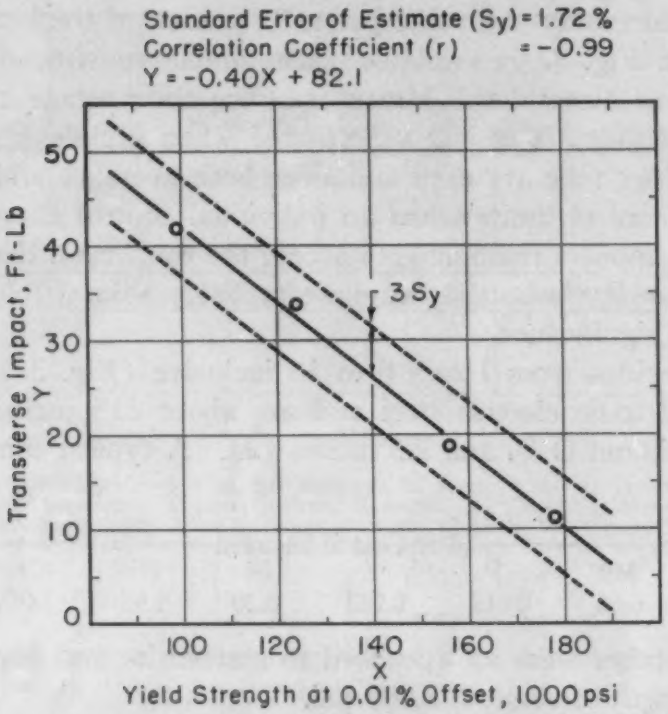


Fig. 38—Shows Relation Between Transverse Impact and Yield Strength in a Quenched and Tempered Seamless Tube (Tube No. 14-2). The Y coordinate of each of the four data points represents the average of about 50 transverse impact values and the X coordinate an average of about 50 yield strength values.

inches long, 7.5 inches O.D., and 2.5 inches I.D., and has a composition quite similar to Forging 2 from the same company.

Information reported in this section made it possible to use transverse impact data for specimens from wrought steel products quenched to martensite and tempered to widely different yield

Table XX
Data Showing Relation Between Transverse Impact and Yield Strength

Company	Tube No.	YS Range (1 unit = 1000 psi)	No. of YS Values	No. of TI Values	Equation of Regression Line	S_Y ft-lbs.	r Correlation Coefficient	Effect of Change of 5000 psi on TI, ft-lbs.
12	1	78-140	345	345	Y = −0.58X + 112.1	4.4	−0.953	2.9
	2	83-147	204	204	Y = −0.61X + 111.0	3.1	−0.979	3.1
13	5	91-151	99	99	Y = −0.86X + 162.4	4.2	−0.977	4.3
14	2	99-178	191	191	Y = −0.40X + 82.1	1.7	−0.990	2.0
	3	106-186	194	194	Y = −0.37X + 77.5	1.2	−0.995	1.9
						Average	−0.979	2.8

YS = Yield strength.
TI = Transverse impact.
S_Y = Standard error of estimate.
Y = Transverse impact in foot-pounds.
X = Yield strength at 0.01% offset (1 unit = 1000 psi).

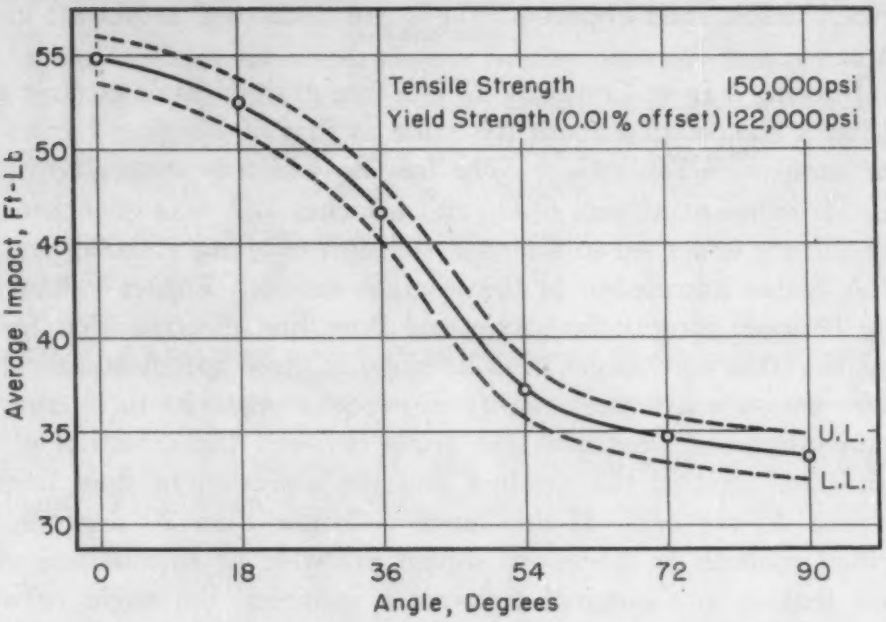


Fig. 39—Shows Relation of Angle Between Longitudinal Axis and Flow Line Direction in Specimens to Average Impact. Data for Forging 4, Company 12. U.L.—Upper limit. L.L.—Lower limit.

strength levels much more effectively (a) in the development of certain specifications and (b) in the study of the effect of various factors on transverse impact quality.

Relation of Angle Between Longitudinal Axis and Flow Line Direction in Specimens to Impact

Metallurgists and engineers have known for a long time that longitudinal impact specimens taken from wrought steel products which have flow lines parallel with their longitudinal axis give higher values than do transverse specimens. Brearley (8) using a rolled slab of 0.23% carbon Bessemer steel observed that as the angle between the direction of the longitudinal axis of the specimens and the direction of flow lines was increased from 0 (longitudinal) to 90 degrees (transverse), impact values were decreased rapidly in the range 15 to 75 degrees but only slightly in the ranges of 0 to 15 degrees and 75 to 90 degrees. This relation has now been determined more quantitatively. Results are plotted in Fig. 39; each circle represents an average of 10 or more values.

As the angle between longitudinal axis and flow line direction in specimens from Forging 4, Company 12, is increased from 0 to 90

degrees, determined impact averages are decreased as shown in the figure.

Forging 4 from Company 12 is a fine-grained basic electric steel and has a composition about the same as that of Forging 1 from the same company (Table IV). The forging which is about 180 inches long, 11 inches maximum O.D., and 3 inches I.D. was quenched and subsequently tempered to a tensile strength of about 150,000 psi.

A better knowledge of the relation between impact values and angle between longitudinal axis and flow line direction led to the conclusion that no changes need be made in those specifications which require transverse impact quality in accepted material to be above a certain minimum, providing the angle between the direction of the longitudinal axis of the product and the direction of flow lines is less than 20 degrees. If this angle is larger than 20 degrees, the specified position of specimens should probably be so modified as to insure that in any nominal transverse specimen the angle between its longitudinal axis and flow line direction shall be always higher than 70 degrees.

Average and Variation of Yield Strength

Obviously the average of yield strength values for specimens from any unit of a wrought steel product and the variation among those values depend on heat treatment. Heat treatments are usually so conducted that yield strength averages for quenched and tempered tubes such as those considered in the present investigation are within 10,000 psi of the middle of the range specified, and standard deviations are less than 2500 psi. Typical results are given in Table XXI.

It is believed that the maximum difference among yield strength values for a large number of specimens from a quenched and tempered tube is rarely less than 5000 psi, most frequently about 10,000 psi, sometimes 15,000 psi, and occasionally as high as 30,000 psi. Maximum and minimum among data available per each of five forgings from Companies 12 and 13 are given in Table XXI; differences range from 7000 to 10,000 psi—average 8000 psi.

Compositions and sizes of Forgings 1 and 2 from Company 12 are listed in Table IV. Forging 5 has a composition and size like that of Forging 3 from the same company and listed in the same table. Forgings 3 and 4 from Company 13 have a composition similar to that of Forging 1 from Company 13; the former is 10 inches

Table XXI
Average and Variation of Yield Strength (at 0.01% Offset) for Each of Five Typical Forgings

Company	Forging No.	No. of Values	Specified Limits (1 unit = 1000 psi) Minimum	Specified Limits (1 unit = 1000 psi) Maximum	Average Yield Strength (1 unit = 1000 psi)	Standard Deviation (1 unit = 1000 psi)	Maximum	Minimum
12	1	22	140	170	150	1.7	154	147
12	2	15	140	170	150	1.6	153	146
12	5	12	110	140	127	1.8	131	124
13	3	18	95	125	112	1.5	118	109
13	4	59	90	120	98	2.4	105	95

Each forging was cut transversely into several sections of equal length—Forging 1 into 11, 2 into 8, 5 into 7, 3 into 9, and 4 into 17 pieces. Specimens 0.505 inch in diameter were taken from midwall positions (Fig. 2) in each section.

maximum O.D., 3.5 inches I.D., and 95 inches long, while the latter is 10 inches maximum O.D., 2.5 inches I.D., and 160 inches long.

Control of Yield Strength Quality

From a statistical point of view, yield strength is usually much more poorly controlled than either transverse reduction of area or transverse impact. Frequently, however, yield strength variation within a practice is such that by using a suitable sampling procedure, one can obtain evidence to show that few values for specimens taken from the practice unit are likely to fall outside limits allowed by specification. Such evidence is given in Fig. 40. When each sample consists of two yield strength values for specimens from the small end of each tube made in Practice 14 by Company 14, ranges show some and averages show considerable lack of control (Fig. 40a); however, when each sample consists of values for specimens from two consecutive heat units, then all ranges and averages fall within the limits (Fig. 40b). These limits are of course much wider than those for Control Chart A but are still sufficiently narrow to indicate that the yield strength of tubes made in practices controlled within these limits is expected to fall practically always below the maximum of 125,000 psi and above the minimum of 110,000 psi specified. Actually, out of 2288 yield strength values for specimens taken from 1144 tubes made in Practice 14, not a single value is above 125,000 psi and only 28 are below 110,000 psi. Of these, 18 are either 108,000 or 109,000 psi and no value is below 105,000 psi. Statistically, one expects on the average about 3 values per thousand to be above or below specification limits.

Tubes produced in Practice 14 have essentially the same com-

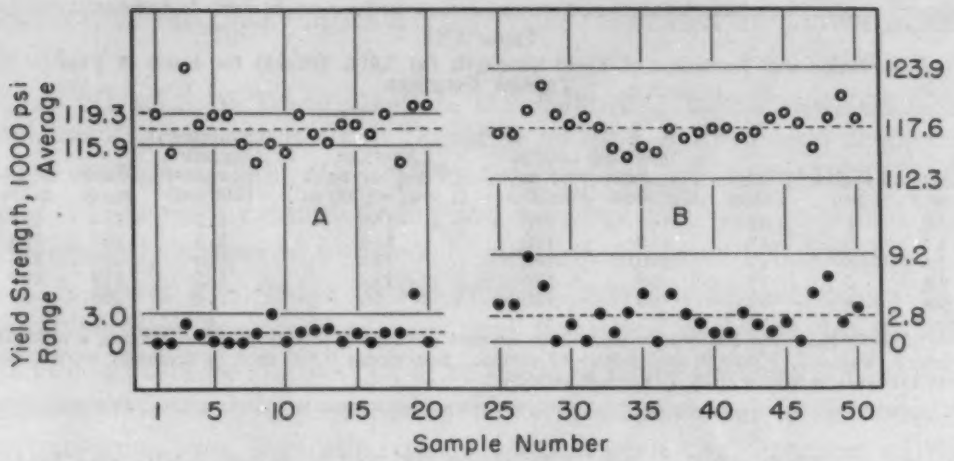


Fig. 40—Shows the Major Portion of Yield Strength Variation Within a Unit Consisting of Small Ends of Tubes From Practice 14, Company 14, to Exist Among Rather Than Within Those Ends. Two yield strength values constitute a sample; these are for 0.357-inch diameter specimens from the small end of one tube (Control Chart A) or from the small end of two tubes from two heats (Chart B).

position and size and received practically the same heat treatment as Heat Units 1 and 2 described on page 735.

Relation of Angle Between Longitudinal Axis and Flow Line Direction in Specimens to (a) Tensile Strength and (b) Yield Strength

Brearley (8), using a rolled slab of 0.23% carbon Bessemer steel, has shown that neither tensile strength nor yield strength is changed significantly as the angle between longitudinal axis and flow line direction in specimens is increased from 0 to 90 degrees. Results presented in Fig. 41 show that Brearley's conclusions relating to the rolled slab apply equally well to the material used by the present authors. This material, Forging 4 from Company 12, is described on page 78. Circles plotted in the figure represent averages of 15 (0°), 14 (18°), 15 (36°), 55 (54°), 60 (72°), and 53 (90°) yield strength values.

Specifications

A detailed description of the development of specifications based on results presented in this paper is given in various reports which are published by the Department of Commerce (20), (21). These specifications are much more efficient and economical than those previously used because they are based on a more precise knowledge

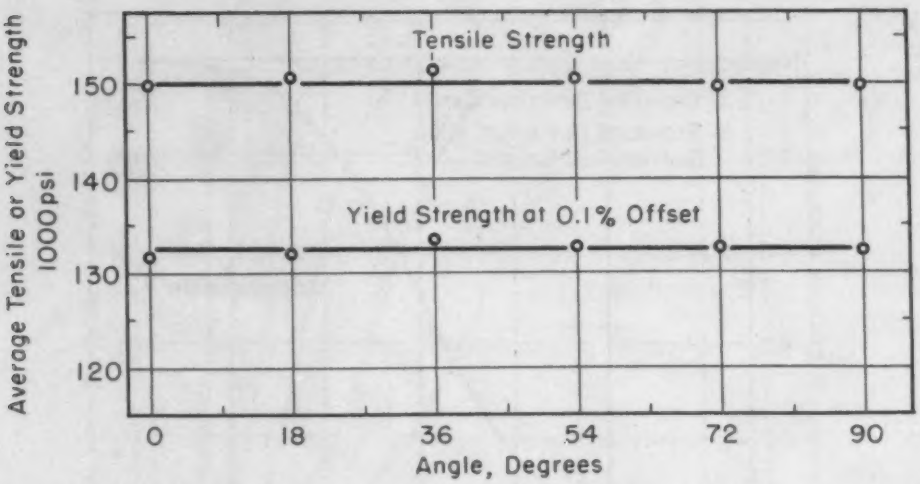


Fig. 41—Shows Relation of Angle Between Longitudinal Axis and Flow Line Direction in Specimens to Average Tensile or Yield Strength. Data for Forging 4, Company 12.

of the probable variation of yield strength, transverse impact, and transverse reduction of area within each unit presented for inspection and because they make provision for the acceptance of "heat units."[19] Such a unit frequently consists of as many as 300 tubes and may sometimes be accepted when only 18 values for each specified property are available; this procedure is justified because of the fact that all tubes in a heat unit are in general essentially alike. Before these newer specifications were developed, not less than one value per specified property per tube was required.

Relation Between Transverse Reduction of Area Quality and Percentage of Material Accepted

The shape of an operating characteristic curve showing the relation between the average transverse reduction of area quality of units presented for inspection and the percentage accepted depends on (a) specification requirements and (b) variation of transverse reduction of area quality within each unit.

Specification A requires that one transverse reduction of area value be obtained per unit and if this is 40% or above, the unit be accepted; otherwise, it must be rejected. If the variation of transverse ductility in each inspected unit were zero, then all material would be accepted when the average is 40% or higher and rejected when lower. (Vertical dashed line A—Fig. 42.) When the quality

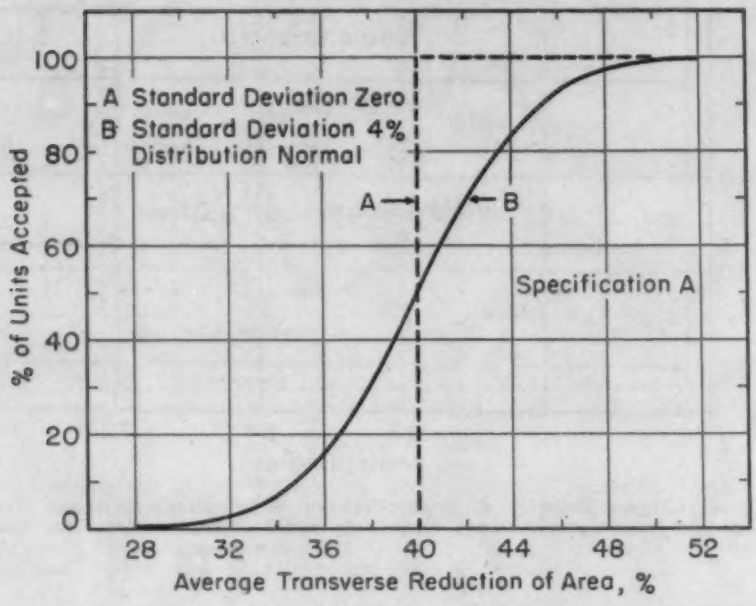


Fig. 42—Relation Between Average Transverse Reduction of Area Quality of Units Inspected and Percentage Accepted. Accept if value 40% or higher; otherwise reject.

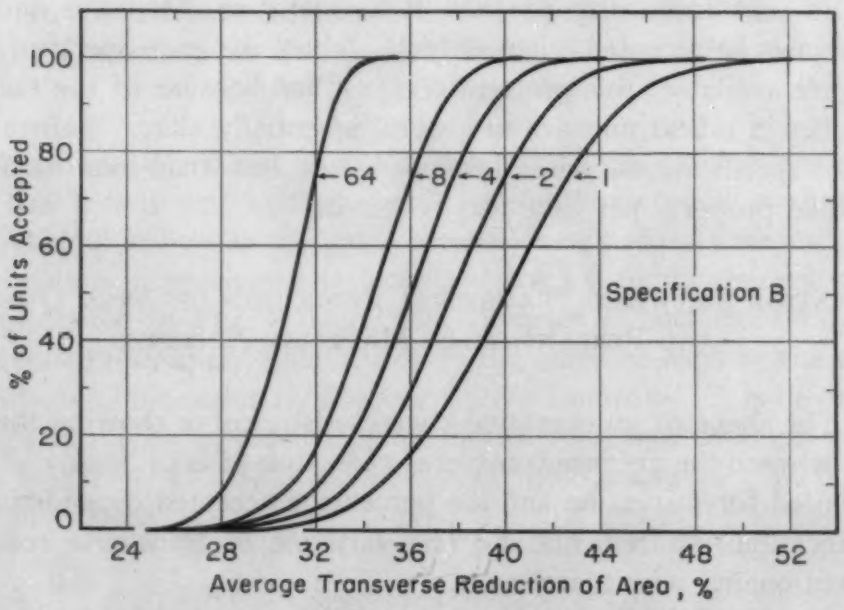


Fig. 43—Operating Characteristic Curves for Specification B.

of each unit of a product, designated as Product B, is such as to be represented by a normal distribution of values with a standard deviation of 4%, then on the average the relation between average quality and percentage accepted is indicated by Curve B; in this instance

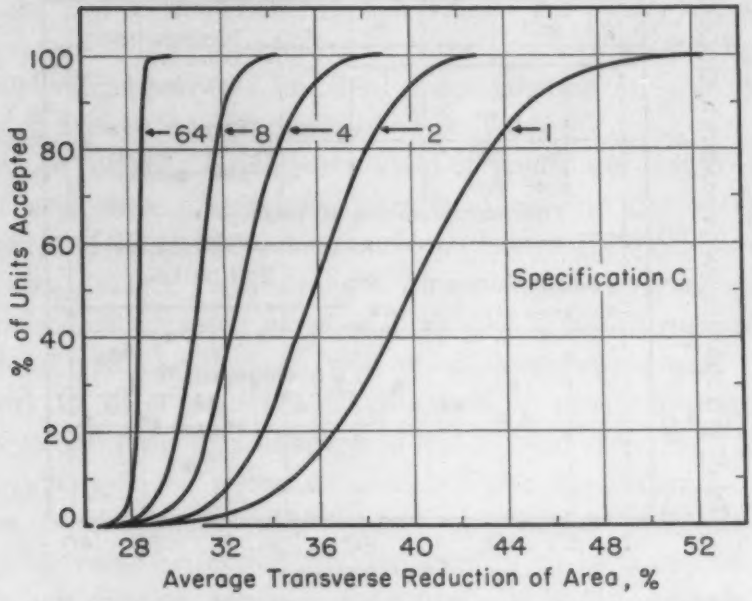


Fig. 44—Operating Characteristic Curves for Specification C.

some rejected material has considerably higher quality than some accepted.

Operating characteristic curves obtained when Product B is submitted under Specifications B and C are given in Fig. 43 and 44. Specification B requires that a unit of product be accepted if a transverse tensile specimen taken from it has a value of 40% or more. Suppose that each of a large number of units of the material presented for inspection has an average of 40%, then 50% of the units is accepted if one value is available per unit, and 50% of the remainder is accepted when two values per unit are available (total accepted 75%), and so on. The total percentage accepted after eight values become available for those units rejected seven times is practically 100% (Curve 8—Fig. 43).

Specification C requires that a unit be accepted if the average of "n" values available per unit is $28 + \frac{12}{\sqrt{n}}$ or above. Suppose the units of Product B previously inspected are now reinspected but that Specification C rather than B is used. If one value per unit is available, 50% of the units are accepted as before; however, when two two values become available per each rejected unit, not 50% but 89% of the rejected units are accepted. (Total accepted 94.5%—Fig. 44, Curve 2.)

From a comparison of the operating characteristic curves of

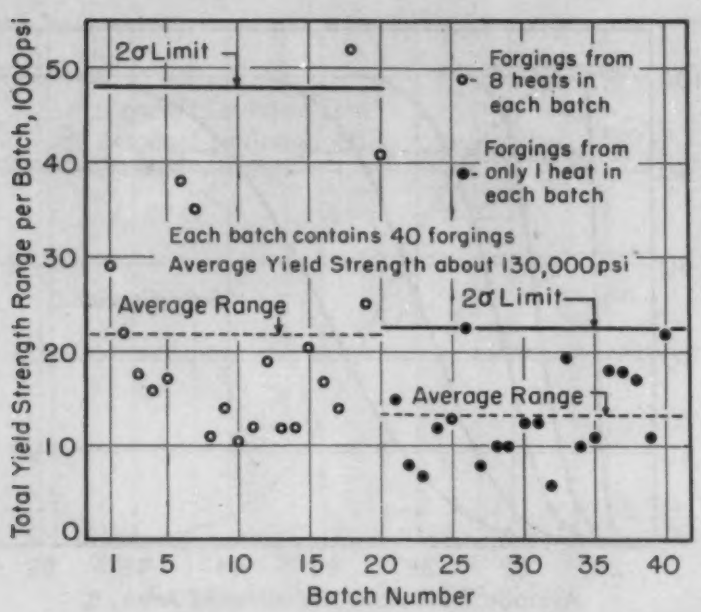


Fig. 45—Shows the Variation of Yield Strength Within a Batch to be on the Average Significantly Less When All Forgings per Batch Are From Only One Heat. Forgings were all from Company 15.

Fig. 43 with those of Fig. 44, it is apparent that Specification C is superior to Specification B.

Modification of Heat Treatment Practice

As a result of information disclosed in this paper, some producers modified their heat treating practices. Tubes consisting of all or a large part of a "heat unit"[19] were segregated into a batch for heat treatment; efforts were made to temper each "batch unit"[35] to an average yield strength lying midway between the minimum and maximum values specified, and the frequency of making reheat treatments was significantly reduced.

The decision to segregate tubes from heat units into batches is based on the observation that tubes from the same heat generally respond similarly to heat treatments while comparable tubes from different heats frequently do not. Typical results showing the effect of changing one procedure from that of using tubes from several heats in one batch to that of segregating tubes from only one heat into each batch are given in Fig. 45. Determined average range

[35] A "batch unit" consists of all forgings or tubes of the same dimensions quenched and subsequently tempered together as a unit.

values are 21,700 psi (before) and 13,100 psi (after), respectively. All quenched and tempered forgings referred to in the figure were supplied by Company 15 and had a composition and size similar to Forging 1 from that company listed in Table IV.

Before the relation between yield strength and transverse reduction of area was determined, specifications for the acceptance of quenched and tempered tubes, such as discussed here, required that over a considerable yield strength range, the transverse reduction of area quality of accepted material be above a certain minimum independent of yield strength. As a result, many producers in making an effort to meet transverse reduction of area requirements frequently submitted tubes having too low a yield strength. Such tubes had obviously to be reheat treated. These specifications have now been modified so as to allow tubes with higher yield strength and lower transverse reduction of area quality to be accepted using the now known relation between yield strength and transverse reduction of area as a basis for such modification, and as a result the number of such reheat treatments as those referred to above has been reduced to practical insignificance. This is because producers now temper their product to a yield strength much closer to the average of the maximum and minimum required and thereby drastically decrease the probability of developing too low a yield strength in tubes.

As a result of the acceptance of the conclusion that reheat treatments normally do not significantly increase the transverse reduction of area quality of tubes quenched to martensite and subsequently drawn to a given yield strength, the practice of making such reheat treatments has been significantly reduced. To what extent reheat treatments of tubes not quenched to martensite before being tempered should be discontinued has not yet been determined.

Summary

1. Conclusions presented in this summary relate to units of quenched and tempered wrought steel products consisting either of tapered solid forgings or tubes and varying considerably in size (minimum 2.5 to 5.5 inches O.D. and 85 inches long, and maximum 17 to 25 inches O.D., 8.5 inches I.D., and 340 inches long). Carbon contents range from about 0.30 to 0.45% and alloying elements from 1.5 to 4.5%.
2. Variation of transverse reduction of area quality within solid

forgings or tubes is much higher than is generally recognized. A maximum difference among 250 transverse reduction of area values for specimens taken from a single forging is rarely less than 18%, say 30% minimum—48% maximum, is frequently about 30%, and sometimes 40% or more. Few determined standard deviations are below 3% or above 8%; the average is about 5%.

3. Transverse reduction of area quality should be thought of as a distribution of transverse reduction of area values which may be represented (a) always by a frequency curve and (b) generally with sufficient precision for most practical purposes by two statistics, an average ($\bar{X}$) and a standard deviation (σ).
4. With few exceptions, comparable tubes or solid forgings coming from a single heat have the same transverse reduction of area quality within the limits of practical significance.
5. Comparable tubes from a similar position in ingots cast from a single heat usually have about the same transverse reduction of area quality. The quality of tubes coming from bottom thirds of ingots is generally slightly lower and occasionally much lower than that of tubes coming from middle or top thirds of ingots.
6. Quite often all the tubes or forgings from several heats made consecutively in a practice have essentially the same transverse reduction of area quality.
7. The relation between yield strength and transverse ductility is such that when yield strength values for tensile specimens taken from units of wrought steel products quenched to martensite and subsequently tempered are higher by 5000 psi in the range between 80,000 and 180,000 psi, transverse reduction of area values are usually lower by about 1.5%.
8. Normally, a commercial heat treatment consisting of a normalize, a quench to martensite and a subsequent temper is sufficient to develop in units of fine-grained wrought steel products a transverse reduction of area quality which cannot be significantly improved by additional heat treatments involving (a) a retemper or (b) a requench and temper, providing the units are always tempered to essentially the same yield strength level.
9. Increasing the angle between longitudinal axis and flow line direction in tensile specimens from 0 to 30 degrees and from 70 to 90 degrees has little effect on the average of reduction of area values for a large number of specimens, but increasing the angle

from 30 to 70 degrees lowers the average quite drastically. Variation among reduction of area values is small when the angle is less than 22 degrees but increases rapidly and becomes quite large as the angle is increased to 54 degrees. Beyond 54 degrees the variation remains large but tends to be decreased.

10. The optimum forging ratio is, in general, probably less than 3 to 1 and may be in some instances less than 2 to 1. It is believed that optimum forging ratio increases with ingot size. Both longitudinal and transverse ductility are improved by optimum forging. An increase of ratio beyond the optimum normally increases the variation of transverse reduction of area quality within a forging and decreases the average. Whether or not excessive forging of perfectly clean steels would reduce transverse ductility has yet to be determined.
11. The average transverse reduction of area quality of midwall material in quenched and tempered tubes having a forging ratio of 3 to 1 and a yield strength of 115,000 psi is significantly lower when the tubes are very large than when they are small; the variation of transverse ductility within the midwall material of these tubes appears to be at least approximately independent of tube size. More effective quenching is believed to be the primary cause of the higher transverse ductility in the smaller forgings. It is believed that if all quenched and tempered tubes had a forging reduction of 3 to 1 and were tempered to a yield strength of 75,000 psi, then the transverse reduction of area quality obtained would be roughly independent of tube size.
12. A positive correlation exists between transverse reduction of area and transverse impact in wrought steel products, providing maximum impact quality is developed by heat treatment and cold brittleness is avoided. A regression line, based on transverse reduction of area and transverse impact data from one product quenched to martensite and tempered to a yield strength of 160,000 psi, shows that when the average of a large number of transverse reduction of area values for specimens from this product is increased by 1%, the average of a large number of transverse impact values for specimens broken at 70 °F is increased by 1.2 foot-pounds.
13. Angular fracture in itself is no certain criterion for low transverse ductility and there is little justification for suspecting the quality of a product simply because the specimen has an angular

fracture, especially if the transverse reduction of area value for that specimen is relatively high. Angular fracture has been observed to depend on the orientation of dendritic pattern and since such orientations are determined by chance, the occurrence of angular fracture should give little concern.

14. Porosity resulting from deep etching should not in itself be considered as a certain criterion for low transverse ductility.
15. On the average, heat treated wrought steel products made of basic electric steel have better transverse ductility than comparable products made of basic open-hearth steel. Sometimes, however, this difference is so small as to be practically insignificant.
16. Discontinuous stringers consisting of hard, angular particles lower average and increase variation of transverse ductility in wrought steel products. These stringers are primarily responsible for tails of frequency curves extending in the direction of lower transverse reduction of area values.
17. The severity of homogenization treatment required to significantly improve transverse ductility is so drastic as to be impracticable commercially.
18. Elongated nonmetallic inclusions and the heterogeneous distribution of elements in solution are together largely responsible for transverse ductility of forgings being lower than longitudinal ductility.
19. The variation among a large number of impact values for specimens broken at 70 °F and taken from a unit quenched to martensite and tempered to a given yield strength increases with decreasing yield strength level. When the unit is tempered to a yield strength level in the range between 95,000 and 145,000 psi, the variation is usually rather well represented by a standard deviation (σ) of about 1.7 foot-pounds; at levels between 145,000 and 170,000 psi and between 170,000 and 180,000 psi, standard deviations of 1.3 and 1.0 foot-pounds, respectively, are probably more appropriate.
20. The transverse impact quality of all tubes quenched to martensite, tempered to the same yield strength, and coming from the same heat is usually alike within the limits of practical significance.
21. Transverse impact values for specimens broken at 70 °F and taken from units of wrought steel products quenched to mar-

tensite before tempering are increased on the average by about 3 foot-pounds when yield strength is lowered by 5000 psi; this relation appears to be valid over a yield strength range extending from 80,000 to 180,000 psi.

22. As the angle between the direction of the longitudinal axis and the direction of flow lines in specimens is increased from 0 to 90 degrees, impact values are decreased. Average values at 18-degree intervals for one product quenched and tempered to a yield strength of 122,000 psi are 55 (0 degrees), 53, 47, 37, 35, and 34 foot-pounds (90 degrees), respectively.
23. The maximum difference among a large number of yield strength values for tensile test specimens from a quenched and tempered tube is rarely less than 5000 psi, usually about 10,000 psi, sometimes 15,000 psi, and occasionally as high as 30,000 psi.
24. Neither tensile strength nor yield strength is changed significantly as the angle between longitudinal axis and flow line directions in specimens is increased from 0 to 90 degrees.
25. Specifications based on results presented in this paper have been developed. These are much more efficient and economical than those previously used.
26. The relation between transverse reduction of area quality and percentage of material accepted by specification has been discussed.
27. As a result of information disclosed in the present investigation, some producers modified their heat treatment practices. These modifications have been described and their significance discussed.
28. Increasing the rate of loading from 2500 to 100,000 psi per minute has no significant effect on either yield strength measured at 0.01% offset or on transverse reduction of area values for specimens taken from a unit of product quenched to martensite and tempered to a tensile strength of 130,000 psi.
29. Increasing tensile specimen size from 0.252 inch diameter to 0.505 inch diameter tends to increase average yield strength and decrease average transverse reduction of area values without significantly affecting average tensile strength.

Acknowledgments

The program of research leading to results published in this

paper was conceived and developed as a result of close co-operation among the following groups:

(a) War Metallurgy Committee of NDRC
(b) An advisory committee functioning under the War Metallurgy Committee
(c) Armed services
(d) Carnegie Institute of Technology
(e) Industrial concerns
(f) Technical advisors.

The authors are indebted to many in each of these groups and wish to express appreciation for their valuable contributions. Advisory committee members consisted of Jerome Strauss, Vanadium Corportion of America; W. G. Hildorf, Timken Roller Bearing Company; F. B. Foley, The Midvale Company; A. P. Spooner, Bethlehem Steel Company; and Col. S. L. Conner, Watervliet Arsenal, N. L. Reed of Watertown Arsenal and Lt. Comdr. B. D. Mills of the Bureau of Ordnance were liaison representatives for the Army and Navy, respectively.

Research assistants whose help has been especially valuable include W. S. Pellini, I. Broverman, C. V. Klimas, P. E. Busby, A. H. Grobe, A. Hanna, C. C. Busby, M. A. Redmerski, and S. Linder. Gratitude is also felt toward C. Miller, D. Stewart, and L. Redmerski, laboratory assistants, for their aid in tabulating data and executing laboratory work.

Advice on statistical problems from E. G. Olds, Carnegie Institute of Technology, and R. F. Passano, Bethlehem Steel Company, is also greatly appreciated.

Finally, the authors wish to thank E. G. Olds, J. W. Spretnak and P. E. Busby for their critical review of the manuscript and for helpful suggestions.

References

1. J. W. Spretnak, K. L. Fetters and E. L. Layland, "Ingot Factors in the Production of Seamless Gun Tubes," TRANSACTIONS, American Society for Metals, Vol. 39, 1947, p. 627.
2. J. W. Spretnak, "Kinetics of Solidification of Killed Steel Ingots," TRANSACTIONS, American Society for Metals, Vol. 39, 1947, p. 569.
3. V. Paschkis, "Theoretical Thermal Studies of Steel Ingot Solidification," TRANSACTIONS, American Society for Metals, Vol. 38, 1947, p. 117.
4. J. W. Spretnak, "Macro Segregation in Some Alloy Steel Ingots," TRANSACTIONS, American Society for Metals, Vol. 40, 1948, p. 897.
5. C. F. Sawyer, J. W. Spretnak and G. Derge, "The Distribution of Oxygen and Nitrogen in an Alloy Steel Ingot," TRANSACTIONS, American Society for Metals, Vol. 40, 1948, p. 922.

6. H. Arkin and R. R. Colton, "An Outline of Statistical Methods," Fourth Edition, 1939, Barnes and Noble, Inc., New York.
7. K. Pearson, "Tables for Statisticians and Biometricians," Third Edition, Biometric Laboratory, University College, London, Cambridge University Press, 1931, p. 165.
8. H. Brearley. Reference to Brearley given in book by L. Aitchison, "Engineering Steels," D. Van Nostrand Company, New York, 1921, p. 31.
9. R. F. Mehl and A. H. Grobe, "Final Report on Acceptance Tests for Plain Carbon Steel Gun Forgings and Other Ordnance Forgings," Serial No. M-466, May 3, 1945, published by the Office of Technical Services, Department of Commerce, Washington 25, D. C.
10. E. J. Janitzky and M. Baeyertz, "The Marked Similarity in Tensile Properties of Several Heat Treated SAE Steels," METALS HANDBOOK, American Society for Metals, 1939, p. 515.
11. D. J. McAdam, Jr., and R. W. Clyne, "The Theory of Impact Testing: Influence of Temperature, Velocity of Deformation, and Form and Size of Specimens on Work of Deformation," *Proceedings,* American Society for Testing Materials, Vol. 38, Part II, 1938, p. 113.
12. *SAE Handbook,* 1946 Edition, p. 334.
13. J. G. Mravec, J. Welchner and W. G. Hildorf, "Final Report on Control of Basic Open Hearth Melting Practice for the Manufacture of Wrought Gun Tubes," Serial No. M-420, December 19, 1944, published by the Office of Technical Services, Department of Commerce, Washington 25, D. C.
14. L. Aitchison, "Engineering Steels," published by MacDonald and Evans, London, 1921, and also by D. Van Nostrand Company, New York, 1921.
15. G. Charpy, "Influence of Hot Deformation on the Qualities of Steel," *Journal,* Iron and Steel Institute, Vol. 98, 1918, p. 7.
16. H. Stryi. Discussion of paper by Kinzel and Crafts, "Inclusions and Their Effect on Impact Strength of Steel," American Institute of Mining and Metallurgical Engineers, Vol. 95, 1931, p. 143.
17. W. J. Priestley, "Effect of Sulphur and Oxides in Ordnance Steel," American Institute of Mining and Metallurgical Engineers, Vol. 67, 1922, p. 317.
18. R. F. Mehl, C. Wells, A. H. Grobe and P. E. Busby, "Final Report on Improvement in Wrought Gun Tubes: Part III—Linear Correlations Among the Tensile and Impact Properties in Quenched-Out Gun Tubes," Serial No. M-556, August 16, 1945, published by the Office of Technical Services, Department of Commerce, Washington 25, D. C.
19. METALS HANDBOOK, American Society for Metals, 1939 Edition, p. 515.
20. C. L. Meyette and V. E. Elliott, "A Method for Determining Origin of Surface Defects in Rolled Steel Products." Presented at the American Institute of Mining and Metallurgical Engineers meeting in New York, February 1948.
21. C. Wells, R. F. Mehl, C. V. Klimas, I. Broverman and P. E. Busby, "Improvement in Wrought Gun Tubes: Part I—Operating Characteristics of Specification WVXS-78," Serial No. M-537, August 6, 1945, Volumes I and II. Published by the Office of Technical Services, Department of Commerce, Washington 25, D. C.
22. R. F. Mehl, C. Wells and C. V. Klimas, "Final Report on Improvement in Wrought Gun Tubes: Part VIII—Operating Characteristics of Specification WVXS-88 and Specification WVXS-95," Serial No. M-564, December 5, 1945. Published by the Office of Technical Services, Department of Commerce, Washington 25, D. C.
23. R. A. Fisher, *Statistical Methods for Research Workers,* Tenth Edition, Oliver and Boyd, London: 98 Great Russell Street, W. C., 1946, p. 121.

DISCUSSION

Written Discussion: By R. J. Stoup, development metallurgist, Spang-Chalfant Division of the National Supply Co., Ambridge, Pa.

Obviously, this paper represents a compilation of a tremendous amount of detail work and the conclusions, based as they are on thousands of determinations and carried through by careful statistical analysis, are not to be readily controverted. During the war, the writer was engaged in the heat treating and testing of gun tubes and it is undoubtedly the consensus of opinion of all those connected with that type of work: that as a result of this and other investigations of the Metals Research Laboratory, specifications have been adopted which permitted from the cannon heat treating plants an increase in both quality and quantity of materiel. It may be well to emphasize the fact, as pointed out by the authors, that their function was not to rationalize the minimum levels for acceptable material set up by the Ordnance Department, but rather to study the causes of variation from test to test and piece to piece.

One of the criteria for acceptable gun tubes has always been the transverse reduction of area. At first glance, it might seem that this property which is measured on a fractured test bar would have little connection with the service life of a gun barrel in which the stresses rarely exceed the yield strength. However, the evidence as compiled by the authors is overwhelming that in properly quenched and tempered forgings, RAT is a measure of the quality of the steel. The reason why this should be so is conceived as follows:

It seems to be well established that final fracture of a sound test bar commences at the center and progresses to the outside. In the course of its progress to the circumference, at some intermediate radius depending on the ductility of the material, the shear strength becomes a factor and the steel possessing high ductility parts along a plane 45° from the tensile stress, giving rise to the various forms of cup and cone fracture. The stress distribution at the neck if interrupted by discontinuities throws the metal into combined states of stress which lead to early failure and consequent low contraction. It has been noted also, on transverse test bars from inclusion-rich material, small X-shaped checks frequently appear on the surface near the fracture and occasionally the break itself can be connected with one of these stress raisers. Such a break is invariably sharp with little contraction and represents a different mode of failure than the more common type which starts in the center.

Drs. Wells and Mehl have shown that strings of inclusions of an angular shape are one type of discontinuity which leads to low RAT values. Transverse reduction of area measurements thus serve a useful purpose in evaluating the cleanliness of the steel when low values are known to be due to the effect of inclusions alone, uncomplicated by extraneous effects due to other heat treatment variables. All other things being equal, it is assumed that the gun tube with the fewest inclusions is the most reliable for service. The reduction of area values represent a method for proof testing a limited area for its inclusion content.

However, in the larger size forgings, there is another effect which may mask the above—that is, the presence of untempered martensite. In water quenching steels of the analysis given in heavy sections, it is common practice to arrest the quench in the vicinity of 300 °F and temper immediately to avoid cracking. The amount of martensite formed is a function of the lowest temperature attained and if the transformation is not completed during the quench, fresh untempered martensite is formed on cooling from the temper. This martensite would act similar to the hard angular inclusions mentioned in this paper.

A re-temper then would be expected to raise the reduction of area values, but it is interesting to note that the authors did not find this to be statistically true. I would like to ask the authors whether the test results on the sizes given in Tables IV and XIII represent only the tests made at the maximum O.D. section or whether the results given include RAT values on the muzzle end also and whether there is any significant difference between them.

Written Discussion: By Edward A. Loria, Fellow, Mellon Institute of Industrial Research, Pittsburgh.

In this outstanding paper, the writer is particularly interested in the sections pertaining to the effects of nonmetallic inclusions on transverse ductility and the heat treatment of gun tubes. The RAT values obtained from tensile test specimens taken from various sections in the ingots studied would serve to evaluate ingot cleanliness and thus provide an indication of ingot quality. The writer[36] has shown the nature of some inclusions in tensile fractures of acid open-hearth forging steel and it is significant to note that even in the case of the more ductile, cup-cone fracture a careful metallographic examination will reveal an inclusion segregate at the center of the cup in at least 50% of such fractures. The occurrence of inclusions in the outer portion of forging ingots can be significant from a quality standpoint, not only in the occurrence of cracking or surface imperfections on machining, but in the effect on transverse mechanical properties. Allen[37] confirms that the inability to develop satisfactory transverse ductility is in a large part due to the presence of nonmetallic material visible in the fractured face of the tensile test specimen. On the influence of ingot size on transverse ductility, it can be said that the amount and size of inclusions and the tendency to form a mixture of large and small inclusions increases in large ingots thereby accentuating the possibility of producing an unfavorable distribution. The total nonmetallic content may affect the quality of gun tubes produced from large ingots to a greater extent notwithstanding the fact that the quality of gun tubes may not be so much related to the amount of inclusion material as to the distribution of that inclusion material. Perhaps the difficulty in determining any measure of inclusion distribution lies in the fact that their effect can be aggravated by

---

[36]H. D. Shephard and E. A. Loria, "The Nature of Inclusions in Tensile Fractures of Forging Steels," TRANSACTIONS, American Society for Metals, Vol. 41, 1949, p. 375.

[37]R. M. Allen, discussion of paper by E. A. Loria and H. D. Shephard, this volume TRANSACTIONS, p. 358.

unfavorable or can be minimized by favorable hot working conditions.

In addition to discontinuous and continuous stringer-type inclusions, untempered martensite and slack-quenched structures may exert a detrimental influence on the transverse ductility of quenched and tempered gun tubes. A fully martensitic structure is recognized as the desirable structure before tempering but if the cooling of the steel during quenching is not sufficiently rapid to retain all of the austenite untransformed down to the low temperature at which the desired martensite is formed, ferrite-pearlite or bainite will appear in the quenched structure. Such slack-quenched gun tubes have been found generally to have inferior mechanical properties, especially with respect to impact strength. In slack quenching where the transformations are occurring under continually dropping temperature rather than isothermally, the bainite decomposition product is formed in two stages, and that austenite retained with it is persistent, i.e., resists decomposition on tempering after quenching; but on cooling from the tempering temperature it may transform to fresh, hard, brittle martensite. This brittle, untempered martensite, as well as the recognized deleterious presence of ferrite or bainite, is partially responsible for much of the poor mechanical behavior of slack-quenched structures. A second tempering to temper this late-formed martensite should correct the situation.

Written Discussion: By Ralph L. Wilson, director of metallurgy, and John Welchner, metallurgical engineer, The Timken Roller Bearing Company, Steel & Tube Div., Canton, Ohio.

The authors are to be complimented on the fine manner in which they analyzed and presented this great amount of important data. The technical literature contains relatively little specific information concerning transverse properties of steel. With the aid of the comprehensive data reported in this paper, more intelligent specifications can be devised and less unnecessary metallurgical testing will be done where transverse or partially transverse properties of wrought steel products are involved.

Of particular interest to the writers is the authors' observations pertaining to nonmetallic inclusions. While it is true that an increase in the continuous and discontinuous stringer type of inclusions definitely lowers the transverse reduction of area, we found that the total nonmetallic content of samples (general cleanliness of the steel) did not affect the RAT of 40-mm gun tubes to the same degree as the 75-mm gun tubes. In fact, with the same relative amount of stringer type of inclusions present, the 40-mm tubes were not adversely affected once the steel became "dirtier" than a certain amount. The 75-mm guns gave progressively lower RAT values as the general cleanliness rating decreased. At present we have no valid explanation for this. (We hope to publish the details of our studies at an early date.)

In our experience as a steel supplier, we find that all too often insufficient samples are taken in an attempt to evaluate the general cleanliness of a heat of steel. From a practical standpoint, enough samples should be taken so that the "average" rating will be within the error of rating of individual samples.

Thus, it is recommended that at least 8 random nonmetallic samples be taken for each heat to be rated and additional samples taken if the heat is below average in cleanliness.

Written Discussion: By J. V. Russell, director, Metallurgical Laboratory, Republic Steel Corp., Chicago.

The authors are to be congratulated on the publication in such concise form of the large mass of data which they accumulated on various gun tubes and forgings. They have presented their conclusions in clear and simple form and they are generally substantiated by a very large amount of testing, the results of which it is gratifying to see handled according to statistical techniques. We do not feel that conclusions arrived at in this manner can be easily denied. We would like to add

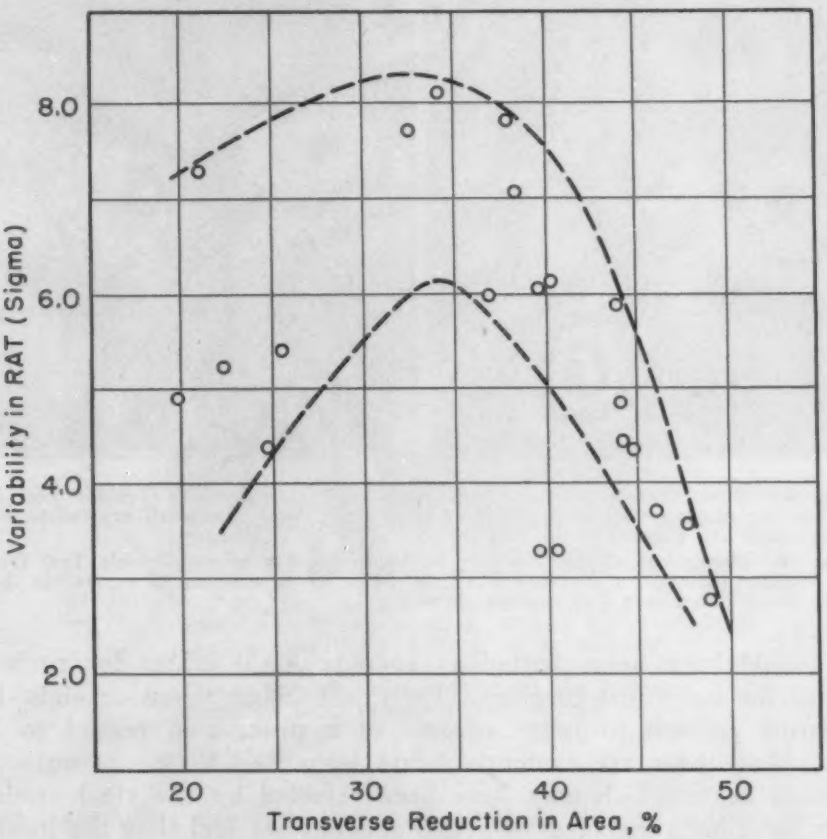


Fig. 46—A Plot of the Data in Table V to Show the Sigma Value for RAT Values as a Function of the Average RAT for the Forging.

our confirmation of certain sections of this paper based on our own experience with relatively large forgings which were produced for this program.

In regard to the authors' statement that the variation of RAT values for good forgings was about the same as that on forgings showing low RAT values, we have plotted in Fig. 46 the data of Table V with the sigma values as a function of the average RAT. This plot shows that

with the highest RAT guns the sigma tends to be low and reaches a maximum at intermediate RAT values and appears to decrease again as very low RAT values are approached. Undoubtedly the authors' conclusions are based on more data than is shown here although we feel that the relation suggested is interesting.

The conclusion is advanced that for a given practice the RAT quality for successive heats falls within limits of statistical control and also, in this case, within specification limits. We would like to point out that in the control charts shown in Figs. 9 and 10 only seven or eight steel heats are reported. Since all forgings from a heat had been demonstrated to be about the same quality we feel that, in this case,

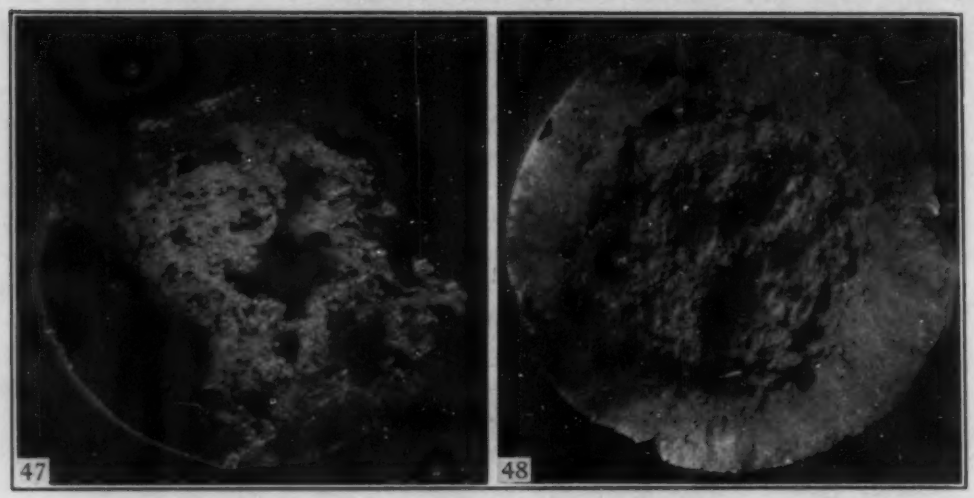


Fig. 47—Photograph of the Fracture Surface of a Transverse Tensile Test from Large Forging Having an Average RAT Value of 36.8%. The small crystalline bands in the fracture and parallel to the forging axis are readily apparent.

Fig. 48—Photograph of the Fracture Surface of a Transverse Tensile Test from a Large Forging Having an Average RAT of 54%. Note absence of crystalline bands and that the fracture is a full cup-cone type.

points should have been plotted as average RAT values for each heat instead of for individual forgings. On this account seven or eight heats seem hardly enough to judge control of a process in regard to RAT quality. Also, these are evidently heats submitted to the manufacturer, and certain heats which may have been rejected by the steel producers may not have been included. On this account we feel that the inference should not be drawn that all heats produced fall within these limits, although those submitted may very well do so.

The relation between RAT and yield strength as derived by the authors is an interesting one and certainly is, as they have stated, a necessary consideration in any specifications involving reduction of area, particularly where close limits are imposed on both. In considering the material and the size of the forgings used in developing this information, it appears that sections used should be considered to be through hardening and consequently the relation is expected to hold only for such sizes. We feel that a similar relation for certain degrees of slack quenching,

i.e., only partially martensitic with varying amounts of bainite present, would be particularly valuable. Many forgings are made of such size and chemical composition that they may in many cases fail to harden completely by the formation of martensite and we wonder if in this case the relation would change. Much the same comment applies where

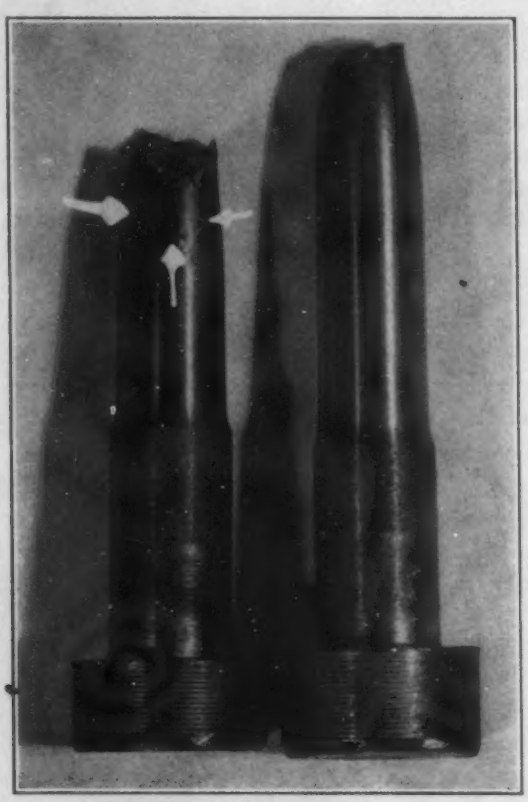


Fig. 49—The Two Test Bars Whose Fractures Are Shown in Figs. 47 and 48. The test of low RAT quality is at the left. The arrows indicate gage length cracks in this specimen. Note that along the forging direction cracks appear and in the plane transverse to the forging direction pits appear.

reheat treatments are described. Here it is shown improvements may be obtained after requenching or redrawing. However, the sections considered here are again relatively small and we feel that for large tubes which might not harden completely on one quench the RAT values might be improved by a re-treatment since, in general, such treatment tends to give deeper hardening than a single quenching and tempering treatment. We feel that this consideration is implied in the authors' discussion and are simply giving our confirmation.

We were particularly impressed by the section devoted to a discussion of the cause of low RAT qualities. The section dealing with factors leading to the occurrence of angular fractures is in close agreement with

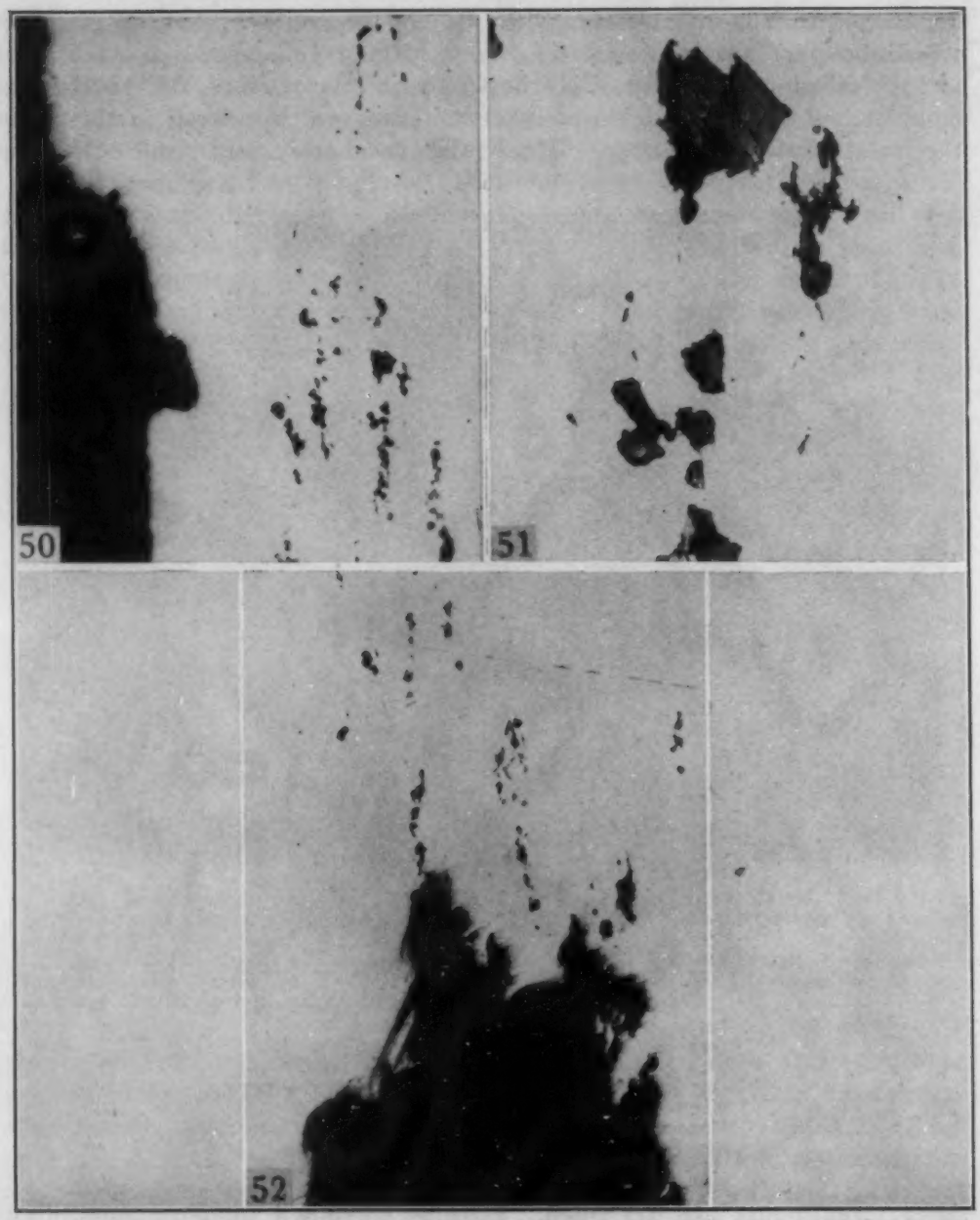


Fig. 50—Oxides Revealed by Carefully Polishing, in the Plane of the Fracture of Fig. 47, Down to a Crystalline Band. × 100.

Fig. 51—The Same Field as in Fig. 50 Except at Higher Magnification. × 500.

Fig. 52—A Group of Oxide Inclusions at the Base of One of the Cracks in the Gage Length of the Specimen Shown in Fig. 49.

our experience. We found that tests showing poor RAT quality generally had such a fracture although it was not necessarily angular, being, in many cases, normal to the axis of the specimen. We found that fractures of this type were generally accompanied by clusters of oxide inclusions. The effect of these clusters on appearance of fractures is

shown in Figs. 47 and 48. The average of eight tests on the material of which Fig. 47 was typical was 36.8% RAT (sigma = 4.34) and average of seven tests on the material of which Fig. 48 was typical was 54% (sigma = 2.24). The small crystalline bands in Fig. 47 were characteristic of low ductility material and appear to be completely absent in Fig. 48 which is a cup-cone break. Another characteristic of material of low RAT was to crack in the gage length as in Fig. 49. Both the crystalline bands and the gage length breaks had associated with them angular oxides as illustrated in Figs. 50, 51 and 52. These inclusions were generally absent in material of high RAT. As a matter of interest, Shephard and Loria[38] illustrate the same condition as suggested by the authors to be a principal factor in low RAT values. We might add also that the condition of heterogeneity referred to by the authors has been observed by us in much the same relation to RAT values.

In connection with the sulphide-rich regions described it has been observed that these regions also may be positively segregated in respect to certain other elements such as carbon, silicon, manganese, chromium and molybdenum.[38] The authors have shown that the presence of these pits after deep etching is not accompanied by an adverse effect on RAT quality but they have demonstrated this at a relatively low strength. Do they have information on the effect of these regions at higher tensile strength? We feel that information on the influence of these areas on quality should be established over a wide range of strength.

Written Discussion: By A. O. Schaefer, executive engineer, The Midvale Co., Nicetown, Philadelphia.

Rarely does the opportunity present itself to anyone to have available for consideration and review the great amount of data contained in the paper and the others in the series being written at Carnegie Institute of Technology. It is indeed fortunate that we have men with the broad experience of the present authors to digest a great quantity of this information for us. The present paper is unique as we understand it in that it summarizes in advance a lot of the detail which will follow in subsequent papers.

The writer of this comment served during the recent War as Chairman of the Development Group on Gun Manufacture, so that he can speak from intimate contact with the research as it progressed. It will be recognized at once that this project started in a modest way, to attempt the explanation of angular fracture and the variations found in what Cyril Wells calls RAT or Reduction of Area Transverse. From this small beginning, the study branched out to cover practically all the variables of steel manufacture and their relationship to transverse tensile and impact properties.

Dr. Wells gave freely of his time during the War, and on several occasions lectured for a full day before the Development Group, keeping them fully informed on the progress of his study. The importance of

---

[38]Convey and Rorery, "Microspectrographic Method for Quantitative Analysis of Steel Segregates," Advance Copy, 1946, *Journal*, Iron and Steel Institute.

this work was recognized from the start by the manufacturing group.

There are several points that, it seems to me, should be emphasized more definitely than they are in the present paper.

In the first place, no one really knows what actual merit reduction of area transverse has as a criterion of the serviceability of steel forgings in general or of gun tubes in particular. The fact remains that this was made the criterion for gun tubes at a period when no one had the time to quibble about it. No one disputes the value of ductility, however, or that it is in fact indicative of quality.

In the same way Charpy Impact Transverse was made a specification requirement for more highly stressed tubes, and the present study was enlarged to include this property.

One of the dangers of a program as broad as this one is that it might be considered to apply to steel forgings in general. I think it should be pointed out that this study really covers a very special type of forging. In most cases, the forging manufacturer is able to adjust his forging method to provide flow lines in an advantageous pattern. This he upsets, expands, draws, or bends, to make the most serviceable part. Optimum ductility as well as impact properties follow flow lines.

However gun tubes, particularly small ones, do not permit the most favorable flow lines. They are forged by a "drawing" operation from the ingot, and can be forged in no other way until we come to sizes large enough to permit hollow forging. Larger hollow forged tubes are not included in the scope of this paper. The reduction of area and impact in transverse planes are obtained then by means which are different from those followed in making most forgings. That is why small ingots giving forging reductions of the order of 2 and 3 to 1 are so often noted.

At the same time it should be realized that we are, in general, reviewing results obtained from steel of the very highest quality, made from selected raw materials, controlled throughout, and with larger discards taken from the ingots. These forgings were made in large quantities. In many cases this permitted the use of ingot molds designed specifically for the job, and in many other special practices.

It is admittedly very difficult and very foolish to dispute statistical mathematics, but I cannot help but feel that the authors have slipped into some generalities which are too broad to apply in all cases. For instance, with regard to the relationship of ingot size to transverse ductility, it is stated that this would have no effect whatsoever provided the forging reduction remained the same, and the quench was as effective, etc. The practical forging manufacturer favors the use of smaller ingots because he knows they naturally tend to a less pronounced dendritic pattern, and because it is easier to obtain clean steel in smaller molds.

We have also the statement that the difference between the transverse reduction of area quality in the product of the basic electric and the basic open-hearth furnace is practically insignificant. This was proven only on pierced tubes at a not very high strength level (Y.S. 115,000 psi). The pierced tubes contained in the investigation represent a product in many ways different from the conventional forged barrel.

The piercing operation, the twist imparted to the stock, and other factors, result in a product which is quite different from the usual forged and bored tube. It is true that there was very little difference between basic open-hearth and electric furnace steel when made into pierced tubes. I do not think there was any comparison made otherwise. When it comes to high strength tubes required to have high transverse impact values, electric furnace steel showed a distinct superiority over open-hearth steel.

The practice of reheat treatment operations has not been discontinued as a result of this research, but the reasons for it are perhaps better understood. It is difficult to establish that we have or have not accomplished a quench completely in the martensite zone. There have been too many instances where a second quench accomplished what a first had not. Sometimes, frankly, a reheat treatment is given merely to permit resubmission under the terms of the specification. It is here that Drs. Wells and Mehl have helped by showing the range of values that may be expected in such properties as reduction of area transverse. Also repeated tempering heats are sometimes found effective for the removal of retained austenite, as well as for final stress removal.

Aside from the great amount of information about forged steel to be gleaned from this work, the greatest practical benefits derived from the application to specifications of the principles revealed are that such values as reduction of area transverse and Charpy impact transverse should be required on a sliding scale based on the actual yield strength obtained and that average and range requirements should be used so that stray values do not necessitate retesting or retreatment. The authors are to be commended for making this great fund of information available to all.

Written Discussion: By James Allison, metallurgist, The Star Drilling Machine Co., Akron, Ohio.

The work described in this paper was probably the most important war-time contribution to gun tube manufacture from the standpoint of cost and time saving, smooth production and clear understanding of the physical test results.

The gun tube specifications at the beginning of the war called for a minimum transverse reduction of area and a minimum and maximum limit of yield strength. For no explainable reason, it was the general experience of most gun tube manufacturers that only about one-half of the gun tubes tested from the majority of heats of steel would pass the transverse reduction of area requirements. Retests were permitted and usually about another one-half of the remaining tubes would pass. The customary practice was to anneal, requench, and draw the tubes which failed on retest. After this treatment about one-half of the retreated tubes, and one-half of the remainder upon still another retest, would pass. This procedure of retreating and retesting had sometimes to be repeated three times to get all guns from a good heat of steel accepted or to reduce the rejects to a negligible percentage. As an average, we had to make twice as many physical tests as were required

by the specification. We found that the tubes of only about one of ten heat lots would pass on the first set of tests. Such erratic results caused large inventories of tubes in process and uncertain delivery schedules.

In April 1943, we began to operate under Specification WVXS 88, one of the specifications which resulted from the work described in this paper. Transverse reduction of area results were subjected to statistical analysis. A sliding scale of minimum reduction of area values for different levels of yield strength was substituted for the single minimum. Immediately the number of tests decreased to one-quarter to one-eighth of those formerly required. The test results from the first heat treating load of a heat of steel gave almost certain proof whether all of the tubes from that heat would pass. Also, it was no longer necessary to draw the tubes to the low limit of yield strength to favor higher reduction of area. As a result, the number of heat treating batches which had to be retreated to bring them within the yield strength limits was reduced to a negligible percentage.

When the trend to higher strength tubes made it necessary to require transverse impact tests, there was some feeling among the manufacturers that this test was subject to too many variables to be practical. As the authors have shown, statistical treatment of the impact test results established a correlation with transverse reduction of area results in tubes quenched to martensite. The impact tests gave protection against slack-quenched tubes being made into guns, and contrary to expectations caused no confusion to production.

The authors are indeed to be congratulated upon this exhaustive study which has clarified both the meaning of transverse reduction of area and impact tests, and the effect of many of the variables of gun tube practice on these physical properties. Also, they are to be congratulated for their timely application of the results of their studies to expedite quality gun tube production during the war.

Authors' Reply

The authors wish to express their appreciation to those who have contributed to the discussion of this paper.

For reasons given by Mr. Stoup and Mr. Loria, one might anticipate that a retemper of certain large quenched and tempered forgings would increase average transverse reduction of area quality. Actually transverse reduction of area quality is sometimes raised quite markedly by a retemper, even though the yield strength is little affected by the retempering treatment. In one instance the average of transverse reduction of area values for 16 specimens from a quenched and tempered forging 25-inch O.D., 8.5-inch I.D., and about 350 inches long is 38.9%; after retempering the average of values for 16 specimens from the same forging is 44.4%, an increase of 5.5%. The yield strength average after tempering is 108,000 psi and 105,000 psi after retempering.

Average and sigma (standard deviation) listed in Columns 8 and 9 of Table VIII are based on (a) data from four 0.357-inch diameter trans-

verse tensile test specimens taken from maximum O.D. ends of forgings supplied by Companies 1, 2, 3, 15, and 16, (b) data from 0.357-inch diameter specimens from minimum O.D. ends of tubes supplied by Company 14, and (c) an equal number of data from 0.505-inch diameter specimens from each end of tubes supplied by other companies, not above mentioned, but referred to in the table. The difference of transverse reduction of area quality between the two ends of any forging randomly selected from those referred to in Table VIII is likely to be insignificant from a practical point of view. Occasionally the smaller diameter end of a quenched and tempered forging is much lower in transverse reduction of area quality than the larger end because of nonmetallic inclusions; sometimes the larger end of the forging is much lower in transverse reduction of area quality than the smaller end because of the smaller end being more drastically cooled during quenching.

The experience of Mr. Wilson and Mr. Welchner shows that both continuous and discontinuous stringer types of inclusions definitely lower transverse reduction of area quality. All seamless tubes referred to here by these two discussers were reduced 15 to 1 or more by hot work, subsequently quenched, and drawn to a yield strength of between 95,000 and 125,000 psi. The authors' experience shows that at least sometimes continuous inclusions of the type, size, and distribution contained in Forging 2 from Company 17 have little effect on average transverse reduction of area quality as determined by standard tensile tests.

Results presented by Mr. Russell are quite valuable and the authors are pleased to note that his conclusions based on these results confirm many of the conclusions drawn by the authors.

In the paper (page 736) the following is stated: "It seems quite probable that all forgings from any arbitrarily selected group of ten or even more consecutively made heats will, if thoroughly tested, be found to have essentially the same transverse reduction of area quality. Hundreds of control charts have been plotted which, considered together, amply support this conclusion. One typical control chart, showing that all the forgings from seven consecutive heats made by Company 17 are probably alike within the limits of practical significance, is plotted in Fig. 9." Of course, the authors agree with Mr. Russell that the results of Fig. 9 do not of themselves form a sufficiently sound foundation on which to base the conclusion that the process is essentially in control with respect to transverse reduction of area quality. These results are typical, however, and the data considered are for forgings from seven consecutively made heats. There are many instances where 6, 8, 10, or even more heats made consecutively in a well-controlled practice appear to have essentially the same transverse reduction of area quality. If space had been unlimited, many more data would have been included in the paper to further support the conclusions drawn.

The authors agree with Mr. Russell that study should be made of the effect of soft, continuous, sulphide stringers, such as were observed in Forging 1 from Company 17, on the transverse reduction of area quality of forgings quenched and tempered to various widely different

tensile strength levels. So far the authors have made this study using forgings drawn to only one tensile strength level of about 100,000 psi.

Thanks are offered to Mr. Schaefer for his discussion. He apparently feels "that the authors have slipped into some generalities which are too broad to apply in all cases." The authors, after a further study of their paper, do not share this feeling. Considerable effort has been expended in attempts to state conditions under which the conclusions drawn are correct and it is hoped that this effort has not been made in vain. Indeed it would be both disappointing and unfortunate if the impression should be given that the conclusions are correct under conditions where actually they are not.

The authors are pleased to have Mr. Allison's comments emphasizing the fact that application of information disclosed as a result of this research has been and still is of interest and value to practical metallurgists.

THE ABRASION RESISTANCE OF METALS

By R. D. Haworth, Jr.

Abstract

A new abrasion testing machine has been devised with which it is possible to determine quantitatively the resistance of metals to either dry or wet abrasion. Weight loss values obtained under several abrasive conditions are presented for a variety of metallic materials. The results show that, in the absence of impact, carbon content is the most effective alloying element in producing resistance to abrasion. With the same abrading material, dry abrasion usually is more severe than wet abrasion. The degree of angularity of the abrading material has a marked effect on the extent of abrasive wear produced.

Ordinary methods of hardness determination show no reliable correlation with abrasion resistance. Hardness of the microconstituents relative to the abrading material together with the size, distribution, and quantity of the hard phases in the structure appear to be determining factors in abrasion resistance. Additionally, under dry abrasive conditions, hot hardness of the aggregate may be an additional important factor.

Introduction

ABRASIVE wear of metals long has been an important problem, the seriousness of which has been increased in recent years by the development of new higher speed mechanisms and by the steadily rising cost of replacing worn parts in terms of maintenance labor and lost production time. In turn, increased attention has been given to the development of better abrasion-resistant materials. Evidence of the gravity of this problem is found in the recent application of special tungsten carbide inserts in mining and earth-moving equipment.

The term abrasion is used with specific reference to the frequently rapid removal of metals by the cutting or scrubbing action

A paper presented before the Thirtieth Annual Convention of the Society, held in Philadelphia, October 23 to 29, 1948. The author, R. D. Haworth, Jr., is supervisor, Abrasion Research, Armour Research Foundation, Chicago. Manuscript received April 15, 1948.

of extraneous abrasive materials. The latter may be materials such as coke, earth, gravel, iron shot, mill scale, ores, or sand. The subject matter of this paper is confined to the abrasive type of wear and more particularly to sliding abrasion in the presence of minor or infrequent heavy impact which would not be sufficient to work harden the surface of the metal.

Studies of abrasion and abrasion resistance are very complex because of the many inherent variables encountered in service. Some of the complexities that must be considered are discussed briefly in the following paragraphs.

Natural materials encountered in various applications range in hardness from talc to corundum (natural aluminum oxide). Silicon carbide, a synthetic material sometimes encountered, has even greater hardness than aluminum oxide. In general, materials with higher hardnesses are more abrasive than softer materials. The reported abrasiveness of materials softer than steel, such as coal, for example, may actually be due to the presence of relatively small amounts of harder materials, such as iron pyrites, shale, or sand.

The type of metal which can be used for a given application is dependent on the degree of impact or pressure involved. Under heavy impact or pressure, austenitic manganese steel work hardens on the surface and resists wear excellently, whereas low shock-resistant materials, such as white iron, are unsuitable for this type of service. On the other hand, for abrasive service accompanied by minor or moderate shock, white iron will outwear austenitic manganese steel by a wide margin (1).[1]

Another important factor in abrasive applications that requires consideration is whether the service is dry or wet. Blake (2) found that dry and wet service were very different, and also that different abrasives would alter and even reverse the order of excellence of the metals tested. Corrosion is often an important factor in the selection of materials for wet abrasion. A material which is inferior to another in a noncorrosive application may be far superior to the other in a corrosive medium. Likewise, a superior metal in wet abrasion may be decidedly inferior in dry abrasion where elevated temperatures, due either to the nature of the application or to frictional heat generated by high speed movement of the metal parts or the abrading material, prevail.

---

[1]The figures appearing in parentheses pertain to the references appended to this paper.

Laboratory Abrasion Testing Devices

The literature abounds with descriptions of devices which have been used for simulating and testing resistance to both metal-to-metal wear and abrasive wear. An extensive bibliography is appended to the paper by H. W. Gillett (3) in the 1937 ASTM *Symposium on Wear of Metals.* This bibliography refers to both abrasion and ordinary wear testing devices. For the purpose of this paper, only the abrasion testing devices are of interest.

Abrasion testing devices which have been used may be classified into five major categories as follows:

1. Fixed abrasive
2. Sand-blast
3. Ball mill
4. Abrasive lap
5. Rotating wheel

1. Typical of the first class are endless belt grinders and grinding wheels. The principal disadvantages of the fixed abrasive testers are that (a) grinding takes place at a uniform rate with no recognition of heterogeneity of the structure which, in loose abrasive applications, may result in undercutting of hard constituents in relatively soft matrices, and (b) the methods lack versatility since abrasive types and grits are limited to those available in bonded form.

2. The sand-blast test, according to Rosenberg (4), does not differentiate between many materials which are known to have widely different "wear-resisting" characteristics. The air pressure in this type of test was found to be very critical. Therefore, variations in line pressure and wear of the blast nozzle exercise a notable effect on the results obtained. With a 30-pound air-blast pressure no difference was noted between a chromium-molybdenum steel, 12% manganese steel, and white iron. Similar tests made with a 60-pound air-blast pressure again showed no difference between the steels but the white iron showed a decidedly higher loss of weight.

3. The laboratory ball mill test has been utilized by numerous investigators. Ellis (5) tested balls of various alloy and carbon contents with several abrasive materials including talc, marble, feldspar, granite, sand, silica, and silicon carbide. The results showed, with the exception of the sand tests, that the abrasion resistance of iron alloys decreased as the carbon content was increased, i.e., plain white iron and 2.5, 7.5, and 15% chromium iron balls all showed a greater

weight loss than steel balls of the same base alloy composition. The superiority of forged steel balls over cast white iron has been confirmed by Norman and Loeb (6) in full-size ball mill tests.

4. The abrasive lap type of tester has been used by Blake (2) and Weiss (7). Their devices are similar and consist essentially of specimens loaded against a circular track rotating in an abrasive slurry. In the device used by Blake the test specimens revolve around a copper lap at a speed of about 119 feet per minute for a total distance of 1.35 miles.

In his monograph on abrasion, Avery (8) lists a large number of values obtained with the device described by Blake. The principal comment on the data is the relatively small difference among some of the materials tested. For example, white iron and SAE 1020 steel are reported to have approximately the same degree of abrasion resistance.

In the device used by Weiss, a rotating gray iron ring carries the abrasive under two stationary, lightly loaded specimens. Weiss used Crystolon (silicon carbide) for his abrasive. The use of silicon carbide produces a vastly accelerated test but the results cannot always be used with complete assurance for applications involving less abrasive materials.

5. The fifth classification of abrasion testing device (rotating wheel) is represented by the Brinell abrasion testing machine (9) which consists of a specimen clamped in a holder against which a disk of open-hearth iron approximately 4 inches in diameter by $\frac{1}{16}$ inch thick is rotated. Sand from a hopper above the device is fed continuously between the specimen and the disk. The disk is rotated at a speed of 45 revolutions per minute (approximately 45 feet per minute) for a predetermined distance, after which the motor is stopped automatically.

Tests made to evaluate the effect of increasing distances of disk travel showed a smaller increase in loss of weight due to the decreasing average pressure per unit of area as the tests progressed. The relative values between good and poor abrasion-resistant materials were, therefore, somewhat affected by the nonuniform decreasing unit pressure between the specimen and disk as the specimens wore. All test runs were made at a pressure of approximately 22 pounds and 200 feet travel of the surface of the disk. Results were reported in terms of depth of the worn groove and by weight loss.

The weight loss of carbon steels was found to decrease propor-

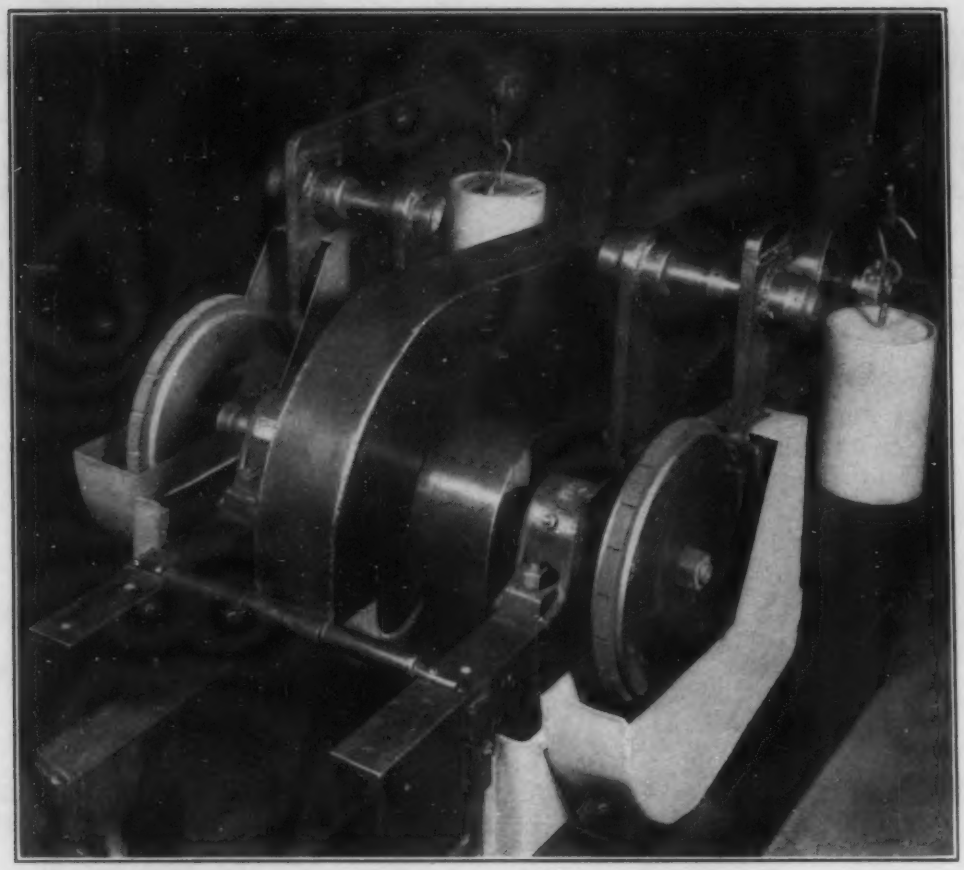


Fig. 1—Abrasion Testing Machine Used in the Investigation.

tionally with increasing hardness; i.e., fully-hardened steels were found to be more abrasion-resistant than the same steels in the annealed condition. A series of plain carbon steels quenched to maximum hardness showed no appreciable change in wear resistance between 0.40 and 1.30% carbon.

Development of a New Abrasion Testing Device

The occasion for developing a laboratory abrasion tester arose during work on liners for the reciprocating pumps used in pumping mud in oil well drilling operations. No apparatus felt to be entirely satisfactory for the purpose had been described in the literature, although the Brinell abrasion machine appeared to approach the required type of abrading action and to have merit both as to simplicity of design and operation.

After several design changes, a considerably modified version

of the Brinell machine was evolved. A photograph of this device is shown in Fig. 1, accompanied by a schematic diagram in Fig. 2. Because the pistons in slush pumps are made of rubber to maintain pressure as the liner wears, the wheel in the machine was made of rubber. The wheel was made thicker and larger in diameter (approximately ½ by 9 inches) than in the Brinell machine. The wheel is notched to help in carrying the abrasive uniformly against the speci-

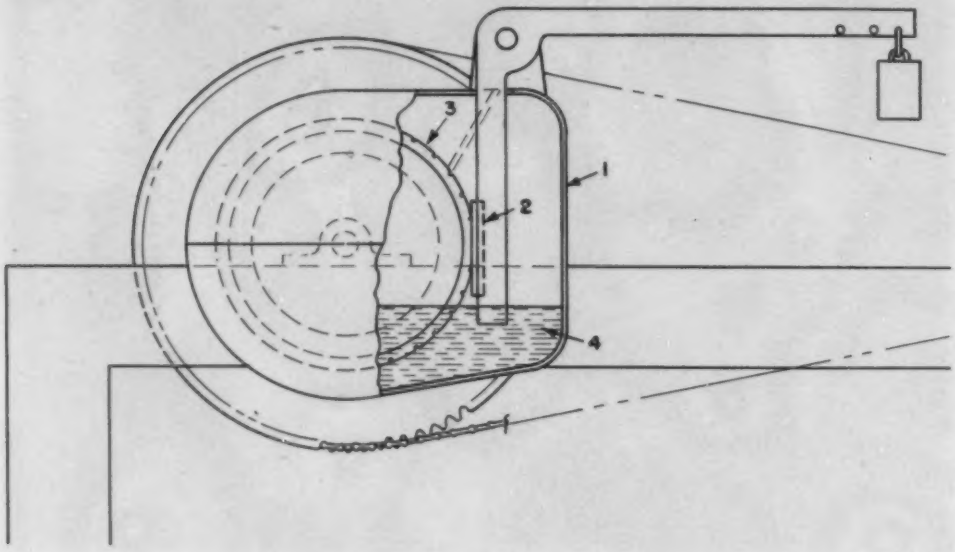


Fig. 2—Schematic Diagram of Abrasion Testing Machine Shown in Fig. 1. Tray —1, specimen—2, abrasive carrying wheel—3, abrasive material—4.

men. The abrasive is placed in a tray beneath the wheel where it is picked up by the wheel. The specimen is held against the periphery of the wheel by means of a weight on the opposite end of the pivoted arm which holds the specimen. The standard specimen size is 3 inches long by 1 inch wide by ½ inch thick.

A high speed photograph of the machine in action with an abrasive slurry and with the retaining cover of the tray removed is shown in Fig. 3. After results obtained with the machine were found to correlate with service data, the machine was applied to other problems involving abrasion. It was found that dry abrasive particles could also be carried by the wheel as illustrated in the high speed photograph in Fig. 4. Correlation with several types of essentially dry abrasive applications, which will be discussed in a later section, was found to be excellent when the tests were properly conducted to simulate the field conditions as nearly as possible.

The device must be used with the abrasive either dry or in

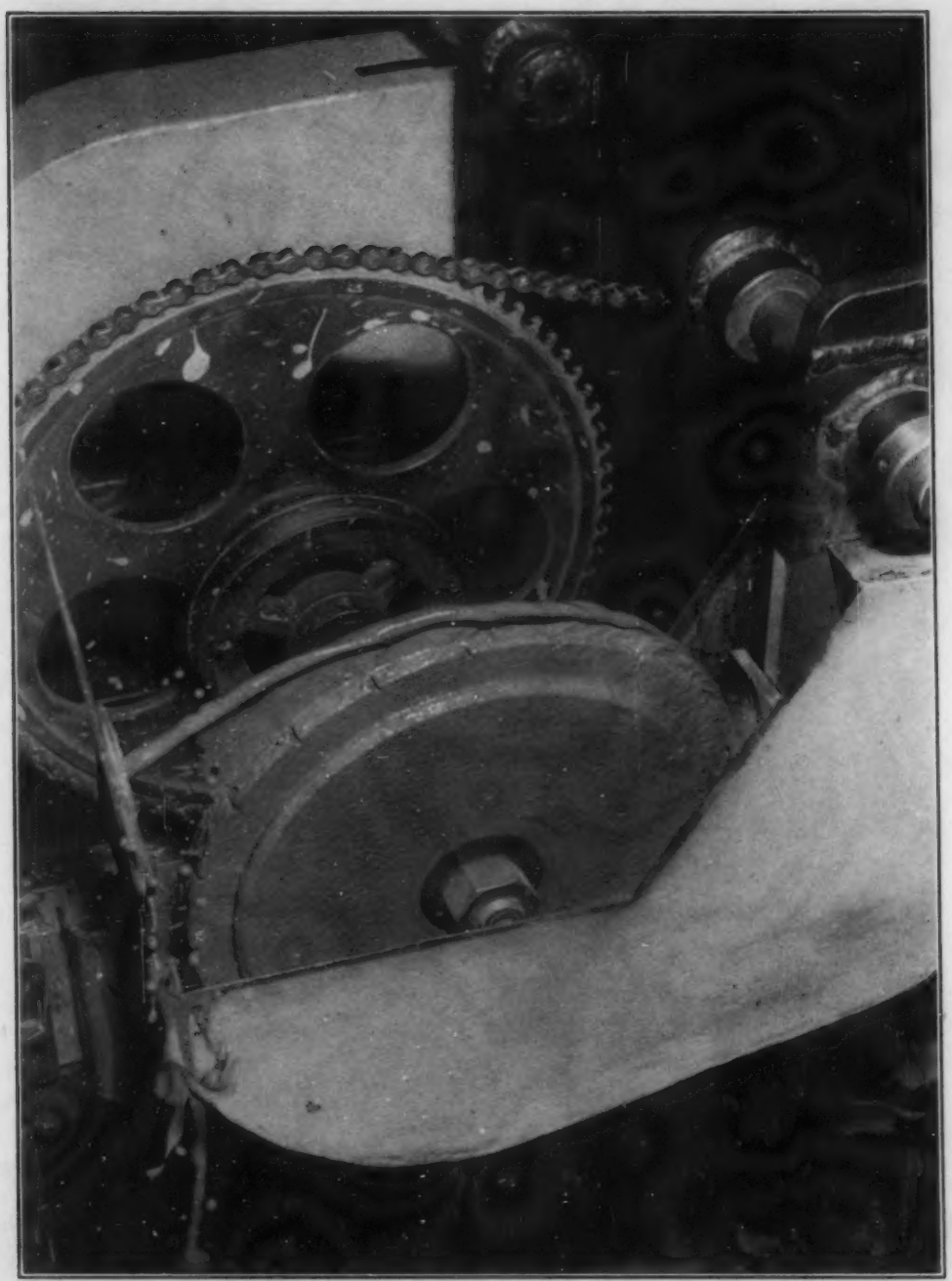


Fig. 3—High Speed Photograph (1/10,000 Sec.) of Abrasion Machine With Retaining Cover Removed Showing Action With a Wet Abrasive Slurry.

slurry form. The wheel will not pick up and carry an intermediate moisture content. However, for almost all types of abrasive service, data from slurry or dry tests or both will probably suffice. The test further does not provide for the effect of impact; but for appli-



Fig. 4—High Speed Photograph (1/10,000 Sec.) of Abrasion Machine Running With Dry Crushed Quartz.

cations involving only light or sporadic impact, the abrasion tests coupled with independent repeated impact tests may be used to

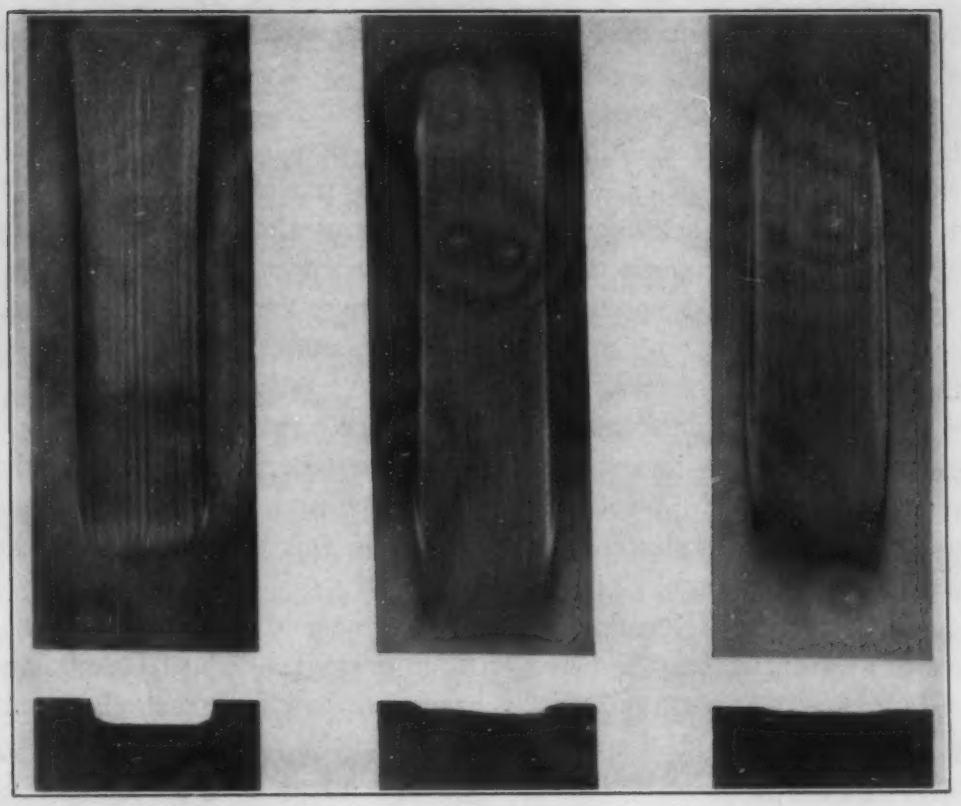


Fig. 5—Typical Abrasive Wear Patterns on Hardened SAE 1045 Steel Obtained in Dry Tests With 28/35 Mesh Crushed Quartz, Crushed Feldspar, and Crude Ottawa Sand From Left to Right. The dark appearance around the grooves is due to temper colors produced in testing.

specify the material with the optimum combination of resistance to both abrasion and impact.

Wheel Material, Pressure, and Speed

The use of a rubber wheel was found to have a number of advantages over the steel wheel used by Brinell. During the progress of a test made with a steel wheel, the area of contact between wheel and specimen gradually increases and the unit pressure correspondingly decreases. With a rubber wheel, on the other hand, due to the resiliency of the rubber, the initial length of the contact area between the specimen and wheel is approximately 2 inches and increases only slightly as a groove is worn in the specimen during the test. The unit pressure on the specimen, therefore, is relatively constant throughout the test, whether the wear pattern is shallow or deep. Typical abrasive wear patterns obtained on hardened SAE 1045 steel

with dry crushed quartz, crushed feldspar, and crude Ottawa sand are shown in Fig. 5.

Perhaps the greatest benefit of the rubber wheel is the lack of high pressure on the individual abrasive particles, again due to the resiliency of the rubber, which permits the particles to imbed in the wheel. When a steel wheel is used with sand, the latter is pulverized as it is carried between the wheel and the specimen. Thus, with a steel wheel the test conditions would change constantly throughout a test, whereas in rubber wheel tests no noticeable breakdown of the sand particles occurs.

The lack of concentrated high pressure on the abrasive particles in the laboratory device produces accurate correlation with many types of abrasive applications where only mild pressure or impact is involved. The simplest illustration of this type of application would be that of sand sliding down a chute.

In order to determine the effect of several variable factors, a series of tests was made using various pressures, wheel speeds, and distances of wheel travel. Fully hardened (water-quenched, untempered) SAE 1045 steel specimens, all from the same heat, were used for these tests. The hardness of the specimens ranged from Rockwell C-59 to C-62.

Table I
Effect of Pressure, Speed, and Test Duration on Abrasive Wear of Hardened SAE 1045 Steel

Hardness 59/62 Rockwell "C"; Abrasive: Dry Crushed Quartz—28/35 Mesh

No.	Wheel Speed rpm	Load on Lever Arm pounds	Distance of Wheel Travel feet	Weight Loss (grams × 10)
1	250	40	2000	67
2	250	40	4000	130
3	250	20	4000	53
4	1035	20	4000	120

The weight loss values shown in Table I are the actual weight losses in grams multiplied by ten. The results are reported in this manner in order to obtain whole numbers for the more abrasion-resistant materials.

The surface speed of the wheel at the lower speed was approximately 600 feet per minute; that at the higher speed, 2450 feet per minute. The approximate load on the test specimen projected over the average wear pattern is approximately 40 psi with the 20-pound load on the lever arm and approximately 60 psi with the 40-pound

load. The area of contact between wheel and specimen is less at the lighter load than at the heavier load. Tests were not made using the 40-pound load on the lever arm at the higher speed (1035 rpm) because of rapid deterioration of the rubber wheel.

The first two values in Table I show almost exact proportionality between weight loss and distance of wheel travel (i.e., duration of test). The third and fourth values, determined at constant load and test duration but at two different speeds, show somewhat more than twice as much weight loss at the higher speed as at the lower speed. The ratio of the speeds is approximately four to one.

Comparison of the second and third values shows a weight loss with the heavier load which is approximately 2½ times the weight loss where the lighter load is used. The disproportionately greater weight loss at the heavier load may be due to the greater area of contact or to the higher temperature developed, or both.

A wheel speed of 250 rpm, a load of 40 pounds, and a distance of 4000 feet were selected as standard test conditions. Under these conditions, the test requires approximately 7 minutes. It is found necessary to vary these test conditions from time to time to obtain more accurate correlation with known field data or to obtain more sensitive distinction among better materials by running longer test distances.

Dry Versus Wet Abrasion

A pronounced aberration in the expected behavior of hardened carbon steels has been observed consistently in dry quartz and sand abrasion tests. Greater weight losses are obtained than in similar steels in the annealed or hot-rolled conditions. In wet abrasion tests, the expected superiority of hardened steels over the softer steels is obtained. Typical comparative values under dry and wet test conditions are shown in Table II.

Table II
Comparison of Dry and Wet Abrasion Tests

28/35 mesh; 250 rpm; 40-lb. load; 4000 feet

Abrasive	Condition of Test	Weight Loss (Grams × 10) Water-Quenched SAE 1045 Steel (Rockwell C 59/62)	Weight Loss (Grams × 10) Hot-Rolled SAE 1020 Steel (Brinell Hardness 131)
Quartz	Dry	131	69
Quartz	Wet	41	60
Ottawa Sand	Dry	21	17
Ottawa Sand	Wet	7	11

A tentative explanation for the dry abrasion superiority of the hot-rolled SAE 1020 steel over that of the water-quenched SAE 1045 steel is that the surface hardness of the hardened steel at the temperature developed during testing may be actually less than that of the hot-rolled material.

This marked indicated inferiority of hardened steels under dry abrasion conditions has not been completely demonstrated in actual service. However, hardened carbon steel Sandslinger liners in actual service showed approximately equivalent life to hot-rolled liners. The reason for the difference between the laboratory and service results may be because the sand used in the foundry contains some moisture which, together with the larger surface area of the liner, probably prevents the liners from reaching the temperature attained by the specimens in the completely dry laboratory abrasion tests.

Temperature Developed in Dry Abrasion Tests

Sufficient heat is generated during the dry sand abrasion tests to produce blue-black temper colors on carbon steel specimens. Attempts were made to measure the temperatures developed by means of a thermocouple spot-welded to the bottom of a groove machined on the back of the specimen. The grooves extended approximately halfway through ¼-inch thick test specimens.

Tests were made at speeds of 250 and 985 rpm using crushed 28/35 mesh Wausau quartzite. Tests were made at 250 rpm with loads of 20 and 40 pounds. A single test was made at 985 rpm with a 20-pound load.

The tests were continued until the specimens were either worn through to the thermocouples or for an excessive period without wearing through to the groove. The test at 250 rpm with a 40-pound load developed a maximum temperature of 620 °F compared to a maximum temperature of 863 °F in the higher speed test. Actual surface temperatures are probably considerably higher than those which were registered by the thermocouples.

Comparative temperature curves are shown in Fig. 6. The data for each condition are not strictly comparable, since all of the specimens were slotted to the same depth. Therefore, the distance from the wearing surface to the thermocouple diminished faster in the high speed test than in the lower speed tests, and faster at the heavier load than at the lighter load in the lower speed tests. However, the

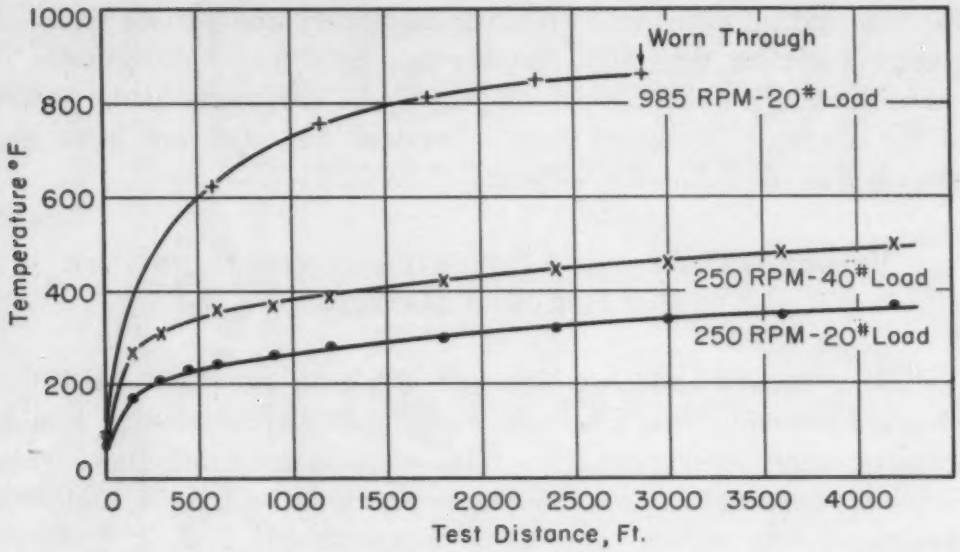


Fig. 6—Temperatures Developed in Dry Crushed Quartz Abrasion Tests.

data show that a considerable temperature is reached, particularly in the higher speed test, which is an aid in explaining some of the observed abrasion results.

Effect of Particle Size

The maximum size of particles which can be used in the device is limited to about ⅛ inch. Early tests showed considerable variation in weight loss of duplicate specimens. This was traced to variable particle size distribution in the abrasive material. Finer particle sizes, particularly of crushed quartz, present a greater multiplicity of cutting edges for an equal volume of abrasive and, therefore, cause more rapid wear than larger particles. Subsequent tests were made with close control over the abrasive particle size. A range of 28/35 mesh was selected as standard.

Abrasion Test Data

Abrasion tests have been run with the test apparatus on a large number of samples of various materials ranging from carbon and alloy steels through highly alloyed cast irons and tungsten carbide inserts. The tests normally are run in duplicate unless the weight loss values do not check within 10%, in which case additional tests are run. This degree of reproducibility has been found to be satisfactory

for practical purposes in correlating laboratory and service data. A greater variation than 10% usually has been found attributable to nonuniformity of the sample, or possibly to variations in the nature of the abrasive. Selected data on various materials are listed and described in the following sections.

Effect of Carbon and Chromium Content and Type of Abrading Material

Since carbon and chromium are the most prevalent hardening elements in commercial cast and wrought alloys intended to combat abrasive wear, their respective roles were investigated thoroughly. Series of steels and irons containing approximately 2, 6, 14, and 30% chromium, with carbon contents of approximately 1, 2, 3, and 4%, were cast into standard abrasion test specimens. The four chromium series have been designated, respectively, AA, BB, CC, and DD. Sufficient specimens were cast and tested to investigate the effect of the following variables.

1. Comparison of dry and wet quartz abrasion.
2. Effect of heat treatment (specimens were compared as cast and hardened).
3. Effect of angularity of grain (crushed quartz vs. sand).
4. Effect of type of abrasive (feldspar vs. quartz vs. alumina).

The test data are shown in Table III including chemical analyses and average weight loss values of two or more tests. The weight loss values again are the actual weight losses in grams multiplied by ten. The results under 100 are reported to the first decimal point. The results obtained under any particular test condition can be expressed as a ratio to a standard or known material by dividing the weight loss of the standard by the weight loss of the sample.

The material referred to as quartz in Table III is a high grade crushed quartzite from Wausau, Wisconsin. In the interests of brevity, however, it will be referred to simply as quartz in subsequent discussion. The feldspar used in the tests was glassmaker's grade of potash (orthoclase) feldspar from North Carolina. The alumina used was a synthetic product produced by the Carborundum Company and marketed under the trade name "Blastite". The sand used was crude Ottawa sand from Ottawa, Illinois.

Under the conditions of the tests, the carbon content of the

Table III
Average Weight Loss of Cast Iron-Chromium Alloys

Particle size—28/35 mesh; Test distance—4000 feet; Weight loss values = grams × 10

Symbol	Treatment	Chemical Analysis C	Si	Mn	Cr	Hardness Rockwell "C"	Abrasive—Wheel Speed (rpm) and Load: Dry Quartz 250/40 #	Wet Quartz 250/40 #	Dry Quartz 1035—20 #	Dry Ottawa Sand 250—40 #	Dry Feldspar 250—40 #	Dry Alumina 250—40 #
SAE 1020	Hot-rolled	0.20	....	....	....	BHN 131	67.4	60.4	52.3	16.9	48.0	90.0
AA1	As-cast	0.89	....	....	1.98	35/42	77.7	42.1	80.0	9.1	34.5	....
AA1	1500° OQ*—300° D†	....	....	....	....	56/60	110	40.0	106	....	32.8	....
AA2	As-cast	1.67	0.66	0.98	1.95	43/47	81.8	40.1	67.7	8.5	14.1	96.0
AA2	1500° OQ—300° D	....	....	....	....	57/62	90.1	25.2	83.5	11.8	16.3	86.0
AA3	As-cast	2.82	0.52	....	1.18	47/51	15.4	6.1	14.9	3.6	3.9	89.2
AA3	1500° OQ—300° D	....	....	....	....	53/58	14.7	6.8	15.6	3.2	6.4	62.0
AA4	As-cast	3.87	0.73	....	1.05	53/57	9.0	4.0	9.4	2.4	3.4	87.3
AA4	1500° OQ—300° D	....	....	....	....	57/61	9.0	4.9	8.8	2.1	5.0	53.4
BB1	As-cast	0.78	....	0.82	6.59	53/58	180	84.3	112	26.6	39.4	134
BB1	1800° OQ—300° D	....	....	....	....	58/63	180	67.9	....	21.3	....	....
BB2	As-cast	1.80	0.30	0.72	6.29	47/52	107	54.2	81.5	12.0	18.2	103
BB2	1800° OQ—300° D	....	....	....	....	59/64	103	23.7	....	11.5	....	....
BB3	As-cast	3.03	0.64	....	7.19	53/58	15.0	7.4	14.4	3.0	2.3	81.0
BB3	1800° OQ—300° D	....	....	....	....	65/69	11.8	4.1	....	3.1	....	....
BB4	As-cast	4.13	0.78	....	6.59	54/59	9.0	6.6	11.1	3.2	3.4	81.0
BB4	1800° OQ—300° D	....	....	....	....	61/67	9.4	5.3	....	3.1	....	....
CC1	As-cast	1.21	....	0.56	14.10	28/34	106	65.5	78.5	13.8	28.2	85.3
CC1	1800° OQ—300° D	....	....	....	....	57/62	145	47.6	91.2	12.6	27.4	....
CC2	As-cast	1.91	0.43	0.66	14.20	43/47	69.4	30.9	44.4	7.3	10.2	89.7
CC2	1800° OQ—300° D	....	....	....	....	63/67	66.9	16.5	37.5	6.8	6.5	97.8
CC3	As-cast	3.19	0.90	....	14.50	53/57	18.7	15.0	10.6	3.8	3.7	57.7
CC3	1800° OQ—300° D	....	....	....	....	66/70	4.7	2.4	4.6	2.0	1.6	86.8
CC4	As-cast	3.85	0.88	....	13.40	54/58	9.4	11.2	5.6	2.9	2.7	48.7
CC4	1800° OQ—300° D	....	....	....	....	65/69	3.3	1.8	3.8	1.5	1.5	47.4
DD1	As-cast	1.25	0.46	0.58	30.10	18/23	66.0	44.9	75.6	7.3	19.1	74.5
DD1	1800° OQ—300° D	....	....	....	....	26/29	78.1	48.5	....	....	....	....
DD2	As-cast	1.96	0.94	0.68	25.25	44/48	66.7	20.3	25.6	5.5	6.9	97.3
DD2	1800° OQ—300° D	....	....	....	....	56/60	74.6	12.8	....	....	....	....
DD3	As-cast	2.85	0.93	....	31.60	56/60	25.9	9.8	16.5	3.9	4.9	73.4
DD3	1800° OQ—300° D	....	....	....	....	61/63	19.4	6.0	....	....	....	....
DD4	As-cast	3.76	1.13	....	31.20	56/60	1.9	3.3	3.7	1.2	0.9	38.1
DD4	1800° OQ—300° D	....	....	....	....	63/65	1.6	2.1	....	....	....	....

*—OQ = oil quench. †—D = draw.

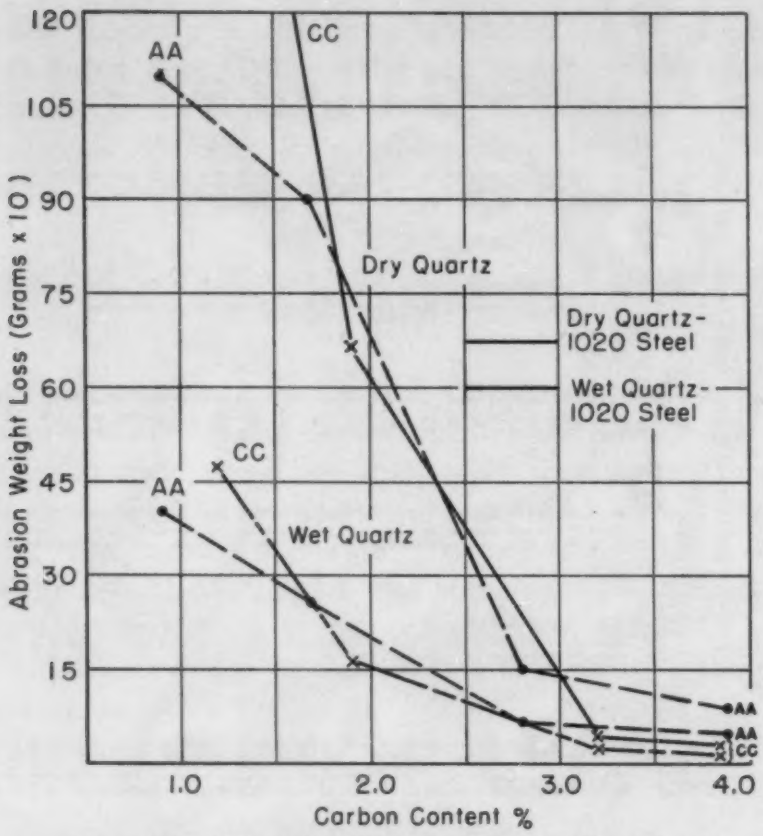


Fig. 7—Effect of Carbon Content on Dry and Wet Abrasion Weight Loss Values of Heat Treated Cast Specimens. AA series contains 1 to 2% Cr; CC series, 14 to 15% Cr.

materials tested is by far the most important factor. For similar carbon content materials, the presence of chromium by itself in the as-cast specimens is of no apparent benefit. In the hardened condition, the lower carbon content materials (up to 2%) showed improvement only in the wet quartz abrasion results; in the dry tests, the hardened specimens showed no appreciable improvement or were even inferior to the same specimens in the softer, as-cast condition. The 3 and 4% carbon test specimens of the 14% chromium alloy showed a decided improvement in the heat treated condition over the corresponding as-cast specimens under both dry and wet abrasive conditions. Both the lower and higher chromium content alloys showed less pronounced improvement in this carbon range as a result of heat treatment.

The effect of carbon content on the abrasion resistance of the AA and CC series in the heat treated condition under both dry and wet quartz abrasion is shown graphically in Fig. 7. For comparison,

the weight loss of hot-rolled SAE 1020 steel is shown by a horizontal line. Under wet quartz abrasion, all of the specimens of the AA and CC series showed less weight loss and hence superior abrasion resistance to the SAE 1020 steel. In the dry quartz abrasion tests, the weight loss line for the 1020 steel intersects the AA and CC lines at approximately 2% carbon. This indicates that carbon contents of more than 2% are required in cast straight chromium alloys to produce dry crushed quartz abrasion resistance superior to that of hot-rolled SAE 1020 steel. It should be borne in mind that these are cast materials; somewhat different properties might be obtained in wrought materials because of greater homogeneity of structure.

Angularity of grain is a potent factor in the abrasiveness of the abrading material. Within limits, angularity appears to be more important than the hardness of the abrading material. For example, the weight loss factors obtained with feldspar, which is softer than quartz, were greater than the respective values obtained with Ottawa sand, which is essentially quartz in rounded granular form. The alumina used was not only angular but also considerably harder than quartz. The alumina values, therefore, showed much less spread between good and poor materials than the results of the other abrading materials. None of the alloys tested were particularly resistant to alumina abrasion. Photographs of grains of feldspar, quartz, and Ottawa sand used in the investigation taken at a magnification of $\times 25$ are shown in Figs. 8a, 8b, and 8c, respectively. In earth moving, mining operations, and the handling of certain types of sands, quartz grains with angularity approaching that of the crushed quartz in Fig. 8b are frequently encountered. The crushed quartz abrasion results, therefore, are of considerable interest.

The influence of angularity becomes much less pronounced as the abrasion resistance of the metal increases. The higher carbon content alloys, for example, show much less spread between the crushed quartz and crude Ottawa sand values than did the lower carbon content materials.

Some of the preceding statements on the effect of various abrasive materials in dry tests are shown graphically for the AA series in the as-cast condition in Fig. 9. As partially illustrated in Fig. 7, the results on this series for similar carbon contents do not differ markedly from those of the other series. For comparison, the weight loss values for similar dry abrasion tests conducted on hot-rolled SAE 1020 steel are shown by horizontal lines. The best alumina

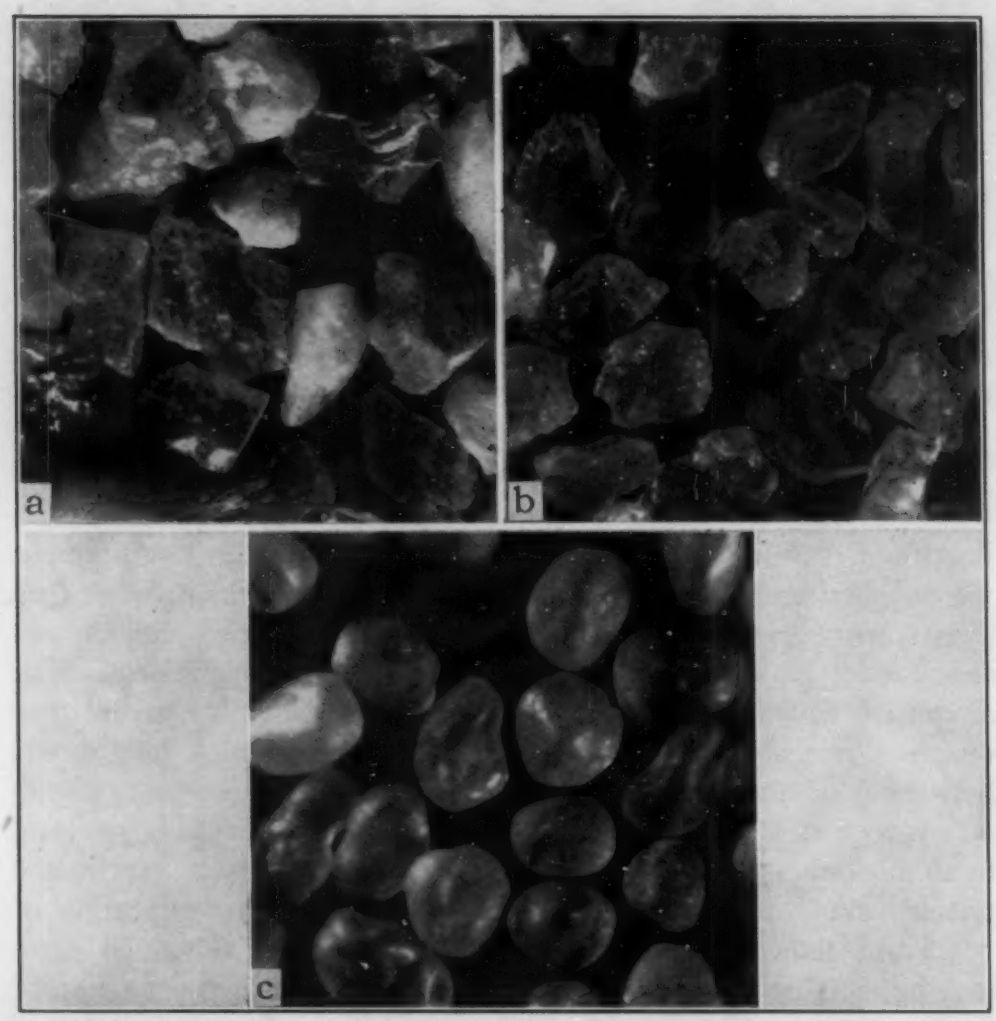


Fig. 8—Enlarged 28/35 Mesh Grains of Crushed Feldspar, Crushed Quartzite and Crude Ottawa Sand. × 25. a—Feldspar. b—Crushed quartzite. c—Crude Ottawa sand.

abrasion results are scarcely better than that of the SAE 1020 steel. The feldspar and Ottawa sand values of the AA alloys are all superior to the respective values obtained on the SAE 1020 steel, whereas the crushed quartz line of 1020 crosses the AA series line at approximately 2% carbon.

The weight loss difference between the dry quartz tests at the two speeds investigated (250 and 1035 rpm) was more pronounced in the lower carbon alloys than in the 3 and 4% carbon alloys. The higher speed values generally showed less weight loss because of the lighter test load used. At the higher chromium contents the disparity between the results at the two speeds increased. Some differ-

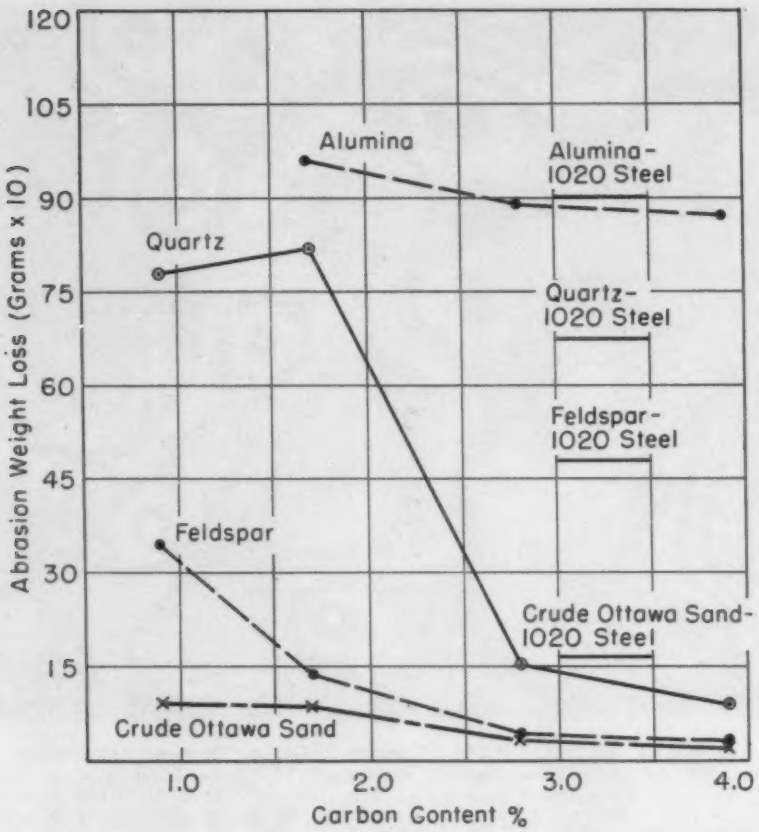


Fig. 9—Effect of Several Abrasive Materials on Dry Abrasion Weight Loss Values of As-Cast AA Series (1 to 2% Cr). Particle size 28/35 mesh.

ence in the order of results was also obtained. For example, alloy CC3 in the as-cast condition was inferior to BB3 at the lower speed but superior at the higher speed.

It is interesting to note that the dry quartz weight loss values of alloys CC4 and DD4 in the as-cast condition are less than those of the corresponding wet quartz values. The reason for these reversals is not clear.

Microstructure and Microhardness

Representative microstructures of the alloys listed in Table III are shown in Figs. 10 to 13. The photomicrographs together with the accompanying Knoop microhardness values partly aid in explaining the observed abrasion results. Only the hardness values of the microconstituents of sufficient size to be tested with a 100-gram load on the indenter are reported. This procedure is in conformity with

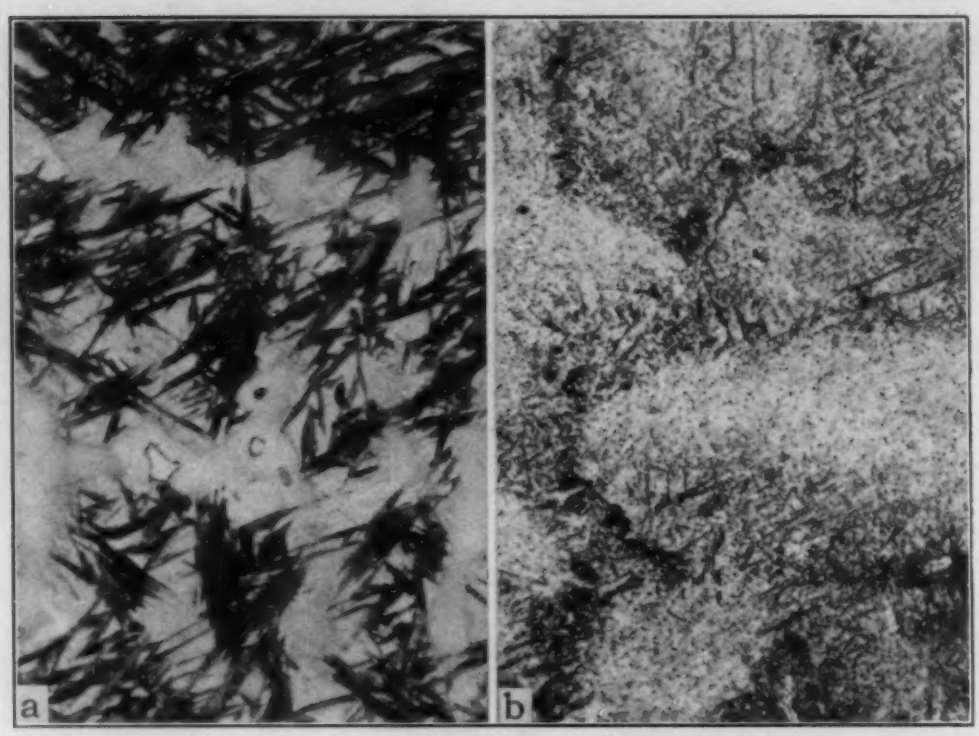


Fig. 10a—BB2 As-Cast. × 500. Etchant—Vilella's Reagent. Structure—cored austenite dendrites partially decomposed to martensite. Microhardness of dark etching cores —K_{100}—569; light envelopes—K_{100}—516. Fig. 10b—BB2—1800 °F Oil Quench, 300 °F Temper. × 500. Etchant—Vilella's Reagent. Structure—principally fine martensite. Microhardness—K_{100}—575.

the findings of Thibault and Nyquist (10) that loads of less than 100 grams produce values inconsistent with those obtained at 100-gram or heavier loads. The microhardness values and the corresponding dry and wet quartz abrasion factors are shown in Table IV.

Table IV
Selected Knoop Microhardness Values—100-Gram Load

Fig. No.	Symbol	Treatment	Average K100 Hardness: Other Structure	Average K100 Hardness: Carbide	Rockwell "C" Hardness	Quartz Weight Loss Values (Grams × 10): Dry	Quartz Weight Loss Values (Grams × 10): Wet
10a	BB2	As-cast	569 (dark) 516 (light)	...	47/52	107	54.2
10b	BB2	1800° OQ	575	...	58/64	103	23.7
11a	CC2	As-cast	390	...	43/47	69.4	30.9
11b	CC2	1800° OQ	588	...	62/66	66.9	16.5
12a	BB3	As-cast	510	810	52/57	15.0	7.4
12b	BB3	1800° OQ	770	980	65/68	11.8	4.1
13a	CC3	As-cast	520	900	53/56	18.7	15.6
13b	CC3	1800° OQ	760	1060	66/70	4.7	2.4

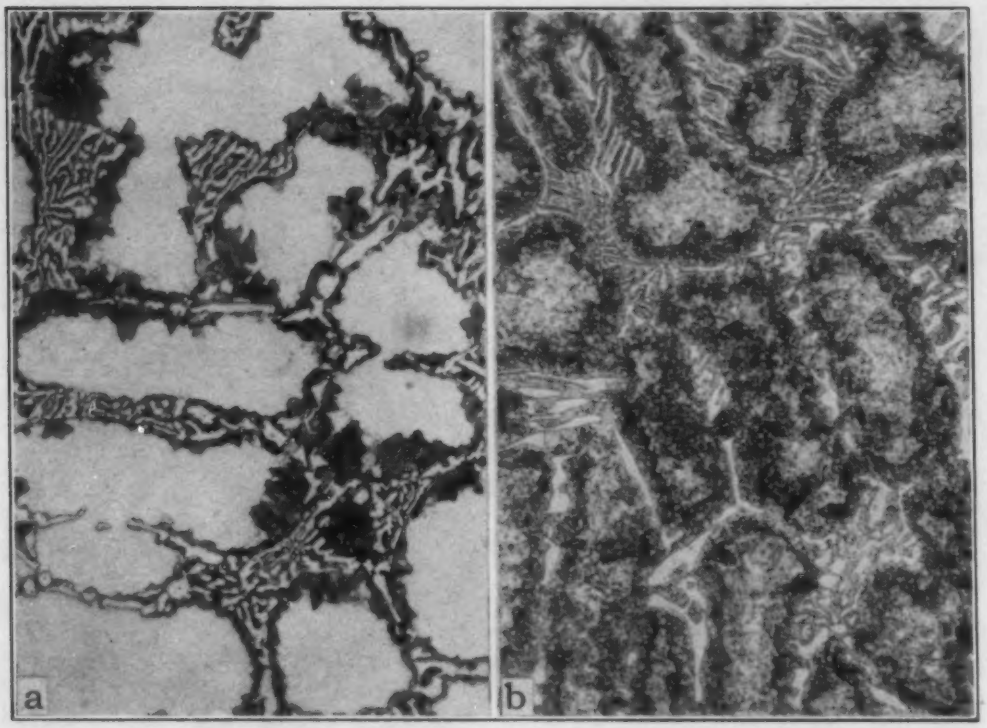


Fig. 11a—CC2 As-Cast. × 500. Etchant—Vilella's Reagent. Structure—austenite dendrites, eutectic regions of carbide and pearlite. Microhardness: Austenite—K_{100}—390. Fig. 11b—CC2—1800 °F Oil Quench, 300 °F Temper. × 500. Etchant—Vilella's Reagent. Microhardness of dendrite cores—K_{100}—588.

The approximate average Knoop hardness value (100-gram load) of quartz, according to Thibault and Nyquist, is 820; that of aluminum oxide, 2000. A value of 560 for orthoclase feldspar was reported by Lysaght (11). Metals consisting predominately of microconstituents with hardness values less than that of the abrading material will wear rapidly; materials with predominating microconstituents harder than the abrasive will resist abrasion more effectively. Since aluminum oxide is considerably harder than any of the microconstituents shown in Table IV, rapid wear with this abrading material results on all of the alloys shown in Table III including those which have excellent resistance to quartz abrasion.

The microstructure of the 1.80% carbon, 6.29% chromium alloy (BB2) is shown in Figs. 10a and 10b in the as-cast and heat treated conditions, respectively. For comparison, the similar carbon (1.91%) alloy containing 14.20% chromium (CC2) is shown in Figs. 11a and 11b, respectively. The quartz abrasion resistance of the higher chromium alloy is somewhat better than that of the lower chromium alloy, but neither is outstanding compared to the higher carbon alloys

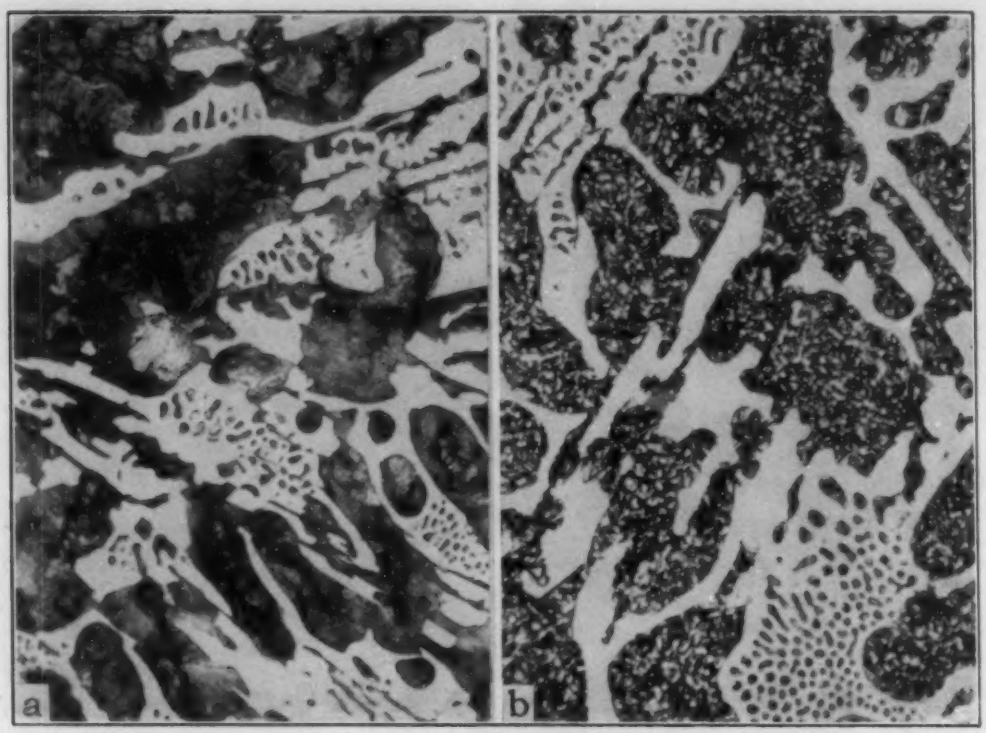


Fig. 12a—BB3 As-Cast. × 500. Etchant—Vilella's Reagent. Structure—primary carbides, eutectic, and pearlite. Microhardness: Carbide—K_{100}—810; Pearlite—510. Fig. 12b—BB3—1800 °F Oil Quench, 300 °F Temper. × 500. Etchant—Vilella's Reagent. Structure—primary carbides, eutectic and austenite-martensite. Microhardness: Carbide—K_{100}—980; Austenite-martensite—770.

shown in Table III. Heat treatment produces no improvement in the dry abrasion tests but a pronounced improvement in the wet quartz tests of both alloys. The Knoop hardness values of the predominating constituents in both alloys are considerably less than that of quartz.

The microstructures of the 3.03% carbon, 7.19% chromium iron (BB3) in the as-cast and heat treated conditions are shown, respectively, in Figs. 12a and 12b. The corresponding microstructures of the 3.19% carbon, 14.50% chromium iron (CC3) are shown in Figs. 13a and 13b, respectively. In the heat treated specimens, the background structures were identified by higher power examination than that used in taking the photomicrographs. In the as-cast condition the quartz abrasion resistance of the higher chromium alloy is less than that of the lower chromium alloy. Heat treatment produces pronounced improvement and a superior material in the higher chromium alloy but somewhat less improvement in the lower chromium alloy. The heat treated counterparts of the pearlitic regions (which

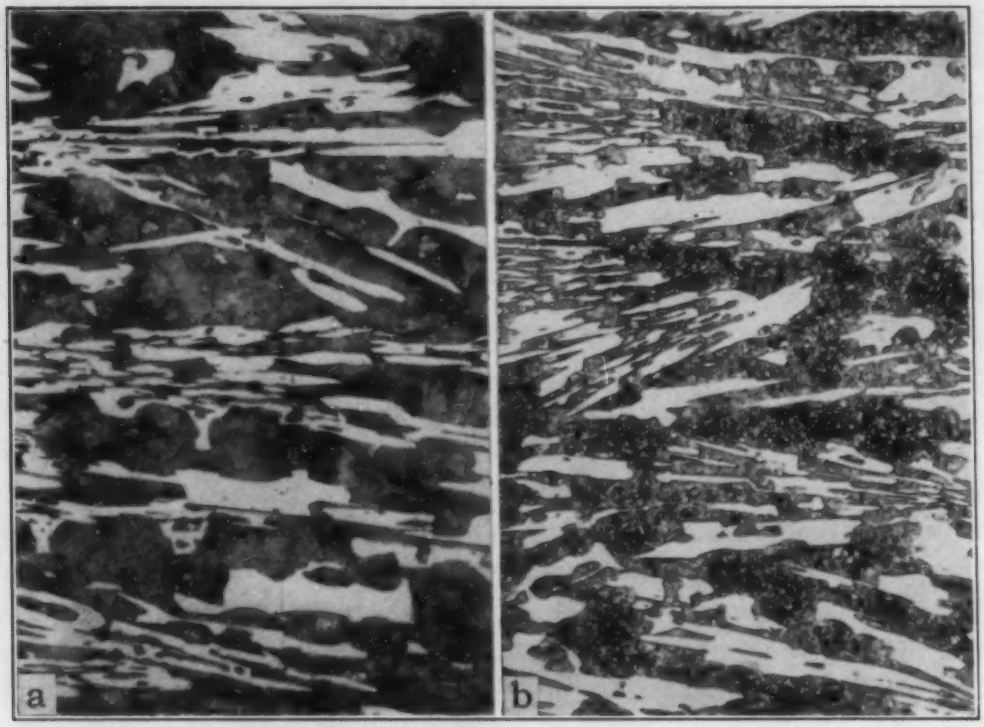


Fig. 13a—CC3 As-Cast. × 500. Etchant—Vilella's Reagent. Structure—primary carbides and fine pearlite. Microhardness: Carbide—K_{100}—900; Pearlite—K_{100}—520. Fig. 13b—CC3—1800 °F Oil Quench, 300 °F Temper. × 500. Etchant—Vilella's Reagent. Structure—primary carbides and austenite-martensite. Microhardness: Carbide—K_{100}—1060; Austenite-martensite—K_{100}—760.

are referred to as matrix for simplicity) and the carbides show an increase in hardness as a result of the heat treatment. However, since the respective carbide and matrix hardness values of the two alloys are nearly identical in the heat treated condition, the relatively greater improvement of the higher chromium alloy as a result of heat treatment cannot be explained on the basis of the microhardness values.

In the heat treated condition, the matrix hardness values of both alloy BB3 and CC3 are slightly less than that of quartz, whereas the carbide hardness is appreciably higher. Since the alloys contain a large proportion of primary carbides and have a high matrix hardness, the resistance to quartz abrasion is good.

The increase in carbide hardness of alloys BB3 and CC3 as a result of heat treatment is probably due to attainment of a state of equilibrium between the alloying elements in the carbide and matrix phases. J. B. Austin in his 1946 Campbell Memorial Lecture (12) reported that the alloy contents of the carbides in cast alloys con-

taining chromium and molybdenum increase sharply as the materials are reheated to progressively higher temperatures. Saturation of the carbide with alloy as a result of reheating produces a harder carbide and may even change the carbide form; i.e., in high chromium alloys the carbides may change from orthorhombic cementite, $(Fe,Cr)_3C$, to a trigonal carbide structure, $(Cr,Fe)_7C_3$. The increase in carbide hardness in alloy CC3 as well as a possible change in the carbide structure may account for the superior abrasion resistance of this alloy in the heat treated condition.

In summation, it appears that the problem of abrasion resistance may be resolvable into three parts: (a) the properties contributed by the harder phases; (b) the properties contributed by the softer phases; and (c) the properties dependent upon the physical constitution of the aggregate; that is, the form, size, and distribution of the harder regions in the matrix and their relative volumes. For wet abrasion an important requirement of the harder constituent and the matrix, if possible, is a hardness level equal to or greater than that of the abrading material. For dry abrasion resistance, the hot hardness of the aggregate may be as much or more of a governing factor than the room temperature hardness, and the latter, therefore, may be of limited usefulness in predicting the behavior of materials in this type of service.

Hard Surfacing

Hard surfacing is a useful and economical operation when properly and logically applied for repair work or on original equipment to obtain longer life. The prime consideration in determining whether a part should be repaired or replaced hinges on whether the cost of the resurfaced part spread over the extended service life is greater or less than the cost of the replacement part installed and its corresponding service life.

The cost of the welding rod used may be of only secondary importance, since the prime costs are frequently the labor cost of application and the loss of production time during replacement of the parts. Therefore, expensive surfacing materials, basically intended for service where resistance to heat or corrosion also is required, are often used in straight abrasive applications where a cheaper rod would serve as well or better. The reason for this misuse is that, in the absence of specific data, the erroneous conclusion is reached that higher cost materials will be more effective in service.

The results of abrasion tests made with dry crushed quartz on various commercial hard surfacing compositions are shown in Table V. Specimens for testing were prepared by both arc and gas (oxy-acetylene) deposition. The arc specimens were deposited at normal recommended amperages.

The most interesting observation from the data of Table V is the superiority of gas over arc-deposited hard-surfaced specimens in thicknesses of ⅛ inch or less. This difference has been substantiated in field tests on Sandslinger tips and Speedmullor plows. The effect is believed to be due to dilution with the base metal because of

Table V
Dry Quartz Abrasion Tests on Hard Surfaced Specimens

Wheel speed—250 rpm; load—40 lbs.;. particle size—28/35 mesh; distance—4000 feet

No.	Nominal Chemical Analysis C	Si	Mn	Cr	Mo	Ni	W	Welding Procedure	Approximate Deposit Thickness	Hardness Rockwell C	Abrasion Weight Loss (Grams × 10)
SAE 1020	0.20	....	....	....	....	....	.....	hot-rolled	.....	BHN 131	72.0
1	1.0	1.2	2.0	6.0	....	....	.....	arc	0.090	58/62	114
2	[c]1.79	....	....	6.70	0.07	0.15	.....	arc	0.090	27/38	88.3
3	[c]1.35	....	....	6.18	....	....	.....	arc	0.090	51/57	63.1
4	[c]1.96	....	....	5.81	....	....	.....	arc	0.110	66/68	56.9
5	4.00	0.70	0.55	4.75	4.0	....	.....	arc	0.150	58/60	55.5
6	[c]2.50	....	....	1.41	....	....	.....	arc	0.090	42/50	55.0
7	[c]3.09	0.90	0.20	8.0	2.5	....	15.00	arc	0.110	56/60	42.0
8	3.75	0.80	....	7.5	1.75	....	.....	arc	0.150	48/60	32.3
9	[c]5.38	1.9	4.0	32.0	....	....	.....	arc	0.090	59/63	26.2
10	3.75	0.80	....	7.5	1.75	....	.....	gas	0.125	60/62	9.8
11	[c]3.31	0.90	0.20	8.0	2.5	....	15.00	gas	0.090	57/60	5.7
12	[c]5.38	1.9	4.0	32.0	....	....	.....	arc	0.180	57/59	5.8
13	[c]4.98	1.9	4.0	32.0	....	....	.....	gas	0.170	59/63	3.6

c = actual carbon analysis on built-up bead.

the higher temperatures attained in arc welding compared to gas welding. Arc-deposited specimens prepared with heavier deposits showed abrasion resistance comparable to gas-welded deposits. Comparative abrasion results for a high chromium alloy arc-deposited in two thicknesses and gas-deposited may be seen by comparing Nos. 9, 12, and 13, respectively, in Table V. The conclusion from these data is that deposit thicknesses of ⅛ inch or more are required by arc deposition in these compositions in order to achieve full abrasion resistance. Even then the abrasion resistance progressively decreases as the deposit is worn away. Light gas deposits, on the other hand, show equal abrasion resistance to heavy arc and gas deposits.

Because almost all of the deposits of the hard surfacing materials shown in Table V were less than ⅛ inch thick and, therefore,

variably affected by the factor of dilution, no reliable conclusions can be drawn from the data regarding the effect of composition on the abrasion results. In general, however, a trend toward increasing abrasion resistance is noted with higher carbon and alloy contents. The results on specimens deposited in sufficient thickness by arc or by gas should be somewhat comparable to similar alloy and carbon content cast materials. It should be emphasized that the abrasion results in Table V were obtained with dry crushed quartz; wet abrasion results and tests made under milder abrasive conditions might show results in a different order.

Special Surface Treatments

Abrasion tests were made with dry and wet crushed quartz on a number of specimens that were given special surface treatments including chromium plating, carburizing, nitriding, and pre-peening (of 12% manganese steel). The results are shown in Table VI in comparison with hot-rolled SAE 1020 steel.

The abrasion values reveal that the rate of metal removal was not notably impeded by any of the surface treatments except chromium plating. In all instances, except the latter, the case was worn through and the greater part of the reported wear took place in the base material.

Pre-peening of austenitic manganese steel to work harden the surface does not appear to be of any value in a strictly abrasive application. The greater wear rate of manganese steel than that

Table VI
Dry and Wet Quartz Abrasion Tests on Special Surface Treatments

28/35 mesh; 250 rpm; 40-lb. load; 4000 ft.

Material	Treatment	Hardness	Case Depth	Weight Loss Values (Grams × 10) Dry Quartz	Wet Quartz
SAE 1020	Hot-rolled	BHN 131	.....	67.4	60.4
SAE 1020	Carburized	Rc 65/69	0.100 in.	110	48.5
Nitralloy G	Nitrided 72 hrs.	*Rc 65/69	0.018 in.	69.7	51.0
SAE 1045	Siliconized	*BHN 217	0.018 in.	72.3	54.3
3% chromium, 12% manganese steel	Quenched	Rc 17/20	.....	94.8	54.4
3% chromium, 12% manganese steel	Pre-peened	Rc 45/53	.....	96.0	68.6
Heavy hard chromium plate	None	Rc 62/65	0.030%	12.0	....

*Converted from Rockwell "A".

of mild steel has been confirmed in certain industrial applications where impact or heavy pressures are not involved. Manganese steel has its primary field of application where toughness rather than straight abrasion resistance is the important requirement.

The results indicate that these surface treatments, except chromium plating, are not effective in increasing abrasion resistance

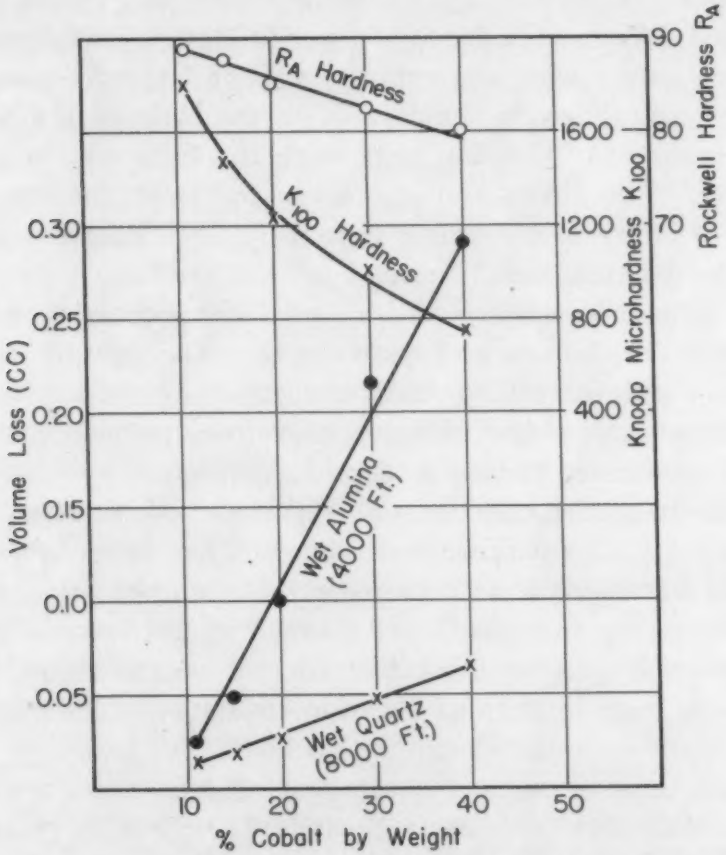


Fig. 14—Volume Loss of Several Cobalt Content Grades of Sintered Tungsten Carbide Under Wet Alumina and Quartz Abrasion.

under the severely abrasive conditions of the tests. Under less severely abrasive conditions, some improvement might be obtained with these treatments, but other means of increasing abrasion resistance appear more promising.

Sintered Tungsten Carbide Compacts

The use of tungsten carbide inserts for increasing the abrasion resistance of mining and road building equipment has received widespread attention recently. The carbides which are most satisfactory

for such applications are not the usual cutting tool carbides, since the latter are not sufficiently shock-resistant for the degree of impact frequently encountered. Higher cobalt binder contents are used than in cutting tools, resulting in increased toughness but at some sacrifice of abrasion resistance.

The effect on abrasion resistance of increasing the cobalt binder content from 11 to 40% by weight is shown in Fig. 14. Because of the great difference in density between tungsten carbide and cobalt, weight loss values were converted to volume loss values in order to make the results directly comparable on the basis of the amount of material removed. Abrasion tests were run both with wet alumiua and quartz. The quartz tests were run for twice the standard test distance of 4000 feet because extremely low weight losses were obtained in the standard distance.

The volume losses increased directly with increasing cobalt content in both the alumina and quartz tests. The rate of increase of volume loss with increasing cobalt content was greater with alumina than with quartz. Alumina tests, therefore, provide greater sensitivity in accelerated testing of carbide materials.

Hardness of the carbides was reported both as Rockwell "A" and Knoop (K_{100}) microhardness values. The latter were average values taken at random without respect to the microstructure. The rapidly increasing microhardness differential between alumina and the carbide materials as the cobalt content was increased explains the sharp decrease in alumina abrasion resistance much more clearly than the relatively minor change in Rockwell "A" hardness.

On the basis of the wet quartz tests, the abrasion resistance of the 11% cobalt carbide is approximately 110 times as great as that of hot-rolled SAE 1020 steel. The 20% cobalt grade is approximately 60 times as abrasion-resistant as the hot-rolled steel.

In order to employ carbide inserts successfully in abrasive applications, the matter of design in incorporating the carbides must be carefully engineered to provide adequate support and cushion against shock and breakage.

Field Test Results

Reliable field test data on abrasive applications are rather difficult to obtain. Reports of service life, even in tests of the same material, are apt to be erratic and colored by the operator's judgment

of when the part is no longer serviceable. Then too, the conditions of service often vary greatly from time to time or at different locations.

For accurate comparisons among materials, the greatest reliability is achieved, when possible, by weight loss measurements over a known, and preferably constant, period of time. This presumes that the test conditions are essentially constant. Where a number of similar parts are used concurrently, variations in field conditions can be largely discounted by simultaneous comparison of standard with experimental materials.

Sandslinger Liners

Accurate field tests on Sandslinger liners were obtained in a commercial steel foundry by means of an automatic timer incorporated in a Sandslinger which recorded only when the unit was in operation. The tests were continued until the liners, which wear locally (see Fig. 15), were worn through. The sand, which contains a high proportion of crude Ottawa sand and is a typical steel foundry mixture, is reasonably consistent in abrasive characteristics.

Service life comparisons of several materials are shown in Table VII. Wrought liners are usually made of ¼-inch stock whereas cast liners are ⅜ inch thick. The results on the cast liners, therefore, are shown corrected to the corresponding thickness of the rolled liners.

Table VII
Sandslinger Liner Field Data Vs. Laboratory Abrasion Tests

	Chemical Analysis								Service Life Tests (Steel Foundry Sands in Commercial Sandslinger)		Laboratory Abrasion Tests (Dry Ottawa Sand—28/35 Mesh—20-Lb. Load—1035 rpm—Rubber Wheel—8000-Ft. Wheel Travel)	
No.	C	Mn	Cr	Ni	Mo	V	Treatment	Hardness Rc	Service Life[1] (Min.)	Ratio (Life Sample) / (Life No. 1)	Weight Loss (Grams × 10)	Ratio (Wt. Loss No. 1) / (Wt. Loss Sample)
1	0.40	1.55	....	...	....	....	hot-rolled	22/28	31	1.0	26.3	1.0
2	0.40	1.55	....	...	....	....	water-quenched	52/55	29	0.9	31.0	0.85
3	Carburized-nitrided SAE 1020						water-quenched	50/58[2]	32	1.0	24.3	1.1
4	3.20	....	0.26	(white iron)			as-cast	44/48	100	3.2	6.3	4.2
5	3.22	1.72	1.77	6.0	....	....	as-cast	58/62	200	6.5	4.2	6.3
6	2.25	....	11.50	...	0.77	0.20	1825 air-cooled	62/67	360	11.6	2.6	10.0

[1]Time to wear through ¼-inch thickness.
[2]Converted from Rockwell "A".

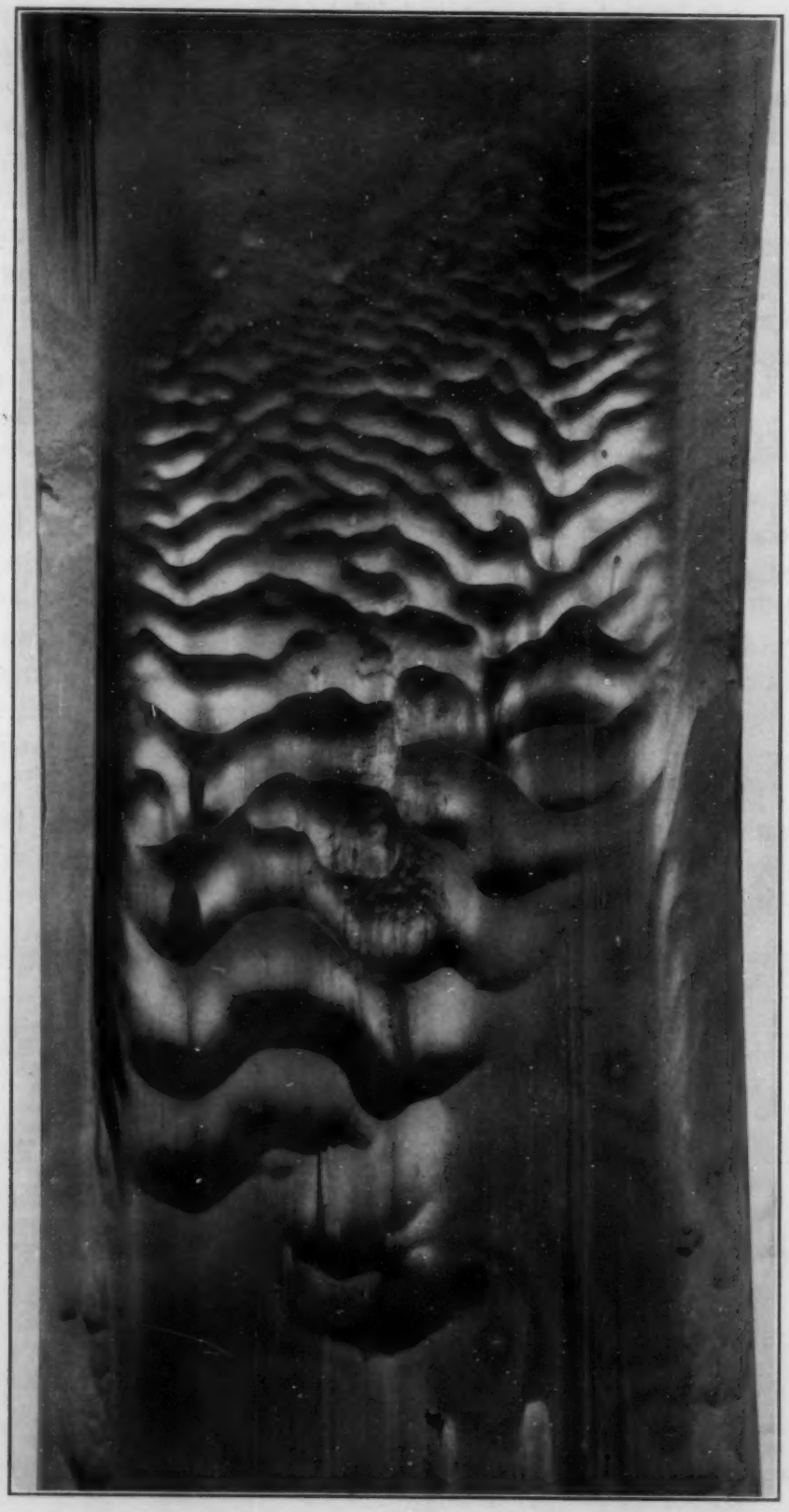


Fig. 15—Section of a Cast Sandslinger Liner Showing Typical Wear Pattern. The above liner of a specially developed composition considerably outlasted carbon steel rolled liners.

Laboratory abrasion test results, obtained with crude Ottawa sand, also are shown in Table VII. The tests were run at 1035 rpm with a 20-pound load on the lever arm. Laboratory results obtained under these testing conditions showed better correlation with preliminary field data than did the results of lower speed tests.

The laboratory test results are essentially in the same order and are nearly of the same relative magnitude as the field test results. The 0.40% carbon, 1.55% manganese steel which showed the lowest liner life in this particular series was selected as the base material for comparison purposes in obtaining the ratios.

While the developments are still in the experimental stages, cast liner materials have been produced as a result of the accelerated laboratory tests which have resulted in service life ratios many times that of the medium carbon steel rolled liner used as a reference material in Table VII.

Blades for Centrifugal Abrading Machines

Another service application where abrasive wear is a serious problem is in the throwing blades of centrifugal-type machines used for cleaning or peening with metallic grit or shot. Typical worn blades may be seen in Fig. 16. The lineal speed of the grit or shot at the discharge end of the blades is approximately 10,000 feet per minute.

Eight blades are used in a wheel in this type of machine. As many as four different materials can be tested simultaneously and thereby directly compared. In order to insure reasonably constant balance, the same materials must be used in diametrically opposed blades.

Representative field test data showing the weight losses on blades which were carefully weighed before and after testing are shown in Table VIII compared with the laboratory abrasion data on the same materials. In making the laboratory tests, grit was used as the abradant because the angularity of the particles produces greater weight loss in a given test period than the rounded globules of shot. It was found necessary to use a steel wheel in the abrasion device in order to obtain satisfactory correlation with service. The reason for this is not clear, since in sand abrasion, correlation with actual service using a steel wheel in the abrasion machine was poor. The tests were run through a distance of 8000 feet at 250 rpm with a 40-pound load on the weight arm.

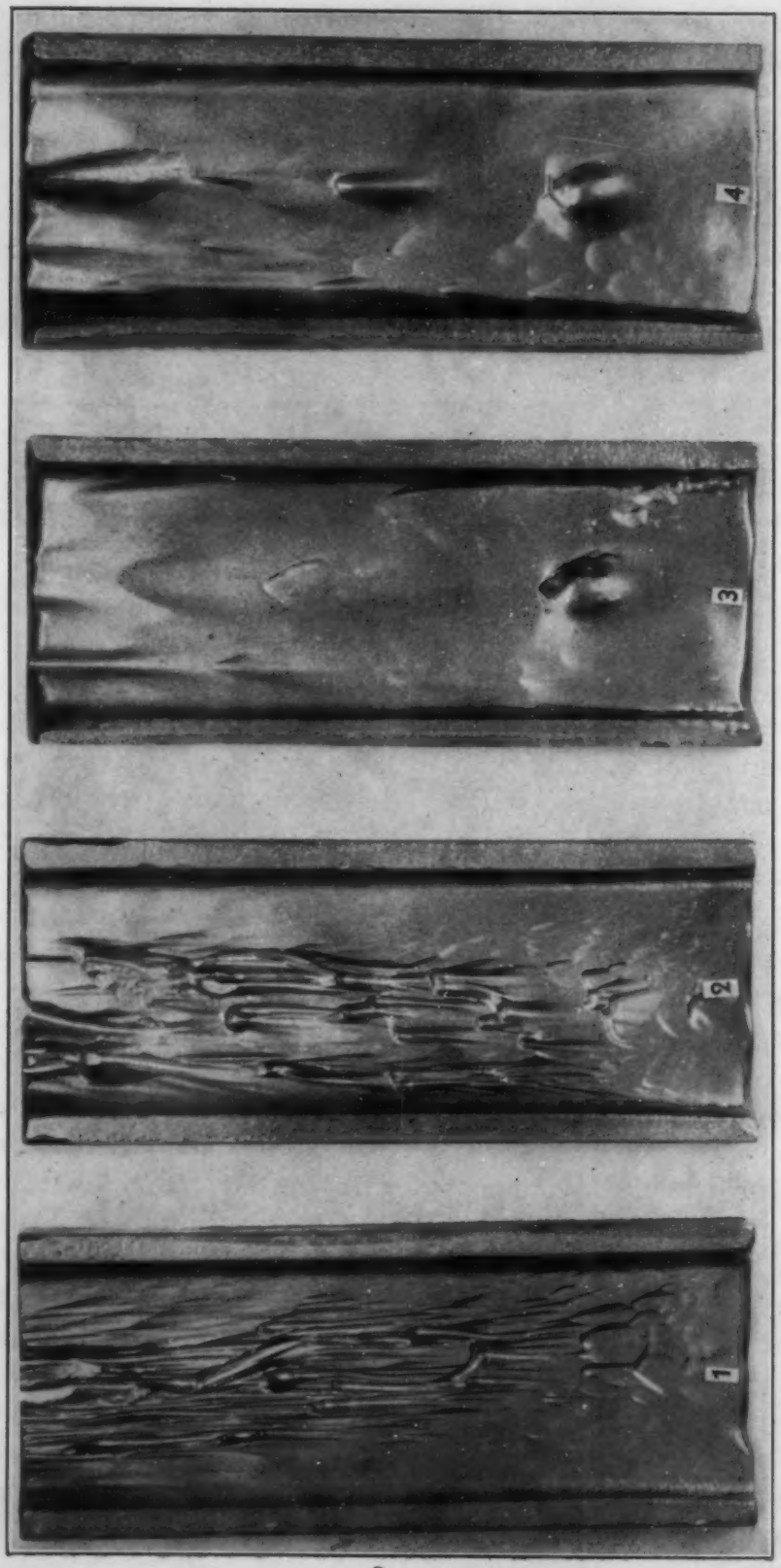


Fig. 16—Typical Worn Blades From a Centrifugal Abrading Machine Used for Shot Cleaning or Peening.

The metallic grit and shot usually is made of chilled high carbon iron although tempered steel shot has recently been advertised. Considerable variation (as great as two to one) has been noted in the abrasiveness of the grit used in the laboratory tests even within single shipments from the same supplier. For this reason, it was found necessary to run a standard test on each 100-pound bag of grit. A large stock of hardened SAE 1045 steel was set aside as a standard material for this purpose.

The blades in Table VIII were all in the as-cast condition. Laboratory grit test results have shown little or no advantage accruing to the heat treatment of any of these materials.

The correlation between the weight loss ratios in the actual machine and in the laboratory device appears satisfactory. Although not normally used in this application, white iron was chosen as the base material for comparison in these tests.

The data show that the material No. 5, which has been used as a standard material for a number of years, is approximately 70% better than sand cast nickel-chromium white iron. A war-born material, No. 3, designed to save molybdenum, is only one-half as effective as the higher molybdenum alloy. Actually the high chromium, low molybdenum alloy, No. 6, showed the best results of these particular materials.

Table VIII
Centrifugal Abrading Machine Blade Tests Vs. Laboratory Tests

	Chemical Analysis						Service Life Tests—S-460 Chilled Iron Shot in Commercial Machine		Laboratory Abrasion Tests—(Chilled Iron Grit—28/35 Mesh—40-Lb. Load—250 rpm—Steel Wheel—8000-Ft. Wheel Travel)	
No.	C	Cr	Mo	Ni	Condition	Hardness Rc	Service Wear (Grams/Hr.)	Ratio (Wt. Loss No. 1)/(Wt. Loss Sample)	Wt. Loss[1] (Grams × 10)	Ratio (Wt. Loss No. 1)/(Wt. Loss Sample)
1	2.77	0.25	(white iron)		as-cast	44/48	19.0	1.0	24.0	1.0
2	3.18	9.60	....	....	as-cast	51/54	7.4	2.6	7.5	3.2
3	1.10	2.16	1.34	....	as-cast	40/46	3.7	5.1	4.4	5.5
4	3.02	1.25	....	4.10	as-cast	49/53	2.8	6.8	4.0	6.0
5	2.57	2.53	7.67	....	as-cast	62/64	1.9	10.0	2.3	10.4
6	3.14	12.14	1.84	....	as-cast	52/56	1.7	11.2	1.9	12.6

[1]Corrected for variations in abrasiveness of grit from bag to bag through use of hardened SAE 1045 steel as standard on each bag.

The grit and shot results in Table VIII, both in service and in laboratory tests, are obviously of a different order than the crude

Ottawa sand results in Table VII. For instance, the nickel-chromium white iron was six times more effective than plain white iron in the service employing cast iron grit or shot, whereas with sand the superiority of the alloy iron was only about twice that of the plain white iron.

Conclusions

The following conclusions have been derived from data obtained with a newly developed laboratory abrasion testing machine. These results have been confirmed at least partially by field tests.

1. Weight loss of carbon and low alloy steels due to dry abrasion increases as both speed and pressure are increased in constant test distances.

2. Under certain dry abrasive conditions, due to the temperatures developed, hardened plain carbon or low alloy steels are no better or are actually inferior to the same steels in the annealed or hot-rolled conditions. In wet abrasive applications, the hardened steels are superior.

3. Angular particles of crushed quartz were found to be considerably more abrasive than rounded particles of quartz sand. Angular particles of crushed feldspar, a naturally softer material than quartz, were found to be more abrasive than the rounded grains of crude Ottawa sand.

4. With similarly shaped particles, abrasiveness increases with the hardness of the abrading material from feldspar to quartz to alumina. Materials with good resistance to quartz abrasion are not necessarily satisfactory in resisting alumina abrasion although the reverse is true.

5. Carbon content is the most important alloying element in providing irons and steels with resistance to feldspar, quartz, or sand abrasion. By comparison, other elements are of secondary importance.

6. Ordinary methods of hardness determination show no correlation with abrasion resistance. However, if the microhardness of one constituent of an alloy is harder and the accompanying structures are roughly equal to that of the abrading material, the abrasion resistance will increase as the hardness and the amount of the hardest constituent are increased.

7. Arc deposition of certain hard surfacing materials in thicknesses of less than ⅛ inch results in sufficient dilution with the base material to cause a sharp reduction in abrasion resistance compared

to heavier arc deposits. The factor of dilution is less pronounced in gas (oxyacetylene) welding and, hence, satisfactory abrasion resistance is obtained in thin deposits.

8. Special surface treatments, i.e., carburizing, nitriding, siliconizing, and cold working, are of little or no apparent value in increasing resistance to dry or wet quartz abrasion. Hard chromium plating has some merit and in some applications may be of considerable value.

9. Certain grades of sintered tungsten carbide have excellent resistance to alumina and quartz abrasion. With increasing cobalt binder content, the abrasion resistance decreases but other properties, notably toughness, improve.

Acknowledgments

The following industrial concerns are gratefully thanked for their financial support and permission to publish certain data: Beardsley and Piper Division of Pettibone-Mulliken Corporation, Harnischfeger Corporation, Harrisburg Steel Corporation, Michiana Products Corporation.

The constant encouragement of certain members of the staff of the Armour Research Foundation enabled the establishment of abrasion research as a specialized activity at the Foundation. Acknowledgments are also due to other members of the staff of the Foundation for the necessary technical assistance in carrying out the research and preparing the paper.

Special mention is made of W. H. Graft, Associate Metallurgist of the Armour Research Foundation, who conceived and largely designed the abrasion testing device.

References

1. J. H. Hall, "Wearing Tests of Twelve Per Cent Manganese Steel," *Proceedings,* American Society for Testing Materials, Vol. 28, 1928, p. 326.
2. J. M. Blake, "Wear Testing of Various Types of Steels," *Proceedings,* American Society for Testing Materials, Vol. 28, Part II, 1928, p. 341-355.
3. H. W. Gillett, "Considerations Involved in the Wear Testing of Metals," *Symposium on Wear of Metals,* American Society for Testing Materials, 1937, p. 3-23.
4. S. J. Rosenberg, "Resistance of Steels to Abrasion by Sand," Transactions, American Society for Steel Treating, Vol. 18, 1930, p. 1093-1124.
5. O. W. Ellis, "Wear Tests on Ferrous Alloys," Transactions, American Society for Metals, Vol. 30, 1942, p. 249-286.
6. T. E. Norman and C. M. Loeb, Jr., "Wear Tests on Grinding Balls," American Institute of Mining and Metallurgical Engineers, *Metals Technology,* T.P. 2319, 1948.

7. C. R. Weiss, "Relative Wear of Metals Due to Abrasion," *Iron Age,* Vol. 129, Part II, 1932, p. 1166.
8. H. S. Avery, "Hard Surfacing by Fusion Welding," A Monograph published by the American Brake Shoe Co., 1947.
9. J. A. Brinell, "Researches on the Resistance of Iron, Steel and Some Other Materials to Wear," *Jernkontorets Annaler,* Vol. 76, 1921, p. 347-398.
10. N. W. Thibault and H. L. Nyquist, "Knoop Hardness Testing," TRANSACTIONS, American Society for Metals, Vol. 38, 1938, p. 271-330.
11. V. E. Lysaght, "The Knoop Indenter as Applied to Testing Nonmetallic Materials Ranging From Plastics to Diamonds," *ASTM Bulletin,* January 1946, No. 138, p. 39.
12. J. B. Austin, "The Effect of Changes in Condition of Carbides on Some Properties of Steel," TRANSACTIONS, American Society for Metals, Vol. 38, 1947, p. 28-69.

DISCUSSION

Written Discussion: By Howard S. Avery, research metallurgist, American Brake Shoe Co., Mahwah, N. J.

This is a welcome contribution to the literature of wear and Messrs. Haworth and Graft are to be complimented on having standardized and

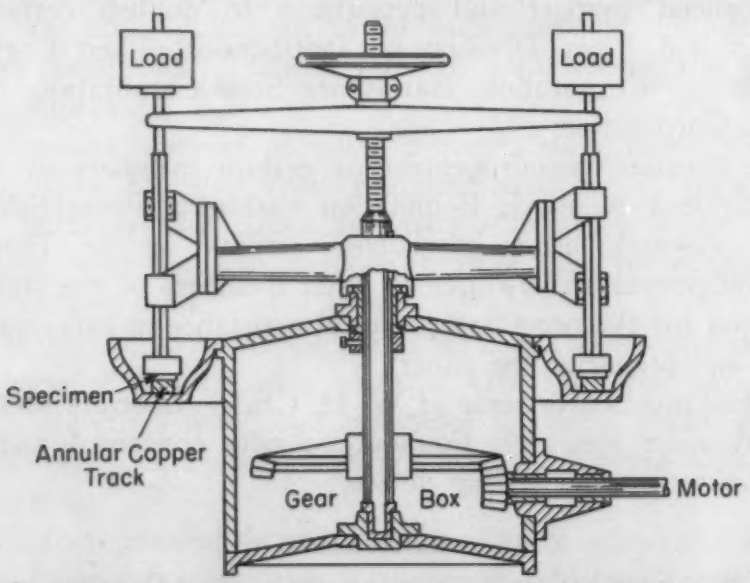


Fig. 17A—Schematic Diagram of American Brake Shoe Company High Microstress Abrasion Testing Device (2), (8).* The usual tests employ No. 50 quartz sand and a 54-psi stress on the specimen. The abrasive is progressively ground finer during the test.

validated a new abrasion testing apparatus. It is easy to make laboratory devices that produce wear, but it is difficult and frequently tedious to refine them to the point of giving reproducible results and to validate such data against field service.

Since the mechanical conditions of a wear test influence the results, it is important to describe these as precisely as possible. Consider the rubber wheel arrangement: Though the superficial unit pressure (60 psi

*The figures appearing in parentheses pertain to the references appended to this paper.

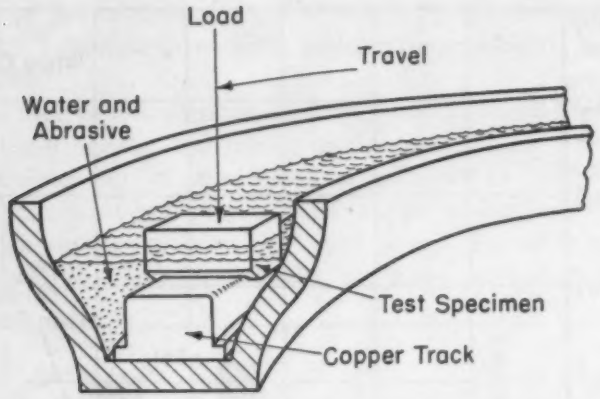


Fig. 17B—Schematic Diagram of American Brake Shoe Company High Microstress Abrasion Testing Device (2), (8).* The usual tests employ No. 50 quartz sand and a 54-psi stress on the specimen. The abrasive is progressively ground finer during the test.

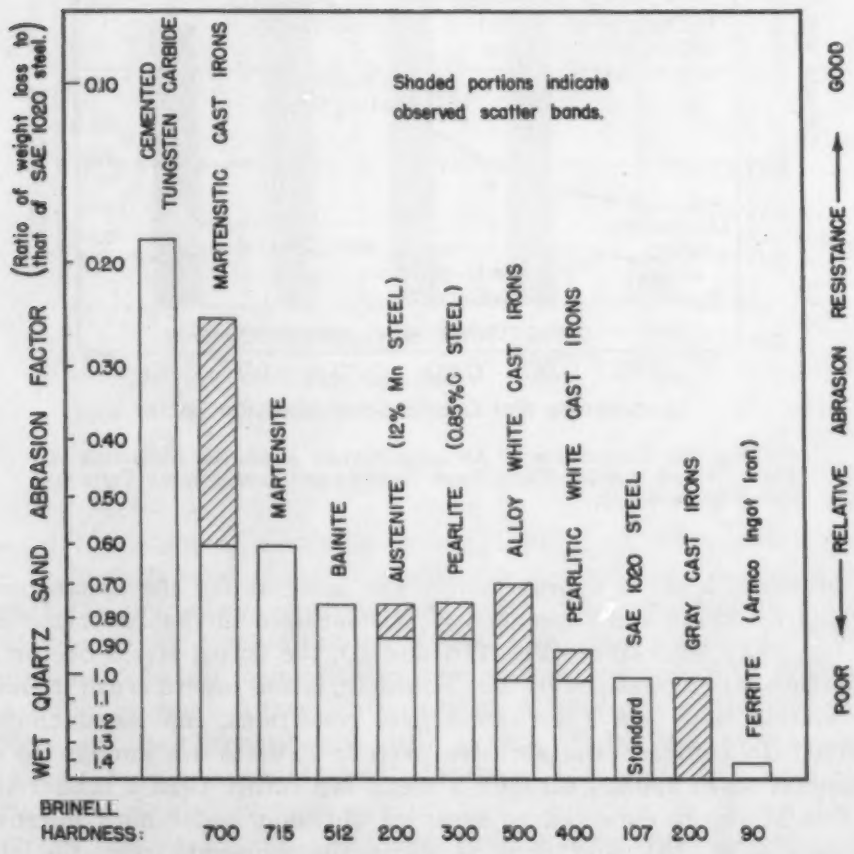


Fig. 18—Relative Abrasion Resistance of Several Common Materials and Structures to the High Microstress Abrasion of the Apparatus in Fig. 17.

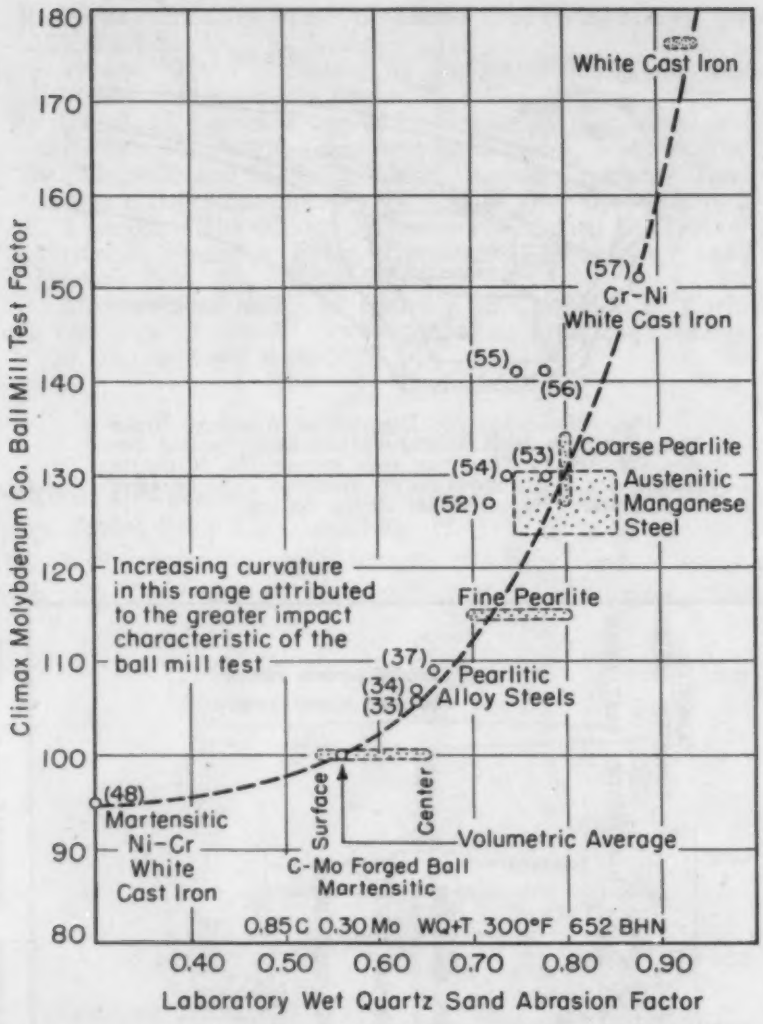


Fig. 19—Correlation of Abrasion Factors From the Apparatus of Fig. 17A and B With Those From Norman and Loeb's Wear Tests on Grinding Balls (6).

with 40-pound load) is approximately the same as for the apparatus first described by Blake and subsequently standardized in the American Brake Shoe Company laboratory (Fig. 17A and B), the actual stress on the abrasive particle, as emphasized by Mr. Haworth, is too low to crush it and thus a correlation with low microstress field conditions, like sand chutes, is expected. In contrast, the abrasive particle stresses are enough to crush the mineral when applied through a metal lap rather than a rubber wheel. This test set-up is expected to measure abrasion under high microstress conditions (Fig. 18), and thus is distinctly different from the rubber wheel test.

One consequence is to reverse the relative performance of white cast iron (Table III) and austenitic manganese steel (Table VI). With the rubber wheel the abrasion factors are about 0.10 and 0.91 respectively,

while with the high stress test they are 0.95 and 0.80. The latter relation has been validated by ball mill tests with which the apparatus has a good correlation. (Fig. 19.)

Despite the distinctive differences in these tests, similar conclusions can be drawn in certain areas. Confining our comments to wet abrasion, where the water cooling action minimizes or eliminates temperature as a variable, we confirm that an increase of abrasive hardness increases the severity of wear on pearlitic white cast iron. In addition to the minerals above 6 on Mohs' hardness scale, we have extended the series

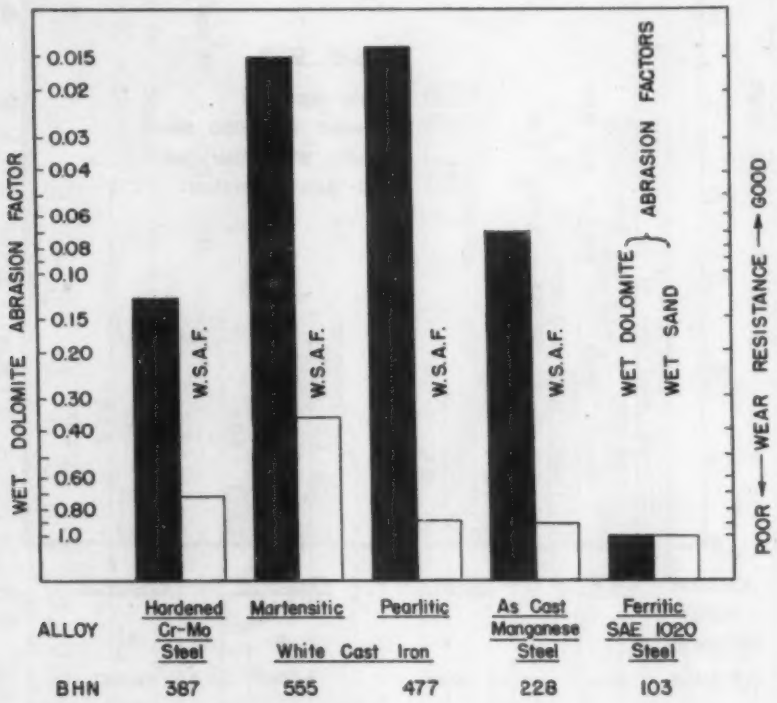


Fig. 20—Comparison of Abrasion by Wet Dolomite (Solid Block Bars) With Abrasion by Wet Quartz Sand (White Bars).

downward to dolomite, which is about Mohs' 3 to 3½. Some results appear in Fig. 20, with direct comparisons against No. 50 quartz sand. Note that the four alloys are relatively much more resistant to dolomite than to quartz in comparison with the soft steel standard. This is attributed to dolomite being softer than all except the SAE 1020 steel. At the other extreme, silicon carbide with a hardness exceeding any of the alloys or their constituents will abrade them, and even tungsten carbide, at a rate comparable to the wear of soft steel.

The relative abrasiveness against four materials is shown for the high stress test in Fig. 21. Against some alloys, cleavage, angularity, size and toughness of the abrasive appear to overshadow the effect of hardness, as a harder abrasive does not always increase the wear rate.

We wish to emphasize that the importance (Mr. Haworth's conclusion No. 5) attached to carbon in irons and steels is justified only with

low stress on the abrasive. The conclusion is invalid for ball mill service and similar conditions where the abrasive is fractured.

It would be better to narrow the conclusion about hardness and abrasion resistance since it is contrary to the author's report on Brinell's wear test and because it lacks confirmation under a variety of conditions. We have observed cases where hardness can be correlated usefully even when dealing with heterogeneous metal structures. However, we concur heartily with the implication that hardness cannot be accepted as a

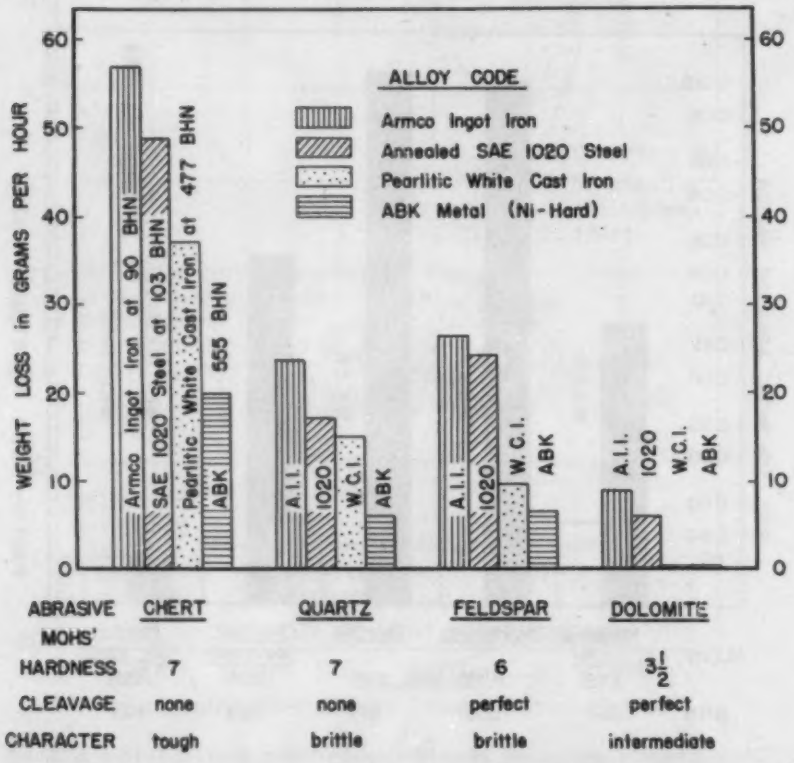


Fig. 21—Relative Abrasiveness of Common Mineral Abrasives Used in the Apparatus of Fig. 17A and B.

criterion of abrasion resistance any more than data from other unvalidated wear tests. The relation should be proven, not assumed. There are circumstances where other qualities, such as toughness, dominate behavior and permit softer constituents or composite structures to outwear harder but brittle materials. In high microstress abrasion the soft austenite of manganese steel will outlast the pearlite-cementite combination of white cast iron, though both constituents are harder. Moreover, neither impact nor work hardening is necessary to demonstrate this.

The better abrasion resistance of gas welds compared with arc welds has been repeatedly confirmed for a variety of hard surfacing alloys. Fig. 22 shows an example for a martensitic iron, together with comparison against other hard facing deposits. Moreover, the effect usually appears when testing the top of a multilayer deposit where dilution with

base metal is negligible. The situation is more complex than the simple mechanism of dilution, though this undoubtedly contributes. Distinctive cooling rates are important and residual stresses perhaps play a part. How far these factors apply to both low and high stress abrasion is an interesting field for future research.

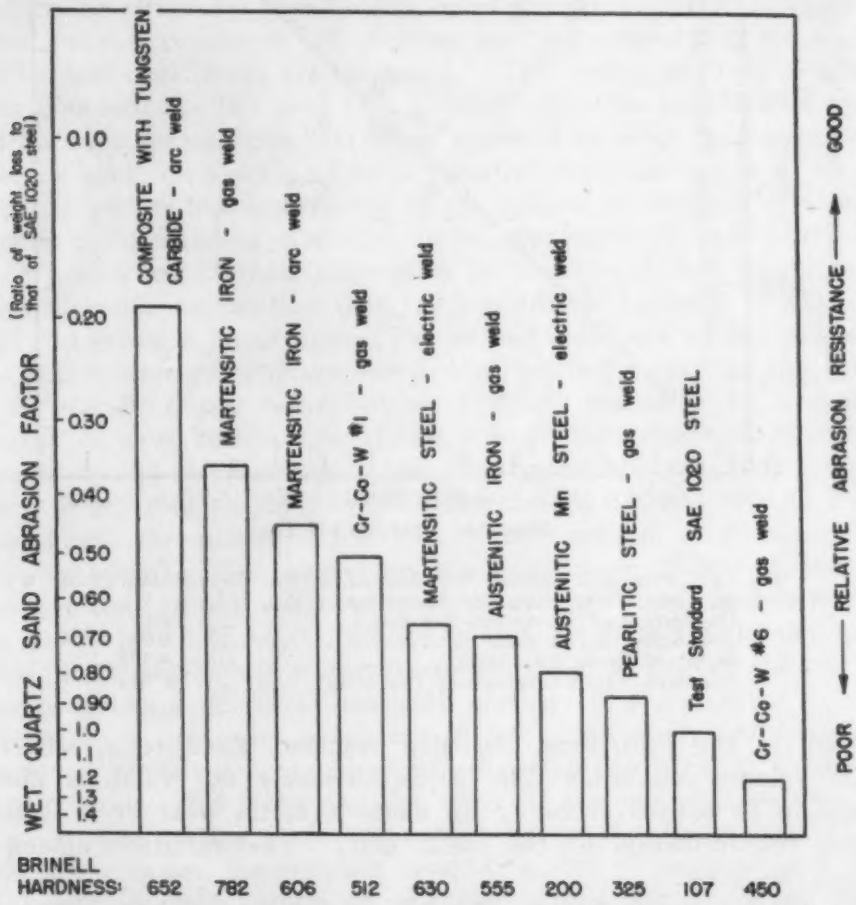


Fig. 22—Relative Abrasion Resistance of Structures Encountered in Hard Facing Deposits. (The chromium-cobalt-tungsten welds differ chiefly in nominal carbon content (8), No. 1 carrying 2.5% carbon, 30% chromium, 14% tungsten and 46% cobalt; and No. 6 about 1.0% carbon, 28% chromium, 4% tungsten, and 55% cobalt.)

Our high stress abrasion experience also confirms that of Mr. Haworth for thin protective layers. These are very useful for mild metal-to-metal wear conditions, but with vigorous abrasion they wear through too soon to be economical.

We should like to ask two questions: In the tests of sintered tungsten carbide, did the softer quartz actually wear the carbide or was the wear confined to the softer matrix? Our observations of composite structures containing hard carbides usually reveal them standing high in relief. The final weight loss data reflect mechanical loss of these as well as abrasive wear because of this complication.

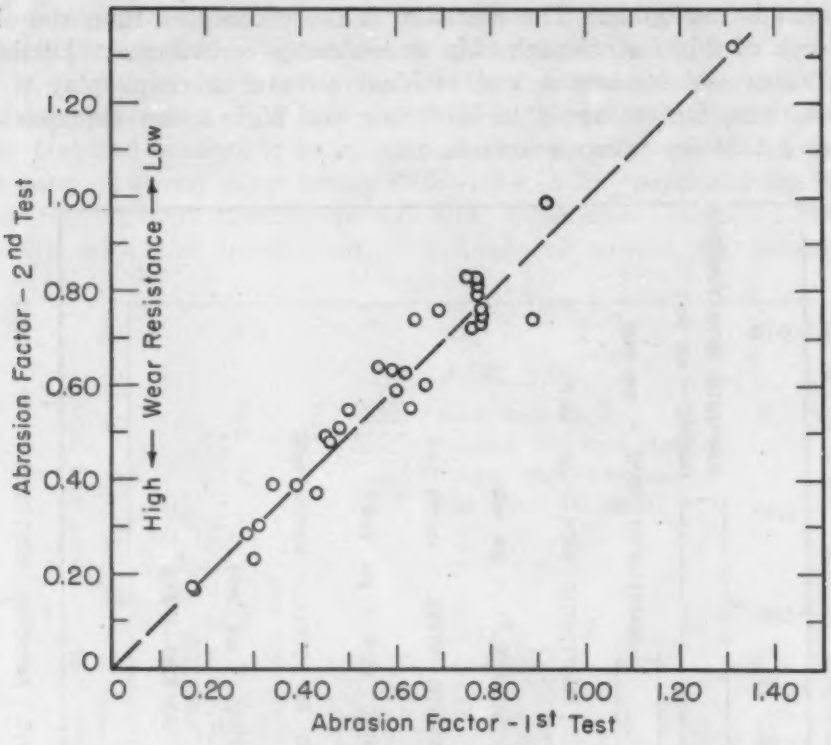


Fig. 23—Proposed Method for Indicating the Reproducibility of a Wear Test, Using Data From the Apparatus of Fig. 17A and B.

Correlation of 1st versus 2nd test	0.97
Reliability of two tests	0.985
Standard Error (one test)	0.028
Standard Error (average of two tests)	0.020

Also, in the centrifugal abrading machine blade tests, where the carbide volume conclusion (No. 5) is obviously not valid, is abrasion believed to be caused primarily by metal-to-metal wear or is it related to sand contamination of the metal grit? The variation among lots suggests the latter.

Finally, we should like to plead for a uniform system of reporting the reproducibility of wear tests. Statistical theory provides mathematical terms for designating test reliability, which might well be employed if enough data are presented. Our suggestion is a plot of the correlation between duplicate tests, similar to Fig. 23. Unfortunately, most wear tests in the literature leave the reader in doubt about the statistical limitations of the data.

Written Discussion: By H. Czyzewski, assistant professor of metallurgical engineering, University of Illinois, Urbana, Ill.

The author has presented a great deal of data on abrasion testing and an examination of his paper shows that this substantial amount of material was extracted from an even larger mass of data. The data presented instead of satisfying the appetite temporarily, actually whet it for additional data. It is hoped that more data will be available to the public in the near future.

This writer would like to discuss a number of general conclusions made by the author and also some specific result interpretations.

It is stated in conclusion 6 that "Ordinary methods of hardness determination show no correlation with abrasion resistance. However, if the microhardness of one constituent of an alloy is harder and the accompanying structures are roughly equal to that of the abrading material, the abrasion resistance will increase as the hardness and the amount of the hardest constituent are increased." This writer has two objections to that conclusion. The first is a general objection to the assumption that a hardness penetration test to be sensitive to wear resistance would have to be made on a scale adjusted for that particular purpose. In one respect the author has contributed to the science of analysis of abrasion resistance by demanding that the micro properties of the constituents and the properties of their aggregates be considered, but he has made the less plausible assumption that the penetration hardness is the micro property of greatest importance. The second objection to this conclusion is that it is inaccurate with respect to the results obtained by the author. That is, the SAE 1020 hot-rolled steel would ordinarily be considered to consist of a microstructure having a large percentage of ferrite and a certain amount of cementite, a carbide. Essentially the same constituents but in differing amounts may be expected in the sample AA1 (0.89% carbon, 1.98% chromium) and in BB1 (0.78% carbon, 0.82% manganese, 6.59% chromium). The aggregate hardness given indicated that the amount of the hardest constituent is increasing if the steels are rated in the above order. However, according to the results for the dry quartz and for most of the other conditions given in Table III the abrasion resistance actually decreases markedly rather than increases.

Table I of the paper gives the effect of pressure, speed and test duration on abrasive wear; however, the material used is a hardened SAE 1045 steel. This work and the study of the temperature developed in dry abrasion testing leads the author to the conclusion that "Under certain dry abrasion temperature conditions, due to temperatures developed, hardened plain carbon or low alloy steels are no better or are actually inferior to the same steels in the annealed or hot-rolled conditions. In wet abrasive application the hardened steels are superior." It is not clear that heating of hardened steels will produce a structure inferior to the structure obtained at the same temperature with annealed or hot-rolled conditions in steel, on the basis of hardness test. Is it not a further index that a property other than hardness is a principal component to be taken into account in these abrasive tests?

Conclusion 3 states that angular particles of crushed quartz are found to be considerably more abrasive than rounded particles of quartz sand. Is there not a corollary conclusion to be made that certain conditions make for a very high degree of sensitivity whereas others tend to make the effect of angularity negligible; for example, see test DD4? The angularity ratios (Dry Ottawa Sand: Dry Quartz) vary in Table II from 1 to 1 to a maximum of 1 to 12. It is further interesting to note that when the sensitivity to angularity is low as in DD4, then the angular

particles of crushed feldspar are not more abrasive than the rounded grains of the crude Ottawa sand, and wet quartz test weight loss exceeds that in the dry quartz test.

This writer has made some arithmetical calculations from Mr. Haworth's test results as follows:

The approximate depth of the abrasion can be determined from density figures (0.28 pound per cubic inch for steels) where the abrasion area is 0.5 inch wide by 2 inches long and the weight loss is 10.0 grams (the index used by Mr. Haworth is grams $\times$ 10 and would be 100 in this case). (The weight losses given in Table III range from 1 to 180 "grams $\times$ 10".)

$$\frac{10 \times 0.00220 \text{ (lb. per gram)}}{2\text{(in.)} \times \tfrac{1}{2}\text{(in.)} \times t} = 0.28$$

$t = 0.075$ inch. (The depths could be ascertained directly from Mr. Haworth's samples.)

If we assume a constant wear rate, it can be computed with respect to time or in the following case with respect to length of abrasion (2 inches, the length of abraded area and also the approximate length of the circumferential divisions of the rubber wheel).

The wear rate per circumferential division is then

$$\frac{0.075 \text{ in. (t)}}{\text{4000 ft. (length of test)} \times 6 \text{ (no. of circumf. div. per ft.)}} = 3 \times 10^{-6} \text{ inches}$$

/circumf. div. which equals approx. 7.6×10^{-6} cm./circumf. div.

In the case of a weight loss of 1 (gram $\times$ 10), the wear rate is 7.6×10^{-6} cm./circumf. div.

The iron (B.C.C.) lattice parameter $a = 2.86$ Angstrom units (10^{-8} cm.); the complex carbide lattice parameters are greater.

Some further calculations give more interesting results. The particles in the 28-35 mesh range have an average diameter of about 0.02 inch. If the circumferential division of the rubber wheel (2 inches by 0.5 inch) is considered to be coated by a close packed single-particle-depth layer there would be a row 25 grains across the 0.5-inch width and 100 rows of grains over the 2-inch length.

If the wear rate is computed on a per grain row basis then $tg = 7.6 \times 10^{-6}$ cm./grain row at the high wear rates of about 100 (grams $\times$ 10), and 7.6×10^{-10} cm./grain row at the low wear rates of 1 (grams $\times$ 10).

Such calculations prompt several questions two of which are given here:

1. Does any "abrasion test" involve predominantly mechanical factors in metal removal? And the more fundamental question,
2. What is the mechanism of abrasive wear?

It should be noted that the results of the calculations are common to most abrasion tests and are not unique with this series.

This writer does not pretend to have all the answers, but even his

small contribution must be delayed pending thesis completion and approval. It is hoped, however, that these questions will promote an intensive analysis of the wear phenomena.

These observations do not detract from the value of simulated service tests now or previously performed, but they do emphasize that nothing more than that can be accomplished without a detailed understanding of wear processes.

Written Discussion: By M. C. Fetzer, research metallurgist, Latrobe Electric Steel Co., Latrobe, Pa.

In dealing with abrasion in which the abrasive particles are considerably harder than martensite, the quantity, distribution and hardness of the carbides control the wear. The relative importance of each of these

Table IX
Effect of Chromium Carbides on Wear

Alloy No.	% C	% Cr	% C_1	% C_2	% C_3	Total	Wear, Grams ×10 — Dry Quartz	Wet Quartz	Dry Alumina	Dry Feldspar	Rockwell C
AA4	3.9	1.0	50	0	0	50	9	5	53	5	59
BB4	4.1	6.6	50	0	0	50	9	5			65
CC4	3.9	13.4	25	20	0	45	3	2	47	1	67
DD4	3.8	31.2	0	40	0	40	2	2			64
DD3	2.8	31.6	0	35	0	30	19	6			62
AA3	2.8	1.2	30	0	0	30	15	7	62	6	55
BB3	3.0	7.2	30	0	0	30	12	4			67
CC3	3.2	14.5	5	20	0	25	5	2	87	2	68
DD2	2.0	25.3	0	25	0	25	74	13			58
CC2	1.9	14.2	0	20	0	20	67	16	98	6	65
AA2	1.7	19.2	15	0	0	15	90	25	86	16	60
DD1	1.3	30.1	0	0	15	15	78	48			27
BB2	1.8	6.3	5	5	0	10	103	24			61
CC1	1.2	14.1	0	10	0	10	145	47		27	60
BB1	0.8	6.6	0	3	0	3	180	68			60
AA1	0.9	2.0	0	0	0	0	110	40		33	58

$C_1 = (Fe, Cr)_3 C$ or cementite with up to 15% Cr.
$C_2 = (Cr, Fe)_7 C_3$ or trigonal chromium carbide with up to 55% Fe.
$C_3 = (Cr, Fe)_4 C$ or cubic chromium carbide containing up to 25% Fe.

three variables depends upon the nature of the test; that is, whether the abrasive particles are fixed or free, and on the hardness of these particles. This may be illustrated by comparing the high carbon, high chromium die steel (2.2% carbon, 13% chromium) with the tungsten (1.4% carbon, 3.7% tungsten) die steel. Of these two, the chromium steel has about 30% exposed chromium carbide whereas the exposed tungsten carbide in the other steel is probably less than 5%. On the other hand, tungsten carbide, WC, is considerably harder than the chromium carbide, $(Cr, Fe)_7 C_3$. Tests on the Brinell abrasion tester (free abrasive particles) show the high carbon chromium steel to be superior to the tungsten steel but with fixed abrasives (as on 120-grit alundum paper) the tungsten steel is better. The difference is due either to the softer abrasive in the Brinell test or to the looseness of the abrasive which could possibly dig out the carbides more readily when the percentage of carbides is small. It therefore appears advisable to compare Mr. Haworth's abrasion results with

the quantity and type of carbide present. Information on the quantity and type of carbide may be approximately determined from the 850 °C level ternary iron-carbon-chromium diagram.[2] The wear results taken are the "Oil-Quenched Steel" in Table III of the paper under discussion. The results are shown in Table IX in order of decreasing total carbide content. Within the scope of the alloys in Table III there are three carbides, C_1, cementite; C_2 trigonal chromium carbide; and C_3, cubic chromium carbide. Only one alloy, DD1, appears to have the cubic chromium carbide present which is insufficient to evaluate it as to wear resistance because of the low percentage present. Otherwise the cementite and trigonal chromium carbide appear to have about the same effect on decreasing wear in proportion as the percentage of each increase. There are, however, indications that the trigonal chromium carbide is more resistant to wear than cementite. This is shown by the quartz results on alloys AA4 and BB4 versus CC4 and DD4 and also by the feldspar results of AA4 versus CC4 and AA3 versus CC3.

It is realized that the comparison is not exact as regards to quantity of carbides and no consideration is given to either distribution but it does throw some light on the factors controlling abrasion.

Written Discussion: By T. E. Norman, metallurgical engineer, Climax Molybdenum Company, Denver, Colo.

The author of this paper is to be congratulated on the development of a testing machine which shows good correlation between laboratory and field results on materials for sandslinger liners and blades for centrifugal abrading machines. Generally the wear testing of metal parts by laboratory methods has presented a problem because of the difficulty in duplicating conditions encountered in actual service.

One of the major contributions of this paper is, I believe, the introduction of the idea that elevated temperature hardness is an important factor in determining the abrasion resistance of materials under conditions involving rapid abrasion by dry or almost dry materials. This offers at least a partial explanation for the fact that white irons containing molybdenum carbides or complex carbides of chromium and molybdenum have given outstanding service in centrifugal abrading machines and in wearing parts for sandslingers.

In applying the results from Mr. Haworth's tests to the choice of materials to withstand other types of abrasion, I feel that considerable caution should be observed at this time. I believe that this is particularly true for applications where actual crushing or grinding of mineral particles is involved. The results and some of the conclusions from Mr. Haworth's tests on alloys containing primary carbides do not agree with those obtained from our wear tests on grinding balls (6)[3] or the American Brake Shoe Company's tests on their abrasion testing machine (8). These latter two methods of testing both involve the actual grinding of mineral particles rather than abrasion without grinding, such as occurs on Mr. Haworth's machine.

[2] METALS HANDBOOK, published by American Society for Metals, 1948, p. 1249.

[3] The figures appearing in parentheses pertain to the author's references.

Where grinding of mineral particles occurs in wet abrasive service, an indenting effect is produced by the mineral particles as they are pinched between two metallic surfaces. Consequently, high localized maximum pressures are involved on the metallic wearing faces which crush these minerals. As a result of the high unit pressures, most massive carbides in a white iron part fail, I believe, by crumbling, so that they offer little if any protection to the matrix of the iron. This hypothesis at least applies to the unalloyed or low alloy grades of white iron which we have studied in our wear tests on grinding balls. It also apparently applies to many of the higher alloy white irons which Avery studied in his wet quartz sand abrasion test (8). This relatively poor performance of ferrous compositions containing massive carbides, when exposed to service involving the grinding of minerals, is quite contradictory to the results obtained by Mr. Haworth on his machine where abrasion without appreciable grinding is involved.

Written Discussion: By Gorham W. Woods, metallurgical engineer, The Lincoln Electric Co., Cleveland.

This is considered a real contribution to the baffling phenomenon of the wear of metals. It is of interest to note that rate of wear on the test samples checks very closely with the rate of wear in actual service. We look forward to reading more publications of this work, especially when procedures are worked out to test samples for resistance to impact with varying degrees of abrasive wear.

We wish to add a word to possibly clarify the discussion of hard surfacing with the electric arc versus the oxyacetylene torch. See pages 839 and 840 (Hard Surfacing Section) and conclusion No. 7.

If a given hard surfacing rod is applied with oxyacetylene and also with the electric arc using normal procedures, the arc deposit will be diluted more by the parent metal than will the gas torch deposit. However, the amount of the dilution may be increased or decreased depending upon the welding procedure that is used.

The carbon content of the deposited metal may be increased if a carburizing oxyacetylene flame is used and it will be decreased with an oxidizing flame. It is possible to put on a thinner deposit with the torch than with the arc.

We wish to emphasize the fact that hard surfacing materials are designed for either arc deposition or gas application, but not for both. Gas rods are usually bare and the best arc electrodes are coated.

There are some nonferrous hard surfacing materials that lose a large amount of their abrasion resistant properties when diluted with iron. Hence these alloys should be deposited by the gas process.

There are many makes of hard surfacing rods that are designed for deposition by the electric arc process. These electrodes are coated to increase ease of deposition and also in some cases to add carbon, etc., to the deposit.

The alloy content of the electrodes is such that after dilution with iron from the base metal, a hard surfacing alloy will be obtained that has the desired resistance to abrasion, and to impact.

If one of the above electrodes were deposited by oxyacetylene, the resulting alloy would no doubt be more resistant to abrasion, but it probably would not have the required resistance to cracking and chipping.

It seems that with any type of surfacing material, the product of the resistance to impact and the resistance to abrasion is a constant. When one property is improved the other one suffers.

When two deposits are compared, both the resistance to abrasion and the resistance to impact should be checked, for invariably a change to increase the toughness will give a deposit that will not stand as much abrasion.

We conclude with the statement that there is a field for gas surfacing and one for arc surfacing, and that there is a complete series of materials for each process from the most ductile to those most resistant to abrasion.

Author's Reply

The author wishes to thank the numerous individuals who have expressed opinions regarding this paper, both verbal and written, for their kind comments, encouragement, and criticism.

We believe, in response to the queries concerning the mechanism of abrasion and wear, that we are merely on the threshold and not the culmination of our research in these interesting and important fields. Our theories, therefore, are somewhat conjectural and are expected to be subjected to modification (and perhaps complete revision) as additional evidence and data are accumulated.

Mr. Avery's discussion and data are highly valued contributions to the paper. Of particular interest is his correlation with Mr. Norman's ball mill data. The instances of disagreement are of as much interest and value, if not more, than those of confirmation.

The action of harder abrasives in generally causing more severe abrasion than softer ones is a logical expectation. However, in both Mr. Avery's and our studies, the effect of abrasive hardness may be overshadowed within limits by the angularity of the abrasive.

Our conclusions regarding hardness and carbon content refer specifically to the results obtained with our rubber wheel tester. Although similar in principle, the use of a metal wheel in the Brinell test probably produces results more nearly comparable to those in ball mill than in sliding abrasive service. Under wet or low speed dry abrasion, indentation hardness may be correlated to some extent with abrasion resistance but only for a given material. For materials of widely differing carbon content, no correlation of abrasion resistance and hardness (except microhardness) is evident in either Mr. Avery's or our results.

We can confirm Mr. Avery's statement that arc-deposited hard surfacing, when present in sufficient depth to make the factor of dilution negligible, is still inferior to gas-deposited material. This difference is not nearly as severe as the dilution effect in thinner arc-deposited layers and for practical purposes may not be important. The difference, when

dilution is negligible, possibly may be attributed to coarser structures and poorer carbide distribution caused by the more intense heat of arc deposition. At any rate, it is agreed that further investigation of the nature of hard surfacing deposits is warranted.

In reply to Mr. Avery's two questions, we feel that the wear of the sintered tungsten carbide specimens undoubtedly occurred chiefly in the soft cobalt matrix. This statement is based on the data which show increasing wear with increased binder content and the fact that deposits of tungsten carbide made with tube-type rods show severe erosion of the matrix around the particles with but little wear of the particles. In service, particles standing in relief might be broken off before their intrinsic abrasion resistance was realized.

In the centrifugal abrading machine blade tests, the wear apparently was caused primarily by the shot and not by sand contamination. Laboratory tests made with crushed shot (grit) correlated well with the field results whereas laboratory sand and quartz data showed no correlation with centrifugal abrading machine blade service. The poor performance of ordinary white iron in this unit is not understood clearly. No plain carbon steel blades were run in the field but laboratory results on ordinary white iron were actually poorer than those on hardened SAE 1045 steel. On the other hand, the performance of nickel-chromium white iron was far superior to that of the hardened steel.

Regarding reproducibility of results, our data normally check within 10% which is considered sufficiently accurate when reporting differences of many times this order. Additional tests are run when reproducibility of the initial tests is poor. The results are averaged or obviously faulty values are disregarded.

Mr. Czyzewski has mentioned a seeming discrepancy in the data with the conclusion that "if the microhardness of one constituent of an alloy is harder than that of the abrading material, the abrasion resistance will increase as the hardness and the amount of the hardest constituent are increased." In the instances of alloys AA1 and BB1 which were considerably higher in carbon content than SAE 1020 steel, constituents harder than ferrite, namely, martensite or other higher temperature transformation products, together with a minor amount of excess cementite admittedly were present. These, however, with the exception of the minor amount of cementite (which, therefore, exerts a negligible influence) are softer than quartz. In the presence of the severely abrasive crushed quartz, factors other than the difference in the hardness between ferrite and martensite appear to be more important.

Under the milder abrasive conditions obtained with crushed feldspar, which is intermediate in hardness between ferrite and martensite, the weight loss values on alloys AA1 and BB1 were lower than that on SAE 1020 steel. These latter results confirm the validity of the questioned conclusion; the quartz results do not invalidate it because only the small amount of poorly distributed cementite was actually harder than the abrasive.

Hot hardness values (shown in the table below) obtained on annealed and on hardened specimens of SAE 1045 steel at several temperatures offer a partial explanation for the observation that "under certain dry abrasive conditions, due to the temperatures developed, hardened plain carbon or low alloy steels are no better or are actually inferior to the same steels in the annealed or hot-rolled conditions."

DIAMOND PYRAMID HOT HARDNESS NUMBERS ON SAE 1045 STEEL—10 KG. LOAD*

Condition	Room Temperature	800° F	1000 °F	1300 °F
Annealed	191	147	92	58
Hardened	592	265	146	63

*Courtesy Climax Molybdenum Corp.

These hardness values were obtained under equilibrium temperature conditions, and therefore might be different from the instantaneous values at the wearing surface. Under severely abrasive dry conditions the extreme surface, perhaps only to a depth of a few molecules, actually may be above the critical temperature. Because of the very short duration of any surface increment at the extreme temperature before it is removed by the abrasive, the solution of carbides in the matrix probably would be much less than in conventional hot hardness tests. The latter, therefore, probably would be of little value in explaining the abrasion results. Instantaneous surface hardness values above the critical temperature may be higher in annealed than in initially hardened plain carbon steels. No method of determining instantaneous hot hardness values is apparent at this time.

Mr. Czyzewski has pointed out that the angularity of silica is a negligible abrasive factor in some of the more abrasion resistant alloys in Table III. The reason for this is that in contact with essentially harder materials, such as the large amounts of primary carbides in specimen DD4, the sharp edges of the crushed quartz are rapidly rounded and, therefore, have relatively less cutting efficiency than against less abrasion resistant materials. The rounding of sharp abrasive grains has been demonstrated clearly by running dry crushed quartz against sintered tungsten carbide for 1 hour at 250 rpm. The grains which were originally jagged, as shown in Fig. 8b, were rounded considerably and were more nearly comparable to the Ottawa sand grains in Fig. 8c. This would indicate that the more abrasion resistant materials wear the abrasive rather than vice versa.

Mr. Czyzewski's calculations are of interest and will be kept in mind during subsequent investigations of the fundamentals of abrasion and wear.

Mr. Fetzer's analysis of our data in regard to the effect of carbide type is interesting and confirms our unpublished findings that alloys containing high percentages of trigonal carbides show superior abrasion resistance. However, the matrix properties of such alloys are equally important. For example, if alloys CC4 and DD4 were annealed, their abrasion resistance would be much poorer than that shown for the respective as-cast or quenched specimens.

As Mr. Norman has pointed out clearly, the principal difference between our machine and almost all other prior abrasion testing devices is the lack of concentrated high localized pressure on the individual abrasive grains. Such high pressure causes crushing of minerals and undoubtedly crumbling of massive carbides.

In our tests, the resiliency of the normally used rubber wheel protects mineral particles from crushing. Breakdown of the abrasive particles is generally negligible in sliding abrasion applications to which the machine has been applied almost exclusively. These applications are more numerous and diversified although perhaps not as important as those involving grinding of mineral particles in respect to tonnage of materials consumed.

In reply to Mr. Woods, the question of combining abrasion and impact tests has been discussed previously and the conclusion reached that such a combined test is impractical. For applications involving severe shock, separate impact tests have been employed. A typical illustration of this approach was in the selection of materials for special wheel excavator teeth. The impact test consisted of a repeated 400 foot-pound blow on the points of actual teeth. Materials without the requisite shock resistance were eliminated quickly in this manner. The more abrasion resistant materials which withstood the impact were recommended for field tests. An additional advantage of the impact tests was that the effects of tooth design modifications also could be evaluated.

A more complete dissertation on the subject of hard facing appeared in a recent issue of *Iron Age*.[4] Included are laboratory and field test data together with chemical analyses which illustrate clearly the effect of dilution produced in arc welding. These results illustrate that other hard surfacing materials in addition to nonferrous compositions lose a large degree of their abrasion resistance when diluted with iron. In these tests both coated arc and uncoated gas welding rods were obtained from the manufacturers. Abrasion tests on specimens gas deposited with both rod materials (the arc rod coating was broken off prior to welding) showed almost identical results.

The conclusion was reached that many manufacturers use the same analysis for arc and gas deposition. Actually, in order to obtain results comparable to gas welding, electrodes intended for deposition in thin layers should contain additional carbon and alloy content in the coating or base metal to compensate for the greater dilution obtained. For heavier deposits ($\frac{3}{32}$ inch or thicker) such compensation is less important. However, in order to obtain consistent results, a fairly uniform deposit thickness should be established. Likewise, to obtain uniform results by gas welding, precautions must be taken to maintain consistent flame characteristics.

---

[4]R. D. Haworth, Jr., "Effect of Welding Practice on Abrasion Resistance of Hard Facings," *Iron Age*, Vol. 162, October 7, 1948, p. 82.

A VERSATILE VACUUM-FUSION APPARATUS

By Manley W. Mallett

Abstract

The vacuum-fusion method is a valuable metallurgical tool for the estimation of gases in metals. Details of the construction and operation of a vacuum-fusion apparatus are given. One unusual feature is that the gas sample is removed from the extraction apparatus by a fully automatic Toepler pump and analyzed in a modified Orsat apparatus. This versatile apparatus is used for gas analysis of plain carbon and certain alloy steels, nonferrous metals, alloys, and powders by vacuum fusion in graphite. In addition, analytical vacuum fusions in oxide (i.e., BeO) crucibles are made and small experimental alloy ingots are prepared.

Analytical difficulties arising from the presence of large inclusions of Al_2O_3, glassy SiO_2, and refractory nitrides are discussed. Vapors of chromium and titanium tend to cause low nitrogen (and perhaps oxygen) analyses.

Introduction

THE development of the modern vacuum-fusion method for the determination of oxygen, hydrogen, and nitrogen is usually ascribed to Oberhoffer and his co-workers whose work was reported in *Stahl und Eisen* at various times from 1922 to 1929, and to Jordan and Eckman (1)[1] of the National Bureau of Standards. The improved version (2) of the Bureau's apparatus still is copied extensively by other investigators. Although early workers used resistance heaters, high frequency induction heating, first used by Jordan and Eckman, is now quite universally employed. Many modifications have been made in the design of crucibles, thermal insulation, and sample storage chambers. Several widely different methods of analyzing the extracted gases are now in use. Most of these variations are summarized in Gmelin's Handbuch (3). Thompson,

[1]The figures appearing in parentheses pertain to the references appended to this paper.

A paper presented before the Thirtieth Annual Convention of the Society, held in Philadelphia, October 23 to 29, 1948. The author, Manley W. Mallett, is research engineer, Battelle Memorial Institute, Columbus, Ohio. Manuscript received March 9, 1948.

Vacher, and Bright (4), in their report on the cooperative study of methods for the determination of oxygen in steel, record the essential features of a number of vacuum-fusion apparatus and compare the results obtained by various laboratories on samples of eight representative steels. Results obtained by chemical methods are also given.

Reeve (5) developed a fractional vacuum-fusion method by which the distribution of the oxygen of a steel among the various oxides, FeO, MnO, SiO_2, and Al_2O_3, could be determined. Hoyt and Scheil (6) applied this modification to the eight Cooperative Steels mentioned above and showed that, when the fractional oxide analysis is used in conjunction with polarized light, a rather complete understanding of the oxide inclusions is obtained.

Sloman (7) has written a very adequate description of the vacuum-fusion method including details of several apparatus now in use in Great Britain. Therefore there is little need, in this paper, for extensive commentary on the method in general.

The vacuum-fusion method was developed primarily for the determination of oxygen in plain carbon steels and was later found to give a rather reliable estimate of the nitrogen (8) and hydrogen content. The method, as applied to ordinary steels of quite low alloy content, gives accurate and reproducible results. However, the method has in many cases been used for analysis of high alloy steels and nonferrous metals and powders (9). Unqualified accounts of the analyses of high alloy materials have appeared from time to time with claims of accuracy of the order of $<\pm 0.001\%$ for both oxygen and nitrogen. It appears that in some cases reproducibility and precision have been mistaken for accuracy. Reasons why these results should be viewed with suspicion will be given in the present paper. At the same time, it will be shown that values obtained for many materials of unusual composition are highly significant and extremely useful.

In 1940, a cooperative project, sponsored by the Crucible Steel Company of America and Battelle Memorial Institute, was set up for the development of a versatile vacuum-fusion apparatus for the analysis of high alloy tool and heat resistant steels and a wide variety of other metals.

Because the apparatus was to be used for the fractional vacuum-fusion method of analysis as well as the total method, several of the features of the fractional apparatus developed at the A. O. Smith

Corporation were included in the design. Reeve's (5) method of analyzing the extracted gas in a separate Orsat apparatus was adopted, as well as an improved modification of the automatic Toepler pump designed at the A. O. Smith Corporation.

The resulting apparatus will be described, and results obtained on a heterogeneous array of materials discussed. The desirability of a versatile and rugged apparatus to produce useful figures will be stressed.

The Apparatus

A photograph of the vacuum-fusion apparatus is shown in Fig. 1 and a schematic diagram in Fig. 2. The essential details of the apparatus may be described as follows. The melting crucible is heated by an induction coil 4-inch I.D. by 4 inches in length containing 4 turns of flattened ¼-inch copper tubing per inch. The coil is energized by a 7½ kw., 300 kc. Lepel High Frequency Laboratories, quenched gap-type converter. The fused-silica furnace tube ($2\frac{9}{16}$-inch I.D. by $2\frac{15}{16}$-inch O.D. by 18 inches) is connected by picein wax to a brass head containing a revolving sample magazine (see Fig. 3) which can hold seven samples (⅝ by 2 inches). It is interesting to note that, although this head has been in continuous use for 7 years, there is no evidence of embrittlement by mercury vapor. This is in marked contrast to the observation of one investigator (10) who reports serious embrittlement in less than 9 months. The head is water-cooled and additional protection of the wax seal is obtained by playing a 10-inch fan on the furnace tube on a level with the induction coil. The coil may be raised or lowered over an 8-inch distance by means of a crank-actuated screw.

A unique feature of the storage head is a pyrex glass baffle disk which turns with the magazine and catches spatter and vaporized metal which ordinarily would deposit on the sight glass in the cover. Thus, a clean window comes into position with each sample. The magazine is keyed to a greased, tapered plug that is indexed and provided with a pointer to indicate which chamber is in line with the sight hole.

The furnace head is connected to a steel manifold (1½-inch I.D.) by a tongue-and-groove joint, sealed with a rubber gasket, and is readily disconnected for changing furnace tubes. The manifold, fabricated from seamless tube turns by welding, is only 12

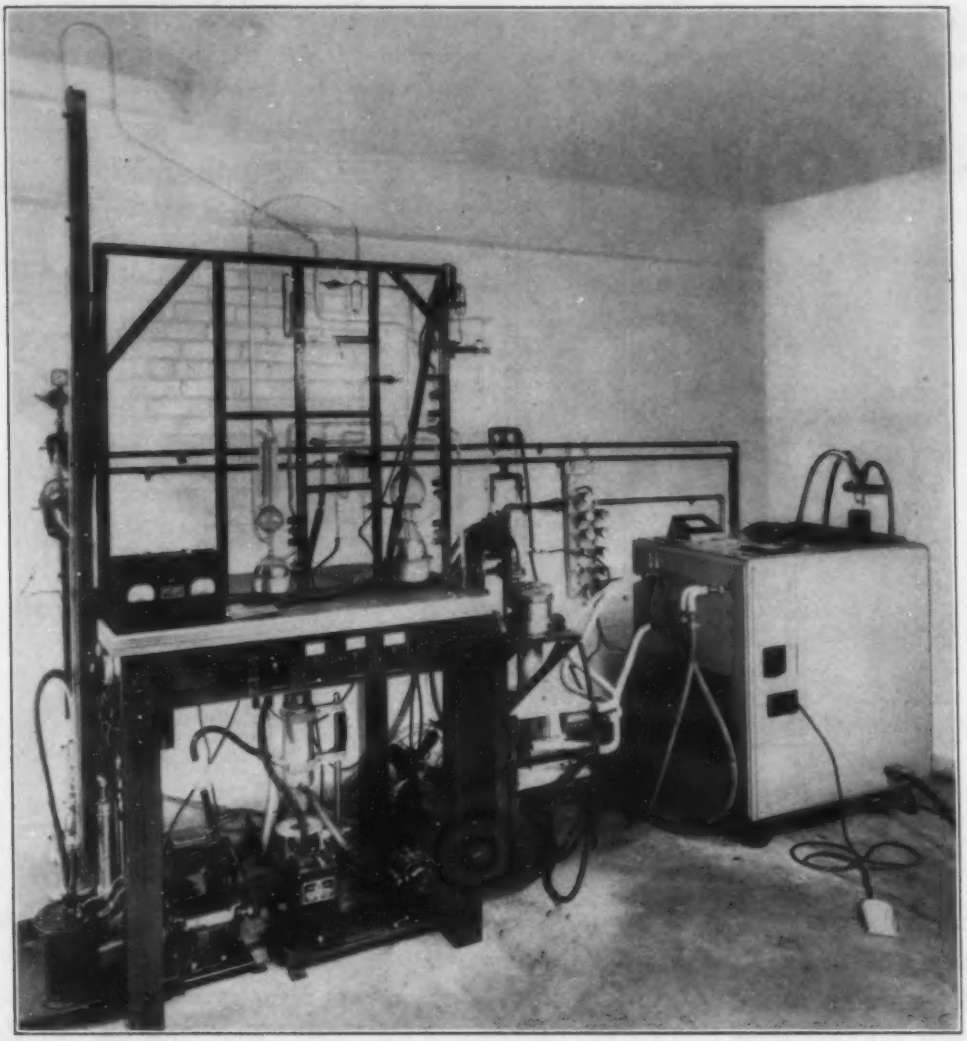


Fig. 1—The Vacuum-Fusion Apparatus.

inches in length. Since it is the same diameter as the inlet end of the vacuum pump, the manifold diminishes the pumping speed very little.

The crucible assembly is placed on a bed of alumina sand (carbon analysis grade), about 1-inch thick, in the bottom of the silica furnace tube. This assembly, shown in Fig. 3, consists of a graphite heater crucible (1-inch I.D. by $1\frac{3}{16}$-inch O.D. by 4 inches) packed in 60-mesh graphite powder contained in a beryllia thimble. Alumina thimbles have been used, but they are less satisfactory because they tend to react with the hot carbon. A smaller melting crucible ($\frac{3}{4}$-inch I.D. by $\frac{15}{16}$-inch O.D. by $3\frac{1}{2}$ inches) is placed inside the heater

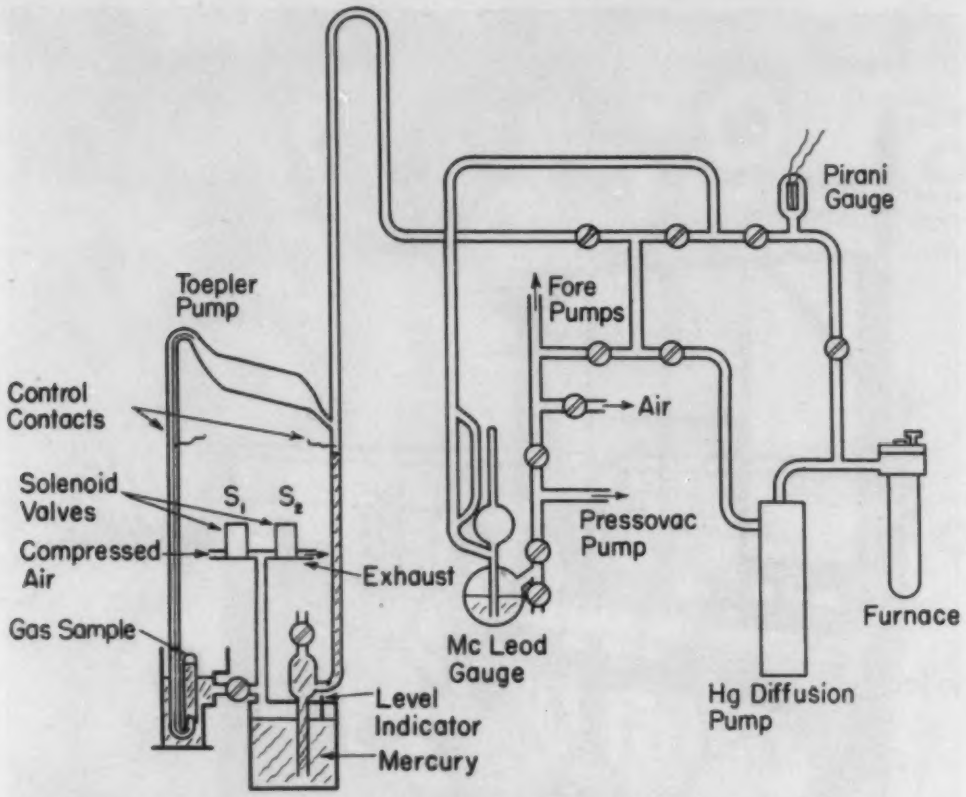


Fig. 2—Schematic Diagram of the Vacuum-Fusion Apparatus.

crucible. After an analysis, the melting crucible is discarded and a new crucible put in place without disturbing the rest of the assembly. A graphite guide tube rests on top of the melting crucible. This is split on one side to prevent induction heating. The graphite guide tube is connected to a silica guide tube 6 to 8 inches in length leading to the furnace head.

A Gaede, all-metal, 3-stage, mercury diffusion pump, type E, is used to evacuate the furnace. This pump has a pumping speed of 15 to 20 liters per second at 10^{-3}-mm. pressure with a back pressure of 20 mm. Hg. The ultimate vacuum obtainable is 10^{-6} mm. Hg. The metal pump coupled with the metal manifold and furnace head comprises a very sturdy and trouble-free assembly. A Pirani gage is connected to the manifold to give a continuous indication of the pressure in the furnace.

A satisfactory substitute for the Gaede pump, which is not generally available, has been assembled by combining a Cenco Supervac all-metal, mercury diffusion pump and a glass one-stage injector-

type mercury pump similar to that described by Kraus (11). The Supervac supplied the high speed diffusion stage needed for rapid pumping, while the injector stage worked well against a back pressure as high as 20 mm. Hg.

Oil diffusion pumps, so widely used for other purposes, were considered as a substitute for mercury pumps, but were rejected for

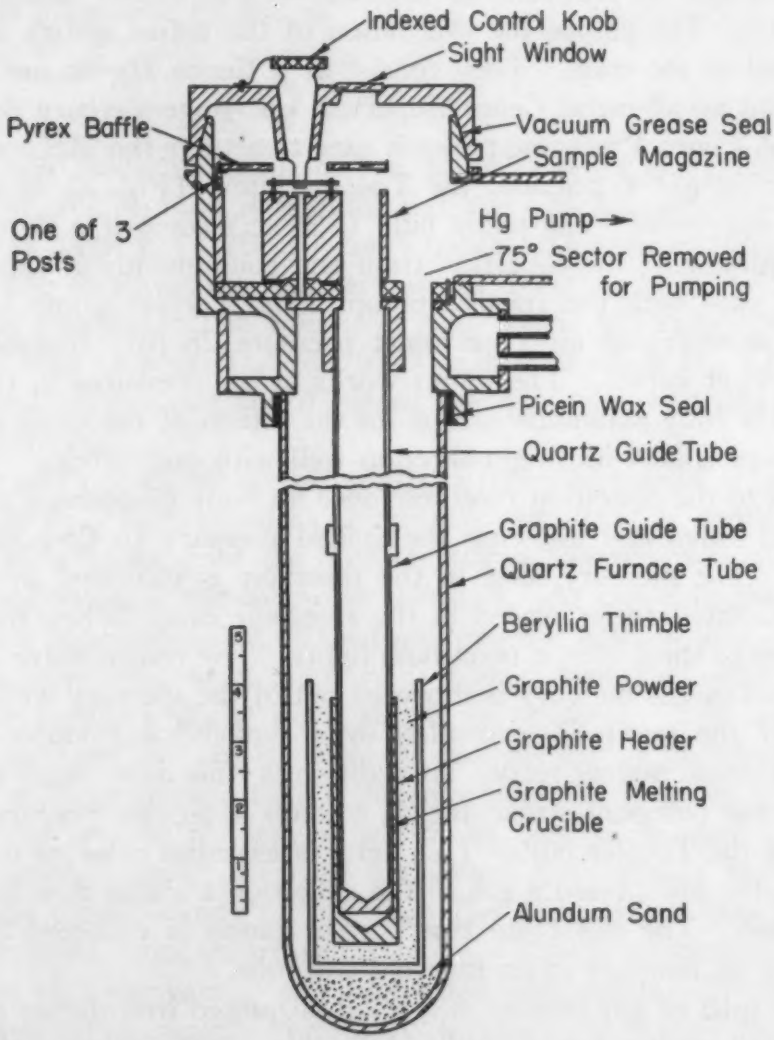


Fig. 3—Diagram of the Vacuum-Fusion Furnace Assembly.

a number of reasons. Because the extracted gases build up a pressure in the collection system, the furnace pump must be capable of working against a back pressure of 15 to 20 mm. Hg. Most oil diffusion pumps are stopped by back pressures of 100 microns or less. In addition, there is the possibility of gaseous products being

produced by the decomposition of the oil in the pump. The oil may also diffuse back into the furnace, reacting with the hot crucible and molten metal, thus vitiating the analytical results.

The collection train consists essentially of a line of 10-mm. pyrex tubing leading to an automatic Toepler pump. Connected to the train is a large range McLeod gage (0.0002-9.0 mm.). This gage may also be connected to the furnace side of the Gaede pump, if desired. The pumps for evacuation of the entire system are also connected to the train. They consist of a Cenco Hyvac mechanical pump and an all-metal Cenco Supervac, one-stage-mercury diffusion pump. A Cenco Pressovac pump is used to actuate the McLeod gage.

During gas extraction, the Toepler pump (Fig. 2) is in continuous operation. The pump bulb (750 cc.) comprises about 75% of the volume of the collection train and consequently is capable of keeping pace with the furnace pump. The Toepler pump is operated by compressed air (maximum pressure 28 psi) controlled by two solenoid valves. The pump works at all pressures in the system and is fully automatic except for the return of the small amount of mercury spilled into the collection well with each stroke. This is returned to the operation reservoir once an hour by opening a stainless steel valve and allowing the spilled mercury to flow back by gravity. The mercury level in the reservoir is indicated by means of an insulated feeler placed in the reservoir cap. When the mercury rises to the feeler, a neon bulb lights. The return valve is then closed and excess mercury is dippered out of the mercury well. The action of the pump is controlled by a double-pole, double-throw, normally open, midget relay. In addition, a time-delay relay is used to delay the pumping stroke for 25 seconds after the mercury empties from the Toepler bulb. This delay is essential in order to allow time for the low pressure gas in the collection train to flow into the pump bulb. The gas from the Toepler pump is collected by displacement of mercury in an inverted test tube.

The tube of gas resting in a small lacquered iron dipper is then stored until analyzed in a modified Bureau of Mines type (Burrell Build-Up Model) Orsat apparatus. This is equipped with a mercury well and a long capillary J-tube for introduction of the sample to the gas burette. About 15 cc. of inert gas is retained in the Orsat apparatus at all times to provide sufficient volume to carry small gas samples through the absorbent solutions. All volumes, of course, are determined by difference. The absorbent solutions used are KOH

(33%) for CO_2, alkaline pyrogallol for O_2, and Cosorbent (Burrell proprietary solution) for CO. The decrease in volume caused by the oxidation of H_2 as the gas passes over CuO (300 °C) is the measure of the H_2 content of the sample. The difference between the residual unabsorbed gas and the original volume of inert gas is the volume of N_2 present. The gas burette has 0.10-ml. graduations and 0.05 ml. can be estimated.

Operation

When analyzing plain carbon steels, five or six samples are loaded in the storage magazine, and the crucible assembly is degassed at 2300 °C (4170 °F) for 4 hours. The temperature is then lowered to the operating temperature of 1650 °C (3000 °F), and a blank is collected. The volume of this gas is generally about 0.60 ml. per hour of which 0.20 ml. is CO and 0.40 ml. is H_2. The samples are then dropped and degassed one at a time with the Toepler pump running.

In many cases the evolution of gas from the sample is over 90% complete in 3 to 5 minutes. However, extraction is continued for 15 to 20 minutes until the Toepler pump has removed all of the extracted gas to a test tube over mercury. At this time the rate of evolution approaches that of the blank gases. Without delay, another sample tube filled with mercury is placed over the outlet of the Toepler pump, and the next sample is dropped. This procedure decreases interference from volatilized metals by minimizing the time for their vaporization from the melt. In systems where the melt must be held for longer periods of time while analysis of the gas is carried on in the collection train, considerable vaporization may take place building up reactive metal films, which tend to getter gases evolved from subsequent samples. This is particularly noticeable in high-manganese and high-chromium steels. If necessary, the extracted gas may be stored over mercury for several days before analyzing. In the meantime, the apparatus is free for further gas extraction or other work.

Analytical Results of Plain Carbon Steels

When the apparatus was first completed, its performance was checked by analyzing samples of the Cooperative Steels (4). As

shown in Table I, the analyses for all eight steels checked, or were satisfactorily close to, the "best" values chosen from the results obtained by a number of laboratories. It appears that for rapidity and accuracy in determining the total oxygen content of plain carbon

Table I
Oxygen Analyses of the Co-operative Steels by the Total Vacuum-Fusion Method

Steel No.	Values from Co-operative Study — Acceptable Range, %	Values from Co-operative Study — "Best" Value, %	Battelle Memorial Institute, %
1	0.016–0.020	0.018	0.018
2	0.012–0.018	0.017	0.015
3	0.014–0.020	0.017	0.017
4	0.001–0.004	0.002	0.003
5	0.007–0.011	0.009	0.011
6	0.005–0.008	0.007	0.007
7	0.100–0.110	0.106	0.100
8	0.015–0.019	0.017	0.017

Table II
A Comparison of Fractional Oxide Analyses Obtained by Battelle Memorial Institute and Hoyt and Scheil

Co-operative Steel No.	Investigators	Weight, % Oxygen — FeO	MnO	SiO_2	Al_2O_3	Total
1	Battelle	0.004	0.011	0.001	0.002	0.018
	Hoyt and Scheil	0.002	0.013	0.001	0.004	0.020
2	Battelle	0.001	0.005	0.005	0.003	0.014
	Hoyt and Scheil	0.001	0.006	0.006	0.001	0.014
3	Battelle	0.002	0.007	0.006	0.003	0.018
	Hoyt and Scheil	0.002	0.011	0.004	0.004	0.021
4	Battelle	0.000	0.000	0.001	0.002	0.003
	Hoyt and Scheil	0.000	0.000	0.001	0.004	0.005
5	Battelle	0.001	0.004	0.003	0.001	0.009
	Hoyt and Scheil	0.000	0.004	0.007	0.001	0.012
6	Battelle	0.001	0.003	0.003	0.002	0.009
	Hoyt and Scheil	0.000	0.003	0.002	0.001	0.006
7	Battelle	0.093	0.005	0.000	0.000	0.098
	Hoyt and Scheil	0.100*	.....	0.003	0.000	0.103
8	Battelle	0.001	0.002	0.005	0.009	0.017
	Hoyt and Scheil	0.000	0.002	0.009	0.005	0.016

*FeO and MnO fractions combined.

steels the vacuum-fusion method is superior to other methods. The Cooperative Steels were also analyzed by the fractional oxide method. In Table II the values obtained are compared with those reported by Hoyt and Scheil (6). Despite the personal factor involved in the sometimes difficult task of deciding when a fraction is complete, a generally good agreement is shown.

In order to compare the vacuum-fusion nitrogen analyses with the chemical method, analyses were made on a number of plain carbon steels which were also analyzed by the wet-digestion method

Table III
Chemical Analysis of Steels Used in the Comparative Study of Nitrogen Analyses

Sample	C	Mn	P	S	Si	Ni	Cr	Mo
B	0.12	0.85	0.104	0.39	0.02	0.02	0.01	0.01
O	0.15	1.13	0.116	0.146	0.02	0.02	0.01	0.01
OI	0.52	0.82	0.014	0.028	0.17	0.02	0.04	0.04
ROH	0.24	0.47	0.010	0.027	0.04	0.06	0.05	0.01
RB	0.09	0.38	0.091	0.030	0.17	0.03	0.01	0.01
DB	0.16	0.48	0.010	0.030	0.06	0.01	0.01	0.01

by laboratories at the American Rolling Mill Company, the National Bureau of Standards, and the Duquesne Steel Works of the Carnegie-Illinois Steel Corporation. The compositions of these steels are given in Table III, and the nitrogen analyses in Table IV. It will be noted that there is as good an agreement between the vacuum-fusion and the chemical method as between the various wet methods themselves. On all samples, the agreement may be considered quite satisfactory. Similar agreement between the two methods is almost invariably obtained whenever plain carbon or low alloy steels are analyzed (12).

Hydrogen is extracted along with the oxygen and nitrogen of the steel sample. The hydrogen values obtained by the vacuum-fusion method are comparable to those obtained by the warm-extraction (13) method. Although hydrogen may be completely extracted by either method, the analysis of the usual sample is often of no significance. Because of the fugitive nature of hydrogen, which can diffuse from steel at room temperature, the hydrogen which damaged a steel may no longer be present at the time of analysis. Recently, the importance of sampling during pouring has been emphasized. Such samples tend to contain much greater quantities of hydrogen, which show better correlation with defects in steel than do the residual amounts present after storage.

Table IV
A Comparative Study of Nitrogen Analyses

	Nitrogen, Weight, %					
	B	O	OI	ROH	RB	DB
Battelle Memorial Institute*	0.010	0.010	0.003	0.003	0.011	0.010
	0.011	0.008	0.002	.....	.....	.....
American Rolling Mill Company**	.....	0.010	.....	0.003	0.011	0.013
National Bureau of Standards**	0.0133	0.0112	.....	0.004	0.0128	0.0125
Duquesne Steel Works, CIL**	0.0116	0.0098	0.003	0.0039	0.0135	0.0107

*Vacuum fusion.
**Wet digestion.

Table V
Vacuum-Fusion Analysis of Various Materials

Material	Weight, % O_2	H_2	N_2
Bronze, Type M	0.002	0.00007	0.001
Cobalt, pellets	0.22	0.01	Trace
Cobalt, electrolytic	0.034	0.003	<0.001
Cobalt, electrolytic	0.16	0.015	Trace
Chromium, 98-99%, carbide free	0.05	0.0003	0.02
Chromium, electrolytic	0.67	0.047	Trace
Chromium, powder	0.05	0.0014	<0.01
Chromium, powder	0.53	0.013	Trace
Chromium alloy, 18 Cr-8Ni+Cb	0.013	0.0003	0.24
Chromium nitride—oxide mixture	2.1	0.32	2.8
Chromium nitride—oxide mixture	1.4	0.002	18.9
Copper, OFHC	0.0007	0.00013	Trace
Copper, electrolytic	0.0015	0.00017	Trace
Duriron	0.003	0.0002	0.001
Duriron, hot cracked pipe	0.014	0.0005	0.002
Ferro-silicon	0.005	0.0003	0.001
Ferro-silicon, 77% Si	0.024	0.003	0.003
Iron, nodulized	1.2	.....	Trace
Iron, powder, from ferric chloride	4.3	0.017	Trace
Iron, powder, Swedish sponge	1.5	0.007	Trace
Iron, powder, malleableized white iron	0.54	0.005	Trace
Magnet metal, iron-iron oxide	13.4	0.34	0.7
Molybdenum, lump	0.003	.....	....
Molybdenum, powder A	0.06	.....	.....
Molybdenum, powder B	0.65	.....	.....
Nickel, electrolytic	0.40	0.019	Trace
Titanium, lump	0.042	0.013	0.02
Titanium oxide, after treatment to remove oxygen	38.0	.....	.....
Tungsten, powder	0.20	0.003	Trace
Weld metal, Unionmelt	0.051	0.0001	0.005

Analysis of High Alloy Steels and Nonferrous Materials

The accuracy obtained on plain carbon steels is about ±0.001% for both oxygen and nitrogen. Table V contains typical analyses of a very wide variety of nonferrous and high alloy materials. The analyses of some of these materials, such as bronze, copper, duriron, ferrosilicon, molybdenum (lump), and weld metal, have an accuracy and precision similar to the plain carbon steels. With higher gas contents, the precision becomes less because the sample size must be diminished to keep the volume of extracted gas under control. In most vacuum-fusion apparatus, a total volume of evolved gas of less than 10 cc. is desirable. The three samples of molybdenum (Table V) illustrate nicely how the significant figure shifts from 0.001% to 0.01% to 0.1% oxygen. From a practical standpoint, a precision of ±0.1% for the molybdenum sample analyzing 0.65% oxygen is entirely adequate, for, after all, the producer of this sample was trying to make a material of about 0.003% oxygen and not one of 0.650% ±0.001% oxygen.

The researcher who submitted the sample of TiO_2, analyzing

38% oxygen, hoping he had produced titanium metal of perhaps 0.04% oxygen content, gladly changed his technique on the next run without insisting that the full stoichiometric amount of oxygen should have been obtained. Of course, the operator of the vacuum-fusion apparatus was somewhat disconcerted when the evolved gas exceeded that anticipated by 1000 fold. This is not pleading the case for sloppy techniques, but rather is pointing out that insistence on extreme precision should be confined to cases where it is justified. Both the nature of the sample and use to be made of the results must be considered. With this in mind, it is seen that many of the analyses reported in Table V are very useful figures, although in many cases they are the product of extemporaneous modifications of the vacuum-fusion method. For instance, the analyses of chromium nitride – chromium oxide mixtures are of samples from a series of attempts to produce material of a high chromium nitride content. The first attempt showed only 2.81% nitrogen while, after a number of modifications, one of the final runs produced 18.9% nitrogen. The vacuum-fusion apparatus proved to be a valuable analytical tool in that investigation.

A correlation was found between vacuum-fusion oxygen results and the properties of magnet materials (iron-iron oxide). A number of other materials listed will be recognized as addition materials for alloys. Their analyses enable one, to some extent, to anticipate their behavior in the bath and their effect upon the final analysis of the melt. For example, the analysis of the sample of electrolytic cobalt that contains 0.16% oxygen and 0.015% hydrogen shows that considerable oxygen must be removed during the melt, while the high hydrogen content predicts considerable boil from this source unless precautions are taken to remove it before melting.

It is evident that very accurate analytical results are obtainable on the class of materials for which the vacuum-fusion method was devised, and, in addition, many valuable approximate analyses are obtainable on a wide variety of other materials for which no other method of gas analysis presently exists.

Techniques for Powders and Nonferrous Metals and Alloys

Samples for vacuum-fusion analysis should, preferably, be in massive form with the smallest possible surface area. Interference caused by large surface areas was found by Thompson and Holm

(14), and substantiated by Sloman and Rooney (15). More recently, Alexander, Murray and Ashley (10) have discussed this point. However, in certain cases, such as when finely divided material is to be used in charging a melt, an analysis which includes surface oxide and adsorbed gases will give a truer value of the gases that will be carried into the melt than would an analysis of "clean" material. With the growth of powder metallurgy, finely divided metals have become quite common.

Loose powders of high gas content tend to blow from the analysis crucible. In analyzing such samples, it was found convenient to compress the powders into metal wafers, ½ inch in diameter by any desired thickness, at 50,000 psi. This converts the powder into a convenient massive piece and eliminates the necessity of adding a foreign material to the sample as is done when the powder is wrapped in foil or enclosed in a metal capsule.

The results shown in Table V give some idea of the typical gas content of a variety of materials, and demonstrate the versatility of the vacuum-fusion method. The only modification required to handle most nonferrous materials is the use of a bath of degassed iron in which to drop the sample. In the case of metals such as W, Mo, Ta, or Ti, the iron fluxes the sample and forms alloys with melting points similar to steel. Any good compilation (16) of binary-alloy data is a convenient guide to the proper ratios of sample to iron in the bath.

The iron bath not only fluxes high melting point materials, but it also carries carbon into metals, such as copper, which have low carbon solubility. The bath also serves to reduce the partial pressure of volatile metals, such as Cr, Ti, etc., and thus decreases interference from their vapors. When melting volatile metals, it is sometimes helpful to vaporize a few grams of tin between samples so as to cover the freshly deposited reactive metal with the rather inert tin and so prevent gettering of evolved gases.

Techniques for handling nickel, cobalt, copper, chromium, manganese, silicon, tungsten, and various alloys have been discussed by Sloman (7). Our experience with these materials has been similar, with the exception of nickel and cobalt which we found to dissolve sufficient carbon (2 to 3%) quite readily.

In addition to analysis in a graphite crucible, the apparatus is useful for work in BeO crucibles. For example, the carbon content of copper was determined by adding CuO to the copper melt, oxidiz-

ing the carbon content to CO_2 and CO. Results of 0.0005 to 0.0010% were obtained. These values fall within the limits of solubility found by Bever and Floe (17). Semi-vitreous BeO crucibles are only very slowly reduced by contact with hot carbon and have been used inside graphite-heater crucibles at temperatures up to 2000 °C (3630 °F). By use of such a crucible assembly, the vacuum-fusion apparatus becomes an excellent set-up for making small experimental melts. It is superior to most vacuum-furnace set-ups in that the entire charge can be stored in the sample magazine while the crucible is brought to temperature and degassed. Metals, such as chromium, which tend to be oxidized (even in a vacuum) by gases given off upon first heating a crucible assembly, are readily melted when dropped into the hot crucible. Additions of volatile metals are made with a minimum loss because of rapid melting.

Inaccuracies in Vacuum-Fusion Analyses

The highly satisfactory results obtained in the vacuum-fusion analysis of plain carbon and low alloy steels have been discussed. Ziegler (18) found that all of the usual oxide compounds found in steels are readily reduced by the carbon of the melt if the particle size was small enough and if the particles were separated by the addition of graphite powder to prevent agglomeration. Unfortunately, the nonmetallic inclusions of an occasional steel sample will be too massive to be reduced in any reasonable extraction time. Thompson and Holm (19) report difficulty with certain samples containing Al_2O_3 particles of greater than normal size, particularly when the melt contained volatile metals.

We have found it impossible to reduce the large particles of Al_2O_3 produced in bomb test samples killed with a large excess of aluminum. The particles floated to the top of the vacuum-fusion melt where their reduction took place too slowly to be completed. Tenenbaum and Brown (20) give a comparison of results obtained by gravimetric and vacuum-fusion methods on this type of sample. While samples containing 0.010% oxygen tend to give but slightly low results, one yielding 0.106% oxygen by the gravimetric method gave only 0.061% by vacuum fusion.

Similar difficulty is also encountered when rather large, clear, globular SiO_2 inclusions are present. On the other hand, mixed sulphide-silicate inclusions of the same size are readily reduced.

Certain steels fall into a borderline class in respect to inclusion size. These steels give accurate results by the total vacuum-fusion method, but give low results by the fractional vacuum-fusion method where the melt is held a rather long time at 1060 to 1320 °C (1940 to 2410 °F) during which time the more refractory oxides float to the top of the melt and agglomerate, forming masses difficult to reduce.

Interference of vaporized manganese with oxygen analyses has been widely discussed, and it is customary to provide a high speed pump to remove gases from the furnace as rapidly as they are evolved in order to minimize this effect. Similar trouble with aluminum vapor (16) has been found. Interference from such metals as chromium, titanium, etc., in oxygen analyses apparently has not been investigated to the same extent, chiefly because chemical methods of checking are laborious, time-consuming, and of doubtful accuracy themselves. However, such interference may exist as is evidenced by the effect of these metals on nitrogen analyses.

Sloman (7) has discussed some of the difficulties encountered in analyzing high silicon steels which tend to form kish in the crucible, giving a mushy semi-solid mass in which bubbles of gas are trapped. This condition can be avoided by dropping the sample into an empty crucible or by analyzing samples in such an order that the per cent of silicon in the melt is never increased, because an increase in silicon causes graphite to precipitate. In addition, silicon seems to soak into the graphite, causing it to swell and crack, probably through the formation of silicon carbide. When the concentration of silicon is kept low, this does not occur.

Phragmen and Treje (21) have shown that the agreement in nitrogen analyses by the chemical and vacuum-fusion methods on low alloy steels does not generally hold for high chromium steels or when titanium is present. Although we have been able to extract a greater portion of the nitrogen from ferrotitanium materials than they indicate, titanium- and zirconium-bearing steels give erratic and low nitrogen results. Finely divided nitride particles seem to be decomposed easily, but the larger nitride inclusions are not entirely decomposed. It appears that the refractory nitrides that remain after completion of the initial boil (CO and H_2) are never completely decomposed. Phragmen and Treje obtained about 4.25% nitrogen from titanium carbide by both vacuum-fusion and chemical methods. This suggests an analogy between the cyano nitrides and the sulphur-

Table VI
Nitrogen Analysis of 25-20, Chromium-Nickel Steels

Sample	Weight, % Nitrogen	
	Vacuum Fusion	Chemical
A	0.046	0.052
B	0.037	0.046
C	0.038	0.057
D	0.036	0.045
E	0.043	0.053
F	0.037	0.046
G	0.044	0.054

silicate inclusions and substantiates the belief that mixed-type inclusions are more readily decomposed than the single-phase type.

To illustrate the effects of titanium further, a sample of 18-8 Ti steel was analyzed by vacuum fusion both at Battelle and at the Crescent Laboratory of the Crucible Steel Company of America. The vacuum-fusion results of both laboratories were in agreement (0.012% nitrogen), but this result was definitely low compared to chemical analysis (CSC) which yielded 0.024% nitrogen.

Vaporized chromium tends to absorb nitrogen evolved from the melt, causing low results. Table VI contains typical results obtained on 25-20 Cr-Ni alloys. The vacuum-fusion nitrogen results rather consistently run about 0.010% lower than those obtained by the chemical method, and less nitrogen is recovered as successive samples are analyzed. Consequently, no more than three samples of high chromium alloys are melted in one run.

The difficulties described above are encountered in but a minor percentage of samples. The vacuum-fusion method is applicable to many metals and alloys with little modification and has proved itself to be a valuable metallurgical tool for estimating the gas content of metals.

Summary

The work presented in this paper may be summarized as follows:

1. A vacuum-fusion apparatus of simple design and rugged construction is described.

2. Vacuum-fusion analyses of plain carbon steels have an accuracy of ±0.001% for both oxygen and nitrogen.

3. The significance of results obtained in the analysis of nonferrous materials of high gas content is discussed.

4. Techniques are given for the analysis of powders, nonferrous metals and alloys.

5. Inaccuracies in vacuum-fusion analyses are discussed, particularly the problems of massive nonmetallic inclusions and metallic vapors.

ACKNOWLEDGMENTS

I wish to express my appreciation for the opportunity afforded me by Battelle Memorial Institute and the Crucible Steel Company of America to develop this apparatus. I am particularly indebted to Dr. S. L. Hoyt, Dr. H. R. Nelson, and Dr. H. W. Russell of the supervisory staff of Battelle Memorial Institute for their valuable advice and suggestions during the construction of the apparatus and for their continued interest in the vacuum-fusion method.

Grateful acknowledgment is made to the A. O. Smith Corporation for their cooperation and assistance in design problems and to the National Bureau of Standards and the Duquesne Steel Works of the Carnegie-Illinois Steel Corporation for an opportunity to compare analytical results with other laboratories.

References

1. L. Jordan and J. R. Eckman, "Gases in Metals: II. The Determination of Oxygen and Hydrogen in Metals by Fusion in Vacuum," Bureau of Standards Scientific Paper No. 514, 1925.
2. H. C. Vacher and L. Jordan, "Determination of Oxygen and Nitrogen in Irons and Steels by the Vacuum-Fusion Method," *Journal of Research,* National Bureau of Standards, Vol. 7, 1931, p. 375-399.
3. "Gmelins Handbuch der anorganischer Chemie," 8th Edition, Eisen 59, Teil F1, Lieferung 1, p. 62-63. Berlin, Verlag Chemie, 1939.
4. J. G. Thompson, H. C. Vacher and H. A. Bright, "Cooperative Study of Methods for the Determination of Oxygen in Steel," *Journal of Research,* National Bureau of Standards, Vol. 18, 1937, p. 259-293.
5. L. Reeve, "Improvements in the Vacuum-Fusion Method for Determination of Gases in Metals," *Transactions,* American Institute of Mining and Metallurgical Engineers, Vol. 113, 1934, p. 82-110.
6. S. L. Hoyt and M. A. Scheil, "Fractional Vacuum-Fusion Analysis for Determination of Oxygen in Steel," *Transactions,* American Institute of Mining and Metallurgical Engineers, Vol. 125, 1937, p. 313-330.
7. H. A. Sloman, Third Report of the Oxygen Sub-Committee, Section II, Part A, "The Determination of Oxygen, Nitrogen, and Hydrogen in Steel," *Journal,* Iron and Steel Institute, Vol. 143, No. 1, 1941, p. 298-312.
8. L. Jordan and J. R. Eckman, "Gases in Metals: III. The Determination of Nitrogen in Metals by Fusion in Vacuum," Bureau of Standards Scientific Paper No. 563, 1927.
9. H. A. Sloman, "The Application of the Vacuum-Fusion Method to the Determination of the Oxygen, Hydrogen and Nitrogen Contents of Non-Ferrous Metals, Alloys and Powders," *Metallurgia,* Vol. 32, 1945, p. 223-227.

10. L. Alexander, W. M. Murray and S. E. Q. Ashley, "Determination of Oxygen in Steel by the Vacuum-Fusion Method," *Industrial and Engineering Chemistry,* Analytical Edition, Vol. 19, No. 6, 1947, p. 417-422.
11. C. A. Kraus, "Mercury Vapor Pumps for Operating Against High Pressures," *Journal,* American Chemical Society, Vol. 39, 1917, p. 2183-2186.
12. T. Swinden, Fourth Report of the Oxygen Sub-Committee, Section I, Part C, "Determination of Nitrogen," by the chemical distillation method, *Journal,* Iron and Steel Institute, Vol. 148, No. 2, 1943, p. 306-320.
13. V. C. F. Holm and J. G. Thompson, "Determinations of Hydrogen in Ferrous Materials by Vacuum Extraction at 800 °C. and by Vacuum Fusion," *Journal of Research,* National Bureau of Standards, Vol. 26, 1941, p. 245-259.
14. J. G. Thompson and V. C. F. Holm, "Hydrogen-Reduction Method for the Determination of Oxygen in Steel," *Journal of Research,* National Bureau of Standards, Vol. 21, 1938, p. 79-86.
15. H. A. Sloman and T. E. Rooney, Fourth Report of the Oxygen Sub-Committee, Section III (b), "The Surface (Oxygen) Film on Iron and Steel and Its Effect on the Determination of Oxygen," *Journal,* Iron and Steel Institute, Vol. 148, No. 2, 1943, p. 327-340.
16. M. Hansen, "Der Aufbau der Zweistofflegierungen," Verlag von Julius Springer, Berlin, 1936.
17. M. B. Bever and C. F. Floe, "Solubility of Carbon in Molten Copper," *Metals Technology,* Vol. 12, T.P. 1802, September 1945, p. 14.
18. N. A. Ziegler, "Reduction of Oxides in the Graphite Vacuum-Fusion Method of Analysis for Oxygen," *Mining and Metallurgy,* Vol. 14, 1933, p. 260.
19. J. G. Thompson and V. C. F. Holm, "Determination of Oxygen in Alloy Steels," *Journal of Research,* National Bureau of Standards, Vol. 21, 1938, p. 87-93.
20. M. Tenenbaum and C. C. Brown, "The Total Oxygen Content of Plain Carbon Open-Hearth Steel During Deoxidation and Teeming," *Transactions,* American Institute of Mining and Metallurgical Engineers, Vol. 162, 1945, p. 685-711.
21. G. Phragmen and R. Treje, "A Comparative Investigation of Methods of Determining the Nitrogen Content in Steels and in Alloys," *Jernkontorets Annaler,* Vol. 124, 1940, p. 511-531.

DISCUSSION

Written Discussion: By Harold E. Cleaves, chief, Chemical Metallurgical Section, Division of Metallurgy, National Bureau of Standards, Washington, D. C.

Mr. Mallett has incorporated many desirable features in his version of the vacuum-fusion apparatus. That satisfactory accuracy is achieved in its operation, is shown by his results on the cooperative steels.

It is interesting to the writer that satisfactorily low furnace pressures and blanks are obtained in Mr. Mallett's furnace despite the use of a beryllia container for the graphite crucible and insulation. A slit graphite shell, resting by edge contact on a beryllia disk, serves in the Bureau apparatus to hold the graphite crucible and graphite powder. Normally the blank is about the same as that reported by Mr. Mallett, but if graphite powder sifts through the slit onto the beryllia disk, as has hap-

pened in a few instances, an increase in the blank and the furnace pressure to 4 or 5 times normal results. Apparently, it is reaction of the carbon with some material other than beryllia, possibly with the silica of the furnace tube, that is responsible for the increased gas evolution.

The interference that Mr. Mallett reports in the determination of nitrogen by vacuum fusion in steels containing titanium has not been observed at the Bureau. Table VII shows the nitrogen values we obtained on some 18 chromium – 10 nickel steels treated with titanium.

Table VII

Nitrogen Values Obtained on 18 Chromium – 10 Nickel Steels Titanium-Treated

Steel No.	Titanium %	Nitrogen	
		Vacuum Fusion %	Chemical Analysis %
S-34	0.26	0.031	0.038
S-21	0.32	0.027	0.031
C-6	0.35	0.012	0.011
S-39	0.36	0.023	0.023
S-25	0.37	0.017	0.021
S-35	0.44	0.012	0.015
C-2	0.50	0.010	0.010
C-5	0.50	0.008	0.008
S-36	0.54	0.022	0.017
C-7	0.57	0.007	0.006
C-8	0.59	0.007	0.007
S-32	0.61	0.016	0.016

The greatest difference between the two methods was observed on steel S-34, the vacuum-fusion result, 0.031%, being lower than the chemical value, 0.038%. However, the next greatest spread in values, on steel S-36, was in the opposite direction, the vacuum-fusion value, 0.022%, being higher than the chemical value, 0.017%.

No interference by titanium was reported by Sloman (Report No. 1504 of the National Physical Laboratory) in determining nitrogen in titanium metal by vacuum fusion. However, he reported that an operating temperature of 1800 °C (3270 °F) is necessary for complete decomposition of the nitride, whereas no increase in nitrogen recovery was observed at the Bureau to result from increase in operating temperature above 1625 °C (2960 °F). We did find that a temperature of 1700 °C (3090 °F) or higher was required for satisfactory recovery of nitrogen from columbium-treated stainless steels, as will be seen from the following results:

Steel No.	Columbium %	Vacuum Fusion at 1625 °C %	Vacuum Fusion at 1700 °C %	Chemical Analysis %
C-3	0.35	0.024	0.032	0.035
C-9	0.52	0.033	0.049	0.052

Written Discussion: By William F. Murphy, metallurgist, Crucible Steel Company of America, Pittsburgh.

The author is to be commended for his work in extending the scope of materials capable of being analyzed by vacuum-fusion gas analysis.

His paper serves to focus attention on the fact that interfering elements require modifications in procedure just as they do in routine chemical analysis.

In 1941, Mr. Mallett constructed a vacuum-fusion apparatus at our Crescent Laboratory. This apparatus was very similar in design to that previously constructed by him at Battelle Memorial Institute. During the past 7 years this apparatus has been operated without any serious difficulty. In agreement with the author's findings we too have had no trouble with mercury causing embrittlement of the furnace head although some amalgamation does seem to have occurred. Our apparatus has been modified in some minor aspects from its original form. For example, we have completely removed the expansion bulb which appears in Fig. 1 on the right side of the table top and which proved to be unnecessary to the successful operation of the apparatus.

Because of the nature of the steels and alloys manufactured by the Crucible Steel Company, our equipment has been used to determine the gaseous elements in a wide variety of materials, both our manufactured products and materials going into these products. As discussed by Mr. Mallett, the results of analyses on such materials must be considered from the viewpoint of the elements in the material.

As an illustration to indicate further the versatility of this type of equipment, the following results are presented. At one time it was necessary to try to determine the difference between two samples of calcium metal which were behaving very differently in use. The samples identified as No. 1 and No. 2 were analyzed by a modification of the regular vacuum-fusion procedure. The temperature of operation was held as well as possible at about 1600 °F (870 °C), but fogging of the sight glass which hindered temperature observation and the necessary intermittent operation of the converter made this difficult.

The behavior of the two calcium materials was very different under approximately similar conditions of temperature and pressure. The No. 1 calcium generally melted rather quietly and distilled into the guide tube where it condensed. The No. 2 calcium erupted rather violently before melting or simultaneously thereto. In this case, too, the metal solidified in the guide tube. The No. 2 calcium gave off a small amount of a material which collected on the sight glass as a reddish brown powder. This might possibly have been calcium nitride which is identified as a brown crystalline material with a melting point of 1650 °F (900 °C). Both materials partially sublimed before melting. The results obtained are given in Table VIII.

Samples No. 6 for both materials were attempts at hot extraction without melting. In both cases the calcium metal sublimed into the guide tube. Considerably higher hydrogen contents were obtained from the hot-extraction analyses.

The fact that calcium distilled from the crucible and solidified in relatively cold parts of the furnace makes it doubtful that all of the gases, hydrogen and nitrogen, were removed from the metal. It is more prob-

able considering that calcium vapors were present that some of the gases recombined with the metal condensing in the guide tube.

Under the conditions of operation it was not expected that any oxygen would be found. But in a few cases small amounts of oxygen were determined. In general, the nitrogen content of the No. 2 material was higher than that of the No. 1 material. The hydrogen content was higher in the latter material.

Table VIII
Results of Vacuum-Fusion Analysis of Two Calcium Metal Samples

Material	Sample	Weight, % O_2	Weight, % H_2	Weight, % N_2
Calcium No. 1	1	0.003	0.01835	0.007
	2	none	0.00788	0.014
	3	none	0.02172	0.010
	4	none	0.02077	0.005
	5	none	0.01794	0.004
	6*	0.002	0.02632	0.007
Calcium No. 2	1	none	0.00956	0.008
	2	0.002	0.01854	0.019
	3	none	0.01354	0.059
	4	none	0.01593	0.043
	5	none	0.01735	0.085
	6*	0.002	0.02388	0.010

*Attempted hot extraction without melting.

Some experiments which were made at Crescent Laboratory of the Crucible Steel Company on small newly cast ingots and aged ingots have led to the same general conclusion with respect to hydrogen analyses as presented by the author.

Mr. Mallet has presented an excellent paper which indicates some of the possibilities for research on the determination of gases in metals and has given us a more thorough understanding of the limiting factors in this kind of analysis.

Written Discussion: By J. C. Lewis, Jr., research metallurgist, Driver-Harris Co., Harrison, N. J.

In consideration of a vacuum-fusion apparatus that handles a wide variety of material, having widely different melting temperatures, a statement might well be made regarding the basis for selection of the temperature used for analysis of a given material.

In the operation described by Hoyt and Scheil, cited as reference (6) in this paper, a temperature schedule was followed which was designed to provide information about the quantities of certain oxides present and was selected on the basis of their respective reduction temperatures.

In my own experience I have found it satisfactory to use a temperature below the melting point by less than about 45 °C (80 °F) for half the degassing time, and above the melting point by about the same amount for the remainder of the time, when running copper-nickel alloys, pure Ni, and nickel-chromium alloys. This selection of temperatures is on the basis that there is often more hydrogen available from the metal just

before it melts, there is greater reaction of oxides and nitrides with the carbon crucible at higher temperatures, and the evaporation of nickel and copper makes it inconvenient to go much higher.

So I should like to know if any more specific statements may be made than that sometimes physical facts dictate the temperature (as in the fractional oxide determination) but otherwise good judgment, justified and modified by experiment, as to what will satisfy the needs in a particular case decides the selection of temperature. Also I should like to know what temperatures were used for the analysis of copper and the higher melting materials, tungsten and molybdenum.

I heartily agree with the author's remarks in his statements about the relationship of precision, absolute accuracy and utility of results.

The apparatus is shown as having a graphite guide tube touching a quartz tube above. I should like to know at what general temperature level this silica-carbon junction begins to be unsatisfactory in this application.

The paper states that "no more than three samples of high chromium alloys are melted in one run". This is of interest and confirms belief that an essential feature of a gas-analysis apparatus is that after one run it may readily be rearranged for another run.

Author's Reply

I wish to thank Mr. Cleaves for his interest in this paper and for the additional data on the effects of titanium and columbium upon vacuum-fusion analysis.

In regard to Mr. Cleaves' observation on the reaction of BeO containers with the graphite-powder insulation, I would like to point out why we use a BeO container rather than the thin-walled slit graphite shell used at the Bureau of Standards. The Lepel converter used on the Battelle apparatus operates at a frequency of about 300 kc. Even extremely thin-walled split cylinders of graphite or molybdenum tend to heat at this frequency. This heating is usually confined to spots or irregular areas where concentrations of eddy currents cause extremely high temperatures which vaporize the graphite shell or melt holes in molybdenum. There is much less of this skin effect at the lower frequencies (30 kc.) used at the Bureau.

About 8 to 10 hours at degassing temperatures is required to break in a new BeO container. A thin layer of Be_2C forms during this period, minimizing further reactions between the BeO and graphite.

Apparently, the question of Ti interference with nitrogen analyses is far from settled. We are very much interested in the analysis of titanium metal for nitrogen and oxygen by vacuum fusion, or, indeed, by any method. To date, our attempts to duplicate Sloman's results have been unsuccessful. In the past, it has been difficult to evaluate methods because standard samples were lacking. For our work, samples of titanium containing known additions of nitrogen and others containing similar additions of oxygen were prepared in a modified Sieverts apparatus. Very satisfactory chemical analyses of the nitrogen standards were

obtained, but the vacuum-fusion values for nitrogen were quite low. Attempts to analyze the oxygen standards by both chemical and vacuum-fusion methods have been very unpromising.

It is of particular interest to me to receive Mr. Murphy's comments after several years' use of an apparatus very similar to that used at Battelle. It is gratifying that no major changes in design were found necessary during this period.

Knowing the great variety of materials used in producing the various alloys of the Crucible Steel Company, I am certain versatility was required of both Mr. Murphy and the equipment in order to analyze these materials.

The data on the gas analysis of calcium add to our store of information on the vacuum-fusion method. Although the results are evidently only semi-quantitative, they indicate a marked difference in nitrogen content which probably accounts for their different behavior in use.

We had a similar experience with calcium silicide which was particularly gassy. By the vacuum-fusion method it analyzed: nil oxygen, 0.016% hydrogen, and 0.07% nitrogen. Chemical analysis later showed the true nitrogen value to be 0.12%. However, the difficulty had already been corrected upon the basis of vacuum-fusion results.

In reply to the discussion by Mr. Lewis, the temperature is chosen so that the gas extraction is made from a molten bath. The method used for materials with high melting points is described in the paper. The temperature also must equal or exceed that required for rapid reduction of the type of oxides or nitrides likely to be present in the sample. In the case of copper, which contains oxides that are easily reduced, an operating temperature of 1300 °C (2370 °F) is quite satisfactory. Higher temperatures result in excessive vaporization of the copper.

In regard to extraction of hydrogen from the solid sample, we have obtained comparable results on steels by "warm" extraction at either 650 or 1000 °C (1200 or 1830 °F) for several hours and by vacuum fusion at 1650 °C (3000 °F) for 20 minutes. It also appears that FeO may be removed from a solid sample in a tin bath at 1060 °C (1940 °F). This temperature is customarily used for reducing FeO in the fractional vacuum-fusion method and often does not result in melting of the sample. In spite of this, a satisfactory separation of FeO from the more refractory oxides seems to be obtained.

The junction of the graphite guide tube with the silica tube is always at least 3 inches above the top of the crucible and does not reach a red heat even at outgassing temperatures. No evidence of a reaction between the graphite tube and the silica tube has been observed.

NATURE AND DETECTION OF GRINDING BURN IN STEEL

By L. P. Tarasov and C. O. Lundberg

Abstract

Unsatisfactory grinding conditions may generate sufficient heat in the work surface to discolor it and to affect the physical condition of a surface layer several thousandths of an inch deep. This paper is concerned with the microstructural and hardness changes that may occur in hardened steel parts when they are burned in grinding, and with their response to macroetching. Most of the results were obtained on high speed and oil-hardening tool steels, but enough work was done with some other steels to show that the same conclusions can be expected to apply to hardened steels in general.

When there is sufficient temperature rise for rehardening to occur, some novel microstructures may be observed. One of these is grain boundary austenitization in a transition region between rehardened and overtempered zones.

Hardness data are presented showing that, even under conditions of rapid stock removal, hardened steel can be ground without appreciable surface softening by adhering to good grinding practice, and that burn can be completely eliminated if necessary. It is also shown that grinding can work harden the surface of hard steel.

Sensitive, nondestructive macroetching techniques are described for detecting hardness changes (and sometimes high stresses) in ground surfaces, which should be useful for inspection and trouble-shooting purposes.

Introduction

EXCESSIVE heat can be generated in a workpiece when grinding conditions are not right. The grinding may be at fault, as when a wheel is too hard or too dull or when the machine is in

A paper presented before the Thirtieth Annual Convention of the Society, held in Philadelphia, October 23 to 29, 1948. The authors, L. P. Tarasov and C. O. Lundberg, are associated with the Research Laboratories, Norton Company, Worcester, Mass. Manuscript received May 17, 1948.

poor condition; or the workpiece may be at fault, as when too much stock is left in spots with the result that deeper cuts are taken at those spots than are allowable. This can happen if the prior machining has not been done with sufficient accuracy or if the distortion in heat treatment has been greater than expected.

Whatever the cause of the excessive heat, both visible and invisible changes may take place in the ground surface. The visible

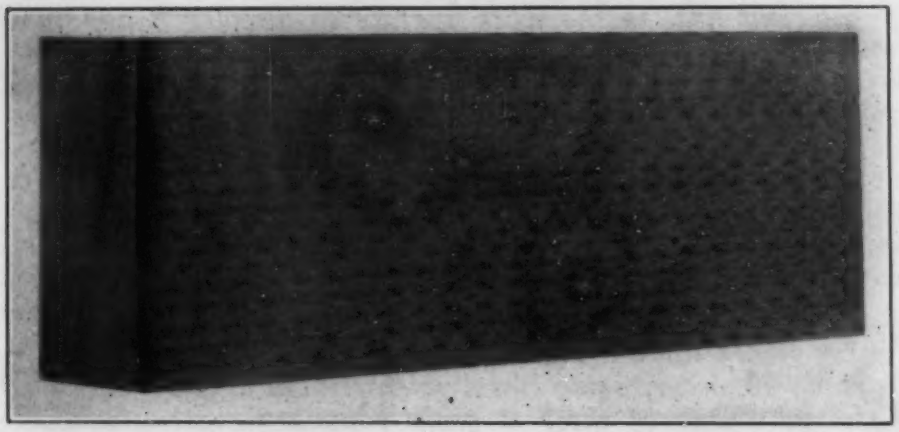


Fig. 1—Burn Marks in Hardened Steel Ground Too Severely. × 1.

manifestation is commonly referred to as burn. This is simply a discoloration of the surface resulting from its oxidation during momentary exposure to high temperatures. The color of the oxide film depends on its thickness, which is of the order of the wave length of light, just as is the case with temper colors. In fact, the only difference between the two is that temper colors result from fairly long exposure, such as 1 hour, to ordinary tempering temperatures, while burn marks of exactly the same colors result from momentary exposure to considerably higher temperatures, although these are still far below the melting point of steel. A typical example of a pronounced burn pattern is shown in Fig. 1.

Whether the surface appears to be burned or not, there may be invisible but significant changes in the surface layers immediately underneath the ground surface. The microstructure and hardness can be materially affected by flashes of heat, as witness the surface softening or even rehardening often observed in hardened steel in cases of severe burn.

These changes can occur even though no burn color is visible after grinding, since any discoloration developed during severe grind-

ing is often cleaned off in finish grinding. Even when the surface is not cleaned up in this fashion, it sometimes happens that the temperature reached momentarily is high enough to cause a little tempering but is still too low to discolor the surface.

Another type of invisible change can occur in the grinding of any metal, not just steel. This is the generation of surface stresses, again the result of momentary heat. The stresses, which are tensile in character and in the plane of the surface, can lead to distortion if the part is sufficiently thin, and they can also be the forerunners of surface cracks, provided the material is hard and fairly brittle. Surface stresses and cracks, and methods of detecting and preventing them, have been discussed elsewhere (1), (2).[1]

Grinding burn, it should be noted, has nothing to do with the type of burning sometimes experienced when steel is heated so close to the melting point in preparation for forging as to cause melting of the more fusible constituents, subsurface oxidation, or segregation of some of the elements present in the steel. That there are two different meanings attached to burn in connection with steel is unfortunate as this is occasionally confusing; however, one meaning has long been accepted in the field of grinding while the other has been accepted just as long in the manufacture of steel, and all that can be done now is to recognize the existence of the distinct meanings of the same word.

From a practical standpoint, grinding burn is injurious only when it affects unfavorably the usefulness of the part in subsequent processing or under service conditions. Thus soft skin on the cutting edges of tools, resulting from overtempering in grinding, is likely to cause a marked decrease in tool life. Bar ends inadvertently hardened by improper use of abrasive cut-off wheels may lead to tool breakage when the bars are machined afterwards. Burn marks in the roots of hardened gear teeth used under extremely high loads, as in aircraft engines, may result in premature failure of the gears. On the other hand, no harm is done when a relatively thick piece of a soft steel like SAE 1020 is burned moderately in grinding. Surface stresses are undoubtedly introduced in this instance but they do not matter, provided they do not distort the piece.

Many instances of burn, however, are not so simple from the standpoint of determining whether or not they injure the ground part. In order to be able to make an intelligent decision in the

[1]The figures appearing in parentheses pertain to the references appended to this paper.

absence of experience with similar parts, it is necessary to perform tests simulating service conditions; otherwise, perfectly satisfactory parts may be rejected on account of burn, or else badly injured parts may pass inspection and lead to trouble in service.

At present, detailed information is lacking on some of the important characteristics of grinding burn in hardened steel and on how it can best be detected. The purpose of this paper is to furnish as much of this information as is now available so that those engaged in grinding hardened steel may be able to correlate more effectively the degree of burn in a given part with its effect on the service life of the part. In this way, it should be possible to determine in each case just how much burn, if any, is permissible. This information should also be helpful in studies of how various physical properties of hardened steel may be affected by grinding, the severity of which can logically be measured in terms of burn depth.

Practically all of the experimental studies described in this paper were performed on high speed steel and on oil hardening tool steel, but the results are general enough that they can be safely extended to other hardened steels. Three methods of detecting burn are discussed: metallographic examination of microstructural changes; microhardness measurements, also in metallographically prepared surfaces; and visible changes brought out in ground surfaces by suitable macroetching techniques. No attempt is made to include the practical aspects of avoiding burn and of trouble shooting as these have been recently covered in another publication (2).

Microstructural and Hardness Changes in High Speed Steel

Heat Treatment—The first type of steel to be discussed will be high speed steel because this was subjected to the most complete metallographic study to determine the cause of certain macroetching peculiarities connected with portions of the surface overtempered in grinding. The steel was standard 18-4-1 bar stock, ⅞ by ⅞ inch, containing 0.75% carbon. Specimens ½ inch thick were cut off and surface ground so that the square sides were flat and parallel. No attention was paid to the slight surface decarburization of the bar, since the edges of the ⅞ by ⅞-inch surfaces were ignored in the various studies conducted on the specimens.

The pieces were oil-quenched from 2350 °F (1290 °C) and

were then double tempered for 2 hours plus 2 hours at 1050 °F (565 °C), the resultant hardness being Rockwell C-63.

Grinding—Ordinarily, microstructural and hardness changes in hardened steel associated with grinding burn are extremely shallow, extending at most only a few thousandths of an inch or so in depth. In order to clarify the exact nature of these changes, the burn effects were made to extend to a considerably greater depth than would normally be encountered in ordinary grinding practice. This was done by intentionally grinding one of the ⅞ by ⅞-inch surfaces of a specimen as abusively as possible. Subsequent comparison with specimens burned much less severely showed that the same changes occurred under the less drastic conditions, but in a much thinner surface layer.

The grinding was done dry with the periphery of an 8 by ½-inch 38A180-O11VBE wheel[2] on a Norton 6 by 18-inch surface grinder. The wheel was purposely much too hard and fine according to the usual wheel recommendations for grinding hardened steel. The wheel speed was 6000 surface feet per minute; the table speed was 65 feet per minute; the crossfeed was 50 mils (0.050 inch); the downfeed was 5 mils per completed crossfeed for a total downfeed of 15 mils. The wheel was dressed smooth as for finish grinding and then it was loaded by grinding some soft steel with it. In a loaded grinding wheel, metal particles fill some of the pores and are smeared over some of the abrasive grains, with the result that during grinding contact the frictional heat becomes much greater.

Under these abusive grinding conditions, the specimens of hardened high speed steel were certain to be deeply burned. Austenitizing temperatures were attained to depths of 2 mils over large areas, while temperatures that resulted in softening penetrated several times as deeply.

Taper Sectioning—Metallographic taper sections very nearly parallel to the severely burned surface were then prepared. Thus a ½-inch length along the taper section might correspond to a depth of 5 mils, a hundred-fold mechanical magnification. Tapering was done by shimming up, with the appropriate leaves of a dismantled feeler gage, one end of the specimen on the magnetic chuck of the surface grinder. A very soft and free-cutting wheel, like 32A46-G12VBEP, was used successfully for tapering, the downfeed

[2]This is a Norton 38 Alundum wheel (white aluminum oxide), 180-grit size, O grade letter, No. 11 structure, vitrified bond of the BE type. The wheel grade or hardness, which is a measure of bond strength, increases in alphabetical sequence.

being kept small, especially toward the end of the operation. Sensitive etching techniques to be described later disclosed no evidence at all of any tempering during the taper grinding.

The taper sectioning was discontinued when about a ¼-inch length of the original ground surface remained. The taper section surface was then mechanically polished in the usual manner to a metallographic finish. The intersection between the two nearly parallel surfaces served as the reference line of zero depth from which the depth below the original ground surface of any point in the taper section itself could be accurately determined. Thus if the mechanical magnification resulting from the taper sectioning was 100, the distance along the taper section from a given point to the reference line, divided by 100, was the depth of that point below the original ground surface.

It should be noted that other experimenters have plated the surface to be taper sectioned in order to protect the very edge of the taper section from rounding and thus preserve the accuracy of the mechanical magnification at the surface. This was done by Nelson (3), who was the first to use taper sectioning as an accurate experimental technique in his study of the actual contours of various surface finishes; and also by Sakmann (4), in his recent study of geometrical and metallurgical changes occurring in steel surfaces as a result of frictional contact. In the present work, it was possible to dispense with plating, since subsurface changes were the object of the investigation, while the rounding, if any, was limited to the taper section of the grinding scratches. The polished portion of the taper section, starting at or near the lower ends of the tapered scratches, was very flat, as shown by focussing at × 1500.

Etching—Various etchants were tried to bring out the burn microstructures clearly and reproducibly. The most satisfactory one turned out to be acid ferric chloride in alcohol. The following is the solution that was used as the standard etchant in this work:

2 ml conc. HCl
4 g $FeCl_3 \cdot 6H_2O$
Methyl alcohol to make 100 ml of reagent.

For convenience this has been termed 2:4 hyfercal (accent on the first syllable), the name being coined by analogy with nital and picral. (The first two letters are for hydrochloric acid, the next three for ferric, the next one for chloride and the last two for alcohol.) The concentrations of the two solutes, given by the two

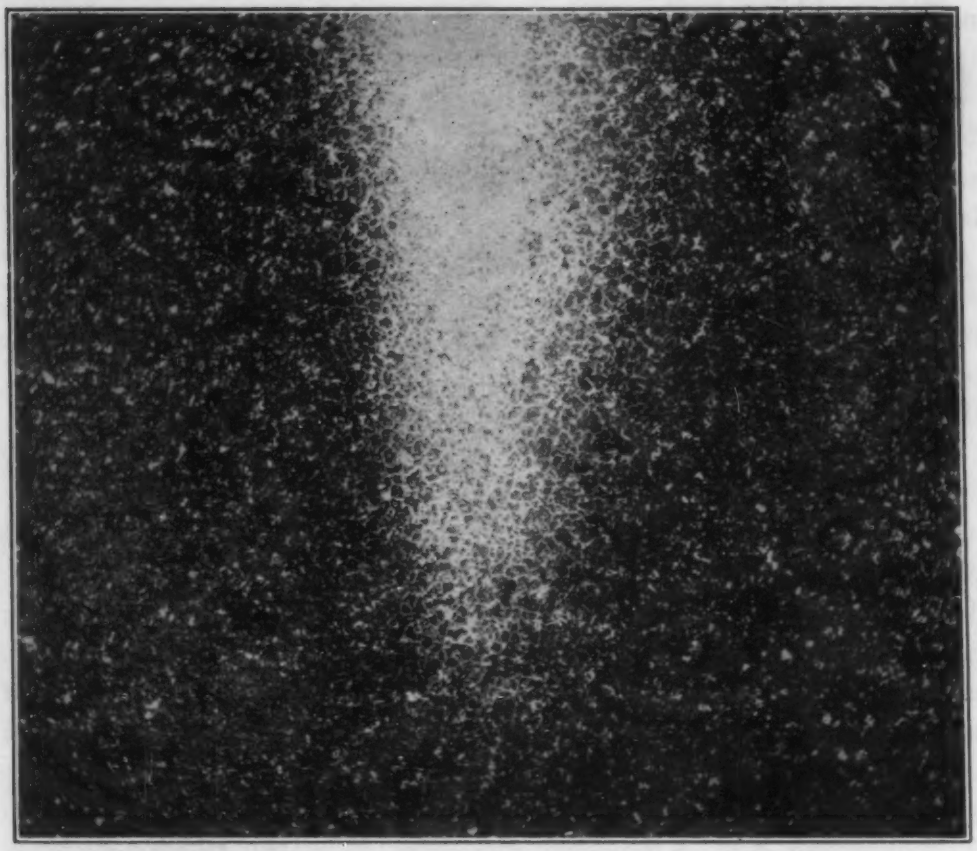


Fig. 2—Microstructure of Severely Burned Area in High Speed Steel. Hyfercal etch. × 100.

numbers, can be varied when necessary. Ethyl alcohol can be substituted for methyl.

In etching, with nital, areas that had been overtempered in grinding, it was found that the correct etching time to reveal slight traces of burn varied a great deal. For a constant etching time, the depth to which overtempering appeared to extend, in a severely ground piece of hardened steel, depended on the way in which it happened to etch that particular time. With hyfercal, on the other hand, the results were very reproducible and it was possible to make reliable comparisons of burn depth in specimens ground under various conditions.

Both high speed and other steels in the hardened and tempered condition etch rapidly in hyfercal, 10 seconds being satisfactory in many instances. This is a marked convenience in connection with high speed steel, since it has to be etched for several minutes in

nital. For etching pearlitic and ferritic structures, hyfercal is generally inferior to nital and other etchants.

As will be shown later, the burn microstructures brought out by etching in hyfercal are the same as can be revealed, usually less satisfactorily or conveniently, with the etchants commonly used for tool steels.

Typical Burn Microstructures—A taper section of a portion of a typical burn streak is shown at × 100 in Fig. 2. The top of the picture is slightly closer to the original ground surface than is the bottom, the vertical magnification resulting from the tapering operation alone being about 100.

The central portion of the burned area was austenitized by excessive grinding heat and then transformed, in large part, to white martensite. Surrounding this is a region in which the highest temperature reached momentarily could only soften the steel. This dark, overtempered structure gradually changes into the lighter colored pre-existing tempered structure of the steel, where the grinding heat did not penetrate. The difference between the overtempered and the original structures is much clearer when the etched surface is viewed directly than when magnified.

To explain the mottled appearance of much of both the rehardened area and its overtempered rim, it is necessary to go to a considerably higher magnification. Micrographs of the structures found in and near a burn spot are shown in Fig. 3 at 1500 diameters. Fig. 3a is the normal microstructure of the hardened and tempered steel where it was not affected at all by grinding heat. The next micrograph, Fig. 3b, is of an overtempered area in the burn spot. A few grains are outlined in white, primarily in the upper portion, and some very fine white grain boundaries can also be seen toward the right. This is the very edge of the transition structure, which is shown much more clearly in Fig. 3c. The white grain boundaries become wider as one moves in the direction of higher and higher temperatures, i.e., to the center of the burn spot. This is evident at the other edge of the transition structure, Fig. 3d, where the white bands on both sides of the dark grain boundaries gradually lose their band-like character and merge into grains of white martensite[3] containing residual dark specks of overtempered martensite.

This sequence of micrographs establishes the nature of the transition microstructure. When a certain maximum temperature

[3]For the sake of brevity, the white structure is generally referred to in this paper as martensite although it undoubtedly contains appreciable amounts of retained austenite.

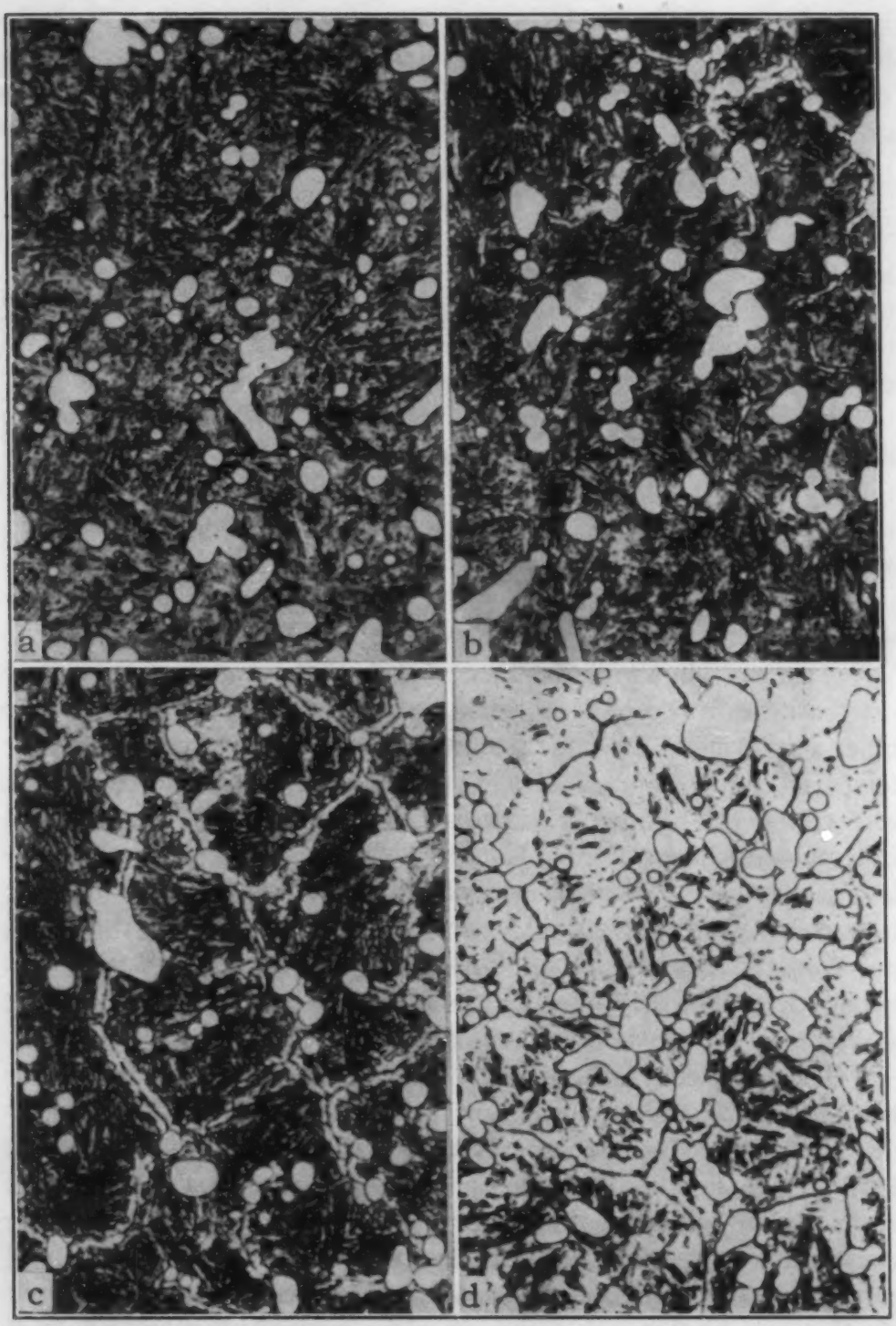


Fig. 3—Burn Microstructures in High Speed Steel. Hyfercal etch. × 1500. (a) Unaffected by grinding heat. (b) Overtempered structure merging into transition structure. (c) Center of transition region. (d) Transition structure merging into almost completely rehardened structure.

is reached momentarily during grinding contact, the grain boundaries begin to austenitize, being more reactive, while the rest of the grain remains in the highly overtempered condition. The nucleation and growth of the austenite at the grain boundaries is evident, especially in Fig. 3c, from the irregular, nodular nature of the white martensite boundaries that formed on rapid cooling. Nearer to the center of the burn spot, austenitization can progress further from the grain boundary, and the less reactive interior of the grain begins to austenitize independently, leaving discontinuous patches of the overtempered structure. As the center of the burn spot is approached even closer, more and more of the dark-etching, overtempered martensite austenitizes, leaving only a relatively few dark specks inside the white grains of untempered martensite formed on cooling. If the temperature reached has been high enough, there will be complete austenitization and no dark specks will be found. The burn spot, shown in Figs. 2 and 3, did not reach a sufficiently high temperature for this to happen, but complete austenitization will be shown later in connection with a burn spot in another specimen.

That the white grain boundary bands in the transition region are martensite can also be established by tempering experiments. Two other specimens of the same steel and burned to the same extent were tempered for 1 hour at 800 °F (425 °C) and 1050 °F (565 °C), respectively. The microstructures after etching for 10 seconds in hyfercal are shown in Fig. 4. The formerly white grain boundary bands have been darkened appreciably by the 800 °F tempering, but they can still be recognized easily. After the 1050 °F treatment, however, it requires some effort to locate the rehardened grain boundaries, since they have been tempered to almost the same shade (upon etching) as the overtempered portions of the grains.

The completely rehardened portion of a burn spot, when one exists, reacts in exactly the same manner to tempering. It is for this reason that tempering severely burned high speed steel at 1050 °F or slightly below helps to overcome at least part of the harm caused by excessive grinding heat. Undesirable surface stresses accompanying burn are undoubtedly relieved by the tempering operation, but the principal effect of tempering after grinding that is severe enough to reharden the surface must be to temper the brittle, freshly formed martensite. Overtempered regions, of course, cannot be restored to their original hardness in this manner.

Before leaving the transition structure, it may be well to discuss

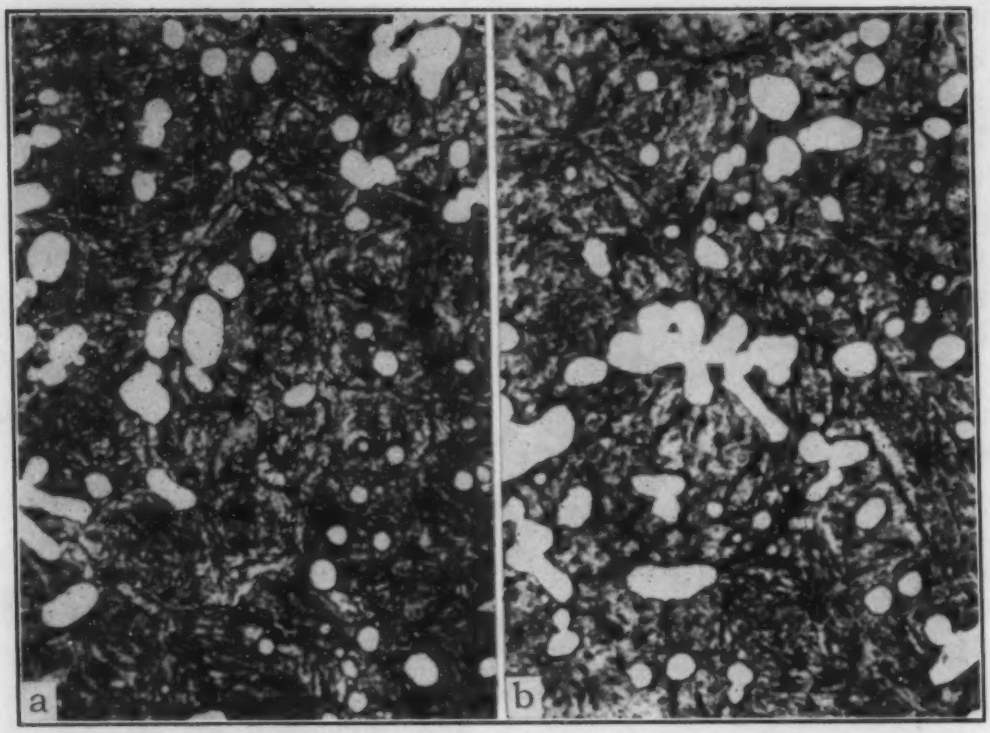


Fig. 4—Transition Structures in High Speed Steel After Tempering for 1 Hour. Hyfercal etch. × 1500. (a) 800 °F. (b) 1050 °F.

briefly its appearance under some other etching conditions that are likely to be used. First of all, prolonging the etching time to 15 seconds in 2:4 hyfercal brings out, as can be seen in Fig. 5a, a slightly darkened spotty structure in the white grain boundary bands, in keeping with their martensitic nature; the portions remaining white, other than the carbide particles, are probably retained austenite, but further work would be needed to establish this point, since the microstructure is so indistinct and on such a fine scale. The softened interiors of the grains have been overetched and do not show the details present after the 10-second etch used to obtain Fig. 3c.

Another quick way of clearly revealing the transition structure is to use Villela's etchant for austenitic grain size, which contains 1 gram picric acid and 5 milliliters hydrochloric acid in 100 milliliters alcohol. Fig. 5b illustrates the structure after a 15-second etch. This gave excellent contrast although the softened grain interiors were overetched in this particular instance. The authors' preference for hyfercal is that it does not stain the fingers as does picric acid.

Fig. 5c depicts the structure after 5 minutes in the reagent originated by Snyder and Graff for revealing grain size in high speed steel, and which consists of 10 milliliters hydrochloric acid and 3 milliliters nitric acid in 100 milliliters alcohol. The only advantage of using hyfercal is that etching with it requires much less time.

Nital gives unsatisfactory results, as shown in Fig. 5d. It was necessary to etch for 15 minutes in 5% nital to bring out the transition structure and even then it could be easily overlooked. Much of the detail made evident by the other etchants is missing.

Acicular Microstructures in Rehardened Areas—Another type of structure is sometimes found in the rehardened zone of a burn spot. This dark-etching acicular martensitic structure, such as is shown in Fig. 6a, appears only under extremely severe grinding conditions, and then not always. When it does appear, it often shades off into lighter and lighter acicular structures, illustrated in Figs. 6b and 6c, until it disappears completely on that side of the burn spot which was away from the leading edge of the grinding wheel.

In a number of instances, it was found that the rehardened areas of *alternate* burn streaks contained the acicular constituent, while the remaining ones did not. The former went about 10% deeper below the severely ground surface than did the latter. A slight variation of this was observed in one of the specimens examined. Here the acicular structure was present in every burn streak, but it was dark in alternate ones, and very light in the others; moreover, the dark structure was always in the deeper streaks. In still another specimen, the dark and light acicular structures were superimposed.

These acicular structures were attributed at first to a straightforward tempering effect. The leading edge of the wheel, slightly rounded by normal wear during grinding, removed most of the stock and obviously caused the observed rehardening; the remaining width of the wheel cleaned up the surface in the succeeding passes as the work was advanced across the wheel and, it was thought, generated enough heat to temper at least some portions of the already rehardened areas.

If only a rise in temperature was needed for the formation of the acicular structure, then it should have been possible to reproduce it by tempering in a furnace at some appropriate temperature a piece known to have been rehardened in grinding. However, at-

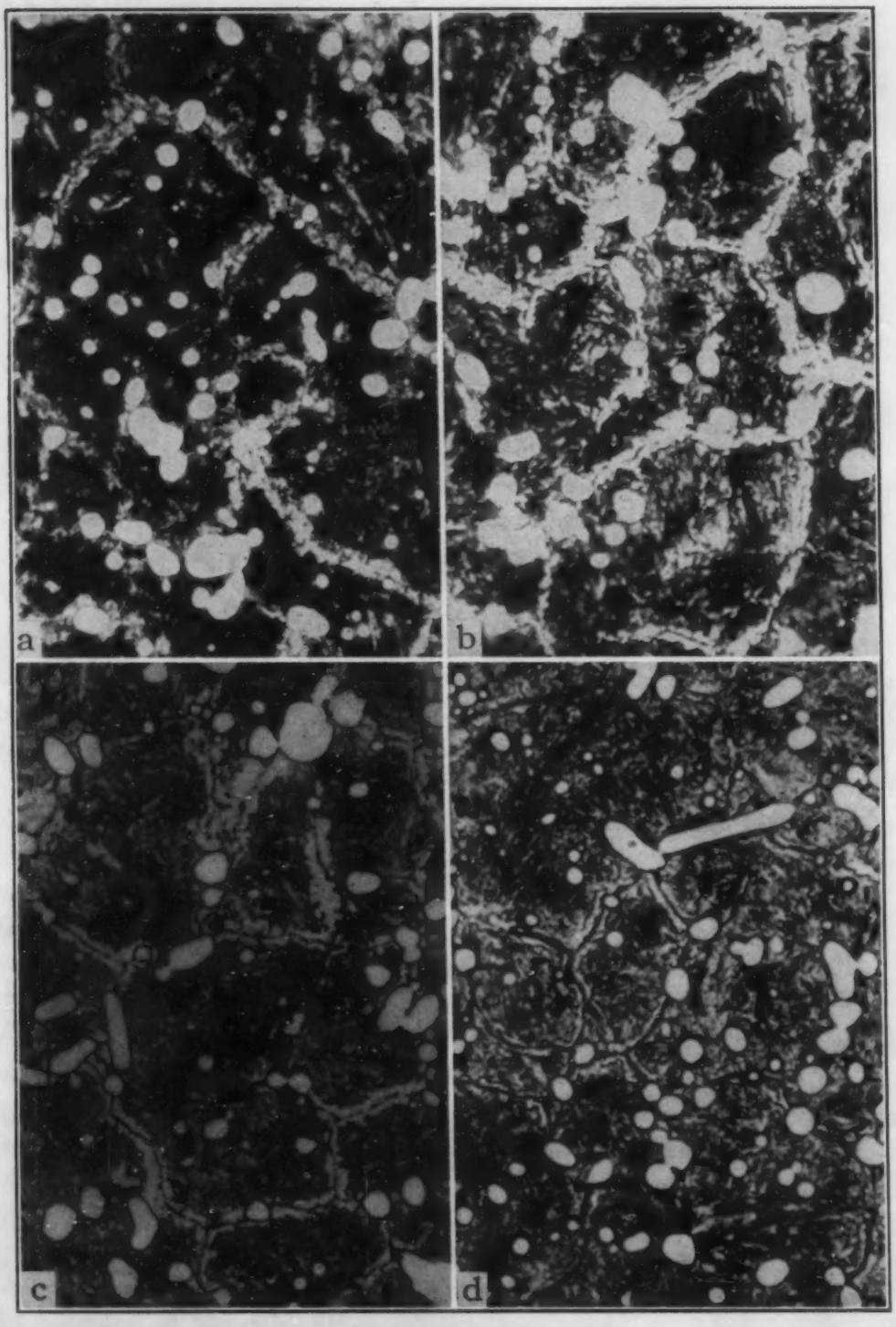


Fig. 5—Transition Structures in High Speed Steel, Using Various Etchants. × 1500. (a) 15 seconds in 2:4 hyfercal. (b) 15 seconds in Villela's etchant. (c) 5 minutes in Snyder and Graff's etchant. (d) 15 minutes in 5% nital.

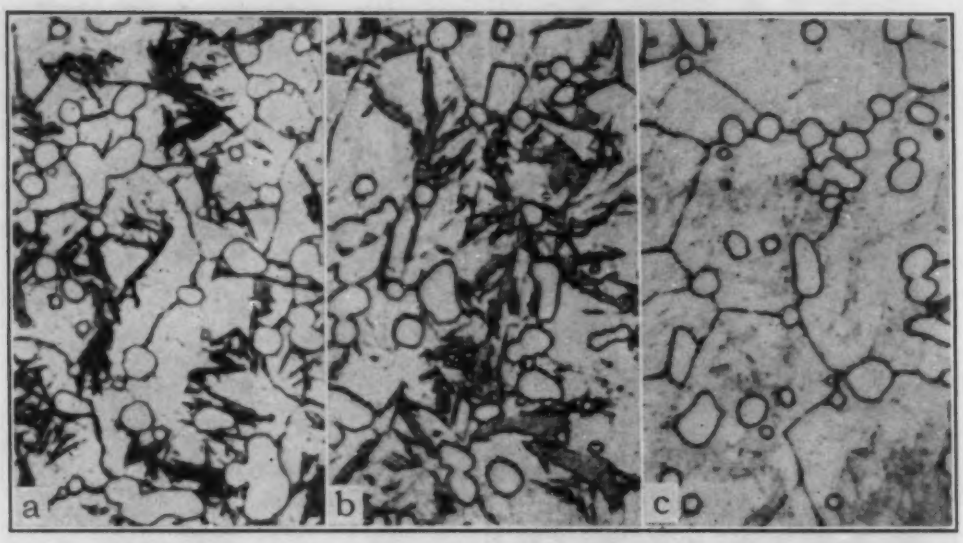


Fig. 6—Acicular Structures Sometimes Found in Close Proximity in Rehardened Areas of High Speed Steel. Hyfercal etch. × 1500. (a) Dark. (b) Light. (c) Barely visible.

tempts to obtain this acicular structure by such tempering failed completely regardless of whether portions of the rehardened areas did or did not contain the acicular structure. All that happened when such specimens were tempered at various temperatures was that the white, rehardened areas became uniformly darkened upon etching, the extent of darkening depending on the tempering conditions.

Similar results were obtained when some new specimens from the same bar of high speed steel were hardened but left in the quenched condition, with a Rockwell hardness of C-65. These were then badly burned, using the abusive grinding technique previously described. Metallographic taper sections again showed the acicular structure in the rehardened areas, but no trace of it could be found further below the ground surface, where the grinding heat was sufficient only to temper the original untempered white martensite formed in the oil quench. With increasing distance below the level of the transition region, the overtempered and uniformly darkened microstructure became progressively lighter etching until the original white martensite structure was reached.

It was thus evident that tempering alone was insufficient to produce the observed acicular structure. The possibility was then examined that the acicular structure appeared on tempering only in those portions of the rehardened zone that had been properly con-

ditioned by exposure to a sufficiently high austenitizing temperature during grinding contact. Wooding (5) recently showed that the higher the austenitizing temperature was for high speed steel, the more acicular was its microstructure after tempering. It was certain from the closely similar depths of the burn streaks in a taper section, some containing the acicular structure and others not, that the austenitizing temperatures must have overlapped considerably in these streaks. In spite of this, it was not possible to create the acicular structure by tempering where it did not already exist.

Thus the occurrence of the acicular structure could not be explained in terms of the austenitizing temperature alone. Since severe grinding is known to create high stresses in the surface layers, it is quite possible that simultaneous generation of high austenitizing temperature and stress are required to condition the rehardened areas so that the acicular structure can form on subsequent tempering. Another possibility is that the surface must be stressed in a particular manner while it is being tempered. Additional experiments would have to be performed to clarify the conditions under which the acicular structure is formed in severely burned specimens.

Hardness Studies—The taper section of one of the severely burned specimens of tempered high speed steel was repolished carefully after the center line of a burn streak had been staked out with a few 1000-gram indentations on the Tukon Hardness Tester, which were deep enough to remain visible after polishing. A row of 100-gram Knoop indentations was then made in the polished taper section along the center line of the burn streak, starting near the intersection of the taper section with the ground surface and continuing to the opposite edge of the specimen. The indentations were spaced 0.010 inch apart, corresponding to a depth change of 0.0001 inch or 100 microinches.

The depth of an indentation was of the order of 50 microinches so that the measured hardness number was actually an average value for a layer of somewhat greater thickness. This was of no practical importance, since the normal hardness variations even in the unburned portion of the specimen were considerably greater than the average change in hardness between two successive indentations in the region of the steepest hardness gradient. A large number of closely spaced indentations in the taper section were necessary for determining the correct location of the average hardness curve.

Since the burn streak extended the complete length of the speci-

men, the taper section gave undistorted mechanical magnification of very close to 100. Had the burn pattern consisted of relatively short, disconnected, trough-like burn spots, such as are usually found in a burned surface, the taper section would most likely not have passed through the deepest point of a burn spot and thus the maximum

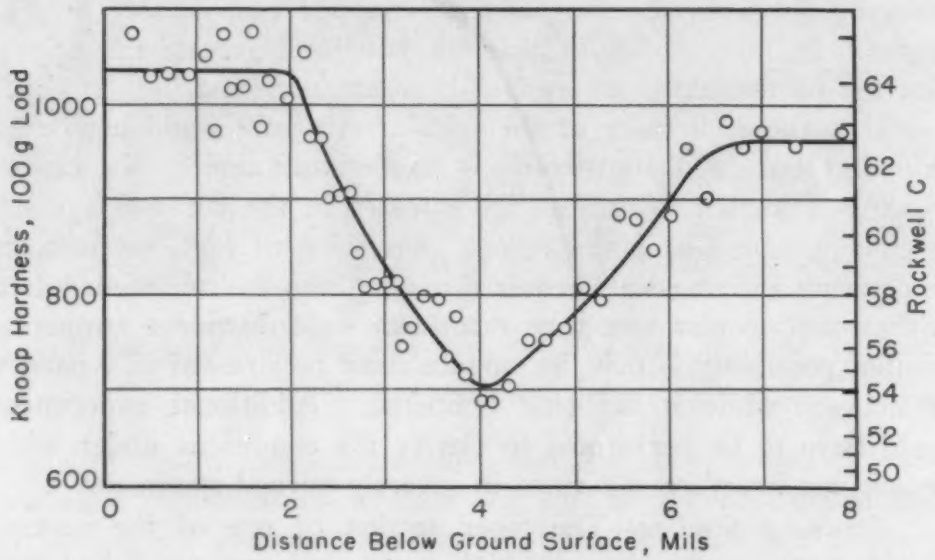


Fig. 7—Hardness Gradient Down Center of Burn Streak in High Speed Steel Resulting From Abusive Grinding.

depth of rehardening or of softening would have been recorded as less than it actually was.

The hardness curve obtained for one of the severely burned specimens of high speed steel is shown in Fig. 7, together with the experimental hardness values to indicate the spread that can normally be expected. The Rockwell C values corresponding to the 100-gram Knoop hardness numbers are indicated at the right. These were obtained from test blocks of the same steel hardened and tempered to various hardness levels. The details of the hardness conversion studies will be published at a later date.

The hardness is seen to drop from the original C-62½ in the interior to a minimum of C-54 and then to rise to C-64 in the rehardened surface layer. Average rather than extreme values are listed. As the grinding conditions are made progressively less severe, the whole curve may be expected to shift bodily to the left, causing first the disappearance of the completely rehardened structure, then of the transition structure, until the lowest point of the curve is at

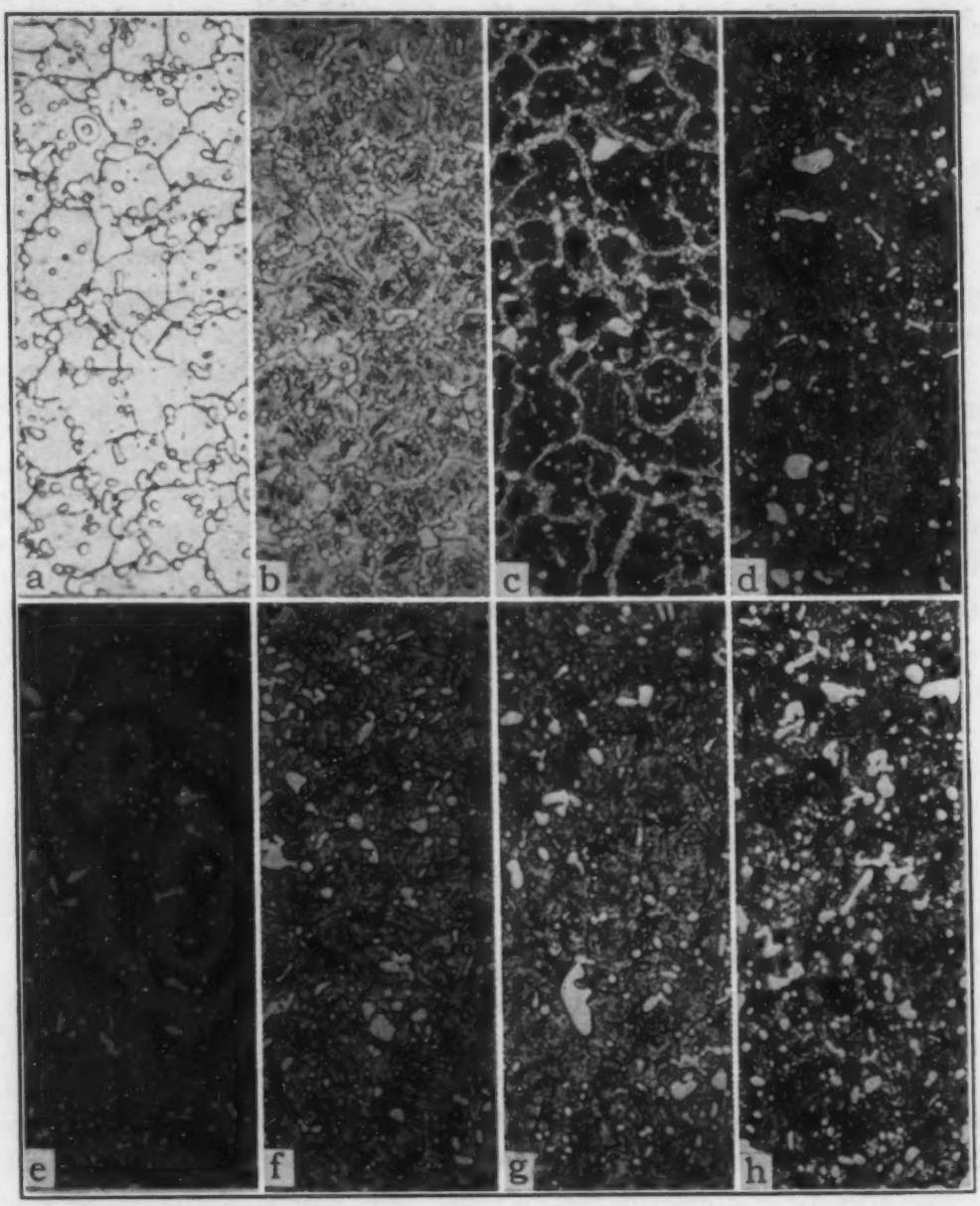


Fig. 8—Representative Microstructures of High Speed Steel for Selected Points on Hardness Curve of Fig. 7. Hyfercal etch. × 500. Depth below ground surface in mils (0.001 inch) and Knoop hardness at 100-gram load are listed in that order for each micrograph. (a) Completely rehardened; 0.6; 1030. (b) Rehardened, but with traces of badly overtempered martensite; 2.2; 970. (c) Transition; 2.5; 910. (d) Badly overtempered, but with traces of grain boundary rehardening; 3.3; 7.70. (e) Badly overtempered, minimum hardness; 4.1; 690. (f) Overtempered, but not as much as (e); 5.1; 810. (g) Slightly overtempered; 5.7; 890. (h) Unaffected by burn; 7.0; 980.

the surface. The maximum drop in hardness from the original value would be about the same. A further reduction in grinding severity would cause the maximum hardness drop to become less.

A variety of burned high speed steel specimens examined by the authors have not shown any greater drop in hardness in the soft skin than that indicated by Fig. 7.

After the hardness measurements were completed, the specimen was etched in hyfercal and a series of micrographs at × 500 was made of representative structures along the line of indentations. These are shown in Fig. 8. The depth below the ground surface given in the caption makes it easy to correlate the microstructures with the various portions of the hardness curve of Fig. 7.

The microstructure of Fig. 8a is of particular interest in that it is typical of the rehardened areas found in the most abusively ground specimens of high speed steel. The authors have never been able to find any traces of eutectic structure, indicative of partial melting, in the white martensite. This means that even under far more adverse grinding conditions than are normally encountered in the grinding of hardened tool steels, the work surface does not melt, at least in a layer thick enough to be visible when highly magnified.

Just below the fully austenitized zone, the hardness begins to drop off as the austenitization becomes less complete. Microstructures similar to those of Figs. 8b and 8c were shown previously at a higher magnification in Fig. 3. Fig. 8d shows that the hardness does not drop to its minimum value when the structure is badly overtempered, but still contains barely detectable traces of grain boundary rehardening.

The remaining micrographs are of the softest region (Fig. 8e) followed by progressively less overtempered regions (Figs. 8f and 8g), and ending with the unaffected steel (Fig. 8h). There is no real difference between the microstructures, and even the degree of darkening does not change a great deal unless the taper surface is viewed directly without magnification.

As for the dark-etching acicular structure, represented by Fig. 6a, its average Knoop hardness at a 100-gram load was found to be 940. The average hardness of white martensite alone was 1030 on the same scale. The corresponding Rockwell C values are 62 and 64.

Microstructural and Hardness Changes in Oil Hardening Tool Steel

Abusive Grinding Conditions—Parallel studies were made of

severely burned oil-hardening tool steel. Its type analysis was: 0.90% carbon, 1.25% manganese, 0.50% tungsten, 0.50% chromium. Blocks ½ inch thick were cut from 1½ by ⅝-inch bar stock. They were hardened by oil quenching from 1450 °F (790 °C), and were then tempered 1 hour at 350 °F (175 °C). All specimens of this steel, used in the present study, were processed the same way.

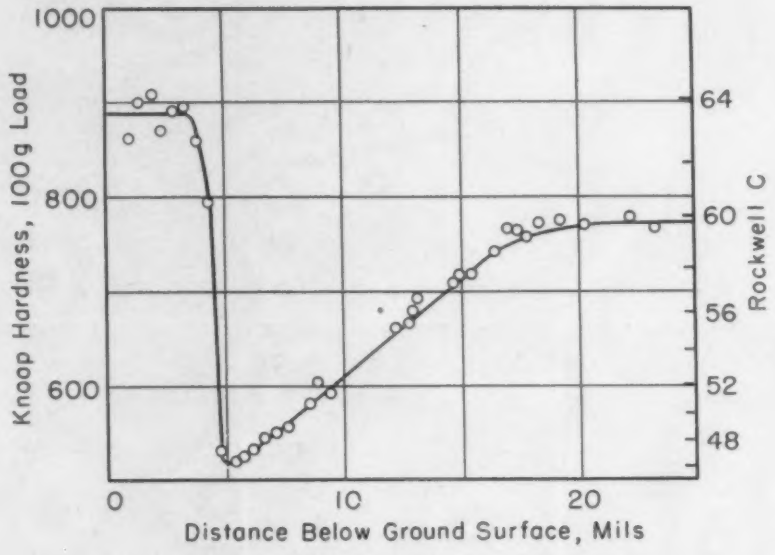


Fig. 9—Hardness Gradient Down Center of Burn Streak in Oil Hardening Tool Steel Resulting From Abusive Grinding.

One of these was ground lengthwise on a 1½ by ⅝-inch face in the same abusive manner as the high speed steel specimens and was then taper sectioned. For convenience in subsequent handling, the piece was cut in half so that it was only ¾ inch long. The taper angle was such that the normal structure of the steel, unaffected by burn, was represented in the taper section used in the hardness and microstructure studies. The tapering had to be done with a much thicker shim than for the high speed steel because the burn effects extended to 20 mils below the ground surface. The difference in burn depth between the two steels was probably caused by uncontrollable variations in the condition of the wheel face.

After the taper section was mounted in Bakelite and metallographically polished, Knoop hardness indentations at 100-gram load were made along the center line of a pronounced burn spot, which had been located by preliminary etching. The hardness data shown in Fig. 9 were obtained, then the specimen was etched for 10 seconds

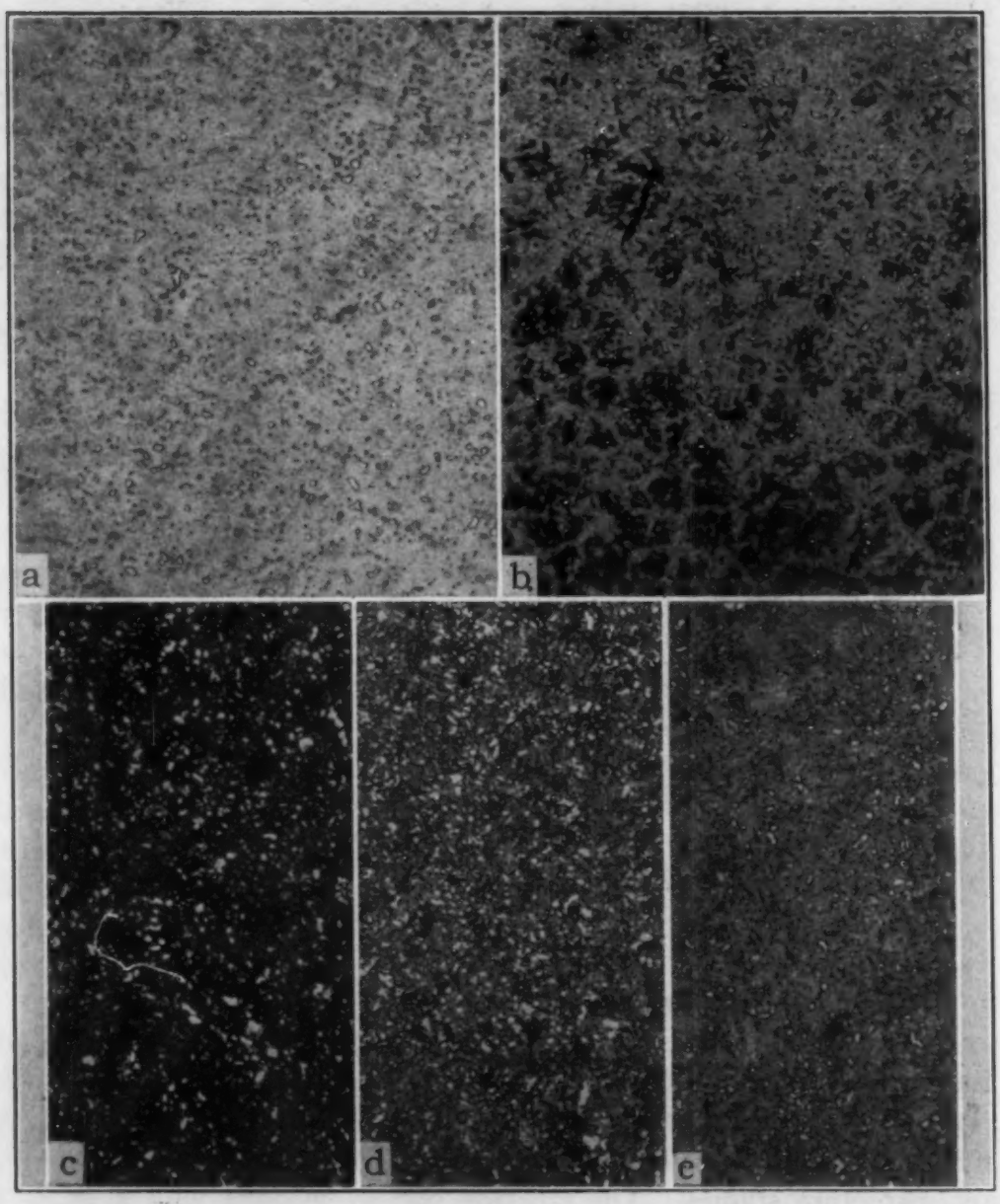


Fig. 10—Representative Microstructures of Oil Hardening Tool Steel for Selected Points on Hardness Curve of Fig. 9. Hyfercal etch. × 500. Depth below ground surface in mils (0.001 inch) and Knoop hardness at 100-gram load are listed in that order for each micrograph. (a) Completely rehardened; 3.4; 890. (b) Rehardened, but with appreciable amounts of badly overtempered martensite and merging into transition structure; 4.3; 800. (c) Badly overtempered, minimum hardness; 5.3; 520. (d) Overtempered; 12.3; 660. (e) Unaffected by burn; 20.4; 770.

in 2:4 hyfercal and the micrographs of Fig. 10 were prepared.

The progression of microstructures with increasing depth below the ground surface follows in a general way that already shown for high speed steel. However, the overtempered structures gradually

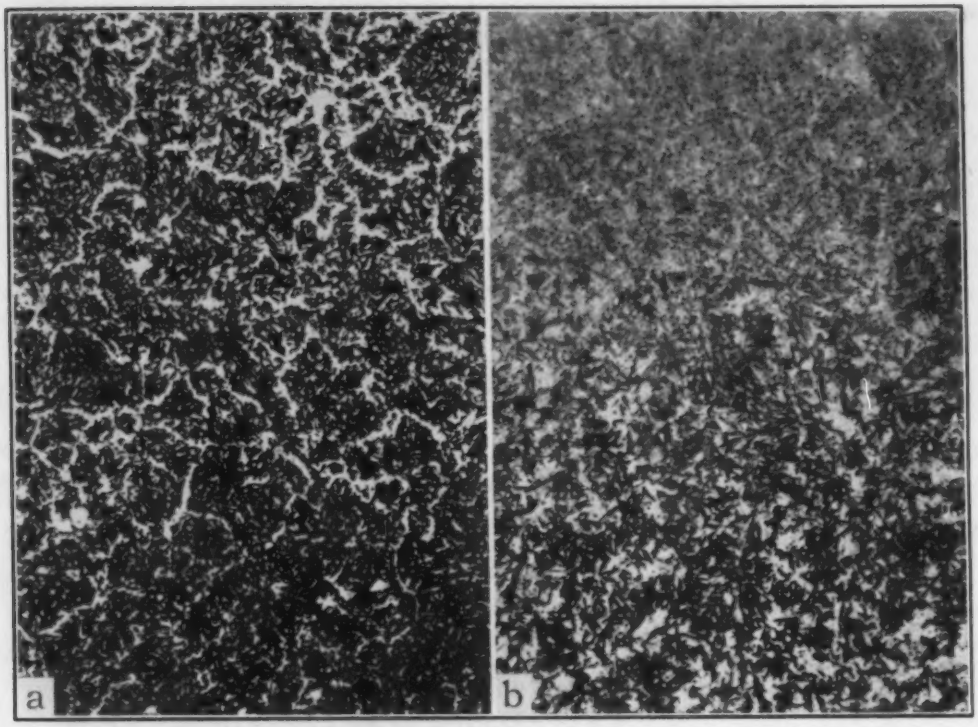
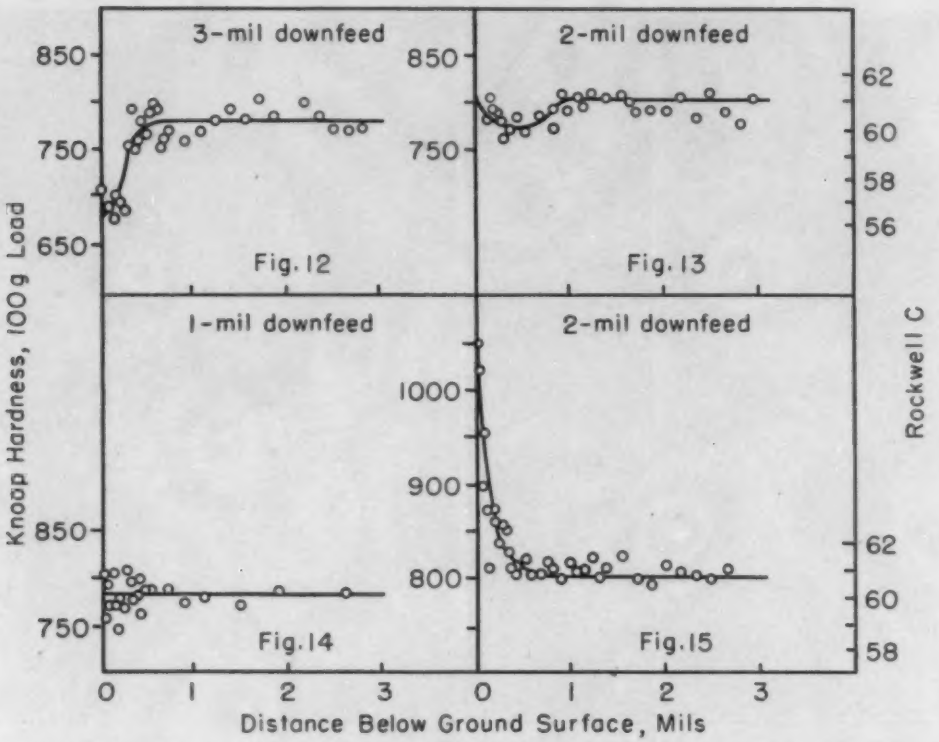


Fig. 11—Severely Burned Area in Oil Hardening Tool Steel. Nital etch. × 500. (a) Transition structure. (b) Acicular structure.

became lighter with increasing distance from the ground surface, while the overtempered high speed steel structures did not differ very much from the original tempered structure. The transition structure, poorly represented in this series by the lower portion of Fig. 10b, is shown far more clearly in Fig. 11a. This happened to be a different specimen of the same steel, etched for 2 minutes in 1% nital. This same specimen also contained in the rehardened areas a considerable amount of acicular structure, varying from dark to light, as can be seen in Fig. 11b.

To return briefly to the hardness gradient for the burn spot, the Knoop hardness dropped from the original 770 to a minimum of 520, while rehardening of the surface increased the hardness there to 890. The corresponding Rockwell C figures are 60 for the original hardness, 46 for the minimum, and 64 for the rehardened surface.

A tentative conversion from Knoop to Rockwell hardness has to be used for this steel since the conversion for oil-hardening tool steel has been found by preliminary experiments to be somewhat different from the conversion for high speed steel. The maximum drop in hardness caused by overtempering is seen to be greater for



Figs. 12 to 15—Surface Hardness Changes in Oil Hardening Tool Steel Ground Correctly With Various Downfeeds. Fig. 12—Moderate softening with 3-mil downfeed. Fig. 13—Barely detectable softening with 2-mil downfeed. Fig. 14—No change in average hardness with 1-mil downfeed. Fig. 15—Work hardening with 2-mil downfeed.

oil-hardening tool steel than for high speed steel, but even so this drop is not as large as frequently assumed.

Normal Grinding Conditions—Other blocks of the same steel were ground in accordance with normal commercial practice, rather than in the extremely abusive fashion purposely followed up to this point so as to obtain the complete range of possible burn microstructures. The 180-grit wheel previously used, which was much too fine and hard, was replaced by one frequently used in toolrooms for surface grinding hardened steels, the complete specifications being 38A46-I8VBE. It was properly dressed with a sharp diamond so that the wheel face was sharp and free-cutting. Downfeeds of 1, 2 and 3 mils for a total of two successive downfeeds were used in various experiments. The other conditions were the same as before: dry grinding; crossfeed—50 mils per pass; full table speed—65 feet per minute; and wheel speed—6000 surface feet per minute.

Metallographic taper sections with a mechanical magnification of 125 were prepared in the manner already described for the abusively ground block of the same steel. Knoop hardness indentations

were made at 100-gram load along the center lines of burn streaks, provided they were present, their location being determined by etching.

With a 3-mil downfeed, which is considered severe for hardened steels, a surface layer 0.4 mil thick was softened, as shown by the curve in Fig. 12. Proceeding from the unaffected interior toward the surface, the Knoop hardness dropped from 780 to 680, corresponding to a drop from Rockwell C-60 to 56. This was the most pronounced softening that could be found in this specimen.

The corresponding drop in hardness in a burn spot of the specimen ground with a 2-mil downfeed was just barely detectable, as shown in Fig. 13. It amounted to a change of only a single point on the Rockwell C scale, yet the burn marks could be clearly brought out by etching in hyfercal or nital. This shows how sensitive are the etching techniques for detecting burn.

As for the 1-mil downfeed, no burn whatsoever could be detected by etching, nor was there any drop in the average hardness in the immediate vicinity of the ground surface (Fig. 14).

To return to the piece ground with a 2-mil downfeed, additional hardness measurements were made between adjacent burn spots. Unexpectedly enough, there was a sharp *increase* in hardness in the vicinity of the ground surface, the results being plotted in Fig. 15. The taper section was then etched in hyfercal and it was found that the Knoop indentations corresponding to the rising portion of the hardness curve were not in a thermally rehardened, white martensite area, as first suspected, but in an area having the tempered martensite microstructure characteristic of the steel a considerable distance below the ground surface. Two such indentations can be seen in the micrograph of Fig. 16. All the indentations of Fig. 15 were located in exactly the same microstructure.

The absence of any subsurface softening that would normally be associated with surface rehardening is corroboratory evidence that something else than thermal hardening is involved. The logical explanation of the observed hardening is that it is caused by cold work arising from the grinding operation. Other instances of this work-hardening effect have been observed in hardened and ground high speed steel, where this phenomenon was responsible for some initial difficulty in the preparation of a conversion table for Knoop hardness (at 100-gram load) to the Rockwell C scale.

Certain peculiarities observed in the hardness curves of Figs.

13 and 14 can be explained in terms of this work hardening effect. With a 2-mil downfeed, the hardness in a burn spot was slightly greater at the surface than just below it although there was no trace of thermal rehardening. Evidently the softening, which should increase as the ground surface is approached, was compensated by the work hardening of a very shallow layer, which did not extend deep enough to take care of all the softening. When the downfeed was only 1 mil, the individual hardness values showed appreciably more



Fig. 16—Appearance of Work-Hardened Tempered Martensite in Oil Hardening Tool Steel. Hyfercal etch. × 500. The Knoop indentations, from left to right, correspond to the points in Fig. 15 for which the hardness numbers are 900 and 955, respectively.

scatter in the vicinity of the surface than at some distance below it, although the average hardness was the same. It is probable that cold work by grinding was responsible for the increased scatter.

From a practical standpoint, these curves prove that when proper grinding conditions are chosen, even severe grinding, such as a 3-mil downfeed, results in relatively little softening; furthermore, this softening can be eliminated by going to a somewhat smaller downfeed, but one which is still commercially feasible.

The curves shown earlier in Figs. 7 and 9, where rehardening extended to considerable depths, are characteristic of poor grinding practice. Although those curves and microstructures were obtained by the use of a wheel that was far too hard and fine, and purposely loaded in addition, similar undesirable results are sometimes obtained with wheels correctly selected for the job but used improperly. As soon as the wheel face is permitted to become dull or loaded, any rough grinding operation is likely to cause considerable burning of

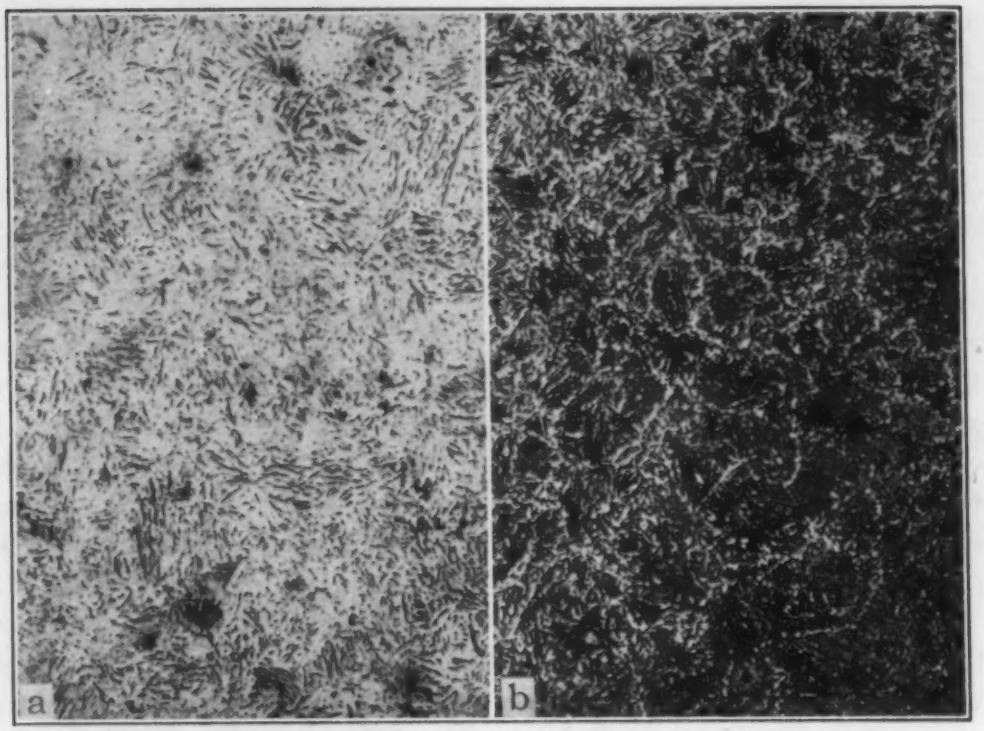


Fig. 17—Severely Burned Area in SAE 1040 Steel. Nital etch. × 500. (a) Residual overtempered structure in rehardened matrix. (b) Transition structure.

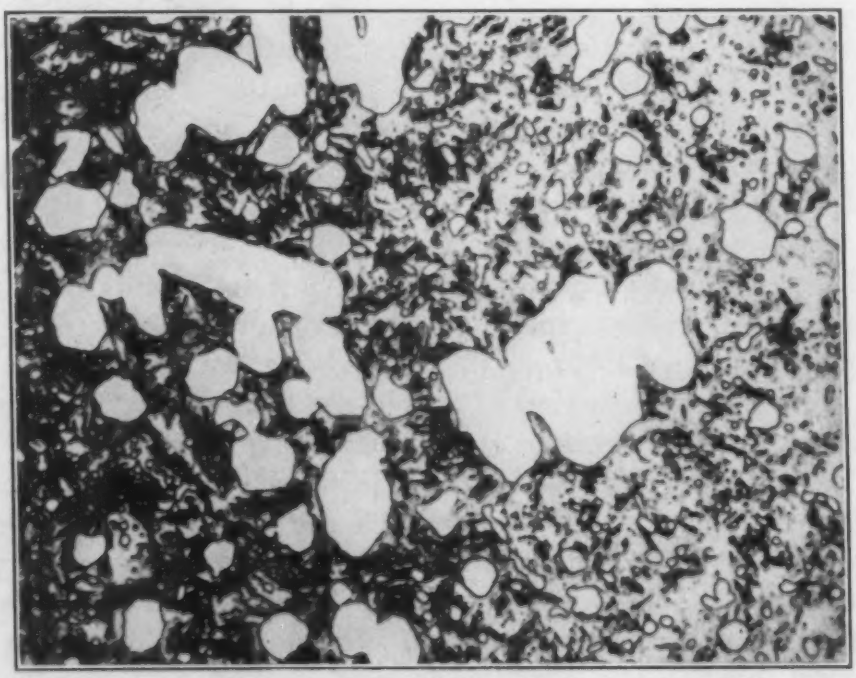


Fig. 18—Residual Overtempered Structure in Rehardened Matrix of Burn Spot in High Carbon, High Chromium Steel. Hyfercal etch. × 1500.

the surface with the accompanying rehardening and overtempering. Important factors in avoiding burn are discussed elsewhere (2) and need not be repeated here.

Microstructural Changes in Other Steels and in Cast Iron

The various burn microstructures found in hardened 18-4-1 high speed steel and oil hardening tool steel are also encountered in other types of hardened steels. SAE 1040, 1095, 52100, oil hardening high carbon and high chromium, and molybdenum-tungsten high speed steels were investigated briefly. Similar microstructural changes can be observed in carburized and hardened steels, although the changes associated with varying carbon content may mask some of the grinding effects and render them more difficult to interpret properly. Some typical microstructures are shown in Figs. 17 and 18.

When the steel is in the soft condition, it is generally impossible to harden it even by abusive grinding. Of course, such grinding will introduce high tensile stresses in the surface which are likely to distort the piece if it is sufficiently thin. However, hardenable steels in the soft condition can be hardened when cut improperly with an abrasive cutting-off wheel. Enough heat can be developed by such an operation, even when it is done wet, to bring the cut surface above the transformation range. A section through the cut surface will etch white for a distance depending on the severity of the cut, while beyond a certain point, it will change to the original, soft microstructure. The white martensite layer may contain darkened streaks resulting from flashes of tempering heat following hardening.

Gray iron can be hardened by excessive grinding heat. This can happen in surface grinding and not just in an abrasive cut-off operation. The light-etching hardened structure can be readily differentiated in Fig. 19 from the neighboring dark-etching pearlite. Knoop hardness measurements proved the light-etching structure to be martensite. The greater ease of hardening pearlite in gray iron by abusive griding can be ascribed tentatively to the presence of graphite flakes, which effectively block the immediate transmission of momentary flashes of grinding heat to the more distant portions of the metal. This would permit the heat to build up, with the result that the temperature reached becomes much higher for the same heat input than it would be in steel.

Attempts to surface harden white cast iron by grinding it in the



Fig. 19—Edge of Hardened Area in Burn Spot in Gray Iron. Nital etch. × 500.

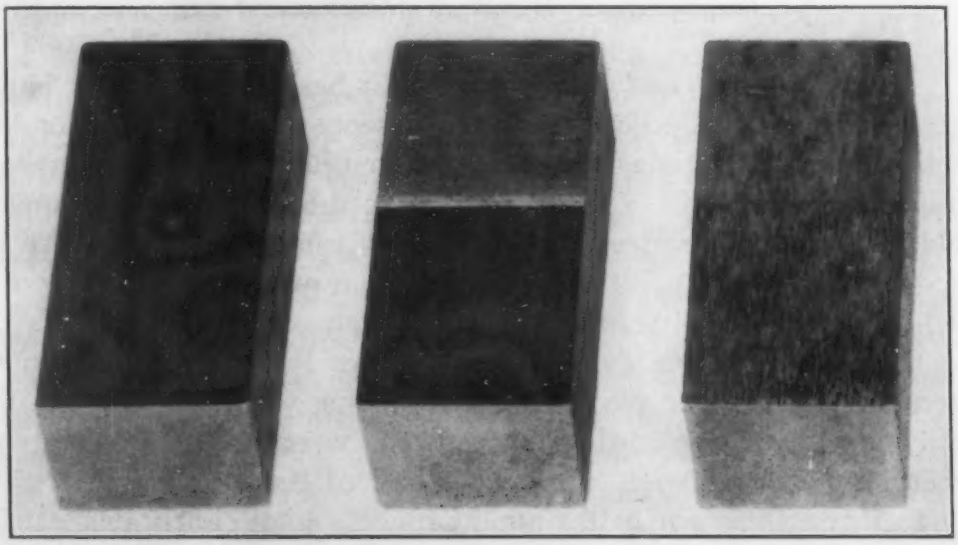


Fig. 20—Samples of Hardened Steel Burned Slightly When Ground Lengthwise as Indicated in the Left-Hand Piece. Burned surface was removed from upper half of middle piece by gentle cross grinding. The piece on the right was cross ground the same way and was then etched in 10% nital to bring out dark burn marks caused by overtempering. × 1.

same way as the gray iron was ground failed completely. This difference in the response to grinding heat is in agreement with the

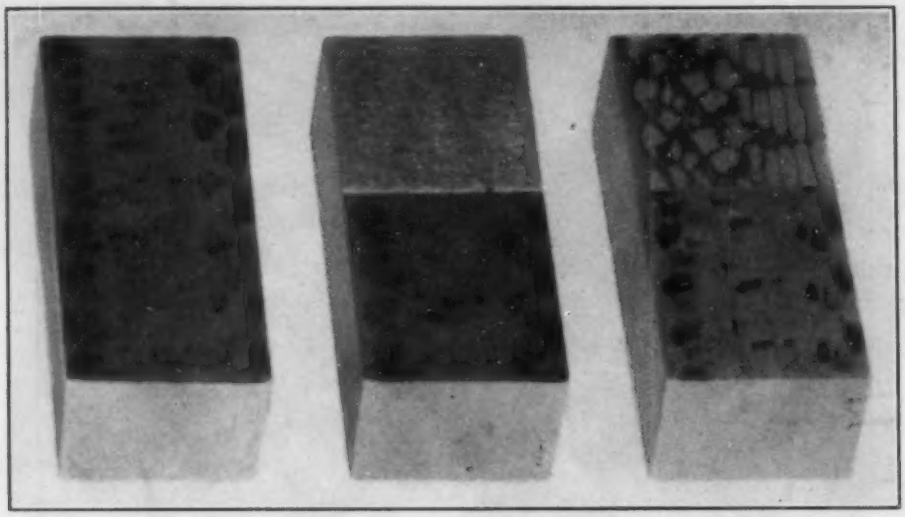


Fig. 21—Similar to Fig. 20 Except That the Pieces Were Burned Much More Severely in Grinding So That the Surface Rehardened in Spots, as Shown by the White Areas.

hypothesis that the graphite flakes in gray iron are an important factor in the observed hardening of the badly burned areas.

Detection of Burn by Macroetching

Overtempering and Rehardening—In heat treated steels, burn effects can be readily detected in the absence of any burn color by etching the ground surface itself, without any need for metallographic examination. The methods to be described first are applicable to steels other than the high speed variety, which require a modified technique to attain satisfactory results. The etching of high speed steels will be dealt with separately.

A 5 or 10% nital etch will often serve to show up burn in a ground surface. The pieces of oil hardening tool steel in Fig. 20, which had been hardened and tempered, were burned moderately when ground lengthwise. The upper half of the piece on the right shows that etching for half a minute in 10% nital clearly delineated the spots that had become overtempered even though a layer 2 mils deep was first removed from the burned surface by gentle cross grinding.

Another set of bars that were ground abusively with a loaded wheel to cause serious visible burn and chatter, and were then processed as before, are shown in Fig. 21. Rehardened spots, which appear white after etching, are present in a dark-etching, over-

tempered background; only the left edge of the bar was not burned, and it etched a light gray, a little darker than the rehardened areas.

When macroetching for burn, nitric acid in water can usually be substituted for nital without any ill effects. Only when the ground surface happens to wet with difficulty is there any advantage in using nital.

Both the sensitivity and contrast of the macroetch can be improved considerably by following with an etch in a weak solution of hydrochloric acid. A procedure that has been widely used involves etching in 5% nital, rinsing, and etching in a 10% solution of hydrochloric acid in alcohol. The best etching time depends on the steel but is generally one to several minutes in each of the acids.

Further improvement in contrast results from changing the solvent for hydrochloric acid from alcohol to acetone. The authors have found that the best results are obtained with 4% nitric acid in water, and 2% hydrochloric acid in acetone. The piece is etched for 15 seconds in the first reagent, washed off with hot water, then with acetone, and finally etched for 15 seconds in the second reagent. This cycle can be repeated once for greater contrast when necessary. Sometimes rubbing the surface vigorously after etching in the nitric acid and rinsing helps to bring out the burn pattern.

Whatever etching procedure is followed, once the etching has been completed, the piece, if it is to be preserved, is washed and then neutralized in some alkaline solution like weak ammonium hydroxide to remove the last traces of acid. It is usually desirable to coat the piece with some rust preventive, since the acids are likely to make the surface more susceptible to rusting.

An example of the extreme contrast obtainable with the last etching procedure is presented in Fig. 22. The two bars of hardened and tempered oil hardening tool steel were badly burned on a surface grinder by plunging the wheel into the work while the table was stationary. The piece on the right was then traverse ground to a level slightly below the bottom of the gouged-out portion, leaving an apparently undamaged surface. However, the burned structure was clearly brought out by etching. Grinding heat had rehardened to a considerable depth the whole area in contact with the wheel, and had overtempered a narrow rim around this area.

The moderately dark spots in the white area resulted from a slight tempering of the freshly formed white martensite during the traverse grinding which removed the visible traces of burn. Since

these spots darkened about the same as the unburned portion of the block, it can be deduced that the tempering of the white martensite that took place was roughly the same as occurred when the oil-quenched steel was originally tempered for 1 hour at 350 °F. Of course, the traverse grinding operation must have momentarily raised the surface temperature in the darkened spots considerably

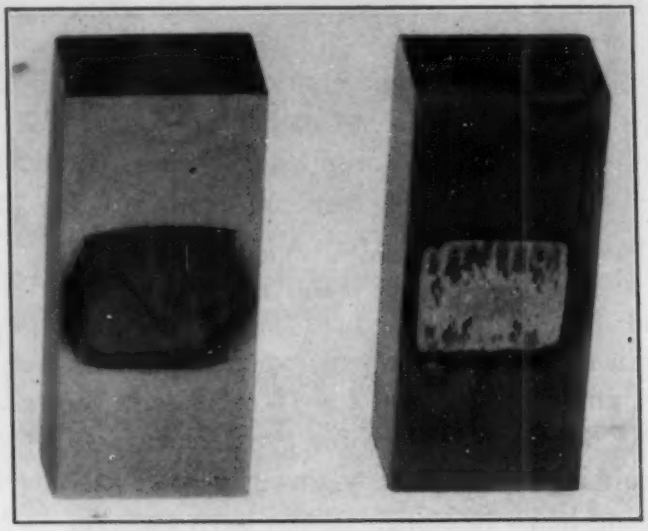


Fig. 22—Samples of Hard Steel Burned Severely by Plunging Grinding Wheel While They Were Stationary. All traces of burn were carefully ground off the piece on the right, which was then etched, as described in the text, to bring out metallurgical changes. × 1.

higher than this to compensate for the great difference in tempering time.

Another example of the advantage of using hydrochloric acid in acetone to sharpen the contrast is furnished by Fig. 23. This is a taper section of a block of the same steel that was severely burned in a traverse grinding operation. The left end of the specimen is at the original, severely ground surface, while the opposite end is 15 mils below it. The depth of rehardening is readily seen to be close to 5 mils, while the softening extends as deep as 14 mils.

The concentrations of the etchants used to develop burn marks in ground surfaces are sufficiently high to take care of hardened steels other than high speed steel. Sometimes, if the surface is unduly rough, it may help to smooth it with fine abrasive cloth.

Macroetching of High Speed Steel—In order to etch successfully the ground surface of high speed steel burned in grinding, it

is necessary to increase the concentration of nitric acid in water to 10% and to prolong the duration of the etches. Two minutes in the nitric acid and 3 minutes in the hydrochloric acid are generally sufficient to darken any overtempered areas that may be present; rehardened areas show up white in a much shorter time.

Scratch Burn—When any hardened steel is etched to see if it has been burned, it is sometimes found that white scratches or

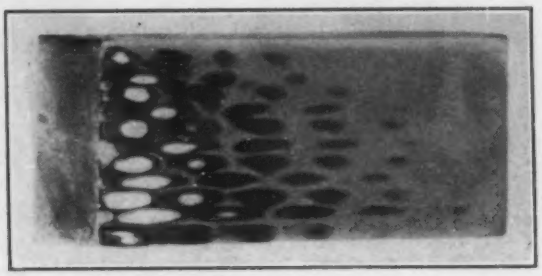


Fig. 23—Taper Section of Severely Burned Hard Steel Specimen, Etched, as Described in Text, to Show Depths of Rehardening and of Softening. × 1.

groups of them can just be distinguished in the dark, overtempered background. There may also be some white, rehardened spots of appreciable extent, but this is not necessary for the occurrence of the white scratches.

If a metallographic taper section is prepared through one of these scratches, as in Fig. 24, it becomes clear that the bottom of the scratch was heated high enough to reharden when it was being cut out, presumably by a dull abrasive grain. The heat was concentrated over the width of the scratch and it dissipated almost immediately into the underlying steel, with the result that only a narrow and extremely thin band of material was rehardened. The scratch proper appears in greatly exaggerated taper section as a dark, slender, out-of-focus groove, ending in and partly surrounded by the white-etching constituent. The depth of rehardening can be estimated as about 20 microinches.

Since the ground surface had been previously found to have a Profilometer roughness of 30 microinches rms, the actual peak-to-valley depth of a scratch like that shown in Fig. 24 was likely to be five times as much (6), or 150 microinches. Thus the depth of rehardening of the scratch valley was only a little over 10% of the actual scratch depth. The total burn depth, including both reharden-

ing and overtempering, was about twice this. Since scratch burn is so shallow, even by comparison with scratch depth, it appears most unlikely that it has any practical significance from the standpoint of injury.

Nondestructive Nature of Etching Procedure—The detection of burn by any of the macroetching procedures that have been described

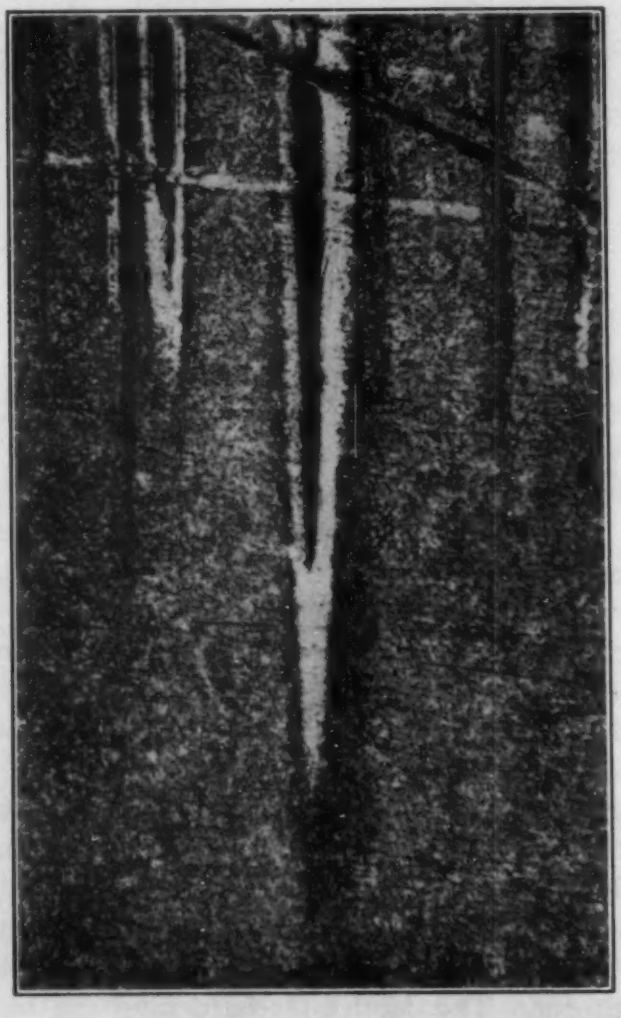


Fig. 24—Taper Section Showing Burn in Bottom of Grinding Scratch. Nital etch. Vertical magnification (mechanical times optical)—× 31,250; horizontal magnification (optical only)—× 250.

is, with some exceptions, a nondestructive process. Although etching discolors the surface, there is no change in dimensions that can be detected with a micrometer caliper. The discoloration can be removed, if necessary, by any method that leaves a good finish but

does not remove any appreciable amount of metal, such as Liquid Honing, which consists of blasting with fine abrasive particles suspended in drops of liquid.

It has been found that parts inspected for burn by etching are frequently more likely to rust at a later date, even though the acid has been properly neutralized. This prevents the use of such etching as a routine inspection tool in those instances where the parts might rust slightly in service and be damaged thereby, an example being antifriction bearings. Aside from such special cases, it has been found by experience that etching for burn does not affect the useful life of the part under service conditions.

No trouble has been encountered from etch-cracking (1) following the use of 2% hydrochloric acid in acetone, such as can occur when a surface severely stressed by grinding is etched in hot 1 : 1 hydrochloric acid. Evidently there is insufficient hydrogen embrittlement, if any, to crack hardened steel when a weak solution of hydrochloric acid in acetone is used for the recommended periods of time.

Effect of Stress on Etching Results—A piece of soft steel can be discolored by severe grinding just as readily as a hard piece. When an annealed specimen of SAE 1020 steel was severely burned in an attempt to harden it by grinding, a metallographic taper section failed to reveal any change whatsoever in the normal annealed microstructure. However, direct visual observation of the same taper surface showed what appeared to be rows of burn spots which gradually disappeared with increasing depth below the burned surface. Although a few of the most distinct spots were outlined in ink, additional microscopic examination at various magnifications, ranging from $\times$ 50 to $\times$ 1500, failed to reveal any difference between the microstructures inside and outside the ink marks.

It was concluded that the spots which could be seen with the unaided eye after the surface was etched were regions of high stress. This was the logical conclusion, since it was known, from their distortion, that high tensile stresses were present in thin strips of the same soft steel when they were similarly burned in grinding; furthermore, it could be expected that highly stressed areas would be more reactive than relatively unstressed areas, with the result that the former would etch more rapidly and appear relatively dark to the eye.

These stress effects are of negligible importance in most hardened steels, since the darkening attributable to overtempering is so

much more pronounced. In hardened and tempered high speed steels, however, the darkening caused by overtempering is much less pronounced, since it occurs against a background of material that has already been tempered at a high temperature. The spots that have been burned have also been stressed, and when the surface is etched, the darkening resulting from the presence of stresses may be about as great as that caused by overtempering. This may lead to a variety of shadings in an etched surface of burned high speed steel, which are quite confusing and difficult to evaluate properly.

Conclusions

When excessive heat is generated in grinding because of unsatisfactory grinding practice or for any other reasons, the momentary temperature rise in hardened steel may be enough to cause rehardening of a surface layer accompanied by softening of the immediately adjacent material. Softening can also occur in the absence of rehardening.

Metallographic examination of such a burned surface, especially in a taper section, may reveal a progression of microstructures, some of which are novel in appearance. A transition structure is often found in which grain boundary austenitization has occurred so that the dark-etching, highly overtempered grains are delineated by light-etching rehardened bands. As the region of complete austenitization is approached, the dark-etching grain centers gradually shrink and then change to discontinuous dark patches and specks in a white matrix.

The maximum hardness drop observed in the most highly overtempered regions in badly burned high speed steel was from Rockwell C-63 to C-54, while the corresponding figures for oil-hardening tool steel were C-60 to C-46.

When grinding is properly conducted, with the wheel face kept sharp, there is no rehardening, and softening can be decreased to a negligible amount under conditions of fairly rapid stock removal; if necessary, all traces of softening can be completely eliminated by decreasing the rate of stock removal. Under good grinding conditions, the hardness of a surface layer a few ten-thousandths of an inch thick can be increased appreciably, even in hardened steel, by work hardening resulting from the action of the grinding wheel, and this may be an advantageous effect.

Soft steel can be hardened by an improperly conducted abrasive cutting-off operation but generally it cannot be hardened by abusive grinding. Gray iron can be hardened much more easily than soft steel by abusive grinding.

Macroetching techniques, nondestructive in character, are available for detecting even faint traces of burn in ground surfaces. Under some circumstances, grinding stresses can also be detected by macroetching.

From a practical standpoint, only that degree of burn can be considered as injurious which affects unfavorably the life of the part under service conditions. To eliminate any burn that does not affect the service life is likely to increase grinding costs without any corresponding benefit.

References

1. L. P. Tarasov, "Detection, Causes and Prevention of Injury in Ground Surfaces," TRANSACTIONS, American Society for Metals, Vol. 36, 1946, p. 389-451.
2. L. P. Tarasov, "Injury in Ground Surfaces," 1947, Norton Company, Worcester, Mass.; also condensed version in *Steel,* Vol. 122, March 22, 1948, p. 71-79.
3. H. R. Nelson, "Surface Contour by Taper Sectioning," *American Machinist,* Vol. 85, 1941, p. 743-747.
4. B. W. Sakmann, "Geometrical and Metallurgical Changes in Steel Surfaces Under Conditions of Boundary Lubrication," *Journal of Applied Mechanics,* March 1947, p. A-43 to A-52.
5. W. H. Wooding, "The Hardened and Tempered Microstructure of High Speed Tool Steel as a Factor in Tool Performance," *Transactions,* American Society of Mechanical Engineers, Vol. 69, 1947, p. 281-306.
6. L. P. Tarasov, "Relation of Surface-Roughness Readings to Actual Surface Profile," *Transactions,* American Society of Mechanical Engineers, Vol. 67, 1945, p. 189-196.

DISCUSSION

Written Discussion: By Howard E. Boyer, chief metallurgist, American Bosch Corp., Springfield, Mass.

Messrs. Tarasov and Lundberg are to be congratulated on their work and presentation of the results relative to the injurious effects which may be imparted to the surfaces of steel by grinding.

The authors have proven beyond any doubt that hardened steel, in particular, can be seriously injured by unsatisfactory grinding conditions. The methods described in this paper for the detection of grinding injury are not only of academic interest, but may be used to advantage in manufacturing operations. No doubt others besides myself have, during the past few years, resorted to etching techniques similar to those described by the authors for detection of burn on high-precision parts. We have

long known that hardness testing machines other than microhardness testers are relatively insensitive and are usually of little value for the detection of surface characteristics.

In my opinion the authors have not placed sufficient emphasis upon the importance of producing hardened steel parts which are free from grinding injury. While it may be true that such injuries can be tolerated in many service requirements it must be remembered that the quality of any parts is seriously impaired by grinding injury.

It has become an accepted fact that most grinding operations tend to impart tension stresses to the surfaces irrespective of whether the material being ground is hard or soft. Considering this condition as one phase and burn as another we have divided burn into two classes which we have termed as primary and secondary. We define primary burn as that which has heated the surface layers just high enough to result in the overtempered condition described by the authors. The term secondary burn we have applied to the condition where the material has been heated to the austenitizing range so that rehardening is affected.

Either condition is likely to cause serious difficulty in certain types of service. Parts which have suffered primary burn possess a soft skin which is extremely susceptible to failure from scuffing or galling. Conditions of this sort usually take place early in the operating life of the part, probably due to the fact that if the part does survive the run-in period that the soft skin will work harden. Parts which possess surface layers of reaustenitized material as affected by secondary burn are readily susceptible to spalling under conditions of heavy-duty service, thus decreasing the service life and frequently leading investigators astray. Therefore it seems obvious that we cannot overemphasize the necessity for adherence to good grinding practice in order that we may comply with present day engineering requirements.

Written Discussion: By T. L. Counihan, chief metallurgist, Hyatt Bearings Division, General Motors Corp., Harrison, N. J.

The authors are performing a valuable service to industry in presenting their paper on the "Nature and Detection of Grinding Burn in Steel". Dr. Tarasov's past papers have been most helpful to many of us and we trust his work will continue, for there are still many unexplored fields in the grinding of metals.

A "grindability" yardstick would be most welcome. We have the end quench test as a measure of hardenability for steels of diverse analyses. No similar measuring rod is available for evaluating the ease or difficulty which may be encountered in grinding steels of different analyses or heat treatments.

We know that differences in grinding characteristics exist between different steel chemistries and heat treatments. It appears that the addition of chromium to steel increases its susceptibility to grinding difficulties. The only difference between AISI 4620 and AISI 4320 steels, for example, is that the latter has 0.40 to 0.60% additional chromium. There is experience, however, that 4320 steel carburized and hardened requires

more careful grinding than 4620 steel carburized and hardened. AISI 52100 steel hardened to the same hardness as the carburized 4320 and 4620 steels offers the greatest difficulty in grinding of all three analyses. I know of no confirmed explanation for these differences in grinding characteristics. It is probable that one will try to explain such differences in grinding characteristics between carburized and hardened 4320 and 52100 steels as due to the dissimilarity in stresses. It is possible that the grinding differences which we try to associate with differences in chemistry, fracture grain size, austenite content, microstructure, and heat conductivity are all directly connected to variations in stress patterns.

The main objective in commenting upon today's paper in this manner is to emphasize the rather scant knowledge we have on matters that pertain to the relationship between metallurgy and grinding characteristics. We are indebted to the authors for furthering knowledge in this direction.

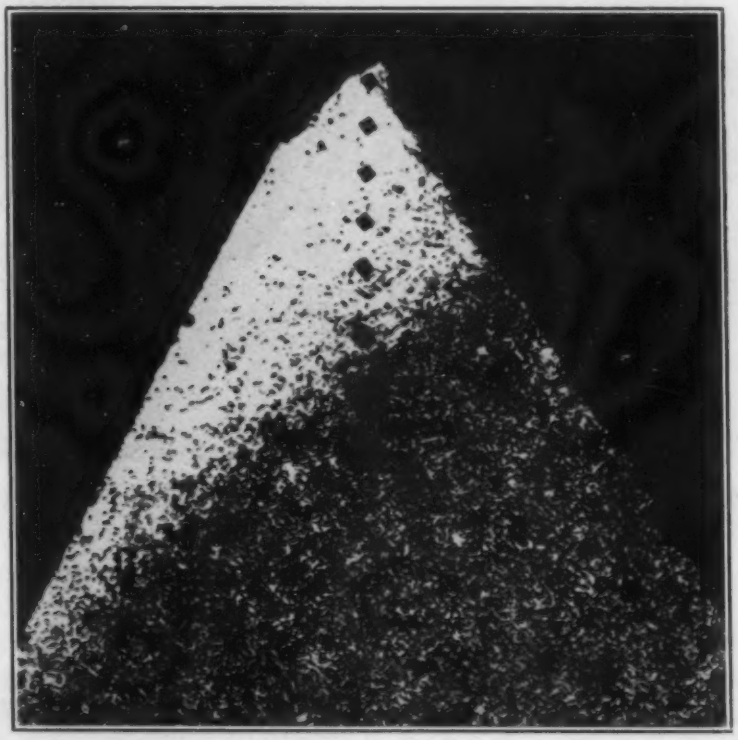


Fig. 25—Carbon Tool Steel Thread Ground in Annealed Condition. Etchant, 2% nital. Microhardness equivalent Rockwell C-68 to C-29. × 125.

Written Discussion: By W. R. Frazer, chief metallurgist, Union Twist Drill Co., Athol, Mass.

We are all aware, through grave experience, that improper selection or use of a grinding wheel, whereby it becomes loaded and dull or removes too much stock per pass, will disastrously affect the temper of tool steels. The authors of this important paper have clearly demonstrated the

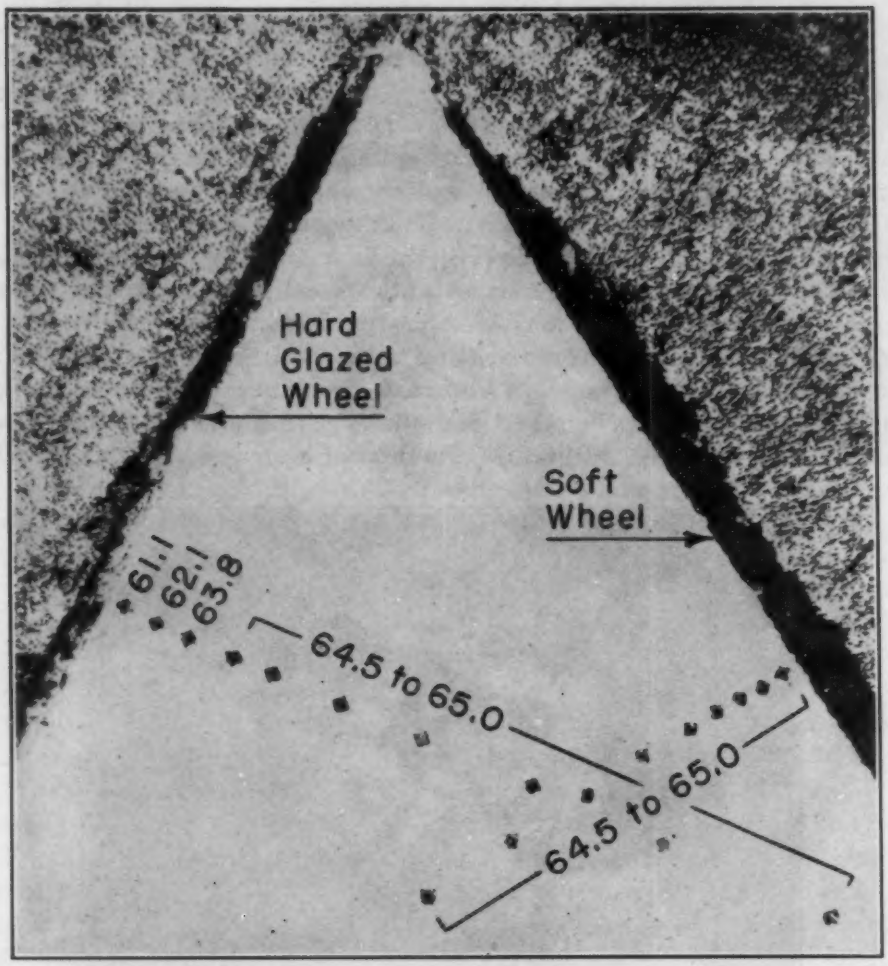


Fig. 26—Hardened and Tempered 18-4-1 High Speed Steel (Rockwell C-64.5). Unetched. Effect of hard glazed wheel vs. soft wheel on microhardness. × 125.

metallurgical and physical changes that can take place under improper grinding conditions.

The authors show that the extremely rapid heating and cooling of the surface immediately in contact with the grinding wheel can develop a temperature within the austenitizing range of the steel. The speed of reaction is so fast that a zone of transition may be present between the rehardened (austenitized) layer and the overtempered area, wherein the transformation to austenite starts at the grain boundary and progressively transforms the entire grain, thereby showing the kinetics of austenite formation.

The structures shown in this paper confirm our observations regarding the complex origin of the severe grinding stresses that often result in cracks which can cause failure of a cutting tool either during its production or during its subsequent use. We would be interested in learning if the authors have observed any relationship between the type of burned structure and grinding cracks, either actually produced by the wheel or

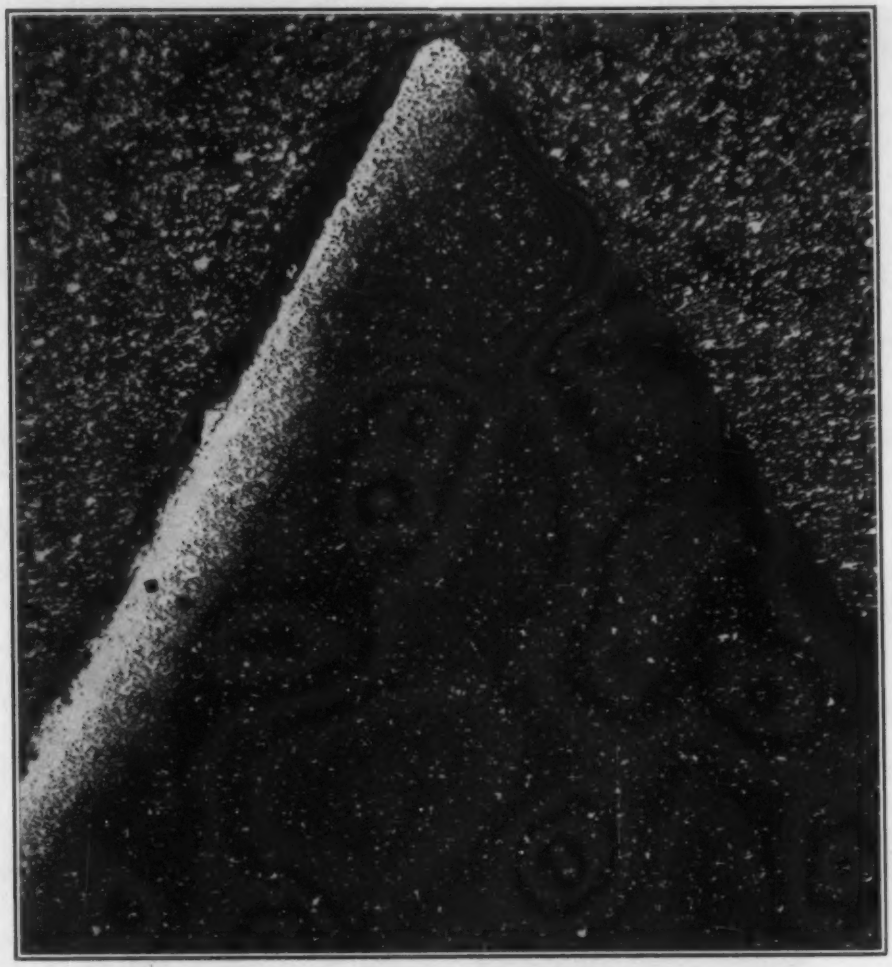


Fig. 27—Same Specimen as Fig. 26. Etched, 2% nital, 1 minute. × 125.

by deep etching after burning. In other words, is a rehardening with its complex stress conditions more likely to develop cracks than a less severely burned but overtempered and softer surface? This question is purely academic since either defect is cause for rejection of a cutting tool.

We would judge from the structure of Fig. 8a that the surface has reached a temperature of approximately 2250 °F (1230 °C). To strengthen the argument that wheel burning is detrimental to the work, it would be interesting if the authors would determine the temperature by checking the grain size and comparing the structures from pieces of the same bar heated to known temperatures by conventional methods.

In our studies to determine the effect of improper grinding on both carbon tool steel and high speed steel, we confirm the authors' observations. In Fig. 25 is shown the hardening produced at the crest of an annealed carbon tool steel tap when improperly ground from the solid, using thread grinding oil as a coolant but allowing the wheel to become dull. The microhardness indentations (Eberbach) show a range from

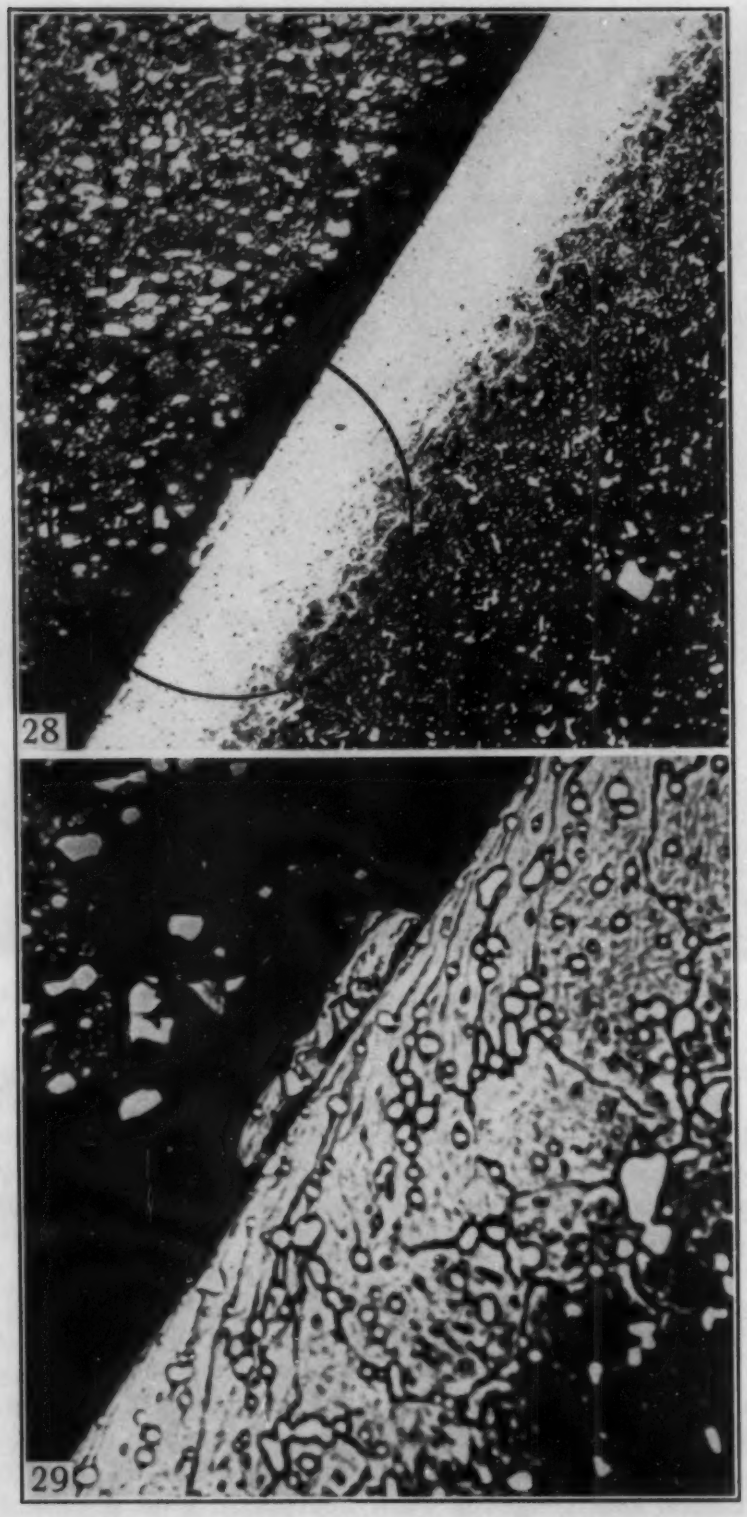


Fig. 28—Same Specimen as Fig. 27. Etched, 2% nital, 1 minute. × 500.

Fig. 29—Enlargement of Fig. 28. Note rehardened surface layer and distortion of grains indicating plastic flow during grinding. Etched, 2% nital, 1 minute. × 1500.

Rockwell C-68 to C-29. In Fig. 26 we show the result of microhardness exploration on a plane through a hardened and tempered piece of 18-4-1 high speed steel (Rockwell C-64.5) that has been ground with different wheels on either side of a 60-degree point. From 0.0006 to 0.0045 inch below the left-hand surface, the microhardness varied from Rockwell C-61.1 to C-63.8 and at 0.0067 inch depth, full hardness was attained. The microhardness impressions on the right-hand side, which was carefully ground, reveal no softening up to 0.0005 inch from the surface.

Fig. 27 shows the etched structure of Fig. 26 at the same magnification. Fig. 28 is a portion of Fig. 27 at a higher magnification, and Fig. 29 is a part of Fig. 28 at still higher magnification. This shows plastic deformation of the grains in the rehardened surface area, which gives some indication of the tremendous pressure developed in the grinding operation. These structures are similar to those observed by the authors.

Written Discussion: By E. S. Rowland, research metallurgical engineer, The Timken Roller Bearing Company, Canton, Ohio.

The metallurgical literature contains practically no information on the effects of grinding on the surface of hardened steel except that contributed by Dr. Tarasov and his associates. More work of this nature may lead to a better understanding of the mechanism of the grinding process.

We were much interested in the evidence of cold work on the surface of the hardened steel when lightly ground. In some experiments with hardened SAE 52100, we found that cold-worked areas resisted tempering to a considerably greater degree than the unaffected metal. A short tempering time in the range of 500 to 600 °F (260 to 315 °C) would leave the cold-worked areas considerably lighter after a normal etch than the unaffected material. The authors might try this as additional evidence of cold work.

Written Discussion: By Charles Nagler, professor of physical metallurgy, Wayne University, Detroit.

The authors are to be complimented on their fine paper concerned with burning in high speed steel and oil hardening tool steel. The fine quality of the work is evident in the set of photomicrographs in Fig. 8 which correlate very well with the hardness gradient curve of Fig. 7.

In the various burn tests carried out by the investigations on the high speed and oil hardening steels, was there any evidence of surface cracks to help substantiate the statement (page 907, paragraph 2), "it is quite possible that simultaneous generation of high austenitizing temperature and stress are required to condition the rehardened areas so that acicular structure can form on subsequent tempering"?

On finished tools, fabricated from oil hardening and water hardening tool steels, finish ground poorly and hot-etched with 50% muriatic acid in water at 165 °F, the ground surface has been found to show the presence of minute cracks that are not visible to the unaided eye.

Written Discussion: By R. G. Kennedy, Jr., research metallurgist, The Cleveland Twist Drill Co., Cleveland.

The authors have contributed several important items to the present

meager stock of knowledge pertaining to the subject of grinding burn.

In our studies of methods of revealing grinding burn, we were interested in developing not only an etchant to reveal microstructural changes in burned areas but also a macroetchant suitable for use in the grinding room. Of the dozen etchants used to reveal grinding burn on tools made of the Mo-W type of high speed steel, the three most successful were:

No. 1	5% HNO_3 in H_2O	3-min. etch
	1:1 HCl	3-sec. dip
No. 2	Hyfercal	2 to 3 min.
No. 3	Saturated Bromine water	1½ to 3 min.

We supplemented the macroetch test with a careful file test made by

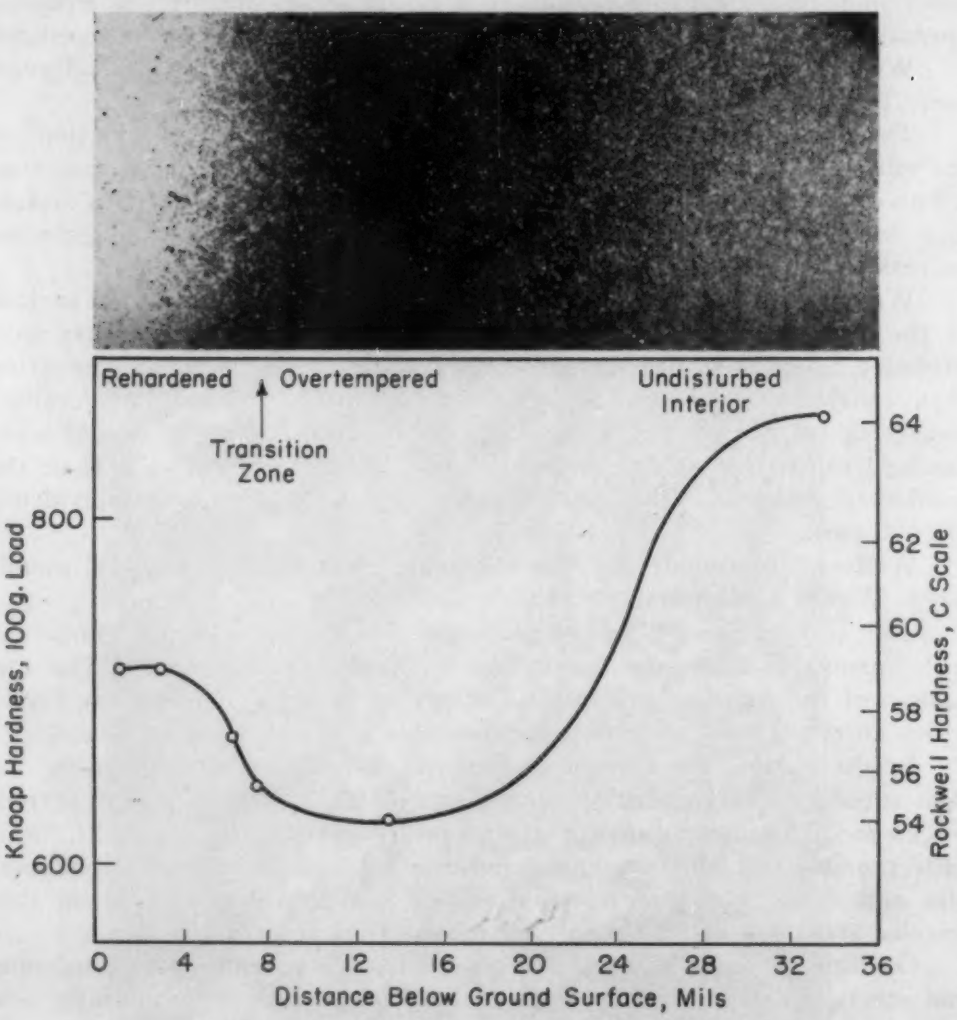


Fig. 30—Hardness Tests of a Specimen Burned in Grinding.

drawing the file in a flat position across the ground surface and comparing the file hardness obtained in this manner with the file hardness made on a cross section of the ground tool where no grinding had been done.

This test, when correctly done, is capable of detecting grinding burn quite well.

We have used the Tukon hardness test to good advantage in detecting grinding burn in cases where it was possible to cut off a cross sectional specimen. In such cases we usually plated the specimens with a heavy chromium plate and mounted them in bakelite containing fine

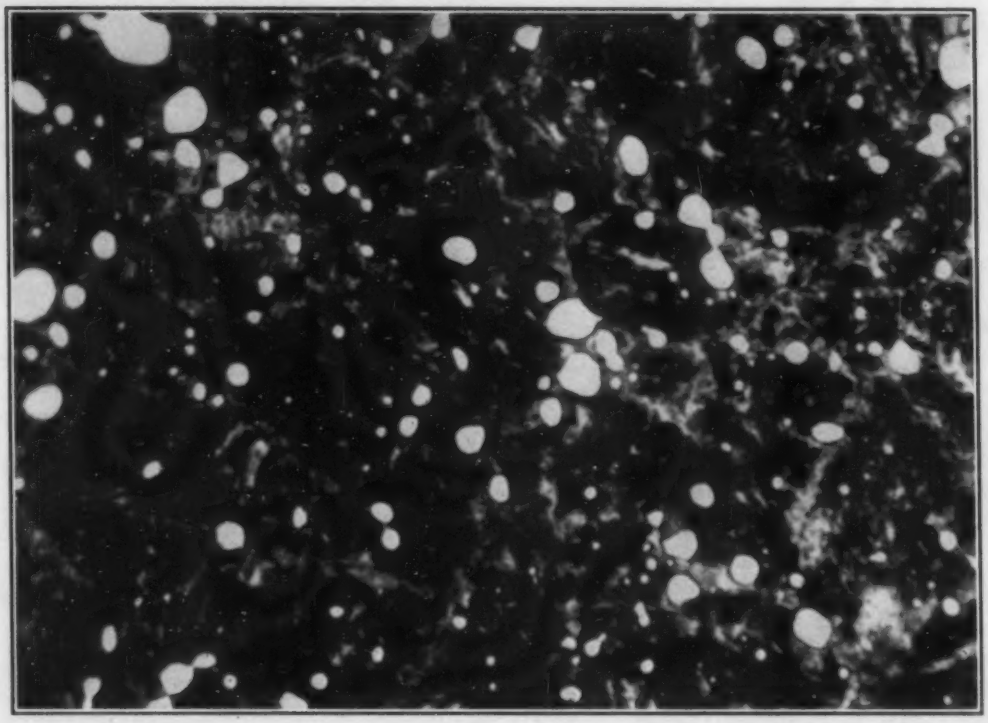


Fig. 31—Transition Structure of Specimen Shown in Fig. 30. Etched, 6% nital. × 2000.

metallic shot to prevent rounding of the edges in polishing. With such a technique we could then make a series of Tukon impressions at 100-gram load, starting in the unburned interior and extending within several microns of the edge. With a cross sectional specimen there is no danger of influencing the Tukon impressions because of hardness variations within the depth of penetration of the Tukon indenter. Our hardness surveys of cross sectional specimens burned in grinding have not shown results in exact agreement with those shown in Fig. 7. Even where grinding burn is severe enough to cause austenitizing to an appreciable depth, we have not obtained Tukon hardness readings in the rehardened area higher than those obtained in the unburned interior. Indeed they have been considerably softer in the rehardened area as Fig. 30 illustrates.

This lower hardness in the rehardened area agrees with Rockwell hardness data on the molybdenum-tungsten high speed steel which we have assembled. It indicates that the rehardened areas (which we find softer) attained a temperature possibly under 2000 °F (1095 °C), or if the temperature reached as high as 2200 °F (1205 °C), the very short dura-

tion of time in this temperature range did not result in enough solution of carbides to attain full hardness.

On the other hand the authors' Fig. 7 shows a Rockwell hardness of C-64 in the rehardened zone and only C-62.5 in the undisturbed interior. The fact that the authors observed an increase in hardness while we have observed a decrease in the rehardened areas indicates that the conditions under which grinding burn was produced were quite different. Another important difference is that we have recorded grinding burn to a depth of over 0.025 inch as compared to about 0.007 inch shown in Fig. 7. The grinding burn shown in the accompanying figure was observed when grinding a slot in a cylindrical specimen, $\frac{3}{32}$ inch in diameter. In our case there was not as much solid metal to carry the heat away from the burned area as there was when the authors produced burn in block specimens, size $\frac{7}{8}$ by $\frac{7}{8}$ by $\frac{1}{2}$ inch.

The transition structures showing grain boundary austenitization are a most important portion of the authors' new data. Here is definite evidence that the transition starts at the grain boundaries rather than in the interior of the grains. The zone in which the transition structures are observed is very narrow. It is not difficult to observe in taper-ground specimens, but can easily be overlooked in specimens cut and polished perpendicular to the burned surface. Fig. 31 shows the transition zone of the structure in our Fig. 30, where burning was observed to a depth of 0.028 inch.

Authors' Reply

We are glad to have Mr. Boyer emphasize the practical aspects of grinding burn, since we purposely mentioned this phase of the subject only briefly to avoid repeating material published elsewhere. Our position with respect to grinding burn is this: it is harmful only when it affects adversely the usefulness of the ground part in service. The purpose of this paper is to describe some techniques of studying burn so that a metallurgist can proceed to determine for himself just what degree of burn may be considered harmful in any given application.

The proposed use of "primary" and "secondary" to describe burn may lead to misunderstanding since these words are likely to be thought of as analogous to "major" and "minor". Actually, "secondary" burn, involving rehardening, is likely to be more injurious than "primary" burn, involving only softening. We prefer to describe the two degrees of burn as overtempering (or softening) burn and rehardening (or sometimes hardening) burn. For convenience, we also sometimes refer to them as dark and white burn, in accordance with their etching characteristics.

Mr. Counihan brings up the subjects of grindability and grinding sensitivity, which at first glance might appear to be unrelated to burn. However, any worthwhile study of these subjects would certainly require a knowledge of how to detect and measure burn inasmuch as this is a measure of actual grinding severity, which is of importance in interpreting grindability and sensitivity from a practical standpoint.

It might be well to point out that the term "grindability", which is now beginning to be used, refers to a particular form of machinability and can be considered to be the measure of the ease with which stock can be removed by grinding.

To avoid possible misunderstanding, it is best to exclude the concept of grinding sensitivity (or susceptibility to cracking) from that of grindability. Two steels can have the same resistance to grinding and yet differ greatly in their susceptibility to cracking under the same grinding conditions. Thus, it is more convenient to have separate terms for two distinct grinding characteristics of a steel.

Studies of grindability and of sensitivity are in progress and it is expected that differences in these characteristics, such as those described by Mr. Counihan, will eventually be related to variations in the microstructural condition of the steels. Although no proof exists as yet, indirect evidence points to retained austenite as being one of the most important factors involved in the sensitivity of steels like 52100.

Dr. Frazer's discussion confirms and extends very nicely our findings with respect to grinding burn. In particular, he has shown that annealed steel can be hardened when threads are ground improperly. This is in contrast to our surface grinding experiments, in which we were unable to harden annealed steel, even by extremely abusive grinding. The geometry of the ground part is responsible for this difference in results. In thread grinding, it is more difficult for the heat to escape from the vicinity of the ground surface into the interior of the steel than in plain surface grinding; hence, a higher temperature can be developed in the surface region of a thread. In a recent experiment, in which the surface grinding conditions were made even more abusive than previously, we succeeded in hardening small areas of annealed 1020 steel. The Knoop hardness at 100-gram load was raised to 350 from the normal value of about 200. Metallographic examination of the surface indicated that the increase in hardness was due not to cold work but rather to the formation of a martensitic structure.

In regard to the relation between the type of microstructure in the burned areas and the formation of cracks, it can generally be expected that cracking will occur more readily when the surface has been rehardened than when it has been only overtempered. The reason is that cracking is more likely to take place when the momentary surface temperature is raised to a higher value.

This is borne out by experiments on oil-hardened tool steel in which the severity of grinding was gradually increased so that more and more etch cracks were found after etching the test pieces in cold sulphuric acid, indicating a corresponding increase in the magnitude of the surface stress introduced by the grinding operation. At the same time, the surface overtempering became more pronounced until the momentary temperature rise became pronounced enough to cause austenitization and consequent rehardening. When the steel happened to be more sensitive than that used in the foregoing experiment, then increased severity of grinding resulted in a corresponding increase in the amount of actual

surface cracking observable immediately after grinding. Here again there was a correspondence between the amount of cracking and the severity of the burn. It should be kept in mind, however, that when hardened steel is not sensitive to cracking it can be ground severely enough to become rehardened and yet it will not crack at all during grinding nor will the surface stresses be high enough to cause etch cracks to form.

The grain size obtained in the rehardened areas of high speed steel does not seem to depend on the maximum temperature reached momentarily. Although no grain size measurements have been made, we have never seen any significant difference between the grain size at the center of a completely rehardened burn spot, where the highest temperature was obviously reached, and the grain size in the transition region, where the temperature was just barely high enough to austenitize the grain boundaries but not the interior portions of the grains. This point is well illustrated by Figs. 8a, b and c. We have also observed that the grain size of a rehardened area is essentially the same as that present in the regions unaffected by grinding heat.

All this leads to the conclusion that when austenitization takes place, there is no time for any grain growth to occur in the extremely short interval that the surface is at a suitably high temperature. The newly formed austenite grains have much the same boundaries as were left in the martensite when it formed from the austenite existing in the hardening furnace. Thus it is not possible to deduce the maximum temperature reached in grinding from the grain size of a rehardened area.

It is worth noting that grinding offers a convenient and rapid method of determining the austenitic grain size of hardened and tempered high speed steel. All that is necessary is to surface grind the specimen abusively enough to cause rehardening and the grain boundaries can be brought out without any difficulty by etching for 10 seconds in hyfercal.

Dr. Rowland's observations on the response of cold-worked areas in hardened steel to subsequent tempering should be kept in mind when interpreting the pattern that may be found upon macroetching to detect burn in a part that was stress-relieved after grinding.

Professor Nagler's question has already been answered in a general way in connection with the reply to Dr. Frazer. More specifically, the formation of the acicular structure in the rehardened areas may or may not be accompanied by surface cracking, depending on the sensitivity of the steel. As for the cracks found after etching severely ground tool steels in hot 1:1 hydrochloric acid, these may be either actual cracks in the surface that have been widened somewhat by the action of the acid, or they may be etch cracks which formed only after etching because of the presence of high stresses in the ground surface. To distinguish between the two possibilities, it is best not to etch in this manner but to subject the ground surface to magnetic particle inspection, which will reveal only cracks that are already present.

The results obtained by Mr. Kennedy with burned molybdenum-tungsten high speed steel corroborate ours except that his rehardened

areas were appreciably softer than the unaffected interior of the steel. Insofar as the method of making Knoop indentations is concerned, a taper section is just as reliable as a cross section taken perpendicular to the ground surface. As was mentioned in the paper, the depth of the indentations was extremely small compared to the variation of hardness with distance below the ground surface. If there were any effect of the underlying material in the taper section of a burned area, the over-tempered zone beneath the rehardened portion would tend to bring the measured hardness of the rehardened area below its correct value rather than to raise it. Thus, the difference between the hardness level of the rehardened region in the molybdenum-tungsten high speed steel and in our steels cannot be ascribed to differences in the type of section used for the Knoop hardness measurements. The difference must then be attributed to the way the steels respond to momentary grinding heat in the rehardening range.

SOLDER FLOW TESTER FOR TINPLATE

By J. J. Sperotto

Abstract

This paper presents a simple and rapid method for comparing the flow of soft solders on sheet metals and is particularly adapted to thin sheets such as tinplate. The method consists essentially of placing a constant volume pellet of solder on a tinplate disk together with an excess of flux and heating the disk above the melting point of the solder. The extent to which the molten solder spreads out on the plate is measured with a planimeter and used for comparison. Incorporated in this method is a means for preventing distortion or buckling of the sample plate during the heating cycle and, also, provision is made for the introduction of an inert gas to reduce oxidation of the plate or solder.

A STUDY of the literature yields little information on solder flow which can be applied to tinplate used in the can manufacturing industry. Most of the experiments were made on metals other than tinplate. This dearth of solder flow data on tinplate with different grades of solder and fluxes, particularly at the beginning of World War II, brought about the need for a rapid method of obtaining this information. The methods reported in the literature were not considered adaptable to tinplate or were too cumbersome and slow.

History

Methods previously reported have been based on the measurement of (a) capillary rise of solder in a hole (1)[1] and between rods or strips (2), (b) the rise of solder on a single strip of plate immersed in the solder, (c) the contact angle of the solder with the plate surface (3), and (d) the spread of solder on a flat surface (1), (2), (4), (5), (6). This latter method was considered more

[1]The figures appearing in parentheses pertain to the references appended to this paper.

A paper presented before the Thirtieth Annual Convention of the Society, held in Philadelphia, October 23 to 29, 1948. The author, J. J. Sperotto, is associated with the General Research Laboratories, American Can Company, Maywood, Illinois. Manuscript received April 21, 1948.

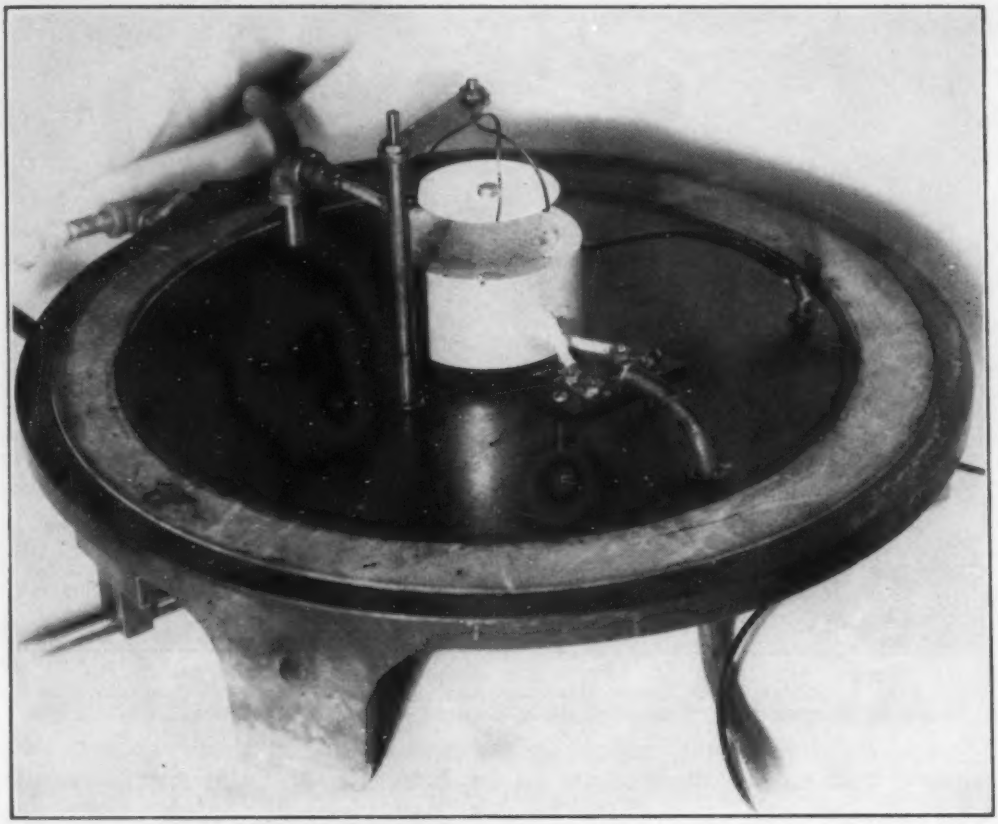


Fig. 1—Solder Flow Tester Showing Bell Jar Base Plate, Hot Plate and Specimen Lowering Device.

versatile and capable of rapid and simple operation and was therefore selected for refinement and adaptation to our specific needs.

In the initial experiments it was found that a disk of tinplate when heated by a hot plate or other means became warped or distorted by the heat. Solder flow under such conditions was erratic on account of the unequal heating of the plate and the fact that the plate surface was not level. This problem led to the development of a hot plate which incorporated a vacuum hold-down feature to prevent the test plates from buckling and warping while being heated. It was also thought desirable to incorporate, in the tester, provision for controlling atmosphere.

Description of the Tester

With the above specifications in mind, the solder flow tester shown in Fig. 1 was constructed consisting of the base plate of a large bell jar, hot plate, mechanical lowering device with tinplate

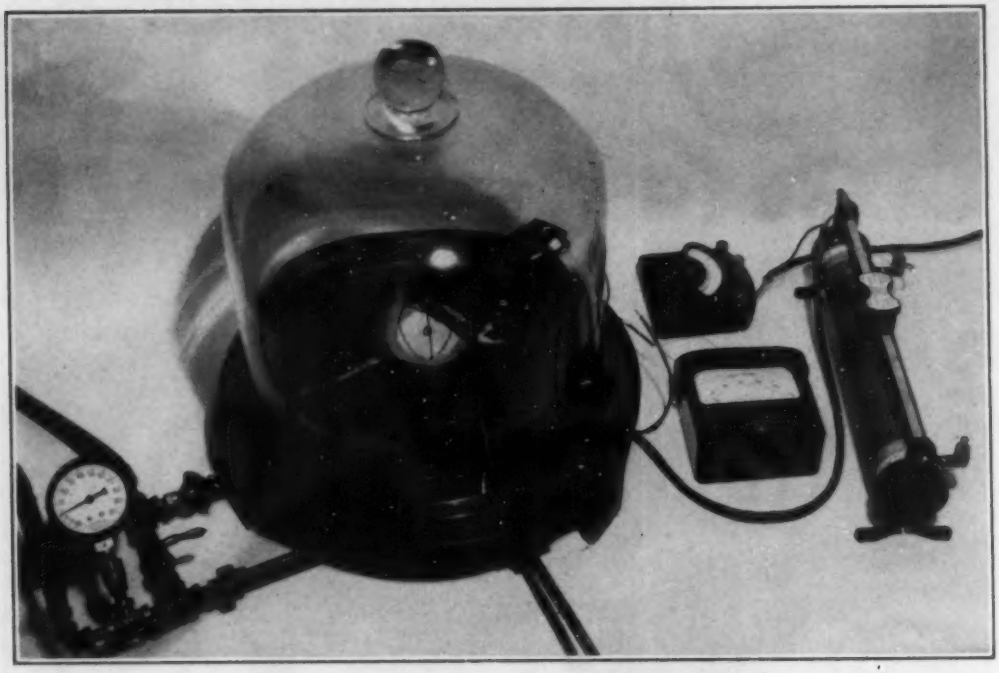


Fig. 2—Solder Flow Tester Showing Auxiliary Equipment for Controlling and Indicating Temperature of the Hot Plate, Gage, Piping and Bell Jar for Gas Control.

sample and solder in position to be lowered, and the thermocouple lead wires. The electrically heated hot plate has a series of small holes in the top. These holes are connected to a source of vacuum which can be applied as desired. The holes are located within the area covered by the sample tinplate disk, which in this case is 2¼ inches in diameter. In operation, vacuum is applied slightly before the tinplate disk with the solder and flux in place is lowered onto the hot plate. The force pushing down on the sample plate caused by the vacuum underneath prevents the plate from buckling or warping while being heated. The disks remain flat after vacuum is released. Fig. 2 presents another view of the set-up showing an ammeter and variable resistance in series with the heating element of the hot plate to control the temperature. A direct-reading temperature indicator gives the temperature of the hot plate. The piping sysem, with a compound gage, permits evacuating the bell jar and introducing an atmosphere of inert gas.

The solder pellets are prepared by punching out circular disks $\frac{5}{16}$ inch in diameter and 0.026 inch in thickness from sheet solder by means of a two-operation die. This procedure maintains a more constant volume of solder in the pellets. Variation in the thickness of the solder pellet is held within ± 0.0002 inch by measuring each pellet

with a micrometer and discarding those which are not within the above limits.

Operation of the Tester

The operation of the tester consists of placing a sample disk of tinplate, with the solder and flux applied onto the lowering device. The bell jar is placed on its base and evacuated. Then an atmosphere of nitrogen is introduced into the jar and the sample plate is lowered onto the heater whose temperature is maintained at 100 °F above the liquidus point of the solder being used in the flow test. The solder quickly melts and is allowed to flow out to its maximum area before the vacuum holding the plate down is released and the tinplate disk is raised up from the hot plate. After a series of solder flow samples has been run, the flow area of each sample is measured with a planimeter, and these measurements are then used as a basis for comparing relative solder flow.

Although the method does not yield an absolute value of the extent of solder flow for a given tinplate, solder and flux, it does serve as a convenient means of comparing solder flow for such variables as type of plate, solder composition, temperature, and to a limited extent, type of flux. In addition, the tester has been found helpful in determining whether soldering difficulties encountered on automatic can-making equipment are the result of tinplates exhibiting poor soldering characteristics or of faulty equipment operation.

Discussion of Results

The results obtained in a series of measurements on solder flow for a 4% tin, 96% lead solder on several types of plate used in can making are given in Table I. Table II lists the results of a similar

Table I
Comparative Flow of 4% Tin, 96% Lead Solder on Commercial Tinplates and Black Plate

	Solder Flow Values Expressed in Square Inches 700 °F (370 °C)—Rosin-Alcohol Flux (1 lb. Rosin per Gallon Alcohol)				
Sample No.	1.25# Hot-Dipped Plate	.75# Elect. Plate	.50# Elect. Plate	.25# Elect. Plate	Black Iron Plate
1	0.43	0.42	0.39	0.32	0.13
2	0.48	0.51	0.50	0.26	0.11
3	0.54	0.47	0.53	0.29	0.11
4	0.46	0.41	0.47	0.36	0.13
Avg.	0.48	0.45	0.47	0.31	0.12

Table II
Comparative Flow of 40% Tin, 60% Lead Solder on Commercial Tinplates and Black Plate

Sample No.	Solder Flow Values Expressed in Square Inches 560 °F (290 °C)—Rosin-Alcohol Flux (1 lb. Rosin per Gallon Alcohol) 1.25# Hot-Dipped Plate	.75# Elect. Plate	.50# Elect. Plate	.25# Elect. Plate	Black Iron Plate
1	0.79	0.42	0.59	0.24	0.11
2	0.53	0.38	0.45	0.25	0.14
3	0.65	0.38	0.44	0.23	0.14
4	0.75	0.43	0.46	0.31	0.13
Avg.	0.66	0.40	0.49	0.26	0.13

series of measurements using a 40% tin, 60% lead solder. The correlation between the data given in Tables I and II and commercial experience in soldering cans, fabricated from the same tinplates and solders, has been found to be sufficiently close to warrant the use of this test procedure to determine the probable performance of various solders and plates under factory operating conditions.

This test procedure has also been used with some success as a means of evaluating the relative efficacy of fluxes. The wide variations in physical properties of fluxes when heated to soldering temperatures make this method less reliable in predicting flux performance on high speed can-making equipment than is the case when solder variables alone are under study. The usefulness of results on fluxes is limited by the tendency of certain fluxes to produce irregular solder flow pattern due to uneven action of the flux on the heated plate. Rosin-alcohol flux gave the most stable flux action of the fluxes tested and was therefore chosen as the standard flux for use in evaluating the solderability of tinplate.

Conclusions

A method is briefly described for comparing the relative solder flow characteristics of various types of tinplate, grades of solder, and different fluxes. It is adaptable for use on tinplate and other light gage metals. The correlation between the results obtained on this tester and the commercial experience in soldering cans is sufficiently close to allow the use of this test procedure to determine the probable performance of tinplate and solder in high speed can manufacturing operations.

References

1. J. B. Russell and J. O. Mack, "Substitute Solders of the 15-85 Tin-Lead Type," *Metals Technology*, American Institute of Mining and Metallurgical Engineers, T.P. 1770, October 1944.
2. F. N. Rhines and W. A. Anderson, "Substitute Solders," *Metals and Alloys*, Vol. 14, November 1941, p. 704-711.
3. A. Latin, "The Influence of Fluxes on the Spreading Power of Tin Solders on Copper," International Tin Research and Development Council, Publication No. 88.
4. A. W. Coffman and S. W. Parr, "Surface Tension of Metals With Reference to Soldering Conditions," *Industrial and Engineering Chemistry*, Vol. 19, December 1927, p. 1308-1311.
5. R. S. Dean and R. V. Wilson, "The Action of Fluxes in Soft Soldering and a New Class of Fluxes for Soft Soldering," *Industrial and Engineering Chemistry*, Vol. 19, December 1927, p. 1312-1314.
6. J. A. Kies and W. F. Roeser, "The Testing and Properties of Low-Tin Solders Listed in Recent Federal Specifications," American Society for Testing Materials, Preprint No. 36 (1943).

DISCUSSION

Written Discussion: By Carl A. Zapffe, consultant, Baltimore.

In view of the multitude of soldering operations possible with stainless steels, and the great sensitivity of solder on these steels to factors causing poor flowability, a natural question is to ask Mr. Sperotto whether he intends to extend this promising method to that field.

Written Discussion: By H. B. Osborn, Jr., technical director, TOCCO Division, The Ohio Crankshaft Co., Cleveland.

I should like to ask the author whether he would care to make any comments on the following points:

1. How does the condition of the surface of the material affect the soldering rate? I rather imagine that the stock as received from the mill is not too smooth and that there will be wide variation in the type of finish.

2. How does the rate of heating affect the flow of solder?

3. What is the effect of temperature on the results with various fluxes and solders?

4. Would the same results apply on tin plate which has been processed by reflowing with induction heating as with the material referred to in this paper?

Author's Reply

Replying to Dr. Zapffe's question, no solder flow tests have been made on stainless steels and none are anticipated.

Replying to Dr. Osborn's questions:

1. Normal temper mill finish variations in commercial deliveries have no significant effect on solder flow. There are, however, more subtle

characteristics of the steel surface which may be important enough to make large differences in solder flow and performance in can making operations, irrespective of tin coating weight. The reasons for this behavior and the exact nature of the factors responsible are not yet adequately understood.

2. This solder flow tester was designed for constant temperature work; therefore, the rate of heating is also constant except for slight variations in sample plate thicknesses. However, when the temperature is less than 75 to 80 °F above the liquidus point of the solder being used, the fluidity or mobility of solder is lowered, which in turn reduces the spread or flow of solder. Temperatures greater than 100 °F above the liquidus point do not make any appreciable difference in solder flow.

3. The effect of temperature on fluxes appears to depend entirely upon the physical properties of the fluxes. Those which are extremely volatile or whose cleaning and fluxing properties are spent quite rapidly produce erratic flow results. This is due to the fact that these fluxes have volatilized off or lost their fluxing properties by the time the solder pellet melts or starts to flow.

4. Electrolytically deposited tin which has been melted by induction heating, resistance heating, and hot air or radiant heating has been used indiscriminately in container manufacture and in our solder flow tests without exhibiting significant differences in solderability or solder flow.

THE INDIUM-BISMUTH PHASE DIAGRAM

By E. A. Peretti and S. C. Carapella, Jr.

Abstract

The system, indium-bismuth, has been investigated using 65 alloys for thermal, X-ray, and metallographic methods of analysis. Thermal data are in substantial agreement with those obtained in a recent investigation by Henry and Badwick. The presence of a eutectic at 66.3 weight per cent indium and 72.1 °C has been confirmed. A peritectic reaction, gamma + liquid ⇆ beta, at 89.0 °C has been detected, which is not in agreement with the eutectic proposed by Henry and Badwick in this region. Between the gamma phase and pure bismuth, a eutectic was established at 33.0 weight per cent indium, which is in agreement with the revised diagram of these investigators. Four phases were found to exist at room temperature. For the first time, the complete course of the solidus and the limits of solid solubility of the indium-rich phase have been determined (20.5 weight per cent bismuth at 72.1 °C and 7.1 weight per cent bismuth at room temperature). The solid solubility regions of the other phases are small.

At the inception of this work, no knowledge of the system, indium-bismuth, was on record. Just recently, Henry and Badwick (1)[1] have reported the findings of their investigation in which they propose two eutectic reactions, one occurring at 66 weight per cent indium and 72.5 °C and the other at 50 weight per cent and 90 °C, and a peritectic reaction Bi + liquid ⇆ γ at 110 °C. The peritectic reaction was later revised (2) to a eutectic reaction. The course of the solvus of the alpha (indium-rich) phase was not established. Two intermetallic compounds were observed in the vicinity of the composition InBi and In_2Bi.

For the present investigation, there were employed thermal analysis, X-ray diffraction techniques, and microscopic examinations.

[1]The figures appearing in parentheses pertain to the references appended to this paper.

A paper presented before the Thirtieth Annual Convention of the Society, held in Philadelphia, October 23 to 29, 1948. Of the authors, E. A. Peretti is an associate professor of metallurgy, and S. C. Carapella, Jr., is a teaching fellow at the University of Notre Dame. Manuscript received March 26, 1948.

Out of the experimental findings, a diagram has been developed, Fig. 1, which differs in part from the diagram of Henry and Badwick.

Experimental Procedure

High purity indium[2] obtained from the Indium Corporation of America and C. P. bismuth[2] obtained from the J. T. Baker Chemical Company were used to prepare the alloys. Each alloy used for thermal analysis weighed 75 grams; twenty-one of them were prepared by accurately weighing the pure constituents on an analytical balance. The remaining alloys were made by diluting with either indium or bismuth. With careful technique, melting losses could be kept to as low as 2 parts in 300,000. No one alloy was used more than three times to make subsequent alloys. Therefore, it is felt that the intended composition could be used without chemical analysis. The alloying constituents, placed in a pyrex tube and covered with mineral oil to minimize oxidation, were melted at 280 °C. Stirring was carried out by means of a glass rod to insure dissolution of the metals.

Thermal data were obtained using an adaptation of a furnace designed to employ the principle described by Smith (3) and the improvement of Edmunds (4) for controlling the rate of heat input or heat extraction. In this investigation, two concentric iron cylinders with constantan wires were used for the thermal regulator instead of the nichrome cylinders and alumel wire as proposed by Edmunds. This was found practical since low temperatures were involved and iron cylinders are available in a variety of sizes. With this apparatus, the heating rate could be controlled to almost a constant value, thus making small heat effects discernible. To detect phase changes, inverse rate curves were plotted. It was advantageous to plot direct rate curves to determine the temperature of these reactions. In cases where pronounced supercooling was noted, extrapolation of the direct rate curve yielded questionable values. For this reason the liquidus temperatures are probably not more accurate than $\pm$ 1 °C. Considering the consistency of the temperature values and the amount of metal involved in the eutectic and peritectic reactions, it is believed that these values are accurate to

[2]The indium had a guaranteed purity of 99.97% with the following analysis: Cu—0.002, Pb—0.006, Sn—0.01, Zn—0.01. The bismuth had the following label analysis: S—0.01, Pb—0.005, Cu—0.005, Ag—0.01, Fe—0.01, Zn—0.005.

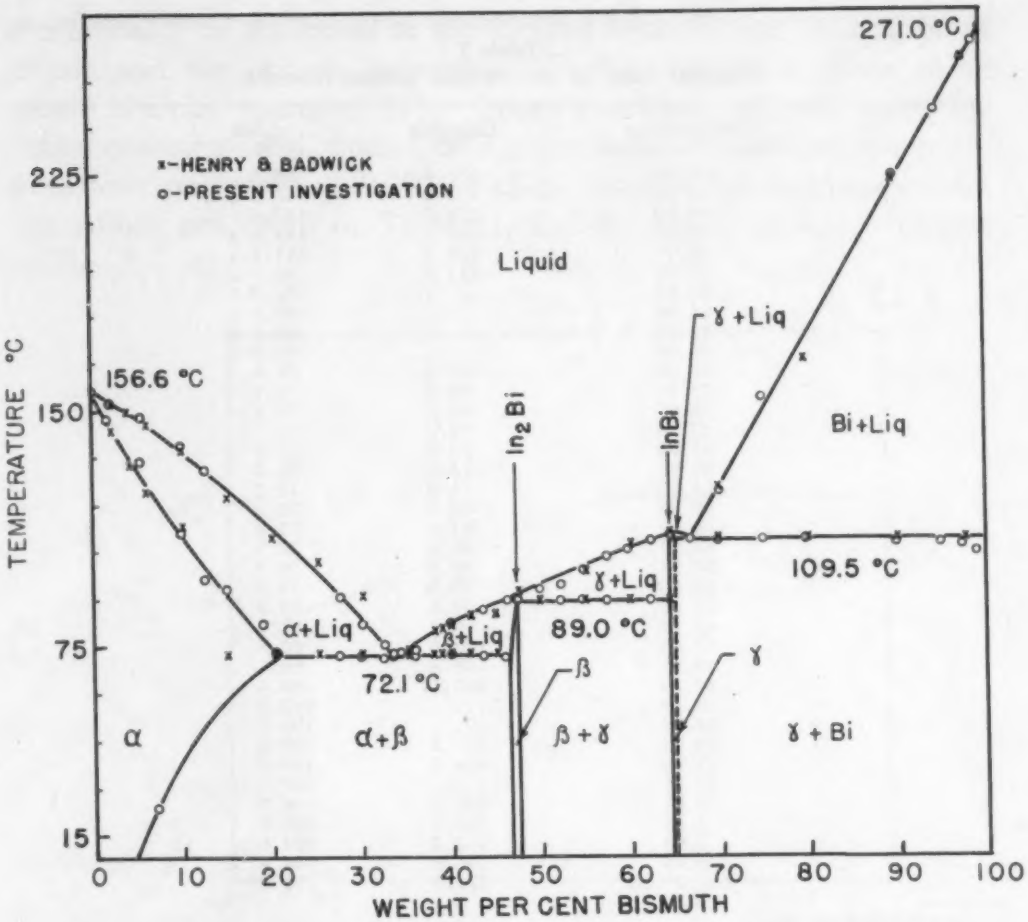


Fig. 1—Phase Diagram of the System Indium-Bismuth.

± 0.5 °C. The values obtained from thermal investigation with the respective alloy compositions are given in Table I and plotted in Fig. 1.

The solidus was located in part by heating curves from alloys worked and homogenized for a week at 68 °C. It was later found satisfactory to record the temperature at which intercrystalline fracture[3] occurred for a given alloy, the solidus temperature. This supplemental test was used since it required small amounts of alloy and a shorter annealing period. A 10-gram specimen was used to form a strip of the approximate dimensions, 0.025 by 2.50 by 0.75 inches. The strip was placed in a Precision Scientific Company furnace, which maintains a circulating air atmosphere, under a tensile load of approximately 30 grams. Next to the specimen was placed a certified

[3]This principle has been successfully employed by C. E. Homer and H. Plummer (5) and F. N. Rhines and W. Pellini (6).

Table I
Thermal Data of the System Indium-Bismuth

Composition Weight % Indium	Liquidus °C	Solidus °C
100.00	156.6	156.6
98.19	153.0	148.5
98.00	152.5	147.4
95.28	147.5	134.4 x
90.71	139.5	111.5 x
87.50	131.6	96.7 x
85.00	.....	94.0 y
85.00	.....	93.1 x
82.00	.....	84.5 y
80.00	.....	73.8 y
80.00	110.6	71.8
72.51	90.8	72.1
70.01	82.2	72.1
67.51	76.0	72.1
67.00	73.0	72.0
65.81	73.6	72.0
63.90	74.0	72.1
59.98	83.9	72.1
56.32	87.0	72.1
53.75	89.6	72.1
52.35	89.5	89.5
50.00	93.0	89.0
47.51	94.6	88.9
45.17	99.7	88.9
42.50	103.8	88.5
39.91	106.2	88.4
37.50	109.1	88.6
35.45	.....	110.0
33.02	.....	109.7
29.93	127.5	109.0
25.00	154.3	109.7
19.96	.....	109.2
9.99	225.3	108.9
4.95	248.6	108.9
2.00	262.3	107.6
0.99	266.9	105.1
100.0 Bi	271.0	271.0

x = Heating curves.
y = Tension-fracture temperature.

thermometer which recorded the temperature of fracture. The temperature of the furnace in the vicinity of the fracture was changed 1 °C every five minutes, thus obtaining an effective heating rate of 0.2 °C per minute. Values obtained by this method, compared with temperatures obtained for the solidus in heating and the value obtained for a eutectic alloy on cooling, checked within ± 1.0 °C. These values are incorporated in Table I and Fig. 1.

X-ray diffraction analyses were used to establish the limits of the alpha, beta and gamma phases.

To determine the solid solubility range of the alpha (indium-rich) phase in the vicinity of the eutectic temperature, X-ray slivers of a series of alloys were homogenized at 68 °C and water-quenched. Debye photograms were taken since the symmetrical back-reflection focusing camera patterns yielded broad and weak reflections, which

can probably be attributed to the thermal factor in low melting point metals and the camera geometry. Photograms were taken using cobalt K-alpha radiation (7). Cohen's method (8) was used for lattice constant calculations. The error in lattice constant computations was one part in 4500. Values obtained for lattice constant evaluations are given in Table II, and the axial ratios are plotted in Fig. 2.

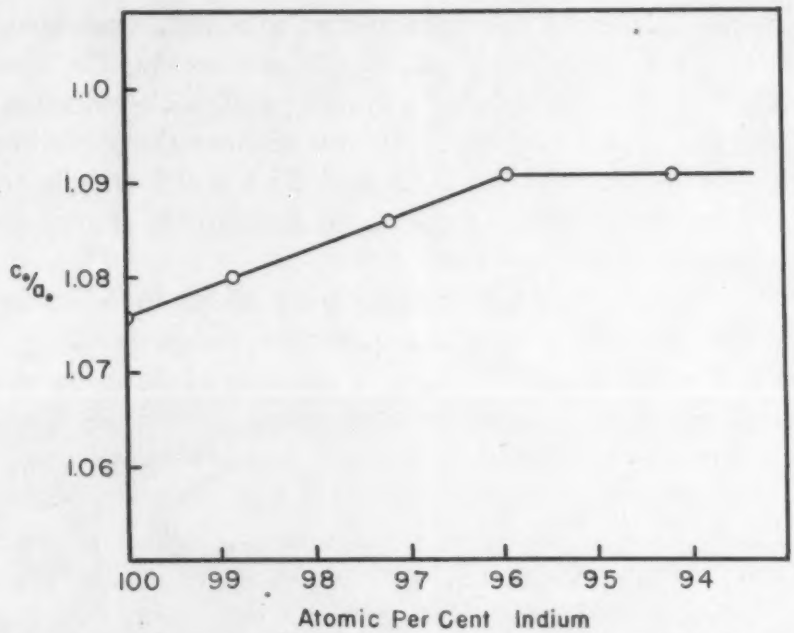


Fig. 2—The Change in Axial Ratio as a Function of the Bismuth Content.

In view of the value obtained from the thermal data for the solubility of bismuth in indium, see Fig. 1, and the fact that a quenched alloy did not show any further change in lattice constant after three months at room temperature, the value obtained, Fig. 2, of the 7.1 weight per cent bismuth alloy does not depict the upper temperature solubility. It is believed that the alloys in this region

Table II
Lattice Constants for the Indium-Rich Alloys

Atomic % Indium	Weight % Indium	c_o	a_o	c_o/a_o
100.00	100.00	4.938	4.590	1.076
98.88	97.99	4.956	4.589	1.080
97.21	95.00	4.985	4.588	1.086
95.95	92.94	5.006	4.588	1.091
94.21	89.88	5.007	4.589	1.091

transform at a rapid rate, and the value obtained represents room temperature equilibrium, instead of that at 68 °C. The same situation has been encountered in the indium-tin system (9).

Since the crystal structure of the beta and gamma phases were not identified, the solubilities of these entities were established, though not very accurately, by observing the change in interplanar spacing as a function of composition. Alloys were prepared in intervals of one per cent in the vicinity of the respective compounds. Filings made of these alloys were placed in a vial, evacuated, sealed and annealed for three days. After furnace cooling the specimens, X-ray patterns were taken using a symmetrical, back-reflection focusing camera and cobalt radiation. In this manner the solubility range for beta was placed between 52.5 and 53.5 $\pm$ 0.5 weight per cent indium. The gamma phase exhibits no measurable change in interplanar spacing.

A satisfactory procedure for preparing alloys for metallographic examination consisted of filing a flat surface, rough grinding on 220, 400 and 600 abrasive papers using a solution of kerosene and paraffin, rough polishing on a canvas cloth using aloxite and liquid soap, then on a kitten's-ear cloth using a paste of Linde powder and liquid soap. Final polishing was done on a Gamal cloth using Gamal abrasive and free application of the liquid soap. Etching was generally done with Vilella's reagent. For identification of the alpha and gamma phases, a chromate solution was used which was found by Rhines (10) to work well with the indium-zinc alloys. Characteristic photomicrographs are presented in Figs. 3 to 15.

Discussion of Results

In general, the thermal data obtained for the liquidus are in good agreement with those of Henry and Badwick. A more complete investigation was undertaken in the critical regions. For the first time, the solvus and the entire solidus of the indium-rich phase have been located, and a peritectic reaction has been established.

By means of thermal analysis the maximum solubility of bismuth in indium has been fixed at 20.5 weight per cent bismuth. X-ray diffraction analysis established the room temperature solubility at 7.1 weight per cent.

Photomicrographs of the alloys in the pure indium to beta region are shown in Figs. 3 to 8. In Fig. 5, large amounts of the beta phase

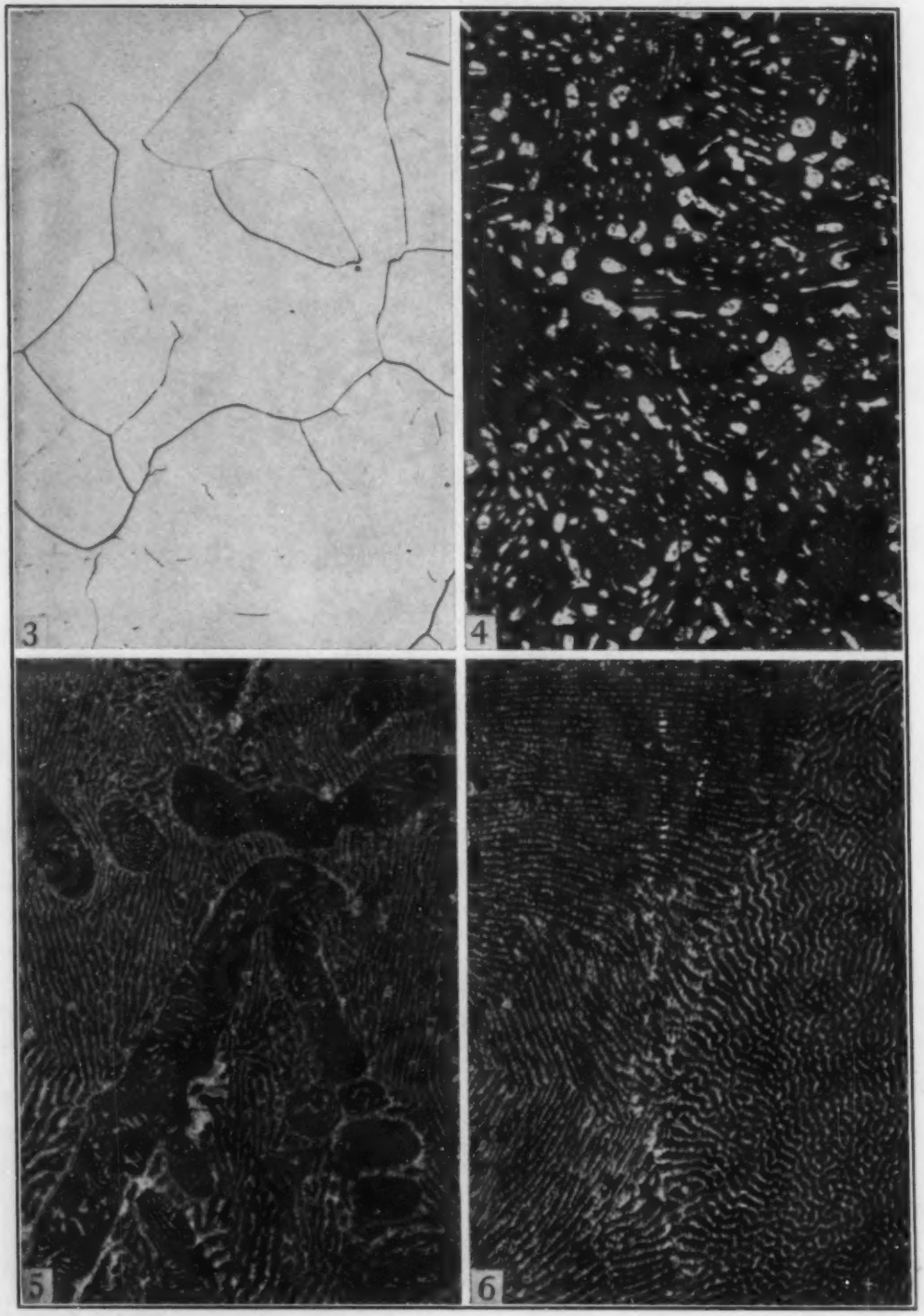


Fig. 3—Pure Indium. Etched electrolytically. × 100. (2 parts methyl alcohol, 1 part concentrated HNO_3.)

Fig. 4—85.0% Indium. Alpha plus beta. Vilella's reagent. × 125.

Fig. 5—67.0% Indium. Alpha and eutectic. Chromate reagent. × 100.

Fig. 6—66.3% Indium. Eutectic. Vilella's reagent. × 250.

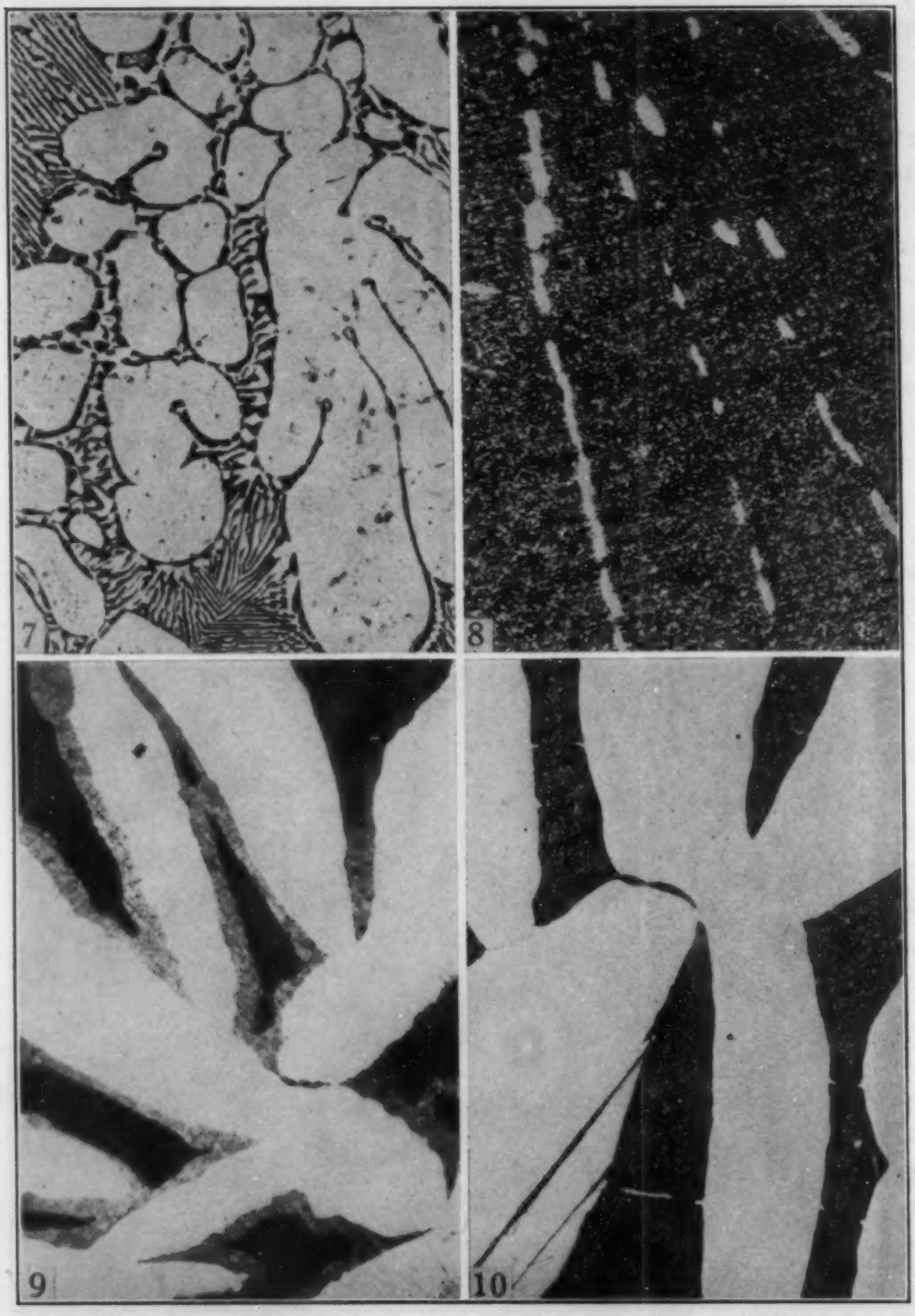


Fig. 7—60.0% Indium. Beta plus eutectic. Chromate reagent. × 75.
Fig. 8—52.35% Indium. Beta plus gamma. Vilella's reagent. × 75.
Fig. 9—42.5% Indium. Beta plus gamma (slowly cooled). Vilella's reagent. × 75.
Fig. 10—42.5% Indium. Beta plus gamma (homogenized at 88 °C for 2 weeks). Vilella's reagent. × 75.

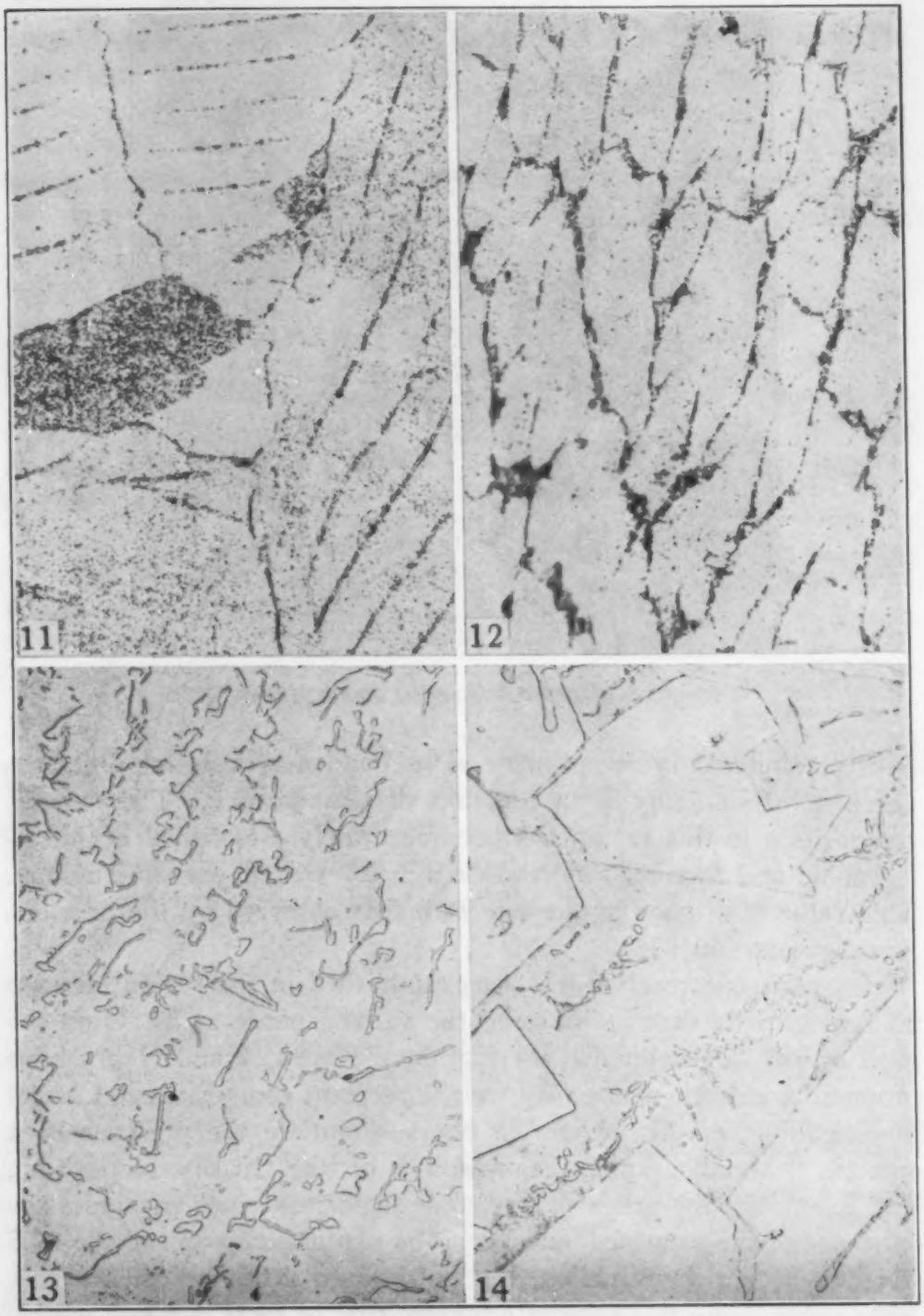


Fig. 11—35.45% Indium. Gamma plus bismuth precipitate. Vilella's reagent. × 75.
Fig. 12—34.2% Indium. Gamma plus eutectic. Vilella's reagent. × 75.
Fig. 13—33.0% Indium. Eutectic (gamma plus bismuth). Vilella's reagent. × 125.
Fig. 14—12.8% Indium. Bismuth plus eutectic. Vilella's reagent. × 175.



Fig. 15—Pure Bismuth. Cast against smooth surface. × 75.

have precipitated in the primary alpha dendrites, resulting from the decrease in solubility as a function of temperature. The eutectic composition in this region has been accurately established by metallographic and thermal means at 66.3 ± 0.1 weight per cent indium. This value is in good agreement with that observed by the previous investigators (66%).

A peritectic reaction has been established in the region between 53.5 weight per cent indium and the gamma phase at 89 °C on the basis of metallographic and thermal data. Badwick and Henry have proposed a eutectic at the fifty weight per cent composition. Careful investigations in this region do not substantiate the presence of a eutectic. Metallographic examination of the In_2Bi composition, Fig. 8, exhibits the presence of gamma dendrites which precludes the existence of the proposed eutectic. The photomicrograph of the 42.5 weight per cent indium alloy, Fig. 9, shows a definite peritectic rim. After maintaining this alloy at a temperature of 88 °C for two weeks, the reaction went to completion. This is illustrated in Fig. 10.

Although the limits of the gamma phase could not be established by means of X-ray measurements, they have been indicated in Fig. 1 on the basis of metallographic examination. Alloys containing pri-

mary gamma and eutectic exhibit a bismuth-rich precipitate along the crystallographic planes, Figs. 11 and 12. On the other hand, alloys in this area whose indium content exceed 35.45 weight per cent indium did not show any precipitate. In the gamma to bismuth region, the eutectic composition has been established at 33.0 weight per cent indium and 109.5 °C, which is in corroboration with the revised diagram of Henry and Badwick.

Summary

The present investigation has accurately established two eutectics, one at 66.3 weight per cent indium and 72.1 °C and the other at 33.0 weight per cent indium and 109.5 °C. A peritectic reaction has been established:

gamma plus liquid ⇆ beta, at 89 °C.

The liquid and solid solubility of the alpha phase have been completely determined for the first time.

Acknowledgment

The authors wish to express their appreciation of the helpful suggestions contributed by Dr. A. R. Troiano, Professor of Metallurgy, University of Notre Dame.

Some of the preliminary work was done while one of the authors (E. A. Peretti) was on the staff of the School of Mines, Columbia University.

References

1. O. Henry and E. Badwick, "The Constitution of the Bismuth-Indium System," *Metals Technology,* American Institute of Mining and Metallurgical Engineers, Technical Publication 2159, April 1947.
2. O. Henry and E. Badwick, "The Constitution of the Bismuth-Indium System," *Metals Technology,* Discussion, Institute of Metals Division, Vol. 14, No. 5, 1947, p. 23.
3. C. S. Smith, "A Simple Method of Thermal Analysis Permitting Quantitative Measurements of Specific and Latent Heats," Temperature, Its Measurement and Control in Science and Industry, American Institute of Physics, 1941, p. 974; Reinhold Publishing Corporation, 330 West 42nd Street, New York City; and *Transactions,* American Institute of Mining and Metallurgical Engineers, Vol. 137, 1940, p. 244.
4. G. Edmunds, Discussion to Paper by Smith, Ibid.
5. C. E. Homer and H. Plummer, "Embrittlement of Tin at Elevated Temperatures," *Journal of the Institute of Metals,* Vol. 64, 1939, p. 169.
6. W. S. Pellini and F. N. Rhines, "Constitution of Lead-Rich Lead-Antimony Alloys," *Transactions,* American Institute of Mining and Metallurgical Engineers, Vol. 152, 1943, p. 65.

7. L. A. Carapella, "A Graphical Method for Selecting Suitable Radiations for Precision Determination of Noncubic Lattice Constants and for Indexing Back-Reflection Lines in X-Ray Photograms," *Journal of Applied Physics,* Vol. 11, No. 12, 1940, p. 800.
8. M. U. Cohen, "Precision Lattice Constants From X-Ray Powder Photographs," *Review of Scientific Instruments,* Vol. 6, 1935, p. 68.
9. C. Fink, E. Jette, S. Katz, F. Schnettler, "The Binary Alloys of Indium and Tin," *Transactions,* American Electrochemical Society, Vol. 75, 1939 p. 463; and Preprint 88-15, October 1945.
10. F. N. Rhines and A. H. Grobe, "Constitution of the System Indium-Zinc," *Transactions,* American Institute of Mining and Metallurgical Engineers, Vol. 156, 1944, p. 253.

DISCUSSION

Written Discussion: By O. H. Henry, professor of metallurgical engineering, and E. L. Badwick, graduate student, Polytechnic Institute of Brooklyn, Brooklyn, N. Y.

It is gratifying to have one's results of an investigation checked by those of others, especially when the latter have been very thorough in their work as evidenced by the work of Dr. Peretti and Mr. Carapella. The only point in difference is the existence of a eutectic or a peritectic in the region between the beta and gamma phases at 89 °C. During the presentation of our paper on bismuth-indium, we stated that the eutectic should rightly be a peritectic, and we quote from the discussion by Dr. Rhines, "I am inclined to think also that the proposal that the reaction at the composition of $BiIn_2$ should be a peritectic is right on the basis of micrographs, for the photographs appear rather characteristic of a peritectic structure."[4] However, the diagram was drawn with a eutectic instead, based upon the experimental cooling curves obtained. Three different melts of the alloy, 50% bismuth – 50% indium, were prepared, and each time the results were the same, namely: melting and freezing of the alloys at 90.2 °C. Why there should be a discrepancy, we honestly do not know.

We should like to know if the authors actually determined the melting point of indium as 156.6 °C, since there is a slight disagreement.[5]

It is felt that the table and the photomicrographs should have been recorded in weight per cent bismuth to conform with that of the diagram. This would facilitate comparing the points on the diagram with that of the table and the photomicrographs.

Written Discussion: By M. Hansen, associate professor of physical metallurgy, Department of Metallurgical Engineering, Illinois Institute of Technology, Chicago.

I would like to offer some comments concerning the microstructure given in Figs. 11 to 13 of the paper. Thermal analysis has shown that the maximum melting point of the composition BiIn is only very slightly

[4]F. N. Rhines, discussion of "The Constitution of the Bismuth-Indium System," by O. H. Henry and E. L. Badwick, *Metals Technology,* Vol. 14, No. 5, T.P. 2222, 1947, p. 23.

[5]F. N. Rhines, W. M. Urquhart and H. R. Hoge, "Constitution of the System Indium-Tin," discussion, TRANSACTIONS, American Society for Metals, Vol. 39, 1947, p. 711.

above the temperature of the eutectic between BiIn or gamma and bismuth and that the concentration of this eutectic lies close to the composition BiIn. As a consequence, we might expect that there will be no well-defined eutectic but a more or less degenerated eutectic structure, as is the case in many other binary systems of a similar constitution. In other words, the gamma crystals solidifying during the eutectic crystallization join the primary gamma crystals, leaving behind the bismuth melt which solidifies simultaneously but separately. And this is what is observed, as shown by Fig. 13 as well as Figs. 12 and 11. Otherwise, the microstructure of the alloy with 34.2% indium (Fig. 12) would show nearly equal amounts of primary gamma and eutectic areas because 34.2% indium lies nearly halfway between the compound and the eutectic. According to the lever rule, the alloy with 34.2% indium consists of 96.5% gamma and 3.5% bismuth, which seems to be in accordance with the structure given in Fig. 12.

I do not agree with the authors that the minute bismuth crystals shown in Fig. 11 are due to a decomposition in the solid state. These tiny bismuth crystals have been separated from the melt in such a way that after the dendritic crystallization of gamma, the remaining melt enriched in bismuth and solidified is a degenerated eutectic at practically the same temperature as the primary gamma crystals. The fact that the bismuth crystals are located within the gamma grains does not contradict this interpretation. Similar structures are known from other systems and also from single crystals of zinc-cadmium and zinc-tin alloys which consist of alternate layers of these metals or solid solutions, respectively.

The composition of the alloy of Fig. 11 is given as that of the compound BiIn. This cannot be true because the structure then should be homogeneous as shown in the diagram. It must be concluded, therefore, that the indium content of the alloy of Fig. 11 is slightly smaller. In such an alloy, with say 0.1 or 0.2% indium less than that of the compound, we have to expect a structure as shown by Fig. 11 which consists of alternate layers of gamma and bismuth. (If the composition of the alloy given in Fig. 11 would be, for instance, 35.27% indium, the amount of bismuth crystals would be about 0.5%.) As the authors state, the alloys have not been analyzed.

If these bismuth particles would be formed by precipitation in the solid state, they should also be present in the alloy of eutectic composition which is, however, not the case, as shown by Fig. 13. I hereby assume that the treatment of these samples has been the same.

The microstructure of the alloy with 12.8% indium given in Fig. 14 is rather unusual. Here we have primary crystals of bismuth surrounded by gamma crystals and also areas of a eutectic arrangement of the constituents. This structure is also due to the fact that the composition of the eutectic lies close to that of the compound and due chiefly to a higher tendency of the compound to crystallize as compared with that of bismuth. The magnification of this photomicrograph seems to be too high in order to be able to draw conclusions as to the relative amounts of both phases which should be about 36% gamma and 64% bismuth.

I would like to add 2 suggestions: (1) The composition of the alloys investigated is given in Table I as well as in the text by weight per cent indium. In the diagram, however, it is given as weight per cent bismuth. It would be more convenient to use the same designation throughout the whole paper. And (2) I would like to suggest for greater convenience to give the composition also in atomic per cent in the table as well as the diagram so that the reader is able to draw the diagram in atomic per cent without any trouble.

Authors' Reply

The authors wish to express their appreciation to those who have contributed discussion to this paper. We can appreciate the fact that Professor Henry and Mr. Badwick failed to obtain two arrest points in the thermal curves for the 50% alloy. We also were unable to observe the upper arrest point for this composition until we started using the Smith apparatus. We did determine the melting point of indium by means of a calibrated thermocouple and a certified Bureau of Standards thermometer and were unable to check exactly the value given by Messrs. Henry and Badwick.

Professor Hansen's point regarding the bismuth-gamma eutectic is well taken, and it may well be that the freezing takes place as he suggests. However, the relative proportion of the two phases in Fig. 12 would also be observed with our interpretation, particularly if the gamma region is wide at the eutectic temperature.

DILATOMETRIC EFFECTS OF HARDENING AND RECRYSTALLIZATION IN THE 60 COPPER – 20 NICKEL – 20 MANGANESE ALLOY

By C. H. Samans, C. C. Brayton, H. L. Drake and L. Litchfield

Abstract

Using the Chevenard differential method, dilatometric studies were made up to 800 °C (1475 °F) on specimens of the 60 copper – 20 nickel – 20 manganese alloy after various thermal and mechanical treatments. The nature of discontinuities found in instantaneous coefficient of thermal expansion versus temperature curves was investigated further by electrical resistance measurements up to 620 °C (1150 °F), and by Rockwell C hardness measurements after heating for constant short times over the entire range of temperatures or for varying times at several constant temperatures. Metallographic evidence also is presented.

These discontinuities are explained satisfactorily on the assumption of the successive formation in the stable solid solution, with increasing temperature, of (a) a low temperature, ordered face-centered tetragonal structure, the most compact; (b) an orthorhombic structure, somewhat less compact; and (c) a high temperature, disordered solid solution, all of copper in MnNi. The hardening is attributed to the effect of the face-centered tetragonal structure, and the minimum conductivity to a balance between the orthorhombic structure and the concentration change in the solid solution. The effect of cold work is to decrease the tendency toward ordering and so to cause the hardening to take place at a higher temperature than in the unworked alloy, after recovery has removed some of the effects of the deformation. The temperature of most rapid recrystallization is shown to be about 525 °C (980 °F) and to follow, at least approximately, the temperature of disordering or re-solution.

A paper presented before the Thirtieth Annual Convention of the Society, held in Philadelphia, October 23 to 29, 1948. Of the authors, C. H. Samans is chief, and C. C. Brayton, L. Litchfield and H. L. Drake are technical assistants, Metallurgical Section, Research Laboratory, American Optical Company, Southbridge, Mass. Manuscript received April 17, 1948.

Introduction

THE hardening characteristics of the 60 copper – 20 nickel – 20 manganese alloy were described first by Dean and his co-workers (1), (2), (3), (4).[1] Since that time the alloy has become available commercially. The present paper correlates the results of dilatometric, electrical resistance, and hardness tests made upon the commercial alloy, and offers an explanation for the effects noted.

Specimen Treatment and Test Procedure

The material used was secured from Driver-Harris Company in the form of 0.250-inch diameter soft wire which analyzed 59.4% copper, 19.8% nickel, 20.8% manganese. This wire was subjected to the following treatments to secure specimens for study:

(a) roll through grooved rolls to 0.159 inch square (reduction in area of 59.5%); and

(b) anneal 30 minutes at 595 °C (1100 °F), water quench, and flat roll to 0.0625 inch (reduction in thickness of 61%); or

(c) anneal 30 minutes at 595 °C (1100 °F), water quench, draw to 0.1305 inch diameter, anneal 30 minutes at 595 °C (1100 °F), water quench, and draw to 0.115, 0.101, or 0.090 inch diameter (reductions in area of 22.5, 40, or 52.5%).

Dilatometric studies were made on a Chevenard differential dilatometer using a Pyros standard, the head of normal sensitivity (magnification: × 278), and a heating rate of about 8.7 °C (15.7 °F) per minute. The tangents to the photographically recorded curves were measured at suitable intervals (usually 25 °C or less) and the instantaneous coefficients of thermal expansion computed from the known constants of the instrument. The results of these computations for all tangent angles already had been tabulated by E. D. Tillyer, A. E. Glancy and J. K. Davis for the constants of the dilatometer used, so this usually laborious portion of the work was simplified greatly.

Electrical resistance measurements were made by heating a coil of wire in a nichrome-wound furnace and measuring resistance with a Wheatstone bridge circuit. No atmosphere control was used.

Rockwell hardness measurements were made on both the C and

[1] The figures appearing in parentheses pertain to the references appended to this paper.

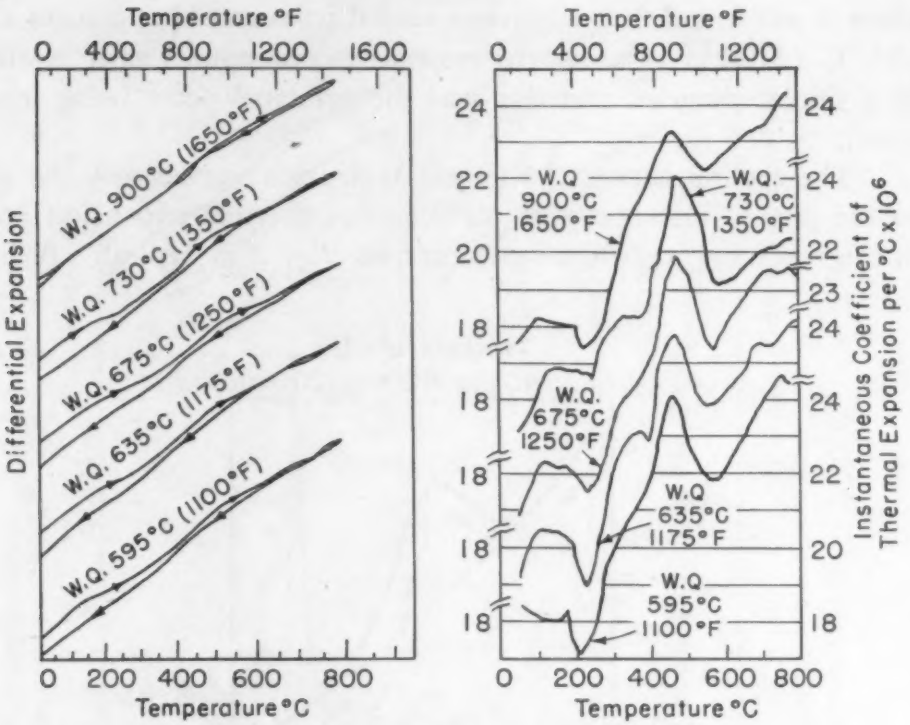


Fig. 1a (Left)—Differential Expansion Curves After Quenching From Various Pretreating Temperatures. The zero points have been separated for clarity.

Fig. 1b (Right)—Instantaneous Coefficient of Thermal Expansion Vs. Temperature Curves After Quenching From Various Pretreating Temperatures. Heating rate 8.7 °C (15.7 °F) per minute.

B scales. Both are shown on one of the graphs by adjusting the scale suitably for the B readings, but usually only the C readings are given.

Dilatometric Results

Differential expansion curves for a series of specimens obtained by water quenching the 0.159-inch square rod after a 1-hour anneal at 595, 635, 675, 730 or 900 °C (1100, 1175, 1250, 1350 or 1650 °F) are shown in Fig. 1a. The derived instantaneous coefficients of thermal expansion are plotted against temperature in Fig. 1b.

It will be seen at once that, although these curves are similar, there are certain differences between them as far as the development of the "hills" at about 150, 350 and 470 °C (300, 660 and 880 °F), and the "valleys" at about 225 and 575 °C (440 and 1070 °F) are concerned. The possible significance of some of these differences, particularly at higher temperatures, was not investigated thoroughly,

since it was found that specimens cooled from any temperature above 595 °C (1100 °F) seemed to respond to subsequent heat treatment in a similar manner, and this was the principal point being investigated.

The cooling curves of all these specimens were nearly the same, so the plot of instantaneous coefficient of thermal expansion (taken during cooling) versus temperature in Fig. 2 is typical. A hypothetical "true" curve also is shown (dotted) and the differences between it and the actual curve have been plotted below to illustrate the effect of the reaction alone. It will be noted also that the "hills" found in the heating curve apparently do not occur in the cooling curve, although the "valleys" do.

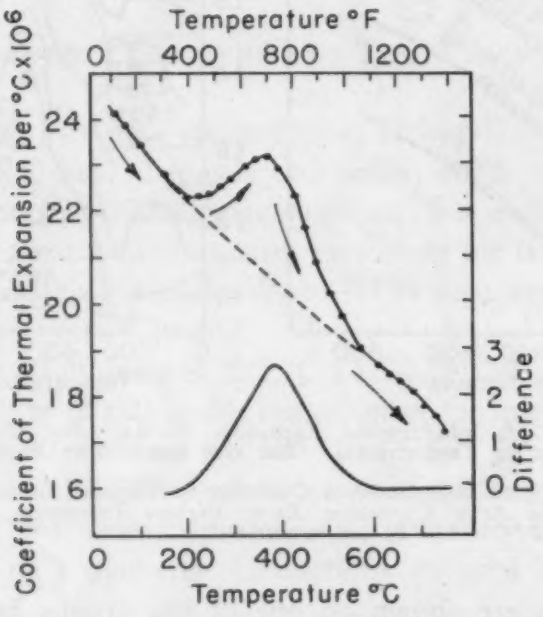


Fig. 2—Instantaneous Coefficient of Thermal Expansion Vs. Temperature Curve Typical of the Cooling Curves in Fig. 1a. The differences between the actual and the hypothetical (dotted) expansion coefficient curve have been plotted below to show the nature of the curve for the reaction alone.

After all the other curves had been obtained, a rebuilding of the dilatometer furnace controls permitted runs to be made with a heating rate of only 0.8 °C (1.4 °F) per minute, less than one-tenth of that used previously. Curves taken under both conditions are compared in Fig. 3 for specimens either water-quenched or furnace-cooled from 900 °C (1650 °F). In addition to making the various discontinuities

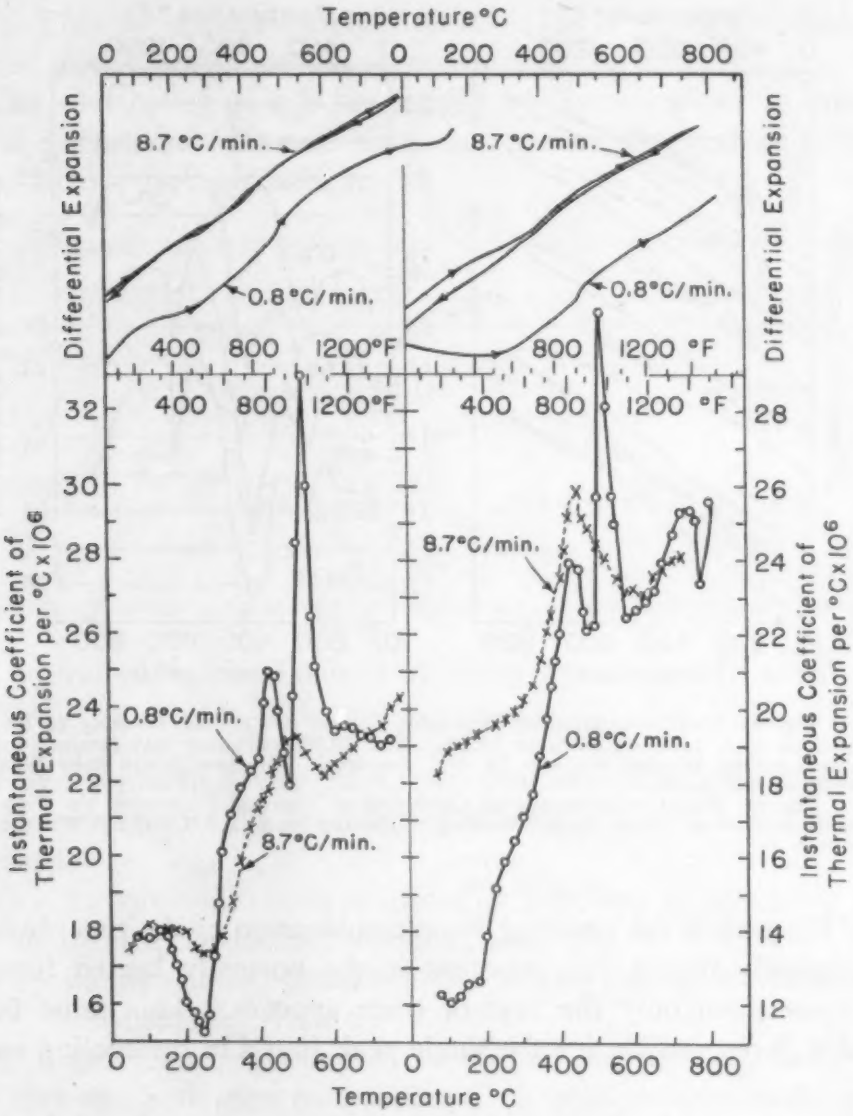


Fig. 3—Comparison of Instantaneous Coefficient of Thermal Expansion Vs. Temperature Curves for Previously Quenched (Left) and Furnace-Cooled (Right) Specimens Taken With Heating Rates of 8.7 °C (15.7 °F) Per Minute and 0.8 °C (1.4 °F) Per Minute.

noted before more pronounced, the slower rate has brought out a new and very pronounced peak at 510 °C (950 °F). The furnace-cooled specimen, furthermore, no longer has the hill found in the water-quenched specimen at about 150 °C (300 °F), and has its first peak at about 440 °C (825 °F) just as in both the slowly heated runs but about 50 °C (90 °F) lower than for the normally heated water-quenched specimen. Because of this, it would seem probable that, in the normally heated water-quenched specimen, the 490 °C

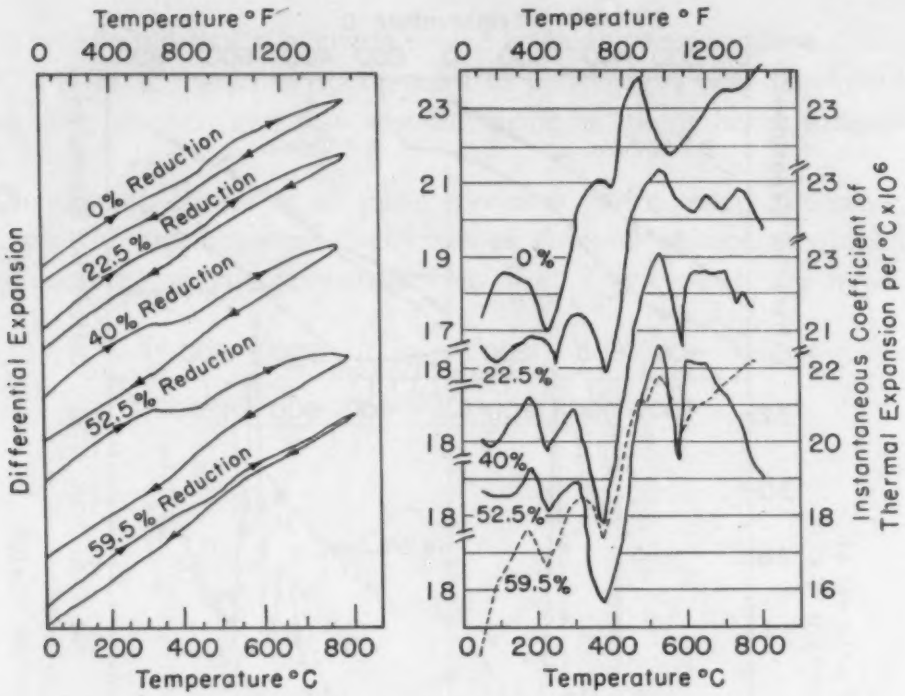


Fig. 4a (Left)—Differential Expansion Curves After Cold Working to Reductions of 0, 22.5, 40, 52.5, or 59.5%. The 59.5% reduction was obtained by square rolling to size, the rest by cold drawing. The zero points have been separated for clarity.

Fig. 4b (Right)—Instantaneous Coefficient of Thermal Expansion Vs. Temperature Curves After Cold Working. Heating rate 8.7 °C (15.7 °F) per minute.

(915 °F) peak is the result of some combination of the two observed in the slowly heated run, whereas in the normally heated furnace-cooled specimen only the first of them appears. This same factor probably is responsible for the single peak found in the cooling curve, Fig. 2.

In order to determine what changes were introduced into the curves by cold working, the series of cold drawn wire specimens was run, again at the 8.7 °C (15.7 °F)-per-minute heating rate. The resulting differential expansion and expansion coefficient versus temperature curves are shown in Fig. 4. The major effects of the cold working are either to introduce or to accentuate (a) the peak at about 175 °C (350 °F), (b) a peak at 300 °C (570 °F), (c) a valley at 375 °C (705 °F), (d) a valley at 550 to 600 °C (1020 to 1110 °F), and (e) a peak at 600 to 650 °C (1110 to 1200 °F). In addition, it will be noted that the principal peak, which occurred at about 475 °C (885 °F) in the quenched specimens, now occurs about 50 °C (90 °F) higher at 525 °C (975 °F) in the cold-worked speci-

mens. This is approximately 100 °C (180 °F) higher than it occurred in the furnace-cooled specimen, Fig. 3.

The dilatometric results, as judged by discontinuities in instantaneous coefficient of thermal expansion versus temperature curves, may be summarized in Table I.

Table I

Pretreatment	Heating Rate	Peaks (°C)				
Quenched from 595 °C (1100 °F) or higher	8.7 °C/min	100-175	350-500		475-500	700
900 °C (1650 °F)	0.8 °C/min	125	350-400	430	510	
Furnace-cooled from 900 °C (1650 °F)	8.7 °C/min			450		
	0.8 °C/min		250-275	440	510	740
Cold-worked 22.5-59.5%	8.7 °C/min	175	300-320		525	600-650
Cooling curve				430		

Softening and Hardening Characteristics During Heat Treatment

From a practical viewpoint, two characteristics are of greatest importance as far as the reactions of this alloy to heat treatment are concerned:

(a) its softening characteristics, for purposes of annealing preparatory to further working; and

(b) its hardening characteristics during aging treatments at constant temperature.

The first of these was investigated by taking the 0.0625-inch thick material, both after cold rolling 61% to a hardness of Rockwell C-22 and after hardening this material to the maximum hardness of Rockwell C-42 at 400 °C (750 °F), as suggested by the work of Dean and his co-workers (4), and heating it for 15 or 30 minutes at 55 °C (100 °F) intervals from 370 to 540 °C (700 to 1000 °F) and thereafter at 28 °C (50 °F) intervals up to 760 °C (1400 °F). The results of Rockwell hardness readings after these heat treatments are shown in Fig. 5. Clearly, the significant softening occurs at about 565 °C (1050 °F), although even at higher temperatures the hardness readings seem to be somewhat higher than would be expected. This latter peculiarity, however, may be only a grain size effect similar to that reported by Cook and Miller (13) for brasses containing small amounts of iron. These results were largely responsible for

the selection of 595 °C (1100 °F) for the pretreatment temperature. It seemed to be the lowest that could be used consistently in plant processing, and therefore was of the greatest interest.

The results of constant temperature treatments on the various types of specimens are given in Figs. 6 to 9.

In securing the data plotted in Fig. 6, the 0.159-inch square material was used after a furnace cool from 30 minutes at 595 °C

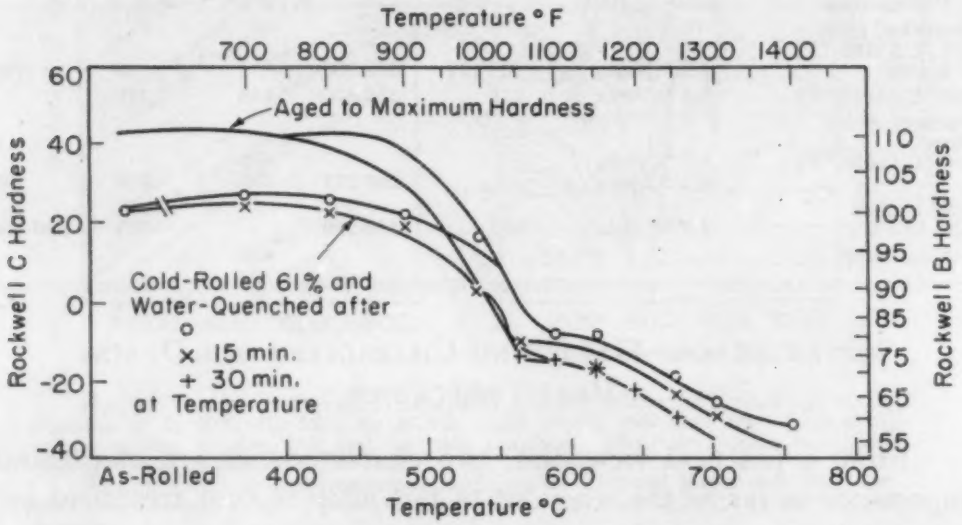


Fig. 5—Change in Rockwell Hardness Vs. Temperature in Specimens Reheated for Constant Times After Initially Hardening to C-22 by Cold Rolling or to C-42 by Cold Rolling and Aging at 400 °C (750 °F).

(1100 °F). The initial hardness ranged from Rockwell C-5 to C-10, and the maximum hardening (Rockwell C-44) occurred at 400 °C (750 °F), although comparable hardening was secured, but in somewhat longer times, at both higher and lower temperatures. At 290 °C (550 °F) Rockwell C-27 was the maximum hardness that could be secured and no definite increase in hardness was noted after 8 hours at 480 °C (900 °F) or after 81 hours at 215 °C (430 °F). At 510 °C (950 °F) and higher, the alloy softened appreciably during the first 15 minutes and thereafter remained substantially constant. When the material was fully hardened (Rockwell C-44) at 400 °C (750 °F), no softening occurred in 168 hours at 205 °C (400 °F) or in 126 hours at 260 °C (500 °F).

The data in Fig. 7 were taken with the same type specimen but after a water quench from 595 °C (1100 °F). The times at this temperature before quenching were varied from 15 to 120 minutes without any noticeable change in the hardness following the subsequent

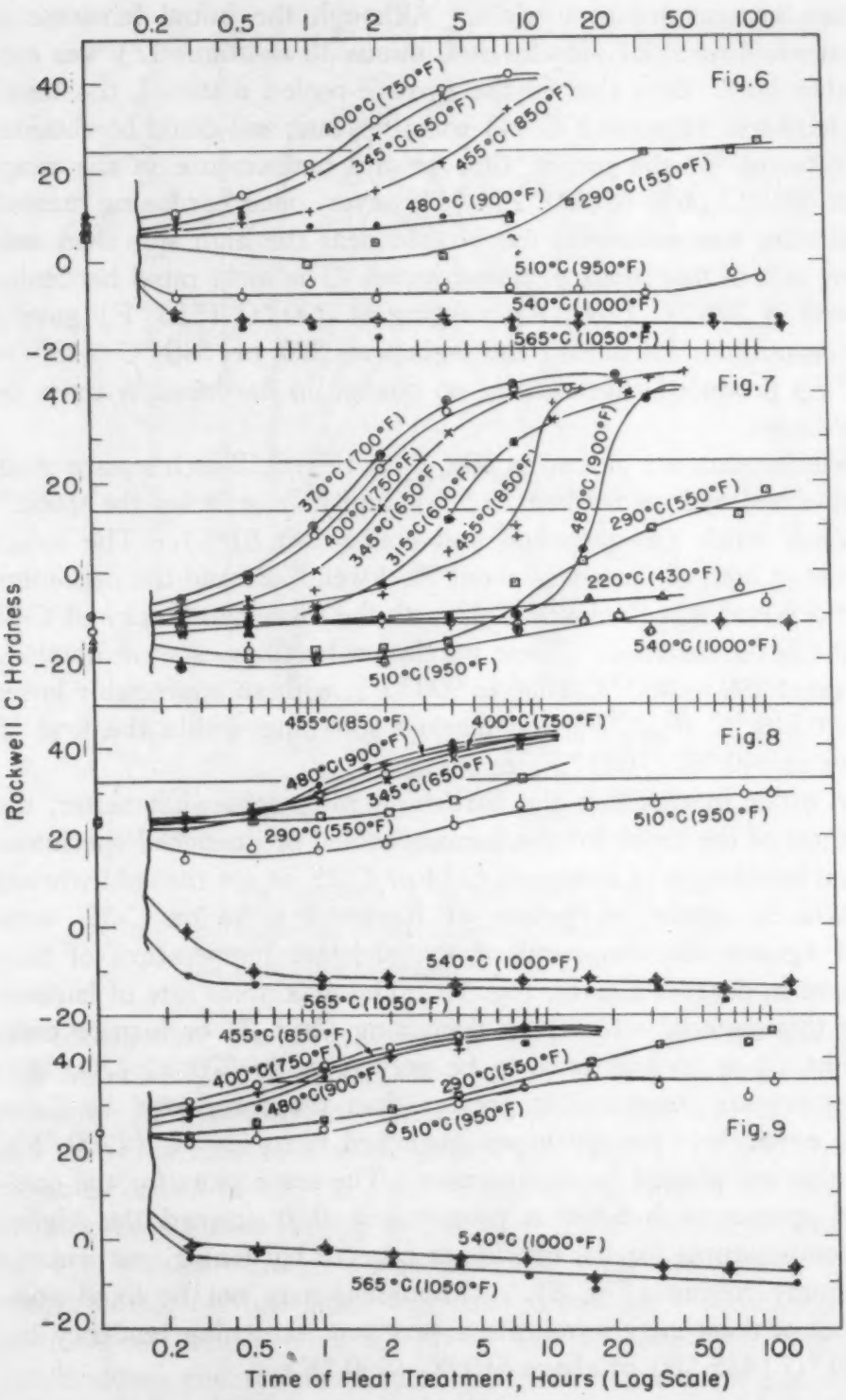


Fig. 6—Change in Rockwell Hardness With Time in Specimens Reheated at Various Constant Temperatures After Furnace Cooling Initially From 30 Minutes at 595 °C (1100 °F) to a Hardness of C-5 to C-10.

Fig. 7—Change in Rockwell Hardness With Time in Specimens Reheated at Various Constant Temperatures After Water Quenching Initially From 595 °C (1100 °F) to a Hardness of Minus C-10 to Minus C-17.

Fig. 8—Change in Rockwell Hardness With Time in Specimens Reheated at Various Constant Temperatures After Square Rolling (59% Reduction in Area) Initially to a Hardness of C-24.

Fig. 9—Change in Rockwell Hardness With Time in Specimens Reheated at Various Constant Temperatures After Flat Rolling (61% Reduction in Thickness) Initially to a Hardness of C-24.

constant-temperature treatments. Although the initial hardness of the quenched material (Rockwell C minus 10 to minus 17) was considerably lower than that of the furnace-cooled material, the maximum hardness (Rockwell C-44) was the same, and could be obtained by treatment for the proper time at any temperature in the range 315 to 480 °C (600 to 900 °F). However, once hardening started, the increase was somewhat more rapid near the high side than near the low side of this range of temperature. The most rapid hardening occurred at 370 °C (700 °F). Aging at 290 °C (550 °F) gave a lower maximum hardness, and aging at 220 or 540 °C (430 or 1000 °F) produced substantially no change in hardness in times up to 100 hours.

Similar data are plotted in Fig. 8 for the 0.159-inch square stock (as-quenched and cold-rolled 59.5%), and in Fig. 9 for the 0.0625-inch thick stock (as-quenched and cold-rolled 61%). The initial hardness of both of these was about Rockwell C-24 and the maximum hardness found was Rockwell C-42 with the former or Rockwell C-47 with the latter material. These maximum hardnesses were obtained by aging at 290 to 480 °C (550 to 900 °F), with an appreciably lower value at 510 °C (950 °F) and marked softening within the first 15 minutes at 540 °C (1000 °F) or higher.

In order to correlate the hardening rates somewhat better, the logarithms of the times for the furnace-cooled or quenched specimens to attain hardnesses of Rockwell C-14 or C-25, or for the cold-worked specimens to attain hardnesses of Rockwell C-33 or C-35, were plotted against the reciprocal of the absolute temperature of heat treatment in degrees Kelvin, Fig. 10. The maximum rate of hardening for this material after water quenching (Fig. 7) or furnace cooling (Fig. 6) is seen at once to be very close to 370 °C (700 °F). These rates are considerably greater than those reported by Dean and his co-workers for specimens quenched from 650 °C (1200 °F), which also are plotted for comparison. The same plots for the cold-worked specimens indicate a pronounced shift toward the higher aging temperatures for the maximum rates of hardening, particularly after square rolling (Fig. 8). Although it may not be fixed positively, all of these curves indicate a very low hardening tendency below 280 °C (535 °F) or above 510 °C (950 °F).

Electrical Resistance Measurements

The results of measurements of relative electrical resistance ver-

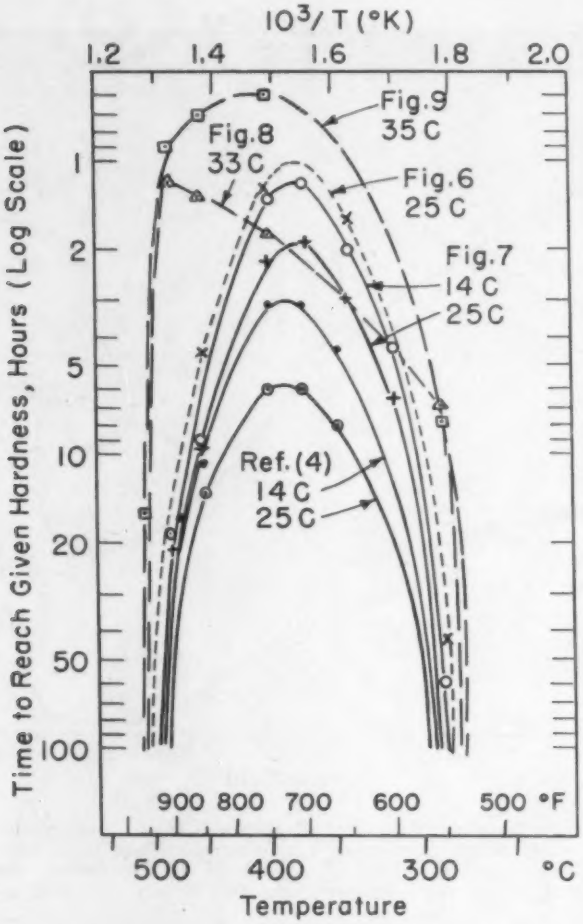


Fig. 10—Plots of the Logarithms of the Time Required to Attain the Hardness Indicated Against the Reciprocal of the Absolute Temperature. The highest point on each curve gives the temperature for most rapid hardening.

sus temperature are shown in Fig. 11. Starting with a value of 1.00 for wire quenched from 20 minutes at 595 °C (1100 °F), the resistance falls steadily to a minimum of 0.945 at 440 °C (825 °F) and then increases to a value of 0.975 at 545 °C (1015 °F). The specimen cooled to 530 °C (985 °F) over a period of 17 hours, and then somewhat more rapidly to 280 °C (535 °F) where the resistance had a minimum value of about 0.943. On further cooling to room temperature, the resistance increased somewhat. Reheating again gave almost the same values up to 280 °C (535 °F). At higher temperatures the resistance decreased still more to a minimum of 0.921 at 425 to 475 °C (800 to 890 °F), then increased fairly rapidly up to about 540 °C (1000 °F). Above this temperature the increase was relatively small.

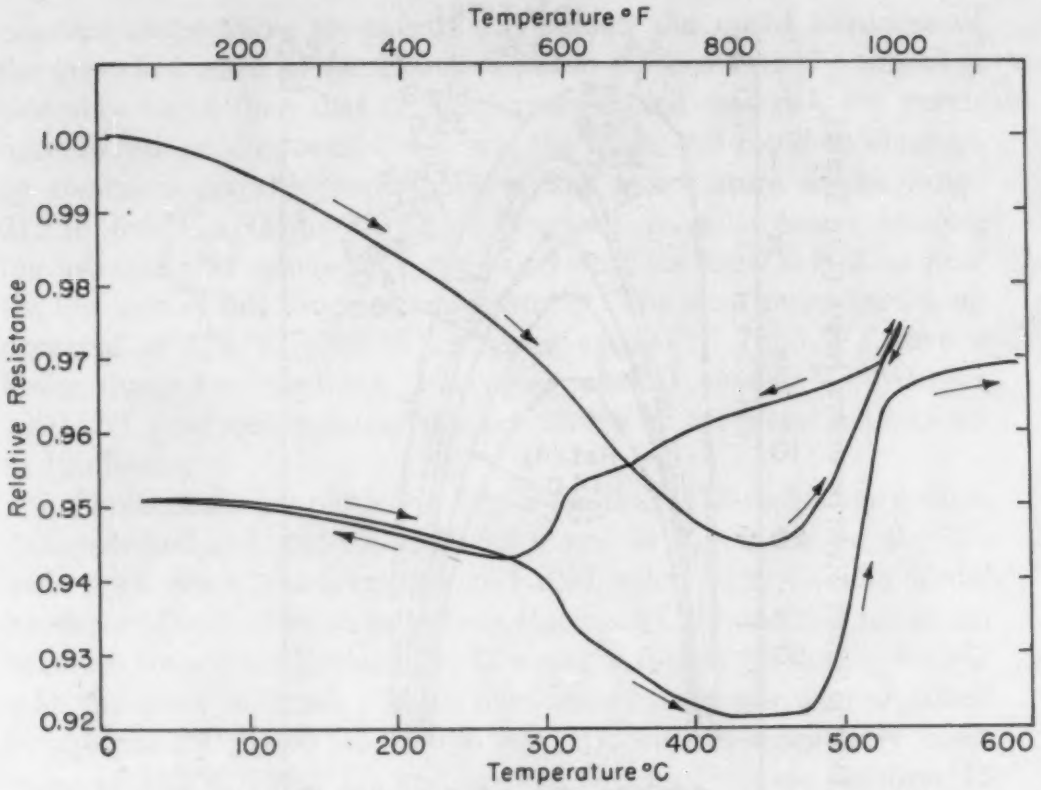


Fig. 11—Variation of Relative Electrical Resistance With Temperature. In making the measurements, the wire, which previously had been quenched from 595 °C (1100 °F), was slowly heated to about 550 °C (1020 °F), held 17 hours, cooled slowly to 150 °C (300 °F) and then overnight to room temperature, and finally reheated to about 650 °C (1200 °F).

Metallography

The photomicrographs (× 200) in Fig. 12 show the effect of reheating 24 hours at various temperatures after quenching from 4 hours at 900 °C (1650 °F). At 525 °C (975 °F) and above, the alloy clearly is a solid solution. However, after reheating at 455 °C (850 °F), there is a small amount and, after reheating at 370 °C (700 °F), there is an appreciable amount of what apparently is a second phase at the grain boundaries. From the data of Fig. 7, both these specimens would be expected to be completely hardened. However, no appreciable difference in hardness between the material in the grains and that at the grain boundaries could be found with a Knoop indenter. Reheating for 24 hours at 200 °C (390 °F) produced no change in the quenched structure.

Fig. 13 shows the effect of reheating at various other temperatures a specimen that previously was fully hardened at 370 °C

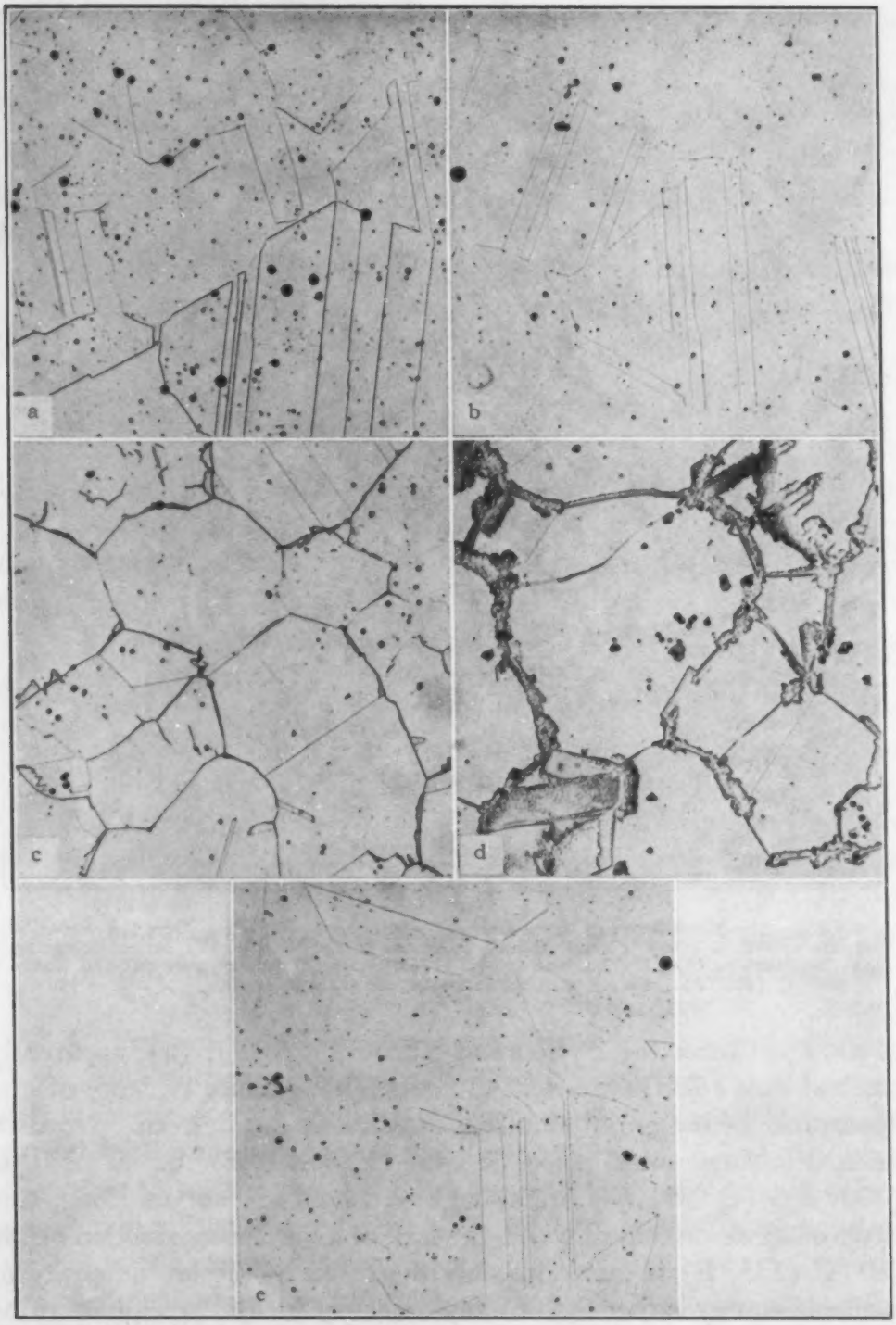


Fig. 12—Metallographic Structures of Specimens Initially (a) Quenched From 4 Hours at 900 °C (1650 °F), and Then Reheated 24 Hours at (b) 525 °C (975 °F), (c) 455 °C (850 °F), (d) 370 °C (700 °F), or (e) 200 °C (390 °F). Etched with nitric and acetic acids in acetone. × 200. The dark spots in the solid solution alloys are etching pits.

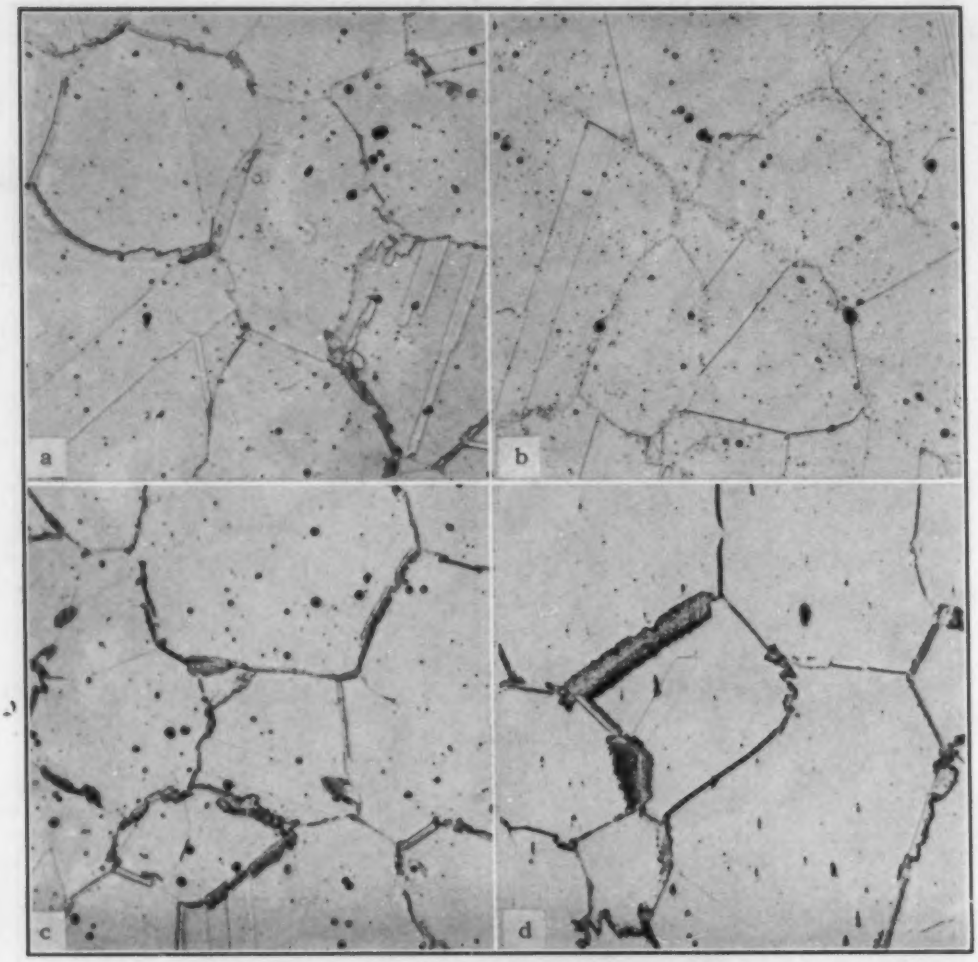


Fig. 13—Metallographic Structures of Specimens Initially Quenched From 4 Hours at 900 °C (1650 °F) and Heated 24 Hours at 370 °C (700 °F), After Reheating (a) 24 Hours or (b) 116 Hours at 525 °C (975 °F), or (c) 24 Hours or (d) 116 Hours at 200 °C (390 °F). Etched with nitric and acetic acids in acetone. × 200.

(700 °F). Reheating 24 hours at 525 °C (975 °F), (a), apparently has had little effect, but after 116 hours, (b), definite evidence of disappearance of the grain boundary constituent can be seen. No such marked change was noted at 455 °C (850 °F) or at 200 °C (390 °F), (c) and (d). Although 116 hours is not too long, this latter observation indicates that the lack of a hardening reaction below 280 °C (535 °F) is more probably the result of the low intensity of available energy rather than of any tendency for the precipitate to be soluble in this region. The apparent difference in amount of grain boundary constituent between the structure in Fig. 12d and those in Figs. 13c and 13d is within the normal variation throughout the specimen.

Discussion of Results

Both the hardness and the resistance data agree that the significant reactions occur between about 280 °C (535 °F) and 510 to 540 °C (950 to 1000 °F). The three regions above 225 °C (435 °F) in Fig. 3, for which the expansion coefficients are increased, evidently correspond, therefore, to

(a) the reaction which is primarily responsible for the hardening and has its maximum rate at about 370 °C (700 °F) in the unworked specimens;

(b) the reaction which is responsible for the minimum resistance and has its maximum rate at about 425 °C (800 °F); and

(c) the disordering or solution reaction, which has its maximum rate at about 510 °C (950 °F).

For all except the slowest heating rates, these three overlap appreciably.

To rationalize these reactions, reference must be made to the studies of Dean and his co-workers (1-4) which have established that:

1. The 60 copper – 20 nickel – 20 manganese alloy can be considered as a part of the pseudo-binary system Cu-MnNi.
2. Although, because of the similarity in sizes of the atoms involved and of the relative sizes of the face-centered cubic lattices of MnNi($a_o = 3.651$ Å) and Cu($a_o = 3.608$ Å), the two probably form a complete series of solid solutions at high temperatures, they have a limited solid solubility of about 22% MnNi in copper at room temperature.
3. The ordered MnNi phase can dissolve up to about 18% copper without losing its general characteristics.

Since, in the present study, the high temperature solubility is confirmed by the metallographic structures in Figs. 12a and 12b, these observations suggest that the formation of a low temperature, ordered phase within the copper-rich solid solution lattice is significantly related to the changes observed.

Although complete information about the ordering characteristics of the solid solution of copper in MnNi is lacking, Valentiner and Becker (5) and Averbach (6) have determined that the composition MnNi (with up to about 2% copper) has a disordered face-centered cubic structure after quenching from 950 °C (1740 °F) and an or-

dered face-centered tetragonal structure after hardening by aging at 500 °C (930 °F). Furthermore, Hansen (7) indicates transformations for MnNi at 590 to 610 °C (1095 to 1130 °F) and at 555 to 585 °C (1030 to 1085 °F), the exact temperatures depending on the composition.

A similar condition exists in the gold-silver-copper alloys, although because of the greater difference in the sizes and natures of these three atoms, somewhat less silver can be dissolved in the gold-copper superlattice, AuCu, than copper in MnNi. The effect of silver on AuCu has been studied by Johansson and Linde (8) and by Hultgren and Tarnopol (9). These investigators found that the addition of silver lowered the temperature of the AuCu order-disorder transformation, and that, in addition to the high temperature, disordered face-centered cubic form, there was a low temperature, ordered face-centered tetragonal form as well as an orthorhombic form which existed and appeared to be stable in the intermediate zone. This latter structure could be thought of as consisting of ten of the face-centered tetragonal cells side by side with the gold and copper atoms reversing positions after five cells. The positions of the silver atoms in this structure were not reported. Whether this orthorhombic form should be considered as a separate phase or merely as a state of aggregation of the tetragonal form, which rearranges according to a definite orientation pattern in order to minimize lattice strains when it grows to some definite size, is perhaps open to some question.

If similar changes are produced by the addition of copper to the MnNi superlattice, the results found can be explained satisfactorily, since in the copper-bearing compound the reactions might be expected to take place at a somewhat lower temperature than in MnNi.

First, consider the water-quenched specimens in Fig. 3. In the quenched alloy the metastable solid solution retains its high temperature spacing. Therefore, although it starts to expand in a normal manner when reheated, the initial tendency, as soon as diffusion makes appreciable atom movement possible, is for the lattice either to reject or to segregate the proper number of copper, manganese and nickel atoms and to compact toward the spacing which would be stable at low temperatures. This would result in the dip noted at 200 to 225 °C (390 to 435 °F), but also would start the formation and growth of face-centered tetragonal ordered regions and, consequently, the hardening reaction. The process must be thought of

as a two-stage one, the regions rich in manganese and nickel being disordered and probably face-centered cubic initially but transforming with time to the ordered face-centered tetragonal form.

The tetragonal structure, although more compact than the metastable, quenched, disordered solid solution, is less compact than the copper-rich, stable, low temperature solid solution, and consequently its formation puts a compressive strain on the solid solution lattice which hardens it and gives it an expansion coefficient somewhat higher than normal. This accounts for the bulge between 225 and 400 °C (435 and 750 °F), a region in which both segregation and ordering probably are taking place simultaneously. Maximum hardening may occur before the ordering transformation is complete because of the overlapping in the reactions noted above. The formation and growth of the face-centered tetragonal form (there may be some question as to whether there is any actual precipitation) undoubtedly is very sluggish, probably since diffusion must be involved.

As the ordered regions continue to form and to grow, the tendency for them to change over into the less compact but more stable orthorhombic structure increases. This reaction, which probably takes the form of a strain-reducing interchange of atoms within the ordered regions, would account for the relatively rapid increase in expansion coefficient which reaches its peak at about 440 °C (825 °F). At about 490 °C (915 °F) these orthorhombic cells start to redissolve in the copper-rich matrix, the maximum rate of solution occurring about 20 °C (35 °F) higher. Solution seems to be complete at about 580 to 600 °C (1075 to 1110 °F).

The bump at about 740 °C (1365 °F) is believed to be connected with grain growth in some manner similar to that found by Cook and Miller (13) for alpha brass. It will be noted that this temperature also corresponds approximately to the removal of the hardness bump in the annealed alloys in Fig. 5.

In Fig. 3, the curve for the quenched alloy, which was secured with the more rapid heating rate, suggests that the ordering of the tetragonal form is so sluggish in comparison with the heating rate that the orthorhombic formation and re-solution stages overlap, giving a peak at about 500 °C (930 °F).

In the furnace-cooled alloys, the room temperature structure must be closer to equilibrium than in the quenched alloys, even though peak hardness has not been reached. Hence, there is no initial dip. However, since it appears much more likely that ordering

starts with the formation of the smaller tetragonal units rather than of the larger orthorhombic units, the sluggishness of the ordering makes the direction of approach to the hardening stage unimportant. On reheating, the remainder of the ordered tetragonal regions form first, producing further hardening, and then aggregate and rearrange into the orthorhombic form, and redissolve in the matrix exactly as before. The peak in the curve taken at the faster rate corresponds to the most rapid formation of the orthorhombic structure because the relatively long time that is required for the initial tetragonal ordering largely has been taken care of during the original cooling so the orthorhombic structure can be formed more rapidly than in the quenched specimens.

The hardness and resistance effects are explained in a similar manner. The resistance of the quenched alloy falls at an increasing rate up to about 350 °C (660 °F), and then at a decreasing rate up to the minimum at about 440 °C (825 °F). During this latter range the hardening tendency is greatest. Above this range the hardening tendency decreases and the resistance increases. Consequently, it appears reasonable that the decreasing resistance corresponds to the rejection from or segregation in the solid solution of the nickel and manganese atoms, and that this is substantially complete at about 440 °C (825 °F), the tendency above this range being toward re-solution. Hardening will depend on the strain and stress distribution induced in the solid-solution lattice by the ordered regions. Although this strain will increase both in the solid solution and in the ordered regions as the size of the latter increases, the tendency would seem to be to relieve it by rearrangement within the ordered regions, without affecting the solid solution to any extent, rather than by forming an interface with the solid solution.

The change in slope of the resistance curve noted between 350 and 440 °C (660 and 825 °F) probably is determined by the effect of the growth of the ordered regions, to a size of about 10 Å, in increasing the resistance by scattering the electron wave as suggested by Mott (10). This range also corresponds to the maximum rate of formation of the orthorhombic structure, indicating that this also is determined by the size of the ordered regions. As expected, the hardening rate decreases and the resistance increases as disordering or re-solution starts at about 440 °C (825 °F), although maximum hardening still can be secured up to at least 480 °C (900 °F) if enough time is given for all possible ordering to take place.

This is excellent evidence also that the formation of the orthorhombic structure, which has its maximum rate at 440 °C (825 °F), does not decrease the hardening effects of the ordering even though it appears to increase the resistance somewhat. The hardness can be decreased only by the solid-solution lattice being raised to a high enough temperature for it to relieve its own strain and thus redissolve the excess nickel and manganese atoms.

During cooling from the maximum temperature of 545 °C (1015 °F) the resistance again falls to a minimum at about 290 °C (555 °F), as excess nickel and manganese atoms are rejected, and then rises slightly, possibly from strain relief.

On heating this slowly cooled material, the resistance retraces the curve from the cooling cycle up to about 290 °C (555 °F) and then decreases rapidly, as additional ordering starts, to a minimum in the range 425 to 475 °C (795 to 885 °F) before rising again because of re-solution. This indicates only the occurrence of ordering which had not taken place during the cooling. Again it is in this range that the hardening occurs.

The most puzzling thing is the apparent grain boundary constituent in the hardened structures in Figs. 12 and 13. Averbach (6) found a similar structure in his 49 manganese – 49 nickel – 2 copper alloy after aging at 500 °C (930 °F), and attributed it to the precipitation of a second phase, although his X-ray evidence, which successfully detected the face-centered tetragonal ordering in the same specimen, apparently gave no evidence of a second phase. Dean and his co-workers (4) also found this constituent, and a similar structure has been observed in the gold-silver-copper alloys by the present authors, so it probably is characteristic of this type of hardening.

In the present work, at least, this constituent cannot be directly responsible for the hardening for two reasons:

(a) the amount of it in the alloy aged 24 hours at 455 °C (840 °F), Fig. 12c, is appreciably less than in the alloy of equal hardness which was aged at 370 °C (700 °F), Fig. 12d; and

(b) no difference in hardness was found with a Knoop indenter between the material within the grains and that at the grain boundaries.

The decrease in amount of this constituent as the temperature increases above 370 °C (700 °F) appears to rule out anything but the copper-enriched solid solution, or the ordered face-centered

tetragonal material, as possible explanations. Of the two, the former seems more logical. With the etching reagent used, viz., 2 parts acetic acid, 2 parts nitric acid, 1 part acetone, any increase in copper content in these regions could cause a relatively great difference in etching rate. The segregation of nickel and manganese atoms into groups, either disordered or ordered, also might give some electrochemical acceleration to the etching.

This would indicate the hardening reaction in this alloy to be discontinuous by comparison with Mehl and Jetter's (14) classification of precipitation hardening. At higher temperatures the rate of segregation of nickel and manganese would be about the same throughout the entire grain and consequently the composition would be more uniform and the selective etching of the grain boundary regions less. It should be pointed out also that, if the effect of diffusion in equalizing composition was the principal reason for the difference between the structures of Figs. 12c and 12d, reheating at 525 °C (975 °F) after aging at 370 °C (700 °F) would be expected to be more rapid in its effect than is indicated in Figs. 13a and 13b.

In rationalizing the effects of cold work on these expansion coefficient curves, two additional facts must be remembered:

1. As shown by Dahl (11) for the Cu_3Au structure and by Dehlinger and Graf (12) for the CuAu structure, plastic deformation tends to destroy the effects of ordering.
2. The effects of cold work generally are relieved in two stages, (a) recovery and (b) recrystallization, both tending to compact the structure and therefore to decrease the expansion coefficient.

Inspection of the curves in Fig. 4b strongly suggests that the dip with its minimum at about 375 °C (705 °F) results from the recovery stage and that the one with its minimum increasing from 580 to 620 °C (1075 to 1150 °F) with decreasing deformation results from recrystallization. It may be significant also that recrystallization appears to start at about the temperature for which re-solution is complete.

Since the specimens were quenched before cold working, the initial stage is a normal expansion followed by a region of decreased coefficient with its minimum at about 225 °C (435 °F) as the solid solution changes composition and contracts to its low temperature stable size. Since the expanding effects of cold work still are present in the solid-solution lattice the normal increase in the coefficient of

expansion then resumes up to about 300 °C (570 °F). Here the compacting effects of recovery begin to appear, and the expansion coefficient decreases until the lattice strain has been reduced to such a point that the formation of the ordered tetragonal structure can begin. Because of this restraining action, the maximum dilatometric effect of the ordering as well as the maximum hardening rate occurs at an appreciably higher temperature than in the unworked material. Once ordering has taken place the subsequent stages of aggregation and transformation to the orthorhombic structure and re-solution take place as before with increasing temperature.

It should be pointed out also that, once recovery has reduced the lattice strains sufficiently, hardening takes place appreciably more rapidly than in either the furnace-cooled or the quenched specimens. Furthermore, there is little real difference between the hardening rates in Figs. 8 and 9 for any temperatures in the range 345 to 480 °C (650 to 900 °F). This is definite evidence that, even though the alloy is heated to a higher temperature than the optimum for the unworked alloys, the restraining influence of the cold work stress distribution controls the hardening rate. It should be noted also that 345 °C (650 °F) is appreciably lower than the temperature of the minimum in the recovery dip, so that recovery need not be complete to permit ordering, and therefore hardening, to begin. Since the apparent minimum in the recovery dip at 375 °C (705 °F) is merely the point at which the expanding effect of ordering balances the contracting effects of recovery, the true minimum may occur at an even higher temperature.

Furthermore, the shapes of the two curves in Fig. 10 indicate that the stress distribution from flat rolling, possibly because it is more nearly unidimensional, is more favorable to rapid hardening, when it is relieved properly, than the distribution from square rolling which undoubtedly is more complex.

Summary and Conclusions

1. Changes with temperature, and time, of the coefficient of thermal expansion, electrical resistance, and hardness of both the cold-worked and heat treated 60 copper – 20 nickel – 20 manganese alloy have been shown to be consistent with the formation, in the stable solid solution, of regions of ordered structures comparable with

those found by others in the compound MnNi as well as in the somewhat similar gold-silver-copper alloys.

2. The four essential stages are postulated as (a) rejection of excess copper, nickel and manganese atoms from the metastable solid solution; (b) ordering of the rejected atoms into a face-centered tetragonal form; (c) aggregation and reordering of the tetragonal regions into an orthorhombic structure; and (d) disordering or re-solution.

3. The ordering reaction, producing the face-centered tetragonal form, is the slowest and therefore the controlling stage. It is responsible for the hardening of the stable solid solution.

4. In cold-worked alloys, the tendency toward ordering is destroyed until after recovery has reduced the lattice strains a sufficient amount.

5. In cold-worked alloys, the recrystallization range follows closely after disordering or re-solution although the recrystallization temperature is decreased with increasing amounts of deformation in the usual manner.

6. The relation between the logarithm of the time to reach a given hardness and 1/T is not linear but increases to a maximum and then decreases.

7. The alloy will soften in relatively short times, even from the fully hardened condition, if heated above 565 °C (1050 °F).

8. The maximum hardening rate is at 370 °C (700 °F) after quenching or furnace cooling, but appreciably higher, at 400 to 480 °C (750 to 900 °F), after cold working, the specific temperature being related to the type of deformation.

9. The apparent grain boundary constituent noted in the fully hardened structure has been explained as an etching effect resulting from discontinuous segregation of manganese and nickel in the solid solution.

Acknowledgments

The authors are grateful to Howard Chace and Dorothy Dennison for their assistance in some of the experimental work, and to E. D. Tillyer and H. R. Moulton for their advice and encouragement. Thanks are also due to the American Optical Company for permission to publish the results.

References

1. R. S. Dean and C. T. Anderson, "The Alloys of Manganese-Copper and Nickel: Hardening in the pseudo-binary system, Cu-MnNi," TRANSACTIONS, American Society for Metals, Vol. 29, 1941, p. 808-812.
2. R. S. Dean and C. T. Anderson, "The Alloys of Manganese-Nickel and Copper: The electrical resistance and temperature coefficient of electrical resistance," TRANSACTIONS, American Society for Metals, Vol. 29, 1941, p. 899-906.
3. R. S. Dean, C. T. Anderson and E. V. Potter, "The Alloys of Manganese-Nickel and Copper: The coefficient of thermal expansion," TRANSACTIONS, American Society for Metals, Vol. 29, 1941, p. 907-912.
4. R. S. Dean, J. R. Long, T. R. Graham and C. W. Matthews, "Age Hardening Copper-Manganese-Nickel Alloys," TRANSACTIONS, American Society for Metals, Vol. 34, 1945, p. 481-502.
5. S. Valentiner and G. Becker, "The System Nickel-Manganese," *Zeitschrift für Physik*, Vol. 93, 1935, p. 795-803.
6. B. L. Averbach, "Electrolytic Manganese, Alloyed with Copper and Nickel," *Metals and Alloys*, Vol. 13, 1941, p. 730-733; *ibid.*, Vol. 14, 1941, p. 47-51.
7. M. Hansen, "Der Aufbau der Zweistofflegierungen," Berlin, 1936. Julius Springer.
8. C. H. Johansson and J. O. Linde, "X-Ray and Electrical Investigations in the Copper-Gold System," *Annalen der Physik*, Vol. 25, 1936, p. 1-48.
9. R. Hultgren and L. Tarnopol, "Effect of Silver on the Gold-Copper Superlattice, AuCu," *Transactions*, American Institute of Mining and Metallurgical Engineers, Vol. 133, 1939, p. 228-237.
10. N. F. Mott, discussion to paper by M. L. V. Gayler, *Journal*, Institute of Metals (London), Vol. 60, 1937, p. 267.
11. O. Dahl, "Cold-Work Deformation and Recovery in Alloys with Orderly Atom Configuration," *Zeitschrift für Metallkunde*, Vol. 28, 1936, p. 133-138.
12. U. Dehlinger and L. Graf, "The Rearrangement of a Solid Metallic Phase," *Zeitschrift für Physik*, Vol. 64, 1930, p. 359-377.
13. M. Cook and H. J. Miller, "The Effect of Different Elements on the Annealing and Grain Growth Characteristics of Alpha Brass," *Journal*, Institute of Metals (London), Vol. 49, 1932, p. 247-261.
14. R. F. Mehl and L. K. Jetter, "The Mechanism of Precipitation from Solid Solution. The Theory of Age Hardening," AGE HARDENING OF METALS, published by the American Society for Metals, Cleveland, 1940.

DISCUSSION

Written Discussion: By J. C. Lewis, Jr., research metallurgist, Driver-Harris Co., Harrison, N. J.

A particularly useful feature of this alloy is the fact that its cooling rate from the annealing temperature of 595 °C (1100 °F) is not critical, in order to put the material into condition either for further working or for hardening; even hardening "on the way down" from the anneal is entirely satisfactory, by merely holding at the hardening temperature for the proper time. The paper explains why this is so. The data and discussion of results presented in the paper provide a useful picture of structure and transformation relationships, satisfactory to the needs of a production metallurgist called on to handle this alloy.

Authors' Reply

Since this work was undertaken primarily to assist the production men in our plant to fabricate this alloy, we are particularly pleased to receive Mr. Lewis' comments. If, as a production man, he, too, finds the work satisfactory, we believe the study has been worth while.

Mr. Lewis' comments on the manner in which the sluggishness of the transformation permits the alloy to be hardened during cooling call attention to one of the unusual features of this alloy. As shown in Fig. 14, however, the structure of the alloy after furnace cooling to room tem-

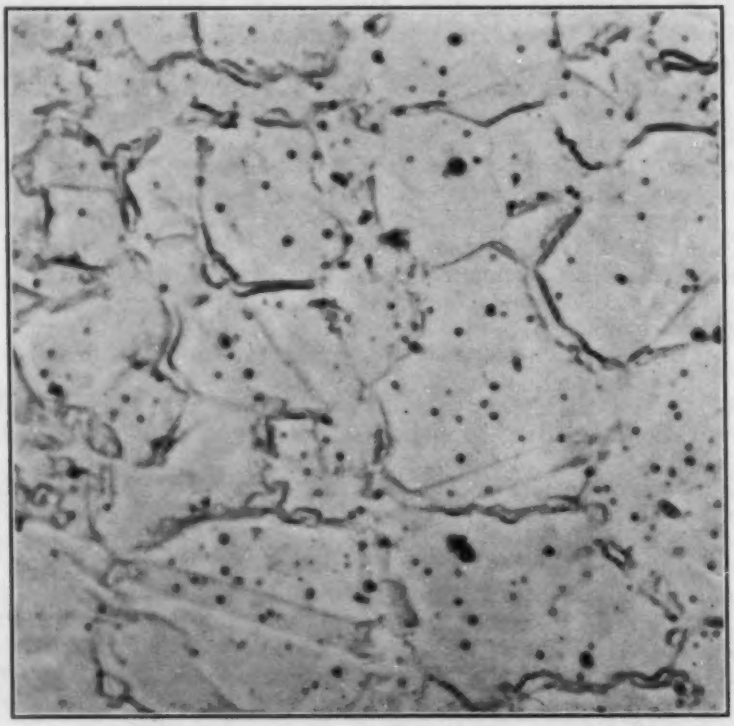


Fig. 14—Metallographic Structure of a Specimen Furnace-Cooled From 1100 °F (595 °C) Over a Period of 15 Hours. Etched with nitric and acetic acids in acetone. × 1000.

perature over a period of about 15 hours is somewhat different from that secured on reheating. The grain boundary constituent here appears much more like a second phase than in any of the quenched and reheated samples. Unfortunately we were unable to check this possibility because of the lack of suitable X-ray equipment.

However, even with the apparently logical explanation of the hardening which we have been able to offer, it is clear that considerable careful work needs to be done before the problem truly can be said to be solved. The X-ray study alone should present an interesting problem in techniques to some ambitious student of the future.

BETA LAMINATIONS IN CARTRIDGE BRASS

By Ralph L. Dowdell, Charles A. Nagler, Morris E. Fine,
Harold P. Klug and Gust Bitsianes

Abstract

This paper deals with strip cartridge brass, laminated in manufacture, so that the resulting cups were unsatisfactory for cartridge cases. The phenomenon had been previously referred to as "phantom laminations in brass" and this research was undertaken to determine the cause of the laminations.

When cartridge brass, containing between 30 and 33% zinc, is cast into commercial cakes in water-cooled molds, there is some segregation. The central portion of the cake contains a cored structure of alpha brass with segregated beta brass as the last to freeze. In the customary rolling practice any residual beta present may be banded in the central portion of the strip.

The beta phase contained in the alpha strip brass for caliber .50 cartridge cases may be dissolved by annealing at 600 °C (1110 °F); however, there is a strong tendency for a mixed grain size. There is usually a finer grain size in the central areas formerly containing beta than in the outside areas, and evidence indicates there is a composition gradient inhibiting grain growth on annealing before any cupping operation.

In order to avoid phantom laminations, it is recommended that beta be eliminated by making use of a longer soaking or annealing practice prior to rolling.

Brass cakes with zinc 2% above normal, containing relatively large amounts of beta, were soaked at 825 °C (1515 °F), and after 4 hours the residual beta was completely dissolved. This high temperature of soaking is not recommended as the only remedy because there are

This research was made possible by contract between the University of Minnesota and the Office of Scientific Research and Development under contract No. OEMsr-1084 and was known as NDRC Research Project NRC-62. The declassification of this material has been approved.

A paper presented before the Thirtieth Annual Convention of the Society, held in Philadelphia, October 23 to 29, 1948. The authors, Ralph L. Dowdell, Charles A. Nagler, Morris E. Fine, Harold P. Klug and Gust Bitsianes, were associated with the Department of Metallurgy, University of Minnesota, Minneapolis. Manuscript received December 15, 1947.

many other combinations of time and temperature which will remove beta before it is banded in strip.

When beta dissolves in alpha no voids are formed, and if cakes are homogenized there will be no difficulties from the harmful effects of phantom laminations.

Introduction

DURING World War II there was considerable difficulty in making brass cartridge cases in sizes of .50 caliber and larger because some of the strip brass was laminated or banded in the vicinity of its central portion.

At that time this phenomenon had been discussed as "ghosts" and "phantom laminations" in a somewhat evasive manner, and this project was carried out to show the nature of these phantom laminations.[1]

This study was completed in May 1944 and is reported at this time for the purpose of recording all important data on cartridge brass and also to show that the ordinary metallographic tools will solve an important alloy problem pertinent to national defense.

Microscopic Investigation

The microstructure at the central portion of cast cakes, containing between 30 and 33% zinc, consists of primary cored alpha with varying amounts of a second phase which is the last to freeze and which has proved in this investigation to be the beta phase of the copper-zinc system. Most of the beta is located along the central portion of the cake as would be expected. Figs. 1, 2, 3, and 4 show the structure of a cast cake.

Ordinary 70-30 brass cakes, 5 inches thick, have small amounts of beta. With this composition there is very much less beta than with 67-33 brass. The beta laminations are more prevalent in cakes with a high zinc content and also cakes of great thickness.

A sample from an original cake, as shown in Fig. 1, was squeezed in a vise so as to cause slipping. Upon micro-examination it was found that there were many characteristic slip lines in the alpha but none in the beta. This structure is shown in Fig. 4, and it indicates a well-accepted fact that beta is harder and less plastic than alpha.

[1]Daniel R. Hull, H. F. Silliman and John R. Freeman, Jr., "Phantom Laminations in Brass," *Transactions*, American Institute of Mining and Metallurgical Engineers, Institute of Metals Division, 1945, p. 203-213.

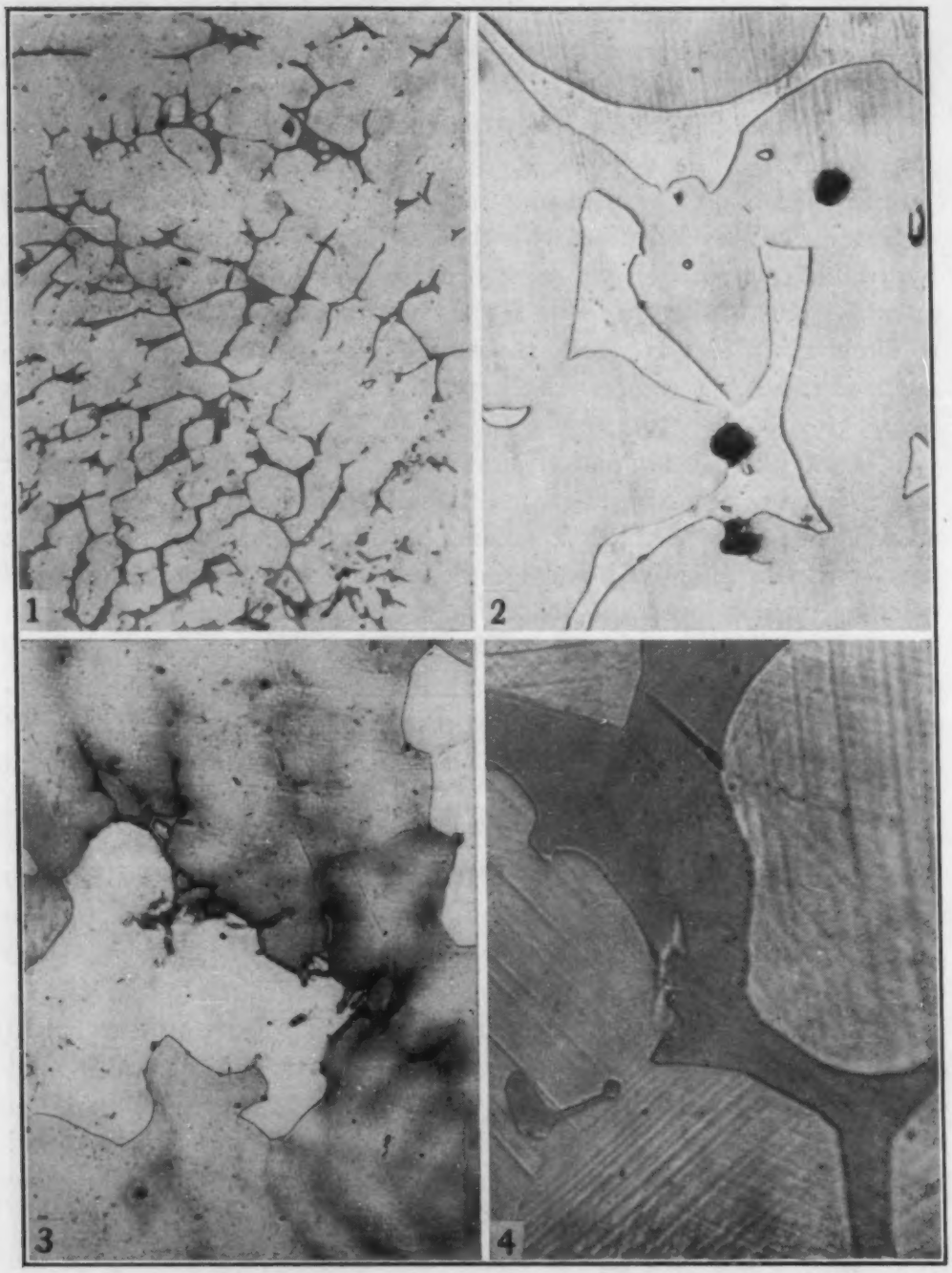


Fig. 1—Cast Cake Showing Beta Inclusions and Voids. Location, center of cast cake. Mild etching reagent to resolve beta; 50% $NH_4OH + H_2O$ for 30 seconds. × 100.

Fig. 2—Same as Fig. 1 at × 1000 Magnification.

Fig. 3—Same as Fig. 1 Etched 5 Seconds in $NH_4OH + H_2O_2$ Which Is a Much More Drastic Etching Reagent. Cored alpha is resolved. Much less beta is apparent than in Fig. 1. × 100.

Fig. 4—Cast Cake Squeezed in a Vise Showing Characteristic Slip Lines in Alpha and None in Beta. Composition: Cu 68.17%, Zn 31.81%, Fe 0.018%. × 1000.

In order to resolve beta in the presence of large amounts of alpha, a better and more selective reagent has been found consisting of 50% NH_4OH and H_2O. With this mild etching reagent, beta is slowly attacked and not easily overetched while the alpha is almost unattacked.

Small amounts of beta in either cast cakes or rolled brass would ordinarily escape detection with the customary etch with ammonium hydroxide in hydrogen peroxide because it is too drastic and causes pitting. This is also true with ferric chloride reagents. If one wishes to show grain size contrast, the ammonium hydroxide-peroxide reagent is ideal, but it is not well suited for the detection of the beta phase.

Since micro-examination showed beta in original cast cakes, it was decided to anneal beta-rich sections from a cast cake in hydrogen at 825 °C (1515 °F) for 2, 4, and 8 hours to see whether or not beta would be dissolved and eliminated and at the same time find whether or not any inclusions would be reduced by the hydrogen treatment. After 2 hours at 825 °C (1515 °F) only a small amount of beta was present and after 4 and 8 hours there was no beta present. This suggests that a soaking practice for the proper time and temperature will eliminate all beta and, consequently, give freedom from laminated beta so that the higher zinc alloy (32% zinc) can be used successfully for the manufacture of cartridge cases.

Fig. 5 shows that all the beta is eliminated by annealing the original casting at 825 °C (1515 °F) for 4 hours, and also that there are no voids formed when beta is dissolved. Fig. 6 shows that the coring of the alpha has been eliminated without grain growth.

If samples of plain cast cakes containing beta are cold-rolled to about 0.020 inch with no annealing whatsoever, the strip is sound but banded or laminated with beta streaks longitudinal to the direction of rolling. These beta laminations are identical with those found from other heats of brass made into strip by commercial practice for the drawing of cartridge cases.

Figs. 7 and 8 are typical of the laminated beta occurring in the middle of commercial strip containing 66.87% copper and 33.12% zinc. These bands of beta are somewhat irregular in width because of the residual distribution of beta in the cast cake.

If cold-rolled brass with structures typical of Figs. 7 and 8 are annealed, the beta laminations can be eliminated by diffusion without the formation of voids or holes. If, however, the specimens are

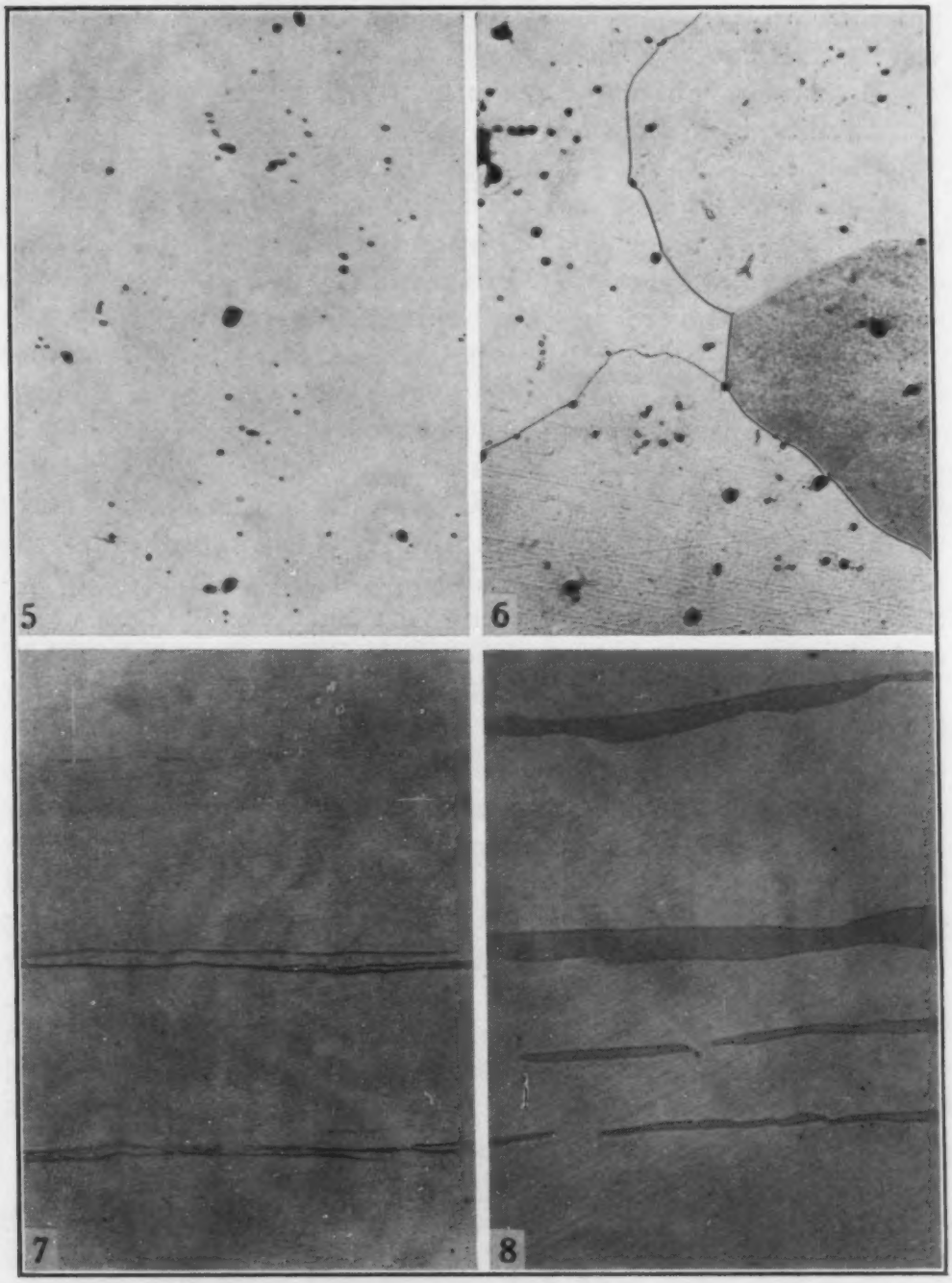


Fig. 5—Cast Cake Showing Elimination of Beta After Annealing in Hydrogen at 825 °C for 4 Hours. No voids formed by the solution of the beta that did not exist before annealing. Most of the gray patches are inclusions not reducible at 825 °C. Etched in 50% $NH_4OH + H_2O$ for 30 seconds. × 100.

Fig. 6—Same as Fig. 5 Except Etched Deeper in 50% $NH_4OH + H_2O$ Mixed 5 to 1 With 1½% Solution of H_2O_2 for 5 Seconds in Order to Show Grain Size. Note freedom from coring and absence of grain growth when compared with Fig. 3. Deep etching dissolves alpha around inclusions so they appear as holes. × 100.

Fig. 7—Cold-Rolled 0.50-Caliber Strip As-Received, 0.256 Inch Thick, From Brass Mill; Longitudinal Section, Unannealed. Light etch in 50% $NH_4OH + H_2O$, 30 seconds. Shows beta banding in alpha. Composition: Cu 66.87%, Zn 33.12%, Fe 0.01%. × 100.

Fig. 8—Same as Fig. 7 at × 1000 Magnification.

pitted from overetching, they will appear as in Figs. 9 and 10 and consequently appear as holes.

A series of annealing experiments was made on cold-rolled strip by annealing in hydrogen at 200, 400, 600, and 800 °C (390, 750, 1110, and 1470 °F) for 2 hours. It was found that the beta laminations could be diffused into the alpha and eliminated by either a 2-hour anneal at 600 or 800 °C, but not at 200 or 400 °C. In some cases recrystallization at 600 °C resulted in a slightly finer grain size at the locations where the beta bands had existed previously. In most cases the size after recrystallization was nearly the same throughout.

When the cold-rolled strip is annealed at 600 °C (1110 °F) in hydrogen for 2 hours the grains are recrystallized and are much finer than when annealed at 800 °C (1470 °F). Fig. 11 shows only alpha and a series of stippled lines where beta had existed previously to the anneal. These lines are also known as "ghosts" or "phantoms" and they are present because beta laminations existed previously to annealing. At the higher annealing temperature, 800 °C (1470 °F), Fig. 9, the stippled lines are not as pronounced as at 600 °C (1110 °F). It should be noted that some of these stippled lines cut across grains and some are intergranular. These lines are not resolved with proper polishing. With overpolishing, pits may be formed. After etching in ammonium hydroxide-peroxide, pits are easily formed. It is likely that the time and temperature of anneal are not sufficient to completely diffuse the high zinc areas originating from the beta bands and that etching attacks these areas at a faster rate and forms the localized pits. This is verified by X-ray analysis.

When beta dissolves in alpha, there are still high zinc areas at the old interfaces of beta and alpha which etch at a faster rate and also pit faster with the result that ghost lines show up on deep etching with NH_4OH-peroxide reagent.

If beta is eliminated, therefore, by soaking the cake before rolling is undertaken, there will be no beta laminations and no ghosts. Why not eliminate beta before it has caused damage?

It is usually conceived that beta is much less plastic than alpha and strain hardens faster; however, in this investigation, structures of about 90% beta have been cold-rolled to 0.020-inch strip without difficulty from cracks. When structures containing beta, similar to Figs. 7 and 8, are given a reverse bend test to failure, they crack at the interface of the beta and alpha. This proves that laminated beta is

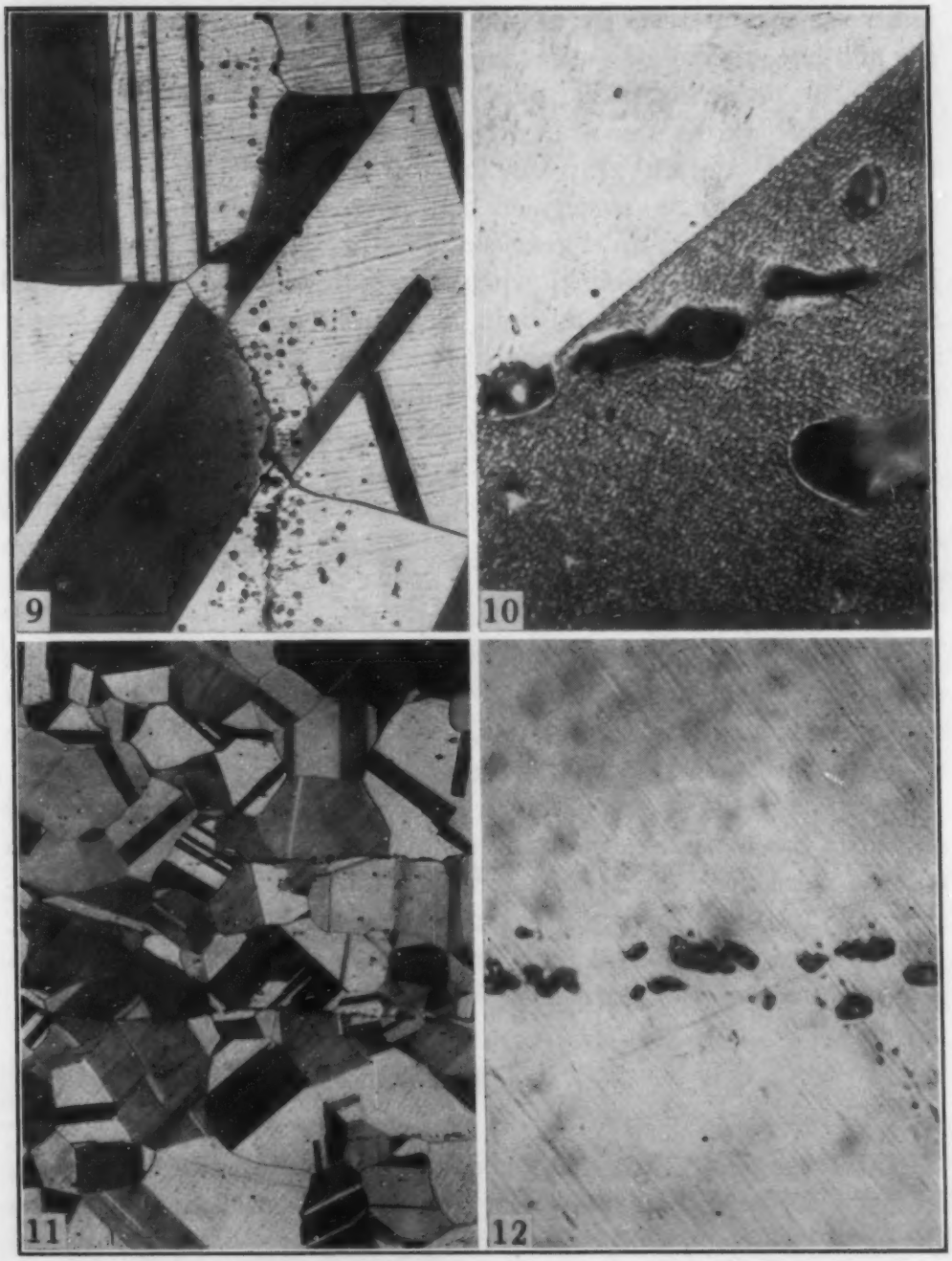


Fig. 9—Cold-Rolled Brass Strip From 0.460 to 0.256 Inch. Composition: Cu 66.87%, Zn 33.12%. This originally contained beta laminations similar to Fig. 7. Treatment: annealed in hydrogen at 800 °C, 2 hours. Etched deeply in 50% $NH_4OH + H_2O_2$, 5 seconds. Shows pitting; as polished there were no voids present. × 100.

Fig. 10—Same as Fig. 9 at × 1000 Magnification.

Fig. 11—Cold-Rolled Brass Strip, Cu 66.87%, Zn 33.12%, From 0.460 to 0.256 Inch. This originally contained beta laminations similar to Fig. 7. Treatment: annealed in hydrogen at 600 °C for 2 hours. Etched deeply in 50% $NH_4OH + H_2O_2$. Shows pitting in stippled lines where beta existed previous to anneal; as polished these pits are not present. × 100.

Fig. 12—Typical Inclusion Stringers in Cold-Rolled Brass, Cu 66.87%, Zn 33.12%, From 0.460 to 0.256 Inch. These inclusions are dark gray-blue in color and are not reduced with hydrogen annealing at 800 °C in 2 hours. They occur in the central portion of the strip brass. × 1000.

undesirable as there is the possibility of rupturing during cold rolling and later during deep drawing.

Inclusion stringers in rolled bars are rather uncommon. Fig. 12, however, shows some relatively short inclusions of rounded particles having a dark gray-blue color. These inclusions occurred generally close to the segregated beta phase but sometimes near the surface of strip brass. Occasionally some inclusions appear cubic in shape. When examined with reflected polarized light, crossed nicols, the inclusions have a bright canary-yellow color. Occasionally a *few* small, isolated inclusions having a reddish color were found and appeared to be cuprous oxide (Cu_2O).

There were relatively few inclusion streaks found in cartridge brass so this factor is considered to be a very minor cause of the failure of cups. It should, however, be pointed out that overetching with $NH_4OH + H_2O_2$ etching reagent allows the inclusions to drop out and appear as holes or voids.

Annealing in hydrogen at temperatures as high as 800 °C (1470 °F) for 2 hours had no reducing effect whatsoever on the stringer inclusions so they may be regarded as unreducible at ordinary annealing temperatures and from their sparse distribution to have no particular bearing on the problem of laminated brass.

Cartridge brass is a relatively clean metal as compared to steel and little trouble is expected from the standpoint of inclusions. In no case were there any *drawn out* inclusions present. When inclusions are found in isolated areas they resemble those shown in Fig. 12 and are a collection of individual inclusions which are not elongated to any great extent during rolling.

X-Ray Diffraction

Two types of X-ray diffraction photographs were taken, the ordinary Debye-Scherrer powder photographs and back-reflection photographs. Samples for the powder photographs were fine slivers of brass, ground to size from the larger pieces, or filings glued onto a fine glass capillary tube with Duco cement. To produce good photographs, annealing was necessary to relieve any strain originally present in the material and that produced by the cold work of grinding and filing. The samples in the powder photographs were rotated at 1 revolution per minute. The samples for the back-reflection photographs were suitable blocks of brass set up on the axis of the

Table I
Data on X-Ray Diffraction Photographs of Cartridge Brass Samples

Film No.	Type (Note 1)	Sample	β Phase Lines Present	Remarks
583	B.R.	Block of No. 0	None	Exploratory
584	B.R.	Block of No. 1	None	Exploratory, lines diffuse
586	B.R.	Block of No. 0	None	Exploratory
587	B.R.	Block of No. 1 (Note 2)	(321)	Lines are diffuse
588	B.R.	Block of No. 1 (Note 2)	(321)	Lines are diffuse
589	P.	Filings of No. 0	None	Lines diffuse
591	P.	Filings of β brass (Special Sample)	All	Lines diffuse
593	P.	Sliver of No. 0	None	Lines diffuse
595	P.	Same as 591 but annealed 2 hours at 400 °C	All	Lines much sharper
597	P.	Same as 589 but annealed 2 hours at 400 °C	None	Lines much sharper
599	B.R.	Block No. 1 (Note 2), annealed 2 hours at 400 °C	None	Overannealed
601	P.	Sliver of No. 0, annealed 2 hours at 400 °C	None	Overannealed
M 6	B.R.	Block No. 1 (Notes 2, 3), annealed 3 hours at 200 °C	All	Beam slipped past one side of sample
M 8	B.R.	Block No. 1 (Notes 2, 3), annealed 2 hours at 175 °C	(321) (222) (310) (220)	
M 9	B.R.	Block No. 1, annealed 2 hours at 175 °C	None	Microscope revealed no β
M16	B.R.	Block No. 0 (Note 2), cold-rolled and annealed 2 hours at 175 °C	(321)	(321 is present but very faint
M37	B.R.	Sliver No. 1 (Notes 2, 3), annealed 2 hours at 175 °C	(321) (220) (110) (211)	

Notes:
1. B.R. = back-reflection photograph; P. = powder photograph.
2. Microscope revealed the presence of β phase in the samples.
3. Samples in banded region ground longitudinally to direction of rolling. Area of high band concentration located with microscope. X-ray beam impinged on this area.

Composition:
Sample 0: Cu 68.29, Zn 31.71, Fe 0.01; Cake as cast.
Sample 1: Cu 66.86, Zn 33.12, Fe 0.01; Caliber .50 strip received in cold-rolled condition from mill.

The minimum amount of the beta phase required to show diffraction lines is estimated at 20% by volume as shown by microscopic examination. When about 30% of beta is present the lines are very clear.

camera and held stationary during the exposure. Some of these samples were large enough so that the beam was completely blocked and only back-reflection lines were obtained. In other cases part of the beam could slide past the sample giving rise to some of the low θ lines of the pattern as well. Both types of photographs were taken with a Buerger precision powder camera using copper Kα radiation obtained by filtering the beam through nickel foil.

Fig. 13 shows the relative positions of the various lines in the patterns of α and β brass as obtained by the powder method using a sample which is a mixture of the two phases with β brass predominating. In the actual photograph the two patterns are superimposed.

Back-reflection photographs from large blocks will show only those lines to the right of the dotted line in the diagram. The various lines are labeled with the indices of the planes producing them. It is seen that the lines for the two phases do not coincide and the positions of most of them with respect to the other phase are unmistakable. Thus the (321) doublet of β brass is especially easy to identify on back-reflection photographs. When enough β brass is present to give lines of sufficient intensity to find them, they are readily identified. Also, if lines in the positions indicated in the β brass pattern are found on a diffraction photograph of a brass sample, it is conclusive evidence of the presence of β brass in the sample.

Nineteen exposures were taken on various samples. Some of these must be regarded as exploratory in nature in order to check on the technique. Table I gives the important data on exposures. Six different samples of cold-rolled strip and one sample of a cast cake show one or more lines of the β brass pattern, indicating its presence in the respective samples.

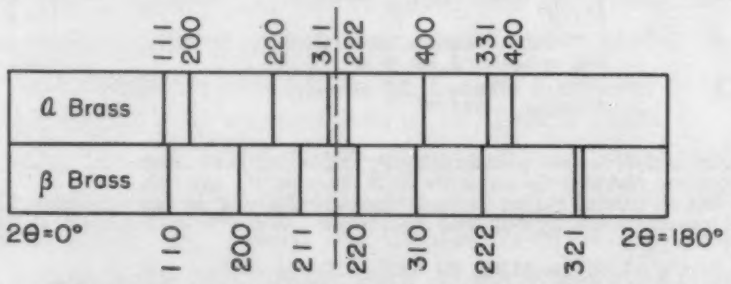


Fig. 13—Diagram of the Relative Positions of the Various Lines in the Patterns of α and β Brass.

High θ lines were measured on four of the films and the lattice constants of the phases were calculated. These results are tabulated in Table II.

Table II
Lattice Constant Data

Film No.	Sample	Lattice constants in Å α phase	β phase
595	Special sample of β brass with some α	3.689	2.944
597	No. 0 showing no β	3.673	.....
M 6	No. 1 showing β	3.683	2.943
M37	No. 1 showing β	3.690	2.944

The reported value of a_o for the saturated α phase is 3.68 Å, and for the β phase in contact with it is $a_o = 2.945$ Å. Film No.

595 is in agreement with these values. Apparently areas in this brass which contain no β phase are not quite saturated as evidenced by the slightly smaller a_o value of 3.673 Å found in film No. 597. When the β phase is present the α phase in its immediate vicinity is apparently saturated as found in films No. M6 and M37. This, of course, is what would be expected.

Thermal Analysis

Temperature-time cooling curves were taken on samples from cast cake and also from cold-rolled strip which showed beta laminations. The ordering transformation from β to β' found at 451 to 454 °C (845 to 850 °F) was recorded, which was added proof that beta is present in the higher zinc brasses in sufficient quantities to cause a heat effect.

Dilatation

In order to determine the magnitude of the volume changes accompanying dissolving of beta stringers or laminations, various brass samples containing beta stringers were heated, annealed, and cooled in a dilatometer. Test pieces about 5 by ½ by ¼ inches were cut from cold-rolled brass strip. The edges of the test pieces were rounded by turning the strips in a lathe. The furnace consisted of a porcelain tube ⅝ inch in diameter surrounded by a larger tube which supported the heating element. Both tubes were enclosed in an insulated cylindrical jacket.

Test strips were located centrally in the furnace and hollow silica connecting tubes were fitted onto machined ends of test pieces. The rear tube (6¾ by ¼ inch diameter) was held in a fixed position by a backstop attached to a rigid bar. The front tube was ground so as to furnish a concave seating for an Ames dial reading to 0.0001 inch. The whole set-up was mounted on a well-aged wooden base. The temperature was determined by means of a chromel-alumel thermocouple in contact with the specimen.

In order to minimize oxidation during heating in the dilatometer, the test pieces were coated by dipping in a colloidal graphite suspension; powdered charcoal was put in the furnace tube; and the ends were plugged with asbestos fiber. One test strip was chromium plated to prevent oxidation and this gave similar results to the uncoated strips. Microscopic examination indicated no diffusion of the chromium into the brass.

Fig. 14 is a graph representing typical data obtained with the dilatometer. This particular specimen used was not the one coated with chromium. The analysis of the sample was 66.87% copper, 33.12% zinc, and 0.01% iron. Estimates of a transverse cross section made with a microscope showed about 0.2% beta to be present. The central portion, of course, had all the beta. This strip was an-

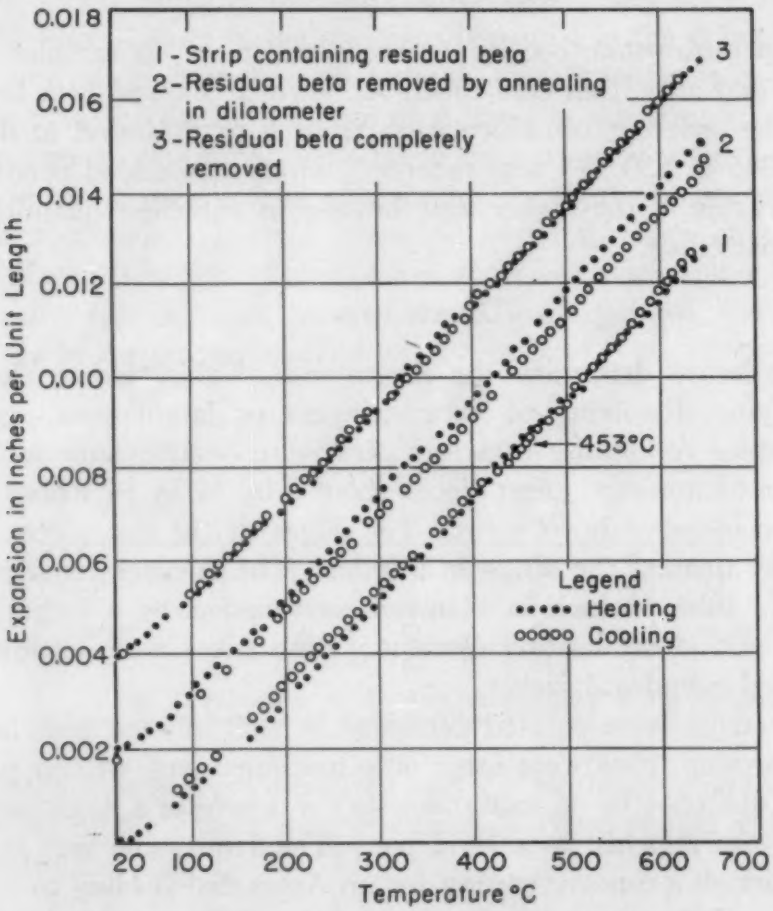


Fig. 14—Linear Thermal Expansion of Cartridge Brass.

nealed for ½ hour at 300 °C (570 °F). The test piece was first heated to 650 °C (1200 °F) and cooled immediately (Curve 1). The change in length of the strip was followed with the Ames dial. The change in slope at 453 °C (845 °F) on heating is due to the β to β' transformation. The cooling curve (Curve 1) returns along the heating curve. Merica[2] obtained similar results with alpha brass

[2]P. D. Merica and L. W. Schad, *Journal*, American Institute of Metals, Vol. 11, No. 3, 1917, p. 396.

samples. From 650 to 453 °C (1200 to 845 °F) the cooling and heating curves are almost coincidental.

In Curve 2 the test strip was heated 4 hours at 630 to 650 °C (1165 to 1200 °F). Measurements were taken every 15 minutes. There was a gradual decrease in length as the beta was dissolved. The change amounted to about 0.0004 inch per inch at 650 °C (1200 °F).

After this anneal the test strip was again heated and cooled. This is plotted in Curve 3. The heating and cooling curves are almost coincidental, indicating that the beta is all dissolved. Microscopic examination of the strip after this experiment did not show the presence of beta nor were there any voids formed as the alloy decreased in size. Data from the chromium plated strip gave similar results; however, the decrease in length was only 0.0003 inch per inch. When beta dissolves in alpha in the vicinity of 650 °C there is a slight decrease in volume showing that alpha is denser than beta.

The results plotted in Fig. 14 are all corrected by subtracting the readings of the apparatus with a fused quartz blank.

Density

Density determinations were made in a special 10 ml. pycnometer bottle. In order to obtain the maximum amount of beta in the samples, a caliber .50 strip containing 66.87% copper, 33.12% zinc, and 0.01% iron was ground down on each side until approximately one-third of the section remained and which measured 0.070 inch thick. These sections of $\alpha + \beta$ brass were stress relieved in H_2 at 300 °C for 1 hour, then washed, rinsed and dried. Three pieces at a time were checked. Distilled water was used, samples boiled and evacuated and allowed to stand 3 hours for equilibrium. Density determinations were found to be 8.472 and 8.480 on the two lots.

The samples were then annealed in H_2 3 hours at 600 to 630 °C and the densities redetermined with the result that they had increased to 8.491 and 8.494 on the respective lots. When beta dissolves in alpha the density increases and its magnitude checks roughly with the results of the dilatation experiments if one considers a much higher concentration of beta in the density samples as compared with the dilatation samples having less beta. It is estimated that the density samples contained from 5 to 10% beta by volume.

Summary

As a result of this investigation it appears that the following conclusions can be made from the evidence found:

1. Cast cakes contain more or less beta, depending on the zinc content of the brass and many metallurgical factors such as size of cake, rate of pouring, gating, rate of cooling, etc. Beta has been shown to exist by microscopic, thermal analysis, dilatometric, and X-ray studies.

2. In the customary rolling practice any residual beta is rolled out and laminated in the brass strip as long stringers, lenticular in shape.

3. Laminated beta is not as ductile as alpha and there may be internal ruptures in some cold-rolled strip which will not add to the soundness of the strip. A duplex structure of alpha and beta is not advantageous to cold mechanical working. Laminated brass on reversed bending shows fracture at the interface between beta and alpha.

4. The laminated beta phase of strip brass is dissolved in alpha when annealed 2 hours at 650 °C but the resulting strip shows phantom lines after deep etching in $NH_4OH+H_2O_2$. These lines are the result of a higher rate of etching in the previously laminated area than in the adjacent area because of higher zinc content. This is shown by microscopic and X-ray evidence.

5. Phantom lines commonly are intergranular, occasionally transgranular, and frequently have a fine grain size along the contact line because of the effect of concentration gradient on grain growth.

6. To insure freedom from laminated beta in the higher zinc alloys, it is recommended that a long soaking or annealing be given the cakes so all beta is eliminated before rolling begins. Four hours at 825 °C (1515 °F) will dissolve all the beta, but a longer time at a lower temperature will result in less dezincification. The dezincification at 825 °C is less harmful than the banded brass.

7. The inclusions contained in cartridge brass are not too continuous and have little to do with the question of laminated brass.

8. When beta is dissolved by annealing there is a slight contraction in volume, as shown by dilatation curves, and there is a slight increase in density. This reaction is too small to form voids. Any voids formed in the vicinity of the phantoms are the result of localized overetching and pitting because of the high zinc areas.

9. There appears to be no reason why 2:1 brass cannot be satisfactorily used for cartridge cases if the beta segregate is removed by soaking the castings before rolling begins.

ACKNOWLEDGMENT

The writers are very appreciative of the suggestions of the Project Liaison Officers, Lieutenant Colonel C. H. Greenall, Commanding Officer, Frankford Arsenal, and Major C. H. Corey, Chief of Ordnance, Technical Division, Army Service Forces, and Project Committee Chairman, L. L. Wyman.

DISCUSSION

Written Discussion: By R. S. Pratt, Bridgeport Brass Co., Bridgeport, Conn.

The authors have presented some interesting data in relation to the difficulties encountered during the war with the so-called "beta laminations" in cartridge brass. Their approach has been from an academic standpoint and it might be desirable to point out certain practical aspects which may have been overlooked.

It seems to have been clearly established that the copper/zinc ratio and the presence or absence of the beta constituent are directly related to the difficulty. It should also be clearly stated that the central laminations revealed in cups or fracture tests are directly related to the solution of the beta phase rather than to the beta itself. Hot-rolled or hot-rolled and cold-rolled strip containing thin plates of beta in the center of the thickness of the strip do not show weakness in fracture tests. This weakness is only developed by temperatures sufficient to cause solution of the beta and the degree of weakening or separation depends on such factors as amount of beta, distribution, and extent of solution. It is possible, for instance, to completely recrystallize the cold-worked brass with very little solution of beta or development of weakness but as soon as the beta is absorbed the weakness is readily apparent in fracture or tensile tests. In order for this picture to be clearly developed it is necessary that the hot-rolled brass be promptly quenched after hot rolling. If the hot-rolled material is allowed to slow cool some of the beta is dissolved during cooling and the weakness may be found in the strip as-hot-rolled or after subsequent cold rolling.

We question if the complete homogenization of full-size castings can be accomplished in 4 hours. However, we do know that the difficulty can be avoided if the castings can be held long enough to complete the homogenization. It was not a practical possibility during the war to spend any such amount of time in preheating. Insofar as commercial brass is concerned, the usual gage is such that we do not need to be concerned about this difficulty, as the additional rolling and annealing operations will permit this type of discontinuity to heal.

The authors have assumed that the stippled lines in the center of the cross section from which the beta has been dissolved (see Fig. 11) are merely etch pits due to a difference in copper content. Whether the lines are due to etching pits or not is immaterial but if fracture tests had been made it could have been seen that the separation occurred at these lines. These lines would also seem to be of significance because they are not usually transcrystalline and the fine boundary grains indicate some resistance to normal grain growth. This condition exists quite generally unless very high annealing temperatures are used and then there appears to be some growth across the stippled lines. We believe that the lines are due to a lack of continuity in the metal structure resulting from the presence of foreign material or voids. If not mechanically separated the discontinuity is readily healed by diffusion across the line in subsequent rolling and annealing operations.

While it is not clear what the actual cause of discontinuity may be, we have found that low copper alloys (68%) may be cast in conventional size cakes in such a way that the difficulty does not occur. Bars cast with a dry mold dressing were found to have much less than the usual amount of residual beta after hot rolling and as a result very few of the typical discontinuities. While this is not a feasible commercial practice it does suggest that the persistence of the beta constituent noted in bars of the same copper content cast in the usual way may be due to some selective absorption of gases during casting.

Authors' Reply

The authors wish to thank Mr. Pratt for his very pertinent remarks, and we are pleased to learn that there is very little disagreement in our findings.

If bend tests were given to brasses which contain bands of beta, the fracture will be at the interface between alpha and beta. The authors worked along that line rather than on fractures after the elimination of the beta. Would it not be feasible to expect some fracturing during the rolling of the combination structure of alpha and beta which would not heal during annealing? If there were no fracturing during the cold rolling of the combination structure, it might be still possible to have fracturing at the interface after annealing because of the higher zinc concentration at those locations. The complete solution to this question might not be answered for some time.

From the oral discussions of Mr. Jackson and Mr. Jamieson, together with Mr. Pratt's, it appears that the segregation of beta in cartridge brass is the "root of all the evil" causing the laminations. The only way that cartridge cases can be properly made is to eliminate the formation of beta in the cake. If that cannot be done, then it will be possible to eliminate beta by annealing after some early stage of reduction.

In conclusion, I wish to again thank Messrs. Pratt, Jackson, and Jamieson, and Dr. Fine and Dr. Nagler for their valuable contributions to this discussion.

MANGANESE-ZINC PHASE DIAGRAM FROM 0 TO 50% ZINC

By E. V. Potter and R. W. Huber

Abstract

The manganese-zinc phase diagram from 0 to 50% zinc was determined by X-ray and thermal analysis methods, using alloys prepared by powder methods.

In addition to the four allotropic forms of manganese (alpha-manganese, beta-manganese, gamma-manganese, and delta-manganese), three other phases (beta, epsilon, and alpha) occur.

The alpha-manganese phase, existing below 705 °C (1300 °F) in pure manganese, showed a 2% solubility for zinc.

The beta-manganese phase, existing in pure manganese between 705 and 1100 °C (1300 and 2010 °F), would dissolve up to 20% zinc, the maximum temperature for this single-phase field decreasing to 554 °C (1030 °F) at 20% zinc.

The gamma-manganese phase, existing between 1100 and 1138 °C (2010 and 2080 °F) in pure manganese, had a solubility for zinc of about 40%. This phase has a face-centered tetragonal structure with an axial ratio of 0.938 at 100% manganese, which gradually becomes more nearly cubic as zinc is added, being cubic with 23% or more of zinc. The gamma-manganese phase decomposes eutectoidally at 554 °C (1030 °F), forming beta-manganese and epsilon, the eutectoid composition being 39% zinc.

The delta-manganese phase exists from 1138 to 1245 °C (2080 to 2275 °F) in pure manganese. Its structure is not known.

The beta phase exists in a very small field near 45% zinc and between 1000 and 650 °C (1830 and 1200 °F). It forms by a peritectic reaction near 1000 °C (1830 °F) from gamma-manganese and melt, and decomposes by a eutectoidal reaction at 650 °C (1200 °F), forming gamma-

Published by permission of the Director, Bureau of Mines, U. S. Department of the Interior.

A paper presented before the Thirtieth Annual Convention of the Society, held in Philadelphia, October 23 to 29, 1948. Of the authors, E. V. Potter is physicist, and R. W. Huber is physical metallurgist, Intermountain Experiment Station, Bureau of Mines, Salt Lake City, Utah. Manuscript received January 30, 1948.

manganese and epsilon. It has a body-centered cubic structure identical with that of the beta phase in the copper-zinc system.

The epsilon phase has an extensive field, existing from 46 to about 90% zinc and between 835 and 250 °C (1535 and 480 °F). It is formed by a peritectic reaction at 835 °C (1535 °F) from the beta phase and melt, and decomposes at low temperatures to form numerous phases, only two of which—beta-manganese and alpha—are found below 70% zinc. The latter are formed by the eutectoidal decomposition of epsilon at 250 °C (480 °F), the eutectoid composition being about 67.5% zinc. Epsilon has a close-packed hexagonal structure and corresponds closely to the epsilon phase in the copper-zinc system.

The alpha phase was not actually observed but has been shown by Schramm to exist below 250 °C (480 °F) above 50% zinc.

The diagram from 0 to 50% zinc determined in this investigation is entirely consistent with that determined by Schramm from 50 to 100% zinc.

Introduction

FOLLOWING the development by the Bureau of Mines of an electrolytic method for producing pure manganese, a number of investigations were undertaken to determine the properties and uses of this metal. A number of binary and ternary alloy systems involving manganese as one constituent were investigated. Among these was the copper-manganese-zinc system. In studying such ternary systems it is advantageous to know the phase diagrams of the three bounding binary systems. The copper-zinc and copper-manganese (1)[1] systems are known, but the manganese-zinc system has been studied only in the range from 0 to 50% manganese (2). To complete this system, an investigation was made in the range from 50 to 100% manganese; the results are reported in this paper.

The lack of information regarding the alloys of manganese and zinc containing over 50% manganese is undoubtedly due to the great difficulty in preparing and heat treating these alloys. Using normal fusion methods, the zinc will melt and boil below the melting point of manganese, and even the high-zinc alloys must be prepared under a cover of sodium and potassium chlorides and borax or in closed porcelain or glass vessels (2). Also, after a satisfactory alloy is obtained, zinc is readily lost during the heat treating. Therefore,

[1]The figures appearing in parentheses pertain to the references appended to this paper.

major problems in investigating this system are that of getting the manganese and zinc to interdiffuse and form a homogeneous alloy and of retaining the zinc in subsequent heat treating. Powder methods offer distinct advantages over fusion methods in satisfactorily solving these difficulties and were used in preparing the alloys for this investigation.

Preparation of Alloys

The manganese powder used in making these alloys was prepared from fresh electrolytic manganese made at the Boulder City, Nevada, station of the Bureau of Mines. This metal was broken into small pieces and milled in a 5-inch Abbe porcelain mill with fresh flint pebbles. The first charge in the mill was ground for several hours to polish the balls and was discarded. Charges of 400 to 500 grams of manganese were used and ground for about 10 minutes, the minus 200-mesh material being screened out and the larger material returned to the mill for another 10 minutes. Fresh manganese was added as needed. The zinc powder assayed 99 plus per cent zinc and was 200 mesh and finer.

These powders were mixed on a weight basis, placed in small bottles, and shaken and rolled for about one-half hour. Fifty to 70 grams of each mixture was placed in a ¼ by 6-inch die and pressed at a pressure of 25 to 30 tons psi, the green compacts being about ¼ inch square. In this condition the specimens, especially above 90% manganese, were quite friable but could be handled satisfactorily with care.

The specimens were sintered in quartz tubes filled with helium. The sintering was started at 400 °C (750 °F), the specimens being held at this temperature for 4 hours, after which the temperature was increased in steps of 100 °C and held for 1 hour at each step up to 1000 °C (1830 °F). It was hoped that the intimate contact of the many small particles of manganese and zinc and the sintering at gradually increasing temperatures would result in satisfactory interdiffusion of the metals without serious loss of zinc. It was found that the alloys above 40% zinc melted partly or completely at 1000 °C (1830 °F), so in subsequent work the maximum sintering temperature was reduced to about 800 °C (1470 °F) for these alloys. The samples were quenched when removed from the furnace.

Microscopic examinations of these alloys were, in general, unsatisfactory, due to the porosity of the specimens; but at the low

zinc contents, particles that appeared to be pure manganese often could be distinguished. To insure maximum homogeneity, the alloys up to 26% zinc were sealed in evacuated quartz tubes with molybdenum liners and reheated to 1000 °C (1830 °F) for 18 hours. Molybdenum liners were used to prevent undesirable reactions between the manganese and the quartz which would occur to an undesirable extent at this temperature and time of heat treatment. Chemical analysis of these alloys before and after sintering checked the theoretical analyses and showed no appreciable loss of zinc. In a few cases, the alloys were prepared from a master alloy containing 15% zinc. After sintering, this alloy was powdered and mixed with either pure manganese or zinc and prepared as described above. Alloys prepared in this way seemed to be no better than those prepared by the more direct and simple procedure.

Procedure

This investigation consisted of two main parts: X-ray investigations and thermal analysis investigations. X-ray methods were used to determine the phases present and to locate the phase boundaries. In some cases, the boundaries were located on the basis of phase identification only, but whenever sufficient accurate parameter data could be obtained, the variation of parameter with composition was also used to locate the phase boundaries. Thermal analysis data were used primarily for determining eutectoid temperatures.

All the X-ray work was done by the powder method. Iron radiation was used, the tube operating at about 40 kilovolts potential with 9-milliampere current. Full circular cameras with a radius of about 7 centimeters were employed, the exposures being about 1 hour. The X-ray specimens were prepared as follows: Powder samples weighing about ½ gram were placed in stainless steel capsules and sealed in evacuated containers for heat treating. Pyrex glass tubing was used below 700 °C (1290 °F) and Vicor or vitreous quartz tubing for higher temperatures. After heat treating, the tubes were removed from the furnace and quenched in a methanol-water mixture, the tubes being broken under the surface of the liquid to insure rapid quenching of the specimen. The sample was dried and screened and a portion of the minus 200-mesh particles cemented on a very fine glass rod, less than 0.25 millimeter, with diluted "Duco" cement. Compositions were checked after heat treating and the loss of zinc was negligible.

At the high temperatures (near 1000 °C), half-hour heat treatments gave very satisfactory diffraction patterns, the alpha doublets being readily resolved. At low temperatures, especially below 500 °C (930 °F), much longer times were used, 300 to 500 hours being used at 200 °C (390 °F). At the high temperatures, the heat treating time was limited primarily by the tendency for the particles to fuse together. At the low temperatures, this did not occur but some oxidation and loss of zinc occurred if the times were too long. Below 500 °C (930 °F), the reactions are quite slow and even after the 200 to 500 hours allowed for some of these alloys, the inconsistencies in the results indicated lack of complete equilibrium. This made it impossible to locate phase boundaries above 20% zinc by parameter measurements, and below 400 °C (750 °F) phase identifications are questionable.

The thermal analyses were made using a special Leeds & Northrup Micromax recording potentiometer, in which the chart drive motor was replaced by a special drive motor controlled by an indicating Micromax potentiometer. Both horizontal and vertical motions were completely reversible, and both were approximately 10 inches and corresponded to 10 or 50 millivolts input. The horizontal scale was the temperature differential between the specimen and a nickel sleeve, and the vertical scale was the temperature. The specimens used in this work were ¾-inch lengths of the sintered bars, these being swaged to approximate rounds (about 0.225 inch in diameter) to fit the nickel sleeve. A hole about ⅜ inch deep was drilled in one end to fit a thermocouple. In this work, the specimen could not be conveniently enclosed and oxidation and loss of zinc occurred. The method was therefore unsatisfactory for high-temperature work, such as locating the liquidus and solidus lines. Sluggishness of the reactions made it difficult to locate many of the other transitions. It was quite satisfactory for determining eutectoid temperatures, however, as some change in composition can be tolerated in such cases and the heat changes associated with these reactions are greater than those occurring with other types of transitions.

Results

The results of this investigation are presented in three parts: X-ray phase identification, X-ray parameter determinations, and thermal analysis determinations. For the most part the various results agree quite well. A diagram showing the composite result

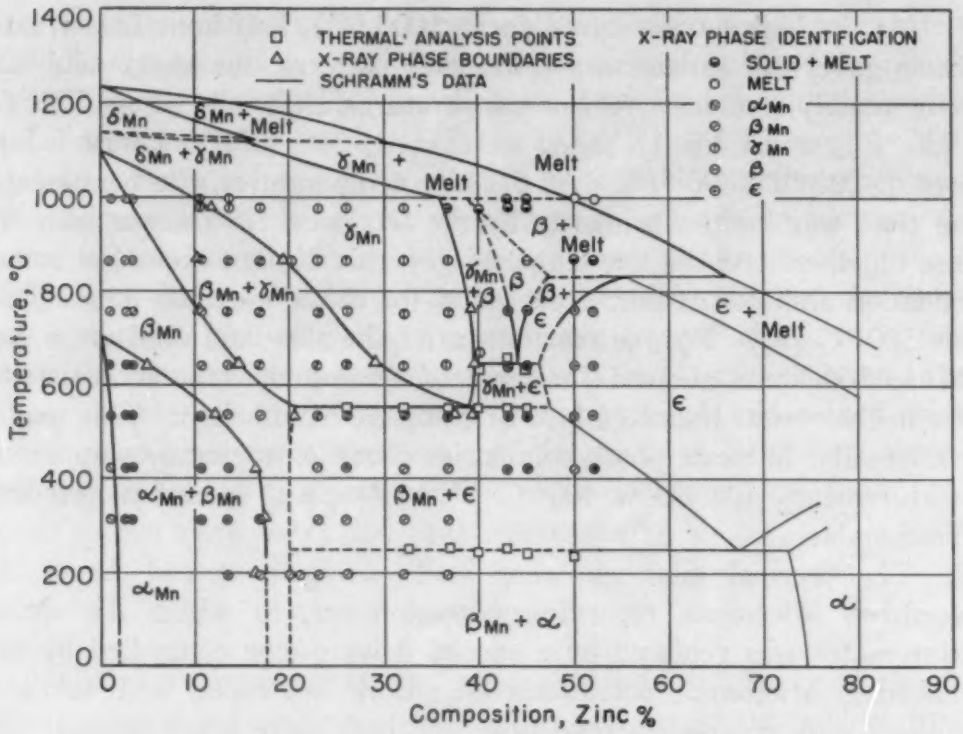


Fig. 1—Manganese-Zinc Phase Diagram.

is given in Fig. 1. The manner in which the various plotted points were obtained is indicated by the legend in the figure. The boundaries determined in this investigation are shown by the heavy solid lines as distinguished from the light solid lines showing the results of Schramm's (2) work. The uncertain boundaries are indicated by the broken lines. Because of the small number of alloys in certain fields, parameter determinations were unreliable, and these phase boundaries were determined solely on the basis of phase identification. In other cases, both X-ray methods could be used and the indicated boundary is that considered to be most probable from both sets of data. The indications agree so closely in all these cases, however, that no significant discrepancies were found. These data indicated the presence of two eutectoids, $\beta \leftrightarrows \gamma\text{-Mn} + \epsilon$ and $\gamma\text{-Mn} \leftrightarrows \beta\text{-Mn} + \epsilon$. X-ray methods are not well adapted for locating the eutectoid temperatures, however, so thermal analysis techniques were used to do this. Thermal analysis data and the X-ray indications agreed well on the temperature at which the $\beta \leftrightarrows \gamma\text{-Mn} + \epsilon$ reaction occurs. X-ray data place it above 649 °C (1200 °F) and thermal analysis data at 646 ± 9 °C. It is shown at 650 °C (1200 °F),

which is consistent with both sets of observations. Thermal analysis data place the γ-Mn $\leftrightarrows$ β-Mn + ϵ reaction at 554 $\pm$ 2 °C; X-ray data are inconclusive. The transition is therefore shown at 554 °C (1030 °F).

The transformation temperatures for pure manganese used in Fig. 1 are given in Table I. Except for the α-Mn $\leftrightarrows$ β-Mn transition, the values given are the most reliable values based on three independent methods, hydrogen solubility, heat content, and thermal analyses. These investigations are discussed in an earlier paper (3). Because of the sluggishness of the α-Mn $\leftrightarrows$ β-Mn transition, there is some uncertainty regarding proper location of this point. The temperature given in the table and used in the diagram is that used in an earlier work (1) and may be in error by 10 or 15 °C.

Table I
Transition Points in Manganese

	°C
α-Mn to β-Mn	705
β-Mn to γ-Mn	1100
γ-Mn to δ-Mn	1138
δ-Mn to melt	1245

X-Ray Phase Identification

The alloys used in these investigations ranged from 1 to 52% zinc and were heat treated at temperatures from 200 to 1000 °C (390 to 1830 °F). The phases found in them, based on X-ray diffraction patterns, are tabulated in Table II. Five of the phases shown in the phase diagram (Fig. 1)—alpha-manganese, beta-manganese, gamma-manganese, beta, and epsilon—were definitely identified in these alloys; two of them—delta-manganese and alpha—were not actually found but other evidence that will be cited later shows that they exist.

The alpha-manganese phase is found in a very small field. It is stable below 705 °C (1300 °F) and up to between 1 and 2% zinc. It is a body-centered cube, having 58 atoms in a unit cell, and in pure manganese its parameter is 8.894 Å.

The beta-manganese phase extends from 0 to 20% zinc. In pure manganese it is stable from 705 to 1100 °C (1300 to 2010 °F), these temperatures decreasing as zinc is added, the upper temperature decreasing to 554 °C (1030 °F) at 20% zinc. It has a cubic struc-

Table II
X-Ray Phase Identification

Composition, Per Cent Zn	Temperature, °C								
	1000	982	871	760	649	538	427	316	200
1.09	β-Mn		β-Mn	β-Mn	α-Mn + β-Mn	α-Mn + β-Mn	α-Mn	α-Mn	
2.76	β-Mn		β-Mn	β-Mn	α-Mn + β-Mn	α-Mn + β-Mn	α-Mn + β-Mn	α-Mn + ?	
3.37	β-Mn		β-Mn	β-Mn	α-Mn + β-Mn	α-Mn + β-Mn	α-Mn + β-Mn	α-Mn + β-Mn	
10.6	γ-Mn + β-Mn	γ-Mn + β-Mn	β-Mn + γ-Mn	β-Mn	β-Mn	β-Mn + α-Mn	α-Mn + β-Mn	α-Mn + β-Mn	α-Mn + β-Mn
13.5	γ-Mn	γ-Mn	γ-Mn + ?	β-Mn + γ-Mn	β-Mn	β-Mn	β-Mn + α-Mn	α-Mn + β-Mn	
16.9		γ-Mn	α-Mn + β-Mn	γ-Mn + β-Mn	β-Mn + γ-Mn	β-Mn		β-Mn + α-Mn	β-Mn
20			γ-Mn						β-Mn
21									β-Mn
23		γ-Mn	γ-Mn	γ-Mn + β-Mn	γ-Mn + β-Mn	β-Mn + γ-Mn	β-Mn + ?	β-Mn + ?	β-Mn
26		γ-Mn	γ-Mn	γ-Mn	γ-Mn + β-Mn	β-Mn + γ-Mn	β-Mn + ε	β-Mn + ?	β-Mn
32		γ-Mn	γ-Mn	γ-Mn	γ-Mn	γ-Mn + β-Mn	β-Mn	β-Mn	β-Mn
36.7		γ-Mn + β	γ-Mn	γ-Mn	γ-Mn*	γ-Mn + β-Mn + ε	β-Mn	β-Mn	β-Mn
40		solid + melt			γ-Mn*				
43	solid + melt	solid + melt		γ-Mn + β	γ-Mn + ε	γ-Mn + ε	β-Mn + ε		
45	solid + melt	solid + melt	β	β + ε	γ-Mn + ε	γ-Mn + ε	ε + β-Mn		
50	melt		solid + melt	ε	ε	ε	β-Mn + ?		
52	melt		solid + melt	ε	ε	ε	ε + β-Mn		

*677 °C.

ture with 20 atoms to the unit cell and in pure manganese its parameter is 6.300 Å.

The gamma-manganese phase extends from 0 to 40% zinc. It is stable only at the higher temperatures, undergoing a eutectoid transformation at about 554 °C (1030 °F), forming beta-manganese and epsilon. The composition of the eutectoid is about 39% zinc. At 100% manganese, gamma-manganese has a tetragonal structure, the parameter being 3.774 Å and the axial ratio 0.938. As zinc is added, the structure gradually changes, becoming cubic near 20% zinc. This will be discussed in more detail later.

The delta-manganese phase is found between 1138 and 1245 °C (2080 and 2275 °F) in pure manganese. It was not found in any of the alloys in this investigation, and has not been observed directly by either X-ray or microscopic means. Apparently it is very unstable at room temperature, as it has never been successfully retained by quenching either in pure manganese or in an alloy. Neither its structure nor the nature of its transition to gamma-manganese is known but its existence has been shown by other methods (1), (3); for the sake of completeness, in Fig. 1 it is shown to decompose eutectoidally, forming gamma-manganese and melt somewhat below 1138 °C (2080 °F).

The beta phase is found between about 39 and 47% zinc and only at high temperatures. It is formed by a peritectic reaction between gamma-manganese and melt occurring near 1000 °C (1830 °F). It decomposes at about 650 °C (1200 °F), forming gamma-manganese and epsilon. It is a simple body-centered cube, with 2 atoms to the unit cell. A 45% zinc alloy quenched from 871 °C (1600 °F) has a parameter of 3.054 Å. This phase has the same structure as that of the beta-brass in the copper-zinc system. The latter has a somewhat smaller parameter, however, varying from 2.94 to 2.95 between 38 and 55% zinc.

The epsilon phase is found above about 46% zinc and extends, according to Schramm (2), up to 90.5% zinc. It is stable only at the higher temperatures. It is formed by a peritectic reaction between beta and melt at 835 °C (1535 °F) and at lower temperatures decomposes in various ways to form a number of phases, beta-manganese and alpha being the only two occurring in the composition range shown in Fig. 1. Epsilon has a close-packed hexagonal structure, with 2 atoms to the unit cell. At 50% zinc, it has a parameter of 2.726 Å and an axial ratio of 1.631.

The alpha phase was not actually observed in any of the alloys used in this investigation. It is formed by the eutectoidal decomposition of epsilon forming beta-manganese and alpha, which, according to Schramm (2), occurs near 250 °C (480 °F). This phase was observed by him in alloys from 23 to 50% manganese, but only after very prolonged slow cooling to room temperature, requiring many weeks. Alpha has a simple face-centered cubic structure with 4 atoms to the unit cell. In the 23% manganese alloy it has a parameter of 3.849 Å.

X-Ray Parameter Determinations

All the alloys listed in Table II did not give good enough diffraction patterns to provide accurate parameter data, even though they were satisfactory for phase identification. The parameters of the various phases were determined whenever possible, however, and these data were used to obtain normal parameter curves and locate phase boundaries.

Alpha-Manganese Phase—The parameters of the alpha-manganese phase are shown in Table III, any other phases also present being indicated. Since only two of the alloys were single-phase, a normal parameter curve for the alpha-manganese phase could not be obtained, and the alpha-manganese, alpha-manganese plus beta-manganese boundary could not be located in this way. The parameter of the alpha-manganese phase in the two-phase alloys is quite uniform and averages about 8.913 Å as compared to 8.894 Å for normal alpha-manganese. The enlargement due to the zinc in solution with the alpha-manganese is about 0.2% and is practically the same as that produced by the copper in the copper-manganese system (1). In each case, their solubility in alpha-manganese is about 2%.

Beta-Manganese Phase—The parameters of the beta-manganese

Table III
Parameters of the Alpha-Manganese Phase

Composition, Per Cent Zn	Temperature, °C				
	649	538	427	316	200*
1.09	β-Mn + 8.914	β-Mn + 8.898	8.897	8.902	
2.76	β-Mn + 8.912	β-Mn + 8.912	β-Mn + 8.913	α-Mn + β-Mn?	
3.37	β-Mn + 8.914	β-Mn + 8.912	β-Mn + 8.913	α-Mn + β-Mn	
10.6	β-Mn	β-Mn + α-Mn	α-Mn + β-Mn	α-Mn + β-Mn	
13.5		β-Mn	β-Mn + α-Mn	α-Mn + β-Mn	α-Mn + β-Mn
16.9				β-Mn + α-Mn	β-Mn

*Equilibrium conditions questionable.

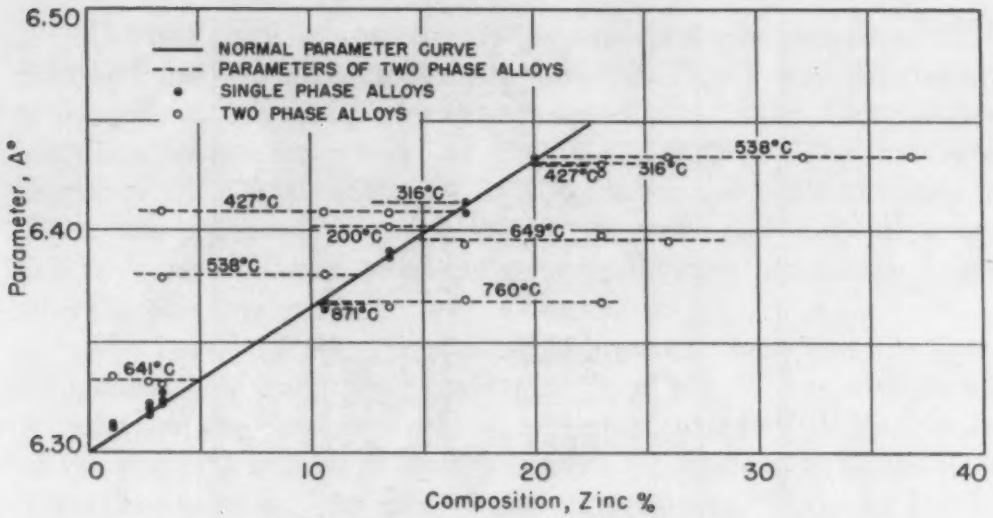


Fig. 2—Parameters of Beta-Manganese Phase.

phase are shown in Table IV, any other phases also present being indicated. In this case, at practically each composition, several single-phase alloys were found. The parameters of these alloys were used to determine the normal parameter curve for the beta-manganese phase. This curve is the solid line in Fig. 2. It passes through 6.300 Å at 0% zinc, this being the accepted parameter value for pure beta-manganese.

The broken horizontal lines represent the parameters of the beta-manganese phase in the two-phase alloys at the designated temperatures. These are necessarily horizontal because the parameters of the phases in the two-phase fields are independent of composition and vary only with temperature. The lines to the left of the normal parameter curve are for the beta-manganese phase in the alpha-manganese plus beta-manganese field. The lines to the right of the normal parameter curve, for temperatures of 871, 760, 649 and 538 °C (1600, 1400, 1200 and 1000 °F), represent the beta-manganese phase in the beta-manganese plus gamma-manganese field; the 427 and 316 °C (800 and 600 °F) lines are for the beta-manganese phase in the beta-manganese plus epsilon field. These lines represent the average or most probable parameter value, determined from the data for the two-phase alloys listed in Table IV; the actual values used are given in Table V. The intersection of these lines and the normal parameter curve determine the composition of the beta-manganese phase at the boundary between the single-phase beta-manganese field and the two-phase fields at the various temperatures. These composition values are listed in Table V and plotted in Fig. 1.

Table IV
Parameters of Beta-Manganese Phase

Composition, Per Cent Zn	Temperature, °C								
	1000	982	871	760	649	538	427*	316*	200†
1.09	6.312		6.313	6.312	α-Mn + 6.335	α-Mn + β-Mn	α-Mn	α-Mn	
2.76	6.317		6.322	6.320	α-Mn + 6.332	α-Mn + β-Mn	α-Mn + β-Mn	α-Mn + ?	
3.37	6.327		6.323	6.322	α-Mn + 6.331	α-Mn + 6.379	α-Mn + 6.409	α-Mn + β-Mn	
10.6	γ-Mn + β-Mn	γ-Mn + β-Mn	γ-Mn + 6.367	6.365	6.368	α-Mn + 6.381	α-Mn + 6.409	α-Mn + β-Mn	
13.5	γ-Mn	γ-Mn	γ-Mn + ?	γ-Mn + 6.366	6.388	6.391	α-Mn + 6.408	α-Mn + β-Mn	α-Mn + 6.402
16.9			γ-Mn + β-Mn	γ-Mn + 6.369	γ-Mn + 6.394	6.413		α-Mn + 6.413	6.408
20									6.433
21									6.430
23			γ-Mn	γ-Mn + 6.368	γ-Mn + 6.398	2 phase 6.430	2 phase 6.430	2 phase 6.431	6.434
26				γ-Mn	γ-Mn + 6.397	γ-Mn + 6.434	ε + 6.450	2 phase 6.442	6.443
32					γ-Mn	γ-Mn + 6.434	6.452	6.461	6.450
36.7						γ-Mn + ε + 6.434	6.459	6.461	6.468
43						γ-Mn + ε	ε + 6.462		
45							ε + 6.462		
50							2 phase 6.462		
52							ε + β-Mn		

*Equilibrium conditions questionable above 20% zinc.
†Equilibrium conditions questionable.

The boundary between the alpha-manganese plus beta-manganese field and the beta-manganese field shown in Fig. 1 was determined in this way and agrees perfectly with the results of the X-ray phase-identification studies except at 200 °C (390 °F). The indicated boundary at 200 °C (390 °F) is considered unreliable, as only a single two-phase alloy was available for parameter determinations and it is very difficult to obtain true equilibrium conditions in the alloys at this low temperature.

The boundary between the beta-manganese field and the beta-manganese plus gamma-manganese field in Fig. 1 was also determined from the data in Table V. The agreement with the results of the phase-identification studies is quite satisfactory although some discrepancies exist. At each of the temperatures, 1000 and 760 °C (1830 and 1400 °F), one of the alloys identified as single-phase beta-manganese is included in the two-phase beta-manganese plus gamma-manganese field. In each case it lies very close to the boundary, however, and would contain only a small amount of gamma-manganese which might not be detectable in the X-ray diffraction patterns. At 871 °C (1600 °F), the boundary indicated in Table V is very obviously in error; it was based on a single parameter determination and was so obviously in error that it was completely neglected in locating the boundary shown in Fig. 1. The lower end of this boundary has been modified slightly to meet the eutectoid line located at 554 °C (1030 °F) by thermal analysis studies. X-ray data on most of the alloys from 20 to 45% zinc at 538 °C (1000 °F) would place the eutectoid temperature below 538 °C

Table V
Beta-Manganese Phase Boundaries

Temperature, °C	Parameter, A	Composition, Per Cent Zn
	α-Mn + β-Mn $\leftrightarrows$ β-Mn	
649	6.333	5
538	6.380	12.2
427	6.409	16.5
316	6.413	17.1
200	6.402*	15.5*
	β-Mn $\leftrightarrows$ β-Mn + γ-Mn	
871	6.367*	10.2*
760	6.368	10.4
649	6.396	14.6
538	6.434	20.4
	β-Mn $\leftrightarrows$ β-Mn + ϵ	
427	6.430*	19.7*
316	6.431*	19.9*

*Not reliable, equilibrium conditions questionable.

(1000 °F). One alloy, however, shows three phases—gamma-manganese, beta-manganese, and epsilon. The presence of the epsilon phase would indicate that the eutectoid temperature is above 538 °C (1000 °F) and the alloy has not had time to reach equilibrium. Because of this uncertainty in locating the eutectoid temperature by X-ray means, it is shown in Fig. 1 at the temperature indicated by the thermal analysis data, some revision of the X-ray boundaries in this part of the diagram being required.

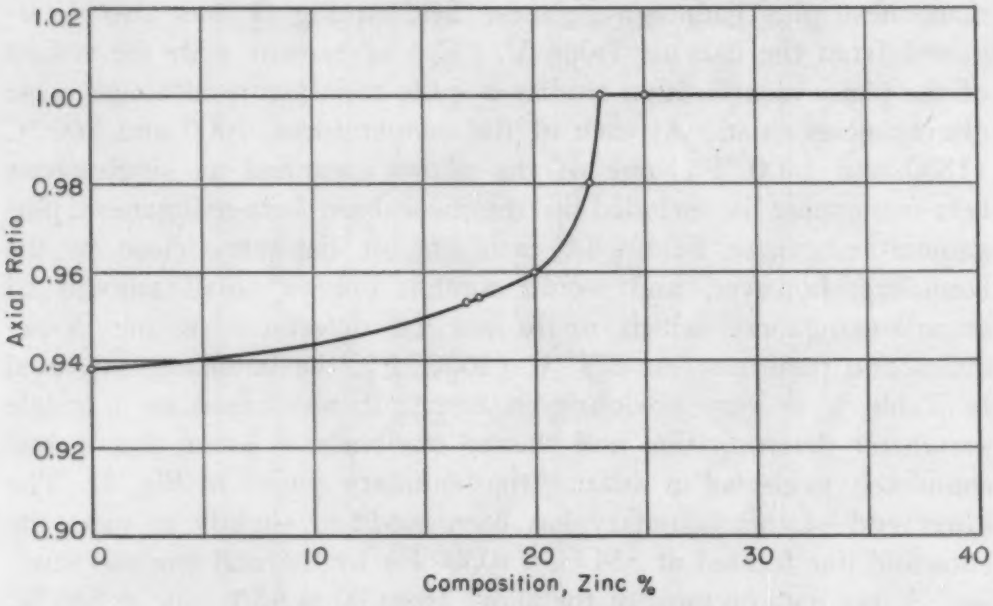


Fig. 3—Axial Ratio of Gamma-Manganese Phase.

The boundary between the beta-manganese field and the beta-manganese plus epsilon field is uncertain. The beta-manganese parameter in the alloys above 20% zinc varies with composition, even though two phases are present. This indicates lack of equilibrium, and the boundary indicated in Fig. 1 is thought to be the most probable one on the basis of the data available.

Gamma-Manganese Phase—The gamma-manganese phase is more complicated than the beta-manganese phase in that it changes from a face-centered tetragonal structure at 100% manganese to a face-centered cubic structure at about 23% zinc. The parameters and axial ratios of this phase for various alloys are given in Table VI and the variation of axial ratio with composition is shown in Fig. 3. This behavior is exactly analogous to that of the gamma phase in the copper-manganese system (1), and since two variables are in-

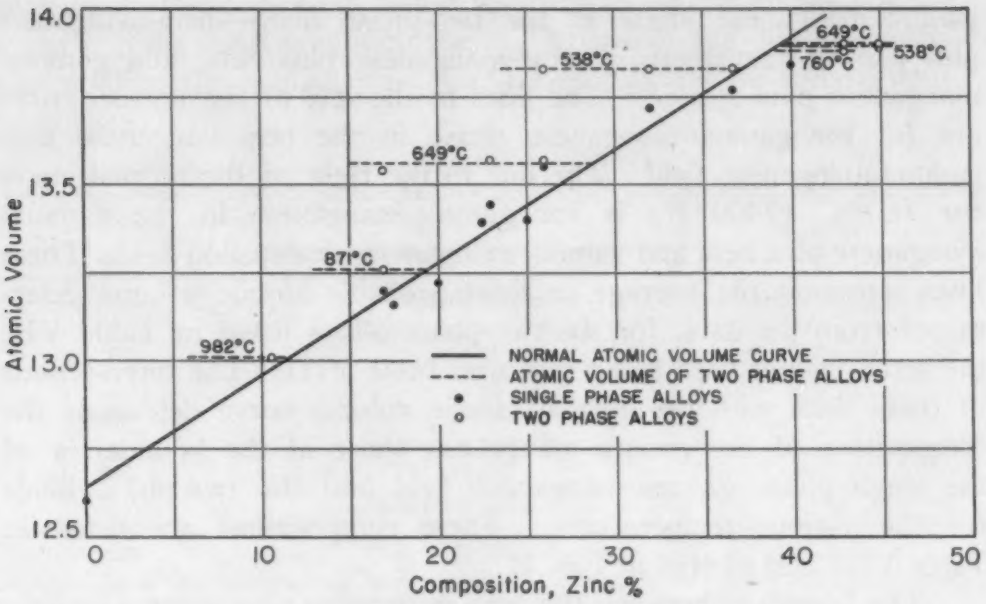


Fig. 4—Atomic Volumes of Gamma-Manganese Phase.

volved, it is more convenient to combine them and deal with atomic volumes rather than axial lengths in determining the phase boundaries.

In Table VII, the atomic volume of the gamma-manganese phase is given for all the alloys where reliable values were obtainable; other phases associated with the gamma-manganese phase are also indicated. Average values of atomic volume for the single-phase alloys were obtained from data in Table VII and plotted against composition in Fig. 4. Since these points were somewhat scattered but showed no definite tendency to curve, these values of atomic volume along with the value of 12.605 for pure gamma-manganese were treated by least square methods to obtain the best-fitting straight line. This normal atomic volume is shown by the solid line in Fig. 4. The broken horizontal lines represent the atomic volumes of the

Table VI
Parameters and Axial Ratios of Gamma-Manganese Phase

Composition, Per Cent Zn	Parameter, a, Å	Axial ratio c:a
0	3.774	0.938
16.9	3.814	0.953
17.5	3.807	0.954
20.0	3.805	0.960
22.5	3.795	0.98
23	3.774	1.00
25	3.770	1.00

gamma-manganese phase in the two-phase fields—beta-manganese plus gamma-manganese, gamma-manganese plus beta, and gamma-manganese plus epsilon. The lines to the left of the normal curve are for the gamma-manganese phase in the beta-manganese plus gamma-manganese field. The line to the right of the normal curve for 760 °C (1400 °F) is for gamma-manganese in the gamma-manganese plus beta and gamma-manganese plus epsilon fields. These lines represent the average or most probable atomic volume determined from the data, for the two-phase alloys listed in Table VII, the actual values used being given in Table VIII. The intersections of these lines with the normal atomic volume curve determine the composition of the gamma-manganese phase at the boundaries of the single-phase gamma-manganese field and the two-phase fields for the various temperatures. These compositions are listed in Table VIII and plotted in Fig. 1.

The boundary between the beta-manganese plus gamma-manganese field and the gamma-manganese field in Fig. 1 is located from the data in Table VIII. Except at 1000 °C (1830 °F), it agrees perfectly with the phase-identification results. At 1000 °C (1830 °F), one of the alloys identified as gamma-manganese plus beta-manganese is slightly in the gamma-manganese field. This discrepancy is of no consequence, however, as only a slight shift in temperature or composition would place this alloy in the two-phase field.

Table VII
Atomic Volume of the Gamma-Manganese Phase

Composition, Per Cent Zn	Temperature, °C					
	1000	982	871	760	649	538
10.6	γ-Mn + β-Mn	β-Mn + 13.01	γ-Mn + β-Mn	β-Mn		
13.5	γ-Mn	13.11	γ-Mn + β-Mn?	β-Mn + γ-Mn	β-Mn	
16.9		13.20	β-Mn + 13.26	γ-Mn + β-Mn	β-Mn + 13.54	β-Mn
17.5	13.16					
20	13.22					
22.5	13.39					
23		13.44	13.45	γ-Mn + β-Mn	β-Mn + 13.57	γ-Mn + β-Mn
25	13.40					
26		13.60	13.52	13.54	β-Mn + 13.57	β-Mn + 13.83
32		13.79	13.72	13.71	13.69	β-Mn + 13.83
36.7		γ-Mn + β	13.78	13.75	13.77	β-Mn + 13.83
40					13.84*	
43				β + 13.88	ε + 13.90	ε + 13.90
45				β + ε	ε + 13.90	ε + 13.89

*677 °C.

The point at 760 °C (1400 °F) on the boundary between the gamma-manganese field and the gamma-manganese plus beta field

is also quite satisfactory. It is not sufficient to determine the boundary but is quite consistent with the indications of the phase-identification studies, the boundary in Fig. 1 being located to satisfy both sets of data.

Table VIII
Gamma-Manganese Phase Boundaries

Temperature, °C	Atomic Volume	Composition, Per Cent Zn
	β-Mn + γ-Mn $\rightleftarrows$ γ-Mn	
982	13.01	11.6
871	13.26	19.5
649	13.56	28.9
538	13.83	37.3
	γ-Mn $\rightleftarrows$ γ-Mn + β	
760	13.88	38.8
	γ-Mn $\rightleftarrows$ γ-Mn + ϵ	
649	13.90	39.5
538	13.895	39.3

The boundary between the gamma-manganese field and the gamma-manganese plus epsilon field located by atomic volumes also agrees satisfactorily with the results of the phase-identification studies. In this region, some revision of the X-ray results is required to make the boundaries conform to the eutectoid line at about 554 °C (1030 °F). This was discussed earlier in connection with the beta-manganese phase boundaries.

Beta Phase—Since only one single-phase beta alloy was found and the field is so limited in extent, the parameter data are insufficient for phase-boundary determinations. The parameter of this one alloy containing 45% zinc was 3.054 Å, the same value as was obtained by Schramm (2) for a 44% zinc alloy. Considering the difficulties involved in obtaining accurate analyses, these results agree very well. The boundaries of the beta-phase field were of necessity located solely on the results of the phase-identification studies and Schramm's work. The exact temperature of the peritectic reaction shown at 1000 °C (1830 °F) in Fig. 1 is not known. It must be above 982 °C (1800 °F), since at this temperature a 36.7% zinc alloy contains both gamma-manganese and beta. It cannot be much over 1000 °C (1830 °F), however, as it would be difficult to obtain phase boundaries consistent with the observed phases and extend the beta field to much higher temperatures.

The extent of the peritectic reaction line located at 835 °C (1535 °F) by Schramm (2) also is not known definitely. He termi-

nated it at about 51% zinc, but it would be very improbable that the boundary between the beta field and the beta plus epsilon field should rise sharply above the 650 °C (1200 °F) eutectoid line, include the 45% zinc alloy at 760 °C (1400 °F) in the beta plus epsilon field, and then bend sharply to the right, meeting the 835 °C (1535 °F) peritectic line at 51% zinc. For this reason the 835 °C (1535 °F) peritectic line has been extended to about 47.5% zinc, making the boundary between beta and beta plus epsilon look more reasonable and still placing the 45% zinc alloy at 871 °C (1600 °F) in the beta field. The composition of the beta eutectoid is not definitely known, but must be close to 44% zinc.

Epsilon Phase—Parameter values could be readily obtained on the epsilon phase. In the epsilon field, the parameter decreased from 2.757 Å at 84% zinc to 2.726 Å at 50% zinc, while the axial ratio increased from 1.609 at 84% zinc to 1.631 at 50% zinc. In the two-phase alloys, however, satisfactory equilibrium conditions were never achieved. Phase boundaries located on the basis of the epsilon parameter in three alloys were inconsistent with phase-identification results and Schramm's results (2). For this reason the exact extent of the eutectoid lines at 650 and 554 °C (1200 and 1030 °F) are not definitely known and the boundaries between the two-phase fields (beta plus epsilon, gamma-manganese plus epsilon, and beta-manganese plus epsilon) and the single-phase epsilon field cannot be located definitely. Our phase-identification results and Schramm's data locate them within close limits, however, placing the right end of the 650 °C (1200 °F) eutectoid line between 45 and 48% zinc and the end of the 550 °C (1020 °F) eutectoid line between 45 and 49% zinc.

Thermal Analysis Determinations

The results of the thermal analysis determinations are shown in Table IX. Variations in zinc content and oxidation unavoidable with the apparatus available made it difficult to locate phase boundaries other than eutectoids with satisfactory certainty, so only the data pertaining to the eutectoid reactions are shown. These values are also shown in Fig. 1.

Three of the alloys showed breaks in the temperature differential curves near 650 °C (1200 °F) where the phase-identification data indicate a eutectoid reaction should occur, the beta phase decomposing on cooling to form the gamma-manganese plus epsilon. The

X-ray data indicate the eutectoid temperature to be between 649 and 760 °C (1200 and 1400 °F), while the average temperature from the thermal analysis data (Table IX) is 646 ± 9 °C. This agreement is satisfactory, the eutectoid temperature shown in Fig. 1 being placed at 650 °C (1200 °F).

Table IX
Thermal Analysis Data

Composition, Per Cent Zn	Eutectoid Temperatures		
	*$\epsilon \leftrightarrows \beta$-Mn + a	γ-Mn $\leftrightarrows \beta$-Mn + ϵ	$\beta \leftrightarrows \gamma$-Mn + ϵ
26	...	552	...
32	255	555	...
36.5	259	552	...
40	247	558	638
43	258	555	662
45	243	554	638
50	235	...	...
Average values	249 ± 6	554 ± 2	646 ± 9

*Indications unreliable. See text regarding this reaction.

Six of the alloys showed breaks in the temperature differential curves near 550 °C (1020 °F) where the phase-identification data indicate another eutectoid reaction to occur, gamma-manganese decomposing to form beta-manganese plus epsilon. In this case, the thermal analysis data place the eutectoid temperature at 554 ± 2 °C, while the X-ray phase identification data show the gamma-manganese plus beta-manganese and the gamma-manganese plus epsilon fields to extend to 538 °C (1000 °F). In one alloy, however, three phases—beta-manganese, gamma-manganese, and epsilon—are found. Since these alloys were originally quenched from high temperatures and reheated, it is very likely that they have not had time to reach equilibrium conditions and have retained their high-temperature structures, the alloy at 36.7% zinc showing three phases being more advanced, its original single-phase, gamma-manganese structure, being partly broken down to form beta-manganese and epsilon. This inconsistency in the X-ray data and the close agreement in the temperature indicated by thermal analysis (Table IX) indicate that the thermal analysis data are the most reliable and the eutectoid is shown in Fig. 1 at 554 °C (1030 °F) in agreement with these results.

Six of the alloys also showed breaks in the temperature differential curve near 250 °C (480 °F) where Schramm (2) placed the eutectoid reaction $\epsilon \leftrightarrows \beta$-Mn + a. These breaks were observed only in alloys originally quenched from high temperatures, however, and it is extremely doubtful if the transition indicated is that between

beta-manganese plus alpha and beta-manganese plus epsilon. More likely, it is due to some higher temperature phases changing to beta-manganese plus epsilon, in which case the average temperature of 249 ± 6 °C (Table IX) has no connection with the eutectoid reaction found by Schramm (2) and the close agreement in the two temperatures is purely accidental and without significance. The observed points are shown in Fig. 1, however, but the eutectoid temperature line is shown dotted to indicate the uncertainty of its proper location.

Summary and Conclusions

The phase diagram of the manganese-zinc alloy system from 0 to 50% zinc was determined by X-ray and thermal analysis methods using alloys prepared by powder methods. The following five phases were observed:

Alpha-Manganese—This is a manganese solid solution existing below 705 °C (1300 °F). It is homogeneous up to about 2% zinc and has a body-centered cubic structure with 58 atoms to the unit cell. Its parameter is 8.894 Å for pure manganese and increases to 8.913 Å with 2% zinc.

Beta-Manganese—This phase is a manganese solid solution existing between 705 and 1100 °C (1300 and 2010 °F) in pure manganese and is homogeneous up to about 20% zinc; the temperature limits decrease as zinc is added, the maximum temperature being 554 °C (1030 °F) at 20% zinc. It has a cubic structure, the parameter increasing from 6.300 Å for pure manganese to 6.433 Å at 20% zinc.

Gamma-Manganese—This phase is a manganese solid solution. In pure manganese it exists between 1100 and 1138 °C (2010 and 2080 °F) and is homogeneous up to about 40% zinc. It decomposes eutectoidally at 554 °C (1030 °F), forming beta-manganese and epsilon. The eutectoid composition is about 39% zinc. It has a face-centered structure, being tetragonal up to 23% zinc and cubic from there to 40% zinc. It has a parameter of 3.774 Å and an axial ratio of 0.938 in pure manganese, the atomic volume being 12.60, increasing to 13.9 at 40% zinc.

Beta—The beta phase exists from about 38 to 47% zinc. The exact limits cannot be determined readily but all the experimental evidence indicates that its field is very small. It forms by a peritectic reaction from gamma-manganese, melts at about 1000 °C (1830 °F),

and decomposes by a eutectoid reaction, forming gamma-manganese plus epsilon at about 650 °C (1200 °F). The peritectoid composition is about 36% zinc and the eutectoid composition about 44% zinc. It has a body-centered cubic structure with 2 atoms to the unit cell and a parameter of about 3.054 Å. It is analogous to the beta phase in the copper-zinc system.

Epsilon—The epsilon phase is homogeneous from about 46 to 90% zinc (see Schramm). It forms by a peritectic reaction from beta plus melt at 835 °C (1535 °F), decomposing in various ways to form many phases at low temperatures, the only reaction occurring in the composition range shown in Fig. 1 being the eutectoidal decomposition at about 250 °C (480 °F), below which beta-manganese and alpha are formed. The peritectoid composition is about 55% zinc and the eutectoid composition about 67.5% zinc. It has a close-packed hexagonal structure with 2 atoms to the unit cell, the parameter decreasing from 2.757 Å at 84% zinc to 2.726 Å at 50% zinc while the axial ratio increases from 1.609 at 84% zinc to 1.631 at 50% zinc.

Two other phases not actually observed are indicated by other data and the results of other investigators. They are:

Delta-Manganese—This phase is a manganese solid solution, existing between 1138 and 1245 °C (2080 and 2270 °F) in pure manganese. Its structure is unknown.

Alpha—This phase is formed by the decomposition of epsilon at 250 °C (480 °F), forming a beta-manganese and alpha. This reaction was shown by an earlier investigation by Schramm (2) on alloys above 50% zinc. This phase has a simple face-centered cubic structure with 4 atoms to the unit cell and its parameter is about 3.849 Å.

Four eutectoid reactions and two peritectoid reactions are indicated. They are:

$$\beta \leftrightarrows \gamma\text{-Mn} + \epsilon \text{ at } 650\ ^\circ\text{C}.$$

This was located by X-ray and thermal analysis methods.

$$\gamma\text{-Mn} \leftrightarrows \beta\text{-Mn} + \epsilon \text{ at } 554\ ^\circ\text{C}.$$

This was indicated by X-ray data and located by thermal analysis methods.

$$\epsilon \leftrightarrows \beta\text{-Mn} + \alpha$$

This is based on an earlier investigation by Schramm (2).

$$\delta\text{-Mn} \leftrightarrows \gamma\text{-Mn} + \text{melt}$$

The nature of this reaction and its temperature are unknown. It is shown as a eutectoid reaction, delta-manganese decomposing to form gamma-manganese plus melt at a temperature below 1138 °C (2080 ° F), only to complete the phase diagram, dotted lines (Fig. 1) being used to indicate the uncertainty.

$$\beta \leftrightarrows \gamma\text{-Mn} + \text{melt}$$

The temperature of this reaction is not definitely known. It must be above 982 °C (1800 °F) and cannot be much over 1000 °C (1830 °F). It is indicated at 1000 °C (1830 °F).

$$\epsilon \leftrightarrows \beta + \text{melt at } 835\ ^\circ\text{C}.$$

This was determined by investigations of Schramm (2) on manganese-zinc alloys containing over 50% zinc.

The results of this investigation up to 50% zinc are in complete accord with Schramm's results (shown by the light lines in Fig. 1) above 50% zinc and complete the data on the manganese-zinc phase diagram.

References

1. R. S. Dean, J. R. Long, T. R. Graham, E. V. Potter and E. T. Hayes, "The Copper-Manganese Equilibrium System," TRANSACTIONS, American Society for Metals, Vol. 34, 1945 p. 443.
2. J. Schramm, "The System Manganese-Zinc with 0 to 50% Manganese," *Z. Metallk.*, Vol. 32, 1940, p. 399-407.
3. E. V. Potter and H. C. Lukens, "Solubility of Hydrogen in Electrolytic Manganese and Transition Points in Electrolytic Manganese," *Metals Technology*, Vol. 13, No. 9, September 1946.

DISCUSSION

Written Discussion: By W. M. Baldwin, Jr., research professor, Department of Metallurgical Engineering, Case Institute of Technology, Cleveland.

There is a point in connection with Fig. 1 which I would appreciate having clarified. In the legend in the upper right-hand corner of this diagram, it is implied that X-ray determinations of the liquid phase, and liquid plus solid regions, were made. Although it is not stated explicitly, it would seem from the description in the second paragraph under "Procedure" that the X-ray determinations were made at room temperature. I have never heard of any X-ray technique, carried on at room temperature, by which a positive identification of these two regions could

be made. Were these two regions identified by specific X-ray technique, or were they identified in the course of preparation of a specimen for general X-ray investigation? This is a minor matter and certainly does not detract from the excellent value of the paper as a whole.

Authors' Reply

The authors thank Dr. Baldwin for his comments concerning this paper.

The legend referred to is misleading and the symbols for the solid + melt and melt fields should have been listed separately in the diagram. These two regions were identified by direct observation of the sintered powder compacts. In the text under preparation of alloys, brief mention is made of the alloys above 40% zinc melting partly or completely at 1000 °C (1830 °F). Some partial melting was also observed at 982 and 871 °C (1800 and 1600 °F).

THE ISOTHERMAL DECOMPOSITION OF MARTENSITE AND RETAINED AUSTENITE

By B. L. Averbach and Morris Cohen

Abstract

The rates of isothermal martensite and retained austenite decomposition have been determined by means of X-ray and precision length measurements. During the first stage of tempering, martensite contracts because of a rejection of carbon until it reaches pseudo-equilibrium with a transition precipitate. This martensite decomposition proceeds according to a modified first-order equation. At the end of the first stage there is still considerable carbon dissolved in the martensite lattice.

Retained austenite also decomposes isothermally at relatively low aging temperatures. It has been shown that the austenite-martensite reaction on hardening does not stop sharply when cooling stops and as much as 5% of retained austenite may transform isothermally into martensite at room temperature. The isothermal austenite decomposition proceeds rapidly during the first 1.5 hours after the quench, but it continues at a diminishing rate for several months. The rate of this reaction is not affected by tempering, although if the tempering temperature and/or time are increased sufficiently the austenite decomposes into bainite with a heat of activation of about 38,000 cal/mol.

THE tempering of high carbon martensitic steel has been studied extensively by means of dilatometric, specific volume, metallographic, magnetic, X-ray, hardness, and electrical resistance methods (1), (2), (3), (4).[1] As a result of these investigations, the tempering process for plain carbon and low alloy tool steels may be summarized as follows:

[1]The figures appearing in parentheses pertain to the references appended to this paper.

This paper is taken from a thesis submitted by B. L. Averbach in September 1947 in partial fulfillment for the degree of Doctor of Science in Metallurgy at the Massachusetts Institute of Technology.

A paper presented before the Thirtieth Annual Convention of the Society, held in Philadelphia, October 23 to 29, 1948. Of the authors, B. L. Averbach is assistant professor, and Morris Cohen is professor of physical metallurgy, Massachusetts Institute of Technology, Cambridge, Mass. Manuscript received April 15, 1948.

1. Immediately after quenching, the hardened steel consists of untempered martensite, retained austenite and undissolved carbides. This presupposes, of course, that decomposition products such as pearlite and bainite are not formed during quenching.
2. Untempered martensite may be considered a supersaturated solution of carbon in alpha iron, with the interstitial carbon atoms located preferentially in such a fashion that the resulting lattice is measurably tetragonal. If the latter structure is heated at temperatures less than approximately 400 °F (205 °C), a carbon-rich transition product (not cementite) is precipitated, and this process has been called the first stage of tempering. During the process of carbon rejection, the martensite lattice contracts in volume and also becomes less tetragonal.
3. At temperatures between about 400 to 600 °F (205 to 315 °C), the retained austenite is decomposed into a structure resembling bainite, and this transformation, which is the second stage of tempering, causes an increase in volume.
4. As the temperature is raised beyond 400 °F, the transition precipitate is converted to cementite and results in the third stage of tempering. It is marked by a considerable decrease in volume, and overlaps the austenite decomposition reaction.

The kinetics of the martensite decomposition, however, are not easily studied by the above methods. Changes in volume, in length, or in other macro-properties, which accompany the various steps in the martensite decomposition are usually too small to be clearly resolved by these techniques, and additional complications arise because of the overlapping effects caused by the presence of retained austenite. In principle, the X-ray method can isolate the martensite phase and is, therefore, unaffected by what happens to the austenite; but lattice determinations lack sufficient precision to establish the kinetics of the reaction because of the broadness of the martensite diffraction lines from a polycrystalline sample. Kurdjumov and Lyssak (5) have improved the precision of this technique greatly by using single crystals of martensite, and thus were able to show that the martensite tetragonality persists on tempering up to 570 °F (300 °C). The lingering tetragonality indicates that even after the first stage of tempering appreciable carbon remains dissolved in the martensite lattice. From specific volume data, these investigators

also catalogued the decomposition as a first-order reaction, but the measurements were not sufficiently precise to establish the kinetic behavior accurately.

In a previous paper (6), the present authors studied the dimensional stability of hardened tool steels as a function of time at 68 °F by a method which could distinguish changes in length as small as 1×10^{-6} in/in. It was shown that such observations yielded the algebraic sum of two reactions at room temperature: (a) the contraction caused by the decomposition of martensite during the first stage of tempering, and (b) the expansion caused by the decomposition of retained austenite into an unspecified product which was more voluminous than the austenite. Obviously, an important extension of this procedure was to temper a series of hardened steels at various temperatures so that accurate changes in length could be observed as a function of temperature as well as time. Such experiments have since been performed, and the results are presented in this paper. However, on tempering at elevated temperatures, the decomposition of the retained austenite assumed a more significant role than had been hitherto appreciated; and this made it essential to measure the retained austenite with greater certainty and absoluteness than was previously possible. Fortunately, a new X-ray method became available (7) which was capable of quantitatively determining austenite even in specimens where none could be found before. For example, earlier X-ray techniques had indicated that, with plain carbon tool steels, refrigeration into liquid nitrogen immediately after the hardening quench could transform practically all of the retained austenite into martensite (8), (9), but the new technique was able to detect and measure 1 to 3% of austenite *after* this treatment.

With precise knowledge of the austenite contents in a given steel after hardening and after subcooling, it became possible to differentiate between the austenite and martensite transformations during tempering merely by measuring changes in length on tempering a pair of specimens, one hardened and the other refrigerated. Such dimensional observations, made in pairs, yielded simultaneous equations which were solvable for the respective contributions of the austenite-decomposition expansion and the martensite-decomposition contraction. In this fashion, the kinetics of the tempering process could be studied in considerable detail.

However, as will be explained shortly, it was not feasible to make the precision length determinations within the first 1½ hours

after the hardening or subcooling operations; yet important changes were suspected during this early period. Consequently, a quenching dilatometer was devised so that change-in-length observations could be started at the exact instant that the specimens reached room temperature and continued to the point where the more accurate length determinations could take over. Thus, by a combination of X-ray measurements of retained austenite, quenching dilatometer observations and precision length determinations, it was possible to obtain a novel insight into the decomposition of both the martensite and austenite during the first and second stages of tempering. Moreover, the kinetics of the latter were found to be sensitive to the conditions of the hardening treatment. Hence, the effect of arrested quenching at different temperatures was also investigated to some extent. In addition, complete hardness data were recorded for correlation with practical heat treatment.

The changes which take place during the third stage of tempering are so large, relatively speaking, that the precision techniques employed for the first two stages of tempering are not necessary. These reactions are being studied dilatometrically at present, and will be reported at a later date.

Precision Length Measurements

Two common tool steels were used in this investigation: one was a plain carbon steel with about 1% carbon and the other a ball bearing steel similar to SAE 52100. Their compositions are listed in Table I. The steels were received in the form of spheroidized bars. The effect of fiber had been studied previously (6) by aging specimens cut from a plate parallel and transverse to the rolling direction. No significant differences in dimensional behavior were found with the two types of specimens, and this has been confirmed by further experiments not yet published. Hence, the length changes measured in the present work are essentially independent of fiber

Table I
Analyses of Steels

Steel	Weight Per Cent						
	C	Si	Mn	S	P	Cr	V
K	1.07	0.23	0.25	0.014	0.011	....	....
T	1.00	0.35	0.37	.....	.....	1.56	0.21

direction, and are believed to reflect the true volume changes accompanying the phase transformations under consideration.

Length determinations were made with a 5000 × gage comparator by a method (6) which permitted measurements on a wide variety of sample lengths with a relative accuracy of about 1.5 microinches per inch. The specimens were in the form of rods ⅜ inch in diameter by 4.0 ± 0.001 inches long, with the ends accurately ground to the contour of a 4-inch diameter sphere. After the machining and grinding, the specimens were austenitized for 30 minutes in a lead pot controlled to ±5 °F and then quenched. Some of these specimens were subcooled immediately in a closed brass tube surrounded by liquid nitrogen at —321 °F (—195 °C). Others were hardened by arresting the quench at various temperatures for 5 minutes, followed by air cooling to room temperature. Any scale accumulation was removed with emery paper in a lathe running at slow speed, and then the specimens were degreased and allowed to remain for an hour on a large copper surface plate in the measuring room, where the ambient was maintained at 68 ± 1 °F. Length determinations were then made. After this, the specimens were aged for over 200 days in oil baths at 100, 150, 200, 250, 300 ± 2 °F, in salt baths at 400 and 500 ± 2 °F, in air at 68 ± 1 °F and in an ice bath at 32 ± 0.5 °F. At periodic intervals, the aging was interrupted by returning the specimens to room temperature for the precision length measurements.

The type of data obtained from such determinations is shown in Fig. 1. A series of specimens of the plain carbon steel (K steel) was austenitized at 1450 °F (790 °C), quenched into water at 68 °F and aged at the temperatures mentioned above. Fig. 1 shows the relative changes of length as a function of time at each aging temperature. Time is taken as beginning at 1½ hours after the completion of the hardening operation, since this period was required to clean the specimens and bring them to thermal equilibrium before precise length measurements could be made. The time scale is actually plotted as elapsed time after this reference point, and any changes (cf. p. 24) during the first 1½ hours after the quench apply as a constant correction to all of the determinations.

The relative changes in length (plotted in microinches per inch) are the averages of at least two specimens treated simultaneously. Over 20 measurements were made on each specimen within the first 1000 hours, but the individual points are not plotted, to avoid confu-

sion. The readings were reproducible to an accuracy of ±2 microinches per inch or 10% of the length change, whichever is the greater. This error did not usually arise from the measurement itself but from the inherent difficulties in reproducing quenching conditions exactly for each set of specimens. The structural reactions under investigation, however, caused length changes which were large compared to this error. No corrections were made for the tempera-

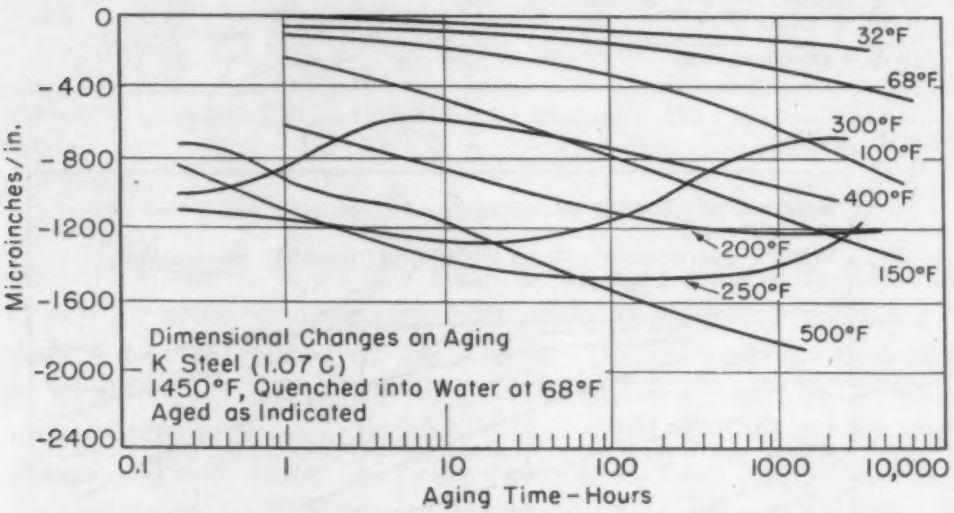


Fig. 1—Relative Changes in Length Observed on Aging Plain Carbon Steel.

ture coefficient of expansion, since both the specimens and the precision length standards used in the measurement had approximately the same coefficient, and the specimens were left on the same surface plate with the standards long enough for both to come to the same ambient temperature.

The data in Fig. 1 indicate a progressive series of shrinkages as the specimens are aged at 32 to 150 °F. Beyond 150 °F an expansion sets in, and occurs sooner the higher the temperature. It is undoubtedly caused by the decomposition of the retained austenite into bainite during the second stage of tempering. Fig. 2 shows the dimensional behavior on aging of a similar set of specimens which had been subcooled to —321 °F (—195 °C) immediately after the hardening quench. The curves clearly demonstrate that, while the expansion effects have been reduced in magnitude, they are still detectable. Apparently, even the refrigerated specimens contain significant quantities of retained austenite, and this is verified by the newer X-ray determinations. Table II lists the percentages of austenite for these (and other) quenching conditions and, accordingly,

Table II
Microconstituents of Plain Carbon Tool Steel

K Steel (1.07% C)—austenitized 1450 °F (790 °C) for 30 minutes

Treatment	Hardness Rockwell C	Volume Per Cent—Retained Austenite*	Volume Per Cent—Martensite	Volume Per Cent—Carbides
Water-quenched to 125 °F, air-cooled to room temperature	65.9	14.1	83.3	2.6
Water-quenched to 68 °F	67.0	9.0	88.4	2.6
Quenched into brine at 23 °F	67.2	8.5	88.9	2.6
Water-quenched to 68 °F, refrigerated immediately to −321 °F	68.0	2.9	94.5	2.6

*10 days after treatment.

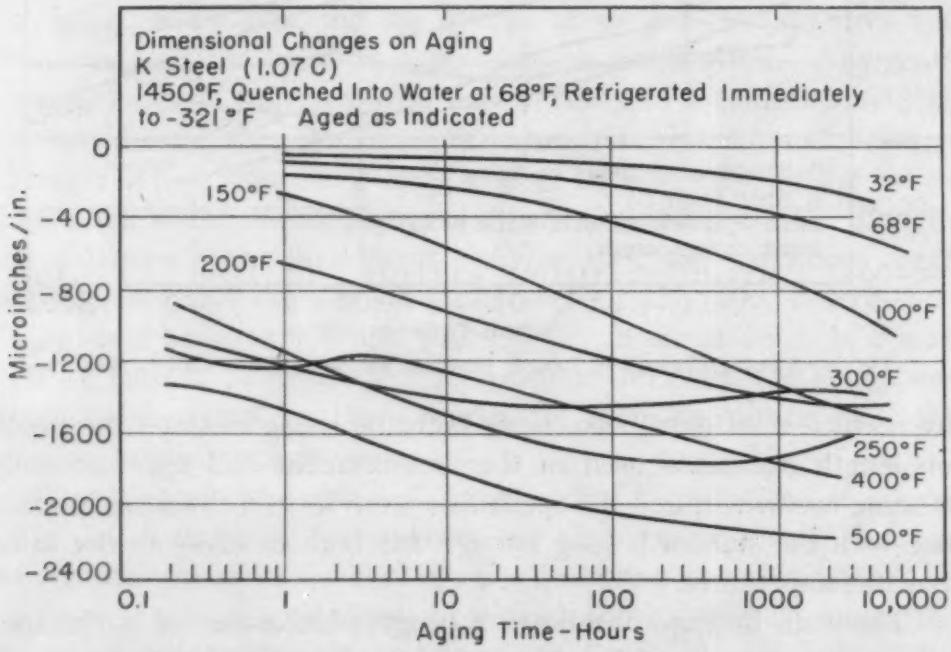


Fig. 2—Relative Changes in Length Observed on Aging Plain Carbon Steel Which Has Been Refrigerated Immediately After the Quench.

the data in Figs. 1 and 2 may be considered as resulting from two mixtures of austenite and martensite of identical chemical composition but with different ratios of the two constituents. The undissolved carbides do not take any part in these reactions.

An analogous set of treatments was performed with the ball bearing steel (T steel). Fig. 3 illustrates the dimensional behavior of this steel after quenching into oil from 1550 °F (845 °C), and here again it is evident that considerable quantities of retained austenite decompose into bainite at the higher aging temperatures. This

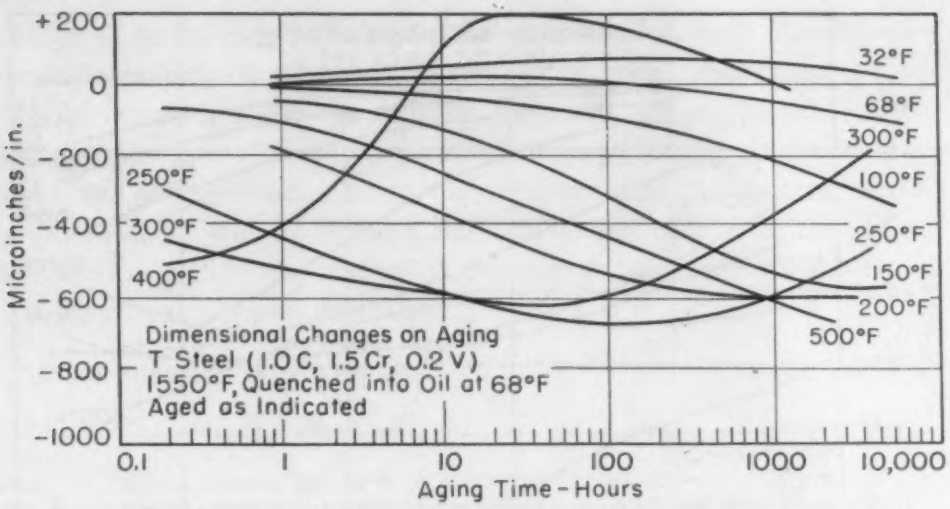


Fig. 3—Relative Changes in Length Observed on Aging Ball Bearing Steel.

steel, in addition, displays a small amount of growth at 32 °F and at 68 °F, which disappears as the aging temperature increases and does not seem related to the austenite-bainite reaction that comes at much higher temperatures. Specimens which are hardened and immediately subcooled to −321 °F (−195 °C) (Fig. 4) shrink correspondingly faster on aging because of their larger martensite-austenite ratios. In this case, the early expansions at 32 and 68 °F are wiped out, although a definite vestige of the later bainitic decomposition still remains. The retained austenite contents for the ball bearing steel after various quenching treatments are given in Table III. It is interesting to note that the plain carbon steel actually contains more retained austenite than the ball bearing steel, but the early expansions at 32 to 68 °F are not visible in the plain carbon

Table III
Microconstituents of Ball Bearing Steel

T Steel (1.0% C, 1.5% Cr, 0.2% V)—austenitized 1550 °F (845 °C) for 30 minutes

Treatment	Hardness Rockwell C	Volume Per Cent—Retained Austenite*	Volume Per Cent—Martensite	Volume Per Cent—Carbides
Quenched into molten salt at 450 °F, air-cooled to room temperature	64.0	10.6	85.4	4.0
Oil-quenched to 250 °F, air-cooled to room temperature	64.4	9.5	86.5	4.0
Oil-quenched to 125 °F, air-cooled to room temperature	64.9	9.0	87.0	4.0
Oil-quenched to 68 °F	66.5	7.0	89.0	4.0
Oil-quenched to 68 °F, refrigerated immediately to −321 °F	67.0	2.0	94.0	4.0

*10 days after treatment.

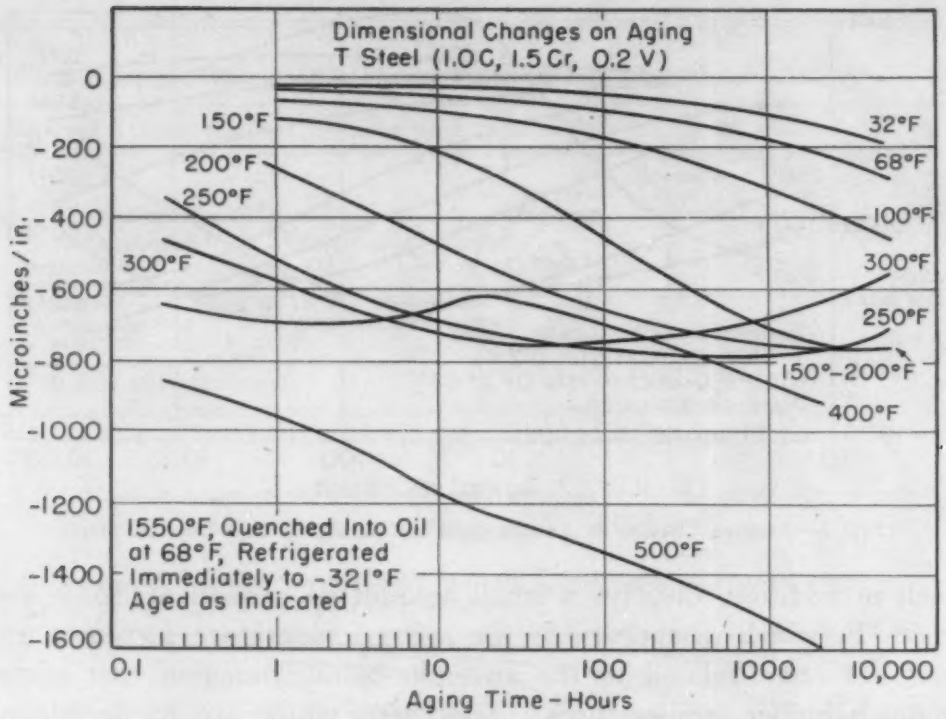


Fig. 4—Relative Changes in Length Observed on Aging Ball Bearing Steel Which Has Been Refrigerated Immediately After the Quench.

steel because of its relatively greater martensite contraction on tempering.

From these data it may be seen qualitatively that retained austenite decomposes in a two-stage process. The first proceeds at relatively low tempering temperatures while the second, which is the usual bainitic decomposition of the second stage of tempering, occurs at temperatures from 250 to 500 °F (120 to 260 °C).

The Decomposition of Martensite

Contraction Due to Martensite Tempering

Previous investigations on the decomposition of high carbon martensite have been handicapped by the inability to account quantitatively for the effects caused by retained austenite, which was always present. In this study, however, it was possible to subtract out the changes caused by the austenite and to analyze each reaction independently. Furthermore, the methods under discussion were sensitive enough not only to reveal the fine detail involved in the

first stage of tempering but also to detect unambiguously the isothermal transformation of austenite proceeding at room temperature.

If we consider a steel containing austenite and martensite (with or without excess carbides), the total change in length observed may be taken as the algebraic sum of the separate changes caused by the decomposition of the martensite and the austenite. For two mixtures containing different ratios of these two constituents, the summation may be expressed as follows:

$$\Delta L_1 = m_1 M + a_1 A \qquad \text{Equation I}$$

$$\Delta L_2 = m_2 M + a_2 A \qquad \text{Equation II}$$

where:

m_1 = volume per cent of martensite in mixture 1 at time = 0
m_2 = volume per cent of martensite in mixture 2 at time = 0
a_1 = volume per cent of austenite in mixture 1 at time = 0
a_2 = volume per cent of austenite in mixture 2 at time = 0
ΔL_1 = unit change in length of mixture 1 up to time = t
ΔL_2 = unit change in length of mixture 2 up to time = t
M = unit change in length caused by partial decomposition in 1% of martensite up to time = t
A = unit change in length caused by partial transformation in 1% of austenite up to time = t

Solving for M, we have:

$$M = \frac{a_2 \Delta L_1 - a_1 \Delta L_2}{a_2 m_1 - a_1 m_2} \qquad \text{Equation III}$$

100 M is the unit change in length that would occur up to time = t in a hypothetical sample of 100% martensite of the type at hand. This formulation assumes, of course, that the martensite and austenite in the two mixtures have the same decomposition kinetics, irrespective of the martensite-austenite ratio. By observing ΔL_1 and ΔL_2 for the two mixtures aged at various times and temperatures it becomes possible to plot 100 M as a function of time and temperature as in Figs. 5 and 6, thus resolving the separate dimensional behavior of the martensite during tempering.

Inasmuch as refrigeration in liquid nitrogen was employed to provide a second mixture of the same type of martensite and austenite that coexisted in the as-hardened structure, it was important to ascertain whether the cold treatment had any influence on the tempering kinetics, aside from the alteration of the martensite-austenite ratio. The martensite decomposition was found to be substantially independent of variations in the rate of subcooling and is, therefore, believed to be relatively insensitive to any stresses that might be

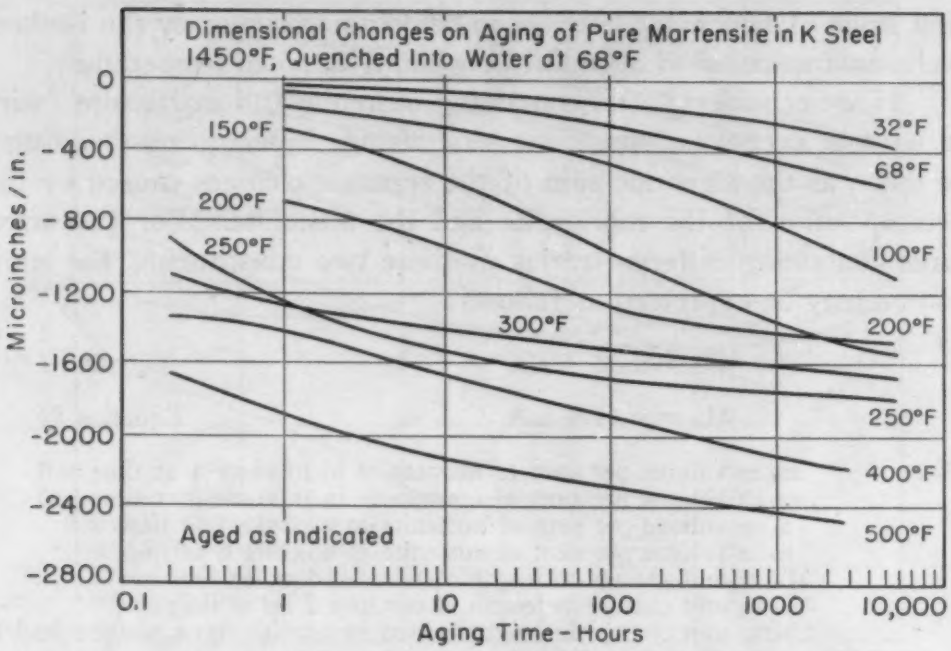


Fig. 5—Changes in Length on Aging 100% Martensite in the Plain Carbon Steel.

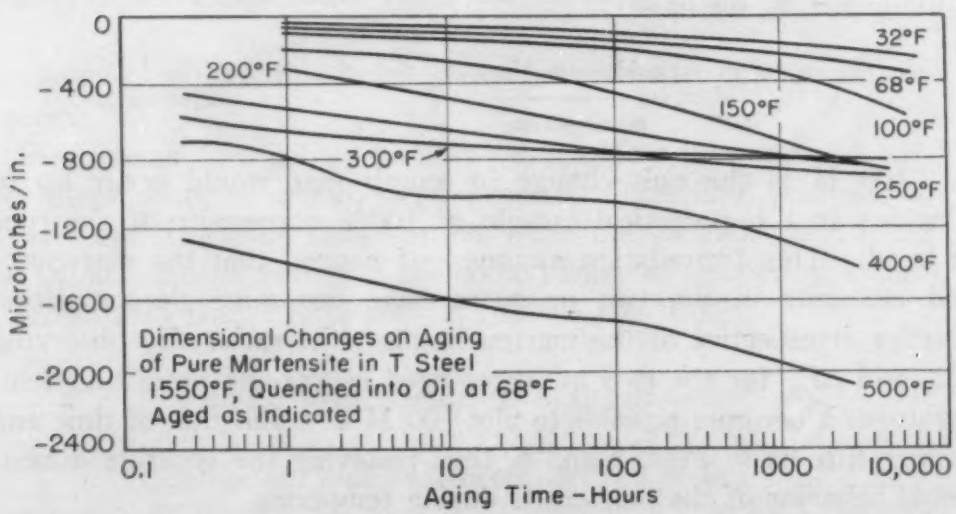


Fig. 6—Changes in Length on Aging 100% Martensite in the Ball Bearing Steel.

set up by the refrigeration. It is possible, however, that the austenite decomposition on tempering is affected to some extent by the subcooling stresses. This extraneous factor may be quite complex, but can be ignored for the steels under consideration because the amount of austenite after refrigeration is small. Moreover, it differs from the austenite content of the as-hardened mixture by only a few

Table IV
Effect of Tempering on Hardness

K Steel (1.07% C)—austenitized 1450 °F, quenched as indicated

Hours at Temperature / Aging Temperature, °F	1	10	100	1000	2000
	Rockwell C				
	Quenched into water at 68 °F				
32	66.8	67.0	67.7	68.3	67.7
68	66.8	67.3	67.5	68.5	69.2
100	66.8	67.6	67.7	68.2	....
150	67.5	68.4	67.8	67.1	66.9
200	68.4	67.3	66.9	65.0	64.7
250	68.4	67.6	65.4	63.2	62.6
300	67.0	64.5	62.5	62.5	62.2
	Quenched into water at 68 °F, refrigerated immediately to −321 °F				
32	67.6	67.6	67.7	68.3	68.8
68	67.6	67.7	68.0	−69.4	68.4
100	67.7	68.3	68.7	69.4	68.4
150	68.6	69.0	68.5	68.3	68.0
200	69.0	68.6	67.0	65.9	65.2
250	68.6	67.6	66.5	64.0	62.5
300	67.3	65.4	64.2	63.5	62.3

per cent and, hence, the conditions in the two structures cannot be far different.

At this point of the investigation, the absolute austenite and martensite contents are only known after 240 hours of aging at room temperature, rather than at $t = 0$. As a first approximation, these values (Tables II and III) may be used for the a's and m's in Equation III. Such a substitution introduces very little error in the calculations for M because the fractional change in the martensite content between $t = 0$ and $t = 240$ hours at 68 °F is quite small. This method forms the basis for the eventual determination of the austenite and martensite contents at $t = 0$ (p. 1048), and then the M values can be recomputed to give still closer approximations. However, the first approximation was considered sufficient for the purposes at hand.

From the contraction curves for 100% martensite in Figs. 5 and 6 several trends may be noted directly. The reaction starts immediately with no apparent incubation period, and when the curves are plotted on a linear scale, it can be seen that the rate of reaction is a maximum at the beginning. That precipitation accompanies the martensite decomposition is supported by Tables IV and V in which the hardness values are tabulated after various combinations of hardening and tempering. It is interesting to note that this reaction is rather similar to the usual precipitation hardening phenomenon observed in nonferrous alloys, with maximum hardening occurring at

Table V
Effect of Tempering on Hardness

T Steel (1.0% C, 1.5% Cr, 0.2% V)—austenitized 1550 °F, quenched as indicated

Hours at Temperature Aging Temperature, °F	1	10	100	1000	3000
	Rockwell C				
	Quenched into oil at 68 °F				
32	66.8	67.1	67.0	67.3	66.7
68	66.9	67.0	67.1	67.5	67.7
100	67.0	67.3	67.4	67.4	66.9
150	67.1	67.4	66.8	65.7	65.3
200	66.9	66.7	65.5	64.2	63.6
250	65.7	64.5	63.8	61.4	60.7
300	64.0	62.6	61.1	60.3	60.3
	Quenched into oil at 68 °F, refrigerated immediately to —321 °F				
32	67.2	67.2	67.2	67.6	67.3
68	67.2	67.2	67.4	68.2	68.5
100	67.6	67.6	67.8	67.2	66.6
150	68.2	68.3	67.6	66.2	66.4
200	68.0	67.3	66.3	64.5	65.3
250	66.1	65.2	64.1	62.1	61.1
300	63.7	62.4	61.0	60.0	60.0

shorter times the higher the aging temperature. The hardening is not caused by the isothermal decomposition of retained austenite, for a comparison of the refrigerated and nonrefrigerated steels indicates that the former undergo equal or greater hardening on aging, and yet contain less austenite.

At 250, 300 and 400 °F (120, 150 and 205 °C), Figs. 5 and 6 also show that the rate of martensite contraction slows up considerably as time progresses and reaches a plateau which delineates the end of the first stage of tempering. At this point, softening is already well advanced, resulting at least partly from the depletion of carbon from the martensite lattice in the formation of the transition precipitate. Beyond the plateau, further contraction sets in, corresponding to the third stage of tempering (conversion of the transition precipitate to cementite). The surprising trend, however, is that the total shrinkage at the plateau does not increase with the aging temperature, but actually seems to vary inversely with the aging temperature.[2] Since the shrinkage measured here accompanies a rejection of carbon from the martensite lattice, the inverse temperature dependence of the first-stage total shrinkage signifies that the amount of precipitation occurring during the first stage becomes smaller the higher the tempering temperature, at least up to 400 °F (205 °C). This probably indicates that the solubility of carbon in the martensite

[2]At 400 °F the plateau designating the completion of the first stage of tempering corresponds to the flattened portion of the curve (Figs. 5 and 6) at the very beginning of the aging. Thus, most of the 400 °F measurements and all of the 500 °F measurements lie beyond the first stage.

lattice coexisting with the transition precipitate increases with increasing temperature. In other words, the plateau is visualized as a period of pseudo-equilibrium between the transition precipitate and partially depleted martensite. Such a postulation for the increasing solubility of carbon in martensite coexisting with the transition precipitate is consistent with the most recent measurements of Kurdjumov and Lyssak (5) on the tetragonality of martensite as a function of tempering temperature. They found that the axial ratio after 1-hour tempering increases slightly or remains practically constant up to 300 °F (150 °C). With the much more sensitive method available here, the indications are that the transition precipitate may be in balance with slightly increasing percentages of carbon in the martensite lattice as the temperature rises, up to the temperature at which the cementite conversion occurs before the time of the earliest observations. All other attempts to explain the plateau phenomena have proved fruitless.

Kinetics of Martensite Decomposition

In analyzing the kinetics of the martensite decomposition, it might first be assumed that the precipitation proceeds by nucleation and growth (10), (11), but such a process starts at a very low rate, usually after an incubation period. In contrast, the martensite decomposition shows no evidence of incubation, and has its maximum reaction rate at the beginning of tempering. Such behavior is typified by a first-order equation:

$$-\frac{dc}{dt} = K_1 c \qquad \text{Equation IV}$$

where: c = concentration of carbon in martensite lattice at time = t, and
K_1 = reaction-rate constant = a function of temperature

However, when compared with the data, even this equation does not provide for a sufficiently rapid rate at the beginning. On the other hand, if K_1 is made large enough to fit the early data for a given tempering temperature, then the equation fails to account satisfactorily for the later retardation of the decomposition. It is apparent that a suitable variation in K_1 with respect to tempering time must be postulated to adapt Equation IV to the experimental curve.

From the very nature of the austenite-martensite transformation, it may be expected that the freshly-formed martensite is in a

state of considerable stress, and that this stressed condition promotes the decomposition of the martensite on tempering. However, stress relief also occurs during the tempering, and its stimulating effect would tend to diminish progressively. Rominski and Taylor (12) have studied stress relief in steel castings as a function of time and temperature, and their results may be expressed as follows:

$$-\frac{d\sigma}{dt} = \frac{K_2}{t^S} \qquad \text{Equation V}$$

where: σ = stress
K_2 = constant = a function of temperature
S = stress relief index = a function of temperature

Hargreaves (13) has found an analogous relationship for the variation of the recovered Brinell impressions in plastically deformed materials after different loading times. Accordingly, the time-dependence of K_1 in Equation IV may be modified by introducing the stress effect of Equation V:

$$-\frac{dc}{dt} = K \cdot \frac{c}{t^S} \qquad \text{Equation VI}$$

where: K = a new constant which is independent of time, but is a function of temperature.

Since the lattice parameters of tetragonal martensite vary linearly with the dissolved carbon content (1), it may be concluded that fractional changes in dissolved carbon due to precipitation are proportional to fractional changes in volume $\left(\frac{dv}{V}\right)$, or in length $\left(\frac{dy}{y}\right)$. Hence, the differential equation for the rate of length change may be written:

$$\frac{dy}{dt} = K\frac{a-y}{t^S} \qquad \text{Equation VII}$$

where: y = contraction in microinches per inch which occurs up to time = t
a = total contraction in microinches per inch at the end of the first stage of tempering.

This equation may be integrated for the isothermal case to yield the following explicit relationship:

$$y = a\left[1 - e^{-Kt^{(1-S)}}\right] \qquad \text{Equation VIII}$$

or in logarithmic form:

$$\log\log\frac{a}{a-y} = (1-S)\log t + \log\frac{K}{2.3} \qquad \text{Equation IX}$$

Before Equation VIII or IX can be evaluated, however, the end point "a" of the reaction must be determined. If the steel is tempered completely to cementite and ferrite, specific volume data on 1.02% carbon martensite indicate that a total shrinkage of a = 6000 microinches/in will occur (1). These data also indicate that the end of the first stage of tempering attained at a temperature of 300 °F (150 °C) is about 30% of this total contraction. The reaction considered here ends with the first stage of tempering, and it is found that a shrinkage value of 1700 microinches/in best fits the 300 °F data for the martensite in Fig. 5. This "a" value is also consistent with the plateau that the 300 °F curve approaches. Furthermore, in keeping with the concept of a temperature-dependent solubility of carbon in the martensite lattice coexisting with the transition precipitate, the value of "a" is expected to decrease as the temperature increases.

Rather than attempt to calculate the variation of "a" with temperature on the basis of ideal solution laws, "a" was simply assumed to be inversely proportional to temperature. The values of "a" were chosen to fit the plateaus at the higher tempering temperatures where the reaction approaches completion, and were extrapolated to the lower temperatures where the reaction is still far removed from completion in 200 days. As shown in Table VI, the variation of "a" with temperature turns out to be quite small in comparison with the total contraction.

With the end point of the reaction thus established, it is possible to verify the proposed kinetics by evaluating Equation IX. If values for $\log \log \frac{a}{a-y}$ are plotted as a function of log t at a given temperature, a straight line should be obtained, having a slope of $(1 - S)$ and an intercept of $\log \frac{K}{2.3}$ at $\log t = 0$. Fig. 7 shows the data for the plain carbon steel (K steel) plotted in this form and it is evident that Equation IX fits quite well. The values of the rate constant "K" and the stress-relief index "S" are also listed in Table VI. The temperature dependence of these constants is indicated in Fig. 8, from which the activation energies given in Table VI may be determined.

An exactly similar procedure was followed with the T steel (1.0% carbon, 1.5% chromium, 0.2% vanadium) except that the "a" values corresponding to the plateaus (Fig. 6) are found to be

about one-half those of the plain carbon steel. A comparison of the hardness data in Tables IV and V also reveals that the precipitation hardening during the first stage of tempering in the T steel is roughly one-half that occurring in the K steel.

The calculated results for the T steel are presented in Table VI.

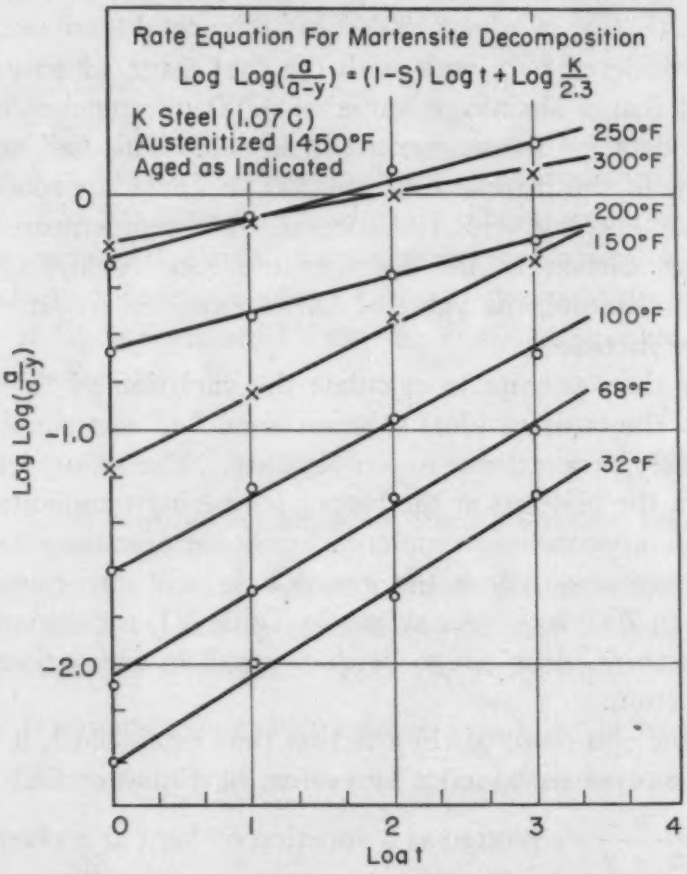


Fig. 7—Rate Equation for Martensite Decomposition in Plain Carbon Steel.

Like the plain carbon steel, the kinetics of the alloy steel conform to Equation IX and plot as straight lines to give the S and K values listed in the Table. The temperature-dependence of these constants is also shown.

Stages of Martensite Tempering

With the aid of Equation IX and the appropriate constants, it is now possible to compute the martensite contraction which takes place during the first 1.5 hours at room temperature. This comes out to be 50 and 30 microinches/in for the K and T steels, respectively.

Table VI
Constants of Rate Equation for Martensite Decomposition

$$\frac{dy}{dt} = \frac{K \cdot (a - y)}{t^S}$$

Tempering Temperature °F	$\frac{1}{T} \times 10^{-3}$	a Microinches/in	S	K	% Carbon in Solution at End of First Stage of Tempering
K Steel (1.07% C)—austenitized 1450 °F 30 minutes—0.90% C in martensite					
32	3.67	2240	0.63	0.0090	0.53
68	3.31	2160	0.65	0.0215	0.54
100	3.21	2100	0.68	0.0590	0.55
150	2.95	2000	0.70	0.163	0.57
200	2.74	1900	0.84	0.477	0.58
250	2.54	1800	0.84	1.270	0.60
300	2.37	1700	0.89	1.390	0.62
400	2.10	1300	....	.....	0.68
T Steel (1.0% C, 1.5% Cr, 0.2% V)—austenitized 1550 °F 30 minutes—0.84% C in martensite					
32	3.67	1035	0.64	0.0183	0.67
68	3.31	1000	0.69	0.0319	0.67
100	3.21	980	0.71	0.0635	0.68
150	2.95	940	0.71	0.167	0.68
200	2.74	900	0.79	0.482	0.69
250	2.54	860	0.84	1.100	0.70
300	2.37	820	0.88	1.530	0.70
400	2.10	740	....	.....	0.72

Heats of Activation for Rate Constants

$$\ln K = \ln A - \frac{Q_K}{RT} \qquad \ln S = \ln B - \frac{Q_S}{RT}$$

Steel	Q_K cal/mol	Q_S cal/mol
K	9050	380
T	7480	495
Average	8250	440

Accordingly, these increments may be added to the ordinates of Figs. 5 and 6 to obtain the contraction relative to the as-quenched martensite. For the most part, this is a small correction, and has no material bearing on the quantitative relationships just discussed.

The last column in Table VI indicates the carbon content of the martensite at the end of the first stage of tempering for each of the two steels. These values are computed on the basis that complete precipitation of carbon into cementite from a 1.02% carbon martensite causes a total shrinkage of 6000 microinches/in (1). If it is assumed that the difference in density between the transition precipitate and cementite is negligible,[3] then the "a" values correspond to proportional percentages of carbon $\left[\frac{1.02}{6000} \times a\right]$ precipitated from the martensite at the end of the first stage of tempering. Subtraction

[3]It can be shown that even if the transition precipitate is taken as Fe_8C, the resulting calculations are little affected.

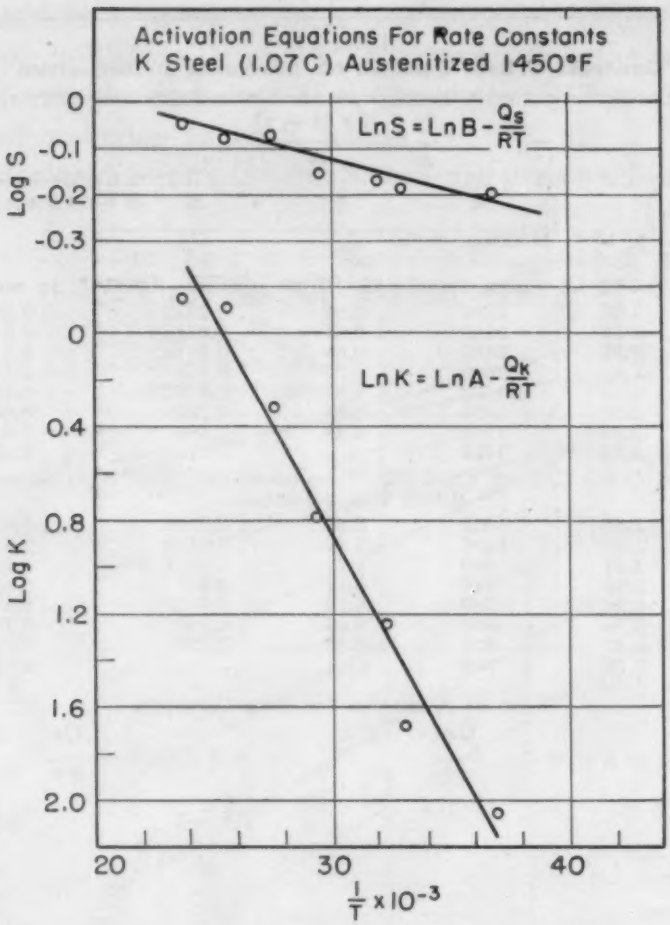


Fig. 8—Activation Equations for Martensite Decomposition in Plain Carbon Steel, Showing Temperature Dependence of the Constants K and S.

of the precipitated carbon from the initial carbon contents of the martensite in the two steels at hand yields the figures in the last column of Table VI. The initial carbon contents in the martensite are 0.90 and 0.84% in the K and T steel, respectively, as determined from the over-all carbon content and the measured amounts of undissolved carbide (assumed to contain 6.7% carbon).[4]

It is significant that the carbon content of the martensite at the end of the first stage of tempering represents such a large fraction of the initial carbon content. This accounts for the substantial con-

[4]The M_s temperatures of the two steels under the austenitizing conditions used were found by the Greninger-Troiano technique to be 400 °F (205 °C) and 420 °F (215 °C) respectively. The 400 °F value checks exactly with the M_s reported by Greninger and Troiano (14) for a 0.90% carbon steel with all the carbon in solution, and confirms the dissolved carbon content determined for the K steel on the basis of the measured amount of undissolved carbide. In the case of the T steel, the 420 °F value was compared with the M_s temperatures determined by Klier and Troiano (15) for a series of chromium steels with all the carbon in solution. The steel in question behaved as if 0.5% chromium were dissolved in addition to the 0.84% carbon determined above.

traction observed during the third stage of tempering when the transition precipitate goes over to cementite (2). The attendant contraction is much too large to be explained by any reasonable difference in density between the two forms of precipitate; but the conversion does permit the further rejection of carbon by the martensite, since the capacity of the martensite to retain carbon in solution is greater when coexisting with the transition precipitate than when coexisting with the more stable cementite. Hence, the volume effect observed during the third stage of tempering is primarily related to the further precipitation of the carbon from the partially depleted martensite, but this process is controlled by the kinetics of the conversion of the transition precipitate to cementite.

The carbon percentage in the martensite at the end of the first stage of tempering not only increases with the temperature but is also greater in the alloy steel than in the plain carbon steel. The latter difference, although slight, may be real, inasmuch as chromium is known to increase the solubility of carbon in ferrite (16). The temperature-dependence indicates an apparent heat of solution of 180 calories/mol for the K steel and 80 calories/mol for the T steel. These small values suggest that true equilibrium is not obtained between the martensite and the transition precipitate at the end of the first stage of tempering. It may be added, however, that the temperature-dependence of the experimentally determined solubility of cementite in alpha iron in this low temperature range is also very small, and likewise indicates evidence of supersaturation (17).

Table VI shows that the two steels have roughly the same reaction-rate constants and stress-relief indices, and also have about the same heats of activation for these factors. Consequently, the smaller martensite contractions in the T steel as compared to the K steel (Fig. 6 versus Fig. 5) are not attributable to a reduction in the rate of martensite decomposition by the alloying elements, but are due rather to the effect of the latter in increasing the tolerance of martensite for carbon in the presence of the transitite precipitate. This decreases the total shrinkage at the end of the first stage of tempering and accounts at least in part for the greater dimensional stability of the ball bearing steel.

If the martensite decomposition is controlled by the diffusion of carbon, the activation energy for the temperature dependence of the reaction-rate constant (Q_K) may be taken as a measure of the activation energy for the diffusion coefficient. Yet the average value of

8250 calories/mol (Table VI) is less than half the 18,000 calories/mol obtained by Snoek (18) for the heat of diffusion of carbon in alpha iron. Either the above premise is incorrect, or the rate of carbon diffusion in high carbon martensite is much faster than in low carbon ferrite.

Isothermal Decomposition of Retained Austenite

Quenching Dilatometer Experiments

In the course of the precision length determinations it was observed that specimens immediately after the hardening treatment were very unstable, and that the length changes involved were very much greater than could be explained by temperature effects or by the previously calculated martensite decomposition during the first 1.5 hours. Rather important austenite changes were suspected, and a quenching dilatometer was constructed to study the interval immediately after the hardening. The dilatometer was essentially that of Flinn, Cook and Fellows (19) except that it was modified to take a thermocouple and a specimen of the same size used for the precision length determinations. The specimen was supported at its lower end by an outer quartz tube cut away to admit free access of the quenching fluid, and was held by spring compression at the upper end against a smaller quartz tube which transmitted the changes in specimen length to the dial gage. The arrangement is photographed in Fig. 9.

For a dilatometer run, the specimen was set into the quartz holder, and austenitized in the small lead pot set on the moving table. To quench, the lead pot was lowered away from the specimen and the quenching bath brought up around it, by swinging the counterweighted table through a U-shaped course controlled by the guide shown in Fig. 9. During the quench, the dial gage and timer remained in the same position and were photographed by a motion picture camera running at 16 frames per second but with shutter speed advanced to 1/80 of a second to stop the motion of the dial. The quenching bath was equipped with a high speed electric stirrer, a cooling coil, and an immersion heater actuated by a potentiometer controller, so that a wide variety of quenching conditions was possible. A vibrator was attached to the quartz tube holder, and floodlights were provided to illuminate the dial sufficiently to be photographed.

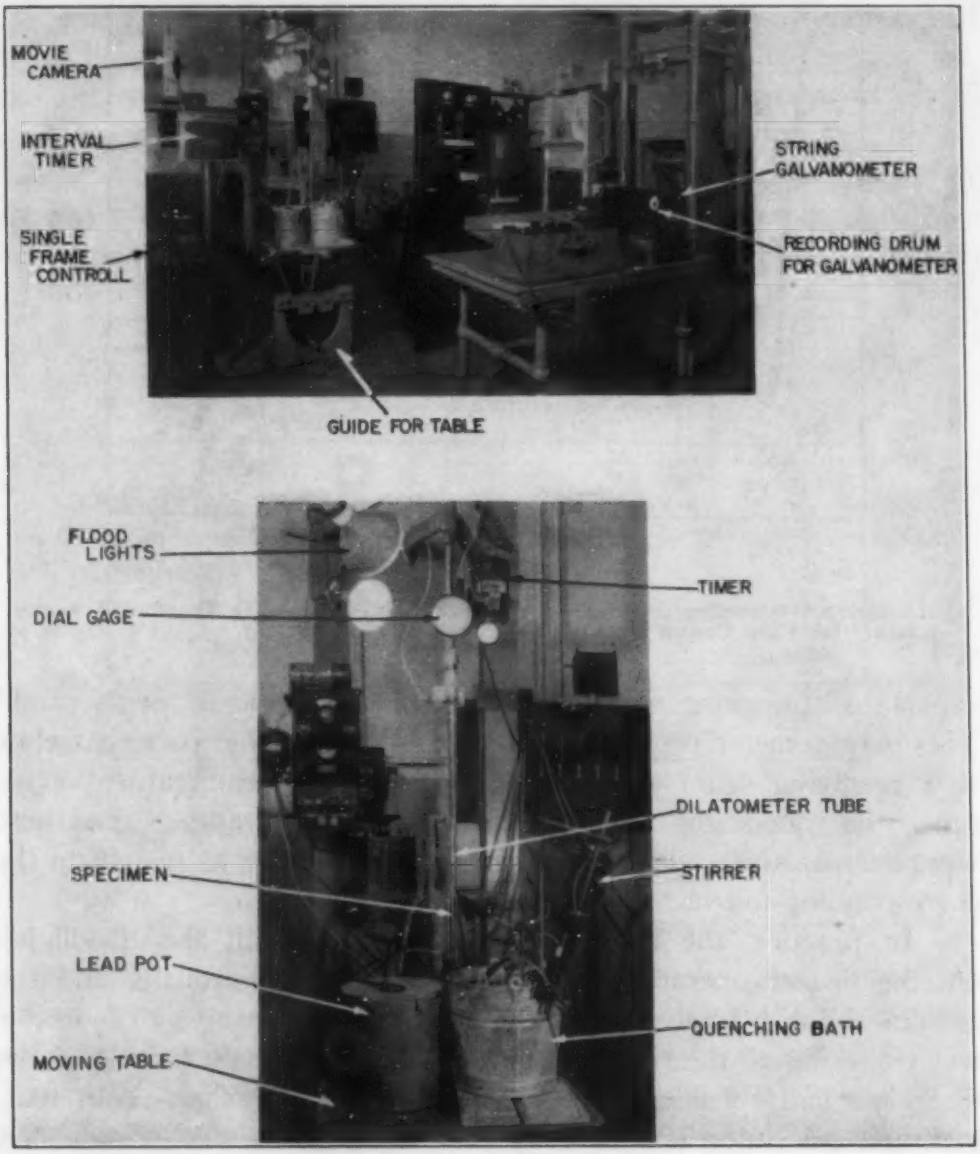


Fig. 9—Quenching Dilatometer Apparatus Showing General Arrangement of the Equipment and a Close-Up of the Specimen. The dial gage and timer are turned 90 degrees from their normal position.

For these experiments, it was of utmost importance to determine when the specimen reached room temperature. A hole ½ inch deep and $\frac{1}{16}$ inch in diameter was drilled into the top of each dilatometer specimen and a 28-gage chromel-alumel thermocouple inserted until it made firm metallic contact. The thermocouple wires were threaded back through the inner quartz tube of the dilatometer to a string galvanometer with a 0.007 second period, which was

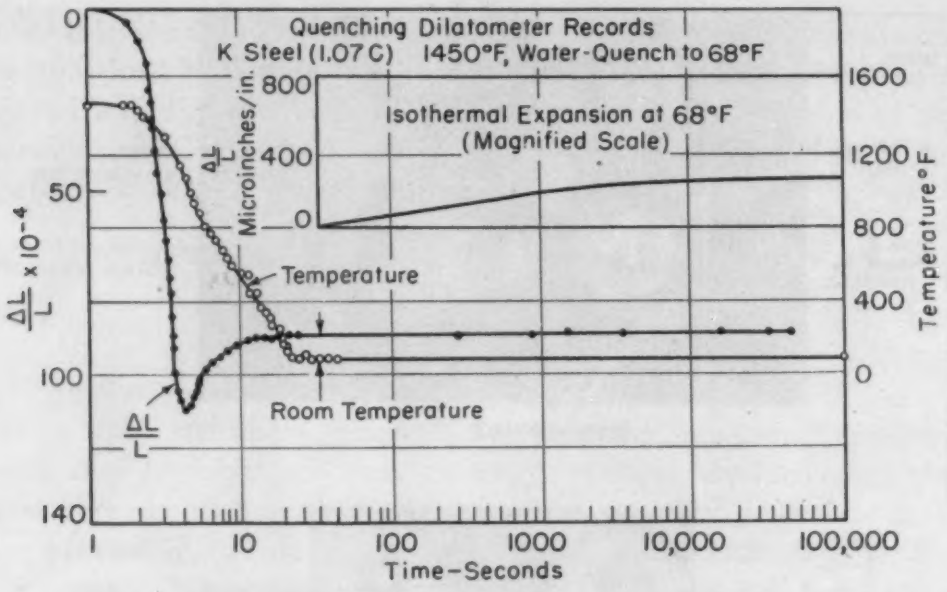


Fig. 10—Quenching Dilatometer Curves Showing Changes in Length and Temperature for Plain Carbon Steel.

capable of following quenching rates up to 10,000 °F per second.[5] This galvanometer produced a trace on photographic paper attached to a revolving drum and provided a record of temperature versus time. The quenching rates for the fairly massive samples used here were comparatively slow and it was an easy matter to match up the corresponding movie record of dilation versus time.

In practice, the specimen was quenched with the floodlights on, the buzzer operating, the stirrer working vigorously, and the camera running freely. At the same time, the string galvanometer was recording on the revolving drum. After the main motion of the dial gage had subsided and the specimen had reached room temperature, an automatic timer was introduced to take single-shot photographic exposures on the same movie film at predetermined intervals during the next 24 hours. In runs where the quenching bath was above room temperature, the arresting time was fixed at 5 minutes after which an electric fan was used to accelerate the air cooling of these specimens to room temperature. Duplicate runs were made for each of the quenching conditions, and it was thereby possible to project the dilatometric changes during the first 1.5 hours after the hardening onto the precision length data obtained with the gage comparator.

[5]The string galvanometer had been previously used by Greninger (20) and was borrowed through the courtesy of Professor John Hobstetter of Harvard University, Cambridge, Mass.

The results for a plain carbon steel specimen (K steel) quenched from 1450 °F (790 °C) into water at 68 °F are plotted in Fig. 10, and the corresponding data for a specimen of ball bearing steel (T steel) oil-quenched from 1550 °F (845 °C) are plotted in Fig. 11. The onset of the hardening reaction is indicated approximately by the sharp minima in the length curves, since the austenite-martensite transformation is attended by a large increase in volume superim-

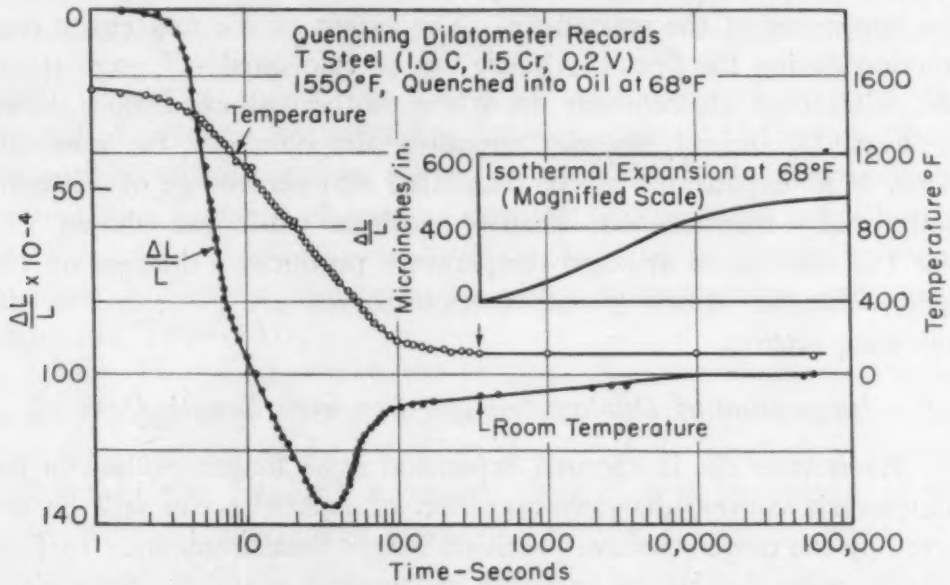


Fig. 11—Quenching Dilatometer Curves Showing Changes in Length and Temperature for Ball Bearing Steel.

posed upon the normal cooling contraction. However, the temperature readings corresponding to these inversions are not to be construed as M_s points since the thermocouple invariably lagged the average temperature of the specimens during the quench. It should be borne in mind that the objective of this procedure was not to study the quenching process but to determine the time when the specimen arrives at room temperature. Because of the location of the thermocouple, the difference between its reading and the average specimen temperature becomes minimal as the ambient is approached. Actually, any possible error is on the conservative side in that the thermocouple may arrive at the ambient after the specimen but not before. Hence, transformations observed after the thermocouple reaches room temperature may be regarded as true isothermal changes rather than as transient cooling effects.

Even on the compressed scale of Figs. 10 and 11, it is evident

that expansion takes place at room temperature following the hardening quench. Of equal importance is the fact that this expansion is continuous with the primary austenite-martensite reaction on cooling. In other words, the hardening process does not appear to stop completely when the cooling stops. Similar results are obtained when the hardening quench is arrested and followed by air cooling to room temperature. The isothermal expansion is caused by decomposition of the retained austenite, but is partially obscured by the simultaneous tempering of the martensite. The extent of the martensite contraction during the first 1½ hours can be calculated (cf. page 1040) and subtracted algebraically from the isothermal expansion shown by Figs. 10 and 11, thereby revealing the effect of the austenite alone. The expansions can be translated into percentage of austenite isothermally transformed because previous work has shown (1) that 1% conversion at room temperature produces a dilation of 140 microinches/in. Such transformation curves are presented in the following section.

Integration of Dilatometric and Precision Length Data

Even after the isothermal expansion is no longer evident in the dilatometric curves, the decomposition of austenite can still be detected by the more sensitive precision length measurements. In fact, the expansion due to the austenite decomposition can be determined uniquely. If the pure martensite contraction curves in Fig. 5 are multiplied by 0.88 (the martensite content of steel K as given in Table II) and then subtracted algebraically from the over-all observed length changes in Fig. 1, the net result is the expansion attributable to the austenite decomposition during the aging of steel K at the temperatures shown. A similar subtraction based on Figs. 6 and 3 yields the austenite contribution in steel T, except that the martensite content happens to be 0.87 (Table III).

To go a step further, the austenite expansions thus derived permit the calculation of the quantitative course of the austenite decomposition on aging. However, to put such calculations on an absolute basis, the austenite must be known at some point in the aging process. Tables II and III give the X-ray determinations of the retained austenite in each case after 240 hours of aging at 68 °F after the hardening quench, when the reaction rate is very small. Then with the aid of the conversion factor of 140 microinches/in per per cent of austenite decomposed at room temperature (Table VII), we can

Table VII
Unit Change in Length Caused by Decomposition of 1% of Austenite at Various Temperatures

Decomposition Temperature °F	$\frac{\Delta L}{L} \times 10^{-6}$
32	140
68	140
100	140
150	137
200	132
250	123
300	114

work backward (from the 240-hour measurement) to find the amount of austenite in the steel at the very beginning of aging. Once the initial retained austenite content is available, the residual austenite content as a function of time at elevated temperatures as well as at 68 °F can be computed from the expansions due to austenite decomposition at various temperatures and the appropriate conversion factors in Table VII.

Figs. 12 and 13 present the retained austenite changes on aging at 68 °F, not only after direct quenching to room temperature but after arrested hardening. It is evident that the isothermal decomposition of the retained austenite, though small compared to the transformation that takes place during the hardening quench, is nevertheless quite detectable by this sensitive method of investigation. Within the first hour after the hardening, 1 to 3% austenite decomposes at room temperature. In both steels, this initial conversion is greatest when the arresting quench is at 125 °F. Beyond 1 or 2 hours, the rate of decomposition diminishes rapidly; yet minor progressive changes of the order of tenths of a per cent are actually detectable for thousands of hours. In 5000 hours at 68 °F, a total of 2.5% austenite decomposes isothermally in the K steel after a direct quench to room temperature, but this figure increases to 5.0% if the hardening quench is arrested at 125 °F, followed by air cooling to room temperature. The corresponding figures for the T steel are 4.5 and 5.5, respectively.

It is also significant to note, from the starting values of the curves in Figs. 12 and 13, that arrested hardening at 125 °F results in an appreciably higher austenite content on arrival at room temperature than does direct quenching. On the other hand, raising the arresting temperature from 125 to 450 °F (martempering) produces no further increase in the initial austenite content. Nevertheless,

variations in this range do affect the rate of austenite decomposition on aging, so that when the X-ray determinations are conducted at some later time, a progressive increase is found in the retained austenite content as a result of raising the arrested hardening temperature from 68 to 450 °F.

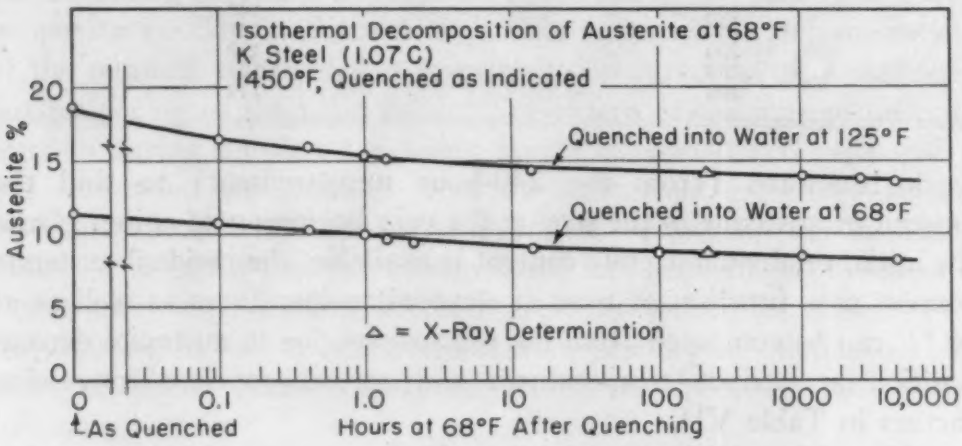


Fig. 12—Isothermal Decomposition of Austenite in Plain Carbon Steel at Room Temperature.

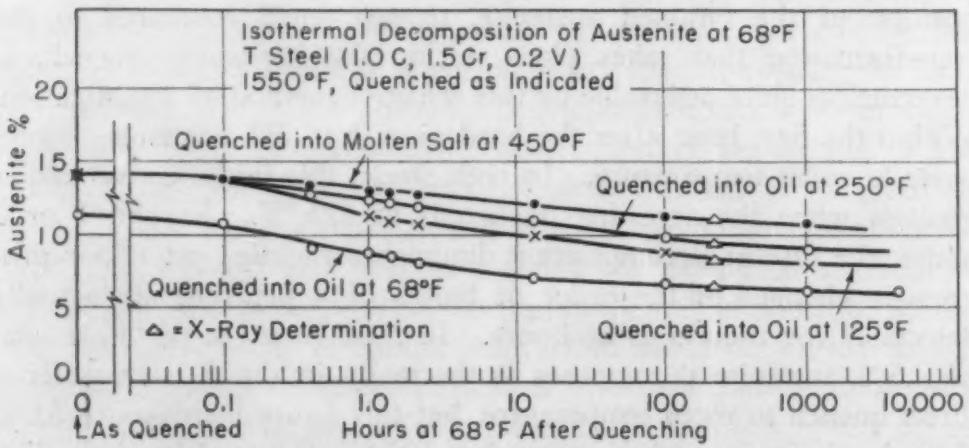


Fig. 13—Isothermal Decomposition of Austenite in Ball Bearing Steel at Room Temperature.

Comparing the K and T steels after direct quenching, it is seen that both materials have nearly the same per cent of austenite immediately after hardening, but the rate of isothermal decomposition is greater in the alloy steel and results in a measurably smaller austenite content than in the plain carbon steel after a short period at room temperature.

Decomposition of the Retained Austenite at Elevated Temperatures

Figs. 14 and 15 show the course of austenite decomposition in the two steels on tempering at various temperatures. It may be recalled that every specimen used for the precision length measurements is aged at 68 °F for 1½ hours before the first determination.

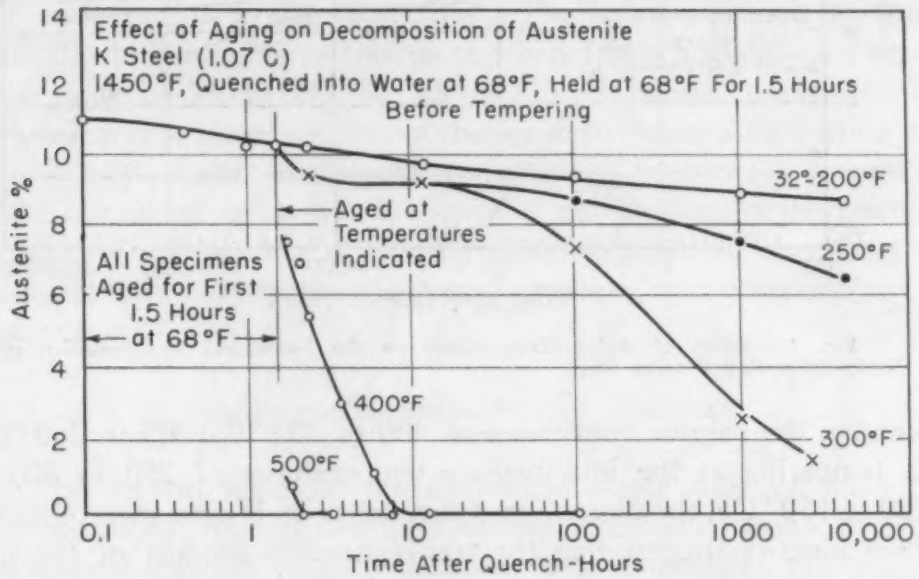


Fig. 14—Effect of Aging Temperature on the Isothermal Decomposition of Austenite in Plain Carbon Steel.

In each case, therefore, the subsequent changes occurring at a given temperature are plotted as continuations of the decomposition which takes place during the initial period at room temperature, the latter being evaluated from the dilatometric runs.

It is surprising to find that the isothermal decomposition of retained austenite is not much affected by the tempering temperature up to about 250 °F (120 °C), where further transformation sets in after prolonged holding. Above 250 °F, the latter mode of transformation occurs more rapidly, the higher the temperature, and becomes the well-known austenite-bainite reaction characterizing the second stage of tempering. The temperature-dependence of this reaction is quite marked, and corresponds to a heat of activation of about 38,000 calories/mol.

It is evident, then, that the isothermal decomposition of retained austenite is in itself a two-stage process. First, there is the low temperature conversion observed at 68 to 200 °F (20 to 95 °C), and

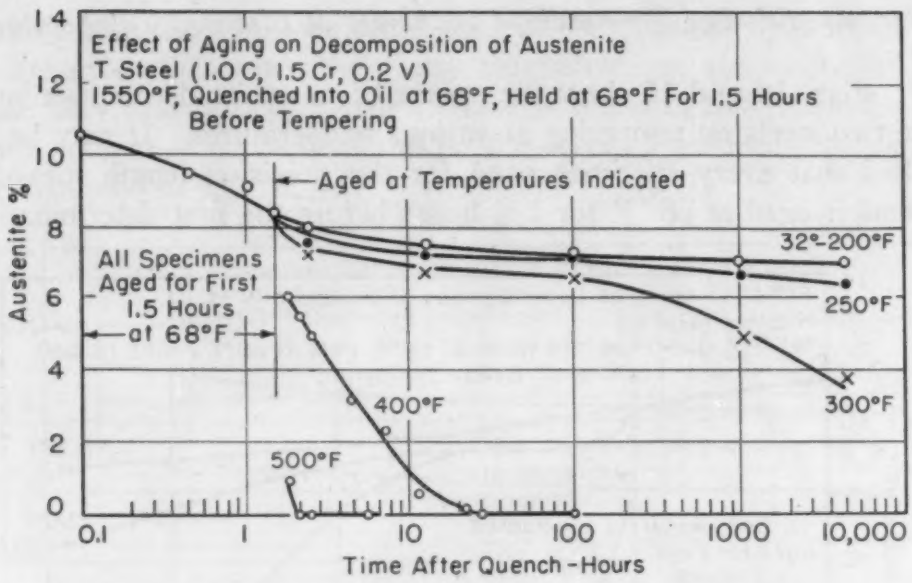


Fig. 15—Effect of Aging Temperature on the Isothermal Decomposition of Austenite in Ball Bearing Steel.

secondly, the bainitic conversion at 400 to 500 °F (205 to 260 °C). On tempering at the intermediate temperatures of 250 to 300 °F (120 to 150 °C), the discrete two-step behavior is even more obvious. These kinetics suggest that the transformation product of the first step is martensite, as proposed recently by the authors (6), notwithstanding the isothermal nature of the process. This far-reaching conclusion is substantiated by the fact that the isothermal decomposition found at room temperature (and at temperatures up to 200 °F) is continuous with the primary austenite-martensite reaction occurring during the hardening quench. There is no pause in the austenite decomposition when the ambient is reached, even though the magnitude of the isothermal reaction is small compared to the cooling reaction. Moreover, it is not likely that an isothermal *bainitic* transformation would set in at the very instant that the cooling *martensitic* transformation ceases. In fact, at the higher tempering temperatures, where the transformation is clearly bainitic, the large heat of activation signifies that bainite formation at room temperature must be fantastically slow and can hardly account for the isothermal decomposition observed after the hardening quench. All these factors point to martensite as the first product of the retained austenite decomposition on tempering. Its formation appears to be merely a residual effect of the main hardening reaction, and occurs most rapidly immediately after the hardening quench. Raising the tem-

pering temperature does not accelerate this "after effect", but does eventually bring in the bainitic conversion as a separate process when the temperature is sufficiently high and/or the time is sufficiently long.

At the present time, the kinetics of retained austenite decomposition cannot be handled in the same quantitative fashion as is possible with the martensite tempering. The bainitic process will undoubtedly be amenable to treatment when further studies are made in the range of 300 to 600 °F (150 to 315 °C) and such experiments are underway. However, the isothermal martensite stage, being inevitably a by-product of the primary hardening reaction, is dominated by the quenching conditions to a greater extent than by the tempering process. This initial phase of tempering is but another facet of the basic austenite-martensite transformation that remains to be explored.

Practical Significance of Results

This investigation on the isothermal martensite and austenite decompositions in hardened high carbon steels emphasizes that the dimensional stability of such materials is a function of the amount and nature of the martensite and austenite present. The contraction due to the aging or tempering of the martensite is quite predictable in terms of experimentally-derived constants. In fact, it is known from previous findings that martensite contractions are additive (6). From a practical standpoint, this means that martensite decomposes according to a basic equation, which can be set up for room temperature, and that any decomposition which occurs during prior tempering has the same effect as though it had all taken place in a much longer time at room temperature. Since temperature and time are related through Equation IX, long-range changes at room temperature in finished gages and precision tools can be neatly anticipated and avoided by tempering for reasonable times at elevated temperatures. The larger the martensite contraction achieved during such tempering, the less shrinkage may be expected in subsequent aging at room temperature. Such effects can be calculated with the aid of Equation IX and the constants in Table VI.

However, if hardness is an important consideration, then the temperature and time of tempering are not interchangeable for optimum results because, although a given extent of martensite de-

composition may be obtained with varied combinations of temperature and time, a comparison of the hardness values (Tables IV and V) for given martensite contractions (Figs. 5 and 6) indicates that higher hardness can be achieved with low tempering temperatures and long times than with high temperatures and short times. On the other hand, the required time to accomplish a predetermined shrinkage increases rapidly as the temperature is decreased, and hence practical heat treatment cannot go too far in this direction, despite the superior hardness attainable. For example, in steel T, a martensite contraction of 640 microinches/in may be produced by tempering for 1 hour at 300 °F, 3 hours at 250 °F, 60 hours at 200 °F, or 300 hours at 150 °F. The corresponding hardness values are Rockwell C-64.0, C-65.1, C-65.8 and C-66.3, respectively.

The rate of martensite shrinkage at a given temperature depends upon the chemistry of the martensite. Comparing the plain carbon and ball bearing steels studied here, the rate of shrinkage is much slower in the latter. This is not because of more sluggish precipitation from the martensite, but because the alloy-bearing martensite has a larger capacity for carbon at the end of the first stage of tempering and hence less precipitation takes place during tempering at the low temperature usually employed for low alloy tool steels.

The decomposition of retained austenite at room temperature causes an expansion effect which tends to counterbalance the martensite shrinkage. However, the austenite behavior is greatly influenced by the quenching conditions because the isothermal transformation is really a hangover of the main hardening reaction. In fact, the isothermal product is now believed to be martensite (bainite is not formed appreciably below 300 °F), and the accompanying expansion is undoubtedly a major factor in the cracking-propensity of hardened tool steels during aging at room temperature after the quench. The desirability of tempering soon after the hardening is thereby indicated.

The amount of retained austenite and its rate of decomposition at low aging temperatures are appreciably affected by arrested hardening. Interrupting the quench for only 5 minutes at 125 °F or above, followed by air cooling to the ambient, increases the quantity of retained austenite. Furthermore, its subsequent decomposition persists for longer periods of time than in the case of direct quenching to room temperature. Thus, deviations in quenching practice may cause significant differences in dimensional behavior.

The expansion due to this isothermal reaction is relatively large considering the small quantities of austenite involved. The magnitude of the effect is easily seen if the austenite decompositions plotted in Figs. 14 and 15 are multiplied by the conversion factors in Table VII. The combination of such austenite expansions and the martensite contractions, previously discussed, accounts quantitatively for the net changes in length actually measured during the aging.

Conclusions

1. The separate contributions of martensite decomposition (contraction) and retained austenite decomposition (expansion) to the phenomenon of dimensional instability on aging or tempering have been quantitatively resolved and analyzed.
2. During the first stage of tempering, martensite decomposition proceeds by the rejection of carbon at an increasing rate with increasing temperatures until the end of the first stage is reached. At this point, the further rejection of carbon from the depleted martensite lattice almost ceases before the formation of cementite begins.
3. The solubility of carbon in martensite at the end of the first stage of tempering increases slightly with increasing temperature and with chromium content. The martensite at the end of the first stage of tempering is visualized as being in pseudo-equilibrium with a transition precipitate.
4. The decomposition of martensite follows a first-order equation with the reaction-rate constant possibly influenced by the stress relief that occurs during the tempering. The kinetics of the process may be represented by the rate equation:

$$-\frac{dc}{dt} = K \cdot \frac{c}{t^S}$$

   Both K and S are temperature-dependent.
5. The heat of activation for the martensite decomposition has been determined as about 8300 calories/mol. This is approximately half of the published heat of diffusion for carbon in ferrite.
6. The austenite-martensite reaction on hardening does not cease completely when the cooling stops. As much as 5% of retained austenite may transform isothermally into martensite at room temperature. This isothermal transformation proceeds rapidly

during the first 1.5 hours after the quench, but continues at a diminishing rate for several months. Its rate is not measurably affected by tempering above room temperature.

7. If the tempering temperature and/or time are increased sufficiently, the well-known decomposition of the austenite into bainite takes place with a heat of activation of about 38,000 calories/mol. This process (i.e., the so-called second stage of tempering) is quite distinguishable from the earlier isothermal decomposition of the austenite into martensite.

Acknowledgments

The authors would like to acknowledge the assistance of the Sheffield Foundation of Dayton, Ohio, for a grant-in-aid which made this work possible. They are also grateful to the Pratt and Whitney Division of Niles-Bement-Pond Company, and to the Taft-Peirce Manufacturing Company for their co-operation and interest in this program. The quenching dilatometer was a gift of the Metallurgical Department of the American Brake Shoe Company and is also gratefully acknowledged.

References

1. S. G. Fletcher and M. Cohen, "The Effect of Carbon on the Tempering of Steel," Transactions, American Society for Metals, Vol. 32, 1944, p. 333-357.
2. D. P. Antia, S. G. Fletcher and M. Cohen, "Structural Changes During the Tempering of High Carbon Steel," Transactions, American Society for Metals, Vol. 32, 1944, p. 290-324.
3. M. Cohen, "Tempering of Tool Steels," Metal Progress, Vol. 51, May 1947, p. 781-788 and June 1947, p. 962-968.
4. W. Fraenkel and E. Heymann, "Zur Kinetik der Anlass Vorgänge im Stahl," *Zeitschrift anorganische Chemie,* Vol. 134, 1924, p. 137.
5. G. Kurdjumov and L. Lyssak, "The Application of Single Crystals to the Study of Tempered Martensite," *Journal,* Iron and Steel Institute, Vol. 156, Part 1, May 1947, p. 29-36.
6. B. L. Averbach, M. Cohen and S. G. Fletcher, "The Dimensional Stability of Steel. Part III—Decomposition of Martensite and Austenite at Room Temperature," Transactions, American Society for Metals, Vol. 40, 1948, p. 728-757.
7. B. L. Averbach and M. Cohen, "X-Ray Determination of Retained Austenite by Integrated Intensities," *Metals Technology,* T.P. 2342, Feb. 1948.
8. S. G. Fletcher and M. Cohen, "The Dimensional Stability of Steel. Part I—Subatmospheric Transformation of Retained Austenite," Transactions, American Society for Metals, Vol. 34, 1945, p. 216-236.
9. S. G. Fletcher, B. L. Averbach and M. Cohen, "The Dimensional Stability of Steel. Part II—Further Experiments on Subatmospheric Transformation," Transactions, American Society for Metals, Vol. 40, 1948, p. 703.

10. W. A. Johnson and R. F. Mehl, "Reaction Kinetics in Processes of Nucleation and Growth," *Transactions*, American Institute of Mining and Metallurgical Engineers, Vol. 135, 1939, p. 416.
11. M. Avrami, "Granulation, Phase Change, and Microstructure," *Journal of Chemical Physics*, Vol. 9, 1941, p. 177.
12. E. A. Rominski and H. F. Taylor, "Stress Relief and the Steel Casting," *Transactions*, American Foundrymen's Association, Vol. 51, 1943, p. 709.
13. F. Hargreaves, "The Ball Hardness and the Cold Working of Soft Metals and Eutectics," *Journal*, Institute of Metals, Vol. 39, 1928, p. 301.
14. A. B. Greninger and A. R. Troiano, "Kinetics of the Austenite to Martensite Transformation in Steel," TRANSACTIONS, American Society for Metals, Vol. 28, 1940, p. 537.
15. E. P. Klier and A. R. Troiano, "Ar" in Chromium Steels," *Transactions*, American Institute of Mining and Metallurgical Engineers, Vol. 162, 1945, p. 175.
16. A.S.M. Metals Handbook, 1939, p. 407A-408.
17. C. Zener, "Equilibrium Relations in Medium Alloy Steels," *Transactions*, American Institute of Mining and Metallurgical Engineers, Vol. 167, 1946, p. 513.
18. J. L. Snoek, "Effect of Small Quantities of Carbon and Nitrogen on the Elastic and Plastic Properties of Iron," *Physica*, Vol. 8, 1941, p. 711.
19. R. A. Flinn, E. Cook and J. A. Fellows, "A Quantitative Study of Austenite Transformation," TRANSACTIONS, American Society for Metals, Vol. 31, 1943, p. 41.
20. A. B. Greninger, "The Martensite Thermal Arrest in Iron-Carbon Alloys and Plain Carbon Steels," TRANSACTIONS, American Society for Metals, Vol. 30, 1942, p. 1.

DISCUSSION

Written Discussion: By Clarence Zener, Institute for the Study of Metals, The University of Chicago, Chicago.

Dimensional arguments alone show that one would not expect the "heat of activation" of the constant K, Q_K, to be comparable to the heat of activation for the diffusion of carbon in iron, Q_C. One can fairly compare the heats of activation only of quantities having the same dimensions in time. The diffusion coefficient has dimensions of (length^2/time). On the other hand, K has dimensions of (time)$^{-(1-s)}$. If we, therefore, introduce a new constant τ by the relation

$$K = 1/\tau^{(1-s)},$$

τ^{-1} will have dimensions of (time)$^{-1}$, and we might, therefore, expect its heat of activation, Q_τ, to be comparable to Q_C. The two heats of activation Q_K and Q_τ are related by

$$Q_\tau = Q_K/(1 - s)$$

From the measurements at the lower temperature one thereby obtains

$$Q_\tau \doteq 3Q_K \doteq 25{,}000 \text{ cal/mol},$$

which value is encouragingly close to Snoek's value for Q_C.

One cannot help but wonder whether the second heat of activation

found by the authors, Qs, is merely a result of certain assumptions in their analyses, rather than being a heat of activation of some real rate process. It is clear that in their Equation V the exponent s cannot be a true constant, but must gradually increase with time, or otherwise the stress σ would become negative. We are accordingly led to consider the following equation, which is slightly more general than Equation VIII:

$$y(t) = a[1 - e^{-f(t/\tau)}]. \qquad \text{Equation A}$$

If the only influence of temperature is through the diffusion coefficient of carbon in iron, then temperature will enter this equation only through

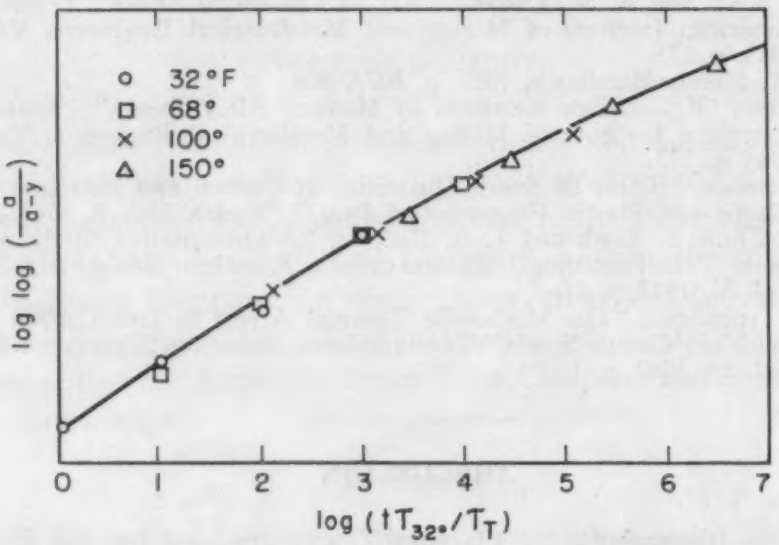


Fig. 16—Replotting of the Four Lowest Temperature Points from the Authors' Fig. 7.

the time of relaxation τ. In this case all the curves in Fig. 7 should lie upon a common curve when plotted as a function of log (t/τ) rather than of log t. Upon taking the heat of activation of τ^{-1} to be 23,000 cal/mol, the experimental points in Fig. 7 for the four lowest temperatures are indeed found to lie upon a common curve, as illustrated in Fig. 16. The observations at the four lowest temperatures are thus consistent with the picture that the only effect of temperature is upon the rate of diffusion of carbon. The invalidity of Equation A at higher temperatures indicates that above 150 °F temperature has an effect other than upon the diffusion rate of carbon.

Written Discussion: By S. L. Hoyt, technical advisor, Battelle Memorial Institute, Columbus, Ohio.

In our work at Battelle on the factors that promote cracking alongside welds in hardenable steels, we have come to understand it as a process which consists, in part, of the retention of austenite in the heat-affected zone. That austenite would thereupon precipitate out its dissolved hydrogen and initiate the crack. Obviously, this involves the transformation of that austenite upon standing at room temperature. We

have run into unexpected resistance to the acceptance of this idea on the basis that retained austenite is held not to transform in that way.

If there is something basically incorrect in our idea, we would naturally like to know about it and I would like to ask the authors if retained austenite cannot actually transform at room temperature.

Written Discussion: By A. R. Troiano, professor of metallurgy, University of Notre Dame, Notre Dame, Ind.

I note, in Fig. 6, that the curves for the isothermal decomposition of martensite at 400 and 500 °F have an anomalous plateau. This cannot be explained by either the effect of the first stage of tempering, or by the decomposition of retained austenite, since this discontinuity occurs after the first stage of tempering, at these temperatures, and the curves have been calculated after subtracting the effect of retained austenite.

Although the temperatures involved seem to be quite low, have the authors considered that this may be due to a change in the nature of the carbide? To check whether this phenomenon or some modification of it may be operative in the lower (32 to 200 °F) temperature range, it might be instructive to observe the behavior of a freshly quenched steel which had 100% martensite on quenching to room temperature.

Authors' Reply

For a strict comparison of heats of activation, it is preferable to consider quantities having the same dimensions. The diffusion coefficient has dimensions of length^2/time, and Dr. Zener has adjusted only the time dimension. Since the jump distance varies only slightly with temperature, this correction is probably adequate. Nevertheless, it should be noted that even with this adjustment of the time parameter, Q_T (25,000 cal/mol) is still considerably different from Snoek's diffusion value of Q_C (18,000 cal/mol), and such a discrepancy suggests that the diffusion of carbon is not the only temperature-dependent factor involved in the tempering process.

Dr. Zener's alternate treatment of our rate data in terms of a relaxation time, τ, is applicable only in the temperature range of 32 to 150 °F. The equation which was developed in the paper, however, reproduces the process over a larger temperature range (32 to 300 °F) and describes the volume changes occurring during the entire first stage of tempering. The alternate treatment is capable of explaining only the initial portions of the process, and also overlooks the possibility that nucleation and growth may be involved. Tempering can logically be assumed to occur by nucleation and growth, and our equation describes such a reaction, with certain modifications that are peculiar to martensite.

The authors cannot provide positive assurance to Dr. Hoyt that his hardenable welding steels contain retained austenite in the heat-affected zone and that this austenite undergoes isothermal transformation at room temperature. Our experimental work has been primarily devoted to the high carbon steels, and although we have some evidence that low carbon steels do retain austenite we have not tested them for isothermal decom-

position. In principle, it would seem that such decomposition might be expected.

In reply to Dr. Troiano, the plateaus in the 400 and 500 °F curves for the decomposition of 100% martensite in Fig. 6 are probably connected with a later step in the tempering of martensite. The composition of the carbon-rich precipitate probably changes during the tempering, but a calculation of the dilation accompanying any reasonable change in the carbide density shows that this effect is small compared to the shrinkage of the martensite lattice as it rejects carbon. The 400 and 500 °F curves were not involved in the main results of the paper, since the first stage of tempering is completed within a few minutes at these temperatures. A more detailed dilatometric study of these later changes is now in progress.

THE DIMENSIONAL STABILITY OF STEEL
PART IV—TOOL STEELS

By B. S. Lement, B. L. Averbach and M. Cohen

Abstract

Dimensional changes which occur in four low alloy and two high alloy tool steels on aging at 68 °F (20 °C) as long as 1 year after selected heat treatments have been determined. The effects of these treatments are explained on the basis of martensite decomposition and retained austenite transformation.

In low alloy tool steels, dimensional stability is increased by the presence of such alloying elements as chromium, tungsten and manganese and by the use of as high a tempering temperature as hardness requirements will permit. Refrigeration, whether carried out prior to or after single tempering at temperatures below about 300 °F (150 °C), increases the rate of contraction over that obtained without refrigeration; however, refrigeration does result in increased hardness. Long-time tempering at low temperatures with or without refrigeration results in a superior combination of hardness and dimensional stability as compared to short-time tempering at high temperatures. Arrested quenching during hardening as compared with direct quenching to room temperature results in lowered dimensional stability; however, by use of higher tempering temperatures after arrested quenching, dimensional stability can be improved at the expense of hardness. The disadvantage of lowered hardness can be avoided by use of long-time tempering and refrigeration cycles after arrested quenching.

In high alloy tool steels, attainment of dimensional stability is rendered difficult if tempering results in secondary hardening. Refrigeration following the original hardening operation, by causing the transformation of a large amount of retained austenite, is helpful in overcoming the difficulty. Multiple tempering, including oil quenching from the tempering temperature, was found

---

A paper presented before the Thirtieth Annual Convention of the Society, held in Philadelphia, October 23 to 29, 1948. Of the authors, B. S. Lement is research assistant, Department of Metallurgy, B. L. Averbach is assistant professor of physical metallurgy, and M. Cohen is professor of physical metallurgy, Massachusetts Institute of Technology, Cambridge, Mass. Manuscript received May 24, 1948.

effective in promoting dimensional stability in high speed steel; whereas a cyclic treatment involving refrigeration, tempering, and oil quenching from the tempering temperature is best for high carbon, high chromium die steel.

OBTAINING adequate dimensional stability in a high precision tool, gage, or die is often a difficult problem because such considerations as steel composition, mechanical properties, and tool design impose practical limitations on the treatments that can be used to confer dimensional stability. To arrive at the over-all optimum treatment requires an intimate knowledge of the several factors affecting dimensional stability. The present investigation was undertaken to determine the influence of various treatments on tool steels, and constitutes Part IV of a series of papers designed to supply quantitative information regarding the dimensional stability of steel.

The published work on dimensional properties of tool steels has been primarily concerned with the behavior during hardening, tempering, and refrigeration, rather than during aging at room temperature after the final treatment. Scott (1)[1] pioneered in this field by investigating the length changes which take place in a wide variety of low alloy tool steels, and more recently Scott and Gray (2) determined the dimensional variations that occur during the heat treatment of two air hardening chromium tool steels. Ameen (3) and Butler (4) also made observations of this type in several tool and die steels, and Gippert and Butler (5) investigated the dimensional changes in high carbon, high chromium die steels caused by subzero refrigeration.

Part I (6) of the present series was concerned mainly with the phenomenon of stabilization which occurs in the retained austenite of hardened steel if allowed to age at room temperature prior to subzero cooling. Such aging lowers the temperature at which the retained austenite starts to transform into martensite on subsequent refrigeration and also reduces the total amount of martensite formed. Charts showing the relationships between the extent of austenite decomposition, the subcooling temperature, and the prior holding time at room temperature were presented.

Part II (7) dealt with the effect of austenitizing temperature, tempering temperature, and tempering time on the stabilization of retained austenite against transformation on subzero cooling. It was found that for low austenitizing temperatures it is possible to transform most of the austenite by cold treatment shortly after the hard-

[1]The figures appearing in parentheses pertain to the references appended to this paper.

ening quench; whereas for high austenitizing temperatures only a fraction of the retained austenite is transformed by subcooling. Moreover, the higher the tempering temperature, or the longer the tempering time, the greater is the degree of stabilization achieved. Essentially complete stabilization can be attained by tempering, but the required tempering temperature increases with the austenitizing temperature.

Part III (8) considered the influence of both the quantity and condition of the martensite as well as of the retained austenite on the dimensional stability. The over-all changes in length observed during aging at room temperature were treated as an algebraic summation of a contraction caused by the decomposition of martensite and an expansion caused by the isothermal transformation of retained austenite into a more voluminous product. The isothermal martensite contraction rate is found to be initially high but it decreases with aging time. During tempering, martensite contracts quite markedly but the subsequent decomposition on aging at room temperature takes place as if all of the reaction occurred at room temperature. Therefore, the martensite reaction is said to be additive. Below the temperature range of the retained austenite decomposition into bainite (the second stage of tempering), tempering transforms a small portion of the retained austenite, but tends to stabilize the remainder against further transformation at room temperature. The degree of such stabilization increases with tempering temperature, so that either a net growth or a net shrinkage can be observed on aging at room temperature, depending on the relative amounts of austenite and martensite and on the previous tempering which they have undergone.

The present paper describes the dimensional behavior of six tool steels during aging at room temperature after various hardening, tempering, and refrigeration treatments. These treatments were designed to reveal the effects of tempering temperature, multiple tempering, refrigeration both prior to and following tempering, arrested quenching including martempering, and combinations of tempering and refrigeration cycles. It should be borne in mind that, for the purposes of this discussion, dimensional stability is defined as the ability of a steel to maintain a given size over a long period of time after it has been heat treated and finished to final dimensions. This does not include the "movement" which occurs during hardening, nor the distortions which may result from stress relief.

Experimental Details

Chemical Composition—The chemical compositions of the six tool steels are listed in Table I. These materials were obtained in the form of ⅜-inch diameter drill rod, annealed and centerless ground.

Table I
Chemical Composition of Steels Investigated

Tool Steel	C	Si	Mn	S	P	W	Cr	V	Mo	Co
Plain Carbon	1.07	0.23	0.25	0.014	0.011	....	....	....	....	....
Ball Bearing	1.04	0.34	0.35	0.012	0.014	....	1.54	0.20	....	....
Tungsten Die	1.24	0.39	0.33	0.007	0.022	1.59	0.76	0.20	0.22	....
Manganese Die	0.94	0.21	1.17	0.016	0.020	0.82	0.59	0.24	....	....
M-2 High Speed	0.79	0.34	0.27	0.010	0.020	5.75	4.18	1.52	4.68	....
High Carbon, High Chromium Die	1.54	0.43	0.30	0.007	0.015	....	12.0	0.77	0.99	0.40

Hardening Treatments—The austenitizing temperatures, time at temperature, and quenching media used for the six steels are given in Table II. Such hardening operations are representative of normal commercial practice for these tool steels. Data on the percentage of austenite retained as a result of direct quenching to room tempera-

Table II
Hardening Treatments and Retained Austenite Contents

Tool Steel	Austenitizing Temperature, °F	Time at Austenitizing Temperature in Minutes	Regular Quenching Medium	Retained Austenite Content, % by Volume*			
				Quenched to +68 °F	Quenched to +68 °F and Cooled to −321 °F	Quenched to +125 °F and Air-Cooled to +68 °F	Salt-Quenched to 450 °F and Air-Cooled to +68 °F
Plain Carbon	1450	30	water	9	3	14	....
Ball Bearing	1550	30	oil	7	2	9	10.5
Tungsten Die	1600	30	oil	13.5	6.5	....	....
Manganese Die	1450	30	oil	8.5	5.5	10.5	11
M-2 High Speed	2220	3	oil	19.5	8	...	....
High Carbon, High Chromium Die	1900	30	air	....	..	....	....

*Austenite determinations made by integrated X-ray intensities (9).

ture, arrested quenching, and refrigeration at −321 °F (−195 °C) are also included in Table II. The retained austenite contents were determined with the aid of a recently published X-ray technique (9) and are somewhat higher than previous determinations because of the increased sensitivity of the newer method.

Method of Measurement—Determination of dimensional sta-

bility was carried out by measuring the changes in length that occur in specimens ⅜ inch diameter by 4.000 ± .001 inches long on aging at 68 °F (20 °C) following heat treatment. The ends of the specimens were spherically ground to a radius of 2 inches, and precision length measurements were made with a gage comparator of × 5000 magnification. In essence, this gage compared the length of the specimen with a 4.120-inch standard block independently calibrated to the nearest microinch. Deviations from this standard could be determined with an accuracy of 5 microinches, which for a 4-inch specimen corresponds to a relative accuracy of about 1 microinch per inch. Changes in length expressed in microinches per inch are reported for 1 day, 1 week, 1 month, 3 months and 1 year of aging at 68 °F following heat treatment. The specimen-length after 1 day of aging at room temperature is arbitrarily selected as the starting point, and hence the change in length for 1 day is reported to be zero in all cases, although variations are known to occur during the first day (10). This procedure was adopted because, as a practical matter, most precision tools and gages are not finish ground, or otherwise brought to final dimensions, within the first day after heat treatment.

Dimensional Stability of Low Alloy Tool Steels

Tempering Following Quenching to Room Temperature—The effect of tempering temperature on the dimensional stability of the plain carbon and ball bearing tool steels was studied in detail. A series of specimens of each material was quenched to room temperature and then tempered in the range of 68 to 500 °F (20 to 260 °C). The length changes observed during aging at room temperature after the tempering are given in Table III.[2]

The dimensional behavior of both the plain carbon and ball bearing steels can be understood on the basis of the internal reactions which are now known to occur (8, 10). As indicated by Table II, the structure of the plain carbon tool steel water-quenched to room temperature consists of about one-tenth retained austenite and nine-tenths untempered martensite. Some of the retained austenite transforms isothermally at 68 °F, causing an expansion; however, this effect is masked by the much faster rate of contraction due to the isothermal decomposition of the larger amount of martensite present,

[2]The dimensional stability data are presented in the form of tables, rather than graphs, to facilitate their utilization in engineering and design problems.

Table III
Effect of Tempering Following Quenching to Room Temperature on Dimensional Stability at +68 °F

Tool Steel	Temper	Rockwell "C" Hardness	Total Change in Length on Aging at 68 °F — Microinches per Inch — 1 Day	1 Week	1 Month	3 Months	1 Year
Plain Carbon	1 hour at 68 °F	66	0	−90	−175	−265	−405
Plain Carbon	1 hour at 150 °F	66.5	0	−26	− 86	−161	−292
Plain Carbon	1 hour at 200 °F	67	0	− 5	− 15	− 36	− 95
Plain Carbon	1 hour at 250 °F	65	0	− 2	− 6	− 11	− 19
Plain Carbon	1 hour at 300 °F	64.5	0	− 2	− 3	− 6	− 10
Plain Carbon	1 hour at 350 °F	63.5	0	− 2	− 3	− 6	− 9
Plain Carbon	1 hour at 400 °F	63	0	0	− 2	− 3	− 7
Plain Carbon	1 hour at 500 °F	61.5	0	0	− 2	− 3	− 3
Ball Bearing	1 hour at 68 °F	64	0	−10	− 42	− 82	−110
Ball Bearing	1 hour at 150 °F	65	0	+ 5	+ 1	− 11	− 38
Ball Bearing	1 hour at 200 °F	65	0	+ 6	+ 10	+ 12	+ 20
Ball Bearing	1 hour at 250 °F	65	0	+ 3	+ 5	+ 7	+ 6
Ball Bearing	1 hour at 300 °F	63.5	0	0	− 1	− 1	− 2
Ball Bearing	1 hour at 350 °F	63	0	0	− 1	− 1	− 2
Ball Bearing	1 hour at 400 °F	62	0	0	− 1	− 1	− 1
Ball Bearing	1 hour at 500 °F	60	0	0	− 1	− 1	− 1
Manganese Die	1 hour at 300 °F	62.5	0	0	− 1	− 1	− 3
Tungsten Die	1 hour at 300 °F	64.5	0	+ 1	0	− 1	− 2

and a net contraction occurs. As a result of tempering, the rates of both these reactions are decreased at room temperature (8). With increased tempering temperature, progressively more martensite decomposition occurs during tempering and the rate of the subsequent martensite decomposition at 68 °F is reduced to that which would occur after an enormously long time of aging at this temperature in the as-hardened condition. The effect of increasing the tempering temperature on the retained austenite is to transform small portions and render the remainder progressively more stabilized against transformation at room temperature. If tempering is carried out above 250 °F (120 °C), the plain carbon steel exhibits a fairly high degree of dimensional stability because the subsequent martensite decomposition and transformation of the retained austenite at 68 °F not only occur at a very slow rate, but tend to counterbalance each other.

Similar reactions take place in the ball bearing steel, but with certain differences in detail. Since, as shown in Table II, the ball bearing steel contains less retained austenite than the plain carbon steel in the as-quenched condition, it might be expected that the ball bearing steel would contract at a somewhat faster rate. Actually what happens in the ball bearing steel is that, for low tempering temperatures, the austenite transformation at room temperature is masked to a lesser extent by the martensite decomposition than in the plain carbon steel, and net expansions result. This occurs even on aging at 68 °F, but only during the first day (8), and hence is

Table IV
Effect of Tempering Following Refrigeration at −321 °F on Dimensional Stability at +68 °F

Tool Steel	Temper	Rockwell "C" Hardness	Total Change in Length on Aging at +68 °F — Microinches per Inch — 1 Day	1 Week	1 Month	3 Months	1 Year
Plain Carbon	1 hour at 68 °F	67	0	−120	−240	−350	−525
Plain Carbon	1 hour at 150 °F	68	0	− 50	−127	−220	−380
Plain Carbon	1 hour at 200 °F	68	0	− 10	− 30	− 58	−145
Plain Carbon	1 hour at 250 °F	68	0	− 2	− 7	− 15	− 21
Plain Carbon	1 hour at 300 °F	67.5	0	− 2	− 4	− 9	− 13
Plain Carbon	1 hour at 350 °F	66	0	− 2	− 4	− 8	− 9
Plain Carbon	1 hour at 400 °F	63.5	0	− 1	− 3	− 5	− 6
Plain Carbon	1 hour at 500 °F	59.5	0	− 1	− 3	− 5	− 5
Ball Bearing	1 hour at 68 °F	65	0	− 50	− 90	−135	−195
Ball Bearing	1 hour at 150 °F	65	0	− 9	− 25	− 42	− 69
Ball Bearing	1 hour at 200 °F	65	0	− 5	− 11	− 18	− 44
Ball Bearing	1 hour at 250 °F	65	0	− 3	− 6	− 9	− 11
Ball Bearing	1 hour at 300 °F	64	0	− 2	− 4	− 6	− 6
Ball Bearing	1 hour at 350 °F	63.5	0	− 2	− 4	− 5	− 6
Ball Bearing	1 hour at 400 °F	60.5	0	− 1	− 3	− 4	− 4
Ball Bearing	1 hour at 500 °F	59	0	0	− 1	− 1	− 1
Manganese Die	1 hour at 300 °F	63	0	− 3	− 6	− 9	− 11
Tungsten Die	1 hour at 300 °F	67.5	0	− 3	− 5	− 7	− 9

not indicated in Table III. The reason for the difference in behavior of the plain carbon and ball bearing steels will be discussed in the following section dealing with the effect of refrigeration. On tempering above 250 °F (120 °C), the rates of the two compensating reactions become very slow and a high degree of dimensional stability is imparted to the ball bearing steel.

Both the tungsten and manganese die steels were tested for dimensional stability after tempering at 300 °F (150 °C). As shown in Table III, these steels are found to possess dimensional stability equivalent to that of the ball bearing steel given the same treatment. Of these four low alloy tool steels, plain carbon tool steel appears to have the lowest dimensional stability after a 300 °F temper.

Tempering Following Refrigeration—The effect of tempering following cold treatment on the dimensional stability of the plain carbon and ball bearing tool steels was also studied in detail, and the results are given in Table IV. Specimens of both steels were quenched to room temperature, cooled immediately to −321 °F (−195 °C), held for 1 hour, returned to room temperature, and tempered in the range of 68 to 500 °F (20 to 260 °C). As shown in Table II, refrigeration results in transformation of the major portion but not all of the retained austenite present in the as-quenched steels.

As compared with the straight quench-and-temper treatment, tempering following refrigeration results in an increased rate of contraction for tempering temperatures up to about 300 °F (150 °C).

The difference in behavior of refrigerated and unrefrigerated steels is readily understood, since the subcooling results in the transformation of most of the retained austenite present in these steels. Thus a larger amount of untempered martensite becomes available for contraction than in the case without the cold treatment and, moreover, there is relatively little austenite present to cause expansion. Tempering above 250 °F (120 °C) substantially retards the rate of decomposition of the martensite at 68 °F and stabilizes what little austenite remains after refrigeration.

The much slower rate of contraction of the ball bearing steel after refrigeration as compared with the plain carbon steel is attributed to the difference in behavior of the martensites in the two steels. It has been shown (10) that whereas completion of the first stage of tempering in the two steels is accomplished in about the same time at a given tempering temperature, the amount of contraction that occurs in the alloy martensite is considerably smaller than that in the plain carbon steel. In other words, despite the fact that the carbon content of both martensites is about the same, less carbon is rejected from the martensite in the ball bearing steel during the first stage of tempering than in the plain carbon steel (10).

From the standpoint of dimensional stability, any reduction in the martensite decomposition is of definite advantage since a slower rate of over-all length change is then attainable, once the retained austenite has been either stabilized or removed by refrigeration. The relationship between steel composition and the rate of martensite shrinkage can be shown by a comparison of specimens that have been refrigerated and allowed to age at room temperature. In Table V,

Table V

Effect of Refrigeration Temperature on Dimensional Stability at +68 °F, Without Tempering

Tool Steel	Refrigeration	Temper	Rockwell "C" Hardness	Total Change in Length on Aging at +68 °F, Microinches per Inch				
				1 Day	1 Wk.	1 Mo.	3 Mos.	1 Yr.
Plain Carbon	None, as-hardened	None	66	0	− 90	−175	−265	−405
Plain Carbon	Cooled to −123 °F	None	67	0	−110	−205	−310	−480
Plain Carbon	Cooled to −321 °F	None	66.5	0	−120	−240	−350	−525
Ball Bearing	None, as-hardened	None	65	0	− 10	− 42	− 82	−110
Ball Bearing	Cooled to −123 °F	None	66	0	− 36	− 73	−110	−173
Ball Bearing	Cooled to −321 °F	None	66	0	− 50	− 90	−135	−195
Manganese Die	None, as-hardened	None	64	0	− 14	− 30	− 48	− 87
Manganese Die	Cooled to −123 °F	None	64.5	0	− 36	− 71	−103	−158
Manganese Die	Cooled to −321 °F	None	65	0	− 50	− 91	−128	−183
Tungsten Die	None, as-hardened	None	66	0	− 52	−101	−156	−259
Tungsten Die	Cooled to −123 °F	None	67.5	0	− 88	−162	−230	−355
Tungsten Die	Cooled to −321 °F	None	67.5	0	− 94	−173	−248	−362

such comparisons are offered for specimens of the four low alloy tool steels which have been refrigerated at —321 °F (—195 °C) to convert as much of the retained austenite as possible to martensite. It is seen here that the martensite in the manganese die steel appears to have about the same rate of decomposition as in the ball bearing steel, while that of the tungsten die steel occupies an intermediate position between these alloy compositions and the plain carbon steel. Evidently, tungsten and manganese, like chromium (10), increase the capacity of martensite to retain carbon at the end of the first stage of tempering, and therefore reduce the extent of precipitation (contraction) during such tempering.

Although refrigeration enhances the contraction tendency as compared with the straight quench-and-temper treatment, it does raise the hardness in some of the steels. The increment in hardness for the plain carbon and tungsten die steels is of the order of 2 to 3 Rockwell C points, whereas no significant improvement is found in the ball bearing and manganese die steels. The hardness increment in the plain carbon steel persists only for tempering temperatures below 400 °F (205 °C). Since increased hardness obtained by refrigeration may be beneficial to wear resistance, it may be advantageous to use such a treatment, provided tempering is then carried out at a temperature which confers a degree of dimensional stability equivalent to that obtained without refrigeration. For example, if the plain carbon steel is tempered at 350 °F (175 °C) after refrigeration, a hardness of Rockwell C-66 is achieved, whereas without refrigeration, such tempering produces a hardness of only Rockwell C-63.5. Yet, essentially the same dimensional stability is attained by the two treatments.

Refrigeration Temperature—The influence of refrigeration temperature on dimensional stability is shown in Table V. Results on specimens after (a) hardening, (b) hardening and subcooling to —123 °F (—92 °C), and (c) hardening and subcooling to —321 °F (—195 °C) are presented. In each steel, cooling to —123 °F results in an increased rate of contraction as compared with the as-hardened state. Likewise, cooling to —321 °F produces an increased rate of contraction as compared with cooling to —123 °F.

Subcooling to —123 °F transforms part of the retained austenite and consequently there is not only less retained austenite to cause expansion but also more untempered martensite to cause contraction on aging at 68 °F. Since the temperature at which the sub-

Table VI
Effect of Refrigeration Following Tempering on Dimensional Stability at +68 °F

Tool Steel	First Temper	Refrigeration	Second Temper	Rockwell "C" Hardness	Total Change in Length on Aging at +68 °F, Microinches per Inch				
					1 Day	1 Wk.	1 Mo.	3 Mos.	1 Yr.
Plain Carbon	1 hr. at 300 °F	Cooled to −123 °F	None	65.5	0	−4	− 8	−10	−14
Plain Carbon	1 hr. at 300 °F	Cooled to −321 °F	None	65.5	0	−6	−10	−14	−17
Plain Carbon	1 hr. at 300 °F	Cooled to −123 °F	1 hr. at 300 °F	65.5	0	−5	− 8	−10	−14
Plain Carbon	1 hr. at 300 °F	Cooled to −321 °F	1 hr. at 300 °F	65.5	0	−5	− 8	−11	−16
Ball Bearing	1 hr. at 300 °F	Cooled to −123 °F	None	64	0	−3	− 5	− 7	− 9
Ball Bearing	1 hr. at 300 °F	Cooled to −321 °F	None	64	0	−2	− 4	− 6	− 8
Ball Bearing	1 hr. at 300 °F	Cooled to −123 °F	1 hr. at 300 °F	63.5	0	−1	− 2	− 4	− 6
Manganese Die	1 hr. at 300 °F	Cooled to −123 °F	None	62.5	0	−3	− 5	− 7	− 8
Manganese Die	1 hr. at 300 °F	Cooled to −321 °F	None	63	0	−5	− 8	−10	−13
Manganese Die	1 hr. at 300 °F	Cooled to −123 °F	1 hr. at 300 °F	62	0	−2	− 5	− 6	− 8
Tungsten Die	1 hr. at 300 °F	Cooled to −123 °F	None	65.5	0	−3	− 6	− 8	−10
Tungsten Die	1 hr. at 300 °F	Cooled to −321 °F	None	65	0	−5	− 8	−11	−14
Tungsten Die	1 hr. at 300 °F	Cooled to −123 °F	1 hr. at 300 °F	64.5	0	−3	− 5	− 7	− 9
Tungsten Die	1 hr. at 300 °F	Cooled to −321 °F	1 hr. at 300 °F	64.5	0	−2	− 4	− 6	− 8

zero austenite transformation ceases is between —250 and —260 °F for these compositions (6), cooling to —321 °F achieves the transformation of all of the retained austenite that is convertible by refrigeration. The greater content of untempered martensite and the elimination of most of the retained austenite cause the increased rate of contraction at room temperature following cooling to —321 °F as compared with the —123 °F treatment.

With increased tempering temperature following refrigeration, it would be expected that the difference in contraction rate at 68 °F of specimens subcooled to —123 °F as compared with —321 °F would tend to be wiped out. This is indicated by the fact that there is only a small difference between the contraction rates of nonrefrigerated and refrigerated (—321 °F) specimens if tempering is carried out at 300 °F (150 °C) or above (Tables III and IV). Accordingly, from a commercial standpoint, subcooling to —123 °F may be used instead of the more difficultly attained lower temperature.

Refrigeration Following Tempering—Based on a comparison of Tables VI and III, it appears that the effect of refrigeration following the straight quench-and-temper treatment is to increase slightly the rate of contraction at 68 °F in the four steels over that obtained

Table VII
Effect of Long-Time Tempering and Refrigeration Cycles on Dimensional Stability of Ball Bearing Tool Steel at +68 °F

Treatment	Tempering and Refrigeration Cycle	Number of Cycles	Rockwell "C" Hardness	Total Change in Length on Aging at +68 °F —Microinches per Inch— 1 Day	1 Wk.	1 Mo.	3 Mos.
VII-A	Tempered 10 hours continuously at 250 °F	1	64.5	0	0	0	0
VII-B	Tempered 1 hour at 250 °F	10	65	0	0	0	−1
VII-C	(1) Tempered 1 hour at 250 °F (2) Cooled to −321 °F	10	64.5	0	−3	−5	−7
VII-D	(1) Cooled to −321 °F (2) Tempered 1 hour at 250 °F	10	65	0	0	0	0

without refrigeration. With the exception of the ball bearing steel, a slight increase in the rate of contraction occurs if a refrigeration temperature of −321 °F (−195 °C) is used instead of −123 °F (−92 °C). Subcooling following tempering evidently converts only a small amount of austenite into martensite, the effect of the cold treatment being considerably curtailed by the stabilization accompanying the temper. As shown in Table VI, a second temper, performed after refrigeration, does not quite reduce the rate of contraction to that obtained by the straight quench-and-temper treatment. Therefore, here again, the cold treatment is not helpful to dimensional stability, except on the basis that somewhat greater hardness may be realized in some cases.

Long-Time Tempering and Refrigeration Treatments—Table VII indicates the effect of four long-time tempering and refrigeration treatments on the dimensional stability of the ball bearing tool steel. These operations were carried out using 250 °F (120 °C) for tempering and −321 °F (−195 °C) for subcooling. Treatments VII-A and VII-B[3] consisted of tempering at 250 °F without refrigeration, whereas treatments VII-C and VII-D involved cycling between 250 and −321 °F. As a result of these combinations, all specimens received the same total of 10 hours' tempering at 250 °F.

All these treatments, with the possible exception of VII-C, confer high dimensional stability on the ball bearing steel. It appears that cyclic refrigeration and tempering does not yield any improvement over cyclic tempering without refrigeration, and that a continuous temper of 10 hours at 250 °F (treatment VII-A) is as good as 10 multiple tempers of 1 hour each at 250 °F (treatment VII-B). Treatments VII-A, VII-B and VII-D result in dimen-

[3]The Roman numeral in the treatment designation refers to the table in which the operation is described.

sional stability better than that achieved by straight hardening and tempering for 1 hour at 300 °F (150 °C), and have the additional advantage of maintaining higher hardness by one or two Rockwell C units. It is important to note that 10 hours at 250 °F yields higher hardness and greater dimensional stability than 1 hour at 300 °F. This trend is discussed in some detail elsewhere (10). Of the two types of refrigeration cycles investigated here, subcooling followed by tempering (treatment VII-D) produces a better combination of hardness and stability than tempering followed by subcooling (treatment VII-C).

Table VIII
Effect of Tempering Directly After Arrested Quenching at 125 °F on Dimensional Stability at +68 °F

Tool Steel	Temper	Rockwell "C" Hardness	Total Change in Length on Aging at 68 °F, Microinches per Inch			
			1 Day	1 Week	1 Month	3 Months
Plain Carbon	1 hour at 250 °F	66	0	+ 1	+ 4	+ 5
Plain Carbon	1 hour at 300 °F	65.5	0	− 2	− 4	− 5
Plain Carbon	1 hour at 400 °F	62.5	0	− 5	−10	−13
Ball Bearing	1 hour at 250 °F	66	0	+19	+40	+64
Ball Bearing	1 hour at 300 °F	65	0	+ 8	+17	+27
Ball Bearing	1 hour at 400 °F	61.5	0	− 1	− 2	− 3
Manganese Die	1 hour at 250 °F	63.5	0	+18	+43	+68
Manganese Die	1 hour at 300 °F	63	0	+ 7	+15	+21
Manganese Die	1 hour at 400 °F	60.5	0	+ 1	+ 3	+ 6

Tempering Directly After Arrested Quenching at 125 °F—The effect of interrupting the quench for 5 minutes and tempering directly without intermediate cooling to room temperature is presented in Table VIII. The quenching media used were water at 125 °F (50 °C) for the plain carbon steel and oil at 125 °F for both the ball bearing and manganese die steels. Tempering was carried out at 250, 300 and 400 °F (120, 150 and 205 °C) after arrested quenching.

Interrupting the quench at 125 °F has been found to stabilize whatever untransformed austenite exists in the low alloy tool steels at this temperature against further transformation when the cooling to room temperature is resumed (11). As shown in Table II, this results in a greater amount of retained austenite as compared with direct quenching to room temperature. If tempering immediately follows the arrested quench at 125 °F, some isothermal transformation may be induced, but after cooling to room temperature more austenite is retained than after a straight quench-and-temper treatment. It is the increased content of retained austenite that is responsible for the relatively large expansions that occur in the ball bearing

and manganese die steels following tempering at 250 and 300 °F. The increased austenite content in the plain carbon steel is not so evident because of the higher rate of contraction due to the martensite decomposition in this steel.

As compared with the straight quench-and-temper treatment, arrested hardening necessitates a higher tempering temperature to stabilize the retained austenite in order that equivalent dimensional stability may be obtained at 68 °F. A temper of 400 °F is required in the case of the ball bearing steel, and a temper of over 400 °F for the manganese die steel. The plain carbon steel appears to require a 275 °F temper following the interrupted quench. Even after a 300 °F temper, isothermal austenite transformation occurs in this steel at 68 °F, but the corresponding expansion is counterbalanced by the martensite contraction that occurs simultaneously. A 400 °F temper markedly upsets the balance in favor of martensite contraction.

Interrupting the quench from the austenitizing temperature is usually practiced for the purpose of minimizing distortion or avoiding cracking. Sometimes arrested hardening is done inadvertently. For example, a piece may be pulled out of the quenching tank and transferred to the tempering furnace before having a chance to cool down to the ambient. The same situation may result from allowing the temperature of the quenching medium to rise appreciably above room temperature. However, whether the arrested quenching is intentional or not, the consequence will usually be detrimental from the standpoint of dimensional stability. The normally predominating contraction of the martensite decomposition is more than offset by the expansion effect due to the excessive amounts of retained austenite, and the steels become dimensionally unstable because of growth rather than shrinkage. A higher tempering temperature will, in general, be required to equal the stability obtained by a straight quench-and-temper treatment but is likely to be disadvantageous because of the lower hardness that results (Table VIII).

Martempering—The dimensional stability of the ball bearing and manganese die steels after interrupting the quench at 450 °F (230 °C) for 3 minutes, air cooling to room temperature, and then tempering in the range of 250 to 400 °F (120 to 205 °C) is shown in Table IX. Such a treatment (called martempering) is practiced commercially to minimize distortion and to prevent cracking. The temperature at which the quench was interrupted, 450 °F, is above the M_s point of both steels.

Table IX
Effect of Martempering (450 °F) on Dimensional Stability at +68 °F

Tool Steel	Temper	Rockwell "C" Hardness	Total Change in Length on Aging at +68 °F, Microinches per Inch			
			1 Day	1 Week	1 Month	3 Months
Ball Bearing	1 hour at 250 °F	65	0	+27	+48	+60
Ball Bearing	1 hour at 300 °F	64	0	0	0	+ 2
Ball Bearing	1 hour at 400 °F	62.5	0	− 2	− 4	− 6
Manganese Die	1 hour at 250 °F	63.5	0	+15	+32	+48
Manganese Die	1 hour at 300 °F	63	0	+ 3	+ 8	+13
Manganese Die	1 hour at 400 °F	60	0	− 1	− 2	− 3

It appears that the influence of martempering on these steels is similar to that of the arrested hardening at 125 °F (50 °C). As shown in Table II, more austenite is retained by martempering than by straight quenching and, therefore, a higher tempering temperature is required to reduce the expansion effect caused by the isothermal austenite transformation which occurs subsequently at room temperature. To achieve dimensional stability equivalent to that of a straight quench-and-temper treatment, the higher tempering temperature necessitated by martempering involves a sacrifice of hardness.

The behavior of the ball bearing steel after martempering again illustrates how dimensional stability at room temperature may depend on a fine balance between the rates of expansion due to austenite transformation and of contraction due to martensite decomposition. Following a temper at 250 °F, this steel expands at a relatively rapid rate (Table IX). With a slightly higher tempering temperature of 300 °F, excellent stability is attained as far as dimensional change is concerned. On the other hand, after a 400 °F temper, the delicate balance is upset and appreciable contraction occurs because the austenite has been sufficiently stabilized or converted so that the contraction accompanying the martensite decomposition becomes the controlling factor in establishing the net dimensional change.

Thus, even though little change in dimensions may be observed at 68 °F after heat treatment, it does not mean that the internal reactions have ceased or are necessarily proceeding at a negligible rate. However, dimensional stability as achieved by balancing relatively rapid rates of these opposing reactions is not particularly desirable. Such a balance is difficult to reproduce in practice, since slight variations in heat treatment may alter the rates of the internal reactions sufficiently to cause an appreciable net expansion or contraction. It is also possible that while the rates of the two reactions are initially equal and opposite, such compensation may not last indefinitely.

Table X

Effect of Tempering and Refrigeration Cycles Following Martempering on Dimensional Stability of Ball Bearing Steel at +68 °F

Treatment	Tempering and Refrigeration Cycle	Number of Cycles	Rockwell "C" Hardness	Total Change in Length on Aging at +68 °F —Microinches per Inch— 1 Day	1 Wk.	1 Mo.	3 Mos.
X-A	(1) Cooled to −321 °F (2) Tempered 1 hour at 250 °F	1	65.5	0	−6	−10	−12
X-B	(1) Cooled to −321 °F (2) Tempered 1 hour at 300 °F	1	64.0	0	−4	− 6	− 7
X-C	(1) Cooled to −321 °F (2) Tempered 1 hour at 400 °F	1	63.0	0	−3	− 5	− 5
X-D	(1) Cooled to −321 °F (2) Tempered 10 hours continuously at 250 °F	1	66	0	−3	− 5	− 6
X-E	(1) Cooled to −321 °F (2) Tempered 1 hour at 250 °F	10*	66	0	0	0	0
X-F	(1) Cooled to −321 °F (2) Tempered 1 hour at 250 °F	10	66	0	−3	− 4	− 5
X-G	(1) Tempered 1 hour at 250 °F (2) Cooled to −321 °F	10	65	0	−2	− 3	− 4

*Only tempering was repeated for 10 cycles.

Tempering and Refrigeration Cycles Following Martempering—The influence of various tempering and refrigeration cycles following martempering, on the dimensional stability of ball bearing tool steel, is presented in Table X. It is found that if this steel is cooled to −321 °F (−195 °C) after martempering and then tempered in the range of 250 to 400 °F (120 to 205 °C) (treatments X-A, X-B, and X-C), contractions occur on subsequent aging at room temperature. The difference in dimensional behavior between martempered specimens given a 250 °F temper with and without an intervening cold treatment is quite pronounced. Considerable expansion occurs if the subcooling is omitted, as was pointed out in connection with Table IX. It is evident that refrigeration results in the transformation of sufficient retained austenite so that a net contraction occurs on aging at room temperature. Tempering at temperatures above 250 °F would, of course, be expected to slow down the rate of contraction at room temperature, since more of the martensite decomposition occurs during the temper; however, this contraction is still appreciable even after a 400 °F temper.

Although tempering above 250 °F improves the dimensional stability, a loss of hardness is involved. In order to determine whether it is possible to attain good dimensional stability along with high hardness in martempered ball bearing tool steel, four long-time tempering and refrigeration treatments were investigated. These con-

sisted of the following operations: Cooling to —321 °F and tempering 10 continuous hours at 250 °F (treatment X-D); cooling to —321 °F and cycling 10 times between 68 and 250 °F (treatment X-E); 10 cycles of cooling to —321 °F and tempering at 250 °F (treatment X-F); and 10 cycles of tempering at 250 °F and cooling to —321 °F (treatment X-G). In each case, the total tempering time at 250 °F was 10 hours. As indicated in Table X, these treat-

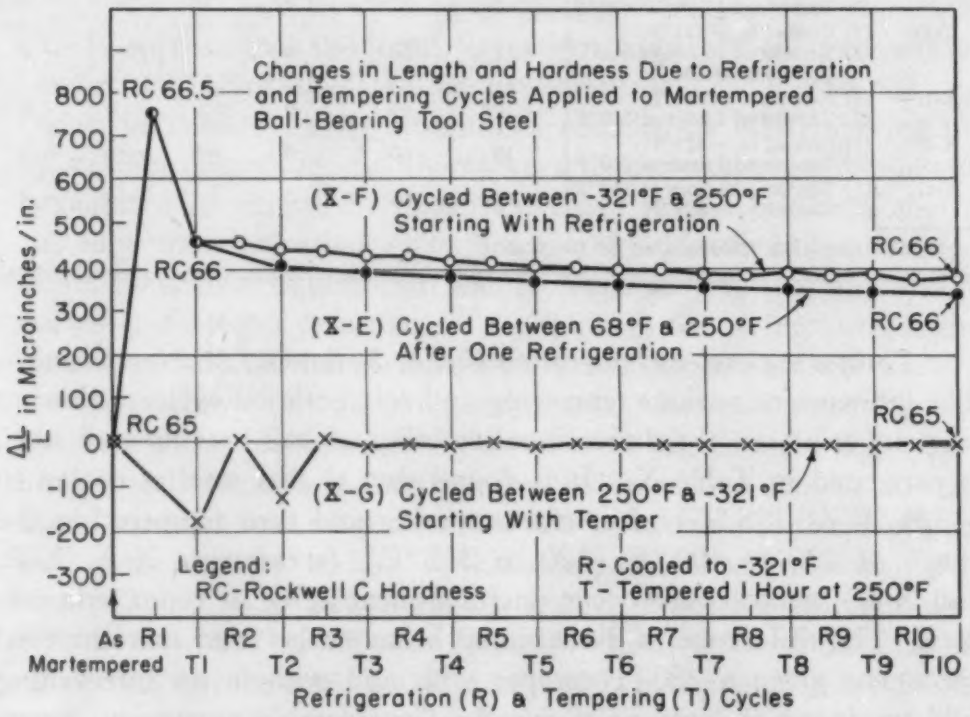


Fig. 1—Cyclic Treatment of Ball Bearing Tool Steel.

ments were found to result in a good combination of dimensional stability and hardness (Rockwell C-65 to C-66).

To ascertain what occurred during each of the long-time treatments, changes in length were observed during each step, and are plotted in Fig. 1. These measurements are all referred to the length of the as-martempered specimens. The first refrigeration as carried out in treatments X-D,[4] X-E, and X-F results in a large expansion of about 760 microinches per inch, which corresponds to the transformation of about 5.5% retained austenite to martensite as calcu-

[4]For the sake of clarity, the changes in length that occurred during treatment X-D are omitted from Fig. 1. The net expansion after this treatment was found to be about the same as after treatment X-E.

lated on the basis that the conversion of 1% of austenite to martensite involves a change of 140 microinches per inch at 68 °F (10). Tempering 1 hour at 250 °F after the first refrigeration as in treatments X-E and X-F causes a marked contraction because of the large amount of untempered martensite available for decomposition. Following the first temper at 250 °F, the changes in length that occur on succeeding steps during treatments X-E and X-F are quite small. After 10 cycles there is a slightly greater net expansion resulting from treatment X-F than from treatment X-E, and is probably due to the fact that a small amount of austenite transforms during the second subcooling (R2) of treatment X-F. After this, the curves remain quite parallel, signifying that the subsequent cycling between —321 and 250 °F merely has the same cumulative tempering effect as cycling between 68 and 250 °F. Tempering 10 hours continuously at 250 °F after refrigeration (treatment X-D) results in about the same net expansion as does 10 multiple 1-hour tempers at 250 °F after refrigeration (treatment X-E). Apparently, cooling from the tempering temperature has no effect on austenite transformation.

Instead of cycling between —321 and 250 °F by first cooling to —321 °F (treatment X-F), if the cycling is reversed by tempering at 250 °F first (treatment X-G), an initial contraction caused by decomposition of the martensite present in the as-martempered steel is observed. On cooling to —321 °F after the first temper, an expansion occurs due to transformation of some austenite. The second temper results in slightly smaller contraction than does the first temper. Likewise, the second refrigeration produces a smaller expansion than does the first refrigeration, and the specimen returns to about its original length in the as-martempered condition. Further cycling has no appreciable effect. Comparing the net expansion of treatment X-G with that of treatment X-F, it turns out that over 2.5% more retained austenite is converted if the cycling is started by subcooling instead of tempering.

The indications are that two refrigeration cycles after martempering are beneficial in removing austenite from the ball bearing steel, but additional cycles are inconsequential. However, the cumulative tempering of 10 hours at 250 °F is important and should remain a part of the treatment, irrespective of how the two subcoolings are introduced. Two appropriate combinations are recommended: (a) temper 1 hour at 250 °F, subcool, repeat tempering and subcooling, temper 8 hours at 250 °F; or (b) subcool, temper 1 hour at 250 °F,

Table XI
Effect of Tempering Following Oil Hardening on Dimensional Stability at +68 °F of Type M-2 High Speed Steel

Treatment	Temper	Rockwell "C" Hardness	Total Change in Length on Aging at 68 °F, Microinches per Inch				
			1 Day	1 Wk.	1 Mo.	3 Mos.	1 Yr.
XI-A	(1) None, as-hardened	65	0	−36	−70	−100	−150
XI-B	(1) 2½ hrs. at 1050 °F—air-cooled	65	0	+22	+35	+ 43	+ 48
XI-C	(1) 2½ hrs. at 1050 °F—air-cooled (2) 1 hr. at 600 °F—air-cooled	64.5	0	+18	+33	+ 46	.....
XI-D	(1) 2½ hrs. at 1050 °F—air-cooled (2) 1 hr. at 900 °F—air-cooled	65	0	+10	+19	+ 30	+ 43
XI-E	(1) 2½ hrs. at 1050 °F—air-cooled (2) 2½ hrs. at 1050 °F—air-cooled (3) 1 hr. at 600 °F—air-cooled	64	0	+ 4	+ 9	+ 12	.....
XI-F	(1) 2½ hrs. at 1050 °F—air-cooled (2) 2½ hrs. at 1050 °F—air-cooled (3) 2½ hrs. at 1050 °F—air-cooled (4) 1 hr. at 600 °F—air-cooled	64.5	0	+ 5	+ 9	+ 11	.....
XI-G	(1) 2½ hrs. at 1050 °F—oil-quenched (2) 1 hr. at 600 °F—air-cooled	64	0	− 7	− 3	+ 1	.....
XI-H	(1) 2½ hrs. at 1050 °F—oil-quenched (2) 2½ hrs. at 1050 °F—oil-quenched (3) 2½ hrs. at 1050 °F—oil-quenched (4) 1 hr. at 600 °F—air-cooled	65	0	− 3	− 5	− 6	.....
XI-I	(1) 2½ hrs. at 1050 °F—oil-quenched (2) 2½ hrs. at 1050 °F—oil-quenched (3) 2½ hrs. at 1050 °F—oil-quenched (4) 1 hr. at 900 °F—air-cooled	65	0	0	0	0	.....

subcool, temper 9 hours at 250 °F. Treatment (a) has the advantage of minimizing the possibility of cracking in refrigeration (because the first temper toughens the steel and reduces the subzero transformation), and should yield dimensions almost exactly the same as those of the martempered steel. On the other hand, treatment (b) involves one less step, removes more austenite, and results in greater hardness. Both treatments should yield the same dimensional stability with respect to room temperature aging. It is interesting to note that, in this way, the advantages of martempering can be combined with high hardness and good dimensional stability.

Dimensional Stability of High Alloy Tool Steels

Tempering of High Speed Steel Following Normal Hardening—The results of various tempering treatments on type M-2 high speed steel are tabulated in Table XI. These data indicate that the dimensional behavior of high speed steel is more complex than that of low alloy tool steels. This is because the tempering temperature of 1050 °F (565 °C), commonly used to obtain secondary hardening, conditions the retained austenite for transformation to martensite on cooling from the tempering temperature. Such tempering can be

considered to involve the same type of hardening reaction that occurs during the original quench from the austenitizing temperature. Notwithstanding this added complexity, the dimensional behavior of high speed steel can be understood if one takes into account what is happening to both the austenite and martensite in any particular heat treatment.

In the as-quenched condition, this high speed steel contains a greater amount of retained austenite than found in the low alloy tool steels previously discussed (Table II). However, following quenching to room temperature (treatment XI-A), a contraction is observed, which indicates that the shrinkage due to martensite decomposition is greater than the expansion due to retained austenite transformation. This is quite similar to the behavior of the low alloy tool steels in the as-quenched condition.

If tempering is carried out at 1050 °F (565 °C) (treatment XI-B), the original martensite is sufficiently decomposed so that its rate of decomposition at room temperature becomes virtually nil. However, on cooling from 1050 °F (565 °C), the austenite transformation starts in the neighborhood of 500 °F (260 °C) and proceeds down to room temperature. At 68 °F the austenite transformation does not stop but continues isothermally just like the austenite in the as-quenched condition. A net expansion is observed after such a temper because the expansion from the austenite transformation is greater than contraction from the decomposition of any martensite which forms on cooling to and at room temperature.

If the 1050 °F (565 °C) temper is followed by a second temper, or stress relieving operation, expansion due to austenite transformation at 68 °F can be reduced, provided the second tempering temperature is properly adjusted. A second temper carried out at 600 °F (315 °C) (treatment XI-C) is not so effective as at 900 °F (480 °C) (treatment XI-D). The 900 °F temper, which is just below the temperature range for appreciable conditioning of the retained austenite for transformation on cooling, partially stabilizes the austenite against subsequent transformation on aging at room temperature. Such a second temper is also advantageous in that the secondary martensite formed as a result of the first temper is partially decomposed and the rate of contraction on subsequent aging at room temperature is decreased.

Double and triple tempers (treatments XI-E and XI-F) at 1050 °F (565 °C), followed by air cooling after each temper,

result in the conditioning and transformation of more and more austenite. However, there is still sufficient austenite left after even a triple temper to cause a net expansion by transformation on aging at room temperature.

By oil quenching instead of air cooling from the tempering temperature a greater amount of austenite transformation can be made to occur during the cooling to room temperature because the stabilizing effect of slow cooling is thereby avoided (11). Thus a larger amount of martensite becomes available for contraction at room temperature and an initial contraction is observed even after a single temper at 1050 °F (565 °C) followed by a stress relief at 600 °F (315 °C) (treatment XI-G). However, austenite transformation is still appreciable after this treatment and the initial contraction is wiped out in 3 months. By oil quenching from 1050 °F (565 °C) each time during a triple temper and ending with a stress relieving operation, the retained austenite can be substantially eliminated and the martensite can be sufficiently decomposed so that high dimensional stability results. Treatment XI-I, in which a 900 °F (480 °C) stress relief follows the triple temper at 1050 °F (565 °C), was found to be more effective in eliminating martensite contraction than treatment XI-H, in which a 600 °F (315 °C) stress relief is used.

Tempering Following Refrigeration of High Speed Steel—Table XII shows the effect of tempering following refrigeration at —321 °F (—195 °C) on the dimensional stability of high speed steel. Tempering first at 1050 °F (565 °C) and then at 600 °F (315 °C) following refrigeration (treatment XII-A) is unable to prevent expansion due to retained austenite transformation at room temperature. Although there is less retained austenite present after refrigeration than in the as-quenched condition (Table II), there is still enough for the conditioning treatment at 1050 °F to result in a surprisingly rapid rate of austenite transformation at room temperature.

As in the case of unrefrigerated high speed steel, this expansion can be eliminated if oil quenching from the temper is employed. A triple temper after refrigeration involving oil quenching each time from 1050 °F (565 °C) (treatments XII-B and XII-C) is highly effective in imparting dimensional stability. Thus, triple tempering with oil quenching appears capable of imparting high dimensional stability after cold treatment as well as after conventional hardening. Refrigeration may be of advantage, however, if the hardening results

Table XII
Effect of Tempering Following Refrigeration on Dimensional Stability at +68 °F of Type M-2 High Speed Steel

Treatment	Refrigeration and Temper	Rockwell "C" Hardness	Total Change in Length on Aging at 68 °F —Microinches per Inch— 1 Day	1 Wk.	1 Mo.	3 Mos.
XII-A	(1) Cooled to −321 °F (2) 2½ hrs. at 1050 °F—air-cooled (3) 1 hr. at 600 °F—air-cooled	64	0	+14	+26	+33
XII-B	(1) Cooled to −321 °F (2) 2½ hrs. at 1050 °F—oil-quenched (3) 2½ hrs. at 1050 °F—oil-quenched (4) 2½ hrs. at 1050 °F—oil-quenched (5) 1 hr. at 600 °F—air-cooled	64	0	0	+ 1	+ 2
XII-C	(1) Cooled to −321 °F (2) 2½ hrs. at 1050 °F—oil-quenched (3) 2½ hrs. at 1050 °F—oil-quenched (4) 2½ hrs. at 1050 °F—oil-quenched (5) 1 hr. at 900 °F—air-cooled	64	0	0	0	0
XII-D	(1) Cooled to −321 °F (2) 2½ hrs. at 1050 °F—oil-quenched (3) Repeat steps (1) and (2) twice (4) Cooled to −321 °F (5) 1 hr. at 600 °F—air-cooled	64.5	0	0	0	0
XII-E	(1) Cooled to −321 °F (2) 2½ hrs. at 1050 °F—oil-quenched (3) Repeat steps (1) and (2) twice (4) Cooled to −321 °F (5) 1 hr. at 900 °F—air-cooled	65	0	− 1	− 2	− 2

in unduly high contents of retained austenite. For instance, it has been shown possible to retain as much as 60% austenite by arrested hardening of high speed steel (12). In such situations it may be advantageous to refrigerate not only after the original hardening operation but also following each oil quench from the tempering temperature (treatments XII-D and XII-E). Such a combination of operations can be applied with advantage to the high carbon, high chromium die steel, as will be discussed later.

Tempering of High Carbon, High Chromium Die Steel Following Hardening—The results of various tempering treatments on high carbon, high chromium die steel are given in Table XIII. In the as-hardened condition, this steel is known to contain a greater amount of retained austenite than the high speed steel. After air hardening, the high carbon, high chromium die steel expands during the first month of aging at 68 °F and contracts from then on (treatment XIII-A). Evidently the amount of expansion due to austenite transformation is greater than the amount of contraction due to martensite decomposition during the first month of aging; however, after this period, the rate of austenite transformation slows down sufficiently so that a net contraction is observed.

Tempering at 500 °F (260 °C) (treatment XIII-B) reduces the

Table XIII
Effect of Tempering Following Air Hardening on Dimensional Stability at +68 °F of High Carbon, High Chromium Tool Steel

Treatment	Temper	Rockwell "C" Hardness	Total Change in Length on Aging at +68 °F, Microinches per Inch — 1 Day	1 Wk.	1 Mo.	3 Mos.	1 Yr.
XIII-A	(1) None, as-hardened	64.5	0	+ 12	+ 14	+ 7	− 11
XIII-B	(1) 2 hrs. at 500 °F—air-cooled	60.5	0	+ 12	− 1	− 4	− 9
XIII-C	(1) 2 hrs. at 950 °F—air-cooled	61.5	0	+ 85	+128	+150	+165
XIII-D	(1) 2 hrs. at 950 °F—oil-quenched	63	0	+ 25	+ 30	+ 33	+ 28
XIII-E	(1) 1 hr. at 950 °F—oil-quenched (2) 1 hr. at 450 °F—air-cooled	62	0	+ 30	+115	+190	.....
XIII-F	(1) 1 hr. at 950 °F—oil-quenched (2) 1 hr. at 950 °F—oil-quenched (3) 1 hr. at 450 °F—air-cooled	63	0	+210	+310	+370	.....
XIII-G	(1) 1 hr. at 950 °F—oil-quenched (2) 1 hr. at 950 °F—oil-quenched (3) 1 hr. at 950 °F—oil-quenched (4) 1 hr. at 450 °F—air-cooled	61	0	+ 80	+150	+185	.....

expansion observed in the untempered condition by partial conversion and stabilization of the retained austenite. If, however, tempering is carried out at 950 °F (510 °C) (treatment XIII-C), a considerable amount of retained austenite becomes conditioned for transformation on cooling, and a large expansion due to austenite transformation continues on aging at room temperature. Oil quenching from 950 °F (510 °C) (treatment XIII-D) markedly reduces this expansion but it still remains relatively large. Single, double, and triple tempering at 950 °F (510 °C), including oil quenching from the temper, do not reduce the expansion even if a 450 °F (232 °C) stress relief is added (treatments XIII-E, XIII-F and XIII-G). Indeed, double tempering at 950 °F (treatment XIII-F) results in a greater amount of expansion than does single tempering (treatment XIII-E) because the contractive effect of the martensite is suppressed by the second tempering. Furthermore, on account of the large amount and nature of the austenite in this steel, multiple tempering including oil quenching does not appear sufficient to overcome expansion, as was possible with the high speed steel. During each temper, a large amount of austenite becomes conditioned for transformation on cooling, and isothermal transformation then proceeds vigorously at room temperature. Theoretically, after a sufficient number of tempers at 950 °F (510 °C) the expansion due to transformation can be eliminated. However, from a practical point of view, it would be advisable to use refrigeration in order to minimize the number of tempers required.

Tempering Following Refrigeration of High Carbon, High

Table XIV
Effect of Tempering Following Refrigeration on Dimensional Stability at +68 °F of High Carbon, High Chromium Tool Steel

Treatment	Refrigeration and Temper	Rockwell "C" Hardness	Total Change in Length on Aging at 68 °F, Microinches per Inch — 1 Day	1 Wk.	1 Mo.	3 Mos.	1 Yr.
XIV-A	(1) Cooled to −123 °F	66	0	−26	−51	− 78	−118
XIV-B	(1) Cooled to −123 °F immediately (2) 2 hrs. at 950 °F—air-cooled	60.5	0	+30	+46	+ 54	+ 60
XIV-C	(1) Cooled to −123 °F after 24 hrs. at room temperature (2) 2 hrs. at 950 °F—air-cooled	60.5	0	+39	+55	+ 65	+ 72
XIV-D	(1) Cooled to −321 °F (2) 1 hr. at 650 °F—oil-quenched	63	0	− 9	− 7	− 12	.....
XIV-E	(1) Cooled to −321 °F (2) 1 hr. at 950 °F—oil-quenched (3) 1 hr. at 950 °F—oil-quenched (4) 1 hr. at 950 °F—oil-quenched (5) 1 hr. at 450 °F—air-cooled	62	0	+55	+97	+135	.....
XIV-F	(1) Cooled to −321 °F (2) 1 hr. at 950 °F—oil-quenched (3) Repeat steps (1) and (2) three times (4) 1 hr. at 450 °F—air-cooled	59.5	0	− 1	− 2	− 2	.....
XIV-G	(1) Cooled to −321 °F (2) 1 hr. at 950 °F—oil-quenched (3) Repeat steps (1) and (2) nine times (4) 1 hr. at 450 °F—air-cooled	58.5	0	− 1	− 2	− 3	.....

Chromium Die Steel—The effect of tempering following refrigeration is shown in Table XIV. Cooling to −123 °F (−90 °C) after hardening (treatment XIV-A) results in a high rate of contraction, which indicates that transformation of sufficient retained austenite has occurred during subcooling so that the martensite contraction predominates over any expansion due to the transformation of the remaining austenite. The rate of this contraction can be greatly reduced by tempering at 650 °F (345 °C) after subcooling (treatment XIV-D).

If tempering is carried out at 950 °F (510 °C) after subcooling (treatment XIV-B or XIV-C), preshrinkage due to martensite decomposition is accomplished while more austenite is conditioned for transformation on cooling to and at room temperature. Hence, a relatively fast rate of expansion occurs at 68 °F. A triple temper at 950 °F following subcooling (treatment XIV-E) is actually found to be less effective than a single temper, ar far as dimensional stability is concerned. This is even more surprising, since oil quenching from the tempering temperature which proved so beneficial for high speed steel was employed.

In an attempt to achieve high dimensional stability in the high

carbon, high chromium steel, multiple cycles involving cooling to —321 °F (—195 °C), tempering at 950 °F (510 °C), and oil quenching to room temperature were tried. As shown in Table XIV, good success was obtained with four such cycles ending up with a 450 °F (230 °C) stress relief (treatment XIV-F). This is as effective as 10 cycles ending with the same stress relieving treatment (treatment XIV-G).

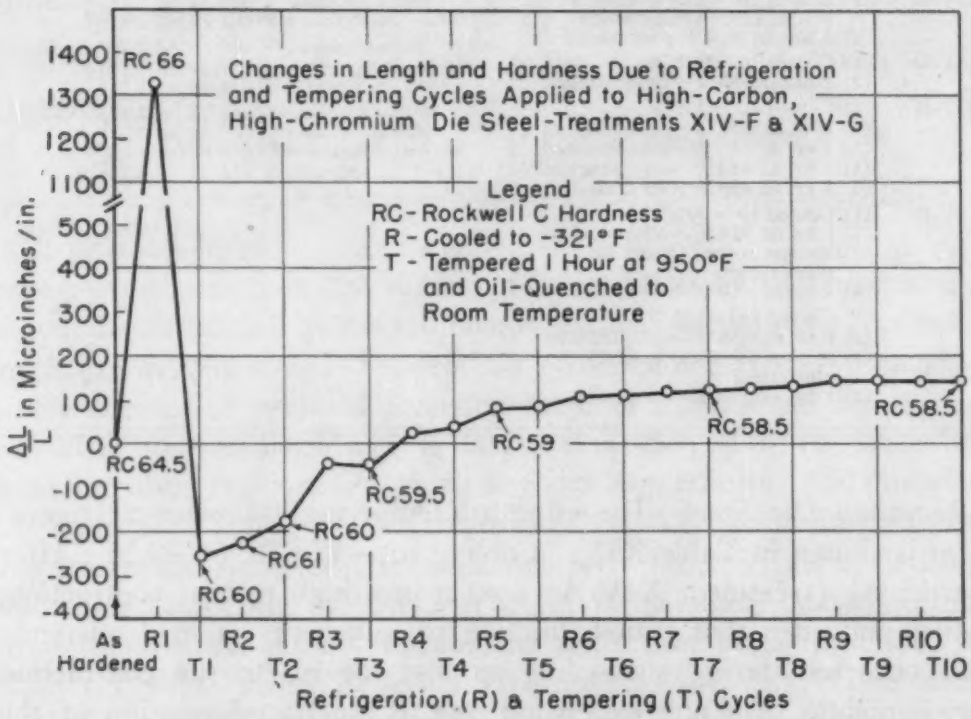


Fig. 2—Cyclic Treatment of High Carbon, High Chromium Die Steel.

To determine the changes occurring during each step of the above refrigeration and tempering cycles, measurements were made after each step of each cycle. These changes are shown in Fig. 2 and refer to the length in the as-hardened condition. The first refrigeration at —321 °F (—195 °C) results in a large expansion of about 1330 microinches per inch, whereas the first temper at 950 °F (510 °C) produces a contraction of 1580 microinches per inch. This huge contraction is caused by decomposition of the martensite present in the as-quenched steel as well as that formed during the first refrigeration. The actual magnitude of the contraction due to martensite decomposition must be larger than 1580 microinches per inch, since there is an expansion due to austenite transformation that takes

place on cooling from 950 °F (510 °C). Succeeding refrigeration and tempering cycles result in progressive expansions. Constant length is attained after about 9 cycles, and it appears that the austenite has been rendered stable as far as transformation on refrigeration or cooling from the tempering temperature is concerned. This achievement is, however, accompanied by a loss of hardness, dropping from Rockwell C-66 in the as-refrigerated condition to Rockwell C-58.5 after 10 cycles.

Discussion of Results

As a result of this investigation certain general recommendations for obtaining dimensional stability in both low and high alloy tool steels can be formulated. These recommendations are based on the knowledge that attainment of dimensional stability depends on minimizing both the contraction due to martensite decomposition and the expansion due to austenite transformation at room temperature. Ideally, both objectives can be accomplished by tempering high enough to cause complete elimination of tetragonal martensite and retained austenite; however, such a procedure involves a sacrifice of hardness and wear resistance which are essential for the proper functioning of tool steels. Thus, in practice, the degree of dimensional stability that can be obtained is limited to some extent by other requirements. It is important that such requirements not be arbitrary, but accurately reflect the service conditions to which gages, dies, or high precision tools are subjected. In this way unnecessary limitations on the attainment of dimensional stability may be avoided.

To minimize the contraction due to martensite decomposition, it is necessary to cause preshrinkage by tempering as high as possible consistent with hardness requirements. A given amount of preshrinkage can be produced at low tempering temperatures if the treatment time is correspondingly long, and higher hardness is thereby attainable than with higher temperatures and shorter times. It is also helpful to select a tool steel composition which tends to decrease the extent of martensite contraction during the first stage of tempering. Alloying elements such as chromium, tungsten, and to some extent manganese perform a useful function in this connection.

To minimize the expansion caused by austenite transformation, it is necessary to stabilize the retained austenite against transformation at room temperature by a tempering operation. For low alloy

tool steels, the higher the tempering temperature the greater the extent of this type of stabilization. High tempering temperatures will convert the austenite into bainite, but the hardness level is adversely affected. However, with high alloy tool steels, a high tempering temperature conditions the retained austenite for transformation into martensite on cooling down to and while at room temperature. Since such high tempering is necessary for imparting secondary hardness, the problem of obtaining good dimensional stability in high alloy tool steel becomes one of substantially reducing the retained austenite content and stabilizing the remainder against isothermal transformation at room temperature. For normally hardened high speed steel, a triple temper with oil quenching from the tempering temperature plus a final stress relief has been found effective in promoting dimensional stability. In high carbon, high chromium steel, cyclic treatments involving refrigeration, tempering, and oil quenching from the tempering temperature are apparently necessary for obtaining high dimensional stability. On the other hand, if there is no objection to leaving appreciable amounts of retained austenite in the finished part, tempering the high carbon, high chromium steel at 500 °F (260 °C) provides fair stability. However, this stability is of the "balanced" type and may not be as reproducible as the more complex cyclic treatments designed to remove the major part of the austenite.

Use of cold treatment is of limited advantage in attaining high dimensional stability in low alloy tool steels, provided that in the hardening operation quenching from the austenitizing temperature is done directly to room temperature. In certain compositions, such as the plain carbon and tungsten die steels, refrigeration does result in higher hardness along with equivalent dimensional stability as compared with the straight quench-and-temper treatment. If, however, arrested hardening or martempering is required for the purpose of avoiding warping or cracking in such steels, refrigeration is definitely beneficial because a larger content of austenite is retained by interrupted quenching than by quenching directly to room temperature. This means that a higher tempering temperature is required to stabilize the extra austenite, and consequently a lowered hardness is involved. Subcooling to transform a sizable portion of this austenite enhances the hardness and allows a lower tempering temperature to be used after interrupted quenching, thus avoiding the sacrifice of hardness.

Conclusions

Low Alloy Tool Steels—1. The higher the tempering temperature, the higher the degree of dimensional stability and the lower the hardness attained after normal hardening treatments.

2. Long-time tempering at low temperatures results in a superior combination of dimensional stability and hardness compared to short-time tempering at high temperatures.

3. The presence of alloying elements such as chromium, tungsten, and manganese in tool steels provides increased dimensional stability by decreasing the amount of martensite contraction that occurs during the first stage of tempering.

4. For tempering temperatures under 300 °F (150 °C), refrigeration prior to tempering results in an increased rate of contraction on aging at room temperature as compared with the straight quench-and-temper treatment.

5. Refrigeration following tempering at 300 °F (150 °C) slightly increases the rate of contraction over that obtained without refrigeration.

6. Arresting the quench above room temperature during hardening necessitates a higher tempering temperature in order to achieve dimensional stability equivalent to that obtained by direct quenching and tempering. A decrease in hardness is thereby involved.

7. However, long-time tempering and refrigeration cycles applied to either the as-quenched or as-martempered condition result in equivalent dimensional stability along with higher hardness as compared with the straight quench-and-temper treatment.

High Alloy Tool Steels—1. The dimensional behavior of high speed and high carbon, high chromium tool steels is more complex than that of low alloy tool steels, since relatively large amounts of austenite are retained and the tempering temperature normally used conditions the retained austenite for transformation on cooling to and at room temperature. For this reason, it is much more difficult to stabilize high alloy tool steels than low alloy tool steels, despite the use of higher tempering temperatures.

2. Refrigeration following hardening aids in promoting dimensional stability by causing the transformation of a large amount of retained austenite.

3. Normally hardened high speed steel can be stabilized without

cold treatment by multiple tempering and oil quenching, instead of air cooling, from the tempering temperature.

4. A cyclic treatment involving refrigeration, tempering, and oil quenching from the tempering temperature is particularly effective in promoting dimensional stability in high carbon, high chromium die steel. Fair stability can be attained by simple tempering at a low temperature, but considerable quantities of austenite remain.

Acknowledgments

This investigation, originally under the sponsorship of the Sheffield Foundation of Dayton, Ohio, was completed in co-operation with the Instrumentation Laboratory of Massachusetts Institute of Technology. The authors wish to thank the Taft-Peirce Manufacturing Company for spherical grinding of specimens and the Pratt and Whitney Division of the Niles-Bement-Pond Company for use of precision gage blocks. They are also indebted to Louis S. Castleman for X-ray determinations of retained austenite contents and to Eugene Blacquier, William C. Clancy, and Walter Fitzgerald for their assistance in various phases of the investigation.

The contribution of Dr. Stewart G. Fletcher of the Latrobe Electric Steel Co. in laying the foundation for the present investigation is gratefully acknowledged.

References

1. H. Scott, "Dimensional Changes Accompanying the Phenomena of Tempering and Aging Tool Steels," Transactions, American Society for Steel Treating, Vol. 9, 1926, p. 277.
2. H. Scott and T. H. Gray, "Dimensional Changes on Hardening High Chromium Tool Steels," Transactions, American Society for Metals, Vol. 29, 1941, p. 503.
3. E. Ameen, "Dimensional Changes of Tool Steels During Quenching and Tempering," Transactions, American Society for Metals, Vol. 28, 1940, p. 472.
4. G. M. Butler, "Study of Dimensional and Other Changes in Various Die Steels Due to Heat Treatment," Transactions, American Society for Metals, Vol. 30, 1942, p. 191.
5. L. E. Gippert and G. M. Butler, "Changes in Size and Toughness of High Carbon - High Chromium Steels Due to Subzero Treatments," Transactions, American Society for Metals, Vol. 39, 1947, p. 540.
6. S. G. Fletcher and M. Cohen, "The Dimensional Stability of Steel. Part I —Subatmospheric Transformation of Retained Austenite," Transactions, American Society for Metals, Vol. 34, 1945, p. 216.
7. S. G. Fletcher, B. L. Averbach and M. Cohen, "The Dimensional Stability of Steel. Part II—Further Experiments on Subatmospheric Transformation," Transactions, American Society for Metals, Vol. 40, 1948, p. 703.

8. B. L. Averbach, M. Cohen and S. G. Fletcher, "The Dimensional Stability of Steel. Part III—Decomposition of Martensite and Austenite at Room Temperature," TRANSACTIONS, American Society for Metals, Vol. 40, 1948, p. 728.
9. B. L. Averbach and M. Cohen, "X-ray Determination of Retained Austenite by Integrated Intensities," T. P. 2342, *Metals Technology*, February 1948.
10. B. L. Averbach and M. Cohen, "The Isothermal Decomposition of Martensite and Retained Austenite," American Society for Metals, Preprint No. 1, 1948.
11. W. J. Harris, "A Quantitative Study of the Austenite to Martensite Transformation," Sc. D. Thesis, Massachusetts Institute of Technology, 1948.
12. P. Gordon, M. Cohen and R. S. Rose, "Effect of Quenching Bath Temperature on the Tempering of High Speed Steel," TRANSACTIONS, American Society for Metals, Vol. 33, 1944, p. 411.

DISCUSSION

Written Discussion: By George A. Roberts, chief metallurgist, Vanadium-Alloys Steel Co., Latrobe, Pa.

It was a pleasure to read the fine collection of data presented in the paper with respect to the stability of high alloy tool steels. That these changes in size can be rationalized on the basis of known tempering phenomena is encouraging. I should like to request that only specific data regarding the as-hardened microstructural characteristics be included for future reference. The data can specifically apply only to the particular hardening temperatures, or, more significantly, grain sizes achieved. Data on the grain size and the relative amounts of solution of carbide will permit future workers in this field to make a valid comparison of results and carry on this basic work to practical applications involving the heat treatment of commercial tools and dies.

Written Discussion: By R. G. Kennedy, Jr., research metallurgist, and J. V. Emmons, chief metallurgist, The Cleveland Twist Drill Co., Cleveland.

The authors are to be congratulated on their carefully collected and analyzed data with regards to the dimensional stability of tool steels.

We have a small amount of data on the dimensional stability of three types of high speed steels which were aged over a 10-year period. Our data may be of interest as supplementary information to the data of Table XI of the authors' paper.

Changes of length in the length of specimens 1 inch in diameter by 7½ inches long were measured by means of a Zeiss horizontal optometer. The specimens were originally hardened in 1938 and were given four ½-hour temperings followed by an air cool after each cycle. The ends of the specimens were carefully lapped parallel, length readings were made, and they were then coated with a rust preventive and stored in a dry closed container for 10 years. The present paper revived our interest in these specimens and they were accordingly remeasured within the past week. Fig. 3 illustrates graphically the expansion which has occurred over the 10-year period for the three types of high speed steels.

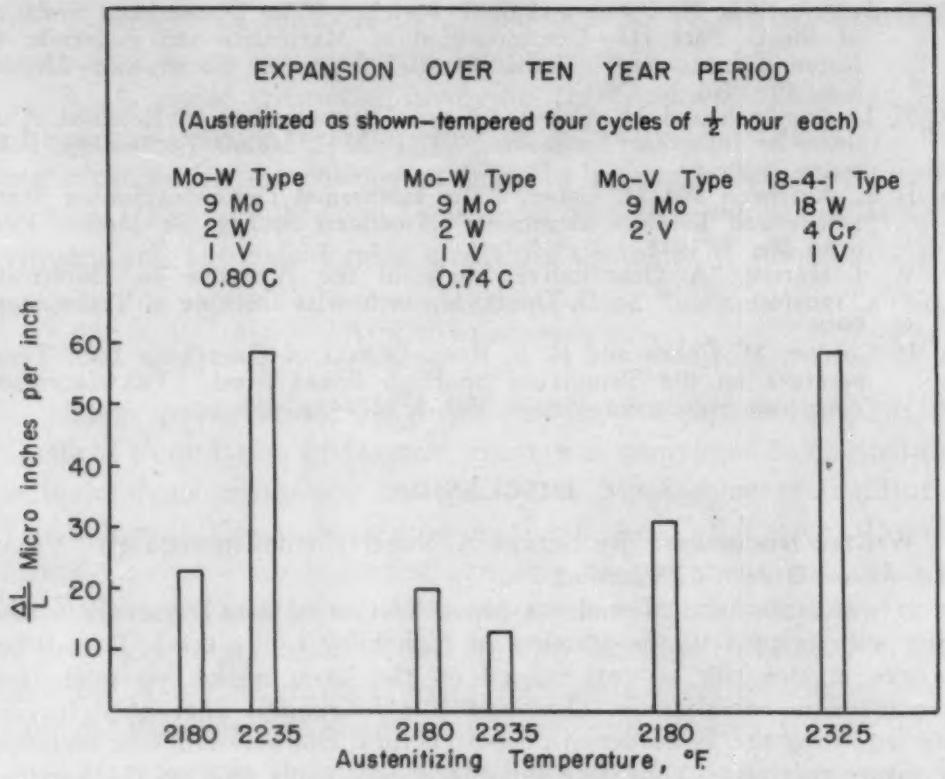


Fig. 3—Graph Showing Expansion Over Ten-Year Period for the Three Types of High Speed Steels.

Written Discussion: By Paul Gordon, Department of Metallurgy, Massachusetts Institute of Technology, Cambridge, Mass.

I should like to ask the authors whether a seeming inconsistency in some of the data in their paper has a ready explanation. The data shown in Table XV for the M-2 high speed steel, the ball bearing steel, and the manganese die steel have been taken from Tables II, V, and XI of the paper.

Table XV

Steel	Condition	Retained Austenite, %	Length Change After 1 Year at 68 °F Microinches per Inch
High speed	As Hardened	19.5	—150
Mn Die	As Hardened	8.5	— 87
Ball Bearing	As Hardened	7	—110

It is seen that the high speed steel underwent a much larger net contraction than either of the other two steels. Is this not contradictory to the general implication of the paper that the greater the amount of retained austenite the smaller the net contraction or the larger the net expansion? It may be argued, of course, that the austenite in the high

speed steel, having a much higher alloy content, would be more resistant to isothermal decomposition at 68 °F than the austenite in the other steels, and thus the contraction due to the decomposition of the martensite would be relatively unopposed by expansion due to austenite transformation. By the same token, however, should not the martensite in the high speed steel also be reluctant to transform, not only because of its high alloy content but also because of its relatively low carbon content? Because the decomposition of the martensite consists of the rejection of some form of carbon-rich phase, lowered carbon content should decrease the probability of the formation of a nucleus of such a phase and thus retard the decomposition.

Authors' Reply

The authors wish to thank Messrs. Kennedy and Emmons for their contribution of supplementary dimensional stability data on four types of high speed steel differing in composition from the M-2 steel used in this investigation. The magnitudes of expansion found for the molybdenum-tungsten type (0.80% carbon) and for the 18-4-1 type, hardened from 2235 and 2325 °F (1225 and 1275 °C), respectively, are about what would be expected from the results of Treatment XI-B. Although the latter consisted of a single 2½-hour temper at 1050 °F (565 °C), it is roughly equivalent to four ½-hour tempers as far as conditioning of the retained austenite is concerned, after normal hardening.

In answer to Dr. Roberts' request for data on grain size and undissolved carbides in the high alloy tool steels, we submit Table XVI.

Table XVI

Steel	Austenitizing Temperature, °F	Fracture Grain Size	Wt. % Carbides	Vol. % Carbides
M-2 high speed	2220	8-9	12	8.7
High-carbon High-chromium	1900	8-9	16	15
	Chemical Composition of Carbides			
	C	Cr	V	Mo	W
M-2 high speed	3.47	1.64	3.80	22.67	29.05
High-carbon High-chromium	9.57	39.69	5.16	3.66	.....

The weight per cent of carbides and their chemical composition were determined by electrolytic extraction. The volume per cent of carbides was measured by the metallographic technique of lineal analysis.

As Mr. Gordon points out, it is surprising to find a greater rate of contraction in high speed steel than in the low alloy steels when tested at room temperature in the as-hardened condition. The explanation of this anomalous behavior lies in the comparative expansions associated with the transformation of a unit quantity of retained austenite in the two cases, as well as in the relative rates of transformation of the retained

austenite. The expansion attending the transformation of 1% austenite at room temperature was found to be only 90 microinches per inch in the high speed steel as compared to 140 microinches per inch in the ball bearing tool steel. Furthermore, the rate of transformation of the retained austenite is slower in the high speed steel because of its much higher alloy content. Both a lower expansion per unit of austenite transformation and a slower rate of transformation could overcompensate sufficiently for the higher austenite content and lower martensite contraction to result in a higher net contraction in the high speed steel as compared to the low alloy steels.

THE TRANSFORMATION AND RETENTION OF AUSTENITE IN SAE 5140, 2340, AND T1340 STEELS OF COMPARABLE HARDENABILITY

By A. R. Troiano

Abstract

Austenite transformation diagrams for steels SAE 5140, 2340, and T1340, of equal hardenability are presented and evaluated, including an examination of the retention of austenite.

In addition, an X-ray diffraction study of retained austenite in Jominy hardenability test bars of these three steels was performed and correlated with the microstructural characteristics of the same bars. All three steels exhibit a gradual increase in the amount of retained austenite, which attains a maximum and then decreases as one proceeds back from the quenched end of the Jominy bar. At all corresponding positions on the bar, SAE 2340 retains slightly more austenite than T1340 and substantially more than 5140. The limitations of the end-quenched hardenability test as a means of comparison of various steels are discussed.

Introduction

DESPITE the wide use of the Jominy hardenability test as a tool for both steel selection and control, relatively few investigations have been devoted to a systematic study and correlation of the structures produced in such test bars with the isothermal transformation characteristics of the austenite in the same steels. Even less information is available in the nature of a correlation of austenite retention in Jominy bars with the general austenite transformation characteristics under controlled conditions.

Of particular interest would be a careful examination of several steels of widely different chemical analyses, having essentially the same Jominy hardenability. Presented here are the results of a determination of the transformation characteristics of a plain chro-

A paper presented before the Thirtieth Annual Convention of the Society, held in Philadelphia, October 23 to 29, 1948. The author, A. R. Troiano, is professor of metallurgy, University of Notre Dame, Notre Dame, Indiana. Manuscript received April 23, 1948.

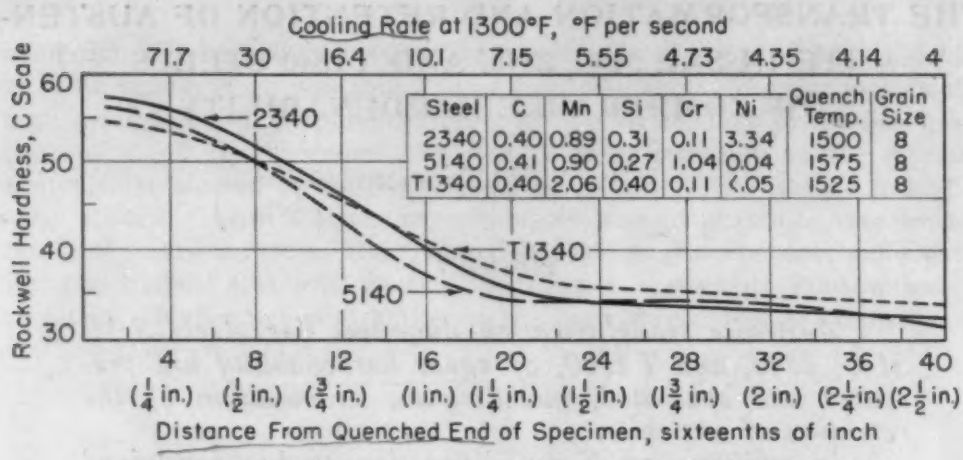


Fig. 1—Jominy End-Quench Test on Steels SAE 5140, 2340 and T1340.

mium, a plain nickel, and a plain manganese steel, all of approximately equal hardenability; as well as a correlation with the structures and state of retained austenite in Jominy bars of the same steels.

Materials and Methods

Three steels of types SAE 5140, 2340, and T1340 were employed in this investigation. The analyses are given in Table I.

Table I
Chemical Composition of Steels Investigated

Type	C %	Mn %	Si %	Cr %	Ni %
SAE 5140	0.41	0.90	0.27	1.04	0.04
SAE 2340	0.40	0.89	0.31	0.11	3.34
SAE T1340	0.40	2.06	0.40	0.11	0.05

The Jominy curves of Fig. 1 demonstrate that the hardenability of these three steels is essentially the same. The total spread is no greater than one may encounter in different heats of the same type of steel.

The methods employed in the determination of the transformation diagrams were much the same as those employed in the many diagrams determined in this laboratory. Briefly, the metallographic specimens were $\frac{3}{16}$ by ½ by ⅛ inch and larger when possible, the dilatometer specimens were 1 by ¼ by $\frac{1}{16}$ inch, X-ray diffraction specimens were ½ by $\frac{1}{16}$ by $\frac{1}{16}$ inch. All steels were normalized at 1650 °F (900 °C) and austenitized for 30 to 40 minutes in a vertical tube furnace provided with a continuous flow of purified

nitrogen. The austenitizing temperature and resulting grain size are indicated on the appropriate transformation diagrams. A_1, A_3, and M_s temperatures were determined by standard metallographic methods.

The retention of austenite in both the metallographic and Jominy bar specimens cannot be properly examined by metallographic techniques. However, X-ray diffraction methods were capable of supplying at least a qualitative concept of the relative amounts of

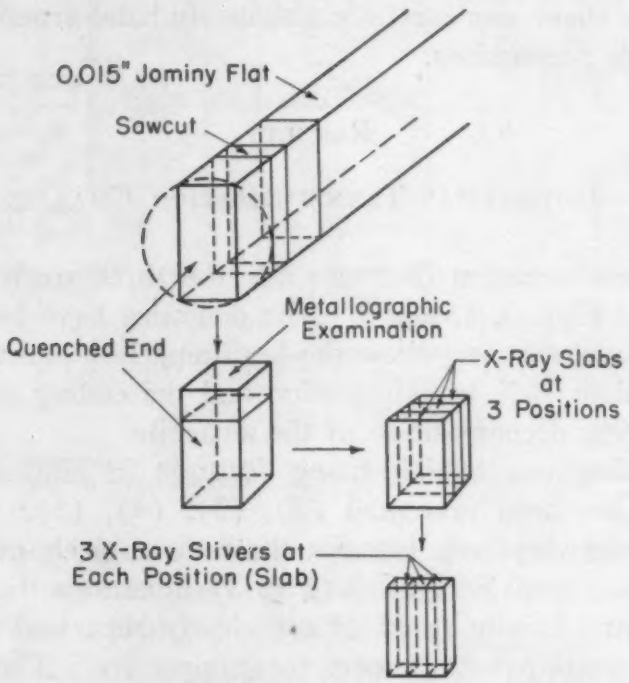


Fig. 2—Method of Sampling Jominy Bar Showing the Geometric Relation of the Various Specimens in Each of the Three Jominy Bars of Fig. 1.

retained austenite present following various isothermal heat treatments as well as at various positions in the Jominy bar.

The general X-ray diffraction techniques employed here have been described in detail elsewhere (1).[1] The method of sampling the Jominy bar for X-ray analysis, in particular, presented some special problems considering that only slight deformation or overheating will decompose the retained austenite. Fig. 2 illustrates the method of sampling and shows the geometric relation of the various specimens in each of the three Jominy bars of Fig. 1. The metallographic examination was made just under the hardness flat. Beneath this and extending to the opposite flat, the X-ray slabs were

[1]The figures appearing in parentheses pertain to the references appended to this paper.

cut approximately $\frac{3}{32}$ inch wide. Thus, for each metallographic specimen, at least three positions at known distances from the quenched end could be examined by X-rays. In addition, each X-ray slab provided three X-ray sliver specimens, thus allowing two check specimens at each position. All cutting of specimens was performed with a thin abrasive wheel submerged under water containing a cutting compound. The X-ray specimens after cutting were approximately $\frac{3}{32}$ inch square by $\frac{5}{8}$ inch long. To minimize the effects of cutting, each sliver was carefully alternately hand-ground and etched to needle-like proportions.

Results

Part I—Isothermal Transformation Characteristics

The transformation diagrams for the three steels investigated are shown in Figs. 3, 4, and 5. The diagrams have been drawn in the conventional manner where the beginning line indicates approximately less than ½% transformation and the ending line somewhat more than 99% decomposition of the austenite.

These diagrams exhibit many features of similar and other steels that have been presented (2), (3), (4), (5). Of greatest interest are the variations between these three steels of comparable hardenability. Steel SAE 5140 (Fig. 3) illustrates the case where the pearlite and bainite reactions are clearly separated with respect to time but overlap with respect to temperature. The top of the bainite reaction in this steel is at approximately 1035 °F (555 °C), and the bainite reaction exhibits the usual dependence upon temperature for the amount of austenite transformed by this reaction. This austenite transformation will vary from zero at the top of the bainite temperature range to 100% at some lower temperature as shown repeatedly in the literature. In the upper temperature range of bainite formation, the remaining austenite will transform by what is presumably a low-temperature pearlite type of reaction.[2] This is indicated in the transformation diagram in the neighborhood of 1000 °F (540 °C), where there are two sets of beginning and ending curves, the first set for bainite and the second set for pearlite. Note that the ending line for the bainite reaction does not indicate

[2]An analysis of the reaction kinetics of the transformation of austenite remaining after partial bainite formation over the entire bainite temperature range is nearing completion. This will include a precise determination of the temperature at which the bainite reaction achieves complete decomposition of the austenite in these as well as other steels.

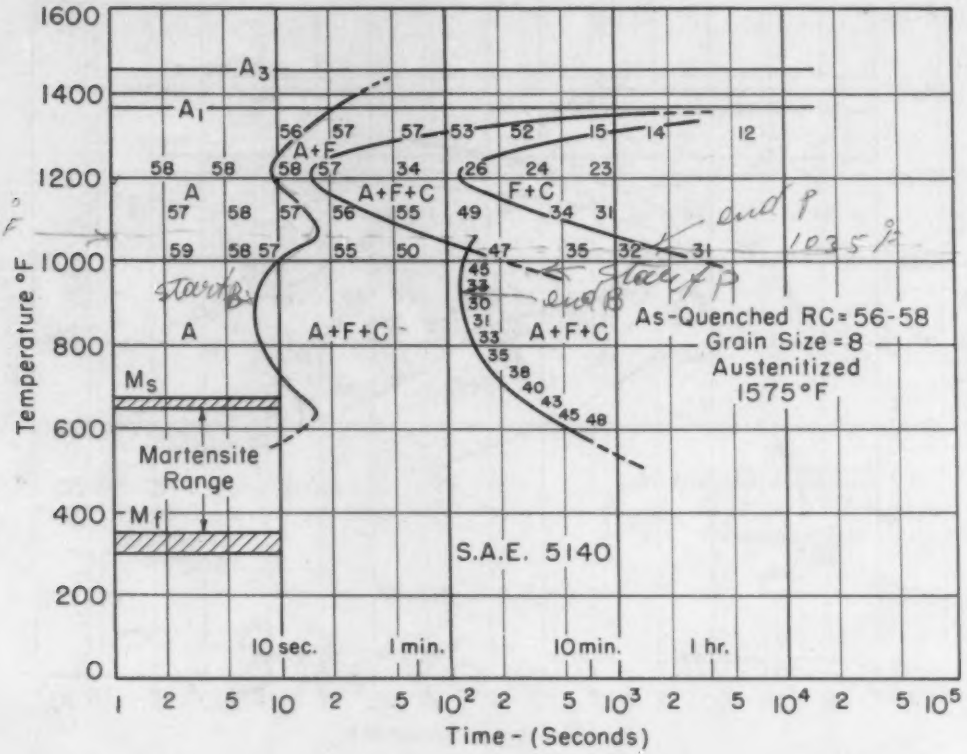


Fig. 3—Transformation Diagram for SAE 5140 Steel. As-quenched Rockwell C-56-58. Grain size—8. Austenitized 1575 °F.

complete decomposition of the austenite. The dilatometer curve of Fig. 6 clearly indicates the time-separation between the bainite and pearlite reactions at 1010 °F (545 °C).

The behavior of steel SAE 2340 (Fig. 4) differs from the above. Here the pearlite and bainite reactions almost completely overlap with respect to both time and temperature; although definitely present, the temperature dependence of the extent of bainite formation is partially masked by the overlapping pearlite reaction (6), as it is in plain carbon steels (3), (7). The top of the bainite range is indicated at approximately 960 °F (515 °C). Thus in the temperature range from approximately 800 to 960 °F (425 to 515 °C), there is a time interval in which both reactions will occur simultaneously. For example, at 935 °F (500 °C) the transformation of the austenite is initiated by the bainite reaction, later the pearlite reaction starts and both proceed simultaneously, following which the bainite reaction ceases (temperature dependence) and the transformation of the austenite is completed by the formation of pearlite. Dilatometric evidence for this phenomenon is apparent in Fig. 7.

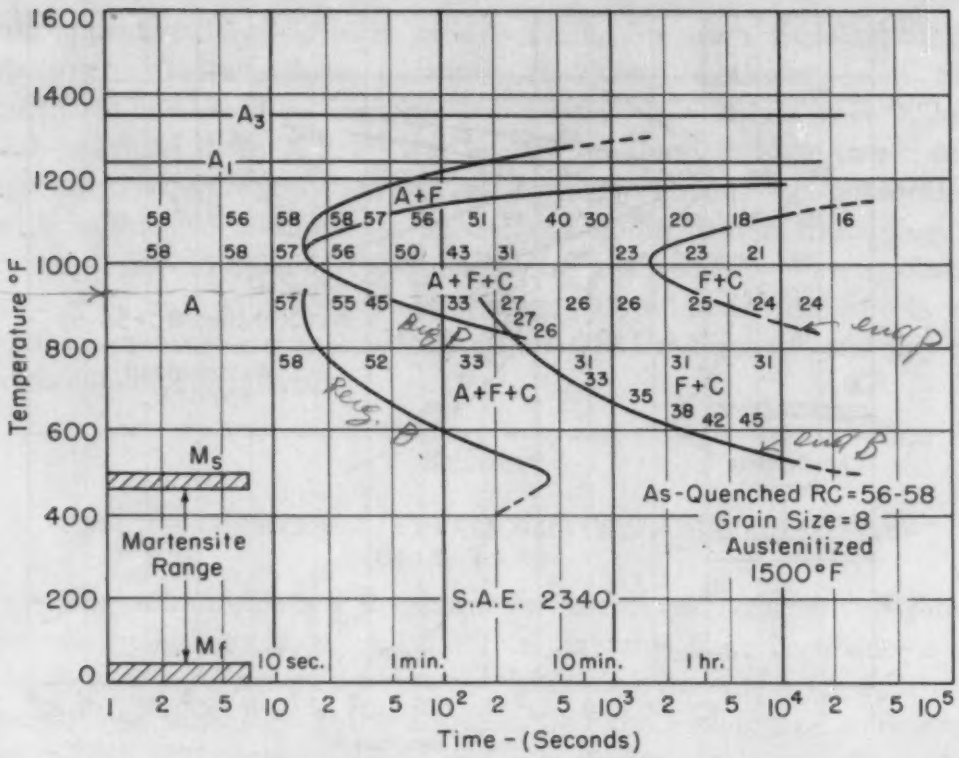


Fig. 4—Transformation Diagram for SAE 2340 Steel. As-quenched Rockwell C-56-58. Grain size—8. Austenitized 1500 °F.

The transformation characteristics of steel SAE T1340 are indicated in Fig. 5. The behavior of this steel may be most briefly described as being between SAE 5140 and SAE 2340. That is, over a portion of the bainite temperature range (1030 to 940 °F) there is overlapping of the pearlite and bainite reactions with respect to time as well as temperature; but approximately below 940 °F (505 °C) to about 775 °F (415 °C), the two reactions are separated with respect to time. The dilation curve of Fig. 8 indicates the nature of the transformation kinetics at approximately the maximum temperature where the pearlite and bainite reactions are separable in this steel. Fig. 9 typifies the microstructure obtained in a temperature region where the two reactions overlap. The light constituent is bainite and possibly some of Hultgren's (5) paraferrite, while the dark-etching constituent is a form of low-temperature pearlite.

Small, water-quenched X-ray diffraction specimens of SAE 5140 and SAE T1340 did not reveal the presence of any retained austenite. On the other hand, similarly treated specimens of SAE 2340 definitely yielded indications of a slight amount of retained austenite. The retention of austenite at room temperature was investigated after

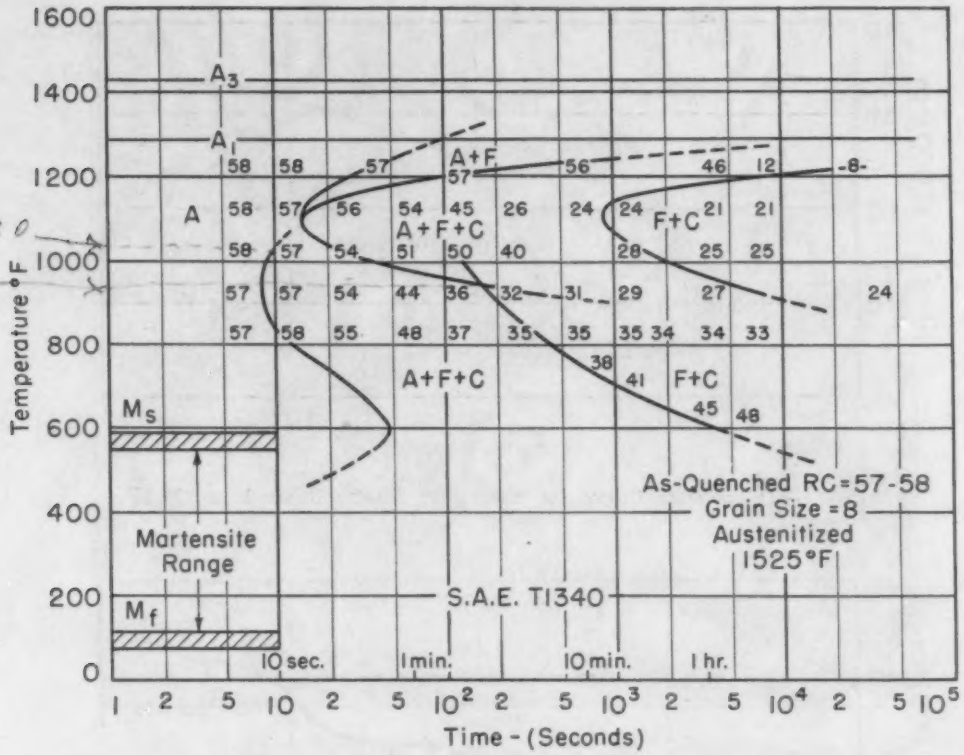


Fig. 5—Transformation Diagram for SAE T1340 Steel. As-quenched Rockwell C-57-58. Grain size—8. Austenitized 1525 °F.

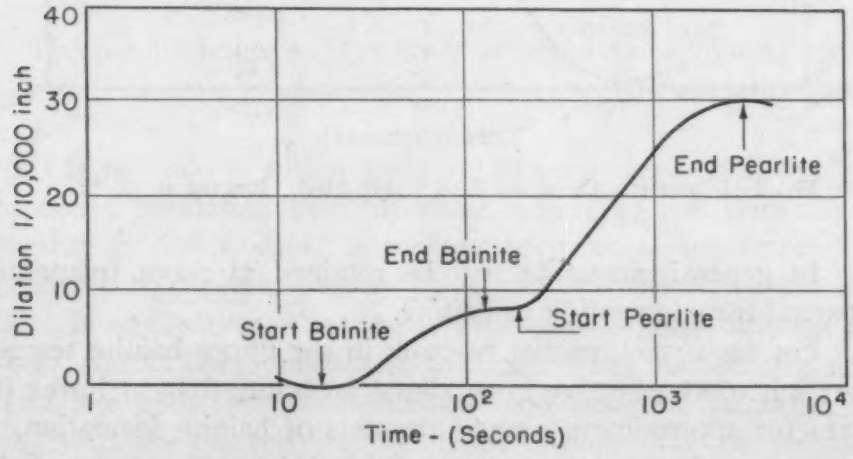


Fig. 6—Dilatometer Curve for SAE 5140 Steel. Reacted at 1010 °F.

partial bainite formation over the entire bainite temperature range. It is a well-established fact that the formation of bainite will enhance the stabilization of austenite. As expected, all three steels exhibited the presence of retained austenite after partial transformation of the austenite to bainite. Results may be summarized briefly as follows:

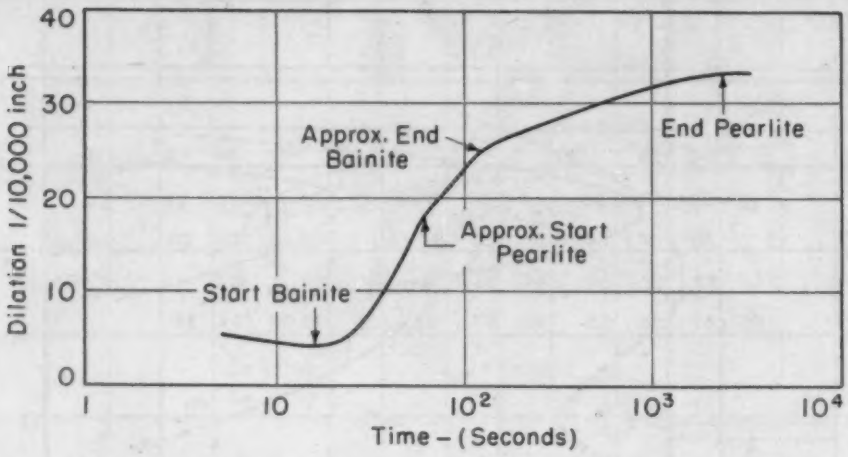


Fig. 7—Dilatometer Curve for SAE 2340 Steel. Reacted at 935 °F.

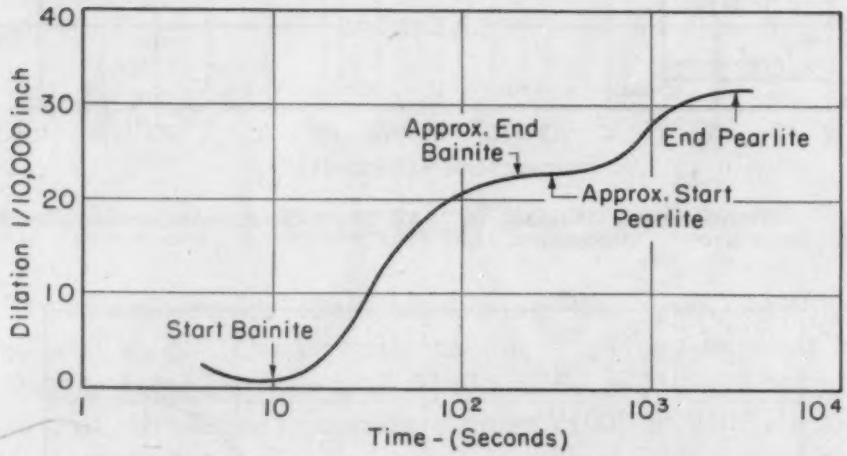


Fig. 8—Dilatometer Curve for SAE T 1340 Steel. Reacted at 935 °F.

1. In general, austenite will be retained at room temperature after partial transformation to bainite.

2. For each steel, partial reaction in the upper bainite temperature range is more effective in retaining austenite than at lower temperatures for approximately equal amounts of bainite formation.

3. For analogous treatments, SAE 2340 will retain slightly more austenite than SAE T 1340, and substantially more than SAE 5140.

4. Overlapping of the pearlite and bainite reactions will reduce the allowable isothermal holding time which will result in austenite retention.

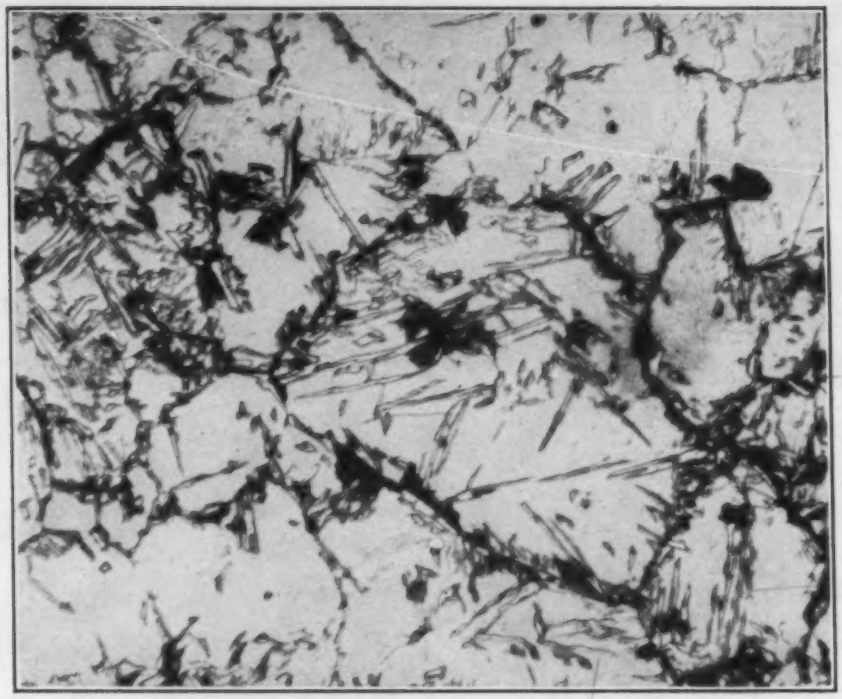


Fig. 9—Photomicrograph of SAE T1340 Steel, Reacted at 1000 °F for 100 Seconds. Etched 4% Nital. × 500.

Part II—The Jominy Bar and Austenite Retention

The results reported here were obtained by sectioning identically the same Jominy specimens that yielded the hardenability curves of Fig. 1.

It is possible to retain austenite at room temperature after partial bainite formation even in steels which do not normally retain austenite on direct, rapid quenching to room temperature. It is a logical step to conceive that a "slack-quench", which usually involves partial decomposition to bainite on cooling, will result in some austenite retention. The Jominy test bar affords an excellent opportunity to examine both the microstructural and austenite retention characteristics at various cooling velocities, which may be subsequently correlated with the condition existing in the interior of a quenched section (8), (9).

The results of the retained austenite investigation in the three Jominy bars are summarized in condensed form in Table II. It should be emphasized that the tabulation of retained austenite is based upon an arbitrary numbering system, where 10 represents the maximum intensity of austenite lines observed in any of the steels

Table II
Retention of Austenite in Jominy Specimens

Distance from Quenched End	X-ray* Retained Austenite	Cooling Velocity from Jominy Chart
	SAE 2340	
1/16 inch	3	600 °F/sec.
1/4	4	72
1/8	5	19
1	7	10
1¼	10	7.2
1½	9	5.6
2	9	4.4
2½	5	4.0
	SAE 5140	
1/16 inch	1	600 °F/sec.
1/4	1	72
1/8	2	19
1	2	10
1¼	1	7.2
1½	0	5.6
	SAE T1340	
1/16 inch	1	600 °F/sec.
1/4	3	72
1/8	4	19
1	5	10
1¼	7	7.2
1½	7	5.6
2	6	4.4
2¼	3	4.1

*Arbitrary numbering system where 10 represents the maximum intensity of the austenite X-ray reflections which were observed within this series of tests. Qualitative only.

at any position in the Jominy bar. The method is qualitative but adequate to indicate the trends. An absolute, quantitative analysis would be highly desirable.[3] It is difficult to estimate the actual volume of austenite retained. However, if one assumes that the minimum quantity of austenite that may be detected by X-ray diffraction methods is of the order of ½ to 1%, it follows that the maximum (see Table II) may be as much as 5 to 10% or more.

It is apparent, from Table II, that the amount of retained austenite increases as one proceeds along the Jominy bar, attains a maximum value and then decreases for all three steels. Steel SAE 2340 retains much more austenite than SAE 5140 and slightly more than SAE T1340 at all corresponding positions on the Jominy bar. In addition, the maximum of retained austenite in SAE 2340 and SAE T1340 occurs in the neighborhood of 1¼ to 1½ inches in the Jominy bar; while for SAE 5140 it occurs at ¾ to 1 inch. Steel SAE 5140 at 1½ inches does not retain any austenite, while SAE 2340 and SAE T1340 each retain almost their maximum of austenite at this position.

[3]Recently, such a method has been developed (10), which unfortunately is not applicable to cases where ferrite, bainite, pearlite, etc., may be present.

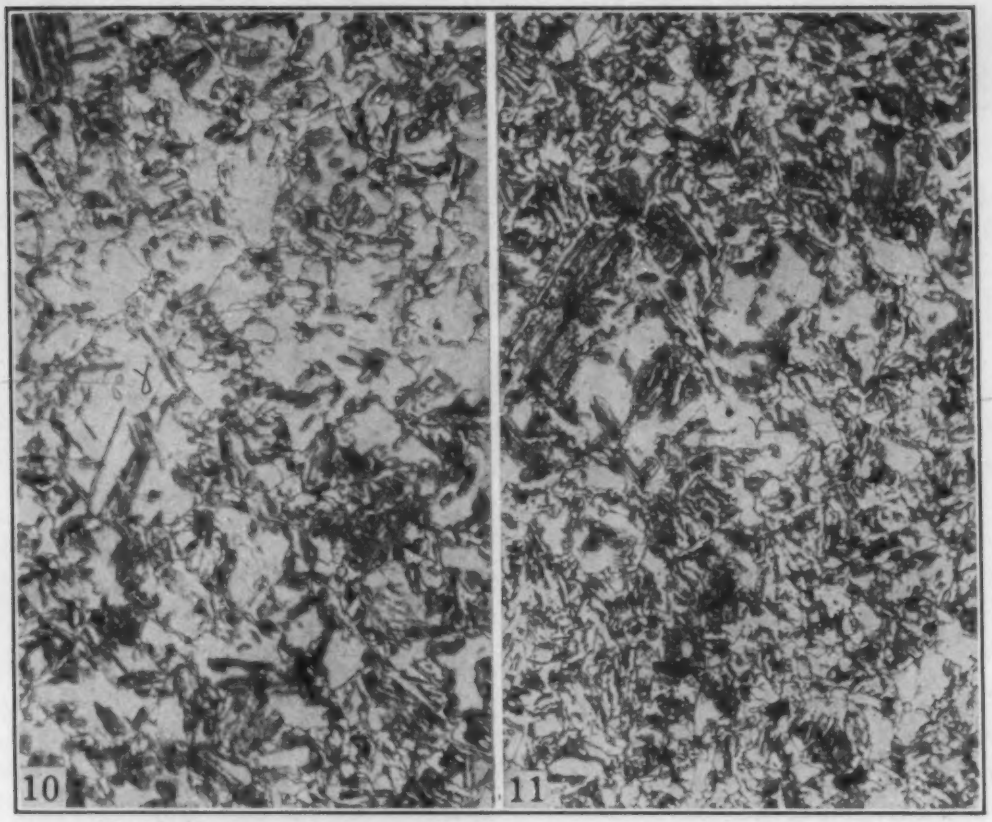


Fig. 10—Photomicrograph of SAE 2340 Steel, 1 Inch from Quenched End of Jominy Bar. Etched 4% Nital. × 500.

Fig. 11—Photomicrograph of SAE 2340 Steel, 1½ Inches from Quenched End of Jominy Bar. Etched 4% Nital. × 500.

In addition to the X-ray analysis, a complete metallographic examination of the three Jominy bars was performed. At all equivalent positions on the Jominy bar beyond ⅜ inch, SAE 5140 indicated the presence of substantially greater decomposition of the austenite to bainite, ferrite, etc., than did SAE T1340, and SAE T1340 in turn slightly more than SAE 2340. Figs. 10 to 13 inclusive demonstrate the type of structures obtained at two corresponding positions on the Jominy bar for SAE 2340 and SAE 5140. At the 1-inch position on the Jominy bar, SAE 2340 steel shows (Fig. 10) approximately 40 to 50% decomposition of the austenite to bainite: at the 1½-inch position (Fig. 11) the structure is composed of approximately 75% bainite. Steel SAE 5140 at 1 inch (Fig. 12) is mostly bainite, and at 1½ inches (Fig. 13) is completely decomposed to bainite, ferrite and some pearlite which is evident as the dark-etching constituent. The matrix in all cases is composed of martensite and the retained austenite. Steel SAE T1340 follows the same

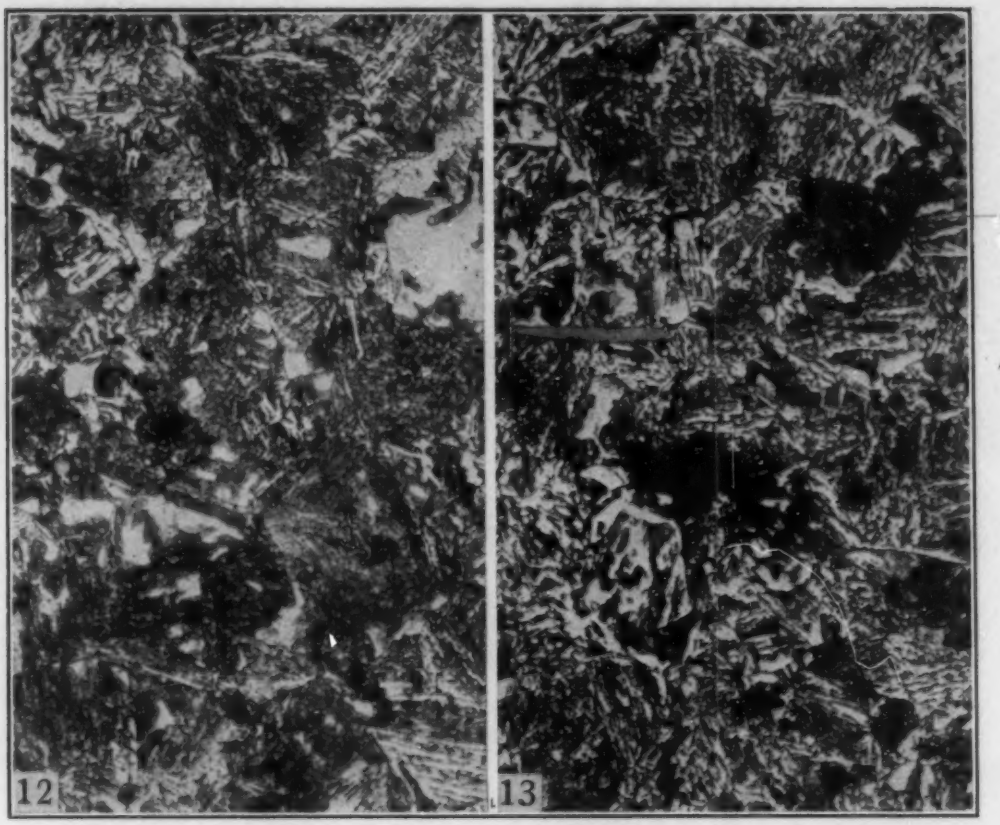


Fig. 12—Photomicrograph of SAE 5140 Steel, 1 Inch from Quenched End of Jominy Bar. Etched 4% Nital. × 500.

Fig. 13—Photomicrograph of SAE 5140 Steel, 1½ Inches from Quenched End of Jominy Bar. Etched 4% Nital. × 500.

general pattern with a transformation behavior which embodies the characteristics of both of the other two steels. It becomes apparent that the microstructural characteristics correlate well with the retention of austenite in the three Jominy bars.

Discussion

No fundamental difference in the mechanisms of decomposition of the austenite in these three steels was observed despite an appreciable apparent difference in external form of the three transformation diagrams.[4] All three steels exhibited a normal type of pearlite transformation, typical bainite reactions as discussed in the text, and characteristic behavior of martensite formation. The important

[4]The diagrams have been drawn in a manner to minimize the apparent differences in form by indicating the beginning and ending times for the reactions even at temperatures where they overlap.

difference lies, in each case, in the relative position of the pearlite and bainite reactions with respect to time and temperature, and also on the temperature of the martensite transformation range. These factors will, of course, exert a vital influence on the nature of the transformation products on cooling at less than the critical cooling velocity. The overlapping of the pearlite and bainite reactions with respect to temperature in SAE 2340 and, to a lesser extent in SAE T1340, appears to be a direct consequence of the effect of nickel and manganese in lowering A_1 and the pearlite range to a greater extent than the bainite range.

It has been shown that partial transformation of austenite to bainite in the upper bainite temperature range is more effective in retaining austenite than are lower temperatures. This phenomenon appears to be consistent with other recent studies on austenite stabilization. It has been demonstrated (11) that tempering retained austenite at successively elevated temperatures progressively increases stabilization on subsequent cooling. It has been suggested that stabilization may be correlated with stress relaxation (12) as the result of the similarity in activation energies for both processes. On the other hand, the effect observed here does not coincide well with other indirect evidence (13), which indicates that M_s may be lowered more than 200 °F in a 0.12% carbon, 3.8% manganese steel, as the temperature of bainite formation is lowered. However, in this latter work it is not possible to separate the time, amount of bainite formed, and temperature variables. In all cases, the lower temperatures involved longer times and more transformation to bainite prior to martensite formation.

The increase in retained austenite as one proceeds back from the quenched end of the Jominy bar is consistent with the isothermal results. More bainite forms as the cooling velocity is decreased. However, factors other than the formation of bainite must contribute to the observed retention of austenite, especially near the quenched end of the Jominy bar. At cooling velocities of 600 °F or 79 °F per second, no bainite is formed on cooling;[5] yet cooling at these velocities promotes stabilization (see Table II). This phenomenon may be accounted for by either or both of two phenomena. One, that stabilization in some steels may be promoted by holding in

[5]A series of small specimens for each steel was cooled at various velocities, the cooling curves recorded and transposed to the isothermal transformation charts indicating that at 79 °F per second or faster, no part of the cooling curve touched any beginning line on the transformation chart. In addition, all specimens were examined metallographically and by X-rays. These data are not reported here since they are in complete agreement with the Jominy bar analysis and add nothing to the conclusions.

the subcritical austenite range without decomposition (14) and second, that stabilization is enhanced by slow cooling through the martensite range. This latter effect, although recognized for some time, has only recently been demonstrated in convincing fashion (10).

The decrease in retained austenite back in the Jominy bar can be directly correlated with the fact that at the slower cooling velocities more decomposition at the higher temperatures occurs on cooling, until eventually no austenite is available for retention and transformation to martensite. The metallographic examination (for example, see Figs. 10 to 13 inclusive) affords vivid confirmation of this conclusion. It is further evident that, although these steels possess similar Jominy hardenability curves, the relative proportions and even the nature of the structures present at corresponding positions on the Jominy bar may be widely different. Obviously, various proportions of the same and/or different constituents may balance to give approximately equal hardness values. The relatively soft retained austenite undoubtedly plays an important role in this behavior in steels SAE T1340 and especially SAE 2340. For example, the expected higher hardness caused by the greater amount of martensite back in the Jominy bar in these steels, as compared to SAE 5140, presumably is masked in part by the larger amount of retained austenite present. It follows that the Jominy curve, as soon as it departs from a straight horizontal line representing essentially 100% martensite, is seriously limited as a tool for comparison of various steels even at comparable hardenability, since variations in structures may exist which are not evident from hardness data alone.

Acknowledgment

The author wishes to acknowledge the helpful assistance of E. F. Bailey. The co-operation of Prof. E. G. Mahin, head, department of metallurgy, University of Notre Dame, is appreciated.

References

1. T. Lyman and A. R. Troiano, "Isothermal Transformation of Austenite in One Per Cent Carbon, High Chromium Steels," *Transactions*, American Institute of Mining and Metallurgical Engineers, Vol. 162, 1945, p. 196.
2. A. R. Troiano, "An Investigation of the Metallographic and Physical Properties of New Types of Gun Steels," Final Report, NRC 36, Office of Scientific Research and Development, April 1944.
3. E. P. Klier and T. Lyman, "The Bainite Reaction in Hypoeutectoid Steels," *Transactions*, American Institute of Mining and Metallurgical Engineers, Vol. 158, 1944, p. 394.

4. T. Lyman and A. R. Troiano, "Influence of Carbon Content upon the Transformations in 3 Per Cent Chromium Steel," TRANSACTIONS, American Society for Metals, Vol. 37, 1946, p. 402.
5. A. Hultgren, "Isothermal Transformation of Austenite," TRANSACTIONS, American Society for Metals, Vol. 39, 1947, p. 915.
6. A. R. Troiano, Discussion to reference 5.
7. W. T. Griffiths, L. B. Pfeil and N. P. Allen, "The Intermediate Transformation in Alloy Steels," Second Report of the Alloy Steels Research Committee, The Iron and Steel Institute, 1939, p. 343.
8. A. L. Boegehold, "Selection of Automotive Steel on the Basis of Hardenability," *SAE Journal,* October 1944, p. 472.
9. G. K. Manning, "End-Quenched Hardenability Versus Hardness of Quenched Rounds," METAL PROGRESS, October 1946, p. 647.
10. B. L. Averbach and M. Cohen, "X-ray Determination of Retained Austenite by Integrated Intensities," Technical Publication 2342, American Institute of Mining and Metallurgical Engineers, 1948.
11. S. G. Fletcher, B. L. Averbach and M. Cohen, "The Dimensional Stability of Steel — Part II — Further Experiments on Subatmospheric Transformation," TRANSACTIONS, American Society for Metals, Vol. 40, 1948, p. 703.
12. J. H. Hollomon, L. D. Jaffee and D. C. Buffum, "Stabilization, Tempering and Relaxation in the Austenite-Martensite Transformation," *Journal of Applied Physics,* Vol. 18, 1947, p. 780.
13. F. Wever and K. Mathieu, "Ueber die Umwandlungen der Manganstähle." *Mitt., Kaiser-Wilhelm Institut für Eisenforschung,* Vol. 22, 1940, p. 9.
14. E. P. Klier and A. R. Troiano, "Ar" in Chromium Steels," *Transactions,* American Institute of Mining and Metallurgical Engineers, Vol. 162, 1945, p. 175.

DISCUSSION

Written Discussion: By E. S. Rowland, research metallurgical engineer, The Timken Roller Bearing Co., Canton, Ohio.

Dr. Troiano is to be congratulated on a fine practical demonstration of the important effect of partial bainite transformation on the stabilization of the untransformed austenite. While Dr. Troiano and others have explored this phenomenon in the past, the practical significance of its influence on the microstructure of slack quenched alloy steel parts has been generally overlooked. This paper should lead the way to a better understanding of such matters.

The author states in his last sentence that the Jominy curve is seriously limited as a tool for comparison of various steels, even at comparable hardenability, once the region of substantially 100% martensite is passed. This statement is based upon the undeniable fact that the three steels investigated had significantly different microstructures on the end-quenched bars at essentially the same hardness levels.

A purely practical viewpont leads the writer to wish that Dr. Troiano had obtained two additional bits of information. First, it would be nice to know that tempering of the Jominy bars in the temperature range of commercial treatment, say 1000 to 1200 °F (540 to 650 °C), would produce significantly different tempered hardenability curves for the three steels. Furthermore, it would be necessary to know that the tempered structures of these three steels at the same as-quenched hardness, but different

microstructures, would produce different mechanical properties. The point of the matter is that unless the tempered properties of the three steels of equivalent hardenability are different in the slack-quenched condition, the end-quenched test is still a satisfactory guide to the selection and application of engineering alloy steels. The Jominy test has proved so satisfactory a practical tool that the writer hesitates to let even this mild and well-meant indictment pass without comment.

Written Discussion: By H. B. Knowlton, supervisor, Materials Engineering, International Harvester Co., Chicago.

Dr. Troiano presents some very interesting and valuable information concerning variations in microstructure produced by quenching three alloy steels having the same hardenability. It might be added that these structures will respond differently to tempering. It would be undesirable, therefore, to purchase alloy steels on the basis of hardenability alone. This would cause great confusion in production heat treating.

The facts brought out in this paper are not debatable. We fear, however, that a very erroneous inference may be drawn, that since the Jominy curve does not tell the whole story with regard to microstructure, the Jominy test is of little value. A recent survey by the SAE steel users subcommittee of the Hardenability Division, showed that the majority of steel users, who replied, reported definite advantages in purchasing steel to Jominy hardenability as well as analysis.

Dr. Troiano does not recommend judging the merits of steel solely on the basis of the type of microstructure produced. There seems to be some trend among others lately to discuss heat treated steels upon the basis of the per cent of martensite in the as-quenched structure. Judging the merits of such steel solely on the basis of the per cent of martensite would be very much worse than judging on Jominy hardenability alone. Martensite is not a definite entity with fixed physical properties. It is a type of structure. According to Burns, Archer and Moore, the hardness of martensite varies from Rockwell C-30 to C-65, depending upon the carbon content. Strength and other properties vary with the hardness.

The merit of a heat treated steel should be judged on the basis of whether it will serve some useful function. The three steels discussed in this paper are commonly used in the automotive industry for heat treated parts such as bolts, studs, shafts, and steering knuckles and arms. Many of these parts are heat treated to about Rockwell C-30 to C-40.

Two types of failure are encountered. Bolts may stretch in assembly if the yield strength is too low. Breakage in service is almost always due to fatigue. What then are the relative effects of hardness and microstructure on the yield strength and the endurance limit in fatigue? There has been a tendency to state that steel should be heat treated so as to produce at least 90% if not 100% martensite in the as-quenched condition. Is this necessary or desirable?

These questions are best answered by the data recently presented by Boegehold[7] and Dolan and Yen[8].

[7]A. L. Boegehold, General Motors Report MR 73 12-29-47.

[8]Dolan and Yen, University of Illinois, March 1948.

Boegehold quenched samples of three different types of 0.41 to 0.43% carbon alloy steel at different rates so as to produce initial hardnesses of Rockwell C-40, C-47 and C-55 with each steel. All samples were tempered to Rockwell C-35. Only the Rockwell C-55 specimens could approach 100% martensite in the as-quenched condition. An as-quenched hardness of Rockwell C-40 would indicate nearer 50% martensite.

As might be expected, the specimens which showed the highest as-quenched hardness, also showed the highest yield strength and the highest fatigue endurance limit after tempering to Rockwell C-35. The difference, however, was much less than would be expected. The yield strength and the endurance limits of the specimens showing the lowest as-quenched hardness were only about 10% lower than those of the specimens showing the highest as-quenched hardness.

In practical commercial heat treating, involving oil quenching, 0.40% carbon low and medium alloy steels such as described in the paper, production of complete martensite at the surface cannot be guaranteed for sections larger than about ¾-inch diameter. Heats having the minimum permissible hardenability will not produce 100% martensite in such sections.

Considering the fact that bending and torsional strength vary with the cube of the diameter of the specimen, it would be possible to compensate for the 10% lower fatigue strength of the steel having the low as-quenched hardness by increasing the diameter by 3%. This might be much more economical than selecting a higher alloy steel which would develop a better type of structure.

Data presented by Dolan and Yen showed that in some cases greater differences in notched fatigue strength of fully quenched and slack-quenched were encountered, but in general the same conclusions may be drawn. Some writers point to greater differences in the so-called impact strength. Dolan and Yen show that the correlation between impact and notched fatigue tests is not too good.

Written Discussion: By Paul Gordon, Massachusetts Institute of Technology, Department of Metallurgy, Cambridge, Mass.

I do not wish to detract from the general excellence of this latest paper by Dr. Troiano whose enviable reputation as a metallurgical experimentalist is well established and just as well deserved. I do, however, wish to call the author's attention to an apparent inconsistency in the interpretation of the curve in Fig. 7. This curve represents the expansion of the 2340 steel held at 935 °F for some 5000 seconds after quenching to this temperature. During the course of the expansion the curve reveals two rather sharp decreases in slope, indicating more or less sudden decreases in the rate of expansion. The first of these changes in slope is described by the author as the beginning of the austenite-to-pearlite reaction, and is cited as evidence that both pearlite and bainite reactions are proceeding simultaneously for a period of time. It is difficult to see how the austenite-pearlite reaction, which results in an appreciable expansion, could manifest its initiation by a decrease in the rate of expansion

of a dilatometer specimen. On the contrary, with the bainite reaction under way, as is presumably the case in Fig. 7, it would seem one should look for an increase in the rate of expansion as an indication of the onset of the pearlite reaction.

Written Discussion: By D. C. Buffum and L. D. Jaffe, Watertown Arsenal, Watertown, Mass.

In connection with the author's observations and remarks on austenite stabilizing during continuous cooling, when no bainite forms, it seems worthwhile to mention some measurements made a few years ago.

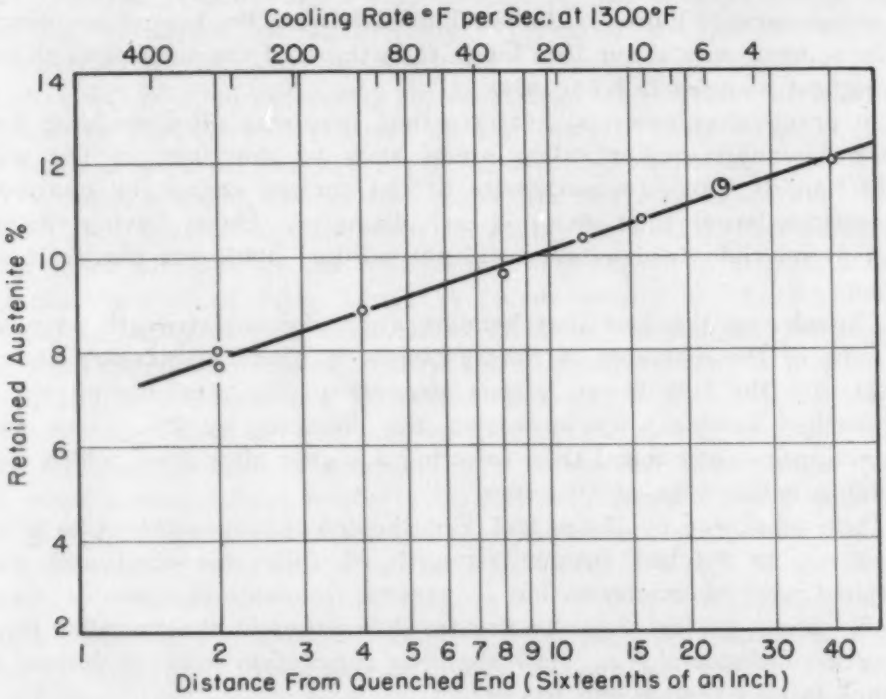


Fig. 13—Retained Austenite in Jominy Specimen.

A Jominy specimen of the following composition was austenitized 4 hours at 1725 °F (940 °C) and end-quenched:

C	Mn	Si	S	P	Ni	Cr	Mo
0.39	1.33	0.39	0.016	0.013	3.31	1.58	0.49

Microscopic examination revealed only martensite and austenite throughout the length of the bar. Determination of the percentage of retained austenite was made by means of X-ray diffraction following the technique of Gardner, Cohen and Antia[6] (except that 18-8 stainless steel was used for calibration). Results are shown in Fig. 13.

It is interesting to note that the amount of retained austenite is a linear function of the logarithm of the distance from the quenched end of

[6]F. S. Gardner, M. Cohen and D. P. Antia, "Quantitative Determination of Retained Austenite by X-Rays," *Transactions*, American Intitute of Mining and Metallurgical Engineers, Vol. 154, 1943, p. 306-317.

the Jominy bar. A plot of per cent austenite versus logarithm of the cooling rate at 1300 °F (705 °C) (as given by the Standard Jominy chart) also was found to be linear.

Author's Reply

It would be sheer folly to deny the role that the Jominy test has played in bringing a measure of order to an almost completely chaotic condition. It would be equally senseless to accept this or any other test as the last word, never subject to change or further interpretation. It was in this spirit that this and similar current studies were undertaken; a philosophy with which I am sure no one disagrees.

Dr. Rowland, quite logically, desires a correlation of the variations in microstructure with mechanical properties. We hope to be able to furnish such information in the near future. All that can be said at the present time is that preliminary impact tests appear to show marked variations with changes in structure at approximately the same hardness level.

Essentially, Mr. Knowlton also would like more data on the physical properties. It is our considered opinion that the physical properties of steel are primarily a function of the microstructure and that the hardness as a standard of comparison has been successful only where it has fortuitously represented essentially equivalent structures. As a vivid example of the difference in a mechanical property that may exist between two microconstituents at equal strength levels, one has only to compare the impact strength of pearlite with that of tempered martensite of the same hardness in the same steel. The impact strength of the tempered martensite will be many orders of magnitude greater. Although most information available at the present time appears to indicate the desirability of 100% martensite in the as-quenched condition, there is reason to suspect that this may not always be the case. Combinations of physical properties have been obtained with lower bainite and mixtures of lower bainite and martensite not possible with tempered martensite. Furthermore, virtually nothing is known of the effect of retained austenite on the physical properties. One may ask, what is the effect of retained austenite per se: how does it behave on tempering as a function of time and temperature: if not completely transformed at the tempering temperature, how will it react on subsequent cooling, etc.?

The results of Boegehold and also Dolan and Yen presented by Mr. Knowlton are quite interesting. Unfortunately, intelligent comment is limited by the fact that these data are not available to us at the moment. We note that the slack-quenched steels did show a 10% decrease in yield and fatigue strength. We suspect that the difference in impact strength would be greater. We are in complete agreement with Mr. Knowlton's comments on the difficulty of obtaining 100% martensite by oil quenching of steels such as those reported here.

With reference to Fig. 7, Dr. Gordon states that it is difficult to see

how the austenite-pearlite reaction, which results in an appreciable expansion, could manifest its initiation by a decrease in the rate of expansion. The key to the explanation of this phenomenon lies in the fact that for the circumstances depicted in Fig. 7, the expansion caused by the bainite reaction is approaching zero in characteristic fashion as the reaction comes to completion. If the pearlite reaction did not overlap, the rate of reaction (expansion) would be zero as in Fig. 6, for example. However, the rate of expansion does not go to zero, but only decreases slightly as the pearlite reaction with its concomitant expansion overlaps slightly and picks up the expansion as the bainite transformation fades out. Thus, there actually is an increase in the expansion over what would normally be present if the pearlite reaction had not been initiated. The problem is merely one of relative rates of partially overlapping expansions.

The data of Buffum and Jaffe constitute a welcome and valuable addition to this paper. It is instructive to note that the retention of austenite follows such a simple relationship with cooling velocity, as long as the critical cooling velocity is exceeded. Our results for 2340 (including some not reported) when plotted in the same manner also yield a straight line roughly parallel to that of Buffum and Jaffe, extending to the position on the Jominy bar where the critical cooling velocity is no longer exceeded. At this point the curve for retained austenite shows a sharp breakup, indicating a change in mechanism; that is, stabilization of austenite by partial bainite formation.

THE MICROSTRUCTURE OF LOW CARBON STEEL

By R. L. Rickett and F. C. Kristufek

Abstract

The microstructure of low carbon steel is considered in terms of (a) isothermal transformation of austenite, (b) precipitation of carbide from ferrite and the influence of prior structure, (c) amount of cold reduction, and (d) effect of annealing variables on the structure after annealing near or below the A_1 equilibrium temperature.

Ferrite forms very rapidly from austenite in such steels, even well above 1335 °F (725 °C), the Ae_1 temperature; transformation of the remaining austenite requires a very long time at 1300 °F (705 °C) and an extremely short time at 1000 °F (540 °C). The resulting microstructure depends upon temperature of transformation and, generally, upon the extent of carbon enrichment of the austenite, due to rejection of ferrite, prior to its transformation.

Appreciable hardening may result from the retention of carbon in solution in ferrite by rapid cooling, with further hardening on holding at ordinary temperature. Much of this carbon may be precipitated by cooling slowly or by reheating after quenching; size and distribution of the resulting carbide particles depend upon the temperature at which they are formed.

Microstructure after customary low temperature annealing, usually at a temperature near or somewhat below the Ae_1, is influenced by prior ferrite grain size and carbide distribution, amount of cold reduction, annealing temperature and time and sometimes by cooling rate.

Introduction

LOW CARBON steel is commonly regarded as a simple material, whose properties and structure are not affected significantly by anything except cold deformation. This erroneous viewpoint probably accounts for the relatively small amount of attention that has been devoted to its metallography as contrasted with that of higher

A paper presented before the Thirtieth Annual Convention of the Society, held in Philadelphia, October 23 to 29, 1948. The authors, R. L. Rickett and F. C. Kristufek, are associated with the Research Laboratory, United States Steel Corp., Kearny, N. J. Manuscript received April 13, 1948.

carbon steel. Although the magnitude of the effects of certain treatments on its structure and properties may be somewhat less than in higher carbon steel, their practical importance may be equally great in the lower carbon material. Moreover, certain phenomena in low carbon steel are absent or relatively unimportant in higher carbon material. There is, therefore, ample reason for studying the microstructures that may be present in low carbon steel and the factors that determine its structure.

The principal constituents of low carbon steel at ordinary temperature are ferrite and cementite (iron carbide), just as in higher carbon steels, except that, in low carbon steel, ferrite is the predominant constituent. Cementite may be present in conjunction with ferrite as pearlite, or it may occur as discrete particles ("carbide particles") which may vary greatly in size, shape and distribution. Microstructure of low carbon steel is determined, therefore, by those factors that influence size and shape of the ferrite grains and type and distribution of carbide particles. Both constituents form from austenite, and their microstructure depends largely upon the temperature at which transformation occurs; cementite may also be formed by precipitation from solid solution in ferrite, which is capable of dissolving approximately 0.03% carbon at 1335 °F (725 °C), less at lower temperature. The structure of both may be further influenced by subsequent cold reduction and annealing. The influence of these various factors has been investigated and is discussed below.

The Iron-Carbon Equilibrium Diagram

Before presenting the experimental results, it may be well to consider certain features of the iron-carbon equilibrium diagram of particular interest in the metallography of low carbon steel; a portion of this diagram (1)[1] is shown in Fig. 1, together with photomicrographs illustrating the phases corresponding to selected portions.

The ferrite field (RTU in Fig. 1) is an extremely important one in the physical metallurgy of low carbon steel. Solubility of carbon in ferrite is greatest, approximately 0.03%, at the eutectoid temperature (1335 °F); at lower temperatures the solubility is less, becoming very slight at ordinary temperatures. Carbon dissolved in ferrite may be kept in solution by quenching as in photomicrograph B, Fig. 1, representing a steel containing 0.02% carbon quenched from within the ferrite field; under equilibrium or near-equilibrium conditions, however, carbon in excess of the lower tem-

[1]The figures appearing in parentheses pertain to the references appended to this paper.

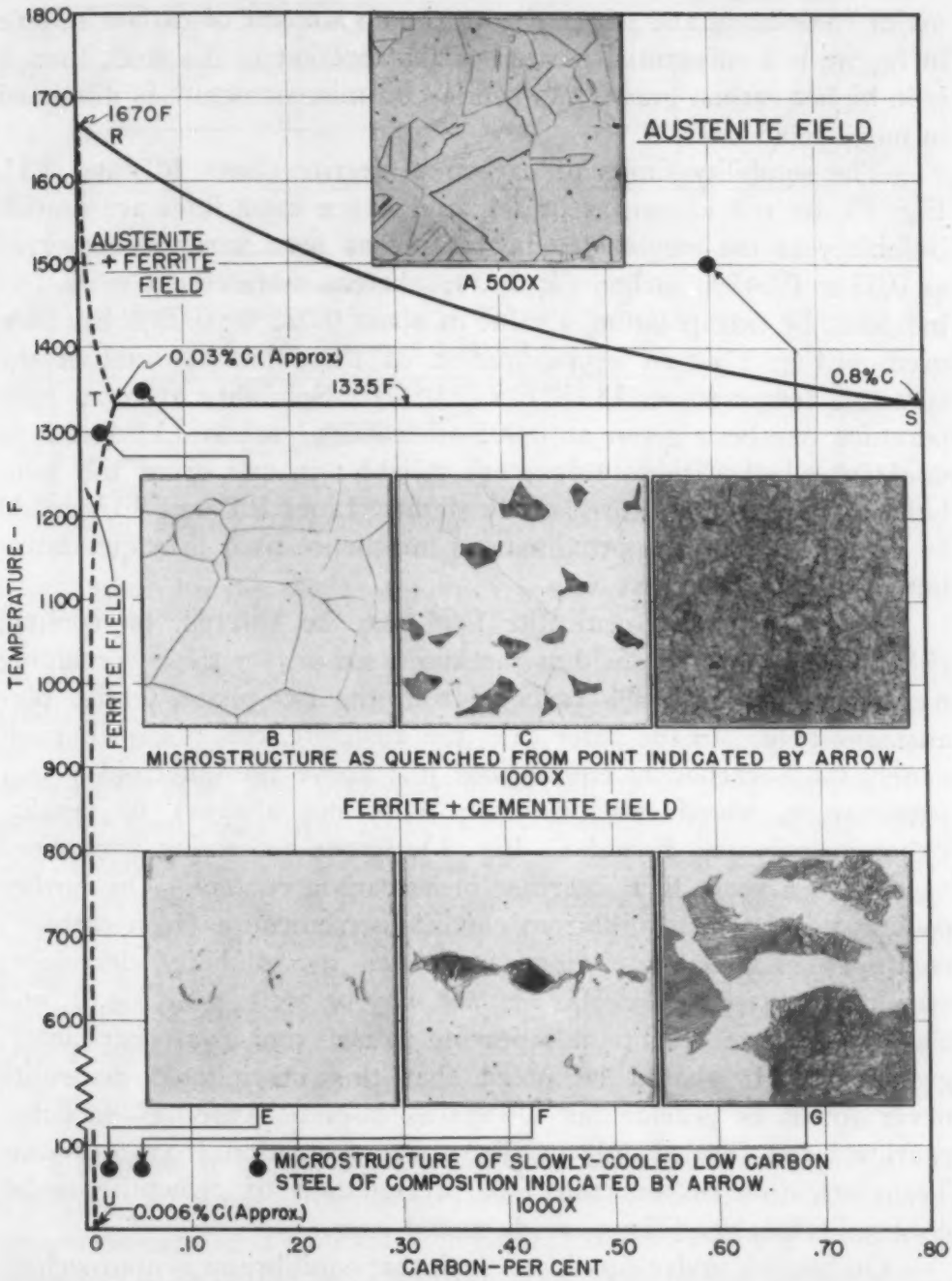


Fig. 1—Portion of Iron-Carbon Equilibrium Diagram and Microstructures Representing Selected Locations. Original magnification of photomicrographs given.

perature solubility limit precipitates during cooling as in E, Fig. 1, a photomicrograph of the same steel as B after air cooling from within the ferrite field. This changing solubility of carbon in ferrite is much more important in low carbon steel, where ferrite is the

major constituent and where the maximum amount of carbon soluble in ferrite is a substantial portion of that present in the steel, than it is in higher carbon grades; its bearing on microstructure is discussed in more detail later.

The solubility limits of carbon in ferrite (lines RT and TU, Fig. 1) are not known accurately and hence these lines are dotted. Solubility at the eutectoid temperature has been variously reported as 0.03 to 0.045% carbon (1, 2, 3), whereas more recent work (4) indicates, by extrapolation, a value of about 0.025%; 0.03% has been used in Fig. 1 as an approximation of the solubility limit at the eutectoid temperature, 1335 °F (725 °C). Solubility at room temperature has been given as 0.005 to 0.008% carbon (1) but it is doubtful whether these values are reliable; in any event the solubility at room temperature is only slight. Lines RT and TU should be regarded only as approximations and hence used in a qualitative but not in a quantitative way.

The ferrite plus cementite field may be entered, on cooling, either from the ferrite field as just discussed or, for steels containing more than about 0.03% carbon, from the two-phase ferrite plus austenite field. In the latter case, the austenite, containing approximately 0.8% carbon at equilibrium just above the eutectoid (Ae_1) temperature, transforms ordinarily (but not always) to pearlite (photomicrographs F and G, Fig. 1), ferrite remaining unchanged except for a very slight decrease in its carbon content. On further cooling under near-equilibrium conditions, cementite (iron carbide) continues to precipitate from ferrite as its solubility decreases; cementite precipitated in this manner may be seen in E, Fig. 1, and also in F, where it surrounds pearlite patches and also occurs intergranularly. It should be noted that this precipitated cementite never forms as pearlite but always as discrete "carbide" particles, pearlite being formed only by direct transformation from austenite. Transformation of austenite and precipitation of cementite under nonequilibrium conditions are discussed later.

On heating under conditions such that equilibrium is approached, the changes that take place are the reverse of those occurring on cooling. To illustrate the effect of such changes in a low carbon steel, specimens were heated at a series of temperatures, then quenched and their hardness measured. The results, shown in Fig. 2, indicate that detectable hardening resulted upon quenching from as low as about 800 °F (425 °C), this hardening being due to solu-

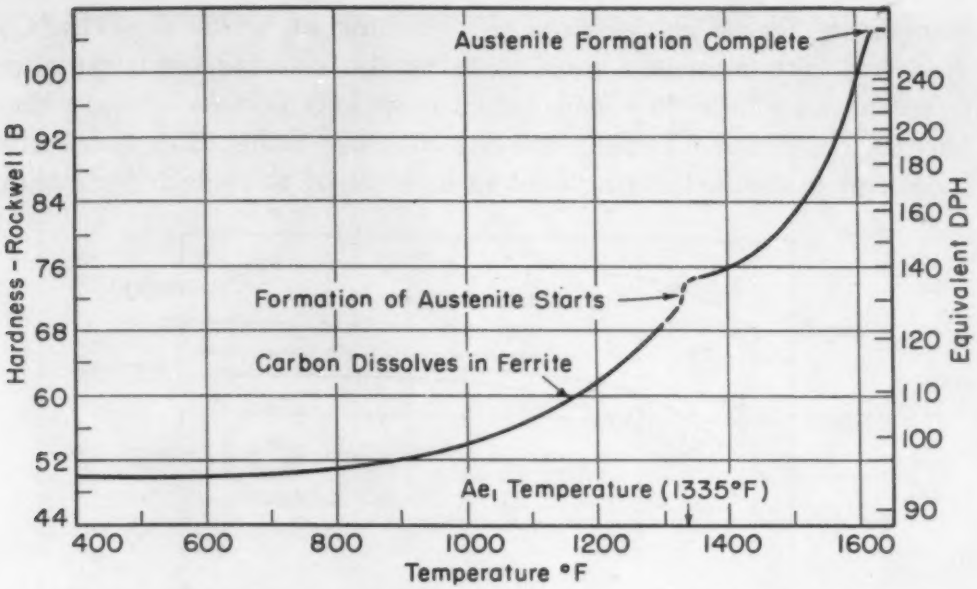


Fig. 2—Effect of Quenching from Various Temperatures on Hardness of Previously Box-Annealed 0.06% Carbon – 0.43% Manganese Rimmed Steel.

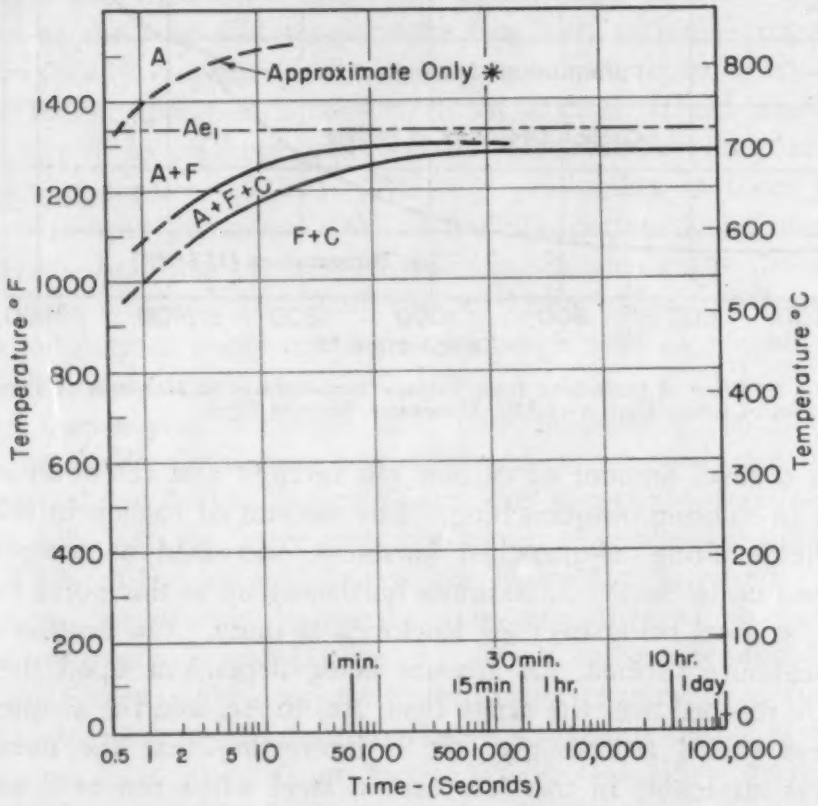
tion of a small amount of carbon (in ferrite) and retention of this carbon in solution on quenching. The amount of carbon in solution, and the resulting as-quenched hardness, increased as temperature increased up to the Ae_1, maximum hardening up to this point for this particular steel being over 20 Rockwell B units. On heating above Ae_1, austenite formed, the amount being dependent upon the temperature reached over the range from Ae_1 to Ae_3 and the as-quenched hardness varied accordingly. It is interesting that the maximum hardness attainable in this low carbon steel when rendered entirely martensitic is approximately Rockwell B-105 (corresponding to about Rockwell C-25).

Transformation of Austenite in Low Carbon Steel

Useful as it is, the equilibrium diagram yields no information as to rate of change of phase nor, directly, any idea as to the resulting microstructure. To obtain such information concerning the transformation of austenite to ferrite plus cementite in low carbon steel, the isothermal method of investigation, employed so successfully for higher carbon steels, was used. The resulting isothermal transformation (IT) diagram for one steel investigated is shown in Fig. 3, and representative microstructures in Figs. 4 and 5.

To obtain the IT diagram in Fig. 3, 0.040-inch thick cold-rolled specimens of a low carbon rimmed steel (0.06% carbon, 0.43%

manganese) were austenitized 10 minutes at 1675 °F (915 °C), quenched into a molten-metal bath at the selected transformation temperature, where they were held for various periods of time, then quenched in brine. Despite the use of these rather thin specimens, some ferrite formed during cooling to most of the selected tempera-



* Taken from work of Blanchard, Parke & Herzig
Trans. ASM, 29 317-335 (1941)

Fig. 3—Isothermal Transformation Diagram (Tentative), Low Carbon Steel. 0.06% Carbon, 0.43% Manganese (Rimmed Steel), Austenitized at 1675 °F.

tures. Moreover, at some levels the steel transformed so rapidly that the time for start and end of transformation could not be determined, nor could the steel be cooled to lower temperatures without transforming completely during cooling. The data are thus somewhat limited and uncertain; for this reason the diagram in Fig. 3 is marked tentative, yet it is sufficiently accurate to show the general transformation behavior of low carbon steel. Similar diagrams for a few other low carbon steels have been determined and the effect of other austenitizing conditions has been investigated, with results in general agreement with the diagram as given in Fig. 3.

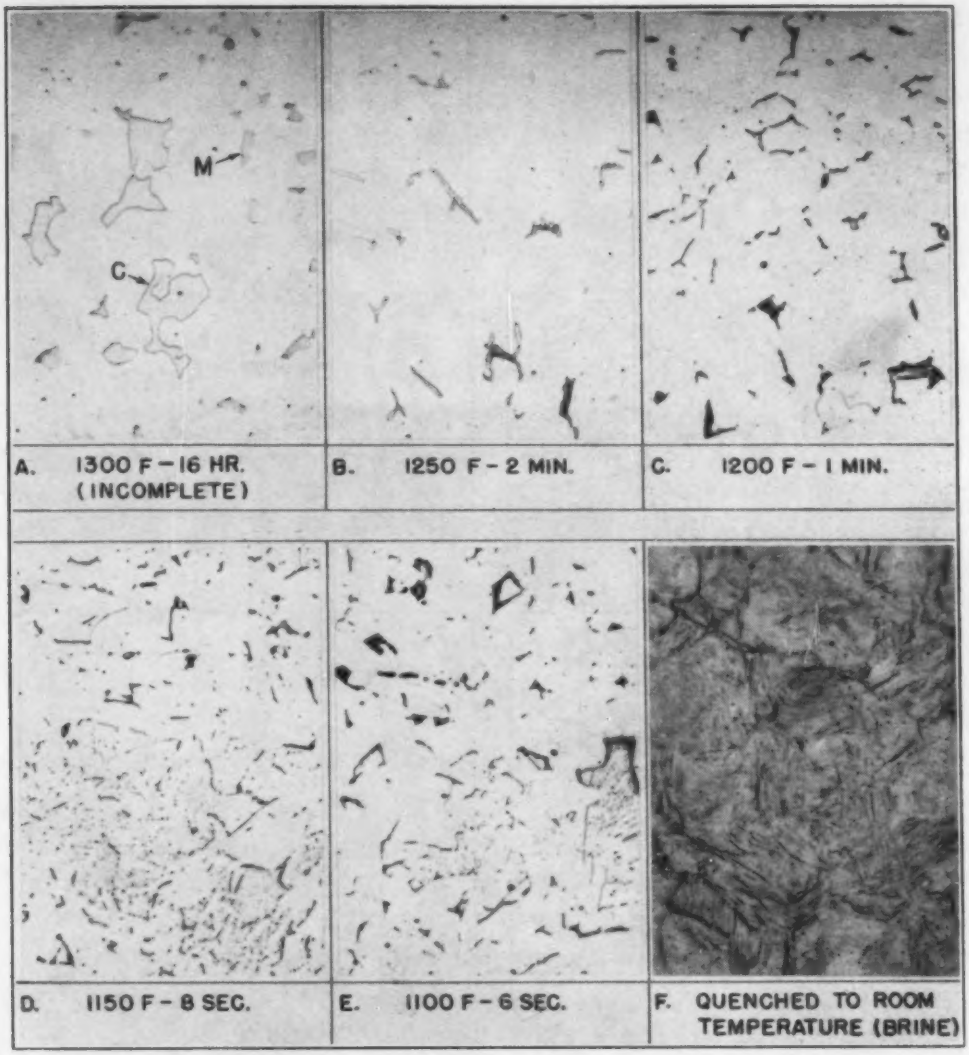


Fig. 4—Microstructure of 0.06% Carbon Rimmed Steel Isothermally Transformed at 1100 to 1300 °F and As-Quenched. Original magnification × 1000. Picral etch. M—martensite. C—cementite.

Principal features of the low carbon steel IT diagram (Fig. 3) that should be noted are: (a) the very short period of time for start of ferrite formation, even at a temperature well above Ae_1; (b) the long time required for completion of transformation at about 1300 °F (705 °C) or above; and (c) the extreme rapidity of transformation at 1100 °F (595 °C) and below. This diagram, although it does not apply directly to continuous cooling, indicates that, to attain complete transformation at a temperature only slightly below the Ae_1, even such a low carbon steel would have to be cooled very slowly. On the other hand, extremely rapid cooling would be required to

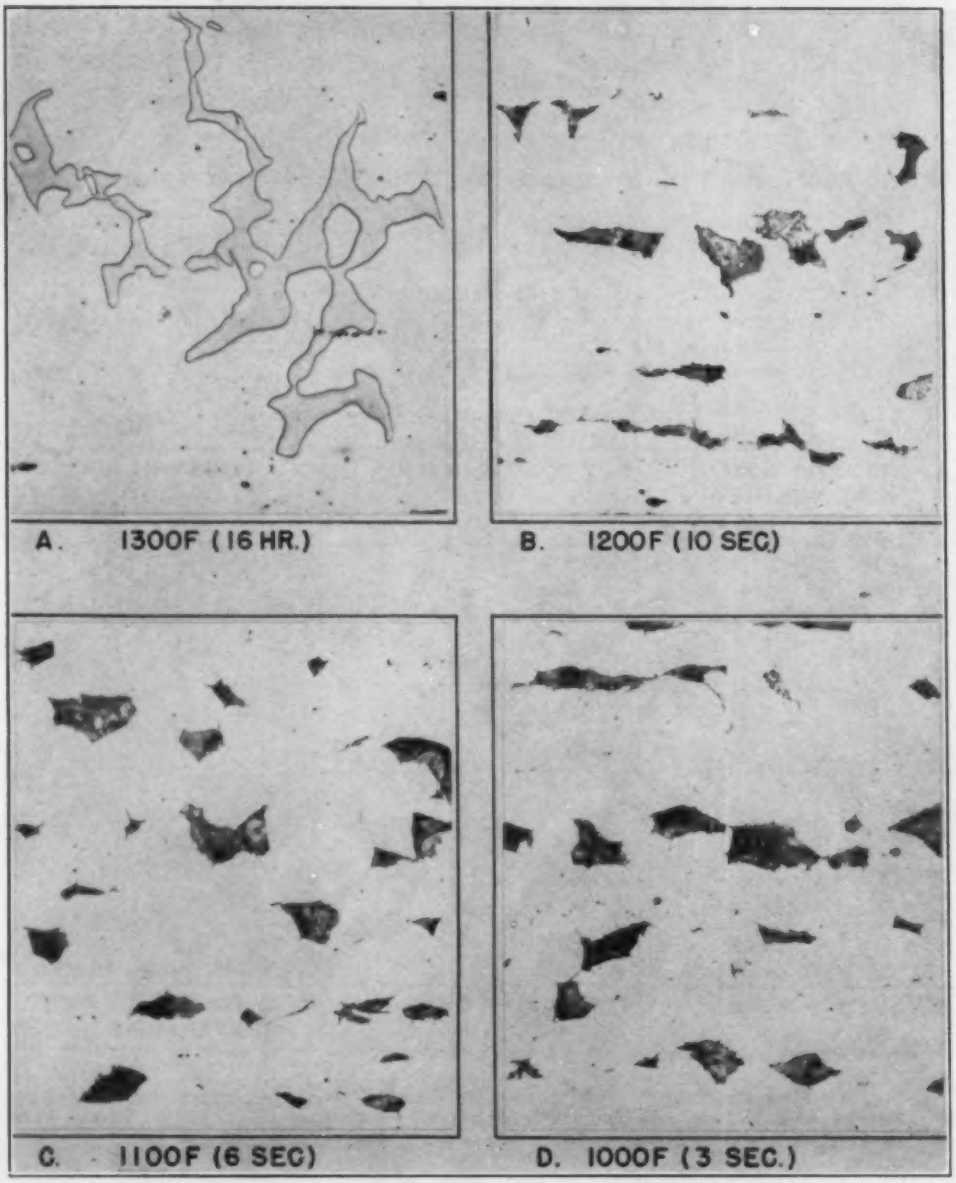


Fig. 5—Microstructure of 0.06% Carbon Rimmed Steel Cooled from 1675 to 1350 °F More Slowly Than in Fig. 4, Then Transformed Isothermally at Temperature Shown. Picral etch. Original magnification × 1000.

avoid complete transformation above about 1000 °F (540 °C). For such a steel, therefore, a marked change in cooling rate would change the transformation temperature range only slightly.

Microstructures resulting from isothermal transformation at selected temperatures from 1300 to 1100 °F (705 to 595 °C) are shown in Fig. 4, the products of transformation in this temperature range being, of course, ferrite and cementite. Upon transformation

at 1300 °F (705 °C) cementite forms as massive particles of irregular shape; this indicates one of the ways in which such undesirably large carbide particles can be formed in low carbon steel. When transformed at 1250 to 1100 °F (675 to 595 °C), cementite particles are smaller and tend increasingly to occur as an aggregate of iron and iron carbide as the transformation temperature decreases. On quenching from the austenitizing temperature directly into brine, martensite and a very small amount of ferrite formed, as seen in Fig. 4F.

As mentioned previously, some ferrite formed during cooling this steel to the isothermal levels selected. To investigate further the effect of carbon enrichment of austenite on type of final transformation product, specimens of the same steel were cooled more slowly than before from the austenitizing temperature to 1350 °F (730 °C) in order to form a substantial amount of proeutectoid ferrite, then transformed isothermally at lower temperatures. The resulting microstructures, Fig. 5, show that at 1300 °F (705 °C) the transformation product again is massive cementite, but that at 1200 to 1000 °F (650 to 540 °C) it is definitely pearlitic, the pearlite becoming finer the lower the transformation temperature, just as in higher carbon steels. It is evident, therefore, that the structure of the ferrite-cementite aggregate depends not only upon the temperature at which it forms but also upon the composition (carbon content) of the austenite from which it is produced.

Thus far in this discussion nothing has been said about the microstructure of ferrite, the principal constituent of low carbon steel. The effect of cooling rate and of prior austenite grain size on the structure of ferrite in a low carbon steel is shown in Fig. 6. Figs. 6A and 6E show the initial austenite grain size, the fine grain size in Fig. 6A having been developed at 1675 °F (915 °C) and the coarse grain size, Fig. 6E, at 2000 °F (1095 °C). Specimens were then cooled in each of three ways from a common temperature, 1675 °F (915 °C); the structures resulting from transformation of fine-grained austenite are shown in B, C and D of Fig. 6, those from coarse-grained austenite in F, G and H. In either series, ferrite grain size becomes finer, and hardness higher, as cooling rate increases. The effect of coarser austenite grain size, for comparable cooling rate, is to produce coarser ferrite grains and to increase the tendency toward Widmanstätten structure. Similar effects of prior austenite grain size and cooling rate on structure of ferrite in a 0.2% carbon

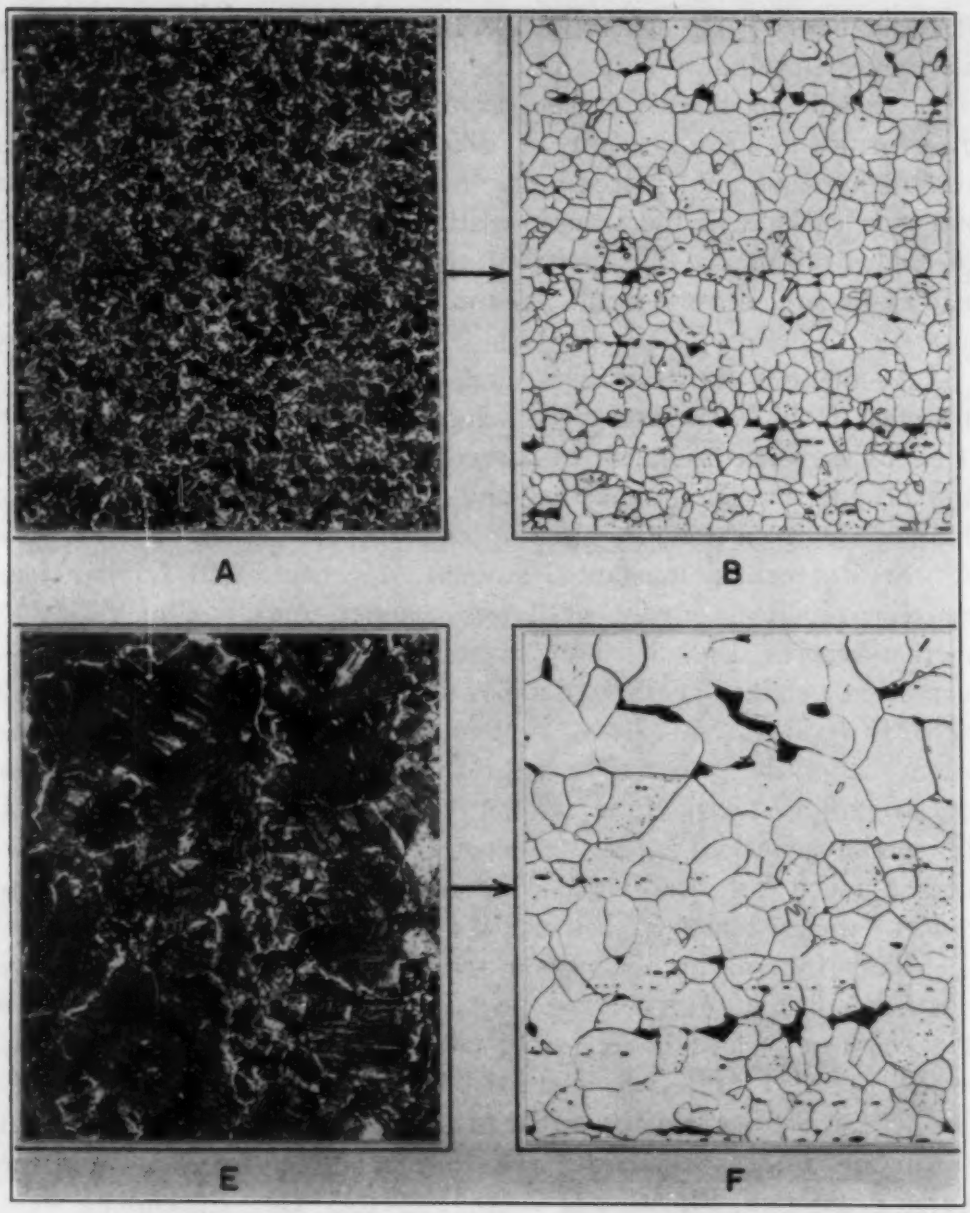


Fig. 6—Effect of Prior Austenite Grain Size and Cooling Rate on Ferrite Grain Structure of 0.05% Carbon Rimmed Steel. Original magnification × 100. A—Fine austenite grain size. B—Furnace-cooled, Rockwell B-42.5. E—Coarse austenite grain size. F—Furnace-cooled, Rockwell B-32.5. A and E quenched, etched in $FeCl_3$. Others etched in nital.

steel have been shown by J. R. Vilella (5).

Ordinarily, the conditions of cooling after ferrite formation is complete have little effect on ferrite grain structure. If cooled very rapidly through the ferrite formation range, however, the metal may be strained sufficiently to cause "exaggerated" grain growth when held subsequently at a sufficiently high temperature or cooled very

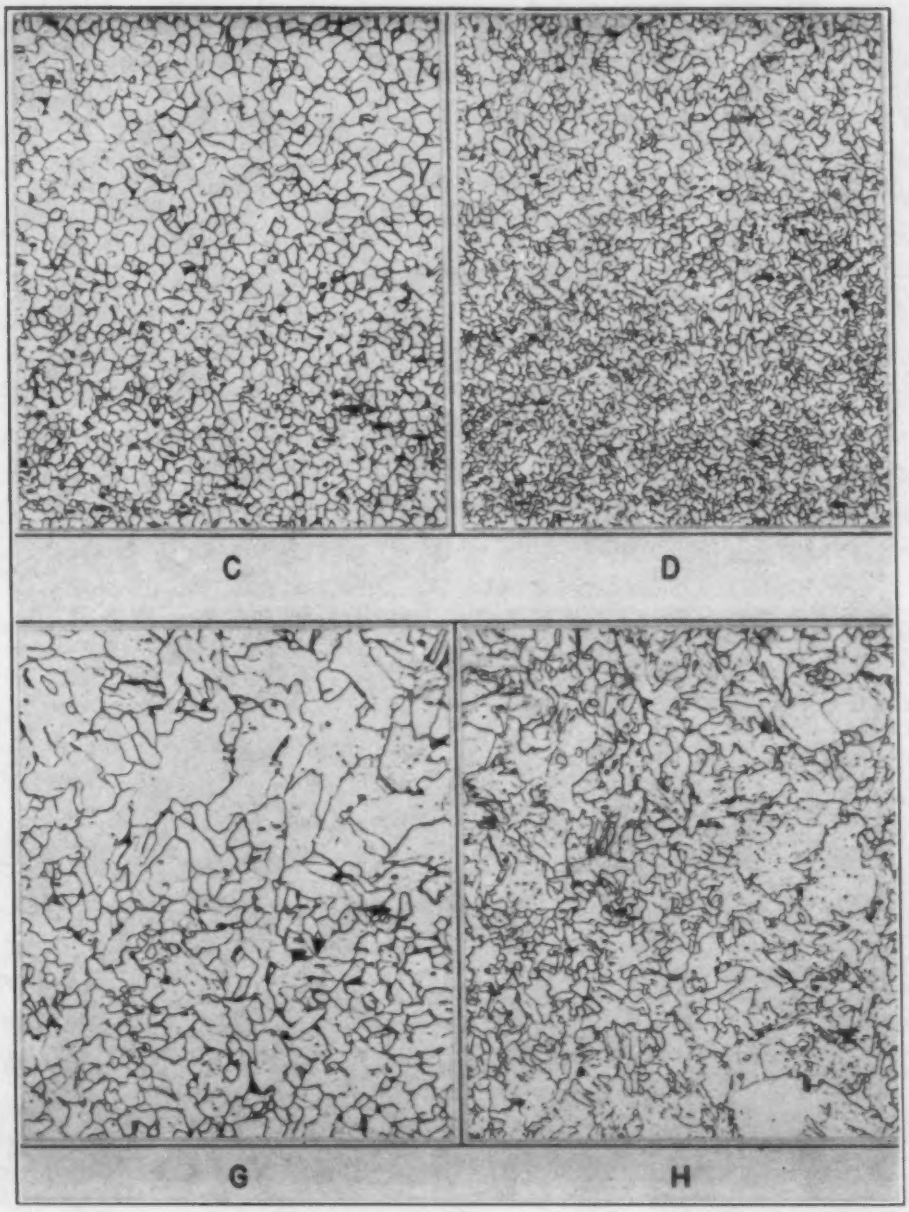


Fig. 6 (continued)—Effect of Prior Austenite Grain Size and Cooling Rate on Ferrite Grain Structure of 0.05% Carbon Rimmed Steel. Original magnification × 100. C—Air-cooled, Rockwell B-51. D—Quenched in lead at 1200 °F, Rockwell B-56. G—Air-cooled, Rockwell B-43. H—Quenched in lead at 1200 °F, Rockwell B-48. Etched in nital.

slowly. Fig. 7 illustrates the effect of fast as compared to slow cooling on subsequent grain growth at 1300 °F (705 °C). Rapid cooling through the ferrite formation range resulted in the structure shown in Fig. 7a, which, on holding 16 hours at 1300 °F (705 °C), coarsened (partially) as seen in Fig. 7b. Slower cooling produced a coarser, more equiaxed initial structure, Fig. 7c, with only slight

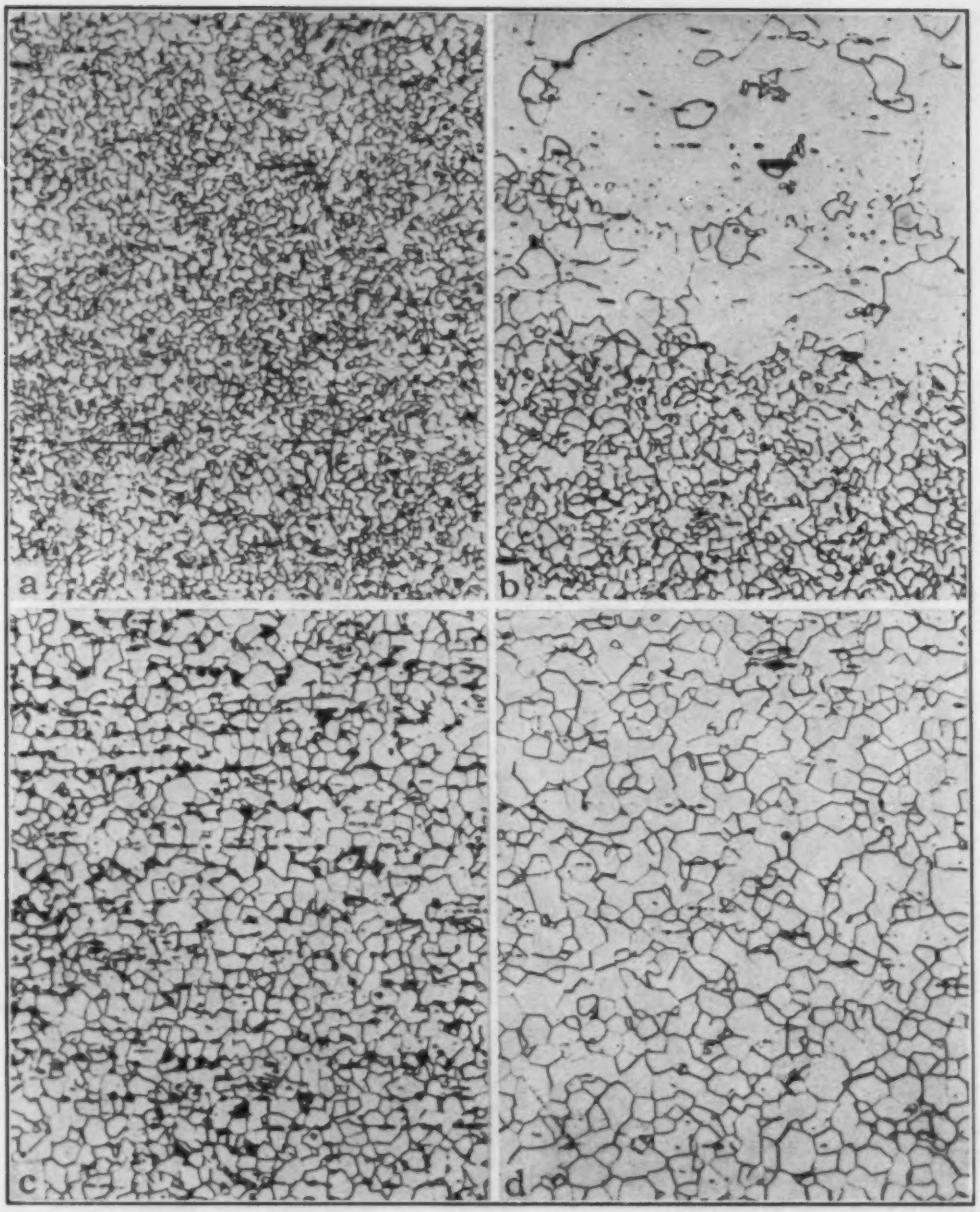


Fig. 7—Effect of Cooling Rate Through Ferrite Formation Range on Grain Structure and Tendency Toward Subsequent Grain Growth of 0.06% Carbon Steel. Nital etch. Actual magnification × 100. a—0.040-inch sheet quenched from 1675 °F into lead at 1300 °F, held 10 minutes. b—Same, except held 16 hours at 1300 °F. c—0.040-inch sheet transferred from furnace at 1675 °F to one at 1350 °F for 5 minutes, then quenched into lead at 1300 °F and held 10 minutes. d—Same as "c" except held 16 hours at 1300 °F.

grain growth on subsequent exposure for 16 hours at 1300 °F (705 °C), Fig. 7d. Samuels (6) has shown that even cooling in air (normalizing) may produce sufficient strain to cause exaggerated grain growth on subsequent annealing.

Solution and Precipitation of Iron Carbide

As shown in Fig. 1, approximately 0.03% carbon is soluble in ferrite at the eutectoid temperature, 1335 °F (725 °C). A steel of this or lower carbon content, therefore, will consist entirely of ferrite, with the carbon in solid solution, if held for sufficient time at this temperature or one near it, or is heated or cooled slowly into this temperature range. In a steel of higher carbon content, the ferrite present will also, under suitable conditions, dissolve carbon up to its solubility limit, the excess carbon ordinarily being present below the Ae_1 as iron carbide (cementite) particles of some sort, or above the Ae_1 in solution in austenite. At lower temperatures the solubility of carbon in ferrite is less than 0.03%, consequently any dissolved carbon in excess of that soluble at equilibrium will tend to precipitate. Precipitation may occur during cooling, or the steel may be cooled rapidly enough to retain the carbon in solution temporarily, precipitation then taking place slowly at ordinary temperature or more rapidly at elevated temperature. Structures resulting from such precipitation of cementite, and the accompanying changes in hardness, are discussed below.

In the first experiments to be discussed, specimens of a steel containing 0.02% carbon were heated for 10 minutes at 1300 °F (705 °C), resulting in nearly complete solution of all cementite present. Specimens were then cooled very rapidly to one of a series of selected temperature levels by quenching in a molten-metal bath, held isothermally for chosen periods of time, then brine-quenched to "fix" the structure as it existed before the final quench. Hardness of the specimens was measured immediately after quenching to room temperature, after which they were examined metallographically; selected microstructures are shown in Fig. 8, and the hardness curves in Fig. 10.

On holding at 1200 °F (650 °C), Fig. 8A, cementite is precipitated as rather massive intergranular particles; the particles formed at 1100 °F (595 °C), Fig. 8B, are similar but smaller in size, whereas at 1000 °F (540 °C), Fig. 8C, they are still thinner and more randomly dispersed in the grain boundaries. At 800 °F (425 °C), Fig. 8D, needle or plate-like cementite particles appear within the grains in addition to chains of particles in the grain boundaries; at lower temperatures, Figs. 8E and 8F, the precipitated particles are finer and more numerous and tend increasingly to occur within the grains rather than in the boundaries.

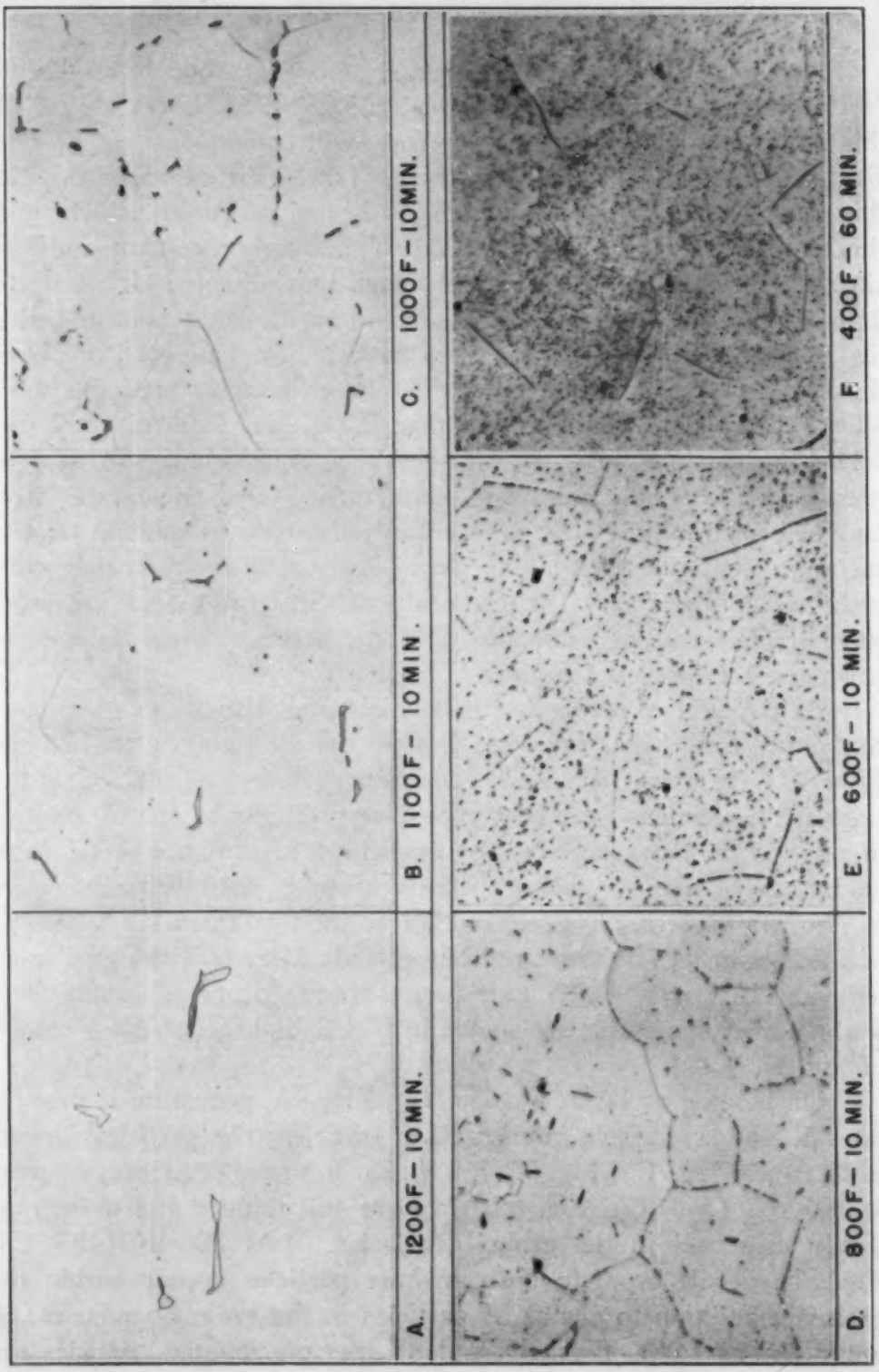


Fig. 8—Microstructure Resulting from Isothermal Precipitation of Cementite in 0.02% Carbon Rimmed Steel. Solution treatment 10 minutes at 1300 °F (cementite nearly all dissolved). Picral etch. Original magnification × 1000.

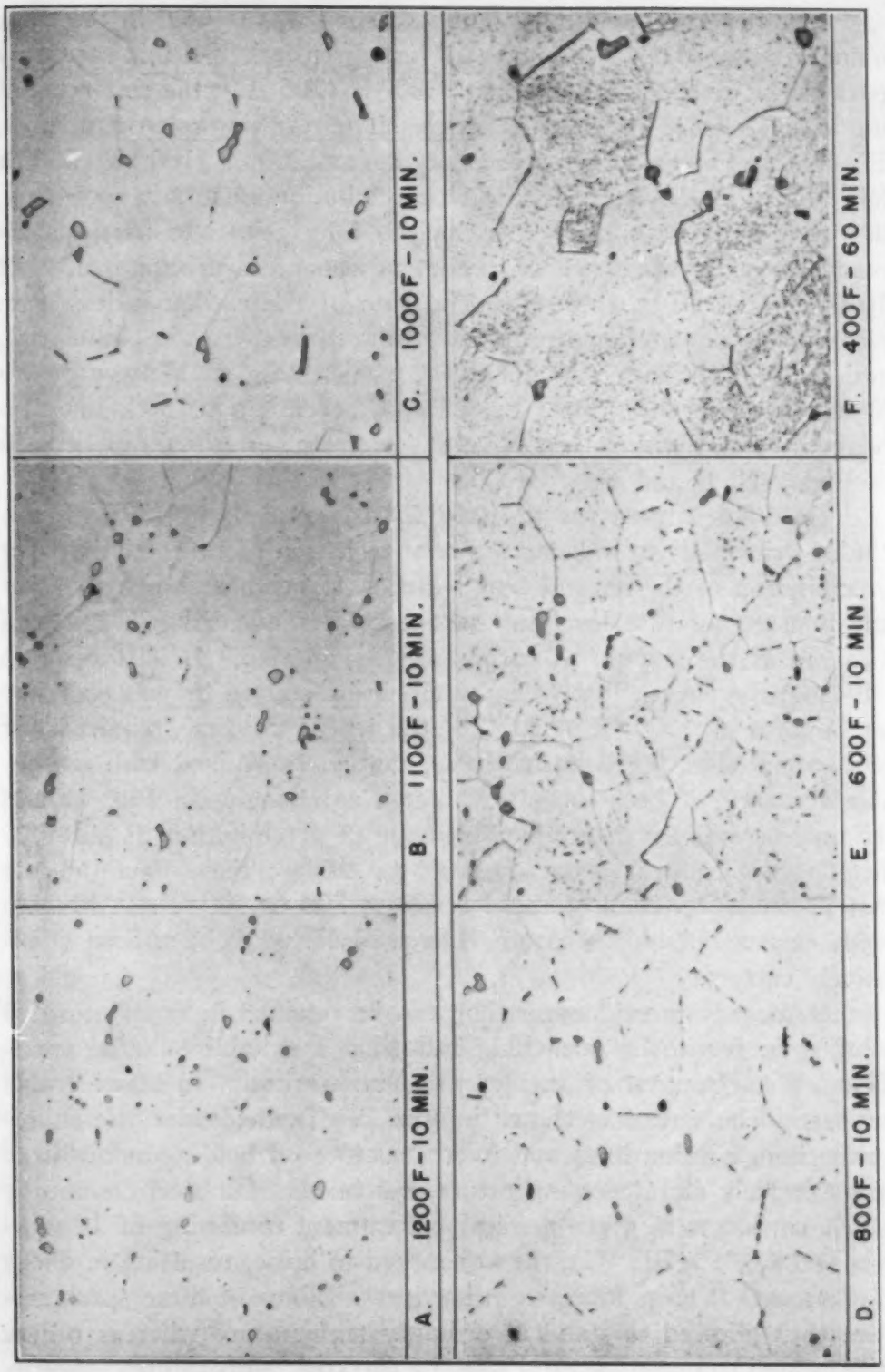


Fig. 9—Microstructure After Isothermal Precipitation of Cementite in 0.06% Carbon Rimmed Steel. Cementite not completely dissolved in solution treatment of 10 minutes at 1300 °F. Picral etch. Original magnification × 1000.

Another steel containing 0.06% carbon was treated in the same manner as the 0.02% carbon steel just discussed. In this case only part of the carbon was soluble at 1300 °F (705 °C), the rest remaining as spheroidized cementite particles. The resulting microstructures, Fig. 9, show no evidence of precipitation at 1200 or 1100 °F (650 or 595 °C) (Figs. 9A and 9B); some precipitation must have occurred, however, and presumably was nucleated by cementite particles already present, upon which the new cementite precipitated. At 1000 °F (540 °C), where diffusion rate of the carbon is less, thin plates of precipitated cementite may be seen in the grain boundaries, and some of the larger, undissolved, particles appear to have grown in length (Fig. 9C); clear evidence of precipitation, both in grain boundaries and within the grains at lower temperatures, can be seen in Figs. 9D, E and F.

Hardness curves for the 0.02% carbon steel, Fig. 10, are included principally to indicate the relative length of time required for precipitation at the several temperatures, it being assumed that for any one temperature level the hardness after quenching is a rough measure of the amount of carbon still in solution. It is difficult to tell from the curves just when precipitation started or was complete but, except at 1200 °F (650 °C), the length of time required for 50% completion, based on hardness, can be determined with reasonable accuracy. These times are plotted as triangles in Fig. 11 and the time periods for detectable beginning of precipitation, as observed metallographically at about × 1000, as circles; these data indicate that precipitation is most rapid at about 700 to 900 °F. Although neither curve is highly accurate, both are believed to be at least qualitatively correct.

As already mentioned, carbon can be retained in supersaturated solution in ferrite by quenching following a suitable solution treatment; this retention of carbon in solution results in considerable increase in hardness, as shown in Fig. 2. To determine the subsequent change in hardness and microstructure on holding at ordinary or moderately elevated temperature, specimens of a steel containing 0.06% carbon were given a solution treatment consisting of 10 minutes at 1300 °F (705 °C), then quenched in brine, resulting in about 15 Rockwell B units increase in hardness. Some of these specimens were then allowed to stand at ordinary temperature whereas others were heated to one of several selected elevated temperatures. Hardness of these specimens was measured periodically, with the results

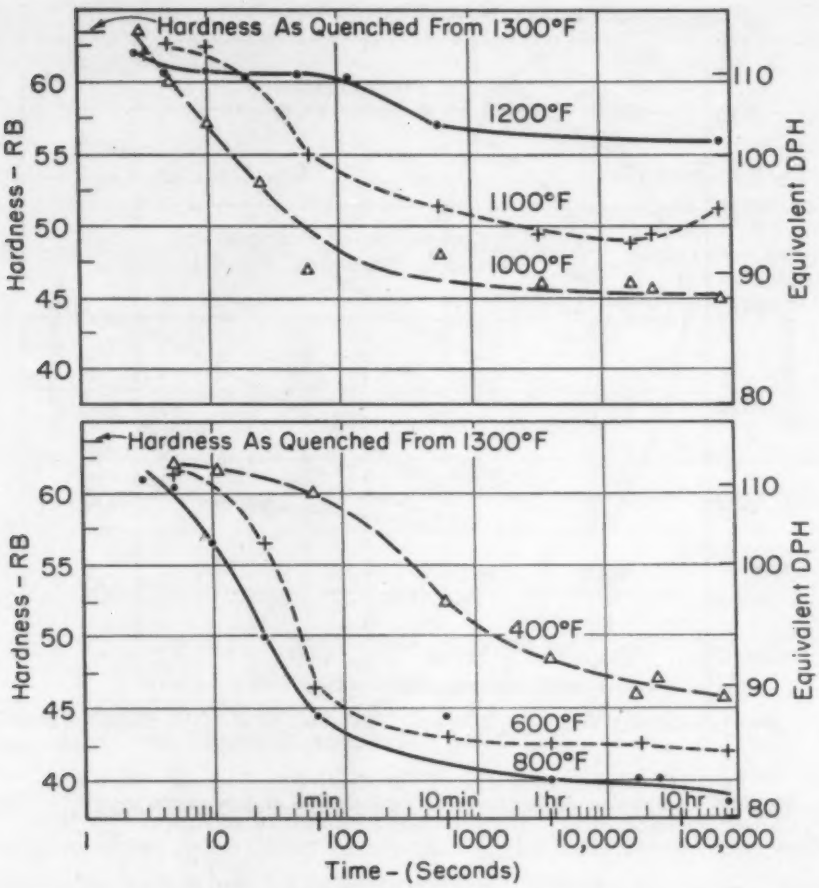


Fig. 10—Change in Hardness of 0.02% Carbon Steel as a Result of Isothermal Precipitation of Cementite After Solution at 1300 °F. (Specimens quenched after isothermal treatment.)

shown in Fig. 12; their microstructure at the end of the test is shown in Fig. 13.

The 70 °F aging curve in Fig. 12 shows that this specimen, already hardened some 15 Rockwell B units by quenching from 1300 °F (705 °C), increases in hardness by an additional 20 Rockwell B units or more when held about 3 months at ordinary temperature, at the end of which period the curve appears to be leveling off. On aging at 210 °F, maximum hardening is much less, 2-3 Rockwell B units, the hardness eventually decreasing below the as-quenched value. Davenport and Bain (7) also investigated this "quench aging" of low carbon steel at temperatures up to 210 °F and obtained similar results, the peak hardness decreasing as aging temperature increases, with the time to reach maximum hardness also decreasing. On holding at higher temperatures, subsequent to quenching from

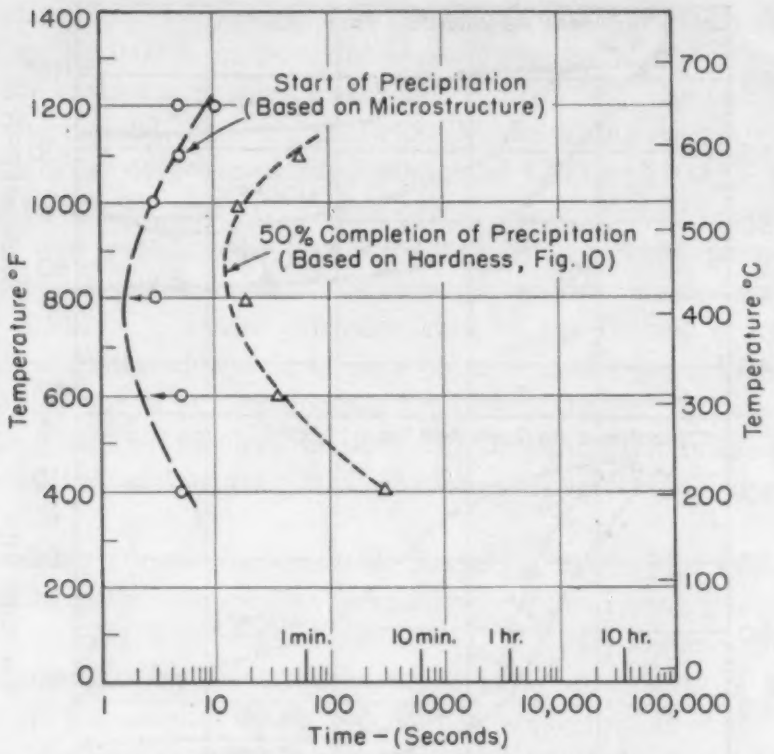


Fig. 11—Approximate Length of Time Required for Start and for 50% Completion of Isothermal Precipitation of Cementite in 0.02% Carbon Rimmed Steel. Prior solution treatment 10 minutes at 1300 °F.

1300 °F (705 °C), Fig. 12, hardness decreases rapidly, eventually approaching that of the steel before solution heat treatment.

In Fig. 13 may be seen the microstructure of this steel after aging or reheating as indicated. These photomicrographs represent the structure in the "rim" portion of the sheet (near the surface) where the carbon content is less than that indicated by the over-all composition, hence carbide particles undissolved during the solution heat treatment are absent or few in number, so that precipitated cementite can be distinguished more easily. In Fig. 13A is the structure as quenched, or as aged at 70 °F, the latter treatment producing no detectable change in microstructure. Long aging at 210 °F resulted in precipitation of particles visible under the microscope, as seen in Fig. 13B. Holding at higher temperatures caused visible precipitation within a shorter period of time, the particles becoming larger, and having a greater tendency to locate in ferrite grain boundaries the higher the temperature, Fig. 13, C to F. In the latter photomicrographs may be seen some relatively large carbide particles; these were not dissolved during the solution treatment. Photo-

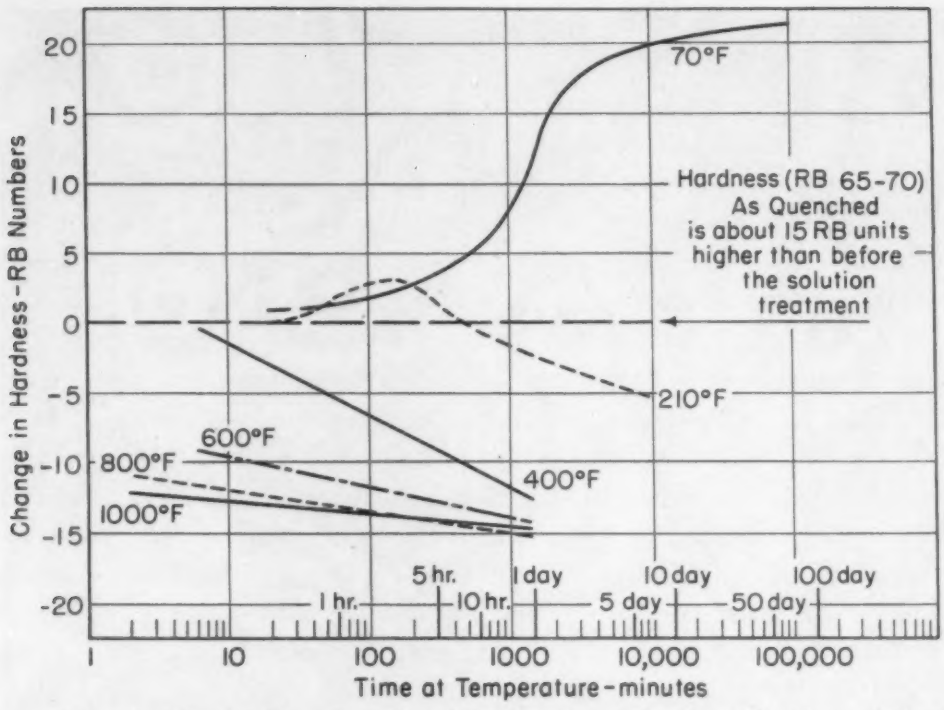


Fig. 12—Effect of Time at Indicated Temperature After Quenching from 1300 °F on Hardness of 0.06% Carbon Rimmed Steel.

micrographs showing similar structures produced by reheating low carbon steel after quenching from below the Ae_1 have been published previously by Whiteley (3), Andrew and Trent (8), and Bates (9).

Cold Reduction and Annealing

The influence of prior structure on the microstructure of cold-reduced, box-annealed low carbon steel is shown in Fig. 14. The initial structures, top row of photomicrographs in Fig. 14, represent a somewhat wider range than is ordinarily encountered in hot-rolled strip; from left to right they comprise: (A) pearlite; (B) massive cementite, some of it enclosing pearlite; (C) massive cementite; (D) coarse, somewhat spheroidized pearlite; (E) finer pearlite and small, dispersed cementite particles, and (F) mostly dispersed fine cementite particles.

The effect of 60% cold reduction is shown by the photomicrographs immediately below those representing the initial microstructures. Areas consisting of pearlite or groups of fine cementite particles are elongated in the direction of rolling, larger cementite particles are broken and the resulting fragments in some instances are

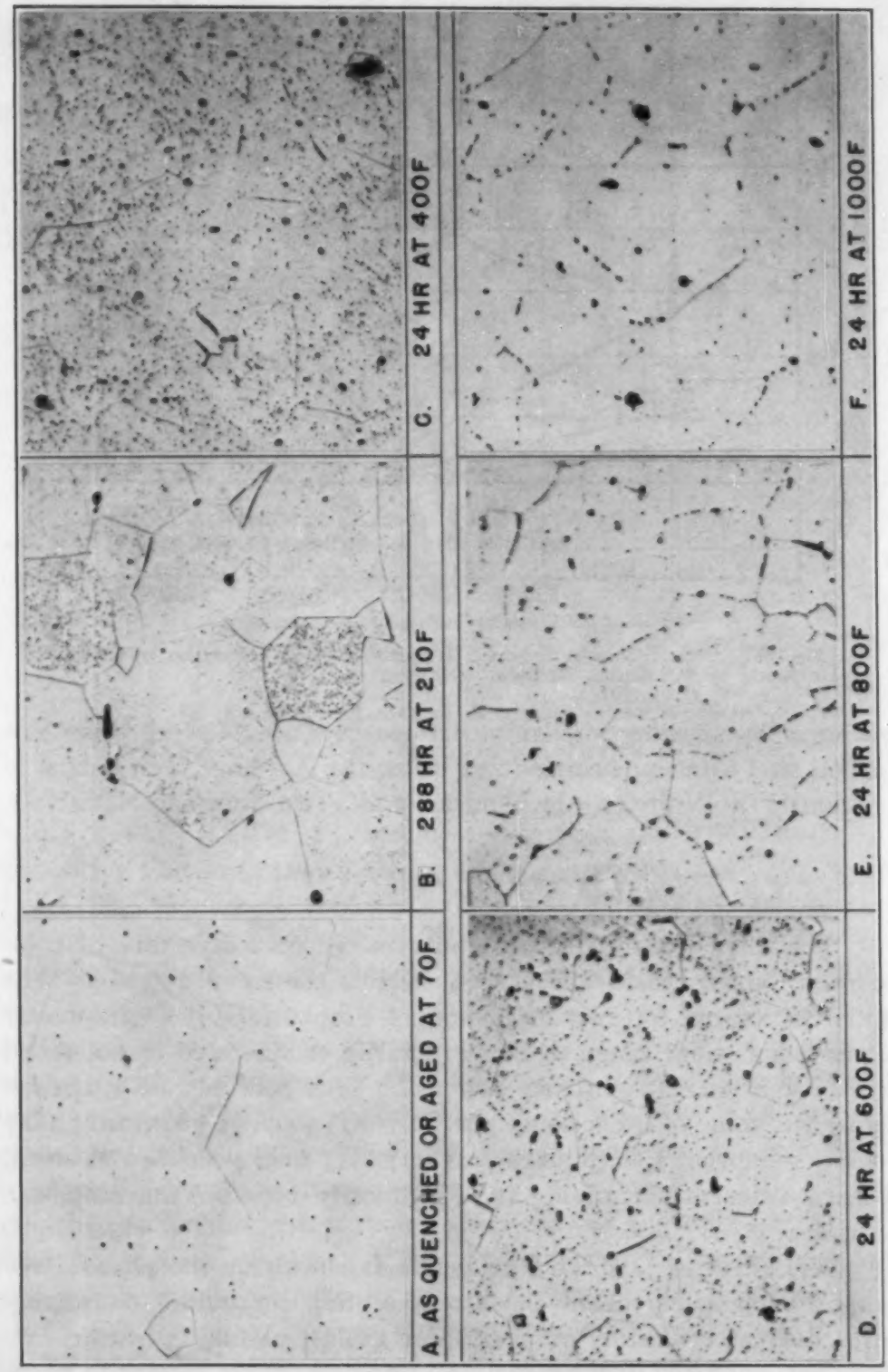


Fig. 13—Effect of Reheating, Following Quench from 1300 °F, on Microstructure of Rim Portion of 0.06% Carbon Rimmed Steel. Picral etch. Original magnification × 1000.

strung out in the rolling direction. The extent to which the structure is altered will depend, of course, upon the amount of cold reduction.

Box annealing, as shown by the two bottom rows of photomicrographs in Fig. 14, results generally in spheroidization of cementite particles, although the larger fragments change very little in shape. Distribution of cementite after annealing is determined largely by its distribution in the prior cold-reduced condition; this is particularly true when the steel is annealed either at a low temperature or for a short time, or regardless of annealing temperature up to the Ae_1, when massive cementite particles are present. The influence of box annealing variables on microstructure, and particularly the effect of annealing above Ae_1, is discussed in more detail below.

There is a definite relationship between grain size of hot-rolled strip and grain structure as subsequently box-annealed after cold reduction, the final grain size being finer the smaller the initial grain size as shown in Fig. 15. The steel represented in Fig. 15 was cold-reduced 60% prior to box annealing; less cold reduction would result in larger, and more cold reduction would lead to finer, grains in the annealed condition as is well known (10). To a lesser extent such variables as time and temperature of annealing will affect ferrite grain size.

Increased box annealing temperature, below the Ae_1, is shown in Fig. 14 to increase the size of iron carbide particles and to result in their more random distribution, except when the prior structure is massive cementite, which is affected very little. Fig. 16 shows the effect of annealing temperature and of time at temperature on microstructure of a steel, the structure of which before cold reduction consisted of ferrite and pearlite. The effect of annealing above Ae_1 (Fig. 16C) is particularly marked; austenite formed at the annealing temperature transforms during subsequent slow cooling to massive cementite particles that tend toward an irregularly-shaped type. The structure formed is largely independent of prior structure or of time at temperature so long as substantially all carbon is dissolved during the anneal. Increased time at lower box annealing temperature, Fig. 16, D to F, coarsens the cementite particles and results in their more random dispersal, provided the initial particles, after cold reduction, are not too large.

In box-annealed low carbon steel containing more than approximately 0.03% carbon, large irregularly-shaped carbides occur only when the steel has been annealed at a temperature above Ae_1

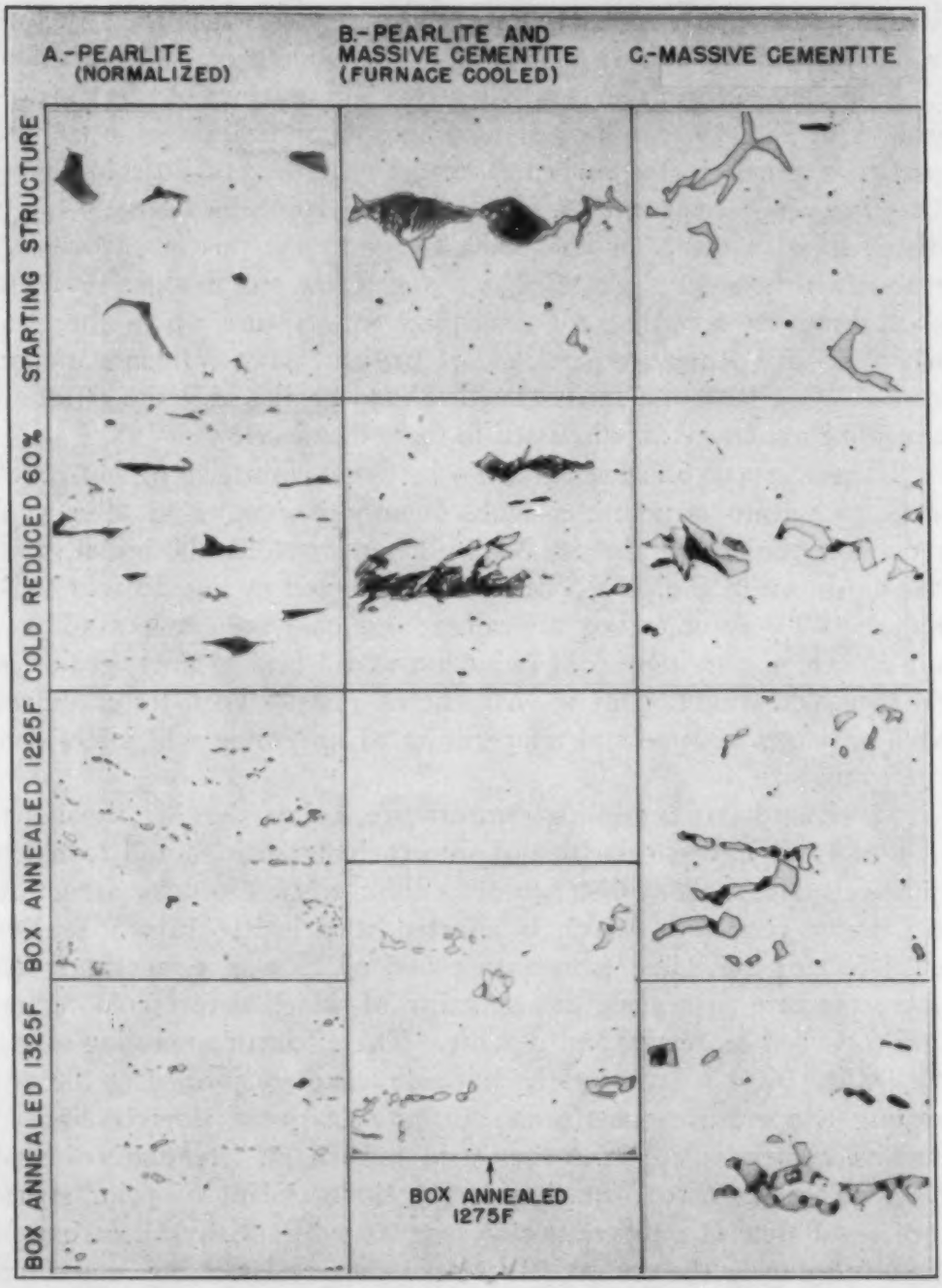


Fig. 14—Effect of 60% Cold Reduction and of Cold Reduction Followed by Box Annealing (16-Hour Soak) on Structure of Approximately 0.06% Carbon Rimmed Steel for Various Initial Conditions. Picral etch. Original magnification × 1000.

(1335 °F), as discussed above. In a lower carbon steel, containing perhaps 0.03% or less, all the cementite may dissolve at a lower temperature so that, on subsequent slow cooling, massive iron car-

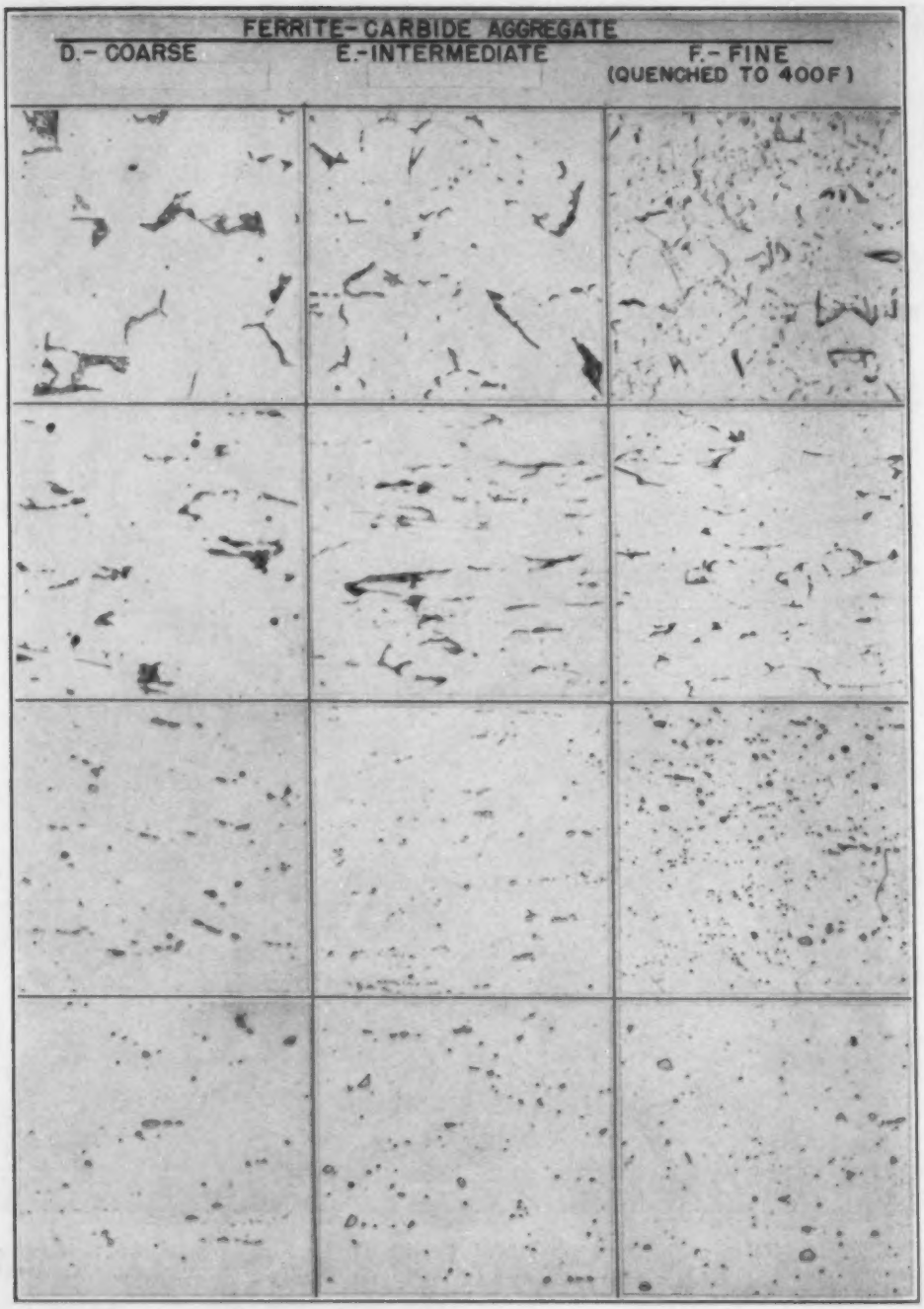


Fig. 14 (continued)—Effect of 60% Cold Reduction and of Cold Reduction Followed by Box Annealing (16-Hour Soak) on Structure of Approximately 0.06% Carbon Rimmed Steel for Various Initial Conditions. Picral etch. Original magnification × 1000.

bide particles will form as shown in Fig. 17. Here, an increase in box annealing temperature from 1100 to 1200 °F (595 to 650 °C) merely coarsened the cementite particles slightly, but on annealing at

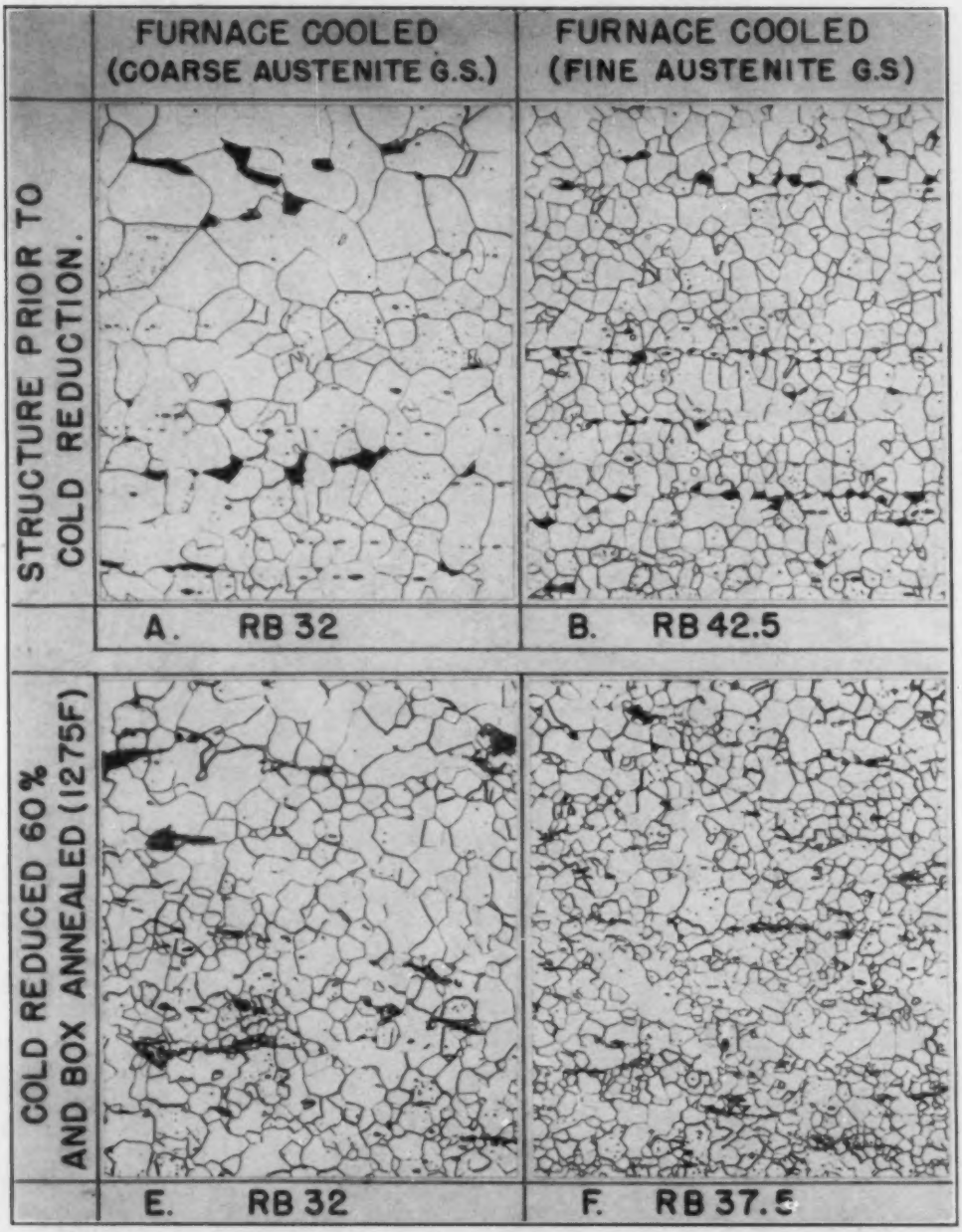


Fig. 15—Relationship Between Initial Ferrite Grain Structure of 0.05% Carbon Rimmed Steel and Cold-Reduced Box-Annealed Structure. Nital etch. Original magnification × 100.

1275 °F (690 °C) extremely large irregular masses of cementite formed. It appears that this massive cementite may form either on transformation of austenite or by precipitation of cementite from solid solution in ferrite, the essential conditions being: (a) that the solution of carbon is essentially complete at the annealing temperature

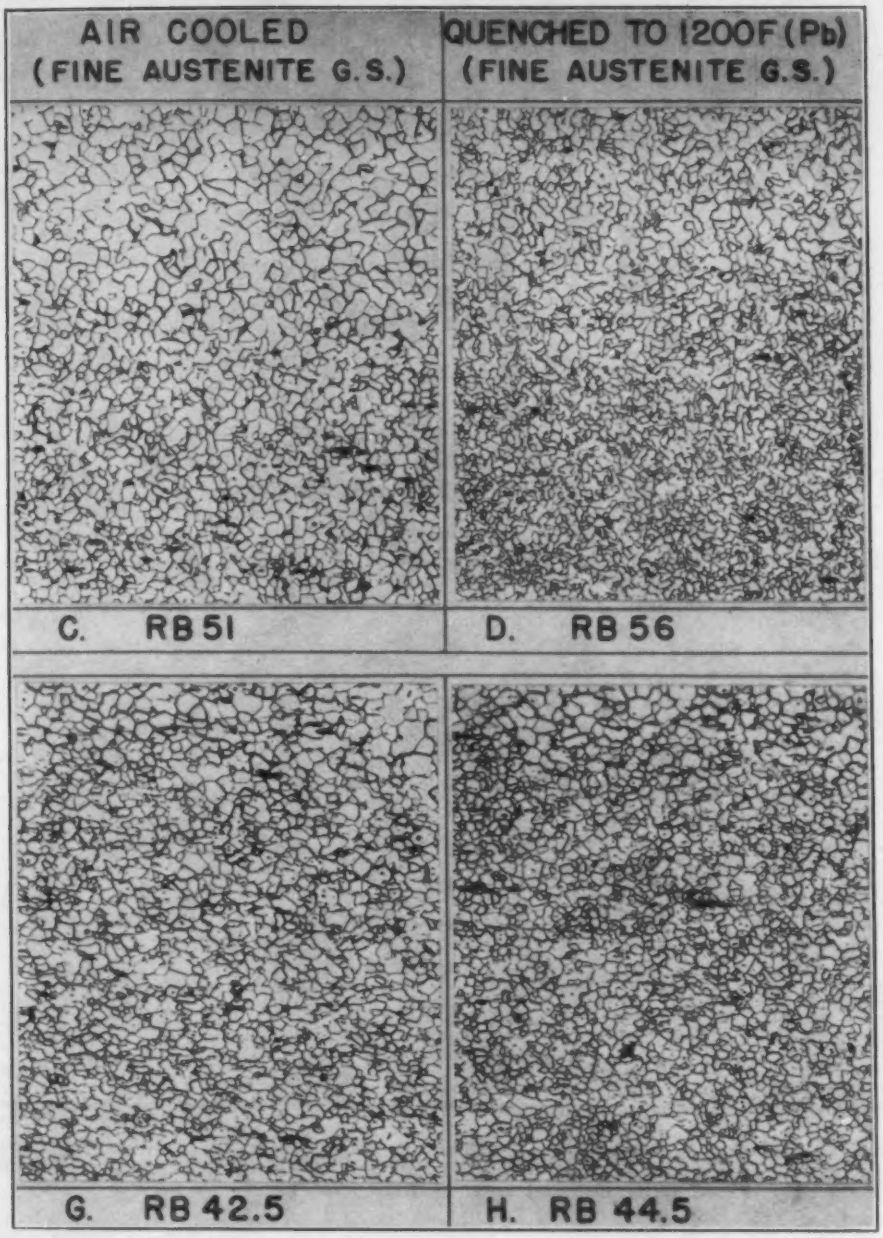


Fig. 15 (continued)—Relationship Between Initial Ferrite Grain Structure of 0.05% Carbon Rimmed Steel and Cold-Reduced Box-Annealed Structure. Nital etch. Original magnification × 100.

so that few if any undissolved carbides remain to nucleate subsequent transformation or precipitation; and (b) that cooling is sufficiently slow that cementite forms initially at a relatively high temperature (not too far below 1300 °F), subsequent precipitation occurring upon the nuclei thus formed. From the type of cementite particles

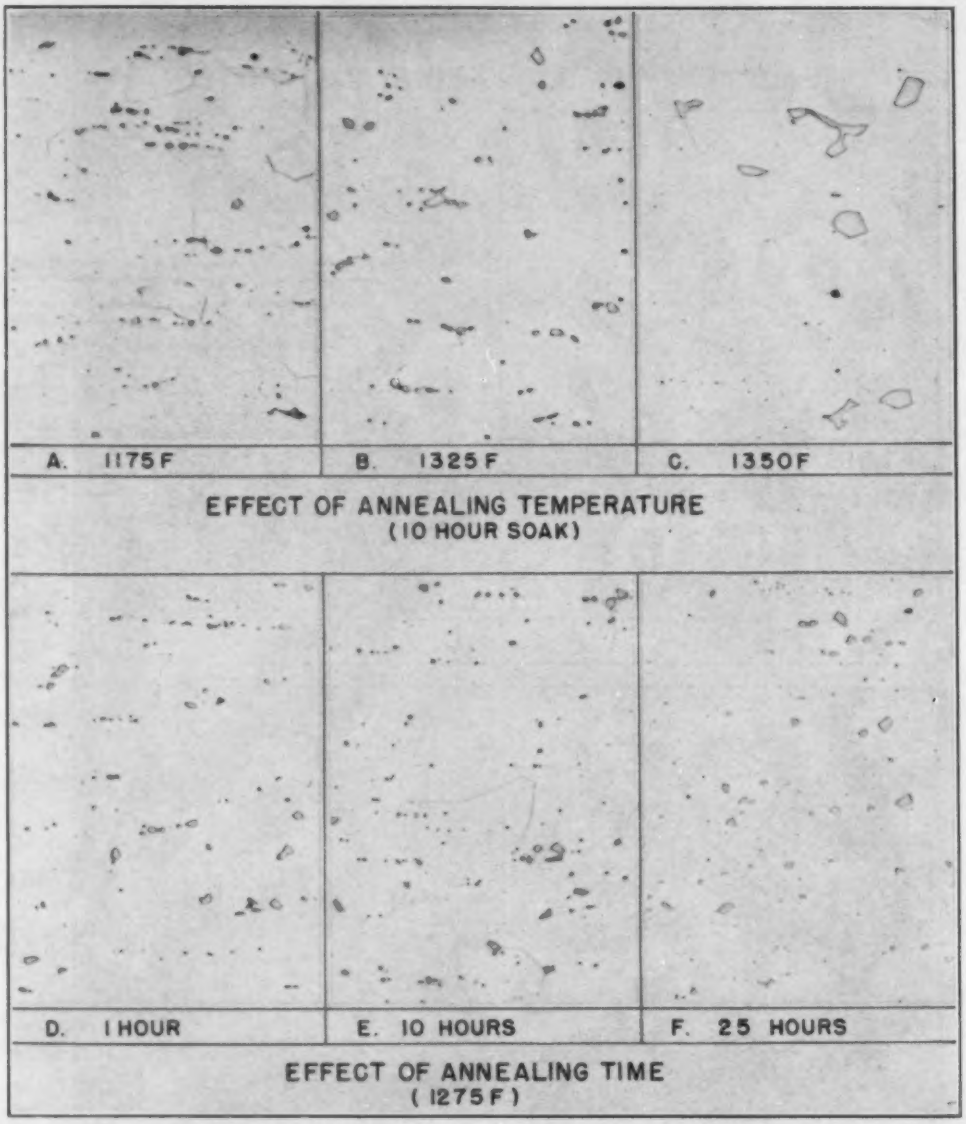


Fig. 16—Effect of Box Annealing Temperature and Time at Temperature on Microstructure of 0.05% Carbon Rimmed Steel Having Pearlitic Carbide Structure Prior to Cold Reduction. Picral etch. Original magnification × 1000.

precipitated isothermally at lower temperatures (Fig. 8) it may be inferred that in an extremely low carbon material, such that on cooling the solubility of carbon in ferrite would not be exceeded until a temperature of perhaps 1000 °F (540 °C) was reached, finer intergranular cementite particles would result from box annealing, regardless of the annealing temperature.

Summary

In general, microstructure of low carbon steel is determined by

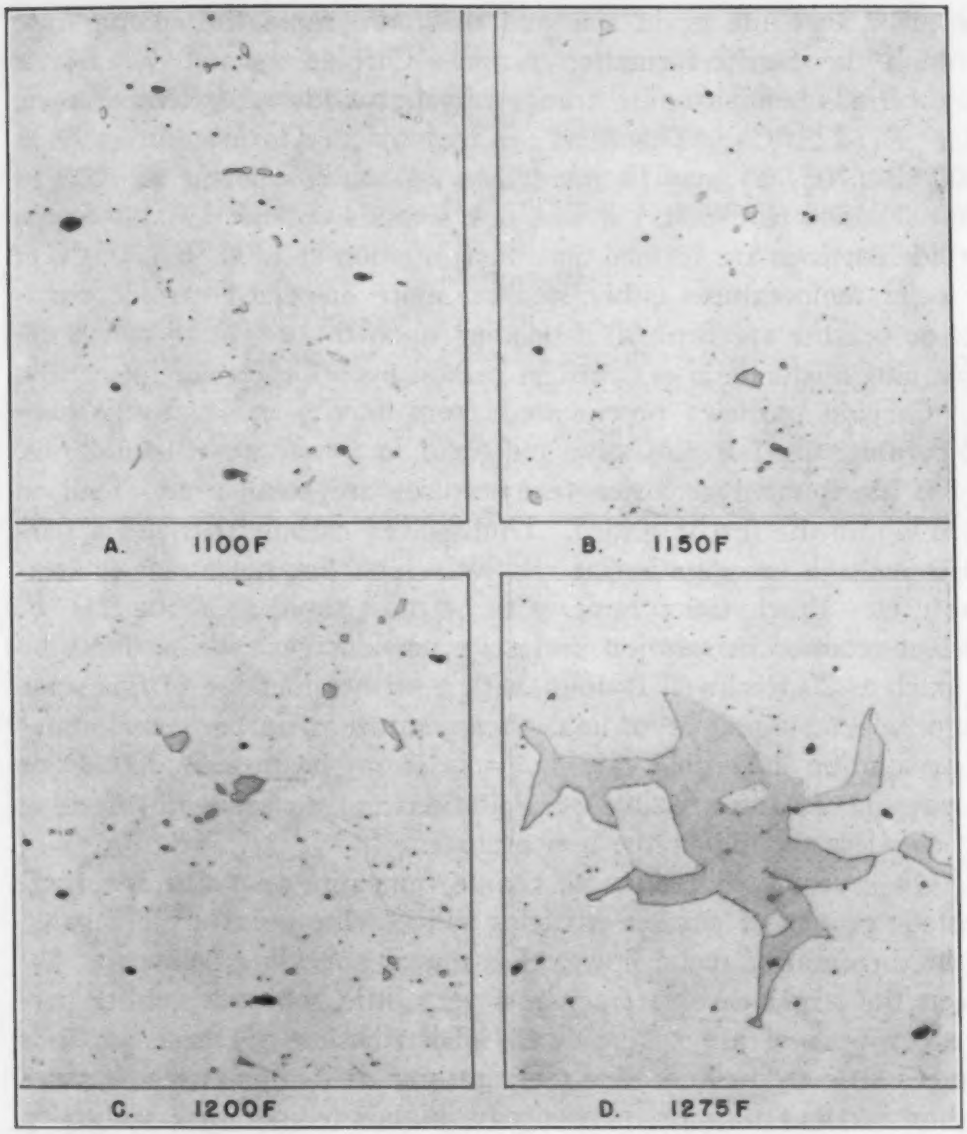


Fig. 17—Effect of Box Annealing Temperature on Microstructure of Nominally 0.03% Carbon Steel. (All box-annealed 16 hours at temperature after 50% cold reduction.) Picral etch. Original magnification × 1000.

those factors that affect size and shape of the ferrite grains and the type and distribution of carbide particles. Both grain structure and carbide distribution are influenced by the conditions under which austenite transforms and by cold working and annealing. The carbide distribution in low carbon steel also may be influenced by the conditions under which carbon precipitates from ferrite.

Ferrite forms rapidly from austenite in a low carbon steel at 1500 °F (815 °C) or below; ferrite grain size is finer the smaller

the prior austenite grain size and the more rapid the cooling rate through the ferrite-formation range. Carbide as well as ferrite may form when austenite transforms below the Ae_1 temperature, 1335 °F (725 °C). The time required to transform completely at 1300 °F (705 °C) may be more than 24 hours, whereas at 1000 to 1100 °F (540 to 595 °C) it is a few seconds or less. Massive-type carbide particles are formed on transformation at 1300 °F (705 °C); at lower temperatures either smaller, more dispersed carbide particles or pearlite are formed, depending upon the extent to which the remaining austenite is enriched in carbon by prior ferrite formation.

Carbide particles precipitated from ferrite at relatively high temperature are fairly massive and occur in ferrite grain boundaries. Those precipitated at lower temperatures are smaller and tend to form within the ferrite grains. Undissolved carbide particles apparently nucleate precipitation at relatively high but not at lower temperatures. Precipitation appears to be most rapid at about 800 °F. Carbon retained in solution in ferrite may increase its hardness by as much as 20 Rockwell B units, with a further increase of this same magnitude on aging at ordinary temperature. Carbon precipitates from solution as visible carbide particles on heating at 200 °F or above; the time for visible precipitation and consequent softening becomes less the higher the temperature.

On severe cold reduction, coarse cementite particles are fragmented; groups of smaller particles and pearlite areas are elongated in the direction of metal flow. Subsequent annealing below the Ae_1 affects the larger carbide fragments very little, whereas smaller particles or pearlite are spheroidized. Distribution of these particles changes little at low annealing temperatures or if time at temperature is short; longer time or, particularly, higher temperature results in more general distribution of these particles, with a tendency for them to locate in ferrite grain boundaries. In general, a fine carbide particle size and random carbide distribution before cold reduction lead to the most uniform carbide dispersal after annealing. Massive carbide particles may form if the steel is annealed above the Ae_1 or if it contains so little carbon that none remains undissolved at the annealing temperature.

Ferrite grain size after annealing depends upon the grain size before cold reduction as well as upon amount of cold reduction, annealing temperature, and time at temperature.

ACKNOWLEDGMENTS

The assistance of C. E. Morgan, W. P. Wallace, T. B. Linn, M. H. Pakkala, L. B. Haberman, J. T. MacKenzie, Jr., S. H. Kalin and H. M. Evers, all former members of the United States Steel Corporation Research Laboratory Staff, is gratefully acknowledged.

References

1. S. Epstein, "Alloys of Iron and Carbon," Vol. I, McGraw-Hill, 1936.
2. W. Köster, "The Influence of Heat Treatment Below A_1 on the Properties of Commercial Iron," *Archiv. Eisenhüttenwesen,* Vol. 2, 1929, p. 503-522.
3. J. H. Whiteley, "The Solution of Cementite in Alpha Iron and its Precipitation," *Journal,* Iron and Steel Institute, Vol. 116, 1927, p. 293-310.
4. R. P. Smith, "Equilibrium of Iron-Carbon Alloys with Mixtures of CO-CO_2 and CH_4-H_2," *Journal,* American Chemical Society, Vol. 68, 1946, p. 1163-1191.
5. J. R. Vilella, "Grain Size: A Review in Simple Terms," *Mechanical Engineering,* Vol. 62, 1940, p. 293-307.
6. M. L. Samuels, "Grain Growth in Normalized Sheet Steel During Box Annealing," *Transactions,* American Institute of Mining and Metallurgical Engineers, Vol. 131, 1938, p. 327-345.
7. E. S. Davenport and E. C. Bain, "The Aging of Steel," TRANSACTIONS, American Society for Metals, Vol. 23, 1935, p. 1047-1093.
8. J. H. Andrew and E. M. Trent, "The Quench Aging of Steel," *Journal,* Iron and Steel Institute, Vol. 138, 1938, p. 241-288.
9. A. A. Bates, "Aging in Low Carbon Steels," TRANSACTIONS, American Society for Steel Treating, Vol. 19, 1932, p. 449-471.
10. A. Hayes and R. S. Burns, "The Cold Rolling of Mild Steel Sheets and Strip," TRANSACTIONS, American Society for Metals, Vol. 25, 1937, p. 129-157.

DISCUSSION

Written Discussion: By G. F. Comstock, assistant director of research, Titanium Alloy Manufacturing Div., National Lead Co., Niagara Falls, N. Y.

This paper is indeed a scholarly description of the structural variations which can be caused by the different ways in which iron carbide or cementite can be made to form from austenite or ferrite by heat treating low carbon steel, but it might be pointed out that other elements than carbon, although completely neglected by the authors, contribute items of considerable importance to the subject included in the title of the paper. Probably the most important of these elements is oxygen, but nitrogen, phosphorus, and sulphur should also be considered. It is rather surprising to find no mention of the contents of these impurities in the samples which the authors used. They certainly occur in all commercial steel, whereas the paper apparently is intended to deal with iron-carbon alloys of ideal purity.

In 0.02 or 0.03% carbon steel, as illustrated in Figs. 8 and 17, considerable oxide and nitride might be expected, and it would be very interesting if the authors could state what evidence they have to prove that the precipitate illustrated so prominently in Figs. 8E and 8F is not an oxide or nitride. These photomicrographs show a most surprising volume of precipitate, if it is only carbide, for a 0.02% carbon steel. Incidentally, it would be helpful if the actual magnification of these illustrations could be given.

The authors should probably not be criticized for neglecting sulphur, as its metallographic appearance is so well known. Phosphorus, however, if segregated as it often is in rimmed steel, or as it occurs in re-phosphorized tin-plate, can lead to the occurrence of quite interesting features in the microstructure of low carbon steel. As these so-called "ferrite ghosts" due to phosphorus have been adequately described in the literature,[2] it should not be necessary to discuss them further, but for a complete treatment of this subject, it is felt that they should at least be mentioned.

Written Discussion: By Peter Payson and A. E. Nehrenberg, Research Laboratory, Crucible Steel Co. of America, Harrison, N. J.

The authors are to be congratulated on this noteworthy contribution to our knowledge of the metallography of low carbon steel. The massive carbides shown in several of the photomicrographs, particularly Fig. 5A, are extremely interesting. We wonder if the authors have any explanation for such growth of carbides. In eutectoid carbon tool steel which has been double annealed to a hardness of 137 Brinell, the coarsest carbide particles are much smaller than some of those shown in the authors' photomicrographs. Is it likely that the mechanism of carbide growth in the authors' rimmed steel is similar to that involved in the formation of massive carbides in abnormal steel?

We have found in low carbon alloy steels of the cold-hubbing type, effects of solution of carbon in ferrite similar to those found by the authors in their steel which is practically free of alloy. The steels we investigated were the 3110 type formerly used widely for mold dies for plastics, and the new 1.5% chromium, 0.5% nickel, 0.2% molybdenum steel which is replacing the 3110 steel. The data on these steels are as follows:

Grade	3110	Formold
Carbon	0.07	0.05
Manganese	0.41	0.40
Silicon	0.22	0.20
Nickel	1.20	0.53
Chromium	0.57	1.35
Molybdenum	....	0.21
Rockwell B, fully annealed	70	64
Rockwell B, as-quenched from 1300 °F	83	73
Rockwell B, as-aged at 80 °F, 24 hours	87	76
Rockwell B, as-aged at 80 °F, 96 hours	93	76

In both these alloy low carbon steels, solution of carbon in the ferrite is at a minimum below about 700 °F, in agreement with the authors' curve, Fig. 2.

[2]Whiteley, *Journal*, Iron and Steel Institute, No. 1, 1920, p. 359. Comstock, *Forging and Heat Treating*, Vol. 7, 1921, p. 60. Schofield, *Journal*, Iron and Steel Institute, No. 1, 1944, p. 119.

Written Discussion: By L. D. Jaffe, M. R. Norton and D. C. Buffum, Watertown Arsenal, Watertown, Mass.

The authors have certainly established their premise that the properties and structure of low carbon steel are markedly affected by other variables besides deformation. Their data concern steels with as low as 0.02% carbon. We have recently been investigating a "steel" of the SAE 3100 series containing 0.002 to 0.003% carbon, as determined by the low-pressure oxidation method. The nitrogen content was less than 0.002%. As-cast, the hardness was approximately Rockwell B-45. Somewhat to our surprise, quenching from the austenite range increased the hardness to Rockwell B-75. By tempering, the hardness was lowered to Rockwell B-56. As might be expected, the material also age-hardened considerably, reaching a hardness as high as Rockwell B-80.

Some microstructural studies have been conducted on this steel and further ones are under way. More angular carbide particles have been observed in a specimen which had been tempered after quenching than in a companion specimen which had been quenched only. (In both cases the samples had received a subsequent aging treatment at 100 °C for 3 hours.) These particles tend to be concentrated within some grains while other grains are devoid of them.

Do the authors have any information on the effect of heat treatment upon the microstructure and hardness of material having a carbon content comparable to the steel just described?

On the basis of Fig. 3, the authors remark that a long period of time is required for completion of transformation at 1300 °F (705 °C) and above. It seems more likely that the Ae_1 (lower boundary of the three-phase equilibrium region) is below 1300 °F (705 °C), rather than at 1335 °F (725 °C). The literature[3] suggests 1290 °F (700 °C) for a steel with 0.06% carbon and 0.43% manganese. Many of the published Ae_1 temperatures for steels are far too high because the methods used did not reveal equilibrium temperatures. Would the authors explain how their Ae_1 was determined?

Authors' Reply

Mr. Comstock rightly points out that elements other than carbon may affect the microstructure of low carbon steel. Carbon and iron are, however, the principal components of ordinary carbon steel and the paper intentionally was confined to a consideration of the constituents arising from these elements. The microstructural features shown are believed to be quite generally applicable to conventional commercial types of low carbon steel.

In reference to Figs. 8 and 17, Mr. Comstock states that considerable oxide and nitride might be expected in the 0.02 to 0.03% carbon steels used. Figs. 8, 10 and 11 are based on material from the "all rim" portion of an ingot containing approximately 0.06% carbon, 0.3% manganese, and an unkown amount of oxygen as poured; both carbon and oxy-

[3] C. Wells, "Constitution of Ternary Alloys. Carbon-Iron-Manganese," ASM METALS HANDBOOK, 1948, p. 1251-1252.

gen were lowered as a result of the rimming action. Fig. 17 happens to be for a steel of the "low-metalloid" type (approximately 0.03% carbon, 0.1% manganese), which is quite highly oxidized, although the behavior illustrated is believed to be due to low carbon rather than to high oxygen. Neither grade of steel commonly contains more than about 0.005% nitrogen and in the absence of aluminum or similar elements this amount probably is completely soluble at most or all of the temperatures covered in Fig. 8. We know of no reliable data on the solubility of oxygen over this temperature range but have no reason to believe that oxygen plays a major part in forming any of the precipitate shown.

The volume of precipitate in Figs. 8E and 8F may appear much greater than it actually is because of the tendency of etching reagents to dissolve small particles and the surrounding metal leaving holes much larger than the particles themselves. In reply to Mr. Comstock's question, the actual magnification in this illustration is approximately × 600. The actual magnification of other photomicrographs in the paper taken originally at × 1000 is from × 525 to × 600 and that of photomicrographs at an original magnification of × 100 in Figs. 6 and 15 is × 70 to × 75.

In reply to Payson and Nehrenberg the authors have no explanation for the growth of massive carbides, such as those in Fig. 5A, other than that suggested in their paper. We have found such carbides in both rimmed and aluminum-killed steels, hence their formation does not appear to be related directly to deoxidation practice. We have not compared the relative "normality" of these two grades.

The solution hardening and "quench aging" effects observed by Messrs. Payson and Nehrenberg and by Messrs. Jaffe, Norton and Buffum in low carbon alloy steels demonstrate that such effects are by no means confined to the common low carbon grades. They are, in fact, not even confined to low carbon steels but may be encountered in higher carbon grades when spheroidized so that a substantial amount of "free" ferrite is present.

The authors have no information regarding the effect of heat treatment upon the microstructure and hardness of "steel" containing as little as 0.002 to 0.003% carbon and 0.002% nitrogen.

Jaffe, Norton and Buffum suggest that the Ae_1 temperature for steel of the type used by the authors is below 1300 °F (705 °C) rather than about 1335 °F (725 °C) as reported. The approximate Ae_1 temperature of several steels containing 0.05 to 0.08% carbon and 0.30 to 0.45% manganese, including rimmed, silicon-killed, and aluminum-killed grades, was determined by heating specimens for periods up to 2 hours in a lead bath at various temperatures, then quenching. The lowest temperature at which austenite formed, as determined by metallographic examination of the quenched specimens, was 1335 to 1345 °F (725 to 740 °C). Based on this evidence, we doubt that the true Ae_1 temperature is much below 1335 °F (725 °C).

INFLUENCE OF NICKEL AND MOLYBDENUM ON ISOTHERMAL TRANSFORMATION OF AUSTENITE IN PURE IRON-NICKEL AND IRON-NICKEL-MOLYBDENUM ALLOYS CONTAINING 0.55% CARBON

By D. A. Scott, W. M. Armstrong and F. A. Forward

Abstract

A metallographic investigation of isothermal transformation of austenite is described for two series of pure iron-nickel-carbon alloys containing 0.55% carbon and 0, 2, 3.75, and 5% nickel. One series contained no molybdenum, the other 0.35% molybdenum. The laboratory procedure for the production of these alloys is described.

In alloys without molybdenum, as the nickel content is increased: the appearance of visible proeutectoid ferrite and of pearlite is retarded; the formation of upper bainite by growth of ferrite plates and subsequent carbide precipitation is more readily observed; the minimum temperature for formation of upper bainite is lowered appreciably.

In alloys containing 0.35% molybdenum, as the nickel content is increased: the appearance of visible proeutectoid ferrite is retarded to a greater degree than in the molybdenum-free alloys; the acicular character of ferrite formed at intermediate temperatures becomes more apparent; the acicular ferrite and feathery bainite reactions as represented on the isothermal curves become more widely separated.

In all 0.35% molybdenum alloys examined: the acicular ferrite reaction is followed by carbide rejection and later by agglomeration and growth of the carbide phase as a separate constituent; the time required for the formation of visible proeutectoid ferrite is approximately 10 times that observed in the molybdenum-free alloys, this multiplying factor being uninfluenced by temperature or nickel content; the similar multiplying factor for bainite is uninfluenced by temperature but is apparently decreased exponentially by increasing nickel contents.

A paper presented before the Thirtieth Annual Convention of the Society, held in Philadelphia, October 23 to 29, 1948. Of the authors, Donald A. Scott is instructor in physical metallurgy, W. M. Armstrong is associate professor of physical metallurgy, and F. A. Forward is professor and head, department of mining and metallurgy, University of British Columbia, Vancouver, Canada. Manuscript received April 17, 1948.

Introduction

THE phenomena accompanying the decomposition of austenite have not been fully or satisfactorily explained despite the fact that they have been examined by many observers. Especially lacking is information on the effect of single elements added to alloys of iron and carbon in which no other residual elements are present to complicate the experimental results. Once this effect of individual elements has been established it should be possible to find the correlated effect of two or more alloys, and, by so doing, some of the phenomena accompanying austenite decomposition may be explained more satisfactorily than they are at present. Studies of this type should provide quantitative data for predicting the form of the isothermal transformation curve for any combination of alloys.

The present investigation is the first of many that will be required to provide this data. The object of this phase of the work is to establish the quantitative effect of nickel on the beginning of isothermal transformation of austenite in two series of pure iron-carbon-nickel alloys containing 0.55% carbon and 0, 2, 3.75 and 5% nickel; one series containing no molybdenum, the other 0.35% molybdenum.

Survey of Previous Work

A significant development in the understanding of transformation of austenite at sub-critical temperatures was the work of Bain and Davenport (1),[1] which resulted in the isothermal transformation diagram. Since this development many workers have investigated austenite transformation experimentally and by means of theory.

An extensive review of the literature on austenite transformation has been listed and discussed in a recent paper by Hultgren (2).

Previous workers, Bain (3), Davenport (4), Lange and Mathieu (5), and Ham (6), have summarized the present knowledge of the effect of nickel on the transformation of austenite in the temperature range of formation of pearlite and bainite. It has been reported that, in general, nickel moves the isothermal transformation curve to the right (longer times) with little change in the shape of the curve except that caused by lowering the eutectoid temperature. Most of the alloys studied by these investigators contained appreciable

[1]The figures appearing in parentheses pertain to the references appended to this paper.

amounts of residual alloying elements such as silicon and manganese, and some of the results are not quantitatively comparable because of varying amounts of residual elements.

The effects of nickel on eutectoid carbon content and eutectoid temperature are shown in Figs. 1 and 2.

The effect of molybdenum on isothermal transformation has

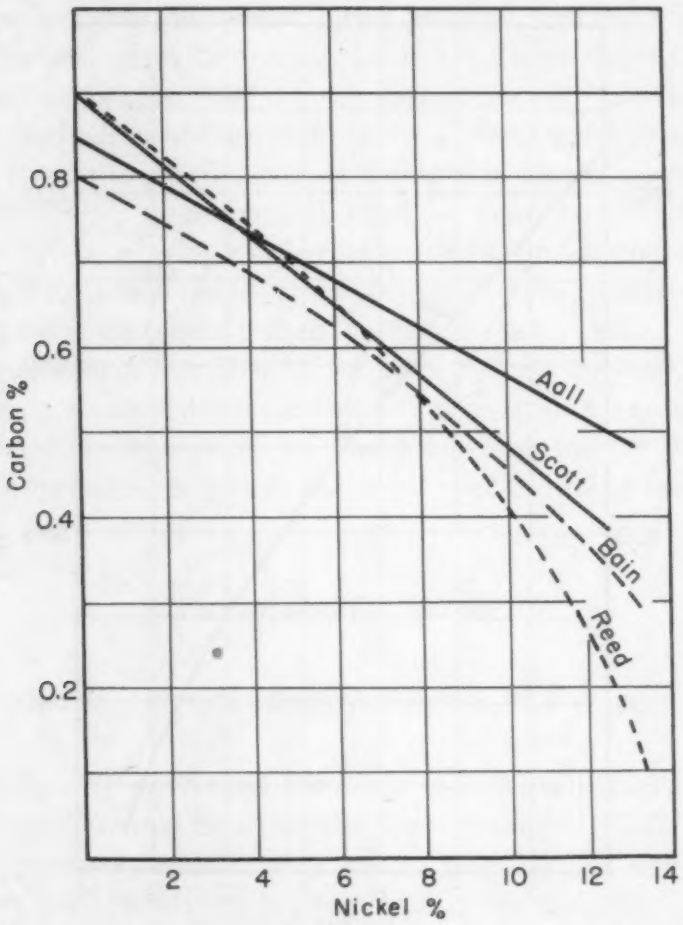


Fig. 1—Change in Eutectoid Carbon Content With Change in Nickel [After Bain (3), Hall (7), Reed (8), and Scott (9)].

been reported by Davenport (4), and Blanchard, Parke, and Herzig (10). Molybdenum has a greater effect on retarding transformation to pearlite than it has on transformation to any other product.

Very little information is available on the interrelated effect of nickel and molybdenum on the isothermal transformation of austenite in pure alloys.

Nickel retards the transformation of gamma to alpha in carbon-

free iron alloys. Ham (6) relates the sluggish reaction in carbon-free nickel alloys to the effect of nickel on increasing isothermal transformation times in alloys containing carbon. Nickel is a so-called ferrite-forming element, with a much lower diffusion rate than iron, carbon (11), (12), and molybdenum (13). In hypoeutectoid steels, ferrite forms from austenite before pearlite and "upper bain-

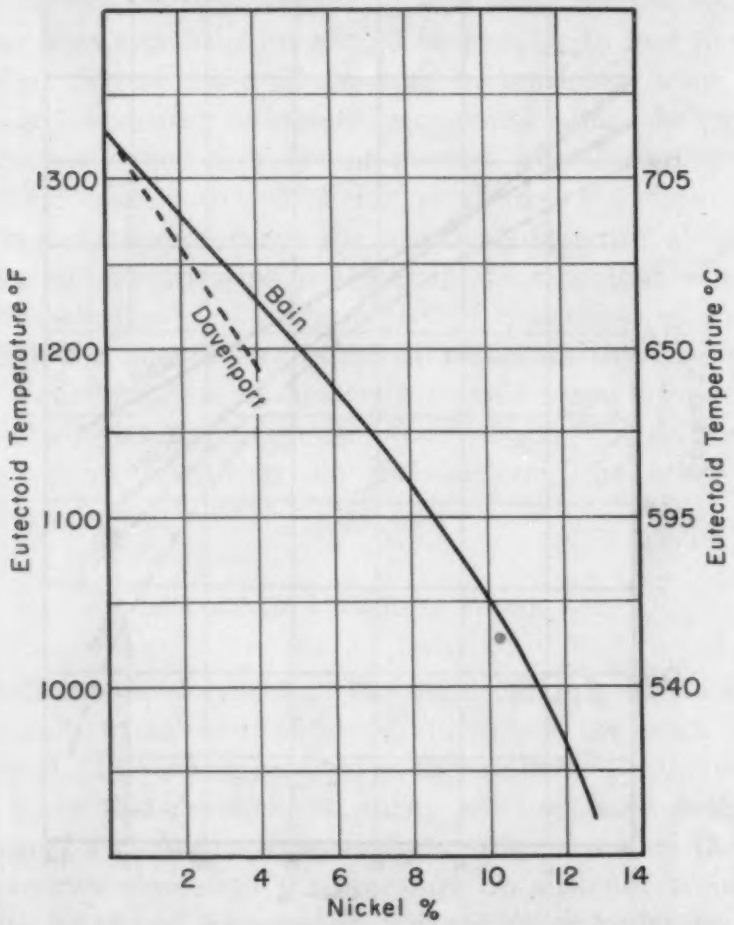


Fig. 2—Change in Eutectoid Temperature With Change in Nickel [After Bain (3) and Davenport (4)].

ite". These authors suggest that the composition of the austenite must increase in carbon and decrease in nickel appreciably before pearlite can form, and hence the delay in ferrite formation in the presence of nickel must, of necessity, delay the pearlite transformation.

The "upper bainite" transformation is initiated by the formation of a ferrite nucleus (14). This would mean that proeutectoid

ferrite and bainite transformations are delayed in a similar manner.

The crystal lattice of bainite is reported (14), (15) to change with respect to form and orientation as the temperature of bainite formation is decreased. There is some evidence that, with decreasing temperature of bainite formation, a gradual change from a body-centered cubic to a tetragonal lattice occurs, suggesting that an increasingly greater amount of carbon is retained in the bainite.

The ferrite, pearlite, and "upper bainite" reactions take place by nucleation and growth processes (15). Some degree of doubt exists as to the exact method of formation of "lower bainite", whether by nucleation and growth, or by a shear mechanism.

Apart from the mechanism of formation of the various transformation products, some method must be found of evaluating the *quantitative* effect of single alloying elements on isothermal transformation. The interrelated effect of pairs (or greater numbers) of alloying elements should then be established. From results so obtained it should be possible to set up a system for predicting the shape of the isothermal transformation curve from a known analysis (including residual elements) or for predicting the necessary alloy additions to produce a given shape of isothermal transformation curve.

Experimental Work

Melting of Alloys

The technique developed for making 200-gram melts is as follows. Using Norway iron as the base material (0.02% carbon, 0.001% manganese, and 0.004% silicon), holes are drilled in one end of small rods, into which are packed pure graphite powder and the required ferroalloy in accurately weighed amounts. The Norway iron bars are placed, packed end down, in dry 1¾ by 2¾-inch cylindrical, high grade alundum melting crucibles, and any required amounts of nickel added in the form of pure shot. A shaped graphite block and lid surrounds the crucible, and the assembly is placed in a globar furnace which is brought up to 2900 °F (1595 °C). After melting, a small amount of calcium-silicon is added as a deoxidizer, and the melt is held at temperature a few minutes. The alloy is poured into a heated graphite mold to make 0.25-inch diameter by 3-inch long pencils, from which small specimens are cut after

Table I
Alloys for Isothermal Transformation

Alloy No.		C	Ni	Mo	Mn	Si	A.S.T.M. Grain Size	Ae Temp. °F*
Norway Iron		0.02			<.001	.004	..	....
1	Weight %	0.50	0.00	....	<.001	<.01	5	1333
	Atomic %							
2	Weight %	0.52	2.11	....	....	....	5	1280
	Atomic %	2.38	1.98					
3	Weight %	0.55	3.78	....	....	....	6	1225
	Atomic %	2.51	3.63					
4	Weight %	0.56	4.89	....	....	....	5	1185
	Atomic %	2.56	4.55					
5	Weight %	0.55	0.00	0.35	....	....	5	1333
	Atomic %	2.51	....	0.199				
6	Weight %	0.55	2.13	0.34	....	....	6	1280
	Atomic %	2.51	1.99	0.194				
7	Weight %	0.51	3.69	0.35	....	....	6	1220
	Atomic %	2.33	3.44	0.199				
8	Weight %	0.59	5.31	0.35	....	....	5	1175
	Atomic %	2.68	4.97	0.199				

*See References (3) and (4).

annealing in a neutral salt bath furnace for 30 minutes at 1550 °F (845 °C).

Alloys prepared in this way and used for isothermal work are listed in Table I.

Isothermal Transformation

Specimens for isothermal transformation were cut approximately 0.05 inch thick from the annealed pencils. Small holes were drilled in the center of each specimen through which 22-gage chromel wire was threaded to serve as a handle for transferring the specimen from one bath to the next. Experiment showed that it required a period of 3 minutes at an austenitizing temperature of 1550 °F (845 °C) to completely austenitize the specimens. In view of this fact, all specimens isothermally treated were heated at least 6 minutes at 1550 °F (845 °C) in a neutral salt bath to insure complete austenitization. Specimens were quenched to, and held for a measured time at, the isothermal transformation temperature in a salt bath, followed by an immediate quench to room temperature in an 8% brine solution. Time was measured from the instant the specimen entered the bath.

One flat face of each of the transformed specimens was smoothed on No. 2 emery paper, the specimen mounted in lucite, polished, etched in nital, and examined at 1300 magnifications. For a detailed survey of some transformation temperatures higher magni-

fications were used for visual observation. Criterion of beginning of transformation was the first visual appearance of any transformation product in a minimum of six random fields on the specimen.

Experimental Results

The effect of nickel on the beginning of transformation of

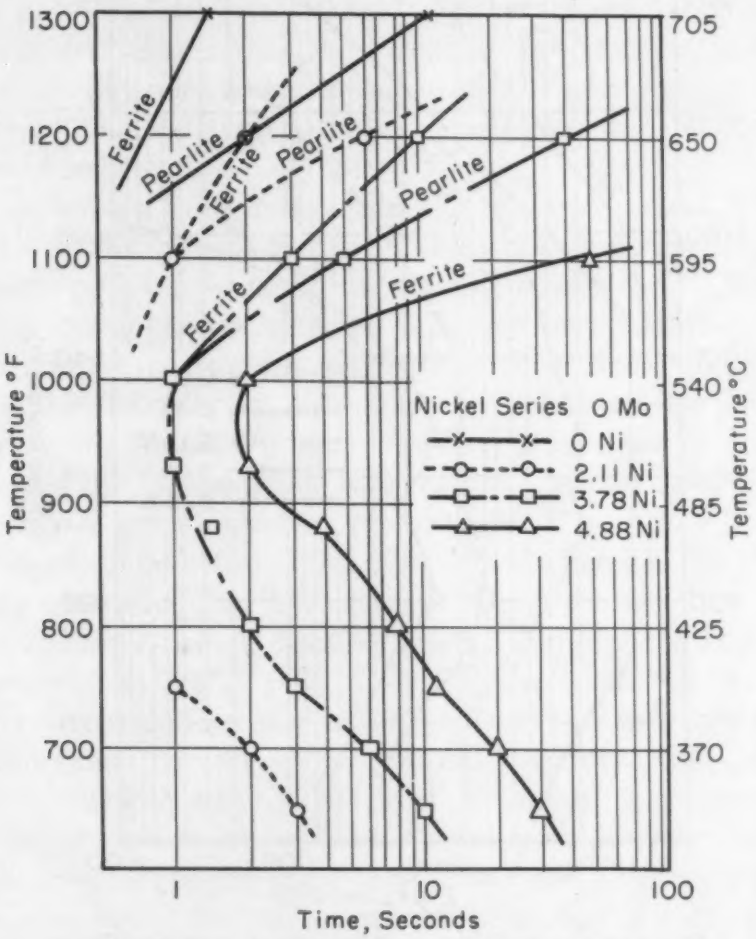


Fig. 3—Effect of Nickel on Beginning of Isothermal Transformation of Austenite in Pure Iron Alloys Containing 0.55% Carbon.

austenite in pure iron-carbon-nickel alloys is shown in Fig. 3, and the effect in similar alloys containing 0.35% molybdenum is shown in Fig. 4.

Alloys Containing No Molybdenum

Nickel increases considerably the time for formation of visible

ferrite and pearlite above 1000 °F (540 °C). The lowest temperature of formation of visible proeutectoid ferrite followed by pearlite is lowered approximately 100 °F between 0% and 5% nickel. Over the same range of compositions the eutectoid and gamma to alpha equilibrium temperatures are lowered approximately 150 °F and 200 °F respectively (16).

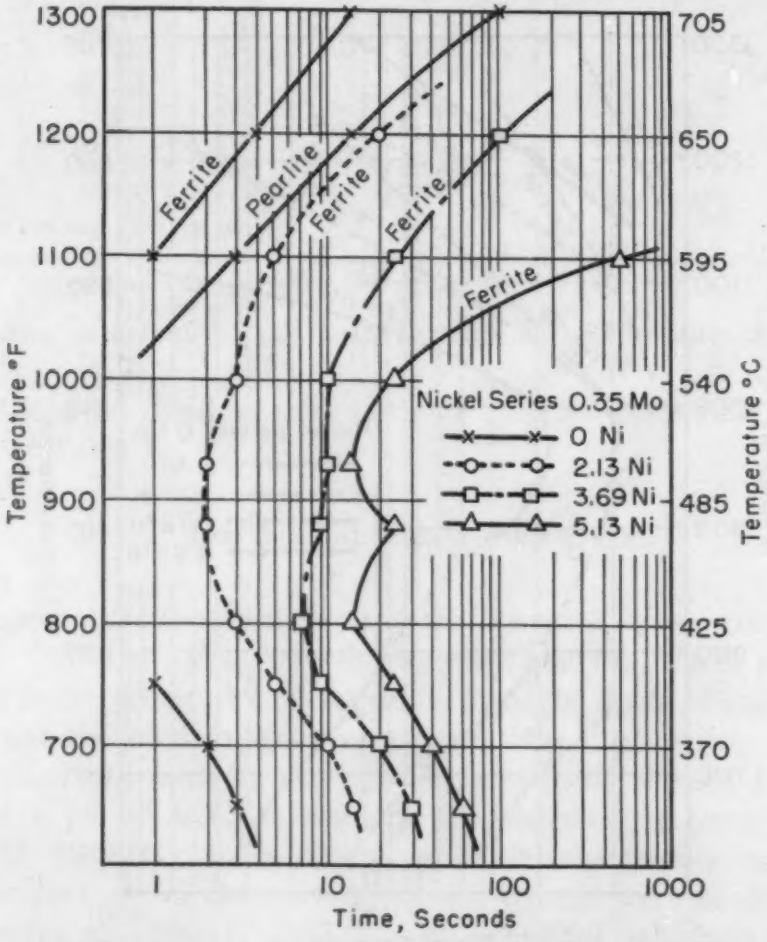


Fig. 4—Effect of Nickel on Beginning of Isothermal Transformation in Pure Iron Alloys Containing 0.55% Carbon and 0.35% Molybdenum.

The ferrite and pearlite curves are depressed in the upper temperature range but the time required for the appearance of these phases is greater than can be accounted for by the lowering of the equilibrium temperatures. This would seem to substantiate the following hypotheses: (a) nickel being partitioned in ferrite rather than in pearlite delays ferrite formation because of low nickel diffusion rate; (b) carbon atoms must diffuse into austenite and nickel

atoms into ferrite at the rate required to give an austenite low enough in nickel and high enough in carbon to allow pearlite formation to begin. The slower ferrite transformation at higher nickel contents and slow diffusion of nickel from austenite to ferrite delays the pearlite reaction much more than it does the ferrite reaction.

Upper bainite forms at temperatures just below the "nose of the S-curve" and, with increasing nickel content, the change from nodular "upper bainite" to feathery "lower bainite" occurs at a much lower temperature. The formation of nodular bainite by growth of ferrite plates and subsequent carbide precipitation is more readily observed. As transformation progresses, the ferrite plates are spheroidized.

Fig. 5 shows a pure iron-carbon alloy held ½ second at 930 °F (500 °C). It shows approximately 50% transformation to pearlite and bainite, growing inwards from grain boundaries. The large white areas in the photomicrograph represent untransformed austenite. This degree of transformation at such a short time interval illustrates the difficulty in obtaining any points on the beginning curve below the "nose" in the pure iron-carbon alloy. A direct quench from the austenitizing bath to room temperature produces no intermediate transformation products.

Fig. 6 shows transformation after 1 second at 930 °F (500 °C) in an alloy containing 2.11% nickel.

Fig. 7 shows bainite formed after holding the 2.11% nickel alloy 3 seconds at 750 °F (400 °C). Compare with Fig. 8 showing bainite formed after 5 seconds at 750 °F (400 °C) in a 3.78% nickel alloy. Individual "feathers" of bainite apparently form as a thin black wedge (nital etch), and grow to about three times their original length and width, at which point growth apparently stops along one crystallographic plane in austenite and then resumes at an angle to the first "feather", presumably along another crystallographic plane.

Fig. 9 shows transformation to bainite after 15 seconds at 750 °F (400 °C) in a 4.89% nickel alloy. The very small black needles indicate the size of the first visible bainite. The first needles appear after 12 seconds, and in the next 3 seconds grow to the size of the largest needle shown in Fig. 9. Fig. 10 shows further growth in the same alloy after 30 seconds at 750 °F (400 °C). Note the parallel acicular growth of the bainite and the angle between adjacent plates.

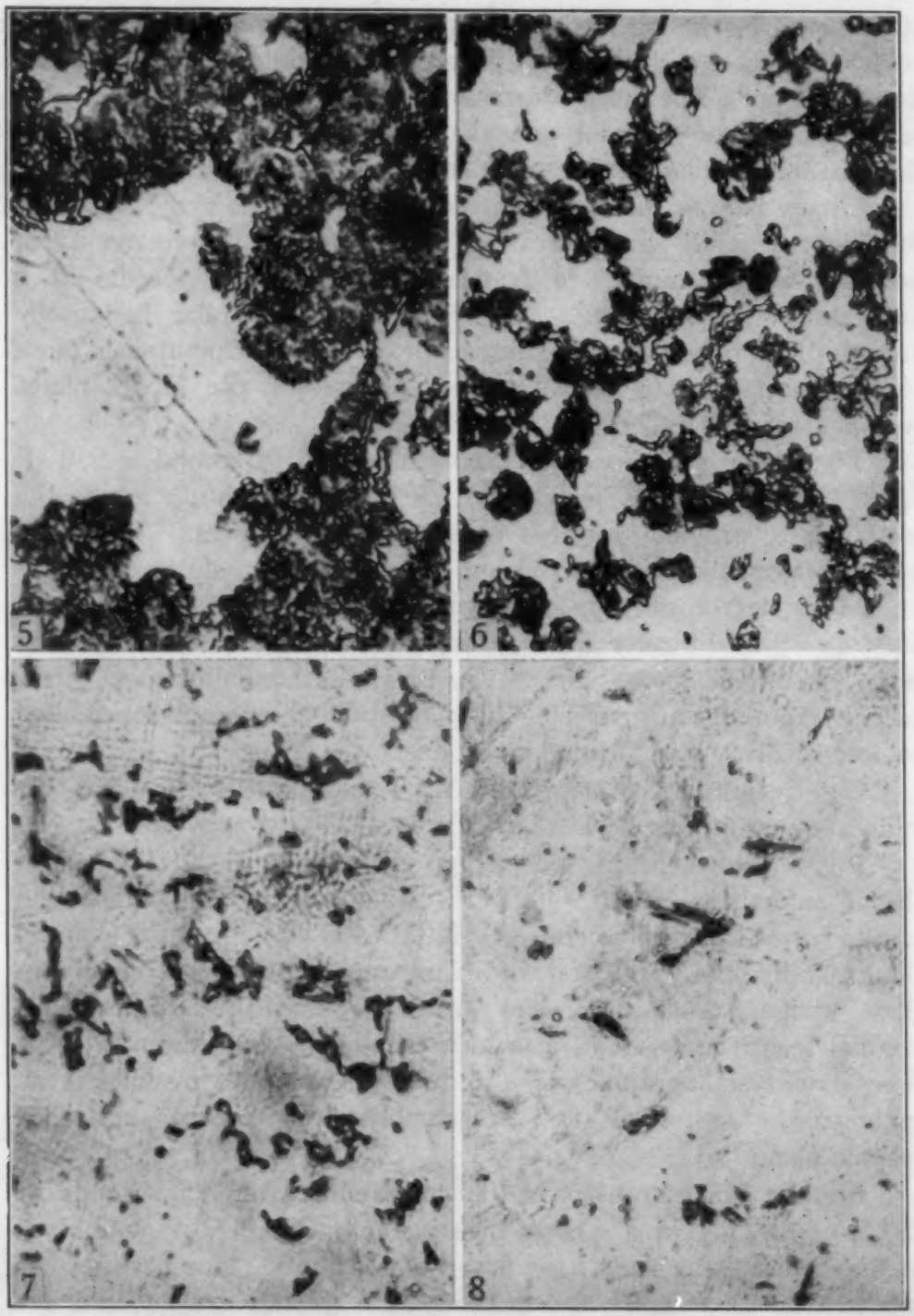


Fig. 5—Pure 0.55% Carbon Alloy Transformed ½ Second at 930 °F (500 °C).
Fig. 6—2% Nickel, 0.55% Carbon Alloy Transformed 1 Second at 930 °F (500 °C).
Fig. 7—2% Nickel, 0.55% Carbon Alloy Transformed 3 Seconds at 750 °F (400 °C).
Fig. 8—3.75% Nickel, 0.55% Carbon Alloy Transformed 5 Seconds at 750 °F (400 °C).
All photomicrographs × 850, nital etch.

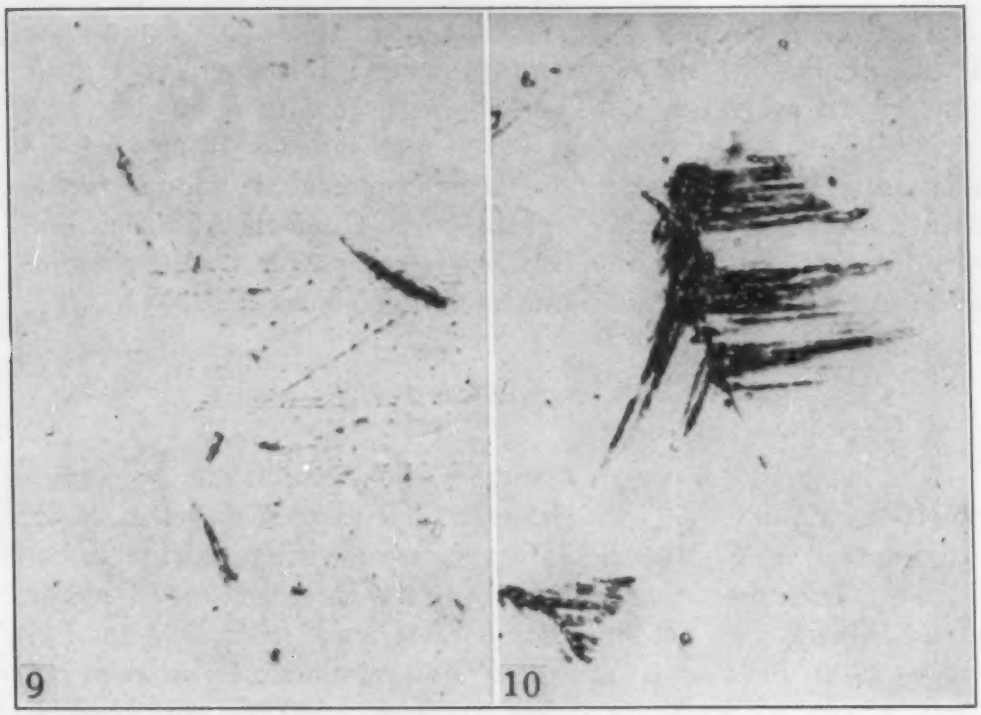
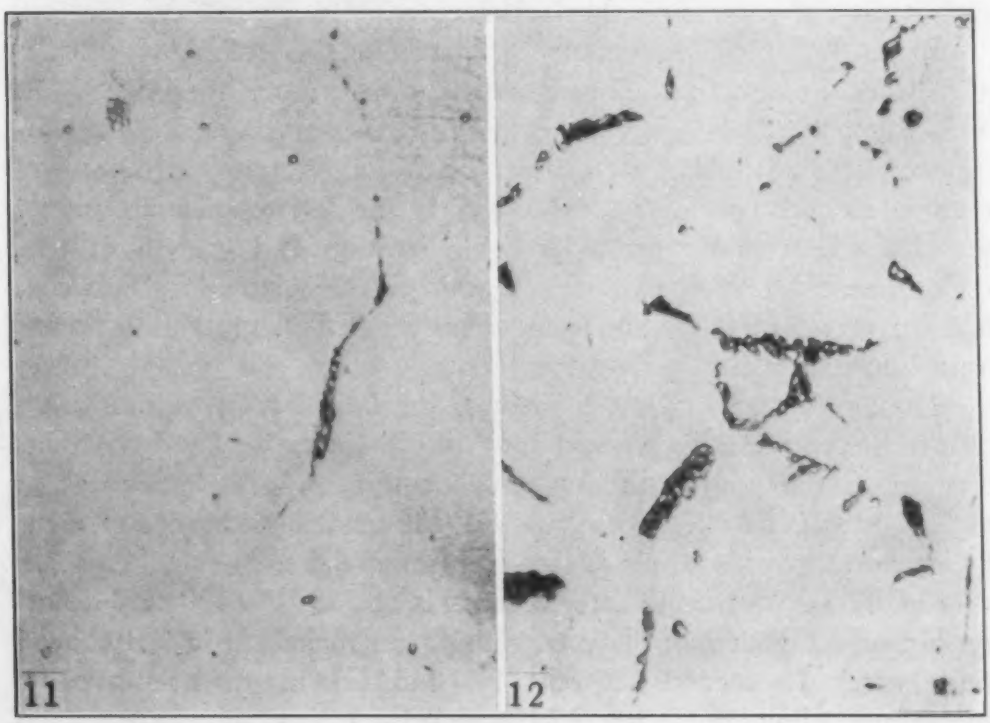


Fig. 9—5% Nickel, 0.55% Carbon Alloy Transformed 15 Seconds at 750 °F (400 °C).
Fig. 10—5% Nickel, 0.55% Carbon Alloy Transformed 30 Seconds at 750 °F (400 °C).
All photomicrographs × 850, nital etch.



Figs. 11 and 12—5% Nickel, 0.55% Carbon Alloy Transformed at 880 °F (475 °C).
× 850, nital etch. Fig. 11—5 Seconds. Fig. 12—10 Seconds.

Figs. 11 to 16 show a series in the 4.89% nickel alloy at 880 °F (475 °C). Fig. 11 shows extent of bainite formation at a grain boundary after 5 seconds. The bainite appears to form first as a series of ferrite spheroids, the dark areas possibly being carbides which are rejected at the ferrite-austenite interface. Parallel ferrite plates grow along crystallographic planes from these nuclei, followed by carbide precipitation between ferrite platelets, and spheroidization of some of the first-formed ferrite platelets.

Alloys Containing 0.35% Molybdenum

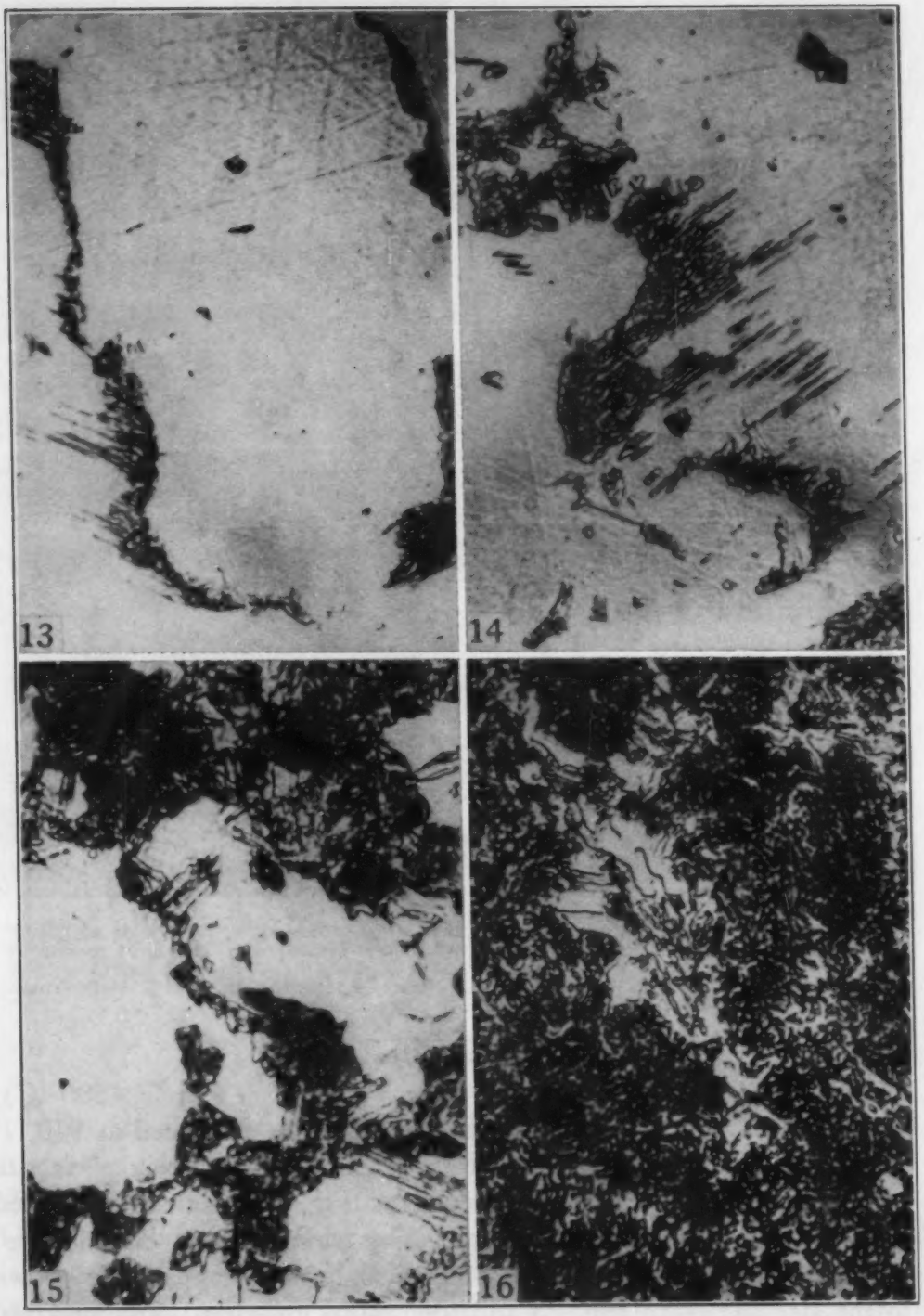
The beginning of visible transformation in iron alloys containing 0.55% carbon, 0.35% molybdenum, and varying nickel is shown by the curves in Fig. 4. The formation of visible pearlite is delayed very much more than is the case in the plain iron-nickel-carbon alloys. Pearlite does not appear in a 3.5% nickel alloy held for 5½ hours at 1100 °F (595 °C); in the 5% nickel alloy, pearlite does not appear after 5½ hours at either 1000 °F (540 °C) or 1100 °F (595 °C). For this reason comparative studies of the pearlite reaction were not made. The effect on the pearlite reaction is, however, much greater than it is on the ferrite reaction.

Increasing nickel produces a "bay" in the curve at 880 °F (475 °C). Ferrite in the intermediate temperature range, 880 °F (475 °C) to 1000 °F (540 °C) is more acicular as the nickel content is increased, and, during growth of the acicular ferrite, carbides are precipitated both within the ferrite and at the ferrite-austenite interface, followed at later times by agglomeration and growth of the carbide phase. This agglomeration and growth occurs first between plates of acicular ferrite and subsequently extends into the untransformed austenite surrounding the ferrite.

The appearance and mechanism of growth of these transformation products in the alloys containing molybdenum differs from that observed in the alloys without molybdenum. In the temperature range 800 to 1000 °F (440 to 540 °C), the tendency towards growth of a separate carbide phase is less in the molybdenum-free alloys.

Fig. 17 shows bainite after 3 seconds at 750 °F (400 °C) in an iron-carbon-molybdenum alloy containing no nickel. Fig. 18 shows bainite after 15 seconds at 650 °F (345 °C) in an iron-carbon-molybdenum alloy containing 2.13% nickel.

Figs. 19 and 20 show pearlite which forms at intermediate



Figs. 13 to 16—5% Nickel, 0.55% Carbon Alloy Transformed at 880 °F (475 °C). × 850, nital etch. Fig. 13—15 seconds. Fig. 14—20 seconds. Fig. 15—30 seconds. Fig. 16—100 seconds.

temperatures in the low nickel alloys containing molybdenum. Fig. 19 shows the 0% nickel alloy after 1 second at 930 °F (500 °C).

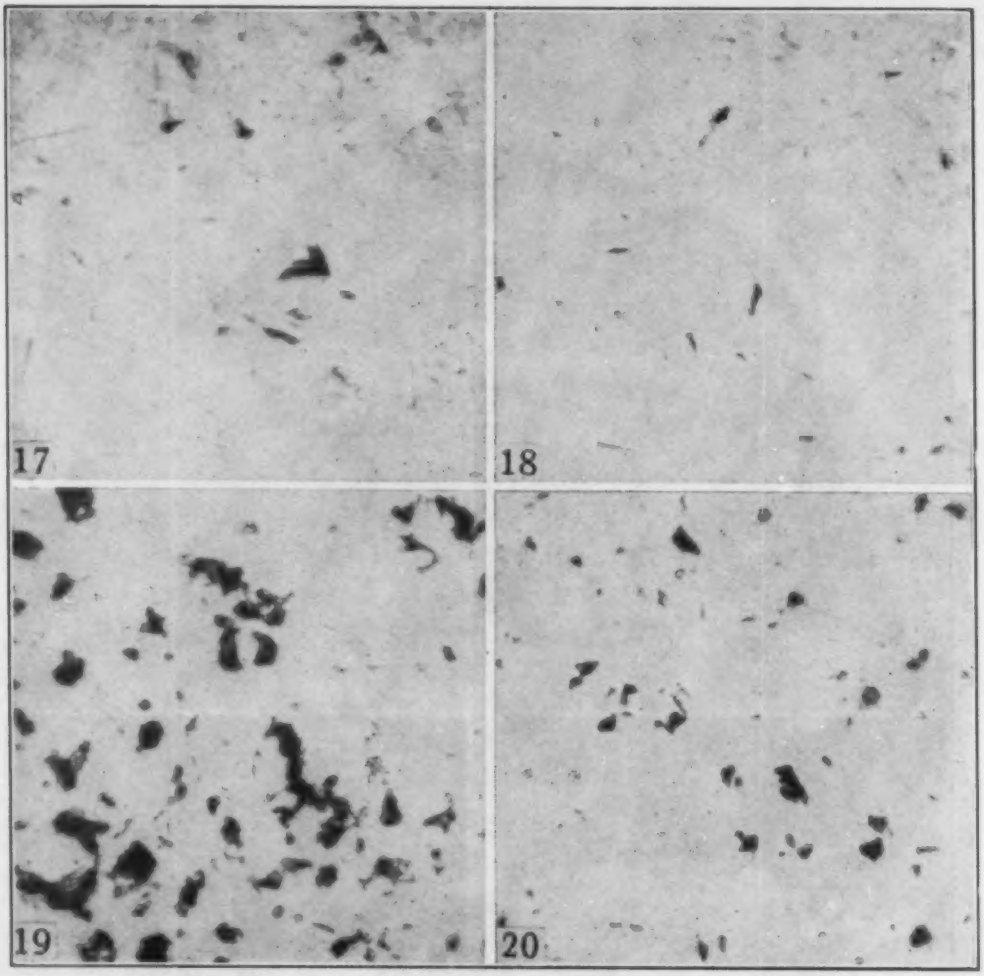
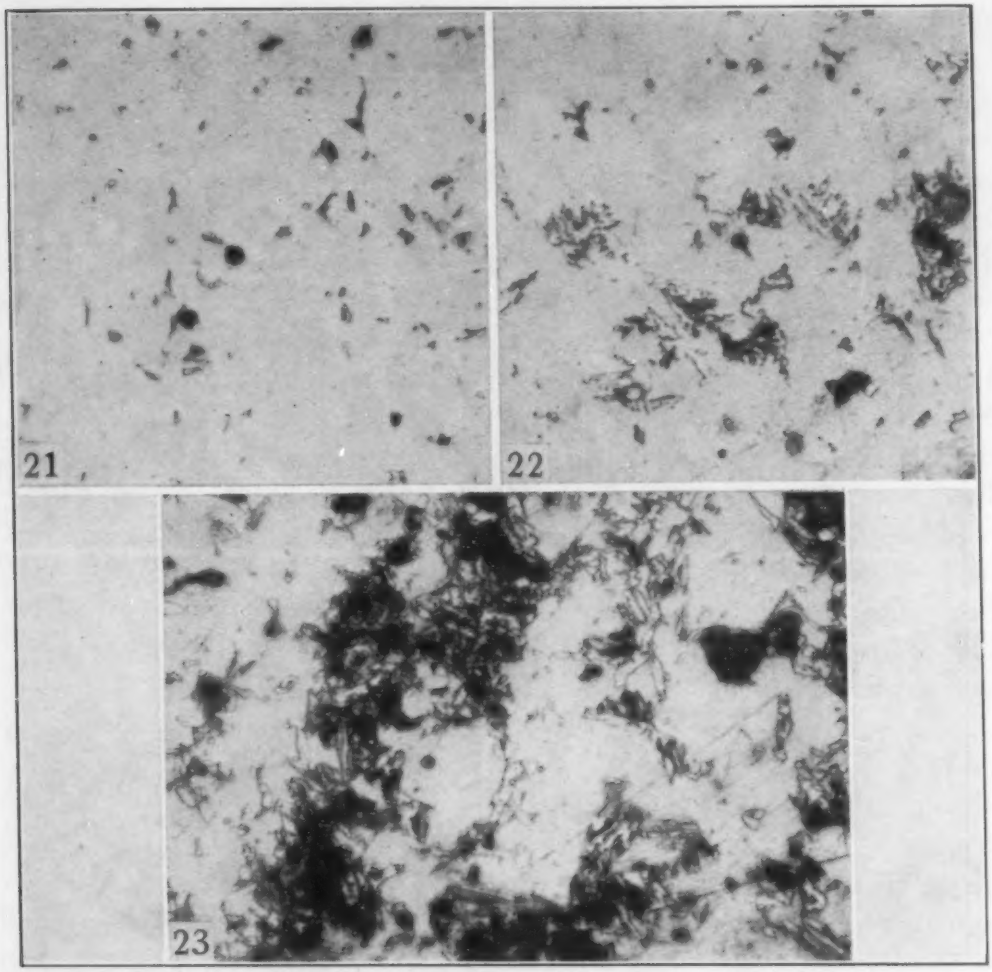


Fig. 17—0% Nickel, 0.55% Carbon, 0.35% Molybdenum Alloy. 3 seconds at 750 °F (400 °C). Fig. 18—2% Nickel, 0.55% Carbon, 0.35% Molybdenum Alloy. 15 seconds at 650 °F (345 °C). Fig. 19—0% Nickel, 0.55% Carbon, 0.35% Molybdenum Alloy. 1 second at 930 °F (500 °C). Fig. 20—2% Nickel, 0.55% Carbon, 0.35% Molybdenum Alloy. 3 seconds at 930 °F (500 °C). All × 850, nital etch.

Fig. 20 shows 2.13% nickel alloy after 3 seconds at 930 °F (500 °C).

Figs. 21 to 23 show the duplicate structure produced at 930 °F (500 °C) in a 3.89% nickel alloy. Fig. 21 shows acicular ferrite which precipitates after 12 seconds. Fig. 22 shows continued transformation at 15 seconds, indicating simultaneous carbide precipitation and ferrite growth. The acicular ferrite apparently grows to the size shown in Fig. 23 and then stops growing. The separate carbide phase has agglomerated and grown considerably.

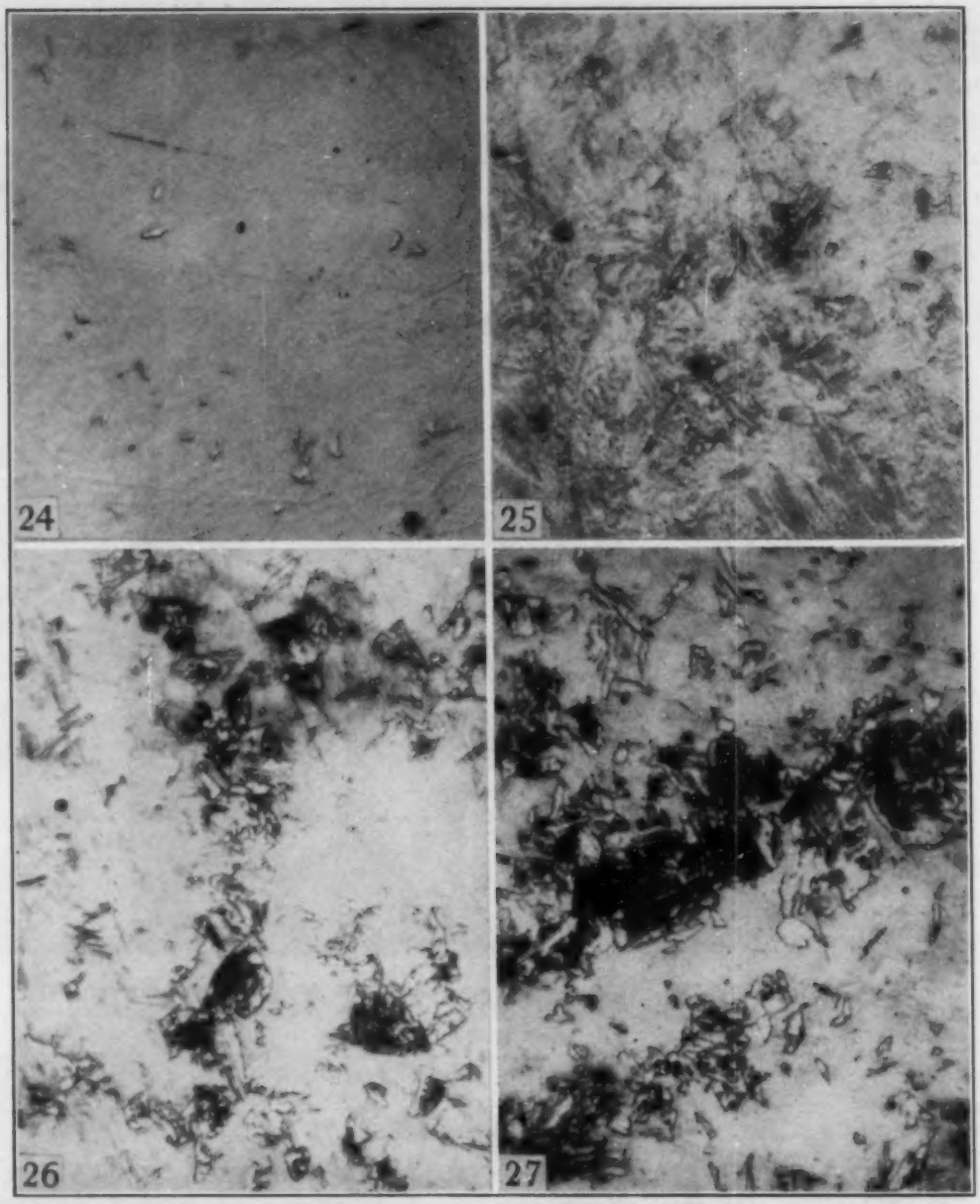
Figs. 24 to 27 show a similar series of duplicate structure produced in the 5.13% nickel alloy after 25, 30, 60, and 120 seconds respectively at 930 °F (500 °C).



Figs. 21 to 23—3.75% Nickel, 0.55% Carbon, 0.35% Molybdenum Alloy at 930 °F (500 °C). Fig. 21—12 Seconds. Fig. 22—15 Seconds. Fig. 23—30 Seconds. All × 850, nital etch.

Discussion of Results

Pearlite—In the alloys investigated, increased nickel content delays the first appearance of visible pearlite more than it does that of visible ferrite. This difference is accentuated by the addition of 0.35% molybdenum, indicating that there is some correlation between the separate effects of nickel and molybdenum on the time required for the appearance of visible pearlite. It is conceivable that the addition of nickel to iron-carbon-molybdenum alloys causes the partition of molybdenum between ferrite and carbide to shift towards the carbide phase, as nickel is the stronger ferrite-former of the two. If this assumption is valid the molybdenum in the austenite at trans-



Figs. 24 to 27—5% Nickel, 0.55% Carbon, 0.35% Molybdenum Alloy at 930 °F (500 °C). Fig. 24—25 Seconds. Fig. 25—30 Seconds. Fig. 26—60 Seconds. Fig. 27—120 Seconds. All × 850, nital etch.

formation temperature, being a strong carbide former, would associate with carbon atoms and decrease the probability of iron carbide nucleus formation. A further retarding influence is provided by the lower diffusion rate of nickel at these temperatures compared with that of carbon or molybdenum (6).

Transition Constituents

The appearance and mechanism of growth of the transformation products in the intermediate temperature range 800 to 1000 °F (440 to 540 °C), in the alloys containing molybdenum, differ from that observed in the alloys without molybdenum. In the molybdenum-free alloys there is less tendency towards separate growth of the precipitated carbide phase. In the alloys containing molybdenum, as the nickel content is increased, two facts become apparent: first, that acicular ferrite is the initial product of transformation; and second, that the amount and stability of this acicular constituent increase. Carbon and molybdenum atoms must be entrapped when this acicular ferrite forms. Continued diffusion of carbon and molybdenum in the ferrite would result in the formation of carbide nuclei, both within the ferrite areas and at the external ferrite-austenite interface. These carbide particles continue to form and agglomerate until their volume approaches that of the acicular ferrite, at which point the transformation ceases and the remaining austenite becomes stable for a considerable time period.

Quantitative Factors

The experimental results indicate that there is a quantitative relation between the relative amounts of nickel and molybdenum present and the time required for the first visible transformation product, which may be either proeutectoid ferrite or bainite. The pertinent data listed in Table II show that:

(a) In the proeutectoid range (see Fig. 28) the time is increased by a factor of 10 when 0.35% molybdenum is present. Within the limits of experimental error it appears that this factor is constant for all temperatures and nickel contents.

(b) In the transition range it is not possible to establish a definite factor. This is probably due to the fact that two transformation reactions occur simultaneously and that accurate measurement of transformation times less than 1 second is not feasible.

(c) In the bainite range the time is increased by the addition of 0.35% molybdenum. This factor is between 2 and 5, and is unaffected by temperature but is decreased exponentially by increasing nickel (see Table II and Fig. 29).

Table II

Times* for Beginning of Transformation of Austenite to Proeutectoid Ferrite and Bainite in 0.55% Carbon-Iron Alloys

		Temperature °F									
Wt. % Ni	Wt. % Mo	1300	1200	1100	1000	930	880	800	750	700	650
0	0	1-2									
	0.35	15									
	Mo Factor	10									
2	0		2	<1	<1	..	..	1	1	2	3
	0.35		20	5	3	..	..	3	5	10	15
	Mo Factor		10	..	..	..	..	..	5	5	5
3.75	0		10	<3	1	1	1-2	2	3	6	10
	0.35		100	25	10	10	9	7	9	20	30
	Mo Factor		10	10	10	10	..	3.5	3	3	3
5	0			50	2	2	4	8	12	20	30
	0.35			500	25	14	25	15	25	40	60
	Mo Factor			10	10	7	6	2	2	2	2

*All times listed are to the nearest second. It should be noted that possibility of experimental error is greater the shorter the transformation time.

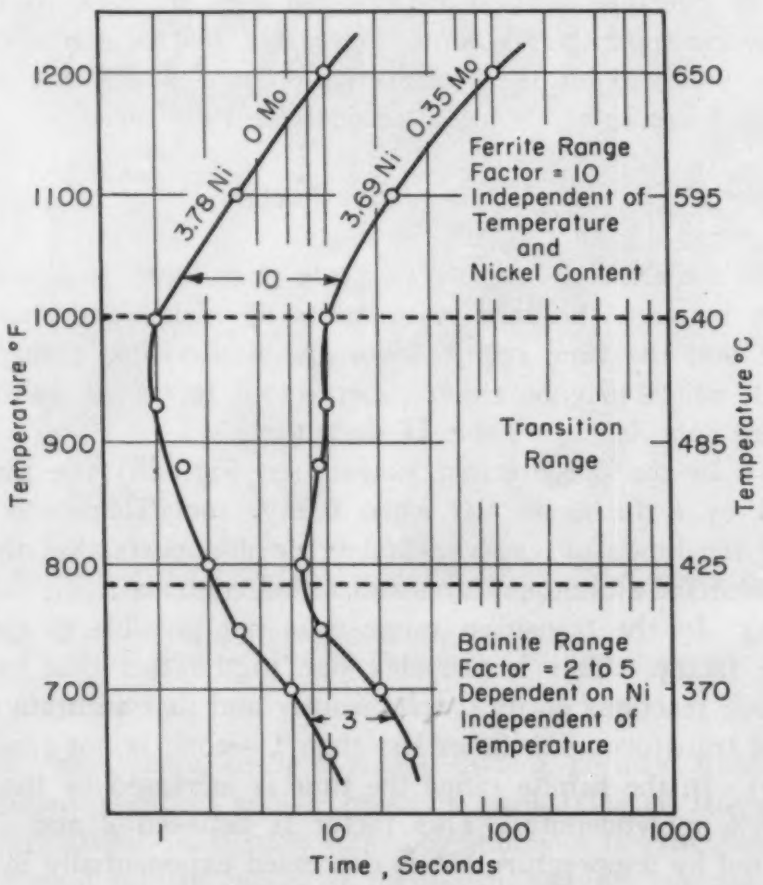


Fig. 28—Comparative Curves of Beginning of Isothermal Austenite Transformation.

Further work is proposed on alloys containing 1 and 6% nickel to complete the curve of Fig. 29. Also, the carbon and molybdenum should be varied to establish curves similar to those in Fig. 29.

This method of presentation indicates a possible approach for evaluating quantitatively the individual and interrelated effects of

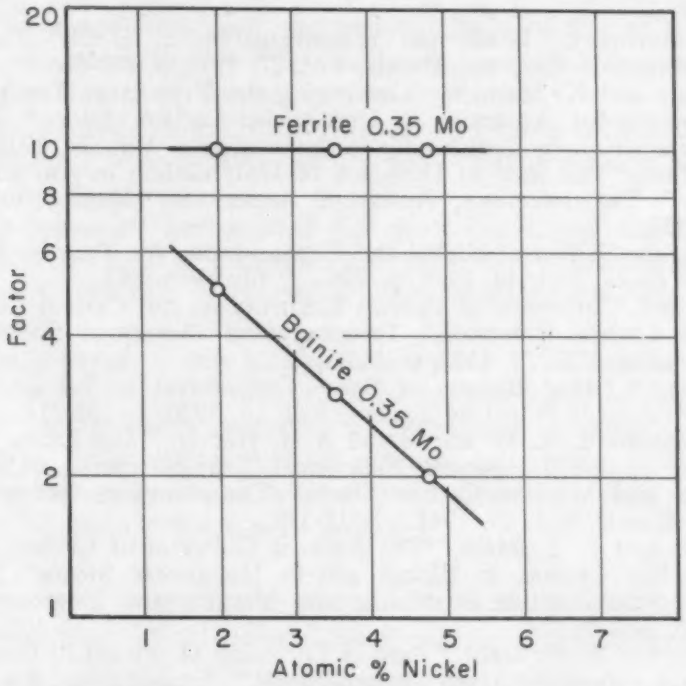


Fig. 29—Plot of Time Factor for Effect of 0.35% Molybdenum on Beginning of Isothermal Transformation of Austenite.

the various alloying elements on the beginning of austenite transformation. From data presented in this way, if one basic curve is known, it may be possible to set up charts or nomograms for calculating the exact times to be expected by adding any alloying elements. It may also be possible to predict the amounts of different alloying elements required to produce an isothermal transformation diagram of any desired shape.

Acknowledgments

This research was made possible by a National Research Council (Ottawa) Bursary held by Mr. Scott, and research grants to the Department of Mining and Metallurgy, University of British Columbia from National Research Council and the University of British Columbia Research Fund.

References

1. E. C. Bain and E. S. Davenport, "Transformation of Austenite at Subcritical Temperatures," *Transactions,* American Institute of Mining and Metallurgical Engineers, Iron and Steel Division, 1930, p. 117.
2. A. Hultgren, "Isothermal Transformation of Austenite," TRANSACTIONS, American Society for Metals, Vol. 39, 1947, p. 915.
3. E. C. Bain, "Functions of Alloying Elements in Steel," A.S.M. Publication, 1939.
4. E. S. Davenport, "Isothermal Transformation in Steels," TRANSACTIONS, American Society for Metals, Vol. 27, 1939, p. 837-886.
5. H. Lange and K. Mathieu, "Concerning the Process of Transformation of Undercooled Austenite in Iron-Nickel-Carbon Alloys," *Mitteilungen, Kaiser-Wilhelm Institut für Eisenforschung,* Vol. 20, 1938, p. 125-134.
6. J. L. Ham, "The Rate of Diffusion of Molybdenum in Austenite and Ferrite," TRANSACTIONS, American Society for Metals, Vol. 35, 1945, p. 331.
7. N. H. Hall, "Effect of Nickel and Chromium on the Pearlite Point," *Stahl und Eisen,* Vol. 44, 1924, p. 256-259 (In German).
8. E. L. Reed, "Influence of Special Elements on the Carbon Content of the Iron-Carbon Eutectoid," TRANSACTIONS, American Society for Steel Treating, Vol. 20, 1932, p. 115-176.
9. H. Scott, "Critical Ranges of Some Commercial Nickel Steels," Bureau of Standards Scientific Papers, Vol. 16, 1920, p. 195-214.
10. J. R. Blanchard, R. M. Parke and A. J. Herzig, "The Effect of Molybdenum on the Isothermal Subcritical Transformation of Austenite in Low and Medium Carbon Steels," TRANSACTIONS, American Society for Metals, Vol. 29, 1941, p. 317-338.
11. C. Wells and R. F. Mehl, "The Rate of Diffusion of Carbon in Austenite in Plain Carbon, in Nickel, and in Manganese Steels," *Transactions,* American Institute of Mining and Metallurgical Engineers, Vol. 140, 1940, p. 279.
12. C. Wells and R. F. Mehl, "Rate of Diffusion of Nickel in Gamma Iron in Low Carbon and High Carbon Steels," *Transactions,* American Institute of Mining and Metallurgical Engineers, Vol. 145, 1941, p. 329.
13. J. L. Ham, R. M. Parke and A. J. Herzig, "The Effect of Molybdenum on the Rate of Diffusion of Carbon in Austenite," TRANSACTIONS, American Society for Metals, Vol. 31, 1943, p. 877.
14. G. V. Smith and R. F. Mehl, "Lattice Relationships in the Decomposition of Austenite to Pearlite, Bainite and Martensite," *Transactions,* American Institute of Mining and Metallurgical Engineers, Vol. 150, 1942, p. 211.
15. R. F. Mehl, "The Physics of Hardenability," A.S.M. Symposium on Hardenability of Alloy Steels, 1939, p. 1.
16. E. C. Bain, "On the Rates of Reaction in Solid Steel," *Transactions,* American Institute of Mining and Metallurgical Engineers, Vol. 100, 1932, p. 13.

THE TRANSFORMATION CHARACTERISTICS OF TEN SELECTED NICKEL STEELS

By J. P. Sheehan, C. A. Julien and A. R. Troiano

Abstract

Presented here is a systematic study of the effect of nickel, in quantities of 5% and more, on the transformation of austenite of several carbon contents.

No pearlite reaction was observed in any of the steels containing 7.5 and 10% nickel for transformation times as long as 4 months.

In general, the bainite reaction displayed its usual characteristics, except where masked by overlapping pearlite formation or altered by concomitant carbide precipitation.

In several of the steels, notably the 7.5% nickel and 1.2% carbon steel, separate initial carbide and subsequent ferrite precipitation was able to transform completely the austenite, as a major type of reaction and not merely as a contributory reaction to any of the generally recognized modes of transformation in steel.

THE effects of manganese, chromium, and molybdenum on the transformation of austenite have received considerably more attention than have the effects of some of the other common alloying elements in steel.

Although some research has been conducted on nickel steels, comparatively little of a systematic nature has been done on the transformation of austenite as affected by nickel. Allen, Pfeil and Griffiths (1)[1] obtained dilatometric data on several low carbon steels containing less than 5% nickel and found that the rate of transformation to both pearlite and bainite was slightly decreased. Lange and Mathieu (2) made a magnetometric study of the course of the austenite transformation in steels containing from 3 to 12% nickel.

[1]The figures appearing in parentheses pertain to the references appended to this paper.

Most of the material presented here has been abstracted from theses submitted by J. P. Sheehan and C. A. Julien in partial fulfillment for the degree of Master of Science, University of Notre Dame, December 1946.

A paper presented before the Thirtieth Annual Convention of the Society, held in Philadelphia, October 23 to 29, 1948. Of the authors, J. P. Sheehan is with the Armour Research Foundation, Chicago; C. A. Julien is with the Naval Research Laboratory, Washington, D. C., and A. R. Troiano is professor of metallurgy, University of Notre Dame, Notre Dame, Ind. Manuscript received May 4, 1948.

Unfortunately they discussed and presented data for only several of these alloys. In most of the other published work, the effect of nickel is often masked or altered by the presence of other alloying elements.

This investigation was undertaken for the purpose of making a systematic study of the effect of nickel, in quantities of 5% and more, on the transformation of austenite of several carbon contents. A series of alloys was selected in which three carbon contents were represented, i.e., 0.50, 0.80, and 1.2% carbon, with each of these containing 5, 7.5 or 10% nickel. An additional steel with 0.25% carbon and 7.5% nickel was also studied. The analyses of the steels are shown in Table I.

The steels were made in an induction furnace, rolled to 1½-inch bars and forged to ⅜-inch flats. Metallographic specimens ⅜ by ⅜ by $\frac{3}{16}$ inch and dilatometric specimens 1 by ¼ by $\frac{1}{16}$ inch were machined from the bars after they had been softened by an 80-hour anneal at 470 °C (880 °F).

Experimental Procedure

Dilatometric Method—A rough survey of the isothermal transformation curves for each steel was made by employing a dilatometer similar to the type used by Davenport and Bain (3). The dilatometer specimens were austenitized for 15 minutes at 1000 °C[2] (1830 °F) in a vertical tube furnace provided with a continuous flow of dried, purified nitrogen to minimize decarburization.

Metallographic Method—The dilatometer was relatively insensitive to the first and last 2 to 3% of the austenite to transform; so microscopic examination was employed for a more precise determination of the beginning and ending curves of the transformation. Specimens were heated for 30 minutes at 1000 °C (1830 °F) in the furnace described above, quenched into salt or lead baths controlled to ±3 °C, and after suitable periods of time quenched into water. In the polishing operation at least $\frac{1}{16}$ inch of material was ground from the face of the specimen that represented a cross section of the forged bar.

Experimental Results

Graphical Presentation—The results of this study are presented

[2]In the 1.2% carbon steels, graphitization occurred during the bar softening anneal. For this reason, a relatively high temperature was used for austenitizing the steels.

Table I
Chemical Compositions of Steels Investigated

	5% Nickel Steels			7½% Nickel Steels			
	0.50% C	0.80% C	1.2% C	0.25% C	0.50% C	0.80% C	1.2% C
Carbon	0.51	0.79	1.26	0.29	0.48	0.79	1.18
Nickel	5.26	5.25	5.30	7.61	7.61	7.53	7.64
Manganese	0.23	0.23	0.21	0.15	0.22	0.21	0.22
Phosphorus	0.006	0.007	0.009	0.010	0.006	0.008	0.008
Sulphur	0.017	0.015	0.019	0.011	0.016	0.016	0.016
Silicon	0.17	0.22	0.23	0.13	0.16	0.22	0.22

	10% Nickel Steels		
	0.50% C	0.80% C	1.2% C
Carbon	0.51	0.77	1.17
Nickel	10.11	10.01	10.30
Manganese	0.21	0.20	0.21
Phosphorus	0.005	0.006	0.009
Sulphur	0.016	0.019	0.019
Silicon	0.16	0.22	0.22

Chromium and molybdenum were 0.04 and 0.01% respectively in each steel.

in the form of typical transformation diagrams which appear in Figs. 1 to 10. The A_1, A_3, and M_s temperature for each steel were determined by the interpretation of microscopic evidence. These temperatures are represented by horizontal lines and where they occur beyond the temperature scale of the diagrams they are merely indicated.

It has already been noted that nickel promotes the formation of graphite in the high carbon steels, thereby accounting for the high austenitizing temperature necessary to redissolve the graphite. On the other hand, nickel lowers the A_1 critical by causing the gamma to alpha transformation in iron to take place at lower temperatures. The M_s temperature is also lowered to the extent of about 18 °C (32 °F) for each 1% nickel, which agrees with the value reported by Chiswik and Greninger (4).

Steels Containing 5% Nickel—The transformation of austenite to pearlite or bainite at any constant temperature between A_1 and M_s is shown on the diagrams by the typical "C" curves denoting the beginning and ending of the transformation.

In the 5% nickel steels, the transformation diagrams for which are shown in Figs. 1, 2, and 3, the austenite transforms to a mixture of pearlite and bainite at high temperatures and to bainite at lower temperatures. The most important characteristic of these nickel steels is the predominating nature of the bainite reaction. Apparently, the formation of bainite is not limited to that temperature region below the pearlitic reaction but actually occurs over almost the entire range between A_1 and M_s. At the so-called "nose"

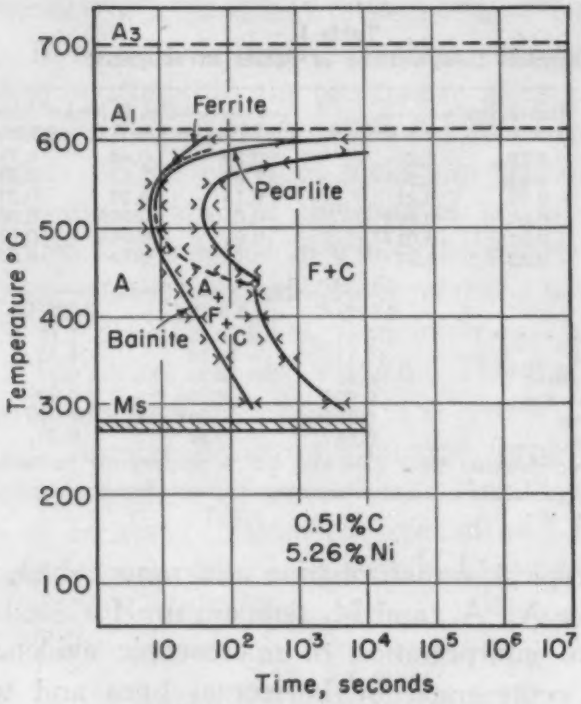


Fig. 1—Transformation Diagram for 5% Nickel Steel With 0.5% Carbon.

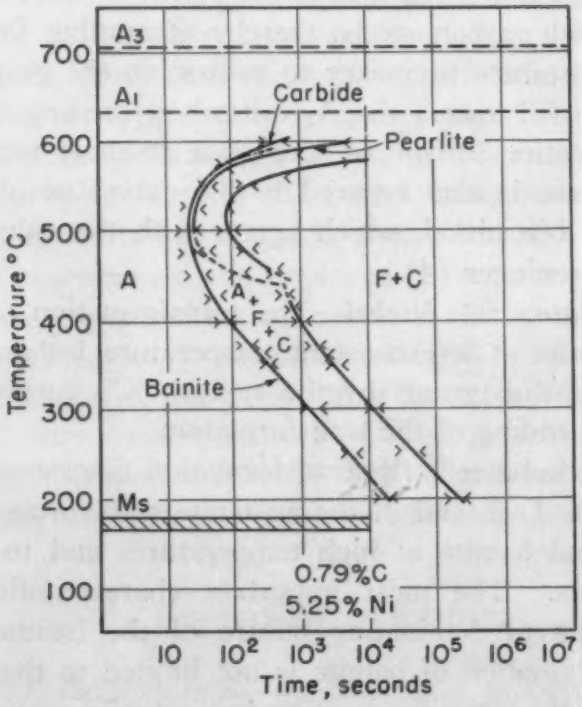


Fig. 2—Transformation Diagram for 5% Nickel Steel With 0.8% Carbon.

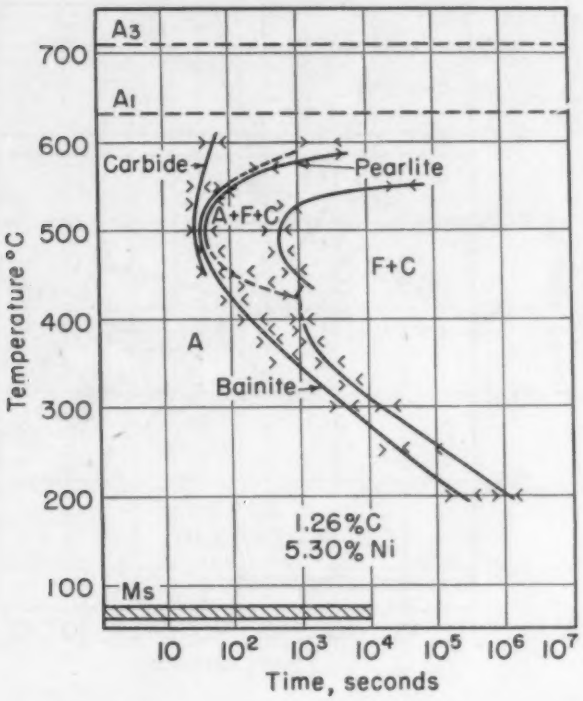


Fig. 3—Transformation Diagram for 5% Nickel Steel With 1.2% Carbon.

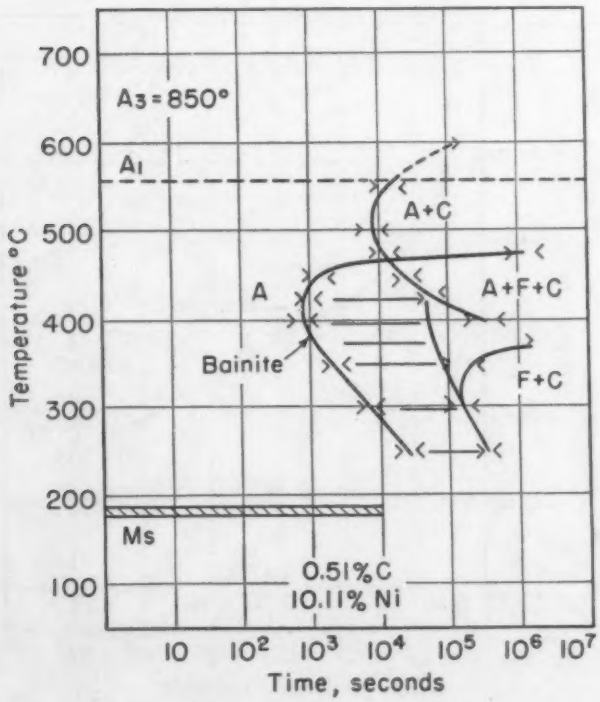


Fig. 4—Transformation Diagram for 10% Nickel Steel With 0.5% Carbon.

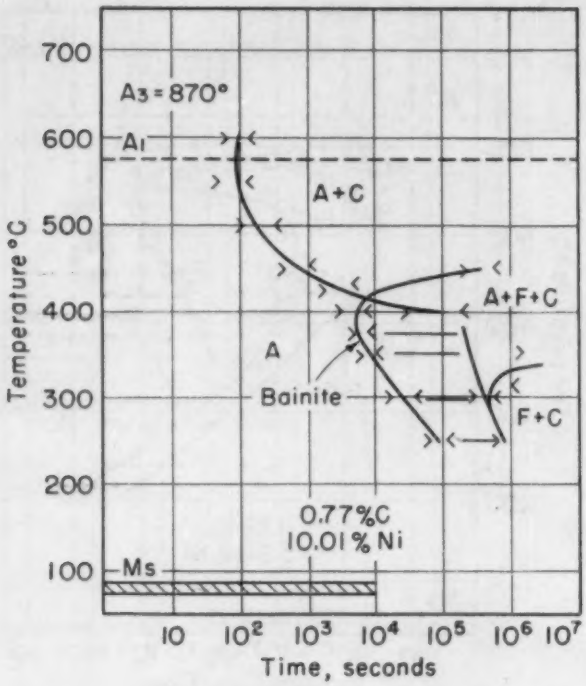


Fig. 5—Transformation Diagram for 10% Nickel Steel With 0.8% Carbon.

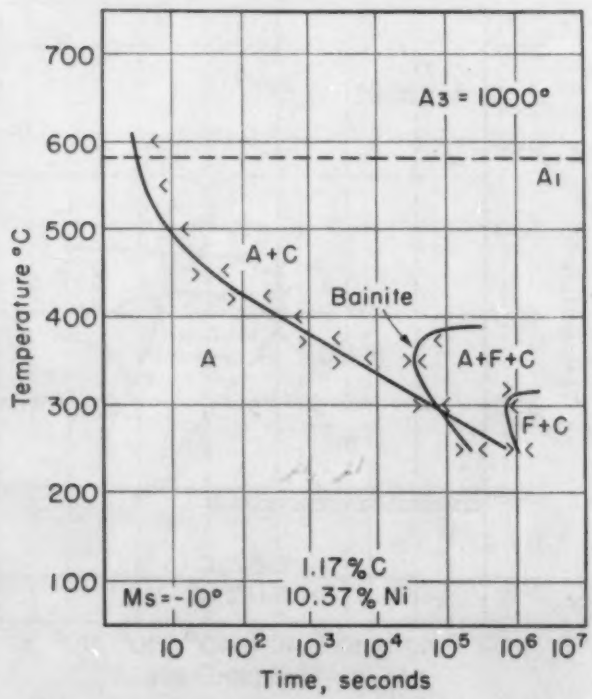


Fig. 6—Transformation Diagram for 10% Nickel Steel With 1.2% Carbon.

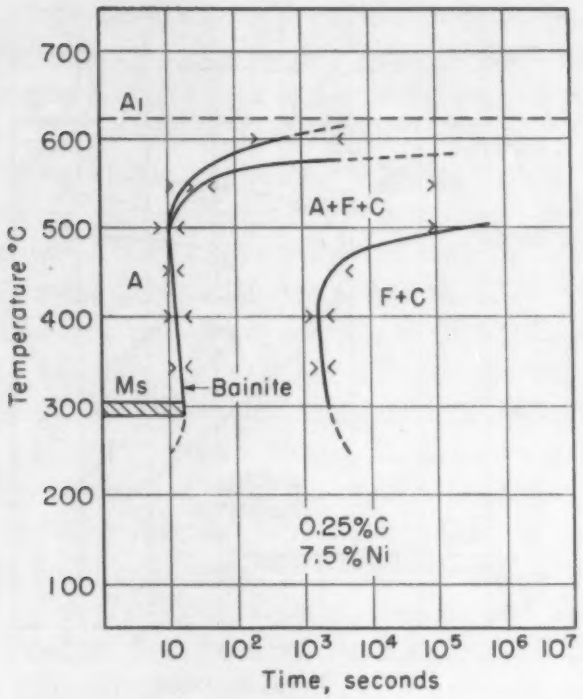


Fig. 7—Transformation Diagram for 7.5% Nickel Steel With 0.2% Carbon.

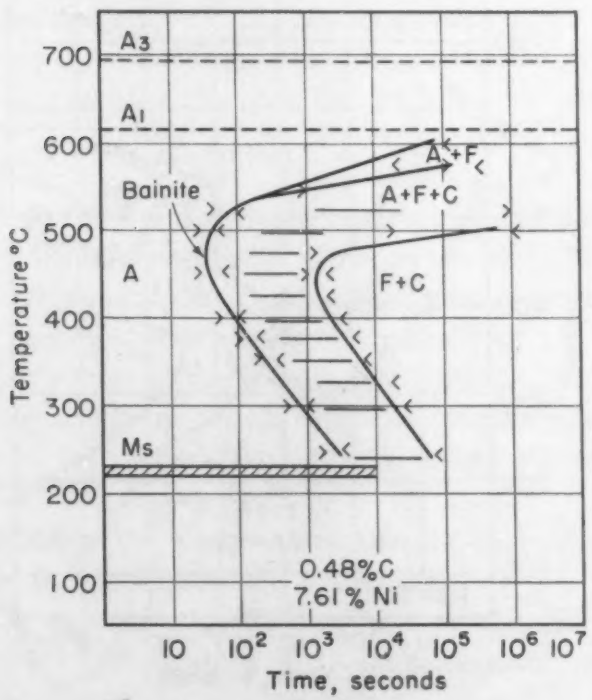


Fig. 8—Transformation Diagram for 7.5% Nickel Steel With 0.5% Carbon.

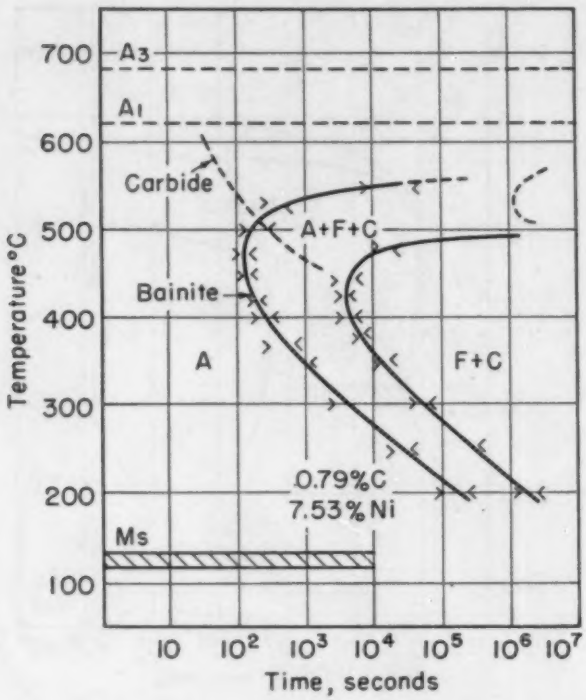


Fig. 9—Transformation Diagram for 7.5% Nickel Steel With 0.8% Carbon.

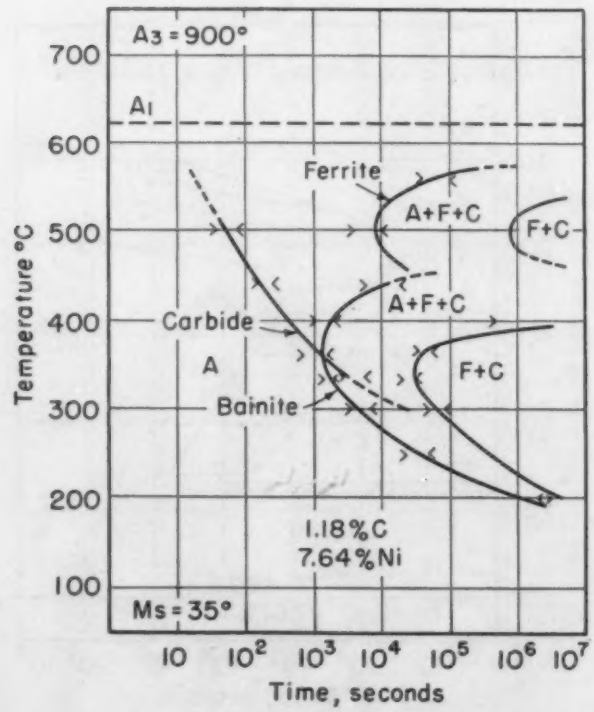


Fig. 10—Transformation Diagram for 7.5% Nickel Steel With 1.2% Carbon.

of the curve, bainite and pearlite form simultaneously, but because of the incomplete nature of the bainite reaction at high temperatures the pearlite reaction finishes the transformation and accounts for the major part of the austenite transformed (5). The proportion of pearlite to bainite in the completely transformed structure changes with temperature. Thus, pearlite predominates at and above the "nose" of the curve but is gradually replaced by bainite below this temperature. In the 5% nickel steels, 437 °C (820 °F) is the lowest temperature at which pearlite appears and the transformation occurs by the bainite reaction alone below this temperature. The curve denoting the beginning of transformation is continuous all the way from 600 °C (1110 °F) down to the M_s temperature. The ending curve, however, shows a distinct discontinuity at the maximum temperature of exclusive bainite formation. This is considered to be significant and will be discussed in greater detail. Photomicrographs illustrating the "duplex" structure of pearlite and bainite formed at or above the nose of the curve in the 0.50 and 0.80% carbon steels are shown in Figs. 11 and 12.

With increasing carbon content the transformation to pearlite and bainite occurs at slightly lower temperatures and longer times. The M_s temperature is also lowered by carbon, thereby expanding the temperature range for isothermal transformation. The steel with 0.80% carbon is hypereutectoid and forms a carbide grain boundary network which precedes the pearlite and bainite reaction at high temperatures. At 600 °C (1110 °F), this carbide network decomposes to graphite and ferrite. The presence of graphite apparently acts as a nucleus for the direct precipitation of carbon from the austenite at the grain boundaries. This decreases the carbon content of the austenite, thus promoting the subsequent formation of ferrite. The resultant microstructure is illustrated in Fig. 13.

Steels Containing 10% Nickel—The powerful effect that nickel has in lowering the temperature range of transformation, and causing the reaction to proceed more slowly, may be best illustrated by considering the 10% nickel steels.

In these steels the pearlite reaction is completely eliminated,[3] and the austenite transforms solely to bainite and pro-bainitic phases. Because of the absence of pearlite, these steels afford an excellent opportunity for investigating the characteristics of the bainite

[3]No pearlite was observed at temperatures from A_1 to the top of the bainite range for the longest times investigated (approximately 4 months) for all three 10% nickel steels.

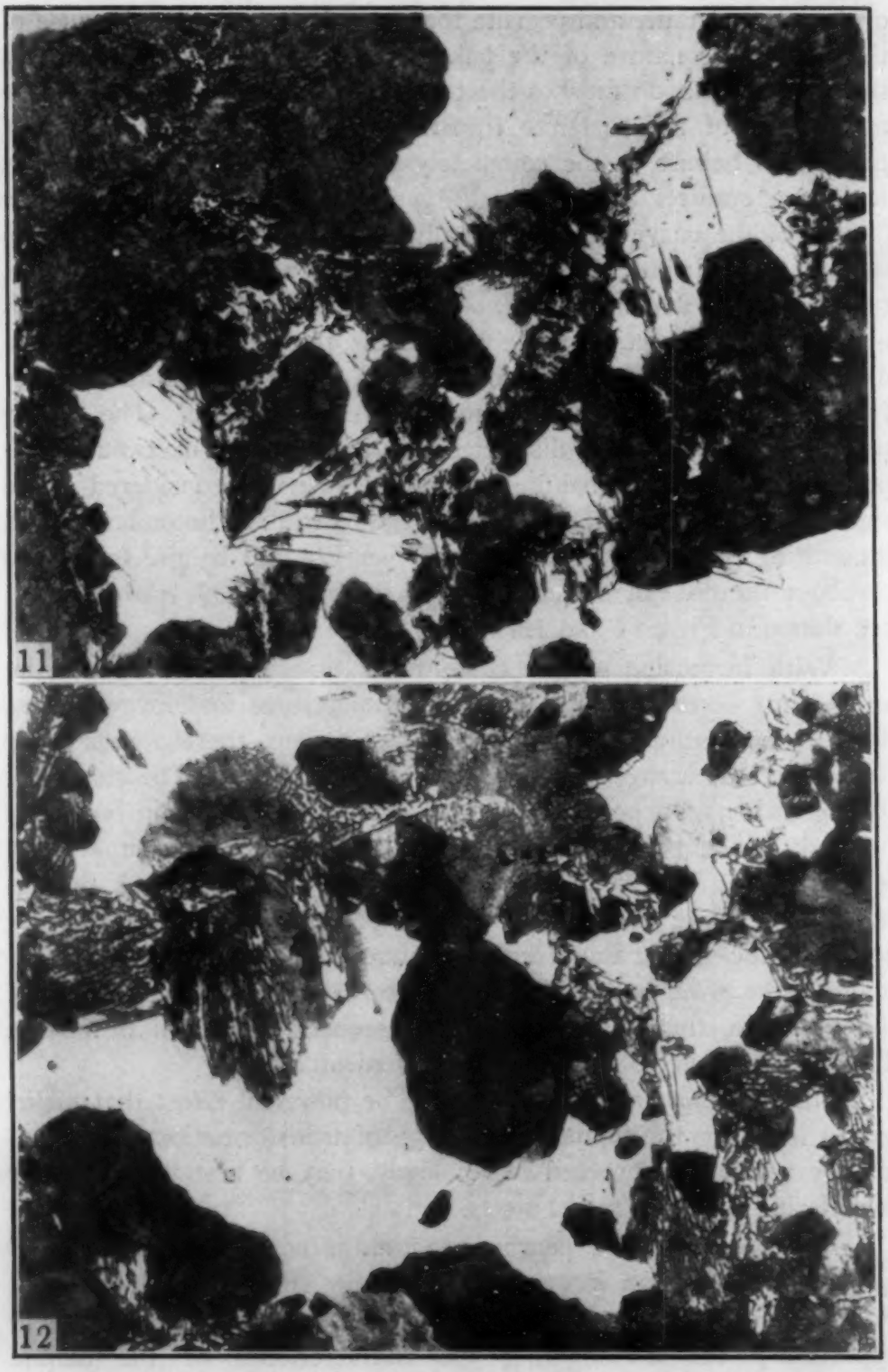


Fig. 11—5% Nickel, 0.5% Carbon Steel. Reacted at 525 °C, 18 seconds. Etched with 2% nital. × 700.

Fig. 12—5% Nickel, 0.8% Carbon Steel. Reacted at 500 °C, 60 seconds. Etched with 2% nital. × 750.

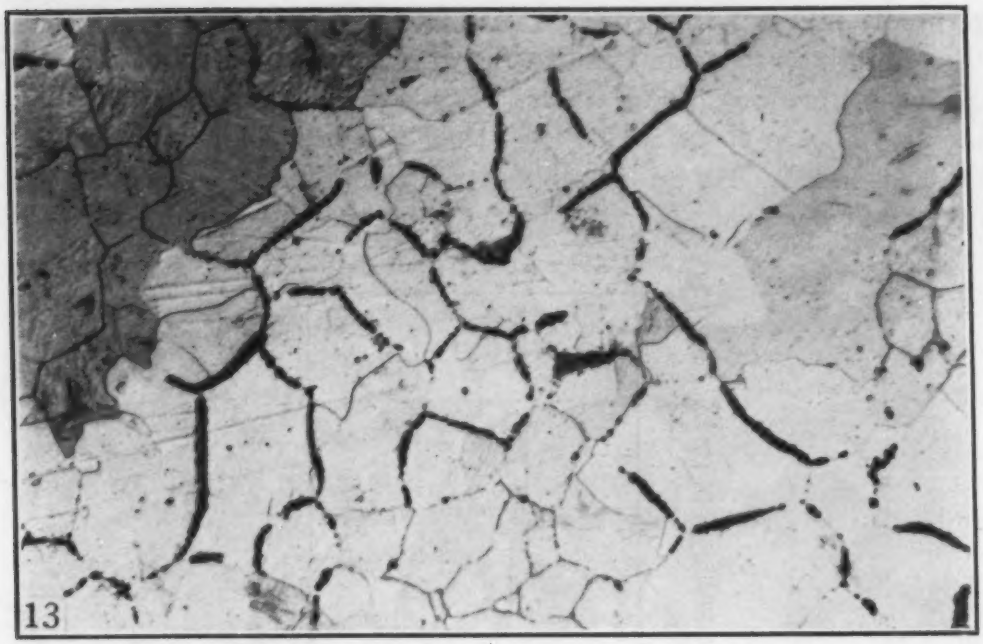


Fig. 13—5% Nickel, 0.8% Carbon Steel. Reacted at 600 °C, 3 hours. Etched with 2% nital. × 500.

reaction and the microstructure of the resultant aggregrates.

Figs. 4, 5, and 6 show the transformation diagrams for the 10% nickel steels. The usual dependence on temperature of the extent of bainite transformation is shown in Fig. 14 where the total dilation is plotted against transformation temperature for two of the steels containing 0.51 and 0.77% carbon. At higher temperatures the total dilation decreases very rapidly because the extent of the reaction also decreases with rising temperature. Photomicrographs of two specimens from the 0.51% carbon steel, transformed in this region for periods of 14 hours and 110 days respectively, are shown in Figs. 15 and 16. A comparison of the relative amounts of austenite remaining in each of these specimens yields convincing metallographic evidence for the incomplete nature of the bainite reaction.

Common to most steels, the microstructural appearance of bainite changes markedly as a function of temperature. For example, in the 0.51% carbon, 10% nickel steel at low temperatures, the bainite has a typical dark-etching, acicular appearance characteristic of low temperature bainite. The structure gradually becomes more granular and lighter etching as the temperature rises, the carbide particles become larger and more widely separated, finally giving rise to a "ferritic" structure such as that in Fig. 16. X-ray diffraction pat-

terns of specimens transformed in this range did not yield any evidence of a gross carbon enrichment of austenite.

The transformation characteristics and the microstructure found in the 0.77% carbon, 10% nickel steel are very similar to those of the above steel. As an example of the complications in microstructure that may arise, Fig. 17 indicates the presence of four types of

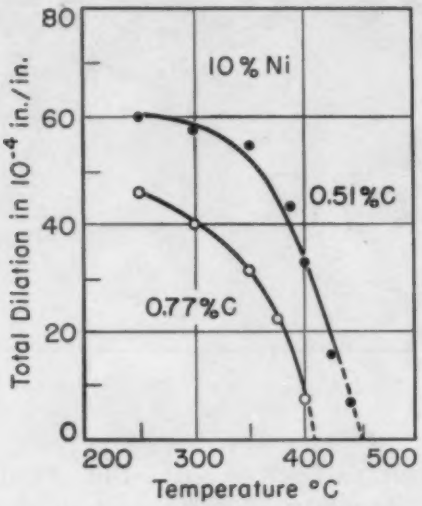


Fig. 14—10% Nickel Steel. Total dilation versus reaction temperature in the bainite temperature range.

carbide distribution near the top of the bainite range. They are: grain boundary network, plate carbide, massive carbide, and the carbide that is part of the bainite.

In the 1.2% carbon, 10% nickel steel, bainite forms only at very low temperatures and after long periods of time. However, plate carbide precipitates very quickly and in considerable quantity in this steel. Fig. 18 illustrates the structure of a specimen transformed at 350 °C (660 °F), where the carbide precipitation precedes the bainite reaction. The bainite, which is the dark, irresolvable structure, occupies the space between the carbide plates.

Steels Containing 7.5% Nickel—The 7.5% nickel steels are of particular interest regarding the presence or absence of pearlite since they represent an intermediate analysis to the 5 and 10% nickel steels.

The transformation diagrams for the four steels are presented in Figs. 7 to 10 inclusive. From an examination of these charts it is apparent that the pearlite reaction is eliminated by 7.5% nickel

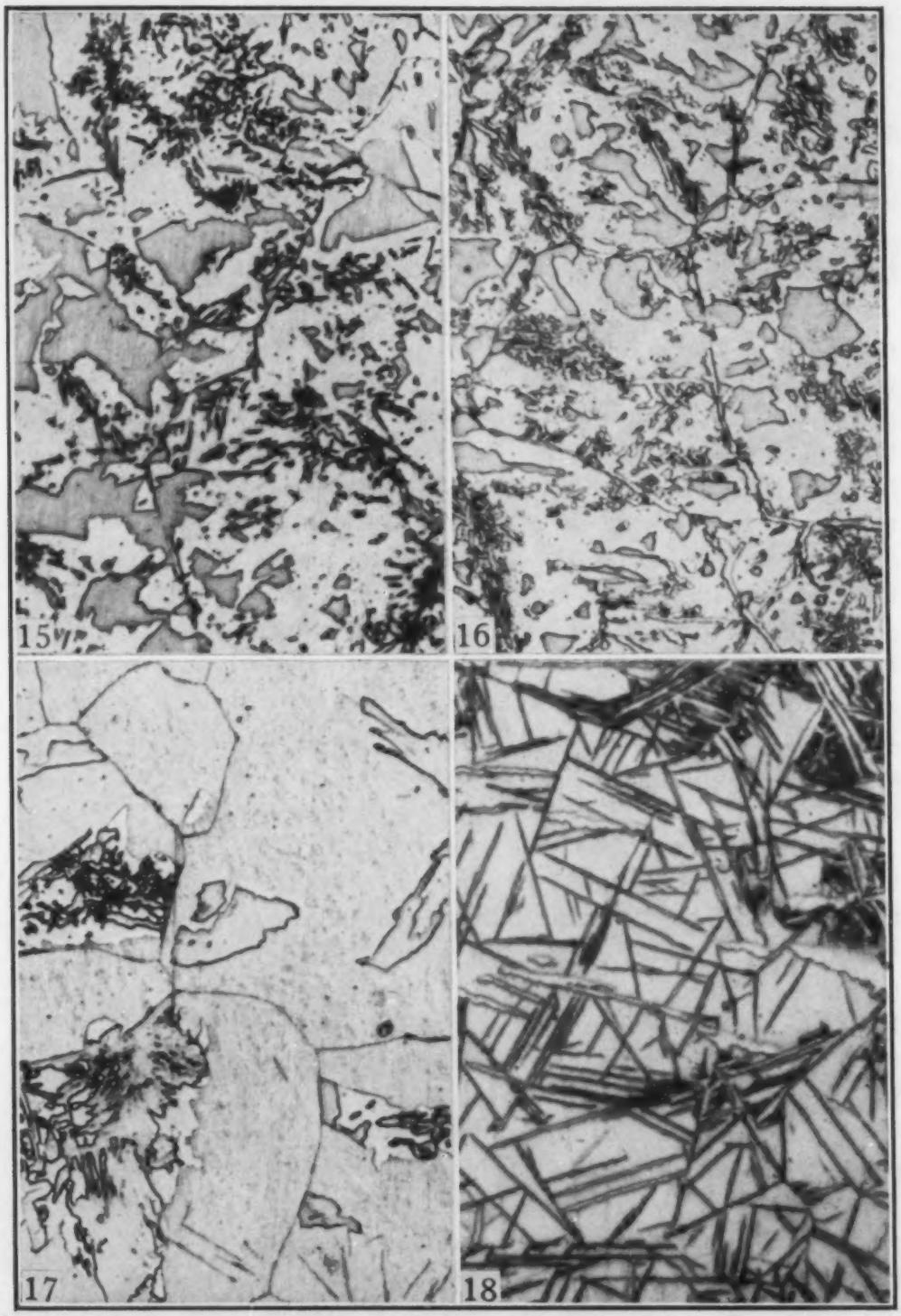


Fig. 15—10% Nickel, 0.5% Carbon Steel. Reacted at 400 °C, 14 hours. Etched with 2% nital. × 600.

Fig. 16—10% Nickel, 0.5% Carbon Steel. Reacted at 400 °C, 110 days. Etched with 2% nital. × 600.

Fig. 17—10% Nickel, 0.8% Carbon Steel. Reacted at 400 °C, 11.5 days. Etched with 2% nital. × 750.

Fig. 18—10% Nickel, 1.2% Carbon Steel. Reacted at 350 °C, 7 days. Etched with 2% nital. × 1200.

and the steels should thus be classified, in this respect, with those containing 10% nickel.

In the 0.79% carbon steel, the normal behavior of the transformation to bainite is altered by the continuous simultaneous precipitation of carbide which changes the composition of the undecomposed austenite. In the upper transformation temperature range of this steel, the decomposition of the austenite is initiated by the precipitation of carbide followed by bainite, whereupon both reactions proceed simultaneously. It follows, that the precipitation of carbide is continuously changing the composition of the remaining austenite, presumably in a manner which allows the bainite reaction to go to completion. Fig. 19 indicates the microstructure resulting from this type of transformation. Note the general heavy carbide network between grains that exhibit complete decomposition as contrasted to the relatively light carbide precipitate between grains that exhibit no decomposition. As the carbide precipitation increases between these latter grains, they will eventually transform.[4] After complete transformation of the austenite, the carbide network is remarkably uniform and heavy. Contrasted to the above is the behavior of the 0.25 and 0.48% carbon steels, where no pro-bainitic carbide is present. Here, although the microstructural characteristics of the bainite are similar, the reaction exhibits the usual normal temperature dependence.

In the upper temperature range of the 1.18% carbon steel, the transformation of the austenite is initiated by the abundant precipitation of plate carbide. This reduces the carbon content of the austenite and the transformation is completed by the precipitation of ferrite, accounting for the entire decomposition of the austenite.[4] Fig. 20 demonstrates the microstructure resulting from this reaction. It is interesting to note that the reaction is displaced, with respect to temperature, above the bainite range and thus does not appreciably influence or mask the normal behavior of bainite. This reaction product was also observed in the 5% nickel, 1.2% carbon steel at 587 °C (1090 °F). Here, it formed above the pearlite region in a very narrow temperature range and is not indicated in Fig. 3. However, in the 7.5% nickel steel the reaction played a major role in the isothermal transformation, extending over a broad temperature range. It appears that this type of transformation represents a mode

[4]It appears that this process is aided by direct precipitation of graphite.

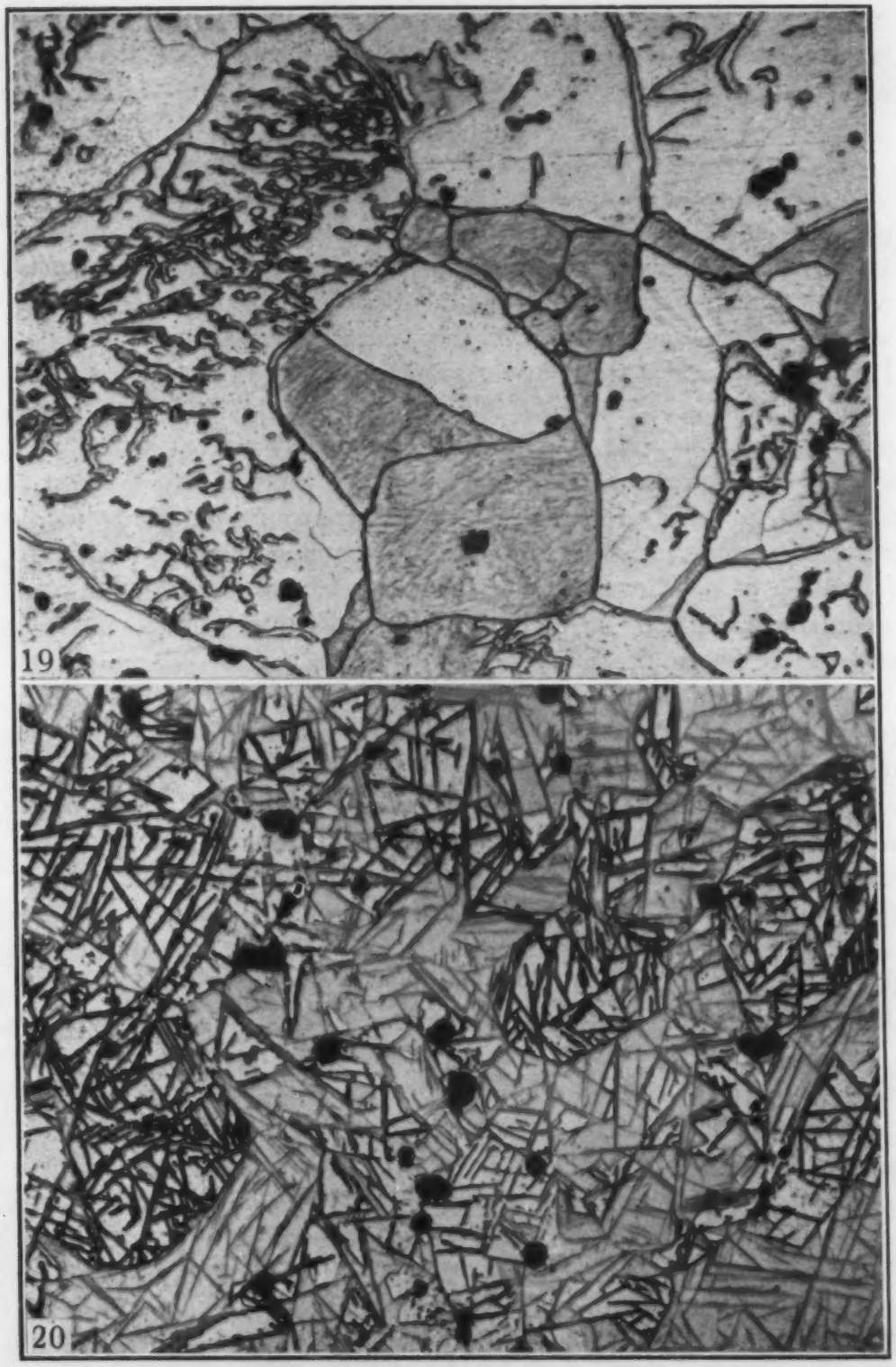


Fig. 19—7.5% Nickel, 0.8% Carbon Steel. Reacted at 525 °C, 22 hours. Etched with 2% nital. × 600.

Fig. 20—7.5% Nickel, 1.2% Carbon Steel. Reacted at 500 °C, 20 hours. Etched with 2% nital. × 600.

of austenite decomposition that does not fit into any of the accepted transformation categories such as those that produce pearlite, bainite or martensite.

Discussion

Many of the reaction sequences and resulting microstructural characteristics observed here are similar to those found in other steels, particularly in chromium (6) and manganese (7) steels; where isolated separate carbide and ferrite reactions have been observed overlapping with both the pearlite and bainite reactions. However, in several steels investigated here, notably the 7.5% nickel, 1.2% carbon steel, separate initial carbide and subsequent ferrite precipitation was able to transform completely the austenite as a major type of reaction and not merely as a contributory reaction to any of the generally recognized modes of transformation in steel. It must be emphasized that this reaction cannot be classified with the formation of pearlite since the austenite changes composition, with a drastic reduction in carbon content until eventually virtually carbon-free ferrite precipitates.

One of the notable features of these steels was the absence of pearlite in steels containing 7.5 and 10% nickel. Presumably this may occur as a consequence of the effect of nickel in lowering A_1 and thus the temperature range of pearlite formation, depressing it well down in the bainite temperature range. Here the bainite with a faster reaction rate will transform the austenite before the pearlite reaction has an opportunity to become operative. A second possibility is that additions of nickel between 5 and 7.5% abruptly increase the time for the initiation of the transformation to pearlite to longer than 4 months, the maximum time investigated.

In general, the bainite reaction behaved in normal fashion, exhibiting the usual dependence on temperature of the amount of austenite transformed by this reaction. The lower the temperature, the greater the amount of austenite transformed by this reaction, varying from zero at the top of the bainite range to 100% at some lower temperature. However, in several steels this effect was masked by the overlapping of the pearlite reaction. The only exception was the 7.5% nickel, 0.79% carbon steel. This steel did exhibit continuous and complete decomposition at all temperatures in the bainite range with no formation of pearlite. However, it was possible to rationalize this behavior on the basis of the concomitant precipitation

of carbide which continuously changed the composition of the remaining austenite as the reaction proceeded, thus actually modifying rather than masking the normal behavior of the transformation to bainite.

The masking of the incomplete nature of the bainite transformation by the overlapping of the pearlite reaction is a quite common occurrence. Occasionally it may be rather difficult to observe, since the beginning curves for both reactions may virtually coincide, presenting a relatively smooth and continuous envelope. In addition, the microstructural evidence may not always be conclusive. However, this phenomenon will invariably manifest itself by a discontinuity in the curves for the end of transformation; as observed, for example, in Figs. 1, 2, and 3 of this investigation, in many of the manganese steels (7), and, in fact, in most of the isothermal transformation diagrams scattered throughout the literature, where in most cases no effort has been made to separate these two reactions.

Acknowledgments

The steels were furnished by the International Nickel Company, and chemical analyses and forging to flat stock by the Republic Steel Corporation. The authors also wish to acknowledge the co-operation of Dr. E. G. Mahin, Head of the Department of Metallurgy, University of Notre Dame.

References

1. N. P. Allen, L. B. Pfeil and W. T. Griffiths, "The Determination of the Transformation Characteristics of Alloy Steels," Second Report of the Alloy Steels Research Committee, The Iron and Steel Institute, 1939, p. 369.
2. H. Lange and K. Mathieu, "Uber den Ablauf der Austenitumwandlung im unterkühlten Zustand bei Eisen-Nickel-Kohlenstoff-Legierungen," *Mitt., Kaiser-Wilhelm Institut für Eisenforschung,* Vol. 20, 1938, p. 125.
3. E. S. Davenport and E. C. Bain, "Transformation of Austenite at Constant Subcritical Temperatures," *Transactions,* American Institute of Mining and Metallurgical Engineers, Vol. 90, 1930, p. 117.
4. H. Chiswik and A. B. Greninger, "Influence of Nickel, Molybdenum, Cobalt, and Silicon on the Kinetics and Ar" Temperatures of the Austenite to Martensite Transformation in Steels," Transactions, American Society for Metals, Vol. 32, 1944, p. 483.
5. A. R. Troiano, Discussion to reference 7.
6. T. Lyman and A. R. Troiano, "Influence of Carbon Content Upon the Transformations in 3% Chromium Steel," Transactions, American Society for Metals, Vol. 37, 1946, p. 402.
7. A. Hultgren, "Isothermal Transformation of Austenite," Transactions, American Society for Metals, Vol. 39, 1947, p. 915.

DISCUSSION

Written Discussion: By E. S. Rowland, research metallurgical engineer, The Timken Roller Bearing Company, Steel & Tube Division, Canton, Ohio.

This is a most interesting piece of work and one could wish that more of this type could follow from the same and other laboratories.

I was much interested in the transformation of austenite directly to carbide and ferrite in the higher temperature ranges of the high nickel, high carbon steels. In what essential features does this type of reaction differ from what obtains in the commercial spheroidization of high carbon steels? In production spheroidize annealing of hypereutectoid steels, the material is heated into the austenite plus carbide range. After temperature equalization, the charge is either cooled through the transformation range at such a rate that few new carbide nuclei are formed and the transformation completes itself by precipitation largely on existing carbide particles, or the transformation is effected isothermally at a temperature where the rate of transformation is such that the same result occurs. In either case the product is spheroidized carbide without passing through the formation and decomposition of pearlite. The conditions seem to be such that the grain boundaries are not preferred as centers of nucleation and growth of pearlite.

It seems to me that the situation reported in this research differs only in that the initial carbide precipitation from the austenite is in an acicular form rather than being prior spheroidized. The average diffusion distances for carbon and alloying elements seem to be of the same order of magnitude and the austenite decomposes by carbide precipitation on the existing carbide phase.

The simultaneous presence of both bainite and pearlite has been observed in our laboratory in the gradation zone of carburized SAE 2512 when quenched in massive sections. The very logical explanation of how this is possible is certainly welcome.

Written Discussion: By L. D. Jaffe, Watertown Arsenal, Watertown, Mass.

It is a little surprising to note that, in the 5% nickel steels, increase in carbon content appears to retard the pearlite reaction somewhat (Figs. 1, 2, 3). This is contrary to previous observations on plain carbon[5, 6, 7] and chromium[8] steels. Would the authors care to comment on this point?

Written Discussion: By Axel Hultgren, professor of metallography, Tekniska Hogskolan, Valhallavagen, Stockholm, Sweden.

This investigation by Dr. Troiano and his collaborators is pioneering into an unknown field of compositions and the observations made present

[5]E. Scheil, "Initiation Time of the Austenite Transformation" (in German), *Arch. Eisenhüttenw.*, Vol. 8, 1935, p. 565-567.

[6]T. Sato, "On the Critical Points of Pure Carbon Steels" (in English), *Technical Reports*, Tohoku Imperial University, Vol. 8, 1929, p. 27-52.

[7]F. Wever, A. Rose and H. Lange, "The Influence of Cooling Velocity on the Transformations of Steels" (in German), *Mitteilungen aus dem Kaiser-Wilhelm Institut für Eisenforschung*, Vol. 19, 1937, p. 289-298; Vol. 20, 1938, p. 55-65.

[8]See authors' reference 6.

several interesting features. It may be that some of them can be interpreted differently but that will probably not surprise the authors.

It so happens that a steel with about 5% nickel and 0.5% carbon has been studied in the writer's laboratory. A higher austenitizing temperature was employed and the TTT-diagram was accordingly displaced somewhat to the right as compared with the authors' Fig. 1, otherwise it was essentially the same. The equilibrium composition of the pearlitic cementite of that steel at 575 °C has been determined. It contained 1.5% nickel. The cementite of bainite, immediately on formation at 450 and 410 °C, held, however, about 4.7% nickel, in agreement with the so-called paratransformation hypothesis (7).[9]

It is not clear what the authors mean when they say, on page 1167, that the A_1 and A_3 temperatures were determined by the interpretation of microscopic evidence. Furthermore, what is meant by A_3 in the case of hypereutectoid steels, as shown in Figs. 2, 3, 4, 5, 6, 9 and 10? An assumption that A_3 should read A_{cm} does not agree with the value of 710 °C in Fig. 3, nor with the trend of the carbide zero transformation curve in that figure.

If one compares the rates of carbide precipitation in Fig. 4 and Fig. 6 it is seen that this rate is considerably accelerated in 10% nickel steel, by increasing the carbon content from 0.5 to 1.2%. From Fig. 4 and from a comparison with Figs. 2 and 5 it may be established that nickel retards the carbide precipitation. This is consistent with the view that the low equilibrium nickel content of cementite in nickel steels, in the higher transformation range, involves diffusion of nickel away from the carbide during precipitation. Furthermore, the formation of appreciable quantities of carbide, which is demonstrated in the paper for the high carbon steels, for the same reason should cause the nickel content of the remaining austenite to rise, as its carbon content is falling. Admittedly, however, this will remain a guess, as long as the nickel content of the precipitated carbide has not been determined for these steels.

The authors emphasize that the completion of the transformation in the upper temperature range, in Figs. 9 and 10, is a consequence of the carbide precipitation, such completion not being reached at lower carbon contents, as in Figs. 7 and 8. Is it not possible that graphite precipitation may be responsible, in some manner, in the former case? In this connection it may be asked whether graphite was not precipitated during transformation of the steel with 10% nickel and 1.2% carbon (Fig. 6).

Authors' Reply

We agree with Dr. Rowland that the high temperature transformation observed in several of these steels may be much the same as that which occurs in the commercial spheroidization of high carbon steels. The fact that the carbide precipitates in plate form in these steels as compared to the spheroids of commercially treated steels may be explained on the

[9]The investigation referred to will, it is hoped, be published during 1949.

basis that commercial spheroidization of high carbon steels invariably involves the initial presence of undissolved carbides which may act as nuclei for subsequent carbide precipitation.

In answer to Dr. Jaffe, we do not feel that the nickel steels necessarily represent an exception to the general rule that increased carbon content accelerates the pearlite reaction. The rather heavy carbide precipitation preceding and accompanying the pearlite reaction in two of the three 5% nickel steels is sufficient to account for the apparent anomaly.

We are pleased to note that Professor Hultgren is extending his investigations on the partition of the alloying elements to nickel steels, and has obtained further confirmation of his original composition hypothesis which appears plausible to us. We have probably overstepped the bounds of convention in naming the upper critical temperatures A_3 rather than A_{cm}. There are many alloy steels whose value of carbon content for eutectoid composition is unknown and thus the upper critical temperature cannot be properly designated as A_{cm} or A_3 according to present conventions; however, there are many problems of greater importance and we have no desire to make an issue of nomenclature at this time. With regard to Fig. 3, we do not feel that it is possible to predict the trend of the carbide line toward the upper critical temperature on the basis of the limited amount of data presented at these high temperatures. This is particularly true since there is a general tendency for all beginning curves to show marked curvature at these high temperatures.

As mentioned in the text, the completion of the transformation at high temperatures in Figs. 9 and 10 was probably aided by the direct precipitation of graphite. A considerable quantity of graphite was also present in the 10% nickel, 1.2% carbon steel resulting from the decomposition of carbide and possibly also by direct precipitation from the austenite.

THE METALLOGRAPHY AND HEAT TREATMENT OF 8 TO 10% NICKEL STEEL

By G. R. Brophy and A. J. Miller

Abstract

This paper describes the preliminary metallographic studies from which were developed a composition range and a heat treatment for a ferritic nickel steel intended for service at —320 °F.

The studies included determinations of thermal expansion characteristics, microstructural changes during heat treatment and notch bar impact tests of low carbon steels containing from 3 to 15% nickel.

The final composition arrived at as the most economical for the purpose is: Carbon 0.12% max., manganese 0.35 to 1.00%, silicon 0.15 to 0.30%, sulphur 0.04% max., phosphorus 0.04% max., nickel 8.0 to 10.0%.

Optimum properties are developed by double normalizing followed by reheating to a temperature within the range between the true and conventional Ac_1 temperatures to convert carbides to high carbon, nickel austenite.

IT is a characteristic of ferritic steels to lose toughness as the temperature is decreased. The embrittlement occurs, usually, rather abruptly, over a more or less narrow temperature range which may be above or below room temperature depending upon such factors as composition, grain size, deoxidation, and heat treatment. These factors have been dealt with in detail in a number of previous investigations (1),[1] but in most cases the scopes of the investigations have been limited to moderately low alloy contents and to temperatures above —200 °F (—129 °C).

The results of these investigations have shown nickel to be outstanding among the commonly used alloying elements as a toughener of ferritic steels at low temperatures. It lowers the temperature range of brittle behavior and reduces the degree of brittleness in that

[1]The figures appearing in parentheses pertain to the references appended to this paper.

A paper presented before the Thirtieth Annual Convention of the Society, held in Philadelphia, October 23 to 29, 1948. The authors, G. R. Brophy and A. J. Miller, are metallurgists, Research Laboratory, The International Nickel Co., Inc., Bayonne, N. J. Manuscript received March 10, 1948.

range. But, to obtain the full effect, the steel must be properly melted and finished with sufficient aluminum to insure not only a fine grain size but a residual content (2); the carbon content should be low in nonquenched steels and heat treatments should provide structural uniformity, fine grain size, and stress relief; finally, the nickel content should be adequate for the intended service temperature.

Until recently, the requirements for low temperature service have been met with the previously developed ferritic nickel steels, but now commercial needs have been extended to —320 °F (—196 °C), a range of temperature heretofore closed to those steels because it is usually below their transition temperatures and there is likelihood of excessive loss of toughness. The effectiveness of nickel in lowering the temperature range of brittle behavior stimulated the study of the behavior at low temperature of ferritic steels with nickel contents above the usual range. This study led to the development of a steel (3), and a heat treatment for it, which adequately meets the requirements for impact values usually set by engineers for low temperature service.

The steel composition range is as follows:

% C	% Mn	% Si	% S	% P	% Ni
0.12 max	0.35/1.00	0.15/0.30	0.04 max.	0.04 max.	8.0/10.0

While an excellent combination of properties at temperatures from normal to —320 °F (—196 °C) was shown to be developed in this steel by simple normalizing treatments, its optimum properties and particularly its quality at low temperatures were reported to be developed fully only after a subsequent, unorthodox treatment which consists of reheating the preconditioned steel to within a limited temperature range between its true and conventional Ac_1 temperatures. During this treatment the carbides present in the structure after normalizing, and which are conducive to lowered toughness, are converted to an austenite which, by virtue of its high carbon and nickel contents, is stable at low temperatures.

The present paper deals with the development of this heat treatment through a metallographic study of low carbon steels containing from 3 to 15% nickel, and a detailed study of the 8 to 10% nickel range which was found (3) to be the most economical content for the development of superior mechanical properties at —320 °F (—196 °C).

Procedure

The exploratory work, initiated in the International Nickel Co.'s Research Laboratory in August 1944, was accomplished on small high frequency furnace melts of steel thoroughly deoxidized with aluminum. The steels were forged to bars of 5/8 to 1-inch sections.

A dilatometric study was conducted on the steel compositions listed in Table I. This comprised a determination of the conventional critical temperature on heating and the transformation temperatures on cooling and formed the basis for heat treatments. For this study specimens 1/4-inch diameter and 4 inches long were used. These were heated in the dilatometer at a rate of 250 °F per hour to a temperature above the Ac_3 temperature for each steel and were cooled at a rate of 75 °F per minute to simulate the cooling rate of moderate steel sections during normalizing. The cooling was accomplished by removing the dilatometer and specimen from the furnace and cooling in an uninsulated sheet metal container. Other dilatometer experiments were conducted at elevated temperatures at the same rates of heating and cooling, and at subzero temperatures by immersing the specimen and dilatometer in refrigerated baths or in liquid nitrogen.

For all dilatometric measurements, the specimens were given a preliminary normalizing at 1650 °F (900 °C) for a degree of homogenization. This was followed by austenitizing at about 100 °F above the respective Ac_3 temperatures for grain refinement and, then, furnace cooling.

Table I
Compositions of Steels

Steel	Composition				
	C	Mn	Si		Ni
16768	0.11	0.48	0.24		3.04
15996	0.09	0.36	0.13		3.77
16769	0.12	0.48	0.22		4.92
15997	0.09	0.37	0.13		5.00
16770	0.10	0.46	0.21		6.68
16127	0.08	0.50	0.17		7.01
16370	0.10	0.48	0.19		7.42
16371	0.09	0.35	0.13		7.93
16128	0.09	0.49	0.15		8.5
L65*	0.10	0.75	....	0.16 Cu	8.6
16129	0.10	0.38	0.12		10.05
16658	0.10	0.50	0.20		11.00
16373	0.08	0.44	0.17		12.92
16671	0.10	0.50	0.20		15.00

*Commercial steel.

Some mechanical property tests were made, consisting primarily of hardness measurements and standard keyhole notch bar impact tests at normal temperatures and at —320 °F (—196 °C). The limiting temperatures were used since the interest was greatest in the embrittlement resulting from that temperature change. The temperature for tests at —320 °F (—196 °C) was obtained by immersing the specimens directly in liquid nitrogen.

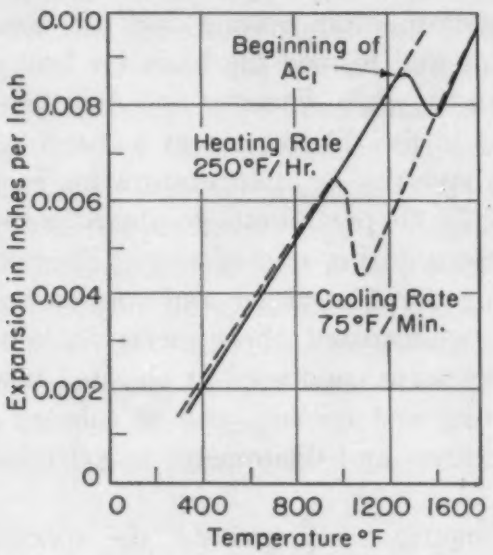


Fig. 1—Dilation Curve of 5% Nickel Steel.

Results

Influence of Nickel on Heating Transformation Temperatures

The fully annealed steels of Table I were subjected to dilation tests and the heating curves constructed. The curves for the 5, 8½, and 15% nickel steels, only, are shown in Figs. 1, 2 and 3, but these will serve to illustrate the whole series. In each steel, the conventional Ac_1 point is marked by the temperature at which the rate of expansion becomes zero (4) while the conventional Ac_3 temperature is marked by the end of contraction. The temperature range between is the accepted critical range in which austenite forms continuously at relatively high rates to cause contraction. Beyond the conventional Ac_3 point, full austenitic expansion is approached only after considerable temperature interval during which the last traces of ferrite are absorbed. The temperature at which full austenitic

expansion is attained, therefore, marks the true Ac_3 temperature.

Again, there is a temperature interval just below the conventional Ac_1 point for each steel during which the previously constant ferritic expansion rate decreases continuously with rising temperatures. Such a change of the ferritic expansion rate could result from one of three causes: namely, tempering of martensite, carbide precipitation, or by austenite formation in quantities too small to do

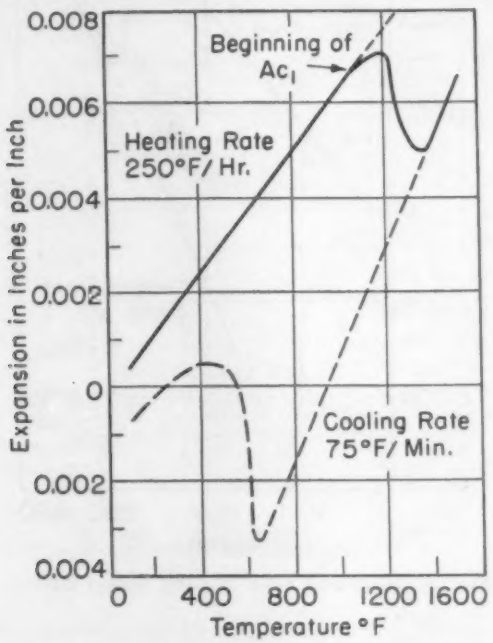


Fig. 2—Dilation Curve of 8.5% Nickel Steel.

more than modify the predominant ferritic expansion. Since the deviation occurs in annealed steels and at a temperature where the carbides would tend to dissolve, it is improbable either that martensite is tempering or that carbides are precipitating. This leaves only the formation of austenite as the probable cause of the negative deviations found.

The temperature at which this deviation is first detected, for the rate of heating used, occurs at lower temperatures as the nickel content is increased. These temperatures, together with the conventional Ac_1 and the true Ac_3 temperatures, for the several nickel contents are listed in Table II and are shown in Fig. 4 as functions of the nickel content. The modifications of the ferritic expansion rates were observed at about 50 °F below the conventional Ac_1 temperature for the nickel contents up to about 7% and at about

150 °F below for nickel contents from 8 to 15%. In these composition ranges the conventional Ac_1 temperatures and the temperatures of deviation are reduced approximately 22 °F for each per cent increase of nickel. The range between 7 and 8% nickel is critical in that the point of deviation is reduced abruptly.

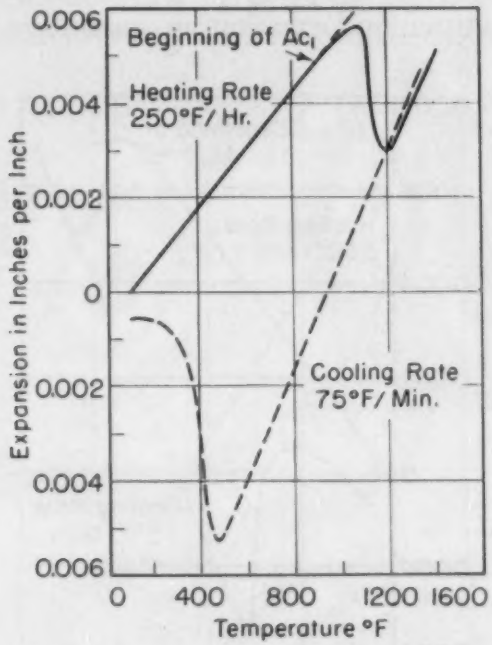


Fig. 3—Dilation Curve of 15% Nickel Steel.

The Influence of Nickel on Cooling Transformation

After fully austenitizing above the Ac_3 temperatures and cooling at the rate of 75 degrees per minute the cooling curves were constructed. Those for the 5, 8½ and 15% nickel steels are given in Figs. 1, 2 and 3 as examples. The coefficient of contraction for

Table II
Critical Temperature Data on Heating and Cooling Steels of 0.10% Carbon and 3 to 15% Nickel

Steel	Ac_1 °F True	Ac_1 °F Conventional	Ac_3 °F	Ar′ °F	Ar″ °F
3.04 Ni	1280	1320	1485	1230	
4.92 Ni	1220	1270	1410	1097	
7.01 Ni	1180	1230	1350	950	690
7.42 Ni	1160	1215	1355	970	...
7.93 Ni	1110	1210	1340	920	...
8.5 Ni	1025	1190	1350	...	650
11.0 Ni	960	1140	1270	...	580
15.0 Ni	900	1055	1200	...	480

austenite is higher than the coefficient of expansion for ferrite. For the 8½% nickel steel, these are, respectively, 11.5×10^{-6} and 6.6×10^{-6}.

The temperatures of transformation on cooling for the complete series of steel are given in Table II. They occur at a relatively high temperature for the lower nickel steels and decrease continuously with increasing nickel to about 8% where, again, an abrupt drop occurs. For the higher nickel steels, the transformation is at low

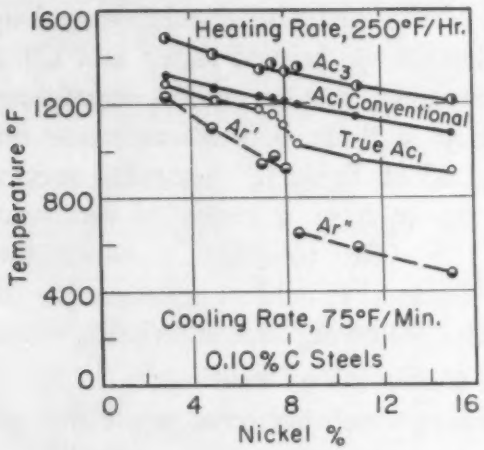


Fig. 4—The Influence of Nickel on Transformation Temperatures.

temperatures and essentially to martensite. These are summarized graphically in Fig. 4 where, it is seen, the abrupt drop in the true Ac_1 temperature at 8% nickel is associated with the abruptly increased austenite stability on cooling. Both discontinuities are importantly associated with the improved low temperature properties of the normalized, low carbon steels of 8 to 15% nickel and particularly to their further improvement and peculiar response to reheating to just above the temperature of deviation but below the conventional Ac_1 temperature.

Interpretation of the Change at the Temperature of Deviation

Zavarin (5) presented strong evidence for the formation of austenite in 3½% nickel steels at temperatures just below the conventional Ac_1 point; and Bleakney and Grosvenor (6) reported a deviation from the ferritic expansion rate in 3½% nickel steel, beginning at about 1000 °F (540 °C), which they attributed to the

beginning of a three-phase equilibrium between ferrite, carbide and austenite. These support the probability of austenite formation as the cause of the expansion deviation noted.

If austenite forms in the temperature range of expansion deviation, it should be possible to demonstrate its formation and presence with dilatometric measurements because austenite formation is accompanied by shrinkage, the amount of which is dependent upon the amount formed. Having formed, it should increase the coefficient of contraction of the steel before transformation on cooling. Also, the carbon content of the austenite should depend upon the temperature of formation within the critical range and should, therefore, influence the temperature of transformation on cooling.

A detailed study of these points was made on the commercial 8½% nickel steel, L65 of Table I. Annealed specimens were heated in the dilatometer to each of a series of temperatures within the range 985 to 1450 °F (530 to 790 °C) which includes the entire critical range (see Table II), held at temperature for two hours and then air-cooled. The following characteristics were determined:

a. the ferritic coefficient on heating;
b. the contraction which occurred while the specimen was held at constant temperature;
c. the coefficient of contraction measured before transformation, from which was calculated the amount of austenite formed at temperature, on the assumption that the increase would be proportional to the amount formed;* and
d. the temperature of transformation, if any, on cooling.

The data so obtained are given in Table III and are shown graphically in Figs. 5a to 5d.

The specimens heated to and held two hours at 985 and 1025 °F (530 and 550 °C) did not contract measurably at temperature. Therefore, it is probable that little or no austenite formed. When, however, the steel was heated to 1075 °F (580 °C) or to 1125 °F (605 °C), a small but definite contraction did occur with time, and it was found that as the heating temperature increased, the contraction increased to a sharp maximum at 1225 °F (665 °C), Fig. 5a, beyond which it was reduced rapidly by the large amount of contraction which

*the equation for calculating the austenite content is:
$6.6(1-X) + 11.5X =$ coefficient of specimen
where $X =$ amount of austenite
$6.6 \times 10^{-6} =$ coefficient of ferrite
and $11.5 \times 10^{-6} =$ coefficient of austenite

occurred previously during heating through the lower temperatures of the critical range. It is concluded that austenite begins to form in appreciable quantities, then, at some temperature between 1025 and 1075 °F (550 and 580 °C).

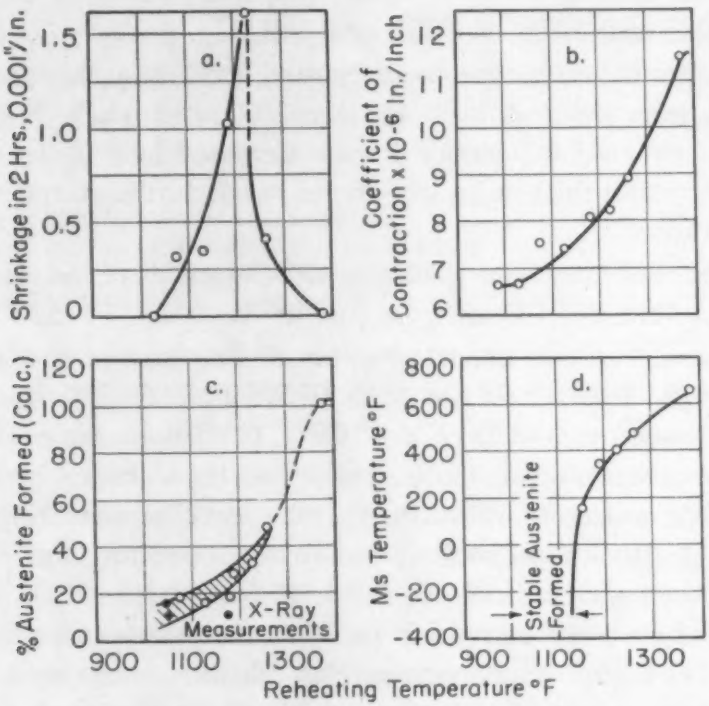


Fig. 5—Graphical Summary of Transformation Characteristics of 8.5% Nickel Steel.

The coefficients of contraction of the specimens heated at 985 °F (530 °C) and at 1025 °F (555 °C) were found to be the same as the coefficients on heating. Those for the specimens heated at 1075 and

Table III
Dilation Characteristics of Annealed 8½% Nickel Steel Reheated to 985 to 1450 °F

Heating Temp. °F	Time	Shrinkage Inch/Inch at Temp.	Martensite Expans. Temp. °F	Coeff.[3] Contraction	% Austenite Calculated
985	2 hrs.	Not observed	Not observed[2]	6.6×10^{-6}	0
1025	2 hrs.	Not observed	Not observed[2]	6.6	0
1075	2 hrs.	0.0003	Not observed[2]	7.5	18
1125	2 hrs.	0.00035	Not observed[2]	7.4	16
1150	2 hrs.	.....	150	...	..
1185	2 hrs.	0.00102	340	8.0	28
1225	2 hrs.	0.00160	400	8.2	32.5
1260	2 hrs.	0.00040[1]	475	8.9	47
1450	10 mins.	.....	650	11.5	100

[1]Full shrinkage attained in 45 minutes. All others still shrinking at 2 hours.
[2]Cooled to —390 °F.
[3]Measured before transformation on cooling.

1125 °F (580 and 610 °C) increased to 7.5 and 7.4×10^{-6} and higher heating temperatures yielded larger coefficients of contraction until the austenitic coefficient of 11.5 was attained at and above the Ac_3 temperature as shown in Table III and Fig. 5b. The changes in coefficient on cooling indicate, again, the first formation of austenite between 1025 and 1075 °F (555 and 580 °C).

The amounts of austenite calculated from the changed cooling coefficients were 18 and 16% for the 1075 and 1125 °F (580 and 610 °C) specimens but increased with increased heating temperature, at first slowly and then more rapidly, to reach 100% at and above the Ac_3 temperature.

Fig. 5c indicates the probable development of an appreciable austenite content upon heating to just above 1025 °F (555 °C).

No transformation occurred upon cooling any of the specimens heated at 985, 1025, 1075 or 1125 °F (530, 555, 580 or 610 °C), even when cooled to —320 °F (—196 °C). Taken alone, this might indicate the absence of austenite, but it has been shown by the other evidence that austenite did form at the two higher temperatures. Martensite expansion on cooling was first noticed to occur at 150 °F in the specimen air-cooled from 1150 °F (620 °C) and, as the heating temperature was increased further, the martensitic expansion commenced at higher temperatures, Fig. 5d, thus reflecting a decrease in the carbon content of the austenite through dilution with ferrite. The austenites formed at 1075 and 1125 °F (580 and 610 °C) must, therefore, be of high carbon content which, with the high nickel, stabilizes them even to —320 °F (—196 °C).

The facts presented establish the temperature of deviation as the practical beginning of the Ac_1 transformation. Austenite evidently begins to form there in small but effective quantities and increases slowly with temperature up to the conventional Ac_1 temperature where the carbides are completely converted to austenite. The amounts are so small that their formation exerts but a small modifying effect upon the dominant ferritic expansion. At the conventional Ac_1 temperature, which marks the end of the Ac_1 range, ferrite is absorbed in the austenite thus increasing the rate of formation of austenite and causing the familiar contraction upon continuous heating through the critical range. The austenite formed in the Ac_1 range has, of necessity, a high carbon content and therefore is of increased stability. The carbon content, and therefore the austenite stability, decreases with higher temperatures of austenite formation.

At and above the Ac_3, the carbon content of the austenite is that of the steel and the austenite stability then is at a minimum.

X-Ray Diffraction Measurements

In support of the interpretation of the dilatometric data, a few quantitative X-ray diffraction measurements were made[2] on specimens of 8½% nickel steel variously treated. The treatments and measurements are as follows:

Normalized 1650 to 1450 °F—no reheating	10% Austenite
Normalized 1650 to 1450 + 800 °F—reheat 1 hour	5% Austenite
Normalized 1650 to 1450 + 1050 °F—reheat 1 hour	12% Austenite
Normalized 1650 to 1450 + 1050 + 800 °F—reheat 1 hour	15% Austenite

Obviously, the austenite remaining after the 1450 °F normalizing treatment is quite unstable, for half of it was decomposed during 1 hour heating at 800 °F (425 °C) and longer heating possibly would have decomposed the balance. On the other hand, the 12% formed at 1050 °F (565 °C) is highly stable, because upon reheating at 800 °F[3] the amount was not decreased, but instead, 15% was measured. It is hardly possible that this second reheating to 800 °F has actually formed more austenite, so the two results, 12 and 15%, may be accepted as check determinations. This amount agrees, within expectance (see Fig. 5c), with the 18% austenite calculated from the coefficient of the specimen heated to the higher temperature of 1075 °F (Table III) where slightly more austenite should be formed. This agreement is excellent in view of the limit of error for quantitative measurement of each method.

Notch Impact Tests

The practical aspects of these changes in austenite composition on the notch impact resistance of 8½% nickel steel are shown in Table IV and Fig. 6.

In the normalized condition there is a content of austenite which is unstable and upon reheating up to 800 °F transforms with an attendant embrittlement which is revealed only by the more sensitive

[2]Through the courtesy of Dr. Kent R. Van Horn, manager, Research Laboratory, Aluminum Co. of America, Cleveland, Ohio.

[3]During the X-ray measurements, it was noticed that a considerable amount of stress relief had been accomplished by the final reheating to 800 °F after double normalizing and reheating to 1050 °F.

Table IV

Influence of Reheating Normalized Commercial 8½% Nickel Steel, Heat L65 (Table I)

Reheat Temp. °F	Rc	Ft. Lbs. +70 °F	Keyhole Notch −320 °F
No reheat	35	33–35	20–21
600	35	31–38	8– 7
800	29	32–34	6– 6
900	26	.....	17–20–21
950	23	.....	24–25–27
1000	23	52–49	18–36
1050	22	51–49	29–26
1100	22	51–59	30–30
1150	23	62–52	9–12
1200	33	84–33	15–13

Steels initially normalized from 1650° and then from 1450 °F.

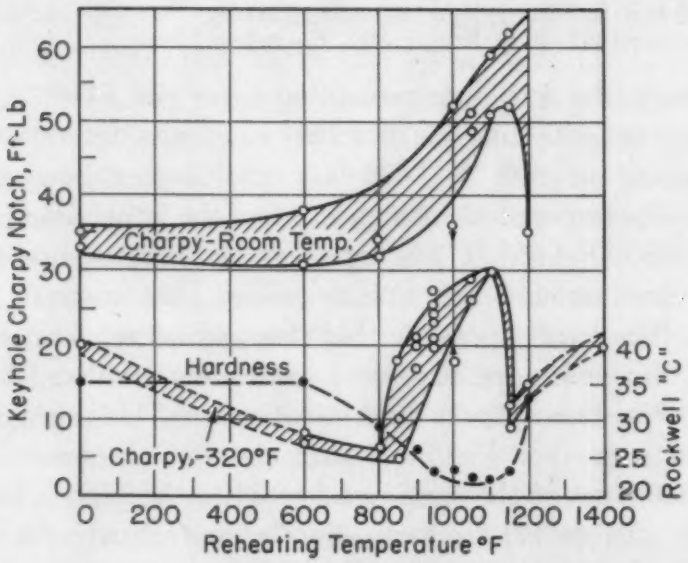


Fig. 6—The Notch Impact Resistance and Hardness of Normalized and Reheated 8.5% Nickel Steel.

low temperature tests. Upon further reheating the steel softens and the notch impact resistances at both normal temperature and at −320 °F (−196 °C) increase sharply but attain maximum values when the steel has been reheated to within the Ac_1 temperature range where the hardness is at a minimum and where stable austenite is formed. When the moderately high carbon unstable austenite forms, the impact resistances fall precipitously to low values particularly at the low testing temperatures, because of the relatively high carbon content martensite formed on cooling. As the austenite is further diluted with respect to carbon, the martensite subsequently formed becomes tougher and the impact values again rise to equal, finally, the normalized values.

Table V
Influence of Reheating Temperature on Charpy Notch Resistances, Double Normalized Steels, Room Temperature and —320 °F

Steel % Ni	Reheating Temp. °F	B.H.N. Before Test	B.H.N. After −320°	Charpy Keyhole Ft.-Lbs. R.T.	Charpy Keyhole Ft.-Lbs. −320°
3.04	1250	126	126	64½	4½
	1275	116	116	66	3
	1300*	116	116	67	3
3.77	1250*	124	124	61	3
4.92	1185	130	128	65	6
	1200	138	...	60	6
	1225*	135	136	63	8–3
	1250	150	156	66	8
6.68	1150	226	231	45	6
	1175*	168	178	58	12
	1200	187	203	44	15–9
8.5	1000	241	240	52	18–36
	1050*	235	235	50	27
	1100	235	235	55	30
10.05	975	227	227	47	34
	990*	217	217	..	44
	1035	212	...	..	40
11.00	985*	235	235	..	38
	1010	249	259	..	38
12.92	925*	273	273	44	35
	975	255	255	..	37
	1000	248	...	..	31
15.00	885	277	277	..	36
	910*	269	269	..	37
	950	248	269	43	30

*At or just above the true Ac_1 temperature from Fig. 2.
Values are averages of two tests except where disagreement occurred.

Below about 7% nickel, the austenite formed at any temperature is comparatively unstable upon cooling and, therefore, the properties of these steels do not respond to reheating to just above their true Ac_1 temperatures as does the 8½% nickel steel. At higher nickel contents, all austenites become more stable, so that the effectiveness and importance of reheating to just above the true Ac_1 is reduced. The data of Table V illustrate this and demonstrate that the steels between 8 and 10% nickel not only are most responsive to the heat treatment but develop maximum low temperature notch impact resistance.

Microstructures

A series of photomicrographs of heat treated structures of the commercial 8½% nickel steel are shown in Fig. 7. These are typical of the composition range of greatest interest.

Fig. 7a represents the normalized structure which consists substantially of martensite and ferrite with, of course, some austenite.

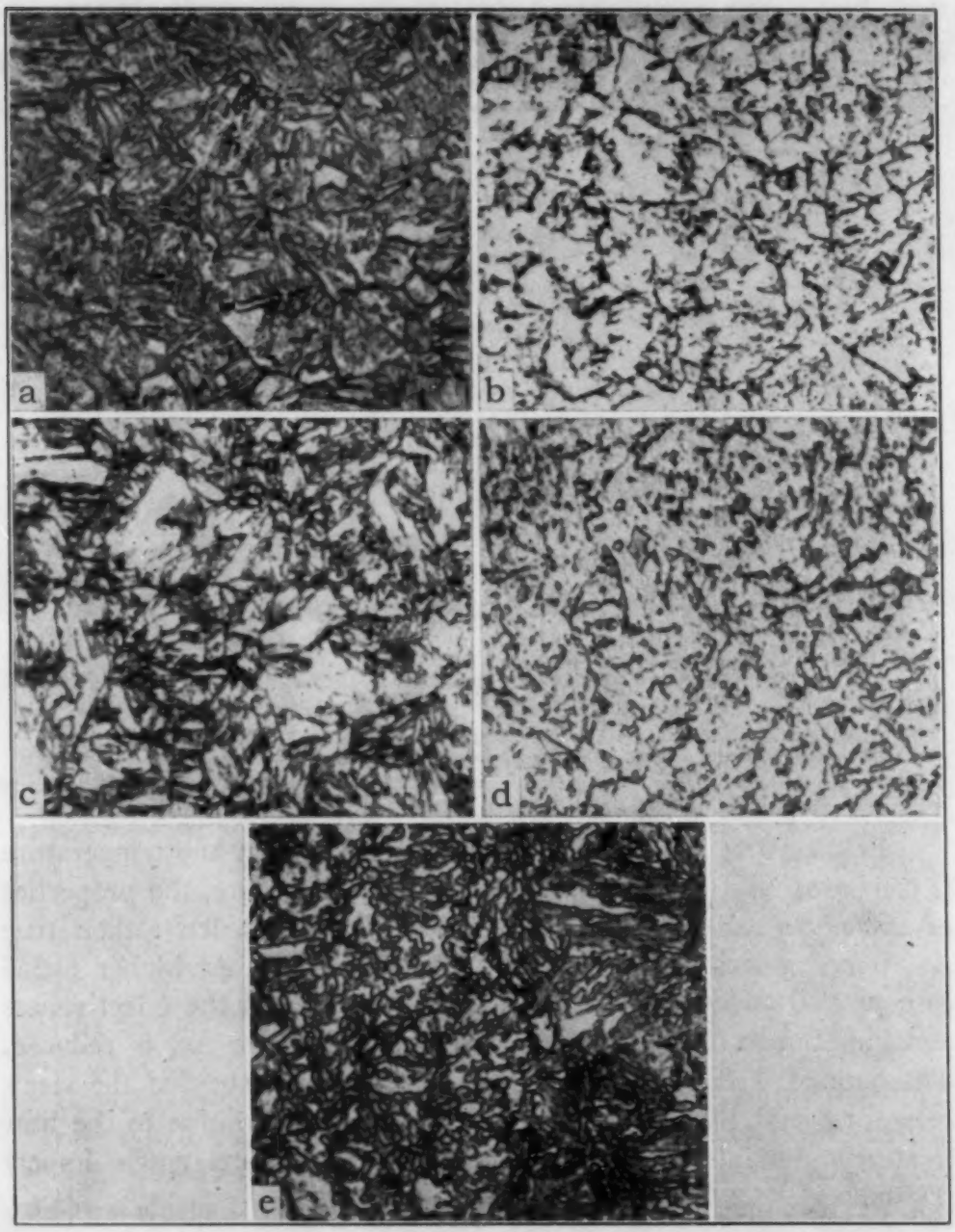


Fig. 7—Structures of 8.5% Nickel Steel (L65). × 1000. a. Normalized 1650 and 1450 °F. Structure composed substantially of martensite and ferrite. Hardness—BHN 330. Charpy at —320 °F—20 ft-lb. b. Normalized 1650 and 1450 °F. Reheated 900 °F. Structure composed substantially of ferrite and carbide. Hardness—BHN 260. Charpy at —320 °F—20 ft-lb. c. Normalized 1650 and 1450 °F. Reheated 1050 °F. Structure composed substantially of ferrite and austenite (and carbide). Hardness—BHN 235. Charpy at —320 °F—27 ft-lb. d. Normalized 1650 and 1450 °F. Reheated 1100 °F. Structure substantially ferrite and austenite. Hardness—BHN 235. Charpy at —320 °F —30 ft-lb. e. Normalized 1650 and 1450 °F. Reheated 1150 °F. Structure substantially ferrite and martensite (and austenite). Hardness—BHN 240. Charpy at —320 °F—10 ft-lb. Etchant for all photomicrographs was picral.

More rapid cooling produces larger amounts of martensite at the expense of ferrite while slower cooling induces the reverse.

The structure shown in Fig. 7b is typical of the normalized steel tempered at temperatures somewhat below the practical Ac_1. The pre-existing martensite has been broken down completely to ferrite and carbide and the structure consists essentially of these constituents. When the reheating temperature slightly exceeds the true Ac_1 temperature most of the carbides are converted to stable austenite and the resulting structure becomes that shown in Fig. 7c, which consists of ferrite, austenite, and any remaining carbides. In this condition the low temperature notch impact resistance approaches the maximum. In this steel it is only after reheating to 1100 °F that the last traces of carbide are converted to stable austenite so that the final structure consists wholly of austenitic islands in a matrix of ferrite, as shown in Fig. 7d. This is the optimum structure for maximum low temperature notch toughness.

The structure of the steel after heating at 1150 °F consists of ferrite, austenite and martensite, as shown in Fig. 7e. The appearance of martensite is due to the fact that at this reheating temperature ausenite is increased in amount over that which forms at 1100 °F (595 °C) through the absorption of ferrite. This dilution decreases the stability of the austenite and permits its partial decomposition to martensite on cooling, with resulting low temperature embrittlement. With still higher reheating temperatures this effect becomes more pronounced; the amount of martensite increases, and the structures approach those of the original normalized steel of Fig. 7a.

The higher nickel contents, to at least 15%, respond, structurally, in a similar manner upon reheating, but, of course, at temperatures which are dependent upon the nickel content, and with increased austenite stability.

Summary and Conclusions

The ferrite to austenite transformation has been shown to occur in nickel steels at temperatures well below the conventional Ac_1 temperatures. These temperatures have been termed the true Ac_1 temperatures and probably mark the practical beginning of a three-phase equilibrium between ferrite, carbide and austenite. This temperature interval is narrow for steels containing up to about 7%

Table VI
Mechanical Properties of 8½% Nickel Steel, Double Normalized and Reheated

0.10% C, 0.75% Mn, 8.63% Ni, 0.23 Si

Reheating Temp. °F	Tensile Strength Lbs./Sq. In.	Yield Point Lbs./Sq. In.	% Elong. 2 Inches	% Red. of Area	Charpy Ft.-Lbs. Keyhole Room Temp.	Charpy Ft.-Lbs. Keyhole −320°
None	168,000	108,000	17	58	31–38	17–20
600	158,000	121,000	17	60	32–38	6– 8
800	130,000	117,000	20	62	32–34	6
1050	115,000	104,000	26	65	49–51	26–29
1150	132,000	71,000	26	63	52–62	9–12
1050 redraw 800	.....	.....	..	..	73–84	31–38

nickel but widens more or less abruptly at about 8% nickel. In this critical nickel content range the stability of austenite is abruptly increased. This is true not only of the austenite formed above the Ac_3 temperatures of these steels but particularly of the austenite formed in the lower portion of the Ac_1 range of temperature which is so stable that the steels may be cooled to −320 °F (−196 °C) essentially without transformation. The stability arises from the fact that the high nickel austenite thus formed is of high carbon content.

The low temperature notch impact resistance of these steels treated to confine the carbides to solution in stable austenite is attractively improved. The improvement approaches a maximum with nickel contents between 8 and 10%, and no advantages commensurate with the added cost are obtained by exceeding this range.

The condition previous to the final treatment is of importance and for best low temperature results the steel should be fine-grained and the carbides have the maximum dispersion which results from liquid quenching from just above the Ac_3 temperature. For moderate sections, however, air cooling yields fully satisfactory results, particularly as the nickel content is increased above 8%. Even fully annealed steels are improved to a useful degree by the conversion of carbides to stable austenite but they suffer in comparison with more rapidly cooled steels because of the lack of dispersion.

The carbon content of the stable austenite formed in the final treatment can vary to a limited extent and is dependent upon the temperature of formation since a three-phase equilibrium is involved; it is quite independent of the carbon content of the steel, which primarily controls only the amount of austenite formed. It has been shown in the previous publication that the low temperature impact resistance of these steels improves with decreasing carbon and, there-

fore, with decreasing austenite, which indicates that the nickel ferrite is tougher than the stable, nickel austenite; and, in turn, the austenite is tougher than the carbide from which it forms. The importance of reheating, to form the stable austenite, therefore, is reduced as the carbon content is lowered but does not disappear even at the lowest practical carbon limit. Conversely, the importance of this treatment increases at higher carbon contents.

While, under some circumstances, higher nickel contents may be advantageous, the steels within the composition range given have attractive mechanical properties. Table VI shows representative properties of an 8½% nickel steel double normalized and variously reheated. The optimum combination of tensile and notch impact resistance is developed by reheating to 1050 to 1075 °F (565 to 580 °C), and it appears to be advantageous to reheat finally to 800 to 900 °F (425 to 485 °C) for stress relief. The preferred treatment is:

Normalize 1650 °F (900 °C)
Renormalize 1450 °F (790 °C)
Reheat 1050 to 1075 °F (565 to 580 °C) and finally
reheat to 800 to 900 °F (425 to 485 °C) for stress relief.

References

1. H. W. Gillette and F. T. McGuire, "Behavior of Ferritic Steels at Low Temperature," Part I, War Metallurgy Committee report, published by American Society for Testing Materials, December 1945.
2. T. N. Armstrong and A. P. Gagnebin, "Impact Properties of Some Low Alloy Nickel Steels at Temperatures Down to —200 °F," TRANSACTIONS, American Society for Metals, Vol. 28, 1940, p. 1-19.
3. T. N. Armstrong and G. R. Brophy, "Some Properties of 8.5% Nickel Steel," presented at the Annual Conference of Petroleum Division, American Society of Mechanical Engineers, held at Houston, Texas, Oct. 5-8, 1947.
4. Steel Standardization Group, "A Review of the Steel Standardization Group's Method for the Determination of Critical Points of Steel," METAL PROGRESS, Vol. 49, 1946, p. 1169.
5. *Transactions*, American Institute of Mining and Metallurgical Engineers, Iron and Steel Division, Vol. 135, 1939, p. 459.
6. *Transactions*, Canadian Mining and Metallurgy, 1944, p. 44, as well as discussion.

DISCUSSION

Written Discussion: B. W. F. Hodges, Works Laboratory, General Electric Co., Schenectady, N. Y.

We have read with interest the excellent paper by Messrs. Brophy and Miller.

Dilation curves, metallographic studies, and mechanical tests, includ-

ing impact tests at —300 °F, have been made in our laboratory. Results obtained agree very closely with those reported by the authors.

We concur with the authors in their conclusion that the ferrite-to-austenite transformation, in nickel steels, begins to occur well below the conventional Ac_1 temperature and that the stable austenite thus formed is responsible for the comparatively high notch-toughness at extremely low temperatures.

In view of the increasing interest in steels for applications that involve shock loading at temperatures as low as —300 °F, this paper is timely and should be welcomed by those responsible for the selection of metals for low temperature service.

Written Discussion: By O. O. Miller, Research Laboratory, United States Steel Corp., Kearny, N. J.

This is an excellent paper on a series of nickel steels which, because of their well-known extreme sluggishness, especially at higher nickel compositions, require unusually painstaking experimental work and great care in interpreting the results. We have recently been investigating a 9% nickel steel containing 0.10% carbon and, though I shall not present our results in any detail, a few remarks comparing some of them with this paper may be of interest.

Our work indicates: (a) an Ae_1 temperature range from 850 to 1115 °F (455 to 600 °C); this is a 3-phase region with ferrite, carbide, and austenite in equilibrium and (b) an Ae_3 temperature of 1300 °F (705 °C). These data indicate that at or near equilibrium, the first austenite forms about 175 °F (100 °C) below the "true" Ac_1 temperature in Fig. 4. This illustrates the extreme sluggishness of these steels, inasmuch as a slow heating rate of 250 °F (140 °C) per hour was employed by the authors in determining Ac_1 and Ac_3.

Our curve for percentage of austenite, at or near equilibrium and determined by microscopic and X-ray measurements, is to the left of the one in Fig. 5c, as would be expected. Otherwise the two curves are similar with the exception that the amount of austenite, reported in Fig. 5c as formed in a 2-hour heating period at 1050 °F (565 °C), is probably the sum of that retained in the annealed specimens used by the authors and that forming in 2 hours at 1050 °F (565 °C). We have made two observations in support of this hypothesis: (a) After a slow cool, such as 50 °F per hour, from austenitizing temperature about 10% austenite is retained to room temperature and much of this is retained on reheating at a moderate or rapid rate to 1050 °F (565 °C) and (b) there is a maximum increase of 3 to 5% austenite during 2 hours at 1050 °F (565 °C).

Though the value of 650 °F (345 °C) for the M_s temperature, in Table III and Fig. 3, is 30 °F lower than we obtained by the microscopic method, the agreement is good considering that the first traces of martensite can be detected by the microscopic method, whereas this is practically impossible by dilatometric measurements.

X-ray measurements, made by them and by us, show that austenite retained in normalized 8.5 or 9% nickel steel partly transforms on heating to 800 °F (425 °C) for a few hours; however, we do not wholeheartedly

support the authors' theory that this transformation is the cause of the observed embrittlement. Is it not possible that temper brittleness may be involved? Regardless of the cause, the material responsible for the brittleness apparently goes into solution, or is otherwise rendered ineffective, when the steel is heated into the Ae_1 temperature range; this suggests, but does not prove, that iron carbide may be involved.

There are five questions which I would like to ask the authors:

1. What were cooling rate and percentage of retained austenite of the annealed 8.5% nickel steel used for dilatometric work?
2. What was the size of the normalized specimens austenitized and air-cooled in X-ray diffraction measurements?
3. What was the length of reheating of specimens used for Table V and Fig. 7?
4. What length of reheating is suggested for the recommendations at end of Summary and Conclusions?

Authors' Reply

We wish to thank Messrs. Hodges and Miller for their kind remarks.

Mr. Hodges evidently has confirmed, in a practical manner, the important points of our paper pertaining to the heat treatment, structure and low temperature properties of a commercial 8 to 10% nickel steel. This is gratifying.

Mr. Miller's more detailed, fundamental study also has confirmed our results, at least qualitatively. The difference between our designated "true Ac_1" temperature and his is recognized but, as emphasized in the paper, the point of deviation marks the practical beginning of the Ac_1 temperature range. The term "true Ac_1" temperature probably should be withdrawn.

The cooling rate used for annealing the 8.5% nickel steel used for the dilatometric specimens was 40 °F per hour. We have not determined the amount of austenite retained in the annealed steel but this may be, as Mr. Miller states, about 10%.

Temper brittleness may be involved in the embrittlement rated in the low temperature tests of the normalized steels reheated to 800 °F. This explanation seems to fit the facts equally as well as the one given in the paper.

The X-ray diffraction specimens were taken from Charpy bars cut from normalized ⅝-inch square bars.

The data for Table V and the photomicrographs of Fig. 7 were obtained from specimens reheated for 2 hours. Reheating for at least this length of time is recommended.

A DIFFUSION METHOD FOR DETERMINING THE AUSTENITIC GRAIN SIZE OF STEEL

By Earl J. Eckel and Stan J. Paprocki

Abstract

This paper describes a method for determining the austenitic grain size in steel by diffusing bronze intergranularly into steel at the austenitizing temperature. A regular metallographic polish followed by a 4% picral etch develops a clear, high contrast microstructure which may be easily evaluated and photographed. The austenitic grain sizes obtained check well with those developed by other methods.

Introduction

THE austenitic grain size of steel has been recognized as one of the important factors determining the properties of steel. In a majority of steels austenite decomposes for the most part above room temperature and the importance of the austenitic grain size is associated with the inheritance effects exhibited by the transformation products.

Inasmuch as it is desirable to study and measure the austenitic grain size at room temperature, some indirect means is required to delineate the grain boundaries. A number of methods have been proposed and used for this purpose. Hawkes[1] has recently reviewed most of the methods in regard to their use for measuring the austenitic grain size of cast steel. For details his paper should be consulted. Suffice to say, Hawkes concluded that the martensitic etch method was the most promising.

Experience in our own laboratories supports Hawkes' results for we too have found the martensitic etch very helpful when other

[1]M. F. Hawkes, "Austenite Grain Size in Cast Steel," American Institute of Mining and Metallurgical Engineers, June 1947, T.P. 2170.

Of the authors, Earl J. Eckel is Associate Professor of Metallurgical Engineering, University of Illinois, and Stan J. Paprocki, formerly a graduate student in Metallurgical Engineering at the University of Illinois, is now associated with Battelle Memorial Institute. A portion of this investigation was submitted in partial fulfillment of the requirements for the degree of Master of Science in Metallurgical Engineering in the Graduate School of the University of Illinois. Manuscript received June 15, 1948.

methods have failed. However, anyone who has used the martensitic etch method realizes that this method often leaves much to be desired because of the lack of clarity. Usually a rather large percentage of the grain boundaries are not distinct. This is not very important if the grain size is uniform but may lead to errors if there is a mixed grain size. Frequently the grain outlines appear clearer under a microscope than in a photomicrograph.

It occurred to us during an investigation using electroplated copper for protection of steel specimens during austenitizing that the well-known intergranular diffusion characteristics of copper might be utilized for determining the austenitic grain size of steel. This investigation was made to exploit some of the possibilities of this idea.

Experimental Procedures

Tests were first made by electroplating steel specimens with copper, packing in charcoal, heating for the desired time at the austenitizing temperature, and quenching. A metallographic polish followed by a picral etch brought out a grain size which was much smaller than that obtained when other grain size measurement methods were used. It was soon evident that a considerable amount of copper diffused intergranularly before the final austenitic grain size was established and that the copper had inhibited further grain growth. By polishing to a greater depth a grain size closer to the true grain size was obtained but this procedure was limited by the depth of the copper diffusion.

It was then apparent that the method should involve two steps, one to set up the austenitic grain size, and the other to carry out the diffusion. Finding a medium in which to heat the specimens that would not lead to an inhibiting action near the surface proved to be very difficult.

A previous investigation revealed that a certain lot of SAE 2340 steel was highly susceptible to grain growth inhibition when heated in air or charcoal. This steel was used in the search for a satisfactory method of protecting the steel specimens during austenitizing. The inhibiting effect was exaggerated by double normalizing. During the first heating some growth took place before the inhibiting action became fully effective and therefore was not as pronounced as after the second heating.

Protection methods such as lead pots, and solid carbonaceous

packing mediums that may be considered satisfactory for ordinary heat treating operations proved to be inadequate.

Satisfactory protection was finally obtained by first grinding one surface of each of two small specimens with 3-grit emery paper, and soldering the surfaces with tin. Then with both specimens heated above the melting point of tin, the tinned surfaces were brought together, making a sandwich. The purpose of the sandwich was to obtain the protection associated with tin and at the same time limit the quantity of tin in contact with the steel. This is necessary because of the rapid solution of iron in tin at high temperatures. The limited amount of tin in the sandwich seemed to form a thin layer of iron-tin compounds that was relatively inactive. Heating times as long as 10 hours at 1800 °F (980 °C) brought no appreciable change in the iron-tin layer. Excessive scaling was prevented by placing the metal sandwich in a small pot and covering it with charcoal.

The effectiveness of the tin as a protective medium is illustrated by Figs. 1 and 2. Fig. 1 shows an unprotected surface and Fig. 2 the protected surfaces of the metal sandwich of the SAE 2340 steel after double normalizing with an austenitizing temperature of 1800 °F (980 °C). Both the depth and degree of the surface change are very pronounced in Fig. 1, while no appreciable surface effect is noticeable in Fig. 2.

The diffusion step as it was finally developed consisted of first placing (in the furnace that was being used to austenitize the steel specimens) a small copper plate ($\frac{3}{16}$ inch thick) which was heavily coated with tin ($\frac{1}{32}$ inch thick) on the top side. The tin was applied with a soldering iron. After 8 minutes in the furnace which was more than enough time for the copper to reach the furnace temperature, approximately ⅓ ml. of a mixture of powdered phosphor copper (15% phosphorus) and brazing flux* was poured on the tinned copper plate. The ratio of the two ingredients did not appear to be critical but we usually used about 1 part of flux to 1 of phosphor copper.

Two minutes were allowed for the flux and phosphor copper to reach furnace temperature and then the metal sandwich was taken from the charcoal and opened. This was done readily by grasping the top section of the sandwich with the tongs and pushing the bottom

*The flux used was Brazo Flux for Bronze Welding, produced by Linde Air Products Company.

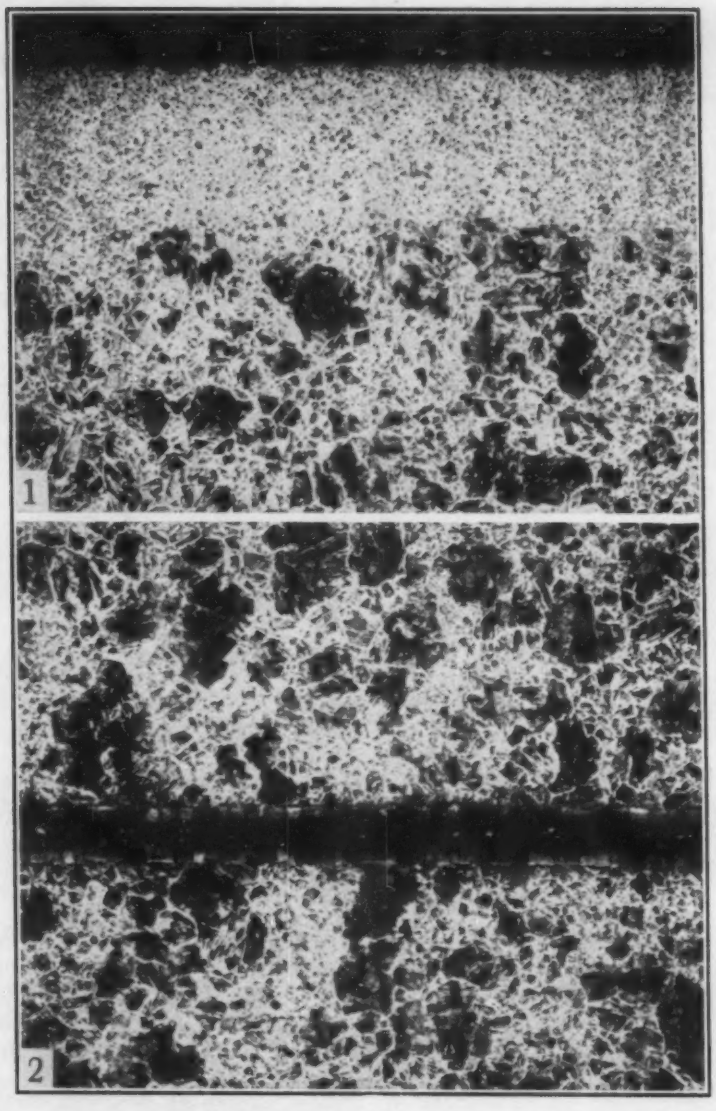


Fig. 1—Section Perpendicular to Top Surface of Metal Sandwich after Double Normalizing. Each heating was 1½ hours in a furnace operating at 1800 °F (980 °C). The metal sandwich was heated in wood charcoal packing. The area shown adjoined the top surface of the metal sandwich which was not protected with tin. 2% Nital etch. × 50.

Fig. 2—Same Section as Shown in Fig. 1 but Area Photographed Is at the Center of the Metal Sandwich at Which the Surfaces Were Protected by a Layer of Tin. 2% Nital etch. × 50.

section off by rubbing it on the furnace hearth. The top section was then placed in the puddle of bronze that had formed on the copper plate. After allowing 30 minutes for intergranular diffusion of the bronze into the steel, the specimen was quenched in water.

It might be well to mention at this time that the purpose of the addition of the flux to the tinned copper plate was to insure wetting

of the steel specimen by the bronze. The phosphor copper addition increased the depth of diffusion and lowered the melting range of the bronze so that the treatment could be carried out at a temperature as low as 1400 °F (760 °C).

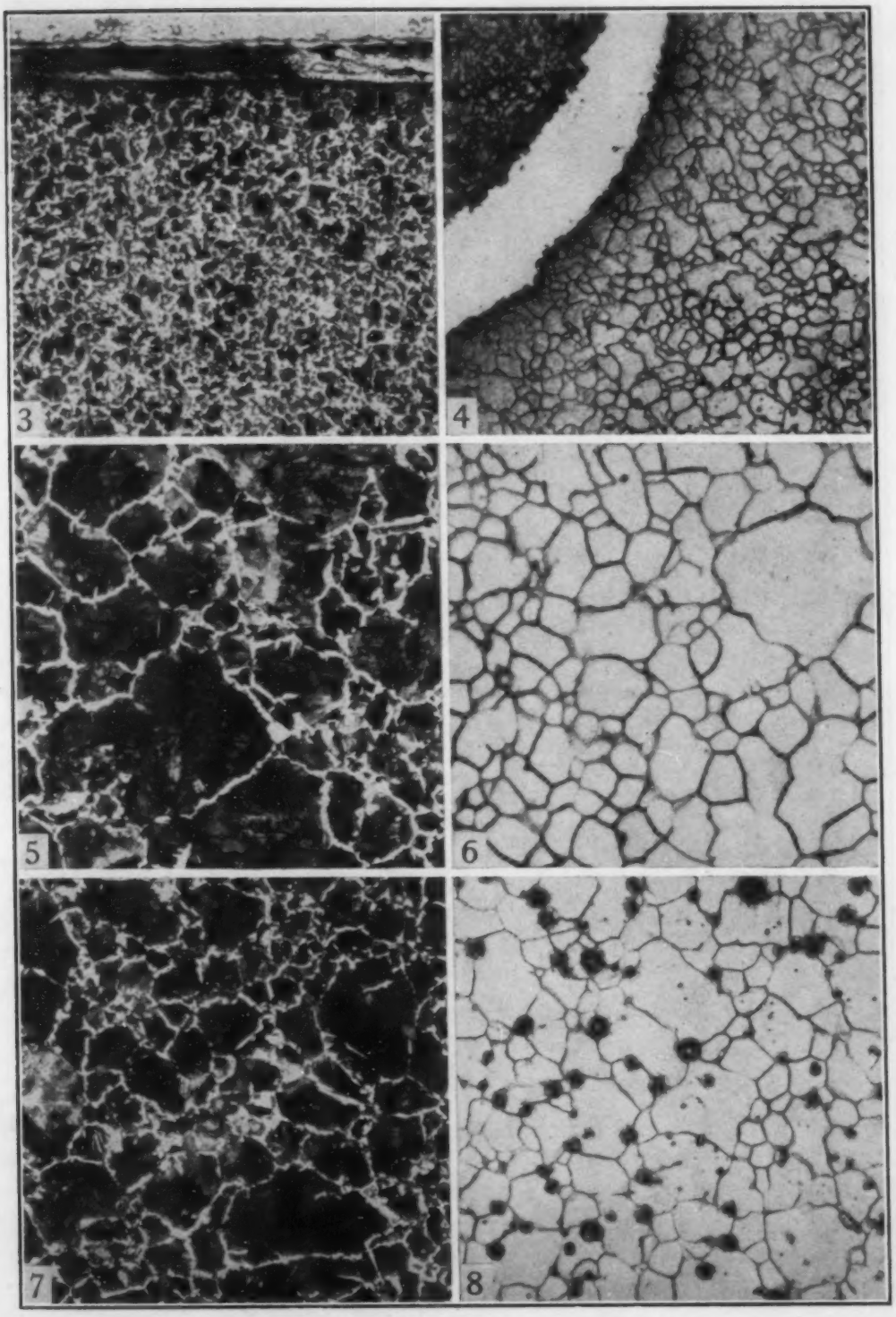
The necessity of "fishing" for the metal sandwiches after they were austenitized in charcoal was eliminated by using small pots made of 2-inch pipe caps and 1¼-inch pipe couplings. The steel sandwich was placed on a ¾-inch thick piece of steel in one cap, a coupling was placed over the metal sandwich and filled with charcoal, and then another cap was set on top of the coupling to reduce the burning rate of the charcoal. At the end of the austenitizing time the top cap and coupling were raised allowing the charcoal to fall, exposing the metal sandwich. Unless the sandwich is in view before it is grasped with the tongs there is danger that it will be inadvertently separated and an unprotected side of a specimen be placed in the molten bronze.

The bronze layer adhering to the specimen after quenching was partially removed by grinding on 3-grit emery paper. This was easily accomplished because of the variation in the depth of the bronze attack on the specimen, and the warpage of the surface as a result of thermal and transformation stresses. Thus some areas were ground to just the right depth for a study of the layer of steel penetrated by bronze.

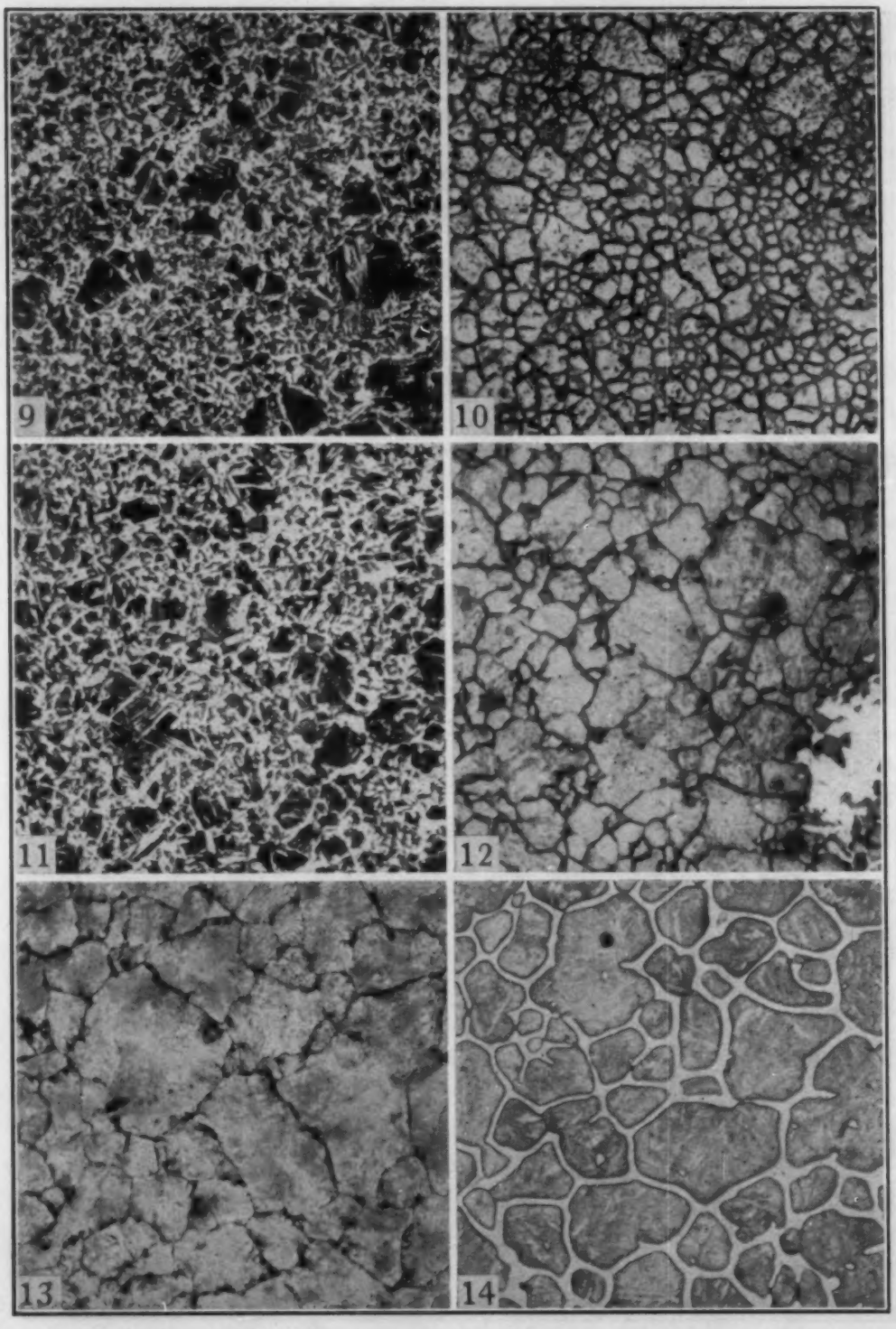
Regular metallographic polishing with a 4 to 8-minute etch by immersion in picral (4%) completed the specimen preparation. Sharply outlined grains similar to a ferritic microstructure were obtained in some areas when the austenitizing temperature ranged from 1400 to 1650 °F (760 to 898 °C). With higher temperatures the boundaries appeared somewhat thicker. The copper-tin rich areas at the prior austenitic grain boundaries were preferentially attacked by the etchant, leaving the martensite quite light.

The diffusion method was then evaluated by developing the austenitic grain sizes in a number of steels at different austenitizing temperatures and checking the results against the grain sizes as determined by other methods. Good checks were obtained in all cases.

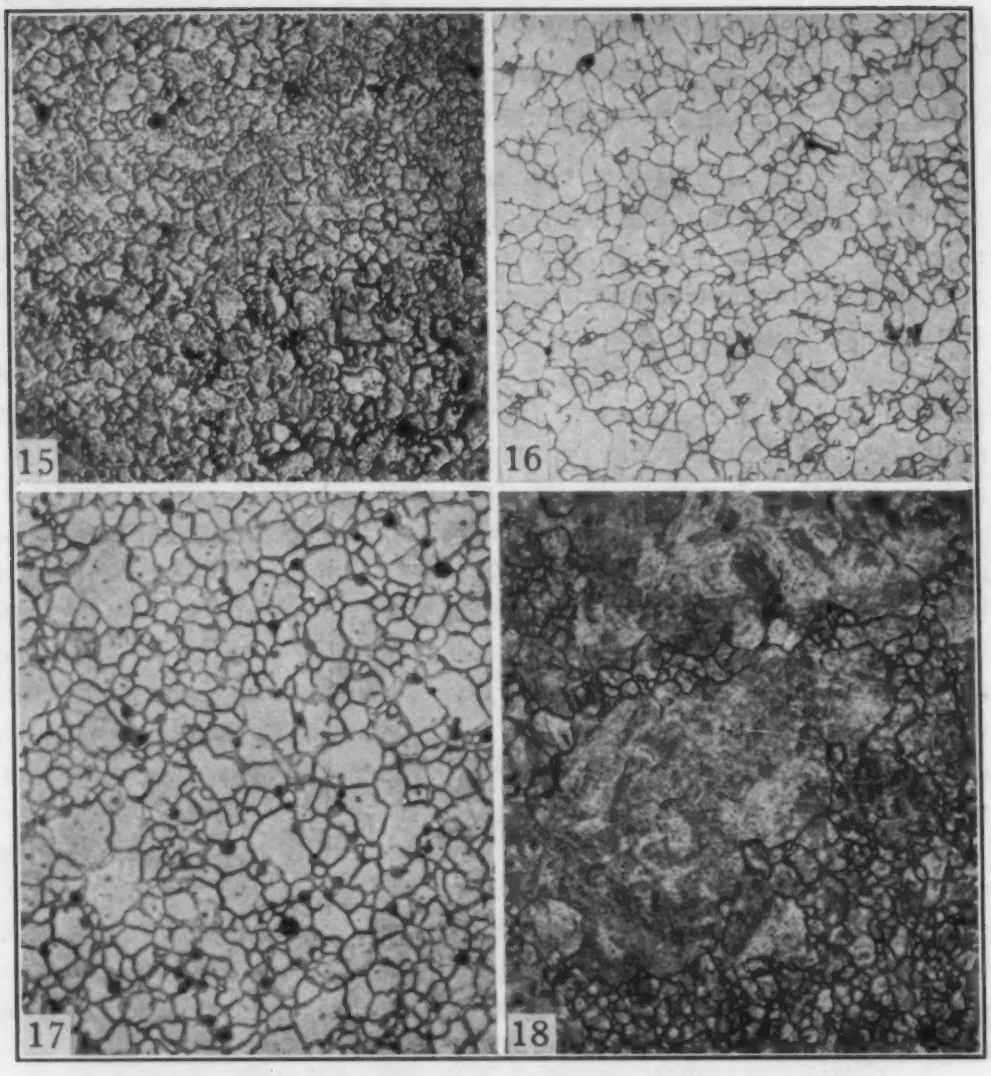
Thus far no attempt has been made to use the diffusion method below 1400 °F (760 °C) or above 1800 °F (980 °C). Several unsuccessful attempts were made to austenitize at one temperature and diffuse the bronze at a lower temperature. For reasons unknown



Figs. 3, 5, and 7—Microstructures Developed by Normalizing. 2% Nital etch. × 100.
Figs. 4, 6, and 8—Microstructures Developed by Diffusion Method. 2% Nital etch. × 100.
Figs. 3 to 6 SAE 1040 Steel. Figs. 3 and 4 Austenitized at 1500 °F. Figs. 5 and 6 Austenitized at 1650 °F.
Figs. 7 and 8 SAE 1137 Steel. Austenitized at 1550 °F.



Figs. 9, 11, and 13—Microstructures Developed by Normalizing. 2% Nital was used for Figs. 9 and 11, and Boiling Sodium Picrate was used for Fig. 13. × 100.
Figs. 10, 12, and 14—Microstructures Developed by the Diffusion Method. 2% Nital etch. × 100.
Figs. 9 to 12 SAE 2340 Steel. Figs. 9 and 10 Austenitized at 1650 °F. Figs. 11 and 12 Austenitized at 1800 °F.
Figs. 13 and 14 1.4% Carbon Steel. Austenitized at 1800 °F.



Figs. 15 to 18—Microstructures Developed by Diffusion Method.
Fig. 15 SAE 52100 Steel. Austenitized at 1550 °F. × 150.
Fig. 16 SAE 1085 Steel. Austenitized at 1400 °F. × 100.
Fig. 17 SAE 4140 Steel. Austenitized at 1550 °F. × 100.
Fig. 18 SAE 4615 Steel. Austenitized at 1800 °F. × 100.

to us the austenitic grain sizes developed tended to be erratic and smaller than when determined by other methods.

The diffusion method was further checked by allowing students in our undergraduate heat treating laboratory course to use it. This not only gave us data on additional steels but also demonstrated the difficulties that might be expected if inexperienced personnel used the method. The most common error encountered in the student work involved confusing a structure developed in the bronze layer on the specimen with that showing the austenitic grain size. Once the

correct microstructure was pointed out to the student, this gave no further trouble.

Results and Discussion of Results

Figs. 3 to 14 illustrate results of the diffusion method as compared with the grain size developed by either ferrite or cementite rejection. The white area shown in Fig. 4 is bronze that was not removed during specimen preparation. Fig. 3 shows a transverse section of a specimen that was given the regular diffusion treatment and then air-cooled while in contact with the copper plate. The purpose of this section was to show any difference in grain size that might exist at the bronze interface. The grain size appears unchanged at the surface.

Fig. 14 shows the very heavy bronze boundaries that were developed in the 1.4% carbon steel at 1800 °F (980 °C). By grinding to a greater depth finer boundaries were obtained but they became incomplete before they were reduced to widths as narrow as those shown in Fig. 8. Although other compositions tended to give somewhat finer boundaries at 1800 °F (980 °C), it was noticed that as a general rule the lower the austenitizing temperature the narrower were the grain boundaries developed.

Figs. 15 to 18 are given to show the results obtained with four other steels. The grain sizes were checked by use of the martensitic etch method but contrast obtained with this method was insufficient for satisfactory photography. Both methods appeared to give the same grain size. The rather dark martensite shown in Fig. 18 is to be expected because of the low carbon content.

Summary

A method has been presented for determining the austenitic grain size of steel by diffusing bronze intergranularly into the steel at the austenitizing temperature.

The austenitic grain sizes obtained by this method are shown to be in good agreement with those found by other methods for all the steels that have been tested.

The advantages of the diffusion method are: (a) It is simple, requiring little time or experience; (b) the procedure is essentially unaffected by the composition of the steel tested; (c) it works well over a wide range of steel compositions; (d) it gives a sharply defined microstructure that may be easily evaluated and photographed.

MECHANISM OF THE RAPID OXIDATION OF HIGH TEMPERATURE, HIGH STRENGTH ALLOYS CONTAINING MOLYBDENUM

By W. C. Leslie and M. G. Fontana

Abstract

The unusually rapid oxidation at high temperatures of 16% chromium, 25% nickel, 6% molybdenum alloy and similar alloys containing over 3% molybdenum and a considerable proportion of iron has been investigated. The structure and composition of the oxide and the microconstituents of 16-25-6 have been studied. A survey has been made of the effects of the more volatile metal oxides on the oxidation of various metals and alloys. The effects produced on the rapid oxidation of 16-25-6 by changes in the alloy composition, by stress, surface finish, coatings, and circulation of the oxidizing atmosphere have been studied. The possibility of a thermal dissociation of MoO_3 was investigated. The rapid oxidation of the alloy has been found to be due to accumulation of gaseous MoO_3 on the metal surface, and the rate of oxidation is accelerated by a thermal dissociation of MoO_3 at temperatures above about 1500 °F (815 °C). The reaction can be prevented by movement of oxidizing gases across the surfaces of the alloy. Stress, surface finish, surface coatings of other metals, and minor changes in composition of the alloy have little or no effect on the oxidation when gaseous molybdenum oxides are present. PbO, V_2O_5, WO_3, and Bi_2O_3 have been found to produce the same effects as MoO_3, when present as gases on the metal surface.

The microconstituents of 16-25-6 are composed of nitrides as well as carbides. No evidence has been found of the formation of sigma phase (FeCr) in this alloy. A surface carburization accompanies the rapid oxidation.

A paper presented before the Thirtieth Annual Convention of the Society, held in Philadelphia, October 23 to 29, 1948. Of the authors, W. C. Leslie is research fellow, The Ohio State University Research Foundation, and M. G. Fontana is professor and chairman, Department of Metallurgy, The Ohio State University, Columbus, Ohio. Manuscript received April 16, 1948.

Introduction

THE object of this investigation was the determination of the nature and cause of the deterioration at high temperatures of 16-25-6 and other similar alloys. By far the greatest portion of the work was concerned with 16-25-6. This alloy is quite widely used in applications where strength at elevated temperatures is important, particularly in aircraft turbo-superchargers and turbo-jet rotors. Under certain specific conditions the deterioration of this and similar alloys at high temperatures consists of a very unusual and distinctive type of oxidation. The compositions of some alloys susceptible to this attack are given in Table I. It may be noted that all of these alloys contain at least 6% molybdenum or at least 5% molybdenum plus tungsten. Although a thin, adherent oxide film generally forms when alloys of this type are heated in oxidizing atmospheres, in some

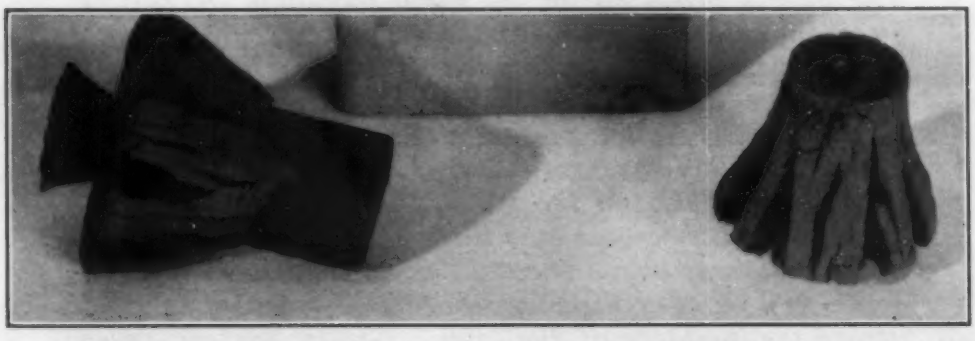


Fig. 1—Typical Effects Produced on Cylinders of 16-25-6 Alloy by Heating in Still, Oxidizing Atmospheres.

instances the oxidation becomes very rapid and large growths of oxide with a "pie-crust" structure appear. These effects are illustrated in Fig. 1. So severe is this attack that the term "catastrophic oxidation" has been applied.

This type of oxidation was observed during heat treatment, creep, and stress-rupture testing of the alloys. The growth of the oxide appeared to initiate at surfaces in contact with oxidized metal, for example, an alloy hearth plate. During heat treatment, white fumes, presumably molybdenum oxides, were observed to distill off the metal and crystallize in the cooler parts of the furnace.

The first step in the investigation was the determination of the circumstances under which the rapid oxidation occurred and the factors which might influence its development, such as temperature,

Table I
Composition of Some High Temperature Alloys Containing Molybdenum

Material	% C	% Mn	% Si	% Cr	% Ni	% Co	% Mo	% W	% Cb	% Other
*16-25-6	0.072	....	2.03	15.86	25.14	.....	7.09	....	....	N_2 0.15
*S-495	0.50	0.73	0.88	14.44	20.52	.....	4.38	3.92	2.76	.....
422-19	0.40	....	0.51	24.75	15.92	Bal.	6.08	....	....	Fe 0.65
*Refractaloy B	0.07	2.0	....	24.4	30.0	.....	8.0	....	....	.....
*N-153	0.38	1.78	0.52	16.20	14.98	12.82	3.01	2.19	1.06	.....
Refractaloy	0.11	1.97	0.25	20.3	20.1	30.2	8.3	3.8	....	Fe 15.3
69A (cast)	0.12	1.35	1.22	11.50	34.71	16.25	16.83	6.0	....	.....
Co-Cr-Ni base	0.52	0.70	0.59	22.54	19.17	Bal.	9.09	....	....	Fe 0.9
Timken "X"	0.13	1.44	0.75	16.80	28.62	30.68	10.50	....	....	N_2 0.098

*Susceptible to rapid oxidation under conditions of tests.

atmosphere, stress, and contact with metal oxides. The effects produced on the metal by the oxidation were studied. The circumstances of formation being known, a study of the possible causes of the reaction and means of prevention was understaken.

To determine the cause, it was necessary to determine if a dissociation of molybdic oxide occurs at high temperatures, since the available data on these oxides were insufficient to enable a conclusion to be drawn. A survey of the effects of other volatile oxides on metals and alloys was made.

The methods studied for preventing the rapid oxidation of 16-25-6 included atmosphere circulation, various coatings, and changes in the alloy composition. The composition and structure of the minor phase in the alloy were investigated in connection with changes in alloy composition.

Survey of Literature

The development of 16-25-6 alloy has been described by Fleischmann (1, 2).[1] The alloy was produced to meet a demand for a forgeable, machinable steel with good strength at high temperatures. Chromium is included in the composition for oxidation resistance, and a maximum of 7% molybdenum is added to increase the high temperature strength. Sufficient nickel is included to keep the alloy austenitic. Nitrogen up to 0.20% is used to stabilize the austenite and to produce some precipitation hardening. Carbon is kept below 0.12% to improve machinability and because of its tendency to remove molybdenum and chromium from the austenitic matrix. The alloy is made up of austenite grains with a minor phase occurring

[1]The figures appearing in parentheses pertain to the references appended to this paper.

in bands. The secondary phase is dissolved in the austenite at about 2150 °F (1175 °C).

A study of the available literature on the oxidation of metals has brought to light no mention of the type of attack illustrated in Fig. 1. Pfeil (3) produced what he termed "disintegrated scale" by coating iron with a wash of litharge and water. Pfeil's method for indicating the mode of scale formation by the use of a distemper of Cr_2O_3 and water painted on the metal surface was employed in this investigation.

The only available determination of the vapor pressure of MoO_3 is that of J. Feiser (5), who determined this pressure between 610 and 1155 °C (1130 and 2111 °F) through the loss in weight by vaporization. The vapor pressure was calculated by three different methods. No essential deviation was found between values obtained by two methods, but the other yielded values for the vapor pressure which were greater by a ratio of 1 : 3.744. It was concluded that this calculation was not accurate because the MoO_3 is in a molecular state which differs from those of the vapors of other oxides, i.e., it is polymerized.

Hagg and Magneli (6) conducted X-ray studies on the oxides of molybdenum and tungsten. Their materials were prepared by heating mixtures of MoO_3 and Mo in vacuum. MoO_3 was found to be stable at 1050 °C (1920 °F) for 35 hours. Beta and beta prime phases were observed near the composition $MoO_{2.90}$. From the density, the composition of beta prime is given as $Mo_{18}O_{52}$. A gamma phase was found by heating a preparation of $MoO_{2.75}$ for 17 hours at 670 °C (1240 °F) and the formula Mo_4O_{11} is suggested for this phase. The delta phase, MoO_2, is reported as being monoclinic. An epsilon phase was detected and is said to result from the decomposition of beta prime or gamma between 850 and 1000 °C (1560 and 1830 °F), but the composition is not given.

Hickman and Gulbransen (8) found that MoO_2 in contact with molybdenum is stable through the range 300 to 700 °C (575 to 1290 °F). Above 400 °C (750 °F) MoO_3 was not observed, only MoO_2 being present. No oxides intermediate between MoO_2 and MoO_3 were found.

A carburization of steel in oxidizing atmospheres has been noted by several investigators. Morrison (9) found an increase of surface carbon in 0.60, 0.70 and 0.93% carbon 18-4-1 steels after heating at 2350 °F (1290 °C) in an atmosphere containing 2.5% O_2. The

carbon content at the surface was increased up to 0.95% and the conclusion was made that oxidation or loss of surface by scaling was dependent on how rapidly the surface attained about 0.95% carbon. The same carburizing effects were noted when a 4% chromium, 2% vanadium and 9% molybdenum steel was used.

Schlegel (10) noted the same phenomenon, but reached a different conclusion. Carburization was observed in an 18-4-1 tool steel after heating at 2350 °F (1290 °C). Both the scaling and the surface carburization increased as the proportion of oxygen in the atmosphere increased. The author concluded that the oxidation is so rapid in the early stages that it does not affect the composition of the carbides, but merely attacks the parent metal. The carbides, being nearly insoluble in the scale, eventually come in contact with the austenitic parent metal and are dissolved. After a certain amount of scale has formed, the oxidizing reaction is slowed down and when this occurs the decarburization reaction becomes effective. This would explain the rapid carburization for short times, the decrease in carburization for longer oxidation periods, and finally decarburization for still longer times.

Stout and Aho (11) produced carburization of the surface of carbon tool steel in oxidizing atmospheres free from carbon compounds, and concluded that the carbon must be supplied by the steel itself. They suggested that the build-up of carbon was dependent on two reaction rates: First, the rate of carbon escape through the scale, and secondly, the scaling rate. The rate of carbon escape is limited by its low solubility and low diffusion rate in that phase. When the rate of scaling is high, the iron is removed so rapidly that most of the carbon cannot escape and is forced back into the austenite; later, when scaling has slowed, the diffusion of carbon outward overtakes the removal of iron, and decarburization results.

Hume-Rothery, Raynor and Little (12) used electrolytic dissolution of steel in HCl to concentrate carbides for X-ray examination and found a continuous series of solid solutions to exist between titanium carbide and titanium nitride. In the discussion of this article, Ransley and Rooksby stated they had found that zirconium nitride and zirconium carbide form a similar series of solid solutions.

Foley (13, 14) has written two reviews of the literature pertaining to sigma phase (FeCr). Sigma may form directly from austenite and the presence of nickel raises the temperatures at which it may be

found. The behavior of manganese resembles that of nickel. A fairly high nitrogen content may aid formation of FeCr, while silicon above 1% may have the effect of three times its weight per cent of chromium, and molybdenum may have the effect of four times its weight per cent of chromium. These factors, the total effect of which is not completely known, made it desirable to test 16-25-6 for sigma phase.

Apparatus

A commercial electric resistance heating furnace was used for many of the tests. Others, including the tests conducted in inert atmospheres and those made under stress, were made in an electric resistance tube furnace. The heating was by six ½-inch Globar elements, with a platinum-platinum 13% rhodium thermocouple used in conjunction with an indicating controller.

For the tests made under stress, standard ¼-inch tensile test specimens were used. The adapters into which the specimen was threaded were made of Inconel, since tests indicated that Inconel is relatively unaffected by MoO_3. The adapters were supported on collars of insulating brick which fitted closely to the inside diameter of the tube. This eliminated a long, unsupported span of metal and ensured that axial loading would be approximated. Loading was by means of an accurately counterbalanced lever; either a 1-to-6 or a 1-to-16 ratio could be used. The load was transmitted from the lever to the adapters by a link-belt chain, which passed over a roller bearing sheave to change direction.

The equipment used in the determination of the dissociation of MoO_3 has been described by Speiser (15). The Knudsen cell used was a hollow cylinder approximately 1 inch diameter by ¾ inch high, fabricated of 10-mil platinum. A hole approximately 0.17 centimeter diameter was drilled in the center of the top face. A circular platinum disk was suspended above the cell to intercept the vapor. The cell and sample were heated by induction in a vacuum of 10^{-5} mm. mercury, the temperature being held constant by supplying a constant energy to the work coil. The temperature of the specimen could be held constant to 0.1%. The weighings of sample, cell and disk were accurate within ± 0.00004 gram, and the dimensions of the disk and cell orifice were measured to ± 0.0005 inch.

Experimental Procedure

The Effects of Metal Oxides—To test the supposition that the rapid oxidation was initiated by metal oxides, 16-25-6 was heated in contact with C.P. metal oxides, oxidized metal surfaces, refractory porcelain, and asbestos board. The metal oxides used were Cr_2O_3, NiO, Fe_3O_4, Fe_2O_3, mill scale, MnO_2, SnO_2, Sb_2O_3, Bi_2O_3, PbO, WO_3, MoO_3 and V_2O_5. The list of metals used included 25Cr – 12Ni alloy, Armco iron, Chlorimet 2 (65% nickel, 32% molybdenum), Chlorimet 3 (60% nickel, 18% molybdenum, 18% chromium), and molybdenum. The last three named were included to test the effect of increasing the concentration of molybdenum oxides on the rapid oxidation of 16-25-6 alloy. All of the tests were conducted at 1650 °F (900 °C) in air, in an electric muffle furnace, with no circulation of atmosphere. The test temperature is not particularly significant, save that it is high enough to make the rapid oxidation possible. The 16-25-6 was surfaced with 120 emery, and placed on the powdered oxide or oxidized metal, which in turn rested on a small square of refractory porcelain. When the more volatile oxides were used, a piece of 16-25-6 was placed on porcelain close by the specimen in contact with the oxide in order to gage the effect of the oxide vapor alone. The tests were observed during heating and were removed after the spongy oxidation began or after sufficient time had elapsed to make it fairly certain that the phenomenon would not occur.

Because of the effects produced on 16-25-6 by contact with volatile metal oxides and oxide vapors, it was considered desirable to conduct a survey of the effects of those oxides on metals and alloys, particularly those used in high temperature applications. The testing methods were the same as those previously described, save that the test temperature varied. Tests with MoO_3 were made between 1500 and 1650 °F (815 and 900 °C), while those with V_2O_5 were between 1200 and 1650 °F (650 and 900 °C). Specimens were oxidized in air with no volatile oxides present, to provide a basis for comparison. Alloys similar in composition to 16-25-6 were tested by heating at 1650 °F in still air.

Metallographic Examination of Oxidized Specimens—The 16-25-6 alloy specimens which displayed the spongy oxide were sectioned, polished, etched in aqua regia in glycerol, and examined in an attempt to ascertain the method of attack and changes in the

microstructure resulting from the very rapid scaling. Chemical analysis of thin metal sections remaining after oxidation was used to supplement the metallographic examinations. These thin sections are illustrated in Fig. 2.

Location of the Oxidation Reaction—Conclusions as to the location of the oxidation reaction could be drawn from the appearance of the scale alone, but the experiments of Pfeil (3) were used to

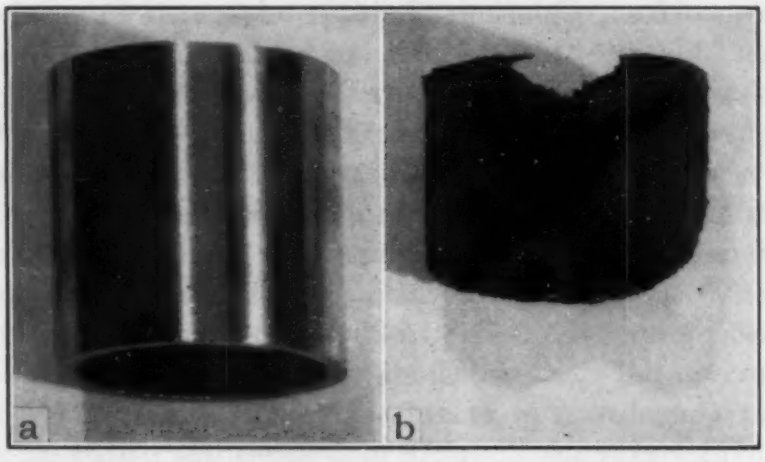


Fig. 2—16-25-6 Alloy Heated in Still Air for 100 Hours at 1650 °F. 2-inch O.D. a—Original specimen. b—Specimen after 100 hours at temperature (bulk oxide removed).

verify these conclusions. Samples of 16-25-6 were ground, painted with spots of a suspension of Cr_2O_3 in polyvinyl alcohol, then heated in air until the bulk oxide appeared. The experiment was repeated, with small bits of refractory porcelain being used in place of the Cr_2O_3 paint.

Examinations of the Oxide—The bulk oxide formed on 16-25-6 is not of the layer type, but appears to be homogeneous throughout the entire thickness. Chemical analysis, petrographic examination and X-ray diffraction were employed. Since a difference in structure between the bulk oxide and the thin oxide film formed on 16-25-6 under conditions of a moving, oxidizing atmosphere might have been significant, electron diffraction examinations were made of thin films. Four specimens were prepared. Three specimens were polished with 4-0 emery paper and oxidized in an electric resistance furnace, in a current of air, at 1650 °F (900 °C) for 2 hours, 15 minutes, and 5 minutes, respectively. The fourth specimen was given a metallographic polish and heated for 5 minutes. The struc-

ture revealed by electron diffraction was compared with that shown for the bulk oxides by the powder method of X-ray diffraction.

Heating in Inert Atmospheres—In order to discover if atmospheric nitrogen had an appreciable effect on the drastic oxidation and also to determine if the attack would proceed in the absence of atmospheric oxygen, 16-25-6 was heated in contact with MoO_3 and V_2O_5 in helium and argon at 1650 °F (900 °C). The heating was done in the tube furnace previously described. The helium used contained about 1.5% nitrogen, so a change was made to welder's grade argon, with a purity of about 99.8%. Before entering the furnace the gas was passed through drying towers containing $CaCl_2$ and P_2O_5. A positive pressure of gas was maintained in the furnace. No oxygen could be detected in the furnace atmosphere by an Orsat apparatus. A further check was made by heating a specimen of 16-25-6 in the furnace tube, without MoO_3 or V_2O_5 being present. Only very light color tints were produced on the metal after 2 hours at 1650 °F (900 °C) and furnace cooling.

X-Ray Diffraction Examinations of MoO_3—When 16-25-6 alloy is heated above about 1500 °F (815 °C), yellowish-white, tinsel-like crystals form in the cool zones of the heating furnace. While this has always been assumed to be MoO_3, it was considered best to verify the fact. MoO_3 powder of 99.6% purity was X-rayed and the diffraction pattern compared with that from the crystals collected from the furnace. The X-ray diffraction photograms were made in a Debye-Scherrer powder camera, 114.6 mm. in diameter, using Cu K_α radiation with a nickel filter.

Determination of the Thermal Dissociation of MoO_3—Molybdic oxide of 99.6% purity was evaporated in the platinum Knudsen cell previously described, at constant temperature, under vacuum, and the weight loss determined. The vapor was intercepted by the platinum disk placed directly above the orifice of the Knudsen cell. The proportion of the vapor which should strike the plate can be calculated accurately, since the cosine law of evaporation is followed. Since the accommodation coefficient of the oxide is unity, molecules which strike the plate will stick. The calculated weight gain will equal the actual weight gain if no changes take place in the vapor phase; if a dissociation of MoO_3 occurred, the actual weight gain would be less than the calculated increase. From the difference, the degree of dissociation can be calculated. Two determinations were made, one at 1728 °F (941 °C), the other at 1530 °F (831 °C),

these temperatures being chosen because they were in the range in which the bulk oxide quickly forms.

Tests of the Effects of Atmosphere Circulation—To compare the oxidation of 16-25-6 alloy in a still atmosphere with oxidation in a moving current of air, specimens of 16-25-6 were heated in a small electric muffle furnace (2.5 liters volume) at 1650 °F (900 °C). For the first test, the furnace was closed and no circulation of atmosphere was attempted. In the second test, dried air was passed through the furnace at the rate of 5 liters per minute. The inlet tube was arranged so that the air stream impinged on the roof. For the third test, the air stream was made to strike the bottom of the furnace. During the second and third tests, the temperature of the specimens was checked with an optical pyrometer and was found to vary not more than ± 15 °F from 1650 °F. The heating period in each case was 100 hours.

Surface Finish and Protective Coatings—It had been indicated (16) that degree of surface finish might be of considerable importance in inhibiting the formation of the spongy oxide; accordingly, specimens were abraded on 2-0 emery, then buffed to a high polish on a rouge wheel. Others were finished with a No. 10 mill file. A third set was abraded on 120 emery cloth, then heated in air over a Meker flame until covered with a dark blue film. The three types were placed in the tube furnace previously described, and heated at 1650 °F (900 °C) in still air.

Previous experiments on the effectiveness of surface coatings in preventing the spongy oxidation have been reported to us (17). These seemed to indicate that chromium plating, chromizing and aluminizing would keep the bulk oxide from forming. It was decided to repeat this work, increasing the severity of the tests. Nickel plating was included. These surface coatings were tested at 1550 °F (840 °C) in still air, both with and without gaseous MoO_3 being present. A specimen of each type of coating was placed on transite board and heated for 136 hours. In a test which would approximate a condition in which unprotected 16-25-6 was present, one specimen of each surface coating was placed on transite board, then a 2-inch length of 16-25-6 tubing was placed around it. It is felt that this ensured fairly equal concentrations of MoO_3 at the surface of each specimen. This test was also made at 1550 °F (840 °C) in still air for 136 hours. Both tests were repeated at 1650 °F (900 °C) for 100 hours.

Examinations of Microconstituents of 16-25-6—Before the microconstituents of an alloy can be studied, other than metallographically, they must be concentrated from the alloy. This was accomplished by the method of Hume-Rothery, Raynor and Little (12). Essentially, this is electrolytic digestion of the alloy in a reagent that selectively dissolves the matrix; this process deposits a residue rich in microconstituents on the bottom of the bath.

X-ray diffraction and chemical analysis were the methods chosen to carry out the investigation. X-ray examination reveals the structure of the compound but, in the case of metal carbides and nitrides, leaves the composition somewhat uncertain. Although chemical analysis cannot be used for the identification of a phase when other phases are present, it can show which elements are concentrated in the microconstituents.

In order to discover if a difference exists between the microconstituents of the solution-quenched alloy and the tempered alloy, concentrates were made from 16-25-6 solution-quenched from 2200 °F (1200 °C) and from specimens which had been solution-quenched and tempered 16 hours at 1600 °F (870 °C). The alloy was digested in 10% HCl, with a current density of about 0.15 ampere per square inch. A carbon cathode was used, surrounded by a porous thimble to prevent contamination of the residue from the 16-25-6 anode. The residues were washed by centrifuging, since they very rapidly clogged filter paper. Washing could not be prolonged because a part of the fines could not be depressed in the centrifuge after each washing and rapid losses occurred.

The X-ray diffraction photograms were taken in a 57.3-mm. Debye-Scherrer camera using filtered chromium radiation.

In an attempt to produce sigma phase in 16-25-6, specimens were heated for 1000 hours at 1550 °F (840 °C). They were examined metallographically by the method outlined by Emmanuel (18). Filings from these specimens were X-rayed, using filtered chromium radiation.

Modifications of 16-25-6—To test the effects on the oxidation of an increased chromium content and a decreased nitrogen content, two trial heats were melted in a 50-pound induction furnace and forged into 1-inch square bars. No difficulty was encountered in preparing the high chromium heat, but the minimum nitrogen which can be obtained in this type of analysis has been found to be 0.085 to 0.095%, with normal melting practice. Compositions of these two

heats are given in Table IV. These heats were made for the authors by the Timken Roller Bearing Company.

Since the low nitrogen heat still contained 0.096% nitrogen, any conclusions drawn from the behavior of this alloy could not be conclusive with regard to the effect of nitrogen; therefore, about 150 grams of this special heat was melted under a vacuum of about 15 microns of mercury. No analysis for nitrogen was made on the resulting ingot, but from other experience it can be stated that a considerable reduction in nitrogen was effected.

Samples from the two special heats were included in most of the tests made on the normal alloy. In addition, standard 0.505-inch tensile specimens were machined from the experimental heats and the tensile properties determined at room temperature.

Results and Discussion

Effects of Metal Oxides—The spongy oxide of 16-25-6 has been formed with the alloy in contact with asbestos board, tile, Fe_2O_3, Fe_3O_4, Armco iron, Chlorimet 2, molybdenum, MoO_3, WO_3, PbO, Bi_2O_3 and V_2O_5; also the rapid oxidation has begun on the surface of the alloy at points removed from contact with other materials. Clearly, contact with any kind of solid surface is not necessary for the initiation of the very rapid oxidation, although contact surfaces or the properties of the other material may have an accelerating effect.

Of the low-melting metal oxides tested, vanadium pentoxide—melting point 690 °C (1275 °F)—was found to cause the most spectacular increases in the rate of oxidation. The bulk oxide formed in this case at temperatures as low as 1200 °F (650 °C). At 1650 °F (900 °C), 24 hours was sufficient for a sample of 16-25-6, weighing about 50 grams, to be completely converted to the oxide.

Tungstic oxide (WO_3), bismuth trioxide (Bi_2O_3), and litharge (PbO) had similar, although less drastic, effects. These results correspond to that of Pfeil (3), but considering the high vapor pressure of PbO, it is hardly likely that lead would accumulate in the scale, slowing down the diffusion of the iron as he concluded. Pfeil stated that the reaction was very rapid at first, then proceeded according to the parabolic rate law. The quantity of PbO present, however, was very small, and it is thought that if the amount of litharge had been greater, the reaction would have proceeded accord-

ing to a linear rate law until the iron was completely consumed.

Heating 16-25-6 alloy in contact with molybdenum metal, in air, at 1650 °F (900 °C) produced a striking result. The molybdenum began to give off fumes almost immediately and in 1.5 hours had produced a swelling about ⅛ inch high on a ⅛-inch thick piece of alloy. The molybdenum, weighing 4.5 grams originally, was about two-thirds converted to the oxide. The swelling shattered forcibly during cooling, leaving a depression in the 16-25-6. Heating in contact with Chlorimet 2 (65% nickel, 32% molybdenum) C.P. MoO_3 and vapors given off by MoO_3, accelerated the formation of the bulk oxide. Contact with the following materials did not cause an increase in the oxidation rate: MnO_2, SnO_2, Sb_2O_3, Cr_2O_3, NiO, mill scale, iron, nickel, chromium, 25Cr – 12Ni alloy, asbestos board, and porcelain.

Contact of 16-25-6 with Fe_3O_4, however, produced a very considerable acceleration of the rate of oxidation. This cannot be explained as due to a low melting point. Analyses of the Fe_3O_4 before and after heating in contact with 16-25-6 show an increase in iron content, which may be interpreted on the basis of the conclusions made by Pfeil (3) who heated pure iron in vacuum at 1000 °F (540 °C) in contact with scale from electrolytic iron, and also separated by a distance of 1 millimeter from the scale. In both cases the iron was oxidized and the iron content of the scale was increased. The author stated that owing to the dissociation pressure of the scale being greater than that of the iron saturated with FeO, oxygen would pass from the scale particles into the furnace atmosphere from which it would be withdrawn by the iron to form new scale, having a higher iron content and lower dissociation pressure than that from which the oxygen was derived. This can be used to explain the oxidation of the 16-25-6 by Fe_3O_4, but by the same token, Fe_2O_3 and mill scale should have produced the same effect, but they did not.

The metals and alloys tested in the presence of MoO_3 and V_2O_5 were iron, nickel, chromium, cobalt, stainless steels Types 304, 309, 316, 322, 329, 410 and 430, SAE4130, Inconel, Hastelloy C, Chlorimet 2 and 3, and Durimet 20. The presence of either of the two oxides increased the rate of oxidation of all the specimens tested, although chromium, nickel and Inconel were only slightly more heavily oxidized than when heated in air alone. Owing to the difficulty of maintaining constant concentrations of oxide vapor over the surfaces

of specimens, no exact quantitative comparisons were made. A more detailed study will be required before it can be stated definitely whether the presence of vapors of these oxides in furnace atmospheres causes the metals to oxidize according to a linear rate law, or merely causes an increase in rate under a parabolic rate law. The distinctive type of oxide formed by 16-25-6 and similar alloys was not found on any of the alloys tested in this series. Iron and alloys of iron with less than 12% chromium formed the familiar layer-type of oxide. Increasing the chromium content decreased the oxidation, but alloys with 18% or more of chromium were still very heavily oxidized, especially when in direct contact with the volatile oxide. Chlorimet 3, Chlorimet 2 and Hastelloy C (55% nickel, 17% molybdenum, 6% iron, 15% chromium, 5% tungsten), while lacking in surface stability, did not form spongy oxides, but were covered with loose yellow-brown powder (probably NiO + molybdenum oxides) with adherent films beneath. The amount of oxidation appeared to be in direct proportion to the amount of molybdenum in the alloy.

Stated briefly, then, contact with oxidized metal surfaces is not necessary for the initiation of the very rapid oxidation of 16-25-6 and similar alloys, but Fe_3O_4 ond volatile metal oxides accelerate the reaction. The rate of the reaction, when 16-25-6 is heated alone, is dependent on the temperature and the concentration of gaseous molybdenum oxides on the metal surfaces. Contact surfaces act to increase concentration of the molybdenum oxides. The lower temperature limit of formation of the spongy oxide, when 16-25-6 is heated alone in still, oxidizing atmospheres, appears to be between 1400 and 1500 °F (760 and 815 °C). The melting point of MoO_3 is 1470 °F (795 °C) and the vapor pressure increases quite rapidly near the melting point. For the rapidly growing, spongy oxide to form, both iron and molybdenum must be present in the alloy. Chromium and nickel appear to inhibit this type of oxidation, at least to some extent. The amount of molybdenum required to develop the reaction is dependent upon the proportions of chromium, nickel and iron, but the minimum is probably between three and four per cent.

The Rapid Oxidation of Alloys Similar to 16-25-6—While this investigation was concerned primarily with 16-25-6 alloy, it is incorrect to assume that the spongy oxide is formed only on this alloy. Cross (16) has reported that the phenomenon was encountered in

high temperature testing of S-497, S-495 and Gamma Columbium, all alloys containing 14 to 17% chromium, and molybdenum 3.5% or higher. The compositions of alloys tested in this program are given in Table I and the results of some oxidation tests are illustrated in Fig. 3. Refractaloy B, S-495 and N-153 were all found to produce the rapidly growing oxide when heated in still air at 1650 °F (900 °C). All contain iron, 3 to 8% molybdenum, and chromium up to 24%, verifying the conclusion drawn in the preceding section, that iron and molybdenum are required for the reaction, and high percentages of chromium are required to halt it. This type of oxidation does not affect Type 316 stainless steel which contains 2% molybdenum.

The effect of tungsten is not known with any degree of certainty, but since it forms the same type of oxides as molybdenum, it could be logically assumed that the effects of its oxides would be analogous to those of molybdenum. This would account for the badly oxidized condition of S-495 and N-153, which contained 4.38% molybdenum, 3.92% tungsten, and 3.01% molybdenum, 2.19% tungsten, respectively. High temperature alloys containing molybdenum and/or tungsten, other than those tested in this investigation, should be tested for susceptibility to this type of oxidation before conclusions are drawn.

In the test made with pure cobalt in contact with MoO_3, it was found that the cobalt oxidized quite heavily, the oxide powdering as it cooled. This was found also to be characteristic of the alloys containing sizable amounts of cobalt, particularly NR-87, 69A, 422-19, and Refractaloy. All the alloys tested were most heavily attacked on the surface in contact with the furnace hearth and the sides immediately above that surface. The sides of specimens which were closest to other specimens were much more heavily oxidized than the sides which were closer to the furnace walls. Another and more striking example of the effects of a high concentration of molybdenum oxide vapors is shown in Fig. 3. A center-hole had been drilled in the top surface of the S-495 specimen for turning in a lathe. When heated, the molybdenum oxide vapors, being heavy, concentrated in the hole and produced the pimple shown.

Oxide Composition and Structure—Petrographic examination of the bulk oxide of 16-25-6 showed it to consist of a spinel with index of refraction between 2.2 and 2.3.

Table II gives chemical analyses of the bulk oxide. In general,

Table II
Chemical Analyses of Bulk Oxides Formed on 16-25-6

Sample	% Fe	% Ni	% Cr	% Mo
12A	39.40	17.88	14.00	3.42
12B	37.98	18.76	14.18	3.32
16B	45.85	17.54	12.12	1.25
17	46.99	14.73	12.37	1.34
40	50.55	10.04	11.48	3.16
Original Metal	49.52 (by diff.)	25.74	15.74	6.49

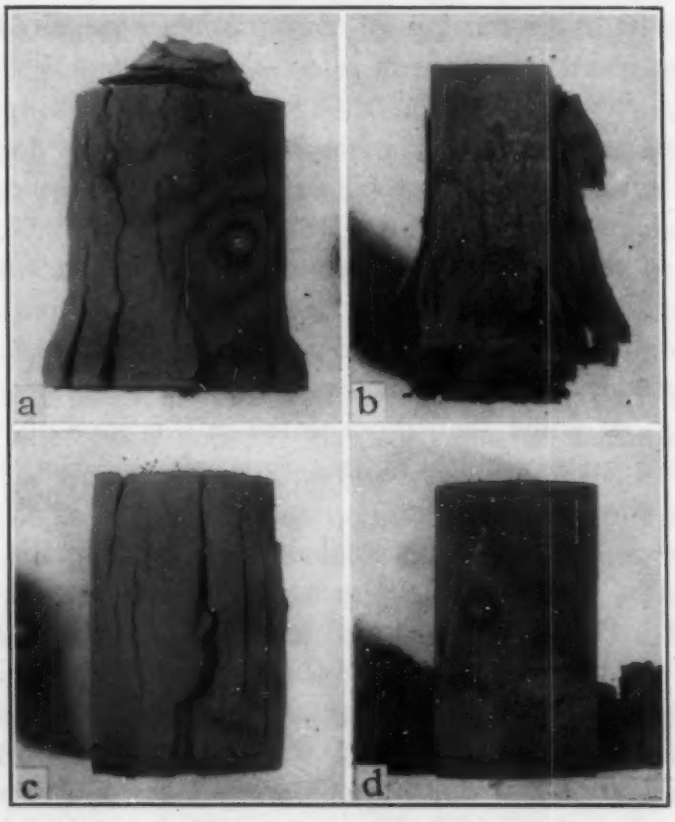


Fig. 3—High Temperature Alloys Heated in Still Air at 1650 °F. a—S-495, 100 hours, 1½-inch diameter. b—Refractaloy B, 150 hours, 1¼-inch diameter. c—N-153, 150 hours, 1½-inch diameter. d—Timken "X", 350 hours, 1-inch diameter.

a reduction of chromium and molybdenum from their proportions in the metal was found. The molybdenum is reduced because of the volatility of the oxide. Table III shows a reduction in the amount of chromium present in thin metal sections left after oxidation, which appears to conflict with a reduction of chromium in the oxide. Although the oxide shows none of the layer effects which are obtained when iron and steel are oxidized, there may be composition

gradients, and this might explain the irreconcilable differences in the chromium content in the oxide and in the remaining metal. Samples for chemical analyses were taken so as to be representative of the whole thickness of the layer, but perhaps analyses of sections of

Table III
Chemical Analyses of Thin Sections of 16-25-6 Left After Oxidation

Sample	% C	% N	% Cr	% Ni	% Mo	% Fe	% Si
Original Metal	0.072	0.15	16.12	25.13	6.12	.....	....
A	0.33	0.098	10.71	26.58	8.28	51.00	2.14
B	0.58	0.061	12.86	25.14	7.09	51.02	2.03

oxide taken parallel to the metal would have proved more illuminating.

By X-ray diffraction, the bulk oxide was determined to be an Fe_3O_4-type spinel with alpha Fe_2O_3. The lattice parameter of the spinel phase was 8.32Å as compared to 8.39Å for pure Fe_3O_4. The shift in lattice parameter of the spinel phase is believed to be due to the substitutional type of solubility of NiO for FeO in $FeO \cdot Fe_2O_3$ and also to a possible replacement of some of the Fe_2O_3 with Cr_2O_3. Either or both of the above types of solubility would cause the decrease in the parameter of the Fe_3O_4 lattice.

The thin oxide films were identified by electron diffraction as an Fe_3O_4-type spinel. The accuracy of the electron diffraction method is not sufficient to distinguish between spinel structures with less than a 2% difference in lattice parameter. The results of the X-ray and electron diffraction examinations do not show a difference between the bulk and thin oxide films which would account for the nonprotective nature of the bulk oxide. The only difference between the two is the presence of alpha Fe_2O_3 in the bulk oxide. This is to be expected on surfaces at temperature for long periods and in contact with sufficient oxygen. It is also possible that a very thin layer of alpha Fe_2O_3 was present on the samples covered with a thin film, but was not detected by electron diffraction.

X-Ray Examinations of MoO_3—The X-ray diffraction photograms made from C.P. MoO_3 and the crystals collected from the cool zone of the furnaces yielded identical patterns. All the lines in the photogram of C.P. MoO_3 were present in the photogram of the crystals formed from the vapors arising from the surface of 16-25-6. It can be safely stated, then, that the crystals which collect in the cool zones of the furnace are MoO_3.

The Type of Attack—No indications have been found that the rapid oxidation proceeds preferentially along grain boundaries. The attack is general in nature.

Mechanism of the Attack—Fig. 4 illustrates the oxidation produced by heating 16-25-6 alloy in a still, oxidizing atmosphere as compared with that produced by heating the alloy for the same length of time in a moving, oxidizing atmosphere at the same temperature.

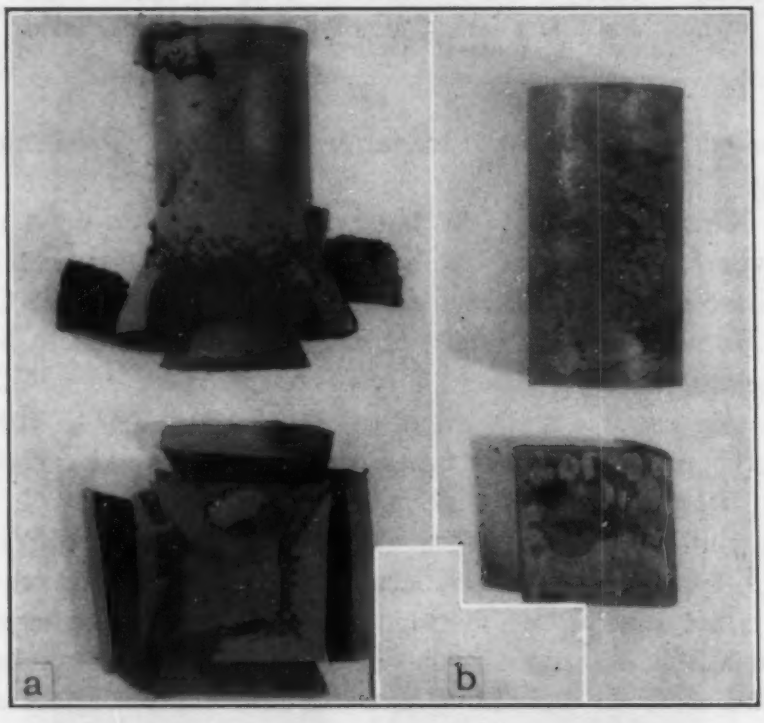


Fig. 4—Effect of Atmosphere Circulation on the Oxidation of 16-25-6 Alloy, 100 Hours at 1650 °F. 1-inch O.D. Left—Heated in still air. Right—Heated in air stream.

The passage of gas across all of the metal surfaces is more important than the velocity of the movement. In particular, the air must circulate through the lower parts of the furnace to remove the heavy molybdenum oxide vapors which gather there. Contact surfaces should be kept to a minimum. Gas-fired furnaces with ample circulation should be best for heat treating the alloy, although electric resistance furnaces are satisfactory if circulation can be assured. In the latter type, it is felt that the best arrangement for preventing the rapid oxidation would be to support the specimens on a grid, with air passing beneath it to remove the oxide vapors.

Any sharp re-entrant angles, holes, or small pits or cavities on

Table IV
Chemical Analyses of Two Modifications of 16-25-6

	% C	% Mn	% P	% S	% Si	% Cr	% Ni	% Mo	% N
Heat No. 1906 High Cr	0.085	1.58	0.020	0.018	0.54	20.75	24.29	5.92	0.18
Heat No. 1908 Low N	0.090	1.76	0.023	0.018	0.54	17.41	24.09	5.80	0.096

the surface, such as might be caused by uncleaned weld beads, will cause the concentration of molybdenum oxide vapor to increase and thus act as foci for the start of rapid oxidation.

The results obtained by spotting the metal surface with Cr_2O_3 paint and also by placing small bits of refractory porcelain on the surface were quite different from those obtained by Pfeil (3). The Cr_2O_3 paint and the pieces of porcelain always remained on the surface of the oxide; they were never buried. This indicates that the growth of the oxide is from the surface of the metal outward, and that the oxidation reaction takes place at the metal-oxide interface. These results had been expected because of the nature of the scale. Corners are never rounded, as in the normal oxidation of iron and steel, but are left vacant, with the oxide growing straight out from each surface. Surface markings on the metal are retained on the oxide.

The "pie-crust" structure of the bulk oxide, with the characteristic deep cracks caused by the nonplastic oxide being pushed outward by new scale forming beneath, allows ample opportunity for oxygen to penetrate to the metal surface. It has been thought that the molybdenum in the alloy might oxidize and volatilize beneath a thin film, pushing the film outward, the process recurring to give the growth of the oxide that is so striking. However, this process would be independent of the concentration of MoO_3 or other volatile oxide in the atmosphere and independent of atmosphere circulation. It has been demonstrated that high concentrations of volatile oxides initiate the rapid growth of the oxide almost immediately, and circulation of atmosphere inhibits the growth; therefore, the reaction is dependent upon conditions outside of the metal. If 16-25-6 is heated in an oxidizing atmosphere in a restricted space, the MoO_3 produced from the metal will quickly begin the oxide growth.

The drastic oxidation of 16-25-6 has been produced in atmospheres of helium and argon by placing the alloy in contact with V_2O_5 or MoO_3. A 24-hour heating period with the alloy in contact with V_2O_5, in helium, at 1650 °F (900 °C) resulted in almost com-

plete oxidation of the specimen. When 16-25-6 was heated in contact with MoO_3 or V_2O_5 in argon of 99.8% purity, the spongy oxide resulted. The molybdenum and vanadium oxides adsorbed on the refractory porcelain tube during previous tests were sufficient to begin the rapid oxidation on an alloy specimen not in contact with the walls of the tube, in argon, even though the furnace had been previously heated to 2300 °F (1260 °C) and air passed through the tube. These results compelled the discarding of any theory for the rapid oxidation which involved atmospheric nitrogen. The phenomenon can occur when the only source of oxygen is MoO_3 or V_2O_5.

The rapid oxidation takes place when molybdenum oxide fumes are present in contact with the metal surface and does not take place when they are absent. Then what is the mechanism of the attack?

When the alloy is heated in an oxidizing atmosphere above about 1475 °F (800 °C), MoO_3 will distill off the surface. This action prevents the formation of an impervious, protective spinel layer and gives the oxide its characteristic "pie-crust" appearance. The oxidation of the alloy by MoO_3 is then unhindered, as passage of oxidizing gases through the scale is not impeded. Attempts to prove thermodynamically that MoO_3 can oxidize the components of the alloy are hindered by the lack of data on MoO_3 and MoO_2 at high temperatures. Seltz, Dunkerly and DeWitt (19) determined the heat capacity of MoO_3 between 70 and 298 °K. The data from which Thompson (20) has derived an equation for change in free energy in the reaction $Mo + O_2 \rightarrow MoO_2$ was obtained only between 918 and 1098 °K. Extrapolation of data obtained over such narrow temperature ranges is seldom good practice, but no other sources of information have been found. There seems to be a complete lack of heat capacity data on liquid and gaseous MoO_3 or MoO_2.

Calculations have been made only at 800 °C (1475 °F), approximately the melting point of MoO_3.

$$2\,Cr_{(s)} + 3MoO_{3(s)} = Cr_2O_{3(s)} + 3MoO_{2(s)}$$
$$\Delta F^\circ = -129{,}000 \text{ cal}$$
$$K = 10^{+26.3}$$

$$Fe_{(s)} + MoO_{3(s)} = FeO_{(s)} + MoO_{2(s)}$$
$$\Delta F^\circ = -24{,}300 \text{ cal}$$
$$K = 10^{+4.59}$$

$$Ni_{(s)} + MoO_{3(s)} = NiO_{(s)} + MoO_{2(s)}$$
$$\Delta F^\circ = -11{,}600 \text{ cal}$$
$$K = 10^{+2.58}$$

These results should be considered no more than indications.

It is certain, however, that MoO_3 will oxidize the components of the alloy at 800 °C (1475 °F).

An explanation of the action of SO_2 in increasing the oxidation of metals (21) has been that sulphates, sulphites or sulphides are formed, then from these compounds a certain amount of secondary oxide is formed, which almost certainly would be more porous than the oxide formed by direct union between oxygen and metal. An analogous situation may exist here; molybdates may form momentarily, then oxides form from these.

If a dissociation of MoO_3 occurred, with release of nascent oxygen, it is logical to assume that the nascent oxygen would greatly increase oxidation of metals. Polymerization of this type of molecule, as assumed by Feiser (5), would be unusual, so it was decided to test the possibility of dissociation by the Knudsen effusion method. If it is assumed that there is no decomposition or dissociation of the liquid in the Knudsen cell, and further that there is an equilibrium between MoO_3 and MoO_2 and O in the cell in the vapor phase and also that there is no recombination of $MoO_2 + O$ on the collector plate, then the equilibrium will be:

$$\begin{array}{ccccc} MoO_3 & \leftrightarrows & MoO_2 & + & O \\ N_o - X & & X & & X \end{array}$$

$$X = \text{moles of O formed} = \frac{\text{calculated weight—weight collected}}{16}$$

N_o = number of moles of MoO_3 evaporated

$$K = \frac{X^2}{N_o - X} = \frac{N_o a^2}{1 - a}$$

where a, the degree of dissociation, equals $\frac{X}{N_o}$. This was found to be 6.73% at 1728 °F (941 °C) and 10^{-5} mm. mercury pressure. The color of the deposit on the collector plate was a dark greenish-blue. It was a smooth, adherent coat that readily dissolved in concentrated ammonia. From a consideration of the additivity of colors, one would expect that the composition of the deposit would be $XMoO_2 \cdot yMoO_3$, or a mixture of the two oxides. A similar reasoning on a change of color was advanced by Hagg and Magneli (6) as evidence of a thermal decomposition of WO_3.

In the second determination, made by identical methods at 1530 °F (831 °C), a dissociation of 0.70% was found. The color of the deposited oxide was greenish-yellow, indicating that very little

decomposition or dissociation took place, which agrees with the data. These results, by the nature of the tests, are minimum figures, and the actual dissociation may be slightly greater. When calculated at a partial pressure of 0.2 atmosphere of oxygen, the dissociation at 1728 °F (941 °C) is 1.24%, and at 1530 °F (831 °C) is 0.6%. Fig. 8 illustrates the good agreement obtained between the partial pressures of oxygen obtained from these determinations and those calculated from the data of Seltz, Dunkerly and DeWitt (19) and Thompson (20), despite the extrapolation involved. It is concluded that the effect of gaseous molybdenum oxides in rapidly attacking the surfaces of metals is enhanced by a thermal dissociation of MoO_3, which becomes appreciable at temperatures above 1500 °F (815 °C). When 16-25-6 and similar alloys are oxidized under conditions involving no circulation of atmosphere, the reaction may be considered as consisting of two processes—a rate process, the oxidation of molybdenum and other components of the alloy:

$$Mo + 3/2\ O \rightarrow MoO_3$$

and an equilibrium process involving the dissociation of MoO_3,

$$MoO_3 \leftrightarrows MoO_2 + O$$

The concentration of molybdenum oxide vapors on the surface of the alloy is critical. The effect produced by a local concentration is illustrated in Fig. 5. This specimen was covered with lime in an attempt to prevent the rapid oxidation. Calcium molybdate is known to have a low vapor pressure, and it was hoped that the lime would absorb the molybdic oxide vapors, but contact of the lime and the metal surface was not continuous, and a pocket of gaseous oxide formed, with the result shown.

At times the oxidation proceeds on narrow fronts, as shown in Fig. 6. In this case, the bulk oxide had begun to form in a still atmosphere, then a change was made to a furnace in which air was circulated. The gaseous oxides were removed from the surface of the metal, but high local concentrations remained beneath the bulk oxide, and the attack took the form of pitting.

Surface Carburization—Metallographic examinations and the analyses of thin metal sections remaining after oxidation, as given in Table III, show that the formation of the spongy oxide is accompanied by a carburization of the metal surface. The carbon contents in the analyses given in Table III are five and eight times that of the original metal. A carburization accompanying rapid oxidation



Fig. 5—Localized Oxidation of 16-25-6 Alloy, 100 Hours at 1650 °F. 1-inch O.D.

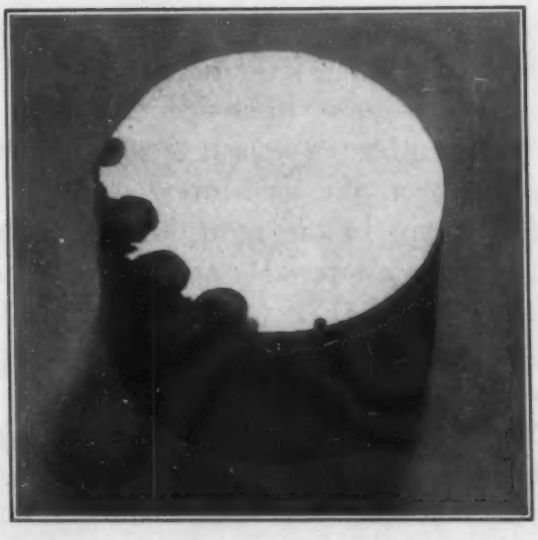


Fig. 6—Section of 1-Inch Round of 16-25-6 After 1000 Hours at 1500 °F in Air.

has been noted before, by Morrison (9), Schlegel (10), and Stout and Aho (11). Because of the low solubility and low diffusion rate of carbon in the scale and the rapid rate of oxidation of the alloy, the carbides are forced back into the austenite as the metal around

the carbide particles is oxidized. If the oxidation were very slow, the rate of diffusion of carbon through the scale would exceed the rate of oxidation and a surface decarburization would result.

The 16-25-6 specimen which was severely oxidized by contact with V_2O_5 for 2 hours at 2200 °F (1200 °C) showed no surface carburization. It is thought that the rate of oxidation greatly exceeded the rate of carbon diffusion into the austenite, so the carbide particles were carried into the scale when the austenite around them was oxidized. These conclusions would postulate a critical rate of oxidation for carburization. If the rate were greater than the diffusion rate of carbon in austenite, the carbon content of the metal surface would remain the same; if greater than the diffusion rate of carbon in scale, but less than that in austenite, the metal surface would be carburized; if the scaling rate were less than the diffusion rate of carbon in austenite and less than the diffusion rate of carbon in the scale, a decarburization would result. The spongy oxidation of 16-25-6 and similar alloys will result in an unchanged or carburized surface, while a thin, adherent oxide coating formed during a long heating period will probably result in a decarburized surface. The carburization will be negligible in its effect on the high temperature strength of the alloy as compared with the reduction of cross sectional area, which the rapid oxidation always entails.

Rapid Oxidation Under Stress—Since the rapid oxidation of the alloy is not intergranular, it was not expected that the oxidation would have any effect on the load-carrying ability of the alloy at high temperatures except in the reduction of cross sectional area. Stress apparently has no appreciable effect on the rate of oxidation, for in tests performed at 1500 °F (815 °C) and 15,000 psi stress, the stressed specimens were no more badly oxidized than unstressed specimens under the same conditions.

Effect of Surface Finish, Preoxidation and Coatings—Degree of surface finish is important only as it affects the concentration of molybdenum oxide vapor on the metal surface. The difference between a high polished surface and one finished with a file is insignificant. Preoxidation likewise has no inhibiting effects. The metal surfaces should be clean, however, as any particles of foreign matter, such as slag around an uncleaned weld bead, will cause a concentration of molybdenum oxide vapor to form beneath them.

In the tests of the four types of surface coatings at 1550 °F (840 °C) in air, no bulk oxide formed on any of the specimens. In

the tests at 1550 °F (840 °C) with MoO_3 present in the atmosphere, a similar result was obtained, nor did any growth of oxide occur on the unprotected 16-25-6 used to produce molybdenum oxide vapors in the furnace. The reason for this is that the specimens were quite small and the furnace fairly large, so the concentration of molybdenum oxide vapors was not sufficiently great. At a higher tempera-

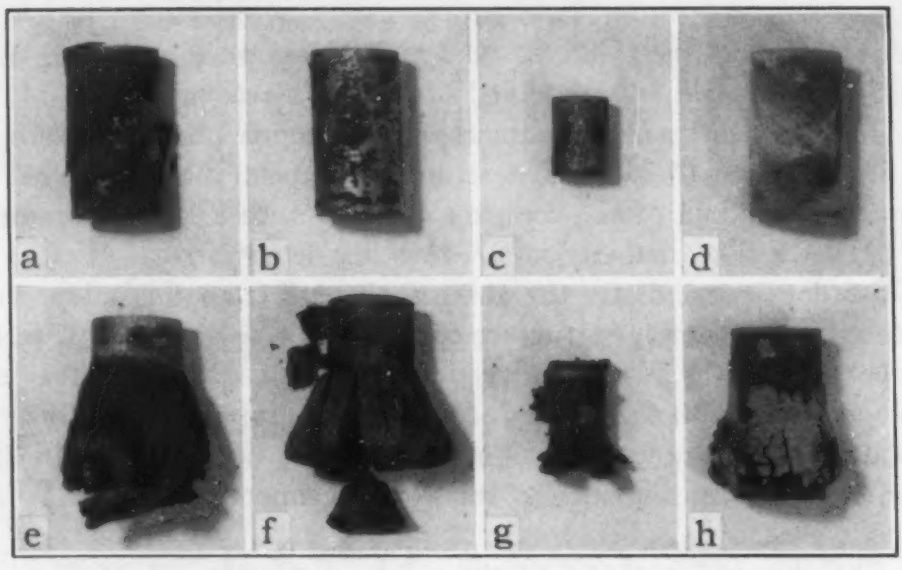


Fig. 7—Tests of Methods of Surface Protection of 16-25-6 Alloy, 100 Hours at 1650 °F. a and e—Chromium plated. b and f—Nickel plated. c and g—Chromized. d and h—Aluminized. a, b, c and d—Heated in still air. e, f, g and h—Heated in still air with MoO_3 vapor.

ture in the same furnace, however, this situation changed. When the specimens were tested at 1650 °F (900 °C) with no unprotected 16-25-6 present, no growth of oxide occurred, as is shown in the upper half of Fig. 7. When unprotected 16-25-6 was present at 1650 °F (900 °C), none of the coatings tested gave protection, as is shown in the lower half of Fig. 7.

The ease with which these coatings were penetrated and the extent of the reaction would make it difficult to provide a coating for 16-25-6 which would give protection under conditions which cause the rapid oxidation of the unprotected alloy. If no volatile oxides are present in the atmosphere or are removed as soon as formed, no coatings are necessary.

The Minor Phase in 16-25-6—Although sigma phase was identified metallographically in 25Cr – 12Ni alloy and in 25Cr – 20Ni alloy after 475 and 1000 hours at 1550 °F (840 °C), no trace of it

Table V
Room Temperature Tensile Test of Modified 16-25-6

Sample	U.T.S.	Yield Point (0.2% Elong.)	Elongation %	Reduction of Area %
1906 (20.75% Cr)	131,900	99,000	27.5	45.9
1908 (0.096% N)	125,000	104,000	26.0	53.8
Normal*	122,500	94,000	25.0	43.1

*Results from Cross and Simmons (22).

could be found in 16-25-6. Only carbides were revealed when 16-25-6 was etched with modified Murakami's reagent.

In X-ray diffraction examinations for sigma phase, the samples of filings from 16-25-6 gave strong base-metal patterns plus the diffraction maxima of the complex carbides with a lattice parameter of 10.80Å. The inability of X-rays to detect sigma (FeCr) in 16-25-6 does not indicate the absence thereof from this alloy, since in the case of a complex structure such as FeCr, less than 10% would not be detected by X-ray diffraction methods. However, this evidence, coupled with the results of the metallographic tests, allows us to state with assurance that sigma phase does not occur in 16-25-6 alloy, or occurs in amounts so small they cannot be detected by the methods used.

The chemical analyses of the microconstituents of 16-25-6 are given in Table VI. Some of these results are quite erratic. The spread in percentages of nickel from 0.56 to 20.06 and of iron from 6.54 to 15.61 indicates that the greater portion of these metals is present through incomplete removal of the austenitic matrix. The microconstituents, then, are largely compounds of molybdenum and chromium. While the nitrogen contents have been fairly uniform, ranging from 1.09 to 1.57%, the carbon content has varied considerably, from 0.87 to 2.03%. Despite the erratic results of the analy-

Table VI
Chemical Analyses of Microconstituents of 16-25-6

Sample	% Fe	% Cr	% Ni	% Mo	% Si	% C	% N
Original Metal	.....	16.12	25.13	6.12	1.03	0.072	0.15
53	10.95	11.45	20.06	35.98	7.96	2.03	1.23
75A	6.66	17.32	20.56	48.40	7.83	0.92	1.57
75B	15.61	13.41	14.67	33.65	6.93	1.49	1.09
75C	6.54	15.30	2.82	46.15	7.72	1.35	1.15
80A	11.75	10.77	16.62	43.80	2.60	0.87	1.20
80B	11.90	15.3	18.6	44.5	5.35	0.91	1.45
Average	10.57	13.93	12.22	42.08	6.40	1.26	1.28

ses, it is very evident that molybdenum, carbon and nitrogen are concentrated in the microconstituents over their proportions in the alloy.

X-ray diffraction examination showed that the microconstituents have a face-centered cubic structure with cell constants of 10.80Å and 10.90Å. These may be classed as carbides of the type M_6C or

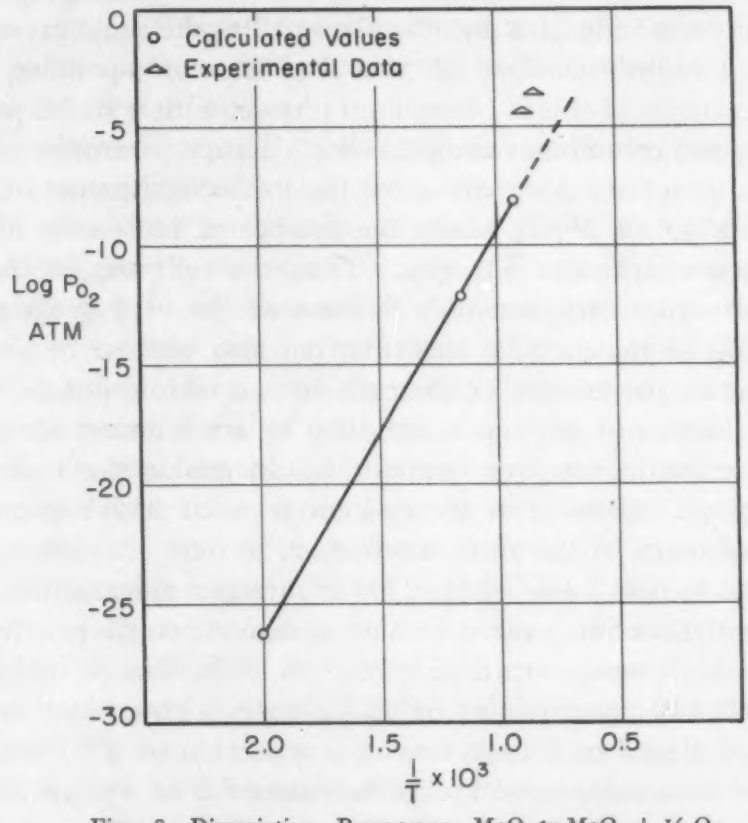


Fig. 8—Dissociation Pressure $MoO_2 \leftrightarrows MoO_2 + \frac{1}{2} O_2$ Versus Temperature.

M_4C, in which chromium, iron, nickel and molybdenum are the probable metal atoms in the structure. Owing to the variation in lattice parameter which may result from a solubility range or from isomorphic replacement of various metallic constituents in these complex carbides, no definite compound can be expected to match the lattice dimensions of the observed phases.

In all cases, the face-centered cubic 10.90Å phase was the major microconstituent in solution-quenched 16-25-6, while the face-centered cubic 10.80Å phase is the major microconstituent of the aged or tempered alloy. It is evident that the carbide present in the alloy is a function of the temperature of formation of the carbides

as well as the composition of the alloy, and probably is also a function of time at temperature, which would determine how closely equilibrium was approached at the temperature of formation.

From the results of the chemical and X-ray examinations, it is concluded that nitrogen may be dissolved in the M_6C or M_4C carbides of 16-25-6 without greatly changing the lattice parameter. Carbon and nitrogen are very similar elements in a crystallographic sense and usually a nitride of a metallic element has the same crystal structure and a slightly smaller cell size than the corresponding carbide. A good example of this is columbium nitride, with a lattice parameter of 4.40Å, and columbium carbide, with a lattice parameter of 4.44Å. A more appropriate designation for the microconstituents of 16-25-6 might be M_6C' or M_4C', where the symbol M represents metal and C′ represents carbon or nitrogen. Thus, the cell sizes of the microconstituents may vary, not only because of the very great range of composition of the metallic elements, but also because of the difference in lattice parameters of the carbide and nitride phases.

A reduction of carbon in the alloy to a minimum, accompanied by a reduction in nitrogen content, would enable the molybdenum to be reduced. Because of the concentration of molybdenum in the microconstituents of the alloy, a reduction in total molybdenum could be accomplished in a low carbon, lower nitrogen alloy without reducing the molybdenum content in the austenite, which is effective in increasing high temperature strength. A reduction of molybdenum content could be accompanied by an increase in chromium content in the ratio of 1 to 3 or 1 to 4, that is, a reduction of 1% in molybdenum could be accompanied by an increase of 3 or 4% in chromium while maintaining the austenitic character of the alloy.

The rapid oxidation has been produced on the 21% chromium 16-25-6 and on low nitrogen 16-25-6 when heated in air in a restricted space. Any difference in the three types has been too slight to be significant. The results of the room temperature tensile tests of the experimental heats are given in Table V. It appears that reducing the nitrogen content as far as possible without resorting to special melting techniques has little or no effect on room temperature strength or ductility, nor do increases in the chromium content from 16 to 21%. It must be emphasized, however, that only a single test was made of each modification, and the metal was made in small experimental heats.

The rapid oxide growth has been produced on vacuum melted,

low nitrogen 16-25-6 quite as readily as on the normal alloy, so it is concluded that nitrogen in the alloy has no effect on the rapid oxidation.

Conclusions

1. It has been found that the very rapid oxidation of 16-25-6 and similar alloys at high temperatures occurs only when specific conditions exist, these conditions being an oxidizing atmosphere and severely restricted circulation.

2. The alloys susceptible to this type of attack contain substantial amounts of molybdenum and iron.

3. The very drastic oxidation of these alloys is caused by the action of MoO_3 as an oxidation catalyst. Thermal dissociation of MoO_3 accelerates the oxidation and this dissociation may be the chief cause of the extremely rapid destruction of the alloys. The only factors which substantially affect the rates of oxidation are temperature and the concentration of molybdenum oxide or other volatile oxide vapors on the surface. The very rapid oxidation can occur when the only source of oxygen is gaseous molybdenum oxides.

4. Preliminary investigation shows appreciable dissociation of MoO_3 at temperatures above 1500 °F (815 °C). In vacuum, the dissociation was determined to be at least 0.7% at 1530 °F (831 °C) and at least 6.7% at 1728 °F (941 °C). At atmospheric pressure the dissociation is at least 1.24% at 1728 °F and 0.6% at 1530 °F.

5. The oxidation is general, rather than intergranular, and the reaction takes place at the metal-oxide interface. Due to the porous nature of the oxide, penetration of oxygen inward is easily accomplished.

6. The spongy oxide has been identified as an Fe_3O_4-type spinel plus alpha Fe_2O_3.

7. Some metal oxides which melt at relatively low temperatures greatly increase the rates of oxidation of iron, nickel, chromium, cobalt and their alloys. Some of these oxides are MoO_3, V_2O_5, PbO, Bi_2O_3 and WO_3.

8. A surface carburization takes place because of the rapid oxidation.

9. Atmospheric nitrogen has no effect on the rapid oxidation, nor does nitrogen in 16-25-6 alloy, in the range of nitrogen composition studied.

10. Increasing the chromium content of 16-25-6 from 16 to 21% has no appreciable effect on the rapid destruction of the alloy.

11. Nickel plating, chromium plating, chromizing and aluminizing are effective in preventing the spongy oxidation when no molybdenum oxide vapors are present. When these vapors are present, as they would be when unprotected 16-25-6 is oxidized, none of the coatings tested were effective. If surface coatings are to be used, all molybdenum-bearing alloys present must be coated for the protection to be effective.

12. The rapid destruction of high temperature alloys containing molybdenum can be prevented in oxidizing atmospheres by ensuring appreciable movement of gas across all surfaces of the metal. The effect of contact surfaces is to inhibit circulation and to increase concentration of molybdenum oxides.

13. The microconstituents of 16-25-6 alloy are of the type M_6C' or M_4C' where M may be iron, nickel, chromium or molybdenum and C′ may be carbon or nitrogen. Sigma phase (FeCr) does not form in 16-25-6, even after 1000 hours at the most favorable temperature for formation.

14. It may be possible to decrease the rate of the oxidation attack on 16-25-6 while maintaining the excellent high temperature properties of the alloy by reducing the carbon to a minimum, reducing the nitrogen and molybdenum and increasing the chromium content.

Acknowledgment

The work reported here was sponsored by the Materials Laboratory, Engineering Division, Air Materiel Command, Wright Field, Dayton, Ohio. The authors wish to express their appreciation for the aid of Dr. Rudolf Speiser, The Ohio State University Research Foundation, in the determination of the dissociation of MoO_3 and for the interest shown by Messrs. Martin Fleischmann, Howard Cross and Ward Simmons.

References

1. M. Fleischmann, "16-25-6 Alloy for Gas Turbines," *Iron Age,* Vol. 157, Jan. 17 and 24, 1946.
2. M. Fleischmann, U. S. Patent 2,398,702, April 16, 1946.
3. L. B. Pfeil, "The Oxidation of Iron and Steel at High Temperatures," *Journal,* Iron & Steel Institute, Vol. 119, 1929, p. 501.
4. J. W. Hickman and E. A. Gulbransen, "An Electron Diffraction Study of

Oxides Formed on Alloys of Iron, Cobalt, Nickel and Chromium at High Temperatures," American Institute of Mining and Metallurgical Engineers, T.P. 2069, *Metals Technology,* Vol. 13, No. 7, October 1946.

5. J. Feiser, "The Vapor Pressure of Molybdenum Trioxide," *Metall und Erz,* Vol. 28, 1931, p. 298.
6. G. Hagg and A. Magneli, "X-Ray Studies on Molybdenum and Tungsten Oxides," *Arkiv fer Kemi, Mineralogie Och Geologi,* Bd. 19A, No. 2, 1944.
7. E. A. Gulbransen and W. S. Wysong, "Thin Oxide Films on Molybdenum," American Institute of Mining and Metallurgical Engineers, T.P. 2226, *Metals Technology,* Vol. 14, No. 5, September 1947.
8. J. W. Hickman and E. A. Gulbransen, "An Electron Diffraction Study of Oxides Formed on Molybdenum, Tungsten, and Alloys of Molybdenum, Tungsten and Nickel," American Institute of Mining and Metallurgical Engineers, T.P. 2144, *Metals Technology,* Vol. 14, No. 3, April 1947.
9. J. G. Morrison, "Some Surface Studies on Treated High Speed Steels," TRANSACTIONS, American Society for Metals, Vol. 29, 1941, p. 470.
10. W. A. Schlegel, "Surface Carbon Chemistry and Grain Size of 18-4-1 High Speed Steel," TRANSACTIONS, American Society for Metals, Vol. 29, 1941, p. 159.
11. R. D. Stout and T. Aho, "Surface Effects Accompanying the Heating of Carbon Tool Steels in Oxidizing Atmospheres," CONTROLLED ATMOSPHERES, published by American Society for Metals, 1942, p. 159.
12. W. Hume-Rothery, G. V. Raynor and A. T. Little, "On the Carbide and Nitride Particles in Titanium Steels," *Journal,* Iron & Steel Institute, Vol. 145, 1942, p. 143.
13. F. B. Foley, "The Sigma Phase in Certain High Chromium Steels," *Metallurgia,* Vol. 34, 1946, p. 139.
14. F. B. Foley, "The Sigma Phase," *Alloy Castings Bulletin,* No. 5, Alloy Castings Institute, 1945.
15. R. Speiser, "The Vapor Pressure of Metals," *Engineering Experiment Station News,* Ohio State University, Vol. 29, No. 5, December 1947, p. 12.
16. H. C. Cross, Private Communication.
17. R. Matters, Private Communication.
18. G. N. Emmanuel, "Metallographic Identification of Sigma Phase in 25-20 Austenitic Alloy," METAL PROGRESS, Vol. 52, 1947, p. 78.
19. H. Seltz, F. I. Dunkerly and B. J. DeWitt, "The Heat Capacities and Entropies of Molybdenum and Tungsten Trioxides," *Journal,* American Chemical Society, Vol. 65, 1943, p. 600.
20. M. de K. Thompson, "The Total and Free Energy of Formation of the Oxides of Thirty-Two Metals," *Electrochem. Soc.,* 1942, New York.
21. U. R. Evans, "Metallic Corrosion, Passivity and Protection," Edward Arnold and Company (London), 1937, p. 104.
22. H. C. Cross and W. F. Simmons, "Final Report on Heat Resisting Metals for Gas Turbine Parts," O.S.R.D. 6563, Ser. No. M-636, Jan. 21, 1946.

DISCUSSION

Written Discussion: By Martin Fleischmann, metallurgical engineer, The Timken Roller Bearing Co., Canton, Ohio.

The authors of this paper did an outstanding piece of work in clearing up a phenomenon which had baffled many investigators ever since the

16-25-6 alloy has found large commercial application in the construction of turbo-superchargers, gas turbines and jet engines.

While the rapid oxidation of the 16-25-6 alloy has been frequently observed in the laboratory and occasionally in the heating furnaces used during the processing of the material into forgings, it never was encountered in actual service in the applications for which it was recommended. There, the rapid circulation of the gases around the material prevent the accumulation of molybdenum oxide and with it the rapid destruction of the alloy as is so clearly shown in the paper.

It may be of interest to mention here that the 16-25-6 alloy in form of long eyebolts has been used very successfully in vertical carburizing retorts at 1700 °F (925 °C) giving many thousand hours of life. These eyebolts not only have to withstand the effect of the carburizing atmosphere but also carry heavy loads at 1700 °F (925 °C) out of the retort and are subjected to repeated oil quenching. This application confirms the first conclusion reached in the paper: that one of the conditions for the disintegration is an oxidizing atmosphere, producing molybdenum oxide.

While we at Timken are especially pleased to see many of our ideas about this subject confirmed in the conclusions reached in this paper, we cannot fully agree with the final suggestion made, recommending an increase in the chromium content and a simultaneous reduction in the carbon, nitrogen and molybdenum of the composition. We feel that the specified amount of nitrogen and molybdenum is necessary to assure the excellent high temperature properties of the material and that a substantial increase in chromium may lead to the formation of sigma phase which should be avoided.

The most effective way to prevent the rapid oxidation in oxidizing atmospheres under severely restricted circulation is the use of protective coatings as shown in the paper. However, if this procedure should not be feasible or should be undesirable and exceptionally high temperature strength is demanded, the choice of a nonferrous material is indicated. As pointed out in the paper, the high temperature alloys susceptible to the rapid oxidation contain substantial amounts of iron together with molybdenum or other metals like tungsten and vanadium necessary to improve their high temperature strength. The deterioration of the alloy at elevated temperatures may be prevented by eliminating most or all of the iron from the composition as indicated in the alloy designated in the paper as Timken "X", where the iron was replaced with cobalt although the molybdenum content of the material had been increased from 6% to better than 10%.

The authors of this paper deserve considerable credit for their clear and precise presentation of a timely subject and for their research pointing the way to the development of superior high temperature alloys.

Written Discussion: By E. E. Reynolds, research associate, Engineering Research Institute, University of Michigan, Ann Arbor, Mich.

The authors are to be commended on their contribution of a valuable study of the oxidation characteristics of 16-25-6 alloy. Although rather unusual oxidation characteristics have been observed during experimental

heat treatment and testing of 16-25-6 alloy, a systematic study of the phenomenon has not previously been presented.

In general, our experience has indicated that the occurrence of the rapid oxidation of 16-25-6 decreases at temperatures above 1850 °F (1010 °C). Do the authors have any information to indicate whether there is a change in the oxidation characteristics at the higher temperatures or was the lack of such rapid oxidation simply due to the use of furnaces with better circulation and shorter time periods at temperature?

An example of severe oxidation similar to that on 16-25-6 influenced by the nickel content of the alloys was encountered during a study[2] of the 1700 and 1800 °F (925 and 980 °C) rupture-test properties of several sheet alloys. Two sets of alloys differing only in nickel content and having the compositions shown in Table VII were tested:

Table VII

	Chemical Composition, Per Cent								
Alloy	C	Cr	Ni	Co	Mo	W	N	B	Fe
J837	0.13	20	4.5	22	4.4	4.6	low	0.34	Balance
J838	0.11	20	15	21	4.4	4.4	low	0.37	Balance
J839	0.12	22	4.5	20	4.5	4.4	0.12	0.56	Balance
J840	0.13	21	15	21	4.3	4.3	0.12	0.45	Balance

The alloys with 4.5% nickel were subject to rapid oxidation and failed from this cause in the rupture tests. J838 and J840, with 15% nickel, had satisfactory oxidation resistance in tests of over 1000 hours duration. The low oxidation resistance of J837 and J839 was verified by heating small samples of the 0.040-inch thick sheet, without stress in still air at 1700 °F (925 °C) and obtaining complete oxidation in 100 hours. A spongy oxide resulted. In the light of the present paper, evidence points to the conclusion that the high percentage of molybdenum and tungsten, coupled with the low nickel of these two alloys, was responsible for the severe oxidation. It also indicates that nickel in these limits has a marked inhibiting effect on the spongy oxidation phenomenon. One added factor in these alloys was that they contained boron, the effect of which on oxidation characteristics is not known.

It is concluded in the paper that the rapid oxidation of 16-25-6 can be prevented by circulation of the atmosphere, thus removing the molybdenum oxides formed. Was any check made after such a treatment to determine the extent of molybdenum depletion in the alloy? The possibility exists that such a loss could seriously alter the properties of the alloy at time periods similar to those used in this investigation.

Written Discussion: By H. V. Kinsey, metallurgical engineer, Department of Mines and Resources, Ottawa, Ontario, Canada.

We have encountered an oxidation phenomenon somewhat similar to that described in this paper and probably attributable to the same

[2] J. W. Freeman, E. E. Reynolds and A. E. White, "The Rupture-Test Characteristics of Heat-Resistant Sheet Alloys at 1700 and 1800 °F," National Advisory Committee for Aeronautics, Technical Note No. 1465, 1948.

cause. However, in view of the fact that the conditions surrounding the phenomenon we observed are different in certain respects, we would appreciate having the authors' comments.

Cast retorts having a nominal analysis of 36% nickel, 17% chromium, 0.4% carbon are used in the ferrosilicon reduction process for magnesium in Canada. These retorts are used in globar heated furnaces and operate at a temperature of 1170 °C (2140 °F). The retorts are supported over their entire length on a hearth. They have a life of from 200 to 400 days. Failure never occurs from oxidation but is always due to cracking.

In an effort to improve retort life, several retorts were cast from metal to which 1.7% molybdenum had been added. These retorts all failed from rapid oxidation in a matter of from 10 to 30 days. The main attack was along the line of contact of the retort with the hearth, where atmosphere circulation was restricted.

Oxidation occurred in a manner similar to that described by the authors, that is, it built up in layers and the final product was many times the thickness of the original metal. It is probably of interest to note that the molybdenum content of this scale is considerably lower than would be expected if no molybdenum were lost during oxidation. Tables VIII and IX illustrate this point.

Table VIII
Chemical Analyses of Oxide and Adjacent Metal

	Per Cent						
	Carbon	Manganese	Silicon	Nickel	Chromium	Molybdenum	Iron
Metal	0.24	0.98	0.71	36.62	15.37	1.59	44.82
Oxide		0.80	0.75	26.06	11.51	0.44	31.83

Table IX
Ratio of Alloy Elements to Chromium in Metal and Oxide

	Per Cent					
	Chromium	Nickel	Iron	Silicon	Manganese	Molybdenum
Metal	1	2.39	2.92	0.046	0.064	0.103
Oxide	1	2.26	2.76	0.065	0.069	0.038

Evidently there has been an appreciable molybdenum loss through the volatilization of its oxide. Under the conditions dealt with by the authors, it is their opinion that at least 3% molybdenum is required for this rapid oxidation to take place. Under the conditions described above, could the 1.59% molybdenum be responsible for the greatly accelerated oxidation that occurs here?

Authors' Reply

The authors appreciate the discussion of the paper by Messrs. Fleischmann, Reynolds and Kinsey.

The thought that the oxidation rate of 16-25-6 could be decreased by

simultaneous reduction of carbon, nitrogen and molybdenum and an increase in chromium content is merely a suggestion based on our findings that carbon, nitrogen and molybdenum are concentrated in the microconstituents of the tempered alloy. Time and funds did not permit a study of this suggestion with regard to corrosion and mechanical properties. The concentration of nitrogen in the microconstituents and the change in the character of the minor phase with a change in temperature of formation indicates a change in solubility of nitrogen in the austenite. The solubility and effects of nitrogen in highly alloyed austenite should be more definitely known and investigation in this field indicated.

With regard to Mr. Reynolds' question on a change in oxidation characteristics at temperatures above 1850 °F (1010 °C), we have not observed such a change. Oxidation at 2000 and 2100 °F (1095 and 1150 °C) with restricted circulation has been found to be extremely rapid.

We are glad to receive evidence that an increase of nickel content increases resistance to this type of oxidation. As noted in the paper, chromium, nickel and Inconel were only slightly more heavily oxidized when heated in the presence of MoO_3 and V_2O_5 than when heated in air.

Although we have made no analyses to determine whether or not depletion of molybdenum occurred in the alloy when heated in a circulating atmosphere, we doubt very much that such a depletion occurs. Only a very thin oxide film forms, and a very small amount of MoO_3 crystallizes in the cooler zones of the furnace. A depletion of molybdenum in this case would entail a diffusion of molybdenum to the surface.

Although we found that about 3% molybdenum in the alloy was required to initiate the rapid oxidation under the test conditions, we now lean toward the view that the reaction will occur whenever a concentration of MoO_3 vapor occurs on the surface of the alloy, regardless of the molybdenum content. We are very glad to note that the evidence presented by Mr. Kinsey supports this view. In addition, we learned during private discussion after presentation of the paper that the rapid oxidation effect has been observed on 16-13-3 stainless steel.

In closing we would like to mention that shortened life of stainless steel parts has been reported in heat resistant applications involving heating with Venezuelan fuel oils containing small amounts of vanadium. The oxide of this element has been found on the failed stainless steel surfaces. Similar effects have also been observed in connection with vanadium oxide catalysts. We believe that the mechanism of the attack in these cases is similar to the one described in the paper.

ISOTHERMAL TRANSFORMATION OF AUSTENITE IN TWO ALLOY STEELS

By Edward A. Loria

Abstract

Two steels containing appreciable amounts of multiple alloying elements have been subjected to isothermal transformation studies in order to illustrate how the pearlite and bainite reactions are altered by alloy composition and austenite heterogeneity. The TTT-diagrams for a chromium-molybdenum-manganese hypoeutectoid steel and a nickel-chromium-molybdenum hypereutectoid steel are presented and evaluated. Both show a full knee for the pearlite reaction and a second, lower knee for the bainite reaction, separated by a bay of extremely slow reaction. The general transformation features of the hypoeutectoid alloy steel upon austenitizing at 1650 °F (900 °C) are discussed and evaluated in terms of the behavior of other steels when possible. The hypereutectoid alloy steel austenitized at 1550 °F (845 °C) displayed undissolved carbides which enhanced the nucleation of the pearlite reaction.

Introduction

THE results of recent investigations on the transformation characteristics of alloy steels indicate that there are two general types of TTT-diagrams which will describe the time-temperature relationship under which the austenite transformation has taken place. In one type of diagram the pearlite and bainite transformations overlap in temperature and/or time, while in the other the transformations are completely separated, both as to temperature and time.

These two types of diagrams occur because alloying elements in steel delay the initiation of transformation and increase the time required for its completion at subcritical temperatures. Although the nature and degree of the effect are different for each element, the effect of variation in chemical composition upon the pearlite transformation is usually much greater proportionally than the effect upon

The author, Edward A. Loria, is Fellow, Mellon Institute of Industrial Research, Pittsburgh. Manuscript received September 28, 1948.

the bainite transformation. Some alloying elements affect the pearlite transformation much more markedly than do others. Such elements as chromium and molybdenum are mainly responsible for the retardation of the pearlite transformation and complete separation of the pearlite and bainite transformation ranges. Other elements, such as nickel, do not delay the initiation of the pearlite reaction, or reduce its rate, in such a marked manner as molybdenum or chromium, but are somewhat more effective in delaying the start of the bainite reaction.

Furthermore, the TTT-diagram for alloy steels becomes more complex in that a proeutectoid constituent resembling ferrite forms down to quite low temperatures in the bainite transformation range, which in itself presents a diversity of phenomena in different alloy steels. This field of the intermediate temperature transformation products is very important practically, for these products occur widely in heat treated steels and a knowledge of the metallographic and rate characteristics within this range should provide the best basis for a rationalization of commercial heat treatment.

The purpose of this paper is to present further data on the isothermal transformation of austenite in steels containing appreciable amounts of several alloying elements and to illustrate how the pearlite and bainite transformations in these steels are altered by alloy composition and austenite heterogeneity. Specifically considered are a chromium-molybdenum-manganese hypoeutectoid steel and a nickel-chromium-molybdenum hypereutectoid steel. In part, the work is a continuation of the report given last year (1)[1] on the nature and mode of formation of the acicular structure found within the intermediate transformation range of two alloy steels.

Experimental Procedure

The compositions of the steels investigated are given in the following tabulation:

Steel	C	Ni	Cr	Mo	Mn	Si	V	P	S
A	0.60	2.75	1.25	0.50	0.60	0.30	0.12	0.035	0.024
B	0.59	....	1.06	0.54	0.96	0.28	0.12	0.032	0.022
C	0.86	2.47	1.21	0.50	0.66	0.38	....	0.040	0.024

The transformation characteristics of steel A were discussed in the previous paper (1) and its chemical composition is repeated here

[1]The figures appearing in parentheses pertain to the references appended to this paper.

only in order to maintain the same code notation for steel B as in the initial paper. Steels B and C were commercially made acid open-hearth steels and were processed in the form of forged rounds.

In order to facilitate machining, both steels received a 1700 °F (925 °C) normalizing and a 1200 °F (650 °C) tempering treatment (Fig. 2). Microscope and hardness specimens were usually ¼ by ½-inch diameter. All austenitizing was done in an atmosphere fur-

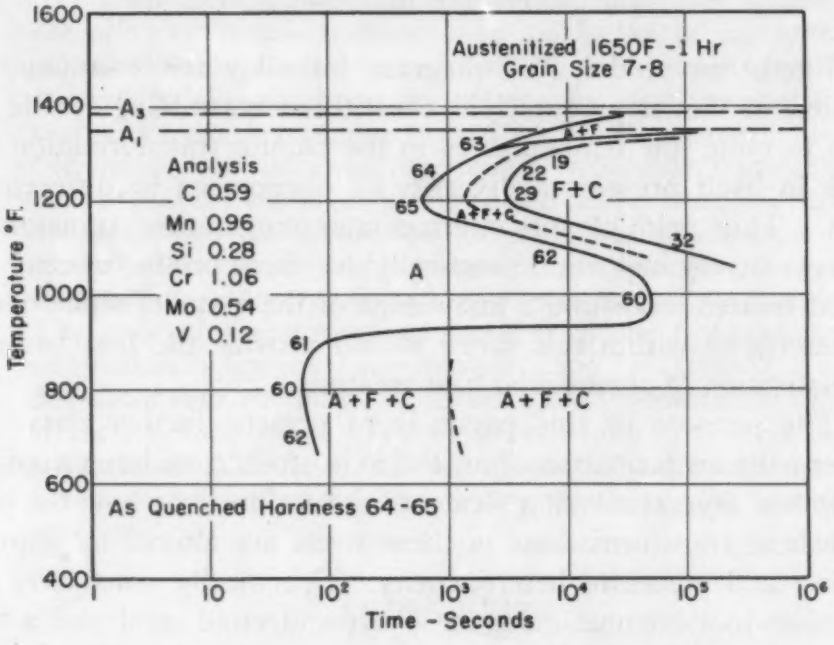


Fig. 1—Transformation Diagram for Alloy Steel B, Austenitized at 1650 °F (900 °C).

nace. Steel B was austenitized for 1 hour at 1650 °F (900 °C) and steel C for 1 hour at 1550 °F (845 °C). These temperatures were selected because they approximate those employed in the commercial heat treatment of these steels. The grain sizes resulting from these austenitizing treatments are indicated on the appropriate transformation charts.

Upon austenitizing, the specimens were quickly transferred to lead baths controlled to ±5 °C and after suitable periods of time quenched into water. The pearlite and bainite reactions were studied by the use of the microscope supplemented by hardness data. The Rockwell C hardness numbers on the transformation charts are virtually self-explanatory. Also, the values for A_1 and A_3 are indicated on the appropriate TTT-diagrams. In general, the over-all accuracy of the microscope determinations is believed to be of the order of

10 to 15 °F. The normal inhomogeneities of commercial steels preclude the possibility of greater accuracy. A_{cm} for high carbon steel C could not be determined by the standard microscopic method since it was virtually impossible to detect and identify the first small particles of carbide to precipitate below A_{cm}.

Results and Discussion

The TTT-diagrams for alloy steels B and C are shown in Figs. 1 and 10. The diagrams have been drawn in the conventional manner where the beginning line indicates approximately less than 1% transformation and the ending line somewhat more than 99% decomposition of the austenite. The thin dotted line within the A + F + C field represents, for each temperature level, the time at which half of the total austenite has transformed.

The TTT-diagram developed for steel B shows a full knee for the pearlite reaction and a second, lower knee for the bainite reaction, separated by a bay of extremely slow reaction. An unusual aspect of this diagram is that the "ferrite line" which marks the start of the separation of proeutectoid ferrite in hypoeutectoid steels is practically nonexistent. The alloying elements in steel B are of sufficient quantities to cause a shift in the eutectoid point to the left in the iron-carbon diagram and to suppress the proeutectoid reaction in the temperature range of pearlite transformation. In other words, the "carbon equivalents" of these elements are almost sufficient to make steel B of eutectoid percentage. Only at temperatures of 1350 °F (730 °C) and above is there evidence of ferrite. Fig. 3 illustrates such a structure on holding at 1350 °F (730 °C) for 24 hours. At 1300 °F (705 °C) and lower temperatures, the austenite transforms directly to an aggregate of ferrite and carbide[2] in the form of pearlite, as can be seen in Figs. 4 to 9. The tip of the pearlite knee or the temperature of most rapid reaction occurs at 1200 °F (650 °C), the resultant structures on holding at this temperature being shown in Figs. 8 and 9. At lower temperatures the time for transformation increases rapidly and the lower the temperature of transformation the finer and stronger and harder is the final structure. In part, steel B resembles those alloy eutectoid steels in which pearlite forms both above and below the pearlite knee; such

[2]The three transformation products of austenite (pearlite, bainite and martensite), although different in structure and properties, are all basically mixtures of ferrite and carbide and are, therefore, all customarily indicated on the TTT-diagrams by the notation F + C.

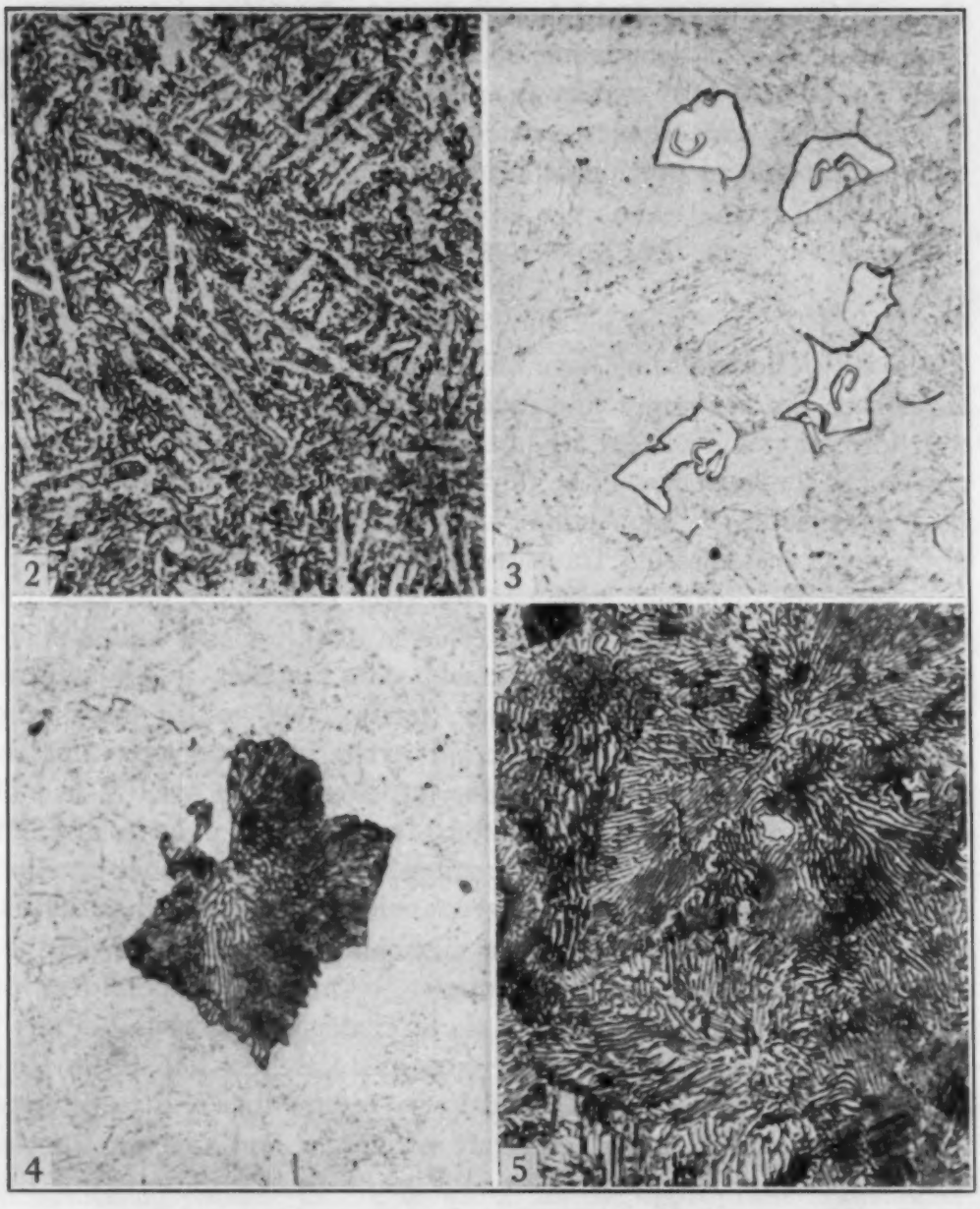


Fig. 2—Alloy Steel B Normalized at 1700 °F, Tempered at 1200 °F.
Fig. 3—Alloy Steel B Transformed at 1350 °F for 24 Hours.
Fig. 4—Alloy Steel B Transformed at 1300 °F for 40 Minutes.
Fig. 5—Alloy Steel B Transformed at 1300 °F for 160 Minutes.
Modified picral etch. × 1000.

alloy steels differ in this way from carbon steels and from nickel and manganese alloy steels in which pearlite forms only at temperatures above the knee. This behavior of pearlite in alloy eutectoid steels has its counterpart in proeutectoid ferrite in low carbon alloy steels, ferrite forming at temperatures both above and below the tempera-

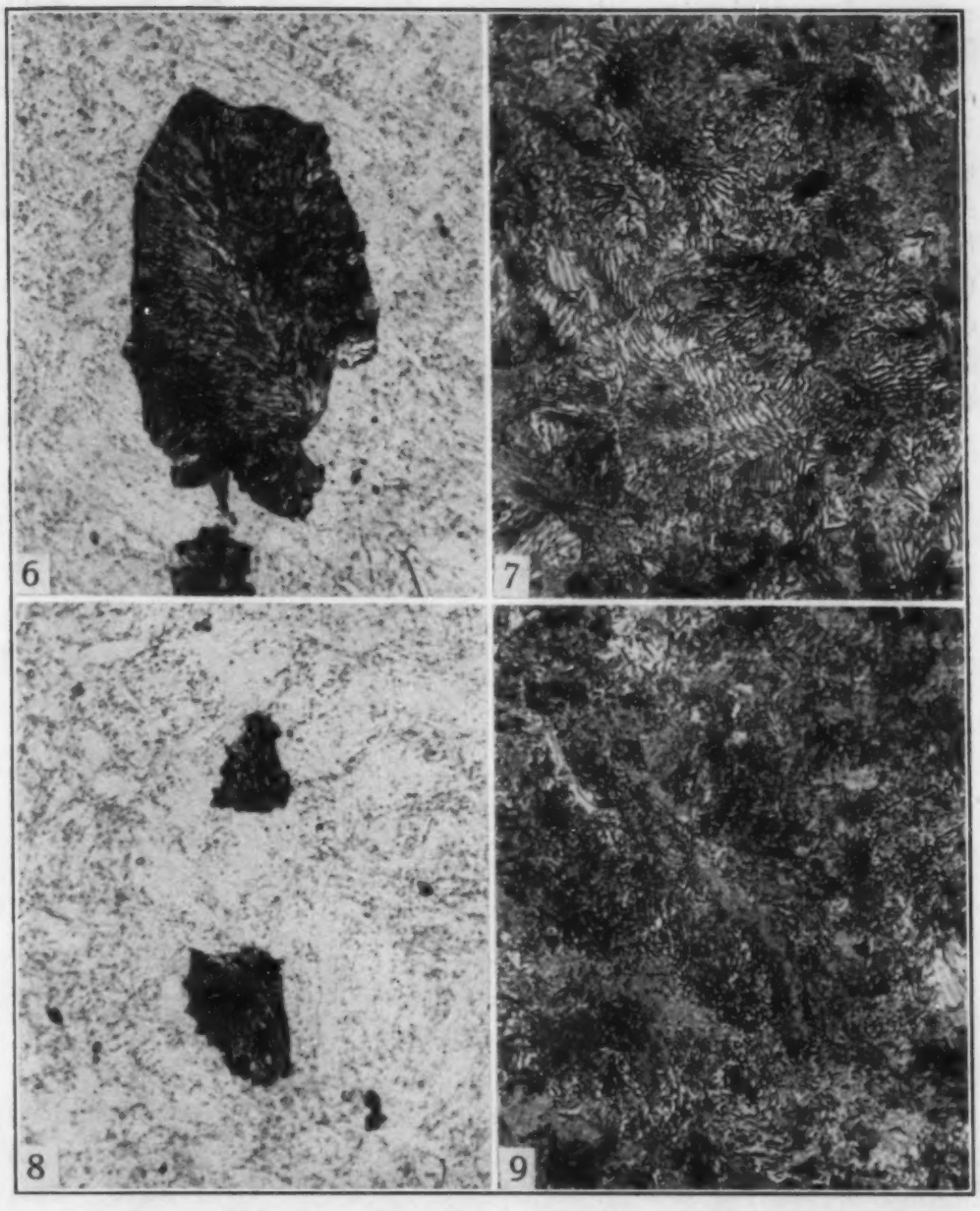


Fig. 6—Alloy Steel B Transformed at 1250 °F for 20 Minutes.
Fig. 7—Alloy Steel B Transformed at 1250 °F for 80 Minutes.
Fig. 8—Alloy Steel B Transformed at 1200 °F for 10 Minutes.
Fig. 9—Alloy Steel B Transformed at 1200 °F for 80 Minutes.
Modified picral etch. × 1000.

ture of the knee and, when the carbon is sufficiently low, exhibiting a knee of its own.

In eutectoid carbon steels the pearlite reaction, proceeding more and more rapidly as the temperature decreases, is replaced at the knee of the TTT-diagram by the formation of bainite, which forms

more and more slowly as the temperature decreases. The knee of the TTT-diagram is thus a point where one reaction is replaced by a fundamentally different one but there is no sensible break in the TTT-diagram at this point in eutectoid carbon steel, as one might expect. Some overlap of the two reactions is always observed with specimens reacted just at the knee showing both pearlite and bainite, but how much of this is to be ascribed to austenite heterogeneity is unknown. On the other hand, in nearly eutectoid steel B and in other alloy steels where the alloy is strong in carbide-forming tendency, the separation of the two processes is very evident.

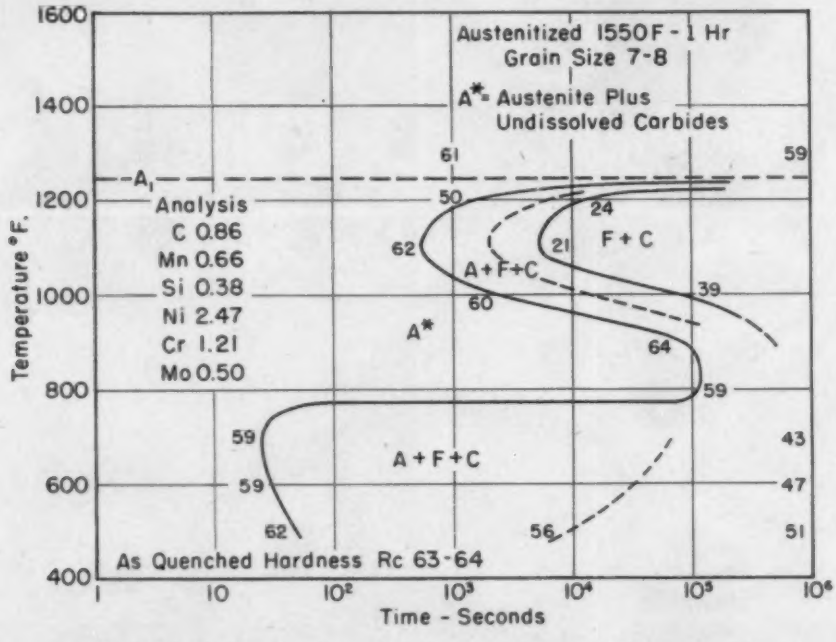


Fig. 10—Transformation Diagram for Alloy Steel C, Austenitized at 1550 °F (843 °C).

The initiation of the bainite reaction in steel B is not delayed to the same degree as the pearlite transformation. As can be seen in Fig. 1, the pearlite knee is transposed far to the right on the time axis by the alloy content while the bainite knee juts out to the left below the 950 °F shelf. In the 700 to 925 °F range, transformation starts rather promptly but is extremely sluggish in going to completion. The nature of these acicular ferrite structures and the complexities of multiple-stage transformation of the austenite were illustrated and discussed in the previous paper (1). Below 700 °F the dark-etching acicular bainites made their appearance and the isothermal transformation more nearly approached completion the lower the temperature.

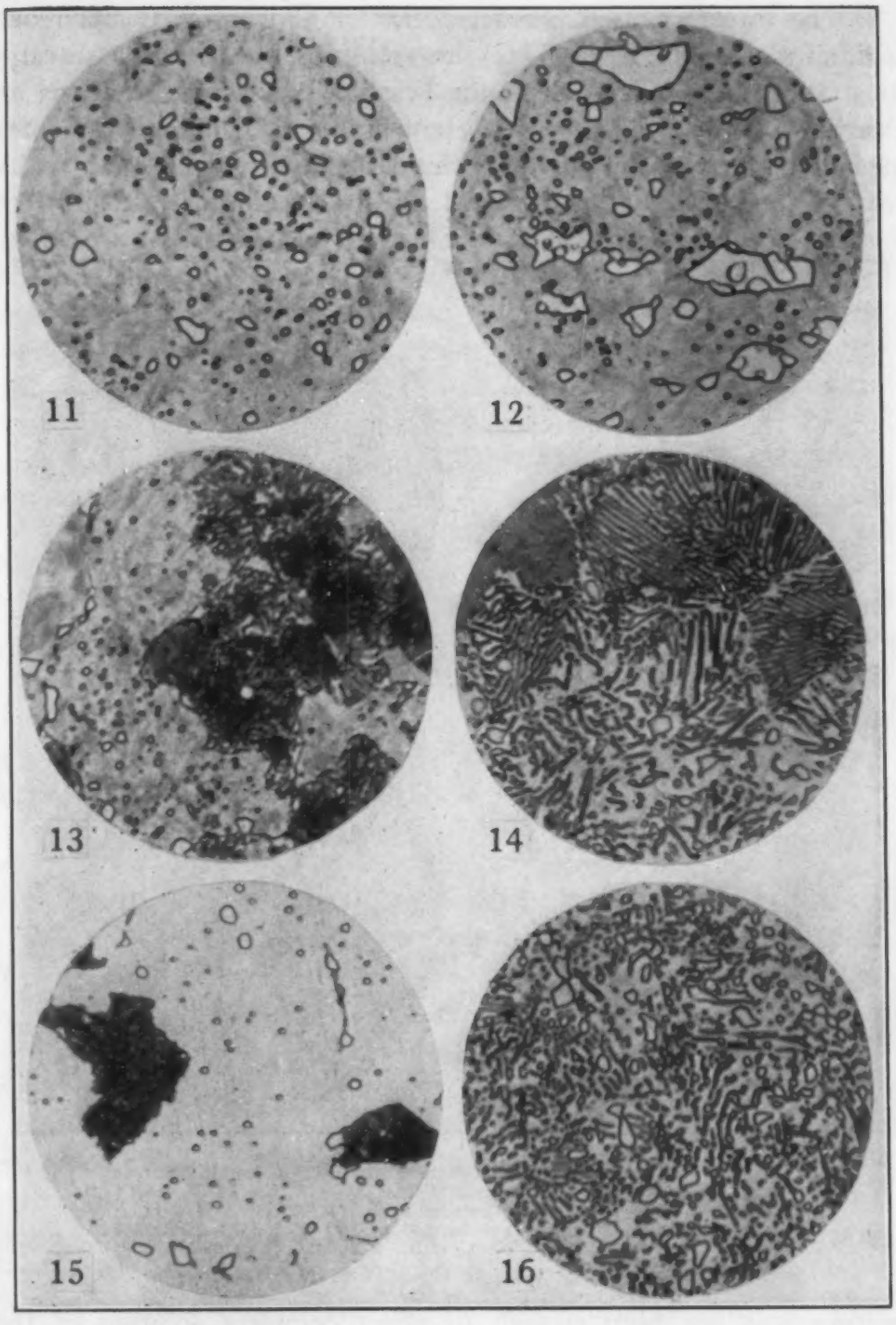


Fig. 11—Alloy Steel C Transformed at 1300 °F for 1 Minute.
Fig. 12—Alloy Steel C Transformed at 1300 °F for 24 Hours.
Fig. 13—Alloy Steel C Transformed at 1200 °F for 30 Minutes.
Fig. 14—Alloy Steel C Transformed at 1200 °F for 3 Hours.
Fig. 15—Alloy Steel C Transformed at 1100 °F for 15 Minutes.
Fig. 16—Alloy Steel C Transformed at 1100 °F for 85 Minutes.
Modified picral etch. × 2000.

The transformation characteristics of alloy steel C upon austenitizing at 1550 °F (845 °C) are set forth in Fig. 10. Steel C illustrates another case where the pearlite and bainite reactions are clearly separated with respect to temperature and there is an intermediate temperature range in which neither reaction will occur within reasonable time. Figs. 11 and 12 show that the austenitizing tem-

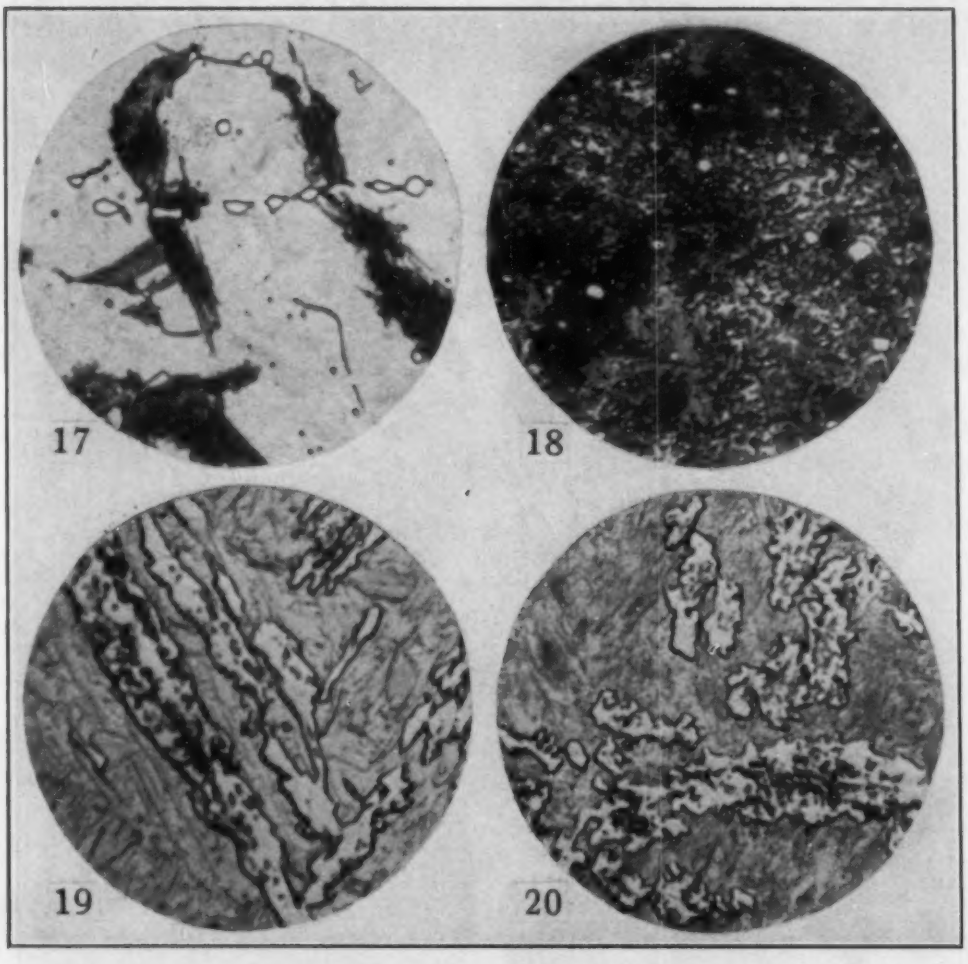


Fig. 17—Alloy Steel C Transformed at 1000 °F for 1 Hour.
Fig. 18—Alloy Steel C Transformed at 1000 °F for 24 Hours.
Fig. 19—Alloy Steel C Transformed at 900 °F for 25 Hours.
Fig. 20—Alloy Steel C Transformed at 800 °F for 34 Hours.
Modified picral etch. × 2000.

perature was not high enough to effect complete solution of the alloy carbides and as a consequence undissolved carbides were found in all of the decomposition products. Figs. 13 to 18 illustrate the transition from coarse to fine pearlite on transformation at various temperatures in the pearlite region. As in steel B, pearlite forms

directly both above and below the knee, very fine pearlite (Fig. 17) being the primary reaction product to temperatures as low as 925 °F. Figs. 19 and 20 depict structures obtained in the intermediate range on isothermal holding for long periods of time. These structures are similar to those shown in the initial paper (1) for steel B in the 700 to 925 °F temperature range. The primary precipitate is the light-etching acicular ferrite and the entrapped particles therein are carbide and austenite (martensite on quench). Whereas in carbon eutectoid steels pearlite forms only at temperatures down to the knee of the TTT-diagram, and bainite below, in the class of steels exemplified by chromium steels, proeutectoid ferrite forms below the knee of the pearlite curve, down to the region where the X-constituent and bainite form, providing an intermediate temperature at which the rate of reaction is very slow.

In steel C the top of the bainite transformation is at approximately 775 °F and two types of structure occur on isothermal transformation at various temperature levels in this region (compare Figs. 21 and 22 with Figs. 25 and 26). Hultgren (2) has stated that in alloy steels of high carbon content the transformation products at lower intermediate temperatures, above 300 °C, form slowly and present structures that are difficult to interpret, because they resemble in certain respects pearlite, in others bainite. He suggested as a possibility that at still lower temperatures (but above M_s in such steels) precipitation of cementite, probably paracementite, may cause martensite to form, as a result of the lowered carbon content, the structure slowly decomposing into a fine mixture of cementite and tempered martensite. In alloy steel C the transformation products form readily but require considerable time for the reactions to go to completion. The structures are complicated in that they resemble the acicular ferrite type of structure at the top of the range (Figs. 21 and 22) and gradually assume the typical dark-etching, acicular appearance of low temperature bainite (Figs. 23 to 26). The low temperature bainite knee in many alloy steels is attended by the initial rejection of a ferrite-like constituent, usually acicular in character, which is sometimes also referred to as bainite, probably inadvisedly. Common to most alloy steels, the microstructural appearance of the bainite changes markedly as a function of temperature (3). At the low temperature of 500 °F (260 °C) only the dark-etching acicular bainite forms, as can be seen in Fig. 25. The structure gradually becomes more granular and lighter etching as the temperature rises;

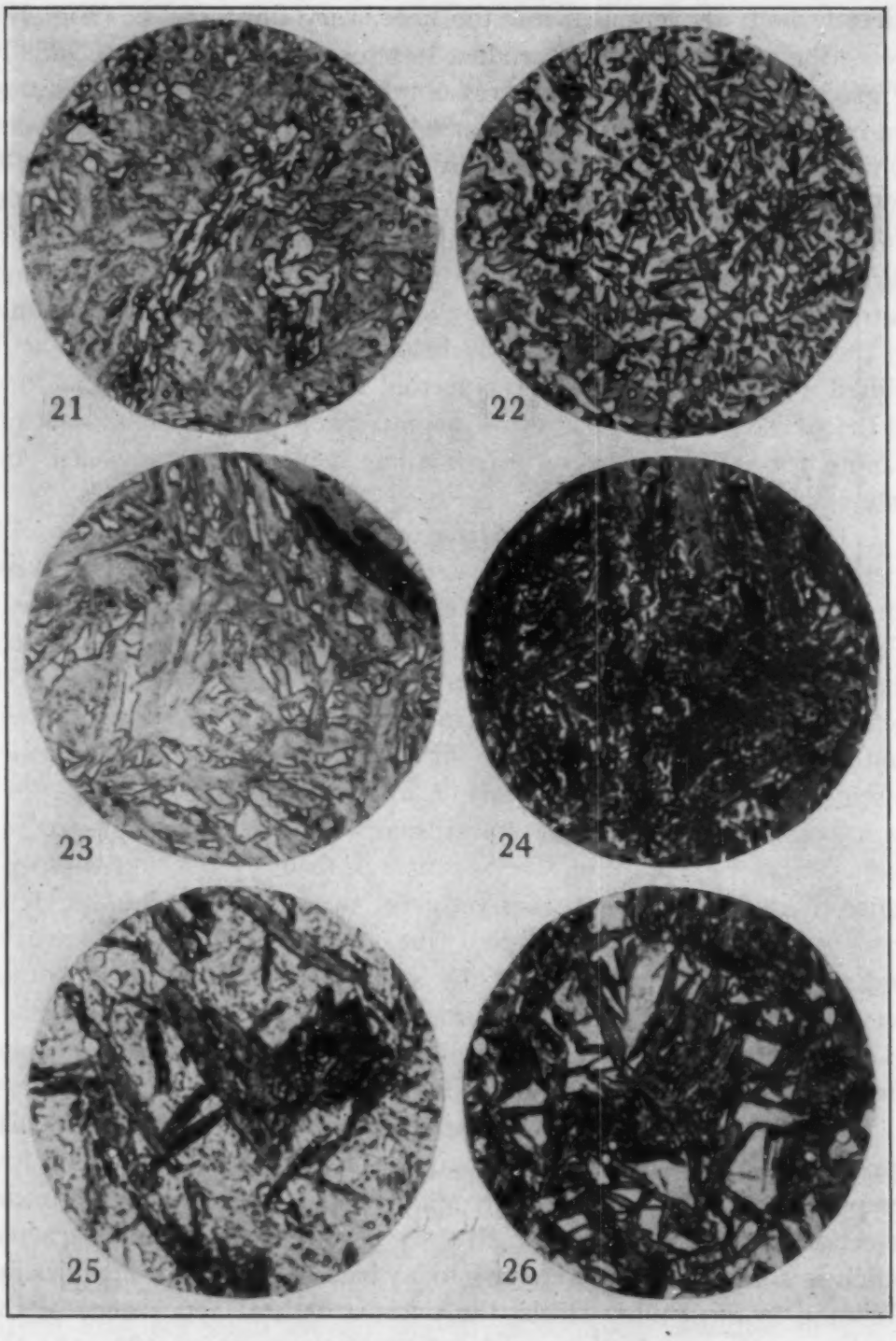


Fig. 21—Alloy Steel C Transformed at 700 °F for 25 Seconds.
Fig. 22—Alloy Steel C Transformed at 700 °F for 26 Hours.
Fig. 23—Alloy Steel C Transformed at 600 °F for 30 Seconds.
Fig. 24—Alloy Steel C Transformed at 600 °F for 336 Hours.
Fig. 25—Alloy Steel C Transformed at 500 °F for 1 Minute.
Fig. 26—Alloy Steel C Transformed at 500 °F for 2 Hours.
Modified picral etch. × 2000.

the carbide particles become larger and more widely spaced finally giving rise to a "ferritic" structure such as that in Fig. 23. The dark-etching acicular bainite also makes its initial appearance on holding test specimens at this temperature (600 °F). The light angular constituent may possibly be some of Hultgren's (2) "para-constituent" which precedes the dark-etching bainite transformation. However, since there is no other evidence of it over the narrow 600 to 700 °F temperature range, it appears more likely that it is the last trace of the acicular ferrite type of transformation product (Fig. 21) which formed at higher temperatures (600 to 750 °F).

A comparison of the position of the pearlite knee for the lower carbon steel B with the high carbon steel C austenitized at 1550 °F (845 °C) indicates that transformation in the latter occurs 100 °F below the former but begins and ends in practically the same interval of time. Thus in the nearly eutectoid steel B containing less alloy and carbon content it is possible to have as great a hardness at the start of the pearlite transformation as in steel C, with fine lamellar pearlite forming instead of the more spheroidal type observed in the latter. This behavior can be rationalized by considering the fact that in steel B there is no precipitation of ferrite preceding the pearlite reaction whereas in steel C excess carbides are present. Effects which contribute to the shifting of the pearlite knee to the left in steel C to a position comparable to that in steel B of lower hardenability are: (a) The presence of many uniformly distributed, undissolved carbide particles which enhance nucleation of the pearlite reaction, (b) the impoverishment of the austenite of alloying elements held by the undissolved carbide particles, which moves the pearlite knee to shorter time, (c) the increase in carbon content decreasing the pearlite reaction as a natural phenomenon. Lyman and Troiano (4) have shown this to be true for a series of 3% chromium steels. These factors were previously cited by Troiano and DeMoss (5) as responsible for a similar behavior observed in low and high carbon Krupp-type carburizing steels and they apply as well to the steels under consideration.

Since the alloy carbides did not readily enter into solution in the austenite at 1550 °F (845 °C), the effect of the alloying elements was lessened in that any portion of the alloy which did not go into solution during the austenitizing treatment and any carbon associated with it did not exert the delaying influence upon austenite transformation that they otherwise would have, and, in fact, actually

hastened the pearlite transformation by reason of nucleation opportunities provided by the undissolved material.

In the intermediate range of hypereutectoid steel C, the usual rules[8] appear to apply to the nucleation and growth of the grain boundary phase and of the Widmanstätten figure, but carbide plates grow from grain-boundary carbide only infrequently, and Widmanstätten precipitation by separate nucleation and growth within the grain is far more pronounced, forming a sharply defined Widmanstätten figure of thin, long plates (1), (6).

References

1. E. A. Loria and H. D. Shephard, "Acicular Transformations in Alloy Steel," TRANSACTIONS, American Society for Metals, Vol. 40, 1948, p. 758-774.
2. A. Hultgren, "Isothermal Transformation of Austenite," TRANSACTIONS, American Society for Metals, Vol. 39, 1947, p. 915-1005.
3. A. R. Troiano, Discussion to Reference 2, p. 994-996.
4. T. Lyman and A. R. Troiano, "Influence of Carbon Content Upon the Transformations in 3% Chromium Steel," TRANSACTIONS, American Society for Metals, Vol. 37, 1946, p. 402-448.
5. A. R. Troiano and J. E. DeMoss, "Transformations in Krupp-type Carburizing Steels," TRANSACTIONS, American Society for Metals, Vol. 39, 1947, p. 788-800.
6. T. Lyman and A. R. Troiano, "Isothermal Transformation of Austenite in One Per Cent Carbon, High Chromium Steels," *Transactions*, American Institute of Mining and Metallurgical Engineers, Vol. 162, 1945, p. 196-222.

[8]The decomposition of austenite at subcritical temperatures, either on cooling or isothermally, is a typical heterogeneous reaction, proceeding by the formation of nuclei and their subsequent growth.

STABILIZATION OF AUSTENITIC STAINLESS STEEL

By Samuel J. Rosenberg and John H. Darr

Abstract

A study was made of the resistance to intergranular attack of twenty-three 18% Cr – 10% Ni austenitic corrosion resisting steels in twelve different initial conditions. Susceptibility to intergranular attack was determined after seven sensitizing treatments, followed by exposure for a maximum of 14 days in a boiling acidified copper sulphate solution.

It was found that maximum susceptibility to intergranular attack was developed by sensitizing either 8 or 21 days at 1020 °F (550 °C). The straight carbon austenitic steels were quite vulnerable to attack, although decrease in carbon content decreased the degree of vulnerability. The columbium- and titanium-treated steels were satisfactorily resistant to attack, provided the Cb/C or Ti/C ratios were sufficiently high. These ratios varied, depending on the initial condition of the steel. The carbon content of the treated steels had no influence upon the resistance to intergranular attack, the predominating factor being the Cb/C or Ti/C ratio.

Introduction

AN undesirable characteristic of the austenitic stainless steels is their susceptibility to intergranular embrittlement after exposure to moderately elevated temperatures. This susceptibility to embrittlement may be decreased or eliminated, i.e., the steels may be stabilized against intergranular embrittlement, by the addition of titanium or columbium, usually in conjunction with a stabilizing heat treatment.

A diversity of opinion as to the relative amounts of titanium or columbium necessary for effective stabilization, the injurious effect of carbon content, and the necessity for stabilizing heat treat-

Publication approved by the Director of the National Bureau of Standards.

A paper presented before the Thirtieth Annual Convention of the Society, held in Philadelphia, October 23 to 29, 1948. Of the authors, Samuel J. Rosenberg is senior metallurgist, and John H. Darr is junior metallurgist, National Bureau of Standards, Washington, D. C. Manuscript received January 10, 1948.

ments, led the Bureau of Aeronautics, Navy Department, to request the National Bureau of Standards to undertake a study of factors affecting the stabilization of the 18-8 type of steels. This paper summarizes the results of such an investigation.

Theory of Sensitization and Stabilization

Intergranular embrittlement (or corrosion—the terms are usually used synonymously) may be considered as a disease of 18-8 steels, although it is not peculiar to these steels alone. Specifically, this type of corrosion is particularly pronounced in some 18-8 steels which have been subjected to moderately elevated temperatures [700 to 1400 °F (370 to 760 °C)] and are either simultaneously or subsequently subjected to corrosive conditions. Exposure to these elevated temperatures causes the precipitation of what are generally conceded to be chromium carbides at the grain boundaries, and steels having such carbide precipitation have been found to be more or less susceptible to intergranular corrosion, whereas steels which do not exhibit this structure are generally immune.

Annealed 18-8 stainless steel [quenched from temperatures in the neighborhood of 1800 to 2000 °F (980 to 1095 °C)] theoretically consists of metastable austenite, in this case a supersaturated solid solution of carbon or of chromium carbide in chromium-nickel austenite. Upon reheating to moderately elevated temperatures, chromium carbide (Cr_4C) precipitates at the grain boundaries. One school of thought believes that this precipitation reduces the chromium content of the metal near the grain boundaries to a level below that necessary to resist corrosion. This appears to be the most prevalent view. Others believe that internal strains resulting from the precipitation of carbides, and from the formation of alpha iron from the metastable austenite, are the cause of intergranular corrosion. Still another belief is that the electrolytic effect resulting from a difference in potential between grains and grain boundaries is responsible. Regardless of the underlying theory, however, it is generally agreed that the presence of chromium carbides distributed in the form of a thin, nearly continuous network at the grain boundaries is an indication of material which is susceptible to intergranular corrosion. The larger isolated carbides which result after sufficient time at temperature has been allowed for coalescence of the precipitated carbides and for replenishment by diffusion of chromium in the de-

pleted areas do not appear to be associated with intergranular corrosion.

The earliest efforts to prevent intergranular embrittlement were directed toward the manufacture of 18-8 with low carbon content, on the theory that precipitation of chromium carbide would thereby be minimized or even eliminated (1), (2), (3)[1]. It was also suggested that a treatment at about 1600 °F (870 °C) resulted in a decreased susceptibility to intergranular corrosion upon subsequent exposure at lower temperatures. This stabilizing (sometimes termed "desensitizing") treatment was presumed to precipitate sufficient chromium carbides as coalesced particles, and also to permit diffusion of chromium, so that the amount of carbon which would be available to precipitate as fine chromium carbides at lower (sensitizing) temperatures would be negligible.

It was also reported that decreasing the austenitic grain size diminished the severity of intergranular attack (4) by providing extra grain boundary area for precipitation of carbides; that cold-rolled material was more resistant to intergranular attack (3) because of the availability of numerous slip planes for the precipitation of carbides upon subsequent heating; and that the addition of elements which caused the formation of delta ferrite was also beneficial (5) in that, because of the lower solubility for carbides, precipitation occurred in the areas of delta ferrite.

The most commonly used method of preventing intergranular corrosion in 18-8 consists of adding a strongly carbide-forming element to the steel. The function of this element is to combine with the carbon, thus allowing the chromium to remain in solid solution in the austenite. To be effective, this alloy carbide should be less soluble in the chromium-nickel austenite than is the chromium carbide. The two elements most frequently used are titanium and columbium (6), (7). It is known that these elements are more strongly carbide forming than is chromium, and evidence is available that the titanium and columbium carbides are considerably less soluble in 18-8 austenite than is chromium carbide. Theoretically, if the carbon of 18-8 stainless is "fixed" by either of these stabilizing elements, that is, precipitated as TiC or CbC, no chromium carbide precipitates at the grain boundaries upon subsequent reheating to sensitizing temperatures and the steel thereafter exhibits no intercrystalline embrittlement upon exposure to a corroding medium.

[1]The figures appearing in parentheses pertain to the references appended to this paper.

The atomic weight of carbon is 12.01 and that of titanium is 47.90, and since titanium forms a carbide corresponding to TiC, it is necessary, theoretically, to have about four times as much titanium as carbon in order to fix all the carbon as titanium carbide. Columbium has an atomic weight of 92.91, and since columbium forms a carbide corresponding to CbC, the theoretical minimum amount of columbium which must be added to fix the carbon is slightly less than eight times the amount of carbon.

Stabilization consists of reheating the Cb or Ti-treated steels within the temperature range 1550 to 1800 °F (845 to 980 °C), usually at about 1600 °F (870 °C). At these temperatures the precipitation of titanium and columbium carbides within the austenitic grains is facilitated. The slight amount of carbon remaining in solid solution after this treatment is (theoretically) insufficient to cause any deleterious effects (in the form of Cr_4C precipitated at the grain boundaries) upon subsequent reheating to sensitizing temperatures.

Materials

Most of the steels used in this investigation were experimental melts, although a few commercial steels were included. The experimental steels were melted in an induction furnace and poured into 3-inch square big-end-up tapered molds equipped with hot tops. Each experimental heat weighed about 75 pounds and all were made in the foundry of the Naval Research Laboratory. The ingots were shaped on all four sides as much as necessary to produce clean surfaces, following which they were hot-forged to slabs about 3 inches wide by 1 inch thick. Some of these ingots were forged at the Rustless Iron and Steel Division, American Rolling Mill Company, Baltimore, Md.; all others were forged at the Naval Research Laboratory. The slabs were surface ground on four sides and rolled into 0.050-inch strip at the American Rolling Mill Company, Middletown, Ohio, the schedule of operations being as follows:

1. Hot roll at 2000 to 2200 °F (1090 to 1205 °C) to 0.125 inch and straighten.
2. Anneal 6 minutes at 1950 to 2000 °F (1065 to 1090 °C) and air cool.
3. Pickle
   (a) 2½ minutes in 10% H_2SO_4 at 190 °F.
   (b) 45 minutes in caustic permanganate at 200 °F.
   (c) 10 minutes in 1½% HF plus 10% HNO_3 at 130 °F.
4. Cold roll to 0.080 inch and straighten.
5. Anneal 6 minutes at 1950 to 2000 °F (1065 to 1090 °C) and air cool.

6. Pickle
   (b) and (c) only under 3 above.
7. Cold roll to 0.050 inch and straighten.

The final strip thus had a cold reduction of 37.5%. Although the sequence of fabrication was not known, all commercial steels were furnished in cold-rolled strip 0.050 inch thick, the same as the experimental steels.

Chemical analyses of all the steels were made on samples cut from the finished strip; these analyses are given in Table I. All experimental steels were made to the base analysis of 18% chromium, 10% nickel, 1¼% manganese, and 0.40% silicon.

During the progress of this investigation some question was raised as to the effect of nitrogen on the Cb/C or Ti/C ratio. Analyses for nitrogen were therefore made, both chemically and by vacuum fusion. It is known that nitrogen combines with both titanium and columbium. The acid soluble and acid insoluble nitrogen can be separated by treatment of the steel with dilute sulphuric acid. For purposes of calculation (as noted in Table I), it was assumed that all of the acid insoluble nitrogen was combined with either titanium or columbium, as the case might be. Considering the fact that the steels which contained no titanium or columbium also contained no acid insoluble nitrogen, this assumption appeared to be quite plausible. The revised percentages of titanium and columbium and the revised ratios of Ti/C and Cb/C were calculated after allowing for the amounts of titanium and columbium combined with the acid insoluble nitrogen and are included in Table I.

Procedure

Specimens 3 inches long by ½ inch wide by 0.050 inch nominal thickness were taken longitudinally to the direction of rolling. A small hole was punched in one end of each specimen so that groups of specimens could be strung on wire for sensitizing treatments. All such treatments were carried out in furnaces of the vertical muffle type, electrically heated, and constructed especially for this work. Inside dimensions of the muffles were 4 inches in diameter by 18 inches long. Temperature variations within the working length of each furnace were less than 10 °F. Each furnace was controlled by an individual recording potentiometer controller.

Corrosion tests for development of intergranular embrittlement

Table I
Analyses of the Test Steels

Steel No.	% C	% Mn	% Si	% Cr	% Ni	% Cb	% Ti	Ratio Cb/C	Ratio Ti/C	% Nitrogen (Vacuum Fusion)	% Nitrogen (Chemical Analysis) Total	Acid Soluble	Acid Insoluble (by Difference)	% (Revised)* Cb	% (Revised)* Ti	Ratio (Revised)* Cb/C	Ratio (Revised)* Ti/C
C-1	0.025	0.70	0.50	19.7	8.8	....	....	....	...	0.041	0.039	0.039	0.000	....	....	...	...
C-10	0.026	0.59	0.40	17.2	12.6	....	....	....	...	0.026	0.026	0.025	0.001	....	....	...	...
S-37	0.044	1.10	0.33	17.8	10.5	....	....	....	...	0.049	0.053	0.053	0.000	....	....	...	...
S-4	0.072	1.13	0.45	18.0	10.2	....	....	....	...	0.036	0.036	0.035	0.001	....	....	...	...
S-23	0.113	1.11	0.37	17.6	10.2	....	....	....	...	0.041	0.039	0.039	0.000	....	....	...	...
S-26	0.068	1.21	0.37	17.8	10.0	0.50	....	7.4	...	0.065	0.061	0.041	0.020	0.37	....	5.4	...
S-6	0.070	1.23	0.54	17.6	10.1	0.61	....	8.7	...	0.056	0.054	0.034	0.020	0.48	....	6.9	...
S-12	0.074	1.23	0.38	17.9	10.0	0.75	....	10.1	...	0.051	0.047	0.024	0.023	0.60	....	8.1	...
C-3	0.060	1.69	0.67	17.7	11.0	0.71	....	11.8	...	0.032	0.035	0.015	0.020	0.58	....	9.7	...
S-27	0.087	1.19	0.40	17.8	10.1	0.76	....	8.7	...	0.059	0.057	0.030	0.027	0.58	....	6.7	...
S-28	0.115	1.22	0.40	17.7	9.9	0.92	....	8.0	...	0.045	0.045	0.022	0.023	0.77	....	6.7	...
S-17	0.117	1.21	0.40	18.0	10.1	1.14	....	9.7	...	0.039	0.040	0.016	0.024	0.98	....	8.3	...
S-18	0.132	1.18	0.40	17.9	10.1	1.47	....	11.1	...	0.044	0.046	0.014	0.032	1.26	....	9.5	...
S-34	0.067	1.17	0.45	17.7	10.2	....	0.26	....	3.9	0.031	0.039	0.001	0.038	....	0.13	...	1.9
S-21	0.071	1.49	0.41	17.9	10.1	....	0.32	....	4.5	0.027	0.031	0.002	0.029	....	0.22	...	3.1
C-6	0.064	1.32	0.40	18.3	10.0	....	0.35	....	5.5	0.012	0.013	0.002	0.011	....	0.31	...	4.8
S-39	0.065	1.23	0.53	18.2	10.1	....	0.36	....	5.5	0.023	0.023	0.001	0.022	....	0.28	...	4.3
C-2	0.070	1.52	0.50	17.8	9.6	....	0.50	....	7.1	0.010	0.010	0.001	0.009	....	0.47	...	6.7
C-8	0.075	1.25	0.52	18.0	10.6	....	0.59	....	7.9	0.006	0.007	0.001	0.006	....	0.57	...	7.6
S-25	0.082	1.23	0.40	17.7	9.9	....	0.37	....	4.5	0.017	0.022	0.001	0.021	....	0.30	...	3.7
S-35	0.107	1.29	0.42	17.5	9.7	....	0.44	....	4.1	0.012	0.016	0.001	0.015	....	0.39	...	3.6
S-36	0.109	1.35	0.48	17.5	10.0	....	0.54	....	5.0	0.022	0.018	0.001	0.017	....	0.48	...	4.4
S-32	0.105	1.44	0.40	18.0	9.9	....	0.61	....	5.8	0.016	0.017	0.001	0.016	....	0.56	...	5.3

Steels designated by the prefix "S" are laboratory melts; those designated by the prefix "C" are commercial melts.

*The revised percentages of Ti and Cb were calculated by assuming that all of the acid insoluble nitrogen was combined as TiN or CbN. According to the atomic weights of these elements, 1 part of nitrogen will combine with 3.43 parts of titanium or 6.64 parts of columbium by weight. Multiplying these figures by the amount of acid insoluble nitrogen in the titanium- and columbium-treated steels, respectively, and subtracting the results from the amounts of titanium and columbium present in the steels gives the revised amounts of titanium or columbium available for combination with carbon. The revised Ti/C and Cb/C ratios were then obtained by dividing the revised percentages of titanium and columbium by the carbon contents.

were conducted in a boiling acidified copper sulphate solution contained in 2-liter wide-mouth Erlenmeyer flasks. These flasks were equipped with ground glass joints for fitting the reflux condensers. Specimens were laid in glass racks so that there was no metallic contact between specimens. No more than seven specimens were placed in an individual flask and material of straight 18-10, 18-10 Cb, and 18-10 Ti was always segregated in different flasks. A minimum of 35 cc of acidified copper sulphate solution per square inch of surface area was used. The solution was changed every 48 hours at which time all specimens were examined; those showing definite evidence of intergranular attack were removed. Where evidence of attack, as indicated by a change in color of the solution, occurred in less than two days, the run was interrupted to remove the failed specimen or specimens and the solution was changed. Maximum time of exposure in the acidified copper sulphate solution was 14 days.

Preliminary tests indicated the necessity of carefully controlling certain factors. The original choice of concentration for the boiling copper sulphate – sulphuric acid solution was 13 g of $CuSO_4 \cdot 5H_2O$, 47 cc of concentrated H_2SO_4, and distilled water to make 1 liter of solution. This solution, which has been used by some investigators, corresponded to 0.8% of $CuSO_4$ and 8.2% of H_2SO_4 and the ratio of $CuSO_4$ to H_2SO_4 proved too low to prevent surface corrosion in many of the steels. Since the resultant corrosion complicated the evaluation of intergranular embrittlement, this solution was discarded in favor of that containing 100 g of $CuSO_4 \cdot 5H_2O$, 100 cc of concentrated H_2SO_4 (sp. gr. 1.84), and 900 cc of distilled water. This solution corresponded to 5.4% of $CuSO_4$ and 15.5% of H_2SO_4 by weight.

The scale which formed on specimens during sensitization was influenced by both time and temperature. In order to eliminate the variable which scale would introduce, it was decided to remove all scale. Polishing was tried and proved to be too time-consuming; pickling was therefore adopted with a schedule of operations as follows:

1. Pickle in 8% H_2SO_4 + 4% HCl at 160 °F for 10 minutes; wash, scrub, and dry.
2. Pickle in 10% HNO_3 + 1% HF at 160 °F for 5 minutes; wash, scrub, and dry.
3. Passivate in 20% HNO_3 at 125 °F for 15 minutes; wash and dry.

To ascertain whether the method of scale removal influenced the susceptibility to intergranular attack, check tests were made on cer-

tain specimens both as pickled and as polished. These tests showed that the method of scale removal had no detectable effect on the specimens which were extremely vulnerable to intergranular embrittlement. With specimens which were moderately vulnerable, it appeared that the extent of intergranular attack was greater in specimens which had been pickled than in specimens which had been polished. Typical microstructures of such specimens after corrosion are shown in Fig. 1. Since it is frequently commercial practice to finish stainless steels by pickling, it appeared logical to test the steels as finished in that manner.

The susceptibility to intergranular attack of the various steels was determined for 12 different initial conditions, as listed in Tables 2 to 24. A few steels were tested in only 5 different initial conditions, as may be seen from the particular table involved.

In the first series of tests (carried out on the cold-rolled steels), specimens from each steel were tested in 16 sensitized conditions. Four sensitizing temperatures were used—840, 1020, 1200, and 1380 °F (450, 550, 650, and 750 °C). Single specimens were held at each sensitizing temperature for 2 hours, 2, 8, and 21 days. After exposure to the boiling copper sulphate solution it was apparent that certain of these sensitizing treatments were quite innocuous and could be discarded. It was decided, therefore, to decrease the number of sensitizing conditions to seven in all—these were 21 days at 840 °F (450 °C); 2 hours, 2, 8, and 21 days at 1020 °F (550 °C); and 2 hours and 2 days at 1200 °F (650 °C). A control specimen, not sensitized, was included in each series.

Evaluation of intergranular embrittlement was made by observations of: (a) change in electrical resistivity, (b) loss in metallic ring when the test specimen was dropped on a steel plate, (c) extent of cracks occurring after bend tests of 180 degrees, and (d) appearance of the corroded sections under the microscope. The interpretation of these various tests was frequently influenced by the personal factor, particularly in cases where only slight evidence of failure existed. Frequently, also, evidence of failure by one method was not corroborated by another.

Results and Discussion

All specimens were examined for carbide distribution subsequent to sensitizing. The type of distribution of the precipitated

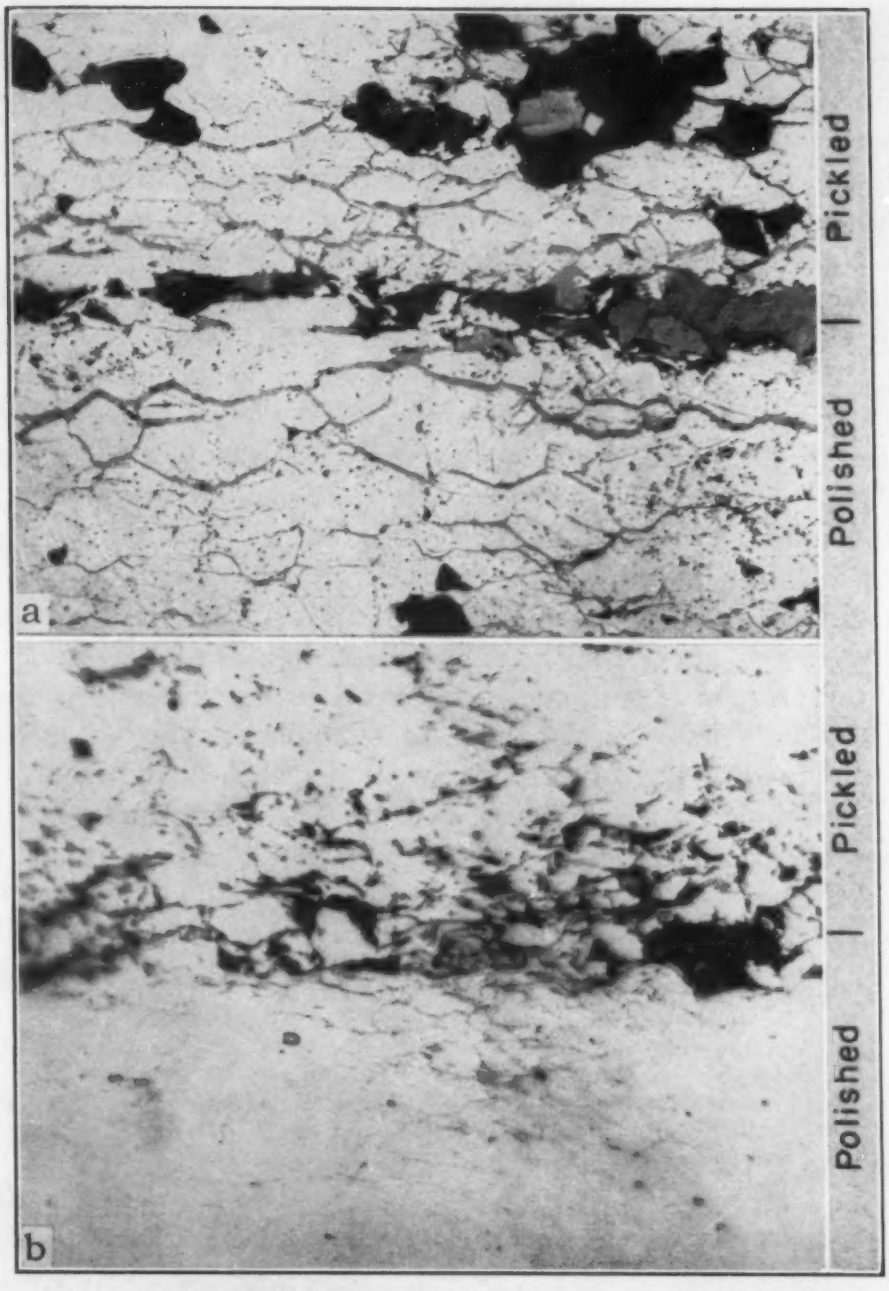


Fig. 1—Effect of Method of Scale Removal on Susceptibility to Intergranular Attack. a—Extremely vulnerable material after 2 days in the boiling acidified copper sulphate solution. Unetched. × 100. b—Less vulnerable material after 6 days in the boiling acidified copper sulphate solution. Unetched. × 500.

carbides was not an infallible indication of the resistance to intergranular attack. Steels in which the carbides were distributed randomly were usually resistant to intergranular attack. However, steels which contained carbides at the grain boundaries, even though

these carbides were distributed as a continuous network, either were or were not susceptible to intergranular attack, depending on the time-temperature relation during sensitization. Frequently the microstructures of susceptible and unsusceptible specimens of the same steel appeared quite similar. A rather striking illustration of this statement is shown in Fig. 2. This figure shows the microstructure of a straight carbon (0.09%) austenitic steel, initially as cold-rolled, after sensitizing 2 hours at 1200 °F (650 °C) (Fig. 2a) and after sensitizing 2 days at 1200 °F (650 °C) (Fig. 2b). Both micrographs show a precipitation of carbides at the grain boundaries and on various slip planes and it is evident that the microstructures resulting from the two treatments are indistinguishable. The behavior of these two specimens after exposure to the boiling acidified copper sulphate solution, however, differed radically. Specimen "a" was exposed 2 days and suffered severe intergranular corrosion (see left side of Fig. 2c). Specimen "b" was exposed 14 days and showed no evidence of intergranular attack (see right side of Fig. 2c).

Since a total of well over 2500 individual specimens was tested, it is obviously impractical to present a detailed account of the test data procured. All data were assembled in tabular form for study. The performance of each specimen was then rated on the basis of each of the four methods of evaluation (electrical resistivity, metallic ring, bend test, and microstructure after corrosion). An arbitrary system of appraisal was used, as follows:

A—Completely immune to intergranular attack
  Electrical resistivity—no increase
  Metallic ring—no impairment
  Bend test—no evidence of cracks
  Microstructure—no evidence of intergranular attack
B—Practically immune to intergranular attack
  Electrical resistivity—not more than 12% increase
  Metallic ring—slightly dead
  Bend test—slight cracks
  Microstructure—slight intergranular attack in extreme surface layers only
C—Moderately vulnerable to intergranular attack
  Electrical resistivity—more than 12% but not more than 25% increase
  Metallic ring—slight
  Bend test—cracked
  Microstructure—moderately severe intergranular attack in surface layers only
D—Vulnerable to intergranular attack
  Electrical resistivity—more than 25% increase
  Metallic ring—dead
  Bend test—broke
  Microstructure—intergranular attack
E—Extremely vulnerable
  Same as D but occurring in a few days.

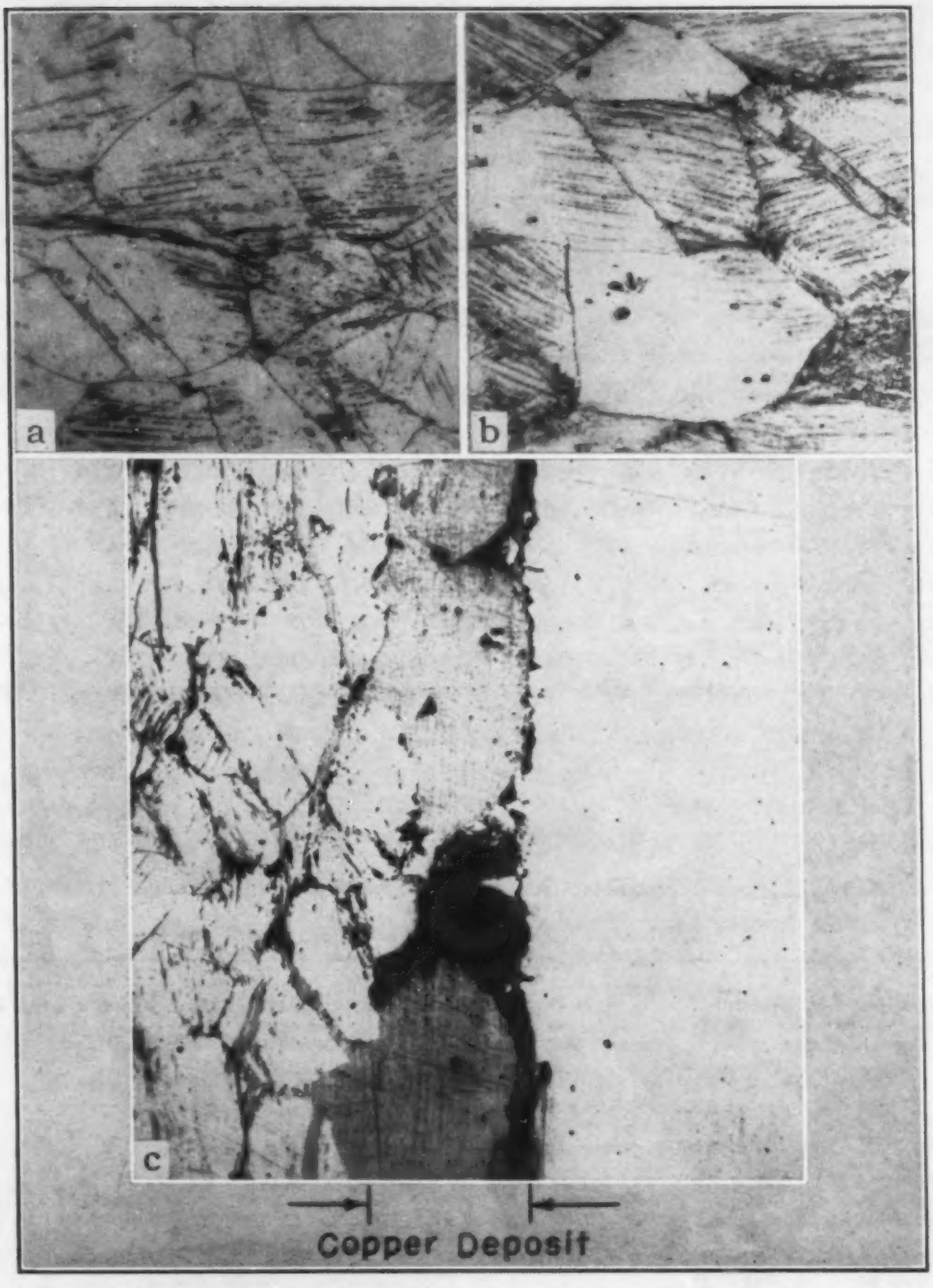


Fig. 2—Structure of Straight Carbon (0.09%) Austenitic Stainless Steel, Initially as Cold-Rolled, Before and After Exposure to the Boiling Acidified Copper Sulphate Solution. a—Sensitized 2 hours at 1200 °F. Heavy carbide precipitation at grain boundaries and on slip planes. Etched electrolytically 10 minutes in 10% sodium cyanide. × 500. b—Sensitized 2 days at 1200 °F (650 °C). Heavy carbide precipitation at grain boundaries and on slip planes. Etched electrolytically in 10% sodium cyanide. × 500. c—After exposure to boiling acidified copper sulphate solution. Specimen "a" (left side of micrograph) was exposed 2 days and suffered severe intergranular attack. Specimen "b" (right side of micrograph) was exposed 14 days and showed no evidence of intergranular attack, yet both had the same type of carbide precipitation. The massive gray globules attached to specimen "a" are particles of copper deposited from the acidified copper sulphate solution. Unetched. × 250.

Table II

Effect of Various Treatments Upon the Susceptibility to Intergranular Attack of Steel C-1

(Carbon = 0.025%—no stabilizing element)

Treatment of Steel Subsequent to Cold Rolling		Sensitizing Treatment							
Annealing	Stabilizing	None	21 Days at 840 °F	2 Hours at 1020 °F	2 Days at 1020 °F	8 Days at 1020 °F	21 Days at 1020 °F	2 Hours at 1200 °F	2 Days at 1200 °F
None	None	A	A	A	D−	E+	D−	A	A
None	½ hour at 1600 °F, A.C.	A	A−	A	C	D−	D−	A	A
½ hour at 1800 °F, W.Q.	None	A	A	A	DE	DE	E	A−	A
½ hour at 1800 °F, W.Q.	½ hour at 1600 °F, A.C.	A	A	A	B	DE	E+	A	A
½ hour at 1800 °F, W.Q.	2 hours at 1600 °F, A.C.	A	A−	A	B	DE	DE	A−	A
½ hour at 1800 °F, A.C.	None	A	A	A	C−	D	CD	A−	A
½ hour at 1800 °F, A.C.	1 hour at 1600 °F, A.C.	A	A	A	C−	D	D	A	A−
3 min. at 1975 °F, W.Q.	None	A	A	A	CD	D	CD	A	A
3 min. at 1975 °F, W.Q.	1 hour at 1600 °F, A.C.	A	A	A	BC	CD	CD	A	A
3 min. at 1975 °F, A.C.	None	A	A	A	B−	DE	C	A	A
3 min. at 1975 °F, A.C.	½ hour at 1600 °F, A.C.	A	A	A	D+	D	D	A	A−
3 min. at 1975 °F, A.C.	2 hours at 1600 °F, A.C.	A	A	A	C−	D−	D+	A−	A−

Table III

Effect of Various Treatments Upon the Susceptibility to Intergranular Attack of Steel C-10

(Carbon = 0.026%—no stabilizing element)

Treatment of Steel Subsequent to Cold Rolling		Sensitizing Treatment							
Annealing	Stabilizing	None	21 Days at 840 °F	2 Hours at 1020 °F	2 Days at 1020 °F	8 Days at 1020 °F	21 Days at 1020 °F	2 Hours at 1200 °F	2 Days at 1200 °F
None	None	A	B+	A	B−	A	A−	A−	A
None	½ hour at 1600 °F, A.C.	A	A	A−	DE	E	E	A−	B−
½ hour at 1800 °F, W.Q.	None	A−	A	A	E+	E	E	AB	C−
½ hour at 1800 °F, W.Q.	½ hour at 1600 °F, A.C.	A	A	A	E+	E	E	A	B−
½ hour at 1800 °F, W.Q.	2 hours at 1600 °F, A.C.	A−	A	A	E+	E	E	A−	BC
½ hour at 1800 °F, A.C.	None	A	A	A	E+	E	E	AB	CD
½ hour at 1800 °F, A.C.	1 hour at 1600 °F, A.C.	A	A	A	E	E	E	AB	C
3 min. at 1975 °F, W.Q.	None	A	A	A	E	E	E	A−	A−
3 min. at 1975 °F, W.Q.	1 hour at 1600 °F, A.C.	A	A	A	E+	E	E	A−	BC
3 min. at 1975 °F, A.C.	None	A	A	A	D+	E	E	A	BC
3 min. at 1975 °F, A.C.	½ hour at 1600 °F, A.C.	A	A	A	D+	E	E	A	C+
3 min. at 1975 °F, A.C.	2 hours at 1600 °F, A.C.	A	A	A	D	E	E	A	C−

The four ratings obtained for each individual specimen were then averaged by assigning numerical values to the ratings (A = 4, B = 3, C = 2, D = 1, E = 0) and converting to the appropriate letter symbol. Plus or minus signs were used to indicate averages falling slightly above or below letters, respectively, and averages falling midway between two letters were denoted by both letters. These averages were then used to prepare Tables II to XXIV, inclusive, which summarize qualitatively the performance of each steel after various annealing, stabilizing, and sensitizing treatments. The averaged letter symbols may be considered as an order of merit, bearing in mind that the differences between A and B are rather slight and those between D and E are very large. Since specimens were exposed to the boiling acidified copper sulphate solution for a maximum time of 14 days, specimens which were rated B and C, and in many cases even D, might have been rated as satisfactory had they been subjected to the corroding solution for the more or less standardized time of only 2 days.

A noteworthy feature shown by these tables is that the sensitizing temperature of 1200 °F (650 °C), which is commonly specified, is too high to effect maximum susceptibility to intergranular attack. Exposure to a sensitizing temperature of 1020 °F (550 °C) is much more effective, provided the time of exposure is quite long. A period of 8 or 21 days at 1020 °F (550 °C) appeared to be the most severe sensitizing treatment of those used. It was not unusual for steels which showed complete immunity to intergranular attack after sensitizing either 2 hours or 2 days at 1200 °F (650 °C) to be definitely

Table IV
Effect of Various Treatments Upon the Susceptibility to Intergranular Attack of Steel S-37
(Carbon = 0.044%—no stabilizing element)

Treatment of Steel Subsequent to Cold Rolling		Sensitizing Treatment							
Annealing	Stabilizing	None	21 Days at 840 °F	2 Hours at 1020 °F	2 Days at 1020 °F	8 Days at 1020 °F	21 Days at 1020 °F	2 Hours at 1200 °F	2 Days at 1200 °F
None	None	A	AB	A	E+	E	D+	AB	A
None	½ hour at 1600 °F, A.C.	A	D	AB	E	E	E	B+	A
½ hour at 1800 °F, W.Q.	None	A	A−	A	E+	E	E	D+	D−
½ hour at 1800 °F, W.Q.	½ hour at 1600 °F, A.C.	A	A	A−	DE	E	E	A	E
½ hour at 1800 °F, W.Q.	2 hours at 1600 °F, A.C.	A	A−	A−	CD	E	E	BC	D

Table V
Effect of Various Treatments Upon the Susceptibility to Intergranular Attack of Steel S-4
(Carbon = 0.072%—no stabilizing element)

Treatment of Steel Subsequent to Cold Rolling		Sensitizing Treatment							
Annealing	Stabilizing	None	21 Days at 840 °F	2 Hours at 1020 °F	2 Days at 1020 °F	8 Days at 1020 °F	21 Days at 1020 °F	2 Hours at 1200 °F	2 Days at 1200 °F
None	None	A	D+	DE	E	E	E	E	A
None	½ hour at 1600 °F, A.C.	B	E	E	E	E	E	CD	A
½ hour at 1800 °F, W.Q.	None	A	A−	A	E	E	E	E	E
½ hour at 1800 °F, W.Q.	½ hour at 1600 °F, A.C.	DE	E	E	E	E	E	E	E
½ hour at 1800 °F, W.Q.	2 hours at 1600 °F, A.C.	D	E	E	E	E	E	E	E+
½ hour at 1800 °F, A.C.	None	A	D	A	E	E	E	E	E
½ hour at 1800 °F, A.C.	1 hour at 1600 °F, A.C.	C−	E	E	E	E	E	E	D
3 min. at 1975 °F, W.Q.	None	A	A	A	DE	E	E	E	E
3 min. at 1975 °F, W.Q.	1 hour at 1600 °F, A.C.	D	E	E+	E	E+	E+	DE	E
3 min. at 1975 °F, A.C.	None	A	A	A	D	E	E	E	E
3 min. at 1975 °F, A.C.	½ hour at 1600 °F, A.C.	C	D	D	E	E	E	E	E
3 min. at 1975 °F, A.C.	2 hours at 1600 °F, A.C.	C+	E+	E+	E+	E	E	E	E

Table VI
Effect of Various Treatments Upon the Susceptibility to Intergranular Attack of Steel S-23
(Carbon = 0.113%—no stabilizing element)

Treatment of Steel Subsequent to Cold Rolling		Sensitizing Treatment							
Annealing	Stabilizing	None	21 Days at 840 °F	2 Hours at 1020 °F	2 Days at 1020 °F	8 Days at 1020 °F	21 Days at 1020 °F	2 Hours at 1200 °F	2 Days at 1200 °F
None	None	A	D	DE	E	E	E	E	A
None	½ hour at 1600 °F, A.C.	C+	E	E	E+	E	E+	D	A
½ hour at 1800 °F, W.Q.	None	A	B+	D+	E	E	E	E	E
½ hour at 1800 °F, W.Q.	½ hour at 1600 °F, A.C.	E+	E+	E	E+	E+	E	E	E
½ hour at 1800 °F, W.Q.	2 hours at 1600 °F, A.C.	D	E	E	E	E	E+	E	BC

vulnerable to intergranular attack after sensitizing for either 8 or 21 days at 1020 °F (550 °C). It is possible that a shorter period of time at a temperature higher than 1020 °F (550 °C), but lower than 1200 °F (650 °C), would be equally effective in causing maximum sensitization. This possibility, however, was not explored during this investigation.

Considering the steels which contained no stabilizing elements (Tables II to VI, inclusive), it is apparent that all of these were quite

Table VII

Effect of Various Treatments Upon the Susceptibility to Intergranular Attack of Steel S-26

(Carbon = 0.068%, Columbium = 0.50%; Cb/C = 7.4)

Treatment of Steel Subsequent to Cold Rolling		Sensitizing Treatment							
Annealing	Stabilizing	None	21 Days at 840 °F	2 Hours at 1020 °F	2 Days at 1020 °F	8 Days at 1020 °F	21 Days at 1020 °F	2 Hours at 1200 °F	2 Days at 1200 °F
None	None	A	B+	A−	D	B+	A	A	A
None	½ hour at 1600 °F, A.C.	A	A	A	D	DE	D+	A	A
½ hour at 1800 °F, W.Q.	None	A	A	A	E+	E	E	A	A
½ hour at 1800 °F, W.Q.	½ hour at 1600 °F, A.C.	A	A	A	D	E+	E+	A	A
½ hour at 1800 °F, W.Q.	2 hours at 1600 °F, A.C.	A	A	A	D+	E+	E	A	A
½ hour at 1800 °F, A.C.	None	A	A	A	DE	E	E+	AB	A
½ hour at 1800 °F, A.C.	1 hour at 1600 °F, A.C.	A	A	A	E+	E+	E+	A−	A
3 min. at 1975 °F, W.Q.	None	A	A	A	C−	E	E	BC	A−
3 min. at 1975 °F, W.Q.	1 hour at 1600 °F, A.C.	A	A	A	D	DE	D	A−	A
3 min. at 1975 °F, A.C.	None	A	A	A	E+	E+	E	A	A−
3 min. at 1975 °F, A.C.	½ hour at 1600 °F, A.C.	A	A	A	DE	E	E+	A−	A−
3 min. at 1975 °F, A.C.	2 hours at 1600 °F, A.C.	A	A	A	D−	E	E+	A−	A−

Table VIII

Effect of Various Treatments Upon the Susceptibility to Intergranular Attack of Steel S-6

(Carbon = 0.070%, Columbium = 0.61%; Cb/C = 8.7)

Treatment of Steel Subsequent to Cold Rolling		Sensitizing Treatment							
Annealing	Stabilizing	None	21 Days at 840 °F	2 Hours at 1020 °F	2 Days at 1020 °F	8 Days at 1020 °F	21 Days at 1020 °F	2 Hours at 1200 °F	2 Days at 1200 °F
None	None	A	B	AB	B+	AB	AB	A−	A
None	½ hour at 1600 °F, A.C.	A	A	A	C−	C−	B	A	A
½ hour at 1800 °F, W.Q.	None	A	A	A	C+	D−	E+	A	A
½ hour at 1800 °F, W.Q.	½ hour at 1600 °F, A.C.	A	A	A	D+	E+	E+	A	A
½ hour at 1800 °F, W.Q.	2 hours at 1600 °F, A.C.	A	A	A	C−	E+	D−	A	A
½ hour at 1800 °F, A.C.	None	A	A	A	BC	D	C	A	A
½ hour at 1800 °F, A.C.	1 hour at 1600 °F, A.C.	A	A	A	D	D−	D−	A	A
3 min. at 1975 °F, W.Q.	None	A	A	A	B+	E	E	A	A
3 min. at 1975 °F, W.Q.	1 hour at 1600 °F, A.C.	A	A	A	C	E	D	A	A
3 min. at 1975 °F, A.C.	None	A	A	A	C	DE	E+	A−	A−
3 min. at 1975 °F, A.C.	½ hour at 1600 °F, A.C.	A	A	A	D	E+	E	A−	A−
3 min. at 1975 °F, A.C.	2 hours at 1600 °F, A.C.	A	A	A	DE	DE	E	A	A−

Table IX

Effect of Various Treatments Upon the Susceptibility to Intergranular Attack of Steel S-12

(Carbon = 0.074%, Columbium = 0.75%; Cb/C = 10.1)

Treatment of Steel Subsequent to Cold Rolling		Sensitizing Treatment							
Annealing	Stabilizing	None	21 Days at 840 °F	2 Hours at 1020 °F	2 Days at 1020 °F	8 Days at 1020 °F	21 Days at 1020 °F	2 Hours at 1200 °F	2 Days at 1200 °F
None	None	A	AB	A−	B+	A	A−	A	A
None	½ hour at 1600 °F, A.C.	A	A	A	A	A	A	A	A
½ hour at 1800 °F, W.Q.	None	A	A	A	A	A	A−	A	A
½ hour at 1800 °F, W.Q.	½ hour at 1600 °F, A.C.	A	A	A	A	A	A−	A	A
½ hour at 1800 °F, W.Q.	2 hours at 1600 °F, A.C.	A	A	A	A	A	A	A	A
½ hour at 1800 °F, A.C.	None	A	A	A	A	A−	A−	A	A
½ hour at 1800 °F, A.C.	1 hour at 1600 °F, A.C.	A	A	A	B+	B	B−	A−	A
3 min. at 1975 °F, W.Q.	None	A	A	A	A	B	D+	A	A
3 min. at 1975 °F, W.Q.	1 hour at 1600 °F, A.C.	A	A	A	B+	B	B	A	A
3 min. at 1975 °F, A.C.	None	A	A	A	A−	AB	C−	A	A
3 min. at 1975 °F, A.C.	½ hour at 1600 °F, A.C.	A	A	A	AB	C−	C	A	A
3 min. at 1975 °F, A.C.	2 hours at 1600 °F, A.C.	A	A	A	C+	C	C	A	A−

Table X

Effect of Various Treatments Upon the Susceptibility to Intergranular Attack of Steel C-3

(Carbon = 0.060%, Columbium = 0.71%; Cb/C = 11.8)

Treatment of Steel Subsequent to Cold Rolling		Sensitizing Treatment							
Annealing	Stabilizing	None	21 Days at 840 °F	2 Hours at 1020 °F	2 Days at 1020 °F	8 Days at 1020 °F	21 Days at 1020 °F	2 Hours at 1200 °F	2 Days at 1200 °F
None	None	A	A−	A	A	A	A−	A	A−
None	½ hour at 1600 °F, A.C.	A	A	A	A	A	A	A	A
½ hour at 1800 °F, W.Q.	None	A	A	A	A	A	A	A	A
½ hour at 1800 °F, W.Q.	½ hour at 1600 °F, A.C.	A	A	A	A	A−	A−	A	A
½ hour at 1800 °F, W.Q.	2 hours at 1600 °F, A.C.	A	A	A	A	A	A	A	A
½ hour at 1800 °F, A.C.	None	A	A	A	A	A	A	A	A
½ hour at 1800 °F, A.C.	1 hour at 1600 °F, A.C.	A	A	A	A	A−	A−	A−	A
3 min. at 1975 °F, W.Q.	None	A	A	A	A	A	A	A	A
3 min. at 1975 °F, W.Q.	1 hour at 1600 °F, A.C.	A	A	A	A	A	A	A	A
3 min. at 1975 °F, A.C.	None	A	A	A	A	A	A	A−	A
3 min. at 1975 °F, A.C.	½ hour at 1600 °F, A.C.	A	A	A	A	A	A	A	A
3 min. at 1975 °F, A.C.	2 hours at 1600 °F, A.C.	A	A	A	A	A	A	A	A

Table XI
Effect of Various Treatments Upon the Susceptibility to Intergranular Attack of Steel S-27
(Carbon = 0.087%, Columbium = 0.76%; Cb/C = 8.7)

Treatment of Steel Subsequent to Cold Rolling		Sensitizing Treatment							
Annealing	Stabilizing	None	21 Days at 840 °F	2 Hours at 1020 °F	2 Days at 1020 °F	8 Days at 1020 °F	21 Days at 1020 °F	2 Hours at 1200 °F	2 Days at 1200 °F
None	None	A	B+	A	B	A	A	A−	A
None	½ hour at 1600 °F, A.C.	A	A	A	C−	C	AB	A	A
½ hour at 1800 °F, W.Q.	None	A	A	A	D	DE	E+	A	A
½ hour at 1800 °F, W.Q.	½ hour at 1600 °F, A.C.	A	A	A	D	E+	E+	A	A
½ hour at 1800 °F, W.Q.	2 hours at 1600 °F, A.C.	A	A	A	CD	E+	D	A	A

Table XII
Effect of Various Treatments Upon the Susceptibility to Intergranular Attack of Steel S-28
(Carbon = 0.115%, Columbium = 0.92%; Cb/C = 8.0)

Treatment of Steel Subsequent to Cold Rolling		Sensitizing Treatment							
Annealing	Stabilizing	None	21 Days at 840 °F	2 Hours at 1020 °F	2 Days at 1020 °F	8 Days at 1020 °F	21 Days at 1020 °F	2 Hours at 1200 °F	2 Days at 1200 °F
None	None	A	B	A−	C−	B+	A−	A−	A
None	½ hour at 1600 °F, A.C.	A	A	A	D+	D+	BC	A	A
½ hour at 1800 °F, W.Q.	None	A	A	A	DE	E	E	A	A
½ hour at 1800 °F, W.Q.	½ hour at 1600 °F, A.C.	A	A	A	D	E+	E+	A	A
½ hour at 1800 °F, W.Q.	2 hours at 1600 °F, A.C.	A	A	A	C−	E+	DE	A	A
½ hour at 1800 °F, A.C.	None	A	A	A	DE	DE	E+	A−	A
½ hour at 1800 °F, A.C.	1 hour at 1600 °F, A.C.	A	A	A	D	DE	D−	B+	A
3 min. at 1975 °F, W.Q.	None	A	A	A	D+	E	E	B−	A
3 min. at 1975 °F, W.Q.	1 hour at 1600 °F, A.C.	A	A	A	CD	E	C−	A−	A
3 min. at 1975 °F, A.C.	None	A	A	A	E+	DE	E	A−	A
3 min. at 1975 °F, A.C.	½ hour at 1600 °F, A.C.	A	A	A	D−	E+	E+	A−	A
3 min. at 1975 °F, A.C.	2 hours at 1600 °F, A.C.	A	A	A	E+	E+	DE	A−	A−

vulnerable to intergranular attack after certain sensitizing treatments. Decrease in carbon content decreased the degree of vulnerability but even the two very low carbon steels tested were quite susceptible to attack. The ratio of chromium to nickel in steel C-1 (Table II) was such that, in the presence of low carbon, appreciable amounts of delta ferrite were present in the microstructure. Steel C-10 (Table III) contained lower chromium and higher nickel so that no delta ferrite existed. This latter steel proved generally to be the more susceptible

Table XIII

Effect of Various Treatments Upon the Susceptibility to Intergranular Attack of Steel S-17

(Carbon = 0.117%, Columbium = 1.14%; Cb/C = 9.7)

Treatment of Steel Subsequent to Cold Rolling		Sensitizing Treatment							
Annealing	Stabilizing	None	21 Days at 840 °F	2 Hours at 1020 °F	2 Days at 1020 °F	8 Days at 1020 °F	21 Days at 1020 °F	2 Hours at 1200 °F	2 Days at 1200 °F
None	None	A	B+	A−	AB	AB	A−	A	A
None	½ hour at 1600 °F, A.C.	A	A	A	A	A	A	A	A
½ hour at 1800 °F, W.Q.	None	A	A	A	A	A	B+	A	A
½ hour at 1800 °F, W.Q.	½ hour at 1600 °F, A.C.	A	A	A	AB	B	AB	A	A
½ hour at 1800 °F, W.Q.	2 hours at 1600 °F, A.C.	A	A	A	A	A	A	A	A
½ hour at 1800 °F, A.C.	None	A	A	A	A	AB	A	A	A
½ hour at 1800 °F, A.C.	1 hour at 1600 °F, A.C.	A	A	A	BC	BC	B+	A	A
3 min. at 1975 °F, W.Q.	None	A	A	A	A−	C+	D+	A	A
3 min. at 1975 °F, W.Q.	1 hour at 1600 °F, A.C.	A	A	A	B+	B	B	A	A
3 min. at 1975 °F, A.C.	None	A	A	A	A−	B−	CD	A	A
3 min. at 1975 °F, A.C.	½ hour at 1600 °F, A.C.	A	A	A	B+	D	C	A−	A
3 min. at 1975 °F, A.C.	2 hours at 1600 °F, A.C.	A	A	A	C−	C	C	A−	A−

Table XIV

Effect of Various Treatments Upon the Susceptibility to Intergranular Attack of Steel S-18

(Carbon = 0.132%, Columbium = 1.47%; Cb/C = 11.1)

Treatment of Steel Subsequent to Cold Rolling		Sensitizing Treatment							
Annealing	Stabilizing	None	21 Days at 840 °F	2 Hours at 1020 °F	2 Days at 1020 °F	8 Days at 1020 °F	21 Days at 1020 °F	2 Hours at 1200 °F	2 Days at 1200 °F
None	None	A	A	A	A−	A−	A−	A−	A
None	½ hour at 1600 °F, A.C.	A	A	A	A	A	A	A	A
½ hour at 1800 °F, W.Q.	None	A	A	A	A	A	A−	A	A
½ hour at 1800 °F, W.Q.	½ hour at 1600 °F, A.C.	A	A	A	A	A	A−	A	A
½ hour at 1800 °F, W.Q.	2 hours at 1600 °F, A.C.	A	A	A	A	A	A	A	A
½ hour at 1800 °F, A.C.	None	A	A	A	A	A	A	A	A
½ hour at 1800 °F, A.C.	1 hour at 1600 °F, A.C.	A	A	A	A−	B+	A−	A	A
3 min. at 1975 °F, W.Q.	None	A	A	A	A	A	B	A	A
3 min. at 1975 °F, W.Q.	1 hour at 1600 °F, A.C.	A	A	A	A	A−	A−	A	A
3 min. at 1975 °F, A.C.	None	A	A	A	A−	A−	B+	A	A
3 min. at 1975 °F, A.C.	½ hour at 1600 °F, A.C.	A	A	A	A	B+	B	A	A
3 min. at 1975 °F, A.C.	2 hours at 1600 °F, A.C.	A	A	A	A	A−	A−	A	A

Table XV
Effect of Various Treatments Upon the Susceptibility to Intergranular Attack of Steel S-34
(Carbon = 0.067%, Titanium = 0.26%; Ti/C = 3.9)

Treatment of Steel Subsequent to Cold Rolling		Sensitizing Treatment							
Annealing	Stabilizing	None	21 Days at 840 °F	2 Hours at 1020 °F	2 Days at 1020 °F	8 Days at 1020 °F	21 Days at 1020 °F	2 Hours at 1200 °F	2 Days at 1200 °F
None	None	A	C+	B	D−	E+	DE	B+	A
None	½ hour at 1600 °F, A.C.	A	E+	D	E	E	E+	A−	A
½ hour at 1800 °F, W.Q.	None	A	A	A	E	E	E	DE	C−
½ hour at 1800 °F, W.Q.	½ hour at 1600 °F, A.C.	A	E	D	E	E	E	B	B
½ hour at 1800 °F, W.Q.	2 hours at 1600 °F, A.C.	A	D	D+	E	E	E	C+	A−
½ hour at 1800 °F, A.C.	None	A	A	A	E	E	E	DE	CD
½ hour at 1800 °F, A.C.	1 hour at 1600 °F, A.C.	A	C	B−	E	E	E	C+	A
3 min. at 1975 °F, W.Q.	None	A	A	A	C+	E	E	E+	E
3 min. at 1975 °F, W.Q.	1 hour at 1600 °F, A.C.	AB	D+	CD	E+	E	E	C−	D+
3 min. at 1975 °F, A.C.	None	A	A	A	B−	E+	E	E+	E
3 min. at 1975 °F, A.C.	½ hour at 1600 °F, A.C.	A	BC	B+	E	E	E	C	E
3 min. at 1975 °F, A.C.	2 hours at 1600 °F, A.C.	A−	B−	B−	DE	E	E	C+	CD

Table XVI
Effect of Various Treatments Upon the Susceptibility to Intergranular Attack of Steel S-21
(Carbon = 0.071%, Titanium = 0.32%; Ti/C = 4.5)

Treatment of Steel Subsequent to Cold Rolling		Sensitizing Treatment							
Annealing	Stabilizing	None	21 Days at 840 °F	2 Hours at 1020 °F	2 Days at 1020 °F	8 Days at 1020 °F	21 Days at 1020 °F	2 Hours at 1200 °F	2 Days at 1200 °F
None	None	A	C−	B	D	DE	D	B+	A
None	½ hour at 1600 °F, A.C.	A	AB	AB	E+	E+	E+	A−	A
½ hour at 1800 °F, W.Q.	None	A	A	A	E	E	E	D	A−
½ hour at 1800 °F, W.Q.	½ hour at 1600 °F, A.C.	A	CD	B	E	E	E	A	A
½ hour at 1800 °F, W.Q.	2 hours at 1600 °F, A.C.	A	A−	AB	E+	E+	E	AB	A−
½ hour at 1800 °F, A.C.	None	A	A	A	E	E	E	D+	B+
½ hour at 1800 °F, A.C.	1 hour at 1600 °F, A.C.	A	B+	A−	CD	D−	D	BC	A
3 min. at 1975 °F, W.Q.	None	A	A	A	D+	E	E	E	DE
3 min. at 1975 °F, W.Q.	1 hour at 1600 °F, A.C.	A	BC	B+	E+	E	E	B−	B
3 min. at 1975 °F, A.C.	None	A	A	A	DE	E+	E+	DE	E+
3 min. at 1975 °F, A.C.	½ hour at 1600 °F, A.C.	A	AB	AB	E+	E	E	BC	CD
3 min. at 1975 °F, A.C.	2 hours at 1600 °F, A.C.	A−	A−	B	D−	E	E	BC	C

Table XVII

Effect of Various Treatments Upon the Susceptibility to Intergranular Attack of Steel S-39

(Carbon = 0.065%, Titanium = 0.36%; Ti/C = 5.5)

Treatment of Steel Subsequent to Cold Rolling		Sensitizing Treatment							
Annealing	Stabilizing	None	21 Days at 840 °F	2 Hours at 1020 °F	2 Days at 1020 °F	8 Days at 1020 °F	21 Days at 1020 °F	2 Hours at 1200 °F	2 Days at 1200 °F
None	None	A	B+	A	A−	B+	A	A	A−
None	½ hour at 1600 °F, A.C.	A	A	A	A	A	A	A	A
½ hour at 1800 °F, W.Q.	None	A	A	A	A−	C−	C−	A−	A
½ hour at 1800 °F, W.Q.	½ hour at 1600 °F, A.C.	A	A	A	AB	B−	BC	A	A
½ hour at 1800 °F, W.Q.	2 hours at 1600 °F, A.C.	A	A	A	B−	BC	BC	A−	A
½ hour at 1800 °F, A.C.	None	A	A	A	BC	C−	CD	AB	A
½ hour at 1800 °F, A.C.	1 hour at 1600 °F, A.C.	A	A	A	BC	BC	B	A	A
3 min. at 1975 °F, W.Q.	None	A	A	A	A	E+	E	A−	A−
3 min. at 1975 °F, W.Q.	1 hour at 1600 °F, A.C.	A	A	A	B	C	BC	A−	A−
3 min. at 1975 °F, A.C.	None	A	A	A	AB	D+	E	A	A−
3 min. at 1975 °F, A.C.	½ hour at 1600 °F, A.C.	A	A	A	AB	D	D	A	A
3 min. at 1975 °F, A.C.	2 hours at 1600 °F, A.C.	A	A	A	C+	C+	CD	A	A−

Table XVIII

Effect of Various Treatments Upon the Susceptibility to Intergranular Attack of Steel C-6

(Carbon = 0.064%, Titanium = 0.35%; Ti/C = 5.5)

Treatment of Steel Subsequent to Cold Rolling		Sensitizing Treatment							
Annealing	Stabilizing	None	21 Days at 840 °F	2 Hours at 1020 °F	2 Days at 1020 °F	8 Days at 1020 °F	21 Days at 1020 °F	2 Hours at 1200 °F	2 Days at 1200 °F
None	None	A	A	A	A	A−	A	A	A
None	½ hour at 1600 °F, A.C.	A	A	A	A	A	A	A	A
½ hour at 1800 °F, W.Q.	None	A	A	A	A−	AB	C−	A	A
½ hour at 1800 °F, W.Q.	½ hour at 1600 °F, A.C.	A	A	A	A−	A−	A−	A	A−
½ hour at 1800 °F, W.Q.	2 hours at 1600 °F, A.C.	A−	A−	A	A	A	A−	A	A
½ hour at 1800 °F, A.C.	None	A	A	A	AB	C	C−	A−	A
½ hour at 1800 °F, A.C.	1 hour at 1600 °F, A.C.	A	A	A	A−	BC	B−	A	A
3 min. at 1975 °F, W.Q.	None	A	A	A	A	D	D−	A	A−
3 min. at 1975 °F, W.Q.	1 hour at 1600 °F, A.C.	A	A	A	AB	B	C−	A	A
3 min. at 1975 °F, A.C.	None	A	A	A	A	D+	E+	A	B
3 min. at 1975 °F, A.C.	½ hour at 1600 °F, A.C.	A	A	A	B+	CD	D	A	A−
3 min. at 1975 °F, A.C.	2 hours at 1600 °F, A.C.	A	A	A	C+	C+	C+	A	A−

Table XIX

Effect of Various Treatments Upon the Susceptibility to Intergranular Attack of Steel C-2

(Carbon = 0.070%, Titanium = 0.50%; Ti/C = 7.1)

Treatment of Steel Subsequent to Cold Rolling		Sensitizing Treatment							
Annealing	Stabilizing	None	21 Days at 840 °F	2 Hours at 1020 °F	2 Days at 1020 °F	8 Days at 1020 °F	21 Days at 1020 °F	2 Hours at 1200 °F	2 Days at 1200 °F
None	None	A	C−	A	AB	A	B−	A	A
None	½ hour at 1600 °F, A.C.	A	A	A	A	A	A	A	A
½ hour at 1800 °F, W.Q.	None	A	A	A	A	A	A	A	A
½ hour at 1800 °F, W.Q.	½ hour at 1600 °F, A.C.	A	A	A	A	A	A	A	A
½ hour at 1800 °F, W.Q.	2 hours at 1600 °F, A.C.	A	A	A	A	A	A	A	A
½ hour at 1800 °F, A.C.	None	A	A	A	A	B+	B+	A	A
½ hour at 1800 °F, A.C.	1 hour at 1600 °F, A.C.	A	A	A	A	A	A−	A−	A
3 min. at 1975 °F, W.Q.	None	A	A	A	A	BC	D	A	A
3 min. at 1975 °F, W.Q.	1 hour at 1600 °F, A.C.	A	A	A	A	A	A−	A	A
3 min. at 1975 °F, A.C.	None	A	A	A	A	B+	D+	A	A
3 min. at 1975 °F, A.C.	½ hour at 1600 °F, A.C.	A	A	A	A	A−	A−	A	A−
3 min. at 1975 °F, A.C.	2 hours at 1600 °F, A.C.	A−	A−	A	A	A−	A	A	A

Table XX

Effect of Various Treatments Upon the Susceptibility to Intergranular Attack of Steel C-8

(Carbon = 0.075%, Titanium = 0.59%: Ti/C = 7.9)

Treatment of Steel Subsequent to Cold Rolling		Sensitizing Treatment							
Annealing	Stabilizing	None	21 Days at 840 °F	2 Hours at 1020 °F	2 Days at 1020 °F	8 Days at 1020 °F	21 Days at 1020 °F	2 Hours at 1200 °F	2 Days at 1200 °F
None	None	A−	B+	A	A	AB	B+	A	A
None	½ hour at 1600 °F, A.C.	A	A	A	A	A	A	A	A
½ hour at 1800 °F, W.Q.	None	A	A	A	A	A	A	A	A
½ hour at 1800 °F, W.Q.	½ hour at 1600 °F, A.C.	A	A	A	A−	A	A	A	A
½ hour at 1800 °F, W.Q.	2 hours at 1600 °F, A.C.	A	A	A	A	A	A	A	A
½ hour at 1800 °F, A.C.	None	A	A	A	A−	A	A	A	A
½ hour at 1800 °F, A.C.	1 hour at 1600 °F, A.C.	A	A	A	A	A	A−	A−	A
3 min. at 1975 °F, W.Q.	None	A	A	A	A	A	A−	A	A
3 min. at 1975 °F, W.Q.	1 hour at 1600 °F, A.C.	A	A	A	A	A	A	A	A
3 min. at 1975 °F, A.C.	None	A	A	A	A	A	B	A	A
3 min. at 1975 °F, A.C.	½ hour at 1600 °F, A.C.	A	A	A	A	A	A	A	A
3 min. at 1975 °F, A.C.	2 hours at 1600 °F, A.C.	A	A	A	A	A−	A−	A	A

Table XXI
Effect of Various Treatments Upon the Susceptibility to Intergranular Attack of Steel S-25
(Carbon = 0.082%, Titanium = 0.37%; Ti/C = 4.5)

Treatment of Steel Subsequent to Cold Rolling		Sensitizing Treatment							
Annealing	Stabilizing	None	21 Days at 840°F	2 Hours at 1020°F	2 Days at 1020°F	8 Days at 1020°F	21 Days at 1020°F	2 Hours at 1200°F	2 Days at 1200°F
None	None	A	CD	B	C−	D+	B+	A	A
None	½ hour at 1600°F, A.C.	A	AB	A	E+	E+	D+	A−	A
½ hour at 1800°F, W.Q.	None	A	A	A	E	E	E	B	A−
½ hour at 1800°F, W.Q.	½ hour at 1600°F, A.C.	A	B−	A−	E	E+	E	A−	A
½ hour at 1800°F, W.Q.	2 hours at 1600°F, A.C.	A	A	A−	DE	DE	E+	A−	A−

Table XXII
Effect of Various Treatments Upon the Susceptibility to Intergranular Attack of Steel S-35
(Carbon = 0.107%, Titanium = 0.44%; Ti/C = 4.1)

Treatment of Steel Subsequent to Cold Rolling		Sensitizing Treatment							
Annealing	Stabilizing	None	21 Days at 840°F	2 Hours at 1020°F	2 Days at 1020°F	8 Days at 1020°F	21 Days at 1020°F	2 Hours at 1200°F	2 Days at 1200°F
None	None	A	E+	D+	DE	C+	B	A	A
None	½ hour at 1600°F, A.C.	A	AB	A−	DE	E	D	A−	A
½ hour at 1800°F, W.Q.	None	A	A	A	E	E	E	D	A
½ hour at 1800°F, W.Q.	½ hour at 1600°F, A.C.	A	C	B	E	E	E	A	A
½ hour at 1800°F, W.Q.	2 hours at 1600°F, A.C.	A	A	A	DE	E+	E	AB	A−
½ hour at 1800°F, A.C.	None	A	A	A	D−	E	DE	B−	A
½ hour at 1800°F, A.C.	1 hour at 1600°F, A.C.	A	B+	A−	D	DE	D	BC	A
3 min. at 1975°F, W.Q.	None	A	A	A	C−	E	E	E	DE
3 min. at 1975°F, W.Q.	1 hour at 1600°F, A.C.	A	B+	AB	D−	E	E	B−	AB
3 min. at 1975°F, A.C.	None	A	A	A	DE	E	E	D−	E+
3 min. at 1975°F, A.C.	½ hour at 1600°F, A.C.	A	B	A	DE	E	E	B+	C+
3 min. at 1975°F, A.C.	2 hours at 1600°F, A.C.	A	B+	B	D−	E	E	B	C+

to intergranular attack except that, in the initially cold-rolled condition, it was practically immune.

The performance of the individual columbium- and titanium-treated steels may be studied by reference to the appropriate table but a more readily comprehensible presentation is given in Table XXV. In this table only the *worst* averaged rating of each steel, as presented in Tables VII to XXIV, inclusive, is used. The steels are arranged in Table XXV in order of Cb/C or Ti/C ratio without regard to the carbon content. It will be observed that, for all 12 ini-

Table XXIII

Effect of Various Treatments Upon the Susceptibility to Intergranular Attack of Steel S-36

(Carbon = 0.109%, Titanium = 0.54%; Ti/C = 5.0)

Treatment of Steel Subsequent to Cold Rolling		Sensitizing Treatment							
Annealing	Stabilizing	None	21 Days at 840 °F	2 Hours at 1020 °F	2 Days at 1020 °F	8 Days at 1020 °F	21 Days at 1020 °F	2 Hours at 1200 °F	2 Days at 1200 °F
None	None	A	B−	A	D−	B+	B+	A	A
None	½ hour at 1600 °F, A.C.	A	A	A	A	A	A	A	A
½ hour at 1800 °F, W.Q.	None	A	A	A	C+	C	E+	A	A
½ hour at 1800 °F, W.Q.	½ hour at 1600 °F, A.C.	A	A	A	A	A	A	A	A
½ hour at 1800 °F, W.Q.	2 hours at 1600 °F, A.C.	A	A	A	A	A	A	A	A
½ hour at 1800 °F, A.C.	None	A	A	A	B−	C+	BC	AB	A
½ hour at 1800 °F, A.C.	1 hour at 1600 °F, A.C.	A	A	A	B	B	A−	A	A
3 min. at 1975 °F, W.Q.	None	A	A	A	B+	E+	E	C+	A
3 min. at 1975 °F, W.Q.	1 hour at 1600 °F, A.C.	A	A	A	A−	A−	B	A	A
3 min. at 1975 °F, A.C.	None	A	A	A	C+	DE	E	A−	A
3 min. at 1975 °F, A.C.	½ hour at 1600 °F, A.C.	A	A−	A	A−	BC	B−	A	A
3 min. at 1975 °F, A.C.	2 hours at 1600 °F, A.C.	A	A	A	C+	BC	C−	A−	A−

Table XXIV

Effect of Various Treatments Upon the Susceptibility to Intergranular Attack of Steel S-32

(Carbon = 0.105%, Titanium = 0.61%; Ti/C = 5.8)

Treatment of Steel Subsequent to Cold Rolling		Sensitizing Treatment							
Annealing	Stabilizing	None	21 Days at 840 °F	2 Hours at 1020 °F	2 Days at 1020 °F	8 Days at 1020 °F	21 Days at 1020 °F	2 Hours at 1200 °F	2 Days at 1200 °F
None	None	A	B+	A	C	AB	B+	A	A
None	½ hour at 1600 °F, A.C.	A	A	A	A	A	A	A	A
½ hour at 1800 °F, W.Q.	None	A	A	A	A	B+	C−	A	A−
½ hour at 1800 °F, W.Q.	½ hour at 1600 °F, A C.	A	A	A	A	A	A	A	A
½ hour at 1800 °F, W.Q.	2 hours at 1600 °F, A.C.	A	A	A	A	A	A	A	A
½ hour at 1800 °F, A.C.	None	A	A	A	B+	B	A	A	A
½ hour at 1800 °F, A.C.	1 hour at 1600 °F, A.C.	A	A	A	A	B	AB	A	A
3 min. at 1975 °F, W.Q.	None	A	A	A	A−	D	D	A	A
3 min. at 1975 °F, W.Q.	1 hour at 1600 °F, A.C.	A	A	A	A−	A−	A−	A	A
3 min. at 1975 °F, A.C.	None	A	A	A	B+	C+	DE	A	A
3 min. at 1975 °F, A.C.	½ hour at 1600 °F, A.C.	A	A	A	A−	B+	B−	A	A
3 min. at 1975 °F, A.C.	2 hours at 1600 °F, A.C.	A	A	A	A−	B	BC	A	A

Table XXV
Qualitative Rating of Resistance of Test Steels to Intergranular Attack*

Steel No.	% C	Ratio Cb/C	Ratio Ti/C	Cold Rolled (37½%) — No Stabilizing Treatment	Cold Rolled (37½%) — Stabilized ½ Hr. at 1600 °F, A.C.	Annealed ½ Hr. at 1800 °F, W.Q. — No Stabilizing Treatment	Annealed ½ Hr. at 1800 °F, W.Q. — Stabilized ½ Hr. at 1600 °F, A.C.	Annealed ½ Hr. at 1800 °F, W.Q. — Stabilized 2 Hrs. at 1600 °F, A.C.	Annealed ½ Hr. at 1800 °F, A.C. — No Stabilizing Treatment	Annealed ½ Hr. at 1800 °F, A.C. — Stabilized 1 Hr. at 1600 °F, A.C.	Annealed 3 Min. at 1975 °F, W.Q. — No Stabilizing Treatment	Annealed 3 Min. at 1975 °F, W.Q. — Stabilized 1 Hr. at 1600 °F, A.C.	Annealed 3 Min. at 1975 °F, A.C. — No Stabilizing Treatment	Annealed 3 Min. at 1975 °F, A.C. — Stabilized ½ Hr. at 1600 °F, A.C.	Annealed 3 Min. at 1975 °F, A.C. — Stabilized 2 Hrs. at 1600 °F, A.C.
S-26	0.068	7.4	...	D	DE	E	E+	E	E	E+	E	DE	E	E	E
S-28	0.115	8.0	...	C−	D+	E	E+	E+	E+	DE	E	E	E	E+	E+
S-6	0.070	8.7	...	B	C−	E+	E+	E+	D	D−	E	E	E+	E	E
S-27	0.087	8.7	...	B	C−	E+	E+	E+	..	..	..	..	..	..	..
S-17	0.117	9.7	...	B+	A	B+	B	A	AB	BC	D+	B	CD	D	C−
S-12	0.074	10.1	...	B+	A	A−	A−	A	A−	B−	D+	B	C−	C−	C
S-18	0.132	11.1	...	A−	A	A−	A−	A	A	B+	B	A−	B+	B	A−
C-3	0.060	11.8	...	A−	A	A	A−	A	A	A−	A	A	A−	A	A
S-34	0.067	....	3.9	E+	E	E	E	E	E	E	E	E	E	E	E
S-35	0.107	....	4.1	E+	E	E	E	E	E	DE	E	E	E	E	E
S-21	0.071	....	4.5	DE	E+	E	E	E	E	D−	E	E	E+	E	E
S-25	0.082	....	4.5	D+	E+	E	E	E+	..	..	..	..	..	..	..
S-36	0.109	....	5.0	D−	A	E+	A	A	C+	B	E	B	E	BC	C−
S-39	0.065	....	5.5	B+	A	C−	BC	BC	CD	BC	E	C	E	D	CD
C-6	0.064	....	5.5	A−	A	C−	A−	A−	C−	BC	D−	C−	E+	D	C+
S-32	0.105	....	5.8	C	A	C−	A	A	B	B	D	A−	DE	B−	BC
C-2	0.070	....	7.1	C−	A	A	A	A	B+	A−	D	A−	D+	A−	A−
C-8	0.075	....	7.9	B+	A	A	A−	A	A−	A−	A−	A	B	A	A−

*This table was prepared from Tables VII to XXIV, inclusive, using only the *worst* averaged rating of each steel in each initial condition. For instance, steel S-26, as cold-rolled and stabilized ½ hour at 1600 °F, was rated "DE" as tested after sensitizing 8 days at 1020 °F (see Table VII). Although for all other conditions of sensitization the ratings were higher than "DE", this worst rating was used in this summary table.

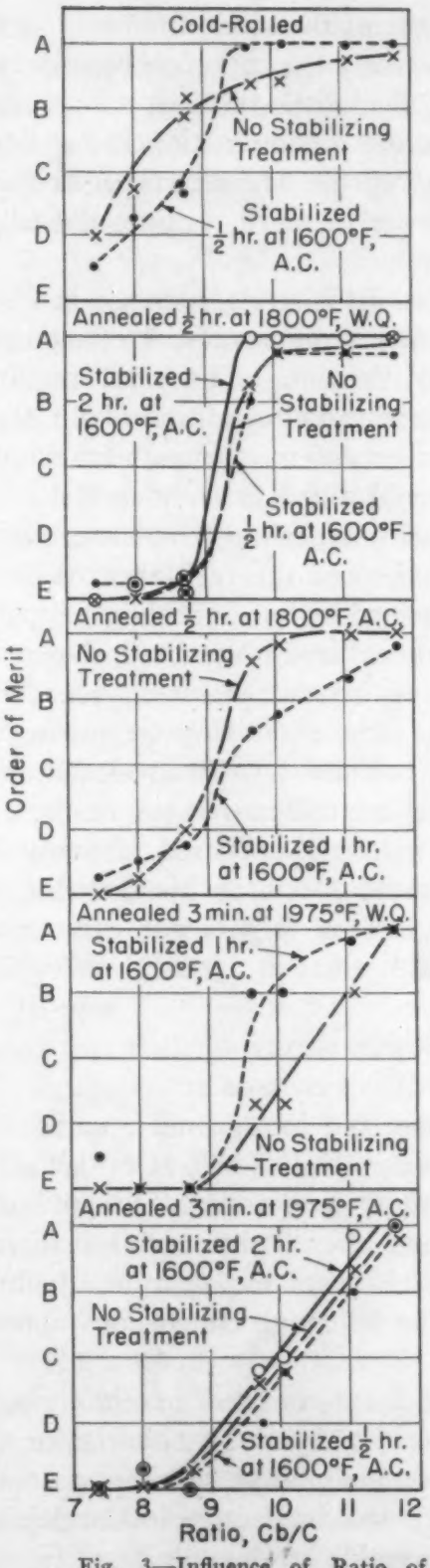


Fig. 3—Influence of Ratio of Cb/C and of Initial Heat Treatment Upon Resistance to Intergranular Attack. (See page 1270 for explanation of significance of letters representing order of merit.)

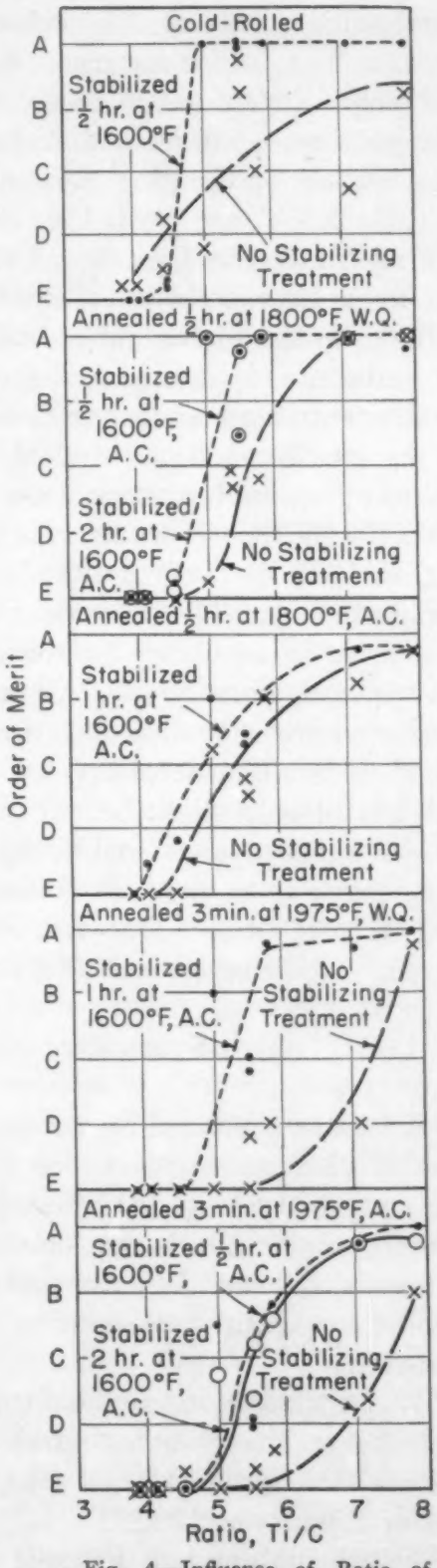


Fig. 4—Influence of Ratio of Ti/C and of Initial Heat Treatment Upon Resistance to Intergranular Attack. (See page 1270 for explanation of significance of letters representing order of merit.)

tial conditions studied, the performance of the steels improves as the Cb/C or Ti/C ratios increase. Apparently the carbon content within the range studied (0.06 to 0.13%) had little, if any, effect upon susceptibility to intergranular attack, the predominating factor being the Cb/C or Ti/C ratio. The ratings of the various steels, as given in Table XXV, are plotted, as an order of merit, against the Cb/C and Ti/C ratios in Figs. 3 and 4.

Regardless of the initial condition of the steels, increase in Cb/C or Ti/C to the higher ratios had a markedly beneficial effect upon the resistance to intergranular embrittlement. The ratio required for substantial immunity varied with the initial condition of the steel. Of the initial conditions studied, those conferring maximum immunity to intergranular attack were as cold-rolled or as quenched from 1800 °F (980 °C) in water. Increase in annealing temperature from 1800 to 1975 °F (980 to 1080 °C) impaired the resistance to intergranular attack. The deleterious effect of higher annealing temperatures upon susceptibility to intergranular attack has been shown by other investigators (8). Air cooling instead of water quenching after annealing was also detrimental. The stabilizing treatment appeared to be quite necessary for the titanium-treated steels but was generally of only slight benefit to the columbium-treated steels. In fact, a superimposed stabilizing treatment appeared actually to be detrimental to the columbium-treated steels as air-cooled from 1800 °F (980 °C). The data indicated no significant differences between stabilizing periods of ½ and 2 hours at 1600 °F (870 °C).

Summary and Conclusions

Data are presented on the resistance to intergranular embrittlement of 23 austenitic corrosion resisting steels (18% Cr – 10% Ni base composition) in 12 different initial conditions. Susceptibility to intergranular attack was determined after 7 different sensitizing treatments, followed by a maximum of 14 days' exposure in a boiling acidified copper sulphate solution. The following conclusions appear warranted:

1. Of the various sensitizing treatments utilized, maximum susceptibility to intergranular attack was developed by either 8 or 21 days at 1020 °F (550 °C). The commonly used sensitizing treatment of 2 hours at 1200 °F (650 °C) was ineffective in developing susceptibility in any but the most vulnerable steels.

2. The straight carbon austenitic corrosion resisting steels were very susceptible to intergranular embrittlement. The susceptibility decreased as the carbon content decreased but, with the exception of one low carbon steel in the cold-rolled condition only, even the very low carbon steels (0.025% C) were vulnerable regardless of heat treatment.

3. In the columbium- and titanium-bearing steels, carbon content within the range of 0.06 to 0.13% had no influence upon the resistance to intergranular attack except insofar as it influenced the Cb/C or Ti/C ratios. Steels having similar ratios of stabilizing element to carbon had approximately the same degree of susceptibility to intergranular attack regardless of the carbon content.

4. Both the columbium- and titanium-treated steels exhibited greater resistance to intergranular attack as cold-rolled or annealed at 1800 °F (980 °C) and water-quenched than as annealed at 1800 °F (980 °C) and air-cooled, or as annealed at 1975 °F (1080 °C) and either water-quenched or air-cooled.

5. Stabilizing heat treatments at 1600 °F (870 °C) had a negligible effect upon the resistance to intergranular embrittlement of the columbium-treated steels. The performance of the titanium-treated steels carrying the higher ratios of Ti/C, however, was markedly improved by such treatments. Variation in time of the stabilizing treatments from ½ to 2 hours had no effect.

6. When properly treated, substantially complete immunity to intergranular attack may be obtained with a minimum ratio of Cb/C = 10 and Ti/C = 5. For more "fool-proof" immunity, it is believed that these ratios should be 12 and 8, respectively.

It should be emphasized that the data and conclusions given in this paper refer only to the susceptibility of the test steels to intergranular attack as developed under test conditions considerably more severe than those normally used.

Acknowledgments

The authors are indebted to Lt. (j.g.) Dennis J. Carney and James Darby, Naval Research Laboratory, for assistance in melting the experimental steels; to G. N. Goller, Rustless Iron and Steel Division, American Rolling Mill Company, Baltimore, Md., for forging many of the steels; to M. E. Carruthers and H. I. White, American Rolling Mill Research Laboratory, Middletown, Ohio,

for assistance in rolling the experimental steels; to J. L. Hague and J. T. Sterling, National Bureau of Standards, for the chemical and vacuum fusion analyses, respectively, and to Albert Lewis, National Bureau of Standards, for assistance in the early phases of the work.

This investigation was made possible by the generous support of the Bureau of Aeronautics, Navy Department, and the friendly co-operation of N. E. Promisel and B. A. Kornhauser of that Bureau.

References

1. B. Strauss, H. Schottky and J. Hinnüber, "The Precipitation of Carbide on Annealing Corrosion Resisting Nonmagnetic Chromium-Nickel Steels," *Zeitschrift für anorganische Chemie,* Vol. 188, 1930, p. 309.
2. Robert H. Aborn and Edgar C. Bain, "Nature of the Nickel-Chromium Rustless Steels," TRANSACTIONS, American Society for Steel Treating, Vol. 18, 1930, p. 837.
3. E. Houdremont and P. Schafmeister, "Prevention of Intergranular Corrosion of Steels With 18% Cr and 8% Ni," *Archiv f. d. Eisenhüttenwesen,* Vol. 1, 1933, p. 187.
4. H. D. Newell, "Influence of Grain Size on the Properties and Corrosion Resistance of the 18-8 Iron-Chromium-Nickel Alloy for Elevated Temperature Service," TRANSACTIONS, American Society for Steel Treating, Vol. 19, 1932, p. 673.
5. P. Payson, "Prevention of Intergranular Corrosion in Corrosion-Resistant Chromium-Nickel Steels," *Transactions,* American Institute of Mining and Metallurgical Engineers, Vol. 100, 1932, p. 306.
6. E. C. Bain, R. H. Aborn and J. J. B. Rutherford, "The Nature and Prevention of Intergranular Corrosion in Austenitic Stainless Steels," TRANSACTIONS, American Society for Steel Treating, Vol. 21, 1933, p. 481.
7. Frederick M. Becket and Russell Franks, "Effects of Columbium in Chromium-Nickel Steels," *Transactions,* American Institute of Mining and Metallurgical Engineers, Vol. 113, 1934, p. 143.
8. L. B. Pfeil and D. G. Jones, "A Contribution to the Study of the Properties of Austenitic Steels," *Journal,* Iron and Steel Institute, Vol. 127, 1933, p. 337.

DISCUSSION

Written Discussion: By John F. Tyrrell and John C. Southard, Solar Aircraft Co., San Diego, Calif.

The authors are to be congratulated on their interesting and informative work on the embrittlement of the austenitic stainless steels and, in particular, for their clear and concise summary of the theories of sensitization and stabilization. The subject is of particular interest to the aircraft industry, since many aircraft engine components operate at temperatures in the range of sensitization and their service life depends in part on their resistance to intergranular embrittlement.

The effect of nitrogen content on the ratio of stabilizing element to carbon was discussed but not included in the summary of results listed in Table XXV. If the ratios, revised to allow for the stabilizing element

combined with nitrogen, are considered in evaluating the results, they illustrate quite effectively one of the reasons why the minimum contents of titanium and columbium have been set higher than the amount theoretically required to fix the carbon.

Table XXVI has been compiled from the data reported in Tables I and XXV and shows rather clearly that when the ratio of stabilizing element to carbon includes the effect of nitrogen, the critical ratio required for stabilization approaches more closely the theoretical value (Cb/C = 7.8, Ti/C = 4.0).

Table XXVI
Qualitative Rating of Resistance to Intergranular Attack After Stabilizing Heat Treatment at 1600 °F

Steel No.	Revised Ratio* Cb/C	Revised Ratio* Ti/C	Cold-Rolled + Stabilization	1800°F ½ Hr.—WQ + Stabilization		1800°F ½ Hr.—AC + Stabilization	1975°F 3 Min.—WQ + Stabilization	1975°F 3 Min.—AC + Stabilization	
S-26	5.4	...	DE	E+	E	E+	DE	E	E
S-28	6.7	...	D+	E+	E+	DE	E	E+	E+
S-27	6.7	...	C−	E+	E+	...	...	...	...
S-6	6.9	...	C−	E+	E+	D−	E	E	E
S-12	8.1	...	A	A−	A	B−	B	C−	C
S-17	8.3	...	A	B	A	BC	B	D	C−
S-18	9.5	...	A	A−	A	B+	A−	B	A−
C-3	9.7	...	A	A−	A	A−	A	A	A
S-34	...	1.9	E	E	E	E	E	E	E
S-21	...	3.1	E+	E	E	D−	E	E	E
S-35	...	3.6	E	E	E	DE	E	E	E
S-25	...	3.7	E+	E	E+	...	...	...	...
S-39	...	4.3	A	BC	BC	BC	C	D	CD
S-36	...	4.4	A	A	A	B	B	BC	C−
C-6	...	4.8	A	A−	A−	BC	C−	D	C+
S-32	...	5.3	A	A	A	B	A−	B−	BC
C-2	...	6.7	A	A	A	A−	A−	A−	A−
C-8	...	7.6	A	A−	A	A−	A	A	A−

*Cb/C and Ti/C ratio revised to allow for nitrogen content. (See authors' Table I.)

Recently an investigation was completed in our laboratory on the effect of nitrogen content on the embrittlement of thirty commercial heats of stabilized austenitic stainless steel sheets purchased to Specification AN-QQ-S 757 from various producers. The results confirmed the data given in Table XXVI, showing that it was necessary to include the effect of nitrogen in determining the critical ratio of stabilizing element to carbon for freedom from sensitization. It is interesting to note that the nitrogen content of the thirteen 18-10-columbium samples examined had an average content of 0.048% nitrogen (range 0.030 to 0.070%) whereas the seventeen 18-10-titanium samples averaged only 0.018% nitrogen (range 0.010 to 0.024%).

Binder, Brown and Franks[2] also show that nitrogen must be included in the calculations of the critical amount of stabilizing element required to fix the carbon in columbium-stabilized grades. They have found, however, that only nitrogen in excess of 0.022% would affect the amount of

[2]W. O. Binder, C. M. Brown and Russell Franks, "Resistance to Sensitization of Austenitic Chromium-Nickel Steels of 0.03% Max. Carbon Content," TRANSACTIONS, American Society for Metals, Vol. 41, 1949, p. 1301.

columbium necessary for stabilization. This would indicate that an average columbium-stabilized alloy should contain at least 0.17% columbium over that required to react with carbon. If the minimum value of effective nitrogen is the same for the titanium-bearing alloys, it is evident that, normally, no extra titanium would be necessary. However, even if all the nitrogen present reacted with titanium, it would still require only 0.06% extra titanium to assure complete fixation of the carbon in an average sample.

It has been emphasized by the authors that the test conditions were much more severe than those normally used. In our experience with approximately 400,000 airplane engine exhaust sets, we have found that there is no apparent difference in the service life of the titanium and columbium-stabilized grades, although the only heat treatment used was a solution anneal at about 1950 °F (1065 °C). Unstabilized grades generally are not satisfactory.

Written Discussion: By R. S. Stewart, assistant chief, Physical Metallurgy, Titanium Alloy Manufacturing Division, National Lead Co., Niagara Falls, N. Y.

The authors are to be commended for their thorough work of evaluating so many of the factors affecting the resistance of austenitic steels to intergranular attack.

The authors have found that sensitizing for 8 or 21 days at 1020 °F (550 °C) provided the most severe effect so far as susceptibility to intergranular corrosion is concerned. It should be emphasized, however, that this heat treatment does not simulate conditions obtained from welding or from any high temperature service for which these steels might be used. For this reason the treatment should not be considered as a substitute for the present practice of sensitizing for 2 hours at 1200 to 1250 °F (650 to 675 °C). The latter treatment seems to be quite adequate for testing purposes if welding is the only consideration.

It is gratifying to note that the nitrogen contents of steels stabilized with titanium or columbium have been taken into consideration in this paper. This is more important in the case of the titanium steels than in the columbium steels, because titanium is a better nitride-forming element than columbium. The data in Table I indicate that even with the lowest titanium to carbon ratio investigated, essentially all the nitrogen is insolubilized, while only about one-half the nitrogen is insolubilized with the highest columbium to carbon ratios. It has recently been shown by Comstock[3] that a titanium to carbon ratio of 2 is sufficient to insolubilize practically all the nitrogen present in either low alloy or stainless steels. It would seem that much of the controversy of the past regarding the minimum titanium or columbium to carbon ratio required for immunity to intergranular susceptibility, under any given condition of heat treatment, could have been avoided had allowance been made for nitrogen. Since the authors recognize the importance of nitrogen, it is difficult to understand why their conclusions are based on titanium or columbium to

[3]George F. Comstock, "The Effect of Titanium on Nitrogen in Steel," METAL PROGRESS, Vol. 54, No. 3, September 1948, p. 319-322.

carbon ratios rather than on the revised ratios which they have calculated, especially so since the nitrogen contents of the steels investigated vary from 0.007 to 0.061%.

Written Discussion: By J. J. Heger, research associate, Research and Development Division, Carnegie-Illinois Steel Corp., Pittsburgh.

Messrs. Rosenberg and Darr are to be commended for this excellent investigation of the intergranular corrosion of the 18-8 stainless steels. The wealth of information that has been developed and reported is a valuable addition to our knowledge of the subject.

As a manufacturer of stainless steels, we naturally are vitally interested in the commercial implications arising from the interpretations of the results of this investigation. Accordingly, we ask consideration of several comments concerning the conclusions reached in this work.

As the authors' data show and as they state in their first conclusion, the commonly specified sensitizing condition of 2 hours at 1200 °F (650 °C) will not develop maximum susceptibility to intergranular attack. Certainly, this observation is not a new one. Indeed, as early as 1933, Bain, Aborn and Rutherford[4] reported that the maximum susceptibility of 18-8 to intergranular attack would be developed by heating for long times at temperatures between 950 and 1050 °F (510 and 565 °C). In other words, the most critical temperature for sensitization decreases with increasing time of exposure at temperature. However, we hasten to add that a majority of the applications requiring resistance to intergranular corrosion do not involve long heating times at these relatively low temperatures. Accordingly, for these applications, which include welding, the sensitizing conditions of 1 or 2 hours at 1200 to 1250 °F (650 to 675 °C) are believed to evaluate best the susceptibility to intergranular corrosion.

An evaluation of the suitability of materials for long-time service in the temperature range of 900 to 1600 °F (480 to 870 °C), in other words, the determination of the composition requirements necessary for complete immunity to intergranular corrosion, is more difficult than one might imagine. The authors have chosen a sensitizing condition of 21 days at 1020 °F (550 °C) and used the results of long-time boils in acidified copper sulphate as their criterion for complete or "fool proof" immunity to intergranular corrosion. Based on these results, they conclude that to obtain complete immunity a Ti/C ratio of 8 or a Cb/C ratio of 12 is necessary. These ratios are somewhat above the commercial minima of 5 and 10, respectively, and the authors' results might be interpreted to indicate that these commercially established minima are unsatisfactory. However, in view of the present consideration now being given to the conservation of alloying elements and the fact that service experience has proven these commercial minima to be entirely satisfactory, we believe that the definition of "complete immunity to intergranular corrosion" should be subjected to careful scrutiny.

Actually, complete immunity is a relative term depending upon the specific criteria employed. We must agree that the authors' criterion of

[4]E. C. Bain, R. H. Aborn and J. J. B. Rutherford, "The Nature and Prevention of Intergranular Corrosion in Austenitic Stainless Steels," TRANSACTIONS, American Society for Steel Treating, Vol. 21, 1933, p. 481.

resistance to acidified copper sulphate solution following a sensitization of 21 days at 1020 °F (550 °C) is a severe one. However, their data show that as the severity of the sensitization conditions increases, the Ti/C and Cb/C ratios necessary to insure resistance to intergranular corrosion also increase until, after the most severe treatment, i.e., 21 days at 1020 °F (550 °C), a Ti/C ratio of 8 or a Cb/C ratio of 12 is required. One, therefore, wonders if this relationship between Ti/C or Cb/C and the sensitizing condition continues, to the extent that conditions more severe than those employed by the authors would require Ti/C and Cb/C ratios higher than 8 and 12 respectively.

Conceivably, this relationship does continue and we offer for consideration the results of corrosion tests in boiling 65% nitric acid on an 18-8 titanium material and an 18-8 columbium material, both of which had been sensitized for 10,000 hours at 1050 °F (550 °C). These results are summarized in Table XXVII.

Table XXVII

	Composition						
	C	Mn	Si	Ni	Cr	Ti	Cb
18-8 Ti	0.07	0.52	0.386	10.40	17.97	0.58	....
18-8 Cb	0.06	1.43	0.444	11.16	17.80	....	0.77

Heat Treatment

Annealed .....1950 °F— ½ hour —Water Quench
Stabilized .....1550 °F— 2 hours—Water Quench
Sensitized .....1050 °F—10,000 hours—Air Cool

Corrosion Rate in Boiling 65% Nitric Acid
(Inches Penetration per Month)

	1st Period	2nd Period	3rd Period	4th Period	5th Period	Average
18-8 Ti	0.0016	0.0047	0.0062	0.0076	0.0083	0.0057
18-8 Cb	0.0044	0.0176	0.0208	.....	.....	0.0143

As will be noted, the corrosion rate of the 18-8 columbium material, which had a Cb/C ratio of 12.8, was so high that the corrosion test was discontinued after but three periods. The corrosion rate of the 18-8 titanium material, although lower than that of the 18-8 columbium material, was still quite high even though the Ti/C ratio was 8.3.

The microstructures of the materials are shown in Figs. 5 and 6. As will be noted, a precipitate has formed at the grain boundaries of both materials and the amount of this precipitate is greater in the 18-8 columbium.

On the basis of these results, we could say that a Ti/C ratio of 8 or a Cb/C ratio of 12 is not sufficient to insure complete or "fool proof" immunity to intergranular corrosion. Perhaps, by further experimentation, we could determine what composition requirements are necessary to insure resistance to intergranular corrosion in nitric acid after a sensitizing condition of 10,000 hours at 1050 °F (565 °C). However, the composition that we could select might not be resistant to intergranular corrosion after 100,000 hours at 1050 °F (565 °C). In other words, since complete immunity to intergranular corrosion, as measured by laboratory

methods, depends so much on the criteria employed, service requirements should be considered before establishing composition limits.

Although not stated by the authors, we understand that this investigation was undertaken to evaluate the suitability of materials for service in aircraft engine exhaust manifolds. If our understanding is correct, we then question the advisability of using the results of acidified copper

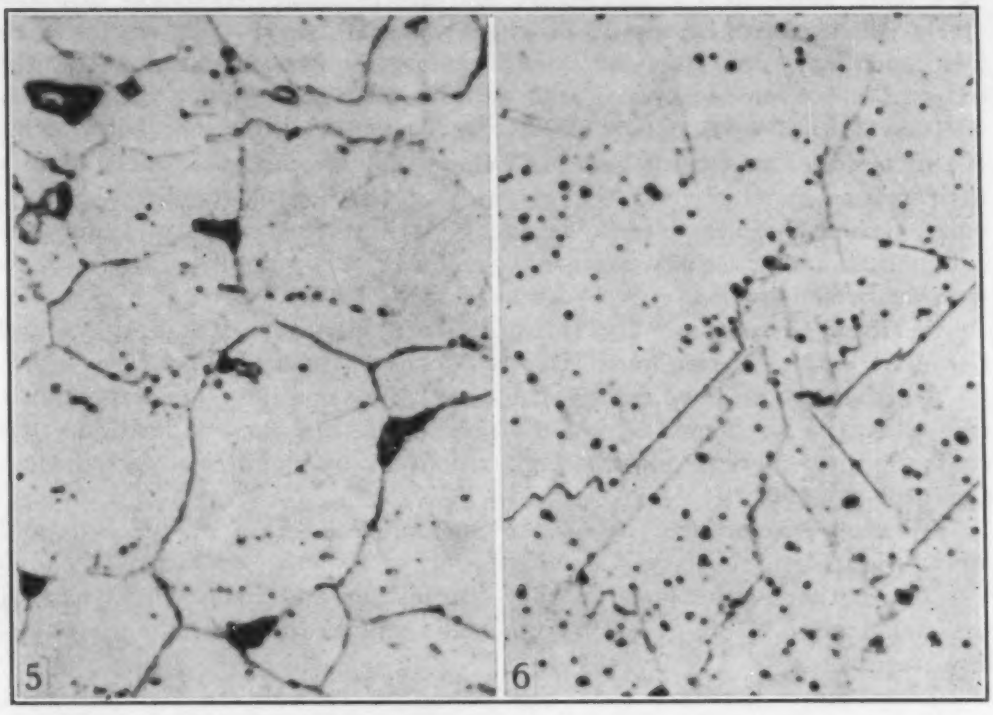


Fig. 5—AISI Type 347 (18-8 Columbium) Stainless Steel, Heated for 10,000 Hours at 1050 °F. Etched electrolytically with 5% chromic acid. × 2000.

Fig. 6—AISI Type 321 (18-8 Titanium) Stainless Steel, Heated for 10,000 Hours at 1050 °F. Etched electrolytically with 5% chromic acid. × 2000.

sulphate tests on sensitized materials as a criterion for such service behavior, unless evidence is available to show a relationship to exist between the corrosive conditions of the acidified copper sulphate solution and the corrosive conditions existing in exhaust manifolds.

The authors' conclusion regarding the low carbon (0.03% max.) 18-8 indicates that this grade is only slightly better than the higher carbon counterparts and thus is of little value. However, we believe that sufficient data are now available to show that these steels have satisfactory resistance to intergranular corrosion after short sensitizing periods. In fact, an examination of the authors' data indicates that after a treatment of 2 hours at 1200 °F (650 °C) steels C-1 and C-10 are comparable in resistance to intergranular attack to both steel C-8, which has a Ti/C ratio of 7.9, and steel C-3, which has a Cb/C ratio of 11.8. Thus for applications involving only short heating times, the low carbon stainless steels may be considered as being satisfactory substitutes for the titanium and columbium-stabilized grades.

We recognize that the low carbon stainless steels are vulnerable to intergranular corrosion after long-time sensitizing treatments; but, as we have just demonstrated, the columbium and titanium-stabilized grades also are vulnerable after prolonged sensitization. We cannot overemphasize that this question of immunity to intergranular corrosion is a relative one and should not be based alone upon the results of severe laboratory tests, since such a philosophy will preclude the usefulness of many steels which otherwise would be entirely satisfactory. Rather, the relative merits of each steel should be compared one with another on the basis of the requirements necessary for satisfactory service behavior, as well as on the basis of behavior under laboratory conditions of testing. If this is done, we cannot help but believe that the authors would modify their second conclusion to the extent that they would credit the 0.03% max. carbon stainless steels as being satisfactory substitutes for the columbium and titanium-stabilized grades in those applications, such as welding, which involve only short heating times.

Written Discussion: By Howard Scott, manager, Metallurgical and Ceramic Dept., Westinghouse Electric Corp., Pittsburgh.

Do the authors have any evidence that the sensitivity to intergranular embrittlement is affected by grain size? There are some indications that coarse-grained 18-8 requires a higher content of stabilizing agents than does fine-grained.

Written Discussion: By Roger Sutton, director of engineering and metallurgy, General Alloys Co., Boston.

The authors have made a very interesting and important study of the stabilization effect of columbium and titanium in the austenitic stainless steel.

I recognize the fact that this paper refers only to the effect of columbium and titanium additions in preventing or controlling carbide precipitation and subsequent intergranular attack. It is believed, however, that this highly specific attack may, in the minds of some readers, be confused with general corrosion rates.

It is thought, among those of us intimately connected with the production and use of austenitic stainless steels, that a preponderance of stabilizing elements, and particularly of columbium, over that required for the complete "tying up" of carbon promotes the formation of an eutectic or an intermetallic compound which is weak, brittle, and highly susceptible to corrosive attack. In fact, research work sponsored by the Alloy Casting Institute indicates that the proper ratio of columbium to carbon is not 10 to 1, but slightly over 7 to 1. This is contrary to the recommendations of the authors that a ratio of 12 to 1 is indicated as more desirable.

Have the authors any data based on over-all corrosion which might further clarify this point?

Authors' Reply

Several of the discussers of this paper emphasize the important effect that nitrogen has upon the resistance to intergranular embrittlement of

Types 321 and 347 stainless steel. Messrs. Tyrrell and Southard, using our revised ratios for Ti/C and Cb/C calculated as explained in Table I, present a table which is quite interesting in its theoretical implications. They recognize, however, that stainless steels do contain nitrogen and that minimum amounts of titanium and columbium must, therefore, be set high enough to allow for combination with nitrogen as well as with carbon if the steels are to be effectively stabilized.

Titanium must be an avid nitride former, since in the Type 321 steels all of the nitrogen except traces (0.001 to 0.002%) were acid insoluble. The actual calculated amounts of titanium thus rendered ineffective for stabilization of carbon by combination with nitrogen are of interest and are given in Table XXVIII.

Table XXVIII

Steel No.	Insoluble Nitrogen, % (Presumably as TiN)	Titanium Used by Insoluble Nitrogen, %
S-34	0.038	0.13
S-21	0.029	0.10
C- 6	0.011	0.04
S-39	0.022	0.08
C- 2	0.009	0.03
C- 8	0.006	0.02
S-25	0.021	0.07
S-35	0.015	0.05
S-36	0.017	0.06
S-32	0.016	0.05

These values may readily be calculated by the formula:

$$\text{Per cent titanium (as TiN)} = 3.43\ (\%\ \text{nitrogen} - 0.001)$$

Tyrrell and Southard mention that Binder, Brown and Franks[2] found that nitrogen only in excess of 0.022% would affect the amount of columbium necessary for stabilization. Their data were secured on steels of higher nickel content (11.75% nickel) than ours, and furthermore, their steels were sensitized 24 hours at 1200 °F (650 °C). Reference to our Table I shows that much larger amounts of nitrogen are soluble in steels treated at higher temperatures (emphasis must be placed on the fact that our analyses were made on the steels as annealed at 1950 to 2000 °F and cold-rolled). Apparently the temperatures at which the steels are treated have some influence on the relative proportions of soluble and insoluble nitrogen, at least in the columbium-treated steels. If so, it is also apparent that reference to the amount of columbium tied up as CbN is meaningless unless the temperatures at which the steels were treated are included.

Mr. Stewart takes us to task for basing our conclusions on titanium or columbium to carbide ratios, rather than on the revised ratios as calculated in Table I. Analyses for nitrogen are not normally reported for stainless steels; at least we are not familiar with any specifications which call for such analyses. For practical purposes, such an analysis does not appear to be necessary; the incorporation of a sufficient additional amount

of columbium or titanium to take care of about, roughly, half of the nitrogen in the columbium steels and all of the nitrogen in the titanium steels is all that is required. We feel that the titanium or columbium to carbon ratios recommended by us satisfies this requirement with safety. If it is assumed that the nitrogen content of the average type 347 steel is 0.050%, and that of the average Type 321 steel is 0.025%, the actual amounts of stabilizing elements which must be added, over and above that theoretically necessary to take care of the carbon, are 0.17% columbium and 0.08% titanium. As a matter of fact, it appears to be common practice among manufacturers to produce rather consistently steels which exceed the commercially accepted minimum ratios of Ti/C = 5 and Cb/C = 10 by fairly wide margins.

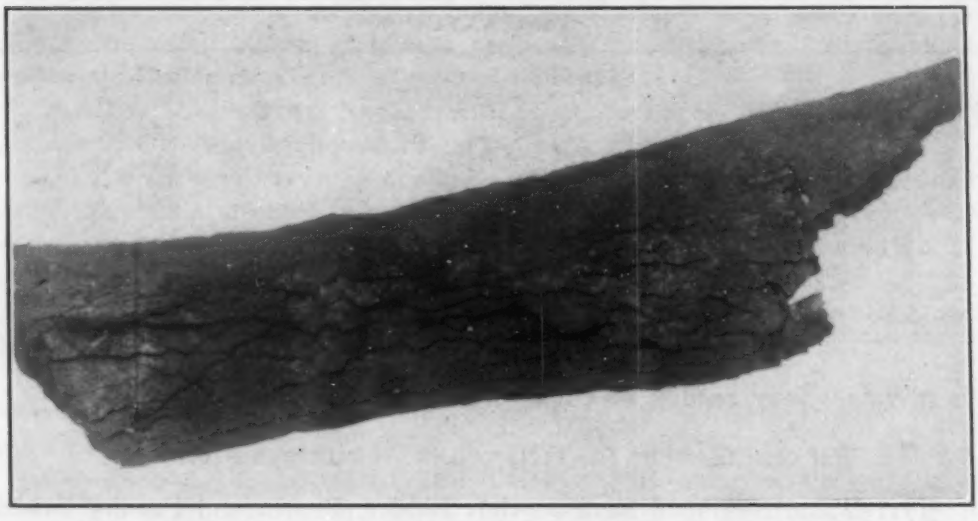


Fig. 7—Appearance of Sample (After Bend Test) Taken From Failed Portion of Exhaust Collector Ring. Material—Type 302 stainless. Approximately × 3.

Both Mr. Stewart and Mr. Heger question the use of a prolonged exposure at 1020 °F (550 °C) as a sensitizing treatment for evaluation of steels suitable for welding. We realize, of course, that such a treatment does not simulate conditions obtained during welding and are in complete agreement with their belief that for such a purpose a 2-hour sensitize at 1200 °F (650 °C) is probably adequate. The purpose of our study, however, was the determination of minimum Ti/C and Cb/C ratios for stabilization against intergranular embrittlement under severe conditions, and for such a purpose the 2-hour sensitize at 1200 °F (650 °C) is wellnigh worthless.

We were surprised and chagrined that Mr. Heger so interpreted our paper that it appeared that prolonged exposure at 1020 °F (550 °C) was a new development for inducing maximum susceptibility to intergranular attack. As a matter of fact, the very excellent paper by Bain, Aborn and Rutherford was given as a reference in our paper and lengthy conversations on the time-temperature relationships during sensitization were

held with R. H. Aborn, Russell Franks and others. We are sorry indeed for what is apparently a sin of omission in our paper.

With reference to Mr. Heger's question as to whether higher Ti/C or Cb/C ratios would be necessary for immunization as the conditions of severity of sensitization increase, we are inclined to believe that such higher ratios would not be necessary. If a steel is made with sufficient titanium or columbium so that, after due allowance is made for all the titanium or columbium that is rendered ineffective for one reason or another, enough is still left to combine effectively with all of the carbon

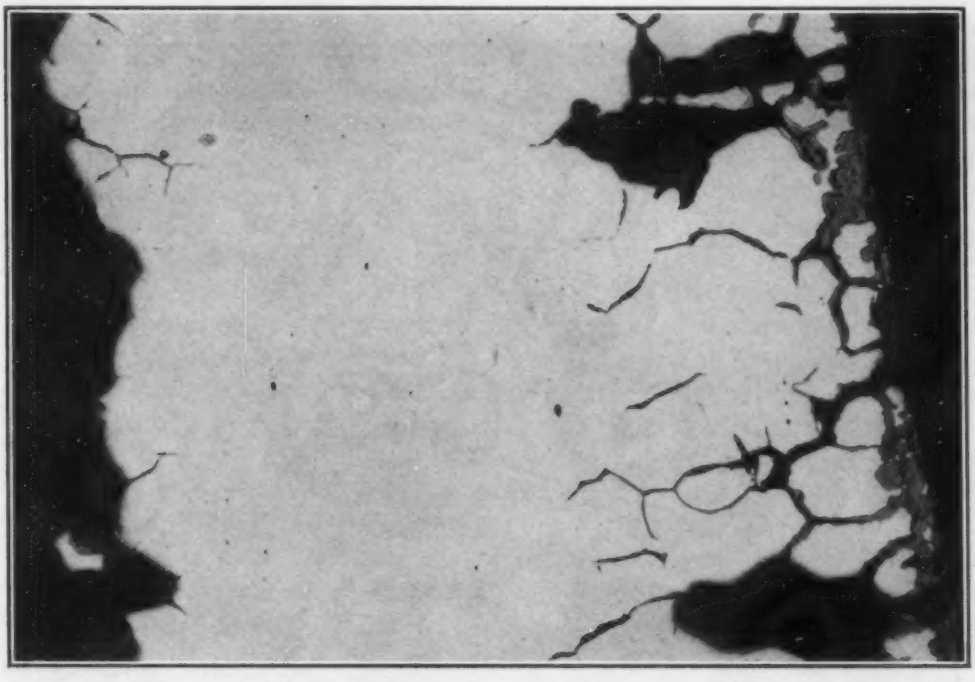


Fig. 8—Photomicrograph of Another Sample Taken From Failed Portion of Exhaust Collector Ring. Material—Type 302 stainless. Right side of photomicrograph shows the inside edge of the sample. This edge was in direct contact with the hot exhaust gases and shows severe intergranular attack. Unetched. × 100.

(except what is apparently the very slight amount soluble at the lower sensitizing temperatures), it is difficult to conceive what good purpose would be served by any additional amounts of these elements insofar as conferring resistance to intergranular embrittlement is concerned. The test data on the two steels offered by Mr. Heger to support his contention that the amounts of titanium or columbium must be increased as the severity of sensitization increases certainly do not prove his point since the boiling nitric acid test, useful as it may be for evaluating general corrosion resistance, has been pretty thoroughly discredited as a test for evaluating susceptibility to intergranular embrittlement. Some recent data substantiating this viewpoint were given by Stewart.[5] Furthermore, as Mr. Heger allows his fancy to move from 10,000 hours to 100,000 hours

[5]Raymond S. Stewart, "Resistance of Sensitized Steels to Boiling Nitric Acid," METAL PROGRESS, Vol. 52, 1947, p. 971.

at 1050 °F (565 °C), presupposing that a steel resistant to embrittlement after the first treatment would not be resistant after the longer treatment, he overlooks the possibility of the healing effects which excessively long exposures have at sensitizing temperatures. Some data on this phenomenon are given in the paper by Bain, Aborn and Rutherford, the very same paper that showed the added severity of sensitizing at 1000 to 1050 °F (540 to 565 °C). On the basis of our present state of knowledge we believe that there can be no serious disagreement with the premise that severity of sensitization (as regards intergranular embrittlement) is dependent upon both time and temperature, and that for any selected

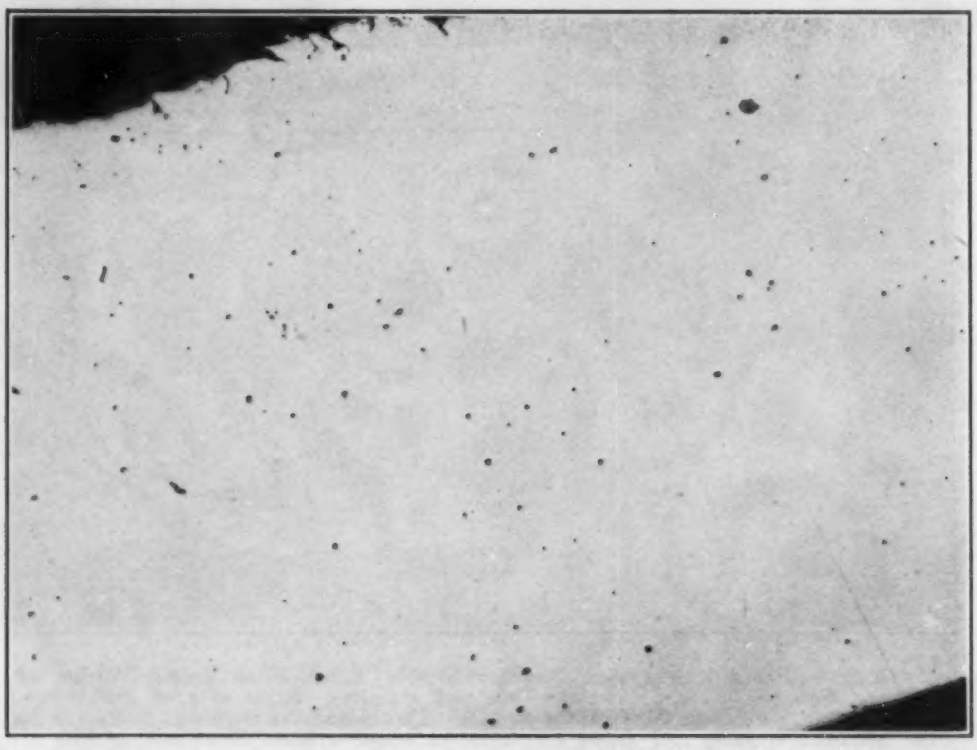


Fig. 9—Photomicrograph of Sample Taken From Another Portion of the Same Exhaust Collector Ring From Which the Samples Shown in Figs. 7 and 8 Were Taken. Material—Type 321 stainless. Lower right side of photomicrograph was in direct contact with the hot exhaust gases. Note freedom from intergranular attack. This sample was exposed for 4 days to the boiling acidified copper sulphate solution. Unetched. × 100.

temperature there is an optimum period of exposure for inducing maximum susceptibility to intergranular attack. Exceeding this length of time should cause the steel to improve. What effect such excessively long holding periods would have upon general or surface corrosion (which property is much better evaluated by the boiling nitric acid test) is not necessarily parallel to intergranular embrittlement. Mr. Heger has made an entirely unwarranted assumption by stating that his data and discussion demonstrate that the columbium and titanium grades are vulnerable to intergranular attack after prolonged sensitization.

With reference to the two low carbon stainless steels which were included in our test program, it is true, as Mr. Heger states, that after sensitizing 2 hours at 1200 °F (650 °C) their performance was comparable to that of steels carrying a Ti/C ratio of 7.9 or a Cb/C ratio of 11.8. However, when sensitized for 8 or 21 days at 1020 °F (550 °C), these low carbon steels failed badly (Tables II and III), whereas the stabilized steels were practically unaffected (Tables X and XX). Obviously these low carbon steels, as well as the stabilized grades carrying the lower Cb/C and Ti/C ratios, are suitable for use in applications where sensitizing conditions are not too severe.

Mr. Heger's reference to aircraft engine exhaust manifolds is, in a very nice way, of course, the same thought which many manufacturers of stainless steel have frequently expressed verbally in a much blunter fashion; namely, "An airplane does not fly through sulphuric acid; why test the steel in sulphuric?" The answer is that resistance to intergranular embrittlement is an important requirement for certain aircraft applications and the sulphuric acid test is a reliable means of evaluating this property. Whether there is or is not a relationship between the corrosive conditions of the acidified copper sulphate solution and the corrosive conditions existing in exhaust manifolds, we are not prepared to state. We are, however, able to state that properly stabilized steels (and hence resistant to the acidified copper sulphate solution) perform satisfactorily in aircraft exhaust collector rings and that the unstabilized grades do not. (See also the last paragraph of discussion by Messrs. Tyrrell and Southard.) Furthermore, intergranular corrosion is a major cause of failure in such applications.

We have recently had occasion to examine some failed collector rings returned from service. Examination showed that, presumably because of a mix-up in material, some parts of these rings had been fabricated of Type 302 stainless and other parts of Type 321; the latter steel (or Type 347) should have been used throughout. Susceptibility to intergranular attack was induced in the Type 302 material adjacent to the welds by the temperature effects during welding and this sensitization was aggravated by the heat effects of the exhaust gases during service. The heat from the exhaust gases was also effective in sensitizing the 302 material remote from the welds and the corrosive action of the exhaust gases was effective in actually developing intergranular corrosion in this material, which ultimately failed from this cause. The 321 material showed no evidence of failure from intergranular corrosion.

The appearance of a sample taken from the Type 302 steel in one of these rings is shown in Fig. 7. The sample showed numerous cracks after a simple bend test and the nature of these cracks will be recognized as typical of those caused by intergranular embrittlement. Metallographic examination of another sample of this steel showed severe intergranular corrosion, particularly at the inside surface (Fig. 8). No evidence of intergranular attack was observed in a sample taken from the Type 321 steel in this ring (Fig. 9), even after a 4-day exposure to the boiling acidified copper sulphate solution. We offer this account and these illus-

trations as evidence that, as far as intergranular embrittlement is concerned, some relationship does exist between the corrosive conditions of the acidified copper sulphate solution and the corrosive conditions in exhaust manifolds.

With reference to the question asked by Howard Scott, our data indicate that superior resistance to intergranular attack was obtained with materials annealed at 1800 °F (980 °C) than when annealed at 1975 °F (1080 °C). We believe this to be an indication that grain size does have an effect, a trend which has been reported by others.

We regret that we are unable to supply Mr. Sutton with any data on the over-all corrosion of our steels, since our study was restricted entirely to intergranular corrosion. The eutectic or intermetallic compound which Mr. Sutton mentioned was not observed in any of our steels. Perhaps this eutectic is peculiar to the cast materials only. The low ratio of columbium to carbon indicated by the work sponsored by the Alloy Casting Institute may be suitable for some uses not mentioned by Mr. Sutton but is, we are certain, much too low for effective stabilization of 18-8 against intergranular embrittlement.

RESISTANCE TO SENSITIZATION OF AUSTENITIC CHROMIUM-NICKEL STEELS OF 0.03% MAX. CARBON CONTENT

By W. O. Binder, C. M. Brown and Russell Franks

Abstract

A basic study of low-carbon austenitic chromium-nickel steels was made to determine the effects of chromium, nickel, carbon, and nitrogen on their susceptibility to intergranular corrosion. The compositions investigated ranged from 16 to 25% chromium, 6.5 to 25% nickel, 0.005 to 0.05% carbon, and 0.002 to 0.15% nitrogen. Additions of up to 3% molybdenum and small amounts of columbium were also investigated.

Complete immunity is essential to the successful service of steel exposed at elevated temperatures for long periods of time. This work substantiates the viewpoint that carbon must be lowered to at least 0.02% if the steels are to be completely free of susceptibility to intergranular attack. The proper addition of columbium to steels of somewhat higher carbon content for complete immunity to intergranular attack must allow for its solubility in the steel and for its combination with carbon and nitrogen.

Steels subjected to high temperatures only during fabrication require somewhat less than complete immunity to intergranular corrosion that more extended heating demands. Partial immunity has been studied from the standpoint of the time-temperature-precipitation characteristics of the steels. The start of carbide precipitation has been found to be influenced by the elements chromium, nickel, and nitrogen. The effects of composition on the resistance to attack after short periods of heating at 650 and 750 °C (1200 and 1380 °F) have been summarized in empirical formulas. The study of the time-temperature-precipitation relationship was extended to steels containing molybdenum.

A paper presented before the Thirtieth Annual Convention of the Society, held in Philadelphia, October 23 to 29, 1948. Of the authors, W. O. Binder and C. M. Brown are metallurgists, Union Carbide and Carbon Research Laboratories, Inc., Niagara Falls, N. Y., and Russell Franks is chief metallurgist, Electro Metallurgical Company's Sales Development and Technical Service Department, Pittsburgh. Manuscript received April 14, 1948.

Introduction

CARBON adversely affects the corrosion resistance of the austenitic chromium-nickel steels. The adverse effect of carbon on corrosion resistance is related to the decreased solubility of carbon in austenite with lowering of temperature. The precipitation of intergranular chromium carbide, which occurs when the steels are heated at temperatures between 400 and 900 °C (750 and 1650 °F), renders them susceptible to grain boundary attack. In this condition, the steel may fail by intergranular corrosion when exposed to relatively weak corrosives.

As a part of the effort to control intergranular susceptibility in the austenitic chromium-nickel steels, a basic study of steels with very low-carbon contents was undertaken at the Union Carbide and Carbon Research Laboratories to determine the effects of carbon, chromium, nickel, and nitrogen. The results obtained from this study tend to substantiate the viewpoint of the earlier workers, and the conclusion is that carbon must be reduced to less than 0.02% if the chromium-nickel stainless steels are to completely resist intergranular corrosion without the addition of a carbide stabilizer. Steels in this classification may be heated for prolonged periods of time in the carbide precipitation range without loss of corrosion resistance.

A large current use for austenitic chromium-nickel steels involves heating for only short periods of time in the carbide precipitation temperature range. This implies a partial degree of immunity to intergranular corrosion. A study of partial immunity has been carried out which has been concerned with the time-temperature-precipitation characteristics of the steels. The start of carbide precipitation has been found to be influenced by the elements chromium, nickel, and nitrogen. An empirical equation, based on a short period of exposure at a given temperature in the carbide precipitation range, has been evolved quantitatively relating these variables. The equation shows that the maximum permissible amount of carbon in these steels is controlled by nickel and chromium. When nickel is increased, the allowable carbon content is diminished, whereas increasing chromium raises the carbon limit. However, the beneficial effect of chromium cannot be fully utilized because the high-chromium steels must contain larger amounts of nickel to maintain an austenitic structure. The effect of nitrogen on intergranular corrosion resistance has been found to be relatively small under these conditions.

The study of the time-temperature-precipitation relationship was also extended to steels containing molybdenum. The addition of 2% molybdenum to 0.02 to 0.03% carbon steels increases the time for damaging carbide precipitation to occur.

Small amounts of columbium may be employed to render the relatively low carbon steels completely resistant to intergranular attack. The proper amount of columbium must allow for its solid solubility in the steel and for its combination with both carbon and nitrogen. Insufficient data for other carbide-forming elements have been obtained to permit inclusion at this time. Their effects are believed qualitatively similar in most respects to the effects of columbium.

Literature Review

Considerable effort has been expended to devise means of eliminating the intergranular susceptibility of these steels. A number of methods have been proposed; namely, lowering of carbon content, cold working the steel and subsequently precipitating the carbides and rendering them harmless by suitable coagulating heat treatments, adjusting the chromium or nickel contents to form an austenitic structure with some delta ferrite, and introducing elements such as columbium and titanium which preferentially combine with carbon and form more insoluble carbides than chromium. Of these methods, only the latter has been widely used in practice.

Since their inception, the carbon content of the austenitic steels has gradually decreased. When introduced some 35 years ago by Strauss and Maurer, the steels contained about 0.25% carbon, but the development of low-carbon ferrochromium has permitted the concurrent manufacture of lower carbon steels. Under the present 0.08% maximum carbon specification, about half of the 18% chromium – 8% nickel steels now manufactured contain 0.05 to 0.07% carbon.

The British Patent, No. 305,564 (1929), issued to F. Krupp A.G., states that, if the carbon content is reduced below 0.07%, no precipitation of carbide occurs in heating for welding operations. Practical experience with steels of this kind has shown that 0.07% carbon as a limiting value is considerably too high. Later investigations by Bain, Aborn and Rutherford (1)[1], and by Strauss, Schottky

[1]The figures appearing in parentheses pertain to the references appended to this paper.

and Hinnüber (2), indicate that carbon lower than 0.07% is necessary.

The estimated carbon solubility limit in 18-8 steels is 0.02% at about 650 °C (1200 °F) according to Bain, Aborn and Rutherford (1). If the precipitation of carbides is related to intergranular corrosion, it might be expected that, if carbon were lowered to this level, the steel would be relatively free from intergranular corrosion when heated at temperatures at which carbon precipitates. That improved resistance is obtainable in this manner has been demonstrated by Krivobok, et al. (3), Becket and Franks (4), and more recently by Uhlig (5). Since the indications were that these very low carbon steels were highly resistant to intergranular attack, this investigation was concerned with the corrosion resistance of steels ranging in carbon from 0.005 to 0.03%.

Test Procedure

The steels used in this investigation were made as small induction furnace heats. The charges consisted of Armco iron, 0.03% maximum carbon ferrochromium, high-nitrogen ferrochromium, electrolytic nickel, low carbon manganese metal, and silicon metal. The chromium content of the steels ranged from 16 to 25% and the nickel from 7 to 25%. The manganese content was held at 1.25% and the silicon at 0.4% for deoxidation purposes and good hot workability. Carbon ranged from 0.005 to 0.05% and nitrogen from 0.002 to 0.15%.

The steels were cast into 2-inch square ingots from which ¼-inch thick plate and 0.04-inch thick strip were obtained by forging and hot rolling. No difficulty was experienced in hot working any of the steels. The samples, after shearing and machining to size, were held 10 minutes at 1075 °C (1970 °F) and air-cooled. They were heated subsequently at several different temperatures in the carbide precipitation temperature range; namely,

(a) 100 hours and 336 hours at 475 °C (890 °F)
(b) 1, 16, and 100 hours at 550 °C (1020 °F)
(c) 1 and 24 hours at 650 °C (1200 °F).

As will be described later, the time and temperature ranges were expanded in certain instances for the purpose of determining the

shape of the time-temperature curve for the beginning of carbide precipitation.

One of the most important considerations in this work has been the accuracy of the carbon analysis. Results obtained by ordinary combustion methods, where the gas was absorbed in a weighed bulb, proved unsatisfactory and a more sensitive method was developed by Messrs. R. M. Fowler, J. H. Harley and E. L. Bennet of the Union Carbide and Carbon Research Laboratories, Inc. In the new method, which is a refinement of the conductivity methods proposed by Cain and Maxwell (6), Ericsson (7), and Newton (8), combustion is carried out as formerly, but the gas is absorbed in a dilute barium hydroxide solution. The change in conductivity of this solution is accurately measured in an a.c. bridge circuit and this reading is converted into per cent carbon. The accuracy of this method has been found to be within plus or minus 0.002% carbon, based on available Bureau of Standards samples.

Two corrosion test media were generally employed—boiling acidified copper sulphate solution (50 g. $CuSO_4 \cdot 5H_2O$, 50 ml. H_2SO_4 (sp. gr. 1.84), 420 ml. H_2O) and boiling 65% nitric acid. These solutions are commonly used in testing steels of this type and are known to produce intergranular attack if the grain boundaries contain finely divided precipitated carbides. In the copper sulphate test, two types of samples were used: one for bend tests, and the other for electrical resistance tests. Each of these samples was taken from the 0.04-inch thick material. The bend samples were ½ inch wide and 3 inches long and the electrical resistance samples were 0.180 inch wide and 6 inches long. At the end of 1, 2, 24, 100, 300, and 700 hours' boiling, the samples were removed and inspected either for evidence of cracking when bent or for a change in electrical resistance. Polished samples 1 inch by 1½ inches prepared from the ¼-inch thick plate were exposed to the boiling 65% nitric acid for five 48-hour periods. Their weight losses were converted into corrosion rates in terms of inch penetration per month.

The steels in the annealed condition were also tested by means of a sensitive magnetic balance in order to detect the presence of ferrite in the structure. Fully austenitic steels required only about 0.15 gram to break the magnetic pull, while completely ferritic steels required over 200 grams. Confirmatory metallographic examinations were also made.

Discussion of Results

Austenite—Austenite-Plus-Ferrite Phase Relationship

As an initial step in the study of the very low-carbon chromium-nickel steels, experiments were made to determine the interrelation among chromium, nickel, carbon, and nitrogen in the formation of a stable austenitic structure. The reduction of carbon in austenitic chromium-nickel steels is accompanied by the formation of ferrite unless the nickel or nitrogen content of the steel is raised or the chromium content is lowered. It is generally felt that the maintenance of an austenitic structure is advisable from the standpoint of workability and corrosion resistance. There is the possibility of using partially ferritic steels in many applications although this work has centered on completely austenitic steels to prevent prejudice to the quality inherent in the wholly austenitic structure.

From the magnetic balance data, taken on samples heated 10 minutes at 1075 °C (1970 °F) and air-cooled, coupled with numerous metallographic examinations, curves were derived to indicate the necessary proportions of chromium, nickel, carbon, and nitrogen required to produce a completely austenitic structure. By employing three-dimensional scatter plots, it was possible to derive an empirical equation relating these elements. It was found that a plane surface satisfactorily divided the austenite field from the austenite-plus-ferrite field within the limits of the experiment. In the range of compositions studied, the equation provides a fairly simple means for determining approximately the structure existing in a given steel. The final equation expressing the relationship is:

$$30\,(\%\text{ carbon}) + 26\,(\%\text{ nitrogen}) + (\%\text{ nickel}) - 1.3\,(\%\text{ chromium}) + 11.1 = 0 \qquad \text{(Equation I)}$$

It is valid within the following composition limits:

Chromium, 18 to 25%
Nickel, 9 to 25%
Carbon, up to 0.05%
Nitrogen, up to 0.15%

The solution of this equation gives the minimum values of carbon, nitrogen, and nickel and the maximum value of chromium to obtain an austenitic structure. The coefficients of the variables indicate the relative austenite-forming power of each of the elements. Nitrogen, for example, is nearly as strong as carbon in this respect.

Chromium-Nickel Steels Completely Immune to Intergranular Corrosion

Effect of Carbon—Complete immunity to intergranular corrosion is required if the steel is to be exposed at elevated temperatures for long periods of time under corrosive conditions. The heat treatment consisting of 100 hours at 550 °C (1020 °F) was selected as a criterion of complete immunity. A low temperature was required, as it was important that the relatively small amounts of carbon in excess of the solubility limit being dealt with here would have an opportunity to precipitate. Temperatures below 550 °C (1020 °F), while they further decrease the solubility of carbon, had the disadvantage that their diffusion coefficient was so low that extremely long periods of heat treatment would be required to cause precipitation, rendering the preparation of test samples laborious and impractical from an experimental standpoint. Diffusion at 550 °C (1020 °F) is rapid enough to bring about complete precipitation of the excess carbon in relatively short periods of time without danger of self-healing from coagulation. A time period of 100 hours was used, as past experience indicated that it was long enough to precipitate nearly all of the carbon present in the steel. Subsequent corrosion tests substantiated the choice of test condition for defining complete immunity, as it was found that, of the test conditions employed, heating 100 hours at 550 °C (1020 °F) caused the most severe corrosion damage.

Although major emphasis was placed on steels containing 18% chromium, the study was carried out in 18 to 25% chromium steels of similar nitrogen content in sufficient detail to evaluate the influence of carbon on the corrosion resistance of a wide variety of austenitic compositions. The effect of carbon content on intergranular corrosion in the 18% chromium steels containing 0.03 to 0.05% nitrogen after heating 100 hours at 550 °C (1020 °F) is shown in Fig. 1. Curves are presented for several nickel levels between about 9 and 12%. As indicated by these data, increasing carbon beyond a certain limiting value causes severe attack in the copper sulphate solution. The amount of nickel present is also important as the depth of penetration at any given carbon level is increased, and the critical carbon content for complete resistance to intergranular attack is decreased by larger amounts of nickel. These values for maximum allowable carbon indicate the extremely low level to which carbon must

be reduced for complete freedom from intergranular attack.

Companion samples to those tested in boiling copper sulphate solution were also tested in boiling 65% nitric acid. The average corrosion rates obtained from these tests are summarized in the curves of Fig. 2. Here, again, the plotted curves are for samples heated 100 hours at 550 °C (1020 °F). In Fig. 2 the marked effect of increasing carbon is evident as the curves rise steeply to very

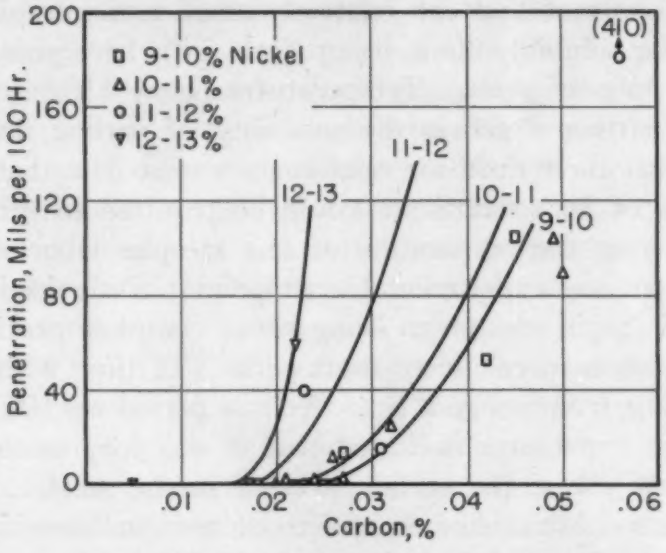


Fig. 1—Influence of Carbon on Depth of Intergranular Penetration in 18% Chromium Steels with 0.03 to 0.05% Nitrogen, Tested in Boiling Acidified Copper Sulphate Solution After Air-Cooling from 1075 °C (1970 °F) and Heating 100 Hours at 550 °C (1020 °F).

high rates with a small increase in carbon content beyond the limiting amount. The corrosion rates for steels with carbon contents within the solubility range are approximately 0.0005-inch penetration per month, which is the same as the rate observed for the annealed steel. Nickel is seen to be an important factor in the nitric acid test, as in the copper sulphate test, in regulating the severity of attack for a given carbon content.

In continuing the investigation, steels with chromium contents greater than 18% were made. At 20 and 25% chromium levels, steels with varying nickel and carbon were tested in the same manner as the 18% chromium steels. Fig. 3 shows the penetration versus carbon curves for the 20% chromium steels in the boiling copper sulphate test for samples heated 100 hours at 550 °C (1020 °F). Fig. 4 contains the nitric acid data obtained for these same steels.

It is observed that the carbon content of the 20% chromium steels must also be reduced to less than 0.020% if the steels are to be free

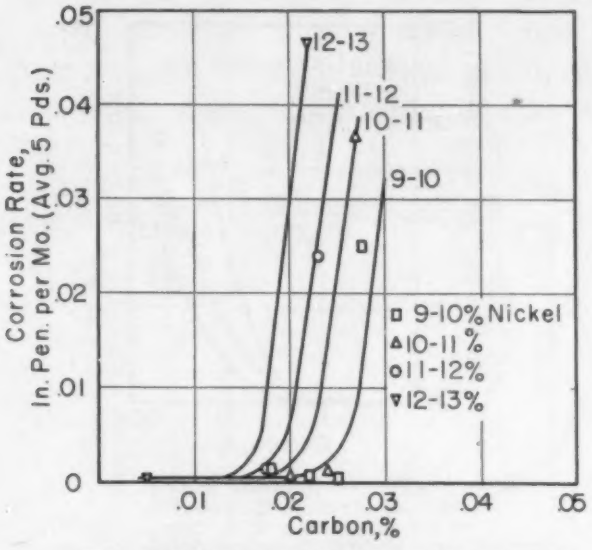


Fig. 2—Influence of Carbon on Average Corrosion Rate in Boiling 65% Nitric Acid of 18% Chromium Steels with 0.030 to 0.050% Nitrogen After Air Cooling from 1075 °C (1970 °F) and Heating 100 Hours at 550 °C (1020 °F).

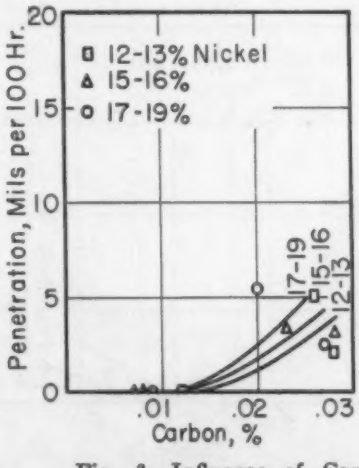


Fig. 3—Influence of Carbon on Depth of Intergranular Penetration in 20% Chromium Steels with 0.030 to 0.050% Nitrogen, Tested in Boiling Acidified Copper Sulphate Solution After Air Cooling from 1075 °C (1970 °F) and Heating 100 Hours at 550 °C (1020 °F).

from intergranular attack in these test media. It is again seen that, by increasing the nickel content at a given carbon level, more severe intergranular attack occurs. Figs. 5 and 6 contain similar data for

the effect of carbon in the 25% chromium steels in the two test media. Again, it is necessary in the 25% chromium range to lower

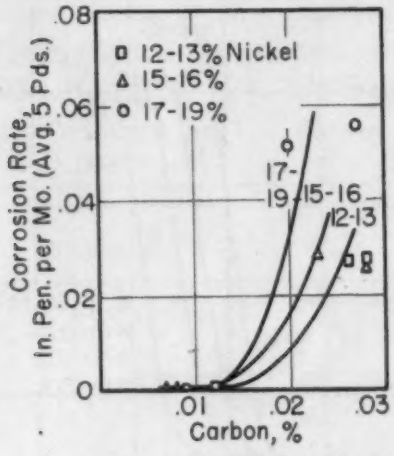


Fig. 4—Influence of Carbon on Average Corrosion Rate in Boiling 65% Nitric Acid of 20% Chromium Steels with 0.030 to 0.050% Nitrogen, After Air Cooling from 1075 °C (1970 °F) and Heating 100 Hours at 550 °C (1020 °F).

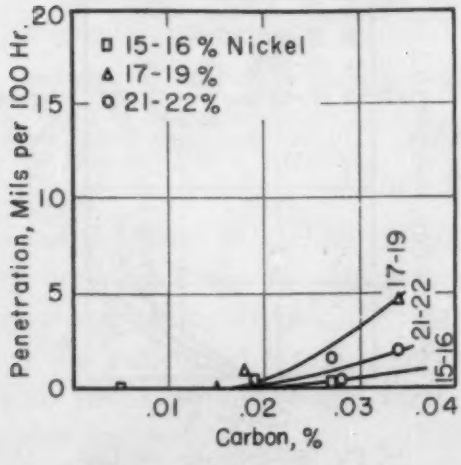


Fig. 5—Influence of Carbon on Depth of Intergranular Penetration in 25% Chromium Steels with 0.030 to 0.050% Nitrogen, Tested in Boiling Acidified Copper Sulphate Solution After Air Cooling from 1075 °C (1970 °F) and Heating 100 Hours at 550 °C (1020 °F).

the carbon content to less than 0.020% to obtain complete immunity from intergranular attack after long heating at 550 °C (1020 °F). In general, the attack in boiling copper sulphate solution is less severe

as the chromium content is increased. However, in boiling nitric acid this benefit from increasing chromium is not observed.

Effect of Nitrogen—Nitrogen is present in all austenitic chromium-nickel steels made by normal melting practices, due to the affinity of chromium for nitrogen. Since nitrogen is very difficult to remove from these steels, it was important to study its effect on

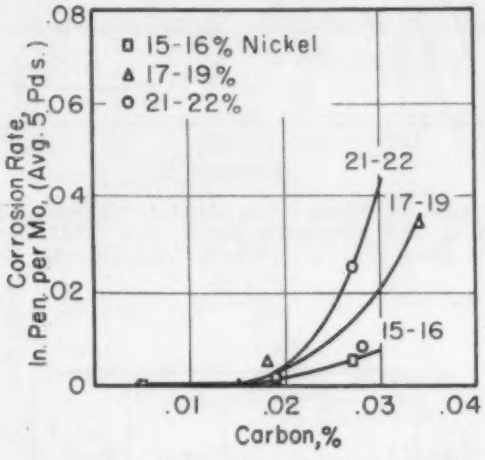


Fig. 6—Influence of Carbon on Average Corrosion Rate in Boiling 65% Nitric Acid of 25% Chromium Steels with 0.030 to 0.050% Nitrogen, After Air Cooling from 1075 °C (1970 °F) and Heating 100 Hours at 550 °C (1020 °F).

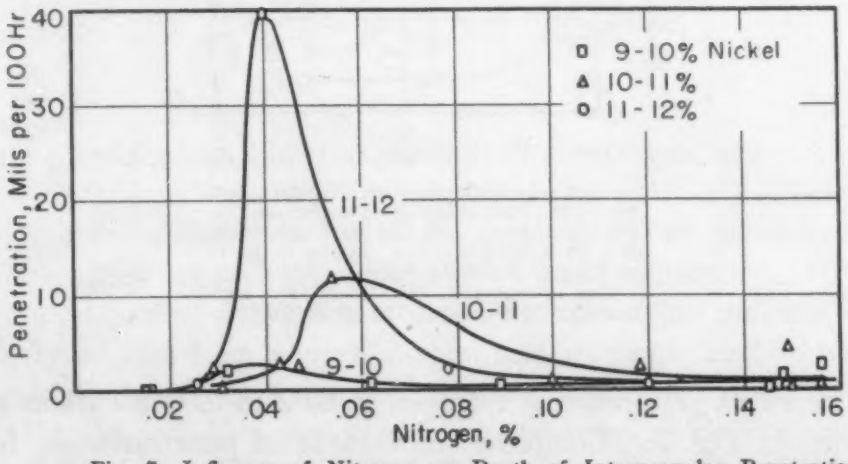


Fig. 7—Influence of Nitrogen on Depth of Intergranular Penetration in 18% Chromium Steels with 0.020 to 0.030% Carbon, Tested in Boiling Copper Sulphate Solution After Air Cooling from 1075 °C (1970 °F) and Heating 100 Hours at 550 °C (1020 °F).

intergranular corrosion resistance. It was expected that, because nitrogen has a pronounced effect on structure, it might cause a change in the limiting carbon content for complete immunity.

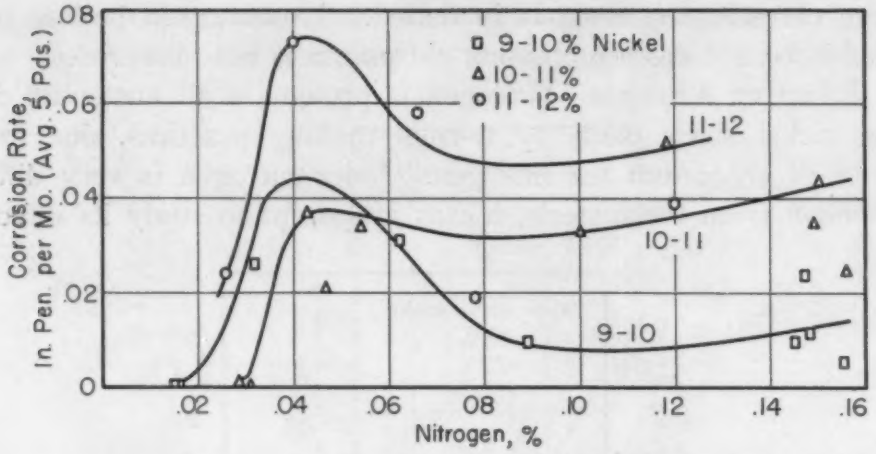


Fig. 8—Influence of Nitrogen on Average Corrosion Rate in Boiling 65% Nitric Acid of 18% Chromium Steels with 0.020 to 0.030% Carbon, After Air Cooling from 1075 °C (1970 °F) and Heating 100 Hours at 550 °C (1020 °F).

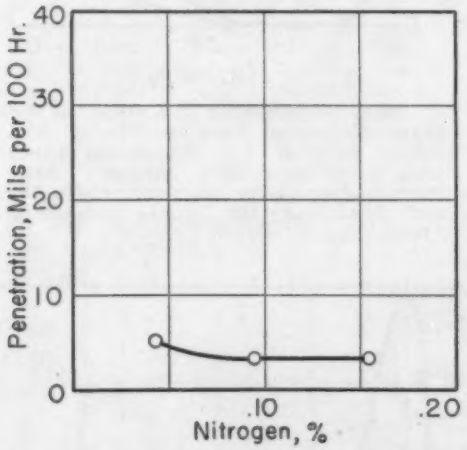


Fig. 9—Influence of Nitrogen on Depth of Intergranular Penetration in 25% Chromium – 18% Nickel Steels with 0.030 to 0.035% Carbon, Tested in Boiling Copper Sulphate Solution After Air Cooling from 1075 °C (1970 °F) and Heating 100 Hours at 550 °C (1020 °F).

The effect of increasing nitrogen in 0.02 to 0.03% carbon steels is shown in Fig. 7. Complete freedom from penetration is found when the nitrogen content is less than about 0.020%. Increasing the nitrogen up to about 0.04 or 0.05% causes increased penetration in the range of 9 to 12% nickel, whereas further increase in the nitrogen content up to about 0.150% reduces the penetration in boiling copper sulphate solution to a value of only 1 to 2 mils. While this effect of nitrogen appears beneficial, it will be shown later that

0.15% nitrogen decreases the resistance of the steel to boiling nitric acid. Here, again, the general influence of raising nickel is to increase the depth of penetration.

Fig. 8 for the nitrogen-bearing steels in boiling nitric acid resembles to some degree the curves of Fig. 7 for the same steels in copper sulphate solution. The corrosion rates rise rapidly up to about 0.04 to 0.06% nitrogen, fall off between about 0.07 to 0.09% nitrogen, and again rise as the nitrogen is further increased. The

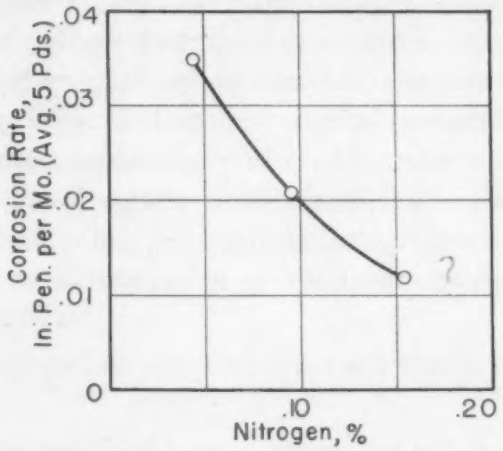


Fig. 10—Influence of Nitrogen on Average Corrosion Rate in Boiling 65% Nitric Acid of 25% Chromium – 18% Nickel Steels with 0.030 to 0.035% Carbon After Air-Cooling from 1075 °C (1970 °F) and Heating 100 Hours at 550 °C (1020 °F).

actual corrosion rates in the 0.07 to 0.09% nitrogen range are on the order of 0.01 to 0.02-inch penetration per month, and although less than the rates observed for steels with somewhat lower or higher nitrogen, they are still too high to be of practical interest. In Fig. 8, the curves plotted for different nickel contents again indicate that the severity of attack at a given carbon and nitrogen level is increased by raising the nickel content.

Figs. 9 and 10 are plotted from the copper sulphate and nitric acid data for the high-nitrogen 25% chromium steels. While these data are too few to give anything but the tentative shape of the curves, the general trend of the results is shown. There is indication that some benefit is obtained with nitrogen increased to 0.15 to 0.18%, but the nitric acid rates are still too great to be of practical interest.

Significance of Tests of Steels Completely Immune to Intergranular Corrosion—The foregoing data indicate that the carbon content of austenitic chromium-nickel steels containing 0.03 to 0.05% nitrogen must be reduced to between 0.015 and 0.02% if complete resistance to intergranular attack is to be attained. The limiting carbon content is lowered by increasing nickel at a given chromium level. Nitrogen increases intergranular susceptibility in the range of compositions studied. Chromium increases the tolerance for carbon, but since the nickel content must be increased to avoid ferrite formation and possible subsequent embrittlement, little advantage regarding increased resistance to intergranular corrosion can be gained from chromium contents higher than about 18%, that is, beyond the chromium content required to give general corrosion resistance. It is evident that, in plain chromium-nickel austenitic steels, the conclusions of the earlier investigations (1, 2, 3, 4, and 5) have been confirmed regarding the maximum carbon content consistent with complete immunity to intergranular corrosion.

Chromium-Nickel Steels Partially Immune to Intergranular Corrosion

The maximum carbon content required for complete immunity is so low that consideration was given to steels having partial immunity. The precipitation of carbides in austenitic chromium-nickel steels is the result of a nucleation and diffusion process; hence, under certain conditions of limited heating, the steels should remain free of intergranular susceptibility as a finite amount of time is usually required to produce nuclei for precipitation. In the case of 0.07% carbon steels, the safe time intervals are extremely short and far too critical for practical control. Much longer time intervals are present in the low-carbon steels, and it should be possible, by means of suitable test procedures, to define compositions wherein limited heating in the carbide precipitation temperature range would not cause intergranular susceptibility.

To establish a suitable test procedure, corrosion data for steels heat treated for 1 and 16 hours at 550 °C (1020 °F) and for 1 and 24 hours at 650 °C (1200 °F) were reviewed. It appeared from these results that the 1 hour at 650 °C (1200 °F) treatment was quite selective, more so than the 1 hour at 550 °C (1020 °F) treatment, and yet not so severe as the 16 or 24-hour treatment. Moreover, it seemed likely that most fabricating heat cycles involving

continuous cooling would produce intergranular carbide precipitation closely approximating that produced by isothermally heating 1 hour at 650 °C (1200 °F).

Samples of all the steels in this investigation were exposed to boiling acidified copper sulphate solution for up to 700 hours after heating 1 hour at 650 °C (1200 °F) to determine their resistance to intergranular corrosion with the results listed in Table I. A three-dimensional plot for chromium, nickel, and carbon was then prepared for all steels up to 0.05% nitrogen to picture the interrelationships involved between composition and corrosion resistance. The data obtained from the boiling copper sulphate tests were imposed on the three-dimensional model. The model then represented a scatter plot in three dimensions which showed that a surface could be described through the numerous data points dividing the region where intergranular attack was found from the region where no attack was found. The general shape of this limiting surface was that of a noncircular cylinder. The equation found to best fit the experimental data is:

$$\frac{6.17}{(\%\ \text{carbon})^{0.88}} + 13.8\ (\%\ \text{chromium}) - 10\ (\%\ \text{nickel}) - 276 = 0$$

(Equation II)

Small regions of uncertainty exist on each side of the given surface, due to errors in the chemical analyses and test procedures. The regions may be represented by a variation of ± 8 in the constant term of Equation II, that is, -276 ± 8. Twenty-two of the steels in Table I fall within this range. Of these steels about one-half were found satisfactory in the corrosion tests, and one-half were unsatisfactory. Outside the range of uncertainty, four steels which were predicted satisfactory failed in one or more of the corrosion tests, and six steels, predicted unsatisfactory, passed the corrosion tests. A schematic drawing of the limiting surface is given in Fig. 11. If two of the three variables are known, substituting in the equation gives the value of the third variable to place the composition *on the limiting surface*. If the function is solved for carbon or nickel, the resulting values are maximum values. Whereas, if the expression is solved for chromium, the resulting value is a minimum, since lower values of chromium move the composition into the intergranular attack region. For optimum corrosion resistance after 1 hour at 650 °C, the composition should fall somewhat below the limiting surface.

Table I

Corrosion Data for Austenitic Chromium-Nickel Steels of Low-Carbon Content Heated 1 Hour at 650 °C

Heat No.	Chemical Composition, %						Corrosion Rate, Inch Penetration per Month in Boiling 65% Nitric Acid				Boiling Acidified Copper Sulphate Heated 10 Min. at 1075 °C, Reheated 1 Hour at 650 °C and Air-Cooled	
							Heated 10 Min. at 1075 °C and Air-Cooled		Heated 10 Min. at 1075 °C, Reheated 1 Hour at 650 °C and Air-Cooled			
	Cr	Ni	Mn	Si	C	N	Fifth 48-Hr. Period	Avg. of Five 48-Hr. Periods	Fifth 48-Hr. Period	Avg. of Five 48-Hr. Periods	Bend Rating†	Per Cent Increase in Electrical Resistance‡
K380	18.54	9.86	1.23	0.48	0.018	0.044	0.00051	0.00055	0.00067	0.00066	0	..
K652	17.83	9.21	1.2*	0.4*	0.022	0.016	0.00070	0.00066	0.00089	0.00081	0	..
K17	17.99	9.71	0.98	0.30	0.025	0.015	0.00045	0.00058	0.00056	0.00075	0	..
L376	18.92	9.70	1.26	0.39	0.027	0.032	0.00067	0.00066	0.00152	0.00105	2	5
K382	18.36	9.97	1.36	0.50	0.042	0.027	0.00063	0.00064	0.0149	0.00620	2–24	..
K383	18.61	9.90	1.26	0.40	0.045	0.026	0.00051	0.00057	0.0125	0.00520	2–24	..
K197	18.57	10.31	1.14	0.33	0.020	0.031	0.00042	0.00055	0.00048	0.00060	0	..
K634	18.51	10.66	1.32	0.37	0.021	0.047	0.00045	0.00053	0.00092	0.00076	0	..
K198	18.37	10.88	1.09	0.32	0.024	0.029	0.00048	0.00056	0.00068	0.00080	0	..
K638	18.35	10.75	1.40	0.36	0.026	0.054	0.00050	0.00055	0.00109	0.00087	0	..
K385	18.48	10.41	1.33	0.51	0.027	0.043	0.00044	0.00055	0.00069	0.00073	0	..
L379	18.54	10.39	1.22	0.42	0.032	0.037	0.00052	0.00060	0.00280	0.00171	3	24
K384	18.48	10.34	1.24	0.44	0.049	0.041	0.00052	0.00057	0.0133	0.00550	3–24	..
K388	18.22	10.95	1.50	0.46	0.050	0.049	0.00050	0.00058	0.0190	0.00780	3–24	..
K199	18.40	11.50	1.09	0.32	0.018	0.036	0.00049	0.00057	0.00050	0.00056	0	..
K393	17.83	11.38	1.40	0.52	0.023	0.040	0.00053	0.00058	0.00082	0.00081	0	..
K395	18.51	11.82	1.32	0.51	0.023	0.026	0.00058	0.00058	0.00098	0.00084	1	..
L382	18.05	11.24	1.23	0.44	0.031	0.031	0.00044	0.00052	0.00370	0.00205	2–300	14
K776	18.19	11.10	0.75	0.42	0.056	0.015	0.00057	0.00059	0.0275	0.0106	2	12
K765	19.30	12.14	0.82	0.46	0.005	0.024	0.00043	0.00044	0.00043	0.00044	0	1
K394	17.92	12.64	1.27	0.50	0.022	0.027	0.00044	0.00053	0.00064	0.00069	0	..
L24	20.68	12.83	1.23	0.56	0.012	0.043	0.00032	0.00036	0.00028	0.00036	0	0
L3	20.29	12.80	1.42	0.51	0.026	0.030	0.00038	0.00041	0.00174	0.00103	2	33
L14	20.52	12.71	1.24	0.54	0.028	0.039	0.00044	0.00053	0.00750	0.00500	2	64
L49	21.22	15.35	0.84	0.34	0.007	0.022	0.00026	0.00034	0.00022	0.00030	0	0
L25	20.22	15.71	0.43	0.43	0.008	0.042	0.00027	0.00034	0.00030	0.00039	0	0
L4	20.10	15.12	1.42	0.54	0.023	0.029	0.00037	0.00039	0.0112	0.00362	2	39
L15	20.36	15.24	1.39	0.47	0.028	0.035	0.00037	0.00039	0.0268	0.0125	3	172
L50	21.16	18.29	0.38	0.27	0.009	0.035	0.00028	0.00035	0.00025	0.00036	0	0
L5	20.10	17.68	1.34	0.57	0.020	0.030	0.00035	0.00040	0.0172	0.00736	3	80
L16	20.61	18.32	1.35	0.52	0.027	0.034	0.00035	0.00042	0.0760	0.0350	3	230

*Approximate analysis.

†Bend Rating: 0 = No cracking. 1 = Surface cracks. 2 = Deep surface cracks. 3 = Broke. B = Brittle.

Note: Results are for 700 hours' boiling except where hyphen appears and then number following hyphen indicates time (hours) when result was observed.

‡Resistance change of 5% or more represents significant penetration.

Table I—(Continued)
Corrosion Data for Austenitic Chromium-Nickel Steels of Low-Carbon Content Heated 1 Hour at 650 °C

Heat No.	Chemical Composition, %						Corrosion Rate, Inch Penetration per Month in Boiling 65% Nitric Acid: Heated 10 Min. at 1075 °C and Air-Cooled		Heated 10 Min. at 1075 °C, Reheated 1 Hour at 650 °C and Air-Cooled		Boiling Acidified Copper Sulphate: Heated 10 Min. at 1075 °C, Reheated 1 Hour at 650 °C and Air-Cooled	
	Cr	Ni	Mn	Si	C	N	Fifth 48-Hr. Period	Avg. of Five 48-Hr. Periods	Fifth 48-Hr. Period	Avg. of Five 48-Hr. Periods	Bend Rating†	Per Cent Increase in Electrical Resistance‡
L51	26.39	15.48	0.28	0.28	0.005	0.041	0.00026	0.00030	0.00038	0.00042	2B	0
L6	25.15	15.00	1.40	0.57	0.019	0.043	0.00023	0.00025	0.00205	0.00145	1B	6
L17	25.34	15.24	1.38	0.63	0.027	0.044	0.00030	0.00035	0.00140	0.00076	2B	9
L389	25.15	15.40	1.25	0.56	0.049	0.049	0.00023	0.00027	0.00105	0.00058	0	3
L52	25.64	17.80	0.67	0.30	0.015	0.029	0.00018	0.00026	0.00027	0.00029	2B	0
L7	25.91	18.82	1.33	0.67	0.018	0.038	0.00033	0.00034	0.00151	0.00085	0	4
L27	25.70	18.50	1.77	0.67	0.019	0.045	0.00024	0.00026	0.00052	0.00035	2B	0
L350	25.35	17.60	1.34	0.59	0.034	0.043	0.00032	0.00034	0.0112	0.00510	2	7
L18	25.44	17.85	1.41	0.59	0.036	0.044	0.00023	0.00029	0.00310	0.00160	2	26
L8	26.00	21.15	1.61	0.62	0.027	0.045	0.00029	0.00030	0.00160	0.00090	1	9
L28	25.29	21.65	1.46	0.65	0.028	0.041	0.00025	0.00029	0.00108	0.00064	1	0
L19	25.40	21.06	1.41	0.66	0.034	0.045	0.00023	0.00027	0.0386	0.0104	2	43
L611	25.77	25.67	1.18	0.57	0.012	0.046	0.00015	0.00022	0.00014	0.00026	0	1
L610	26.19	23.87	1.25	0.58	0.019	0.039	0.00018	0.00021	0.00013	0.00020	0	1
L20	25.11	25.26	1.18	0.68	0.017	0.068	0.00021	0.00024	0.00023	0.00026	1	0
L722	18.3*	6.5*	1.2*	0.4*	0.025	0.089	0.00071	0.00085	0.00109	0.00092	0	0
L723	18.3*	6.5*	1.2*	0.4*	0.030	0.115	0.00074	0.00088	0.00111	0.00092	0	0
L725	18.3*	6.5*	1.2*	0.4*	0.033	0.132	0.00136	0.00144	0.00135	0.00147	0	1
L724	18.3*	6.5*	1.2*	0.4*	0.033	0.146	0.00091	0.00099	0.00096	0.00099	0	1
L348	18.16	7.65	1.30	0.52	0.034	0.088	0.00072	0.00091	0.00089	0.00093	2–300	3
L347	18.47	7.63	1.22	0.43	0.036	0.031	0.00076	0.00086	0.00090	0.00089	2	4
L349	17.80	7.38	1.22	0.49	0.041	0.136	0.00112	0.00115	0.00109	0.00114	0	3
L726	18.3*	8.0*	1.2*	0.4*	0.030	0.113	0.00064	0.00072	0.00069	0.00074	0	0
L727	18.3*	8.0*	1.2*	0.4*	0.032	0.144	0.00070	0.00076	0.00074	0.00081	0	0
K380	18.54	9.86	1.23	0.48	0.018	0.044	0.00051	0.00055	0.00067	0.00066	0	..
K17	17.99	9.71	0.98	0.30	0.025	0.015	0.00045	0.00058	0.00056	0.00075	0	..
K652	17.83	9.21	1.2*	0.4*	0.022	0.016	0.00070	0.00066	0.00089	0.00081	0	..
L376	18.92	9.70	1.26	0.39	0.027	0.032	0.00047	0.00054	0.00152	0.00105	2	5
K381	18.30	9.72	1.38	0.48	0.025	0.062	0.00052	0.00055	0.00068	0.00072	0	..
L385	18.62	9.36	1.07	0.42	0.024	0.089	0.00070	0.00076	0.00129	0.00110	0	1
L388	18.16	9.33	1.22	0.42	0.028	0.145	0.00068	0.00072	0.00115	0.00102	0	2
L729	18.3*	9.0*	1.4*	0.4*	0.029	0.147	0.00060	0.00068	0.00068	0.00074	0	0
L386	18.25	9.61	1.32	0.44	0.025	0.148	0.00072	0.00076	0.00148	0.00116	0–1	2
L378	18.62	9.35	1.25	0.40	0.026	0.156	0.00070	0.00071	0.00140	0.00109	0	0
K119	18.36	9.43	1.25	0.39	0.031	0.057	0.00060	0.00067	0.00310	0.00194	2–24	..

*Approximate analysis.
†Bend Rating: 0 = No cracking. 1 = Surface cracks. 2 = Deep surface cracks. 3 = Broke. B = Brittle.
Note: Results are for 700 hours' boiling except where hyphen appears and then number following hyphen indicates time (hours) when result was observed.
‡Resistance change of 5% or more represents significant penetration.

Table I—(Continued)
Corrosion Data for Austenitic Chromium-Nickel Steels of Low-Carbon Content Heated 1 Hour at 650 °C

Heat No.	Chemical Composition, %						Corrosion Rate, Inch Penetration per Month in Boiling 65% Nitric Acid: Heated 10 Min. at 1075 °C and Air-Cooled		Heated 10 Min. at 1075 °C, Reheated 1 Hour at 650 °C and Air-Cooled		Boiling Acidified Copper Sulphate Heated 10 Min. at 1075 °C, Reheated 1 Hour at 650 °C and Air-Cooled	
	Cr	Ni	Mn	Si	C	N	Fifth 48-Hr. Period	Avg. of Five 48-Hr. Periods	Fifth 48-Hr. Period	Avg. of Five 48-Hr. Periods	Bend Rating†	Per Cent Increase in Electrical Resistance‡
L387	18.78	9.42	1.27	0.50	0.032	0.036	0.00045	0.00055	0.00175	0.00125	1	3
L377	18.54	9.25	1.18	0.46	0.034	0.105	0.00061	0.00069	0.00275	0.00173	1	7
L728	18.3*	9.0*	1.2*	0.4*	0.039	0.115	0.00059	0.00068	0.00073	0.00074	0	2
K382	18.36	9.97	1.36	0.50	0.042	0.027	0.00063	0.00064	0.0149	0.00620	2–24	..
K383	18.61	9.90	1.26	0.40	0.045	0.026	0.00051	0.00057	0.0125	0.00520	2–24	..
K643	18.45	10.58	0.21	0.37	0.006	0.012	0.00056	0.00060	0.00054	0.00057	0	..
L411	19.70	10.25	0.94	0.45	0.011	0.073	0.00041	0.00046	0.00044	0.00048	0	1
K198	18.37	10.88	1.09	0.32	0.024	0.029	0.00048	0.00056	0.00068	0.00080	0	..
K197	18.57	10.31	1.14	0.33	0.020	0.031	0.00042	0.00055	0.00048	0.00060	0	..
K385	18.48	10.41	1.33	0.51	0.027	0.043	0.00044	0.00055	0.00069	0.00073	0	..
K634	18.51	10.66	1.32	0.37	0.021	0.047	0.00045	0.00053	0.00092	0.00076	0	..
K638	18.35	10.75	1.40	0.36	0.026	0.054	0.00050	0.00055	0.00109	0.00087	0	..
L380	18.25	10.15	1.24	0.40	0.030	0.100	0.00055	0.00065	0.00315	0.00191	1	8
K636	18.22	10.88	1.28	0.39	0.022	0.118	0.00060	0.00063	0.00191	0.00128	0	..
K641	18.02	10.97	1.27	0.40	0.030	0.149	0.00066	0.00070	0.00230	0.00140	0	..
K637	18.60	10.66	1.36	0.38	0.024	0.150	0.00064	0.00064	0.00202	0.00130	0	..
L381	18.21	10.62	1.16	0.44	0.028	0.156	0.00068	0.00072	0.00072	0.00073	0	..
L379	18.54	10.39	1.22	0.42	0.032	0.037	0.00052	0.00060	0.00280	0.00171	3	24
K123	18.35	10.47	1.20	0.40	0.033	0.153	0.00073	0.00075	0.00530	0.00250	3	..
K121	18.29	10.53	1.24	0.45	0.035	0.127	0.00062	0.00065	0.00680	0.00280	0	..
K386	18.29	10.60	1.35	0.38	0.041	0.039	0.00049	0.00053	0.00400	0.00230	2–24	..
K384	18.48	10.34	1.24	0.44	0.049	0.041	0.00052	0.00057	0.0133	0.00550	3–24	..
K388	18.22	10.95	1.50	0.46	0.050	0.049	0.00050	0.00058	0.0190	0.00780	3–24	..
K117	18.36	10.56	1.38	0.44	0.054	0.038	0.00053	0.00062	0.00325	0.00189	1	..
K766	18.54	11.63	0.82	0.37	0.010	0.053	0.00049	0.00053	0.00048	0.00059	0	2
K767	17.93	11.54	0.82	0.37	0.015	0.049	0.00043	0.00049	0.00043	0.00049	0	1
K199	18.40	11.50	1.09	0.32	0.018	0.036	0.00049	0.00057	0.00050	0.00056	0	..
K395	18.51	11.82	1.32	0.51	0.023	0.026	0.00058	0.00058	0.00098	0.00084	1	..
K393	17.83	11.38	1.40	0.52	0.023	0.040	0.00053	0.00058	0.00082	0.00081	0	..
K387	17.90	11.04	1.22	0.44	0.030	0.066	0.00055	0.00061	0.00090	0.00092	0	..
K639	18.32	11.44	1.35	0.36	0.026	0.078	0.00054	0.00057	0.00171	0.00115	0	..
K640	18.08	11.22	1.21	0.35	0.028	0.120	0.00059	0.00064	0.00123	0.00092	0	..
L382	18.05	11.24	1.23	0.44	0.031	0.031	0.00044	0.00052	0.00370	0.00205	2–300	14
K392	18.78	11.32	1.26	0.47	0.033	0.028	0.00046	0.00052	0.00179	0.00116	2–48	..
K776	18.19	11.10	0.75	0.42	0.056	0.015	0.00057	0.00059	0.0275	0.0106	2	12
K765	19.30	12.14	0.82	0.46	0.005	0.024	0.00043	0.00044	0.00043	0.00044	0	1
L384	18.31	12.50	1.22	0.46	0.033	0.176	0.00055	0.00062	0.00275	0.00170	2	4

*Approximate analysis.
†Bend Rating: 0 = No cracking. 1 = Surface cracks. 2 = Deep surface cracks. 3 = Broke. B = Brittle.
Note: Results are for 700 hours' boiling except where hyphen appears and then number following hyphen indicates time (hours) when result was observed.
‡Resistance change of 5% or more represents significant penetration.

A second three-dimensional diagram was prepared involving carbon, nickel, and up to 0.15% nitrogen at a constant level of 18% chromium. Again points were located in space according to the respective compositions of the steels and these points were designated as passing or not passing the copper sulphate test after 1 hour at 650 °C (1200 °F). The surface formed through the scatter of

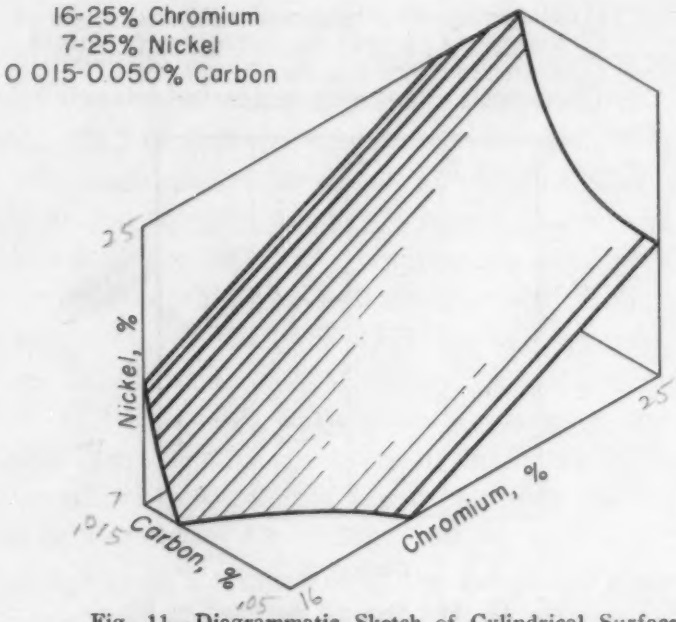


Fig. 11—Diagrammatic Sketch of Cylindrical Surface Separating Regions of Composition Susceptible to, and Free from, Intergranular Attack After Heating 1 Hour at 650 °C (1200 °F). No attack occurs in compositions falling behind the surface. The small regions of experimental error existing on each side of this surface are not shown. The axes extend from 0.015 to 0.05% carbon, from 7 to 25% nickel, and from 16 to 25% chromium. This figure is not drawn to scale.

points in space was again determined to be cylindrical with the same function existing between carbon and nickel as the directrix of the cylinder. The cylinder was observed, however, to be practically parallel to the intersection of the 0% carbon and 0% nickel planes, indicating that, as closely as could be determined, varying nitrogen had no effect on the intergranular corrosion resistance of steels heated 1 hour at 650 °C (1200 °F). Modification of the above function for the limiting intergranular corrosion surface to include a nitrogen term is, therefore, unnecessary because the coefficient of the nitrogen term would be zero.

The fact that nitrogen apparently does not affect the intergranular corrosion resistance after heating for 1 hour at 650 °C

(1200 °F) has an interesting corollary. If nitrogen is added to the steel, the nickel content may be reduced, and an austenitic structure will be maintained. A reduction in the nickel content permits the carbon to be carried at a higher level without moving the composition into the intergranular corrosion region. This is probably best illustrated by Fig. 12. Line AB represents the trace of the intergranular

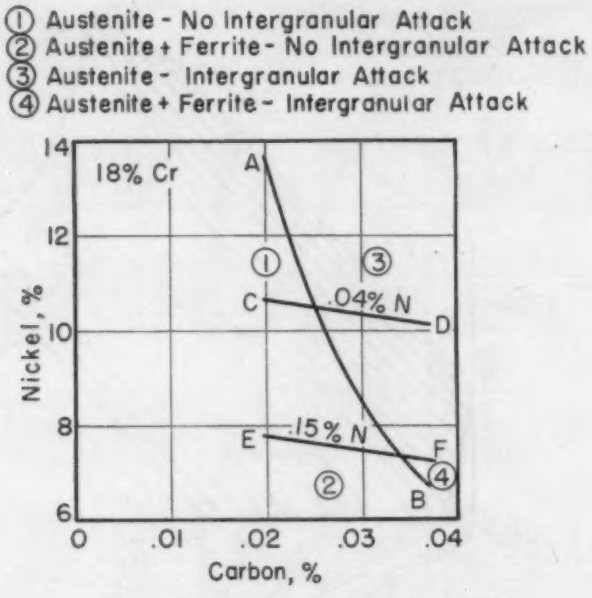


Fig. 12—Plot Showing the Effect of Nitrogen in Enlarging the Range of Compositions Which Are Austenitic and Free from Intergranular Attack After Heating 1 Hour at 650 °C (1200 °F).

attack surface on the 18% chromium plane. It is seen that, when the nitrogen content is raised, the austenite — austenite-plus-ferrite line CD moves in the direction of lower nickel, to position EF, thereby enlarging the area of composition where austenitic steels are free from intergranular attack after heating 1 hour at 650 °C (1200 °F). It should be pointed out, however, that the enlargement of the area due to increased nitrogen is somewhat less at higher temperatures than at 650 °C (1200 °F). Further data on the effect of nitrogen are presented later in the paper.

The results obtained from boiling nitric acid tests conducted on companion samples agree closely with those of the boiling acidified copper sulphate test. In some cases the corrosion rate increased after heat treatment at 650 °C (1200 °F), even though no attack occurred in the acidified copper sulphate solution. However, the

maximum rate did not exceed about 0.002-inch penetration per month in the fifth 48-hour test period, and a maximum average rate of about 0.0013-inch penetration per month for five periods may be expected for steels defined by Equation II. The actual nitric acid data are given in Table I.

Further Study of the Time-Temperature-Precipitation Relationship—While the foregoing equation defines steels having suitable corrosion resistance after heating 1 hour at 650 °C (1200 °F), it gives no information about the time-temperature-precipitation characteristics of the steel at other times and temperatures. It is known, for example, that carbide precipitation occurs most rapidly in the austenitic chromium-nickel steels at about 750 °C (1380 °F) and less rapidly as the temperature is decreased below this temperature or is increased above it. The temperature of 750 °C (1380 °F) appears to provide optimum conditions for nucleation and diffusion. At higher temperatures, the nucleation rate is less rapid, and at lower temperatures the diffusion rate of chromium and carbon is less rapid than at 750 °C (1380 °F). The general shape of the precipitation curve roughly approximates the shape of the letter "C". The portion of the curve where precipitation begins earliest will be defined here as the nose of the curve.

Knowledge as to the location of the nose of the curve is a guide in estimating the susceptibility of a steel to intergranular precipitation. If the nose is located too close to the point of zero time, short periods of heating, such as experienced in fabrication heat cycles, will cause carbide precipitation to occur. Obviously, the steel would be less susceptible to intergranular attack if it were possible to shift the nose of the curve farther away from zero time. Because of the importance of time-temperature data, the shape of the curve was determined for a number of the steels. While it would have been desirable to develop the curve for each steel, the time and labor required to establish such curves made it impossible to do so except in relatively few cases. Sufficient data were obtained, nevertheless, to indicate the general characteristics of the very low-carbon steels, and to permit the determination of an empirical equation for calculating the time to the nose of the curve from knowledge of composition of the steel.

The method of developing these curves follows: Samples, 0.04 inch thick, for electrical resistance tests were prepared and annealed by heating 10 minutes at 1075 °C (1970 °F) followed by air-cooling.

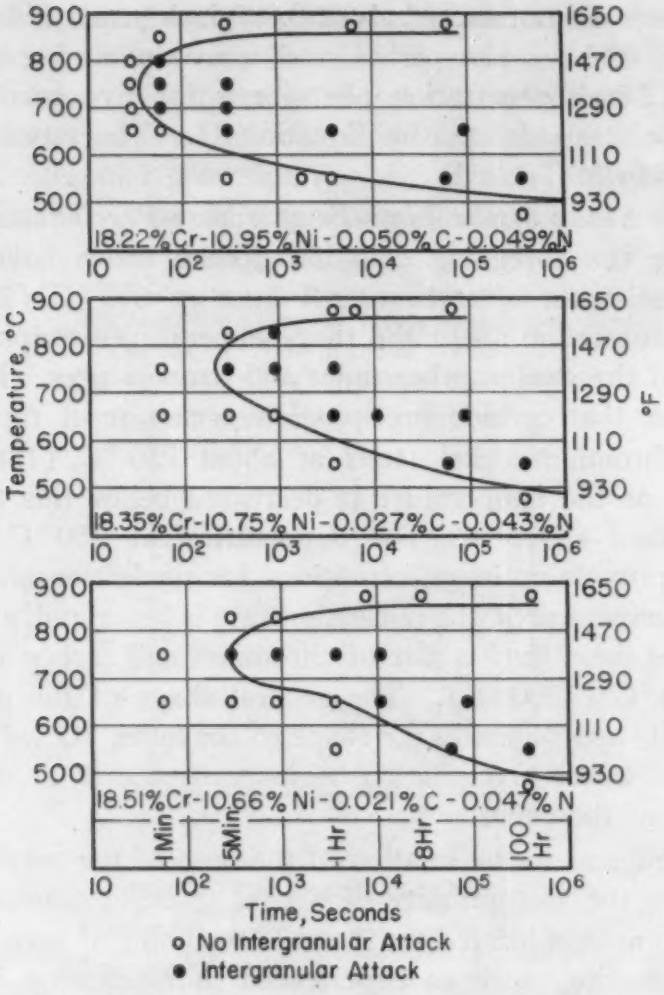


Fig. 13—Time-Temperature-Precipitation Curves Showing the Effect of Changing Carbon Content in Austenitic 18% Chromium Steels Containing 10.5 to 11.0% Nickel. Tests made in boiling acidified copper sulphate solution.

These samples were then heated at temperatures in the range 475 to 870 °C (890 to 1600 °F) for various periods of time. They were exposed to the boiling acidified copper sulphate solution for periods up to 700 hours, and the corrosion damage was determined by measuring the change in electrical resistance of the sample and by bend tests. A scatter plot was then prepared on temperature versus log time co-ordinates, and a curve constructed to separate the regions subject to, and free from, intergranular attack as indicated by the corrosion data. The presence of intergranular attack was taken as the criterion of carbide precipitation.

The curves in Fig. 13 are for 18% chromium steels with 10.5

to 11.0% nickel, about 0.04% nitrogen, and carbon from 0.050 to 0.021%. In the 0.050% carbon steel, the minimum time for precipitation is about 37 seconds. For the 0.021% carbon steel, the nose time is about 270 seconds, indicating how lowering the carbon increases the time for precipitation. In each case the temperature corresponding to the minimum time is approximately 750 °C (1380 °F). It will be observed that, in the 0.021% carbon steel, the curve retreats rather sharply to 650 °C (1200 °F) and then falls

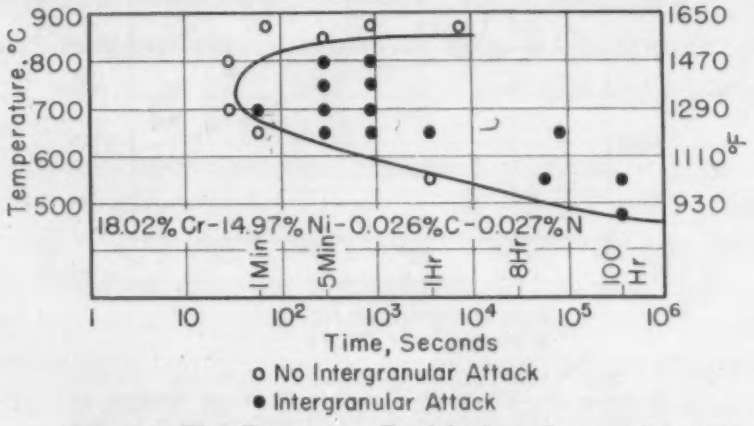


Fig. 14—Time-Temperature-Precipitation Curve for 18% Chromium – 15% Nickel – 0.026% Carbon Steel. Tests made in boiling acidified copper sulphate solution.

continuously to lower temperatures. This behavior cannot be fully explained at this time, but the formation of some ferrite on holding below 650 °C (1200 °F) may be responsible for the change of direction, since the solubility of carbon is less in ferrite than in austenite.

Fig. 14 contains the curve for a steel containing about 18% chromium and 15% nickel. The effect of nickel on decreasing the time for precipitation is clearly seen by comparing this curve with the second curve of Fig. 13, which represents a steel of nearly the same composition, containing 10.75% nickel.

The curves of Fig. 15 are presented to indicate that nitrogen moves the nose of the curve to the left. The power of nitrogen to cause this movement is, however, much smaller than the power of carbon. It is important to observe that nitrogen is influential at 750 °C (1380 °F) in contrast with its lack of influence after heating 1 hour at 650 °C (1200 °F) as previously shown.

The effect of chromium on the shape of the curve is given in Fig. 16 for an austenitic 25% chromium – 21% nickel steel. The

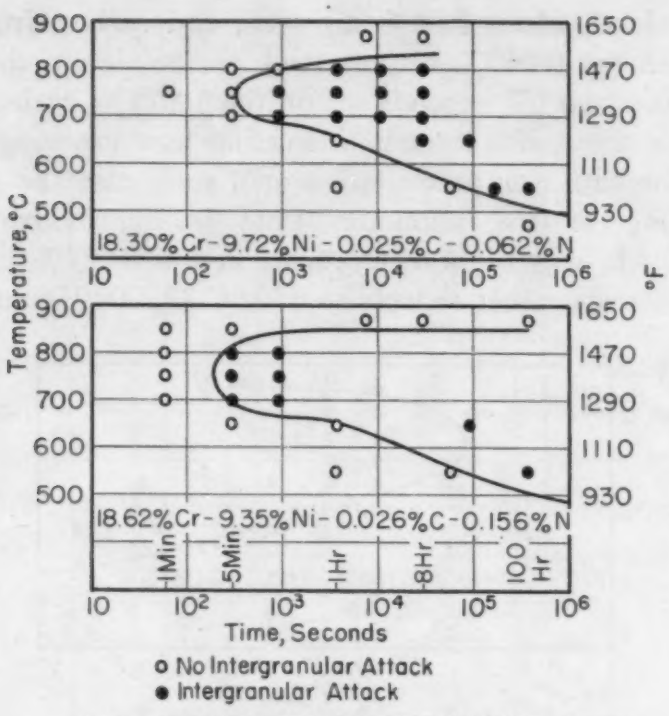


Fig. 15—Time-Temperature-Precipitation Curves Showing the Effect of Changing Nitrogen Content in Austenitic 18% Chromium – 9% Nickel – 0.025% Carbon Steels. Tests made in boiling acidified copper sulphate solution.

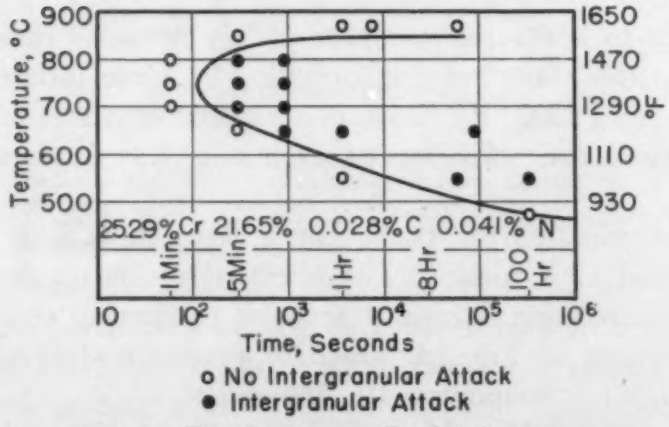


Fig. 16—Time-Temperature-Precipitation Curve for 25% Chromium – 21% Nickel – 0.028% Carbon Steel. Tests made in boiling acidified copper sulphate solution.

minimum time for precipitation to occur in this steel is 110 seconds, which indicates that there is no advantage to be gained in increasing the time for precipitation in higher-alloy steels.

The data for these curves and for several others similarly determined have been studied from a quantitative point of view. Factors

have been derived by a method of successive approximations which express the respective effects that the four elements have in determining the time to the nose of the curve. These factors have been combined into an equation which predicts the time, t, in seconds, to the nose of the curve. The equation follows:

$$t = 63.5\ (\%\ \text{chromium}) - [50.5\ (\%\ \text{nickel}) + 6820\ (\%\ \text{carbon}) + 1037\ (\%\ \text{nitrogen})] - 178$$

(Equation III)

The data on which this function is based were obtained on steels with carbon and nitrogen contents greater than 0.020% and for nickel contents at least great enough to form a substantially austenitic steel at the chromium level in question.

The calculated minimum times for precipitation to start, in austenitic steels meeting the 1 hour at 650 °C (1200 °F) test, range between about 120 and 270 seconds. This difference in time is due to the possibility of selecting a variety of carbon and nickel contents satisfying Equation II, with shorter times occurring for the high-nickel, low-carbon combinations. An example of the change in nose time due to variations in carbon and nickel content follows: An 18% chromium – 10.5% nickel – 0.025% carbon steel has a nose time of 220 seconds, whereas an 18% chromium – 13.5% nickel – 0.02% carbon steel has a nose time of 110 seconds, each steel containing 0.04% nitrogen. An increase in nose time can be obtained by adjusting the nickel and nitrogen contents as was mentioned previously. For example, an 18% chromium – 7.6% nickel – 0.025% carbon – 0.15% nitrogen steel has a nose time of 250 seconds.

In order to check the applicability of Equations II and III, a steel composition was selected for welding tests. This composition, approximately 18% chromium, 11% nickel, 0.025% carbon, with normal manganese, silicon and nitrogen, was chosen as being able to resist intergranular attack after the 1 hour at 650 °C (1200 °F) heat treatment. The experimental weld was made by butting together the prepared faces of two ½-inch thick plates, each about 2 inches wide and 15 inches long, and joining them in a single pass by the Unionmelt process. The electrode was of the same composition as the plate metal. This technique was used, since it was believed that conditions for intergranular precipitation would be intensified by the narrow plate width and high heat input of the single-pass weld. Had wider plates been used, more rapid cooling through the carbide precipitation temperature range would have resulted, due

to the increased quenching effect of the greater mass of metal.

Samples taken from the experimental weld showed no signs of intergranular susceptibility when submitted to corrosion tests in the as-welded condition or after stress relieving 2 hours at 870 °C (1600 °F). The appearance of samples tested for five 1-hour periods in a 10% nitric acid – 3% hydrofluoric acid solution at 70 °C (160 °F) is shown in Fig. 17. In boiling 65% nitric acid, the average corrosion rate of 0.0006-inch penetration per month for as-welded and stress-relieved samples is the same as for unwelded plate samples of this steel, as given in Table II.

Table II

Boiling 65% Nitric Acid Corrosion Data for Unionmelt Weld in ½-Inch Thick Plate of Low-Carbon Austenitic 18% Chromium-Nickel Steel

	Chemical Composition, %	
	Plate and Electrode	Weld Metal
Cr	17.92	.....
Ni	10.97	.....
Mn	1.10	.....
Sn	0.41	.....
C	0.026	0.026
N	0.031	0.035

Sample	Condition	Corrosion Rate Inch Penetration per Month Average 5 Periods
Welded Plate	As-welded	0.00057
Welded Plate	Welded, heated 2 hr. at 870 °C and air-cooled	0.00062
Plate	Heated 10 min. at 1075 °C and air-cooled	0.00063
Plate	Heated 10 min. at 1075 °C and air-cooled, reheated 2 hr. at 870 °C and air-cooled	0.00060

Two other welding tests were also made. The results are given pictorially in Fig. 17. In one case, a plate of about the same composition and size as that mentioned above was welded by the multiple-pass hand arc method. The plate metal was again free from intergranular corrosion in the as-welded or the stress-relieved condition, but the weld metal was severely corroded, due to an increase in its carbon content during welding. The second case involved the hand arc welding of Type 304 steel plates, containing 0.06% carbon, of the same size as the previous 0.025% carbon steel plates. The corrosion tests on samples from this weldment showed severe granulation in both the as-welded and stress-relieved conditions.

In summary, it is fair to say that Equation II, developed for selecting steels having partial immunity, provides a sound first approximation of the composition balance required. Obviously, any

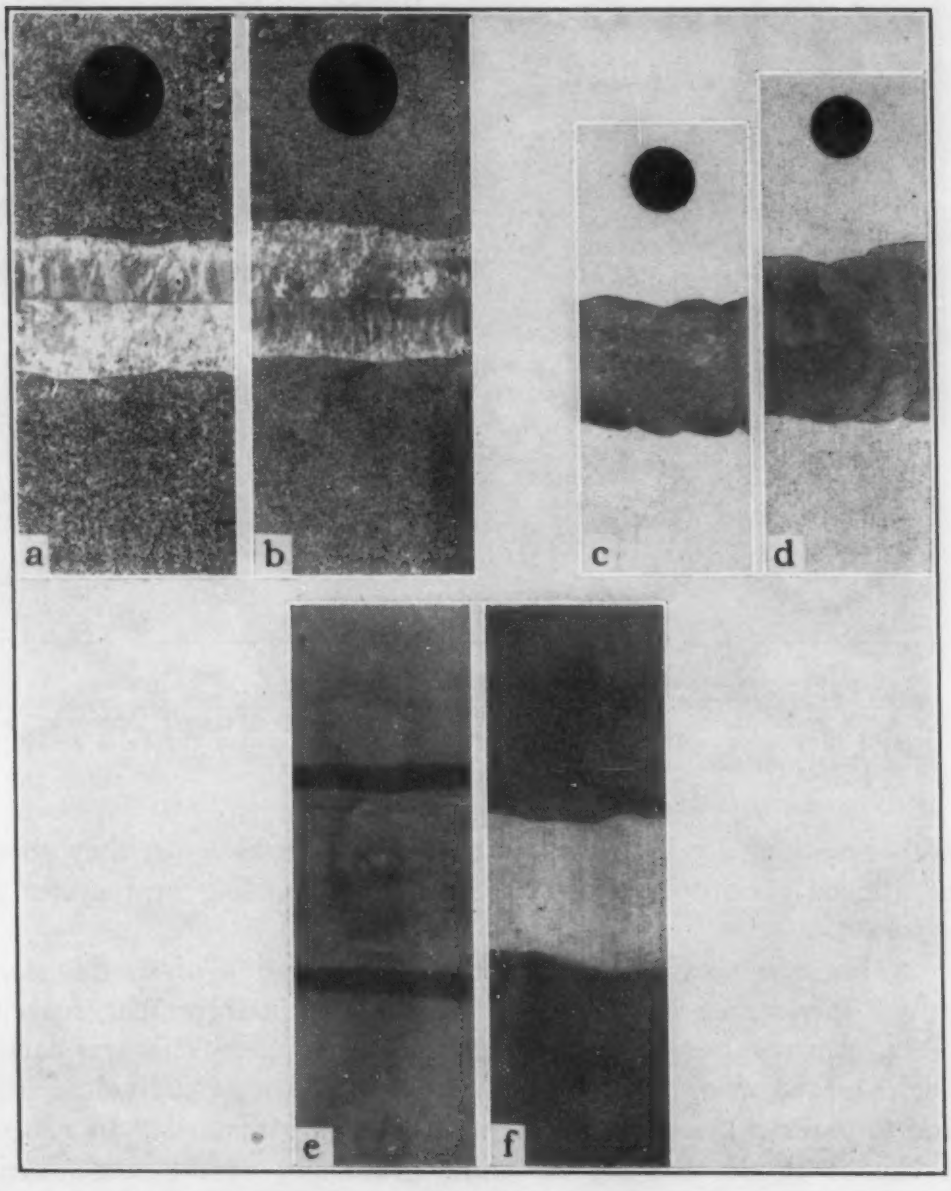


Fig. 17—Appearance of Welds in ¼-Inch Thick Plate After 1 Hour in 10% Nitric Acid – 3% Hydrofluoric Acid Solution at 70 °C (160 °F). a and b—Union-melt welds. c, d, e, f—Hand-arc welds. a, c and e—As-welded. b, d and f—Stress-relieved.

Composition	C	Mn	Si	N	Cr	Ni
a and b	0.026	1.10	0.41	0.031	17.92	10.97
c and d	0.026	1.32	0.36	0.035	18.38	11.68
e and f	0.062	1.10	0.41	0.034	18.06	8.51

selection of steels on the basis of the 1 hour at 650 °C (1200 °F) criterion should be accompanied by a calculation of the minimum time for precipitation to begin, so that the final composition will best withstand the heating cycle to which it will be subjected. Since

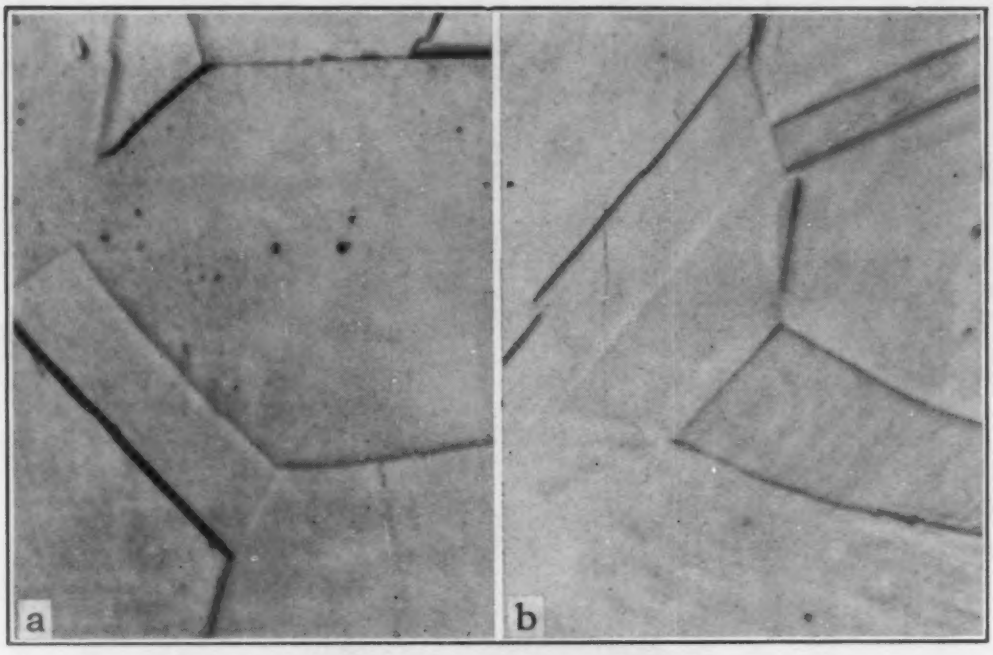


Fig. 18—Metallographic Structure of Steel Containing 17.90% Chromium, 12.60% Nickel, 0.005% Carbon, and 0.002% Nitrogen. Etchant: Aqua regia in glycerine. × 2000. a—Heated 10 minutes at 1075 °C (1970 °F) and air-cooled. Austenite. b—Heated 10 minutes at 1075 °C (1970 °F) and air-cooled, reheated 100 hours at 550° C (1020 °F). Austenite.

both equations are based on isothermal heat treatments, they should be applied conservatively where continuous cooling heat cycles are involved.

Microstructure—Throughout the investigation of the resistance of the low-carbon chromium-nickel steels to intergranular susceptibility, considerable metallographic work was done. This was carried out in order to have a check on the grain size of individual heats and to observe the precipitated grain boundary material. In general, it can be stated that the austenitic grain size of the steels varied between about 4 and 6. The structure was not greatly different from the structure observed in ordinary austenitic chromium-nickel steels except that, since these steels contain lower carbon, the amount of carbide precipitate was proportionally reduced. When the carbon content of a fully austenitic steel was reduced to less than 0.015 to 0.020%, no intergranular carbide precipitate was found, even after long holding in the precipitation temperature range.

Fig. 18 shows the structure of a steel containing about 18% chromium, 13% nickel, 0.005% carbon, and 0.002% nitrogen. In the annealed condition and after heating 100 hours at 550 °C

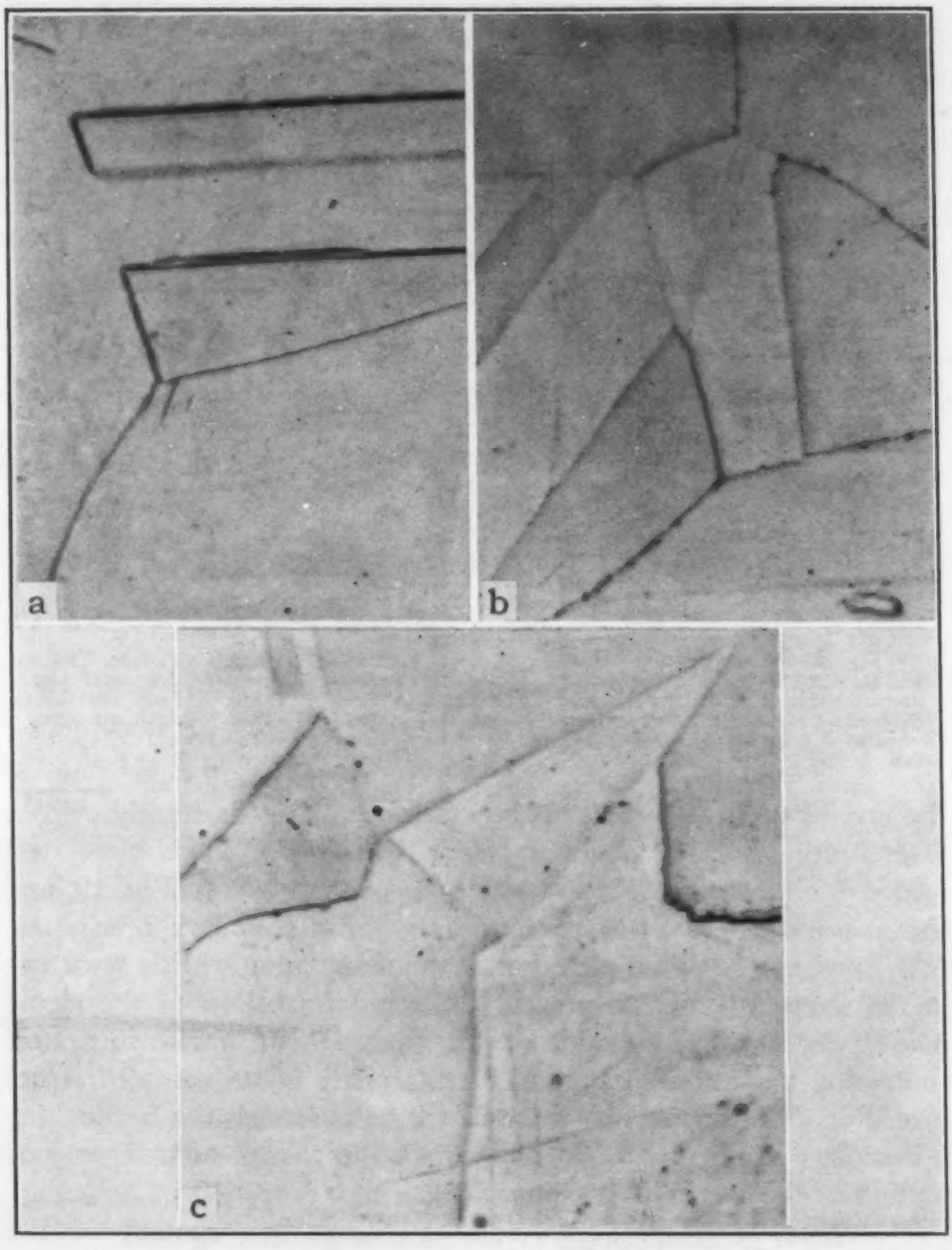


Fig. 19—Metallographic Structure of Steel Containing 17.83% Chromium, 11.38% Nickel, 0.023% Carbon, and 0.040% Nitrogen. Etchant: Aqua regia in glycerine. × 2000. a—Heated 10 minutes at 1075 °C (1970 °F) and air-cooled. Austenite. b—Heated 10 minutes at 1075 °C (1970 °F) and air-cooled, reheated 100 hours at 550 °C (1020 °F). Austenite + carbide. c—Heated 10 minutes at 1075 °C (1970 °F) and air-cooled, reheated 1 hour at 650 °C (1200 °F). Austenite.

(1020 °F), the grain boundaries are free from precipitated material.

A steel containing about 18% chromium, 10.75% nickel, 0.025% carbon, and 0.03% nitrogen is illustrated in Fig. 19. In this steel

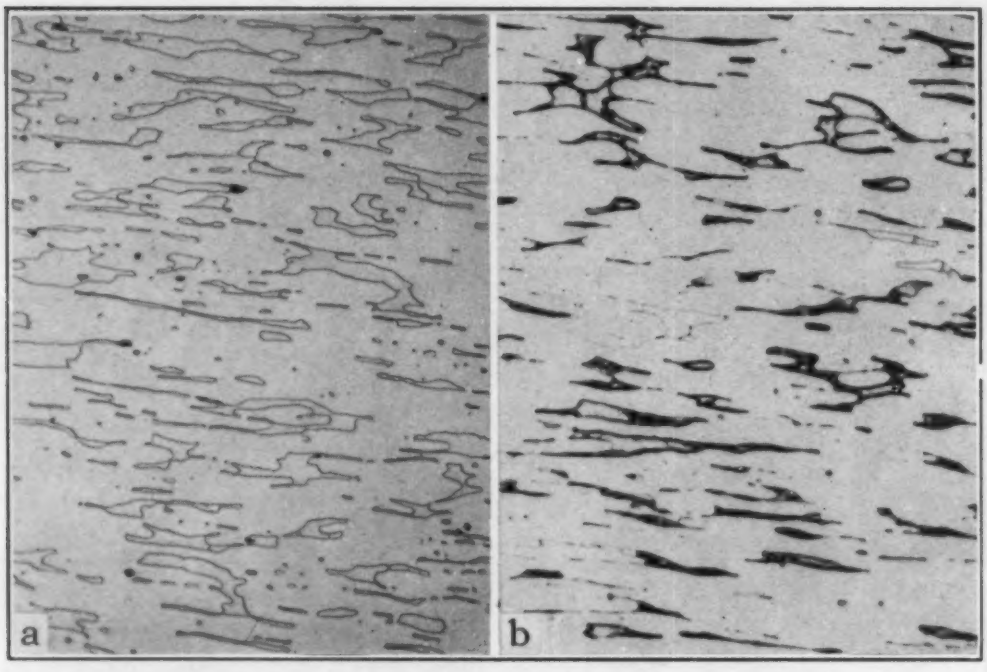


Fig. 20—Metallographic Structure of Steel Containing 26.39% Chromium, 15.48% Nickel, 0.005% Carbon, and 0.041% Nitrogen. Etchant: Electrolytic 5% nital after electropolishing. × 250. a—Heated 10 minutes at 1075 °C (1970 °F) and air-cooled. Austenite + delta ferrite. b—Heated 10 minutes at 1075 °C (1970 °F) and air-cooled, reheated 1 hour at 650 °C (1200 °F). Austenite + sigma + delta ferrite.

the precipitation of carbide at the grain boundaries is readily evident after heating for 100 hours at 550 °C (1020 °F). This same steel heated for 1 hour at 650 °C (1200 °F) is also given in Fig. 19, and the micrograph shows a freedom from grain boundary precipitate.

Emphasis has been placed on maintaining an austenitic structure in the steels in order to prevent the rapid formation of the sigma phase. To briefly illustrate the decomposition of ferrite in a steel containing a substantial amount of this phase in its annealed structure, Fig. 20 is presented. Here it will be observed that heating for 1 hour at 650 °C (1200 °F) has caused the change of a large proportion of the ferrite into sigma phase.

Mechanical Properties—Reducing the carbon content of the austenitic 18% chromium-nickel steels, as illustrated by the data in Table III, causes a small decrease in yield and tensile strengths in the annealed condition when compared with 0.06% carbon Type 304 steel. The ductility, however, is practically unaffected.

Welds in these steels also possess satisfactory mechanical properties as shown in Table IV. These data, obtained on Unionmelt welded ½-inch thick plate, show that the impact strength of the weld

is of a high order even when tested at —183 °C (—295 °F) in either the welded or stress-relieved condition.

In order to determine whether the steels were subject to embrittlement after short heating periods, impact tests were made on samples heated at 550, 650, and 870 °C (1020, 1200, and 1600 °F).

Table III
Mechanical Properties of Low-Carbon Austenitic 18% Chromium-Nickel Steels, Annealed Condition

Composition, %						Yield Strength 0.2% Offset	Tensile Strength	Elongation
Cr	Ni	Mn	Si	C	N	psi	psi	in 2 In., %
Type 304 (0.06% C)						31,000	86,000	63
17.99	9.71	0.98	0.30	0.025	0.015	28,000	82,000	50
18.78	11.32	1.26	0.47	0.028	0.028	25,000	77,000	58
17.92	12.64	1.27	0.50	0.022	0.027	27,000	77,000	61
17.90	12.60	....	....	0.005	0.002	26,000	67,000	56

Tests made on 0.035 to 0.040-inch thick strip.

The data are shown in Table V. No change in impact toughness was observed after 336 hours' heating at any of the test temperatures. Only a small loss in toughness was found when the heating was prolonged to 1 month at 870 °C (1600 °F).

Table IV
Mechanical Properties of Low-Carbon Austenitic 18% Chromium-Nickel Steel Unionmelt Weld in ½-Inch Thick Plate

Plate and Electrode Composition, %						Condition	Yield Strength 0.2% Offset psi	Tensile Strength psi	Elongation in 1 in. %	Red. in Area %	Izod Impact, ft-lb. Room Temp.	Izod Impact, ft-lb. —183 °C
Cr	Ni	Mn	Si	C	N							
17.92	10.97	1.10	0.41	0.026	0.031	1	29,000	68,000	54	59	72	39
17.92	10.97	1.10	0.41	0.026	0.031	2	.....	.....	..	..	75	40

1 = As-welded. 2 = Welded and heated 2 hours at 870 °C.

Summary of Tests of Steels Partially Immune to Intergranular Corrosion—Empirical formulas have been derived to allow steels containing carbon, chromium, nickel, and nitrogen to be balanced with respect to composition so as to resist intergranular carbide precipitation for 1 hour at 650 °C (1200 °F) and about 200 seconds at 750 °C (1380 °F). The isothermal nature of the tests has been described and the results of these tests show that it is possible to produce an effective degree of resistance to intergranular corrosion

Table V
Effect of Heating at 550, 650 and 870 °C on Toughness of Austenitic Low-Carbon 18% Chromium-Nickel Steel

Composition, %						Test Temp.	Izod Impact Value, ft-lb.				
Cr	Ni	Mn	Si	C	N	°C	1 Hr.	4 Hr.	100 Hr.	336 Hr.	720 Hr.
18.48	10.41	1.33	0.51	0.027	0.043	550	..	..	98	96	..
						650	..	..	94	94	..
						870	96	96	96	94	71

at carbon levels that are greater than the 0.015 to 0.020% maximum carbon content required for complete immunity.

Molybdenum-Bearing Chromium-Nickel Steels

The above study of the austenitic chromium-nickel steels gave rise to the question of how other alloying elements affect the composition and time-temperature relationships. One element of interest is molybdenum as it is introduced into steels of this type to increase their resistance to corrosion in reducing media. The commercial grades of molybdenum-bearing steels are known to be susceptible to intergranular corrosion and require stabilization with columbium if the steel cannot be annealed after fabrication. In view of the widespread usage of these steels in the chemical industry, it is important to know the extent to which they can be rendered resistant to intergranular attack by lowering carbon. With this purpose in mind, steels containing about 0.03% carbon, 18% chromium, 10 to 15% nickel, up to 3% molybdenum, together with normal amounts of manganese and silicon, were tested after heating at 475, 550, and 650 °C (890, 1020, and 1200 °F).

It appeared from the results of corrosion tests in boiling acidified copper sulphate solution on samples exposed for relatively long periods of time at 475, 550, and 650 °C (890, 1020, and 1200 °F) that heating at 650 °C (1200 °F) produced a marked susceptibility to intergranular attack. Therefore, the same test procedure as previously described for the austenitic chromium-nickel steels was adopted to establish the compositions of austenitic chromium-nickel-molybdenum steels having partial immunity to intergranular corrosion.

The results of these tests on samples heated 1 hour at 650 °C (1200 °F), shown in Table VI, were plotted on a three-dimensional model where molybdenum, carbon, and nickel were the variables and

chromium and nitrogen the constants. The shape of the limiting surface was again cylindrical, differing from the surface shown in Fig. 11 only in that the slope of the directrix was greater. This indicates that molybdenum is more powerful than chromium in increasing the time before damaging precipitation takes place. The empirical equation for this surface was calculated, and when combined with Equation II gave the following results:

$$\frac{6.17}{(\%\ \text{carbon})^{0.88}} + 13.8\ [(\%\ \text{chromium}) + 2.25\ (\%\ \text{molybdenum})] - 10\ (\%\ \text{nickel}) - 276 = 0 \qquad \text{(Equation IV)}$$

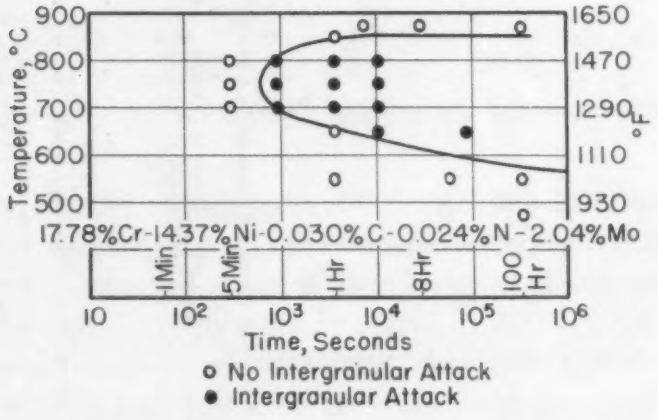


Fig. 21—Time-Temperature-Precipitation Curve for an Austenitic 18% Chromium – 15% Nickel – 2% Molybdenum – 0.030% Carbon Steel. Tests made in boiling acidified copper sulphate solution.

These data are in agreement with the widely-held opinion that molybdenum imparts increased resistance to intergranular corrosion.

Fig. 21 shows the time-temperature-precipitation curve for a steel containing 17.78% chromium, 14.37% nickel, 0.030% carbon, 0.024% nitrogen, and 2.04% molybdenum. About 600 seconds is observed to be the minimum time for precipitation to occur in the 2% molybdenum steel which is an increase of 350% in nose time when compared with a steel containing 18% chromium, 10.5% nickel, and 0.03% carbon. In view of the marked increase in time for carbide precipitation to start in the molybdenum-bearing steels, it would be expected that compositions predicted on the basis of 1 hour at 650 °C (1200 °F) tests would be amenable to welding.

The results of actual welding tests are of interest here. A steel containing 18.19% chromium, 13.95% nickel, 0.020% carbon, 0.03%

Table VI
Corrosion Data for Molybdenum-Bearing Austenitic Chromium-Nickel Steels of Low-Carbon Content

Heat No.	Composition, % Cr	Ni	Mn	Si	C	N	Mo	Cond. of Metal	Boiling Acidified Copper Sulphate: Bend Rating†	Per Cent Increase in Elect. Resist.‡	Corrosion Rate Inch Penetration per Month in Boiling 65% Nitric Acid: Fifth 48-Hr. Period	Avg. of Five 48-Hr. Periods
L2	18.02	14.97	1.43	0.47	0.026	0.027	....	a	0	4	0.00046	0.00055
								b	3–300	210	0.051[3]	0.0208[3]
								c	2–300	43	0.00340	0.00197
								d	3	1600	0.0700	0.0333
K969	18.3*	12.5*	1.4*	0.4*	0.026	0.028	1.01	a	0	0	0.00073	0.00073
								b	2–1	8	0.00200	0.00130
								c	2–1	0	0.00081	0.00074
								d	2	29	0.0540	0.0168
L711	18.3*	12.25*	1.4*	0.4*	0.072	0.029	2.1*	a	0	1	0.00084	0.00075
								b	2–1	2	0.0125	0.0110
								c	2–300	10	0.0375[2]	0.0216[2]
								d	3–24	7400	0.041[1]	0.041[1]
L710	18.3*	13.5*	1.4*	0.4*	0.053	0.029	2.1*	a	0	0	0.00072	0.00071
								b	2–2	2	0.0181	0.0117
								c	1–300	3	0.044[3]	0.0205[3]
								d	3–24	2800	0.044[1]	0.044[1]
L709	18.3*	13.75*	1.4*	0.4*	0.031	0.027	2.1*	a	0	4	0.00065	0.00059
								b	0	1	0.00540	0.0027
								c	0	0	0.00410	0.00260
								d	2–100	10	0.053[4]	0.019[4]
L310	18.05	11.82	1.09	0.29	0.033	0.025	2.16	a	0	0	0.00078	0.00063
								b	0	0	0.00087	0.00067
								c	0	0	0.00100	0.00080
								d	2–300	42	0.0870[4]	0.0400[4]
L323	17.96	13.62	1.23	0.43	0.018	0.032	2.23	a	0	0	0.00126	0.00090
								b	0	0	0.00146	0.00098
								c	0	0	0.00218	0.00130
								d	1	10	0.0290[4]	0.0335[4]
L311	17.78	14.37	1.28	0.40	0.030	0.024	2.04	a	0	0	0.00102	0.00078
								b	0	0.3	0.00110	0.00081
								c	0	0	0.00320	0.00178
								d	2–300	31.5	0.0740[2]	0.0398[2]
L715	18.3*	14.75*	1.4*	0.4*	0.069	0.026	3.1*	a	0	2	0.00098	0.00088
								b	1	0.5	0.0032	0.00231
								c	2	8	0.048[4]	0.0218[4]
								d	3–24	11,200	0.040[1]	0.040[1]
L714	18.3*	15.0*	1.4*	0.4*	0.046	0.027	3.1*	a	0	0	0.00078	0.00079
								b	0	0.5	0.0036	0.00237
								c	0	3	0.00990	0.00500
								d	2–24	3.4	0.029[1]	0.029[1]
L713	18.3*	15.5*	1.4*	0.4*	0.036	0.026	3.1*	a	0	2	0.00097	0.00086
								b	0	0	0.00232	0.00151
								c	0	2	0.00610	0.00300
								d	2–100	18	0.044[2]	0.030[2]
L477	18.24	13.27	1.30	0.51	0.031	0.032	3.30	a	0	2	0.00106	0.00101
								b	0	1.4	0.00314	0.00165
								c	2	9	0.0436	0.0276
								d	2–1	692	0.154[1]	0.154[1]
L712	18.3*	15.75*	1.4*	0.4*	0.028	0.030	3.1*	a	0	2	0.00074	0.00068
								b	0	1	0.00177	0.00122
								c	0	0	0.00410	0.00210
								d	1	2	0.080[1]	0.080[1]

*Approximate composition. a = Heated 10 min. at 1075 °C and air-cooled. b = Heated 10 min. at 1075 °C and air-cooled, reheated 100 hr. at 550 °C. c = Heated 10 min. at 1075 °C and air-cooled, reheated 1 hr. at 650 °C. d = Heated 10 min. at 1075 °C and air-cooled, reheated 24 hr. at 650 °C.

†Bend Rating: 0 = No cracking. 1 = Surface cracks. 2 = Deep surface cracks. 3 = Broke. *Note:* Results are for 700 hours' boiling except where hyphen appears and then number following hyphen indicates time (hours) when result was observed.

‡Resistance change of 5% or more represents significant penetration.

[1]First period rate and average of 1 period. [2]Second period rate and average of 2 periods. [3]Third period rate and average of 3 periods. [4]Fourth period rate and average of 4 periods.

Table VII

Boiling 65% Nitric Acid Corrosion Data for Unionmelt Welds in ½-Inch Thick Plate of Low-Carbon Molybdenum-Bearing Austenitic 18% Chromium-Nickel Steels

	Chemical Composition, %	
	Plate and Electrode	Weld Metal
Cr	18.19	.....
Ni	13.95	.....
Mn	1.26	.....
Si	0.37	.....
C	0.020	0.023
N	0.025	0.031
Mo	2.02	.....

Sample	Condition	Corrosion Rate Inch Penetration per Month Average 5 Periods
Welded Plate	As-welded	0.00116
Welded Plate	Welded, heated 2 hr. at 870 ° C and air-cooled	0.00091
Plate	Heated 10 min. at 1075 °C and air-cooled	0.00118
Plate	Heated 10 min. at 1075 °C and air-cooled, reheated 2 hr. at 870 °C and air-cooled	0.00116

nitrogen, and 2.02% molybdenum was welded by the Unionmelt process in the same manner as previously described. Samples taken from this weld showed no signs of intergranular attack when exposed to 10% nitric acid – 3% hydrofluoric acid at 70 °C (160 °F) in the as-welded or stress-relieved condition. In boiling 65% nitric acid the welded samples had corrosion resistance equal to that of the base metal. The detailed results of the corrosion tests are listed in Table VII.

The presence of molybdenum in austenitic chromium-nickel steels reduces their resistance to boiling 65% nitric acid. While its presence can be noted in the annealed condition, the influence of molybdenum is most noticeable after heating in the carbide precipitation temperature range. The tests on samples heated 1 hour at 650 °C (1200 °F), given in Table VI, show that the corrosion resistance of the steel depends not only on the molybdenum content but also on the nickel content. Fig. 22 has been plotted to show the influence of increasing nickel in steels containing 2 and 3% molybdenum.

In these very low-carbon steels, it was felt important to investigate the stability of the austenitic phase after exposure to elevated temperatures. Impact toughness tests were made on samples of the steels after heating at 550, 650, and 870 °C (1020, 1200, and 1600 °F). The results indicate that heating two weeks at 550 and 650 °C (1020 and 1200 °F) does not affect the high toughness of

the steels. At 870 °C (1600 °F) steels containing 1 to 2% molybdenum retain their toughness up to at least 100 hours' exposure, whereas the 3% molybdenum steel falls to about 65 ft-lb. As shown in Fig. 23, heating at 870 °C (1600 °F) for 1 month lowers the toughness of the 1 and 2% molybdenum steels to between 45 and 55 ft-lb. and that of the 3% molybdenum steel to 25 ft-lb. These remarks apply to steels containing sufficient nickel to render them austenitic. The loss of toughness in steels containing smaller amounts of nickel is

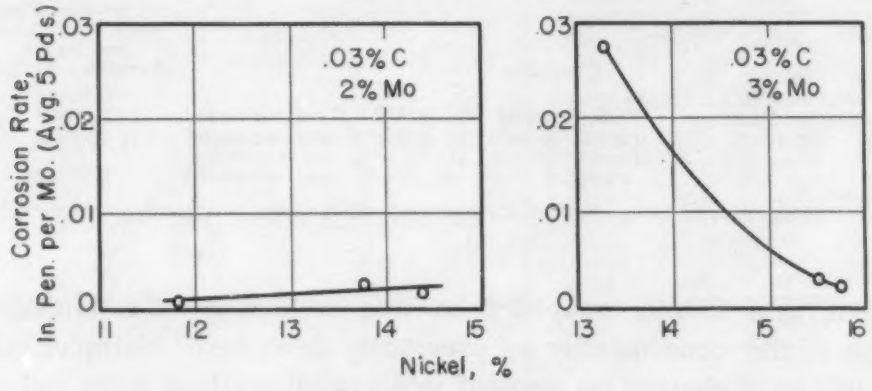


Fig. 22—Influence of Nickel on Average Corrosion Rate in Boiling 65% Nitric Acid of Low-Carbon 18% Chromium Steels Containing 2 and 3% Molybdenum, After Heating 1 Hour at 650 °C (1200 °F).

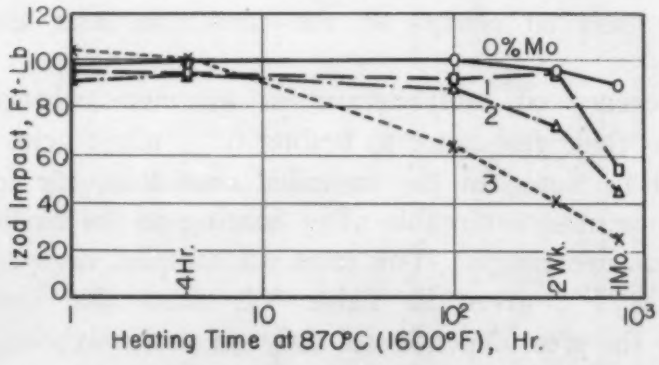


Fig. 23—Effect of Heating at 870 °C (1600 °F) on Izod Impact Strength of Austenitic 18% Chromium-Nickel Steels Containing 0 to 3% Molybdenum and 0.030% Carbon.

more rapid. From these data it would appear that the molybdenum content is not critical for short periods of heating.

It is important to prohibit the formation of ferrite because sigma phase occurs more rapidly in steels containing some delta ferrite than in homogeneous austenitic steels. As a guide in adjusting composi-

tion with respect to nickel in the molybdenum-bearing steels, Fig. 24 is included. The curve drawn in this figure was derived from metallographic and magnetic balance data. It shows that, for each 1% molybdenum added, about 1.7% additional nickel must be added to maintain an austenitic structure.

Fig. 25 reveals the development of sigma phase on heating at 870 °C (1600 °F) in a steel containing a small amount of ferrite in the annealed condition. It is noted that after 4 hours' heating there is a marked decomposition of the ferrite. After 100 hours the formation of sigma is nearly complete. The impact toughness of this steel in the annealed condition was 99 ft-lb. After 4 hours at

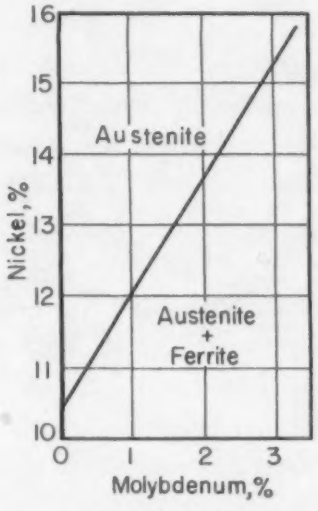


Fig. 24—Relationship Between Nickel and Molybdenum in 18% Chromium – 0.03 to 0.05% Nitrogen – 0.030% Carbon Steels in Forming Austenite.

870 °C (1600 °F) it was 92 ft-lb., dropping to 41 ft-lb. in 100 hours, and to 9 ft-lb. after one month.

The addition of molybdenum to the 0.03% carbon-chromium-nickel steels is helpful to a significant extent in delaying the start of carbide precipitation. This is true in spite of the fact that these steels must contain higher percentages of nickel than steels without molybdenum, to prevent the formation of a partially ferritic structure. When sufficient nickel is present, the steels have good nitric acid resistance and remain tough after short exposures at temperatures between 550 and 870 °C (1020 and 1600 °F).

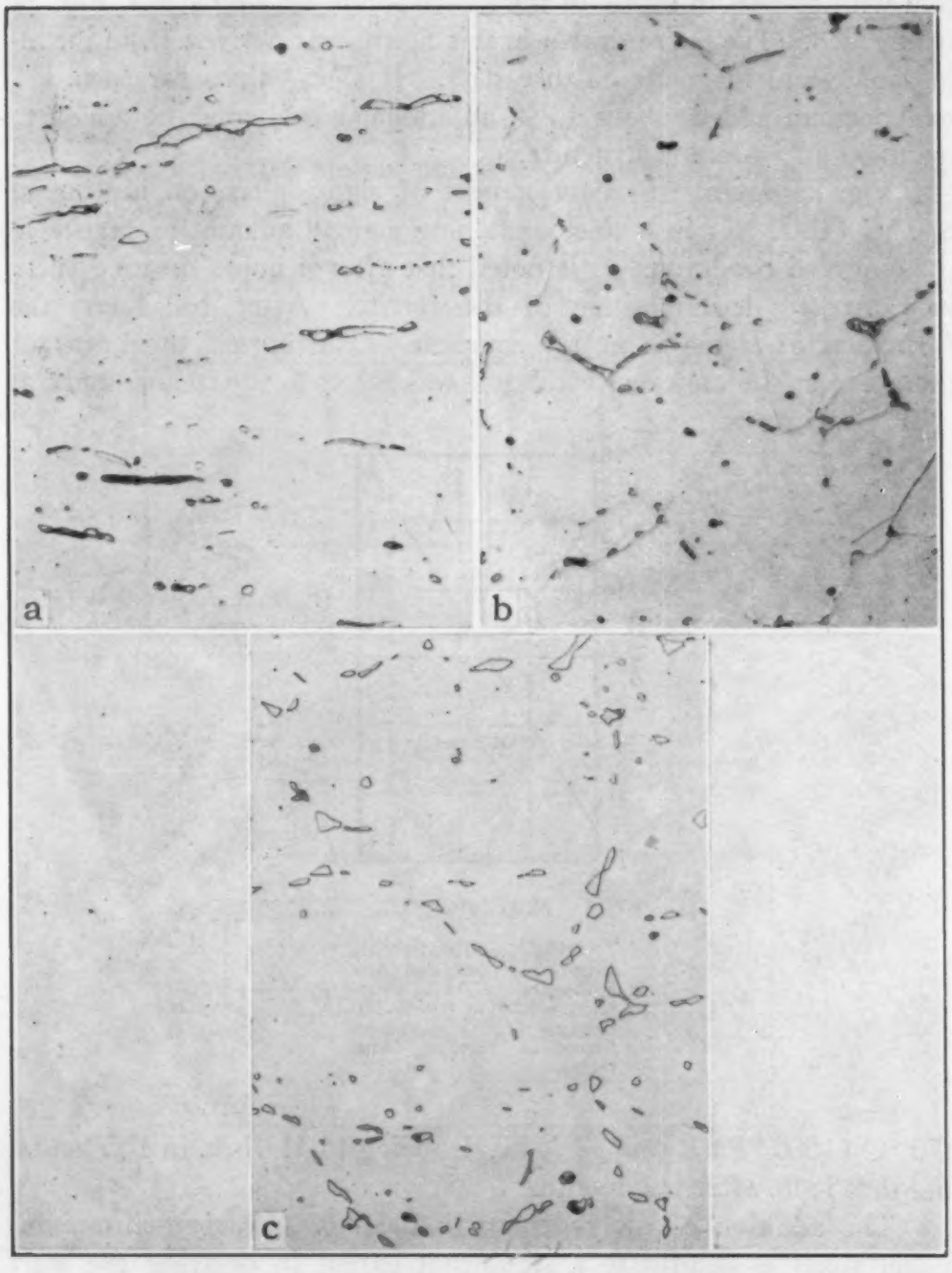


Fig. 25—The Development of Sigma Phase in a Steel Containing 18.24% Chromium, 13.27% Nickel, 0.031% Carbon, 0.032% Nitrogen and 3.30% Molybdenum. Etchant: Aqua regia in glycerine + copper chloride. × 500. a—Heated 10 minutes at 1075 °C (1970 °F) and air-cooled. Austenite + delta ferrite. b—Heated 10 minutes at 1075 °C (1970 °F) and air-cooled, reheated 4 hours at 870 °C (1600 °F). Austenite + delta ferrite + sigma. c—Heated 10 minutes at 1075 °C (1970 °F) and air-cooled, reheated 100 hours at 870 °C (1600 °F). Austenite + sigma.

Columbium-Bearing Chromium-Nickel Steels

The foregoing data have indicated the low level to which carbon must be reduced to obtain complete freedom from intergranular attack in the austenitic 18 to 25% chromium-nickel steels. Therefore, the question of adding small amounts of stabilizing agents to steels with carbon contents somewhat higher than 0.015 to 0.020% is logically introduced, and work centering about the addition of columbium was undertaken.

Several heats of steel containing 18% chromium, 10 to 12% nickel, 1.3% manganese, 0.4% silicon, 0.020 to 0.040% carbon, 0.030 to 0.150% nitrogen, and varying amounts of columbium were made for this portion of the investigation. A nickel content of 11.75%, to render stabilized steels completely austenitic, was established from magnetic tests. The columbium steels were annealed at 1075 °C (1970 °F), air-cooled and then heated as before at temperatures of 475, 550, and 650 °C (890, 1020, and 1200 °F). Tests were made in both acidified copper sulphate solution and in boiling 65% nitric acid.

In these low-carbon steels only small amounts of columbium are required and due regard must be given to the columbium which exists in solid solution as well as that combined as columbium carbide and columbium nitride. This problem was solved by analyzing the steels and the precipitate formed on heating at 650 °C (1200 °F). Heating for 24 hours at 650 °C (1200 °F) proved to be a decisive means of differentiating between steels containing sufficient and insufficient amounts of columbium. Samples of several steels were heat treated 24 hours at 650 °C (1200 °F) and analyzed for total carbon, nitrogen, and columbium, as well as for combined carbon, nitrogen, and columbium. The latter information was obtained from the analysis of the residue remaining after dissolving a sample in copper-potassium chloride solution. The results of these analyses are plotted in Figs. 26, 27, and 28.

In Fig. 26 are plotted values of insoluble columbium, that is, columbium combined with carbon and nitrogen, against total columbium as determined for steels subject to intergranular attack. A straight line drawn through the points intersects the total columbium axis at 0.093%. The slope of this line should be 45 degrees, since the amount of combined columbium is proportional to the amount of columbium present in excess of the solubility limit. The line

drawn in Fig. 26 has a slope of 45 degrees, and it is seen that the determined values fall relatively uniformly around this line. The fact that the line does not pass through zero indicates that a small amount of columbium, about 0.1%, is soluble in austenite at this carbon level and it is not available for combining with carbon and nitrogen. In very low-carbon steels this amount of columbium

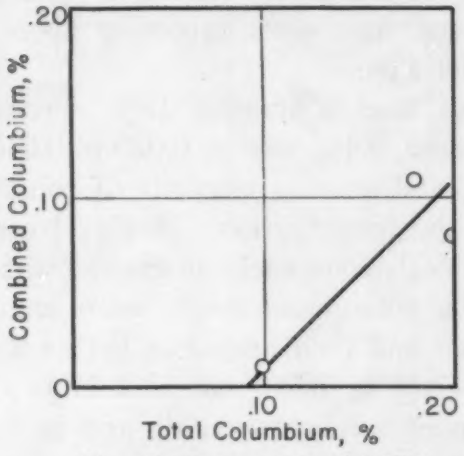


Fig. 26—Data on the Solubility of Columbium in Austenitic 18% Chromium – 11.75% Nickel Steels After Heating 24 Hours at 650 °C (1200 °F).

represents a substantial proportion of the columbium added to the steel for stabilization purposes.

Figs. 27 and 28 are plots of total carbon against carbon combined with columbium and of total nitrogen against nitrogen combined with columbium for steels that did not show intergranular corrosion. In each of these figures the lines intersect the total carbon and total nitrogen axes. The values at these intersections represent the amounts of carbon and nitrogen soluble in the steel, 0.013% and 0.022% respectively, which may be compared with the data for limiting carbon and nitrogen previously discussed for the plain chromium-nickel steels.

When the above facts are considered, it is apparent that columbium must be added to the steel in a total amount which is the sum of the amount in solid solution, plus the amount combined with carbon in excess of 0.013%, plus the amount combined with nitrogen in excess of 0.022%. This may be expressed as follows:

$$\% \text{ total columbium} = 0.093 + 7.7\ (\% \text{ carbon} - 0.013) + 6.6\ (\% \text{ nitrogen} - 0.022) \qquad \text{(Equation V)}$$

where 7.7 and 6.6 are respectively the combining ratios for columbium carbide and columbium nitride. Clearly, it is impossible to give a fixed value for the simple ratio of columbium to carbon in these low-carbon steels. For example, a steel with 0.020% carbon

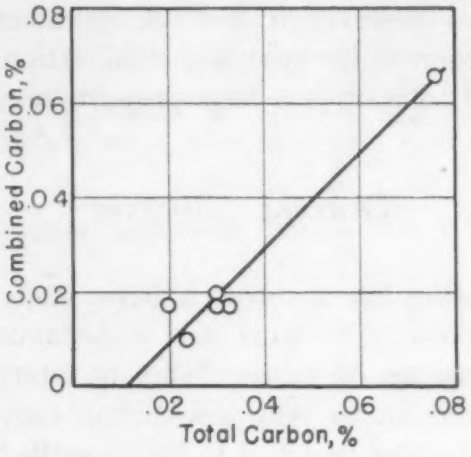


Fig. 27—Data on the Solubility of Carbon in Austenitic 18% Chromium–11.75% Nickel Steels After Heating 24 Hours at 650 °C (1200 °F).

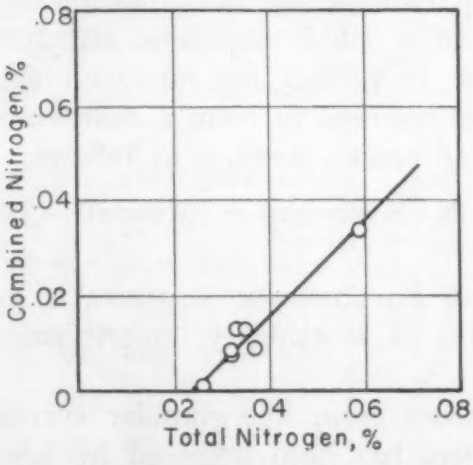


Fig. 28—Data on the Solubility of Nitrogen in Austenitic 18% Chromium–11.75% Nickel Steels After Heating 24 Hours at 650 °C (1200 °F).

and 0.04% nitrogen from the above relation requires 0.25% columbium while a 0.040% carbon – 0.040% nitrogen steel requires 0.42% columbium.

The results of corrosion tests on a series of low-carbon columbium-bearing steels varying in columbium content are of interest. It may be observed in Table VIII that steels containing sufficient

columbium to satisfy Equation V are resistant to intergranular attack in both boiling nitric acid and boiling acidified copper sulphate solutions after prolonged heating at 550 °C (1020 °F). Steels containing less columbium than required, while susceptible to attack after prolonged heating, show satisfactory resistance after short periods of heating. However, it does not appear effective to add less columbium than required for complete stabilization because the 0.1% columbium in solid solution is a large proportion of the total amount required.

General Summary

This investigation has involved a basic study of the austenitic chromium-nickel steels. The work was undertaken to determine the influence of composition on susceptibility to intergranular corrosion with particular attention to very low-carbon contents. It was desired to know the factors that had to be controlled in order to eliminate intergranular corrosion.

As an initial step in the study, experiments were made to determine the interrelation among chromium, nickel, carbon, and nitrogen in the formation of a stable austenitic structure. An empirical equation, developed to predict the minimum amounts of carbon, nitrogen, and nickel required to form a completely austenitic structure in 18 to 25% chromium steels, is as follows:

$$30\,(\%\text{ carbon}) + 26\,(\%\text{ nitrogen}) + (\%\text{ nickel}) - 1.3\,(\%\text{ chromium}) + 11.1 = 0 \qquad \text{(Equation I)}$$

The maintenance of an austenitic structure is generally advisable from the standpoint of workability, embrittlement, and corrosion resistance.

Complete freedom from intergranular corrosion of austenitic chromium-nickel steel has been achieved by lowering the carbon contents to 0.015 to 0.020%. This value for carbon in austenitic 18 to 25% chromium-nickel steels, having complete resistance to intergranular attack, was obtained by means of corrosion tests on samples heated for 100 hours at 550 °C (1020 °F). It was observed that the limiting value for carbon depends on the alloy content of the steel with higher nickel restricting, and higher chromium extending somewhat, the maximum carbon content. The above carbon limit refers to steels containing a maximum of about 0.05% nitrogen.

The proper amount of columbium, to attain complete immunity

Table VIII
Corrosion Data for Columbium-Bearing Austenitic Chromium-Nickel Steels of Low-Carbon Content

Heat No.	Composition, % Cr	Ni	Mn	Si	C	N	Cb	Cond. of Metal	Boiling Acidified Copper Sulphate — Bend Rating†	Boiling Acidified Copper Sulphate — Per Cent Increase in Elect. Resist.‡	Corrosion Rate Inch Penetration per Month in Boiling 65% Nitric Acid — Fifth 48-Hr. Period	Corrosion Rate Inch Penetration per Month in Boiling 65% Nitric Acid — Avg. of Five 48-Hr. Periods
K118	18.39	10.44	1.38	0.40	0.032	0.037	0.29	a	0	..	0.00055	0.00060
								b	0	..	0.00119	0.00093
								c	0	..	0.00072	0.00067
								d	0	..	0.00141	0.00099
K120	18.09	10.15	1.41	0.46	0.032	0.058	0.33	a	0	2	0.00063	0.00064
								b	1	13	0.00206	0.00140
								c	0	..	0.00080	0.00074
								d	0	4	0.00194	0.00127
K122	18.24	10.18	1.42	0.43	0.034	0.115	0.35	a	0	..	0.00069	0.00069
								b	2–300	..	0.0510	0.0320
								c	0	..	0.00147	0.00109
								d	1	..	0.00700	0.00400
K203	18.05	10.65	1.14	0.46	0.030	0.112	0.57	a	0	0	0.00056	0.00066
								b	0	0	0.00550	0.00340
								c	0	..	0.00083	0.00083
								d	0	0	0.00250	0.00180
K124	18.48	10.53	1.39	0.40	0.034	0.147	0.31	a	0	0	0.00067	0.00069
								b	2–24	161	0.0710	0.0533
								c	1	..	0.00256	0.00162
								d	2–400	0	0.0123	0.00670
K809	18.3*	10.5*	1.2*	0.4*	0.023	0.026	0.12	a	0	2	0.00045	0.00054
								b	1	1	0.00202	0.00144
								c	0	4	0.00078	0.00075
								d	0	2	0.00305	0.00168
K808	18.3*	10.5*	1.2*	0.4*	0.023	0.026	0.17	a	0	2	0.00044	0.00047
								b	0	1	0.00121	0.00093
								c	0	3	0.00071	0.00070
								d	0	3	0.00345	0.00198
K807	18.3*	10.5*	1.2*	0.4*	0.026	0.028	0.19	a	0	4	0.00046	0.00054
								b	0	1	0.00205	0.00138
								c	0	4	0.00082	0.00081
								d	0	4	0.00259	0.00161
K964	18.3*	10.5*	1.2*	0.4*	0.023	0.029	0.28	a	0	0.5	0.00061	0.00066
								b	0	0	0.00111	0.00088
								c	0	0	0.00220	0.00124
								d	0	2	0.00500	0.00310
K200	18.37	10.94	1.10	0.44	0.024	0.034	0.42	a	0	0	0.00074	0.00071
								b	0	0	0.00093	0.00079
								c	0	..	0.00103	0.00080
								d	0	0	0.00300	0.00150
K201	18.36	11.75	1.11	0.46	0.027	0.036	0.38	a	0	1	0.00055	0.00057
								b	0	1	0.00139	0.00108
								c	0	..	0.00092	0.00075
								d	0	1	0.00220	0.00131
K202	18.05	12.20	1.17	0.41	0.020	0.035	0.37	a	0	0	0.00058	0.00059
								b	0	0	0.00087	0.00074
								c	0	..	0.00084	0.00070
								d	0	0	0.00188	0.00120

*Approximate composition. a = Heated 10 min. at 1075 °C and air-cooled. b = Heated 10 min. at 1075 °C and air-cooled, reheated 100 hr. at 550 °C. c = Heated 10 min. at 1075 °C and air-cooled, reheated 1 hr. at 650 °C. d = Heated 10 min. at 1075 °C and air-cooled, reheated 24 hr. at 650 °C.

†Bend Rating: 0 = No cracking. 1 = Surface cracks. 2 = Deep surface cracks. *Note:* Results are for 700 hours' boiling except where hyphen appears and then number following hyphen indicates time (hours) when result was observed.

‡Resistance change of 5% or more represents significant penetration.

to intergranular corrosion in steels containing in excess of 0.02% carbon, must allow for that which combines with carbon and nitrogen and that which remains in solid solution in the austenite. In very low-carbon steels, the amount of columbium remaining in solid solution represents a substantial proportion of the total amount of columbium. The total columbium required for complete immunity is:

$$\%\ \text{total columbium} = 0.093\% + 7.7\ (\%\ \text{carbon} - 0.013) + 6.6\ (\%\ \text{nitrogen} - 0.022) \qquad \text{(Equation V)}$$

Complete immunity to intergranular corrosion is essential to the successful service of steel exposed at elevated temperatures for long periods of time. Steels, which are subjected to high temperatures only during fabrication, require somewhat less than the complete immunity to intergranular corrosion that more extended heating demands. The foregoing study has indicated that the compositions required for partial immunity may contain somewhat higher carbon.

Steels with partial resistance to intergranular corrosion have been defined as those remaining free from attack after an isothermal heat treatment of 1 hour at 650 °C (1200 °F). Such a criterion ultimately may be found to apply to a greater or lesser degree in fabrication practices because of the differences between isothermal test heat treatments and actual continuous cooling cycles. The time before initiation of intergranular precipitation has been found to vary with temperature in the form of a "C" curve with the nose at about 750 °C (1380 °F). Because the nose time is relatively short, reliable experimental testing is difficult and exposure of 1 hour at 650 °C (1200 °F) is preferred as the criterion of susceptibility. The effects of composition on the nose time at 750 °C (1380 °F) and on the resistance to attack after exposure at 650 °C (1200 °F) have been summarized in empirical formulas. These expressions indicate that (with respect to tolerance for carbon) chromium and molybdenum are beneficial, that nickel beyond the amount required to produce the wholly austenitic condition is harmful, and that nitrogen may be substituted in part for nickel with some improvement. The maximum carbon content should not be more than about 0.03%.

An empirical equation, based on samples heated 1 hour at 650 °C (1200 °F), has been developed for calculating the composition of steels resistant to intergranular attack after limited heating in the carbide precipitation range. The equation showing the respective effects of the alloying elements investigated is given on the next page:

Table IX
Typical Compositions of Austenitic Chromium-Nickel Steels Resistant to Intergranular Corrosion After 1 Hour at 650 °C (1200 °F)

Nitrogen	<0.05%
Manganese	1.25%
Silicon	0.40%

Chemical Composition, %			Minimum Calculated Time for Start of Carbide Precipitation, Seconds
Cr	Ni	C	
18	10.5	0.025	220
18	13.5	0.020	110
20	13.2	0.025	215
20	16.2	0.020	100
25	20.0	0.025	195
25	23.0	0.020	75

$$\frac{6.17}{(\%\ \text{carbon})^{0.88}} + 13.8\ [(\%\ \text{chromium}) + 2.25\ (\%\ \text{molybdenum})] - 10\ (\%\ \text{nickel}) - 276 = 0 \qquad \text{(Equation IV)}$$

Nitrogen was found to have practically no effect within the range of tests conducted on samples heated 1 hour at 650 °C (1200 °F). A limited number of welding tests have been made which, in part, verify the applicability of the above equation.

The use of Equation IV should be accompanied by a calculation of the minimum time for precipitation to start, so that the final composition will best withstand the heating cycle to be encountered. The calculation is carried out according to Equation III, which has been determined from an analysis of time-temperature-precipitation curves for a number of steels. The time, t, in seconds, to the nose of the curve is expressed by the following equation:

$$t = 63.5\ (\%\ \text{chromium}) - [50.5\ (\%\ \text{nickel}) + 6820\ (\%\ \text{carbon}) + 1037\ (\%\ \text{nitrogen})] - 178 \qquad \text{(Equation III)}$$

Table IX was prepared to illustrate various compositions of austenitic steels in accord with Equation I, partially resistant to intergranular corrosion as specified by Equation IV.

The addition of 2% molybdenum to austenitic 18% chromium-nickel steels containing 0.02 to 0.03% carbon greatly increases the time for damaging carbide precipitation to occur. This means that there is a greater tolerance for carbon in molybdenum-bearing steels.

Conclusions

This study of very low-carbon austenitic chromium-nickel steels has indicated that immunity to intergranular attack may be attained by lowering carbon content and adjusting the composition of the steels to avoid intergranular carbide precipitation. It may be concluded that:

1. Complete immunity may be obtained if the carbon is held below 0.015 to 0.020%, depending on the balance of the composition.
2. Complete immunity may be obtained with a small addition of columbium if carbon is in the neighborhood of 0.03%.
3. Partial immunity may be obtained in steels of balanced composition with the carbon content not more than about 0.03%.
4. In 18% chromium-nickel steels containing 2% molybdenum, partial immunity may be obtained with carbon at about 0.03%.

Acknowledgments

The authors are pleased to express their appreciation of the co-operative aid given them by Messrs. Walter Crafts, chief metallurgist, C. R. Bishop, James Thompson, and Dr. W. D. Forgeng, of the Union Carbide and Carbon Research Laboratories, Inc.

References

1. E. C. Bain, R. H. Aborn and J. J. B. Rutherford, "The Nature and Prevention of Intergranular Corrosion in Austenitic Stainless Steels," Transactions, American Society for Steel Treating, Vol. 21, 1933, p. 481.
2. B. Strauss, B. H. Schottky and J. Hinnüber, "Carbide Precipitation During Tempering of Corrosion-Resistant Non-Magnetic Chromium-Nickel Steels," *Ztsch. f. anorg. u. allg. Chem.*, Vol. 188, 1930.
3. V. N. Krivobok, with the assistance of E. L. Beardman, H. J. Hand, T. O. A. Holm, A. Reggiori and R. S. Rose, "Further Studies in Chromium-Nickel-Iron and Related Alloys," Transactions, American Society for Steel Treating, Vol. 21, 1933, p. 22.
4. F. M. Becket and R. Franks, "Effects of Columbium in Chromium-Nickel Steels," *Transactions,* American Institute of Mining and Metallurgical Engineers, Vol. 113, 1934, p. 143.
5. H. H. Uhlig, "The Role of Nitrogen in 18-8 Stainless Steel," Transactions, American Society for Metals, Vol. 30, 1942, p. 947.
6. J. R. Cain and L. C. Maxwell, "An Electrolytic Resistance Method for Determining Carbon in Steel," *Journal,* Industrial and Engineering Chemistry, Vol. 11, 1919, p. 852.
7. G. Ericsson, "Method for the Determination of the Lowest Carbon Contents in Steel," *Jernkont. Ann.*, Vol. 128, 1944, p. 579.
8. R. G. Newton, "An Improved Electrical Conductivity Method for the Estimation of CO_2 and Other Reactive Gases," *Ann. Botany,* Vol. 49, 1935, p. 381.

DISCUSSION

Written Discussion: By C. M. Sheridan, associate director of research, Allegheny Ludlum Steel Corp., Brackenridge, Pa.

Messrs. Binder, Brown and Franks are to be congratulated on their methodic approach to this subject and the accompanying problems. On the whole, their results are in agreement with those of our work; however, there are divergencies which are apparent after consideration of additional information.

Fig. 29[2] shows the effect of nitrogen on the corrosion resistance of

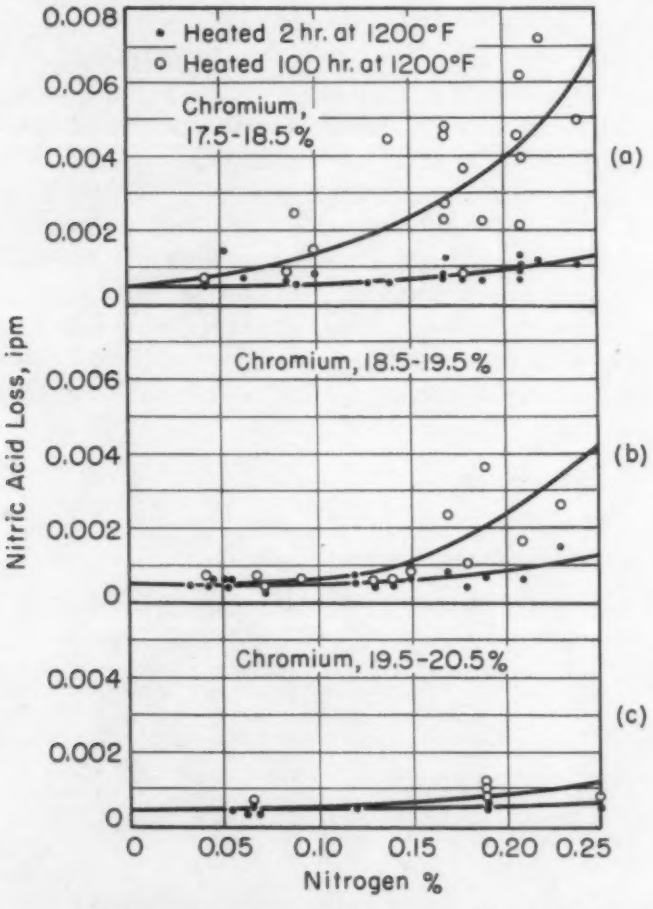


Fig. 29—Effect of Nitrogen on the Corrosion Resistance of 0.03% Carbon Stainless Steels With Varying Chromium Content.

low carbon stainless steels with chromium content ranging from a mean of 18 to 20%. Although increased nitrogen tends to increase the corrosion loss in boiling nitric acid, the effect is much less pronounced with increased chromium and, in fact, is practically negligible in alloys containing 20% chromium. The effect of nickel as shown by the authors again con-

[2]G. C. Kiefer and C. M. Sheridan, "Effect of Composition on Low Carbon Austenitic Cr-Ni Stainless Steels," paper presented at May 1948 meeting of American Iron and Steel Institute.

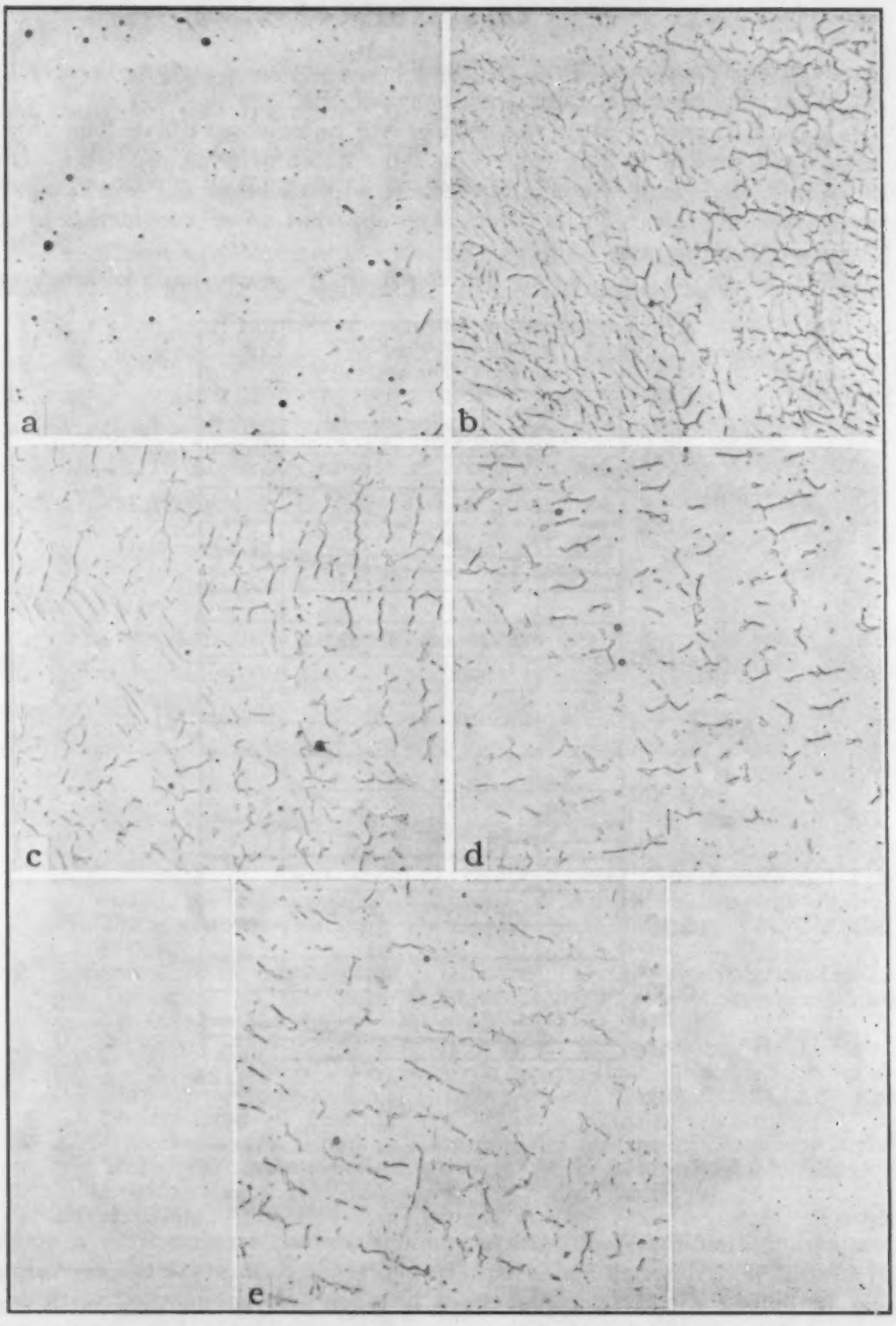


Fig. 30—Etch Electrolytic NaCN, × 200. Showing amount of ferrite in cast structure of alloys with varying compositions.

	C	Mn	Si	Cr	Ni	N_2
Fig. 30a—BU-82	0.031	0.48	0.38	18.88	9.33	0.18
Fig. 30b—BU-85	0.031	0.59	0.42	20.11	9.09	0.049
Fig. 30c—BV-37	0.034	0.50	0.49	19.65	11.02	0.078
Fig. 30d—BV-46	0.035	0.47	0.63	20.11	8.27	0.14
Fig. 30e—BU-91	0.066	0.53	0.26	18.89	9.11	0.085

firms what has long been recognized in austenitic steels containing higher carbon. It is realized also that there is a limit to the relative amounts of chromium and nickel or more precisely, austenite and ferrite-forming elements, in a one-phase alloy when optimum workability is to be had. Since nitrogen may be substituted in part for nickel but does not appear to decrease the corrosion resistance as markedly, there exists the possibility of making an alloy with a chromium content of approximately 20% and lower than normal nickel, substituting in part nitrogen. Fig. 30 shows the cast microstructure of alloys with varying amounts of chromium, nickel and nitrogen. Fig. 30e shows the structure of an alloy approximating the composition of a normal commercial austenitic steel, with the exception of the slightly higher nitrogen. The potency of nitrogen as an austenite former becomes apparent at once. In passing, it might be mentioned that the only alloy showing ferrite after rolling and annealing was Fig. 30b, containing 20% chromium, 9% nickel and 0.05% nitrogen.

Corrosion tests were conducted on some of these heats and the results listed in Table X bear out further conclusions on the effect of nitrogen on corrosion rates in boiling 65% nitric acid. It is apparent from this table that nitrogen may be added to a low nickel steel, rendering it essentially austenitic without impairing the corrosion resistance. Although both heats disintegrated in nitric acid after 100 hours at 595 and 550 °C (1100 and 1025 °F), they were passable after 1 hour's treatment at each temperature and the losses were relatively low after 100 hours' treatment at 650 °C (1200 °F).

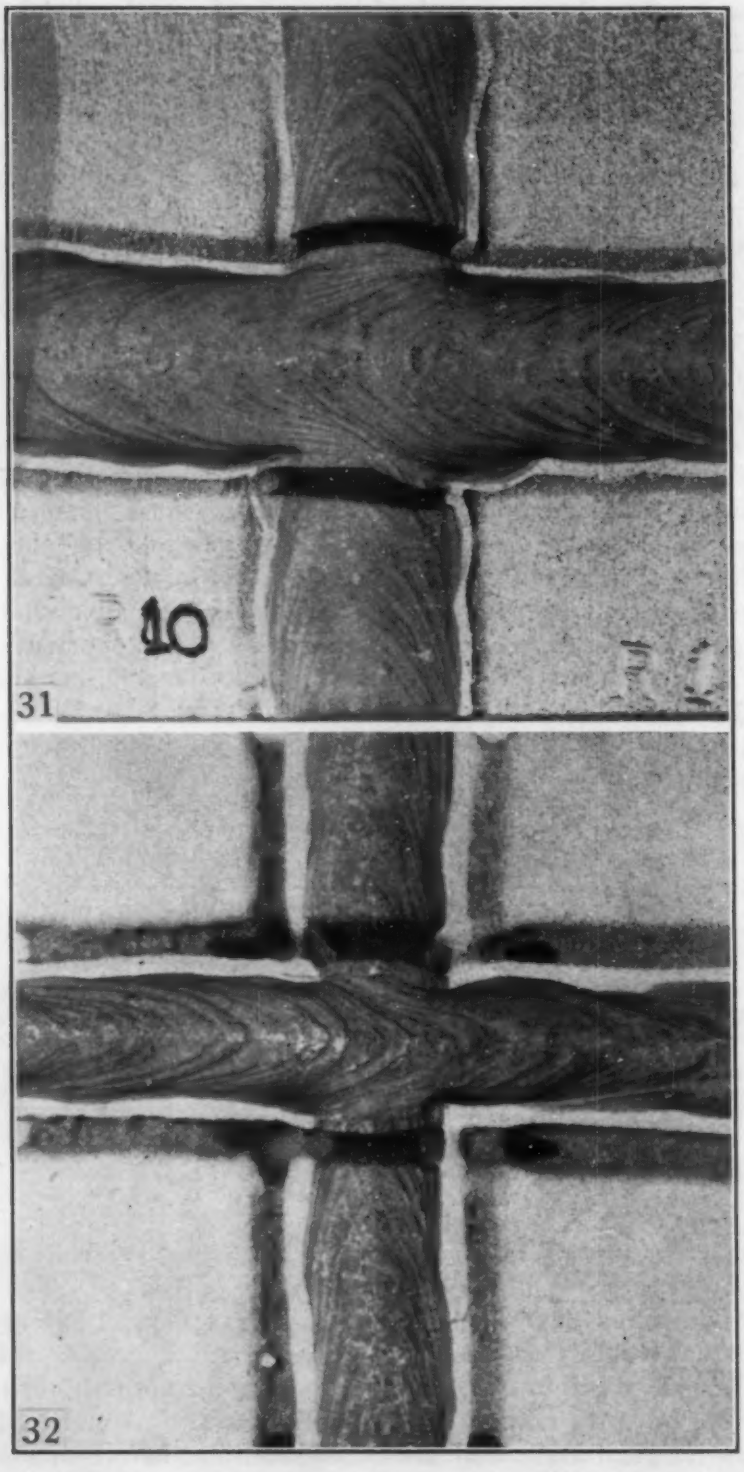
Table X

Heat No.		Corrosion Rates, Inches Penetration Per Minute After— Annealed	Ann. + 1 Hr. At 1200°F	Ann. + 100 Hr. At 1200°F	Ann. + 1 Hr. At 1100°F	Ann. + 100 Hr. At 1100°F	Ann. + 1 Hr. At 1025°F	Ann. + 100 Hr. At 1025°F
BU-82	Last period	0.00062	0.00060	0.0029	0.00049	*	0.00056	*
	Average of 5	0.00061	0.00058	0.0020	0.00048	*	0.00066	*
BU-85	Last period	0.00049	0.00045	0.0037	0.00050	*	0.00042	*
	Average of 5	0.00051	0.00055	0.0022	0.00050	*	0.00053	*

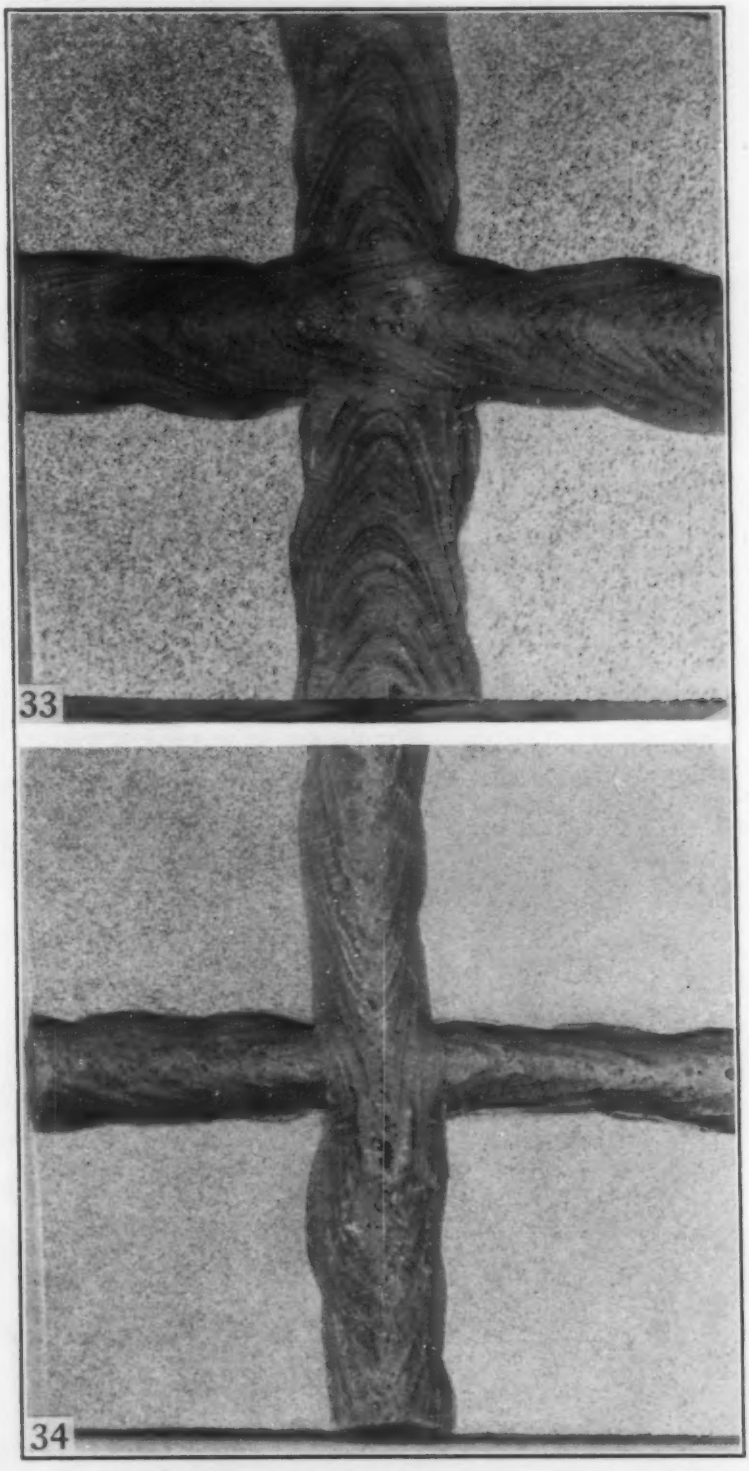
Heat No.	Composition— C	Cr	Ni	N_2
BU-82	0.031	19.88	9.33	0.18
BU-85	0.031	20.11	0.09	0.049

*Disintegrated.

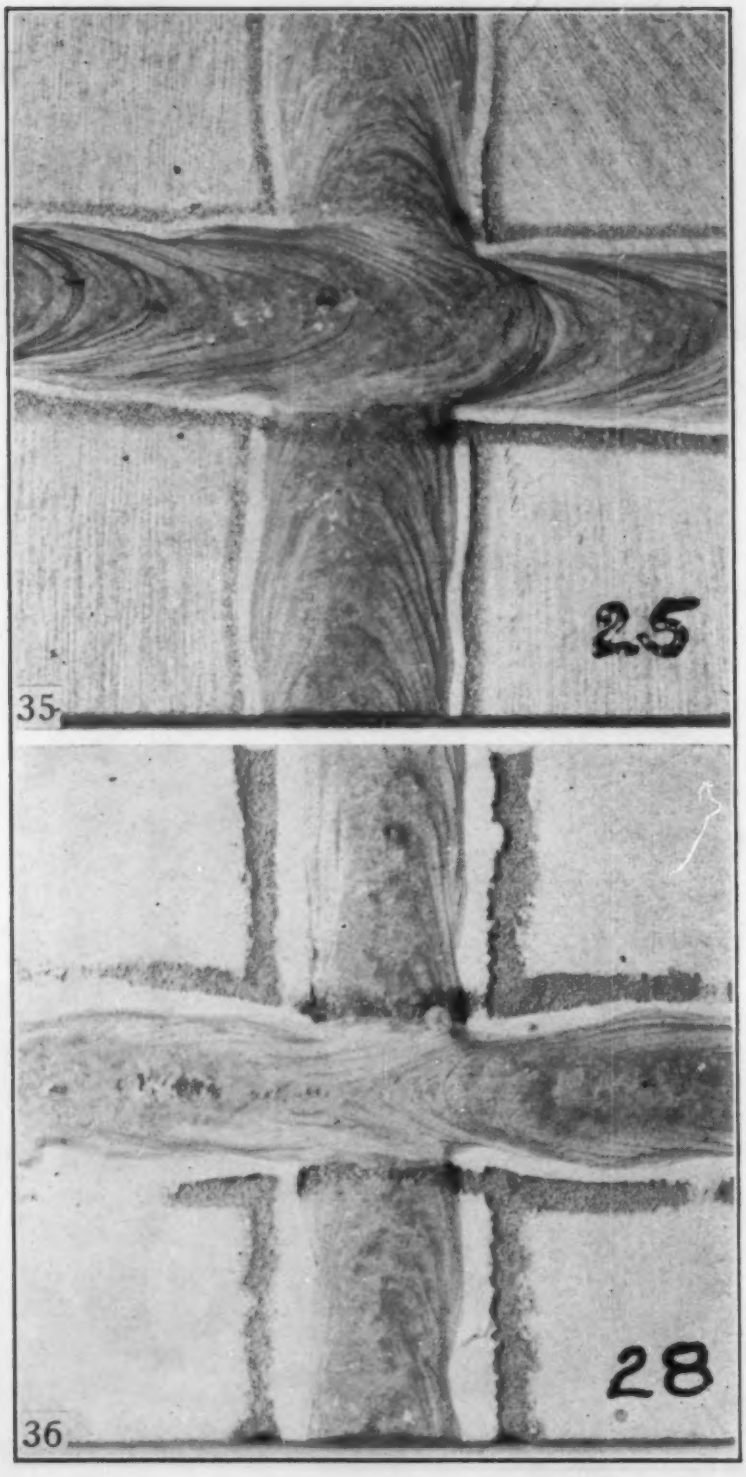
The "C" curves developed by the authors offer an interesting and novel approach to this problem and it is hoped they will facilitate the study of carbide precipitation. It is surprising to note the shape of the curve for the steel containing 0.021% carbon as shown in Fig. 13. From the authors' original statement under the heading, Effect of Carbon, and in Fig. 1, they state that the solubility curve for carbon shows increasing solubility with increasing temperature and passes through the point located at 550 °C (1020 °F) and 0.02% carbon. From this it would normally be expected that the curve for this steel would not extend much



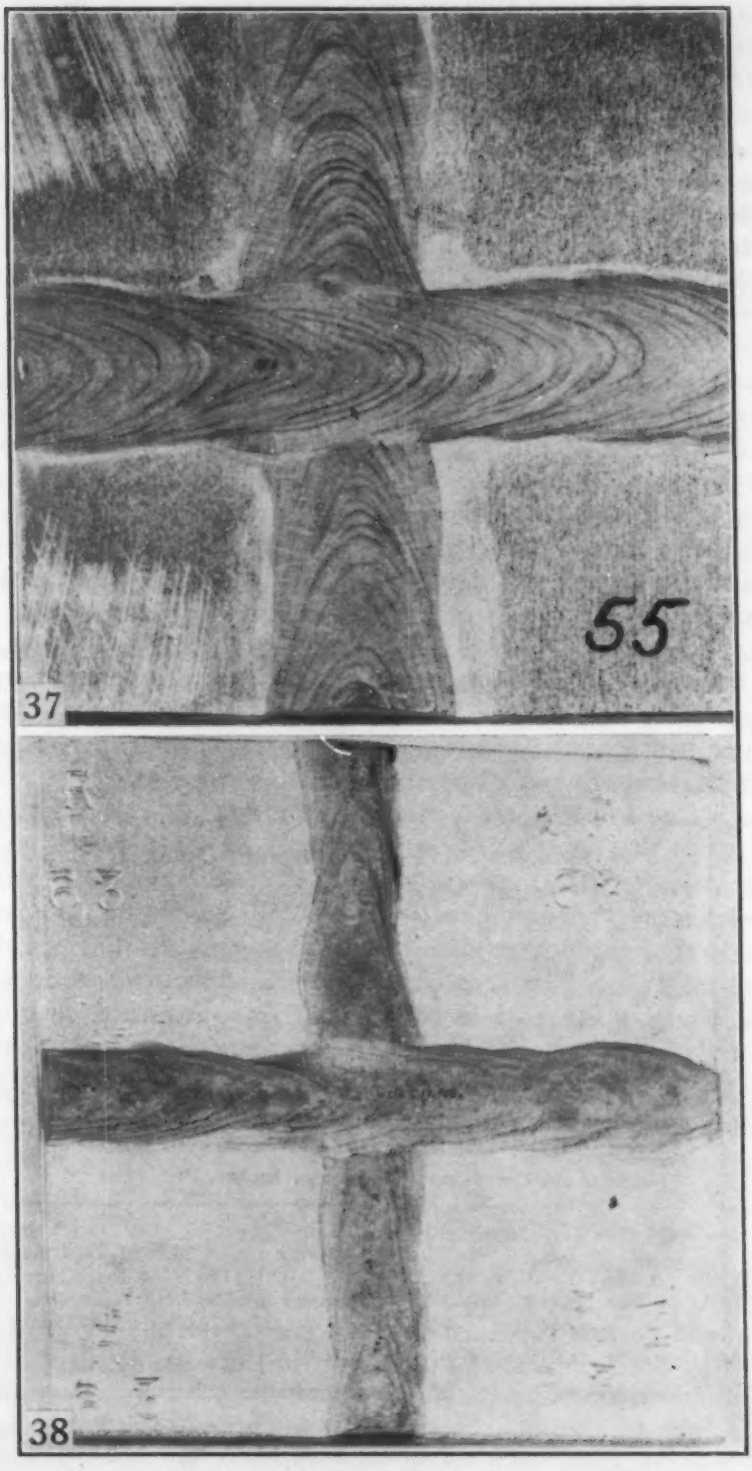
Figs. 31 and 32—Appearance of Metal-Arc Welded Type 304 (0.06% Carbon) Plate and Sheet Respectively, After Three 4-Hour Periods in 10% Nitric – 3% Hydrofluoric Acid Solution at 80 °C (175 °F). As-welded condition. Note severe intergranular corrosion on base metal heat-affected zones and heat-affected zones in first weld seams. × 1.5.



Figs. 33 and 34—Appearance of Metal-Arc Welded Type 304 ELC (0.03% Carbon) Plate and Sheet Respectively, After Nitric–Hydrofluoric Acid Etch Test. As-welded condition. No localized intergranular corrosion attack. × 1.5.



Figs. 35 and 36—Appearance of Metal-Arc Welded Type 316 (0.07% Carbon) Plate and Sheet Respectively, After Nitric–Hydrofluoric Acid Etch Test. As-welded condition. Note intergranular corrosion on base metal heat-affected zones. Somewhat lighter attack can be seen on heat-affected zones of first weld seams. × 1.5.



Figs. 37 and 38—Appearance of Metal-Arc Welded Type 316 ELC (0.03% Carbon) Plate and Sheet Respectively, After Nitric–Hydrofluoric Acid Etch Test. As-welded condition. No localized intergranular corrosion attack. × 1.5.

above 540 to 595 °C (1000 to 1100 °F) unless there is a sudden increase in the slope of the solubility curve. If these curves represent reaction curves for the precipitation of carbides, they should become asymptotic to the horizontal temperature line representing the solubility of carbon for that steel being studied. Obviously, this is not the case since curves for all steels, regardless of carbon content, become asymptotic at approximately 850 °C (1560 °F).

Written Discussion: By Hilmer Ebling and M. A. Scheil, A. O. Smith Corp., Milwaukee.

The authors are to be commended by bringing forth valuable information concerning the low carbon types of stainless steel which have been used commercially for the past few years. Their basic research in the field of austenitic chromium-nickel alloys has added greatly to the knowledge and limitations of these alloys. We hope that they can continue to further investigate the low carbon alloys. Most commercial heats of steel are usually confined to rather narrow ranges of alloying elements, thereby limiting our information about the specific effects of these elements. Our use of these low carbon stainless steels has been chiefly confined to Type 316 and we have used some of the first commercial heats rolled to sheet and plate. In our experience with this type of stainless steel we have found that mill processing of the steel is a very important factor influencing the corrosion behavior of the steel. For example, many of our low carbon Type 316 heats of steel were completely austenitic which, according to Fig. 24, should have a structure of austenite and ferrite. We know that a casting of low carbon Type 316 with 0.028% carbon, 18.4% chromium, 11.1% nickel and 2.55% molybdenum has about 20% ferrite. A wrought material with 0.02% carbon, 17.7% chromium, 10.7% nickel and 2.6% molybdenum was found to be completely austenitic. From this we can conclude that the degree of mechanical working influences the structure of the material. The resultant austenitic structure produced by the mechanical working must be in equilibrium since it is not decomposed to austenite and ferrite after subsequent annealing heat treatments. This brings up a question in our minds as to whether the microstructure of

Table XI
Nitric Acid Corrosion Resistance, Inches Per Year

Material	Period 1	2	3	4	5	Avg.	Heat Treatment
Slab	0.009	0.014	0.031	0.042	0.061	0.031	1100°F—2 hours, furnace-cooled.
¼-in. Sheet	0.011	0.009	0.011	0.010	0.012	0.011	
Slab	0.010	0.017	0.030	0.053	0.122	0.046	Stabilized at 1625°F for 2 hours—heat, and cooled on ASTM-A70 ¾-inch steel plate.
¼-in. Sheet	0.011	0.008	0.010	0.009	0.011	0.012	

the 0.25-inch thick plate used for nitric acid tests and the 0.040-inch thick strip used for Strauss tests were of similar microstructure and exhibited the same corrosion behavior.

On a few occasions we have had the opportunity of running a nitric acid test on slab material and the finished rolled sheets of the same heat.

Our tests always show an improvement in the corrosion resistance in nitric acid of the final product over the slab material. An example of this is illustrated in Table XI.

The analysis of the above heat was as follows: 0.026% carbon, 1.74% manganese, 0.43% silicon, 17.53% chromium, 11.99% nickel and 2.63% molybdenum. Other heats similarly tested sometimes showed much greater improvement in corrosion resistance in nitric acid than the above heat.

In our experience in testing many heats of low carbon Type 316 stainless steels we have not found any heats which would show satisfactory corrosion resistance in nitric acid after sensitizing for 2 hours at 650 °C (1200 °F), furnace cool. We base our satisfactory corrosion resistance to nitric acid as an average of 0.035 inch per year or less with no single period over 0.050 inch per year. In the nitric acid tests, it is interesting to note that heats having 0.03% carbon maximum, 17 to 19% chromium, 11 to 14% nickel and 2.0 to 3.0% molybdenum exhibited no preferential attack in the heat-affected zones produced by welding in the as-welded condition in materials of thickness $\frac{5}{64}$ to $\frac{1}{4}$ inch. A number of Strauss tests were made in the as-welded condition on many heats of this composition and all were found to be satisfactory after 2 hours at 650 °C (1200 °F), furnace cool. The resistance to intergranular attack was judged by the bend test made on sheet stock about $\frac{7}{64}$ inch thick. Our Strauss tests were made in boiling Aborn's solution[3] which we consider to be a severe test. Some of these test specimens were exposed to the boiling Aborn's solution for as long as 216 hours without producing any intergranular attack. These tests were substantiated by tests made at one of the mills which cooperated with us on low carbon Type 316 material. It was also their experience that when the carbon content was 0.03% or less, none of the material was sensitized after 650 °C (1200 °F) for 2 hours. Their tests were run for 72-hour periods in boiling Aborn's solution and none of the tests showed intergranular attack after this treatment.

We have made a few tests on these materials sensitized for various lengths of time at 480 and 550 °C (900 and 1020 °F). One heat having 0.028% carbon, 1.62% manganese, 0.42% silicon, 17.95% chromium, 13.49% nickel and 2.80% molybdenum showed no intergranular attack after 1000 hours at 480 °C (900 °F). The sample was boiled for 300 hours in Aborn's solution and showed no intergranular attack in the bend test. However, the same heat after being sensitized for 500 hours at 550 °C (1020 °F) proved to be free of intergranular attack after 300 hours in boiling Aborn's solution, but after 1000 hours' sensitizing time, the specimen showed intergranular attack. Another heat containing 0.040% carbon, 1.28% manganese, 0.51% silicon, 17.30% chromium, 12.98% nickel and 2.30% molybdenum was tested similarly and resulted in no intergranular attack being exhibited after 1000 hours at 480 °C (900 °F). However, this heat showed a slight attack after being sensitized for 300 hours at 550 °C

[3]Composition of Aborn's solution: 13 grams $CuSO_4 \cdot 5H_2O$ and 47 ml conc. H_2SO_4 (Sp. Gr. 1.84) per liter of water.

(1020 °F) and exhibited very severe cracking after 1000 hours at 550 °C (1020 °F. This shows that 100 hours is not long enough to precipitate nearly all the carbon present in the steel and much longer times are needed to adequately test this material at these lower sensitizing temperatures.

We have also observed the development of sigma phase after long-time treatments at 870 °C (1600 °F). However, none of our commercial heats have shown noticeable embrittlement because of sigma formation in a 2-hour treatment at 885 °C (1625 °F). This was shown by bending the specimen 180 degrees without cracking. We have had one experi-

Table XII
Nitric Acid Corrosion Data

Heat No. 1

C	Mn	Si	Cr	Ni	Mo
0.048	1.28	0.51	17.30	12.98	2.30

Stabilized at 1625 °F—2 Hours at Heat

Cooling Rate from Stabilizing Temp.	Period 1	Period 2	Period 3	Period 4	Period 5	Average
To 1000 °F in 10 minutes	0.011	0.016	0.024	0.035	0.055	0.028
To 1000 °F in 60 minutes	0.014	0.046	0.086	0.196	0.185	0.105
To 1000 °F at 100 °F per hour	0.032	0.252	0.318	.....	.....	.....

Rates in I.P.Y.

Heat No. 2

C	Mn	Si	Cr	Ni	Mo
0.028	1.62	0.42	17.95	13.49	2.80

Stabilized at 1625 °F—2 Hours at Heat

Cooling Rate from Stabilizing Temp.	Period 1	Period 2	Period 3	Period 4	Period 5	Average
To 1000 °F in 10 minutes	0.007	0.007	0.011	0.013	0.018	0.011
To 1000 °F in 60 minutes	0.009	0.008	0.012	0.017	0.027	0.015
To 1000 °F at 100 °F per hour	0.010	0.013	0.025	0.038	0.073	0.032

Rates in I.P.Y.

Heat No. 3

C	Mn	Si	Cr	Ni	Mo
0.021	0.71	0.33	18.35	12.67	2.85

Stabilized at 1625 °F—2 Hours at Heat

Cooling Rate from Stabilizing Temp.	Period 1	Period 2	Period 3	Period 4	Period 5	Average
To 1000 °F in 10 minutes	0.006	0.006	0.006	0.006	0.008	0.006
To 1000 °F in 60 minutes	0.009	0.005	0.007	0.007	0.009	0.007
To 1000 °F at 100 °F per hour	0.005	0.007	0.005	0.007	0.009	0.007

Rates in I.P.Y.

mental heat of 10% maximum nickel Type 317 which contained a large amount of ferrite in the structure. This heat, analyzing 0.06% carbon, 18.55% chromuim, 9.57% nickel and 3.58% molybdenum, showed severe loss in ductility after being heat treated for 2 hours at 870 °C (1600 °F). This loss in the ductility was accompanied by a loss of magnetic properties, showing that the conversion of ferrite to sigma was nearly complete

in the 2-hour treatment. A bend test made on the material in this condition failed after bending to about 90 degrees over a ⅛-inch diameter pin.

We are interested in learning from the authors more about the reasons for the differences in corrosion attack caused by the nitric acid test and the Strauss test. It was noted that in the 650 °C (1200 °F) treatment for 2 hours all production heats we have tested performed poorly in nitric acid, showing a very distinct intergranular and general attack. The same heat treatment in the Strauss test showed no intergranular attack. It is evident from the Strauss test results that it is not caused by carbide precipitation. The high corrosion rate exhibited after this heat treatment in the nitric acid test is probably caused by some other phase at the grain boundary.

It is conceivable that an initial stage of sigma formation may be taking place at the grain boundary. The formation of a low temperature sigma phase on the grain boundary could cause a chromium depletion similar but not as severe as the carbide precipitation. In view of this we might assume that the chromium depletion caused by sigma formation at low temperature and short times is not sufficiently severe to cause intergranular attack from the Strauss solution, but will exhibit severe attack in nitric acid.

Because of the difference between the nitric acid test and the Strauss test to detect intergranular attack during the early stages of sensitization, we are of the opinion that the authors should investigate the time-temperature-precipitation curve for a few of their alloys using the boiling nitric acid test as the criterion. We have noted in our work that as the temperatures approach 870 °C (1600 °F) for stabilization or stress annealing purposes, the cooling rate from this temperature through the range to 540 °C (1000 °F) can very materially affect the corrosion rate in boiling nitric acid. As an indication of this effect, Table XII shows the importance of carbon on the cooling rate from 885 °C (1625 °F) of three heats of low carbon Type 316.

Written Discussion: By N. E. Carruthers, supervising metallurgist, and G. E. Linnert, senior research engineer, Research Division, Armco Steel Corp., Middletown, Ohio, and Baltimore, Md.

The authors' interesting work on very low carbon austenitic chromium-nickel steels is an outstanding contribution to the published literature. In their attack on the carbon problem, they are dealing with what is probably the most serious shortcoming of austenitic chromium-nickel steels. The desirability of avoiding intergranular carbide precipitation by producing steels of very low carbon content rather than by the addition of a stabilizing element has been recognized for a long time. Although the production of very low carbon steels (0.015 to 0.020% carbon) possessing complete immunity to intergranular carbide precipitation does not appear to be commercially practicable at present, recent developments in melting technique now make possible the manufacture of steels containing about 0.03% maximum carbon which display a degree of immunity adequate for the many applications wherein the steels are subjected to high temperatures for relatively short times during fabrication, as, for

example, during welding. The need for this kind of material may become acute if the current heavy drain on our columbium supply is suddenly increased by the demands of an emergency.

Our experience with many commercial heats of very low carbon steels confirms the observation that 0.03% maximum carbon content imparts adequate immunity to harmful intergranular carbide precipitation which may occur in certain fabricating operations. This enhanced resistance also

Table XIII

Results of Nitric-Hydrofluoric Acid Etch Test on Metal-Arc Welded Specimens in As-Welded Condition

Spec. No.	Material	Chemical Composition C	Cr	Ni	Mo	N	Base Metal Immunity Factor[1]	Appearance of Etched Specimen
Type 304 Base Metal—Type 308 Welding Electrodes								
1	½-Inch Plate	0.064	18.22	8.97		0.046	−54	Intergranular Attack
	Electrode Deposit	0.070	20.32	9.74				
2	⅛-Inch Sheet	0.064	18.22	8.97		0.046	−54	Severe Intergranular Attack
	Electrode Deposit	0.070	20.32	9.74				
Type 304 ELC Base Metal—Type 308 ELC Welding Electrodes								
3	½-Inch Plate	0.029	18.47	9.17		0.014	+ 4	No Intergranular Attack
	Electrode Deposit	0.031	19.07	9.62				
4	⅛-Inch Sheet	0.029	18.47	9.17		0.014	+ 4	No Intergranular Attack
	Electrode Deposit	0.031	19.07	9.62				
Type 316 Base Metal—Type 316 Welding Electrodes								
5	½-Inch Plate	0.066	17.60	12.50	2.20	0.035	−31	Intergranular Attack
	Electrode Deposit	0.072	18.83	12.90	2.35			
6	⅛-Inch Sheet	0.066	17.60	12.50	2.20	0.035	−31	Severe Intergranular Attack
	Electrode Deposit	0.072	18.83	12.90	2.35			
Type 316 ELC Base Metal—Type 316 ELC Welding Electrodes								
7	½-Inch Plate	0.031	18.34	13.26	2.51	0.012	+32	No Intergranular Attack
	Electrode Deposit	0.030	17.78	13.45	2.58			
8	⅛-Inch Sheet	0.029	17.41	12.45	2.30	0.019	+28	No Intergranular Attack
	Electrode Deposit	0.030	17.78	13.45	2.58			

[1]Immunity factor is secured by solving Equation II or Equation IV as proposed by Binder, Brown and Franks.

Equation II: $$\frac{6.17}{(\%\ \text{Carbon})^{0.82}} + 13.8\ (\%\ \text{Chromium}) - 10\ (\%\ \text{Nickel}) - 276 = \text{Immunity Factor}$$

Equation IV: $$\frac{6.17}{(\%\ \text{Carbon})^{0.82}} + 13.8\left[(\%\ \text{Chromium}) + 2.25\ (\%\ \text{Molybdenum})\right] - 10\ (\%\ \text{Nickel}) - 276 = \text{Immunity Factor}$$

permits welding many types of equipment in the field, without hazard of subsequent failure through intergranular corrosion.

Work conducted in our laboratories has included an investigation of the corrosion resistance of 0.03% maximum carbon material after welding. The complete results of this investigation are to be published at a future date. However, it appears timely to offer some results of welding tests conducted with regular Type 304 (18-8) and Type 316 (18-12 Mo) grades, and their extra low carbon counterparts, for comparison with the weld test data presented by the authors.

Butt-type joints were made in both ½-inch thick plate and ⅛-inch thick sheet by the metal-arc welding process employing flux-coated electrodes of compositions similar to the base metals. The ½-inch thick plate received a single-bevel preparation and was joined using five passes from $\frac{5}{32}$ and $\frac{1}{8}$-inch size electrodes. The ⅛-inch thick sheet contained square-

butt joints welded with a bead from a $\frac{5}{32}$-inch electrode deposited on each side. Each specimen contained two weld seams at right angles to each other because this condition frequently arises in practice and because it permits a study of the heat effect of the second weld seam on the first weld seam. Among the specimens removed from each welded plate was a 2-inch square specimen from the center where the weld seams intersected. This piece was tested for susceptibility to intergranular corrosion by exposing it to 10% nitric–3% hydrofluoric acid solution at 80 °C (175 °F) for three 4-hour periods. Test results on eight specimens are summarized in Table XIII, and photographs of the specimens are shown in Figs. 31 to 38, respectively.

The results show that the regular Type 304 and Type 316 materials undergo marked intergranular attack in this severe corrosive medium, while the materials containing about 0.03% carbon show no evidence of sensitization. The immunity factors were computed for the base metals as proposed by the authors in their Equations II and IV and appear in Table XIII. It is of interest to note that the sensitized materials showed high negative factors while the materials which were immune had positive factors.

In conclusion it may be noted that while the electrodes used to weld the 0.03% maximum carbon steels listed in Table XIII were of the extra low carbon variety, equally good success has been obtained with regular electrodes of the columbium-containing grades, such as Types 347 and 316 Cb.

Written Discussion: By Samuel J. Rosenberg, metallurgist, Department of Commerce, National Bureau of Standards, Washington, D. C.

We can, in a small measure, offer some confirmation of one particular statement contained in this excellent paper. The authors indicate that increasing the nickel content of these low carbon steels renders them more susceptible to intergranular attack after sensitization. Two low carbon steels (0.025 and 0.026% carbon) were included in a study of intergranular embrittlement of austenitic stainless steels conducted at the National Bureau of Standards and it is pertinent to note that one of these steels, containing 8.8% nickel, was definitely less susceptible to intergranular attack than the other, which contained 12.6% nickel.

The authors' Equation I was used to determine the structures of these two low carbon steels, and the results of the calculations confirmed the metallographic examination in that the 8.8% nickel steel contained delta ferrite and the 12.6% nickel steel did not.

The statement that the presence of intergranular attack was taken as a criterion of carbide precipitation, mentioned in connection with the authors' Figs. 13, 14, 15, 16 and 21, is true in its literal sense; i.e., if intergranular attack develops after exposure to the boiling acidified copper sulphate solution, the steels must have contained precipitated carbides. The unwary reader, however, may interpret the authors' statement as also being true in the reverse sense; e.g., if intergranular attack does not develop, the steels do not contain precipitated carbides. This, of course, is not true.

The curves shown in Figs. 13, 14, 15, 16 and 21 should be useful in serving as a guide to the time the various steels may be exposed at the different sensitizing temperatures without becoming susceptible to intergranular attack. Some mention should have been made, however, of the healing effects of long periods of exposure. An extension of these tests to longer periods of time might close these curves into fields. Although the right-hand boundaries of such fields would be of no interest for the purpose for which the authors developed these figures (for application to welding), they would be of interest for use in high temperature applications.

It is rather surprising to note the difference in the effect of nickel on the behavior of the 2 and 3% molybdenum steels in boiling nitric acid, as is indicated in Fig. 22. Can the authors advance an explanation for this?

Is it possible that the micrographs in Fig. 18 have been mixed? The clear second phase shown in Fig. 25c appears quite similar to delta ferrite, although the authors indicate it to be sigma. We have had no experience with the etchant used by the authors and a few words on the use of this etchant in differentiating between delta ferrite and sigma, as well as its effect on precipitated carbides, would be appreciated.

Written Discussion: By C. Sykes, The Brown-Firth Research Laboratories, Sheffield, England.

The authors have produced a considerable body of data of great interest, and from the practical angle, the curves defining maximum permissible time-temperature treatments for avoidance of intercrystalline corrosion are of special interest. Using the 700-hour test in the sulphuric acid – copper sulphate solution, these curves indicate that some intercrystalline corrosion is to be expected at the 0.02% carbon level in 18-11 chromium-nickel steels, after 5 minutes' exposure at 750 °C (1380 °F) or 6 minutes at 650 °C (1200 °F) and that these times decrease to about ¾ and 1½ minutes at the 0.05% carbon level. Economic and satisfactory commercial production of the very low carbon materials is doubtful, but the figures deduced from this stringent 700-hour test suggest that it should be possible to weld the thinner gages of 0.05% carbon sheet material without introducing any significant intercrystalline corrosion tendency. If, in addition, allowance is made for the fact that successful service application is seldom likely to call for complete resistance to the 700-hour test, the more general 72-hour test normally proving adequate, the practical field becomes even less restricted. Application of this test to a large number of commercial casts of 18-10 chromium-nickel steel after treatment for 2 minutes at 650 °C (1200 °F) has, in the writer's experience, produced no failure at the 0.06% carbon level. Even with 30 minutes' treatment at 650 °C (1200 °F) about half the 0.06% carbon and two-thirds of the 0.05% carbon casts successfully passed the 72-hour test. Thus welding of the 0.06% carbon 18-10 material in the thinner gages of sheet, to, say, 16 gage, should be satisfactory for very many applications, and this has, in fact, been borne out by the behavior of such material in service.

For still greater resistance, recourse must be had to stabilization, and small additions of columbium or titanium have been successfully used. It is unfortunate that the authors have not found it possible to include some data for titanium-bearing materials in the present survey, because, although additions of this element can give rise to a lowered resistance to hot, strong nitric acid solutions, as used in the Huey type of test,[4] this is not reflected in the response to most conditions of service. Indeed, useful improvement can result from the titanium addition, as in the case of dilute sulphuric acid solutions, where it has been shown that the titanium-bearing steel possesses better resistance than the unstabilized material. At the same time titanium possesses a definite superiority over columbium from the point of view of hot working.

In their consideration of the molybdenum-bearing materials, the use of a 700-hour test in the sulphuric acid – copper sulphate solution, following treatment for 24 hours at 650 °C (1200 °F), again tends to induce a pessimistic outlook. Working with 18% chromium – 8% nickel – 2.5% molybdenum steels, a very large tonnage of material with carbon up to 0.07% and without either titanium or columbium stabilization has been consistently fabricated in the weld plant, and used under drastic service conditions with complete satisfaction. Such a composition is, of course, duplex, but it is considered that too great an emphasis has been laid on the desirability of a purely austenitic structure and the avoidance of sigma phase. Fabrication does not normally necessitate extended exposure to temperatures in the region of 870 °C (1600 °F) and in practice the writer has met with no mechanical difficulties arising from sigma with this type of steel. In a very few special instances, some evidence of lower corrosion resistance adjacent to welds has been found, not associated with intercrystalline corrosion, but probably related to phase changes. Its occurrence, however, has been limited to slow development under such severe conditions that the normal material, remote from the welds, was itself attacked, though to a lesser degree. For such conditions, consideration should be given to modified or alternative materials, but it is neither necessary nor desirable that a wholesale changeover should be made to the higher nickel fully austenitic type, particularly since this might lead to very real problems at the hot working stages of production.

In regard to the more detailed results, the beneficial effect of nickel in relation to the 65% nitric acid test (Figs. 2, 4 and 6) would appear to be much more consistently evident than for the sulphuric acid – copper sulphate test (Figs. 1, 3 and 5). The statement (page 1311) to the effect that in boiling nitric acid no benefit occurs from rising chromium content is not strictly in accordance with these curves. For example, they indicate that 0.02 to 0.025% carbon, 12 to 13% nickel material would show an improvement of about 2 to 1 as chromium rises from 18 to 20%, and of about 10 to 1 as it further increases from 20 to 25%. While this over-all increase in resistance may be much less than the corresponding increase toward the sulphuric acid – copper sulphate test, it should not be entirely

[4]R. S. Stewart, "Resistance of Sensitized Stainless Steels to Boiling Nitric Acid," METAL PROGRESS, Vol. 52, 1947, p. 971-973.

neglected, since it might provide a pointer of importance where conditions of service involve resistance to critical concentrations of nitric acid.

Finally, in relation to the columbium additions, the writer would suggest that while the data indicate 0.1% columbium as the approximate equilibrium amount remaining in solution with the residual carbon and nitrogen concentrations for the steels and additions studied, this should not be taken as a fixed solubility limit for the very low carbon steels. Greater additions would presumably result in further precipitation of carbide and nitride and solution of columbium to new equilibrium values. The important point, however, remains, that with these small additions to low carbon steels, solubility effects become increasingly important in determining the necessary columbium-carbon ratios for stability.

Written Discussion: By Hallock C. Campbell, associate director, research and engineering, Arcos Corp., Philadelphia.

The authors' interpretation of the effect of nitrogen (Figs. 7 and 8) is open to constructive criticism. The unexpected maxima in their nitrogen curves are more probably an evidence of experimental error than a true effect of the nitrogen.

The data for Figs. 1 through 10 are not given (presumably because of space limitations), but the heats involved seem to be certain of the heats appearing in Table I. The carbon content in Figs. 7 and 8 ranges from 0.020 to 0.030%, which is too wide a range to be considered a unit. According to the authors' curves in Fig. 1, a change in carbon of only 0.005% will change the penetration of an 11 to 12% nickel sample by 40 mils per 100 hours, which would be sufficient to account for all of the maxima in Fig. 7. Similarly it is evident from Fig. 2 that a small variation in carbon would also account for all of the maxima in Fig. 8.

When the carbon contents of the points in Figs. 7 and 8 are critically examined with this in mind, no rational pattern can be discerned. The highest points are not high in carbon, which is an item in favor of the authors' theory, but these points are significantly lower in chromium. Several points with nearly identical carbon, chromium and nitrogen contents can be found, which differ noticeably in penetration. Other sets of points can be found which should differ in penetration (because of carbon variations at given chromium, nickel and nitrogen levels) but which do not. The conclusion seems to be inescapable that the authors' data are not sufficiently self-consistent to warrant drawing the elaborate curves of Figs. 7 and 8.

The authors are urged to submit their present data to a statistical analysis, correcting all points to a common carbon level (by interpolation in Figs. 1 and 2, for example, as a first approximation) and to a common chromium level. The writer believes they will find the effect of nitrogen to be very slight, with no valid evidence for the present maxima.

Written Discussion: By F. J. Phillips and R. Smith, Wood Works, Carnegie-Illinois Steel Corp., McKeesport, Pa.

Messrs. Binder, Brown and Franks are to be complimented for their comprehensive study of the intergranular corrosion of the 0.03% maxi-

mum carbon stainless steels. They have wisely and logically distinguished between the requirements needed for complete immunity and those needed for partial immunity to intergranular corrosion. Moreover, they have properly emphasized those requirements needed for partial immunity by their use of "C" curves.

For the past several years, Carnegie-Illinois has been actively engaged in an investigation of the intergranular corrosion resistance of a considerable number of commercially melted and processed heats of 0.03% maximum carbon 18-8, 18-8 columbium, 18-8 molybdenum, and 18-8 molybdenum-columbium. In a very broad sense the results of our investigations agree with those presented in the preprint of the paper by Messrs. Binder, Brown and Franks. However, in certain instances, we had difficulty in interpreting these results; and in order to avoid any misconception which might arise regarding the corrosion resistance of the low carbon stainless steels, we wish to discuss these interpretations.

In general, it appears to us that an improved technique could have been used in drawing curves to fit the experimental points shown on the graphs. In Fig. 1, for example, the position of the curves would appear to require further explanation. The curve for the 10 to 11% nickel steels does not intersect the experimental points shown and ignores completely the two points off to the right which should have served to stabilize or tie-down the end of the curve. Similarly in Fig. 2 we are curious as to why only three heats were used to establish the curve for the same 10 to 11% nickel steels when, as indicated in Fig. 1 and Table I, a total of seven heats was available?

We believe a second example of questionable plotting technique is illustrated by Figs. 3 and 6 where the scatter of points is such that if the curves had been fitted to the experimental points of the ten laboratory heats plotted, it would have been observed that the interrelation between carbon and nickel content was indeterminate. When data secured by us on ten commercial 18-8 0.03% carbon maximum heats (9 to 12% nickel) were plotted in a manner similar to that used by the authors, the interrelation between carbon and nickel content was again not apparent. Consequently, without additional information, we hesitate to accept the statement at the bottom of page 1307 that "the critical carbon content for complete resistance to intergranular attack is decreased by larger amounts of nickel".

After careful study of the data presented in Table I, it was observed that 20 heats and their respective data have been duplicated. Thus, after deleting the 20 duplicates and those heats which do not meet the chemical composition limitations specified by the authors, 49 heats were available for developing Equation II which is intended to predict intergranular corrosion behavior based on chemical composition. Since, according to the authors, the predicted intergranular behavior of 32 of the heats fell within the range of uncertainty or failure, the behavior of only 17 heats was predicted satisfactorily. The equation, therefore, suffers from the reliability viewpoint when it is realized that the coefficient of determination

is 30.4. To remove the statistical nomenclature, this means that the variables of Equation II (carbon, chromium, nitrogen and nickel) explain only 30.4% of the behavior observed in the intergranular tests summarized in Table I of this paper. We believe this percentage figure is low for quantitative information.

The authors are to be commended for their application of the "C" curves to the intergranular corrosion behavior of the low carbon 18-8 steels. In 1933 this novel method of presentation was used by E. C. Rollason[5] in the development of stabilized stainless steels. We question, however, the license taken by the authors on pages 1322 and 1323 in their explanation of the curves as a guide for minimum times required to suppress carbide precipitation. The literature supports our own experience that the mere presence of intergranular carbides does not necessarily mean failure through intergranular corrosion, and any technique based on this assumption is not well founded. Therefore, all references to the "C" curves should be with respect to intergranular corrosion on which these curves are based and not to the presence or absence of carbides.

In regard to complete immunity, we have observed that all the low carbon (0.016 to 0.030% carbon, 0.03 to 0.15% nitrogen) 18-8 steels we have tested to date exhibited unsatisfactory corrosion resistance to boiling nitric acid after having been heat treated 24 hours at 1100 °F (595 °C). However, following a 2-hour heat treatment at 540, 595, 650, 675, 815 and 885 °C (1000, 1100, 1200, 1250, 1500 and 1625 °F), all these materials were satisfactory in the boiling nitric acid. Furthermore, weld tests on several of the low carbon 18-8 steels have in every case been satisfactory after the boiling nitric acid and 500-hour $CuSO_4 - H_2SO_4$ tests.

Regarding the 18-8 molybdenum steels, the authors are probably correct in concluding that partial immunity may be obtained with carbon under 0.03%, in view of the data presented, which indicated that molybdenum increased the time at temperature before damaging carbide formation occurred. However, we do not believe that these data should be interpreted to mean that molybdenum will stabilize 18-8 steels in the same sense as we think of columbium and titanium as stabilizing elements. In fact, the corrosion data on our commercial low carbon (0.016 to 0.030% carbon) 18-8 molybdenum steels have been cause for discouragement when testing in 65% boiling nitric acid after a heat treatment such as 2 hours at 675 °C (1250 °F). Boiling copper sulphate – sulphuric acid corrosion tests on similarly treated materials have been satisfactory; furthermore, based on limited data, it appears the material can be satisfactorily welded without fear of intergranular corrosion in the heat-affected zone.

It is not clear from the statements made on page 1331 and data contained in Table V whether the impact values were obtained by breaking the test piece at room temperature or at the indicated elevated temperatures. It seems unlikely that the test pieces were broken at 870 °C (1600 °F), although this inference is given.

With reference to Equation V, the authors again have attempted to

[5]E. C. Rollason, "Intergranular Corrosion of 18-8 Austenitic Stainless Steels," *Journal*, Iron and Steel Institute, Vol. 127, No. 1, 1933.

present a quantitative evaluation with somewhat meager information. Equation V allegedly allows computation of columbium content necessary for immunity to intergranular corrosion, and the variables included are carbon, nitrogen and columbium. Inasmuch as it is known that in the 18-8 titanium steels the formation of titanium carbide is influenced by such factors as heat treating temperatures, times and prior cold work, we question if these additional variables should not have been considered by the authors in their derivation of Equation V. It would appear to us that the aforementioned mathematical evaluation may be applicable only when the conditions used by the authors are employed.

We believe preliminary results in the evaluation of the low carbon stainless steels are now at a stage where, from the practical viewpoint, there exists adequate immunity to intergranular corrosion for a wide variety of applications that are denied if we accept the limitations imposed by arbitrary laboratory acceptance tests. The ultimate levels of usefulness of these compositions can best be established by comparative tests under actual service conditions, and it is in this direction that future work should be planned. We concur with the authors of this paper in their wisdom of showing that immunity to intergranular corrosion is a relative condition, and we again commend them for making this distinction.

Written Discussion: By T. D. Radcliffe, Eastern Materials Representative, Standard Oil Company of California, Evanston, Ill.

This paper deserves and stimulates extensive study, which I regret not having given it. I wish to ask the authors several questions endeavoring to do so from the refinery engineers' and operators' viewpoint.

1. Your low carbon alloys were made in induction furnaces, which in some cases, have given superior quality alloys as compared to other melting practices. Can equal quality, cleanliness, freedom from oxides and dirt be obtained in other commercial processes? I believe it can and has with proper methods and care. These questions will be raised by the steelmaker, as they have been repeatedly, as necessity forced users to request lower carbon alloys. The steelmaker has his process limitations.

2. The second question is one concerning temperature. In the summary on page 1344, "Complete immunity . . . is essential to the successful service . . . at elevated temperatures . . .", is stated. This statement is too broad and should be revised, as wrought Type 304 and even higher carbon coarse-grained cast alloy has operated for years in some refinery services at temperatures in the carbide precipitation range, and as high as 675 °C (1250 °F). Intergranular corrosion occurred chiefly when the equipment was cold and exposed to moisture and corrosive salts, or on rare occasions, in the cooler sections under similar vapor conditions. Admittedly there are vapor and liquid services for which Type 304 is entirely unsuitable, due to rapid attack at operating temperatures.

3. There is the question of the effect at temperature and resulting stabilization, carbide precipitation, spheroidization and variations in susceptibility. In services for which the alloys are suitable, what is the effect of years under operating conditions on the rate of attack and can this be indicated by short-time tests at the most critical temperatures,

preferably under comparable operating conditions? Some of these remarks are outside the limits of the paper, which I also believe is true of the statement quoted in the summary, if taken literally.

Authors' Reply

We acknowledge with pleasure the considerable amount of discussion that has been elicited by our paper, for it reveals the marked interest in the properties of 0.03% maximum carbon 18-8 steels. It is believed that such interest as displayed here is indicative of a rapid commercial development for these steels.

Mr. Sheridan's comments with regard to the high-nitrogen steels bear out our conclusions in regard to the substitution of nitrogen for nickel, as indicated by Fig. 12 in the paper. We are in agreement that for long heating periods the high-nitrogen steels are subject to increased attack in boiling nitric acid. We made no attempt here to develop the carbon solubility curve versus temperature, but it is our opinion that the slope of the curve is very steep up to about 700 to 750 °C.

Messrs. Ebling and Scheil discuss the influence of mill processing on the structure and nitric acid corrosion resistance of 0.03% carbon Type 316 stainless steels, and we agree that this is an important factor to consider when adjusting the composition to produce a fully austenitic structure. However, assuming that we are discussing relatively thin plate, we are quite amazed that a steel containing 17.7% chromium, 10.7% nickel, 2.6% molybdenum, and as little as 0.02% carbon, could be rendered fully austenitic by hot working and annealing. It is believed that some other factor besides mill processing is responsible for the austenitic condition, and the opinion is that the steel is probably high in nitrogen. In our tests, no significant differences in microstructure were noted between 0.25-inch thick plate samples used for nitric acid tests and the 0.04-inch thick strip samples used for the acidified copper sulphate tests. Their experiences in testing 0.03% carbon Type 316 stainless steels in boiling nitric acid and in boiling acidified copper sulphate solution agree closely with ours. Samples of low carbon Type 316 steel heated 1 hour at 650 °C (1200 °F) show corrosion rates in excess of 0.002-inch penetration per month in the fifth period, becoming greater as the molybdenum content is raised from 2 to 3%, whereas in boiling acidified copper sulphate solution similarly heated, samples remain unaffected for at least 700 hours' boiling. As shown in Fig. 22, the nickel content of the steel must be sufficient to produce a fully austenitic structure if optimum resistance to nitric acid is required after heating in the carbide precipitation temperature range. Our tests show that the length of time required to produce damaging carbide precipitation, as measured by the acidified copper sulphate test, is a function of composition as well as of temperature. Since molybdenum delays the time for damaging carbide precipitation to occur in acidified copper sulphate solution, we agree that for steels containing molybdenum the heating time should exceed 100 hours in the lower temperature ranges in evaluating the resistance of these steels for

Table XIV

Results of Corrosion Tests in Boiling 65% Nitric Acid on Austenitic 18% Chromium-Nickel Steels Containing 0 to 3% Molybdenum, Less Than 0.01% Carbon and Less Than 0.015% Nitrogen

	Composition, %		
Chromium	19.58	18.68	18.64
Nickel	14.63	18.08	19.15
Manganese	0.28	0.45	1.32
Silicon	0.20	0.39	0.40
Carbon	0.003	0.004	0.006
Nitrogen	0.010	0.008	0.014
Molybdenum	.....	1.88	2.94
Condition	Corrosion Rate, In. Pen. Per Mo. Average Five Periods		
Annealed[1]	0.00047	0.00040	0.00046
Annealed +10 minutes at 650°C	0.00071	0.00067	0.00074
Annealed + 1 hour at 650°C	0.00046	0.00039	0.0293[3]
Annealed + 8 hours at 650°C	0.00068	0.0209	0.0810[3]
Annealed +10 minutes at 750°C	0.00041	0.00054	0.00915
Annealed + 1 hour at 750°C	0.00044	0.00052	0.0373[3]
Annealed + 8 hours at 750°C	0.00048	0.00039	0.00061
Annealed +24 hours at 750°C	0.00040	0.00038	0.00078

[1]Heated 15 minutes at 1150°C and water-quenched.
[2]Average of four periods.
[3]First period.

long-time service at elevated temperature, but as indicated in the paper, steels for such service must contain less than about 0.02% carbon or have columbium present in the proper amount to combine with carbon and nitrogen, and this is demonstrated by Messrs. Ebling and Scheil's experience with molybdenum-bearing steels containing 0.028 to 0.04% carbon. That the high corrosion rate of the molybdenum-bearing steels in nitric acid is due in part to the formation of an intermetallic compound, possibly sigma phase at the grain boundaries, is an interesting viewpoint to us, as it is in line with what we believe might be taking place. So far, however, our attempts to identify the phase changes or composition changes near and at the grain boundaries have failed to provide the information needed to prove that this viewpoint is correct. In this connection, it should be pointed out that when the sigma phase is readily identified in the microstructure, the time period producing maximum corrosion damage in nitric acid has been exceeded. The data shown in Table XIV indicate that some other mechanism than carbide precipitation is required to explain the loss of corrosion resistance of the molybdenum-bearing steels in boiling nitric acid. The importance of lowering carbon in steels to be stress-relieved after fabrication is quite forcibly shown by the data in Table XII, and it is seen that if slow cooling is carried out after stress-relieving, the carbon content should not exceed about 0.03% for good corrosion resistance in nitric acid.

The discussion presented by Messrs. Carruthers and Linnert is an important addition to our knowledge of the 0.03% maximum carbon steels, and we are looking forward to the publication of the complete results of their investigation. The data they give here substantiate the viewpoint that these steels are resistant to intergranular corrosion in the welded condition if their compositions are properly controlled. Further

information of this kind will help to show the degree to which the criterion for partial resistance to intergranular corrosion, proposed in the paper, actually does apply to fabrication practices.

As Mr. Rosenberg points out, the statements in connection with Figs. 13 to 16, and Fig. 21, should not be interpreted as meaning that there is no carbide precipitation if the steel does not exhibit intergranular attack in the test media. No emphasis was placed on the healing effect of long periods of heating, beyond the mere mention of this possibility on page 1307, since it was not studied in detail. We can cite one instance of the healing effect in connection with Fig. 16. Here additional samples heated 1 hour at 750 and 800 °C (1380 and 1470 °F) were not attacked in the copper sulphate solution. These results indicate that it would take a relatively long time to produce healing at lower temperatures. However, it is agreed that information of this kind would be useful for high temperature applications. Fig. 21 indicates that there is no damaging carbide precipitation in the 0.03% carbon-molybdenum steels after heating 1 hour at 650 °C (1200 °F). The high corrosion rate of the 3% molybdenum steel in nitric acid is, therefore, believed to be due to some other cause, as discussed in connection with the question raised by Messrs. Ebling and Scheil. As shown previously, the 3% molybdenum steels are more easily damaged than the 2% molybdenum steels by heating in the temperature range of 650 to 750 °C (1200 to 1380 °F). Because it is known that sigma phase develops far more rapidly in the 3% molybdenum steels than in the 2% molybdenum steels, it is conceivable that the formation of this phase is responsible for the damage. The micrographs in Fig. 18 are correctly presented. The etchant used to develop the structure shown in Fig. 25 was made up as follows:

15 cc HCl saturated with $CuCl_2$; 5 cc HNO_3; 20 cc glycerine

This etchant is applied by swabbing. In the chromium-nickel-molybdenum steels sigma phase is outlined, and there is some slight attack on the delta ferrite. It should be pointed out that in the plain chromium-nickel steels the etchant attacks both sigma and the delta ferrite. When the interpretation of the structure is doubtful, magnetic balance tests readily show whether the outlined phase is sigma or delta ferrite.

We were glad to receive Dr. Sykes' comments, since they reflect the viewpoint taken in Great Britain in connection with the intergranular corrosion problem. It is evident from his discussion that in Great Britain the trend is toward higher carbon and lower nickel steels than in this country. We admit that the laboratory test conditions employed in our investigation are stringent, but they were so designed to reveal any shortcomings that the steels might display in critical long-time service. We did not wish to imply that no benefits occur from raising chromium with respect to nitric acid resistance. Truly, the higher chromium steels show lower corrosion rates than lower chromium steels under similar test conditions, and for many practical purposes this point should be kept in mind, as pointed out by Dr. Sykes. It cannot be disregarded that the higher chromium steels are still susceptible to intergranular attack.

With respect to Mr. Campbell's discussion concerning the influence

Table XV
Results of Corrosion Tests in Boiling 65% Nitric Acid on Very Low Carbon Chromium-Nickel Steels

Heat No.	Composition, %						Corrosion Rate, In. Pen. Per Mo.—Avg. 5 Periods—Condition	
	Cr	Ni	Mn	Si	C	N	1	2
	Influence of Increasing Carbon in 9 to 12% Nickel Steels Containing Less Than 0.032% Nitrogen							
K652	17.83	9.21	1.2*	0.4*	0.022	0.016	0.00089	0.00118
K17	17.99	9.71	0.98	0.30	0.025	0.015	0.00068	0.00070
L376	18.92	9.70	1.26	0.39	0.027	0.032	0.0259[4]	0.00250
K382	18.36	9.97	1.36	0.50	0.042	0.027	0.086	0.0121
K383	18.61	9.90	1.26	0.40	0.045	0.026	0.062	0.0142
K197	18.57	10.31	1.14	0.33	0.020	0.031	0.00088	0.00065
K198	18.37	10.88	1.09	0.32	0.024	0.029	0.00112	0.00122
K199	18.40	11.50	1.09	0.32	0.018	0.030	0.00162	0.00084
K395	18.51	11.82	1.32	0.51	0.023	0.026	0.0240	0.00189
L382	18.05	11.24	1.23	0.44	0.031	0.031	0.023[3]	0.0220
K776	18.19	11.10	0.75	0.42	0.056	0.015	0.0148	0.0459
K765	19.30	12.14	0.82	0.46	0.005	0.024	0.0047	0.00046
K394	17.92	12.64	1.27	0.50	0.022	0.027	0.0467	0.00254
	Influence of Increasing Nickel in 18% Chromium, 0.022 to 0.026% Carbon Steels Containing Less Than 0.029% Nitrogen							
K17	17.99	9.71	0.98	0.30	0.025	0.015	0.00068	0.00070
K198	18.37	10.88	1.09	0.32	0.024	0.029	0.00112	0.00122
K395	18.51	11.82	1.32	0.51	0.023	0.026	0.0240	0.00189
K394	17.92	12.64	1.27	0.50	0.022	0.027	0.0467	0.00254
L2	18.02	14.97	1.43	0.47	0.026	0.027	0.0208	0.0333
	Influence of Increasing Nickel in 18% Chromium, 0.032 to 0.034% Carbon Steels Containing 0.11 to 0.15% Nitrogen							
L725	18.3*	6.5*	1.2*	0.4*	0.033	0.132	0.00330	0.00370
L724	18.3*	6.5*	1.2*	0.4*	0.033	0.146	0.0101	0.00290
L727	18.3*	8.0*	1.2*	0.4*	0.032	0.144	0.00570	0.00300
L377	18.54	9.25	1.18	0.46	0.034	0.105	0.0197[4]	0.0114
K123	18.35	10.47	1.20	0.40	0.033	0.153	0.0500	0.0166
	Influence of Increasing Nickel in 20% Chromium, 0.026 to 0.028% Carbon Steels Containing 0.030 to 0.035% Nitrogen							
L3	20.29	12.80	1.42	0.51	0.026	0.030	0.0279[3]	0.00670
L15	20.36	15.24	1.39	0.47	0.028	0.035	0.0260[3]	0.0296[3]
L16	20.61	18.32	1.35	0.52	0.027	0.034	0.0557[3]	0.0440[3]

[1] = Heated 10 minutes at 1075°C and air-cooled + 100 hours at 550°C and air-cooled.
[2] = Heated 10 minutes at 1075°C and air-cooled + 24 hours at 650°C and air-cooled.
[3] = Average of 3 periods.
[4] = Average of 4 periods.
* = Approximate analysis.

of nitrogen, the main point here is that nitrogen is not so influential as carbon in rendering the steel susceptible to intergranular attack in acidified copper sulphate solution. It is quite evident though that increasing nitrogen at the 0.02 to 0.03% carbon level produces high rates of attack in nitric acid after heating 100 hours at 550 °C (1020 °F). On the other hand, nitrogen has practically no effect on the corrosion resistance of the steel in these test media after heating 1 hour at 650 °C (1200 °F).

We are well aware that quantitative inconsistencies exist within the experimental data upon which Messrs. Phillips and Smith base their criticism. Considering the many factors involved in a large investigation, as well as some of the vagaries of quantitative corrosion testing, it is not unexpected that they would exist. However, the fact still remains, if one studies carefully the trends, that there is considerable evidence to show qualitatively at least that as the nickel content is increased the

corrosion rate rises after heating at 550 °C (1020 °F). The many incidents in which this trend has been noted lead us to interpolate our data to the extent shown in the paper. Naturally, our interpretation is open to outside criticism as it has been in the case of Messrs. Phillips and Smith. To help reveal the basis for our point of view, we submit Table XV which shows several series of steels that vary in carbon or nickel, but in which chromium and nitrogen are held as constant as the information available permits. Regarding their comments on the validity of Equation II, a check of the data in Table I shows that there are 49 heats containing less than 0.05% nitrogen available for developing the equation. Of these, 14 were within the ±8 uncertainty region, and 2 falling outside the uncertainty range were incorrectly predicted. This leaves 33 out of a total of 35 falling outside the ±8 region predicted correctly, which is 94% of the total. In the case of steels containing more than 0.05% nitrogen, there are available 30 steels for establishing the limiting equation. Seven of these fall within the ±8 region, and 8 falling outside this region were incorrectly predicted. This means that out of 23 steels, 15 were predicted correctly, which is 65% of the total. These calculations indicate that the resistance of a steel to intergranular corrosion, after heating 1 hour at 650 °C (1200 °F) and air cooling, can be predicted with reasonable success by the use of Equation II. They further substantiate our viewpoint that the equation represents the limiting composition, and for optimum resistance the composition should fall below the surface represented by Equation II. We agree that the presence of intergranular carbides does not necessarily mean that intergranular attack will occur and do not wish to imply that this is the case. However, when intergranular corrosion developed in acidified copper sulphate solution, we assumed that the attack was caused by the formation of intergranular carbides. Our experience with 18-8 type steels falling within the range of 0.016 to 0.03% carbon and 0.03 to 0.15% nitrogen indicates that in some cases heating for 2 hours at 600 and 650 °C (1110 and 1200 °F) would cause the development of intergranular corrosion. We agree that the data should not be interpreted to mean that molybdenum stabilizes the 18-8 steel to the same extent as titanium or columbium, and the point of view taken in writing conclusion 4 is that molybdenum imparts immunity for only short periods of heating. The impact tests were conducted at room temperature. The comments regarding Equation V are well taken, and these points must be considered when utilizing the information. The opinion is that since columbium carbide is very insoluble in austenite, the factors of heat treating temperature within the normal commercial ranges, time, and prior cold work, are not so important as in the case of more soluble carbides.

The comments made by Mr. Radcliffe are of interest and there is every indication that the 0.03% carbon 18-8 steels can be furnished equal in quality to the higher carbon grades. We do not wish to imply that for all service at elevated temperature complete immunity to intergranular attack is essential. In each case the degree of resistance required will be dictated by the actual corrosive conditions involved.

DELTA FERRITE FORMATION AND ITS INFLUENCE ON THE FORMATION OF SIGMA IN A WROUGHT HEAT RESISTING STEEL

By John J. Gilman, Pun Kien Koh and Otto Zmeskal

Abstract

The formation of high temperature ferrite in a wrought heat resisting steel was studied metallographically. The structural stability at 1200 to 1600 °F (650 to 870 °C) was studied for the case of an initial structure high in ferrite (22 to 23%) and for the case of an initial structure low in ferrite (2 to 3%). It was found that the presence of ferrite markedly accelerated the formation of sigma. However, it was also found that cold work had an even more pronounced effect.

Sigma was identified by X-ray diffraction and the pattern compared with those of other investigators.

Introduction

ALL high strength, high temperature steels used at the present time have austenitic matrices. This structure facilitates fabrication and enhances the service life. Depending on the balance of ferrite-forming elements and austenite-forming elements, and the heat treatment, variable amounts of ferrite may be present. Also, intermetallic compounds of varying sizes, compositions, and distributions are generally present.

Since these alloys are planned for applications requiring strength over a relatively long time at temperatures in the range of 1200 to 1600 °F (650 to 870 °C), the structural changes occurring at these temperatures are of great importance. The change that can most influence the properties of these steels is that resulting in the formation of the sigma phase. The chromium contents of wrought heat

A paper presented before the Thirtieth Annual Convention of the Society, held in Philadelphia, October 23 to 29, 1948. Of the authors, John J. Gilman was formerly instructor in metallurgical engineering, Illinois Institute of Technology, now Campbell Fellow at Columbia University, New York; Pun Kien Koh was formerly research metallurgist, Standard Oil Company of Indiana, now research metallurgist, Allegheny Ludlum Steel Corporation, Brackenridge, Pa., and Otto Zmeskal is director, Department of Metallurgical Engineering, Illinois Institute of Technology, Chicago. Manuscript received April 14, 1948.

resisting alloy steels are high enough to permit the formation of sigma, and the presence of elements such as silicon, columbium, titanium, tungsten and molybdenum promotes its formation. It is generally conceded that sigma phase adversely affects the impact resistance of these steels. The literature on sigma phase has been well reviewed (1).[1]

The purpose of this investigation was to present data showing the influence of solution treatment temperature and time on the formation of delta ferrite and the influence of different amounts of delta ferrite and of cold work on the formation of the sigma phase.

The steel used, known as 19-9DL, is a commercially available wrought heat resisting steel. It was supplied as bar stock, stress-relieved at 1200 °F (650 °C). Its analysis follows:

	Per Cent
Carbon	0.27
Chromium	18.82
Nickel	9.59
Molybdenum	1.34
Tungsten	1.39
Columbium	0.54
Titanium	0.32
Manganese	1.20
Silicon	0.66
Sulphur	0.01
Phosphorus	0.02

Solution Treatments

Two series of specimens were employed in this study. The first determined the effect of solution treatment temperature (1800 to 2400 °F) (980 to 1315 °C) on the amount of delta ferrite formed in 1 hour (Figs. 2 to 7).[2] The second series determined the effect of increasing time (2 to 256 minutes) on the amount of delta ferrite formed at one temperature (2350 °F) (Figs. 8 to 13).

All specimens were cut from $\frac{11}{16}$-inch diameter bar stock and were approximately ¼ inch in thickness. The temperatures of solution treatment were carefully checked and controlled. The specimens shown in Figs. 2 to 7 were held at temperature for 1 hour. In both series, the specimens were water-quenched from the solution temperature.

Effect of Temperature of Solution Treatment—The initial struc-

[1]The figures appearing in parentheses pertain to the references appended to this paper.

[2]Photomicrographs throughout this paper were made of longitudinal sections.

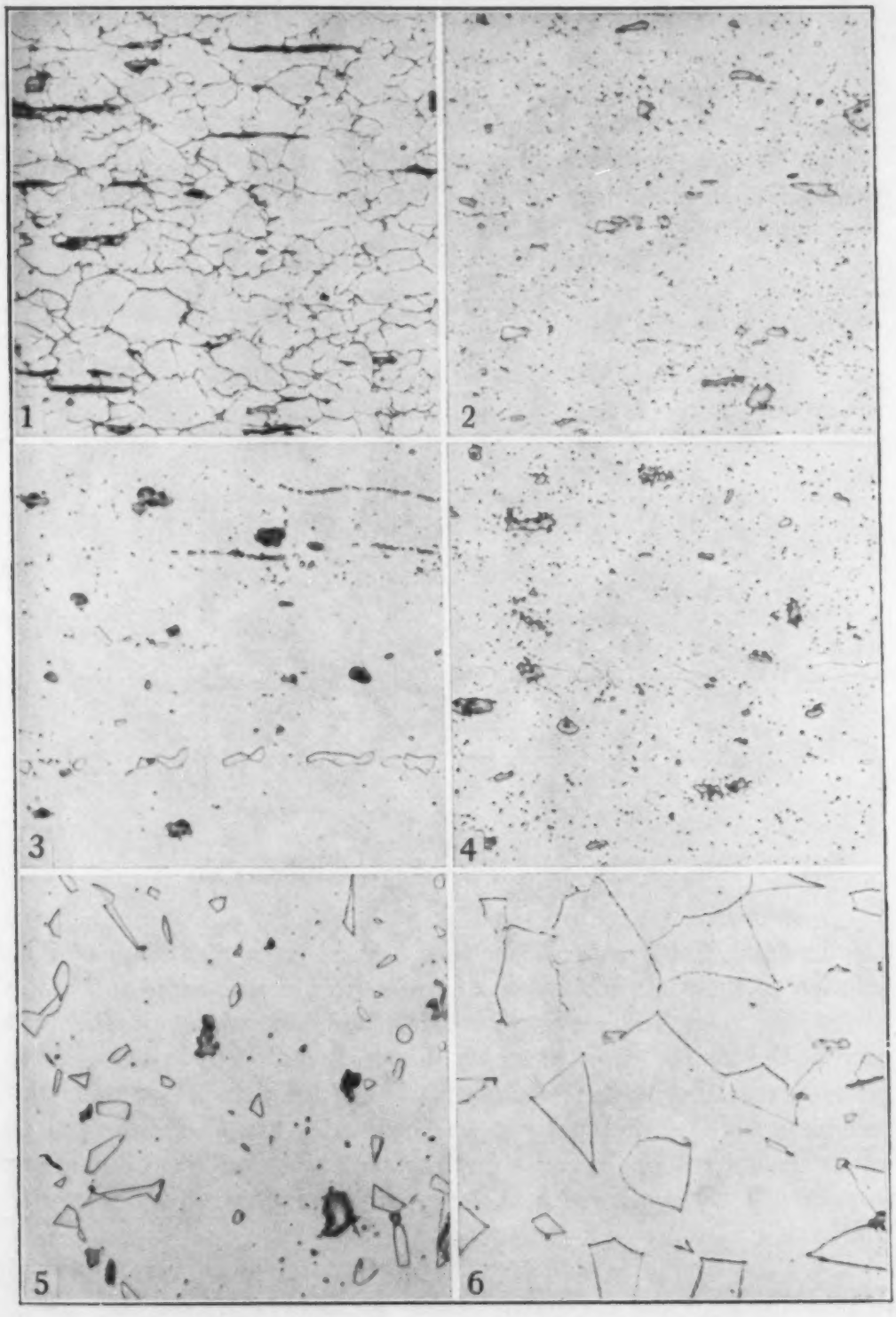


Fig. 1—Hot Cold-Rolled and Stress-Relieved. Glyceregia etch.
Fig. 2—Solution-Treated at 1800 °F. Oxalic acid etch. × 500.
Fig. 3—Solution-Treated at 2000 °F. Oxalic acid etch. × 500.
Fig. 4—Solution-Treated at 2100 °F. Oxalic acid etch. × 500.
Fig. 5—Solution-Treated at 2200 °F. Oxalic acid etch. × 500.
Fig. 6—Solution-Treated at 2400 °F. Oxalic acid etch. × 500.

ture, shown in Fig. 1, consisted of stringers of precipitated particles in an austenitic matrix.

Delta ferrite was formed in increasing amounts as the solution temperature was raised from 1800 to 2400 °F (980 to 1315 °C) as shown by the microstructures of Figs. 2 to 16 and the results of magnetic determinations (Fig. 7). The increase in delta ferrite was rapid above 2200 °F (1205 °C).

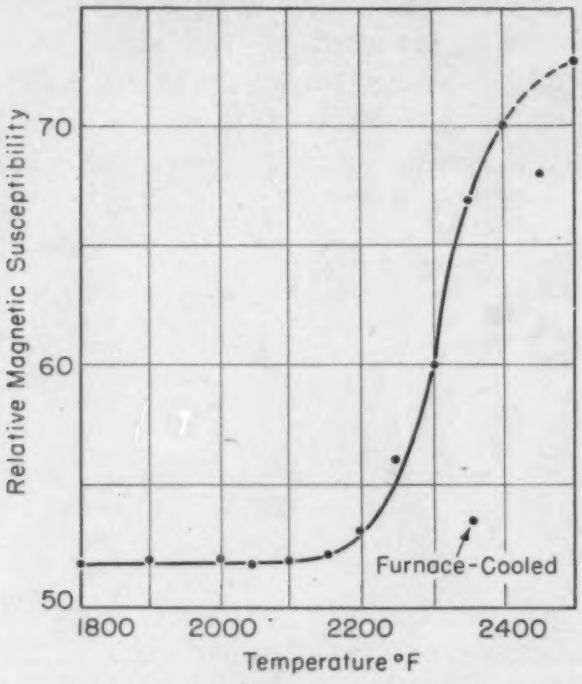


Fig. 7—Effect of Solution Treatment Temperature on Delta Ferrite in 19-9DL.

Initially, the structure contained several types of carbides. The solution of the fine carbides was coincident with the rapid formation of ferrite. Some of the large carbides, however, were not dissolved even at the temperatures at which the steel was partly molten. It is believed that the more refractory carbides are rich in titanium and columbium. The titanium-rich carbo-nitrides are easily recognized under the microscope because of their pink tint and typically square form. The columbium-rich carbides are characterized by irregular contours.

A clustering of small carbides about large ones was observed to take place in the specimen treated at 2100 °F (1150 °C) (Fig. 4). This was probably a result of dissolution of carbon from the large carbides into the matrix and reprecipitation by combination with other elements in the austenite.

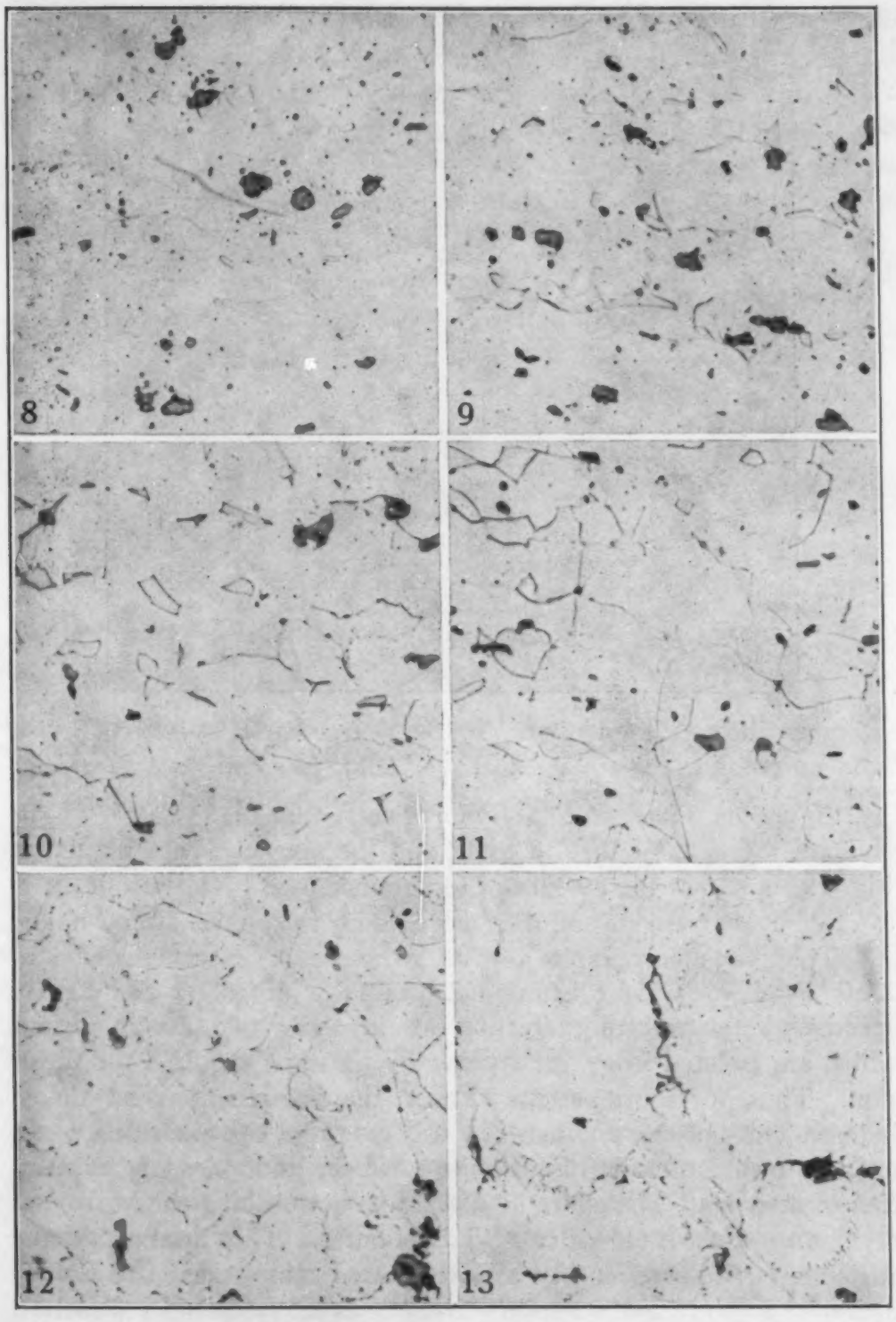


Fig. 8—Held 2 Minutes at 2350 °F. Oxalic acid etch. × 500.
Fig. 9—Held 8 Minutes at 2350 °F. Oxalic acid etch. × 500.
Fig. 10—Held 32 Minutes at 2350 °F. Oxalic acid etch. × 500.
Fig. 11—Held 64 Minutes at 2350 °F. Oxalic acid etch. × 500.
Fig. 12—Held 128 Minutes at 2350 °F. Oxalic acid etch. × 500.
Fig. 13—Held 256 Minutes at 2350 °F. Oxalic acid etch. × 500.

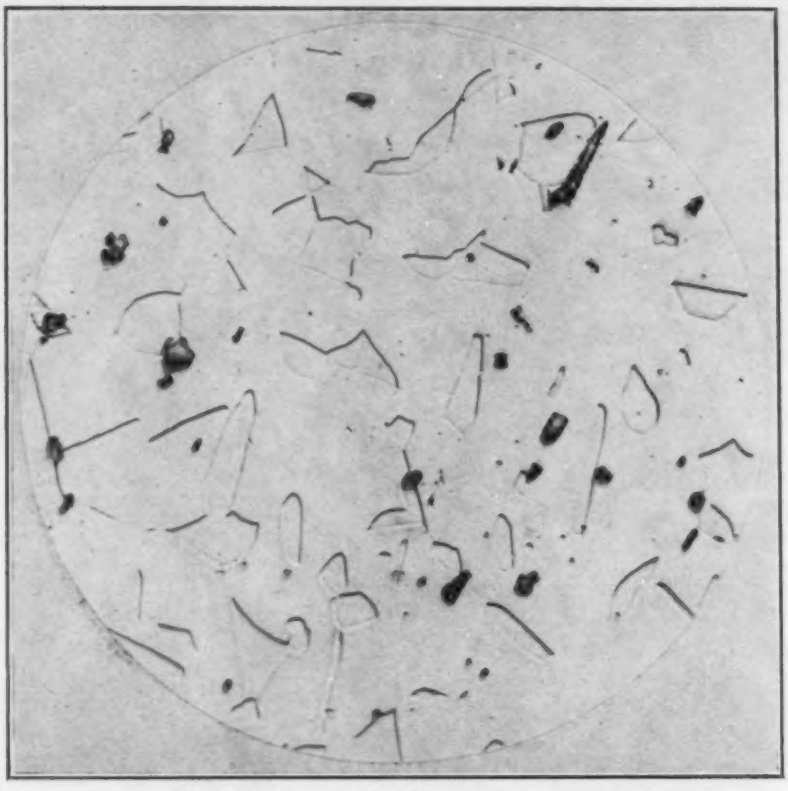


Fig. 14—Solution-Treated at 2350 °F for 1 Hour. Oxalic acid etch. Conical illumination. × 500.

Effect of Time at a Solution Temperature of 2350 °F—The photomicrographs of Figs. 8 to 12 and the magnetic data plotted in Fig. 15 show that the amount of ferrite increased rapidly from 2-3% to 22-23% after 1 hour and then more slowly to 25-26% after 2 hours.

The photomicrographs of the structure of specimens held at 2350 °F (1290 °C) for 128 and 256 minutes (Figs. 12 and 13, respectively) illustrate an interesting case involving two phase reactions which are isolated from one another by the time required for diffusion. Thus, for short periods of time, the two reactions act almost independently of one another. In this case, the two reactions were: one, the transformation of austenite to ferrite; and two, the dissolution of carbides. The curve in Fig. 15 is approaching the horizontal asymptote at the time value of 128 minutes. This means that the austenite-ferrite reaction had almost reached completion. An examination of Figs. 12 and 13 shows that not as many carbides dissolved in 128 minutes as in 256 minutes. Therefore, although the austenite-ferrite equilibrium had almost been reached in 128 minutes at temperature, this equilibrium was for a carbon composition lower than

the saturation value. As the carbides continued to dissolve, additional carbon in solid solution shifted the equilibrium and ferrite began to transform to austenite. From an areal analysis of the photomicrographs, the decrease in ferrite was determined to be about 10%; from 37-38% to 27-28%.

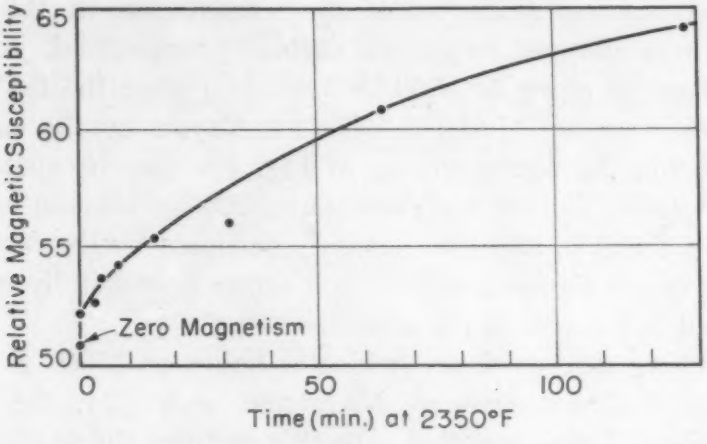


Fig. 15—Rate of Formation of Delta Ferrite in 19-9DL at 2350 °F.

Another change that occurred when the specimens were held for very long times at 2350 °F (1290 °C) was precipitation at the austenite-ferrite interface. A specimen held 1 hour at 2350 °F (1290 °C) had no precipitate at this interface, as shown by the absolutely clear and smooth sides of the ferrite when illuminated conically (Fig. 14). Fig. 13 shows the jagged interface that resulted wherever a particle of precipitate formed, depleting the matrix of some element and shifting the austenite-ferrite equilibrium.

Aging Treatments

Two solution temperatures were used: one to result in a low ferrite content, and the other in a high ferrite content.

The temperatures used for aging were 1200, 1400 and 1600 °F (650, 760 and 870 °C). At each temperature, specimens were held for 0.1, 0.5, 1, 10, and 100 hours. After aging, all specimens were quenched in water. The temperatures of aging were carefully controlled in each case. They did not vary more than 3 or 4 degrees during the periods of aging.

Aging of Structures High in Ferrite Content—The effects of

aging on the specimens solution-treated at 2350 °F (1290 °C) for 1 hour are shown in Figs. 16 to 22.

It can be seen that precipitation of carbides began at the austenite-ferrite interface and proceeded into the ferrite. At the same time, the ferrite was transforming to austenite, as shown by the magnetic data plotted in Fig. 23. When the precipitation at the ferrite sites was complete, grain boundary precipitation in the austenite began and was followed by general carbide precipitation.

One hour of aging at 1600 °F (870 °C) gave the first evidence of the transformation of sigma. This is shown by the small white globules within the ferrite grains in Fig. 19. In the specimen held at 1600 °F (870 °C) for 10 hours (Fig. 20) substantial amounts of sigma had formed in the sites formerly occupied by the ferrite. The black color of the sigma in this picture shows how rapidly it is etched as compared to the rest of the structure.

By etching the specimen held 100 hours at 1400 °F (760 °C) with a modified concentrated Murakami etch (2), the structure shown in Fig. 21 was revealed. In this picture, the particles of the sigma phase can be clearly distinguished from carbide particles. With natural coloring, the difference in appearance was vivid because some particles of the sigma phase were stained bright red, some green, and some brownish-red, while the carbides were black. It was noticed that many of the carbides in the austenite, visible after etching electrolytically in 10% oxalic acid, were unattacked by the Murakami etchant.

The concentrated Murakami etch consisted of a solution of 60 milliliters of water and 30 grams of potassium hydroxide which was saturated with potassium ferricyanide. The specimen was etched by immersion for a few seconds with the temperature of the etching solution at approximately 120 °F. The clarity of detail in Fig. 22 establishes the superiority of this etch for revealing sigma in alloys of this type. The color of the sigma in this specimen was light blue. The carbides were blackened. It can be seen that some of them agglomerated in the former ferrite areas.

Because there has been some doubt why, during aging of duplex austenite-ferrite structures, the carbides precipitate preferentially in the ferrite, this point will be discussed further.

The process of carbide precipitation was complicated by the fact that the ferrite was transforming to austenite almost simultaneously with the precipitation of carbides. This can be seen from a compari-

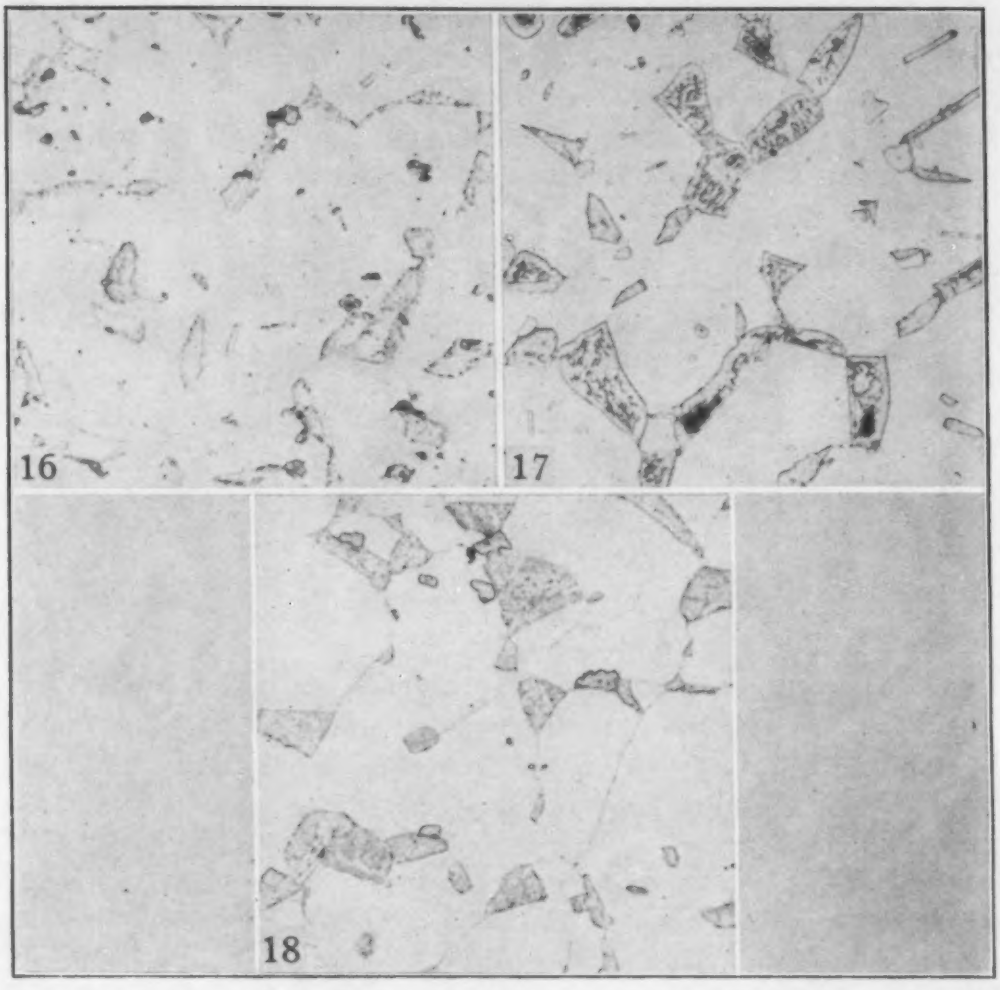


Fig. 16—Solution-Treated at 2350 °F. Aged 0.1 hour at 1400 °F.
Fig. 17—Solution-Treated at 2350 °F. Aged 0.5 hour at 1400 °F.
Fig. 18—Solution-Treated at 2350 °F. Aged 1 hour at 1400 °F.
All specimens oxalic acid etched. × 500.

son of the photomicrographs of the variously aged specimens and the relative magnetic susceptibility of the same specimens (Fig. 23).

It may be that the reason for the rapid precipitation at the ferrite sites was the retreating ferrite-austenite interface. That is, precipitation was able to take place at the interface sooner than at other points in the specimen because of the high energy there during the transformation of ferrite to austenite. From this standpoint, then, the movement of the precipitate inward in the ferrite was limited by the transformation.

Another possible explanation is that the precipitate appeared first in the ferrite because of the more rapid rate of diffusion in fer-

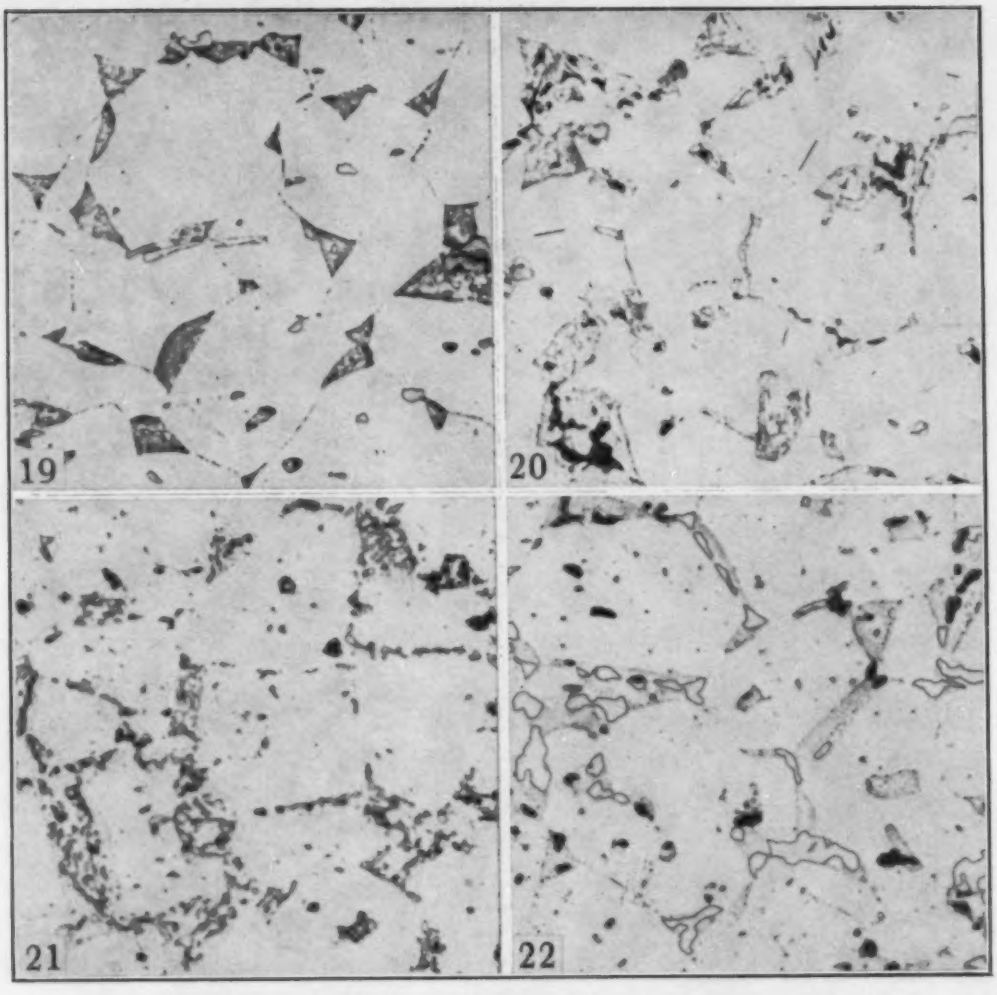


Fig. 19—Solution-Treated at 2350 °F. Aged 1 hour at 1600 °F.
Fig. 20—Solution-Treated at 2350 °F. Aged 10 hours at 1600 °F.
Both specimens oxalic acid etched. × 500.
Fig. 21—Solution-Treated at 2350 °F. Aged 100 hours at 1400 °F.
Fig. 22—Solution-Treated at 2350 °F. Aged 100 hours at 1600 °F.
Both specimens—modified Murakami etched. × 500.

rite as compared to austenite (3), (4), (5, disc.). However, it seems unlikely that such a large amount of precipitate could have come from the ferrite alone.

The most likely explanation is that there was segregation of the various elements in the two phases at the solution treatment temperature. The alloying elements chromium, molybdenum, tungsten, columbium, and titanium would tend to concentrate in the ferrite because they are more soluble in the body-centered lattice than in the face-centered lattice of austenite. Carbon, being more soluble in the face-centered lattice, would tend to concentrate in the austenite. When the alloy was aged after quenching, the ferrite transformed to

an austenite that was low in carbon content, but high in alloy content. Carbon diffused into these low carbon regions and immediately combined with the alloying elements to form the precipitate. The concentration of alloying elements at the former ferrite regions was probably the factor that caused the rapid formation of sigma at those sites also.

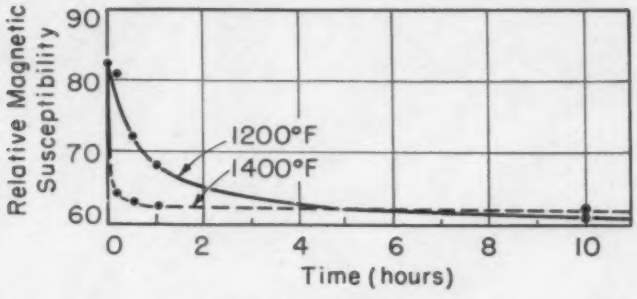


Fig. 23—Decomposition of Delta Ferrite in 19-9DL During Aging After Solution Treatment at 2350 °F.

In examining the structures of the specimens where precipitation was complete, it should be remembered that the dark areas do not represent ferrite containing carbides; they represent carbides in the sites of ferrite that transformed to austenite.

Aging of Structures Low in Ferrite Content—The effects of aging on the specimens solution-treated at 2050 °F (1120 °C) are shown in Figs. 24 and 25. The only ferrite that these structures contained prior to aging was an occasional stringer (2 to 3%).

Sigma appeared only in the specimens aged 100 hours at 1400 and 1600 °F (760 and 870 °C). Also, the amounts were much smaller than in the specimens that initially contained 22 to 23% ferrite. Thus, the presence of ferrite in the initial structure either directly or indirectly promoted the formation of the sigma phase. One would hesitate to say that the phase formed from the ferrite directly because by the time it could be clearly identified the ferrite had long since transformed. This does not mean that it could not have been a part of the original precipitation; it merely suggests that the formation of sigma followed the precipitation of carbides rather than accompanied it.

Long-Time Aging Treatments

Two initial structures were used for the study of long-time aging treatments. One was the hot cold-rolled and stress-relieved struc-

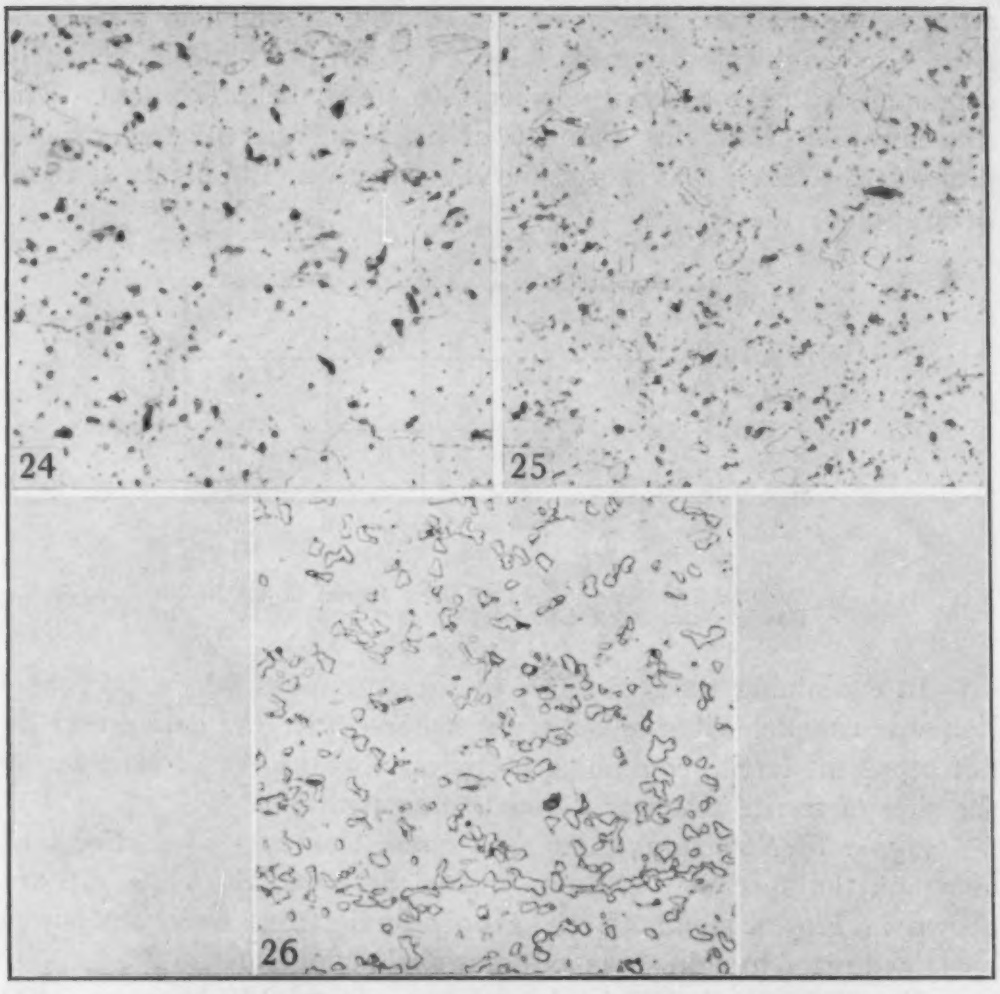


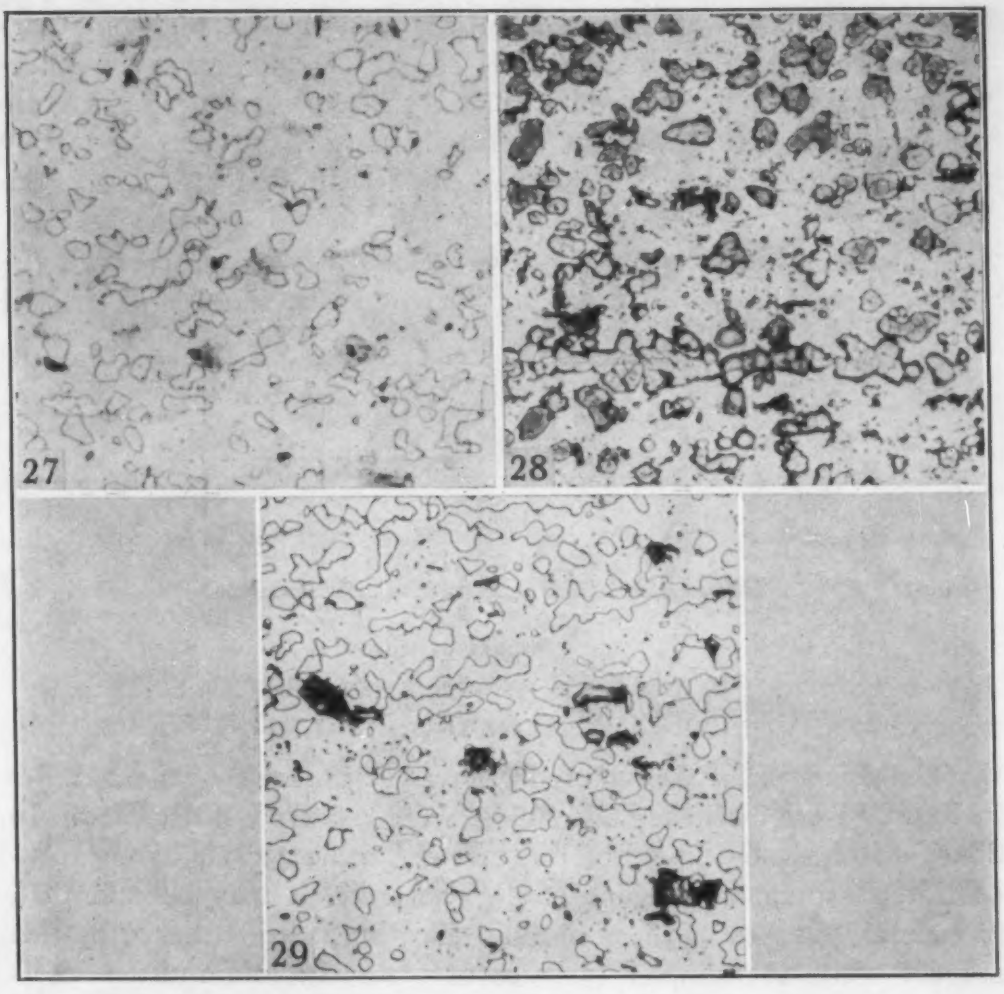
Fig. 24—Solution-Treated at 2050 °F. Aged 100 hours at 1400 °F.
Fig. 25—Solution-Treated at 2050 °F. Aged 100 hours at 1600 °F.
Both specimens oxalic acid etched. × 500.

Fig. 26—Hot Cold-Rolled and Stress-Relieved. Aged 100 hours at 1500 °F. Oxalic acid etch. ×500.

ture; the other was the structure produced by solution treatment at 2350 °F (1290 °C).

The lengths of time used were: 1, 10, 100, 500 and 1000 hours. In addition, one of the specimens solution-treated at 2350 °F (1290 °C) was held for 2000 hours at temperature. The aging temperature was 1500 °F (815 °C) and the specimens were air-cooled following aging.

Initial Condition—Hot Cold-Rolled and Stress-Relieved—Initially, these specimens were low in ferrite, and their hardness (Rockwell B-97 as compared to Rockwell B-87 for the annealed material) showed that they had been cold-worked 5 to 10%.



Figs. 27, 28, 29—Hot Cold-Rolled and Stress-Relieved. Aged 1000 hours at 1500 °F. × 500. Fig. 27—Oxalic acid etch. Fig. 28—Murakami etch. Fig. 29—Modified Murakami etch.

A large amount of sigma was produced in the specimen held at 1500 °F (815 °C) for 100 hours (Fig. 26). The stringers formed by some particles of sigma indicate that the stringers of the former phase promoted the formation of the sigma phase in some way and thereby had their traces outlined.

After heating 500 hours at 1500 °F (815 °C) the alloy was less magnetic than it was initially.

Twenty-five to 30% of sigma was produced by heating 1000 hours at 1500 °F (815 °C) as shown by Fig. 27.

Etching electrolytically with normal Murakami's reagent (10 grams of potassium hydroxide—10 grams of potassium ferricyanide —100 milliliters of water) produced the structure shown in Fig. 28.

The sigma phase was stained mostly reddish-brown, but some particles were blue. The thickness of the coating built up is the determining factor in the coloring. The crack-like markings which are sometimes associated with the sigma phase (2), (6) may be merely cracks in the etching film. The carbides in this structure were blackened.

Etching with concentrated Murakami's reagent created the microstructure shown in Fig. 29. Viewing with white light showed

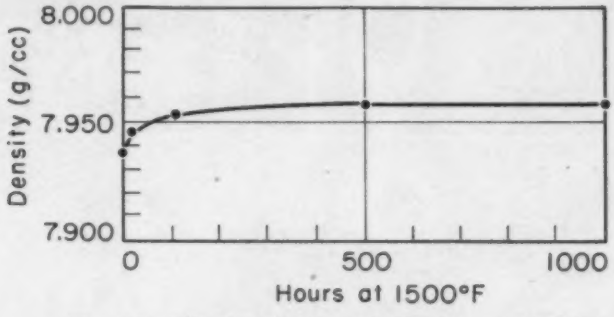


Fig. 30—Effect of Prolonged Heating at 1500 °F on the Density of 19-9DL.

that the sigma phase was colored yellow. Also, some of the carbides in Fig. 29 were blackened and others were relatively unattacked. In 25-20 stainless steel none of the carbides are attacked by the concentrated Murakami reagent (6). Therefore, it may be said that, in general, complex carbides in multi-alloy steels are attacked by this reagent while the simpler carbides in plain chromium-nickel steels are not.

Sigma is more dense than austenite. This is shown by Fig. 30; a plot of density versus time at 1500 °F (815 °C).

Initial Condition—Solution-Treated to Give High Ferrite—Initially these specimens contained approximately 20% of ferrite.

After 1000 hours at 1500 °F (815 °C) the particles of sigma were quite large, but comparison of Fig. 27 with Fig. 31 will show that the amount of sigma is greater in Fig. 27. From the previous section on aging, it will be recalled that the presence of ferrite in the initial structure promoted the formation of sigma when cold work was absent. Sigma formed more rapidly in a material that was low in ferrite but that was cold-worked, than in an initially high-ferrite material that was fully annealed. Therefore, while ferrite in the initial structure promotes the formation of sigma, cold work in the initial structure has a more pronounced effect.

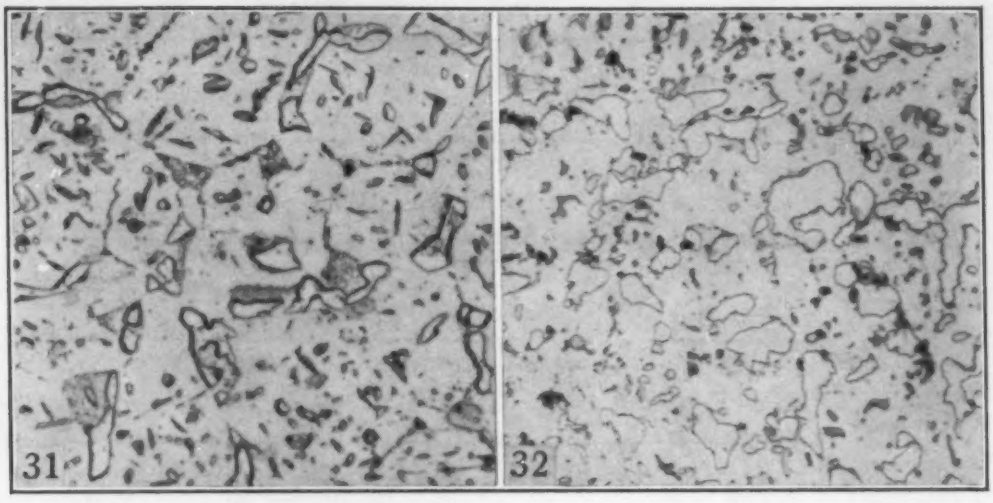


Fig. 31—Solution-Treated at 2350 °F. Aged 1000 hours at 1500 °F. Oxalic acid etch. × 500.

Fig. 32—Solution-Treated at 2350 °F. Aged 2000 hours at 1500 °F. Modified Murakami etch. × 500.

Fig. 32 shows the amount of sigma produced by holding a specimen at 1500 °F (815 °C) for 2000 hours. The particles of sigma in this structure were sufficiently large so that microhardness measurements could be made. However, the particles were crushed by the penetrator and the values are therefore only approximate. The sigma particles had a Knoop hardness number of about 500, and the austenitic matrix had a number of about 275.

X-Ray Diffraction Study

All exposures were made in a Debye-Scherrer camera of 7.16 cm. radius. The specimens were cut and ground to a wedge shape and were then deeply etched before exposure, to remove the surface layers distorted by grinding. Each wedge was placed in the camera in such a way that its chisel edge half blocked the X-ray beam. Unfiltered chromium radiation was used.

Precise identification of the sigma phase is not possible at the present time because its crystallographic structure is not known. The structure is very complex but seems to be related somewhat to the body-centered cubic structure of the ferrite.

The only lines visible on the film of the hot cold-rolled and stress-relieved specimen were those of austenite. The diffraction technique did not produce the lines of the carbides in the specimen;

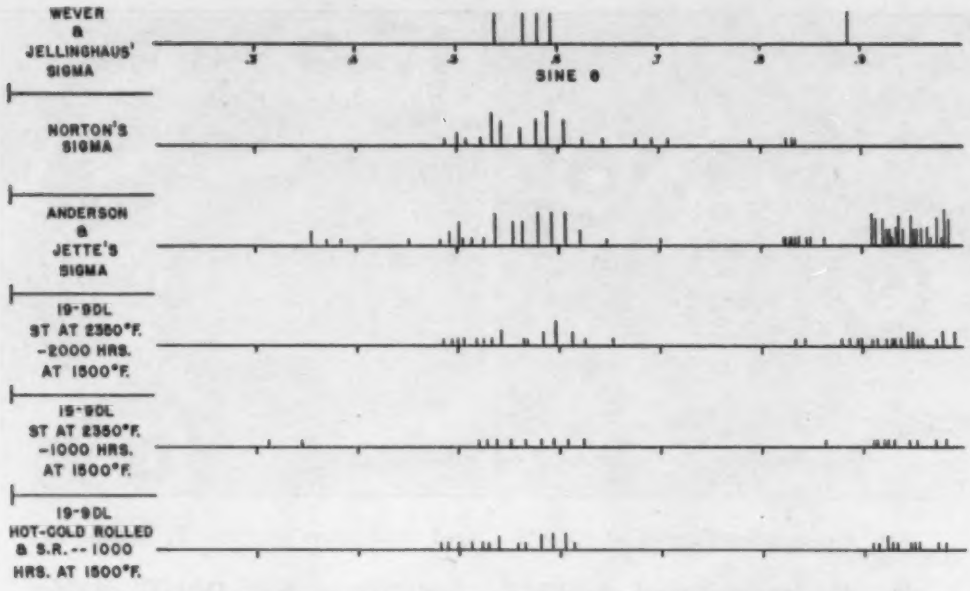


Fig. 33—Comparison of Unknown Lines in 19-9DL with Sigma Patterns Published by Other Authors.

therefore, most of the lines in the pictures were assumed to be from austenite, ferrite or sigma (although large agglomerated carbides may have produced additional lines in some of the films). Twenty-three additional lines appeared on the diffraction film of the hot cold-rolled and stress-relieved specimen that had been heated 1000 hours at 1500 °F (815 °C).

The diffraction pattern of the specimen that was solution-treated at 2350 °F (1290 °C) showed lines of both ferrite and austenite plus a few lines probably due to carbides. After the specimen had been heated 2000 hours at 1500 °F (815 °C) 33 unknown lines appeared.

A plot was made of the sine θ values of the various lines of some of the specimens together with those found in the literature (7), (8), (9), and is presented in Fig. 33. The heights of the lines indicate the relative intensities of the diffracted beams. However, "weak" and "very weak" lines were plotted as though they had the same intensity because of the difficulty in correctly judging their intensities.

It can be seen from Fig. 33 that the phase encountered was sigma, but it is strange that there is not more precise matching of the various patterns. Perhaps, as suggested by Bradley and Goldschmidt (10), a transition structure precedes the stable sigma structure. Also, the mode of formation from austenite may be different than from ferrite. Further investigation is necessary.

Summary and Conclusions

Photomicrographs showing the progressive formation of delta ferrite at high solution treatment temperatures were presented.

Reasons for the preferential precipitation of carbides in the ferrite sites of duplex ferrite-austenite structures were discussed.

The sigma phase was investigated and the following conclusions made:

1. Sigma forms from austenite as well as ferrite.
2. The presence of ferrite in the initial structure hastens the formation of sigma. The reason may be one or more of the following:
   a. The crystallographic structure of ferrite resembles that of sigma more closely than does the structure of austenite.
   b. The atomic mobility is greater in ferrite than in austenite.
   c. Preferential precipitation of carbides in the ferrite sites concentrates the alloying elements locally or distorts the ferrite lattice and thereby facilitates the formation of sigma.
3. Cold work accelerates the formation of sigma to a greater extent than does the presence of ferrite in the initial structure.
4. There is no general method at present for the identification by etching of sigma that is reliable for all alloys.
5. The complex structure of the sigma phase was confirmed.

Acknowledgment

The authors wish to thank Mr. F. Garratt of the Universal-Cyclops Steel Corporation for supplying the steel used in this research.

References

1. F. B. Foley, "The Sigma Phase," *Alloy Casting Bulletin,* No. 5, July 1945, p. 1.
2. C. O. Burgess and W. D. Forgeng, "Constitution of Fe-Cr-Mn Alloys," *Transactions,* American Institute of Mining and Metallurgical Engineers, Vol. 131, 1938, p. 277.
3. G. E. Claussen, "Diffusion of Elements in Solid Iron," Transactions, American Society for Metals, Vol. 24, 1936, p. 640.
4. C. E. Birchenall and R. F. Mehl, "Self-Diffusion in Iron," *Mining and Metallurgy,* November 1947, p. 555.
5. F. E. Harris, "Discussion—The Diffusion Rates for Carbon in Austenite," *Metals Technology,* October 1947, T.P. No. 2258, p. 10.
6. G. N. Emmanuel, "Metallographic Identification of Sigma Phase in 25-20 Austenitic Alloy," Metal Progress, July 1947, p. 78.

7. P. Payson and C. H. Savage, "Changes in Austenitic Chromium-Nickel Steels During Exposures at 1100 to 1700 °F.," TRANSACTIONS, American Society for Metals, Vol. 39, 1947, p. 404.
8. A. G. H. Andersen and E. R. Jette, "X-Ray Investigation of the Fe-Cr-Si Phase Diagram," TRANSACTIONS, American Society for Metals, Vol. 24, 1936, p. 375.
9. F. Wever and W. Jellinghaus, "Zur Kenntnis des Zweistoffsystems Eisen-Chrom," *Mitt. K-W Inst. Eisenforschung,* Vol. 13, 1931, p. 143.
10. A. J. Bradley and H. J. Goldschmidt, "An X-Ray Investigation of Iron-Nickel-Chromium Alloys," *Journal,* Iron and Steel Institute, Vol. 144, No. II, 1941, p. 273.

DISCUSSION

Written Discussion: By C. T. Evans, Jr., chief metallurgist, Elliott Co., Jeannette, Pa.

This is one of the first attempts to explore fundamentals of microstructure and phases in the special heat resisting alloys currently in use for gas turbines, jet engines, etc. The authors are to be congratulated in achieving a milestone in this field.

The photomicrographs are excellent, although one cannot help but sympathize with the authors' problems of interpretation of such complex structures. Fig. 14, with the conical illumination, is an outstanding example.

It would be of interest to know how the magnetic susceptibility characteristics were determined. It also occurs to me that magnetic readings are not much help in determining whether the ferrite phase is transforming to sigma or austenite since both sigma and austenite are nonmagnetic phases. Accordingly, I would be inclined to judge the metallographic and X-ray diffraction data as more indicative as to which phase, austenite or sigma, was actually the transformation product.

I have attempted to correlate the work in this paper with a similar study on 19-9 W-Mo alloy performed by the N.A.C.A. Aircraft Engine Research Laboratory at Cleveland, Ohio. The analysis of the material was as follows:

	%		%
C	0.084	Cr	18.50
Mn	0.44	Ni	8.78
Si	0.61	W	1.38
S	0.013	Mo	0.28
P	0.013	Cb	0.47
		Ti	0.38

It will be noted that the analysis is quite similar to 19-9 DL except for lower carbon and molybdenum.

The exact history of the bar stock was not revealed but it was probably hot-rolled and stress-relieved for about 4 hours at 1200 °F (650 °C), followed by air cooling. Even in this condition, 19-9 W-Mo contains a high percentage of delta ferrite, as is shown by Figs. 32 to 35. Around 30% ferrite in the original structure is a good estimate.

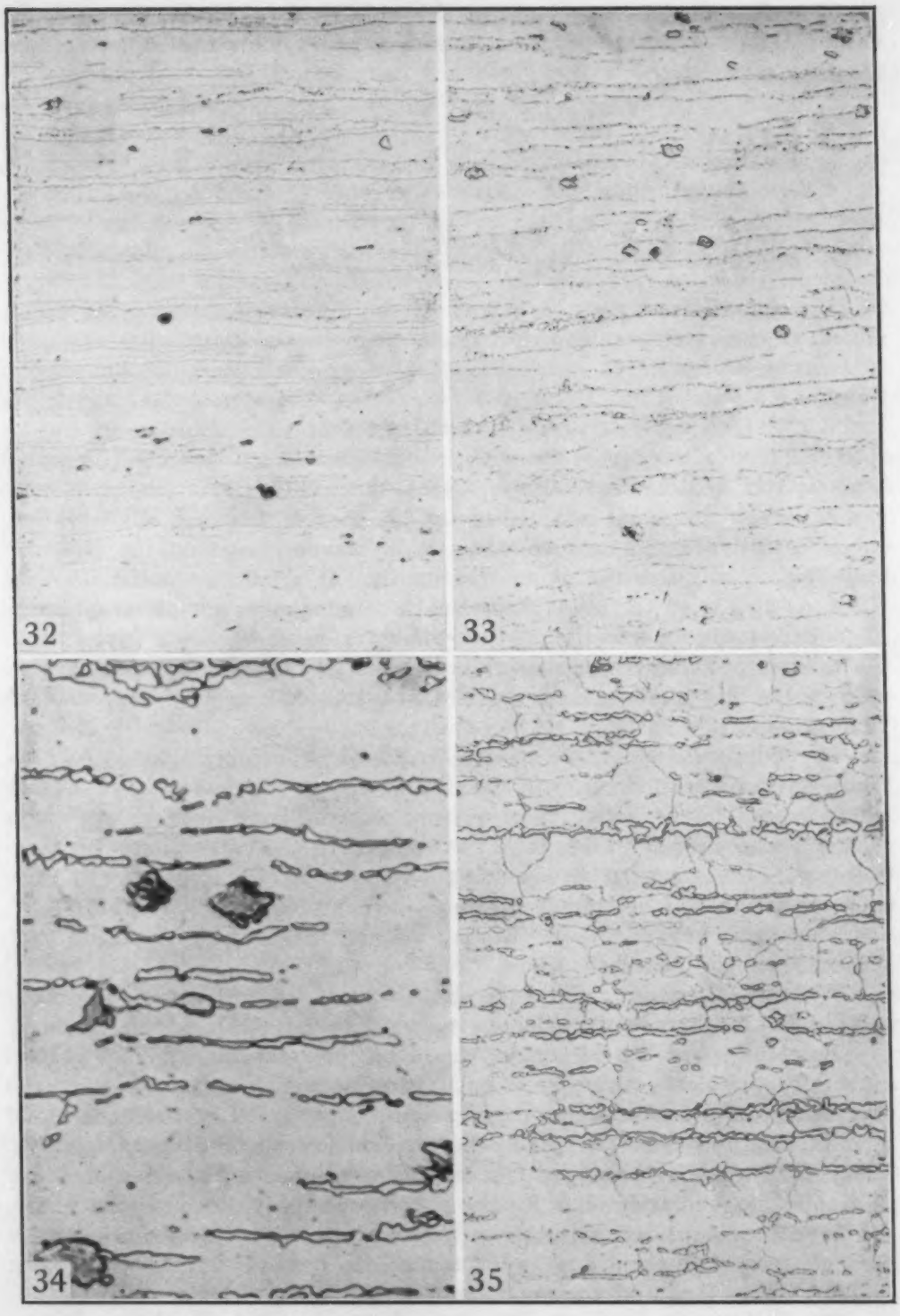


Fig. 32—Photomicrograph of Specimen in the As-Received Condition. Held for 72 hours at 1400 °F. Etched Vilella's reagent. × 250.

Fig. 33—Photomicrograph of Specimen Held 72 Hours at 1500 °F. Etched Vilella's reagent. × 250.

Fig. 34—Same Specimen as Fig. 33. × 1000.

Fig. 35—Photomicrograph of Specimen Held 2 Hours at 2400 °F, Water-Quenched, 1500 °F for 92 Hours. Etched Vilella's reagent. × 250.

The Cleveland laboratory then determined X-ray diffraction patterns with a Geiger-counter spectrometer, on samples with the following heat treatments:

Prior Treatment	Aging Temperature °F	Time Hours
As-received	....	..
As-received	1400	72
2300 °F—2 hours. Water quench	1500	91
2400 °F—2 hours. Water quench	....	..

No sigma lines appeared in any of the diffraction patterns as determined at room temperature. Instead, the only transformation appeared to be that of ferrite to austenite. This does not check the findings of Gilman, Koh and Zmeskal on 19-9 DL, who found sigma after 100 hours at 1400 °F (760 °C) in a sample which had first been solution treated at 2350 °F (1290 °C) and who likewise found sigma in a slightly cold-worked sample after holding for 100 hours at 1500 °F (815 °C).

Although the work is not directly comparable, because of the differences in analyses and heat treatments, it is surprising that the N.A.C.A. found no sigma after the aging treatments. It should be noted that the N.A.C.A. also tried to reveal sigma in these specimens metallographically. Their private communication to the writer of April 16, 1948, advises that the following etchants were employed: Vilella's reagent; Vilella's reagent followed by Murakami's reagent; and 1:1 HCl followed by 10% alkaline ferricyanide.

In addition, N.A.C.A. technical note of November 1947 (TN No. 1488), giving hot diffraction data, shows that: "The alloy 19-9 W-Mo when heated began to transform from a two-phase mixture of body-centered and face-centered cubic structures to a single phase of face-centered cubic structure between 1400 and 1450 °F (760 and 790 °C). The transformation was completed between 1450 and 1500 °F (790 and 815 °C)".

This same report shows that no change in thermal expansion rate accompanied the phase change.

Written Discussion: By John M. Thomas, research associate, Engineering Research Institute, University of Michigan, Ann Arbor, Mich.

The authors are to be congratulated on their careful study of several aspects of the sigma phase problem, a problem which certainly is in need of systematic and thorough investigations in order to remove the cloud of uncertainty which still surrounds its identification and characteristics. In the University of Michigan laboratories, we made up a series of alloys of iron, chromium, and nickel for the purpose of studying the sigma phase. We have done considerable experimental work on these alloys, much of it paralleling work the authors have presented. I would like to offer some of our observations and comments on the subject.

The authors report the coloring produced to be dependent upon the thickness of the coating built up when a modified Murakami's reagent is used to etch sigma phase. This is similar to what we have found in some of our alloys. In an alloy of 45% chromium, balance iron, which had been

aged at 1400 °F (760 °C), the interference phenomenon, such as is observed in tempering steel or in oil films, was clearly visible and the color at any one particular position on the sample was dependent only upon the time of etching.

However, experience with other compositions, such as an alloy of 25% chromium, 6% nickel, balance iron, in which the sigma was consistently colored light blue, using the same etchant, seems to indicate that the color is also dependent upon the composition of the sigma phase. This probably led to Burgess and Forgeng's[3] statement that sigma phase is colored light blue when etched with modified Murakami's reagent, in which they were dealing with iron-chromium-manganese alloys. Failure to reproduce this color in some of the chromium-nickel alloys initially caused us considerable concern, and probably has been confusing to other investigators.

Another identification clearly shown in photomicrographs by Burgess and Forgeng[3] was the anisotropic behavior of the sigma phase in plane-polarized light, which under the crossed nicols would cause a change from light to dark upon rotation of the specimen. We have never been able to duplicate this phenomenon in sigma phase using the 45% chromium or iron-chromium-nickel alloys, and are curious to know if the authors have checked their 19-9 DL specimens for this behavior.

The authors present a graph showing the density increase of 19-9 DL accompanying the transformation of austenite and ferrite to sigma phase. The amount indicated is about 0.25%, which I presume is for the cold-worked alloy which formed between 25 and 30% of sigma after 1000 hours at 1500 °F (815 °C). In the 45% chromium alloy mentioned previously, which can be aged at 1400 °F (760 °C) to form almost 100% sigma phase, the density increase on transformation from ferrite to sigma was found to be about 0.90%. Upon solution treating to re-form ferrite, the density decreased exactly the same amount as it had increased. An alloy of 40% chromium, 15% nickel, balance iron, which when solution-treated at 1900 °F (1040 °C) had about 60% alpha and 40% gamma phase transformed to about 30% gamma and 70% sigma phase on aging at 1400 °F (760 °C). The density increase accompanying this transformation was about 0.55%, with an equivalent decrease upon re-solution treating at 1900 °F (1040 °C) to its original condition. These figures seem to be in fairly good agreement with the findings of the authors.

An interesting thought on the subject of this change in specific volume is the effect it may have on time-elongation measurements in high-temperature creep tests. If the amount of sigma phase formed is in excess of about 3%, it may quite radically affect the characteristics of the creep curve, depending upon the rate of transformation.

The authors suggest that the crack-like markings associated with the sigma phase may be cracks in the etching film. This possibility should not be ruled out. However, it is not difficult to conceive of them being actual cracks. If only the film cracked, it seems that a new film would

[3]C. O. Burgess and W. D. Forgeng, "Constitution of Iron-Chromium-Manganese Alloys," *Transactions*, American Institute of Mining and Metallurgical Engineers, Vol. 131, 1938, p. 277-302.

immediately form of some other color than black due to the rapid action of the modified Murakami's reagent on the sigma phase. The sigma phase is extremely brittle at room temperature, as borne out by the authors' experience in having the material crumble when attempting to make microhardness measurements. Our own experience with the 45% chromium alloy aged at 1400 °F (760 °C) was that it cracked severely in a transcrystalline manner upon cooling from the aging temperature, and the corners of a specimen could be crumbled away with one's fingernail. The stresses necessary to cause cracking of the brittle material could be thermal stresses set up when cooling the specimen from the aging temperature, when etching in hot solution and then cooling, or when polishing, or they could be mechanical stresses set up during polishing. Burgess and Forgeng[3] also showed photomicrographs of an iron-chromium-manganese alloy in which a very light etch using a 10% aqueous solution of hydrochloric acid revealed countless unmistakable transcrystalline cracks in the sigma phase.

The results of two elevated temperature tests on sigma may be of interest. A Charpy impact specimen and a tensile test bar were machined from the 45% chromium alloy in the hot-rolled condition. Each was held at 1400 °F (760 °C) for 22 hours, which was sufficient to transform it into sigma phase, and then tested at that temperature. The Charpy impact value was 8 foot-pounds, although the specimen shattered badly. The tensile bar withstood a stress of 18,000 psi at 1400 °F (760 °C) before a very brittle fracture occurred in the threads of the specimen. The measured permanent deformation of the gage section was zero.

Written Discussion: By Peter Payson and Lo Ching Chang, Research Laboratory, Crucible Steel Co. of America, Harrison, N. J.

These authors have introduced the very interesting idea that sigma in some steels may form by a two-step transformation—that is, ferrite to austenite and then to sigma. The prevalent opinion is that sigma forms from ferrite, generally, and that in some steels of suitable composition, sigma may form from austenite but only after quite long holding periods at temperatures between about 1200 and 1600 °F (650 and 870 °C).

Since in our laboratory we are very much interested in sigma formation, we thought it worthwhile to make several determinations to see if we could find evidence to support the proposed hypothesis.

We used one steel somewhat similar to that used by the authors. This analyzed:

C	Mn	Si	Ni	Cr	Mo	Cb
0.18	3.3	0.70	7.3	19.0	2.9	1.0

In the as-rolled condition, this steel contained a small amount of ferrite, but when it was quenched from 2350 °F (1290 °C), it contained a large amount of ferrite. In other words, in the heating to 2350 °F (1290 °C), some austenite is converted to ferrite and this increased amount is retained at room temperature when the steel is cooled fairly rapidly. However, when the steel after being heated at 2350 °F (1290 °C) was transferred directly to a furnace at 1400 °F (760 °C) and held at this tempera-

ture, it could be observed that in a relatively short time an appreciable amount of ferrite changed back to austenite. The retained ferrite in the rapidly cooled sample was also transformed to austenite when the sample was reheated at 1400 °F (760 °C). The progress of the transformation is shown in Fig. 36. The top curve shows the change in magnetism with time at 1400 °F (760 °C), and the lower curve shows the change in room temperature hardness. At the end of 30 minutes at 1400 °F (760 °C), the

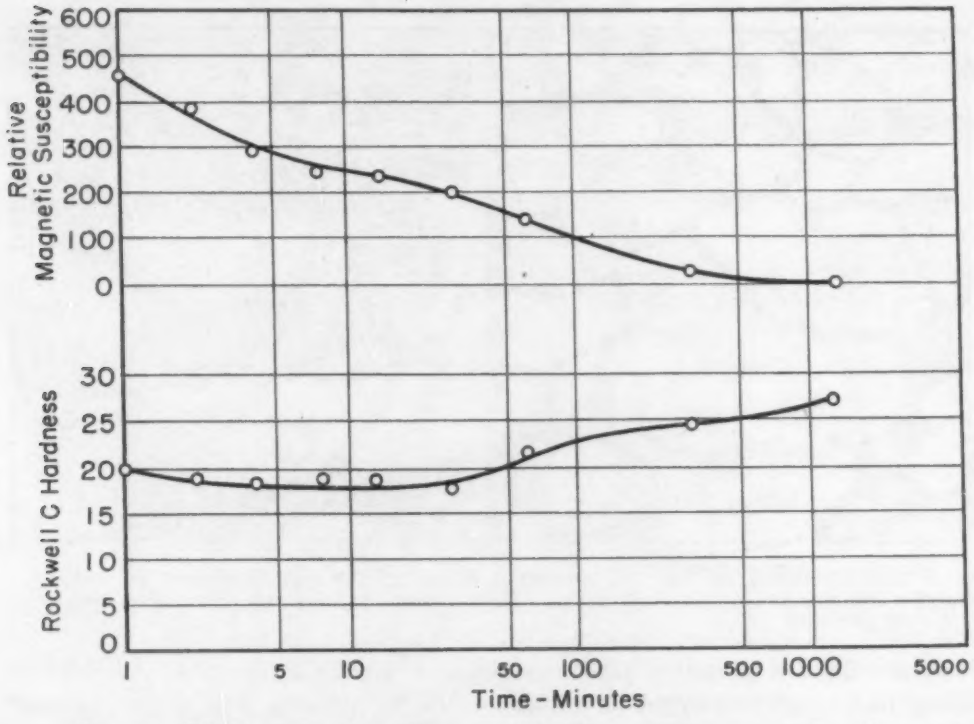


Fig. 36—Effect of Heating Time at 1400 °F on Changes in Magnetism and Hardness of 0.18% Carbon, 3.3% Manganese, 0.70% Silicon, 7.3% Nickel, 19.0% Chromium, 2.9% Molybdenum, 1.0% Columbium Steel Quenched from 2350 °F.

magnetism has dropped appreciably but the hardness has hardly changed. The structure of the steel at the end of 30 minutes at 1400 °F (760 °C) is shown in Fig. 37a. Obviously there has been a change in the ferrite but the X-ray diffraction pattern of this sample shows only ferrite and austenite and, therefore, it is safe to conclude that austenite is the new phase in the areas that were formerly ferrite.

With increasing time at 1400 °F (760 °C) there is a continued decrease in magnetism but there is also an increase in hardness. Since both austenite and sigma are nonmagnetic, the decrease in magnetism may mean the transformation of ferrite to either austenite or sigma, or both. The increase in hardness definitely implies the formation of sigma. The structure also shows sigma as may be seen in Fig. 37b, and this is confirmed by the X-ray diffraction pattern. However, we were not able to detect the change from austenite to sigma. Rather, we believe that some of the ferrite first transforms to austenite and then the remaining ferrite prob-

ably enriched by the ferrite-forming elements molybdenum, columbium and chromium transforms to sigma.

We also used a sample of the important commercial valve steel XCR which analyzed:

C	Mn	Si	Ni	Cr	Mo
0.42	0.81	0.72	4.7	23.3	2.6

This steel unlike the one previously discussed contains an appreciable amount of ferrite at the rolling temperature and the room temperature

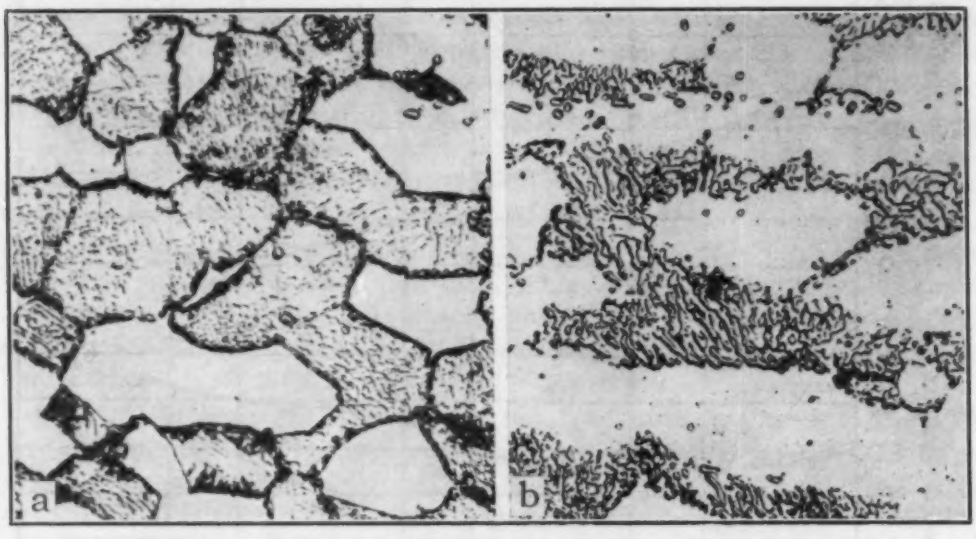


Fig. 37—Steel of Fig. 36, Quenched from 2350 °F and Reheated at 1400 °F. a—for 30 minutes; b—for 20 hours. Etched with hydrochloric-picric acid reagent. × 1000 (reduced 50%).

structure of the as-rolled steel consists of ferrite, austenite and carbide. When this steel is heated at 1400 °F (760 °C), there is a slight decrease in magnetism during the first hour of heating and practically no change in room temperature hardness. Also during this period there is no evidence of sigma in the X-ray diffraction pattern. We must conclude, therefore, that during the first hour of heating some of the ferrite transforms to austenite. Beyond the first hour of heating at 1400 °F (760 °C) there is a more marked drop in magnetism but this is accompanied by a marked increase in hardness and the appearance of sigma lines in the X-ray diffraction pattern. The changes in microstructure are not easy to follow in this steel but our tentative conclusion is that after the first formation of a small amount of austenite from the ferrite the ensuing formation of sigma is from the remaining ferrite and not from the austenite.

The delineation of the phases in the microstructures of these complex high alloy steels is extremely difficult and the concentrated Murakami reagent used by the authors does not always give satisfactory results. It is likely that some etching technique will be developed which will make it possible to trace the structural changes accurately and thus make the kinetics of sigma formation more clear than it now is.

We hope the authors of this paper will continue their study of sigma formation. The subject is not only of academic interest but since sigma is an important constituent of one of the most prominent automotive exhaust valve steels, it is also of considerable practical interest.

Written Discussion: By G. J. Guarnieri, research metallurgist, Cornell Aeronautical Laboratory, Inc., Buffalo.

Information of the type presented in this paper should be of interest to metallurgists and engineers utilizing austenitic stainless steels at both normal and elevated temperatures. Since such steels are usually considered nonheat-treatable in the normal sense of the word, it would seem that more effort should be made in utilizing the sigma constituent under controlled conditions as a hardener of the austenitic matrix. Such experiments of the type here presented provide preliminary information needed for any such controlled manipulation of sigma phase.

Work being done on Type 310 stainless sheet material indicates that the short-time, high-temperature, load-carrying ability of such an alloy may be improved by promotion of a fine sigma phase dispersion in its matrix by suitable aging treatments. Cold working prior to aging not only accelerates the sigma formation as indicated by the authors, but also promotes a finer distribution and less acicular type of constituent. The result may mean in some cases improved strength with ample ductility.

Written Discussion: By Howard S. Avery, research metallurgist, American Brake Shoe Co., Mahwah, N. J. (Chairman, Technical Research Committee of the Alloy Casting Institute.)

Occasionally interest is expressed in the sigma phase because of its hardness. Pertinent to this is a brief investigation recently completed as part of the Alloy Casting Institute research program at Battelle Memorial Institute. This work was aimed at producing a hardenable stainless steel with greater alloy content than is compatible with hardening in the 12% chromium types.

Using low carbon 29% Cr–9% Ni as the base composition, it was possible to attain a hardness of 350 to 490 BHN by means of aging between 1000 and 1600 °F (540 and 870 °C), which promoted sigma formation. However, this hardening was associated with extreme brittleness, with an expectation of mechanical properties much inferior to those of the hardened 12% chromium steels.

Corrosion resistance, after aging at 1000 °F (540 °C), was also poor, the corrosion rate in 65% boiling nitric acid being about ten times that of the same alloy in the solution heat treated condition. These observations, coupled with British reports of impaired resistance to sulphuric acid corrosion[4] because of sigma formation, suggest that sigma precipitation hardening is probably undesirable in chromium-nickel-iron corrosion resistant alloys.

Written Discussion: By R. D. Wylie, metallurgist, The Babcock & Wilcox Co., Barberton, Ohio.

[4]Smith and Bowen, "The Occurrence and Some Effects of Sigma Phase in a Molybdenum Bearing Chromium-Nickel Austenitic Steel," *Journal*, Iron and Steel Institute, Vol. 158, March 1948, p. 295-305.

In recent years fabricators and electrode manufacturers using and producing austenitic welding electrodes for welding pressure vessels operating at high temperature have been increasingly aware of the presence of microfissures in austenitic weldments. These fissures appear to lower the room temperature and high temperature ductility of such material. Several investigators[5, 6] have proposed that the presence of a small amount of delta ferrite in the weldment may inhibit either the formation or the effect of such fissures. It is for this reason that investigations such as the one conducted by Messrs. Gilman, Koh and Zmeskal are of primary interest in the field of welding metallurgy. The authors are to be commended for the thoroughness with which their investigation was made.

A similar study is in progress in the Works Control Laboratory of the Babcock & Wilcox Company in Barberton, Ohio, using weld metal samples of the following analysis:

	%
Carbon	0.09
Manganese	1.67
Silicon	0.62
Chromium	19.48
Nickel	9.93
Columbium	1.04
Sulphur	0.008
Phosphorus	0.011

The weld metal pads were prepared with $\frac{5}{32}$-inch diameter 19-9 Cb electrodes with beads deposited upon a plate of a similar composition to the weld metal. Sufficient layers were deposited to permit the machining of standard tensile specimens from the weld pad. Such a specimen will contain metal which has received numerous heat treatments. Some of the structure will remain "as-cast", other portions will have been reheated to temperatures below the melting point and quenched, while still other parts of the specimen will have been reheated several times at successively lower temperatures.

It was found as the authors indicated in Fig. 7 of the paper that successively higher heat treating temperatures above 1600 °F (870 °C) produced increasing quantities of delta ferrite and increased the magnetic permeability. Further samples treated in a laboratory furnace at temperatures from 1750 to 2400 °F (955 to 1315 °C) produced a similar effect, except at a temperature of approximately 2250 °F (1230 °C) where there appeared to be a definite drop in the quantity of ferrite present in the microstructure and a similar drop in magnetic properties. This phenomenon has not been explained.

The transformation structures and rates of their formation and dissociation are being studied at temperatures from 1050 to 2400 °F (565 to

---

[5]A. L. Feild, F. K. Bloom and G. E. Linnert, "The Effect of Variations in Chromium-Nickel Ratio and the Molybdenum Content of Austenitic (20 Cr – 10 Ni) Electrodes on Properties of Armor Weldments," NDRC Report, OSRD No. 303X, December 14, 1943.

[6]H. C. Campbell and R. D. Thomas, "The Effect of Alloying Elements on the Tensile Properties of 25-20 Weld Metal," *The Welding Journal*, Vol. 25, No. 11, Research Supplement, November 1946, p. 760-S to 768-S.

1315 °C). The complete data have not been accumulated as yet, but from initial data these conclusions have been drawn:

1. Sigma phase appears to transform progressively from the delta ferrite at temperatures from 1050 to 1600 °F (565 to 870 °C) with the rate of formation a maximum at about 1550 °F (845 °C). The rate of formation seems to be a function of the initial concentration of alloying elements, especially chromium, in the ferrite. The first ferrite formed from the melt is relatively pure iron and when quenched, as in welding, little or no diffusion will take place so that the ferrite remaining at room temperature will still have a low alloy concentration. When held for even very short periods of time at a temperature of 2350 °F (1290 °C) the diffusion of large amounts of such alloying elements as chromium, silicon, molybdenum and columbium into the delta ferrite occurs very rapidly. G. E. Claussen[7] showed relative diffusion rates for chromium in solid iron at 2020 and 2380 °F (1105 and 1305 °C) which indicate that the rate of diffusion of chromium is increased from 30 to 70 times as the temperature is raised. This indicates that the ferrite present after heating at 2020 °F (1105 °C) would probably have a much lower initial concentration of alloying than that formed at 2380 °F (1305 °C). Therefore, one would expect that the higher alloyed ferrite would transform to sigma more rapidly than the ferrite having a low initial concentration of alloying elements. This was substantiated in the authors' paper and in our investigation.

2. The authors' suggestion of an initial transformation of the delta ferrite to austenite prior to the formation of sigma phase is rather hard to justify, especially at temperatures of 1200 and 1400 °F (650 and 760 °C). If the ferrite conforms to the same pattern as the iron-chromium alloys, which is quite likely, the minimum transformation temperature has been given by numerous investigators[8] as 1490 °F (810 °C). At 1600 °F (870 °C) such a transformation is more likely, but should again depend upon the chromium concentration of the ferrite. The presence of carbon does not lower the critical transformation temperature but merely increases the area within the gamma loop. The presence of nickel in the delta ferrite is questionable because if there were sufficient nickel some intermediate transformation to martensite would be expected and as yet no such transformation has been reported.

3. We have noticed the behavior of columbium carbide in this investigation and believe that at temperatures above 1500 °F (815 °C) in the presence of delta ferrite and/or sigma phase there is some dissociation of columbium carbide with an accompanying diffusion of columbium into the ferrite or sigma.

In closing, we agree with the authors that more investigation is necessary, particularly with respect to the effect of delta ferrite and sigma phase on the high temperature properties of these materials.

[7] G. E. Claussen, "The Diffusion of Elements in Solid Iron," TRANSACTIONS, American Society for Metals, Vol. 23, 1935, p. 640-648.

[8] A. B. Kinzel and Walter Crafts, "The Alloys of Iron and Chromium"—Vol. 1: Low Chromium Alloys, The Engineering Foundation Monograph Series, McGraw-Hill Book Co., New York, 1937, p. 31-45.

Authors' Reply

The data Mr. Evans contributed are of great interest. Molybdenum is a powerful promoter of sigma phase, and we believe that the reduction of the quantity of this element by a factor of four to five in 19-9 W-Mo, as compared to 19-9 DL, accounts for the lack of sigma phase found in the steel. It is possible, however, that much longer times than the 91 hours used will develop sigma phase in this steel, and this is now being determined.

With the acid etches described by Mr. Evans it is very difficult to distinguish between ferrite and sigma. We do not advise the use of the etching procedure by which acid is followed by alkali as the sigma tends to dissolve out.

Our magnetic determinations were made by measuring the forces required to pull a standard Alnico magnet away from the specimens cut to a standard size. The magnet was suspended from one arm of an analytical balance, and the specimen was held in a copper vise. As Mr. Evans points out, magnetic measurements alone are not much help in determining whether ferrite is transforming to austenite or to sigma; however, when made in conjunction with X-ray diffraction, hardness, density, and metallographic measurements, they are very helpful indeed.

The authors find Messrs. Payson and Chang's photomicrographs of great interest. The manner in which the sigma growth seems to have followed the traces of the ferrite in the structures is significant. However, the evidence is not clear-cut as to whether the sigma formed from ferrite or from austenite. There seems to be some lack of balance between the magnetic changes and the appearance of the microstructures.

The authors wish only to state that it is possible, in some steels, for the sigma phase to form from austenite and yet have its formation accelerated by the presence of former ferrite which served to concentrate sigma-forming elements locally. That is, sigma need not form directly from ferrite for ferrite to promote its formation.

The exact sequence of the reaction which leads to the transformation of some of the steel to the sigma phase depends on the balance of the steel toward austenite stability for a given temperature and composition. In steels which have austenite of high stability the sigma forms directly from the austenite, as was shown by Payson and Savage for 25 chromium – 20 nickel stainless steel. Some steels have stable duplex ferrite-austenite structures in the sigma formation temperature range. In these steels, we believe that sigma forms directly from the ferrite. In 19-9 DL, the ferrite is highly unstable in the sigma formation range and we believe that sigma forms not from ferrite but from austenite which was formerly ferrite. The steel that Messrs. Payson and Chang used seems to have behaved in an intermediate manner. This could be expected because of the rather favorable compositional balance of the steel toward ferrite stability.

We would like to emphasize, as Payson and Chang have stated, the caution that must be observed in examining microstructures of these com-

plex steels. As many as four phases may be present simultaneously and as each has an etching rate different from the others, proper etching requires much skill. Also, as Mr. Thomas pointed out, the alkaline etchants usually used for these steels seem to be quite sensitive to variations in composition as well as to different phases. Thus, what appears to be ferrite may be highly alloyed austenite, etc.

The most satisfactory etchant known to us, for four-phase structures (austenite, ferrite, sigma, carbides) is the modified Murakami's reagent. Its behavior is quite erratic, however. We suggest alkaline sodium picrate, used electrolytically, as another satisfactory reagent which is useful in that it usually attacks sigma more rapidly than carbides and may, therefore, be used to aid in identification.

Mr. Thomas asked whether we observed in 19-9 DL the color changes observed by Burgess and Forgeng in iron-chromium-manganese alloys when the specimen was rotated in polarized light. We did not observe that any changes in color occurred. It seems unlikely that the crack-like markings on the etched sigma phase in alloys like 19-9 DL, where the amount of sigma is less than 50%, are due to actual cracks in the sigma phase. Acid etching reagents have never shown cracks in sigma. Alkaline reagents will produce crack-like markings on the ferrite of ferrite-austenite duplex structures in which no sigma is present; these crack-like markings occur at long etching treatments and widen into bands as the time of etching is further prolonged. Furthermore, in sigma structures, in which the sigma actually seems to have cracks in it, it is difficult to conceive how these cracks can heal up so perfectly on solution treatment, as the density data of Mr. Thomas indicates they do. Surely the presence of cracks would change the density, and not allow an almost exact return to the density of the austenite phase.

We welcome Mr. Guarnieri's remarks on the value of sigma phase for promoting increased high temperature strength properties of stainless steels. The 19-9 DL alloy has had a successful commercial history. A good example of a commercially successful application, of designed-for-sigma phase hardening, is afforded by the valve steel, XCR, containing 24% chromium, 5% nickel, 0.40% carbon, and 3% molybdenum.

However, as Mr. Avery points out, brittleness and lower corrosion resistance in certain media are obstacles which limit the general application of sigma-hardened steels.

In point 2 of Mr. Wylie's discussion it is maintained that 1490 °F (810 °C), the temperature for the alpha-gamma transformation in the binary iron-chromium alloys, is also to be expected as the minimum transformation temperature in 19-9 DL. As given in "The Alloys of Iron and Chromium", Volume II, page 270, the transformation temperature in an 18% chromium – 8% nickel alloy is 675 °F. It is to be expected that the other elements in 19-9 DL will raise this temperature but hardly much over 1100 °F (595 °C). We cannot agree with Mr. Wylie as to his statement that "the presence of nickel in the delta ferrite is questionable", since the equilibrium diagrams available at present all show that high quantities of nickel can be present in ferrite.

PREDICTING THE EFFECT OF COMPLEX TEMPERING CYCLES

By J. L. Waisman and W. T. Snyder

Abstract

A method has been developed for predicting the effect of a complex tempering cycle on the hardness of quenched steels. The technique involves the division of any complicated tempering cycle into a series of small isothermal "steps" and the integration of the hardness effects of all such steps.

Experimental isothermal tempering data are presented for two medium carbon alloy steels. These data are used to illustrate predictions of the effects on hardness of variations in heating and cooling rate, and of fluctuations at the tempering temperature.

The data are compared with a general relationship proposed by Hollomon and Jaffe in a recently published paper, and, within limits, excellent agreement is obtained.

A CONSIDERABLE amount of work has been done during the past two decades which has clarified concepts of the mechanism of steel hardening and tempering and of the engineering advantages of such heat treatment. It has now been widely recognized that, for the alloy constructional steels, the best combination of tensile, impact and fatigue strengths is obtained by "through hardening" and tempering. A large amount of metallurgical effort has been expended in providing data to enable the engineer and metallurgist to predict the "as-quenched" hardness gradient to be expected from a steel when various shapes and sizes are quenched into a variety of quenching media. The "as-quenched" hardness gradient is used as a measure of the microstructure. Knowing the hardened structure, the engineer can estimate the range of static, impact, and fatigue properties which can be produced in a part after tempering to a given hardness, and proceeds to specify the hardness to which each part is to be tempered.

A paper presented before the Thirtieth Annual Convention of the Society, held in Philadelphia, October 23 to 29, 1948. Of the authors, J. L. Waisman is metallurgist, Douglas Aircraft Company, Inc., Santa Monica, California, and W. T. Snyder is chief engineer, Herff Jones Company, formerly metallurgist, Douglas Aircraft Company, Inc., Chicago. Manuscript received March 24, 1948.

In selecting the tempering time to secure a specified hardness, most heat treating departments follow a "rule-of-thumb" method, by arbitrarily allowing 2 hours at the tempering temperature for each inch of maximum cross section. The selection of tempering temperature is then made by "experience" or by use of a chart such as is shown in Fig. 1.

Under most production conditions, such a procedure is entirely adequate for producing acceptably heat treated parts. Frequently, however, unorthodox tempering cycles may be desired or equipment

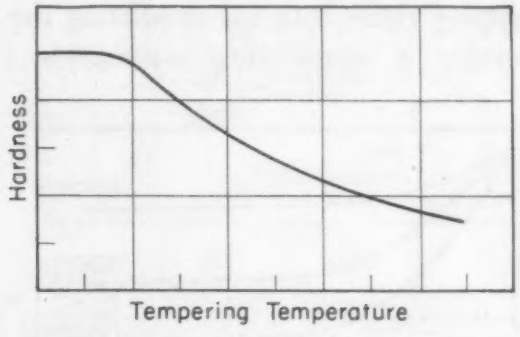


Fig. 1—Typical Chart Used for the Selection of Tempering Temperatures.

breakdowns may produce undesired fluctuations in the tempering cycle. For example, a furnace may be extremely slow in heating or cooling. Or, the furnace may go out of control and either overshoot or undershoot the desired temperature. In each case, modifications of the time at the tempering temperature may be required for developing the specified hardness.

Until recently, little information was available which would make it possible to predict the effect of unusual or complex tempering cycles. An excellent recent paper presented by Hollomon and Jaffe[1] has presented an analytical technique which, it appears, will enable the metallurgist to make such predictions based on a small amount of experimental data.

This paper presents a similar graphical method employed by the authors for making such predictions and includes the experimental data necessary for predicting the effect of tempering cycles for two medium carbon alloy steels. A comparison is made between the authors' experimental results, and predictions of these results made, using the technique presented by Hollomon and Jaffe.

[1] "Time-Temperature Relations in Tempering Steel," by J. H. Hollomon and L. D. Jaffe, American Institute of Mining and Metallurgical Engineers, Technical Publication No. 1831, *Metals Technology*, September 1945.

Authors' Method

The authors have employed the following technique in making their predictions: First, data on isothermal tempering effects are accumulated. This is accomplished by selecting significant temperatures in the tempering range and tempering groups of quenched samples for various times at each of these temperatures. (A description of a typical procedure is included in the appendix.) The data are conveniently plotted as time-hardness curves as shown in Fig. 2.

In order to employ these data for predicting the effects of other than isothermal cycles, a simplifying assumption is required. It

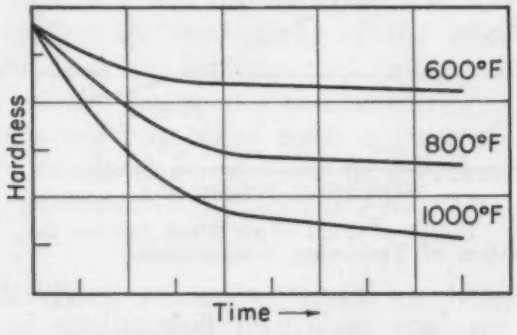


Fig. 2—Chart Showing Hardness Curves.

must be assumed that hardness is the sole criterion of "degree of tempering". This statement implies that although a given hardness can be produced by a large variety of tempering cycles, all such cycles are equivalent. For example, if a hardness of Rockwell C-34 could be produced in a quenched and tempered steel either by tempering at 950 °F for 4 hours or tempering at 1000 °F for 1 hour, it is assumed that each cycle produces exactly the same structure. Further, if the quenched specimen has been tempered at 950 °F for 4 hours and is suddenly heated to 1000 °F, the specimen will immediately act just like a sample of the same hardness which has already been tempered at 1000 °F for 1 hour.

With this assumption the way is now clear for predicting the effect of complex cycles; it is only necessary to divide any cycle into a series of isothermal steps. The progress of tempering during each isothermal heating is determined from the time-hardness curve for that temperature. The transition from one curve to another is made by assuming an instantaneous heating (or cooling) from one

temperature to another, and therefore by passing from one curve to another at equal hardness lines.

A typical breakdown of this type is shown in Fig. 3. The upper portion of this figure shows a simple tempering cycle broken down into its components. This cycle includes a 1-hour dwell in temperature range A, and 1 hour in range B during heating. Four hours

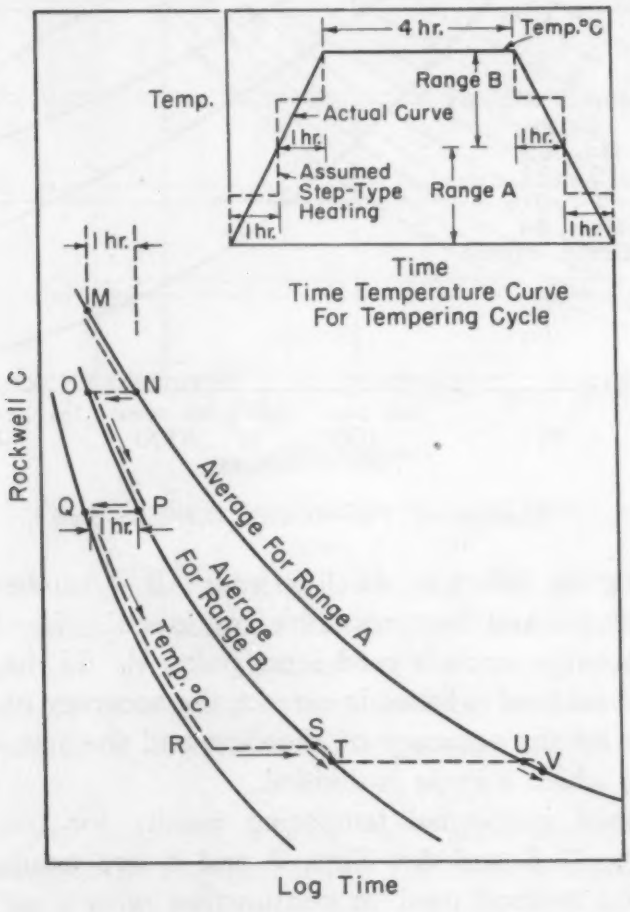


Fig. 3—Method of Integrating Effect of Heating, Soaking and Cooling.

are spent at temperature C. During cooling, 1 additional hour is spent in each of the temperature ranges B and A. Referring now to the lower portion of Fig. 3, the effect of each component part of the cycle can be determined. Line MN shows the hardness decrease which would result from heating in temperature range A. A horizontal line NO is now drawn, since the hardness of any particle at the beginning of the time dwell in range B is assumed to be the same as it was at the end of the dwell in range A. Next, the line OP is

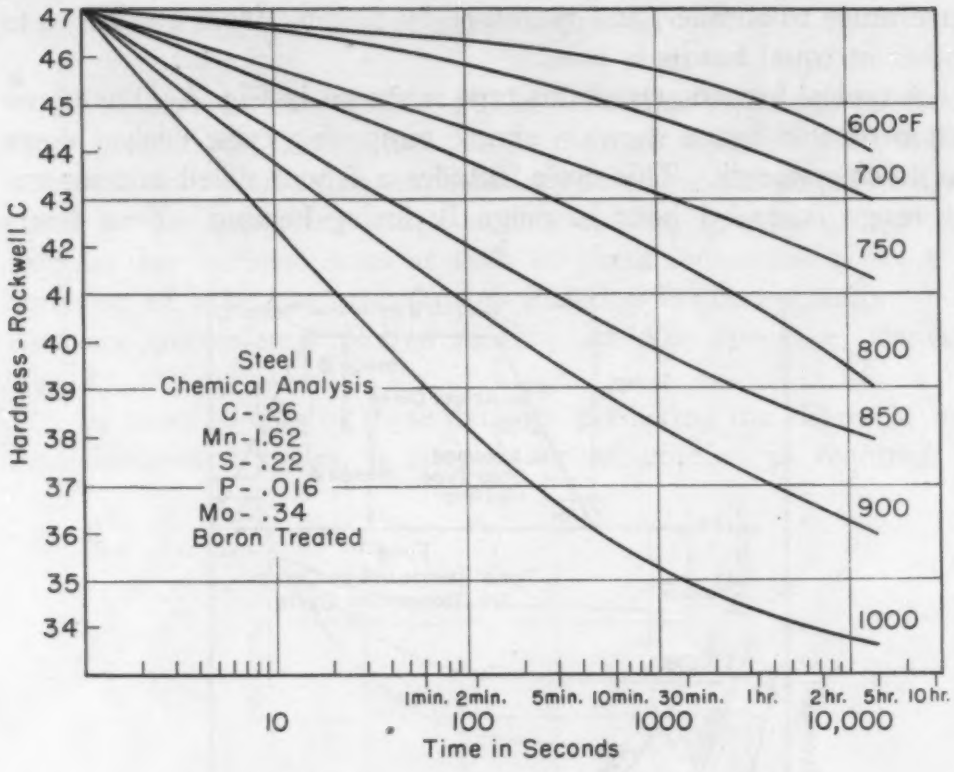


Fig. 4—Experimental Time-Hardness Curve for Steel 1.

drawn, showing the effect of dwell in range B. Another horizontal line is now drawn and the procedure continued. The hardness at the end of the entire cycle is read from point V. If the assumption upon which the method is based is correct, the accuracy of the method is limited only by the accuracy of the data and the size of temperature steps into which a cycle is divided.

The authors' isothermal tempering results for two steels are shown in Figs. 4, 5 and 6. Figs. 7 and 8 are examples of the accuracy of the method used in conjunction with Fig. 5 for predicting the effects of complex cycles. In these figures the actual hardnesses resulting from a series of complex tempering cycles are compared with the predicted hardness. It is apparent that good correlation is obtained.

It is obvious, however, that for steels and temperature ranges where secondary hardening accompanies tempering, the method outlined would not be valid, since equivalent hardnesses may not always be equivalent structures. One other caution is appropriate here for those wishing to make use of this or similar techniques. No implication has been intended that hardness and structure alone determine

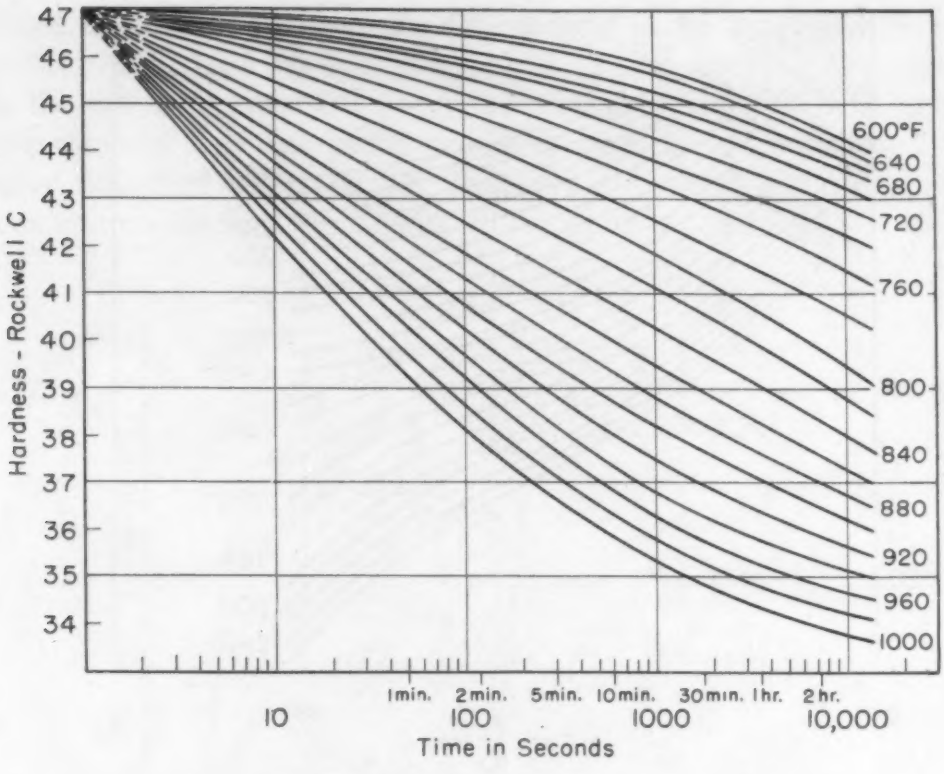


Fig. 5—Idealized Time-Hardness Curves for Steel 1.

the mechanical properties of a heat treated steel part. It is recognized that for many conditions the residual stresses in a part may play an important part in determining its strength characteristics. In such cases, caution must be employed to see that manipulations of a tempering cycle do not cause dangerous residual stresses.

Comparison of Authors' Data with Empirical Functional Relationship Developed by Hollomon and Jaffe

Hollomon and Jaffe have demonstrated that for a variety of steels showing no secondary hardening, the following relationships are valid:

$$H = f\,[T\,(c + \log t)\,] \qquad \text{Equation I}$$

where H is the hardness in any units, T is the absolute temperature, c is a constant for the steel in question, and t is the time in any units.

Except for hardnesses below Rockwell C-25 and hardnesses within 3 points of the "as-quenched" hardness, and except for steels con-

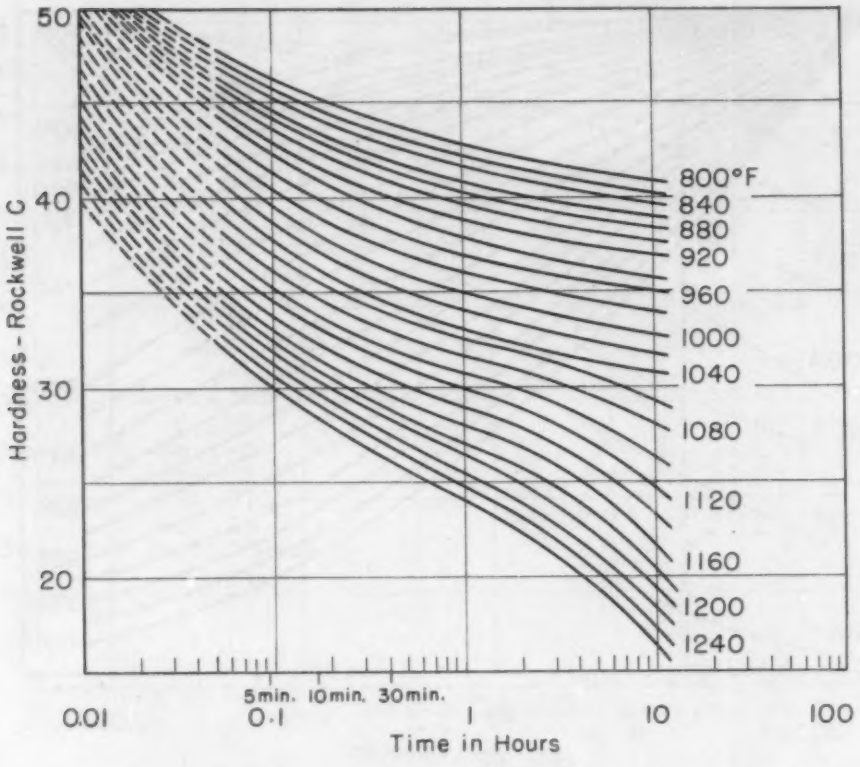


Fig. 6—Idealized Time-Hardness Curves for Steel 2. (SAE 4140)

taining large quantities of carbide-forming elements, the above functional relationship takes a form typified by this equation:

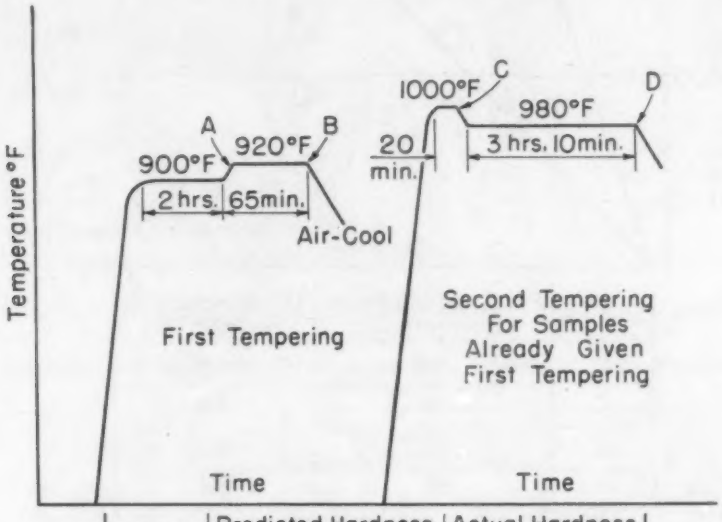
$$R_c = H_c - 0.00457T\ (13.0 + \log t) \qquad \text{Equation II}$$

where R_c is the Rockwell "C" hardness of the steel, H_c is an experimentally determined characteristic of the steel termed "characteristic hardness", T is the absolute temperature on the Kelvin scale, and t is the tempering time in seconds.

Equation I gives an infinite series of time-temperature combinations which will yield the same hardness. The test of validity for Equation I is that a plot of hardness versus the function $T\ (c + \log t)$ should give a smooth curve with reasonably small scatter. Fig. 9 is such a plot of the authors' data previously shown in Fig. 4. The plot was made after "c" was calculated on the basis of several time-temperature combinations known to give the same hardness. The curve is smooth and the scatter well within the range of experimental error.

Fig. 10 is a reproduction of a chart presented by Hollomon and Jaffe for rapid solutions of Equations I and II. By the use of this chart, predictions were made for the hardness which would be pro-

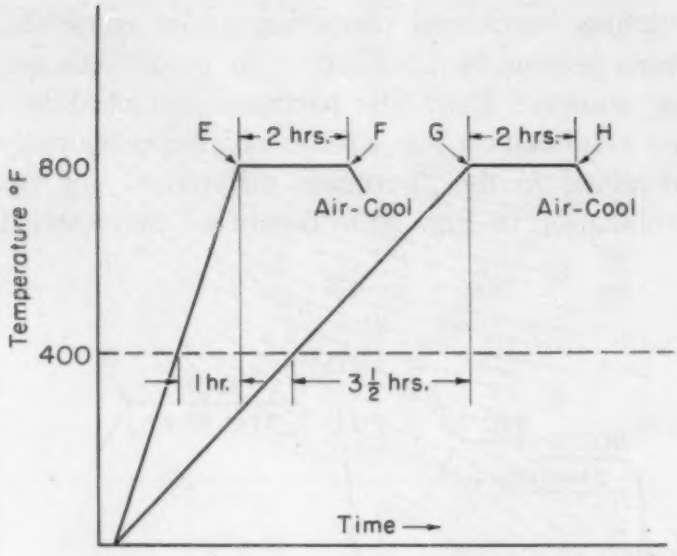
duced during various isothermal tempering cycles employed by the authors in the tests previously described. The predictions were made in the following manner: First, the hardness produced by a given time-temperature combination was determined experimentally. This value was then added to the "hardness difference" for that time-temperature combination in Fig. 10 to obtain a "characteristic hard-



Sample	Predicted Hardness Rockwell C	Actual Hardness Rockwell C
A	36½	36½
B	36	35
C	35½	35½
D	34	33½

Fig. 7—Effect of Complex Cycle and Double Tempering on Rockwell Hardness. Comparison of actual and calculated values. Four samples started through cycle. Each of four removed at various stages as shown.

ness". For any other time-temperature combination the predicted hardness is determined by reading the "hardness difference" corresponding to the new time and temperature in Fig. 10. This number is then subtracted from the "characteristic hardness" previously determined, to give the predicted hardness. For example, for steel 1, Fig. 5, tempering for 1 hour at 800 °F gives a hardness of Rockwell C-40.5. According to Fig. 10, 1 hour at 800 °F corresponds to a hardness difference of 53. Adding 53 and 40.5 gives a "characteristic hardness" of 93.5. Now, to predict the hardness which would be developed by tempering at 1000 °F for 15 minutes, we check Fig. 10 and find that this time-temperature combination corresponds



Sample	Predicted Hardness Rockwell C	Actual Hardness Rockwell C
E	44	44
F	39	39
G	41	40½
H	38	38

Fig. 8—Effect of Variations in Heating Time on Rockwell Hardness. Comparison of actual and calculated values.

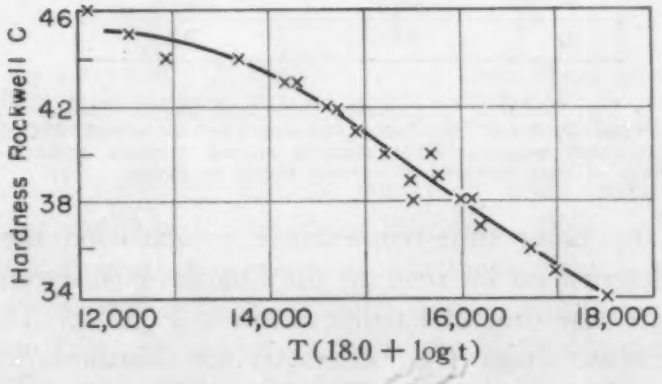


Fig. 9—Check on Functional Relationship of Hollomon and Jaffe.
$H = f\ [T(C + \log t)]$
Where H is the hardness
t is the tempering time in seconds
C is a constant characteristic of the steel
T is the Absolute Temperature °K

to a "hardness difference" of 59.5. Subtracting this value from the "characteristic hardness" of 93.5 gives us the predicted hardness of

Table I
Comparison of Experimental Hardness Determinations with Predictions after Hollomon and Jaffe

(Steel 1)
Rockwell "C" Hardness

Tempering Temperature	Time Hours	Actual Hardness	Predicted Hardness
600 °F	¼	45½	50½
	1	45	48½
	4	44½	47½
800 °F	¼	42	42
	1	40½*	40½
	4	39	38½
900 °F	¼	38½	38
	1	37	36½
	4	36	34½
1000 °F	¼	35	34
	1	34	32
	4	33	30

*This value was used to establish H_c.

Table II
Comparison of Experimental Hardness Determinations with Predictions after Hollomon and Jaffe

(Steel 2)
Rockwell "C" Hardness

Tempering Temperature	Time Hours	Actual Hardness	Predicted Hardness
800 °F	½	44	44½
	2	42½*	42½
	12	40½	40½
1025 °F	½	34½	35
	2	33	33
	12	30½	30½
1250 °F	½	23½	23½
	2	22	22½
	12	15½	20½

*This value was used to establish H_c.

Rockwell C-34. The actual hardness obtained, Fig. 5, is Rockwell C-35.5.

Tables I and II show a series of such comparisons for steels 1 and 2. Most of the predictions are within 1 point of the true values; some predictions differ from the true value by 2 points; and an occasional deviation of 3 to 5 points is observed. The larger deviations are for hardnesses close to the "as-quenched" hardnesses or for the structures softer than Rockwell C-20. Considering that experimental error is at best 1 point Rockwell C, this agreement is remarkably good.

A method for predicting the hardness of tempered steels for which no experimental data are available is also tentatively advanced by Hollomon and Jaffe, in terms of data correlating the "character-

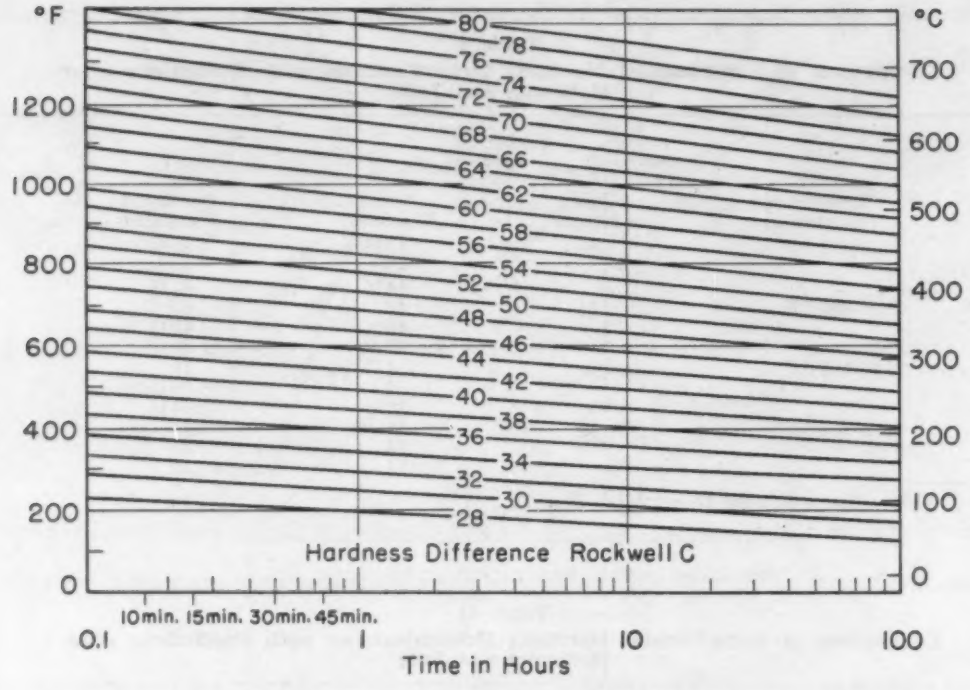


Fig. 10—Chart for Finding Time-Temperature Combinations Giving Equivalent Tempering Presented by Hollomon and Jaffe in Paper Reference in Text.

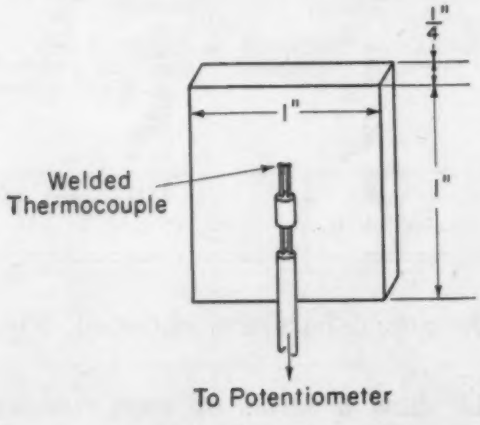


Fig. 11—Size of Typical Sample and Location of Thermocouple on Temperature Check Sample.

istic hardness" with carbon content. Using these data, a "characteristic hardness" of 88 would be predicted for steel 2 (AISI4140). The use of Fig. 10 in conjunction with experimental data shows the correct value to be 96.5. Use of the 88 value would therefore have resulted in a large error in predictions. This result confirms the conclusions of Hollomon and Jaffe that such predictions based on no experimental data are undependable.

Conclusions

1. An accurate method based on empirical data has been developed for predicting the effect of simple and complex tempering cycles on the hardness of a quenched steel.

2. For two medium alloy steels tested, accurate predictions of hardnesses developed in simple and complex tempering cycles are possible, based on a limited amount of experimental data and the use of a functional relationship developed by Hollomon and Jaffe.

3. Where no experimental tempering data are available for a steel, dependable predictions cannot be made using the Hollomon and Jaffe functional relationship.

Appendix

Experimental Procedure

Fig. 11 shows the size of a typical specimen used in the tempering tests. A group of these specimens was heated to production hardening temperatures and quenched. After careful wet grinding, the hardness of each specimen was determined. A number of specimens were then placed in a small electrical-resistance-element heated furnace operating at a predetermined temperature in the tempering range. The heating-up times of all groups of specimens were checked by inserting a "dummy specimen" with thermocouple attached as shown in Fig. 11. Specimens were withdrawn at intervals and air-cooled. They were then reground on No. 240 emery paper and their hardness redetermined. At least 15 readings were taken on each specimen.

Heating-up times were approximately 5 minutes. Certainly the first of these 5 minutes has a negligible softening effect. Therefore, if we assume that the effect of the heating time for these specimens is equivalent to 2 minutes at temperature, the error of this assumption cannot exceed plus or minus 2 minutes. Each actual time at temperature is therefore increased by 2 minutes before plotting curves of the type shown in Figs. 4, 5 and 6.

Acknowledgments

The authors wish to thank the officials of the Douglas Aircraft Company, Inc., Santa Monica, California, for permission to publish these data.

DISCUSSION

Written Discussion: By J. A. Kavenaugh, technical advisor, Revere Copper and Brass Inc., Los Angeles.

The information and procedure presented in this paper is the type so greatly needed to bring the recent advancements in theoretical metallurgy to the working level of the engineer. The authors have shown a method whereby much of the guesswork may be eliminated in predicting the properties of steels under unorthodox tempering cycles.

However, the chart given in Fig. 10 must be made with some assigned or average value of the constant C of Equation I. Since this constant is characteristic of the steel, the chart in Fig. 10 must be a series of curves whose slope is governed by an assigned value. This is shown by the fact that although the steels in Tables I and II are apparently quite similar in time-hardness curves, steel No. 2 shows little divergence between the predicted and actual hardness, whereas steel No. 1 shows a marked increase in divergence as either the time or temperature is increased, indicating that the assigned value of C used in Fig. 10 is entirely too high for the steel. Does this mean that separate charts are necessary for steels with different values of C?

Written Discussion: By H. E. Hostetter, Climax Molybdenum Company of Michigan, Detroit.

The authors have shown good judgment in cautioning that hardness and structure (presumably the structure revealed by routine metallographic technique) are not the only factors affecting the mechanical properties of a heat treated steel part. The authors have recognized the possibility of detrimental residual stresses. In addition it should be recognized that a steel susceptible to temper embrittlement can, at a given hardness, vary appreciably in impact properties as a result of changes in the tempering treatment.

Insofar as prediction of hardness is concerned, there are at least two factors which in practical application would significantly affect the results obtained by the method described in this paper. These factors are: (a) the effect of as-quenched structure on the rate of softening during tempering, and (b) the effect of composition on the hardness after tempering.

The authors used specimens 1 by 1 by ¼ inch which should have been practically 100% martensite prior to tempering. In commercial practice, parts made of the widely used low alloy steels often contain considerably less martensite in the as-quenched condition. The effect of as-quenched structure on the hardness after tempering is illustrated in Table III obtained with a Jominy specimen of AISI 8650 steel.

The data in Table III show that a 2-hour temper at 900 °F of parts made of this steel, having 60% martensite as-quenched, would result in a hardness about three points Rockwell C lower than predicted on the basis of tests made on samples containing 90 to 100% martensite before tempering.

Variation in the carbon and alloy contents within the specified limits for a given grade of steel can also have significant effects on the hardness

Table III

Composition: 0.51% C, 0.71% Mn, 0.25% Si, 0.45% Cr, 0.57% Ni, 0.20% Mo
Austenitizing Treatment: 30 minutes at 1550 °F

Distance from Quenched End ⅛ Inches	% Martensite As-Quenched	Hardness—Rockwell C	
		As-Quenched	Tempered 2 Hr., 900 °F
2	100	61.0	40.5
5	95	57.5	40.5
6	90	56.5	40.3
7	80	53.8	39.3
8	60	50.5	37.3
9	30	46.3	36.0

after tempering, as Crafts and Lamont have shown.[2] Even residual elements may appreciably affect the hardness after tempering. The effect of 0.05% molybdenum, which is within the limit permitted by the AISI for residual molybdenum, is shown in Table IV obtained with Jominy specimens.

Table IV

	0.00 Mo	0.05 Mo
Carbon	0.61%	0.63%
Manganese	0.77	0.79
Silicon	0.25	0.25
Chromium	0.80	0.79
Molybdenum	0.00	0.05

Austenitizing Treatment: 20 minutes at 1550 °F

Distance from Quenched End ⅛ Inches	Hardness—Rockwell C			
	As-Quenched		Tempered 1½ Hr., 1000 °F	
	0.00 Mo	0.05 Mo	0.00 Mo	0.05 Mo
2	64.8	65.0	36.0	37.0
3	63.3	64.3	36.0	37.3
4	62.5	63.8	35.5	37.0
5	61.5	63.3	35.5	37.3
6	59.8	62.3	35.0	37.0
7	56.0	61.5	33.3	36.8
8	51.0	60.3	31.5	35.8
9	45.3	57.3	30.3	35.0
10	41.0	54.5	29.0	33.5
11	38.5	49.5	28.0	32.8

The data in Table IV show that for a given as-quenched hardness the 0.05% molybdenum steel was about 1 to 1.5 points Rockwell C harder after the tempering treatment. For a given part, as represented by a given location on the Jominy specimen, the effect of molybdenum on the hardness after tempering can be much greater.

To illustrate the error that could occur in prediction of hardness, the following example is considered for the 0.00 molybdenum and the 0.05 molybdenum steels. Tempering time – hardness curves might be constructed based on tests made on small specimens of the 0.05% molybdenum steel having as-quenched hardness of Rockwell C-65 (2/16-inch position on the Jominy specimen). Such curves would indicate a hardness

[2]Walter Crafts and John L. Lamont, "The Izod Impact Strength of Heat Treated Alloy Steel," *Transactions*, American Institute of Mining and Metallurgical Engineers, Vol. 172, 1947.

of Rockwell C-37 after tempering for 1½ hours at 1000 °F. If a steel of 0.00% molybdenum, but otherwise the same composition, was obtained and made into parts quenched at a rate corresponding to the 8/16-inch position on the Jominy specimen, the hardness after the same tempering treatment would be Rockwell C-31.5 instead of the predicted Rockwell C-37.

If the authors' method for prediction of hardness after tempering is to be used with a satisfactory degree of precision in commercial heat treating practice, the tempering time – hardness curves must be based on samples having about the same as-quenched structure and composition as the parts for which hardness is to be predicted. As indicated in this discussion, significant errors may result if the parts differ from the samples within commercial limits of as-quenched structure and composition.

Authors' Reply

In reply to Mr. Kavenaugh's question, Fig. 10, which shows the combinations of time and temperature giving various hardnesses, is taken from the paper by Hollomon and Jaffe previously referred to. It was based on assuming the constant "C" as 19.5, where the time is in hours. Hollomon and Jaffe have shown that although C varies somewhat from steel to steel, this variation has very little effect on calculated values.

The deviations of predicted and actual values pointed out by Mr. Kavenaugh are a reflection on the lack of complete accuracy in the relationship involved. This deviation is particularly serious for hardnesses close to the as-quenched hardness or hardnesses below Rockwell C-25. Even within the applicable range occasional deviations of 2 to 3 points Rockwell "C" must be expected.

Mr. Hostetter's data and comments are welcomed. He is quite right in pointing out that inaccuracies do arise in making predictions of the hardness of parts based on data accumulated for other "as-quenched" structures on slightly different chemistries. The way to avoid such inaccuracies is, as Mr. Hostetter suggests, to use only data for the chemistry and "as-quenched" structure in question. Two other possibilities also suggest themselves for cases where data are not available for the exact chemistry and structure in question. Taking one "as-quenched" part from the material in question, check its hardness, temper for one time-temperature combination, and recheck the hardness. Using the available data for the same type of steel, make a graphical correction of the curve family. This family can now be used for a fairly accurate prediction of the effect of complex cycles. Another possibility is to use the hardness data for the sample part after tempering, and make the prediction based on the Hollomon and Jaffe technique previously outlined.

SIMPLE ELECTROLYTIC POLISHING PROCEDURES FOR MOLYBDENUM METALLOGRAPHIC SPECIMENS

By William C. Coons

Abstract

Electrolytic polishing techniques for the metallographic preparation of both sintered and cast molybdenum specimens have been developed. The actual polishing time required is approximately 1.5 minutes, whereas by conventional methods upwards of an hour's time is required to prepare comparable surfaces.

The apparatus necessary to perform the electrolytic polishing is extremely simple, consisting merely of two to six 1½-volt dry cells connected in series, a 200 cc porcelain dish, a stainless steel cathode, and a bare-end copper wire as the anode lead for contacting the specimen.

The electrolyte for sintered molybdenum is 35 ml concentrated sulphuric acid plus 140 ml distilled water and for both cast and sintered molybdenum 50 ml concentrated hydrochloric acid, 20 ml concentrated sulphuric acid, and 150 ml methyl alcohol (95%).

Two new methods of etching molybdenum are advanced, namely, 0.5% oxalic acid used electrolytically and a polish and an etch buff.

MOLYBDENUM, because of its intermediate hardness (Brinell Hardness Number—BHN-150 to 250), is a metal which one would expect could be polished as readily as the ordinary straight carbon steels. However, metallographers who have polished molybdenum by conventional methods have undoubtedly discovered that such is not the case.

The author[1] previously outlined procedures and suggested materials whereby most metals and their alloys could be prepared for microscopic examination with considerable ease. Molybdenum can

[1]William C. Coons, "A Universal Metallographic Polishing Procedure," Metal Progress, Vol. 49, May 1946, p. 956.

These procedures were developed while operating under contract NOrd 9829 with the Bureau of Ordnance, U. S. Navy.

The author, William C. Coons, is metallographist, The Silver Spring Laboratory, The Kellex Corp., Silver Spring, Md. Manuscript received October 16, 1948.

be hand-polished by those techniques, perhaps as well as by any other method, but the task is rather difficult and time-consuming, particularly if a surface is desired which is entirely free of worked surface metal.

In a laboratory report,[2] the surface brightening of molybdenum was stated to be possible by using the molybdenum as the anode in an electrolytic bath of an aqueous solution of concentrated sulphuric acid. Although no other details were given, reference was made to "Le Materiel Telephonique", a French patent No. 707,526 (1930). At first, the only interest in this information was in respect to obtaining an oxide-free surface on molybdenum sheet in conjunction with a program unrelated to metallography. With this objective in mind, an oxidized, scratched, and pitted piece of molybdenum was treated for several minutes in an electrolyte of concentrated sulphuric acid and distilled water combined in unmeasured proportions. This treatment removed the oxide and in some areas polished the specimen sufficiently well to merit an examination on the microscope.

After viewing the polished areas at magnifications in excess of 500, it was realized that, with a few modifications, an extremely rapid and simple method for the preparation of molybdenum metallographic specimens was a possibility.

Precise and predetermined procedures were tried on numerous specimens of sintered and cast molybdenum and excellent results were obtained on all specimens with the exception of those containing molybdenum carbides. This problem was eventually overcome by the development of a different electrolyte.

Material and Procedures

The types of molybdenum specimens employed in the development of the electrolytic polishing method are listed below:

1. Molybdenum sheet, 0.035 inch thick — sintered and wrought.
2. Molybdenum sheet, 0.035 inch thick—sintered, wrought and recrystallized. (Recrystallization temperature unknown—spot-welded area.)
3. Numerous specimens of sintered and wrought and sintered, wrought and recrystallized molybdenum ranging from 0.035-inch thick sheet to 3/8-inch round bar stock.

[2] E. C. Pierce, "Physical and Chemical Properties of Molybdenum—Abstract and Bibliography," Research Laboratory, Climax Molybdenum Company of Michigan.

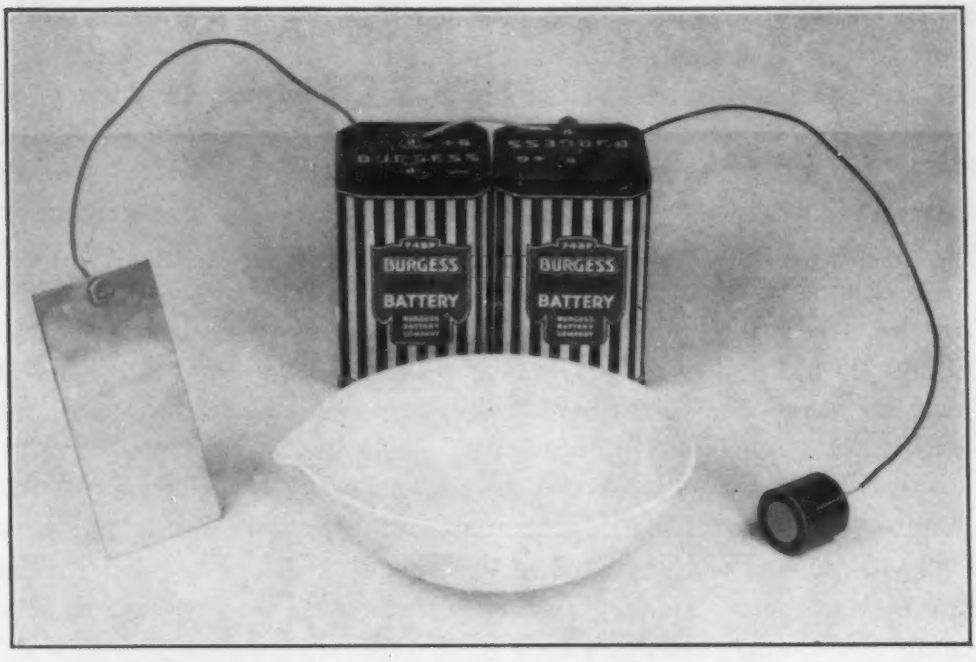


Fig. 1—Electrolytic Polishing Set-Up for Molybdenum Specimens.

4. Cast molybdenum containing oxide at grain boundaries.
5. Cast and wrought molybdenum containing molybdenum carbides.

All specimens were mounted in 1-inch bakelite mounts and were large enough to extend into the mount at least 0.25 inch. Subsequent to mounting, the specimens were ground on a 320-grit belt. Then a small hole was drilled into the curved portion of each mount until contact was made with the molybdenum.

The electrolytic set-up, Fig. 1, consisted of two 6-volt dry cells connected in series, a 200 cc porcelain dish, a 1.5-inch wide by 3-inch long by 0.062-inch thick stainless steel sheet as the cathode and a bare end copper wire (anode lead) to insert in the aforementioned small hole in the bakelite mount. Thus, the surface to be polished was parallel to the face of the cathode sheet during the electrolytic polishing. As will be recognized, this set-up is the same as employed in most every laboratory for the electrolytic etching of conventionally polished specimens.

An electrolyte was prepared by adding one portion (35 ml) of concentrated sulphuric acid to four portions (140 ml) of distilled water. The acid was added to the water slowly to avoid bubbling and splattering. A freshly prepared solution should be thoroughly

mixed before using. It was determined that the temperature of the electrolyte should be maintained at about 125 °F for best results.

As previously mentioned, this solution did not produce good results on molybdenum-containing carbides. The carbides, because of selective attack, were entirely or partially removed, with the result that the surfaces were badly pitted. It was recalled that a solution consisting of 10 ml of concentrated hydrochloric acid in alcohol would etch, without pitting, stainless steel containing carbides. A solution was prepared by adding 50 ml of concentrated hydrochloric acid to 150 ml of alcohol (methyl). Using this solution and four 6-volt dry cells in series, polishing of molybdenum was effected without removing the carbides. However, the surface was considerably etched. The final step in the development of this electrolyte was obvious. Twenty ml of concentrated sulphuric acid was added very slowly to the hydrochloric acid and alcohol solution. Excellent results were then obtained both on sintered molybdenum and on cast molybdenum-containing carbides.

The electrolytes are thus,

Number 1—for sintered molybdenum (sintered molybdenum generally does not contain carbides. In the rare instances where it does solution number 2 below should be used.)

35 ml concentrated sulphuric acid
140 ml distilled water

Number 2—for sintered and cast molybdenum

50 ml concentrated hydrochloric acid
20 ml concentrated sulphuric acid
150 ml methyl alcohol (95%)

The polishing procedures required for optimum results in the shortest possible time are as follows:

1. Rough polish on 0 metallographic polishing paper—15 seconds. Normally this step follows the aforementioned 320-grit grinding operation.
2. Rough polish the specimens on 00 metallographic paper —15 seconds.
3. Rough polish the specimens on a canvas-covered polishing wheel using 600-mesh carborundum as the abrasive —20 seconds.
4. Electrolytically polish for 25 to 35 seconds in the recommended electrolyte (number 1 for sintered molybdenum

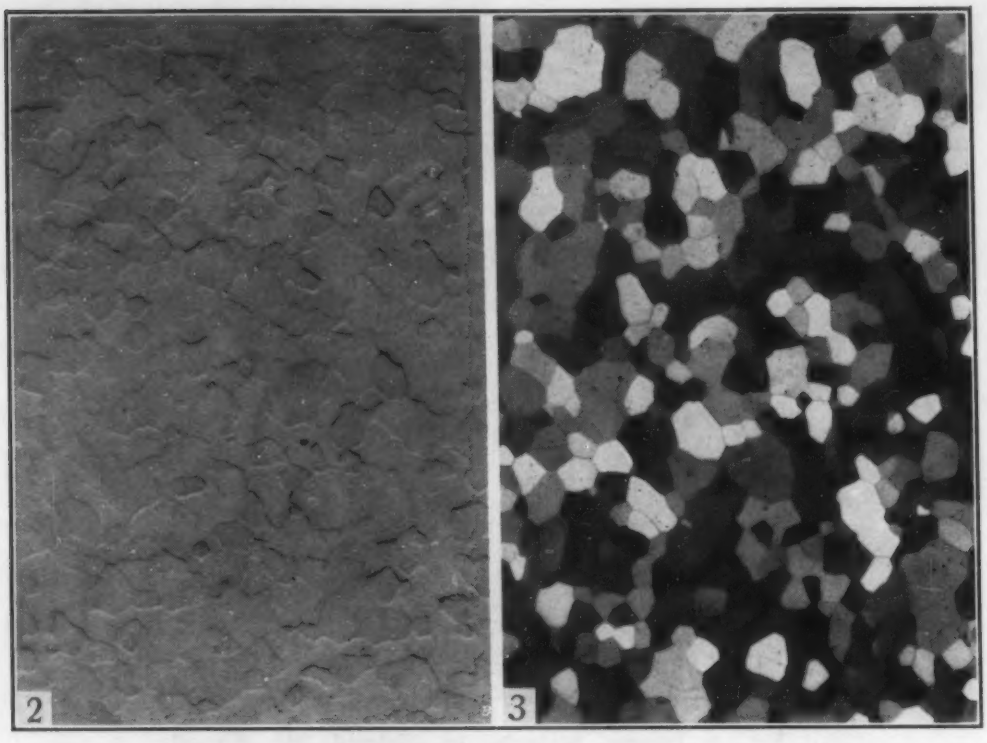


Fig. 2—Overexposed Print of a Photomicrograph of Recrystallized Sintered Molybdenum Showing an Equiaxed Grain Structure. Conical illumination on as polished surface. × 160.

Fig. 3—Same Specimen as Fig. 2. Electrolytically etched in a 0.5% aqueous solution of oxalic acid for 8 seconds after electrolytic polishing. Direct illumination. × 160.

and number 2 for both sintered and cast molybdenum) maintained at a temperature of 125 °F.

5. A blue film, molybdic oxide, covers the specimens after electrolytic polishing in solution number 1 and sometimes through the use of solution number 2 when the solution is contaminated with water. If the latter occurs carbides will be attacked and the solution should be discarded. The blue film can be removed by a 10-second dip in concentrated ammonium hydroxide.
6. Rinse the specimens with water and alcohol and dry in an air blast. The specimens are then ready for examination or etching. The total approximate time required for the actual polishing of any molybdenum specimen is 1.5 minutes.

After polishing has been completed specimens may be etched with the conventional 10% NaOH plus 30% $K_3Fe(CN)_6$ solution. However, a procedure found to slightly etch and clearly delineate

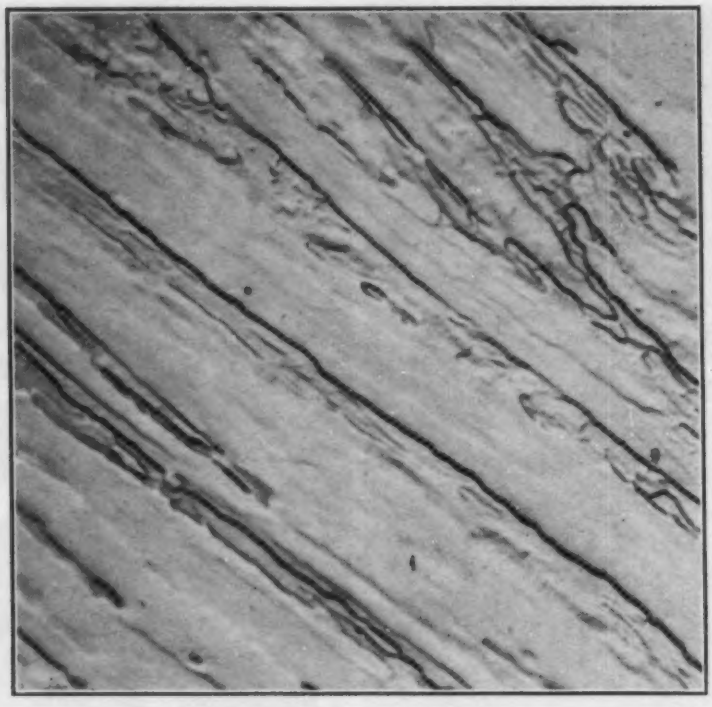


Fig. 4—Fibrous Structure of Sintered and Wrought 0.035-Inch Thick Molybdenum Sheet. Electrolytically polished for 25 seconds followed by a 5-second polish and etch buff. Conical illumination. × 800.

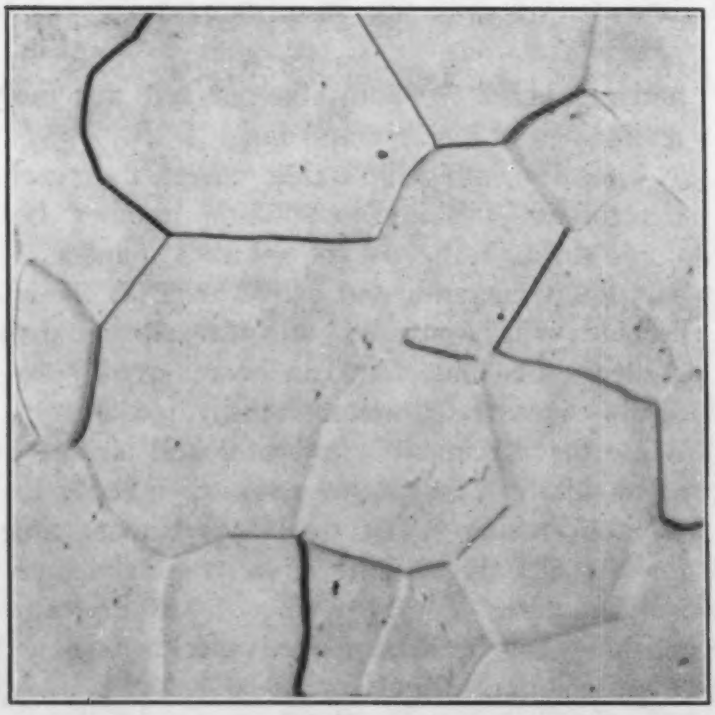


Fig. 5—Wrought 0.035-Inch Thick Sintered Molybdenum Sheet After Recrystallization. Electrolytically polished for 25 seconds followed by a 5-second polish and etch buff. Conical illumination. × 800.

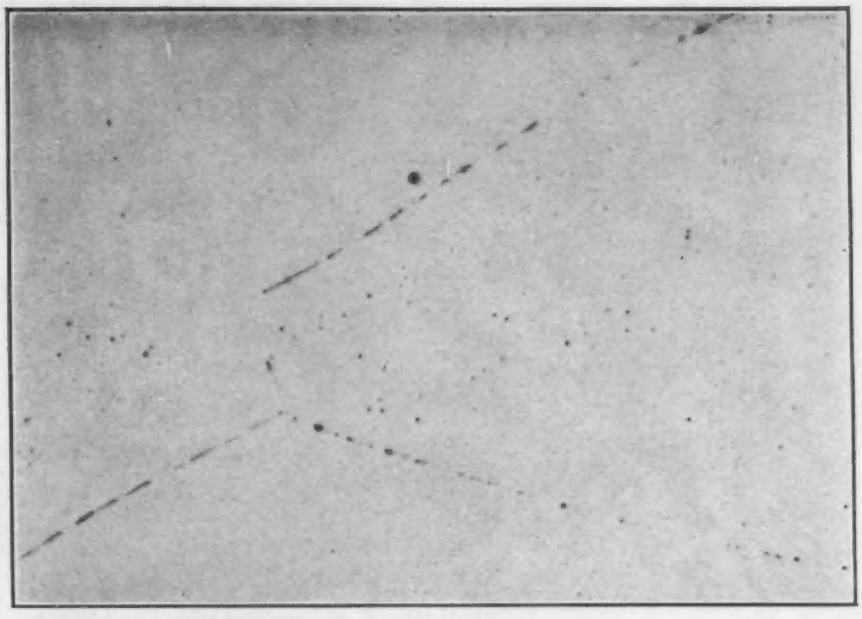


Fig. 6—Cast Molybdenum Containing Oxide at the Grain Boundaries and Within the Grains. Electrolytically polished for 25 seconds. Direct illumination. × 1000.

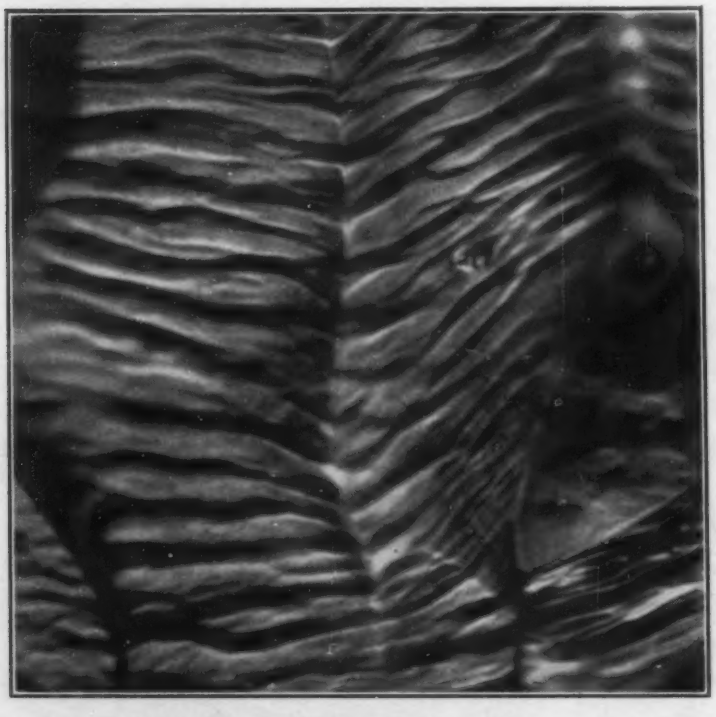


Fig. 7—Fractograph of Sintered and Wrought Molybdenum. Intergranular surfaces revealing considerable slip. × 800.



Fig. 8—Slip As Observed on a Polished Longitudinal Cross Section Surface of Sintered and Wrought Molybdenum. Electrolytically polished for 25 seconds followed by a 10-second polish and etch buff. Conical illumination. × 800.

the structures of molybdenum specimens is suggested. Buff the specimens on a cloth-covered wheel for 3 to 5 seconds, using undiluted "C-RO" metallographic polishing compound to which has been added a mixture of 10 grams of NaOH, 30 grams of $K_3Fe(CN)_6$ and 100 cc of distilled water. One part of the etchant is added to 5 parts of the "C-RO" polishing compound. Conical illumination should be used when examining specimens prepared in this manner. A similar technique for tungsten was advanced by Harry W. Woods.[8]

Electrolytic etching in a 0.5% aqueous solution of oxalic acid also will produce excellent grain contrast and when used for 5 seconds it will reveal considerable detail without serious overetching.

[8]Harry W. Woods, "Attack Method for Preparing Tungsten," METAL PROGRESS, Vol. 51, February 1947, p. 261.

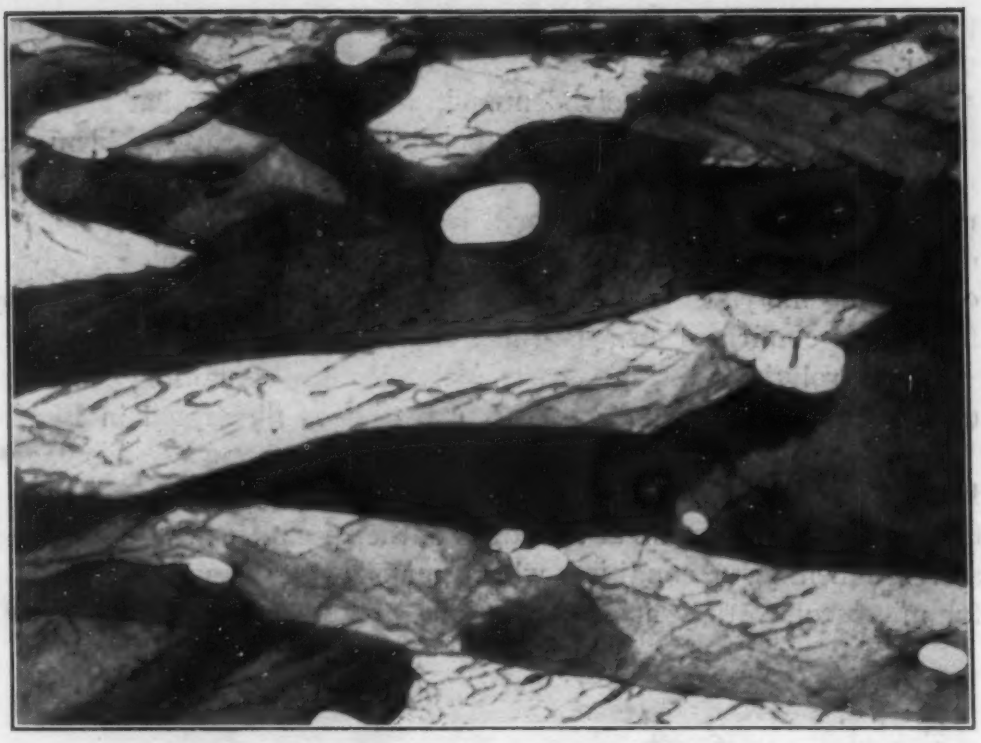


Fig. 9—Cast and Wrought Molybdenum Containing Carbides. Electrolytically polished for 35 seconds followed by etching for 5 seconds in a 0.5% aqueous solution of oxalic acid. Note slip lines. Direct illumination. × 1000.

Results

The reader's attention is directed to the figures and the accompanying captions.

All the photomicrographs, with the exception of Fig. 9, were taken of surfaces electrolytically polished in electrolyte number 1. The actual polishing time required for each specimen varied between 1 and 2 minutes and the polishing necessitated very little labor.

Fig. 2, in addition to being photographed with oblique illumination, was purposely overexposed in printing to emphasize the fact that scratches were nonexistent. The same specimen as etched electrolytically for 5 seconds in a 0.5% oxalic acid and water solution is shown in Fig. 3.

Typical molybdenum structures are illustrated in Figs. 4 and 5.

Oxide inclusions, Fig. 6, were not materially affected and minute amounts at the grain boundaries readily could be detected. However, when polishing molybdenum suspected of containing oxide inclusions the electrolytic process should be limited to the shortest

possible time necessary for adequate results, otherwise pitting may occur.

To reveal slip in molybdenum it was paramount that a perfect polish be obtained. Electrolytic polishing solved this problem admirably. Referring to Fig. 5, which is a photomicrograph of recrystallized molybdenum, it will be observed that there is no evidence of slip. In contrast Figs. 7 and 8 vividly present the effects of working molybdenum. Slip on intergranular surfaces exposed by fracture is confirmed on a polished cross section of the grains.

Electrolytic polishing cast molybdenum containing carbides using electrolyte number 2 produced results as illustrated in Fig. 9.

As with all polishing techniques there are certain disadvantages. Electrolytic polishing of molybdenum is no exception. Excessive electrolytic action occurs at the edges of the specimens, causing pitting and roughening, a condition which renders the samples unsuitable for microscopic study at such locations.

Conclusions

Three new techniques are advanced in this paper pertaining to the preparation of molybdenum specimens for examination on the microscope. They are, namely (a) electrolytic polishing, (b) a polish etch method for slight delineation of grain boundaries and slip, and (c) a 0.5% oxalic acid electrolytic etch.

THE EFFECT OF SILICON ON THE ACTIVITY OF SULPHUR IN LIQUID IRON

By J. P. Morris and A. J. Williams, Jr.

Abstract

A study has been made of the equilibrium conditions at 1615 °C (2940 °F) in the reaction between hydrogen gas and sulphur dissolved in liquid iron and iron-silicon alloys.

At sulphur concentrations of 1% or less in iron, the experimental results can be represented by the relation,

$$K_{1615\,^{\circ}C} = \frac{p_{H_2S}}{p_{H_2} \times \%S} = 0.00256$$

This value for the equilibrium constant is only about one-half the generally accepted value.

Silicon dissolved in the iron had a pronounced effect on the equilibrium conditions. In experiments run at the same H_2S concentration in the gas phase, the sulphur content of the metal at equilibrium decreased as the silicon content was increased. This means that the activity of sulphur in iron is increased by the addition of silicon. At a silicon content of 4%, the activity coefficient of sulphur was about twice that for sulphur dissolved in pure iron.

Introduction

THE purpose of this investigation was to determine the effect of silicon on the activity of sulphur dissolved in liquid iron. This has been done by making a study of the conditions of equilibrium in the reaction between hydrogen gas and sulphur dissolved in liquid iron and in iron-silicon alloys. Very little is known concerning the effect of one alloying element upon the activity of another when the two are in solution in liquid iron. Such information should be

Contribution from the Central Experiment Station of the Bureau of Mines, Pittsburgh.

Of the authors, J. P. Morris is an associate chemist, Metallurgy of Steel Section, Bureau of Mines, Central Experiment Station, Pittsburgh, and A. J. Williams, Jr., formerly a metallurgist at the Central Experiment Station of the Bureau of Mines, is now associated with Battelle Memorial Institute, Columbus, Ohio. Manuscript received July 30, 1948.

useful in arriving at a better understanding of the reactions occurring during the production and refining of iron and steel. In this investigation the measurements showed that the addition of about 4% silicon doubled the activity of sulphur in iron.

Previous work on the reaction between hydrogen gas and sulphur dissolved in iron has been reported by Chipman and Ta Li (1)[1] and by White and Skelly (2). The results of these two investigations do not agree and, furthermore, in both, the melts of iron were contaminated in varying degrees by silicon. For these reasons it was necessary to repeat the work done on iron, taking steps to prevent contamination of the melts by silicon.

Experimental Method

The principle of the method was as follows: Molten iron or an iron-silicon alloy was brought to equilibrium at a constant temperature with a mixture of H_2 and H_2S of constant composition by bubbling the gas directly through the metal. Samples of the melt were taken at intervals throughout the test so that the course of the reaction could be followed. Equilibrium was assumed to have been attained or at least closely approached when the composition of the liquid metal remained constant over a period of one or more hours.

The hydrogen and hydrogen sulphide used were the commercial gases. The hydrogen was manufactured by the electrolytic process and contained oxygen as the chief impurity. This was removed by passing the gas over heated copper turnings and drying. The hydrogen sulphide was used without purification. The gas mixtures were prepared as used by introducing a stream of H_2S into a jet of H_2 by means of the mixing bulb shown in Fig. 1. Each gas was metered separately before mixing, using capillary-type flowmeters with butyl phthalate manometers. The butyl phthalate in the H_2S flowmeter was saturated with H_2S prior to the start of each experiment.

The rate of hydrogen flow was approximately 1050 milliliters per minute in all tests. This flow gave sufficiently rapid approach to equilibrium without causing excessive splashing of the metal. The flow was easily controlled by means of a pressure regulator on the cylinder and a manually operated needle valve mounted beside the flowmeter. Precise control of the H_2S was more difficult because

[1]The figures appearing in parentheses pertain to the references appended to this paper.

of the small rate of flow, but was accomplished satisfactorily by supplying the H_2S to a needle valve from a tank filled to a pressure of a few pounds. The two flowmeters were used only to keep the rates of flow constant, the actual ratio of H_2S to H_2 being determined in each test by analysis.

After considerable preliminary work with crucibles and gas-bubbling tubes of various materials, it was obvious that only refractories with low silica contents would be suitable. Both porcelain and the ordinary grade of alumina crucibles rapidly imparted silicon

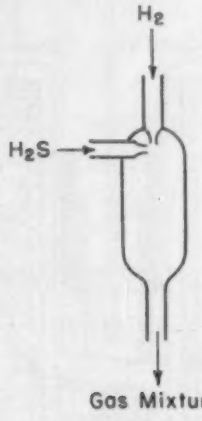


Fig. 1 — Mixing Bulb for Preparation of Hydrogen Sulphide – Hydrogen Mixtures.

to the metal. In several experiments the gas mixtures were impinged onto the surface of the metal through porcelain tubes, and even though the tubes did not touch the metal, and crucibles low in silica were used, the silicon pick-up amounted to as much as 1% in 5 hours. The crucibles and gas tubes finally selected were made of high-purity alumina sintered to a very dense, translucent structure. Contact with liquid iron for periods of 8 or 9 hours resulted in little visible attack on this material and in practically no silicon contamination of the iron. Except for several experiments in which impure alumina sampling tubes were accidentally broken off in the metal, silicon contamination from all sources amounted to only 0.01 to 0.02% during a run. Contamination of the melts by aluminum was negligible also. Spectrographic analyses of samples from several melts, including one that contained 4.7% silicon, indicated the presence of less than 0.02% aluminum. The alumina crucibles were 1.75 inches outside diameter, 1.50 inches inside diameter, and

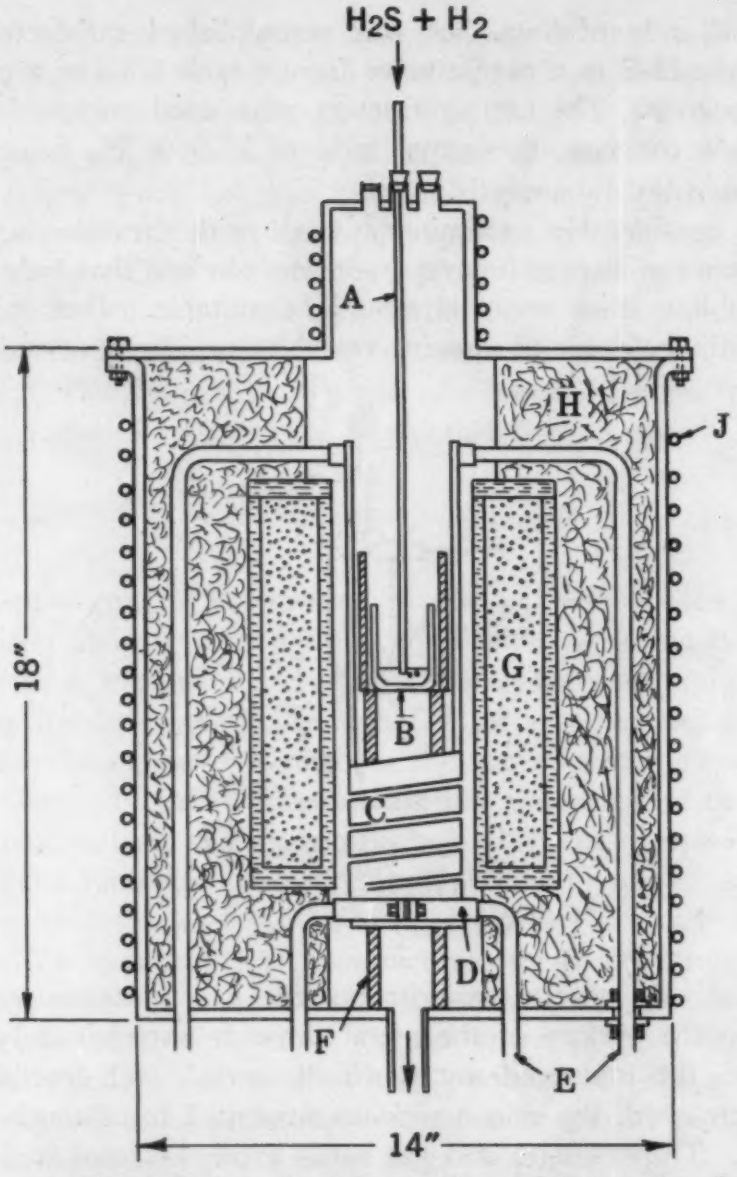


Fig. 2—Furnace Arrangement. A—gas bubbling tube. B—sintered alumina crucible and melt. C—spiral graphite heating element. D—water-cooled copper contact clamp. E—water-cooled electrical leads. F—alundum support for crucible. G—insulating jacket (graphite filled with lampblack). H—insulating brick. J—cooling coil for steel shell.

2.37 inches high. The gas tubes were thermocouple protection tubes 24 inches long and 0.25 inch outside diameter, having 2 holes with a bore of 0.055 inch.

For making the melts, an Arsem-type furnace was used that had a graphite heating element 13 inches long, 3 inches outside diameter, and 2.5 inches inside diameter cut in the form of a spiral with turns 0.75 inch wide. The arrangement within the furnace is shown in

Fig. 2. There was little contamination of the melts by carbon as a result of using graphite in the furnace, analyses of a number of final metals showing the presence of only 0.01 to 0.02% carbon.

In carrying out the tests a charge of 50 grams of electrolytic iron was melted and brought to the operating temperature in a hydrogen atmosphere. Then the tip of the gas-bubbling tube was immersed in the liquid metal and the H_2S flow was started. Next, sufficient FeS was added to the melt to bring the sulphur content near to the expected equilibrium value. This was necessary to shorten the time needed for attaining equilibrium. To prepare an iron-silicon melt, the required amount of silicon was added to the liquid iron either shortly after the iron had melted or later in the run, as desired. The metal temperature and the gas composition were held constant for the duration of the test, which was usually 7 to 8 hours. Samples of the liquid metal for analysis were taken at intervals of about 1 hour.

Iron sulphide and silicon additions to the melt were made in the following manner: The material, in granular form, was placed in a glass bulb attached by rubber tubing to one end of a 2-foot length of steel tubing. The free end of the steel tube was pushed down into the furnace through a close-fitting rubber stopper, and the addition was made by tilting the glass bulb. Air was excluded by passing a rapid stream of hydrogen through the bulb and steel tube as the tube was inserted into the furnace. The iron sulphide was made by heating together electrolytic iron powder and flowers of sulphur in a hydrogen atmosphere. Afterwards the product was melted in hydrogen, crushed, screened to −10, +48 mesh, and analyzed. The silicon used was a commercial grade analyzing about 97% silicon. Almost 100% efficiencies were obtained in these additions.

Samples of the liquid metal for analysis were taken as follows: A 3-inch length of refractory 2-hole thermocouple tubing (0.3 inch outside diameter with 0.086-inch holes) was cemented to one end of a 2-foot length of seamless steel tubing. With hydrogen flowing through the tube to exclude air, the refractory end of the tube was pushed down into the furnace through a rubber stopper. The tip of the refractory tube was momentarily immersed in the liquid metal, and samples were drawn into the two holes by applying suction. By allowing the tube to cool in the upper part of the furnace, surface oxidation of the sample was avoided. Two-hole tubing was used

so that duplicate samples of metal could be taken simultaneously. The weights of samples taken in this manner varied from 0.5 to 2.0 grams in each hole with the average being about 1 gram.

Temperature measurements were made at 10 to 15-minute intervals with a disappearing filament-type optical pyrometer. It was found that consistent readings could be obtained by sighting on the surface of the metal close to the base of the bubbling tube. The pyrometer was calibrated by making simultaneous temperature measurements with a platinum platinum-rhodium thermocople immersed in the metal and protected by a sintered alumina sheath. The calibration of the thermocouple was checked at the freezing point of electrolytic iron, which was assumed to be 1535 °C (2795 °F). Temperature control of the furnace was manual, but once a steady state was reached very little adjustment was necessary. All of the experiments described in this report were run at 1615 °C (2940 °F). The temperature measurements are believed to be accurate within ±10 °C.

The bubbling procedure used in this investigation had several advantages. First, the bubbling action stirred the metal and brought it into close contact with all of the gas. Also, passing the gas mixture directly into the metal prevented pick-up by the gas of carbon and silicon from the furnace refractories and consequent contamination of the melt. Furthermore, the possibility of thermal diffusion affecting the composition of the gas mixture was eliminated until after the gas had passed out of the reaction zone. If the gas mixture had been introduced in some other manner into the furnace, it is possible that thermal diffusion would have set up a concentration gradient between the hot and cold regions of the furnace, decreasing the H_2S concentration in the reaction zone and causing the sulphur content of the melt at equilibrium to be less than it would have been if no thermal segregation had occurred.

Methods of Analysis

Metal samples were analyzed for sulphur by the standard gravimetric procedure (3). Errors due to segregation were avoided by using an entire sample from one hole of the sampling tube in each analysis. As a precautionary measure when a sample dissolved too rapidly, the action of the acid was slowed by placing the beaker in an ice bath. Duplicate analyses, using the two samples from one sampling tube, usually checked within 0.01% sulphur.

Silicon analyses were made by double dehydration with HCl prior to precipitation of the sulphur.

Gas analyses were made on samples taken in a calibrated bulb placed in the gas line between the mixing unit and the furnace. Usually three analyses were made in each experiment; these were spaced 1 to 2 hours apart during the latter half of the run. In the earlier experiments gas samples were analyzed by a method similar to the evolution procedure used in steel analysis. The method gave consistent results, but there was some uncertainty regarding standardization of the KIO_3 titrating solution since it was found that the titer depended somewhat upon the amount of starch used and also upon the weight of sulphur involved. For this reason a gravimetric procedure was eventually adopted. In this method gas samples were taken in a cylindrical bulb with a capacity of 1839 milliliters. The analysis was made by displacing the gas in the bulb with nitrogen, absorbing the H_2S in an ammoniacal solution of hydrogen peroxide, and precipitating the sulphur as $BaSO_4$. Blank determinations on the hydrogen peroxide were run with each analysis.

Gas compositions are expressed as the ratio of the partial pressure of hydrogen sulphide to the partial pressure of hydrogen. In calculating this ratio from the chemical analysis, it has been assumed that the two gases behave ideally at 1615 °C (2940 °F) and that the ratio of the partial pressures is equal to the molar ratio. A correction has been made for dissociation of H_2S into H_2, S_2, and S. Under the conditions of these experiments, this correction amounts to about 1%. The results of a typical set of analyses of gas samples taken during one test are as follows: 0.00287, 0.00287, and 0.00285 (test E-38).

Experimental Results

Effect of Preheating Gas—The bubbling tube was heated for several inches above the charge by radiation from the furnace walls and served as a preheater for the entering gas. Because of the high gas velocity within the tube, the gases may not have been heated to the same temperature as the metal by the time they had reached the metal. For this reason it was desirable to determine whether or not additional preheating would affect the final results. Two experiments (E-30 and E-33) were run in which additional preheating

was employed. These were carried out in the following manner: The web between the two holes in the bubbling tube was removed for a distance of 1 inch back from the tip that was to be immersed in the metal. A small molybdenum wire with heavier copper leads was threaded down one hole of the tube and up through the other. By passing current through the wire, the lower 2 inches of the bubbling tube was heated to approximately the same brightness as the metal. Equilibrium was closely approached in both of these experiments, and it was evident from a comparison with other tests that the additional preheating had little effect on the results.

Rate of Approach to Equilibrium—The rate of approach to equilibrium is illustrated in Fig. 3 by the results of tests E-39 and E-44. These experiments were run at nearly the same $H_2S:H_2$ ratio, but they approach equilibrium from opposite directions. The dashed line is a calculation of the upper curve to the same gas composition as the lower curve. Fig. 3 shows that the rate of approach to equilibrium is rather slow at the low H_2S concentrations used in these experiments, but that the final sulphur content of the metal is independent of the direction of approach.

Results with Pure Iron—The data obtained with pure iron at 1615 °C (2940 °F) are shown in Table I. A final sulphur value

Table I
Experimental Results With Pure Iron

Test No.	Time, Hours	$\frac{H_2S}{H_2} \times 10^3$	Initial Sulphur, %	Final Sulphur, %	$K = \frac{p_{H_2S}}{p_{H_2} \times \%S}$
E-35	4.75	0.96	0.36	0.36	0.00267
E-34	4.58	1.67	0.64	0.65	0.00257
E-31	2.83	2.14	0.83	0.84	0.00255
E-32	3.67	2.19	0.78	0.83 (rising)	0.00264 −
E-30	6.75	2.34	0.72	0.88 (rising)	0.00266 −
E-33	2.92	2.36	0.85	0.89 (rising)	0.00265 −
E-44	7.28	3.04	1.10	1.22	0.00249
E-39	7.50	3.10	1.38	1.26 (falling)	0.00246 +
E-40	7.32	4.41	2.02	1.90	0.00232
E-36	8.00	5.76	1.97	2.52	0.00229

marked "rising" or "falling" indicates that equilibrium was not reached and that the sulphur content of the metal was changing slowly at the end of the run. The last column gives values for the equilibrium constant K for the reaction

$$H_2 \text{ (gas)} + S \text{ (in liquid iron)} = H_2S \text{ (gas)}$$

$$K = \frac{p_{H_2S}}{p_{H_2} \times \%S}$$

K in this relation is a constant over the composition range in which the solution obeys Henry's law, that is, over the range in which the activity of sulphur is directly proportional to its concentration. This range is probably a very limited one owing to the great differences in character between solvent and solute. The experimental values of K show a tendency to decrease as the sulphur content of the metal increases. However, up to about 1% sulphur, K is constant within the limits of experimental error. Over this range its average value was found to be 0.00256.

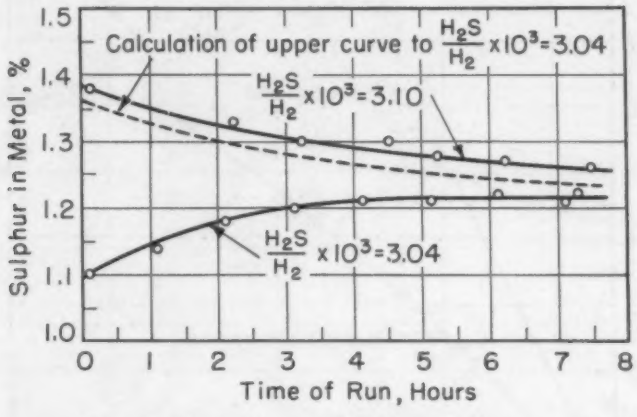


Fig. 3—Variation of Sulphur Content of Melt With Time.

A comparison of these results with those obtained by Chipman and Ta Li (1) and by White and Skelly (2) is shown in Fig. 4. Both of the latter investigations were made at lower temperatures, but the results at 1615 °C (2940 °F) can be calculated from their equations for temperature dependence of K. These equations and the values of K at 1615 °C (2940 °F) are shown as follows:

Chipman and Ta Li:

$$\log K = \frac{-4500}{T} + 0.095$$

$$K_{1615\,^\circ C} = 0.00515$$

White and Skelly:

$$\log K = \frac{-4526}{T} - 0.20$$

$$K_{1615\,^\circ C} = 0.00251$$

Fig. 4 shows that our results do not agree well with those of Chipman and Ta Li. The reasons for such a wide discrepancy are

not clear, but it will be shown later that at least part of the difference is due to contamination of their melts by silicon. They reported the silicon content of three of their melts as being 0.41, 0.81, and 0.86%, respectively. It is possible, too, that the effect of silicon contamination is greater at the temperature where most of Chipman and Ta Li's experiments were run than at the higher temperature used in this investigation. Other considerations of their work are

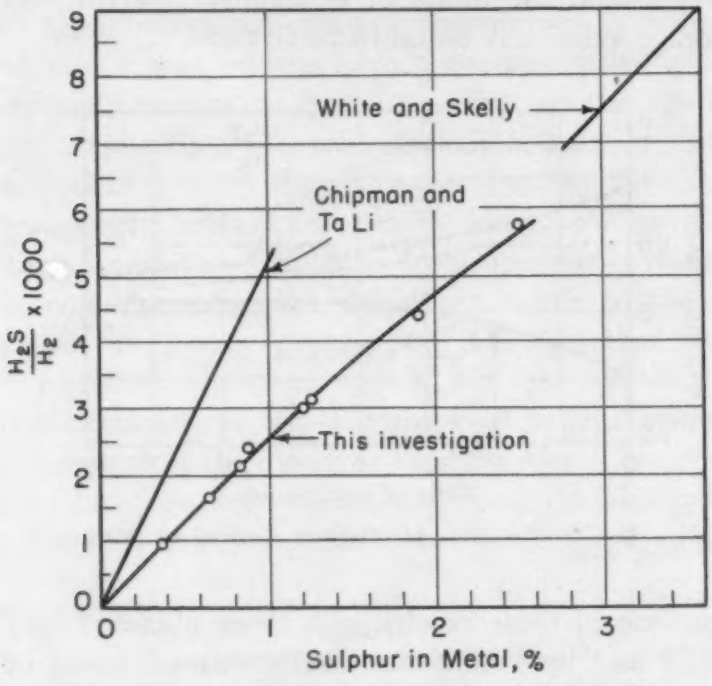


Fig. 4—Comparison of the Data Obtained for Iron-Sulphur Alloys at 1615 °C With the Results of Other Investigators.

(a) in view of the slowness of approach to equilibrium, their experiments were run for too short a time and (b) their precautions for preventing thermal diffusion in the gas mixture may have been inadequate.

A comparison with the results of White and Skelly is difficult to make because of the wide spread in their values. The plot of their results shown in Fig. 4 represents their experiments that had the least silicon contamination (1.1 to 1.6% silicon). Apparently, this plot, if extrapolated to lower sulphur contents in the metal, agrees very well with the present work on pure iron. However, all of the experiments represented by the plot were run at high $H_2S:H_2$ ratios where the relation between H_2S concentration in the gas phase and sulphur concentration in the metal is not linear. At

lower $H_2S:H_2$ ratios the curve probably would lie to the left of our curve. This would be more in line with the results obtained in the present investigation for melts of corresponding silicon contents, as will be shown later. When consideration is given to the high silicon contents of their melts and to the relatively high $H_2S:H_2$ ratios used in many of their experiments, White and Skelly's work seems to be in better agreement with the present work than that of Chipman and Ta Li.

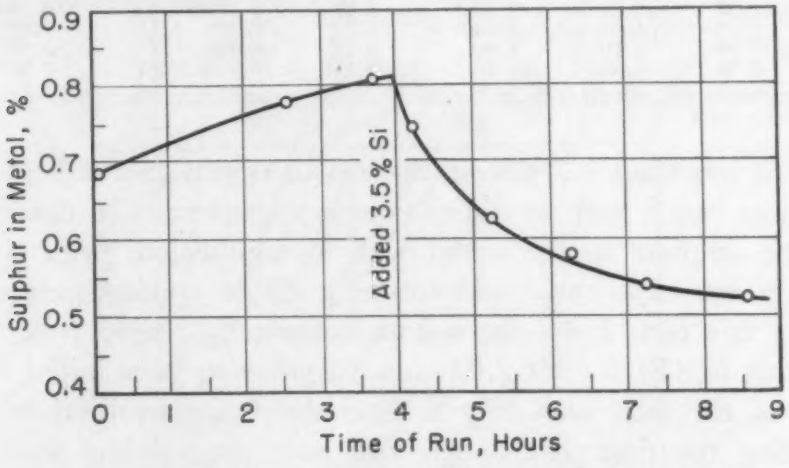


Fig. 5—Influence of Silicon Addition on Sulphur Content of Metal Reacting With H_2S-H_2 Mixture of Constant Composition.

Results with Iron-Silicon Alloys—The influence of silicon on the equilibrium conditions in the reaction between hydrogen and sulphur dissolved in iron is illustrated in Fig. 5 by the results of test E-29. During the first 4 hours of this run no silicon was present and the metal was picking up sulphur from the gas. After the addition of about 3.5% silicon, however, the sulphur content of the liquid metal dropped rapidly. This test shows that at a constant H_2S concentration in the gas phase, equilibrium will be established at a lower sulphur content in an iron-silicon alloy than in pure iron.

The results obtained with iron-silicon alloys are summarized in Table II. In experiments E-25 and E-41 the silicon contents of the melts were the result of contamination by broken sampling tubes. In the remaining experiments, silicon additions were made directly to the liquid iron. In all of the latter tests there was a gradual loss of silicon during the run. For example, in test E-42 the silicon content fell from 4.91 to 4.64% in 7.4 hours. At lower silicon concentrations, the rate of loss was proportionately less. In melts

Table II
Experimental Results With Iron-Silicon Alloys

Test No.	Length of Run, Hours	Silicon at Equil., %	$\frac{H_2S}{H_2} \times 10^3$	Initial Sulphur, %	Final Sulphur, %	$K = \frac{p_{H_2S}}{p_{H_2} \times \%\ S}$
E-25	3.67	0.50	0.70	0.23	0.24	0.00292
E-41	7.33	0.60	3.12	1.09	1.16	0.00269
E-32	4.25	1.16	2.19	0.83	0.75 (falling)	0.00292+
E-38	7.37	2.30	2.86	0.77	0.79	0.00362
E-37	7.58	2.33	1.67	0.50	0.43	0.00388
E-26	4.13	2.56	2.54	0.91	0.77 (falling)	0.00330+
E-29	4.37	3.34	2.20	0.81	0.52 (falling)	0.00423+
E-23	2.28	3.45	1.44	0.49	0.34 (falling)	0.00424+
E-24	2.37	3.79	2.87	1.01	0.70 (falling)	0.00410+
E-42	7.38	4.64	2.82	0.59	0.50	0.00564
E-45	7.00	4.70	1.64	0.25	0.29	0.00566
E-46	7.39	9.40	2.73	0.171	0.155	0.0176

containing less than 5% silicon, the loss of silicon over a 1 or 2-hour period was small, and no difficulty was experienced in determining when the sulphur in the metal was in equilibrium with the gas.

Only one experiment was run at a silicon content greater than 5%. In this test, E-46, the silicon content decreased from 9.65% at the start to 8.81% after 7.4 hours. Apparently, the initial sulphur content of the melt was only a little above the equilibrium value, and during the first part of the run both the sulphur and silicon contents decreased. At 9.4% silicon the sulphur content reached a minimum value of 0.155%, and the melt was assumed to be at equilibrium at this point. Later, as the silicon loss continued, the sulphur content rose slowly.

The mechanism of the silicon loss noted above is not known. A small amount of silicon may have volatilized directly, and some loss may have occurred by oxidation when some of the metal samples were taken. There is also the possibility that the silicon loss took place by volatilization of silicon sulphide from the melt. The presence of silicon sulphide in the outgoing gas would mean that the H_2S concentration was lower than that of the entering gas. If the sulphur in the melt were in equilibrium with the outgoing gas rather than the entering gas, then the calculated equilibrium constant would be too high, as gas analyses were made only on the entering gas. Calculations show that the observed effect of silicon on the activity of sulphur in iron cannot be accounted for entirely by the formation of a silicon-sulphur compound in the gas phase. For example, in test E-42 at 4.7% silicon in the melt, if all of the silicon loss were assumed to occur by volatilization of SiS, the decrease in H_2S concentration would be about 7%; or if SiS_2 were

assumed to form, the decrease would be 14%. The corrected equilibrium constants would be 0.00525 for the assumption of SiS and 0.00485 for SiS_2, whereas the equilibrium constant for silicon-free iron was found to be 0.00256. Few data are available concerning the properties of SiS or SiS_2; and as there are other possible ways in which the silicon loss may have occurred, no attempt has been

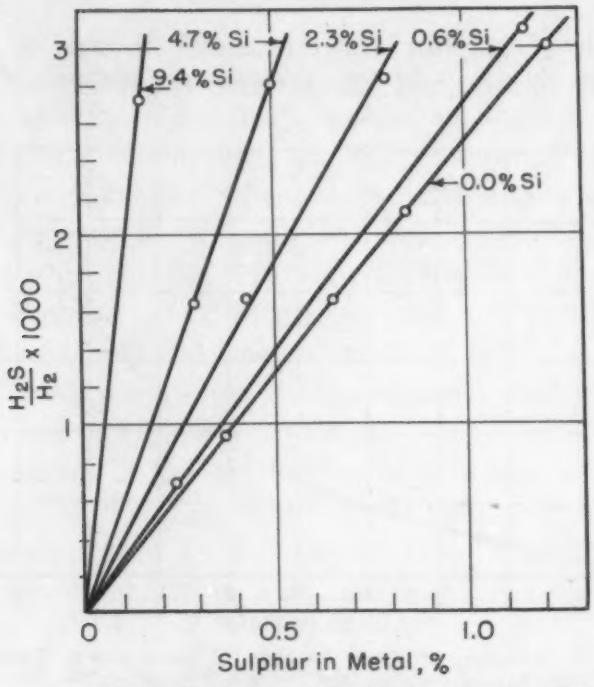


Fig. 6—Variation of Equilibrium Sulphur Content of Metal With the H_2S-H_2 Ratio as Affected by the Silicon Content at 1615 °C.

made to correct the data for errors due to silicon sulphide volatilization.

A comparison of the results of the experiments in which equilibrium was attained is shown in Fig. 6. Each curve in the figure represents a set of experiments run at approximately the same silicon content. With the aid of these curves the relation between silicon content and activity coefficient of sulphur can be determined.

If the reaction between gas and metal is written

$$H_2 \text{ (gas)} + S \text{ (in liquid metal)} = H_2S \text{ (gas)}$$

$$\text{Then } K = \frac{p_{H_2S}}{p_{H_2} \times a_S}$$

It has been shown already that K is equal to 0.00256 when the standard state for sulphur is chosen so that in dilute solution in

pure iron the activity of sulphur is equal to the percentage of sulphur. Using this same standard state, the activity (a_S) and the activity coefficient (γ_S) of sulphur in solutions containing silicon can be calculated from the following equations:

$$a_S = \gamma_S \times \%S = \frac{1}{0.00256} \frac{p_{H_2S}}{p_{H_2}}$$

Over the range of sulphur concentrations shown in Fig. 6, the curves are nearly linear and the activity coefficient of sulphur for

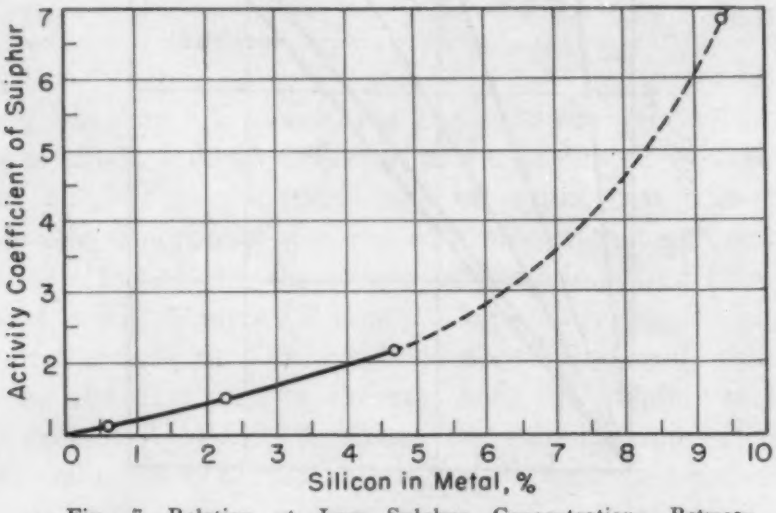


Fig. 7—Relation at Low Sulphur Concentrations Between Activity Coefficient of Sulphur and Silicon Content of the Melt at 1615 °C.

a given silicon content is approximately constant. A plot of activity coefficient of sulphur against per cent silicon in the metal is shown in Fig. 7.

Chipman (4) has suggested that elements such as silicon, carbon, and phosphorus may affect the activity of sulphur in liquid iron by forming compounds with the iron, thereby reducing the mole fraction of free iron in the solution. In the case of silicon there is some evidence in favor of this viewpoint. For example, the large heat of solution of silicon in liquid iron indicates that strong chemical forces exist between the components. The data in this report offer no conclusive evidence as to the nature of the compounds present, if any. Computations show, however, that the reduction in free iron resulting from the formation of only simple molecules, such as FeSi or Fe_3Si together with FeS or Fe_3S, would not be sufficient to explain the observed effect of silicon on sulphur activity. If the

sulphur is present as FeS, iron-silicon molecules as large as Fe_6Si or Fe_7Si would be required. It seems likely that factors other than compound formation are involved and that a reliable theoretical explanation of the experimental results cannot be made at the present time.

Conclusions

The experimental data have shown that silicon has a pronounced effect on the activity of sulphur dissolved in liquid iron. This factor must be considered, therefore, in any theoretical treatment of reactions involving sulphur when appreciable amounts of silicon are present in the metal; for example, the distribution of sulphur between metal and slag in the blast furnace or the desulphurization of hot metal with alkalies. It is very likely that other elements dissolved in the metal also influence the behavior of sulphur. In the case of carbon, preliminary experiments have shown that it affects sulphur activity in a manner similar to silicon. Because of the importance of sulphur control in the production of iron and steel, the need for additional data of this kind is apparent. The authors hope that this work can be continued so that the effect of other alloying elements on the activity of sulphur in iron can be determined.

Acknowledgment

The authors are indebted to Dr. R. C. Buehl, under whose direction this work was undertaken, for his helpful and constructive suggestions.

References

1. John Chipman and Ta Li, "Equilibrium in the Reaction of Hydrogen with Iron Sulphide in Liquid Iron and the Thermodynamics of Desulphurization," Transactions, American Society for Metals, Vol. 25, June 1937, p. 435-465.
2. J. White and H. Skelly, "The Determination of the Equilibrium Constant of the Reaction Between Molten Iron and Hydrogen Sulphide," *Journal,* Iron and Steel Institute, Vol. 155, February 1947, p. 201-212.
3. Chemists of the Subsidiary Company of the U. S. Steel Corporation, "Sampling and Analysis of Carbon and Alloy Steels," Reinhold Publishing Corporation, New York, N. Y., 1938.
4. John Chipman, "The Physical Chemistry of Liquid Steel," *Basic Open-hearth Steel Making,* Chapter 16, The American Institute of Mining and Metallurgical Engineers, New York, 1944, p. 490.

TIME-TEMPERATURE RELATIONSHIPS IN THE ANNEALING OF COPPER-BASE ALLOYS

By A. L. Simmons

Abstract

This paper presents the results of grain size and hardness determinations after annealing seven alpha copper-base alloys (copper, three copper-zinc alloys, and three nickel silvers) for periods up to 5 hours following reductions by cold rolling of 30 and 50%.

Introduction

ALTHOUGH a considerable amount of information has been published previously on the annealing of copper-base alloys, it is thought that the information contained in this paper may also be of interest, inasmuch as it refers to data obtained during an investigation carried out with the object of improving practice in an actual rolling mill.

Seven alloys were used, each being cold-rolled 30 and 50% reduction in thickness, these reductions being the limits of the range normally employed prior to annealing when cold rolling with two-high mills. Samples were then annealed for periods of time ranging from 5 minutes to slightly over 5 hours, and hardness and grain size determinations made. The results are presented in the form of tables.

Experimental

Materials—The compositions of the alloys used are given in Table I. They all complied with the chemical analysis requirements of the relevant British Standard Specifications listed. The assays shown were determined by normal chemical methods. Impurities were determined spectrographically and were well within specification requirements.

The alloys were obtained from normal foundry and rolling mill production.

The author, A. L. Simmons, is senior metallurgist, Government Ammunition Factory, Victoria, Australia. Manuscript received July 28, 1948.

Table I
Analyses of Materials Used

Alloy	Analysis, % Cu	Ni	Mn	Zn	British Standard Spec. No.
Copper, Tough Pitch	99.98	....	....	Rem.	1036
Cap Copper	95.5	....	....	Rem.	S.T.A. 17
Gilding Metal	89.9	....	....	Rem.	S.T.A. 19
Cartridge Brass	69.0	....	....	Rem.	S.T.A. 18
10% Nickel Silver	63.0	9.63	0.18	Rem.	790
20% Nickel Silver	63.0	19.1	0.26	Rem.	790
18% Nickel Silver	55.0	17.9	0.05	Rem.	S.T.A. 7, NS. 2

Ingots for rolling were obtained as follows: Tough pitch copper was in the form of purchased 250-pound wire bars. All the alloys were melted in Ajax-Wyatt furnaces from electrolytic copper, nickel and zinc as required, and clean process scrap. The copper-zinc alloys were cast into water-cooled molds to give ingots 3 inches thick, 11.75 or 14.50 inches wide, and 32 inches long after cropping; similar molds were used for the nickel silvers except that the thickness was 1.75 inches and the width 8.50, 10.50 or 12.25 inches.

The nickel silvers were cold-rolled to 0.675 inch thick and annealed, then cold-rolled to 0.35 inch and 0.030 to 0.040 inch removed from each side by slab milling. Following this the alloys were alternately annealed and cold-rolled to the required size.

The copper and the copper-zinc alloys were hot-rolled to approximately 0.30 inch, slab milled to remove 0.030 to 0.040 inch from each side, then alternately cold-rolled and annealed until the finished size was obtained.

All rolling was done with two-high mills, annealing being carried out after cold reductions of 30 to 40%.

The material was received for test purposes in the form of annealed and pickled strip 4 to 5 inches wide, a nominal 0.042 inch thick. One portion of this strip was then further cold-rolled a nominal 30% and another portion a nominal 50% reduction in thickness. The strip was cut into test pieces 1.25 or 1.50 inches square.

Annealing — Annealing was carried out as follows: The furnace used was an electrically heated muffle 15 inches long with a door opening 7 inches wide and 4.50 inches high. Temperature control was obtained by means of a calibrated Cambridge millivoltmeter-type indicating controller and chromel-alumel thermocouple, together with a manually operated throttling control to reduce hunting. To provide still closer control the muffle was provided with a large brass block to act as a heat storage reservoir; this block was 12 inches long,

5 inches wide and 2 inches high, and weighed about 22 pounds. With this arrangement the temperature could be controlled easily to within plus and minus 2° C.

For each annealing temperature the furnace was heated to the desired temperature and allowed to reach a steady condition. Five test pieces 1.25 or 1.50 inches square were changed into the hot furnace in a very light holder, being supported separately and vertically, and placed on top of the brass block close to the tip of the thermocouple, which was bare and located 1 inch above the block. At the end of predetermined periods, after charging, one test piece was taken out and quenched in water.

The annealed test pieces were pickled, if necessary, and polished prior to measuring hardness and grain size.

Table II
Loads Used for Vickers Hardness Tests

Alloy	Thickness (Inch)	Range of Hardness (VPN)	Load (Kg.)
Copper, Tough Pitch	0.042	All tested	5
	0.028	Over about 45	5
	0.021	Under about 45	2½
Cap Copper and Gilding Metal	0.042 0.028 0.021	All tested	5
Cartridge Brass	0.042	Over about 170	10
	0.028 0.021	Under about 170	5
Nickel Silvers	0.042	All tested	10
	0.028 0.021	Over about 80	10
		Under about 80	5

The temperatures used covered the range of 250 to 850 °C (480 to 1560 °F) by 50 °C intervals. Times were 5, 10, 20, 80 and 320 minutes after charging. These times, of course, do not represent actual times at temperature; the time taken to reach temperature was not greater than about 3 minutes as a maximum, but varied with furnace temperature, and was usually about 1 to 2 minutes.

Measurements—Thickness of the strip was measured with an ordinary micrometer reading to 0.0001 inch.

Hardness determinations were made with a Vickers hardness tester using a 136-degree diamond pyramid indenter. The loads used were in accordance with the requirements of British Standard Specification 427-1931, which states that the maximum load shall be such that the thickness of the specimen shall be at least one and a

half times the diagonal of the impression. These loads are given in Table II; a load of 10 kilograms was used wherever possible.

Hardness values reported in each case are the mean of at least four readings. In some cases the number of readings taken was as many as twelve. Variations in hardness for any one specimen in most cases were within two points VPN, but in extreme cases the variation reached twelve points; however, this occurred only with material as-rolled or material annealed at temperatures of the order 250 to 300 °C (480 to 570 °F), where recovery would occur. In reporting the results none of the mean values contains individual determinations which could reasonably be suspected of being in error, i.e., if for a minimum of four determinations the deviation of an individual determination from the mean is more than four times the mean deviation excluding this determination, then this determination has been rejected.

Grain size was determined with a comparison microscope at a magnification of 75 diameters, using grain size comparison charts according to the method laid down in ASTM specification E 2 - 44 T, paragraph 7 (a). Several fields were examined on a cross section of each specimen.

Results

Results are summarized in Tables III to XVI inclusive. Hardness values have been reported to the nearest whole number VPN only.

In the grain size columns a blank space means no observations were made; R, that recrystallization has begun; AC, recrystallization almost complete; a number, such as "0.025", the average grain size in millimeters according to ASTM specification E 2 - 44 T; M, a mixed grain size of such nature that no accurate figure can be given for the average value; "+", greater than the figure given; "—", less than the figure given.

In the case of some grain size determinations, e.g., 20% nickel silvers, diameters which do not correspond to the ASTM charts are given. In these cases the grain size was too small to obtain a reasonable figure with the charts available, and a magnification of 150 has been used rather than the 75 specified, e.g., "0.018" is obtained from comparison with a 0.035-millimeter chart at twice the normal specimen magnification.

The bold-face figures in the tables correspond to the normal

Table III
Tough Pitch Copper

Original annealed condition: Hardness, 46–48 VPN; Grain Size, 0.065 mm.
Cold-rolled to a reduction in thickness of 30–33%; Hardness after rolling, 101–109 VPN
Normal range of annealed hardness, 42–45 VPN

Temp.	Time in Furnace—Minutes									
	5		10		20		80		320	
°C	VPN	g.s.	VPN	g.s.	VPN	g.s.	VPN	g.s.	VPN	g.s.
250	107		107		107		105	AC	86	−0.035
300	107		104	0.035	77	0.035	49	0.035	45	0.035
350	98	0.035	46	0.035	45	0.035	45	0.035	45	0.035
400	49	0.035	45	0.035	45	0.035	43	0.035	45	0.035
450	45	0.035	45	0.035	44	0.035	46	0.035	45	0.035
500	44	0.035	44	0.035	44	0.035	43	0.035	40	M (0.035 approx.)
550	43	0.035	44	0.035	44	0.035	42	M (0.035 approx.)	41	M (0.035 approx.)
600	45	M (0.035 approx.)	45	M (0.035 approx.)	45	+0.035	43	−0.045	43	−0.045
650	44	−0.045	44	−0.045	44	0.045	43	0.045	43	0.045
700	44	0.045	44	0.045	44	0.045	45	0.045	42	0.045
750	42	0.045	42	0.045	44	0.045	42	0.045	42	0.045

Table IV
Tough Pitch Copper

Original annealed condition: Hardness, 46–48 VPN; Grain Size, 0.065 mm.
Cold-rolled to a reduction in thickness of 48–51%; Hardness after rolling, 110–118 VPN
Normal range of annealed hardness, 42–45 VPN

Temp.	Time in Furnace—Minutes									
	5		10		20		80		320	
°C	VPN	g.s.	VPN	g.s.	VPN	g.s.	VPN	g.s.	VPN	g.s.
250	118		118		117		96	R	59	−0.025
300	117		79	R	54	−0.025	49	−0.025	49	−0.025
350	62	−0.025	51	−0.025	49	−0.025	49	−0.025	48	−0.025
400	50	−0.025	50	−0.025	47	−0.025	47	−0.025	44	−0.025
450	47	−0.025	50	−0.025	47	−0.025	45	−0.025	47	−0.025
500	47	−0.025	47	0.025	46	0.025	45	0.025	43	0.025
550	47	0.025	47	0.025	44	0.025	44	+0.025	44	0.035
600	44	+0.025	44	0.035	44	0.035	44	0.035	43	0.035
650	46	0.035	46	0.035	44	0.035	43	0.035	44	0.035
700	44	0.035	44	0.035	46	0.035	45	0.035	39	0.035
750	46	−0.035	43	−0.045	43	0.045	39	0.045	36	0.045

Table V
Cap Copper

Original annealed condition: Hardness, 49–50 VPN; Grain Size, 0.035 mm.
Cold-rolled to a reduction in thickness of 31–33%; Hardness after rolling, 118–121 VPN
Normal range of annealed hardness, 49–52 VPN

Temp.	Time in Furnace—Minutes									
	5		10		20		80		320	
°C	VPN	g.s.	VPN	g.s.	VPN	g.s.	VPN	g.s.	VPN	g.s.
250	120		118		118		121		118	
300	121		116		117		117		116	
350	120		121		116		114		109	
400	117		114		108	AC	55	0.025	51	−0.035
450	114		65	−0.025	53	+0.025	50	+0.035	51	+0.035
500	58	−0.025	53	0.025	50	−0.035	50	+0.035	49	+0.035
550	54	0.025	52	+0.025	51	0.035	49	0.035	49	+0.035
600	52	0.025	50	+0.025	49	0.035	48	+0.035	47	−0.045
650	52	−0.035	48	0.035	50	+0.035	47	+0.035	47	0.045
700	50	0.035	50	+0.035	48	+0.035	48	M	44	M
750	49	M	49	M	48	M	46	M	44	M

Table VI
Cap Copper

Original annealed condition: Hardness, 49–50 VPN; Grain Size, 0.035 mm.
Cold-rolled to a reduction in thickness of 48–50%; Hardness after rolling, 129–132 VPN
Normal range of annealed hardness, 49–52 VPN

Temp.	Time in Furnace—Minutes									
	5		10		20		80		320	
°C	VPN	g.s.	VPN	g.s.	VPN	g.s.	VPN	g.s.	VPN	g.s.
250	130		131		131		131		128	
300	128		125		128		125		123	
350	128		126		123		110	AC	63	+0.025
400	128		120		69	−0.025	54	−0.025	51	0.025
450	120		56	−0.025	53	0.025	53	+0.025	51	0.025
500	57	−0.025	54	0.025	54	0.025	51	+0.025	47	+0.025
550	55	−0.025	53	0.025	50	0.025	49	0.025	49	+0.025
600	51	−0.025	48	0.025	49	+0.025	47	−0.035	47	0.035
650	53	0.025	49	+0.025	49	−0.035	46	0.035	45	M
700	48	−0.035	47	+0.035	47	0.045	46	M	44	M
750	46	0.045	47	M	46	M	43	M	44	M

Table VII
Gilding Metal

Original annealed condition: Hardness, 58–60 VPN; Grain Size, −0.065 mm.
Cold-rolled to a reduction in thickness of 35–37%; Hardness after rolling, 126–131 VPN
Normal range of annealed hardness, 55–70 VPN

Temp.	Time in Furnace—Minutes									
	5		10		20		80		320	
°C	VPN	g.s.	VPN	g.s.	VPN	g.s.	VPN	g.s.	VPN	g.s.
250	131		130		131		130		133	
300	129		131		129		126		126	
350	127		126		126		125		75	0.010
400	129		123		104	R	63	−0.015	61	−0.015
450	114		63	0.015	58	0.015	57	0.015	56	+0.015
500	67	0.015	58	+0.015	57	+0.015	56	0.025	55	+0.025
550	60	+0.015	57	−0.025	56	0.025	54	+0.035	51	0.035
600	56	−0.015	55	+0.025	54	+0.025	51	0.035	51	0.065
650	54	+0.025	54	+0.035	53	0.045	51	+0.065	49	0.120
700	54	+0.035	54	−0.065	51	0.090	49	0.120	46	+0.150
750	55	0.065	52	+0.065	48	+0.090	46	0.150	46	+0.200

Table VIII
Gilding Metal

Original annealed condition: Hardness, 58–60 VPN; Grain Size, −0.065 mm.
Cold-rolled to a reduction in thickness of 50–53%; Hardness after rolling, 142–145 VPN
Normal range of annealed hardness, 55–70 VPN

Temp.	Time in Furnace—Minutes									
	5		10		20		80		320	
°C	VPN	g.s.	VPN	g.s.	VPN	g.s.	VPN	g.s.	VPN	g.s.
250	146		148		147		148		146	
300	142		144		144		142		125	
350	145		137		125		86	R	66	0.015
400	129		94	R	70	0.015	66	−0.015	64	0.015
450	74	−0.015	64	−0.015	65	0.015	61	0.015	58	+0.015
500	68	−0.015	62	0.015	61	0.015	59	−0.025	56	0.025
550	62	0.015	60	0.025	58	0.025	56	+0.025	52	0.035
600	59	+0.015	54	0.025	54	+0.025	51	0.045	49	0.065
650	57	0.025	54	0.035	52	−0.065	49	+0.065	46	0.090
700	55	0.035	52	+0.045	50	0.065	47	0.120	46	0.150
750	53	−0.090	51	0.090	46	+0.150	48	−0.200	41	+0.200

Table IX
Cartridge Brass

Original annealed condition: Hardness, 56–59 VPN; Grain Size, 0.090 mm.
Cold-rolled to a reduction in thickness of 30–34%; Hardness after rolling, 151–156 VPN
Normal range of annealed hardness, 65–75 VPN

Temp.	Time in Furnace—Minutes									
	5		10		20		80		320	
°C	VPN	g.s.	VPN	g.s.	VPN	g.s.	VPN	g.s.	VPN	g.s.
250	163	R	162	R	157	R	161	R	155	R
300	157	R	155	R	152	R	150	R	128	R
350	157	R	142	R	124	R	93	AC	83	AC
400	138	R	93	AC	82	0.025	77	AC	**72**	**0.025**
450	89	AC	80	AC	**73**	**0.025**	**69**	**+0.025**	**69**	**0.035**
500	**74**	**−0.025**	**72**	**−0.025**	**67**	**0.035**	**66**	**+0.035**	64	0.045
550	**71**	**+0.025**	**67**	**0.035**	**65**	**0.045**	64	+0.065	57	−0.090
600	64	+0.035	62	0.045	59	−0.065	55	+0.065	56	0.090
650	61	0.065	55	0.090	57	+0.090	56	−0.120	55	0.120
700	52	0.090	56	0.090	51	−0.120	51	0.150	51	0.150

Table X
Cartridge Brass

Original annealed condition: Hardness, 56–59 VPN; Grain Size, 0.090 mm.
Cold-rolled to a reduction in thickness of 49–51%; Hardness after rolling, 178–190 VPN
Normal range of annealed hardness, 65–75 VPN

Temp.	Time in Furnace—Minutes									
	5		10		20		80		320	
°C	VPN	g.s.	VPN	g.s.	VPN	g.s.	VPN	g.s.	VPN	g.s.
250	197		196		190		201		169	
300	190		190		169		119		103	R
350	195		124		104	R	93	R	86	AC
400	99	R	92	R	88	AC	84	−0.025	79	0.025
450	91	AC	81	+0.015	77	−0.025	**72**	**+0.025**	**68**	**0.035**
500	81	+0.015	**74**	**0.025**	**69**	**−0.035**	**67**	**+0.035**	62	+0.045
550	**74**	**−0.025**	**66**	**0.035**	64	+0.035	64	−0.065	58	−0.090
600	62	+0.035	62	+0.045	59	+0.045	55	−0.090	54	−0.120
650	62	0.045	57	0.065	54	+0.090	51	−0.120	51	+0.120

Table XI
10% Nickel Silver

Original annealed condition: Hardness, 81–83 VPN; Grain Size, 0.045 mm.
Cold-rolled to a reduction in thickness of 31–33%; Hardness after rolling, 182–189 VPN
Normal range of annealed hardness, 75–90 VPN

Temp.	Time in Furnace—Minutes									
	5		10		20		80		320	
°C	VPN	g.s.	VPN	g.s.	VPN	g.s.	VPN	g.s.	VPN	g.s.
250	187		186		187		186		186	
300	187		184		185		188		180	
350	182		184		181		179		177	
400	183		176		175		172		165	
450	177		166		163		142		108	R
500	169		154		128	R	101	R	95	AC
550	117	AC	97	AC	96	0.010	**90**	**+0.015**	**87**	**−0.025**
600	127	AC	92	+0.015	**83**	**−0.025**	**86**	**0.025**	**76**	**M**
650	**85**	**0.025**	**83**	**+0.025**	**78**	**0.035**	70	+0.045	69	+0.065
700	**81**	**0.025**	71	−0.045	70	0.045	68	0.065	66	+0.090
750	72	0.045	69	−0.065	65	0.065	66	+0.065	60	+0.090
800	68	0.065	66	+0.090	66	0.120	62	0.120	56	+0.120

Table XII
10% Nickel Silver

Original annealed condition: Hardness, 81–83 VPN; Grain Size, 0.045 mm.
Cold-rolled to a reduction in thickness of 50%; Hardness after rolling, 203–209 VPN
Normal range of annealed hardness, 75–90 VPN

Temp.	Time in Furnace—Minutes									
	5		10		20		80		320	
°C	VPN	g.s.	VPN	g.s.	VPN	g.s.	VPN	g.s.	VPN	g.s.
250	213		212		217		218		223	
300	212		214		212		213		206	
350	210		215		213		205		202	
400	207		202		198		181		165	
450	198		178		164		122		114	R
500	159		126		119	R	104	AC	101	−0.015
550	116	R	107	AC	101	0.015	95	+0.015	85	−0.025
600	103	−0.015	94	0.015	92	−0.025	84	−0.035	78	0.045
650	89	0.025	82	+0.025	78	0.035	73	+0.045	71	0.065
700	81	+0.025	76	−0.045	71	0.045	69	0.065	67	−0.120
750	73	0.045	67	0.065	67	+0.065	68	−0.090	61	0.120
800	67	−0.090	68	0.090	64	−0.120	63	−0.150	61	+0.150
850	67	−0.120	60	−0.150	61	−0.200	62	0.200	59	+0.200

Table XIII
20% Nickel Silver

Original annealed condition: Hardness, 94–96 VPN; Grain Size. 0.025 mm.
Cold-rolled to a reduction in thickness of 30–32%; Hardness after rolling, 183–191 VPN
Normal range of annealed hardness, 80–100 VPN

Temp.	Time in Furnace—Minutes									
	5		10		20		80		320	
°C	VPN	g.s.	VPN	g.s.	VPN	g.s.	VPN	g.s.	VPN	g.s.
250	194		193		199		196		197	
300	196		196		192		198		197	
350	194		197		193		193		194	
400	193		187		181		179		178	
450	182		177		172		180		169	
500	170		165		168		160		146	
550	169		163		164		132	R	106	0.012
600	152		114	R	100	+0.012	94	−0.022	93	−0.022
650	100	0.012	97	+0.012	93	0.018	89	−0.022	85	0.022
700	88	0.018	90	−0.022	87	−0.022	88	0.022	87	+0.022
750	91	−0.022	90	−0.022	89	−0.022	88	0.022	83	+0.022
800	89	−0.022	88	0.022	86	0.022	88	0.022	82	+0.022
850	87	0.022	85	+0.022	86	+0.022	79	−0.032	69	0.032

Table XIV
20% Nickel Silver

Original annealed condition: Hardness, 94–96 VPN; Grain Size, 0.025 mm.
Cold-rolled to a reduction in thickness of 50%; Hardness after rolling, 205–210 VPN
Normal range of annealed hardness, 80–100 VPN

Temp.	Time in Furnace—Minutes									
	5		10		20		80		320	
°C	VPN	g.s.	VPN	g.s.	VPN	g.s.	VPN	g.s.	VPN	g.s.
250	208		206		207		209		215	
300	214		211		215		218		222	
350	213		213		214		213		212	
400	209		208		203		207		207	
450	204		195		194		191		187	
500	217		183		182		167		142	
550	181		160		141		109	−0.008	103	0.008
600	127	R	106	−0.008	105	−0.008	99	+0.008	95	0.012
650	102	0.008	98	+0.008	96	0.012	95	+0.018	87	0.022
700	98	0.018	90	−0.018	91	−0.018	85	−0.022	86	0.022
750	92	+0.018	89	+0.018	88	−0.022	85	−0.022	82	0.022
800	90	+0.012	85	−0.022	86	−0.022	84	0.022	83	+0.022
850	87	−0.022	85	+0.022	84	+0.022	87	0.032	81	+0.032

Table XV
18% Nickel Silver

Original annealed condition: Hardness, 89–91 VPN; Grain Size, 0.045 mm.
Cold-rolled to a reduction in thickness of 33–34%; Hardness after rolling, 193–198 VPN
Normal range of annealed hardness, 80–100 VPN

Temp.	Time in Furnace—Minutes									
	5		10		20		80		320	
°C	VPN	g.s.	VPN	g.s.	VPN	g.s.	VPN	g.s.	VPN	g.s.
250	204		199		198		200		205	
300	195		197		197		198		198	
350	198		193		192		194		193	
400	193		189		188		182		181	
450	181		172		170		165		159	
500	172		164		161		140		115	AC
550	147		119	R	102	AC	97	+0.015	94	0.025
600	157		95	+0.015	95	+0.015	90	0.025	88	0.035
650	95	+0.025	92	+0.025	92	0.035	82	−0.045	80	+0.045
700	92	0.025	90	0.035	86	0.045	78	−0.065	74	−0.090
750	86	0.035	80	−0.045	80	0.045	76	0.065	71	0.120
800	79	0.045	78	+0.065	80	0.090	74	+0.090	67	0.120

Table XVI
18% Nickel Silver

Original annealed condition: Hardness, 89–91 VPN; Grain Size, 0.045 mm.
Cold-rolled to a reduction in thickness of 50%; Hardness after rolling, 218–221 VPN
Normal range of annealed hardness, 80–100 VPN

Temp.	Time in Furnace—Minutes									
	5		10		20		80		320	
°C	VPN	g.s.	VPN	g.s.	VPN	g.s.	VPN	g.s.	VPN	g.s.
250	226		230		227		229		233	
300	223		229		227		231		233	
350	226		230		232		232		231	
400	223		218		221		218		214	
450	214		215		200		185		163	
500	197		173		154		126		116	R
550	172		123		112	AC	106	0.010	102	0.010
600	111		98	0.010	102	+0.010	95	0.025	88	0.035
650	98	0.010	94	+0.015	90	0.025	86	+0.035	81	0.045
700	99	0.015	89	0.025	88	0.035	81	0.045	78	+0.065
750	91	+0.025	87	+0.035	77	0.045	78	−0.090	76	0.090
800	83	0.045	81	+0.045	78	+0.045	76	−0.090	70	0.150
850	80	+0.045	79	0.065	74	+0.090	70	−0.150	66	+0.150

range of hardness aimed for on finish-annealed material according to this factory's practice.

A small range in the figure for per cent reduction will be noticed. This is due to unavoidable slight variations (of the order one or two ten-thousandths of an inch) in thickness of strip both before and after rolling.

Discussion of Results

The following information is deduced from a study of the experimental results:

Hardness—As would be expected, the general trend for any one alloy at any one reduction is a decrease of hardness with increase of temperature and/or time.

There are two exceptions to this: (a) For cartridge brass at an annealing temperature of 250 °C, and for the nickel silvers at temperatures up to and including 350 °C (660 °F), there is an increase in hardness over the as-rolled figures due to recovery prior to recrystallization. This is not shown with the copper, cap copper or gilding metal for the temperatures used, although it is possible that recovery may occur for temperatures less than 250 °C (480 °F).

(b) There is an occasional anomalous figure where the hardness is higher or lower than would be expected from its position on the table, e.g., Table III, 700 °C (1290 °F), 80 minutes, or Table XVI, 750 °C (1380 °F), 20 minutes. This can be put down probably to experimental error, not in the averaged hardness figure given, but possibly to slight differences in the per cent reduction on the particular test sample.

Recrystallization—An approximate figure for the temperature at which recrystallization is complete can be obtained by noting the sudden drops in hardness and first occurrence of a definite grain size measurement for either constant temperature or constant time. These results are given in Table XVII.

Table XVII
Approximate Temperatures for Completion of Recrystallization, °C

Alloy	% Reduction	Time—Minutes 5	10	20	80	320
Copper	30	300–350	250–300	250–300	250	250–
	50	300–350	300–350	250–300	250–300	250–
Cap Copper	30	450–500	400–450	400	350–400	350
	50	450–500	400–450	350–400	350	300–350
Gilding Metal	35	450–500	400–450	400–450	350–400	300–350
	50	400–450	400–450	350–400	350–400	300–350
Cartridge Brass	30	450	450	350–400	400	350
	50	450	400–450	400	350–400	350
10% Nickel Silver	30	600	550	500–550	500–550	500
	50	550–600	550	500–550	500	450–500
20% Nickel Silver	30	600–650	600–650	550–600	550–600	500–550
	50	600–650	550–600	550–600	500–550	500–550
18% Nickel Silver	30	600–650	550–600	550	500–550	500
	50	600–650	550–600	550	500–550	500–550

Again, the general behavior is what would be expected, namely, (a) An increase in the annealing time for a given reduction, or the reduction for a given time of annealing shows a general tedency to lower the temperature at which recrystallization is complete. There are minor exceptions to this.

(b) With copper-zinc alloys, increasing the zinc content raises the temperature at which recrystallization is complete.

Table XVIII
Annealing Conditions for Commercial Practice

Alloy	Requirement	% Reduction	Time—Minutes 5	10	20	80	320
Copper	Annealed (42/45 VPN)	30	450–750	400–750	350–750	350–750	300–750
		50	600–750+	600–750+	550–750	450–700	400–650
Cap Copper	Annealed (49/52 VPN)	30	600–700	550–700	500–650	450–550	400–550
		50	600–650	600–650	550–650	500–550	400–550
Gilding Metal	Annealed (55/70 VPN)	35	500–700	450–600	450–550	400–500	400–500
		50	500–700	450–550	400–550	400–550	350–500
Cartridge Brass	Deep Drawing (65/75 VPN, 0.025/0.045 mm.)	30	500–550	500–550	450–550	450–500	400–450
		50	550	500–550	500	450–500	450
10% Nickel Silver	Deep Drawing (75/90 VPN, 0.025/0.045 mm.)	30	650–700	650	600–650	550–600	550–600
		50	650–700	650–700	650	600	550–600
20% Nickel Silver	Annealed (80/100 VPN)	30	650–850+	650–850+	600–850+	600–800	600–800
		50	700–850+	650–850+	650–850+	600–850+	600–850
18% Nickel Silver	Annealed (80/100 VPN)	30	650–750	600–750	600–750	550–650	550–650
		50	650–850	600–800	600–700	600–700	600–650

(c) The addition of nickel to copper-zinc alloys considerably raises the temperature at which recrystallization is complete.

Grain Size—Once recrystallization is complete there is an increase in grain size with increase in time and/or temperature. More specific effects are:

(a) For any one given alloy there is a tendency for 50% reduction to give a slightly finer grain size, for the same annealed hardness, than is obtained after 30% reduction. This is more marked with the copper, cap copper, and gilding metal than with the other alloys.

(b) The addition of nickel to the copper-zinc alloys produces a marked refinement of grain size in the annealed condition.

(c) The bold-face figures in Tables III to XVII represent the hardness of commercial quality "annealed" material. Some alloys allow a wide range of hardness required, while others are "sensitive" in this respect. The effect of 50% reduction rather than 30% also varies with the alloy. It may raise or lower, or restrict or widen the range of temperature to give the desired hardness, depending on the alloy.

A summary of conditions necessary to produce commercial quality annealed material is given in Table XVIII.

Acknowledgment

A considerable amount of the experimental work has been carried out by Mr. F. R. Hindell, whose assistance is very gratefully acknowledged.

The author would also like to express his appreciation to Mr. J. D. O'Shea, Manager, Government Ammunition Factory, for permission to publish the results of this investigation.

References

British Standard Specifications:

1. B.S. 427-1931, "British Standard Tables of Diamond Pyramid Hardness Numbers", November 1931.
2. B.S. 790-1938, "British Standard Specification for Nickel Silver Sheets and Strip of 10 to 30% Nickel Content", February 1938.
3. B.S. 1036-1942, "Electrolytic Tough Pitch High Conductivity Copper".
4. B.S./S.T.A.7, NS.2, "Services' Schedule of Non-Ferrous Metals and Alloys for Armaments and General Engineering Purposes", December 1942 et seq. Group 2—Nickel and Its Alloys, November 1943.
5. B.S./S.T.A.17, "Services' Specification for 'Cap Copper Alloy' Strip for Detonator Shells and Percussion Caps", December 1942.
6. B.S./S.T.A.18, "Services' Specification for Brass Strip for Q.F. and S.A. Cartridge Cases and for Caps", December 1942.
7. B.S./S.T.A.19, "Services' Specification for 'Gilding Metal' Strip for Bullet Envelopes", September 1943.

American Society for Testing Materials Specifications:

8. E2-44T, "Tentative Methods of Preparation of Micrographs of Metals and Alloys", Paragraph 7(a), Method of Measurement of Grain Size for Material in Which the Grains Are Equiaxed.

INDEX OF AUTHORS

Volume XLI

Transactions of American Society for Metals

1949

A

Armstrong, W. M. 1145
Averbach, B. L. 1024, 1061

B

Beidler, E. I. 460
Binder, W. O. 1301
Bitsianes, Gust 985
Brayton, C. C. 961
Brophy, G. R. 1185
Brown, B. F. 519
Brown, C. M. 1301

C

Carapella, S. C., Jr. 947
Cohen, Morris 35, 1024, 1061
Coons, William C. 1415
Cromwell, Frances Jane..... 609

D

Daniels, F. W. 419
Darr, John H. 1261
DeVries, Gerrit 678
Dowdell, Ralph L. 985
Drake, H. L. 961
Dunn, C. G. 419
Duwez, Pol 194

E

Eckel, Earl J. 1204

F

Fetters, K. L. 303
Fine, Morris E. 985
Fontana, M. G. 480, 1213
Forward, F. A. 1145
Franks, Russell 1301

G

Geil, G. W. 609
Gilman, John J. 1371
Goldsmith, J. R. 565
Grant, Nicholas J. 95
Gregg, C. C. 293
Guarnieri, Glen 167
Guy, A. G. 125

H

Harrington, R. H. 443
Hawkes, M. F. 519
Haworth, R. D., Jr. 819
Helzel, M. M. 303
Huber, R. W. 1001

J

Jaffee, R. I. 460
Jordan, Charles B. 194
Julien, C. A. 1165

K

Klug, Harold P. 985
Koh, Pun Kien 1371
Kopelman, Bernard 293
Kristufek, F. C. 1113

L

Landgraf, F. K. 396
Lane, Joseph R. 95
Lement, B. S. 1061
Leslie, W. C. 1213
Light, J. O. 141
Litchfield, L. 961
Loria, E. A. 328, 375, 1248
Lundberg, C. O. 893

M

Mallett, Manley W. 870
McAdam, D. J., Jr. 609
Mehl, Robert F. 715
Meinhart, W. L. 565
Merchant, M. Eugene..... 647
Miller, A. J. 1185
Miller, James 167
Morris, J. P. 1425

N

Nagler, Charles A. 985

P

Paprocki, Stan J. 1204
Pennington, W. A. 213
Peretti, E. A. 947
Phebus, R. L. 259
Potter, E. V. 1001
Potter, R. K. 692

R

Ramsey, R. H. 460
Rickett, R. L. 1113
Rosenberg, Samuel J. 1261

S

Samans, C. H. 961
Sawyer, C. F. 365
Scott, D. A. 1145
Sheehan, J. P. 1165
Shephard, H. D. 328, 375
Simmons, A. L. 1440
Snyder, W. T. 1400
Sperotto, J. J. 940
Spretnak, J. W. 303, 365

T

Tarasov, L. P. 893
Troiano, A. R. 1093, 1165

W

Waisman, J. L. 1400
Wells, Cyril 715
Wilder, A. B. 141
Williams, A. J., Jr. 1425
Wishart, H. B. 692

Z

Zambrow, J. L. 480
Zapffe, C. A. 259, 396
Ziegler, N. A. 565
Zlatin, Norman 647
Zmeskal, Otto 1371

INDEX OF SUBJECTS AND AUTHORS OF PAPERS

VOLUME XLI

TRANSACTIONS OF AMERICAN SOCIETY FOR METALS

1949

A

Abrasion Resistance of Metals—*By R. D. Haworth, Jr.* 819
Aging in Gas Turbine-Type Alloys—*By Nicholas J. Grant and Joseph R. Lane* 95
Aircraft Alloys at Very Low Temperatures; Mechanical Properties, Including Fatigue—*By J. L. Zambrow and M. G. Fontana* 480
Alloy Steel Ingots; Distributions of Nonmetallic Inclusions in Some Killed —*By K. L. Fetters, M. M. Helzel and J. W. Spretnak* 303
Alloy Steels; Isothermal Transformation of Austenite in Two—*By E. A. Loria* 1248
Alloys in Powder Metallurgy; Application of the Theory of Diffusion to the Formation of—*By Pol Duwez and Charles B. Jordan* 194
Aluminum; Effect of Single Addition Metals on the Recrystallization, Electrical Conductivity and Rupture Strength of Pure—*By R. H. Harrington* 443
Annealing of Copper-Base Alloys; Time-Temperature Relationships in the —*By A. L. Simmons* 1440
Annual Address of the President 9
Annual Dinner of ASM 26
Annual Meeting of ASM 7
Annual Report of the Secretary 17
Annual Report of the Treasurer 13
Application of the Theory of Diffusion to the Formation of Alloys in Powder Metallurgy—*By Pol Duwez and Charles B. Jordan* 194
Austenite in Pure Iron-Nickel and Iron-Nickel-Molybdenum Alloys Containing 0.55% Carbon; Influence of Nickel and Molybdenum on Isothermal Transformation of—*By D. A. Scott, W. M. Armstrong and F. A. Forward* 1145
Austenite in Two Alloy Steels; Isothermal Transformation of—*By E. A. Loria* 1248
Austenite, Retained—*By Morris Cohen* 35
Austenitic Chromium-Nickel Steels of 0.03% Max. Carbon Content; Resistance to Sensitization of—*By W. O. Binder, C. M. Brown and Russell Franks* 1301
Austenitic Grain Size of Steel; Diffusion Method for Determining—*By Earl J. Eckel and Stan J. Paprocki* 1204
Austenitic Stainless Steel; Stabilization of—*By Samuel J. Rosenberg and John H. Darr* 1261

B

Basic Reasons for Good Machinability of "Free Machining" Steels—*By M. Eugene Merchant and Norman Zlatin*..... 647
Beta Laminations in Cartridge Brass—*By Ralph L. Dowdell, Charles A. Nagler, Morris E. Fine, Harold P. Klug and Gust Bitsianes* 985
Bismuth-Indium Phase Diagram—*By E. A. Peretti and S. C. Carapella, Jr.* 947
Brass (Cartridge); Beta Laminations in—*By Ralph L. Dowdell, Charles A. Nagler, Morris E. Fine, Harold P. Klug and Gust Bitsianes* 985

C

Campbell Memorial Lecture—23rd; Retained Austenite—*By Morris Cohen* 35
Carbon-Molybdenum Steels; Effect of Vanadium on the Properties of Cast Carbon and—*By N. A. Ziegler, W. L. Meinhart and J. R. Goldsmith* 565
Carbon Steel (Low); Microstructure of—*By R. L. Rickett and F. C. Kristufek* 1113
Cartridge Brass; Beta Laminations in—*By Ralph L. Dowdell, Charles A. Nagler, Morris E. Fine, Harold P. Klug and Gust Bitsianes* 985
Cast Carbon and Carbon-Molybdenum Steels; Effect of Vanadium on the Properties of—*By N. A. Ziegler, W. L. Meinhart and J. R. Goldsmith* 565
Cast Iron; Cause and Cure of Inverse Chill and Hard Spots in—*By C. A. Zapffe and R. L. Phebus* 259
Cast Steels; Microstructure and Mechanical Properties of—*By M. F. Hawkes and B. F. Brown* 519
Cause and Cure of Inverse Chill and Hard Spots in Cast Iron—*By C. A. Zapffe and R. L. Phebus* 259
Chromium-Nickel Steel; Influence of Low Temperatures on the Mechanical Properties of 18-8—*By D. J. McAdam, Jr., G. W. Geil and Frances Jane Cromwell* 609
Chromium-Nickel Steels of 0.03% Max. Carbon Content; Resistance to Sensitization of Austenitic—*By W. O. Binder, C. M. Brown and Russell Franks* 1301
Complex Tempering Cycles; Predicting the Effect of—*By J. L. Waisman and W. T. Snyder* 1400
Copper-Base Alloys; Time-Temperature Relationships in the Annealing of—*By A. L. Simmons* 1440
Copper (60) – 20 Nickel – 20 Manganese Alloy; Dilatometric Effects of Hardening and Recrystallization in the—*By C. H. Samans, C. C. Brayton, H. L. Drake and L. Litchfield* 961
Corrugated Diaphragms; Forming and Heat Treatment of—*By R. I. Jaffee, E. I. Beidler and R. H. Ramsey* 460
Cylinders (Hollow); Residual Stresses and Microstructure in—*By H. B. Wishart and R. K. Potter* 692

D

Decarburization of Steel with Mill Scale; Thermodynamics in the—*By W. A. Pennington* 213
Deep Hardening Steels; End-Quenched Bar for—*By Gerrit DeVries* 678
Delta Ferrite Formation and Its Influence on the Formation of Sigma in a Wrought Heat Resisting Steel—*By John J. Gilman, Pun Kien Koh and Otto Zmeskal* 1371
Density Variations in Some Killed Steel Ingots—*By C. F. Sawyer and J. W. Spretnak* 365
Detection and Nature of Grinding Burn in Steel—*By L. P. Tarasov and C. O. Lundberg* 893
Diaphragms; Forming and Heat Treatment of Corrugated—*By R. I. Jaffee, E. I. Beidler and R. H. Ramsey* 460
Diffusion Method for Determining the Austenitic Grain Size of Steel—*By Earl J. Eckel and Stan J. Paprocki* 1204
Diffusion Theory Application to the Formation of Alloys in Powder Metallurgy—*By Pol Duwez and Charles B. Jordan* 194
Dilatometric Effects of Hardening and Recrystallization in the 60 Copper – 20 Nickel – 20 Manganese Alloy—*By C. H. Samans, C. C. Brayton, H. L. Drake and L. Litchfield* 961
Dimensional Stability of Steel—Part IV—Tool Steels—*By B. S. Lement, B. L. Averbach and Morris Cohen* 1061
Distributions of Nonmetallic Inclusions in Some Killed Alloy Steel Ingots —*By K. L. Fetters, M. M. Helzel and J. W. Spretnak*..... 303

E

Effect of Orientation on Knoop Hardness of Single Crystals of Zinc and Silicon Ferrite—*By F. W. Daniels and C. G. Dunn* 419
Effect of Silicon on the Activity of Sulphur in Liquid Iron—*By J. P. Morris and A. J. Williams, Jr.* 1425
Effect of Single Addition Metals on the Recrystallization, Electrical Conductivity and Rupture Strength of Pure Aluminum—*By R. H. Harrington* 443
Effect of Vanadium on the Properties of Cast Carbon and Carbon-Molybdenum Steels—*By N. A. Ziegler, W. L. Meinhart and J. R. Goldsmith* 565
Election of Officers of ASM 24
Electrical Conductivity, Recrystallization, and Rupture Strength of Pure Aluminum; Effect of Single Addition Metals on the—*By R. H. Harrington* 443
Electrolytic Polishing Procedures for Molybdenum Metallographic Specimens—*By William C. Coons* 1415
End-Quenched Bar for Deep Hardening Steels—*By Gerrit DeVries* 678

F

Factors Affecting Subsurface Defects in Large Forging Steel Ingots—*By E. A. Loria and H. D. Shephard* 328
Fatigue of Aircraft Alloys at Very Low Temperatures—*By J. L. Zambrow and M. G. Fontana* 480
Forging Steel Ingots; Some Factors Affecting Subsurface Defects in Large—*By E. A. Loria and H. D. Shephard* 328
Forging Steels; Nature of Inclusions in Tensile Fractures of—*By H. D. Shephard and E. A. Loria* 375
Forming and Heat Treatment of Corrugated Diaphragms—*By R. I. Jaffee, E. I. Beidler and R. H. Ramsey* 460
Fractographic Examination of Tungsten—*By C. A. Zapffe and F. K. Landgraf* 396
Free Machining Steels; Basic Reasons for Good Machinability of—*By M. Eugene Merchant and Norman Zlatin* 647

G

Gas Turbine-Type Alloys; Aging in—*By Nicholas J. Grant and Joseph R. Lane* 95
Grain Size of Steel; Diffusion Method for Determining the Austenitic —*By Earl J. Eckel and Stan J. Paprocki* 1204
Grinding Burn in Steel; Nature and Detection of—*By L. P. Tarasov and C. O. Lundberg* 893

H

Hardening and Recrystallization in the 60 Copper–20 Nickel–20 Manganese Alloy; Dilatometric Effects of—*By C. H. Samans, C. C. Brayton, H. L. Drake and L. Litchfield* 961
Hard Spots in Cast Iron; Cause and Cure of Inverse Chill—*By C. A. Zapffe and R. L. Phebus* 259
Heat Resisting Steel; Delta Ferrite Formation and Its Influence on the Formation of Sigma in a Wrought—*By John J. Gilman, Pun Kien Koh and Otto Zmeskal* 1371
Heat Treated Wrought Steel Products; Transverse Mechanical Properties in—*By Cyril Wells and Robert F. Mehl* 715
Heat Treatment and Forming of Corrugated Diaphragms—*By R. I. Jaffee, E. I. Beidler and R. H. Ramsey* 460
Heat Treatment and Metallography of 8 to 10% Nickel Steel—*By G. R. Brophy and A. J. Miller* 1185

High Temperature Applications; Nickel-Base Alloys for—*A. G. Guy* 125
High Temperature Deformation Characteristics of Several Sheet Alloys; Short-Time—*By James Miller and Glen Guarnieri* 167
High Temperature, High Strength Alloys Containing Molybdenum; Mechanism of the Rapid Oxidation of—*By W. C. Leslie and M. G. Fontana* 1213
Hollow Cylinders; Residual Stresses and Microstructure in—*By H. B. Wishart and R. K. Potter* 692

I

Inclusions in Tensile Fractures of Forging Steels; Nature of—*By H. D. Shephard and E. A. Loria* 375
Indium-Bismuth Phase Diagram—*By E. A. Peretti and S. C. Carapella, Jr.* 947
Influence of Low Temperatures on the Mechanical Properties of 18-8 Chromium-Nickel Steel—*By D. J. McAdam, Jr., G. W. Geil and Frances Jane Cromwell* 609
Influence of Nickel and Molybdenum on Isothermal Transformation of Austenite in Pure Iron-Nickel and Iron-Nickel-Molybdenum Alloys Containing 0.55% Carbon—*By D. A. Scott, W. M. Armstrong and F. A. Forward* 1145
Ingots; Density Variations in Some Killed Steel—*By C. F. Sawyer and J. W. Spretnak* 365
Ingots; Distributions of Nonmetallic Inclusions in Some Killed Alloy Steel—*By K. L. Fetters, M. M. Helzel and J. W. Spretnak* 303
Ingots; Some Factors Affecting Subsurface Defects in Large Forging Steel—*By E. A. Loria and H. D. Shephard* 328
Inverse Chill and Hard Spots in Cast Iron; Cause and Cure of—*By C. A. Zapffe and R. L. Phebus* 259
Iron-Nickel (Pure) and Iron-Nickel-Molybdenum Alloys Containing 0.55% Carbon; Influence of Nickel and Molybdenum on Isothermal Transformation of Austenite in—*By D. A. Scott, W. M. Armstrong and F. A. Forward* 1145
Isothermal Decomposition of Martensite and Retained Austenite—*By B. L. Averbach and Morris Cohen* 1024
Isothermal Transformation of Austenite in Pure Iron-Nickel and Iron-Nickel-Molybdenum Alloys Containing 0.55% Carbon; Influence of Nickel and Molybdenum on—*By D. A. Scott, W. M. Armstrong and F. A. Forward* 1145
Isothermal Transformation of Austenite in Two Alloy Steels—*By E. A. Loria* 1248

K

Killed Alloy Steel Ingots; Distributions of Nonmetallic Inclusions in Some —*By K. L. Fetters, M. M. Helzel and J. W. Spretnak* 303
Killed Steel Ingots; Density Variations in Some—*By C. F. Sawyer and J. W. Spretnak* 365
Knoop Hardness of Single Crystals of Zinc and Silicon Ferrite; Effect of Orientation on—*By F. W. Daniels and C. G. Dunn* 419

L

Large Forging Steel Ingots; Some Factors Affecting Subsurface Defects in—*By E. A. Loria and H. D. Shephard* 328
Liquid Iron; Effect of Silicon on the Activity of Sulphur in—*By J. P. Morris and A. J. Williams, Jr.* 1425
Low Carbon Steel; Microstructure—*By R. L. Rickett and F. C. Kristufek* 1113
Low Temperature Influence on the Mechanical Properties of 18-8 Chromium-Nickel Steel—*By D. J. McAdam, Jr., G. W. Geil and Frances Jane Cromwell* 609

Low Temperatures; Mechanical Properties, Including Fatigue, of Aircraft Alloys—*By J. L. Zambrow and M. G. Fontana* 480

M

Machinability of "Free Machining" Steels; Basic Reasons for—*By M. Eugene Merchant and Norman Zlatin* 647
Manganese (20) – 60 Copper – 20 Nickel Alloy; Dilatometric Effects of Hardening and Recrystallization in the—*By C. H. Samans, C. C. Brayton, H. L. Drake and L. Litchfield* 961
Manganese-Zinc Phase Diagram from 0 to 50% Zinc—*By E. V. Potter and R. W. Huber* 1001
Martensite and Retained Austenite; Isothermal Decomposition of—*By B. L. Averbach and Morris Cohen* 1024
Mechanical Properties and Microstructure of Cast Steels—*By M. F. Hawkes and B. F. Brown* 519
Mechanical Properties of 18-8 Chromium-Nickel Steel; Influence of Low Temperatures on the—*By D. J. McAdam, Jr., G. W. Geil and Frances Jane Cromwell* 609
Mechanical Properties in Heat Treated Wrought Steel Products—*By Cyril Wells and Robert F. Mehl* 715
Mechanical Properties, Including Fatigue, of Aircraft Alloys at Very Low Temperatures—*By J. L. Zambrow and M. G. Fontana* 480
Mechanism of the Rapid Oxidation of High Temperature, High Strength Alloys Containing Molybdenum—*By W. C. Leslie and M. G. Fontana* 1213
Metallography and Heat Treatment of 8 to 10% Nickel Steel—*By G. R. Brophy and A. J. Miller* 1185
Metal Powders; Some Wetting Properties of—*By Bernard Kopelman and C. C. Gregg* 293
Microstructure and Mechanical Properties of Cast Steels—*By M. F. Hawkes and B. F. Brown* 519
Microstructure and Residual Stresses in Hollow Cylinders—*By H. B. Wishart and R. K. Potter* 692
Microstructure of Low Carbon Steel—*By R. L. Rickett and F. C. Kristufek* 1113
Mill Scale; Thermodynamics in the Decarburization of Steel with—*By W. A. Pennington* 213
Molybdenum and Nickel Influence on Isothermal Transformation of Austenite in Pure Iron-Nickel and Iron-Nickel-Molybdenum Alloys Containing 0.55% Carbon—*By D. A. Scott, W. M. Armstrong and F. A. Forward* 1145
Molybdenum; Mechanism of the Rapid Oxidation of High Temperature, High Strength Alloys Containing—*By W. C. Leslie and M. G. Fontana* 1213
Molybdenum Metallographic Specimens; Simple Electrolytic Polishing Procedures for—*By William C. Coons* 1415

N

Nature and Detection of Grinding Burn in Steel—*By L. P. Tarasov and C. O. Lundberg* 893
Nature of Inclusions in Tensile Fractures of Forging Steels—*By H. D. Shephard and E. A. Loria* 375
Nickel and Molybdenum Influence on Isothermal Transformation of Austenite in Pure Iron-Nickel and Iron-Nickel-Molybdenum Alloys Containing 0.55% Carbon—*By D. A. Scott, W. M. Armstrong and F. A. Forward* 1145
Nickel-Base Alloys for High Temperature Applications—*By A. G. Guy* 125
Nickel (20) – Copper – 20 Manganese Alloy; Dilatometric Effects of Hardening and Recrystallization in the—*By C. H. Samans, C. C. Brayton, H. L. Drake and L. Litchfield* 961
Nickel Steel (8 to 10%); Metallography and Heat Treatment of—*By G. R. Brophy and A. J. Miller* 1185

Nickel Steels; Transformation Characteristics of Ten Selected—*By J. P. Sheehan, C. A. Julien and A. R. Troiano* 1165
Nonmetallic Inclusions in Some Killed Alloy Steel Ingots; Distributions of—*By K. L. Fetters, M. M. Helzel and J. W. Spretnak* 303

O

Orientation Effect on Knoop Hardness of Single Crystals of Zinc and Silicon Ferrite—*By F. W. Daniels and C. G. Dunn* 419

P

Polishing Procedures for Molybdenum Metallographic Specimens; Simple Electrolytic—*By William C. Coons* 1415
Powder Metallurgy; Application of the Theory of Diffusion to the Formation of Alloys in—*By Pol Duwez and Charles B. Jordan* 194
Predicting the Effect of Complex Tempering Cycles—*By J. L. Waisman and W. T. Snyder* 1400
President's Annual Address 9
Pure Aluminum; Effect of Single Addition Metals on the Recrystallization, Electrical Conductivity and Rupture Strength of—*By R. H. Harrington* 443
Pure Iron-Nickel and Iron-Nickel-Molybdenum Alloys Containing 0.55% Carbon; Influence of Nickel and Molybdenum on Isothermal Transformation of Austenite in—*By D. A. Scott, W. M. Armstrong and F. A. Forward* 1145

R

Rapid Oxidation of High Temperature, High Strength Alloys Containing Molybdenum; Mechanism of the—*By W. C. Leslie and M. G. Fontana* 1213
Recrystallization, Electrical Conductivity and Rupture Strength of Pure Aluminum; Effect of Single Addition Metals on the—*By R. H. Harrington* 443
Recrystallization and Hardening in the 60 Copper–20 Nickel–20 Manganese Alloy; Dilatometric Effects of—*By C. H. Samans, C. C. Brayton, H. L. Drake and L. Litchfield* 961
Residual Stresses and Microstructure in Hollow Cylinders—*By H. B. Wishart and R. K. Potter* 692
Resistance to Sensitization of Austenitic Chromium-Nickel Steels of 0.03% Max. Carbon Content—*By W. O. Binder, C. M. Brown and Russell Franks* 1301
Retained Austenite—*By Morris Cohen* 35
Retained Austenite and Martensite; Isothermal Decomposition of—*By B. L. Averbach and Morris Cohen* 1024
Retention and Transformation of Austenite in SAE 5140, 2340 and T 1340 Steels of Comparable Hardenability—*By A. R. Troiano* 1093
Rupture Strength, Recrystallization and Electrical Conductivity of Pure Aluminum; Effect of Single Addition Metals on the—*By R. H. Harrington* 443

S

SAE 5140, 2340 and T 1340 Steels of Comparable Hardenability; Transformation and Retention of Austenite in—*By A. R. Troiano* 1093
Secretary's Annual Report 17
Sensitization of Austenitic Chromium-Nickel Steels of 0.03% Max. Carbon Content; Resistance to—*By W. O. Binder, C. M. Brown and Russell Franks* 1301
Sheet Alloys; Short-Time High Temperature Deformation Characteristics of Several—*By James Miller and Glen Guarnieri* 167

Short-Time High Temperature Deformation Characteristics of Several Sheet Alloys—*By James Miller and Glen Guarnieri*..... 167
Sigma in a Wrought Heat Resisting Steel; Delta Ferrite Formation and Its Influence on the Formation of—*By John J. Gilman, Pun Kien Koh and Otto Zmeskal* 1371
Silicon and Zinc Ferrite; Effect of Orientation on Knoop Hardness of Single Crystals of—*By E. W. Daniels and C. G. Dunn*..... 419
Silicon Effect on the Activity of Sulphur in Liquid Iron—*By J. P. Morris and A. J. Williams, Jr.* 1425
Simple Electrolytic Polishing Procedures for Molybdenum Metallographic Specimens—*By William C. Coons*..... 1415
Single Addition Metals on the Recrystallization, Electrical Conductivity and Rupture Strength of Pure Aluminum; Effect of—*By R. H. Harrington* 443
Solder Flow Tester for Tinplate—*By J. J. Sperotto*..... 940
Some Factors Affecting Subsurface Defects in Large Forging Steel Ingots—*By E. A. Loria and H. D. Shephard*..... 328
Some Wetting Properties of Metal Powders—*By Bernard Kopelman and C. C. Gregg* 293
Stability of Steels at Elevated Temperatures—*By A. B. Wilder and J. O. Light* 141
Stabilization of Austenitic Stainless Steel—*By Samuel J. Rosenberg and John H. Darr* 1261
Stainless Steel; Stabilization of Austenitic—*By Samuel J. Rosenberg and John H. Darr* 1261
Steel; Dimensional Stability of—Part IV—Tool Steels—*By B. S. Lement, B. L. Averbach and Morris Cohen*..... 1061
Steel Ingots; Density Variations in Some Killed—*By C. F. Sawyer and J. W. Spretnak* 365
Steel Ingots; Some Factors Affecting Subsurface Defects in Large Forging—*By E. A. Loria and H. D. Shephard*..... 328
Steels at Elevated Temperatures; Stability of—*By A. B. Wilder and J. O. Light* 141
Subsurface Defects in Large Forging Steel Ingots; Some Factors Affecting—*By E. A. Loria and H. D. Shephard*..... 328
Sulphur in Liquid Iron; Effect of Silicon on the Activity of—*By J. P. Morris and A. J. Williams, Jr.*..... 1425

T

T 1340, SAE 5140 and 2340 Steels of Comparable Hardenability; Transformation and Retention of Austenite in—*By A. R. Troiano*..... 1093
Technical Program and Reports of Officers, ASM—30th Annual Convention, Philadelphia, October 23 to 29, 1948..... 1
Tempering Cycles; Predicting the Effect of Complex—*By J. L. Waisman and W. T. Snyder*..... 1400
Tensile Fractures of Forging Steels; Nature of Inclusions in—*By H. D. Shephard and E. A. Loria*..... 375
Thermodynamics in the Decarburization of Steel with Mill Scale—*By W. A. Pennington* 213
Time-Temperature Relationships in the Annealing of Copper-Base Alloys —*By A. L. Simmons*..... 1440
Tinplate; Solder Flow Tester for—*By J. J. Sperotto*..... 940
Tool Steels—Part IV—Dimensional Stability of Steel—*By B. S. Lement, B. L. Averbach and Morris Cohen*..... 1061
Transformation and Retention of Austenite in SAE 5140, 2340 and T 1340 Steels of Comparable Hardenability—*By A. R. Troiano*..... 1093
Transformation Characteristics of Ten Selected Nickel Steels—*By J. P. Sheehan, C. A. Julien and A. R. Troiano*..... 1165
Transformation of Austenite in Two Alloy Steels; Isothermal—*By E. A. Loria* 1248

Transverse Mechanical Properties in Heat Treated Wrought Steel Products—*By Cyril Wells and Robert F. Mehl*..... 715
Treasurer's Annual Report 13
Tungsten; Fractographic Examination of—*By C. A. Zapffe and F. K. Landgraf* 396

V

Vacuum-Fusion Apparatus; Versatile—*By Manley W. Mallett*..... 870
Vanadium Effect on the Properties of Cast Carbon and Carbon-Molybdenum Steels—*By N. A. Ziegler, W. L. Meinhart and J. R. Goldsmith* 565
Versatile Vacuum-Fusion Apparatus—*By Manley W. Mallett*..... 870

W

Wetting Properties of Metal Powders—*By Bernard Kopelman and C. C. Gregg* 293
Wrought Heat Resisting Steel; Delta Ferrite Formation and Its Influence on the Formation of Sigma in a—*By John J. Gilman, Pun Kien Koh and Otto Zmeskal*..... 1371
Wrought Steel Products; Transverse Mechanical Properties in Heat Treated—*By Cyril Wells and Robert F. Mehl*..... 715

Z

Zinc and Silicon Ferrite; Effect of Orientation on Knoop Hardness of Single Crystals of—*By F. W. Daniels and C. G. Dunn*..... 419
Zinc-Manganese Phase Diagram from 0 to 50% Zinc—*By E. V. Potter and R. W. Huber*..... 1001